

2012

ANNUAL PROGRESS REPORT

DOE Hydrogen and Fuel Cells Program

U.S. Department of Energy
1000 Independence Avenue, S.W.
Washington, D.C. 20585-0121

FY 2012
PROGRESS REPORT FOR THE DOE
HYDROGEN AND FUEL CELLS PROGRAM

December 2012
DOE/GO-102012-3767

Approved by Sunita Satyapal, Director, Hydrogen and Fuel Cells Program

NOTICE

This report was prepared as an account of work sponsored by an agency of the United States government. Neither the United States government nor any agency thereof, nor any of their employees, makes any warranty, express or implied, or assumes any legal liability or responsibility for the accuracy, completeness, or usefulness of any information, apparatus, product, or process disclosed, or represents that its use would not infringe privately owned rights. Reference herein to any specific commercial product, process, or service by trade name, trademark, manufacturer, or otherwise does not necessarily constitute or imply its endorsement, recommendation, or favoring by the United States government or any agency thereof. The views and opinions of authors expressed herein do not necessarily state or reflect those of the United States government or any agency thereof.

Available electronically at <http://www.osti.gov/bridge>

Available for a processing fee to U.S. Department of Energy
and its contractors, in paper, from:

U.S. Department of Energy
Office of Scientific and Technical Information
P.O. Box 62
Oak Ridge, TN 37831-0062
Phone: (865) 576-8401
Fax: (865) 576-5728
E-mail: <mailto:reports@adonis.osti.gov>

Available for sale to the public, in paper, from:

U.S. Department of Commerce
National Technical Information Service
5285 Port Royal Road
Springfield, VA 22161
Phone: (800) 553-6847
Fax: (703) 605-6900
E-mail: orders@ntis.fedworld.gov
Online ordering: <http://www.ntis.gov/ordering.htm>



Printed on paper containing at least 50% wastepaper, including 20% postconsumer waste

Table of Contents

| | | |
|--------|---|-------|
| I. | Introduction | I-1 |
| II. | Hydrogen Production | II-1 |
| II.0 | Hydrogen Production Sub-Program Overview | II-3 |
| II.A | Distributed Biomass-Derived Liquids Production | II-11 |
| II.A.1 | Pacific Northwest National Laboratory: Biomass-Derived Liquids Distributed (Aqueous Phase) Reforming | II-11 |
| II.A.2 | National Renewable Energy Laboratory: Distributed Bio-Oil Reforming | II-15 |
| II.B | Biomass Gasification | II-19 |
| II.B.1 | Gas Technology Institute: One Step Biomass Gas Reforming-Shift Separation Membrane Reactor | II-19 |
| II.C | Separations | II-23 |
| II.C.1 | Media and Process Technology Inc.: Development of Hydrogen Selective Membranes/Modules as Reactors/Separators for Distributed Hydrogen Production | II-23 |
| II.C.2 | H2Pump, LLC: Process Intensification of Hydrogen Unit Operations Using an Electrochemical Device | II-28 |
| II.D | Electrolysis | II-31 |
| II.D.1 | Giner Electrochemical Systems, LLC: PEM Electrolyzer Incorporating an Advanced Low-Cost Membrane | II-31 |
| II.D.2 | Proton OnSite: High Performance, Low Cost Hydrogen Generation from Renewable Energy | II-35 |
| II.D.3 | National Renewable Energy Laboratory: Renewable Electrolysis Integrated Systems Development and Testing | II-39 |
| II.D.4 | National Renewable Energy Laboratory: Hour-by-Hour Cost Modeling of Optimized Central Wind-Based Water Electrolysis Production | II-43 |
| II.D.5 | Proton OnSite: Low-Cost Large-Scale PEM Electrolysis for Renewable Energy Storage | II-46 |
| II.E | Hi-Temp Thermochemical | II-49 |
| II.E.1 | Science Applications International Corporation: Solar High-Temperature Water Splitting Cycle with Quantum Boost | II-49 |
| II.E.2 | Argonne National Laboratory: Membrane/Electrolyzer Development in the Cu-Cl Thermochemical Cycle | II-56 |
| II.E.3 | Sandia National Laboratories: Solar Hydrogen Production with a Metal Oxide-Based Thermochemical Cycle | II-60 |
| II.E.4 | University of Colorado: Solar-Thermal ALD Ferrite-Based Water Splitting Cycle | II-64 |
| II.F | Photoelectrochemical | II-68 |
| II.F.1 | Stanford University: Directed Nano-Scale and Macro-Scale Architectures for Semiconductor Absorbers and Transparent Conducting Substrates for Photoelectrochemical Water Splitting | II-68 |
| II.F.2 | National Renewable Energy Laboratory: Semiconductor Materials for Photoelectrolysis | II-74 |
| II.F.3 | Lawrence Livermore National Laboratory: Characterization and Optimization of Photoelectrode Surfaces for Solar-to-Chemical Fuel Conversion | II-79 |
| II.F.4 | University of Nevada, Las Vegas: Characterization of Materials for Photoelectrochemical (PEC) Hydrogen Production | II-84 |
| II.F.5 | MVSystems, Incorporated: Photoelectrochemical Hydrogen Production | II-89 |
| II.F.6 | Midwest Optoelectronics, LLC: Critical Research for Cost-Effective Photoelectrochemical Production of Hydrogen | II-93 |
| II.F.7 | University of Texas at Arlington: Photoelectrochemical Materials: Theory and Modeling | II-98 |

Table of Contents

| | | |
|--------|---|--------|
| II. | Hydrogen Production (Continued) | |
| II.G | Biological | II-103 |
| II.G.1 | National Renewable Energy Laboratory: Biological Systems for Hydrogen Photoproduction | II-103 |
| II.G.2 | National Renewable Energy Laboratory: Fermentation and Electrohydrogenic Approaches to Hydrogen Production | II-108 |
| II.G.3 | J. Craig Venter Institute: Hydrogen from Water in a Novel Recombinant Oxygen-Tolerant Cyanobacterial System | II-113 |
| II.G.4 | University of California, Berkeley: Maximizing Light Utilization Efficiency and Hydrogen Production in Microalgal Cultures | II-118 |
| II-H | Production | II-122 |
| II.H.1 | Giner Electrochemical Systems, LLC: Unitized Design for Home Refueling Appliance for Hydrogen Generation to 5,000 psi | II-122 |
| II.H.2 | Proton Energy Systems: Hydrogen by Wire - Home Fueling System | II-126 |
| III. | Hydrogen Delivery | III-1 |
| III.0 | Hydrogen Delivery Sub-Program Overview | III-3 |
| III.1 | Sandia National Laboratories: Hydrogen Embrittlement of Structural Steels | III-9 |
| III.2 | Argonne National Laboratory: Hydrogen Delivery Infrastructure Analysis | III-13 |
| III.3 | Oak Ridge National Laboratory: Vessel Design and Fabrication Technology for Stationary High-Pressure Hydrogen Storage | III-17 |
| III.4 | Lawrence Livermore National Laboratory: Failure Analysis, Permeation, and Toughness of Glass Fiber Composite Pressure Vessels for Inexpensive Delivery of Cold Hydrogen | III-22 |
| III.5 | Savannah River National Laboratory: Fiber Reinforced Composite Pipeline | III-27 |
| III.6 | Lincoln Composites, Inc.: Development of High Pressure Hydrogen Storage Tank for Storage and Gaseous Truck Delivery | III-32 |
| III.7 | Concepts NREC: Development of a Centrifugal Hydrogen Pipeline Gas Compressor | III-35 |
| III.8 | Mohawk Innovative Technologies, Inc.: Oil-Free Centrifugal Hydrogen Compression Technology Demonstration | III-40 |
| III.9 | FuelCell Energy, Inc.: Electrochemical Hydrogen Compressor | III-44 |
| III.10 | Oak Ridge National Laboratory: Composite Technology for Hydrogen Pipelines | III-47 |
| III.11 | Lawrence Livermore National Laboratory: LLNL/Linde 875 bar Liquid Hydrogen Pump for High Density Cryogenic Vessel Refueling | III-51 |
| IV. | Hydrogen Storage | IV-1 |
| IV.0 | Hydrogen Storage Sub-Program Overview | IV-3 |
| IV.A | Metal Hydrides | |
| IV.A.1 | Northwestern University: Efficient Discovery of Novel Multicomponent Mixtures for Hydrogen Storage: A Combined Computational/Experimental Approach | IV-11 |
| IV.A.2 | University of Hawaii: Fundamental Studies of Advanced High-Capacity, Reversible Metal Hydrides | IV-18 |
| IV.A.3 | Ohio State University: Lightweight Metal Hydrides for Hydrogen Storage | IV-22 |
| IV.A.4 | University of Illinois at Urbana-Champaign: Reversible Hydrogen Storage Materials - Structure, Chemistry, and Electronic Structure | IV-27 |
| IV.A.5 | Brookhaven National Laboratory: Aluminum Hydride | IV-31 |
| IV.A.6 | Savannah River National Laboratory: Electrochemical Reversible Formation of Alane | IV-35 |
| IV.A.7 | Delaware State University: Hydrogen Storage Materials for Fuel Cell-Powered Vehicles | IV-39 |
| IV.B | Chemical Hydrogen Storage | IV-44 |
| IV.B.1 | University of Oregon: Hydrogen Storage by Novel CBN Heterocycle Materials | IV-44 |
| IV.B.2 | Los Alamos National Laboratory: Fluid Phase Chemical Hydrogen Storage Materials | IV-48 |
| IV.B.3 | University of Oregon: Novel Carbon(C)-Boron(B)-Nitrogen(N)-Containing H ₂ Storage Materials | IV-51 |

| | | |
|---------|---|--------|
| IV. | Hydrogen Storage (Continued) | |
| IV.B | Chemical Hydrogen Storage (Continued) | |
| IV.B.4 | Hawaii Hydrogen Carriers, LLC: Development of a Practical Hydrogen Storage System Based on Liquid Organic Hydrogen Carriers and a Homogeneous Catalyst | IV-55 |
| IV.C | Hydrogen Sorption | IV-60 |
| IV.C.1 | Texas A&M University: A Biomimetic Approach to Metal-Organic Frameworks with High H ₂ Uptake | IV-60 |
| IV.C.2 | University of California, Los Angeles: A Joint Theory and Experimental Project in the Synthesis and Testing of Porous COFs for Onboard Vehicular Hydrogen Storage | IV-67 |
| IV.C.3 | University of Missouri: Multiply Surface-Functionalized Nanoporous Carbon for Vehicular Hydrogen Storage | IV-72 |
| IV.C.4 | Northwestern University: New Carbon-Based Porous Materials with Increased Heats of Adsorption for Hydrogen Storage | IV-78 |
| IV.C.5 | Pennsylvania State University: Hydrogen Trapping through Designer Hydrogen Spillover Molecules with Reversible Temperature and Pressure-Induced Switching | IV-82 |
| IV.C.6 | National Renewable Energy Laboratory: Weak Chemisorption Validation | IV-89 |
| IV.C.7 | HRL Laboratories, LLC: Room Temperature Hydrogen Storage in Nano-Confined Liquids | IV-95 |
| IV.C.8 | Lawrence Berkeley National Laboratory: Hydrogen Storage in Metal-Organic Frameworks | IV-97 |
| IV.C.9 | Oak Ridge National Laboratory: The Quantum Effects of Pore Structure on Hydrogen Adsorption | IV-100 |
| IV.C.10 | Northwestern University: Metal- and Cluster-Modified Ultrahigh-Area Materials for the Ambient Temperature Storage of Molecular Hydrogen | IV-105 |
| IV.C.11 | National Renewable Energy Laboratory: Hydrogen Sorbent Measurement Qualification and Characterization | IV-109 |
| IV.D | H ₂ Storage Engineering Center of Excellence | IV-114 |
| IV.D.1 | Savannah River National Laboratory: Hydrogen Storage Engineering Center of Excellence | IV-114 |
| IV.D.2 | National Renewable Energy Laboratory: System Design, Analysis, Modeling, and Media Engineering Properties for Hydrogen Energy Storage | IV-119 |
| IV.D.3 | Los Alamos National Laboratory: Chemical Hydride Rate Modeling, Validation, and System Demonstration | IV-126 |
| IV.D.4 | Jet Propulsion Laboratory: Key Technologies, Thermal Management, and Prototype Testing for Advanced Solid-State Hydrogen Storage Systems | IV-129 |
| IV.D.5 | Pacific Northwest National Laboratory: Systems Engineering of Chemical Hydride, Pressure Vessel, and Balance of Plant for Onboard Hydrogen Storage | IV-134 |
| IV.D.6 | United Technologies Research Center: Advancement of Systems Designs and Key Engineering Technologies for Materials-Based Hydrogen Storage | IV-140 |
| IV.D.7 | General Motors Company: Thermal Management of Onboard Cryogenic Hydrogen Storage Systems | IV-147 |
| IV.D.8 | Ford Motor Company: Ford/BASF SE/UM Activities in Support of the Hydrogen Storage Engineering Center of Excellence | IV-151 |
| IV.D.9 | Oregon State University: Microscale Enhancement of Heat and Mass Transfer for Hydrogen Energy Storage | IV-156 |
| IV.D.10 | Lincoln Composites, Inc.: Development of Improved Composite Pressure Vessels for Hydrogen Storage | IV-160 |
| IV.E | Storage Testing, Safety and Analysis | IV-164 |
| IV.E.1 | Argonne National Laboratory: System Level Analysis of Hydrogen Storage Options | IV-164 |
| IV.E.2 | H ₂ Technology Consulting LLC: Best Practices for Characterizing Engineering Properties of Hydrogen Storage Materials | IV-170 |
| IV.E.3 | National Institute of Standards and Technology: Neutron Characterization in Support of the DOE Hydrogen Storage Sub-Program | IV-176 |

| | | |
|---------|--|--------|
| IV. | Hydrogen Storage (Continued) | |
| IV.E | Storage Testing, Safety and Analysis (Continued) | |
| IV.E.4 | Strategic Analysis, Inc.: Hydrogen Storage Cost Analysis, Preliminary Results | IV-182 |
| IV.E.5 | Pacific Northwest National Laboratory: Early Market TRL/MRL Analysis | IV-186 |
| IV.F | Tanks | IV-191 |
| IV.F.1 | Oak Ridge National Laboratory: High Strength Carbon Fibers | IV-191 |
| IV.F.2 | Oak Ridge National Laboratory: Lifecycle Verification of Polymeric Storage Tank Liners | IV-197 |
| IV.F.3 | Oak Ridge National Laboratory: Development of Low-Cost, High Strength Commercial Textile Precursor (PAN-MA) | IV-200 |
| IV.F.4 | Pacific Northwest National Laboratory: Synergistically Enhanced Materials and Design Parameters for Reducing the Cost of Hydrogen Storage Tanks | IV-205 |
| IV.G | Cross-Cutting | IV-208 |
| IV.G.1 | University of Nevada, Las Vegas: HGMS: Glasses and Nanocomposites for Hydrogen Storage | IV-208 |
| IV.H | Basic Energy Sciences | IV-210 |
| IV.H.1 | University of Pennsylvania: From Fundamental Understanding to Predicting New Nanomaterials for High-Capacity Hydrogen Storage | IV-210 |
| IV.H.2 | University of Texas at Dallas: Novel theoretical and experimental approaches for understanding and optimizing hydrogen-sorbent interactions in metal organic framework materials | IV-213 |
| IV.H.3 | Virginia Commonwealth University: Design and Synthesis of Chemically and Electronically Tunable Nanoporous Organic Polymers for Use in Hydrogen Storage Applications | IV-216 |
| IV.H.4 | Oak Ridge National Laboratory: Atomistic Mechanisms of Metal-Assisted Hydrogen Storage in Nanostructured Carbons | IV-220 |
| IV.H.5 | Savannah River National Laboratory: Elucidation of Hydrogen Interaction Mechanisms with Metal-Doped Carbon Nanostructures | IV-226 |
| IV.H.6 | University of California, Riverside: Synthetic Design of New Metal-Organic Framework Materials for Hydrogen Storage | IV-229 |
| IV.H.7 | University of Missouri: New Pathways and Metrics for Enhanced, Reversible Hydrogen Storage in Boron-Doped Carbon Nanospaces | IV-233 |
| IV.H.8 | Carnegie Institute of Washington: Novel Molecular Materials for Hydrogen Storage Applications | IV-236 |
| IV.H.9 | Colorado School of Mines: Energy Storage in Clathrate Hydrogen Material | IV-239 |
| IV.H.10 | Pennsylvania State University: Exploration of Novel Carbon-Hydrogen Interactions | IV-243 |
| IV.H.11 | Ames Laboratory: Complex Hydrides - A New Frontier for Future Energy Applications | IV-245 |
| IV.H.12 | Brookhaven National Laboratory: Atomistic Transport Mechanisms in Aluminum-Based Hydrides | IV-249 |
| IV.H.13 | Northwestern University: Theory of Hydrogen Storage in Complex Hydrides | IV-253 |
| IV.H.14 | University of California, Santa Barbara: Computational studies of hydrogen interactions with storage materials | IV-256 |
| IV.H.15 | Washington University: In Situ NMR Studies of Hydrogen Storage Systems | IV-259 |
| IV.H.16 | Pacific Northwest National Laboratory: Activation of Hydrogen with Bi-Functional Ambiphilic Catalyst Complexes | IV-263 |
| IV.H.17 | University of California, Davis: Heavy Cycloadditions: Reactions of Diagailene with Cyclic Polyolefins | IV-267 |
| IV.H.18 | University of Pennsylvania: Mechanistic Studies of Activated Hydrogen Release from Ammonia-Borane | IV-270 |
| IV.H.19 | Florida International University: Influence of Pressure on Physical Property of Ammonia Borane and its Re-Hydrogenation | IV-274 |

| | | |
|--------|---|-------|
| V. | Fuel Cells | V-1 |
| V.0 | Fuel Cells Sub-Program Overview | V-3 |
| V.A | Analysis/Characterization | V-11 |
| V.A.1 | National Renewable Energy Laboratory: Analysis of Laboratory Fuel Cell Technology Status – Voltage Degradation | V-11 |
| V.A.2 | Strategic Analysis, Inc.: Mass-Production Cost Estimation for Automotive Fuel Cell Systems | V-16 |
| V.A.3 | Strategic Analysis, Inc.: Stationary Fuel Cell System Cost Analysis | V-20 |
| V.A.4 | Argonne National Laboratory: Performance of Automotive Fuel Cell Systems with Low-Pt Nanostructured Thin Film Catalysts at High Power Densities | V-25 |
| V.A.5 | Oak Ridge National Laboratory: Characterization of Fuel Cell Materials | V-32 |
| V.A.6 | National Institute of Standards and Technology: Neutron Imaging Study of the Water Transport in Operating Fuel Cells | V-37 |
| V.A.7 | Los Alamos National Laboratory: Technical Assistance to Developers | V-43 |
| V.A.8 | National Renewable Energy Laboratory: Enlarging the Potential Market for Stationary Fuel Cells Through System Design Optimization | V-47 |
| V.A.9 | Battelle: Stationary and Emerging Market Fuel Cell System Cost Analysis | V-51 |
| V.A.10 | Lawrence Berkeley National Laboratory: A Total Cost of Ownership Model for Design and Manufacturing Optimization of Fuel Cells in Stationary and Emerging Market Applications | V-53 |
| V.B | Impurities | V-57 |
| V.B.1 | National Renewable Energy Laboratory: Effect of System Contaminants on PEMFC Performance and Durability | V-57 |
| V.B.2 | Hawaii Natural Energy Institute: The Effect of Airborne Contaminants on Fuel Cell Performance and Durability | V-63 |
| V.C | Membranes | V-68 |
| V.C.1 | University of Central Florida: Lead Research and Development Activity for DOE’s High Temperature, Low Relative Humidity Membrane Program | V-68 |
| V.C.2 | Giner Electrochemical Systems, LLC: Dimensionally Stable High Performance Membrane (SBIR Phase III) | V-71 |
| V.C.3 | FuelCell Energy, Inc.: High-Temperature Membrane with Humidification-Independent Cluster Structure | V-76 |
| V.C.4 | Ion Power Inc.: Corrugated Membrane Fuel Cell Structures | V-80 |
| V.D | Catalysts | V-84 |
| V.D.1 | 3M Company: Advanced Cathode Catalysts and Supports for PEM Fuel Cells | V-84 |
| V.D.2 | UTC Power: Highly Dispersed Alloy Catalyst for Durability | V-95 |
| V.D.3 | 3M Company: Durable Catalysts for Fuel Cell Protection during Transient Conditions | V-100 |
| V.D.4 | National Renewable Energy Laboratory: Extended, Continuous Pt Nanostructures in Thick, Dispersed Electrodes | V-107 |
| V.D.5 | Argonne National Laboratory: Nanosegregated Cathode Catalysts with Ultra-Low Platinum Loading | V-111 |
| V.D.6 | Brookhaven National Laboratory: Contiguous Platinum Monolayer Oxygen Reduction Electrocatalysts on High-Stability Low-Cost Supports | V-117 |
| V.D.7 | Los Alamos National Laboratory: The Science and Engineering of Durable Ultralow PGM Catalysts | V-121 |
| V.D.8 | Lawrence Berkeley National Laboratory: Molecular-Scale, Three-Dimensional Non-Platinum Group Metal Electrodes for Catalysis of Fuel Cell Reactions | V-126 |
| V.D.9 | National Renewable Energy Laboratory: Tungsten Oxide and Heteropoly Acid Based System for Ultra-High Activity and Stability of Pt Catalysts in PEM Fuel Cell Cathodes | V-133 |
| V.D.10 | Illinois Institute of Technology: Synthesis and Characterization of Mixed-Conducting Corrosion Resistant Oxide Supports | V-138 |

| | | |
|--------|--|-------|
| V. | Fuel Cells (Continued) | |
| V.D | Catalysts (Continued) | |
| V.D.11 | Northeastern University: Development of Novel Non-PGM Electrocatalysts for Proton Exchange Membrane Fuel Cell Applications | V-143 |
| V.D.12 | General Motors Company: High-Activity Dealloyed Catalysts | V-149 |
| V.D.13 | University of South Carolina: Development of Ultra-Low Platinum Alloy Cathode Catalyst for PEM Fuel Cells | V-153 |
| V.D.14 | National Renewable Energy Laboratory: High Aspect Ratio Nano-Structured Pt-based PEM Fuel Cell Catalysts (EERE Post-Doc Fellowship). | V-159 |
| V.D.15 | Pacific Northwest National Laboratory: Development of Alternative and Durable High Performance Cathode Supports for PEM Fuel Cells | V-162 |
| V.E | Degradation Studies | V-168 |
| V.E.1 | Argonne National Laboratory: Polymer Electrolyte Fuel Cell Lifetime Limitations: The Role of Electrocatalyst Degradation | V-168 |
| V.E.2 | Los Alamos National Laboratory: Durability Improvements through Degradation Mechanism Studies. | V-175 |
| V.E.3 | Nuvera Fuel Cells, Inc.: Durability of Low Platinum Fuel Cells Operating at High Power Density | V-182 |
| V.E.4 | UTC Power: Improved Accelerated Stress Tests Based on Fuel Cell Vehicle Data | V-186 |
| V.E.5 | Los Alamos National Laboratory: Accelerated Testing Validation | V-190 |
| V.E.6 | Ballard Power Systems: Development of Micro-Structural Mitigation Strategies for PEM Fuel Cells: Morphological Simulations and Experimental Approaches | V-195 |
| V.E.7 | E. I. du Pont de Nemours and Company: Analysis of Durability of MEAs in Automotive PEMFC Applications | V-201 |
| V.F | Transport Studies | V-206 |
| V.F.1 | Plug Power Inc.: Air-Cooled Stack Freeze Tolerance | V-206 |
| V.F.2 | Lawrence Berkeley National Laboratory: Fuel Cell Fundamentals at Low and Subzero Temperatures | V-211 |
| V.F.3 | Sandia National Laboratories: Development and Validation of a Two-Phase, Three-Dimensional Model for PEM Fuel Cells | V-217 |
| V.F.4 | Nuvera Fuel Cells, Inc.: Transport Studies Enabling Efficiency Optimization of Cost-Competitive Fuel Cell Stacks | V-222 |
| V.F.5 | CFD Research Corporation: Water Transport in PEM Fuel Cells: Advanced Modeling, Material Selection, Testing, and Design Optimization | V-226 |
| V.F.6 | Giner Electrochemical Systems, LLC: Transport in PEMFC Stacks | V-230 |
| V.F.7 | General Motors Company: Investigation of Micro- and Macro-Scale Transport Processes for Improved Fuel Cell Performance | V-235 |
| V.G | Portable Power | V-242 |
| V.G.1 | Arkema Inc.: Novel Materials for High Efficiency Direct Methanol Fuel Cells | V-242 |
| V.G.2 | University of North Florida: New MEA Materials for Improved Direct Methanol Fuel Cell (DMFC) Performance, Durability, and Cost | V-246 |
| V.G.3 | Los Alamos National Laboratory: Advanced Materials and Concepts for Portable Power Fuel Cells | V-250 |
| V.H | Hardware | V-257 |
| V.H.1 | TreadStone Technologies, Inc.: Low-Cost PEM Fuel Cell Metal Bipolar Plates | V-257 |
| V.I | Balance of Plant | V-261 |
| V.I.1 | W.L. Gore & Associates, Inc.: Materials and Modules for Low-Cost, High-Performance Fuel Cell Humidifiers | V-261 |
| V.I.2 | Dynalene Inc.: Large Scale Testing, Demonstration and Commercialization of the Nanoparticle-Based Fuel Cell Coolant (SBIR Phase III). | V-266 |

| | | |
|-------|--|--------|
| V. | Fuel Cells (Continued) | |
| V.I | Balance of Plant (Continued) | |
| V.I.3 | Tetramer Technologies, LLC: New High Performance Water Vapor Membranes to Improve Fuel Cell Balance of Plant Efficiency and Lower Costs (SBIR Phase I) | V-270 |
| V.J | Distributed Energy | V-272 |
| V.J.1 | Intelligent Energy: Development and Demonstration of a New-Generation High Efficiency 10-kW Stationary Fuel Cell System | V-272 |
| V.J.2 | Acumentrics Corporation: Development of a Low-Cost 3-10 kW Tubular SOFC Power System | V-277 |
| V.J.3 | Versa Power Systems: Advanced Materials for Reversible Solid Oxide Fuel Cell (RSOFC), Dual-Mode Operation with Low Degradation | V-281 |
| V.J.4 | InnovaTek: Power Generation from an Integrated Biomass Reformer and Solid Oxide Fuel Cell (SBIR Phase III) | V-285 |
| V.J.5 | IdaTech, LLC: Research and Development for Off-Road Fuel Cell Applications | V-289 |
| V.J.6 | UTC Power: 150 kW PEM Stationary Power Plant Operating on Natural Gas | V-291 |
| V.K | Cross-Cutting | V-295 |
| V.K.1 | University of Akron: Development of Kilowatt-Scale Coal Fuel Cell Technology | V-295 |
| V.K.2 | University of Southern Mississippi: Alternative Fuel Cell Membranes for Energy Independence | V-300 |
| V.K.3 | Colorado School of Mines: Biomass Fuel Cell Systems | V-305 |
| V.K.4 | University of Connecticut Global Fuel Cell Center: Improving Reliability and Durability of Efficient and Clean Energy Systems | V-310 |
| VI. | Manufacturing R&D | VI-1 |
| VI.0 | Manufacturing R&D Sub-Program Overview | VI-3 |
| VI.1 | National Renewable Energy Laboratory: Fuel Cell Membrane Electrode Assembly Manufacturing R&D | VI-7 |
| VI.2 | W. L. Gore & Associates, Inc.: Manufacturing of Low-Cost, Durable Membrane Electrode Assemblies Engineered for Rapid Conditioning | VI-11 |
| VI.3 | Rensselaer Polytechnic Institute: Adaptive Process Controls and Ultrasonics for High-Temperature PEM MEA Manufacture | VI-17 |
| VI.4 | National Institute of Standards and Technology: Non-Contact Sensor Evaluation for Bipolar Plate Manufacturing Process Control and Smart Assembly of Fuel Cell Stacks | VI-24 |
| VI.5 | BASF Fuel Cell: High Speed, Low Cost Fabrication of Gas Diffusion Electrodes for Membrane Electrode Assemblies | VI-28 |
| VI.6 | Quantum Fuel Systems Technologies Worldwide, Inc.: Development of Advanced Manufacturing Technologies for Low Cost Hydrogen Storage Vessels | VI-31 |
| VI.7 | National Institute of Standards and Technology: Cause and Effect: Flow Field Plate Manufacturing Variability and its Impact on Performance | VI-36 |
| VI.8 | National Institute of Standards and Technology: Optical Scatterfield Metrology for Online Catalyst Coating Inspection of PEM (Fuel Cell) Soft Goods | VI-41 |
| VII. | Technology Validation | VII-1 |
| VII.0 | Technology Validation Sub-Program Overview | VII-3 |
| VII.1 | National Renewable Energy Laboratory: Controlled Hydrogen Fleet and Infrastructure Analysis | VII-11 |
| VII.2 | Air Products and Chemicals, Inc.: Validation of an Integrated Hydrogen Energy Station | VII-18 |
| VII.3 | National Renewable Energy Laboratory: Technology Validation: Fuel Cell Bus Evaluations | VII-22 |
| VII.4 | Air Products and Chemicals, Inc.: California Hydrogen Infrastructure Project | VII-26 |
| VII.5 | Hawaii Natural Energy Institute: Hawaii Hydrogen Power Park | VII-30 |
| VII.6 | University of Central Florida: Florida Hydrogen Initiative (FHI) | VII-33 |

Table of Contents

| | | |
|---------|--|---------|
| VII. | Technology Validation (Continued) | |
| VII.7 | California State University, Los Angeles: Sustainable Hydrogen Fueling Station, California State University, Los Angeles | VII-38 |
| VII.8 | National Renewable Energy Laboratory: Renewable Electrolysis Integrated System Development and Testing | VII-40 |
| VII.9 | National Renewable Energy Laboratory: Stationary Fuel Cell Evaluation | VII-44 |
| VII.10 | National Renewable Energy Laboratory: Next Generation H2 Station Analysis | VII-46 |
| VIII. | Safety, Codes & Standards | VIII-1 |
| VIII.0 | Safety, Codes & Standards Sub-Program Overview | VIII-3 |
| VIII.1 | Sandia National Laboratories: Hydrogen Safety, Codes and Standards R&D – Release Behavior | VIII-9 |
| VIII.2 | Sandia National Laboratories: Risk-Informed Safety Requirements for H2 Codes and Standards Development | VIII-15 |
| VIII.3 | National Renewable Energy Laboratory: Component Standard Research and Development | VIII-18 |
| VIII.4 | Sandia National Laboratories: Hydrogen Materials and Components Compatibility | VIII-22 |
| VIII.5 | Sandia National Laboratories: Component Testing for Industrial Trucks and Early Market Applications | VIII-25 |
| VIII.6 | National Renewable Energy Laboratory: National Codes and Standards Coordination | VIII-28 |
| VIII.7 | National Renewable Energy Laboratory: Codes and Standards Outreach for Emerging Fuel Cell Technologies | VIII-33 |
| VIII.8 | Los Alamos National Laboratory: Leak Detection and H2 Sensor Development for Hydrogen Applications | VIII-36 |
| VIII.9 | Los Alamos National Laboratory: Hydrogen Fuel Quality Research and Development | VIII-42 |
| VIII.10 | Pacific Northwest National Laboratory: Hydrogen Safety Panel | VIII-45 |
| VIII.11 | Pacific Northwest National Laboratory: Hydrogen Safety Knowledge Tools | VIII-49 |
| VIII.12 | Pacific Northwest National Laboratory: Hydrogen Emergency Response Training for First Responders | VIII-52 |
| IX. | Education | IX-1 |
| IX.0 | Education Sub-Program Overview | IX-3 |
| IX.1 | South Carolina Hydrogen and Fuel Cell Alliance: Development of Hydrogen Education Programs for Government Officials | IX-7 |
| IX.2 | Ohio Fuel Cell Coalition: Raising H2 and Fuel Cell Awareness in Ohio | IX-11 |
| IX.3 | University of California, Berkeley: Hydrogen Technology and Energy Curriculum (HyTEC) | IX-13 |
| IX.4 | Connecticut Center for Advanced Technology, Inc.: State and Local Government Partnership | IX-16 |
| X. | Market Transformation | X-1 |
| X.0 | Market Transformation Sub-Program Overview | X-3 |
| X.1 | Hawaii Natural Energy Institute: Hydrogen Energy Systems as a Grid Management Tool | X-7 |
| X.2 | Pacific Northwest National Laboratory: Fuel Cell Combined Heat and Power Industrial Demonstration | X-10 |
| X.3 | National Renewable Energy Laboratory: Direct Methanol Fuel Cell Material Handling Equipment Demonstration | X-15 |
| X.4 | South Carolina Hydrogen and Fuel Cell Alliance: Landfill Gas-to-Hydrogen | X-20 |
| XI. | Systems Analysis | XI-1 |
| XI.0 | Systems Analysis Sub-Program Overview | XI-3 |
| XI.1 | National Renewable Energy Laboratory: Infrastructure Analysis of Early Market Transition of Fuel Cell Vehicles | XI-11 |
| XI.2 | Argonne National Laboratory: Life-Cycle Analysis of Vehicle and Fuel Systems with the GREET Model | XI-15 |

| | | |
|--------|--|---------|
| XI. | Systems Analysis (Continued) | |
| XI.3 | National Renewable Energy Laboratory: Hydrogen Refueling Infrastructure Cost Analysis | XI-19 |
| XI.4 | National Renewable Energy Laboratory: Comparing Infrastructure Costs for Hydrogen and Electricity | XI-23 |
| XI.5 | National Renewable Energy Laboratory: Infrastructure Costs Associated with Central Hydrogen Production from Biomass and Coal | XI-27 |
| XI.6 | Oak Ridge National Laboratory: Sensitivity Analysis of H ₂ -Vehicles' Market Prospects, Costs and Benefits | XI-31 |
| XI.7 | National Renewable Energy Laboratory: Effects of Technology Cost Parameters on Hydrogen Pathway Succession | XI-35 |
| XI.8 | Oak Ridge National Laboratory: Impact of DOE Program Goals on Hydrogen Vehicles: Market Prospect, Costs, and Benefits | XI-39 |
| XI.9 | National Renewable Energy Laboratory: Resource Analysis for Hydrogen Production | XI-43 |
| XI.10 | National Renewable Energy Laboratory: Cost, Energy Use, and Emissions of Tri-Generation Systems | XI-47 |
| XI.11 | Argonne National Laboratory: Employment Impacts of Early Markets for Hydrogen and Fuel Cell Technologies | XI-52 |
| XII. | American Recovery and Reinvestment Act | XII-1 |
| XII.0 | American Recovery and Reinvestment Act Activities | XII-3 |
| XII.1 | Delphi Automotive Systems, LLC: Solid Oxide Fuel Cell Diesel Auxiliary Power Unit Demonstration | XII-9 |
| XII.2 | Sprint Nextel: Demonstrating Economic and Operational Viability of 72-Hour Hydrogen PEM Fuel Cell Systems to Support Emergency Communications on the Sprint Nextel Network | XII-12 |
| XII.3 | National Renewable Energy Laboratory: Analysis Results for ARRA Projects: Enabling Fuel Cell Market Transformation | XII-16 |
| XII.4 | FedEx Freight: Fuel Cell-Powered Lift Truck FedEx Freight Fleet Deployment | XII-21 |
| XII.5 | Sysco of Houston: Fuel Cell-Powered Lift Truck Sysco Houston Fleet Deployment | XII-24 |
| XII.6 | GENCO Infrastructure Solutions: GENCO Fuel Cell-Powered Lift Truck Fleet Deployment | XII-28 |
| XII.7 | Plug Power Inc.: Highly Efficient, 5-kW CHP Fuel Cells Demonstrating Durability and Economic Value in Residential and Light Commercial Applications | XII-30 |
| XII.8 | Plug Power Inc.: Accelerating Acceptance of Fuel Cell Backup Power Systems | XII-34 |
| XIII. | Small Business Innovation Research | XIII-1 |
| XIV. | Acronyms, Abbreviations and Definitions: | XIV-1 |
| XV. | Primary Contacts Index | XV-1 |
| XVI. | Hydrogen and Fuel Cells Program Contacts | XVI-1 |
| XVII. | Project Listings by State | XVII-1 |
| XVIII. | Project Listings by Organization: | XVIII-1 |

I. INTRODUCTION

I.0 Introduction

The Department of Energy's Hydrogen and Fuel Cells Program (the Program) conducts comprehensive efforts across a range of technical and non-technical areas to enable the widespread commercialization of hydrogen and fuel cell technologies in diverse sectors of the economy. The Program is coordinated across the Department of Energy (DOE or the Department), incorporating activities in the offices of Energy Efficiency and Renewable Energy (EERE), Science (SC), Nuclear Energy, and Fossil Energy (FE), and it is aligned with DOE's strategic vision and goals. The Program's efforts will help boost the competitiveness of U.S. manufacturing, reduce our dependence on foreign oil, and create jobs for American workers.

With emphasis on applications that will most effectively strengthen our nation's energy security and improve our stewardship of the environment, the Program engages in research, development, and demonstration (RD&D) of critical improvements in hydrogen and fuel cell technologies, as well as diverse activities to overcome economic and institutional obstacles to commercialization. The Program addresses the full range of challenges facing the development and deployment of the technologies by integrating basic and applied research, technology development and demonstration, and other supporting activities.

In Fiscal Year (FY) 2012, Congress appropriated approximately \$136 million for the DOE Hydrogen and Fuel Cells Program.¹ The Program is organized into distinct sub-programs focused on specific areas of RD&D, as well as other activities to address non-technical challenges. More detailed discussions of Program activities and plans can be found in the *Hydrogen and Fuel Cells Program Plan*, as well as in the plans of the program offices—EERE's *Fuel Cell Technologies Program Multi-Year RD&D Plan*; FE's *Hydrogen from Coal RD&D Plan*; and SC's *Basic Research Needs for the Hydrogen Economy*. All of these documents are available at www.hydrogen.energy.gov/roadmaps_vision.html.

In the past year, the Program made substantial progress toward its goals and objectives. Highlights of the Program's accomplishments are summarized below. More detail can be found in the sub-program chapters of this report.

PROGRESS AND ACCOMPLISHMENTS, BY SUB-PROGRAM

Fuel Cells

The Fuel Cells sub-program continued to reduce the projected high-volume manufacturing cost of automotive fuel cells, which in 2012 was estimated to be \$47/kW. This represents a reduction of 36% since 2008 and more than 80% since 2002. The 36% reduction since 2008 stems in part from a reduction in platinum group metal (PGM) loading and an increase in cell power density, allowing the design of smaller and less expensive stacks. Newly developed de-alloyed PtNi and PtCo catalysts exceeded the 2017 mass activity target of 0.44 A/mg_{PGM} with 0.46 A/mg_{PGM} for PtCo and 0.52 A/mg_{PGM} for PtNi. The PtCo catalyst also meets durability targets and the PtNi catalyst has demonstrated high-performance operation in MEAs.

Modified catalysts with highly active and durable oxygen evolution met all performance milestones in 2012. By enhancing oxygen evolution capability, these catalysts suppress excursions to high voltage, and thus mitigate corrosion that would occur during startup, shutdown, and fuel starvation conditions. Additionally, a humidifier containing a novel composite membrane and including an integrated module design is projected to meet the cost target of \$100 (for a humidifier in an automotive fuel cell system) when manufactured at high volumes.

¹This includes \$101 million for the Fuel Cell Technologies Program within the Office of Energy Efficiency and Renewable Energy and \$35 million for hydrogen and fuel cell-related research in the Basic Energy Sciences program within the Office of Science.

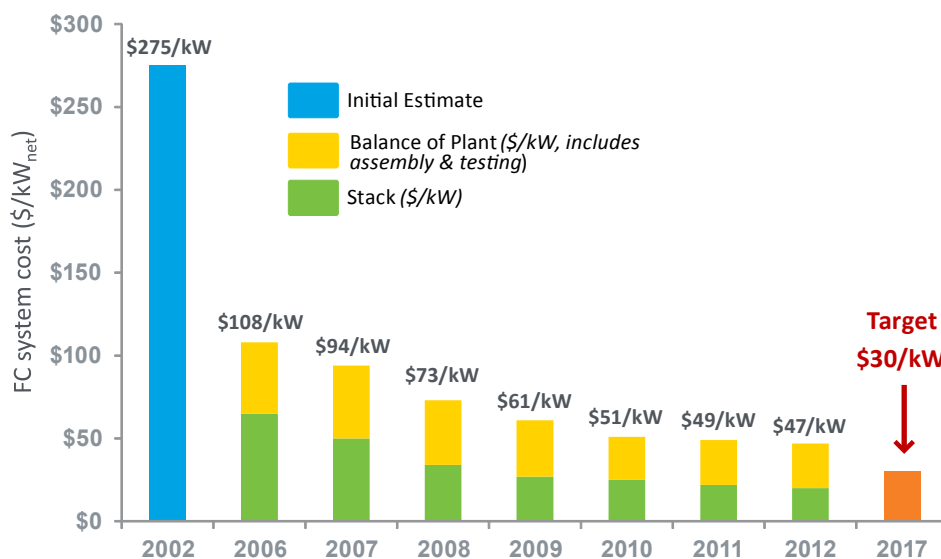


FIGURE 1. Current modeled cost of an 80-kW automotive fuel cell system, based on projections to high-volume manufacturing (500,000 units/year).²

Hydrogen Production

In FY 2012, the Hydrogen Production sub-program continued to focus on developing technologies to enable the long-term viability of hydrogen as an energy carrier for a range of applications, including stationary power, backup power, specialty vehicles, transportation, and portable power. Progress continued in several key areas, including biomass gasification, reforming of bio-derived liquids, electrolysis, solar-thermochemical hydrogen production, photoelectrochemical (PEC) hydrogen production, and biological hydrogen production. Key examples of progress include:

- Developed an electrolyzer system that incorporates low-cost stack components into a high-efficiency hydrogen production system; this system completed over 100 hours of field testing at the National Renewable Energy Laboratory (NREL) test facility for renewable integration, verifying improvements brought about through sub-program investments. (Giner Inc. and NREL)
- Demonstrated extended durability in high-efficiency III-V crystalline systems for PEC hydrogen production from a baseline of about 20 hours up to more than 100 hours, achieved through innovative theory-inspired surface ion nitride treatments of the crystalline surfaces for passivation against corrosion; the enhanced stability was demonstrated under operating conditions consistent with solar-to-hydrogen conversion efficiencies exceeding 10%. (NREL)
- Achieved improved hydrogen fermentation rates by optimizing reactor design and operating conditions, resulting in a two-fold increase in hydrogen production through higher cellulose feedstock loading. This will serve as the foundation for future efforts to scale-up hydrogen fermentation systems. (NREL)

²DOE Hydrogen and Fuel Cells Program Record #12020, http://hydrogen.energy.gov/pdfs/12020_fuel_cell_system_cost_2012.pdf.

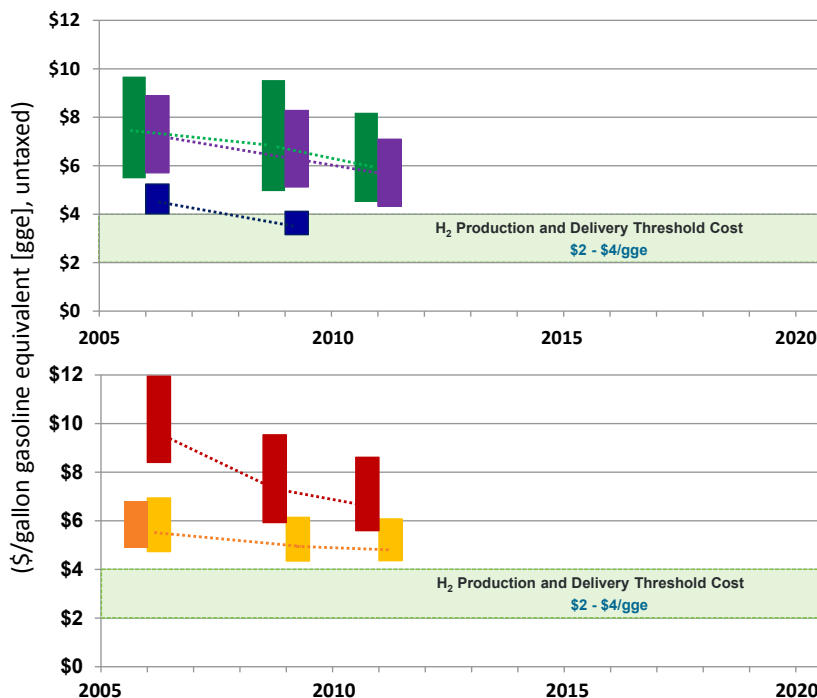
Projected High-Volume Cost of Hydrogen Production¹ (Delivered²)—Status

Distributed Production (near term)

- Electrolysis
Feedstock variability: \$0.03 - \$0.08 per kWh
- Bio-Derived Liquids
Feedstock variability: \$1.00 - \$3.00 per gallon ethanol
- Natural Gas Reforming³
Feedstock variability: \$4.00 - \$10.00 per MMBtu

Central Production (longer term)

- Electrolysis
Feedstock variability: \$0.03 - \$0.08 per kWh
- Biomass Gasification
Feedstock variability: \$40- \$120 per dry short ton
- Nuclear⁴
Feedstock variability: \$0.03 - \$0.08 per kWh



Notes: [1] Cost ranges for each pathway are shown in 2007\$ based on high-volume projections from H2A analyses, reflecting variability in major feedstock pricing and a bounded range for capital cost estimates. [2] Costs include total cost of production and delivery (dispensed, untaxed). Forecourt compression, storage and dispensing added an additional \$1.82 for distributed technologies, \$2.61 was added as the price of delivery for central-production technologies. All delivery costs were based on the Hydrogen Pathways Technical Report (NREL, 2009). [3] Analysis of projected costs for natural gas reforming indicated that the threshold cost can be achieved with current technologies or with incremental improvements made by industry. FCT Program funding of natural gas reforming projects was completed in 2008. [4] High-temp electrolysis activities are ongoing under the Next Generation Nuclear Plant Program.

FIGURE 2. Hydrogen Production Cost Status. Significant progress has already been made in several hydrogen production pathways. The Hydrogen Threshold Cost represents the cost at which hydrogen fuel cell electric vehicles are projected to become competitive on a cost-per-mile basis with competing vehicles (gasoline hybrid-electric vehicles) in 2020.

Hydrogen Delivery

In FY 2012, Hydrogen Delivery sub-program activities continued to focus on reducing the cost and increasing the energy efficiency of hydrogen delivery, to enable the widespread use of hydrogen as an energy carrier. Key examples of progress include:

- Design and construction of a custom-built trailer (shown in Figure 3) capable of holding four 40-foot pressure vessels and an additional 30-foot pressure vessel. This new design has the potential to increase overall capacity by roughly 18%, from about 615 kg in the current U.S. Department of Transportation (DOT)–approved design, to more than 725 kg. (Lincoln Composites)
- Analysis of the cost and power requirements of refueling station compression and pumping technologies, and of the various configurations of high-pressure tube-trailers within DOT-specified weight and size constraints. Two compression options to reduce station capital cost by at least 15% were identified: (1) a high-pressure (900-bar) liquid pump combined with an evaporator to gasify the hydrogen before dispensing (the combined pump/vaporizer cost is less than half the cost of the corresponding gas compressor); and (2) a high-pressure tube trailer that can reduce compression needs at the station, especially in early markets where the utilization of the station compressor would be low. This has the

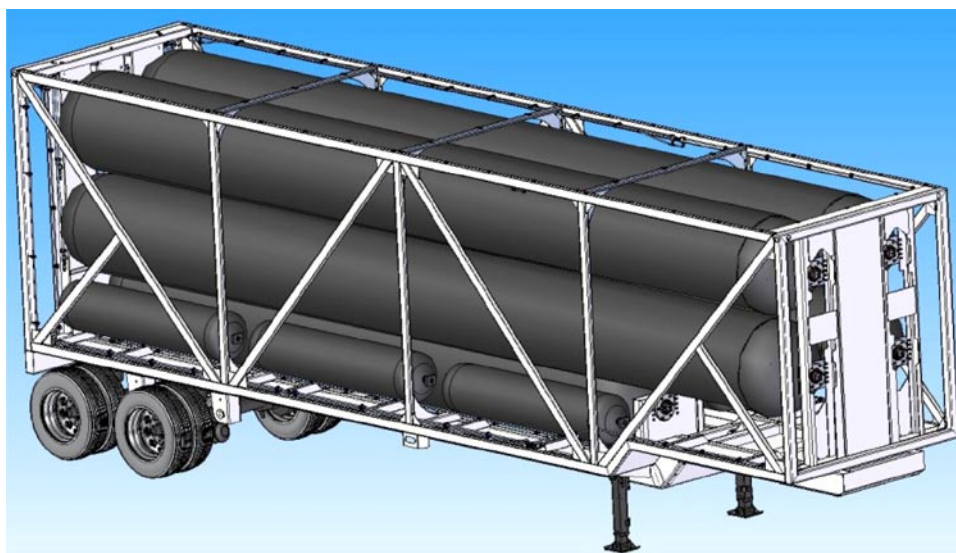


FIGURE 3. Carbon fiber composite tube trailer pressure vessel and International Organization for Standardization container (source: Lincoln Composites).

potential to reduce the impact of station capital cost on overall hydrogen cost by up to 20%, assuming 50% utilization. (Argonne National Laboratory [ANL])

Hydrogen Storage

In FY 2012, the Hydrogen Storage sub-program continued to pursue hydrogen storage materials discovery, including metal hydrides, chemical hydrogen storage, and sorbents, in addition to advanced tank development and total systems engineering to meet DOE onboard hydrogen-storage targets. The sub-program is also initiating efforts for early market fuel cell applications and has developed targets for material handling and portable power applications, which can be found in the *Fuel Cell Technologies Program Multi-Year Research, Development, and Demonstration Plan (MYRD&D Plan)*.

Accomplishments in novel hydrogen storage materials development included:

- Validating hydrogen excess uptake in a metal organic framework material synthesized by Northwestern University (NU-100)—the validated excess capacity of ~8 wt% at 50 bar and 77 K for the NU-100 metal organic framework is among the highest confirmed to date. (NREL)
- Achieving a 30% improvement in hydrogen wt% uptake when normalized to surface area through boron incorporation into porous carbon. (University of Missouri)

The Hydrogen Storage Engineering Center of Excellence partners continued to make progress toward successful completion of Phase II, in preparation for Phase III, including:

- Terminating work on metal hydride systems due to low probability of these materials meeting the required properties in the 2017 timeframe and identification of required onboard reversible metal hydride material properties, through use of the integrated Hydrogen Storage SIMulator vehicle model.
- Conducting failure modes and effects analysis for both adsorbent and chemical hydrogen material systems, identifying potential failure modes requiring further consideration.
- Developing an advanced composite pressure vessel for cryo-sorbents with 11% lower weight, 4% greater internal volume, and 10% lower cost (compared with the baseline established during phase I of the Hydrogen Storage Center of Excellence in 2011).

Accomplishments in developing lower-cost compressed hydrogen tanks include:

- Demonstrating carbonized fiber from low-cost textile-grade polyacrylonitrile blended with methyl acrylate comonomer, which meets the 2012 milestone of at least 300 KSI strength and 30 MSI modulus. (Oak Ridge National Laboratory)
- Developing a pressure vessel design to achieve a 20% reduction in carbon fiber requirement. (ANL)

The sub-program also launched the Hydrogen Storage Materials Database (<http://hydrogenmaterialssearch.govtools.us/>), a comprehensive database to collect and disseminate materials data and accelerate advanced hydrogen storage materials R&D. To date, researchers from more than 60 countries have accessed the database, and the tool was presented as part of the President's Materials Genome Initiative.

Manufacturing R&D

In FY 2012, Manufacturing R&D projects continued in the following areas: novel electrode deposition processes for membrane electrode assembly (MEA) fabrication, reduction in the number of assembly steps to produce low-cost MEAs, flow field plate manufacturing variability and its impact on performance, and fabrication technologies for high-pressure composite hydrogen-storage tanks. Key accomplishments include the following:

- In the area of MEA manufacturing, scaling up the microporous layer ink for full-length and full-width roll coating was found to cause severe bubble formation, leading to variable viscosities in the ink. By modifying additives and processes, the problem was solved and the cost of the microporous layer was reduced by 37% compared with the benchmark. This also resulted in a 3x increase in capacity. (BASF)
- Imaged polymer electrolyte membrane thickness and discrete defects (bubbles, scratches, divots) using optical diagnostics on a full scale weblane—detecting defects on the order of ~10–100 μ in membranes at standard web speeds of 30 feet per minute. (NREL)

Basic Research

The Basic Energy Sciences program in the DOE Office of Science supports fundamental scientific research addressing critical challenges related to hydrogen storage, hydrogen production, and fuel cells. These basic research efforts complement the applied R&D projects supported by other offices in the Program. Progress in any one area of basic science is likely to spill over to other areas and bring advances on more than one front. The subjects of basic research most relevant to the Program's key technologies are:

- Hydrogen Storage: Nanostructured materials; theory, modeling, and simulation to predict behavior and design new materials; and novel analytical and characterization tools.
- Fuel Cells: Nanostructured catalysts and materials; integrated nanoscale architectures; novel fuel cell membranes; innovative synthetic techniques; theory, modeling, and simulation of catalytic pathways, membranes, and fuel cells; and novel characterization techniques.
- Hydrogen Production: Longer-term approaches such as photobiological and direct photochemical production of hydrogen.

By maintaining close coordination between basic science research and applied R&D, the Program ensures that discoveries and related conceptual breakthroughs achieved in basic research programs will provide a foundation for the innovative design of materials and processes that will lead to improvements in the performance, cost, and reliability of fuel cell technologies and technologies for hydrogen production and storage. This is accomplished in various ways—for example, through bi-monthly coordination meetings between the participating offices within DOE, and at the researcher level by having joint meetings with participation from principal investigators who are funded by the participating offices.

Technology Validation

The Technology Validation sub-program demonstrates, tests, and validates hydrogen and fuel cell technologies and uses the results to provide feedback to the Program's R&D activities. The sub-program has been focused on conducting demonstrations that emphasize co-development and integration of hydrogen infrastructure with fuel cell electric vehicles (FCEVs) to permit industry to assess progress toward technology readiness.

In 2012, NREL completed the data collection and analysis portion of the National Fuel Cell Electric Vehicle Learning Demonstration—a government-industry cost-shared project initiated in 2004 with four automobile and energy company teams. A comprehensive final report was published in July 2012. In the course of the project, data were collected on a total of 183 FCEVs and 25 hydrogen fueling stations. FCEVs in the project traveled 3.6 million miles, and 151,000 kg of hydrogen was either produced or dispensed (with some of this hydrogen being used in vehicles outside the Learning Demonstration). Over 500,000 individual vehicle trips were analyzed, and 99 different CDPs were produced to validate the current status of FCEV technology (see Figure 4 for the status of specific performance metrics). FCEVs met or exceeded the 250-mile driving-range goal; fuel cell system efficiencies were demonstrated in the range of 53–59% (at 25% net power), which is close to the DOE target of 60%; and results indicated fuel cell durability in excess of 2,500 hours (>75,000 miles). The final report represents the last of a number of significant and groundbreaking accomplishments by NREL during the project, including the establishment of the HSDC, the methodology of securely aggregating business sensitive performance data into useful public data, and the development of many unique and innovative data products for FCEVs and hydrogen fueling stations.

| Vehicle Performance Metrics | Gen 1 Vehicle | Gen 2 Vehicle | 2009 Target | 2010 – 2011 Results |
|---|---------------|---------------|-------------|---------------------|
| Fuel Cell Stack Durability | | | 2,000 hours | |
| Maximum Team Projected Hours to 10% Voltage Degradation | 1,807 hours | 2,521 hours | | -- |
| Average Fuel Cell Durability Projection | 821 hours | 1,062 hours | | 1,748 hours |
| Maximum Hours of Operation by a Single FC Stack to Date | 2,375 hours | 1,261 hours | | 1,582 hours |
| Driving Range | | | 250 miles | |
| Adjusted Dynamometer (Window Sticker) Range | 103-190 miles | 196-254 miles | | -- |
| Median On-Road Distance Between Fuelings | 56 miles | 81 miles | | 98 miles |
| <i>Fuel Economy (Window Sticker)</i> | 42 – 57 mi/kg | 43 – 58 mi/kg | no target | -- |
| <i>Fuel Cell Efficiency at ¼ Power</i> | 51 – 58% | 53 – 59% | 60% | -- |
| <i>Fuel Cell Efficiency at Full Power</i> | 30 – 54% | 42 – 53% | 50% | -- |

FIGURE 4. Summary of key performance metrics for the Learning Demonstration. *Outside of this project, DOE independent panels estimated that producing hydrogen from distributed reforming of natural gas would cost approximately \$2.75–\$3.50/kg H₂ (2006 study) and producing hydrogen from distributed electrolysis would cost approximately \$4.90–\$5.70/kg H₂ (2009 study)—both analyses assume a build-out rate of 500 stations/year, with stations producing 1,500 kg of H₂/day.³*

³ *Distributed Hydrogen Production from Natural Gas: Independent Review*, NREL, October 2006, <http://hydrogen.energy.gov/pdfs/40382.pdf>; and *Current (2009) State-of-the-Art Hydrogen Production Cost Estimate Using Water Electrolysis: Independent Review*, NREL, 2009, <http://hydrogen.energy.gov/pdfs/46676.pdf>.

In addition to its light-duty vehicle demonstrations, since 2010, the sub-program has been collecting and analyzing data from 17 second-generation fuel cell buses. As of August 2012, one of these buses had exceeded 12,000 hours of operation, and efficiencies up to twice as high as those of diesel buses have been demonstrated.

The Fountain Valley Renewable Energy Tri-Generation Station—the world’s first facility capable of co-producing hydrogen, heat, and power—has operated for more than 1,000 hours in power and power-and-hydrogen modes, and over 5 million standard cubic feet of digester gas has been processed to produce more than 5,000 kg of hydrogen and over 1 million kWh of electricity. The system has achieved an overall efficiency of 54% when co-producing hydrogen and power.

NREL is demonstrating commercially available low-temperature electrolyzer technologies (proton exchange membrane and alkaline electrolyzers) to evaluate their response to commands to increase and decrease stack power (which enable them to shorten frequency disturbances on an alternating current microgrid). The quick response and precise control offered by variable electrolyzer stack operation have been shown to be superior to the control capabilities of many conventional generators. NREL is demonstrating that electrolyzers can perform repeated high cyclic power variations (20–100% of rated stack power) to model performance with wind and solar power. To date, NREL has completed 7,000 hours of operation to help quantify performance differences between constant and variable stack power operation.

Safety, Codes and Standards

In FY 2012, the Safety, Codes and Standards sub-program continued to support R&D to provide the technical basis for codes and standards development, with projects in a wide range of areas, including fuel specification, separation distances, materials and components compatibility, and hydrogen sensor technologies. The sub-program also continued to promote collaboration among diverse stakeholders in order to harmonize regulations, codes, and standards, and it continued to create and enhance safety knowledge tools for emergency responders and authorities having jurisdiction. Key FY 2012 accomplishments include:

- Publishing the compressed hydrogen materials compatibility (CHMC) testing and data application standard, Canadian Standards Association CHMC 1 Part 1.
- Developing accelerated test methods for measurement of hydrogen-assisted fatigue crack growth; this accelerated test greatly reduces the cost barriers that prevent qualification of new materials for hydrogen service.
- Conducted two fire training classes at the Los Angeles City and County Fire Department, with approximately 300 first responders in attendance; to date, more than 23,000 code officials and first responders have been reached through the sub-program’s efforts.

Education

The Education sub-program facilitates hydrogen and fuel cell demonstrations and supports commercialization by providing technically accurate and objective information to key target audiences both directly and indirectly involved in the use of hydrogen and fuel cells. Funding from FY 2010 appropriations supported the sub-program’s activities during FY 2012. Key accomplishments in FY 2012 included:

- Initiating a northeast cluster group for collaboration between states and developing roadmaps for seven states in the cluster.
- Organizing an event to “match” suppliers with manufacturers.
- Launching a monthly newsletter that reaches over 7,500 subscribers.
- Continuing to train middle school and high school teachers through “H2 Educate!”, reaching a cumulative total of 9,700 teachers, in 35 states; 90% of participants felt that the training resources increased the effectiveness of their lesson plans.

Market Transformation

To ensure that the benefits of the Program's efforts are realized in the marketplace, in FY 2012 the Market Transformation sub-program continued to facilitate the growth of early markets for fuel cells used in portable, stationary, and specialty-vehicle applications. Market Transformation activities are helping to reduce the cost of fuel cells by enabling economies of scale through early market deployments; these early deployments also help to overcome a number of barriers, including the lack of operating performance data, the need for applicable codes and standards, and the need for user acceptance. FY 2012 activities primarily involved continuation of projects initiated with FY 2010 appropriations. The Market Transformation sub-program is currently focused on building upon past successes in material handling equipment (e.g., lift trucks) and emergency backup power applications, which received support from Recovery Act funding. The sub-program is seeking to expand on these successes by exploring other potential and emerging applications for market viability. These Recovery Act projects are highly leveraged, with more than half of project funding provided by partner resources, and they are providing valuable data on the status of the technologies in real-world operation that will be used to validate the benefits and potential needs for further R&D (for more information, see the "American Recovery and Reinvestment Act Projects" section, below). Specific accomplishments by the Market Transformation sub-program in FY 2012 include:

- Demonstrating and validating a fuel cell mobile lighting system that combines high-pressure (5,000-psi) hydrogen storage, efficient lighting, and a 5-kW PEM fuel cell; the mobile lighting system was field tested at industry and government installations and demonstrated at various entertainment industry award events, including the Oscars, the Golden Globe Awards, and the Screen Actors Guild Awards.
- Developing and publishing guidelines for federal facilities managers to procure energy from stationary fuel cell power systems, including the use of innovative financing mechanisms that require little or no capital investment.
- Conducting modeling and simulation for evaluating onboard fuel cell rechargers for battery-electric road vehicles.

Systems Analysis and Integration

The Systems Analysis sub-program supports decision-making by providing a greater understanding of technology gaps, options and risks, and examining the interaction of individual technologies and components and their contributions to the performance of larger systems—e.g., the entire hydrogen fuel system, from production to utilization. The sub-program also analyzes cross-cutting issues, such as the integration of hydrogen and fuel cell systems with the electrical sector and the use of renewable fuels. Particular emphasis is given to assessing stationary fuel cell applications and the implications of various approaches to establishing hydrogen infrastructure. The Systems Analysis sub-program made several significant contributions in FY 2012, including:

- Analyzing infrastructure costs for hydrogen fueling and electric vehicle charging, which showed that the capital intensities of the two infrastructure systems are roughly comparable, on a cents-per-mile basis. (NREL)
- Evaluating potential cost reductions for early market hydrogen fueling stations, utilizing diverse stakeholder input to NREL's cost calculator; results will be published at the end of 2012. (NREL)
- Developing and releasing the JOBS FC model, which enables analysis of the impacts of fuel cell market deployments on employment and revenue generation; the model was used to estimate the impact of American Recovery and Reinvestment Act (ARRA) deployments of fuel cells (this analysis was supplemented with calculations that capture economic impacts from expenditures unique to the ARRA program that are not modeled in JOBS FC)—preliminary results indicate that nearly 700 net jobs were created in 2011 as a result of ARRA funding for fuel cell deployments (Figure 5). (ANL and RCF Economic and Financial Consulting)

Employment Impacts of ARRA Fuel Cell Deployments Including Backup Power Fuel Cells and Fuel Cell–Powered Forklifts

- PRELIMINARY ANALYSIS -

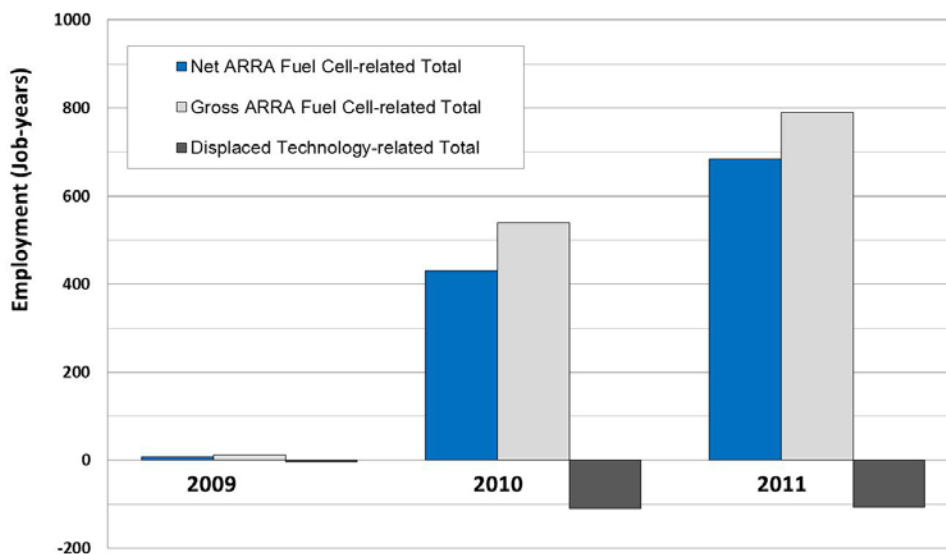


FIGURE 5. Preliminary analysis of employment impacts from ARRA fuel cell deployments, using the JOBS FC model (supplemented with calculations that capture economic impacts from expenditures unique to the ARRA program that are not modeled in JOBS FC) (source: ANL).

- Modifying the GREET model to enable greenhouse gas emissions to be evaluated on a well-to-wheels basis for hydrogen produced from natural gas extracted by hydraulic fracturing. (ANL)
- Conducting a natural gas workshop, involving multiple stakeholders, to gain valuable insight for potential synergies with hydrogen (a summary report and proceedings are available online at www.hydrogenandfuelcells.energy.gov/wkshp_nat_gas_h2_infrastructure.html)

American Recovery and Reinvestment Act Projects

The American Recovery and Reinvestment Act (Recovery Act or ARRA) has been a critical component of the Program's efforts to accelerate the commercialization and deployment of fuel cells in the marketplace. With approximately \$41.9 million from the Recovery Act and \$54 million in cost-share funding from industry participants—for a total of nearly \$96 million—these efforts have deployed more than 1,100 fuel cells, primarily in backup power and forklift applications, exceeding the original ARRA target of 1,000 units. As of the end of October 2012, over 90% of Recovery Act funds had been spent, and more than 1 million hours of operation had been achieved.

Successful DOE deployments of fuel cells (including deployments from ARRA funding as well as Market Transformation projects) have led to industry orders of more than 3,600 fuel cell forklifts and more than 1,400 fuel cell backup power systems, with no additional DOE funding. For example, as a result of deployments of fuel cell lift trucks at the Sysco food distribution center in West Houston, Texas, Sysco is planning to deploy 900 or more fuel cells at seven sites over the next 24 months. Success in these early markets is helping to pave the way for longer term success of fuel cells in larger markets, such as transportation. Additional information about the Program's Recovery Act projects can be found in a newly published fact sheet (www.hydrogenandfuelcells.energy.gov/pdfs/fct_recovery_act_highlights.pdf).

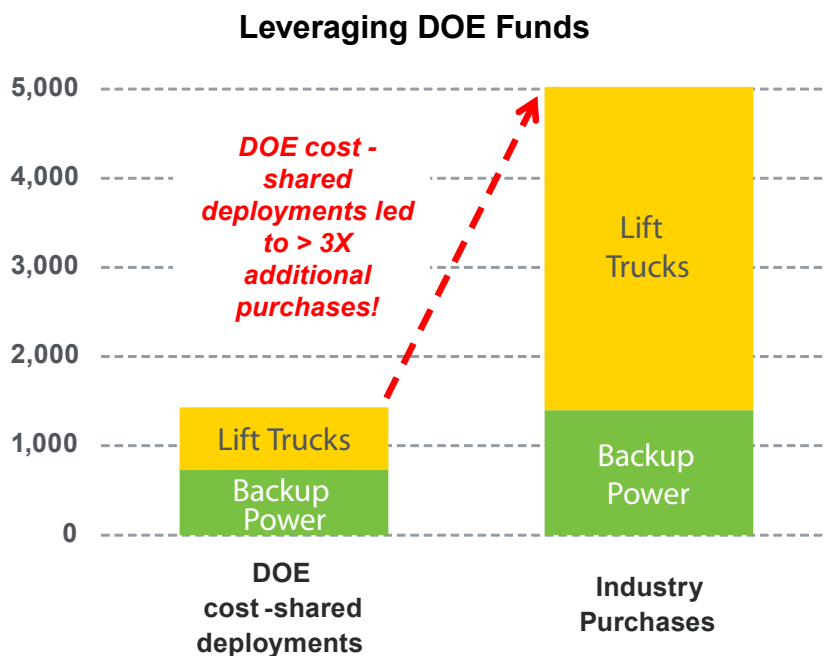


FIGURE 6. Early market deployments of approximately 1,400 fuel cells have led to more than 5,000 additional purchases by major companies (including Coca-Cola, Sprint, Sysco, FedEx, and others) *with no additional DOE funding*.

OTHER PROGRAM ACTIVITIES AND HIGHLIGHTS FROM FY 2012

Tracking Commercialization

One indicator of the robustness and innovative vitality of an RD&D program is the number of patents applied for and granted, and the number of technologies commercialized. The Program continued to assess the commercial benefits of Program funding by tracking the commercial products and technologies developed with the support of the EERE Fuel Cell Technologies Program (FCT Program). R&D efforts funded by the FCT Program have resulted in 363 patents and 36 hydrogen and fuel cell technologies entering the market.⁴ (See Figures 7 and 8.)

Awards & Distinctions

- Dr. Thomas Jaramillo from Stanford University was honored with a **Presidential Early Career Award for Scientists and Engineers (PECASE)** for his innovations in solar hydrogen production and for excellence in mentoring at the university level. Dr. Jaramillo was one of only 96 researchers across the nation honored with this award, which is the highest honor bestowed by the U.S. Government on science and engineering professionals in the early stages of their careers. To date, this was the first and only PECASE award presented to a researcher funded by DOE's Office of Energy Efficiency and Renewable Energy.
- Researchers at Brookhaven National Laboratory won an **R&D 100 Award** for work funded by the FCT Program on platinum monolayer electrocatalysts for fuel cell cathodes. The award was one of only 100 given out this year by *R&D Magazine* for the most outstanding technology developments with promising commercial potential.

⁴ *Pathways to Commercial Success: Technologies and Products Supported by The Fuel Cell Technologies Program*, Pacific Northwest National Laboratory, September 2012, www.hydrogenandfuelcells.energy.gov/pdfs/pathways_2012.pdf.

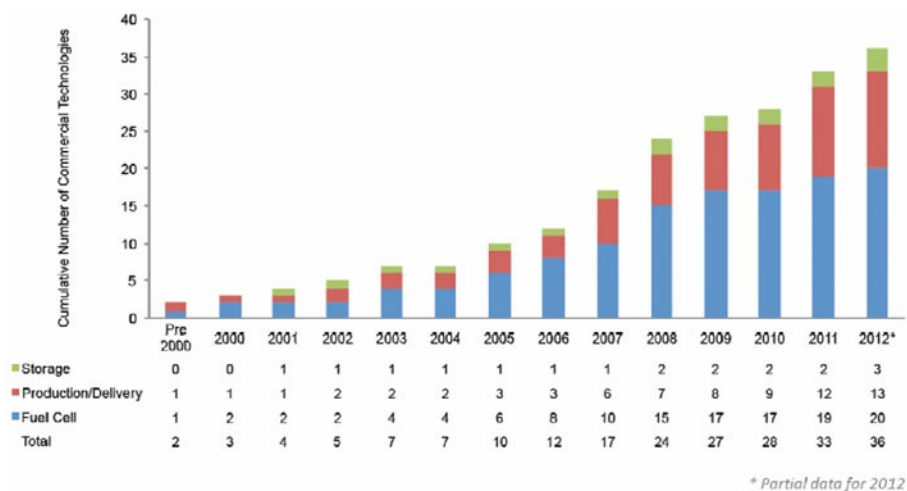


FIGURE 7. Cumulative number of commercial products on the market as a result of funding by the DOE Fuel Cell Technologies Program (source: Pacific Northwest National Laboratory).

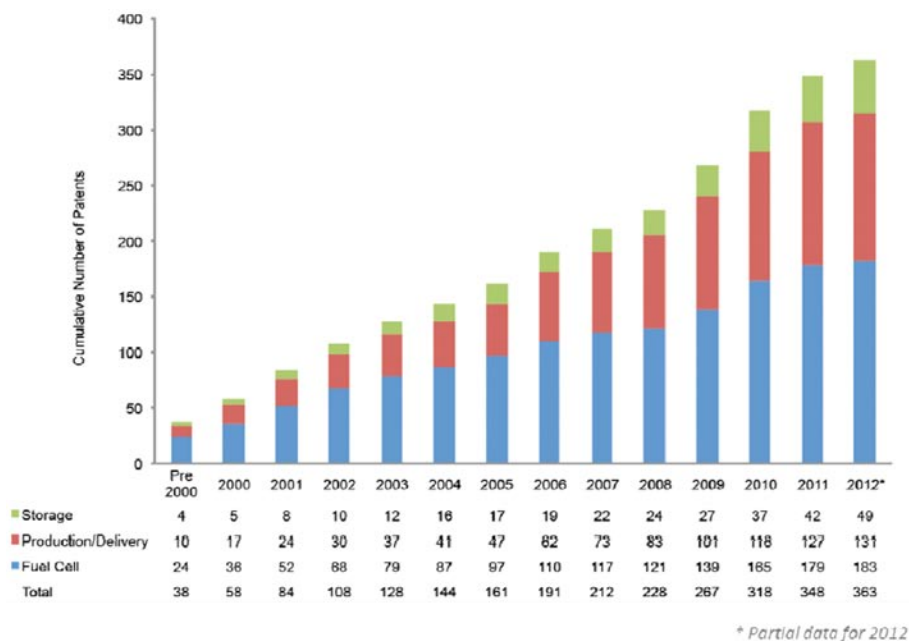


FIGURE 8. Cumulative number of patents awarded as a result of funding by the DOE Fuel Cell Technologies Program (source: Pacific Northwest National Laboratory).

- Dr. Vijay Ramani, a principal investigator for the FCT Program with the Illinois Institute of Technology, and Dr. Adam Weber, the program manager for Lawrence Berkeley National Laboratory’s hydrogen and fuel cell activities, were among the recipients of the **2012 Supramaniam Srinivasan Young Investigator Award** from the Electrochemical Society. Dr. Ramani and his team are currently researching the synthesis of multi-functional electrolyte and electrode materials for polymer based electrochemical systems; Dr. Weber has conducted research for the FCT Program in the areas of fuel cells, electrochemistry, energy storage, and the manufacturing of hydrogen and fuel cell technologies.
- Dr. Fernando Garzon, a long time principal investigator supported by the FCT Program (most recently working on ultra-low platinum group metal catalysts), was elected **President of the Electrochemical Society (ECS)**.

- Lawrence Livermore National Laboratory received a **Pollution Prevention Award** from the National Nuclear Security Administration for their demonstration of hydrogen-powered vehicles, which was supported by the FCT Program.
- Sandia National Laboratories received the Federal Laboratory Consortium's **Excellence in Technical Transfer Award** for their fuel cell mobile lighting project, which demonstrated the ability to meet the needs for portable, indoor lighting that can be operated safely and continuously without ventilation.
- Dr. Radoslav Adzic, an inventor of an innovative nanocatalyst for fuel cell electric vehicles, was named the **2012 Inventor of the Year** by the New York Intellectual Property Law Association for work he and his team did that will effectively reduce the cost required to produce hydrogen fuel cells.

Key Reports/Publications

Every year, the Hydrogen and Fuel Cells Program commissions a number of key reports, providing vital information to industry and the research community. Some of these are released on an annual basis—such as the *Market Report*, the commercialization report (*Pathways to Commercial Success*), and the *State of the States* report—while others are published when studies are complete, projects have ended, or key milestones have been reached.

- The *2011 Fuel Cell Technologies Market Report* indicates that commercial markets for fuel cell technologies expanded significantly over the previous year and forecasts continued growth through 2012, especially in the material-handling industry, www.hydrogenandfuelcells.energy.gov/pdfs/2011_market_report.pdf. (Breakthrough Technologies Institute, Inc.)
- *Pathways to Commercial Success*, the Program's annual commercialization report, indicates that FCT Program funding has resulted in 363 patents and 35 hydrogen and fuel cell technologies entering the market, www.hydrogenandfuelcells.energy.gov/pdfs/pathways_2012.pdf. (Pacific Northwest National Laboratory)
- *State of the States: Fuel Cells in America 2012*, the third annual report on state activities, details fuel cell and hydrogen activities and policies in the 50 states and the District of Columbia, www.hydrogenandfuelcells.energy.gov/pdfs/state_of_the_states_2012.pdf. (Fuel Cells 2000)
- *Business Case for Fuel Cells 2011* illustrates how top American companies are using fuel cells in their business operations to advance their sustainability goals, save millions of dollars in electricity costs, and reduce carbon emissions by hundreds of thousands of metric tons per year, www.hydrogenandfuelcells.energy.gov/pdfs/business_case_fuel_cells_2011.pdf. (Fuel Cells 2000)
- The *National Fuel Cell Electric Vehicle Learning Demonstration Final Report* documents the results of a technology validation project that collected data from more than 180 fuel cell electric vehicle, which made more than 500,000 trips, traveled 3.6 million miles, and completed more than 33,000 fill-ups at hydrogen fueling stations across the country, www.nrel.gov/hydrogen/pdfs/54860.pdf. (NREL)
- *Fuel Quality Issues in Stationary Fuel Cell Systems* assesses impurities encountered in stationary fuel cell systems, the effects of those impurities on fuel cells, and the effectiveness and cost of impurity removal strategies, www.hydrogenandfuelcells.energy.gov/pdfs/fuel_quality_stationary_fuel_cells.pdf. (ANL)
- *Procuring Fuel Cells for Stationary Power: A Guide for Federal Facility Decision Makers* offers step-by-step guidance on implementing a fuel cell stationary power project, www.hydrogenandfuelcells.energy.gov/pdfs/fed_facility_guide_fc_chp.pdf. (Oak Ridge National Laboratory)
- *Executive Summaries for the Hydrogen Storage Materials Centers of Excellence*, summarizes activities performed, accomplishments, and recommendations from each of the centers, which operated from 2005–2010 to develop advanced hydrogen storage materials in the areas of chemical hydrogen storage

materials, hydrogen sorbents, and reversible metal hydrides, www.hydrogenandfuelcells.energy.gov/pdfs/executive_summaries_h2_storage_coes.pdf. (Specific final reports for each Center of Excellence are also available, at www.hydrogenandfuelcells.energy.gov/hydrogen_publications.html#h2_storage.)

- ***Recommended Best Practices for the Characterization of Storage Properties of Hydrogen Storage Materials*** provides an introduction to and an overview of the recommended best practices for making measurements of the hydrogen storage properties of materials, www.hydrogenandfuelcells.energy.gov/pdfs/best_practices_hydrogen_storage.pdf. (H2 Technology Consulting)
- ***2011 Hydrogen and Fuel Cell Manufacturing R&D Workshop Report*** summarizes the results of a workshop that brought together key industry, university, and government representatives to discuss the critical issues facing aspects of manufacturing of hydrogen and fuel cell products, www.hydrogenandfuelcells.energy.gov/pdfs/mfg2011_wkshp_report.pdf. (NREL)
- ***Flow Cells for Energy Storage: Workshop Summary Report*** documents the results of a workshop held to understand the applied R&D needs and the grand challenges for the use of flow cells as energy storage devices, www.hydrogenandfuelcells.energy.gov/pdfs/flow_cells_2012_workshop_report.pdf. (Lawrence Berkeley National Laboratory)
- ***Summary Report: Natural Gas and Hydrogen Infrastructure Opportunities Workshop*** documents the results of a workshop that convened industry and other stakeholders to discuss current status and state-of-the-art technologies for natural gas and hydrogen infrastructure; identify key challenges preventing or delaying widespread deployment of natural gas and hydrogen infrastructure; identify synergies between natural gas and hydrogen fuels; and determine roles and opportunities for both government and industry stakeholders, www.transportation.anl.gov/pdfs/AF/812.PDF. (ANL)
- Proceedings from the ***Biogas and Fuel Cells Workshop*** include the agenda and all presentations from workshop, which focused on discussions of biogas and waste-to-energy technologies for fuel cell applications. The overall objective was to identify opportunities for coupling renewable biomethane with highly efficient fuel cells to produce electricity; heat; combined heat and power; or combined heat, hydrogen and power for stationary or motive applications, www.hydrogenandfuelcells.energy.gov/wkshp_biogas_fuel_cells.html.

New Financial Assistance Awards and Funding Opportunities

- **\$5 Million awarded to two projects to reduce the cost of advanced fuel cells.** These three-year projects will lower the cost of advanced fuel cell systems by developing and engineering cost-effective, durable, and highly efficient fuel cell components.
- **\$2.4 million (not yet awarded) for five projects to collect and analyze performance data for hydrogen fueling stations and advanced refueling components.** Projects located in California, Illinois, and Connecticut will track the performance and technical progress of innovative refueling systems at planned or existing hydrogen fueling stations to find ways to lower costs and improve operation.
- **\$6 Million funding opportunity announced for FCEV data collection.** This funding opportunity announcement (FOA) closed in June, and award negotiations are underway. The projects selected for funding will collect data from next-generation FCEVs as they are operated in real-world conditions, to identify ways to lower costs and improve fuel cell durability and overall vehicle performance.
- **\$2.5 million funding opportunity announced to deploy fuel cell-powered baggage vehicles at U.S. airports.** This FOA closed in July, and award negotiations are underway. These efforts will focus on demonstrating first-generation fuel cell-powered baggage towing tractors operating under real-world conditions, and collect and analyze data to test their performance and cost-effectiveness.
- **FOA for Small-Business Innovation Research (SBIR) includes opportunities for research in fuel cell catalysts.** Topic 10 C of the SBIR FOA is “Innovative Approaches Toward Discovery and/or Development

of Ultra-Low- and Non-PGM Catalysts for PEMFCs and Non-PGM Catalysts for AFCs.” The deadline for receipt of Phase I “letters of intent” was in September 2012.

- **Request for proposals (RFP) issued for deployment of fuel cell-based auxiliary power units for refrigerated trucks.** DOE’s Pacific Northwest National Laboratory issued an RFP for the analysis and demonstration of fuel cell-based auxiliary power units, or APUs, for refrigerated trucks. The project aims to accelerate market deployment of fuel cell-based APUs. The RFP closed in November 2012. This work will be supported by prior-year FCT Program funds made available through down-selections or no-go decisions.

Requests for Information (RFI)

- **Hydrogen Storage for Material Handling and Portable Power Applications** gathered feedback from stakeholders regarding the proposed performance, durability, and cost targets for hydrogen storage sub-systems designed for material handling and portable power fuel cell applications. This RFI closed in June 2012.
- **Fuel Cells for Material Handling and Backup Power Applications** collected feedback from stakeholders regarding the proposed performance, durability, and cost targets for fuel cells designed for backup power and material handling applications. This RFI closed in June 2012.
- **Commercial Readiness of Hydrogen and Fuel Cell Technologies** collected information from stakeholders regarding transportation electrification using fuel cells, specifically onboard refrigeration auxiliary power for heavy duty road vehicles, fuel cell rechargers for battery electric vehicles used for transporting cargo or passengers, and technology deployment opportunities for other on- or off-road transportation markets. This RFI closed in March 2012.
- **High-Accuracy Meters for Hydrogen Fueling Equipment** gathered feedback from stakeholders regarding the current and near-term status and availability of high-accuracy meters that can perform under hydrogen fueling conditions and meet measurement accuracy requirements. This RFI closed in September 2012.

INTERNATIONAL ACTIVITIES

International Partnership for Hydrogen and Fuel Cells in the Economy

The United States is a founding member of the International Partnership for Hydrogen and Fuel Cells in the Economy (IPHE),⁵ which includes 17 member countries (Australia, Brazil, Canada, China, France, Germany, Iceland, India, Italy, Japan, New Zealand, Norway, the Republic of Korea, the Russian Federation, South Africa, the United Kingdom, and the United States) and the European Commission. The IPHE is a forum for governments to work together to advance worldwide progress in hydrogen and fuel cell technologies. IPHE also offers a mechanism for international R&D managers, researchers, and policymakers to share program strategies. In FY 2012, the 17th Steering Committee Meeting was held in South Africa on May 3 and 4. An IPHE Workshop titled “Hydrogen—A Competitive Energy Storage Medium to enable the large scale integration of renewable energies” was held November 15 and 16 in Seville, Spain, following the 18th Steering Committee Meeting, also in Seville, on November 14.

International Energy Agency

The United States is also involved in international collaboration on hydrogen and fuel cell R&D through the International Energy Agency (IEA) implementing agreements; the United States is a member of both the Advanced Fuel Cells Implementing Agreement (AFCIA)⁶ and the Hydrogen Implementing Agreement

⁵ <http://www.iphe.net/>

⁶ www.ieafuelcell.com

(HIA).⁷ These agreements provide a mechanism for member countries to share the results of research, development, and analysis activities. The AFCIA currently includes seven annexes: Molten Carbonate Fuel Cells, Polymer Electrolyte Fuel Cells, Solid Oxide Fuel Cells, Fuel Cells for Stationary Applications, Fuel Cells for Transportation, Fuel Cells for Portable Power, and Systems Analysis. The participating countries are Australia, Austria, Belgium, Denmark, Finland, France, Germany, Italy, Japan, Korea, Mexico, Sweden, Switzerland, and the United States. The IEA HIA is focused on RD&D and analysis of hydrogen technologies. It includes 11 tasks: Hydrogen Safety, Biohydrogen, Fundamental and Applied Hydrogen Storage Materials Development, Small-Scale Reformers for On-site Hydrogen Supply, Wind Energy and Hydrogen Integration, High-Temperature Production of Hydrogen, Advanced Materials for Hydrogen from Water Photolysis, Near-Market Routes to Hydrogen by Co-Gasification with Biomass, Large Scale Hydrogen Delivery Infrastructure, Distributed and Community Hydrogen for Remote Communities, and Global Hydrogen Systems Analysis. The United States participates in all of these tasks. Members of the HIA include: Australia, Denmark, the European Commission, Finland, France, Germany, Greece, Iceland, Italy, Japan, Korea, Lithuania, New Zealand, Norway, Spain, Sweden, Switzerland, Turkey, Taiwan, United Nations Industrial Development Organization-International Center for Hydrogen Energy Technologies, and the United States.

EXTERNAL COORDINATION, INPUT, AND ASSESSMENT

Hydrogen and Fuel Cell Technical Advisory Committee (HTAC)

As required by the Energy Policy Act of 2005, HTAC was created in 2006 to advise the Secretary of Energy on issues related to the development of hydrogen and fuel cell technologies and to provide recommendations regarding DOE's programs, plans, and activities, as well as on the safety, economic, and environmental issues related to hydrogen and fuel cells. HTAC members include representatives of domestic industry, academia, professional societies, government agencies, financial organizations, and environmental groups, as well as experts in the area of hydrogen safety.

HTAC met three times in FY 2012—twice in person and once via webinar. In March 2012, HTAC released its fourth annual report, which summarizes hydrogen and fuel cell technology domestic and international progress in RD&D projects, commercialization activities, and policy initiatives. A major HTAC activity in FY 2012 was the Hydrogen Production Expert Panel Workshop, which was conducted by a new HTAC subcommittee. The workshop was held in May 2012, with opening remarks provided by Secretary of Energy Steven Chu. The panel was charged with providing recommendations to DOE regarding both policy and investments in R&D to enable the widespread production of affordable, low-carbon hydrogen—taking into consideration relevant market and business forces, technology barriers, and policy barriers, as well as the impact of safety codes and standards. A report from the workshop is expected to be published in early 2013. More information about HTAC, including the latest annual report, is available at: http://www.hydrogen.energy.gov/advisory_htac.html.

Federal Inter-Agency Coordination

The Hydrogen and Fuel Cell Interagency Task Force (ITF), mandated by the Energy Policy Act of 2005, includes senior representatives from federal agencies supporting hydrogen and fuel cell activities, with the DOE/EERE serving as chair. Recently, efforts by the ITF have focused on facilitating federal deployment of hydrogen and fuel cells in emerging technology applications such as stationary power and specialty vehicles. The Hydrogen and Fuel Cell Interagency Working Group, co-chaired by DOE and the White House Office of Science and Technology Policy, continues to meet monthly to share expertise and information about ongoing programs and results, to coordinate the activities of federal entities involved in hydrogen and fuel cell RD&D, and to ensure efficient use of taxpayer resources. In January 2012, the Task Force and the Working Group

⁷ www.ieahia.org

released their *Interagency Action Plan*, www.hydrogen.gov/interagency_action_plan.html. Examples of successful inter-agency coordination include:

- Announcement in January that 16 GM Equinox FCEVs would be deployed in Hawaii, as a result of collaboration between DOE, the Department of Defense (DOD), NREL, the University of Hawaii, and the University of California at Irvine. Data collected from the FCEVs will be used for early market evaluation.
- DOD-DOE collaboration to deploy fuel cells for emergency backup power. DOE and DOD are collaborating on a project to install and operate 18 fuel cell backup power systems at eight defense installations across the country. The departments are testing how the fuel cells perform in real-world conditions, identifying improvements manufacturers can make to enhance the value proposition, and highlighting the benefits of fuel cells for emergency backup power applications.

The National Academies

The National Research Council (NRC) of the National Academies provides ongoing technical and programmatic reviews and input to the Hydrogen and Fuel Cells Program. The NRC has conducted independent reviews of both the Program⁸ and the R&D activities of the U.S. DRIVE Partnership.⁹ Formerly known as the FreedomCAR and Fuel Partnership, the U.S. DRIVE (Driving Research and Innovation for Vehicle efficiency and Energy sustainability) partnership works on an extensive portfolio of advanced automotive and energy infrastructure technologies, including batteries and electric-drive components, advanced combustion engines, lightweight materials, and hydrogen and fuel cell technologies. In FY 2012, a new review of U.S. DRIVE was initiated and FCT Program representatives presented recent activities to the NRC.

FY 2012 Annual Merit Review and Peer Evaluation

The Program's Annual Merit Review (AMR) took place May 14-18, 2012, providing an opportunity for the Program to obtain expert peer reviews of the projects it supports and to report its accomplishments and progress. For the fourth time, this meeting was held in conjunction with the annual review of DOE's Vehicle Technologies Program. During the AMR, reviewers evaluate the Program's projects and make recommendations; DOE uses these evaluations, along with other review processes, to make project funding decisions for the upcoming fiscal year. The review also provides a forum for promoting collaborations, the exchange of ideas, and technology transfer. This year, more than 1,800 participants attended, and the Hydrogen and Fuel Cells Program had 163 oral presentations and 65 poster presentations. More than 200 experts peer-reviewed 145 of the Program's projects—conducting a total of over 900 individual project reviews, with an average of more than six reviewers per project. The report summarizing the results and comments from these reviews is available at www.hydrogen.energy.gov/annual_review12_report.html. In 2013, the AMR will be held May 13–17 in Arlington, Virginia.

Funds Saved through Active Project Management

The AMR is a key part of the Program's comprehensive approach toward active management of its projects. Termination of underperforming projects—identified through the AMR as well as through other go/no-go decisions (with criteria defined in the project scope of work)—helped the Program redirect \$6.8 million in funding in FY 2012, \$13.8 million in FY 2011, and nearly \$30 million over the past four years.

⁸ *The Hydrogen Economy: Opportunities, Costs, Barriers and R&D Needs*, National Research Council and National Academy of Engineering, National Academies Press, 2004.

⁹ *Review of the Research Program of the FreedomCAR and Fuel Partnership: First Report*, National Research Council, National Academies Press, 2005, http://www.nap.edu/catalog.php?record_id=11406; *Review of the Research Program of the FreedomCAR and Fuel Partnership: Second Report*, National Research Council, National Academies Press, 2008, http://www.nap.edu/catalog.php?record_id=12113; *Review of the Research Program of the FreedomCAR and Fuel Partnership: Third Report*, National Research Council, National Academies Press, 2010, www.nap.edu/catalog.php?record_id=12939.

IN CLOSING...

The Program will continue to pursue a broad portfolio of RD&D activities for fuel cell applications across multiple sectors. Efforts will span the full spectrum of technology readiness, including: early market applications that are already viable or are expected to become viable in the next few years, such as forklifts, backup power, and portable power applications; mid-term markets that are expected to emerge in the 2012-2015 timeframe, such as residential combined heat and power systems, auxiliary power units, fleet vehicles, and buses; and longer-term markets that are expected to emerge in the 2015-2020 timeframe, including light-duty passenger vehicles and other transportation applications. The Program will also continue to pursue activities to enable commercialization and stimulate the markets for hydrogen and fuel cells as they achieve technology readiness. Supporting these markets will not only help to achieve the economic, environmental, and energy security benefits that fuel cells provide in those specific applications, but it will complement the Program's longer-term R&D efforts by helping to increase current sales and manufacturing volumes, providing essential cost reductions—through economies of scale—for many of the same technologies that will be used in longer-term applications. Supporting earlier markets can also reduce many non-technological barriers to the deployment of hydrogen and fuel cell technologies and lay the groundwork for the larger infrastructure and supply base that will be needed for fuel cell electric vehicles. Communication and outreach remain critical to all these efforts, and the Program actively pursues opportunities to publicize its activities and progress, releasing more than 70 news items in FY 2012, including DOE press releases, progress alerts, success stories, and blogs.

Finally, in 2012 several individual sub-program chapters of the updated *Fuel Cell Technologies Program Multi-Year Research, Development, and Demonstration Plan (MYRD&D Plan)* were published, and they are currently available online (www.hydrogenandfuelcells.energy.gov/mypp/index.html). These updated chapters include a number of revised technical targets. Final updates of the remaining chapters are expected to be complete early in 2013. The *MYRD&D Plan* describes the planned research, development, and demonstration activities for hydrogen and fuel cell technologies. It was first published in 2005, and elements of it have been revised periodically to reflect progress in the technologies and revisions to developmental timelines and targets.



Sunita Satyapal
Director
Hydrogen and Fuel Cells Program
U.S. Department of Energy

II. HYDROGEN PRODUCTION

II.0 Hydrogen Production Sub-Program Overview

INTRODUCTION

The Hydrogen Production sub-program supports research and development (R&D) of technologies that will enable the long-term viability of hydrogen as an energy carrier for a diverse range of end-use applications including stationary power (e.g., backup power and combined heat-and-power systems), transportation (e.g., specialty vehicles, cars, trucks, and buses), and portable power. A portfolio of hydrogen production technology pathways utilizing a variety of renewable energy sources and renewable feedstocks is being developed under this sub-program.

Three DOE offices are engaged in R&D relevant to hydrogen production, including:

- The Fuel Cell Technologies (FCT) Program, within the Office of Energy Efficiency and Renewable Energy (EERE), is developing technologies for distributed and centralized renewable production of hydrogen. Distributed production options under development include reforming of bio-derived renewable liquids and electrolysis of water. Centralized renewable production options include water electrolysis integrated with renewable power generation (e.g., wind, solar, hydroelectric, and geothermal power), biomass gasification, solar-driven high-temperature thermochemical water splitting, direct photoelectrochemical water splitting, and biological processes.
- The Office of Fossil Energy (FE) is advancing the technologies needed to produce hydrogen from coal-derived synthesis gas, including co-production of hydrogen and electricity. Separate from the Hydrogen and Fuel Cells Program, FE is also developing technologies for carbon capture and sequestration, which will ultimately enable hydrogen production from coal to be a near-zero-emissions pathway.
- The Office of Science's Basic Energy Sciences (BES) program conducts research to expand the fundamental understanding of biological and biomimetic hydrogen production, photoelectrochemical water splitting, catalysis, and membranes for gas separation.
- The Office of Nuclear Energy (NE) has been conducting efforts in development of high-temperature electrolysis, under the Next Generation Nuclear Plant (NGNP) project, which also includes evaluations of other end-user applications and energy transport systems. The Nuclear Hydrogen Initiative was discontinued as a separate program in Fiscal Year (FY) 2009 after the selection of steam electrolysis as the hydrogen production pathway most compatible with the NGNP.

GOAL

The goal of the Hydrogen Production sub-program's portfolio is to develop low-cost, highly efficient hydrogen production technologies that utilize diverse domestic sources of energy, including renewable resources (EERE), coal with sequestration (FE), and nuclear power (NE).

OBJECTIVES

The objective¹ of the EERE hydrogen production portfolio is to reduce the cost of hydrogen dispensed at the pump to a cost that is competitive on a cents-per-mile basis with competing vehicle technologies (based on current analysis, this translates to a hydrogen threshold cost of \$2–4 per gallon gasoline equivalent [gge] by

¹Note: Targets and milestones were recently revised; therefore, individual project progress reports may reference prior targets. Some targets are still currently under revision, with updates to be published in FY 2013.

2020²). Technologies are being researched to achieve this goal in timeframes appropriate to their current stages of development.

The objectives of FE's efforts in hydrogen production are documented in the *Hydrogen from Coal Program Research, Development and Demonstration Plan* (September 2010).³ They include proving the feasibility of a near-zero emissions, high-efficiency plant that will produce both hydrogen and electricity from coal and reduce the cost of hydrogen from coal by 25 percent compared with current technology, by 2016. The objectives of NE's efforts in hydrogen production are documented in the *Technology Roadmap for Generation IV Nuclear Energy Systems* (December 2002).⁴ They include the development of high-temperature thermochemical process for hydrogen production compatible with NGNP.

FY 2012 TECHNOLOGY STATUS AND PROGRESS

In FY 2012, significant progress was made by the EERE Hydrogen Production sub-program on several important fronts. For example:

- A Hydrogen Production Expert Panel workshop was held to assess technology status of production technologies and formulate recommendations for enabling pathways forward for the widespread production of affordable low-carbon hydrogen.
- A new version of the Hydrogen Analysis (H2A v3) Model was published with updated economic data and assumptions, and with all costs converted to 2007 dollars to be consistent with the cost basis for the DOE FCT Program's cost threshold for hydrogen production and delivery.
- Updated economic and cost-sensitivity analyses using H2A v3 were performed incorporating the most up-to-date information on pathway technologies and technology-readiness projections; the resulting case studies were used to revise the pathway-dependent cost status and targets for the Hydrogen Production sub-program's chapter of the *Multi-Year Research, Development and Demonstration Plan (MYRD&D Plan)*, currently in final review.
- Important technical advances were made by the principle investigators in all the hydrogen production projects in the sub-program portfolio.

More details of the technology status and progress are provided in following sections.

Hydrogen Production Expert Panel

A Hydrogen Production Expert Panel—composed of world leaders in hydrogen production technologies from industry, academia and the national laboratories—was established as a subcommittee of the Hydrogen & Fuel Cell Technical Advisory Committee (HTAC). In May 2012, Secretary of Energy Steven Chu kicked off a workshop held by the panel to formulate recommendations to HTAC on enabling pathways for the widespread production of affordable low-carbon hydrogen, both for near- and long-term markets. The objectives of the workshop were to: (1) evaluate current status of hydrogen production technologies; (2) identify remaining technological and economic challenges; (3) prioritize R&D needs; and (4) strategize how to best leverage R&D among U.S. Department of Energy Offices and with other agencies. A summary report resulting from the workshop is under final review by the Hydrogen Production Expert Panel for submission to HTAC.

² Hydrogen Threshold Cost Calculation, Hydrogen and Fuel Cells Program Record #11007, U.S. Department of Energy, 2012, http://www.hydrogen.energy.gov/pdfs/11007_h2_threshold_costs.pdf.

³ Hydrogen from Coal Program Research Development and Demonstration Plan, Office of Fossil Energy, U.S. Department of Energy, September 2010, http://fossil.energy.gov/programs/fuels/hydrogen/2010_Draft_H2fromCoal_RDD_final.pdf.

⁴ *A Technology Roadmap for Generation IV Nuclear Energy Systems*, Office of Nuclear Energy, U.S. Department of Energy, December 2002, http://www.ne.doe.gov/genIV/documents/gen_iv_roadmap.pdf.

Production Cost Status and Targets

The status and targets for the projected cost of hydrogen production based on the pathway-specific H2A v3 case studies completed in FY 2012 are shown in Table 1. The technoeconomic assumptions used in these case studies can be found online for each pathway at http://www.hydrogen.energy.gov/h2a_production; and these cases are also fully documented in the FCT Program's new *MYRD&D Plan* (currently in final review). As a note, the 2006 report *Distributed Hydrogen Production from Natural Gas*⁵ provided the basis for DOE to discontinue R&D of steam methane reforming for hydrogen production—verifying that the use of existing steam methane reforming technologies in distributed hydrogen production could already meet the cost target at high-volume production; targets for this pathway are not included in Table 1. Also, targets for hydrogen production efforts in FE and NE (also not included in Table 1), along with information on the status of the technologies, are described separately in the previously cited RD&D and roadmap documents for these programs.

TABLE 1. Cost Status and Targets for Hydrogen Production*

| | \$/gge (production costs only) | 2011 Status | 2015 Target | 2020 Target | Ultimate Production Target |
|--------------------|--|------------------------|------------------------|------------------------|---------------------------------------|
| Distributed | Electrolysis from grid electricity | \$4.20 | \$3.90 | \$2.30 | \$1-\$2 |
| | Bio-derived Liquids (based on ethanol reforming case) | \$6.60 | \$5.90 | \$2.30 | |
| Central | Electrolysis From renewable electricity | \$4.10 | \$3.00 | \$2.00 | |
| | Biomass Gasification | \$2.20 | \$2.10 | \$2.00 | |
| | Solar Thermochemical | NA | \$14.80 | \$3.70 | |
| | Photoelectrochemical | NA | \$17.30 | \$5.70 | |
| | Biological | NA | NA | \$9.20 | |

*H2A v3 technoeconomic assumptions used in the projected cost status and targets for hydrogen production are consistent with the FCT Program's new MYRD&D Plan – currently in final review; apportionment of threshold cost: \$1-2/gge for production, \$1-2/gge for delivery is consistent with a Hydrogen and Fuel Cells Program record currently in final review; new H2A v3 case studies are published at http://www.hydrogen.energy.gov/h2a_production.

Reductions in the projection costs for hydrogen production in several of the nearer term pathways have been realized through continued technical progress in these technologies, as illustrated in Figure 1. Specific technical progress achieved in FY 2012 in both the nearer and longer term hydrogen production pathways is addressed in the following sections.

Separation Processes and Biomass Gasification

Projects in the separations area focused on the development of hydrogen separation membranes for use in a water-gas shift membrane reactor, and on the development and demonstration of a biogas cleanup system. Biomass gasification efforts focused on the development of a one-step biomass gas reforming-shift separation membrane reactor. Technical progress included:

- Demonstrated palladium-copper alloy thin film (~5 μm) membranes with a hydrogen (H₂) permeance of 10-15 m³/m²/hr/bar at 350°C (i.e., 50-75 scfh, at 20 psig) and a selectivity of H₂/N₂ of 200 to >1,000, meeting the DOE 2015 cost vs. performance target of 0.6 scfh, at 20 psi per unit dollar cost. (Media & Process Technology, Inc.)

⁵ *Distributed Hydrogen Production from Natural Gas*, National Renewable Energy Laboratory, October 2006, <http://www.hydrogen.energy.gov/pdfs/40382.pdf>

Projected High-Volume Cost of Hydrogen Production¹—Reductions and Status

Distributed Production (near term)

Electrolysis

Feedstock variability: \$0.03 - \$0.08 per kWh

Bio-Derived Liquids

Feedstock variability: \$1.00 - \$3.00 per gallon ethanol

Natural Gas Reforming³

Feedstock variability: \$4.00 - \$10.00 per MMBtu

Central Production (longer term)

Electrolysis

Feedstock variability: \$0.03 - \$0.08 per kWh

Biomass Gasification

Feedstock variability: \$40- \$120 per dry short ton

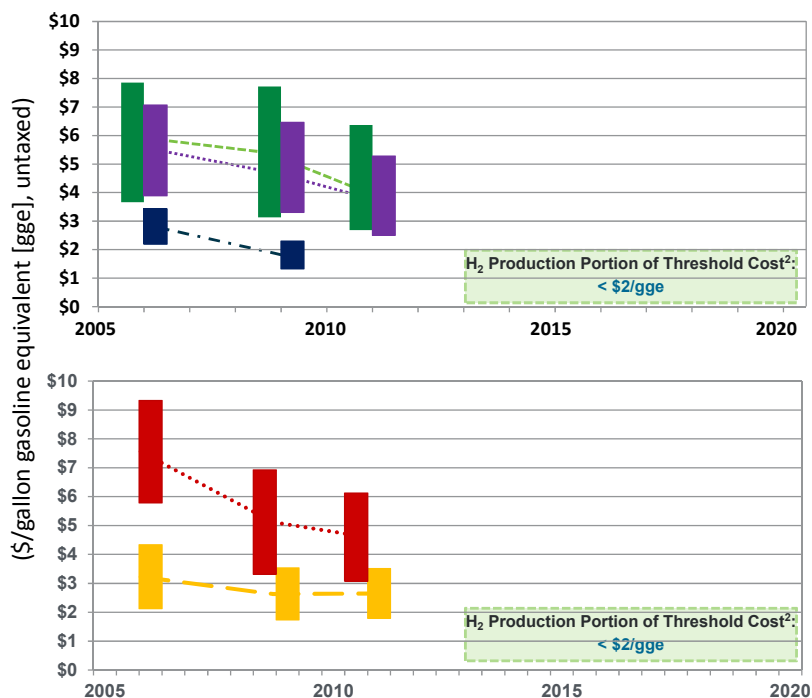


FIGURE 1. Hydrogen Production Cost Status. Significant progress has already been made in several hydrogen production pathways. The Hydrogen Threshold Cost represents the cost at which hydrogen fuel cell electric vehicles are projected to become competitive on a cost-per-mile basis with competing vehicles (gasoline hybrid-electric vehicles) in 2020. Notes: (i) Costs shown do not include taxes. Costs of forecourt compression, storage, and dispensing are not included for distributed technologies, and plant-gate production costs (not including transportation, compression, storage, and dispensing) are shown for centralized technologies. Projections of distributed costs assume station capacities of 1,500 kg/day. Projections of centralized production costs assume capacities of $\geq 50,000$ kg/day. Cost ranges for each pathway are shown in 2007 dollars, based on high-volume projections from H₂A analyses, reflecting variability in major feedstock pricing and a bounded range for capital cost estimates. (ii) DOE funding of natural gas reforming projects was completed in 2009 due to achievement of the threshold cost. Incremental improvements will continue to be made by industry.

- Fabricated a 12 cubic foot/minute, skid-mounted, field-deployable prototype biogas clean-up system for removal of H₂S and siloxane contaminants to less than ppmv levels using an optimized sorbent formulation. (TDA Research Inc.)
- Demonstrated through H₂A modeling the potential for an up to 35% increase in H₂ recovery (compared to conventional pressure swing adsorption separation technology) in a one-step membrane reactor for biomass gas reforming, with a projected high volume cost of \$1.82/kg H₂ compared to \$2.00/kg H₂ with a pressure swing adsorption unit. (Gas Technology Institute)

Bio-Derived Liquid Pathways

Projects in this area addressed hydrogen production through catalytic steam reforming of pyrolysis oil, and aqueous phase reforming of pyrolysis oil at moderate temperatures. Technical progress included:

- Constructed an integrated bench-scale system for the production of 100 L/h hydrogen from pyrolysis bio-oil, including all the basic unit operations as the design for a 1,500 kg/day hydrogen plant, and on-going demonstration of 100 hours of commercial catalyst performance for catalytic autothermal reforming. (National Renewable Energy Laboratory, NREL)
- Identified Pt-Co/ZrO₂ catalysts having potential to improve H₂ yields from water soluble components of bio-oil up to 2-3x the yields with other Pt-based catalysts for aqueous phase reforming. (Pacific Northwest National Laboratory)

Electrolysis Hydrogen Production

The major emphases of the electrolysis projects were on cost reduction and efficiency improvement through cell and stack optimization, higher-pressure operations, and validation of integration with renewable resources. Technical progress included:

- Completed 5,000-hour life-test with dimensionally stable membranes (DSM™) operating at 80°C and 300 psid, for use in advanced electrolyzer stacks with an order of magnitude cost reduction in membrane supports, compared with legacy designs without DSM™. (Giner Inc.)
- Manufactured an electrolyzer system incorporating low-cost stack components into a high-efficiency hydrogen production system, and completed >100 hours of field testing at the NREL test facility for renewable integration, verifying improvements brought about through sub-program investments. (Giner Inc. and NREL)
- Fabricated over 3,000 cells utilizing new flow field design resulting in >20% part cost savings (corresponding to a 12% stack cost reduction over a three year period), and assembled these improved cells into production stacks. (Proton Onsite)

Photoelectrochemical (PEC) Hydrogen Production

The broad focus of projects in this area was on developing viable PEC material systems and prototypes with improved efficiency and durability. Technical progress included:

- Demonstrated extended durability in high-efficiency III-V crystalline systems for PEC hydrogen production from a baseline of ~20 hours up to >100 hours, achieved through innovative theory-inspired surface ion nitride treatments of the crystalline surfaces for passivation against corrosion; the enhanced stability was demonstrated under operating conditions consistent with solar-to-hydrogen (STH) conversion efficiencies exceeding 10%. (NREL)
- Verified 420 hours durability in low cost thin-film copper-gallium-diselenide PEC photoelectrodes under simulated sunlight, operating at a current density equivalent to 5% STH conversion, exceeding the 300 hours target for 2012, and up from the baseline of 200 hours in 2011. This result indicates the viability of lower-cost thin-film material systems for efficient PEC water splitting. (MVSystems/University of Hawaii)
- Demonstrated highly stable H₂ evolution by core-shell MoO₃-MoS₂ nanowires, with no degradation observed in acidic electrolyte through 10,000 cycles of testing at 10 mA/cm² (i.e., conditions consistent with STH conversion efficiencies >12%). This result indicates the long-term viability of theory-inspired nano-structured devices for PEC water splitting. (Stanford U.)

Biological Hydrogen Production

Projects in this area encompassed a portfolio of photobiological and fermentative production methods that use various algal, cyanobacterial, and bacterial microorganisms that produce hydrogen through splitting water or using biomass resources. Technical progress included:

- Achieved improved hydrogen fermentation rates through optimizing reactor design and operating conditions, resulting in a 2-fold increase in hydrogen production through higher cellulose feedstock loading. This will serve as the foundation for future efforts to scale up hydrogen fermentation systems. (NREL)
- Identified and characterized the gene mutation that enabled light utilization efficiency of 25% in the *tla3* mutant strain of algae. These findings will be applied to reducing chlorophyll antenna size to increase the utilization efficiency of incident solar light energy. (UC Berkeley)
- Increased hydrogen evolution activity from ~50 nmol H₂/mg lysate/hour to ~200 nmol H₂/mg lysate/hour through the genetic modification of an environmentally-isolated hydrogenase enzyme. This is

a significant step in improving the mechanisms of hydrogen production in microbes. (J. Craig Venter Institute, in collaboration with NREL)

- Demonstrated light-induced hydrogen production by a cyanobacterial hydrogenase expressed in algae. This is a critical step in engineering algae to produce high levels of hydrogen using the more oxygen-tolerant hydrogenases of other species. (NREL)

Solar-Thermochemical Hydrogen Production

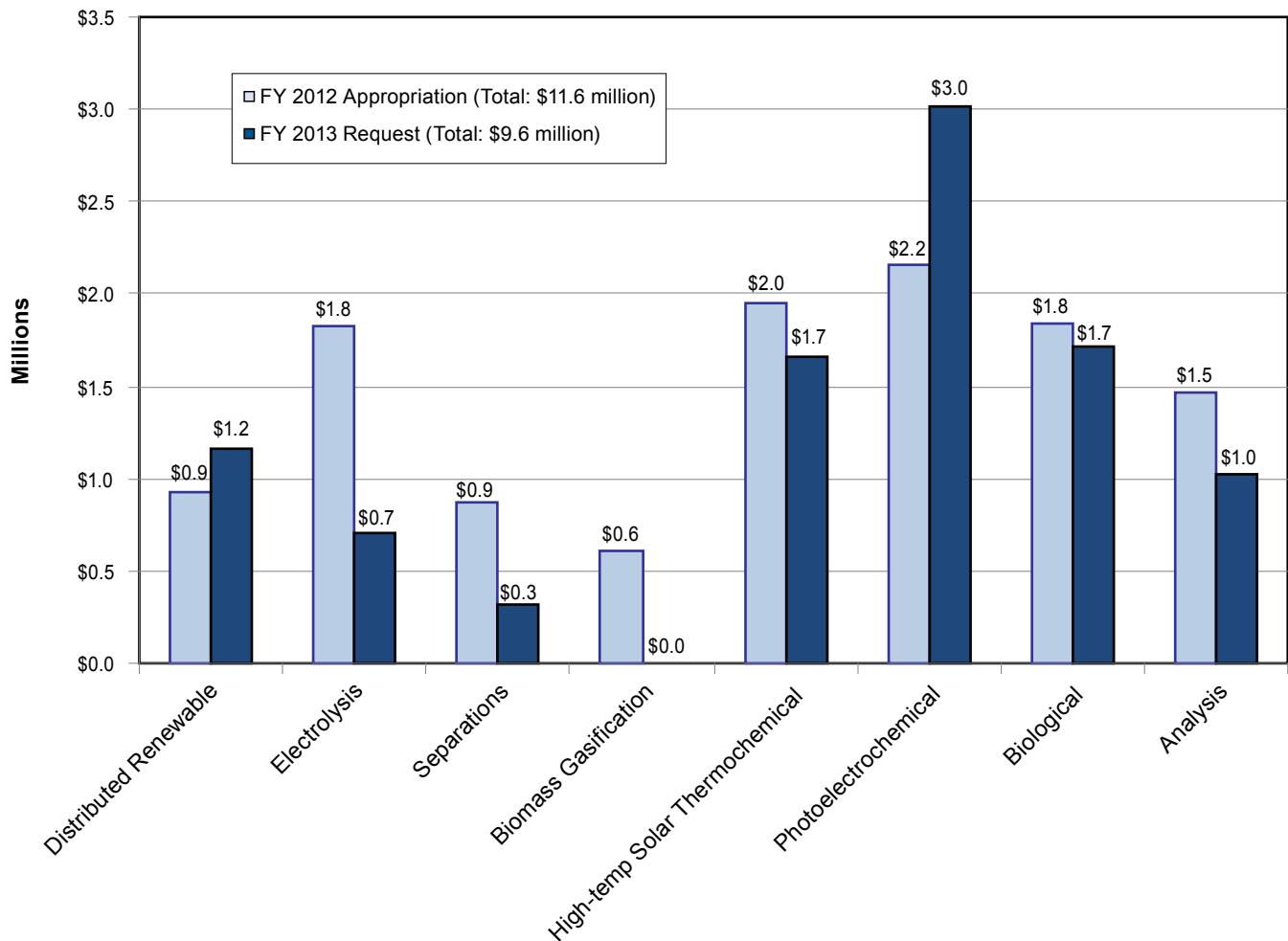
Efforts in these projects were directed toward improving reactor designs, improving voltage and overall efficiency, and addressing membrane crossover issues. Technical progress included:

- Experimentally verified by Raman spectroscopy that hercynite reaction materials follow a redox mechanism through stable aluminates; and demonstrated hydrogen production at reduced temperatures as low as 1,360°C for up to 23 thermal reduction cycles using this novel material. (U. of Colorado, Boulder)
- Developed a phase-change thermal energy storage approach using NaCl for the sulfur-ammonia thermochemical hydrogen production reaction cycle to allow 24/7 operation of the cycle. The molten NaCl approach will provide a large amount of thermal capacity (481 kJ/kg) at temperatures up to 800°C. (SAIC)
- Designed a particle bed reactor featuring particle cycling, high solar utilization, and theoretical solar efficiency >30% over a broad range of direct normal insolation levels from 1,000 W/m² (corresponding to full midday sun) down to 400 W/m². (Sandia National Laboratories)
- Demonstrated of a Faradaic efficiency >95% in the electrolysis step for the CuCl reaction cycle, with a stable cell potential at 0.7 V and the current density of 0.5 A/cm² using a Nafion[®]-based membrane. No copper deposits on any of the cell components were observed after a 36 hour test, indicating a significant mitigation of copper-crossover as a primary technological barrier. (Argonne National Laboratory)

BUDGET

The FY 2012 appropriation for the Hydrogen Production and Delivery sub-program of the FCT Program was \$17.4 million. Funding was distributed approximately 67% to 33% between Production and Delivery, respectively (the same distribution used in FY 2011). Production funding has increasingly focused on early development, long-term, renewable pathways such as photoelectrochemical, biological, and solar-thermochemical hydrogen production. This trend, as shown in the budget breakdown chart in Figure 2, is expected to continue in FY 2013 as projects focused on separations, biomass gasification, and electrolysis transition from the R&D portfolio to Small Business Innovation Research and Technology Validation funding venues. \$9.6 million in funding is planned for Hydrogen Production from the FY 2013 request.

Hydrogen Production Funding



FY 2013 PLANS

General Hydrogen Production sub-program plans for FY 2013 include:

- Continue the emphasis on addressing major challenges in hydrogen production. Performance and durability enhancements in materials and systems will remain a priority, and cost reductions will be achieved through process optimization for all production pathways and technologies. Additional efforts will also address reducing the cost of materials and capital equipment.
- Continue to develop and update case studies for hydrogen production pathways using H2A v3 to identify and address cost barriers and technical challenges.
- Continue to develop and refine materials characterization protocols and performance metrics for early development technologies.
- Use recommendations from the HTAC Hydrogen Production Expert Panel to inform portfolio planning (including coordination with other agencies and DOE Offices to leverage R&D investments in hydrogen production technologies).
- Continue EERE coordination with the Office of Science, which plans approximately \$50 million in basic research related to hydrogen and fuel cell technologies. Through Basic Science activities, a fundamental

understanding of issues related to hydrogen production (particularly in the longer-term R&D areas of photoelectrochemical and biological processes) can help address the challenges of hydrogen production. Coordination of the solar-hydrogen-related fundamental research activities in the Office of Science's Solar Fuels Innovation Hub with the hydrogen production systems-oriented R&D in EERE will be a high priority.

- Initiate new starts in Production Analysis and R&D through competitive funding opportunity announcements.

Some important pathway-specific milestones planned for FY 2012 in the Hydrogen Production sub-program projects include:

- Extend lifetime measurements of GaInP₂/GaAs devices for photoelectrochemical production of hydrogen and determine the durability benchmarked against the target of a 500-hour operational lifetime under conditions equivalent to 10% STH efficiency.
- Verify bipolar plate designs for electrolyzer stacks with sufficient performance and durability to enable cost projections based on early prototypes meeting production target of \$3.70/kg.
- Advance the studies of integrated systems for biological hydrogen production, first improving hydrogen production by fermentation of biomass-based substrates by at least 20%, then demonstrating that a prototype microbial reverse-electrodialysis electrolysis cell reactor can produce hydrogen using the fermentation effluent without grid electricity inputs.

Sara Dillich

Hydrogen Production & Delivery Team Lead (Acting)
Fuel Cell Technologies Program
Department of Energy
1000 Independence Ave., SW
Washington, D.C. 20585-0121
Phone: (202) 586-7925
Email: Sara.Dillich@ee.doe.gov

II.A.1 Biomass-Derived Liquids Distributed (Aqueous Phase) Reforming

David King (Primary Contact), Yong Wang,
Ayman Karim, Christopher Howard, Sarah Widder
Pacific Northwest National Laboratory (PNNL)
P. O. Box 999
Richland, WA 99352
Phone: (509) 375-3908
Email: david.king@pnl.gov

DOE Manager

HQ: Sara Dillich
Phone: (202) 586-7925
Email: Sara.Dillich@ee.doe.gov

Project Start Date: October 1, 2004

Project End Date: Project continuation and direction
determined annually by DOE

Fiscal Year (FY) 2012 Objectives

- Develop aqueous phase reforming (APR) catalysts and technology to convert bio-derived liquids to hydrogen that meets the DOE 2012 cost target of \$3.80/gge, verified by H2A analysis
- Identify primary compounds in bio-oil that are extractable into an aqueous phase
- Determine the effectiveness of aqueous phase reforming in producing hydrogen from these water-soluble compounds
- Estimate cost of hydrogen production using best catalytic results, given a defined feedstock cost

Technical Barriers

This project addresses the following technical barriers from the Production section (3.1.2) of the Fuel Cell Technologies Program Multi-Year Research, Development and Demonstration Plan:

- (A) Reformer Capital Cost
- (D) Feedstock Issues
- (E) Greenhouse Gas Emissions

Technical Targets

TABLE 1. Progress towards Meeting Technical Targets for Distributed Production of Hydrogen from Bio-Derived Renewable Liquids

| Characteristics | Units | 2012 Status | 2017 Target |
|------------------------------------|--------|-------------|-------------|
| Capital Cost | \$/gge | 1.77 | 0.40 |
| Storage, compression, dispensing | \$/gge | 2.00 | 0.35 |
| Fixed operation and maintenance | \$/gge | 0.44 | 0.40 |
| Feedstock Cost | \$/gge | 27.08 | 1.55 |
| Variable operation and maintenance | \$/gge | 0.29 | 0.30 |
| Total hydrogen cost | \$/gge | 31.84 | 3.00 |

gge – gasoline gallon equivalent

FY 2012 Accomplishments

- Aqueous fraction of bio-oil has been examined as low-cost bio-liquid feedstock for APR
- New catalyst leads, especially 5% Pt-1.5% Co/ZrO₂, have been identified and have potential to improve H₂ yield and economics
- Demonstrated that meeting the 2017 target <\$3.00/kg H₂ (produced and dispensed) will be very challenging, and a much lower feedstock cost than 2012 H2A value of \$1.12/gal is required to meet the target



Introduction

This project focuses on the APR of biomass-derived liquids for the production of hydrogen. We target the development of catalysts and catalytic processes to meet the 2017 DOE target of <\$3.00/gge (dispensed). Our H2A analysis has indicated that the primary driver for the cost of H₂ produced from bio-derived liquids is feedstock cost, assuming good catalytic APR performance. As a result, in FY 2011 we switched from relatively purified (and more expensive) bio-liquids, such as glycerol and sorbitol, to pyrolysis oil. Pyrolysis oil (bio-oil) is lower cost and potentially has much higher availability than other bio-derived liquids. Our specific plan is to carry out APR on the water soluble fraction of bio-oil. This fraction is most conveniently generated by addition of water to the initial bio-oil product. It contains lower molecular weight species and a higher fraction of oxygen-containing functional groups than the water-insoluble fraction. As a result, the water soluble fraction is expected to have a greater potential for successful APR to produce hydrogen. In FY 2012 we proposed to

continue the work initiated in FY 2011, with a greater focus on examining alternative catalysts for H₂ production.

Approach

We started by obtaining a source of non-stabilized bio-oil, and mixed it with water in order to generate a water-soluble fraction. We then proceeded to identify the major compounds, and classes of compounds present in this fraction by high performance liquid chromatography (HPLC). From that, we identified one representative compound from each of the classes of compounds identified: 1-propanol (alcohols, mono-oxygenates); glycerol (polyols); acetic acid (carboxylic acids).

We carried out a preliminary evaluation of catalyst performance in a high throughput combinatorial reactor with each of the three compounds identified above. We used our standard testing conditions of relatively low temperatures (225-265°C) and sufficient pressure (about 30 bar) to maintain liquid phase operation. In one set of experiments we examined performance at 300°C. The purpose of the combinatorial testing was to examine possible alternate catalysts to our Pt-Re/C catalyst, which was deemed inadequate to meet the H₂ cost target. The work examined several catalysts based on bimetallic combinations of metals. We also compared performance with ZrO₂ support in place of carbon. Subsequent studies with single unit reactor testing are scheduled for completion prior to the end of FY 2012, examining performance with the surrogate mixture of aqueous soluble bio-oil and then an actual feedstock sample. Finally, the results will be included in the H2A analysis.

Results

Bio-oil generated from pyrolysis of pine saw dust (480°C, 1.6 sec residence time) was mixed with water at a ratio 4 parts H₂O:1 part bio-oil by weight. The sample was shaken vigorously to form a single phase, and then centrifuged to generate the aqueous and non-aqueous phases. Figure 1 shows that a large fraction of the total carbon in the bio-oil was soluble in the water fraction. Table 2 provides the distribution of identified products comprising the bio-oil (accounting for ~70% of the carbon available), as identified by HPLC. The majority of the products are oxygenated hydrocarbon, primarily having four or fewer carbon atoms in the molecule.

Table 2 shows that it is possible to categorize the products according to oxygen content and type: poly-oxygenates (polyols, sugars); mono-oxygenates (alcohols, aldehydes and ketones); and carboxylic acids. We selected one molecule from each group to carry out further tests to screen improved catalyst formulations: glycerol, 1-propanol, and acetic acid.

Segregation of bio-oil carbon, by phase (wt% C in raw bio-oil)

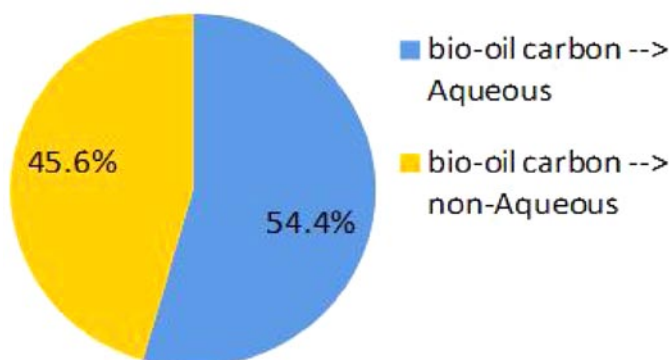


FIGURE 1. Segregation of bio-oil carbon between water and oil fractions; water/oil = 4/1 (wt)/(wt)

TABLE 2. Major Species Identified in the Aqueous Fraction of Bio-Oil by HPLC Analysis

| Poly-Oxygenates | Mono-Oxygenates | Carboxylic Acids |
|-----------------|-----------------|------------------|
| glycerol | 1-butanol | acetic acid |
| glycolic acid | isobutanol | propionic acid |
| ethylene glycol | 1-butanol | |
| glycolaldehyde | ethanol | |
| levoglucosan | 1-propanol | |
| sorbitol | | |
| glucose | | |
| xylose | | |

Based on our work in FY 2011, we found that several molecules in the bio-oil were not reactive toward hydrogen formation, and that acetic acid was difficult to reform and moreover tended to deactivate the 5% Pt-3% Re/C catalyst, reversibly. The primary effort in FY 2012 was to make progress was to develop catalysts that were more active and selective toward H₂. For this reason, we carried out a high throughput screening effort to identify better catalysts. Our first effort was to screen catalysts using glycerol as feedstock, representing the poly-oxygenate class of molecules. Figure 2 shows the possible reaction pathways available to even a seemingly simple three-carbon molecule. The cause of these divergent pathways is a competition between the desired C-C bond cleavage which leads to production of H₂ and CO (and with subsequent water gas shift, the CO shifts to CO₂ and a second molecule of H₂ is generated); and a pathway based on loss of water from the molecule (dehydration), which does not produce hydrogen but rather leads to more saturated

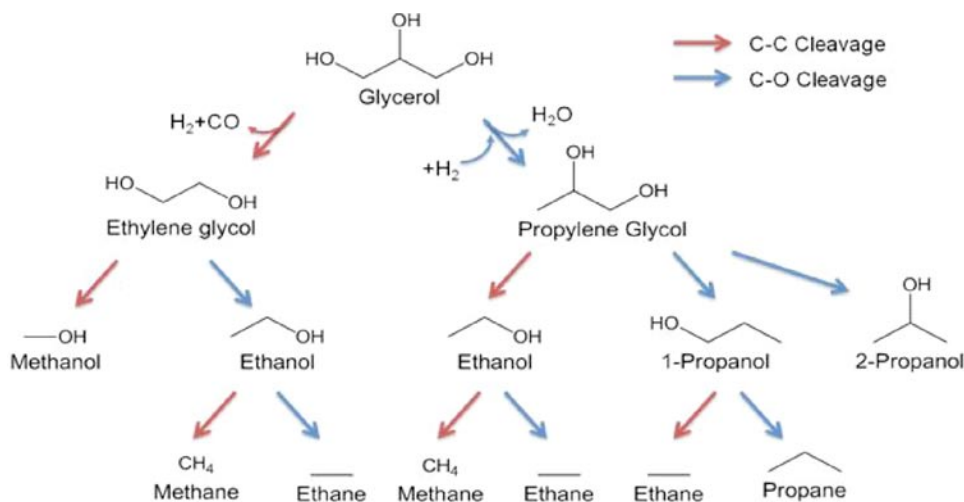


FIGURE 2. Facilitating C-C bond breaking is the key to hydrogen production from glycerol

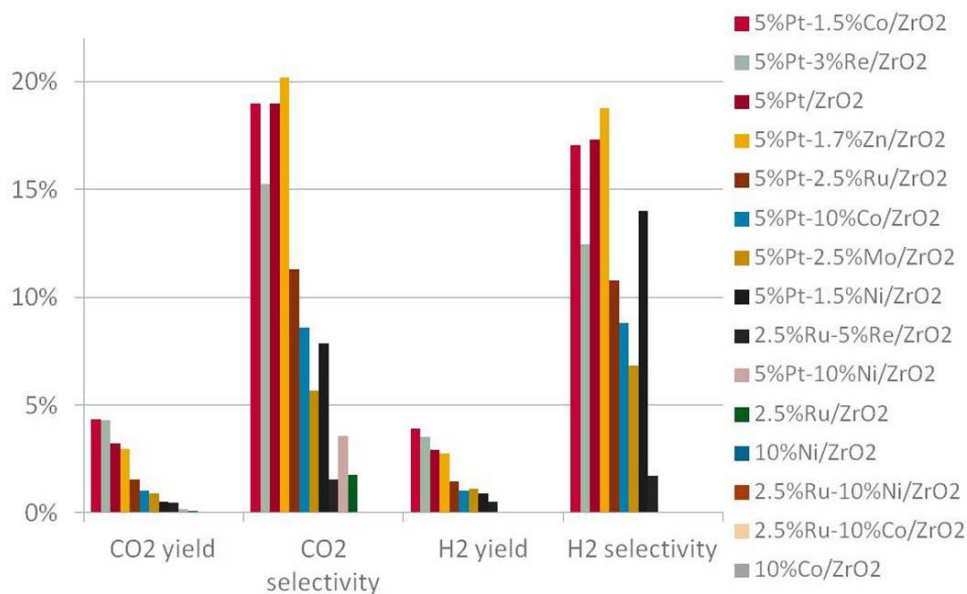


FIGURE 3. Catalyst combinatorial screening for maximum activity and C-C/C-O cleavage: glycerol APR for selected mono- and bi-metallic catalysts supported on ZrO₂

hydrocarbons. Our screening tests were aimed at identifying catalysts that produce the maximum amount of hydrogen. The results of the high throughput test are shown in Figure 3. One thing to notice is that although there were many catalysts screened, fewer provide data in the figure, indicating that many catalysts, including (notably) the single, non-precious metal catalysts, show poor APR activity. A figure of merit was generated (not shown) based on the product of the values for CO₂ yield, CO₂ selectivity, H₂ yield, and H₂ selectivity. The figure of merit was found to be highest for 5% Pt-1.5% Co/ZrO₂, 5% Pt-3% Re/ZrO₂, and 5% Pt/ZrO₂. The new bimetallic combination was the addition of the Pt-Co catalyst.

Studies for 1-propanol APR showed similar behavior and catalyst ranking, although at best 1-propanol generated 1 mole of H₂. This is determined by the fact that ethane was a common product, (rather than ethylene), indicating that one of the two potential molecules of H₂ formed reacted with the C₂ fragment to form ethane. Operation at higher temperature (300°C) did not have any effect on improving selectivity or generating methane, the latter which could be subsequently reformed. Examination of acetic acid performance showed that only the Pt-Re/C catalyst showed the ability to recover activity after being exposed to acetic acid. The remainder of

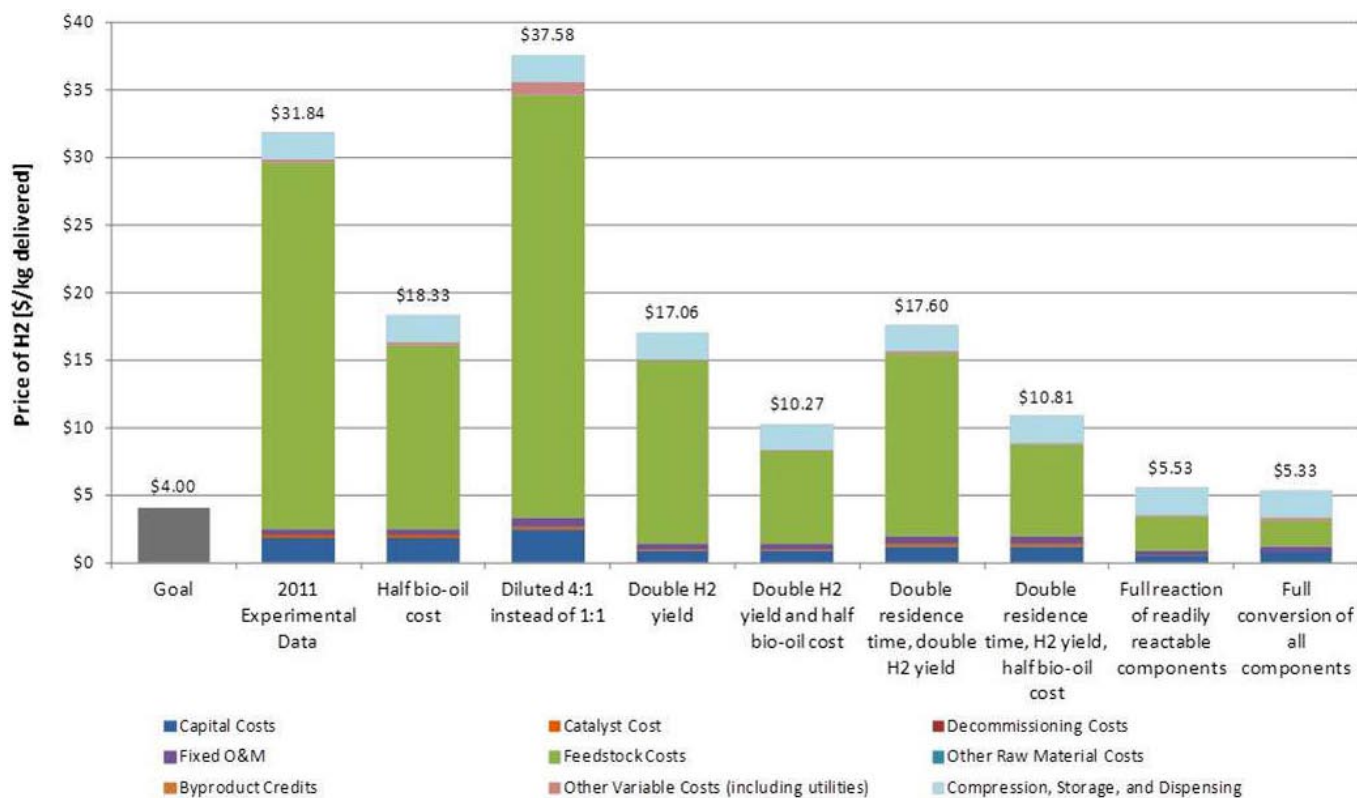


FIGURE 4. H₂Av3 sensitivity analysis

the catalysts showed irreversible deterioration of the catalyst following exposure to acetic acid.

The APR performance with the aqueous fraction of bio-oil is summarized in the H₂Av3 analysis (Figure 4). Part of this summary is based on FY 2011 performance, as FY 2012 studies have not yet been completed. A number of scenarios are considered to determine effects of various factors on H₂ production cost. As expected, a big factor is high feedstock cost. This is based mainly on poor H₂ yield from many of the molecules in the feed, and poses an inherent problem in meeting the delivery target. Improved catalysts are expected to make at best a partial improvement to the H₂ cost, but not to the extent that the \$3.00/kg target can be met.

Conclusions and Future Directions

- Aqueous fraction of bio-oil has been examined as low cost bio-liquid feedstock for APR, and shown to comprise poly-oxygenates, mono-oxygenates, and carboxylic acids, predominantly C₆ or lower. Of these, only the poly-oxygenated components have potential for significant hydrogen production. The theoretical maximum yield of hydrogen with this aqueous bio-oil feed is relatively low in comparison to glycerol, sorbitol, or other predominantly polyol-based feedstocks.

- New catalyst leads, especially Pt-Co/ZrO₂, have been identified and have significant potential to improve H₂ yield and economics compared with FY 2011 results.
- Meeting the target of \$3.00/kg H₂ (produced and dispensed) will be very challenging. The theoretical best H₂ yield case will likely exceed this target, given the feedstock composition and the low potential H₂ yield from mono-oxygenates. A lower feedstock cost than 2012 H₂Av3 value of \$1.12/gal is required to meet the target.
- Concluding work in FY 2012 will be to complete testing with best catalyst of aqueous phase bio-oil, and provide a report and H₂A analysis summarizing findings.
- There are no plans to continue this work in FY 2013, given the challenges to meet the H₂ cost target for 2017.

FY 2012 Publications/Presentations

- Liang Zhang, Ayman M. Karim, Zhehao Wei, David L. King, Yong Wang. Correlation of Pt-Re surface properties with reaction pathways for the aqueous-phase reforming of glycerol. *J. Catal.* 287 (2012) 37-43.

II.A.2 Distributed Bio-Oil Reforming

Stefan Czernik (Primary Contact), Richard French,
Michael Penev

National Renewable Energy Laboratory (NREL)
15013 Denver West Parkway
Golden, CO 80401
Phone: (303) 384-6135
Email: Stefan.Czernik@nrel.gov

DOE Manager

Sara Dillich
Phone: (202) 586-1623
Email: Sara.Dillich@ee.doe.gov

Subcontractor:

University of Minnesota, Minneapolis, MN

Project Start Date: October 1, 2004

Project End Date: September 30, 2012

Technical Targets

TABLE 1. Progress toward Meeting DOE Distributed Hydrogen Production Targets

| Distributed Production of Hydrogen from Bio-Derived Renewable Liquids | | | |
|---|--------|------------------|------------------|
| Process Characteristics | Units | 2012 DOE Targets | 2012 NREL Status |
| Production Energy Efficiency | % | 72 | 62 |
| Total Hydrogen Production Costs | \$/gge | 3.80 | 4.80–6.60* |

*Based on hydrogen production cost of \$2.80–4.60/gasoline gallon equivalent (gge) assuming bio-oil cost ranges from \$100–\$236/ton. Allowance for compression, storage, and distribution is \$2.00/gge.

FY 2012 Accomplishments

- Demonstrated hydrogen production by auto-thermal reforming using an integrated bench-scale system including WGS and electrochemical separation.
- Produced hydrogen at 100 L/h on the integrated bench-scale system and obtained a yield of 9.1 g H₂/100 g bio-oil.
- Demonstrated >30 h of hydrogen production on the integrated bench-scale system.



Introduction

Renewable biomass is an attractive near-term alternative to fossil resources because it has near zero life-cycle carbon dioxide (CO₂) impact. The most recent assessment says that more than 1 billion tons of biomass could be available in the United States each year at less than \$60/ton [1]. This cost may increase to \$72/ton when transportation, drying, and grinding are included. This biomass could be converted to 100 million tons of hydrogen, enough to supply the light-duty transportation needs of the United States. This work addresses the challenge of distributed hydrogen production with a targeted total dispensed hydrogen cost of \$3.80/kg by 2012 [2]. Pyrolysis is used to convert biomass to a liquid that can be transported more efficiently and has the potential to be used in automated operation conversion systems [3,4]. “Bio-oil” can then be converted to hydrogen and CO₂ in a distributed manner at fueling stations.

The thermally reactive compounds in bio-oil tend to decompose thermally and may form carbonaceous deposits and/or aromatic hydrocarbons, which are more difficult to convert to hydrogen. Thus, conventional fixed-bed reformers

Fiscal Year (FY) 2012 Objectives

- By 2012, develop and demonstrate distributed reforming technology for producing hydrogen from bio-oil at \$4.10/kilogram (kg) purified hydrogen.
- Demonstrate integrated performance at bench scale including bio-oil vaporization, partial-oxidation (POX) reforming, water-gas shift (WGS), and hydrogen separation.
- Demonstrate production of hydrogen at a rate of 100 liters per hour (L/h) for 100 hours.

Technical Barriers

This project addresses the following technical barriers from the Production section of the Fuel Cell Technologies Program Multi-Year Research, Development and Demonstration Plan:

- (A) Fuel Processor Capital
- (C) Operation & Maintenance
- (D) Feedstock Issues

have not been proven efficient for this highly reactive feedstock. Reactors that fluidize or circulate the catalyst are much more suited for this application [5] but are not the optimal choice for small-scale and unattended operation. The objective of this project is to develop a system that will provide distributed production of hydrogen from bio-oil at filling stations. To accomplish this we are developing a simple fixed-bed reactor suitable for unsupervised automated operation.

Approach

This research project is focused on developing a compact, low-capital-cost, low/no maintenance reforming system that will enable achievement of the cost and energy efficiency targets for distributed reforming of renewable liquids. In this project, we are evaluating the following steps in the process:

- **Bio-oil volatilization** using ultrasonic atomization. Blending with alcohol is being used to control the physical and chemical properties of the liquid, primarily to achieve an acceptable viscosity.
- **Heterogeneous auto-thermal reforming of bio-oil derived gas and vapor.** Nickel and precious-metal reforming catalysts have been tested. Platinum has proven to be the most effective.

Earlier experiments were carried out using a micro-scale continuous flow tubular reactor coupled with a molecular-beam mass-spectrometer gas analyzer or a bench-scale quartz-tubular reactor with full mass balances and chromatographic gas analysis. This year, a series of tests was conducted using an integrated bench-scale reactor system that included evaporation, vapor filtration, partial-oxidation reforming, WGS, and hydrogen separation to provide a more complete and realistic assessment of the performance of the process.

Results

Integrated bench-scale auto-thermal reforming tests were carried out in the system shown in Figure 1. Poplar pyrolysis bio-oil diluted with 10 wt% methanol was fed at 60–120 g/h using a high-pressure syringe pump (Isco) and 60 kHz ultrasonic nozzle (Sono-Tek) to the top of a 37 mm internal diameter (ID), 150 mm long tubular stainless steel evaporation chamber where it was mixed with air and nitrogen. This was placed on top of a 40 mm ID, 250 mm long 2 μ m stainless-steel mesh filter vessel. Both vessels operated at 400°–600°C. The resulting vapors passed with additional steam into an Incolloy 800 vessel containing a 40 mm by 300 mm bed containing 0.5% platinum-on-alumina reforming catalyst (200 g, BASF) operating at 800°–900°C. The product gas was further processed in a 22-mm

ID by 30-cm fixed bed of high-temperature (350°C) WGS catalyst (190 g, iron/chrome, Sud Chemie), and then on to an electrochemical separator (H₂ Pump), which separated a pure hydrogen stream from the wet, mixed product gas. Water was removed from the remaining product gas in the condenser. The outlet gas flow rate was measured by a dry test meter. The concentrations of CO₂, CO, and CH₄ in the product gas were monitored by a non-dispersive infra-red analyzer (Model 300 from California Analytical Instruments); the hydrogen concentration was tracked by a TCM4 thermal conductivity monitor. In addition, the gas was analyzed every four minutes by an on-line Varian (Model 4900) micro gas chromatograph, which provided concentrations of H₂, CO, CO₂, CH₄, C₂H₄, O₂, and N₂. The temperatures in the system, as well as the flows, were recorded and controlled by an OPTO 22 data acquisition and control system. Based on the flows and compositions of the process streams, mass balances as well as the yields of hydrogen generated from the feed were calculated.

Some integrated testing was achieved in which it was found that the WGS reactor reduced the CO concentration in

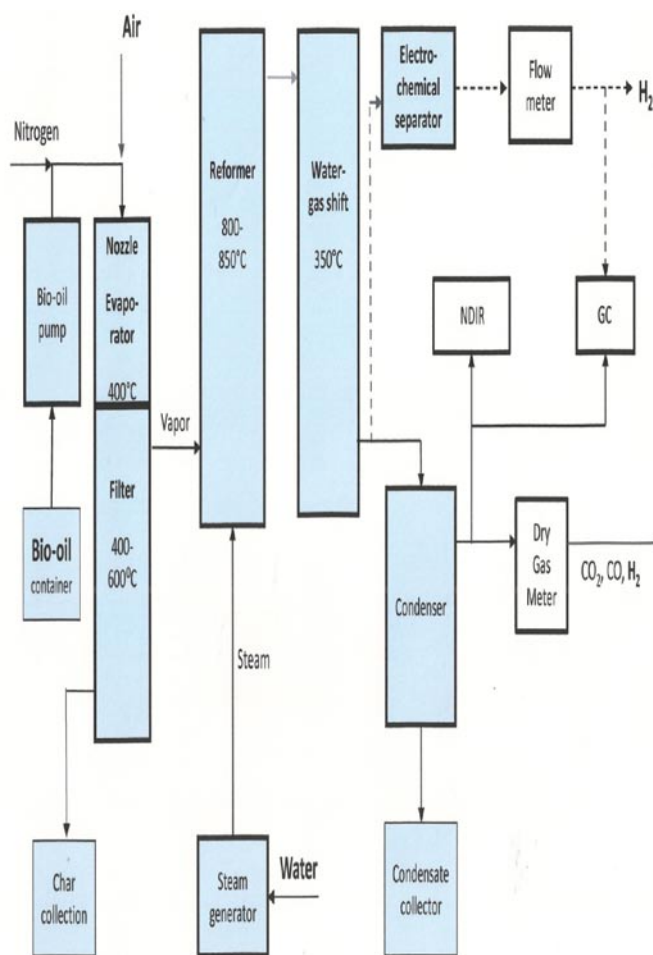


FIGURE 1. Schematic of integrated bio-oil to hydrogen system

the product by about a factor of 4 for at least a short period of time. Also, the hydrogen separator did initially produce a pure hydrogen stream. However, after achieving initially promising yields at the end of FY 2011, it was necessary to start using a new batch of oil. This oil proved more difficult to vaporize, tending to form deposits in the top of the evaporator, leaving more char cenospheres in the filter, and giving more re-deposition of vapor on the filter. It eventually proved possible to get more reliable performance from this oil by raising the evaporator and filter temperatures to about 600°C, and carefully controlling the oil flow rate and the nozzle power and temperature. However, the char yield from this oil was still high, so the best yield obtained from this oil was 9.1 g H₂/100 g oil versus 10.1 g H₂/100 g oil for the previous batch. Some data are shown in Figure 2. This experiment was performed at 850°C with an O/C of 1.5 and an S/C of 3.0 at a gas hourly space velocity of 1,950 h⁻¹. These data show effective CO reduction by the WGS catalyst.

Recent changes in estimated biomass costs have had a large effect on the estimated cost of this process. Previous economic assessments were based on a biomass cost of \$30/ton. Figure 3 shows recent cost estimates for this project; the range of costs is based on different costs for biomass pyrolysis oil (\$100–\$236/ton) from different costs of biomass (\$30–\$72/ton) and different-sized plants (500–2,000 dry tons per day). This shows that although the lower yield from the lower-quality oil used in 2012 had some effect on cost, the largest effect on the cost is the cost of the bio-oil which is about 59% of the hydrogen production cost. In practice, biomass will be available at a range of costs, from about

\$30–\$72/ton, and eventual commercial plant sizes are still uncertain. To meet the DOE targets it would be necessary to have low-cost biomass, a very cost-efficient pyrolysis process and continued progress in development of the POX reforming technology.

In the near future, tests will continue to demonstrate 100 hours of operation on the integrated system. This will

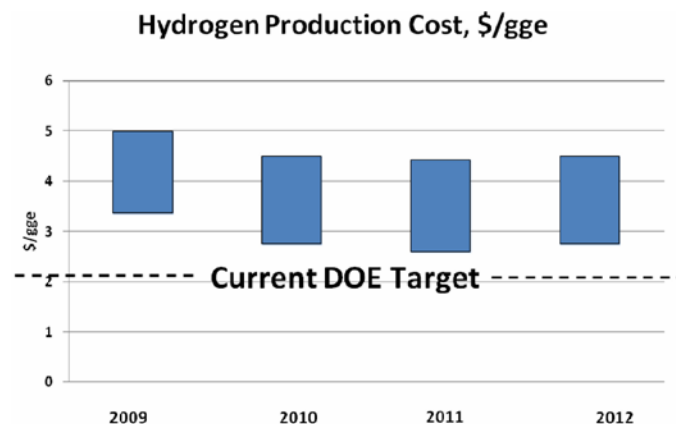


FIGURE 3. Hydrogen production cost estimates from 2009–2012 for distributed bio-oil reforming. The hydrogen cost values correspond to bio-oil prices in a range of \$100–\$236/ton. Increase in cost from 2011 to 2012 is due to a lower yield of hydrogen produced from a new batch of bio-oil (contains higher fraction of non-volatile compounds). For a 1,500 kg/day hydrogen plant with \$236/ton oil, the total production cost was estimated to be \$4.60/gge. Compression, storage, and dispensing are assumed to add \$2.00/gge to the total cost of hydrogen.

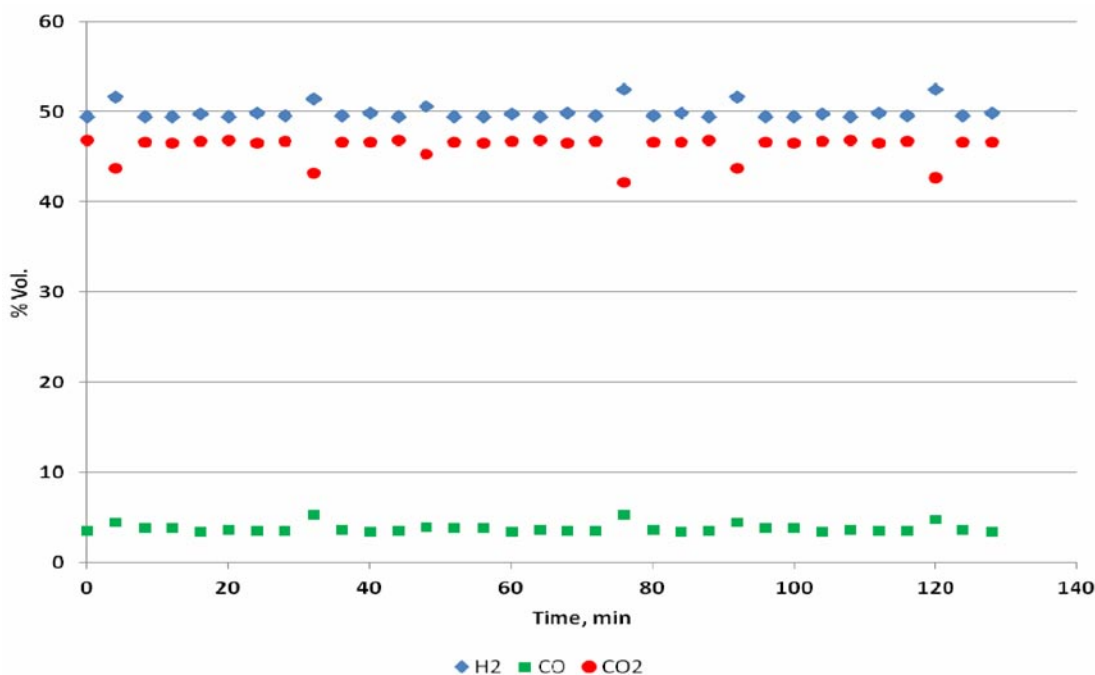


FIGURE 2. Product gas composition from auto-thermal reforming with WGS of poplar bio-oil using BASF 0.5% Pt/Al₂O₃ catalyst

demonstrate the performance of the reforming and WGS catalysts and the hydrogen separator over a longer time period, revealing any effects of organic and inorganic poisons on the components of the integrated system.

Since this work has shown the importance of bio-oil properties to the hydrogen yield, any continuing funding for FY 2013 will be used to explore the dependence of system performance on bio-oil composition, measured as the hydrogen yield and carbon-to-gas conversion. Two different bio-oils and a lignin-free bio-oil will be analyzed to determine elemental and proximate composition as well as average molecular weight (related to volatility). These three liquids will be processed in the bench-scale integrated reforming system to determine process performance data (mass balances, hydrogen yields). Based on those tests, the relationship between the amount of non-volatile fraction and the hydrogen yield will be established. If further additional funding is available, a pressurized system will be constructed to assess how much improvement in reforming kinetics can be achieved at a pressure of about 200 psig (14 bar)—a pressure that is typically used for methane steam reforming. This could reduce reactor size and catalyst use, thus reducing hydrogen production costs.

Conclusions and Future Directions

- Operation of the integrated bench-scale reactor using 90 wt% bio-oil/10 wt% methanol mixtures produced a hydrogen yield of 9.1 gH₂/100 g bio-oil, demonstrated hydrogen production at 100 L/h, and demonstrated the initial effectiveness of water-gas shift and electrochemical separation. Except for the gas compression, this system includes all the same basic unit operations as the design for the 1,500 kg/day hydrogen plant.
- For the new batch of bio-oil, the hydrogen yield achieved so far was 9.1 g/100 g bio-oil and the bio-oil carbon-to-gas conversion was >85%.
- It was demonstrated that the composition of the bio-oil can have a substantial impact on the hydrogen yield.
- Tests will continue to obtain 100 hours of operation at 100 L/h hydrogen production.
- If funded, integrated bench-scale tests of pyrolysis oils with different compositions will be carried out in order to determine the effect of bio-oil composition on hydrogen yield.
- If funded, a pressurized bench-scale auto-thermal bio-oil reformer will be constructed and the effect of pressure on bio-oil reforming will be tested.

FY 2012 Publications/Presentations

1. Czernik, S., “Distributed Bio-Oil Reforming,” 2012 DOE Fuel Cell Technologies Program Annual Merit Review, May 17, 2012, Washington, D.C.

References

1. Perlack, R.; Stokes, B. (Leads). U.S. Billion-Ton Update: Biomass Supply for a Bioenergy and Bioproducts Industry, U.S. Department of Energy, ORNL/TM 2011/224, August 2011.
2. U.S. Department of Energy. *Fuel Cell Technologies Program, Multi-Year Research, Development and Demonstration Plan*, Section 3.1 Hydrogen Production, 2011 Interim Update. U.S. Department of Energy, Office of Energy Efficiency and Renewable Energy: Washington, D.C.
3. Czernik, S., Elam, C., Evans, R., Milne, T. “Thermochemical Routes to Hydrogen from Biomass—A Review.” In *Science in Thermal and Chemical Biomass Conversion*, Bridgwater AV, Boocock DGB, eds., CPL Press: Newbury, UK, 2006, pp.1752–1761.
4. Evans, R.J., Czernik, S., French, R., Marda, J. “Distributed Bio-Oil Reforming,” *DOE Hydrogen Program FY2007 Annual Progress Report*, 2007.
5. Czernik, S., French, R., Feik, C., Chornet, E. “Hydrogen by Catalytic Steam Reforming of Liquid Byproducts from Biomass Thermoconversion Processes.” *Industrial & Engineering Chemistry Research*. 2002, 41(17), 4209–4215.

II.B.1 One Step Biomass Gas Reforming-Shift Separation Membrane Reactor

Michael Roberts (Primary Contact),
Razima Souleimanova
Gas Technology Institute (GTI)
1700 South Mount prospect Rd,
Des Plaines, IL 60018
Phone: (847) 768-0518
Email: roberts@gastechnology.org

DOE Managers

HQ: Sara Dillich
Phone: (202) 586-7925
Email: Sara.Dillich@ee.doe.gov
GO: Katie Randolph
Phone: (720) 356-1759
Email: Katie.Randolph@go.doe.gov

Contract Number: DE-FG36-07GO17001

Subcontractors:

- National Energy Technology Laboratory (NETL), Pittsburgh, PA
- Schott North America, Duryea, PA
- ATI Wah Chang, Albany, OR

Project Start Date: February 1, 2007
Project End Date: June 30, 2013

Technologies Program Multi-Year Research, Development and Demonstration Plan:

- (L) Impurities
- (N) Hydrogen Selectivity
- (O) Operating Temperature
- (P) Flux

Technical Targets

This project is directed at developing a membrane reactor that can be closely-coupled with a gasification reactor while having a sufficiently high hydrogen flux to achieve a hydrogen production cost of \$2-4/gge (without delivery) per the DOE 2012 technical target.

FY 2012 Accomplishments

- Best candidate membrane was chosen: Pd₈₀Cu₂₀ membrane of 5 μm in thickness.
- Process development and economic analysis with best candidate membrane shows process's potential to be economically feasible.
- Fabrication of demonstration membrane module is initiated.



Fiscal Year (FY) 2012 Objectives

GTI together with its partners, NETL, Schott North America and ATI Wah Chang are working to determine the technical and economic feasibility of using the membrane gasifier to produce hydrogen from biomass. Specifically, the team plans to:

- Reduce the cost of hydrogen from biomass to \$2-4/gasoline gallon equivalent (gge) H₂ [1] (excluding delivery).
- Develop an efficient membrane reactor that combines biomass gasification, reforming, shift reaction and H₂ separation in one step.
- Develop hydrogen-selective membrane materials compatible with the biomass gasification conditions.
- Demonstrate the feasibility of the concept in a bench-scale biomass gasifier.

Technical Barriers

This project addresses the following technical barriers from the Hydrogen Production section of the Fuel Cell

Introduction

GTI has developed a novel concept of membrane reactor for clean, efficient, and low-cost production of hydrogen from biomass-derived syngas. GTI's approach is presented in Figure 1 and shows a hydrogen-selective membrane closely coupled with a reforming or gasification reactor for direct extraction of hydrogen from the syngas.

The specific objective of the project is to develop high temperature metallic or glass membranes that can be used closely-coupled with a biomass gasifier. The technical feasibility of using the membrane reactor to produce hydrogen from a biomass gasifier will be evaluated. GTI with its project team (Schott Glass, NETL, and Wah-Chang) has been evaluating potential membranes (metal, ceramic and glass) suitable for high temperature, high pressure, and the harsh environment of a biomass gasifier. The project team has been screening and testing each type of material, investigating its thermal and chemical stability, and conducting durability tests.

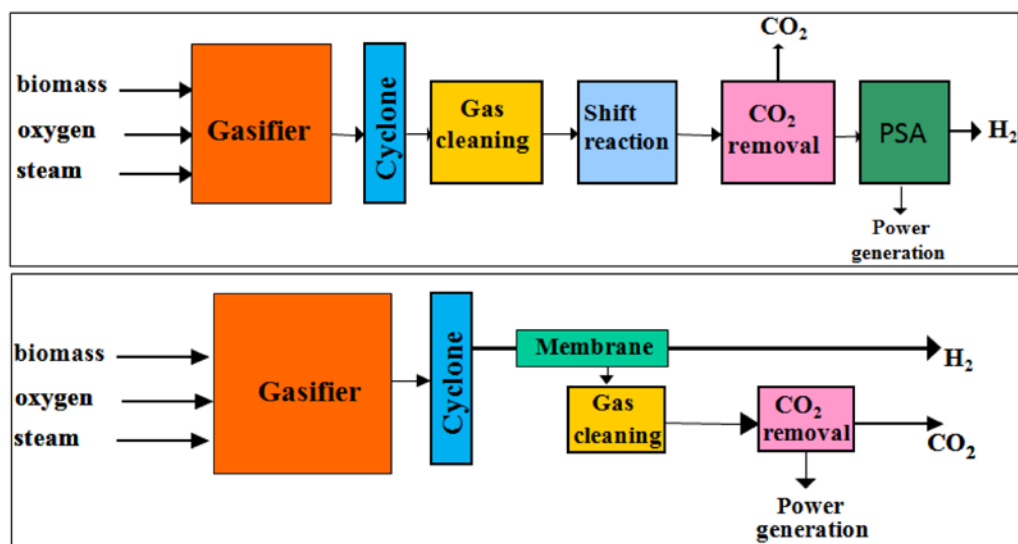


FIGURE 1. Conventional Hydrogen Production from Biomass Gasification and Biomass Gasifier with Close-Coupled Membrane

Approach

To conduct commercially successful research, GTI has developed a plan where efforts are concentrated in four major areas: membrane material development, membrane module development, membrane process development and membrane gasifier scale up. The initial focus of the project has been concentrated on membrane material development. Metallic and glass-based membranes have been identified as hydrogen selective membranes under the conditions of the biomass gasification, temperatures above 700°C and pressures up to 30 atmospheres. Membranes are synthesized by arc-rolling for metallic type membranes and incorporating Pd into a glass matrix for glass membranes. Testing for hydrogen permeability properties have been completed and the effects of hydrogen sulfide and carbon monoxide were investigated for perspective membranes. The initial candidate membrane chosen in 2008 was selected for preliminary reactor design and cost estimates. The overall economics of hydrogen production from this new process will be assessed and compared with traditional hydrogen production technologies from biomass. The final deliverable of the project will be a gasification membrane reactor system that is expected to meet or exceed the DOE's cost target for hydrogen production from biomass. This will be demonstrated by a bench-scale gasification membrane reactor that can process approximately 2–10 kg/hr of woody biomass for hydrogen production.

Results

Based on the timeline of the project, GTI and partners from NETL and Schott researched new candidates for hydrogen-selective membranes.

NETL continued to research hydrogen-selective Pd alloys for high temperature use. Permeable alloys have desirable characteristics for hydrogen membrane applications including high permeability, high temperature strength and cost, but are very susceptible to poisoning of surface catalytic sites and surface corrosion. Therefore, methods of protecting these materials are needed. One possibility being investigated is an inorganic, nonmetallic coating that can protect these alloys at the conditions of interest. Potential inorganic coating systems are being investigated in the literature and synthesis of new tertiary alloy formulations based on Pd metal is in progress.

This year, due to relocations, membrane testing facilities at NETL continued to have a very limited availability.

A niobium-based alloy was identified that may offer high temperature stability under the conditions of interest. These alloys offer good resistance to the corrosive conditions of the post-gasifier environment, however, their hydrogen permeability is still not known. The alloy, a Pd-Cr composition was tested up to 750°C to investigate its potential application for this project. The test was conducted using 100% H₂. Over the range of 650 to 750°C, its permeability was approximately 60% of the permeability of Pd.

SCHOTT continued development of glass ceramic membranes based on results of membranes synthesized by them and tested by GTI. Five new glass melts were completed. All compositions were melted in platinum crucibles and were stable glasses. X-ray fluorescence analyses revealed excellent correspondence between input major oxide wt% and measurements on as-cast glass. Two “alloy” melts were also produced to see what the effects of introducing another metal in addition to the Pd into the base glass had on the performance of the glass. These melts

produced reasonably stable glasses, although one of them revealed evidence of small crystals in the as-cast glass as suggested by a somewhat matte-like appearance, instead of a purely glassy surface. The crystals could be either unmelted material or crystals that formed during the casting and annealing process. In any event, all samples were then ceramized under reducing conditions, ground and polished and sent to GTI for analysis. Glass membranes obtained from SCHOTT were tested for hydrogen permeation by GTI. Unfortunately, these new samples did not yield high H permeation at 800°C during testing.

GTI continued to test membranes fabricated by GTI and other team members as they became available. Pd₈₀Cu₂₀ with 5 microns thickness was tested for hydrogen permeation. Due to small thickness and frailty of metallic foil, there were problems with sealing. The results obtained before the seal failure showed high hydrogen fluxes but no stable state was achieved. These results need to be repeated. Membranes obtained from Schott were tested for hydrogen permeation: low hydrogen permeation was observed (0.04 SCFH/FT²).

Based on all results obtained during this time period, the best membrane candidate based on overall performance is Pd₈₀Cu₂₀ chosen earlier as an initial candidate, but with 5 microns in thickness. Based on inverse dependence of hydrogen permeation with thickness, we expect to increase hydrogen flux several times. For Pd₈₀Cu₂₀ membrane with 120 μm in thickness hydrogen flux at conditions (850°C, pressure difference 85 psi) is about 26 SCFH/FT². The membrane with 5 μm in thickness predicted by Sievert's law will achieved about 600 SCFH/FT² (26*120/5=624).

The fabrication of a membrane module that is compatible with the biomass gasifier is in progress. The module must be reliable, durable and cost effective. GTI fabricated the membrane module in planar design for initial candidate membrane (Pd₈₀Cu₂₀). Sealing was developed to withstand high temperatures and high pressures of operation. Figure 2 shows a section view schematic of the membrane module inside the pressure vessel.

The preliminary process design for a plant to produce hydrogen from a biomass feed using a hydrogen permeable membrane that was previously completed was subjected to a Pinch Analysis to optimize the heat integration and to minimize external heating and cooling demands. A heat exchange network (HEN) analysis then allowed individual heat exchangers to be specified and sized so that the exchanger capital cost estimation could be updated. The pressures in the various pieces of equipment in the process were then updated to make sure that pressure drop driving forces were available for these heat exchangers and all other equipment, and the sizes of the pumps and compressors in the process were updated. The updated process design was documented in a set of twelve drawings to show all the required process equipment.

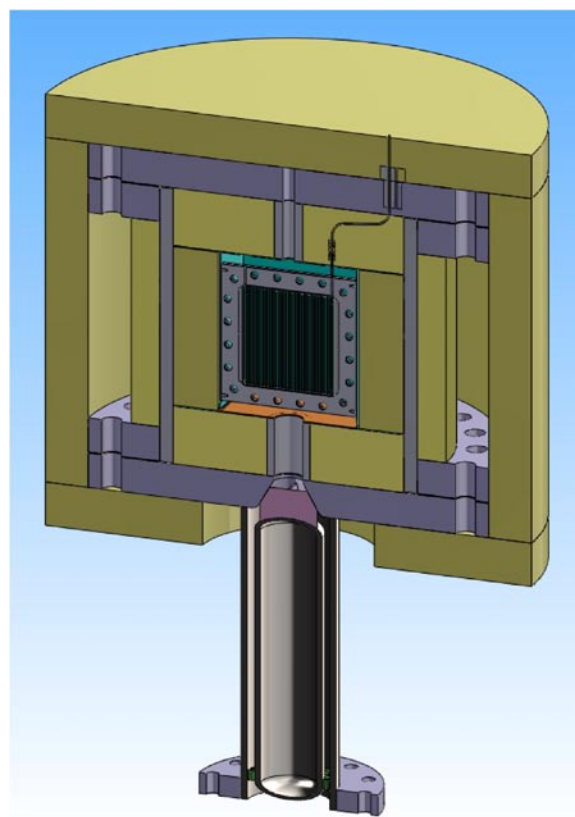


FIGURE 2. Membrane Module Unit in Pressure Vessel

Then, the focus was on engineering design and costing of the process plant that fed 2,000 tons/day of biomass and delivered high-pressure hydrogen product using a hydrogen permeable membrane. Optimum values for gasification temperature, reforming temperature and permeate pressure were used, based on optimization studies previously completed. The ASPEN model of the process was then used to determine the stream flow rates and/or process heat duties for all the process steps so that equipment sizes could be estimated. A Pinch Analysis and HEN analysis was completed so that individual heat exchangers could be sized. The sizes of pumps, vessels, conveyors, compressors, reactors, etc. were based on the flow rates and heat balance from the ASPEN model. This analysis resulted in a listing of the sizes for all major pieces of equipment in the process plant. This compares with a total of 121.5 MM\$ previously estimated from a less complete process design basis, with hydrogen delivered at 1,000 psi.

The more accurate costing increased the capital cost somewhat. If hydrogen is produced at 300 psi, the new capital cost is 129.2 MM\$, compared with the old estimate of 118.0 MM\$. The new capital and operating costs for the membrane process were input into version 3 of the H2A program [2]. This version updates the base year of the

analysis from 2005 to 2007. A revised cost of hydrogen production of \$1.82/kg was obtained, as detailed in Table 1.

TABLE 1. Hydrogen Cost of Production Estimate

| Cost Component | H2 Cost, \$2007/kg |
|----------------------|--------------------|
| Capital Cost | 0.68 |
| Decommissioning | 0.00 |
| Fixed O& M | 0.20 |
| Feedstock Cost | 0.51 |
| Other Raw Material | 0.11 |
| By-Product Credits | 0.00 |
| Other Variable Costs | 0.32 |
| Total | 1.82 |

A tornado diagram was prepared to show the sensitivity to several key process variables as shown in Figure 3.

The main conclusions for Task 2 “Process Development and Techno-Economic Analysis” are:

- Economic optimization was conducted for the variables of reforming (membrane) temperature, permeate pressure, and hydrogen recovery level for membranes 5 microns in thickness. Optimum permeate pressure is about 0.2 bar. Optimum membrane/water-gas shift temperature is at 1,382°F (750°C) or less.
- 2012 Membrane Model Case has recovery of 115% of original H₂. Pressure swing adsorption (PSA) Future Case [3] had about 80% recovery. Over 115% of the hydrogen produced in the gasifier can be recovered due to water-gas shift for membrane.
- Projected using H2A version 3 Cost of hydrogen production with membrane (\$1.82/kg) is less than the cost with PSA (\$2.00/kg).

Conclusions and Future Directions

- GTI and partners will continue to fabricate membrane module for hydrogen separation.
- GTI will test feasibility of membrane module closely-coupled with biomass gasifier.

FY 2012 Publications/Presentations

1. Oral presentation, PD070 Roberts, 2012 Annual Merit Review, Washington, D.C., May 13–17, 2012.

References

1. Presentation on 2011 Annual Merit Review by DOE.
2. https://apps1.hydrogen.energy.gov/cfm/register.cfm?model=02D_Future_Central_Hydrogen_Production_via_Biomass_Gasification_version_3.0.xls.
3. P. Spath, A. Aden, T. Eggeman, M. Ringer, B. Wallace, and J. Jechura, “Biomass to Hydrogen Production Detailed Design and Economics Utilizing the Battelle Columbus Laboratory Indirectly-Heated Gasifier,” NREL/TP-510-37408, May 2005.

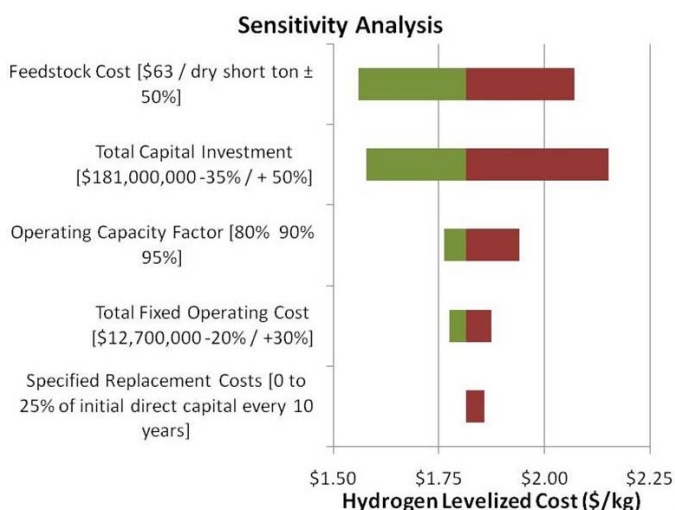


FIGURE 3. Sensitivity Analysis

II.C.1 Development of Hydrogen Selective Membranes/Modules as Reactors/Separators for Distributed Hydrogen Production

Paul KT Liu

Media and Process Technology Inc. (M&P)
1155 William Pitt Way
Pittsburgh, PA 15238
Phone: (412) 826-3711
Email: pliu@mediaandprocess.com

DOE Managers

HQ: Sara Dillich
Phone: (202) 586-7925
Email: Sara.Dillich@ee.doe.gov

GO: Katie Randolph
Phone: (720) 356-1759
Email: Katie.Randolph@go.doe.gov

Contract Number: DE-FG36-05GO15092

Subcontractor:

University of Southern California

Project Start Date: July 1, 2005

Projected End Date: December 31, 2012

- Permeate Flux/Selectivity: cost vs. performance target to meet our end user requirements; in particular for cost sensitive applications
- Stability: lack of long-term membrane and membrane reactor performance data under our target field conditions

Technical Targets

Technical targets for dense metallic membranes for 2010 are listed below:

- Flux Rate – 250 scfh/sq foot at 20 psig pressure
- Membrane Material and All Module Costs – \$1,000/sq. foot of membrane
- Durability – 2,680 hours of testing have been completed
- Operating Capability – 400 psi
- Hydrogen Recovery – >80% (of total gas)
- Hydrogen Quality – 99.99%

FY 2012 Accomplishments

- Completed the foil evaluation to choose a promising palladium alloy for asymmetric membrane development. Commercially available palladium-copper (Pd-Cu), palladium-silver (Pd-Ag) and palladium-gold (Pd-Au) foils along with the Pd foil (as control) were evaluated for their stability of cooling in hydrogen. The Pd-Cu foil shows structural stability through multiple cooling cycles in H₂ (i.e., >60 cycles), not Pd-Ag and Pd-Au.
- Developed palladium-copper alloy membranes that meet the cost vs. performance target set by DOE. Pd-Cu thin film (~5 μm) was successfully deposited on our commercial ceramic substrate with a H₂ permeance of 10-15 m³/m²/hr/bar at 350°C (i.e., 50-75 scfh @ 20 psig) and the selectivity of H₂/N₂ of 200 to >1,000, meeting the DOE 2015 cost vs. performance target.
- Verified the cooling stability in the presence of hydrogen. More than 10 PdCu membranes are currently undergoing cooling stability testing, i.e., cooling from 350°C to room temperature in the presence of H₂. Several of them have experienced >85 cycles with no signs of performance degradation.
- Designed and constructed membrane bundles which can accommodate (i) heat transfer requirement and (ii) flexibility in catalyst volume to membrane surface area ratio. Our unique membrane bundling configuration permits a membrane reactor that can be integrated with internal cooling coils without significant modifications

Fiscal Year (FY) 2012 Objectives

The water-gas shift (WGS) reaction becomes less efficient when high CO conversion is required, such as for distributed hydrogen production applications. Our project objective include:

- Develop a highly efficient and low temperature membrane-based WGS reaction process in a bench scale first, test it at a pilot scale, and finally demonstrate it in a field test unit.
- Screen our existing membranes and then tailor them specifically for the proposed process and reactor.
- Determine hydrogen production cost and define the system integration requirements for commercialization.
- Reduce the capital and operating costs for distributed hydrogen production applications.

Technical Barriers

Although various hydrogen selective membranes have been developed and reported in the literature, their use as a membrane reactor for hydrogen production has not been demonstrated commercially. Major technical barriers include:

- Testing/Analysis: few commercial scale membrane- and membrane reactor-based processes in operation

- to the membrane housing and module for the exothermic WGS reaction. In addition, the bundling configuration allows flexibility in catalyst volume to surface area ratio.
- Assembling a test system for the field test. We currently are assembling the test unit/system around the membrane reactor to perform the field test in the 3rd and 4th quarter of 2012. The reformer and the membrane subunit have been fully tested to meet syngas productivity and separation and purification requirements (i.e., 16 liter/min syngas and <10 ppm CO).
- Continuing the long term thermal stability test of the Pd and Pd-Cu membranes. Thermal stability testing of our Pd membrane bundle is continuing as part of the test requirement to verify that the DOE performance specification is met. Stability for >9,000-10,000 hours at 350°C has been demonstrated for Pd and >600 hrs for PdCu membranes.



Introduction

Membrane separation has been traditionally considered to be a simple, low cost and compact process. Thus, the membrane process has been considered under this project as a WGS reactor/separators for enhancing the hydrogen production efficiency for distributed hydrogen production. In this project, we have focused on the development of the technology components required for integrating a membrane reactor process for distributed hydrogen production. During 2010-2011, we completed the development and produced a test quantity of Pd membrane bundles for packaging into the membrane reactor to be field tested in 2011-2012. The project target of producing a hydrogen product stream with <<10 ppm CO has been achieved. Finally, we have identified a pathway to develop a Pd-based hydrogen membrane with cooling stability in the presence of hydrogen through evaluation of a series of Pd-alloy foils, which will be pursued in FY 2011-2012.

Approach

Our overall technical approach includes three steps as follows:

- Bench-Scale Verification
 - Evaluate membrane reactor: use existing membrane and catalyst via math simulation
 - Experimental verification: use upgraded membrane and existing catalyst via bench unit

- Validate membrane and membrane reactor performance & economics
- Pilot Scale Testing
 - Prepare membranes, module, and housing for pilot testing
 - Perform pilot scale testing
 - Perform economic analysis and technical evaluation
 - Prepare field testing
 - Field Demonstration
 - Fabricate membranes and membrane reactors and prepare catalysts
 - Prepare site and install reactor
 - Perform field test
 - Conduct system integration study
 - Finalize economic analysis and refine performance simulation

Results

1. Preparation of Palladium-Copper Alloy

Membranes with Improved Material Stability: Although the Pd membranes we developed demonstrated excellent functional performance and thermal stability at the target application temperature, i.e., 350°C, its cooling stability in a hydrogen rich environment is poor. This result is consistent with those reported in the literature (discussed in Sec. 2). Our screening study conducted in 2010-2011 showed that Pd alloy with 40% Cu was superior to the foils made with Pd-Ag, Pd-Au, and pure Pd. During this year, we have focused on the deposition of the Pd-Cu thin film on porous ceramic substrate. Pd-Cu thin film (~5 μm) was successfully deposited on our commercial ceramic substrate with an H₂ permeance of 10-15 m³/m²/hr/bar at 350°C (i.e., 50-75 scfh @ 20 psig) and the selectivity of H₂/N₂ of 200 to >1,000, meeting the DOE 2015 cost vs. performance target. Table 1 presents a summary of the Pd/Cu alloy membranes prepared during this year.

TABLE 1. Summary of the Pd/Cu Alloy Membranes Prepared

| Sample ID | Permeance [M ³ /m ² /hr/bar] @350°C | | | | Cu [wt%] | Thickness [μm] |
|-------------|---|----------------|-------------|-------------------------------|----------|----------------|
| | H ₂ | N ₂ | Selectivity | n th Cooling Cycle | | |
| PdCu-500-51 | 11.9 | 0.044 | 271 | 65 | 44.5 | 5.0 |
| PdCu-500-52 | 10.3 | 0.075 | 138 | 65 | 45.3 | 4.7 |
| PdCu-500-53 | 9.1 | 0.007 | 1,379 | Fail | 45.4 | 5.4 |
| PdCu-500-54 | 11.4 | 0.008 | 1,354 | Fail | 43.3 | 3.8 |
| PdCu-500-57 | 10.9 | 0.010 | 1,136 | 16 | 42.8 | 3.0 |
| PdCu-500-58 | 11.5 | 0.053 | 219 | 16 | 44.3 | 5.1 |
| PdCu-500-60 | 7.9 | 0.032 | 248 | 26 | 40.3 | 5.0 |
| PdCu-500-62 | 6.2 | 0.010 | 616 | 6 | 41.5 | |
| PdCu-500-63 | 10.6 | 0.015 | 695 | 3 | 43.2 | |
| PdCu-500-64 | 15.4 | 0.038 | 403 | 3 | 45.0 | |

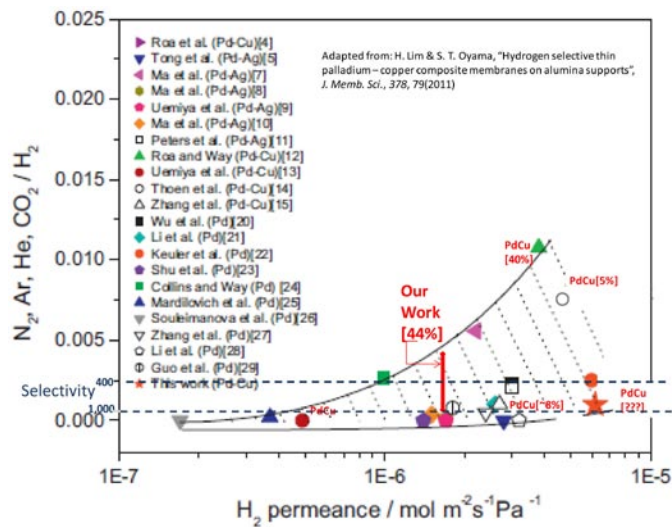


FIGURE 1. Hydrogen Permeances and Selectivity for PdCu Asymmetric Ceramic Membranes: Ours vs. Literature Study

Evidently our deposition technique allows us to deposit a rather consistent layer thickness (i.e., 3-5 μm) and Cu content (~44 wt%). In comparison with the performance of the supported Pd/Cu membranes published in the literature shown in Figure 1, our Pd/Cu membrane demonstrates excellent balance in the performance vs. selectivity.

2. Long-Term Thermal Stability and Thermal Cycling in the Presence of H_2 : Thermal cycling in the presence of H_2 is an important feature required of a commercially viable Pd membrane based upon our discussion with our end user. In this regard, work has been on-going over the past one year on the development of a Pd-alloy membrane that can tolerate thermal cycling in the presence of hydrogen. Figure 2 shows the N_2 permeance stability (leak rate) of the Pd alloy membrane. In all, 85 thermal cycles were conducted with little change in the H_2 permeance and only modest fluctuation in the N_2 permeance. In comparison, no other supported Pd membranes have demonstrated stability with an extended number of cooling cycles in an H_2 -charged environment

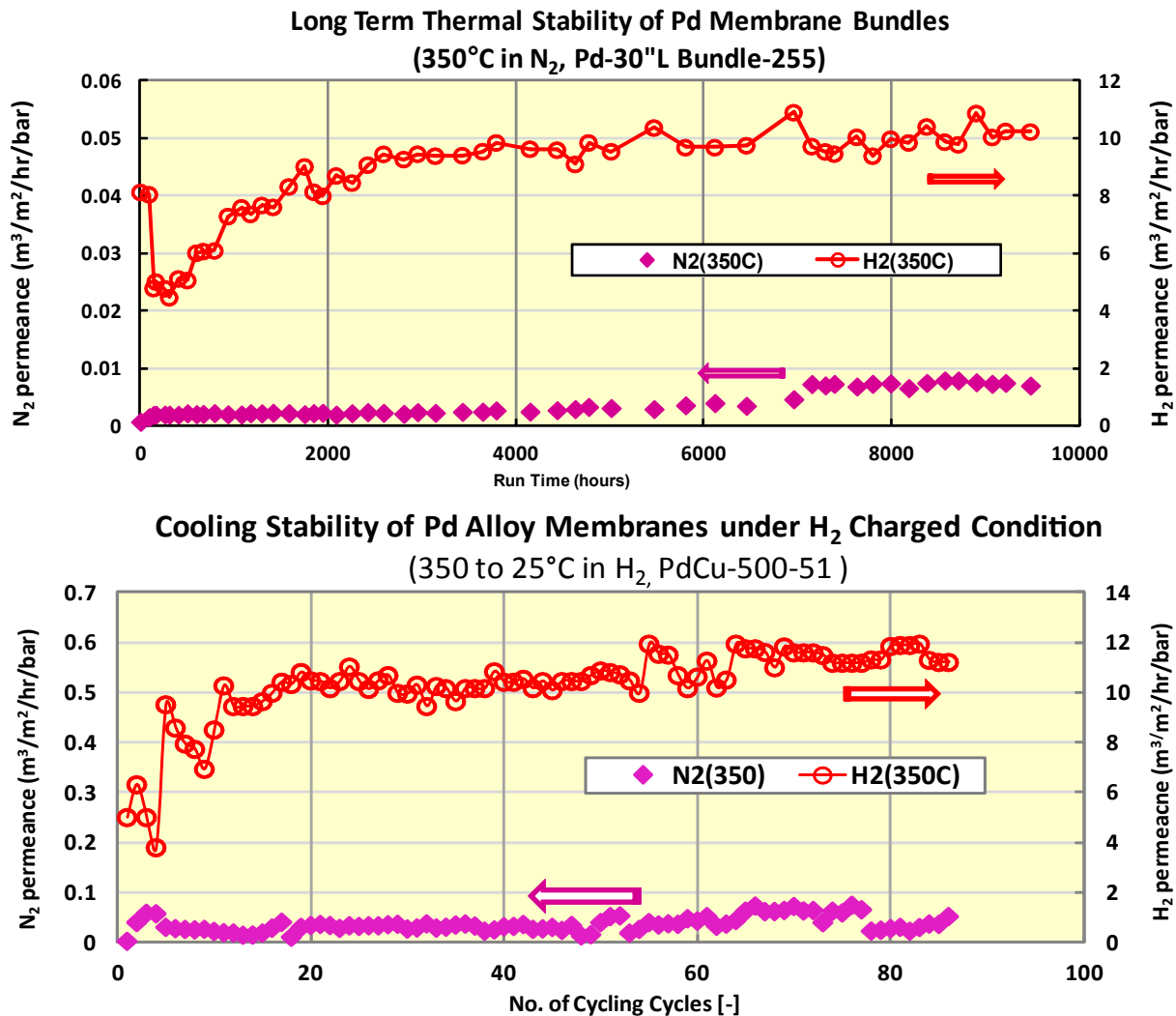


FIGURE 2. Palladium Membrane Stability: Long-Term Thermal Treatment and Cooling under Hydrogen Charged Atmosphere

as ours, in particular for the Pd membranes with ceramic substrate. In addition to thermal cycling stability, it is also important to establish the long-term membrane performance stability at high temperature. During this year, we continued our long-term performance stability testing of the palladium membrane, Pd-30” Bundle-255, at 350°C in the presence of H₂ and N₂. Figure 2 shows the performance of the single tube bundle after ca. 10,000 hours of service. As can be seen, after

the slight increase in the N₂ permeance of the -255 membrane at ca. 8,000 hours, the N₂ permeance stabilized. Overall, the Pd-based membranes we have been developing show very good long term stability in the presence of H₂ and N₂ at the expected minimum operating temperature of 350°C.

3. Development and Construction of Membrane Reactors with Internal Cooling Features: Membrane bundles which can accommodate (i) heat transfer requirement and (ii) flexibility in catalyst volume to membrane surface area ratio are essential for a commercially viable membrane reactor, targeting exothermic WGS shift reaction. Our unique membrane bundling configuration as shown in Figure 3 permits a membrane reactor that can be integrated with internal cooling coils without significant modifications to the membrane housing and module. In addition, the bundling configuration allows flexibility in catalyst volume to surface area ratio. These bundles will be used for our field test to demonstrate its commercial viability.

4. Design, Construction, and Installation of a Hydrogen Production System for Field Test: Once the membrane reactor was constructed, we began the design, construction, and installation of the peripheral subsystem components for the field test. The reformer and the membrane subunit have been fully tested to meet syngas productivity and separation and purification requirements (i.e., 16 liter/min syngas and <10 ppm CO). As presented in Figure 4, the Pd membrane installed in the system is able to enrich the membrane from 62% to >99.9% purity. CO less than 10 ppm was obtained. With the post treatment, the CO contaminant level is expected to be << 10 ppm as reported in the previous annual report. The entire testing system is expected to be



FIGURE 3. Fabrication of a Membrane Reactor for Pd Ceramic Composite Membrane with Integral Cooling Coil for the Target Exothermic WGS Reaction

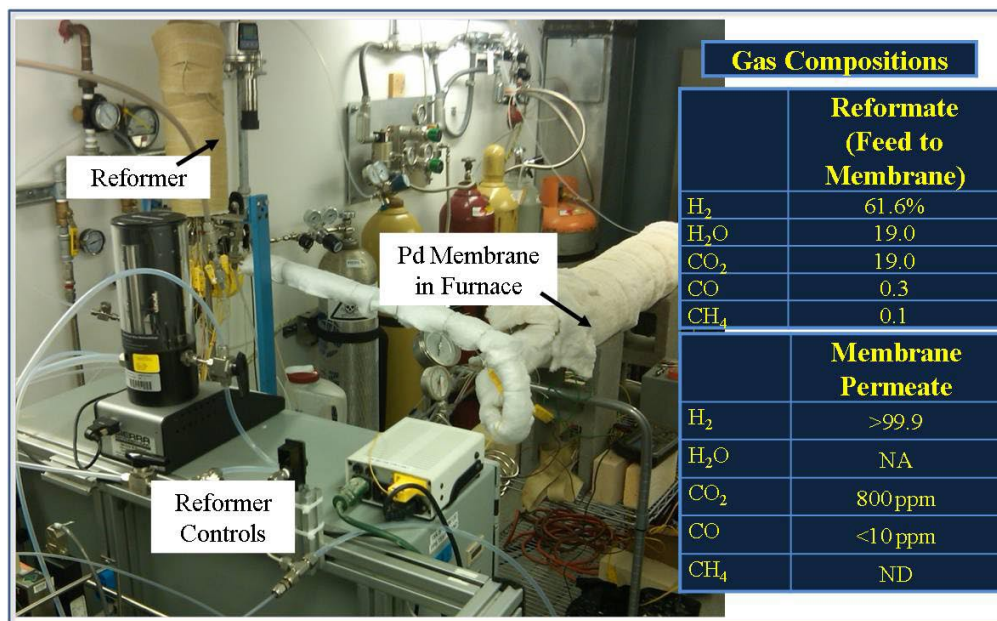


FIGURE 4. Reformer and Hydrogen Selective Membranes Installed and Fully Tested for the Field Test Unit

completely installed by the end June and ready for field test beginning July.

Conclusions and Future Directions

- Performance stability during thermal cycling in the presence of hydrogen is essential for the Pd membrane to be viable for portable power generation applications. Through a screening study with the commercially available Pd alloy foils, PdCu was identified as a promising alloy candidate. PdCu shows no sign of degradation for >60 cycles while PdAg shows degradation from the 2nd cycle in our screening study.
- During this year, we have successfully deposited the PdCu alloy thin film (~5 μm) on our commercial ceramic substrate as an asymmetric Pd alloy membrane in terms of performance, and thermal and cooling stability.
- The Pd alloy membrane thus developed meets the cost performance target set by DOE for 2015, i.e., 0.6 scfh @ Δp=20 psi/unit \$ membrane cost. In general, the permeance is 10-15 m³/m²/hr/bar with the selectivity of ≥~1,000 at 350°C.
- The Pd alloy membranes developed demonstrated performance stability during cooling from 350°C to room temperature in H₂ for >85 cycles as of today.
- A full-scale membrane reactor packed with our PdCu membrane bundle and equipped with an internal cooling device has been designed and is currently under fabrication. The reformer and the membrane subunits have been fully tested. The entire system is scheduled to be ready for field test by the 2nd quarter 2012.

Our FY 2012-13 activities will be focused on the areas below:

1. Complete the field test system assembly which is equipped with a full-scale PdCu membrane bundle and integrated with internal cooling coils by the 2nd quarter 2012.
2. Conduct a field test for 1 month (i.e., ~700 hrs) in the 3rd quarter 2012. The target performance is 99.999% purity and >83% recovery of H₂.
3. Upgrade the permeance of the 3rd generation Pd alloy membrane we have developed by the end of 2012 to the level similar to our existing 2nd generation Pd membrane, i.e., H₂ permeance increase from 15 to 25 m³/m²/hr/bar.

FY 2012 Publications

1. M. Abdollahia, J. Yua, P. K.T. Liu, R. Ciora, M. Sahimia, and T.T Tsotsis, “Ultra-pure hydrogen production from reformat mixtures using a palladium membrane reactor system”, *Journal of Membrane Science*, 390–391,32 (2012) .

II.C.2 Process Intensification of Hydrogen Unit Operations Using an Electrochemical Device

Glenn Eisman (Primary Contact), Dylan Share,
Chuck Carlstrom
H2Pump LLC
11 Northway Lane North
Latham, NY 12110
Phone: (518) 783-2241
Email: glenn.eisman@h2pumpllc.com

DOE Manager
HQ: Richard Farmer
Phone: (202) 586-1623
Email: Richard.Farmer@ee.doe.gov

Contract Number: DE-SC0002185

Subcontractor:
PBI Performance Products, Inc., Rock Hill, SC

Project Start Date: Phase II: August 15, 2010
Project End Date: August 15, 2012

Learnings gained from these studies will be applied to the membrane fabrication process as well as toward the electrochemical cell architecture to meet the following key targets:

- 300 psid pressure operation at 160°C
- CO₂ tolerance
- High efficiency (70%)

FY 2012 Accomplishments

- 300 psid compression demonstrated at 160°C for over 4,000 hours on a PBI-based 50-cm² electrochemical pump
- Materials processing finalized at PBI Performance Products
- Large-scale membrane and electrode fabrication process developed
- Cell hardware scale up completed and validated using low temperature membranes
- Stack design demonstrated to over 2,300 pressure cycles

Fiscal Year (FY) 2012 Objectives

Develop and demonstrate a multi-functional hydrogen production technology based on a polybenzimidazole (PBI) membrane which exhibits:

- High efficiency (70%)
- Up to 100 scfh pumping capability
- CO₂ and CO tolerance
- 300 psig (differential) pressurization capability
- \$3/kg operating costs

Technical Barriers

This project addresses the following technical barriers from the Production section of the Fuel Cell Technologies Program Multi-Year Research, Development and Demonstration Plan:

- (A) Reformer Capital Costs
- (D) Feedstock Issues
- (E) Greenhouse Gas Emissions

Technical Target

This project is focused on fundamental chemical and mechanical engineering studies on PBI proton exchange membranes and electrochemical cell hardware, respectively.



Introduction

One of the barriers to fuel cell acceptance is the lack of a simple, reliable, cost-effective and robust process to purify, pump, and pressurize hydrogen. This challenge is magnified by impurities and that hydrogen generation often occurs at near ambient pressure. Technical means of pressurizing the hydrogen is especially daunting for low to moderate flow rates. If the pressurization, purification, and recovery of hydrogen from any source, including from hydrogen-intensive industrial processes, can be developed into a single unit operation, it would be an attractive and enabling option for recycling hydrogen. H2Pump plans to leverage its extensive experience in electrochemical separation and pressurization systems to meet the project objectives with a high temperature membrane-based electrochemical hydrogen pump. The solutions will be based on developing a chemically and mechanically robust membrane in conjunction with advancements in cell hardware.

The significance of a successful project would be that impure hydrogen from a variety of sources could be simply, reliably, and inexpensively processed for further use. The hydrogen could be reused in the existing process as recycle, or in new applications including as a source of hydrogen for fuel cells. It is the reduction of multiple unit operations in

combination with the high temperature membrane operating at high differential pressure that will enable the benefits of this novel electrochemical approach.

Approach

H2Pump has shown that electrochemical methods to recover, purify, and pressurize hydrogen could be a viable option for low to moderate volumes of hydrogen-containing gases streams. The main challenge for this specific application is the lack of a proton conducting membrane which exhibits carbon dioxide and carbon monoxide tolerance and at the same time be able to pressurize the hydrogen from atmospheric pressure to 300 psid. Working closely with PBI Performance Products, the approach to address this challenge is to enhance the polybenzimidazole membrane properties via chemical and thermal cross-linking methods. Concurrently, H2Pump will work on cell hardware architecture to mechanically support the high temperature, CO₂ and CO tolerant membrane. The effort will focus on the structural integrity of all of the membrane and electrode components, plate materials and geometries, sealing mechanisms, and compression requirements. H2Pump will also investigate operating modes and the impact on performance of various membrane–electrode interface concepts.

Membrane modifications will be tested using 50-cm² single-cell hardware as a test platform. Design guidelines developed with the 50-cm² lab-scale pumps will be scaled up to the larger format to meet the program targets. Stack hardware development will take place concurrent to the membrane development using low-temperature (LT) membranes as a test platform. Results from the membrane and stack development effort will be combined to produce a large format high-temperature (HT) stack. This large format HT stack will be tested independently and then in combination with a reformer.

Results

During this reporting period there have been significant accomplishments in stack hardware design and scale up as well as completion of the HT membrane electrode assembly (MEA) architecture.

Stack Hardware

Stack hardware has been designed, built, and tested on the large format (920 cm²) using LT membranes. Large-scale HT PBI membranes were not used due to their unavailability in this period. Furthermore, the cell and stack hardware were designed to be able to accommodate both types of membranes, and as such, the LT membranes provided a means to accelerate stack engineering prior to the HT membranes being available. First generation PBI 920-cm²

membranes have been successfully prepared and assembled into a short stack and are awaiting testing and evaluation.

Stack hardware design has been improved for high differential pressure performance using the LT membrane. Figure 1 shows how the first generation large format stack hardware had pressure induced lift-off causing loss of performance at high pressures. Figure 2 data shows how the second generation design does not exhibit pressure induced performance limitations at high pressure. Pressure cycle testing was also performed as part of the qualification testing. Over 2,300 pressure cycles have been completed on this hardware without failure or degradation.

PBI MEAs

Three generations of PBI MEA architectures have been tested. Figure 3 shows the significant durability improvement

Nernst Corrected Polarization Curve Rev. 1 – 5 mil membrane

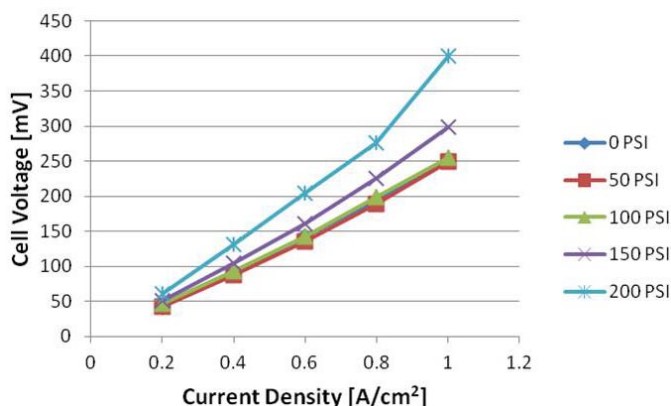


FIGURE 1. First Generation Stack Hardware

Nernst Corrected Polarization Curve Current Rev. - 2 mil membrane

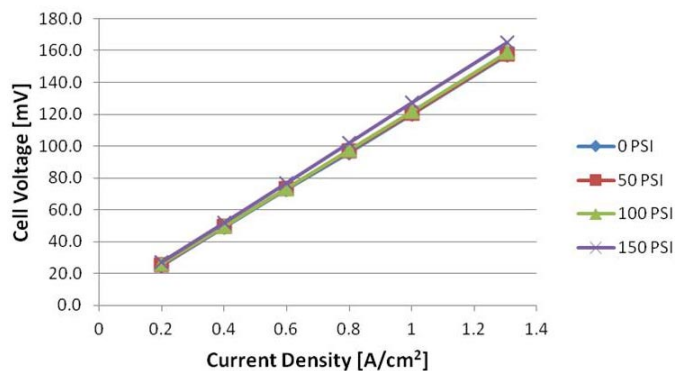


FIGURE 2. Second Generation Stack Hardware

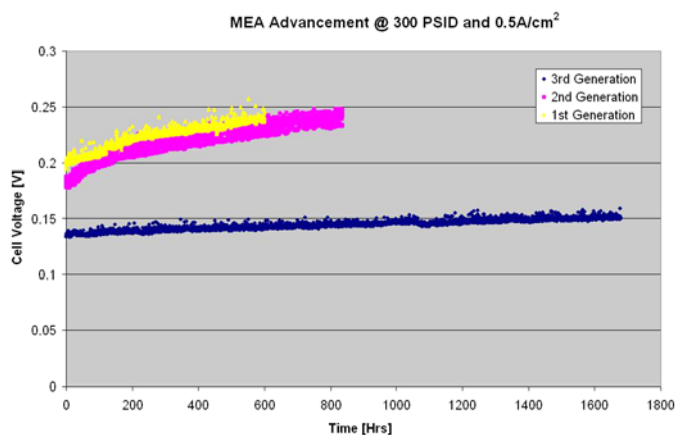


FIGURE 3. PBI MEA Architecture Advancements

the third generation has over the first two generations. Multiple 50-cm² PBI single cells have operated longer than 1,000 hours at 300 psid (differential pressure). One cell has even exceeded 4,000 hours at 300 psi differential pressure. Pressures of 400 psid with the PBI membrane have been achieved on a cell for short durations without damage or loss of performance.

The large format HT membrane and electrode fabrication process has been finalized and a novel, proprietary sealing method has been developed that utilizes commercially available, low cost sheet elastomer. Large format PBI-based MEAs have been produced using the selected sealing, electrode, and membrane fabrication process.

Reformer-Pump Integration

The reformer module has been built and tested independent of the pump module.

All major subsystems have completed verification testing in preparation for the sustained 36-hour test of the integrated unit. Gas analyses using gas chromatography methods have been used to determine reference gas compositions at various points within the integrated system. These results will be compared to the actual gas compositions of the integrated unit during the final demonstration.

Conclusions and Future Directions

- In collaboration with our partner, PBI Performance Products, PBI membrane has been successfully modified and is now stable in the targeted operating environment.
- 920-cm² stack hardware has been developed and successfully tested using LT membranes. Large-scale HT PBI membrane testing is underway.
- Enhancement of the membrane – electrode interface optimization successfully completed and has been scaled up to large format.
- 300 psid pressure operation has been demonstrated on multiple cells for up to 4,000 hours.
- Scale up of the membrane and electrode assemblies as well as the hardware has been completed.
- Gas quality and analytical tests will continue to be performed to further assess the performance of the 300 psid pump cells.
- Reformer-pump integration and preparation for final demonstration underway.
- H2A analysis to be completed.

FY 2012 Publications/Presentations

1. Eisman, G., Carlstrom, C “Process Intensification of Hydrogen Unit Operations Using an Electrochemical Device” Proceedings of the DOE Hydrogen and Fuel Cell Annual Merit Review Meeting, Crystal City, VA., May, 2012.

II.D.1 PEM Electrolyzer Incorporating an Advanced Low-Cost Membrane

Monjid Hamdan (Primary Contact), Tim Norman
Giner, Inc. (Formerly Giner Electrochemical Systems, LLC.)
89 Rumford Ave.
Newton, MA 02466
Phone: (781) 529-0526
Email: mhamdan@ginerinc.com

DOE Managers

HQ: Erika Sutherland
Phone: (202) 586-3152
Email: Erika.Sutherland@ee.doe.gov
GO: David Peterson
Phone: (720) 356-1747
Email: David.Peterson@go.doe.gov

Contract Number: DE-FG36-08GO18065

Subcontractors:

- Virginia Polytechnic Institute and University, Blacksburg, VA
- Parker Hannifin Ltd donnick hunter Division, Hemel Hempstead, United Kingdom

Project Start Date: May 1, 2008
Project End Date: January 31, 2013

Fiscal Year (FY) 2012 Objectives

Develop and demonstrate advanced low-cost, moderate-pressure polymer electrolyte membrane (PEM)-based water electrolyzer system to meet DOE targets for distributed electrolysis:

- Develop high-efficiency, low-cost membrane
- Develop long-life cell-separator
- Develop lower-cost prototype electrolyzer stack and system
- Demonstrate prototype at the National Renewable Energy Laboratory (NREL)

Technical Barriers

This project addresses the following technical barriers from the Hydrogen Production section of the Fuel Cell Technologies Program Multi-Year Research, Development and Demonstration Plan:

- (G) Cost - Capital Cost
- (H) System Efficiency

Technical Targets

Giner Progress toward Meeting DOE Targets for Distributed Electrolysis Hydrogen Production¹

| Characteristics | Units | 2015/2017 Target | 2012 Giner Status |
|---------------------------------------|-----------------------|------------------|--|
| Hydrogen Production Cost ² | \$/kg H ₂ | 3.30/<2.70 | 3.64 |
| Electrolyzer Capital Cost | \$/kg H ₂ | 0.70/0.30 | 0.60 ³ (1.06) ⁴ |
| Electrolyzer Energy Efficiency | % (LHV ⁵) | 69/74 | 66 ⁶ |

¹ Using H2A model rev 2.1.1. Based on electricity cost of \$0.04/kWh.

² Production only (H₂ compression, storage, and delivery expected to add \$2.00/kg).

³ Electrolyzer stack

⁴ Electrolyzer system (stack & BOP)

⁵ Lower heating value

⁶ Does not include H₂-dryer. Stack efficiency measured at 74% LHV.

FY 2012 Accomplishments

Membrane:

- Demonstrated enhanced dimensionally stable membrane (DSM™) performance.
- Completed 5,000-hour life-test with DSM™ (@80°C, 300 psid).
- DSM™ operating lifetime estimated at 55,000 hours.
- Reduced membrane support cost by one order of magnitude.

Cell-Separator:

- Demonstrated reduced hydrogen embrittlement in titanium/carbon cell-separator.
- Projected longevity of the carbon/titanium cell-separators (>60,000 hours).

Electrolyzer Stack and System Design:

- Completed fabrication of full-scale electrolyzer stack utilizing low-cost components.
- Reduced electrolyzer stack costs by 60%.
- Commercialized electrolyzer stack in 2011. Electrolyzer stacks field tested at customer locations (>1,000 hours).
- Completed fabrication of electrolyzer system incorporating a high-efficiency H₂-dryer.
- Extensive safety review of electrolyzer system completed.

- Completed modeling of electrolyzer capital and operating costs; performed economic analysis using the DOE H2A model illustrating cost-reductions.
- Delivered and demonstrated prototype electrolyzer system at NREL.



Introduction

The DOE has identified hydrogen production by electrolysis of water at forecourt stations as a critical technology for transition to the hydrogen economy, and as the hydrogen economy matures, for hydrogen production at centralized locations using renewable energy sources. However, state-of-the-art electrolyzers are not economically competitive for forecourt hydrogen production due to their high capital and operating costs. The cost of hydrogen produced by present commercially available electrolysis systems is estimated to be \$4.80/kg-H₂, considerably higher than the DOE target of <\$3.00/kg-H₂ by 2017 [1]. Analysis of electrolyzer systems performed by Giner and others using DOE's H2A model indicate that the major cost elements are the cost of electricity, the capital costs of electrolyzer stacks and systems, and the high cost of hydrogen compression, storage, and delivery.

Giner, Inc. (Giner) has developed proton exchange membrane (PEM)-based electrolyzer technology that operates at differential pressure for producing hydrogen at moderate to high pressure directly in the electrolyzer stack, while oxygen is evolved at near-atmospheric pressure. The goals of the project are to reduce the cost of the stack and system, improve electrolyzer efficiency, and to demonstrate electrolyzer operation at moderate pressure.

Approach

To reduce the cost of producing hydrogen, Giner is improving electrolyzer stack efficiency and reducing stack cost through development of an advanced low-cost, high-strength, membrane that utilizes a perforated polyimide support imbibed with perfluorosulfonic acid (PFSA) ionomer. Giner is also reducing stack capital cost and increasing stack life through development of a long-life bipolar stack cell-separator, decreasing stack costs by initiating scale-up to a larger active area, and reducing the system capital cost by applying commercial production methods to PEM-based electrolyzer systems. In each of the key development areas, Giner and its team members are conducting focused development of advanced components in laboratory-scale hardware, followed by life-testing of the most promising candidate materials.

Successful development of the advanced electrolyzer stack and system will result in a high-efficiency; low-capital-

cost electrolyzer that will meet the DOE cost targets for hydrogen production, assuming high-volume production. This will provide competitively priced hydrogen for delivery at forecourt stations to enable transition to the hydrogen economy.

Results

DSM™ Membrane Performance

To improve electrolyzer efficiency, Giner has developed an advanced supported membrane having an ionic resistance comparable to that of a 0.0020 to 0.0035 inch-thick Nafion® [2] membrane, but having significantly improved mechanical properties. This advanced membrane is referred to as a DSM™ due to the membrane support that minimizes changes in dimensions (swelling/contraction) under high-pressure operation and with changes in water content. The support structure utilized in the development of the DSM™ consists of a polyimide (Kapton®) base film with a definable open pattern. The support structure is then imbibed with 1100-equivalent-weight PFSA ionomer to a thickness of 3 mil (0.003"). Initially, Giner fabricated the membrane support structures using a laser-drilling procedure. In 2011, a more cost-effective technique of fabricating the support structures via chemical-etching was implemented by Giner, reducing the cost of the membrane by one order of magnitude.

Polarization scans of the DSM™ were conducted in scaled-up, 27-cell electrolyzer stack hardware, through a current density range of 0-1,750 mA/cm², a differential pressure of 300 psid, and a temperature of 80°C. The average cell voltage was measured at 1.757 V/cell corresponding to a voltage efficiency of 74% LHV (87% higher heating value) at a current density of 1,500 mA/cm², Figure 1. During testing, the DSM™ exceeded the criterion for performance:

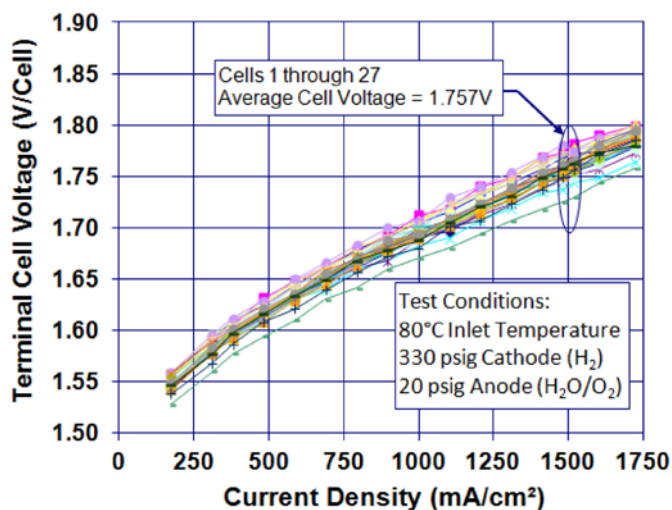


FIGURE 1. Membrane Performance in Full-Scale Electrolyzer Stack Hardware

exhibiting lower cell voltages and thus higher cell efficiencies than that of a Nafion® 1135 membrane.

Durability of the DSM™ was also demonstrated in the scaled-up, hardware via fluoride release rate (FRR) measurements at constant-current operation. Since PFSA ionomer is used as the membrane material and in the binder for the catalyst layer, the loss of fluoride is used as a measurement of membrane degradation. An FRR rate of $3.7 \mu\text{g F}^- \text{ ion/hr}$ or less than $10 \text{ micrograms F}^- \text{ ion/L}$ (<10 ppb) was present in the cathode effluent (electro-osmotically transported water) at the end of 1,000 and 5,000-hour life tests. Based on electrolysis FRR results, the lifetime of the DSM™ is projected to be between 45,000 and 55,000 hours.

Cell-Separator Development

The cell separator is a gas-impermeable conductive sheet that separates the hydrogen and oxygen compartments in the bipolar stack. The separator must be highly conductive, as well as resistant to hydrogen embrittlement and to corrosion in an oxidizing environment. Giner's legacy high-pressure naval electrolyzers use a complex multi-layer cell-separator incorporating a conductive compliant member and sheets of niobium and zirconium metal. Zirconium is used due to its high resistance to hydrogen embrittlement. Giner has previously evaluated a low-cost, dual-layer titanium cell-separator. Although performance was comparable to that of niobium/zirconium cell-separators, lifetimes were limited to 5,000 hours due to hydrogen embrittlement.

The most promising approach for long-term implementation has been achieved by coating titanium with a low-cost electrically conductive, embrittlement-resistant carbon coating. The challenge was the development of a pinhole-free, highly adherent coating with the required characteristics. Under the cell-separator development task, Giner demonstrated performance of a carbon/titanium cell

separator in scaled-up 290-cm² electrolyzer stack hardware. Performance is comparable to that of the niobium-zirconium separator. In addition, life expectancy of the carbon/titanium separator, determined via hydrogen-uptake analysis over a 5,000-hour period, indicates lifetimes exceeding the 50,000-hour system requirement.

Electrolyzer Stack and System Fabrication

In addition to the use of chemically etched DSM™ and carbon/titanium cell-separators, the electrolyzer stack includes several modifications to Giner's legacy hardware; (1) an increase in cell active area from 160 to 290 cm², effectively reducing the number of cells required to produce a given amount of hydrogen, thus reducing the stack manufacturing labor, (2) an overall decrease in the parts count per cell (from 41 to 10), (3) a 75% reduction in anode and cathode catalyst loadings, (4) molded thermoplastic cell frames, resulting in a cost reduction of 95% as compared to machining this component, (5) a 33% reduction in cell frame thickness, thus reducing the anode and cathode support materials and costs by 33%, and (6) a low-cost carbon-steel end plate. As a result of the component and membrane development during this program, the overall projected capital cost of the electrolyzer stack alone has decreased from greater than \$1,000/kW in 2007 to <\$350/kW in 2011 (Figure 2).

The electrolyzer system, shown in Figure 3, required detailed planning with respect to system layout and fabrication sequence. Several factors, including specific codes and standards that are pertinent to hydrogen electrolyzer systems, were considered during the system

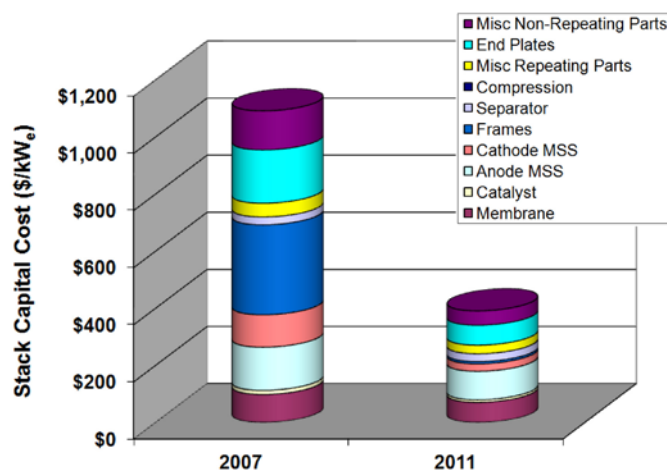


FIGURE 2. Electrolyzer Stack Capital Costs



FIGURE 3. Electrolyzer System

layout. To meet these requirements, the system was designed with three separate compartments; the oxygen (O₂), the hydrogen (H₂), and the electrical (controller and power supply) compartments. The O₂ compartment contains the oxygen gas-phase separator, a circulating liquid pump, and the deionized water feed tank. The H₂ compartment encloses a novel high-efficiency (97%) hydrogen dryer assembly, high- and low-pressure hydrogen gas-phase separators, a heat exchanger, cooling fans, and various flow valves. The electrolyzer stack is powered via a high-efficiency power supply rated at 94% located in the electrical compartment.

The system build, undertaken at the Parker facility, was delivered and tested at NREL's National Wind Technology Center in 2012. A breakdown of the system performance and efficiencies during the initial evaluation period is shown in Table 1. At an operating current density of 1,500 mA/cm², the electrolyzer stack exhibits an energy efficiency of 46.6 kWh/kg, the overall system (not including the H₂-dryer); 50.5 kWh/kg, and with the H₂-dryer; 54.0 kWh/kg. The H₂-dryer utilizes dry hydrogen as a carrier gas. Although the H₂-dryer operates at a high efficiency as compared to the industrial

standard (~10% loss), this is not indicative of a forecourt station where nitrogen is typically used as a carrier gas. It is thus feasible to operate scaled-up systems of this type in the range of 50.5 kWh/kg. During testing at NREL, the voltage performance of the electrolyzer stack was verified, in addition to H₂-dryer losses of less than 3%.

Conclusions and Future Directions

Significant progress has been made in DSM™ membrane development. Giner has demonstrated membrane reproducibility and durability as well as a significant improvement in electrolyzer cell efficiency. The progress made during this program is in line with achieving DOE's 2017 efficiency targets. In addition, development efforts conducted under this project have resulted in significant cost reductions of PEM-based electrolyzer stacks and systems, an increase in the life of the low-cost cell-separators, and improved BOP components efficiency. The future objectives are to:

- Complete evaluation of prototype electrolyzer system at NREL.
- Continue investigation of low-cost stack and system components.
- Conduct optimization studies for stack and system, including the H₂-dryer.
- Develop a high-pressure (>5,000 psi) electrolyzer stack design utilizing low-cost components developed during this project

TABLE 1. Electrolyzer System Performance

| Hydrogen Production & Losses | Units | 1,500 mA/cm ² | 1,750 mA/cm ² |
|--|-----------------------|--------------------------|--------------------------|
| Stack H ₂ -Production | kg-H ₂ /kg | 0.445 | 0.519 |
| Membrane permeation losses (-0.6%) | | -0.003 | -0.003 |
| Phase-Separator (-0.14%) | | -0.0006 | -0.0007 |
| H ₂ -Dryer (- 3 to 4%) | | -0.018 | -0.021 |
| Total H₂-Production (@STP) | | 0.424 | 0.494 |

| Power Consumption | Units | 1,500 mA/cm ² | 1,750 mA/cm ² |
|---|-------|--------------------------|--------------------------|
| Electrolyzer Stack | kW | 20.6 | 24.2 |
| Direct current power supply & control (assuming 94% eff.) | | +1.23 | +1.45 |
| PLC Rack | | 0.05 | 0.05 |
| Electrolyzer water pump | | 0.30 | 0.30 |
| Heat exchanger fans A & B | | 0.05 | 0.05 |
| H ₂ sensor circuit pump | | 0.12 | 0.12 |
| Total Energy Consumption (No Dryer) | | 22.3 | 26.2 |
| H ₂ -Dryer | | 0.53 | 0.67 |
| Total Energy Consumption (w/Dryer) | | 22.9 | 26.8 |

| Overall Efficiencies | Units | 11,500 mA/cm ² | 1,750 mA/cm ² |
|---|--------|---------------------------|--------------------------|
| Electrolyzer Stack (includes permeation) | kWh/kg | 46.6 | 46.9 |
| System (No Dryer) | | 50.5 | 50.8 |
| System (w/Dryer) | | 54.0 | 54.2 |

Special Recognitions

1. 2012 DOE Hydrogen and Fuel Cells Program R&D Award

FY 2012 Publications/Presentations

1. M. Hamdan, *PEM Electrolyzer Incorporating an Advanced Low-Cost Membrane*. 2012 Hydrogen Annual Program Merit Review Meeting. Presentation #pd_030_hamdan, May 16, 2012.
2. M. Hamdan, *Unitized Design for Home Refueling Appliance for Hydrogen Generation to 5,000 psi*. 2012 Hydrogen Annual Program Merit Review Meeting. Presentation #pd_065_norman, May 15, 2012.

References

1. Multi-Year Research, Development and Demonstration Plan. Hydrogen Production. DOE, Pg 3.1-14 (2011 Interim Update) <http://www1.eere.energy.gov/hydrogenandfuelcells/mypp/pdfs/production.pdf>
2. Nafion® and Kapton® are registered trademarks of E.I. du Pont de Nemours and Company

II.D.2 High Performance, Low Cost Hydrogen Generation from Renewable Energy

Dr. Katherine Ayers (Primary Contact),
Andy Roemer
Proton Energy Systems d/b/a Proton OnSite
10 Technology Drive
Wallingford, CT 06492
Phone: (203) 678-2190
Email: kayers@protononsite.com

DOE Managers
HQ: Erika Sutherland
Phone: (202) 586-3152
Email: Erika.Sutherland@ee.doe.gov
GO: Dave Peterson
Phone: (720) 356-1747
Email: David.Peterson@go.doe.gov

Contract Number: DE-EE000276

Subcontractors:

- Entegris, Inc., Chaska, MN
- The Electrochemical Engine Center at Penn State, University Park, PA
- Oak Ridge National Laboratory, Oak Ridge, TN

Project Start Date: September 1, 2009

Project End Date: September 30, 2013

Technical Barriers

This project addresses the following technical barriers from the Production section of the Fuel Cell Technologies Program Multi-Year Research, Development and Demonstration Plan:

- (G) Capital Cost
- (H) System Efficiency
- (J) Renewable Electricity Generation Integration

Technical Targets

TABLE 1. Proton Energy Systems Progress Towards Meeting Technical Targets for Distributed Water Electrolysis Hydrogen Production

| Characteristics | Units | 2012 Target | 2017 Target | Proton Status |
|--------------------------------|---------|-------------|-------------|---------------|
| Hydrogen Cost | \$/gge | <3.70 | <3.00 | 3.46 |
| Electrolyzer Capital Cost | \$/gge | 0.70 | 0.30 | 0.64 |
| Electrolyzer Energy Efficiency | % (LHV) | 69 | 74 | 67 |

gge - gasoline gallon equivalent; LHV - lower heating value
Note: Estimates are based on H2A v2.1, for electrolysis only (compression-storage-delivery not included). Model assumes \$0.05/kWh.
Electrolyzer cost based on 1,500 kg/day capacity, 500 units/year; Efficiency based on system projections and demonstrated stack efficiency of 74% LHV efficiency

Fiscal Year (FY) 2012 Objectives

- Improve electrolyzer cell stack manufacturability through:
 - Consolidation of components
 - Incorporation of alternative materials and manufacturing methods
 - Improved electrical efficiency
- Reduce cost in electrode fabrication through:
 - Reduction in precious metal content
 - Alternative catalyst application methods
- Design scale up for economy of scale including:
 - Scale up of the design to a large active area cell stack platform
 - Development and demonstration of a robust manufacturing process for high volume plate production
- Quantification of the impact of these design changes via the H2A model.

FY 2012 Accomplishments

- Over 3,000 cells utilizing the new flow field design resulting in >20% part cost savings (12% stack cost savings) have been fabricated and assembled into production stacks.
- Composite bipolar plates from Entegris exhibited stability over >3,000 hours of operation.
- Alternative flow field manufacturing methods were validated and an additional 50% cost reduction in the subassembly was realized for an overall stack cost reduction of 40% vs the 2008 baseline.
- Penn State comprehensive electrolyzer cell model was utilized to characterize updated flow field geometry.
- Achieved >5,000 hrs of stable performance with a 3-cell prototype stack utilizing alternate electrode structures and new flow field components.
- Nitrided separators showing stable in cell performance at >5,000 hrs.
- Initiated design effort to scale up existing 0.1 ft² stack up to 0.6 ft².



Introduction

This project addresses the DOE Hydrogen and Fuel Cells Program objective for distributed production of hydrogen from proton exchange membrane (PEM) water electrolysis. The DOE technical targets for hydrogen cost as well as electrolyzer efficiency and capital cost will be directly addressed through the advancement of key components and design parameters. When added together, the bipolar assemblies and membrane electrode assemblies (MEAs) constitute over half of the total cell stack cost. Significant cost reductions of these components as demonstrated with this research are required in order to reach the targets. Further optimization of cell stack components results in efficiency gains at the system level and ultimately a reduction in the cost to produce hydrogen. The efforts of the last year culminated in the build of a 0.1 ft² prototype stack utilizing the selected materials, coatings and manufacturing methods for the bipolar assembly. The prototype 0.1 ft² cell stack design has operated with stable performance for >5,000 hrs (Figure 1). Based on the performance of the prototype stack, and the projected cost savings of this cell stack architecture, the decision was made to scale this architecture up to 0.6 ft². Lessons learned during the prototype design and build will be leveraged during the scale up design activity.

Approach

The scope of work for this project allowed for research and development in several key areas relating to cell stack cost reduction. Topics included: 1) catalyst formulation; 2) flow field design and materials, 3) computational performance modeling, and 4) flow field coating development.

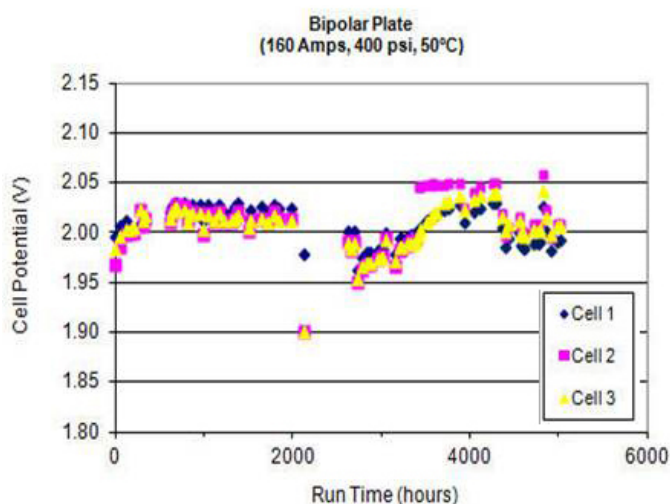


FIGURE 1. Voltage Trend for Composite Bipolar Assembly

Advancements in flow field design are intended to be advantageous for low cost, high volume manufacturing. Alternatives to the current flow field design included either 1) composite bipolar plates or 2) unitized flow fields, which consolidate parts and reduce the amount of required precious metal plating. The early investigations into the cost and manufacturability of the various design alternatives resulted in a final down select to a unitized flow field. This approach integrated the function of several components into a single low-cost component, which also reduced the assembly labor. Computational modeling of an electrolyzer cell will allow for optimization studies to be performed around flow field material and architecture. Cell performance can be quantified in ways not typically possible with standard physical test experiments. Alternate coating strategies are also being investigated which eliminate metal plating. Validation of all of the previously mentioned design changes will be achieved through cost analysis based on the H2A model.

Results

The comprehensive computational model of an electrolyzer cell developed at Penn State was previously shown to be capable of predicting performance parameters based on the geometry of the flow fields and specified operating conditions. Learnings from this model were used for refinement of the updated flow field geometry for improved water flow distribution within the cell and better thermal management.

The down-selected design from the manufacturing study was utilized to make prototype parts and were inspected according to print before assembly into a 0.1 ft² test stack. The stack passed all acceptance testing protocol and performance resulted in passing of the Go/No-Go review for the first phase of the project, kicking off the 0.6 ft² scale up design task and the build of a full-scale prototype production stack of the 0.1 ft² design. Previous work also demonstrated a 55% reduction in the amount of precious metal used in the anode catalyst layers of the MEA. The application technique represents an improvement over existing production techniques in that it allows for improved registration and uniformity while also enabling higher speed throughput. The 0.1 ft² prototype stack was fabricated utilizing the reduced anode catalyst fabrication method.

Nitriding was studied extensively during this period to protect the part from oxidative corrosion and hydrogen embrittlement. Performance of a variety of nitrided parts was evaluated for resistance to H₂ uptake, corrosion resistance, and performance under electrolysis conditions (Figure 2). Additionally, a comprehensive examination of Ti residual stress levels and the effect on H₂ uptake is in progress. Characterization at Oak Ridge National Laboratory (ORNL) showed that samples maintained similar thicknesses of the nitrided layer after electrolysis operation. Thermal nitriding

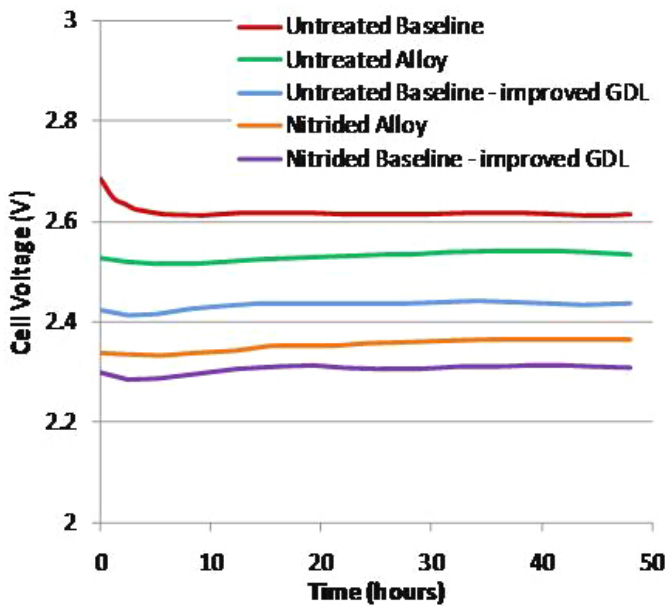


FIGURE 2. Performance of Surface Coatings vs. Untreated Flow Field Material

was also explored at ORNL and samples were tested for 500 hours in the electrolysis environment without evidence of corrosion. These results validate the potential for multiple options for plate fabrication and coating while eliminating noble metal coatings or plating. Commercial suppliers of thermal nitride coatings have been identified and evaluations were initiated. Sample thermally nitrided parts have been

manufactured and initial prototype parts were analyzed at ORNL (Figure 3). Some discoloration has been observed on operated nitrided parts and this behavior has recently become a focus of investigation. ORNL is playing a key role in understanding and characterizing the nitride coatings. Selected samples have been examined after longer operating times to determine overall life based on any signs of corrosion or material degradation.

The overall reduction in cell stack cost was calculated from the bill of materials for the existing 0.6 ft² design, currently in pre-production, and quotations for the modified parts. Figure 4 shows the eliminated cost for the new design. The numbers are very consistent with the 0.1 ft² design, which showed an actual cost reduction of 44%. Using the H2A model, this capital cost savings translates to an overall cell stack capital cost of less than \$0.50/kg for the new large format design. Combined with Proton’s parallel efforts in efficiency improvements and system scale up, the cost status for hydrogen production based on the H2A model is \$3.64/kg, at an electricity cost of \$0.05/kWh.

Conclusions and Future Directions

- Initial cost reductions on the cathode flow field are successfully being produced and fielded in commercial cell stacks.
- Ongoing tests have shown that alternative conductive materials can remain stable in the corrosive environment of operational electrolyzer cells for tests over

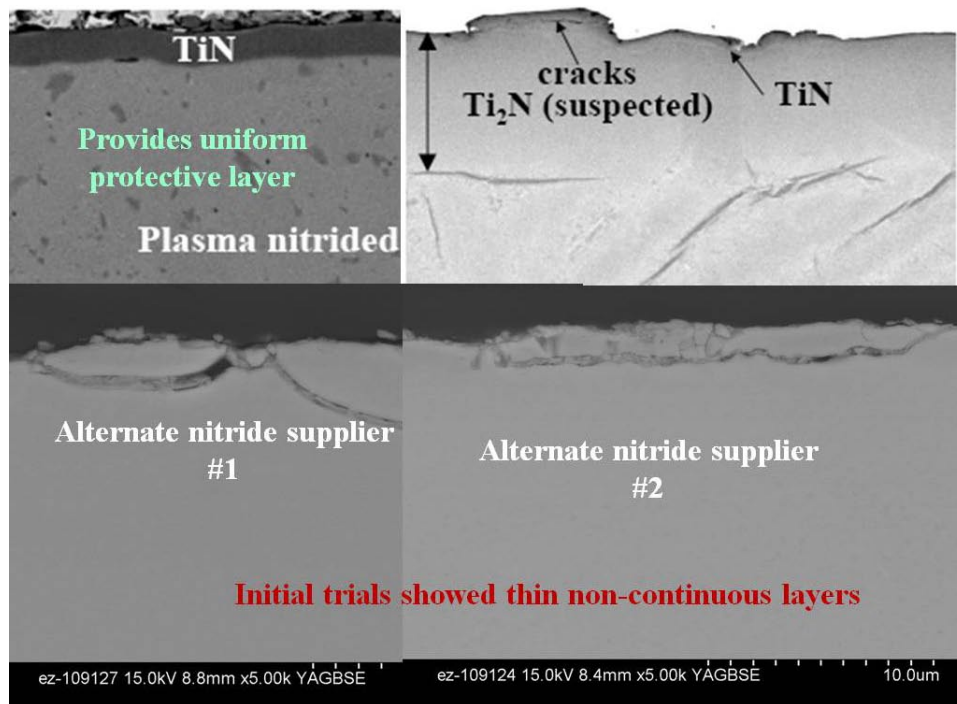


FIGURE 3. Image of Nitrided Part and Analysis of Composition vs. Layer Depth and Operation

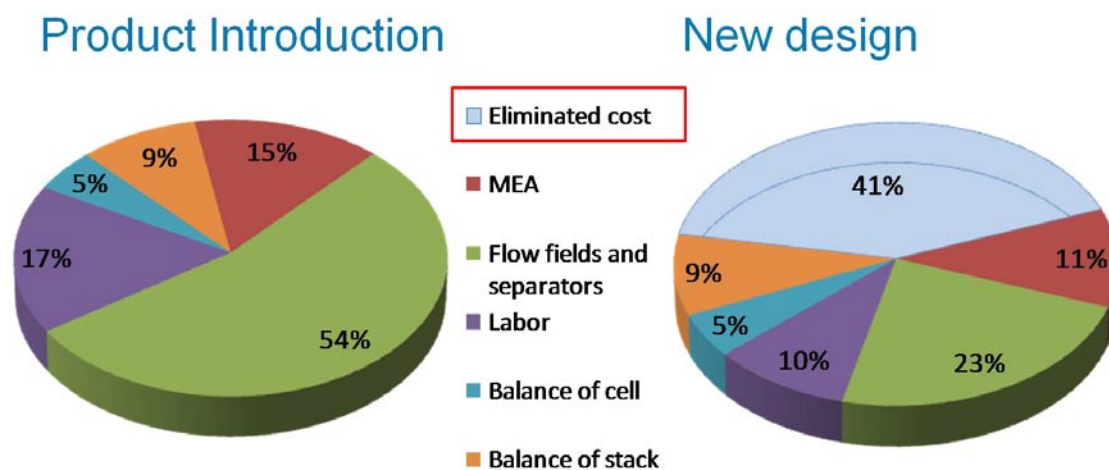


FIGURE 4. Large Format Cell Stack Cost Reduction Based on New Design

5,000 hours. Further analysis is required to determine durability projections and progress towards the 50,000 hour minimum operational life of Proton cell stacks, but no obvious degradation has been observed. A component manufactured from this alternate material was utilized in the 0.1 ft² prototype stack.

- A unitized flow field plus frame assembly was selected as the path to the consolidated bipolar plate assembly, with initial predictions of over 50% part cost reduction being attained. This unitized flow field will be implemented in the 0.6 ft² design.
- Electrolyzer cell performance can be predicted with the use of a comprehensive computational model and flow distribution across the bipolar assembly can be modeled to provide valuable insights on design and flow requirements. The Penn State model will be utilized to guide any changes to the flow field geometry of the 0.6 ft² scaled up design.

- Nitride coatings fabricated by different methods appear to be very stable in electrolysis conditions and may enable reduction in metal coatings. Further process development will be performed to determine the best approach for manufacturability. Qualification of an alternate lower cost nitriding process is currently in progress.

Special Recognitions

1. Hydrogen and Fuel Cells Program Sub-Program Award, for outstanding technical contributions in Hydrogen Production, presented at Annual Merit Review, May 14–18, 2012.

II.D.3 Renewable Electrolysis Integrated Systems Development and Testing

Kevin Harrison

National Renewable Energy Laboratory (NREL)
15013 Denver West Parkway
Golden, CO 80401
Phone: (303) 384-7091
Email: Kevin.Harrison@nrel.gov

DOE Manager

HQ: Eric Miller
Phone: (202) 287-5829
Email: Eric.Miller@hq.doe.gov

Contributors:

Chris Ainscough and Michael Peters

Subcontractor:

Marc Mann, Spectrum Automation Controls, Arvada, CO

Project Start Date: October 1, 2003

Project End Date: Project continuation and direction determined annually by DOE

systems. Insights gained from this work benefit the hydrogen-based industry and relevant stakeholders as the market for this equipment and products continues to expand. Results from the project have demonstrated opportunities to improve the efficiency of an integrated, renewably coupled electrolysis system. Finally, this project validates stack and system performance of DOE-awarded systems to help meet the following DOE hydrogen production and delivery targets:

- By 2012, reduce the cost of central production of hydrogen from wind water electrolysis to \$3.10/gallon of gasoline equivalent (gge) at plant gate (\$4.80/gge delivered). By 2017, reduce the cost of central production of hydrogen from wind water electrolysis to <\$2.00/gge at plant gate (<\$3.00/gge delivered).
- System efficiency (currently being reevaluated): 69% by 2012 and 74% by 2017 (lower heating value*).

* Note that the highest efficiency obtainable on the basis of lower heating value (LHV) of hydrogen is $33.3/39.4 \approx 84\%$

FY 2012 Accomplishments

- Designed and installed a new test facility and supporting infrastructure for validation and performance testing of DOE-awarded electrolyzer systems
- Operated electrolyzer stacks ~5,500 hours with variable wind profile to compare stack decay rate with that of a stack operating under constant power
 - Comparing steady-state and variable stack operation enables better understanding of long-term impacts on stack and system efficiency
- Completed frequency mitigation testing of alkaline and polymer electrolyte membrane (PEM) electrolyzers on an alternating current (AC) microgrid
 - Both commercially available technologies provided sub-second response to significantly reduce the magnitude and duration of the disturbance
- Designed, built and began testing a volumetric mass flow system for high-accuracy determination of electrolyzer system efficiency



Introduction

Renewable electrolysis is inherently distributed, but large-scale wind and solar installations are becoming more common and will take advantage of economies of scale. Renewable electricity sources, such as wind and solar, can be closely—and in some cases directly—coupled to the

Fiscal Year (FY) 2012 Objectives

- Validate stack and system efficiency and contributing sub-system performance of DOE-awarded advanced electrolysis systems
- Collaborate with industry to optimize and demonstrate the commercialization of integrated renewable electrolysis systems
- Develop and demonstrate unique integration opportunities for renewable electrolysis systems in the area of energy storage, grid support and industrial gas end-uses

Technical Barriers

This project addresses the following technical barriers from the Hydrogen Production section of the Fuel Cell Technologies Program's Multi-Year Research, Development and Demonstration Plan (2011 Interim Update):

(H) System Efficiency

(J) Renewable Electricity Generation Integration

Technical Targets

This project is conducting applied research and development to reduce integration barriers between renewable electricity sources and state-of-the-art electrolyzer

hydrogen-producing stacks of electrolyzers to improve system efficiency and lower the capital costs of this near-zero-carbon pathway.

Large-scale hydrogen production using renewable electricity is well positioned to produce near-zero greenhouse-gas-emission vehicle fuel in the coming years as hydrogen-powered electric vehicles are introduced into the marketplace. An integrated system with advanced sensing and communications will enable grid operators to take advantage of the controllable nature of distributed and central water electrolysis systems to maintain grid stability.

Approach

The Xcel Energy/NREL Wind-to-Hydrogen (Wind2H2) research, development, and demonstration project is advancing the integration of renewable electricity sources with state-of-the-art electrolyzer technology. Real-world data from daily system operation are revealing opportunities for improved system design and unique hardware configurations to advance the commercialization of this technology. Lessons learned and data-driven results provide feedback to industry and to the analytical and modeling components of this project (see “Hour-by-Hour Cost Modeling of Optimized Central Wind-Based Water Electrolysis Production,” Genevieve Saur and others).

In areas with large hydrogen production, even small increases in system efficiency result in significant reductions in the cost of hydrogen. DOE is funding electrolyzer manufacturers to design and build improved stacks and system balance of plant to reduce the cost of electrolytically produced hydrogen. This project provides independent testing and verification of the technical readiness of these advanced electrolyzer systems by operating them from the grid and renewable electricity sources.

Results

Much of the effort over the past year was focused on completing the installation of a new facility and the required infrastructure to accommodate testing of DOE-awarded electrolyzer systems. The new test facility takes advantage of some of the existing Wind2H2 infrastructure but also required a new facility, power and safety and support systems.

Some of the capabilities of the new test facility include the following:

- 75 kVA, 208 V, 3-phase power and 100 kVA, 480 V, 3-phase power
- Up to 10 MΩ-cm resistive deionized water (flow rate: 2 gallon per minute)
- Two combustible gas detectors integrated into the Wind2H2 system

- Alarm at 10% lower flammability limit of hydrogen-in-air
- Activation of high-flow exhaust fan follows gas detector alarm signal
- Local monitoring and archiving of the following data:
 - Stack temperature, voltage, and current
 - AC input voltage, current and power
 - Mass flow – hydrogen product (see volumetric mass flow device below)
 - Mass flow – hydrogen waste (e.g., drying)

NREL is conducting side-by-side testing and comparison of stack voltage decay rates between constant and variable power operation. Two 34-cell stacks of an H-Series PEM electrolyzer from Proton Onsite are being operated with a highly variable wind profile, achieving almost 5,500 hours of operation between November 2010 and April 2012. The third stack has operated over the same time with a constant stack power. All three stacks have the same average current. Varying wind current profile is operated for hundreds of hours continuously and only interrupted to operate all three stacks at their full-current point for a few consecutive days to enable comparison of their steady-state voltage. Table 1 summarizes the preliminary results over the roughly 5,500 hours of operation and shows the variable stacks exhibiting a higher decay rate than that of the constant current stack. However, it is possible that the stack with the lowest decay rate may have been randomly selected.

TABLE 1. Average Cell Decay Rates for Electrolyzer Stacks

| Mode | Average Decay $\mu\text{V}/\text{cell-h}$ |
|----------|---|
| Variable | 11.6 |
| Variable | 10.5 |
| Constant | 8.9 |
| Hours | 5,474 |

It is worth noting that before delivery to NREL, the electrolyzer stacks currently under test faced severe abuse with no hydration for about a year in a warehouse. Furthermore, this testing is intended only to reveal relative stack decay rates between a variable wind profile and constant current operation, if there is any difference. Normal stack decay rates of today’s PEM stacks are 2–5 $\mu\text{V}/\text{cell-h}$. However, some of the latest PEM stack designs have even shown no appreciable voltage decay over 20,000 h of life testing.

Management of distributed power systems is expected to become more commonplace as grids and devices become “smarter” and distributed renewable resources become a larger proportion of our energy supply. A critical element for the advancement of smart-grid technologies is managing distributed resources, which includes renewable electricity

generation, distributed energy storage, and taking advantage of active (or controllable) loads to provide grid support services like frequency and voltage regulation.

NREL operated both of the commercially available low-temperature electrolyzer technologies (PEM and alkaline) on an AC microgrid, shown in Figure 1, to evaluate their response to commands to increase and decrease stack power that shorten frequency disturbances. Results show that both the PEM and alkaline electrolyzers are capable of adding or removing stack power to provide sub-second response that reduces the duration of frequency disturbances.

Figure 2 compares a control test where electrolyzers are not triggered to shed load with the separate alkaline and

PEM response tests where the electrolyzers are commanded to reduce stack power by 10 kW. In each of the three tests shown in Figure 2, the load simulator instantly applies 10 kW of resistive load to initiate a frequency disturbance on the grid. High-resolution monitoring of the AC microgrid frequency (nominally 60 Hz) generates a control signal for the electrolyzer when the frequency exceeds ± 0.2 Hz. Similar tests were performed by removing load from the AC microgrid and commanding the electrolyzers to add 25 kW of stack power to mitigate an over-frequency disturbance. Both the alkaline and PEM technologies performed similarly in those tests as well.

Accurately measuring hydrogen mass flow from an electrolyzer, fuel cell, compressor, and hydrogen dispenser is challenging. Commercially available mass flow sensors are expensive and their accuracy can vary significantly depending on the type of transducer employed. This project, under its role as the DOE test and validation facility for advanced electrolyzer systems, designed, built and began testing a volumetrically-based mass flow device.

The design of the mobile mass flow device took advantage of industry partner feedback. The device calculates the mass flow from (or to) a piece of equipment by accurately measuring the pressure and temperature and by knowing the water volume of the composite overwrapped pressure vessel and interconnecting tubing. Using the National Institute of Standards and Technology equations-of-state for hydrogen, the onboard controller determines the mass flow by subtracting the initial from the final mass of hydrogen in the pressure vessel and how long it took to reach the final mass. Preliminary data from the mass flow device for 30+ samples are promising and have resulted in standard deviations of 0.002–0.004 kg per hour while sampling an electrolyzer with a nominal flow rate of 0.5 kg per hour.



FIGURE 1. Frequency regulation experimental system where electrolyzers are powered by diesel generators on an AC microgrid

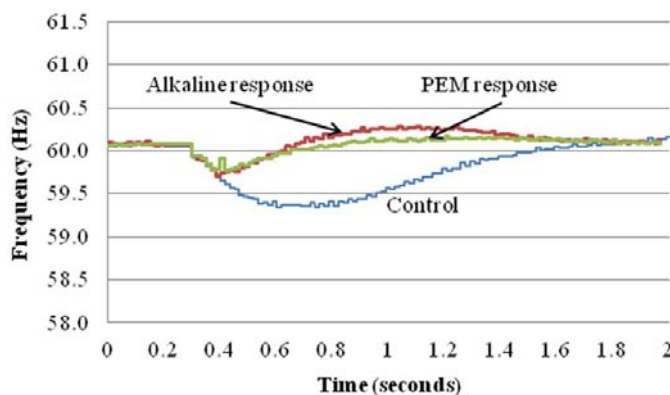


FIGURE 2. Resulting mitigation effects using electrolyzers to stabilize the frequency of an AC microgrid

Conclusions and Future Direction

NREL’s newest hydrogen test facility and supporting infrastructure, co-located at the Wind2H2 project, is complete and awaiting the prototype electrolyzer from Giner and their sub-contractor Parker Hannifin. Long-duration testing of three PEM electrolyzer stacks reached roughly 5,500 hours. The preliminary stack decay rate of the variably powered stacks is greater than that of the constant power stack. However, it is possible that the worst-performing stacks were randomly selected at the beginning of the test. By testing the response of these commercially available electrolyzer systems, NREL has shown that distributed and central electrolysis systems have another potential (economic) value stream because of their ability to quickly increase or decrease stack power, which could be used to improve grid stability. Finally, the volumetric mass flow device has shown low variability (2–4 g/hour) during initial testing of a 0.5 kg/hour electrolyzer.

In the coming year the team will complete the following:

- Install, commission and perform 100 hours of initial testing of a DOE-awarded system from Giner/Parker to complete an EE-1 Joule milestone
- Achieve more than 7,500 hours of stack testing using a variable (wind-based) power profile on two (of three) electrolyzer stacks; switch constant power stack with variable profile stack and re-start test
- Substantiate volumetric mass flow measurements by conducting variance and error analysis and integrating a master meter or gravimetric measurement approach

II.D.4 Hour-by-Hour Cost Modeling of Optimized Central Wind-Based Water Electrolysis Production

Genevieve Saur (Primary Contact),
Chris Ainscough.

National Renewable Energy Laboratory (NREL)
15013 Denver West Parkway
Golden, CO 80401-3305
Phone: (303) 275-3783
Email: genevieve.saur@nrel.gov

DOE Manager

HQ: Erika Sutherland
Phone: (202) 586-3152
Email: Erika.Sutherland@ee.doe.gov

Project Start Date: October 1, 2010
Project End Date: Project continuation and direction
determined annually by DOE

can approach the DOE 2015 centralized cost per gasoline gallon equivalent (\$/gge) target of \$3.10/gge only when taking advantage of wind energy incentives such as the production tax credit, investment tax credit, and Treasury grant [1]. See Table 1 for more details. Using 2010 wind electricity prices, a Class 6 wind resource could produce hydrogen at \$3.60/gge (all hydrogen costs in 2007 dollars, exclusive of compression, storage, and dispensing costs), without the wind incentives. With the incentives, the cost of hydrogen drops to approximately \$2.60/gge.

TABLE 1. Progress toward Meeting Technical Targets for Distributed Water Electrolysis Production

| Characteristics | Units | 2015 Target | 2020 Target | Status |
|-----------------|--------|-------------|-------------|----------------------------------|
| Hydrogen cost | \$/gge | 3.10 | <2.00 | 2.76–4.79 (with wind incentives) |

Fiscal Year (FY) 2012 Objectives

- Corroborate recent wind electrolysis cost studies using a more detailed hour-by-hour analysis.
- Examine consequences of different system configuration and operation for four scenarios, at 42 sites in five electricity markets across the contiguous United States.
- Initiate understanding of sizing implications between electrolyzers and wind farms.
- Identify areas for further analysis and cost reduction.
- Determine the sensitivity of the cost of hydrogen to various inputs, such as turbine cost, electrolyzer efficiency, electrolyzer capital cost, capacity factors, and availability.

Technical Barriers

This project addresses the following technical barriers from the Production section (3.1) of the Fuel Cell Technologies Program’s Multi-Year Research, Development and Demonstration Plan:

- (G) Capital Cost
- (H) System Efficiency
- (J) Renewable Electricity Generation Integration

Technical Targets

This analysis shows that using current prices for electricity from Class 3–6 wind resources, the hydrogen cost

FY 2012 Accomplishments

- Completed hourly analysis of a central wind electrolysis production facility (50,000 kg/day), at 42 sites in five electricity markets across the contiguous 48 states.
- Determined that Class 3–6 wind sites can produce renewable hydrogen for \$2.76–\$4.79/gge.
- Published a technical paper: G. Saur, and C. Ainscough, *U.S. Geographic Analysis of the Cost of Hydrogen from Electrolysis*. NREL/TP-5600-52640. Golden, CO: NREL; December 2011.
- Developed an interactive website allowing exploration of results and self-guided what if analysis: http://www.nrel.gov/hydrogen/production_cost_analysis.html.



Introduction

This work is aimed at understanding the barriers and costs associated with large-scale (50,000 kg/day) wind-based hydrogen generation plants. Such plants can take electrical energy from the wind or from the grid and use it to split water molecules into hydrogen and oxygen. The hydrogen can then be used for a variety of purposes, including vehicle fuel, fertilizer feedstocks, petroleum upgrading, metal processing, and other industrial processes. The hydrogen can also be stored, converted back to electricity, and sold to an electric utility.

Approach

The approach used in this analysis was to review a range of wind sites from Class 1 to 6 for their ability to produce hydrogen economically by electrolysis. Forty-two sites were chosen across the contiguous 48 states including five different electricity markets. Further, each site was analyzed under four different scenarios, defined as follows:

- Cost balanced: \$ grid purchased electricity = \$ wind electricity sold.
- Power balanced: kilowatt-hour (kWh) grid purchased electricity = kWh wind electricity sold.
- Same as A, but no purchase of summer peak electricity.
- Same as B, but no purchase of summer peak electricity.

In addition to these scenarios, sensitivities to various inputs were analyzed, including wind turbine capital cost, wind electricity costs, electrolyzer efficiency, electrolyzer capital cost, capacity factor, and availability.

Results

This analysis found that in power-balanced scenarios, the cost of hydrogen can range from nearly \$5.84/gge down to \$3.92/gge, depending on the class of the wind site. It is only at wind sites of Class 4 or better that such a plant begins to approach DOE technical targets for hydrogen cost production. This analysis included electricity prices in the California, New England, Texas, Midwest, and Pennsylvania, New Jersey, Maryland markets. See Figure 1 for more detail on how hydrogen cost varies by wind class.

In places with low-cost electricity, <\$0.08/kWh, hydrogen can be produced for approximately \$3.82–\$4.77/gge. This is true of both power and cost-balanced scenarios. Scenarios purchasing no summer peak electricity resulted in lower

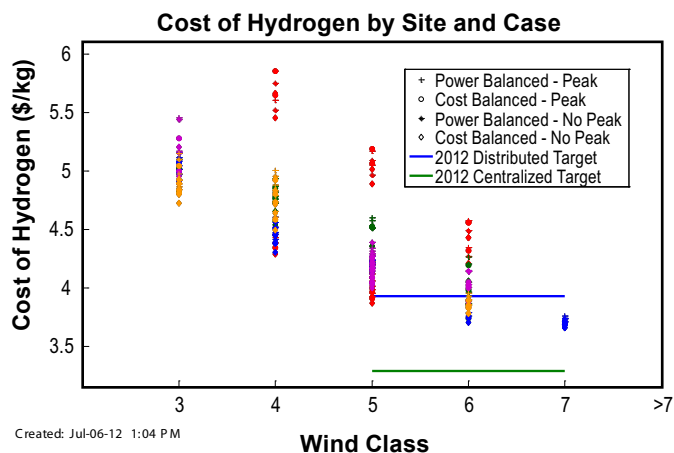


FIGURE 1. The cost of wind-based hydrogen varies greatly by wind resource class. Class 5 and better are required to approach DOE cost targets.

hydrogen costs but could also result in unmet hydrogen demand. See Figure 2 for more detail on how hydrogen cost varies by wind electricity cost.

The required installed wind capacity needed to produce 50,000 kg of hydrogen per day varies greatly with the wind class, which also affects the cost of wind electricity. The installed capacity can be as low as 200 megawatt (MW) (Class 6), and as much as 850 MW (Class 1). See Figure 3 for more detail on how hydrogen cost varies by wind farm size.

Sensitivity analysis was run to see what effect electrolyzer efficiency, availability, capital cost, wind capital cost, and wind availability have on the cost of hydrogen. This analysis showed that the largest hurdles to hydrogen cost from water electrolysis remain wind turbine capital cost and electrolyzer efficiency.

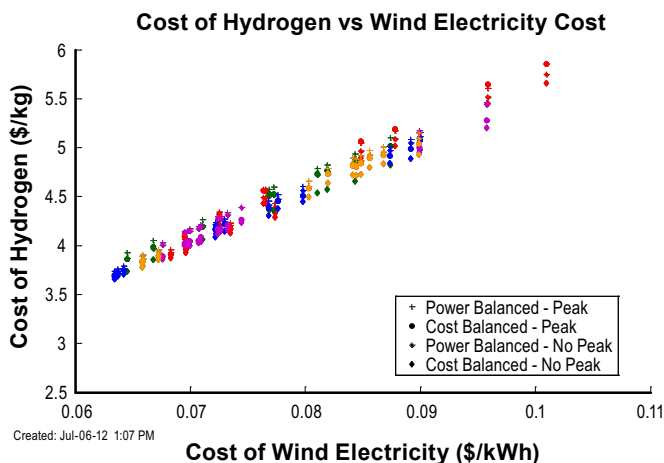


FIGURE 2. The overall cost of wind electricity has a strong influence on the cost of wind-based hydrogen, regardless of the analysis scenario.

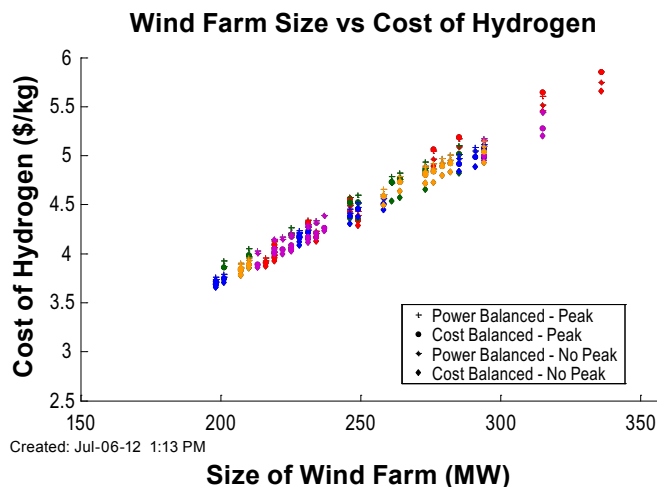


FIGURE 3. The installed capacity of a wind farm needed to produce 50,000 kg/day of hydrogen varies with the wind class. Lower quality winds require greater installed capacity, and thus result in more costly hydrogen.

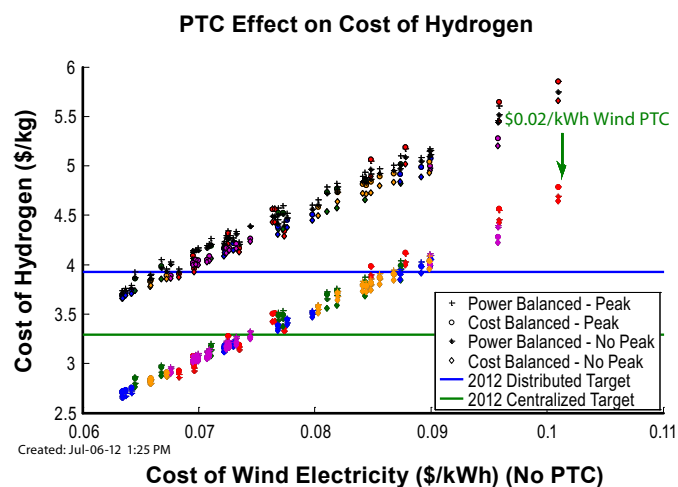


FIGURE 4. The effect of wind power incentives such as the production tax credit (PTC), investment tax credit, and Treasury grant can reduce the cost of wind-based hydrogen by approximately \$1/kg.

In summary, the presence of wind power incentives has a significant impact on the cost of hydrogen produced by central wind electrolysis of approximately \$1/kg as shown in Figure 4. With these incentives, wind sites with good resource quality may meet DOE cost targets.

Conclusions and Future Direction

No future work is currently funded. However if funding were available, the following additions to this analysis would be pursued.

- Add more sites on land
- Add additional electricity markets
- Add offshore wind sites
- Examine solar integration
- Add emphasis on smaller or forecourt-sized renewable electrolysis targeted to the vehicle end use market, with 700 bar storage
- Explore other optimal electricity/hydrogen production balance scenarios
- Explore other electrolyzer types in close collaboration with manufacturers

FY 2012 Publications/Presentations

1. *Hour-by-Hour Cost Modeling of Optimized Central Wind-Based Water Electrolysis Production*, presented at DOE Annual Merit Review, May 14-18, 2012, Washington, D.C.
2. Saur, G. and C. Ainscough, *U.S. Geographic Analysis of the Cost of Hydrogen from Electrolysis*. NREL/TP-5600-52640. Golden, CO: NREL; December 2011.

References

1. Saur, G. and C. Ainscough, *U.S. Geographic Analysis of the Cost of Hydrogen from Electrolysis*. NREL/TP-5600-52640. Golden, CO: NREL; December 2011.

II.D.5 Low-Cost Large-Scale PEM Electrolysis for Renewable Energy Storage

Dr. Katherine Ayers (Primary Contact),
Chris Capuano

Proton Energy Systems d/b/a Proton OnSite
10 Technology Drive
Wallingford, CT 06492
Phone: (203) 678-2190
Email: kayers@protononsite.com

DOE Manager

HQ: Erika Sutherland
Phone: (202) 586-3152
Email: Erika.Sutherland@ee.doe.gov

Contract Number: DE-SC0001338

Subcontractors:

- 3M, Minneapolis, MN
- University of Wyoming, Laramie, WY

Project Start Date: June 19, 2010 (Phase 1)
Project End Date: August 18, 2013 (with Phase 2 continuation)

- Updated H2A analysis based on the actual 435 psi system cost and operation projected to 50,000 kg/day.
- Analysis of greenhouse gas and petroleum reductions that will occur with the successful implementation of the proposed technology.

Technical Barriers

This project addresses the following technical barriers from the Production section of the Fuel Cell Technologies Program Multi-Year Research, Development and Demonstration Plan:

- (G) Capital Cost
- (H) System Efficiency
- (J) Renewable Electricity Generation Integration

Technical Targets

TABLE 1. Proton Energy Systems Progress Towards Meeting Technical Targets for Distributed Water Electrolysis Hydrogen Production

| Characteristics | Units | 2012 Target | 2017 Target | Proton Status |
|--------------------------------|---------|-------------|-------------|---------------|
| Hydrogen Cost | \$/gge | <3.70 | <3.00 | 3.46 |
| Electrolyzer Capital Cost | \$/gge | 0.70 | 0.30 | 0.64 |
| Electrolyzer Energy Efficiency | % (LHV) | 69 | 74 | 67 |

gge - gasoline gallon equivalent; LHV - lower heating value
Note: Estimates are based on H2A v2.1, for electrolysis only (compression-storage-delivery not included). Model assumes \$0.05/kWh.
Electrolyzer cost based on 1,500 kg/day capacity, 500 units/year; Efficiency based on system projections and demonstrated stack efficiency of 74% LHV efficiency.

Fiscal Year (FY) 2012 Project Objectives

- Demonstrate optimal membrane electrode assembly (MEA) efficiency through:
 - Refinement of catalyst compositions based on identified design spaces from Phase 1.
 - Rapid screening of additional metal candidates through combinatorial methods to determine optimal anode catalyst composition.
 - Fabrication of identified materials as both traditional and nano-structured thin-film electrode (NSTF)-type electrodes.
 - Integration of new catalyst materials with advanced thinner membranes.
- Reduce catalyst loading through:
 - Formulation optimization of metal oxide based inks.
 - Improved electrode application processes for uniform distribution.
 - Application of NSTF structures.
 - Demonstration in Proton's large active area format.
- Demonstrate 1,000 hours system operation at >69% efficiency.
- Develop a concept design to scale the system to 50,000 kg/day H₂ production including:
 - Definition of the requirements for operation and maintenance.

FY 2012 Accomplishments

- Completed anode formulation optimization demonstrating >50% reduction in catalyst loading and passed internal concept review to build qualification stack.
- Synthesized initial matrix of alternate metal oxide compositions for screening based on refinement of Phase 1 results.
- Combinatorial study completed for several metal combinations and candidates downselected for powder synthesis.
- Tooling procured for large active area electrodes.
- NSTF electrodes successfully applied to alternative membranes.
- 50,000 kg/day concept design completed and quoted.



Introduction

This project addresses the DOE Hydrogen Program objective for distributed production of hydrogen from proton exchange membrane (PEM) water electrolysis. The DOE technical targets for hydrogen cost as well as electrolyzer efficiency and capital cost will be directly addressed through the advancement of key components and design parameters. For renewable applications such as grid energy storage, a continuum of options from distributed hydrogen generation to centralized production at capacities on the order of 50,000 kg/day will be needed. The majority of the electrolysis efficiency losses arise from the oxygen evolution overpotential and the membrane ionic resistance. To reach a target system operating efficiency of 69%, new catalyst and membrane materials are needed. Especially for these large scales, it is necessary to minimize the use of precious metals. Many learnings from fuel cell materials research can be applied to enable the required advancements. Design studies are also needed for PEM electrolysis at this scale to understand the capital costs, environmental impact, and operation and maintenance requirements.

Approach

This project addresses crucial elements of Proton's technology roadmap, with a focus on improving MEA performance. The oxygen evolution catalyst and membrane are therefore the two key areas of focus. Critical issues include long-term stability of the membrane under electrolysis conditions, particularly as it relates to long-term creep with a thinner membrane, and stability of the catalyst to dissolution. Continuation of the work completed in Phase 1 includes: 1) refinement of the mixed metal oxide catalyst composition for increased activity while maintaining voltage stability, 2) initial reductions in catalyst loading of 50% or greater based on implementation of improved manufacturing processes at Proton, 3) integration of optimized catalyst compositions into nanostructured thin films to demonstrate an additional order of magnitude reduction in catalyst loading and development of high speed manufacturing capability, 4) use of reinforced membranes in order to reduce membrane thickness and ionic resistance without decreasing durability, and 5) projection of these improvements to 50,000 kg/day production levels including cost modeling, impact on reduction of greenhouse gas emissions, and conceptual system design.

Catalyst compositions were made using two techniques. Iteration on promising compositions from Phase 1 were manufactured as nanopowders through fusion of soluble metal salt precursors at high temperatures. Nanopowders will be screened through fabrication of bench-scale MEAs. New candidates were made through ink jet printing and sintering,

and were screened through a fluorescence technique to determine the relative amount of oxygen evolution at a given overpotential. The approach is shown in Figure 1. The conceptual 50,000 kg/day system design was developed through sizing calculations of the major system components and consultation with relevant industries such as chlor-alkali to determine typical redundancy factors and margins. Items such as power conversion components, water treatment facilities, pressure vessels, and storage tanks were quoted through suppliers well versed in the relevant sizes. Cell stack costs were estimated based on a module similar to Proton's largest active area platform and known design improvements validated at a prototype level.

Results

Building from initial feasibility studies under a previous DOE project, significant progress has been made towards production implementation of reduced catalyst loading. Improvements in print uniformity were accomplished through formulation optimization of the ink carrier solution. With the optimized formulation, improved mass activity was observed as shown in Figure 2. Initial cells have been placed on durability testing, with a full scale validation stack expected within the next month. NSTF electrodes have also been fabricated at 3M and are being sent to Proton for testing.

The nanopowder catalyst candidates fabricated at Proton are being fabricated into MEAs for performance testing. For the combinatorial approach, the baseline formulation was



FIGURE 1. Ink jet printer used for combinatorial studies and sample print

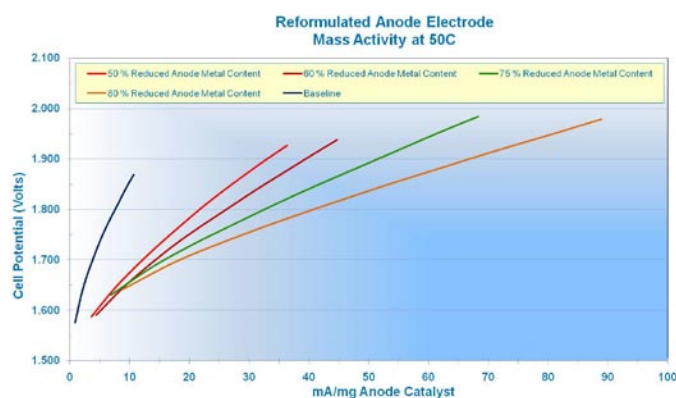


FIGURE 2. Mass activity for various catalyst loadings with improved formulation

provided to University of Wyoming as a comparison point. Trimetallic compositional matrices were printed for several candidates including combinations of Ir, Ru, Pt, Sn, Nb, and Mn. All compositions contained two of the catalytic metals (Ir, Pt, and Ru) and one of the structural metals (Sn, Nb, and Mn). This approach has been proven to be successful in developing catalysts for photoelectrochemical activity and was thus applied for electrolysis. Screening was completed for electrochemical activity and the fluorescence technique was demonstrated to be effective in determining areas of high activity. Polarization curves also show improvement for an initial candidate as shown in Figure 3. Final downselect is ongoing, to be completed within the next month.

The 50,000 kg/day design concept is shown in Figure 4. Power supplies were sized for voltage and current output based on optimal integration with grid input, for minimal efficiency loss. Cell stack voltage was then determined and the module size scaled to leverage Proton's existing design principles. The number of components such as phase separators, pumps, and tanks were determined based on optimization of cost, reliability considerations, and available sizes. The overall concept was estimated to result in a capital cost of \$0.49/kg.

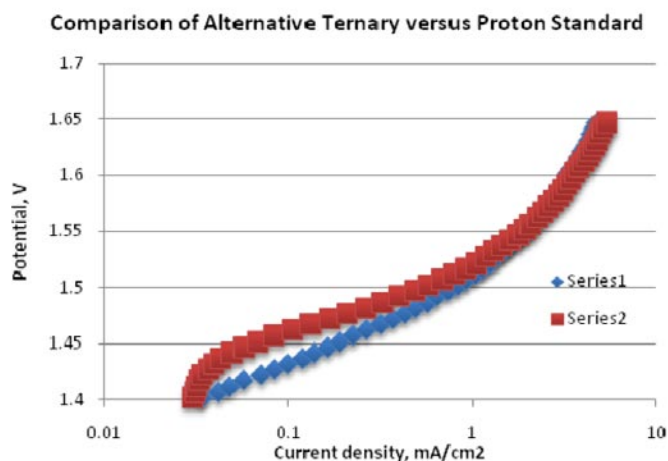
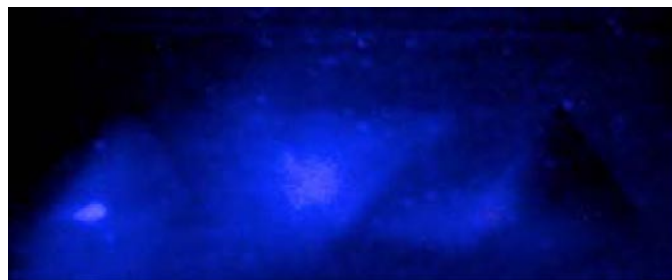


FIGURE 3. Fluorescence screening of combinatorial matrices and polarization curve for discrete sample

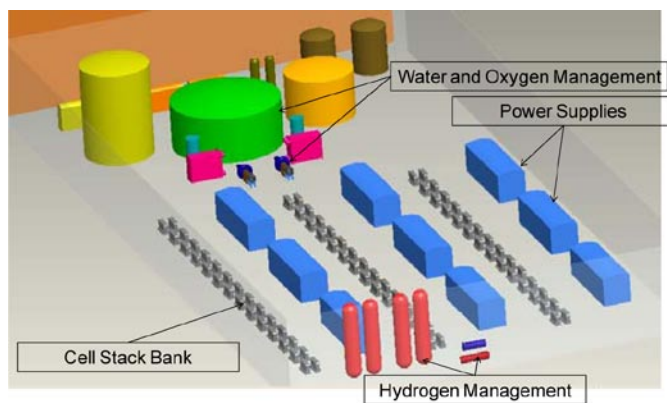


FIGURE 4. 50,000 kg/day plant concept

Conclusions and Future Directions

- Manufacturing transition for initial reduction in catalyst loading in progress:
 - Reproducibility and manufacturability demonstrated.
- Catalyst activity and durability screening ongoing:
 - Proton compositional testing in progress at MEA level.
 - U. Wyoming compositions evaluated and undergoing final downselect.
 - Synthesis scale up to be initiated for Wyoming candidates.
- Electrode and stack scale up initiated:
 - Tooling obtained for large active area stack.
 - Reduced loading validation stack to be tested.
- 50,000 kg/day initial concept design complete:
 - Add stack balance of materials as inputs.
 - Conduct environmental impact assessment.
 - Update with MEA electrical efficiencies and operational data as testing progresses.

II.E.1 Solar High-Temperature Water Splitting Cycle with Quantum Boost

Robin Taylor (Primary Contact), Roger Davenport, David Genders¹, Peter Symons¹, Lloyd Brown², Jan Talbot³, Richard Herz³

Science Applications International, Corp. (SAIC)
10210 Campus Point Drive
San Diego, CA 92121
Phone: (858) 826-9124
Email: taylorro@saic.com

¹Electrosynthesis Co., Inc. (ESC)

²Thermochemical Engineering Solutions (TCHEME)

³University of California, San Diego (UCSD)

DOE Managers

HQ: Sara Dillich

Phone: (202) 586-7925

Email: Sara.Dillich@ee.doe.gov

GO: Katie Randolph

Phone: (720) 356-1759

Email: Katie.Randolph@go.doe.gov

Contract Number: DE-FG36-07GO17002

Subcontractors:

- Electrosynthesis Co., Inc., Lancaster, NY
- Thermochemical Engineering Solutions, San Diego, CA
- University of California, San Diego

Project Start Date: September 1, 2007

Project End Date: August 31, 2014

Technologies Program Multi-Year Research, Development and Demonstration Plan:

- (U) High-Temperature Thermochemical Technology
- (V) High-Temperature Robust Materials
- (W) Concentrated Solar Energy Capital Cost
- (X) Coupling Concentrated Solar Energy and Thermochemical Cycles

Technical Targets

Table 1 presents the progress made, to date, in achieving the DOE technical targets as outlined in the §3.1.4 Multi-Year Research, Development and Demonstration Plan – Planned Program Activities for 2005-2015 (updated September 2011), Table 3.1.9: Solar-Driven, Thermo-chemical High-Temperature Thermochemical Hydrogen Production.

TABLE 1. Progress towards Meeting Technical Targets for Solar-Driven High-Temperature Thermochemical Hydrogen Production

| Characteristics | Units | U.S. DOE Targets | | | Project Status |
|--|-----------------------|------------------|------|------|--|
| | | 2008 | 2012 | 2017 | |
| Solar-Driven High-Temperature Thermochemical Cycle Hydrogen Cost | \$/gge H ₂ | 10.00 | 6.00 | 3.00 | \$7.74 ^a (2015) \$4.65 ^a (2025) |
| Heliostat Capital Cost (installed cost) | \$/m ² | 180 | 140 | 80 | 97 ^b |
| Process Energy Efficiency ^c | % | 25 | 30 | >35 | 22.5% /41% ^d |

gge – gasoline gallon equivalent

^a Electrolytic system projected costs based on latest H2A analysis.

^b Based on SAIC glass-reinforced concrete structure with 10 sq.m. area and low production quantity.

^c Plant energy efficiency is defined as the energy of the hydrogen produced (lower heating value) divided by the sum of the energy delivered by the solar concentrator system plus any other net energy imports (electricity or heat) required for the process.

^d Plant energy efficiency without/with credit for excess electricity produced.

Fiscal Year (FY) 2012 Objectives

- Reduce the energy consumption of the electrolytic hydrogen production step by 20% by decreasing the voltage.
- Demonstrate the molten salt is liquid and will flow (low viscosity) so it is easily pumped.
- Demonstrate the NH₃ can be separated from the SO₃ by thermal decomposition thus avoiding potentially uneconomic gas separation processes.
- Develop a fully functioning and converging Aspen Plus[®] modeling of the Sulfur Ammonia (SA) cycle.
- Update the solar concentrating system to match the thermochemistry.

Technical Barriers

This project addresses the following technical barriers from the Production section (3.1.4) of the Fuel Cell

FY 2012 Accomplishments

- Improvements to electrocatalysts and high temperature operation have achieved cell voltages as low as 0.64 V at 50 mA/cm² and 0.85 V at 300 mA/cm².
- A 500 hour durability test was initiated to demonstrate the long-term stability of the electrolytic cell materials.
- Economic modeling initially showed that the minimum annualized cost was at current densities <100 mA/cm²; however, we may have to operate at higher current densities in order to minimize the effect of sulfite diffusing across the membrane.

- Lab results continue to prove the feasibility of the all- (liquid/gas) molten salt mixture of $(\text{NH}_4)_2\text{SO}_4 + \text{K}_2\text{SO}_4 + 4 \text{K}_2\text{S}_2\text{O}_7 + \text{Na}_2\text{SO}_4 + 4 \text{Na}_2\text{S}_2\text{O}_7$ chemistry for the high-temperature oxygen evolution sub-cycle.
- A thermochemical reactor and residual gas analysis equipment was used to show ammonia and sulfur trioxide can be evolved separately with a 25-50°C temperature difference.
- The melting points, densities and viscosities of the molten salt mixtures were measured; it was proven that the salts have low viscosities and can be easily pumped.
- The Aspen Plus® SA process modeling has been significantly improved and is now a robust fully functioning process tool.
- The Aspen Plus® model and the H2A economic model continued to be used to optimize and trade-off SA cycle configurations.
- A phase change storage approach was identified to allow 24/7 operation of the process, using NaCl, and will continue to be evaluated.



Introduction

Thermo-chemical production of hydrogen by splitting water with solar energy is a sustainable and renewable method of producing hydrogen. However, the process must be proven to be efficient and cost effective if it is to compete with conventional energy sources.

Approach

To achieve the project objectives, the Bowman-Westinghouse “sulfur-family” hybrid thermochemical water splitting cycle (*aka* “Hybrid Sulfur, HyS” cycle) was modified by introducing ammonia as the working reagent, thus producing the sulfur-ammonia, or “SA,” cycle. The purpose of the modification is to attain a more efficient solar interface and less problematic chemical separation steps. Several versions of the SA cycle were developed and evaluated experimentally as well as analytically using the Aspen Plus® chemical process simulator.

Two approaches were considered for the hydrogen production step of the SA cycle, namely: photocatalytic and electrolytic oxidation of ammonium sulfite to ammonium sulfate in an aqueous solution. Also, two sub-cycles have been considered for the oxygen evolution side of the SA cycle, namely: zinc sulfate/zinc oxide and potassium sulfate/potassium pyrosulfate sub-cycles. The laboratory testing and optimization of all the process steps for each version of the SA cycle were then carried out. Once the optimum configuration of the SA cycle has been identified and the

cycle has been validated in closed-loop operation in the lab, it will be scaled up and tested on-sun.

Results

Cycle Evaluation and Analysis

During the past year, work focused on the electrolytic SA cycle, which is summarized in the following equations:

- 1 Chemical Absorption: 25-50°C
 $\text{SO}_{2(\text{g})} + 2\text{NH}_{3(\text{g})} + \text{H}_2\text{O}_{(\text{l})} \rightarrow (\text{NH}_4)_2\text{SO}_{3(\text{aq})}$
- 2 Electrolytic: 80-150°C
 $(\text{NH}_4)_2\text{SO}_{3(\text{aq})} + \text{H}_2\text{O}_{(\text{l})} \rightarrow (\text{NH}_4)_2\text{SO}_{4(\text{aq})} + \text{H}_2$
- 3 Solar Thermal: 400-450°C
 $(\text{NH}_4)_2\text{SO}_{4(\text{aq})} + \text{K}_2\text{SO}_{4(\text{l})} \rightarrow \text{K}_2\text{S}_2\text{O}_{7(\text{l})} + 2\text{NH}_{3(\text{g})} + \text{H}_2\text{O}_{(\text{g})}$
- 4 Solar Thermal: 550-850°C
 $\text{K}_2\text{S}_2\text{O}_{7(\text{l})} \rightarrow \text{K}_2\text{SO}_{4(\text{l})} + \text{SO}_{3(\text{g})}$
- 5 Solar Thermal: 850-1,000°C
 $\text{SO}_{3(\text{g})} \rightarrow \text{SO}_{2(\text{g})} + \frac{1}{2} \text{O}_{2(\text{g})}$

The electrolytic oxidation of the ammonium sulfite solution occurs more efficiently at higher temperatures requiring the development of a system capable of running at higher pressures. Reactions (3) and (4) form a sub-cycle by which potassium sulfate is reacted with ammonium sulfate in the low-temperature reactor, to form potassium pyrosulfate. That substance is then fed to the medium-temperature reactor where it is decomposed to SO_3 and K_2SO_4 again, closing the sub-cycle. The potassium sulfate and pyrosulfate form a miscible liquid melt that facilitates the separations and the movement of the chemicals in reactions (3) and (4). The oxygen production step (5) occurs at high temperature over a catalyst. Separation of the oxygen from SO_2 occurs when they are mixed with water in reaction (1). The net cycle reaction represented by reactions 1-5 is decomposition of water to form hydrogen and oxygen. All of the reaction steps described above have been demonstrated in the laboratory and shown to occur without undesirable side reactions. However, we are working to ensure that there are none in the electrolytic step and the SO_3 decomposition. Figure 1 shows a schematic of the electrolytic SA cycle.

Electro-Oxidation of Aqueous Ammonium Sulfite Solutions

Optimization of the electrolytic process continued at ESC. New catalysts and electrode materials have been screened at 80°C, with the most promising materials including spinels ($\text{M}_x\text{N}_{3-x}\text{O}_4$ where $\text{M}, \text{N} = \text{Fe}/\text{Ni}/\text{Co}$), platinum/cobalt mixtures and alternate felts. These materials were further screened in a new high-pressure reactor which was built for this project and is shown in Figure 2. Current potential curves were generated at 125°C for anolyte

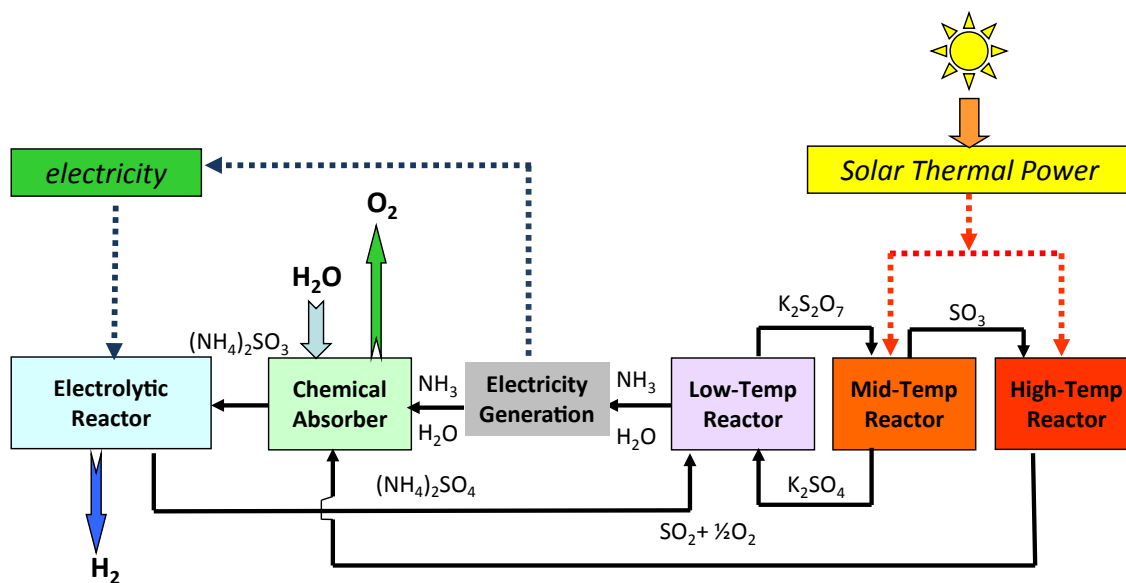


FIGURE 1. Schematic of the electrolytic SA cycle

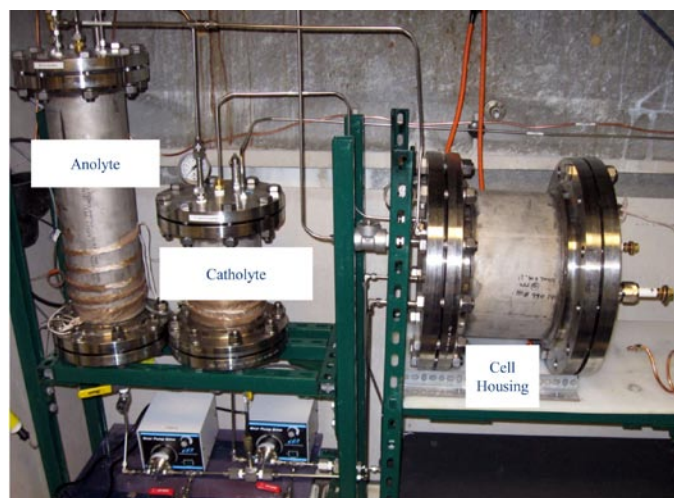


FIGURE 2. Pressure vessels required for electrochemical cell operation at high temperature

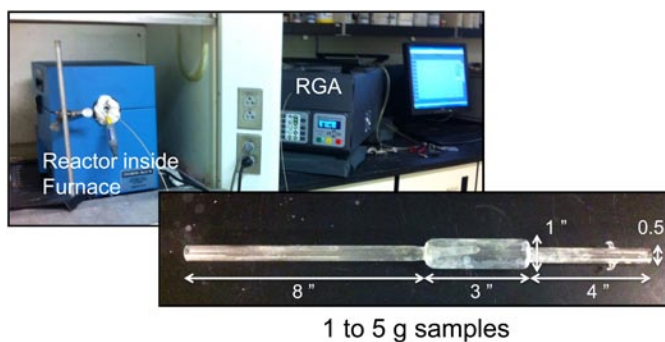


FIGURE 3. Thermochemical reactor system

compositions made up to simulate 0-90% conversions. These show that a voltage penalty of as low as 60 mV should be possible over this conversion range.

A 500-hour durability test was initiated at a current density of 50 mA/cm² and a temperature of 127°C. This ran for approximately 50 hours at which time it became apparent that the sulfite flux across the Nafion[®] membrane was too high. The resulting high concentration of sulfite on the cathode side of the cell resulted in reduced hydrogen current efficiencies. As a result of this testing, we have screened a number of alternate membrane materials and have identified a promising material that shows lower sulfite fluxes. Moreover we have shown that the high flux rates across the Nafion[®] -

type membranes occur after prolonged exposure to high temperature. The new membranes have been exposed to these same temperatures for up to three days and have maintained reasonable flux rates. Long-term testing will be initiated using these membranes.

High-Temperature Cycle Step Evaluation

Evaluation of the all-liquid/gas high-temperature cycle steps continued. A larger reactor system was built, as shown in Figure 3, to use up to ~10 g of reactants to study the evolution of gaseous products under more realistic operating conditions. A residual gas analyzer was used to detect the gases from the reaction. As shown in Figure 4, experiments were conducted to show the evolution of ammonia and water vapor at ~465°C, followed by evolution of sulfur trioxide at 500°C. The viscosity of the molten salt streams which would be entering and exiting the mid-temperature reactor was measured. The melting points and densities were also

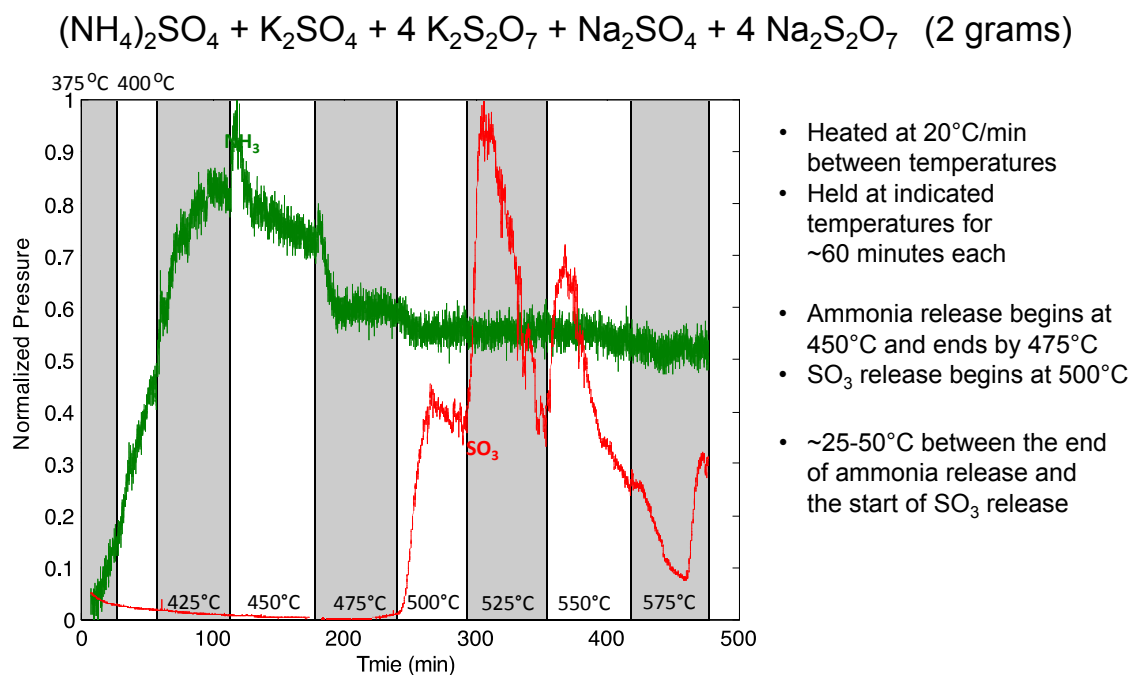


FIGURE 4. Residual gas analysis of oxygen generation half cycle

measured. It was determined that it should be easy to pump these molten salts with viscosities below ~ 8 cP as shown in Figure 5.

Aspen Plus[®] Process Analysis

UCSD developed a new Aspen Plus[®] model of the plant. A process heat integration analysis, or pinch analysis, of the plant was performed in order to place heat exchangers at optimal positions. Thermodynamic data from the literature were incorporated into the mid-temperature reactor, which decomposes molten pyrosulfates to sulfates and releases gaseous SO_3 . Calculator blocks were utilized to obtain power requirements for the electrolyzer and the overall efficiency of the plant. Design specifications were placed in strategic areas of the model to aid convergence.

Energy from the solar-thermal heated reactors is recovered from the $\text{SO}_2 + \text{O}_2$ gas product of the high-temperature reactor and from the $\text{NH}_3 + \text{H}_2\text{O}$ gas product of the low-temperature reactor. The gas product from the high-temperature reactor is used to preheat the SO_3 feed to the high-temperature reactor and the molten salt feed to the mid-temperature reactor. Energy recovery from the gas product of the low-temperature reactor is used to generate the electrical power for the electrolyzer, which produces the hydrogen product of the plant. The first option considered for this energy recovery is a single-flow condensing turbine that expands the $\text{NH}_3 + \text{H}_2\text{O}$ vapor stream from 9 bar to a sub-atmospheric pressure maintained by a condenser. Another option is a standard Rankine steam power plant. The steam

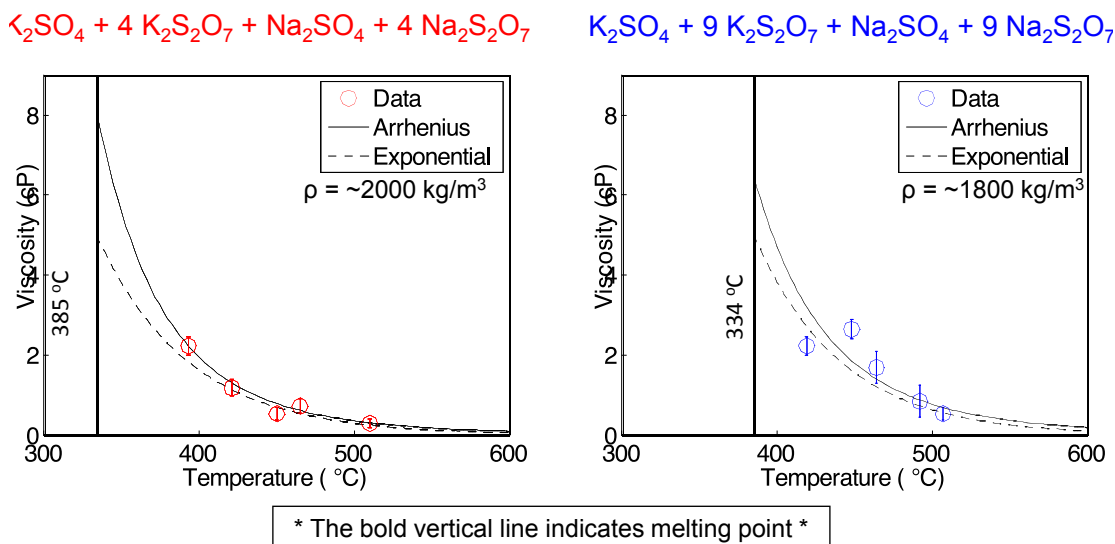
for this power plant would be produced by heat exchange from the $\text{NH}_3 + \text{H}_2\text{O}$ vapor stream. Both options generate more power than needed for the electrolyzer. However, there are operational considerations that may make the steam power plant a preferred option. Further analysis of these trade-offs are required.

The total heat requirements of the solar reactors along with the total hydrogen product were exported to a calculator block that computes the overall efficiency of the plant. Currently, the overall process efficiency is 23%. The efficiency can be increased with further research into heat integration and different modes of power generation.

Process Flowsheet Alternatives

In addition to the process flowsheet from previous years, alternative configurations have been investigated using Aspen Plus[®]. The major alternatives are a different power recovery scheme and use of electricity to power the high temperature step, SO_3 decomposition.

The direct power recovery scheme proposed previously employs an expansion turbine in the ammonia vapor stream from the mid-temperature reactor. The alternative employs heat transfer from this same stream into a Rankine power plant. From an efficiency standpoint, there is little difference between the two schemes. The direct system has less heat exchange losses but the indirect scheme permits recovery of the heat of solution and heat of reaction from the recombination of SO_2 with aqueous ammonium hydroxide forming ammonium sulfite. Work will continue on both



- Viscosity of $\text{K}_2\text{SO}_4 + 4 \text{K}_2\text{S}_2\text{O}_7 + \text{Na}_2\text{SO}_4 + 4 \text{Na}_2\text{S}_2\text{O}_7$ ranged from 0.53 - 2.2 cP from 419 - 507 °C
- Viscosity of $\text{K}_2\text{SO}_4 + 9 \text{K}_2\text{S}_2\text{O}_7 + \text{Na}_2\text{SO}_4 + 9 \text{Na}_2\text{S}_2\text{O}_7$ ranged from 0.29 - 2.3 cP from 393 - 510 °C
- We measured melting points, densities, and viscosities

FIGURE 5. Data showing molten salts can be easily pumped

schemes but the final selection between the two will be based on process economics. The direct scheme is much simpler but requires the power recovery to operate on a corrosive stream. Also, salt carryover into the ammonia stream must be rigorously avoided to prevent solids plate-out in the turbine.

The high-temperature step of the process uses less than 15% of the total thermal energy requirement. Since the process generates more electricity than required by the electrolysis step and since there is no credit given for export of excess electricity production, it made sense to consider electric heating to accomplish SO_3 decomposition. Use of an electrically heated decomposer (Joule Heating) may even make economic sense even if credit were given for export of excess electricity. The SO_3 reactor could be easily heated to above 1,500°C using silicon carbide heating elements thus increasing the conversion of SO_3 to SO_2 . The practical limit is about 1,200°C as above this temperature the reaction does not require catalysis so a quench would be required to retain the chemical conversion obtained at higher temperatures. The main advantages of Joule Heating are that solar costs would be reduced. Also, given a suitable thermal energy storage system, the complete chemical plant could operate continuously, independent of time of day or fluctuations in insolation due to passing clouds.

The cost of a solar installation is strongly dependent upon the highest temperature required. Not only are cavity radiation losses (proportional to T^4) lower, but the solar

field components are less expensive due to less stringent pointing accuracy requirements. Joule heating would remove the high temperature step from the top of a solar tower, increasing safety and reducing heat losses. Moreover, the reactor design would be considerably simplified. Instead of heating individual catalyst filled tubes or being forced to an atmospheric pressure decomposer design, a packed bed reactor could be designed with internal silicon carbide heating elements.

Probably the main advantage of using electric heat is that operation of the hydrogen plant would be completely decoupled, insofar as thermal energy storage allows, from diurnal and short-term fluctuations in solar insolation. Using the sodium chloride latent heat storage method described below, the chemical plant, both the electrolytic hydrogen generating system and the thermal oxygen generating system, can be operated around the clock under steady-state conditions.

Heat Storage

To allow the chemical plant to operate 24/7, storage of solar energy is needed. The most efficient form of storage is direct thermal storage. To provide the needs of the medium-temperature reactor, a maximum temperature of about 800°C is needed. SAIC has identified a unique phase change storage approach using molten NaCl that provides large amounts of

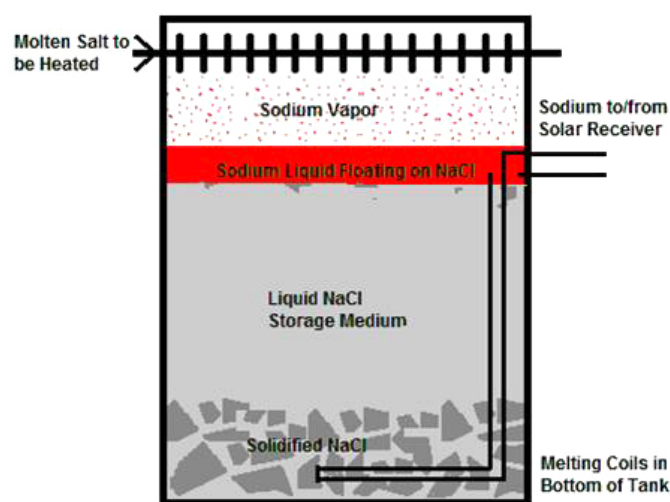


FIGURE 6. Schematic of a conceptual NaCl heat storage system

thermal capacity (481 kJ/kg) at this temperature, as well as providing an efficient means of extracting the heat from the storage to the molten salts. The storage consists of a stainless steel tank holding a volume of NaCl, with some head space above to accommodate the expansion/contraction of the salt as it changes phase. A schematic of the conceptual system is shown in Figure 6. A thin layer of liquid sodium metal (Na) floats on top of the molten NaCl and the head space is filled with Na vapor at its vapor pressure, which runs from about 0.5 to 1.5 bar over the temperature range expected. Pipes carrying the molten salt materials to be heated pass through the headspace in contact with the Na vapor, and the sodium acts as a heat pipe to transfer heat from the NaCl to the pipes. Solid NaCl that forms at the bottom of the Na pool sinks to the bottom (there is about a 30% reduction in volume upon solidification), so the Na remains in contact with liquid NaCl as the entire heat capacity of the storage is used. To re-melt the NaCl, pipes containing liquid sodium are placed at the bottom of the tank, and circulation from the solar receiver heats and re-melts the NaCl.

Solar Field Optimization

Further activity on the solar field configuration was delayed while waiting for the improvements to the Aspen Plus[®] model to be completed, so that it could be used for optimization of the heat interfaces to the solar field. These activities are ongoing.

Economic Analysis

H2A was used to evaluate the optimum operating conditions for the electrolytic portion of the system. The preliminary analysis evaluated the capital costs and electrical operating costs for the electrolysis process. Test data on the voltage versus current density was used. Using the H2A

defaults for the cost of the electrolytic cell and electricity, the conclusion was that the least-cost condition occurred at 50-75 mA/cm². Practical aspects of the electrolytic process, such as movement of sulfite through the membrane, may limit operating conditions to higher current densities. Also, we believe that the H2A capital cost values are low for the electrolytic cell, which would drive the optimum to higher current densities.

Conclusions and Future Directions

In summary:

- Improvements to electrocatalysts and high-temperature operation have improved the electrolytic cell performance. A 500-hour durability test was initiated but showed that extended operation at high temperature resulted in unacceptably high sulfite transfer rates. We have recently identified membranes that appear to have a significantly lower sulfite flux even after treatment at high temperature. The 500-hour durability test will be re-started to demonstrate long-term stability of this process.
- Lab results for the oxygen evolution sub-cycle using molten salt mixtures show ammonia and sulfur trioxide can be evolved separately with a 25-50°C temperature difference, thus avoiding difficult gas separation processes. The melting points, densities and viscosities of the molten salt mixtures were measured to prove that they have low viscosities and can be easily pumped.
- The Aspen Plus[®] SA process modeling was significantly improved and in conjunction with the H2A economic model, continue to be used to optimize and trade-off SA cycle configurations.
- Solar configuration evaluations were performed with the focus remaining on a central receiver system. A phase-change storage approach is being evaluated to allow 24/7 operation.

Activities planned for the upcoming year include:

- Continue with the electrolytic cell long-term (500 hour) test at higher current density and higher voltage. This would demonstrate the cathode stability in the presence of sulfite.
- Develop improved anode electrocatalysts that allow operation at low temperature while achieving low voltage.
- Continue evaluation of alternate membranes that can operate at high temperature with acceptable sulfite flux.
- Identify cathodes that preferentially evolve hydrogen in the presence of sulfite.
- Electrochemical cell design optimization and scale up.
- Develop a bench-scale, pressurized molten salt flow system to study rates of gas evolution.

- Continue refinement of the Aspen Plus[®] model to optimize the chemical process, including heating of the SO₃ reactor using electrical power.
- Evaluate NaCl phase change storage and its potential for supplying heat to the process on a 24/7 basis. Optimize the solar heliostat field configuration to supply the needed solar energy.
- Update the H2A analysis to include the optimized chemical plant configuration and solar field and storage configuration, and use H2A to identify the projected improvements possible due to advancing development in the various process and design areas.
- After completion of phase 1, the next phase of the project will involve bench-scale laboratory validation of the closed-loop SA cycle.

FY 2012 Publications/Presentations

1. Taylor, R., Genders, D., Brown, L., Talbot, J., Herz, R., Davenport, R., Presentation at the STCH Hydrogen Production Technology Team Review Meeting, La Jolla, California, July 10, 2012. (PowerPoint presentation).
2. Wang, M., “Study of the Thermochemistry for Oxygen Production for a Solar Sulfur-Ammonia Water-Splitting Process,” MS thesis, University of California, San Diego (2012).
3. Taylor, R., Davenport, R., Talbot, J., Genders, D., Brown, L., Herz, R., Overview and Status of the Sulfur Ammonia Thermochemical Hydrogen Production System for Splitting Water, Presentation at the 19th World Hydrogen Energy Conference 2012, Toronto, Ontario, Canada, June 3–7, 2012.
4. Taylor, R., Davenport, R., Solar Field Design and Integration for Thermochemical Hydrogen Production Systems, Poster presentation at the 19th World Hydrogen Energy Conference 2012, Toronto, Ontario, Canada, June 3–7, 2012.
5. Littlefield, J., Wang, M., Adoum, M., Talbot, J., Herz, R., Brown, L., Process Modeling and Thermochemical Experimental Analysis of the Solar Sulfur Ammonia Hydrogen Production Cycle, Presentation at the 19th World Hydrogen Energy Conference 2012, Toronto, Ontario, Canada, June 3–7, 2012.
6. Littlefield, J., Wang, M., Talbot, J., Herz, R., Brown, L., Process Modeling and Thermochemical Experimental Analysis of the Solar Sulfur Ammonia Hydrogen Production Cycle, submitted to *Energy Procedia* (2012).
7. Wang, M., Talbot, J., Herz, R., Brown, L., “Melting Point and Viscosity of Molten K₂SO₄ + K₂S₂O₇ + Na₂SO₄ + Na₂S₂O₇ Mixtures”, submitted to *Journal of Chemical and Engineering Data* (2012).
8. Genders, D., Symons, P., Brown, L., Electrochemical Oxidation of Ammonium Sulfite for the Sulfur Ammonia Thermochemical Hydrogen Production System, Poster presentation at the 19th World Hydrogen Energy Conference 2012, Toronto, Ontario, Canada, June 3–7, 2012.
9. Davenport, R., Taylor, R., Genders, D., Brown, L., Talbot, J., Presentation at the 2012 U.S. DOE Hydrogen and Fuel Cell Program and Vehicle Technologies Program Annual Merit Review and Peer Evaluation Meeting, Washington, D.C., May 14–18, 2012. (PowerPoint presentation).
10. Littlefield, J., Herz, R., Brown, L., Solar Thermochemical Hydrogen Production Plant Design, Technical poster presented at the University of California, San Diego Jacobs School of Engineering Research Expo, La Jolla, California, April 12, 2012.
11. Taylor, R., Davenport, R., Woodard, K., Production of Hydrogen from Solar Energy, Technical paper and presentation at the 2011 World Energy Engineering Congress, Chicago, Illinois, October 13, 2011.
12. Taylor, R., Genders, D., Brown, L., Presentation at the STCH Technical Progress Meeting, Livermore, California, July 13, 2011. (PowerPoint presentation).
13. Luc, W., Woodard, K., Presentation at the SAIC and UCSD Team Internship Program (TIP) Presentations, Scaled Hydrogen Reactor Design and Electrode Catalyst Electrophoretic Deposition, Jacobs School of Engineering, UCSD, La Jolla, California, September 28, 2011. (PowerPoint presentation).

II.E.2 Membrane/Electrolyzer Development in the Cu-Cl Thermochemical Cycle

M.A. Lewis (Primary Contact), S. Ahmed,
Serguei Lvov¹, Chinbay Fan²

Argonne National Laboratory

9700 S. Cass Avenue

Argonne, IL 60439

Phone: (630) 881-5973

Email: lewism@cmt.anl.gov

¹Pennsylvania State University, University Park, PA

²Gas Technology Institute (GTI), Des Plaines, IL

DOE Manager

HQ: Sara Dillich

Phone: (202) 586-7925

Email: Sara.Dillich@ee.doe.gov

Start Date: October 2010

Projected End Date: September 2012

FY 2012 Accomplishments

- Showed that both a Nafion[®]-based membrane and a porous polyethylene (PPE) membrane inhibited copper transport from the anode to the cathode.
- Demonstrated that the hydrogen production efficiency exceeded >95% when the cell potential was stable at 0.7 V and the current density was 0.5 A/cm² using a Nafion[®]-based membrane and observed no copper deposits on any of the cell components after a 36 h test.
- Fabricated a full-scale, single-cell electrolyzer which had a current density of 0.18 A/cm² for a cell voltage of 0.7 V.
- Continued collaborations with Atomic Energy of Canada Limited and a group of Canadian universities.



Fiscal Year (FY) 2012 Objectives

- Identify methods that prevent copper deposition at the cathode of the electrolyzer while meeting targets for cell potential (0.7 V) and current density 0.3 A/cm² in 2012.
- Start development of a full size electrolyzer, 300 cm².
- Continue collaborative work on the thermal reactions with Canada.

Technical Barriers

This project addresses the following technical barriers from the Hydrogen Production section of the Fuel Cell Technologies Program Multi-Year Research, Development and Demonstration Plan:

(U) High-temperature Thermochemical Technology

(V) High-Temperature Robust Materials

(W) Concentrated Solar Energy Capital Cost

Technical Targets

The technical targets are the cost of hydrogen production and the process energy efficiency.

- For 2017, these are \$2.00 per gasoline gallon equivalent (gge) H₂ and >35% (lower heating value), respectively.

Introduction

The U.S. Department of Energy's Office of Energy Efficiency and Renewable Energy is supporting the development of hydrogen production technologies that use solar heat. One approach involves thermochemical cycles whose heat source is the solar power tower, which is near commercialization and provides heat near 550°C now and at higher temperatures in the future. The CuCl cycle is unique because its maximum temperature is less than 550°C. The three major reactions in the Cu-Cl cycle are shown below.



All reactions have been verified at the temperatures shown. Note that the maximum temperature is less than 550°C. No separations or phase changes are specified in this high level representation.

Because there is a potential for catastrophic failure of the electrolysis cell if copper crossover and deposition occur and because the electrical energy consumed during electrolysis is a major component of the energy usage, our focus has been on optimizing the electrolyzer's performance, i.e., maximizing current density for a given voltage while eliminating parasitic reactions. Copper crossover must be minimal. Cell voltage needs to be as low as possible to reduce energy usage and the current density has to be as high as possible to minimize capital costs and maximize hydrogen production efficiency.

Approach

The approach for improving electrolyzer performance was threefold: (1) further improve membrane properties to reduce copper crossover, (2) modify the electrolyzer's hardware and operating parameters to increase current density for cell potentials of 0.7 V and less, and (3) develop a methodology to study long-term durability of the electrolyzer and determine degradation mechanisms. To improve the very thin (1-mm thick) porous polyethylene membrane's mechanical stability, various coatings were applied and tested. The Nafion[®]-based membrane is a hot pressed material and differences in pressing procedures were investigated. Different procedures and configurations were investigated for fabricating membrane electrode assemblies. Various changes in hardware and operating parameters, such as flow rates, catalysts and catalyst loadings, as well as anolyte and catholyte compositions are being investigated to determine their effect on cell performance and their potential to reduce costs and/or increase efficiency. For example, we identified changes in flow field designs as having an impact on performance with the porous polyethylene membrane. Some tests with the Nafion[®]-based membrane gave very stable cell potentials while a few did not. Electrochemical impedance spectroscopy will be used to determine degradation mechanisms with the goal of improving lifetime performance. A 6.45 cm² single cell was used for this work.

In addition, a full-size, 300-cm² active area, single cell was fabricated. It is expected that different challenges, e.g., sealing and minimization of shunt current, will need to be addressed but that the work on membranes, degradation mechanisms, etc., will extend to larger scale work.

Results

Characterization of Membranes (S.Lvov, PI)

Potential membrane materials were screened using permeability of dissolved Cu(II) species and conductivity at 25°C. The methods and equipment were carefully verified. Details of the equipment and methods will be published elsewhere. Table 1 contains a comparison of these properties, selectivity values (defined as the ratio of conductivity to permeability, or the ratio of hydrogen transport to copper transport), as well as current costs for Nafion[®] 117, Nafion[®]-

TABLE 1. Properties of Membranes for Possible Use in the Cu-Cl Electrolyzer

| Property | Conductivity (S/cm) | Permeability x 10 ⁻⁸ (cm ² /s) | Selectivity x 10 ⁶ (S·s/cm ²) | Today's Cost (\$/m ²) |
|----------------------------|---------------------|--|--|-----------------------------------|
| Nafion [®] 117 | 0.083 | 1.8 | 4.61 | 550 |
| Nafion [®] -based | 0.057-0.076 | 0.15-1.92 | <39.5 | >550 |
| PPE | 0.050 | 1.6 | 3.1 | 10* |

*Does not include coating costs

based and PPE. Cost is also a factor in the evaluation of the various membranes. As can be seen, the cost of the porous polyethylene is about 55 times less than that of Nafion[®]117. However, the cost for the Nafion[®]-based membranes will be greater than that of Nafion[®]117 because of additional processing. While PPE is the least expensive, it may require a coating for additional mechanical stability and that cost is unknown. Several coatings have been tried but none has proven completely satisfactory.

Electrolyzer Performance with Nafion[®]-Based Membranes (S.Lvov, PI)

A schematic of the electrolyzer is shown in Figure 1. The ancillary equipment was redesigned to allow for recycling the solutions and to maintain a safe working environment and reliable operation. Fabrication was completed in late 2011. Teflon[®] or perfluoroalkoxy components replaced all metallic components. Teflon[®] diaphragm pumps replaced unreliable peristaltic pumps. The HCl concentration in the anolyte and catholyte was reduced from 11M to 6 or 7M. The CuCl concentration was 2M. Additional heating tapes, insulation and oil baths for bringing the recycled solutions to test temperature were incorporated into the design. H₂ production was measured by weighing the water displaced by the exit gas after drying and HCl removal. Additional information on the apparatus and test protocol will be published elsewhere.

Figure 2 shows a polarization curve using the Nafion[®]-based membrane for two flow rates after a 24-h test. The tests were run at 80°C, atmospheric pressure, and 0.8 mg/cm² Pt loading on the Nafion[®]-based membrane. The flow field was serpentine. At the target voltage of 0.7 V, the measured current densities were 0.46 and 0.51 A/cm² for flow rates of 59 and 130 mL/min, respectively. These values exceed our 2012 milestone value and approach our 2015 target. Figure 3 shows that the hydrogen production efficiency was 95-100% for the 24 hour period, i.e., the experimental values were within a few percent of the values predicted by Faraday's Law. Such hydrogen production efficiency indicates there were no parasitic losses due to reduction of copper ions. No copper deposits were visually observed on any of the components of the cell after the tests. A subsequent test was run for 36 h with the same results. However, one test showed decreasing current density with time. The mechanism for the degradation of performance is not understood at this time and electrochemical impedance spectroscopy will be employed in future tests.

Electrolyzer Performance with PPE Membrane (C. Fan, PI)

Tests were conducted at 0.7 V with this membrane in a small electrolyzer, active area of 6.45 cm², at 80°C with deionized water as the catholyte and 2 mol CuCl in 10 mol/L HCl as the anolyte. Of the two flow fields studied,

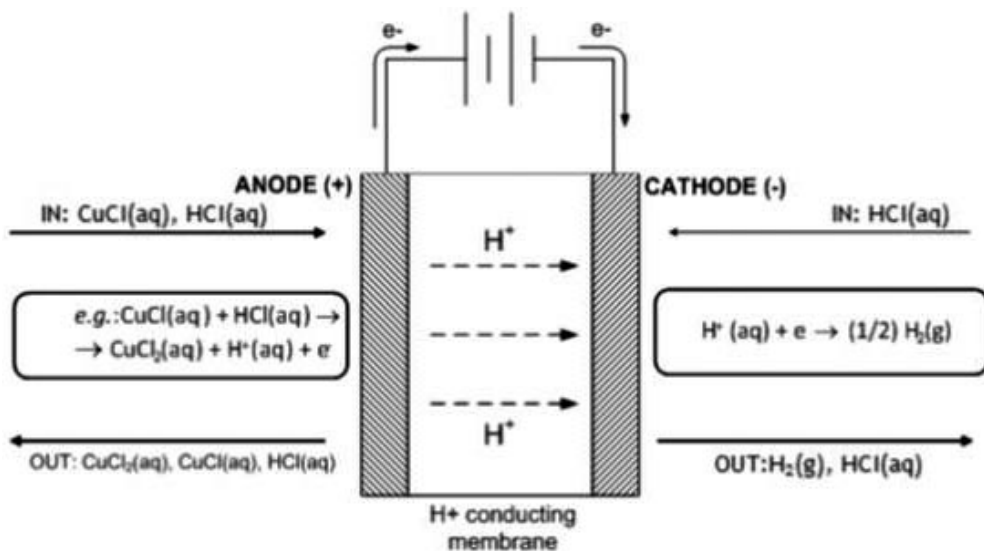


FIGURE 1. Schematic of the electrolysis cell for the CuCl cycle

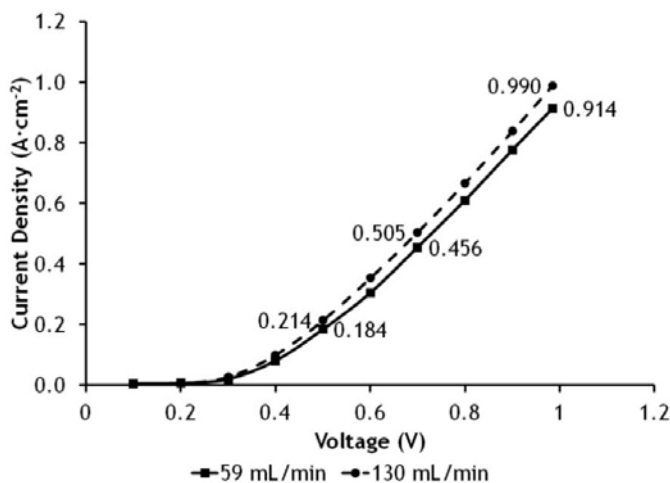


FIGURE 2. Polarization curve for the CuCl electrolysis with Nafion®-based membranes at two flow rates after 24 h

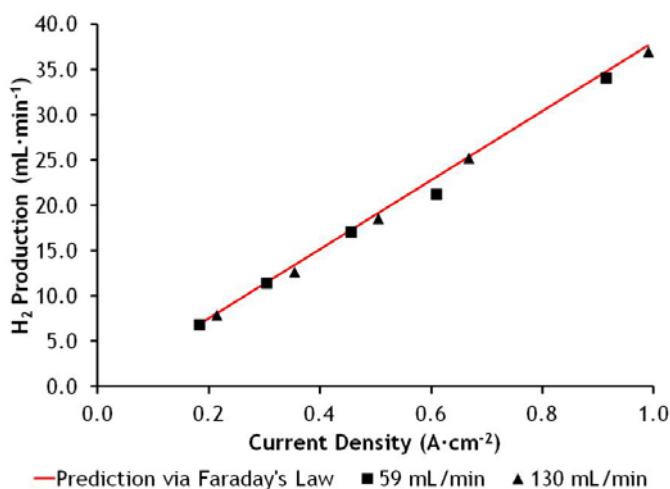


FIGURE 3. Hydrogen production efficiency versus time for the experiment described in Figure 2

the serpentine flow field had a slightly lower current density (0.12 A/cm²) than the carbon felt design (0.16 A/cm²) when the Pt loading was 0.5 mg/cm² on both the anode and cathode. The type of coating on the membrane had a significant effect. For example, for the same Pt loading on the carbon felt cathode (0.5 mg/cm² but none on the anode), the current density was 0.3 A/cm² when the PPE membrane was coated with a ceramic and 0.19 A/cm² when coated with Nafion®. When PPE was coated with Nafion® and the Pt loading was decreased from 2.0 to 0.5 mg/cm², the current density was only marginally impacted as it decreased from 0.19 to 0.18 A/cm². These results suggest that a carbon felt flow field, a ceramic coating on PPE, and 0.5 mg Pt/cm²

are preferred to a serpentine flow field and no coating or a Nafion® coating on the PPE membrane.

GTI's primary focus is the development of a 300 cm²-size electrolyzer, dimensions 14.6 cm by 20.8 cm. Figure 4 shows GTI's polarization curve for a single cell. The current density was 0.18 A/cm² at 0.7 V. Conditions for this test were 62°C, 1 bar, PPE membrane with Nafion® coating, 0.5 mg/cm² Pt on cathode and anode, carbon felt on both anode and cathode, water as catholyte and 1 mol CuCl in a 10 mol/L HCl as anolyte, 1 L/min flow rate. Changes in operating conditions are being investigated to increase current densities in these full-scale electrolyzers. In addition, work is in progress to develop a multi-cell stack. Issues that

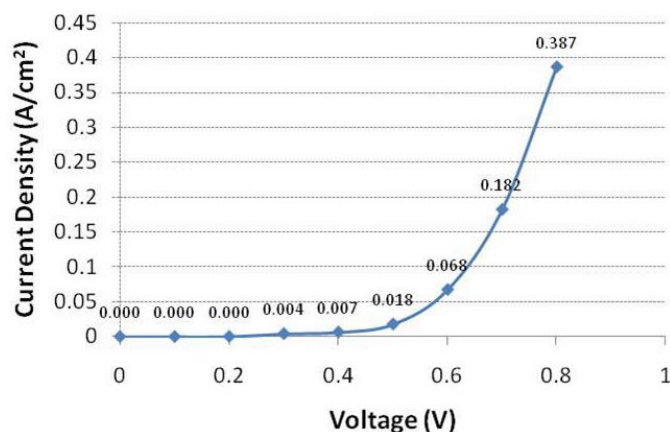


FIGURE 4. Polarization curve for a single cell electrolysis cell with 300 cm² of active area

are being addressed include sealing of the cell, distributing mass of the anolyte/catholyte evenly through all cells in the stack, maintaining good electric contact within each cell and minimizing shunt current.

Collaborations

Atomic Energy of Canada Limited and five Canadian universities are working on the development of the CuCl cycle. The collaboration consists of an informal information exchange. Significant progress has been made recently. For example, Atomic Energy Canada Limited invented a new electrolyzer design that inhibited essentially all diffusion of dissolved copper species to the catholyte for up to 341 h. The measured dissolved copper concentration remained stable at 1-2 ppm during the entire run time.

An integrated demonstration is planned for 2013-2014 at the University of Ontario Institute of Technology. A building is dedicated for this purpose. The equipment for the hydrolysis and oxychloride decomposition reactions and other processes, such as crystallization, are now undergoing hot tests prior to their integration. Direct contact cooling of the molten CuCl in water has been tested. Steam was generated from the direct quench. The molten CuCl droplets solidified and subsequently disintegrated into small pieces within two seconds. No steam explosion was observed.

Conclusions

- Achieved current densities that exceed our 2012 milestone when the cell voltage was 0.7 V using the Nafion®-based membrane.
- Conducted electrolyzer tests that showed no visible copper deposition in/on the cell components.
- Successfully tested a single cell electrolyzer with an active area of 300 cm² and started fabrication of a full scale multi-cell stack.

Future Directions

- Extend duration of the electrolyzer tests with the Nafion®-based membrane.
- Develop methods to improve the mechanical stability of the PPE membrane.
- Continue improvement of the electrolyzer's performance by investigating other compositions for the anolyte and catholyte, flow rates, flow field design, electrode surface, mass transport media, etc. to obtain higher current densities at 0.7 V.
- Fabricate and test a multi-cell stack full size electrolyzer and improve its performance to meet the current density milestone.
- Investigate the degradation mechanisms in the electrolyzer and develop methods to mitigate these.
- Continue collaboration with staff at Atomic Energy of Canada Limited and six Canadian universities; sharing experimental data and approaches to leverage R&D funds.

FY 2012 Publications/Presentations

1. CuCl Electrolysis for Hydrogen Production in the Cu-Cl Thermochemical Cycle, R. Sharna, M. Fedkin, and S. Lvov, *J. Electrochem. Soc.*, 158(3) B266-B275 (2011).
2. G.F. Naterer et al., Clean Hydrogen Production with the Cu-Cl Cycle - Progress of International Consortium, I: Experimental Unit Operations, *Int. J. Hydrogen Energy*, 36, 15472-15485 (2011).
3. M.A. Lewis et al., Recent Advances in the U.S. R&D Program for the Cu-Cl Cycle, Ontario Research Foundation Workshop, Chalk River, Canada, Nov. 9, 2011.
4. M.A. Lewis et al., Electrolyzer Development for the Cu-Cl Thermochemical Cycle, Ontario Research Foundation Workshop, Oshawa, Ontario, Canada, May 10, 2012.

II.E.3 Solar Hydrogen Production with a Metal Oxide-Based Thermochemical Cycle

Anthony McDaniel (Primary Contact),
Ivan Ermanoski

Sandia National Laboratories (SNL)
MS9052
PO Box 969
Livermore, CA 94550
Phone: (925) 294-1440
Email: amcdani@sandia.gov

DOE Manager

HQ: Sara Dillich
Phone: (202) 586-7925
Email: Sara.Dillich@ee.doe.gov

Subcontractors:

- Nathan Siegel, Bucknell University, Lewisburg, PA.
- Alan Weimer, University of Colorado, Boulder, CO.

Project Start Date: October 1, 2008

Project End Date: Project continuation and direction determined annually by DOE

Fiscal Year (FY) 2012 Objectives

- Discover and characterize suitable materials for two-step, non-volatile metal oxide thermochemical cycles.
- Design and test particle conveying concepts for a novel reactor/receiver concept.
- Test construction materials for compatibility between ceria and reactor components at high temperature and low oxygen partial pressure.
- Calculate theoretical system efficiency for various reactor/receiver operating scenarios.
- H2A technoeconomic analysis of dish-based particle reactor/receiver concept.

Technical Barriers

This project addresses the following technical barriers from the Production section (3.1.4) of the Fuel Cell Technologies Program Multi-Year Research, Development and Demonstration Plan:

- (U) High-Temperature Thermochemical Technology
- (V) High-Temperature Robust Materials
- (X) Coupling Concentrated Solar Energy and Thermochemical Cycles

Technical Targets

This project is conducting fundamental studies on materials suitable for use in concentrated solar power applications and designing reactor concepts that when combined will produce H₂ from thermochemical water splitting cycles. Insights gained from these studies will be applied toward the design and optimization of solar-driven reactors that meet the following DOE hydrogen production targets:

- Cost: \$2-\$4/gasoline gallon equivalent H₂
- Process energy efficiency: >35%

FY 2012 Accomplishments

- Developed a detailed kinetic model for ceria redox that can be used to establish theoretical cycle performance metrics in SNL-designed reactors.
- Synthesized and characterized transition metal-doped ceria materials which demonstrate increased redox capacity and lower effective thermal reduction temperature compared to undoped ceria.
- Validated particle conveyor concept by demonstrating a sustained mass flow rate of 30 g/s particles for 1 hour.
- Verified no adverse reactivity between ceria (active material) and materials of construction such as alumina (to 1,550°C), SiC (to 1,400°C), or Haynes 214 alloy (to 1,200°C) for a period of 3 hours.
- Evaluated theoretical system efficiency under low direct normal insolation (DNI). Particle reactor design achieves efficiencies that meet the 2012 DOE target of 30% for DNI between 400 W/m² and 1,000 W/m².
- Initiated H2A analysis of a 100,000 kg/day H₂ plant based on 22,000 dish-type receivers.



Introduction

The conversion of solar radiation into a chemical fuel such as hydrogen is an engineering challenge, however, unlike solar-derived electricity or heat, it is easier and more efficient to transport and store hydrogen. This point is important because energy demand is rarely matched to incident solar radiation, either spatially or temporally. Two-step solar-driven thermochemical cycles based on non-volatile metal oxides are an attractive technology for producing hydrogen because of the potential to operate

at high solar-to-chemical conversion efficiency with moderate operational demands on land and water resources. Conceptually, heat derived from concentrated solar energy thermally reduces a metal oxide at temperatures between 1,300°C and 1,500°C, producing O₂ (step 1). The reduced metal oxide is then taken off sun and oxidized at temperatures below 1,000°C by exposure to H₂O, thus producing H₂ fuel (step 2) and completing the cycle. The ultimate commercial success of solar thermochemical hydrogen production is contingent upon developing suitable redox active materials and incorporating them into an efficient solar reactor/receiver.

Approach

Thermochemical reactors are heat engines that convert concentrated solar energy (heat) to chemical work. Our approach is to use a novel reactor design that achieves unprecedented solar-to-hydrogen fuel conversion efficiency. It is based on a moving bed of packed particles that embodies *all* of the design attributes essential for achieving high efficiency: (1) inherent sensible solid-solid heat recovery between the reaction steps; (2) spatial separation of pressure, temperature, and reaction products within the device; (3) continuous on-sun operation; and (4) direct absorption of solar radiation by the redox active material. In addition, the design is mechanically simple and can accommodate virtually any reactive material in particle form.

We are currently developing a high-temperature particle conveying and reactor system, and discovering active materials suitable for two-step cycle chemistry. Recent efforts have focused on ferrites and cerium oxide, which are representative of two important material classes that are defined by how the metal oxide chemistry is manifested in the solid state. The material discovery work involves expanding our understanding of the underlying thermodynamics and kinetics in order to make performance improvements and/or formulate new compositions that directly impact overall process efficiency. Additional research efforts are directed towards system-level challenges associated with dish and central-receiver based thermochemical platforms, which we address through system performance calculations and economics models.

Results

Materials Development: Cerium oxide has recently gained attention as a suitable material for use in high-temperature thermochemical water splitting cycles [1,2]. Originally disregarded because of the high temperature required to operate the cycle stoichiometrically ($T > 2,000^\circ\text{C}$), it was later discovered that the non-stoichiometric oxide could be marginally effective at lower temperatures ($T \sim 1,500^\circ\text{C}$) due to fast redox kinetics and high thermal stability. However, even at the lower reduction temperature,

it is not likely that unmodified ceria used as a working fluid in a two-step thermochemical cycle will be able to achieve the DOE cost targets for H₂ production because the redox capacity is too low. Therefore, we have been investigating the use of transition metal dopants to: (1) destabilize the ceria crystal structure in order to decrease the temperature required for effective thermal reduction, and (2) increase the redox capacity (i.e., H₂ production rate per cycle) by synthesizing ceria solid solutions with other redox active cations.

Preliminary results of this effort are illustrated in Figure 1 for a 10 mol-% mixture of Fe₂O₃ in CeO₂. Samples prepared by the sol-gel method were reduced and oxidized in a stagnation flow reactor equipped with a 500 W CW near-infrared diode laser for sample heating (thermal flux closely approximates conditions found in solar concentrators). Here the O₂ production rate was measured as a function of time and temperature during thermal reduction *after* oxidation by O₂ (red curve) or H₂O (blue curve) at 800°C. The O₂ redox capacity of the material can be measured by the area under each curve, and by proxy the H₂ production rate inferred. It is clear by the data presented in Figure 1 that adding iron oxide to ceria increases the total amount of O₂ evolved and decreases the temperature at which O₂ evolution begins (see dashed lines with arrows). Unfortunately this behavior is only evident for O₂ redox cycles and not H₂O redox cycles, which indicates that this particular dopant is not an effective additive for water splitting. We have characterized the effects of doping several aliovalent first-row transition metal cations into ceria, as well as mixtures of ceria and zirconia, with mixed results. We find that certain compound formulations do indeed increase the H₂ production capacity, but reduce thermal stability by inducing sintering and slow the oxidation

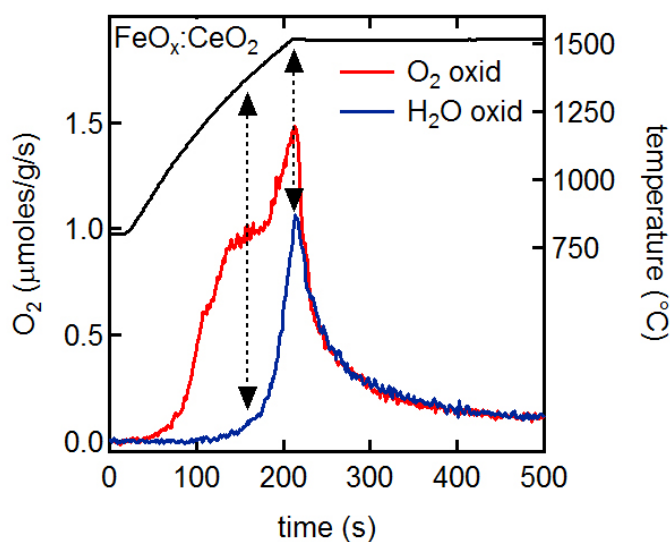


FIGURE 1. The rate of oxygen production measured during thermal reduction as a function of time after O₂ oxidation (red curve) and H₂O oxidation (blue curve) for iron oxide doped ceria

kinetics. In the future, we will investigate non-stoichiometric oxides in the perovskite family of materials.

Reactor Development: Significant progress in the development of the elevator/recuperator section of the reactor was achieved by adopting an innovative nested auger design for vertical conveyance of particles (Figure 2), and testing multiple surrogate materials (75- μm silica sand, 200- μm sand, corn flour, and corn grits). Conveying efficiency was found to differ considerably between materials depending on cohesive strength, internal friction, and wall friction of the material. The surrogate materials were chosen to test different particle sizes, effective densities, and cohesive strengths, which are all known to effect particle transport. In addition, experiments with return particle flow through a finned tube representative of a heat exchanger showed a critical dependence on particle size. Flow was essentially unimpeded for larger particles (75 μm), but was completely hindered for smaller particles (5 μm) except under severe mechanical agitation. We are now able to specify an optimal particle size for conveyance in a bench-scale prototype.

We also investigated the compatibility of ceria with prospective reactor materials, specifically, alumina and alumina-coated silicon carbide. Alumina was found not to react with ceria up to 1,550°C in stagnant air. Alumina-coated silicon carbide was tested up to 1,450°C, and also found to be unreactive. These experiments showed that a minimal thickness of alumina coating is needed before the surface can be passivated. When coating thickness is insufficient, ceria reacts vigorously with the underlying SiC/SiO₂. However, thicker coatings were found to be increasingly unstable. The optimal coating thickness and deposition method will need to be determined if SiC is to be used as a reactor material.

The most relevant performance metric that impacts H₂ production cost is the annual average efficiency. We have previously calculated this efficiency using a simple model



FIGURE 2. Nested auger design prototype for particle conveyance

for the reactor operating at off-design point conditions, i.e., low or high DNI. To better estimate the annual average efficiency we improved the design-point efficiency model, which has enabled the assessment of multiple off-design point performance parameters. The results of these calculations are summarized in Figure 3. The main conclusion from these calculations is that increased efficiency under low DNI can be achieved due to the opposing dependencies of radiation losses, recuperator effectiveness, and thermal reduction pressure. As the oxide flow rate is decreased to maintain the thermal reduction temperature, heat recovery effectiveness increases and oxygen partial pressure (p_{O_2}) decreases, leading to an increased extent of reduction of the oxide. At the same time, the *absolute* amount of power lost through the aperture via radiation remains constant (i.e. the *relative* radiation loss increases). Therefore, for a wide range of DNI the gains from increased heat recovery effectiveness and increased extent of reduction more than offset the increase in the relative radiative losses. This yields a substantially flat solar efficiency making the reactor exceptionally well-suited for real world operation.

H2A Systems Analysis: Analysis for the particle bed reactor includes several elements that build on one another to produce the final economic model. We begin with an annual average efficiency calculation of a single dish-based particle reactor operating in Daggett, CA. The reactor uses an 88-m² parabolic dish collector with optical performance modeled after the pre-commercial units developed by Stirling Energy Systems at SNL over the last decade. The reactor uses cerium oxide particles as the reactive media and we assume sensible heat recuperation of 90%. This level of recuperation is only possible in the particle reactor concept since it includes counterflow heat transfer between solids (absolutely unique to this reactor design).

The system-level hydrogen production is assumed to be 100,000 kg/day, requiring a total of over 22,000 dishes.

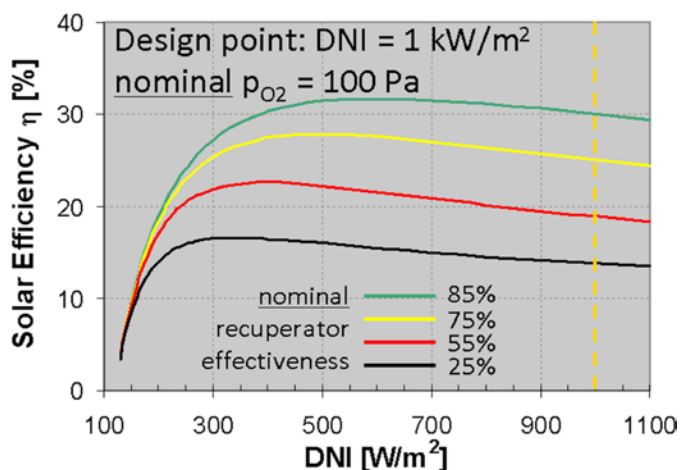


FIGURE 3. Efficiency of the particle reactor under decreased DNI (for detailed discussion see text)

Each of these dishes is connected to a central facility by hydrogen and water piping. Water is delivered under pressure to each dish, and hydrogen is pumped from each dish to the central facility at a pressure of 300 psia. The energy losses associated with pumping both the water and the hydrogen through the field are accounted for in the resultant cost of electricity on an annual basis. Economic assumptions and capital cost estimates are included to complete the model. Our baseline assumptions are consistent with those reported by TIAX [3]. Although our economic analysis is not yet complete, preliminary results indicate a significant amount of uncertainty in the projected cost of H_2 . This is also consistent with other results derived from the TIAX report, e.g. the ferrite process proposed by the University of Colorado is predicted to have a hydrogen cost between \$2.7-\$15.02/kg H_2 [3]. In this case as in ours, most of the uncertainty is tied to the performance of the reactor itself, which is an issue we need to formally address as we continue our assessment of the particle reactor concept.

Conclusions and Future Directions

- Screen a large family of perovskite-type oxides for use in two-step, high-temperature thermochemical water splitting cycles.
- Continue with the staged development of a high-temperature reactor prototype sized for 5 kW_{th} that will be tested on-sun at the National Solar Test Facility.
- Design beam-down optics for both dish and central-receiver based reactors.

FY 2012 Publications/Presentations

1. Scheffe, J.R.; McDaniel, A.H.; Allendorf, M.D.; Weimer, A.W. "Kinetic analysis of the oxidation of $Co_{0.9}Fe_{2.1}O_4/ZrO_2$ for thermochemical H_2 production." In review at E&ES.
2. Arifin, D.; Aston, V.A.; Liang, X.; McDaniel, A.H.; Weimer, A.W. "CoFe₂O₄ on porous Al₂O₃ nanostructure for solar thermochemical CO₂ splitting." In revision at E&ES.
3. N.P. Siegel, J.E. Miller, I. Ermanoski, R.B. Diver, and E.B. Stechel, "System Performance Estimation of Two-Step Solar Thermochemical Fuel Production processes", in preparation.
4. I. Ermanoski, N.P. Siegel, and E.B. Stechel, "A New Reactor Concept for Efficient Solar Thermochemical Fuel Production", submitted to Journal of Solar Energy Engineering.
5. I. Ermanoski and N.P. Siegel, "Packed Bed Reactor for Solar Thermochemical Fuel Production", presented at IEA SolarPACES 2011.

References

1. W.C. Chueh, C. Falter, M. Abbott, D. Scipio, P. Furler, S.M. Haile, and A. Steinfeld, *Science*, 2010, 330, 1797–1801.
2. W.C. Chueh and S.M. Haile, *Philosophical Transactions of the Royal Society A: Mathematical, Physical and Engineering Sciences*, 2010, 368, 3269–3294.
3. "Support for Cost Analyses on Solar-Driven High Temperature Thermochemical Water-Splitting Cycles", DOE report number DE-DT0000951, prepared by TIAX LLC, 2011.

II.E.4 Solar-Thermal ALD Ferrite-Based Water Splitting Cycle

Alan W. Weimer (Primary Contact), Darwin Arifin,
Xinhua Liang, Victoria Aston and Paul Lichty
University of Colorado
Campus Box 596
Boulder, CO 80309-0596
Phone: (303) 492-3759
Email: alan.weimer@colorado.edu

DOE Manager

HQ: Sara Dillich
Phone: (202) 586-7925
Email: Sara.Dillich@ee.doe.gov

Contract Number: DE-FC36-05GO15044

Project Start Date: March 31, 2005

Project End Date: Project continuation and direction
determined annually by DOE

Fiscal Year (FY) 2012 Objectives

- Demonstrate the “hercynite cycle” feasibility for carrying out redox.
- Initiate design, synthesis and testing of a nanostructured active material for fast kinetics and transport.
- Demonstrate the “hercynite cycle” on-sun.

Technical Barriers

This project addresses the following technical barriers from the Production section, page 3.1-26 of the Fuel Cell Technologies Program Multi-Year Research, Development and Demonstration Plan:

- (U) High-Temperature Thermochemical Technology
- (V) High-temperature Robust Materials
- (W) Concentrated Solar Energy Capital Cost
- (X) Coupling Concentrated Solar Energy and Thermochemical Cycles

Technical Targets

The technical targets for solar-driven thermochemical conversion are summarized in Table 1. The projected thermal efficiency for the developed process is 55.5% lower heating value (LHV), thus exceeding the >35% requirement for the 2017 case. For a solar to receiver annual average efficiency of 40.2%, the overall solar to H₂ efficiency is estimated at 22.3% (LHV). Current results indicate that it is possible to achieve

TABLE 1. Technical Targets for Solar-driven High-Temperature Thermochemical Hydrogen Production

| Characteristics | Units | 2012 Target | 2017 Target |
|--|-----------------------|-------------|-------------|
| Plant Gate H ₂ Cost | \$/gge H ₂ | \$6 | \$3 |
| Installed Heliostat Capital Cost | \$/m ² | \$140 | \$80 |
| Process Energy Efficiency (thermal, LHV) | % | 30 | >35 |

gge – gasoline gallon equivalent

reduction times of <30 seconds and oxidation times with oxygen of <30 seconds. Oxidation with steam requires longer times, but it has been found that increased steam partial pressure substantially increases the rate of reaction. Methods to decrease redox cycle time are a focus of current research.

FY 2012 Accomplishments

- Demonstrated redox cycles with oxygen oxidation at less than 2 minutes.
- “Hercynite cycle” reaction mechanism through stable aluminate compounds verified by Raman spectroscopy.
- Designed active material nanostructures fabricated by atomic layer deposition demonstrated stable activity after the first cycle up to 25 cycles.



Introduction

Two-step solar thermochemical processes based on non-volatile metal oxide cycles have the potential to operate at high thermal efficiencies, are chemically simple, and require less land and water to operate than competing biomass, artificial photosynthesis and photovoltaic-driven electrolysis. Traditionally, two types of non-volatile metal oxide redox chemistries are utilized in solar thermochemical CO₂ splitting. The first is based on non-stoichiometric oxides of which ceria is a representative example. Such redox materials are thermally reduced without undergoing phase change, as the lattice is able to accommodate the strain induced by oxygen vacancy formation. These materials are thermally quite stable, although the extent of reduction, and hence cycle capacity, is small compared to other reducible oxides.

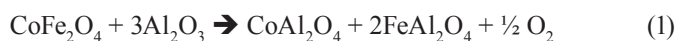
The second prototypical chemistry utilizes materials of the spinel structure that form solid solutions upon reduction. The most common are ferrites where Fe³⁺ in M_xFe_{3-x}O₄ is partially reduced to Fe²⁺; here M can be any number of transition metals that form spinel type oxides with iron though Co, Zn, and Ni are the most studied.

In these redox cycles, the ferrite spinel is heated until it decomposes into a mixture of metal oxide solid solutions that are thermodynamically stable at temperatures above which the spinel decomposes. Thus, thermal reduction yields a solid solution of oxides with mixed valence (M^{2+} , Fe^{2+} , and Fe^{3+}). While these materials theoretically exhibit greater redox potential than non-stoichiometric oxides, in practice deactivation induced by irreversible processes such as sintering or the formation of liquid phases and metal vaporization lead to loss of active oxide.

In this work, we examine a novel chemistry for a two-step, non-volatile metal oxide H_2O splitting cycle that shuttles iron oxidation states ($Fe^{2+/3+}$) between $CoFe_2O_4$ and $FeAl_2O_4$ spinel compounds within a nano-engineered material. This chemistry is dramatically different than current metal oxide cycles that exploit oxygen non-stoichiometry in ceria or solid solution behavior in ferrites. The engineered material was prepared using atomic layer deposition (ALD) and maintained structural integrity over 6 heating cycles under conditions that mimic a concentrated solar power application, namely an oxidation temperature of $1,000^\circ C$, reduction at $1,460^\circ C$, and a heating rate of $16^\circ C/s$ from low to high temperature. Oxygen uptake and release behavior was similar to that of ceria. Raman spectroscopy was used to verify cycle chemistry. These properties provide for a technical foundation to achieve the DOE technical targets and enable the hydrogen economy.

Approach

So called the “hercynite cycle”, reduction chemistry occurs via a reaction between decomposition products of the $CoFe_2O_4$ and Al_2O_3 , forming the corresponding stable aluminates $CoAl_2O_4$ and $FeAl_2O_4$ according to the following oxygen evolution reaction:



During subsequent oxidation by H_2O , the cobalt ferrite spinel and alumina reform and H_2 is produced:



The oxygen evolution reaction Eq. (1) occurs to a greater extent at a temperature $150^\circ C$ lower than a similarly prepared $CoFe_2O_4$ -coated m- ZrO_2 (conventional ferrite) because compound formation is thermodynamically more favourable than solid solution formation. While lowering the reduction temperature is an important consideration for solar thermochemical technologies, perhaps more intriguing is the idea of binding the reduced iron in a compound that is more stable than solid solution.

Inspired by these initial observations, we deposited a nanometer thick film of $CoFe_2O_4$ on a porous thin-walled (15 nm) skeletal Al_2O_3 support to study the CO_2 splitting

capability of this material for use in a concentrated solar power application. The reactive structure is depicted schematically in Figure 1 along with optical images of sample material photographed in the oxidized and reduced states, and an field emission scanning electron microscope (FESEM) image of the alumina support before thermal cycling. The cartoon in Figure 1 implies that the $CoFe_2O_4$ film is located on the exterior surface of the support shell, but the ALD process ensures that the ferrite film covers all gas-accessible surfaces on and within the porous material. As a result, the cobalt ferrite mass loading is relatively high (20%) and the reactive structure maintains a high effective surface area and low bulk density prior to high-temperature thermal cycling.

The main benefit of this reactive structure that sets it apart from prior work is that we can better engineer the spinel-alumina interface. Ideally we would like to irradiate only redox active material, any excess Al_2O_3 would reduce process efficiency by heating of inert carrier. Deposition of $CoFe_2O_4$ on either high surface area Al_2O_3 powders or monoliths would be undesirable because too much inert material would end up in the structure. Perhaps more important than wasting heat, a large excess of alumina would lead to diffusion of Co and Fe deeply into the bulk and undoubtedly have a detrimental impact on the redox kinetics. The porous Al_2O_3 skeletal support with 15-nm wall thickness addresses both of these concerns.

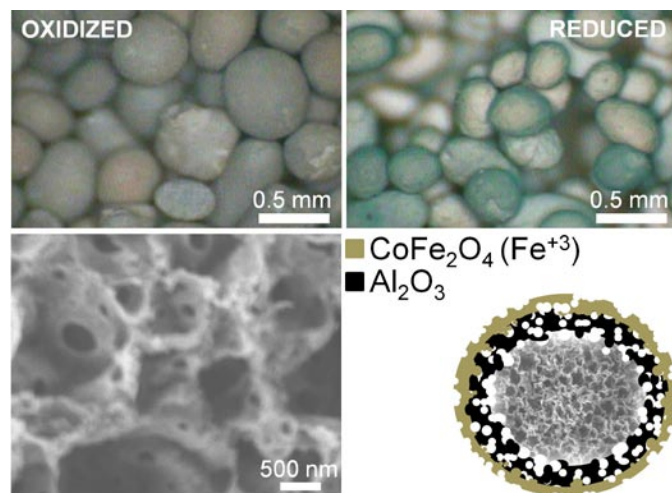


FIGURE 1. Optical image showing 0.5-mm diameter spheroids of porous Al_2O_3 shells coated in nanometer thick $CoFe_2O_4$. Color changes from brown to green when hercynite forms upon thermal reduction (top). FESEM image of the porous Al_2O_3 structure prepared by ALD (bottom left). Schematic illustrating the conceptual layout of the nano-engineered reactive structure, not drawn to scale, and the spinel compound that forms upon calcination (bottom right). A representative FESEM image of the skeletal structure is incorporated into the schematic. The coverage of $CoFe_2O_4$ on the alumina scaffold is not limited to the outer surface; it coats all gas-accessible surfaces on and within the porous structure (see text).

Results

An important measure of a material's suitability for a thermochemical water splitting cycle is the extent to which oxygen exchange occurs upon heating and cooling. This activity was assessed by exposing the nano-engineered material to a gas flow containing 2,000 ppm O_2 in helium and rapidly heating and cooling the material while monitoring the O_2 uptake and release behaviour. The results of this experiment are presented in Figure 2. Starting at $t = 0$ s, a constant background of O_2 is measured by the mass spectrometer. At several time intervals spaced roughly 350 s apart, a laser irradiates the sample raising the temperature from 1,000°C to 1,460°C in 30 s. After a 100 s dwell at 1,460°C, the laser power is turned off and the sample is allowed to cool through conductive, convective, and radiative processes. Testing was carried out for a total of 25 cycles.

According to the data in Figure 2, during the initial part of the heating interval the O_2 signal increases to a peak that is 47% above background, then quickly falls back to baseline before the 100 s dwell time at high temperature expires. O_2 evolution in a gaseous environment where the oxygen activity is relatively high (0.001 atm) indicates favorable thermodynamics for reduction at conditions relevant to solar-driven thermochemistry. Of equal importance is the observation that the material reabsorbs oxygen on cooling, which is evidenced by the O_2 signal dropping below the 2,000 ppm background level for a short period of time after

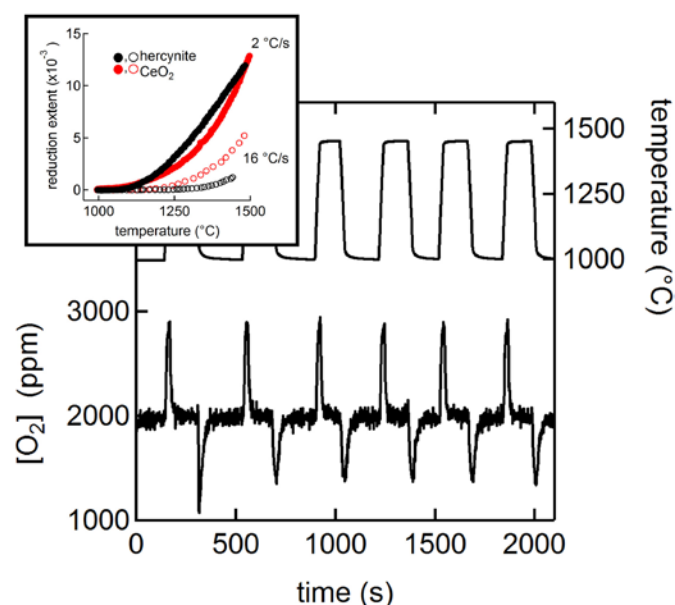


FIGURE 2. Oxygen uptake and release behaviour as a function of time and temperature measured in the presence of a constant 2,000 ppm O_2 background partial pressure indicates thermodynamics for hercynite reduction are favorable for solar-driven thermochemical cycles (see text). The reduction extent as a function of temperature for ceria and hercynite at two different heating rates is shown in the inset.

laser irradiation. To a first approximation, the area under the desorption peak is equal to that of the absorption peak (~ 100 $\mu\text{moles } O_2/\text{g}$ of material). Furthermore, the O_2 redox behavior is reproducible over 6 heating cycles indicating that the material remains chemically active and is structurally stable (i.e., no significant irreversible loss of activity, surface area, physical dimension, or metal oxide).

Optical images of the sample taken before and after thermal redox cycling (Figure 1) show that the material maintains its semi-spherical shape, however, noticeable shrinkage occurs during repeated exposures to 1,460°C. Brunauer-Emmett-Teller analysis on similarly cycled materials confirms internal structural changes that are consistent with loss of porosity and sphere volume as the surface area is reduced from 44 m^2/g (as prepared) to 1.6 m^2/g (cycled). This is due to collapse of the micropores and mesopores in the alumina material resulting from grain growth at these extreme temperatures. Nonetheless, after the first cycle, the oxygen capacity did not diminish after 23 thermal reductions, amounting to 20 hours at 1,000°C and 2 hours at 1,460°C, implying that the activity of the material is not affected by loss of internal surface area and that all structural changes occurred during the first cycle. A more rigorous and detailed study investigating the effect of porosity and the thermal stability of the material is currently underway.

The graph inset to Figure 2 reveals another important feature of our engineered reactive structure. Here we plot the reduction extent as a function of temperature for two different heating rates. The reduction extent is calculated by taking the ratio of evolved oxygen, integrated as a function of time on a molar basis, to the total amount of oxygen present in the fully oxidized material. There are two pieces of information available in Figure 2; (1) by comparing a slow heating rate (2°C/s) to a fast heating rate (16°C/s) possible kinetic limitations to O_2 redox become evident, and (2) the reduction extent for a given temperature provides information on cycle capacity (i.e., how much fuel can be produced per a mole of material). For comparison, reduction data are also presented for CeO_2 particles (nominally 5- μm diameter) in Figure 2.

Clearly the 2°C/s heating rate produces more O_2 at a given temperature than the 16°C/s rate, which is likely due to a transport limitation within the reactive structure. However, the nanostructured ferrite performance compares comparably to that of CeO_2 which, unlike iron oxide, is known to possess high oxygen ion conductivity and rapid exchange kinetics. Therefore it is conceivable that by reducing the thickness of the Al_2O_3 skeletal structure, diffusion limitations may be further mitigated allowing greater utilization of the redox active Fe cation and faster redox kinetics.

To support our hypothesis that the reactions embodied by Eqs. 1 and 2 are correct, we analyzed the chemical

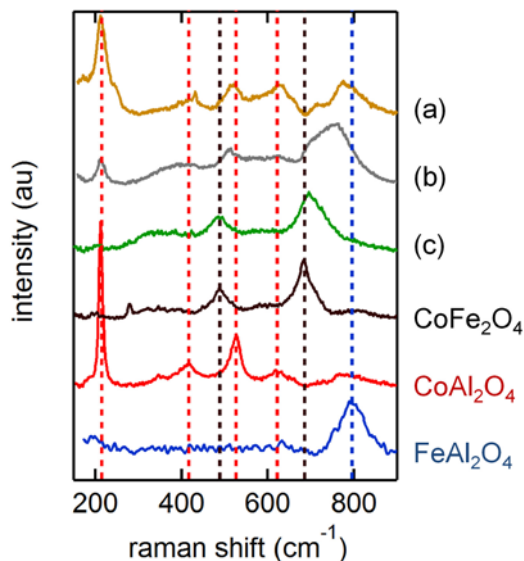


FIGURE 3. Surface Raman spectra recorded for ferrite and aluminate reference materials compared to unknown compositions of nano-engineered CoFe_2O_4 -coated Al_2O_3 material prepared by thermal reduction in helium (a), or oxidation in CO_2 (b), or oxidation in O_2 (c).

composition of the nanostructured materials using surface Raman spectroscopy. Several representative samples were oxidized in either O_2 or CO_2 , or reduced in pure helium, and then thermally quenched before ex situ examination in a Raman microscope. Presented in Figure 3 are Raman spectra for three of our endpoint compounds, CoFe_2O_4 , CoAl_2O_4 , and FeAl_2O_4 , along with spectra measured from samples taken at various states of oxidation (labelled a-c in the figure). Material fully oxidized in O_2 (c) exhibits spectral features indicative of CoFe_2O_4 , with two main excitation peaks observed at 476 and 686 cm^{-1} which agrees with literature assignments for this compound. Raman spectra for material in the fully reduced state (a) show a mixture of phonon modes that can be attributed to cobalt aluminate and hercynite. Furthermore, the strong resonance features of CoFe_2O_4 are not detectable in (a) indicating that the reduction reaction has gone to completion in the near surface region of the ferrite. Also of note is the relative stability of the reduced compound (FeAl_2O_4) in air at room temperature. Samples were removed from the reactor and stored for several days before transport to the Raman microscope without special handling to avoid air exposure.

Conclusions and Future Directions

- The “hercynite cycle” active materials follow a redox mechanism through stable aluminates which is predicted to provide for a chemically robust process.
- Our CoFe_2O_4 -coated Al_2O_3 material is capable of producing appreciable amounts of H_2 after thermal reduction at a temperature as low as 1,360°C, with consistent oxidation behavior up to 25 thermal reductions. This observation is approximately 100°C to 150°C lower than values reported for ferrite or CeO_2 -based systems, respectively.
- The nanostructured active materials can be improved to reduce diffusional resistances and work is underway to develop such materials.

Patents Issued

1. “Metal Ferrite Spinel Energy Storage Devices and Methods for Making and Using Same,” U.S. Patent 8,187,731 (2012).

FY 2012 Publications/Presentations

1. Arifin, D., V.J. Aston, X.H. Liang, A.H. McDaniel and A.W. Weimer, “ CoFe_2O_4 on Porous Al_2O_3 Nanostructure for Solar Thermochemical CO_2 Splitting,” *Energy and Environmental Science*; in-press, DOI:10.1039/C2EE22090C (2012).
2. Martinek, J., C. Bingham, and A.W. Weimer, “Computational Modeling and On-sun Model Validation for a Multiple Tube Solar Reactor with Specularly Reflective Cavity Walls, Part 1: Heat Transfer Model,” *Chemical Engineering Science*; **81**, 298 - 310 (2012).
3. Martinek, J., C. Bingham, and A.W. Weimer, “Computational Modeling of a Multiple Tube Solar Reactor with Specularly Reflective Cavity Walls, Part 2: Steam Gasification of Carbon,” *Chemical Engineering Science*, **81**, 285 - 297 (2012).
4. Scheffe, J.R., M.D. Allendorf, E.N. Coker, B.W. Jacobs, A.H. McDaniel and A.W. Weimer, “Hydrogen Production via Chemical Looping Redox Cycles Using Atomic Layer Deposition-Synthesized Iron Oxide and Cobalt Ferrites,” *Chemistry of Materials*, **23** (8), 2030-2038 (2011).

II.F.1 Directed Nano-Scale and Macro-Scale Architectures for Semiconductor Absorbers and Transparent Conducting Substrates for Photoelectrochemical Water Splitting

Thomas F. Jaramillo (Primary Contact),
 Arnold J. Forman, Zhebo Chen
 Dept. of Chemical Engineering, 381 N-S Axis
 Stanford University
 Stanford, CA 94305
 Phone: (650) 498-6879
 Email: jaramillo@stanford.edu

DOE Manager
 HQ: Eric Miller
 Phone: (202) 287-5829
 Email: Eric.Miller@hq.doe.gov

Contract Number: DE-AC36-08GO28308
 Subcontract Number: NFT-9-88567-01

Subcontractor:
 Board of Trustees of the Leland Stanford Junior University,
 Stanford, CA

Project Start Date: December 18, 2008
 Projected End Date: September 30, 2012

Fiscal Year (FY) 2012 Objectives

The main objective of this project is to develop third-generation materials and structures with new properties that can potentially meet DOE targets (2013 and 2018) for usable semiconductor bandgap, chemical conversion process efficiency, and durability.

- Develop a transparent conducting high surface area electrode (HSE) as a broadly applicable substrate for photoelectrochemical (PEC) devices utilizing scalable fabrication methods.
- Improve efficiency of charge transport limited PEC materials (e.g., $\alpha\text{-Fe}_2\text{O}_3$) by integrating them into the HSE substrate and demonstrate efficacy.
- Develop efficient PEC materials consisting of nanostructured MoS_2 with a wider bandgap, improved band alignment with respect to H_2 and O_2 evolution potentials and improved surface catalysis for the hydrogen evolution reaction.
- Develop durable MoS_2 photo-cathodes.

Technical Barriers

This project addresses the following technical barriers from the Production section of the Fuel Cell Technologies Program Multi-Year Research, Development and Demonstration Plan:

- (Y) Materials Efficiency
- (Z) Materials Durability
- (AA) PEC Device and System Auxiliary Materials
- (AB) Bulk Materials Synthesis

Technical Targets

The focus of this project is the development of a broadly applicable substrate platform that enables the ability to integrate novel third-generation solar absorbers as well as charge transport limited solar absorbers into a complete PEC device. If successful, this project will address the following DOE technical targets as outlined in the Fuel Cell Technologies Program Multi-Year Research, Development and Demonstration Plan.

TABLE 1. Progress towards Meeting Technical Targets for PEC Hydrogen Production

| Characteristics | Units | 2013 Target | 2018 Target | 2012 Status |
|--|-------|-------------|-------------|-------------|
| Usable semiconductor bandgap | eV | 2.3 | 2.0 | 1.8 |
| Chemical conversion process efficiency | % | 10 | 12 | TBD |
| Plant solar-to-hydrogen efficiency | % | 8 | 10 | TBD |
| Plant durability | hr | 1,000 | 5,000 | TBD |

TBD – to be determined

FY 2012 Accomplishments

- Developed and optimized a facile, scalable spray deposition route (patent pending) to fabricate HSEs of transparent conducting oxide (TCO) materials.
- Demonstrated a robust synthetic methodology that enables tunable control of surface area from ~1 to over 100x relative to a planar substrate as determined using extensive electrochemical characterization.
- Use of the HSE substrate as a support for $\alpha\text{-Fe}_2\text{O}_3$ (a minority carrier charge transport limited PEC material)

yields performance enhancement over planar $\alpha\text{-Fe}_2\text{O}_3$ devices.

- Engineered nanoscale mesoporous architectures of MoS_2 to overcome thermodynamic structural limitations in bulk form to achieve a higher density of catalytically active sites for electrochemical hydrogen evolution.
- Determined band structures for quantum confined MoS_2 nanoparticles to show better conduction and valence band alignment for H_2 and O_2 evolution potentials



Introduction

The production of hydrogen (H_2) currently represents 2-3% of worldwide energy consumption due to the critical role of H_2 in large scale industrial processes such as ammonia synthesis and petroleum refining [1,2]. PEC water splitting is a promising route towards producing H_2 using only renewable resources (sunlight and water) [3]. Producing H_2 by this approach can reach costs as low as \$2-\$3/gasoline gallon equivalent [4] and represents a way to store solar energy to better match the intermittent solar collection profile with variable point-of-use energy demand profiles. To realize these competitive economics with PEC water splitting, it is necessary to create higher efficiency and lower cost devices than what is currently available today.

Successful development of an economical system to split water from solar irradiation requires optimizing multiple components that make up a complete PEC device, including discovery of efficient, earth-abundant, and stable photoelectrode materials and electrocatalysts, as well as appropriate architectural supports, followed by integration of these components into a complete system

Approach

One of the major limitations to efficient PEC device development is achieving high solar absorption while maintaining short charge transport distances in a typical planar electrode geometry. Thick samples improve light absorption at the expense of charge transport, while thin samples improve charge transport at the expense of light absorption. This challenge is general to thin-film solar technologies [5]. One method to decouple the two phenomena is to utilize transparent, HSE supports coated with ultra-thin layers of light absorbing material. HSEs enable the fabrication of high optical density devices without using thick absorber layers, thereby mitigating efficiency losses due to transport of both minority and majority charge carriers. This approach has been successfully demonstrated in dye-sensitized solar cells which often employ high surface area TiO_2 [6]. Furthermore, HSE architectures reduce local current densities by increasing interfacial surface area, decreasing

the kinetic overpotential required to turn over a reaction and further enhancing the efficiency of electrodes used in both solar applications as well as non-solar applications such as electrocatalysis. Development of these HSEs is therefore an enabling technology at both the fundamental and applied research levels. To further address the broad range of materials currently being studied for PEC water splitting, it is necessary to develop HSEs with tunable physical and electronic properties in order to optimize the light absorption, charge transport, and mass transport properties of a complete device.

While many materials have previously been studied for PEC water splitting, no one material currently meets the requirements of high efficiency and low cost. To develop novel solar absorber materials, we engineer nanostructures of MoS_2 , [7] a material which demonstrates promising photoactivity in bulk form, [8] but is otherwise hampered by a bandgap that is too small, misaligned conduction and valence bands with respect to the H_2 and O_2 evolution potentials, and poor catalysis. By nanostructuring MoS_2 , the electronic properties can be modified through quantum confinement, [9,10] and the catalytic activity for H_2 evolution can be dramatically enhanced by exposing a greater number of active edge sites [11,12].

Results

Previously, we successfully developed a synthetic route towards fabricating high surface area TCO substrates with hierarchical (nanometer-scale and micron-scale) porosity utilizing a scalable spray deposition technique. The design is applicable to a broad range of compositions, such as indium tin oxide, fluorine-doped tin oxide, aluminum zinc oxide. Figure 1a illustrates a schematic representation of the resulting film morphology from this scalable fabrication process. The amount of mixture sprayed onto the appropriate conductive substrate controls the final surface area of the HSE. These TCO HSEs are capable of enabling PEC materials to simultaneously address three of the DOE technical barriers for Production (Y, AA, AB). Compared to more classical HSE fabrication techniques such as lithographic patterning, spray deposition offers significant cost savings and scalability – absolute necessities for an emerging solar energy technology seeking to generate copious domestic fuel.

We have made significant progress in the development of HSE supports, including synthetic methods, characterization and most notably, in the utilization of the HSE as a PEC support. Spray fabrication conditions for the HSE have been optimized to yield high reproducibility and large area coverage (10's to 100 cm^2) in the laboratory setting. Electrochemical characterization of the HSEs yielded limitations when the active area was defined and sealed with an o-ring in a compression cell configuration, resulting in

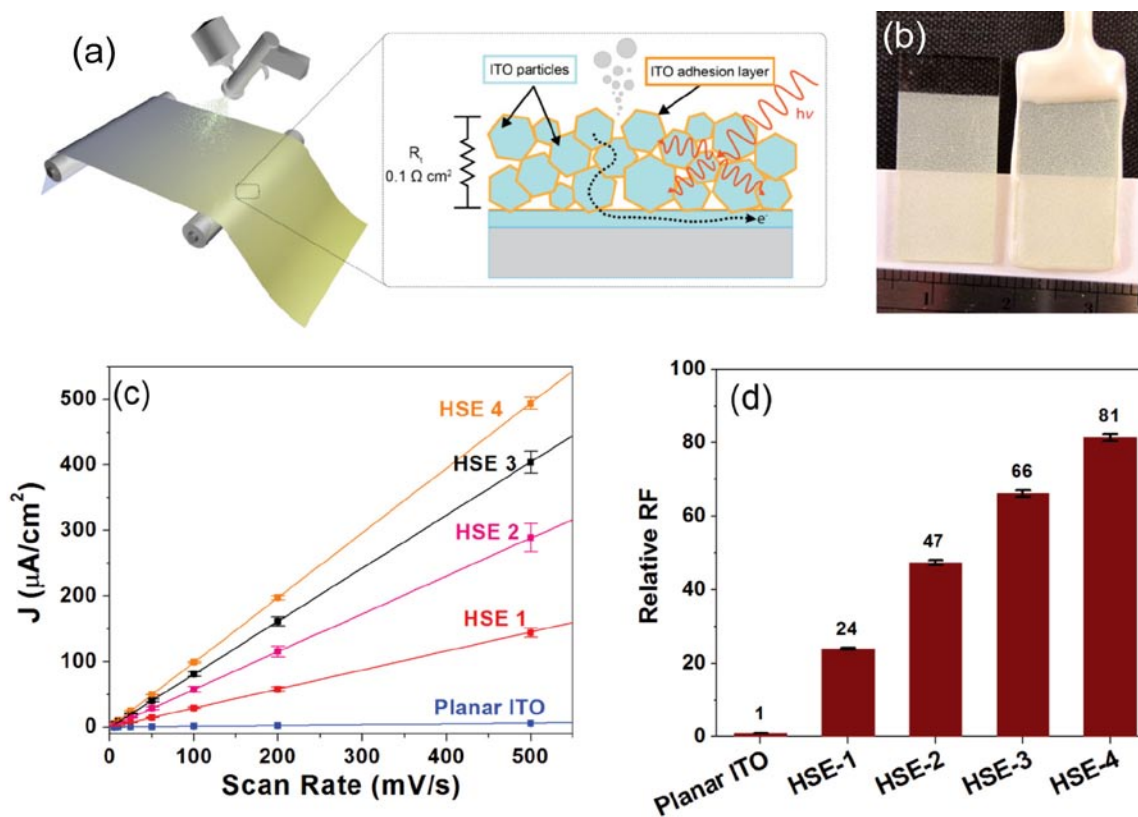


FIGURE 1. Transparent conductive HSEs are fabricated via spray deposition to yield substrates with tunable surface areas (a). Improved electrode mounting methods include conductive paint and insulating epoxy (b) resulting in non-diffusion limited performance (c) and high precision, high accuracy synthetic tunability of the roughness factor (d).

electrolyte leaking and erroneous diffusion limited signals. These problems have been eliminated by contacting the HSEs with conductive paint and defining and sealing the active area with insulating epoxy (Figure 1b). The result of this improved methodology is that the data interpretation for electrochemical surface area characterization is more straightforward – there are no diffusion limitations observed, as evidenced by the linear relationship between current density and scan rate (Figure 1c). The absence of diffusion limitations through the HSE bodes well for subsequent (photo)catalytic applications. The end result of the refined synthesis and electrode mounting procedures is that discrete roughness factors ranging from ~ 1 to >100 can be targeted with great accuracy and precision (Figure 1d) depending on the needs of the final application.

Hematite ($\alpha\text{-Fe}_2\text{O}_3$) was chosen as a proof-of-concept material to test the enhancement afforded by the HSE scaffold for charge transport limited PEC materials. Hematite films were fabricated by dropcasting an ethanolic solution containing FeCl_3 and Ti-butoxide (1:10, Ti:Fe) followed by annealing at 550°C in air following the work of Li *et al.* [13]. For comparison, three samples were fabricated (Figure 2a): 1) HSE substrate with hematite layer. This resulted in a conformal, well adhered film with a high

optical density. 2) Planar substrate with identical hematite loading ($\mu\text{g}/\text{cm}^2_{\text{device}}$) to sample 1. This resulted in a thick, cracked film which delaminated from the substrate. 3) Planar substrate with hematite film thickness (nm) identical to sample 1. This resulted in a thin, low optical density film. The PEC performance of these three samples is presented in Figure 2b. Sample 1 on the HSE substrate shows the best performance, maintaining the expected photocurrent onset of ~ 1 V vs. reversible hydrogen electrode with a superior photocurrent due to high light absorption and charge extraction within the HSE. Samples 1 and 2 have an identical hematite loading, absorb the same number of incoming photons and should therefore be capable of generating the same photocurrent. However, because this high loading is placed on a planar substrate, the actual hematite film thickness is very large, resulting in physical instability and delamination from the substrate. The result is that sample 2 is unstable and gives no PEC signal. The take home message here is that it is desirable to have high loadings of material (per geometric device area) to achieve high optical densities and correspondingly high photocurrents. However, there is an upper stability limit when loading thicker films onto planar substrates which does not allow the desired loadings to be achieved. Yet, our HSE scaffolds do not encounter this same

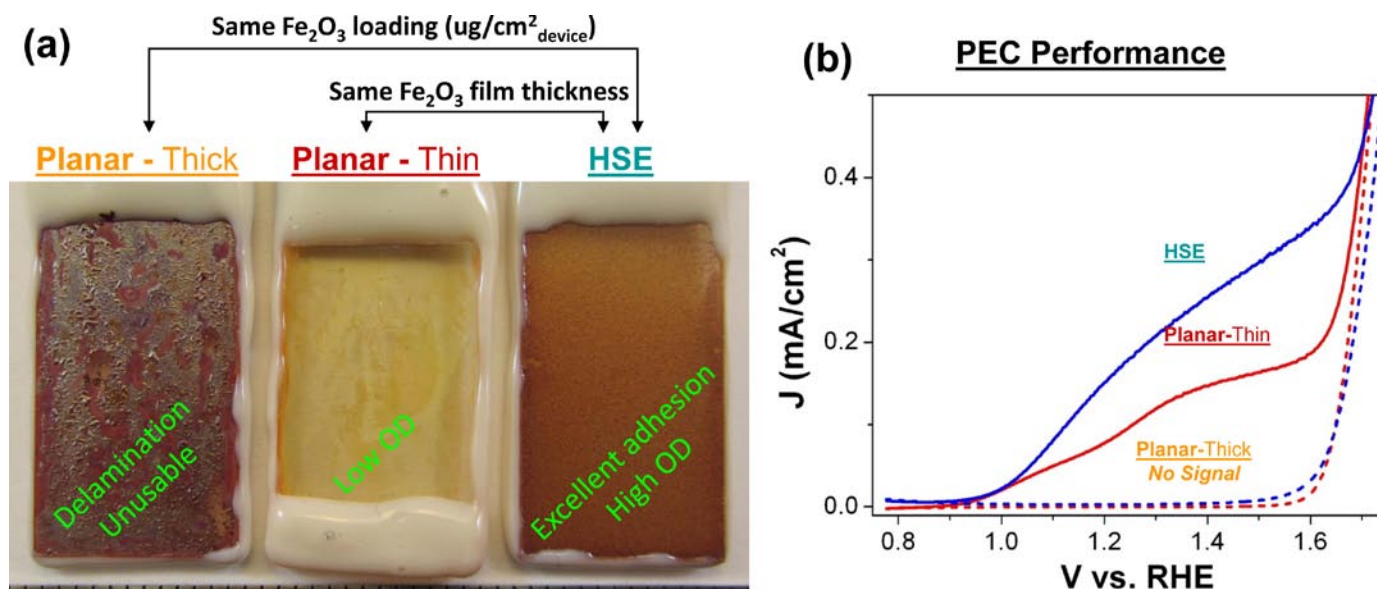


FIGURE 2. Optical photograph of hematite films on planar and HSE substrates (a), see text for synthetic details. (b) Current-voltage curves in the dark (dotted lines) and under 1 sun of illumination (solid lines) for the samples presented in (a).

loading limitation and can offer high optical densities of stable, delamination-free active layers.

Comparison of samples with an identical thickness of hematite, samples 1 and 3, indicates that the HSE substrate offers practical performance enhancement through increased light absorption (Figure 2b). It is clear, however, that there is room for further improvement of the HSE device as the current is only $\sim 2x$ that of sample 3, while the loading is $\sim 12x$ higher. Proposed routes to improvement include further optimization of the dropcasting procedure and introduction of an interfacial layer between the HSE and hematite layers [5,14-16]. Initial work in our labs using interfacial layers of SiO₂ and TiO₂ has shown promising results and must be further optimized to achieve full conformal coverage on the HSE.

Although hematite is an excellent material to study whose performance can be enhanced by the HSE, it is ultimately limited by a mismatched conduction band with respect to the hydrogen evolution potential. In order to engineer materials with more appropriate band structures that sufficiently straddle the water splitting potentials, we leverage the effects of quantum confinement to tune the electronic properties of MoS₂ [17]. We have previously demonstrated the synthesis of MoS₂ nanoparticles using a micelle encapsulation approach that exhibit a blueshift in the absorption onset with smaller size. This corresponds to an enlargement in the bandgap up to ~ 1.8 eV for MoS₂ nanoparticles of only a few nm in diameter. In order to further assess the flatband potential (E_{fb}) of the nanoparticles, we fabricated thin film electrodes. A number of fabrication techniques were explored such as dip coating, drop

casting, and spin coating, but spray coating yielded the most homogeneous films on a variety of substrates. Spray deposited films of nanoparticles on fluorine-doped tin oxide enabled PEC characterization and assessment of E_{fb} by photocurrent onset. When coupled to the optical absorption measurements, we were able to approximate the band structure (Figure 3), showing that the smallest nanoparticles appear to possess conduction and valence bands that adequately straddle the water splitting potentials.

We further enhanced the catalytic properties of MoS₂ for H₂ evolution (Figure 4a) by engineering its surface structure to display an increased density of active edge sites. In order to achieve this result, it is necessary to overcome a limitation in which the formation of these edge sites are thermodynamically unfavored compared to the formation of extended non-active basal planes at bulk length scales greater than a few tens of nanometers. To address this challenge, we synthesized highly ordered and extended films of a mesoporous double-gyroid MoS₂ architecture with features on the order of just $\sim 3-4$ nm. This highly interconnected porous morphology (Figure 4b) not only provided a high surface area for catalysis, but its high curvature limited the formation of extended basal planes and increased the density of catalytically active edge sites (Figure 4c), enabling excellent H₂ evolution.

Conclusions and Future Directions

In order to reach our goal of developing a fully operational PEC water splitting device, we have produced a high surface area transparent conducting electrode and demonstrated its ability to enhance efficiency for PEC. We

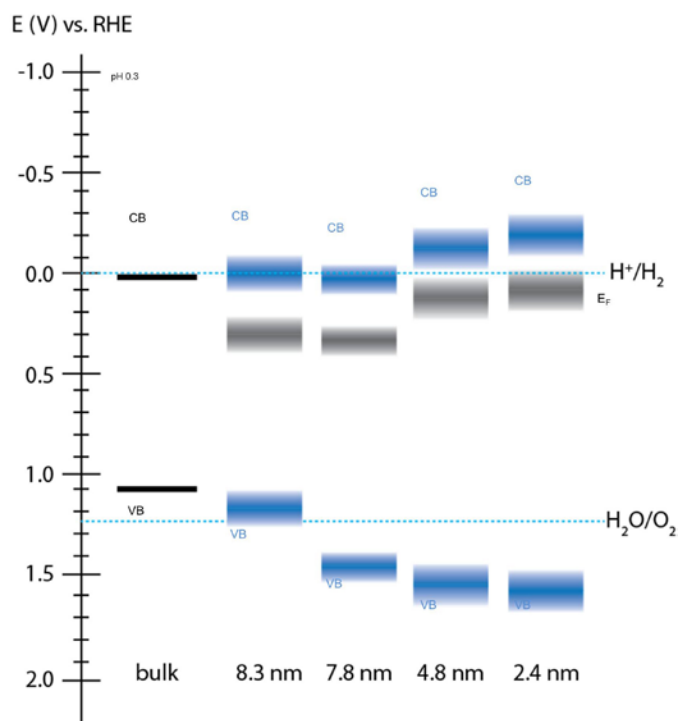


FIGURE 3. Band diagram comparing the position of the conduction and valence bands of several films of MoS₂ nanoparticles (nanoparticle size denoted in the figure) compared to bulk MoS₂ [17].

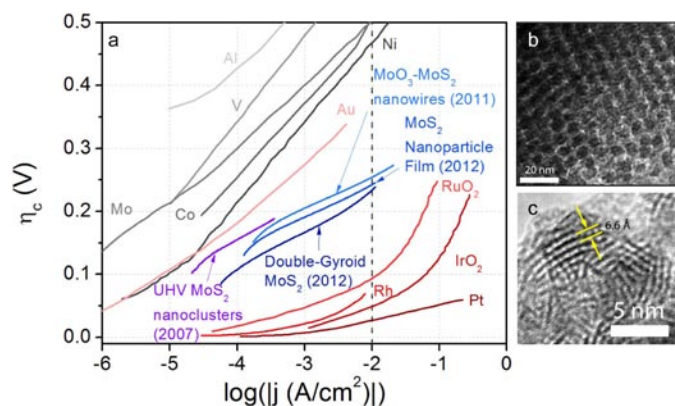


FIGURE 4. Tafel plot of numerous materials for electrochemical H₂ evolution (a). Transmission electron microscopy image of mesoporous double-gyroid architecture (b) and layered MoS₂ domains within the structure (c).

have also developed a third-generation light absorber material (MoS₂) and further enhanced its electrocatalysis. Specifically, we have achieved the following:

- A low-cost, scalable, facile route to fabrication of high surface area transparent conducting electrodes has been developed, a manuscript submitted and a patent application is pending.

- Physical and electronic characterization of these electrodes indicates tunable roughness factors from ~1 to >100 over large substrate areas.
- HSE scaffolds have been used to demonstrate enhanced PEC performance for Hematite thin films. Further improvements are underway.
- Developed quantum confined nanoparticles of MoS₂ with band structures that adequately straddle the redox potentials for water splitting.
- Engineered the surface structure of MoS₂ for enhanced electrocatalytic H₂ evolution.

The next step in our work is to tune the solid-solid interface by addition of hetero-layers. We will accomplish this task through various objectives:

- Identify appropriate methods and materials for deposition of thin, conformal interfacial layers onto HSEs.
- Evaluate and iteratively improve PEC devices which incorporate both interfacial layers and thin semiconductor films.
- Continue to identify and evaluate charge-transport limited PEC materials which benefit from the HSE architecture.
- Incorporate MoS₂ nanoparticles into the HSE and characterize their water splitting properties with respect to light absorption, charge transport, and stability.

Special Recognitions & Awards/Patents Issued

1. DOE Hydrogen and Fuel Cells Program R&D Award to Prof. Thomas F. Jaramillo (PI)
2. Arnold J. Forman, Zhebo Chen, and Thomas F. Jaramillo, "Synthesis of High Roughness Factor Transparent Conducting Oxide Thin Films" (patent application pending).

FY 2012 Publications/Presentations

1. A.J. Forman, Zhebo Chen, and Thomas F. Jaramillo, "Development of a High Surface Area Transparent Conducting Oxide Electrode" (submitted).
2. Jakob Kibsgaard, Zhebo Chen, Benjamin N. Reinecke, and Thomas F. Jaramillo, "Engineering the surface structure of MoS₂ to preferentially expose active edge sites for electrocatalysis" (submitted).
3. I.S. Cho, Z. Chen, A.J. Forman, D.R. Kip, P.M. Rao, T.F. Jaramillo, X. Zheng, "Branched TiO₂ Nanorods for Photoelectrochemical Hydrogen Production," *Nano Letters*, Vol. 11, No. 11, pp. 4978-4984, 2011.
4. Zhebo Chen, Dustin Cummins, Benjamin N. Reinecke, Ezra Clark, Mahendra K. Sunkara, and Thomas F. Jaramillo, "Core-shell MoO₃-MoS₂ Nanowires for Hydrogen Evolution: A functional Design for Electrocatalytic Materials" *Nano Letters*, Vol. 11, pp. 4168-4175, 2011.

5. T.F. Jaramillo, A.J. Forman, Z. Chen, I. Thomann, B.A. Pinaud, I.S. Cho, D.R. Kim, P.M. Rao, B.M. Clemens, X. Zheng, M. Brongersma, "Bridging the gap between optical absorption and charge transport in metal oxide materials for the synthesis of solar fuels," Spring Meeting of the Materials Research Society (MRS), San Francisco, CA, April 13, 2012.

6. T.F. Jaramillo, "Tailoring Electrocatalyst Materials at the Nano-Scale: Controlling Activity, Selectivity, and Stability for Energy Conversion Reactions,"

- University of California, Santa Barbara, Dept. of Chemistry and Chemical Engineering, Santa Barbara, CA, March 7, 2012.
- Massachusetts Institute of Technology (MIT), Energy Initiative Seminar Series, Cambridge, MA, December 2011.
- California Institute of Technology, Chemical Engineering Department Seminar, Pasadena, CA, October 2011.
- University of New Mexico, Chemical and Nuclear Engineering Department Seminar, Albuquerque, NM, October 2011.
- Catalysis for Sustainable Energy (CASE) Seminar Series, Technical University of Denmark, Lyngby, DK, August 2011.

7. T.F. Jaramillo, A.J. Forman, Z. Chen, B.A. Pinaud, J.D. Benck, S.-H. Baeck, Y. Gorlin, E. Cave, K.P. Kuhl, "Advanced electrode and photo-electrode structures for the synthesis of fuels from sunlight," Fall Meeting of the Materials Research Society (MRS), Boston, MA, November 2011.

8. Zhebo Chen, Dustin Cummins, Benjamin N. Reinecke, Ezra L. Clark, Mahendra K. Sunkara, and Thomas F. Jaramillo, "MoS₂ Nanostructures as Efficient, Stable, and Earth-Abundant Catalysts for Hydrogen Evolution in Acid," 2011 Annual Meeting of the American Institute of Chemical Engineers, Minneapolis, MN, October 19, 2011.

9. Zhebo Chen and Thomas F. Jaramillo, "Quantum Confined MoS₂ Nanoparticles for Band Gap Engineered Photoelectrochemical Water Splitting," 220th meeting of the Electrochemical Society, Boston, MA, October 13, 2011.

10. T.F. Jaramillo, "Semiconductors and catalysts for the production of solar fuels," Haldor Topsøe Catalysis Forum: Catalysis & Future Energy, Munkerpugaard, DK, Aug. 2011.

11. T.F. Jaramillo, "Tailoring electrocatalyst materials at the nano-scale: Controlling activity and selectivity for energy conversion reactions," Lawrence Livermore National Laboratory, Livermore, CA., July 2011.

12. Zhebo Chen, Jakob Kibsgaard, and Thomas F. Jaramillo, "Nanostructured MoS₂ for Solar Hydrogen Production," 2011 Materials Research Society Spring Meeting, San Francisco, CA, April 29, 2011.

References

1. A. Midilli and I. Dincer: Key strategies of hydrogen energy systems for sustainability. *Int. J. Hydrog. Energy* **32**, (2007).
2. M. Balat: Potential importance of hydrogen as a future solution to environmental and transportation problems. *Int. J. Hydrog. Energy* **33**, (2008).
3. M.G. Walter, E.L. Warren, J.R. McKone, S.W. Boettcher, Q. Mi, E.A. Santori and N.S. Lewis: Solar Water Splitting Cells. *Chem. Rev.* **110**, (2010).

4. B.D. James, G.N. Baum, J. Perez and K.N. Baum: *Technoeconomic Analysis of Photoelectrochemical (PEC) Hydrogen Production* (2009).

5. F. Le Formal, M. Grätzel and K. Sivula: Controlling Photoactivity in Ultrathin Hematite Films for Solar Water-Splitting. *Advanced Functional Materials* **20**, (2010).

6. A. Yella, H.-W. Lee, H.N. Tsao, C. Yi, A.K. Chandiran, M.K. Nazeeruddin, E.W.-G. Diau, C.-Y. Yeh, S.M. Zakeeruddin and M. Graetzel: Porphyrin-Sensitized Solar Cells with Cobalt (II/III)-Based Redox Electrolyte Exceed 12 Percent Efficiency. *Science* **334**, (2011).

7. Our applied research on the photoelectrochemistry of MoS₂ is funded through this program; our more fundamental research on MoS₂ is currently supported by Center on Nanostructuring for Efficient Energy Conversion (CNEEC) at Stanford University, an Energy Frontier Research Center funded by the U.S. Department of Energy, Office of Science, Office of Basic Energy Sciences under Award Number DE-SC0001060.

8. H. Tributsch and J.C. Bennett: Electrochemistry and photochemistry of MoS₂ layer crystals. *J. Electroanal. Chem.* **81**, (1977).

9. J.P. Wilcoxon and G.A. Samara: Strong quantum-size effects in layered semiconductor - MoS₂ nanoclusters. *Phys. Rev. B* **51**, (1995).

10. J.P. Wilcoxon, P.P. Newcomer and G.A. Samara: Synthesis and optical properties of MoS₂ and isomorphous nanoclusters in the quantum confinement regime. *J. Appl. Phys.* **81**, (1997).

11. T.F. Jaramillo, K.P. Jørgensen, J. Bonde, J.H. Nielsen, S. Horch and I. Chorkendorff: Identification of active edge sites for electrochemical H₂ evolution from MoS₂ nanocatalysts. *Science* **317**, (2007).

12. Z. Chen, D. Cummins, B.N. Reinecke, E. Clark, M.K. Sunkara and T.F. Jaramillo: Core-shell MoO₃-MoS₂ Nanowires for Hydrogen Evolution: A Functional Design for Electrocatalytic Materials. *Nano Lett.* (2011).

13. G. Wang, Y. Ling, D.A. Wheeler, K.E.N. George, K. Horsley, C. Heske, J.Z. Zhang and Y. Li: Facile Synthesis of Highly Photoactive α -Fe₂O₃-Based Films for Water Oxidation. *Nano Lett.* **11**, (2011).

14. Y. Liang, T. Tsubota, L. P. A. Mooij and R. van de Krol: Highly Improved Quantum Efficiencies for Thin Film BiVO₄ Photoanodes. *The Journal of Physical Chemistry C* **115**, (2011).

15. T. Hisatomi, H. Dotan, M. Stefiik, K. Sivula, A. Rothschild, M. Grätzel and N. Mathews: Enhancement in the Performance of Ultrathin Hematite Photoanode for Water Splitting by an Oxide Underlayer. *Adv. Mater.* **24**, (2012).

16. Y. Liang, C. S. Enache and R. van de Krol: Photoelectrochemical Characterization of Sprayed α -Fe₂O₃ Thin Films: Influence of Si Doping and SnO₂ Interfacial Layer. *International Journal of Photoenergy* **2008**, (2008).

17. W. Kautek and H. Gerischer: Photoelectrochemical Reactions and Formation of Inversion Layers at n-Type MoS₂-, MoSe₂-, and WSe₂-Electrodes in Aprotic solvents. *Ber. Bunsen-Ges. Phys. Chem. Chem. Phys.* **84**, (1980).

II.F.2 Semiconductor Materials for Photoelectrolysis

John Turner (Primary Contact), Todd Deutsch, Heli Wang, Adam Welch, Mowafak Al-Jassim, Houwen Tang

National Renewable Energy Laboratory
15013 Denver West Parkway
Golden, CO 80401
Phone: (303) 275-4270
Email: John.Turner@nrel.gov

DOE Manager
HQ: Eric Miller
Phone: (202) 287-5829
Email: Eric.Miller@ee.doe.gov

Subcontractors:

- Stanford University, Palo Alto, CA
- University of Nevada Las Vegas (UNLV), Las Vegas, NV

Project Start Date: 2005

Project End Date: Project continuation and direction determined annually by DOE

the Multi-Year Research, Development and Demonstration Plan PEC hydrogen production goals are as follows:

- Bandgap of 2.3 eV
- 10% conversion efficiency
- 1,000 hour lifetime

FY 2012 Accomplishments

- Demonstrated significantly enhanced photocurrent densities, 5 mA/cm² under bias, on n-InGaN provided by our Los Alamos National Laboratory (LANL) synthesis partner. This material has the potential to be the first non-tandem semiconductor to use visible light to split water with high efficiency (barrier Y).
- Identified a surface nitrogen ion implantation technique that completely passivated corrosion (barrier Z) on p-GaInP₂ surfaces that were tested at -10 mA/cm², a current density equivalent to 12.3% solar-to-hydrogen (STH) efficiency (barrier Y), for several hours in sulfuric acid.
- Observed that co-doping hematite with both titanium and magnesium led to higher photocurrents than titanium doping alone. This experimental result validated theoretical findings that charge compensation from co-doping of durable oxide materials (barrier Z) should yield materials with more favorable electronic properties (barrier Y) than those using a single dopant.
- Surface validation study, in collaboration with UNLV and Lawrence Livermore National Laboratory (LLNL), made progress in establishing baseline spectra of as-grown p-GaInP₂ surface. UNLV analyzed air-excluded sample provided by NREL and used the baseline results to compare against samples that have been subjected to corrosion testing (barrier Z).

Fiscal Year (FY) 2012 Objectives

Identify, synthesize, and characterize new semiconductor materials that have the capability of meeting the criteria for a viable photoelectrochemical (PEC) hydrogen-producing device, either as a single absorber or as part of a high-efficiency multi-junction device.

Technical Barriers

This project addresses the following technical barriers from the Production section (3.1) of the Fuel Cell Technologies Program Multi-Year Research, Development and Demonstration Plan:

- (Y) Materials efficiency
- (Z) Materials durability
- (AB) Bulk materials synthesis
- (AC) Device configuration Technical Targets

Technical Targets

This project is a materials discovery investigation to identify a single semiconductor material that meets the technical targets for efficiency and stability. This project made progress towards the stability target and achieved over 100 hours of corrosion-free operation on a material that exceeds the efficiency target. The 2013 technical targets from



Introduction

Photoelectrochemistry combines a light harvesting system and a water splitting system into a single, monolithic device. A semiconductor immersed in aqueous solution comprises the light-harvesting system. The catalyzed surface of the semiconductor is one part of the water splitting system, and the other part is another electrode in a separate compartment. The key is to find a semiconductor system that can efficiently and sustainably collect solar energy and direct it towards the water splitting reaction.

The goal of this work is to develop a semiconductor material set or device configuration that (i) splits water into

hydrogen and oxygen spontaneously upon illumination, (ii) has a STH efficiency of at least 5% with a clear pathway to a 10% water splitting system, (iii) exhibits the possibility of 10-year stability under solar conditions and (iv) can be adapted to volume-manufacturing techniques.

Approach

Our approach has two tracks, i) the study of current material sets used in commercial solar cells as well as related materials, and ii) the discovery of new semiconducting materials using advanced theoretical calculations to identify promising candidates, closely coupled with synthesis and state-of-the-art characterization. A major component of (i) focuses on III-V semiconductor materials that meet the efficiency target and engineering the surface to meet the durability target. Area (ii) has focused on chalcogenide and Cu, W, Ti, and Bi based multinary oxides.

Results

III-V Nitride Materials

$\text{In}_x\text{Ga}_{1-x}\text{N}$ is a promising alloy that has recently seen advances in synthesis techniques that achieve high-quality thin films over the entire alloy range. High solar conversion efficiencies should be possible with these epilayer single-crystal semiconductors and previous work on III-nitrides has shown that it is a remarkably stable material set [1]. A unique feature of this material system is the broad range of band gaps achievable, that spans between that of InN (0.7 eV) and GaN (3.4 eV).

Recent n-InGaN semiconductors exhibited significantly enhanced photocurrent densities as compared to previous InGaN materials. The samples were grown by our collaborator, Todd Williamson, at LANL by energetic neutral atom beam lithography and epitaxy on sapphire and silicon substrates. Under a moderate bias, the water oxidation photocurrent magnitudes were up to 5 mA/cm^2 (Figure 1).

Durability of n-InGaN grown on silicon substrates was evaluated by looking for a decline in photocurrent under a constant applied bias. In 0.5M sulfuric acid, the electrodes were biased at 1.3 V vs. Ag/AgCl and after an hour the photocurrent declined to 10% of its original value. The durability of this material is lower than anticipated for a nitride semiconductor, but the electrode viability can likely be extended through the application of a surface catalyst or by varying the electrolyte composition.

Protection Strategies for High-Efficiency III-V Materials

A tandem semiconductor configuration consisting of a photovoltaic p/n-GaAs bottom cell and a PEC p-GaInP₂ top cell has demonstrated (unbiased) solar-to-hydrogen conversion

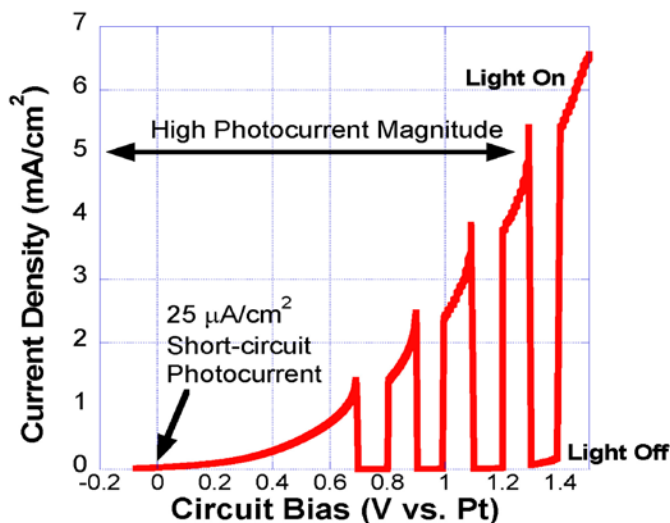


FIGURE 1. Two-electrode chopped-light photocurrent density vs. circuit bias for n-InGaN on sapphire in 0.5M H_2SO_4 . The light source was a 250-Watt tungsten lamp calibrated to AM1.5G using a 2.0 eV reference cell. The photocurrent density of 5 mA/cm^2 at 1.2 V applied bias (vs. a Pt counter electrode) is about 50% of the theoretical maximum for this 2.2 eV band gap material. Though this material exhibited a photocurrent at zero bias, indicating spontaneous photoelectrolysis at true short-circuit, the magnitude was low.

efficiencies well over the Multi-Year Research, Development and Demonstration Plan STH efficiency target of 10% but is prone to corrosion [2]. III-V nitride semiconductors, however, have exhibited excellent durability in a PEC environment in the past [3]. Thus surface nitridation of p-GaInP₂ was investigated as a means of reducing corrosion in the aqueous electrolyte. Thin films of p-GaInP₂ grown by metal organic chemical vapor deposition on a p-GaAs substrate were nitrided by implantation with low-energy N_2^+ ions at room temperature. Control and nitrided samples were tested for durability by applying a constant current of -10 mA/cm^2 , a current density equivalent to 12.3% STH efficiency, in 3M H_2SO_4 for long durations under Air Mass 1.5 Global (solar spectrum, AM1.5G) illumination. After the durability tests the electrodes were disassembled and optical profilometry was used to measure the volume of material lost from the surface due to corrosion during operation. One electrode survived 115 hours with no detectable degradation (Figure 2). Several of the nitrided samples entirely resisted corrosion over 24 hours of testing, where similarly tested untreated samples experienced around $1 \mu\text{m}$ of material loss from their surfaces (Figure 3). The respective electrolytes were analyzed by inductively coupled plasma mass spectrometry (ICP-MS) to determine concentrations of indium and gallium in solution to quantify semiconductor corrosion. The ICP-MS results correlated well with the optical profilometry data, with only trace quantities of analyte detected in the nitride-treated durability electrolytes. The nitrogen ion implantation led to only a modest reduction in photoconversion efficiency. Surface nitridation by ion bombardment could hence be an

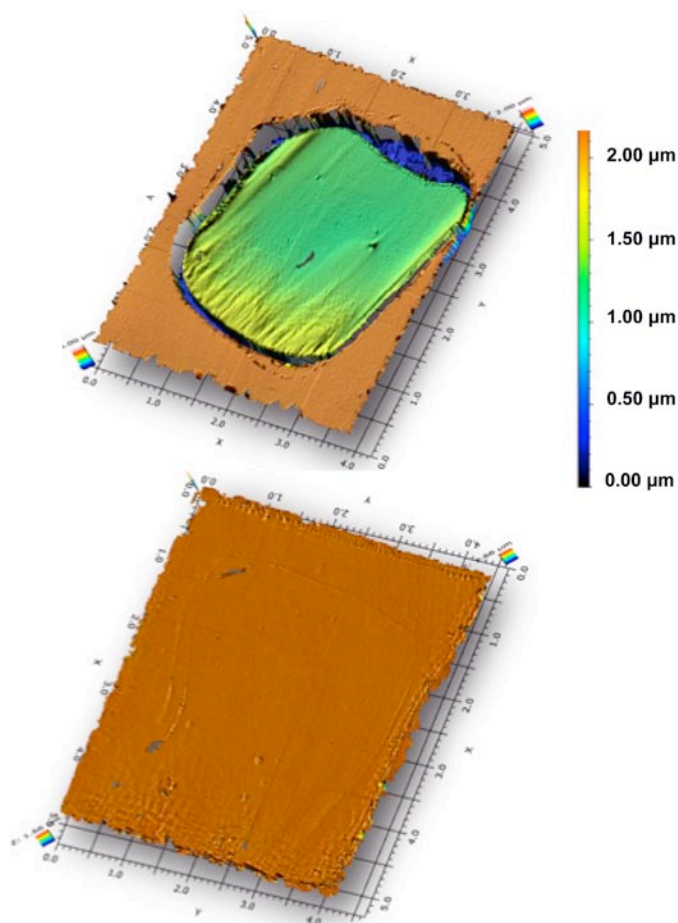


FIGURE 2. Optical profilometry of p-GaN/P₂ electrode surfaces after durability analysis in sulfuric acid. The image on the top is of a sample that had no surface passivation treatment and experienced etching of about 1 μm of material from the surface in the area not masked by epoxy (i.e. exposed to the electrolyte). The nitride treated sample on the bottom exhibited no detectable damage after passing -10 mA/cm² of photocurrent for 115 hours, the equivalent to 12.3% STH conversion.

effective passivation treatment to ensure durability for a highly efficient PEC material, ultimately yielding a viable device capable of converting sunlight and water to a benign solar fuel.

NREL Synthesis of Metal Oxide Alloy Thin Films

α -Fe₂O₃ (hematite) is an n-type semiconducting material that exhibits several potential advantages for PEC hydrogen production. It has an ideal band gap (2.0-2.2 eV), is composed of abundant, non-toxic elements, and can be synthesized via low-cost routes. However, the intrinsic poor conductivity of α -Fe₂O₃ has hindered its PEC performance. Previous studies have shown that the incorporation of Ti can enhance the PEC performance of α -Fe₂O₃. Ti incorporation in hematite is limited by solubility, where too high a concentration can lead to TiO₂ crystallites that compromise the material's

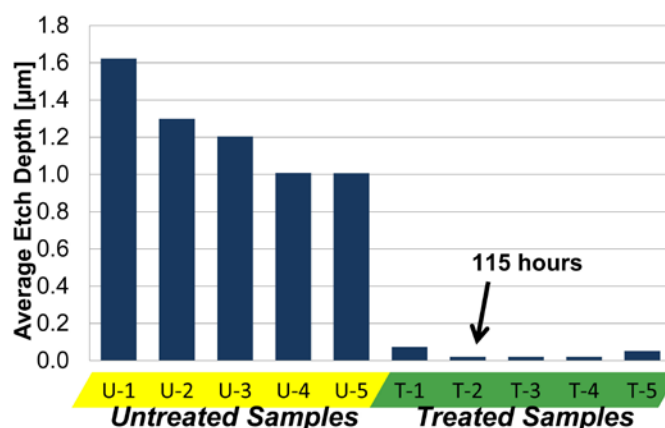


FIGURE 3. Optical profilometer determined etch depths for p-GaN/P₂ electrode surfaces subjected to continuous operation of -10 mA/cm² under AM1.5 G illumination for 24 hours (or longer where noted). The untreated electrodes had a significant fraction of their overall 2 μm thickness removed while the nitrided electrodes exhibited little or no loss of material.

electronic properties. By co-incorporating Mg with Ti, charge compensation can be achieved that allows an increase in the solubility of Mg and Ti. It also provides a mechanism to tune the carrier density while simultaneously reducing the density of charge defects. Our previous work has shown that charge-compensated donor-acceptor co-alloying is an effective approach to improve the electronic properties of a host material [4].

Samples were synthesized by radio frequency reactive co-sputtering of Fe₂O₃, Ti, and MgO targets to deposit Fe₂O₃, (Fe_{0.87}Ti_{0.10}Mg_{0.03})₂O₃, (Fe_{0.84}Ti_{0.09}Mg_{0.07/2})₂O₃, (Fe_{0.79}Ti_{0.09}Mg_{0.12/2})₂O₃ on F-doped tin oxide coated glass substrates. We compared the PEC properties in neutral solutions and while the co-incorporated films did exhibit up to a tenfold increase in photocurrent magnitude at the same potential, all of the films had poor photoconversion properties. Under 5 sun illumination from a tungsten lamp, the photocurrent densities at +0.8 V vs. Ag/AgCl ranged from 5 μA/cm² for pure hematite to 50 μA/cm² for (Fe_{0.84}Ti_{0.09}Mg_{0.07/2})₂O₃. For a viable PEC water splitting system, the photocurrent density should be about 10 mA/cm² under one sun. While the results serve as an experimental confirmation of charge-compensating co-alloying in a novel host material, the method of synthesis and alloying missed the mark. Typical hematite samples are reported in literature to be capable of generating a few mA/cm² under bias at 1 sun. Improving the performance of status quo hematite by co-doping would be a remarkable result. However, as synthesized, none of the films were viable to serve as photoelectrodes.

Advanced Materials Characterization and Support

Through a “surface validation study” framework, we collaborate with UNLV and LLNL, experts in surface spectroscopy and theoretical modeling, respectively. The

goals of this study are to i) study the PEC corrosion in III-V materials, an ideal system for elucidating the corrosion pathway and developing a remediation strategy, ii) identify the chemical character and mechanism of successful protective treatments, iii) apply lessons learned to other inexpensive systems that are more difficult to model and observe.

Semiconductor samples that are exposed to air or electrolyte will react and leave a modified surface that prevents unambiguous correlation with experimental effects and surface chemistry. UNLV (C. Heske, M. Weir, K. George, L. Weinhardt) used a suite of spectroscopic techniques to establish a benchmark electronic character of as-grown p-GaInP₂ sample surfaces. UNLV performed ion-stimulated desorption in order to gently clean air-exposed GaInP₂ surfaces and also analyzed non-air-exposed samples that were provided by NREL. Understanding the baseline spectra will allow UNLV to prepare surfaces that have had air and electrolyte exposure, a required condition for PEC testing, and deconvolute chemical changes due to corrosion from those due to environmental interaction during handling and transit. UNLV also analyzed nitrogen ion implanted GaInP₂ by X-ray emission spectroscopy (XES) at the Advanced Light Source at Lawrence Berkeley National Laboratory synchrotron and detected nitride bonds that are likely responsible for the resistance to corrosion.

The Quantum Simulations group at LLNL (T. Ogitsu, B. Wood, W.-I. Choi), used theoretical calculations to help interpret and complement X-ray absorption spectroscopy experiments on bulk GaP, InP, and GaInP₂ performed by UNLV. There was very good agreement between the theoretically derived and experimentally observed XES under standard conditions which validated the complex model. The next steps are to push the complexity of the models to match the non-standard surfaces and conditions encountered in these real PEC systems. These models should provide insight into experimental spectroscopic observations of corroded GaInP₂ surfaces.

Conclusions

- InGaN is capable of high photon conversion efficiency yielding improved photocurrent densities but the stability must be addressed for it to be a possible candidate for economical PEC water splitting.
- Nitrogen ion implantation of p-GaInP₂ has demonstrated the ability to stop corrosion of the semiconductor surface for 115 hours of simulated 12% STH operational conditions. This result demonstrates significant progress towards the near-term technical targets for efficiency (10%) and durability (1,000 hours) for this material.
- Leveraging the expertise of our collaborators in the surface validation study has led to progress in understanding the chemical state of as-grown and corroded III-V surfaces.

Future Direction

- Test nitrogen ion implanted GaInP₂/GaAs tandem cells at short-circuit until failure and compare results against near-term technical targets.
- Further investigate the role of ion implantation in stabilizing PEC interface through surface validation collaboration; apply treatment to other PEC systems.
- Develop photoreactor and protocols for benchmarking efficiency and durability of PEC materials under real solar conditions.

FY 2012 Publications

1. “Electronic and optical properties of CoX₂O₄ (X=Al, Ga, In) alloys” C. Feng, W-J Yin, J. Nie, X. Zu, M.N. Huda, S-H Wei, M.M. Al-Jassim, J.A. Turner, and Yanfa Yan, *Appl. Phys. Lett.* **100**, 023901 (2012).
2. “Mott insulators: An early selection criterion for materials for photoelectrochemical H₂ production” Muhammad N. Huda, Mowafak M. Al-Jassim, and John A. Turner, *J. Renewable Sustainable Energy* **3**, 053101 (2011).
3. “Phase separation in Ga and N co-incorporated ZnO films and its effects on photo-response in photoelectrochemical water splitting” Sudhakar Shet, Kwang-Soon Ahn, Ravindra Nuggehalli, M.M. Al-Jassim, J.A. Turner, and Yanfa Yan, *Thin Solid Films*, **519**(18), 5983-5987 (2011).
4. “Doping properties of monoclinic BiVO₄ studied by first-principles density-functional theory” Wan-Jian Yin, Su-Huai Wei, M.M. Al-Jassim, J.A. Turner, and Yanfa Yan, *Phys. Rev. B*, **83**(15), 155102 (2011).
5. Nanoporous black silicon photocathode for H₂ production by photoelectrochemical water splitting” Jihun Oh, Todd G. Deutsch, Hao-Chih Yuan, Howard M. Branz, *Energy Environ. Sci.* **4**, 1690-1694 (2011).
6. “Synthesis and characterization of titanium-alloyed hematite thin films for photoelectrochemical water splitting” Houwen Tang, M.A. Matin, Heli Wang, Todd Deutsch, Mowafak Al-Jassim, John Turner, Yanfa Yan, *J. App. Phys.* **110**, 123511 (2011).
7. “Cobalt-phosphate (Co-Pi) catalyst modified Mo-doped BiVO₄ photoelectrodes for solar water oxidation” Satyananda Kishore Pilli, Thomas E. Furtak, Logan D. Brown, Todd G. Deutsch, John A. Turner, Andrew M. Herring, *Energy Environ. Sci.* **4**, 5028-5034 (2011).
8. “Light induced water oxidation on cobalt-phosphate (Co-Pi) catalyst modified semi-transparent, porous SiO₂-BiVO₄ electrodes” Satyananda Kishore Pilli, Todd Deutsch, Thomas E. Furtak, John Turner, Logan D. Brown, and Andrew M. Herring. *Phys. Chem. Chem. Phys.*, Accepted Manuscript, March 06 (2012). DOI: 10.1039/C2CP40673J.

FY 2012 Presentations

1. “Toward economical solar hydrogen production: Surface passivation of GaInP₂ by plasma nitridation” 242nd American

Chemical Society National Meeting, Denver, CO, August 28 – September 1. (Welch) *Contributed*

2. “Semiconducting Materials for Photoelectrochemical Water Splitting”, 242nd American Chemical Society National Meeting, Denver, August 29, 2011. (Turner) *Invited*

3. “Photoelectrochemical Water Splitting”, DOE Laboratory Energy R&D Working Group (LERDWG), September 21, 2011. (Turner) *Invited*

4. “Surface nitridation of p-GaInP₂ for durable photoelectrochemical water splitting” 220th ECS meeting, Oct.12, 2011. (Wang) *Invited*

5. “Hydrogen Production from Photoelectrochemical Cells: Theoretical considerations and experimental results”, Colorado School of Mines, October 27, 2011. (Turner) *Invited seminar*

6. “Challenges and Opportunities in Photoelectrochemical Water Splitting”, University of California, Davis, November 1, 2011. (Turner) *Invited seminar*

7. “Hydrogen Production from Photoelectrochemical Cells: Economic and Theoretical Considerations and Experimental Results”, 2011 DOE PHOTOSYNTHETIC SYSTEMS RESEARCH MEETING, November 7, 2011. (Turner) *Invited plenary*

8. “Hydrogen Production from Photoelectrochemical Cells: Economic and Theoretical Considerations and Experimental Results”, University of Texas at Arlington, November 17, 2011. (Turner) *Invited seminar*

9. “Coupled Photoanode/Photocathode Systems for Unassisted Solar Water Splitting” 2011 Materials Research Society Fall Meeting, Boston, Massachusetts. November 28 – December 2, 2011. (Deutsch) *Invited*

10. “Hydrogen Production from Photoelectrochemical Cells”, Physics@FOM Conference, Holland, January 17, 2012. (Turner) *Invited plenary*

11. “Frontiers, Opportunities and Challenges for a Hydrogen Economy”, International Energy and Sustainability Conference 2012, Farmingdale State College, March 22, 2012. (Turner) *Invited plenary*

12. “Semiconductor Systems for Solar Photoelectrolysis” Colorado School of Mines, April 27th, 2012. (Deutsch) *Invited seminar*

References

1. O. Khaselev and J.A. Turner, *Science* **280**, 425 (1998).

2. T.G. Deutsch, K.A. Koval, J.A. Turner, *J. Phys. Chem. B* **110**, 25297 (2006).

3. J.R. Mileham, S.J. Pearton, C.R. Abernathy, J.D. Mackenzie, R.J. Shul, S.P. Kilcoyne, *J. Vac. Sci. Technol. A* **14**, 836 (1996).

4. S. Shet, K.-S. Ahn, Y. Yan, T. Deutsch, K.M. Chrustowski, J. Turner, M. Al-Jassim, N. Ravindra, *J. Appl. Phys.* **103**, 073504 (2008).

II.F.3 Characterization and Optimization of Photoelectrode Surfaces for Solar-to-Chemical Fuel Conversion

Tadashi Ogitsu (Primary Contact), Woon Ih Choi,
Brandon Wood

Lawrence Livermore National Laboratory (LLNL)
7000 East Ave., L-413
Livermore, CA 94550
Phone: (925) 422-8511
Email: ogitsu@llnl.gov

DOE Manager
HQ: Eric Miller
Phone: (202) 586-5000
Email: Eric.Miller@ee.doe.gov

Project Start Date: March 1, 2010
Project End Date: Project continuation and direction
determined annually by DOE

Fiscal Year (FY) 2012 Objectives

- Develop theoretical tool chest for modeling photoelectrochemical (PEC) systems, including experimental validation using model III-V systems.
- Compile publications database of research on relevant photoelectrode materials.
- Uncover key mechanisms of surface corrosion of semiconductor photoelectrodes.
- Understand dynamics of water dissociation and hydrogen evolution at the water-photoelectrode interface.
- Evaluate electronic properties of the surface and water-electrode interface.
- Elucidate relationship between corrosion and catalysis.
- Provide simulated X-ray spectra to the University of Nevada, Las Vegas (UNLV) for interpretation of experimental results and validation of theoretical models.
- Share research insights with the PEC Working Group members.

Technical Barriers

This project addresses the following technical barriers from the Hydrogen Production section (3.1) of the Fuel Cell Technologies Program Multi-Year Research, Development and Demonstration Plan:

- (Z) Materials Durability
- (Y) Materials Efficiency

Technical Targets

This project is conducting fundamental theoretical studies of mechanisms of corrosion and catalysis in III-V semiconductor-based photoelectrode materials for PEC hydrogen production. Insights gained from these studies will be applied toward the optimization and design of semiconductor materials that meet the following DOE 2013 PEC hydrogen production targets:

- Usable semiconductor bandgap: 1.8-2.3 eV
- Chemical conversion process efficiency: 10%
- Plant solar-to-hydrogen efficiency: 8%
- Plant durability: 1,000 hrs.

FY 2012 Accomplishments

- Continued with compilation, review, and sharing of available information on III-V electrode materials, catalysts, and related subjects (ongoing).
- Performed quantum molecular dynamics of water-electrode interfaces:
 - Summarized studies on III-V surface morphology.
 - Published discussion of effect of surface oxidation and hydroxylation in a peer-reviewed journal.
- Investigated simple model Hamiltonian approach for feasibility of theoretical screening of co-catalysts.
- Group discussion of results pointed to supporting evidence for hole-trap corrosion mechanism, which is one of three possible corrosion mechanisms identified in FY 2011.
- Continued collaborations with unfunded external collaborators to develop theory/computational tool chest for PEC hydrogen research.
- Continued joint theoretical/experimental study on III-V electrode surface (continue through FY 2012 and beyond).



Introduction

Certain III-V based photoelectrochemical cells, notably the GaInP₂/GaAs tandem cell developed at the National Renewable Energy Laboratory (NREL), are known to demonstrate high solar-to-hydrogen conversion efficiencies that already exceed the DOE FY 2013 goal. However, durability of these cells has remained the key unresolved

issue so far. The primary purpose of this project is to perform a detailed investigation into the microscopic properties of the water-electrode interface, and to use this information to identify correlations with device performance, as measured in terms of solar-to-hydrogen conversion efficiency and corrosion resistance. The results will provide key feedback to collaborators at NREL, helping them develop a coherent performance optimization scheme for III-V based photoelectrodes. State-of-art X-ray spectroscopic measurements performed by the UNLV team will bridge remaining gaps in the knowledge obtained from our atomistic modeling, facilitating comparison with actual electrode properties. In FY 2012, we had four major accomplishments [1]. First, our findings on the surface morphology and its chemical properties were summarized and published in a peer-reviewed journal [2]. Second, key evidence that supports one of three corrosion mechanisms identified in FY 2011 was found. Third, we adapted and tested a simple model Hamiltonian-based method, which can be used to screen for good co-catalyst materials in a computationally efficient manner. Fourth, calculation procedures for X-ray absorption spectroscopy (XAS) and X-ray emission spectroscopy (XES) of phosphorous L-edge and nitrogen K-edge spectra were established, with preliminary results showing excellent agreement with experiments [3]. The last accomplishment is particularly significant in light of recent activity at NREL, which found that specific nitrogen surface treatments can improve the durability of GaInP₂ electrode beyond 1,000 hours [4]. The NREL results have motivated a shift in focus for FY 2013, during which we will investigate the chemical and physical state of nitrogen incorporated into the electrode surface, using both simulations and interpretation of the UNLV-generated X-ray spectroscopic measurements. The results will be used to provide feedback to NREL in order to optimize the nitrogen treatment process.

Approach

Further progress in semiconductor-based PEC photoelectrodes requires in-depth understanding of the complex relationship between surface stability and catalytic activity. This in turn relies on knowledge of the fundamental nature of the electrode-water interface, and of the chemical pathways explored during surface-active hydrogen evolution. As such, we are carrying out finite-temperature ab initio molecular dynamics simulations and energetics calculations based on density-functional theory to understand the chemical, structural, and electronic properties of water/electrode interfaces under equilibrium conditions, as well as to understand the competing chemical reaction pathways visited during photocatalysis. Our approach uses (001) surfaces of InP, GaP and GaInP₂, which have known water-splitting activity, as model semiconductor electrodes. We are investigating on effect of the foreign chemical species on the stability and reactivity of the electrode surfaces, as suggested

by our collaborators in J. Turner and T. Deutsch's group at NREL [5], as well as independent reports in the literature that surface oxygen may play a key role in motivating both the surface photocorrosion and the catalytic water splitting reaction [6,7]. Accordingly, we are evaluating the stability, structure and reactivity of the III-V(001)/water interfaces in the presence of surface oxygen, hydroxyl, and nitrogen, in order to correlate the results to experimentally observed surface compositions and morphologies. We also provide ab-initio derived X-ray spectroscopic data to enable direct comparison with experimental results from Prof. C. Heske's group at UNLV. This information is intended to suggest a strategy for device improvement.

Results

Over 800 papers related to PEC hydrogen research have been collected, indexed, and stored. Those deemed especially relevant to III-V semiconductor-based approaches have been summarized and shared with members of the III-V Surface Validation Team (LLNL/NREL/UNLV) of the DOE Photoelectrochemical Hydrogen Production Working Group using a limited-access community web forum and traditional email communication. Particular emphasis was put on GaInP₂, In₂O₃, and the growth interface between the two, since these are expected to be crucial for identifying the agent responsible for corrosion resistance and hydrogen evolution.

Detailed studies of InP and GaP (001) surfaces, and in particular, of the effect of surface oxide and hydroxyl on material properties, were summarized and published in a peer reviewed journal [2]. Specifically, the paper details the relationship between local atomic configurations, electronic structure, and chemical properties of these surfaces. Based on observations of general trends widely observed across various types of surface morphologies, we proposed that despite their structural and morphological complexity, the most important chemical properties of real electrode surfaces could be described by a simple local model. This represents a crucial development, as it allows us to dramatically simplify our models of real photoelectrode surfaces without loss of generality. The local bond-topological model also simplifies the calculation of X-ray spectra of the III-V photoelectrode surfaces, which are an important bridge that can connect the microscopic photoelectrode properties to actual measured device performance. Our paper also identified a few local atomic configurations whose specific electronic signatures point to a possible role in photocorrosion due to hole trapping. Notably, this hole trapping mechanism was one of the three possible mechanisms we identified in FY 2011.

During a PEC Working Group teleconference held in FY 2012, we proposed a "dark" current experiment, in which electrons are provided by the power source to the cathode rather than via photoillumination. This allows one to identify whether cathodic hole transport, which is relevant only in

the case of photoillumination where electrons and holes are co-generated, plays a role in the corrosion mechanism. If hole trapping is the major source of corrosion, the rate of corrosion should be greatly suppressed in a dark current experiment. We were able to determine that the NREL team had already conducted such experiments in 1998 (for an unrelated purpose) [8], and that they indeed observed a reduced rate of corrosion when applying current in the dark. This supports our assertion that the hole-trapping corrosion mechanism is the major contributor for III-V based photocathode. Developing a robust method to eliminate the hole-trap levels is the rational next step. One possibility would be to induce controlled growth of a high-quality surface oxide that avoids the local atomic configurations responsible for the hole trapping.

As was highlighted at the 2012 Annual Merit Review, T. Deutsch (NREL) has successfully shown that by using specific ion energies and durations, nitrogen bombardment of GaInP₂ surfaces can yield significant enhancements in durability, with one nitrogen-treated sample showing durability in excess of 1,000 hours. At this moment, the underlying mechanism of the enhanced durability is not understood. To this end, the spectroscopy team at UNLV recently performed a series of measurements (including XES) and found that the aforementioned sample showed a strong nitrogen-related peak with a shape indicating a unique but unidentifiable chemical environment. Simultaneously, at LLNL, we established the calculation procedures for P L_{2,3}-edge XAS (see Figure 1) and XES of GaP and InP [1], N K-edge of GaN. We anticipate that the information obtained from these analysis will allow us to properly interpret the measured spectra, which will be crucial in understanding the stabilization mechanism due to low energy nitrogen bombardment [5].

Finally, during FY 2012, we began investigating a new method for quickly screening the feasibility of candidate co-catalysts, based on a model Hamiltonian approach developed by Santos and others [9]. This method is based on Markus-Hush theory and the Anderson-Newns model,

and is able to simultaneously address H⁺ solvation, charge transfer reactions, and chemisorption very simply and with relatively low computational cost. In the original paper, it was demonstrated that the protonation of a Pt surface under bias could be described using this approach, yielding qualitatively correct descriptions of the free energy profile (indicative of exothermic, barrierless reaction) and of the barrier suppression mechanism (strong hybridization between Pt *d* and proton *s* levels). We have applied this method to examining protonation of a GaInP₂ surface under an applied bias potential and have confirmed that the model gives qualitatively correct behavior. In particular, we were able to properly predict protonation to be an exothermic reaction, with a large kinetic barrier that can be traced to poor hybridization between the proton and the GaInP₂ surface (see Figure 2). The fact that we are able to successfully discriminate between the free energy profile of a good catalyst (Pt) from a bad one (untreated GaInP₂ surface) indicates that the method may be used to efficiently screen candidate low-cost co-catalyst materials.

Conclusions and Future Directions

- The studies of surface chemistry and morphology performed during FY 2010 and FY 2011 were summarized and published in a peer-reviewed journal.
- Group discussions during a PEC Working Group teleconference led to finding evidence that specifically supports a hole-trapping mechanism as a major source of cathodic corrosion of III-V photoelectrodes.
- Computational procedures for accurate XAS/XES calculations for P L-edge, O K-edge, and N K-edge spectra were established.
- A simple model Hamiltonian approach to screen candidate co-catalysts was shown to be feasible.
- The compilation of past studies will continue in order to refine our growing understanding of the relevant issues of photoelectrochemistry, particularly with respect to III-V surfaces, their oxides, and interfaces between them.

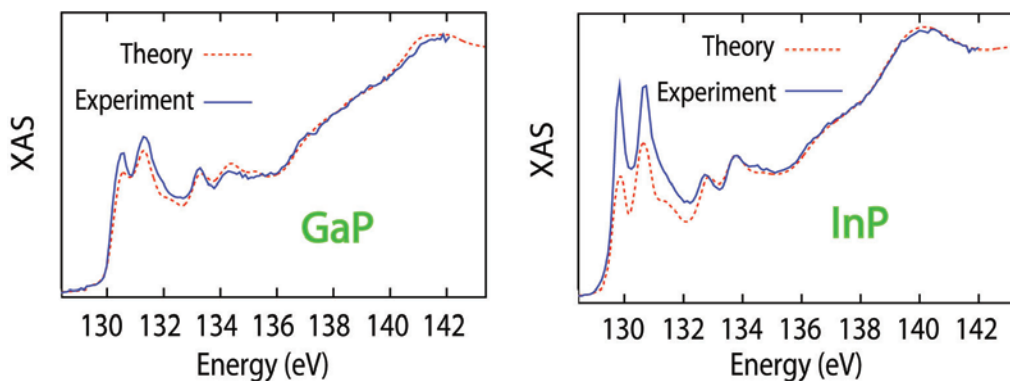


FIGURE 1. P L_{2,3}-edge XAS of bulk GaP and InP

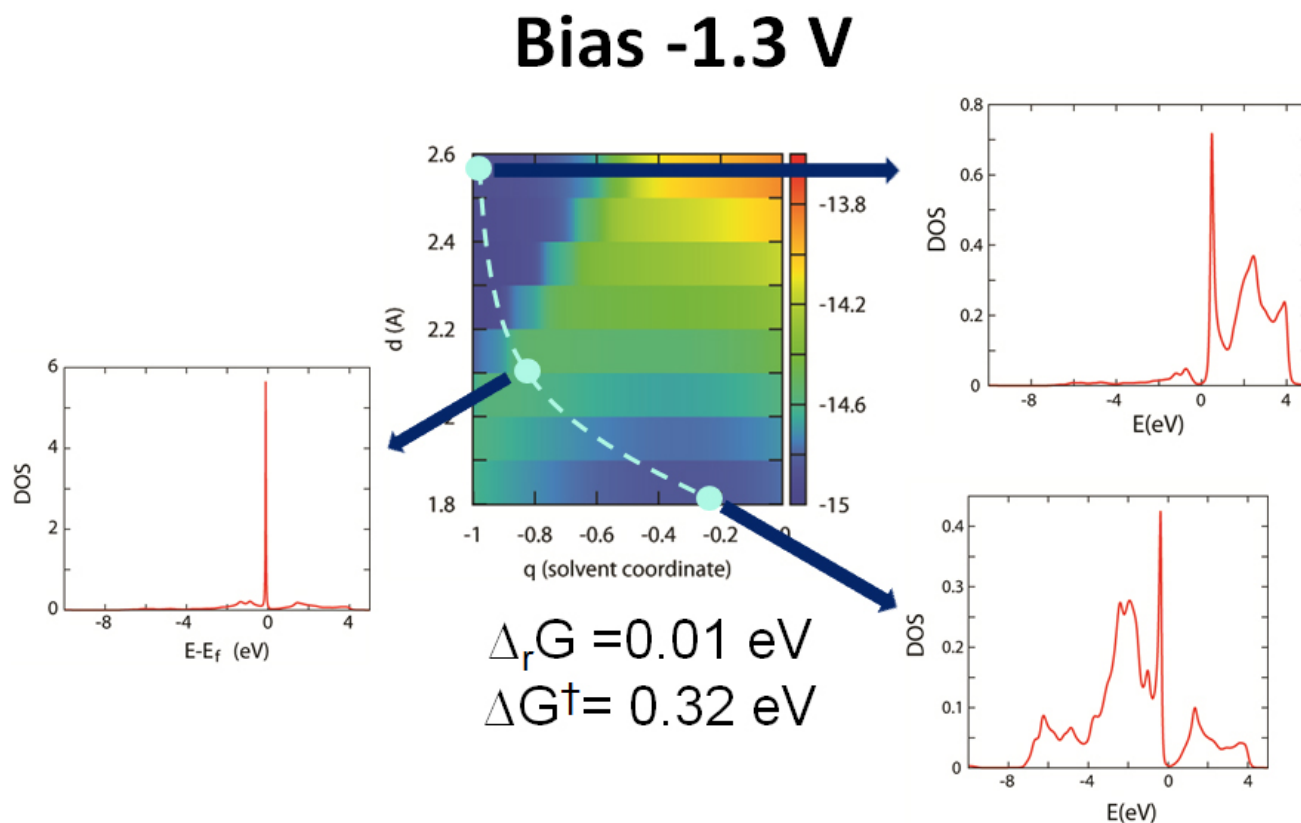


FIGURE 2. Free energy profile of protonation of GaInP₂ surface under a bias potential, calculated using the method described in reference [9]

- In FY 2013, our major focus will be to investigate on the state of nitrogen in nitrogen-bombarded GaInP₂. Successful identification of the optimal state of nitrogen will lead to improve durability of this electrode with minimal compromise of the solar-to-fuel conversion efficiency.
- We are currently summarizing the interface *ab initio* simulations performed in FY 2010-FY 2012 for publication in a high-profile peer-reviewed journal.

FY 2012 Publications/Presentations

Publications

1. T. Ogitsu, B. Wood, W. Choi, *DOE Fuel Cell Technology Hydrogen Program Annual Merit Review* (2012).
2. B. Wood, T. Ogitsu, and E. Schwegler, *J. Chem. Phys.* **136**, 064705 (2012).

Presentations

1. The Molecular Foundry Annual Users Meeting in Berkeley, Oct 2011.
2. 220th ECS meeting in Boston, Oct 2011.

3. Workshop for U.S.-Japan DOE-METI Collaboration on Clean Energy Technology Action Plan in Pleasanton, CA, in Feb. 2012.
4. American Physical Society March Meeting in Boston, March 2012 (two presentations).
5. 2012 Materials Research Society Spring Meeting in San Francisco, April 2012.
6. DOE EERE Fuel Cell Technology Annual Merit Review in Arlington, May 2012.
7. Materials Simulation in Petaflops era in Kashiwa, Japan, June-July 2012 (two invited talks).
8. 19th International Conference on Photoelectrochemical Conversion and Storage of Solar Energy at Caltech, July-Aug 2012 (two presentations).

References

1. T. Ogitsu, B. Wood, W. Choi, *DOE Fuel Cell Technology Hydrogen Program Annual Merit Review* (2012).
2. B. Wood, T. Ogitsu, and E. Schwegler, *J. Chem. Phys.* **136**, 064705 (2012).
3. C. Heske *et al.*, *DOE Fuel Cell Technology Hydrogen Program Annual Merit Review* (2012).
4. T. Deutsch *et al.*, *DOE Fuel Cell Technology Hydrogen Program Annual Merit Review* (2012).

5. T.G. Deutsch, C.A. Koval, and J.A. Turner, *J. Phys. Chem. B* **110**, 25297 (2006).

6. A. Heller, *Science* **223**, 1141 (1984).

7. J. Vigneron, M. Herlem, E. M. Khoumri, and A. Etcheberry, *Appl. Surf. Sci.* **201**, 51 (2002).

8. T. Deutsch, C. Koval, and J. Turner, *J. Electrochem. Soc.* **145**, 3335 (1998).

9. E. Santos *et al.*, *Phys. Rev. B* **79**, 235436 (2009).

II.F.4 Characterization of Materials for Photoelectrochemical (PEC) Hydrogen Production

Clemens Heske
Department of Chemistry
University of Nevada, Las Vegas
4505 S. Maryland Parkway
Las Vegas, NV 89154-4003
Phone: (702) 895-2694
Email: heske@unlv.nevada.edu

DOE Manager
HQ: Eric Miller
Phone: (202) 287-5829
Email: Eric.Miller@hq.doe.gov

Project Start Date: November 4, 2011
Project End Date: September 30, 2012

- Aid the collaboration partners in the development and modification of novel candidate materials.
- Monitor deliberately introduced modifications of PEC candidate materials in view of the electronic and chemical structure.

FY 2012 Accomplishments

- Performed non-invasive cleaning procedure using low-energy Ar⁺ ion treatment on an air-exposed GaInP₂ film, removing all surface C and most surface O. This process allows determination of the true surface electronic structure including the electronic surface band gap, band edge energies, and the work function.
- Worked with collaborators at NREL to reduce ambient-air-related surface adsorbates to preserve the relevant surfaces for water splitting. Achieved a dramatic reduction in the amount of surface contaminants.
- Used synchrotron-based N K X-ray emission spectroscopy (XES) to determine both the relative amount and the chemical environment of N-treated GaInP₂ films to elucidate differences between effective and ineffective treatments.
- Found good agreement of experimental and theoretical X-ray absorption spectroscopy (XAS) in GaP and InP, in close collaboration with our partners at LLNL.
- In situ gas cell for XES/XAS studies was tested and is operational, a liquid/solid interface electrochemical cell is in development.

Fiscal Year (FY) 2012 Objectives

Enhance the understanding of PEC materials and interfaces and promote break-through discoveries by:

- Utilizing and developing cutting-edge soft X-ray and electron spectroscopy characterization.
- Determining electronic and chemical structures of PEC candidate materials.
- Addressing materials performance, materials lifetime, and capital costs through close collaboration with the National Renewable Energy Laboratory (NREL) and other partners from the PEC working group.

Technical Barriers

This project addresses the following technical barriers from the Production section of the Fuel Cell Technologies Program Multi-Year Research, Development and Demonstration Plan:

- (Y) Materials Efficiency
- (Z) Materials Durability
- (AA) PEC Device and System Auxiliary Material

Technical Targets

- Collaborate closely with partners at NREL, Lawrence Livermore National Laboratory (LLNL), and others within the DOE PEC working group to determine the electronic and chemical structure of candidate materials for solar water splitting.



Introduction

This project is embedded into the Department of Energy's efforts to develop materials for PEC water splitting. If successful, PEC will provide an important route to convert the energy supplied by solar irradiation into a transportable fuel. In order to achieve this goal, suitable materials need to be developed that simultaneously fulfill several requirements, among them chemical stability and optimized electronic structure, both for absorption of the solar spectrum and for electrochemical water splitting at a solid/electrolyte interface. This project experimentally derives the chemical and electronic structure information to (a) judge the suitability of a candidate material, (b) show pathways towards a deliberate optimization of a specific material, and (c) monitor whether deliberate modifications of the material indeed lead to the desired changes in electronic and chemical structure.

Approach

A unique “tool chest” of experimental techniques is utilized that allows addressing all technical barriers related to electronic and chemical properties of various candidate materials. With these techniques, it is possible to derive surface and bulk band gaps, the energy level alignment at interfaces, the chemical stability of the materials, and the impact of alloying and doping.

The tool chest includes photoelectron spectroscopy with X-ray (XPS [1]) and ultraviolet photoelectron spectroscopy (UPS) excitation to determine the occupied electronic states (core levels and valence electrons), and inverse photoemission spectroscopy (IPES) to determine the unoccupied electronic states. These techniques, performed in the lab at UNLV, are surface-sensitive and allow a detailed determination of the electronic and chemical surface structure. They are complemented by XES and XAS spectroscopy, performed at Beamline 8.0 of the Advanced Light Source, Lawrence Berkeley National Laboratory. XES and XAS also probe the occupied and unoccupied electronic states, but with an increased information depth. Furthermore, they also give insight into the chemical structure, again complementary to the electron-based techniques performed in the lab at UNLV.

Results

In collaboration with our partners at NREL (T. Deutsch, A. Welch, and J. Turner), we have conducted an investigation of GaInP₂ thin film surfaces. Results were immediately shared with the collaboration partners and discussed in detail through PowerPoint presentations, at phone conferences, and working group meetings. Among the multitude of data obtained, this report focuses on the ion treatment and other methods to remove or reduce surface contamination, so that the underlying electronic structure of the “true” GaInP₂ surface can be determined and used as a benchmark for the study of surfaces exposed to controlled environments (including air, oxygen, and water/electrolyte). Further results, including the N K XES spectra and the comparisons of experimental and theoretical XAS spectra for GaP and InP, are shown in the annual review presentation (the theoretical work was performed by our partners at LLNL).

The surface sensitivity of XPS implies that small amounts of C and O at the surface can have a large effect on the apparent (as-measured) electronic structure (i.e., surface adsorbates attenuate the underlying relevant electronic structure of GaInP₂). Therefore, a low-energy (50 eV) Ar⁺ ion treatment series was performed to remove these contaminants without altering the GaInP₂ surface, thereby revealing the relevant electronic structure of the active PEC material. Note that this treatment is quite different from conventional “sputter-cleaning”, in which significantly higher ion energies (500 to 5,000 eV) have to be used.

Table 1 lists the exposure times for each treatment (as well as the cumulative treatment time) of this series.

TABLE 1. Exposure Times for Each Low-Energy Ion Treatment

| Treatment Number | Length of Time Under 50 eV Ar ⁺ Ion Treatment | Cumulative Time Under 50 eV Ar ⁺ Ion Treatment |
|------------------|--|---|
| As Received | 0 | 0 |
| 1 | 15 minutes | 15 minutes |
| 2 | 30 minutes | 45 minutes |
| 3 | 30 minutes | 75 minutes |
| 4 | 1 hour | 135 minutes |
| 5 | 2 hours | 255 minutes |
| 6 | 2 hours | 375 minutes |
| 7 | 2 hours | 495 minutes |
| 8 | 4 hours, 30 minutes | 765 minutes |

As a first step, we examine the Mg K_α XPS survey spectra for this ion-treatment series, as shown in Figure 1. The spectra are normalized to the same background and offset for visibility. Most notable here is the increase of the various Ga, In, and P signals, while both C and O decrease as a function of treatment time. The surface contaminants are clearly being removed, and no longer attenuating the signal from the underlying film of interest.

Further surface analysis is based on selected detail spectra, as displayed in Figure 2. In the O 1s region, we note that the O signal does not simply decrease with increasing ion treatments, but also shifts toward lower binding energy. This change is likely the result of two separate O species on the film, one of which is both more abundant and more

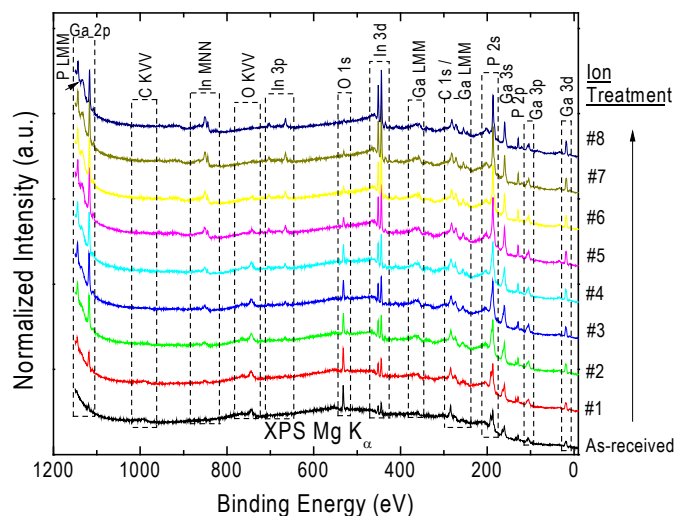


FIGURE 1. XPS Mg K_α survey spectra of a single GaInP₂ thin film sample after various low-energy Ar⁺ ion treatment steps, as listed in Table 1. Spectra were normalized to the background and offset for visibility.

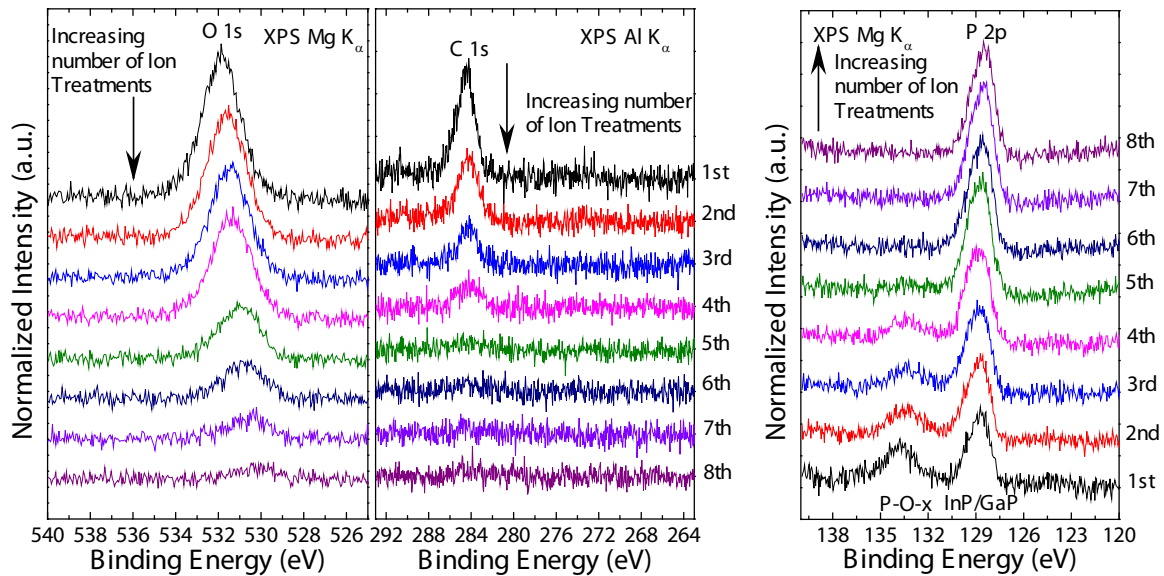


FIGURE 2. XPS detail spectra of the O 1s ($Mg K_{\alpha}$), C 1s ($Al K_{\alpha}$) and P 2p ($Mg K_{\alpha}$) regions of the $GaInP_2$ thin film during the low-energy Ar^+ ion treatment. Spectra were normalized to the background and offset for visibility. Changes in the spectra mirror the surface concentrations of the respective species.

easily removed with ion treatment. The O signal is not fully removed, in contrast to the C signal, which becomes indistinguishable from the background starting at the 5th treatment step. The P 2p spectra clearly show two different P species, one associated with the $GaInP_2$ film (~ 128 eV) and one at higher binding energy (~ 134 eV) with a surface oxide that is removed with ion treatment.

One of the most powerful and unique abilities in our “tool chest” is the use of UPS to measure the valence band and the use of IPES to derive the corresponding information for the conduction band [2]. These two techniques can be combined to determine the electronic surface band gap, as shown in Figure 3. Simultaneous optimization of the two band edge positions (with respect to the Fermi energy) and the band gap is essential for PEC materials - all three can be derived from these measurements and are indicated with vertical lines (for the band edges) and numerical values (for the band gap) in Figure 3. The band gap narrows with successive ion treatments, largely due to the valence band maximum shifting towards the Fermi energy with treatment time. Since the bulk band gap for $GaInP_2$ is 1.75 eV, as compared to the final electronic surface band gap of 1.31 eV, we ascribe this difference to an ion-induced modification of the electronic surface structure (beyond the simple removal of surface adsorbates), which strongly indicates the need for optimal surface preservation between growth and characterization, so that the need for additional surface cleaning steps is minimized.

We have thus worked with our collaborators at NREL to eliminate air exposure of the $GaInP_2$ films between growth and characterization. For this purpose, John Geisz and Waldo

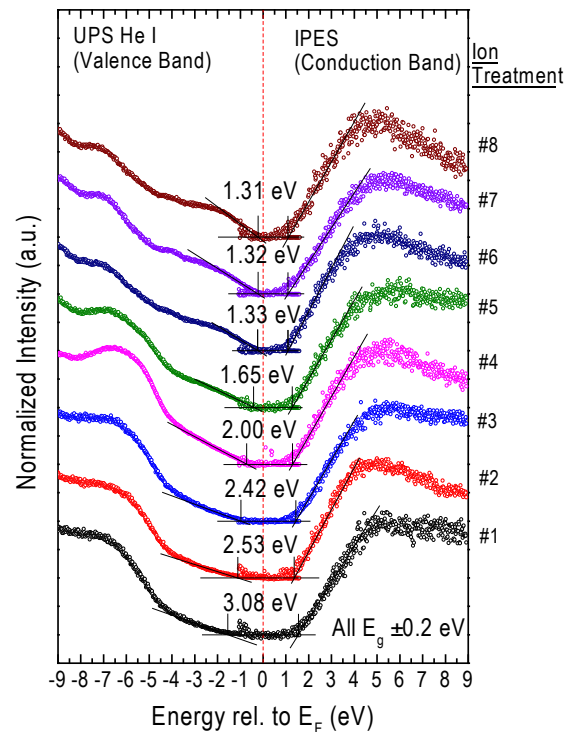


FIGURE 3. UPS (left) and IPES (right) of the $GaInP_2$ thin film during low-energy Ar^+ ion treatment. Both spectra were calibrated to the Fermi energy of a Au reference sample to align energy scales. Drawn lines indicate either the valence band maximum (UPS) or conduction band minimum (IPES) and are used to determine the band gap.

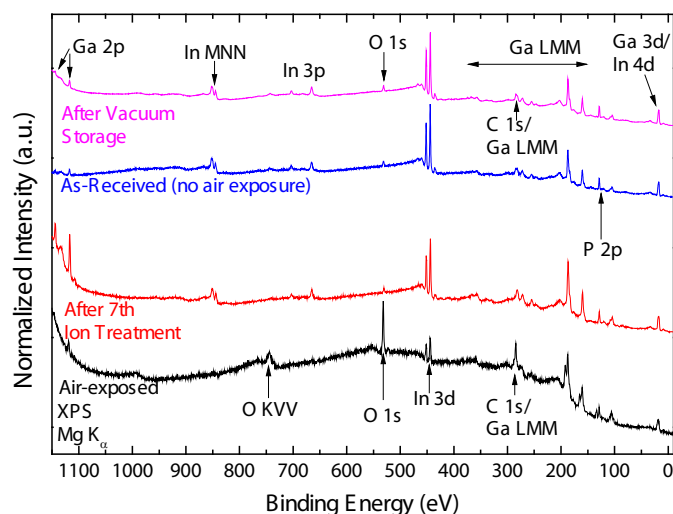


FIGURE 4. XPS Mg K_{α} survey spectra of two GaInP₂ thin films with modified sample handling. The first film is shown before (black) and after (red) low-energy Ar⁺ ion treatment while the second is shown as received (blue) and after storage in UHV (magenta).

Olavaria (NREL) attached an N₂-purged glove bag to their synthesis reactor and removed the sample into this glove bag where it was packaged using a vacuum seal device. At UNLV, the package was opened in a N₂ glove box and introduced to ultra-high vacuum (UHV) for analysis.

While the analysis of this sample is still ongoing, Figure 4 demonstrates the effectiveness of this change in sample handling. Mg K_{α} XPS survey spectra are shown for the above-discussed ion-treated sample, both as-received and after the 7th ion-treatment step, while the newer sample is plotted as-received and after a few weeks of storage in UHV. The differences in the films are most apparent for the significantly reduced C 1s (~285 eV) and O 1s (~530 eV) signals and the significantly increased In and Ga signals (comparable to those after the 7th ion treatment). We expect this cleaner starting point to allow us to reach our goal of measuring the “benchmark” electronic structure of GaInP₂ films.

Conclusions and Future Directions

Conclusions

- Successfully maintained operations of our multi-chamber UHV spectroscopy.
- Conducted experiments with our partners at NREL and select partners of the DOE PEC working group, in particular focusing on the establishment of suitable surface-cleaning procedures of GaInP₂ thin films and the analysis of their electronic and chemical surface properties.

- Conducted experiment-theory comparisons of XAS spectra of GaP and InP, together with our theory partners at LLNL.
- In situ gas cell tested and operational, liquid/solid interface electrochemical cell for XES/XAS studies in development.

Future Directions

- We will determine the benchmark electronic and chemical properties of GaInP₂ thin film surfaces as a baseline and will study the impact of controlled surface exposures (air, oxygen, water/electrolyte) on these characteristics.
- We will further correlate our results with theoretical calculations from our partners at LLNL, extending these activities to XES measurements as well.
- We will continue our development of a liquid/solid interface electrochemical cell for XES/XAS studies.

FY 2012 Publications/Presentations

1. “What electronic structure should a PEC device have (and can we measure it)?”, C. Heske, SPIE Optics & Photonics Conference, San Diego, August 12–16, 2012 (invited oral).
2. “Electronic surface structure of GaInP₂ Thin Films used for Photoelectrochemical Water Splitting”, K. George, M. Weir, S. Krause, I. Tran, K. Horsley, M. Blum, L. Weinhardt, C. Heske, T. Deutsch, J. Turner, T. Ogitsu, B. Wood, R. Wilks, M. Baer, and W. Yang, Symposium on Materials for Catalysis in Energy, Materials Research Society Spring Meeting, April 2012 (contributed oral).
3. “Passivation of Photoelectrochemical Water Splitting Electrodes Based on III-V Compound Semiconductors via Surface Nitridation”, T. Deutsch, A. Welch, A. Lindeman, M. Baer, L. Weinhardt, M. Weir, K. George, C. Heske, and J. Turner, Symposium on Materials for Catalysis in Energy, Materials Research Society Spring Meeting, April 2012 (contributed oral).
4. “Using soft x-rays to look into (buried) interfaces of energy conversion devices”, C. Heske, Department of Physics, Northern Arizona University, February 28, 2012 (invited oral).
5. “Spektroskopie der elektronischen Struktur von Grenzflächen in Solar- und anderen Zellen”, C. Heske, Zentrum für Sonnenenergie- und Wasserstoff-Forschung Baden-Württemberg (ZSW), Stuttgart, February 15, 2012 (invited oral).
6. “How can a synchrotron help to make solar devices better?”, C. Heske, Institute for Chemical Technology and Polymer Chemistry (ITCP), Karlsruhe Institute of Technology (KIT), Nov. 25, 2011 (invited oral).
7. “Wie man mit weicher Röntgenstrahlung die lokale chemische Umgebung ausspäht”, C. Heske, Institute for Technical Chemistry - Thermal Waste Treatment Division (ITC-TAB), Karlsruhe Institute of Technology (KIT), Nov. 23, 2011 (invited oral).

References

1. D. Briggs and M. P. Seah, *Practical Surface Analysis*, John Wiley and Sons, Chichester, 1990.
2. M. Baer, L. Weinhardt, B. Marsen, B. Cole, N. Gaillard, E. Miller, and C. Heske, *Appl. Phys. Lett.* **96**, 032107 (2010).
3. M. Baer, S. Nishiwaki, L. Weinhardt, S. Pookpanratana, O. Fuchs, M. Blum, W. Yang, J.D. Denlinger, W.N. Shafarman, and C. Heske, *Appl. Phys. Lett.* **93**, 244103 (2008).

II.F.5 Photoelectrochemical Hydrogen Production

Arun Madan

MVSystems, Incorporated (MVS)
500 Corporate Circle, Suite L
Golden, CO 80401
Phone: (303) 271-9907
Email: ArunMadan@aol.com or
amadan@mvsystemsinc.com

DOE Managers

HQ: Eric Miller
Phone: (202) 287-5829
Email: Eric.Miller@ee.doe.gov

GO: David Peterson
Phone: (720) 356-1747
Email: David.Peterson@go.doe.gov

Contract Number: DE-FC36-07GO17105, A00

Subcontractor:

University of Hawaii at Manoa (UH), Honolulu, HI

Project Start Date: September 1, 2007

Project End Date: December 31, 2012

Fiscal Year (FY) 2012 Objectives

- Work closely with the DOE Working Group on Photoelectrochemical (PEC) Hydrogen Production for optimizing PEC materials and devices.
- Develop new PEC film materials compatible with high-efficiency, low-cost hydrogen production devices.
- Demonstrate functional multi-junction device incorporating materials developed.
- Explore avenues toward manufacture-scaled devices and systems.

Technical Barriers

This project addresses the following technical barriers from the Photoelectrochemical Hydrogen Production section of the Fuel Cell Technologies Program Multi-year Research, Development and Demonstration Plan:

- (Y) Materials Efficiency
- (Z) Materials Durability
- (AA) PEC Device and System Auxiliary Material
- (AB) Bulk Materials Synthesis
- (AC) Device Configuration Designs

Technical Targets

Table 1 lists the technical targets for PEC hydrogen production using amorphous silicon carbide-compound (a-SiC), metal oxide-compound (i.e. WO_3) and I-III-VI₂ (copper chalcopyrite-based) films.

FY 2012 Accomplishments

1. Improvement in performance of the hybrid photovoltaic (PV)/a-SiC device:
 - Increase of photocurrent density up to 2 mA/cm², or equivalent solar-to-hydrogen efficiency (STH) of ~2.5%, by surface modification using Ru nanoparticles.
2. Improvement in performance of the metal oxide photoelectrode, including:
 - Durability of WO_3 (tungsten oxide) sputtered material has been improved to 600 hrs.
 - Photocurrent density in copper tungsten oxide (CuWO_4 , 2.2 eV) is increased to ~1.2 mA/cm² @1 V (V vs. saturated calomel electrode), an order of magnitude higher than in 2011.
 - Bifacial monolithic integration is demonstrated.
3. Improvement in performance of the I-III-VI₂ photoelectrode, including:
 - Novel coplanar hybrid device achieved 3.53 mA/cm² (or 4.34% STH efficiency).
 - Durability of CuGaSe_2 PEC cell is increased to 420 hrs.
 - Device design pathway developed to quantify material development goals to obtain 10% and 20% STH efficiency.



Introduction

Based on its potential to meet long-term goals, research and development (R&D) centering on multi-junction hybrid photoelectrode technology defines the scope of this collaborative project. Within this scope, particular emphasis is put in the development of low-cost photoactive materials integrated with a-Si-based solar cells as a driving force with photocurrents greater than 4 mA/cm², and with sufficient durability to meet lifetime requirement, i.e., ≥500 hours. In addition to the materials R&D activities, development of laboratory-scale demonstration devices and generation of preliminary energy/economic analysis for hydrogen

TABLE 1. Technical Targets

| Task # | Milestone | a-SiC | WO ₃ | I-III-VI ₂ |
|---|--|--------------|-----------------|-----------------------|
| Year 1 | Material photocurrent ≥ 3 mA/cm ² | Achieved | Achieved | Achieved |
| | Durability ≥ 100 hr | Achieved | Achieved | 10% Achieved |
| Year 2 | Material photocurrent ≥ 4 mA/cm ² | Achieved | 90% Achieved | Achieved |
| | Durability ≥ 200 hr | Achieved | Achieved | Achieved |
| | Device STH efficiency $\geq 5\%$ | 32% Achieved | 60% Achieved | 62% Achieved |
| Passed Go/No-Go decision evaluation in November, 2010 | | | | |
| Year 3* | Device STH efficiency $\geq 5\%$ | 32% Achieved | 60% Achieved | 85% Achieved |
| | Durability ≥ 300 hr | Achieved | 83% Achieved | 66% Achieved |
| Year 4 | Device STH efficiency $\geq 5\%$ | 50% Achieved | 60% Achieved | 87% Achieved |
| | Durability ≥ 500 hr | 62% Achieved | Achieved | 84% Achieved |
| | Completion of Final Energy/ Economics report on scale up and commercialization toward a \$22/kg-H ₂ plant production cost | | | |

* As of writing this report.

production cost based on the developed PEC technology is included in the project scope as second-level priorities. To support the device-demonstration activities, appropriate auxiliary components are being developed for incorporation in PEC photoelectrode designs, including attention to the necessary process integration techniques.

Approach

The general approach of this collaborative effort focuses on the DOE PEC Working Group's "feedback" philosophy integrating state-of-the-art theoretical, synthesis and analytical techniques to identify and develop the most promising materials classes to meet the PEC challenges in efficiency, stability and cost. Materials modeling, bulk-film optimization, film-surface enhancement, along with comprehensive material and device characterization is being employed to facilitate the R&D process. Specifically, the feedback approach is being applied to our focus material classes, including the metal oxide, copper-chalcopyrite- and silicon-based compounds, to enhance understanding of fundamental performance parameters, and expedite development of process-compatible forms of these materials. The most promising candidate materials are being identified, with the short-term goal of demonstrating laboratory-scale water-splitting devices, and with a long-term goal of transferring the fabrication processes toward the commercial scale.

Results

During this reporting period (June 2011–June 2012), extensive studies of the three materials classes under investigation have focused on understanding and improving PEC behavior, specifically by applying our theoretical,

synthesis and analytical techniques in identifying relevant aspects of structural, optoelectronic and electrochemical properties.

1. Amorphous Silicon Carbide-Based Compound Films

The surface barrier at a-SiC/electrolyte interface impedes photocurrent to be extracted from the hybrid PV/a-SiC device. In order to reduce the surface barrier, surface modification using Ru nanoparticle was performed. The Ru nanoparticle catalyst was fabricated at University of Hawaii by sputtering technique. It was observed that the sputter time of 10-20 sec gave best treatment results. The Ru-coated hybrid PV/a-SiC device is of configuration of SnO₂/pin/pin/a-SiC(p)/a-SiC(i)/Ru. Prior to Ru deposition, SiO₂ on a-SiC(i) surface was removed in 5% hydrofluorhydric acid solution for 90 sec. The current density vs. potential characteristics were measured in pH2 buffer electrolyte and in 2-electrode setup using a RuO₂ counter electrode. The illumination intensity conformed with AM1.5G spectrum. The 2-electrode current-voltage characteristics obtained before and after Ru nanoparticle treatment are shown in Figure 1. It was observed that such treatment led to a systematic photocurrent density increase, up to 2 mA/cm² without bias. Also, measurement after the durability test showed that the current density recovered to nearly its original value. Subsequent illuminated open-circuit potential measurements confirmed the anodic flat band potential shift of ca. 500 mV, an ideal situation for photocathode systems. Improvement was also confirmed by the National Renewable Energy Laboratory with outdoor test conditions.

2. Oxide Mineral-Based Compound Films

With an electronic band-gap of 2.2 eV and more favorable surface energetics for water splitting than most

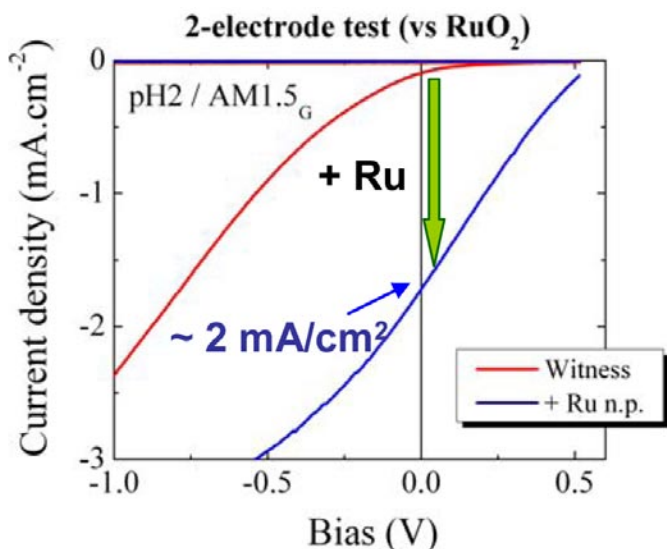


FIGURE 1. The 2-electrode current density-potential characteristics in pH2 buffer solution on hybrid devices

oxide systems (i.e. WO_3 , TiO_2 , Fe_2O_3), copper tungstate (CuWO_4) is a material-class that merits further investigation. We reported last year on the effect of thermal treatment on the crystallographic, surface energetics and PEC properties of reactively co-sputtered CuWO_4 . A major improvement was observed on CuWO_4 films after a post-annealing at 500°C in argon for 8 hours, exhibiting a photocurrent density of approx. $400 \mu\text{A}/\text{cm}^2$ at 1.6 V vs. saturated calomel electrode. More importantly, electrochemical impedance spectroscopy study indicated that CuWO_4 transport properties must be improved in order to achieve better performing photoanodes. This issue was addressed this year by adding conductive carbon nanotubes (CNTs) directly into the matrix of CuWO_4 photoanodes. To do so, CuWO_4 -CNT nanocomposites were obtained via spray pyrolysis deposition process using a solution containing all building blocks (i.e. Cu, W precursors and CNT) required to fabricate this unique system (Figure 2).

Subsequent current-voltage characteristics pointed out a net improvement in photocurrent generation, with a maximum current density of c.a. $1 \text{ mA}/\text{cm}^2$. This corresponds to a doubling of the photocurrent density when compared with CuWO_4 witness samples.

3. I-III-VI₂ (Copper Chalcopyrite-Based) Films

The largest technical barrier in this material class is a misalignment of the energy band levels in the semiconductor-electrolyte interface in the baseline material CuGaSe_2 with a relatively low bandgap of 1.65 eV. This makes monolithic integration with PV driving devices difficult, and the misaligned band levels result in a high required voltage bias from PV cells. Material development is focused on modifying the group I (Cu, Ag) to group VI (S, Se) bond to

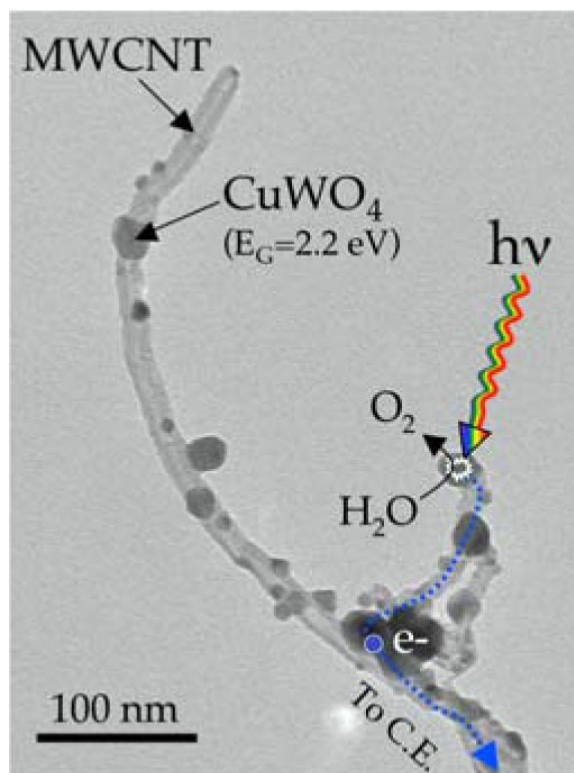


FIGURE 2. Micrograph of a CuWO_4 -CNT nanocomposite used for PEC hydrogen production

more favorably align the energy levels and raise the bandgap. The validation of the novel coplanar device achieving 4.34% STH efficiency using low-cost a-Si PV cells lays out a design pathway towards DOE project goals. The coplanar device cannot achieve much more than 5% STH, and so material advances are needed to allow bandgaps closer to the ideal bandgap of 2.0-2.1 eV. With the addition of either silver or sulfur to raise the bandgap to $\sim 1.8 \text{ eV}$, one PV cell can be buried beneath it and required voltage bias should be reduced, allowing performance beyond the 5% STH threshold. Further raising the bandgap (towards 2.1 eV) will allow a second PV cell to be buried and can potentially extend performance beyond the 20% STH range. Current durability success with CuGaSe_2 achieving 420 hrs of continuous operation at $4 \text{ mA}/\text{cm}^2$ is very promising. Surface treatments of nano- and micro-scale catalysts are being explored to further extend durability towards 1,000 hrs. These same catalytic treatments are, of course, also expected to improve device performance.

Conclusions and Future Directions

Surface treatment of the hybrid PV/a-SiC device using Ru nanoparticles was found to reduce the photocurrent onset and enhance photocurrent up to $\sim 2 \text{ mA}/\text{cm}^2$ at zero potential. In metal oxide-based compound such as CuWO_4 , the post-deposition annealing improves its conductivity and

photo-response while the bandgap remains unchanged (2.1 eV). Finally, a STH efficiency of ~4.3% is achieved in the novel co-planar integrated a-Si (PV)/CuGaSe₂ (PEC) device. Incorporation of Ag and/or S in baseline CuGaSe₂ cells remains the highest priority in the I-III-VI₂ material class to achieve >5% STH efficiency and beyond. The hybrid PV/a-SiC device, and other two-photoelectrode thin film materials (WO₃ and Copper Chalcopyrite) show excellent durability in electrolyte for ≥200 hours.

FY 2012 Publications/Presentations

1. Nicolas Gaillard, Yuancheng Chang, Artur Braun and Alexander DeAngelis, Copper Tungstate (CuWO₄)–Based Materials for Photoelectrochemical Hydrogen Production, 2012 MRS Spring Meeting, mrss12-1446-u02-08.
2. Yuancheng Chang, Artur Braun, Alexander Deangelis, Jess Kaneshiro, and Nicolas Gaillard, Effect of Thermal Treatment on the Crystallographic, Surface Energetics, and Photoelectrochemical Properties of Reactively Cosputtered Copper Tungstate for Water Splitting, *J. Phys. Chem. C*, 25490–25495, DOI: 10.1021/jp207341v (2011).
3. J.M. Kaneshiro, A. Deangelis, X. Song, N. Gaillard and E.L. Miller “I-III-VI₂ (Copper Chalcopyrite-based) Thin Films for Photoelectrochemical Water-Splitting Tandem-Hybrid Photocathode) MRS Proceedings 1324 (2011) mrss11-1324-d15-08 doi:10.1557/opl.2011.964.
4. J. Kaneshiro, Dissertation Thesis, University of Hawai‘i at Mānoa, 2012.
5. PHOTOELECTROCHEMICAL HYDROGEN PRODUCTION, 2012’ DOE H₂ Annual Merit Review meetings, Washington, D.C., May 13, 2012 (presented by Jian Hu and Nicolas Gaillard).

II.F.6 Critical Research for Cost-Effective Photoelectrochemical Production of Hydrogen

Liwei Xu (Primary Contact)¹, Anke E. Abken²,
William B. Ingler³, John Turner⁴

¹Midwest Optoelectronics LLC (MWOE)
2801 W. Bancroft Street
Mail Stop 230
Toledo, OH 43606
Phone: (419) 215-8583
Email: xu@mwoe.com

²Xunlight Corporation (Xunlight)

³University of Toledo, Toledo, OH (UT)

⁴National Renewable Energy Laboratory, Golden, CO (NREL)

DOE Managers

HQ: Eric Miller
Phone: (202) 287-5829
Email: Eric.Miller@ee.doe.gov

GO: David Peterson
Phone: (720) 356-1747
Email: David.Peterson@go.doe.gov

Contract Number: DE-FG36-05GO15028

Subcontractors:

- Xunlight Corporation, Toledo, OH
- University of Toledo, Toledo, OH
- National Renewable Energy Laboratory, Golden, CO

Project Start Date: April 1, 2005

Project End Date: June 30, 2013

- Two approaches are taken for the development of efficient and durable photoelectrochemical (PEC) cells:
 - An immersion-type PEC cell in which the photoelectrode is immersed in electrolyte.
 - A substrate-type PEC cell in which the photoelectrode is not in direct contact with electrolyte.

Technical Barriers

This project addresses the following technical barriers from the Photoelectrochemical Hydrogen Production section (3.1.4) of the Fuel Cell Technologies Program Multi-Year Research, Development and Demonstration Plan (MYPP):

- (Y) Materials Efficiency
- (Z) Materials Durability
- (AA) PEC Device and System Auxiliary Material
- (AC) Device Configuration Designs
- (AD) Systems Design and Evaluation

Technical Targets

This project focuses on the development of photoelectrode materials and triple junction tf-Si-based PEC cells required to achieve or exceed DOE's technical targets. The status of this project towards the DOE MYPP objective for PEC production of hydrogen for 2013 is:

Accomplishments

- TCCR coatings were developed (Task 1).
 - After extensive study of many different types of material classes for TCCR application, cobalt oxide has been identified as the major material class of

Objectives

- To develop critical technologies required for cost-effective production of hydrogen from sunlight and water using thin film (tf)-Si based photoelectrodes.

TABLE 1. Progress towards Meeting Technical Targets for Immersion-Type PEC Cells and Systems

| DOE Barriers | Performance Measure | Units | DOE 2013 Targets | 2010 Go/No-Go | MWOE current Status |
|-------------------------|------------------------------------|-----------------|--------------------|---------------|--|
| Y. Materials Efficiency | Solar-to-Hydrogen (STH) efficiency | % Efficiency | 8 | N/A | 4.0 (immersion-type) |
| Z. Materials Durability | Durability | Hours | ≥1,000 | ≥700 | 1,000 (Co ₃ O ₄) 330 (PEC) |
| | Cost | gge | \$2-3 | N/A | TBD |
| | Deposition temperature | °C | ≤250 (MWOE Target) | ≤300 | 200 |
| | Transparency of TCCR | % Trans-mission | ≥90 (MWOE Target) | ≥85 | 95 |
| | Voltage drop across TCCR layer | V | ≤0.15 | ≤0.35 | 0.086 |

gge = gasoline gallon equivalent; TCCR = transparent, conducting and corrosion resistant; TBD = to be determined

study, moving into the Phase Two of the project period.

- $\text{In}_2\text{O}_3\text{-Co}_3\text{O}_4$ has also shown promising results, will be optimized for TCCR performance.
- Successfully transferred the results from the lab to the prototype roll-to-roll production machine to deposit cobalt oxide film on large area a-Si triple junction cells. The PEC electrodes with cobalt oxide coating have been used to build the immersion-type PEC systems (Task 1 and 4).
- Have achieved 4.1% initial solar to hydrogen conversion efficiency and over 330 hours life time for immersion type PEC cells (Task 3).
- Various immersion-type PEC module designs have been built to optimize the STH conversion efficiency, to extend the lifetime and reduce the cost. Reasonable STH efficiency has been obtained and further improvements are under way (Task 4).
- Worked with Dr. Nocera's group at the Massachusetts Institute of Technology and Sun Catalytix on solar water splitting project, by providing triple junction a-Si solar cells. Their research results were published in Science Magazine and were selected as one of Top 50 Innovations of Year 2011 by Time Magazine ("Artificial Leaf") (Task 4).



Introduction

In this project, MWOE and its subcontractors are jointly developing the critical technologies for cost-effective production of hydrogen from sunlight and water using tf-Si-based photoelectrodes. These tf-Si based electrodes include triple junction cells with either amorphous silicon germanium alloy (a-SiGe) or microcrystalline silicon ($\mu\text{-Si}$) as the narrow band gap absorber material.

In this project two separate approaches have been pursued for the development of immersion- and substrate-type PEC photoelectrodes:

- In one approach, triple-junction tf-Si based photoelectrodes (a-Si/a-SiGe/a-SiGe or a-Si/a-SiGe/ $\mu\text{-Si}$) are used to generate the voltage bias necessary for hydrogen generation. A TCCR coating is deposited on top of the photoelectrode to protect the semiconductor layers from corrosion while forming an ohmic contact with the electrolyte.
- The second approach uses a hybrid structure, in which two tf-Si-based junctions (middle and bottom junctions of the present triple-junction tf-Si cell) provide a voltage bias of about 1.1 V, and a third junction (the top junction) forms a rectifying junction between a photo-active

semiconductor and the electrolyte. This approach was down-selected during a Go/No-Go review in Dec 2010.

Approach

Five technical tasks are being performed under this grant to accomplish the project objectives:

- Task 1: TCCR coating for a triple-junction tf-Si-based photoelectrode.
- Task 2: Hybrid multi-junction PEC electrode having semiconductor-electrolyte junction.
- Task 3: Understanding and characterization of photo-electrochemistry.
- Task 4: Development of device designs for low-cost, durable and efficient immersion-type PEC cells and systems.
- Task 5: Development of device designs for large area, substrate-type PEC cells.

During the Go/No-Go review in Dec 2010, it was decided that the immersion-type PEC work (Task 4) will proceed into the second phase and the substrate-type PEC work (Task 5) would come to an end. It was also determined the TCCR work (Task 1) will proceed and the photo-active semiconductor work (Task 2) will be halted.

Results

The immersion-type PEC system utilizing a-Si triple junction solar cell should be a very efficient and low-cost approach for renewable hydrogen generation. The most challenging part of this approach is to develop a TCCR coating to protect the tf-Si solar cells in electrolyte. The focus of Task 1 has been to identify promising materials to use as the TCCR layer. After extensive studies of various material classes for this purpose, cobalt oxide and cobalt oxide co-deposited with other metal oxides have been identified as the most promising material that we would focus on moving into Phase II of this project. Over the past year the film properties were further optimized in Xunlight's roll-to-roll deposition system. This prototype production system allows large-area PEC electrode fabrication, including the deposition of TCCR layer without breaking the vacuum. Cobalt oxide has been sputtered on a-Si triple junction solar cells at 200°C. Reducing the sputtering power from 1.5 kW (Run 4) to 0.8 kW (Run 5) leads to transmission values of 90-100% in a wavelength range between 300-900 nm (Figure 1). The average thickness of these Co_3O_4 layer is ~70 nm. The oxygen flow was varied between 100-140 sccm and it seems that the transmission of the Co_3O_4 layer does not change with the oxygen flow in the sputtering gas. Under one-sun condition, the voltage drop on the cobalt oxide layer is only 0.086 V, which is excellent since this indicates

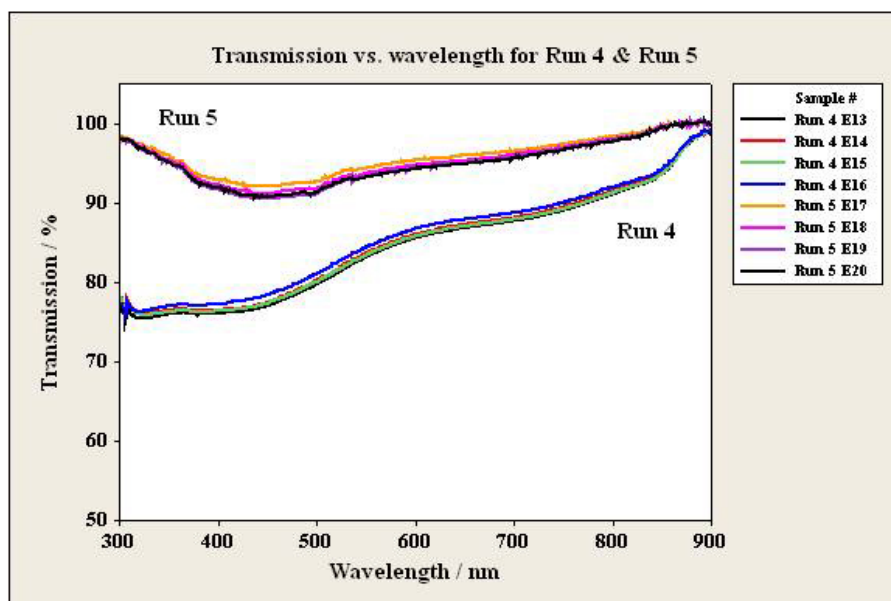


FIGURE 1. Transparency of cobalt oxide films (TCCR layer) deposited in Xunlight's roll-to-roll deposition system for large-area fabrication of PEC electrodes

that almost all the voltage generated by the solar cell can be used for water splitting and hydrogen generation. All of the above performance metrics meet or exceed the DOE goals and MWOE project goals. Cobalt oxide films deposited on fluorine-doped tin oxide (TEC 15) have been shown to be electrochemically stable for over 1,000 hrs under an applied bias of 1.8 V which reassembles the operating conditions for an immersion-type PEC cell assembly. With the roll-to-roll deposition system, not only can we optimize the deposition conditions for cobalt oxide, we can also adjust the solar cell deposition conditions and optimize the solar cell and TCCR layer deposition parameters for PEC performance instead for solar-to-electricity performance. This is a great advantage that we have comparing to many other groups that have to rely on commercially available solar cells which are always optimized for solar to electricity performance.

Under Task 4, we have focused our efforts in two major areas during last year. The first area was to develop immersion-type PEC electrodes with good STH efficiency and life time. We have fabricated PEC electrodes with cobalt oxide coating on the oxygen generating side and porous Ni catalyst on the hydrogen generation side. We have achieved a 4.1% initial STH efficiency and over 330 hrs of lifetime with a 2.5 cm² electrode (Figure 2). This efficiency was calculated by the actual measurement of hydrogen gas collected over time under AM 1.5 illumination (1 sun). It seems the main cause for performance decay overtime is the edge corrosion of the cell by electrolyte. We have been addressing this issue by applying a clear coat at the edge and employ some special design for the electrode holder in the large area PEC module design.



FIGURE 2. The experiment set-up for measuring the STH efficiency of the PEC electrodes

The second area that we have focused on was to design and develop PEC system with our large-area PEC electrodes. The basic design (Figure 3) uses an insert to hold the PEC electrode and to separate the unit into two chambers with an open void at the bottom for ion flow in the electrolyte. An insert holds the PEC electrode which allows for easy



FIGURE 3. Prototype PEC module design with four inch by four inch PEC electrodes

replacement of different PEC electrode materials. A STH conversion efficiency of 2.5 has been achieved with the PEC module in actual outdoor condition. Figure 4 shows the PEC module in operation under normal outdoor condition. We are working on exploring different PEC module designs to further improve the performance.

We have worked with Dr. Nocera's group at the Massachusetts Institute of Technology and Sun Catalytix on solar water splitting project, by providing triple junction a-Si solar cells. Their related research results were published in Science Magazine and were selected as one of Top 50 Innovations of Year 2011 by Time Magazine. MWOE has received many requests for collaboration on PEC hydrogen generation research projects from multiple research groups around the World, including University of Texas at Austin, Toyota Technical Center in Ann Arbor, University of California at San Diego, Energy Research Institute at

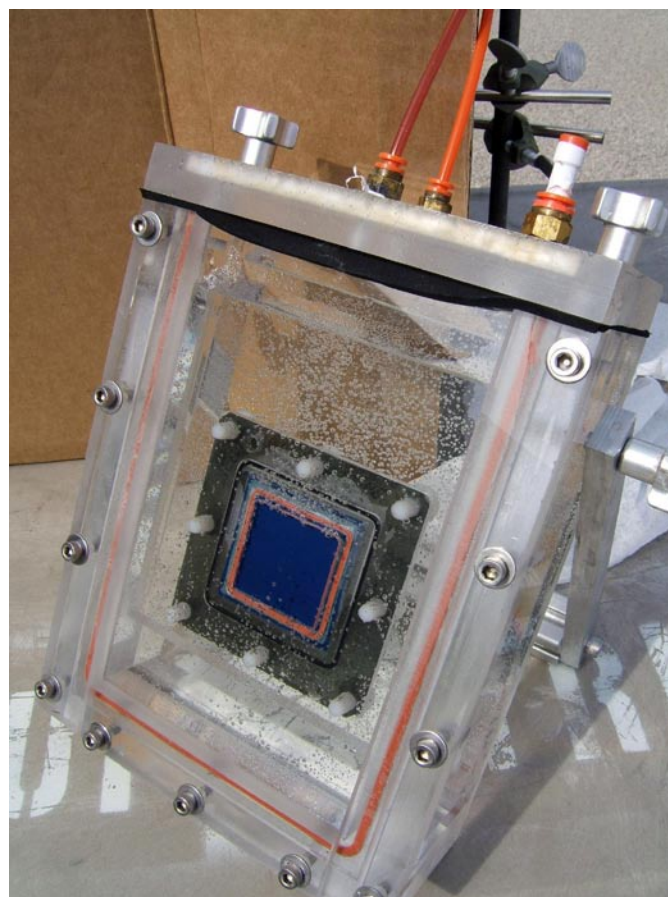


FIGURE 4. An immersion-type PEC module in operation under actual outdoor conditions

Nanyang Technological University in Singapore, Imperial College London in England. As far as we know, MWOE/Xunlight is the only company in the world which can supply triple junction solar cells which are ideal for renewable water splitting and hydrogen generation.

Conclusions and Future Directions

- Continue to improve the STH conversion efficiency for the large-area immersion-type PEC system, understand the different factors which could affect the efficiency such as cell uniformity, optimum operating voltage and operating current of the solar cell, the effect of the TCCR characteristics on the PEC performance, and the hydrogen and oxygen generation catalyst, etc.
- Experiment with different fabrication methods for PEC electrode with respect to solar cell and indium tin oxide deposition conditions, electrode preparation and different conditions for applying TCCR coating both in the lab and in the large scale roll-to-roll deposition system.

- Continue to develop different module designs to optimize the STH efficiency, extend lifetime and reduce cost.
- Develop more TCCR materials in addition to Co_3O_4 .
- Develop 1'x1' commercial size PEC system and carry out test in real life conditions.
- Collaborate with different research groups around the world to further PEC hydrogen generation research and development.
- Carry out the preliminary techno-economic analysis of the immersion-type PEC system.

II.F.7 Photoelectrochemical Materials: Theory and Modeling

Muhammad N. Huda (Primary Contact), Yanfa Yan*,
Todd Deutsch*, Mowafak M. Al-Jassim* and
A. John A. Turner*

Department of Physics
University of Texas at Arlington
Arlington, TX 76019
Phone: (817) 272-1097
Email: huda@uta.edu

*National Renewable Energy Laboratory

DOE Manager
HQ: Eric L. Miller
Phone: (202) 287-5892
Email: Eric.Miller@ee.doe.gov

Subcontractor:
University of Texas at Arlington, Arlington, TX

Project Start Date: September 2009
Project End Date: August 2012

Fiscal Year (FY) 2012 Objectives

For FY 2012, the main goal of this project was to improve materials efficiency by understanding and hence tuning the following by theoretical/computational modeling

- optical gaps and
- absorption probabilities
- conduction properties

This allows us to devise materials selection criteria for photoelectrodes for photoelectrochemical (PEC) energy conversion.

Technical Barriers

This project addresses the following technical barriers from the Production section of the Fuel Cell Technologies Program Multi-Year Research, Development and Demonstration Plan:

- (Y) Materials Efficiency
- (Z) Materials Durability

Technical Targets

This project is intended to provide (i) a theoretical understanding of the performance of current PEC materials and provide feedback and guidance for performance

improvement; (ii) materials prediction for photocatalysts by computational approach.

FY 2012 Accomplishments

- Theoretically studied the Cu-based delafossites materials and their nano-crystal phases to predict efficient photocatalysts for hydrogen production.
- We have shown that a set of unique and highly stable delafossite nano-crystals can be designed with tunable band gap.
- We have further investigated the optical absorption probabilities of these nano-crystals and determined a fundamental barrier in efficient optical absorptions for these oxide materials.



Introduction

Numerous metal oxides have been tried as photocatalysts for the last four decades to produce hydrogen [1-4] by water splitting through PEC process. Simple band engineering approaches to tune the band structure of naturally occurring oxides have not been so far very successful to generate hydrogen efficiently [5]. Alternate strategies, such as nanostructured photocatalysts have shown promises to split water to produce hydrogen [6-8]. Favorable focus on the nanostructure materials are due to the fact that their electronic structures are tunable, charge carrier scatterings are small and in many cases relatively low cost synthesis procedures available. However, to facilitate and control any redox reaction, such as to split water efficiently, the basic understanding of the nature of ‘band’ gap of the nanostructures and the electrons excitation across the gap is essential. The present study of the self-passivated and charge compensated nano-structures were performed with density functional theory (DFT) [9,10] and time-dependent DFT (TDDFT) [11,12]. These are very useful methods to study the ground state electronic structure and excitation energy, respectively, for the nanostructures.

Cu delafossites, CuMO_2 ($M =$ group 13 and 3 metals), have received great attention recently. These are stable in most aqueous solutions and have good p -type conductivity [13]. PEC response to split water for hydrogen has already been demonstrated for Cu-delafossites [16,17]. Recent theoretical studies have revealed that due to their crystal structure, Cu-delafossites have some undesirable features for PEC applications, such as indirect band gap and very weak optical absorption at the minimum band gap [14,15].

However, though the absorption can be improved by breaking the inversion symmetry of the crystals, [15] even after doping or alloying the band gap of delafossites remained indirect [16]. One way to go beyond this limitation is to consider nano-crystals. As the energy levels of the nano-structures are discrete and dispersionless, these structures do not suffer from indirect band gap problem. So it would be interesting to see if the minimum gap of nano-crystals enhances the optical absorptions.

Approach

CuYO_2 nano-crystals have been considered here as the prototype delafossite. These nanostructures were modeled in such a way that the basic structural features of delafossite have been retained. In delafossite structures, O and Cu form linear bonds along the c -axis, and O– M (M = transition metal atoms, such as Y) form distorted octahedrons. These octahedrons are connected by the Cu–O chain. All the nano-crystals considered here have oxygen terminated surfaces on both the lower and upper face (Figure 1). Upon several testing, it has been found that Y-terminated structures (either on both or one side) are heavily distorted and are less stable.

For the present report, *Gaussian03* code [17] has been used to calculate the electronic structures of CuYO_2 nano-crystals. Hybrid density functional theory with B3LYP

functional [18–20] was used with the LANL double ζ basis set and effective core potential [21] to study the delafossite nanocrystals. Hybrid functionals are in general found to be relatively accurate in reproducing the band gaps of semiconductors and insulators [22] for both DFT and TDDFT [23]. Full geometry optimizations with different spin-states were performed to obtain the lowest energy configurations. In addition, to obtain a better description of the optical gap or the electron transition energies from occupied to unoccupied states, we have used TDDFT as implemented in Gaussian03 [24]. All computations were performed at the high performance supercomputing center facilities of the University of Texas at Arlington.

Results

A charge compensated ionic structure, $\text{Cu}_m\text{Y}_n\text{O}_l$, should have $m+3n-2l=0$; where 1, 3 and -2 are the oxidation states of Cu, Y and O atoms in delafossite structure, respectively. Though the overall structure is neutral, a charge uncompensated nanocrystal will have local charged ions and which would lead to charged defect-states in the highest occupied molecular orbital–lowest unoccupied molecular orbital (HOMO-LUMO) gap. Another interesting aspect of these nano-crystals is, in addition to charge compensation, the top and the bottom layer of the nano-crystals are self-passivated by extra Y–Y bonds (Figure 1), which are not found in the corresponding bulk structure [14]. These self-passivated and charge compensated metal-oxide nano-crystals are a unique set of nano-materials with very high chemical stability. It is very challenging to model such nano-crystals with basic delafossite features. Figures 1(a) and (b) show the relaxed structures of two of the charge compensated nanocrystals, and the top views are shown in Figure 1(c) and (d). Extra Y–Y bonds are seen here, which saturate the Y–O octahedrons and resulting in no unpassivated dangling bonds. Even at this small level, the basic delafossite structure, i.e., O–Cu–O linear chain-like bonds bounded by O–Y octahedrons are visible.

Binding Energies: The binding energies were calculated with respect to the infinite separation limit of the constituent atoms at their ground state spin configurations. First of all, the binding energies per atom are considerably high, implying that in general these nano-crystals are stable. Binding energy per atom is slightly higher for $\text{Cu}_6\text{Y}_{14}\text{O}_{24}$, which is charge compensated with zero dipole moment. It has binding energy of 5.408 eV/atom. On the other hand charge neutral, but non-zero dipole moment structure has little lower binding energy, for instance 5.390 eV/atom for $\text{Cu}_8\text{Y}_{16}\text{O}_{28}$. In fact this has a little higher dipole moment of 14.820 Debye which contributes to the polar nature of the structure. On the other hand, the charge uncompensated structure, such as $\text{Cu}_8\text{Y}_{16}\text{O}_{24}$, has relatively much lower binding energy of 5.165 eV/atom. To see how much charge imbalance affects the stability, we further show binding energy of another

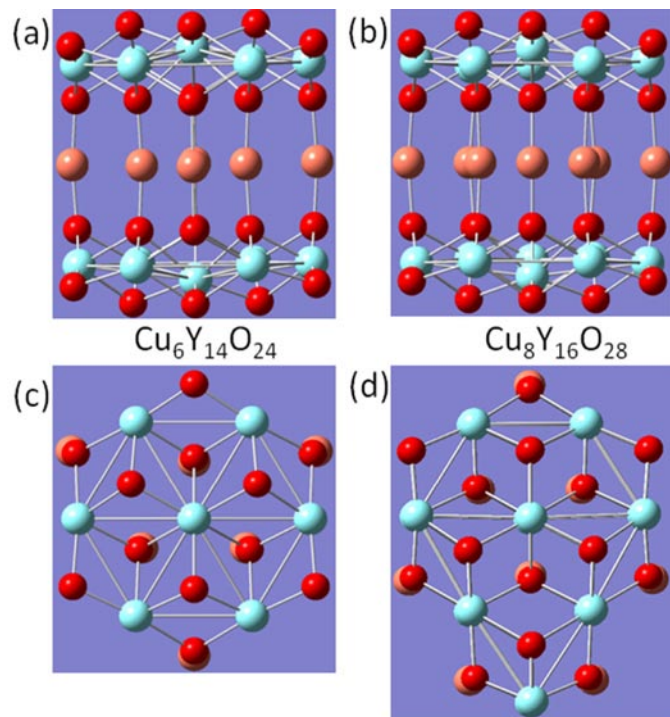


FIGURE 1. Relaxed structures of two charge compensated delafossite nanostructures: (a) $\text{Cu}_6\text{Y}_{14}\text{O}_{24}$ and (b) $\text{Cu}_8\text{Y}_{16}\text{O}_{28}$. Structures in (c) and (d) are the top-views of structures presented in (a) and (b), respectively. Orange, red and light green balls represents Cu, O and Y atoms, respectively.

non-charge balanced structure, $\text{Cu}_8\text{Y}_{18}\text{O}_{32}$, 5.351 eV/atom. However, in the former case the unsaturated charge is +8, in the later the it is only -2 . It can be argued here that *the more charge balanced a structure is, the higher the binding energy*.

HOMO and LUMO: Figure 2(a) shows the structure of the topmost five occupied orbitals for $\text{Cu}_8\text{Y}_{16}\text{O}_{28}$ structures. This structure is especially chosen for the fact that it is a charge compensated structures with non-zero dipole moment, hence will represent a more general case. Here the HOMO is mainly situated around the Cu atoms in the middle with some contributions from O-atoms which are bonded with Cu. The outer O-atoms (top and bottom surfaces) do not have any significant contributions to these top occupied orbitals. The shape of the HOMO around the Cu atoms is clearly indicative of $3d_{z^2}$ orbital. The same is true for the HOMO-1 orbital which is only 35 meV lower than the HOMO. These features can be directly compared with the bulk delafossite structures where valence band maximum is mainly composed by Cu-d with O-p hybridization [14]. From HOMO-2 orbital and further below, the $3d_{z^2}$ structure is no longer seen; rather mixed components of $3d$ orbitals get prominent. As expected, Y has practically no contribution to these orbitals. In case of ionization, an electron will be taken out from the HOMO. Our calculated adiabatic ionization potential is 6.557 eV which is very high.

Similarly, we have also studied the first five unoccupied orbitals, i.e., LUMO, LUMO+1, etc. and are presented in Figure 2(b). Unlike the position of HOMO, LUMO is mainly situated on one side of the structure and have major contributions from all the three types of atoms, while the

contribution from corner Y atoms is higher. The almost sole contribution from Y atoms was found at LUMO+1 which is 170 meV higher than LUMO. It does not distribute itself throughout the structure, rather situated in two corners. LUMO+2 and above have considerably higher energies, hence may not contribute much on the chemical properties of this structure. It is important to note, the distribution of HOMO is almost over all the Cu atoms, however LUMO is only on the Y atoms which are in one side of the structure. The apparent asymmetric distribution of LUMO could be highly structure dependent. If an extra electron is received by this LUMO, the electron will occupy an unfilled Y-orbital, and the corresponding electron affinity is considerably higher, 1.818 eV.

Next we discuss briefly HOMO and LUMO for a charge uncompensated structure, $\text{Cu}_8\text{O}_{24}\text{Y}_{16}$, as shown in Figure 3(a) and (b), respectively. In contrast to the charge compensated structure discussed above, Cu atoms do not contribute much to the HOMO for $\text{Cu}_8\text{O}_{24}\text{Y}_{16}$. The largest contribution to both HOMO and LUMO comes from the under-coordinated Y atoms. This under-coordination of Y atoms is also responsible for the distorted Cu-Y bond as seen in here. Hence these HOMO and LUMO can mainly be considered as charge defect states. Here again, the Y-O octahedrons do not contribute to the HOMO and LUMO. The atomic sites and the relative sizes of HOMO and LUMO do not differ much for this charge uncompensated structure. The energy difference between the HOMO and LUMO is only 0.582 eV.

Optical gaps by TDDFT: The first excitation energy calculated by TDDFT [24] with non-zero oscillator strength would give an estimation of the optical gap for the nano-

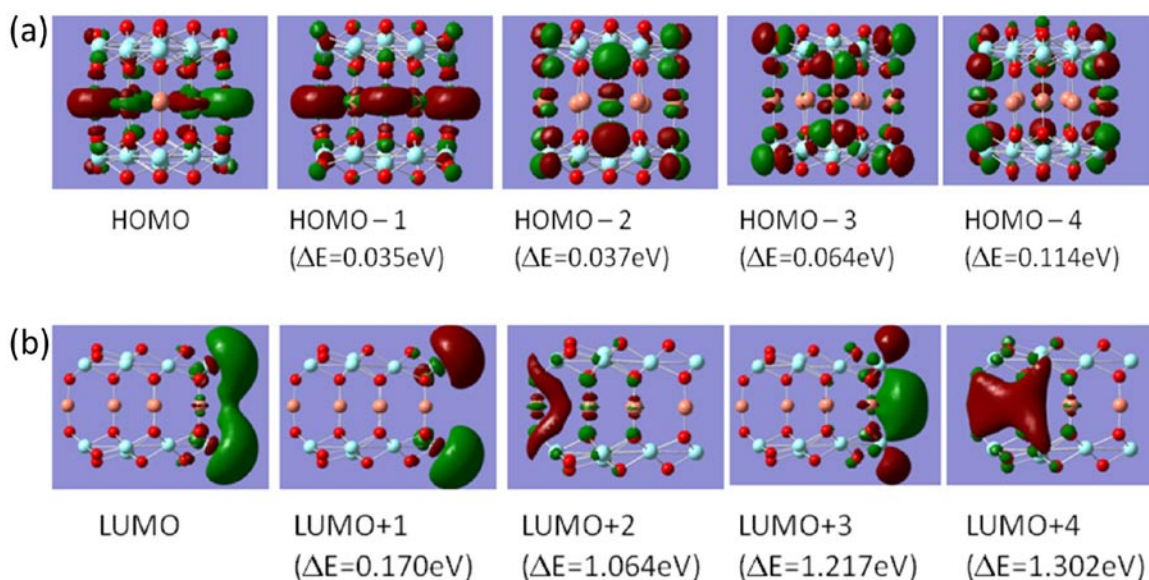


FIGURE 2. (a) Valence band (HOMO) composition for CuYO-52 ($\text{Cu}_8\text{Y}_{16}\text{O}_{28}$) nano-structures is shown here. HOMO- n refers to the n th orbital below the HOMO. ΔE is the energy difference between the HOMO and HOMO- n orbitals. Here we have shown the first five occupied orbitals. (b) Similarly, LUMO is shown here for the same structure. Here LUMO+ n refers to the n th orbital above the LUMO.

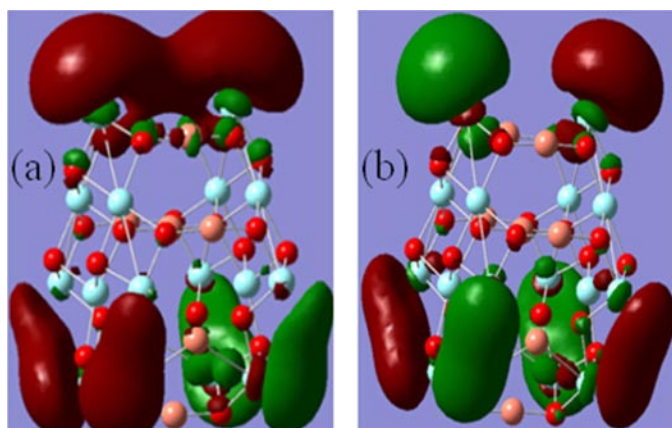


FIGURE 3. (Color online) (a) HOMO and (b) LUMO of fully optimized $\text{Cu}_8\text{Y}_{24}\text{O}_{16}$ structure is shown here.

crystals. For example, the first excitation energy for $\text{Cu}_8\text{Y}_{16}\text{O}_{28}$ was found to be 2.734 eV which is less than its hybrid DFT HOMO-LUMO gap of 3.165 eV. Interestingly, this transition is not allowed as the oscillator strength was found to be zero here. This can be compared to the bulk CuYO_2 where the optical absorption is symmetry forbidden at the minimum direct gap as well [15]. In fact, for $\text{Cu}_8\text{Y}_{16}\text{O}_{28}$ the first five excitations have all zero oscillator strength, implying that none of the low energy transition is possible. Similarly, the first excitation probabilities (oscillator strengths) of other structures were also found to be zero. However, for $\text{Cu}_6\text{Y}_{14}\text{O}_{24}$ the third excitation showed non-zero oscillator strength at energy of 2.931 eV, which is 0.020 eV higher than the first excitation gap. For charge uncompensated structure, like $\text{Cu}_8\text{Y}_{16}\text{O}_{24}$, the oscillator strength in the first excitation energy was very small, almost zero. However, this excitation is between the charge defect states, and predominantly on the Y-site.

Conclusions and Future Directions

A set of self-passivated and charge-compensated nano-crystalline delafossites structures have been presented here. The goal was to (i) model these nano-crystals and find out their stability, and (ii) whether the nanocrystals would enhance the suppressed optical absorption found in delafossite bulk crystals. It has been found that the $\text{C}_m\text{Y}_n\text{O}_l$ nano-crystals have, in general, high binding energies which are more than 5 eV/atom. The stability of these delafossite nano-crystals is ensured by the Y-Y bonds to passivate the terminating surfaces. The HOMO-LUMO gaps are, in general, higher for the charge-compensated structures. For instances, both the charge-compensated structures has gaps more than 2.7 eV calculated by TDDFT. Interestingly, the absorption probabilities for the first few excitation energies are zero for these nano-crystals. This implies that the enhancement of optical absorption at nano-level compared to bulk can be challenging. This conclusion may apply for

other metal-oxide nano-crystals with inversion symmetries. To test this hypothesis, we will further investigate optical absorptions of other nanocrystals in the next year, such as $\alpha\text{-Fe}_2\text{O}_3$ and MoS_2 . Other future plans include:

- Transport properties calculation.
- Electron hopping to the surface, and transfer of electrons from the surface will be studied.
- Doped nano-crystals will be considered.
- Detail orbital analysis will be performed to understand and predict other nano-structures for photo-catalysts.

FY 2012 Publications/Presentations

1. *Mott insulators: An early selection criterion for materials for photoelectrochemical H_2 production.* **M.H. Huda**, M.M. Al-Jassim and J.A. Turner. *Journal of Renewable and Sustainable Energy*, **3**, 053101 (2011).
2. *The effect of Bi alloying in Cu delafossites.* M.N. Huda, Y. Yan and M.M. Al-Jassim, *Journal of Applied Physics*, **109**, 113710 (2011).
3. *The electronic structures of Cu delafossites nanocrystals for PEC hydrogen production: A density functional theory study.* **M.N. Huda**, Y. Yan and M.M. Al-Jassim. American Physical Society Meeting, Dallas, Texas (2011).
4. *A first principle study of noble metal atoms doped in Si nanocrystals.* M.N. Huda and C.L. Mayfield. 23rd Annual Workshop on Electronic Structure Methods, University of Pennsylvania (2011).

References

1. O. Khaselev and J.A. Turner, *Science* **280** (5362), 425-427 (1998).
2. E.L. Miller, N. Gaillard, J. Kaneshiro, A. DeAngelis and R. Garland, *International Journal of Energy Research*, n/a-n/a (2010).
3. K. Rajeshwar, *J Appl Electrochem* **37** (7), 765-787 (2007).
4. F.E. Osterloh, *Chemistry of Materials* **20** (1), 35-54 (2007).
5. M.N. Huda, Y.F. Yan, C.Y. Moon, S.H. Wei and M.M. Al-Jassim, *Physical Review B* **77** (19), 195102 (2008).
6. Y. Li and J.Z. Zhang, *Laser Photonics Rev* **4** (4), 517-528 (2010).
7. A.S. Arico, P. Bruce, B. Scrosati, J.-M. Tarascon and W. van Schalkwijk, *Nat Mater* **4** (5), 366-377 (2005).
8. Y. Kanai, Z. Wu and J.C. Grossman, *J Mater Chem* **20** (6), 1053-1061 (2010).
9. P. Hohenberg and W. Kohn, *Physical Review* **136** (3B), B864 (1964).
10. W. Kohn and L.J. Sham, *Physical Review* **140** (4A), A1133 (1965).
11. E. Runge and E.K.U. Gross, *Phys Rev Lett* **52** (12), 997-1000 (1984).
12. M.A.L. Marques and E.K.U. Gross, *Annual Review of Physical Chemistry* **55** (1), 427-455 (2004).

13. H. Kawazoe, M. Yasukawa, H. Hyodo, M. Kurita, H. Yanagi and H. Hosono, *Nature* **389** (6654), 939-942 (1997).
14. M.N. Huda, Y.F. Yan, A. Walsh, S.H. Wei and M.M. Al-Jassim, *Physical Review B* **80** (3), 035205 (2009).
15. M.N. Huda, Y. Yan, A. Walsh, S.-H. Wei and M.M. Al-Jassim, *Applied Physics Letters* **94** (25), 251907 (2009).
16. M.N. Huda, Y. Yan and M.M. Al-Jassim, *Journal of Applied Physics* **109** (11), 113710 (2011).
17. Gaussian 03, M.J. Frisch, et al., (Gaussian, Inc., Wallingford, CT, 2003).
18. A.D. Becke, *The Journal of Chemical Physics* **98** (7), 5648-5652 (1993).
19. P.J. Stephens, F.J. Devlin, C.F. Chabalowski and M.J. Frisch, *The Journal of Physical Chemistry* **98** (45), 11623-11627 (1994).
20. C. Lee, W. Yang and R.G. Parr, *Physical Review B* **37** (2), 785-789 (1988).
21. P.J. Hay and W.R. Wadt, *The Journal of Chemical Physics* **82** (1), 270-283 (1985).
22. J. Muscat, A. Wander and N.M. Harrison, *Chemical Physics Letters* **342** (3-4), 397-401 (2001).
23. D. Jacquemin, E.A. Perpète, I. Ciofini and C. Adamo, *Journal of Chemical Theory and Computation* **6** (5), 1532-1537 (2010).
24. F. Furche and R. Ahlrichs, *The Journal of Chemical Physics* **117** (16), 7433-7447 (2002).

II.G.1 Biological Systems for Hydrogen Photoproduction

Maria L. Ghirardi (Primary Contact), Paul W. King, Kathleen Ratcliff and David Mulder
National Renewable Energy Laboratory (NREL)
1617 Cole Blvd.
Golden, CO 80401
Phone: (303) 384-6312
Email: maria.ghirardi@nrel.gov

DOE Manager

Eric Miller
Phone: (202) 287-5829
Email: Eric.Miller@hq.doe.gov

Subcontractors:

- Dr. Sergey Kosourov, Institute of Basic Biological Problems, RAS, Pushchino, Russia
- Dr. Eric Johnson, Johns Hopkins University, Baltimore, MD

Project Start Date: October 1, 2000

Project End Date: Project continuation and direction determined annually by DOE

Fiscal Year (FY) 2012 Primary Objectives

- Develop and optimize aerobic, high solar-to-hydrogen (STH) photobiological systems for the production of H₂ from water by:
 - engineering a H₂-producing catalyst ([FeFe]-hydrogenase) that has an extended half-life following exposure to O₂
 - introducing a more O₂-tolerant hydrogenase into the green alga, *Chlamydomonas reinhardtii*
- Further optimize and utilize an anaerobic, limited STH working platform to study biochemical and engineering factors that affect H₂ photoproduction by biological organisms; focus on the effect of an altered chloroplast adenosine triphosphate (ATP) synthase on the rates of H₂ photoproduction.

Technical Barriers

This project addresses the following technical barriers from the Production section of the Fuel Cell Technologies Program's Multi-Year Research, Development and Demonstration Plan.

(AH) Rate of H₂ production

(AI) Continuity of H₂ production

Technical Targets

TABLE 1. Progress toward Meeting Technical Targets for Photobiological Hydrogen Production

| Parameters | Current Status | 2013 Targets | Maximum Potential |
|--|----------------|--------------|-------------------|
| Duration of continuous photoproduction: | | | |
| – Aerobic, high STH (O ₂ -tolerant) | 4.5 min | 30 min | 12 hours |
| – Anaerobic, low STH (S-deprivation) | 50-150 days | | Indefinite |
| – Aerobic, low STH (S-deprivation) | 10 days | | Indefinite |
| Cost (\$/kg H ₂) | | | |
| – Aerobic, high STH | | | \$2.99 |
| – Anaerobic, low STH | | | \$6.02 |

FY 2012 Accomplishments

- Successfully expressed a more O₂-tolerant clostridial hydrogenase (Ca1) in a double hydrogenase knock-out mutant of *Chlamydomonas reinhardtii* and observed *in vivo* H₂ photoproduction.
- Reached a No-Go decision concerning a mutagenesis approach to generate targeted random mutants in *Chlamydomonas*.
- Demonstrated long-term H₂ photoproduction by sulfur-deprived algal cultures immobilized into alginate films, using cycles of +S/-S or continuous flow of medium with low concentrations of sulfate.
- Successfully generated an inducible system for expression of chloroplast genes and tested its efficacy in expressing an Orange Fluorescent Protein.
- Tested transformants containing altered atpE genes using immobilized cells under sulfur-deprivation conditions.



Introduction

Green algae can extract electrons from water and generate H₂ under illumination, using the concerted activities of the photosynthetic electron transport chain and the enzyme [FeFe]-hydrogenase. This pathway evolves O₂ as a by-product, which irreversibly inhibits the [FeFe]-hydrogenase catalytic center. The continuity of H₂ photoproduction is one of the major technical barriers to developing photobiological H₂-production systems that use water as the source of electrons (technical barrier AI). A second major barrier to efficient algal H₂ production is the low rate of the reaction (technical barrier AH), which is

dependent on many intracellular regulatory factors, including the down-regulation of photosynthetic electron transport from water under H₂-producing conditions.

Our current project addresses the O₂ sensitivity and low rates of algal H₂-production by using molecular engineering to alleviate these barriers and testing the results through the sulfur-deprivation platform. The latter allows us to measure the effects of molecular engineering on sustained hydrogen production, although at low STH conversion levels.

Approach

Task 1. Molecular Engineering Approaches to Increase the O₂ Tolerance of H₂ Photoproduction

This task has two major objectives: (a) the engineering of increased O₂ tolerance in [FeFe]-hydrogenases through random mutagenesis, targeted to regions that control O₂ access to the catalytic site; and (b) the expression of a functional, more O₂-tolerant clostridial [FeFe]-hydrogenase in *Chlamydomonas reinhardtii*.

The targeted mutagenesis approach is guided by extensive computational studies of gas diffusion in the *Clostridium pasteurianum* Cpl [FeFe]-hydrogenase (that has a solved crystal structure). These studies previously identified a hydrophobic cavity separated from the catalytic H-cluster by a high-energy barrier. However, site-directed mutagenesis of barrier residues designed to reduce O₂ transport did not yield enzymes with higher O₂-tolerance. Alternative computational and mutagenesis approaches were devised in order to target residues present in the regions around the diffusion barriers (but not in the barrier *per se*), and high-throughput assays were developed in FY 2012 to test the hypothesis. However, due to the complexity of the O₂ effect on hydrogenases as observed by our previous efforts, combined with a limited budget for FY 2012, we concluded that, in order to meet programmatic milestones for increased oxygen tolerance it would be more feasible to focus on introducing known, more O₂-tolerant enzymes into *Chlamydomonas*. If an additional budget is available in the future, we will return to pursuing the targeted random mutagenesis approach for engineering.

Our studies aimed at expressing a more O₂-tolerant hydrogenase from *Clostridium acetobutylicum* (Ca1) in *C. reinhardtii* have benefited enormously from recent findings from a DOE Office of Science project under Dr. Ghirardi, which provided us with a *Chlamydomonas* strain that lacks the two native algal hydrogenases. This strain, together with our efforts at optimizing Ca1 gene expression in *Chlamydomonas* during FY 2012, has been used in our current efforts to demonstrate *in vivo* H₂ photoproduction by a transformant expressing only Ca1. The availability of this transformant will allow us to observe the effects of a more O₂-tolerant hydrogenase in algal H₂ production and overall

physiology and guide further studies aimed at developing hydrogenases with even higher O₂ tolerance.

Task 2. Use of the Sulfur-Deprivation Platform to Test Additional Biochemical and Engineering Barriers to H₂ Photoproduction

To induce sustained H₂ photoproduction, we collaborated with the University of California in 2000 and developed a physiological switch that is based on removing sulfate from the algal growth medium. This procedure has become a platform for testing the performance of a variety of algal mutants, growth conditions, immobilization surfaces and other engineering factors that may affect the overall H₂ yield. In FY 2012, our efforts focused on (a) increasing the duration of H₂ photoproduction using immobilized algal cells; and (b) developing inducible mutants that express an altered ATP synthase gene that prevents down-regulation of electron transport rates during H₂ photoproduction.

Results

Task 1. Molecular Engineering Approaches to Increase the O₂ Tolerance of H₂ Photoproduction

Computational simulations identified differences in the geometries and energies of the gas diffusion barriers protecting the H-cluster of [FeFe]-hydrogenases, indicating that diffusion itself may not be the limiting step for inactivation. Based on these studies, we identified targets for mutagenesis that may increase the energy barriers and allow diffusion to become the rate-limiting step, without affecting the maturation of these hydrogenases. In order to test the validity of this hypothesis, we developed a chemochromic, high-throughput assay, based on the oxidation of methyl viologen by H₂-producing algae and adapted it to a microwell format. The assay was tested with *Escherichia coli* strains expressing hydrogenase mutants that are unable to produce H₂ and it was further optimized. The selected *E. coli* strain, Rosetta-2 (DE3) was chosen as a host for mutated hydrogenases due to its low background endogenous hydrogenase activity (which is catalyzed by native [NiFe]-hydrogenases) and it was shown to successfully express the mutated [FeFe]-hydrogenases upon IPTG (isopropyl β-D-1 thiogalactopyranoside) induction.

More recently, we successfully expressed the clostridial Ca1 hydrogenase in wild-type *Chlamydomonas*, using a *psaD* promoter and terminator based-expression system. The data obtained from these transformed strains, however, have been challenging to interpret. Low expression levels of Ca1 relative to the native algal hydrogenases (HYDA1 and HYDA2) made testing the resulting effects of Ca1 expression on O₂ sensitivity highly variable, and thus difficult to interpret. However, O₂-inhibition assays revealed double decay kinetics, suggesting that the more

O₂-tolerant Ca1 enzyme was expressed and active in the transformed alga. At the beginning of FY 2012, we shifted our transformation experiments to a new host, a double hydrogenase knock-out strain of *C. reinhardtii* that has recently been developed (Meuser et al. 2012. Biochem. Biophys. Res. Commun. 417:704) through a project funded by the DOE's Office of Science Basic Energy Sciences Program. We have since demonstrated successful genome incorporation and expression of Ca1 (Figure 1). At this point, we have postponed our random mutagenesis efforts in order to allocate our resources to pursue this more promising approach.

Although successful Ca1 transformants have been obtained to date, the expression levels are low and may be less stable. As a consequence, we have been unable to accumulate enough cells to test their O₂ tolerance. We have since generated additional transformants and will be measuring their O₂ tolerance to complete milestone 3.3.5 by the end of September 2012.

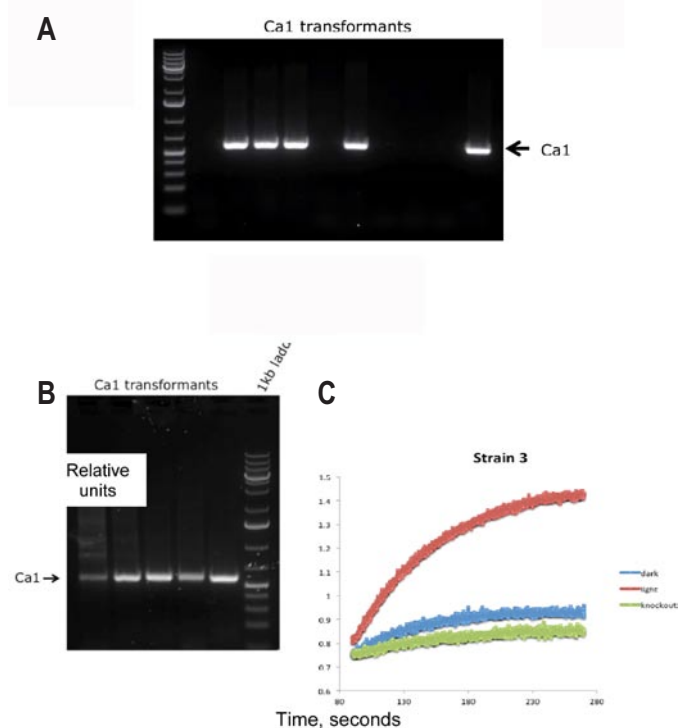


FIGURE 1. (A) Polymerase chain reaction of positive transformants demonstrating the incorporation of the Ca1 gene into the *Chlamydomonas* genome; (B) Reverse-transcriptase polymerase chain reaction of ribo nucleic acid extracted from positive transformants for Ca1, demonstrating that the Ca1 gene is transcribed in the transformants; (C) Initial rates of H₂ production by one of the transformants (upper curve) upon illumination, as measured by the Clark electrode; control curves represent, respectively, H₂-production activity of the transformant in the dark, and H₂ production by the parental strain, the double hydrogenase knock-out mutant upon illumination.

Task 2. Use of the Sulfur-Deprivation Platform to Test Additional Biochemical and Engineering Barriers to H₂ Photoproduction

Sulfur-deprived algal cells immobilized into alginate films in the presence of 0.1% polyethylenimine (PEI) have previously been shown to photoproduce H₂ for a total period of about 10 days. In order to increase the period of H₂ photoproduction, we used two approaches that had been proven successful in extending H₂ production by cells in suspension: (a) perform cycles of +S/-S; and (b) continuously add low concentrations of sulfate to the medium. Figure 2 demonstrates that approach (a) resulted in H₂ photoproduction for a total period of about 150 days, with a total H₂ accumulation of ~0.56 mol/m². Approach (b) proved more successful when applied to strain EJ12F3 (Figure 3A), a mutant on the ATP synthase subunit atpE that is constitutively expressed in the host strain (see following). The process resulted in H₂ photoproduction for a period of about 53 days, with a total H₂ accumulation of 0.8 moles/m² (for comparison, the wild-type accumulated 0.32 moles H₂/m²). The longest period of H₂ photoproduction was detected in the wild-type strain supplied continuously with TAP-S-P medium containing only the residual amounts of sulfates and phosphates. In this case, the alginate film produced 0.27 moles H₂/m² for about 92 days (Figure 3B). Under these conditions, EJ12F3 also demonstrated the highest H₂ photoproduction rate (Figure 3B). In the absence

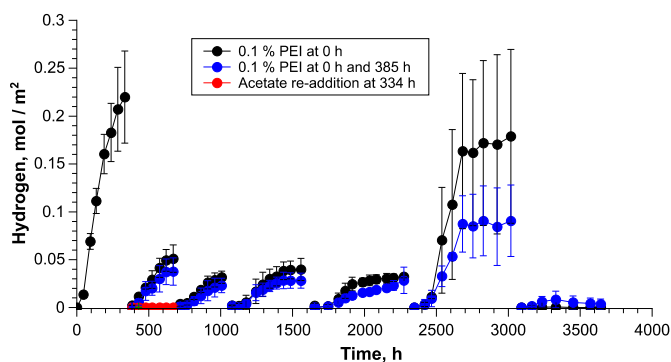


FIGURE 2. Continuous hydrogen photoproduction by sulfur/phosphorus-deprived *C. reinhardtii* cultures entrapped in alginate films. All films were pre-treated for 5 min with 0.1% PEI at the beginning of the experiment, washed in distilled water and transferred to anaerobic vials containing TA-S-P medium. At the beginning of each cycle (except the first one), alginate films were transferred into aerobic vials containing normal tandem affinity purification medium. After 3 days (~72 h), the films were transferred back to anaerobic vials with TA-S-P medium. For better stability, some films were additionally treated with 0.1% PEI for 5 min at the end of the first aerobic phase (~385 h, blue circles). In addition, acetate was re-added back to a third set of vials in the end of the first H₂ photoproduction cycle (at t = 334 h), and the vials were sparged with argon for 20 min. In these vials, the experimental medium was not replaced but acetate was re-added in the concentration equal to its initial concentration in the tandem affinity purification medium.

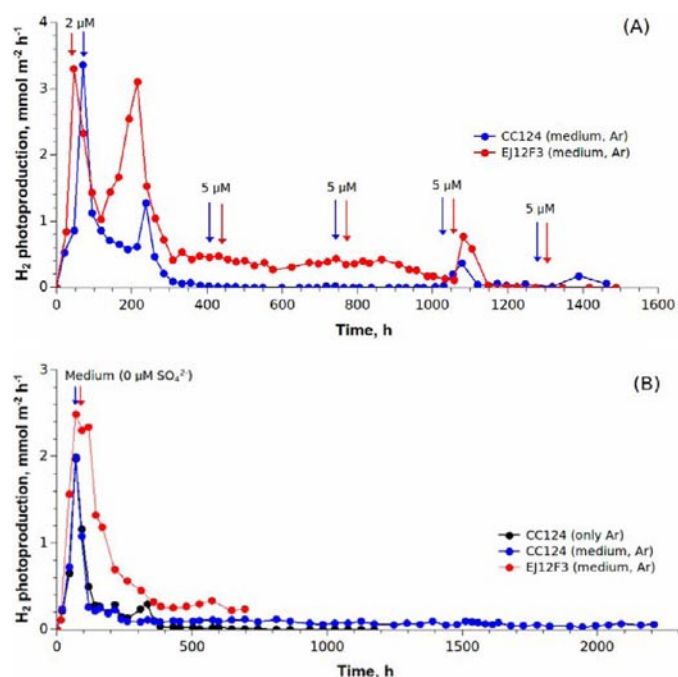


FIGURE 3. Continuous hydrogen photoproduction by sulfur-deprived *C. reinhardtii* wild-type (CC124) and ATP-synthase mutant (EJ12F3) cultures entrapped within thin alginate films. (A) Additional sulfate was added to the cultures at different points, as shown by the arrows. (B) Experiments were done under continuous flow of TAP –S –P medium without re-addition of sulfates, except the experiment marked «only Ar» where only argon was supplied to the bioreactor.

of continuous TAP –S –P flow, the alginate film produced only 0.17 moles/m².H₂ gas for about 48 days.

The sulfur-deprivation process is being used to test the performance of ATP synthase mutants designed to dissipate the proton gradient that is established during electron transfer from H₂O to H₂ and that is known to down-regulate electron transfer (and thus H₂ production). Mutants in the *atpE* subunit defective in its C-terminal were expressed in *Chlamydomonas* strain FUD17 that lacks native *E* subunit. The expression of *atpE* in these initial strains was *constitutive*, which resulted in lower or no growth under photoautotrophic conditions. The H₂-photoproduction activity of a series of slow-growing mutants was tested under sulfur-deprivation conditions and two different light intensities, 90 and 150 μE m⁻² s⁻¹. The results demonstrate that (i) the host strain FUD, when complemented with a non-mutated *atpE* subunit (wtF) produces substantially more H₂ than the usual wild-type strain used in our laboratory, CC124; (ii) all mutants that were tested showed H₂-production levels similar to the wild-type when cultivated under 90 μE m⁻² s⁻¹ but lower H₂-production levels when exposed to 150 μE m⁻² s⁻¹; and (iii) the decrease in H₂ production at higher level intensity compared to wtF was a function of the number of amino acid residues that were mutated. The results suggest that the mutations may have affected other cellular activities as well.

New mutants were designed and are being tested to function under regulation of an inducible promoter, to allow the dissipation of the proton gradient to occur only under H₂-producing conditions. The inducible promoter was tested with an Orange Fluorescent Protein and was shown to efficiently express this protein as a function of its expression level.

Conclusions and Future Direction

Task 1. Continue the characterization of *C. reinhardtii* transformants harboring the Cal expression construct, and improve the expression of the heterologous gene through random mutagenesis of promoter, transit peptide and linker, as needed.

Task 2. Will be discontinued due to budget restrictions.

FY 2012 Publications/Presentations

Publications

- Blankenship, R.E., D.M. Tiede, J. Barber, G.W. Brudvig, G. Fleming, M. Ghirardi, M.R. Gunner, W. Junge, D.M. Kramer, A. Melis, T.A. Moore, C.C. Moser, D.G. Nocera, A.J. Nozik, D.R. Ort, W.W. Parson, R.C. Prince and R.T. Sayre. **2011**. “Comparing Photosynthetic and Photovoltaic Efficiencies and Recognizing the Potential for Improvement”. *Science* 332, 805-809.
- Yacoby, I., Pochekaïlov, S., Toporik, H., Ghirardi, M.L., King, P.W. and Zhang, S. “Photosynthetic electron partitioning between [FeFe]-hydrogenase and ferredoxin:NADP⁺-oxidoreductase. *Proc. Natl. Acad. Sci. USA*, 108, 9396-9401.
- Tekucheva, D.N., T.V. Laurinavichene, M. Seibert, A.A. Tsygankov (2011) “Immobilization of purple bacteria for light-driven H₂ production from starch and potato fermentation effluents.” *Biotechnology Progress Journal Online*. <http://dx.plos.org/10.1371/journal.pone.0025851> October 17.
- Laurinavichene, T.V., Belokopytov B.F., Laurinavichius, K.S., Khusnutdinova, A.N., Seibert, M., Tsygankov, A.A. **2012**. “Towards the integration of dark- and photo-fermentative waste treatment. 4. Fed-batch sequential fed-batch dark and photofermentation using starch as substrate”. *Int. J. Hydrogen Energy* 37: 8800-8810.
- Kosourov, S.N., Batyrova, K.A., Petushkova, E.P., Tsygankov, A.A., Ghirardi, M.L. and Seibert M. **2012**. “Maximizing the hydrogen photoproduction yields in *Chlamydomonas reinhardtii* cultures: the effect of the H₂ partial pressure”. *Int. J. Hydrogen Energy* 37:8850-8858.
- Johnson, EA. **2012**. “Monitoring foreign gene incorporation into the plastome of *Chlamydomonas reinhardtii* by multiplex qPCR” *Photosynthesis Research*, *submitted*.
- Johnson, EA. **2012**. “Expression of monomeric Kusabira Orange in the chloroplast of *Chlamydomonas reinhardtii*”. *Photosynthesis Research*, *submitted*.

Presentations

1. Presentation to the research group at the Institute for Marine and Environmental Technology (IMET) at the University of Maryland (June 2011, Johnson).
2. Presentation at the Natural and Artificial Photosynthesis meeting (November 2011, King).
3. Seminar presentation at the Colorado State University, in Fort Collins, CO (November 2011, Ghirardi).
4. Oral presentation at the Western Photosynthesis Conference in Pacific Grove, CA, (January 2012, Ghirardi).
5. Invited talk to the Department of Life Sciences and Systems Biology at the University of Torino (March 2012, King).
6. Invited Talk at the Metal Hydrides in Biology Meeting-Oxford UK (March 2012, King).
7. Invited talk to the CEA Bioenergy Conference in Paris (February 2012, King and Ghirardi).
8. Organization and presentation at a joint symposium between NREL and French researchers working on algal biohydrogen and biofuels at NREL (April 2012, Ghirardi).

II.G.2 Fermentation and Electrohydrogenic Approaches to Hydrogen Production

Pin-Ching Maness (Primary Contact), Katherine Chou, and Lauren Magnusson
 National Renewable Energy Laboratory (NREL)
 15013 Denver West Parkway
 Golden, CO 80401
 Phone: (303) 384-6114
 Email: pinching.maness@nrel.gov

DOE Manager
 HQ: Eric Miller
 Phone: (202) 287-5829
 Email: Eric.Miller@hq.doe.gov

Subcontractor:
 Bruce Logan, Pennsylvania State University,
 State College, PA

Start Date: October 1, 2004
 Projected End Date: Project continuation and
 direction determined annually by DOE

Technical Targets

TABLE 1. Progress toward Meeting DOE Technical Targets in Dark Fermentation

| Characteristics | Units | Current Status | 2015 Target | 2020 Target |
|--|-----------------------------------|----------------|-------------|-------------|
| Yield of H ₂ from glucose | Mole H ₂ /mole glucose | 2–3.2 | 6* | -- |
| Feedstock cost | Cents/lb glucose | 13.5 | 10 | 8 |
| Duration of continuous production (fermentation) | Time | 17 days | 3 months | -- |
| MEC cost of electrodes | \$/m ² | \$2,400 | \$300 | \$50 |
| MEC production rate | L-H ₂ /L-reactor-d | 1 | 1 | --- |

*Yield of H₂ from glucose: DOE has a 2015 target of an H₂ molar yield of 6 (4 from fermentation and 2 from MEC) from each mole of glucose as the feedstock, derived from cellulose.

Feedstock cost: The DOE Biomass Program is conducting research to meet its 2015 target of 10 cents/lb biomass-derived glucose. NREL's approach is to use cellulolytic microbes to ferment cellulose and hemicellulose directly, which will result in lower feedstock costs.

Fiscal Year (FY) 2012 Objectives

- Optimize sequencing fed-batch parameters in converting cellulose to hydrogen by the cellulolytic bacterium *Clostridium thermocellum*; aimed at lowering feedstock cost.
- Improve plasmid stability in *C. thermocellum*; aimed at metabolic pathway engineering to improve hydrogen molar yield via fermentation.
- Complete analysis of fermentation effluent as the first step in examining gas production from an actual fermentation effluent.
- Generate hydrogen without an external energy input in a microbial reverse-electrodialysis electrolysis cell (MREC).

Technical Barriers

This project supports research and development on DOE Technical Task 6, subtasks “Molecular and Systems Engineering for Dark Fermentative Hydrogen Production” and “Molecular and Systems Engineering for microbial electrolysis cell (MEC)” and it addresses barriers AX, AY, and AZ.

(AX) H₂ Molar Yield

(AY) Feedstock Cost

(AZ) System Engineering

FY 2012 Accomplishments

- Conducted sequencing fed-batch reactor experiments and demonstrated scalability of the system, with both total hydrogen output and volumetric rate of hydrogen production proportional to the amount of cellulosic substrate added in the bioreactor containing the cellulose-degrading bacterium *C. thermocellum*. The improved rates of H₂ production were realized via retaining those microbes that were adapted to degrade cellulose.
- Plasmid stability was improved by approximately 150-fold by ensuring the compatibility of the deoxyribonucleic acid (DNA) restriction profiles between *C. thermocellum* and the plasmid used for its transformation. This finding will serve as the foundation for a future genetic engineering effort with this microbe.
- Fermentation wastewater produced from NREL (from a sequencing fed-batch fermentation reactor fed with 5 g/L cellulose) was analyzed in terms of volatile fatty acids (VFAs), alcohols, carbohydrates, and proteins. In the soluble chemical oxygen demand (COD) (10,810 ± 21 mg/L), protein (33%) was a main component, with fewer carbohydrates present (12%). Alcohols and VFAs accounted for 18% and 28% of the soluble COD, respectively. Only 9% of the soluble COD could not be identified.

- Hydrogen gas was successfully produced without an external electrical energy input in an MREC using salinity gradient energy. In order to generate salinity gradient energy, we used ammonium bicarbonate salts, which can be regenerated using low-temperature waste heat as a saline solution in the reverse electrodialysis (RED) stack. The maximum hydrogen production rate was $1.6 \text{ m}^3 \text{ H}_2/\text{m}^3\cdot\text{d}$, with a hydrogen yield of $3.4 \text{ mol H}_2/\text{mol acetate}$ at an essentially infinite salinity ratio (SR) (distilled water as the low concentration solution).



Introduction

Biomass-derived glucose feedstock is a major operating cost driver for economic H_2 production via fermentation. The DOE Fuel Cell Technologies Program is taking advantage of the DOE Biomass Program's investment in developing less expensive glucose from biomass to meet its cost target of 10 cents/lb by 2015. Meanwhile, one alternative and viable approach to addressing the glucose feedstock technical barrier (AY) is to use certain cellulose-degrading microbes that can ferment biomass-derived cellulose directly for H_2 production. One such example is the cellulose-degrading bacterium *Clostridium thermocellum* (*C. thermocellum*), which was reported to exhibit one of the highest growth rates using crystalline cellulose [1]. Another technical barrier to fermentation is the relatively low molar yield of H_2 from glucose ($\text{mol H}_2/\text{mol sugar}$; technical barrier AX), which results from the simultaneous production of waste organic acids and solvents. Biological pathways maximally yield 4 moles of H_2 per 1 mole of glucose (the biological maximum) [2]. However, most laboratories have reported a molar yield of 2 or less [3,4]. Molecular engineering to block competing pathways is a viable option toward improving H_2 molar yield. This strategy had resulted in improved H_2 molar yield in *Enterobacter aerogenes* [5].

A promising parallel approach to move past the biological fermentation limit has been developed by a team of scientists led by Prof. Bruce Logan at Pennsylvania State University (PSU). In the absence of O_2 , and by adding a slight amount of negative potential (-250 mV) to the circuit, Logan's group has produced H_2 from acetate (a fermentation byproduct) at a molar yield of 2.9–3.8 (versus a theoretical maximum of 4) in a modified microbial fuel cell called an MEC [6]. It demonstrates for the first time a potential route for producing eight or more moles of H_2 per mole glucose when coupled to a dark fermentation process. Indeed, in FY 2009 the team reported a combined molar yield of 9.95 when fermentation was coupled to MEC in an integrated system [7]. Combining fermentation with MEC could therefore address technical barriers AX and improve the techno-economic feasibility of H_2 production via fermentation.

Approach

NREL's approach to addressing feedstock cost is to optimize the performance of the cellulose-degrading bacterium *C. thermocellum*. To achieve this goal, we are optimizing the various parameters in a sequencing fed-batch reactor to improve longevity, yield, and rate of H_2 production. To improve hydrogen molar yield, we are selectively blocking competing metabolic pathways in this organism via genetic methods. Through a subcontract, PSU is testing the performance of an MEC using both a synthetic effluent and the real waste stream from lignocellulosic fermentation generated at NREL.

Results

Lignocellulose Fermentation

Cellulose is a solid substrate, and with continuous feeding the system will eventually suffer from clogging of feed lines and over-exhaustion of the feed pump. A more feasible strategy for cellulose fermentation is to feed the substrate at a predetermined interval in lieu of continuous feeding. This strategy can be realized via the use of a sequencing fed-batch bioreactor. This method also simultaneously retains the acclimated microbes to increase the rate of hydrogen production. We carried out the experiment in a Sartorius bioreactor with a working volume of 2 L. The medium was continuously sparged with N_2 at a flow rate of 16 ccm and agitated at 100 rpm. The hydraulic retention time (HRT) tested was 48 h with a daily carbon loading of 2.5, 5.0, or 10.0 g/L of cellulose, four cycles each. The reactor was initiated by running the fermentation using cellulose at 2.5 g/L for 24 h, turning off the agitation for 1 h during which the unfermented substrate along with the attached microbes settled, then removing 1 L of the clear supernatant and adding back 1 L of fresh medium replenished with cellulose (2.5, 5.0, or 10.0 g/L). We completed a total of 12 cycles, four cycles for each carbon loading condition (Table 2).

Initial results indicate that when cellulose substrate loading was increased from 2.5 g/L to 5.0 g/L, both total hydrogen output and volumetric rate of hydrogen production increased proportionally. This finding demonstrates the scalability of the system between two substrate loadings, a very important criterion in a scale-up process. However, proportionally less hydrogen is produced with cellulose at 10 g/L compared to the other loadings; largely this is because not all the substrate was consumed at this loading. The operating principle of sequencing fed-batch fermentation is to have a small amount of excess cellulose substrate to retain acclimated microbes during each cycle of draining and feeding. The excess substrate hence lowers both the total hydrogen output and the hydrogen molar yield (Table 2), as the latter is calculated based on substrate added, not substrate consumed.

TABLE 2. Rate and Yield of Hydrogen Production in Sequencing Fed-Batch Bioreactor with *Clostridium thermocellum* Fermenting Cellulose Substrate

| Cellulose Concentration | Amount of H ₂ produced | Max H ₂ production rate | H ₂ Yield | H ₂ /CO ₂ |
|-------------------------|-----------------------------------|------------------------------------|----------------------------------|---------------------------------|
| (g/L/day) | (mmol) | (mmol/L-h) | (mol H ₂ /mol hexose) | |
| 2.5 | 18.5 | 1.2 | 1.2 | 1.2 |
| 5 | 35.3 | 2.6 | 1.1 | 1.3 |
| 10 | 51.9 | 3.5 | 0.84 | 1.4 |

Metabolic Engineering

The ultimate goal of this approach is to develop tools to inactivate genes encoding competing metabolic pathways, thus redirecting more cellular flux to improve H₂ molar yield. Transformation in this organism has been challenging, likely due to either an inefficiency of the plasmids used or an active restriction system in the host thus destroying the incoming plasmid. NREL established an active collaboration with the researchers from the University of Manitoba, Canada. Using their proprietary plasmid along with optimized protocols, in 2011 we successfully generated via conjugation two mutant lines in *C. thermocellum* harboring the plasmid. However, we discovered later that the plasmids were lost in the *C. thermocellum* transformants after several sub-culturings, likely attributed to an incompatibility of the DNA restriction system between the host and the plasmid [8]. To circumvent this issue, we (1) tested the effect of *dcm* gene knockout in *E. coli* S17-1; and (2) compared two recipient hosts of *C. thermocellum*: ATCC 27405 and DSM 1313. The *E. coli dcm* gene encodes a DNA methylase that specifically methylates the internal cytosine residues of DNA in the sequences of CCAGG and CCTGG at the C⁵ position. Results of colony formation in different strains are summarized in Table 3. When using DSM 1313 as the recipient, conjugating with a Δdcm *E. coli* mutant results in a more than 150-fold increase in the number of colonies growing on a chloramphenicol (Cm, 30 mg/mL) plate (comparing rows 2 and 3, Table 3). While using the same Δdcm *E. coli* strain for conjugation, DSM 1313 conjugants formed more than 450 colonies on a Cm plate, whereas wild-type ATCC 27405 conjugants formed only five colonies on the same plate (comparing rows 1 and 3, Table 2). Based on our data, we concluded that Δdcm *E. coli* and DSM 1313 render better conjugation efficiency for future metabolic engineering efforts. This finding also confirmed the observation reported by Guss et al. [8].

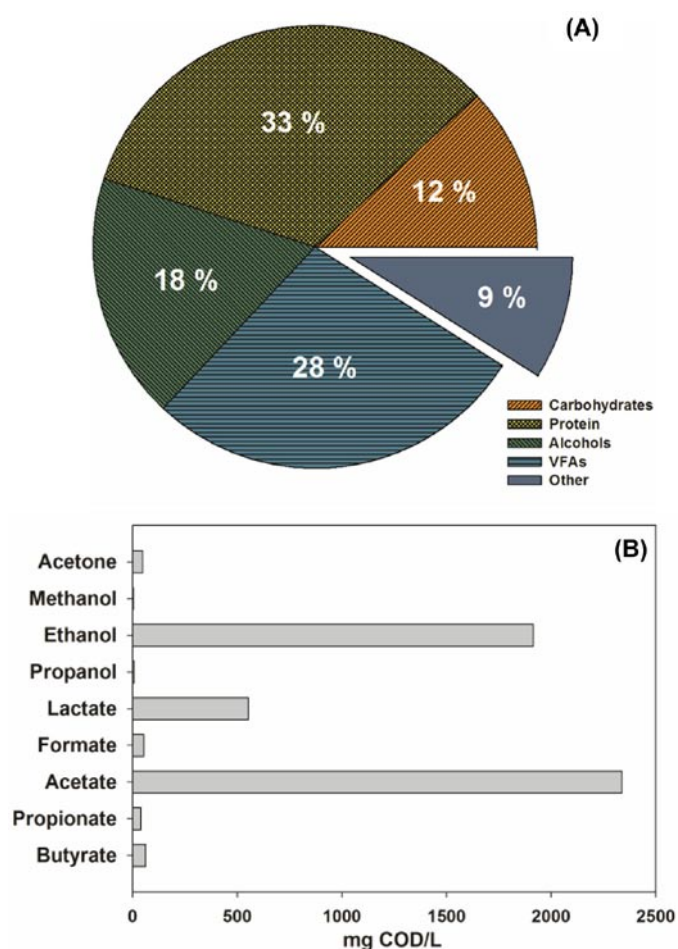
Microbial Electrolysis Cell

Fermentation wastewater produced from NREL was analyzed and found to be composed of proteins,

TABLE 3. *E. coli* and *Clostridium thermocellum* Conjugation Efficiencies

| Conjugation Pair | Cm (μ g/mL) | Growth (Colonies) |
|--------------------------------------|------------------|-------------------|
| 1. <i>E. coli (dcm-)</i> /ATCC 27405 | 30 | 5 |
| 2. <i>E. coli (dcm+)</i> /DSM 1313 | 30 | 3 |
| 3. <i>E. coli (dcm-)</i> /DSM1313 | 30 | >450 |

carbohydrates, alcohols, VFAs, and some organic particulates. The total COD of the fermentation effluent was $11,035 \pm 5$ mg/L and the soluble COD was $10,810 \pm 21$ mg/L, which means that 98% of the effluent consists of soluble organic matter. The soluble COD portion was analyzed in terms of VFAs, alcohols, carbohydrates, and proteins (Figure 1A). Soluble COD contained high concentrations of protein (3,600 mg/L, 33% of the soluble COD) and carbohydrates (1,250 mg/L, 12%). Alcohols and VFAs accounted for 46% of the soluble COD (alcohols 1,974 mg/L, VFAs 3,047 mg/L). Alcohols and VFAs were mainly ethanol (1,915 mg/L) and acetate (2,338 mg/L) (Figure 1B). Only 9%

**FIGURE 1.** (A) Composition of the soluble COD ($10,810 \pm 21$ mg/L) and (B) each alcohol and VFA concentration

of the soluble COD was not identified by this analysis. Due to the various techniques used and measurement errors in each technique, it is possible that this value could be smaller.

Salinity-gradient energy from ammonium bicarbonate (NH_4HCO_3) salts was used as the voltage source for making hydrogen gas in an MEC. A RED stack of alternating ion exchange membranes was placed between the anode and the cathode chambers, producing an MREC. A high concentration (HC) NH_4HCO_3 solution was added into the RED stack, with alternating membrane chambers containing a low concentration (LC) solution of this chemical. The HC solution contained 1.4 M NH_4HCO_3 , and the LC solution of NH_4HCO_3 was adjusted to produce different salinity ratios (SRs) of 100, 200, 400, 800, and infinite (distilled water in the LC solution). Current and hydrogen gas were successfully generated in the MREC using only the NH_4HCO_3 solution and no external power supply. The MREC performance was relatively insensitive to the SRs. The peak volumetric current densities varied over a small range of $137 \pm 8 \text{ A/m}^3$ to $152 \pm 8 \text{ A/m}^3$ for the different SRs. Total hydrogen generation ranged from 27 mL H_2 ($Y = 2.8 \text{ mol H}_2/\text{mol acetate}$, $\text{SR} = 200$) to 30 mL H_2 ($Y = 3.4 \text{ mol H}_2/\text{mol acetate}$, $\text{SR} = \text{infinite}$) over each fed-batch cycle. Energy recovery was 10% based on total energy applied, with an energy efficiency of 22% based on the consumed energy in the reactor. A reduction in the HC solution (1.4 M to 0.1 M) with a fixed LC solution ($\text{SR} = \text{infinite}$) decreased current generation and increased the time needed to complete a fed-batch cycle (Figure 2A). The coulombic efficiency substantially decreased with HC solution, from $\eta_{CE} = 72\%$ using the 1.4 M HC solution to $\eta_{CE} = 50\%$ using the 0.1 M HC solution. The reduction in current decreased the recovery of hydrogen gas from 30 mL H_2 to 17 mL H_2 (93%–94% H_2 , 6%–7% CO_2) and decreased the gas production rate from $1.6 \text{ m}^3 \text{ H}_2/\text{m}^3 \cdot \text{d}$ to $0.5 \text{ m}^3 \text{ H}_2/\text{m}^3 \cdot \text{d}$ (Figure 2B).

Conclusions and Future Direction

- Using cellulose as the substrate, we successfully demonstrated scalability of cellulose fermentation in the sequencing fed-batch mode. We determined that both hydrogen output and volumetric rate of hydrogen production doubled when the cellulose substrate loading was increased from 2.5 g/L to 5.0 g/L with a HRT of 48 h.
- We knocked out the *dcm* gene in *E. coli* S17-1 (the conjugation host) to have a more compatible DNA methylation system with *C. thermocellum* (both strains become *dcm*). This improved plasmid transfer and maintenance in *C. thermocellum* by at least 150-fold. The outcome should aid in future site-directed mutagenesis of competing pathways to improve hydrogen molar yield.
- The fermentation wastewater was mostly composed of soluble organic matter including proteins, carbohydrates, alcohols, and VFAs. The fact that most of the material is

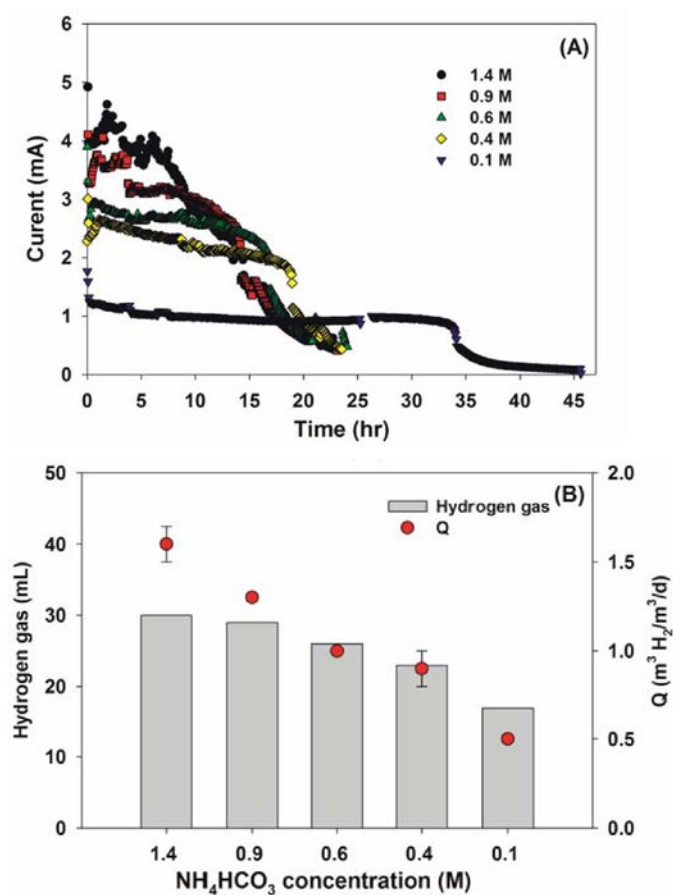


FIGURE 2. MREC performance with different HC concentration: (A) current generation and (B) gas production

soluble will help in converting this material into current and hydrogen gas in the MEC.

- Hydrogen gas was successfully produced without an external energy input in an MREC using salinity gradient energy.

In the future, we will continue to optimize sequencing fed-batch fermentation by testing HRTs of 4 h, 8 h, 12 h, and 24 h. Depending on the HRT, various volumes of liquid replacement will be tested (up to 50% of working volume) aimed at improving both rates and output of hydrogen production as well as cellulose consumption. We will continue to develop genetic tools for molecular engineering in *C. thermocellum* to alter its metabolic pathway to improve H_2 molar yield. We will redesign the plasmid by reducing its size (removing non-essential features) and replacing origin of replication suitable for an electroporation protocol to improve transformation efficiency. In future MEC tests, fermentation wastewater will be supplied to the prototype MEC in order to examine hydrogen production from an actual fermentation effluent. The MEC will be operated in continuous flow mode with the optimum operation conditions that were obtained

with synthetic wastewater (sodium acetate). Also, increased power (more positive anode potentials) will be evaluated in order to enhance treatment efficiency of fermented wastewater. The MREC will be redesigned to examine the scalability of the MREC without an external energy input, and operating conditions such as hydraulic retention times, salinity ratios, and concentrations of the saline solution will be optimized.

FY 2012 Publications/Presentations

1. Thammannagowda, S.; Magnusson, L.; Jo, J.H.; Maness, P.C.; and Seibert, M. 2011. Renewable hydrogen production from biomass. *Enchyclo. Biol. Chem.*
2. Levin, D.; Jo, J.; and Maness, P.C. 2012. Biohydrogen production from cellulosic biomass. Book chapter in “Integrated Forest BioRefineries” (ed. L. Christopher). Royal Society of Chemistry, Cambridge, UK.
3. Nam, J.Y. and Logan, B.E. 2011. Enhanced hydrogen generation using a highly saline catholyte in a two chamber microbial electrolysis cell. *Int. J. Hydrogen Energy* 36(23): 15105-15110.
4. Nam, J.Y.; Cusick, R.D.; Kim, Y.; and Logan, B.E. 2012. Hydrogen generation in microbial reverse-electrodialysis electrolysis cells using a heat-regenerated salt solution. *Environ. Sci. Technol.* 46(9): 5240-5246.
5. Maness, P.C. “The hydrogen production network in *Clostridium thermocellum*.” 2011. SIM Annual Meeting and Exhibition. July 24–28, 2011, New Orleans, LA.
6. Maness, P.C. and Logan, B. 2012. DOE Fuel Cell Technology Program Review, May 2012, Washington, DC. Presentation PD038.

References

1. Zhang, Y.P.; Lynd, L.R. (2005). Cellulose utilization by *Clostridium thermocellum*: bioenergetics and hydrolysis product assimilation. *Proc. Natl. Acad. Sci. USA* **102**, 7321-7325.
2. Hawkes, F.R.; Dinsdale, R.; Hawkes, D.L.; Hussy, I. (2002). Sustainable fermentative hydrogen production: Challenges for process optimisation. *Intl. J. Hydrogen Energy* **27**, 1339–1347.
3. Logan, B.E.; Oh, S.E.; Kim, I.S.; Van Ginkel, S. (2002). Biological hydrogen production measured in batch anaerobic respirometers. *Environ. Sci. Technol.* **36**, 2530–2535.
4. Van Ginkel, S.; Sung, S. (2001). Biohydrogen production as a function of pH and substrate concentration. *Environ. Sci. Technol.* **35**, 4726–4730.
5. Rachman, M.A.; Furutani, Y.; Nakashimada, Y.; Kakizono, T.; Nishio, N. (1997). Enhanced hydrogen production in altered mixed acid fermentation of glucose by *Enterobacter aerogenes*. *J. Ferm. Eng.* **83**, 358–363.
6. Cheng, S.; Logan, B.E. (2007). Sustainable and efficient biohydrogen production via electrogenesis. *Proc. Natl. Acad. Sci. USA.* **104**, 18871-18873.
7. Lalaurette, E.; Thammannagowda, S.; Mohagheghi, A.; Maness, P.C.; Logan, B.E. (2009). Hydrogen production from cellulose in a two-stage process combining fermentation and electrohydrogenesis. *Intl. J. Hydrogen Energy* **34**, 6201-6210.
8. Guss, A.; Olson, D.G.; Caiazza, N.C.; Lynd, L.R. (2012). Dcm methylation is detrimental to plasmid transformation in *Clostridium thermocellum*. *Biotechnol. Biofuels* **5**, 30-41.

II.G.3 Hydrogen from Water in a Novel Recombinant Oxygen-Tolerant Cyanobacterial System

Philip D. Weyman (Primary Contact),
Isaac T. Yonemoto, Hamilton O. Smith

J. Craig Venter Institute
10355 Science Center Dr.
San Diego, CA 92121
Phone: (858) 200-1815
Email: pweyman@jcvl.org

DOE Managers

HQ: Eric Miller
Phone: (202) 287-5829
Email: Eric.Miller@hq.doe.gov

GO: Katie Randolph
Phone: (720) 356-1759
Email: Katie.Randolph@go.doe.gov

Contract Number: DE-FC36-05GO15027

National Laboratory Collaborators:

- Karen Wawrousek, Scott Noble, Jianping Yu, and Pin-Ching Maness
- National Renewable Energy Laboratory (NREL), Golden, CO

Project Start Date: May 1, 2005

Project End Date: January 30, 2014

Fiscal Year (FY) 2012 Objectives

Develop an O₂-tolerant cyanobacterial system for sustained and continuous light-driven H₂-production from water.

Technical Barriers

This project addresses the following technical barriers from the Hydrogen Production section (3.1.4) of the Fuel Cell Technologies Program Multi-Year Research, Development and Demonstration Plan:

(AH) Rate of Hydrogen Production

(AI) Continuity of Photoproduction

Technical Targets

| Characteristics | Current Status | 2011 Target | 2018 Target |
|--|---------------------------|--|---|
| Duration of continuous H ₂ photoproduction in air | Zero to 30 seconds in air | Produce a cyanobacterial recombinant evolving H ₂ through an O ₂ -tolerant hydrogenase | H ₂ production in air for 30 min |

FY 2012 Accomplishments

JCVI

- Re-engineered transcriptional regulation of hydrogenase to achieve four-fold higher activity (from 0.5 to 2 nmol H₂*mg protein⁻¹*h⁻¹).
- Examined the effect of transcriptional modifications on hydrogenase maturation and found that proper regulation of accessory genes is essential for optimal hydrogenase maturation.
- Created mutants of the environmentally-derived hydrogenase small subunit with four-fold improved activity that is biased toward hydrogen evolution.

NREL

- Determined that the putative maturation genes *hypABCDEFG* likely are involved in the maturation of the Casa Bonita strain (CBS) O₂-tolerant hydrogenase. This is supported by similar expression profiles in response to CO for both maturation genes and the hydrogenase structural genes.
- A *Synechocystis* recombinant harboring 10 CBS genes was constructed (including four hydrogenase genes and six maturation genes), with the expression of both HypE and HypF verified by protein immunoblots. A very low level of *in vitro* hydrogenase activity was detected in the recombinant compared to zero-hydrogenase activity in the untransformed control.



Introduction

Photobiological processes are attractive routes to renewable H₂ production. With the input of solar energy, photosynthetic microbes such as cyanobacteria and green algae carry out oxygenic photosynthesis, using sunlight

energy to extract reducing equivalents from water. The resulting reducing equivalents can be fed to a hydrogenase system yielding H₂. However, one major difficulty is that most hydrogen-evolving hydrogenases are inhibited by O₂, which is an inherent byproduct of oxygenic photosynthesis. The rate of H₂ production is thus limited. Certain photosynthetic bacteria are reported to have an O₂-tolerant evolving hydrogenase, yet these microbes do not split water, and require other more expensive feedstocks.

To overcome these difficulties, we propose to construct novel microbial hybrids by genetically transferring O₂-tolerant hydrogenases from other bacteria into cyanobacteria. These hybrids will use the photosynthetic machinery of the cyanobacterial hosts to perform the water-oxidation reaction with the input of solar energy, and couple the resulting reducing equivalents to the O₂-tolerant bacterial hydrogenase, all within the same microbe. By overcoming the sensitivity of the hydrogenase enzyme to O₂, we address one of the key technological hurdles to cost-effective photobiological H₂ production which currently limits the production of hydrogen in algal systems.

Approach

Our goal is to construct a novel microbial hybrid taking advantage of the most desirable properties of both cyanobacteria and other bacteria, to serve as the basis for technology to produce renewable H₂ from water. To achieve this goal, we use the following two approaches. The first approach is to transfer known O₂-tolerant hydrogenases from anoxygenic photosynthetic bacteria *Thiocapsa roseopersicina* and *Rubrivivax gelatinosus* to cyanobacteria. Since only a very limited number of O₂-tolerant hydrogenases are available, our second approach is to identify novel O₂-tolerant hydrogenases from environmental microbial communities and transfer them into cyanobacteria.

Results

JCVI

Previously, we reported the successful expression in cyanobacteria of active, oxygen-tolerant NiFe hydrogenases. These NiFe hydrogenases included the stable hydrogenase from *Thiocapsa roseopersicina* and a novel, environmentally-derived NiFe hydrogenase, HynSL, (previously named HyaAB). Although active hydrogenases were expressed indicating co-expression of all required accessory proteins, the activity was low. We hypothesized that improved plasmid design may increase activity. The original expression plasmid, pRC41, expressed the environmentally-derived hydrogenase under the regulation of one promoter at the beginning of the 13 gene construct (Figure 1A). With such a long transcript (~13-kb), genes

encoded at the end of the operon, such as the *hyp* genes, may not be expressed in sufficient quantity to allow for maximal activity of the environmental hydrogenase in cyanobacteria. These genes at the end of the operon are required for maturation of the hydrogenase and must be transcribed at the optimal level.

In order to achieve higher expression throughout the gene cluster, we have re-engineered the expression plasmid to create an additional three promoters spaced throughout the operon (Figure 1A). We also inserted a sequence encoding the StrepII peptide tag onto the N-terminus of the last gene in the cluster, *hypE*, so that we could monitor expression at the end of the gene cluster.

The presence of one additional promoter preceding the last three genes in the cluster, Nstrep3 (Figure 1A) did not significantly improve hydrogenase activity in cyanobacteria, but it did increase expression of the last gene in the cluster, *hypE* (Figure 1C). The redesigned plasmid with three additional promoters spread throughout the gene cluster, Nstrep5, had approximately four-fold increase in activity over the single promoter version, Nstrep1. This increase in activity was consistent with an increase in total abundance of HynL and HypE protein (Figure 1C). Overall, in both Nstrep1 and Nstrep 5 constructs, most of the HynL protein was found in the pre-processed or immature form, suggesting that optimization of hydrogenase maturation remains a key challenge for heterologous expression. One surprising result was that construct Nstrep3 had increased processing of PreHynL to HynL without a corresponding increase in activity (Figure 1C). This suggests that relative strengths of the promoters we employ to achieve optimum expression must be optimized.

In a parallel approach to increasing activity in the environmentally-derived hydrogenase, we made three mutants that differ in the amino acids that ligate the iron-sulfur clusters to the hydrogenase small subunit. In the first mutant (Figure 2A diagram 2), an amino acid near the proximal cluster was modified from histidine to cysteine which is expected to change the ligation of the cluster to the protein. In the second mutant (Figure 2A diagram 3), an amino acid near the medial cluster was changed from proline to cysteine. This is expected to change the cluster from 3Fe4S to 4Fe4S. Research in other labs suggests that this mutation will remove energy barriers in the flow of electrons from the electron transfer site to the catalytic center. The third mutant combines both of these single mutations into one single strain (Figure 2A diagram 4). We found that neither of the single mutations increased activity individually, but when combined, hydrogen evolution activity increased by approximately four-fold (Figure 2B). To determine if this was a specific change in enzyme bias or a more general increase in the activity of the enzyme, we also measured hydrogen uptake activity. We found that while uptake activity was slightly elevated in constructs 2 and 3, the increase was not

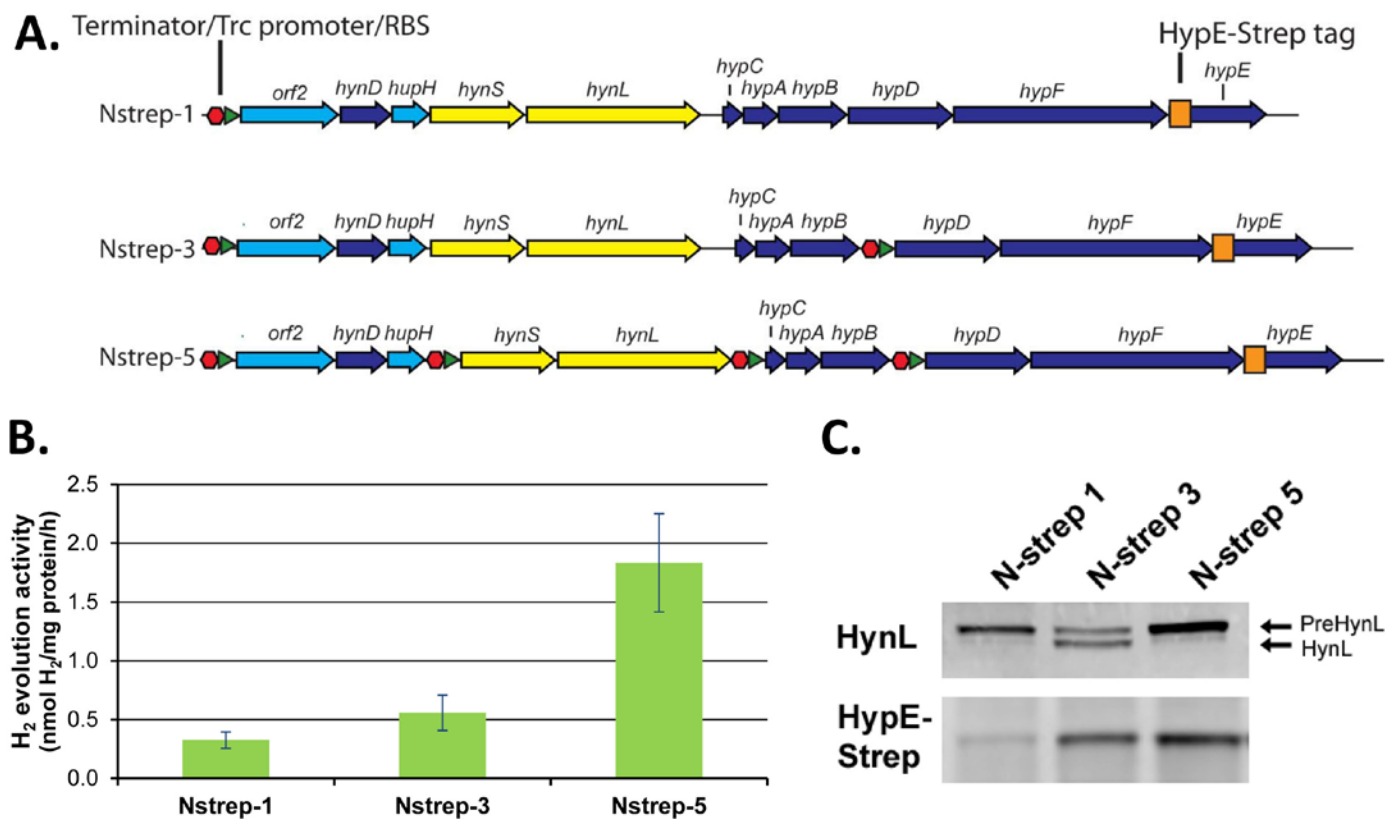


FIGURE 1. Transcriptional re-engineering of the environmentally-derived hydrogenase: (A) Diagram of hydrogenase structural and accessory genes, terminator/promoter cassettes (red hexagon/green triangle), and *hypE* N-terminal StrepII-tag (orange square). (B) *In vitro* hydrogen evolution activity of transcriptionally-modified constructs described in A. (C) Western blots of cyanobacterial extracts from B using anti-HynL or anti-StrepII antisera.

significant and the uptake activity of the mutants was similar to wild type (Figure 2C).

NREL

The overarching goal of the NREL work is to construct a cyanobacterial recombinant harboring the O₂-tolerant hydrogenase from *Rubrivivax gelatinosus* CBS (hereafter “CBS”) using *Synechocystis* sp. PCC 6803 as a model host for sustained photolytic hydrogen production. A prerequisite for success is to gain better understanding of the CBS hydrogenase and its underlying maturation machinery to ensure transfer of the correct genes into *Synechocystis* to confer hydrogenase activity. One strategy to probe the function of the six putative *hypABCDEF* maturation genes is to test if their expression follows the same induction profile as the CBS hydrogenase genes (*cooMKLXUH*), the latter is specifically induced by CO. RT-qPCR was used to examine transcript levels and fold changes of these genes under various conditions. In this case, we chose to grow CBS in three gaseous conditions: with argon gas (un-induced condition), with CO (induced condition), or with CO₂ (a product of CO oxidation). As seen in Figure 3, the *hypA*, *B*, and *D* genes are specifically induced in the presence of

CO, by as high as ~450 fold (*hypB*) compared to the argon gas control, and the *cooH* gene was used as a positive control. Very little transcript abundance was detected in CO₂ atmosphere. While *hypC*, *E*, and *F* are not shown in Figure 3, transcription of these genes was also specifically induced by CO; however, the fold change in mRNA level could not be calculated because the *hypC*, *E*, and *F* transcripts were not abundant enough to be detected in the un-induced condition (in argon gas). Protein immunoblots also confirmed the expression of both HypE and HypF proteins only upon induction by CO (data not shown). These results clearly show that the *hypABCDEF* genes are specifically induced in the same condition in which the CBS O₂-tolerant hydrogenase is induced (both by CO), and strongly suggests that these six *hyp* genes are involved in the production of an active CBS O₂-tolerant hydrogenase and should therefore be transferred into *Synechocystis* host along with the CBS hydrogenase.

Working toward building the cyanobacterial recombinant, we have generated a *Synechocystis* strain containing the four codon-optimized CBS hydrogenase genes (*cooLXUH*). Using this strain as the recipient, we first transformed five codon-optimized *hypABCDE* genes into its genome. Correct gene insertion was verified by polymerase

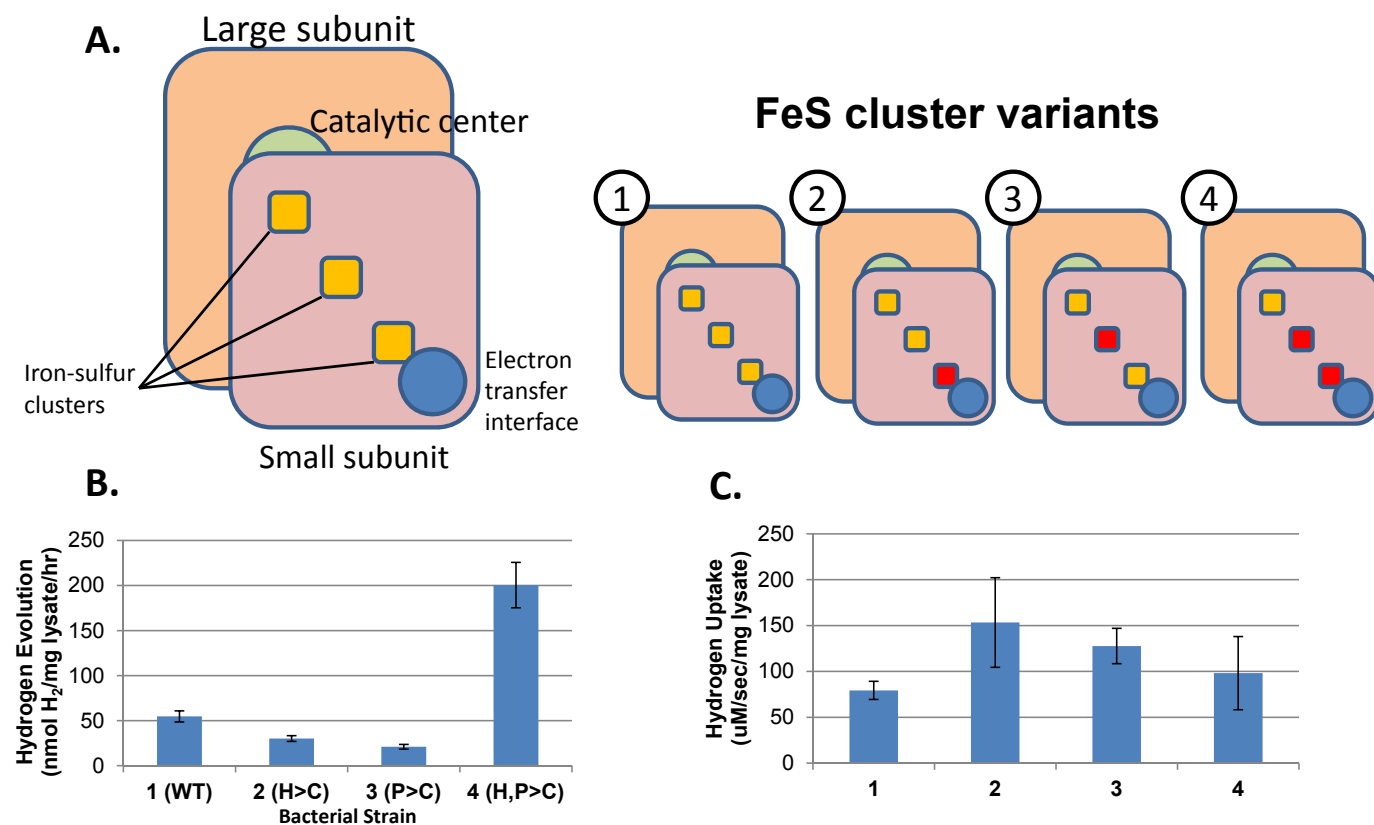


FIGURE 2. Modification of activity bias in mutants of hydrogenase small subunit: (A) Diagram of point mutations. Construct 1 shows the wild type, 2 shows a His to Cys mutation in the proximal cluster, 3 shows a Pro to Cys mutation in the medial cluster, and 4 shows the double mutant with both mutations from 2 and 3. (B) *In vitro* hydrogen evolution activity in extracts from *E. coli* strains expressing the wild type environmental hydrogenase or strains containing the point mutants. (C) *In vitro* hydrogen uptake activity in extracts from *E. coli* strains expressing the wild type environmental hydrogenase or strains containing the point mutants.

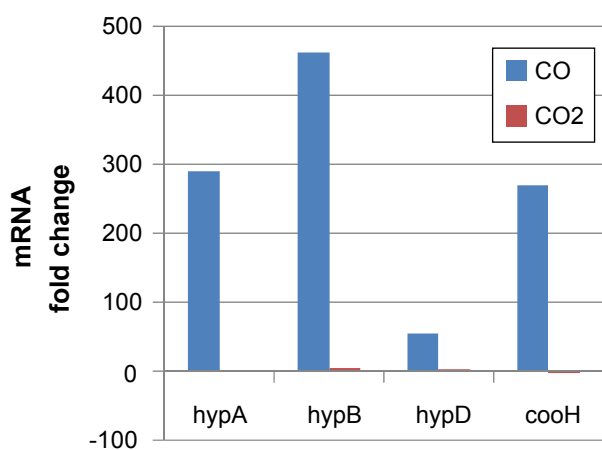


FIGURE 3. Expression profiles of the CBS hydrogenase maturation genes. RT-qPCR was used to detect changes in *hypABCDEF* gene transcript abundance. An un-induced control under argon gas was used to calculate fold change of transcripts using the $\Delta\Delta C_t$ method. The *cooH* gene, encoding the hydrogenase catalytic subunit, was used as a positive control.

chain reaction (data not shown) and the expression of HypE was verified by protein immunoblot (Figure 4A). This was

then followed by transforming the codon-optimized CBS *hypF* gene into the above recombinant, with HypF expression also confirmed via immunoblot (Figure 4B). A schematic of the genotype of the *Synechocystis* strain heterologously expressing 10 CBS genes is illustrated in Figure 4C. The recombinant yielded very low level of hydrogenase activity, *in vitro*, when assayed using methyl viologen reduced by sodium dithionite. Albeit low, the untransformed control exhibited no hydrogenase activity.

Conclusions

JCVI

- By increasing the frequency of promoters driving the expression of hydrogenase genes, we have achieved four-fold higher activity from the environmentally-derived hydrogenase expressed in cyanobacteria.
- We mutated the DNA sequence of the hydrogenase small subunit to change the ligation of FeS clusters. The resulting mutant has increased activity in the direction of hydrogen production.

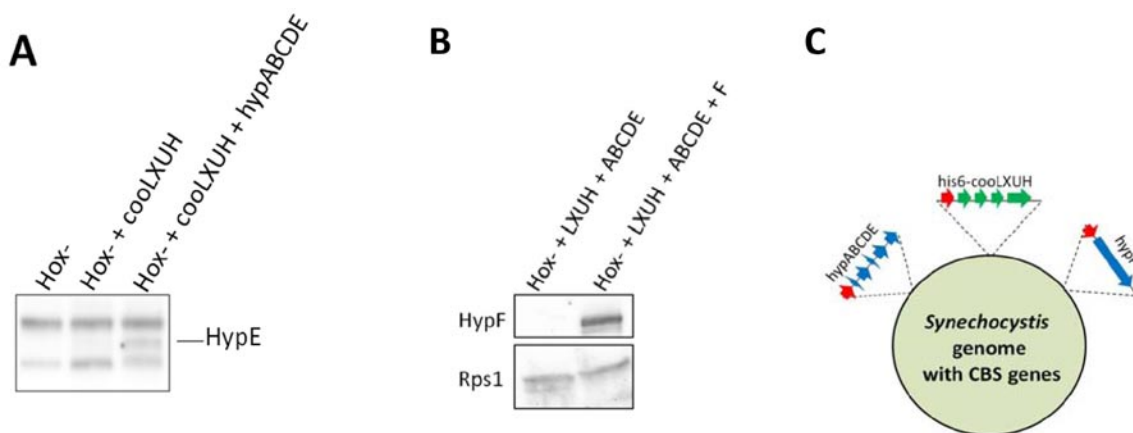


FIGURE 4. (A) Expression of HypE in the recombinant *Synechocystis* strain harboring *coolXUH* and *hypABCDE* as revealed by immunoblot. (B) Expression of HypF in the recombinant *Synechocystis* strain harboring *coolXUH*, *hypABCDE*, and *hypF*, as revealed by immunoblot. (C) Schematic of CBS hydrogenase genes integrated into the genome of *Synechocystis*. Red arrows denote promoters, green arrows are the CBS hydrogenase structural genes *coolXUH*, and blue arrows represent the putative hydrogenase maturation genes, *hypABCDE*.

NREL

- Using both RT-qPCR and protein immunoblots, we successfully demonstrated that the CBS *hypABCDE* genes are likely involved in the assembly and maturation of the CBS O₂-tolerant hydrogenase. The maturation genes and hydrogenase genes display similar induction profiles upon the addition of CO, but not in the argon and CO₂ gas controls.
- We constructed a *Synechocystis* recombinant harboring all ten CBS genes: four hydrogenase genes and six maturation genes. The recombinant displayed low levels of hydrogenase activity when assayed with methyl viologen reduced by sodium dithionite. Albeit low, its untransformed control displayed no hydrogenase activity.

Future Directions

JCVI

- We will continue to modify the environmentally-derived hydrogenase by using additional promoters and by varying the relative promoter strengths throughout the gene cluster to optimize maturation of the enzyme.
- We will combine transcriptional modification approaches and point mutant approaches to further increase hydrogenase activity.

NREL

- We will identify additional hydrogenase maturation genes using the sequenced genome of CBS. Following initial characterization of gene expression and function, candidate maturation genes will be transferred into *Synechocystis* host to express a functional O₂-tolerant hydrogenase.
- We will engineer stronger promoter and shorter transcript size, and optimize growth conditions to maximize the expression of the heterologous hydrogenase in *Synechocystis*.

FY 2012 Publications/Presentations

- Carrieri, D., K. Wawrousek, C. Eckert, J. Yu, and P.C. Maness. 2011. The role of the bidirectional hydrogenase in cyanobacteria. *Biores. Technol.* 102: 8368-8377.
- Hu, P., J. Lang, K. Wawrousek, J. Yu, P.C. Maness, and J. Chen. 2012. Draft genome sequence of *Rubrivivax gelatinosus* CBS. *J. Bacteriol.* 194: 3262.
- 2012 DOE Hydrogen Program Annual Merit Review – Washington, DC, May 2010, Oral Presentation PD039 (Weyman and Maness).
- Noble, SL, Wawrousek K, Yu J, Maness PC. (2012 June) “Genetic Engineering of *Synechocystis* sp. PCC 6803 for Sustained Hydrogen Production” Poster presentation at Gordon Research Conference on Iron-Sulfur Enzymes, Mount Holyoke College, MA (Noble).

II.G.4 Maximizing Light Utilization Efficiency and Hydrogen Production in Microalgal Cultures

Tasios Melis

University of California, Berkeley
Dept. of Plant & Microbial Biology
111 Koshland Hall
Berkeley, CA 94720-3102
Phone: (510) 642-8166
Email: melis@berkeley.edu

DOE Managers

HQ: Eric Miller
Phone: (202) 287-5829
Email: Eric.Miller@ee.doe.gov
GO: Katie Randolph
Phone: (720) 356-1759
Email: Katie.Randolph@go.doe.gov

Contract Number: DE-FG36-05GO15041

Start Date: December 1, 2004
End Date: November 30, 2013

Fiscal Year (FY) 2012 Objectives

- Publish the work on the *TLA2* gene and show its *modus operandi* as to how it confers a truncated Chl antenna size in *Chlamydomonas reinhardtii*.
- Provide physiological and genetic characterization of the *tla3* mutant, including mapping of the plasmid insert site and cloning of the gene affected in the *tla3* mutation.

Technical Barriers

This project addresses the following technical barriers from the Biological Hydrogen Production section of the Fuel Cell Technologies Program Multi-Year Research, Development and Demonstration Plan:

(AG) Light Utilization Efficiency

Technical Targets

The Fuel Cell Technologies Program Multi-Year Plan technical target for this project was to reach a truncated Chl antenna size of about 150 Chl molecules in unicellular green algae by 2015. Progress was achieved ahead of schedule enabling us to reach this goal by 2012.

Approach

- Perform *Chlamydomonas reinhardtii* genomic deoxyribonucleic acid (DNA) mapping at the site of plasmid DNA insertions, followed by identification of open reading frames (ORFs = putative genes) that have been affected by the plasmid insertion.
- Perform complementation-type transformations of the *tla* mutant with each of the affected ORFs to rescue the mutation and, thus, identify the gene that confers a TLA property.
- Clone and characterize the gene(s) that affect the “Chl antenna size” property in *Chlamydomonas reinhardtii*.

FY 2012 Accomplishments (TLA1-MOV34/MPN effort)

- Bioinformatic analysis tentatively identified the truncated light-harvesting chlorophyll antenna-1 (TLA1) protein as a variant of the MOV34/MPN containing proteins.

FY 2012 Accomplishments (TLA2-ΔFTSY effort)

- Physiological characterization of the *tla2* mutant was completed.
- Genetic analysis and multiple crosses of the *tla2* mutant were completed.
- Mapping of the plasmid insert site in the *tla2* mutant was completed.
- Of the five genes adversely affected by the plasmid insertional mutagenesis, gene Cre05.g241450 encoding the CpFTSY protein complemented the mutation.
- The unique functional role of the CpFTSY protein in algae was elucidated.
- Patent application on the function of the TLA2-CpFTSY gene filed.

FY 2012 Accomplishments (TLA3 effort)

- Physiological and genetic characterization of the *tla3* mutant was completed.
- Mapping of the plasmid insert site in the *tla3* mutant was completed.
- The gene affected in the *tla3* mutation is known.
- A Western blot analysis remains to be done for project completion.

TABLE 1. *Chlamydomonas reinhardtii* cellular chlorophyll content, photosystem chlorophyll antenna size and energy utilization efficiency in wild type, *tla1*, *tla2* and *tla3* mutant strains, as determined by spectrophotometric kinetic analysis (n = 5, ±SD).

| | wild type | <i>tla1</i> | <i>tla2</i> | <i>tla3</i> | Long-term goal |
|--|-----------|-------------|-------------|-------------|----------------|
| Chl/cell mol x10 ⁻¹⁵ | 2.4 ±0.5 | 0.9 ±0.06 | 0.93 ±0.1 | 0.7 ±0.1 | |
| Chl-PSII | 222±26 | 115±36 | 80±30 | 50±30 | 37 |
| Chl-PSI | 240±4 | 160±12 | 115±10 | 105±10 | 95 |
| Light Utilization Efficiency (Solar to Chemical) | ~3% | ~10% | ~15% | ~25% | ~30% |



Introduction

The goal of the research is to generate green algal strains with enhanced photosynthetic productivity and H₂-production under mass culture conditions. To achieve this goal, it is necessary to optimize the light absorption and utilization properties of the cells [1-4]. A cost-effective way to achieve this goal is to reduce the number of Chl molecules that function in the photosystems of photosynthesis.

The rationale for this work is that a truncated light-harvesting Chl antenna size in green algae will prevent individual cells at the surface of the culture from over-absorbing sunlight and wastefully dissipating most of it (Figure 1). A truncated Chl antenna size will permit sunlight to penetrate deeper into the culture, thus enabling many more cells to contribute to useful photosynthesis and H₂-production (Figure 2). It has been shown that a truncated Chl antenna size will enable about 3-4 times greater solar energy conversion efficiency and photosynthetic productivity than could be achieved with fully pigmented cells [5].

Approach

The focal objective of the research is to identify genes that control the Chl antenna size of photosynthesis and, further, to elucidate how such genes confer a truncated Chl antenna size in the model green alga *Chlamydomonas*

reinhardtii. Identification of such genes in *Chlamydomonas* will permit a subsequent transfer of this property, i.e., “truncated Chl antenna size”, to other microalgae of interest to the DOE Fuel Cell Technologies Program. This objective has been successfully approached through DNA insertional mutagenesis/screening and biochemical/molecular/genetic analyses of *Chlamydomonas reinhardtii* cells.

Results

The *tla2* mutant plasmid insert site has been cloned and the nuclear-encoded and chloroplast-localized FTSY gene (TLA2-CpFTSY) was identified as causing the *tla2* mutation. The TLA2-CpFTSY gene deletion, causing the *tla2* phenotype, was cloned by mapping the insertion site and upon successful complementation with the *C. reinhardtii* TLA2-CpFTSY gene, whose occurrence and function in green microalgae has not hitherto been investigated. Functional analysis showed that the nuclear encoded and chloroplast-localized CrCpFTSY protein specifically operates in the assembly of the peripheral components of the Chl *a-b* light-harvesting antenna. Figure 3 shows TLA2-CpFtsY

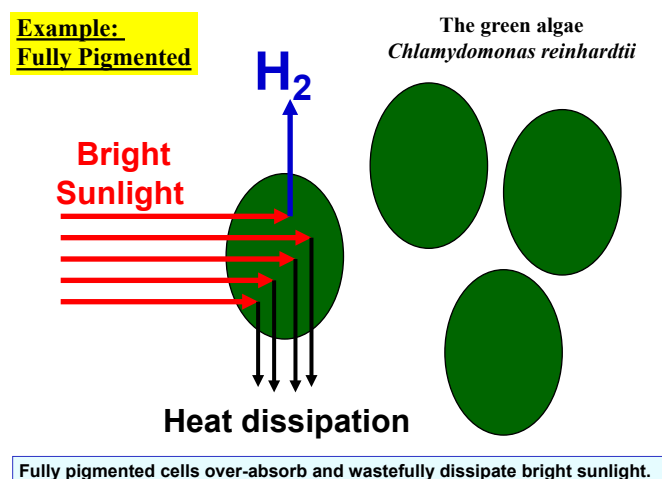


FIGURE 1. Schematic presentation of the fate of absorbed sunlight in fully pigmented (dark green) algae. Individual cells at the surface of the culture over-absorb incoming sunlight (i.e., they absorb more than can be utilized by photosynthesis), and ‘heat dissipate’ most of it. Note that a high probability of absorption by the first layer of cells would cause shading of cells deeper in the culture.

TABLE 2. Progress achieved vs the DOE targets. Chlorophyll antenna size in wild type and mutants (minimum possible = 130 Chl molecules).

| Year | 2000 | 2003 | 2005 | 2007 | 2008 | 2010 | 2011 | 2012 | 2015 |
|---|-----------------|-----------------|-----------------|----------------|-----------------|------|-------------|------|------|
| Targets (Chl Antenna Size) | 600 (wild type) | | 300 | | | 200 | | | 150 |
| TLA strain identified | 600 (wild type) | 300 <i>tla1</i> | 195 <i>tla2</i> | | 150 <i>tla3</i> | | | | |
| Gene cloning and functional elucidation | | | | TLA1-Mov34-MPN | | | TLA2-CpFTSY | TLA3 | |

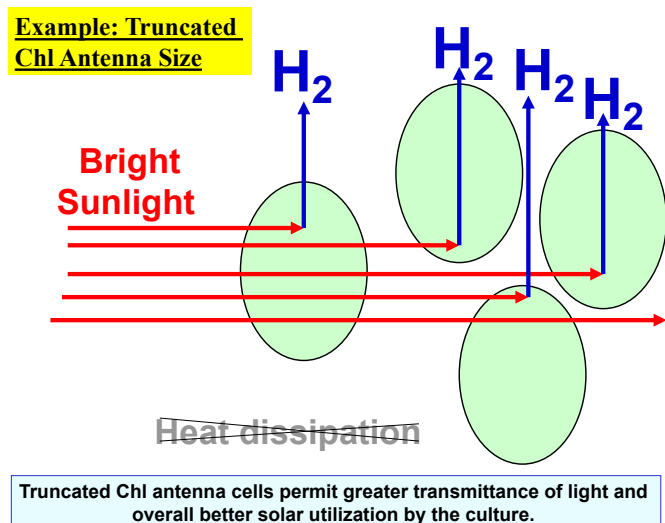


FIGURE 2. Schematic of sunlight penetration through cells with a truncated chlorophyll antenna size. Individual cells have a diminished probability of absorbing sunlight, thereby permitting penetration of irradiance and H₂-production by cells deeper in the culture.

protein amino acid sequence and polypeptide structure revealing domains that are critical for its function [6].

In higher plants, a *cpfts* null mutation inhibits assembly of both the light-harvesting complex and photosystem

complexes, thus resulting in a seedling-lethal phenotype. The work shows that *cpfts* deletion in green algae, but not in higher plants, can be employed to generate *tla* mutants. The latter exhibit improved solar energy conversion efficiency and photosynthetic productivity under mass culture and bright sunlight conditions. This molecular and genetic analysis has been completed and results have been published.

Work further described the isolation and biochemical and physiological characterization of a new mutant of *Chlamydomonas reinhardtii*, termed *tla3*. Properties of the *tla* “truncated Chl antenna size” strains so far isolated are summarized in Tables 1 and 2, and Figure 3. The *tla3* mutant has the smallest yet Chl antenna size known in green algae.

Future efforts will be directed toward the cloning and characterization of gene(s) responsible for the *tla* phenotype in the *tla3* mutant, as well as *tla*-type cyanobacteria.

Conclusions

- Significant progress was achieved in terms of characterization of “truncated Chl antenna size” mutants, cloning of the respective *TLA* genes, and elucidation of the properties of the proteins encoded by these genes.
- Results and analyses on the molecular mechanism for the regulation of the Chl antenna size by the *TLA1* gene [7] and by the *TLA2* gene [6] were published.

TLA2-CpFtsY amino acid sequence and protein structure

MQTTVGRKCVASSAAGRSRNVTVFRRCSSRGGPVKVVANAGGEAGPGFLQRLGRVIKEKA
AGDFDFFAGTSKTRERLGLVDEMLALWSLEDYEDSLEELEEVLI SADFGPRTALKIVD
RIREGVKAGRVS AEDIRASLKAAIVELLTARGRSSELKLGPRPAVVLI VGVNGAGKTT
TVGKIAYKYGKEGAKVFLIPGDTFRAAAEOQLA EWSRRAGATIGAFREGARPQAVIASN
LDDLQRQRTCKDASDVYDLILVDTAGRLHTAYKLM EELALCKAAVSNALPGQPDETLVL
DGTTGLNMLNQAKEFNEAVRLSGLILTKLDGTARGGAVVS VVDQLGLPVKFIGVGETAE
DLQPFDPFAEALFPKVKEPATAGTK



◆ : nucleotide binding domains; cTP: chloroplast transit peptide;
 HB: helical bundle domain

FIGURE 3. Top, Amino acid sequence of the *C. reinhardtii* chloroplast-localized FTSY protein. Domains of the CrCpFtsY protein are defined as follows: amino acids 1 to 36, transit peptide (green font). Amino acids 66 to 147, helical bundle domain (Pfam), SRP54-type protein (blue font). Amino acids 162 to 370, GTPase domain (Pfam), SRP54-type protein (orange font). Amino acids 164 to 183, P-loop nucleotide binding motif. Amino acids 170 to 176, 258 to 262, and 322 to 325, homologous nucleotide binding (red underlined). Bottom, Domain presentation of the CrCpFtsY protein. CpTP, Chloroplast transit peptide; HB, helical bundle domain; GTPase, GTPase domain. (From [6])

- Completion of the work on the *TLA3* gene is nearly at hand.

Future Directions

- Complete the Western blot analysis for the *tlA3* mutant and proceed to peer-reviewed publication of the results.
- Demonstrate feasibility of the TLA concept in cyanobacteria. (Currently in progress.)
- Advance the exploration of the “*extended photosynthetically active radiation*” (ePAR) concept. (Proprietary design not disclosed.)

FY 2012 Publications/Presentations

Peer Reviewed Publications

1. Blankenship RE, Tiede DM, Barber J, Brudvig GW, Fleming G, Ghirardi ML, Gunner MR, Junge W, Kramer DM, Melis A, Moore TA, Moser CC, Nocera DG, Nozik AJ, Ort DR, Parson WW, Prince RC, Sayre RT (2011) Comparing photosynthetic and photovoltaic efficiencies and recognizing the potential for improvement. *Science* 332:805-809 .
2. Mitra M, Ng S, Melis A (2012) The *TLA1* protein family members contain a variant of the plain MOV34/MPN domain. *Amer J Biochem Mol Biol.* 2(1): 1-18.
3. Melis A (2012) Photosynthesis-to-Fuels: From sunlight to hydrogen, isoprene, and botryococcene production. *Energy Environ. Sci.* 5(2): 5531-5539.
4. Kirst H, Garcia-Cerdan JG, Zurbriggen A, Melis A (2012) Assembly of the light-harvesting chlorophyll antenna in the green alga *Chlamydomonas reinhardtii* requires expression of the *TLA2-CpFTSY* gene. *Plant Physiol* 158: 930–945.
5. Mitra M, Dewez D, García-Cerdán JG, Melis A (2012) Polyclonal antibodies against the TLA1 protein also recognize with high specificity the D2 reaction center protein of PSII in the green alga *Chlamydomonas reinhardtii*. *Photosynth Res* 112:39-47.

Patent Application Filed

1. Melis A and Kirst H (2012) Suppression of *TLA2-CpFTSY* gene expression for improved solar energy conversion efficiency and photosynthetic productivity in algae.

References

1. Kok B (1953) Experiments on photosynthesis by *Chlorella* in flashing light. In: Burlew JS (ed), *Algal culture: from laboratory to pilot plant*. Carnegie Institution of Washington, Washington, D.C., pp 63-75.
2. Myers J (1957) *Algal culture*. In: Kirk RE, Othmer DE (eds), *Encyclopedia of chemical technology*. Interscience, New York, NY, pp 649-668.
3. Radmer R, Kok B (1977) Photosynthesis: Limited yields, unlimited dreams. *Bioscience* 29: 599-605.
4. Mitra M, Melis A (2008) Optical properties of microalgae for enhanced biofuels production. *Optics Express* 16: 21807-21820.
5. Melis A, Neidhardt J, Benemann JR (1999) *Dunaliella salina* (Chlorophyta) with small chlorophyll antenna sizes exhibit higher photosynthetic productivities and photon use efficiencies than normally pigmented cells. *J. appl. Phycol.* 10: 515-525.
6. Kirst H, Garcia-Cerdan JG, Zurbriggen A, Melis A (2012) Assembly of the light-harvesting chlorophyll antenna in the green alga *Chlamydomonas reinhardtii* requires expression of the *TLA2-CpFTSY* gene. *Plant Physiol* 158: 930–945.
7. Mitra M, Ng S, Melis A (2012) The *TLA1* protein family members contain a variant of the plain MOV34/MPN domain. *Amer J Biochem Mol Biol.* 2(1): 1-18.

II.H.1 Unitized Design for Home Refueling Appliance for Hydrogen Generation to 5,000 psi

Timothy Norman (Primary Contact),
 Monjid Hamdan
 Giner, Inc. (formerly Giner Electrochemical Systems, LLC)
 89 Rumford Avenue
 Newton, MA 02466
 Phone: (781) 529-0556
 Email: tnorman@ginerinc.com

DOE Manager
 HQ: Eric L. Miller
 Phone: (202) 287-5829
 Email: Eric.Miller@hq.doe.gov

Contract Number: DE-SC0001486

Project Start Date: August 15, 2010
 Project End Date: August 14, 2012

FY 2012 Accomplishments

Membrane

- Developed high-pressure, high-strength membranes compatible with 5,000 psi operation

Completed Electrolyzer Stack Fabrication for 5,000 psi Operation

- Innovative design to reduce stack material costs:
 - Cell Frames
 - Completed cell frame stress analysis and method for high pressure reinforcement
 - Utilizes thermoplastics vs. metal (high-cost)
 - Reduce parts count/cell
 - Carbon cathode support structures
 - Multi-functional part
 - Eliminates 20+ component parts
 - Enables high pressure operation
 - Single piece separator
 - Eliminates hydrogen embrittlement
- Evaluated overboard and crossover sealing to 1.25X operating pressure (6,250 psi)

Electrolyzer System Fabrication Initiated, Near Completion

- Integrated electrolyzer subsystems to minimize the number of balance-of-plant (BOP) components
- Improved safety and reliability



Introduction

U.S. automakers have invested significant resources in the research and development of hydrogen fuel cell vehicles. However, to enable the widespread use of fuel cell vehicles, an additional major investment will be required to construct an infrastructure for hydrogen production and delivery to fueling stations. In order to facilitate this transition, it has been recommended that high-pressure hydrogen, generated at 5,000 psig for home refueling of fuel cell vehicles, be implemented as an intermediary approach. An improved, low-cost process for producing high-pressure hydrogen from water by electrolysis will significantly advance

Fiscal Year (FY) 2012 Objectives

- Detail design and demonstrate subsystems for a unitized electrolyzer system for residential refueling at 5,000 psi to meet DOE targets for a home refueling appliance (HRA)
- Fabricate and demonstrate unitized 5,000 psi system
- Identify and team with commercialization partner(s)

Technical Barriers

This project addresses the following technical barriers from the Hydrogen Production section of the Fuel Cell Technologies Program Multi-Year Research, Development and Demonstration Plan:

- (G) Cost - Capital Cost
- (H) System Efficiency

Technical Targets

Giner Progress toward Meeting DOE Targets for Distributed Electrolysis Hydrogen Production

| Characteristics | Units | 2017–2020 Targets | Giner Status |
|--------------------------------|----------------------|-------------------|--------------|
| Hydrogen Cost | \$/kg H ₂ | 2.00–4.00 | 2.99* |
| Electrolyzer Capital Cost | \$/kg H ₂ | 0.30 | 0.99 |
| Electrolyzer Energy Efficiency | % (LHV) | 74 | TBD |

*Using H2A model rev 2.1.1; LHV – lower heating value

the development of the hydrogen economy, providing hydrogen for fuel cell vehicles at a price competitive with that of gasoline on a per-mile basis. The ability to produce hydrogen economically, the relatively low capital cost of the electrolyzer unit, and the low maintenance cost of the unit will allow widespread distribution of hydrogen home fueling appliances deemed necessary for the introduction of fuel cell vehicles.

The project focuses on the development of high-pressure, low-cost electrolyzer stack and BOP components. Giner has a matured proton exchange membrane (PEM)-based electrolyzer technology for producing hydrogen at moderate to high pressure directly in the electrolyzer stack, while oxygen is evolved at near-atmospheric pressure. In this system, liquid water, which is a reactant as well as coolant, is introduced into the anode (O_2) side of the electrolyzer at near atmospheric pressure; high-pressure hydrogen is removed from the cathode or product side. In addition to reliability, and long maintenance intervals, safety is also a primary concern in this design due to the flammability and reactivity concerns of hydrogen and oxygen.

Approach

Giner is currently conducting a multi-year development project for DOE that aims to reduce commercial electrolyzer costs while simultaneously raising the efficiencies of the PEM-based water electrolyzer units operating in the range of 400 psi. Future extension of this technology to pressures of 5,000 psig is feasible with modifications to the electrolyzer stack, providing the ability to safely operate in a differential hydrogen/oxygen pressure mode. Based on an innovative electrolyzer stack concept and recent developments in high strength membrane, Giner has designed a PEM-based water electrolyzer system for home refueling applications that will be able to deliver hydrogen at pressures of 5,000 psi. High-pressure hydrogen can be generated in low-cost moderate-pressure electrolyzer stacks by means of external reinforcement to the individual cell frames. Utilizing external cell reinforcement eliminates the need for bulky and costly stack parts and facilitates a method for fabricating an electrolyzer stack and system that can safely operate at a high pressure. In addition, a reduction of major system components and system cost is realized.

Results

Membrane Evaluation: PEM electrolyzer gas permeation models developed by Giner and based on single-cell testing at various operating pressures, temperatures, and membrane thicknesses, show that improved stack efficiency is obtained while operating the electrolyzer stack in a differential pressure mode (hydrogen pressure over oxygen pressure) as opposed to balanced pressure in which both hydrogen and oxygen gases are generated at the same pressure. As

illustrated in Figure 1, Faradaic losses, in terms of current density, during differential pressure operation of a 10 mil thick 1100 equivalent weight (EW) perfluorosulfonic acid (PFSA) membrane, is lower than that of a similar membrane tested at balanced pressure. Although not shown, this is true for all membrane thicknesses, operating pressures, and temperatures. The decrease in efficiency at balanced pressure operation is directly related to increased oxygen concentrations gradients across the membrane. Utilizing engineered membranes developed at Giner, the performance of the electrolyzer is optimized for the selected operating pressure (and temperature).

Electrolyzer Stack Fabrication: The HRA has been designed for on-demand operation. The system is designed with a small 2-kWe electrolyzer stack, providing a vehicle tank fill of 0.5 kg of hydrogen over a 12 hour period. This will provide 30 miles of driving range based on current fuel cell vehicle fuel economy estimates of 60 miles/kg- H_2 . Differential pressure operation required redesign of the electrolyzer stack hardware. Giner's initial design included the use of a pressure containment dome; the gas pressure in the pressure dome is matched to that of the electrolyzer's hydrogen and oxygen product streams to provide external stack reinforcement. In 2012, Giner developed a modified stack design that utilizes a metal containment ring externally attached to the electrolyzer-stack's cathode (H_2) cell frames. The simplified design eliminates the need for a containment dome; in addition, this technique enables high pressure operation with the use of low- and moderate-pressure PEM-based electrolyzer stacks without the need for expensive internal cell reinforcement or metal frames. Low-cost is maintained by utilizing previously designed injection molded thermoplastic cell frames and cell components.

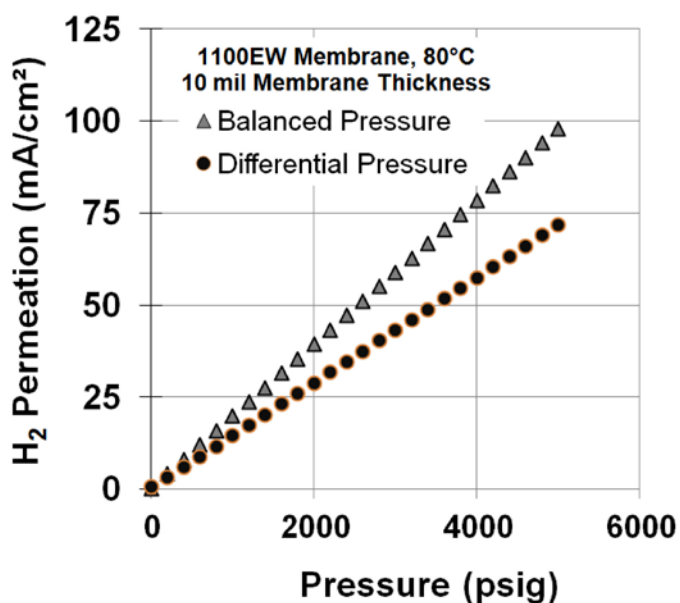


FIGURE 1. Faradaic Losses: Balanced vs. Differential Pressure Operation

In addition to the use of external cell-frame reinforcement, the electrolyzer stack includes several modifications developed under a separate DOE project (PEM Electrolyzer Incorporating an Advanced Low-Cost Membrane) that further reduce stack cost. This includes (1) an overall decrease in the parts count per cell (2) a 75% reduction in anode and cathode catalyst loadings, (3) molded thermoplastic cell frames, resulting in a cost reduction of 95% as compared to machining this component, (4) a reduction in cell frame thickness, thus reducing the anode and cathode support materials and costs, and (6) and a modified anode membrane support material that enables high-pressure operation that can exceed 5,000 psi. The design and fabrication of the electrolyzer stack, utilizing the

external cell reinforcement, has been completed and is shown in Figure 2. The electrolyzer stack was successfully proof pressure tested to 6,250 psi.

Preliminary Design of a 5,000 psi “Unitized” Electrolyzer System for Home Refueling: The HRA depicted in Figure 3 features: (1) a 2-kW differential pressure electrolyzer stack that produces hydrogen at up to 5,000 psi and oxygen at ambient pressure, (2) a water tank, sized for approximately 12 hours of electrolyzer operation at rated power levels, (3) an integrated deionized water loop used to maintain water purity and temperature control of the electrolyzer stack during operation, (4) a small hydrogen dryer to maintain a hydrogen gas dew point of <-40°C, (5) sensors for monitoring the production gases to prevent/detect formation of flammable mixtures, and (6) the integration, where feasible, of electrolyzer subsystems to minimize the number of BOP components. An automated control system also provides safe automated operation.

The reactant water is supplied to the anode side of the electrolyzer stack at ambient pressure. Oxygen generated on the anode side of the electrolyzer stack is then separated from water in the oxygen gas separator which also serves as the water reservoir. Water is circulated from the oxygen gas separator to the anode of the electrolyzer stack and back to the oxygen gas separator. The circulating pump operates at low differential pressure, as it must only overcome the pressure drop in the feed loop. During electrolyzer operation water is transferred from the anode side of the electrolyzer stack to the cathode side due to electrically-osmotic transport. Water loss due to electro-osmotic drag is collected in the hydrogen gas phase separator and returned to the electrolyzer feed loop after it has been degassed. Cooling to the electrolyzer stack is provided by the heat exchanger located in the electrolyzer water feed loop. The cooling loop

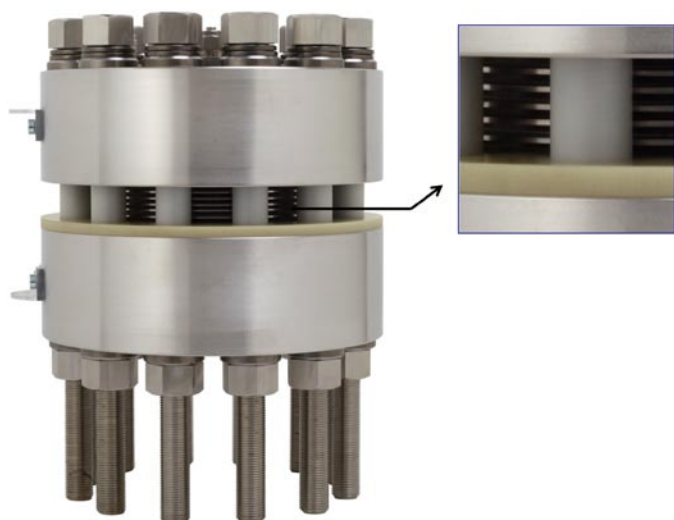


FIGURE 2. High Pressure Electrolyzer Stack with Reinforced Cell Frames

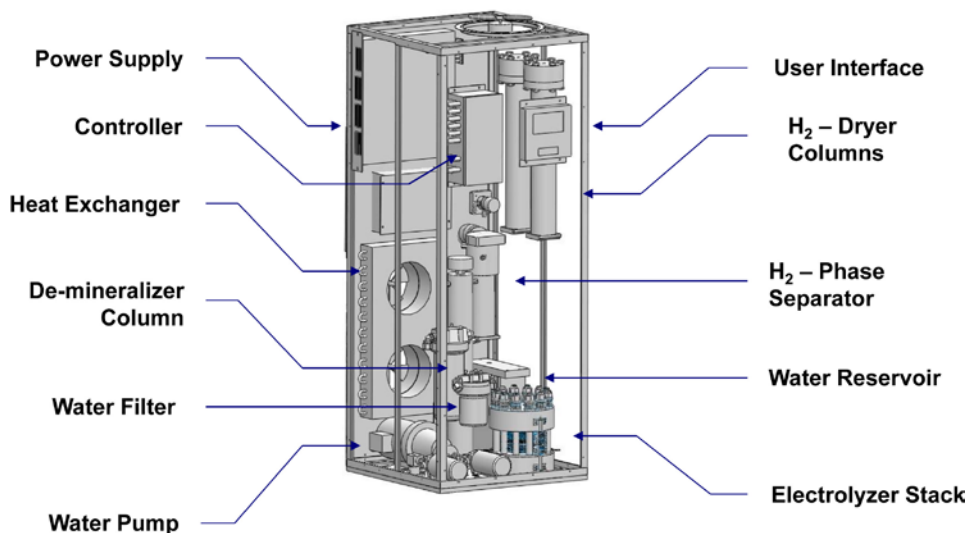


FIGURE 3. Electrolyzer (HRA) System Layout

and the heat exchanger are common between the electrolyzer stacks and the de-ionized water loop. Hydrogen generated on the cathode side is separated from crossover water in the hydrogen gas phase separator prior to entering the drying hydrogen unit.

At the end of the electrolysis cycle, which occurs when the water in the HRA system is nearing depletion, power is no longer available, or at a predetermined time or pressure, the electrolyzer subsystem is shut down. In addition to the normal end-of-cycle operation, the control system automatically shuts down electrolyzer operation when abnormal conditions are detected. The conditions that trigger electrolyzer subsystem shut down include: low water in the electrolyzer feed loop, low water flow rate, high temperatures ($>80^{\circ}\text{C}$), over pressure ($>5,000$ psig), and gas detection alarms. In addition, any cell in the electrolyzer stack exhibiting a low or high voltage will activate a system shutdown.

Performance: The specific energy consumption of the electrolyzer stack, based on a 10-mil membrane is shown in Figure 4. Although Figure 4 includes the affect of a Nernstian voltage penalty due to pressurization from 300 psi to 5,000 psi, the higher power consumption is largely due to faradaic losses related to hydrogen permeation. As shown in Figure 4, an additional 5 kWe per kg of H_2 is required

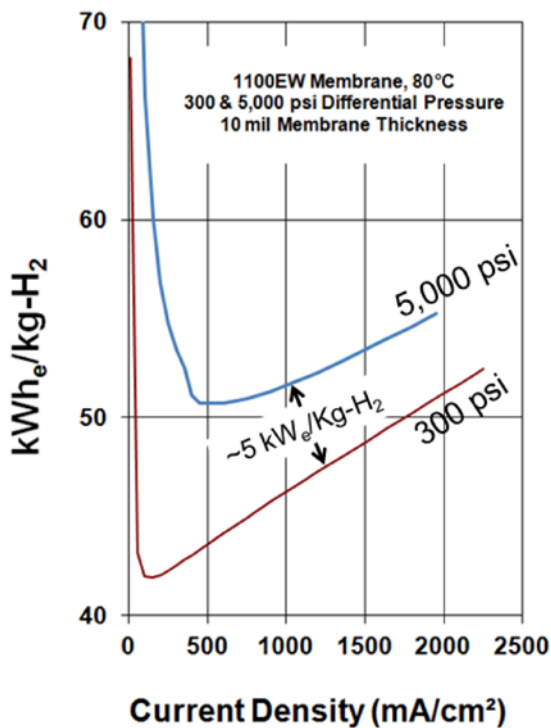


FIGURE 4. Specific Energy Consumption of Electrolyzer Stack

when operating the electrolyzer stack from 300 to 5,000 psi with a 10-mil thick 1100 EW PFSA membrane. At operating current densities above 500 mA/cm^2 , internal resistance losses become dominate. This can be reduced by properly engineering the membrane thickness for pressure and temperature conditions. Giner's current membrane design is expected to result in an electrolyzer stack power consumption of 51-52 $\text{kWh}_e/\text{kg-H}_2$ at an operating at a current density of between 1,000 and 1,500 mA/cm^2 .

Conclusions and Future Directions

The technology will be able to provide onsite residential hydrogen refueling at a cost that meets the DOE target of \$2.00–\$4.00/kg- H_2 by 2017. In addition to unitizing the major components, the design incorporates numerous cost-saving (and reliability enhancing) simplifications. These design features eliminate the need for bulky and costly stack and system parts, and facilitate a method for producing a low-cost electrolyzer system that can safely operate at a hydrogen pressure of 5,000 psi in a residential setting. Future objectives are:

- Complete fabrication of the full-scale HRA system sized for a hydrogen production rate of 0.5 kg H_2 (at 5,000 psi) per 12-hour operational period
- Conduct performance and durability testing of HRA prototype
- Conduct optimization studies: stack and system
- Complete a preliminary design and economic analysis of a future commercial HRA system
- Develop marketing strategy and partnerships for wide scale adoption of technology.

FY 2012 Publications/Presentations

1. T. Norman, and M. Hamdan, *Unitized Design for Home Refueling Appliance for Hydrogen Generation to 5,000 psi*. 2012 Hydrogen Annual Program Merit Review Meeting, Presentation #pd_065 norman, May 15, 2012.

II.H.2 Hydrogen by Wire - Home Fueling System

Luke T. Dalton
 Proton Energy Systems
 10 Technology Drive
 Wallingford, CT 06492
 Phone: (203) 678-2128
 Email: ldalton@protonenergy.com

DOE Manager
 HQ: Eric L. Miller
 Phone: (202) 287-5829
 Email: Eric.Miller@hq.doe.gov

Contract Number: DE-SC0001149

Project Start Date: August 15, 2010
 Project End Date: August 14, 2012

FY 2012 Accomplishments

- Completed prototype and final design of cell and stack components.
- Verified design of cell stack embodiment hardware.
- Completed full-scale stack pressure testing to 520 bar (7,500 psig).
- Verified gas diffusion at full differential pressure.
- Completed system component procurement and fabrication.
- Completed hydrogen phase separator fabrication and proof pressure testing.
- Completed system integration and system checkout.
- Demonstrated 350 bar (5,000 psig) differential pressure electrolysis.



Fiscal Year (FY) 2012 Objectives

- Develop enabling technologies for 350-bar hydrogen home fueling
- Design key electrolysis cell stack and system components
- Fabricate, inspect and assemble prototype components
- Demonstrate prototype 350-bar hydrogen generation
- Demonstrate prototype 350-bar home fueling technologies

Technical Barriers

This project addresses the following technical barriers from the Production section of the Fuel Cell Technologies Program Multi-Year Research, Development and Demonstration Plan:

- (G) Capital Cost
- (H) System Efficiency

Technical Targets

TABLE 1. Progress towards Meeting Technical Targets for Hydrogen Production via Distributed Water Electrolysis

| Characteristics | Units | 2012 Target | 2012 Status |
|--------------------------------|-----------------------|-------------|-------------------|
| Hydrogen Cost | \$/gge ¹ | 3.70 | 5.99 ² |
| Electrolyzer Capital Cost | \$/gge | 0.70 | 2.62 ² |
| Electrolyzer Energy Efficiency | % (LHV ³) | 69 | 57 ⁴ |

¹gge – gasoline gallon equivalent

²Based on H2A model modified for residential (non-commercial) application

³LHV – lower heating value

⁴Includes generation and compression to 350 bar with stack efficiency of 66% LHV

Introduction

Based upon the results of the Phase 1 study, the fundamental requirements for a hydrogen home fueling appliance have been defined. The conclusion of the Phase 1 study indicated that an overnight-fill proton exchange membrane (PEM) electrolysis device that fills the vehicle directly to a maximum of 350 bar with no mechanical compressor or secondary hydrogen storage can cost-effectively supply the daily hydrogen for a typical commuter operating a fuel cell vehicle. The case for including the hydrogen home fueling concept in the overall mix of fueling infrastructure is strong. The home fueler can grow in production volume and geographic distribution with individual vehicles as they are placed in the market with more flexibility than centralized fueling stations. Existing utility infrastructure (water, electricity) can be utilized within their existing capacities to cover the distribution aspect of the fueling infrastructure.

The goal of this Phase 2 project was to design and demonstrate the key hardware for 350-bar hydrogen home fueling based on PEM electrolysis. Proton Energy Systems has previously demonstrated durable PEM electrolysis equipment generating hydrogen at 165 bar. In addition, Proton has also demonstrated the ability of sub-scale prototypes to seal at the required proof pressure for 350-bar operation. Building upon this past work, designs have been developed utilizing Proton's reliable PEM electrolysis cell stack and system technologies for hydrogen generation and vehicle fueling at 350-bar.

Approach

The approach to the Phase 2 project was threefold. First, utilize the data and modeling results from the Phase 1 project to provide approximate sizing for the hydrogen generation rate. Second, build upon Proton's proven cell stack design and development experience to undertake the designs required for 350-bar operation. Third, utilize Proton's strong engineering processes that rely on a phased approach, with stage reviews, key written guidelines, and design output documentation to guide the successive levels of design refinement and demonstration. To that end, the project was organized into four main tasks: (1) Prototype System Design and Fabrication, (2) Prototype Stack Design, (3) Prototype Component Verification, and (4) Prototype System Testing.

Task 1 utilized engineering best practices to design and fabricate the prototype fueling system. This includes producing the plumbing and instrumentation diagram, electrical schematics, bill of materials, control schemes and component specifications for the prototype system. In addition, Task 1 included the procurement, fabrication, and acceptance testing of the prototype system. Task 2 included producing the component designs and assembly models for the cell stack in three-dimensional computer-aided design format. Moreover, it included completing design feasibility pressure testing using both sub-scale and full-scale active area components. Task 3 incorporated work on verifying the functionality of key components within the cell stack design and one or two custom components within the system design. Task 4 included assembling and checking the first electrolysis-ready version of the new prototype stack design. Furthermore, it includes integrating the prototype stack into the prototype system and operating in electrolysis to generate hydrogen at 350 bar.

Results

Now in the second year of this project, the team has made excellent progress toward the overall goals of the project. At the time of writing, the team has completed all of Tasks 1, 2 and 3. Task 4 is also 80% complete and the overall project is on schedule to meet the deliverables at the end of Year 2.

Within Task 1, Prototype System Design and Fabrication, activities in Year 2 first focused on completion of the system bill of materials which allowed ordering and subsequent receipt of all the major components for the prototype system. The prototype system design is based upon Proton's commercial HOGEN[®] HP high pressure hydrogen generator which delivers hydrogen at pressures of up to 2,400 psi. This high pressure system is also derivative of Proton's highly successful HOGEN S-series product with over 400 units now in operation. Based upon the completed prototype design review, the system was assembled and after completion fully checked out to verify operational status. The final

programming of the system's programmable logic controller and data acquisition system was also completed and verified including identification and verification of all input/output communication channels. A picture of the completed system is shown in Figure 1. The plumbing and instrumentation diagram and electrical schematics were updated concurrently with assembly to reflect the final system configuration. A key development effort as part of the system design was the 350-bar hydrogen/water phase separator. The final phase separator configuration was fully fabricated and proof pressure tested (Figure 2). The phase separator was then integrated into the system and its testing completed during the full system checkout. System acceptance testing included leak checking, ground continuity testing, and hi-pot testing.

Within Task 2, Prototype Stack Design, the design of the 350-bar cell stack was completed during this past year. Based upon work completed in Year 1, cell frame and embodiment components were procured and full pressure testing of the stack design was achieved at proof pressures above the required 520 bar (7,500 psig). The design work then moved to cell active area design and was supported by component and full pressure testing during the verification work outlined in Task 3. The prototype and final design reviews were



FIGURE 1. Prototype test system and data acquisition

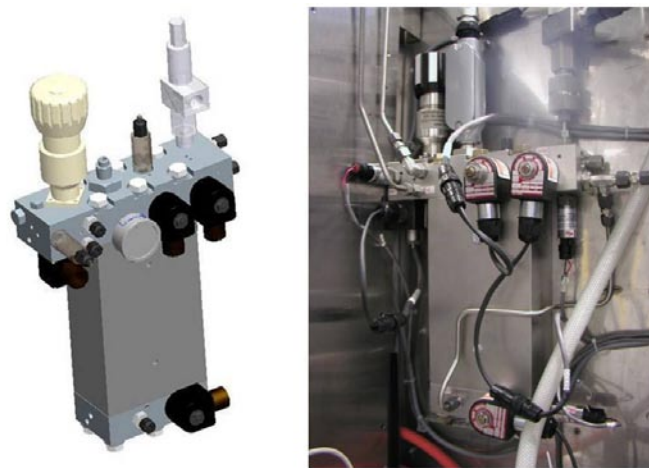


FIGURE 2. Phase separator design and fabricated unit

subsequently completed as the iterative design process honed and refined the final 350-bar cell stack design.

Activities in Task 3 involved the detailed design verification inspections and tests of the components. Non-operational stacks were built to verify sealing to proof pressure and proper distribution of load through the components. Pressure imaging in the sealing as well as the active area of the cell was used to verify uniform load within allowable margins of safety. Flow testing of single- and multiple-cell stacks was conducted and compared to similar lower pressure cell designs to confirm acceptable pressure drop. Proton exchange membrane materials suitable for use in the membrane electrode assembly component were also characterized at differential pressures up to 350 bar (Figure 3). Final activity during this task was the fabrication of an operational single-cell stack suitable for integration and testing in the prototype test bed.

The activities completed during Task 4 started with testing of the water circulation pump and system power supply. Final integration of the thermal management and data collection equipment was also completed. A key element of the system control is the management of the high pressure water collected from the production of 350-bar hydrogen. A hydrogen/water phase separator simulator was developed to mimic the operation of an actual phase separator in order to set the programmable logic control parameters without actually generating 350-bar hydrogen. This ultimately enabled rapid integration of the operating cell stack into the system with minimal premature shutdowns and adjustments. Finally, the single-cell 350-bar stack was installed, the system testing initiated and the milestone of hydrogen

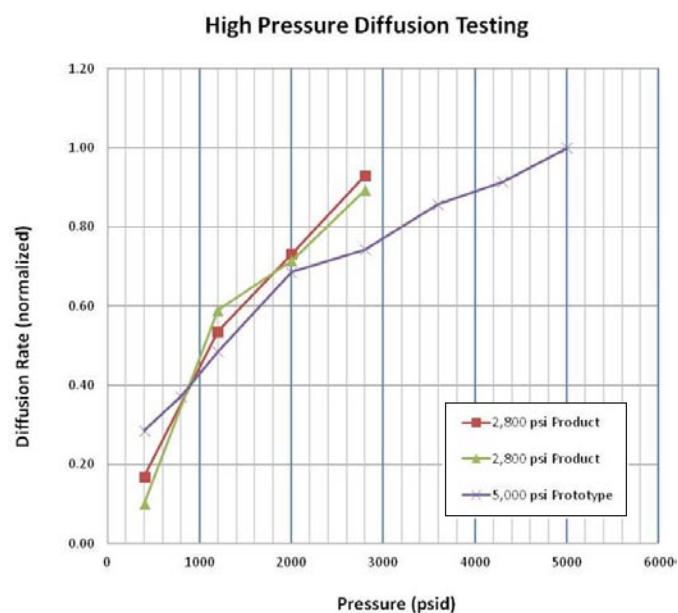


FIGURE 3. Cross-cell diffusion testing at up to 350-bar differential pressure

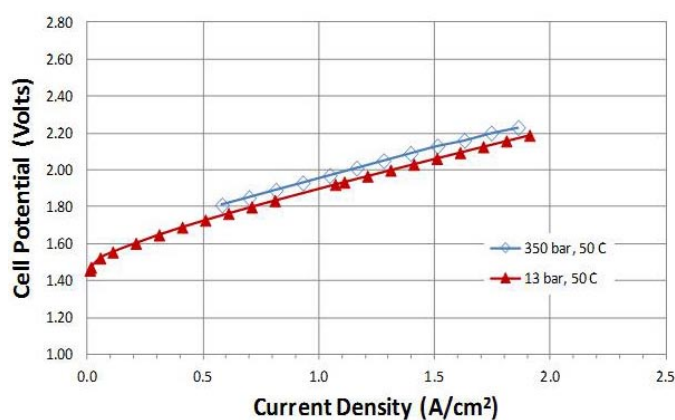


FIGURE 4. Polarization data during 350-bar (5,000 psig) hydrogen generation compared with 13-bar hydrogen generation

production at 350-bar pressure and full differential pressure was achieved during this period (Figure 4). This achievement sets the stage for additional testing and optimization of operational protocols during the remainder of the project.

Conclusions and Future Directions

All of the diligent design and development work of the project team resulted in achievement of the initial demonstration of a 350-bar capable electrolysis stack and system. This accomplishment creates a foundation from which the hydrogen output and pressure can be scaled up and also design improvements can be made to improve the efficiency and economics of this small-scale high-pressure hydrogen generator system.

In summary, the following tasks have been completed for the 350-bar electrolysis fueling system development effort and the parallel 350-bar electrolysis cell stack development:

- All prototype system components have been ordered and procured.
- The prototype system is complete, including full system operational checkout.
- The high pressure cell stack design is finalized including overboard seal testing to proof pressures above 500 bar.
- All prototype cell and stack embodiment components have been ordered and procured.
- Design and verification of cell stack components is completed, including seal and active area full differential pressure testing.
- The operational prototype cell stack has been assembled and acceptance tested.
- The prototype system and operational stack have been integrated and operationally tested.
- 350-bar hydrogen generation from water electrolysis at full differential pressure has been achieved.

FY 2012 Publications/Presentations

1. Anderson, E., Dalton, L., Carter, B., and Ayers, K., “Elimination of mechanical compressors using PEM-based electrochemical technology,” Paper ASR 14.5 presented at the World Hydrogen Energy Conference 2012, Toronto, CA, June 6, 2012.

III. HYDROGEN DELIVERY

III.0 Hydrogen Delivery Sub-Program Overview

INTRODUCTION

The Hydrogen Delivery sub-program supports research and development (R&D) of technologies that enable low-cost, efficient, and safe delivery of hydrogen to the end-user in order to achieve a threshold cost of \$2–\$4 per gallon gasoline equivalent (gge) of hydrogen (produced, delivered, and dispensed), which represents the cost at which hydrogen fuel cell electric vehicles (FCEVs) are projected to become competitive on a cost-per-mile basis with competing vehicles (gasoline-powered hybrid-electric vehicles) in 2020.¹ The Hydrogen Delivery sub-program addresses all hydrogen distribution activities from the point of production to the point of dispensing. R&D activities address challenges to the widespread adoption of hydrogen technologies in the near term through development of tube trailer and liquid tanker technologies as well as forecourt compressors, dispensers, and bulk storage, and in the mid- to long-term through development of pipeline technologies. Strategic analysis is used by the sub-program to identify cost, performance and market barriers to commercial deployment of hydrogen technologies, and to inform program planning and portfolio development.

GOAL

The goal of this sub-program is to reduce the costs associated with delivering hydrogen to a point at which its use as an energy carrier in fuel cell applications is competitive with alternative transportation and power generation technologies.

OBJECTIVES²

The key objective of this sub-program is to develop low-cost, efficient, and safe technologies for delivering hydrogen from the point of production to the point of use—including stationary fuel cells and FCEVs. This objective applies to all of the possible delivery pathways. Interim and ultimate targets for various delivery components are being updated in the *Fuel Cell Technologies Program Multi-Year Research, Development, and Demonstration Plan (MYRD&D Plan)*. Key objectives for specific delivery components include:

- **Tube Trailers:** Reduce the cost of compressed gas delivery via tube trailer by increasing vessel capacity and lowering trailer cost on a per-kilogram-of-hydrogen-transported basis.
- **Pipeline Technology:** Develop mitigation strategies for combined material fatigue and hydrogen-induced embrittlement in steel pipelines; advance the development and acceptance of alternative composite pipe materials that can reduce installed pipeline costs; and develop lower-cost, higher-reliability compression technology for hydrogen transmission by pipeline.
- **Liquefaction:** Reduce the capital and operating costs of hydrogen liquefiers and bulk liquid storage vessels.
- **Forecourt Technologies:**
 - Compression: Develop lower-cost, higher-reliability hydrogen compression technology for terminal and forecourt applications.
 - Storage: Develop lower-capital-cost off-board bulk storage technology.
- **Analysis:** Conduct comprehensive analyses on potential near- and longer-term hydrogen delivery options, comparing the relative advantages of each and examining possible transition scenarios between the two timeframes.

¹Hydrogen Threshold Cost Calculation, Hydrogen and Fuel Cells Program Record #11007, US Department of Energy, 2012, http://www.hydrogen.energy.gov/pdfs/11007_h2_threshold_costs.pdf

²Note: Targets and milestones were recently revised; therefore, individual project progress reports may reference prior targets. Some targets are still currently under revision, with updates to be published in Fiscal Year (FY) 2013.

FY 2012 STATUS AND PROGRESS

In FY 2012 the Delivery sub-program published updated hydrogen delivery scenario analysis models (HDSAM) version 2.3 and version 2.3.1. In addition, updated cost and performance targets for delivery technologies were developed and published in the Delivery chapter of the *MYRD&D Plan*, which was released in September 2012. The Delivery chapter is organized by technology pathway: tube trailers and bulk storage, pipeline technology, and forecourt technology, followed by pathway analysis work.

The projected 2011 costs for the delivery of hydrogen by currently available technologies range from \$2.50/gge to \$9/gge, depending on the quantity and distance transported.³ These projections include the costs of compression, storage, and dispensing at the refueling site and are based on HDSAM assumptions. In order to achieve the threshold cost of \$2–\$4/gge, the goal of the Delivery sub-program is to reduce the delivery cost of hydrogen to <\$2/gge by 2020.⁴ Progress towards current goals and targets to achieve this ultimate goal are summarized in Table 1.

TABLE 1. Delivery Targets and Status

| Delivery Element | Targets (2015/2020) ⁵ | Status ⁵ |
|--|--|--|
| Tube Trailers | Reduce capital cost to <\$728/kg by 2015 and <\$574/kg by 2020 Increase capacity to 700 kg by 2015 and 940 kg by 2020 | Capital cost: \$510/kg Capacity: 726 kg |
| Pipelines | Reduce cost/mile (8 in. diameter pipe installed) to <\$735,000 by 2015 and <\$710,000 by 2020 | Installed steel pipeline cost: \$3 million/mile Cost contribution: \$1.7/kg H ₂ Compressor cost contribution: \$0.1/kg H ₂ |
| Forecourt Compression (1,000 kg/day station) | Reduce uninstalled capital cost to \$400K/\$240k for 700 bar dispensing | Capital cost: \$530K for 700 bar compression |
| Pipeline Compression | Reduce the uninstalled capital cost for 3,000-kW compressor to <\$2.3 million by 2015 and <\$1.9 million by 2020 | Capital cost: \$2.7 million |
| Forecourt Storage (1,000 kg/day station) | Reduce high pressure tank cost to \$1,200 per kg of stored H ₂ by 2015 and \$1,000 by 2020 | Storage tank cost: \$1,450 per kg of stored H ₂ |

Tube Trailers and Bulk Storage

Tube trailers and bulk storage are a critical near-term technology. Until there is significant expansion of the hydrogen pipeline infrastructure, truck transport and storage at the forecourt will be the primary means of distribution to fueling stations. In the last decade, the hydrogen-carrying capacity of tube trailers has more than doubled and the per-kilogram cost has fallen more than 40%. This year, Lincoln Composites was able to further improve on this progress.

- A custom-built trailer shown in Figure 2 capable of holding four 40-foot pressure vessels and an additional 30-foot pressure vessel was designed and constructed. This new design has the potential to increase overall capacity by roughly 18% from about 615 kg in the current Department of Transportation-approved design to more than 725 kg. A prototype trailer (minus vessels, plumbing, and fire protection) was received this year. (Lincoln Composites)
- Pathways were identified for steel-lined reinforced-concrete hydrogen pressure vessels to achieve the DOE 2020 cost target through development of advanced vessel manufacturing technology and materials.

³ *Hydrogen Delivery Cost Projections*, Hydrogen and Fuel Cells Program Record #12022, U.S. Department of Energy, under review in 2012.

⁴ *Hydrogen Production and Delivery Cost Apportionment*, Hydrogen and Fuel Cells Program Record #12001, U.S. Department of Energy, under review in 2012.

⁵ *Fuel Cell Technologies Program MYRD&D Plan* (Section 3.2, *Hydrogen Delivery*), U.S. Department of Energy, September 2012, www.hydrogenandfuelcells.energy.gov/mypp/index.html.

Feasibility of multi-pass, multi-layer friction-stir welding for steel vessel fabrication was demonstrated by successfully joining a 15-mm-thick (0.6 in.) steel plate, which nearly tripled the thickness of steel that can be welded by the conventional friction-stir welding. (Oak Ridge National Laboratory)

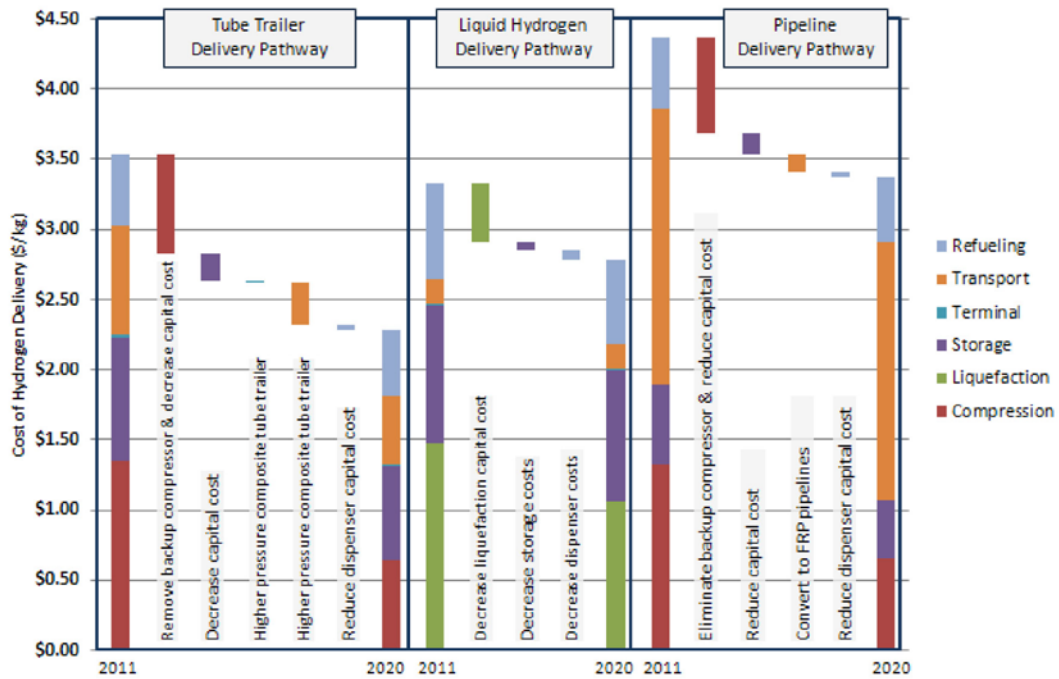


FIGURE 1. This chart shows the projected reduction in hydrogen delivery cost for various pathways based on preliminary analysis (FY 2011–FY 2012) due to technological advancement. Projections are based on HDSAM V2.31 for a well-established hydrogen market demand for transportation (10% market penetration). The specific scenarios examined assume central production of hydrogen that serves a city of moderately large size (population of about 1.5 million).

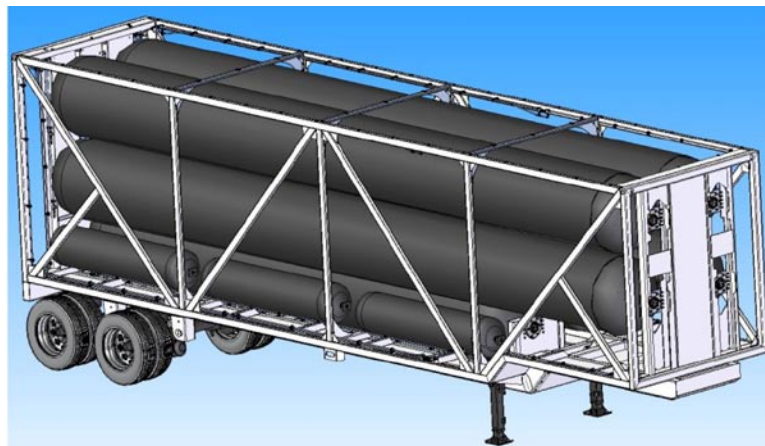


FIGURE 2. Lincoln Composites carbon fiber composite tube trailer pressure vessel and International Organization for Standardization container.

Pipeline Technologies

Pipeline technologies will enable the low-cost delivery of hydrogen in the future. Progress in both the characterization and development of pipeline materials and centrifugal pipeline compressors has been achieved through projects funded by the Hydrogen Delivery sub-program. Testing of fiber-reinforced polymer materials for pipelines is facilitating the adoption of these materials for hydrogen service applications by providing performance data to inform the development of the codes and standards needed for their commercial use. In the area of centrifugal compression, advanced seals have been developed which allow for the compression of hydrogen. Specific accomplishments for this year include:

- Fatigue testing for both flawed and unflawed samples of fiber-reinforced polymer pipe was completed to address the effects of third-party damage. The 40% through-wall flaws resulted in a 28% lower burst pressure of the flawed samples than the unflawed samples. (Savannah River National Laboratory)
- A physics-based model for accelerated fatigue crack growth of steels in hydrogen gas with oxygen impurities was developed. This model enables the extrapolation of data over a range of hydrogen pressure, oxygen concentration, load-cycle frequency, and load ratio (R_K). The model also demonstrates that the threshold level of oxygen required for mitigating accelerated fatigue crack growth of X52 steel in 21 MPa hydrogen gas is a function of load-cycle frequency and R_K . (Sandia National Laboratories)
- The fabrication, assembly and validation testing of a single-stage, oil-free centrifugal pipeline compressor system (Figure 3) was completed, and initial validation tests were performed at 30,000 rpm. The system, which includes advanced Ti-based rotors to achieve the tip speeds needed to meet DOE's 2015 targets for pipeline compression technology, will be tested in FY 2013 at 60,000 rpm in a dedicated test cell currently under construction. (Mohawk Innovative Technology)

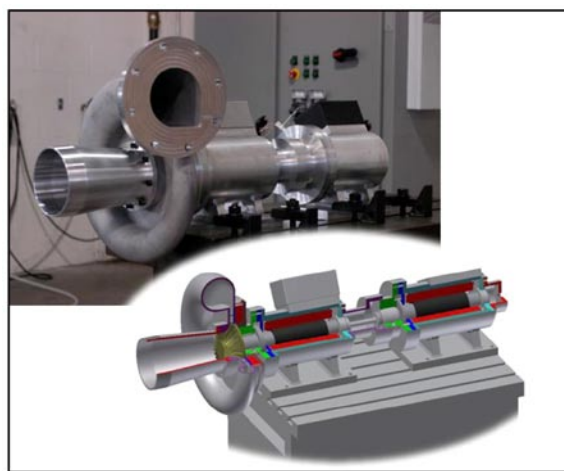


FIGURE 3. MiTi single-stage compressor driven by two 100-kW oil-free motors.

Forecourt Technologies

Improvements in the reliability and cost of forecourt compression and dispensing technologies are needed for the commercialization of hydrogen technologies. Cost improvements can be realized through efficiency improvements and reliability improvements as well as through new designs and materials. Progressive technologies in this area include electrochemical compression and liquid ionic compression. Recent progress includes:

- The maximum hydrogen pressure from a single-stage electrochemical compressor was increased to 12,800 psi (880 bar) from 7,000 psi (480 bar), and at the same time, 98% hydrogen recovery was achieved in a single cell. A 6,000-hour life at an elevated current density of 750 mA/cm² (as compared with 200 mA/cm²) was also demonstrated. (FuelCell Energy)

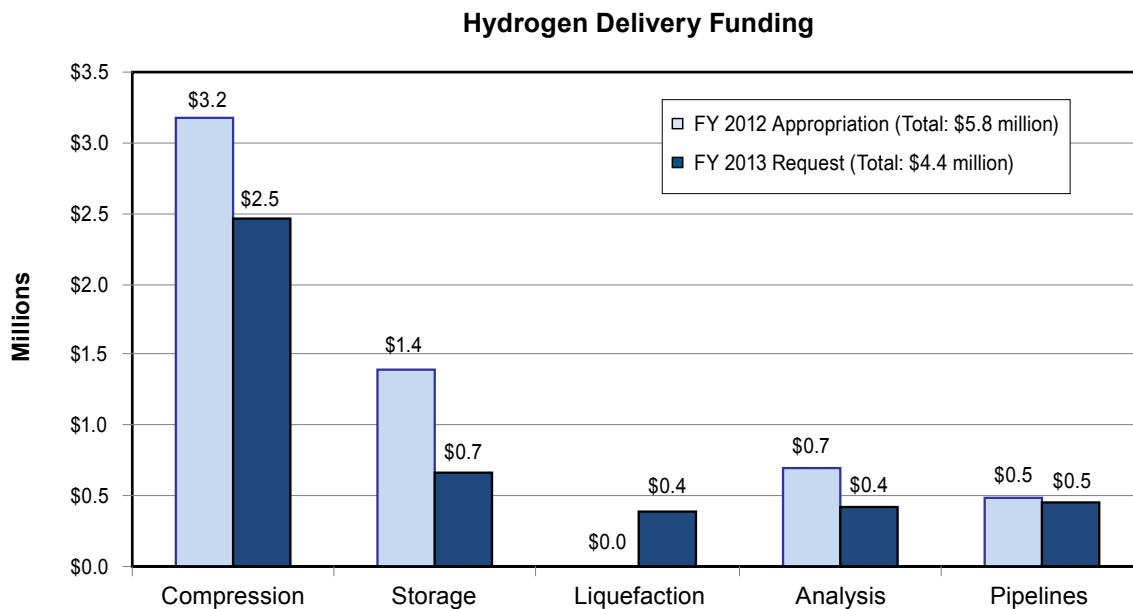
Analysis

Analysis efforts continue to identify areas in most critical need of R&D advances. Additionally, analysis is used to optimize technology pathways in order to reduce the final as-dispensed cost of hydrogen. Progress this year included evaluation of the current cost and power requirement of refueling station compression and pumping technologies and various configurations of high-pressure tube-trailers (within U.S. Department of

Transportation–specified weight and size constraints, including tube fill pressure, tube diameter/thickness, number of tubes and tube material). Two compression options to reduce station capital cost by at least 15% were identified: (1) a high-pressure (900-bar) liquid pump to increase pressure, combined with an evaporator to gasify the hydrogen before dispensing (the combined pump/vaporizer cost is more than 50% lower than the corresponding gas compressor cost); and (2) a high-pressure tube trailer, which can reduce compression demand at the station, especially in early markets where the utilization of the station compressor capital is low (this has the potential to reduce the impact of station capital cost on overall hydrogen cost by up to 20%, assuming 50% utilization). (Argonne National Laboratory)

BUDGET

The FY 2012 appropriation provided \$5.8 million for the Hydrogen Delivery sub-program, and \$4.4 million is planned for FY 2013 (based on the President’s budget request), with an emphasis on reducing near-term technology costs, increasing tube trailer capacity, and lowering the cost of pipeline delivery pathways.



FY 2013 PLANS

In FY 2013, the Hydrogen Delivery sub-program portfolio will focus on two key areas:

1. *Long-term technologies expected to have market impact in 10–20 years.* In FY 2013, the Delivery sub-program portfolio will continue efforts on technologies for transmitting hydrogen as a cold, pressurized fluid—including magnetic refrigeration and electrochemical compression. Some work will also continue on the testing and characterization of materials and systems for pipelines and pipeline compression; however, with the decreased funding scenario, more emphasis will be given to near-term technologies that can have an immediate impact.
2. *Near-term technologies that reduce hydrogen delivery costs for emerging hydrogen and fuel cell applications (e.g., forklifts and backup power) and early adopter FCEV markets.* In FY 2013, the emphasis will be on development of delivery options to reduce the cost of 700-bar hydrogen compression at light-

duty vehicle refueling stations, and on identification of material needs and challenges for delivery and forecourt technologies. New projects in FY 2013 will address technologies to reduce station costs and improve the reliability of forecourt compression and dispensing technologies.

Erika Sutherland
Hydrogen Production and Delivery Team
Technology Development Manager
Fuel Cell Technologies Program
Department of Energy
1000 Independence Ave., SW
Washington, D.C. 20585-0121
Phone: (202) 586-3152
Email: Erika.Sutherland@ee.doe.gov

III.1 Hydrogen Embrittlement of Structural Steels

Daniel Dedrick (Primary Contact), Brian Somerday
Sandia National Laboratories
P.O. Box 969
Livermore, CA 94550
Phone: (925) 294-1552
Email: dededri@sandia.gov

DOE Manager
HQ: Erika Sutherland
Phone: (202) 586-3152
Email: Erika.Sutherland@ee.doe.gov

Project Start Date: January, 2007
Project End Date: Project continuation and direction determined annually by DOE

cycling through the use of code-based structural integrity models. This structural integrity analysis can determine limits on design and operating parameters such as the allowable number of pressure cycles and pipeline wall thickness. Efficiently specifying pipeline dimensions such as wall thickness also affects pipeline cost through the quantity of material required in the design.

FY 2012 Accomplishments

A physics-based model for accelerated fatigue crack growth of steels in hydrogen gas with oxygen impurities was developed that enables the extrapolation of data over a range of hydrogen pressure, oxygen concentration, load-cycle frequency, and load ratio (R_K). This model demonstrates that the threshold level of oxygen required for mitigating accelerated fatigue crack growth of X52 steel in 21 MPa hydrogen gas is a function of load-cycle frequency and R_K .



Fiscal Year (FY) 2012 Objectives

- Determine the threshold level of oxygen impurity concentration required to mitigate accelerated fatigue crack growth of X52 steel in hydrogen at gas pressures up to 3,000 psi (21 MPa)
- Measure the fatigue crack growth (da/dN vs. ΔK) relationship at constant H_2 gas pressure in X65 pipeline girth weld supplied by industry partner

Technical Barriers

This project addresses the following technical barriers from the Hydrogen Delivery section of the Fuel Cell Technologies Program Multi-Year Research, Development and Demonstration Plan:

- (D) High Capital Cost and Hydrogen Embrittlement of Pipelines (Section 3.2.4)
- (K) Safety, Codes and Standards, Permitting (Section 3.2.4)

Technical Targets

The principal target addressed by this project is the following (from Table 3.2.2):

- Pipeline Reliability/Integrity

The salient reliability/integrity issue for steel hydrogen pipelines is hydrogen embrittlement. One particular unresolved issue is the performance of steel hydrogen pipelines that are subjected to extensive pressure cycling. One of the objectives of this project is to enable safety assessments of steel hydrogen pipelines subjected to pressure

Introduction

Carbon-manganese steels are candidates for the structural materials in hydrogen gas pipelines, however it is well known that these steels are susceptible to hydrogen embrittlement. Decades of research and industrial experience have established that hydrogen embrittlement compromises the structural integrity of steel components. This experience has also helped identify the failure modes that can operate in hydrogen containment structures. As a result, there are tangible ideas for managing hydrogen embrittlement in steels and quantifying safety margins for steel hydrogen containment structures. For example, fatigue crack growth aided by hydrogen embrittlement is a well-established failure mode for steel hydrogen containment structures subjected to pressure cycling. This pressure cycling represents one of the key differences in operating conditions between current hydrogen pipelines and those anticipated in a hydrogen delivery infrastructure. Applying code-based structural integrity models coupled with measurement of relevant material properties allows quantification of the reliability/integrity of steel hydrogen pipelines subjected to pressure cycling. Furthermore, application of these structural integrity models is aided by the development of physics-based models, which provide important insights such as the effects of gas impurities (e.g., oxygen) and the hydrogen distribution near defects in steel structures.

Approach

The principal objective of this project is to enable the application of code-based structural integrity models for evaluating the reliability/integrity of steel hydrogen pipelines. The new American Society of Mechanical Engineers (ASME) B31.12 code for hydrogen pipelines includes a fracture mechanics-based integrity management option, which requires material property inputs such as the fracture threshold and fatigue crack growth rate under cyclic loading. Thus, one focus of this project is to measure the fracture thresholds and fatigue crack growth rates of technologically relevant line-pipe steels in high-pressure hydrogen gas. These properties must be measured for the base materials but more importantly for the welds, which are likely to be most vulnerable to hydrogen embrittlement.

A second objective of this project is to enable development of physics-based models of hydrogen embrittlement in pipeline steels. The focus of this effort is to establish phenomenological models of hydrogen embrittlement in line-pipe steels using evidence from analytical techniques such as electron microscopy. These phenomenological models then serve as the framework for developing sophisticated finite-element models, which can provide quantitative insight into the effects of environmental, material, and mechanical variables. Such predictive materials science models can enable the extrapolation of material data inputs required for structural integrity models.

Results

The fatigue crack growth rate (da/dN) vs. stress-intensity factor range (ΔK) relationship is a necessary material-property input into damage-tolerant integrity management models applied to steel hydrogen pipelines. One such integrity management methodology for steel hydrogen pipelines was recently published in the ASME B31.12 code. The measurements of crack propagation thresholds and fatigue crack growth relationships in this task support the objective of establishing the reliability/integrity of steel hydrogen pipelines.

The X52 line-pipe steel was selected for this task because of its recognized technological relevance for hydrogen pipelines. The X52 steel from the round robin tensile property study (FY 2008) was tested for the following reasons: (1) some characterization of the material was already provided from the round-robin study, (2) ample quantities of material were still available, and (3) the X52 steel was in the form of finished pipe, which is the most relevant product form and also allows samples to be extracted from the electric resistance seam weld.

The hydrogen-affected fatigue crack growth relationship (da/dN vs. ΔK) for the structural steel is the basic element in pipeline integrity management models. The ASME B31.12

code requires measurement of the fatigue crack growth relationship for pipeline steels at the hydrogen gas operating pressure. Previous results for pipeline and pressure vessel steels have demonstrated that gas species such as oxygen can favorably affect the fatigue crack growth relationship in hydrogen gas [1]. However, these studies have not systematically examined important variables such as the impurity partial pressure, hydrogen partial pressure, ΔK level, R ratio (K_{min}/K_{max}), and load-cycle frequency. Since the retarding effect of oxygen and other gas impurities on hydrogen-assisted fatigue crack growth may have technological benefits, the windows of variables that promote this positive effect need to be defined more quantitatively.

In the fourth quarter of FY 2011 and the first quarter of FY 2012, the effects of oxygen on the fatigue crack growth relationship for X52 base metal in hydrogen gas were measured for three hydrogen/oxygen gas mixtures: $H_2/10$ vppm O_2 , $H_2/100$ vppm O_2 , and $H_2/1,000$ vppm O_2 , in which the hydrogen gas partial pressure was approximately constant at 21 MPa. The da/dN vs ΔK relationships were measured at an R_k ratio (K_{min}/K_{max}) of 0.1 in all environments and at an additional R ratio of 0.5 in the $H_2/1,000$ vppm O_2 environment (Figure 1). Based on these trends, a model concept was conceived and developed in the second quarter of FY 2012, in which the onset of hydrogen-accelerated fatigue crack growth in the different hydrogen environments could be predicted.

The model was developed based on the following assumptions: 1) the onset of hydrogen-accelerated fatigue crack growth is activated by hydrogen uptake at the crack tip, which is impeded by oxygen adsorption on the crack-tip surface, 2) the rate of oxygen adsorption on the crack tip surface is governed by oxygen diffusion in the hydrogen

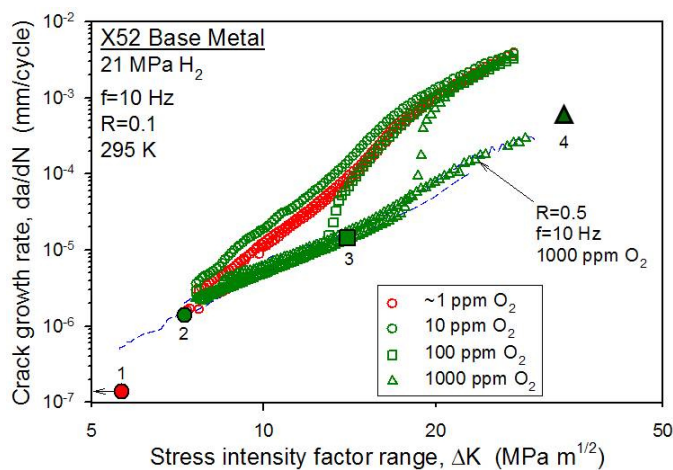


FIGURE 1. Fatigue crack growth rate (da/dN) vs stress-intensity factor range (ΔK) data for X52 steel in H_2/O_2 gas mixtures, high-purity hydrogen, and air. The symbols labeled 1, 2, 3, and 4 represent model predictions for the mechanical da/dN level required for $\theta_0 < 1$.

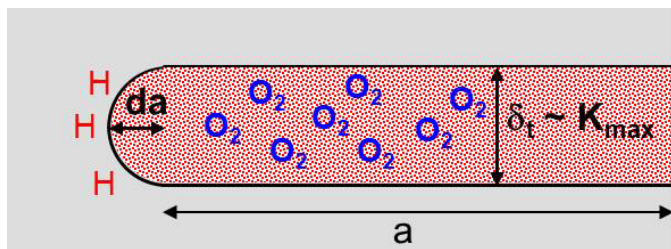


FIGURE 2. Schematic depicting the interactions between a mixed hydrogen/oxygen gas and a crack tip in steel opened at maximum load

gas, and 3) the extent of oxygen adsorption on the crack-tip surface depends on the area of new crack-tip surface created during each load cycle. These model elements are depicted in the schematic displayed in Figure 2. Prior to hydrogen-accelerated crack growth, the crack propagates in a manner dictated solely by mechanical driving forces. This “mechanical” crack growth rate, da/dN , is represented by the crack growth rates measured in an inert environment, i.e., air (blue dashed line in Figure 1). During this mechanical crack growth, the crack advances incrementally each load cycle, and the crack growth increment is equal to the measured da/dN . At the maximum load, the assumed relationship between the crack growth increment (da) and crack tip profile is shown in Figure 1. The new crack tip surface created during the load cycle is assumed to have a semicircular profile. The amount of oxygen adsorbed on this new crack tip surface is given by a simple mass balance: the adsorbed oxygen is equal to the flux of oxygen to the crack tip. The flux of oxygen in the crack channel is calculated using basic diffusion equations as well as the assumptions of steady state and a pressure equal to zero at the crack tip. The height of the crack channel is calculated from a fracture mechanics relationship between K_{max} and the crack opening. Based on these assumptions and relationships, an analytical expression was determined that relates the mechanical crack growth rate, da/dN , to the oxygen surface coverage, θ_o :

$$\frac{da}{dN} = \frac{Dp_o}{\theta_o \pi \nu RT} 0.6(1 - \nu_p^2) \frac{1}{E\sigma_0} \left(\frac{\Delta K}{\sqrt{a}(1 - R_K)} \right)^2$$

In this expression, D is the diffusivity of O_2 in the H_2 “matrix”, p_o is the partial pressure of oxygen in the bulk gas, ν is the load-cycle frequency, R is the gas constant, T is temperature, E is elastic modulus, σ_0 is yield strength, and a is the crack length. Although the original relationship was expressed in terms of K_{max} , this variable was replaced by the equivalent quantity $\Delta K/(1 - R_K)$ in order to include the R_K ratio.

Assuming that hydrogen uptake into the steel proceeds when oxygen delivered to the crack tip cannot cover the entire surface, i.e., $\theta_o < 1$, the model can predict the mechanical da/dN at the onset of accelerated crack growth.

Such predictions are indicated by the symbols labeled 1, 2, 3, and 4 in Figure 1. Considering points 2 and 3, these predictions represent the mechanical da/dN required for hydrogen uptake in the cases of bulk oxygen concentrations equaling 10 vppm and 100 vppm. As shown in Figure 1, the predicted mechanical da/dN levels are approximately equal to the levels at the onset of accelerated cracking for these two cases. Considering point 4, this is the predicted da/dN for hydrogen uptake when the bulk hydrogen concentration is 1,000 vppm and the R_K ratio is 0.5. The model accurately predicts that da/dN at the point of hydrogen uptake and accelerated crack growth is beyond the final point in the measured data set. The correlation between model predictions and experimental data is consistent with the notion that the onset of accelerated crack growth is controlled by the mechanical crack growth rate, which in turn governs the extent of oxygen adsorption on the freshly exposed crack tip. The prediction represented by point 1 is for the case of 1 vppm oxygen. In this case, the mechanical da/dN for hydrogen uptake is substantially lower than the da/dN at the onset of accelerated crack growth. The interpretation here is that thresholds for two mechanical variables must be exceeded for accelerated crack growth: a threshold level of da/dN for hydrogen uptake and a threshold level of K_{max} to activate the embrittlement. For the high-purity hydrogen case, oxygen does not hinder hydrogen uptake, but accelerated cracking is not activated until a critical K_{max} is reached.

The oxygen-diffusion model provides insights into the mechanical variables that dictate the onset of accelerated crack growth for steel in hydrogen/oxygen environments. This model can also be used to quantify the mechanical variables that affect the onset of accelerated cracking for components such as pipelines that contain hydrogen with small concentrations of oxygen. For example, the model demonstrates that higher R_K ratios lead to higher mechanical da/dN for hydrogen uptake and accelerated crack growth. This indicates that the onset of accelerated crack growth is displaced to higher mechanical da/dN when the components operate at higher pressure ratios (p_{min}/p_{max}). Thus, the reliability/integrity of a component containing hydrogen/oxygen is enhanced at higher pressure ratios.

The hydrogen diffusion model was developed in collaboration with Prof. Petros Sofronis (University of Illinois/International Institute for Carbon-Neutral Energy Research) and Prof. Reiner Kirchheim (University of Göttingen/International Institute for Carbon-Neutral Energy Research).

In the third quarter of FY 2012, fatigue crack growth specimens were prepared from the girth weld in a section of X65 steel pipe supplied by ExxonMobil (Figure 3). The fatigue crack growth rate, da/dN , vs. stress-intensity factor range, ΔK , relationship for the girth weld in hydrogen gas will be measured from these specimens.



FIGURE 3. X65 steel girth weld supplied by industry partner

Conclusions and Future Directions

- The development of a physics-based model for accelerated fatigue crack growth of steels in hydrogen gas with oxygen impurities enables the extrapolation of data over a range of hydrogen pressure, oxygen concentration, load-cycle frequency, and load ratio (R_K). This model demonstrates that the threshold level of oxygen required for mitigating accelerated fatigue crack growth of X52 steel in 21 MPa hydrogen gas is a function of load-cycle frequency and R_K .
- (future) Measure the fatigue crack growth (da/dN vs ΔK) relationship at constant H_2 gas pressure in X65 pipeline girth weld supplied by industry partner.

Sandia National Laboratories is a multi-program laboratory managed and operated by Sandia Corporation, a wholly owned subsidiary of Lockheed Martin Corporation, for the U.S. Department of Energy's National Nuclear Security Administration under contract DE-AC04-94AL85000

FY 2012 Publications/Presentations

1. "The Effect of Trace Oxygen on Gaseous Hydrogen-Accelerated Fatigue Crack Growth in a Low-Strength Pipeline Steel", B. Somerday, C. San Marchi, K. Nibur, P. Sofronis, and R. Kirchheim, 2012 TMS Annual Meeting & Exhibition, Orlando FL, March 2012.
2. "Gaseous Hydrogen-Assisted Fatigue Crack Growth in X52 Linepipe Steel", B. Somerday, C. San Marchi, and K. Nibur, MS&T 2011, Columbus OH, October 2011.

References

1. C. San Marchi and B.P. Somerday, *Technical Reference on Hydrogen Compatibility of Materials*, SAND2008-1163, Sandia National Laboratories, Livermore, CA, 2008.

III.2 Hydrogen Delivery Infrastructure Analysis

Amgad Elgowainy (Primary Contact),
Marianne Mintz and Krishna Reddi

Argonne National Laboratory
9700 South Cass Avenue
Argonne, IL 60439
Phone: (630) 252-3074
Email: aelgowainy@anl.gov

DOE Manager

HQ: Erika Sutherland
Phone: (202) 586-3152
Email: Erika.Sutherland@ee.doe.gov

Project Start Date: October 2007

Project End Date: Project continuation and direction
determined annually by DOE

elements of an optimized delivery system which could meet DOE's long-term delivery cost target.

FY 2012 Accomplishments

- Evaluated current cost and power requirement of refueling station compression and pumping technologies
- Evaluated various configurations of high-pressure tube-trailers within U.S. Department of Transportation (DOT) specified weight and size constraints, including:
 - Tube fill pressure
 - Tube diameter/thickness
 - Number of tubes
 - Tube material (steel vs. composite)
- Characterized and examined hydrogen delivery and refueling cost for forklift markets



Fiscal Year (FY) 2012 Objectives

- Identify cost drivers of current technologies for hydrogen delivery to early market applications of fuel cells
- Evaluate role of high-pressure tube-trailers in reducing hydrogen delivery cost
- Identify and evaluate benefits of synergies between hydrogen delivery options to various markets (e.g., forklift market, fuel cell vehicle market)

Technical Barriers

This project directly addresses technical barrier A (which implicitly includes barriers B, C, D, F, H and J) in the Delivery Technical Plan, as well as barriers B, C, D and E in the Systems Analysis Plan of the Fuel Cell Technologies Multi-Year Research, Development and Demonstration Plan. These are:

- (A) Lack of Hydrogen/Carrier and Infrastructure Options Analysis
- (B) Stove-Piped/Siloed Analytical Capability
- (C) Inconsistent Data, Assumptions and Guidelines
- (D) Insufficient Suite of Models and Tools
- (E) Unplanned Studies and Analysis

Technical Targets

The project is using a computer model to evaluate alternative delivery infrastructure systems and components. Insights from the model are being used to help identify

Introduction

Initiated as part of the H2A project, the Hydrogen Delivery Scenario Analysis Model (HDSAM) is an Excel-based tool that uses a design calculation approach to estimate the contribution of individual components of delivery infrastructure to hydrogen cost, energy use and greenhouse gas emissions. The model links individual components in a systematic market setting to develop capacity/flow parameters for a complete hydrogen delivery infrastructure. Using that systems level perspective, HDSAM calculates the full, levelized cost (i.e., summed across all components) of hydrogen delivery, accounting for losses and tradeoffs among the various component costs. A graphical user interface permits users to specify a scenario of interest. A detailed user's guide assists users in defining scenarios and running HDSAM. Users can specify their own inputs to the model or select default inputs – which are based on data from the literature, from vendors of specific delivery components or from stakeholder inputs, or derived from basic engineering design calculations. The quality of the data and the direction of the analysis are vetted in formal interaction with partners from other national laboratories and independent consultants and via briefings to the hydrogen delivery technical team.

From our previous analyses, the refueling station was found to contribute about half of total delivery cost in a mature fuel cell vehicle (FCV) market and refueling station compression and storage were shown to constitute the bulk of station capital cost. Thus, the focus of our analysis this FY was on identifying circumstances that tend to elevate

fueling station investment and leveled cost in early markets (e.g., diseconomies of scale, underutilization of capital, and high risks) and examining the cost and power requirements of current compression technologies for hydrogen refueling. We also evaluated different configurations of high-pressure tube-trailers and their viability for hydrogen delivery to early markets, hydrogen delivery and refueling for forklift applications, and potential synergies and differences between materials handling and FCV markets.

Results

Compression Analysis

Four vendors of piston and diaphragm compressors were surveyed to obtain information on capital costs and power requirements as a function of throughput and dispensing pressure. Figure 1 shows the cost of purchasing a single compressor unit from each vendor as a function of throughput for 350-bar and 700-bar dispensing pressures. The figure reveals an apparent lack of production cost economy with increased throughput. The figure also shows a high compression cost per unit of throughput as well as a large variation in the cost of a single compressor unit between vendors at the same throughput, especially for 700-bar dispensing. The large variation in compressor cost between vendors reflects the different compression technologies but does not address the comparative reliability of these technologies. This is a subject that requires further investigation. We also identified that the cost of a high-pressure (900 bar) liquid pump combined with a vaporizer is more than 50% less than the cost of an equivalent gas compressor. However, the liquid pump option shifts much of the packaging cost to upstream of the refueling station at the liquefaction plant.

High-Pressure Tube Trailer Analysis

Figure 2 shows the relationship between the increase in hydrogen payload of high-pressure (250 bar) composite tubes within an International Organization for Standardization (ISO) container (8 ft wide x 8 ft high x 40 ft long) and the corresponding increase in the cost of these tubes. The payload increase is achieved through packaging more tubes in the ISO container via various inline (NxN) and staggered (NxN-1) arrangements of smaller tube diameters, thus improving the volume utilization of the container at any given pressure. The figure shows that the capital cost of the tubes increase is nearly linear with the payload increase up to a certain payload, above which the volume utilization of the container levels off. We note that the increase in the payload of the tubes would lead to less frequent deliveries, reduced delivery cost and smoother operation at the refueling sites. We also note that improving the volume utilization via packing more tubes in the ISO container requires that the tubes be made of light-weight material (e.g., carbon fiber composites) to comply with the U.S. DOT weight limit of 80,000 lbs. gross combination weight. Figure 3 shows the maximum payload of hydrogen in an ISO container at different loading pressures for steel and composite tubes. While the payload of the composite tubes increases with pressure up to 430 bar, the corresponding payload of the steel tubes drops with pressure to satisfy the aforementioned weight constraint of 80,000 lb. We conclude that high-pressure tube trailers require light weight material to achieve significant increase in hydrogen payload at increased loading pressure. Furthermore, the high-pressure tube trailer can reduce the compression demand at the refueling station, especially in early markets where the utilization of the station compressor is low. This option has the potential to reduce the refueling station capital cost by up to 20% at 50% utilization.

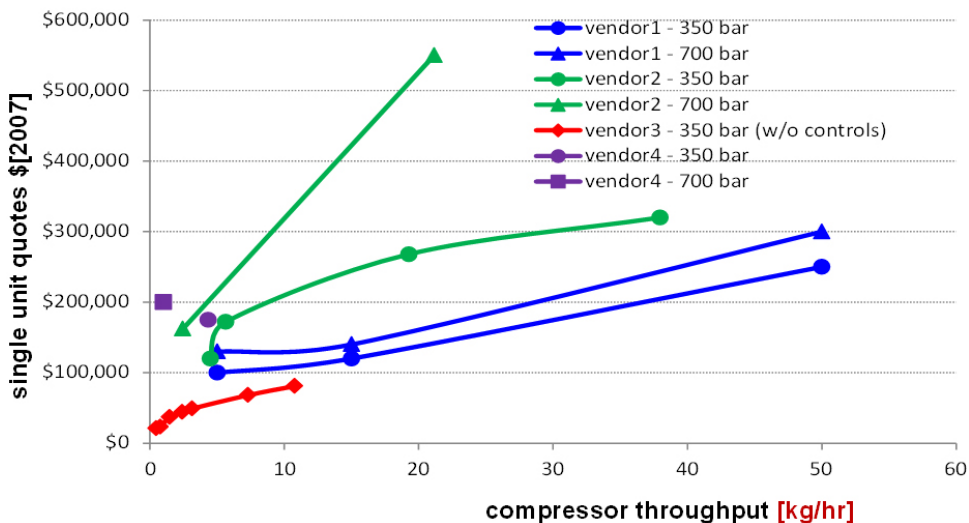


FIGURE 1. Cost of Single Unit Hydrogen Refueling Compressors

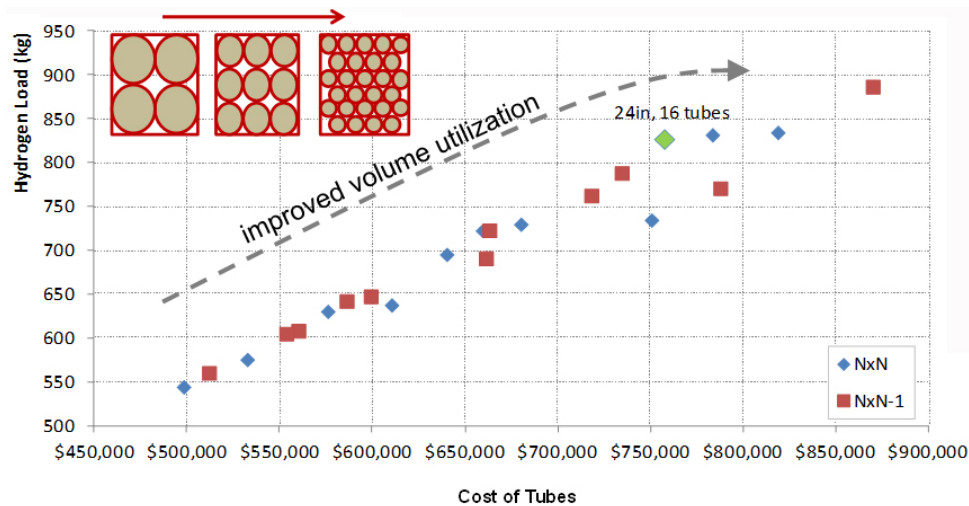


FIGURE 2. Cost of High-Pressure Composite Tubes (250 bar) as a Function of Payload

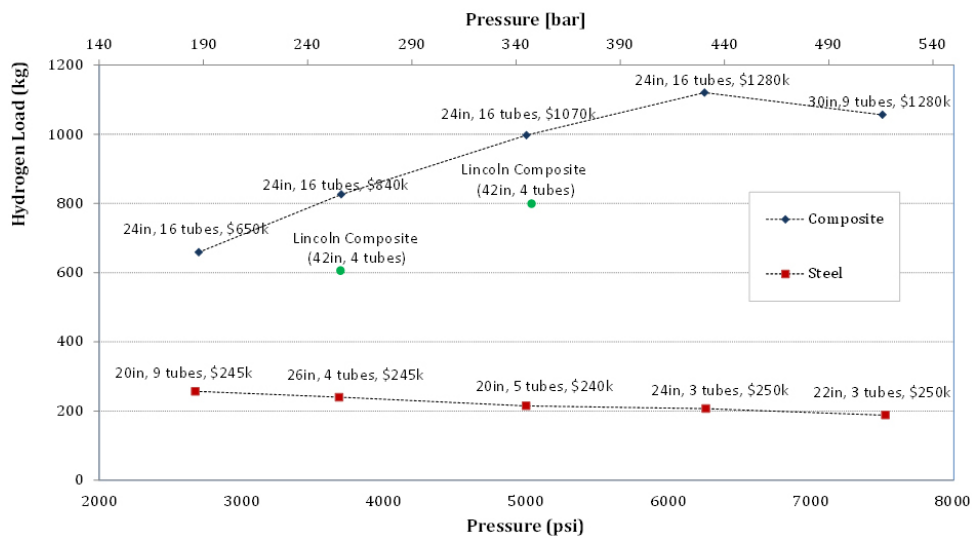


FIGURE 3. Effect of Hydrogen Loading Pressure on Tube Trailer Payload

Hydrogen Delivery for Forklift Applications

Hydrogen delivery for forklift applications was examined to identify potential synergies with hydrogen delivery for vehicle fueling. Table 1 presents selected results (i.e., capital cost, the cost contribution per kg of dispensed hydrogen, and the monthly lease of installed refueling equipment) for two levels of daily forklift refueling demand. With the cost contribution of refueling equipment dropping from \$2.50 to \$2.00 per kg of dispensed hydrogen, results show some economies of scale with increases in daily demand for hydrogen refueling. This is in addition to a \$6 per kg “delivery charge” for producing, liquefying and delivering hydrogen for onsite use.

TABLE 1. Forklift Refueling Cost Estimates

| Daily Refueling Demand | 150 kg/day | 300 kg/day |
|---|------------------------|----------------------|
| Total installed capital | \$850,000 | \$1,300,000 |
| Other Capital (including site preparation) | \$200,000 | \$400,000 |
| Cost contribution of refueling | \$2.5/kg _{H2} | \$2/kg _{H2} |
| Monthly Lease of installed equipment (recover investment in 7 years) | \$15,000 | \$20,000 |
| Monthly Lease of installed equipment (recover investment in 10 years) | \$10,000 | \$15,000 |

The following are some lessons learned from studying fuel cell forklift fueling:

- Hydrogen is available and can be delivered at a cost of ~\$6/kg
- Current technology favors high volume delivery in liquid form
- There is a business case for demand volumes >150 kg/day
- The desired delivery frequency is ~2-3 deliveries/month
- Lease of the installed equipment is a preferred option

However, there are profound differences between refueling forklifts and FCVs. The incumbent technology for fuel cell forklifts is the battery-operated forklift, while FCVs compete against gasoline internal combustion engine vehicles. The refueling frequency for forklifts is every 4-6 hours with relatively flat hourly demand, while vehicles refuel every 300-400 mi with wide variations in desired refueling times (and locations for vehicles that do not return to base each day). FCVs also require high pressure fills at 700 bar with -40°C precooling, while fuel cell forklifts typically refuel at 350 bar with no precooling requirements. Finally, the utilization of the refueling capital investment is expected to be much lower for early deployment of FCVs as compared with a forklift fleet refueled in a central location. All of these differences provide additional challenges with respect to the cost of refueling FCVs.

Conclusions and Future Directions

The hydrogen delivery infrastructure for refueling FCVs as well as forklifts in early markets has been examined. The analysis identified synergies and differences between these two fuel cell applications. Hydrogen is available and can be delivered to these two markets at a reasonable cost when refueling demand exceeds 150 kg/day. The preferred delivery mode for volume deliveries is trucking hydrogen in liquid form. However, liquefying hydrogen suffers from a high electric energy requirement for liquefaction, with potentially high greenhouse gas emissions if the electricity

generation mix relies on fossil sources. Our analysis shows that underutilization of refueling capital and the cost of high-pressure dispensing present major challenges to reducing the cost of hydrogen for FCVs. The need for high-pressure (700 bar) hydrogen for dispensing into FCVs exacerbates the compression requirement at the refueling sites, which is the single most significant contributor to refueling cost. High-pressure tube-trailers can deliver hydrogen with up to 1,000 kg of payload of may reduce the compression requirement at the refueling stations in early markets.

For the remainder of FY 2012, efforts will be directed toward further study of fueling compressor options (the most costly of all refueling components), particularly large throughput compressors. The cost and performance of large throughput compressors will be examined for loading tube trailers and for storing and dispensing hydrogen at large refueling stations. Liquid delivery, today's most favored mode, will also be examined in detail. HDSAM will be updated and employed to examine the impact of these delivery options for early and future markets. Strategies to optimize refueling station and pathways with the greatest potential to achieve significant cost reductions for hydrogen delivery and refueling will be identified for both automotive and non-automotive fuel cell applications.

FY 2012 Publications/Presentations

1. Elgowainy, A., M. Mintz, and M. Gardiner (2012) *Hydrogen Delivery Infrastructure: Analysis of Conventional Delivery Pathway Options*, in *Handbook of Hydrogen Energy*, CRC Press, S.A. Sherif, D.Y. Goswami, E.K. Stefanakos and A. Steinfield, eds., ISBN: 9781420054477.
2. Elgowainy, A., M. Mintz, D. Steward, O. Sozinova, D. Brown and M. Gardiner (2011) *Liquid Hydrogen Production and Delivery from a Dedicated Wind Power Plant*, Argonne National Laboratory Report ANL-11/33, Oct.
3. Paster M.D., R.K. Ahluwalia, G. Berry, K. Day, A. Elgowainy, S. Lasher, K. McKenney, M. Gardiner, (2011) *Hydrogen Storage Technology Options for Fuel Cell Vehicles: Well-to-Wheel Costs, Energy Efficiencies, and Greenhouse Gas Emissions*, Intl. J. of Hydrogen Energy, doi:10.1016/j.ijhydene.2011.07.056.

III.3 Vessel Design and Fabrication Technology for Stationary High-Pressure Hydrogen Storage

Zhili Feng (Primary Contact), Wei Zhang,
John Wang and Fei Ren

Oak Ridge National Laboratory (ORNL)
1 Bethel Valley Rd, PO Box 2008, MS 6095
Oak Ridge, TN 37831
Phone: (865) 576-3797
Email: fengz@ornl.gov

DOE Manager

HQ: Sara Dillich
Phone: (202) 586-7925
Email: Sara.Dillich@ee.doe.gov

Subcontractors:

- Global Engineering and Technology LLC, Camas, WA
- Ben C. Gerwick Inc., Oakland, CA
- MegaStir Technologies LLC, Provo, UT
- University of Michigan, Ann Arbor, MI

Project Start Date: October 1, 2010

Project End Date: Project continuation and direction determined annually by DOE

Fiscal Year (FY) 2012 Objectives

- Develop a high-fidelity cost modeling tool for composite pressure vessels designed based on relevant industry standards and codes
- Quantify the significant cost reduction attainable by composite vessel technology through the optimal use of steels and concretes and the optimization of vessel geometry
- Demonstrate a novel steel vessel manufacturing technology based on ORNL-patented multi-pass, multi-layer friction stir welding (MM-FSW) of thick steel section

Technical Barriers

This project addresses the following technical barriers from the Hydrogen Delivery section (3.2) of the Fuel Cell Technologies (FCT) Program Multi-Year Research, Development and Demonstration Plan:

- (F) Gaseous Hydrogen Storage and Tube Trailer Delivery Cost
- (G) Storage Tank Materials and Costs

Technical Targets

This project aims at developing and demonstrating the novel design and fabrication technology for low-cost and high-safety composite steel/concrete pressure vessel for stationary gaseous hydrogen storage. The flexible and scalable composite vessel design can meet different stationary storage needs (e.g., capacity and pressure) at hydrogen fueling stations, renewable energy hydrogen production sites, and other non-transport storage sites. As shown in Table 1, the current generation composite vessel made using the existing design and manufacturing technology can readily exceed DOE’s 2015 cost target. Moreover, with the successful development of advanced manufacturing technology such as the highly-automated friction stir welding process, the next generation vessel has a high potential to meet DOE’s 2020 capital cost target.

TABLE 1. Progress towards Meeting Technical Targets for Stationary Gaseous H₂ Storage Tanks (for fueling sites, terminals, or other non-transport storage needs)

| Pressure | DOE 2015 Target* | Current generation composite vessel | DOE 2020 Target* | Next generation composite vessel |
|---------------------|--------------------------------|-------------------------------------|--------------------------------|----------------------------------|
| 345 bar (5,000 psi) | \$884 per kg of H ₂ | \$800 per kg of H ₂ | \$735 per kg of H ₂ | \$680 per kg of H ₂ |

*DOE targets for 345 bar pressure were linearly interpolated between the targets at 160 and 430 bar (cost target data from the draft of 2011 FCT Program Technical Plan for Hydrogen Delivery, currently being finalized).

FY 2012 Accomplishments

- Designed a high-pressure composite vessel comprising inner layered steel tanks and outer reinforcement pre-stressed concrete for stationary gaseous hydrogen storage at an estimated capital cost about 10% below the relevant DOE technical target for 2015.
- Identified the pathways to achieve the DOE 2020 target through development of advanced vessel manufacturing technology and materials.
- Demonstrated the feasibility of MM-FSW for steel vessel fabrication by successfully joining a 15-mm-thick (0.6 in.) steel plate, which nearly tripled the thickness of steel weldable by the conventional FSW.



Introduction

Off-board bulk stationary storage of hydrogen is a critical element in the overall hydrogen production and

delivery infrastructure. Stationary storage is needed at fueling stations, renewable energy hydrogen production sites, central production plants, and terminals, etc. The capacity and hydrogen pressure of the stationary storage vessel are expected to vary considerably depending on the intended usage, the location and other economic and logistic considerations. For instance, the storage vessel at a hydrogen fueling station may have a higher pressure but smaller storage capacity when compared to that at a renewable energy hydrogen production site. Therefore, it is important the storage vessel is flexible and scalable to meet different storage needs (i.e., capacity and pressure). Moreover, as it provides the surge capacity to handle hourly, daily, and seasonal demand variations, the stationary storage vessel endures repeated charging/discharging cycles. Therefore, the hydrogen embrittlement in structural materials, especially the accelerated crack growth due to fatigue cycling, needs to be mitigated to ensure the vessel safety.

In this project, ORNL leads a diverse multidisciplinary team consisting of industry and academia to develop and demonstrate an integrated design and fabrication technology for cost-effective composite steel/concrete high-pressure hydrogen storage vessel that can meet different stationary hydrogen storage needs. Safety and economics are two prevailing drivers behind the composite hydrogen storage technology.

Approach

A schematic drawing of the composite pressure vessel in hydrogen fueling station is illustrated in Figure 1, where the salient design features of the composite storage vessel technology are highlighted. The particular vessel design in this figure comprises four inner steel tanks and an outer

reinforcement pre-stressed concrete sleeve. The shell section of each steel tank is a layered structure. The innermost layer directly exposed to the high-pressure hydrogen is made of an austenitic stainless steel (e.g., American Iron & Steel Institute 316L or 304L), which excels as a hydrogen embrittlement and permeation barrier. The other layers are made of high-strength low alloy steel (e.g., ASTM SA724), which costs about four times less than the stainless steel. Finally, the steel tanks are encased in the pre-stressed concrete sleeve, which bears the structural loads at an even lower cost when compared to structural steel. The optimal use of commodity materials (i.e., stainless steel, structural steel and concrete) is essential to the cost-effectiveness and safety of composite pressure vessel. The layered steel vessel technology is proven and accepted in industry standards and codes (e.g., American Society of Mechanical Engineers Boiler and Pressure Vessel Code). It has significant cost and safety advantages over the conventional single-section steel vessel. Moreover, the layered steel vessel is amiable to the advanced fabrication technology based on FSW for further reducing fabrication cost. Sensors will be embedded into both inner steel tanks and outer concrete sleeve to ensure the safe and reliable operation in field. The composite vessel shown in Figure 1 has the modular design with scalability and flexibility for meeting different storage pressure and capacity needs.

Results

The major tasks in FY 2012 include: (1) development of a high-fidelity cost modeling tool for composite pressure vessel and performing the cost optimization study using the model tool, (2) preliminary assessment of steel/concrete interface through finite element modeling of stress and displacement, and (3) demonstration of ORNL-patented MM-FSW for

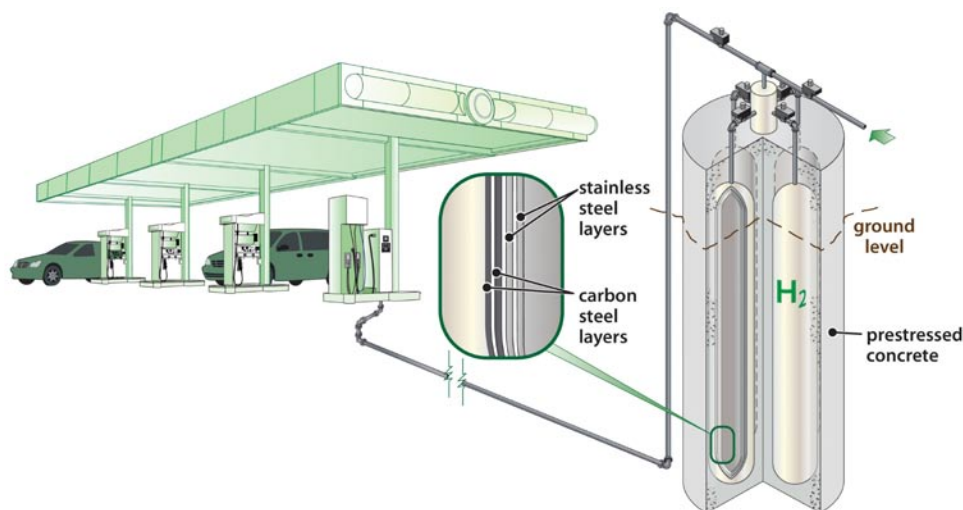


FIGURE 1. Schematic of a composite vessel comprising inner layered steel tanks and outer pre-stressed concrete confinement at hydrogen fueling station

joining of thick steel sections. The key results from this year’s substantial development are as follows.

Composite vessel cost modeling and optimization: The baseline composite vessel is designed to contain 1,500 kg of H₂ per system, which is sufficient to refill around 260 fuel cell passenger cars (based on 5.6 kg H₂ tank per car). The design pressure is chosen at 345 bar (5,000 psi) to match the pressure of Type-III hydrogen tank used in fuel cell cars and forklift trucks. It is noted that due to its modular design, the storage vessel can be flexibly adopted for other pressure levels, i.e., low (160 bar), moderate (430 bar) and high (820 bar), and other storage volumes.

To obtain real-world representative cost estimate of composite vessel, ORNL partnered with Global Engineering

and Technology and Ben C. Gerwick, two leading engineering design firms in the field of steel pressure vessels and pre-stressed concrete structures, respectively. The high-fidelity cost modeling tool was developed using the bottom-up cost estimate approach comprising the following steps. First, the composite vessel dimensions (e.g., thickness of steel and concrete walls) were calculated using the formula from relevant industry codes for the given user inputs (e.g., pressure, load carrying ratio between concrete and steel, and inner diameter). Second, a detailed, step-by-step manufacturing process flow was established for the composite vessel. Schematics of manufacturing steps for layered steel tank and pre-stressed concrete sleeve are illustrated in Figures 2(a) and 2(b), respectively. Finally, the component cost for each manufacturing step was calculated

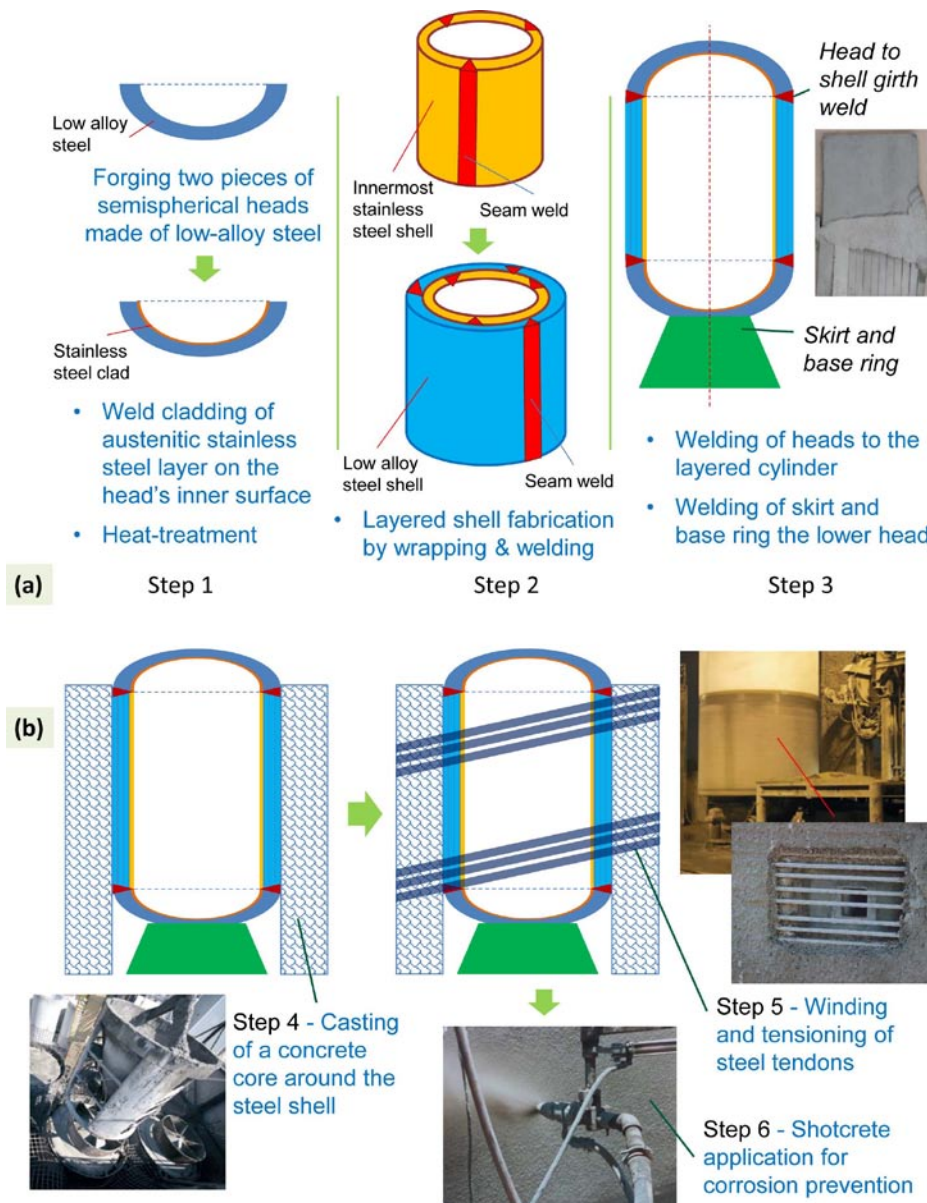


FIGURE 2. Schematics of manufacturing steps for (a) layered steel tank, and (b) pre-stressed concrete sleeve

by considering bill of materials and labor to obtain the total vessel cost.

Figure 3 compares the costs attainable through different composite vessel design and manufacturing technology to the DOE capital cost targets. The leftmost three columns correspond to DOE’s latest cost targets obtained by linearly interpolation to 345 bar pressure. Base Case 1 given in column 4 represents the current industry status based on the conventional steel pressure vessel technology. This base case steel vessel, which includes a stainless steel liner as a hydrogen embrittlement and permeation barrier, has an estimated capital cost of \$1,350/kg of H₂. Columns 5 through 7 correspond to the group of composite vessels with 50%-50% load carrying ratio between steel and concrete (so-called Case 2). In particular, Baseline Case 2 (or simply Case 2) is the first design which is used to establish the detailed cost modeling tool. Built on the results of Case 2, a cost optimization study is performed to reach the “Current (generation) Case 2,” which can be manufactured with the existing technology for an estimated cost of \$800/kg of H₂. Optimized Case 2 represents the next generation composite vessel where the cost reduction is achievable through further technology development including the automated MM-FSW. Finally, it is also studied Case 3 vessel with 30% steel and 70% concrete, which increases the usage of pre-stressed concrete to bear the structural loads. Case 3 does not seem to result in reduction in the total vessel cost since the needs for ultra-high strength concrete and additional longitudinal tensioning add significant cost that outweighs the cost saving due to the thinning of the steel tank.

Through the detailed cost modeling and optimization study, it is shown that the 50/50 composite vessel using the existing design and manufacturing technology can readily exceed DOE’s 2015 cost target. Moreover, it is highly feasible for the composite vessel to meet DOE’s 2020 cost target through the development of advanced vessel manufacturing technology and materials, as discussed in a later section.

It is noted the high-fidelity cost modeling tool for the steel/concrete composite vessel technology is currently being refined and finalized. The refinements include the following. First, a high-productivity electrosag strip cladding process is being considered for manufacturing of the stainless steel liner, which can significantly reduce the liner cost when compared to the conventional weld overlay process. Second, the cost savings achievable through the use of friction stir welding for layered steel shell manufacturing are being quantified based on published data from relevant literature. Finally, the refined cost modeling tool is being applied to study the new vessels for three pressure levels (160, 430 and 860 bar) relevant to the hydrogen production and delivery infrastructure. The final cost study results will be published in an ORNL report entitled “Manufacturing Cost Analysis of Novel Steel/Concrete Composite Vessel for Stationary Storage of High-Pressure Hydrogen.”

Assessment of steel/concrete interface: Due to the different mechanical properties between steel and concrete, the steel/concrete interface is one of the most critical locations in a composite vessel. In collaboration with University of Michigan, a finite element analysis was performed to study the deformation compliance across the

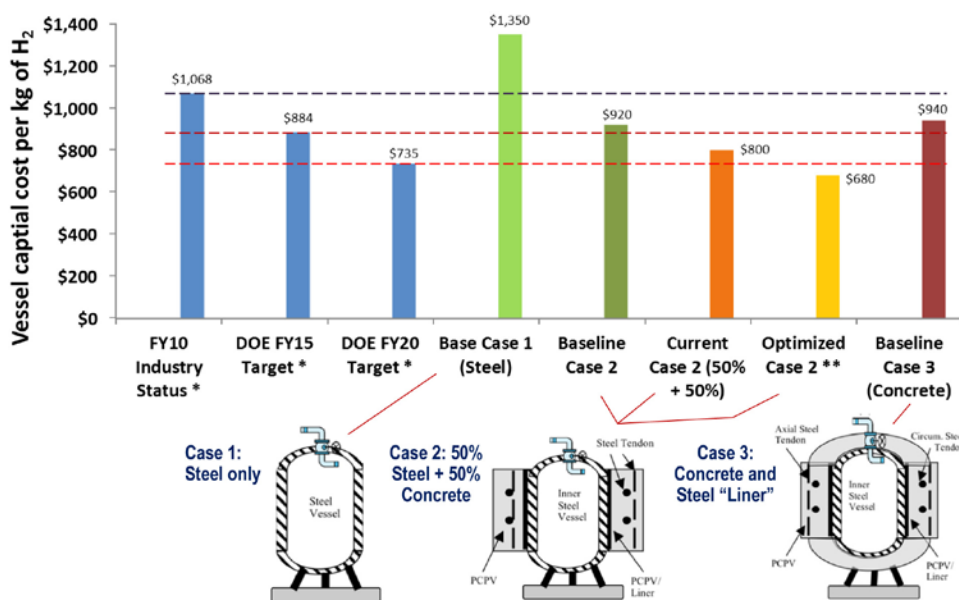


FIGURE 3. Comparison of the capital costs attainable through different composite vessel design and manufacturing technology to the DOE cost targets

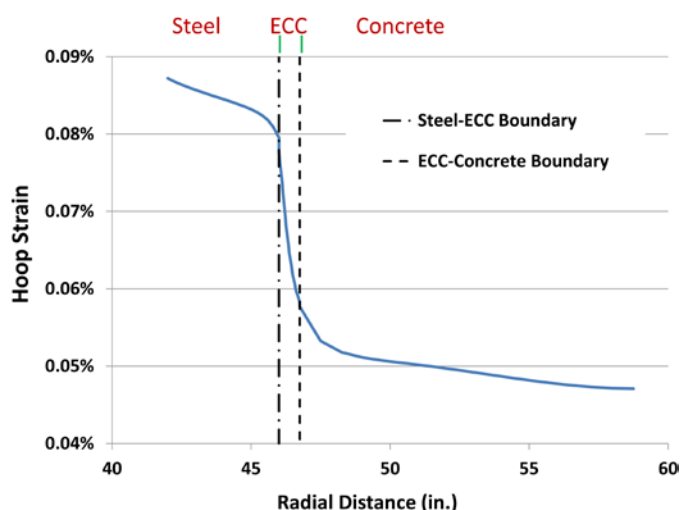


FIGURE 4. Finite element analysis results showing the hoop strain distribution across the steel/concrete interface, indicating a buffer layer of ECC can effectively reduce the tensile strain in the concrete material

steel/concrete interface. A ductile, engineered cementitious composite (ECC) [1] was used as a soft buffer layer between the steel and the concrete. Figure 4 shows the calculated hoop strain profile across the steel/concrete interface under the influence of both external pre-stressing and internal pressurization. As shown in this figure, the tensile strain decreased rapidly within the ECC layer, which limited the tensile strain exerted in the concrete due to internal pressurization. In other words, by utilizing the ductile ECC as soft buffer layer to absorb the majority of deformation, the concrete is exposed to much less tensile strain, thus significantly minimizing the risk of concrete brittle failure under tension.

Manufacturing technology: The detailed cost analysis in the previous task identified that a major pathway for further reducing the total composite vessel cost is the development of advanced welding process to displace the labor-intensive, conventional arc welding construction of steel shells. The highly-automated FSW process, being developed in this project, is expected to significantly reduce the labor cost while improving the weld quality at the same time. In FY 2012, the development effort was focused on the scale up of FSW for thick-section steel structures. The novel MM-FSW process (ORNL Patent US 7,762,447 B2) was successfully developed to weld 15-mm-thick (0.6 in.) pressure vessel steel plates, nearly tripling the thickness of steel that was weldable by the single-pass FSW [2]. Mechanical testing of the friction stir welded thick steel plate is ongoing. Moreover, the MM-FSW technology will be further developed to scale up to the expected wall thickness of the hydrogen storage steel tank.

Conclusions and Future Directions

- Through the detailed engineering calculations and cost optimization study, it is shown that the composite steel/concrete vessel can be fabricated using the existing technology for an estimated capital cost about 10% below the DOE 2015 target. Moreover, with the successful development of advanced manufacturing technology and materials, the next generation composite vessel has a high potential to meet DOE's 2020 capital cost target.
- The feasibility of MM-FSW for steel vessel fabrication is demonstrated by successfully joining a 15-mm-thick (0.6 in.) steel plate, nearly tripling the thickness of steel that can be welded by the single-pass FSW.
- Future directions in FY 2013 and subsequent years will be focused on the manufacturing and testing of mock-up composite storage vessel, which are crucial for enabling the near-term impact of the developed storage technology on high-pressure gaseous hydrogen storage market (especially stationary storage for hydrogen fueling station).

FY 2012 Publications/Presentations

1. W. Zhang *et al.*, "Vessel Design and Fabrication Technology for Stationary High-Pressure Hydrogen Storage," invited talk at Zhejiang University, China in Oct. 2011, hosted by Professor Jingyang (JY) Zheng.
2. W. Zhang *et al.*, DOE Hydrogen Delivery Tech Team (DTT) Meeting, Southfield, MI, March 2012.
3. W. Zhang *et al.*, 2012 DOE Annual Merit Review, Fuel Cell Technologies Program, Washington, DC, May 2011.
4. W. Zhang *et al.*, "Design Analysis of Composite Vessel for High-Pressure Hydrogen Stationary Storage," abstract accepted to the 2012 International Hydrogen Conference.
5. Y.C. Lim *et al.*, "Mechanical properties and microstructure characterization of multilayered multipass friction stir steel weld," abstract submitted to 2013 TMS Annual Meeting.

References

1. Li, V.C., "High-Ductility Concrete for Resilient Infrastructure", *Journal of Advanced and High-Performance Materials*, pp.16-21, 2011.
2. Feng, Z. Steel, R. Packer, S. and David, S.A. 2009. "Friction Stir Welding of API Grade 65 Steel Pipes," ASME PVP Conference, Prague, Czech Republic.

III.4 Failure Analysis, Permeation, and Toughness of Glass Fiber Composite Pressure Vessels for Inexpensive Delivery of Cold Hydrogen

Andrew Weisberg (Primary Contact),
Salvador Aceves
Lawrence Livermore National Laboratory (LLNL)
P.O. Box 808, L-792
Livermore, CA 94551
Phone: (925) 422-0864
Email: saceves@llnl.gov

DOE Manager
HQ: Erika Sutherland
Phone: (202) 586-3152
Email: Erika.Sutherland@ee.doe.gov

Subcontractor:
Spencer Composites Corporation (SCC), Sacramento, CA

Project Start Date: October, 2004
Project End Date: October, 2012

FY 2012 Accomplishments

Developed a deep understanding of composite pressure vessel (CPV) failure analysis and anomalous toughness degradation in ring-opening metathesis polymerization (ROMP) castings.



Introduction

This project has developed the key missing component necessary for LLNL's "cold glass" delivery approach: trailer-scale pressure vessels. Other technologies can build low-temperature-capable pressure vessels, but their vessels are either much too costly or too heavy for delivery trailers.

Only CPVs are light enough to carry compressed hydrogen in sufficient quantity to achieve LLNL's optimized delivery costs within the volume and mass limitations of a trailer. LLNL's target (below \$1/kg, not including forecourt storage, compression, or dispensing) must pay for energy and capital to refrigerate, plus operating and capital costs of the trailer cab (including labor to drive and load/unload).

Development effort required to produce trailer payloads filled with economical CPVs can be categorized on the manufacturing readiness level (MRL) scale [1]. When first proposed in 2007, this CPV development effort expected to advance from MRL 4 (proven manufacturing feasibility) to MRL 8 (manufacturing processes that operate at target cost, quality, and performance). Across the past two and a half years this MRL characterization encountered setbacks, which caused its MRLs to be revised from MRL 3 (manufacturing process identified) to MRL 7 (proven manufacturing processes). Careful study of these setbacks has produced a new understanding of vessel failure mechanisms. This new understanding is the focus of this report.

Approach

Because the processes that build plastics into composites and liners do not scale from one size to another without posing significant risks to CPV performance and cost, only proof at full scale of a CPV technology will prove that LLNL's trailer design is practical. Due to the severe cost scaling of tooling to build such CPVs, LLNL's system integration and subsequent development efforts have focused on 23" diameter, 18 CPVs per International Organization for Standardization (ISO) container cross section, as full scale. Considerable development risk reduction testing has

Fiscal Year (FY) 2012 Objectives

- Optimize hydrogen delivery by tube trailer
- Develop materials and manufacturing for low-temperature hydrogen delivery
- Quantify performance and economics of delivery pressure vessels

Technical Barriers

This project addresses the following technical barriers from the Hydrogen Delivery (3.2) section of the Fuel Cell Technologies Program Multi-Year Research, Development and Demonstration Plan:

- (F) Gaseous Hydrogen Storage and Tube Trailer Delivery Cost
- (G) Storage Tank Materials and Costs

Technical Targets

TABLE 1. Progress towards Meeting Technical Targets for Hydrogen Delivery

| Characteristic | 2005 value (Table 3.2.2) | DOE Targets FY2012/2017 | LLNL + SCC 2012 status |
|--|-----------------------------|----------------------------|---------------------------|
| Delivery Capacity (kg H ₂) | 280 | 700/1,100 | 1,100 |
| Operating Pressure (psi) | 2,640 | <10,000 | <10,000 |
| Purchased Capital Cost (\$) | \$165,000 | <\$300,000 | <\$291,000 |

been performed with 3” diameter subscale vessels, and with strength test coupons.

Results

Hydrogen delivery by trailer cannot meet DOE targets for dollars-per-kilogram without new technology. This project performs research and development on an approach to delivering centrally-produced hydrogen that can achieve DOE targets with high likelihood.

Reaching these objectives demands significant learning because the expertise necessary to determine the safety of our new technology is scarce. In particular, neither regulators nor aerospace experts have valid precedents for large pressure vessels designed to operate economically at near-cryogenic temperatures, on highways, built from unprecedented materials.

In pursuit of a fundamental reduction in the manufacturing cost of pressure vessels, a new category of plastics with properties and manufacturing process advantages was researched. This category will be termed “ROMP” catalyzed, which stands for ring opening metathesis polymerization. Among the features of this plastic are low thermal expansion and full property retention at temperatures

as low as 77 K. These plastics are expected to form both liner and matrix of a new generation of inexpensive pressure vessels.

Failure Analysis

Even CPVs built and operated with thousands of person-years of aerospace experience gained over 40 years with ‘proven’ processes using graphite fibers, familiar polymers, and stainless steel connections fail for unknown reasons. A deep understanding of failure modes is necessary for improved vessel safety.

In collaboration with National Aeronautical and Space Administration (NASA) White Sands Test Facility (WSTF), National Institute of Standards and Technology (NIST), and Department of Transportation (DOT), LLNL produced the first expert-consensus methodology in nearly 30 years to plan how to determine the root causes of a CPV failure. This procedure makes selective use of many new techniques, which it triages for affordability in a better adaptation to motor vehicle CPVs. The procedure prunes the branches of an LLNL-supplied fault tree (Figure 1), as thoroughly as data will allow, to determine the root cause of a CPV failure.

The current LLNL effort seeks novel hydrogen CPVs that will not fail in service, and expects to develop interest at DOT

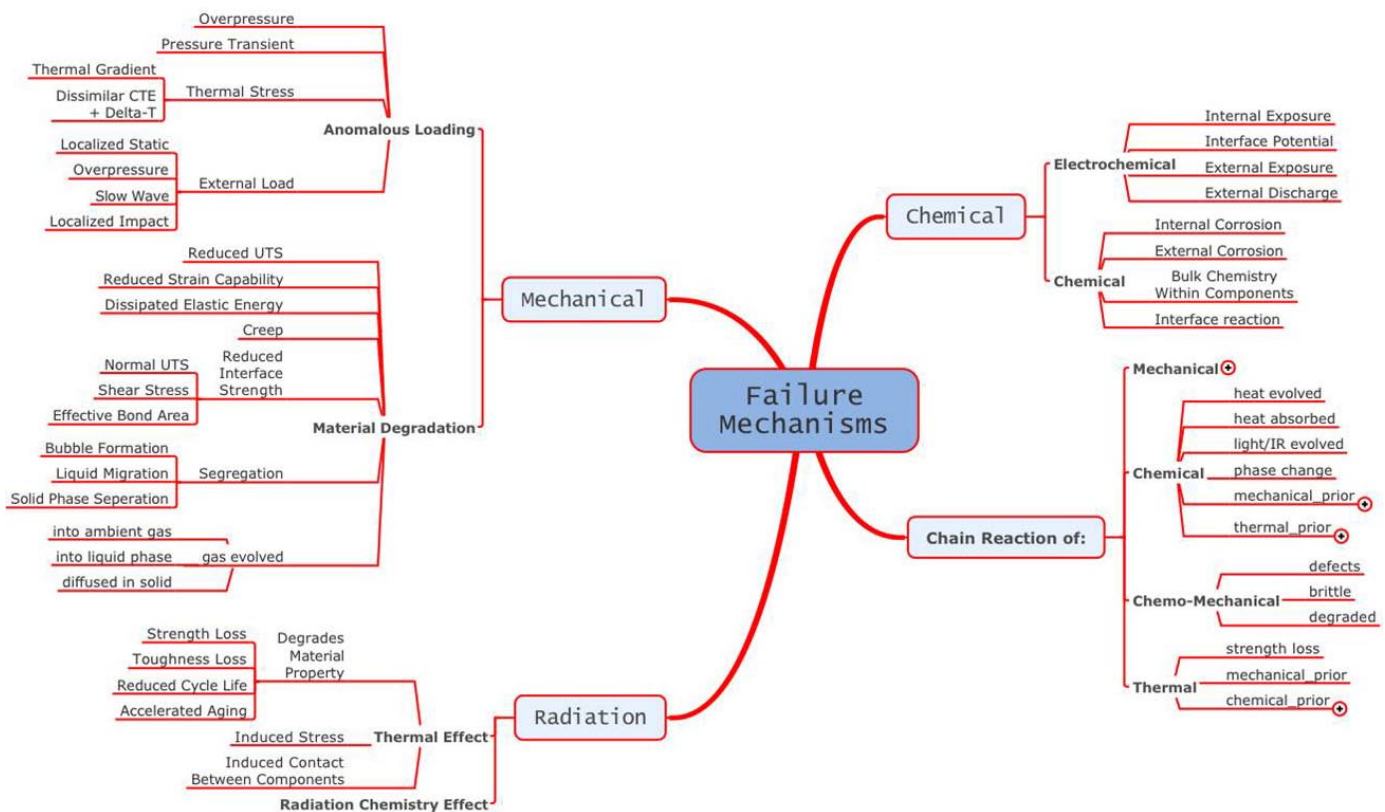


FIGURE 1. Expert-consensus methodology plans how to determine the root causes of a CPV failure, based on using a wide variety of affordable tests to prune branches on the above fault tree, which was prepared by LLNL in support of a multi-agency CPV failure analysis collaboration with NASA WSTF, NIST, and DOT.

for a hydrogen delivery trailer solicitation. This argument depends on quantitative data, including empirical probabilities of failure collected from multiple ‘identical’ CPVs and sorted into failure modes. In particular, the challenges of a probability of disaster limited in the low parts-per-million have focused LLNL on two branches on the CPV fault tree: manufacturing defects and stress rupture. LLNL’s efforts to date have reduced the risk of unpredictable burst strength and should reduce the risk of inadequate cycle life.

Permeation

Permeation of hydrogen through plastics poses a risk to this project. While the only ROMP permeation data (collected at LLNL in 1997 with flat coupons at ambient temperature) indicates extremely low permeation (several orders of magnitude too low to have a negative effect on the proposed delivery approach), it is still important to accurately quantify permeation by conducting full-scale tests.

LLNL has been working with SCC on conducting safe, remotely operated, full-scale CPV permeation tests. A suitable site that contractor personnel can secure for weeks against tampering and intruders was leased by SCC to practice initial ‘coffin’ emplacement and determine manpower costs for long endurance permeation tests. One LLNL coffin is shown emplaced in the trench dug at that site in Figure 2.

Toughness and Toughness Decay

Applications for ROMP chemistry were originally sought in the 1980s. However, their utility as resins for inexpensive polymers failed because their toughness decayed over time. Adding anti-oxidants was a partial solution that maintained higher toughness than toughened epoxies for

a month after casting. If their initial toughness persisted, ROMP formulations would be thirty times as tough as toughened epoxies.

In an effort to organize the hypotheses collected to explain anomalous toughness decay in cast ROMP liners, LLNL developed a tree diagram (Figure 3). Hypotheses in Figure 3 are color coded to distinguish their experimental validation over the course of this project. Green font hypotheses were proven to occur and be responsible for faulty ROMP processing. Blue font hypotheses were proven, yellow were disproven except for highly localized defects due to unclean molds and gaps in seals that retained air at mold parting lines. Orange font hypotheses turned out to be both true and untrue in different senses. The purple font hypothesis appears to be caused by the same driving force that appears in the turquoise font, which represents the root cause of anomalous embrittlement: the differential shrinkage between liquid resin and solidified ROMP, by a novel mechanism this project has come to call ‘nanocracking’.

Detective work with scanning electron microscopy (SEM) explained a sequence of events that evolve gases and liquids from catalyzing gel. The key to identifying these events was careful observation of the “smoking gun crater” (Figure 4). Observation revealed that there was material missing between the walls of such crater because a gel had torn itself apart here while shrinking and then a bubble had forced itself out through a smooth wall caused by strength anisotropy and not by imposed stress, and finally the almost conical volcano had further shrunk to form sharp facets. All this must have happened before the liner failed, in the final phases of its solidification inside a mold, where the catalysis wave ran out of liquid to knit and could not make up for the volume loss of solidification. Any gas pressure would attempt to burst out of a gel under tension. Solids with such stress-



FIGURE 2. Photographs show ‘coffin’ emplacement and steel deck plate covering operations at SCC’s leased permeation test site. The coffin provides a clean environment for transportation (over dirt roads) and plumbing and data collection from a CPV under long duration testing with dangerous high-pressure fluids.

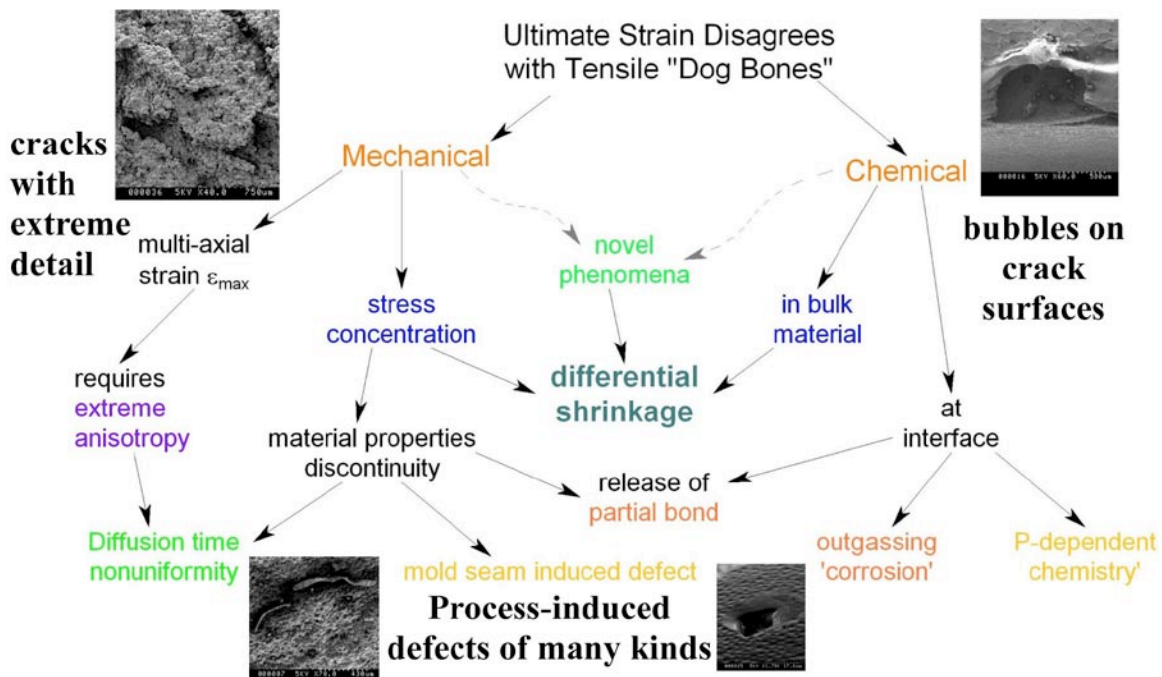


FIGURE 3. A tree diagram organizes the possible hypotheses collected to explain anomalous toughness phenomena in cast ROMP liners. Orange font hypotheses turned out to be both true and false in different contexts. Green hypotheses were proved to occur and be responsible for CPV failures. Yellow hypotheses were not responsible, blue proved to occur, purple responsible, and turquoise the root cause of all responsible hypotheses.

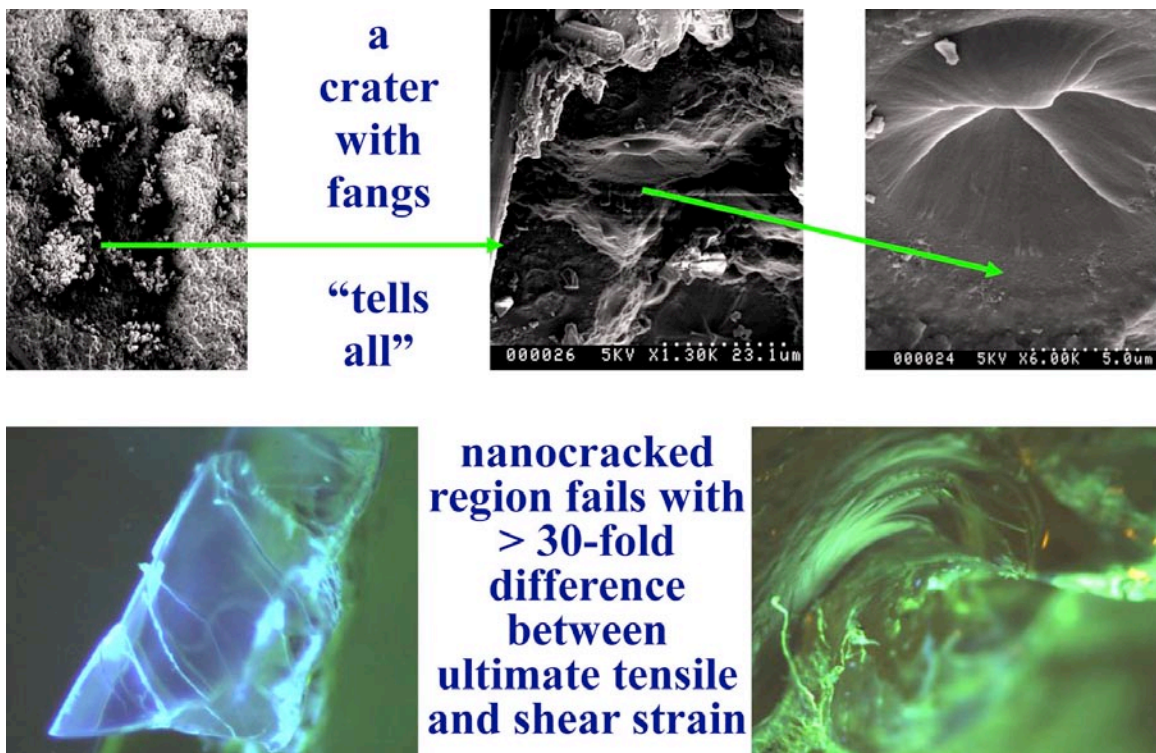


FIGURE 4. Micrographs pivotal to the discovery of new materials science taken in the course of debugging anomalous toughness. Specimens of ROMP liners, their production during deliberate failure, subsequent preparation, and conclusions based on these micrographs are briefly described in the text.

concentrating defective regions built into them were bound to fail if those regions came under subsequent tension even slightly perpendicular to some surface nanocrack.

With toughness loss explained, the remedy was to drive catalysis waves away from solid surfaces and into free surfaces, whereat solidification shrinkage allows the cast surface to recede rather than crack. The team learned to bias catalysis direction by mold design and active thermal control, and to control liner bending during curing. SCC found a technique to detect nanocracked surfaces without breaking liners, sectioning portions of a crack surface, coating specimens with ~50 nanometers of metal to conduct electricity, or even using an SEM. LLNL found some nanocracked regions interior to cast parts where catalysis waves had arrived from different directions at different times. LLNL isolated one of these regions wherein the nanocracked volume appears faintly as a hazy tree under bright light. Successful liner geometries and molding processes were found which did not put nanocracked regions in tension.

This research is continuing with investigation of toughness in ROMP at low temperatures. Countermeasures against toughness loss are under development at SCC, and the likelihood that uncatalyzed molecules must be kept in nanopores to preserve extreme toughness could be tested later this year by correlating Sharpe toughness with weight loss from different cure cycles. Meanwhile a more precise toughness measurement is about to be exercised by LLNL

experiments in a 0.5% accurate impact test rig at NASA WSTF. Figure 5 illustrates that rig, its potential for tests that produce shrapnel, and the exercises that LLNL has already conducted at SCC to determine the drop weight and practice cool down operations in preparation for those tests.

Conclusions and Future Directions

- Considerable scientific effort has generated significant understanding of ROMP failure mechanisms, and further effort will be capable of limiting significant hydrogen delivery cost uncertainties. Subscale and full-scale CPV permeation tests are planned without government funding at leased facilities that have already been exercised to plan safe, long-duration-under-pressure experiments.
- Further quantitative understanding of cold strength at various reduced temperatures is anticipated at multiple glass fiber manufacturers from testing subscale glass fiber pressure vessels in expendable Dewars.
- Joint DOE/DOT demonstration program remains a possibility suitable for discussion early in 2013.

References

1. Manufacturing Readiness Level chart (and accompanying 72 page category descriptions) provided by Department of Defense web site www.dtic.mil/whs/directives/corres/pdf/500002p.pdf.

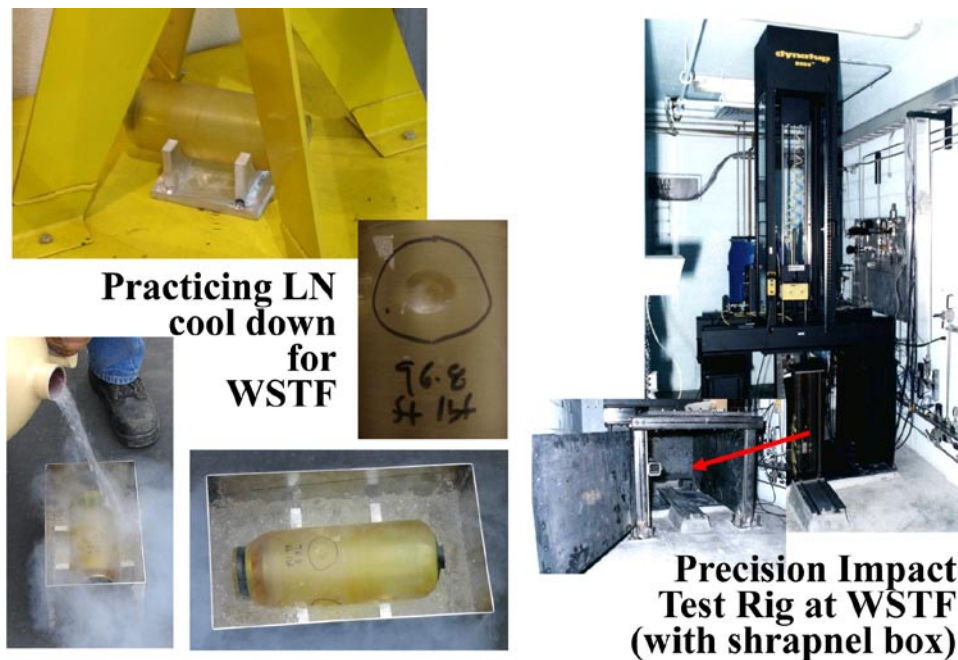


FIGURE 5. Preparations for cold liner toughness measurements yet to be performed at NASA WSTF include a medley (on the left) showing practice for safe cold liner handling, impact fracture, and cooling in liquid nitrogen. Coarse toughness measurements made in the ASTM International drop tower inside SCC facilities at the upper left were performed to specify drop weights for WSTF impact testing.

III.5 Fiber Reinforced Composite Pipeline

George Rawls
Savannah River National Laboratory (SRNL)
Materials Science & Technology
773-41A/173
Aiken, SC 29808
Phone: (803) 725-5658
Email: george.rawls@srnl.doe.gov

DOE Manager
HQ: Sara Dillich
Phone: (202) 586-7925
Email: Sara.Dillich@ee.doe.gov

Project Start Date: October 1, 2006
Project End Date: October 1, 2016

- Transmission pipeline total capital cost \$735k per mile (2015)
- Transmission pipeline total capital cost \$715k, per mile (2020)
- H2 Delivery Cost <\$0.90/gasoline gallon equivalent
- H2 pipeline leakage: <780 kg/mi/y (2020)

FY 2012 Accomplishments

In FY 2012, the SRNL project has focused on supporting the development of a life management methodology for FRP materials and the American Society of Mechanical Engineers (ASME) B31.12 Codification of FRP. The materials testing effort has centered on the fatigue damage of FRP for both flawed and unflawed conditions. Initial meetings were held with the ASME B31.12 Piping Committee to initiate the codification process. A functions and requirements document was also developed for a proposed integrated hydrogen demonstration project.

- FRP Materials Testing
 - Fatigue testing has been completed for both flawed and unflawed samples
 - Proposal developed for extending the service life of FRP
- FRP Codification into ASME B31.12
 - Codification workshop with all stakeholders
 - Presented technical data on FRP to B31.12 Committee
- Proposal to DOE for FRP Demonstration Project
 - Developed a concept plan for an integrated hydrogen delivery project



Fiscal Year (FY) 2012 Objectives

Fiber Reinforced Composite Pipeline (FRP)

- Successfully adapt spoolable FRP currently used in the oil and natural gas industry to use high-pressure hydrogen delivery systems.
- Development of data needed for life management and codification FRP.

Technical Barriers

This project addresses the following technical barriers from the Hydrogen Delivery section of the Fuel Cell Technologies Program Multi-Year Research, Development and Demonstration Plan:

- (D) High Capital Cost and Hydrogen Embrittlement of Pipelines
- (IV) Hydrogen Leakage and Sensors
- (K) Safety, Codes and Standards, Permitting

Technical Targets

This project is focused on the evaluation of FRP for hydrogen service applications. Assessment of the structural integrity of the FRP piping and the individual manufacturing components in hydrogen will be performed. Insights gained will support qualifications of these materials for hydrogen service including:

- Transmission pipeline reliability: Acceptable for hydrogen as a major energy carrier

Introduction

The goal of the overall project is to successfully adapt spoolable FRP currently used in the oil industry for use in high-pressure hydrogen pipelines. The use of FRP materials for hydrogen service will rely on the demonstrated compatibility of these materials for pipeline service environments and operating conditions. The ability of the polymer piping to withstand degradation while in service, and development of the tools and data required for life management are imperative for successful implementation of these materials for hydrogen pipeline.

Approach

To achieve the objective an FRP life management plan was developed. The plan was a joint document developed by SRNL and the ASME to guide generation of a technical basis for safe use of FRP in delivery applications. The plan addresses the needed material evaluations and also focuses on the needed information for codification of FRP into the ASME B31 Code of Pressure Piping. The B31.12 Hydrogen Piping Code is the existing code that provides a consensus standard for the safe and reliable implementation of the piping in hydrogen service. This plan is designed to provide the needed information to support the codification of FRP. The B31.12 Code addresses the initial construction of piping systems. The plan also identifies the tasks needed for the post construction management of FRP to insure structural integrity through end of life. The plan calls for detailed investigation of the following areas:

- System Design and Applicable Codes and Standards
- Service Degradation of FRP
- Flaw Tolerance and Flaw Detection
- Integrity Management Plan
- Leak Detection and Operational Controls Evaluation
- Repair Evaluation

Results

Burst Testing

SRNL has completed the first areas of the Life Management Plan. Codes and standards for the high-pressure piping, process, and transport pressure vessels were reviewed and design margins and qualification techniques evaluated.

SRNL and Oak Ridge National Laboratory (ORNL) have collaborated on evaluating the service degradation of FRP in high-pressure hydrogen. Initial laboratory testing indicated that there is not a degradation mechanism connected with the use of hydrogen in FRP. The codes and standard development organizations would like additional long-term data on this question to ensure the long-term life management of FRP.

SRNL has begun an investigation to determine the flaw tolerance of FRP products. Creep data on glass fiber was also reviewed to evaluate the effect of creep life on the glass fiber. The results indicate that a design margin of at least 3.5 is required to address long-term creep effects for a 20+ year design life. The use of the fiberglass creep data has been effective in evaluating the effect of flaw tolerance using a short-term burst test. Multiple tests have been completed to evaluate the effect of flaw tolerance on FRP samples. FRP designed to a recognized national consensus standard were used in the evaluation. Flaws for various depths were machined into the samples and burst tests have been performed.

To address third-party damage the sensitivity of FRP to flaws must be established. The flaw testing was performed over a range of flaw sizes to determine the flaw tolerance of the FRP. The results of the multi-layer FRP tests are provided in Figure 1. Tests were conducted for increasing flaw depths up to 40% through wall. A 28% reduction in burst pressure from the unflawed condition to a 40% through wall flaw was observed. With the 40% through-wall flaw there is still a margin of approximately 3 above the rated pressure of the FRP multi-layered product. The margin on burst of 3 provides an acceptable remaining product life to detect and repair flaws in FRP systems. Additional burst tests were conducted in on FRP samples with 40% through wall flaws to determine the variability between different samples. The results of the additional tests show that the variability between the tests is low and that all tests provide an acceptable design margin. The results for increasing the flaw length and width are also shown in Figure 1. The flaw with increased length showed no additional loss in design margin above the base flaw length. The flaw with increased width showed a small additional loss in design margin above the base flaw width. Two FRP samples were exposed to the high- and low-PH solutions and burst tested. The results are shown in Figure 2. The failure pressure for the chemically exposed samples fell within the variability of the unexposed data.

From the flawed samples, it was observed that as the flaw depth increased the failure mode changed from a local failure to a more global failure mode. The series of photos shown in Figure 2 illustrates these failure modes. The first photo from the left shows the failure of the unflawed sample indicating a global failure of the pipe. The next three photos illustrate how the failure mode changed as the flaw depth increased. The last photo on the right shows the 40% through-wall flaw. In the 40% through-wall photo, the failure encompasses most of the pipe circumference. Based on this data it was determined that the 40% through flaw was a reasonable upper limit to set for flaw detection.

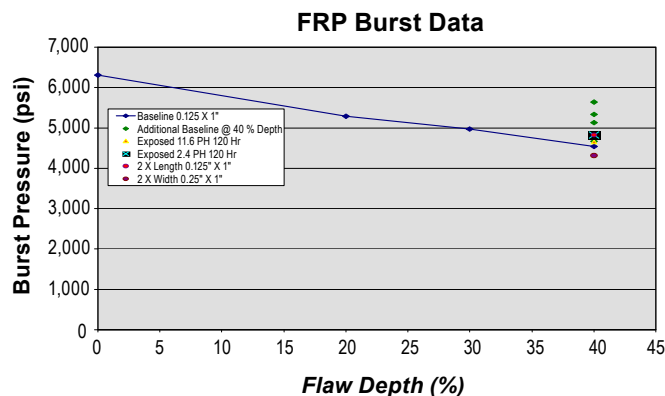




FIGURE 2. Photo Illustrating Failure Mode of FRP

Fatigue Testing

Fatigue testing of FRP was started at SRNL during FY 2012 and it is planned to continue this effort during FY 2013. The fatigue testing is directly tied to the FRP life management plan. During FY 2012 fatigue tests were performed on flawed and unflawed specimens.

Two fatigue tests have been performed on flawed FRP samples. The FRP samples were cycled with compressed nitrogen at 1,500 psi which is the rated pressure of the FRP product. The flaw size used for fatigue testing was 1 inch long, 0.125 inch wide, and at a 40% depth into the structural layer. This was the same flaw size as used for the previous flawed burst test. The pressure cycle interval was a minimum of 1 minute with a 30 second hold time at 1,500 psi. The hold time was specified at rated pressure to ensure that the test specimen had a portion of load at levels affecting the creep rupture strength of the fiber. The two flawed samples failed after 2,830 and 4,862 full design pressure cycles.

The failure of the flawed specimen occurred when the existing flaw propagated through the structural glass layer. The specimen started to delaminate at the bottom of the engineered flaw, as shown in Figure 3. When the flaw depth reached the polyethylene liner, loss of the pressure boundary occurred. The thin polymer liner is not intended to be pressure retaining. The pressure load is supported entirely by the glass composite.

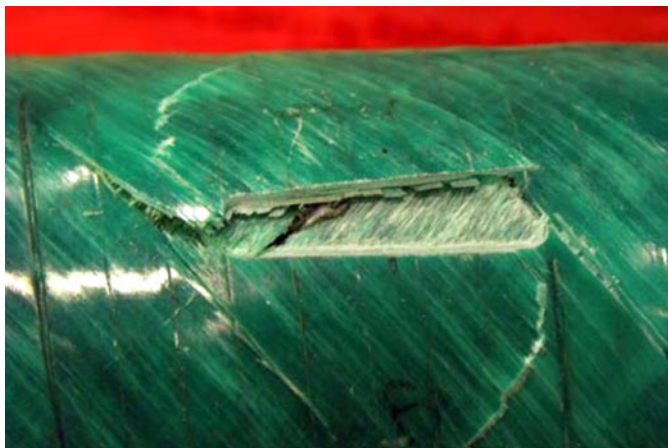


FIGURE 3. Fatigue Failure of Flawed FRP Specimen

An additional fatigue test was performed on an unflawed FRP sample. The unflawed sample was cycled for 8,077 full design pressure cycles. An 8,000 cycle limit was chosen because it represents a bounding value above the design current fatigue cycle limit for FRP of 20 years at 1 cycle per day. The unflawed sample was then burst tested and failed at 4,935 psi which shows a 22% reduction as compared to previously burst tested unflawed sample without fatigue damage. A photo of the failure location is shown in Figure 4.

The results of these tests show that FRP is susceptible to some level of fatigue damage. At the levels initially measured FRP still offers a viable alternative to metallic piping. The additional tests proposed for FY 2013 will focus on data needs for FRP piping design and codification.

B31.12 Codification

The workshop to discuss ASME B31.12 Codification of Fiber Reinforced Piping was held on August 16, 2011. The workshop was attended by DOE, ASME, SRNL, ORNL, FRP manufacturers, and Aiken County.

The technical background for Codification of FRP based on the work performed by SRNL and ORNL for the hydrogen delivery project was presented to the B31.12 Committee on March 15, 2012. An outline of the proposed B31.12 Code



FIGURE 4. Burst Failure Following 8077 Rated Pressure Fatigue Cycles

section has been submitted to the B31.12 Code Committee and included the following elements:

- Scope – Establish the design limits for the product
 - Product form
 - Design pressure limits
 - Design temperature limits
 - Design life
- Material – Additional controls on resins and fibers will be required
 - Fibers
 - Resin system
 - Liner material
- Design – Design to ASTM D2992 for the pressure design basis
 - Design pressure basis
 - Maximum and minimum design temperature
 - Protective layer
- Fabrication
 - Manufacturing specification to control resin and fiber
 - Supplementary code fabrication requirements – (mechanical joint vs. wrapped joint)
- Examination
 - Qualification of nondestructive testing personnel
 - Manufacturing examination requirements
 - Supplementary code examination requirements – acceptable flaw size
- Testing
 - Qualification tests – burst, fatigue, stress rupture, flaw environmental, and permeability
 - Production tests – quality control burst tests on random production samples
- Inspection
 - Supplementary code inspection requirements

Extended Design Life for FRP

Current FRP standards are limited to a 20-year design life. Because pipelines are a large capital investment a 20-year design life could be a limiting factor in the FRP application. SRNL has started to investigate extending the current accepted 20-year service life for FRP. Based on the results of the data from the burst test and review of the available creep rupture data for glass fiber there appears to be sufficient design margin to extend the design life for some FRP product from 20 to approximately 50 years. A comparison of the difference in the required design margin between 20 and 50 years is shown in Figure 5. The required decrease in fiber stress is from 0.32 to 0.3, a change of

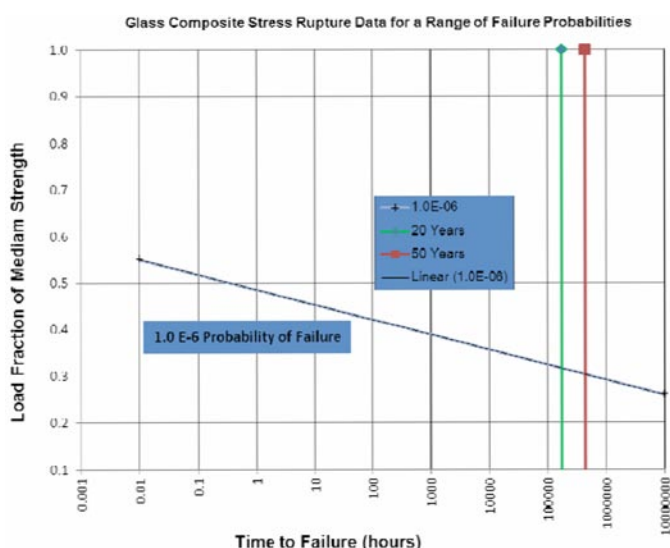


FIGURE 5. Extended Design Life for FRP

approximately 6%. Other standards are also starting to address increased design life for glass composite. The current draft International Organization for Standardization Standard 15399 is proposing a design life of up to 50 years for composite components.

Integrated Hydrogen Demonstration Project

SRNL in partnership with Aiken County Economic Development Partnership, Center for Hydrogen Research, ORNL and ASME has developed a project proposal to partner with industry and government to provide an integrated hydrogen delivery demonstration project. The objective of the project is to install at least 1,000 feet of FRP operating in hydrogen service at a design pressure of 1,500 psi. The pipeline would serve as a test and surveillance facility as a final proof of concept for FRP in hydrogen service. The proposed location of the project is SRNL with demonstration portions at the Sage Mill Central Hydrogen Facility located at Aiken County’s Sage Mill Industrial Park. The facility will have an integrated educational component for the public. An artist conception on the project is provided in Figure 6.

Conclusions and Future Directions

Conclusions

- FRP is an attractive technology with potential to support the DOE goal to reduce overall pipeline installation cost.
- FRP fabricated to American Petroleum Institute (API) 15HR is the most relevant standard reviewed to date for the fabrication of FRP for hydrogen service. This standard can be tailored to address the need for hydrogen pipelines.



FIGURE 6. Integrated Hydrogen Demonstration Project

- Burst tests show that for piping with flaws up 40% through the wall and up to 2-inch length and 0.25 inch width maintain a factor of 3X on rated pressure.
- Fatigue testing of both flawed and unflawed piping sections has been conducted. These tests have shown that fatigue cycles will affect the life of FRP. Additional fatigue testing is needed.
- The current SRNL recommendation is to develop a performance-based design specification to be included in ASME B31.12.
- SRNL has started working directly with the ASME B31.12 Committee to draft code requirements for FRP.
- A proposal for an FRP demonstration project has been presented to DOE. SRNL will partner with ASME, ORNL and Aiken County to provide a demonstration project to support codification and life management of FRP.
- Evaluate B31.8S (Managing System Integrity of Gas Pipelines) for changes needed to address FRP in hydrogen service.
- Perform additional fatigue testing for FRP piping up to the full cyclic design life for pipelines.
- Perform long-term stress rupture tests for flawed FRP samples.
- Evaluate non-mechanical joints for pipeline application.
- Develop draft sections for ASME B31.12 Code for Hydrogen Piping and Pipeline and submit to Code Committee for review.

Future Work

- Perform long-term stress rupture tests for flawed FRP samples.
- Perform additional burst testing of flawed FRP samples on aged samples.
- Recommend performance qualification tests for FRP in hydrogen service to the ASME B31.12 Committee.

FY 2012 Publications/Presentations

1. Gaseous Hydrogen Embrittlement of Materials in Energy Technologies, Chapter 1, Hydrogen Production and Containment, Woodhead Publishing, 2012.
2. ASME Codification of Fiber Reinforced Composite Pipelines, Workshop with Stakeholders, Aiken, SC, August 2011.
3. SRNL FRP Piping Project, Presentation to Hydrogen Delivery Technology Team, Detroit, MI, March 2012.
4. Fiber Reinforced Composite Pipelines, Presentation to ASME B31.12 Committee, Orlando, FL, March 2012.

III.6 Development of High Pressure Hydrogen Storage Tank for Storage and Gaseous Truck Delivery

Jon Knudsen (Primary Contact), Don Baldwin

Lincoln Composites
5117 N.W. 40th Street
Lincoln, NE 68524
Phone: (402) 470-5039
Email: jknudsen@lincolncomposites.com

DOE Managers

HQ: Erika Sutherland
Phone: (202) 586-3152
Email: Erika.Sutherland@ee.doe.gov
GO: Katie Randolph
Phone: (720) 356-1759
Email: Katie.Randolph@go.doe.gov

Contract Number: DE-FG36-08GO18062

Project Start Date: July 1, 2008
Project End Date: April 30, 2013

(G) Storage Tank Materials and Costs

Technical Targets

This project has focused primarily on the design and qualification of a 3,600 psi pressure vessel and International Organization for Standardization (ISO) frame system to yield a storage capacity solution of approximately 8,500-L of water (Figure 1). Original scope of project was to increase working pressure in current design. Together with DOE, scope has been changed to work towards increasing available volume at the 3,600 psi working pressure.

FY 2012 Accomplishments

Lincoln Composites designed and received a custom-built trailer, see Figure 2, capable of holding four 40-foot pressure vessels and an additional 30 foot pressure vessel. This new design has the potential to increase overall capacity by roughly 18%. Prototype trailer, minus vessels, plumbing, fire protection was received in the first quarter of 2012.

Fiscal Year (FY) 2012 Objectives

The objective of this project is to design and develop the most effective bulk hauling and storage solution for hydrogen in terms of:

- Cost
- Safety
- Weight
- Volumetric Efficiency

Technical Barriers

This project addresses the following technical barriers from the Hydrogen Delivery section of the Fuel Cell Technologies Program Multi-Year Research, Development and Demonstration Plan:

- (E) Low Cost, High Capacity Solid and Liquid Hydrogen Carrier Systems



FIGURE 1. Assembled ISO Container without Outer Panels

TABLE 1. Progress towards Meeting Technical Targets for Hydrogen Storage

| Characteristic | Units | 2010 Target | 2015 Target | 2015 Target (Draft) | 2020 Target (Draft) | Status | Comments |
|----------------------------|----------|----------------|-----------------|---------------------|---------------------|----------------|--|
| Storage Costs | \$/kg | \$500/kg | \$300/kg | \$300/kg | | \$500/kg | |
| Volumetric Capacity | kg/liter | 0.030 kg/liter | >0.035 kg/liter | >0.035 kg/liter | | 0.018 kg/liter | |
| Delivery Capacity, Trailer | kg | 700 kg | 1,100 kg | 700 kg | 940 kg | 616 kg | Potential to see 726/775 kg with new Titan5/Titan 5+ |

Introduction

Hydrogen holds the long-term potential to solve two critical problems related to energy use: energy security and climate control. The U.S. transportation sector is almost completely reliant on petroleum, over half of which is currently imported, and tailpipe emissions remain one of the country's key air quality concerns. Fuel cell vehicles operating on hydrogen produced from domestically available resources would dramatically decrease greenhouse gases and other emissions, while also reducing our dependence on oil from politically volatile regions of the world.

Successful commercialization of hydrogen fuel cell vehicles will depend upon the creation of a hydrogen delivery infrastructure that provides the same level of safety, ease, and functionality as the existing gasoline delivery infrastructure. Today, compressed hydrogen is shipped in tube trailers at pressures up to 3,000 psi (about 200 bar). However, the low hydrogen-carrying capacity of these tube trailers results in high delivery costs.

Hydrogen rail delivery is currently economically feasible only for cryogenic liquid hydrogen; however, almost no hydrogen is transported by rail. Reasons include the lack of timely scheduling and transport to avoid excessive hydrogen boil-off and the lack of rail cars capable of handling cryogenic liquid hydrogen. Hydrogen transport by barge faces similar issues in that few vessels are designed to handle the transport of hydrogen over inland waterways. Lincoln Composites' ISO tank assembly will not only provide a technically feasible method to transport compressed hydrogen over rail and water, but a more cost and weight efficient means as well.

Approach

In Phase 1 of this project, Lincoln Composites will design and qualify a large composite pressure vessel and ISO frame that can be used for storage and transport of compressed hydrogen over road, rail or water.



FIGURE 2. Prototype Titan5 Trailer Delivered

The baseline composite vessel will have a 3,600 psi service pressure, an outer diameter of 42.8 inches and a length of 38.3 feet. The weight of this tank will be approximately 2,485 kg. The internal volume is equal to 8,500 liters water capacity and will contain 150 kg of compressed hydrogen gas. The contained hydrogen will be approximately 6.0% of the tank weight (5.7% of the combined weight).

Four of these tanks will be mounted in a custom-designed ISO frame, resulting in an assembly with a combined capacity of 600 kg of hydrogen. Installing the compressed hydrogen vessels into an ISO frame offers a benefit of having one solution for both transportable and stationary storage. This decreases research and development costs as well as the amount of infrastructure and equipment needed for both applications.

The large size of the vessel also offers benefits. A limited number of large tanks is easier to package into the container and requires fewer valves and fittings. This results in higher system reliability and lower system cost. The larger diameter also means thicker tank walls, which will make the vessel more robust and damage tolerant.

Phase 2 of the project was originally scoped to evaluate using the same approximate sized vessel(s) and ISO frame at elevated pressures. In the past year, Lincoln Composites determined that there are concerns with moving forward with higher pressure delivery modules. The market is difficult to forecast at this time and the cost to fully qualify a higher pressure module estimated at \$5 MM to complete. Based on this, it was determined that Lincoln Composites would work with our current product and move forward with increasing the potential volume per load as well as improvements in safety. Other projects include the evaluation, testing and qualification of an improved fire protection systems as well a laboratory to begin looking at the effects of hydrogen on liner materials.

Results

Lincoln Composites has worked directly with DOE in determining the need to progress in the qualification of a 5,000 psi is not feasible at this time. The high cost to complete this qualification and lack of market needs has put this development on hold. Lincoln Composites is therefore concentrating efforts on the further development of our current module.

Lincoln Composites has designed a Titan5 trailer capable of increasing total payload capacity by 18% as compared with current Titan module that is in production, see Figure 3 for illustration. This new module will utilize the same four cylinders with the addition of a single 30' tank placed lower in the assembly utilizing space between the axels of the trailer.

Lincoln Composites has also began the design and evaluation of more robust fire protection system utilizing

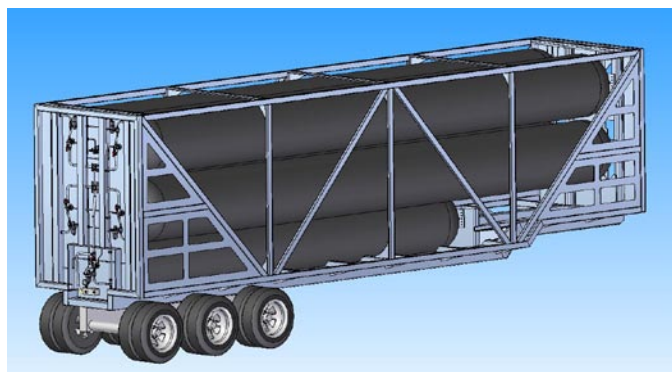


FIGURE 3. Drawing of Titan5

memory metal as a trigger mechanism for de-pressurizing the tank in the case of a fire. This also greatly reduces the cost of the system in both components and labor for assembly. The reduction of components in the system affects the potential number of failure modes that could occur and thus making for a more reliable product.

The installation of a 100% hydrogen testing facility is nearly complete. This laboratory will be used to fully investigate new materials with the potential for them to be integrated into liners. Specifically, these alternate materials will be quantified and qualified as a means to reduce the permeation rates that are present in current Type 4 cylinders.

To further enhance product offering, the development/design of a Titan5 with additional capacity has been initiated. This design will utilize the Titan5 as a baseline with the addition of 6 smaller tanks on either side of the 30' single tank at the bottom of the module. See Figure 4 for illustration of this design. This configuration has the potential to increase capacity by 26% when compared to the standard 4 cylinder module. This translates to an overall payload of 775 kg of hydrogen.

Conclusions and Future Directions

- Proposed objectives for Phase 1 of this project were completed in the fourth quarter of 2009. This includes successful completion of a large 3,600 psi pressure vessel able to contain 8,500 liter water capacity. The successful qualification of an entire assembly into an ISO container was also completed. The delivery of a Titan5 trailer was realized that, when fully completed, will add an additional 18% capacity with respect to our current production module.

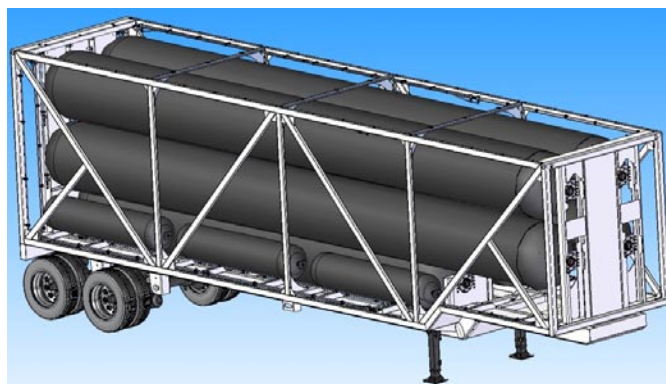


FIGURE 4. Drawing of Titan5 with Additional Capacity

- Future work will consist of completing the prototype Titan5 trailer with pressure vessels, plumbing and fire protection to demonstrate a working module. Plans to perform testing with 100% hydrogen on liner materials will move forward as a means to reduce permeation. Completion of the testing of enhanced fire protection to be completed within the next nine months.
- Completion of the qualification and implementation of a safer and more reliable fire production system. This to include a new trigger mechanism for de-pressurizing systems in case of fire.

FY 2012 Publications/Presentations

- 2012 DOE Hydrogen Program Annual Merit Review, May 17, 2012.

III.7 Development of a Centrifugal Hydrogen Pipeline Gas Compressor

Francis A. Di Bella, P.E.
 Concepts ETI, Inc., d.b.a. Concepts NREC
 285 Billerica Road, Suite 102
 Chelmsford, MA 01824-4174
 Phone: (781) 937-4718
 Email: fdibella@concepts-nrec.com

DOE Managers

HQ: Erika Sutherland
 Phone: (202) 586-3152
 Email: Erika.Sutherland@ee.doe.gov

GO: Katie Randolph
 Phone: (720) 356-1759
 Email: Katie.Randolph@go.doe.gov

Contract Number: DE-FG36-08GO18059

Subcontractors:

Texas A&M University, College Station, TX
 HyGen Industries, Eureka, CA

Project Start Date: June 1, 2008
 Project End Date: May, 2013

site(s) to forecourt stations. Compressing from 350 psig to 1,000 psig or greater. Reduce initial installed system equipment cost to less than \$9 M (compressor package of \$5.4 M) for 240,000 kg/day system.

- Reduce package footprint and improve packaging design.
- Reduce maintenance cost to below 3% of total capital investment. Increase system reliability to avoid purchasing redundant systems.

Fiscal Year (FY) 2012 Objectives

- Procure compressor components for one-stage prototype compressor
- Assemble prototype components
- Prepare test plan for prototype testing

Technical Barriers

This project addresses the following technical barriers from the Delivery section (3.2) of the Fuel Cell Technologies Program Multi-Year Research, Development, and Demonstration Plan [1]:

(B) Reliability and Costs of Hydrogen Compression

Overall Project Objectives

- Develop and demonstrate an advanced centrifugal compressor system for high-pressure hydrogen pipeline transport to support DOE's strategic hydrogen economy infrastructure plan. Delivering 100,000 to 1,000,000 kg/day of 99.99% hydrogen gas from generation

Technical Targets

The project has met the following DOE targets as presented in DOE's 2007 Technical Plan for Hydrogen Delivery Projects [1] (Table 1).

TABLE 1. Progress towards Meeting Technical Targets for Delivery of Hydrogen via Centrifugal Pipeline Compression

| Progress Towards Meeting Technical Targets for Delivery of Hydrogen via Centrifugal Pipeline Compression | | | | |
|--|--------------------|----------------------------|--|---------------|
| (Note: Letters correspond to DOE's 2007 Technical Plan-Delivery Sec. 3.2-page 16) | | | | |
| Characteristic | Units | DOE Target | Project Accomplishment | STATUS |
| Hydrogen Efficiency (f) | [btu/btu] | 98% | 98% | Objective Met |
| Hyd. Capacity (g) | kg/day | 100,000 to 1,000,000 | 240,000 | Objective Met |
| Hyd. Leakage (d) | % | <0.5 | 0.2 (per Flowserve Shaft Seal Spec.) | Objective Met |
| Hyd. Purity (h) | % | 99.99 | 99.99 (per Flowserve Shaft Seal Spec) | Objective Met |
| Discharge Pressure (g) | psig | >1,000 | 1,285 | Objective Met |
| Comp. Package Cost (g) | \$M | 6.0 +/- 1 | 4.0 +/- 0.5 | Objective Met |
| Main. Cost (Table 3.2.2) | \$/kWhr | 0.007 | 0.005 (per <u>CN</u> Analysis Model) | Objective Met |
| Package Size (g) | sq. ft. | 350 (per HyGen Study) | 260 (per <u>CN</u> Design) | Objective Met |
| Reliability (e) | # Systems Required | Eliminate redundant system | Modular systems with 240K kg/day with no redundancy required | Objective Met |

Accomplishments for Phases I and II (completed from 2008 to 2010) and Phase III (in progress)

Developed computer models to aid in analysis of hydrogen compressor:

- System Cost and Performance Model
 - Identifies hydrogen compressor package performance and component cost with respect to a variety of compressor-gearbox configurations.
- System Reliability and Maintenance Cost Model
 - Estimates comparative reliabilities for piston and centrifugal compressors for pipeline compressors developed.
 - Failure mode and effects analysis for component risk and reliability assessment.
 - Estimates operation and maintenance costs for compressor system.
 - Uses Federal Energy Regulatory Commission operation and maintenance database as the basis for determining the maintenance costs for a centrifugal compressor.
- Anti-surge algorithm developed to assist in controls analysis and component selection of preliminary design (completed) and detailed design of pipeline compressor module (in progress), including:
 - Compressor design conditions confirmed by project collaborators.
 - $P_{inlet} = 350$ psig, $P_{outlet} = 1,250$ psig; flow rate = 240,000 kg/day.
 - A six-stage, 60,000 revolutions per minute (rpm), 3.6 (max) pressure ratio compressor with a mechanical assembly of integrally geared, overhung compressor impellers.
 - Stress analysis completed.
 - Volute (compressor housing) design in progress for two-stage prototype.
 - Rotordynamics completed to verify shaft-seal-bearing integrity at operating speeds.
- Completed critical component development (compressor rotor, shaft seal, bearings, gearing, safety systems) and specifications for near-term manufacturing availability.
- Completed detailed design and cost analysis of a complete pipeline compressor and a laboratory-scale prototype for future performance lab verification testing.
- Completed a one-stage laboratory prototype compressor system to verify mechanical integrity of major components at full power ratings per stage.
- Procuring system components for one-stage prototype compressor.



Introduction

The DOE has prepared a Multi-Year Research, Development, and Demonstration Plan to provide hydrogen as a viable fuel for transportation after 2020, in order to reduce the consumption of limited fossil fuels in the transportation industry. Hydrogen fuel can be derived from a variety of renewable energy sources and has a very high BTU energy content per kg, equivalent to the BTU content in a gallon of gasoline. The switch to hydrogen-based fuel requires the development of an infrastructure to produce, deliver, store, and refuel vehicles. This technology development is the responsibility of the Production and Delivery sub-programs within the DOE. The least expensive delivery option for hydrogen involves the pipeline transport of the hydrogen from the production sites to the population centers, where the vehicles will see the highest demand, and thus, have the greatest impact on reducing the U.S. dependency on fossil fuel. The cost to deliver the hydrogen resource to the refueling stations will add to the ultimate cost per kg or per gallon equivalent that needs to be charged for the hydrogen fuel. Therefore, it is necessary that the cost to deliver the hydrogen be as kept as low as possible, which implies that the cost of the compressor stations, their installation costs, and their efficiency in pumping the hydrogen fuel to the refueling stations must be kept less than \$2/gasoline gallon equivalent (2010 goal).

The delivery cost target can be met if the compressor system can be made more reliable (to reduce maintenance costs), more efficient (to reduce operation costs), and be a smaller, more complete modular package (to reduce the compressor system equipment, shipment, and its installation costs). To meet these goals, the DOE has commissioned Concepts NREC with the project entitled: The Development of a Centrifugal Hydrogen Pipeline Gas Compressor.

Approach

A three-phase approach has been programmed to implement the technical solutions required to complete a viable hydrogen compressor for pipeline delivery of hydrogen. The three phases include: Phase I-Preliminary Design, Phase II-Detailed Design of a both a Full-Scale and Prototype Hydrogen Compressor, and Phase III-The Assembly and Testing of the Prototype Compressor.

The technical approach used by Concepts NREC to accomplish these goals is to utilize state-of-the-art aerodynamic/structural analyses to develop a high-performance centrifugal compressor system for pipeline service. The centrifugal-type compressor is able to provide high pressure ratios under acceptable material stresses for relatively high capacities – flow rates that are higher than

what a piston compressor can provide. Concepts NREC’s technical approach also includes the decision to utilize commercially available, and thus, proven bearings, shaft seal technology, and high-speed gearing to reduce developmental risk and increase system reliability at a competitive cost.

The engineering challenge to implement this technical approach is to design a compressor stage that can achieve the highest acceptable pressure ratio and thermodynamic efficiency per stage, while also using as few stages as possible and employing the smallest diameter impeller necessary. Ultimately, the major constraint is imposed by the limitations of the maximum stress capability of impeller material. This constraint is further aggravated by the need for the material selection to consider the effects of hydrogen embrittlement on the strength of the material. The selection of a rotor material that can enable the high tip speeds to be achieved while avoiding damage from hydrogen embrittlement was selected as the major technical challenge for the project.

Concepts NREC has met all of these engineering challenges in order to provide a pipeline compressor system that meets DOE’s specifications for near-term deployment.

The project team includes researchers at Texas A&M, led by Dr. Hong Liang, who are collaborating with Concepts NREC to confirm the viability of aluminum alloys for this compressor application. Also assisting with a collegial collaboration of suggestions are several national laboratories, including: Sandia National Laboratories (fracture mechanics testing; Dr. Chris San Marchi), Savannah River National Laboratory (specimen “charging” with hydrogen plus tensile testing with H₂; Dr. Andrew Duncan and Dr. Thad Adams), and Argonne National Laboratory (Dr. George Fenske).

Results

The engineering analysis has resulted in the design of the pipeline compressor package shown in Figure 1. The complete modular compressor package is 29 ft long x 10 ft

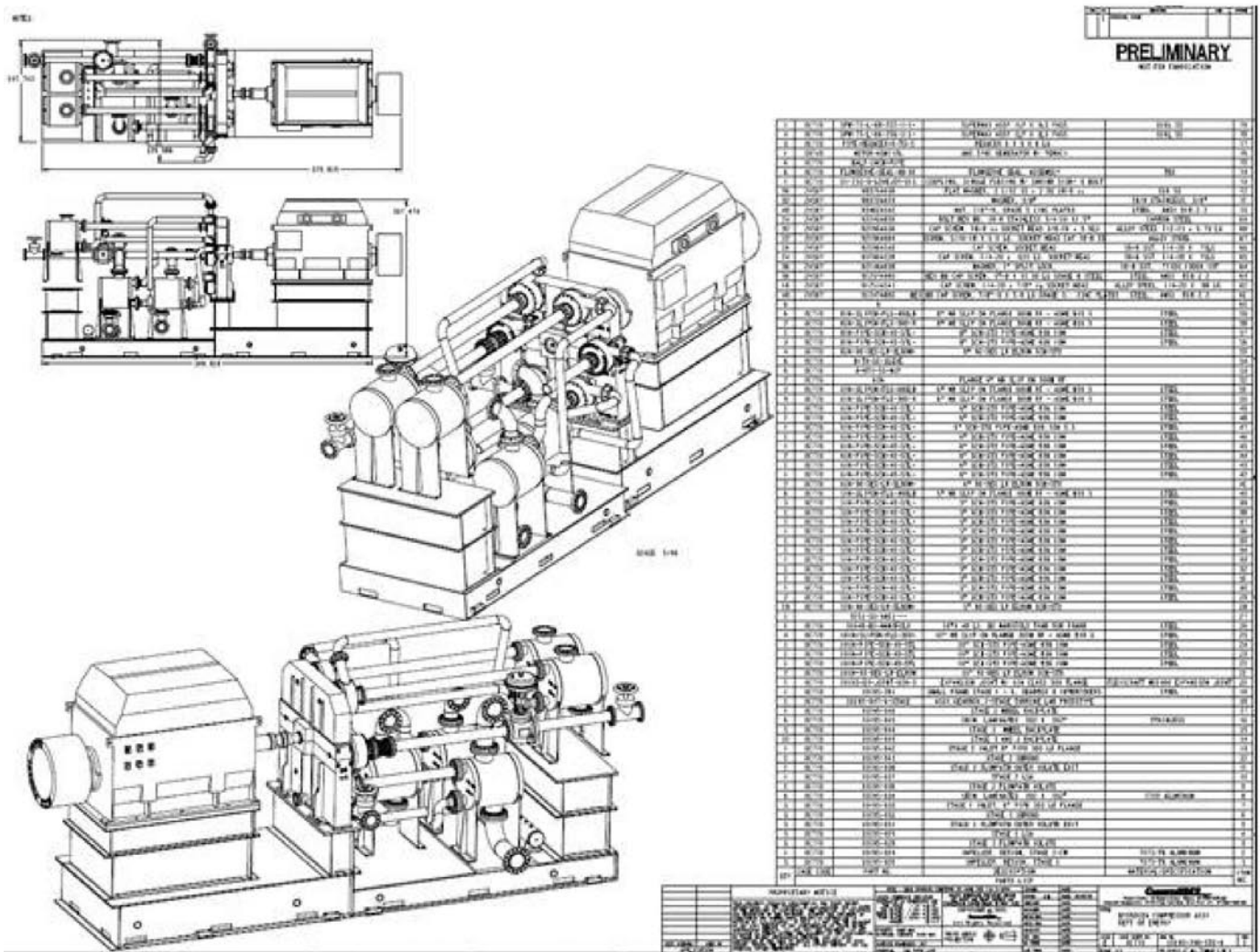


FIGURE 1. Pipeline Hydrogen Centrifugal Compressor: 240,000 kg/day; 350 to 1,285 psig

tall x 6 ft wide at the base x 8 ft wide at the control panel, approximately one-half of the footprint of a piston-type, hydrogen compressor.

The compressor selection uses six stages, each operating at 60,000 rpm with a tip speed of less than 2,100 ft/s. Each compressor rotor and drive shaft is 8 inches in diameter and has an overall stage efficiency of between 79.5 and 80.5%, for an overall compressor efficiency of 80.3%. The first and last stages have a slightly different length, which helps to improve the rotordynamics for the last stages. Each compressor impeller is a single, overhung (cantilevered) impeller attached to a drive shaft that includes a shaft seal, bearing, and drive pinion (Figure 2) integrated with the gearbox drive. The impeller rotor is designed without a bored hub, in order to reduce the hub “hoop” stresses. This requires the impeller to be mechanically attached to the high-strength steel alloy, a drive shaft with a patented design attachment system that enables the rotor to be removed from the gearbox without removing the drive shaft so it does not disturb the shaft seal and bearings. A gas face seal will provide the isolation of the hydrogen from the lubricating oil. The 1,400 hp per stage can be sustained by using two tilting pad hydrodynamic bearings on either side of a 2.5-inch-long drive-pinion gear. The face seal and bearings are commercially available from Flowserve and KMC, respectively. The pinion and bull gear is part of a custom gearbox manufactured by Artec Machine Systems representing NOVAGEAR (Zurich, Switzerland) and utilizes commercially available gear materials that are subjected to stresses and pitch line speeds that meet acceptable engineering practice.

The material chosen for the compressor rotor and volute is an aluminum alloy: 7075-T6. The choice is based on its mechanical strength-to-density ratio or (S_{yield}/ρ), which can be shown to be a characteristic of the material’s ability to

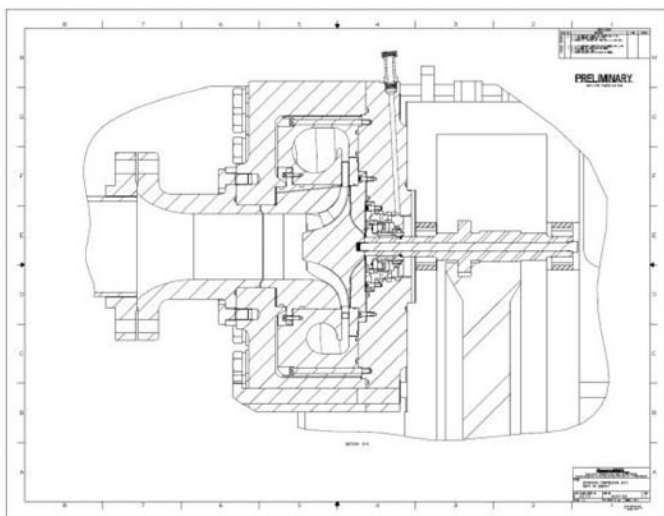


FIGURE 2. Mechanical Detailed Assembly of One Stage, Prototype Compressor

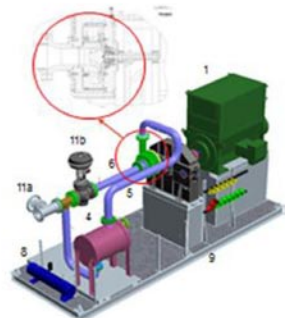
withstand centrifugal forces. This aluminum alloy has a strength-to-density ratio that is similar to titanium and high-strength steels at the 140°F (max) operating temperatures that will be experienced by the hydrogen compressor. However, unlike titanium and most steels, aluminum is recognized by the industry as being very compatible with hydrogen.

Aluminum also helps to reduce the weight of the rotor, which leads to an improved rotordynamic stability at the 60,000 operating speed. A rotor stability and critical speed analysis has confirmed that the overhung design is viable. The first stage compressor rotor has been manufactured and successfully spun to 110% of its 60,000 operating speed. A subsequent fluorescent penetrant inspection and strain measurements of the rotor after the spin test indicated no creep or micro-crack design flaws as a result of the test.

The one-stage prototype compressor has been chosen for laboratory testing in Phase III of the project. The laboratory prototype is shown in Figures 3a and 3b. The compressor components are being manufactured, and the balance of the system components are being purchased. The system will be assembled and tested starting in 2012 and into 2013.

Single-stage Laboratory Prototype System for Testing

The Phase III of the project will test each of the hydrogen compressor components by first constructing a 1-stage prototype test platform. The principal design approach has been to utilize commercially available components in order to minimize the need for individual testing of the components that unique to a hydrogen compressor. Thus the major concern: that an aluminum rotor can be designed to operate at 2,100 ft/s has been accomplished and there only remains the testing under load in a hydrogen environment.



Detail of One Stage (of Six) of Hydrogen as Used on the Prototype

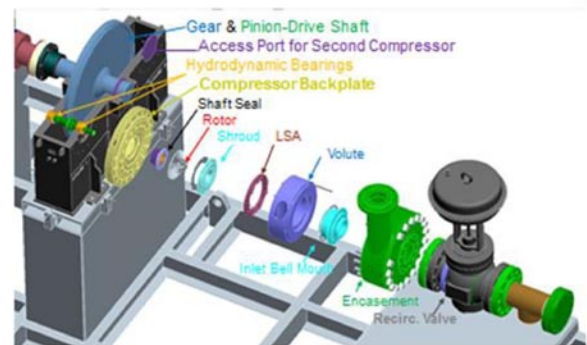


FIGURE 3. Detail Specification for the One-Stage Prototype Compressor

**Accomplishment and Progress (4):
Aluminum Volute (Flow Diffuser), Shroud, LSA (Exit Vane Diffuser) and Enclosure
Have Been Manufactured & Remaining Machine Parts on Order**

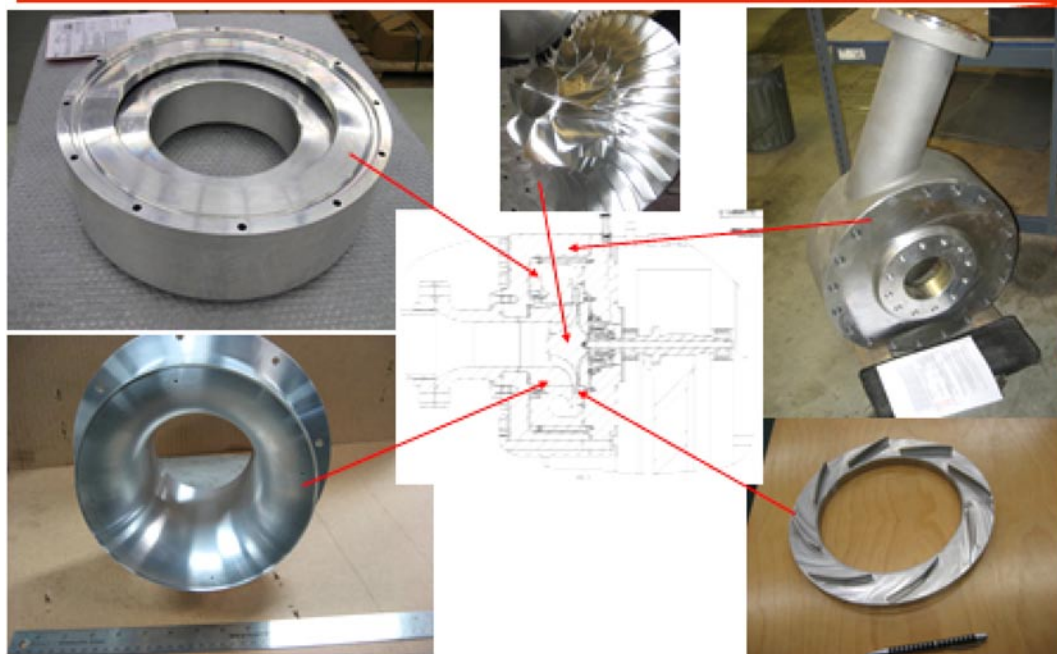


FIGURE 4. Components Prepared for the One-Stage Laboratory Prototype Compressor

Conclusions and Future Directions

The advanced, six-stage, intercooled, centrifugal compressor-based system can provide 240,000 kg/day of hydrogen from 350 to 1,280 psig high (6,300 kW_e) for pipeline-grade service. The system is 1/4 to 1/3 the size of existing industrial systems at projected cost of less than 80% of DOE's target and a maintenance cost that is less than the \$0.01/kWh. This has been accomplished by utilizing a state-of-the-art aerodynamic and structural analysis of the centrifugal compressor impeller to provide high pressure ratios under acceptable material stresses.

Phase III System Component Procurement, Construction, and Validation Testing (January 2011 to May, 2013)

- Continue component procurement for the one-stage prototype hydrogen compressor system.
- Assembly of the one-stage centrifugal compressor system.
- Conduct aerodynamic testing and assessment of mechanical integrity of the compressor system.
- Prepare a plan for placement of the prototype compressor for continued testing, including the deployment in an industrial gas user or a university research laboratory.

Patents Issued

1. Patent application filed on several innovations for centrifugal compressor design; filed March, 2010 (provision file March, 2009: SN 60/896985): "Centrifugal Compressor Design for Hydrogen Compression".

FY 2012 Publications/Presentations

1. "Development of a 240,000 kg/day Hydrogen Pipeline Centrifugal Compressor for the Department of Energy's Hydrogen Delivery and Production Program," IMECE2012-88965.

References

1. DOE Multi-Year Research, Development, and Demonstration Plan.

III.8 Oil-Free Centrifugal Hydrogen Compression Technology Demonstration

Hooshang Heshmat
 Mohawk Innovative Technology, Inc. (MiTi)
 1037 Watervliet Shaker Road
 Albany, NY 12205
 Phone: (518) 862-4290
 Email: HHeshmat@miti.cc

DOE Managers
 HQ: Erika Sutherland
 Phone: (202) 586-3152
 Email: Erika.Sutherland@ee.doe.gov
 GO: Katie Randolph
 Phone: (720) 356-1759
 Email: Katie.Randolph@go.doe.gov

Contract Number: DE-FG36-08GO18060

Subcontractor:
 Mitsubishi Heavy Industries, Ltd, Compressor Corporation,
 Hiroshima, Japan

Project Start Date: September 25, 2008
 Project End Date: May 30, 2013

centrifugal compressor. The project addresses the following DOE technical targets from the Hydrogen Delivery section of the Fuel Cell Technologies Program Multi-Year Research, Development and Demonstration Plan (see Table 1).

TABLE 1. Technical Targets for Hydrogen Compression

| Category | 2005 Status | FY 2012 | FY 2017 |
|---|------------------|----------|---------|
| Reliability | Low | Improved | High |
| Energy Efficiency | 98% | 98% | >98% |
| Capital Investment (\$M) (based on 200,000 kg of H ₂ /day) | \$15 | \$12 | \$9 |
| Maintenance (% of Total Capital Investment) | 10% | 7% | 3% |
| Contamination | Varies by Design | | None |

FY 2012 Accomplishments

- Completed fabrication, assembly and validation testing of two 100-kW, oil-free motors.
- Completed fabrication and assembly of the single-stage compressor.
- Performed initial check-out testing of the motors and single-stage compressor system.
- Made preliminary selection of materials for the centrifugal hydrogen compressor.



Fiscal Year (FY) 2012 Objectives

Design a reliable and cost-effective centrifugal compressor for hydrogen pipeline transport and delivery:

- Eliminate sources of oil/lubricant contamination
- Increase efficiency by using high rotational speeds
- Reduce system cost and increase reliability

Technical Barriers

This project addresses the following technical barriers from the Hydrogen Delivery section of the Fuel Cell Technologies Program Multi-Year Research, Development and Demonstration Plan:

- (B) Reliability and Costs of Hydrogen Compression
- (I) Hydrogen Leakage and Sensors

Technical Targets

This project is directed towards the design, fabrication and demonstration of the oil-free centrifugal compression technology for hydrogen delivery. This project will identify the key technological challenges for development and implementation of a full-scale hydrogen/natural gas

Introduction

One of the key elements in realizing a hydrogen economy is the deployment of a safe, efficient hydrogen production and delivery infrastructure on a scale that can compete economically with current fuels. The challenge, however, is that hydrogen, the lightest and smallest of gases with a lower viscosity than natural gas, readily migrates through small spaces. While efficient and cost-effective compression technology is crucial to effective pipeline delivery of hydrogen, today's positive displacement hydrogen compression technology is very costly, and has poor reliability and durability, especially for components subjected to wear (e.g., valves, rider bands and piston rings). Even so called "oil-free" machines use oil lubricants that migrate into and contaminate the gas path. Due to the poor reliability of compressors, current hydrogen producers often install duplicate units in order to maintain on-line times of 98-99%.

Such machine redundancy adds substantially to system capital costs. Additionally, current hydrogen compression often requires energy well in excess of the DOE goal. As such, low capital cost, reliable, efficient and oil-free advanced compressor technologies are needed.

Approach

The MiTi team will meet project objectives by conducting compressor, bearing and seal design studies; selecting components for validation testing; fabricating the selected centrifugal compressor stage and the corresponding oil-free bearings and seals; and conducting testing of the high-speed, full-scale centrifugal compressor stage and oil-free compliant foil bearings and seals under realistic pressures and flows in air and helium (used as a simulant gas for hydrogen). Specific tasks include: (1) Compressor design analysis – oil-free, multi-stage, high-speed centrifugal compressor system; (2) Mechanical component detailed design – oil-free bearings, seals and shaft system; (3) Detailed design and fabrication of a full-scale single-stage centrifugal compressor – for aerodynamic design verification and component reliability testing; (4) Compressor performance testing – with air and helium; (5) System design refinement; and (6) Project management and reporting.

Results

The MiTi hydrogen compressor design consists of three frames operating at the same speed with a rotor tip velocity of 1,600 fps. The system capacity is 500,000 kg/day with a pressure ratio (PR) of approximately 2.4. The mock-up of a single frame of the compressor system is shown in Figure 1. As discussed in prior reports, a single-stage compressor system has been developed to verify aerodynamics of the proposed oil-free centrifugal compressor system. The design of the single-stage compressor was described in the previous annual report.

Fabrication of the components and final assembly of the single-stage compressor and test rig has been completed (Figure 2) and initial performance verification testing has been initiated. The single-stage, 200-kW drive compressor system, consists of two 100-kW motors coupled together. The first objective of testing was to demonstrate the performance of the individual motors before testing the coupled system. Each motor was tested to full speed (60,000 rpm). Test data for one of the motors are provided in Figure 3. Testing was conducted at speeds ranging from 10,000 rpm to 60,000 rpm and stable motor speed control was demonstrated. Foil bearing temperatures were carefully monitored during testing and stable bearing performance was observed during operation. Bearing temperatures were less than 150°F at full speed. During testing, cooling air was supplied externally at a rate of 15 scfm. In the final single-stage compressor, bearing cooling gas will be taken from the compressor



FIGURE 1. Mock-up of a single frame of MiTi hydrogen compressor exhibited at the 2012 ARPA-E Energy Innovation Summit at the Gaylord National Convention Center, National Harbor, MD.

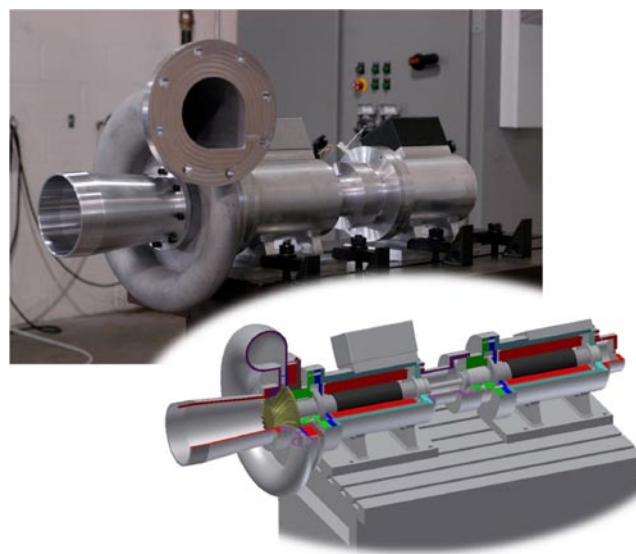


FIGURE 2. MiTi single-stage compressor driven by two 100 kW oil-free motors. Design details are shown in the inset.

bleed rather than externally provided. Rotor vibrations were recorded during full-speed testing using fiber-optic proximity probes. The maximum rotor motions measured at full speed were 0.0002". This represents extremely low vibrations as it is approximately equivalent to the mechanical run-out of the rotor.

Following successful testing of the individual motors, a bladeless compressor wheel was attached to one of the

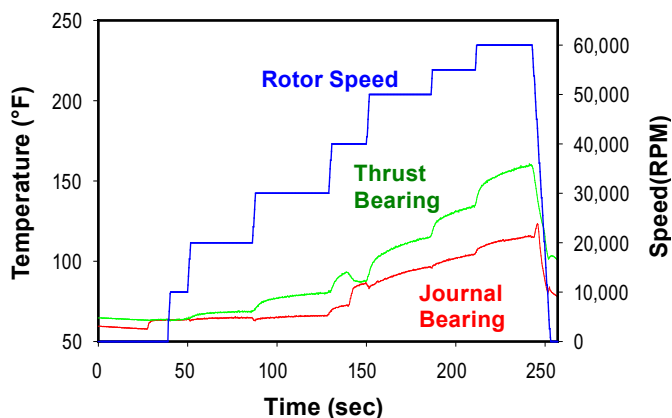


FIGURE 3. Each oil-free motor was performance tested independently up to 60,000 rpm. Both motors were thermally and dynamically stable. Maximum bearing temperature was less than 160°F and no extraneous vibration modes were observed.

motors. The bladeless wheel was designed to have the same mass, center of gravity and inertial properties as the bladed compressor wheel. Bladeless wheel testing is a cost-effective method to demonstrate rotor dynamics and system stability before testing with more delicate and costly components such as bladed compressor wheels. The bladeless wheel testing was successful and the compressor performed as predicted. Stable operation and low foil bearing temperature were observed. Testing with the bladeless wheel was limited to 40,000 rpm for safety reasons. Testing beyond 40,000 rpm with a compressor wheel, bladed or bladeless, will be conducted after construction of the dedicated test cell with proper safety provisions.

After testing with the bladeless wheel, the bladed compressor wheel and volute were installed and tested (see Figure 2). Bearing temperatures were found to be lower in the bladed wheel (Figure 4) due to additional cooling flows, which were provided by the compressor bleed air that was not available with the bladeless wheel. Rotor vibrations with the bladed wheel were less than levels measured with the bladeless wheel and no vibration issues were observed. Testing with the bladed wheel was limited to 30,000 rpm for safety reasons. Further testing will resume when the dedicated test cell is completed. (Operation of the single stage compressor can be viewed at the following website: <http://www.youtube.com/watch?v=dPn0uLIdtS8>).

The dedicated test cell that will house the 200-kW single-stage compressor testing is in the process of being constructed. When completed, the test rig will be relocated in the test cell and compressor testing will resume with air and helium per the ASTM International PTC-10 standard.

MiTi has conducted a thorough literature review in order to select the most appropriate materials for use in the high-speed, centrifugal, hydrogen compressor. The material of choice requires high strength, low density, high resistance to

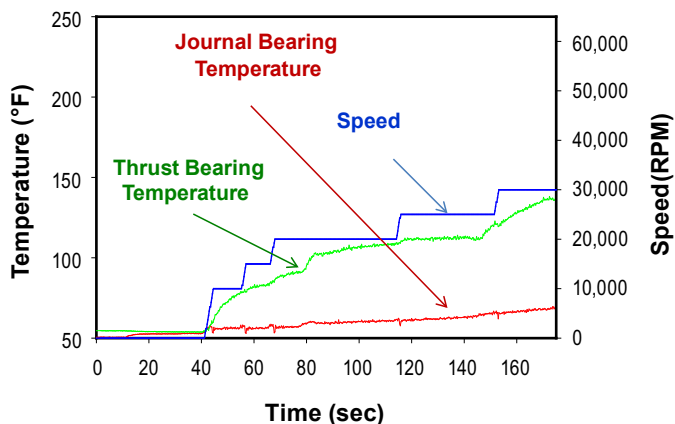


FIGURE 4. Compressor testing was successfully demonstrated up to 30,000 rpm for several 3-min test cycles. Testing to full speed of 60,000 rpm requires a dedicated reinforced test cell.

fatigue, and an acceptable level of toughness and ductility. The data on possible materials have been discussed with experts at Sandia National Laboratories and the University of Illinois and were previously presented to the DOE. Further search of the literature was conducted recently for a separate funded project. The additional data has provided sufficient information to allow for the selection of a suitable material for the rotating group. MiTi has selected beta titanium alloys as the most appropriate material for the hydrogen compressor over other possible candidates such as high-strength steels and aluminum alloys. Beta titanium exhibits superior strength and fatigue life, particularly when exposed to hydrogen. Two beta titanium alloys were considered for the rotating group of the hydrogen compressor. Both Ti-10-2-3 and Ti Beta C are available in bar stock form and possess the necessary strength and fatigue properties (measured in air and not hydrogen). The effect of hydrogen on mechanical properties of these alloys is not well studied but limited data exist. MiTi has been able to locate one study [1] which compared Ti-10-2-3 and Ti Beta C both before and after exposure to low concentrations of hydrogen. Despite the fact that both materials are beta titanium alloys, the effect of hydrogen exposure was very different. The particular Ti-10-2-3 evaluated in that study experienced a 45% drop in yield strength but gained ductility when exposed to hydrogen, while the effect of hydrogen exposure on Ti beta C was nearly opposite. For the hydrogen compressor application, the increase in ductility is more critical than the improvement in yield strength exhibited. Therefore, MiTi recommends the Ti-10-2-3 alloy for this application.

While Ti-10-2-3 has been selected as the most appropriate material for the rotating group, this material is not available in thin foil form for the foil bearings. Therefore, following a similar material selection study, Ti-15-3 has been identified as an excellent candidate for the foil bearings and seals. This material is available in thin stock

and has demonstrated excellent properties in the hydrogen environment.

Mechanical properties of beta titanium alloys are highly dependent on the exact method of heat treatment, exposure time, temperature and hydrogen concentration in service. Further data are needed in order to make a final confident selection. In the meantime, MiTi recommends a coating such as TiN or CrN to be applied to all surfaces exposed to hydrogen to further reduce the likelihood of embrittlement and degradation of mechanical properties.

Mitsubishi Heavy Industries (MHI), Compressor Corporation, has completed the design analysis of their single-entry compressor concept. The design analysis included computational fluid dynamics (CFD) performance analysis on several different design iterations. For each design concept, different axial clearances had been investigated in order to determine the sensitivity of clearance on performance. In addition to aerodynamic performance with CFD, MHI has also conducted finite element analysis (FEA) to investigate the structural integrity of the proposed impeller concepts. The FEA results revealed unacceptable local and membrane stresses in some of the impeller designs. Several modifications were evaluated to reduce the local and membrane stresses: for example, increasing the thickness of the compressor blades at the root, thereby increasing blade stiffness without unnecessary blade mass, and reducing blade lean to improve stress levels at the blade root. A successful design of the final impeller geometry has been achieved. MHI is currently designing a single-stage compressor system based on their single entry compressor design. MiTi and MHI have engaged in frequent email discussions and monthly video teleconferences to aid the collaborative effort.

Conclusions and Future Directions

During this reporting period, fabrication and assembly of the single-stage centrifugal hydrogen compressor were completed. The single-stage compressor system includes two 100-kW oil-free motors designed and fabricated at MiTi. The two motors are coupled using MiTi's proprietary mechanical coupling technology. All components of the motors and

compressor, including permanent magnets, electronic drive system, sensors, compressor wheel, shafting, oil-free foil bearings, and others were acquired or manufactured. Each component was performance tested prior to incorporation into the final system. Initial validation tests of the motors indicated that each motor was capable of operating at the design speed of 60,000 rpm. Both motors independently evaluated, were thermally and dynamically stable. The compressor system driven with the oil-free motors were tested up to 30,000 rpm. The results were encouraging and no difficulties were experienced. Testing of the compressor system to 60,000 rpm requires a dedicated test cell, which is currently under construction. Once the test cell is available and testing can be performed with proper safety precautions, the compressor system will be evaluated with air and helium used as a simulant gas for hydrogen. The following tasks are planned for the remainder of FY 2012 and FY 2013:

- Single-stage performance testing in air and helium (as a simulant gas for hydrogen).
- Comparison between single-entry and double-entry compressor designs.
- Design refinements.
- Final report.

FY 2012 Publications/Presentations

1. "Oil-Free Bearings and Seals for a Centrifugal Hydrogen Compressor," invited presentation, International Tribology Conference, Hiroshima, Japan, December 2011.
2. "Oil-Free Compression for Hydrogen Delivery and Transportation," Hydrogen Delivery Technology Team Meeting, January 5, 2012, Columbia, MD.
3. "Oil-Free Centrifugal Hydrogen Compression Technology Demonstration," DOE Hydrogen Program Annual Merit Review and Peer Evaluation Meeting, May 2012, Arlington, VA.

References

1. HJ Christ, A Senemmar, M. Decker and K Prubner, "Effect of Hydrogen on Mechanical Properties of Beta-Titanium Alloys," *Sadhana*, 28(2003)453-465.

III.9 Electrochemical Hydrogen Compressor

Ludwig Lipp (Primary Contact), Pinakin Patel
FuelCell Energy, Inc.
3 Great Pasture Road
Danbury, CT 06813
Phone: (203) 205-2492
Email: llipp@fce.com

DOE Managers
HQ: Erika Sutherland
Phone: (202) 586-3152
Email: Erika.Sutherland@ee.doe.gov
GO: Katie Randolph
Phone: (720) 356-1759
Email: Katie.Randolph@go.doe.gov

Contract Number: DE-EE0003727

Subcontractor:
Sustainable Innovations, LLC, Glastonbury, CT

Start Date: July 15, 2010
End Date: July 14, 2013

- Multi-stage compression of hydrogen from near-atmospheric pressure to 6,000-12,000 psi.
- Ensure no possibility of lubricant contamination of the hydrogen from compression (DOE 2015 target).
- Reduce EHC specific energy consumption.
- Scale up EHC to a capacity of 2-4 lb/day H₂.

The ultimate goal of the project is to meet the DOE targets for forecourt compressors [1].

FY 2012 Accomplishments

- Hydrogen pressure: Reached 12,800 psi hydrogen pressure in a single-stage EHC cell (Figure 1).
- Hydrogen recovery: Achieved 98% hydrogen recovery in a single cell.

Fiscal Year (FY) 2012 Objectives

- Develop a solid-state electrochemical hydrogen compressor (EHC) building block capable of compressing hydrogen from near-atmospheric pressure to 2,000-3,000 psi.
- Study feasibility of an EHC multi-stage system capable of compressing hydrogen from near-atmospheric pressure to 6,000-12,000 psi.
- Increase compression efficiency to 95% (DOE 2015 target).

Technical Barriers

This project addresses the following technical barrier from the Hydrogen Delivery section (3.2) of the Fuel Cell Technologies Program Multi-Year Research, Development and Demonstration Plan:

(B) Reliability and Cost of Hydrogen Compression

Technical Targets

This project is directed at developing a solid-state EHC. The EHC is an enabling device for low-cost hydrogen delivery. Goals include the following:

- Single-stage compression of hydrogen from near-atmospheric pressure to 2,000-3,000 psi.

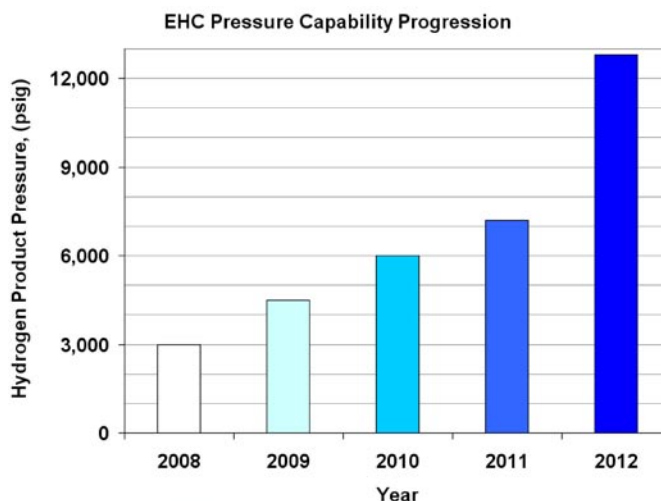


FIGURE 1. Met DOE 2015 Pressure Target for Forecourt Compressors

- Capital cost: Increased hydrogen flux up to 1,200 mA/cm² and reduced EHC cell part count by 20% (Figures 2 and 3).
- Durability: Demonstrated 6,000 hour life at elevated current density (750 mA/cm² – Figure 4).



Introduction

With the depletion of fossil fuel reserves and a global requirement for the development of a sustainable economy, hydrogen-based energy is becoming increasingly important. Production, purification and compression of hydrogen represent key technical challenges for the implementation of a hydrogen economy, especially in the transportation sector

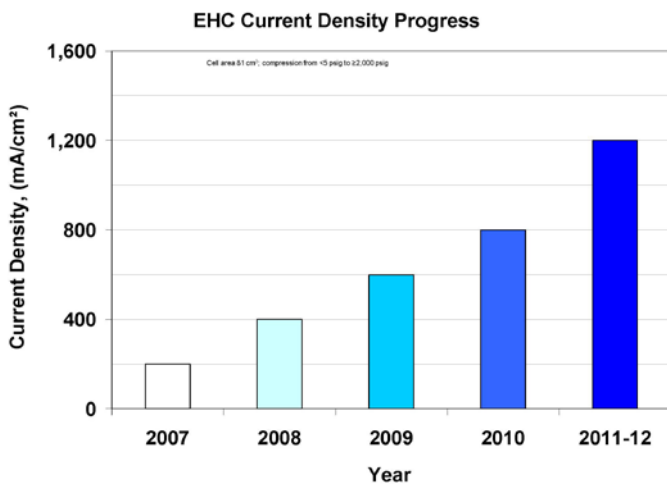


FIGURE 2. Six-Fold Increase in Current Density Leads to Significant Cost Reduction

where onboard storage of pure hydrogen may be required at pressures up to 10,000 psi and compression of the hydrogen fuel up to 12,000 psi.

The level of maturity of current hydrogen compressor technology is not adequate to meet projected infrastructure demands. Existing compressors are inefficient and have many moving parts, resulting in significant component wear and therefore excessive maintenance. New technologies that achieve higher operational efficiencies, are low in cost, safe and easy to operate are therefore required. This project addresses high-pressure hydrogen needs by developing a solid-state EHC.

Approach

The approach to address the project goals consists of the following major elements:

- Increase hydrogen recovery efficiency by improving flow field design.
- Reduce capital cost by increasing the hydrogen flux.
- Reduce operating cost by improving membrane and electrode design.
- Develop a multi-stage system concept for compression to 6,000-12,000 psi.

To this end, the approach includes the design, fabrication and evaluation of improved cell architecture, and the development and demonstration of critical sealing technology to contain the high-pressure hydrogen within the EHC.

Results

A major focus of this year’s efforts was to increase the pressure capability of the EHC cell beyond the previously demonstrated 6,000 psi. The design, fabrication and testing

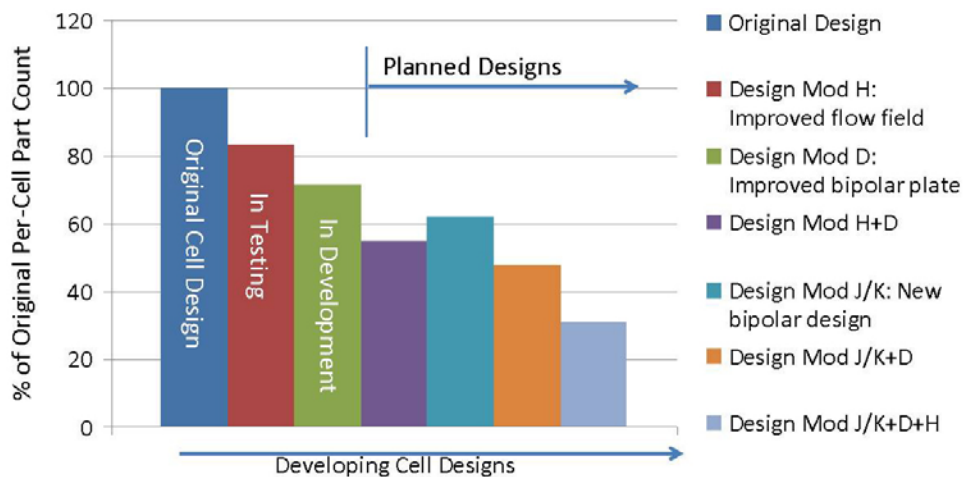


FIGURE 3. Reducing Cell Part Count for EHC Cost Reduction

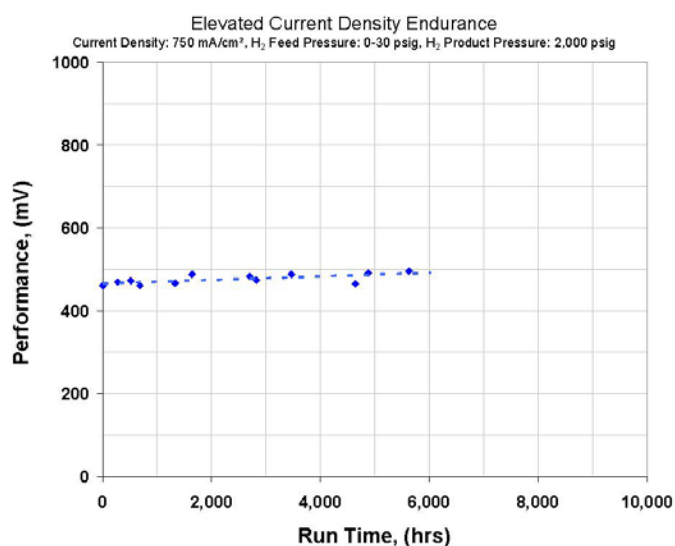


FIGURE 4. 6,000 Hour Endurance Demonstrated at Elevated Current Density

efforts resulted in an increase in pressure capability to 7,500 psi. The lessons learned from this cell were implemented in a subsequent design, which reached a maximum pressure of 12,800 psi, as shown in Figure 1. The hydrogen was being fed at near-atmospheric pressure. Improvements that enabled these results include seals with higher pressure capability and an improved MEA support structure. The new pressure record meets the DOE 2015 compression target for forecourt compressors (12,000 psi) [1]. This design, when scaled up and implemented in a stack, is expected to bring significant savings in capital and operating costs compared to a multi-stage system. The high-pressure single-stage design comes with a higher technology risk and will require significant additional development (beyond the current project).

Efforts to improve the internal fluids management resulted in a cell that was capable of operating continuously at a hydrogen recovery rate of 98%. It was compressing hydrogen from near-atmospheric pressure to 3,000 psi and has been operated for >1,000 hours. This is an important step towards meeting the DOE 2015 target of 95% compression efficiency. These features will be incorporated into a planned larger-area cell design.

Capital cost was reduced in two different ways. First, the operating current density of the EHC cell was increased from a previous maximum of 800 mA/cm² to a peak current density of 1,200 mA/cm², as shown in Figure 2. This was possible due to a higher performance MEA and a lower cell resistance at high pressure. The 50% increase in current density translates to a 50% higher hydrogen flux from the same size hardware, therefore significantly reducing the equipment cost. The second way cost reduction was achieved

was by lowering the EHC cell part count by 20% in a new cell design that incorporates an improved flow field. Further reductions in part count are underway, as shown in Figure 3. They are focused on improved bipolar plate designs and its combination with the improved flow field. Mass manufacturability is an important criterion that is being taken into account in the selection of the improved component designs.

Durability is a critical parameter in the life-cycle cost. Therefore, a cell running at an elevated current density of 750 mA/cm² was endurance tested for 6,000 hours. As can be seen in Figure 4, cell performance was essentially stable throughout the test. This suggests that the current cell hardware is capable of long-term operation at 2,000 psid. This is providing valuable design input for the planned EHC scale up.

Conclusions and Future Directions

The feasibility of reaching DOE's pressure target of 12,000 psi has been demonstrated in a single-stage EHC cell. The hydrogen flux through the EHC was increased by up to 50%, which translates to a lower capital cost. A 20% reduction in EHC cell part count also contributes to reduced cost. Durability of the EHC cell architecture has been demonstrated in a 6,000 hour test, confirming its robustness. The following summarizes critical performance parameters that were advanced during this reporting period:

| Parameter | 2011 Value | 2012 Value |
|--------------------------|------------------------|--------------------------|
| Output Pressure | 7,000 psi | 12,800 psi |
| Current Density | 800 mA/cm ² | 1,200 mA/cm ² |
| Endurance | 3,000 hours | 6,000 hours |
| % of Original Part Count | 100% | 80% |

Future efforts will include further improvements in cell architecture for a lower cost design, which will then be incorporated into an advanced, 200-cm² EHC cell and short stack. The scaled up short stack will be designed for a capacity of 2-4 lb/day H₂ to meet the objective of the project.

FY 2012 Publications/Presentations

1. L. Lipp, "Electrochemical Hydrogen Compressor", 2012 DOE Hydrogen Program Merit Review and Peer Evaluation Meeting, Arlington, VA, May 14–18, 2012.

References

1. HFCIT MYRDD Plan, Table 3.2.2 "Technical Targets for Hydrogen Delivery", section on Forecourt Compressors, page 3.2-14.

III.10 Composite Technology for Hydrogen Pipelines

Barton Smith (Primary Contact), Barbara J. Frame and Lawrence M. Anovitz

Oak Ridge National Laboratory (ORNL)
P. O. Box 2008
Oak Ridge, TN 37831
Phone: (865) 574-2196
Email: smithdb@ornl.gov

DOE Manager

HQ: Sara Dillich
Phone: (202) 586-7925
Email: Sara.Dillich@ee.doe.gov

Start Date: January 2005

Project End Date: Project continuation and direction determined annually by DOE

- Transmission and delivery reliability: Acceptable for H₂ as a major energy carrier
- Hydrogen pipeline leakage: < 80 kg/mi/y (2020)

FY 2012 Accomplishments

- Completed cyclic fatigue testing on FRP pipeline specimen using H₂ pressurizations to maximum allowable working pressure (MAWP) – Test results show that the pipeline retains performance similar to that of newly manufactured pipe following thermal cycling, pressurization-depressurization cycling and blowdown testing.
- Codes and standards acceptance – Participated in codification kickoff meeting with ASME at SRNL (August 2011) and contributed summary of ORNL testing and analysis on FRP pipelines for joint preparation of proposal to ASME for inclusion of composite hydrogen pipeline in B31.12, Part PL.

Fiscal Year (FY) 2012 Objectives

- Complete high-pressure cyclic fatigue tests to verify that a combination of H₂ environment and stress does not adversely affect composite pipeline integrity and service life.
- Identify the requisite data, provide data, and contribute to the codification of hydrogen composite pipelines, in collaboration with Savannah River National Laboratory (SRNL), American Society of Mechanical Engineers (ASME), et al.

Technical Barriers

This project addresses the following technical barriers from the Hydrogen Delivery section of the Fuel Cell Technologies (FCT) Program Multi-Year Research, Development and Demonstration Plan [1]:

(D) High Capital Cost and Hydrogen Embrittlement of Pipelines

Technical Targets

The long-term project objective is to achieve commercialization and regulatory acceptance of fiber-reinforced polymer (FRP) pipeline technology for hydrogen transmission and distribution. Accordingly, the project tasks address the challenges associated with meeting the DOE hydrogen delivery performance and cost targets [2]:

- Transmission pipeline total capital cost: \$735k per mile (2015), \$710k per mile (2020)
- Hydrogen delivery cost: <\$2.00/gge by 2020



Introduction

Pipelines could be a feasible long-term solution for delivering large quantities of gaseous hydrogen over long distances and distributing it in urban and rural settings. However, there are hydrogen compatibility issues in steel pipelines, and the capital costs for pipeline installation must be dramatically reduced. Composite pipeline technology is a promising alternative to low-alloy high-strength steel pipelines from both performance and cost considerations. For instance, FRP pipelines are engineered composite pipelines that are widely used in upstream oil and gas operations and in well interventions. FRP pipelines typically consist of an inner non-permeable liner that transports the fluid (pressurized gas or liquid), a protective layer applied to the liner, an interface layer between the protective layer and the reinforcement layers, multiple glass or carbon fiber reinforcement layers, an outer pressure barrier layer, and an outer protective layer. The pipeline has large burst and collapse pressure ratings, high tensile and compression strengths, and tolerates large longitudinal and hoop strains. Thousands of feet of continuous pipe can be unspooled and trenched as a seamless entity, and adjoining segments of pipeline can be joined in the trench without welding using simple connection techniques. The emplacement requirements for FRP pipelines are dramatically less than those for metal pipe; installation can be done in narrower trenches using light-duty, earth-moving equipment. This enables the pipe to be installed in areas where right-of-way restrictions are severe. In addition, FRP

pipe can be manufactured with fiber optics, electrical signal wires, power cables or capillary tubes integrated within its layered construction. Sensors embedded in the pipeline can be powered from remote locations and real-time data from the sensors can be returned through fiber optics or wires. This allows the pipeline to be operated as a smart structure, providing the unique advantage of lifetime performance and health monitoring.

Approach

The challenges for adapting FRP pipeline technology to hydrogen service consist of evaluating the constituent materials and composite construction for hydrogen compatibility, identifying the advantages and challenges of the various manufacturing methods, identifying polymeric liners with acceptably low hydrogen permeability, critiquing options for pipeline joining technologies, ascertaining the necessary modifications to existing codes and standards to validate the safe and reliable implementation of the pipeline, and determining requirements for structural health monitoring and embedded real-time measurements of gas temperature, pressure, flow rate, and pipeline permeation.

These challenges are being addressed by performing bench-scale tests of FRP pipelines and constituent materials to determine their long-time compatibility with hydrogen, identifying pipeline liner materials that exhibit good performance in hydrogen environments, evaluating current methods for pipeline joining with consideration of the unique requirements for hydrogen service, and assessing the state-of-the-art in integrated sensing technologies for composite structures.

Results

We performed a cyclic fatigue test on an FRP pipeline specimen using high-pressure H₂ to assess the effect of the combination of H₂ environment and pressure-induced fatigue on pipeline integrity and service life. Fatigue testing via gas pressurization-depressurization cycling will provide information valuable for codification of composite reinforced polymer pipelines for hydrogen service. The pipeline specimen was a 4-ft-long Fiberspar LPJ 2.5-inch inside diameter (ID) 1,500(E) LinePipe™, with the open ends capped with Fiberspar steel joint connectors. A series of three viton o-rings in each connector served to pressure-seal the connector end cap to the high-density polyethylene (HDPE) liner (gas barrier) in the pipeline. We affixed strain gages at multiple locations along the pipeline length to record hoop-direction strains during the pressurization-depressurization cycles. Before beginning the pressure cycling we performed three temperature cycles between room temperature and 60°C, at 1,500 psig H₂ pressurization, which is the specified MAWP for the pipeline. Immediately following the temperature cycling, which conditioned the

pipeline and saturated the liner and reinforcement layers with H₂, we performed 50-plus pressurization cycles (500-1,500 psig) at room temperature. When the pressure cycling was completed we raised the pipeline temperature to 60°C and subjected the pipeline to a pressure blowdown test from 1,500 psig to atmospheric pressure ($\Delta p/\Delta t > 6,000$ psi/min). We then performed a pressure-decay leak measurement and inspected the liner for blistering or delamination. The pressure-decay leak measurement was supplemented with a leak measurement using a thermal conductivity-type gas leak detector with H₂ sensitivity $\sim 1 \times 10^{-5}$ cc/s. No increase in leak rate attributable to the cyclic fatigue test was detected and there was no visible damage to the liner. Following leak testing, the pipeline specimen was shipped to Fiberspar for standard quality assurance testing to verify performance of the product against new, unused product. These quality assurance tests revealed that the pipe retained performance that was indistinguishable from that of newly manufactured pipe.

At the recommendation of the FCT Program Delivery Tech Team, we updated our capital cost estimate for installation of an FRP hydrogen pipeline. We used the H2A Delivery Scenario Analysis Model, version 2.3.1, to guide us in the determination of pipeline parameters. We assumed a pipeline transmission distance of 300 miles and hydrogen inlet and outlet pressures of 1,000 psia (69 bar) and 700 psia (48 bar), respectively (no compressor substations). The peak hydrogen flow rate was specified as 135,000 kg/day, and a calculation using the Panhandle B pipeline equation predicted that four 4.5-inch ID FRP pipelines with HDPE liners would provide a flow rate equivalent to one 8-inch ID steel pipeline. The pipeline flow efficiencies used in Panhandle B were 0.92 for steel and 0.98 for HDPE. To calculate costs we used the current pricing sheet for Fiberspar's 4.52-inch ID, 1,500 psi rated, HDPE-lined FRP linepipe, with 316 stainless steel connectors at 2,100-foot intervals, and factored in a mean labor cost of \$5 per foot for trenching and installation. The material cost for four 300-mile-long pipelines with connectors was estimated at \$138M, and the trenching and installation cost was estimated at \$32M. We did not include an estimate for inspection and testing—requirements which are undefined at present. The total material and labor cost is then \$170M, for a total capital investment of approximately \$570,000 per mile, excluding permitting and right-of-way costs.

Table 1 compares this estimate with those of our earlier (2007) cost estimate for FRP hydrogen pipelines, the cost estimate for an 8-inch-diameter natural gas pipeline, and the 2020 cost target for a hydrogen transmission pipeline. Our earlier cost estimation was about 40% lower than the present estimate because in it we did not allow for the cost of stainless steel connectors and because the present estimate reflects a slight increase in the cost of raw materials used in the pipelines. The present cost estimate is about 25% lower than that for the equivalent steel pipeline and is about 20%

TABLE 1. Estimates for total capital investment for hydrogen pipelines compared with 2020 cost target technical and an estimate for hydrogen loss from FRP pipelines compared with 2020 technical target

| Gaseous Hydrogen Delivery | | | | |
|--|---|---|--|---|
| Transmission Pipeline | | | | |
| | 2007 Estimate for FRP Pipeline | 2009 Estimate for Natural Gas Pipeline | 2012 Estimate for FRP Pipeline | 2020 Target |
| Total capital investment, in \$/mile (excluding costs for ROW and permitting) | 346,000³ | 765,000⁴ | 570,000 | 710,000² |
| H₂ leakage, in kg H₂/mile/y | | | <60⁵ (<0.1%)⁶ | <780² (<0.5%)⁶ |

ROW - right of way

² Fuel Cells Technology Program Multi-Year Research, Development and Demonstration Plan—Hydrogen Delivery, Table 3.2.3, Technical Targets for Hydrogen Delivery Components (2012, draft).³ Smith, Frame, Eberle, Anovitz and Armstrong, 2007 AMR, presentation PD14, May 16, 2007.⁴ Elgowainy, Mintz and Brown, 2011 AMR, presentation PD14, May 10, 2011 (for 8-inch steel pipeline).⁵ Estimate based on FRP pipeline leak rate from Smith, Frame and Anovitz, 2009 AMR, presentation PDP24, May 19, 2009, and connector leak rate from Adams, 2008 AMR, presentation PD20, June 11, 2008.⁶ Leakage expressed as a percentage of total hydrogen transmitted; 2020 target from Table 3.2.2 Technical Targets for Hydrogen Delivery, in Fuel Cells Technology Program Multi-Year Research, Development and Demonstration Plan—Hydrogen Delivery, October 2007.

below the 2020 cost target. In addition, our calculation of the anticipated loss due to permeation through the pipeline wall and leakage through the o-rings at the connectors is 13 times smaller than the technical target.

Conclusions and Future Directions

Conclusions from this year's work:

- Initial cyclic fatigue testing on FRP pipeline specimens using H₂ pressurizations showed that a combination of H₂ environment and pressure-induced stress does not measurably affect pipeline integrity and service life.
- Our estimate for total capital investment for pipeline emplacement—based on current pricing for commercially available FRP pipelines and realistic pipeline operational parameters—indicates that FRP polymer pipelines could meet the FCT Program's 2020 cost and leakage targets for a transmission pipeline.

Respecting the very limited amount of funding that might be available in the next project year, we intend to focus our efforts on outlining a concrete research plan for providing the data required to close the knowledge gap between the work done and work that needs to be done to qualify composite pipelines for H₂ service. These knowledge gaps, which are in effect the barriers to technology adoption through codification, are:

- Processes by which testing procedures can be directed and coordinated to provide the requisite performance data for H₂ pipeline codes and standards.
- Test data on fatigue due to cyclic pressurization during H₂ service.
- Test data from studies done to assess environmental effects on FRP pipeline systems in hydrogen service (all H₂ evaluations to date have been done in lab settings):
 - Tests conducted with and without water exposure
 - Tests conducted on potential impacts of geotechnical phenomena
 - Tests conducted with real third-party damage
 - Microanalysis and chemical analysis to determine effects of environment on pipeline structure
 - Hydrogen delivery “test loop” that includes all the delivery infrastructure relevant to full pipeline emplacement and operation (i.e., a few miles of pipeline with fittings, compressors, etc., in varying terrains and environments)
 - Harmonization of results obtained in the lab and in field installation
- Identification of gas purity requirements and pipeline gas purity data.
- Expanded knowledge of H₂ performance in commercial products—testing to date focused mainly on FRP pipeline products offered by two domestic manufacturers.

FY 2012 Publications/Presentations

1. 2012 DOE Hydrogen Program Annual Merit Review, Arlington, Virginia, May 17, 2012, presentation PD024.
2. Keynote address on “Commercial Deployment of FRP Hydrogen Pipelines,” presented at Composite Conference 2012, August 13–17, 2012, Las Cruces, NM.

References

1. Fuel Cells Technology Program Multi-Year Research, Development and Demonstration Plan–Hydrogen Delivery, page 3.2-19 (2007).

III.11 LLNL/Linde 875 bar Liquid Hydrogen Pump for High Density Cryogenic Vessel Refueling

Salvador M. Aceves (Primary Contact), Gene Berry, Francisco Espinosa-Loza, Guillaume Petitpas, Vernon Switzer, Stan Tuholski
Lawrence Livermore National Laboratory (LLNL)
7000 East Avenue, L-792
Livermore, CA 94551
Phone: (925) 422 0864
Email: saceves@llnl.gov

DOE Manager
HQ: Erika Sutherland
Phone: (202) 586-3152
Email: Erika.Sutherland@ee.doe.gov

Subcontractors:
Linde LLC, Hayward, CA
Engineering, Procurement & Construction (EPC),
Lakewood, CO

Start Date: October 1, 2009
Project End Date: Project continuation and direction determined annually by DOE

FY 2012 Accomplishments

- Developed a vessel fill model and demonstrated agreement with BMW experimental data
- Located an appropriate site for liquid hydrogen (LH₂) pump installation at LLNL
- Completed topographical, soil, and utility scans of selected location
- Received institutional approval for pump installation



Introduction

Cryogenic pressure vessels have demonstrated highest performance for automotive hydrogen storage, with storage density (43 gH₂/L), weight fraction (7.3%), cost (\$11.3/kWh), and safety advantages (~8X lower expansion energy than compressed gas and secondary protection from vacuum jacket) [1,2]. One of the outstanding challenges for cryogenic pressure vessels is refueling. Today's hydrogen storage technologies (compressed and liquid hydrogen) operate at fixed temperature. Cryogenic pressure vessels, however, drift across the phase diagram depending on the level of use, cooling down and depressurizing when driven and heating up and pressurizing when parked. The challenge is demonstrating rapid, inexpensive refueling that minimizes evaporative losses regardless of the initial thermodynamic state of the vessel.

Approach

LLNL has identified a promising technology for cryogenic pressure vessel refueling: a liquid hydrogen (LH₂) pump. Manufactured by Linde, a leading supplier of cryogenic equipment, this pump takes liquid hydrogen at low pressure (near atmospheric) and delivers it at high pressure (up to 875 bar), high flow rate (100 kg/hour), low temperature (30-60 K), high density (>80 g/L), and low evaporative losses

Fiscal Year (FY) 2012 Objectives

- Demonstrate rapid refueling of cryogenic vessels
- Refuel cryogenic vessels even when warm and/or pressurized
- Refuel at high density (>80 kgH₂/m³)

Technical Barriers

This project addresses the following technical barrier from the Delivery section of the Fuel Cell Technologies Program Multi-Year Research, Development and Demonstration Plan:

(J) Refueling Site Operations

TABLE 1. Progress toward Meeting DOE Hydrogen Delivery Technical Targets

| Pressurized LH ₂ pump | | | | |
|---------------------------------------|-------------|-------------|-------------|----------------------------------|
| DOE targets for forecourt compressors | Units | 2010 Target | 2015 Target | Pressurized LH ₂ pump |
| Reliability | - | Improved | High | High |
| Compression energy efficiency | % | 94 | 95 | 99 |
| Installed capital cost | k\$(/kg/hr) | 4 | 3 | 5 |
| H ₂ fill pressure | Peak psi | 6,250 | 12,000 | 12,700 |

(less than 3% of dispensed H₂). Pumped hydrogen can be directly dispensed into a cryogenic pressure vessel, even when warm and/or pressurized. In this project we plan to install a LH₂ pump in the LLNL campus and demonstrate its virtues for rapid and efficient cryogenic vessel refueling.

Results

In an effort to evaluate the potential for future LH₂ pump high density refueling, LLNL has developed a model for vessel fill processes. Based on REFPROP [3], the model considers real gas hydrogen properties and enables quick calculation of relevant thermodynamic properties. The model is based on experimental measurements of outlet temperature vs. pressure performed at Linde, and has been validated against experimental BMW data for an existing 300 bar pump, demonstrating good agreement for a wide range of experimental conditions (Figure 1).

Aside from model validation, FY 2012 effort has mainly focused on site location and institutional approvals for LH₂ pump installation. The LH₂ pump and dewar (3,000 gallons, 800 kg LH₂ storage capacity) make a large package (12-m long by 4-m wide, Figure 2) and need to be installed in a location that permits access by LH₂ delivery truck.

With assistance from LLNL's facilities group, an appropriate location for the pump in the southern end of the LLNL campus has been identified. The site is within the future Livermore Valley Open Campus, a joint LLNL-Sandia partnership established to enhance industrial collaboration. The pump may therefore be publicly accessible in the future if so decided by laboratory/DOE management. A soil study and a topographical survey has been conducted (Figure 3).

All institutional approvals have been granted, and detailed design is about to start. Detailed design will include

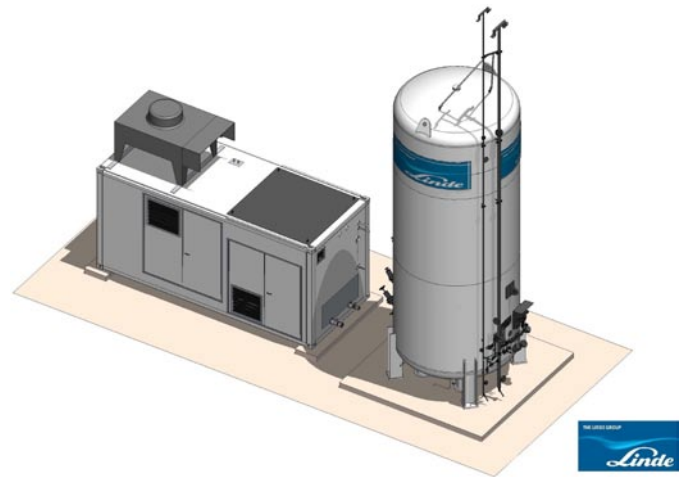


FIGURE 2. Rendering of the future LLNL LH₂ pump fabricated by Linde

plans for demolition, tree removal, fence removal and rebuild, electric supply (480 and 120 volts), telephone line, foundation, bollard installation, road construction, grading, and paving.

The design was conducted during the month of August. The design package will then be approved by LLNL in September, immediately followed by construction. Pump installation by Linde is finally expected for January of 2013.

Conclusions and Future Directions

- Rapid, low-loss refueling of cryogenic vessels is possible through pressurized LH₂ dispensing
- LH₂ pump model has been developed and validated against BMW experimental data
- LLNL facilities program has approved the proposed plan
- Detailed design is under way, to be quickly followed by construction
- Pump installation is planned for January 2013
- LH₂ pump will enable up to 30% higher density refueling and will open to research a large region of the H₂ phase diagram (Figure 4)

References

1. Aceves, S.M., Espinosa-Loza, F., Ledesma-Orozco, E., Ross, T.O., Weisberg, A.H., Brunner, T.C., Kircher, O., "High-density automotive hydrogen storage with cryogenic capable pressure vessels," *International Journal of Hydrogen Energy*, Vol. 35, pp. 1219-1226, 2010.
2. Ahluwalia, R.K. Hua, T.Q. Peng, J.-K. Lasher, S, McKenney, K. Sinha, J., Gardiner, M. "Technical assessment of cryo-compressed hydrogen storage tank systems for automotive applications," *International journal of hydrogen energy*, Vol. 35, pp. 4171-4184, 2010.

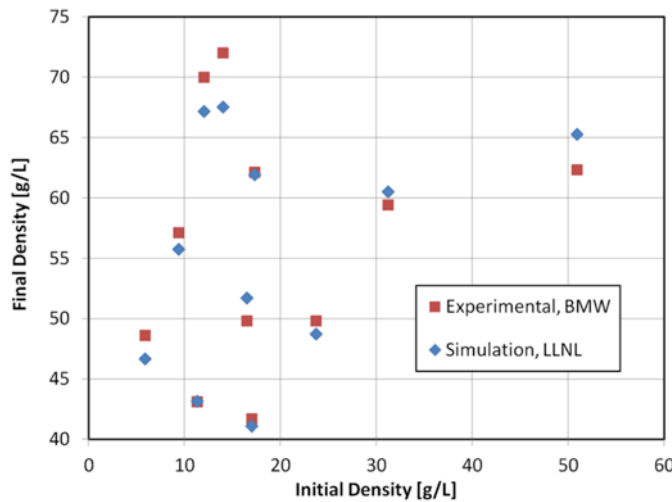


FIGURE 1. Validation of REFPROP-based model for Linde's LH₂ pump vs. experimental data from BMW



FIGURE 3. Topographical area of the construction site indicating the future location of the LH₂ pump (red rectangle near the middle of the figure)

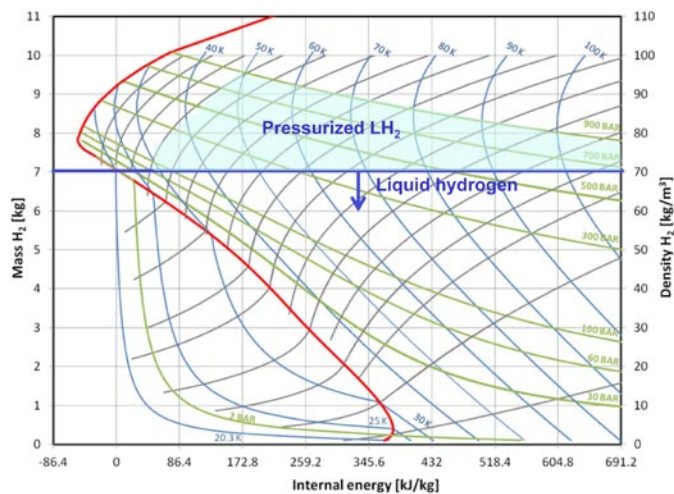


FIGURE 4. Hydrogen phase diagram indicating the operating region for LH₂ (below 70 g/L) and the region opened to research by the LH₂ pump

3. Lemmon, E.W., McLinden, M.O., Huber, M.L., “REFPROP: NIST reference fluid thermodynamic and transport properties,” National Institute of Standards and Technology, 2004. NIST Standard reference database 23, version 7.1.

FY 2012 Publications/Presentations

1. Cryogenic Hydrogen Storage, Delivery, and Safety, Salvador Aceves, Invited Presentation, Annual Congress of the Mexican Society of Mechanical Engineers, San Luis Potosi, Mexico, September 2011.
2. Compact Hydrogen Storage in Cryogenic Pressure Vessels, Salvador M. Aceves, Francisco Espinosa-Loza, Elias Ledesma-Orozco, Guillaume Petitpas, in Handbook of Hydrogen Energy, Edited by S.A. Sherif, E.K. Stefanakos, and D.Y. Goswami, CRC Press, Taylor & Francis, 2012.
3. Web-Based Resources Enhance Hydrogen Safety Knowledge, Weiner, S.C., Fassbender, L.L., Blake, C., Aceves, S.M., Somerday, B.P., and Ruiz, A., Accepted for Publication, International Journal of Hydrogen Energy, 2012.
4. Hydrogen Safety Training for Researchers And Technical Personnel, Aceves, S.M., Espinosa-Loza, F., Petitpas, G., Ross, T.O and Switzer, V.A., International Journal of Hydrogen Energy, 2012.
5. Modeling of sudden hydrogen expansion from cryogenic pressure vessel failure, Petitpas, G. and Aceves, S.M., International Journal of Hydrogen Energy, 2012.
6. Vehicle refueling with liquid hydrogen thermal compression, Guillaume Petitpas, Salvador M. Aceves, Nikunj Gupta, International Journal of Hydrogen Energy, Vol. 37, Issue 15, pp. 11448-11457, 2012.

IV. HYDROGEN STORAGE

IV.0 Hydrogen Storage Sub-Program Overview

INTRODUCTION

The Hydrogen Storage sub-program supports research and development (R&D) of materials and technologies for compact, lightweight, and inexpensive storage of hydrogen. In Fiscal Year (FY) 2012, the sub-program focused on system engineering for transportation applications while continuing R&D efforts in materials-based storage including metal hydrides, chemical hydrogen storage materials, and hydrogen sorbents. Additionally, work was directed at reducing the cost of compressed gas storage systems (i.e., physical storage) as a near-term commercialization pathway. The storage portfolio, including Basic Energy Sciences, currently includes projects involving 22 universities, 11 companies, and 13 federal laboratories and involves work in hydrogen storage materials discovery; materials-based system engineering; advanced high-pressure tank R&D; and system performance and costs analyses.

GOAL

The sub-program's goal is to develop and demonstrate commercially viable hydrogen storage technologies for transportation and early market fuel cell applications including stationary power, backup power, portable power, and material handling equipment.

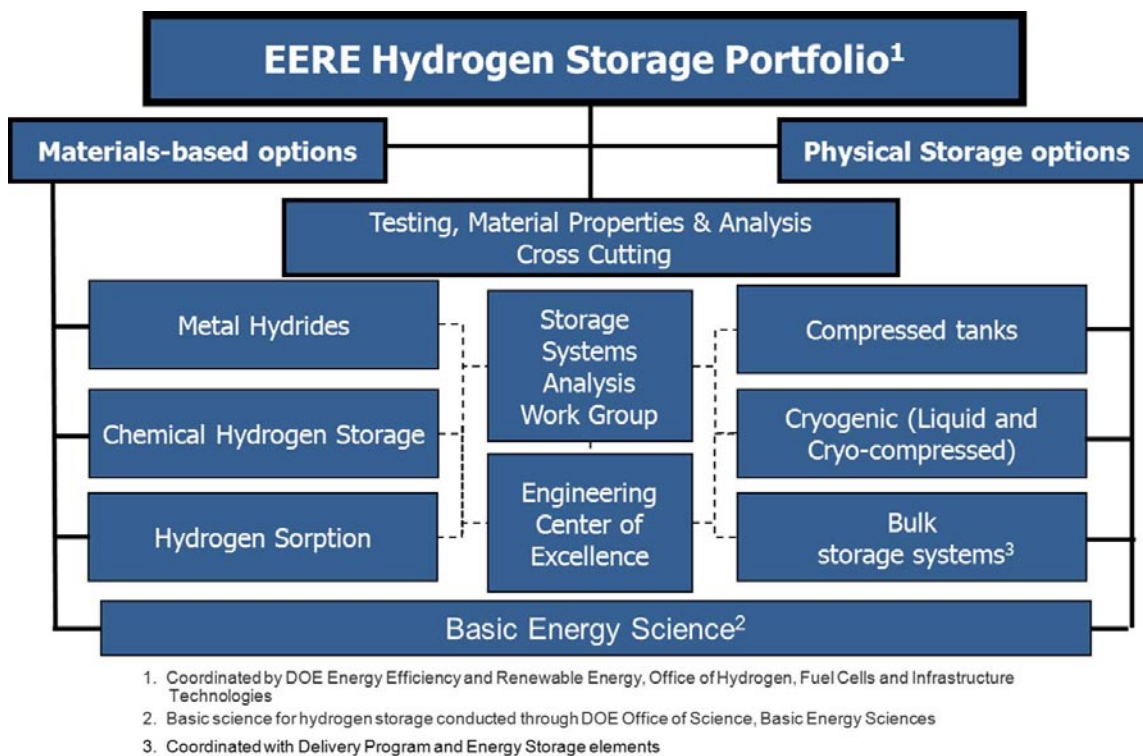
OBJECTIVES¹

The objective for the storage sub-program regarding light-duty vehicles is to store sufficient hydrogen onboard the vehicle to allow for a driving range of more than 300 miles (500 km), while meeting packaging, cost, safety, and performance requirements to be competitive with current vehicles. Although automakers have made progress in demonstrating some vehicles able to travel more than 300 miles on a single fill using high-pressure tanks, this driving range must be achievable across different vehicle models without compromising space, performance, or cost. By 2017, the sub-program aims to develop and verify onboard automotive hydrogen storage systems achieving 1.8 kWh/kg system (5.5 wt%), 1.3 kWh/L system (0.040 kg hydrogen/L) and \$12/kWh (\$400/kg H₂). These targets will allow some hydrogen-fueled vehicle platforms to meet customer performance expectations, while the ultimate targets of 2.5 kWh/kg system (7.5 wt%), 2.3 kWh/L system (0.070 kg hydrogen/L), and \$8/kWh (\$266/kg H₂) are intended to facilitate the introduction of hydrogen-fueled propulsion systems across the majority of vehicle classes and models. Advanced storage materials and concepts will be needed to meet the 2017 and ultimate targets.

The storage sub-program also aims to develop hydrogen storage for early market fuel cell applications including stationary and backup power, portable power, and material handling equipment. This effort is focused on developing technologies that provide enough hydrogen to enable efficient operation of fuel cells to meet customer-driven performance metrics in a safe, convenient, and cost-effective manner. These metrics include capacity (i.e., run-time), durability, and operability. The storage sub-program is currently working to finalize the technical and cost targets for these applications.

In pursuit of high level goals and targets for hydrogen storage, there are many requirements for achieving technical success, including improvements in volume, weight, cost, durability, cycle life, and transient performance. The full set of detailed hydrogen storage targets can be found in the *Multi-Year Research, Development, and Demonstration Plan (MYRD&D Plan)* www.hydrogenandfuelcells.energy.gov/mypp. These targets are based on the requirements of the application—not the current status of the technologies—and

¹ Note: Targets and milestones were recently revised; therefore, individual project progress reports may reference prior targets. Some targets are still currently under revision, with updates to be published in FY 2013.



in the transportation case, they account for differences in vehicle architecture between conventional vehicles and fuel cell vehicles.

FY 2012 STATUS AND PROGRESS

The hydrogen storage sub-program continues to pursue hydrogen storage materials discovery, including metal hydrides, chemical hydrogen storage, and sorbents, in addition to advanced tank development and total systems engineering to meet DOE onboard storage targets. The sub-program is also initiating efforts for early market fuel cell applications and has developed targets for material handling and portable power applications which can be found in the *MYRD&D Plan*. While there are several targets the sub-program is working towards, for transportation applications, system gravimetric and volumetric capacity, system cost, durability, and charging/discharging rates are important criteria to judge progress. System cost, in particular, is one of the most important barriers to commercialization of hydrogen fuel cell vehicles. On a routine basis the program assesses technical progress by evaluating the variable-volume manufacturing costs of compressed gas storage as shown in Figure 1. The 2012 high-volume (i.e., 500,000 units) manufacturing cost is \$15/kWh while the carbon fiber composite overwrap layer continues to contribute the majority of the costs. The sub-program also has system capacity projections made for the various onboard hydrogen storage technologies under development. The current projected storage system gravimetric and volumetric capacities are shown relative to the 2017 targets in Figures 2 and 3. Confidence in the accuracy of the projection improves with the maturity of the technology; for instance, there is higher confidence in projections for relatively mature compressed gas systems than for much less mature complex hydride systems. The range bars shown in Figures 2 and 3 represent the ranges of volumetric and gravimetric capacity projections conducted for all the onboard storage technologies during the given year. The point within the bars is the average (mean) capacity for the technologies analyzed within the given year.

In FY 2012, the hydrogen storage sub-program started four new projects covering chemical hydrogen storage, sorbents, and advanced tank design. The University of Oregon, in collaboration with Pacific Northwest National Laboratory (PNNL), the University of Alabama, and Protonex, will develop and analyze a new class

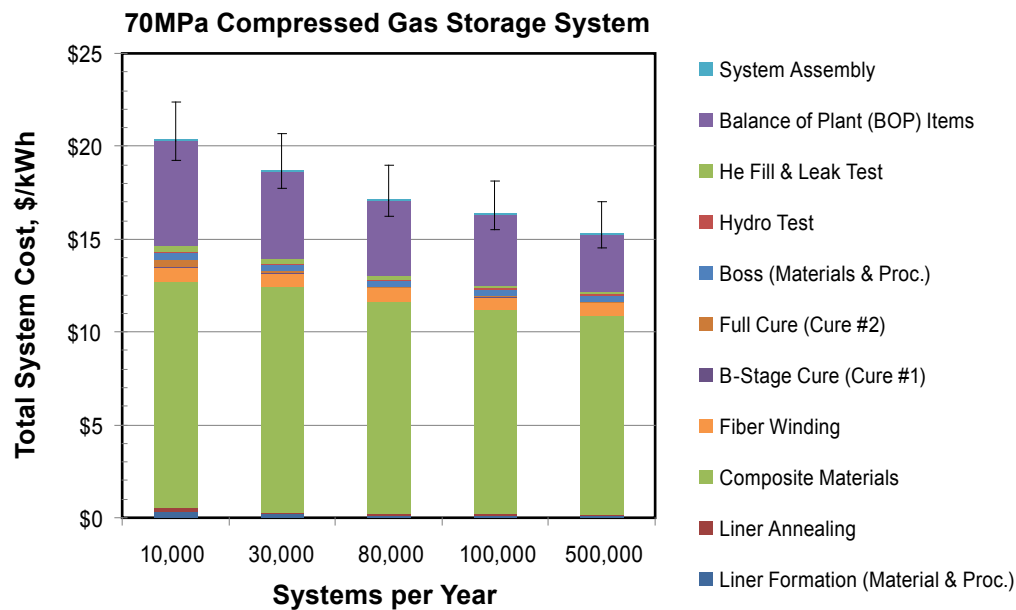
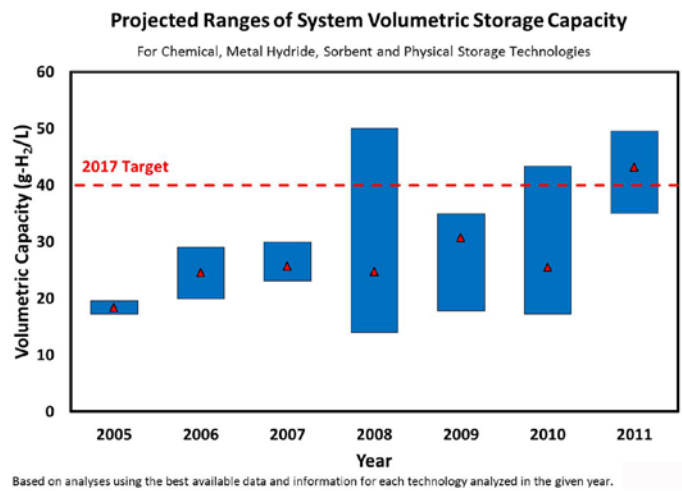
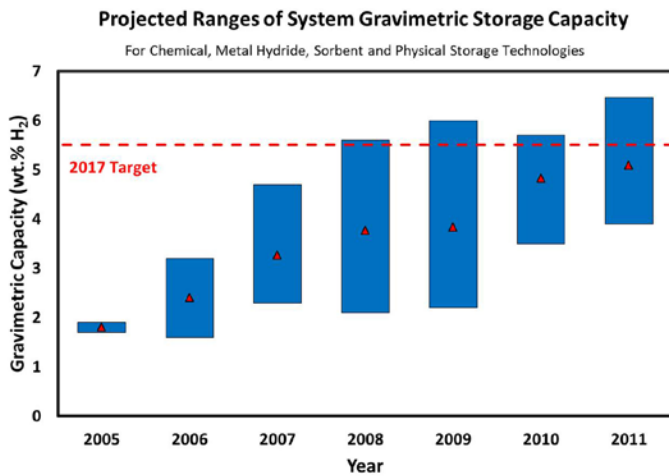


FIGURE 1. Projected cost, at various annual manufacturing capacities and in 2007\$, of compressed hydrogen storage systems, sized to deliver 5.6 kg of hydrogen to the vehicle fuel cell powerplant using two 700 bar, Type IV tanks. Cost analysis performed by Strategic Analysis, Inc. in 2012.



FIGURES 2 and 3. Status of projected hydrogen storage system gravimetric and volumetric capacities versus 2017 onboard system targets. (Note that all systems were sized to provide 5.6 kg of useable hydrogen and that the plotted data points are the average value for all technologies and systems analyzed during each year while the bars correspond to the range of maximum and minimum values obtained for the year. Also note that systems with predicted capacities exceeding the gravimetric targets do not necessarily meet all other targets.)

of boron- and nitrogen-containing carbon heterocycle compounds (CBN), capable of high hydrogen capacities. The CBN materials to be synthesized are liquid phase and high capacity, and will include potentially reversible combinations which couple endothermic and exothermic hydrogen release to potentially enable onboard recharging with hydrogen. HRL Laboratories will explore ambient temperature hydrogen sorption in nanoconfined liquids. Solvent liquids within porous scaffolds have been shown to have greatly enhanced gas solubilities over that of bulk liquids. HRL will leverage this observed phenomenon and its experience with nano-scaffolds to develop materials that meet the DOE’s hydrogen storage targets. Lawrence Berkeley National laboratory, in collaboration with the National Institute of Standards and Technology and General Motors, will

develop coordination polymer (metal organic framework) compounds with high gravimetric and volumetric capacity and high isosteric adsorption enthalpies. The focus of this work will center on the synthesis of high valent metal coordinatively unsaturated cation structures with high micropore volume. PNNL, in collaboration with Toray, Lincoln Composites, AOC, and Ford Motor Company, will produce and test enhanced materials and manufacturing methods to reduce the cost of high-pressure storage tanks. As carbon fiber accounts for nearly 75% of overall tanks costs, the team will develop and implement design approaches that will reduce the carbon fiber content consistent with structural design criteria.

Materials Development

In FY 2012 the sub-program continued efforts in developing and improving hydrogen storage materials with potential to meet the 2017 onboard storage targets. In the area of chemical hydrogen storage materials, much of the focus was on developing liquid phase, such as slurries or solutions, in keeping with the findings of the Hydrogen Storage Engineering Center of Excellence. For hydrogen sorbents, efforts were focused on increasing the isosteric heat of adsorption to increase the adsorb capacity at higher temperatures. For metal hydrides, efforts emphasized reducing the desorption temperatures and improving kinetics. Also in FY 2012, the Hydrogen Storage sub-program launched a comprehensive hydrogen storage materials database (<http://hydrogenmaterialssearch.govtools.us/>) to collect and disseminate materials data and accelerate advanced hydrogen storage materials research and development.

Metal Hydrides

- Demonstrated the first example of the reversible, solid-state dehydrogenation of a borohydride at temperatures below 250°C (200°C dehydrogenation; 100°C, 50 atm re-hydrogenation). (University of Hawaii)
- Demonstrated a carbon-Ni catalyst that significantly enhanced the hydrogen desorption kinetics of complex hydrides. (Northwestern University)

Chemical Hydrogen Storage Materials

- Synthesized an additive hexylamineborane ($\text{H}_3\text{C}(\text{CH}_2)_6\text{NH}_2\text{BH}_3$, hexyl-AB) that has 3-4 wt% usable H_2 and maintains fluid phase at room temperature. Also demonstrated that 20 wt% AB in hexyl-AB (6 wt% H_2) transforms from a slurry to liquid upon dehydrogenation at 140°C. (Los Alamos National Laboratory/University of Ottawa)
- Developed ammonia borane silicon oil slurry (45 wt% AB, 7 wt% H_2) that remains a liquid-slurry before and after dehydrogenation. (PNNL)
- Optimized dehydrogenation/trimerization reaction of the six-member ring CBN material with cheap and relatively environmentally benign catalyst FeCl_2 . (University of Oregon).
- Improved synthesis of the CBN-heterocyclic materials reducing processing steps by 50% and increased overall yield by five fold to 51% from commercially available starting materials. (University of Oregon)

Hydrogen Sorption Materials

- Synthesized a boron substituted templated carbon and with the use of a Ru-based catalyst, noted a 15 wt% improvement in hydrogen uptake over baseline materials. Moreover, the kinetics for the weak chemisorption effect were improved by a factor of 25 over that of similar materials with 95% of the adsorption process taking place within 10 minutes. (National Renewable Energy Laboratory, NREL)
- Initiated a startup by leveraging work within the H_2 storage sub-program that won DOE's National Clean Energy Business Plan Competition. NuMat Technologies employs rapid computational discovery, efficient synthesis technology and supercritical activation to design sorbents that will obviate the high pressures presently required for gas storage. (Northwestern University)

- Completed and established measurement, qualification, and characterization facilities as an outgrowth of its lead role of the Hydrogen Sorption Center of Excellence. Assisted materials-research groups to characterize and qualify samples for hydrogen-storage properties, and validated H₂ excess uptake in a metal organic framework (MOF) material synthesized by Northwestern University (NU-100). The validated excess capacity of ~8 wt% at 50 bar and 77 K for the NU-100 MOF is amongst the highest confirmed to date. (NREL)
- Continued efforts to incorporate boron into carbon utilizing X-ray photoelectron spectroscopy and Fourier transform infrared spectroscopic techniques to confirm the existence of B-C bonds in a material that has double the isosteric enthalpy of adsorption vs. unmodified material. The result of this modification is a 30% improvement in hydrogen wt% uptake when normalized to surface area. (University of Missouri)

Engineering

In FY 2012, the Hydrogen Storage Engineering Center of Excellence (HSECoE) completed hydrogen storage system level models for cryo-sorbents and liquid-phase off-board regenerable chemical hydrogen storage material systems. The HSECoE successfully transitioned from Phase 1 into Phase 2 and began conducting thorough tradeoff analyses comparing various novel system designs and candidate storage materials. Based on these results, the center chose MOF-5 as the base material for the cryo-sorbent system and ammonia borane (AB) for the chemical hydrogen storage system. In addition, the HSECoE began component level testing and model validation as the center moves towards final prototype design, construction, and testing in Phase 3.

- Based on the integrated Hydrogen Storage SIMulator vehicle model, the HSECoE:
 - Terminated work on metal hydride systems due to low probability of these materials meeting the required properties in the 2017 timeframe.
 - Identified ideal onboard reversible metal hydride material properties. (HSECoE)
- Completed down-select of adsorbent materials with selection of MOF-5. (HSECoE)
- Completed down-select of chemical hydrogen materials with selection of exothermic materials (AB). (HSECoE)
- Performed a failure modes and effects analysis for both adsorbent and chemical hydrogen material systems identifying potential failure modes not previously considered including adsorbent bed packing and impurity effects and chemical hydrogen material settling/flocculation and balance of plant (BOP) compatibility issues. (HSECoE)
- HSECoE identified primary technical barriers limiting advancement of materials-based hydrogen storage systems as:
 - Metal hydrides (heat transfer design, media compaction, media thermal conductivity, lowered mass of BOP components).
 - Chemical hydrogen materials (media slurry agent/solvent with 50 wt% capacity, media kinetics, novel impurity trapping).
 - Adsorbents (Type-4 vessels at cryogenic temperatures, media thermal conductivity improvement, flow through cooling, media compaction, minimized tank outgassing, potential low pressure Type-1 tank).
- Developed an advanced composite pressure vessel for cryo-sorbents with 11% lower weight, 4% greater internal volume, and 10% lower cost than the baseline vessel established in Phase I. (Lincoln)
- Performed vehicle-level tradeoff analyses to better understand the impact of key engineering designs, for example, the tradeoffs between mass, onboard hydrogen storage capacity, and vehicle range. (NREL)
- Developed and validated advanced vessel thermal isolation design capable of limiting parasitic heat load on a full tank to <2 W, a 38% improvement over the current state of art, resulting in increased dormancy

(“hold”) times for the idle vehicle over the entire operating range, -40°C to 60°C. (Jet Propulsion Laboratory)

- Completed a demonstration of a flow through cooling system and validated detailed models for super activated carbon. (Savannah River National Laboratory)

Advanced Physical Storage

In FY 2012, the sub-program continued to emphasize its efforts on reducing the cost of compressed hydrogen gas storage tanks by initiating new efforts on low-cost, high-strength carbon fiber. Lightweight compressed gas storage vessels requiring a composite overwrap to contain hydrogen gas are considered the most likely near-term hydrogen storage solution for the initial commercialization of fuel cell electric vehicles, as well as for other early market applications. Carbon fiber composite overwraps can currently contribute as much as 75% or more to the overall cost of advanced Type-IV tanks. In addition to the new effort initiated with PNNL mentioned above, the Hydrogen Storage sub-program supported efforts at Oak Ridge National Laboratory (ORNL) to reduce the cost of polyacrylonitrile-based (PAN) fibers used as precursors to produce high-strength carbon fibers. The ORNL efforts focused on advanced precursor materials and processing since precursors have been shown to contribute approximately 50% of the total cost of high-strength carbon fibers. The team investigated the use of low-cost textile-grade fibers made from PAN blended with a methyl acrylate comonomer (PAN-MA) as lower cost precursors and continued development of melt-spinnable PAN precursors and processing techniques to replace the current more costly wet processing methods. A broad-based topic on “development of fibers, resins and/or composite additives” to reduce the cost of high-pressure hydrogen storage cylinders was included in the FY 2012 Small Business Innovation Research (SBIR) release 3 solicitation through which two new awards are anticipated. Additionally the project by Applied Nanotech, Inc. developing lightweight, high-strength carbon nanotube reinforced composite overwraps for tanks was selected to continue as a Phase II SBIR award.

In December 2012, DOE participated in a workshop to identify strategies and R&D needs for lowering the cost of high-strength carbon fiber and carbon fiber composite systems (<http://www.compositesworld.com/news/2011-carbon-fiber-workshop-reviews-low-cost-carbon-fiber-in-energy>). The input garnered from this activity will aid in identifying key challenges, priorities, and needs for carbon fiber composites and in development of future solicitations for R&D in these areas.

- Demonstrated carbonized fiber from low-cost textile-grade PAN-MA met the 2012 milestone of at least 300 KSI strength and 30 MSI modulus and identified areas for further refinement and improvement of properties. (ORNL)
- Demonstrated the ability to melt-spin PAN precursor fibers with the target denier (for fibers 10 to 20 microns in diameter) with a one-step spinning/drawing process. (ORNL)

Testing & Analysis

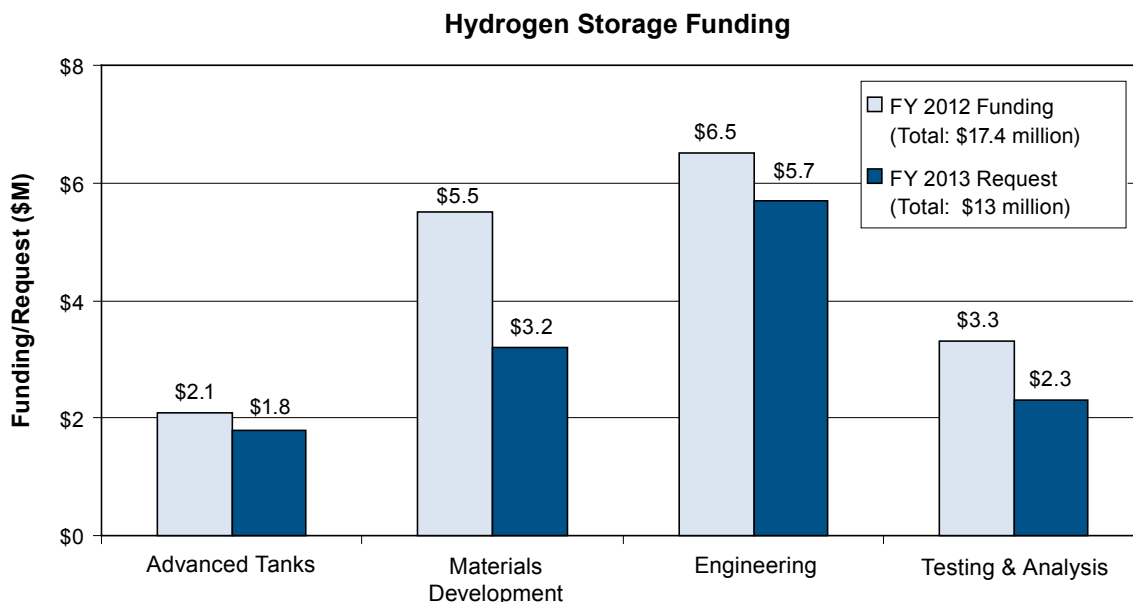
In FY 2012, the Hydrogen Storage sub-program continued carrying out assessments of hydrogen storage technologies to meet hydrogen fuel cell applications. A new effort was initiated with Strategic Analysis Inc. (SA) to develop cost models and carry out cost analyses of hydrogen storage technologies. Two national laboratories (Argonne National Laboratory [ANL] and NREL) will contribute as partners with SA.

- Completed an assessment of the technology and manufacturing readiness levels of hydrogen storage technologies to meet the requirements of identified early market hydrogen fuel cell applications. (PNNL)
- Updated the onboard analyses of the MOF-5 system (powder and pellets) with adiabatic para LH₂ refueling. Determined the intrinsic capacities, thermodynamics, dormancy, H₂ refueling dynamics, and discharge dynamics with the potential benefits of para-to-ortho conversion in the onboard storage tank. (ANL)

- Developed a model of the onboard hydrogen discharge reactor for the single-component liquid CBN hydrogen storage material and surmised that a more rapid or dispersed catalyst is needed to meet the required conversion in <10 s at 150°C. (ANL)
- Developed design to achieve 20% reduction in carbon fiber requirement. (ANL)
- Developed design to reduce or eliminate pre-cooling in fast fill of 700-bar compressed hydrogen storage tanks. (ANL)
- Developed and updated cost analysis model for the compressed hydrogen storage system. (SA)
- Conducted preliminary cost analyses for the 700 bar system with capacity of 5.6 kg of useable hydrogen, at varying manufacturing volumes using input from vehicle manufacturers to validate the cost model. (SA)
- Initiated analysis of using “wet-wind” versus using “pre-preg” in the composite cylinder manufacturing process. Determined that the following areas of the analysis require further work and scrutiny before the cost model can be finalized for further analyses: 1) carbon fiber composite mass requirement, 2) pre-preg fiber cost and comparison with wet-winding, 3) average winding speed, 4) BOP cost (particularly at low manufacturing rates), 5) complete assembly analysis, and 6) sensitivity studies: 350 bar and multiple vessels analyses. (SA)
- Updated and completed sections (Introduction, Kinetics, Capacity, Thermodynamics and Cycle-life) of the Best-Practices Document on the Characterization of Hydrogen Storage Materials were posted on the DOE website. Two additional sections on engineering related properties (Thermal and Mechanical Properties) are estimated to be 85 and 15% complete respectively. (H2 Technology Consulting through NREL)

BUDGET

\$13 million from the President’s FY 2013 budget request is planned for hydrogen storage—compared with \$17.4 million from the FY 2012 congressional appropriation. In FY 2013, the Hydrogen Storage sub-program will continue to focus on materials discovery, system engineering for materials-based storage technologies, R&D to lower the cost of high-pressure storage systems, and systems analysis. The sub-program will also initiate activities focused on hydrogen storage for early market applications.



FY 2013 PLANS

The technology portfolio for Hydrogen Storage emphasizes materials R&D to meet system targets for onboard and early market applications. While a focus on light-duty vehicle applications will continue, increased emphasis will be placed on new materials and novel concepts to meet performance requirements for early market applications. In FY 2013, goals and objectives for hydrogen storage for early market applications will be released. The increased emphasis on developing lower-cost physical storage technologies will continue to be expanded. Specifically, the sub-program will use the SBIR program and coordinate with other efforts (e.g., Vehicle Technologies, Defense Advanced Research Projects Agency, etc.) on development of approaches to produce low-cost carbon fiber for composite cylinders. System engineering and analysis will continue through the HSECoE, ANL, and SA. Coordination with basic science efforts, including theory, characterization, and novel concepts, will continue during FY 2013. The sub-program will also coordinate with the National Science Foundation and Advanced Research Projects Agency–Energy through activities such as workshops and joint meetings.

Ned Stetson

Hydrogen Storage Team Lead
Fuel Cell Technologies Program
Department of Energy
1000 Independence Ave., SW
Washington, D.C. 20585-0121
Phone: (202) 586-9995
Email: Ned.Stetson@ee.doe.gov

IV.A.1 Efficient Discovery of Novel Multicomponent Mixtures for Hydrogen Storage: A Combined Computational/Experimental Approach

Prof. Christopher Wolverton (Primary Contact),
Prof. Vidvuds Ozolins¹, Prof. Harold H. Kung,
Dr. Jun Yang²

Department of Materials Science & Engineering
Northwestern University
Evanston, IL 60208
Phone: (847) 467-0593

Email: c-wolverton@northwestern.edu

¹University of California, Los Angeles

²Ford Motor Company

DOE Managers

HQ: Ned Stetson

Phone: (202) 586-9995

Email: Ned.Stetson@ee.doe.gov

GO: Katie Randolph

Phone: (720) 356-1759

Email: Katie.Randolph@go.doe.gov

Contract Number: DE-FC36-08GO18136

Project Start Date: September 1, 2008

Project End Date: July 31, 2013

Fiscal Year (FY) 2012 Objectives

The objective of this project is to discover novel mixed hydrides for hydrogen storage, which enable the DOE 2010 system-level goals. Our goal is to find a material that desorbs 8.5 wt% H₂ or more at temperatures below 85°C. The research will combine first-principles calculations of reaction thermodynamics and kinetics with material and catalyst synthesis, testing, and characterization. We will combine materials from distinct categories to form novel multicomponent reactions. Examples of systems to be studied include mixtures of complex hydrides and chemical hydrides and novel multicomponent complex hydride materials and reactions.

Technical Barriers

This project addresses the following technical barriers from the Storage section of the Fuel Cell Technologies Program Multi-Year Research, Development and Demonstration Plan:

(P) Lack of Understanding of Hydrogen Physisorption and Chemisorption

- (A) System Weight and Volume
- (E) Charging/Discharging Rates

Technical Targets

This study is aimed at fundamental insights into new materials and the thermodynamic and kinetic aspects of hydrogen release and reabsorption from them. Insights gained from these studies will be applied toward the design and synthesis of hydrogen storage materials that meet the following DOE 2010 hydrogen storage targets:

- Specific energy: 1.5 kWh/kg
- Energy density: 0.9 kWh/L

FY 2012 Accomplishments

- H₂ desorption and decomposition pathways have been studied in
 - 5LiBH₄ + 2Mg(BH₄)₂ (~5.8 wt% desorbed)
 - Mg(BH₄)₂ + Mg(NH₂)₂ (~8.3 wt% desorbed)
 - (NH₄)₂B₁₂H₁₂. (~4.5 wt% desorbed)
- Partial reversibility (~1-2.5 wt%) found in 5LiBH₄ + 2Mg(BH₄)₂ and (NH₄)₂B₁₂H₁₂
- Proposed new metal-carbon catalyst: Tested on NaAlH₄, and applied to Mg(BH₄)₂ + Mg(NH₂)₂, 2LiBH₄+5Mg(BH₄)₂ and LiBH₄; effective catalyst - lowers desorption temperature, improves dehydrogenation rate, and suppresses formation of borane and NH₃
- Down-select the mixed borohydride/amide systems as promising hydrogen storage material (lack of reversibility and B-N bonds in products)
- Predicted a new metastable Mg₃(B₃H₆)₂ intermediate in decomposition of Mg(BH₄)₂, but showed that recently-proposed Mg(B₃H₈)₂ is not stable.
- Prototype electrostatic ground state plus density functional theory combined experimental measurements are used in unique way to solve amorphous AlB₄H₁₁ polymeric structure (with J.C. Zhao, Ohio State University)
- Using the predictive models of defects, kinetics of mass transport: mass transport in LiBH₄ is very low (much lower than that in NaAlH₄)



Introduction

The long-term DOE targets for hydrogen storage systems are very challenging, and cannot be met with existing materials. The vast majority of the work to date has delineated materials into various classes, e.g., complex and metal hydrides, chemical hydrides, and sorbents. However, very recent studies indicate that mixtures of storage materials, particularly mixtures between various classes, hold promise to achieve technological attributes that materials within an individual class cannot reach. Our project involves a systematic, rational approach to designing novel multicomponent mixtures of materials with fast hydrogenation/dehydrogenation kinetics and favorable thermodynamics using a combination of state-of-the-art scientific computing and experimentation. Specifically, we focus on combinations of materials from distinct categories to form novel multicomponent reactions.

Approach

We use the accurate predictive power of first-principles modeling to understand the thermodynamic and microscopic kinetic processes involved in hydrogen release and uptake and to design new material/catalyst systems with improved properties. Detailed characterization and atomic-scale catalysis experiments elucidate the effect of dopants and nanoscale catalysts in achieving fast kinetics and reversibility. And, state-of-the-art storage experiments give key storage attributes of the investigated reactions, validate computational predictions, and help guide and improve computational methods. In sum, our approach involves a powerful blend of: 1) H₂ storage measurements and characterization, 2) state-of-the-art computational modeling, 3) detailed catalysis experiments, and 4) an in-depth automotive perspective.

Results (Selected Examples)

I. High-resolution desorption data for the following three prioritized mixtures: (NH₄)₂(B₁₂H₁₂), 2LiBH₄ + 5Mg(BH₄)₂, and Mg(NH₂)₂ + Mg(BH₄)₂

Our recent experimental efforts focused on obtaining high-resolution desorption and recharging data as well as phase identification for the following three prioritized mixtures: (NH₄)₂(B₁₂H₁₂), 2LiBH₄ + 5Mg(BH₄)₂, and Mg(NH₂)₂ + Mg(BH₄)₂. Building off of the temperature-programmed desorption mass spectrometry (TPDMS) data previously obtained, we focused on phase identification via in situ X-ray diffraction (XRD) and Fourier transform infrared (FTIR) experiments as well as water displacement desorption (WDD) to establish reversibility. The XRD measurements were performed in a flowing nitrogen (200 sccm) environment using a sapphire substrate with a temperature

ramp of 1°C/min from 50 to 550°C after a 1-hour room-temperature scan. For the variable temperature scans, each scan was integrated for 10 minutes, providing averaged data over a 10°C window. Phases were identified using the MDI JADE software package and the ICDD Powder Diffraction Database. For the FTIR experiments, both diffuse reflectance infrared Fourier transform spectroscopy (DRIFTS) and photo acoustic (PAS) FTIR methods were used. DRIFTS measurements allowed us to explore local environment changes with changes in temperature. The samples to be measured via DRIFTS were contained in a sample holder under flowing argon. The chamber containing the sample holder was purged with nitrogen and the sample temperature ramped at a rate of 5°C/min from room temperature to 450°C. Every minute, 16 sample scans were collected during the temperature ramp and a powdered KBr background was used. For the PAS measurements, the sample holder was purged with helium while the enclosure was purged with nitrogen. All PAS measurements were taken at room temperature, with a carbon black background and collected 32 sample scans for each spectrum. Because of the different WDD conditions used, the details of the measurements are only given in the relevant section below.

1. **2LiBH₄ + 5Mg(BH₄)₂**: The LiBH₄/Mg(BH₄)₂ mixture was prepared by ball milling as-purchased LiBH₄ and Mg(BH₄)₂ in a 2:5 molar ratio. Our XRD measurements (Figure 1) revealed that the mixture resembled a physical mixture of LiBH₄ and Mg(BH₄)₂, though the peaks corresponding to LiBH₄ were partially convoluted with the substrate. The measurements revealed several steps of decomposition: 1) consumption of LiBH₄ and partial consumption of Mg(BH₄)₂ (decreasing intensity of peaks) between 200-250°C, 2) full consumption of Mg(BH₄)₂ and possible MgB₂ or MgH₂ formation (250-300°C), and 3) above 350°C, the formation of MgB₂, and the formation of peaks corresponding to an unidentified phase (at 2θ = ~30-40°). This reaction path differs from that predicted by thermodynamics, which we attribute to kinetic limitations in the system. This conclusion is supported by the difference in observed desorption onset versus the predicted temperature (approximately 200°C vs. -29°C).

We used WDD to examine the reversibility of this mixture, as well. The experiment was performed by ramping the sample from room temperature to 350°C at 5°C/min and holding for approximately 2 hours. To recharge the system, the temperature was maintained and the sample exposed to 138 bar ultra-high purity (UHP) hydrogen for approximately 18 hours. The process was then repeated for each cycle. We found indications of limited reversibility under the conditions used (Figure 2).

2. **Mg(NH₂)₂ + Mg(BH₄)₂**: The Mg(NH₂)₂/Mg(BH₄)₂ mixture was produced by ball milling as-purchased Mg(BH₄)₂ with Mg(NH₂)₂ synthesized from

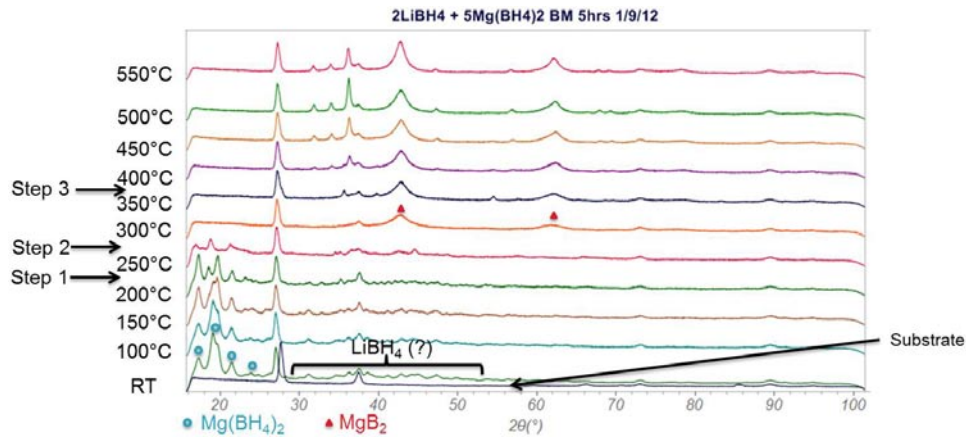


FIGURE 1. XRD measurements of ball milled $2\text{LiBH}_4 + 5\text{Mg}(\text{BH}_4)_2$

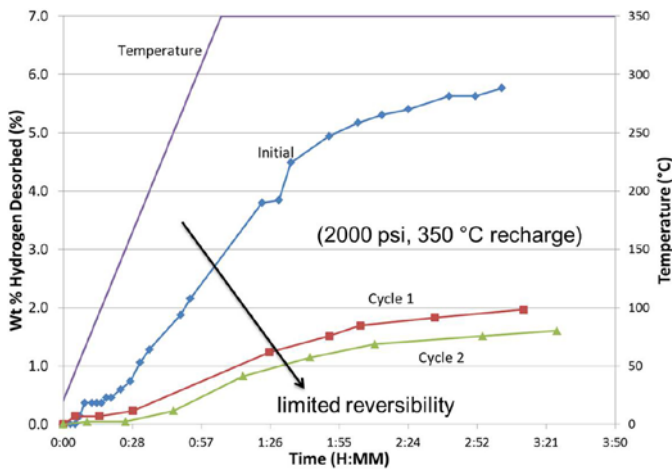


FIGURE 2. Reversibility studies of mixed $2\text{LiBH}_4 + 5\text{Mg}(\text{BH}_4)_2$

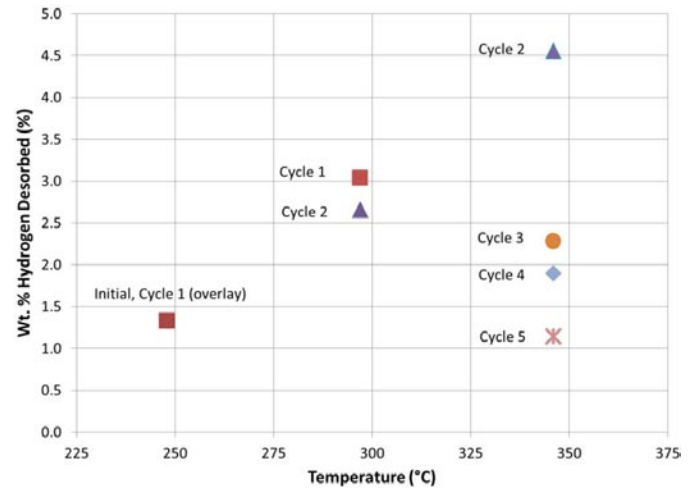


FIGURE 3. Partial reversibility of $(\text{NH}_4)_2\text{B}_{12}\text{H}_{12}$

MgH_2 and 20 bar NH_3 . Like the $\text{LiBH}_4/\text{Mg}(\text{BH}_4)_2$ mixture, we reported previously that the onset of hydrogen desorption occurs at $\sim 200^\circ\text{C}$, a significantly lower temperature than the pristine constituents, with a second hydrogen release event at roughly 400°C . Northwestern and Ford collaborated closely in the identification of the reaction products and pathway, with Ford providing available XRD and infrared data to assist in the determination of reaction products via computational methods, including PEGS to determine new structures. However, further study of the system via WDD found it to be irreversible under the conditions tested: 1) ramp to 250°C at $5^\circ\text{C}/\text{min}$, cool to room temperature for recharge with 114 bar UHP hydrogen, 2) ramp to 380°C at $5^\circ\text{C}/\text{min}$, maintain for recharge with 138 bar UHP hydrogen.

3. $(\text{NH}_4)_2(\text{B}_{12}\text{H}_{12})$: This compound was synthesized and kindly provided to Ford by J.C. Zhao (Ohio State University). We reported previously that hydrogen

desorption begins at roughly 250°C , and occurs in two primary steps. Our TPDMS results indicated that little NH_3 is released and undetectable quantities of diborane or borazine are produced during decomposition. We found evidence of partial reversibility up to 350°C via WDD cycling experiments (Figure 3). The WDD experiment was carried out as follows:

- Initial desorption to 250°C at $5^\circ\text{C}/\text{min}$ and holding for approximately two hours.
- Recharge overnight at the above temperature with 138 bar UHP hydrogen.
- Cool sample to room temperature, purge excess hydrogen from the system.
- Ramp sample to 250°C at $5^\circ\text{C}/\text{min}$ and hold for two hours (Cycle 1, 250°C in (Figure 3)).
- After the two hours at 250°C , the sample was ramped up to 300°C at $5^\circ\text{C}/\text{min}$ and held (Cycle 1, 300°C in Figure 3).

- Recharge overnight at 300°C under 138 bar UHP hydrogen.
- Repeat process for subsequent temperatures.

II. Characterizing carbon/Ni catalysts for LiBH₄ dehydrogenation

The effect of carbon on the dehydrogenation kinetics of LiBH₄. In view of the observed favorable dehydrogenation and hydrogenation kinetics of carbon-based catalysts on NaAlH₄, we initiated the study of carbon and Ni/carbon catalysts on the dehydrogenation of LiBH₄ and the results are shown in Figure 4. The dashed curves are the dehydrogenation profiles of physical mixtures of LiBH₄ mixed with carbon containing 2% Ni; which was loaded on using the precursor bis(cyclooctadiene)nickel(0). The weight loading of LiBH₄ in the physical mixture of LiBH₄ and Ni containing carbon was 47% and 68% respectively for curve **a** and curve **c**. For curve **b**, the loading of LiBH₄ in the mixture was 48% but the carbon contained no Ni. Curve **d** is the profile for 100% LiBH₄ and shows that dehydrogenation kinetics was very sluggish; similar to what was reported in the literature. The data clearly show that the dehydrogenation kinetics were enhanced with increasing carbon content in the physical mixture and for a given ratio of carbon and LiBH₄ (compare black dash and pink solid curves), the presence of Ni mildly enhanced the dehydrogenation rate.

LiBH₄-carbon-Ni composite synthesized with a one-step infusion. Since it appears that the contact between carbon and LiBH₄ is important, we explored ways to increase the contact area between LiBH₄ and carbon in the mixture. Figure 5 shows the data for a composite sample where the LiBH₄ is in more intimate contact with the carbon than just that of a physical mixture. The curve labeled Composite is for a sample, containing 70 wt% LiBH₄, that

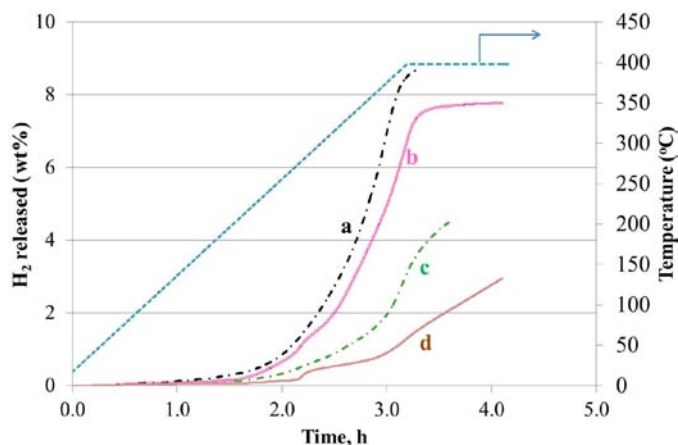


FIGURE 4. Dehydrogenation profile of carbon (Norit SX Ultra Cat) and LiBH₄ physical mixture; (a) 47% LiBH₄ and 53% carbon containing 2% Ni, (b) 48% LiBH₄ and 52% carbon, (c) 68% LiBH₄ and 32% carbon containing 2% Ni, and (d) 48% LiBH₄.

was made by mixing a tetrahydrofuran (THF) solution of bis(cyclooctadiene)nickel(0) and LiBH₄ with carbon (Norit, SX Ultra Cat). The THF solvent was removed by evacuation at room temperature for an extended time period and then by an additional 25 min evacuation at 60°C. Compared with a physical mixture, the composite began decomposing at a substantially lower temperature. Although we have yet to firmly establish that hydrogen release was the cause for the increase in pressure in the reactor, particularly at low temperatures, the low boiling point of THF (66°C) and the fact that we had previously established effective THF removal by room temperature evacuation of a THF solution containing bis(cyclooctadiene)nickel(0) and Norit carbon, led us to believe that at least some of the pressure increase was due to hydrogen evolution.

LiBH₄-Y carbon composite made by multi-step infusion (Composite C1 and C2). In order to further enhance the contact between LiBH₄ and carbon, we modified the preparation procedure of the composite by using a multiple impregnation technique. In this technique, the total volume of LiBH₄ in THF solution was divided into small portions, and each portion was dried onto the carbon consecutively. In this way, most of the solution would be in the pores of the carbon, such that selective deposition on the external surface of the carbon is minimized.

For these composites, a higher surface area carbon material was used, which was a carbon molecular sieve (Y carbon; Inc) with a surface area of 3,200 m²/g. Its surface area is even higher than a single graphene sheet (2,630 m²/g), possibly due to the presence of defects. For these samples, the LiBH₄ was introduced using the glass apparatus shown in Figure 6, which afforded addition of a THF-LiBH₄ solution to carbon in dry nitrogen; and drying by evacuation without

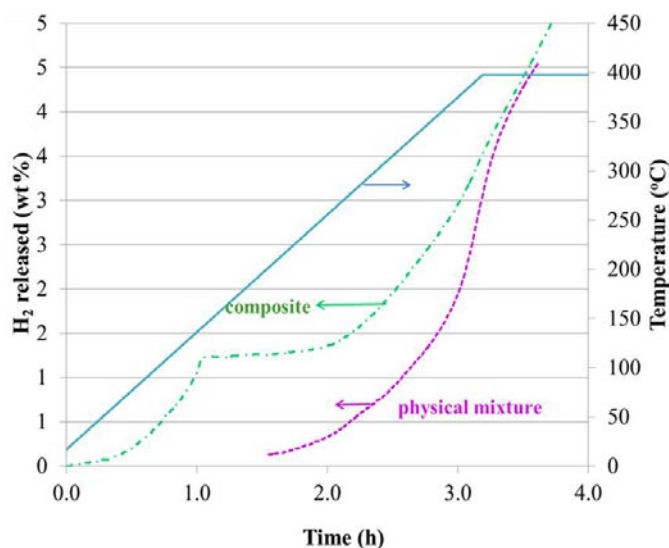


FIGURE 5. Comparison of the dehydrogenation kinetics of a physical mixture and a composite of Norit carbon and LiBH₄.

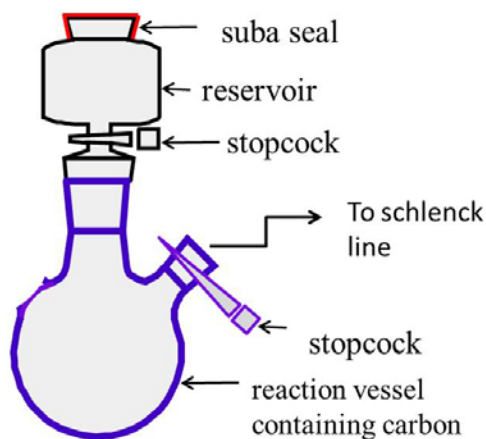


FIGURE 6. Synthesis glassware

the need to transfer the sample. Aliquots of the THF-LiBH₄ solution, enough to fill the pore volume of the carbon, was introduced into the reservoir using a syringe pump, and then dripped into the reaction vessel, all without exposure to air. Then the solvent was removed by evacuation at around 40°C. After drying, another aliquot was introduced and the procedure was repeated until the desired amount of LiBH₄ was added (about 30 wt%).

The decomposition profile of this sample (labeled composite C1) is shown in Figure 7. Because of some uncertainties of the amount of LiBH₄ added, due to splashing of the LiBH₄ solution onto the reactor wall, the Y axis is labeled as approximate H₂ released. The dehydrogenation kinetics was enhanced significantly for this sample than a physical mixture of carbon and LiBH₄. Very interestingly, low temperature H₂ release was observed.

This experiment was repeated with an improved procedure that reduced splashing of the LiBH₄ onto the wall of the reaction vessel, and composite C2 was prepared. The decomposition profile of this sample is shown in Figure 8a.

A series of dehydrogenation and rehydrogenation experiments was conducted using composite C2 and the temperature sequence of these operations is shown in the scheme depicted in Figure 8b. The black solid lines denote the hydrogenation portion of the experiment, and the dehydrogenation portions are denoted by the dashed lines. Different colored curves of the data in Figure 8a and 8c correspond to the dehydrogenation steps of the same color depicted in Figure 8b. Figure 8c is the magnified low-temperature portions of the data in Figure 8a.

When the composite C2 was first heated with a temperature ramp of 2°C/min to 250°C and maintained at that temperature for 5 min (curve I), a low-temperature H₂ release was observed similar to that seen for composite C1, indicating that the synthesis of the composites is repeatable. When the sample at this point was rehydrogenated at 240°C

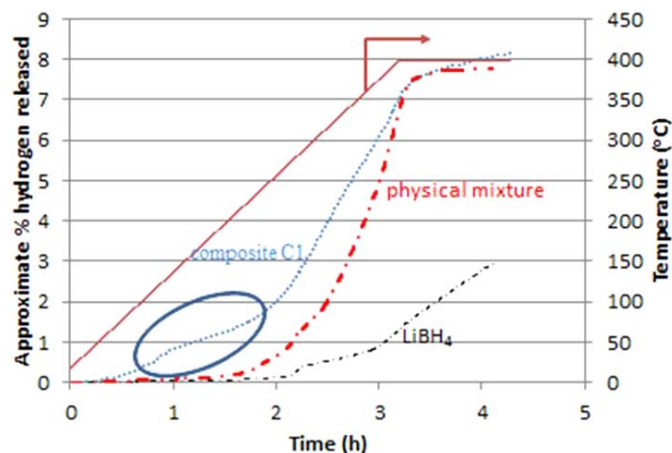


FIGURE 7. Comparison of the dehydrogenation of composite C1 (LiBH₄ infused into Y carbon) and a physical mixture of Norit carbon and LiBH₄

with 12.8 bar H₂, subsequent dehydrogenation experiment showed a very low but detectable level of H₂ release (curve II, Figure 8a and Figure 8c). At this point, the sample was cooled to room temperature and dehydrogenation was conducted again at 2°C/min ramp to 400°C and the sample was kept at 400°C for 37 min (curve III). Little H₂ release was observed below 200°C but the rate of release was accelerated above 250°C. The total H₂ release from the three dehydrogenation experiments was 10.2 wt% of LiBH₄. The dehydrogenated sample was rehydrogenated at 13.8 bar and 390°C for 0.5 h and cooled down to room temperature and evacuated. The dehydrogenation profile of this rehydrogenated sample is shown in curve IV (Figures 8a and 8c). There was still some H₂ released below 200°C but the amount was very small. The total H₂ released for the rehydrogenated sample was 2.5%. Since the pressure of the rehydrogenation experiment was very low, it is not clear whether the sample had picked up the maximum amount of H₂. When the hydrogenation was repeated with a slightly higher pressure of 15.3 bar at 390°C, the dehydrogenation profile obtained was similar (curve V of Figure 8a and 8c). The uptake of hydrogen during rehydrogenation was fast. At this point, we believe that more extensive rehydrogenation can be obtained using a much higher H₂ pressure.

The dehydrogenation and rehydrogenation results using the composite of carbon-LiBH₄ are promising but the current synthesis procedure is cumbersome. We plan to investigate alternate, easier methods to form these composite with the same or better hydrogen storage properties. In addition, addition of Ni and Pd will be explored to enhance low temperature dehydrogenation kinetics.

III. Mass transport in lithium borohydride

LiBH₄ has a high volumetric and gravimetric (18.4 wt%) hydrogen density and has shown partial reversibility, but the kinetics remain very slow at temperatures below

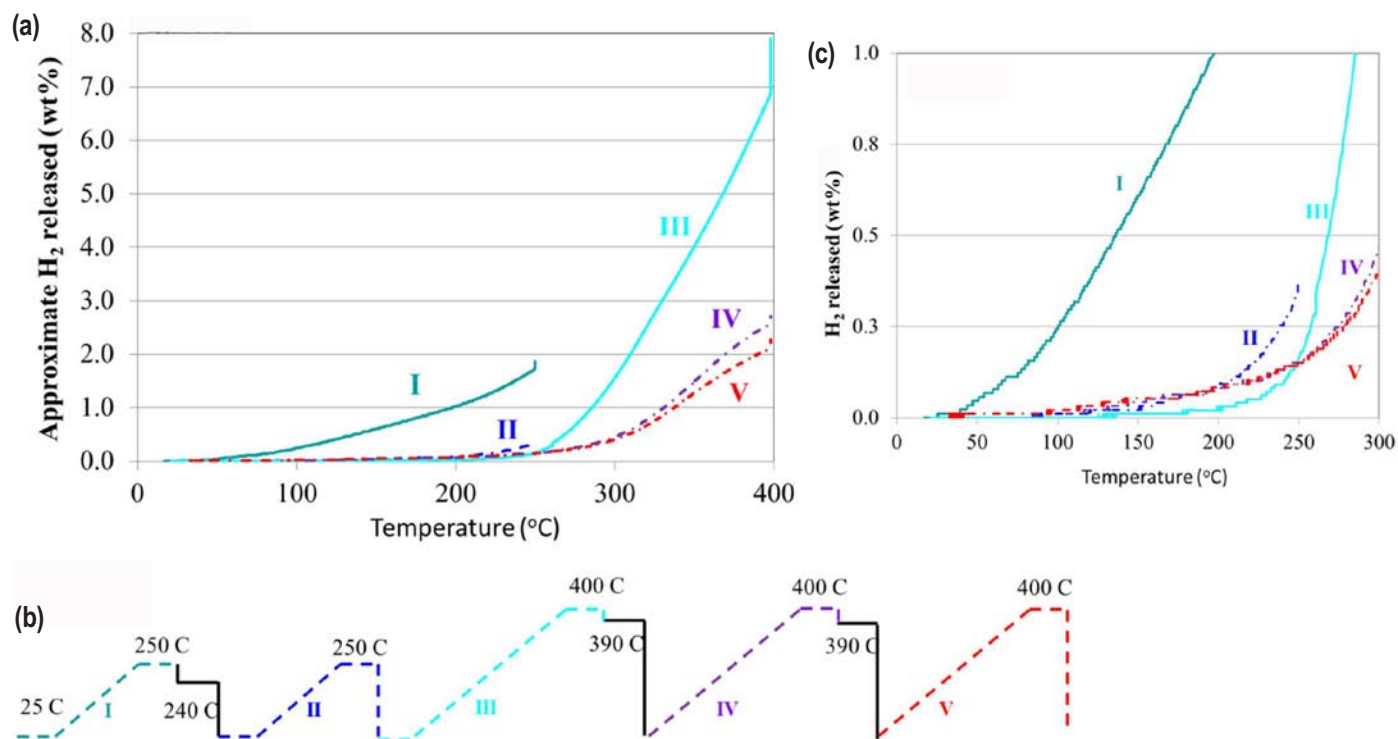
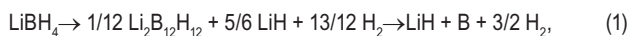


FIGURE 8. Dehydrogenation and hydrogenation of composite C2

its melting point of approximately 280°C. Even though the thermodynamic properties of pure LiBH₄ are not suitable for onboard storage, we have predicted several destabilized reactions involving LiBH₄ with equilibrium reaction temperatures below the melting point of LiBH₄. Thermodynamically, these reactions are allowed at temperatures compatible with proton exchange membrane fuel cells, but almost all of them are inhibited kinetically and require melting of the reactants to show appreciable hydrogen release rates. It is natural to hypothesize that slow rates of mass transport in the solid state is a key reason for the slow hydrogen release kinetics in solid. Hence, understanding of the kinetics of solid-state mass transport could provide clues for developing effective catalytic doping strategies.

Thermodynamically, the solid-state dehydrogenation reaction is predicted to occur in the following two-step process:



Our calculation shows that the total reaction enthalpy is $\Delta H = 83 \text{ kJ}/(\text{mol H}_2)$ at $T=0 \text{ K}$, in line with the experimentally determined value of $\Delta H = 74 \text{ kJ}/(\text{mol H}_2)$. The calculated enthalpies of the first-step and second-step reactions are 61 and 141 kJ/(mol H₂), respectively.

We have completed a systematic study of mass transport in solid LiBH₄ and its decomposition products, Li₂B₁₂H₁₂ and

LiH, using the mass transport model recently developed by us. This formalism is based on local equilibrium assumptions at interfaces where diffusion is driven by concentration gradients across the phases participating in Reaction (1). Defect formation energies are calculated from the density-functional theory, and both charged and neutral defects are taken into account. Chemical potentials are set by local equilibrium assumptions at the interfaces shown in Figure 9, and lead to nonzero mass fluxes through the participating phases.

Our results show that defects with the highest concentration in the products LiH and Li₂B₁₂H₁₂ are compensating intrinsic defect pairs, the creation of which does not involve exchange of atoms with any of the coexisting phases in Reaction (1). Hence, their concentration is uniform throughout the sample and they have zero concentration gradients and negligible mass fluxes. In LiH, the dominant defects are Schottky pairs of [H]⁺ and [Li]⁻ vacancies, while in Li₂B₁₂H₁₂ they are Frenkel pairs of Li⁺ interstitials and [Li]⁻ vacancies. In the reactant LiBH₄, negatively charged Li vacancies ([Li]⁻), positively charged Li interstitials (Li⁺), positively charged BH₄ vacancies [BH₄]⁺, and neutral BH₃ vacancies [BH₃] have the highest concentrations. Among them, only the neutral [BH₃] vacancies have an appreciable concentration gradient, while the others are mutually compensating intrinsic defects with small gradients (see Figure 10).

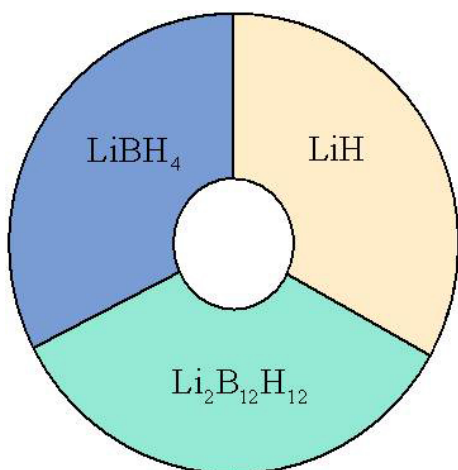


FIGURE 9. Schematic reaction morphology for reaction (1) showing the possible interfaces, which in turn determine the mass fluxes through the reactant and product phases

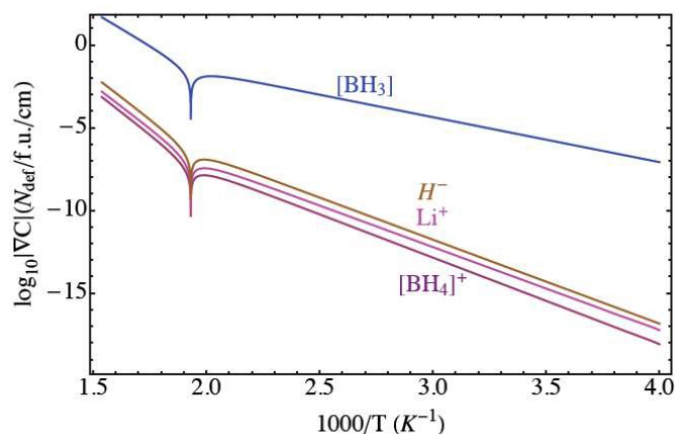


FIGURE 10. The calculated concentration gradients in LiBH_4

The structure of the neutral $[\text{BH}_3]$ vacancy is shown in Figure 11. It shows that removing a BH_3 complex leaves behind a negatively charged H^- anion occupying the vacant site. Compared with the $[\text{AlH}_3]$ vacancy diffusion mechanism in NaAlH_4 , the $[\text{BH}_3]$ vacancy diffusion in LiBH_4 is blocked by the negative H^- anion left behind after creating the $[\text{BH}_3]$ vacancy. We conclude that mass transport in solid LiBH_4 is very slow and likely represents a key rate-limiting process of the dehydrogenation reaction based on this material. In the future studies, we plan to investigate catalytic strategies for accelerating diffusion by either using reactants with faster rates of mass transport or by doping with elements to create additional anion vacancies.

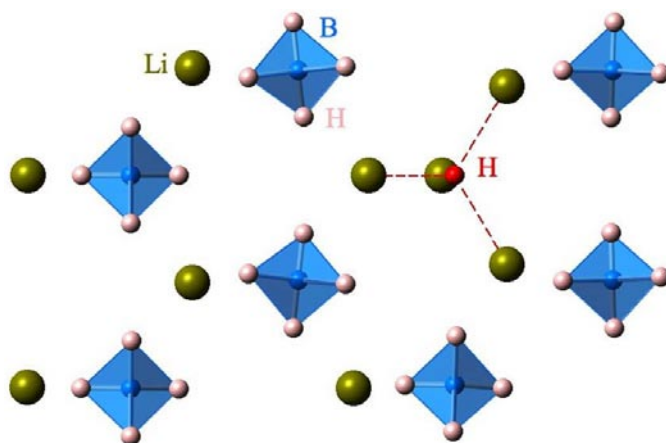


FIGURE 11. Structure of the neutral $[\text{BH}_3]$ vacancy in LiBH_4 . The H^- anion is shown as red, Li^+ cations are dark green, B atoms are blue, and H atoms are pink. Red dashed lines indicate that the H^- anion is tetrahedrally coordinated with the surrounding Li^+ cations.

Future Directions

- Experimentally characterize storage properties/reactions of $(\text{NH}_4)_2\text{B}_{12}\text{H}_{12}$ and other predicted reactions; Optimize reversibility conditions for $5\text{Mg}(\text{BH}_4)_2 + 2\text{LiBH}_4$ mixture.
- Extend experimental catalyst studies to other predicted promising materials; explore optimal morphology of carbon/metal catalysts.
- Focus experimental efforts on rehydriding reactions/reversibility (subject to pressure limitations of experimental equipment).
- Focus computational efforts on kinetics, defects, diffusion/mass transport/hydrogen dissociation in promising predicted reactions.
- Down-select decision: End work on borohydride/amide combinations. (No reversibility from computational or experimental work; B-N bonds in product.)

IV.A.2 Fundamental Studies of Advanced High-Capacity, Reversible Metal Hydrides

Craig M. Jensen (Primary Contact) and
Marina Chong

University of Hawaii
Department of Chemistry
Honolulu, HI 96822
Phone: (808) 956-2769
Email: jensen@hawaii.edu

DOE Managers

HQ: Ned Stetson
Phone: (202) 586-9995
Email: Ned.Stetson@ee.doe.gov
GO: Katie Randolph
Phone: (720) 356-1759
Email: Katie.Randolph@go.doe.gov

Contract Number: DE-FC36-05GO15063

Project Start Date: April 1, 2005
Project End Date: September 30, 2012

developed a system of for the full reversible dehydrogenation of $\text{Mg}(\text{BH}_4)_2$ to MgB_2 that has shown a record, >12 wt% reversible hydrogen capacity but requires further development to meet kinetic performance targets within the target temperature.

FY 2012 Accomplishments

During the past year we have provided the first example of the reversible, solid-state dehydrogenation of a borohydride at temperatures below 250°C (200°C dehydrogenation, 100°C, 50-atm re-hydrogenation).



Introduction

The development of high capacity, hydrogen storage materials that can be recharged under moderate conditions is a key barrier to the utilization of hydrogen as an onboard energy carrier. Towards this end we have examined mixed metal borohydride complexes as hydrogen storage materials. Our initial focus was on anionic transition metal complexes. Our structural characterizations of these complexes have shown that they are best viewed as Group I and II salts anionic transition metal borohydride complexes. Through studies utilizing X-ray diffraction (XRD), nuclear magnetic resonance (NMR), and vibrational spectroscopy, we have clearly established the coordinative interaction between the BH_4^- anions and the metal centers. The anionic character of these borohydrides has been found to result in an increased stability and a reduced volatility when compared to neutral transition metal borohydride complexes. Our efforts are currently focused on determining whether the thermodynamic parameters of these complexes will allow them to undergo reversible dehydrogenation.

In the course of these investigations we have found that that ball-milled mixtures of MgB_2 and catalytic additives undergo full hydrogenation to $\text{Mg}(\text{BH}_4)_2$ at high pressures. In consideration of the >14 wt% hydrogen that is potentially cyclable with this system, it has become the focus of our efforts in the area of borohydride complexes. More recently, we have studied the dehydrogenation of $\text{Mg}(\text{BH}_4)_2$ under mild conditions and observed the, clean, reversible dehydrogenation of $\text{Mg}(\text{BH}_4)_2$ to $\text{Mg}(\text{B}_3\text{H}_8)_2$ as seen in equation 1 (dehydrogenation, 200°C; re-hydrogenation, 250°C under 120 atm of H_2). Our findings have provided



Fiscal Year (FY) 2012 Objectives

The objective of this project is to develop a new class of reversible materials that have the potential to meet the DOE kinetic and system gravimetric storage capacity targets. During the past year, our investigations have focused on the study of novel, high hydrogen capacity, borohydrides that can be reversibly dehydrogenated at low temperatures.

Technical Barriers

This project addresses the following technical barriers from the Hydrogen Storage section of the Fuel Cell Technologies Program Multi-Year Research, Development and Demonstration Plan:

- (A) System Weight and Volume
- (E) Charging/Discharging Rates
- (J) Thermal management
- (P) Lack of Understanding of Hydrogen Physisorption and Chemisorption

Technical Targets

During the past year, work on this project was currently exclusively devoted borohydride materials that have demonstrated available hydrogen capacities of >10 wt% hydrogen. In our previous work on this project we have

the first example of the **reversible**, solid-state dehydrogenation of a borohydride occurring at temperatures below 300°C.

Our studies of the mixed metal borohydride complexes showed that they evolve high weight percentages of hydrogen at low temperatures (100-150°C). Our finding of the reversible dehydrogenation of magnesium borohydride at moderate temperatures suggested that reversibility of our novel anionic transition metal borohydrides which previously thought to be “irreversible” should be investigated under the same conditions found for the reversible cycling of $\text{Mg}(\text{BH}_4)_2$ to $\text{Mg}(\text{B}_3\text{H}_8)_2$.

Approach

Having demonstrated the reversible elimination of >12 wt% hydrogen from $\text{Mg}(\text{BH}_4)_2$, we sought to develop methods for hydrogen cycling in this system under less forcing conditions. In order to accomplish this, we required a more detailed understanding of the dehydrogenation reaction pathway. Thus we have monitored both the dehydrogenation and re-hydrogenation reactions by XRD and magic angle spinning boron-11 (MAS ^{11}B) NMR spectroscopy and conducted quantitative thermal volumetric pressure-composition-temperature measurements. In order to further explore the low temperature reversible dehydrogenation of $\text{Mg}(\text{BH}_4)_2$, we planned to prepare $\text{Mg}(\text{B}_3\text{H}_8)_2$ through an alternative method and examine the hydrogenation of mixtures of the triborane and two equivalents of MgH_2 under the conditions we have previously utilized in our re-hydrogenation studies. Furthermore, we have hypothesized that stability of the corresponding metal hydride formed in the dehydrogenation of Group I borohydrides may explain in part the trend in barriers to their reversibility. In order to probe these possibilities we planned to explore hydrogenation $\text{Mg}(\text{B}_3\text{H}_8)_2$ in mixtures containing MgH_2 , LiH, and NaH.

Results

Synthesis and Evaluation of Novel Borohydrides

As discussed above, our previous studies have indicated that the dehydrogenation of $\text{Mg}(\text{BH}_4)_2$ at 200°C results in selective dehydrogenation to $1/3 \text{Mg}(\text{B}_3\text{H}_8)_2 + 2/3 \text{MgH}_2$ and that this process can be reversed at 250°C under 120 atm of H_2 . In order to verify this finding, we sought to prepare $\text{Mg}(\text{B}_3\text{H}_8)_2$ through an alternative method, and examine the hydrogenation of mixtures of the triborane and MgH_2 under the conditions we have previously utilized in our re-hydrogenation studies. Finding the syntheses reported in the literature for $\text{Mg}(\text{B}_3\text{H}_8)_2$ to be irreproducible, we have developed a reliable, high yield synthesis for $\text{Mg}(\text{B}_3\text{H}_8)_2$. In accordance with equation 2, our method entails the reaction of the tetrahydrofuran (THF) adduct of borane, 25°C



$\text{BH}_3\cdot\text{THF}$ with magnesium-mercury amalgam in THF solution at room temperature which results in the immediate precipitation of pure $\text{Mg}(\text{B}_3\text{H}_8)_2$ as a white crystalline powder in >95% yield.

Our synthesis of pure $\text{Mg}(\text{B}_3\text{H}_8)_2$, allow us to explore the hydrogenation the triborane with stoichiometric quantities of different metal hydrides. The metal hydrides (LiH, NaH, and MgH_2) were chosen for their varying degrees of thermodynamic stabilities. Mixtures of the triborane and hydride were hydrogenated under 7 MPa H_2 at 200°C for 2 days and the resulting products were analyzed by solid-state ^{11}B NMR spectroscopy. Surprisingly, hydrogenation of the mixtures of $\text{Mg}(\text{B}_3\text{H}_8)_2$ and either LiH and NaH resulted in the exclusive formation of $[\text{BH}_4]^-$. Initial attempts at the hydrogenation of a 2:1 mixture of MgH_2 and $\text{Mg}(\text{B}_3\text{H}_8)_2$ were found to instead give rise to $\text{MgB}_{12}\text{H}_{12}$ and other boranes. However, we found if mixtures of MgH_2 and $\text{Mg}(\text{B}_3\text{H}_8)_2$ are ball-milled prior to reaction, that the predominant product is $\text{Mg}(\text{BH}_4)_2$ and that $\text{MgB}_{12}\text{H}_{12}$ is obtained in only minor amounts. The production of the $\text{MgB}_{12}\text{H}_{12}$ side product can be completely eliminated by increasing the $\text{MgH}_2:\text{Mg}(\text{B}_3\text{H}_8)_2$ ratio to 4:1. The speed at which the triborane species hydrogenates to borohydride was investigated and found to occur within 2 hours at 100°C.

We also studied the hydrogenation of mixtures of $\text{Mg}(\text{B}_3\text{H}_8)_2$ and either LiH, NaH, or MgH_2 by differential scanning calorimetry (DSC) in collaboration with Dr. S. Orimo at the Institute for Materials Research at Tohoku University. A hydrogen pressure of 5 MPa was applied as the temperature was ramped to 200°C at a rate of 5°C/s. Regardless of metal hydride species, all experiments with $\text{Mg}(\text{B}_3\text{H}_8)_2$ exhibited a quick endothermic step beginning at about 60°C (Figure 1). ^{11}B NMR analysis of the material immediately after this step confirmed that

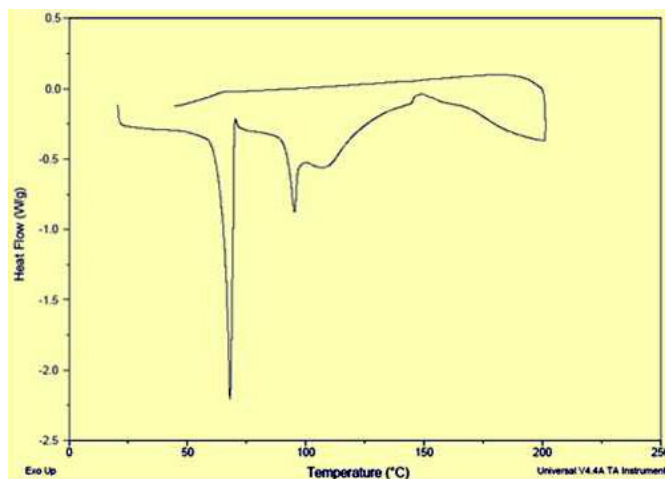


FIGURE 1. DSC scan of $\text{Mg}(\text{B}_3\text{H}_8)_2 + 2 \text{MgH}_2$ heated under 5 MPa H_2

the $[\text{B}_3\text{H}_8]^-$ anions were still intact. Next, a large broad exothermic peak was consistently observed with a maximum at about 130°C . ^{11}B NMR analysis after this step showed that the boron in the sample had converted predominantly to $[\text{BH}_4]^-$. Hydrogenation of $\text{Mg}(\text{B}_3\text{H}_8)_2$ (Figure 2) without any metal hydride present displayed the same endothermic peak at around 60°C , suggesting that it may be attributed to the melting of the triborane. For comparison, NaB_3H_8 was hydrogenated under the same conditions in mixtures containing either NaH or MgH_2 . NaB_3H_8 was found to melt at a lower temperature and two overlapping exothermic steps were observed at higher temperature. The detection of $\text{Na}_2\text{B}_{12}\text{H}_{12}^-$ along with NaBH_4^- in the MAS ^{11}B NMR analysis of the NaB_3H_8 hydrogenation reaction products implies that while $\text{Mg}(\text{B}_3\text{H}_8)_2$ + metal hydride readily forms $\text{Mg}(\text{BH}_4)_2$ in a single step after melting, the hydrogenation of NaB_3H_8 is somewhat more complex, resulting in the formation of more than one boron species.

In addition, to releasing high weight percentages of hydrogen at low temperatures ($100\text{--}150^\circ\text{C}$), our studies have indicated that the alkali metal salts of anionic manganese and zirconium borohydride complexes undergo elimination of hydrogen with little or no tandem production of diborane. However, there have been conflicting reports regarding the levels diborane that are released during the thermal dehydrogenation of the scandium borohydride complexes, $\text{MSc}(\text{BH}_4)_4$ ($\text{M} = \text{Li}, \text{Na}, \text{K}$). In order to resolve this controversy, we established a collaboration with the group of Prof. Zuetzel at EMPA to quantify the amount of diborane produced during the thermal decomposition of $\text{MSc}(\text{BH}_4)_4$ ($\text{M} = \text{Li}, \text{Na}, \text{K}$). The dehydrogenation of samples of the scandium borohydrides that were synthesized at the University of Hawaii was studied by specialty infrared equipment at EMPA that was designed for the detection and quantification of diborane emission from borohydrides. This method has proven much more reliable and reproducible

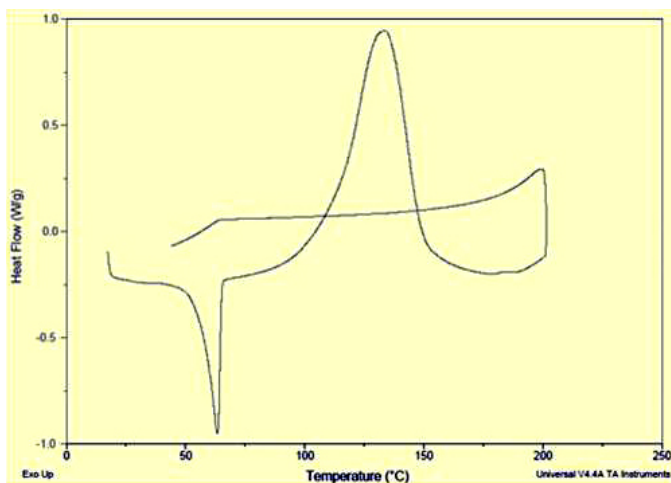
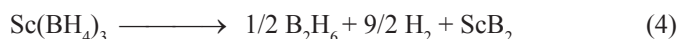
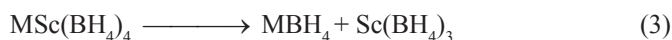


FIGURE 2. DSC scan of $\text{Mg}(\text{B}_3\text{H}_8)_2$ heated under 5 MPa H_2

than determinations that have been made using flow meter/mass spectrometer equipment. These studies have shown that about 0.5 equivalents of diborane are released during the dehydrogenation of $\text{MSc}(\text{BH}_4)_4$ $\sim 150^\circ\text{C}$. Our previous studies have shown that a second hydrogen release occurs at higher temperatures that match the characteristic hydrogen release temperatures of the corresponding simple alkali metal borohydride, MBH_4 . These results indicate thermal decomposition of the scandium borohydrides proceeds according to equations 3 and 4.



Conclusions

We have established that $\text{Mg}(\text{BH}_4)_2$ is selectively dehydrogenated to $\text{Mg}(\text{B}_3\text{H}_8)_2$ 200°C while cleanly releasing 2.9 wt% H_2 . This reaction has now been demonstrated to be reversible at 100°C under 50 atm of H_2 thus provides the first example of direct hydrogen cycling of a borohydride under mild conditions. The rapid re-hydrogenation kinetics are, at least in part, due to the fact that $\text{Mg}(\text{B}_3\text{H}_8)_2$ is in the liquid state above 60°C . This finding points to the possibility of finding mild, proton exchange membrane fuel relevant conditions for the reversible dehydrogenation of borohydrides that avoid the thermodynamic sinks such as $[\text{B}_{12}\text{H}_{12}]^{2-}$.

We have also found that the thermal decomposition of $\text{MSc}(\text{BH}_4)_4$ ($\text{M} = \text{Li}, \text{Na}, \text{and K}$) at 150°C gives rise to MBH_4 and $\text{Sc}(\text{BH}_4)_3$. The resulting neutral, $\text{Sc}(\text{BH}_4)_3$ is unstable and rapidly decomposes to produce diborane. Thus the $\text{MSc}(\text{BH}_4)_4$ family of borohydrides will not undergo reversible dehydrogenation and can be excluded as potential application as reversible hydrogen storage materials.

Future Directions

We plan to explore the adjustment of conditions to maximize trade off between cycling capacity and temperature/pressures required for reversible dehydrogenation of $\text{Mg}(\text{BH}_4)_2$ under moderate conditions.

FY 2012 Publications/Presentations

Publications

1. "Reversible Dehydrogenation of Magnesium Borohydride to Magnesium Triborane in the Solid State Under Moderate Conditions", Marina Chong, Ahbi Kamkamkar, Tom Autrey, Shin-ichi Orimo, Satish Jalihatgi, and Craig M. Jensen; (invited contribution for themed issue on Hydrogen) *Chem. Commun.* **2011**, 47, 1330.
2. "Homogeneous Dehydrogenation of Liquid Organic Hydrogen Carriers Catalyzed by an Iridium PCP Pincer Complexes",

Zhouhui Wang, Jack Belli, and Craig Jensen, *Faraday Discuss* **2011**, *151*, 297.

3. “High-Yield Direct Synthesis of LiAlH_4 from LiH and Al in the Presence of TiCl_3 and Me_2O ”, Xiangfeng Liu, Henrietta W. Langmi, Shane D. Beattie, Felix F. Azenwi and G. Sean McGrady, and Craig M. Jensen, *J. Am. Chem. Soc.* **2011**, *133*, 15593.

Presentations

1. ”Development of Processes for the Reversible Dehydrogenation of High Capacity Hydrogen Carriers”; Craig Jensen; Peking University; Beijing, China.; October 20 2011.

2. ”Development of Processes for the Reversible Dehydrogenation of High Capacity Hydrogen Carriers”; [Craig Jensen](#), Godwin Severa, Marina Chong, Zhouhui Wang, Ewa Rönnebro, Tom Autrey, and Ahbi Kamkamkar; Symposium on Complex Hydrides for Hydrogen Storage, Low Carbon Earth Summit 2011.; Dalian China, October 23–24, 2011.

3. “Development of Processes for the Reversible Dehydrogenation of High Capacity Hydrogen Carriers”; Craig Jensen; Nankai University; Tainjin, China; October 26 2011.

4. ”Development of Processes for the Reversible Dehydrogenation of High Capacity Hydrogen Carriers”; Craig Jensen; Yanshan University; Qinhuangdao, China; October 27 2011.

5. “Development of Processes for the Reversible Dehydrogenation of High Capacity Hydrogen Carriers”; Craig Jensen; Institute of Metals Research; Chinese Academy of Science; Shenyang, China, October 31, 2011.

IV.A.3 Lightweight Metal Hydrides for Hydrogen Storage

Ji-Cheng Zhao (Primary Contact), Xuenian Chen,
Sheldon G. Shore

The Ohio State University, Department of Materials Science
and Engineering,
286 Watts Hall, 2041 College Road
Columbus, OH 43210
Phone: (614) 292-9462
Email: zhao.199@osu.edu

DOE Managers

HQ: Ned Stetson
Phone: (202) 586-9995
Email: Ned.Stetson@ee.doe.gov

GO: Katie Randolph
Phone: (720) 356-1759
Email: Katie.Randolph@go.doe.gov

Contract Number: DE-FC3605GO15062

Project Start Date: January 1, 2005

Project End Date: August 31, 2011 (No-cost
extension to December 31, 2012)

studies will be applied towards the design and synthesis of hydrogen storage materials that may meet the following DOE 2010 hydrogen storage targets:

- Cost: \$3-7/gasoline gallon equivalent at pump
- Specific energy: 1.5 kWh/kg (4.5 wt% H)
- Energy density: 0.9 kWh/L (0.028 kg/L)

FY 2012 Accomplishments

- In collaboration with both Northwestern University and National Institute of Standards and Technology (NIST), we have identified the structure of the aluminoborane, $\text{AlB}_4\text{H}_{11}$.
- We studied the formation mechanism of $\text{AlB}_4\text{H}_{11}$.
- We determined the formation mechanism of the diammoniate of diborane, DADB; and based on the mechanistic understanding we developed a convenient synthetic method for pure DADB.
- The stability of DADB in different solvents was investigated systematically.



Fiscal Year (FY) 2012 Objectives

- Develop a high-capacity lightweight hydride for reversible vehicular hydrogen storage, capable of meeting or exceeding the 2010 DOE FreedomCAR targets.
- Synthesize and study aluminoborane compounds for hydrogen storage.
- Synthesize and study other lightweight, high-capacity boron hydride for hydrogen storage.

Technical Barriers

This project addresses the following technical barriers from the Storage section of the Fuel Cell Technologies Multi-year Research, Development and Demonstration Plan.

- (D) Durability/Operability
- (E) Charging/Discharging Rates
- (J) Thermal Management
- (P) Lack of Understanding of Hydrogen Physisorption and Chemisorption

Technical Targets

This project is conducting synthesis and structure studies of the aluminoborane compounds. Insights gained from these

Introduction

The DOE defines onboard hydrogen storage for mobile vehicles as a “Grand Challenge”. It is one of the biggest hurdles to the implementation of hydrogen-powered vehicles. Metal hydrides have the advantages of the highest volumetric density, relatively low working pressure, and reasonable working temperature range. The disadvantage of current reversible hydrides is a significant weight penalty. Metal borohydrides have among the highest gravimetric hydrogen storage capacities with the potential to meet the DOE gravimetric density targets and to offset the system weight penalties. However, desorption temperature, reversibility and formation of gaseous borane compounds during desorption are challenging issues for these materials. This project attempts to develop a high-capacity lightweight hydride for reversible vehicular hydrogen storage, capable of meeting or exceeding the 2010 DOE/FreedomCAR targets.

Approach

- Explore aluminoborane compounds such as $\text{AlB}_4\text{H}_{11}$ and other high-capacity, lightweight boron hydrides for hydrogen storage.
- Study the structure and the formation mechanisms of $\text{AlB}_4\text{H}_{11}$ using multiple techniques such as solution nuclear magnetic resonance (NMR), infrared (IR),

neutron vibrational analysis (NVS), and first-principles predictions.

Results

1. The Study of the Structure and Formation Mechanism of $\text{AlB}_4\text{H}_{11}$

The aluminoborane compound, $\text{AlB}_4\text{H}_{11}$, has shown attractive properties as potential hydrogen storage material [1]. The properties of $\text{AlB}_4\text{H}_{11}$ are quite different from other borane compounds, suggesting a potentially unique structure. The previous structure proposed by Himpsl and Bond [2] based on the analogue to pentaborane (B_5H_{11}) is inconsistent with the IR and ^{11}B NMR spectra of $\text{AlB}_4\text{H}_{11}$ [1]. Hence, the determination of the $\text{AlB}_4\text{H}_{11}$ structure is significant for the understanding of its stability and hydrogenation/dehydrogenation properties.

The amorphous nature of $\text{AlB}_4\text{H}_{11}$ and its insolubility in organic solvents prevent us from determining its structure using X-ray diffraction (XRD), neutron diffraction, solution NMR, or mass spectrometry techniques. Solid-state NMR and vibrational spectra were found to be insufficient for even speculating on its structure. Instead, a novel combination of experimental measurements (NMR, IR, and NVS) with a theoretical prediction method (the Monte-Carlo based prototype electrostatic ground state (PEGS) search with density functional theory (DFT) calculations) are used to identify local structures of this amorphous $\text{AlB}_4\text{H}_{11}$ phase. The structure identification is a closely coupled theoretical and experimental study involving the Ohio State University, Northwestern University, and NIST.

Among the predicted structures (Figure 1), Str-00 is the most stable one which has the best overall agreement with experimental observations. The $\text{AlB}_4\text{H}_{11}$ structure contains

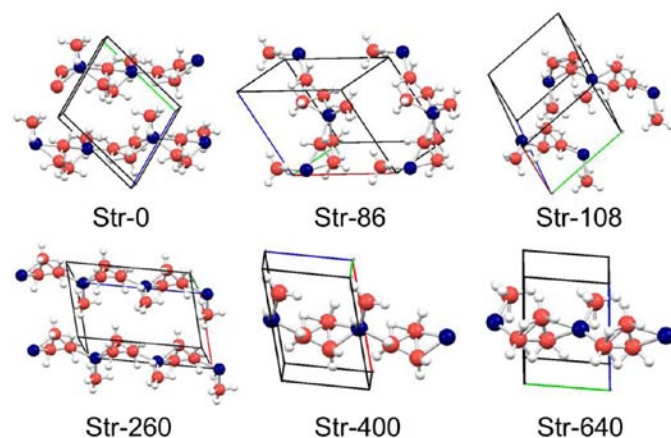


FIGURE 1. PEGS+DFT theoretically predicted $\text{AlB}_4\text{H}_{11}$ crystal structures. The number in the nomenclature is the energy difference relative to the theoretically predicted lowest-energy $\text{AlB}_4\text{H}_{11}$ structure. Al = blue, B = orange, H = white gray.

distinct $[\text{BH}_4]$ and $[\text{B}_3\text{H}_7]$ units without any $[\text{AlH}_4]$ units. It forms a $-\text{[B}_3\text{H}_7]-\text{Al}(\text{BH}_4)-$ polymer chain with the $[\text{BH}_4]$ units twisted relative to each other perpendicular to the chain direction and bonded to Al, and a chain backbone consists of $[\text{B}_3\text{H}_7]$ and Al where the $[\text{B}_3\text{H}_7]$ unit exhibits a triangular boron configuration.

In order to further confirm the predicted structure, we compare the simulated ^{11}B NMR spectra of the predicted structures and the experimental solid state ^{11}B NMR spectrum [1]. The ^{11}B NMR spectra of the four predicted 2-fu structures (they are labeled as Str-0, Str-86, Str-108 and Str-260, respectively, in Figure 1) have been simulated using the Gauge Including Projector Augmented Waves method as implemented in the Quantum ESPRESSO package [3]. The simulated ^{11}B NMR indicates that two sets of signals are separately located at higher and lower fields, which is consistent with the solid ^{11}B NMR spectrum of $\text{AlB}_4\text{H}_{11}$. The simulated chemical shifts vary from structure to structure but are generally comparable with the experimental $\text{AlB}_4\text{H}_{11}$ solid-state spectrum that has two broad signals located at around δ -38.8 and -51.0 ppm respectively at a roughly 2:1 ratio [1]. Three boron signals for the lowest energy structure (Str-0) are located at higher field (δ -58.48, -60.96, and -61.82 ppm) and five boron signals at lower field (δ -33.45, -41.29, -46.50, -46.61, and -47.61 ppm). The ratio of the two sets of signals (5:3) is close to the experimental value (2:1). Two broad peaks created by stacking together the two sets of the simulated NMR signals closely resemble the experimental solid-state ^{11}B NMR spectrum of $\text{AlB}_4\text{H}_{11}$ with the peaks positions only differ by about 8~10 ppm (higher field) (Figure 2).

Two sets of boron signals are predicted for Str-86 with one set (two signals) located at δ -59.41 and -70.40 ppm and

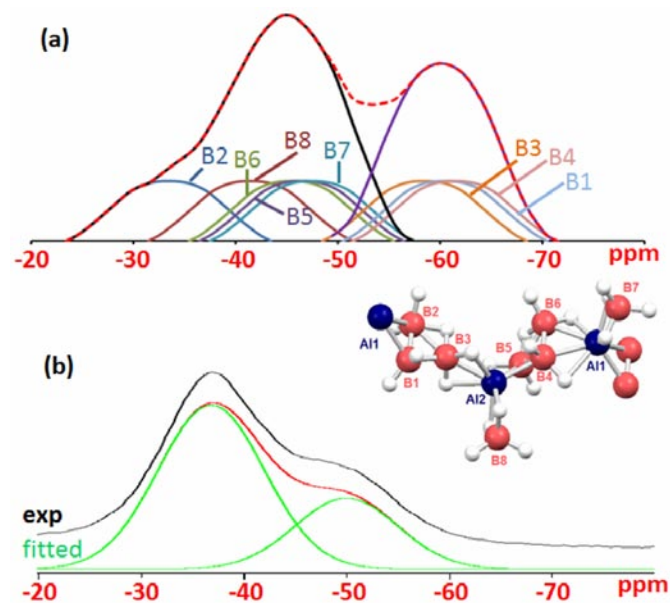
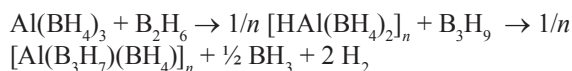


FIGURE 2. ^{11}B NMR spectra of $\text{AlB}_4\text{H}_{11}$ (a) simulated based on the predicted Str-0 and (b) experiment

the other set (six boron signals) at δ -30.5 to 44.13 ppm. The intensity ratio of the two sets is 3:1. Both Str-108 and Str-260 have four boron signals at higher field and four boron signals at lower field with the integrated peak intensity ratio of 1:1.

As we discussed above, the comparison of the simulated ^{11}B NMR spectra of these structures with the solid-state ^{11}B NMR spectrum of $\text{AlB}_4\text{H}_{14}$ indicates that the lowest-energy structure (Str-0) has the best merit in terms of both peak shapes and the peak intensity ratio, thus we believe Str-0 is the best representation of the $\text{AlB}_4\text{H}_{11}$ structure.

We also studied the formation mechanism of $\text{AlB}_4\text{H}_{11}$. The reaction of $\text{Al}(\text{BH}_4)_3$ and diborane was monitored by ^{11}B and $^{11}\text{B}\{^1\text{H}\}$ NMR spectroscopy. The two starting materials, $\text{Al}(\text{BH}_4)_3$ and diborane, are each alone stable at 100°C in benzene solution. The ^{11}B and $^{11}\text{B}\{^1\text{H}\}$ NMR spectra of the mixture of $\text{Al}(\text{BH}_4)_3$ and diborane indicate that when reaction starts, two sets of small peaks simultaneously appear at nearly the signal of $\text{Al}(\text{BH}_4)_3$ (δ -33.4, -36.89 -38.1, -43.6, and -44.7 ppm) and at δ -52.6 and 53.8 ppm. The low-field peaks at around δ -33.4 to -44.7 ppm are related to an intermediate of $[\text{HAl}(\text{BH}_4)_2]_n$ with different states of aggregation [4], and the high-field peaks at δ -52.6 and -53.8 ppm might be related to a B_3H_7 group, which might not exist alone, but interacting with $[\text{HAl}(\text{BH}_4)_2]_n$ once it is formed. Therefore, the formation mechanism of $\text{AlB}_4\text{H}_{11}$ is probably: 1) B_2H_6 initially pulls a BH_3 unit from $\text{Al}(\text{BH}_4)_3$ to form $[\text{HAl}(\text{BH}_4)_2]$ and B_3H_7 with one H_2 elimination; 2) two intermediates of $[\text{HAl}(\text{BH}_4)_2]$ and B_3H_7 interact in an unknown way once they are formed; and 3) a $-\text{[B}_3\text{H}_7\text{]-Al}(\text{BH}_4)\text{-[B}_3\text{H}_7\text{]-}$ polymer chain is formed as shown in Scheme 1.



SCHEME 1. The formation mechanism of $\text{AlB}_4\text{H}_{11}$

The proposed mechanism is derived from both the ^{11}B NMR spectra and the literature work. It was reported that when $\text{Al}(\text{BH}_4)_3$ reacted with CO at ambient temperature, the CO molecule pulled a BH_3 moiety from $\text{Al}(\text{BH}_4)_3$ to form $[\text{HAl}(\text{BH}_4)_2]_n$ and $\text{CO}\cdot\text{BH}_3$ [4]. Comparing the reaction of $\text{Al}(\text{BH}_4)_3$ with CO at room temperature and with B_2H_6 at 100°C , it is reasonable to assume that B_2H_6 performed the same function as CO to pull a BH_3 group out from $\text{Al}(\text{BH}_4)_3$ to form a B_3H_7 unit and $[\text{HAl}(\text{BH}_4)_2]$. For the room-temperature reaction with CO, two signals of BH_4^- were detected at δ -38.0 and -43.3 ppm, since two states of aggregation of $[\text{HAl}(\text{BH}_4)_2]_n$ ($n = 1$ or 2) were formed. This was supported by the formation of monomer and dimer compounds, $[\text{HGa}(\text{BH}_4)_2]$, and $[\text{HGa}(\text{BH}_4)_2]_2$, in a similar reaction of $\text{Ga}(\text{BH}_4)_3$ with CO. Thus, an elevated-temperature reaction with B_2H_6 could lead to higher oligomers of $[\text{HAl}(\text{BH}_4)_2]$; and the small peaks observed at δ -33.4 to -44.7 ppm are believed to represent polymeric $[\text{HAl}(\text{BH}_4)_2]_n$ with more than two different states of oligomers. These polymer species probably have limited solubility in the reaction media

at this stage, so they were decreasingly detected in ^{11}B NMR spectroscopy as the reaction proceeded.

The reaction of B_2H_6 with a BH_3 unit to produce B_3H_7 , followed by conversion to triborane, B_3H_7 , with a H_2 molecule elimination has been extensively investigated both theoretically and experimentally [5]. The triborane could be stabilized by coordination with bases. Three boron atoms in B_3H_7 display one or two signals over a wide range when B_3H_7 is coordinated to different bases. In adducts of $\text{CO}\cdot\text{B}_3\text{H}_7$ and $\text{PH}_3\cdot\text{B}_3\text{H}_7$, one boron signal appeared at δ -51.2 ppm which is close to the small peaks observed in ^{11}B NMR in this experiment [6]. It is worthy to note that, although the existent format of B_3H_7 in the reaction system is unknown, it seems to interact with $[\text{HAl}(\text{BH}_4)_2]_n$. So we presumed the small peaks at δ -52.6 and -51.3 ppm were associated with a B_3H_7 group which interacted with $[\text{HAl}(\text{BH}_4)_2]_n$ in some way. At an initial stage, these species could be detected in ^{11}B NMR spectra. The assignment is confirmed by simulation B NMR spectra in which the chemical shifts of borons in the B_3H_7 group have a wide range from δ -30.5 ppm to -70.4 ppm. Another mechanism was also proposed [1].

2. Formation Mechanism and New Synthetic Method of DADB

DADB, an isomer of ammonia borane (AB) with 19.6 wt% hydrogen, has recently been studied as a potential hydrogen storage material. DADB was first observed in the 1920s in a mixture with ammonia borane (NH_3BH_3 , AB) produced when ammonia reacted with diborane [7]. Though DADB has been known for almost a century, a convenient synthetic method for pure DADB has not been developed partly due to a lack of understanding of its formation mechanism. Many factors such as steric effects and solvent properties were considered and discussed in the literature, but were found to be insufficient to explain the formation mechanism of DADB [8]. Conflicting conclusions were drawn for different systems concerning different factors. To develop a more satisfactory explanation, we studied the formation mechanism of DADB and then employed the understanding to develop a convenient method to synthesize it.

We derived a new three-step mechanism for the formation of DADB in the reaction of ammonia with THFBH_3 . Ammonia reacted with tetrahydrofuran (THF)- BH_3 first to produce AB and THF; then the formed AB reacts with another molecule of $\text{THF}\cdot\text{BH}_3$ to produce ammonia diborane ($\text{NH}_3\text{BH}_2(\mu\text{-H})\text{BH}_3$, AaDB) – an intermediate; in the third step, another ammonia molecule reacts with AaDB to produce either AB or DADB. In step 3, dihydrogen bond, an attractive interaction between a protonic and a hydridic hydrogen, plays an important role in the formation of DADB, which was never recognized before for the formation of DADB. For the first time, we were able to catch the intermediate of AaDB by ^{11}B NMR (Figure 3) [9].

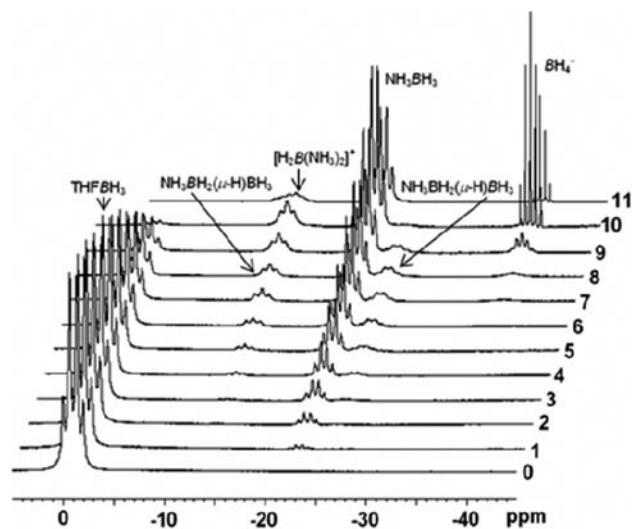
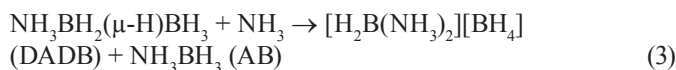
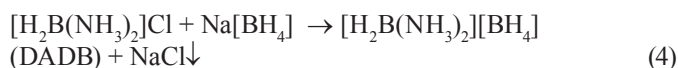


FIGURE 3. ^{11}B NMR spectra of the reaction of NH_3 with a $\text{THF}\cdot\text{BH}_3$ solution at -78°C



The understanding of the formation mechanism of DADB leads to the conclusion that pure DADB could not be produced by the reaction between ammonia and $\text{THF}\cdot\text{BH}_3$. DADB is consisted of an cation of $[\text{H}_2\text{B}(\text{NH}_3)_2]^+$ and an anion of $[\text{BH}_4]^-$. The ionic nature of DADB along with the mechanistic understanding prompted us to synthesize pure DADB through a metathesis reaction between $[\text{H}_2\text{B}(\text{NH}_3)_2]\text{Cl}$ and NaBH_4 in an appropriate solvent (reaction 4).



After examining the reaction conditions especially by screening many solvents, we found that liquid ammonia is the best solvent for reaction 4. This convenient preparative method for DADB takes advantage of a modified synthesis of the cationic borane complex $[\text{H}_2\text{B}(\text{NH}_3)_2]\text{Cl}$ which was first synthesized by Shore and Parry in a reaction of DADB with NH_4Cl [10]. Cationic borane complexes can also be prepared by a reaction of amines with halogen substituted boranes. When ammonia monochloroborane ($\text{NH}_3\text{BH}_2\text{Cl}$), formed readily as gaseous HCl is added to a solution of AB in diethyl ether, is dissolved in liquid ammonia it is converted quantitatively to $[\text{H}_2\text{B}(\text{NH}_3)_2]\text{Cl}$. The formation of $[\text{H}_2\text{B}(\text{NH}_3)_2]\text{Cl}$ was verified by ^{11}B NMR and confirmed by XRD [11].

We also determined the stability of pure DADB. We found that DADB is stable in liquid ammonia but decomposes in organic solvents at room temperature. Its instability in THF was demonstrated using variable-temperature ^{11}B NMR

experiments from -40°C to room temperature (Figure 4). DADB was stable at lower temperatures, slowly converting to AB as the temperature was raised (-10°C). Once AB was formed, it could not revert back to DADB when the temperature was lowered. This instability of the DADB in organic solvents at ambient temperature, not widely known, has led to confusion about the purity of the samples.

Conclusions and Future Directions

- In collaboration with Northwestern University and NIST, we have now identified the structure of $\text{AlB}_4\text{H}_{11}$, an amorphous chain compound containing both BH_4 and B_3H_7 units. This structure features were supported by the following observations: 1) both $[\text{BH}_4]^-$ and $[\text{B}_3\text{H}_8]^-$ ^{11}B NMR signals were observed in a liquid ammonia solution of $\text{AlB}_4\text{H}_{11}$, 2) good agreement between the simulated phonon density of states and the experimental IR and NVS results, and 3) good agreement between the predicted and simulated ^{11}B NMR spectra.

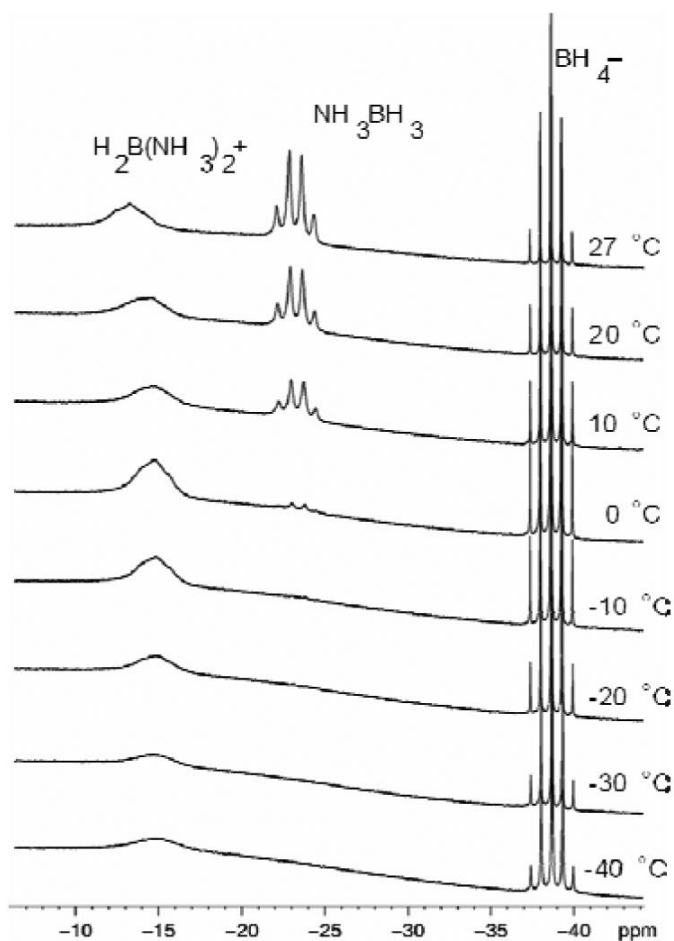


FIGURE 4. Variable temperature ^{11}B NMR spectra of DADB from -40°C to 27°C with 10°C intervals

- The formation mechanism of $\text{AlB}_4\text{H}_{11}$ was studied by monitoring the reaction procedure using ^{11}B NMR spectroscopy and two plausible mechanisms were derived.
- Simple and efficient method for the preparation of the DADB was developed. The DADB was found to be unstable in organic solvents at room temperature.
- The formation mechanism of the DADB was determined to be a three step process.
- A final report of this entire project will be written at the end of 2012 as a conclusion of this project.

FY 2012 Publications/Presentations

1. X. Chen, Y. Zhang, Y. Wang, D.A. Knight, W. Zhou, T.B. Yisgedu, Z. Huang, H.K. Lingam, B. Billet, T.J. Udovic, G.M. Brown, S.G. Shore, C. Wolverton, and J.-C. Zhao "Structure determination of an amorphous compound $\text{AlB}_4\text{H}_{11}$ " *Chem. Sci.*, DOI: 10.1039/c2sc21100a (2012).
2. Z. Huang, M. Eagles, S. Porter, B. Billet, R.L. Corey, M.S. Conradi and J.-C. Zhao, "Thermolysis and solid state NMR studies of NaB_3H_8 , $\text{NH}_3\text{B}_3\text{H}_7$ and $\text{NH}_4\text{B}_3\text{H}_8$ " *Dalton Trans.* DOI:10.1039/C2DT31365K.
3. X. Chen, X. Bao, J.-C. Zhao, S.G. Shore "Experimental and computational study of the formation mechanism of the diammoniate of diborane: the role of dihydrogen bonds" *J. Am. Chem. Soc.* **2011**, 133, 14172-14175.
4. X. Chen, X. Bao, S.G. Shore, J.-C. Zhao "Large-scale and facile preparation of pure ammonia borane through displacement reactions" *Chem. Eur. J.* DOI: 10.1002/chem.201201342 (2012).
5. X. Chen, J. Gallucci, C. Campana, Z. Huang, H. Lingam, S.G. Shore, J.-C. Zhao "Anti and Gauche Conformers of an Inorganic Butane Analogue, $\text{NH}_3\text{BH}_2\text{NH}_2\text{BH}_3$ " *Chem. Commun.* **2012**, 48, 7943-7945.
6. H. Lingam, X. Chen*, J.-C. Zhao, S.G. Shore "A convenient synthesis and a NMR study of the diammoniate of diborane" *Chem. Eur. J.* **2012**, 18, 3490-3492.
7. T.B. Yisgedu, Z. Huang, X. Chen, H.K. Lingam, G. King, A. Highley, S. Maharrey, P.M. Woodward, R. Behrens, S.G. Shore, J.-C. Zhao "The structural characterization of $(\text{NH}_4)_2\text{B}_{10}\text{H}_{10}$ and thermal decomposition studies of $(\text{NH}_4)_2\text{B}_{10}\text{H}_{10}$ and $(\text{NH}_4)_2\text{B}_{12}\text{H}_{12}$ " *Inter. J. Hydrogen Energy* **2012**, 37, 4267-4273.
8. T.B. Yisgedu, X. Chen, H. Lingam, Z. Huang, A. Highley, S. Maharrey, P.M. Woodward, R. Behrens, S.G. Shore, J.-C. Zhao "Synthesis, Structural Characterization, and Thermal Decomposition Study of $\text{Mg}(\text{H}_2\text{O})_6\text{B}_{10}\text{H}_{10}\cdot 4\text{H}_2\text{O}$ " *J. Phys. Chem. C.* **2011**, 115, 11793-11802.
9. Z. Huang, X. Chen, T.B. Yisgedu, E.A. Meyers, S.G. Shore, J.-C. Zhao "Ammonium octahydrotriborate ($\text{NH}_4\text{B}_3\text{H}_8$): new synthesis, structure, and hydrolytic hydrogen release" *Inorg. Chem.* **2011**, 50, 3738-3742.
10. Z. Huang, X. Chen, T.B. Yisgedu, J.-C. Zhao, S.G. Shore "High-capacity hydrogen release through hydrolysis of NaB_3H_8 " *Inter. J. Hydrogen Energy* **2011**, 36, 7038-7042.
11. X. Chen*, H.K. Lingam, J.-C. Zhao, S.G. Shore "The roles of dihydrogen bonds in amine borane chemistry" Boron Americas XIII Meeting, Purdue University, USA, June 3–6, 2012.
12. X. Chen*, X. Bao, J.-C. Zhao, S.G. Shore "The formation mechanism of the diammoniate of diborane: the role of dihydrogen bonds" IME Boron XIV Conference, Niagara Falls, CA, September 15–19, 2011.
13. X. Chen*, X. Bao, J.-C. Zhao, S.G. Shore "Dihydrogen bond effects in amine borane chemistry"(INOR-1001) 241st ACS National Meeting, Anaheim, USA, March 27–31, 2011.

References

1. (a) J.-C. Zhao, D.A. Knight, G.M. Brown, C. Kim, S.-J. Hwang, J.W. Reiter, R.C. Bowman, Jr., J.A. Zan, J.G. Kulleck; *J. Phys. Chem. C.* **2009**, 113, 2. (b) X. Chen, Y. Zhang, Y. Wang, D.A. Knight, W. Zhou, T.B. Yisgedu, Z. Huang, H.K. Lingam, B. Billet, T.J. Udovic, G.M. Brown, S.G. Shore, C. Wolverton, and J.-C. Zhao; *Chem. Sci.*, DOI: 10.1039/c2sc21100a (2012).
2. F.L. Himpsl, Jr., A.C. Bond *J. Am. Chem. Soc.* **1981**, 103, 1098.
3. P. Giannozzi, S. Baroni, N. Bonini, M. Calandra, R. Car, C. Cavazzoni, D. Ceresoli, G.L. Chiarotti, M. Cococcioni, I. Dabo, A. Dal Corso, S. Fabris, G. Fratesi, S. de Gironcoli, R. Gebauer, U. Gerstmann, C. Gougousis, A. Kokalj, M. Lazzeri, L. Martin-Samos, N. Marzari, F. Mauri, R. Mazzarello, S. Paolini, A. Pasquarello, L. Paulatto, C. Sbraccia, S. Scandolo, G. Sclauzero, A.P. Seitsonen, A. Smogunov, P. Umari, R.M. Wentzcovitch, *J. Phys.: Condens. Matter* **2009**, 21, 395502.
4. A.J. Downs, L.A. Jones, *Polyhedron*, **1994**, 13, 2401.
5. (a) J.F. Stanton, W.N. Lipscomb, R.J. Bartlett, *J. Am. Chem. Soc.* **1989**, 111, 5165. (b) R. Greatrex, N.G. Greenwood, S.M. Lucas, *J. Am. Chem. Soc.* **1989**, 111, 8721. (c) S.A. Fridmann, T.P. Fehlner, *J. Am. Chem. Soc.* **1971**, 93, 2824. (d) S.A. Fridmann, T.P. Fehlner, *Inorg. Chem.* **1972**, 11, 936. (e) W.N. Lipscomb, H.F. Stanton, W.B. Connick, D.H. Magera, *Pure Appl. Chem.* **1991**, 63, 335. (f) R.E. Enrione, R. Schaeffer, *J. Inorg. Nucl. Chem.* **1961**, 18, 103. (g) L.H. Long, *J. Inorg. Nucl. Chem.* **1970**, 32, 1097. (h) H. Fernández, J. Grotewold, C.M. Previtali, F.F. Bioquímica, *J.C.S. Dalton*, **1973**, 2090. (i) B. Brellocks, H. Binder, *Angew. Chem. Int. Ed.* **1988**, 27, 262.
6. (a) C.W. Yoon, P.J. Carroll, L.G. Sneddon, *J. Am. Chem. Soc.* **2009**, 131, 855. (b) H. Beall, C.H. Bushweller, *Chem. Rev.* **1976**, 15, 741. (c) L.D. Brown, W.N. Lipscomb, *Inorg. Chem.* **1977**, 16, 1. (d) V.L. Bishop, G. Kodama, *Inorg. Chem.* **1981**, 20, 2724. (e) G. Kodama, *Inorg. Chem.* **1975**, 14, 452.
7. (a) A. Stock and E. Kuss, *Ber. Dtsch. Chem. Ges.*, 1923, **56**, 789. (b) E. Z. Wiberg, *Anorg. Allg. Chem.*, 1928, **173**, 199.
8. (a) S.G. Shore, C.W. Hickam Jr., D. Cowles, *J. Am. Chem. Soc.*, **1965**, 87, 2755. (b) D.E. Young, S.G. Shore, *J. Am. Chem. Soc.*, **1969**, 91, 3497. (c) R.W. Parry, *J. Organomet. Chem.* **2000**, 614, 5. (d) E. Mayer, *Inorg. Chem.* **1972**, 11, 866. (e) E. Meyer, *Inorg. Chem.* **1973**, 12, 1954.
9. X. Chen, X. Bao, J.-C. Zhao, S.G. Shore, *J. Am. Chem. Soc.* **2011**, 133, 14172-14175.
10. S.G. Shore and R.W. Parry, *J. Am. Chem. Soc.*, **1958**, 80, 8.
11. H.K. Lingam, X. Chen, J.-C. Zhao, S. G. Shore, *Chem. Eur. J.* **2012**, 18, 3490.

IV.A.4 Reversible Hydrogen Storage Materials – Structure, Chemistry, and Electronic Structure

Ian Robertson (Primary Contact) and
Duane Johnson

University of Illinois, Department of Materials Science
and Engineering
1304 West Green Street
Urbana, IL 61801
Phone: (217) 333-6776
Email: ianr@illinois.edu

DOE Managers

HQ: Ned Stetson
Phone: (202) 586-9995
Email: Ned.Stetson@ee.doe.gov
GO: Katie Randolph
Phone: (720) 356-1759
Email: Katie.Randolph@go.doe.gov

Contract Number: DE FC36-05GO15064

Project Start Date: March 1, 2005
Project End Date: Project continuation and direction
determined annually by DOE

Insights gained from these studies will be applied toward the design and synthesis of hydrogen storage materials that meet the following DOE hydrogen storage targets:

- Cost: to be determined
- Specific energy: 1.3 kWh/kg
- Delivery pressure - 50 and 150 bar for materials-based storage systems

FY 2012 Accomplishments

- Discovered that the hydrogen desorption mechanism is a two-step process, with diffusion from the bulk involving a lower barrier than the H₂ surface desorption. To calculate catalyzed H₂ surface desorption, we found that magnetic degrees of freedom must be carefully addressed to describe the crossover of magnetic states during desorption.
- The catalytic effect of Ti-substitutional dopant on H₂ desorption from bulk MgH₂(110) surfaces was determined, including (110)/(001) step edges, and for nanoparticle MgH₂, which also addresses size effects associated with ball-mill processing.
- The efficiency of ball-milling on dispersing catalytic species has been determined using three-dimensionally electron tomography.
- The three-dimensional structure of carbon nano-scaffolds was determined and shown to be composed of a layered structure with different orientations. This has implications for the fill capacity.

Fiscal Year (FY) 2012 Objectives

- Understand the processes controlling uptake and release of hydrogen from on-board solid-state systems.
- Understand the catalytic processes operating in on-board solid-state systems.

Technical Barriers

This project addresses the following technical barriers from the Hydrogen Storage section (3.3.4) of the Fuel Cell Technologies Program Multi-Year Research, Development and Demonstration Plan:

- (A) System Weight and Volume
- (D) Durability/Operability
- (P) Lack of Understanding of Hydrogen Physisorption and Chemisorption

Technical Targets

Catalytically Enhanced Hydrogen Storage Systems:

This project is conducting fundamental studies of the role of catalyst species in nanoparticles as well as the role of nanostructures for confinement of the storage medium.



Introduction

The atomic and molecular processes, by which hydrogen is adsorbed and desorbed from solid-state storage systems, both in bulk and nanoparticle form, are being investigated by using a combination of first-principle calculations and advanced characterization techniques. The dispersion of catalytic species and its function in the charging and discharging cycle are of particular interest. In addition, in the case of nanoparticle systems in which the storage material is confined within a nanoscale scaffold structure, the microstructure as a function of the number of cycles is being investigated to understand how the storage capacity degrades with the number of cycles. This investigation of the fundamental processes seeks to inform the design and development of onboard solid-state storage systems

to achieve the DOE targets as well as understand system changes during cycling, which pertains to system durability.

Approach

We utilize advanced characterization tools especially state-of-the-art transmission electron microscope (TEM) including three-dimensional electron tomography to investigate the structural and compositional changes in nano-scaffold systems as well as the dispersion of catalyst species by ball milling. Scanning tunneling microscopy is used to explore the interaction of a pure metal surface with and without catalyst species for both atomic and molecular hydrogen. In parallel, we use density functional theory (DFT) calculations to determine the role of transition-metal catalysts to increase H_2 absorption and desorption kinetics in both bulk and nanoparticle MgH_2 . This also addresses size effects associated with ball-mill processing of materials. The nudged-elastic band method is used to determine the kinetic energy barriers of reaction pathways of H_2 desorption.

Results

In collaboration with Professor Eric Majzoub, University of Missouri, $LiBH_4$ -infiltrated nanoporous carbon scaffold hydrogen storage materials are being investigated as a function of hydrogen charging and discharging cycles. The nanoporous carbon scaffolds have been found to be complex with differing column size, orientations, and curvatures all within domains that can vary from their neighbors. These observations have implications related to the fill capacity of the structures and are being correlated with processing parameters. Annealing of $LiBH_4$ above $200^\circ C$ causes the formation of granular coatings composed of cubic or cuboid nanoscale growths with dimensions of ≈ 10 - 20 nm on the outer surfaces of many scaffold particles. Following annealing these nano-crystals can be found micrometers from the host scaffold, Figure 1. The size distribution of the dispersed nano-crystals implies different migration rates along the holey carbon support substrate and that larger crystals are formed by particle agglomeration. Preliminary results, including the cubic structure of the ejected material, and first-principle calculations performed by Majzoub suggest LiH is a likely candidate for the ejected material [1]. These results have implications regarding the long-term stability of such storage materials.

In our preliminary TEM analysis of $MgH_2 + 0.05 Ni$, milled for 1, 5, and 10 hours, and $MgH_2 + 0.05 NiCl_2$, milled for 1 hour, no appreciable differences were observed in the size distribution of the Mg particles, regardless of milling time or form of the catalyst. The shape of the $NiCl_2$ -doped material, however, was very angular and sharp compared to those doped with Ni only. The morphology of the Ni particles depended on milling time, changing from irregular shaped, spherical and elongated to predominately spherical.

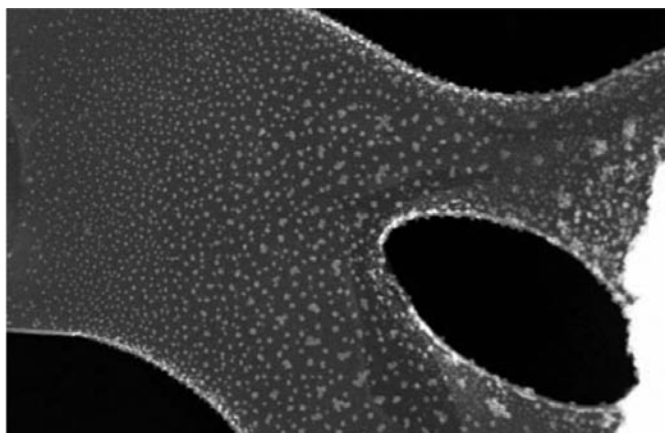


FIGURE 1. High-angle annular dark-field scanning transmission electron microscope images of a $LiBH_4$ -infiltrated carbon scaffold particle heated to $200^\circ C$, showing long-range ejection of nanocrystals from the scaffold surface along the holey carbon support grid.

The density of Ni particles also decreased with increased milling time. Energy-dispersive X-Ray spectroscopy (EDS), Figure 2, reveals that the Ni catalyst becomes increasingly delocalized and dispersed with increasing milling time. After 10 hours of milling time, few Ni particles remain, and the diffuse Ni background has increased and appears to be almost uniformly dispersed. Point spectra confirm a roughly stoichiometric ratio of Ni and Mg (0.05:1) in regions where no distinct Ni particles are observed. These observations have implications for the role of catalytic species at enhancing hydrogen charging and discharging.

Previous studies have shown that the overall desorption enthalpy of H_2 from MgH_2 nanoparticles only decreases significantly when the particle size decreases below 5 formula units. Recently, using DFT simulations of desorption enthalpies, we reported that there is no size effect for initial H_2 desorption from MgH_2 surface with(out) defects versus MgH_2 amorphous nanoparticles. All the data are shown in Figure 3. We have considered both singly- and doubly-bonded H . Figure 3 shows that a singly-bonded H is removed from an amorphous MgH_2 nanoparticle of 31 formula units with a desorption energy of 148 $kJ/(mol-H_2)$ in reference to free H_2 . Because a singly-bonded H cannot be found on $MgH_2(110)$, where only doubly-bonded H exist, a step surface was constructed. The desorption energy of singly-bonded H from this step surface is 140 $kJ/(mol-H_2)$ – within 6% of the nanoparticle result. For doubly-bonded H , we found a similar result, i.e., 240 $kJ/(mol-H_2)$. The lack of a size effect in the initial H -desorption can be understood by the fact that $Mg-H$ bond is local in nature. This result provides insight to the fundamental mechanisms of hydrogen uptake and release.

Kinetic barriers in nanoparticles, in principle, may be reduced due to the free surface and altered bonding. Nonetheless, from Figure 4, we find that the desorption enthalpies for a nanoparticle are unaffected and, for the

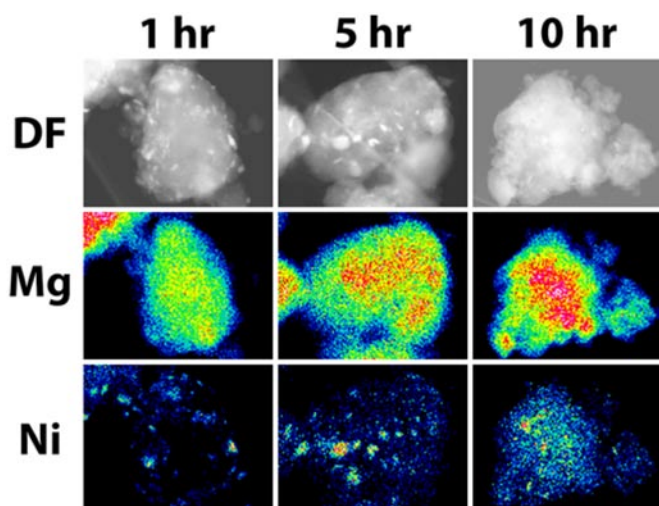


FIGURE 2. High-angle annular dark-field scanning transmission electron microscope images of $\text{MgH}_2 + 0.05 \text{ Ni}$ specimens and their corresponding EDS chemical maps of Mg and Ni. As milling time increases, the Ni becomes increasingly delocalized and dispersed throughout the Mg. At 1 hour, the Ni still resides mostly in distinct Ni nanoparticles. By 5 hours, distinct Ni nanoparticles still account for most of the nickel, but a diffuse background of Ni is visible throughout most of the Mg. By 10 hours, few nanoparticles of Ni remain, with most of the Ni dispersed.

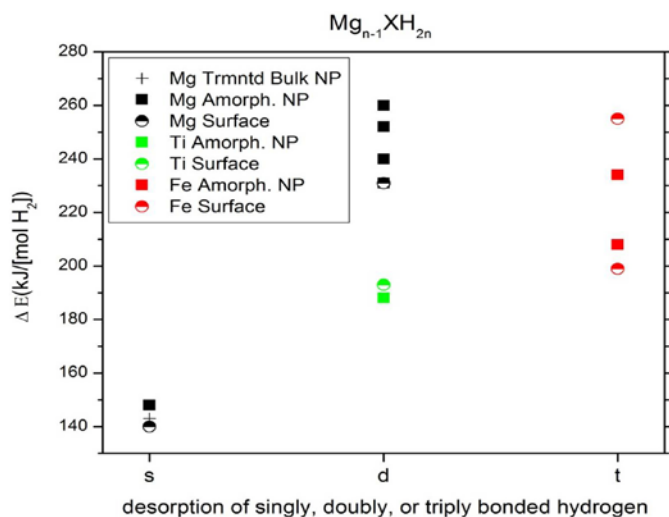


FIGURE 3. Desorption energies of singly-, doubly- and triply-bonded H from various structures. “Mg Trmtd Bulk NP” is the bulk-terminated $\text{Mg}_{31}\text{H}_{62}$ after relaxation. “Mg Surface” refers to (110)/(001) step edge and (110) surface. “Ti Surface” is the relaxed (110) surface with a single Ti substitutional dopant for Mg. “Fe Surface” is the reconstructed (110) surface with Fe substituting Ti.

desorption pathways thus far investigated, the barriers (1.85 eV) are also similar to the bulk MgH_2 (1.83 eV), see publications. Therefore, only doping can affect the enthalpies and barriers.

For doped bulk surfaces, we found that a single Ti dopant is effective in reducing the kinetic barrier by 0.41 eV.

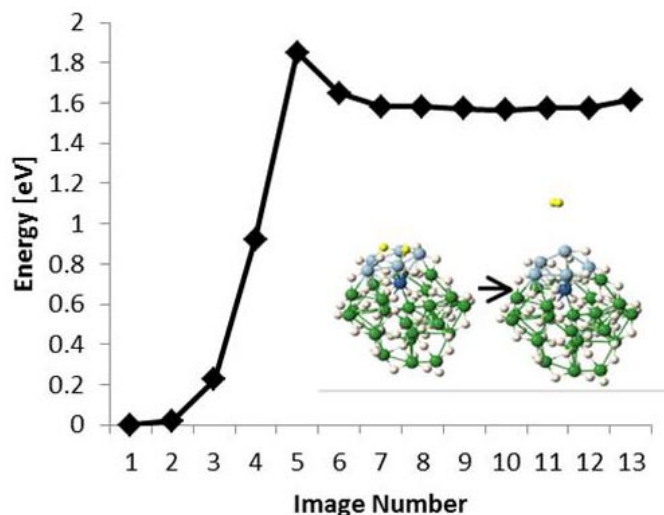


FIGURE 4. Kinetic barrier (nudged elastic band) results for H-desorption from undoped nanoparticle $\text{Mg}_{31}\text{H}_{62}$ with 1.85 eV barrier, which is similar to undoped $\text{MgH}_2(110)$ bulk surface.

We revealed a mechanism involving concerted motion of H_2 surface desorption and H bulk diffusion to reduce the barrier. We also found that magnetic degrees of freedom must be carefully addressed to describe the crossover of magnetic states during catalyzed H_2 surface desorption, from early to late stage (see 2012 publications for details). The overall kinetic barrier is 1.42 eV. In contrast, without such crossover of magnetic moment, the barrier is 1.46 eV for the same initial state with a magnetic moment of $0 \mu_B$ (Ti having H coordination 8) and 1.84 eV for a degenerated state with a magnetic moment of $2 \mu_B$ (Ti having H coordination 6). Thus, we have shown the catalytic effect of a single Ti substitution on kinetic barrier reduction is due to the concerted motion of surface H_2 desorption and bulk H diffusion. We will next study the effect of other transition-metal dopants either embedded or supported on surfaces of MgH_2 as well as dopant nanoparticles and other metal hydrides on the adsorption/desorption processes.

Conclusions and Future Directions

- Found that a single Ti dopant in MgH_2 is effective in reducing the kinetic barrier by 0.41 eV and revealed a mechanism involving concerted motion of H_2 surface desorption and H bulk diffusion to reduce the barrier.
- Found no size effect for initial H_2 desorption from MgH_2 surface with(out) defects versus MgH_2 amorphous nanoparticles.
- Found that storage material may be ejected from nano-scaffold structures during the discharge cycle.
- Demonstrated the microstructural and compositional changes associated with ball milling.

- Despite there being no size effect for the binding of H, the appearance of singly and weakly bonded H will be studied further because it is relevant to nanoparticle systems and high-indexed surfaces produced under ball-milling experiments.
- Nano-particle doping studies similar to the bulk cases will be completed. For comparison, other defects such as vacancies (prominent in ball-milled materials) will be introduced and their impact determined.
- The structural and compositional changes in ball-milled MgH_2 with Ni will be completed.
- The structure of nano-scaffold systems as a function of charging/discharging cycles will be completed.

FY 2012 Publications/Presentations

1. J.M. Reich, Lin-Lin Wang, and Duane D. Johnson, "Surface and particle-size effects on hydrogen desorption from catalyst-doped MgH_2 ," (2012), submitted – responding to reviews.
2. Lin-Lin Wang and D.D. Johnson, "Hydrogen Desorption from Ti-doped $\text{MgH}_2(110)$ Surfaces: Catalytic effect on reaction pathways and kinetic barriers," *J. Phys. Chem. C* 116, 7874–7878 (2012).

Presentations

1. Duane D. Johnson and Lin-Lin Wang, "Defect-Mediated Properties in Bulk and Nanoparticle Metallic Alloys: Quantitative Prediction of Phase Stability, Mechanical Properties and Kinetics," (invited) SYMPOSIUM: Phase Stability, Diffusion, Kinetics and their Applications, Materials Science & Technology Meeting 16–20 October 2011, Columbus, Ohio.

2. Duane D. Johnson and Lin-Lin Wang, "Defect and Chemically Mediated Catalytic Behavior," (invited) Data-rich Approaches in Catalysis Science, Spring ACS 2012 National Meeting, San Diego, CA, 25–29 March 2012.
3. Lin-Lin Wang, Duane D. Johnson, Teck L. Tan, Configurational Thermodynamics of Alloyed Nanoparticles, American Physics Society March 2012 Meeting, Boston, MA.
4. Duane D. Johnson, "Data Discovery versus Data Mining," (invited) in USC-DOE conference on "Materials Genome: Simulations, Synthesis, Characterization and Manufacturing", Los Angeles, 4–6 April, 2012.
5. Duane D. Johnson, "Materials Design, Synthesis, and Characterization: coupling theory and experiment with data discovery," (invited) Argonne National Laboratory, 21 May 2012.
6. Duane D. Johnson, "Reaction Pathways for Solid-State Transformations: a proper nudged-elastic band," (invited) symposium in honor of Warren Pickett's 65th Birthday, UC Davis, 24 June 2012.
7. S. House, I.M. Robertson and D. Graham, "Applications of Electron Microscopy to Complex Metal Hydrides," M&M 2011.
8. Ian M. Robertson, Josh Kacher, Grace Liu, Stephen House, "In-situ TEM studies of the response of a Material to an External Stimulus" MS&T 2011, Narayan Symposium. Invited.

References

1. Majzoub, E.H., X.F. Liu, D. Peaslee, and C.Z. Jost, *Controlling the Decomposition Pathway of LiBH_4 via Confinement in Highly Ordered Nanoporous Carbon*. *J Phys Chem C*, 2010. 114(33): p. 14036-14041.

IV.A.5 Aluminum Hydride

Jason Graetz (Primary Contact), James Wegrzyn
 Brookhaven National Laboratory (BNL)
 Building 815
 Upton, NY 11973
 Phone: (631) 344-3242
 Email: graetz@bnl.gov

DOE Manager
 HQ: Ned Stetson
 Phone: (202) 586-9995
 Email: Ned.Stetson@ee.doe.gov

Project Start Date: October 1, 2011
 Project End Date: Project continuation and
 direction determined annually by DOE

Fiscal Year (FY) 2012 Objectives

Develop onboard vehicle storage systems using aluminum hydride that meets all of DOE's targets for proton exchange membrane fuel cell vehicles.

- Produce aluminum hydride material with a hydrogen storage capacity greater than 9.7% gravimetric (kg-H₂/kg) and 0.13 kg-H₂/L volumetric.
- Develop practical and economical processes for regenerating aluminum hydride.
- Assist in developing aluminum hydride slurry storage systems for better than 6% hydrogen gravimetric material density, 0.07 kg-H₂/L volumetric hydrogen storage capacity, and well-to-wheels efficiencies greater than 60%.

Technical Barriers

This project addresses the following technical barriers from the Hydrogen Storage section of the Fuel Cell Technologies Program Multi-Year Research, Development and Demonstration Plan:

- (A) System Weight and Volume
- (B) System Cost
- (E) Charging/Discharging Rates

Technical Targets

Table 1 is a listing of the 2015 DOE hydrogen storage targets along with BNL's current 2012 aluminum hydride project status. The well-to-wheels efficiency listed in the table under the column for 2012 Status was taken from an

independent analysis of an aluminum hydride storage system by Argonne National Laboratory. The 0.0582 gravimetric storage parameter listed in Table 1 is a measured value from decomposing 60-wt% slurry consisting of 9.7-wt% aluminum hydride particles. It does not take into account the balance-of-plant weight. In FY 2012 progress was realized in meeting the refueling target by formulating 60-wt% alane slurry using di-ethylene glycol as the liquid carrier. At 25°C the slurry viscosity was measured to be 1,500 centipoise.

TABLE 1. Progress in Meeting Technical Hydrogen Storage Targets Aluminum Hydride Regeneration

| Storage Parameter | Units | 2015 Target | 2012 Status |
|------------------------------|-----------------------|-------------|-------------|
| Gravimetric | wt% H ₂ | 0.055 | 0.0582 |
| Volumetric | kg H ₂ /L | 0.040 | 0.070 |
| Full Flow Rate (temperature) | (g/s)/kW °C | 0.02 80 | 0.02 80 |
| Well-to-Wheels Efficiency | kW-H ₂ /kW | 60% | 55% |
| Refueling Time | min | 3.3 | TBD |

TBD – to be determined

FY 2012 Accomplishments

- Measured the viscosities for four different ATK/solvent slurries as a function of composition, shear rate and temperature.
- Identified the 60% by wt. ATK in a 40% by wt. di-ethylene glycol di-butyl ether (DGDE) slurry as having viscosities less than 1,500 centipoise at 25°C.
- Demonstrated 96% hydrogen release in 88 seconds at 180°C for a catalyzed 60% by wt. ATK in a 40% by wt. DGDE slurry.
- Demonstrated 96% hydrogen release in 2,860 seconds at 100°C for a catalyzed 60% by wt. ATK in a 40% by wt. DGDE slurry.



Introduction

The FY 2012 objective was to achieve DOE's 2015 system fill target of 5 kg of H₂ in 3.3 minutes. Since aluminum hydride exists only as a solid, this objective was directed towards formulating a "pumpable" 6% by H₂ wt. AlH₃ slurry. In order to meet this 1.5 kg H₂ per minute target, the slurry had to be stable against phase separation and sedimentation with a viscosity less than 1,500 centipoise (cP). This year a pumpable 6% by H₂ wt. AlH₃ slurry was formulated with viscosities less than 1,500 cP; however,

further work is needed to improve these slurries against phase separation due to particle sedimentation.

Approach

AlH_3 can be classified as a kinetically stabilized material. A nucleation and growth chemistry model was used in the past to describe the decomposition rates of AlH_3 . This chemical model was useful in defining both an induction period (IP) along with a kinetic decomposition period. However, under isothermal conditions, a statistical approach was also found to be helpful in describing the AlH_3 decomposition rate. The statistic of choice is the hyperbolic secant probability distribution function, which can be written as:

$$f(t) = (1/2t_k) \text{sech}[(\pi/2)(t-t_m)/t_k]. \quad [1]$$

In the above equation t_m is the time when the decomposition rate reaches its peak value, and $(1/2t_k)$ is the peak kinetic decomposition rate. The integration of the probability distribution function $f(t)$ over time yields the cumulative distribution function $F(t)$. This function is however more convenient to work with than the probability density function, since it is the percent loss of hydrogen as a function of time. Integrating over time Equation [1] yields the following expression for the cumulative distribution function $F(t)$:

$$F(t) = (2/\pi) \tan^{-1}(\exp[(\pi/2)(t-t_m)/t_k]). \quad [2]$$

The IP is now defined as the time when $F(t) = 0.02$. In other words, the time it takes for the first 2% decomposition. Setting $F(t) = 0.02$, replacing (t) with IP and solving for IP gives the following:

$$\text{IP}^{2\%}(t_m, t_k) = t_m + (2t_k/\pi) \ln \{ \tan(0.01\pi) \} = t_m - (2t_k/\pi) 3.4601. \quad [3]$$

The time required for 96% release of hydrogen after the induction period is:

$$\Delta t(96\%) = (2t_k/\pi) \ln \{ \tan(0.49\pi) \} - (2t_k/\pi) \ln \{ \tan(0.01\pi) \} = (4t_k/\pi) 3.4601. \quad [4]$$

Note that $\ln \{ \tan(0.49\pi) \} = 3.4601$ and $\ln \{ \tan(0.01\pi) \} = -3.4601$.

This model implies that surface coatings can increase the induction period by increasing t_m (see Equation [3]). Eqn. [4] shows that the time release of hydrogen Δt (96%) depends only on t_k and not t_m . Recall that $(1/2t_k)$ is the peak decomposition rate. Thus, the increase in IP from increasing t_m essentially has no effect on the time it takes to release the remainder (96%) of the hydrogen. The results of this study support this model, since it shows that surface coatings can improve the stability of AlH_3 against decomposition; but once decomposition has started, the rate is then controlled by catalysts and the sample temperature.

Results

This year's results were the measurements the viscosities and decomposition rates of several different types of 6-wt% H_2 alane slurries. The primary goal was to formulate 6-wt% H_2 alane slurries with viscosities around 1,500 centipoise. Another goal was to determine changes in aluminum hydride decomposition rates because of the slurry form. The aluminum hydride used in this study was supplied by Savannah River National Laboratory. It goes by the name of the company who made the material—ATK. The reason for using ATK-alane was that this was the alane material under consideration by DOE's Hydrogen Storage Engineering Center of Excellence. Figure 1 is an electron micrograph of the as-received ATK-alane material. No attempt was made to improve slurry properties by optimizing particle size distributions. The aluminum hydride particles were mixed (as-received) with the liquid carriers without changing their particle size.

Tests were conducted on the 6-wt% H_2 slurries by blending as-received ATK particles with several different types of liquid carriers. However, both the viscosities and kinetics of the slurry were modified by various chemical additive packages. The chemical additives tested this year were triton based ionic surfactants (X-10 and X-100), as well as the known alane de-stabilizers (LiH and/or Ti). The use of surfactants did lower the slurry's viscosities at low temperatures ($T < 25^\circ\text{C}$), but had little effect at higher temperatures. Since the surfactant study is considered preliminary, more data is needed before any conclusion

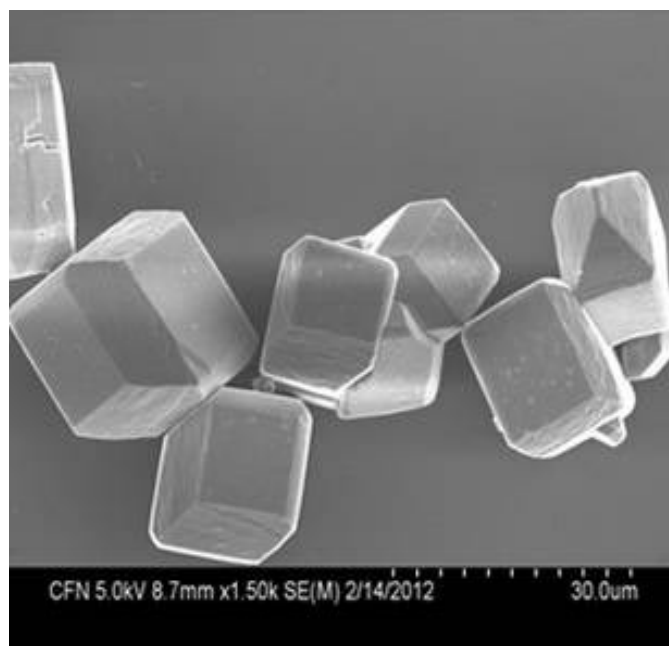


FIGURE 1. Electron micrograph of the as-received ATK aluminum hydride particles

can be reached. On the other hand, the addition of LiH and Ti increased quite significantly the alane's decomposition rate. This was most noticeable for the DGDE-based slurry. Figure 2 shows the per cent loss of hydrogen as a function of time. In this experiment the test reactor is lowered into a constant temperature 180°C oil bath. The liquid carrier in the test was (DGDE) with Ti and LiH additions. The figure lists both the experimental data along with the model as given by equation 2. The half-life was 74 seconds ($t_m=74$ sec) and where the maximum decomposition rate was $1/(2 \cdot t_k)$ where $t_k=20$ sec). One reason for the deviation between model and experiment is shown by Figure 3. This figure gives the internal temperature as a function of time of the test reactor as it's lowered into the temperature 180°C bath. One sees a

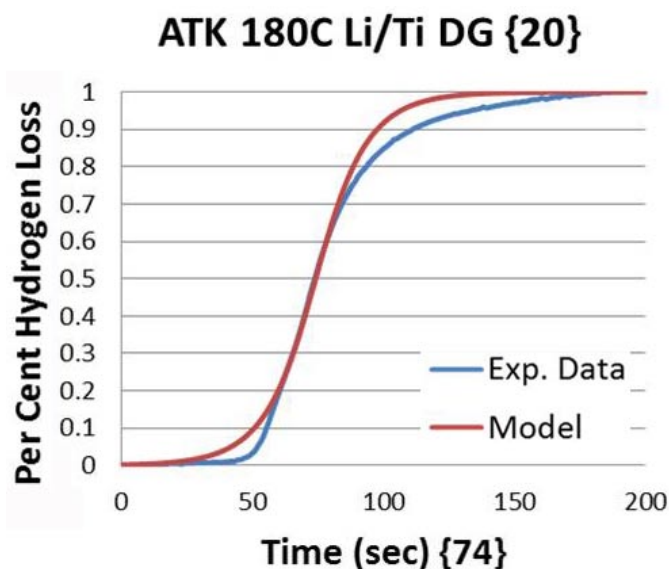


FIGURE 2. Comparison of the model (Eqn. 2; with $t_k=20$ seconds and $t_m=74$ seconds) against the experimental data of the time release of hydrogen at 180°C for a 60% by wt. ATK slurry in DGDE that was activated with Ti and LiH.

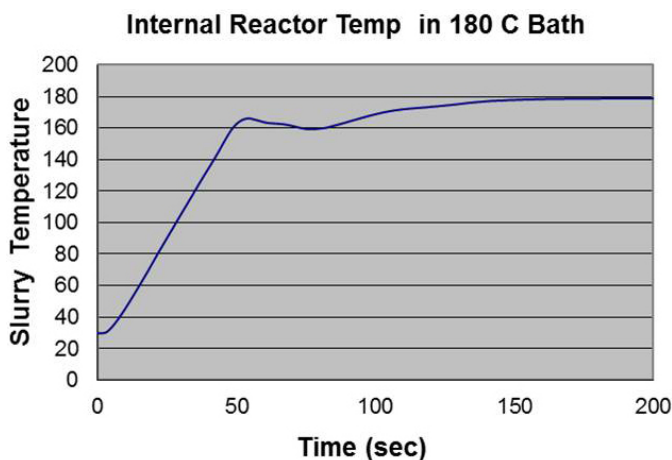


FIGURE 3. Slurry temperature as a function of time when placed in a 180°C oil bath

nearly linear increase in the alane sample temperature for the first 50 seconds. After the first 50 seconds, the sample cooling due to its endothermic nature is clearly evident. The isothermal model of Equation 2 does not account for the endothermic cooling, and thereby predicts higher hydrogen losses than actually measured.

Figure 4 shows the probability distribution of hydrogen loss for 6-wt% H₂ slurries with four different liquid carriers (DGDE, H350, C50S, and mineral oil); as well as the hydrogen loss for dry ATK particles (ATK-Ref). H350 and C50S are both high temperature, heat transfer fluids that were purchased from Julabo USA, Inc. The common material name for H350 is di-benzltoluene, and for C50S the common material name is di-methylsiloxane. The most notable fact about the data of Figure 4 is that the (DGDE) slurry showed increased alane decomposition in relation to powdered ATK-Ref. dry particles. All other slurries had slower kinetic decomposition rates than ATK-Ref. These tests were run without the addition of any catalysts. More tests are needed to understand these results. It is speculated that the higher decomposition rates with DGDE slurries are related to surface/solvent chemistry, since DGDE completely wets aluminum hydride. Since neither H350, C50S and mineral oil completely wet the aluminum hydride particles, these slurries appear to be more stable against decomposition than the dry ATK particles. The effect of changing particle/solvent surface tension on alane decomposition rates is at this time an open question. Also, at 120°C these measured decomposition rates are such that endothermic effects (as seen in Figure 3 at 180°C) were not observed, and the isothermal model is appropriate.

Figure 5 lists the viscosity data as function of shear rate for four different 6-wt% H₂ slurries. The data was taken at 25°C using a Brookfield DV-E viscometer. No surfactants

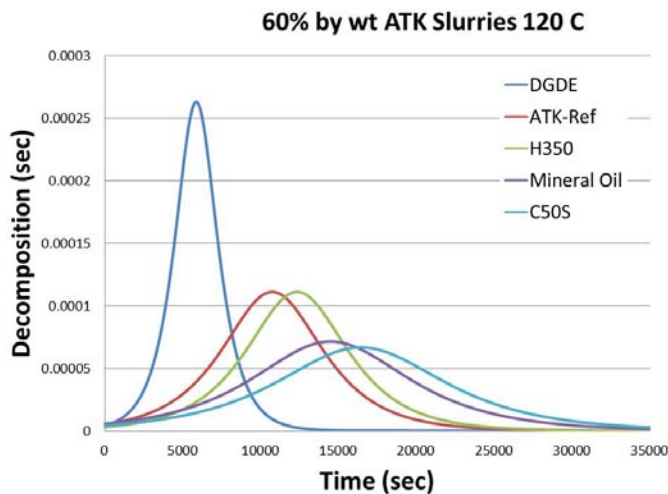


FIGURE 4. Plots at 120°C of the decomposition probability distribution functions (Eqn. 1) as function of time for four ATK slurries and dry material

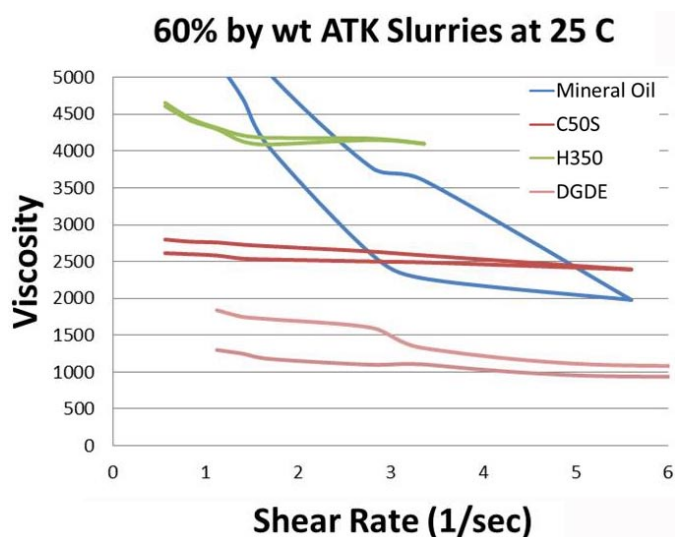


FIGURE 5. Viscosity measurements of four different 60% by wt ATK slurries at 25°C

were used to reduce the slurry's viscosity in these tests. The data presented in Figure 5 shows that the 60% by wt. DGDE alane slurry had the lowest viscosity tested. It had measured viscosities below 1,500 cP over all the test range of shear rates. Although the viscosity target can be met, further research is needed to improve the stability of these slurries. This research would entail reducing the aluminum hydride particle size, and also employ liquid carriers with densities above 1.20 gm/cm³. This combination would significantly improve slurry stability by reducing particle sedimentation velocity.

Conclusions and Future Directions

- Develop a 100 gram/week capability for synthesizing 1-10 micron AlH₃ particles.
- Improve the stability of AlH₃ slurries by lowering slurry sedimentation rate by reducing particle sizes and increase the liquid carrier density.
- For the lower temperature range ~0°C maintain slurries viscosities <1,500 cP.
- Optimize procedures for activating AlH₃ slurries for enhanced hydrogen release.

FY 2012 Presentations

1. "Tailoring aluminum hydride for mobile hydrogen storage systems" World Hydrogen Energy Conference, Toronto, June, 2012.
2. "Synthesis and Regeneration of Aluminum Hydride", *International Energy Agency (IEA) Task 22 Experts Meeting*, Heidelberg, Germany, May, 2012.
3. "Conversion Electrodes for Lithium Batteries" 243rd of the *American Chemical Society Meeting*, San Diego, March, 2012.
4. "Recent Developments with Aluminum Hydride", *Materials Challenges in Alternative and Renewable Energy (MCARE)*, Clearwater, Florida, February, 2012.

IV.A.6 Electrochemical Reversible Formation of Alane

Ragaiy Zidan¹ (Primary Contact),
Douglas A. Knight¹, Scott Greenway²

¹Savannah River National Laboratory
999-2W Room 121
Savannah River Site
Aiken, SC 29808
Phone: (803) 646-8876
Email: ragaiy.zidan@srnl.doe.gov

²Greenway Energy

DOE Manager

HQ: Ned Stetson
Phone: (202) 586-9995
Email: Ned.Stetson@ee.doe.gov

Project Start Date: October 1, 2006

Project End Date: October 1, 2012

TABLE 1. Alane Compared with 2015 Target

| Storage Parameter | 2015 Target | AlH ₃ |
|----------------------|------------------------------------|---|
| Gravimetric Capacity | 0.055 kg H ₂ /kg System | 0.1 kg H ₂ /kg AlH ₃ |
| Volumetric Capacity | 0.04 kg H ₂ /L System | 0.149 kg H ₂ /L AlH ₃ |

FY 2012 Accomplishments

- Demonstrated the use of a hydrogen-pressurized electrochemical cell, producing alane at a higher rate and minimal amount of dendrites.
- Demonstrated the use of spent aluminum to produce alane and regenerate the starting material (LiAlH₄-based electrolyte).
- Used saturated solutions to have solid aluminum adducts to precipitate, allowing efficient separation.
- Produced several of gram quantities of high purity alane at an improved energy efficiency.



Fiscal Year (FY) 2012 Objectives

- Identify means for achieving energy efficiency improvements of over 50%.
- Perform electrochemical production of alane and alane adducts in a pressurized electrochemical cell and demonstrate production of α -alane.
- Demonstrate the formation of alane and the regeneration of the starting materials, using spent aluminum and identify electro-catalytic additive.
- Produce larger quantities of alane (several grams).

Technical Barriers

This project addresses the following technical barriers from the Storage section of the Fuel Cell Technologies Program Multi-Year Research, Development and Demonstration Plan:

- (A) System Weight and Volume
- (B) System Cost
- (C) Efficiency
- (R) Regeneration Processes Scale Up

Technical Targets

In this project studies are being conducted to lower cost and improve efficiency of the electrochemical method to form AlH₃. This material has the potential to meet the 2015 technical target for on-board hydrogen storage as shown in Table 1.

Introduction

The DOE is supporting research to demonstrate viable materials for onboard hydrogen storage. Aluminum hydride (alane – AlH₃), having a gravimetric capacity of 10 wt% and volumetric capacity of 149 g H₂/L and a desorption temperature of ~60°C to 175°C (depending on particle size and the addition of catalysts) has the potential to meet the 2010 and 2015 DOE targets [1,2].

The main drawback for using alane as a hydrogen storage material is unfavorable thermodynamics towards hydrogenation. Past attempts to regenerate alane under mild conditions were reported, including attempts based on electrochemical methods [3,4]. However, recent results on the regeneration of alane reported by Zidan and others [5] were the first to show a reversible cycle utilizing electrochemistry and direct hydrogenation, where gram quantities of alane were produced, isolated and, characterized. This regeneration method is based on a complete cycle that uses electrolysis and catalytic hydrogenation of spent Al(s). This cycle avoids the impractical high pressure needed to form AlH₃ and the chemical reaction route of AlH₃ that leads to the formation of alkali halide salts, such as LiCl or NaCl, which become a thermodynamic sink because of their stability. During FY 2012, the electrochemical synthesis of alane described in Zidan and others [5] has been improved using a higher efficiency set up while increasing the alane production rate. Improvements are achieved by the use of LiAlH₄ etherates (e.g. Et₂O and DME) and a hydrogen-pressurized

electrochemical cell. In the hydrogen-pressurized cell, electrochemical alane was formed at higher rate than in the ambient cell. Aluminum from dehydrogenated aluminum hydride (spent aluminum) was used to form alane as well as regenerate the starting electrolyte.

Approach

Experimentally, the electrolysis was carried out as described in the electronic supplementary information of Zidan and others [3]. However, LiAlH_4 was used instead of NaAlH_4 . Both, tetrahydrofuran (THF) and diethyl ether (Et_2O) were used as aprotic solvents for the alane regeneration. Research on the electrochemical properties of MAlH_4 ($\text{M} = \text{Na}, \text{Li}$) in THF and Et_2O has been reported [7,8] but these studies were not directed at the regeneration and characterization of alane. Also, the work of Senoh and others [7,8] was performed with Ni electrodes different to this work in which Al is used as working electrode. Our group work is aimed at advanced studies involve the use of a modified Parr reactor designed to perform the electrolysis under a moderate pressure of hydrogen in order to observe how this might affect both the production rate of alane and the formation of any byproducts such as Li_3AlH_6 and aluminum dendrites that tend to foul the electrochemical cell. Similarly, further studies involve improved separation of alane from the alane-THF adduct and other alane-etherates adducts as well as an investigation of using spent aluminum to produce alane and regenerate the starting material to close the alane production cycle.

Results

As mentioned above, a modified Parr reactor was used for electrochemical reactions under pressurized hydrogen. The Parr reactor used is shown in Figure 1. The factory sealed electrodes featured in this design along with the



FIGURE 1. The modified Parr reactor as a pressurized electrochemical cell shown as it looks in operation. With factory-sealed electrodes and Swagelok fittings, this reactor is rated to 2,500 psig operating pressure.

various selected Swagelok fittings allow for an operating pressure of up to 2,500 PSIG; well beyond our proposed pressures of 500-1,000 psig when used with hydrogen and only 70 psig when being used with the dimethyl ether solvent system.

A promising observation with the hydrogen-pressurized reactions was realized when aluminum anode in a cell at 500 psig hydrogen with a 1.5 V potential would be rapidly consumed. The Al electrode degradation after a 12 hour run is shown in Figure 2a. The majority of the electrode deterioration occurs at the surface of the solvent as is interfaces with the pressurized hydrogen. This should make it possible to design a cell that will accommodate electrodes that are made of spent alane (aluminum metal) and recycle this into the reaction. An early version of this electrode is pictured in Figure 2b, showing each electrode as a hollow glass frit that holds the aluminum powder and allows for the reaction solution to flow through.

The cathode also is fabricated from another fritted electrode. This time, the electrode is filled with catalyzed aluminum powder. With this type of set up, the catalyzed aluminum (Al^*) is expected to react with the LiH byproduct (formed during the electrolysis of LiAlH_4 and while under pressurized hydrogen) and reform LiAlH_4 as per the reaction: $\text{LiH} + \text{Al}^* + \text{H}_2 \rightarrow \text{LiAlH}_4$

This type of reaction has been recently reported as a process for regeneration of LiAlH_4 [9].

We have shown this will fit with our proposed electrochemical cell using the spent alane. In our study, alane containing a catalytic amount (~0.2 mole %) of Ti-catalyst was thermally decomposed to remove all hydrogen, leaving the activated catalyzed aluminum. This activated catalyzed aluminum was then transferred into a Parr reactor containing LiH in THF. After 12 hours of stirring the spectrum of the Fourier transform infrared analysis of the solution had shown



FIGURE 2. a) The aluminum anode from a hydrogen-pressurized cell showing the decomposition that occurs near the solvent/hydrogen interface. b) First generation of proposed fritted electrodes to house spent alane (aluminum powder) in the anode and activated spent alane (aluminum powder with Ti-catalyst) to recycle the alane as it is used in hydrogen delivery.

the appearance of an Al-H stretch at $1,650\text{ cm}^{-1}$, indicative of the presence of LiAlH_4 .

Based on our initial results of this cycling reaction in the electrochemical cell more experimental work and cell design needs to be conducted to achieve a more efficient cycle. The initial porous frit electrode proved to be too small to be useful in this operation. None-the-less, this design was only the first of a new line of modified porous electrodes with the most recent and much larger porous electrodes ready now for future experiments.

The study on the economical isolation of the alane from the THF continues. Latest results show that the alane-THF adduct can be crystallized out of a toluene solution containing the electrolytic solution. It was found that the solid material $\text{AlH}_3\cdot 2\text{THF}$ appears quite readily after this solution is heated to $\sim 70^\circ\text{C}$. The resulting solid, shown in Figure 3a, was found to be considerably stable, being insoluble in several solvents; including THF. This material demonstrates an easy route to isolate the solid alane material and is

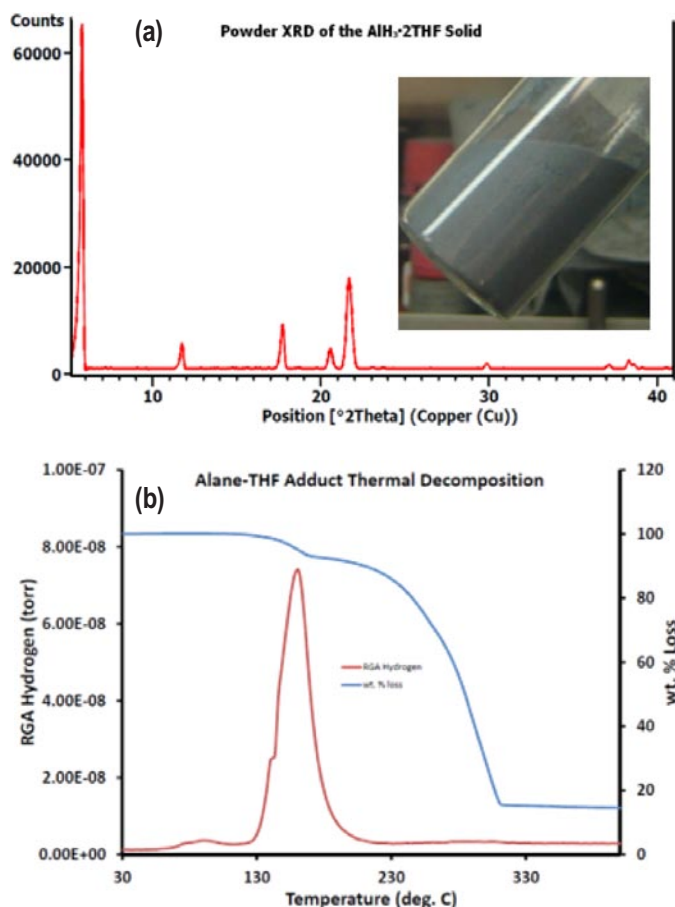


FIGURE 3. a) A sample of the crystallized alane/THF adduct and the powder pattern indicative of alane-2THF adduct; still with the typical alane-grey appearance. This material shows added stability as it remains insoluble in several solvents, including THF. b) The TGA of this alane/THF adduct showing a combination release of hydrogen and THF.

currently being investigated as an intermediate to the alpha alane recovery. The thermal decomposition of this material (Figure 3b) shows an apparent release of hydrogen prior to the THF loss. Calculations of the recorded weight loss and residual gas analysis (RGA) indicate, however, that the THF release onset coincides with the release of hydrogen.

In a related study, electrochemical cells were run that contained saturated lithium aluminum hydride (LAH, LiAlH_4) in THF. This concentrated LAH/THF electrolyte was obtained by gently heating and stirring a mixture of excess LAH in THF using a Parr pressure reactor set at 75°C . After filtering out the undissolved LAH, the resulting solution was somewhat viscous but relatively clear. The cell, shown in Figure 4a is fitted with an aluminum anode and a palladium cathode. The maximum current flow was the highest ever recorded for these types of reactions at some 200 mA, peaking at four hours into the experiment. After only around seven hours of applied current, the anode area in



FIGURE 4. a) Showing a glass frit-divided electrochemical cell with an aluminum anode and palladium cathode in place. b) The saturated LAH-THF solution forces the alane-THF adduct to precipitate at the anode as a grey-white solid.

the electrochemical cell, shown in Figure 4b, was filled with a grey solid. Analysis of this solid revealed it was composed mainly of alane-2THF. As suspected, the saturated solution forced the alane adduct to solidify as it was formed in the solution. The solution also contained a considerable amount of alane as the dissolved THF adducted material. The same saturated solution using etherates will be conducted in the future. While the aluminum anode remained unchanged (in the absence of pressurized hydrogen) the palladium cathode lacked any dendrite formation and, instead, was covered with a fine black coating of activated aluminum. Both of these results combined have shown great results in the advancement of the electrochemical generation of alane.

Conclusions and Future Directions

- Perform electrochemical production of alane and alane adducts based on etherates in a pressurized solvent environment and demonstrate production of α -alane.
- Investigate the recycling of LiH into LAH in situ during electrochemical production of alane.
- Work with industrial partners to lower the cost of alane production for use as high energy density storage materials in near term portable power systems.
- Continued production of gram quantities of alane with improving energy efficiency.

Patents Issued

1. Two Steps Hydrogen System Based on Dehydriding and Hydrolysis Enhanced by Novel Additives to Alane and Activated Al, *Pending*.
2. Novel Method for Synthesizing Alane without the Formation of Adducts and Free of Halides, *Pending*.
3. Enhancing Electrochemical Methods for Producing and Regenerating Alane by Using Electrochemical Catalytic Additive, *Pending*.

FY 2012 Publications [PU]/Presentations [PR]

1. Michael J. Martínez-Rodríguez, Brenda L. García-Díaz, Joseph A. Teprovich Jr., Douglas A. Knight, Ragaïy Zidan, “Advances in the Electrochemical Regeneration of Aluminum Hydride” *Applied Physics A*, 2011 Vol106, Issue 3, pp.545-550 [PU].
2. Long V. Dinh, Douglas A. Knight, Mark Paskevicius, Craig E. Buckley and Ragaïy Zidan “Novel methods for synthesizing halide-free alane without the formation of adducts” *Applied Physics A*, 2012 Vol. 107, No. 1, 173-181 [PU].

3. Joseph A. Teprovich Jr., Theodore Motyka, Ragaïy Zidan” Hydrogen system using novel additives to catalyze hydrogen release from the hydrolysis of alane and activated aluminum” *Int. J. of Hydrogen Energy* 2012 Vol. 3, Issue 2, 1594-1603 [PU].
4. “Advances in Materials and Methods for Hydrogen Storage” Gordon Research Conference July 17–22, 2011 Stonehill College Easton, MA Invited Speaker [PR].
5. “Progress in the Electrochemical Formation of Alane” MRS San Francisco, March 2011, Invited Speaker [PR].
6. “Development and Characterization of Novel Hydrogen Storage Materials” IEA January 16 2011 Fremantle, Copenhagen, Denmark, September 2011 [PR].

References

1. G. Sandrock, J. Reilly, J. Graetz, W.M. Zhou, J. Johnson and J. Wegrzyn, *J. Alloys Compd.*, 2006, 421, 185-189.
2. J. Graetz and J.J. Reilly, *Journal of Physical Chemistry B*, 2005, 109, 22181-22185.
3. H. Clasen, Germany Pat., 1141 62315. H. Clasen, Germany Pat., 1141 623, 1962.2, 1962.
4. N.M. Alpatova, T.N. Dymova, Y.M. Kessler and O.R. Osipov, *Russ. Chem. Rev.*, 1968, 37, 99.
5. Ragaïy Zidan, Brenda L. Garcia-Diaz, Christopher S. Fewox, Ashley C. Stowe, Joshua R. Gray and Andrew G. Harter *Chem. Commun.*, 2009, 3717-3719, 114.
6. Improving Electrochemical Methods for Producing and Regenerating Alane by the Addition of Halides to Electrolyte, *Patent pending*.
7. H. Senoh, T. Kiyobayashi, N. Kuriyama, K. Tatsumi and K. Yasuda, *J. Power Sources*, 2007, 164, 94-99.
8. H. Senoh, T. Kiyobayashi and N. Kuriyama, *Int. J. Hydrogen Energy*, 2008, 33, 3178-3181.
9. (a) Graetz, Jason; Wegrzyn, James; Reilly, James J.; *JACS* (2008), 130(52), 17790-17794. (b) Lacina, David; Yang, Liu; Chopra, Irinder; Muckerman, James; Chabal, Yves; Graetz, Jason; *Phys. Chem. Chem. Phys.*, (2012), 14(18), 6562-6569.

IV.A.7 Hydrogen Storage Materials for Fuel Cell-Powered Vehicles*

Andrew Goudy
Delaware State University
1200 N. Dupont Highway
Dover, DE 19901
Phone: (302) 857-6534
Email: agoudy@desu.edu

DOE Managers
HQ: Ned Stetson
Phone: (202) 586-9995
Email: Ned.Stetson@ee.doe.gov.
GO: Katie Randolph
Phone: (720) 356-1759
Email: Katie.Randolph@go.doe.gov

Contract Number: DE-FC36-06GO86046

Start Date: July 1, 2006
Projected End Date: May 30, 2013

*Congressionally directed project

Fiscal Year (FY) 2012 Objectives

The objectives of this project are to:

- Identify complex hydrides, such as the $\text{LiNH}_2/\text{MgH}_2$ system and the $\text{LiBH}_4/\text{MgH}_2$ system, that have great hydrogen storage potential.
- Develop new catalysts and engineering techniques for increasing reaction rates and lowering reaction temperatures.
- Perform kinetic modeling studies and develop methods for improving kinetics and lowering reaction temperatures using MgH_2 as a model system.

Technical Barriers

This project addresses the following technical barriers taken from the Hydrogen Storage section of the Fuel Cells and Infrastructure Technologies Program Multi-Year Research, Development and Demonstration Plan:

- (A) System Weight and Volume
- (D) Durability/Operability
- (E) Charging/Discharging Rates

Technical Targets

This project is conducting fundamental studies of complex borohydride materials and other promising hydrogen

storage materials. Insights gained from these studies will be applied toward the design and synthesis of hydrogen storage materials that meet DOE's 2015 goal of 5.5 weight percent hydrogen storage for the system. Table 1 summarizes the targets.

TABLE 1. Technical Targets

| Storage Parameter | Units | Target |
|--|---------|--------|
| System Gravimetric Capacity: Usable, specific-energy from H_2 (net useful energy/max system mass) | kW.h/kg | 1.5 |
| System Volumetric Capacity: Usable energy density from H_2 (net useful energy/max system volume) | kW.h/L | 1.2 |
| Storage System Cost | \$/kWh | 6 |

FY 2012 Accomplishments

- Several borohydride systems have been kinetically modeled and the rate controlling process has been identified.
- The desorption properties of a $\text{MgH}_2/\text{LiBH}_4$ system have been determined. Temperature-programmed desorption (TPD) results show that NbF_5 and Nb_2O_5 catalysts are more effective in lowering desorption temperatures than MgNi_2 . Kinetics measurements show that NbF_5 is vastly superior to the other catalysts in improving reaction rates and that desorption is faster than that from MgH_2 .
- We have compared the dehydriding kinetics of several borohydride systems at constant pressure driving forces and found that a mixture of $\text{Mg}(\text{BH}_4)_2/\text{Ca}(\text{BH}_4)_2$ releases hydrogen faster than either individual borohydride. Modeling results indicate that the rate of hydrogen release from $\text{Mg}(\text{BH}_4)_2$, during the first 80% of the reaction, is diffusion controlled while in $\text{Ca}(\text{BH}_4)_2$ the reaction rate is phase boundary controlled. In the mixture the rate appears to be under the mixed control of both processes.
- Mixtures with initial molar compositions of $(\text{LiNH}_2 + \text{MgH}_2)$ and $(2\text{LiNH}_2 + \text{MgH}_2)$ were studied with and without the presence of 3.3 mol% potassium hydride dopant. TPD analyses showed that the potassium hydride doped samples had lower onset temperatures than their corresponding pristine samples.
- The addition of potassium hydride dopant was found to have a 25-fold increase on the desorption rates of the $(2\text{LiNH}_2 + \text{MgH}_2)$ mixture, however it had almost no effect on the desorption rates of the $(\text{LiNH}_2 + \text{MgH}_2)$ mixture. The catalyzed $(2\text{LiNH}_2 + \text{MgH}_2)$ mixture reacted faster than the catalyzed $(\text{LiNH}_2 + \text{MgH}_2)$ mixture.

- The design, fabrication and demonstration of a hydride-based hydrogen storage system for fuel cell is underway. Results show that the heat removal rate can be increased by increasing the effective thermal conductivity by mixing the metal hydride with conductivity-enhanced materials such as aluminum foam or graphite.



Introduction

There has been considerable interest in complex hydrides such as borohydrides and amides because they have been determined to have great potential to meet DOE's goals for hydrogen storage. Current efforts in our research lab are focused on performing hydrogen storage studies on some new destabilized complex hydrides that have been predicted by first principles calculations to be suitable hydrogen storage materials. We will develop methods for the synthesis, characterization, and modeling of these new complex hydrides as well as developing new catalysts and engineering techniques for increasing reaction rates and lowering reaction temperatures. We will also extend these studies to include carbon materials, metal organic frameworks (MOFs) and possibly other nanostructured and porous materials as potential hydrogen storage materials. Once a suitable material has been identified for hydrogen storage it will be necessary to design, fabricate and test a hydride-based hydrogen storage system for fuel cell applications. Efforts are currently underway with a partner institution to design a hydrogen storage system and test it using a suitable material. This phase of the research will include using flow, reaction kinetics and thermal modeling, followed by system design, fabrication and performance evaluation.

Approach

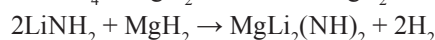
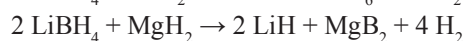
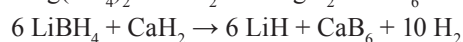
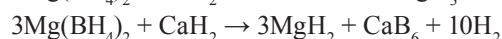
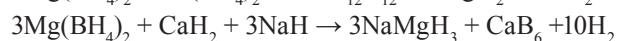
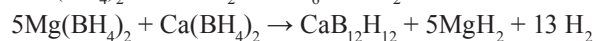
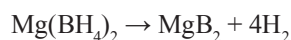
To achieve the project objectives, it was first necessary to design suitable methods using MgH_2 as a model system. These methods included:

- Synthesis of new materials by mechanical alloying using ball milling.
- Determining thermal stability using thermogravimetric analysis or TPD.
- Using X-ray diffraction to determine phase purity and crystal structure.
- Using pressure-composition isotherm analyses to determine thermodynamic stability.
- Finding catalysts for making the hydriding faster and reversible.
- Determining kinetic rate curves using constant pressure driving forces.

- Performing modeling to gain understanding of the mechanism.
- Studying other classes of promising hydrogen storage materials.

Results

First principles calculations have predicted that the following systems may be thermodynamically suitable for hydrogen storage.



Therefore several of these systems were studied thermodynamically and kinetically to confirm the theoretical predictions. A system of particular interest was the $\text{Mg}(\text{BH}_4)_2/\text{Ca}(\text{BH}_4)_2$ system. Calculations showed that a mixture of the two components would have better thermodynamic properties than those of either constituent. TPD curves were constructed for the $\text{Mg}(\text{BH}_4)_2/\text{Ca}(\text{BH}_4)_2$ mixture in the stoichiometric ratio of 5:1, along with those for pure $\text{Mg}(\text{BH}_4)_2$ and pure $\text{Ca}(\text{BH}_4)_2$. The curves shown in Figure 1 indicate that the mixture releases hydrogen at a lower temperature than $\text{Mg}(\text{BH}_4)_2$ or $\text{Ca}(\text{BH}_4)_2$. The kinetics of the $\text{Mg}(\text{BH}_4)_2/\text{Ca}(\text{BH}_4)_2$ mixture as well as those of the pure $\text{Mg}(\text{BH}_4)_2$ and $\text{Ca}(\text{BH}_4)_2$ components were also performed. Figure 2a contains plots in which the kinetics of the borohydrides are compared. It can be seen that the $\text{Mg}(\text{BH}_4)_2/\text{Ca}(\text{BH}_4)_2$ mixture has faster kinetics than either $\text{Mg}(\text{BH}_4)_2$ or $\text{Ca}(\text{BH}_4)_2$.

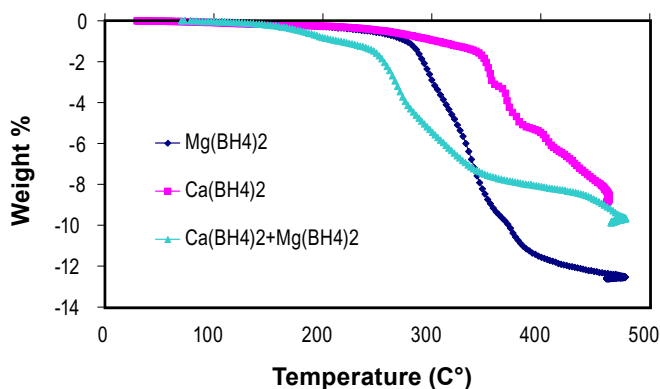


FIGURE 1. TPD profiles for $\text{Mg}(\text{BH}_4)_2$, $\text{Ca}(\text{BH}_4)_2$ and a mixture of the two compounds. A mixture of $\text{Mg}(\text{BH}_4)_2/\text{Ca}(\text{BH}_4)_2$ releases hydrogen at a lower temperature than either individual borohydride.

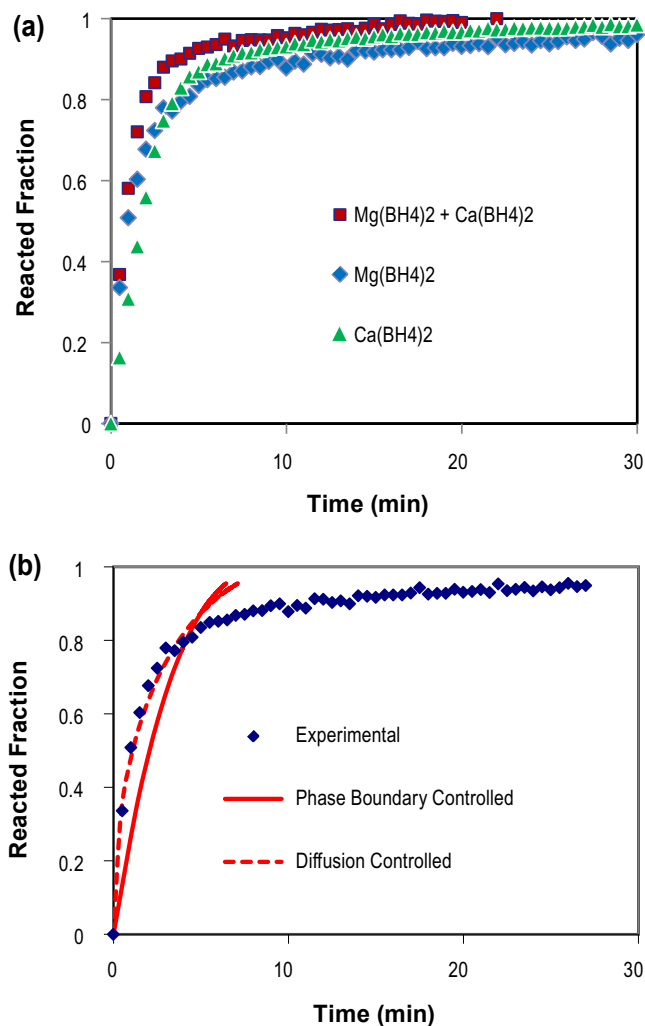


FIGURE 2. Figure 2a shows that the mixture desorbs hydrogen faster than either pure component. Figure 2b shows that the rate-controlling process for hydrogen desorption from $\text{Mg}(\text{BH}_4)_2$ is diffusion. Different processes controlled the kinetics for desorption from $\text{Ca}(\text{BH}_4)_2$ and the $\text{Mg}(\text{BH}_4)_2/\text{Ca}(\text{BH}_4)_2$ mixture.

An attempt was also made to determine the rate-controlling process in these samples by doing kinetic modeling. The theoretical equations that were used are shown below:

$$\frac{t}{\tau} = 1 - (1 - X_B)^{1/3} \quad (1)$$

$$\text{Where } \tau = \frac{\rho_B R}{b k_s C_{Ag}}$$

$$\frac{t}{\tau} = 1 - 3(1 - X_B)^{2/3} + 2(1 - X_B) \quad (2)$$

$$\text{Where } \tau = \frac{\rho_B R^2}{6bD_e C_{Ag}}$$

Where t is the time at a specific point in the reaction, X_B is the fraction of the metal reacted. R is the initial radius of

the hydride particles, ' b ' is a stoichiometric coefficient of the metal, C_{Ag} is the gas phase concentration of reactant, D_e is the effective diffusivity of hydrogen atoms in the hydride, r_B is the density of the metal hydride and k_s is a rate constant.

The model based on Eq. (1) will have chemical reaction at the phase boundary controlling the reaction rate whereas a model based on Eq. (2) is one in which diffusion controls the overall reaction rate. Both equations were fitted to the kinetic data for $\text{Mg}(\text{BH}_4)_2$, $\text{Ca}(\text{BH}_4)_2$ and $\text{Mg}(\text{BH}_4)_2 + \text{Ca}(\text{BH}_4)_2$. Figure 2b contains modeling plots for $\text{Mg}(\text{BH}_4)_2$, based on the kinetics data in Figure 2a. In the graph, one curve is an experimental curve, a second curve is based on the overall rate being controlled by diffusion, and a third curve is calculated based on chemical reaction controlling the rate. The plots in Figure 2b show a good fit for a diffusion controlled model up to 80% of the reaction but not beyond. This means that the process controlling hydrogen desorption of this reaction at the later stage of the reaction is different from that at the beginning. Kinetic modeling was also done on $\text{Ca}(\text{BH}_4)_2$ and $\text{Mg}(\text{BH}_4)_2 + \text{Ca}(\text{BH}_4)_2$ mixture. The results indicate that the rate of hydrogen release from $\text{Mg}(\text{BH}_4)_2$, during the first 80% of the reaction, is diffusion controlled while in $\text{Ca}(\text{BH}_4)_2$ the reaction rate is phase boundary controlled. In the mixture the rate appears to be under the mixed control of both processes.

Another system that was studied was $\text{LiBH}_4\text{-MgH}_2$. This system shows excellent hydrogen storage capacity but it still has the problem of sluggish kinetics. In order to improve the hydrogen desorption kinetics, mixtures of $\text{LiBH}_4\text{-MgH}_2$ (2:1) were doped with 4 mol% NbF_5 , Nb_2O_5 , and Mg_2Ni . The hydrogen desorption kinetics of these mixtures were compared using constant pressure thermodynamic forces in which the ratio of the equilibrium plateau pressure to the opposing plateau was the same for all the reactions studied. Figure 3 contains plots of reacted fraction versus time for hydrogen desorption from the samples. It can be seen from the plots that the un-catalyzed borohydride sample mixture has the slowest hydrogen desorption rate. The addition of

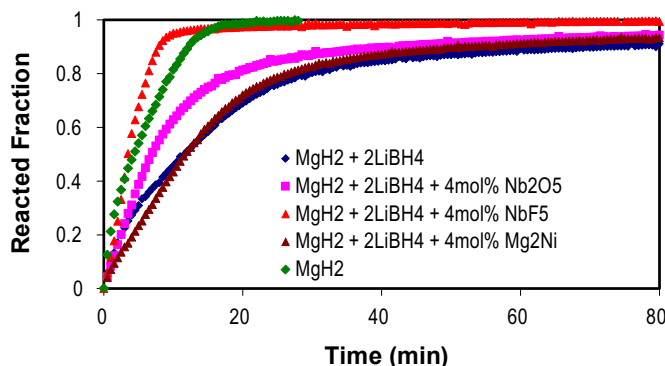


FIGURE 3. Kinetics measurements done at $N = 3$ and 450°C show that NbF_5 is vastly superior to the other catalysts in improving reaction rates.

4 mol% Mg_2Ni to the $2\text{LiBH}_4\text{-MgH}_2$ mixture does not have any significant effect on the reaction kinetics. However, the niobium-based catalysts are very effective in improving the kinetics of the mixture. The sample mixture doped with 4 mol% NbF_5 in particular has exceptionally fast desorption reaction kinetics. Under the conditions used, the NbF_5 -catalyzed mixture releases approximately 80% of its hydrogen in 6.5 minutes, whereas the Nb_2O_5 -catalyzed mixture takes 20 minutes and the un-catalyzed borohydride sample takes 30 minutes to release the same percentage of hydrogen. It is interesting to note that the NbF_5 -catalyzed borohydride mixture is the only one to release hydrogen faster than pure MgH_2 . These results showed NbF_5 to be vastly superior to the other catalysts for improving the kinetics of the composite mixture with the hydrogen desorption rates being in the order: $\text{NbF}_5 \gg \text{Nb}_2\text{O}_5 > \text{Mg}_2\text{Ni}$. Desorption enthalpies that were obtained from van't Hoff plots indicated that the thermodynamic stabilities of the catalyzed mixtures were in the order: $\text{NbF}_5 < \text{Nb}_2\text{O}_5 < \text{Mg}_2\text{Ni}$. Modeling studies indicated that chemical reaction at the phase boundary was the most likely process controlling the reaction rates for the catalyzed mixtures.

Another system that was studied was $\text{LiNH}_2\text{-MgH}_2$. Lithium amide and magnesium hydride are lightweight materials with high hydrogen-holding capacities and thus they are of interest for hydrogen storage. Mixtures with initial molar compositions of $(\text{LiNH}_2 + \text{MgH}_2)$ and $(2\text{LiNH}_2 + \text{MgH}_2)$ were ball milled with and without the presence of 3.3 mol% potassium hydride dopant. TPD analyses of the mixtures showed that the potassium hydride doped samples had lower onset temperatures than their corresponding pristine samples. The dehydrogenation kinetics of the doped and pristine mixtures was compared at 210°C . In each case a constant pressure thermodynamic driving force was applied in which the ratio of the plateau pressure to the

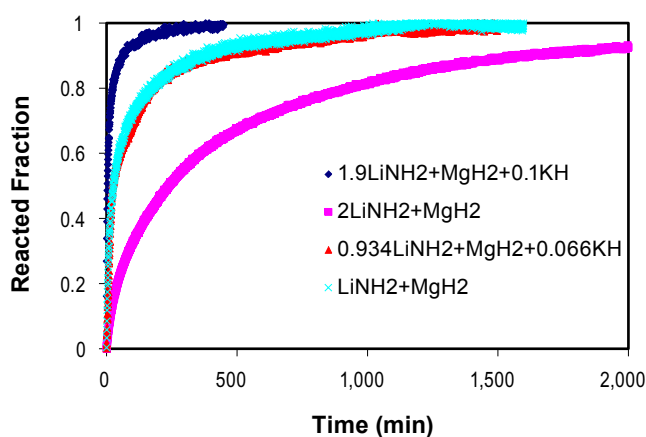


FIGURE 4. Desorption kinetics were done at 210°C and $N = 10$. There is a dramatic improvement in the desorption rates in the $2\text{LiNH}_2 + \text{MgH}_2$ system but virtually no improvement in the $\text{LiNH}_2 + \text{MgH}_2$ system.

applied hydrogen pressure was set at 10. It can be seen from Figure 4 that the doped ($1.9\text{LiNH}_2 + \text{MgH}_2 + 0.1\text{KH}$) sample has the fastest desorption reaction kinetics while its pristine ($2\text{LiNH}_2 + \text{MgH}_2$) sample has the slowest desorption reaction kinetics. The KH seems to have no effect on the desorption kinetics of ($0.934\text{LiNH}_2 + \text{MgH}_2 + 0.066\text{KH}$) when compared with its pristine sample, ($\text{LiNH}_2 + \text{MgH}_2$). The doped and pristine samples both take approximately the same time for hydrogen desorption. Activation energies were determined by the Kissinger method. Results showed the potassium hydride doped mixtures to have lower activation energies than the pristine mixtures.

Another project has been ongoing entitled “Design, Fabrication and Demonstration of a Hydride-Based Hydrogen Storage System for Fuel Cell Applications.” The overall objective is to improve the rate at which the hydrogen gas can be charged into a hydride-based hydrogen storage tank, and to improve the hydrogen storage density. A mathematical model is being used to predict the temperature at selected locations within the storage tank. A series of experiments have been performed to compare the temperature at these locations with the numerically predicted value. All of this work is being done by our partners at the University of Delaware.

Conclusions and Future Directions

- The results of this study show that the rate of hydrogen desorption from $\text{Mg}(\text{BH}_4)_2$ can be increased by mechanically alloying it with $\text{Ca}(\text{BH}_4)_2$. Modeling studies indicate that the rate of hydrogen release from $\text{Mg}(\text{BH}_4)_2$, during the first 80% of the reaction, is diffusion controlled while in $\text{Ca}(\text{BH}_4)_2$ the reaction rate is phase boundary controlled. In the mixture the rate appears to be under the mixed control of both processes.
- Kinetics and modeling studies on a $2\text{LiBH}_4/\text{MgH}_2$ system show that the hydrogen desorption rates are in the order: $\text{Mg}_2\text{Ni} < \text{Nb}_2\text{O}_5 \ll \text{NbF}_5$. All of these findings indicate that NbF_5 is vastly superior to the other materials for catalyzing the $2\text{LiBH}_4/\text{MgH}_2$ system. The modeling studies indicate that chemical reaction at the phase boundary is the likely rate-controlling process in all of the catalyzed mixtures.
- Kinetics studies on a $\text{LiNH}_2/\text{MgH}_2$ system have shown that KH is a very effective catalyst for the desorption of hydrogen from the $\text{MgH}_2\text{-}2\text{LiNH}_2$ system but not so effective for $\text{MgH}_2\text{-LiNH}_2$ system.

In FY 2013, the following work is planned:

- Continue to perform absorption and desorption kinetics and modeling studies on several catalyzed $\text{MgH}_2/\text{Amide}$ and $\text{MgH}_2/\text{LiBH}_4$ based destabilized systems using constant pressure driving forces.

- Continue the cycling studies on amide and borohydride reactions.
 - Use techniques such as residual gas analysis to determine if dehydrogenation is accompanied by the release of other gaseous byproducts such as ammonia and diborane.
 - Extend the studies to include carbon materials and MOFs.
 - Continue to collaborate with Sonjong Hwang at Cal Tech in solid state nuclear magnetic resonance analyses of reaction intermediates in hydriding/de-hydriding reactions.
 - Continue with the design, fabrication and demonstration of a hydride-based hydrogen storage system that is on-going with our collaborators at the University of Delaware.
3. Andrew Goudy, Adeola Ibikunle, Saidi Sabitu and Tolulope Durojaiye, “Thermodynamics and Kinetics of Complex Borohydride and Amide Hydrogen Storage Materials” Proceedings of the MCARE Conference, 2012.
 4. Andrew Goudy, “Thermodynamics, Kinetics and Modeling Studies on Hydrogen Storage Materials”, Low Carbon Earth Summit, Dalian, China, October 2011.
 5. Synthesis of New Naphthalene Linkers for the Incorporation in Hydrogen Storing Metal Organic Frameworks Bryan Wakefield, Andrew Goudy, Samuel Orefuwa, Lewis Q. Lott, Dante Alexander, Andre Kerr, ACS Meeting, Washington, D.C., 2011.
 6. Andrew Goudy, “Thermodynamics and Kinetics of Complex Borohydride and Amide Hydrogen Storage Materials”, Materials Challenges in Alternative & Renewable Energy, Clearwater Beach, FL, 2012.
 7. Hongwei Yang, Samuel Orefuwa and Andrew Goudy, “Solvent-Assisted Mechanochemical Synthesis of Metal-Organic Framework $\text{Cu}_3(\text{BTC})_2$ for Hydrogen Storage” MRS Fall meeting, April 9 – April 13, 2012, San Francisco, CA.

FY 2012 Publications/Presentations

1. Samuel A. Orefuwa, Hongwei Yang, and Andrew J. Goudy, “Rapid Solvothermal Synthesis of an Isoreticular Metal Organic Framework with Permanent Porosity for Hydrogen Storage”, Micropor. Mesopor. Mater., 153 (2012) 88–93.
2. Durojaiye T, Goudy A, “Desorption kinetics of lithium amide/magnesium hydride systems at constant pressure thermodynamic driving forces”, Int. J. Hyd. Energy, 37 (2012) 3298-3304.

IV.B.1 Hydrogen Storage by Novel CBN Heterocycle Materials

Shih-Yuan Liu
University of Oregon
Department of Chemistry
1253 University of Oregon
Eugene, OR 97403-1253
Phone: (541) 346-5573
Email: lsy@uoregon.edu

DOE Managers
HQ: Grace Ordaz
Phone: (202) 586-8350
Email: Grace.Ordaz@ee.doe.gov
GO: Katie Randolph
Phone: (720) 356-1759
Email: Katie.Randolph@go.doe.gov

Contract Number: DE-FG36-08GO18143

Project Start Date: September 1, 2008
Project End Date: September 30, 2012

- (E) Charging/Discharging Rates
- (R) Regeneration Processes

Technical Targets

This project is developing new liquid phase materials for hydrogen storage that can be readily regenerated. Insights gained from these studies will be applied toward the design and synthesis of hydrogen storage materials that meet the following DOE 2017 hydrogen storage targets:

- Specific energy: 1.8 kWh/kg (5.5 wt%)
- Energy density: 1.3 kWh/L (4.0 vol%)

FY 2012 Accomplishments

- Optimized first-fill synthesis of 6-membered N-Me fuel system (**1'**).
- Characterized thermodynamics of H₂ release from N-Me (**1'**).
- Optimized dehydrogenation/trimerization reaction of **1** with cheap and relatively environmentally benign FeCl₂.
- Explored various strategies to regenerate spent fuel materials using less energetically costly reagents.



Fiscal Year (FY) 2012 Objectives

The objective of this project is to develop novel boron-nitrogen heterocycles as liquid-phase hydrogen storage materials with storage capacities and thermodynamic properties that have the potential to lead to rechargeable systems capable of meeting DOE targets. We seek to:

- Develop new materials that:
 - are structurally well-defined along the desorption/absorption processes
 - exhibit appropriate enthalpy of H₂ desorption
 - are liquids at operating temperatures
 - possess high H₂ storage capacities
- Identify catalysts that will release hydrogen from these materials at temperatures <200°C.
- Develop conditions that will readily recharge the spent fuel.

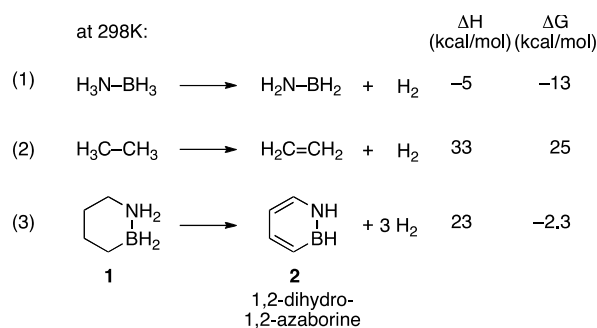
Technical Barriers

This project addresses the following technical barriers from the Hydrogen Storage section of the Fuel Cell Technologies Program Multi-Year Research, Development and Demonstration Plan:

- (A) System Weight and Volume
- (C) Efficiency

Introduction

Hydrogen storage is a vital component in the development of a hydrogen-based energy infrastructure. Boron nitrogen containing compounds, e.g., ammonia-borane (H₃N–BH₃ or AB), have attracted much attention as chemical H₂ storage materials because of their high gravimetric hydrogen densities and fast kinetics of H₂ release. This project is developing structurally well-defined liquid carbon-boron-nitrogen (CBN) hydrogen storage materials (i.e., heterocycles containing carbon, boron, and nitrogen) that have the potential to be reversibly regenerated using molecular hydrogen. A liquid phase, hydrogen storage system that can be regenerated using molecular hydrogen is highly desired for many reasons, including versatility, lower cost and improved efficiency, and durability. Such a storage material will allow onboard hydrogen storage. It can also be applied as an off-board energy carrier for vehicle and stationary applications that takes advantage of the existing liquid fuels infrastructure.



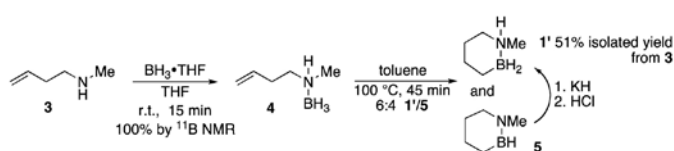
Approach

In order to accomplish reversibility, neutrality in free energy of the hydrogen release process (i.e., $\Delta G \sim 0$ kcal/mol) at the operating temperature is pivotal. The dehydrogenation of AB is exergonic by -13 kcal/mol at 298 K (eq 1). In contrast to AB, the dehydrogenation of its isoelectronic organic counterpart, ethane (CH_3-CH_3), is endergonic by $+25$ kcal/mol (eq 2). The coupling of endothermic dehydrogenation from CC with exothermic dehydrogenation from BN in a cyclic six-membered framework could lead to a reversible H_2 storage system. Indeed, high-level computational analysis indicates that the release of H_2 from CBN heterocycles such as **1** has favorable overall thermodynamics conducive to reversibility, (e.g., see eq 3). The potential for reversible hydrogen release/uptake and the relatively high gravimetric hydrogen density of CBN heterocycle materials (e.g. 7.1 wt% for **1**) render their preparation and development an important goal. This project is investigating several CBN heterocycle materials for H_2 storage applications using a synergistic theoretical and experimental approach. Synthesis will be a crucial component of this project given the relatively unexplored nature of these CBN heterocycles. The structurally well-defined nature of these CBN heterocycle materials will facilitate their characterization and mechanistic investigation of the proposed desorption/absorption processes.

Results

Optimized First-Fill Synthesis of **1'**

We have further optimized the synthesis of **1'** and now report the gram-scale overall yield from amine **3** to be 51% (Scheme 1). This was achieved by careful monitoring of the “ring-closing” step: utilizing a shorter reaction time (45 min vs 1 hour) and a slightly lower temperature (100°C vs 110°C) promoted the formation of **1'** and reduced the formation of the species **5**. The resulting mixture could be separated by distillation and **5** could be converted to **1'** by sequential treatment with KH and HCl.



SCHEME 1. Optimized synthesis of **1'**

Experimental Measurement of Thermodynamics of H_2 Release from **1'**

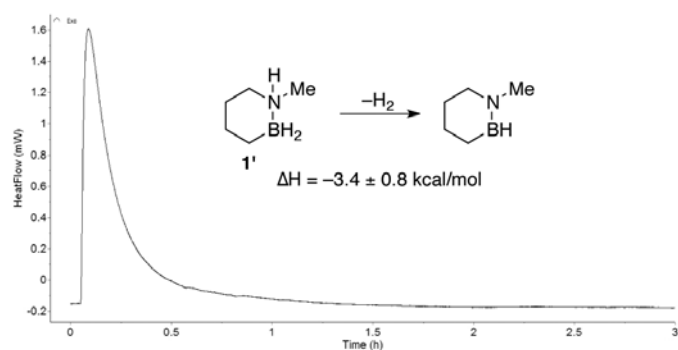
We have found the optimal catalyst for our calorimetric dehydrogenation experiments, $\text{Cl}_2(\text{PPh}_3)_3\text{Ru}$ at 10 mol % loading, and used it to perform thermodynamic measurements for the dehydrogenation of the N-Me model fuel **1'** (Scheme 2). We measured the enthalpy of dehydrogenation to be -3.4 ± 0.8 kcal/mol compared to a predicted $\Delta H = -4.9$ kcal/mol (G3/MP2). This is more exothermic by 2.02 kcal/mol than the value we previously measured for the N-tBu substituted model fuel (-1.38 ± 0.12 kcal/mol).

Dehydrogenation of **1** Using FeCl_2

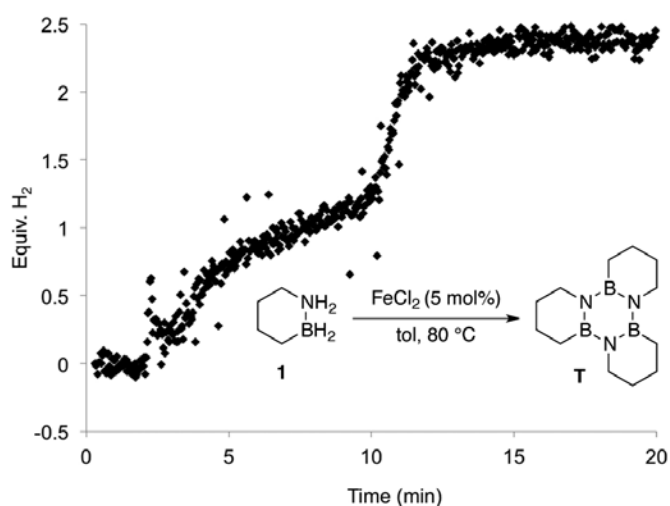
Last year we reported the discovery that CoCl_2 , efficiently promoted hydrogen loss from our CBN fuel materials. More recently, we were pleased to find that FeCl_2 enabled clean dehydrogenation and trimer formation from **1** at a reasonable rate and yield under the same conditions (80°C , 5 mol% catalyst loading). Interestingly, the shape of the FeCl_2 promoted H_2 release curve shown in Scheme 3 differs considerably from CoCl_2 . The loss of the first equivalent of H_2 takes place within seven minutes of the start of the reaction, slow compared to cobalt. The loss of the second equivalent of H_2 proceeds more quickly and the reaction is complete within 12 minutes.

Potential Regeneration Pathways

We previously reported conditions to regenerate the spent fuel trimer **T** via treatment with excess MeOH and



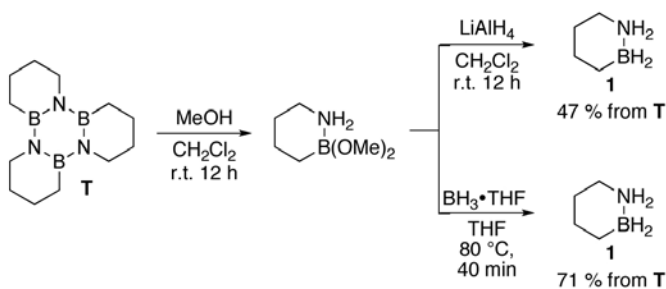
SCHEME 2. Representative calorimeter heat flow trace for the dehydrogenation of **1'**



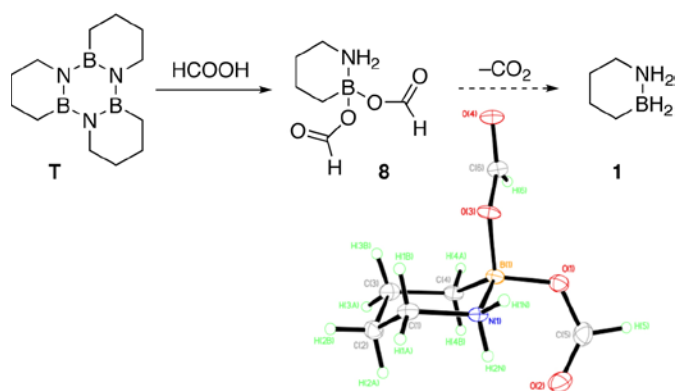
SCHEME 3. Burette measurement of hydrogen release from **1** catalyzed by FeCl_2

subsequent addition of 2 equivalents LiAlH_4 to generate the parent fuel **1** in 47% overall yield (Scheme 4). In an effort to optimize the yield of the regeneration sequence and utilize milder hydride sources, we found that treatment of the $\text{B}(\text{OMe})_2$ intermediate with $\text{BH}_3\cdot\text{THF}$ at 80°C for 40 minutes afforded the fully charged fuel **1** in 71% yield over two steps. We also attempted digestion of the trimer with formic acid, which is synthetically available from the hydrogenation of CO_2 . We found that treatment of **T** with 7 equiv. formic acid smoothly generated the monomeric bisformate adduct **8** (Scheme 5). We are currently working to find conditions to regenerate the fully charged fuel **1** by decarboxylation (i.e., loss of CO_2) of species **8** and thus eliminate the need for high-energy reagents (e.g., LAH, KH, BH_3).

We have also pursued lower-energy regeneration strategies predicated on avoiding the formation of strong B-O bonds. Hydrazine has been used to “digest” and regenerate the polymeric reaction products (e.g. polyborazylene) of the dehydrogenation of ammonia borane [1]. When excess hydrazine was added to **T** without additional solvent and heated to 90°C overnight, approximately 25% conversion to the bishydrazine adduct was observed by ^{11}B NMR. When



SCHEME 4. Regeneration of spent-fuel trimer **T**



SCHEME 5. Digestion of trimer **T** with formic acid

two equivalents of hydrazine (per B equivalent) were added to a toluene solution of **T** and heated at 150°C overnight, approximately 25% of conversion to monohydrazine adduct was observed. In both cases, no other boron-containing products formed, but we were unable to increase the yield to useable levels. *Ortho*-benzenedithiol has also been used for the digestion of polyborazylene [2]. Treatment of **T** with one equiv. benzenedithiol (per boron equivalent) in tetrahydrofuran at 90°C for 24 hours resulted in <10% conversion to the boron-sulfur adduct **8** (identified by ^{11}B NMR comparison to a sample of **8** synthesized from **1**) in addition to ~5% of an unidentified boron-containing product.

Conclusions and Future Directions

In summary, we have optimized the synthesis of 6-membered N-substituted material **1'** concluding the materials optimization portion of our Phase II goals. We measured the enthalpy of hydrogen release from **1'** and found it to be -3.4 ± 0.8 kcal/mol compared to a predicted $\Delta H = -4.9$ kcal/mol (G3/MP2). We also pursued alternative spent-fuel regeneration strategies using less energy-intensive reagents. We successfully digested the spent fuel trimer using formic acid, which is synthetically available from the hydrogenation of CO_2 and may enable regeneration of fully charged fuel by a decarboxylation reaction.

Future work includes:

- Continue develop/optimize conditions/catalysts for H_2 desorption, specifically the H_2 desorption from the carbon portions of the fuel.
- Continue develop more efficient conditions for recharging the spent fuel material.

Selected FY 2012 Publications/Presentations

1. Luo, W.; Zakharov, L.N.; Liu, S.-Y. "1,2-BN Cyclohexane: Synthesis, Structure, Dynamics, and Reactivity" *J. Am. Chem. Soc.* 2011, *133*, 13006-13009.
2. Campbell, P.G.; Marwitz, A.J.V.; Liu, S.-Y. "Recent Advances in Azaborine Chemistry" *Angew. Chem. Int. Ed.* 2012, *51*, 6074-6092.
3. "Hydrogen Storage by Novel CBN Heterocycle Materials"; Copenhagen, Denmark, *International Energy Agency, Hydrogen Implementing Agreement, Task 22 Expert Meeting*, September 5, 2011.
4. "Developing the Basic Science and Applications of Boron(B)-Nitrogen(N)-Containing Heterocycles"; Université de Pau, Pau, France, *Seminar*, November 24, 2011.
5. "Developing the Basic Science and Applications of Boron(B)-Nitrogen(N)-Containing Heterocycles"; Université Paul Sabatier, Toulouse, France, *Seminar*, November 28, 2011.
6. "Developing the Basic Science and Applications of Boron(B)-Nitrogen(N)-Containing Heterocycles"; Okayama, Japan, 6th *International Green Elements Science Symposium*, December 3, 2011.
7. "Developing the Basic Science and Applications of Boron(B)-Nitrogen(N)-Containing Heterocycles"; The University of Tokyo, Tokyo, Japan, *Seminar*, December 6, 2011.
8. "Developing the Basic Science and Applications of Boron(B)-Nitrogen(N)-Containing Heterocycles"; San Diego, CA, *American Chemical Society National Meeting 243 Session "ACS Award for Creative Work in Synthetic Organic Chemistry: Symposium in Honor of Gregory C. Fu"* (ORGN 442); *Invited Lecture*, March 27, 2012.
9. "Hydrogen Storage by Novel CBN Heterocycle Materials"; Washington DC, *DOE Annual Merit Review*, May 17, 2012.
10. "Hydrogen Storage by CBN Heterocycle Materials"; Calgary, Canada, *National Meeting of the Canadian Society for Chemistry Session "Recent Advances in Hydrogen Activation, Production and Storage"*; *Invited Lecture*, May 30, 2012.
11. "Hydrogen Storage by CBN Heterocycle Materials"; Baltimore, MD, *Remsen Symposium; Invited Lecture*, May 31, 2012.

References

1. Sutton, A.D.; Burrell, A.K.; Dixon, D.A.; Garner, E.B.; Gordon, J.C.; Nakagawa, T.; Ott, K.C.; Robinson, J.P.; Vasiliu, M. *Science* **2011**, *331*, 1426–1429.
2. Davis, B.L.; Dixon, D.A.; Garner, E.B.; Gordon, J.C.; Matus, M.H.; Scott, B.; Stephens, F.H. *Angew. Chem. Int. Ed.* **2009**, *48*, 6812–6816.

IV.B.2 Fluid Phase Chemical Hydrogen Storage Materials

Benjamin L. Davis (Primary Contact),
Tessui Nakagawa, Biswajit Paik, and
Troy A. Semelsberger
Materials Physics and Applications, Materials Chemistry
Los Alamos National Laboratory (LANL), MS J514
P.O. Box 1663
Los Alamos, NM 87545
Phone: (505) 500-2463
Email: bldavis@lanl.gov

DOE Manager
Grace Ordaz
Phone: (202) 586-8350
Email: Grace.Ordaz@hq.doe.gov

Partner
Tom Baker, University of Ottawa, Ontario, Canada

Project Start Date: October 1, 2010
Project End Date: Project continuation and direction
determined annually by DOE

capacities as well as discharging rates. Subsequent work at LANL has shown that these RTIL-based fuels could also be regenerated off-board without separating the spent fuel from the RTIL. Successful development of fluid systems should meet the following DOE 2017 and Hydrogen Storage Engineering Center of Excellence (HSECoE) targets:

- Gravimetric Capacity (1.8 kWh/kg)
- Volumetric Capacity (1.3 kWh/L)
- H₂ Discharge Rate (minimum full flow rate 1.5 kg H₂/min)
- H₂ Purity (99.97 % H₂)
- Start-Up Time to Full Flow (5 s @ 20°C, 5 s @ -20°C)
- Shelf Life: Loss of Usable H₂ (0.05 g/hr-kg H₂ stored)
- HSECoE: 40 wt% AB dissolved or slurried

FY 2012 Accomplishments

- Additive amine-boranes with 3-4 wt% usable H₂ and maintain fluid phase after H₂ release.
- 20 wt% AB in hexylamine-borane (6.0 wt% H₂ material) transforms from a slurry to a liquid upon H₂ release.
- Developed ¹¹B nuclear magnetic resonance (NMR) solubility quantification method and measured AB, polyborazylene (PB) solubility in a variety of RTILs.
- Identified, removed, and measured the impact of water on AB solubility and stability in RTILs.
- Developed a method for measuring the known impurities of AB dehydrogenation (borazine, diborane, and ammonia) and hydrogen in a single flow-thru apparatus. Evaluation of several fuel blends indicates the impurity profile is AB/RTIL composition dependent.



Introduction

Chemical hydrogen storage (CHS) involves storing H₂ in molecular chemical bonds where an on-board chemical reaction is used to release H₂. Currently the resulting spent fuel may be regenerated off-board using chemical processing. CHS provides a diversity of options to enable H₂ for transportation as well as other niche and stationary applications. Especially attractive, CHS offers the potential for no direct H₂ handling by the consumer, as well as low pressure storage concepts.

Researchers at LANL and the University of Ottawa are focused on the development of liquid AB fuels that integrate with the HSECoE. We are currently studying the formation, stability, and catalytic release of H₂ from these materials.

Fiscal Year (FY) 2012 Objectives

Develop fluid, pumpable ammonia-borane (AB)-based fuels with high-H₂ content.

Technical Barriers

This project addresses the following technical barriers from the Storage section of the Fuel Cell Technologies Program Multi-Year Research, Development and Demonstration Plan:

- (A) System Weight and Volume
- (D) Durability/Operability
- (E) Charging/Discharging Rates

Technical Targets

A significant barrier to the application of off-board regenerable hydrogen storage materials is on- and off-boarding of the fuel and spent fuel, respectively. A fluid, pumpable fuel that remains liquid through dehydrogenation to the spent fuel form is desired for readily engineered fueling concepts. This project is exploring other compositions of AB/room temperature ionic liquid (RTIL) systems; the original concept was developed within Center of Excellence in Chemical Hydrogen Storage by Professor Larry Sneddon of the University of Pennsylvania. This work showed great promise with excellent gravimetric and volumetric

Approach

A serious drawback of AB-based pumpable fuels is product precipitation during hydrogen removal. To address this concern, we developed a solubility quantification method based on ^{11}B NMR to screen RTIL for their ability to solubilize AB (to maximize capacity) and its dehydrogenation products (to avoid precipitation). In addition, we identified amineborane additives which can improve the solubility properties of the dehydrogenation products. To meet the other technical targets for fuel stability and H_2 purity, we identified/removed impurities in commercially available RTIL and developed a method to measure the known gaseous effluents from the decomposition of AB/RTIL fuel blends.

Results

One technique for mitigating product precipitation is to find a solvent or solvents that dissolve the reactant and product. To this end, we developed a method for quantifying the solubility of boron species using ^{11}B NMR which would allow us to correlate the reactant/product solubility with RTIL components (cations, anions). The solubility results for AB and PB (derived from borazine decomposition) indicate RTIL composition only affects AB dissolution (Figure 1).

At this time we have not performed extensive solubility evaluations to determine which RTIL would be optimal for AB/RTIL fuel blends. It is clear from this initial survey, however, that we will not be able to make a solution of AB in RTIL that meets the HSECoE's minimum target of 40 wt%. Slurries of AB in RTIL are being pursued as a consequence.

We hypothesized that the insolubility of PB, a material similar to the products previously characterized after the dehydrogenation of AB/RTIL fuels [1], was related to the extensive polymeric networks that are possible. To improve the solubility AB/RTIL dehydrogenation

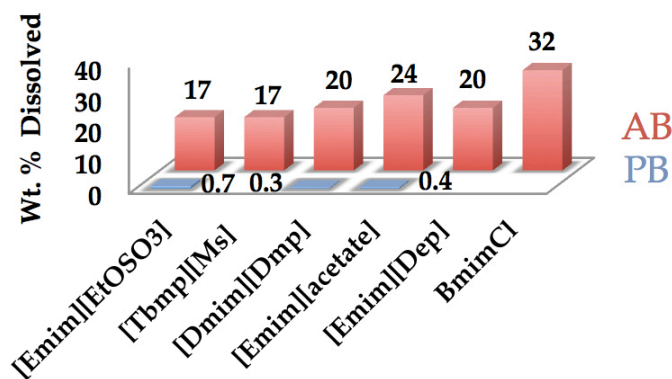


FIGURE 1. Solubility (wt%) of AB and PB in RTIL using ^{11}B NMR method. Emim = ethyl, methyl imidazolium, Bmim = butyl, methyl imidazolium, Tbmp = tributylmethylphosphonium, EtOSO₃ = ethylsulfonate, Ms = methylsulfonate, Dmp = dimethylphosphonate, Dep = diethylphosphonate.

products, we designed functionalized amineborane additives that should react with AB given sufficient activation energy or a catalyst. The first generation additives are hexylamineborane, $\text{H}_3\text{C}(\text{CH}_2)_5\text{NH}_2\text{BH}_3$ (hexyl-AB), and 3-methoxypropylamineborane, $\text{H}_3\text{CO}(\text{CH}_2)_3\text{NH}_2\text{BH}_3$ (methoxy-AB), whose analogous synthetic preparation is described in the literature [2].

To assess whether hexyl-AB and methoxy-AB additives would impart greater solubility on AB dehydrogenation products, we first heated each in a closed vessel at 130°C for 12 hours. In each case a liquid product formed, even after cooling to room temperature. AB/BmimCl under the same conditions results in a solid product. When 1:1 molar mixtures of hexyl-AB or methoxy-AB with AB are heated under the same conditions, a liquid product also results (Figure 2). This is a significant result, as 1:1 mixtures of hexyl-AB:AB store 6 wt% H_2 , which is equal to the HSECoE minimum requirement of 40 wt% AB dissolved/slurried.

The ultimate goal of amineborane additives is to broaden the liquid range of the AB/RTIL fuel, which we define as the amount of hydrogen released per gram of fuel before product precipitation. To assess the methoxy-AB additive, we prepared a 23 wt% AB/BmimCl solution where ~60 mg of RTIL was substituted for methoxy-AB and measured the release of hydrogen at 90°C . A 23 wt% AB/BmimCl solution without additive was used as a control. Greater than 10 mM of H_2 /gram of fuel was released when methoxy-AB additive was used, compared to ~7.5 mM for the control. This 30% greater H_2 release is consistent with the H_2 stored in methoxy-AB.

While formulating AB/RTIL fuel blends, we recognized that many RTIL are hygroscopic and this dissolved water might be an issue for H_2 capacity after cycling, accurate solubility measurements, and long-term storage. To reduce the influence water may have, we utilized Karl Fisher titrations to accurately measure water content in



FIGURE 2. 1:1 molar mixture of hexyl-AB, heated for 12 h @ 130°C . Picture was acquired at room temperature.

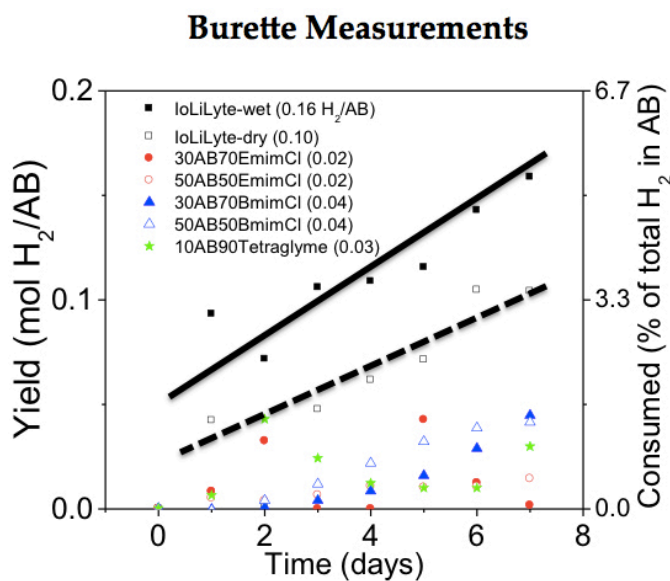


FIGURE 3. Short-term stability measurements of AB/RTIL fuel blends. Measurements of H_2 were made at room temperature. Note significant reduction in H_2 formation with the dried RTIL (dashed best fit line) as compared to the as-received 'wet' fuel (solid best fit line). IoLiLyte is a tradename by lolitec (Tuscaloosa, AL) for Emim EtOSO₃.

commercially sourced RTILs and then verify the extent of dryness after a water removal procedure was applied. With the dried RTILs, we then determined AB solubility and found improvements in almost all cases (Table 1). No dry RTIL, however, was able to dissolve 40 wt% AB, the HSECoE's minimum target. Water removal also impacted short term room temperature stability measurements (Figure 3).

TABLE 1. Water content in as-received and dried RTIL. Subsequent AB wt% solubility.

| RTIL | As Received H ₂ O content (ppm) | Dried RTIL H ₂ O content (ppm) | AB wt% dissolved in dried RTIL |
|------------------------|--|---|--------------------------------|
| EmimEtOSO ₃ | 1,600 | 80 | 27 |
| DmimDmp | 4,000 | 250 | 32 |
| EmimAcetate | 1,500 | 100 | 31 |
| BmimCl | 10,000 | 320 | 31 |
| BmimOTf | 450 | <30 | 4.4 |

Lastly, to help the HSECoE select a AB/RTIL fuel blend that is compatible with their developing filtration technologies, we developed a method to measure the known impurities (ammonia, borazine, and diborane) in the H_2 effluent when AB/RTIL is decomposed. Using a calibrated thermogravimetric analysis-infrared-mass spectrometry system, several compositions of AB, AB/RTIL, and additives were decomposed (Figure 4). While mass balance indicates there are some unaccounted species, the variable distribution

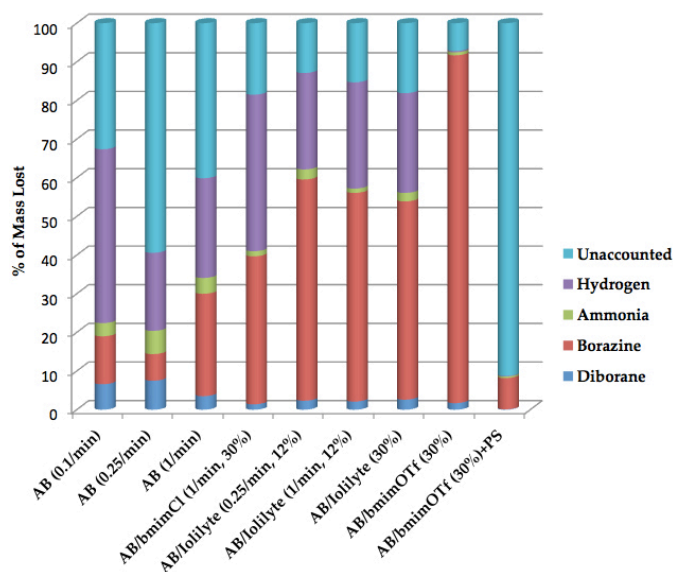


FIGURE 4. Gaseous measurements of borazine, diborane, ammonia, and hydrogen from decomposed samples of AB and AB/RTIL at different ramp rates, loadings, and compositions. Data was acquired on a calibration thermogravimetric analysis-infrared-mass spectrometry coupled system.

of products suggests that fuel composition may be used to tailor impurity profiles.

Conclusions and Future Directions

- Solubility measurements of AB and PB in RTIL indicate there is no clear path to >40 wt% AB/RTIL solutions or a solvent system for preventing PB precipitation; slurries of AB in RTIL will be required to meet gravimetric targets for H_2 stored.
- Amineborane additives show promise for altering the solubility of AB dehydrogenation products, yielding liquid products with AB after extensive heating in some cases. Future work will focus on non-volatile amineborane derivatives.
- Some quality control is required with commercially sourced RTILs, since impurities such as water have an impact on room temperature stability and maximum dissolved AB.
- A method for measuring known impurities (ammonia, borazine, diborane) and evolved H_2 from decomposed AB and AB/RTIL fuel blends was developed. This is a useful tool for the HSECoE to gauge which fuel blends will be compatible with their filtration systems.

References

- Sneddon et al., *Inorg. Chem.*, **2009**, *48*, 9883.
- Framery et al., *Heteroatom Chem.*, **2000**, *11*, 218.

IV.B.3 Novel Carbon(C)-Boron(B)-Nitrogen(N)-Containing H₂ Storage Materials

Shih-Yuan Liu

University of Oregon
Department of Chemistry
1253 University of Oregon
Eugene, OR 97403-1253
Phone: (541) 346-5573
Email: lsy@uoregon.edu

In collaboration with:

- Dr. Tom Autrey, Dr. Abhi Karkamkar, and Mr. Jamie Holladay
Pacific Northwest National Laboratory
- Dr. David Dixon
The University of Alabama
- Dr. Paul Osenar
Protonex Technology Corporation

DOE Managers

HQ: Grace Ordaz
Phone: (202) 586-8350
Email: Grace.Ordaz@ee.doe.gov

GO: Katie Randolph
Phone: (720) 356-1759
Email: Katie.Randolph@go.doe.gov

Contract Number: DE-EE0005658

Project Start Date: March 5, 2012
Project End Date: March 14, 2015

Technical Targets

This project is developing and characterizing new CBN materials for hydrogen storage. Insights gained from these studies will be applied toward the design and synthesis of hydrogen storage materials that meet the following DOE 2017 hydrogen storage system targets:

- Specific energy: 1.8 kWh/kg (5.5 wt%)
- Energy density: 1.3 kWh/L (4.0 vol%)

FY 2012 Accomplishments

- Identified three classes of CBN materials for synthesis and characterization (liquid, reversible, high-capacity).
- Synthesized a CBN material that is a single-component liquid carrier.
- Developed catalytic conditions for the release of H₂ from the liquid carrier at 80°C



Introduction

Approaches to store H₂ in chemical bonds provide a means for attaining high energy densities. Molecular complexes containing protic and hydridic hydrogen such as ammonia borane (AB) provide between 8 to 16 wt% H₂ at acceptable temperatures in a kinetically controlled decomposition. AB shows promise to meet a number of important technological targets such as high volumetric and gravimetric density of H₂, fast kinetics, thermal stability, facile synthesis at large scale and safe handling under atmospheric conditions. Some of the challenges involving AB include: volatile impurities (e.g., ammonia, diborane, borazine) and the economics of spent fuel regeneration [1-4].

This project is developing hydrogen storage materials that contain the element carbon in addition to boron and nitrogen. The inclusion of carbon can be advantageous for developing chemical H₂ storage materials that are structurally well defined (thus has good potential to be liquid phase), exhibit thermodynamic properties conducive to reversibility, and demonstrate good storage capacities.

Approach

This project will develop new CBN H₂ storage materials that have the potential to meet the DOE goals for motive and non-motive applications. Specifically, we will be focusing on three basic systems: 1) liquid-phase systems that release H₂ in a well-defined and high-yield fashion, minimizing the

Fiscal Year (FY) 2012 Objectives

This project seeks to develop a class of chemical hydrogen storage materials containing the elements carbon, boron, and nitrogen (CBN materials). The project will focus on compounds that show potential to meet the Department of Energy's vehicular technical targets and/or can be applied to near-term market applications. The preferred materials to be developed will exhibit good storage capacity, be liquid, reversible, have good release kinetics at moderate temperature.

Technical Barriers

This project addresses the following technical barriers from the Hydrogen Storage section of the Fuel Cell Technologies Program Multi-Year Research, Development and Demonstration Plan:

- (A) System Weight and Volume
- (C) Efficiency
- (E) Charging/Discharging Rates

formation of NH_3 and $\text{B}_3\text{N}_3\text{H}_6$, 2) reversible storage systems that could be potentially regenerated onboard, 3) high H_2 -content storage systems that can be used in slurries and regenerated off-board (see Figure 1). Computational chemistry studies will direct our research and reduce risk by accelerating progress. Finally, we will demonstrate the material in conjunction with a fuel cell. These new materials will be prepared and characterized by our interdisciplinary team comprised of the University of Oregon, the University of Alabama, Pacific Northwest National Laboratory, and Protonex (a small business fuel cell manufacturer).

Results

Synthesis of CBN Compounds

We synthesized compound **B** (Figure 1) *via* conditions adapted from our previously reported “first-fill” synthesis of compound **F**. *Bis*-(trimethylsilyl)crotylamine **1** was reacted with borane-triethylamine, producing **2** through intramolecular hydroboration (Scheme 1). The resulting crude mixture containing **2** was reacted with potassium hydride, followed by treatment with $\text{HF}\cdot\text{pyridine}$, yielding carrier **B** in 51% yield from **1**. Compound **B** is indeed a liquid at room temperature (melting point -16°C).

Release of Hydrogen from Liquid Carrier **B**

As with **AB** and other amine-boranes, release of hydrogen from **B** can be induced thermally, or at lower temperatures using catalysts. At 150°C , two equivalents of hydrogen are released from each molecule of **B** within one hour. The release of hydrogen triggers a trimerization reaction (Scheme 1b) and produces trimer **3**, which is also a liquid at room temperature. Thus the hydrogen desorption from liquid material **B** does not involve a phase change. The reaction was monitored by automated gas burette in addition to NMR spectroscopy.

First-row transition metal-halide salts such as CoCl_2 and FeCl_2 can catalyze the hydrogen desorption reaction. The reaction can be

performed at temperatures as low as 50°C in the presence of catalysts. Among the surveyed catalysts, the most active catalyst proved to be CoCl_2 (Figure 2a). At the polymer electrolyte membrane fuel cell waste heat temperature of 80°C , the reaction can be completed in just over five minutes using CoCl_2 as the catalyst. Though cobalt(II) chloride was most effective, we focused further efforts using iron(II) chloride because of its much reduced cost. To demonstrate the potential utility of our material as a simple-to-operate, single-component liquid system, we performed a large-scale dehydrogenation of liquid fuel **B** without additional solvent using 5 mol% FeCl_2 as a catalyst. Figure 2b shows that 2 equiv of H_2 were released from the neat material in ca. 20 min at 80°C . At the conclusion of the reaction, the spent fuel trimer was isolated in 95% yield.

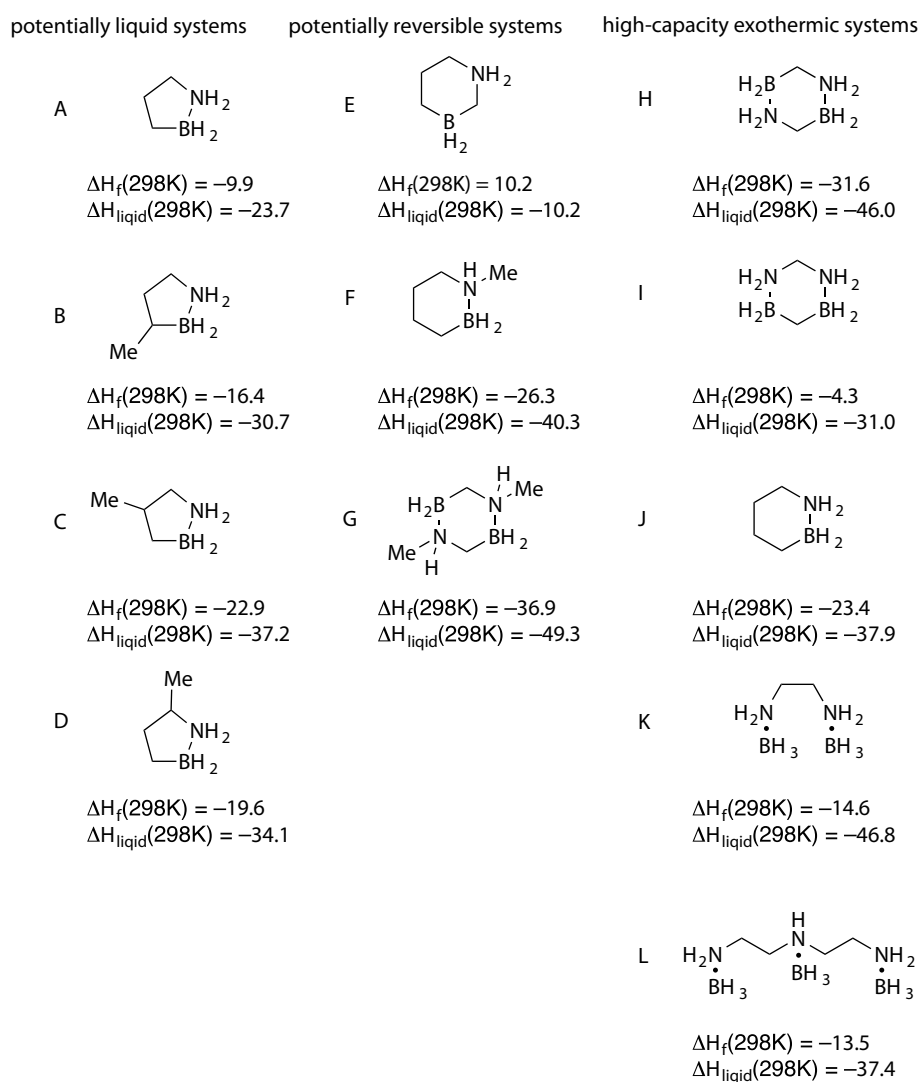
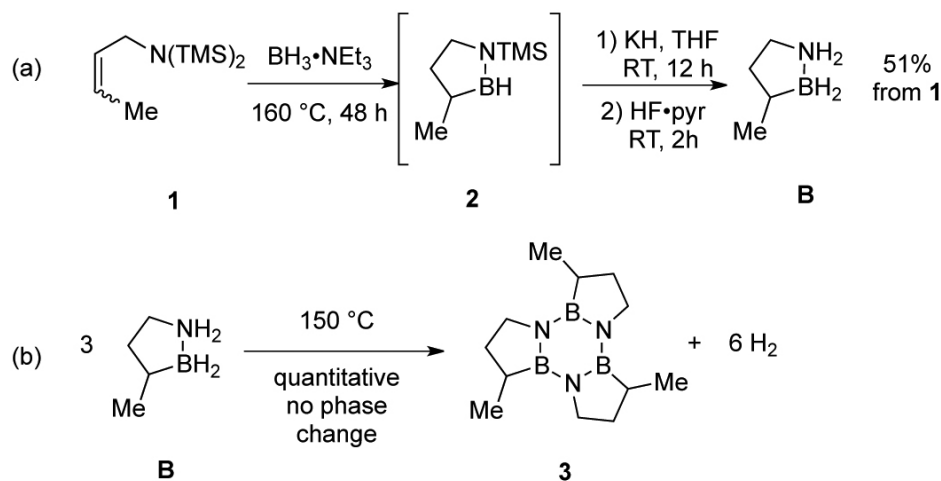


FIGURE 1. Selected synthetic targets and their gas phase heats of formation calculated at the G3MP2 level. Liquid phase heats of formation obtained from calculated boiling points using COSMO-RS. Energy values are in kcal/mol.



SCHEME 1. Synthesis of liquid fuel **B** and its thermal H_2 desorption reaction

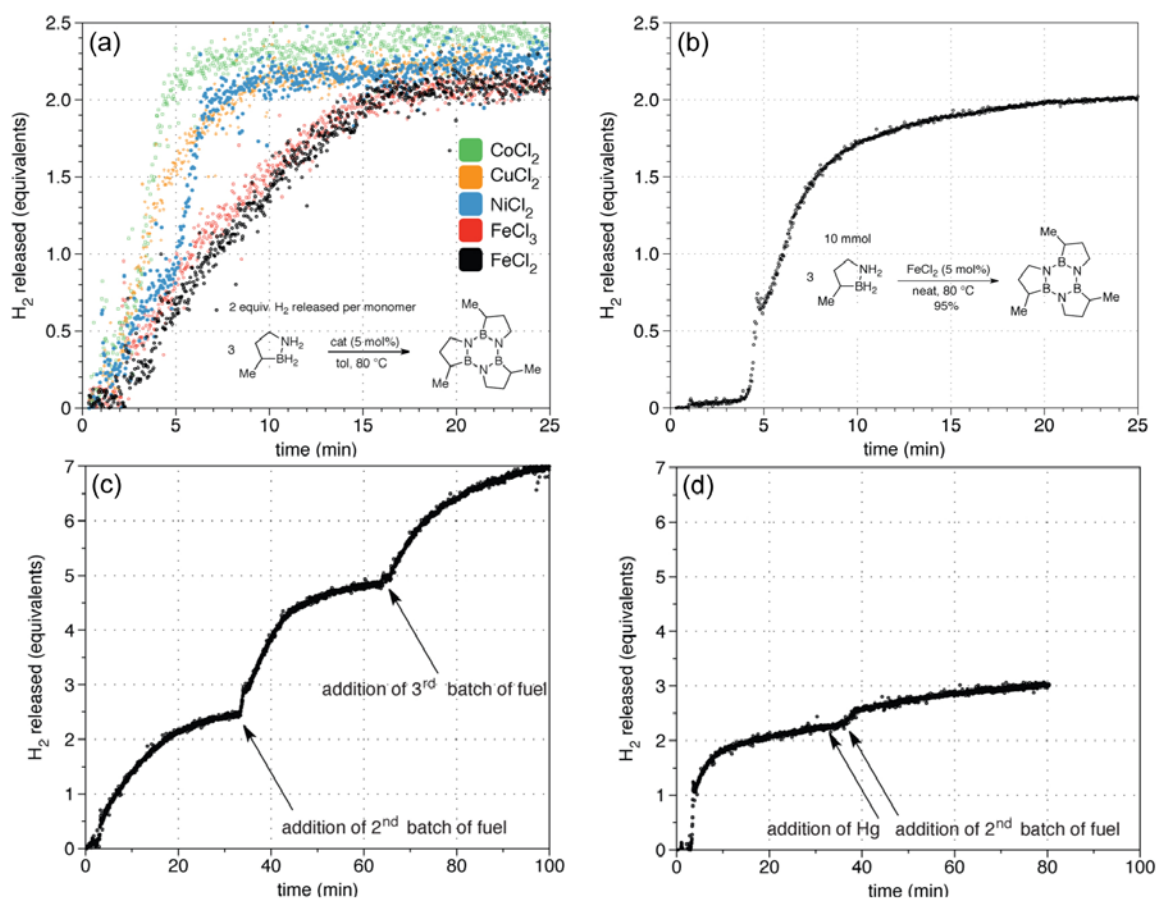
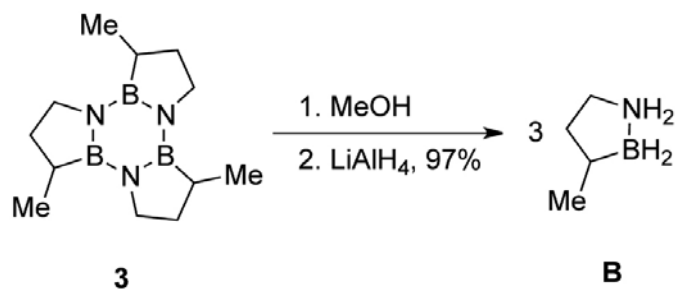


FIGURE 2. Automated gas burette analysis of a) catalyst screening survey for hydrogen desorption of **B** at 80 °C, b) large scale dehydrogenation of **B** using $FeCl_2$ as a catalyst, c) hydrogen desorption via sequential addition of charged fuel to $FeCl_2$ catalyst, d) hydrogen desorption with Hg poisoning of the $FeCl_2$ catalyst.

The $FeCl_2$ pre-catalyst changed form during the course of the reaction, becoming an amorphous black powder. At 5 mol% loading, the catalyst could be reused without loss of

activity (Figure 2c). Adding fresh fuel **B** to the reaction flask after dehydrogenation of the old batch had completed resulted in immediate H_2 desorption from the new batch of fuel



SCHEME 2. Conversion of spent fuel trimer **3** back to the charged fuel **B**

(tested up to three times). To probe the nature of the active catalyst species, Hg was added to the reaction mixture, and a reduced rate of hydrogen release was observed, suggesting a heterogeneous catalysis mechanism (Figure 2d vs 2c).

Regeneration of B from Spent Fuel Trimer

We determined that trimer **3** can be “digested” at room temperature by stirring with methanol then reduced with lithium aluminum hydride to furnish the charged liquid fuel **B** in high yield (Scheme 2). The described regeneration scheme is not yet optimal from an energetic point of view (i.e., the use of highly energetic LiAlH_4 ultimately needs to be avoided).

Conclusions and Future Directions

In summary, we developed the synthesis of a new single-component liquid phase hydrogen storage material **B** based on the CBN heterocycle approach. We found that liquid carrier **B** released two equivalents of hydrogen in less than 20 minutes at 80°C in the presence of catalytic amounts of first-row transition metals without a phase change. A preliminary regeneration scheme was also demonstrated.

Future work includes:

- Continue develop and demonstrate the synthesis of remaining CBN heterocycle targets illustrated in Figure 1.
- Provide detailed characterization for compound **B** (e.g., thermogravimetric analysis, residual gas analysis, viscosity, thermodynamic parameters).
- Investigate the dehydrogenation mechanism of CBN heterocycles.

Selected FY 2012 Publications/Presentations

1. Luo, W.; Campbell, P.G.; Zakharov, L.N.; Liu, S.-Y. “A Single-Component Liquid-Phase Hydrogen Storage Material” *J. Am. Chem. Soc.* **2011**, *133*, 19326-19329.

* This paper is included for completeness sake. It was published before the grant was funded. Highlighted in *Chemical & Engineering News (C&EN)* (2011, November 28, page 35), C&EN online (2011, <http://cen.acs.org/articles/89/web/2011/11/Liquid-Future-Hydrogen-Fuel.html>), in *Nature Chemistry* **2012**, *4*, 5, and in *Nature Climate Change* **2012**, *2*, 23.

2. “Hydrogen Storage by Novel CBN Heterocycle Materials”; Heidelberg, Germany, *International Energy Agency, Hydrogen Implementing Agreement, Task 22 Expert Meeting*, May 8, 2012.

3. “Hydrogen Storage by Novel CBN Heterocycle Materials”; Washington, DC, *DOE Annual Merit Review*, May 17, 2012.

References

1. McWhorter, S.C. Read, G. Ordaz, N. Stetson. “Materials-Based Hydrogen Storage: Attributes for Near-Term, Early Market PEM Fuel Cells” *Current Opin. Sol. State Mat. Sci.* **2011** *15*, 29-38.
2. A. Staubitz, A.P. Robertson, I. Manners. “Ammonia-borane and related compounds as dihydrogen sources” *Chem. Rev.* **2010**, *110*, 4079-4124.
3. C.L. Aardahl, D. Rassat. “Overview of systems considerations for on-board chemical hydrogen storage” *Int. J. Hydrogen. Energy.* **2009**, *34*, 6676-6683.
4. A.D. Sutton, A.K. Burrell, D.A. Dixon, E.B. Garner, III, J.C. Gordon, T. Nakagawa, K.C. Ott, J.P. Robinson, and M. Vasiliu. “Regeneration of Ammonia Borane Spent Fuel by Direct Reaction with Hydrazine and Liquid Ammonia” *Science*, **2011**, *331*, 1426-1429.

IV.B.4 Development of a Practical Hydrogen Storage System Based on Liquid Organic Hydrogen Carriers and a Homogeneous Catalyst*

Craig Jensen¹ (Primary Contact), Daniel Brayton¹, and Scott Jorgensen²

¹Hawaii Hydrogen Carriers, LLC
531 Cooke Street
Honolulu, HI 96813
Phone: (808) 339-1333
Email: hhcllc@hotmail.com

²General Motors Technical Center

DOE Managers

HQ: Ned Stetson
Phone: (202) 586-9995
Email: Ned.Stetson@ee.doe.gov

GO: Katie Randolph
Phone: (720) 356-1759
Email: Katie.Randolph@go.doe.gov

Contract Number: DE-EE0005020

Project Start Date: July 1, 2011
Project End Date: June 30, 2013

*Congressionally directed project

(H) Balance-of-Plant (BOP) Components

(F) Thermal management

(R) Regeneration Processes

Technical Targets

1. Identification of a low-cost, LOC that, in the presence of low loading of a homogeneous pincer catalyst, will release >7 wt% H₂ at sufficiently high rates and low temperatures in a practical, onboard dehydrogenation reactor to meet the demands of an onboard fuel cell.
2. Identification of a LOC/pincer catalyst combination of sufficiently high hydrogen cycling capacity that rapidly dehydrogenates **without** also undergoing LOC degradation upon cycling.
3. Utilization of the advantages of the liquid hydrogen storage medium to eliminate thermal management problems associated with solid-state hydrogen absorbing materials.
4. Design of a space, mass and energy efficient tank and reactor system to house the LOC and facilitate hydrogen release that can be easily interfaced with a fuel cell.

Fiscal Year (FY) 2012 Objectives

The objective of this project is to optimize a hydrogen storage media based on a liquid organic carrier (LOC) for hydrogen and design a commercially viable hydrogen delivery system based on this LOC media. The project consists of two parts: Part 1 (conducted at Hawaii Hydrogen Carriers, LLC [HHC]) has the objective to develop an optimized catalyst/organic carrier combination; and Part 2 (conducted at General Motor Research Center) has the objective of designing of a space, mass and energy efficient tank and reactor system to house the carrier and release hydrogen.

Technical Barriers

This project addresses the following technical barriers from the Hydrogen Storage section of the Fuel Cell Technologies Program Multi-Year Research, Development and Demonstration Plan:

- (A) System Weight and Volume
- (B) System Cost
- (C) Efficiency
- (E) Charging/Discharging Rates

FY 2012 Accomplishments

We have shown the homogeneous pincer catalysts to be effective for the rapid dehydrogenation of the 5-membered, nitrogen-containing ring of methylperhydroindole (MPHI), perhydro-indolizidine (PHI), and ethylperhydrocarbazole (EPHC). MPHI has been identified as the most promising candidate LOC among this group as it has the best combination of high performance and low cost. Additionally, our modeling studies have shown that the most effective heat transfer occurs in helical reactors which allow the design of a short, easy to package reactor which in turn reduces heat loss in the system. In consultation with other DOE contract holders (Oregon State University), we were able to significantly reduce both our engineering time and the mass and volume of the unit by use of micro-channel heat exchangers.



Introduction

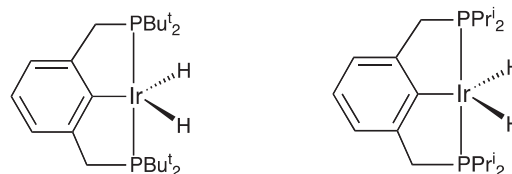
For decades, hydrogen has been targeted as the utopian fuel of the future on account of its abundance and environmental friendliness. However, a major difficulty

in the utilization of hydrogen as a fuel for vehicles is the problem of onboard storage because hydrogen is problematic to store at high density. While this is a major problem for vehicles, it is also a significant problem for portable power as it adds to both the cost and inconvenience of frequent delivery and change-over of hydrogen supply for all fuel cell applications. Thus a high density, high stability method for storing hydrogen is essential to the implementation of fuel cells in all but a few niche applications. Another major concern about hydrogen is putting an infrastructure in place. While this could be done for any form of hydrogen carrier, the barrier to implementing a LOC would be significantly lower than others because it is a similar type of chemical to the current distribution system. The tanks, piping and refinery systems used to make and deliver gasoline are appropriate for LOCs. In addition to the easy adaption to existing infrastructure, LOCs have many other enormous practical advantages. Cheap, abundant LOCs can reversibly release 7-8 wt% hydrogen. They can be economically manufactured in the massive quantities required to meet the anticipated demand and would eliminate the thermal management problems commonly associated with the systems based on solid-state hydrogen absorbing materials. The technology has the potential to exceed the performance of carbon-emitting technologies such as direct methanol fuel cell. We have recently discovered catalysts that enable this technology that has remained a tantalizing but impractical possibility for over the last 60 years. This project targets the development of a commercially viable LOC-based hydrogen storage and delivery system. The project consists of two parts: 1) development of an optimized catalyst/carrier combination; and 2) the design of a space, mass, energy efficient tank and reactor system to house the carrier and release the hydrogen.

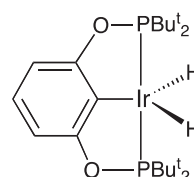
Although promising hydrogen cycling performances have been demonstrated, these previous LOC studies utilized very high loadings of heterogeneous and precious metal catalysts in order to achieve acceptable dehydrogenation kinetics at temperatures that are near the operating temperatures of proton exchange membrane (PEM) fuel cells ($\leq 150^\circ\text{C}$). The high cost of the massive quantities of precious metals precludes the commercialization of these systems.

In order to overcome the barrier to practicality that is imposed by the heterogeneous catalysts, we have developed alternative homogeneous catalysts. Homogeneous catalytic systems typically operate at significantly lower temperatures and show much greater product specificity than their heterogeneous counterparts. In 1997, we discovered that the “pincer” complex, $\text{IrH}_2\{2,6\text{-C}_6\text{H}_3\text{-CH}_2\text{P}(\text{Bu}^t)_2\}_2$ (**1**), catalyzes the dehydrogenation of cycloalkanes to arenes. This was the first report of a homogeneous catalyst for this reaction. The unique reactivity of this especially robust and active catalyst can be ascribed to the tridentate “PCP pincer” ligands which contain two coordinating, neutral phosphorus

centers as well as an anionic, coordinating carbon site. It has been found that the electronic environment of the catalytic metal center of the pincer complex is highly sensitive to minor changes in the PCP pincer ligand. Following our report that (**1**) catalyzes the dehydrogenation of aliphatic groups, the related PCP pincer complexes, $\text{IrH}_2\{2,6\text{-C}_6\text{H}_3\text{-CH}_2\text{PPri}_2\}_2$ (**2**) and $\text{IrH}_2\{\text{C}_6\text{H}_3\text{-2,6-(OPBu}^t)_2\}$ (**3**) were shown to



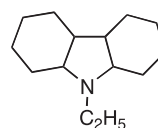
$\text{IrH}_2\{2,6\text{-C}_6\text{H}_3\text{-CH}_2\text{P}(\text{Bu}^t)_2\}_2$ (**1**) $\text{IrH}_2\{\text{C}_6\text{H}_3\text{-2,6-(CH}_2\text{PPri}_2\}_2$ (**2**)



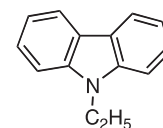
$\text{IrH}_2\{\text{C}_6\text{H}_3\text{-2,6-(OPBu}^t)_2\}$ (**3**)

have incremental improvement in catalytic efficiency. It is now well established that dihydro PCP pincer iridium complexes can selectively dehydrogenate aliphatic groups under much milder conditions than those required for the corresponding heterogeneous catalysts, such as platinum on alumina, without harm to other functional groups of an organic molecule.

More recently, we found **1** and the related complexes, **2**, and **3**, to be highly active catalysts for the dehydrogenation of amines, EPHC and other



N-ethylperhydroethylcarbazole (EPHC)



N-ethylcarbazole (EPHC)

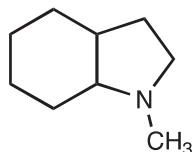
heterocyclic LOCs. We have recently synthesized the novel AsCAs pincer complex, $\text{IrH}_2\{\text{C}_6\text{H}_3\text{-2,6-(OAsBu}^t)_2\}$ (**4**), and found it to be a highly active dehydrogenation catalyst for LOCs. At 150°C , **4** catalyzes the dehydrogenation of EPHC at rates that are nearly double those achieved with **3**. Furthermore, it exhibited acceptable activity at 125°C , at temperatures at which the PCP catalysts are completely inactive.

Approach

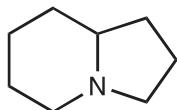
Clearly, our studies of the LOC/pincer catalyst systems have demonstrated the potential of these systems to serve as

the basis of a practical hydrogen storage system. However, further studies must be conducted to find the system and conditions that gives the best combination of high cycling capacity, rapid dehydrogenation kinetics, and lack of LOC degradation upon cycling. In order to accomplish this we will conduct the following four sub-tasks:

Task 1.1: Isothermal kinetic studies of the pincer complex catalyzed dehydrogenation of the candidate LOCs, perhydro-ethylcarbazole, perhydro-methylindole, PHI, and aminomethyl-cyclohexane (AMC).



perhydro-methylindole



perhydro-indolizidine

Task 1.2: In cases where incomplete dehydrogenation of the LOC is observed, studies of the dehydrogenation reaction in the presence of a hydrogen acceptor (transfer dehydrogenation) will be carried out to determine if the reaction is limited by kinetic or thermodynamic constraints.

Task 1.3: Studies to determine if the formation of unwanted side products that arise in some LOC systems can be controlled by the addition of additive.

Task 1.4: Cycling studies to determination if LOC/ catalyst combinations that have acceptable dehydrogenation kinetics and capacity will undergo cycling without degradation of LOC and/or catalyst.

Additionally, the practical advance of LOC systems awaits the design of a deployable reactor to house the LOC and facilitate the hydrogen release that can be easily interfaced with a fuel cell. This task consists of the following four sub-tasks:

Task 2.1 Model Development: The first part is to devise a notional model of the entire system. In part 2, one or more reactor model(s) are developed in detail using COMSOL. As the model or models are completed, they will be validated in part 3 to be certain the fluid mechanics, heat transfer, and reaction proceed as would be expected based on the standard engineering concepts. Part 4 will entail a basic estimate of the cost of the system.

Task 2.2 Function Evaluation: Our experience indicates that the system function and cost is often fixed by the full flow condition. To ensure efficient use of resources, we will evaluate this functionality first. Once the reactor “runs” at the full flow condition it will be evaluated at idle. Once these extremes have been evaluated, the mid-speed/mid-load condition will be evaluated and finally transient performance will be evaluated.

Task 2.3 System Optimization: This sub-task is centered on improving both the engineering and the storage materials.

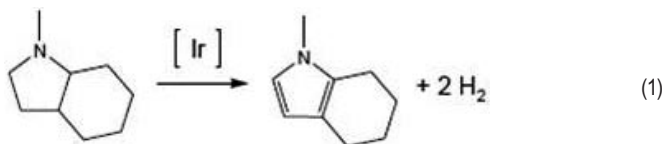
Based on what we have learned about the system function, we will look for both reactor and balance of plant aspects where cost effective change is possible. It may also be possible to: further improve the design; reduce reactor and BOP size; or improve operation conditions.

Task 2.4 Final Simulations: This subtask is analogous to sub-task 2.2. Steady-state and transient simulations will both be done with multiple reactions paths so that both efficiency and selectivity can be evaluated. At the conclusion of the simulations the data will be evaluated, and documented.

Results

Task 1.1 Isothermal Kinetic Studies: The unsaturated, candidate LOCs, methylindole, indolizidine, and ethylcarbazole were obtained from commercial sources. The saturated, perhydro LOCs were prepared through hydrogenation of the commercially obtained materials with the appropriate metal (Ru or Pd) on carbon at high temperature (120-150°C) and high pressure (69 bar). The PCP pincer catalysts were prepared using standard Schlenk techniques using the methods reported in the literature. Catalysts were then checked for activity under well-established protocols, specifically for the conversion of cyclooctane to cyclooctene with a hydrogen acceptor molecule, tert-butylethylene. The high purity of the perhydro-LOCs and pincer complexes was established by comparison to literature reports by the appropriate technique (gas chromatograph-mass spectrometry, ^1H , ^{13}C , and ^{31}P nuclear magnetic resonance) and found acceptable. Once the LOCs and pincer catalysts were in hand, isothermal studies were carried out in order to elucidate any discrepancies in the literature. We found that heating to 180°C (rather than 150°C as previously reported) was required to achieve practical levels of dehydrogenation of N-EPHC within a 24 hour period.

Once the benchmarking of the EPHC “standard” LOC was completed, we initiated the isothermal kinetic studies of the $\text{IrH}_2\{\text{C}_6\text{H}_3-2,6-(\text{OPBu}^t)_2\}$ catalyzed dehydrogenation of MPHI in the 150-200°C temperature range. As seen below in equation 1, it was observed that only the 5-membered, nitrogen-containing ring undergoes rapid dehydrogenation and the 6-membered ring does not undergoes appreciable dehydrogenation at relevant rates.



An activation energy of 133 kJ/mol and frequency factor of $9.457 \times 10^{10} \text{ M}^{-1}\text{s}^{-1}$ were derived from an Arrhenius plot of the kinetic data. Although we determined an activation energy of 111 kJ/mol and a frequency factor of $1.26 \times 10^8 \text{ M}^{-1}\text{s}^{-1}$ for EPHC, it should be noted that only

limited data can be obtained for EPHC as the rate of the catalytic dehydrogenation is prohibitively slow below 180°C and the pincer catalyst undergoes thermal decomposition at significant rates above 200°C.

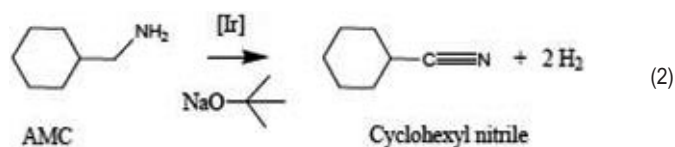
Our studies of the dehydrogenation of AMC at temperatures up to 200°C showed that while the dehydrogenation of the methylamino group to nitrile (as seen in equation 2) occurs at relevant rates, the dehydrogenation of the saturated 6-membered ring does not. Thus AMC has been eliminated as a potential LOC.

We have also found that at temperatures up to 200°C, only the 5-membered ring of PHI undergoes rapid dehydrogenation while the 6-membered ring does not undergoes dehydrogenation at relevant rates. In view of the much higher cost (>50x) PHI and similarity of its dehydrogenation behavior to MPHI, we have eliminated PHI as a candidate LOC.

Higher rates of dehydrogenation of EPHC were not observed in preliminary studies in which the phosphorous pincer complex was replaced by the arsenic pincer complex, $\text{IrH}_2\{\text{C}_6\text{H}_3\text{-2,6-(OAsBu}^t_2)_2\}$. Thus the combination of the EPHC and arsenic pincer complex have been ruled out for further cycling studies.

Task 1.2 Differentiation of Thermodynamic vs. Kinetic Limitations: Work on this task has not been initiated.

Task 1.3 Additive Intervention of Side Reactions: As seen in equation 2, we have found that



addition of hindered base (sodium tert-butoxide) inhibits the unwanted imine condensation side reaction during the dehydrogenation of AMC. However, it was found that the level of dehydrogenation was only 33% and not 95-97% as reported in the literature.

Task 1.4 Cycling Studies: We found that ruthenium, one of the cheapest metals that was screened, is an effective catalyst for the hydrogenation of carbazole-related compounds. However, it was also discovered that ruthenium is not an effective catalyst for the hydrogenation of similar indole compounds but instead catalyzes a previously unknown carbon-carbon bond cleavage reaction.

Task 2.1 Model Development: Four notional models of the entire system have been devised and developed in detail using COMSOL and validated in terms of the fluid mechanics, heat transfer, and reaction progress. Our studies show that the more effective heat transfer in helical reactors allows the design of a short, easy to package reactor which in turn reduces heat loss in the system. Basic estimate of

the system cost have been carried out and show that the reactor could be constructed from parts currently in standard production and thus insures price reasonableness of the reactor.

Task 2.2 Function Evaluation: The basic function of four reactor types have been investigated. We found the reactor length in steady-state operation to have a profound impact of kinetics. In consultation with other DOE contract holders (Oregon State University), we were able to significantly reduce both our engineering time and the mass and volume of the unit by use of micro-channel heat exchangers.

Task 2.3 System Optimization: We have begun to introduce several designs to this step. We are presently carrying out exact reactor simulations and working on BOP issues.

Task 2.4 Final Simulations: Work on this task has not yet been initiated.

Conclusions

Our isothermal kinetic studies have shown the pincer catalysts to be effective for the rapid dehydrogenation of only the 5-membered, nitrogen-containing ring of MPHI, PHI, and EPHC. EPHC has been down-selected as the LOC for use in our system since significantly higher rates of catalysis were observed for the dehydrogenation of MPHI and PHI. In view of the much higher cost (>50x) PHI and similarity of its dehydrogenation behavior to MPHI, we have also eliminated PHI as a candidate LOC. Our studies of the dehydrogenation of AMC have shown that while the dehydrogenation of the methylamino group to nitrile occurs at relevant rates, the dehydrogenation of the saturated 6-membered ring does not. Thus AMC has also been eliminated as a potential LOC. Higher rates of dehydrogenation of EPHC were not observed in preliminary studies of the arsenic pincer complex, $\text{IrH}_2\{\text{C}_6\text{H}_3\text{-2,6-(OAsBu}^t_2)_2\}$. Thus the arsenic pincer complex has been ruled out for further cycling studies.

Four notional models of the entire system have been devised and developed in detail using COMSOL. Our studies show that the most effective heat transfer occurs in helical reactors that allow the design of a short, easy to package reactor which in turn reduces heat loss in the system. Basic estimate of the cost system have been carried out and show that the reactor could be constructed from part currently in standard production and thus insures price reasonableness of the reactor. Reduction of enthalpy and conservation of waste heat from both the reactor and other sources on the vehicle are key to a high hydrogen capacity system. In consultation with other DOE contract holders (Oregon State University), we were able to significantly reduce both our engineering time and the mass and volume of the unit by use of micro-channel heat exchangers.

Future Directions

LOC Screening and Evaluation: We plan to continue the isothermal kinetic studies of the PCP pincer complex catalyzed dehydrogenation of LOCs. Our studies of MPHI and EPHC have shown that the “outer rings” (the 6-member rings that do not containing the nitrogen atom) undergo very little dehydrogenation. We will determine whether this phenomenon is due to kinetic or thermodynamic constraints using the Task 2 procedure. However, in view of the low levels of dehydrogenation that has been found to occur in the outer rings, we have decided to screen perhydro-indolizidine and other candidate LOCs that have two 5-membered ring systems and appropriate physical properties. We also plan to carry out cycling studies on methylperhydro-indole and/or a better performing alternative LOC.

Reactor Design: We plan to finish the down-selection of reactor design using calculations of dynamic performance to select the best option. We will also carry out a trade-off analysis of hydrogen-hydrocarbon separator options. Finally, we will determine the properties required to meet different DOE targets.

FY 2012 Presentations

1. “Development of Processes for the Reversible Dehydrogenation of High Capacity Hydrogen Carriers at Practical Conditions”; Craig M. Jensen, Godwin Severa, Marina Chong, Zhouhui Wang, Ewa Rönnebro, Tom Autrey, and Ahbi Kamkamkar, 1st Low Carbon Earth Summit 2011, Forum 7 Clean and Sustainable Energy, Complex Hydrides; Dalian, October 24–26 2011.
2. “Development of Liquid Organic Hydrogen Carriers”, Daniel Brayton and Craig M. Jensen, Materials Challenges in Alternative & Renewable Energy 2012, Clearwater, Florida, February 26–29, 2012.

IV.C.1 A Biomimetic Approach to Metal-Organic Frameworks with High H₂ Uptake

Hong-Cai (Joe) Zhou

Dept. of Chem., Texas A&M University
P.O. Box 30012
College Station, TX 77842-3012
Phone: (979) 845-4034
Email: zhou@mail.chem.tamu.edu

DOE Managers

HQ: Ned Stetson
Phone: (202) 586-9995
Email: Ned.Stetson@ee.doe.gov

GO: Jesse Adams
Phone: (720) 356-1421
Email: Jesse.Adams@go.doe.gov

Contract Number: DE-FC36-07GO17033

Project Start Date: July 1, 2007
Project End Date: June 30, 2013

of MOFs with gas-adsorption affinity around 15 to 20 kJ/mol for hydrogen.

- The overall objective is to achieve the DOE 2010 and 2017 system goals, primarily the gravimetric and volumetric storage goals, at or near-ambient temperatures and moderate pressure for onboard vehicular hydrogen storage (Table 1).

TABLE 1. Technical System Targets: Onboard Hydrogen Storage for Light-Duty Vehicles

| Storage Parameter | Units | 2010 | 2017 | Ultimate |
|--|---------------------------------------|-------------|-------------|-------------|
| System Gravimetric Capacity: Usable, specific-energy from H ₂ (net useful energy/max system mass) | kWh/kg (kg H ₂ /kg system) | 1.5 (0.045) | 1.8 (0.055) | 2.5 (0.075) |
| System Volumetric Capacity: Usable energy density from H ₂ (net useful energy/max system volume) | kWh/L (kg H ₂ /L system) | 0.9 (0.028) | 1.3 (0.040) | 2.3 (0.070) |

Fiscal Year (FY) 2012 Objectives

- Design, synthesis, and characterization of metal-organic frameworks (MOFs) with potential anchors for active metal centers introduction.
- Design, synthesis, and optimization of porous polymer frameworks (PPNs) with different functionalities.
- These functionalized MOFs and PPNs demonstrate much enhanced H₂ affinity through optimized, cooperative binding. The results can be a great help in designing advanced porous materials to reach the DOE 2010 and ultimately 2017 hydrogen storage goal.

Technical Barriers

This project addresses the following technical barriers from the Hydrogen Storage section of the Fuel Cell Technologies Program Multi-Year Research, Development and Demonstration Plan:

- (P) Lack of Understanding of Hydrogen Physisorption and Chemisorption
- (Q) Reproducibility of Performance

Technical Targets

- The focus of the proposed research is the use of concepts evident in metalloproteins to guide the synthesis

FY 2012 Accomplishments

- High-surface-area MOFs (PCN-82 and PCN-88) with potential anchors for metal incorporation were synthesized, the calculated heat of adsorption for PCN-82 is 6.6 kJ/mol at zero loading, and this value compares favorably with MOFs lacking special sorption sites.
- Highly stable Zr-MOF with metalloporphyrin ligand (PCN-223) was synthesized and initial metal-insertion study was carried out, these materials exhibit high surface area and high heat of adsorption for H₂.
- Low-cost PPN enriched with phenol groups (PPN-43) was synthesized, phenol group can be served as anchor for metal incorporation, therefore high heat of adsorption for H₂.
- A series of biphenyl ring PPNs have been designed and synthesized, these materials are relatively low cost, but exhibit high surface areas and high heats of adsorption for H₂.



Introduction

In the past decade, there has been an escalation of interest in the study of MOFs due to their fascinating structures and intriguing application potential. Their exceptionally high surface areas, uniform yet tunable pore sizes, and well-defined adsorbate-MOF interaction sites

make them suitable for hydrogen storage. Various strategies to increase the hydrogen capacity of MOFs, such as using pore size comparable to hydrogen molecules, increasing surface area and pore volume, utilizing catenation, and introducing coordinatively unsaturated metal centers (UMCs) have been widely explored to increase the hydrogen uptake of the MOFs. Recently, inelastic neutron scattering and neutron powder diffraction as well as computational studies suggest that the choice of both metal centers and ligands can play an important role in tailoring the gas-framework interactions. Additionally, those ligands containing phenyl rings have been proved favorable for hydrogen desorption. MOFs with hydrogen uptake approaching the DOE 2010 gravimetric storage goal under reasonable pressure but cryo-temperature (typically 77 K) were reported. However, the weak interaction between hydrogen molecules and MOFs has been the major hurdle limiting the hydrogen uptake of MOFs at ambient temperature.

Approach

Our strategy to enhance H₂ uptake was as follows:

- (1) prepared the catenation isomer pair to evaluate the contribution from catenation to the hydrogen uptake of a MOF material. Catenation can be utilized to reduce pore sizes in porous MOFs and has also been explored as an efficient method to improve the hydrogen uptake of MOFs.
- (2) Synthesized porous MOFs with high hydrogen adsorption capacities based on different coordinatively UMCs. The implementation of coordinatively UMCs into porous MOFs has been considered one of the most attractive ways to improve their affinities to hydrogen.
- (3) Hydrogen storage studies in MOFs containing nanoscopic cages based on double-bond-coupled di-isophthalate linkers. Those ligands containing phenyl rings in MOFs have been proved favorable for hydrogen adsorption.
- (4) Design and synthesize porous MOFs based on an anthracene derivative which can provide additional hydrogen binding sites to increase the hydrogen uptake.
- (5) Obtained stable MOFs with high surface areas by the incorporation of mesocavities and microwindows.
- (6) Constructed MOFs with “close-packing” alignment of open metal sites, which can increase the number of nearest neighboring open metal sites of each H₂-hosting void in a three-dimensional (3-D) framework so that they can interact directly with the guests (H₂ molecules) inside the void.
- (7) Built up porous lanthanide MOFs and studied their potential application in gas adsorption.
- (8) Prepared an unprecedented linkage isomer pair of MOFs and studied the impact of pore size on H₂ storage capacity in MOFs.
- (9) Incorporated polyynes unit into MOFs, which has higher H₂ affinity.
- (10) Construct stable and high-surface-area Zr-MOFs, study the effect on gas uptake by introducing different metals into their porphyrin linkers.
- (11) Design and synthesize PPNs with high chemical stability suitable for further

decoration. (12) Incorporated metal ions into PPNs, which can enhance the isosteric heats of hydrogen-adsorption.

Results

In the past year, we have prepared a series of MOFs and PPNs and explored their potential applications in hydrogen storage. Table 2 shows the comparison of hydrogen heat of adsorption, uptake at low pressure, and Brunauer-Emmett-Teller (BET) surface area of selected MOFs and PPNs. Next we will discuss in detail the results of H₂ uptakes of these materials.

TABLE 2. Comparison of Hydrogen Heat of Adsorption, Uptake at Low Pressure, and BET Surface Area of Selected MOFs and PPNs

| Material | ΔH_{ads} (kJ/mol) | Uptake at 77 K and 1 bar (wt%) | BET surface area (m ² /g) |
|----------------------|----------------------------------|--------------------------------|--------------------------------------|
| PCN-82 | 6.6 | 2.7 | 4,488 |
| PCN-88 | 6.0 | 2.6 | 3,300 |
| PCN-223-Zr; -Fe; -Ni | 8.7; 8.0; 8.5 | 1.6; 1.5; 1.2 | 2,200 (Fe) |
| PPN-43 | 8.6 | 1.2 | 1,040 |
| PPN-10 | 8.4 | 1.0 | 1,128 |
| PPN-12 | 5.8 | 1.7 | 3,420 |
| PPN-13 | 8.2 | 1.4 | 1,026 |
| PPN-14; 15; 16 | 7.1; 7.9; 8.7 | 1.6; 1.2; 1.2 | 1,910; 873; 794 |

a. High-surface-area MOF (PCN-88) with pre-designed single-molecule trap (SMT) for pyrazine derivatives

A newly designed tetratopic carboxylic acid ligand 5,5'-(naphthalene-2,7-diyl)diisophthalic acid (H₄L) was synthesized by Pd-catalyzed coupling reactions between 2,7-dibromonaphthalene and diethyl 5-(4,4,5,5-tetramethyl-1,3,2-dioxaborolan-2-yl)isophthalate. H₄L reacted with Cu(NO₃)₂·2.5H₂O under solvothermal conditions affording PCN-88, which has a 3-D framework structure containing the pre-designed SMT units (Figure 1a).

After activation at 100°C under reduced pressure, PCN-88 retained its crystallinity as confirmed by powder X-ray diffraction (PXRD). The N₂ and Ar adsorption isotherms at 77 and 87 K further revealed its permanent porosity. A two-step adsorption was observed in N₂ and Ar isotherms, with BET and Langmuir surface areas of 3,308 and 3,845 m²/g, respectively.

In the low pressure region, the hydrogen-uptake capacity is largely controlled by the hydrogen affinity towards the framework, which can be quantified by heat of adsorption. Variable-temperature measurements reveal an isosteric heat of adsorption of 6.0 kJ/mol for PCN-88 at zero loading, as a result, PCN-88 can take up a remarkable 320 cm³/g (2.7 wt%) of H₂ at 77 K and 1 bar (Figure 1b). The value is among the highest of reported porous materials at low pressure. Work is

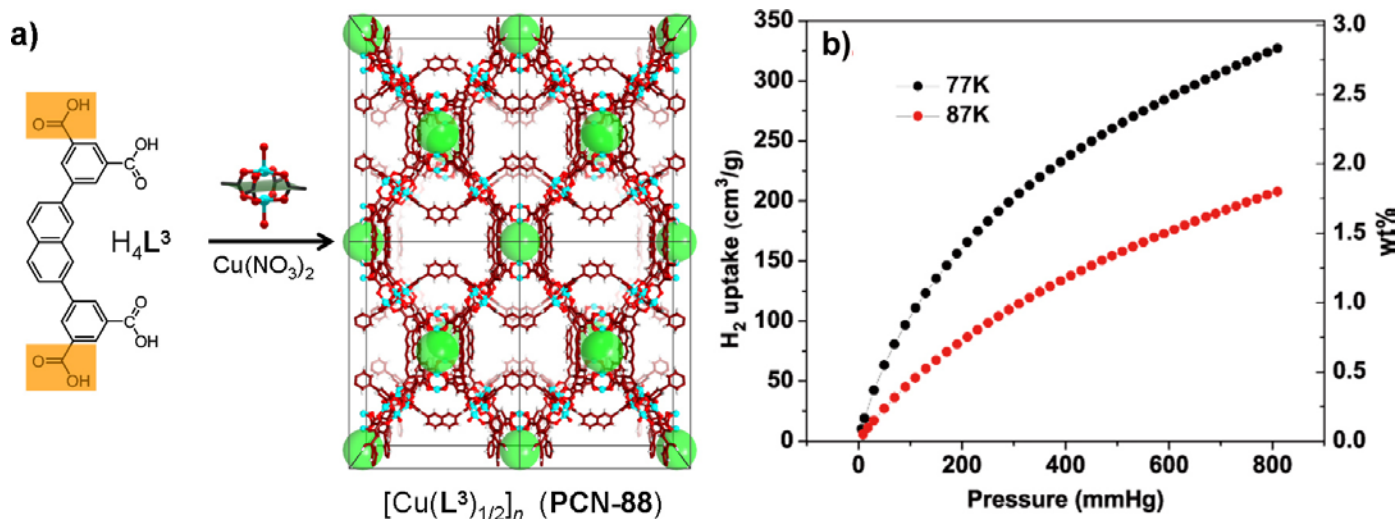


FIGURE 1. (a) Schematic representation of the construction of PCN-88 and its 3-D framework structure. (b) Low-pressure hydrogen isotherms of PCN-88 at 77 and 87 K.

continuing on introducing pyrazine derivatives into SMT and their heats adsorption for H_2 .

b. Highly porous MOF sustained with 12-connected nanoscopic octahedra

The tetra-carboxylate ligand, bpbcd, with a 90°-angle-carbazole-3,6-dicarboxylate moiety as opposed to the widely used 120°-angle-isophthalate, was synthesized by a Cu(I)-catalyzed reaction between dimethyl 9H-carbazole-3,6-dicarboxylate and 1,4-dibromo-2,5-dimethoxybenzene followed by hydrolysis. Solvothermal reaction of H_4 bpbcd and $Cu(NO_3)_2 \cdot 2.5H_2O$ in the presence of HBF_4 afforded green block crystals PCN-82 (Figure 2a).

The N_2 sorption for freeze-dried PCN-82 at 77 K exhibited a reversible Type-I isotherm as shown in Figure 2b, a characteristic of microporous materials. PCN-82 exhibits exceptionally high N_2 uptake (ca. 1,100 cm^3/g). By applying the BET model (up to $P/P_0 \approx 0.05$), the apparent surface area is estimated to be $\sim 4,488$ m^2/g (calculated $\sim 4,307$ m^2/g) and Langmuir surface area $\sim 4,859$ m^2/g , which is similar to MOF-177 (BET $\sim 4,500$ m^2/g).

Variable-temperature measurements reveal an isosteric heat of adsorption of 6.6 kJ/mol for PCN-82 at zero loading, this value compares favorably with MOFs lacking special sorption sites; their heats of adsorption are typically in the 4–5 kJ mol. The excellent performance of PCN-82 can be attributed to the availability of open metal sites, microporous nature and exceptionally high surface area, as a result, PCN-82 can take up a remarkable 300 cm^3/g (2.6 wt%) of H_2 at 77 K and 1 bar (Figure 2c). Work is ongoing to introduce different functionalities onto benzene linkers to improve their heat adsorption for H_2 .

c. Highly stable mesoporous zirconium MOFs with metalloporphyrin ligand

Solvothermal reactions of metalloporphyrin M-TCPP (TCPP = tetrakis(4-carboxyphenyl)porphyrin, M = Fe, Mn, Co, Ni, Cu, Zn, H₂), $ZrCl_4$ and benzoic acid yielded needle shaped single crystals of PCN-223. Different from the well-known 12-connected Zr_6 cluster observed in the UiO-series of MOFs, only eight edges of the Zr_6 octahedron are bridged by carboxylates from TCPP ligands in PCN-223, while the remaining positions are occupied by terminal –OH groups (Figure 3a).

The porosity of PCN-223 has been examined by nitrogen adsorption experiments at 77 K. The typical type IV isotherm of PCN-223(Fe) exhibits a steep increase at the point of $P/P_0 = 0.3$, suggesting meso-porosity. A N_2 uptake of 1,009 cm^3/g and a BET surface area of 2,200 m^2/g have been observed for PCN-223(Fe), the pore volume of 1.56 cm^3/g is also in good agreement with the calculated pore volume of 1.63 cm^3/g . Other PCN-223 MOFs with different porphyrin centers also displayed similar type IV N_2 sorption isotherms and gave surface area, N_2 uptake, and total pore volume up to 2,312 m^2/g , 1,067 cm^3/g , and 1.65 cm^3/g , respectively.

The PXRD patterns remain intact upon immersion in water, boiling water, as well as 2M, 4M, 8M, and even concentrated hydrochloric acid (HCl) aqueous solutions for 24 h, suggesting no phase transition or framework collapse happening during these treatments (Figure 3b). More importantly, the N_2 sorption isotherms remained almost the same upon all treatments, which further confirmed the intactness of the tested frameworks. Strikingly, PCN-223(Fe) survived even after the treatment with concentrated HCl,

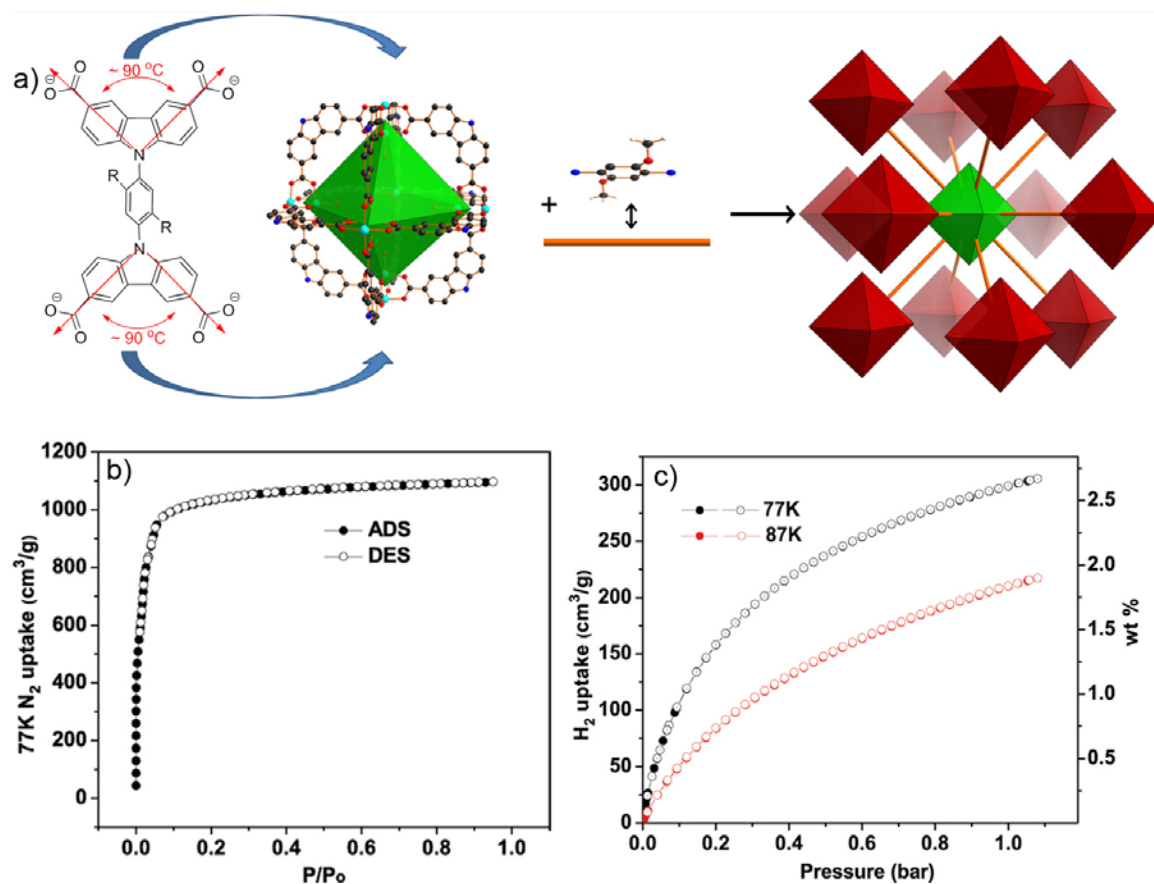


FIGURE 2. (a) Schematic representation of the construction of PCN-82 and its 3-D framework structure. (b) 77 K N₂ isotherm for PCN-82. (c) Low-pressure hydrogen isotherms of PCN-82 at 77 and 87 K.

a strong acid, which has rarely been observed for MOF materials, showing its exceptionally high chemical stability.

Variable-temperature measurements reveal isosteric heats of adsorption of 8.7, 8.0, and 8.5 kJ/mol for PCN-223(Zr), PCN-223(Fe), and PCN-223(Ni), respectively, at zero loading (Figure 3c, 3d). The high value can be partially attributed to the incorporated metal centers in the porphyrin ligand.

d. Functionalized PPN design and synthesis

The advantages of phenolic resin are high density of phenol, high stability, easy to scale up, et al. These properties are extremely important for practical gas storage applications. To render these properties into porous polymers, we designed and synthesized a tetrahedral polyphenol 4,4',4'',4'''-methanetetrayltetraphenol. With this tetrahedral monomer reacted with formaldehyde, we successfully synthesized a PPN-43 with remarkable density of phenol group. PPN-43 exhibits BET surface area as high as 1,040 m²/g, by measuring H₂ uptake at various temperatures, H₂ heat of adsorption for PPN-43 was calculated to be 8.6 kJ/mol at zero loading.

Considering its superb physicochemical property, our group is working on optimizing reaction conditions to further improve the surface area; and the study of using phenol group as an anchor for multivalent metals incorporation is also underway.

Oxidative Eglinton coupling of terminal alkynes has been proven very efficient in polymerization reactions. We designed and synthesized a series of biphenyl ring tetrahedral monomers, the two phenyl rings are in a perpendicular position by the substitution at 2,2',6,6' positions. We successfully synthesized a series of PPNs, among them; PPN-12 shows a BET surface area as high as 3,420 m²/g (Figure 4a). PPN-13 with all fluorine substitution has the highest heat of adsorption for H₂. We also tried to release the phenol groups in PPN-14, and convert it into phenolic lithium (Figure 4b). Although surface area significantly decreased with this procedure, the increase of heat of adsorption is obvious (Figure 4d). Work is continuing in our group to optimize the reactions and incorporate other functionalities to further improve heat of adsorption.

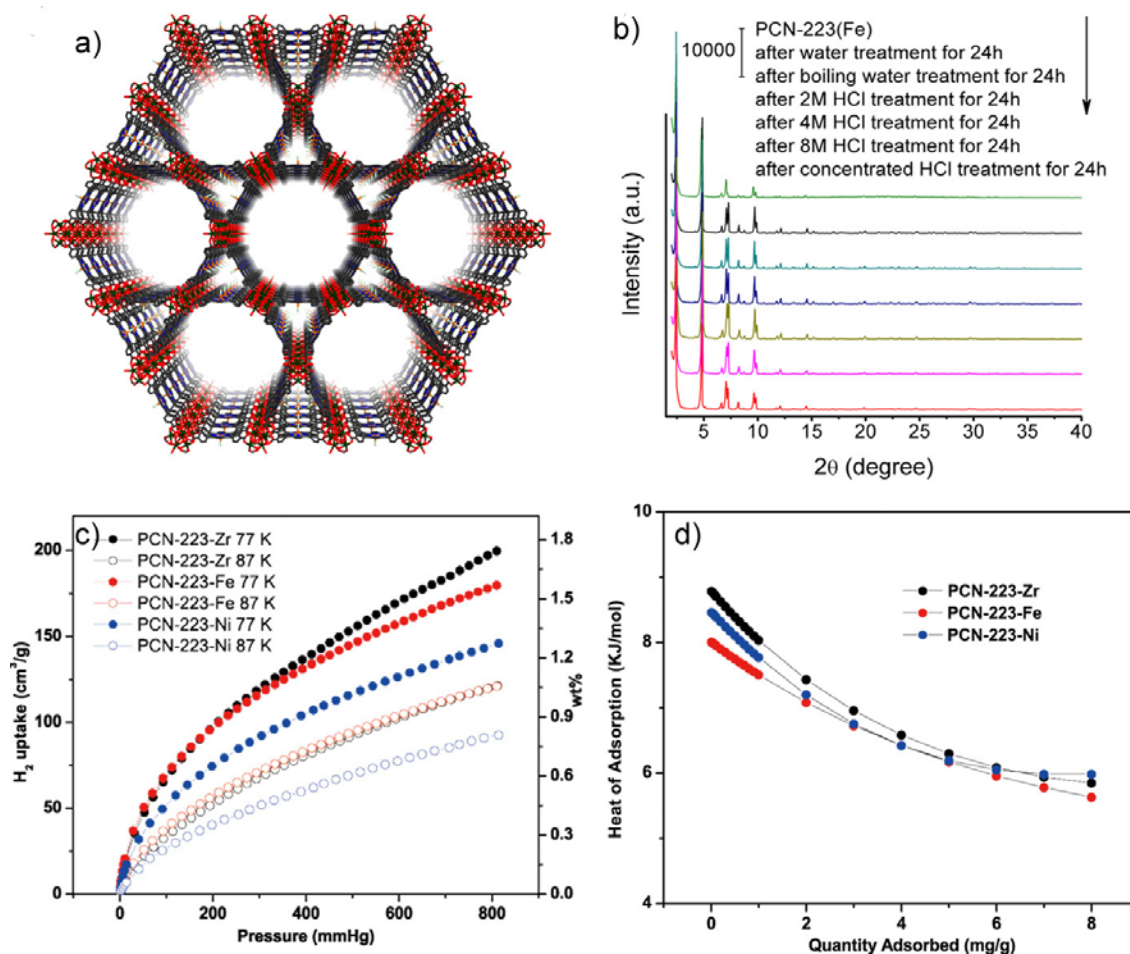


FIGURE 3. (a) Crystal structure and underlying network topology of PCN-223(Fe). (b) Powder X-ray diffraction pattern upon treatments with water, boiling water, 2M, 4M, 8M and even concentrated HCl. (c) Low-pressure hydrogen isotherms of PCN-223 at 77 and 87 K. (d) Calculated heats of adsorption of PCN-223.

Conclusions and Future Directions

Conclusions:

- Two MOFs (PCN-82 and PCN-88) with exceptionally high surface areas (4,488 and 3,300 m²/g) have been designed and synthesized. They all have high heat of adsorption and potential anchors for metal incorporation.
- A series of high-surface-area Zr-MOFs were synthesized by using metalloporphyrin ligands, these MOFs are stable even in strong acidic conditions. Initial study shows that metal incorporation leads to high heat of adsorption for H₂.
- A phenolic PPN was synthesized, the phenol group can serve as an anchor for multivalent metal incorporation.
- A series of biphenyl PPNs were designed and synthesized by using triple bond coupling reaction, the biphenyl ring is “locked” by introducing functional groups at 2 & 2' positions, therefore leading to high-surface-area PPNs, and high heat of adsorption for H₂.

Future Directions:

- Further enhancement of H₂-MOF interaction by doping coordinatively unsaturated metal centers (heat of adsorption 15 kJ mol⁻¹). Based on theoretical calculations, main group metals such as Li, Mg and Ca and multivalent metals, such as V³⁺, Fe³⁺, Ti³⁺, etc. will be tested.
- Working with partners, test H₂ uptake at temperatures higher than 77 K.
- Preparation of MOFs with high surface area and optimized cage size with newly designed ligands based on theoretical calculations.
- Incorporation of entatic-state metals based on theoretical guidance.
- Preparation of new PPNs containing active metals.

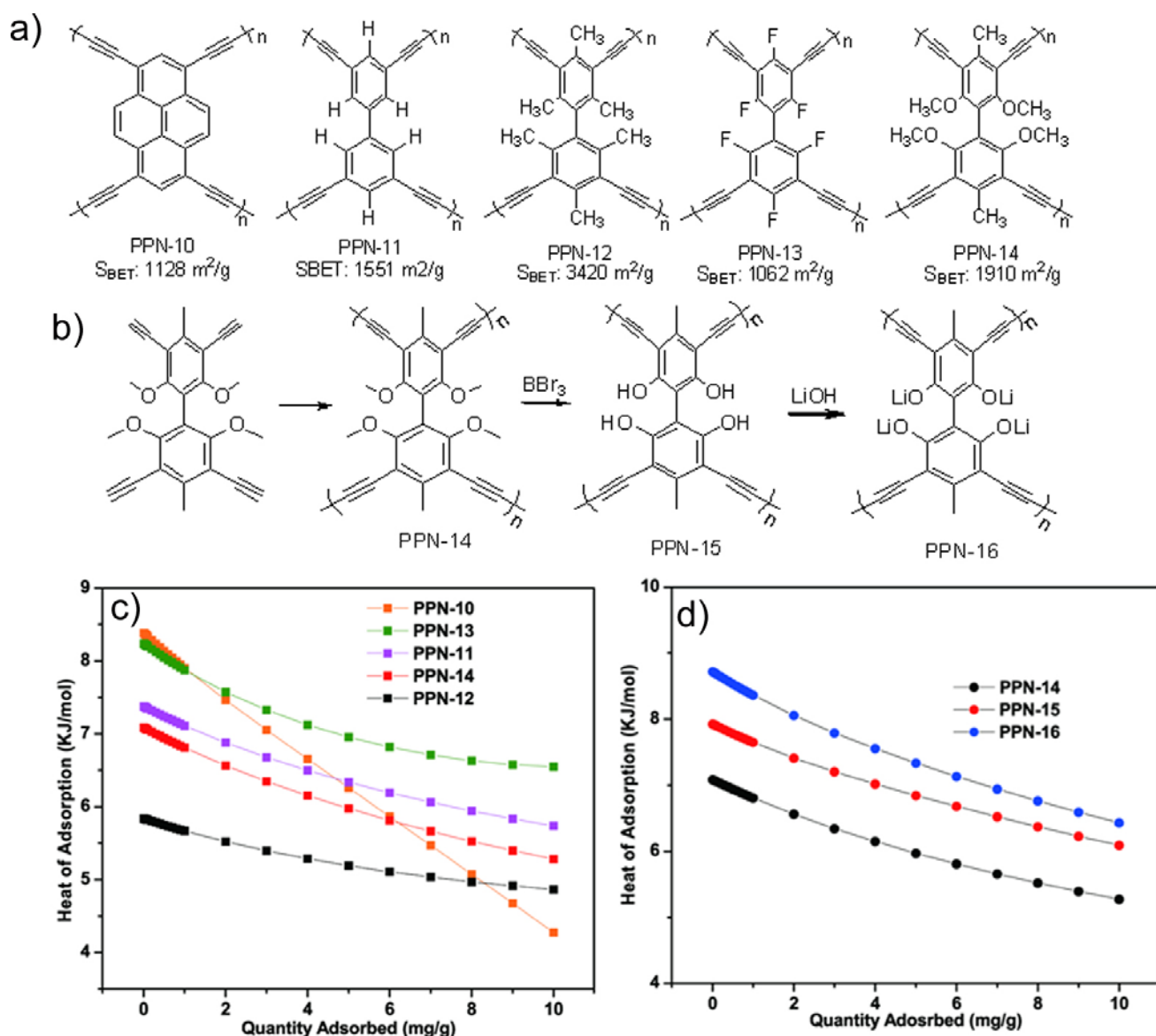


FIGURE 4. (a) The structure of biphenyl ring PPNs with their calculated BET surface areas. (b) Synthetic scheme of PPN-15 and 16. (c) The calculated H_2 heats of adsorption for PPN-10, 11, 12, 13, and 14. (d) The calculated H_2 heats of adsorption for PPN-14, 15, and 16.

FY 2012 Publications/Presentations

Publications

1. "Highly Stable Porous Polymer Networks with Exceptionally High Gas-Uptake Capacities", Yuan, D.; Lu, W.; Zhao, D.; Zhou, H.-C., *Adv. Mater.* **2011**, *23*, 3723–3725.
2. "Sulfonate-Grafted Porous Polymer Networks for Preferential CO_2 Adsorption at Low Pressure", Lu W.; Yuan D.; Sculley J.; Zhao D.; Krishna R.; Zhou, H.-C., *J. Am. Chem. Soc.* **2011**, *133* (45), 18126–18129.
3. "Isomerism in Metal-Organic Frameworks: "Framework Isomers", Makal, T. A.; Yakovenko, A.; Zhou, H.-C., *J. Phys. Chem. Lett.*, **2011**, *2*, 1682–1689.

4. "A Robust Metal-Organic Framework with An Octatopic Ligand for Gas Adsorption and Separation: A Combined Characterization by Experiments and Molecular Simulations", Zhuang, W.; Yuan, D.; Liu, D.; Zhong, C.; Li, J.-R.; Zhou, H.-C., *Chemistry of Materials*, **2011**, *24* (1), 18–25.
5. "Pressure-Responsive Curvature Change of a "Rigid" Geodesic Ligand in a (3,24)-Connected Mesoporous Metal-Organic Framework", Yuan, D.; Zhao, D.; Zhou, H.-C., *Inorg. Chem.* **2011**, *50* (21), 10528–10530.
6. "A Porous Metal-Organic Framework with Helical Chain Building Units Exhibiting Facile Transition from Micro- to Mesoporosity", Park, J.; Li, J.-R.; Sañudo, E.C.; Yuan, D.; Zhou, H.-C., *Chem. Commun.*, **2012**, *48* (6), 883 – 885.

7. “Stepwise Adsorption in a Mesoporous Metal-Organic Framework: Experimental and Computational Analysis” Yuan, D.; Getman, R.B.; Wei, Z.; Snurr, R.Q.; Zhou H.-C. *Chem. Comm.*, **2012**, *48*, 3297-3299.
8. “A Highly Porous and Robust (3,3,4)-Connected Metal-Organic Framework Assembled with a 90°-Bridging-Angle-Embedded Octa-carboxylate Ligand”, Lu, W.; Yuan, D.; Makal, T. A.; Li, J.-R.; Zhou, H.-C., *Angew. Chem. Int. Ed.*, **2012**, *124* (7), 1612-1616.
9. “Highly Potent Bactericidal Activity of Porous Metal-Organic Frameworks”, Zhuang, W.; Yuan, D.; Li, J.-R.; Luo, Z.; Zhou, H.-C.; Bashir, S.; Liu, J., *Adv. Healthcare Mater.*, **2012**, *1*, 225–238.

Presentations

1. “MOFs, MOPs, and PPNs: Porous Materials through Rational Design”, University of California at Berkeley, Oct. 18, 2011, Berkeley, California.
2. “MOFs, MOPs, and PPNs: Preparation and Application”, University of North Carolina, Chapel Hill, Nov. 8, 2011, Chapel Hill, North Carolina.
3. Featured Speaker, “MOFs, MOPs, and PPNs: Porous Materials through Rational Design”, ACS Southwest Regional Meeting, Nov. 10, 2011, Austin, Texas.
4. “Optically Controlled Hydrogen Adsorption in MOFs and MOPs”, Jinhee Park and Hong-Cai Zhou, 2011 Southwest Regional ACS meeting, Nov. 12, 2011, Austin, Texas.
5. “Metal-organic frameworks constructed from infinite zinc chains”, Yangyang Liu, and Hong-Cai Zhou, 2011 Southwest Regional ACS meeting, Nov. 12, 2011, Austin, Texas.
6. “New interweaving MOF possessing the Pt₃O₄-net topology based on a metalloligand”, Zhangwen Wei and Hong-Cai Zhou, 2011 Southwest Regional ACS meeting, Nov. 12, 2011, Austin, Texas.
7. “MOFs, MOPs, and PPNs: Preparation and Application”, Sichuan University, Nov. 17, 2011, Nov. 17, 2011, Chengdu, Sichuan, China.
8. “MOFs, MOPs, and PPNs: Preparation and Application”, Sichuan Normal University, Nov. 17, 2011, Nov. 17, 2011, Chengdu, Sichuan, China.
9. “MOFs, MOPs, and PPNs: Preparation and Application”, National University of Singapore, Nov. 22, 2011, 2011, Singapore.
10. “MOFs, MOPs, and PPNs: Preparation and Application”, Nanyang Technological University, Nov. 23, 2011, 2011, Singapore.
11. “MOFs, MOPs, and PPNs: Preparation and Application”, Agency for Science Technology & Research (A*Star), Nov. 24, 2011, 2011, Singapore.
12. “Building Metal-Organic Frameworks, One Cavity at a Time”, Invited Speaker – University of South Florida, Mar 8, 2012, Tampa, FL.

IV.C.2 A Joint Theory and Experimental Project in the Synthesis and Testing of Porous COFs for Onboard Vehicular Hydrogen Storage

Omar M. Yaghi

Department of Chemistry and Biochemistry
University of California - Los Angeles
607 Charles E. Young Drive East
Los Angeles, CA 90095
Phone: (310) 206-0398
Email: yaghi@chem.ucla.edu

DOE Managers

HQ: Ned Stetson
Phone: (202) 586-9995
Email: Ned.Stetson@ee.doe.gov
GO: Katie Randolph
Phone: (720) 356-1759
Email: Katie.Randolph@go.doe.gov

Contract Number: DE-FG36-08GO18141

Project Start Date: September 1, 2008

Project End Date: July 31, 2012

Technical Targets

This project consists of several fundamental studies on COFs. Insights gained from these studies will be applied toward the design and synthesis of hydrogen storage materials that meet the following DOE 2015 hydrogen storage targets:

- Volumetric density: 40 g L⁻¹
- Gravimetric density: 5.5 wt%

FY 2012 Accomplishments

- Synthesized new air stable COFs through imine condensation (COF-320 and 340).
- Performed metalation experiments of COFs (COF-301, phenanthroline-COFs).
- Synthesized two low density COFs with triptycene unit (0.15-0.21 g cm⁻³).
- Predicted binding energy with different first row transition metals.
- Predicted H₂ isotherms and Q_{st} values of metalated COF-322, 330 and 333 (298 K, up to 100 bar).



Fiscal Year (FY) 2012 Objectives

- Design optimal frameworks with potential metal binding sites for metal impregnation.
- Predict H₂ uptake isotherm for designed frameworks using our newly developed force field.
- Implement metalation experiments and evaluate the H₂ adsorption property.
- Synthesize new covalent organic frameworks (COFs) with ultra-high surface area (>5,000 m² g⁻¹).

Technical Barriers

This project addresses the following technical barriers from the Storage section (3.3.4.2) of the Fuel Cell Technologies Program Multi-Year Research, Development and Demonstration Plan:

- (A) System Weight and Volume
- (C) Efficiency
- (E) Charging/Discharging Rates
- (P) Lack of Understanding of Hydrogen Physisorption and Chemisorption

Introduction

Storage of hydrogen in porous materials is a promising approach to achieve the DOE system requirements for use of H₂ as a transportation fuel. After the first report of successful H₂ storage in metal-organic frameworks (MOFs), the Yaghi group has succeeded in incrementally increasing the gravimetric and volumetric capacities in order to reach the highest H₂ uptake capacity, albeit at 77 K. However, for onboard vehicular H₂ storage it is necessary to improve the adsorption enthalpy of porous materials to achieve significant capacities at room temperature. Therefore, we are currently focusing our efforts on discovering highly porous materials with strong affinity for H₂.

Approach

To meet the DOE 2015 revised targets by physisorption, adsorbents must have high surface area (>3,500 m² g⁻¹) and relatively high density (>0.75 g cm⁻³). We have previously demonstrated how to design high surface area MOFs and COFs [1]. However, in many cases, these materials do not show steep H₂ uptake in the low-pressure region, because

the binding energy based on non-covalent interactions (electrostatic and dispersion) is generally smaller than 10 kJ mol^{-1} [2,3]. In contrast, it is known that orbital interaction (i.e. the interaction between hydrogen and the d-orbital of transition metals) is stronger than van der Waals interaction, where the values may be greater than 20 kJ mol^{-1} . This prompts us to prepare COFs with metal binding sites and to impregnate COFs for the enhancement of the adsorption enthalpy. From the preliminary metal impregnation experiments, it seems that larger pore materials are better to implement the metal impregnation because metals and metal salts are solvated. In this year, we prepared expanded version of COF-300 with metal binding sites. In parallel with the synthesis, H_2 loading curves for the pristine and metalated COF materials were calculated.

Results

Metal impregnation is one of the most promising strategies to improve the adsorption enthalpy of COFs. However, our initial attempts at COF-301 indicate poor metalation yield. A similar problem was also observed in MOFs that have potential metal binding sites in their structures. Possible explanations for the low metalation yield include (1) low coordination ability of metal ions, (2) unfavorable conformation of the metal binding sites (i.e. a bipyridine linker can rotate), (3) steric hindrance due to the solvation of metal salts and the presence of counter anions, and (4) structural decomposition of the frameworks. Because the bipyridine moiety in the framework structure can rotate, it is likely that relatively large pore volume (large pore diameter) is critical to successful incorporation of the guest metal, which was not considered in simulation calculations. Before the metal impregnation experiments are carried out, it is necessary to prepare COFs with large pores. To this end, we designed and prepared expanded versions of COF-300 by condensation reactions.

Preparation of imine COF and its metalation reaction. We have demonstrated the condensation of the tetrahedral building block tetra-(4-anilyl)methane (Figure 1, **1**) with the linear linking unit terephthalaldehyde (**2**) to produce a material with an extended three-dimensional framework structure (COF-300) [4]. To increase the storage space in COF materials, expansion of linker **2** is a good approach. Therefore the structures of organic linkers that can be easily synthesized and/or commercially available were investigated. It is intuitively found that linker **7** is a good candidate to expand the pore while introducing the potential metal binding sites. However, it is difficult to add aldehyde groups to the 3 and 8 positions. It could be possible to make linker **5** according to a literature procedure, but our final decision rather was to synthesize linker **6** due to the greater density of potential metal binding sites compared to **5**. In addition, the preparation of an expanded version of phenanthroline linker (**8**) was synthesized.

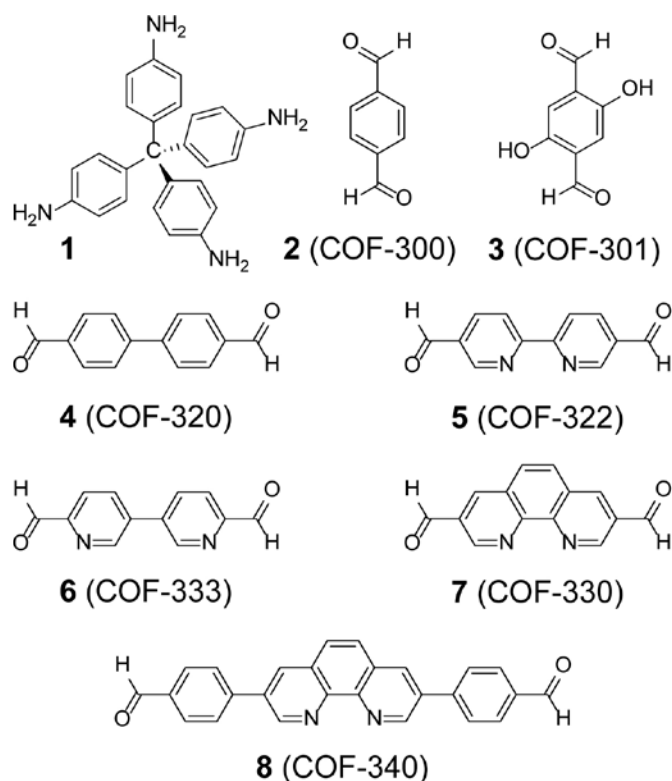


FIGURE 1. Molecular structures of tetrapoic (**1**) and ditopic building units (**2-8**), which form COF materials. The name of each COF is shown in parentheses.

The synthesis of COFs was carried out by solvothermal synthesis of a suspension of linker **1** and ditopic linker (**4**, **6**, or **8**) in a mixture of organic solvents. For a comparison of the porosity, a new COF (COF-320) using linker **4** was also newly synthesized. Synthetic conditions of these COFs were similar to COF-300, but these conditions are not optimized yet. Typically, a mixture of 1,4-dioxane and aqueous acetic acid with starting materials were heated at 120°C . All resulting materials are insoluble in water and common organic solvents such as: hexanes, methanol, acetone, tetrahydrofuran, and *N,N*-dimethylformamide. Therefore, the resultants are an extended structure.

The crystallinity of COF-320 and 340 was confirmed by powder X-ray diffraction (PXRD) analysis (Figure 2, top). Although its atomistic connectivity (including the degree of interpenetration) is not determined yet due to the limited numbers of diffraction peaks, it is important to note the position of the first peak located at lower angle when extended linkers were employed. This clearly demonstrates the successful pore expansion. Assuming that the connectivity (topology) of these COFs is in a diamond net, it is possible to build modeled structures (Figure 2, bottom). The simulated PXRD patterns are similar to those of experimental data, so that the full refinement of these COF will be performed in the future. With regard to COF-333, the solid material did not diffract well; although there are a few

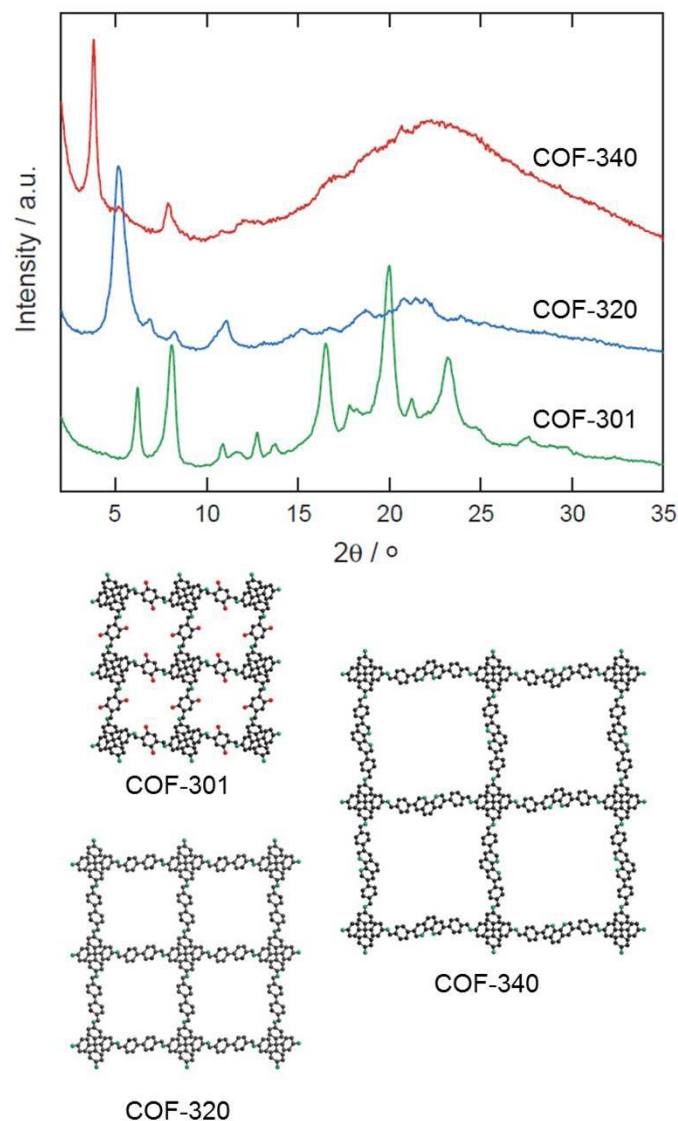


FIGURE 2. (top) PXRD patterns for COF-320 (blue) and COF-340 (red). As a reference, PXRD pattern for COF-301 was overlaid in green. (bottom) Modeled structure of COF-301, 320, and 340 based on the PXRD pattern.

weak diffraction lines observed. Further modification of the synthetic condition will be made to obtain crystalline solid.

The permanent porosity of COF-320 was demonstrated by measuring N_2 adsorption at 77 K. The application of the Brunauer-Emmett-Teller (BET) model results in a surface area of $1,620 \text{ m}^2 \text{ g}^{-1}$, which is higher than COF-300 and 301. However, low-pressure H_2 uptake at 77 K by COF-320 was not exceptional (Figure 3). The uptake at 1 bar and 77 K was 0.6 wt%, which is smaller than COF-300 (1.1 wt%). Currently the reason is not clear why the H_2 uptake is so small; however, it is likely that the activation conditions are not optimized yet. In the case of COF-340, N_2 isotherms using activated samples were also recorded. Unexpectedly N_2 uptake was very low (BET surface area = $35 \text{ m}^2 \text{ g}^{-1}$),

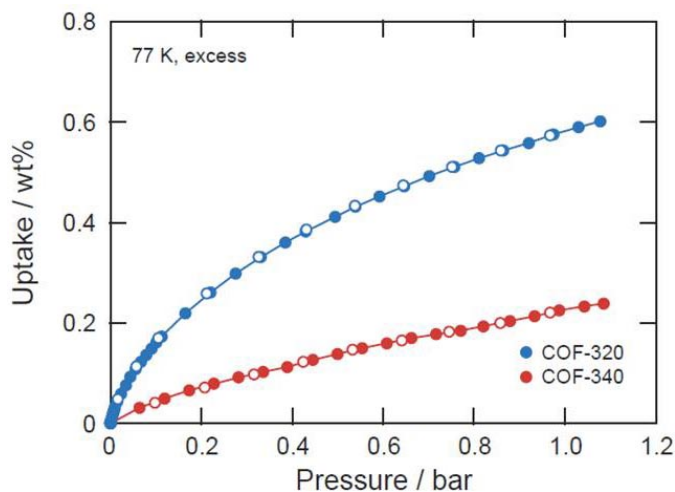


FIGURE 3. Excess H_2 isotherms of COF-320 (blue) and 340 (red) at 77 K

although the PXRD pattern indicates that the crystallinity still remains after the sample activation. Since the pore diameter of COF-340 is even greater than COF-320, this may be due to the presence of oligomers (i.e. fragments of COFs) in the pore. Currently investigation of the optimal condition to make crystalline COF-340 with reasonable porosity is now in progress.

Simulation of H_2 uptake at 298 K for COF-320, COF-322, COF-330 and COF-333. In the simulation side, the isotherms at the high pressure range for COF-320, COF-322, COF-330 and COF-333 were calculated and these are compared to the H_2 uptake of COF-300 at 298 K. It was found that the uptake for the other COFs at room temperature are very similar to each other but even higher than COF-300 (Figure 4). The maximum excess H_2 uptakes for these COFs in gravimetric units are listed in Table 1. Table 1 implies that all the compounds have a similar property. COF-320, COF-322 and COF-333 have very similar surface areas, which are greater than $7,000 \text{ m}^2 \text{ g}^{-1}$, while COF-300 and COF-330 show lower values. This should be due to the smaller pore diameter and/or larger volume of organic linker per volume.

Next the Q_{st} value for each compound was estimated. Since all the COFs contain C, H, and N and have an imine bond, it is expected that the interaction between framework and H_2 is also similar. The degree of this interaction should be derived from the Q_{st} . Obtained initial Q_{st} values for all pristine COFs are summarized in Table 1. The values of Q_{st} are ranging from 4.3 and 5.8 kJ mol^{-1} , leading to the fact that these COFs have essentially similar binding energy of H_2 . COF-300 has the lowest gravimetric uptake, while it showed the highest Q_{st} because of the small pore diameter. In this case, the potential energy surface for the pore overlaps and makes the H_2 interacts strongly with framework; however, it is well known that the small pore provides limited amount of H_2 uptake.

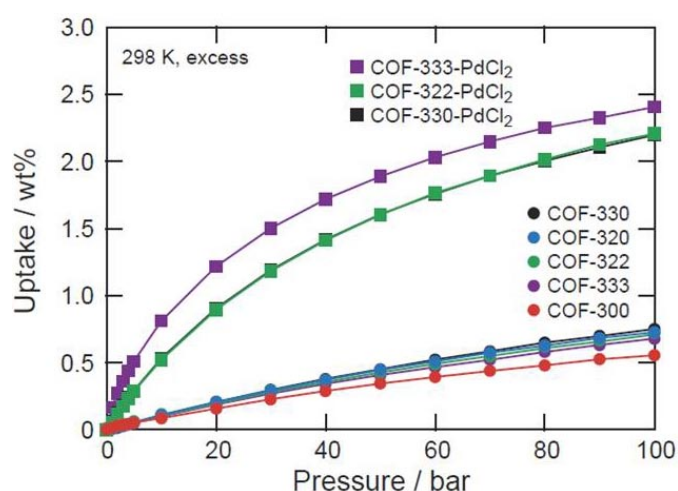


FIGURE 4. Predicted excess H_2 isotherms of COF-300, 320, 322, 330, and 333 and metalated versions of COF-322, 330, and 333 at 298 K. The values of COF-330 and COF-333 are very similar.

Next, total and excess uptake for the metalated versions of COF-330 and COF-333 at 298 K was estimated. The excess gravimetric uptake at 298 K is shown in Figure 4. In this case, the H_2 uptake in gravimetric unit is very similar to each other; metalated COF-330 and COF-333 take up 2.2 and 2.4 wt% (excess uptake) of H_2 at 100 bar, respectively. The same trend was observed by the total uptake in gravimetric units; the uptake at 100 bar and 298 K is 3.1 and 3.2 wt% for metalated COF-330 and COF-333, respectively (Table 1).

The total volumetric uptake for these two compounds was also estimated (Table 1). It should be noted that both frameworks show much greater H_2 uptake; COF-330 has 2.5 times higher uptake at 100 bar than bulk H_2 , while COF-333 has 3 times higher uptake. This clearly proves the advantage of metalation of the frameworks, although these values should be improved more. The total uptake of metalated COF-333 and 330 in volumetric unit is shown

in Table 1. These values are higher than bulk density of H_2 (7.6 g L^{-1}) so that it is presumed that H_2 molecules are effectively trapped by metal moieties introduced in the pore.

The initial Q_{st} values for these compounds were also calculated. The Q_{st} for metalated COF-333 (19 kJ mol^{-1} and 12.4 kJ mol^{-1} in average between 1-100 bar) is higher than other materials shown in this report. Note that metalated COF-333 also demonstrates the highest total uptake in volumetric unit. COF-333 and COF-322/330 have the same topology, the same connectivity and almost the same atoms, although the density of metal binding sites is double. On the contrary, the spatial location of the metals is different; for COF-333 the metal sites are on the corners of the pore, while metal sites for COF-322/330 are in the middle of the linker. Since it is unlikely that the density of metal in the framework affects the Q_{st} value, metals sites on the corners may interact more strongly. As a result, the stronger binding energy of H_2 can show improved H_2 uptake behavior despite COF-333 having a smaller surface area.

Conclusions and Future Directions

We originally performed the metalation reactions using COF-301 and phenanthroline-COFs; however, the results implied that the pore diameter is critical to successful incorporation of the guest metal. Therefore, in the middle of this year, the synthesis of new COFs with large pores was implemented by connecting ditopic and tetratopic building units through imine condensation (COF-320 and 340). In parallel with the synthesis, the binding energy with all first row transition metals was estimated to be the best candidates. Since the results indicate these transition metals and $PdCl_2$ show greater metal- H_2 interaction, H_2 loading curves for the expanded version of COF-300 with and without $PdCl_2$ were calculated. In addition to this, two low density COFs with triptycene units ($0.15\text{-}0.21 \text{ g cm}^{-3}$) were designed and synthesized.

TABLE 1. Summary of linker, and predicted surface area, H_2 uptake, and initial Q_{st} data for materials in this study

| Compound | Linker | BET area ($\text{m}^2 \text{g}^{-1}$) | Excess uptake (wt%) | Total uptake (wt%) | Total uptake (g L^{-1}) | Q_{st} (kJ mol^{-1}) |
|-------------------|--------|---|---------------------|--------------------|------------------------------------|-----------------------------------|
| COF-300 | 1 + 2 | 3,820 | 0.55 | 1.4 | 7.9 | 5.8 |
| COF-320 | 1 + 4 | 7,850 | 0.73 | 2.5 | 8.0 | 4.4 |
| COF-322 | 1 + 5 | 7,300 | 0.71 | 2.4 | 8.1 | 4.4 |
| COF-330 | 1 + 7 | 5,990 | 0.75 | 2.2 | 8.3 | 4.7 |
| COF-333 | 1 + 6 | 7,710 | 0.68 | 2.4 | 7.9 | 4.3 |
| COF-322- $PdCl_2$ | 1 + 5 | 5,550 | 2.2 | 3.3 | 16 | 9.2 |
| COF-330- $PdCl_2$ | 1 + 7 | 3,930 | 2.2 | 3.1 | 17 | 9.9 |
| COF-333- $PdCl_2$ | 1 + 6 | 2,990 | 2.4 | 3.2 | 21 | 19 |

- Optimize the activation conditions for the best surface area. H_2 isotherms and Q_{st} data will be compared to the predicted data.
- Characterize metalated materials (metal binding fashion, surface area, H_2 uptake, Q_{st})
- Develop the van der Waals-Force Field for the entire row of early transition metals from our current results.
- Use 2PT approach to calculate phase diagrams for H_2 inside the pores including counter anions.
- Optimize the metalation condition and loading amount for high-pressure H_2 tests at room temperature.

Special Recognitions & Awards/Patents Issued

1. TOP 2 most cited chemist worldwide (ISI Thomson)

FY 2012 Publications

1. S. Wan, F. Gándara, A. Asano, H. Furukawa, A. Saeki, S.K. Dey, L. Liao, M.W. Ambrogio, Y.Y. Botros, X. Duan, S. Seki, J.F. Stoddart, O.M. Yaghi, "Covalent Organic Frameworks with High Charge Carrier Mobility," *Chem. Mater.* **2011**, *23*, 4094-4097.

2. F.J. Uribe-Romo, C.J. Doonan, H. Furukawa, K. Oisaki, O.M. Yaghi, "Reticular Synthesis of Mesoporous Covalent Hydrazone Frameworks," *J. Am. Chem. Soc.* **2011**, *133*, 11478-11481.
3. J.L. Mendoza-Cortes, S.S. Han, W.A. Goddard, "High H_2 Uptake in pure, Li-, Na-, K-Metalated Covalent Organic Frameworks and Metal Organic Frameworks at 298 K," *J. Phys. Chem. A* **2012**, *116*, 1621-1631.
4. J.L. Mendoza-Cortes, "Design of Molecules and Materials for Applications in Clean Energy, Catalysis and Molecular Machines through Quantum Mechanics, Molecular Dynamics and Monte Carlo Simulations," California Institute of Technology, 2012, Ph.D. thesis.

References

1. H.M. El-Kaderi, J.R. Hunt, J.L. Mendoza-Cortés, A.P. Côté, R.E. Taylor, M. O’Keeffe, O.M. Yaghi, *Science*, **2007**, *316*, 268-272.
2. H. Furukawa, O.M. Yaghi, *J. Am. Chem. Soc.*, **2009**, *131*, 8876-8883.
3. J.L. Mendoza-Cortes, S.S. Han, W.A. Goddard, *J. Phys. Chem. A*, **2012**, *116*, 1621-1631.
4. F.J. Uribe-Romo, J.R. Hunt, H. Furukawa, C. Klock, M. O’Keeffe, O. M. Yaghi, *J. Am. Chem. Soc.*, **2009**, *131*, 4570.

IV.C.3 Multiply Surface-Functionalized Nanoporous Carbon for Vehicular Hydrogen Storage

P. Pfeifer (Primary Contact), C. Wexler, P. Yu, G. Suppes, F. Hawthorne, S. Jalisatgi, M. Lee, D. Robertson

University of Missouri
223 Physics Building
Columbia, MO 65211
Phone: (573) 882-2335
Email: pfeiferp@missouri.edu

DOE Managers

HQ: Ned Stetson
Phone: (202) 586-9995
Email: Ned.Stetson@ee.doe.gov
GO: Jesse Adams
Phone: (720) 356-1421
Email: Jesse.Adams@go.doe.gov

Contract Number: DE-FG36-08GO18142

Subcontractors:

Midwest Research Institute, Kansas City, MO

Project Start Date: September 1, 2008

Project End Date: November 30, 2013

Fiscal Year (FY) 2012 Objectives

- Fabricate high-surface-area, multiply surface-functionalized carbon (“substituted materials”) for reversible hydrogen storage with superior storage capacity (strong physisorption).
- Characterize materials and storage performance. Evaluate efficacy of surface functionalization, experimentally and computationally, for fabrication of materials with deep potential wells for hydrogen sorption (high binding energies).
- Optimize gravimetric and volumetric storage capacity by optimizing pore architecture and surface composition (“engineered nanospaces”).

Technical Barriers

This project addresses the following technical barriers from the Hydrogen Storage section of the Fuel Cell Technologies Program Multi-Year Research, Development and Demonstration Plan:

- (A) System Weight and Volume
- (B) System Cost

- (E) Charging/Discharging Rates
- (J) Thermal Management
- (P) Lack of Understanding of Hydrogen Physisorption and Chemisorption

Technical Targets

This project aims at the development of surface-engineered carbons, made from corncob or other low-cost raw materials, which simultaneously host high surface areas, created in a multi-step process, and a large fraction of surface sites with high binding energies for hydrogen, created by surface functionalization with boron, iron, and lithium. Targets are surface areas in excess of 4,500 m²/g, average binding energies in excess of 12 kJ/mol, and porosities below 0.8, toward the design of materials that meet the following 2017 DOE hydrogen storage targets:

- Gravimetric storage capacity: 0.055 kg H₂/kg system
- Volumetric storage capacity: 0.040 kg H₂/liter system

Accomplishments

- Demonstrated that boron substitution of high-surface area carbon raises binding energy (isosteric heat of adsorption) from ~7 kJ/mol to ~17 kJ/mol at zero coverage, and from 6 kJ/mol to 10 kJ/mol at high coverage. Demonstrated reproducibility of the high binding energy on samples from different lots.
- Manufactured boron-substituted carbons by deposition and thermolysis of B₁₀H₁₄ on high-surface-area activated carbon, without significant reduction in surface area (~15%), by multiple methods. 1-step doping gave a reduction in total pore volume of ~20%; 5-step doping gave virtually no reduction.
- Measured hydrogen adsorption as a function of boron concentration. Observed systematic increase in adsorption (excess adsorption per surface area) with increasing boron concentration. At room temperature (303 K) and 200 bar, the increase is 40% for B:sample = 8.9 wt% (annealed at 600°C), and 10% for B:sample = 6.7 wt% (annealed at 1,000°C).
- Developed experimental estimates of the thickness of adsorbed hydrogen films on boron-free (undoped) carbon at different temperatures. The estimated thickness at room temperature and liquid nitrogen temperature is ~0.6 nm (2012) and ~0.4 nm (2010), respectively, both independent of the gas pressure.
- A 5.3-liter hydrogen sorption tank, densely packed with 1.5 kg of high-performance U. Missouri carbon

(undoped, powder), designed for operation anywhere between room temperature and dry-ice temperature and at 0-100 bar, was put into commission and tested for storage capacity and charge/discharge kinetics. Packing was maximum (random close packing). Storage capacity at 296 K and 100 bar was 0.031 kg H₂/kg carbon (3.0 material wt%).



Introduction

High-surface-area carbons from corncob, as developed by our team, are outstanding starting materials for the development of functionalized materials which store hydrogen, by strong physisorption, reversibly at high gravimetric and volumetric storage capacity. An earlier carbon exhibited a gravimetric storage capacity of 0.11 kg H₂/kg carbon at 80 K and 50 bar. This project is a systematic effort to achieve comparable results at 300 K, by increasing surface areas from currently ~3,000 m²/g to ~6,000 m²/g, and substituting carbon with boron and other elements that increase the binding energy for hydrogen (electron donation from H₂ to electron-deficient B, and other charge-transfer mechanisms). Earlier high surface areas and high binding energies were hosted by sub-nm pores in narrowly spaced “stacks of large graphene sheets.” New high-surface-area, boron-substituted materials are manufactured by thermolysis of volatile boron carriers in pores of stacks of graphene sheets. New surface area, created by chemical means (controlled oxidation) in the form of “stacks of small graphene sheets” (large ratio of edge sites to in-plane sites), is expected to be able to add as much as another 3,000 m²/g. A significant effort of the project goes into conversion of these materials, most of which currently are powders, into monoliths, without loss of surface area and high-binding-energy sites. Monoliths have lower porosity and, as a result, higher volumetric storage capacity than powders.

Approach

The approach is an integrated fabrication, characterization, and computational effort. Structural characterization includes determination of surface areas, pore-size distributions, and pore shapes. Storage characterization includes measurements of hydrogen sorption isotherms and isosteric heats. Computational work includes adsorption potentials and simulations of adsorbed films for thermodynamic analysis of experimental isotherms. Comparison of computed and experimental isotherms validates theoretical adsorption potentials and experimental structural data.

Results

Increase of binding energy and hydrogen uptake on boron-doped samples

High-surface-area boron-substituted (“doped”) carbons were prepared by using as precursor (boron-free carbon) the U. Missouri sample 3K-600C, coating the precursor with a monolayer or less of decaborane, B₁₀H₁₄ (liquid/vapor deposition), thermal decomposition of the adduct, and annealing of the decomposition product [1]. Sample 3K-600C is our best-performing undoped carbon, with 30% and 20% higher gravimetric excess hydrogen adsorption than the commercial carbon MSC-30 (Maxsorb, Kansai Coke and Chemicals, Ltd) at 100 bar and 80 K and 303 K, respectively [2]. Representative results for doped samples are collected in Table 1 and Figure 1. They demonstrate that the doping method developed preserves much of the structural integrity of the precursor: reduction of surface area upon doping is ~15% or less (Table 1); reduction of volume in pores <2.0 nm is about 20%; and reduction in the total pore volume is about 0-20% (Figure 1). Sample 3K-H79 (I,A), which gave negligible reduction in total pore volume, suggests that multiple doping by small amounts is better than single doping by a large amount. The increase in binding energy and hydrogen uptake on boron-doped samples, as predicted by theory [3], can be observed in three different ways:

(i) The hydrogen excess adsorption per unit surface area (“areal excess adsorption”) systematically increases with increasing boron concentration (Figure 2, bottom). At 303 K and 200 bar, the increase relative to the undoped precursor is 10% and 40% at boron concentration 6.7 and 8.9 wt%, respectively. The top performer, 3K-H60 (I,A), outperforms the undoped precursor even at the level of gravimetric excess adsorption (Figure 2, top), illustrating that the higher binding energy in the doped sample can more than make

TABLE 1. Preparation of boron-doped carbons. Brunauer-Emmett-Teller (BET) surface areas (Σ) and void fractions (porosity, ϕ) are from N₂ adsorption at 77 K. Boron concentrations (B:sample) were measured by prompt gamma neutron activation analysis at the University of Missouri Research Reactor. Annealing at 1,000°C [3K-H60 (I,B)] reduced the boron content by ~25% relative to annealing at 600°C [3K-H60 (I,A)], with unknown decomposition products, but unchanged surface area and pore-size distribution.

| Sample | Precursor | Annealing temp. | B conc. (wt%) | BC _x | Σ (m ² /g) | ϕ |
|-----------------------------|----------------------|-----------------|---------------|--------------------|------------------------------|--------|
| 3K-600C | Not applicable (N/A) | N/A | 0.0 | BC _∞ | 2,500 | 0.76 |
| 3K-H60 (I,A), 1-step doping | 3K-600C | 600°C | 8.9 | BC _{9.21} | 2,100 | 0.74 |
| 3K-H60 (I,B), 1-step doping | 3K-600C | 1,000°C | 6.7 | BC _{12.5} | 2,100 | 0.72 |
| 3K-H79 (I,A), 5-step doping | 3K-H78 (I,A) | 600°C | 7.1 | BC _{11.8} | 2,200 | 0.78 |

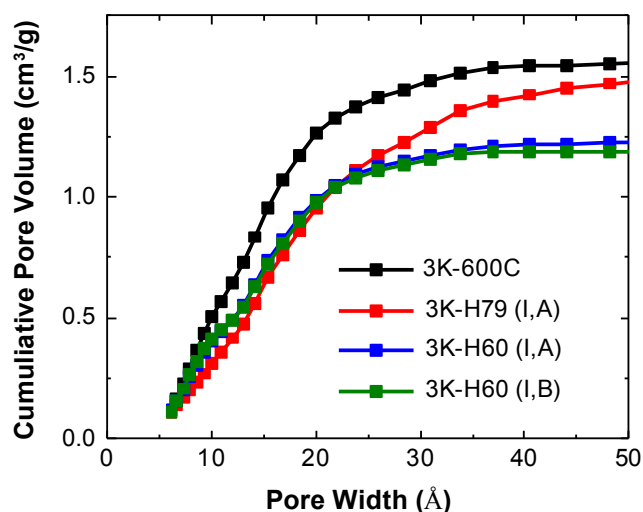


FIGURE 1. Cumulative pore-size distribution of doped materials and undoped precursor in Table 1. Sample 3K-H79 (I,A), from 5-step doping, with ~1.4 wt% boron added per step, exhibits the smallest loss in surface area and largest retention of total pore volume.

up for a lower surface area. Areal excess adsorption is a direct measure of the binding energy because it depends only on how strongly the surface adsorbs hydrogen, but not on pore volume and surface area of the sample. If high-binding-energy sites were present only as a small fraction of all surface sites, the areal excess adsorption isotherm of the doped surface would rise over the isotherm of undoped surface at low pressure (high-binding-energy sites are filled first), but then approach the isotherm of the undoped surface at higher pressures. Figure 2 shows that this is not the case; instead the isotherm of the doped surface rises above the isotherm of the undoped surface at *high pressures*, signaling the presence of high binding energies on a majority of surface sites (high *average* binding energy).

(ii) Isothermic heats of adsorption (enthalpy of adsorption), ΔH , of hydrogen on boron-doped and undoped samples were determined, from Clausius-Clapeyron analysis of adsorption isotherms at 273 K and 303 K (Figure 3). The boron-doped sample gave $\Delta H \sim 17$ kJ/mol at zero coverage and $\Delta H \sim 10$ kJ/mol at high coverage (Figure 3, bottom), exhibiting that the surface hosts a small fraction of sites with binding energies as high as 17 kJ/mol, and a majority of sites with binding energy of 10 kJ/mol (*average* binding energy). The undoped sample gave $\Delta H \sim 7$ kJ/mol at zero coverage and $\Delta H \sim 6$ kJ/mol at high coverage, and corresponding high and average binding energies. (Estimates of binding energies are equated to ΔH values in this report; more accurate estimates involve addition of zero-point and thermal energies [4].) This demonstrates that the U. Missouri boron-doping procedure successfully raises the binding energy, from ~6 kJ/mol to ~10 kJ/mol, uniformly across a majority of surface sites—in excellent agreement with theory, which predicts, on undoped/

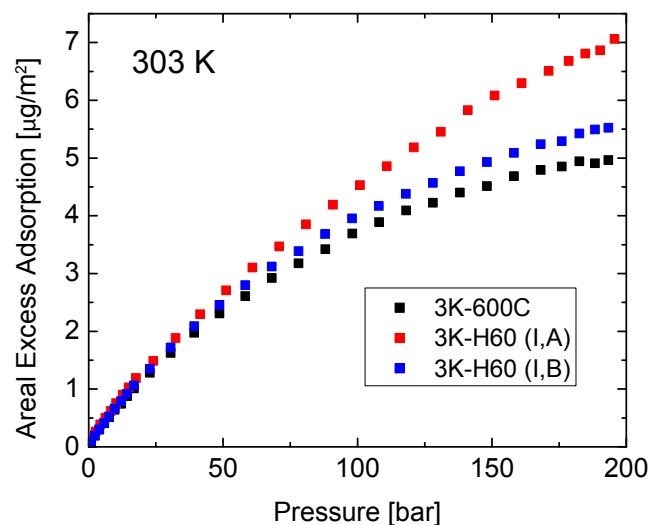
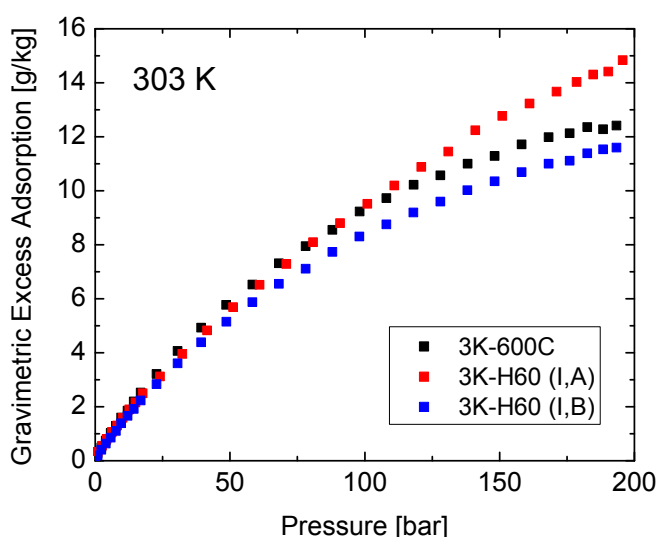


FIGURE 2. Hydrogen sorption at room temperature for materials in Table 1, as a function of boron concentration. Top: gravimetric excess adsorption. Bottom: areal excess adsorption (gravimetric excess adsorption divided by BET surface area; compares excess adsorption on identical surface areas). The higher the areal excess adsorption at a given pressure and temperature, the higher is the binding energy. Thus, the samples ordered from high to low binding energy are: 3K-H60 (I,A) > 3K-H60 (I,B) > 3K-600C. The corresponding boron concentrations are: 8.9 > 6.7 > 0.0 wt%.

doped graphene sheets, an increase from 5 kJ/mol (0 wt% B) to 10-12 kJ/mol (10 wt% B) [3].

(iii) As the temperature is lowered from 303 K to 273 K, gravimetric excess adsorption in Figure 3, top, increases by about 90% for the boron-doped sample and about 45% for the undoped sample, both at high pressure (200 bar) and low pressure (50 bar). These increases are consistent with that the binding energy of the doped material, E_d , is approximately twice the binding energy of the undoped material, E_u . The analysis is as follows. For given E_d , E_u , and temperatures

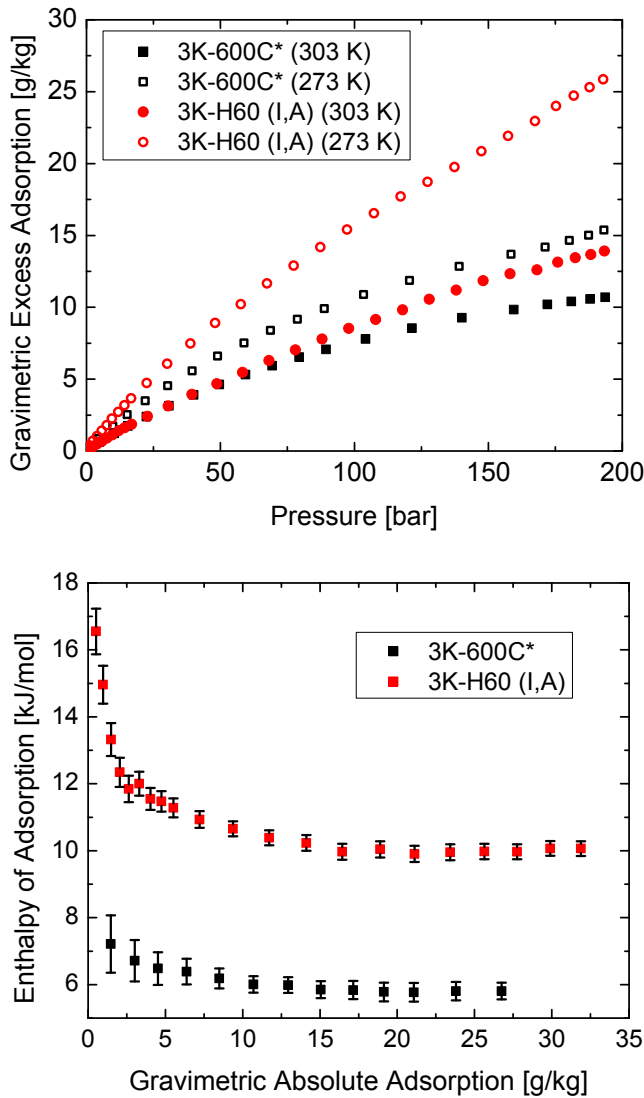


FIGURE 3. Isostatic heat of adsorption (bottom) from adsorption isotherms at 273 K and 303 K (top). The isosteric heats refer to the temperature $[(273\text{ K}) \cdot (303\text{ K})]^{1/2} = 288\text{ K}$. Gravimetric excess adsorption was converted into absolute adsorption (“coverage”), using a hydrogen film thickness of 0.6 nm (smallest film thickness such that the calculated ΔH does not rise at high coverage); gas pressure at constant coverage (isosteric variation of film) was calculated from interpolated absolute adsorption; and the Clausius-Clapeyron equation was evaluated with so-determined pressures at constant coverage [4]. Plotted isosteric heats are the average over four different interpolation models for absolute adsorption, and error bars represent the variation from the different models. The boron-doped sample 3K-H60 (I,A) is from Table 1; the undoped sample 3K-600C* is from a remanufactured lot of the precursor 3K-600C in Table 1. A remanufactured lot of 3K-H60 (I,A) gives an isosteric heat curve similar to the one here, with $\Delta H \sim 10\text{ kJ/mol}$ at high coverage.

$T_1 < T_2$, the respective ratios R_d, R_u of gravimetric excess adsorption at T_1 to gravimetric excess adsorption at T_2 are approximately:

$$R_d \approx \chi(E_d, T_1) / \chi(E_d, T_2) = (T_2 / T_1)^{1/2} \exp[E_d(T_1^{-1} - T_2^{-1}) / R] \quad (1)$$

$$R_u \approx \chi(E_u, T_1) / \chi(E_u, T_2) = (T_2 / T_1)^{1/2} \exp[E_u(T_1^{-1} - T_2^{-1}) / R] \quad (2)$$

$$R_d / R_u \approx \exp[(E_d - E_u) (T_1^{-1} - T_2^{-1}) / R] \approx (T_1 / T_2)^{1/2} R_u \quad (3)$$

$$R_d \approx (T_1 / T_2)^{1/2} (R_u)^2 \quad \text{if } E_d = 2E_u \quad (4)$$

In Eqs. (1, 2), gravimetric excess adsorption is approximated by absolute adsorption, valid at low pressure; absolute adsorption is calculated from the Langmuir isotherm for mobile adsorption with Langmuir constants $\chi(E_d, T)$ and $\chi(E_u, T)$, respectively, evaluated at low pressure and high temperature, and evaluated with $\alpha(T_1) = \alpha(T_2)$ for the footprint area of one hydrogen molecule [5]; and R is the gas constant. Equation (3) follows from (1, 2), where in the second part $E_d = 2E_u$ has been used. This gives the “doubling of the binding energy” relation (4). Experimentally, $R_d = 1.89$ and $R_u = 1.43$ at 50 bar (Figure 3, top). Theoretically, $R_d \approx 1.94$ from $R_u = 1.43$ and (4). The remarkable agreement of the experimental and theoretical value for R_d shows that a doubling of the binding energy, from $\sim 5\text{ kJ/mol}$ to $\sim 10\text{ kJ/mol}$ according to (ii), indeed accounts for the observed increase of 90% on the doped sample.

Hydrogen storage on undoped carbon in 5.3-liter tank

A 5.3-liter hydrogen sorption tank, constructed by the University of Missouri and Midwest Research Institute under a Defense Logistics Agency contract [6], was filled with undoped high-performance U. Missouri carbon and tested for storage capacity and charge/discharge kinetics, including temperature evolution during, at room temperature (Figure 4). To the best of our knowledge, this is the first fully operational sorption-based hydrogen tank in the U.S., allowing comparison of projected storage capacity (based on adsorption of hydrogen on small, typically a few 100 mg, samples in the laboratory) and actual storage capacity, measured by a flow meter on a tank holding of the order of a kilogram of sorbent. This amounts to a scale-up by a factor of 10^4 . The agreement between projected storage capacity (“tank capacity from 300 mg sample”) and actual storage capacity (“total hydrogen in tank from flow meter”), both in terms of gravimetric storage capacity, is better than within 1%, across the entire pressure range (Figure 4b). The agreement demonstrates that the 1.5 kg carbon has outstanding sample homogeneity. Storage capacities at 296 K and 100 bar from Figure 4b are: 0.031 kg H_2 /kg carbon (3.0 material wt%), 0.047 kg H_2 (whole tank), and 0.0088 kg H_2 /liter internal tank volume. To the best of our knowledge, these values are unprecedented for sorption at room temperature.

How densely was the carbon powder packed in the tank? The answer is obtained from the relation between the void fraction in the tank and the void fraction in individual sorbent particles, with packing fraction f (fraction of tank volume that is occupied by particles):

$$\phi_{\text{tank}} = (1 - f) + f \phi_{\text{cryst}} \quad (5)$$

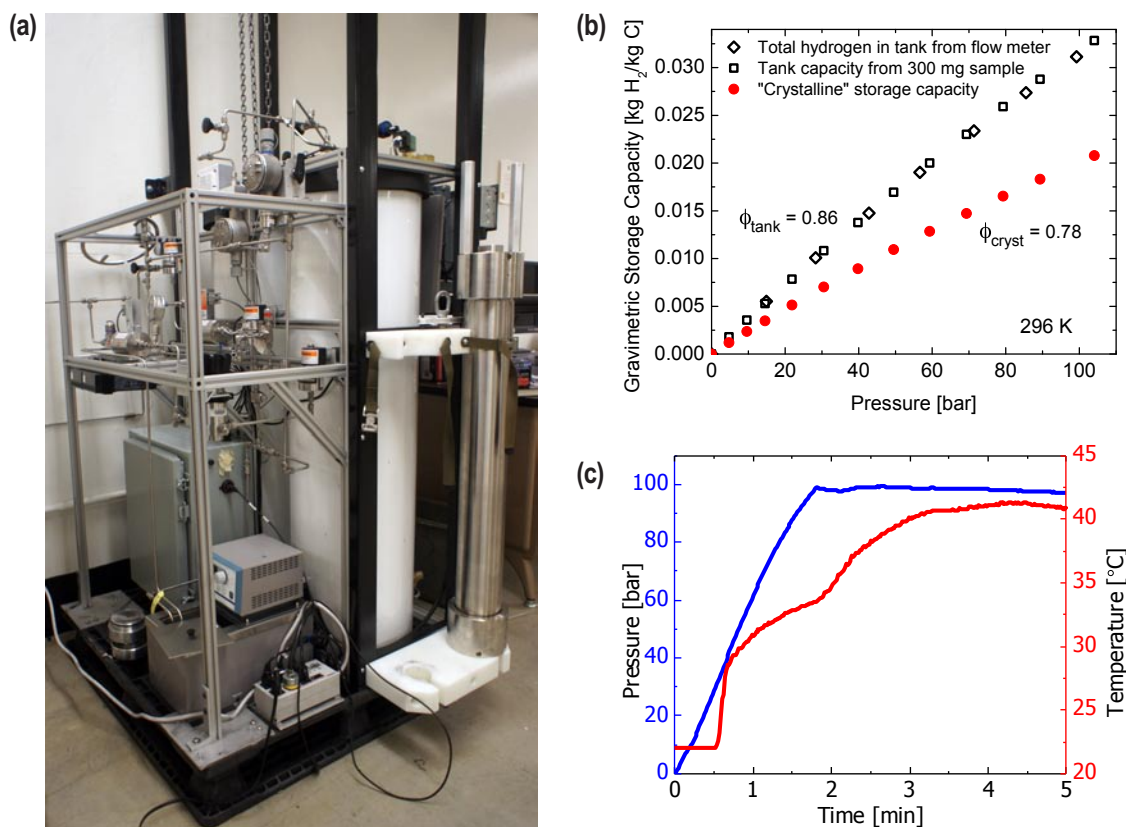


FIGURE 4. (a) Two cylindrical 5.3-liter tanks, designed to operate individually or as joint 10.6-liter tank, between room temperature and dry-ice temperature and pressure 0-100 bar. One of the tanks was filled with 1.5 kg of carbon powder, similar to 3K-600C (Table 1), but degassed at 120°C instead of 600°C. Degassing was done in situ. Surface area (Σ) and void fraction (ϕ_{cryst}) of the carbon was 2,700 m²/g and 0.78, from N₂ adsorption at 77 K. We refer to the void fraction in individual sorbent particles as “crystalline” in analogy to the void fraction in metal-organic frameworks and other porous solids, and in contradistinction to the void fraction after packing of sorbent particles in a bed or tank, ϕ_{tank} . (b) Gravimetric storage capacity of the tank at 296 K, (i) measured by flow meter; (ii) calculated from gravimetric excess adsorption, G_{ex} , measured on a 300-mg sample, and the tank void fraction, ϕ_{tank} ; (iii) calculated from G_{ex} and void fraction ϕ_{cryst} (“crystalline” storage capacity). Gravimetric storage capacity from G_{ex} and ϕ was calculated as $G_{\text{ex}} + (\rho_{\text{gas}}/\rho_{\text{skel}})\phi(1-\phi)$ with $\rho_{\text{skel}} = 2.0 \text{ g/cm}^3$ [7]. The tank void fraction was $\phi_{\text{tank}} = 1 - m_{\text{sorbent}}/(\rho_{\text{skel}} V_{\text{tank}}) = 0.86$. (c) Pressure and temperature evolution in the tank during a fast-fill cycle.

The values $\phi_{\text{tank}} = 0.86$ and $\phi_{\text{cryst}} = 0.78$ in Figure 4 yield $f = 0.64$. This is, within experimental uncertainty, equal to the theoretical maximum, $f = 0.63$, for random close packing of spherical particles of identical size. The only way to achieve a higher packing fraction would be to convert the powder into monoliths, ideally with $f = 1$, which would give $\phi_{\text{tank}} = \phi_{\text{cryst}}$, a mass of 2.3 kg carbon in the tank, and the following storage capacities at 296 K and 100 bar: 0.021 kg H₂/kg carbon (Figure 4b), 0.049 kg H₂ (whole tank), and 0.0092 kg H₂/liter internal tank volume. This illustrates that a decrease in ϕ_{tank} leads to a drop in gravimetric storage capacity (because more sorbent fits into the tank) and a rise in volumetric storage capacity (because the tank holds less nonadsorbed gas) [7]. In the present case, the drop is large and the rise is small because the tank, as is, resides on the flat part of the volumetric-vs.-gravimetric storage capacity curve in Ref. [7].

The kinetic data, Figure 4c, shows that the tank can be filled in ~3 minutes (end of temperature rise). Gravimetric storage capacity as a function of time (not shown) showed that the tank was 95% full in 3.3 minutes. The temperature inside the tank (center of the cylinder) rose from initially 22°C to a maximum of 41°C (Figure 4c), due to heat of adiabatic compression and heat of adsorption (no attempt was made to measure the two effects separately). The cusp in the pressure and temperature curve at 2 min is the result of that the hydrogen flow was stopped when the pressure reached 100 bar. As the flow of room-temperature gas, acting as a coolant, stopped, the temperature began to rise more rapidly. During the interval 2.5-3.3 min, the hydrogen flow resumed at a low rate to maintain the target pressure of 100 bar. At 3.3 min, the flow was stopped permanently, which gave rise to a second, less pronounced cusp in the temperature curve. The overall temperature profile suggests that heat transfer

via convection in the gas phase is faster than heat transfer via heat conduction through the sorbent and tank walls.

Conclusions and Future Directions

- Established increase in binding energy of molecular hydrogen on boron-doped carbon, by a factor of two on average surface sites and a factor of three on exceptional surface sites, and established correspondingly enhanced adsorption of hydrogen, by 40%, on such surfaces at room temperature, relative to undoped surfaces.
- Demonstrated record-breaking performance of a kg-scale hydrogen tank, based on adsorption of hydrogen on undoped carbon at room temperature, with gravimetric storage capacity of over 50% and volumetric storage capacity of over 20% of the 2017 DOE hydrogen storage targets, both relative to material.
- Future work: Overall goal: manufacture, characterize, and optimize B-doped carbon monoliths, by direct deposition of $B_{10}H_{14}$ into/onto carbon monoliths, for achievement, at room temperature, of 2017 DOE hydrogen storage targets. In support of this agenda: (a) Optimize B-doping—with precursor 3K-600C—in the region B:sample 0-10 wt% for maximum areal excess adsorption of H_2 at room temperature, under variation of B-delivery (1-step vs. 5-step doping), annealing (600-1,000°C), and removal of B via high-temperature reaction with H_2 . (b) Investigate—with precursor 3K-600C and optimal path from (a)—the region B:sample 10-20 wt%. Find saturation limit, i.e., lowest B concentration above which further boron does not improve H_2 adsorption. (c) Produce and characterize B-doped samples—with precursors different from 3K-600C, but optimal path from (a, b)—in high-performance region of B concentration. Precursors: U. Missouri monoliths and powders 2.5K, 3.5K, 4K, 5K [1]. (d) Perform H_2 storage and associated kinetic measurements on B-doped monoliths under oxygen-free conditions in U. Missouri 0.5-liter hydrogen test fixture [1]. (e) Monitor quality of doped materials by (i) isosteric heat determinations at room temperature; (ii) determination of binding energies from Henry-law analysis of low-pressure room-temperature adsorption isotherms; (iii) Fourier transform infrared spectroscopy, X-ray photoelectron spectroscopy, and nuclear magnetic resonance spectroscopy under oxygen-free conditions; (iv) computational simulations on select B-doped structures. (f) Investigate low-temperature performance (77 K) of select B-doped materials.

FY 2012 Publications/Presentations

- J. Romanos, “Nanospace Engineering of Porous Carbon for Gas Storage.” Ph.D. Dissertation, University of Missouri (2012)
- M. Beckner, “Hydrogen Adsorption Studies of Engineered and Chemically Modified Activated Carbons.” Ph.D. Dissertation, University of Missouri (2012).
- J. Romanos, M. Beckner, T. Rash, L. Firlej, B. Kuchta, P. Yu, G. Suppes, C. Wexler, and P. Pfeifer, “Nanospace Engineering of KOH Activated Carbon.” *Nanotechnology* **23**, 015401 (2012).
- B. Kuchta, L. Firlej, A. Mohammadhosseini, P. Boulet, M.W. Beckner, J. Romanos, and P. Pfeifer, “Hypothetical High-Surface-Area Carbons with Exceptional Hydrogen Storage Capacities: Open Carbon Frameworks.” *J. Am. Chem. Soc.* **134**, 15130-15137 (2012).
- J. Romanos, M. Beckner, D. Stalla, A. Tekeci, G. Suppes, S. Jalisatgi, M. Lee, F. Hawthorne, J. D. Robertson, L. Firlej, B. Kuchta C. Wexler, P. Yu, P. Pfeifer, “Infrared Study of Boron-Carbon Chemical Bonds in Boron Doped Activated Carbon.” *Carbon*, under review (2012).
- R.J. Olsen, M. Beckner, J. Romanos, P. Lewellyn, B. Kuchta, P. Pfeifer, and C. Wexler, “Experimental Determination of Adsorbed Film Volumes.” *Adsorption*, under review (2012).
- P. Pfeifer, C. Wexler, P. Yu, G. Suppes, F. Hawthorne, S. Jalisatgi, M. Lee, D. Robertson, and S. Chakraborti, “Multiply Surface-Functionalized Nanoporous Carbon for Vehicular Hydrogen Storage.” *2012 DOE Hydrogen and Fuel Cells Program Annual Merit Review and Peer Evaluation*, Arlington, VA, May 13-17, 2012.

References

- P. Pfeifer *et al.*, In: *DOE Hydrogen Program, FY 2011 Annual Progress Report*, ed. by S. Satyapal (U.S. Department of Energy, Washington, DC, 2011), p. 444-449.
- P. Pfeifer, DOE Hydrogen Storage Technical Team Meeting, USCAR, Southfield, MI, Sept. 15, 2011.
- L. Firlej, S. Roszack, B. Kuchta, P. Pfeifer, and C. Wexler, *J. Chem. Phys.* **131**, 164701 (2009).
- P. Pfeifer *et al.*, In: *DOE Hydrogen Program, FY 2010 Annual Progress Report*, ed. by S. Satyapal (U.S. Department of Energy, Washington, DC, 2011), p. 474-480.
- J. Burress *et al.*, *Nanotechnology* **20**, 204026 (2009).
- Defense Logistics Agency, Contract NSWC-N00164-08-C-GS37 (2008-11).
- P. Pfeifer *et al.*, In: *DOE Hydrogen Program, FY 2009 Annual Progress Report*, ed. by S. Satyapal (U.S. Department of Energy, Washington, DC, 2009), p. 646-651.

IV.C.4 New Carbon-Based Porous Materials with Increased Heats of Adsorption for Hydrogen Storage

Randall Snurr (Primary Contact), Joseph Hupp,
Mercouri Kanatzidis, SonBinh Nguyen

Northwestern University
2145 Sheridan Road
Evanston, IL 60208
Phone: (847) 467-2977
Email: snur@northwestern.edu

DOE Managers

HQ: Ned Stetson
Phone: (202) 586-9995
Email: Ned.Stetson@ee.doe.gov

GO: Katie Randolph
Phone: (720) 356-1759
Email: Katie.Randolph@go.doe.gov

Contract Number: DE-FG36-08GO18137/A001

Project Start Date: September 1, 2008
Project End Date: August 31, 2012

Technical Targets

TABLE 1. Progress towards Meeting Technical Targets for Hydrogen Storage

| Characteristic | 2017 Targets | NU 2012 Status |
|-----------------------------|---|---|
| System Gravimetric Capacity | 0.055 kg H ₂ /kg system at ambient T and 100 bar | 0.14 kg H ₂ /(kg sorbent + H ₂) at 77 K and 70 bar |
| System Volumetric Capacity | 0.040 kg H ₂ /L system at ambient T and 100 bar | 0.045 kg H ₂ /L sorbent at 77 K and 70 bar |

FY 2012 Accomplishments

- Obtained external validation of 8 wt% excess hydrogen uptake in NU-100 at 77 K and 50 bar.
- Developed a new MOF material with over 6 wt% excess hydrogen uptake at 77 K and 35 bar.
- Demonstrated a high-throughput computational screening method capable of screening thousands of hypothetical MOF targets.



Fiscal Year (FY) 2012 Objectives

- Obtain external validation of hydrogen uptake at 77 K in the metal-organic framework (MOF) NU-100, which was measured in our labs last year
- Develop high surface area materials for cryogenic hydrogen storage
- Develop high surface area materials containing functional groups that can bind hydrogen at room temperature
- Use computational modeling to understand existing materials and design new materials for hydrogen storage

Technical Barriers

This project addresses the following technical barriers from the Hydrogen Storage section of the Fuel Cell Technologies Program Multi-Year Research, Development and Demonstration Plan:

- (A) System Weight and Volume
- (F) Charging/Discharging Rates
- (P) Lack of Understanding of Hydrogen Physisorption and Chemisorption

Introduction

One option for storing hydrogen on vehicles is to use tanks filled with porous materials that act as “sponges” to take up large quantities of hydrogen without the need for extremely high pressures. The materials must meet many requirements to make this possible. This project is developing two related classes of porous materials to meet these requirements. All materials are synthesized from molecular constituents in a building-block approach. This allows us to create a wide variety of materials in a tailorable fashion. The materials have extremely high surface areas, to provide many locations for hydrogen to adsorb. In addition, they are designed to contain cations that create large electric fields to bind hydrogen strongly but not too strongly.

Approach

The approach in this project is to introduce cations into MOFs and polymeric-organic frameworks to increase the hydrogen heats of adsorption, which will, in turn, increase the amount of hydrogen that can be stored near room temperature. Many MOFs have enough surface area to meet the DOE hydrogen storage targets if the entire surface were covered with a monolayer of hydrogen. However, at room temperature, the energetic interactions between hydrogen and the surfaces are too weak to bind hydrogen. Thus, we are

focused on increasing these energetic interactions. A variety of synthetic chemistries are being explored to increase the chances of success. In addition, molecular modeling is used to help explain experimental observations and provide guidance to the synthetic efforts.

Results

Previously we had reported [1] on the design, synthesis, and computational modeling of a micro- and mesoporous MOF material, NU-100, that displayed an extraordinarily high internal surface area and very high uptake of molecular hydrogen at 77 K. Experimentally we had obtained a Brunauer-Emmett-Teller (BET) surface area of 6,160 m²/g, in good agreement with predictions from modeling (i.e. ~6,600 m²/g). In addition, we measured an excess uptake of 99 mg of H₂ per gram of NU-100, corresponding to 9.0 wt% at 77 K, and we estimated the total hydrogen uptake (at the pressure of maximum excess H₂ sorption) to be 164 mg/g, or 14.3 wt%. During the past year, we worked closely with Phil Parilla at NREL to obtain external validation of these hydrogen uptake numbers. At NREL we observed a maximum excess uptake of 87 mg of H₂ per gram of NU-100, corresponding to 8.0 wt%. These values are ~12% lower than found earlier at Northwestern (with a separate preparation of NU-100). The differences can be traced to difficulties in fully activating the material and in maintaining a moisture-free environment, rather than to measurement discrepancies. The activation problems were reflected in surface area measurements that likewise returned values ~12% lower than obtained under optimum experimental conditions.

We also investigated the question of whether phenyl rings or carbon-carbon triple bonds are better for creating ultra-high surface area materials that can be functionalized for high hydrogen uptake. In the course of investigating this question, we synthesized a new MOF, NU-111, from a new hexa-carboxylic acid linker that contains triple bond spacers [2]. The material has an experimental BET surface area of 5,000±80 m²/g and a total pore volume of 2.38 cm³/g. The material was sent to NREL for high-pressure hydrogen uptake measurements, and the results are shown in Figure 1B. The excess hydrogen uptake of NU-111 is 21 mg/g at 1 bar and 69 mg/g at 32 bar. By using the N₂-derived pore volume (2.38 cm³/g) and the bulk phase density of H₂, the total H₂ uptake at 110 bar and 77 K was calculated to be 135 mg/g (Figure 1C). The uptake of NU-111 is within range of the system gravimetric target for onboard H₂ storage, 5.5 wt% (= 58 mg/g), albeit at cryogenic rather than ambient temperature. The simulated H₂ isotherm of NU-111 is in only qualitative agreement with the experimental H₂ measurements using the classical force field model (Figure 1B). However, incorporating the Feynman-Hibbs corrections for quantum diffraction effects results in excellent agreement with the experimental isotherm. The

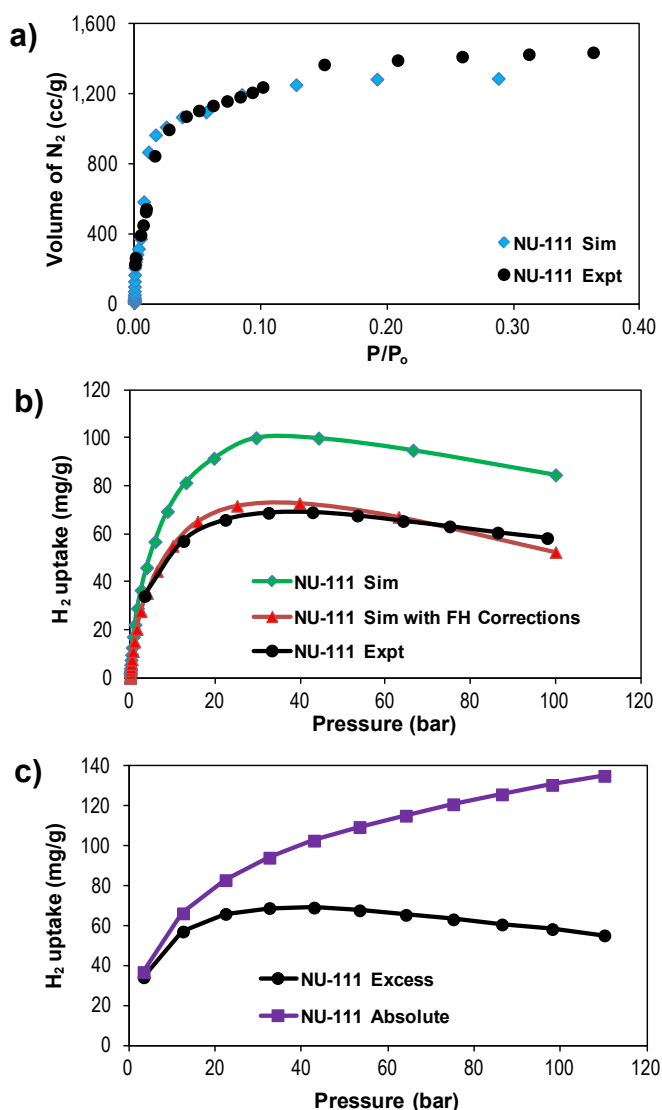


FIGURE 1. Adsorption isotherms in NU-111 at 77 K: a) N₂ isotherms, b) excess H₂ isotherms, showing comparison of simulation and experiment, c) excess and absolute (total) H₂ isotherms

stability of NU-111 was examined by running multiple cycles of high-pressure hydrogen adsorption at room temperature, and it showed no loss of capacity. In addition, the N₂ isotherms for NU-111 was measured before sending the sample to NREL and upon receiving the sample back from NREL. The N₂ isotherm showed no loss of porosity during the shipping and measurements.

Significant efforts were devoted to introducing divalent metal cations into MOFs and porous organic polymers. A variety of synthetic strategies were tested to introduce cations via linker functionalization. Successful metal incorporation was demonstrated in multiple types of materials. The observed H₂ heats of adsorption increase upon metal incorporation, but at present they are lower than expected

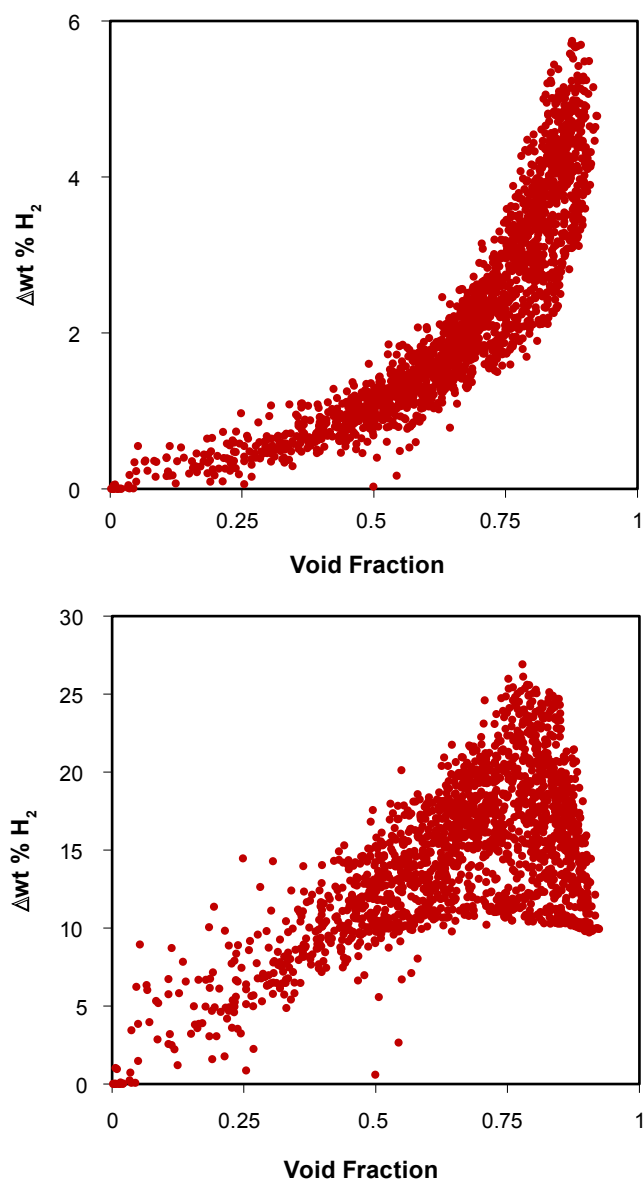


FIGURE 2. Preliminary results from high-throughput computational screening of MOFs, showing that deliverable gravimetric capacity increases with void fraction and that deliverable volumetric capacity has a maximum around 0.75 void fraction

from our computational work, perhaps due to residual solvent molecules blocking access to the metal atoms.

In the computational part of the project, we pursued three goals. First, we tested how the degree of metal functionalization (metal loading) affects hydrogen storage in MOFs. As expected, higher metal loading leads to an increase in the absolute (total) H_2 uptake. The deliverable capacity (defined in this work as hydrogen uptake at a pressure of interest minus hydrogen uptake at 2 bar) does not necessarily increase with higher metal loading. From the results so far, it is difficult to make any generalization

except to say that for each material there will be an optimum metal loading and that higher metal loading is not always better for the deliverable hydrogen capacity. Second, we investigated how incorporation of Mg-alkoxide functionality affects the rate of hydrogen diffusion in MOFs. Using molecular dynamics simulations, we calculated the diffusion coefficients of hydrogen in several MOFs of different topology. The main conclusion is that the Mg-alkoxide groups have only a small effect on hydrogen diffusion (less than one order of magnitude) and should not adversely affect rates of hydrogen uptake and release.

Finally, we demonstrated a method for high-throughput computational screening of MOFs for hydrogen storage. This work builds on our related work on natural gas storage [3] and previous work from this project on modeling hydrogen adsorption in metal-functionalized MOFs [4]. We combined these methods to screen over 16,000 MOFs with Mg-functionalized linkers for their ability to store and deliver hydrogen. In addition to identifying promising synthetic targets, the method provides useful structure/property relationships, as shown in Figure 2.

Conclusions and Future Directions

Conclusions

- We obtained external validation of 8 wt% excess hydrogen uptake in NU-100 at 77 K and 50 bar.
- We developed a new MOF material, NU-111, with over 6 wt% excess hydrogen uptake at 77 K and 35 bar.
- We tested a variety of synthetic strategies for introducing exposed divalent cations into MOFs and porous organic polymers as a means to increase the hydrogen enthalpy of adsorption.
- We demonstrated a high-throughput computational screening method capable of screening thousands of hypothetical MOF targets. This is a promising strategy for identifying new MOFs that may meet DOE hydrogen storage targets.

Future Directions

- Test hydrogen uptake in recently synthesized materials.
- Complete modeling study of hydrogen diffusion in Mg-functionalized MOFs.
- Write up results for publication.

FY 2012 Publications/Presentations

1. A.P. Katsoulidis, M.G. Kanatzidis, "Phloroglucinol microporous polymeric organic frameworks with -OH functional groups and high CO_2 capture capacity," *Chem. Mater.*, **23**, 1818-1824, (2011).

2. A.P. Katsoulidis, M.G. Kanatzidis, “Mesoporous hydrophobic polymeric organic frameworks with bound surfactants. Selective adsorption of C₂H₆ versus CH₄,” *Chem. Mater.*, **24**, 471-479 (2012).
3. D. Yuan, R.B. Getman, Z. Wei, R.Q. Snurr, H.-C. Zhou, “Stepwise adsorption in a mesoporous metal-organic framework: Experimental and computational analysis,” *Chem. Commun.* **48**, 3297-3299 (2012).
4. R.B. Getman, Y.-S. Bae, C.E. Wilmer, R.Q. Snurr, “Review and analysis of molecular simulations of methane, hydrogen, and acetylene storage in metal-organic frameworks,” *Chem. Rev.* **112**, 703-723 (2012).
5. A.P. Katsoulidis, J. He, M.G. Kanatzidis, “Functional monolithic polymeric organic framework aerogel as reducing and hosting medium for Ag nanoparticles and its application to the capture of iodine vapors” *Chem. Mater.*, **24**, 1937-1943 (2012).
6. M.H. Weston, O.K. Farha, B.G. Hauser, J.T. Hupp, S.T. Nguyen, “Synthesis and metalation of catechol-functionalized porous organic polymers,” *Chem. Mater.*, **24**, 1292-1296 (2012).
7. O.K. Farha, C.E. Wilmer, I. Eryazici, B.G. Hauser, P.A. Parilla, K. O’Neill, A.A. Sarjeant, S.T. Nguyen, R.Q. Snurr, J.T. Hupp, “Designing higher surface area metal-organic frameworks: Are triple bonds better than phenyls?” *J. Am. Chem. Soc.*, **134**, 9860-9863 (2012).

References

1. O.K. Farha, A.Ö. Yazaydin, I. Eryazici, C.D. Malliakas, B.G. Hauser, M.G. Kanatzidis, S.T. Nguyen, R.Q. Snurr, J.T. Hupp, “De novo synthesis of a metal-organic framework material featuring ultra-high surface area and gas storage capacities,” *Nature Chem.* **2**, 944-948 (2010).
2. O.K. Farha, C.E. Wilmer, I. Eryazici, B.G. Hauser, P.A. Parilla, K. O’Neill, A.A. Sarjeant, S.T. Nguyen, R.Q. Snurr, J.T. Hupp, “Designing higher surface area metal-organic frameworks: Are triple bonds better than phenyls?” *J. Am. Chem. Soc.*, **134**, 9860-9863 (2012).
3. C.E. Wilmer, M. Leaf, C.Y. Lee, O.K. Farha, B.G. Hauser, J.T. Hupp, R.Q. Snurr, “Large-scale screening of hypothetical metal-organic frameworks,” *Nature Chem.*, **4**, 83-89 (2012).
4. R.B. Getman, J.H. Miller, K. Wang, R.Q. Snurr, “Metal alkoxide functionalization in metal-organic frameworks for enhanced ambient temperature hydrogen storage,” *J. Phys. Chem C* **115**, 2066-2075 (2011).

IV.C.5 Hydrogen Trapping through Designer Hydrogen Spillover Molecules with Reversible Temperature and Pressure-Induced Switching

Angela D. Lueking (Primary Contact), Jing Li, Sarmishtha Sircar, Cheng-Yu Wang, Qixiu Li, Yonggang Zhao, Qihan Gong, Zhijuan Zhang, Haohan Wu, Milton W. Cole

The Pennsylvania State University (PSU)
120 Hosler
University Park, PA 16802
Phone: (814) 863-6256
Email: adl11@psu.edu

DOE Managers

HQ: Ned Stetson
Phone: (202) 586-9995
Email: Ned.Stetson@ee.doe.gov

GO: Jesse Adams
Phone: (720) 356-1421
Email: Jesse.Adams@go.doe.gov

Contract Number: DE-FG36-08GO18139

Subcontractor:

Rutgers University, Piscataway, NJ

Project Start Date: January 1, 2009

Project End Date: June 30, 2013

Technical Targets

TABLE 1. System Gravimetric Capacity 2010/2017 Target (0.045/0.055) of Metal-Doped "Spillover" Materials

| Sample | Pressure (bar) | Hydrogen in excess of He at 298 K (kg H ₂ /kg) ^a | Enhancement Relative to Physisorption (%) ^b |
|----------------------------------|----------------|--|--|
| <u>Pt-Doped Carbon Samples</u> | | | |
| PtC(INER) ^{c,d} | 1-20 | 0.012 | 780 (at 20 bar) |
| PtC/ACo ^d | 1-20 | 0.014 | |
| PtC (Maxsorb) | 70-72 | 0.0079-0.0091 ^e | |
| PtAC (PtC) | 1.01 | 0.00027 | |
| Pt-oxCA (Pt ₂ oxCA) | 1.02 | 0.00014 | |
| <u>Direct Doped MMOF Samples</u> | | | |
| Pt/MMOF-NH ₂ -03 | 69.6 | 0.0047 | 430 |
| Pt/MMOF-NH ₂ -04 | 70.1 | 0.0019 | 100 |
| Pt-IRMOF8 | 1.02 (20) | 0.00032 (0.00079) | 1,200 (65) |
| <u>Preformed bridge samples</u> | | | |
| PtCA/IRMOF8 | 66-70 | 0.0063-0.0026 | 89 to (-27) |
| PtC/IRMOF8 | 71.1 | 0.00317 | -15 |
| PtC/CuTDPAT-air exposure | 71.9 | 0.0026 | -42 |
| PtC/CuTDPAT | 1.02 | 0.00044 | 600 |

^a Samples are referenced to He measurement at same pressure; Values do not include He adsorption.

^b (uptake - expected physisorption [same conditions])/expected physisorption

^c Provided by C. S. Tsao (Institute of Nuclear Energy Research, Taiwan).

^d Uptake is determined gravimetrically. Temperature-programmed desorption also done.

^e Range is for six separate sample preparations and measurements.

^f Value includes He adsorption for comparison with literature.

Fiscal Year (FY) 2012 Objectives

- Synthesize designer microporous metal-organic frameworks (MMOFs) mixed with catalysts to enable H-spillover for H₂ storage at 300 K-400 K and moderate pressures.
- Develop methods to reliably introduce catalyst into MMOFs.
- Demonstrate spectroscopic evidence for hydrogen spillover.

Technical Barriers

This project addresses the following technical barriers from the Hydrogen Storage section of the Fuel Cell Technologies Program Multi-Year Research, Development and Demonstration Plan:

- (A) System Weight and Volume
- (D) Durability: Min/max temperature/maximum pressure
- (E) Charging/Discharging rates
- (P) Lack of Understanding of Hydrogen Physisorption and Chemisorption
- (Q) Reproducibility of Performance

FY 2012 Accomplishments

- Developed and tested over 20 new MMOF structures (since project onset), with variations in surface chemistry, porosity, and metal incorporation.
- Tested four methods to introduce catalyst into MMOF samples, of which the 'pre-bridge' method provides best means to keep MMOF structure and surface area intact (see Table 2).
- Quantified advantages of differential volumetric system in measuring hydrogen uptake.
- Published spectroscopic evidence of spillover to CuBTC MMOF framework from hydrogen spillover catalyst, demonstrating unexpected hydrogenation site.
- Provided Pt-doped carbon samples to the National Renewable Energy Laboratory (NREL) for round-robin testing.
- Participated in "Weak Chemisorption" workshop.

TABLE 2. Development of MMOF Catalyst Doping Methods

| Doping Technique Sample Name from PSU *Literature Report | Comparison of X-Ray Diffraction Quality (Before vs. After Doping) | Brunauer-Emmett-Teller (BET) Specific Surface Area (m ² /g) Before/After doping (%) |
|---|---|--|
| <u>Physical Mixing/Ball Milling</u> PtC/IRMOF8-iv | New Peak | 1384/380 (28%) |
| <u>Bridging Technique</u> PtC/IRMOF8-x *PtC/IRMOF1—Ref 1 *PtC/IRMOF8—Ref 1 *PtC/COF1—Ref 2 *PtC/CuBTC—Ref 2 *PtC/MIL101—Ref 2 | Different ND† ND ND ND ND | 1384/310-760 (22-55%) 1021/890 (87%) 548/466 (85%) 628/582 (93 %) 1,296/1,116 (86%) 3,023/2,580 (85%) |
| <u>Direct Doping</u> Pt/IRMOF8 Pt/MMOFNH2 *Pt/IRMOF8-Ref 3 *Pd/MIL101(Al)—Ref 4 | Missing Peak Different Intact Intact | 1,384/674 (49%) 1,250/350-370 (30%) 1,430/1,175 (82%) 1,200/380 (31%) |
| <u>Prebridging Technique</u> PtC/IRMOF8 PtCA/IRMOF8 PtC/CuTDPAT *PtC/IRMOF1—Ref 5 *PtMWNT/IRMOF1—Ref 6 | Intact Intact Intact Intact Intact | 1,384/1,471 (106%) 1,384/1,421 (103%) 1,938/1,748 (90%) 1,820/730 (40%) 1,758/1,692 (96%) |

† Not Determined



Introduction

The term *hydrogen spillover* has been used to describe a synergistic effect between high-surface area adsorbents and associated catalysts. The associated catalyst may act to dissociate molecular H₂ into atomic H species, which may then chemisorb to the support. This process occurs at moderate temperature (i.e. 300 K) and generally leads to a much higher uptake than expected for the metal catalyst or high-surface area adsorbent alone. Spillover materials using MMOFs have been reported to have high uptake at ambient temperature: bridged ('br') PtC/IRMOF8 achieved 4 wt% excess adsorption at 100 bar and 298 K [1]. Independent groups have demonstrated up to 4.2 wt% at 6.9 MPa after extended equilibration for brPtC/IRMOF-8 [7]. Subsequent reports on spillover materials at room temperature have varied from less than physisorption to almost 9 wt%, demonstrating difficulties in reproducibility and invoking controversy. These uptakes approach DOE goals; however, as the process is highly dependent upon synthesis, measurement, and catalytic particle size [8,9], the process remains poorly understood. It is anticipated that optimization of the MMOF structure, surface chemistry, and porosity will further increase uptake via spillover. Meeting DOE hydrogen storage targets at moderate temperature will have significant engineering advantages for mobile applications, as temperature of operation has implications for system weight, cost, and wells-to-wheels efficiency.

Approach

The project relates to materials development and optimization of catalyst, surface chemistry, crystal and pore structure, and system parameters for the hydrogen spillover phenomenon. For surface chemistry, different MMOFs were mixed with catalyst to test hydrogen storage and the effect of functional groups. We are investigating novel methods to incorporate a hydrogen dissociation catalyst into MMOFs, such that the hydrogen spillover mechanism can be applied to well-defined MMOF structures. For carbon-based catalysts, acid, base, and high temperature after-treatments were used to have various surface functional groups and to test hydrogen uptake. We are utilizing both gravimetric and differential volumetric adsorption methods to quantify hydrogen uptake, the former allows for precise catalyst activation whereas the latter allows for high-pressure measurements and is more accurate than conventional volumetric techniques. In addition, we are complementing hydrogen adsorption measurements with spectroscopy to identify the active sites that bind with spilled over hydrogen.

Results

In Phase 1 of the project, we have developed and tested some 20 new MOF structures, investigated the roles of pretreatment and reactor configuration on the PtC catalyst (Section I, below), verified spillover to MOFs with spectroscopic evidence (Section II), conducted extensive reproducibility tests on standard samples including the effect

of measurement, synthesis, and pretreatment conditions, and as of January 2012, tested four methods to incorporate the catalyst into the MOF (Section III), using methods that do not degrade the structure of the MOF yet maintain high catalytic activity. Highlights of results I-III are discussed below.

I. Optimization of PtC Catalysts.

We have found surface oxidation (using KOH activation) to be essential to observe high uptake in PtC catalyst via spillover [10]. Interestingly, high uptake was observed only when trace water was present in the system during catalyst reduction, which we attribute to a modification of Pt-C interfacial surface chemistry, as evidenced by X-ray photoemission spectroscopy (XPS) and Fourier transform infrared (FTIR) data. At 300 K, the hydrogen uptake of multiple preparations of activated PtC_{KOH} was 1.4 wt% at 20 bar (Figure 1), exceeding the above benchmarks. As the sample was reduced in H₂ in situ and the uptake significantly exceeded the stoichiometric amount attributable to the catalyst, the uptake is attributed to spillover. Temperature-programmed desorption with mass spectroscopy showed no evidence of water desorption as the sample was heated; the rate of hydrogen desorption was slow at ambient temperatures but could be increased with mild heating to

~100°C. The isotherm showed a significant portion of the uptake was at low-pressure (1.1 wt% at 100 mbar), providing a material with high catalytic activity for subsequent introduction of this PtC into MOF materials (see, e.g. PtC@CuTDPAT in Section III). In addition, our group provided gravimetric measurements of an oxidized Pt-doped activated carbon material (PtC_{INER}, Table 1) in support of inelastic neutron scattering studies conducted by Tsao et al. [11]. Uptake of this PtC_{INER} exceeded 1.0 wt% at 20 bar and 298 K (also exceeding benchmarks), with the majority of the uptake occurring at low pressure (Figure 2). The similar isotherm shape of PtC_{KOH} and PtC_{INER} are surprising given the extreme differences in catalyst content, structure, and introduction method, and will be explored in the upcoming year. These Pt-doped activated carbons only show dependence on the method by which they are measured (reactor size, gas flow, and history), which will be verified in the upcoming year.

II. Spectroscopic Evidence of Spillover to MMOFs

Spectroscopic evidence for spillover was a primary recommendation of the 2010 NREL-led spillover commission. In early studies conducted as a part of this work, a CuBTC (BTC=benzene tricarboxylate) MOF exhibited a 3.5-fold increase at 298 K and 20 bar after addition of a

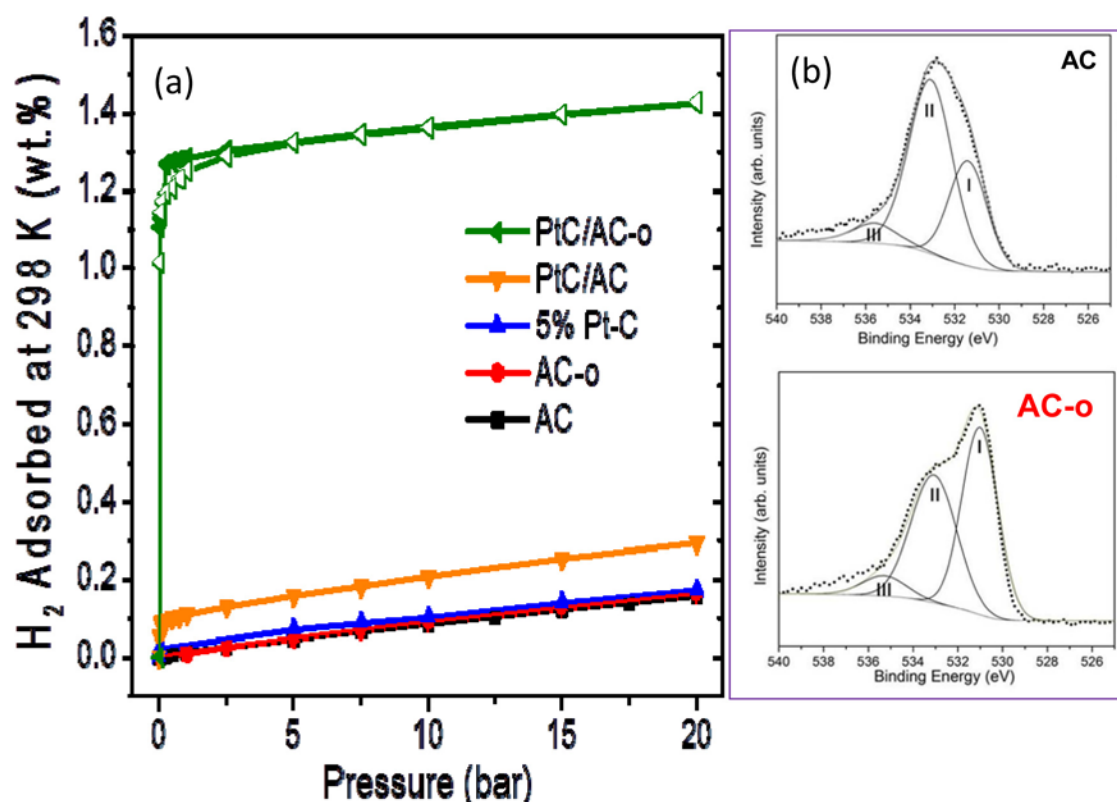


FIGURE 1. Oxidation of an activated carbon significantly increases low-pressure hydrogen spillover, as measured by gravimetric adsorption (a) in hydrogen at 298 K. XPS demonstrates changes in oxygen-carbon binding after oxidation and after introduction of trace water during the pretreatment step (b).

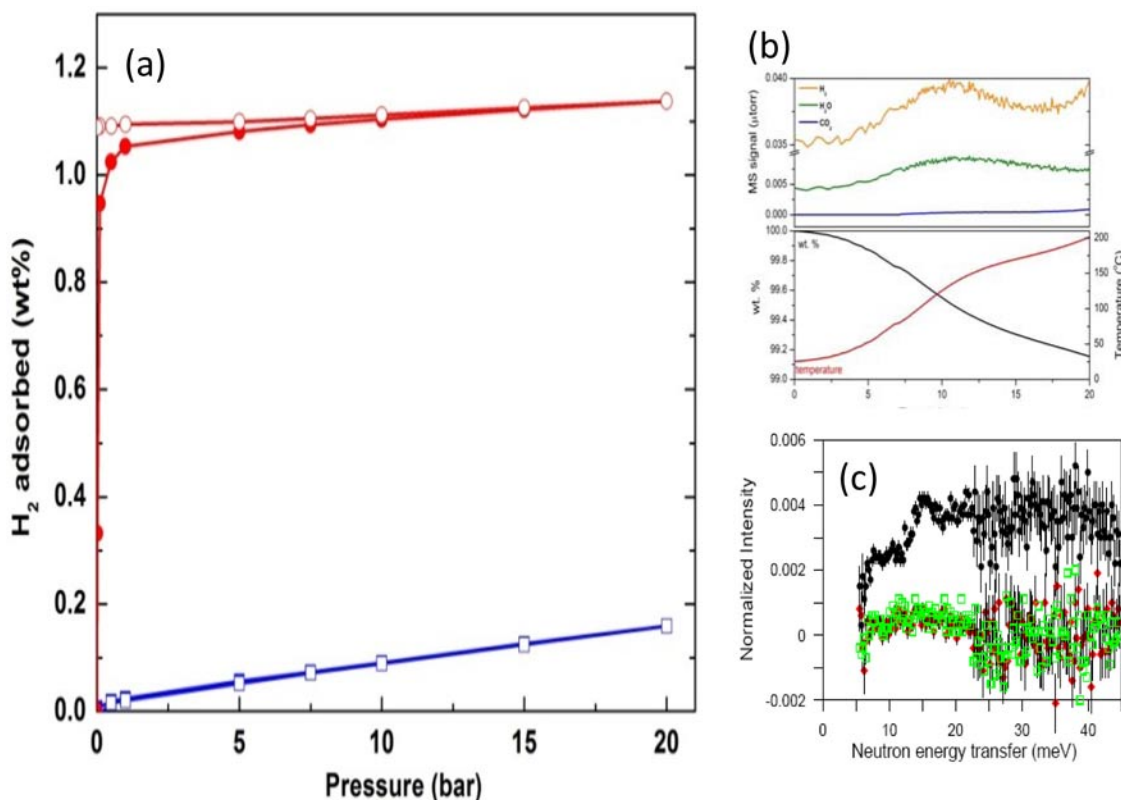


FIGURE 2. (a) A Pt-doped oxidized activated carbon provided by the Institute of Nuclear Energy Research, Taiwan had high gravimetric hydrogen uptake at 298 K (red) versus the activated carbon precursor (blue). (b) Only trace water is detected during temperature-programmed desorption. These results were used to support (c) inelastic neutron scattering measurements, which demonstrated this sample had a reduction in the H₂ modes after spillover occurred at 298 K.

carbon-spillover catalyst (PtC), from 0.17 to 0.61 wt% [12], exceeding the above benchmarks. Maintaining the structural integrity of the MOF upon mixing with the catalyst was important to achieve demonstrable chemisorption to the CuBTC. The rates of adsorption and temperature dependence were suggestive of irreversible chemisorption, making this material not viable for practical applications but an ideal candidate for early ex situ spectroscopic studies. FTIR of the hydrogenated PtC/CuBTC conclusively demonstrated hydrogenation of the carboxylate group of the BTC supported Pt ligand [12], providing the first published spectroscopic evidence for spillover to a MOF (Figure 3).

III. Development of New MMOFs and Catalyst-Doping

The best candidate MOF for future studies is Cu-TDPAT [a.k.a. Cu₃(TDPAT)(H₂O)₃, where H₆TDPAT = 2,4,6-tris(3,5-dicarboxylphenylamino)-1,3,5-triazine]. Cu-TDPAT is the smallest member of (3,24)-connect nets of *rht* topology made of a three-armed hexacarboxylate ligand and 24 M₂(COO)₄ paddle-wheel based supramolecular building blocks, as shown in Figure 4 (inset). The Cu-TDPAT framework is highly porous and contains three different types of cages, cuboctahedron (cub-*O_h*), truncated tetrahedron (T-*T_d*),

and truncated octahedron (T-*O_h*). The pore volume, BET and Langmuir surface areas are estimated to be 0.93 cc/g, 1,938 and 2,608 m²/g, respectively, calculated from N₂ adsorption isotherms (77 K). Cu-TDPAT is featured with a high density of both open metal sites (1.76/nm³) and Lewis basic sites (3.52/nm³), as well as high thermal and water stability. At 77 K and 67 bar, Cu-TDPAT takes up 4.83 (excess) and 6.77 (total) wt% of H₂, respectively. At 298 K and 60.9 bar, these numbers are 0.61 (excess) and 1.04 (total) wt%, respectively. The hydrogen adsorption is further enhanced upon a pre-bridging method we have recently developed to incorporate the PtC catalyst into the material during synthesis, with catalyzed uptake exceeding other common doping methods by a factor of 5 at 1 bar and ambient temperature (e.g. compare Pt/AC@CuTDPAT to Pt/CuTDPAT in Figure 4). Compared to other low-pressure measurements of doped MOF systems from the literature (see Figure 4), uptake of pre-bridged Pt/AC@CuTDPAT shows the highest uptake to date, and the slope of the low-pressure isotherm is high, suggesting high-pressure measurements (which are in progress) will also exceed the other materials. The high uptake of Pt/AC@CuTDPAT can be attributed to the doping technique, which typically maintains 90-110% of the surface area of the original MOF. In contrast, common

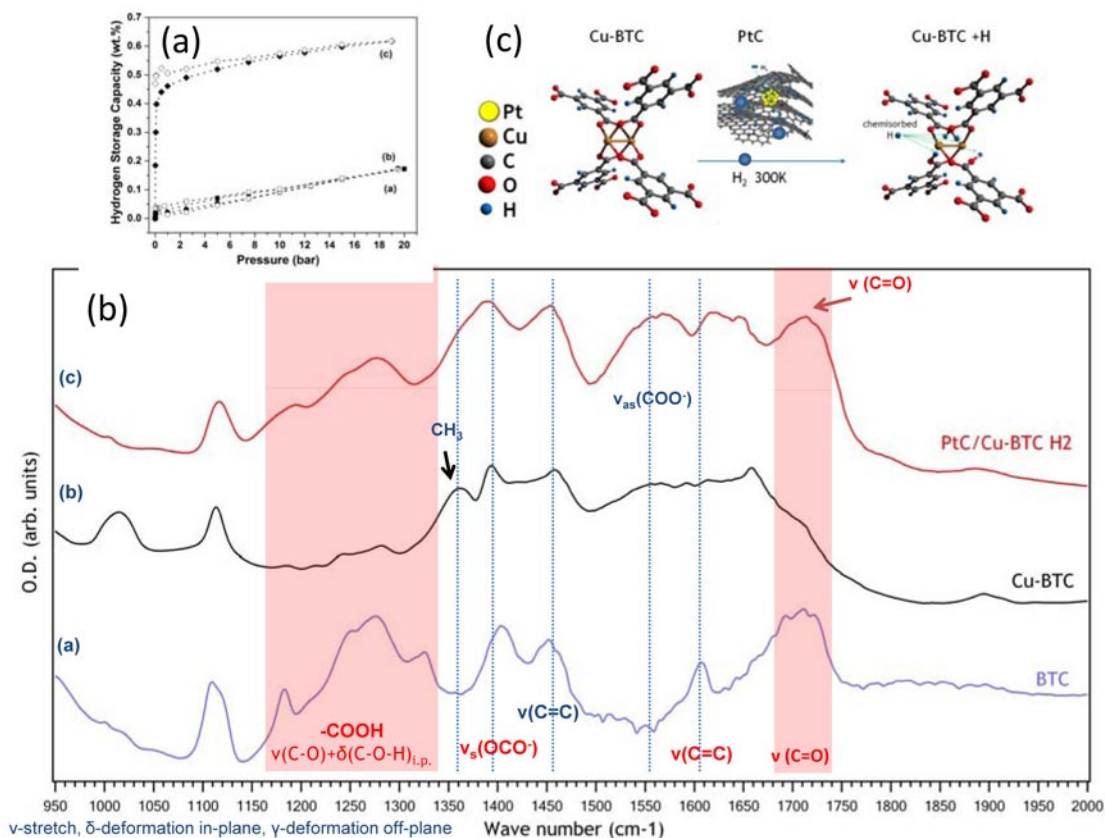


FIGURE 3. Introduction of a Pt/C spillover catalyst via mixing with CuBTC significantly increases low-pressure gravimetric hydrogen uptake at 298 K, achieving 0.61 wt% at 20-bar (a). FTIR spectra (b) demonstrate that this induces chemisorption to the Cu corners of the MOF by hydrogenating the carboxylate group, as demonstrated in the schematic (c).

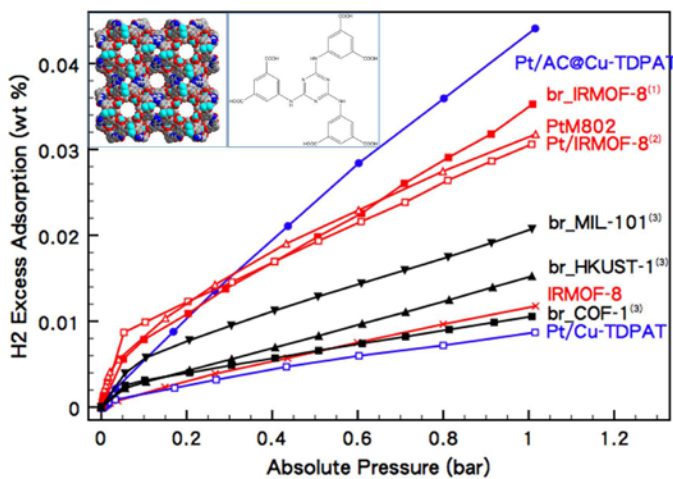


FIGURE 4. Room temperature H₂ uptake of "prebridged" Pt/CuTDPAT (blue circles) relative to direct-doped Pt/CuTDPAT (blue squares). The latter doping technique degrades structure and significantly decreases N₂ BET surface area. The inset shows the CuTDPAT crystal structure and the H₂TDPAT ligand. Other doped MOFs from the literature are included for comparison (1) Li, Y.; Yang, F.H.; and Yang, R.T. J. Phys. Chem. C. 2007, 111, 3405-3411; (2) Wang, L.F.; Stuckert, N.R.; Chen, H.; and Yang, R.T. J. Phys. Chem. C. 2011, 115, 4793-4799; (3) Li, Y. and Yang, R.T. AIChE Journal. 2008, 54, 269-279.

catalyst doping techniques, when applied to MOFs, may degrade surface area by as much as 20-70%, and may lead to complete amorphitization of structure. Clearly, the developed doping procedure yields the best room temperature uptake among all samples investigated. This method to incorporate the catalyst will be used to explore other MOF structures, with varying surface chemistry.

Conclusions and Future Directions

- Hydrogen spillover is verified with spectroscopic measurements. However, results with Pt-doped activated carbons suggest co-catalysts, trace water, and/or reactor configuration may play a role in systematically achieving high uptake via spillover. Future work will deduce role of energy propagation and co-catalysts in optimizing hydrogen spillover.
- Type and form of oxygen groups on carbon substrate affects Pt particle size and ultimate spillover on carbon materials (Figures 1 and 2). Future work will explore role of oxygen group and catalyst activators in optimizing spillover.

- A method to introduce a hydrogen dissociation catalyst into MMOF materials has been developed and tested. The new method provides substantial improvements over other common methods in terms of maintaining MMOF surface chemistry, structure, and surface area (Table 2). The doping method will be optimized in the upcoming year.
- PtC@CuTDPAT, produced via this new doping method, has the highest uptake via spillover at 1 bar (Figure 4), relative to all previously studied catalyst-doped MMOFs. The uptake is reversible and recoverable for three adsorption-desorption cycles, and XRD after adsorption shows the MMOF structure matches the as-synthesized CuTDPAT. Future studies will measure the uptake of PtC@CuTDPAT at high pressure and explore reproducibility of synthesis and measurement.
- Time permitting, this new catalyst doping method will be used to revisit effect of surface chemistry/structure on a variety of MMOFs that were previously tested after physical mixing with a hydrogen dissociation catalyst.
- Finalize papers on: (1) methods validation and reproducibility in differential volumetric analyzer; (2) development of direct-doping studies and instability of MMOFs; and (3) cross-comparison of catalyst doping techniques for MMOF materials.

Special Recognitions & Awards/Patents Issued

1. A. Lueking was selected as an Incoming Marie Curie Fellow for her work related to spillover.

FY 2012 Publications

1. Sircar, S.; Wu, H.; Li, J.; Lueking, A.D., Effect of Time, Temperature, and Kinetics on Hysteretic Adsorption-Desorption of H₂, Ar, and N₂ in the Metal-Organic Framework Zn₂(bpdC)₂(bpee), *Langmuir* 27 (23), 14169-14179, 2011.
2. Tsao, C.S.; Liu, Y.; Chuang, H.Y.; Tseng, H.H., Chen, T.Y.; Chen, C.H., Yu, M.S.; Li, Q., Lueking, A.D, Chen, S.H.. Hydrogen Spillover effect of Pt-doped Activated Carbon Studied by Inelastic Neutron Scattering. *J. Phys. Chem. Lett.* 2, 2322-2325, 2011.
3. Li, Q.; Lueking, A.D. Effect of Surface Oxygen Groups and Water on Hydrogen Spillover in Pt-Doped Activated Carbon. *J. Phys. Chem. C.* 115, 4273-4282, 2011.
4. Noa, K.E.; Lueking, A.D.; Cole, M.W., Imbibition transition: gas intercalation between graphene and silica. *J Low Temp Phys* 163, 26-33, 2011.
5. Lee, J.Y.; Pan, L.; Huang, X.Y.; Emge, T.J.; Li, J. A Systematic Approach to Build Highly Porous, Non-interpenetrating Metal Organic Frameworks with Large Capacity in Adsorbing H₂ and CH₄. *Adv. Func. Mater.*, 21, 993-998, 2011.

6. Liu, X.M.; Rather, S.; Li, Q.; Lueking, A.D., Zhao, Y.; Li, J. Hydrogenation of CuBTC framework with the introduction of a PtC hydrogen spillover catalyst. *J Phys. Chem. C*, 116 (5), 3477-3485, 2012.
7. Cole, M.W.; Gatica, S.M.; Kim, H.Y.; Lueking, A.D.; Sircar, S. Gas Adsorption in Novel Environments, Including Effects of Pore Relaxation. *J. Low Temp. Phys.* 166 (5-6), 231-241, 2012.

FY 2012 Presentations and Reports

1. Lueking, A.D. (invited) "Hydrogen storage in metal-organic frameworks via spillover and gate-opening mechanism". International Workshop: Adsorption at the nanoscale, a new frontier in fundamental science and applications Sep 21–24, 2011 at the University of Missouri, Columbia, MO.
2. Wang, C.Y. (speaker); Li, Q. Sircar, S. Liu, X. Lueking, A.D., Li, J. Cole, M. "Hydrogen Trapping through Designer Hydrogen Spillover Molecules with Reversible Temperature and Pressure-induced Switching" (Invited/Report) Hydrogen Storage Tech Team Meeting, Detroit, MI, September 15, 2011.
3. Lueking, A.D. (speaker), "Hydrogen Trapping through Designer Hydrogen Spillover Molecules with Reversible Temperature and Pressure-Induced Switching," (Report), Annual Merit Review Meeting, Washington, DC, May 12, 2011.
4. Lueking, A.D. (speaker), "Effect of Equilibration Time and Reduced Conditions on Adsorption to "Gate-Opening Metal-Organic Frameworks", AIChE Annual Meeting, Minneapolis, MN, October 19, 2012.
5. Lueking, A.D. (Invited speaker), "Nanomaterials for Gas Storage and Separations via a Trapping Mechanism," James and Catherine Patten Seminar, University of Colorado at Boulder, November 1, 2012.
6. Lueking, A.D. (Invited speaker), "Spectroscopic Evidence for Hydrogen Spillover," NREL working group on Weak Chemisorption, National Renewable Energy Laboratory, Golden, CO, February 2, 2012.
7. Li, J. (Invited speaker), "Microporous Metal Organic Frameworks: Porosity, Functionality and Potential Applications," Institute of Chemistry, Chinese Academy of Sciences, Beijing, China, April 30, 2012.
8. Li, J. (Invited speaker), "Functional Porous Materials: Design, Synthesis, Characterization and Applications", University of Texas at Dallas, Dallas, TX, April 5, 2012.
9. Li, J. (Invited speaker), "Designing and Functionalizing MMOFs for Energy Related Applications", Institute of Chemistry, Chinese Academy of Sciences, Beijing, China, April 30, 2012.
10. Li, J. (Invited speaker), "Microporous Metal Organic Frameworks: Porosity, Functionality and Gas Adsorption Properties", Jilin University, Changchun, China, May 3, 2012.
11. Li, J. (Invited speaker), "Porosity and Functionality in Metal Organic Framework Structures", Changchun Institute of Applied Chemistry, Chinese Academy of Sciences, Changchun, China, May 4, 2012.

References

1. Li, Y. and Yang, R.T. *J. Am. Chem. Soc.* 2006, 128, 8136-8137.
2. Li, Y. and Yang, R.T. *AIChE Journal*. 2008, 54, 269-279.
3. Wang, L.F.; Stuckert, N.R.; Chen, H.; and Yang, R.T. *J. Phys. Chem. C*. 2011, 115, 4793-4799.
4. Zlotea, C.; Campesi, R.; Cuevas, F.; Leroy, E.; Dibandjo, P.; Volkringer, C.; Loiseau, T.; Férey, G.; and Latroche, M. *J. Am. Chem. Soc.* 2010, 132, 2991-2997.
5. Lee, S.Y. and Park, S.J. *International Journal of Hydrogen Energy*. 2011, 36, 8381-8387.
6. Yang, S.J.; Cho, J.H.; Nahm, K.S.; and Park, C. R. *International Journal of Hydrogen Energy*. 2010, 35, 13062-13067.
7. Tsao, C.S.; Yu, M.S.; Wang, C.Y.; Liao, P.Y.; Chen, H.L.; Jeng, U.S.; Tzeng, Y.R.; Chung, T.Y.; and Wu, H.C. *J. Am. Chem. Soc.* 2009, 131, 1404-1406.
8. Stadie, N.P.; Purewal, J.J.; Ahn, C.C.; and Fultz, B. *Langmuir*. 2010, 26, 15481-15485.
9. Stuckert, N.R.; Wang, L.; and Yang, R.T. *Langmuir*. 2010, 26, 11963-11971.
10. Li, Q.; Lueking, A.D. Effect of Surface Oxygen Groups and Water on Hydrogen Spillover in Pt-Doped Activated Carbon. *J. Phys. Chem. C*. 2011, 115, 4273-4282.
11. Tsao, C.S.; Liu, Y.; Chuang, H.Y.; Tseng, H.H., Chen, T.Y.; Chen, C.H., Yu, M.S.; Li, Q., Lueking, A.D, Chen, S.H.. Hydrogen Spillover effect of Pt-doped Activated Carbon Studied by Inelastic Neutron Scattering. *J. Phys. Chem. Lett.* 2011, 2, 2322-2325.
12. Liu, X.M.; Rather, S.; Li, Q.; Lueking, A.D., Zhao, Y.; Li, J. Hydrogenation of CuBTC framework with the introduction of a PtC hydrogen spillover catalyst. *J Phys. Chem. C*, 2012, 116 (5), 3477-3485.

IV.C.6 Weak Chemisorption Validation

Thomas Gennett (Primary Contact), Lin Simpson, Jeffrey Blackburn, Katherine Hurst, Philip Parilla, Chaiwat Engtrakul, Steve Christensen
National Renewable Energy Laboratory (NREL)
1617 Cole Blvd.
Golden, CO 80401-3393
Phone: (303) 384-6628
Email: thomas.gennett@nrel.gov

DOE Managers

HQ: Ned Stetson
Phone: (202) 586-9995
Email: Ned.Stetson@ee.doe.gov

GO: Jesse Adams
Phone: (720) 356-1421
Email: Jesse.Adams@go.doe.gov

Subcontractors:

- University of Hawaii (Craig M. Jensen), Honolulu, HI
- University of New Mexico (Plamen Atanassov), Albuquerque, NM
- Max Planck (Michael Hirscher), Stuttgart, Germany
- Institut de Chimie et des Matériaux (ICPME) (Michel Latroche), Paris, France
- H2 Technology Consulting LLC (Karl Gross), Alamo, CA

Project Start Date: October 1, 2011

Project End Date: Project continuation and direction determined annually by DOE

- Provide highly accurate hydrogen storage measurement support to the sorption community in order to validate exceptional results.
- Coordinate additional work for the Best Practices document and for the characterization of hydrogen storage materials.

Technical Barriers

This project addresses the following technical barriers from the Storage section of the Fuel Cell Technologies Program's Multi-Year Research, Development and Demonstration Plan:

- (A) Cost
- (B) Weight and Volume
- (C) Efficiency
- (E) Refueling Time
- (M) Hydrogen Capacity and Reversibility
- (N) Understanding of Hydrogen Physi- and Chemisorption
- (O) Test Protocols and Evaluation Facilities

Technical Targets

This project is validating experimentally observed weak chemisorption. Insights gained from this work may be applied toward the future design and synthesis of hydrogen storage materials that meet the following DOE 2017 hydrogen storage system targets:

- Specific energy: 1.8 kWh/kg
- Energy density: 1.3 kWh/L

The specific technical objectives include:

- Verify at least 30% increase in hydrogen uptake over baseline sorbent material at room temperature conditions based on the effects of weak chemisorption/spillover.
- NREL will complete compiling the sorption test results for at least two different materials each prepared by at least two independent laboratories with sorption measurements made for each in at least three separate laboratories. Results will include at least two spectroscopic characterizations for each sample as well. These results are to be compiled into a report for publication either on the DOE Hydrogen and Fuel Cells' website or in a peer reviewed journal by September 30, 2012.

Fiscal Year (FY) 2012 Objectives

- Evaluate the weak chemisorption/spillover process as a means to achieve DOE 2017 Hydrogen Storage goals:
 - Lead sample exchange and measurement validation efforts for weak chemisorption.
 - Perform round robin with "standard" high specific surface area sorbents to ensure all participating laboratories are measuring similar hydrogen storage capacities for both volumetric and gravimetric measurements.
 - Evaluate universal reproducibility of enhanced adsorption weak chemisorption/spillover effects.
 - Determine type of interaction of the carbon-based support with the spillover hydrogen.
 - Establish if weak chemisorption/spillover is a viable process for hydrogen storage.
 - Communicate validated results to the community at large.

Accomplishments

- Completed synthesis of three different spillover samples and distributed to the different labs for evaluation.
 - Verified a >30% enhancement of hydrogen storage in Pd catalyst on templated carbon (Pd/TC) materials via volumetric measurements (NREL and ICPME).
- Synthesized and characterized weak chemisorption/spillover materials at four different laboratories (NREL, ICPME, Max Planck, Penn State)
- Demonstrated direct spectroscopic evidence of a reversible room temperature sorption/desorption apparently from a unique C-H interaction via diffuse reflectance infrared Fourier transform spectroscopy (DRIFTS) and nuclear magnetic resonance (NMR) spectroscopies.
 - DRIFTS measurements up to 100 bar hydrogen overpressure for Ru-BCx (BCx is a boron-substituted carbon material formed by the pyrolyzation of triethylborane) and Pd/TC showed a unique reversible infrared stretch that was tentatively assigned to spillover hydrogen.
 - NMR measurements of the Ru-BCx and Pd/TC showed reversible room temperature carbon substrate-hydrogen interaction upon exposure to up to 100 bar hydrogen overpressure.
- Reported detailed findings and recommendations on hydrogen spillover results.
 - International Energy Association Hydrogen Implementation Agreement (IEA-HIA) Task 22 meetings in Copenhagen Denmark and Heidelberg Germany.
 - DOE Fuel Cell Technologies Annual Merit Review, Washington, D.C.
 - Ceramic Society Materials Challenges in Alternative and Renewable Energy, March 2012.
 - Session organizer and presenter at American Chemical Society Meeting, (August 2011) and IEA-HIA Task 22 Hydrogen Storage Meeting (September 2011).
 - Annual Hydrogen Storage Tech Team presentation April 2012.
- Completed required deliverables for the Best Practices document.
- Submitted for publication five separate peer-review journal articles related to our efforts.



Introduction

The ultimate goal of the Hydrogen Storage sub-program is the development of hydrogen storage systems that meet or exceed the DOE's goals for the onboard hydrogen storage in hydrogen-powered vehicles. With the tremendous interest in weak chemisorption materials for hydrogen storage, NREL and DOE have dedicated considerable resources working with partner institutions to synthesize specific materials and to develop/perform the requisite measurements in order to establish the capacity, kinetics and overall performance of these materials. The key critical issues that must be resolved for these materials include reproducibility of material synthesis, understanding the kinetics of H transport on receptor surfaces, and which chemical reactions are desired and which are not. In addition, weak chemisorption properties are intricately linked to more standard H₂ storage mechanisms, so information gained on the hydrogen-substrate interactions should help accelerate viable sorbent development.

Approach

Organized and led an international group with IEA and International Partnership for the Hydrogen Economy members to validate weak chemisorption synthesis and measurement results. This past year participants included: Angela Lueking (Penn State), Michael Hirscher (Germany), Michel Latroche (France), Thomas Gennett (NREL), Craig Brown (National Institute of Standards and Technology), Craig Jensen (University of Hawaii), Mike Miller (Southwest Research Institute®) and Channing Ahn (California Institute of Technology). Our approach included the synthesis and characterization of a series of materials with an unexplained enhancement of hydrogen sorption in the presence of catalysts that is thought to be caused by hydrogen spillover. The materials selected are Pd/TC, Pt/TC, and Ru/BCx. These materials were synthesized and validated across laboratories. As we move forward we will utilize volumetric measurements for verified capacity measurements. Then through spectroscopic evaluation of the materials with DRIFTS and NMR we will determine correct peak assignments in order to determine if spillover hydrogen spectroscopic modes are in regions expected for room temperature hydrogen desorption. There will then be a coordination of efforts for Inter-laboratory comparison of characterization of results and eventually a reconciliation of spillover propagation mechanisms to thermodynamic parameters.

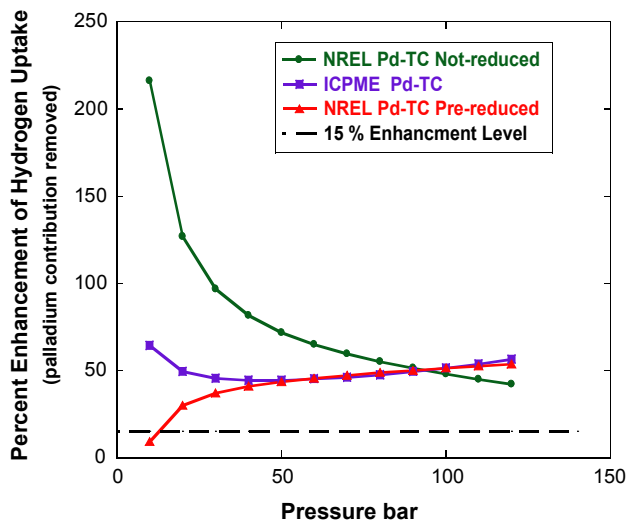
Results

1. Confirmed hydrogen sorption enhancement in Pd/TC materials of greater than 30% enhancement. NREL and ICPME were able to achieve a similar enhancement in

hydrogen sorption on Pd incorporated into a TC matrix. This adsorption was beyond that expected for palladium hydride formation, Pd-H₂, possibly from the addition of the Pd. This was confirmed on two separate samples (Figure 1).

2. DRIFTS determination of new hydrogen-substrate interactions for an apparent spillover material. Using

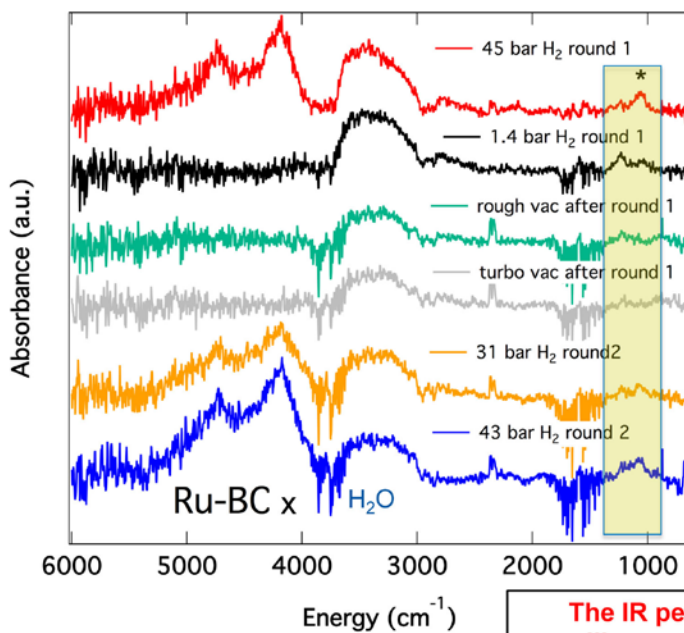
infrared spectroscopy to identify distinct substrate-hydrogen interactions is an essential component of our work as we look to establish the energetics associated with the spillover hydrogen. Figure 2 shows DRIFTS spectra for several samples charged with molecular deuterium and treated at various temperatures.



- greater than 45 percent increase in hydrogen uptake over baseline sorbent material at room temperature conditions is demonstrated.
- Data from two separate laboratories (purple and red traces) are shown.
- false enhancement can be observed when the metal oxide is initially present in the Pd-TC materials (green isotherm).

A multi-laboratory verification of a reversible enhanced hydrogen sorption via spillover at room temperature

FIGURE 1. Multi-laboratory comparison of volumetric data which illustrates a greater than 45% reversible hydrogen sorption enhancement attributed to a possible “spillover” type process



Sample degassed To 250 °C

First dose shows water formation similar to observed with TPD

Upon evacuation, peaks at 1070 and 1230 cm⁻¹ “disappear”

No degas prior to second dose.

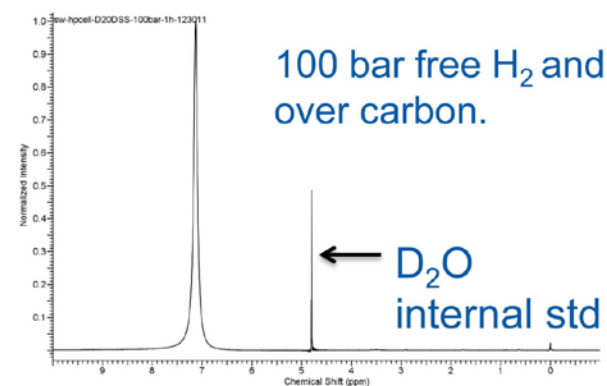
Peaks reappear at 1070 and 1230 cm⁻¹

The IR peaks, apparently from spillover process, are reversible

FIGURE 2. DRIFTS spectra for RuBCx sample which illustrates the reversibility of the new C-H peaks that appear in the infrared spectrum

3. ^1H NMR evidence for spillover hydrogen on a Ru-BCx material. NREL synthesized over 4 grams of ruthenium-decorated BCx TC materials and out of that batch both DRIFTS and NMR experiments were performed. The NMR results are illustrated in Figure 3. This unique peak shape is currently undergoing deconvolution to establish the type of carbon substrate-hydrogen interaction.

4. In August 2012, we will initiate synchrotron spectroscopic investigation of hydrogen-matrix interactions on the Ru-BCx sorbent in order to ascertain optimized storage capacity limits. Through a successful competitive proposal we have been awarded access to the Stanford Synchrotron Radiation Laboratory/Stanford National Accelerator Laboratory facility at Stanford University. With the use of our model materials system, it will be the most sensitive to changes in sp^2 to sp^3 bonding and will enable X-ray absorption spectroscopy and X-ray emission spectroscopy. These measurements can be correlated with states in the metal of choice regarding hydrogen adsorption, dissociation, and migration.



Signal shifted upfield 2.2 ppm (from 7.1 to 4.9 ppm) Chemical shift and broadening indicate physisorbed H_2 interacting with BCx.

NMR Signal is reversibly split on RuBCx with hydrogen dose as compared to BCx blanks

No new signals observed for ^{11}B NMR.

Possible new reversible C-H interaction observed

Conclusions and Future Direction

- Reconcile spillover propagation mechanisms:
 - Reconcile mechanism with metal-mediated processes with different substrate matrices.
 - Investigate new weak bond or localized catalytically activated interaction.
 - Use metal dispersion effects to establish whether current enhancements are localized or if there is evidence of long-range interactions.
 - Determine specifics of new C-H interaction on RuBCx material through currently on-going Stanford Linear Accelerator Center investigation.
- Determine ultimate spillover capacity possible with optimized interactions and substrate chemistry:
 - Evaluate effects of pore structure.
 - Design materials to enhance diffusion across substrate surface away from metal sites.
 - Determine whether PdBCx shows comparable enhancement to Pd/TC.

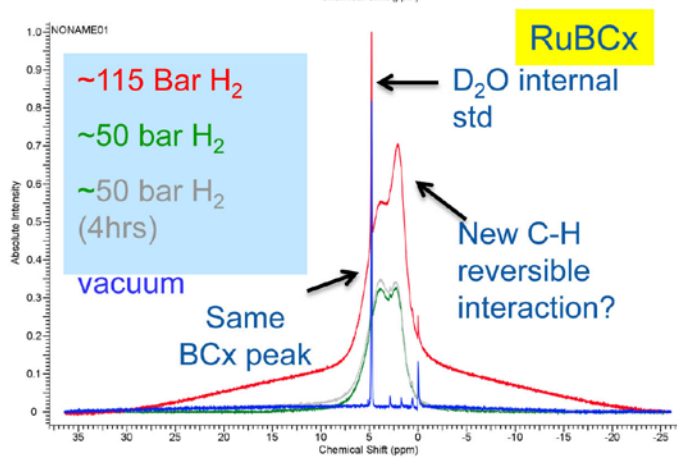
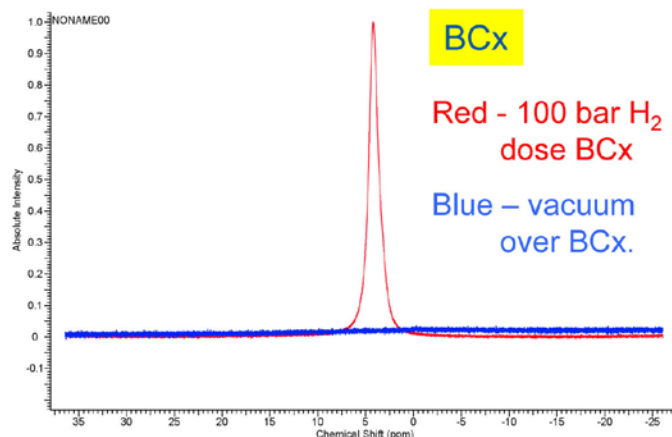


FIGURE 3. ^1H NMR data of BC_x material that illustrates the appearance of a new C-H interaction upon exposure of the sample to hydrogen overpressures at room temperature

- Establish ability to quantify hydrogen adsorption via DRIFTS and/or NMR spectroscopic techniques:
 - Investigate whether or not volumetric enhancements match new spectroscopic data.
 - Analyze Pd-TC and Pd-BCx materials via DRIFTS and NMR.
- Expand NMR work:
 - Deconvolute the observed features resultant from room temperature hydrogen sorption.
 - Perform variable temperature analysis of the BCx samples to verify the dynamic behavior.
 - Characterize the features in the RuBCx spectrum:
 - Quantification by line fitting
 - Characterization by T_1 analysis
 - Further analysis by study of ^{13}C -labeled materials with magic-angle-spinning solid-state NMR
 - Coupling constant and off resonance analysis.
- Complete the remaining sections, and update the other sections within Best Practices document.
- Stanford Linear Accelerator Center Work
 - Study, as a function of H_2 over-pressure, the sorbent near edge X-ray absorption fine structure (NEXAFS) via X-ray Raman scattering.
 - Correlate changes in the unoccupied density of states (from the NEXAFS) that support a transition away from sp^2 towards sp^3 bonding upon hydrogen uptake.
 - Probe the chemical states of the metal catalyst as a function of H pressure using X-ray emission spectroscopy.
 - Establish the experimental characterization protocol to determine the optimized reversible room temperature hydrogen capacity for a matrix based upon the results from the Stanford Linear Accelerator Center
- **Report detailing findings and recommendations at:** Tech Team update, (October 2012), Final analysis and recommendations will be presented at the 2013 Annual Merit Review Meeting and within several peer-reviewed journal submissions.

Validation and recommendations of weak chemisorption processes from this project will enable the hydrogen sorption community to accelerate development of room temperature hydrogen storage materials for light-duty vehicle and other early market applications.

FY 2012 Publications/Presentations

Publications

1. “Accelerating the Understanding and Development of Hydrogen Storage Materials: A review of the five year efforts of the three DOE Hydrogen Storage Materials Centers of Excellence.” K. Ott, L. Klebanoff, L.J. Simpson and N. Stetson. Submitted Metallurgical and Materials Transactions A (2012).
2. “Hydrogen Sorption Center of Excellence Final Report,” Lin Simpson Director, April 2012, http://www1.eere.energy.gov/hydrogenandfuelcells/pdfs/hydrogen_sorption_coe_final_report.pdf
3. “Executive Summaries for the Hydrogen Storage Materials Centers of Excellence; Hydrogen Sorption Center of Excellence Executive Report,” Lin Simpson Director, April 2012, http://www1.eere.energy.gov/hydrogenandfuelcells/pdfs/executive_summaries_h2_storage_coes.pdf
4. “Critical and precise calibration required to avoid large systematic errors in volumetric apparatus: isothermal case” submitted to *Review of Scientific Instruments*, P.A. Parilla, K.E.Hurst, L.J. Simpson, K.J. O’Neill, T Gennett.
5. “A Dynamic Calibration Technique for Temperature Programmed Desorption Spectroscopy ” accepted pending revision to *Review of Scientific Instruments*, K.E. Hurst, M.J. Heben, J.L. Blackburn, T. Gennett, A.C. Dillon and P.A. Parilla.
6. “Spectroscopic Identification of Hydrogen Spillover Species in Ruthenium-modified High Surface Area Carbons by Diffuse Reflectance Infrared Fourier Transform Spectroscopy” submitted to *J. Phys. Chem. C.*, Jeffrey L. Blackburn, Chaiwat Engtrakul, Justin B. Bult, Katherine E. Hurst, Yufeng Zhao, Qiang Xu, Philip A. Parilla, Lin J. Simpson, Craig Brown, Thomas Gennett.
7. “Sodium-Doped Carbon Nanotubes as Potential Hydrogen Storage Materials” C. Engtrakul, C.J. Curtis, L.M. Gedvilas, L.J. Simpson, P.A. Parilla, M.J. Heben, T. Gennett, accepted for publication in *J. Materials Chemistry*.
8. *Manipulation of Hydrogen Binding Energy and Desorption Kinetics by Boron Doping of High Surface Area Carbon*, Justin B. Bult, Justin Lee, Kevin O’Neill, Chaiwat Engtrakul, Katherine E. Hurst, Yufeng Zhao, Lin Simpson, Phillip Parilla, Thomas Gennett, Jeffrey L. Blackburn, submitted to *Chemistry of Materials*.
9. “Synthesis of Novel Lithiated BC_6 Materials with Enhanced H_2 Binding Sites” C. Engtrakul, J.L. Blackburn, J.B. Bult, K.J. O’Neill, P.A. Parilla, T. Gennett, L.J. Simpson. in preparation.
10. “Energetics of hydrogenation of single-walled carbon nanotubes and Graphene” Q. Xu, J.L. Blackburn, L.J. Simpson, T. Gennett, Y. Zhao, in preparation.
11. “Multi-Institutional Comparison of Volumetric H_2 Adsorption Measurements on Carbon Sorbents”, K.E. Hurst, K.J. O’Neill, J.L. Blackburn, T. Gennett, and P.A. Parilla, in preparation.

Presentations

1. Invited Talk: *Weak hydrogen chemisorption validation*, Thomas Gennett, DOE Fuel Cell Technologies Program Annual Merit Review, May, 2012, Washington, D.C.

2. Invited Talk; *Capacity, Kinetics and Evaluation of the Spillover Hydrogen Sorption Process*, Thomas Gennett, IEA-HIA Task 22 Hydrogen Storage, Heidelberg, Germany, May 2012.
3. Invited Talk: “*Capacity, Kinetics and Evaluation of the Spillover Hydrogen Sorption Process*” Thomas Gennett, DOE Technical Advisory Board Meeting, Dearborn, Mi, April 2012.
4. Invited Talk: “*Capacity, Kinetics and Evaluation of the Spillover Hydrogen Sorption Process*” Thomas Gennett, MRS Meeting, San Francisco, CA, April 2012.
5. Invited Talk: “*Capacity, Kinetics and Evaluation of the Spillover Hydrogen Sorption Process*” Thomas Gennett, Materials Challenges In Alternative & Renewable Energy, American Ceramic Society, February, 2012.
6. Invited Talks: Spillover Workshop Winter February 2012, Denver, CO. Organizer and Invited NREL Presentations:
 - a. “*Inter-Laboratory Comparison: Testing Measurement Reproducibility and Accuracy*” Phil Parilla, Katherine Hurst, Lin Simpson, Jeffrey Blackburn, Chai Engtrakul, Thomas Gennett.
 - b. “*Capacity, Reproducibility, and Kinetics of the Weak Chemisorptive (spillover) Hydrogen Sorption Process*, Thomas Gennett.
 - c. *Spectroscopic Identification of Hydrogen Spillover Species in Ruthenium-modified High Surface Area Carbons by Diffuse Reflectance Infrared Fourier Transform Spectroscopy* Jeffrey L. Blackburn,* Chaiwat Engtrakul, Justin B. Bult, Katherine E. Hurst, Yufeng Zhao, Qiang Xu, Philip A. Parilla, Lin J. Simpson, Craig Brown, Thomas Gennett.
 - d. *High Surface Area Boron Doped Carbon with Slow Hydrogen Desorption Kinetics*. Justin Bult, Jeffrey Blackburn,, Kevin O’Neill, Katherine Hurst, Chaiwat Engtrakul, Philip Parilla, Lin Simpson and Thomas Gennett.
7. Invited Talk: “*Capacity, Reproducibility, and Kinetics of the Weak Chemisorptive (spillover) Hydrogen Sorption Process*” Phil Parilla, Katherine Hurst, Lin Simpson, Justin Lee, Jeffrey Blackburn, Chai Engtrakul, Thomas Gennett, IEA-HIA Task 22 Meeting, Copenhagen, Denmark, September, 2011.
8. Invited Talk: *In situ spectroscopic identification of hydrogen binding sites on carbon-based hydrogen sorption materials* JL Blackburn, C Engtrakul, KE Hurst, JB Bult, J Lee, KJ O’Neill, PA Parilla, LJ Simpson, T Gennett 2011 American Chemical Society Fall National Meeting.
9. Invited Talk: *Weak hydrogen chemisorption validation*, Thomas Gennett, 2011 American Chemical Society Fall National Meeting.
10. Invited Talk: *Overview of hydrogen sorbents*; Lin Simpson, Thomas Gennett, Philip Parilla, Jeffrey Blackburn, Chaiwat Engtrakul, Yufeng Zhao, Katherine Hurst, Justin Bult, Kevin O’Neill 2011 American Chemical Society Fall National Meeting.
11. Invited Talk: Common errors found in volumetric hydrogen capacity measurements and how to avoid them Philip A Parilla, Kevin J O’Neill, Katherine E Hurst, Richard Knott, Thomas Gennett, Jeffery L Blackburn, Chaiwat Entrakul, Justin B Bult, Lin J Simpson, 2011 American Chemical Society Fall National Meeting.

IV.C.7 Room Temperature Hydrogen Storage in Nano-Confined Liquids

John J. Vajo

HRL Laboratories, LLC
3011 Malibu Canyon Road
Malibu, CA 90265
Phone: (310) 317-3745
Email: jjvajo@hrl.com

DOE Managers

HQ: Ned Stetson
Phone: (202) 586-9995
Email: Ned.Stetson@ee.doe.gov

GO: Katie Randolph
Phone: (720) 356-1759
Email: Katie.Randolph@go.doe.gov

Contract Number: DE-EE0005659

Project Start Date: March 05, 2012

Project End Date: March 14, 2015

Approach

Our approach is to use a composite consisting of a liquid solvent for molecular hydrogen that is nano-confined within a porous scaffold. Nano-confined liquids have been shown to have hydrogen solubilities that are enhanced by up to 50 times compared with bulk solubilities [1]. These enhanced solubilities enable a nano-confined solvent/porous scaffold composite hydrogen storage material with a material basis hydrogen storage density of 6% hydrogen by weight and 50 g/L that operate at room temperature and at pressures <350 bar (Figure 1). These materials could be readily used in current compressed hydrogen tank designs with minimal changes to vehicle engineering and delivery infrastructure, thus facilitating technology transition. The room temperature design also addresses critical shortcomings of current high capacity metal hydride (high temperature) and cryo-adsorbent (coolant and boil off) materials, resulting in significant cost reductions. We will investigate a variety of scaffold material compositions, including those based on carbon (e.g., mesoporous carbon and carbon aerogel) and aluminosilicates (e.g., MCM-41 and zeolites), and hydrogen dissolving liquids to maximize storage capacity. The enthalpy of the stored hydrogen as well as the effect of scaffold pore size will be explored. Storage capacity measurements together with simulations will be used to understand the mechanism of hydrogen storage in nano-confined liquids and optimize performance.

Fiscal Year (FY) 2012 Objectives

- Develop techniques for volumetric measurements of hydrogen solubility in volatile liquid solvents in both bulk form and nano-confined liquid/scaffold composites.
- Demonstrate volumetric measurements of hydrogen solubility in bulk hexane at pressures up to 100 bar.

Technical Barriers

This project addresses the following technical barriers from the Hydrogen Storage section (3.3) of the Fuel Cell Technologies Program Multi-Year Research, Development and Demonstration Plan:

- (A) System Weight and Volume
- (C) Efficiency
- (E) Charging/Discharging Rates

Technical Targets

This project is conducting initial studies of enhanced hydrogen solubility in nano-confined liquid solvents. Results from these studies will be applied to developing nano-confined liquid/nano-porous scaffold composite hydrogen storage materials that meet the following DOE targets:

- Specific energy: 6 wt% hydrogen (system)
- Energy density: 50 g/L hydrogen (system)

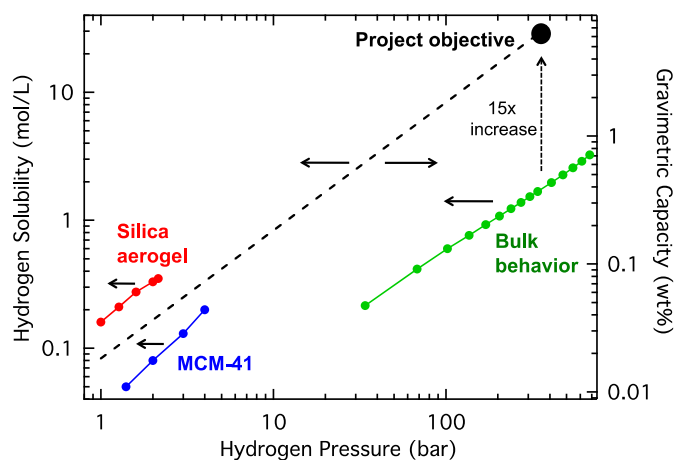


FIGURE 1. Hydrogen storage in nano-confined solvent/porous scaffold composites. Hydrogen solubility (left axis) versus pressure is shown for bulk hexane and nano-confined hexane/silica aerogel and nano-confined hexane/MCM-41 composites. Solubilities for hexane/silica aerogel and hexane/MCM-41 composites indicate ~50x and ~8x enhancements over the bulk, respectively. The project objective and progression (dashed line) are shown in terms of both solubility and hydrogen gravimetric capacity (right axis) based on an ~15x solubility enhancement and a 4 cm³/g pore volume scaffold.



FY 2012 Accomplishments

- Developed protocols for measuring hydrogen solubility using Sieverts apparatus at pressures between ~10 bar and 50 bar.
- Measured the solubility of hydrogen in n-hexane up to 70 bar using two different Sieverts apparatus and compared with published state-of-the-art measurements.

Future Directions

- We will extend our solubility measurement protocols from bulk liquids to nano-confined solvent/scaffold composites.
- We will develop methods for preparing nano-confined solvent/scaffold composites with specific liquid compositions.
- We will measure the solubility of hydrogen in a nano-confined solvent/scaffold composite, such as hexane/MCM-41.
- We will optimize the confined liquid and the scaffold to maximize hydrogen storage capacities.

FY 2012 Publications/Presentations

1. J.J. Vajo, Room temperature hydrogen storage in nano-confined liquids, Research Performance Progress Report for DOE/EERE, covering March 5, 2012 to June 30, 2012; submitted July 15, 2012.
2. J.J. Vajo, Room temperature hydrogen storage in nano-confined liquids, Poster presentation at the 2012 DOE Fuel Cell Technologies Program Annual Merit Review, May-2012, Crystal City, Virginia.

References

1. V. Rakotovoao, R. Ammar, S. Miachon, M. Pera-Titus, "Influence of the mesoconfining solid on gas oversolubility in nanoliquids", *Chem. Phys. Lett.*, **485**, 299-303 (2010).

IV.C.8 Hydrogen Storage in Metal-Organic Frameworks

Jeffrey Long (Primary Contact),
Martin Head-Gordon

Lawrence Berkeley National Laboratory
1 Cyclotron Road
Berkeley, CA 95720
Phone: (510) 642-0860
Email: jrlong@berkeley.edu

DOE Managers

HQ: Ned Stetson
Phone: (202) 586-9995
Email: Ned.Stetson@ee.doe.gov
GO: Jesse Adams
Phone: (720) 356-1421
Email: Jesse.Adams@go.doe.gov

Subcontractors:

- National Institute of Standards and Technology, Gaithersburg, MD (Craig Brown)
- General Motors Corporation, Warren, MI (Anne Dailly)

Project Start Date: April 1, 2012
Project End Date: March 31, 2015

- Quantify site-specific interactions of hydrogen with newly synthesized materials using inelastic neutron scattering
- Finish calculations of the binding of H₂ with the M-BTT linker and compare with experimental values for primary and secondary binding sites
- Assess performance of different computational methods for the M-BTT-H₂ binding problem
- Commence calculations of H₂ binding to carboxylate-substituted aromatic linkers decorated with light metal ions.
- Validate the excess adsorption measurement and data acquisition system through measurements on benchmark materials such as activated carbons and MOF-177

Technical Barriers

This project addresses the following technical barriers from the Hydrogen Storage section of the Fuel Cell Technologies Program Multi-Year Research, Development and Demonstration Plan:

(A) System Weight and Volume

Technical Targets

Specific efforts are focused on the research and development of onboard systems that allow for a driving range greater than 300 miles. Materials are sought with the potential for meeting the 2017 DOE targets of reversible uptake and, subsequently, the “ultimate full fleet” targets (see Table 1).



Fiscal Year (FY) 2012 Objectives

- Demonstration of the ability to prepare five mixed functionality ligands
- Development of *in silico* pore surface screening
- Preparation of metal-organic frameworks with high metal:ligand ratios
- Demonstrate ability to locate and uncover detailed descriptions of high-enthalpy H₂ binding sites in high-valent metal-organic frameworks
- Extract vital structural snapshots of the D₂-M²⁺ in systems exhibiting coordinatively unsaturated metal centers using neutron diffraction

TABLE 1. Progress towards Meeting Technical Targets for Onboard Hydrogen Storage for Light-Duty Vehicles

| Storage Parameter | Units | 2017 Target | Ultimate Target | 2012 Status [†] |
|--|--|----------------|-----------------|---|
| System Gravimetric Capacity: Usable, specific-energy from H ₂ (net useful energy/max system mass) [*] | kWh/kg (kg H ₂ /kg system) | 1.8 (0.055) | 2.5 (0.075) | (0.016 kg H ₂ /kg adsorbent) |
| System Volumetric Capacity: Usable, energy density from H ₂ (net useful energy/max system volume) | kWh/L (kg H ₂ /L system) | 1.3 (0.040) | 2.3 (0.070) | (0.011 kg H ₂ /L adsorbent) |

^{*} Generally the full mass (including hydrogen) is used; for systems that gain weight, the highest mass during discharge is used. All capacities are net useable capacity able to be delivered to the power plant. Capacities must be met at end of service life.

[†] Since the project deals with the development of storage materials, the performance status is given in terms of storage capacity for storage materials, not the whole storage system.

Approach

Metal-organic frameworks are promising solid sorbents for storage of H₂ at room temperature. They can be tailored to incorporate a large number of selected metal ions, thereby tuning the H₂ binding energy. The overall aim of the project is to synthesize new metal-organic frameworks capable of achieving the -20 kJ/mol adsorption enthalpy required for use as hydrogen storage materials operating under 100 bar at ambient temperatures.

This research involves investigators with a range of capabilities—including synthesis and characterization of new materials, electronic structure calculations, neutron diffraction and scattering studies, and high-pressure gas sorption measurements. The team performs work in four areas: Task 1) Synthesis of Metal-Organic Frameworks (Long-LBNL), Task 2) Characterization of Framework-H₂ Interactions (Brown-NIST), Task 3) First-Principles

Calculations of Hydrogen Binding Enthalpies (Head-Gordon-LBNL), Task 4) High-Pressure H₂ Adsorption Measurements (Dailly-GM).

FY 2012 Accomplishments

- Five new ligands with carboxylate and pyridine functionalities have been prepared (Figure 1).
- Opposing surface area distribution program has been written and submitted for publication [1].
- A number of new metal-organic frameworks containing accessible metal centers (Ni²⁺, Fe²⁺, Co²⁺, Ti³⁺) have been prepared. The Ni²⁺ framework (Figure 2) displays an H₂ binding enthalpy approaching the year two target of -12 kJ/mol (Figure 3).

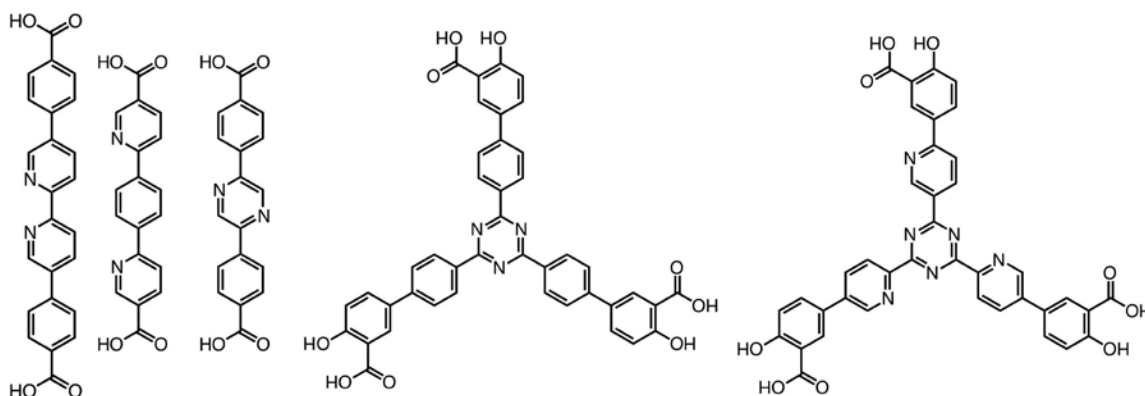


FIGURE 1. New di- and tritopic ligands containing both carboxylate and pyridine functional groups

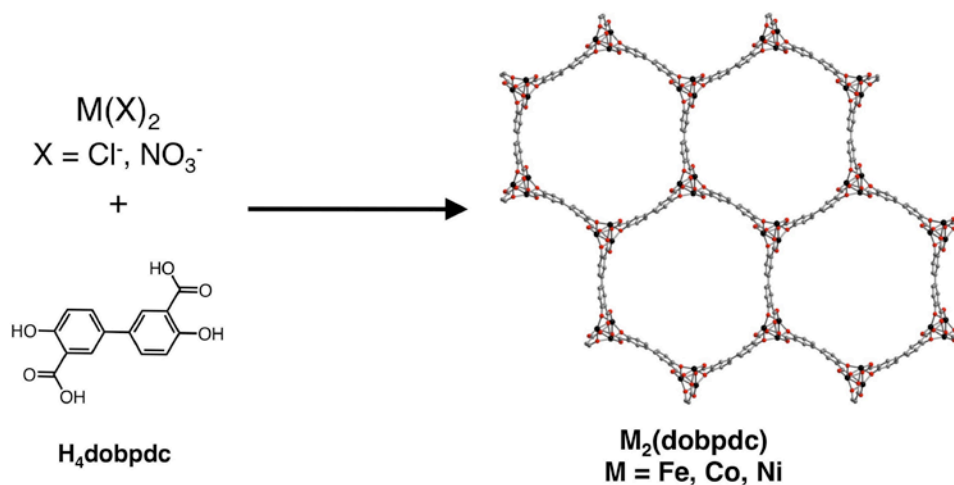


FIGURE 2. Recently synthesized metal-organic frameworks are expanded analogues of MOF-74 and feature high surface areas and a high density of open metal sites

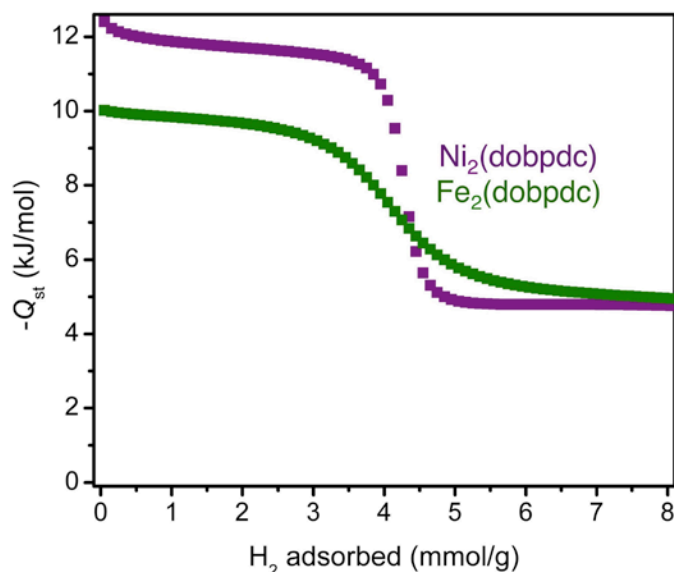


FIGURE 3. Isosteric heat of H_2 adsorption in $Fe_2(dobpdc)$ and $Ni_2(dobpdc)$. The heat of adsorption in the Ni^{2+} material approaches the year 2 target of -12 kJ/mol.

Future Directions

- Metal-organic frameworks containing the mixed functionality ligands reported herein will be synthesized and post-synthetically loaded with metal cations.
- Further analysis of the recently synthesized Ni^{2+} , Co^{2+} , Ti^{3+} frameworks by powder neutron diffraction, infrared spectroscopy, and high pressure H_2 adsorption experiments will be performed to obtain insight into which combination of surface area, pore volume, and open metal cations sites will lead to optimal room temperature H_2 storage properties.

- We will utilize a number of techniques, including neutron diffraction and inelastic neutron scattering to explore site-specific interactions of hydrogen with newly synthesized materials and the energetics of those binding events.
- We will reveal atomically detailed information about these adsorbates, extracting vital structural snapshots of the D_2-M^{2+} in systems exhibiting coordinatively unsaturated metal centers. The site-specific adsorption sites in these systems will be identified from sequential loadings corresponding to a progression from strong to weak adsorption sites, mirroring the site-specific enthalpy of adsorption.
- Continue calculations of H_2 binding to carboxylate-substituted aromatic linkers decorated with light-metal ions.
- Commence integrated quantum mechanics/molecular mechanics modeling of metal-organic framework systems to go beyond isolated linkers.
- Perform excess adsorption measurements on newly synthesized metal-organic framework samples.

FY 2012 Publications/Presentations

1. "Opposing Surface Area Distribution (OSAD) as a Characterization Tool for Microporous Metal-Organic Frameworks" Sumida, K.; Rogow, D.L.; Herm, Z.R.; Long, J.R. *Langmuir* submitted.

References

1. "Opposing Surface Area Distribution (OSAD) as a Characterization Tool for Microporous Metal-Organic Frameworks" Sumida, K.; Rogow, D.L.; Herm, Z.R.; Long, J.R. *Langmuir* submitted.

IV.C.9 The Quantum Effects of Pore Structure on Hydrogen Adsorption

Raina Olsen
 Oak Ridge National Laboratory
 One Bethel Valley Road
 P.O. Box 2008, MS-6115
 Oak Ridge, TN 37831-6115
 Phone: (573) 999-2371
 Email: olsenrj@ornl.gov

DOE Manager
 HQ: Grace Ordaz
 Phone: (202) 586-8350
 Email: Grace.Ordaz@ee.doe.gov

Technical Advisor
 James Morris
 Phone: (865) 630-0020
 Email: morrisj@ornl.gov

Project Start Date: October 31, 2011
 Project End Date: October 31, 2013

is studied. This sample has already been synthesized by the ALL-CRAFT group at the University of Missouri [1]. The purpose of this project is to investigate the mechanism(s) at work in this sample, with the ultimate goal of identifying novel techniques to increase volumetric and gravimetric storage in inexpensive carbon materials.

FY 2012 Accomplishments

- Measured inelastic neutron scattering spectra from variants of the sample of interest, demonstrating significant differences between quantum states measured in different carbon samples.
- Measured inelastic neutron scattering spectra from an oriented graphite sample, identifying important aspects missing from current theory and developing use of inelastic scattering as a sample characterization technique.
- Completed numerical solutions of the three-dimensional Schrodinger equation for pores composed of expanded graphite, revealing the physical origin of several features of measured quantum states.



Fiscal Year (FY) 2012 Objectives

- Neutron characterization of variants of sample of interest
- Measurement of quantum states in idealized oriented carbon adsorbent
- Demonstrate theoretical origin of measured quantum states

Technical Barriers

This project addresses the following technical barrier from the Hydrogen Storage section (3.3) of the Fuel Cell Technologies Program Multi-Year Research, Development, and Demonstration Plan:

(A) System Weight and Volume

Technical Targets

In this project, a carbon adsorbent with unusually high volumetric storage (Table 1) compared to similar samples

Introduction

It seems unlikely that modest improvements in current hydrogen storage systems using well-understood techniques, such as increasing the surface area or binding energy of adsorbants, will be able to reach the ultimate DOE goals for gravimetric and volumetric storage. Instead, a major technological breakthrough is needed. The ALL-CRAFT group at the University of Missouri has produced a carbon adsorbent, HS;0B, with several unusual and desirable characteristics [1,2]. In particular, its volumetric storage is 40-75% higher than similar carbon adsorbents. While its gravimetric performance is 40-55% smaller than similar carbons, it is notable that these values are achieved with a sample surface area of only 700 m²/g, which is nearly a quarter of comparable nanoporous materials. The most unusual feature of the cryogenic excess isotherm is the lack

TABLE 1. Volumetric and gravimetric performance of sample of interest (HS;0B) compared with an industry standard activated carbon (MSC-30)

| Characteristic | Units | 2017 Target (System) | HS;0B | | MSC-30 | |
|---------------------|---------------------------------------|----------------------|-----------------|----------------|-----------------|----------------|
| | | | 300 K 90 bar | 80 K 90 bar | 300 K 90 bar | 80 K 90 bar |
| Volumetric Storage | g H ₂ /L sample | 40 | 14.7 | 58.4 | 8.5 | 41.6 |
| Gravimetric Storage | wt% (g H ₂ /g sample *100) | 5.5 | 1.24 | 4.90 | 2.26 | 11.1 |

of a peak, indicating the film can still easily accommodate more molecules, despite the large amount adsorbed for the surface area [1,2]. If the same performance could be attained in a similar material with maximal surface area, the 2017 targets could be easily achieved at cryogenic temperatures, even when the mass and volume of the system is included, and the system would be close to meeting targets at room temperature. Several samples with similarly unusual properties have been reported in the literature [3-6], indicating the presence of adsorption mechanism(s) which are not currently understood. Thus it is also possible that a robust understanding of these samples could lead to more impressive gains, bringing ultimate targets into reach.

Because the performance of HS;0B cannot be explained with classical adsorption theory and because the measured quantum states of hydrogen molecules adsorbed in the sample are significantly different than in comparable carbon samples, a logical hypothesis is that there is a quantum effect at work in the sample. Work accomplished as part of this project uses both experimental and theoretical techniques to investigate this hypothesis.

Approach

This project seeks answers to several major questions about the system under study. Preliminary work has shown HS;0B has a unique structure, and structure can have a significant effect on quantum states. Thus a number of experimental techniques are used to study the structure of variants of HS;0B in order to learn how they are different from other carbon samples and from one another. If a quantum mechanism is at work, it is essential that the quantum states of hydrogen molecules adsorbed both in the sample of interest and in similar carbon samples be understood. Inelastic neutron scattering (INS) is an invaluable tool for study of this problem [7]. Incident neutrons lose energy while exciting transitions in the quantum states of adsorbed molecules. INS has been used in this work both to study variants of HS;0B, as well as an idealized carbon sample with large, clean, flat surfaces whose orientation relative to incident neutrons can be controlled. In addition, the theoretical origins of the measured quantum states of both HS;0B and other carbon samples have been studied with both analytical and numerical techniques. This work enables use of INS data collected as an additional method of pore characterization, and advances understanding of the mechanism(s) of action in HS;0B.

Results

Currently, INS spectra have been collected during two experiments from six powdered carbon adsorbents, including three variants of HS;0B and three other carbons used for comparison purposes. Figure 1 shows a spectrum around the first rotational peak at an energy transfer of 14.7 meV, which

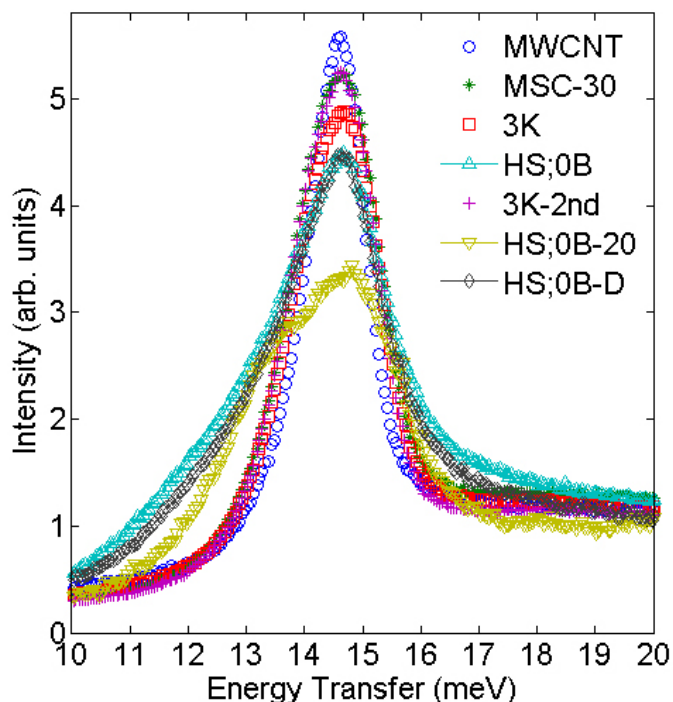


FIGURE 1. INS spectra collected from three HS;0B variants and several comparable carbon samples, including a sample of multi-walled carbon nanotubes (MWCNTs) and two activated carbons (MSC-30 and 3K, with the later measured twice). Temperature is 15 K, and each sample contains hydrogen at ~85% coverage. All spectra have been normalized by the amount of hydrogen.

represents a transition in the highly quantized rotational motion of the two hydrogen atoms about their mutual center of mass. All samples also have a tail (called the roto-recoil tail [8]) extending from the rotational peak on the high energy side, which represents a continuous spectrum of transitions in the translational motion of the hydrogen molecules along the adsorption plane. The three carbons used for comparison purposes all have spectra quite similar to one another, with minor differences which we have related to surface heterogeneity [8]. The spectra of the three HS;0B variants are significantly different from the other carbons. All show asymmetric broadening on the low energy side, but there are also significant differences between the three samples, both in the broadening and in the amount of recoil on the high energy side.

INS spectra have also been collected from an idealized carbon substrate with pores of infinite width, where the alignment of the adsorption surfaces with respect to the scattering neutrons can be controlled. Figure 2 shows this sample, which was constructed from 29 parallel sheets of an exfoliated graphite foil. The purpose of this experiment was to refine physical understanding of the motion of the adsorbed hydrogen molecules. Figure 3 shows the experimental geometry for the experiment and several key results. There are stark differences in the spectra based on the



FIGURE 2. Sample with oriented adsorption planes used for INS experiment.

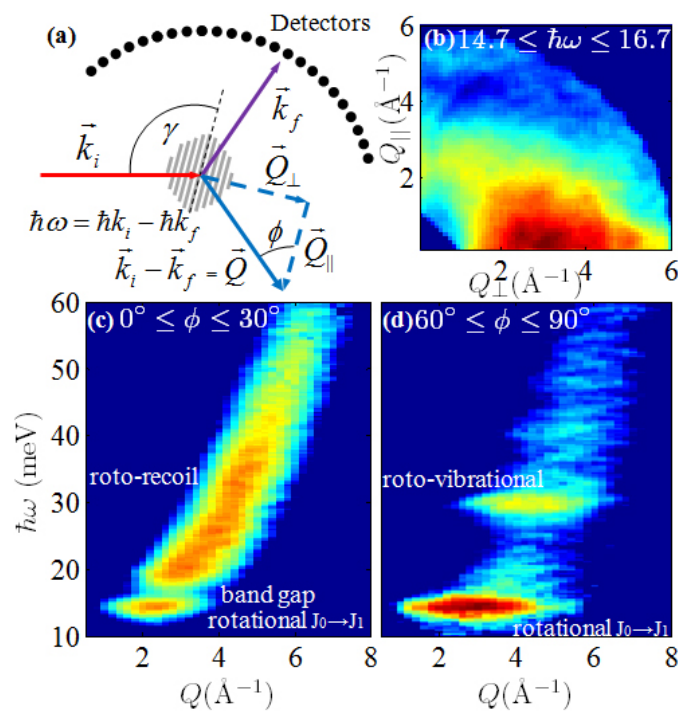


FIGURE 3. (a) Experimental geometry for IINS measurements of an oriented carbon sample, with energy transfer ($\hbar\omega$) and momentum transfer relative to the adsorption plane (Q) defined. (b) Spectrum of the main rotational peak as a function of Q_{\parallel} and Q_{\perp} . (c) Spectrum with the momentum transfer tending to be parallel or (d) perpendicular to the adsorption plane. Intensity is plotted on a log scale, temperature is 15 K, and the sample contains hydrogen at 25% coverage.

direction of momentum transfer (Q) relative to the adsorption plane. When Q tends to be parallel to the plane (Figure 3c), a continuous spectrum of transitions in the translational motion along the plane, the roto-recoil tail, extends from the main rotational peak at 14.7 meV. In contrast, when Q tends to be perpendicular to the plane (Figure 3d), roto-vibrational transitions are observed instead, where vibration refers to the bound motion of the molecule in the adsorption potential. The intensity, Q -dependence, and energy of the main rotational peak also varies significantly with the direction of momentum transfer (Figure 3b). While some of these results were expected, others were not.

To understand these experimental results, numerical solutions of the Schrodinger equation [9] have been performed for various two- and three-dimensional adsorption potentials. Figure 4 shows a representative quantum state for a hydrogen molecule adsorbed on a graphene plane. Previous work in the field has treated motion parallel to the plane and motion perpendicular to the plane separately. However, current results show an important relationship between these two types of motion, with highly coupled states where the vibrational wavefunction changes with the position of the molecule along the plane. This effect is caused by the corrugation of adsorption plane, which causes the distance of the potential minimum from the plane to vary with position. This coupling also results in non-zero angular momentum of the hydrogen center of mass, making it likely that this translational motion also couples to the rotational motion of the hydrogen atoms about their mutual center of mass. Indeed, a preliminary four-dimensional solution (with two translational and two rotational degrees of freedom) does show roto-translational coupling. Previous work in the field has also ignored this aspect of the problem in developing analysis techniques to use INS as a characterization method. So far, these theoretical results are consistent with the unexpected features observed in INS spectra.

To understand how this coupling is dependent on features of the potential, extensive solutions of an idealized two-dimensional adsorption potential have also been performed. The degree of coupling increases with both the degree of corrugation and the width of the potential. It is difficult to see how the amount of corrugation may be increased significantly in a carbon material by varying pore structure. However, calculations [7] have shown that for slit-shaped pores composed of two parallel sheets of graphene, the width of the potential is significantly larger with pore sizes between 7.5 and 9 Å. (Above 9 Å, the two walls are essentially independent adsorption potentials, whereas below 7.5 Å the adsorption potential is narrower because the two walls are quite close.) Pore size distributions of HS;0B generally show a peak around 8-9 Å. Pores of this size are also just large enough to allow bi-layer adsorption [10], and interaction between two nearby layers may be another significant source of quantum adsorption effects

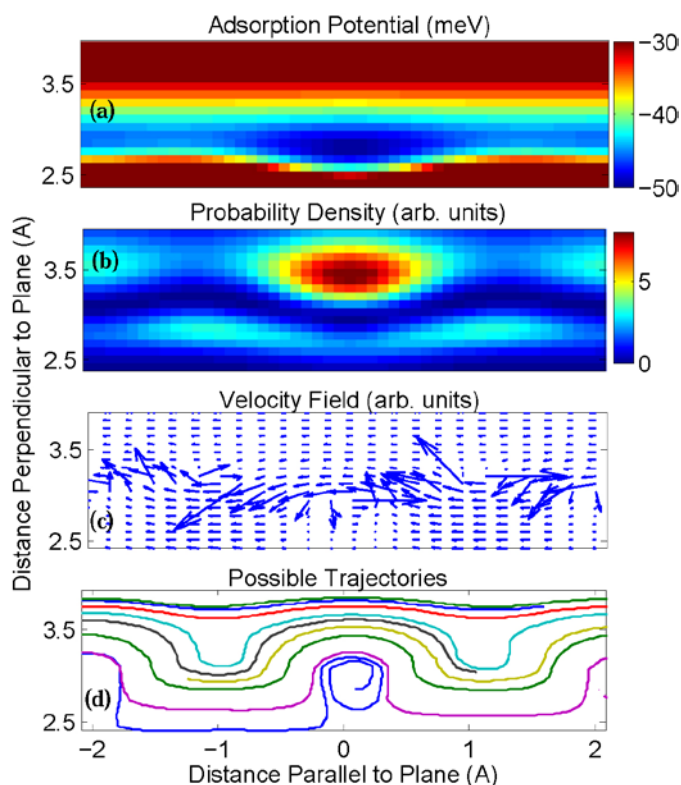


FIGURE 4. (a) Adsorption potential above the center of a hexagonal graphene unit cell, showing corrugation. (b) Probability density of a state which shows strong coupling between motion parallel and perpendicular to the plane. (c) Velocity field calculated from the wavefunction, which shows the magnitude and direction of the velocity at each point. The molecule has a net motion to the left, but the coupling creates areas where the velocity reverses direction, resulting in non-zero angular momentum of the molecular center of mass which varies with position. (d) Several representative classical trajectories calculated using the velocity field and an arbitrary initial position, which show rotational motion. All plots show a two-dimensional cut of a three-dimensional function.

Conclusions and Future Directions

- Based on work done so far, it seems likely that at least some of the unique characteristics of HS;0B are due to its average pore width of approximately 8-9 Å. Additional methods of pore characterization, including Raman scattering, X-ray diffraction, transmission electron microscopy, and pore size distributions measured with CO₂ will be used to verify these results and explore any other structural features which may affect the storage capabilities of this sample.
- Experimental INS work done with an oriented carbon sample shows that certain assumptions made during analysis of INS spectra from carbon samples in previous work need to be refined. These results will be used to develop INS as a more sensitive pore characterization technique, and applied to INS spectra which have also been collected from variants of HS;0B.

- Numerical solutions of the three-dimensional Schrodinger equation for an adsorbed hydrogen molecule show that coupling between the motion parallel and the motion perpendicular to the plane has a significant effect on the quantum states, and varies as a function of pore width. These solutions also show the coupling creates curved paths, making it likely that translational motion will also couple to rotational motion. Solutions of the five-dimensional Schrodinger equation will be done to explore this effect, and its relationship to the INS spectra measured for HS;0B and other carbon samples.

FY 2012 Publications/Presentations

- Raina Olsen, "The Quantum Effects of Pore Structure on Hydrogen Adsorption" 2012 Annual Merit Review, Washington, D.C., May 16, 2012.
- Raina Olsen, "Recoiling and Bound Quantum Excitation Spectrum of Adsorbed Hydrogen as an Assessment of Planarity" 6th Workshop on Characterization of Porous Materials, Delray Beach, FL, April 30, 2012.
- Raina Olsen, "Quantum Excitations of Adsorbed Hydrogen Studied by Inelastic Neutron Scattering" Carbons for Energy Applications, Atlanta, GA, March 30, 2012.
- Raina Olsen, "The Stationary States of Adsorbed Hydrogen" 2012 March Meeting of the American Physical Society, Boston, MA, March 1, 2012.

References

- P. Pfeifer et al., 2010 DOE Hydrogen Program Review, "Multiply Surface-Functionalized Nanoporous Carbon for Vehicular Hydrogen Storage," (http://www.hydrogen.energy.gov/pdfs/review10/st019_pfeifer_2010_o_web.pdf).
- R.J. Olsen, *Investigations of Novel Hydrogen Adsorption Phenomena* (PhD thesis), University of Missouri Columbia (2011).
- D.F. Quinn, "Supercritical adsorption of 'permanent' gases under corresponding states on various carbons," *Carbon* **40**, 2767-2773 (2002).
- J. Li et al., "Adsorption of hydrogen on porous materials of activated carbon and zeolite NaX crossover critical temperature," *Journal of Supercritical Fluids* **49**, 196-202 (2009).
- D. Saha et al., "Hydrogen adsorption equilibrium and kinetics in metalorganic framework (MOF-5) synthesized with DEF approach," *Separation and Purification Technology* **64**, 280-287 (2009).
- D. Saha et al., "Equilibrium, kinetics, and enthalpy of hydrogen adsorption in MOF-177," *International Journal of Hydrogen Energy* **33**, 7479-7488 (2008).
- R.J. Olsen et al., "Sub-nanometer characterization of activated carbon by inelastic neutron scattering," *Carbon* **49**, 1663-1671 (2011).
- R.J. Olsen et al., "Recoiling and bound quantum excitations of adsorbed hydrogen observed by inelastic neutron scattering," *Physical Review B*, under review.

9. S.A. Chin et al., “An arbitrary order diffusion algorithm for solving Schrodinger equations,” *Computer Physics Communication* **180**, 1700-1708 (2009).

10. B. Kuchta et al., “Numerical estimation of hydrogen storage limits in carbon based nanospaces,” *Carbon* **48**, 223-231 (2010).

IV.C.10 Metal- and Cluster-Modified Ultrahigh-Area Materials for the Ambient Temperature Storage of Molecular Hydrogen

Joseph E. Mondloch (Primary Contact),
Joseph T. Hupp, Omar K. Farha
Northwestern University
2145 Sheridan Road
Evanston, IL 60208
Phone: (847) 467-4932
Email: mojo0001@gmail.com

DOE Managers

HQ: Grace Ordaz
Phone: (202) 586-8350
Email: Grace.Ordaz@ee.doe.gov

GO: Gregory Kleen
Phone: (720) 356-1672
Email: Gregory.Kleen@go.doe.gov

Contract Number:

This research was supported in part by the Department of Energy (DOE) Office of Energy Efficiency and Renewable Energy (EERE) Postdoctoral Research Awards under the EERE Fuel Cell Technologies Program administered by Oak Ridge Institute for Science and Education (ORISE) for the DOE. ORISE is managed by Oak Ridge Associated Universities under DOE contract number AC05-06OR23100.

Project Start Date: November 1, 2011

Project End Date: Project continuation and direction determined annually by DOE

Fiscal Year (FY) 2012 Objectives

- Synthesis of –OH and –NH₂ functionalized ultrahigh-area sorbents
- Develop strategies to introduce metal cations into ultrahigh-area sorbents
- Evaluate materials performance of metal functionalized ultrahigh-area sorbents

Technical Barriers

This project addresses the following technical barriers from the Hydrogen Storage section of the Fuel Cell Technologies Program Multi-Year Research, Development and Demonstration Plan:

- (A) System Weight and Volume
- (E) Charging/Discharging Rates
- (P) Lack of Understanding of Hydrogen Physisorption and Chemisorption

Technical Targets

This project consists of developing ultrahigh-area sorbents capable of being modified with divalent metal cations. These materials aim to meet the DOE 2017 hydrogen storage targets:

- System Gravimetric Capacity: 1.8 kWh/kg (0.055 kg H₂/kg system)
- System Volumetric Capacity: 1.3 kWh/L (0.040 kg H₂/L system)

FY 2012 Accomplishments

- Synthesis of ultrahigh-area sorbents and –OH and –NH₂ functionalized sorbents
- Atomic layer deposition (ALD) and solution-based metallation of –OH and –NH₂ functionalized sorbents
- Initial materials performance analysis for increased Q_{st}



Introduction

Ultrahigh-area physisorption-based sorbents—for example, metal-organic frameworks (MOFs) and porous organic polymers (POPs)—are attractive candidates for the storage of molecular hydrogen (H₂). MOFs and POPs are built up from well-defined molecular components and key material properties such as pore size and functionality can often be readily controlled. On a materials basis, some of these sorbents meet the DOE's technical targets for both gravimetric and volumetric capacity, albeit at cryogenic temperatures. A crucial challenge for physisorption-based sorbents has therefore been storage of H₂ at or near room temperature. Storing H₂ at or near room temperature will require sorbents that can bind H₂ more effectively.

Approach

Our approach relies on introducing coordinatively unsaturated metal cation sites into (–OH or –NH₂) functionalized ultrahigh-area (i.e., ≥3,000 m²/g) physisorption-based sorbents. Recent computational evidence has suggested that divalent metal cations are capable of achieving the binding energies (isosteric heat of adsorption (Q_{st}) ~20–30 kJ/mol) necessary to store H₂ at room temperature [1]. We are pursuing three metallation strategies: (i) introduction of divalent metal cations via ALD; (ii) introduction of small metal-oxo(hydroxy) clusters via ALD;

and (iii) introduction of divalent metal cations via precedent solution chemistry [2].

ALD is an intriguing vapor phase deposition technique that, at least in principle, is capable of depositing divalent metal ions and small metal-oxo(hydroxy) clusters on ultrahigh aspect ratio structures such as MOFs and POPs. The unique feature of ALD is that it relies on self-limiting chemical surface reactions, allowing precise, atomic level control over both the location and number of metal (and –oxo(hydroxy)) species deposited. This in turn will allow precise tuning of the H_2 binding energies within metallated MOF or POP sorbents.

Results

As an ultrahigh-area platform, we synthesized the well-known MOF, MIL-101; shown in Figure 1a is the $[Cr_3(F,OH)(H_2O)_2O(bdc)_3]$ building block that MIL-101 is built up from [3]. MIL-101 is thermally stable ($\sim 275^\circ C$), has ultrahigh surface areas ($\sim 4,000\text{ m}^2/\text{g}$) and large pores (29 and 34 Å)—attributes which are desirable for metal modification. Functionality was introduced into MIL-101 post-synthetically. Dehydration of MIL-101 exposed coordinatively unsaturated Cr^{III} centers and subsequent addition of ethylenediamine (ED) or 3-aminopropane-1,2-diol (APD) from solution yields MIL-101 derivatives with $-NH_2$ or $-OH$ functionality respectively. As expected, the surface area for both ED-MIL-101 and APD-MIL-101 decrease with respect to MIL-101, while still remaining porous (Figure 2). The decreasing Barrett, Joyner and Halenda pore-size-distributions (Figure 2) are also consistent with the $-NH_2$ moieties of ED and APD binding to cus Cr^{III} centers in MIL-101 [3].

Subsequently ED-MIL-101 and APD-MIL-101 were subject to treatment with $Zn(Et)_2$ in an ALD reactor. Zn metallation was quantified by inductively coupled plasma-optical emission spectroscopy, the Zn:Cr ratios were slightly higher than expected, a result which is most likely due to the ALD process scavenging any unreacted hydroxyl sources present within ED-MIL-101 and APD-MIL-101 (e.g., bdc, H_2O , etc...). H_2 isotherms were measured at 77 and 87 K and the Q_{st} were extracted using a virial analysis. Figure 3 depicts the Q_{st} at constant H_2 coverage for APD-MIL-101 and Zn-modified APD-MIL-101. A slight increase in Q_{st} was observed at zero H_2 coverage for the Zn-modified material vs. the parent, APD-MIL-101 (note that the error bars in the measurement are smaller than the plotted data points). The results suggest that ALD may be an effective synthetic strategy to incorporate divalent metals into MOFs and therefore lead to increased Q_{st} if more favorable synthetic conditions can be found. In particular, the Zn metallated APD-MIL-101 lost much of its surface area ($\sim 75\%$) and was not crystalline (Figure 3).

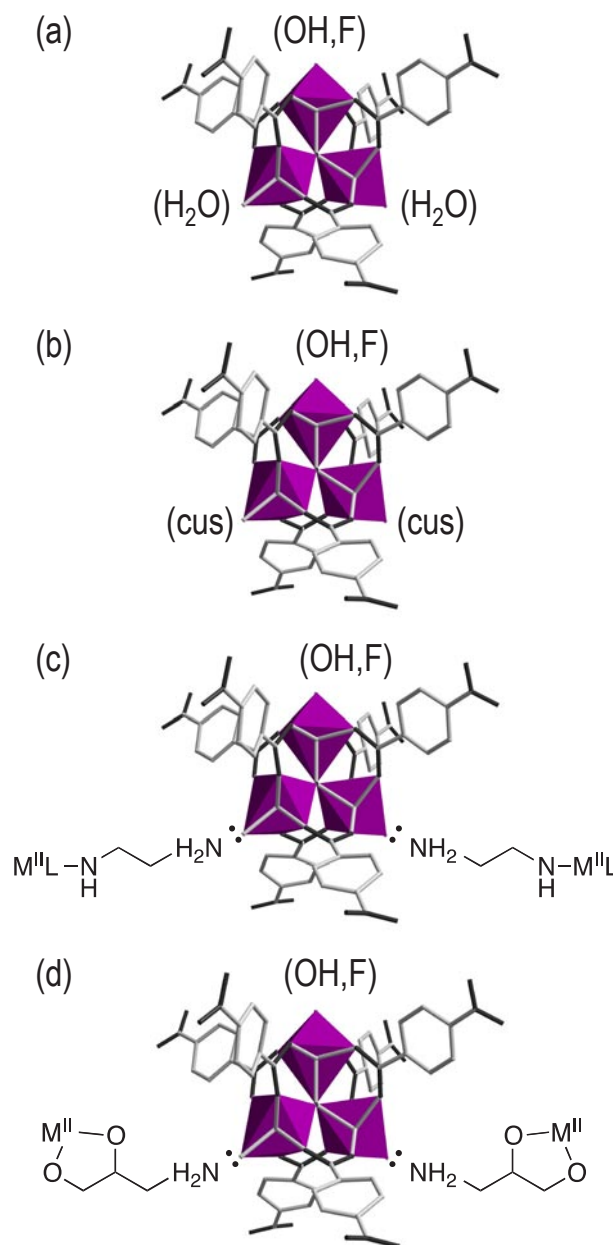


FIGURE 1. Representations of (a) MIL-101, (b) dehydrated MIL-101, (c) post-synthesis metallated ED-MIL-101 and (d) post-synthesis metallated APD-MIL-101. Coordinatively unsaturated Cr^{III} sites are represented by cus, while divalent metal cations are represented as M^{II} .

We also metallated APD-MIL-101 with $Mg(CH_3)_2$ from a dry, O_2 -free solution of toluene. The 77 and 87 K H_2 isotherms were collected and the Q_{st} are plotted in Figure 3. Again we observed a slight increase in the Q_{st} , with a large loss in surface area ($\sim 75\%$) and loss of crystallinity in the X-ray diffraction.

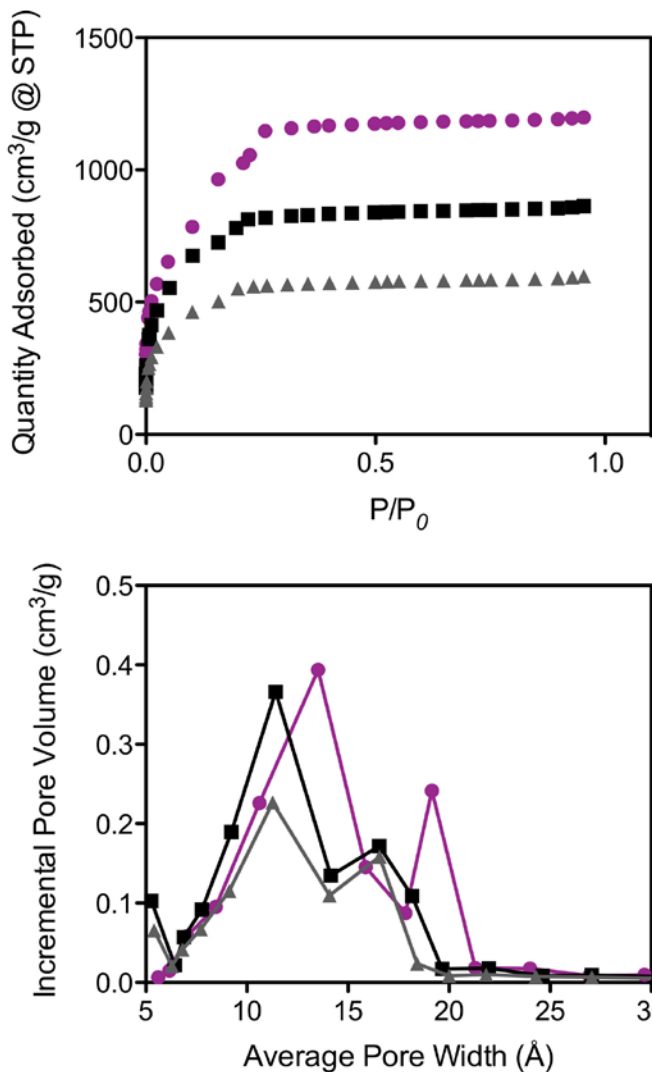


FIGURE 2. N_2 gas adsorption isotherms (top) and Barrett, Joyner and Halenda pore size distributions (bottom) for MIL-101 (purple circles), ED-MIL-101 (black squares) and APD-MIL-101 (gray triangles)

Conclusions and Future Directions

Conclusions

- $-NH_2$ and $-OH$ functionalized sorbents with surface areas of $\sim 2,000$ - $2,800$ m^2/g have been synthesized and characterized
- Divalent metals (Zn and/or Mg) have been incorporated into ED-MIL-101 and APD-MIL-101
- Q_{st} heats of adsorption have been obtained for all metalated (and parent) materials

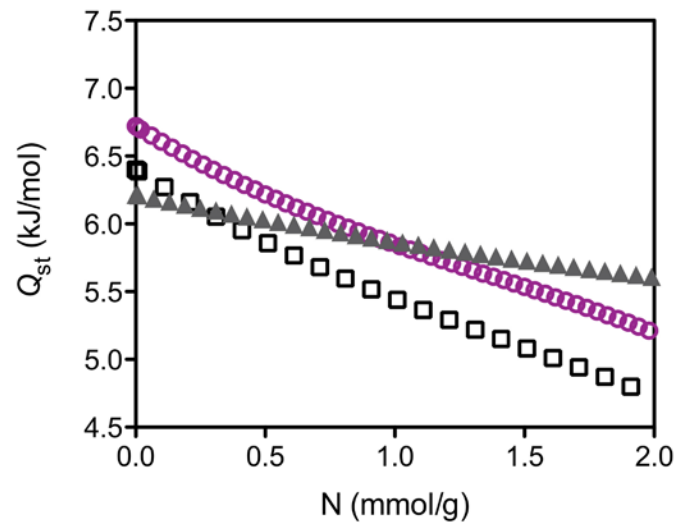


FIGURE 3. Q_{st} at constant H_2 coverage for APD-MIL-101 (gray triangles), Zn-APD-MIL-101 (purple circles) and Mg-APD-MIL-101 (black squares)

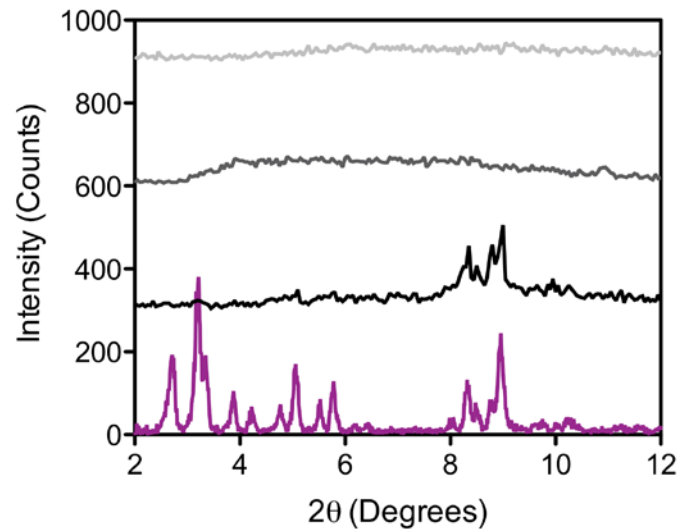


FIGURE 4. Powder X-ray diffraction patterns for MIL-101, APD-MIL-101, Zn-APD-MIL-101 and Mg-APD-MIL-101 (from bottom to top)

Future Directions

- Find synthetic conditions which retain the MOF crystallinity and surface area after post-synthesis metallation
- Build small metal-oxo(hydroxy) clusters in ED-MIL-101 and APD-MIL-101 via ALD
- Experimentally screen additional metals for enhanced Q_{st}
- Synthesis of $-NH_2$ and $-OH$ functionalized POPs and subsequent metallation

Special Recognitions & Awards/Patents Issued

1. DOE EERE postdoctoral research awardee.

FY 2012 Publications/Presentations

1. Mondloch, J.E.; Farha, O.K.; Hupp, J.T. "Metal- and Cluster-Modified Ultrahigh-Area Diamond Network Materials for the Ambient Temperature Storage of Molecular Hydrogen" Presented at Annual DOE EERE Postdoctoral Research Meeting, Washington, D.C., 2012.

References

1. Getman, R.; Miller, J.; Wang, K.; Snurr, R. "Metal Alkoxide Functionalization in Metal-Organic Frameworks for Enhanced Ambient-Temperature H₂ Storage" *J. Phys. Chem. C* **2011**, *115*, 2066.
2. Mulfort, K.L.; Farha, O.K.; Stern, C.L.; Sarjeant, A.A.; Hupp, J.T. *J. Am. Chem. Soc.* "Post-Synthesis Alkoxide Formation within Metal-Organic Framework Materials: A Strategy for Incorporating Highly Coordinatively Unsaturated Metal Ions" *J. Am. Chem. Soc.* **2009**, *131*, 3866.
3. Hwang, Y.K.; Hong, D.-Y.; Chang, J.-S.; Jung, S.H.; Seo, Y.-K.; Kim, J.; Vimont, A.; Daturi, M.; Serre, C.; Férey, G. "Amine Grafting on Coordinatively Unsaturated Metal Centers of MOFs: Consequences for Catalysis and Metal Encapsulation" *Angew. Chem. Int. Ed.* **2008**, *47*, 4144.

IV.C.11 Hydrogen Sorbent Measurement Qualification and Characterization

Philip A. Parilla (Primary Contact), Lin Simpson,
Jeffrey Blackburn, Katherine Hurst,
Chaiwait Engtrakul, Justin Bult, Thomas Gennett
National Renewable Energy Laboratory (NREL)
15013 Denver West Pkwy
MS 3211
Golden, CO 80228
Phone: (303) 384-6506
Email: Philip.Parilla@nrel.gov

DOE Managers

HQ: Ned Stetson
Phone: (202) 586-9995
Email: Ned.Stetson@ee.doe.gov
GO: Jesse Adams
Phone: (720) 356-1421
Email: Jesse.Adams@go.doe.gov

Subcontractors:

H2 Technology Consulting LLC, (Karl Gross) Alamo, CA

Collaborators:

- Caltech, USA – Channing Ahn group
- Institut de Chimie et des Matériaux, France
– Claudia Zlotea
- Max Planck, Germany – Michael Hirscher group
- Northwestern University, USA – Joe Hupp group
- Penn State, USA – Angela Lueking group
- Southwest Research Institute®, USA – Mike Miller

Project Start Date: October 1, 2011

Project End Date: Project continuation and direction
determined annually by DOE

- Identify the major error sources that will dominate the measurement.
- Recommend improved instrumentation and procedures to minimize such errors.

Technical Barriers

This project addresses the following technical barriers from the Storage section of the Fuel Cell Technologies Program Multi-Year Research, Development and Demonstration Plan:

- (A) System Weight and Volume
- (B) System Cost
- (C) Efficiency
- (E) Charging/Discharging Rates
- (K) System Life-Cycle Assessments
- (P) Lack of Understanding of Hydrogen Physisorption and Chemisorption
- (Q) Reproducibility of Performance

Technical Targets

This project supports the following overall DOE objective: “Capacity measurements for hydrogen-storage materials must be based on valid and accurate results to ensure proper identification of promising materials for DOE support”. This project focuses on this through the FY 2012 Objectives as listed above. Insights gained from these studies will be applied toward the design and synthesis of hydrogen storage materials that meet the following DOE hydrogen storage targets:

- Specific energy: 1.8 kWh/kg
- Energy density: 1.3 kWh/L

The specific technical objectives include:

- Disseminate measurements qualification and validation improvements to the hydrogen community.
- Work with hydrogen-storage material-synthesis researchers to measure, at least, 15 external samples.

FY 2012 Accomplishments

- Completed round-robin analysis of standard samples:
 - Achieved <5% error on hydrogen capacity measurements on the same standard sorbents at three different laboratories.

Fiscal Year (FY) 2012 Objectives

- Assist materials-research groups to characterize and qualify their samples for hydrogen-storage properties:
 - Measure external samples at NREL to compare results with source group’s and/or third-party’s results.
 - Discover sources of measurement discrepancies and advise on corrective actions, if needed, for source group.
- Analyze for, identify, and recommend corrective actions for major sources of measurement error in volumetric and temperature programmed desorption (TPD) systems:
 - Analyze realistic models for random and systematic errors.

- Measured over 20 external samples from outside laboratories. This surpasses the milestone of measuring 15 external samples.
- Collaborated with outside labs to investigate and verify operation of their hydrogen capacity equipment.
- Developed realistic models for the data analysis for volumetric systems, both for isothermal and non-isothermal conditions. Used models to understand both systematic and random error sensitivities.
- Identified the major error sources that dominate the measurement. We conclude that the most dominant errors are systematic errors!
- Developed recommended procedures to be used to improve measurement accuracy.
- Reported detailed findings and recommendations on hydrogen capacity measurements:
 - IEA-HIA Task 22 meeting Copenhagen, Denmark
 - DOE Fuel Cell Technologies Annual Merit Review, Washington, D.C.
 - Spillover Workshop, Winter 2012, Golden, CO
 - Summer ACS Meeting, 2011, Denver, CO
 - Spring MRS Meeting, 2011, San Francisco, CA
- Continued to manage and collaborate on the Best Practices document with its seven sections: Introduction, Capacity, Kinetics, Thermodynamics, Cycle-Life, Thermal Properties, Mechanical Properties measurements



Introduction

The ultimate goal of the Hydrogen Storage sub-program is the development of hydrogen storage systems that meet or exceed the DOE's goals for the onboard hydrogen storage in hydrogen-powered vehicles. In order to develop new materials to meet these goals, it is extremely critical to accurately measure the materials properties relevant to the specific goals otherwise the metrics are meaningless and achieving of goals uncertain. In particular, capacity measurements for hydrogen-storage materials must be based on valid and accurate results to ensure proper identification of promising materials for DOE support. A previous round-robin study had discovered major discrepancies among the different participating laboratories for capacity measurements on a standard material, both for room-temperature and liquid-nitrogen capacity determinations [1]. This study emphasizes the importance of maintaining a quality assurance effort within the hydrogen storage community. This project focuses on maintaining a world-class measurement facility for determining hydrogen storage capacities of novel research materials, understanding the experimental issues, procedures, and analysis to ensure accurate measurements, and assisting

the hydrogen storage community in performing and understanding these measurements. NREL's main focus is on the volumetric capacity measurement technique; this is also known as the manometric and Sieverts technique. NREL also has extensive experience in the TPD (or thermal desorption spectroscopy) technique.

Approach

NREL continues with a multiyear intensive effort to improve measurement quality and accuracy, understand the sources of and correct for measurement error, work with external groups to provide measurements and verify results, collaborate with the hydrogen community to improve measurements, and manage and coordinate with the "Best Practices" document project to disseminate recommended practices and procedures. In previous FYs, this effort was folded into the main materials-development project. This effort has its roots even before the Hydrogen Sorption Center of Excellence (HSCoE), but the effort accelerated during its existence as NREL was the main measurement resource for the HSCoE. The approach can be divided into two components: 1) work with external groups to measure samples and to examine their measurement techniques and procedures; and 2) in general analyze for, identify, and recommend corrective actions for major sources of measurement error in volumetric systems.

With respect to working with external groups, NREL actively seeks out collaborations for comparison studies, helps out with DOE projects to ensure robust measurements, and tests very promising results for verification. Additionally, NREL works with external groups to discover sources of measurement discrepancies and advise on corrective actions, if needed. This entails sending standardized samples to external labs to test instrumentation and experimental procedures, examining data and data analysis protocols to discover possible avenues to improve measurement techniques, and making recommendations to labs for improvements. With respect to measurement error, NREL analyzes realistic models for random and systematic errors, identifies the major error sources that will dominate the measurement, and recommends improved instrumentation, protocols and data analysis to minimize such errors.

Results

1. Completed inter-laboratory comparison for spillover research project. NREL collaborated with measurement experts from six laboratories for this comparison. This was an investigation to ensure instrumentation and procedures were in agreement among the laboratories participating before the spillover study began in earnest using two types of standardized samples. Reasonable agreement among the laboratories was seen typically with less than 5% discrepancy. Figure 1 shows results

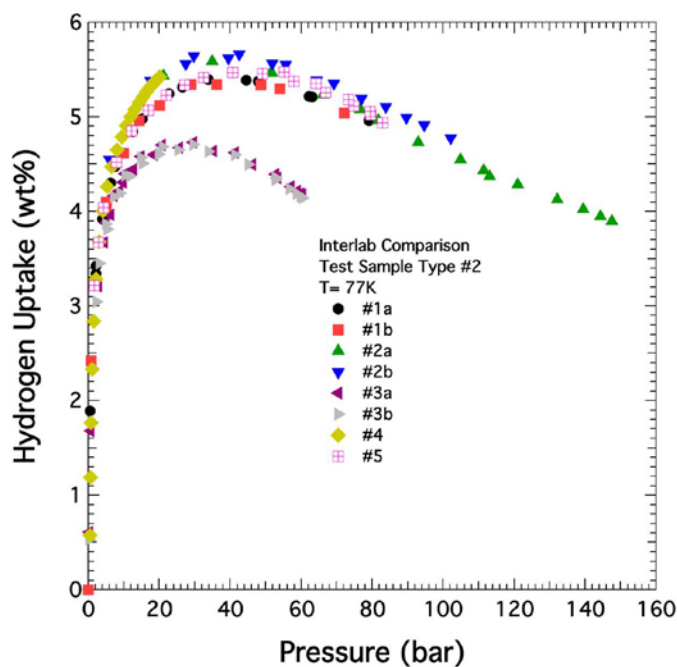


FIGURE 1. PCT data from inter-laboratory comparison study for sample type 2 at 77 K shows very good agreement among the labs except for lab #3. NREL helped Lab #3 identify measurement issues by using this material as a diagnostic tool.

for liquid nitrogen measurements for one of the standard sample types. There is one outlier lab shown in the figure (3a and 3b in the legend); this lab was not part of the main inter-laboratory comparison but was an external lab whose equipment and protocols was being diagnosed (see number 3 herein) and shows the importance of these efforts to try and improve the measurement art in the scientific community.

2. Measured over 20 external samples from outside laboratories. This surpasses the milestone of measuring 15 external samples. Each sample typically undergoes ~5 measurements using different techniques in the course of a typical analysis. Techniques include multiple pressure-concentration-temperature (PCT) isotherms, Brunauer-Emmett-Teller isotherm for surface-area analysis, TPD during degas, TPD after PCT, density and cycle-life PCT. Sample material types included templated carbon with and without catalysts, boron-substituted carbon material with and without catalysts, and metal-organic framework materials. Data from these external samples are considered proprietary and cannot be shown here.
3. Collaborated with outside labs to investigate and verify operation of their hydrogen capacity equipment. Figure 1 shows the data from one such lab (3a and 3b in the legend) and this measurement was used to help diagnose their equipment and protocols.

4. Developed realistic models for the data analysis for volumetric systems, both for isothermal and non-isothermal conditions. The importance of using realistic models should not be underestimated. Volumetric mass-balance models in the scientific literature, although ideally correct, typically do not account for real-world measurement situations. Most volumetric systems contain many more moles in the gas phase than the moles sorbed onto the sample thus requiring very accurate mass-balance accounting. Examples of real-world issues absent in the models include valves that change volume with operation and can transport gas between volumes, assumptions of non-measured pressure values, and the absence of temperature gradients or unrealistic temperature gradients.
5. Identified the major error sources that dominate the measurement. We conclude that the most dominant errors are systematic errors! The main sources of systematic error are improper “null” calibration, inadequate data analysis models (mass-balance models), ignorance of the large error associated with non-uniform temperature fluctuations, and ignorance of the importance of having adequate sample mass. The null calibration is the main factor in determining the accuracy of the mass-balance accounting. This can be seen in Figure 2a, which shows the total number of moles in an idealized volumetric system as a function of pressure. There are three curves, one is for an empty system, the second for the system with 100 mg of an idealized sample that adsorbs 1 wt% hydrogen (Figure 2b) at 100 bar, and the third with 1,000 mg of the same idealized sample. The null calibration is effectively equivalent to the empty curve and that “null” curve must be subtracted from the other curves to yield the adsorption results. The 100 mg curve is barely distinguishable from the null curve and shows both the importance in determining the null calibration accurately and of using an adequate sample mass as the 1,000 mg curve is easily distinguished. Error analyses performed to date include the null miscalibration, reference volume miscalibration, non-uniform temperature fluctuations, digital error, and helium adsorption during calibration.
6. Developed recommended procedures to be used to improve measurement accuracy. These include:
 - It is extremely important to measure the null calibration as accurately as possible (~1/1,000 to 1/10,000)
 - The system should be tested (and occasionally retested) with no sample to determine its ability to measure ‘zero’ adsorption (isothermal and non-isothermal conditions)
 - The system should be tested with a known material to check the absolute calibration

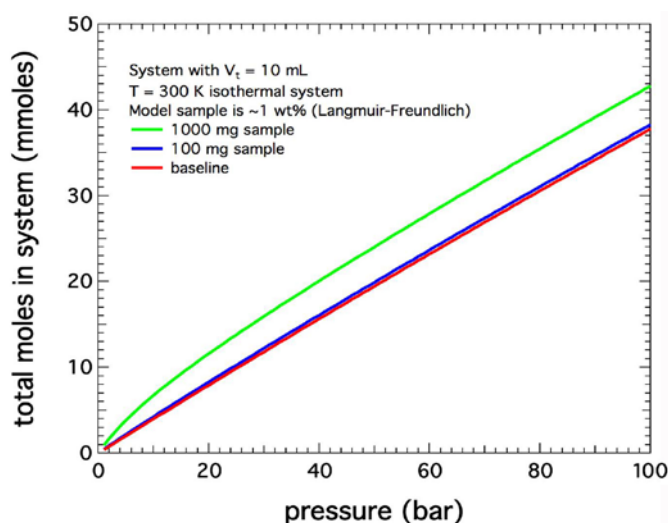


FIGURE 2A. Model data for an idealized 10 mL volumetric measurement system shows the number of total moles in the system as a function of pressure. The three curves show the number of moles with no sample (red), 100 mg of an idealized 1 wt% sample (blue) and 1,000 mg of the same sample (green). This shows the importance of accurately calibrating the system and having adequate sample mass as the red and blue curve are barely distinguishable (see text for discussion).

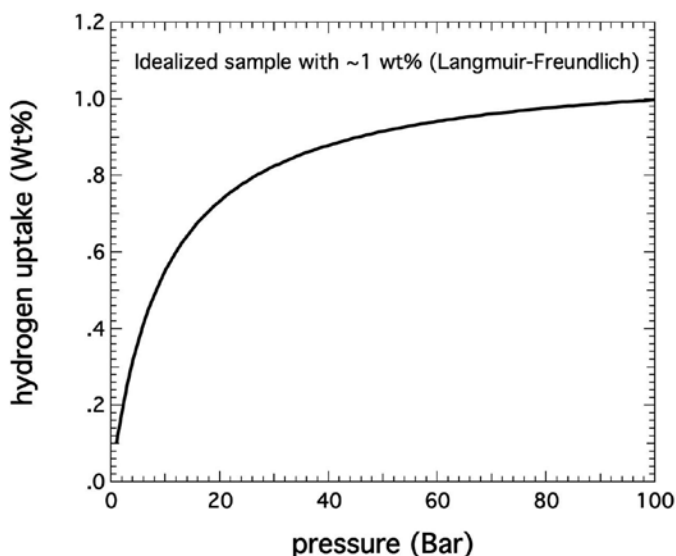


FIGURE 2B. Model sample data used for the example of Figure 2a shows an idealized sample material with 1 wt% hydrogen adsorption at ~100 bar.

- The system’s temperature profile should be controlled and monitored (pressure stability test)
- Use the highest sample mass as possible for measurements

Conclusions and Future Directions

- The hydrogen-storage community will benefit from efforts to ensure accurate capacity measurements. Increased quality-control efforts will ensure that the proper emphasis will be placed on new hydrogen-storage materials. There is sufficient cause to believe that inaccurate measurements may have misdirected emphasis.
- Direct collaboration among the laboratories performing capacity measurements has improved measurement accuracy and the quality of published results thereby allowing for more effective utilization of the available research and development resources.
- Several key aspects of the measurement equipment and protocols have been identified to minimize experimental error. Recommendations addressing these issues have been made to improve measurement quality.
- The hydrogen-storage community will continue to benefit from these efforts in the future and help ensure high quality research. NREL will continue to assist in these efforts and provide expertise for the hydrogen-storage community. NREL will adjust its measurement program to meet the needs for the DOE program, such as expanding its capabilities towards a wider range of temperature and/or pressure or facilitating new materials.

Special Recognitions & Awards/Patents Issued

1. NREL Team of the Month (November, 2011) - Katherine Hurst, Jeffrey Blackburn, and Philip Parilla, for One Time Special Effort related to hydrogen storage work.

FY 2012 Publications/Presentations

1. Two papers submitted: 1 on volumetric measurements; 1 on TPD calibration:

- “Critical and precise calibration required to avoid large systematic errors in volumetric apparatus: isothermal case” *submitted to Review of Scientific Instruments, P.A. Parilla et al.*
- “A Dynamic Calibration Technique for Temperature Programmed Desorption Spectroscopy” *submitted to Review of Scientific Instruments, K.E. Hurst et al.*

2. Two papers in preparation on volumetric measurements focusing on proper modeling, error analysis and methodology:

- “Realistic modeling and error analysis for non-isothermal volumetric apparatus” *in preparation, P.A. Parilla et al.*
- “Modeling and error analysis for a differential Sieverts apparatus” *in preparation, P.A. Parilla et al.*

3. One paper published in JACS by Northwestern University:

- “Designing Higher Surface Area Metal–Organic Frameworks: Are Triple Bonds Better Than Phenyls?”, *Farha, Omar; Wilmer, Christopher; Eryazici, Ibrahim;*

Hauser, Brad; O'Neill, Kevin; Parilla, Philip; Sarjeant, Amy; Nguyen, SonBinh; Snurr, Randall; Hupp, Joseph; J. Am. Chem. Soc., **2012**, 134 (24), pp 9860–9863

4. Invited Talk Spring 2011 MRS – P.A. Parilla: “*Round-Robin Results on Measuring Materials For Hydrogen Storage and Critical Calibration Issues*”

5. Invited Talk Summer 2011 ACS – P.A. Parilla: “*Common Errors Found In Volumetric Hydrogen Capacity Measurements And How To Avoid Them*”

6. Invited Talk Fall 2011 IHA – P.A. Parilla: “*Improving the reproducibility and uptake kinetics of chemisorptive (spillover) materials*” (This talk had substantial content on the round-robin results and measurement issues and errors.)

7. Talk at Spillover Workshop Winter 2012: “*Inter-Laboratory Comparison: Testing Measurement Reproducibility and Accuracy*”

References

1. Zlotea et. al., International Journal of Hydrogen Energy 34 (2009) 3044.

IV.D.1 Hydrogen Storage Engineering Center of Excellence (HSECoE)

Donald L. Anton (Primary Contact),
Theodore Motyka, Bruce Hardy and
David Tamburello
Savannah River National Laboratory (SRNL)
Bldg. 999-2W
Aiken, SC 29808
Phone: (803) 507-8551
Email: DONALD.ANTON@SRNL.DOE.GOV

DOE Managers

HQ: Ned Stetson
Phone: (202) 586-9995
Email: Ned.Stetson@ee.doe.gov
GO: Jesse Adams
Phone: (720) 356-1421
Email: Jesse.Adams@go.doe.gov

Technical Advisor

Robert Bowman
Phone: 818-354-7941
Email: rcbjr1967@gmail.com

Subcontractors:

- Pacific Northwest National Laboratory (PNNL)
- United Technologies Research Center (UTRC)
- General Motors Corp (GM)
- Ford Motor Corp. (FMC)
- National Renewable Energy Laboratory (NREL)
- Los Alamos National Laboratory (LANL)
- Jet Propulsion Laboratory (JPL)
- University of Michigan (UM)
- California Institute of Technology (Cal Tech)
- Oregon State University (OSU)
- Lincoln Composites LLC
- University of Québec, Trios Rivieres (UQTR)

Project Start Date: February 1, 2009
Project End Date: July 31, 2014

Fiscal Year (FY) 2012 Objectives

- Develop system models that will lend insight into overall fuel cycle efficiency.
- Compile all relevant materials data for candidate storage media and define future data requirements.
- Develop engineering and design models to further the understanding of onboard storage energy management requirements.
- Develop innovative onboard system concepts for metal hydride, chemical hydride, and adsorption hydride materials-based storage technologies.

- Design components and experimental test fixtures to evaluate the innovative storage devices and subsystem design concepts, validate model predictions, and improve both component design and predictive capability.
- Design, fabricate, test, and decommission the subscale prototype components and systems of each materials-based technology (adsorbents, metal hydrides, and chemical hydrogen storage materials).

Technical Barriers

This project addresses the following technical barriers from the Hydrogen Storage section of the Fuel Cell Technologies Program Multi-Year Research, Development and Demonstration Plan:

- (A) System Weight and Volume
- (B) System Cost
- (C) Efficiency
- (D) Durability/Operability
- (E) Charging/Discharging Rates
- (G) Materials of Construction
- (H) Balance of Plant Components
- (J) Thermal Management
- (K) System Life Cycle Assessments
- (L) High Pressure Conformality
- (P) Lack of Understanding of Hydrogen Physisorption and Chemisorption
- (S) By-Product/Spent Material Removal

Technical Targets

This project directs the modeling, design, build and demonstration of prototype hydrogen storage systems for each metal hydride, chemical hydride and hydrogen sorption material meeting as many of the DOE Technical Targets for light-duty vehicular hydrogen storage. The current status of these systems vs. the Onboard Hydrogen Storage System Technical Targets are given in Table I.

FY 2012 Accomplishments

Center Wide Accomplishments

- Completed assessment of metal hydrides for further evaluation in phase 2. Terminated work on metal hydride system due to low probability of these materials meeting the required properties in the 2017 timeframe.

TABLE I. System Status vs. Technical Targets

| | Technical Target | Units | 2010 | 2015 | Ultimate | Metal Hydride | Chemical Hydride | Adsorbent |
|----------------|---------------------------------|--|-------|-------|----------|---------------|------------------|--------------|
| Non-Quantified | Permeation & Leakage | scc/hr | # | # | # | s | s | s |
| | Toxicity | | # | # | # | s | s | s |
| | Safety | | # | # | # | s | s | s |
| Mandatory | Gravimetric Density | kgH ₂ /kgSystem | 0.045 | 0.055 | 0.075 | 0.012 | 0.038 | 0.039 |
| | Min. Delivery Temp. | °C | -40 | -40 | -40 | -40 | -40 | -40 |
| | Max. Delivery Temp. | °C | 85 | 85 | 85 | 85 | 85 | 85 |
| | Min. Delivery Pressure (PEM) | bar | 5 | 5 | 3 | 5 | 5 | 5 |
| | Max. Delivery Pressure | bar | 12 | 12 | 12 | 12 | 12 | 12 |
| | Min. Operating Temperature | °C | -30 | -40 | -40 | -30 | - | -30 |
| Desirable | Max. Operating Temperature | °C | 50 | 60 | 60 | 50 | 50 | 50 |
| | Min. Full Flow Rate | [gH ₂ /s]/kW | 0.02 | 0.02 | 0.02 | 0.02 | 0.02 | 0.02 |
| | System Cost* | \$/kWh net | 4 | 2 | 1.80 | 49.0 | 25.6 | 18.5 |
| | On-Board Efficiency | % | 90 | 90 | 90 | 78 | 97 | 95 |
| | Volumetric Density | kgH ₂ /liter | 0.028 | 0.040 | 0.070 | 0.012 | 0.034 | 0.024 |
| | Cycle Life | N | 1000 | 1500 | 1500 | 1000 | 1000 | 1000 |
| | Fuel Cost* | \$/gge | 3.7 | 2.6 | 2.3 | 7.3 | - | 4.88 |
| | Loss of Useable Hydrogen | [gH ₂ /hr]/kgH ₂ | 0.1 | 0.05 | 0.05 | 0.1 | 0.1 | 0.44 |
| | WPP Efficiency | % | 60 | 60 | 60 | 44.1 | 37.0 | 40.1 |
| | Fuel Purity | % | 99.97 | 99.97 | 99.97 | 99.97 | 99.97 | 99.99 |
| | Transient Response | sec. | 0.75 | 0.75 | 0.75 | 0.75 | 0.49 | 0.75 |
| | Start Time to Full Flow (-20°C) | sec. | 15 | 15 | 15 | 15 | 1 | 15 |
| | Fill Time | min. | 4.2 | 3.3 | 2.5 | 10.5 | 5.4 | 4.2 |
| | Start Time to Full Flow (20°C) | sec. | 5 | 5 | 5 | 5 | 1 | 5 |

* Previous Values

non-quantified

s - satisfactory

PEM = polymer electrolyte membrane

- Completed down-select of adsorbent materials with selection of metal-organic framework (MOF)-5.
- Completed down-select of chemical hydride materials with selection of fluid phase material.
- Completed down-select of chemical hydride materials with selection of exothermic materials.
- Completed failure modes and effects analysis for both adsorbent and chemical hydride systems identifying potential failure modes not previously considered including adsorbent bed packing and impurity effects and chemical hydride settling/flocculation and balance of plant (BOP) compatibility issues.
- Identified primary technical barriers limiting advancement of materials based hydrogen storage systems as:
 - Metal Hydrides (heat transfer design, media compaction, media thermal conductivity, lowered mass of BOP components).
 - Chemical Hydrides (media slurry agent/solvent with 50 wt% capacity, media kinetics, novel impurity trapping).
 - Adsorbents (Type 4 vessels at cryogenic temperatures, media thermal conductivity improvement, flow through cooling, media compaction, minimized tank outgassing, potential low pressure Type 1 tank).
- Identified Phase 3 Go/No-Go targets
- Initiated Phase 3 testing requirements system sizing analysis.
- Upgraded HSECoE.org website and added metal hydride models for public download and use.

SRNL Technical Accomplishments

- Completed a demonstration of a flow through cooling system and validated detailed models for super activated carbon.
- Developed external, publically accessible, website and disseminated the metal hydride acceptability envelope and the metal hydride heat transfer model.
- Designed and evaluated heat transfer technologies for cooling the adsorbent during the charging phase and heating it during the discharge phase.
- Evaluated detailed and system level performance for modified forms of MOF-5. These modified forms include pellets at different levels of compaction and amended MOF-5 which contained additives to enhance thermal conductivity.
- Used system models to identify suitable hydrogen refueling and desorption schemes for cryo-adsorbent systems.
- Used system models to design adsorbent systems.
- Identified optimal operation conditions for adsorbent system using MOF-5 or MaxSorb (including compacted forms).

- Evaluated media and gas thermodynamic properties required for modeling framework.



Introduction

The HSECoE brings together all of the materials and hydrogen storage technology efforts to address onboard hydrogen storage in light-duty vehicle applications. The effort began with a heavy emphasis on modeling and data gathering to determine the state of the art in hydrogen storage systems. This effort spanned the design space of vehicle requirements, power plant and BOP requirements, storage system components, and materials engineering efforts. These data and models will then be used to design components and sub-scale prototypes of hydrogen storage systems which will be evaluated and tested to determine the status of potential system against the DOE 2010 and 2015 technical Targets for hydrogen Storage Systems for Light-Duty Vehicles.

Approach

A team of leading North American national laboratories, universities, and industrial laboratories, each with a high degree of hydrogen storage engineering expertise cultivated through prior DOE, international, and privately sponsored projects has been assembled to study and analyze the engineering aspects of condensed phase hydrogen storage as applied to automotive applications. The technical activities of the Center are divided into three system architectures: adsorbent, chemical hydride and metal hydride matrixed with six technologies areas: Performance Analysis, Integrated Power Plant/Storage System Analysis, Materials Operating Requirements, Transport Phenomena, Enabling Technologies and Subscale Prototype Construction, Testing and Evaluation. The project is divided into three phases; Phase 1: System Requirements and Novel Concepts, Phase 2: Novel Concept Modeling Design and Evaluation and Phase 3: Subscale System Design, Testing and Evaluation.

SRNL Technical Results

SRNL and its sub-recipient UQTR to date have met and or exceeded their FY 2012 objectives for all of their major technical goals within the HSECoE. These objectives fall within the areas of: Transport Phenomena, Adsorbent System Level Modeling, Material Operating Requirements and System Architecture. Transport Phenomena and Adsorbent System Modeling results are shown below for adsorbent systems.

Transport Phenomena

- Numerical models were validated against data from the UQTR flow-through cooling experiments. The predicted

and measured volume average temperatures compared well, see Figure 1. Discrepancies are due to experimental error and modeling assumptions about the homogeneity of the adsorbent bed.

- New test facilities are being prepared at UQTR to conduct flow-through tests at higher gas flowrates.
- A vessel for flow-through cooling experiments with a structured adsorbent is being constructed at UQTR. The adsorbent will be in the form of pellets stacked in a honeycomb array, see Figure 2.
- In conjunction with the UQTR structured adsorbent experiments, a numerical model that represents the charging and discharging process is being developed by SRNL.
- UQTR produced 17 kg of activated carbon for experimental usage within the HSECoE.
- A numerical model has been developed for non-conductive heating of the adsorbent bed. Experiments are being designed and necessary property measurements are being made. This technique has the potential to

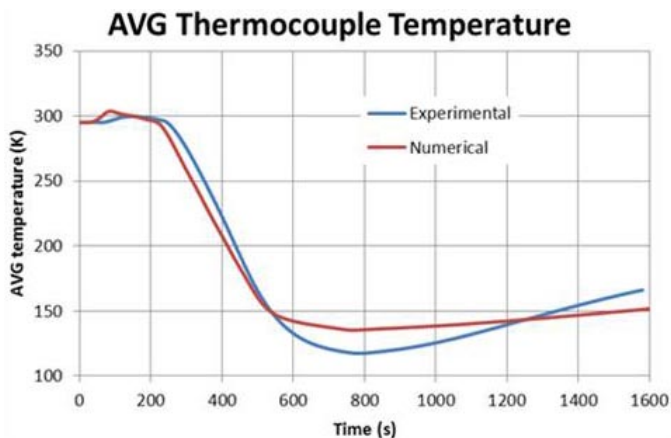


FIGURE 1. Average temperatures for hydrogen charging of the flow-through system predicted by the detailed numerical model and those measured in experiments performed at UQTR.

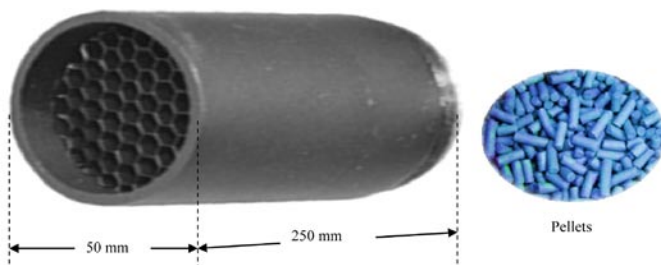


FIGURE 2. Honeycomb insert for stacking MOF-5 pellets for structured bed. The diameter and length of the pellets is 6 mm.

affect rapid hydrogen discharge even for low bed thermal conductivities.

- Development of the Modular Adsorption Tank Insert (MATI) concept for adsorbent bed heat exchangers continues as a joint effort between UQTR, OSU and SRNL. The effort includes design, optimization and planned experiments.
- Continued evaluation, fitting and incorporation of Ford data for compacted forms of MOF-5.

Adsorbent System Level Modeling

- The Matlab[®]-version of the cryo-adsorbent system models has been updated to include the following design options, with additional testing and debugging extending into the next quarter. All subroutines have expansion capabilities should additional options be needed. (Figures 3 and 4 show just two examples [MOF-5 in Type I tanks] out of dozens of modeling comparisons that were analyzed using the system models):
 - Dubinin-Astakhov (D-A) Parameters for hydrogen storage within several cryo-adsorbents.

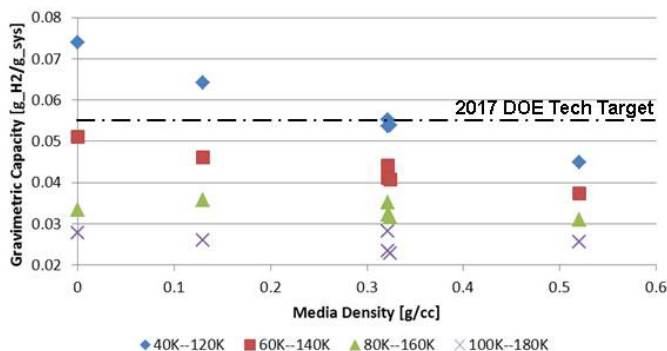


FIGURE 3. System model gravimetric capacity trends for compacted MOF-5 in an aluminum Type I tank at $P_{full_tank} = 60$ bar. Zero density corresponds to comparable cryo-compressed systems.

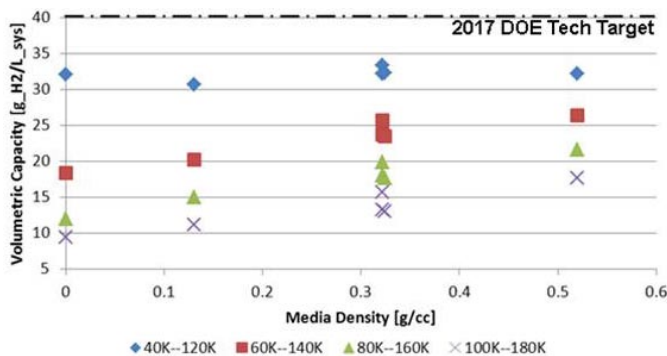


FIGURE 4. System model volumetric capacity trends for compacted MOF-5 in an aluminum Type I tank at $P_{full_tank} = 60$ bar. Zero density corresponds to comparable cryo-compressed systems.

- Internal tank heat exchanger concepts, where the mass and volume of the heat exchanger is adaptable based on the properties of the cryo-adsorbent.
- Expanded tank sizing estimator with a wide range of dimensional options and design types.
- The system model have been extended to include thermo-physical property correlations for $0.1 \text{ bar} < P < 450 \text{ bar}$ and $20 \text{ K} < T < 450$.
 - Included para-ortho conversion correlations based on temperature.
 - Provides for direct system level comparisons between cryo-compression of gas-only storage and cryo-adsorbent based storage.
- Ongoing collaborative efforts:
 - Working with UQTR, GM, and Ford to update the D-A Parameter estimates and proof-of-concept tank designs.
 - Working with PNNL to update the tank sizing estimator and improve on its accuracy for multiple tank types.
 - Working with OSU to improve the accuracy of the MATI design subroutine within the system model analysis.
 - Working with JPL to redesign the hydrogen conditioning heat exchanger for multiple passes to work with the warm hydrogen stream leaving the MATI for use in the desorption loop.
 - Working with PNNL to decrease the mass and volume of the system BOP components.
 - Working with NREL and PNNL to add costing estimates to the system model analyses.

Conclusions and Future Directions

Metal hydride efforts were terminated based on the judgment that no known material was near capable of meeting either the 2017 or ultimate targets in a system configuration. Ultimately, a metal hydride is needed which will have a capacity of 10-11 wt% hydrogen and an enthalpy of 25-27 KJ/mole H₂ to avoid the requirement of consuming a significant portion of the stored hydrogen. No metal hydride is foreseen to meet this very demanding target.

Chemical hydride efforts centered on slurry/solvent ammonia-borane materials development and utilizing flow through reactor development with dynamic temperature control, high flow gas liquid separation and impurity trapping. Further studies were conducted on endothermic vs. exothermic chemical hydrides with the identification of various start stop cycles deeply inhibiting attainment of the onboard efficiency target.

Adsorbent system efforts centered on compaction and thermal management during both fill and discharge segments

of operation. Identification of flow through cooling during fueling and resistive heating during discharge were identified and verified numerically. The overall system operating temperature and pressure ranges were analyzed with various options for optimum system performance identified. Cryogenic pressure vessel designs were developed and materials and tank testing equipment constructed and used to design potential tank concepts.

Future technical work by SRNL in the adsorbent area will include:

- Examining the performance of the MATI using the system models.
- Validating, tuning and refining the detailed models to make them applicable for scale up and alternative applications of hydrogen storage technology.
- Continuing the flow-through cooling experiments, investigating MOF-5 in powder and compacted forms, as applicable.
- Optimizing the adsorbent system with respect to pressure work, enthalpy of hydrogen discharge flow, dormancy conditions and thermal interaction with the container wall.
- Selecting an adsorbent, and form thereof, for use in the prototype.
- Designing the prototype and develop an experimental test matrix.

FY 2012 Publications/Presentations

1. B. Hardy, C. Corgnale, R. Chahine, M-A Richard, S. Garrison, D. Tamburello, D. Cossement and D. Anton. “*Modeling of adsorbent based hydrogen storage systems.*” International Journal of Hydrogen Energy, Volume 37, Issue 7, April 2012, Pages 5691-5705.
2. C. Corgnale, B. Hardy, S. Garrison, D. Tamburello, D. Anton. “*Acceptability envelope for metal hydride-based hydrogen storage systems.*” International Journal of Hydrogen Energy, Volume 37, Issue 3, February 2012, Pages 2812-2824.
3. S. Garrison, M. Gorbounov, D. Tamburello, B. Hardy, C. Corgnale, B. vanHassel, D. Mosher and D. Anton. “*Optimization of internal heat exchangers for hydrogen storage tanks using metal hydrides.*” International Journal of Hydrogen Energy, International Journal of Hydrogen Energy, Volume 37, Issue 3, February 2012, Pages 2850-2861.
4. M. Bhourri, J. Goyette, B. Hardy, D. Anton. “*Numerical modeling and performance evaluation of multi-tubular sodium alanate hydride finned reactor.*” International Journal of Hydrogen Energy, Volume 37, Issue 2, January 2012, Pages 1551-1567.
5. B. Hardy, C. Corgnale. “*Adsorbent Based Hydrogen Storage System Models.*” Invited presentation at the 2012 World Hydrogen Energy Conference, Toronto, Canada, June 4, 2012.

IV.D.2 System Design, Analysis, Modeling, and Media Engineering Properties for Hydrogen Energy Storage

Matthew Thornton (Primary Contact), Lin Simpson, Aaron Brooker, and Jonathon Cosgrove
National Renewable Energy Laboratory (NREL)
1617 Cole Boulevard
Golden, CO 80401
Phone: (303) 275-4273
Email: Matthew.Thornton@nrel.gov

DOE Managers

HQ: Ned Stetson
Phone: (202) 586-9995
Email: Ned.Stetson@ee.doe.gov
GO: Jesse Adams
Phone: (720) 356-1421
Email: Jesse.Adams@go.doe.gov

Project Start Date: February 2, 2009
Project End Date: September 30, 2014

storage vessels that meet the following DOE 2015 hydrogen storage for light-duty vehicle targets:

- Cost: to be determined
- Specific energy: 0.055 kg H₂/kg system
- Energy density: 0.040 kg H₂/L system
- Charging/discharging rates: 3.3 min
- Well to power plant efficiency: 60%

FY 2012 Accomplishments

- Developed a vehicle model framework and test cycle matrix to aid in the analysis and understanding of hydrogen storage system requirements for light-duty vehicles.
- Integrated the hydrogen storage simulator (HSSIM) vehicle model with the center fuel cell and hydrogen storage models to create a model framework that could be used across the center to evaluate all storage system designs on a common basis and with consistent assumptions.
- Used the vehicle model and the center modeling framework to evaluate the performance of specific storage system designs across all material classes and assess the impact on vehicle performance to help guide specific system designs and focus engineering solutions that will overcome barriers to meeting the technical targets.
- Performed vehicle-level tradeoff analyses to better understand the impact of key engineering designs, for example, the tradeoff between mass, onboard hydrogen storage capacity, and vehicle range.
- Used Hydrogen Delivery Scenario Analysis Model (HDSAM) to calculate preliminary greenhouse gas (GHG) emissions and well-to-power plant (WTPP) efficiency figures for baseline physical storage systems and candidate materials-based storage systems for each material class.
- Identified potential materials for analysis and provided storage system design guidance to help meet DOE storage targets with adsorption materials.



Fiscal Year (FY) 2012 Objectives

- Perform vehicle-level modeling and simulations of various storage systems configurations.
- Lead the storage system energy analysis and provide results.
- Compile and obtain media engineering properties for adsorbent materials.

Technical Barriers

This project addresses the following technical barriers from the Hydrogen Storage section of the Fuel Cell Technologies Program's Multi-Year Research, Development and Demonstration Plan:

- (A) System Weight and Volume
- (B) System Cost
- (C) Efficiency
- (E) Charging/Discharging Rates
- (I) Dispensing Technology
- (K) Systems Life-Cycle Assessments

Technical Targets

This project is conducting simulation and modeling studies of advanced onboard materials-based hydrogen storage technologies. Insights gleaned from these studies are being applied toward the design and synthesis of hydrogen

Introduction

Overcoming challenges associated with onboard hydrogen storage is critical to the widespread adoption of hydrogen-fueled vehicles. The overarching challenge is

identifying a means to store enough hydrogen onboard to enable a driving range greater than 300 miles within vehicle-related packaging, cost, safety, and performance constraints. By means of systems analysis and modeling, hydrogen storage system requirements for light-duty vehicles can be assessed. With these findings and through collaboration with our Hydrogen Storage Engineering Center of Excellence (HSECoE) partners, optimal pathways for successful hydrogen storage system technology can be identified to enable future commercialization of hydrogen-fueled vehicles.

Approach

An array of tools and experience at NREL are being used to meet the objectives of the HSECoE. Specifically, extensive knowledge of multiple vehicle simulations, well-to-wheels analysis, and optimization are being employed and integrated with fuel cell and material-based hydrogen storage system models developed by other HSECoE partners. This integrated model framework allows for the evaluation of various hydrogen storage options on a common basis. Engineering requirements are defined from these studies thus enabling the design of hydrogen storage vessels that could meet DOE performance and cost targets in a vehicle system context.

In the area of media engineering, attaining the objectives of the HSECoE relies on NREL's leadership in developing custom analytical instrumentation for hydrogen sorption analysis. These tools are used to thoroughly characterize hydrogen storage sorbents so that an optimized storage vessel specific to the sorption material may be efficiently engineered. NREL uses these methods to analyze sorption materials identified by the HSECoE as holding promise for application in commercial on-vehicle refuelable hydrogen storage systems capable of meeting DOE targets.

Results

The following will provide results from work completed this year to support the HSECoE with a focus on five main tasks. In collaboration with our original equipment manufacturer (OEM) partners, NREL (1) worked on the development of HSSIM and final structure of a test cycle matrix used to support the overall modeling effort; (2) worked on the integration of the vehicle model with the center fuel cell and hydrogen storage models to create a model framework; (3) worked with the systems architects to perform simulations and tradeoff studies to help with the high-level storage systems design and engineering, including mass and volume trade-offs; (4) performed energy analysis on specific system designs being considered by the HSECoE; and (5) continued work in the area of adsorbent materials characterization and analysis.

To gain a better understanding of the interactions that exist between various materials-based hydrogen storage systems and the vehicle system as well as the engineering

challenges that exist when integrating one of these systems with a vehicle, NREL has developed a vehicle-level model designed to be sensitive to these issues. The HSSIM vehicle model was developed as a specialized tool that could be used to assist in the design and engineering of materials-based hydrogen storage systems being considered by the HSECoE. This tool is designed to not only allow for understanding key trade-offs, but also to have a seamless integration with the HSECoE fuel cell and detailed hydrogen storage system models and to evaluate progress towards the DOE's hydrogen storage technical targets. This model has been integrated with a fuel cell model developed by Ford Motor Company in a HSECoE common modeling framework developed by United Technologies Research Center and other HSECoE partners (Figure 1).

The HSSIM vehicle model is designed to evaluate high-level attribute improvements. To accomplish this, the inputs, such as the glider and powertrain components, are also defined at a high level. The vehicle glider is defined with a specific frontal area, drag coefficient, mass, center of gravity, front axle weight fraction, and wheelbase. The wheels are defined by inertia, a rolling resistance coefficient, coefficient of friction, and radius. The inputs for the motor are power, peak efficiency, mass per unit of power, cost per unit of power, and time to full power. The battery inputs include power, energy, mass per unit of energy, and round trip efficiency. Auxiliary loads are assumed to be a specified constant plus an amount required for the fuel cell and hydrogen storage systems. These inputs match the DOE's technical target units, such as battery kilograms per kilowatt hour, so that the impact of improvements can be evaluated over time as the targets change.

A key part of the vehicle model was working with the center OEMs on developing a test matrix that will be used to evaluate all the storage systems being considered across the center on a common basis. The test matrix was structured to evaluate the performance of the storage systems against the technical targets under standard and realistic transient driving conditions. The matrix was also designed to exercise a given system from full to empty to provide an understanding of its performance over the entire range of fill conditions. Therefore, the test cases were designed to repeat a drive cycle or set of drive cycles until the storage system being evaluated was empty. Standard drive cycles are typically not long enough to achieve this and would not even deplete a buffer tank in some systems. The important point here is that when evaluating the complex dynamics of hydrogen storage system, this approach of repeating drive cycles to create test cases is critical to gaining the feedback necessary to refine and improve the systems.

As shown in Table 1, the center test matrix includes five test cases:

The first case combines repeats of the urban dynamometer driving schedule (UDDS) and the highway fuel

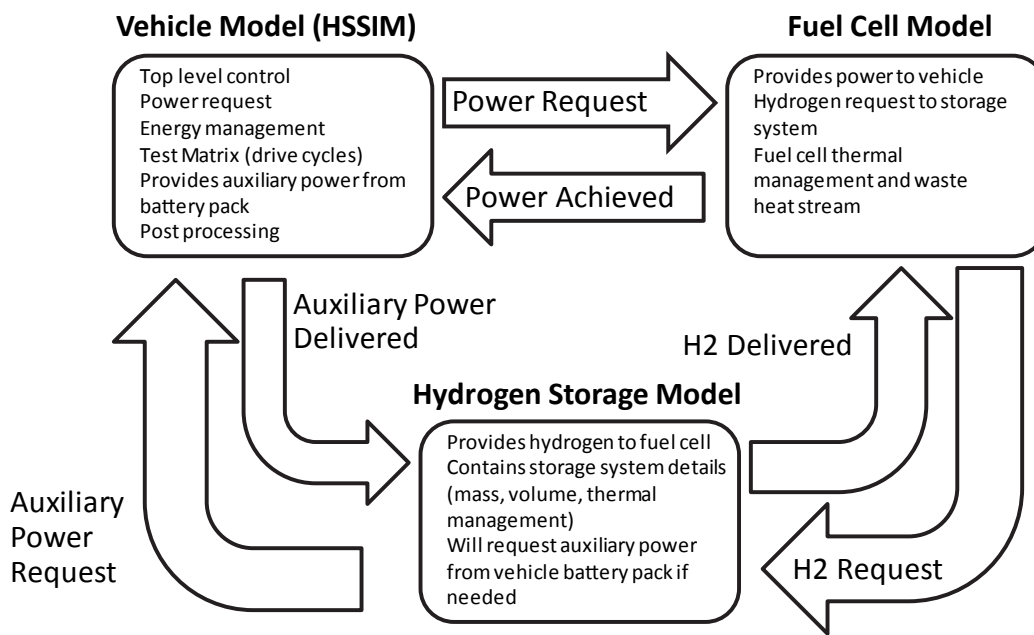


FIGURE 1. HSECoE integrated modeling framework

TABLE 1. Test matrix used across the center to evaluate the performance of all the storage systems

| Case | Test Schedule | Cycles | Description | Test Temp (°F) | Distance per cycle (miles) | Duration per cycle (minutes) | Top Speed (mph) | Average Speed (mph) | Max. Acc. (mph /sec) | Stops | Idle | Avg. H2 Flow (g/s)* | Peak H2 Flow (g/s)* | Expected Usage |
|------|---|---------------|---|----------------|----------------------------|------------------------------|-----------------|---------------------|----------------------|-------|------|---------------------|---------------------|--|
| 1 | Ambient Drive Cycle - Repeat the EPA FE cycles from full to empty and adjust for 5 cycle post-2008 | UDDS | Low speeds in stop-and-go urban traffic | 75 (24 C) | 7.5 | 22.8 | 56.7 | 19.6 | 3.3 | 17 | 19% | 0.09 | 0.69 | 1. Establish baseline fuel economy (adjust for the 5 cycle based on the average from the cycles) 2. Establish vehicle attributes 3. Utilize for storage sizing |
| | | HWFET | Free-flow traffic at highway speeds | 75 (24 C) | 10.26 | 12.75 | 60 | 48.3 | 3.2 | 0 | 0% | 0.15 | 0.56 | |
| 2 | Aggressive Drive Cycle - Repeat from full to empty | US06 | Higher speeds; harder acceleration & braking | 75 (24 C) | 8 | 9.9 | 80 | 48.4 | 8.46 | 4 | 7% | 0.20 | 1.60 | Confirm fast transient response capability – adjust if system does not perform function |
| 3 | Cold Drive Cycle - Repeat from full to empty | FTP-75 (cold) | FTP-75 at colder ambient temperature | -4 (-20 C) | 11.04 | 31.2 | 56 | 21.1 | 3.3 | 23 | 18% | 0.07 | 0.66 | 1. Cold start criteria 2. Confirm cold ambient capability – adjust if system does not perform function |
| 4 | Hot Drive Cycle - Repeat from full to empty | SC03 | AC use under hot ambient conditions | 95 (35 C) | 3.6 | 9.9 | 54.8 | 21.2 | 5.1 | 5 | 19% | 0.09 | 0.97 | Confirm hot ambient capability - adjust if system does not perform function |
| 5 | Dormancy Test | n/a | Static test to evaluate the stability of the storage system | 95 (35 C) | 0 | 31 days | 0 | 0 | 0 | 100% | 100% | | | Confirm loss of useable H2 target |

economy test (HWFET) until the storage systems is depleted. This is used to determine the vehicle-level fuel economy and from that figure the vehicle range. The fuel economy is calculated using the current Environmental Protection Agency five-cycle procedure of adjusting and weighting

the UDSS and HWFET to provide one fuel economy figure that represents real-world use—it is not the raw figures that come directly from running the cycles. Similarly, the range is then calculated from the adjusted and weighted UDSS and HWFET figure and not simply the cycles miles achieved until

the storage systems is empty. Again, this test matrix is key to providing a means to evaluate the fuel economy, range, and other vehicle level performance features of the storage systems on a common and comparable basis.

NREL used these model outputs from the framework to evaluate the current status of various materials-based systems being evaluated by the HSECoE. Because this work is in progress, the results presented here are preliminary and may change over time as the storage systems are refined and the models are adjusted accordingly. That is, the intent is to show how the model outputs can be used to evaluate and compare different storage systems and support engineering solutions to particular barriers. The intent, at least at this time, is not to develop an argument for which system or materials class has the most promise for actual vehicle application. Vehicle-level results will be presented for a select group of these systems (i.e., this is not a comprehensive set of systems being evaluated under the HSECoE nor is it a complete set of storage models induced in the framework). For the model application, example results discussed in this section's simulations were run with the AX-21 and MOF-5 adsorbent systems, the NaAlH₄ and TiCrMn metal hydride systems, and the fluid ammonia borane (AB) chemical hydride system. In addition, 350-bar and 700-bar compressed gas systems are included for comparison to the materials-based systems.

For the following discussion, model applications and results reported are based on Test Case 1 of the framework exclusively (i.e. UDSS and HWFET combined test cycles). In addition, a midsize car class was selected as the initial baseline simulations within the framework. The intent was to be representative of a high sales volume midsize car, such as the Ford Fusion, Chevrolet Malibu, or Toyota Camry. The attributes associated with this size vehicle are a frontal area of 2.2 m², drag coefficient of 0.29, and tire size of P195/65R15. The electric motor was sized to 100 kW with 85% efficiency from the motor to the road. Consistent with most fuel cell vehicles, the vehicle includes a 20 kW/1 kWh battery pack for hybridization for capturing regenerative

braking and assistance with propulsion. The state of charge of the battery is maintained between 40% and 80%, with the target state of charge varying throughout the cycle depending on driving conditions. The vehicle glider weight (excluding the hydrogen storage system and other drive components) is 1,104 kg. The motor and power electronics combined weight is 105 kg, the battery system weight is 51 kg, the fuel cell system with cooling weight is 214 kg, and the hydrogen storage systems weight varied. The remaining weight is the vehicle glider and other supporting subsystems. All of the following results are based on the vehicle configuration above, but the model is capable of simulating both larger and smaller vehicle classes and configurations.

For the example systems included in Table 2, the fuel economy for materials-based systems ranged from 49.3 miles per gallon gasoline equivalent (mpgge) for the MOF-5 system to 36.4 mpgge for the NaAlH₄ system. The NaAlH₄ system performed the worst in terms of fuel economy due its requirement for high temperature conditions to release hydrogen from the hydride material. As a result, the system burns hydrogen to create the needed temperatures for the storage system so that hydrogen can be released for use in the fuel cell. The use of hydrogen for system thermal management results in poor onboard efficiency and subsequently poor fuel economy, as up to 23% of the stored hydrogen is not used to generate tractive power. Alternatively, the fluid AB and MOF-5 systems performed better in this example due to their high gravimetric efficiency resulting in lower overall systems and vehicle mass and therefore better fuel economy. As a result, the MOF-5 system also offers the best range results of 276 miles based on the above vehicle configuration and 5.6 kg nominal usable hydrogen storage capacity. The NaAlH₄ system had a range of 204 miles, which is well below the target of 300 miles. All of the other systems in this example were near the 300-mile range target (ranging from 257 to 276 miles). This included the other metal hydride system. The compressed gas systems demonstrated slightly better, but comparable fuel economy and range relative to these example material-based systems.

TABLE 2. Vehicle Level Performance Summary

| Hydrogen Storage System | Adjusted Fuel Economy (mpgge) | Range (mi) 5.6 kg H2 | On-Board Efficiency (%) UDSS/HFET | Gravimetric Density (wt%) | Volumetric Density (g/l) |
|-------------------------|-------------------------------|----------------------|-----------------------------------|---------------------------|--------------------------|
| AX21 press FCHX | 48.7 | 273 | 97 | 4.3 | 25.2 |
| MOF5 Cmpct- FCHX | 48.3 | 271 | 97 | 3.5 | 24.1 |
| MOF5 Press FCHX | 49.3 | 276 | 98 | 4.6 | 25.3 |
| Fluid AB | 45.3 | 254 | 96 | 4.6 | 38.9 |
| Alane | 42.6 | 239 | 88 | 4.6 | 38.9 |
| NaAlH ₄ | 36.4 | 204 | 77 | 1.2 | 11.4 |
| TiCrMn | 45.9 | 257 | 100 | 1.1 | 26.5 |
| 350-bar Compressed Gas | 49.9 | 280 | 100 | 4.8 | 17.0 |
| 700-bar Compressed Gas | 49.9 | 279 | 100 | 4.7 | 25.0 |

The MOF-5 adsorbent system and the fluid AB chemical hydride system both had a gravimetric density of 4.6 weight percent (i.e., the percent of hydrogen mass to the overall storage system mass; the DOE 2017 technical target for gravimetric density is 5.5 weight percent). These were the best performing materials-based systems and were comparable to the compressed gas systems, which had gravimetric densities of 4.7–4.8 weight percent. That said the fluid AB system outperformed the compressed gas systems and all of the other materials-based systems in terms of volumetric density with nearly 40g of hydrogen per system liter. The DOE's 2017 technical target for volumetric density is 40 g/L. For all the example materials-based systems included here, the MOF-5 system performed the best in terms of fuel economy, range, and gravimetric density and was comparable or better than the compressed gas systems. Also note the fluid AB system performed best in terms of volumetric density, but it is important to remember that the fluid AB system is an off-board regenerable system that is accompanied by unique refilling challenges, logistics, and costs that are not captured in the above analysis.

Another example application was working the center system architects to provide high-level feedback on the performance and design of their given material systems. The

focus of this activity was an example of a trade-off study quantifying the relative range impacts resulting from a fixed volume study. Table 3 shows the results from the application of this type of study to four adsorbent systems.

In this fixed volume study four different adsorbent system designs were evaluated in conjunction with three different volume levels. The four adsorbent systems included powdered MOF-5 operating at 60 bar and 80 K full tank conditions with an assumed aluminum tank, powdered MOF-5 operating at 60 bar and 40 K full tank conditions with an assumed carbon-fiber tank, compacted MOF-5 0.52 g/cc operating at 200 bar and 80 K full tank conditions with an assumed aluminum tank and compacted MOF-5 0.52 g/cc MOF-5 operating at 200 bar and 40 K full tank conditions with an assumed carbon-fiber tank. Each system was simulated in a mid-sized passenger vehicle using the integrated modeling framework for case one to provide range and fuel economy for three volume assumptions; 140 liters, 205 liters and 253 liters. These three volume levels were based on assumptions from the DOE 2017 hydrogen storage technical targets and represent the high, medium and low range of practical storage systems volume for passenger vehicles. For comparison, the usable capacity in the 350 bar

TABLE 3. Range and Vehicle Level Performance Results for Fixed Volume Study

| Hydrogen Storage System | Adjusted Fuel Economy (mpgge) | Usable H2 (kg) | Range (mi) Usable H2 | Gravimetric Capacity Weight Percent | Volumetric Capacity (g/l) | Volume (L) |
|--------------------------------|-------------------------------|----------------|----------------------|-------------------------------------|---------------------------|------------------|
| Powder MOF-5 60-bar 80 K Al | 51.11 | 2.00 | 102.20 | 2.80 | 12.86 | 140 ¹ |
| Powder MOF-5 60-bar 40 K CF | 51.30 | 4.20 | 215.50 | 6.61 | 29.84 | 140 |
| 0.52g/cc MOF-5 200-bar 80 K Al | 50.47 | 3.35 | 169.10 | 2.68 | 23.94 | 140 |
| 0.52g/cc MOF-5 200-bar 40 K CF | 50.62 | 4.60 | 232.90 | 4.18 | 32.59 | 140 |
| Powder MOF-5 60-bar 80 K Al | 50.95 | 2.80 | 142.70 | 3.15 | 13.67 | 205 |
| Powder MOF-5 60-bar 40 K CF | 50.97 | 6.70 | 341.50 | 7.97 | 32.64 | 205 |
| 0.52g/cc MOF-5 200-bar 80 K Al | 49.93 | 5.35 | 267.10 | 2.92 | 26.11 | 205 |
| 0.52g/cc MOF-5 200-bar 40 K CF | 50.18 | 7.30 | 366.30 | 4.61 | 35.51 | 205 |
| Powder MOF-5 60-bar 80 K Al | 50.73 | 3.60 | 182.60 | 3.39 | 14.18 | 253 |
| Powder MOF-5 60-bar 40 K CF | 50.89 | 8.60 | 437.60 | 8.68 | 33.96 | 253 |
| 0.52g/cc MOF-5 200-bar 80 K Al | 49.32 | 6.85 | 337.90 | 3.02 | 27.05 | 253 |
| 0.52g/cc MOF-5 200-bar 40 K CF | 49.71 | 9.30 | 462.30 | 4.77 | 39.56 | 253 |

compressed gas storage system for the Ford Focus fuel cell vehicle was 4 kg with an external volume of about 230 liters.

This study shows that the volume target is much more sensitive to range than the gravimetric target. That is, storage systems that had high mass but allowed for more onboard hydrogen storage through compaction or low temperature operation had small fuel economy penalties but were accompanied by much higher ranges due to their ability to store more hydrogen onboard for a given volume. This information has been used by the adsorbent system architect and modeler to help refine their system designs.

NREL also continued to support the HSECoE by performing energy analyses on various storage system designs that have become available. These analyses provide the center system architects and other partners with high-level estimates about the overall energy inputs required by a given system, including WTPP efficiency (%), hydrogen cost (\$/kg) and GHG emissions (carbon dioxide equivalent) on a gram per mile basis.

The HDSAM was used to estimate the above parameters for each system. To date the HDSAM model has been run for NaAlH₂ metal hydride system and the AX-21 and MOF-5 sorbent systems to produce preliminary WTPP efficiency, GHG emissions, and hydrogen cost figures. NREL is currently working with the center adsorbent and chemical hydride system architects to obtain these data and perform HDSAM runs for a fluid AB, Alane and various MOF-5 adsorbent storage systems.

For media engineering, NREL worked with engineering center partners to identify potential materials and configurations that can be optimized with the appropriate thermal conductivity, sorption, and mechanical properties needed for integration in a hydrogen storage system. Specific efforts included optimizing activated carbon pellet synthesis and capacities. Comparison of results between MSC-30, Missouri 3K, and pyrolyzed polyether ether ketone (PEEK) powders and pellets indicated similar behavior to MOF-5. Potentially, slightly higher volumetric capacities could be obtained with optimized PEEK materials, but is not warranted due to the additional material and synthesis costs. This work also identified that carbon fibers improve pellet structure and thermal conductivities.

NREL also measured hydrogen sorption using a He cryostat cooler to provide variable temperature capabilities. Initial analysis indicates that He and hydrogen measurements as a function of pressure of the empty sample holder provides a reasonable measure of zero adsorption at both 303 K and 75 K (Figure 2). Additional measurements at other temperatures will be performed to identify issues and limits on the experimental parameters. Hydrogen adsorption and desorption results for different temperatures and pressures were also obtained. Direct comparison between the use of water and liquid nitrogen baths to control temperature and the use of a He cryostat were made at 303 K and 75 K. In

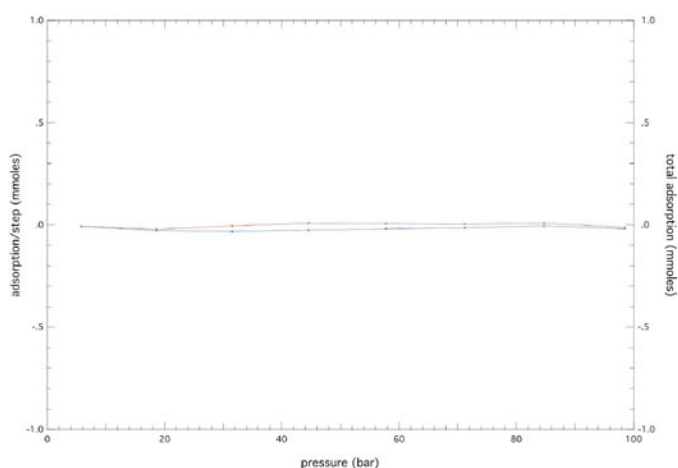


FIGURE 2. Hydrogen adsorption of empty sample holder at 303 K. The data show that the instrument is providing a reasonable measure of zero adsorption as a function of pressure. Red: Adsorption per step (left axis) Blue: Total Adsorption (right axis).

general the results from the measurements using the baths typically have uncertainties less than 20%. However, with the present cryostat configuration that limits sample size and has slightly higher volumes, the measurements have uncertainties above 20%. Significant modifications to the sample holder and cryostat configuration are required to reduce uncertainties.

Future Direction

- Continue to run vehicle simulations to support engineering design and support the center modeling framework refinements and enhancements:
 - Run vehicle simulations to support high-level storage system design and engineering tradeoffs.
 - Run vehicle simulations to support storage systems sizing analyses.
- Evaluate storage system impacts on vehicle performance (e.g., fuel economy, range).
- Evaluate storage system progress toward tech targets. Run HDSAM to evaluate (fluid AB, Alane and various MOF-5 adsorbent storage systems):
 - WTPP efficiency
 - GHG emissions
 - H₂ cost
- Provide additional material characterization specifically related to sorbents optimized for engineered hydrogen storage systems.

FY 2012 Publications/Presentations

1. Matthew Thornton, Aaron Brooker, Jonathon Cosgrove, National Renewable Energy Laboratory; Michael Veenstra, Ford Motor Company; Jose Miguel Pasini, United Technologies Research

Center, “Development of a Vehicle Level Simulation Model for Evaluating the Trade-off between Various Advanced On-board Hydrogen Storage Technologies for Fuel Cell Vehicles”, SAE Paper 2012-01-1227, April 2012, Detroit Michigan.

2. System Design, Analysis, Modeling, and Media Engineering Properties for Hydrogen Energy Storage, Matthew Thornton, DOE Annual Merit Review Meeting, May 15, 2012, Washington, D.C.

IV.D.3 Chemical Hydride Rate Modeling, Validation, and System Demonstration

Troy A. Semelsberger (Primary Contact),
Biswajit Paik, Tessui Nakagawa, Ben Davis, and
Jose I. Tafoya

Los Alamos National Laboratory
MS J579, P.O. Box 1663
Los Alamos, NM 87545
Phone: (505) 665-4766
Email: troy@lanl.gov

DOE Managers

HQ: Ned Stetson
Phone: (202) 586-9995
Email: Ned.Stetson@ee.doe.gov

GO: Jesse Adams
Phone: (720) 356-1421
Email: Jesse.Adams@go.doe.gov

Project Start Date: February 2009

Project End Date: February 2014



Introduction

Hydrogen storage systems based on chemical hydrides require a chemical reactor to release the hydrogen from the storage media, which is a fundamental difference from the other modes of hydrogen storage, adsorbents and metal hydrides. This hydrogen-release reactor is crucial to the performance of the overall storage system, especially in meeting the DOE targets for hydrogen generation rate, transient operation, and startup times. The reactor must be designed to achieve these targets while meeting the constraints of the overall system volume and weight targets.

LANL will also address the unique requirements of onboard automotive hydrogen storage systems. For example, these systems require fast startup, operation over a wide dynamic range (10:1 turndown or greater), and fast transient response to meet the demands of a drive cycle. The LANL team will develop novel reactor designs and operation strategies to meet these transient demands. In addition, the shelf life and stability of the hydrogen storage media is crucial for an automotive system, especially pertaining to safety and cost. Starting with the kinetics models, the LANL team will develop mathematical models for the aging characteristics of candidate hydrogen storage media (for example, complex metal hydrides or chemical hydrides) subjected to a range of environmental factors. These models can be incorporated into system-level models of performance and cost and also used for the development of accelerated aging protocols necessary for later testing.

Results

Reaction Characteristics of Fluid-Phase AB Compositions

Experiments were performed to determine the reaction characteristics of fluid-phase IL compositions as a function of IL (e.g., EmimCl, Tebmp MS, EmimAC, BmimCl, etc.). The reaction characteristics of interest are the reaction selectivity, chemical compatibility and total mass loss. The collected data allow for determining the maximum reactor operating temperature that will maximize the selectivity of the dehydrogenation reaction. Shown in Figure 1 are two examples of AB/IL compositions that demonstrate differing reaction selectivities. The fluid-phase composition of AB/EmimAc (Figure 1a) demonstrated a chemical incompatibility with ammonia borane for temperatures greater than 100°C.

Fiscal Year (FY) 2012 Objectives

- Investigate reaction characteristics of various fluid-phase ammonia-borane (AB)-ionic liquid (IL) compositions
- Identify and quantify hydrogen impurities and develop novel impurity mitigation strategies
- Design, build, and demonstrate a subscale prototype dehydrogenation reactor using chemical hydrides (technology area lead)
- Develop an onboard fluid-phase chemical hydrogen storage system; system designer

FY 2012 Accomplishments

- Designed and built novel fluid-phase chemical hydrogen reactors
- Identified reactor operating limits for various fluid-phase chemical hydrogen storage media
- Quantified impurities generated from fluid-phase AB compositions
- Developed boundary conditions of borazine adsorption unit to meet engineering center of excellence targets

The total mass loss for the AB/EmimAc composition is well above of what the maximum that can be expected for the dehydrogenation of AB reaction (~15.2 wt%). The total mass loss for this composition was greater than 60 wt%. The additional mass loss is attributed to the chemical incompatibility of EmimAc with AB (confirmed via gas phase Fourier transform infrared). The mass loss curve also suggests that the dehydrogenation kinetics of AB is comparable to the kinetics of AB reacting with EmimAc. The convoluted kinetics results in a system that cannot be controlled through reactor temperature or space-time. In contrast, the composition of AB/IoliLyte (Figure 1b) shows two clearly distinct kinetics regions. The first event occurring from 75–150°C is the dehydrogenation of AB. The second event is the side reaction of AB and iolilyte and occurs at a temperature greater than 180°C. The width of the temperature plateau between the two events is a measure of the flexibility in the reactor operating temperature. In short, the maximum operating temperature for the AB/Iolilyte composition would be around 170°C in order to isolate the dehydrogenation reaction from the unwanted side reaction.

Chemical Compatibility of AB/IL with Bladder Tank Material

Preliminary investigations are under way to investigate the chemical compatibilities of various 20 wt% AB fluid-phase compositions (solutions and slurries). No physical degradation of the bladder material has been observed after three months of room temperature soaking.

Borazine Adsorption Unit

The Hydrogen Storage Engineering Center of Excellence has imposed a mass and volume target on the automotive-

scale borazine adsorption unit. The mass and volume design constraints are 4 kg and 3.6 L. The adsorption unit must be able to achieve an 1,800 mile replacement interval. The design constraints allow the required borazine adsorption capacity, the monolayer coverage and the adsorbent surface area to meet the mass target. Shown in Figure 2 are the required adsorbent masses for a borazine adsorption unit as a function of borazine impurity production (kg borazine/kg AB), adsorbent surface area, and borazine coverage. A surface coverage of one monolayer is equivalent to the entire surface area being covered and a 0.25 monolayer is indicative of one fourth of the surface being covered. The general trend is, the higher the surface coverage the lower the mass and volume of the adsorption unit. Physical adsorbents tend to be equilibrium limited and require large volume and mass. Currently, in order to meet the mass target of the borazine adsorption unit, surface areas greater than 2,000 m²/g and surface coverages greater than one monolayer are required.

Novel Fluid-Phase Reactor Designs

We have developed a novel helical reactor design that is expected to promote gas-liquid separation and prevent liquid slugging from occurring. Eliminating liquid slugging will result in a more efficient and compact reactor. Shown in Figure 3 is one example of our novel reactors. Additional reactors have been designed and built, but are not shown. The reactors will be validated in the coming FY.

Summary

- Successfully designed and built novel fluid-phase reactors (currently being evaluated)

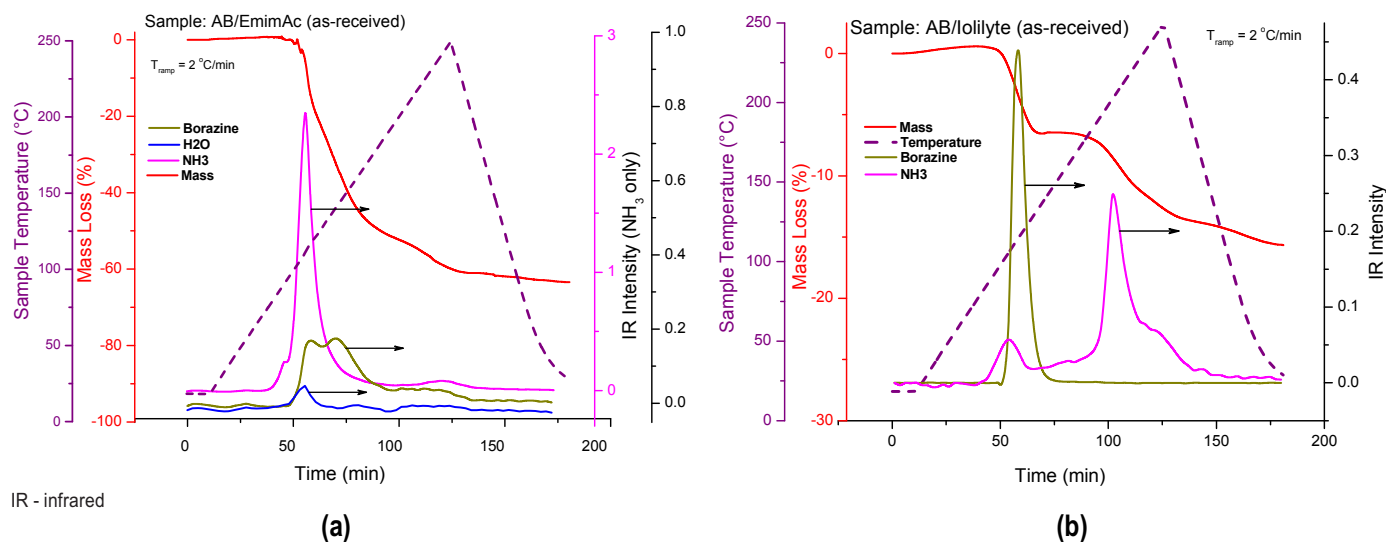


FIGURE 1. Dehydrogenation of fluid-phase AB/IL compositions (a) AB/EmimAc (b) AB/Iolilyte (temperature ramp rate = 2°C/min)

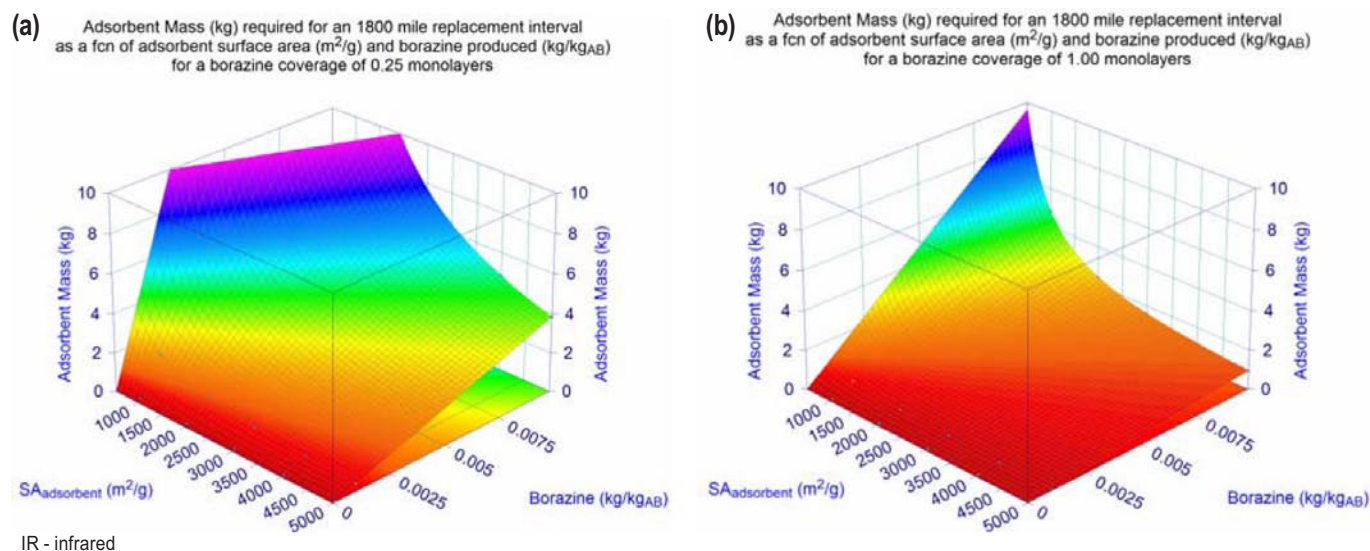


FIGURE 2. Adsorbent mass as a function of adsorbent surface area and borazine production for an 1,800 mile replacement frequency for (a) 0.25 monolayer surface coverage and (b) 1.00 monolayer surface coverage

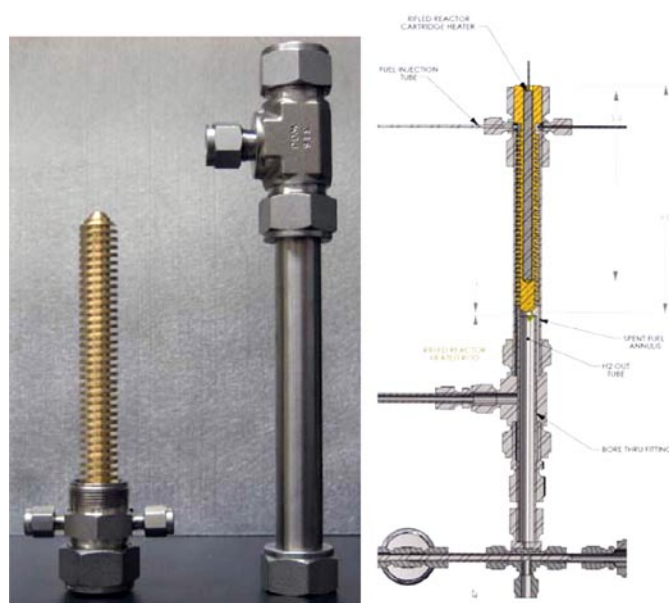


FIGURE 3. Novel reactor design for handling fluid-phase chemical hydrogen storage media

- Identified reactor operating limits of a number of fluid-phase AB/IL compositions that maximize hydrogen selectivities
- Quantified gas phase impurities produced from a number of AB/IL compositions
- Developed and designed automotive scale fluid-phase chemical hydrogen storage system
- Identified the boundary conditions of the required borazine adsorption unit

Future Directions

Borazine Adsorbents

- Develop and optimize the most promising borazine adsorbent

Reactor Design and Testing

- Quantify and compare performances of novel reactors

Shelf-Life Studies

- Continue shelf-life studies on viable chemical hydrogen storage media

Subscale Component Design and Validation

- Gas-liquid separator
- Reactor
- Hydrogen purification train

FY 2012 Publications and Presentations

1. “Overview of LANL’s Engineering Research Efforts for Chemical Hydrogen Storage” WHEC 2012, Toronto CA, *Invited Speaker*.
2. “Chemical Hydride Rate Modeling, Validation, and System Demonstration” 2012 Annual Merit Review, Washington, D.C., May 2012.

IV.D.4 Key Technologies, Thermal Management, and Prototype Testing for Advanced Solid-State Hydrogen Storage Systems

Joseph W. Reiter (Primary Contact),
Alexander Raymond, Channing C. Ahn (Caltech),
Bret Naylor, Otto Polanco, Rajeshuni Ramesham,
and Erik Lopez

Jet Propulsion Laboratory (JPL)
4800 Oak Grove Drive, Mail Stop 79-24
Pasadena, CA 91109-8099
Phone: (818) 354-4224;
Email: Joseph.W.Reiter@jpl.nasa.gov

DOE Managers

HQ: Ned Stetson
Phone: (202) 586-9995
Email: Ned.Stetson@ee.doe.gov

GO: Jesse Adams
Phone: (720) 356-1421
Email: Jesse.Adams@go.doe.gov

Subcontractor:

California Institute of Technology, Pasadena, CA

Project Start Date: February, 2009
Project End Date: September, 2014

Fiscal Year (FY) 2012 Objectives

- Identify state-of-art concepts and designs for cryosorbent-based hydrogen storage systems
- Discover and characterize technical barriers to system development toward DOE targets
- Develop means and/or identify trajectories to overcome barriers using modeling techniques
- Describe and develop enabling technologies toward achieving targets
- Design, fabricate, and test hardware components for model validation

Technical Barriers

This project addresses the following technical barriers from the Hydrogen Storage section of the Fuel Cell Technologies Program Multi-Year Research, Development and Demonstration Plan (referenced to 2017 targets, as revised 2009):

- (A) System Weight and Volume: $5.5\% \text{ wt}_{\text{sys}}, 55 \text{ gH}_2/\text{kg}_{\text{sys}}, 40 \text{ gH}_2/\text{L}_{\text{sys}}$
- (C) Efficiency: 90% Onboard

- (D) Durability/Operability: $<1\%$ degradation @ 1,500 cycles, etc.
- (E) Charging/Discharging Rates: 3.3 min fill, 0.02 g/kW-s minimum full flow
- (G) Materials of Construction
- (H) Balance-of-Plant Components
- (J) Thermal Management

Technical Targets

The JPL effort is currently focused on delivering beyond state-of-art cryogenic systems technologies and optimizations for the various cryo-adsorbent storage options being examined by the Center of Excellence. Table 1 summarizes recent progress and gives the current status for JPL tasks and milestones as measured against the specific targets that guide them.

TABLE 1. Current (FY 2012) Status of Target-Relevant JPL Tasks

| Task Area | 2012 Status | Main Relevant Target(s) (2017) | Comments |
|--|--|--|--|
| Advanced Vessel Thermal Isolation Design | Complete. Model validated, showing $<2 \text{ W}$ heat leak @ 77 K, improved from over 3 W | Loss of useable H_2 $<0.05 \text{ g/h/kg}$ | "Subscale" 77 K dormancy validation experiments planned late FY 2012 |
| Outgassing of COPV Tank-Wall Materials | Partially Complete. Initial experimental results show strong temperature dependence. | Loss of Useable H_2 $<0.05 \text{ g/h/kg}$ Permeation and Leakage | Inadequate instrumental resolution and sensitivity; new bench-top facility to be ready fourth quarter of FY 2012 |
| Downstream Cryogenic H_2 Heat Exchanger | Complete. Design satisfies targets at all but coldest (-40°C) environment for 77 K fuel supply | Min Delivery Temperature $> -40^\circ\text{C}$ Onboard Efficiency $>90\%$ | Bench-top cryogenic validation experiments in design stage; expected operation early FY 2013. Modeled device is 1.1 kg, 1.0 L |
| COPV Cryogenic Burst Test | Incomplete. Task shifted to later in FY due to resource allocation. | Safety Operational Cycle Life ($>5,000$ cycles) | Facility nearing completion; COPV tank articles have been provided by Lincoln Composites; initial burst at 77 K expected early FY 2013 |

COPV - Carbon-overwrapped pressure vessel

FY 2012 Accomplishments

- Advanced Vessel Thermal Isolation Design:** In 2012, JPL performed detailed thermo-mechanical design of an advanced vessel isolation system for automotive use

and experimentally validated the design at 80 K. The validated results indicate the design approach is capable of limiting parasitic heat load on a full tank to <2 W, a 38% improvement over the current state of the art. This improved performance is expected to consequently result in increased dormancy (“hold”) times for the idle vehicle over the entire operating range, $-40^{\circ}\text{C} < T_{\text{amb}} < 60^{\circ}\text{C}$.

- **Vacuum Outgassing of COPV Materials:** As part of the effort to characterize the dormancy behavior of a vacuum-insulated COPV, JPL obtained outgassing data for carbon fiber tank-wall materials in vacuum over the range $170\text{ K} < T < 350\text{ K}$. Initial results from this “ad-hoc” experimental effort indicate a clear “vacuum spoiling” effect and a temperature-dependent outgassing rate.
- **Cryogenic Fuel Energy Management:** JPL developed a coupled, detailed analytical model for a downstream H₂ fuel heat exchanger, necessary for cryo-adsorbent storage systems to raise the temperature of fuel supplied to the fuel cell. JPL’s design utilizes both ambient air and fuel cell waste heat as necessary via a closed coolant loop. The compact design (1.1 kg, 1.0 L – a “soda bottle”) has been modeled for 40 K and 80 K storage temperatures at steady-state and transient (cold-start) conditions, and satisfies DOE targets at all but the coldest ambient temperature (-40°C).
- **Cryogenic COPV Burst Testing:** in FY 2012, JPL completed the facility design for providing 15 kpsi burst for a medium-sized (5–20 L) Type 4 COPV at 77 K. Due to parallel tasks, resource allocation forced a shift of the completion to FY 2013, although procurements and some fabrication are taking place in the current FY. The facility has been designed to flexibly perform repeated burst events as well as provide a pressure cycling capacity with some modification.



Introduction

Since the inception of the Hydrogen Storage Center of Excellence (HSECoE) in FY 2009, JPL has been engaged in developing advanced, enabling technologies for vehicular hydrogen storage systems to meet DOE/U.S. DRIVE technical targets. To this end, JPL also serves the Center as Technology Area Lead for the Enabling Technologies team, providing technology management and coordination for overcoming technical gaps and incorporating emergent technologies and approaches.

During FY 2012, JPL’s technical effort has been primarily concerned with low-temperature thermal management and related technologies for cryo-adsorbent storage system options with emphasis in three areas: 1) parasitic heat transfer reduction in pursuit of the 2017 loss of useable H₂ target of $<0.05\text{ g h}^{-1}\text{ kg}^{-1}$ useable H₂; 2)

downstream hydrogen heating to achieve the minimum delivery temperature target $T_{\text{min}} > -40^{\circ}\text{C}$ for hydrogen delivered by the storage system, and 3) demonstration of cryogenic burst failure performance of COPVs to address the safety and operational cycle life targets. These are the primary targets influenced by each activity; except for burst testing (shifted to FY 2013), the current state of the art was either extended in relation to the primary targets, or it was shown that the technical targets could be fully satisfied. In practice, each task area also addresses several additional subsequent targets in a cross-cutting fashion.

Approach

JPL has identified and filled a need for critical cryo-system engineering in Phase 2 of the Center’s project. This renewed effort has allowed efficient use of manpower and resources following the de-scope of the metal hydride system in 2011 and suits the direction of the Center very well, supporting the development of gap-mitigating technologies critical to the implementation of a cryo-adsorbent-based onboard storage option. JPL’s approach involves bootstrapping into advanced technology development via modeling and bench-top proof-of-concept validation. The FY 2012 technology program has been generally guided by the following technical milestones:

- Experimentally validate model results for high-isolation cryo vessel design at 77 K
- Measure and characterize outgassing from COPV materials from $300\text{ K} > T > 77\text{ K}$
- Refine coupled downstream heat exchanger (HX) model and predict performance for relevant drive cycles, conditions; fuel at 77 K and 40 K, 1.6 g/s (max)
- Implement cryo-burst facility and determine burst limit for sample COPV at 77 K

Results

As a direct result of discharging gaseous hydrogen at storage temperatures below 80 K, a heat exchanger is required downstream of the storage vessel. This device must enable the storage system to meet the required technical targets (fuel T_{min} : -40°C ; flowrate: $1.6\text{ g}\cdot\text{s}^{-1}$; T_{amb} : -40 to 60°C) and be very compact. A coolant-coupled HX design was selected during mid-2011 to utilize the existing vehicle radiator and the large coolant flow rate to the fuel cell to mitigate frost formation while pre-heating H₂ fuel using waste heat. JPL’s HX model assumes an off-the-shelf shell/tube configuration for the device, and predicts coupled inlet and outlet temperatures of three fluid streams: H₂, glycol-water (55/45) coolant, and ambient air. The model assumes a constant fuel cell $T_{\text{FC}} = 80^{\circ}\text{C}$ for the purposes of efficiency calculations, a conservative decision that actually minimizes available waste heat. Furthermore, it is assumed

that cryogenic hydrogen is discharged from a full tank via isenthalpic expansion, giving the coldest possible fuel stream; this is also a conservative assumption. The steady-state predictive results show near-total compliance with targets for the prototype HX design at both 80 K and 40 K, as the colder storage temperature is only marginally more challenging from a fuel-heating perspective. Figure 1 shows these results, plotting fuel delivery temperature against fuel flowrate for several ambient temperatures. Only the coldest environment (-40°C) prevents the fuel from heating to the minimum requirement; optimization beyond the off-the-shelf design may enable even this requirement to be met. Figure 2 shows a visualization of the modeled device in a representatively sized benchtop storage system, indicating to good effect the

truly compact nature of such a device (1.1 kg, 1.0 L, most of which is thermal insulation).

The advanced Kevlar™ “web” suspension design JPL introduced in 2011 was compared to the current state-of-art design using a detailed thermo-mechanical model that was later validated to within 10% by experimental data. In the model, the G-10 fiber-reinforced plastic (FRP) standoffs of the state-of-art vessel and the Kevlar™ 29 cords of the advanced design were both sized for driving loads and conservatively designed for robust performance over long life. Thermally, the use of tensile cords to limit parasitic heating of the inner vessel is responsive to the fact that conduction of G-10 FRP is ~60% of the total heat load of such a vessel, while the use of Kevlar™ can limit conduction to below 40% of the total. This approach improves the thermal design by attacking the “low hanging fruit” of conduction while avoiding a more difficult (i.e., expensive) radiation optimization. Modeling the multi-layer insulation blanket was via the “Lockheed equation” with gas effects for an assumed vacuum pressure of 10⁻⁴ torr, 40% more conservative than the absolute minimum. In the experimental setup, vessel heat load was simulated by a heated aluminum test coupon in a vacuum chamber suspended from a cold boundary by either G-10 FRP or Kevlar™ 29 cord. Radiation was controlled by multi-layer insulation wrapped around the test coupon. Heat flows were measured for cold side temperatures of 80 and 150 K and hot side temperatures of -25, 10, and 45°C. The results of this experimental validation

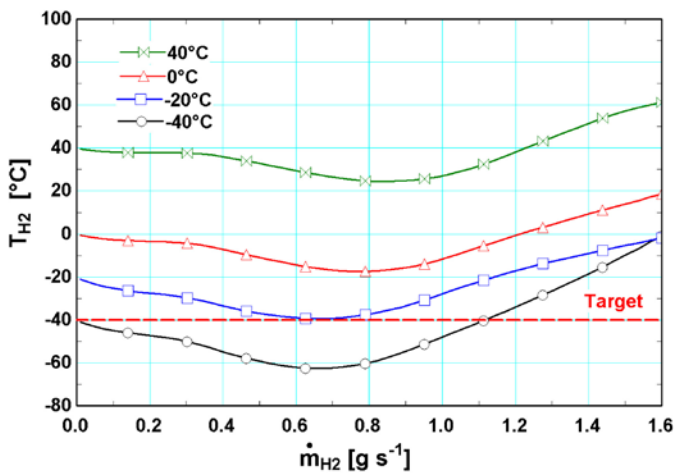


FIGURE 1. Curves showing performance of JPL’s Downstream Fuel HX design; here, fuel delivery temperature at the fuel cell is plotted against fuel flowrate for several ambient temperatures. The 80 K storage case is shown here; the results for 40 K are categorically similar.

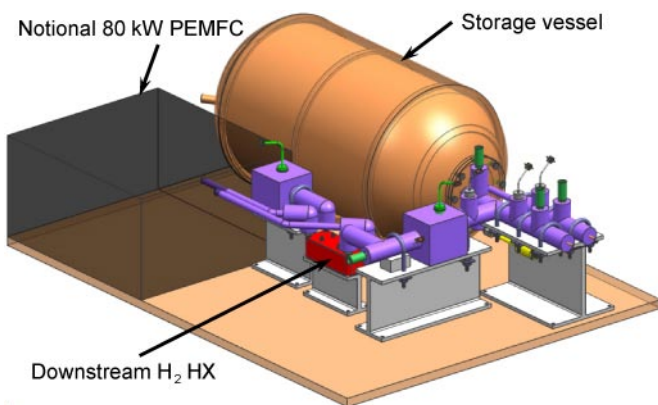


FIGURE 2. Computer-aided design visualization of JPL’s Downstream Fuel HX design, showing the compact device (in red) installed in a representative hydrogen storage system. Sizes of components were defined by a design that optimally satisfies the 2017 targets using technology known to the Center in 2011.

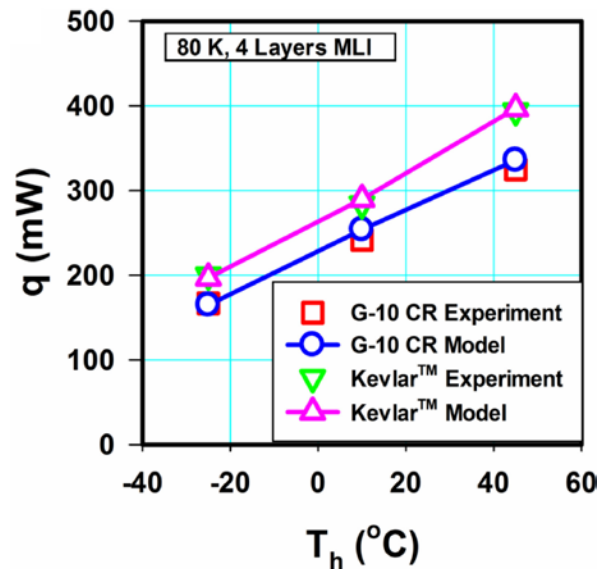


FIGURE 3. Curves indicating the correlation of model and experimental data for JPL’s advanced thermal architecture design at 80 K. There is very good agreement (within 10%) between predictions and experimental results for both Kevlar™ and G-10 materials. The mostly linear form of the curves shows the effect of T_{hot} on total heat transfer. The results are similarly well correlated for the 150 K storage temperature as well as for varying MLI layer count, indicating a robust design.

are shown in Figure 3. Dormancy cases were evaluated for the advanced vessel design using the validated model, showing an increase in “hold” time from 2 to 3 days for a full tank and no driving; these results are shown in Figure 4. In addition, an initial outgassing study of COPV material was performed as part of this effort to quantify the impact of volatile contaminant species on the integrity of the vessel’s vacuum insulation, a critical system parameter. While the ad-hoc nature of the experimental setup yielded mostly qualitative results, a rise in pressure with increasing temperature was apparent. This result will be further investigated and quantified with a new experimental setup and approach.

Conclusions and Future Directions

JPL’s conclusions from work in FY 2012 represent the initial steps in Phase 2 of the Center’s top-level research project, in which key technologies were actively developed with a focus on bench-top component testing and model validation.

- A detailed thermo-mechanical design of an advanced vessel thermal isolation system has shown that thermal load on a cryogenic tank can be reduced by almost 40%; this result has been experimentally validated via coupon-

scale testing at 80 K. Follow-on work has already begun, and will include validation of performance models at appropriate (i.e., larger) scales and environmental conditions. These data, along with demonstrated manufacturability methods for the advanced isolation system, will be provided to the Center and to DOE.

- Initial outgassing data for carbon fiber tank-wall materials were obtained over a temperature range of 170 K < T < 350 K; the results indicate that outgassing is a potential source of vacuum-spoiling species. Next steps involve completion, calibration, and commissioning of the new high-resolution test facility, after which higher-quality outgassing data will be acquired for a range of materials over a larger temperature range.
- A fully-coupled Downstream Fuel HX model was developed and utilized to obtain refined results showing potential mass/volume reductions of the HX device; this design was visualized using a computer-aided design model in a representative storage system. In FY 2013, this work will be supported by experimental verification via a new bench-top facility; this campaign may use the “full-sized” article, as it is already compact.
- An initial design review for a cryo-burst facility is complete, including safety reviews, burst energy calculations, and facility use; the test procedure was

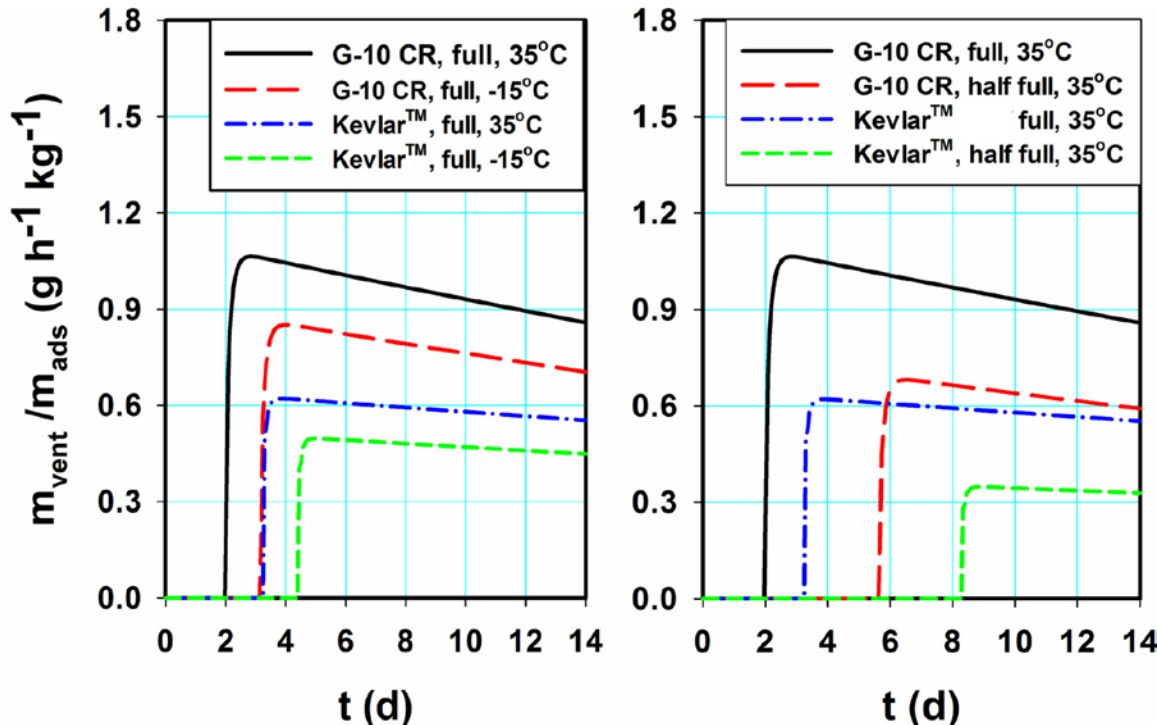


FIGURE 4. Plots comparing the validated dormancy performance of the advanced JPL design over the current state-of-art G-10 design, showing an improvement in dormancy times for a full (5.6 kg useable H₂) tank from 2 to 3 d with no driving of the vehicle. Here the curves indicate H₂ vent rates as heat ingress causes adsorbed H₂ to pressurize the vessel via thermal desorption. The effects of a “half-full” tank are also shown on the right hand side.

developed with assistance from industry (Lincoln Composites, National Aeronautical and Space Administration, etc.) and procurements have begun. By early FY 2013, the burst facility will have conducted its first burst of a small COPV provided by Lincoln Composites, on the way to additional tests examining cycled vs. un-cycled burst strength and other variations. Plans may be implemented to allow pressure-cycle testing to be conducted on this same facility at cryogenic temperatures.

FY 2012 Publications/Presentations

1. Reiter, J.W., Raymond, A., and Ramesham, R. Outgassing Rate and Species Measurement for Cryogenic Carbon Fiber Hydrogen Storage Vessels. Oral Presentation. AIChE Annual Meeting, October 16–21, 2011. Minneapolis, MN.
2. Raymond, A. and Reiter, J. “Modeling and Testing of Cryo-adsorbent Hydrogen Storage Tanks with Improved Thermal Isolation.” Proceedings of the 2011 Cryogenic Engineering Conference, in press.

IV.D.5 Systems Engineering of Chemical Hydrogen, Pressure Vessel, and Balance of Plant for Onboard Hydrogen Storage

Jamie D. Holladay (Primary Contact),
Kriston P. Brooks, Ewa C.E. Rönnebro,
Kevin L. Simmons and Mark R. Weimar.
Pacific Northwest National Laboratory (PNNL)
902 Battelle Blvd
Richland, WA 99352
Phone: (509) 371-6692
Email: Jamie.Holladay@pnnl.gov

DOE Managers

HQ: Ned Stetson
Phone: (202) 586-9995
Email: Ned.Stetson@ee.doe.gov

GO: Jesse Adams
Phone: (720) 356-1421
Email: Jesse.Adams@go.doe.gov

Contract Number: DE-AC05-76RL01830

Project Start Date: February 1, 2009

Project End Date: January 31, 2014

- Demonstrate the performance of economical, lightweight vessels for an adsorbent system and containment vessel for a chemical hydride system.
- Guide design and technology down selection, Go/No-Go decision-making, and address vehicle and market impact through cost modeling and manufacturing tradeoff assessments of the three HSECoE prototype storage systems.
- Achieving the objectives will enable PNNL, Savannah River National Laboratory (SRNL), and other HSECoE partners to demonstrate onboard hydrogen storage with the potential to meet 2017 DOE technical targets. This technology and design knowledge will be transferred to the participating automotive original equipment manufacturers and non-proprietary information and models will be made available to the fuel cell community, thus advancing the hydrogen market sector and production of future hydrogen-powered vehicles.

Technical Barriers

This project addresses the following technical barriers from the Storage section of the Fuel Cell Technologies Program Multi-Year Research, Development and Demonstration Plan:

General to All Storage Approaches

- (A) System Weight and Volume
- (B) System Cost
- (C) Efficiency
- (E) Durability/Operability
- (F) Charging/Discharging Rates
- (G) Materials of Construction
- (H) Balance of Plant (BOP)
- (I) Dispensing Technology
- (J) Thermal Management
- (K) System Life-Cycle Assessments
- (O) Hydrogen Boil-Off

Off-Board Regenerable Specific

- (S) By-Product/Spent Material Removal

Technical Targets

The Center activities being conducted at PNNL range from process and reactor modeling and component design/

Fiscal Year (FY) 2012 Objectives

The Pacific Northwest National Laboratory (PNNL) objectives address the critical engineering challenges currently limiting onboard hydrogen storage systems for light-duty fuel cell vehicles. Each of the project's objectives and tasks have been established to advance the state of the art in analysis, design and engineering for chemical hydride storage, pressure/containment vessel construction for metal hydride and cryogenic adsorbent systems, and component miniaturization for all systems to achieve PNNL, Hydrogen Storage Engineering Center of Excellence (HSECoE), and DOE goals.

- Demonstrate performance that meets DOE targets for key components (heat exchanger, pumps, and volume exchange tank) of a chemical hydrogen storage system through the use of system modeling and component validation testing.
- Reduce system volume and mass while optimizing system storage capability and performance through value engineering of heat exchangers and balance-of-plant (BOP) components.
- Mitigate materials incompatibility issues associated with hydrogen embrittlement, corrosion, and permeability through suitable materials selection for vessel materials, heat exchangers, plumbing and BOP components.

engineering to technology application and prototype fabrication for demonstration. The final ultimate goal for the PNNL scope is to demonstrate, with Los Alamos National Laboratory (LANL), a scaled chemical hydrogen storage system that meets the 2015 DOE storage performance targets. As a snapshot of progress to date, the spider chart in Figure 1 represents the principal 2017 DOE performance targets and status toward achieving those targets as a percentage with 1a representing exothermic systems with ammonia borane (AB) as the surrogate and 1b representing endothermic systems with alane as the surrogate. The DOE has established an initial in-process review gate of 60% for each of the targets except system cost; the dashed line represents this 60% threshold.

FY 2012 Accomplishments

- Completed development of Simulink® AB Slurry storage system model and integrated it with the fuel cell vehicle system model.
- Completed sensitivity analysis for both AB and alane slurries by doing both a tornado plot type analysis (change one parameter at a time) and Box-Behnken type of sensitivity analysis (vary multiple parameters).
- Demonstrated feasibility of 45 wt% AB slurry: slurry performance is well below upper limit of flow ability before and after hydrogen release.
- Measured key AB slurry properties including viscosity, yield stress, hydrogen release kinetics, and qualitative flocculation/settling before and after hydrogen release.
- Demonstrated 3+ months with no apparent flocculation or settling of a 40 wt% AB slurry.
- Identified key BOP components including a pump and heat exchanger which are a 44% mass reduction and 60% mass reduction, respectively.

- Identified optimal liner thickness to minimize mass and cost while retaining fatigue resistance at cryogenic temperatures.
- Developed cryogenic test plan to test polymer liners for Type-IV vessels and completed testing on seven material candidates.
- Completed sensitivity analysis of mass relative to pressure and volume for Type-I and Type-III vessels. The analysis revealed that changing hydrogen pressure had a larger impact on mass than changing the tank volume at cryogenic conditions.
- Developed cost model tool that will analyze the cost of a pressure vessel at different pressures and different temperatures. The user inputs material, vessel Type (I, III, or IV) pressure, temperature, volume and the model provides manufacturing and material costs.



Introduction

Multiple onboard vehicle-scale hydrogen storage demonstrations have been done, including several studies to examine characteristics that impact systems engineering. However, none of these demonstrations have simultaneously met all of the DOE hydrogen storage sub-program goals. Additionally, engineering of new chemical hydride approaches is in its infancy, with ample opportunity to develop novel systems capable of reaching the DOE targets for storage capacity. The goal of the HSECoE, led by SRNL, is to develop and demonstrate low-cost, high-performing, onboard hydrogen storage through a fully integrated systems design and engineering approach. Toward this end, PNNL is working with HSECoE partners to design and fabricate a

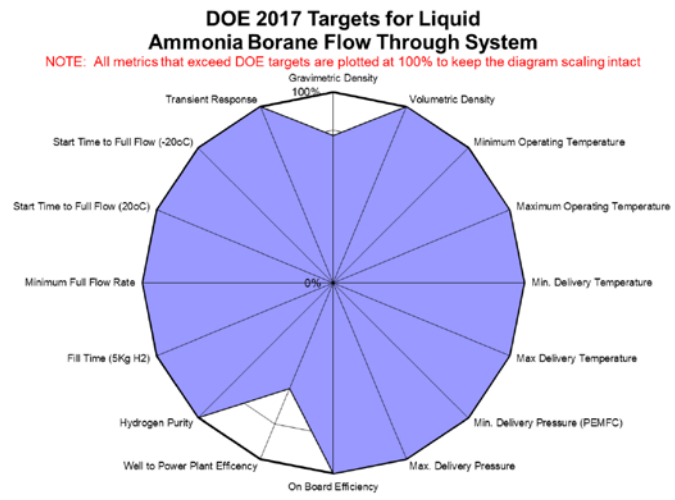
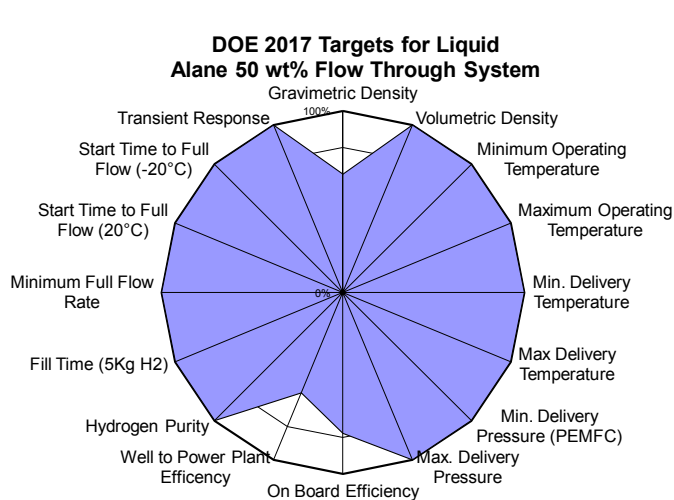


FIGURE 1. a) Progress towards achieving DOE performance targets for an exothermic material slurry with AB as surrogate. b) Progress towards achieving DOE performance targets for endothermic material slurry with alane as surrogate.

system based on slurry chemical hydride storage media. This system will be demonstrated at LANL in Phase 3.

Approach

As part of the HSECoE PNNL actively contributes to all five technology areas and targets six key objectives to optimize performance characteristics and reduce the size, weight, and cost of a H₂ storage system. This is being accomplished through engineering and integrated design approach, including application of advanced materials (structural and H₂ storage), and assessments of manufacturing and cost impact based on established models/approaches for technology tradeoff or “viability” studies.

PNNL serves multiple leadership roles within the HSECoE technology area structure to help facilitate collaboration across the center partnership and to feed technical results to other Center partners. Achieving the objectives enables PNNL, SRNL, and other HSECoE partners to demonstrate onboard hydrogen storage with the potential to meet DOE technical targets. This technology and design knowledge will be transferred to the participating automotive original equipment manufacturers, thus advancing the hydrogen market sector and production of future hydrogen-powered vehicles. As appropriate, the models, catalogues, and lessons learned will be made available to the fuel cell community to accelerate fuel cell technology commercialization.

Results

Chemical Hydride Modeling

In the past year the models were updated for both endothermic and exothermic surrogate materials (alane and AB, respectively). The Simulink[®] models were integrated into the fuel cell vehicle model framework and operated to predict the performance of the hydrogen storage system. Finally, the models were exercised to gain a better understanding of the operating envelope of storage material properties that will meet DOE targets. The model updates included improved kinetic data, additional heat losses, and impacts of viscosity. The heat losses included were for the reactor, the phase separator, the pump, and recycle tubing. These components are assumed to be insulated with one inch of kaowool insulation and heat losses are associated with conduction through this insulation and natural convection to the environment. For the endothermic system a recuperator was added to the Simulink[®] model to maximize efficiency. These models were integrated with the fuel cell vehicle model framework, and four drive cycles were simulated (city and highway fuel economy [UDDS and HWFET], high-power and acceleration [US06], cold-start city, and air conditioning [SC03]). The simulations showed, among

other things, that for endothermic materials like alane, the heat required to maintain full conversion during each of the four drive cycles resulted in onboard efficiencies of less than the DOE 2017 target of 90%. Furthermore, using the current BOP, a storage material such as alane must be loaded to an unrealistic value of 82 wt% slurry to meet the system gravimetric targets. In contrast, the exothermic chemical hydrides model demonstrated that they could meet the DOE onboard efficiency targets for all four drive cycles. The DOE 2017 gravimetric target has not been achieved either, but it is improved from that of the endothermic systems. The impact of varying the heat of reaction, kinetics (pre-exponential factor), chemical hydride mass loading, activation energy, and viscosity was completed by varying a single parameter for a tornado type plot and by varying multiple parameters for a Box-Behnken type of sensitivity analysis. These data will be used by the DOE to develop operating envelopes for directing future materials discovery work.

Chemical Hydride Slurry Development

The focus of PNNL’s efforts for the chemical hydride slurry was on the AB surrogate for the exothermic slurry and to increase the loading of AB in the selected liquid carrier while maintaining required performance with respect to flow ability (pump ability). An endothermic slurry is being developed by Brookhaven National Laboratory and the Engineering Center is using their results. For the AB slurry, PNNL evaluated four candidate carrier liquids, seven synthesis techniques and is in the process of examining six additives. We have out-selected development on three carrier liquids, six synthesis techniques, and three additives. We have demonstrated a 40 wt% AB slurry that showed no settling or flocculation after 3+ months and our kinetic tests indicate that the release kinetics were similar to that of the solid AB; however, with a reduced induction period. We believe the induction period reduction was due to improved thermal conductivity of the slurry compared to a solid pellet of AB. The spent fuel did exhibit settling after several hours which will need to be addressed in the system design. The viscosity and yield stress for fresh and spent fuel was also measured (Table 1) and are well within the viscosity limit of 1,500 cP. The results indicate that both the fresh and spent slurry are Bingham plastics.

TABLE 1. Plastic viscosity and yield stress of 45% AB slurry before and after hydrogen release. These results indicate that the slurry is a Bingham plastic.

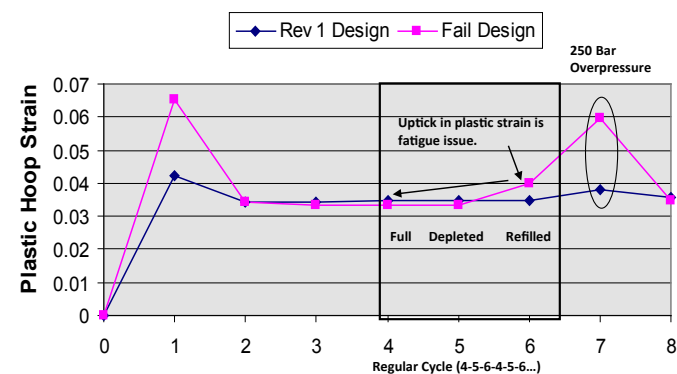
| Rheology properties of 45% AB slurry at 25°C | AB slurry before H-release | AB slurry after H-release |
|--|----------------------------|---------------------------|
| Plastic viscosity (cP) | ~ 617 | ~ 442 |
| Yield stress (Pa) | ~ 48 | ~ 3.7 |

Component Testing

PNNL has begun validating key components (pumps and heat exchanger [HX]) for the chemical hydrogen storage system. PNNL has identified a new pump which is capable of pumping slurries with viscosity up to 50,000 cp, at pressures up to 65 bar, and that has a mass and volume of ~2.5 kg and 1.5 L respectively. This represents a mass reduction of 44% compared to our original system. The HX we identified has a mass and volume of 1.32 kg and 1.3 L which is a 60% and 50% reduction respectively from our baseline system. We have completed initial testing of a test system composed of the prototypic pump, HX, piping, valves, and pressure sensors at room temperature and at -20°C using slurries composed of polyethylene particles and silicon oil and polyimide particles and silicon oil at appropriate loadings to simulate the fresh and spent AB slurry, respectively. No clogging was observed, but tests are on-going.

Vessels

PNNL developed models for estimating the mass of Type-III and -IV tanks subjected to cycling cryogenic temperatures and pressures in the 80-180 K and 200 bar nominal (250 bar max) range. The ring model represents a section of the cylindrical portion of a tank, with aluminum liner and carbon fiber composite overwrap. The quarter-symmetry ring is subjected to a particular pressure and temperature history that covers the autofrettage stage followed by the normal fill-depletion-refill cycle expected of an automotive hydrogen fuel tank. The results of the model determine if a set of wall thicknesses is sufficient or not (Figure 2). We found that an aluminum liner thickness of 9 mm was sufficient. The ring finite element model was employed to evaluate the Type-IV tanks, with the goals of checking the amount of load carried by the liner (minimal) and the amount of strain predicted in the liner material (about



200L, 200 Bar Cryo (77-120K)
 Fail design 7.5mm Al liner, 7.2 mm shell
 Rev 1 design 9.0mm Al liner, 7.2mm shell

FIGURE 2. Type-III wall cylinder finite element analysis to find the optimal tank thickness.

7.5% maximum) for comparison against cryogenic material test data.

PNNL developed cryogenic (80 K) testing capability for mechanical properties of materials. Staff tested eight candidate liner materials for cryogenic strength and elongation. Staff completed HDPE, Halar, Kynar homopolymer and Kynar copolymer materials, Kel F, polytetrafluoroethylene, and nylon. In addition, dynamic mechanical analysis for these materials was conducted. Figure 3 contains the results for Halar, Kynar homopolymer, Kynar copolymer, and high-density polyethylene (HDPE). Halar and HDPE have the lowest glass transition temperatures and storage modulus making them the best candidates at this time.

The Center determined that in addition to the Type-III and -IV tanks, a model for Type-I pressure vessels was needed for determining mass and cost as a function of pressure (40 K and 60 bar to 80 K and 200 bar). Therefore, PNNL developed the model for determining wall thicknesses and mass as a function of pressure, temperature, tank radius, and volume. The data from the model is being used as a first order of costing for Type-I tanks and then compare the masses and costs against other tank types for a tradeoff study. The model has been incorporated into the cost model.

Costing

This year the manufacturing and cost analysis task began development of a manufacturing process model to evaluate cost differences between Type-I, Type-III, and Type-IV pressure vessels at different temperatures and pressures

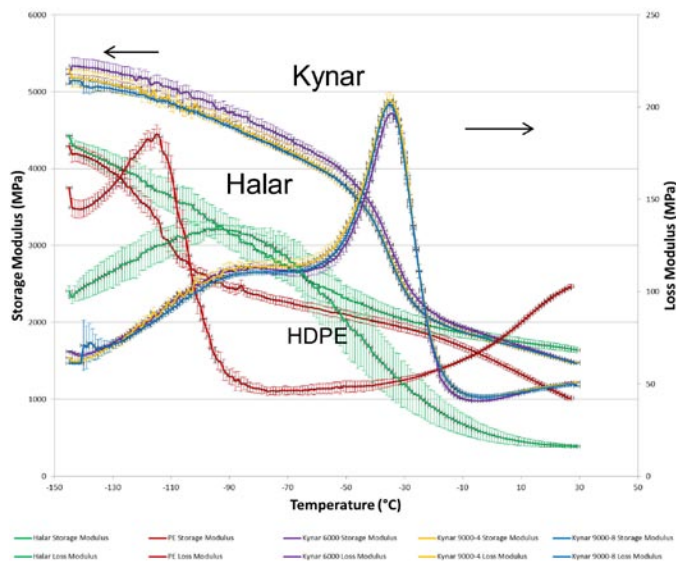


FIGURE 3. Dynamic mechanical analysis for Halar, Kynar homopolymer, Kynar copolymer, and HDPE. Halar and HDPE have the lowest glass transition temperatures and storage modulus making them the best candidates at this time.

(Figure 4). The goal for this model was to provide a high level difference between Type-I and Type-III/IV tanks costs with operating temperatures from -250 to 40°C and from 20 to 200 bar. We have incorporated manufacturing processes based on information from Lincoln Composites, the Jet Propulsion Laboratory, and literature for the Type-III and Type-IV tanks that details the steps required to manufacture the liners and wind the composites onto the tank in addition to capital costs, labor cycle time, quality assurance, insulation (from discussions with the Jet Propulsion Laboratory), installing and processing the vacuum shell, and installing the balance of plant. Only those steps associated with filling the tank with adsorbent and HX are not currently populated.

Conclusions and Future Directions

- Chemical Hydrogen System – Modeling and Validation Exothermic Slurry (AB)
 - Modeled fraction AB critical to meeting DOE mass target
 - Onboard efficiency target can be met with >8 cold-starts/day
 - Performed tornado type (vary one parameter) and Box Benken type (vary multiple parameters) sensitivity analysis
- Chemical Hydrogen System – Modeling and Validation Endothermic Slurry (Alane)

- Alane cannot meet DOE targets for mass or onboard efficiency for the system specified and conditions evaluated
- Performed sensitivity tests
- Performed tornado type (vary one parameter) and Box Benken type (vary multiple parameters) sensitivity analysis.
- Chemical Hydrogen System – BOP
 - Identified key components to reduce mass/volume for pump, radiator (heat exchanger) and performance validation initiated
 - 45 wt% AB slurry demonstrated: Slurry pre- and post-H₂ release
 - Kinetics similar to solid AB without the induction period
 - Viscosity and yield stress for both fresh and spent slurries acceptable
- Vessels
 - Completed the HSECoE tank needs survey for bench top tank production
 - Modeled various cases of Type-I, -III, and -IV tanks of pressure and temperature
 - Tested of Type-IV liner materials at cryogenic temperatures
 - Evaluated mass comparisons between Type-I, -III, and -IV

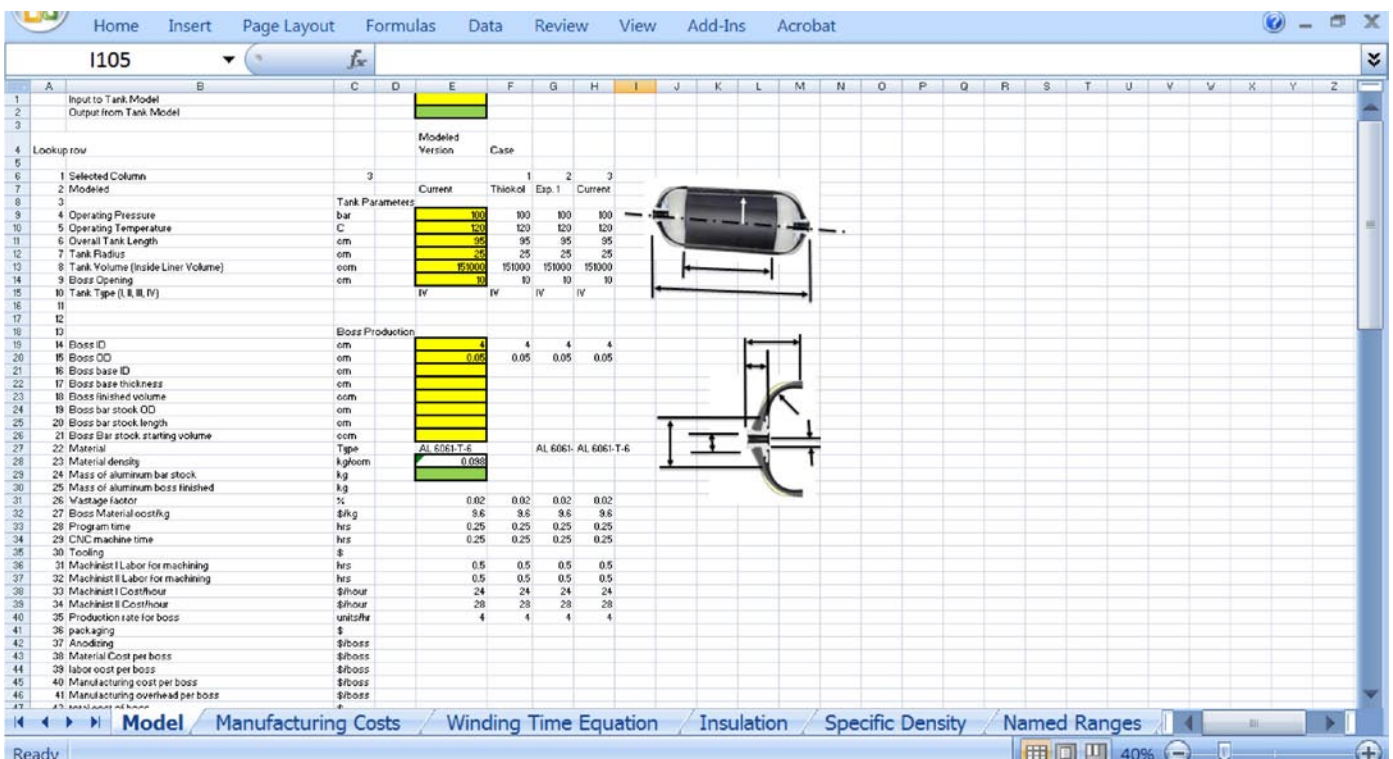


FIGURE 4. Sample page of the cost model which combines costs with predictive models.

- Cost Analysis
 - Updated metal-organic framework-5 cost analysis
 - Cost analysis being combined with vessel design models

Future Work for FY 2013

Chemical Hydrogen System

- Detailed Design, Engineering and Analysis
 - Update component models based on validation testing
 - Complete sensitivity analysis
- Validate Volume Exchange Tank
- Complete Solid-Liquid Slurry Development
 - Additives
 - Scale up synthesis

Pressure Vessel

- Pressure Vessel Engineering
 - Reduce cost, mass
 - Maintain safety
- Materials Compatibility/Reactivity
 - Finalize H₂-wetted material compatibility in components
- Determine BOP and pressure vessel materials compatibility

Cost Analysis

- Work with partners, vendors on reducing cost
- Update analysis with detailed design

FY 2012 Publications/Presentations

Publications List

- 1. Devarakonda MN, KP Brooks, E Ronnebro, and SD Rassat.** 2012. "Systems Modeling, Simulation and Material Operating Requirements for Chemical Hydride Based Hydrogen Storage." *International Journal of Hydrogen Energy* 37(3):2779-2793.
- 2. Brooks KP, MN Devarakonda, SD Rassat, and JD Holladay.** 2011. "Systems Modeling of Chemical Hydride Hydrogen Storage Materials for Fuel Cell Applications." *Journal of Fuel Cell Science and Technology* 8(6):Article No. 061021.
- 3. Majzoub EH, and E Rönnebro.** 2012. "Methodology of Materials Discovery in Complex Metal Hydrides Using Experimental and Computational Tools." *Materials Science and Engineering R*, 73 (2012) 15-26.
- 4. Devarakonda MN, KP Brooks, and JD Holladay.** 2011. "A Solvated Ammonia Borane Model for Chemical Hydrogen Storage

in Fuel Cell Applications." PNNL-SA-84798, Pacific Northwest National Laboratory, Richland, WA. Submitted

5. Devarakonda MN, KP Brooks, E Rönnebro, SD Rassat, and JD Holladay. 2011. "Chemical Hydrides for Hydrogen Storage in Fuel Cell Applications." In *SAE World Congress 2012*. Pacific Northwest National Laboratory, Richland, WA.

Presentations List

- 1. Rönnebro E.** 2011. "Fluid Phase Chemical Hydrides-presentation at F2F meeting for the Hydrogen Storage Engineering Center of Excellence." Presented by Ewa Ronnebro (Invited Speaker) at Hydrogen Storage Engineering Center of Excellence Project Meeting, Santa Fe, NM on October 13, 2011. PNNL-SA-83480.
- 2. Brooks K., S Rassat, M Devarakonda, T. Semelsberger.** 2011. "System Modeling of Chemical Hydride Storage Systems." Presented by Kriston Brooks (Invited Speaker) at Hydrogen Storage Engineering Center of Excellence Project Meeting, Santa Fe, NM on October 13, 2011.
- 3. Brooks K., S Rassat, M Devarakonda.** 2011. "Enabling Technology: Slurry Reactor/Gas Phase Separator Concepts." Presented by Kriston Brooks (Invited Speaker) at Hydrogen Storage Engineering Center of Excellence Project Meeting, Santa Fe, NM October 13, 2011.
- 4. Simmons K.** 2011. "Pressure Vessel Breakout Session." Presented by Kevin Simmons (Invited Speaker) at Hydrogen Storage Engineering Center of Excellence Project Meeting, Santa Fe, NM on October 13, 2011.
- 5. Weimar M, M Veenstra, K Simmons.** 2011. "HSECoE On-Board Hydrogen Storage Cost Estimates." Presented by Mark Weimar (Invited Speaker) at Hydrogen Storage Engineering Center of Excellence Project Meeting, Santa Fe, NM on October 13, 2011.
- 6. Simmons K, N. Klymyshyn, J Reiter, N Newhouse, J Makinson, M Veenstra, J Khalil, D Tamburello.** 2012. "DIT11-HSECoE Pressure Vessel and Containment TTR Highlights." Presented by Kevin Simmons (Invited Speaker) at Project review of the Hydrogen Storage Engineering Center of Excellence, Detroit, MI on February 16, 2012.
- 7. Ronnebro E.** 2012. "Materials Operating Requirements for Fluid Phase Chemical Hydrides ." Presented by Ewa Ronnebro (Invited Speaker) at Review of Hydrogen Storage Engineering Center of Excellence, Detroit, MI on February 16, 2012.
- 8. Brooks K, M Devarakonda, T Semelsberger.** 2012. "System Modeling of Chemical Hydride Storage Systems." Presented by Kriston Brooks (Invited Speaker) at Review of Hydrogen Storage Engineering Center of Excellence, Detroit, MI on February 16, 2012.
- 9. Brooks K, K Simmons, M Devarakonda, T Semelsberger.** 2012. "System Modeling and Balance of Plant for the Chemical Hydride Storage Systems." Presented by Kriston Brooks (Invited Speaker) at Review of Hydrogen Storage Engineering Center of Excellence, Detroit, MI on February 16, 2012.
- 10. Rönnebro E. Karkamkar A. Choi YJ. Chun J. Westman M.** 2012. "Materials Engineering of Fluid Phase Chemical Hydrides for Automotive Applications". Presented by Ewa Ronnebro (Invited Speaker) at American Chemical Society, Fuel Chemistry Division, San Diego, CA, March 26, 2012.

IV.D.6 Advancement of Systems Designs and Key Engineering Technologies for Materials Based-Hydrogen Storage

Bart van Hassel (Primary Contact),
Jose Miguel Pasini, Andi Limarga, John Holowczak,
Igor Fedchenia, John Khalil, Reddy Karra,
Ron Brown, Randy McGee

United Technologies Research Center (UTRC)
411 Silver Lane
East Hartford, CT 06108
Phone: (860) 610-7701
Email: vanhasba@utrc.utc.com

DOE Managers

HQ: Ned Stetson
Phone: (202) 586-9995
Email: Ned.Stetson@ee.doe.gov

GO: Jesse Adams
Phone: (720) 356-1421
Email: Jesse.Adams@go.doe.gov

Contract Number: DE-FC36-09GO19006

Project Start Date: February 1, 2009
Project End Date: June 30, 2014

- (A) System Weight and Volume
- (C) Efficiency
- (D) Durability/Operability
- (E) Charging/Discharging Rates
- (H) Balance of Plant (BOP) Components
- (J) Thermal Management

Technical Targets

The goals of this project mirror those of the HSECoE to advance hydrogen storage system technologies toward the DOE Hydrogen Program's 2017 storage targets [1].

TABLE 1. Current status of three system-related targets

| Characteristic | Units | HSECoE Goals | Storage System Type | UTRC 2012 Status |
|----------------------|-------------------|--------------|---------------------|------------------|
| Gas Liquid Separator | kg | 5.4 | Chemical Hydride | 5.9 |
| | L | 19 | | 2.7 |
| Ammonia Filter | kg | 1.2 | Chemical Hydride | 1.1 |
| | L | 1.6 | | 1.6 |
| SAC Density | g/cm ³ | >0.6 | Adsorbent | 0.76 |
| | m ² /g | 2,800 | | 1,698 |

SAC – super activated carbon

Fiscal Year (FY) 2012 Objectives

- Collaborate closely with the Hydrogen Storage Engineering Center of Excellence (HSECoE) partners to advance materials-based hydrogen storage system technologies.
- Develop vehicle/power plant/storage system integrated system modeling elements to improve specification of storage system requirements and to predict performance for candidate designs.
- Engineer and test specialty components for H₂ storage systems.
- Assess the viability of onboard purification for various storage material classes and purification approaches.
- Compact super activated carbon and metal-organic framework (MOF) materials without binder.
- Conduct risk assessments during the progression of the phased HSECoE efforts.

Technical Barriers

This project addresses the following technical barriers from the Storage section (3.3.4) of the Fuel Cell Technologies Program Multi-Year Research, Development and Demonstration Plan:

FY 2012 Accomplishments

Accomplishments of the current project comprise:

- Used Simulink® framework and metal hydride system model to identify ideal onboard reversible metal hydride material properties.
- Identified high contact resistance in combination with slow two-step hydrogen absorption kinetics as obstacle to meet 2017 DOE refueling time target if using sodium aluminum hydride (SAH) pellets integrated with a heat exchanger tube.
- Selected gas-liquid separator (GLS) for chemical hydride system and designed test rig.
- Developed high capacity and regenerable H₂ purification cartridge that enables NH₃ removal down to 0.1 ppm, as required by the SAE J2719 APR2008 guideline.
- Evaluated porous metal filters for containment of cryo-adsorbent material into storage tank and for particulate mitigation.
- Performed Qualitative Risk Analysis of HSECoE designs/materials.

- Developed method to assess thermal conductivity anisotropy of compacted H₂ storage materials.
- Improved volumetric capacity and thermal conductivity of MOF-5 through uniaxial compaction and additives.
- Improved volumetric capacity and thermal conductivity of super activated carbons MaxSorb and IRH-33 through spark plasma sintering and additives.



Introduction

Physical storage of hydrogen through compressed gas and cryogenic liquid approaches is well established, but has drawbacks regarding weight, volume, cost and efficiency which motivate the development of alternative, materials-based methods of hydrogen storage. Recent worldwide research efforts for improved storage materials have produced novel candidates and continue in the pursuit of materials with overall viability. While the characteristics of the storage materials are of primary importance, the additional system components required for the materials to function as desired can have a significant impact on the overall performance. Definition, analysis and improvement of such systems components and architectures, both for specific materials and for generalized material classes, are important technical elements to advance in the development of superior methods of hydrogen storage.

Approach

UTRC's approach is to leverage in-house expertise in various engineering disciplines and prior experience with metal hydride system prototyping to advance materials based H₂ storage for automotive applications. UTRC continued to focus during the third year of the HSECoE project on developing tools for comparing H₂ storage systems on a common basis that could also be used by a wider audience. UTRC screened H₂ storage system improvement ideas resulting from compaction, thermal conductivity enhancement, H₂ purification, compact and low weight heat exchanger design, and gas liquid separator technology. Results contributed to the quantification of ideal on-board reversible metal hydride properties that would enable meeting the DOE 2017 system targets [1].

Results

UTRC, in collaboration with Savannah River National Laboratory, General Motors, Lincoln Composites and the Pacific Northwest National Laboratory (PNNL), performed a study with the aim of quantifying the ideal metal hydride properties of an onboard reversible metal hydride storage system that would be capable of meeting the DOE 2017

targets for onboard hydrogen storage systems for light-duty vehicles [1]. Figure 1 shows the gravimetric capacity of metal hydride materials as a function of the hydrogenation enthalpy. It also shows two targeted areas, one enclosed by a green line for regular metal hydrides and one enclosed by a blue line for destabilized metal hydrides. Details about the results of this analysis can be found in [2,3].

DOE targets [1] are specific, quantitative, and timely and have to be met simultaneously. One important target is the onboard efficiency target that specifies that 90% of the hydrogen that has been stored in the hydrogen storage system needs to be delivered to the fuel cell. This greatly limits the hydrogenation enthalpy of metal hydrides that can be considered for this application. UTRC estimated that this target can only be met when the hydrogenation enthalpy is less than 30 kJ/mole-H₂ for regular metal hydrides. Such a material will make hydrogen available to the fuel cell at the minimum delivery pressure of 5 bar at 60°C by using waste heat from the fuel cell. Such a metal hydride should have a minimum gravimetric capacity of 11 wt% in order for the hydrogen storage system to be able to meet DOE's weight and volume targets for light-duty vehicles. The hydrogenation enthalpy can also not be too low as the equilibrium pressure of the material would be too high and require a much heavier pressure vessel. It was decided in this study to limit the hydrogen pressure in the storage system to less than 100 bar in order to maintain the benefit of a lower pressure H₂ storage system that would require less carbon fiber than high pressure physical storage systems and that would require less compression energy and have safety benefits. Metal hydrides with a higher hydrogenation enthalpy (>30 kJ/mole-H₂) will not be able to meet the onboard efficiency target as more than 10% of the stored hydrogen would need to be combusted in order to generate heat for H₂ desorption before the H₂ could be made available to the fuel cell. Such a combustion system increases the weight of the H₂ storage system and this has to be compensated for by having a H₂ storage material with an even higher gravimetric capacity (dashed green line). A similar box has been drawn in Figure 1 for destabilized metal hydride materials. The difference in hydrogenation entropy in comparison to the regular metal hydride materials causes the blue box to be in a different location. Currently, the HSECoE is not aware of any metal hydride materials that fit within the green or blue box and the onboard reversible metal hydride system development was discontinued within the HSECoE for this light-duty vehicle application. Some materials appear to be close to the desired regions but either will result in a H₂ storage system with a lower than targeted onboard efficiency when used in combination with a conventional proton exchange membrane fuel cell system or will be heavier or larger in volume than the DOE targets allow.

As part of an orderly completion of the onboard reversible metal hydride work, heat transfer characteristics were determined of SAH pellets integrated with a heat

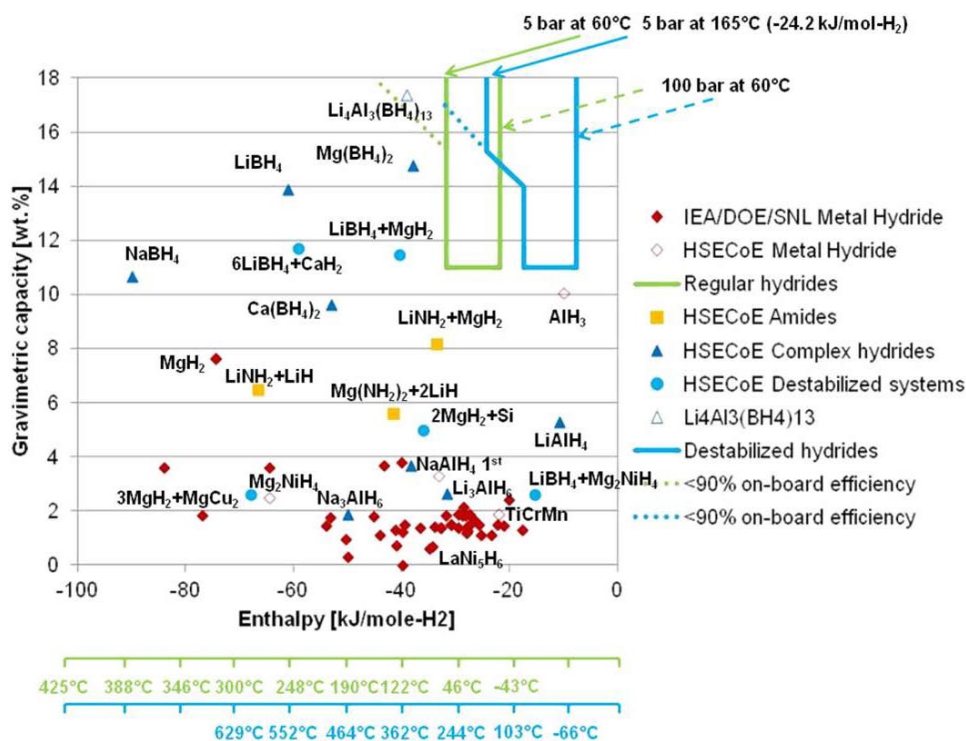


FIGURE 1. Ideal metal hydride properties for light-duty vehicle application

exchanger tube. The results show that the contact resistance between the SAH pellets and the heat exchanger tube was significant and this in combination with the relatively slow two step H₂ adsorption mechanism limited the H₂ adsorption rate that could be achieved. Reaching 90% of the storage capacity in DOE’s 2017 refueling time target of 3.3 minutes was not feasible. A more detailed comparison between the experimental data and a COMSOL model is being pursued.

A fluid-based chemical hydride system, such as for instance ammonia borane (AB) dissolved in ionic liquids (Los Alamos National Laboratory) or suspended in a slurry (PNNL), requires a GLS. It separates hydrogen gas produced during AB thermolysis from the fluids that will also contain the AB thermolysis byproducts (e.g. BNH_x). UTRC selected a passive GLS design with a low profile and no moving parts that deploys three different separation mechanism: coalescence, gravity and centrifugal action. UTRC also designed a laboratory system for testing the GLS performance, as shown in Figures 2 and 3, which has the following key components: 1) feed tank with mixing impeller, 2) Coriolis mass flow meter, 3) metering pump, 4) tube-in-tube heat exchanger (heating), 5) GLS, 6) drain with actuated drain valve, 7) magnetic level indicator, 8) sloped bottom collection tank, 9) tube-in-tube heat exchanger (cooling), 10) coalescing filter, 11) transfer pump, 12) vent silencer. Construction of the GLS test facility is in progress. UTRC will report out on the ability of this GLS and its modified form(s) to reach the performance target of producing a H₂

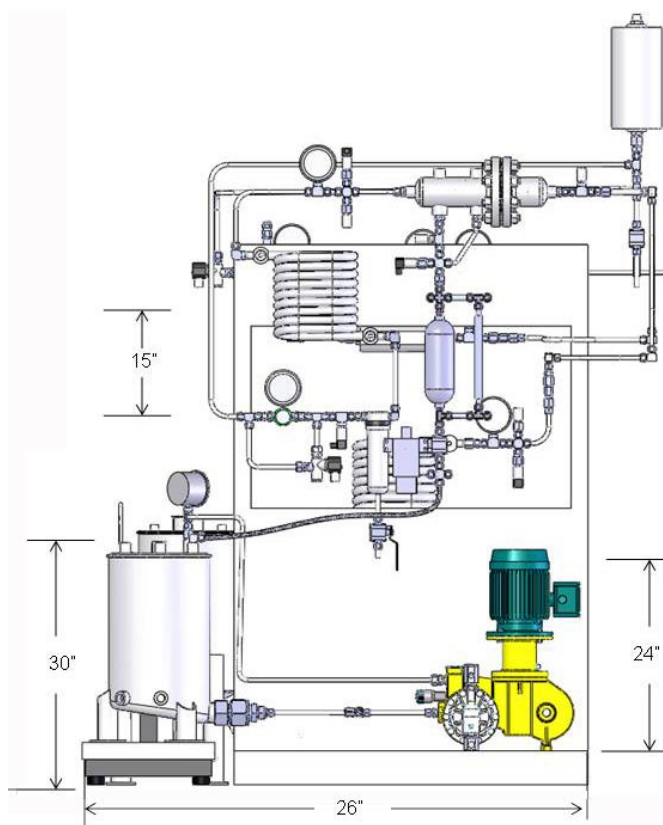


FIGURE 2. Front view gas liquid separator test rig

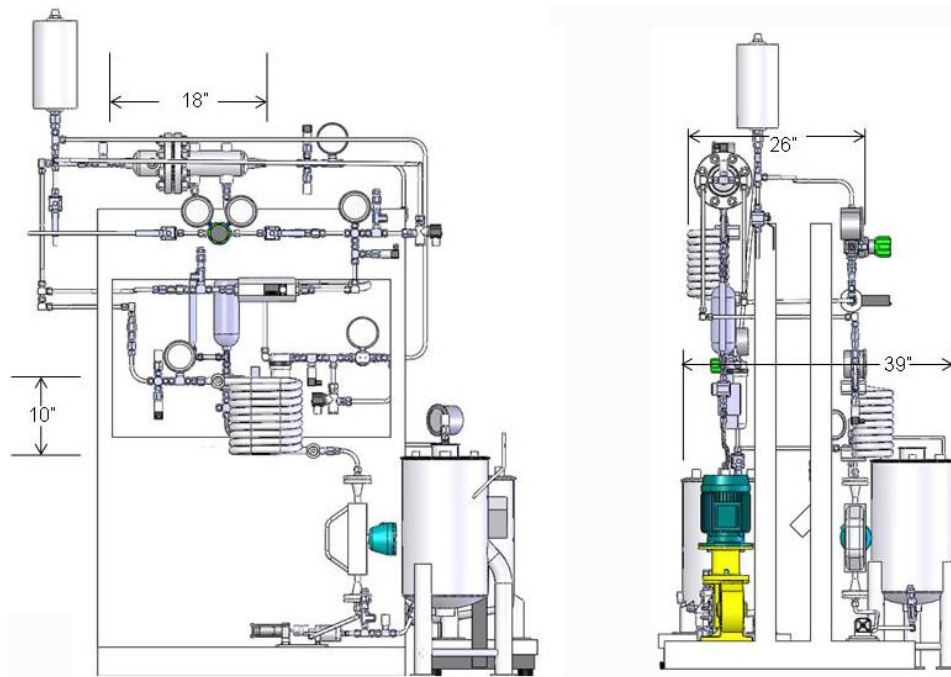


FIGURE 3. Back and side view of gas liquid separator test rig

gas with less than 100 ppm aerosol when handling a fluid comprising 720 mL/min liquid phase and 600 slpm of H₂ gas phase (from 40 wt% AB @ 2.35 Eq H₂ and max H₂ flow of 0.8 g/s H₂) that has a viscosity less than 1,500 cp with a GLS mass and volume less than 5.4 kg and 19 liters, respectively.

Hydrogen produced during AB thermolysis contains various impurities [4]. One of those impurities is ammonia (NH₃), which has to be removed down to 0.1 ppm level according to the SAE International J2719 guideline [5]. UTRC developed a high capacity regenerable ammonia adsorbent in collaboration with Université du Québec à Trois-Rivières (UQTR), Canada. The sorbent comprises metal chlorides (e.g. ZnCl₂, MgCl₂, and MnCl₂) that have been deposited on the super activated carbon IRH-33. Its dynamic sorption capacity is shown in Figure 4 as a function of the number of cycles. The sorbent makes it possible to scrub NH₃ down to 0.1 ppm with a replacement/regeneration interval of 1,800 miles of driving at an inlet concentration of 500 ppm while having a mass and volume of 1.2 kg and 1.6 liters, respectively, which is an important goal for the chemical hydride system development within the HSECoE.

H₂ quality from cryo-adsorption systems is impacted by adsorbent particulates that can get entrained into the hydrogen that is being supplied to the fuel cell system. UTRC evaluated the performance of porous metal particulate filters to mitigate particulates and for containing the adsorbent material in its storage tank. The particulate concentration was measured by means of a Engine Exhaust Particle Sizer™ spectrometer on the outlet of a packed bed of MaxSorb powder inside a sample cylinder with and without the filter.

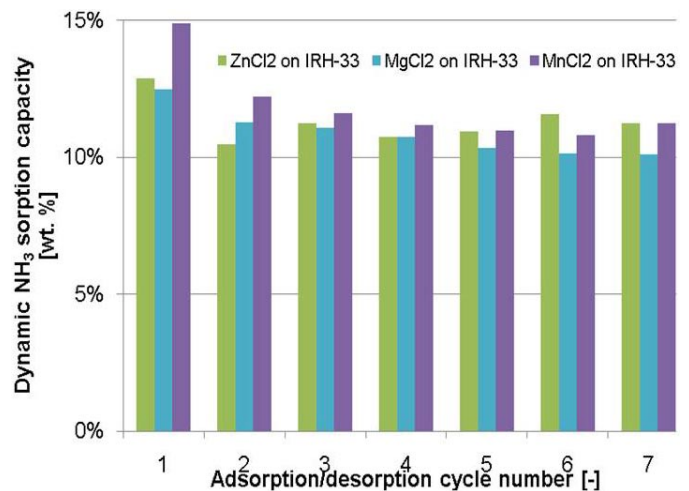


FIGURE 4. High capacity and regenerable NH₃ adsorbent based on IRH-33 + metal chlorides

The results indicate that a 0.5 μm porous metal filter is capable of reducing the particulate concentration to a level of 400 μg/m³, which is below the SAE J2719 guideline [5] of 1,000 μg/m³.

Adsorbents like MaxSorb, IRH-33 and MOF-5, which are being considered for the cryo-adsorption system, have a high specific surface area on a gravimetric basis but a relative low specific surface area on a volumetric basis when deployed as a powder due to their low tap density. UTRC evaluated several methods for compacting these materials in

order to reduce the volume of the storage system: 1) uniaxial compaction, 2) uniaxial compaction inside an aluminum foam, 3) vibration packing, 4) filter press and 5) spark plasma sintering (SPS). Uniaxial compaction was found to be applicable to MOF-5 and thermal conductivity samples were prepared that contained 10 wt% expanded natural graphite (ENG) worms and had a density of $(0.604 \pm 0.004) \text{ g/cm}^3$ after compaction at 25 MPa. SPS was successful in compacting MaxSorb and IRH-33 to densities $>0.6 \text{ g/cm}^3$ but all other techniques that were evaluated yielded densities equal to the tap density of 0.3 g/cm^3 of those SACs due to spring-back. SPS processing conditions were optimized in order to minimize loss of specific surface area on a gravimetric basis upon compaction. The results for IRH-33 are shown in Table 2. SPS was found to be scalable to large size samples, as shown in Figure 5. Samples with a 4-cm diameter and 2-cm thickness were successfully prepared and were used for thermal conductivity measurements.

UTRC developed a test method to assess the thermal conductivity anisotropy of compacted materials after introducing ENG worms [6]. The method is based on performing measurements according to the transient plane source method in each of the orthogonal directions of the sample and a subsequent inverse analysis with a COMSOL multiphysics model of the experiment in order to extract thermal conductivity parameters. The method was applied to MOF-5 with 10 wt% ENG worms at room temperature. The results from the analysis are shown in Table 3. The thermal conductivity of the MOF-5 sample with ENG was a factor 5-12 higher in the direction perpendicular to the compaction direction. This has been ascribed to the alignment of ENG platelets perpendicular to that compaction direction, which was first observed in $\text{MgH}_2 + \text{ENG}$ composites [7]. UTRC observed similar improvements of the thermal conductivity with IRH-33 + ENG composite samples that had been compacted through SPS.

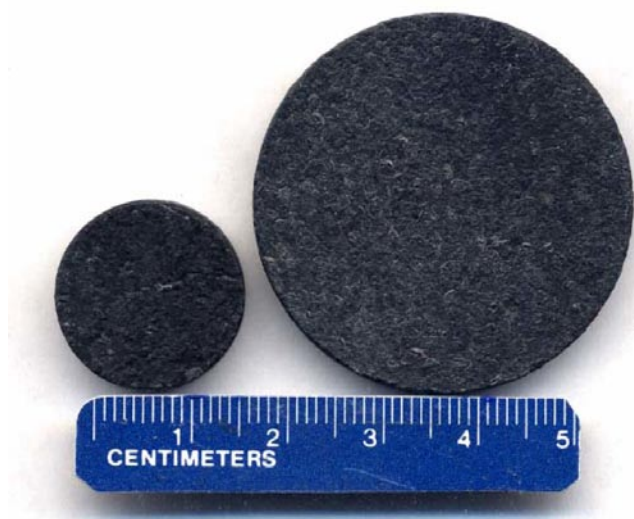


FIGURE 5. SPS of SAC IRH-33

TABLE 3. Thermal conductivity anisotropy of compacted MOF-5 + 10 wt% ENG worms at a density of $(0.604 \pm 0.004) \text{ g/cm}^3$

| Parameter | 95% confidence interval | Unit |
|-----------|-------------------------|--------|
| k_x | $3.32 < 3.45 < 3.58$ | W/m/K |
| k_y | $1.44 < 1.49 < 1.55$ | W/m/K |
| k_z | $0.280 < 0.286 < 0.292$ | W/m/K |
| C_p | $1,395 < 1,438 < 1,484$ | J/kg/K |

UTRC developed a plan for measuring the dust explosion characteristics of MOF-5 powder in air and air/ H_2 mixtures, building on its experience with such tests from a separate DOE contract. UTRC performed a limited number of experiments to assess the risks associated with AB dissolved in or mixed with ionic liquids. AB phase separated from the three ionic liquids that were evaluated and an AB mixture with ionic liquids that would stay liquid before and after

TABLE 2. SPS results of SACIRH-33

| Material | Form | Temp. (°C) | Pressure (MPa) | Density (g/cm^3) | Surface Area | | Micropore Vol. (cm^3/g) | Mesopore Vol. (cm^3/g) | Total Vol. ($P/P_0=0.9$) (cm^3/g) |
|----------|---------------------|------------|----------------|-----------------------------|---------------------------|------------------------------|---|--|---|
| | | | | | (m^2/g) | (m^2/cm^3) | | | |
| IRH-33 | Granular | N.A. | | 0.22 | 2,334 | 513 | 0.81 | 0.85 | 1.44 |
| | Pellet (HRI binder) | | | 0.84 | 1,381 | 1,160 | 0.49 | 0.18 | 0.68 |
| | SPS | 900 | 40 | 0.63 | 1,558 | 982 | 0.56 | 0.44 | 0.92 |
| | | 900 | 80 | 0.76 | 1,698 | 1,290 | 0.60 | 0.34 | 0.92 |
| | | 1000 | 40 | 0.70 | 1,401 | 981 | 0.50 | 0.40 | 0.82 |
| | | 1200 | 10 | N.A. | 1,400 | N.A. | 0.51 | 0.65 | 0.94 |
| | | 1200 | 40 | 0.84 | 1,046 | 879 | 0.37 | 0.31 | 0.63 |
| | | 1200 | 80 | 1.13 | 993 | 1,122 | 0.35 | 0.17 | 0.52 |
| | | 1200 | 80 | 0.94 | 1,094 | 1,028 | 0.38 | 0.22 | 0.59 |

thermolysis was not found. Kidde-Fenwal made flammability test equipment available to UTRC. It will be used to evaluate the flammability of AB in a slurry form with silicone oil, as is going to be prepared by PNNL. In collaboration with members of the HSECoE, UTRC participated in face-to-face failure mode and effect analysis (FMEA) of both the proposed chemical hydride and cryo-adsorption system. The focus of both FMEAs was to identify additional experiments that would need to be performed in order to make sure that each of HSECoE's systems would meet the DOE requirements.

Conclusions and Future Directions

Conclusions derived from the work in FY 2012 are:

- System engineering shows that onboard reversible metal hydride materials need to meet stringent requirements in terms of gravimetric capacity and hydrogenation enthalpy in order to meet the DOE 2017 targets for light-duty vehicles. HSECoE discontinued such a system development when such materials could not be identified.
- GLS became a new unit operation in the chemical hydride system as a result of selecting AB in a fluid form for Phase 2 of HSCoE. UTRC is taking the lead on this topic and selected a passive GLS design with low profile and is building a test rig.
- The NH₃ impurity in H₂ produced from the thermolysis of AB can be effectively removed with a high capacity and regenerable adsorbent filter that comprises metal chlorides deposited on the super activated carbon IRH-33 from UQTR.
- ENG 'worms' are effective additives that increase the thermal conductivity of not only metal hydride materials but also adsorbents like MOF-5, and IRH-33.
- SPS is an effective technique that can be used to compact super activated carbon while minimizing the loss of its gravimetric specific surface area.

Future work will comprise:

- Graphical user interface development of Simulink[®] framework in order to promote wider usage.
- Lead Integrated Power Plant/Storage System Modeling technical area.
- Qualitative risk assessments of each of the remaining materials based hydrogen storage systems and tests in support of the qualitative risk assessment.
- Engineering and testing of specialty components for H₂ storage systems and their experimental evaluation, such as the gas liquid separator in the chemical hydride system.
- Experimental evaluation of NH₃ filter connected to H₂ generated from the thermolysis of liquid AB.

FY 2012 Publications/Presentations

1. Bart A. van Hassel, Daniel A. Mosher, José Miguel Pasini, Mikhail Gorbounov, John Holowczak, Xia Tang, Robert Brown, Bruce Laube, and Lawrence Pryor, "Engineering improvement of NaAlH₄ system," *Int. J. Hydrogen Energy* **37**, 2756–2766 (2012).
2. José Miguel Pasini, Bart A. van Hassel, Daniel A. Mosher and Michael J. Veenstra, "System modeling methodology and analyses for materials-based hydrogen storage," *Int. J. Hydrogen Energy* **37**, 2874–2884 (2012).
3. Matthew Thornton, Jon Cosgrove, Aaron Brooker, José Miguel Pasini, and Michael J. Veenstra, "Development of a vehicle level simulation model for evaluating the trade-off between various advanced on-board hydrogen storage technologies for fuel cell vehicles," SAE Technical Paper 2012-01-1227, *SAE 2012 World Congress & Exhibition*, April 2012, Detroit, MI, USA (2012).
4. Bart A. van Hassel, J.M. Pasini, D. Mosher, M. Gorbounov, J. Holowczak, I. Fechenia, J. Khalil, F. Sun, X. Tang, R. Brown, B. Laube and L. Pryor, "Advancement of Systems Designs and Key Engineering Technologies for Materials-Based Hydrogen Storage", Gordon Research Conference, July 17–22, 2011 Stonehill College, Easton, Massachusetts.
5. Igor Fechenia and Bart A. Van Hassel. "Solution of Inverse Thermal Problem for Assessment of Thermal Parameters of Engineered H₂ Storage Material", COMSOL Conference, Boston, October 13–15, 2011.
6. Bart A. van Hassel, D. Mosher, J.M. Pasini, M. Gorbounov, J. Holowczak, X. Tang, R. Brown, Fanping Sun, Igor Fedchenia and A.E. Kuczek, Engineering progress in materials based H₂ storage for light-duty vehicles, IEA HIA Task 22, Copenhagen, Denmark, September 4–8, 2011.
7. Bart A. van Hassel, D. Mosher, J.M. Pasini, M. Gorbounov, J. Holowczak, X. Tang, R. Brown, Fanping Sun, Igor Fedchenia and A.E. Kuczek, Engineering progress in materials based H₂ storage for light-duty vehicles, IEA HIA Task 22, Copenhagen, Heidelberg, May 6–10, 2012.
8. Bart A. van Hassel, J.M. Pasini, R.C. McGee, J.R. Karra, A.M. Limarga, J. Holowczak, I. Fedchenia, J. Khalil, J.C. Rampone and R. Brown, Advancement of Systems Designs and Key Engineering Technologies for Materials Based Hydrogen Storage, Annual Merit Review, Crystal City, Virginia, May 14–18, 2012.
9. José Miguel Pasini, Claudio Corgnate, Bart A. van Hassel, Theodore Motyka, Sudarshan Kumar, and Kevin L. Simmons, "Metal hydride material requirements for automotive hydrogen storage systems," *submitted to Int. J. Hydrogen Energy*.

References

1. <http://www1.eere.energy.gov/hydrogenandfuelcells/mypp/pdfs/storage.pdf>
2. Bart A. van Hassel, J.M. Pasini, R.C. McGee, J.R. Karra, A.M. Limarga, J. Holowczak, I. Fedchenia, J. Khalil, J.C. Rampone and R. Brown, Advancement of Systems Designs and Key Engineering

Technologies for Materials Based Hydrogen Storage, Annual Merit Review, Crystal City, Virginia, May 14–18, 2012.

3. José Miguel Pasini, Claudio Corgnale, Bart A. van Hassel, Theodore Motyka, Sudarshan Kumar, and Kevin L. Simmons, “Metal hydride material requirements for automotive hydrogen storage systems,” *submitted to Int. J. Hydrogen Energy*.

4. T.A. Semelsberger, Ben Davis, Biswajit Paik, Jose Tafoya, Gerie Purdy, and Tessui Nakagawa, Chemical Hydride Rate Modeling, Validation, and System Demonstration, Annual Merit Review, Crystal City, Virginia, May 14–18, 2012.

5. Information Report on the Development of a Hydrogen Quality Guideline for Fuel Cell Vehicles, SAE International Surface Vehicle Information Report, J2719 APR2008, Revised 2008-04.

6. Igor Fechenia and Bart A. Van Hassel. “Solution of Inverse Thermal Problem for Assessment of Thermal Parameters of Engineered H₂ Storage Material”, COMSOL Conference, Boston, October 13–15, 2011.

7. A. Chaise, P. de Rango, Ph. Marty, D. Fruchart, S. Miraglia, R. Olive's, S. Garrier, Enhancement of hydrogen sorption in magnesium hydride using expanded natural graphite, *International journal of hydrogen energy*, 34 (2009), pp. 8589 – 8596.

IV.D.7 Thermal Management of Onboard Cryogenic Hydrogen Storage Systems

Mei Cai (Primary Contact), Darsh Kumar, Senthil Kumar, Niket Kaisare, Martin Sulic, Jerry Ortman, and Amlan Chakraborty
General Motors R&D Center (GM)
30500 Mound Road
Warren, MI 48090
Phone: (586) 596-4392
Email: mei.cai@gm.com

DOE Managers

HQ: Ned Stetson
Phone: (202)586-9995
Email: Ned.Stetson@ee.doe.gov
GO: Jesse Adams
Phone: (720) 356-1421
Email: Jesse.Adams@go.doe.gov

Contract Number: DE-FC36-09GO19003

Project Start Date: February 1, 2009
Project End Date: June 30, 2014

Fiscal Year (FY) 2012 Objectives

Main objectives of this project are:

- To develop system models and detailed transport models for onboard hydrogen storage systems using adsorbent materials, and to determine system compliance with the DOE technical targets.
- To develop storage media structures with optimized engineering properties for use in storage systems.
- To design and build an experimental vessel for validation of cryo-adsorption models.

Technical Barriers

This project addresses the following technical barriers from the Hydrogen Storage section of the Fuel Cell Technologies Program Multi-Year Research, Development, and Demonstration Plan:

- (A) System Weight and Volume
- (C) Efficiency
- (E) Charging/Discharging Rates
- (J) Thermal Management

Technical Targets

In this project, studies are being conducted to develop metal-organic framework (MOF)-5 based storage media with optimized engineering properties. This material has potential to meet 2017 technical target for onboard hydrogen storage as shown Table 1.

TABLE 1. 2017 Technical Targets for Onboard Hydrogen Storage

| Storage Parameter | 2017 Target (system) | MOF-5 (material) |
|---|----------------------|------------------|
| System Gravimetric Capacity | 0.055 | 0.187 |
| System Volumetric Capacity ¹ | 0.040 | 0.028 |

¹Volumetric capacity is based on powdered MOF5

FY 2012 Accomplishments

- Developed a two-dimensional (2-D) model of refueling of MOF-5 pellet with Dubinin-Ashtakohov (D-A) adsorption isotherm that includes effects of expanded natural graphite (ENG) additive and anisotropic thermal conductivity.
- Demonstrated that over 96% of the hydrogen from MOF-5 bed can be extracted.
- Completed the design, built, and installation of a cryo-vessel with automated control instrumentation.
- Designed an effective helical coil heat exchanger for hydrogen desorption process to be used in an MOF-5 bed with a hydrogen supplying rate of 1 g/s.
- Completed low temperature thermal conductivity measurements of MOF-5 pellets with density of 0.3 and 0.5 g/cm³ respectively, and with 0, 5 and 10 wt% ENG for improved thermal conductivity.



Introduction

The DOE is supporting research to demonstrate viable materials for onboard hydrogen storage. Onboard hydrogen storage systems based on cryo-adsorbents are of particular interest due to high gravimetric hydrogen capacity and fast kinetics of the sorbent materials at low temperatures and moderate pressure. However, cryo-adsorbents are generally characterized by low density and thermal properties. As part of the Hydrogen Storage Engineering Center of Excellence (HSECoE) team, the GM team is building system models and detailed transport models to optimize the cryo-adsorbent fuel tank.

Over FY 2012, models have been developed for the MOF adsorbent material, MOF-5, with a focus on optimization of heat exchanger design with the objective of minimizing the heat exchanger mass while meeting DOE targets. In addition, models for MOF-5 intra-pellet hydrogen transport to optimize pellet shape and pellet permeability and thermal conductivity for refueling have been developed. Examination of the low density and thermal conductivity properties of MOF-5 lead to compaction of the adsorbent with addition of a thermal enhancer by up to 10 wt%. Samples of various densities and thermal enhancement were studied over a large temperature range.

Approach

Based on the previous work done with AX-21 system, continued modeling effort was carried out for the design of an optimized heat exchanger to be used in the MOF-5 system. The goal of this design is to extract 5,600 g of hydrogen during a 5,600 s time discharge period with a maximum hydrogen flow rate of 1 g/s to supply the fuel cell stack. All the required heat for achieving this goal should be supplied by the internal element in a helical coil shape. Two scenarios were studied in details, in which the initial bed pressure was set to 60 and 200 bars respectively, for systems with a thermal conductivity of 0.3 and 0.5 W/mK respectively. For each system, two contact heat fluxes, 919 and 1,546 W/m², were also examed. For all the case studies, the final bed pressure was set to 4 bars. The optimal pellet size was calculated through modeling based on previously reported excess adsorption data on neat MOF-5 pellets [1,2]. Parameters used for the baseline case study are: isotropic thermal conductivity of a MOF-5 pellet with 10 wt% ENG, permeability of 1.2×10^{-14} m², D-A adsorption isotherm parameters for neat MOF-5 and pellet dimensions of $h=d=1$ cm. MOF-5 pellets with densities of 0.3 and 0.5 g/cm³ respectively were used for the permeability modeling study. The anisotropic thermal conductivity modeling of MOF-5 + ENG pellets was aimed to examine the effect on refueling time across the radial and axial direction of the pellet. Low temperature thermal conductivity experiments were also carried out on a series of MOF-5 pellets, with the densities of 0.3 and 0.5 g/cm³ respectively, each one of them contains 0, 5 and 10 wt% ENG respectively for the thermal enhancement. The ENG were introduced into the system by mixing MOF-5 and ENG with a shaker mill with no additional mixing medium. Pellets were primarily prepared by Ford and supplied to GM for measurement; additional pellets were also prepared by GM for validation purpose. The thermal conductivity of pellet was measured with a P670 Thermal Transport System from Quantum Design, over a range of 4–350 K.

Results

A. Three-Dimensional (3-D) Modeling for Hydrogen Desorption on MOF-5

Figure 1 demonstrates the bed temperature profile and amount of extracted hydrogen during the discharge with an initial bed pressure of 200 bars and bed thermal conductivity of 0.5 W/mK. Figure 1A shows that the average final bed temperature remains in an acceptable range of 150-160 K whereas maximum bed temperature lies below 240 K. Minimum bed temperature lies in between 80-105 K. Further investigation confirmed that there is uniform temperature distribution throughout the bed which significantly affects the desorption efficiency. Figure 1B indicates the amount of extracted total hydrogen (gas phase + adsorbed phase)

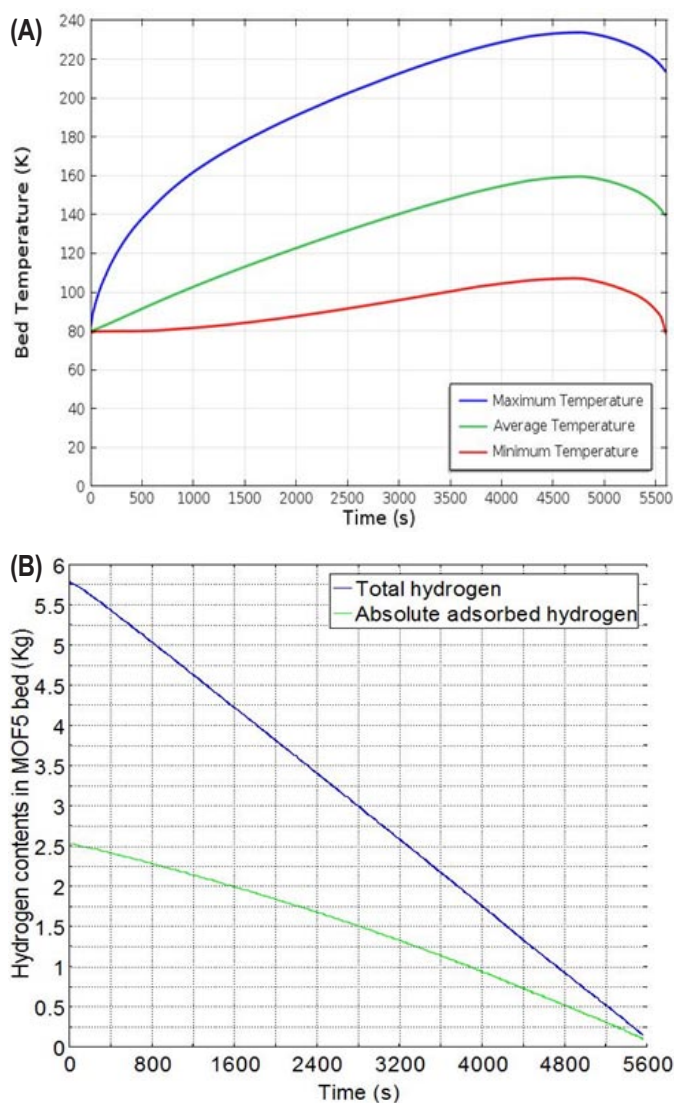


FIGURE 1. (A) Temperature profiles; and (B) amount of hydrogen extraction in MOF-5 bed.

and absolute adsorbed hydrogen during the time period. It is evident that the system can effectively extract over 96% of hydrogen from the bed. Table 2 further shows the comparison of hydrogen extraction process in two models for AX-21 and MOF-5. Both models are proven to be efficient and accurate since the modeled desorption efficiencies are very close to that of the theoretical values. The total hydrogen desorption efficiency of MOF-5 is significantly higher than that of AX-21 (>96% vs. >92%). Another important aspect is that the heat applied into the discharging is comparatively lower in MOF-5 system than that in AX-21 system. Furthermore, the results indicate that the bed volume with higher initial pressure is comparatively lower in MOF-5 than that of AX-21. There are also significant design alterations in the heating coil with the exception for a 60 bar system. A significant decrease in coil length and turns were also observed for the MOF-5 system with higher initial pressure of 200 bars, compared to AX-21 system.

TABLE 2. Comparison of Simulation and Theoretical Results for 5.6 kg of Deliverable H₂

| | 60 bar and 80K | | 200 bar and 80K | |
|--|----------------|-----------|-----------------|-----------|
| | AX-21 bed | MOF-5 Bed | AX-21 bed | MOF-5 Bed |
| THEORETICAL (D-A METHOD) HYDROGEN AVAILABILITY FOR EXTRACTION | | | | |
| % extracted H ₂ | 92.1 | 96.7 | 94.1 | 98.4 |
| RESULTS FROM SIMULATION | | | | |
| % extracted H ₂ | 91.8 | 96.6 | 92.6 | 97.5 |
| Required Heat (W) | 1,760 | 1,546 | 1,374 | 919 |
| Mass of the bed (kg) | 59 | 30 | 36 | 16 |
| Total bed volume (L) | 212.52 | 217.23 | 140.08 | 125.24 |
| HEATING ELEMENT SPECIFICATION | | | | |
| Turn of the coil | 12.13 | 12.40 | 8 | 6.63 |
| Length of the coil (m) | 13.33 | 13.63 | 8.80 | 7.30 |

B. 2-D Modeling of Pellet Size, Permeability, and Thermal Conductivity Effect on Refueling

Various pellet sizes were studied for the effect of refueling time. Stick like pellets with aspect ratios of $h/d \gg 2$ were found to be the most suitable size to achieve the fast refueling time at a relatively high storage volume. Likewise, flat “hockey puck” pellets are also likely to provide low refueling time. Conversely, short pellets ($h/d \approx 0.5$) show the longest refueling times. In addition, a random packed bed of such pellets is not recommended based on simulation studies.

Based on previous study, pellet compaction to 0.51 gm/cm³ provides a good compromise between the volumetric and gravimetric capacities [1]. Permeability was measured for MOF-5 pellets at different compaction

levels (0.3 to 0.5 gm/cm³). Three values were modeled: a baseline of 1.2×10^{-14} m² (corresponding to 0.51 g/cm³ MOF-5 pellet), a high value of 2.1×10^{-13} m² (0.301 g/cm³ pellet), and a low value of 5.1×10^{-16} m². The results showed that pellet permeability had a negligible impact on the amount of hydrogen adsorbed and the volume-averaged temperature. Even for the lowest value of permeability, the pressure equilibrates within 0.1 seconds. We conclude that the pellet permeability does not have any impact on the refueling behavior of a single pellet with quiescent boundary conditions. These results may not be extrapolated to refueling of an adsorbent bed because pressure drop and flow rate through the bed may depend on the bed permeability.

Anisotropic thermal conductivity of MOF-5 pellets with 10 wt% ENG was also modeled. Figure 2 shows the effect of radial thermal conductivity λ_r on the refueling. The axial conductivity was kept at the nominal value of λ_z while two cases of $\lambda_r = \{2, 4\} \times \lambda_z$ were studied. The results show that increasing the radial thermal conductivity decreases the refueling time from 15.7 seconds in the base case to 9.3 and 5.1 seconds, respectively. We consider the refueling time here to be the point at which 95% of the pellet’s volumetric storage capacity has been reached.

C. Low Temperature Thermal Conductivity Measurements

Figure 3 shows improvement in thermal conductivity while increasing the amount of ENG and the pellet density. In this study, pellets with 0.3 g/cm³ are proven not strong for handling, which resulted in limited data collection. In addition, structural integrity of 0.3 g/cm³ pellets decreased with increasing wt% ENG. Noticeable variances in the thermal conductivity profile were observed over the temperature range studied, indicating there is a lack of the consistency between pellets. These variances are attributed

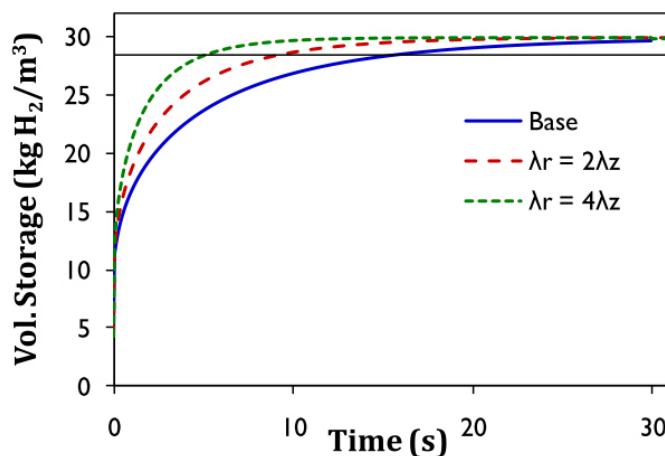


FIGURE 2. Effect of radial thermal conductivity on pellet refueling. The solid line corresponds to $\lambda_r = \lambda_z$; the axial thermal conductivity is kept at a nominal value of λ_z and the radial value is increased in the two dashed lines.

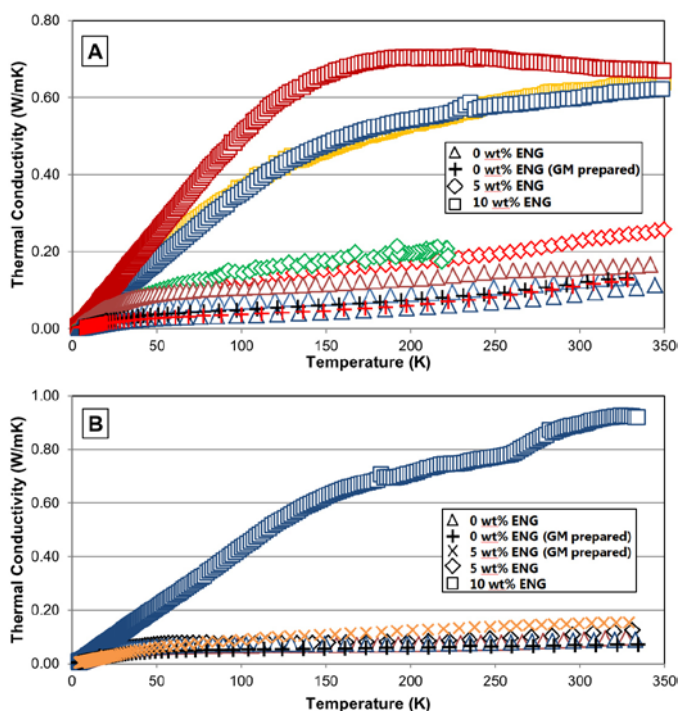


FIGURE 3. MOF-5 pellets (A) 0.5 g/cm^3 series; (B) 0.3 g/cm^3 series with 0, 5, and 10 wt% expanded natural graphite (ENG).

to slight difference in density or wt% ENG or orientation of ENG within each pellet. Typically, the lowest density pellet within a series exhibited the lowest k value, as expected. As shown in Figure 3, one interesting observation is that the pellets with 0.3 g/cm^3 did not improve in k value as significantly as the pellets with 0.5 g/cm^3 over the range of 0 to 5 wt% ENG. However, the difference between 0.3 and 0.5 g/cm^3 pellets is only slight at ENG levels of 10 wt%. This is mainly due to the graphite which plays a more significant role in the thermal conductivity over the temperatures studied.

Future Directions

- Include D-A adsorption isotherm parameters for MOF-5 pellet with 10% ENG in pellet model; obtain improved measurement of pellet permeability for model.
- Modeling of a 3-D flow through hydrogen charging system in MOF-5 bed for a 3-L vessel.
- Design and fabrication of a 3-L vessel for MOF-5 charging and discharge experiments – model validation with simulation results.
- Design and modeling of heat exchangers – liquid N_2 cooling during adsorption and fuel cell waste heat for desorption.
- Experimental validation of flow-through and heat exchanger models.

FY 2012 Publications/Presentations

1. S Kumar et al. Thermal Management of On-Board Cryogenic Hydrogen Storage Systems, DOE Annual Merit Review, 2012, Washington, D.C.
2. A Chakraborty; S Kumar. Heat Exchanger Design for Adsorbent Systems : Model and Results, HSE CoE face to face meeting, Santa Fe, NM, November, 2011.
3. A Chakraborty; S Kumar. Thermal Management and Desorption Modeling of a Cryo-adsorbent Hydrogen Storage System, International Journal of Hydrogen Energy, manuscript submitted, 2012.
4. M Sulic; S Kumar; M Cai. Cycling and Engineering Properties of Highly Compacted Sodium Alanate Pellets, International Journal of Hydrogen Energy, manuscript submitted, 2012.
5. M Sulic; S Kumar; M Cai. Controlled Degradation of Highly Compacted Sodium Alanate Pellets, International Journal of Hydrogen Economy, manuscript submitted, 2012.
6. M. Raju; S. Kumar. Optimization of Heat Exchanger Designs in Metal Hydride based Hydrogen Storage Systems, International Journal of Hydrogen Economy, 37, 2767, 2012.
7. S Kumar; M Raju; VS Kumar. System Simulation Models for On-board Hydrogen Storage Systems, International Journal of Hydrogen Economy, 37, 2862, 2012.
8. N Kaisare. Modeling of Cryo-adsorption of Hydrogen on MOF-5 Pellets: effect of pellet properties on moderate pressure refueling, Internal GM report, 2012.
9. VS Kumar. 2-D Model for Non-isothermal Adsorption of Hydrogen in Cylindrical Adsorbent Pellets, Internal GM report, 2011.
10. S Kumar. Metal Hydride Material Requirements for Hydrogen Storage in Fuel Cell Vehicles, Internal GM report, 2012.

References

1. Purewal, J.J.; Liu, D.; Yang, J.; Sudik, A.; Siegel, D.J.; Maurer, S.; Muller, U., Increased volumetric hydrogen uptake of MOF-5 by powder densification. International Journal of Hydrogen Energy 2012, 37, (3), 2723-2727.
2. Sudik, A.; Veenstra, M.; Müller, U.; Maurer, S.; Gaab, M.; Purewal, J.; Liu, D.a.; Xu, C.; Siegel, D.; Ni, J., Adsorbent Materials for HSECoE, In Hydrogen Storage Technical Team Review, 2012.

IV.D.8 Ford/BASF SE/UM Activities in Support of the Hydrogen Storage Engineering Center of Excellence

Michael Veenstra (Primary Contact, Ford),
 Andrea Sudik (Ford), Donald Siegel (UM),
 Justin Purewal (UM), Chunchuan Xu (UM),
 Yang Ming (UM), Manuela Gaab (BASF SE),
 Stefan Maurer (BASF SE), Ulrich Müller
 (BASF SE), Jun Yang (Ford)

Ford Motor Company
 2101 Village Road
 Dearborn, MI 48121
 Phone: (313) 322-3148
 Email: mveenstr@ford.com

DOE Managers

HQ: Ned Stetson
 Phone: (202) 586-9995
 Email: Ned.Stetson@ee.doe.gov

GO: Jesse Adams
 Phone: (720) 356-1421
 Email: Jesse.Adams@go.doe.gov

Contract Number: DE-FC36-GO19002

Subcontractors:

- University of Michigan, Ann Arbor, MI
- BASF SE, Ludwigshafen, Germany

Project Start Date: February 1, 2009
 Project End Date: June 30, 2014

Technologies Program Multi-Year Research, Development and Demonstration Plan:

- (A) System Weight and Volume
- (B) System Cost
- (C) Efficiency
- (D) Durability/Operability
- (E) Charging/Discharging Rates
- (H) Balance of Plant (BOP)
- (J) Thermal Management

Technical Targets

The outcomes of this project affect vehicle and system level models, cost analysis, and materials property assessment/optimization. Insights gained from these studies are applied towards the engineering of hydrogen storage systems that meet the following DOE 2010 and ultimately 2017 hydrogen storage targets (Table 1).

TABLE 1. Technical Targets

| Storage Parameter | Units | 2010 | 2017 |
|---|-----------------------|--------|--------|
| System Gravimetric Capacity | kg-H ₂ /kg | 0.045 | 0.055 |
| System Volumetric Capacity | kg-H ₂ /L | 0.028 | 0.040 |
| Storage System Cost | \$/kWh _{net} | TBD | TBD |
| System Fill Time (for 5 kg H ₂) | min | 4.2 | 3.3 |
| Minimum Full Flow Rate | (g/s)/kW | 0.02 | 0.02 |
| Min/Max Delivery Temperature | °C | -40/85 | -40/85 |
| Min. Delivery Pressure (Fuel Cell) | Atm | 5 | 5 |

TBD – to be determined

Fiscal Year (FY) 2012 Objectives

This project addresses three of the key technical obstacles associated with the development of a viable hydrogen storage system for automotive applications:

- (Task 1) Create accurate system models that account for realistic interactions between the fuel system and the vehicle powerplant.
- (Task 2) Develop robust cost projections for various hydrogen storage system configurations.
- (Task 3) Assess and optimize the effective engineering properties of framework-based hydrogen storage media (such as metal-organic frameworks [MOFs]).

Technical Barriers

This project addresses the following technical barriers from the Hydrogen Storage section of the Fuel Cell

FY 2012 Accomplishments

- Task 1. System Modeling
 - Benchmarked the system modeling results in comparison to other hydrogen vehicle and storage analyses by Argonne National Lab (ANL) and identified the areas of differing assumptions or modeling approaches.
 - Enhanced the framework and validated the elements of the universal Hydrogen Storage Engineering Center of Excellence (HSECoE) Simulink® model with further refinement to the fuel cell model to ensure the waste heat and temperature polarization effects appropriately represent integration with the hydrogen storage system.

- Completed a detailed failure mode and effects analysis (FMEA) for the adsorbent and chemical hydrogen storage systems with the respective design teams.
- Task 2. Cost Analysis
 - Supported the benchmarking and development of the HSECoE material-based hydrogen storage system cost projection models.
 - Decomposed the pressure vessel for the purpose of adsorbent system design trade-offs and sensitivity cost assessments.
 - Developed initial estimator tool and references to be utilized for cost manufacturing models with projection capability based on a set of key cost drivers.
- Task 3. Assessment/Optimization of Framework-Based Storage Media
 - Led the HSECoE adsorbent efforts as the system architect through the identification of research gaps, development of SMART (specific, measurable, attainable, relevant, timely) milestones, completed material selection, and coordinated team.
 - Validated powder MOF-5 isotherm model parameters at higher pressure (i.e. up to 200 bar), and at temperatures within the anticipated operating window.
 - Assessed the impact of thermal conductivity aids on principal hydrogen storage engineering properties (e.g., gravimetric capacity, gas permeability, crush strength, etc.).
 - Established relationship between density and gas transport through permeation and diffusivity.



Introduction

Widespread adoption of hydrogen as a vehicular fuel depends critically on the development of low-cost, onboard hydrogen storage technologies capable of achieving high energy densities and fast kinetics for hydrogen uptake and release. As present-day technologies are unlikely to attain established DOE targets for onboard hydrogen storage technologies, interest in materials-based approaches have garnered increasing attention. To hasten development of these ‘hydride’ materials, the DOE established three centers of excellence for materials-based hydrogen storage research. While the centers have made substantial progress in developing new storage materials, challenges associated with the engineering of the storage system around a candidate storage material remain largely unresolved.

Approach

Ford-UM-BASF is conducting a multi-faceted research project that addresses three of the key challenges associated with the development of materials-based hydrogen storage systems.

Systems Modeling (Task 1): We are evaluating and developing system engineering technical elements with a focus on hydrogen storage system operating models which will result in a set of dynamic parameters for optimizing the storage system as it interacts with the fuel cell system.

Cost Analysis (Task 2): We are performing hydrogen storage manufacturing cost analyses for various candidate system configurations and operating strategies to facilitate potential cost reductions and manufacturing optimization for the storage system designs.

Sorbent Media Assessment & Optimization (Task 3): We are characterizing the “effective engineering properties” for MOFs in order to devise optimal strategies for their use in an adsorbent system.

Results

Below is a description of our technical results for each task and how these results relate to achieving the DOE targets.

Task 1. System Modeling

During this past year, the System Modeling Team focused on the key tasks that were necessary to ensure robustness in the models and system designs. First, Ford led a benchmarking analysis and facilitated a face-to-face design review at United States Council for Automotive Research with ANL and the HSECoE. The review provided an excellent assessment of the commonalities and differences between the ANL and HSECoE modeling assumptions for various material-based hydrogen storage systems. As part of the benchmarking analysis, an evaluation matrix was completed to compile the model results from ANL and HSECoE for each of the baseline systems as identified at the phase 1 milestone: sodium alanate, liquid ammonia borane, and adsorbent MOF-5. The matrix included a summary comparison to the DOE storage system technical targets, a system bill of material with weights and volumes, and a schematic for the system. The HSECoE architects were able to use the results of this effort to reconfirm and/or improve their model assumptions based on the independent comparative assessment. In addition, the modeling effort continued with further refinement in the fuel cell model to ensure the waste heat was correctly represented for the integration with the hydrogen storage systems. In particular, the idle and dynamic UA (overall heat transfer coefficient x heat transfer surface area) values in the fuel cell stack model were modified and verified against vehicle test data.

The modeling team also initiated a target sensitivity study to assess the effects of the storage system gravimetric and volumetric ratios on the vehicle fuel economy and driving range using the HSECoE framework. These results provide a quantitative correlation between the storage targets and vehicle effects which will guide the optimization of the system design. Another key accomplishment was the leading and completion of the FMEA for the adsorbent and chemical hydride systems. The HSECoE team recognized the FMEA as tool that can be used to evaluate risk, reduce failure modes, and guide the validation test plan. The functions within the FMEA were directly aligned with the DOE system targets and the effects along with the severity were completed based on prior original equipment manufacturer assessments. The result of the FMEA was the development of the risk priority number (RPN) which is the product of the severity, occurrence, and detection ratings. The RPN number allows the team to identify the key causes of high risk failures. Figure 1 provides a graphical Pareto summary of the adsorbent system RPN ratings. The team will utilize the FMEA to take action on the high RPN items and then reevaluate the rating after the action has been taken which should reduce the system risk and increase the probability of successfully achieving the desired functions. The same process was accomplished for the chemical hydrogen system based on liquid ammonia borane media.

Task 2. Cost Analysis

The Manufacturing and Cost Analysis Team during the past year developed the initial cost projections for the leading material-based storage systems within the HSECoE and conducted a cost workshop to evaluate the assumptions. As conducted with the system modeling review, an evaluation matrix was constructed to understand the key differences between the TIAX and HSECoE cost structure and assumptions. For the adsorbent system, a Pareto analysis

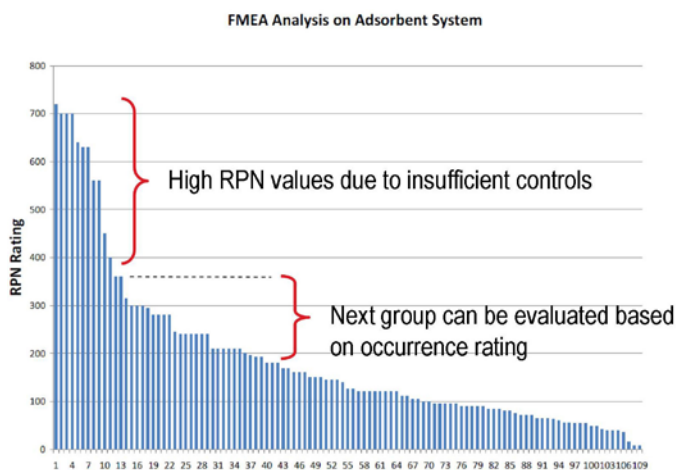


FIGURE 1. Adsorbent FMEA Pareto Chart of RPNs

identified the following key cost differences: pressure vessel fiber carbon fiber, MOF media, balance-of-plant design requirements and quantities. The overall cost results for the MOF system was similar at a cost of \$3,019 (\$16.18/kWh) for TIAX and \$2,871 (\$15.4/kWh) for HSECoE. As part of this cost task, a detailed break-down of the tank manufacturing process was formulated in a cost model based on input from Lincoln Composites and other tank suppliers. The activity-based process steps were developed for different tank types including the effects of the MOF integration into the tank. Material estimating models were also developed to assess the system effects from pressure and temperature for the adsorbent system operating condition trade-off studies.

Task 3. Sorbent Media Assessment & Optimization

System Architect Role: During the previous year, the HSECoE adsorbent system architect position transitioned to Don Siegel along with the additional responsibilities of coordinating the design and research priorities for the adsorbent team. In particular, SMART milestones and GANTT charts were developed for each HSECoE partner within the adsorbent team. The official material selection of MOF-5 for the HSECoE was completed and documented. The system design status was progressed using several face-to-face meetings, monthly teleconferences, and individualized modeling reviews.

Materials Engineering: We had previously collected several isotherms between 77 and 295 K and 0 to 100 bar for powder MOF-5, and fit this data to the Dubinin-Astakov model. Using this same approach, we have determined the isotherm parameters for a series of MOF-5 compacts with varying density and expanded natural graphite (ENG) content. In particular, we have collected adsorption isotherms at no less than three different temperatures including 77, 200, and 298 K for 0.3 or 0.5 gcm⁻³ compacts with 0, 5, or 10 wt% ENG. Here, we describe data for 0.3 gcm⁻³ MOF-5, however, the same process was applied for the determination of 0.5 gcm⁻³ MOF-5 data. The excess gravimetric hydrogen uptake (n_{ex}) for 0.3 gcm⁻³ compacted MOF-5 with 0, 5, or 10 wt% ENG additive as a function of temperature (77 to 295 K) and pressure (0 to 100 bar) is shown in Figure 2. The excess gravimetric capacity data for neat 0.3 gcm⁻³ MOF-5 at 77 K (Figure 2, top) shows a maximum uptake of approximately 6 wt% at 40 bar. This value is the same as the (uncompacted) powder MOF-5. The excess volumetric capacity based on the bulk density for the MOF-5 compact ($\rho=0.30$ gcm⁻³) is 18 g·H₂/L, 225% larger than for powder MOF-5 ($\rho=0.13$ gcm⁻³). Therefore, densification of MOF-5 is indeed beneficial for improving the volumetric capacity of MOF-5 without significantly reducing gravimetric capacity. The addition of 5 or 10 wt% ENG (Figure 2, middle for the 5 wt% case) results in a small decrease in excess gravimetric capacity. In particular, the maximum excess adsorption values for 0.3 gcm⁻³ MOF-5 with 5 or 10 wt% ENG is 5.2 or

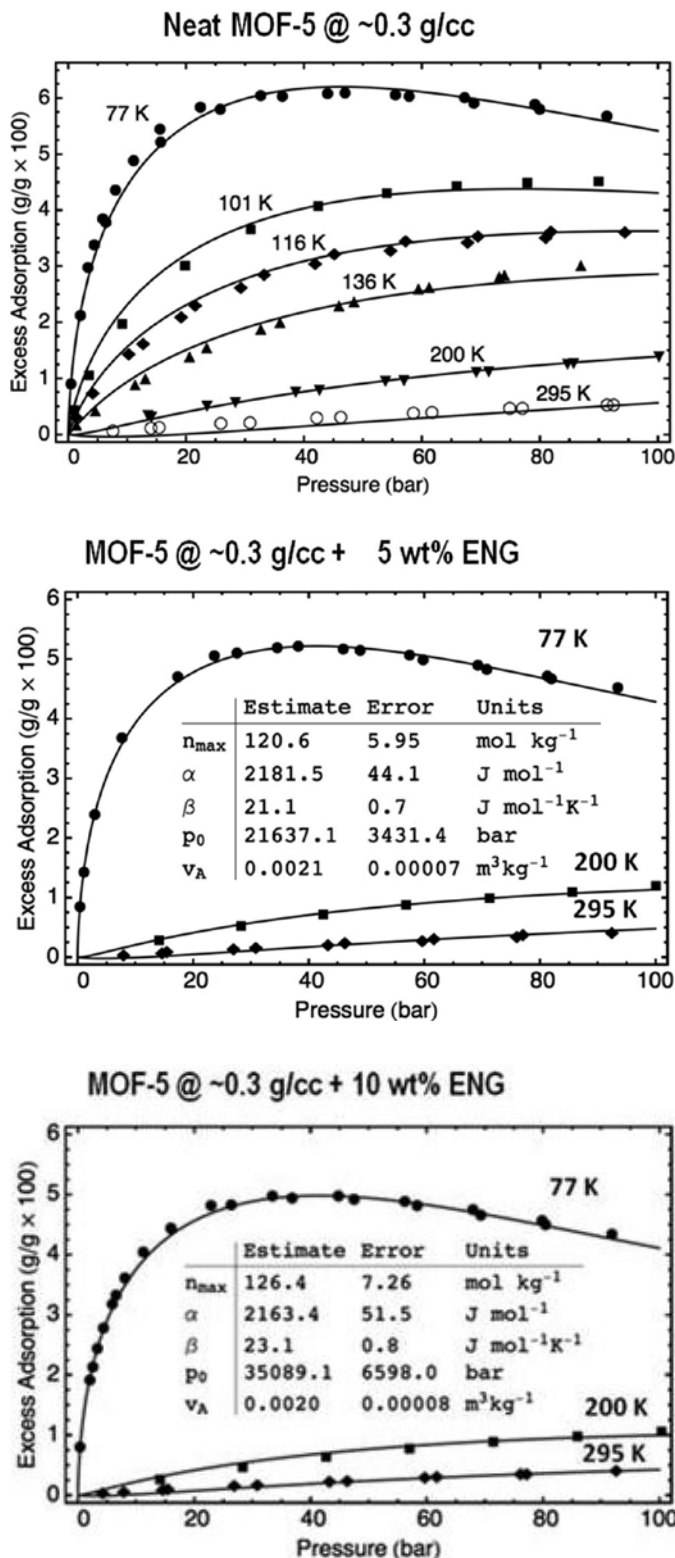


FIGURE 2. Excess hydrogen adsorption isotherms for compacted MOF-5 ($\rho=0.3 \text{ gcm}^{-3}$)

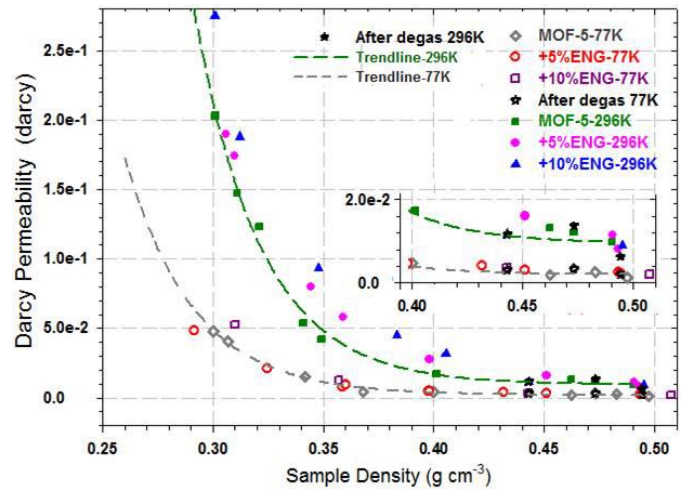


FIGURE 3. Darcy permeability of hydrogen versus sample density

5.0 wt%, a 13% or 17% decrease relative to the neat 0.3 gcm^{-3} (or powder) MOF-5. Despite this decrease in gravimetric capacity, we have previously shown that the thermal conductivity for 0.3 gcm^{-3} MOF-5 can be improved by 200% or 500% with the addition of 5 or 10 wt% ENG (Figure 2, bottom for 10 wt% ENG).

Permeation Measurements: Hydrogen permeation testing was conducted on MOF-5 pellets using the incompressible gas approach and the Darcy equation. The Darcy permeability (κ) of neat MOF-5, MOF-5 + 5 wt% ENG and MOF-5 + 10 wt% ENG samples was determined for various densities at 77 K and 296 K as shown in Figure 3. The results indicate the permeability decreases exponentially with the density of the pellet. In addition, the permeability measured at 296 K is higher than that measured at 77 K for the same sample. At 77 K, the permeability of neat MOF-5, MOF-5 + 5 wt% ENG, and MOF-5 + 10 wt% ENG samples are not significantly different.

Conclusions and Future Directions

- Task 1. System Modeling
 - Complete storage system and powerplant model validation and framework refinement based on component bench tests within the Phase 2 testing.
 - Provide the necessary system model results and optimization studies for the Phase 3 prototype design and scalability evaluation to correlate with the onboard design.
- Task 2. Cost Analysis
 - Develop complete set of material assumptions and predictive usage cost model for the critical components within the adsorbent and chemical hydride systems.

- Establish comprehensive activity-based manufacturing cost models for the storage system materials and components with the HSECoE systems.
- Task 3. Sorbent Media Assessment and Optimization
 - Complete any required material property characterization such as high-pressure and/or low-temperature measurements to support modeling efforts.
 - Continue to assess impact of thermal conductivity aids on material properties and system attributes.
 - Investigate mechanical stability of compacts with respect to cycling and/or mechanical vibration along with subsequent effects on the material properties.
 - Develop tank assembly feasibility and MOF-5 integration concepts.
 - Study degradation effects of MOF-5 upon exposure to air/moisture, and identify the extent to which these can be reversed by various activation procedures.
 - Evaluate uptake robustness by analyzing pellet variations and impurities.
 - Select material and operating conditions for Phase 3 design and sub-scale testing.
 - Pursue experimental validation of sorbent bed and system models through neutron imaging and/or other experimental characterization efforts.

Special Recognitions & Awards/Patents Issued

Matthew Thornton, National Renewable Energy Laboratory; **Michael Veenstra**, Ford Motor Company; and **José Miguel Pasini**, United Technologies Research Center were recognized with a DOE Hydrogen and Fuel Cells Program R&D Award at the 2012 AMR for their outstanding contributions to the development of the integrated modeling framework for the Hydrogen Storage Engineering Center of Excellence (HSECoE).

FY 2012 Publications/Presentations

1. J.J. Purewal, D. Liu, J. Yang, A. Sudik, D.J. Siegel, S. Maurer, U. Müller, “Increased volumetric hydrogen uptake of MOF-5 by powder densification,” *International Journal of Hydrogen Energy*, v 37, n 3, p 2723-2727, February 2012.
2. J.M. Pasini, B. Van Hassel, D. Mosher, and M. Veenstra, “System modeling methodology and analyses for materials-based hydrogen storage,” *International Journal of Hydrogen Energy*, v 37, n 3, p 2874-2884, February 2012.
3. D. Liu, J. Purewal, J. Yang, A. Sudik, S. Maurer, U. Mueller, J. Ni, D. Siegel, “MOF-5 Composites Exhibiting Improved Thermal Conductivity,” *International Journal of Hydrogen Energy*, v 37, n 7, p 6109-6117, April 2012.
4. M. Thornton, M. Veenstra, J.M. Pasini, “Development of a Vehicle Level Simulation Model for Evaluating the Trade-off between Various Advanced On-board Hydrogen Storage Technologies for Fuel Cell Vehicles”, 2012 SAE World Congress, April 2012.
5. M. Veenstra, Ford/BASF/UM “Activities in Support of the Hydrogen Storage Engineering Center of Excellence,” 2012 DOE Hydrogen Program Annual Merit Review Meeting, Arlington VA, May 2012.
6. D.J. Siegel, “Development of an Advanced Hydrogen Storage System Based on Adsorbent Media,” 2012 World Hydrogen Energy Conference, June 2012, Toronto, Canada.
7. C. Xu, J. Yang, M. Veenstra, A. Sudik, J.J. Purewal, B.J. Hardy, J. Warner, S. Maurer, U. Müller, and D.J. Siegel “Hydrogen Permeation and Diffusion in Densified MOF-5 Pellets,” *International Journal of Hydrogen Energy*, 2012, submitted for final review.
8. J.J. Purewal, D. Liu, J. Yang, A. Sudik, M. Veenstra, J. Yang, S. Maurer, U. Müller, and D.J. Siegel “Improved Hydrogen Storage and Thermal Conductivity in High-Density MOF-5 Composites,” *Journal of Physical Chemistry C*, 2012, submitted for review.
9. Justin Purewal, Dongan Liu, Andrea Sudik, Stefan Maurer, Ulrich Mueller, Don Siegel. “Improved Hydrogen Storage and Thermal Conductivity in High-density MOF-5 Composites”. 2012 MRS Spring Meeting & Exhibit- Symposium P: Advanced Materials and Nanoframeworks for Hydrogen Storage and Carbon Capture, April 2012, San Francisco, California.

IV.D.9 Microscale Enhancement of Heat and Mass Transfer for Hydrogen Energy Storage

Kevin Drost (Primary Contact), Goran Jovanovic,
Vinod Narayanan, Brian Paul

School of Mechanical, Industrial and Manufacturing
Engineering

Rogers Hall

Oregon State University (OSU)

Corvallis, OR 97331

Phone: (541) 713-1344

Email: Kevin.Drost@oregonstate.edu

DOE Managers

HQ: Ned Stetson

Phone: (202) 586-9995

Email: Ned.Stetson@ee.doe.gov

GO: Jesse Adams

Phone: (720) 356-1421

Email: Jesse.Adams@go.doe.gov

Contract Number: DE-FC36-09GO19005

Project Start Date: February 1, 2009

Project End Date: June 30, 2014

Fiscal Year (FY) 2012 Objectives

Use microchannel processing techniques to:

- Demonstrate reduction in size and weight of hydrogen storage systems.
- Improve charge/and discharge rates of hydrogen storage systems.
- Reduce size and weight and increase performance of thermal balance of plant components.

Technical Barriers

This project addresses the following technical barriers from the Hydrogen Storage section (3.3.4) of the Fuel Cell Technologies Program Multi-Year Research, Development and Demonstration Plan:

- (A) System Weight and Volume
- (E) Charging/Discharging Rates
- (H) Balance of Plant (BOP) Components

Technical Targets

The Phase II technical targets and Go/No-Go criteria for the Microscale Enhancement of Heat and Mass Transfer for Hydrogen Energy Storage project are:

- Ability to develop and demonstrate a Modular Adsorption Tank Insert (MATI) designed for a system consisting of 100% densified media and capable of allowing less than 3 min. refueling time and H₂ release rate of 0.02 g H₂/(sec. kW) with a mass less than 9.4 kg and a volume less than 4.2 liters. (Barriers A and E)
- Ability to develop and demonstrate a 1-kW catalytic combustor to augment partial hydrogen preconditioning by an existing fuel cell radiator with >90% efficiency having a mass less than 0.5 kg and volume less than 0.5 liters. (Barrier H)

FY 2012 Accomplishments

Key developments and technical accomplishments for the reporting period are:

- Developed a technology development road map for the MATI (Barriers A and E).
- Initiated separate effects and integrated testing of the MATI (Barriers A and E).
- Completed modeling to support the development of conduction enhancements for adsorbing media (Barriers A and E).
- Validated Aluminum as a material of construction for the MATI (Barriers A and E).
- Completed a design and production cost estimate for the MATI (Barriers A and E).
- Completed system design for a microchannel combustor/heat exchanger to provide hydrogen preheating in an adsorption hydrogen storage system (Barrier H).



Introduction

Hydrogen storage involves coupled heat and mass transfer processes that are significantly impacted by size, weight, cost, and performance of system components. Micro-technology devices that contain channels of 10-500 microns in characteristic length offer substantial heat and mass transfer enhancements by greatly increasing the surface-to-volume ratio and by reducing the distance that heat or molecules must traverse. These enhancements often

result in a reduction in the size of energy and chemical systems by a factor of 5-10 over conventional designs, while attaining substantially higher heat and mass transfer efficiency. In cooperation with the DOE Hydrogen Storage Engineering Center of Excellence, the OSU Microproducts Breakthrough Institute and groups at the Pacific Northwest National Laboratory, Savannah River National Laboratory, and Los Alamos National Laboratory, we are developing:

- 1) advanced tank inserts for enhanced heat and mass transfer during charge and discharge of adsorbent hydrogen storage systems; and
- 2) microchannel-based thermal balance of plant components such as combustors, heat exchangers, and chemical reactors.

Approach

To meet the Phase II goals, our technical approach is to reduce the relevant barriers to heat and mass transfer within each high-priority hydrogen storage component using microchannel technology. Our specific approach involves:

- 1) The optimization of the performance of a single unit cell (i.e., an individual microchannel) and then “Number Up” using appropriate simulation tools that we then validate by experimental investigation; and
- 2) Develop microlamination methods as a path to “numbering up” by low-cost high-volume manufacturing. We are applying this approach to both the MATI and the microcombustor applied to hydrogen preheating.

Results

We identified two high-value applications of microchannel technology. The first is the development of a MATI for cooling during charging, heating during discharging, and hydrogen distribution. This system will be applying the modular tank insert to cryogenic adsorption hydrogen storage. The second application is the development of an integrated microchannel combustor and heat exchanger that can be used for preheating hydrogen going to the fuel cell to facilitate cold starts and aggressive driving conditions. Results relative to these two applications are summarized in the following.

MATI – A tank insert that integrates storage media, microchannel heat exchangers, and microchannel hydrogen distribution plates allows convenient use of densified adsorption media with in-excess-of 94% of the tank volume being densified media. The concept separates the cooling process from the charging process, allowing flexibility in cooling strategies, and the MATI can provide heating during discharge, avoiding the need to use electric energy for discharge heating. A schematic of a single cell is presented in Figure 1. The full-sized MATI would consist of a number of cells along with headers for cooling fluid and hydrogen distribution. Progress to date on the development of the microchannel-based tank insert includes:

- MATI Technology Development Road Map—The technology development road map included two phases. The first phase involved modifying the hydrogen distribution plates to introduce the stored hydrogen (at 20 to 40°C) at the highest temperature region of the MATI, maximizing cooling impact. The second phase involved, after having identified aluminum as the material of construction, applying aluminum fins in the densified media to enhance conductivity. The second phase involves applying aluminum fins in the densified media to enhance conductivity and using aluminum as the material of construction. The impact of the two phases on weight is summarized in Figure 2.
- Initiated separate effects and integrated testing—Cryogenic test apparatus have been assembled for experimental investigations of charging and discharging a MATI. The separate effects tests focus on testing individual phenomena such as convective heat transfer coefficient and pressure drop during both single-phase and phase-change cooling. Integrated testing involves experimental investigations of the complete charging and discharge cycles including hydrogen distribution and adsorption and the removal of the heat of adsorption using liquid nitrogen. Both the separate effects and integrated test apparatus have been assembled and are now being used to conduct preliminary experimental investigations (Figure 3). Testing will be completed by 6/30/2013.
- Completed modeling to support the development of conduction enhancements for adsorbing media—Simulation models have been developed to model all relevant phenomena associated with the charging

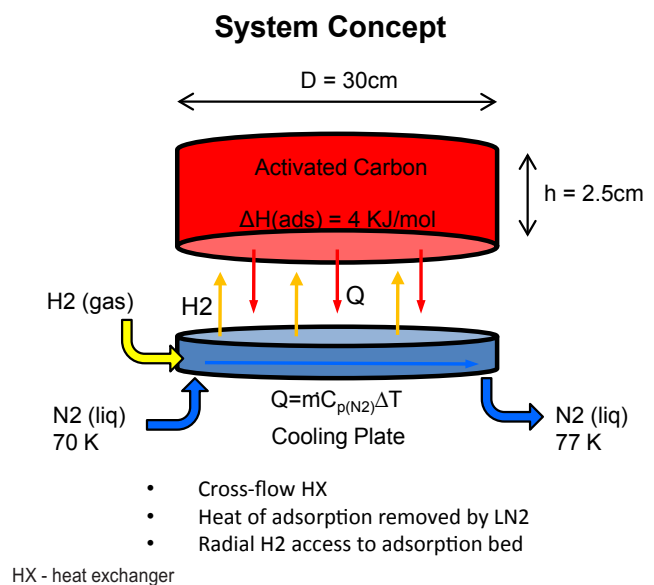
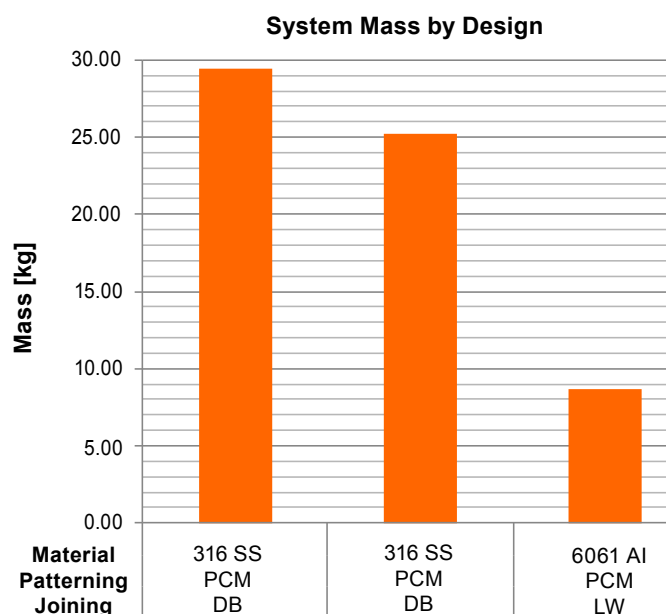


FIGURE 1. MATI Concept

**Development Plan**

Phase 1 – S.S. MATI with combined cooling and H₂ distribution plates produced using photochemical machining (PCM) and diffusion bonding (DB)

Phase 2 – S.S. S.S. with separate cooling and H₂ distribution plates produced using PCM and DB

Phase 3 – Al with separate cooling and H₂ plates and enhanced media conductivity produced using PCM and laser welding (LW)

FIGURE 2. Predicted MATI system weight for the three development phases

and discharging of the MATI. Where possible, these models have been validated against published data. As experimental data becomes available for the MATI, they will be validated against our experimental results. A two-dimensional version of the model has been used to evaluate the required conductivity enhancement of the adsorbent bed, so that we can use a 5-cm spacing between cooling plates. The modeling results show that the average bed conductivity needs to be increased to 3.0 W/mK and that this can be accomplished with the use of embedded aluminum fins in the adsorbing media.

- Validated aluminum as a material of construction for the MATI—We are currently using stainless steel as the assumed material for fabricating the MATI. Stainless steel has been widely used for microlaminated devices and is well understood. However aluminum is significantly lighter and less expensive than stainless steel. Consequently, we have investigated the feasibility of using aluminum as the substrate material for microlamination. Results show that aluminum can be successfully used as a material of construction for microlaminated devices. Both patterning and bonding have been demonstrated.
- MATI Fabrication, Weight, and Cost Analysis—A design of a full-scale MATI has been completed and a fabrication strategy identified. These have formed the

basis for a system weight and volume estimate and a bottoms-up cost estimate. The results of the cost estimate are presented in Figure 4.

Integrated Microscale Combustor/Heat Exchanger

(μ CHX)—The μ CHX (Figure 4) will be used to safely and efficiently preheat hydrogen discharged from the adsorption hydrogen storage system before it enters the fuel cell. In cold conditions, the fuel cell produces insufficient heat to heat the hydrogen to the required inlet temperature for the fuel cell. In these cases a small fraction of the hydrogen will be combusted to preheat the balance of the hydrogen to a temperature appropriate for fuel cell operation. Combining the combustion and heat exchanger systems and using microchannels for enhanced heat and mass transfer can drastically reduce the size and weight required for this function, while simultaneously increasing efficiency. In addition, a substantial safety benefit of a microscale combustor is that flames cannot be sustained in the sub-millimeter microchannels. During the previous reporting period we documented the results of our system design, weight, and cost estimate that showed that the μ CHX System would be perhaps 1/10 the size of the best alternative design with the same heating load, a system efficiency of 92%, and production cost on the order of \$120 per unit for an annual production rate of 500,000 units. During the current reporting period we:

- Completed Unit Cell Experimental Validation of μ CHX Performance and Weight Estimates—We completed a wide range of tests of a single unit cell. The results showed an efficiency of 92% and that 130-140 W of thermal energy was being transferred to the metal hydride heat transfer oil, which is consistent with our size and weight estimates reported above.
- Completed Design of the μ CHX for Adsorption System Hydrogen Preheating—We have modified the design of the μ CHX for the hydrogen preheating application. The significant changes are in heating load (0.5 kW) and application (heating hydrogen initially at cryogenic temperatures). The key design issue was to avoid freezing of the products of combustion (water) in the recuperation section of the device. The new design is slightly less efficient (90%) and much smaller than the oil heating application described above.

Conclusions and Future Directions

Key conclusions resulting from our research include:

- The use of the modular adsorption tank insert allows convenient use of densified adsorption media with in excess of 94% of the tank volume being densified media. The concept separates the cooling process from the charging process, allowing flexibility in cooling

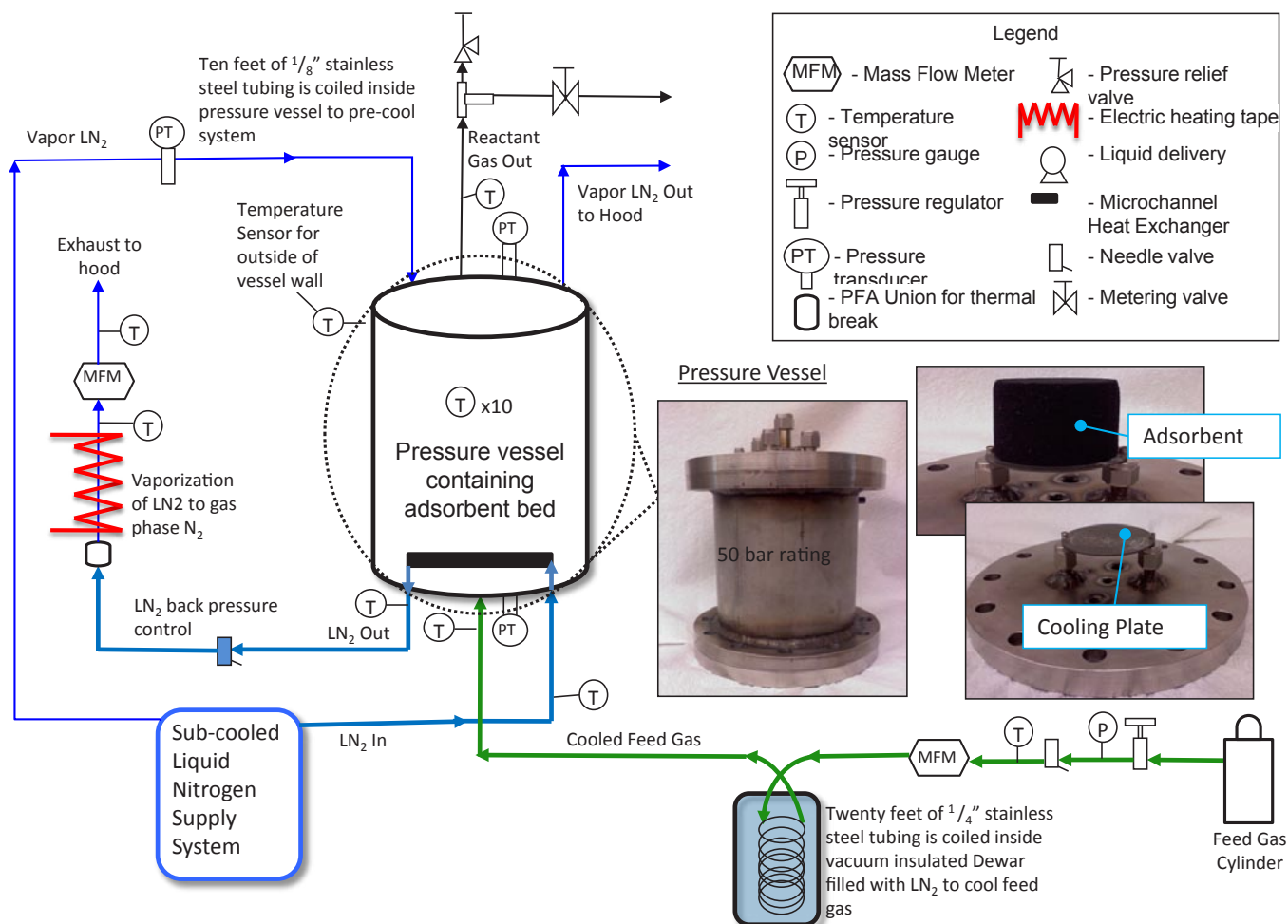


FIGURE 3. Integrated Test Apparatus

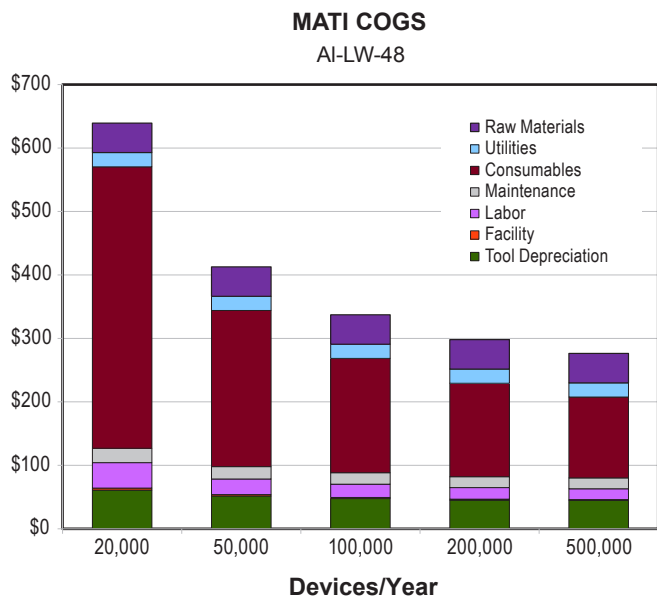


FIGURE 4. Cost of goods sold (COGS) of the MATI as a function of production volume

strategies, and the MATI can provide both cooling during charging and heating during discharge with a weight under 9.5 kg for a hydrogen storage system containing 5.6 kg of hydrogen.

- The μ CHX can provide hydrogen preheating, increasing the flexibility of the storage system in with a minimal impact on system weight and size.

The future direction of our research on the application of microchannel technology to hydrogen storage includes:

- Complete demonstration of a 5-cm diameter MATI including heat removal rates, hydrogen distribution, and durability.
- Complete the demonstration of a .5-kW μ CHX.

FY 2012 Publications/Presentations

- Haley, D.B., and Narayanan, V., 2011, "Performance Characterization of a Microscale Hydrogen Combustor Recuperator and Oil Heat Exchanger," IMECE2011-64176, Proceedings of the ASME 2011 IMECE, Denver CO, November 11–17, 2011.

IV.D.10 Development of Improved Composite Pressure Vessels for Hydrogen Storage

Norman Newhouse (Primary Contact), Jon Knudsen, John Makinson

Lincoln Composites, Inc.
5117 NW 40th Street
Lincoln, NE 68524
Phone: (402) 470-5035
Email: nnewhouse@lincolncomposites.com

DOE Managers

HQ: Ned Stetson
Phone: (202) 586-9995
Email: Ned.Stetson@ee.doe.gov

GO: Jesse Adams
Phone: (720) 356-1421
Email: Jesse.Adams@go.doe.gov

Contract Number: DE-FC36-09GO19004

Project Start Date: February 1, 2009
Project End Date: June 30, 2014

storage system using adsorbant materials. The targets apply to the storage system, of which the vessel is a part. Insights gained from these studies will be applied toward the design and manufacturing of hydrogen storage vessels that meet the following DOE hydrogen storage targets:

- | | 2010 | 2017 |
|-------------------------|-----------------------------|-----------------------------|
| • Gravimetric capacity: | >4.5% | >5.5% |
| • Volumetric capacity: | >0.028 kg H ₂ /L | >0.040 kg H ₂ /L |
| • Storage system cost: | to be determined | to be determined |

FY 2012 Accomplishments

- Phase 1 improvements, which resulted in the following values for the pressure vessel itself, can be incorporated into Phase 2 and 3 components:
 - 11% lower weight
 - 4% greater volume
 - 10% lower cost
- Phase 2 lab test vessel has been designed to requirements established by HSECoE partners. A total of 21 lab test vessels were manufactured for testing and use by HSECoE partners.
- Cryogenic testing of liner and fiber materials to confirm selection and properties.



Fiscal Year (FY) 2012 Objectives

- Improve the performance characteristics, including weight, volumetric efficiency, and cost, of composite pressure vessels used to contain hydrogen in adsorbants.
- Evaluate design, materials, or manufacturing process improvements necessary for containing adsorbants.
- Demonstrate these improvements in prototype systems through fabrication, testing, and evaluation.

Technical Barriers

This project addresses the following technical barriers from the Hydrogen Storage section of the Fuel Cell Technologies Program Multi-Year Research, Development and Demonstration Plan:

- (A) System Weight and Volume
- (B) System Cost
- (G) Materials of Construction

Technical Targets

This project is conducting fundamental studies for the development of improved composite pressure vessels for hydrogen storage, and developing an optimized vessel for use by HSHCoE partners in demonstrating a functioning vehicle

Introduction

Lincoln Composites is conducting research to meet DOE 2010 and 2017 Hydrogen Storage goals for a storage system by identifying appropriate materials and design approaches for the composite container. At the same time, the pressure vessels must continue to maintain durability, operability and safety characteristics that already meet DOE guidelines for 2010 and 2017. There is a continuation of work with HSECoE partners to identify pressure vessel characteristics and opportunities for performance improvement. Lincoln Composites is working to develop high-pressure vessels as are required to enable tank design approaches to meet weight and volume goals and to allow adsorbant materials that operate at cryogenic temperatures to operate efficiently.

Approach

Lincoln Composites established a baseline design using HSECoE team operating criteria as a means to compare and evaluate potential improvements in design, materials and process to achieve cylinder performance improvements for weight, volume and cost. Lincoln Composites then down-selects the most promising engineering concepts to meet Go/No-Go requirements for moving forward. The design and materials improvements will be incorporated into pressure vessel designs to support HSECoE partner systems in phases 2 and 3.

The following areas are being researched and documented:

- Evaluation of alternate fiber reinforcement
- Evaluation of boss materials and designs
- Evaluation of resin toughening agents
- Evaluation of alternate liner materials
- Evaluation of damage vs. impact
- Evaluation of stress rupture characteristics
- Evaluation of in situ non-destructive examination methods to detect damage

Results

Phase 1 efforts resulted in projected improvements to the pressure vessel of 11% lower weight, 4% greater internal volume, and 10% lower cost. These were achieved by:

- Confirmation of higher strength boss material (weight reduction ≈3%).
- Qualification of alternate fiber reinforcements (cost reduction ≈5%).
- Reduction of carbon fiber safety factors (cost reduction ≈5%, weight reduction ≈4%, volume increase ≈2%).
- Use of thinner liner (weight reduction ≈4%, volume increase ≈2%).

The reduction in safety factor will result in a corresponding reduction in minimum burst pressure. However, reliability under stress rupture conditions, which the safety factor addresses, is still projected to be over 0.999999 for the life of the pressure vessel. The cyclic fatigue life of the composite and liner are significantly higher than required by standards, and will not be affected by changing fiber manufacturer or boss material, or by using a thinner liner. The proposed changes will not otherwise adversely affect performance.

A bench-top test vessel was designed, analyzed, and fabricated based on consensus input from HSECoE partners as follows:

| Dimension | Value |
|---|-------------------------------------|
| Design Pressure | 200 bar |
| Maximum Operating Pressure | 250 bar |
| Minimum Operating Pressure | Vacuum, <1e-5 torr |
| Internal Liquid Volume (dimensional priority) | ~6 Liters |
| Internal Liner Inside Diameter | 16.6 cm (6.54 inches) |
| Vessel Outside Diameter | 2:1 aspect ratio for a 6 Liter tank |
| Temperature Range | 20 K to 373 K |

Figure 1 shows a cross-section of the test vessel structural elements, along with stresses calculated using finite element analysis. Figure 2 shows a completed test vessel. A total of 21 test vessels have been manufactured to date. Three were burst to confirm the design, and three were used for cryogenic testing and leak testing. The remainder are available to HSECoE partners to support their activities.

A Type 3 design was evaluated that had the same internal dimensions as the Type 4 design, so that it could be used interchangeably with the Type 4 design. It was designed with a 316L stainless steel liner so that it could be welded and yet maintain strength. However, there was not an expression of interest in using it in Phase 2.

A Type 1 design was prepared with the same internal dimensions. It was designed to open in the center to allow assembly of internal components, but the weight of the design made it impractical.

Liner materials were investigated to determine suitability for cold temperature use. The baseline material, high-density polyethylene (HDPE), was compared with modified ethylene vinyl alcohol, HDPE with nano-additives, polyamide, and

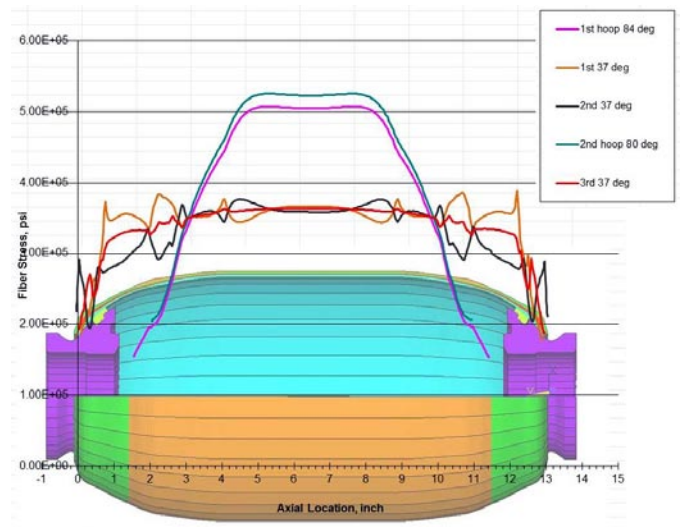


FIGURE 1. Test vessel cross-section and calculated stresses



FIGURE 2. HSECoE Phase 2 test vessel

Teflon®. The HDPE material has shown to be the best suited of the materials tested, but additional evaluation is planned. Figure 3 shows impact test results.

Toray T700 will continue as the baseline reinforcing fiber, but two alternate fibers of similar strength have been identified. A prototype tank has been fabricated with T700 fiber and the baseline resin and is awaiting a burst test at cryogenic conditions, using liquid nitrogen as the pressurizing media, to confirm suitable performance at cryogenic temperatures. Testing of baseline epoxy resin material has confirmed its suitability for use at cryogenic temperatures. Testing of prototype and Phase 2 test vessels has confirmed basic suitability of the design and materials, but additional effort is planned for developing a more robust liner material.

Consideration was given to cylinder types moving forward into Phase 3. A Type 4 tank is the lightest weight, while a Type 1 is the heaviest. Type 1 tanks are generally less expensive than Type 3 and Type 4 tanks, although if stainless steel is required due to use at cryogenic temperatures, their cost would increase over the use of ferritic steels.

At lower pressures, and resultant thinner walls, Type 3 and Type 4 tanks may need additional reinforcement for durability, although this added fiber could be an inexpensive fiber such as glass. At cryogenic temperatures, some steel materials and polymer materials are brittle. Aluminum and composite materials are less affected. Thermal coefficient of expansion differences between a liner and composite must be considered when evaluating stresses.

The ability to install internal components is a consideration in the tank design. Earlier in Phase 2, consideration was given to a larger diameter opening, with components inserted after cylinder manufacture. However, current plans include the use of full diameter pucks or cylinders of sorbent materials, which must be considered in the vessel design and manufacture.

A Type 4 tank could have the components installed inside the liner initially, then it would be welded together, and

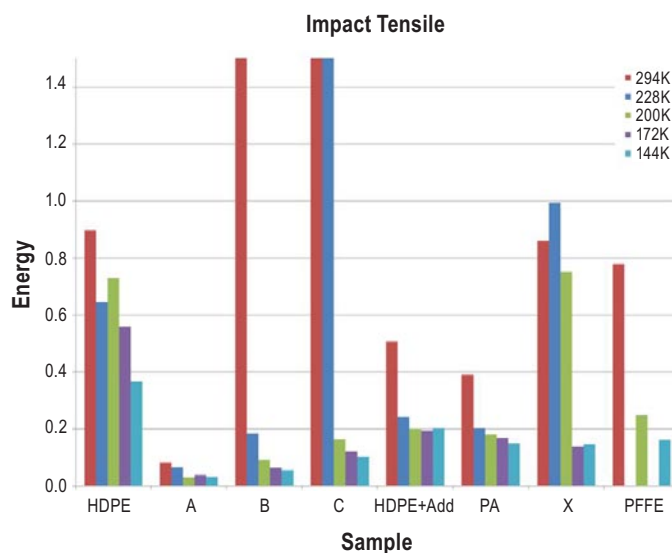


FIGURE 3. Liner material impact testing results

the tank wound and cured. Cure temperature would be below the activation temperature of the sorbent material. Activation of the sorbent material would be done after tank manufacture is completed. The activation temperature of the sorbent material is not expected to adversely affect the tank.

A Type 1 tank would need to be designed to be joined after the sorbent material is installed. There are issues with accomplishing this. A conventional weld in an aluminum alloy would degrade the strength, and heat treatment is not an option. Friction stirred welding is being investigated as an option. Welding of stainless steel might be possible, but the resulting part would be expensive and heavy.

Conclusions and Future Directions

- Significant improvements in the cost, weight, and volumetric performance have been identified.
- Basic suitability for cryogenic service has been demonstrated for the baseline design and materials.
- Additional research is indicated to identify a more robust liner material for a Type 4 vessel. A Type 1 vessel may be considered as an option in Phase 3 to allow all other system components to be demonstrated while the Type 4 liner.
- Research and development will be continued for system design and optimization, including:
 - Insulation evaluation
 - Permeation and outgassing at temperature
 - Evaluation of component installation within the pressure vessel
 - Evaluation of pressure relief devices
 - Evaluation of qualification test requirements

- Continuing effort will be made to address the best options for the pressure vessel for Phase 3, including the means to assemble internal components, and will consider parallel solutions to balance performance with risk.

FY 2012 Publications/Presentations

1. 2012 DOE Hydrogen Program Annual Merit Review, May 15, 2012

Special Recognitions & Awards/Patents Issued

1. Filing of a patent application on a thermal insulation shell system for composite pressure vessel is being evaluated.

IV.E.1 System Level Analysis of Hydrogen Storage Options

Rajesh K. Ahluwalia (Primary Contact), T. Q. Hua,
J-K Peng, Hee Seok Roh, and Romesh Kumar

Argonne National Laboratory
9700 South Cass Avenue
Argonne, IL 60439
Phone: (630) 252-5979
Email: walia@anl.gov

DOE Manager
HQ: Grace Ordaz
Phone: (202) 586-8350
Email: Grace.Ordaz@ee.doe.gov

Start Date: October 1, 2004
Projected End Date: September 30, 2014

Objective

The overall objective of this effort is to support DOE with independent system level analyses of various H₂ storage approaches, to help to assess and down-select options, and to determine the feasibility of meeting DOE targets.

Fiscal Year (FY) 2012 Objectives

- Model various developmental hydrogen storage systems.
- Provide results to Hydrogen Storage Engineering Center of Excellence for assessment of performance targets and goals.
- Develop models to “reverse-engineer” particular approaches.
- Identify interface issues, opportunities, and data needs for technology development.

Technical Barriers

This project addresses the following technical barriers from the Hydrogen Storage section of the Hydrogen, Fuel Cells and Infrastructure Technologies Program Multi-Year Research, Development and Demonstration Plan:

- (A) System Weight and Volume
- (B) System Cost
- (C) Efficiency
- (E) Charging/Discharging Rates
- (J) Thermal Management
- (K) System Life Cycle Assessments

Technical Targets

This project is conducting system level analyses to address the DOE 2015 technical targets for onboard hydrogen storage systems:

- System gravimetric capacity: 1.8 kWh/kg
- System volumetric capacity: 1.3 kWh/L
- Minimum H₂ delivery pressure: 5 bar
- Refueling rate: 1.5 kg/min
- Minimum full flow rate of H₂: 0.02 g/s/kW

FY 2012 Accomplishments

- Analyzed the carbon fiber (CF) requirement using ABAQUS for Type-4 700-bar compressed hydrogen tank. Developed the integrated end cap vessel (IECV) concept to reduce CF usage and cost. Optimized the hoop winding angle layer by layer to reduce the total amount of filament windings.
- Simulated 700-bar fast fill scenario using ANSYS CFX for a Type-4 tank with an enhanced thermal conductivity liner.
- Updated the onboard analyses of the metal-organic framework (MOF-5) system (powder and pellets) with adiabatic para LH₂ refueling. Determined the intrinsic capacities, thermodynamics, dormancy, H₂ refueling dynamics, and discharge dynamics with the potential benefits of para-to-ortho conversion in the onboard storage tank.
- Developed a model of the onboard hydrogen discharge reactor for the single-component liquid carbon-boron-nitrogen (CBN) hydrogen storage material that is being investigated as a potential H₂ storage medium at the University of Oregon.
- Performed off-board analysis of ammonia-borane (AB) regeneration using hydrazine that is produced via the benzophenone process to close the fuel cycle.



Introduction

Several different approaches are being pursued to develop onboard hydrogen storage systems with the goal of meeting the DOE targets for light-duty vehicle applications. Each approach has unique characteristics, such as the thermal energy and temperature of charge and discharge, kinetics of the physical and chemical process steps involved, and requirements for the materials and energy interfaces

between the storage system and the fuel supply system on the one hand, and the fuel user on the other. Other storage system design and operating parameters influence the projected system costs as well. We are developing models to understand the characteristics of storage systems based on the various approaches, and to evaluate their potential to meet the DOE targets for onboard applications, including the off-board targets for energy efficiency.

Approach

Our approach is to develop thermodynamic, kinetic, and engineering models of the various hydrogen storage systems being developed under DOE sponsorship. We then use these models to identify significant component and performance issues, and to assist DOE and its contractors in evaluating alternative system configurations and design and operating parameters. We establish performance criteria that may be used, for example, in developing storage system cost models. We refine and validate the models as data become available from the various developers. We work with the Hydrogen Storage Systems Analysis Working Group to coordinate our research activities with other analysis projects to assure consistency and to avoid duplication. An important aspect of our work is to develop overall systems models that include the interfaces between hydrogen production and delivery, hydrogen storage, and the fuel cell or internal combustion engine hydrogen user.

Results

Physical Storage

We analyzed the 5.6-kg 700-bar compressed hydrogen Type-4 tank to determine the amount of T700S CF needed to meet the 2.25 safety factor. We first constructed the dome shape based on a geodesic path along the isotenoid in a cylindrical tank for a given length-to-diameter ratio. We then performed netting analyses to estimate the needed helical and hoop layer thicknesses. Finally, we performed three-dimensional finite element analyses using ABAQUS with the Wound Composite Modeler extension. A 5° azimuthal strip was modeled with the proper axisymmetric and cyclic boundary conditions. The helical layer thickness and winding angle were varied element by element in the dome section. Changing the helical layer thickness had little effect on hoop stress because the helical winding angle was small ($\alpha_c = 15^\circ$) in the cylindrical section. It was found that the minimum helical and hoop thicknesses were 10.4 mm and 14.8 mm, respectively.

We developed and analyzed the IECV concept (Figure 1) for Type-4 compressed hydrogen storage tanks. The end caps are first fabricated separately by resin transfer molding and are made of the same CF (T700S) and resin material that is used in the tank overwrap. The end caps are then integrated

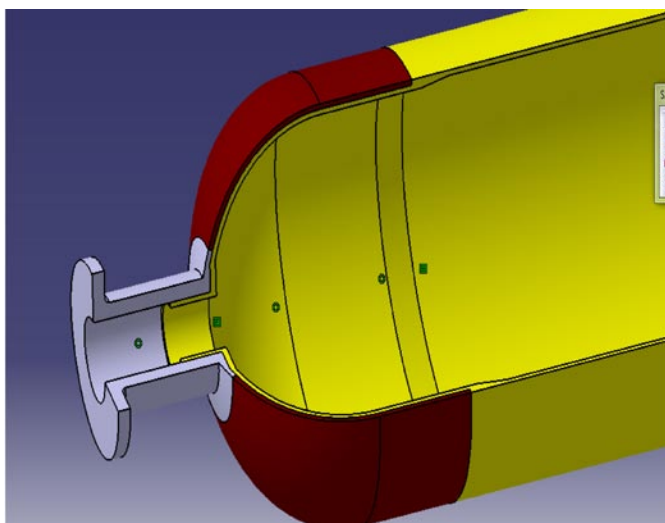


FIGURE 1. The integrated end cap vessel concept for Type-4 tanks

with the high-density polyethylene (HDPE) liner and the aluminum boss using the blow molding method. Finally, the tank is reinforced by conventional helical and hoop winding of the fibers. In this design, the end caps absorb a significant portion of the axial stress in the dome, so that the amount of helical windings needed is substantially less than that in a conventional tank that is reinforced by filament wound fibers only. For the 5.6-kg 700-bar compressed hydrogen tank, our finite element analysis showed that the required helical thickness in the IECV is 5.5 cm, about half the 10.4-cm thickness needed in the baseline design, thereby reducing the needed total CF-composite weight by 18%. Further improvements in the end cap design could result in additional weight reduction. In addition to reducing helical winding using the IECV concept, we also investigated means to reduce the amount of hoop winding material. This can be accomplished by varying the hoop fiber winding angle. In the baseline design where the hoop angle is 90°, the stress at the innermost layer is ~15% higher than that in the outermost layer. Our analysis showed that the stress distribution could be made more uniform across the layers by changing the fiber angle in the layers, which would result in smaller helical and hoop layer thicknesses. This suggests that the amount of filament windings could be reduced by an additional 10% by optimizing the hoop winding angles.

700-bar Fast-Fill Simulation

We investigated the effect of the thermal conductivities of the liner and the carbon fiber on the tank temperature (gas, liner, and CF) during fast fill for 700-bar nominal operating pressure. We used the commercial code ANSYS CFX 13.0 to simulate the thermal hydraulic behavior of the H₂ gas tank filling at 1.5 kg/min at 20°C and -40°C inlet temperatures. The Type-4 tank in our model has a 5-mm thick HDPE liner and a 2.6-cm thick T700S CF overwrap.

We assumed 5 W/m²·K external heat transfer coefficient and 20°C ambient temperature. It was found that a five- to ten-fold increase in the HDPE thermal conductivity would have the potential to reduce the liner temperature by up to 20°C. A similar increase in CF thermal conductivity (which is already ~20 times that of HDPE) has little impact. Figure 2a shows the time variation of the average gas temperature during and after refueling. The peak liner temperature was below 85°C with a five-fold increase in the liner thermal conductivity, even with the fuel initially at ambient temperature (20°C), as shown in Figure 2b.

Hydrogen Storage in MOF-5

We updated an analysis of onboard hydrogen storage in MOF-5 (Basolite Z 100-H) powder (130 kg·m⁻³) and pellets (310 and 510 kg·m⁻³). We extended the H₂ equation of state in REFPROP to account for para/ortho conversion. We

validated the extended equation of state against the available tabulated values of H₂ properties (enthalpy, density, etc.) as a function of pressure and temperature for ortho and para hydrogen. Figure 3 shows the principal components of the reference onboard hydrogen storage system with adiabatic refueling, in which the MOF tank is evaporatively cooled during refueling with LH₂. During discharge, the heat of desorption and any temperature swing in the sorbent bed is provided by recirculating the hydrogen through a small external heat exchanger. The composite pressure vessel consists of T700S CF (2,550 MPa tensile strength) wound on an Al 6061-T6 alloy liner, and it is thermally insulated with multi-layer vacuum super insulation in a 3-mm thick Al 6061-T6 alloy vacuum shell. We conducted fatigue analyses to estimate the required liner thickness to meet the target life of 5,500 pressure cycles (SAE J2579 requirement). The thickness of the insulation was determined so as to limit the heat transfer rate from the ambient to 5 W.

We analyzed the MOF-5 system performance assuming that the system is charged with liquid para H₂, which converts to the equilibrium para-ortho composition solely as a function of the prevailing pressure and temperature (i.e., without any kinetic limitations). The analysis showed that the endothermic heat of para-ortho conversion (~700 J/g-H₂ converted at 20–40 K) sufficiently increases the allowable temperature swing such that the recoverable fraction of sorbed H₂ approaches unity for temperatures above about 80 K. The system can reach lower temperatures with equilibrium H₂ than with normal H₂. We concluded that additional external cooling would not be needed for the system to reach the theoretical gravimetric and volumetric

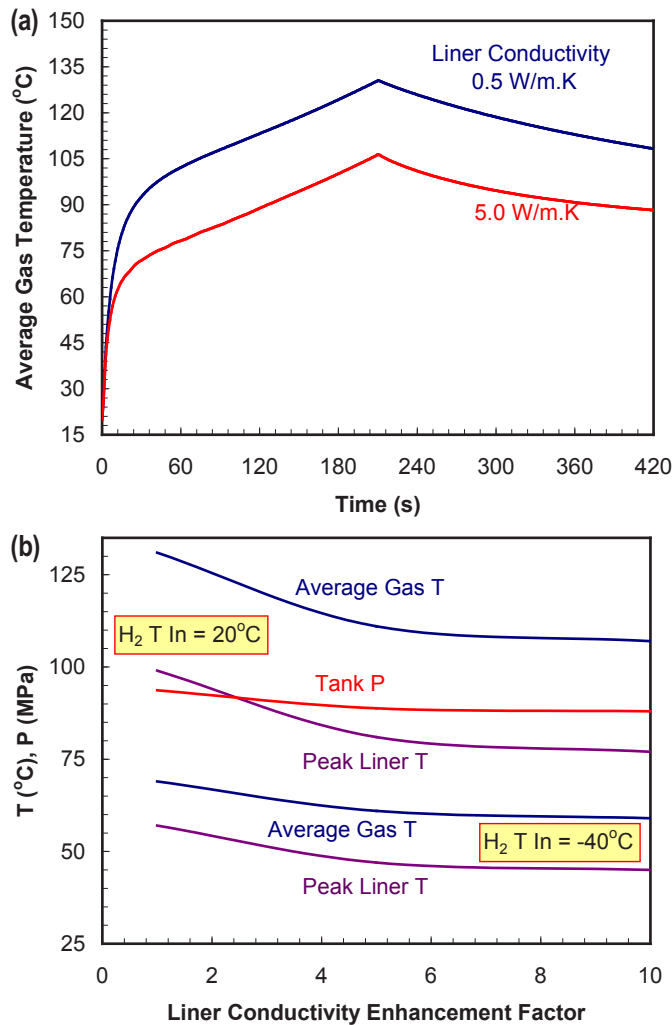


FIGURE 2. (a) Time variation of gas temperature during fast-fill of 700-bar tanks; (b) Changes in gas/liner temperatures with changing liner thermal conductivity

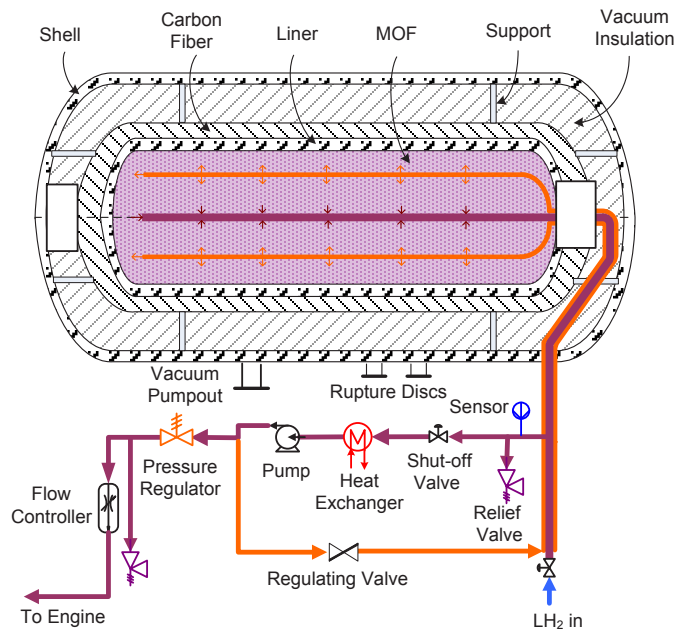


FIGURE 3. Onboard MOF-5 storage system with para LH₂ refueling

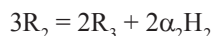
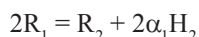
capacities if the para-to-ortho conversion occurs inside the MOF bed. The analysis showed that for MOF-5 powder at 150 atm storage pressure, without para-to-ortho conversion, the allowable temperature swing at 60 K nominal storage temperature is 18 K, whereas with equilibrium H₂, the endothermic conversion allows a temperature swing of 36 K at a 10 K lower storage temperature. At a storage pressure of 150 atm, the system gravimetric capacity increases from 6.5 wt% without conversion to 7.1 wt% with conversion to equilibrium. The corresponding volumetric capacity increases from 34.9 kg·m⁻³ to 40.9 kg·m⁻³. With MOF-5 pelletized to a bulk density of 310 kg·m⁻³, the corresponding storage capacities increase from 4.6 wt% to 5.5 wt% and from 29.5 kg·m⁻³ to 37.6 kg·m⁻³. With further compaction of the MOF-5 to a bulk density of 510 kg·m⁻³, the H₂ storage capacities increase from 3.3 wt% to 4.1 wt%, and from 24.1 kg·m⁻³ to 32.9 kg·m⁻³.

We also evaluated the kinetics of the para-to-ortho conversion. We found that the gas phase kinetics is too slow for any significant conversion during the refueling process (3–5 min duration). We also determined that the kinetics is sufficiently rapid on a commercially available catalyst (APACHI-1) that the equilibrium conversion can be achieved in 3–5 minutes. There is some literature data that suggests that para-to-ortho conversion occurs within minutes on MOF-74 [1]; however, the kinetics on MOF-5 is largely unknown.

Dormancy in MOF-5 H₂ storage systems is a function of the amount of H₂ and the pressure and temperature at the start of the dormancy event. The effect of the para-to-ortho conversion is to extend dormancy by about 20% if the tank is initially more than 75% full, with shorter dormancy increases for smaller initial amounts of H₂ (because of the lower thermal mass of the system).

Chemical Storage

We developed an onboard hydrogen discharge reactor model for the single-component liquid CBN material (BN-methylcyclopentane) being investigated as a potential hydrogen storage material at the University of Oregon [2]. The material is liquid at ambient conditions and does not undergo a phase change upon dehydrogenation. We analyzed the H₂ release data and formulated a 2-step, self-inhibited catalytic reaction model described by the reactions,



where $\alpha_1 = 1$, and $\alpha_2 = 3$. Figure 4a compares the model prediction of H₂ release rate with the data at 80°C and 5-mol% FeCl₂ catalyst loading. Both the model and data exhibit a double peak in reaction rate that is consistent with self-inhibited catalytic behavior. Figure 4b shows the good

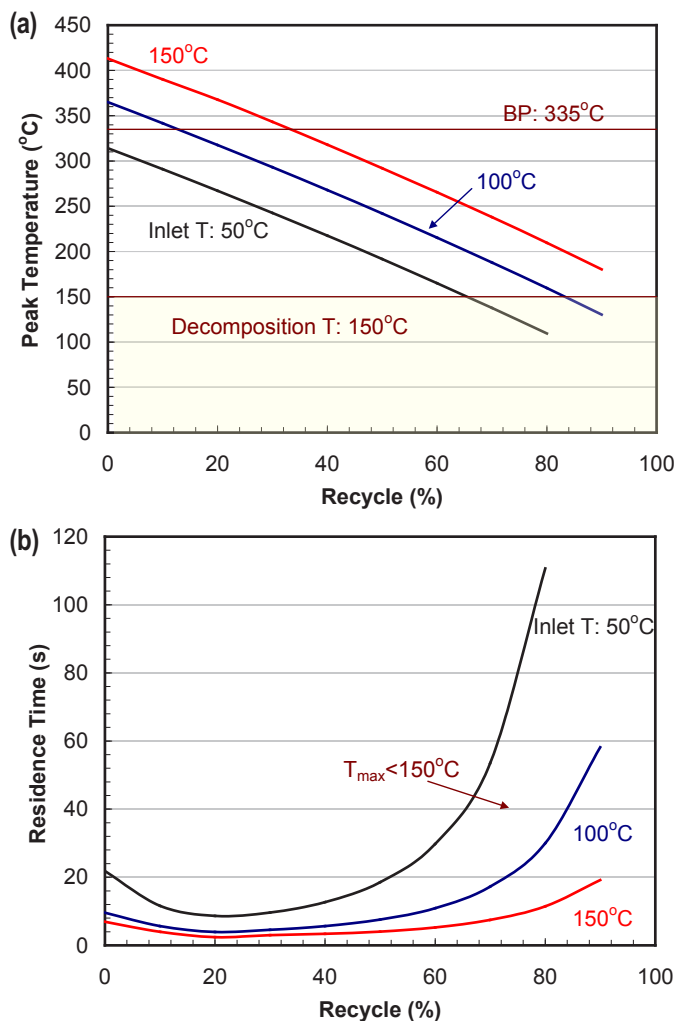


FIGURE 4. (a) Peak reactor temperature for CBN in the hydrogen discharge reactor; (b) Residence time for CBN in the hydrogen discharge reactor as a function of the fraction of spent fuel recycled to the hydrogen discharge reactor

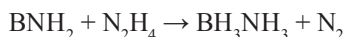
fit between the model results and the experimental data for cumulative hydrogen release.

We modeled the performance of an onboard CBN tube-in-shell reactor for hydrogen discharge. We considered a one-dimensional, steady flow of CBN inside the heat exchanger tubes, and ethylene glycol heat transfer fluid on the shell side. A single-tube, multi-pass tube arrangement was selected to further enhance the tube-side heat transfer coefficient by maintaining a high Reynolds number and a stable two-phase flow. The model results indicated that heat transfer alone was not sufficient to control the peak temperature of the exothermic dehydrogenation reaction. The peak temperature can be controlled, however, by partial recycling of the spent liquid fuel back to reactor. The higher the recycle ratio, the lower is the peak temperature, as shown in Figure 4a for various inlet temperatures. A 65% to 85% recycle of spent CBN is needed, however, to keep the maximum reactor temperature below 150°C, the decomposition temperature of

fresh fuel. Figure 4b shows the residence time of the fuel in the reactor as a function of the spent fuel recycle ratio. For 65% to 85% recycle and inlet temperatures of 50 to 100°C, the residence time is about 40 s. The residence time can be reduced with the use of more active and/or dispersed catalyst, a topic currently being investigated at the University of Oregon.

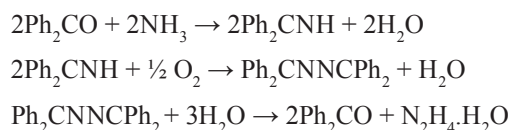
Off-Board Regeneration of AB using Hydrazine

We analyzed the off-board regeneration process for ammonia borane in a single-pot scheme, in which the spent AB is reacted with hydrazine (N_2H_4 , limiting reagent) in liquid ammonia [2].

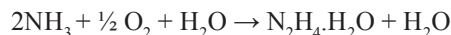


Previously, two flow sheets were constructed to close the cycles by considering the commercial processes (Bayer Ketazine and PCUK) for producing hydrazine. The Bayer Ketazine process requires large amounts of electricity to produce NaOH and Cl_2 , which are the feed materials for hydrazine production. The PCUK process consumes a large amount of steam in making hydrogen peroxide. We constructed a third flowsheet for hydrazine production using benzophenone (Figure 5). This process [3,4] requires only ammonia as a feed material for the production of hydrazine. All reagents and catalysts are recycled in a closed loop. Although this process has been thoroughly reviewed, it has

not yet been commercialized. All reagents and catalysts are recycled in a closed loop. A mixture of ammonia and air ($NH_3:O_2 = 4:1$) is passed through benzophenone under pressure (~1-8 atm) in the presence of zinc chloride and cuprous chloride catalysts at 200°C. The reaction produces benzophenone azine; the reaction mixture is diluted with ethanol to precipitate azine and the catalysts. Unreacted benzophenone and some of the catalysts remain in the ethanol solution, from which the ethanol is subsequently distilled off to return the unreacted benzophenone and catalysts to the reaction step. The precipitated catalysts are recovered by washing with benzene to dissolve the azine. The solution is distilled to remove benzene, and the azine is hydrolyzed in the presence of a strong acid, such as sulfuric acid, to yield hydrazine and benzophenone, which is recycled. The reactions are as follows:



The net reaction is



We analyzed the AB regeneration process using hydrazine produced via the benzophenone pathway. Results of the analysis showed a well-to-tank (WTT) efficiency of ~18%, a notable increase over the ~8% and ~12% WTT

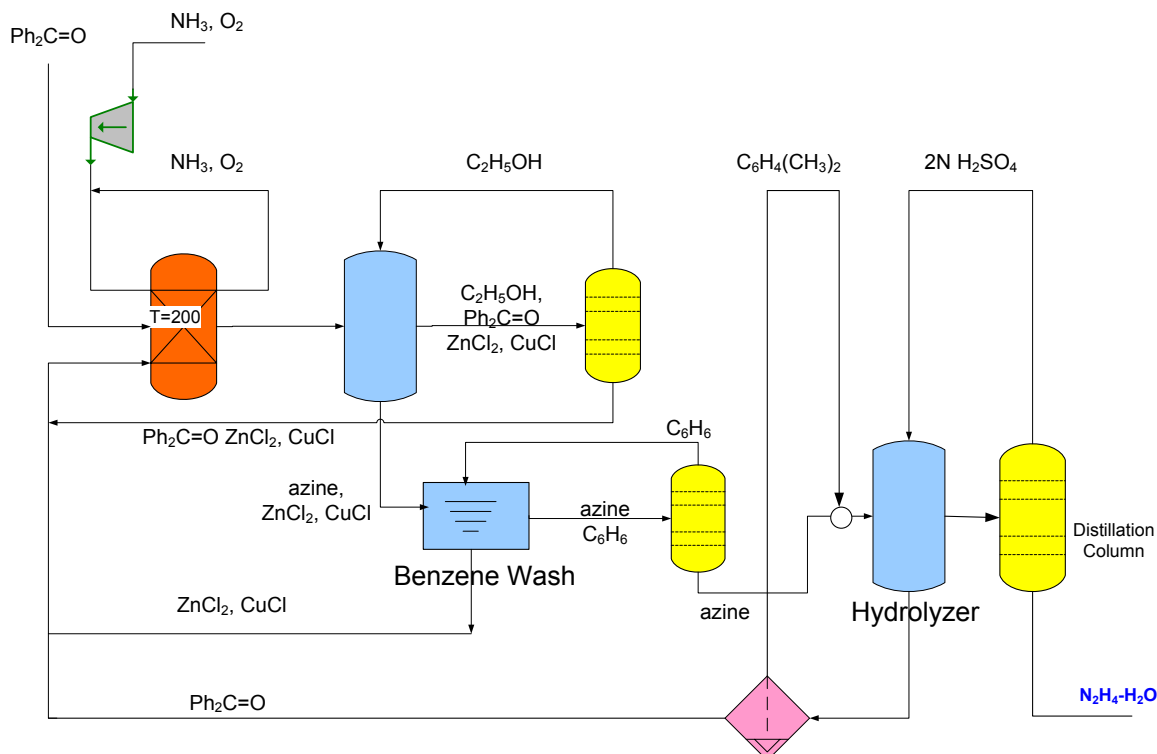


FIGURE 5. The benzophenone process for hydrazine production

efficiencies using the Bayer Ketazine and the PCUK pathways, respectively, for producing hydrazine.

Conclusions and Future Directions

- We project that an onboard MOF-5 system with adiabatic liquid para H₂ refueling and 5.6 kg recoverable H₂ can achieve 7.1 wt% gravimetric capacity and 40.9 g/L volumetric capacity at 150 atm. The loss-free time and hydrogen loss rate are functions of the amount of hydrogen stored and the pressure and temperature at the start of the dormancy event.
- We estimate that the IECV design for Type-4 tanks has the potential to reduce the amount of CF composite usage by ~18% for 700-bar hydrogen storage. We further estimate that optimizing the hoop winding angle layer by layer can bring about an additional 10% savings in the amount of filament windings.
- We estimate that partial recycling of the spent CBN liquid fuel back to reactor is needed to control the peak reactor temperature. A 65% to 85% recycle of the spent fuel would keep the maximum reactor temperature below 150°C, the decomposition temperature of fresh fuel. We estimate that for 65% to 85% recycle and inlet temperatures of 50 to 100°C, the needed residence time is about 40 s.
- We estimate that a five- to ten-fold increase in the HDPE thermal conductivity has the potential to reduce the liner temperature by up to 20°C for 700-bar fast fill at 1.5 kg/min.
- We estimate WTT efficiency of ~18% for regenerating AB using hydrazine produced via the benzophenone process. This WTT efficiency is a notable increase over the ~8% and ~12% WTT efficiencies of AB regeneration using hydrazine produced by the Bayer Ketazine and the PCUK pathways, respectively.
- In FY 2013, we will extend our analysis of Type-4 tank to optimize the end cap design, analyze the effect of mismatch in the coefficient of thermal expansion between the resin and the CF at cold/cryo temperatures, investigate improvements in CF composite mechanical properties with tailored mechanical properties of the epoxy matrix, and investigate differences in tensile strength and translation efficiency for pre-preg versus wet winding.
- In FY 2013, we will analyze a complete CBN onboard system to determine the key performance metrics, and off-board regeneration of CBN for three different chemistries.

- Also in FY 2013, we will perform reverse engineering for onboard hydrogen storage systems based on metal hydrides or chemical hydrogen. The primary goal of the analyses will be to determine the range of materials properties that are needed for the systems to meet the DOE onboard performance targets.

FY 2012 Publications/Presentations

1. R.K. Ahluwalia, T.Q. Hua and J.K. Peng, "On-Board and Off-Board Performance of Hydrogen Storage Options," *International Journal of Hydrogen Energy*, 37 (2012) 2891-2910.
2. T.Q. Hua and R.K. Ahluwalia, "Alane Hydrogen Storage for Automotive Fuel Cells – Off-Board Regeneration Processes and Efficiencies," *International Journal of Hydrogen Energy*, 36 (2011) 15259-15265 .
3. R.K. Ahluwalia and T.Q. Hua, "Hydrogen Storage in Ammonia Borane Dissolved in an Ionic Liquid," *International Journal of Hydrogen Energy*, 36 (2011) 15689-15697.
4. T.Q. Hua and R.K. Ahluwalia, "Hydrogen Storage in Ammonia Borane – Off-board Regeneration Processes and Efficiencies," *International Journal of Hydrogen Energy*, 37 (2012) 14382-14392.
5. T.Q. Hua, R.K. Ahluwalia and J.K. Peng "Analysis of Hydrogen Storage Options for Automotive Fuel Cells," 12th China Hydrogen Energy Conference, Wuhan, China, October 2011.
6. T.Q. Hua, R.K. Ahluwalia and J.K. Peng "Analysis of Hydrogen Storage Options for Automotive Fuel Cells," Shanghai Jiao Tong University, Shanghai, October 2011.
7. R.K. Ahluwalia, J.K. Peng and T.Q. Hua, "Enhanced Cryogenic Hydrogen Storage in MOF-5 with Para-to-Ortho Conversion," Storage System Analysis Working Group Meeting, Argonne National laboratory, February 2012.

References

1. S. FitzGerald et al., "Quantum dynamics of adsorbed normal- and para- H₂, HD, and D₂ in the microporous framework MOF-74 analyzed using infrared spectroscopy," *Physical Rev. B* 2010 (81), 104305.
2. W. Luo, P.G. Campbell, L.N. Zakharov, S-Y Liu, "A single-component liquid phase hydrogen storage material," *J. Am. Chem. Soc.*, 2011 (133) 19326 - 19329.
3. H. Hayashi, A. Kainoh, M. Katayama, K. Kawasaki, T. Okazaki. "Hydrazine production via azine," *Ind. Eng. Chem.* 1976; *Pro. Res. Dev.*, 15 (4).
4. M. Hayashi, "Hydrazine synthesis: commercial routes, catalysis and intermediates," *Res. Chem. Intermed.*, 1998; 24 (2): 183-196.

IV.E.2 Best Practices for Characterizing Engineering Properties of Hydrogen Storage Materials

Karl J. Gross (Primary Contact),
Russell Carrington¹, Steven Barcelo¹,
Abhi Karkamkar², Justin Purewal³, Pierre Dantzer⁴,
Shengqian Ma and Hong-Cai Zhou⁵, Kevin Ott⁶,
Tony Burrell⁶, Troy Semeslberger⁶, Yevheniy Pivak⁷,
Bernard Dam⁷, Dhanesh Chandra⁸

H2 Technology Consulting LLC
P.O. Box 1302
Alamo, CA 94507
Phone: (510) 468-7515
Email: kgross@h2techconsulting.com

¹ University of California Berkeley

² Pacific Northwest National Laboratory

³ California Institute of Technology

⁴ Université Paris-Sud

⁵ Texas A&M University

⁶ Los Alamos National Laboratory

⁷ VU University Amsterdam and the Delft University of
Technology

⁸ University of Nevada, Reno

DOE Managers

HQ: Ned Stetson

Phone: (202) 586-9995

Email: Ned.Stetson@ee.doe.gov

GO: Jesse Adams

Phone: (720) 356-1421

Email: Jesse.Adams@go.doe.gov

Project Start Date: February 7, 2007

Project End Date: Project continuation and direction
determined annually by DOE

- (A) System Weight and Volume
- (C) Efficiency
- (D) Durability/Operability
- (E) Charging/Discharging Rates
- (J) Thermal Management
- (Q) Reproducibility of Performance

Technical Targets

The goal of this project is to prepare a reference document detailing the recommended best practices and limitations in making critical performance measurements on hydrogen storage materials. This reference document will provide a resource to improve the accuracy and efficiency of critical measurements to aid the projects and ultimately the entire sub-program to achieve or exceed the technical storage targets.

In particular this project is focused on the following target related performance measurements:

- Kinetics - targets: system fill time for 5-kg hydrogen, minimum full-flow rate and start time to full-flow
- Capacity - targets: gravimetric and volumetric capacity
- Thermodynamic Stability - targets: maximum/minimum delivery pressure of H₂ from tank and impact on capacity and kinetic related targets
- Cycle-Life Properties - targets: cycle life and cycle life variation
- Heat Transfer Properties - targets: system fill time for 5-kg hydrogen, minimum full-flow rate and start time to full-flow

Fiscal Year (FY) 2012 Objectives

- To prepare a reference document detailing best practices and limitations in measuring hydrogen storage properties of materials.
- The document will be reviewed by experts in the field.
- The final document will be made available to researchers at all levels in the DOE hydrogen storage sub-program.

Technical Barriers

This project addresses the following technical barriers from the Hydrogen Storage section of the Fuel Cell Technologies Program Multi-Year Research, Development and Demonstration Plan:

FY 2012 Accomplishments

- Contributions to this project from world experts have been received including written materials, examples, presentation or editorial review of draft documents.
- External review (U. Nottingham, U.K.) of Thermodynamics section completed.
- All input and edits incorporated into final version of Hydrogen Storage Materials Properties section.
- Final Introduction section 100% complete.
- Final Kinetics section 100% complete.
- Final Capacity section 100% complete.
- Final Thermodynamic section 100% complete.
- Final Cycle-Life Properties section 100% complete.

- Posted final “Recommended Best Practices for the Characterization of Storage Properties of Hydrogen Storage Materials” sections 1-5 to DOE website for world-wide access. Please download the current document from: http://www1.eere.energy.gov/hydrogenandfuelcells/pdfs/best_practices_hydrogen_storage.pdf
- Thermal Properties section 90% complete.
- Thermal Properties section currently being reviewed by international experts.



Introduction

The Hydrogen Storage sub-program goal is the development of hydrogen storage materials that meet or exceed the DOE’s targets for the onboard hydrogen storage in a hydrogen-powered vehicle. The growth of research efforts in this field and new approaches to solving storage issues has brought the talents of a wide-range of researchers to bear in solving the grand challenge of hydrogen storage. There is a need to have common metrics and best practices for measuring the practical hydrogen storage properties of new materials that are being developed within the DOE Hydrogen Storage sub-program as well as at an international level. H2 Technology Consulting is tasked with creating a clear and comprehensive resource that will provide detailed knowledge and recommendations for best practices in the measurements of these properties.

Approach

This project is a combined approach of documenting the experience the primary contact and other experts in the field have with these measurement, incorporating examples from the literature, performing experimental measurements to demonstrate important issues, and finally, condensing key information into a concise reference guide. Each section covers such topics as the overall purpose of the measurements, some basic theory, experimental consideration, methods of measurement, and many details on both material properties and experimental factors that may strongly influence the final results and conclusions. Participation from other experts in the field is being sought out for input, relevant examples, and critical review at all levels.

Results

This year work was completed on the “Recommended Best Practices for the Characterization of Storage Properties of Hydrogen Storage Materials” document sections 1-5 covering the measurement of materials related

hydrogen storage properties. The final version including a preface, introduction, kinetics, capacity, cycle-life, and thermodynamics measurement sections is now posted on the DOE website.

This year’s main focus was on the new Engineering Properties document of the Best Practices Project. The first section of this document covers the best practices in making Engineering Thermal Properties measurements. It includes:

- A review of measurement techniques currently being used for measuring thermal conductivity and heat capacity properties of hydrogen storage materials.
- An evaluation of common thermal property measurement methods used in other applied materials fields that are appropriate for hydrogen storage materials.
- Important issues in making the measurements and analyzing the data that contribute to errors in the results.
- The specific need for data to support scale-up system design.
- How the measurement methods need to be tailored for new materials being developed to address heat transfer issues.

For this new work collaborations were established with the following international experts in the field: Ewa Rönnebro, Pacific Northwest National Laboratories; Bart van Hassel, United Technologies Research Center; Lars Röntzsch, Fraunhofer Institute for Manufacturing Technology and Advanced Materials, Dresden, Germany; Michel Latroche, Institut de Chimie et des Matériaux de Paris Est CNRS, France; Patricia De Rango, Institut Néel CNRS, Grenoble, France; Mike Veenstra and Jun Yang of Ford Motor Co., USA; Bruce Hardy, of Savannah River National Laboratory; David Grant, of the University of Nottingham, United Kingdom; and Daniel Dedrick, Sandia National Laboratories. In addition, the work has been coordinated and has received important scientific input through our contract monitor Phil Parilla at the National Renewable Energy Laboratory.

The objective of this subtask is to review measurement techniques currently being used for measuring thermal properties of hydrogen storage materials. As this has not been done extensively in this field, the task will include an evaluation of common thermal property measurement methods used in other applied materials fields that may be appropriate for hydrogen storage materials. A focus will be on clarifying problem areas in these measurements and to establish some common methods.

The following are some examples of the content of this new Engineering Thermal Properties section.

Thermal Conductivity: Thermal conductivity is a property of a conducting medium and, like the viscosity, is primarily a function of temperature [1]. Thermal conductivity k (sometimes given by the symbol λ), in ($\text{W}\cdot\text{K}^{-1}\cdot\text{m}^{-1}$), describes the ability of a material to transfer heat. This

transfer of heat is defined by Equation 1 (This equation is called Fourier's law):

Equation 1

$$Q_x = -kA \frac{dT}{dx}$$

where Q_x is the heat transfer rate in the x direction, in W; A is the area normal to direction of heat flux, in m^2 ; dT/dx is the temperature gradient in the x direction, in $K \cdot m^{-1}$, and k is the thermal conductivity, in $W \cdot K^{-1} \cdot m^{-1}$. The negative sign indicates that the flux is down the gradient, and it can be shown from irreversible thermodynamics that the coefficient k is always positive.

Multiplied by a temperature difference (in Kelvin, K) and an area (in square meters, m^2), and divided by a thickness (in meters, m), the thermal conductivity predicts the rate of energy loss (in watts, W) through a piece of material. Thermal conductivity and conductance are analogous to electrical conductivity ($A \cdot m^{-1} \cdot V^{-1}$) and electrical conductance ($A \cdot V^{-1}$).

In its most simple form, the measurement of thermal conductivity of a solid involves applying heat to one end of a sample of a uniform shape and measuring Q_x and dT/dx to determine k by means of Equation 1. This is shown diagrammatically in Figure 1.

There are many different methods to measure thermal conductivity. The method selected should be appropriate for the general type of material (gas, liquids, solids, powders) and the temperature range for which the material will be used. Some common measurement methods that are presented in detail in the document are:

- Guarded Hot Plate Method (ASTM C 177)
- Concentric Cylinders Method
- Concentric Spheres Method
- Thermal Probe Method (ASTM D 5334)

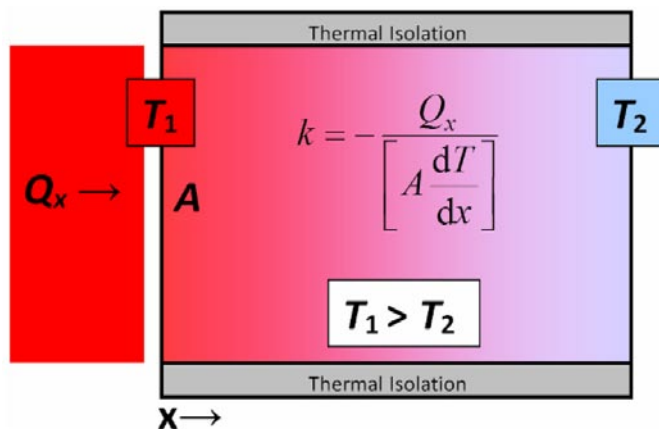


FIGURE 1. Schematic diagram a simple thermal conductivity measurement of a solid

- Transient Plane Source (TPS) Method
- Divided Bar Method (ASTM E1225-87)
- Hot-Wire Method (ASTM C1113) for Gases and Liquids
- Flash Method

Figure 2 illustrates the wide range of thermal conductivities for common materials and shows the generally applicable range of thermal conductivity for common measurement methods. For example, for highly conductive ceramics, metals or diamond composites, the laser flash method is often employed. Whereas, the thermal conductivity of refractory materials is typically determined on large samples using hot wire instruments.

For hydrogen storage systems based on hydrogen storage materials the hydrogen gas itself may play a very important role in the systems' heat transfer. The thermal conductive of several gases as a function of gas pressure are presented in Figure 3 [3]. With the decrease in the pressure, the thermal conductivity of the gas decreases because of the increase in the mean free path of the gas molecules (Smoluchowski effect [4]).

Knowing the thermal conductivity of hydrogen storage materials under operating conditions is important because during charging or hydrogen release the interaction of hydrogen and the storage materials often produces or consumes large amounts of heat. Without sophisticated means of heat transfer, this heat will cause a significant rise in temperature which, among other things, will have a strong impact on hydrogen uptake or delivery rates.

The accurate determination of the effective thermal conductivity and heat capacity of storage materials, additives, and system components is also critical for modeling and design of advanced systems. An example of materials and system modeling is given below for an advanced metal-hydride system that includes an aluminum foam heat transfer solution. A test system as shown in Figure 4 was built and data from those tests were used to validate a numerical model that was developed to be able to simulate the behavior of metal hydride tanks [5].

Simulation results for charging the bed are shown in Figure 5 and compared with measured data.

The flow rate and hydrogen capacity (mass transfer) of the simulations were in relatively good agreement with the experimental results and demonstrated the need for adequate heat transfer. Such modeling relies on accurate values of the thermal properties of the hydrogen storage materials and system components.

Two possible solutions for improving thermal conductivity are 1) to compress the hydrogen storage materials, and 2) to add a second material with high thermal conductivity.

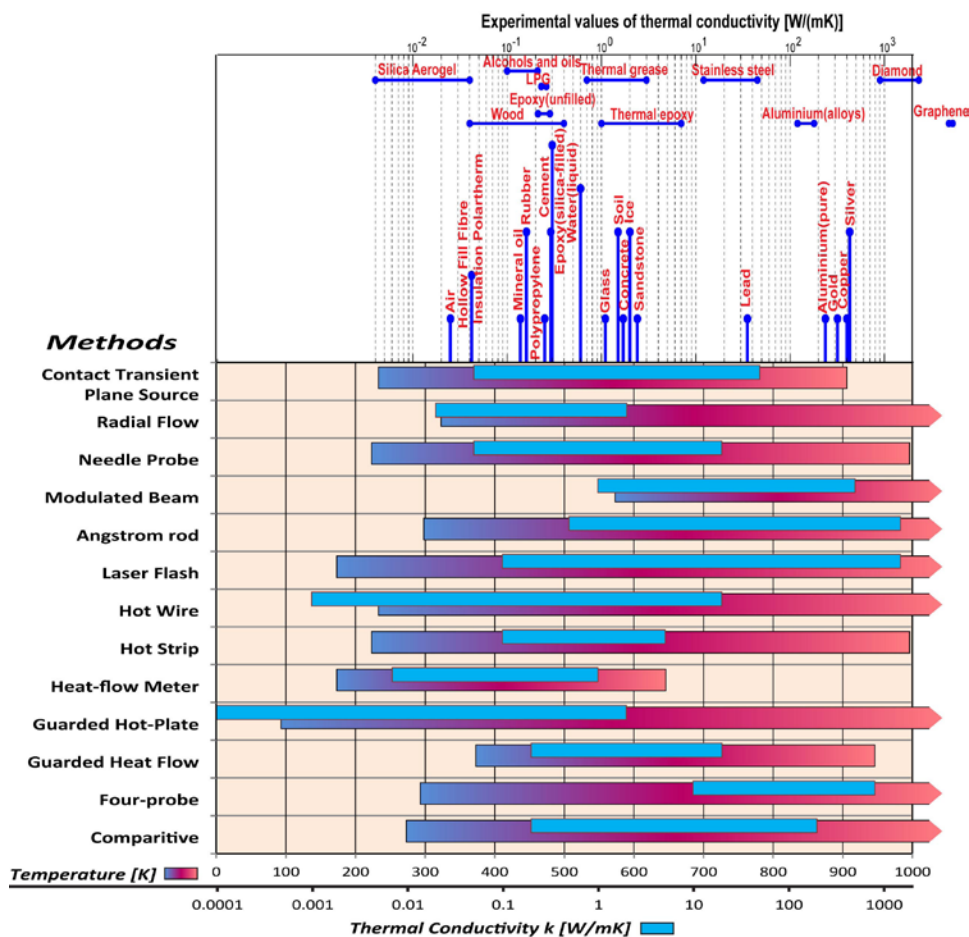


FIGURE 2. Example materials and common measurement methods for different ranges of thermal conductivity [2]

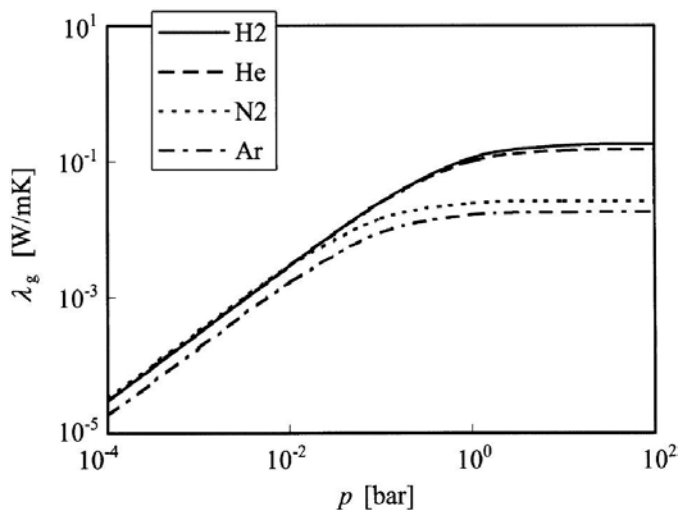


FIGURE 3. Effect of the pressure on the thermal conductivity of different gases [3]

Both methods were explored by Fedchnia et al. for both hydrides and physisorption materials [6]. In that study, three

materials, Ti-doped sodium aluminum hydride, an 8:3 mixture of lithium hydride and magnesium amide, and a metal organic framework were mixed with expanded natural graphite ‘worms’, and uni-axially pressed in a square die to compact the material into cube shaped samples. A hot disk thermal constants analyzer (Figure 6) was used to measure thermal conductivity. The analyzer supplies a constant power to an initially isothermal sample via a sensor located in the middle between two cubes shaped samples and follows, during a limited heating period, the resulting temperature increase using the same sensor also as a resistance thermometer.

The measurements revealed significant anisotropy in the thermal conductivity of these compacted powders. The study also found that there are several important considerations in performing an accurate analysis of thermal conductivity data. These are:

- Analytical solutions for the hot disc in infinite media becomes prohibitive for material exhibiting anisotropic properties.
- It also does not allow inclusion of the heat transfer coefficient for the boundary between the sensor and the material.

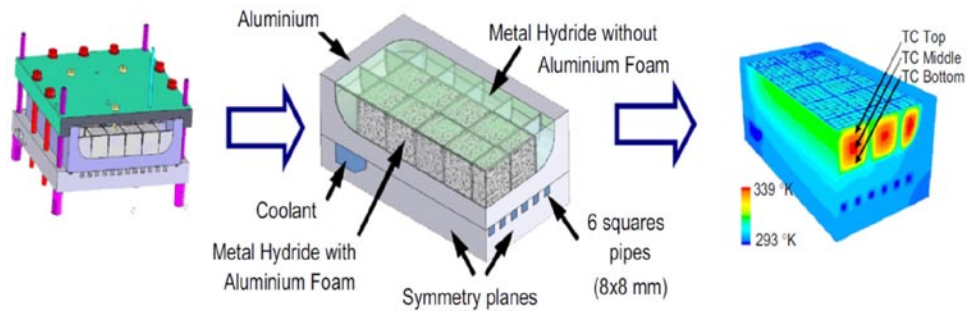


FIGURE 4. AB₅ hydride bed (left), its modeled geometry (center), and calculated temperature contours of temperatures (right) during absorption [5]

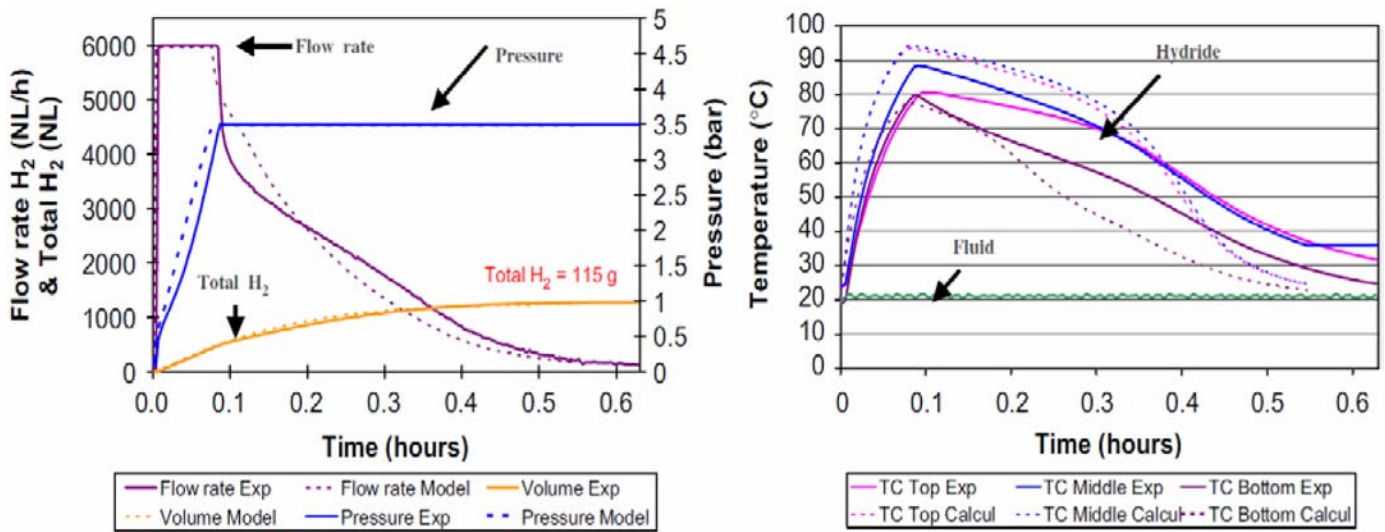


FIGURE 5. Experimental results vs. model results. The experimental results are plotted in continuous lines and the simulation results are plotted as dashed lines [5].

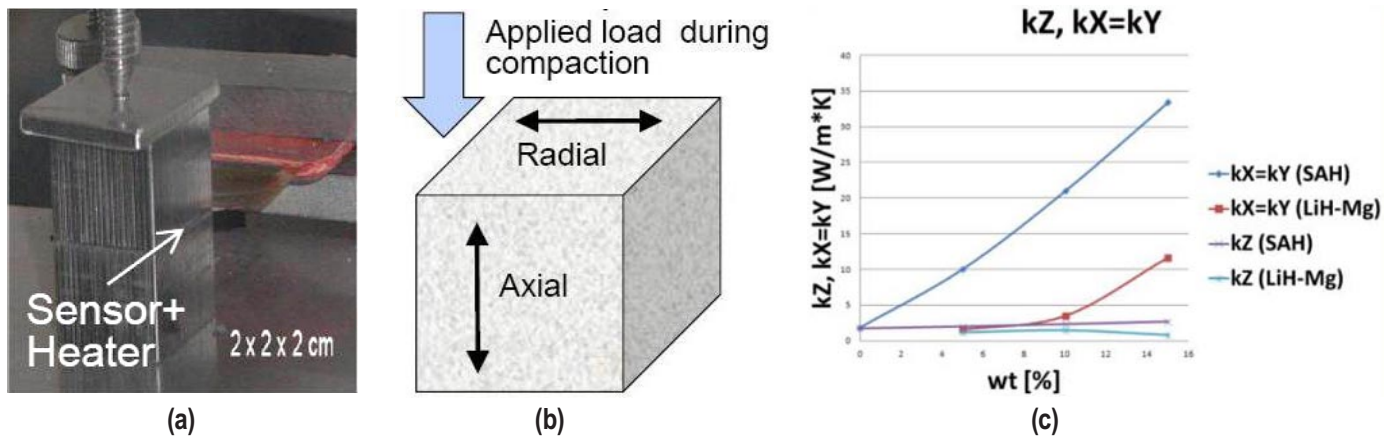


FIGURE 6. (a) Thermal measurement system, (b) Material compaction process, and (c) Thermal conductivity of sodium alanate as a function of thermal additives and direction [6]

- This becomes important for the materials modified by the applied stress. Not accounting for this leads to the wrong relation between the heat applied from the hot disc and the heat transfer properties of the material.
- Also, only thermal diffusivity can be estimated from the analytical model, heat capacity must be measured in a separate experiment.

Conclusions and Future Directions

In FY 2012 we were able to establish important collaborations and technical assistance from experts in the field. We were able to finalize the “Recommended Best Practices for the Characterization of Storage Properties of Hydrogen Storage Materials” sections 1-5 in a timely manner. We are currently working on completing the final version of the Engineering Thermal Properties measurements section and have initiated work on the Engineering Mechanical Properties measurement section.

FY 2012 Publications/Presentations

1. Gross, K.J., Carrington, R., Purewal, J., Barcelo, S., Karkamkar, Dantzer, P., Ma, S., Zhou, H.C., Ott, K., Burrell, T., Semeslberger, T., Pivak, Y., Dam, B., and Chandra, D. “Best Practices for Characterizing Hydrogen Storage Properties of Materials”, IEA HIA Experts Meeting, January 16 – 20, 2011, Fremantle, Australia.
2. Gross, K.J., Carrington, R., Purewal, J., Barcelo, S., Karkamkar, A., Ma, S., Zhou, H.C., Dantzer, P., Ott, K., Burrell, T., Semeslberger, T., Pivak, Y., Dam, B. and Chandra, D., “International standardized testing practices for hydrogen storage materials” IEA HIA Task 22 Expert Workshop for fundamental and applied hydrogen storage materials development, Copenhagen, Denmark, Sept. 6 2011.
3. Gross, K.J., “Best Practices in Characterizing Today’s Most Advance Hydrogen Storage Materials”, Materials Challenges In Alternative & Renewable Energy, Clearwater, Fla., USA, February 29, 2012.

References

1. Welty, J.R. and Wicks, C.E., “Fundamentals of momentum, heat, and mass transfer”, Ed. John Wiley, 4th ed. (2001), New York, U.S.A.
2. Adapted from: Evitherm.org article, “Measurement Methods”, <http://www.evitherm.org/>, <http://www.evitherm.org/default.asp?ID=308>, and Wikipedia article “Thermal Conductivity”, http://en.wikipedia.org/wiki/Thermal_conductivity. http://en.wikipedia.org/wiki/Thermal_conductivity.
3. Asakuma, Y., Miyauchi, S., Yamamoto, T., Aoki, H., Miura, T., “Homogenization method for effective thermal conductivity of metal hydride bed”, *Int. J. of Hydrogen Energy*, 29 (2004) p.209 – 216.
4. Griesinger A, Spindler K, and Hahne E., “Measurement and theoretical modeling of the effective thermal conductivity of zeolites”, *Int J. Heat Mass Transfer*, 42 (1999) p. 4363–74.
5. Botzung, M., Chaudourne, S., Gilliaa, O., Perret, C., Latroche, M., Percheron-Guegan, A., and Marty, P., “Simulation and experimental validation of a hydrogen storage tank with metal hydrides”, *Int. J. of Hydrogen Energy*, 33 (2008) p. 98 – 104.
6. Fedchenia, I.I., and van Hassel, B.A., “Solution of Inverse Thermal Problem for Assessment of Thermal Parameters of Engineered H2 Storage Materials”, paper, Comsol Conference, Boston (2011).

IV.E.3 Neutron Characterization in Support of the DOE Hydrogen Storage Sub-Program

Terrence J. Udovic (Primary Contact),
Craig M. Brown, Dan A. Neumann
NIST Center for Neutron Research
National Institute of Standards & Technology (NIST)
100 Bureau Dr., MS 6102
Gaithersburg, MD 20899-6102
Phone: (301) 975-6241
Email: udovic@nist.gov

DOE Managers
HQ: Ned Stetson
Phone: (202) 586-9995
Email: Ned.Stetson@ee.doe.gov
GO: Jesse Adams
Phone: (720) 356-1421
Email: Jesse.Adams@go.doe.gov

Project Start Date: June 2010
Project End Date: Project continuation and direction
determined annually by DOE

of interest in a variety of materials ranging from H₂ adsorbed in nanoporous materials to H chemically bonded in complex-hydride materials. Insights gained from these studies will be applied toward the design and synthesis of hydrogen-storage materials that meet the following DOE 2017 storage targets:

- Specific energy: 1.8 kWh/kg
- Energy density: 1.3 kWh/L
- Cost: \$2-\$4/kWh net

FY 2012 Accomplishments

- Manuscript published on detailed measurements of temperature dependence of hydrogen adsorbed structures in Fe-MOF74 and its oxidized form.
- Manuscript accepted for publication concerning hydrogen spillover on single-walled carbon-nanohorns in collaboration with the Oak Ridge National Laboratory (ORNL) and Rice University.
- Manuscript submitted for publication concerning spillover speciation in an effort led by NREL.
- Manuscript published on synthesis and characterization of first metal hydrazinoborane and its hydrazine borane adduct.
- Manuscript submitted for publication on structural characterization of X-ray diffraction (XRD)-amorphous, aluminoborane compound AlB₄H₁₁.
- Manuscript published on BH₄⁻ reorientational mechanism in high-temperature hexagonal LiBH₄ phase.
- Manuscript submitted for publication on confinement effects on LiBH₄ and NaAlH₄ sequestered in ordered nanoporous carbon frameworks.

Fiscal Year (FY) 2012 Objectives

- Support the DOE-funded hydrogen-storage projects by providing timely, comprehensive characterization of materials and storage systems using state-of-the-art neutron methods.
- Direct partner synthesis efforts based on the understanding gained through the use of these methods.
- Demonstrate the fundamental characteristics of useful hydrogen-storage materials.

Technical Barriers

This project addresses the following technical barriers from the Storage section (3.3) of the Fuel Cell Technologies Program Multi-Year Research, Development and Demonstration Plan:

- (A) System Weight and Volume
- (P) Lack of Understanding of Hydrogen Physisorption and Chemisorption

Technical Targets

NIST provides important materials metrologies for DOE-funded projects using neutron-scattering measurements to understand and characterize hydrogen-substrate interactions



Introduction

To obtain the DOE levels of hydrogen storage in a timely manner, it is imperative that trial-and-error testing of materials be avoided. Thus, the focus must be upon the rational design of new systems. From a thorough understanding of the physics and chemistry that governs the hydrogen-substrate interactions, we will be able to make a more concerted effort to push the frontiers of new materials. The key to improving materials is a detailed understanding of the atomic-scale locations of the hydrogen and determining how it gets there and how it gets out. Neutron scattering is perhaps the premier technique for studying hydrogen and the

NIST Center for Neutron Research is currently the leading facility in the U.S. for studying these materials.

Approach

NIST provides important materials characterization for DOE-funded, hydrogen storage projects using neutron-scattering measurements to probe the amount, location, bonding states, dynamics, and morphological aspects of (i) molecular hydrogen in carbon-based materials such as polymers, metal organic frameworks (MOFs), and carbonaceous materials such as carbon nanohorns, and (ii) atomic hydrogen in a variety of complex hydride materials including those containing boron and nitrogen, as well as their intermediates and by-products. NIST works directly with DOE and other partners that produce novel hydrogen storage materials to analyze the most promising samples and to help determine and resolve the fundamental issues that need to be addressed.

Results

In collaboration with U. California Berkeley, U. Maryland, U. Florida, Australian Nuclear Science and Technology Organisation, and the Rutherford Appleton Laboratory, we used several neutron-based techniques, including neutron powder diffraction (NPD) and neutron vibrational spectroscopy (NVS), to determine the hydrogen adsorption properties of Fe-MOF74 (Figures 1-2) and its oxidized derivative [1]. These two MOFs, which possess one-dimensional hexagonal channels decorated with unsaturated iron coordination sites, exhibit high initial isosteric heats of adsorption of $-9.7(1)$ and $-10.0(1)$ kJ mol $^{-1}$, respectively. NPD has allowed the identification of three D $_2$ binding sites within the two frameworks, with the closest contacts corresponding to Fe–D $_2$ separations of 2.47(3) and 2.53(5) Å, respectively. NVS spectra, obtained from *p*-H $_2$ (*para*-H $_2$) and D $_2$ -*p*-H $_2$ mixtures adsorbed in Fe $_2$ (dobdc), reveal weak interactions between two neighboring adsorption sites, a finding that is in

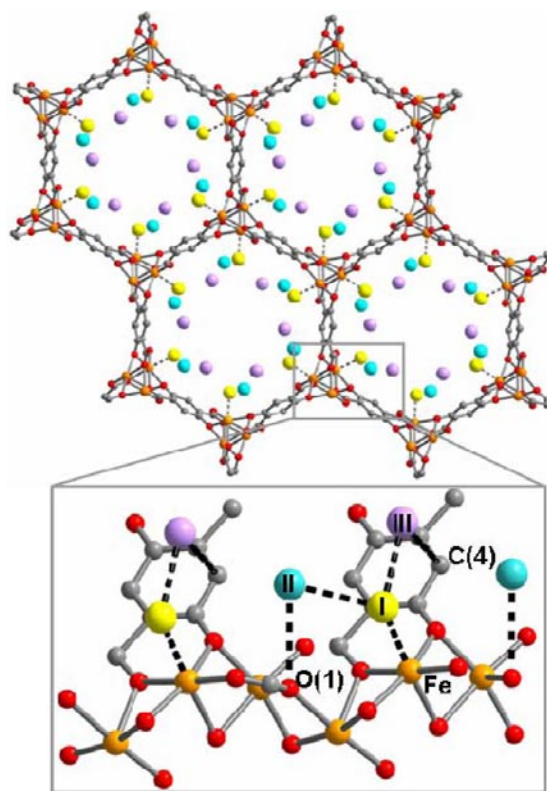


FIGURE 1. Fe-MOF74 loaded with 2.25 D $_2$ per Fe $^{2+}$, viewed along the [001] direction. Orange, gray, and red spheres represent Fe, C, and O atoms, respectively. The box contains a close-up view of the framework wall, showing the closest D $_2$ -D $_2$ and D $_2$ -framework interactions (drawn as dotted lines) along the channel. Three D $_2$ sites, determined by NPD, are labeled as I, II, and III in order of binding strength.

opposition to a previous report of possible ‘pairing’ between neighboring H $_2$ molecules.

In collaboration with U. Delaware, U. Indianapolis, Rice U., Chase Corp., ORNL, and Siberian State Tech. U., NVS and Sievert’s method measurements were combined with temperature-cycling to assess the role of temperature-

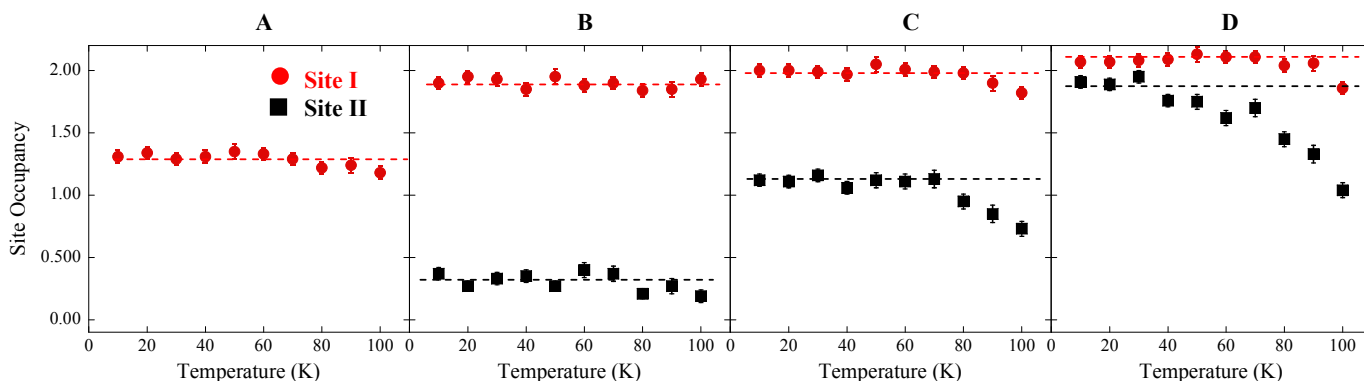


FIGURE 2. Occupancy of H $_2$ in Fe-MOF74 at site I (red) and II (black) plotted as a function of temperature for four different D $_2$ loadings, including (A) 0.5, (B) 1.0, (C) 1.5, and (D) 2.0 D $_2$ molecules per Fe $^{2+}$.

activated, metal-assisted hydrogen storage in Pt-decorated single-wall carbon nanohorns (Pt-SWCNHs) [2]. NVS measurements on single samples of SWCNHs decorated with 2–3 nm Pt nanoparticles showed a 0.17% mass fraction loss of molecular hydrogen after the sample was loaded at 77 K then cycled to room temperature (at a pressure of about 0.5 MPa) and back to 4 K. However, no loss in hydrogen was observed when it was cycled only up to 150 K. Control samples using undecorated SWCNHs did not display any loss of adsorbed H₂ measured at 4 K after cycling to room temperature. Similar measurements involving temperature cycling of Pt-decorated SWCNHs charged with 5 MPa of H₂ at 77 K using a Sievert's apparatus also indicated a measurable quantity ($\approx 0.08\%$ mass fraction) of metal-assisted hydrogen adsorption caused by cycling samples to room temperature. These measurements present evidence for additional excess storage measured at low temperatures induced by metal-assisted activated processes at room temperature. Density functional theory (DFT) calculations were performed to predict signature NVS spectra for C–H libration and bending modes for various conformations of carbon with hydrogen attached in different configurations. However, NVS spectra revealed a near-continuum spectrum, different from the predicted sharp peaks by our DFT calculations, indicating a lack of one preferred binding site if chemically-bonded H occurred in these samples.

In collaboration with U. Maryland, U. Penn, and GM, the first example of a metal hydrazinoborane, LiN₂H₃BH₃ (Figure 3), and its hydrazine borane (N₂H₄BH₃, HB) adduct, LiN₂H₃BH₃·2N₂H₄BH₃, were synthesized, and their structures and bonding were characterized [3] via XRD, molecular dynamics simulated annealing methods, and NVS. The metal hydrazinoboranes exhibit dramatically improved dehydrogenation over pristine HB with nearly complete dehydrogenation in a mild temperature range (323–498 K) with minimal toxic gas (i.e., NH₃ or N₂H₄) release. The metal cation replaces one H on the middle N in the HB molecule, leading to the formation of [NH₂NHBH₃]⁻. In particular, the extent and purity of H₂ released from LiN₂H₃BH₃ exceed

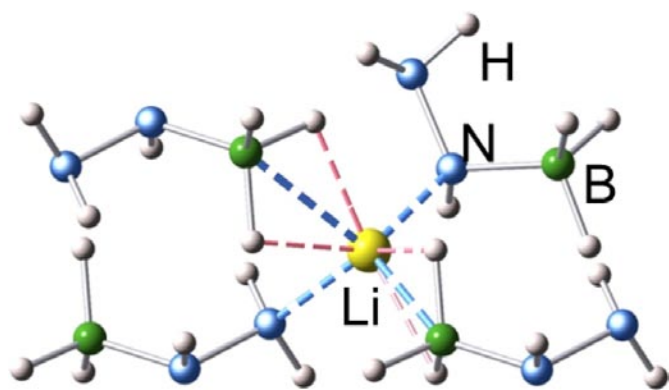


FIGURE 3. The local structure of LiN₂H₃BH₃

even the best performance reported for hydrolysis of HB with catalysts. The electronic and structural changes from N₂H₄BH₃ to [N₂H₃BH₃]⁻ are likely the main reasons for the observed improved hydrogen release properties for the metal hydrazinoboranes.

In collaboration with Ohio State U., Northwestern U., U. Maryland, the Savannah River National Laboratory, and ORNL, we used NVS to help characterize the novel, XRD-amorphous, aluminoborane compound AlB₄H₁₁. The structure was identified by coupling a first-principles, DFT-based approach with infrared (IR), NVS, and NMR measurements. The AlB₄H₁₁ structure was found to contain distinct [BH₄]⁻ and [B₃H₇]⁻ units without any [AlH₄]⁻ units. It forms a –[B₃H₇]⁻–Al(BH₄)⁻ polymer chain with the [BH₄]⁻ units twisted relative to each other perpendicular to the chain direction and bonded to Al, and a chain backbone consisting of [B₃H₇]⁻ and Al where the [B₃H₇]⁻ unit exhibits a triangular boron configuration. The computed lowest-energy structure shows good agreement with IR, NVS, and NMR spectra.

In collaboration with U. Maryland, quasielastic neutron scattering (QENS) spectra were measured for LiBH₄ in the high-temperature hexagonal crystal phase. The elastic incoherent structure factor (EISF) associated with the rapid BH₄⁻ anion reorientations was determined at 400 K, 410 K, and 420 K for momentum transfers as high as 4.2 Å⁻¹ (Figure 4). The results strongly suggest a BH₄⁻ reorientational mechanism approaching quasi-free, trigonal-axis rotation of

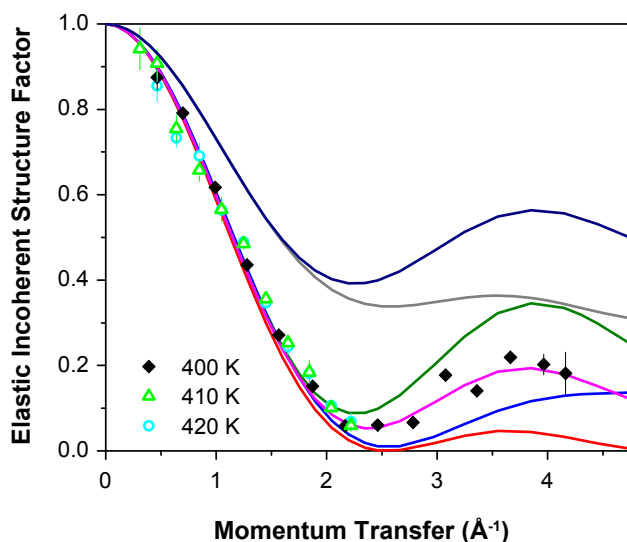


FIGURE 4. EISF data derived from QENS measurements for LiBH₄ at 400 K (black diamonds), 410 K (green triangles), and 420 K (cyan circles) compared with calculated curves for various BH₄⁻ reorientation models, from top to bottom: (dark blue) uniaxial three-fold reorientational jumps, (gray) continuous rotation of three H's around the trigonal axis with a fixed axial H, (green) tetrahedral tumbling among four sites, (magenta) continuous rotation around the trigonal axis combined with jump exchanges with the axial H, (blue) cubic tumbling among eight sites, and (red) isotropic rotational diffusion.

three borohydride H atoms, combined with reorientational jump exchanges between these delocalized “orbiting” H atoms and the remaining axial borohydride H atom [4]. This mechanism is consistent with previously reported diffraction and spectroscopy studies.

Continuing a collaboration with U. Missouri-St. Louis, Washington U.-St. Louis, Sandia National Laboratories, and Caltech, a comparison was made between LiBH_4 sequestered inside an ordered-nanopore carbon (NPC) scaffold and bulk LiBH_4 . Consistent with NMR observations of two translationally distinct BH_4^- populations for LiBH_4 in NPC with 4-nm diameter cylindrical pores, analysis of QENS spectra reveal two reorientationally distinct populations of BH_4^- anions. Such a spectrum at 400 K is shown in Figure 5. The quasielastic scattering from this material is best represented by two Lorentzian functions, with linewidths differing by nearly an order of magnitude. Analogous to the translationally slower interior and more rapid interface BH_4^- anions observed by NMR, the narrower and broader Lorentzian components are associated with the reorientational motions of the less mobile, more bulk-like interior and more mobile, interface BH_4^- anions, respectively. Activation energies for reorientation of 15 ± 1 kJ/mol and 11.3 ± 0.8 kJ/mol for the former and latter BH_4^- populations were determined from an Arrhenius plot of the Lorentzian linewidths. The respective reorientation jump rates from the Arrhenius fits varied from $\sim 2.6 \times 10^9$ s⁻¹ and 5.6×10^{10} s⁻¹ at 193 K to $\sim 3.5 \times 10^{11}$ s⁻¹ and 2.1×10^{12} s⁻¹ at 400 K. The reorientation rates and activation energy of the less mobile population are similar to those for bulk LiBH_4 . The well-behaved Arrhenius

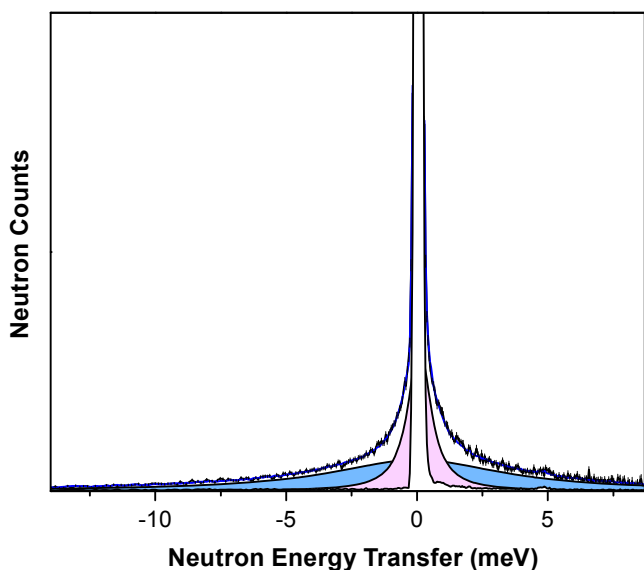


FIGURE 5. QENS spectrum of LiBH_4 in NPC at 400 K and 3 \AA^{-1} momentum transfer. The spectrum is fit to an elastic line with instrumental resolution (white) and two Lorentzian functions (narrower: pink and broader: blue) that reflect two different BH_4^- reorientational dynamics.

-type dependence of the two Lorentzian linewidths from 193 K to 400 K are inconsistent with the presence of a solid-solid phase transition in this region.

Conclusions and Future Directions

- Neutron methods have provided crucial, non-destructive characterization tools for the DOE Hydrogen Storage Sub-Program.
- The Fe-MOF74 system provided a rare opportunity to observe reduction-oxidation chemistry at the unsaturated metal sites in a MOF.
- Our measurements confirm the loss of adsorbed H_2 and significant metal-assisted hydrogen storage on Pt-SWCNHs that are activated at $T > 150$ K, which is consistent with hydrogen spillover.
- The first example of a metal hydrazinoborane was synthesized and characterized. Further studies need to be conducted in expanding the range of metals used, tuning the reactivity of B–H and/or N–H through inducing polar species such as strong electropositive cations or highly active anions, exploring the role of dopants or catalysts in controlling dehydrogenation, and understanding the dehydrogenation mechanism.
- The successful characterization of $\text{AlB}_4\text{H}_{11}$ demonstrates the usefulness of the structure prediction approach for determining the local structures of even XRD-amorphous compounds.
- We continued to characterize various aspects of nanoconfinement in an attempt to understand its effect on the hydrogen cycling of LiBH_4 and were able to observe two dynamically distinct populations of BH_4^- anions associated with LiBH_4 regions next to and away from the pore walls.
- We will continue to support the DOE Hydrogen Storage Sub-Program where needed.

Special Recognitions & Awards/Patents Issued

1. Craig M. Brown received the 2012 Arthur S. Flemming Award, administered by George Washington University, for his seminal contributions to our understanding of new materials suited for hydrogen energy storage in next-generation, clean automobiles.
2. Wendy L. Queen won the NIST chapter of Sigma-Xi Postdoctoral Poster Competition (Materials Category) for her poster: “Reducing Energy Costs of Industrial Gas Separations Using Metal-Organic Framework Based Solid Adsorbents”.

FY 2012 Publications/Presentations

1. N. Verdál, W. Zhou, V. Stavila, J.-H. Her, M. Yousufuddin, T. Yildirim, and T.J. Udovic, “Alkali and Alkaline-Earth Metal Dodecahydro-*Closo*-Dodecaborates: Probing Structural Variations via Neutron Vibrational Spectroscopy,” *J. Alloys Compds.* 509S, S694 (2011).

2. N. Verdal, T.J. Udovic, J.J. Rush, R.L. Cappelletti, and W. Zhou, "Hydrogen Dynamics of the Dodecahydro-*Closo*-Dodecaborate Crystals", Proc. Am. Chem. Soc., Div. Fuel Chem. 56, (2) 181 (2011).
3. N. Verdal, T.J. Udovic, J.J. Rush, V. Stavila, H. Wu, W. Zhou, and T. Jenkins, "Low-Temperature Tunneling and Rotational Dynamics of the Ammonium Cations in $(\text{NH}_4)_2\text{B}_{12}\text{H}_{12}$ ", J. Chem. Phys. 135, 094501 (2011).
4. N. Verdal, H. Wu, T.J. Udovic, V. Stavila, W. Zhou, and J.J. Rush, "Evidence of a Transition to Reorientational Disorder in the Cubic Alkali-Metal Dodecahydro-*Closo*-Dodecaborates," J. Solid. State Chem. 184, 3110 (2011).
5. J.-H. Her, H. Wu, N. Verdal, W. Zhou, V. Stavila, and T.J. Udovic, "Structures of the Strontium and Barium Dodecahydro-*Closo*-Dodecaborates," J. Alloys Compds. 514, 71 (2012).
6. N. Verdal, T.J. Udovic, and J.J. Rush, "The Nature of BH_4^- Reorientations in Hexagonal LiBH_4 ," J. Phys. Chem. C 116, 1614 (2012).
7. N. Verdal, T.J. Udovic, and J.J. Rush, "Correction to 'The Nature of BH_4^- Reorientations in Hexagonal LiBH_4 ,'" J. Phys. Chem. C 116, 5275 (2012).
8. Y.S. Chua, H. Wu, W. Zhou, T.J. Udovic, G. Wu, Z. Xiong, M.W. Wong, and P. Chen, "Monoammoniate of Calcium Amidoborane - Synthesis, Structure and Hydrogen-Storage Properties," Inorg. Chem. 51, 1599 (2012).
9. M.M. Barsan, I.S. Butler, D.F.R. Gilson, R.O. Moyer, Jr., W. Zhou, H. Wu, and T.J. Udovic, "Raman, FTIR, Photoacoustic-Infrared and Inelastic Neutron Scattering Spectra of Ternary Metal Hydride Salts A_2MH_5 (A=Ca, Sr, Eu; M=Ir, Rh) and their Deuterides," J. Phys. Chem. A 116, 2490 (2012).
10. H. Wu, W. Zhou, F.E. Pinkerton, T.J. Udovic, T. Yildirim, and J.J. Rush, "Metal Hydrazinoborane $\text{LiN}_2\text{H}_3\text{BH}_3$ and $\text{LiN}_2\text{H}_3\text{BH}_3 \cdot 2\text{N}_2\text{H}_4\text{BH}_3$: Crystal Structures and High-Extent Dehydrogenation," Energy Environ. Sci. 5, 7531 (2012).
11. W.L. Queen, E.D. Bloch, C.M. Brown, M.R. Hudson, J.A. Mason, L.J. Murray, A.J. Ramirez-Cuesta, V.K. Peterson, and J.R. Long, "Hydrogen Adsorption in the Metal-Organic Frameworks $\text{Fe}_2(\text{dobdc})$ and $\text{Fe}_2(\text{O}_2)(\text{dobdc})$," Dalton Trans. 41, 4180 (2012).
12. Y. Liu, C.M. Brown, D.A. Neumann, D.B. Geohegan, A.A. Puzos, C.M. Rouleau, H. Hu, D. Styers-Barnett, P.O. Krasnov, B.I. Yakobson "Inelastic Neutron Scattering and High Pressure Gas Adsorption Measurements of Hydrogen Spillover on Pt-decorated Single-Walled Carbon Nanohorns," Carbon 50, 4953 (2012).
13. W.L. Queen, C.M. Brown, M.R. Hudson, K. Sumida, E.D. Bloch, L.J. Murray, J.R. Long, D.K. Britt, and O.M. Yaghi "Gas Adsorption in Metal-Organic Frameworks With Coordinatively Unsaturated Metal Sites", 2011 Meeting of the American Crystallographic Association, New Orleans, LA (May 2011).
14. N. Verdal, T.J. Udovic, V. Stavila, and J.J. Rush, "Characterization of Destabilized and Ultra-Stable Hydrogen Storage Materials Using Neutron Scattering Techniques," Hydrogen-Metal Systems Gordon Conference, Stonehill College, Easton, MA (Jul. 2011).
15. C.M. Brown, "Probing Adsorption in Microporous Materials using Neutrons," BraggSpeaks, ANSTO, Sydney, Australia (Jul. 2011) (Invited).
16. C.M. Brown, "Physical Aspects of Gas Adsorption in Microporous Materials," PACRIM9, Cairns, Australia (Jul. 2011) (Invited).
17. N. Verdal, T.J. Udovic, J.J. Rush, R.L. Cappelletti, and W. Zhou, "Hydrogen Dynamics of the Dodecahydro-*Closo*-Dodecaborate Crystals," National Meeting of the American Chemical Society, Denver, CO (Aug. 2011).
18. W.L. Queen, "Utilizing Neutron Scattering Techniques in the Characterization of Metal-Organic Frameworks", University of California Berkeley, Berkeley CA, (Aug. 2011) (Invited).
19. W.L. Queen, C. M. Brown, and M. R. Hudson, "Physical Aspects of H_2 Storage in Microporous Materials", 2011 Fall National Meeting of the American Chemical Society, Denver, CO (Aug. 2011) (Invited).
20. C.M. Brown, "Probing Adsorption in Microporous Materials using Neutrons," University of Sydney Chemistry Department School Seminar, Sydney, Australia (Aug. 2011) (Invited).
21. C.M. Brown, "Probing Adsorption in Microporous Materials using Neutrons," Monash University Faculty of Engineering Seminar, Melbourne, Australia (Sep. 2011) (Invited).
22. C.M. Brown, "Probing Adsorption in Microporous Materials using Neutrons," CSIRO Seminar, Melbourne, Australia (Sep. 2011) (Invited).
23. C.M. Brown, "Probing Adsorption in Microporous Materials using Neutrons," University of Adelaide Chemistry and Physics Seminar, Adelaide, Australia (Sep. 2011) (Invited).
24. C.M. Brown, "Gas Storage in Porous Materials," IUPAC International Conference on Novel Materials, Shanghai, China (Oct. 2011) (Keynote and Session Chair).
25. C.M. Brown, "Structure and Properties of Advanced Materials through Neutron Scattering," Geophysical Laboratory Seminar, Carnegie Institute, Washington, DC (Nov. 2011) (Invited).
26. W.L. Queen, C.M. Brown, M.R. Hudson, E.D. Bloch, and J.R. Long, "Reducing Energy Costs of Industrial Gas Separations Using Metal-Organic Framework Based Solid Adsorbents", 19th Annual Postdoctoral Poster Competition sponsored by the NIST Chapter of Sigma Xi, Gaithersburg, MD (Feb. 2012).
27. T.J. Udovic, "Neutron Scattering Studies of the Structure, Spectroscopy, and Reorientational Dynamics of Borohydride-based Materials," Spring Meeting of the Materials Research Society, San Francisco, CA, (Apr. 2012) (Invited).
28. C.M. Brown, "Gas Storage in Porous Materials," Advanced Seminar on "Perspectives for Neutron Science in Novel & Extreme Conditions," Zaragoza, Spain (May 2012) (Invited).
29. N. Verdal, X. Liu, T.J. Udovic, and E.H. Majzoub, "Understanding the Destabilizing Mechanism of Nanoporous Carbon Using Inelastic Neutron Scattering," American Conference on Neutron Scattering, Washington, DC (Jun. 2012).
30. W.L. Queen, M.R. Hudson and C.M. Brown, "What Neutrons Tell Us about Industrially Important Adsorption Processes," American Conference on Neutron Scattering, Washington, DC (Jun. 2012).

References

1. Y. Liu, *et al.*, Carbon **50**, 4953 (2012).
2. W. Queen, *et al.*, Dalton Trans. **41**, 4180 (2012).
3. H. Wu, *et al.*, Energy Environ. Sci. **5**, 7531 (2012).
4. N. Verdal, *et al.*, J. Phys. Chem. C **116**, 1614 (2012).

IV.E.4 Hydrogen Storage Cost Analysis, Preliminary Results

Brian D. James (Primary Contact),
Andrew B. Spisak, Whitney G. Colella
Strategic Analysis, Inc.
4075 Wilson Blvd. Suite 200
Arlington, VA 22203
Phone: (703) 778-7114
E-mail: bjames@sainc.com

DOE Managers
HQ: Grace Ordaz
Phone: (202) 586-8350
Email: Grace.Ordaz@ee.doe.gov
GO: Katie Randolph
Phone: (720) 356-1759
Email: Katie.Randolph@go.doe.gov

Contract Number: DE-EE0005253

Project Start Date: September 30, 2012

Project End Date: September 29, 2016

Fiscal Year (FY) 2012 Objectives

- Develop cost models of carbon fiber hydrogen storage pressure vessels.
- Explore the sensitivity of pressure vessel cost to design parameters including hydrogen storage quantity, storage pressure, and the number of vessels.
- Validate pressure vessel cost model results and sensitivities against measured data for industry partner costs.
- Develop cost models for the off-board recycle cost of spent chemical hydrogen storage media (hydrogen depleted materials from the alane and ammonia borane onboard storage systems).

Technical Barriers

This project addresses the following technical barriers from the Hydrogen Storage section of the Fuel Cell Technologies Program Multi-Year Research, Development and Demonstration Plan:

- (B) System Cost
- (H) Balance of Plant (BOP) Components
- (K) System Life-Cycle Assessments

Technical Targets

This project conducts cost modeling to attain realistic, process-based system costs for a variety of hydrogen storage systems. These values can help inform future technical targets for System Storage Cost.

- System Storage Cost: to be determined

FY 2012 Accomplishments

- Prepared a cost model and completed a preliminary cost analysis of onboard compressed hydrogen storage pressure vessels. Preliminary analysis identifying a total cost of \$13.11 kilowatt-hour (kWh) of hydrogen energy for a 70 megapascal (MPa, 10,000 pounds per square inch, psi), 5.6 kilograms (kg) hydrogen (H₂) pressure vessel system produced at a rate of 500,000 systems per year.
- Conducted a pressure vessel sensitivity study to explore the cost effect of tank storage capacities of 4 to 8 kg of H₂ per tank and manufacturing rates of 10,000, 30,000, 80,000, 130,000, and 500,000 vessels per year.
- Initiated cost analysis of the off-recycle process of spent ammonium borane (BNH₂) back into an ammonia borane (AB or BH₃NH₂) slurry suitable for use in a vehicular onboard H₂ storage system.
- Initiated cost analysis of the off-recycle process of aluminum (spent alane) back into an alane slurry suitable for use in a vehicular onboard alane (AlH₃) H₂ storage system.



Introduction

To better assess differing technologies for fuel cell vehicle (FCV) hydrogen storage, it is important to have an understanding of the potential cost of each technology, and the primary drivers underlying those costs. The aim of this project is to obtain realistic, process-based system costs for a variety of hydrogen storage systems and to use those cost models to determine sensitivity to design parameters, manufacturing methods, system components, and materials costs. Through this process, it is possible to demonstrate the impact of DOE technical targets and barriers on the overall system cost. These results can be used to gauge and guide future DOE Research and Development efforts by identifying the most fruitful research paths to cost reduction.

During the first year of the project, onboard hydrogen storage in pressurized carbon composite pressure vessels was selected for analysis. While this system has been previously

analyzed by DOE, the objective is to update and expand the cost analysis while also validating the cost analysis methodology and results against industry estimates, thereby increasing confidence for future cost analysis projects. Additionally, two off-board chemical hydride recycle systems were selected for cost analysis: regeneration of ammonia borane and alane from their respective spent fuel. The vehicular onboard components of these systems have been previously analyzed. However, an assessment of the off-board recycle costs is needed to allow DOE to assess the full cost of the storage method.

Approach

To generate cost estimates for the compressed hydrogen pressure vessel system, a Design for Manufacturing and Assembly (DFMA[®])-style analysis was conducted. Key system design parameters and an engineering system diagram describing process flows were obtained from a combination of industry partners, Argonne National Laboratory (ANL), and members of the DOE's Hydrogen Storage Engineering Center of Excellence (HSECoE) [1]. From this system design, the physical embodiment of the system was developed, including materials, scaling, dimensions, and design. Based on this physical embodiment, the manufacturing process train was modeled to attain the cost to manufacture each part. Industry partners were consulted to assess current and future manufacturing procedures and parameters. Cost was based on the capital cost of the manufacturing equipment, machine rate of the equipment, equipment tooling amortization, part material costs, and other financial assumptions. Once the cost model was complete for the system design, sensitivity data for the modeled technology are obtained by varying the key parameters. These results are shared with ANL, the National Renewable Energy Laboratory, and industry partners to obtain feedback and further refine the model.

The analysis explicitly includes fixed factory expenses such as equipment depreciation, tooling amortization, utilities, and maintenance as well as variable direct costs such as materials and labor. However, because this analysis is intended to model manufacturing costs, a number of components that usually contribute to the original equipment manufacturer price are explicitly not included in the modeling. The following costs are excluded in this analysis: profit and markup, one-time costs such as non-recurring research/design/engineering, and general expenses such as general and administrative costs, warranties, advertising, and sales taxes.

The off-board recycle cost analysis for the alane and AB systems is based on a less-detailed cost analysis methodology. For each of the systems, a process flow diagram is developed based on input from ANL. The AB recycle system is based on the Los Alamos National

Laboratory one-pot process using hydrazine to recycle spent AB (BN₂) back into AB (BH₃NH₃) [2-4]. Since hydrazine is a major cost contributor in the recycle process, hydrazine cost is independently analyzed based on the benzophenone process, which converts ammonia, oxygen, and water into hydrazine [5]. The alane recycle system is based on the dimethylethylamine (DMEA) process [6]. Both recycle systems are nominally sized for a central plant with an equivalent capacity of 100 metric tons per day of hydrogen. A modified form of the H2A hydrogen production cost analysis spreadsheet [7] is used to assess recycle cost. While we do not seek to compute hydrogen production costs, the H2A model is based on a discounted cash flow tool that applies to this recycle analysis. Furthermore, the H2A model is a transparent and familiar tool to the hydrogen community. Recycle cost are computed per kg of H₂ eventually releasable onboard the vehicle. Capital cost of the systems are estimated by a summation of major subsystem identified on the process flow diagram, and are based on hand-book [8] capital cost correlations for the type of subsystem and pertinent scaling factors (such as flow rate, pressure, temperature, etc.).

Results

The pressure vessel baseline system was defined with the following parameters and characteristics:

| | |
|--|----------------------------------|
| H ₂ Stored (usable and dispensable as fuel) | 5.6 kg |
| H ₂ Stored (total) | 5.77 kg |
| Rated Pressure | 700 bar (10 kpsi, 70 MPa) |
| Number of Tanks | 1 |
| Pressure Vessel Type | Type 4 |
| Liner Thickness | 5 millimeters (mm) |
| End Caps | Foam, energy-absorbing |
| Boss Material | 316 stainless steel |
| Water Volume (interior) | 145 L |
| Vessel External Diameter | 563 mm |
| Vessel External Length | 900 mm |
| Carbon Fiber Type | T-700S carbon fiber |
| Carbon Fiber Tensile Strength | 4.9 gigapascals (GPa) (711 kpsi) |
| Carbon Fiber Modulus | 230 GPa (33.4 Mpsi) |
| Safety Factor | 2.25 |
| Translation Efficiency | 80% |
| Fiber Strength Rating | 100% |

For the modeled baseline system, costs are broken down into three broad categories:

- (1) manufacturing and tooling
- (2) BOP and assembly
- (3) materials

Figure 1 shows preliminary results for the baseline compressed gas system. Note that research is ongoing, with assumptions continuing to be vetted and improved after discussion with industry and the HSECoE. The results show that materials cost declines only very slightly with manufacturing rate (~13% over a production increase from 10,000 systems/year to 500,000 systems/year) while manufacturing and tooling cost declines dramatically (~60% over the same range).

The results from sensitivity studies demonstrated the effects of varying tank design parameters. Figure 2 shows the variation of system cost with usable H₂ storage capacity at different annual production rates. The H₂ storage cost per unit of energy (\$/kWh) decreases steadily and approximately linearly as usable H₂ storage capacity increases. At the same

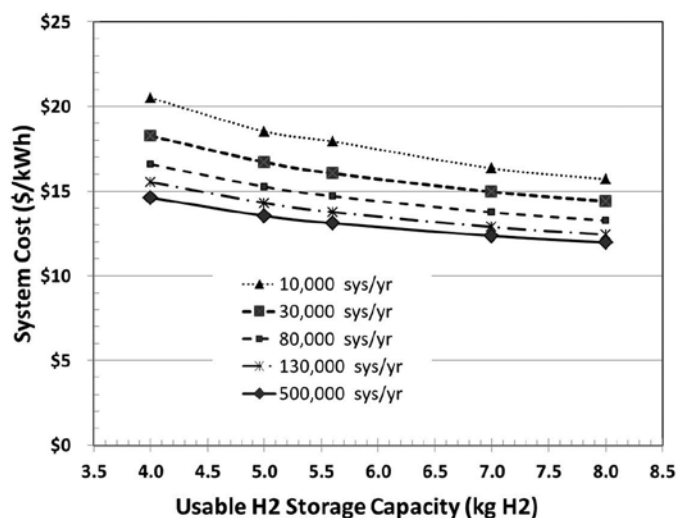


FIGURE 1. System Cost Breakdown for Multiple Manufacture Rates

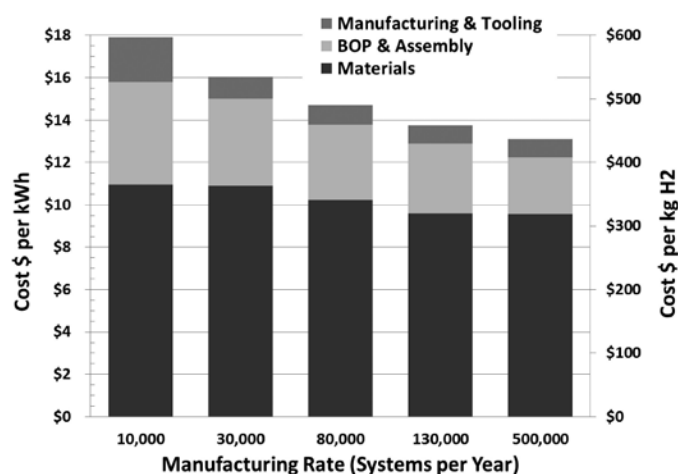


FIGURE 2. Pressure Vessel System Useable H₂ Storage Capacity Sensitivity

storage capacity, the H₂ storage cost per unit energy also decreases with increase annual production rate.

Process flow diagrams for the alane and AB off-board recycle systems have been identified and are being used to generate capital costs estimates for each plant. The DOW report [9] pertaining to AB recycle has been an invaluable aid in the analysis. Based on the parameters in that report, the AB recycle cost is preliminarily estimated at \$47.23 per kg of hydrogen releasable on the vehicle assuming a hydrazine price of \$5.51/kg (all in 2007 dollars). While this is a prohibitively high cost, sensitivity analysis indicates that the recycle cost is highly sensitive to hydrazine price. Thus, AB recycle cost might be acceptable if hydrazine was reduced to <\$1/kg. Cost analysis of the potentially low cost benzophenone process for hydrazine production is not yet complete. Preliminary results from the alane recycle process are also not yet available.

Conclusions and Future Directions

Based upon the work conducted this year, the following conclusions and future directions are revealed:

- Carbon fiber pressure vessels are highly sensitive to carbon fiber cost. Thus accurate estimation of the carbon fiber price and the mass of fiber required in each vessel is very important.
- 700 bar pressure vessel system costs (for a single vessel holding 5.6 kg of usable H₂ fuel) are expected to range from ~\$18/kWh (at 10,000 systems per year) to ~\$13 Wh (at 500,000 systems per year).
- Industry validation of the required pressure vessel carbon fiber mass is needed for confidence in the cost projections.
- A sensitivity analysis regarding tank size (4-8 kg H₂), lower pressure (300 bar), and number of pressure vessels within the system (1, 2, or 3) is helpful to better understand cost tradeoffs.
- The AB recycle system is particularly sensitive to the price of hydrazine. If hydrazine is only available at current market price (~\$5.51/kg), the AB recycle cost is prohibitively expensive (~\$47 per kg of H₂ eventually releasable onboard the vehicle).
- The AB and alane recycle analyses will be concluded.

FY 2012 Publications/Presentations

1. "Preliminary Pressure Vessel Cost Analysis," presentation to the DOE Hydrogen Storage Tech Team, 15 March 2012.
2. "Hydrogen Storage Cost Analysis, Preliminary Results," presentation at the 2012 DOE Hydrogen and Fuel Cells Program Review, Washington, D.C., 15 May 2012.

References

1. “Technical assessment of compressed hydrogen storage tank systems for automotive applications,” T.Q. Hua, R.K. Ahluwalia, J.-K. Peng, M. Kromer, S. Lasher, K. McKenney, K. Law, J. Sinha, *International Journal of Hydrogen Energy* 36 (2011) 3037-3049. (doi:10.1016/j.ijhydene.2010.11.090)
2. Sutton, A.D., “Efficient Regeneration of Ammonia Borane”, ACS Meeting, Aug 20 2009.
3. Sutton et al., “Regeneration of Ammonia Borane Polyborazylene”, US Patent Application 2010/0272622 A1, October 28, 2010.
4. “Off-board Regeneration of Ammonia Borane for Use as a Hydrogen Carrier for Automotive Fuel Cells,” Thanh Hua, Rajesh Ahluwalia, submission for publication in the *International Journal of Hydrogen Energy*, 2 April, 2012.
5. “Hydrazine Production from Ammonia via Azine.” Hiromu Hayashi et. al., *Industrial and Engineering Chemistry Product Research and Development*, Vol. 15 No. 4 (1976) 299-303.
6. “Alane hydrogen storage for automotive fuel cells - Off-board regeneration processes and efficiencies,” Thanh Q. Hua, Rajesh K. Ahluwalia, *International Journal of Hydrogen Energy*, Volume 36, Issue 23, November 2011, Pages 15259–15265. (doi:10.1016/j.ijhydene.2011.08.081)
7. “H2A Hydrogen Production Analysis Model Version 3,” Darlene Steward, National Renewable Energy Laboratory, presented at 2012 DOE Hydrogen and Fuel Cells Program Review, Washington, DC, May 15, 2012.
8. Peters, Max S., Timmerhaus, Klaus D., West, Ronald E., *Equipment Costs Plant Design and Economics for Chemical Engineers – 5th Edition*, (New York, NY: McGraw-Hill, 2002). <http://www.mhhe.com/engcs/chemical/peters/data/ce.html>
9. “Low-Cost Precursors to Novel Hydrogen Storage Materials”, Final Report, Suzanne W. Linehan, Arthur A. Chin, Nathan T. Allen, Robert Butterick, Nathan T. Kendall, I. Leo Klawiter, Francis J. Lipiecki, Dean M. Millar, David C. Molzahn, Samuel J. November, Puja Jain, Sara Nadeau, Scott Mancroni, The Dow Chemical Company, December 31, 2010, Prepared for U.S. Department of Energy, Office of Energy Efficiency and Renewable Energy Hydrogen Program, Hydrogen Storage, Under Contract DE-FC36-05GO15053.

IV.E.5 Early Market TRL/MRL Analysis

Ewa C.E. Rönnebro
Pacific Northwest National Laboratory (PNNL)
902 Battelle Blvd
Richland, WA 99352
Phone: (509) 372-6877
Email: Ewa.Ronnebro@pnnl.gov

DOE Manager
HQ: Ned Stetson
Phone: (202) 586-9995
Email: Ned.Stetson@ee.doe.gov

Project Start Date: October, 2010
Project End Date: September, 2012

Fiscal Year (FY) 2012 Objectives

- Determine methodology for Technology Readiness Level/Manufacturing Readiness Level (TRL/MRL) analysis of technology and manufacturing readiness of early market motive and non-motive hydrogen storage technologies.
- Prepare and send out questionnaire to developers and manufacturers of hydrogen storage technologies for self-assessment to assign TRL/MRL.
- Analyze TRL and MRL of early market hydrogen storage technologies.
- Deliver a TRL/MRL analysis to reveal state of the art of technology and manufacturing readiness and to identify research and development (R&D) gaps.

Technical Barriers¹

This project aids the DOE in understanding the technology readiness levels and manufacturing needs for hydrogen storage technology for use in fuel cell motive and non-motive early market applications. The findings will be used to identify technology gaps in the following:

- System Weight and Volume
- System Cost
- Durability/Operability
- Charging/Discharging Rates
- Materials of Construction
- Manufacturing

¹The technical barriers listed in the DOE Fuel Cell Technologies Program Multi-Year Research, Development and Demonstration Plan pertain to light-duty vehicles and are not applicable to this project.

Technical Targets

To assess technology and manufacturing readiness of early market hydrogen storage technologies, PNNL requested developers and manufacturers to assign TRL and MRL to their technologies based on a self-assessment. The TRL/MRL levels are related to above technical barriers, although they are not quantifiably addressed in this report.

FY 2012 Accomplishments

- Developed a TRL/MRL questionnaire and sent out to technology developers and manufacturers to perform a self-assessment to learn technology readiness for manufacturing.
- Analyzed questionnaire results with assigned TRL/MRL to each hydrogen storage technology based on material and application to identify state of the art.
- Performed a TRL/MRL analysis to reveal technology and manufacturing readiness levels and identify gaps to provide programmatic recommendations to DOE.



Introduction

Fuel cells (FCs) are considered a key future energy efficient power generation technology. The DOE's Fuel Cell Technologies Program (FCTP) is focused on key challenges concerning fuel cells and hydrogen technologies including hydrogen production, delivery, distribution and storage. Recently, the FCTP has broadened its focus from light-duty vehicle application to include near-term market applications, and hydrogen storage is necessary for these fuel cell applications [1,2]. The focus of this report is hydrogen storage for near-term commercial fuel cell applications. The report documents the methodology and results of an effort to identify hydrogen storage technologies' technical and manufacturing readiness for early market motive and non-motive applications and to provide a path forward toward commercialization. Motive applications include materials handling equipment (MHE) and ground support equipment, such as forklifts, tow tractors, and specialty vehicles such as golf carts, lawn mowers and wheel chairs. Non-motive applications are portable, stationary or auxiliary power units and include portable laptops, backup power, remote sensor power, and auxiliary power for recreational vehicles, hotels, hospitals, etc.

The Technology Readiness Assessment (TRA) is based on a combination of TRL and MRL designations that enable evaluation of hydrogen storage technologies in varying levels of development [3,4]. This approach provides a logical

methodology and roadmap to enable the identification of hydrogen storage technologies, their advantages/disadvantages, gaps and R&D needs on an unbiased and transparent scale that is easily communicated to interagency partners.

Approach

To assess the state of the art of hydrogen storage technologies for motive and non-motive early market applications, PNNL performed a Technology Readiness Assessment (TRA) to learn market and technology readiness and to provide a path forward to bring the hydrogen technologies to maturity. The technology development model is illustrated in Figure 1.

PNNL prepared a questionnaire to assign TRL and MRL for each hydrogen storage technology. The definitions of TRL/MRL are provided in Table 1. The manufacturing status is established from eight risk elements: technical maturity, design, materials, cost & funding, process capability, personnel, facilities and manufacturing planning. The questionnaire was sent to hydrogen storage technology developers and manufacturers who were asked to perform a self-assessment. We included both domestic and international organizations including U.S. national laboratories, U.S.

companies, European companies and Japanese companies. PNNL collected the data and performed an analysis to deduce the level of maturity and to provide program recommendations. The TRA report documents the process used to conduct the TRA, reports the TRL and MRL for each assessed technology and provides recommendations based on the findings.

Results

For the TRL/MRL analysis, we targeted technology developers and manufacturers, both U.S. and foreign, with an advanced hydrogen storage material in a subsystem or system. Out of 32 requests for self-assessments, 25 invitees participated. The requests for participation were sent out by email during summer/fall 2011 and the TRA-analysis was performed in winter/spring 2011-2012. Following is a summary of key results of PNNL’s TRA-analysis of each hydrogen storage technology and intended application.

Metal Hydrides TRL/MRL Analysis

Metal hydrides’ technical maturity, based on 12 replies, is between TRL 3 and 9, indicating that there are metal

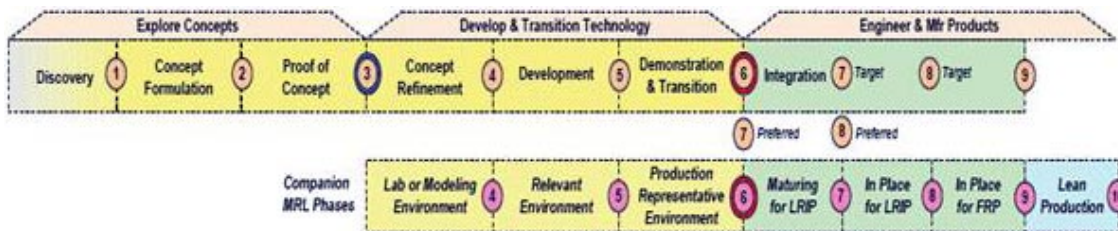


FIGURE 1. Technology Development Model

TABLE 1. Definitions of Technology and Manufacturing Readiness Levels (TRL and MRL)

| Levels | TRL | MRL |
|--------|---|--|
| 1 | Basic principles observed and reported | |
| 2 | Technology concept and/or application formulated | |
| 3 | Analytical and experimental critical function and/or characteristic proof of concept | |
| 4 | Component and/or breadboard system validation in laboratory environment | Capability to produce the technology in a laboratory environment |
| 5 | Component and/or brassboard system validation in relevant environment | Capability to produce prototype components in a production-relevant environment |
| 6 | System/subsystem model or prototype demonstration in a relevant environment | Capability to produce systems or subsystems in a production-relevant environment |
| 7 | System prototype demonstration in an operational environment | Capability to produce systems, subsystems or components in a production-representative environment |
| 8 | Actual system completed and qualified through test and demonstration | Pilot Line Capability demonstrated; ready for Low Rate Initial Production |
| 9 | Actual system operated over the full range of expected mission (operating) conditions | Low Rate Initial Production demonstrated; capability in place to begin Full Rate Production |
| 10 | | Full Rate Production demonstrated and lean production practices in place |

hydride materials with advanced maturity and that are ready for commercialization with great potential for early market applications. The manufacturing readiness is between MRLs 3 and 10, signifying that the metal hydride technologies' manufacturing process has been developed for certain applications and that low rate initial production (LRIP) and even full rate production (FRP) are in progress.

The participants provided the following intended applications and TRL/MRL for metal hydrides:

- material handling equipment with TRL 7-9 and MRL 4-7
- portable applications with TRL 9 and MRL 10
- stationary storage with TRL 4-9 and MRL 4-9
- storage for both high-pressure and low-pressure needs with TRL 5-9 and MRL 5-8
- auxiliary power units with TRL 4 and MRL 4
- mobile/vehicular applications with TRL 4-6 and MRL 4-7

Chemical Hydrogen Storage Materials TRL/MRL Analysis

The chemical hydrogen storage materials' technical maturity, based on three replies, is between TRL 3 and 5 for three different materials, i.e. magnesium hydride slurry, ammonia borane and sodium borohydride. Prototypes have been demonstrated for single-use/disposable hydrogen storage for portable and emergency power applications. In addition, one of the technologies has been integrated in breadboard evaluation. The manufacturing readiness is low at MRL 2, indicating that the manufacturing concept has been defined but not developed. Before reaching LRIP, integrated systems need to be demonstrated to transition the technologies.

Sorbents TRL/MRL Analysis

We could identify one sorbent technology developer with an advanced sorbent material, AX-21/Maxsorb, in large-scale quantities; the application is for cryosorption and intended for storage and transportation. The technical maturity was indicated as TRL 6, which indicates that a prototype has been demonstrated in a relevant environment, but a fully integrated system has not been built. The manufacturing readiness is low at MRL 2, indicating that a manufacturing concept has been defined but not developed.

Hydrogen Storage Cylinder TRL/MRL Analysis

Based on nine replies from tank developers and manufacturers, the TRL for hydrogen storage cylinders is 4-9. Pressure vessels for gaseous and cryo-compressed hydrogen storage are an advanced technology, which is not surprising since there are already commercially available products using hydrogen storage cylinders with fuel cells,

such as MHEs, including forklift fleets. The pressure vessel technology is suitable for early market applications, especially motive applications.

The participants provided the following intended applications and TRL/MRL for hydrogen storage cylinders:

- Type 1 cylinder for hydrogen powered industrial trucks with TRL 9 and MRL 7
- Type 3 cylinder for gaseous hydrogen storage with TRL 8-9 and MRL 5-8
- Type 4 cylinder for gaseous hydrogen storage with TRL 4-5 and MRL 4-6
- Cryogenic pressure vessel for vehicles with TRL 5-6 and MRL 4-6

Conclusions and Future Directions

PNNL performed a technology and manufacturing readiness assessment based on existing DOE TRA and MRA procedures adapted for hydrogen storage technologies to learn the current readiness for early market applications. The manufacturing status could be established from eight risk elements: technical maturity, design, materials, cost & funding, process capability, personnel, facilities and manufacturing planning.

PNNL assisted in identifying candidates for the self-assessments, providing a questionnaire to company points of contact, and collected the data. The replies were validated to ensure consistency and the data was analyzed to establish the status of hydrogen storage technologies based on given TRL/MRL. The replies were anonymous and the assigned TRL/MRL is not tied to any company name.

Key Conclusions

The following key conclusions on hydrogen storage technology maturity could be made based on the TRL/MRL analysis:

- The highest TRLs for existing technologies are for metal hydrides with TRL 7–9 and gaseous storage with TRL 8–9; these are most promising for early markets.
- For metal hydrides, the highest risk elements for manufacturing readiness were identified as process capability, facilities and manufacturing planning.
- Integration of metal hydrides in motive applications is underway, specifically MHE applications, i.e. forklifts, in several global demonstration and deployment projects.
- Materials development programs are needed to replace the expensive rare-earth metal hydrides typically used in MHE applications with low-cost, abundant metals.
- Hydrogen storage cylinders (Types 1 and 3) have been demonstrated in relevant environments for compressed gas storage and LRIP is in progress, ready for FRP if

demand increases. Funded efforts to decrease cost are already in progress.

- Cryo-compressed hydrogen storage has TRL 5–6 with systems validated in relevant environments and one integrated prototype demonstrated onboard a vehicle. MRL 4–5 was given, indicating a low level of readiness for LRIP.
- Metal hydrides for stationary storage of auxiliary power units could also have an impact on early markets, but systems integration efforts would be necessary as a first stage.
- Chemical hydrogen storage canisters/cartridges are to a limited extent commercially available for non-motive applications, especially portable power, but market demand is low and technology transition programs are recommended.
- Chemical hydrogen storage materials are still in need of technology development and appear to be more suitable for mid-term or long-term markets with a few exceptions.
- Sorbent materials have not advanced beyond TRL 2, except for one material which has TRL 5, but is not yet ready for transition to LRIP. An integrated system needs to be demonstrated to proceed toward LRIP, and sorbents appear to be more suitable for mid-term to long-term markets.

Recommendations and Future Directions

Based on the TRA analysis with assignments of TRL and MRL of hydrogen storage technologies based on metal hydrides, chemical hydrogen storage materials, sorbent materials and pressure cylinders, and also specific applications, the following programmatic recommendations are made.

- Metal hydrides are identified to have the greatest impact on the early markets for MHE and ground support equipment, such as forklifts and trucks, provided that funds are provided for systems integration, demonstration and deployment in relevant environments and this is a recommended area for DOE support.
- To reach early commercialization of advanced metal hydride-based technologies, focus needs to be on process capability, facilities and manufacturing planning to reach LRIP and market and technology transformation programs are recommended.
- Chemical hydrogen storage materials are identified to have greatest impact on the early market for portable power and consumer electronics if using one-use cartridges for disposal or recycling. Only a few products are commercially available, main reason due to low consumer demand. It is recommended that DOE supports technology transition projects to advance the technology and lower cost. An infrastructure project to implement

solutions for recycle systems would bring cost down and provide the user with a familiar system similar to that for batteries.

- Many chemical hydrogen storage materials and complex metal hydrides show promise for commercialization, but may realistically be for mid-term to long-term markets since materials development is still in progress and is therefore not recommended for early market demonstrations, rather materials and technology development programs.
- Gaseous hydrogen storage cylinders are already commercially available for a variety of applications, but demand is low. Therefore, a market transformation program would help increase demand for fuel cells and hydrogen storage.
- Infrastructure for hydrogen refueling is a concern for hydrogen storage technology manufacturers and it's necessary to increase the efforts to provide an infrastructure and DOE support is recommended.
- This study was aimed at hydrogen storage for fuel cell applications; however, it was revealed that hydrogen storage is also used in other technologies, such as heat exchangers and thermal energy storage materials, that are viable technologies in need of support by DOE to be further developed and integrated in the hydrogen infrastructure.
- It is important to routinely perform TRA/MRA analysis of hydrogen storage technologies in parallel with the ongoing TRA/MRA analysis of fuel cells, to monitor progress and to identify gaps and R&D needs. It is recommended that an ongoing TRA/MRA activity on hydrogen storage technologies is established and that participation in this activity is a requirement for all co-funded demonstration activities.

FY 2012 Publications/Presentations

1. Ewa Rönnebro, Technology and Manufacturing Readiness of Early Market Motive and Non-Motive Hydrogen Storage Technologies for Fuel Cell Applications, Technical Report prepared for U.S. DOE EERE FCTP, PNNL-21473, June 2012.

References

1. DOE – U.S. Department of Energy. 2011a. *The Department of Energy Hydrogen and Fuel Cells Program Plan – An Integrated Strategic Plan for the Research, Development and Demonstration of Hydrogen and Fuel Cell Technologies*. September 2011. U.S. Department of Energy, Washington, D.C. Accessed March 2, 2012 at http://www.hydrogen.energy.gov/pdfs/program_plan2011.pdf.
2. DOE – U.S. Department of Energy. 2011b. *Pathways to Commercial Success: Technologies and Products Supported by the Fuel Cell Technologies Program*. DOE Energy Efficiency and Renewable Energy. U.S. Department of Energy, Washington, D.C. September, 2011. Accessed March 2, 2012 at http://www1.eere.energy.gov/hydrogenandfuelcells/pdfs/pathways_2011.pdf.

3. DoD – U.S. Department of Defense. 2010. *Manufacturing Readiness Level Deskbook*, Department of Defense Manufacturing Technology Program. July 30, 2010. U.S. Department of Defense, Washington, D.C. Accessed March 2, 2012, at http://www.dodmrl.com/MRL_Deskbook_30_July_2010.pdf.

4. DOE – U.S. Department of Energy. 2009a. *U.S. Department of Energy Technology Readiness Assessment Guide*, DOE G 413.3-4, 10-12-09. U.S. Department of Energy, Washington, D.C. Accessed March 6, 2012, at <https://www.directives.doe.gov/directives/0413.3-EGuide-04a/view>.

IV.F.1 High Strength Carbon Fibers

Felix L. Paulauskas, Bob Norris (Primary Contact),
Amit Naskar, Soydan Ozcan, and Ken Yarborough
Oak Ridge National Laboratory (ORNL)
MS 6053
Oak Ridge, TN 37831-6053
Phone: (865) 576-1179
Email: norrisrejr@ornl.gov

DOE Manager

HQ: Ned Stetson
Phone: (202) 586-9995
Email: Ned.Stetson@ee.doe.gov

Subcontractors:

- Ana Paula Vidigal, Paolo Correira, José Contreiras
Fibras Sinteticas de Portugal (FISIPE), SA, Lavradio,
Portugal
- Donald G. Baird, James E. McGrath, Jianhua Huang,
Myoungbae Lee, Yu Chen, and Ozma Lane
Virginia Polytechnic Institute and State University (VT),
Blacksburg, VA

Project Start Date: November 2006

Project End Date: Project continuation and direction
determined annually by DOE

Fiscal Year (FY) 2012 Objectives

- Demonstrate spinning of a 50 m continuous ~15 filament tow of ~10-12 micron fibers from high molecular weight (MW, >200,000) dope that can be easily spooled and de-spooled for conversion at ORNL's Precursor Development System and yielding 15 Msi modulus and 150 ksi strength.
- Demonstrate spinning of a 1,000 m continuous ~100 filament tow of ~10-12 micron fibers from high MW (>200,000) dope that can be easily spooled and de-spooled for conversion at ORNL's Precursor Development System and yielding 15 Msi modulus and 150 ksi.

Technical Barriers

High-strength carbon fibers account for approximately 65% of the cost of the high-pressure storage tanks. This project addresses the following technical barriers from the Storage section of the Fuel Cell Technologies Program Multi-Year Research, Development and Demonstration Plan:

- (A) System Weight and Volume
- (B) System Cost

(D) Durability/Operatability

(G) Materials of Construction

High strength carbon fiber enables the manufacture of durable, lightweight, compressed hydrogen storage vessels for use in high-pressure storage. Unfortunately, current high-strength carbon fiber products are far too expensive to meet DOE goals for storage system costs.

Technical Targets

Working targets are approximate equivalence with Toray T-700 at substantially reduced production costs:

- 700 ksi ultimate tensile strength
- 33 Msi tensile modulus
- Production cost reduction of at least 25% versus baseline

FY 2012 Accomplishments

- Improved spinning equipment and techniques have been developed and demonstrated for producing initial sample quantities necessary for establishing feasibility of our approach for evaluating sample precursor chemistries and converting melt-spun polyacrylonitrile (PAN) precursor. A number of "engineering" obstacles associated with spinning samples into a pressure chamber and properly winding for feasibility demonstration purposes have been resolved and approaches for further scaling up to the next level of development have been identified.
- Melt-spun PAN-based precursor fiber has been produced in sufficient quality and quantity to begin carbon fiber conversion investigations. Mechanical data for the precursor fiber indicates strength and modulus is lower, but approaching levels typical for precursor utilized in production of commercial PAN-based carbon fiber, giving us confidence in our approach.



Introduction

The exceptional strength-to-weight ratio of carbon fiber composite tanks makes them prime candidates for use with materials-based, cryogenic, or high-pressure gas for both vehicular and stationary storage applications. Cost is the primary issue with composite tank technology. A critical challenge lies in the cost of the fiber and the manufacture of composite tanks. Current projections of the manufactured cost per unit for high production volumes are significantly higher than storage system targets, and it is estimated that

about 40-70% of the unit cost is due to the base cost of the carbon fiber (approximately 40% of the fiber cost is due to the precursor and the remainder due to thermal processing). Research and development (R&D) is needed as composite storage technology is most likely to be employed in the near term for transportation applications and will be needed for most materials-based approaches for hydrogen storage.

Currently, composite tanks require high-strength fiber made from carbon-fiber grade PAN precursor. Manufacturing R&D is needed to develop lower cost, high quality PAN or alternate precursors and reduced energy or faster conversion processes for carbon fiber, such as microwave and/or plasma processing. Developing and implementing advanced fiber processing methods has the potential to reduce cost by 50% as well as provide the technology basis to expand U. S. competitiveness in high-strength fiber manufacturing [1].

This project will leverage previous and ongoing work of the U.S. DRIVE's program to develop a low-cost, high-strength carbon fiber. This project will seek to develop carbon fibers with properties equivalent to Toray's T700/24k fiber (24k tow, 700 ksi ultimate tensile strength, 33 Msi tensile modulus), and reduce production costs by at least 25%.

Approach

This project is structured into tasks focused on precursor development and conversion process improvements. Development and demonstration of melt-spinnable PAN is the project's primary precursor option. This requires concurrent activities in both development of melt-stable PAN copolymer and blends as well as the processes necessary to successfully spin the formulations into filamentary tows. Backup options include textile PAN, polyolefins, and incorporation of nanomaterials. Demonstrating and down-selecting a precursor capable of meeting performance targets utilizing conventional conversion processing defines the pathway for the balance of project activities. In conversion, critical processability parameters include: (i) highly controlled stretching, especially during pre-treatment and stabilization; (ii) residence time in various conversion modules; (iii) optimal graphitization for maximum strength; (iv) uniform treatment of fibers throughout the tow; and (v) characterization of filaments at various stages of conversion operation. Related ORNL work in advanced processing technologies addresses these issues, with a focus on increasing line speed in a reduced footprint, with reduced energy consumption. Means to adapt these emerging processes will be developed and evaluated for applicability to meeting requirements of this project area. As the alternative approaches are demonstrated, the energy efficiency and overall economics of the complete system will be evaluated and forecast for production scale up.

Results

Melt processing of PAN is a difficult issue, although Virginia Tech and others have made modest progress over the last decade [2-6]. One of the principal problems is that PAN degrades even without main chain scission or weight loss, and this essentially precludes melt processing. Reactions of the side groups have been discussed in many reports [7-10]. These degradative reactions can take place both in an intramolecular manner, but also via inter-molecular branching and gelation, which quickly alters the capacity for these materials to be melt fabricated. At 200-220°C, the material can quickly increase in viscosity, thus rendering an intractable material in a very short time. Ideally, one would like to maintain constant viscosity for a required period, and practical considerations suggest that this should be at least 30 minutes or longer.

During this period, the project team with sponsor encouragement decided to put precursor chemistry development work on hold in order to focus limited resources on demonstrating feasibility of the melt spinning approach. For this demonstration effort, some baseline high molecular weight PAN-based formulations are being utilized that, while representative of the processing requirements ultimately required to meet program goals, probably cannot be converted themselves into carbon fiber meeting those performance goals. Significant "engineering" obstacles have been encountered in utilizing the very simple experimental equipment available in this project; a number of these hurdles have been overcome during this period and we have identified solutions for resolving others we expect to encounter on the pathway to our goals. Examples already implemented include improved spinneret design and construction, improved filtration, means for maximizing small sample utilization with integration of purging materials for maintaining open holes as the sample is expended, enhanced extrusion barrel heating, larger spinning pressure chamber, indexed take-up winding patterns, etc. As we continue to resolve these issues, we have gained confidence that the approaches we have proposed do have great potential for meeting program goals given appropriate levels of resources.

As example of our recent progress, Figure 1 shows the original and improved spinning systems developed and employed at Virginia Tech for this work. A demonstration PAN/VA formulation was melt-spun with the new spinning system. The resulting filament package generated on the new system is shown in Figure 2. The spinneret used had 18 holes and it is estimated that the filament tow collected with the same extrusion and take-up speeds (and thus the same/similar fiber size) was about 130 ft (40 meters) in length. The fiber sample was shipped to ORNL for carbon fiber conversion evaluation.

Figure 3 provides the scanning electron microscope images, cross-sectional view, of the melt-spun (VT) fibers produced in comparison with commercial wet-spun fibers.

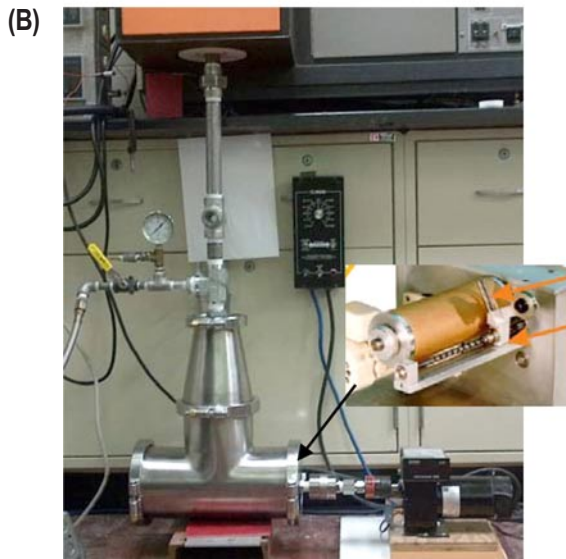
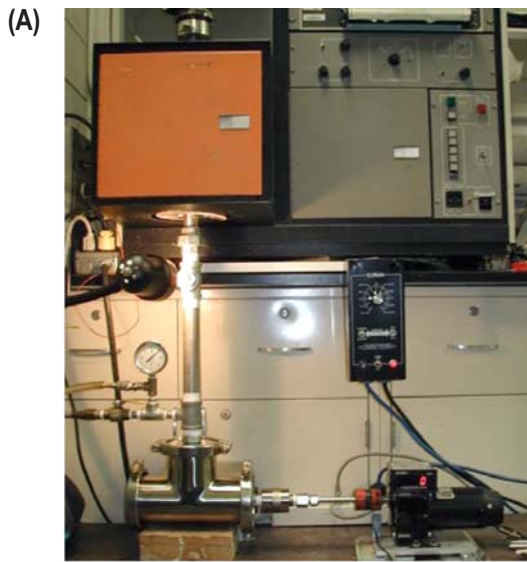


FIGURE 1. Picture of original pressurized fiber spinning system (A) and new system (B). A new take-up device with traverse fiber guide was installed inside the pressure chamber of the new system.

It can be seen that melt-spun fiber has a substantially more circular cross section, with no discrete outer sheath layer as observed by prior researchers who used water as plasticizers. The number and size of the voids also seemed to be acceptable. Figure 4 shows the surface of the melt-spun fibers and commercial PAN fibers. It seems that the surface of the VT fiber is comparable to that of the commercial wet-spun fibers.

The tensile mechanical properties of the PAN fibers are presented in Figures 5-7. Compared with our previous fiber samples (VT-1, 2), we got improvement in both tensile strength and modulus for the fibers generated in the most recent quarter of this reporting period (VT-3). Compared with wet-spun commercial products, the strength of VT-3 is still lower than that of the commercial product. The modulus of



FIGURE 2. Melt-spun PAN/VT fibers generated with new system/winder with traverse fiber guide

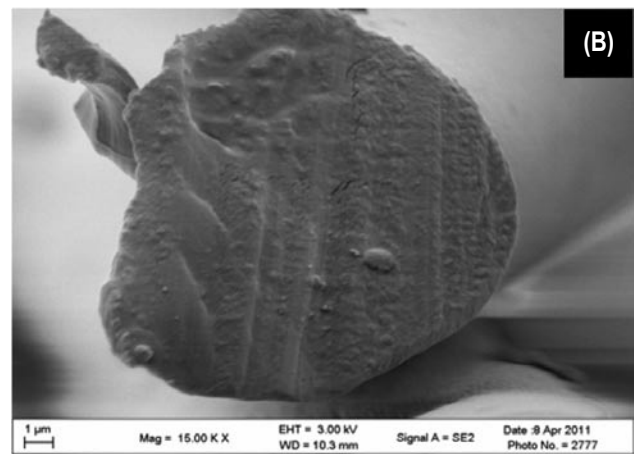
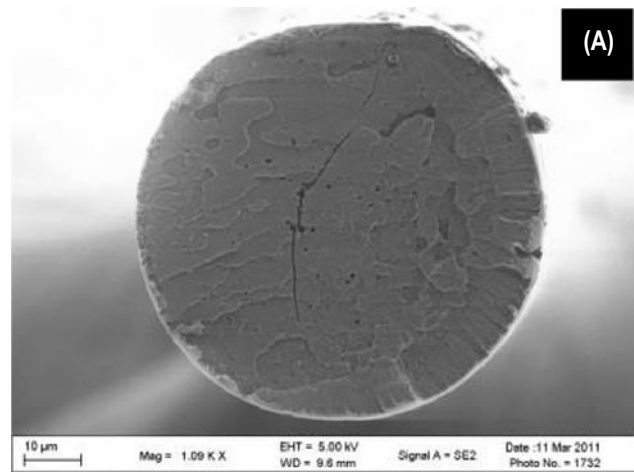


FIGURE 3. Cross-section of VT melt-spun PAN fibers (A) and commercial wet-spun PAN fibers (B)

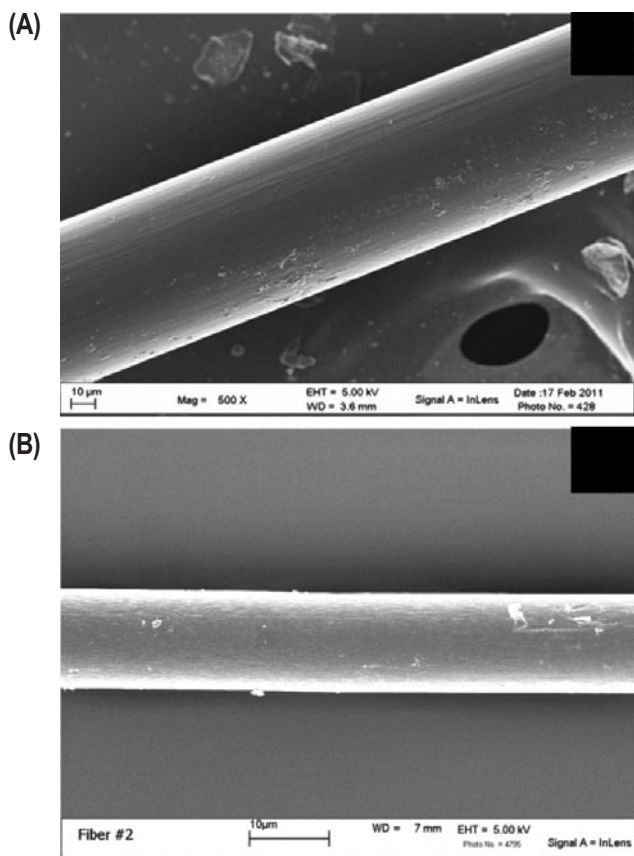


FIGURE 4. Surface of VT melt-spun PAN fibers (A) and commercial wet-spun PAN fibers (B)

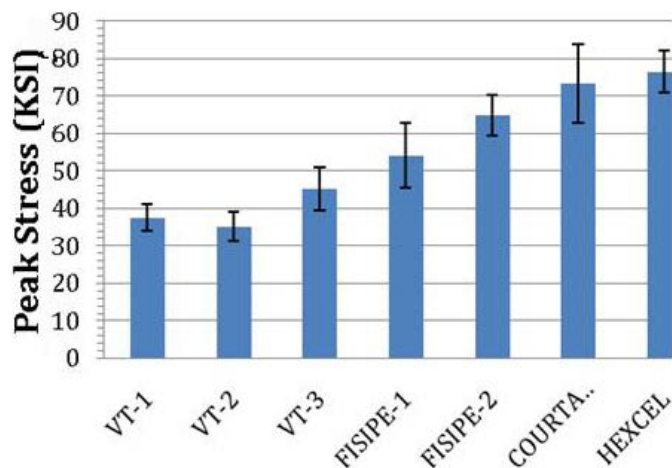


FIGURE 5. Tensile strength of PAN fibers

our fibers is, however, at the average level of the commercial PAN fibers. The elongation of our melt-spun fibers is also close to that of the commercial products.

It is not unusual for precursor fibers to be stretched progressively in steps as opposed to being fully stretched

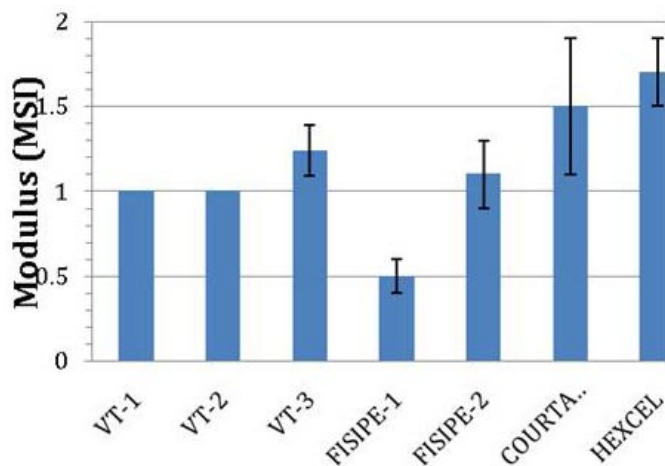


FIGURE 6. Tensile modulus of PAN fibers

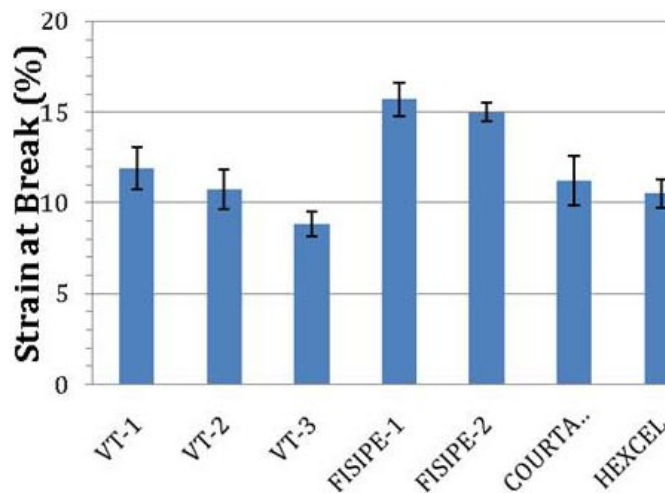


FIGURE 7. Elongation of PAN fibers

coming out of the spinneret. Although initially we were working towards getting the necessary drawing in the initial spinning process, we are now focused on a multi-stage approach more consistent with what BASF employed in its earlier melt-spinning development work. In order to perform the second stage (or post-spinning) stretch process, a steam chest including two rolls connected to two adjustable speed motors was designed and constructed (see Figure 8). The PAN/VA filaments with diameter of about 33 microns, corresponding to a stretch ratio of about 2.8, were generated for this purpose. Saturated steam with pressure of 30 psi (corresponding to temperature of 134°C) was used. We were able to stretch the as-spun fibers to a limited draw ratio (up to 2), but we have difficulty to stretch the fiber further (fibers broke when attempting to get higher stretch ratios). We are currently working on this issue and trying to increase the stretch ratio to the level that BASF reached (6.4 or higher).

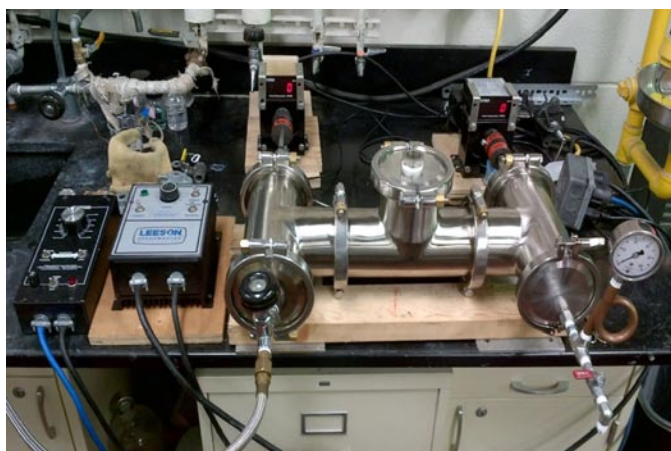


FIGURE 8. Picture of steam chest used to stretch PAN fibers (second stage stretch)

In the last quarter of this reporting period, melt-spun PAN-based precursor fiber has been produced in sufficient quality and quantity to begin carbon fiber conversion investigations. Utilizing ORNL's thermal analysis equipment and its unique suite of very small-scale, but very accurate tensioning systems married with oxidation ovens and carbonization furnaces frequently referred to as the Precursor Evaluation System, ORNL was able to develop conversion protocols and demonstrate both oxidation and carbonization processes. Although the mechanical data was again somewhat lower than for commercially available materials, the properties were consistent with first data from earlier developmental efforts where ORNL progressively increased properties for less costly alternative precursor formulations from below commercial baseline to property levels essentially comparable to those of commercial products. Current plans are to continue improving the precursor spinning, drawing, and conversion processes necessary to meet go-forward milestone levels agreed to as the stage-gate for resuming the larger development effort. Project participants and sponsors are optimistic on meeting these levels in the next year and then pushing forward with the integrated plan bringing all elements of the process – precursor chemistry, spinning, drawing, conversion, (potentially ORNL advanced conversion techniques), post treatment, etc. – necessary to meet cost and performance requirements for this application.

Conclusions and Future Directions

Significant progress has been made in demonstrating melt spinning processes and producing precursor fiber in sufficient quality and quantity to begin carbon fiber conversion investigations. Mechanical properties of the melt-spun precursor fiber are approaching those of commercially produced fibers. Initial conversion protocols have been developed and demonstrated, indicating that we are indeed

taking an effective approach and making progress towards the stage-gate milestone established for taking this initiative to the next level of development.

Near-term objectives are for Virginia Tech to produce longer and more uniform tows that are then drawn in a secondary step as previously described. ORNL will characterize fiber and conduct more extensive conversion trials on precursor filaments generated using its precursor evaluation system. We expect to achieve carbon fiber tensile properties of 15 Msi elastic modulus and 150 ksi tensile strength with 1st generation filaments. With this data, we will have accomplished the previously established stage-gate milestone for moving into the next stage of development and demonstration of this technology.

In this next stage of development, we will resume working the precursor chemistry we believe necessary to enhance baseline properties and move towards the ultimate goals of 33 Msi modulus and 700 ksi strength. We will need to scale the spinning processes up so that we can work with larger tow sizes and more continuous tows in further enhancing the conversion processes and providing feedback to the chemistry and fiber forming development. The filaments at various steps of the conversion process will be fully characterized and the data used to commence optimization of precursor chemistry and the filament generation process. In order to fully address application requirements, we will also need to evaluate and implement appropriate post treatment operations including surface treatment and sizing for the fiber. We will also evaluate whether advanced plasma-based conversion processes (oxidative stabilization and carbonization) under development at ORNL are appropriate for these fibers in reducing costs while meeting performance goals. As the technology is being successfully demonstrated at the Carbon Fiber Technology Facility in Oak Ridge, ORNL will concentrate on the commercialization strategy for technology transfer and implementation.

FY 2012 Publications/Presentations

1. Felix L. Paulauskas, "High Strength Carbon Fibers", presentation at 2012 DOE Hydrogen Program and Vehicle Technologies Annual Merit Review and Peer Evaluation Meeting, May 14–17, 2012.
2. Felix L. Paulauskas, "High Strength Carbon Fibers and Status Report", presentation at Hydrogen Storage Tech Team Meeting, June 21, 2012.

References

1. Hydrogen, Fuel Cells and Infrastructure Technologies Program Multi-Year Research, Development and Demonstration Plan Planned program activities for 2005-2015, October 2007 update.
2. Wiles, K.B., V.A. Bhanu, A.J. Pasquale, T.E. Long, and J.E. McGrath, *Journal of Polymer Science: Part A: Polymer Chemistry*, Vol. 42, 2994-3001 (2004).

3. Bhanu, V.A. P. Rangarajan, K. Wiles, M. Bortner, S. Sankarapandian, D. Godshall, T.E. Glass, A.K. Banthia, J. Yang, G. Wilkes, D. Baird, and J.E. McGrath, *Polymer*, 43, 4841-4850, (2002).
4. Godshall, D., P. Rangarajan, D.G. Baird, G.L. Wilkes, V.A. Bhanu, and J.E. McGrath, *Polymer* 44 (2003), 4221-4228.
5. Rangarajan, P., V.A. Bhanu, D. Godshall, G.L. Wilkes, J.E. McGrath, and D.G. Baird, *Polymer* 43, 2699-2709 (2002).
6. Bortner, Michael J., Vinayak Bhanu, James E. McGrath, and Donald G. Baird, *Journal of Applied Polymer Science*, 93(6), 2856-2865 (2004).
7. Peng, Fred M., "Acrylonitrile Polymers," in Mark, Herman F.; Bikales, Norbert M.; Overberger, Charles G.; Menges, Georg; Editors. *Encyclopedia of Polymer Science and Engineering*, Vol. 1: A to Amorphous Polymers. (1986), 843 pp, pages 426-470, and references therein.
8. Back, Hartwig, C, and Knorr, Raymond S. "Acrylic Fibers," in Mark, Herman F.; Bikales, Norbert M.; Overberger, Charles G.; Menges, Georg; Editors. *Encyclopedia of Polymer Science and Engineering*, Vol. 1: A to Amorphous Polymers. (1986), 843 pp, pages 334-388, and references therein.
9. Capone, Gary J.; Masson, James C. *Fibers, acrylic*. *Kirk-Othmer Encyclopedia of Chemical Technology* (5th Edition) (2005), 11 188-224.
10. Frushour, Bruce G.; Knorr, Raymond S. *Acrylic fibers*. *International Fiber Science and Technology Series* (2007), 16(*Handbook of Fiber Chemistry* (3rd Edition)), 811-973.

IV.F.2 Lifecycle Verification of Polymeric Storage Tank Liners

Barton Smith (Primary Contact) and
Lawrence M. Anovitz

Oak Ridge National Laboratory
P.O. Box 2008
Oak Ridge, TN 37831
Phone: (865) 574-2196
Email: smithdb@ornl.gov

DOE Manager

HQ: Ned Stetson
Phone: (202) 586-9995
Email: Ned.Stetson@ee.doe.gov

Start Date: June 2008

Projected End Date: Project continuation and
direction determined annually by DOE

Fiscal Year (FY) 2012 Objectives

- Continue temperature cycling and permeation measurements on tank liner polymers, and use permeation data to assess ability of tank liners to retain a steady-state hydrogen discharge rate that does not exceed 110% of the 75 normal cubic centimeters per minute (Ncc)/min permeation requirement of SAE International J2579 § 5.2.2.1.3
- Develop a method for temperature cycling on pressurized Type-4 storage tank sections to provide a lifecycle evaluation of the polymer liner when it is in contact with the composite matrix layer.

Technical Barriers

This project addresses the following technical barriers from the Hydrogen Storage section of the Fuel Cells Technology Program Multi-Year Research, Development and Demonstration Plan [1]:

- (D) Durability/Operability (of onboard storage systems – lifetime of at least 1,500 cycles)
- (G) Materials of Construction (vessel containment that is resistant to hydrogen permeation)
- (M) Lack of Tank Performance Data and Understanding of Failure Mechanisms

Technical barriers D and G are applicable to all storage approaches. Technical barrier M is specific to compressed gas systems.

Technical Targets

This project addresses the following technical targets for onboard hydrogen storage systems R&D [2]:

- Operational cycle life (1/4 tank to full) – FY 2017: 1,500 cycles; Ultimate: 1,500 cycles
- Environmental health and safety
- Permeation and leakage: Meets or exceeds applicable standards
- Loss of useable H₂ (g/h/kg H₂ stored): FY 2017: 0.05; Ultimate: 0.05

FY 2012 Accomplishments

- We observed that repetitive temperature cycling decreases H₂ permeability in specimens of extruded high-density polyethylene (HDPE) by increasing the size of the crystalline regions in the polymer.
- A new and improved temperature cycling and permeation measurement system is now online, providing temperature cycling between –40°C and 85°C, faster temperature cycles of ~20 minutes (40% shorter than cycling time in original apparatus), a maximum differential hydrogen pressure across specimen of ~900 bar (13,000 psia), and using less hydrogen and substantially less electrical power.



Introduction

Modern high-pressure hydrogen storage tanks use a polymeric liner as a permeation barrier to hydrogen, typically HDPE or polyamide. Storage tank liners can be stressed by cyclical excursions between temperature extremes, and the cumulative effects of repeated stress could harm the tank's durability. Ultra-high environmental temperatures can promote large hydrogen permeation rates and hydrogen saturation in the liner material. Ultra-low environmental temperatures can possibly induce microcracking. In addition, increasing the pressure of gas in such a tank during filling necessarily raises the temperature of the gas and the pressure-load-bearing carbon-fiber reinforced shell. Over the course of hundreds of fill cycles during the lifetime of the tank, these environmental stresses could affect the permeability characteristics of the liner and failure modes for the liner's performance—based on the interaction of high pressure and extreme temperature cycling—might be introduced. Hydrogen leakage through a liner microcracked by extreme temperature cycling could accelerate under

sustained high temperature and pressure, or hydrogen saturation of the reinforcement layers external to the liner could put backpressure on the liner as the tank pressure decreases during vehicle operation, thereby causing the liner to separate from the reinforcement layers. Minimum temperatures during winter months in northern states may reach well below 0°C, tank precooling before filling could reach -40°C, and maximum temperatures after filling during summer months may reach 85°C. Thus, the purpose of this project is to cycle typical tank liner materials between these temperature extremes to determine whether such a degradation in properties occurs, and, if so, its extent.

Approach

To address this tank liner durability issue, ORNL is performing hydrogen permeation verification measurements on storage tank liner materials using specially designed experimental facilities that provide rapid thermal cycling of polymeric liner specimens between -40 and 85°C at rates of about two to three temperature cycles per hour. This cycling is done while the liner specimens are differentially pressurized to 430 or 860 bar (6,250 or 12,500 psi). (Pressures as high as ~1,000 bar and temperatures near the polymer softening points could be accommodated in the future.)

We are using relevant portions of the test protocol specified in SAE J2579 [3] to guide the implementation of durability test cycling measurements of high-pressure polymeric tank liners. The J2579 test protocol for compressed hydrogen storage systems prescribes long-term thermal cycling at high pressures of hydrogen. The requirement is to subject tank liner specimens to as many as 5,500 thermal cycles over the temperature range 40 to 85°C at hydrogen pressurizations of 43 MPa (6,250 psia) and then 86 MPa (12,500 psia). Testing at 43 and 86 MPa, with cycling between 40 and 85°C, requires an automated temperature control strategy.

The permeation coefficient measurements occur at regular intervals intermittent during the temperature cycling. The hydrogen flux is to be measured at four temperatures (-40, -10, 30 and 85°C) at each measurement interval, when practicable. The first measurements occur after the completion of 250, 500, 750, 1,000, 1,250 and 1,500 cycles. The remaining measurements occur at 500 cycle intervals until a trend in permeation increase/decrease is observed or 5,500 temperature cycles have been reached, whichever occurs first.

Results

In the previous project year, permeation measurements on a specimen of extruded HDPE cut from the cylindrical portion of a tank liner, made during high-pressure hydrogen temperature cycling, showed progressive changes in the

slope, E_A , and pre-exponential scaling factor, P_0 , of the Arrhenius curves. As the number of temperature cycles increased, both the activation energy and the magnitude of the scaling factor decreased, implying that structural changes were taking place in the polymer as the temperature was cycled. Characterization of the polymer using neutron scattering (small angle neutron scattering, ultra-small angle neutron scattering), differential scattering calorimetry (DSC) and helium pycnometry indicated that temperature cycling slightly increases both the average size of the crystalline regions in the polymer and the polymer density. This year we repeated the temperature cycling on a specimen of extruded HDPE from the same liner but this time we used high-pressure argon gas instead of hydrogen. The results were very similar to those observed in the specimen cycled in hydrogen; this specimen also exhibited increased crystallinity, implying that it is the temperature cycling that is primarily responsible for the increases in crystallinity. The increases in density might be attributable to the differential pressurization, which effects a plastic compression of the specimen during testing.

Projections of the potential effect of temperature cycling on a complete tank liner, using modeling based on the permeation coefficients obtained as a function of temperature cycling history, predict that hydrogen leakage through the tank liner will not significantly increase during the tank lifecycle and will remain below the maximum allowable leak rate (see Figure 1).

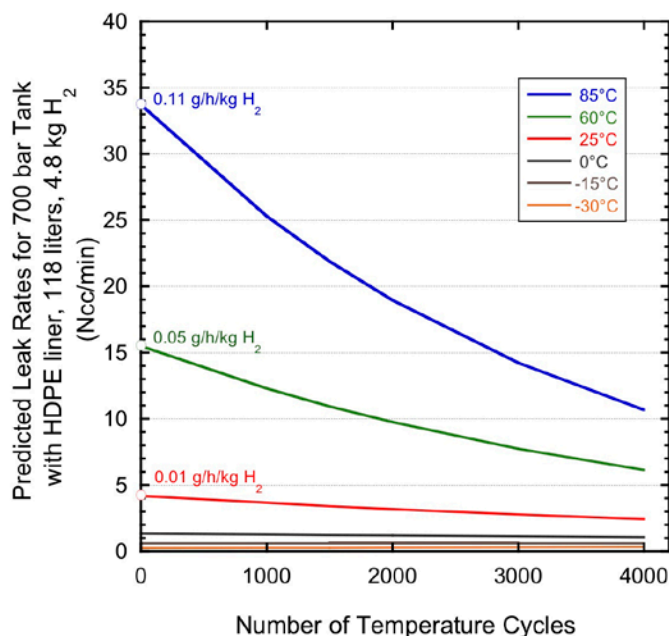


FIGURE 1. Prediction of tank liner durability (changes in hydrogen leak rates) using modeled permeability coefficients P to calculate leak rates in an HDPE-lined cylindrical tank with hemispherical end caps. A family of curves corresponding to predicted leak rates at varying temperatures are plotted as a function of the number of temperature cycles the tank is expected to experience due to fill operations and variations in ambient temperature.

Conclusions and Future Directions

To obtain a quantitative prediction of the leak rate for an actual tank liner, we used the dimensional specifications for a hydrogen storage tank rated for 700-bar service with a volumetric capacity of 118 liters (4.8 kg H₂ capacity). The HDPE tank liner is cylindrical with approximately hemispherical end caps, and the liner wall thickness is about 7 mm. We used the values of P_0 and E_A obtained from measurements during the temperature cycling to model the behavior of the permeation coefficients P as a function of temperature and the number of cycles. This modeling shows that at all temperatures the values of the hydrogen permeation coefficients decrease with cycle count. Thus the hydrogen leak rate of the tank liner should decrease with the number of temperature cycles. In this analysis the tank leak rate remains below 75 Ncc/min at all temperatures for the duration of 4,000 temperature cycles. Furthermore, for all liner temperatures less than about 60°C, the loss of useable hydrogen remains below 0.05 g/h/kg H₂ for a fully filled tank (350 bar pressurization).

Future research will focus on measurements on additional tank liner materials, primarily those that promise to be significantly less expensive and with lower hydrogen permeation. Based on comments made by reviewers at the 2012 Annual Merit Review and by members of the Hydrogen Storage Tech Team, we have crafted our research plan to address the findings made in the present year and to accelerate the rate at which we can evaluate the materials. We would like to expand the scope of our investigation of the durability of the tank liners to an investigation of the durability of the tank liners when they are in physical contact with the reinforcement structure *in toto*. It is widely known by manufacturers of Type-4 composite tanks that the liner permeability of the tank liner tends to be significantly less in practice than predicted based on permeation coefficients and liner thickness. The fiber-epoxy reinforcement, which is the structural support for the liner, appears to enhance the liner's ability to retain hydrogen at high pressures. To adequately assess this contribution and to determine whether it persists during temperature cycling requires a lifecycle analysis of the structure.

We will continue to perform some post-cycling analysis of the specimens to determine the type of structural changes that take place in the polymers. DSC measurements, scanning electron microscopy/back scattered electron microscopy, transmission electron microscopy (using microtome sectioning), and perhaps some additional small angle neutron scattering, ultra-small angle neutron scattering (neutron scattering) will be used. This analysis will allow us to determine the implications of the structural changes during the lifecycle of the tank liner.

FY 2012 Publications/Presentations

1. 2012 DOE Hydrogen Program Annual Merit Review, Arlington, Virginia, May 17, 2012, presentation ST053.

References

1. Fuel Cells Technology Program Multi-Year Research, Development and Demonstration Plan—Hydrogen Storage, pages 3.3-12–3.3-14 (2011, interim update).
2. Fuel Cells Technology Program Multi-Year Research, Development and Demonstration Plan—Hydrogen Storage, Table 3.3.1, “Technical System Targets: Onboard Hydrogen Storage for Light Duty Vehicles,” page 3.3-8 (2011, interim update).
3. SAE J2579, “Technical Information Report for Fuel Cell and Other Hydrogen Vehicles (January 2009),” Fuel Cell Standards Committee, SAE International.

IV.F.3 Development of Low-Cost, High Strength Commercial Textile Precursor (PAN-MA)

C.D. Warren and Felix L. Paulauskas

Oak Ridge National Laboratory
 1 Bethel Valley Road
 Oak Ridge, TN 37831
 Phone: (865) 574-9693
 Email: warrencd@ornl.gov
 Email: paulauskasfl@ornl.gov

DOE Manager

HQ: Ned Stetson
 Phone: (202) 586-9995
 Email: Ned.Stetson@ee.doe.gov

Contributors:

- Hippolyte Grappe (ORNL)
- Fue Xiong (ORNL)
- Ana Paula Vidigal (FISIPE)
- Jose Contrerias (FISIPE)

Project Start Date: April 21, 2011

Project End Date: July 31, 2013

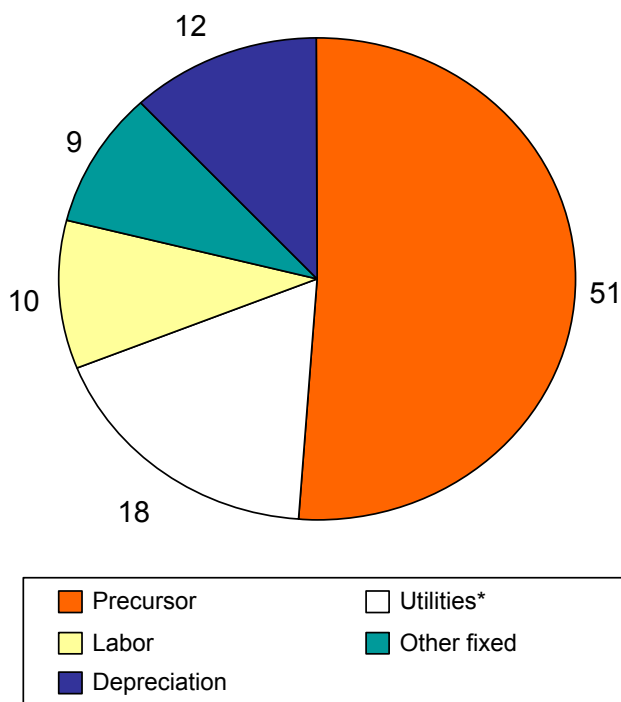


FIGURE 1. Carbon Fiber Production Costs

Fiscal Year (FY) 2012 Objectives

- Down-select from 11 polymer candidate polymer compositions to three for spinning fibers.
- Evaluate three fiber compositions to yield guidance for selecting the best fiber composition.
- Demonstrate at least 300 KSI breaking strength and 30 MSI modulus. (Gate Milestone)
- Down-select to one to two fiber compositions for property optimization.

Technical Barriers

This project addresses the following technical barriers from the Storage section of the Fuel Cell Technologies Program Multi-Year Research, Development and Demonstration Plan:

(B) Storage System Costs

(A) System Gravimetric Capacity

Technical Targets

The hydrogen storage team has been conducting a project to develop lower cost carbon fiber precursors to reduce the cost of carbon fiber for hydrogen storage tanks. Precursors

account for a little more than half of the finished carbon fiber cost and the cost of carbon fiber can account for up to 75% of the storage tank cost (Figure 1). This proposed effort is to develop a solution spun textile grade polyacrylonitrile with methyl acrylate (PAN-MA) precursor with strengths in the range of 550-750 KSI. This project is for a shorter-term, lower-risk approach to addressing the same issue as is being addressed by the melt-spun polyacrylonitrile (PAN) project. Ideally, the fiber developed in this proposal could be ready for commercialization within two to three years to meet programmatic needs. The melt-spun PAN when developed could be ready for market introduction a few years later. Both precursors would be suitable for applications in a wide range of other industries.

TABLE 1. Progress towards Meeting Technical Targets for PAN-MA-Based Lower Cost Carbon Fiber for Hydrogen Storage Tanks

| | Strength (KSI) | Modulus (MSI) | Estimated Production Costs |
|--|----------------|---------------|----------------------------|
| Current Market Fibers | 750 | 38 | \$15-20/lb |
| Target | 650-750 | 35-38 | \$10-12/lb |
| Current Status of Candidate Precursors | 350-400 | 25-35 | \$10-12/lb |

FY 2012 Accomplishments (as of 1 July 2012)

- Down-selected from multiple polymer compositions down to 11 candidate compositions.
- Down-selected from 11 polymer candidate compositions down to three for spinning fibers for carbonization trials.
- Evaluated two of the three fiber compositions to yield guidance for selecting the best fiber composition. The third fiber composition is currently being evaluated.
- Demonstrated at least 300-400 KSI breaking strength and 27-36 MSI modulus from the first fiber composition.
- Demonstrated at least 300-400 KSI breaking strength and 25-36 MSI modulus from the second fiber composition.



Introduction

During the past several years, the Vehicle Technologies Program has been developing technologies for the production of lower cost carbon fiber for use in body and chassis applications in automobiles. Program goals target materials that have tensile strengths in excess of 250 KSI and modulus of at least 25 MSI. Past work included the development of a vinyl acetate co-monomered, lower cost precursor and methods for manufacturing precursors into finished carbon fiber. The basic premise of the project was to be able to use PAN material produced in a high volume textile production process for a carbon fiber precursor rather than the specialty material that is typically used for carbon fiber precursors. A textile line that formerly made knitting yarn has been retrofitted to commercialize that fiber.

The previously developed fiber has strengths slightly below 500 KSI, which is far above strengths suitable for automotive structural applications but insufficient for many higher demanding applications with higher performance requirements such as the manufacture of hydrogen storage tanks. In order to preserve the cost advantages of using a high volume PAN fiber, and simultaneously meet the needs of higher performance applications, it was proposed to develop the capability to use methyl-acrylate based, textile grade, PAN as a carbon fiber precursor and to manufacture that precursor on a textile line.

The purpose of this project is to take one precursor technology, textile-based PAN, while using a higher performance formulation, from the technical feasibility stage and scale up to technology demonstration. This project will result in the determination of the best polymer formulation and conversion protocol (time-temperature-tension profiles) to produce the best carbon fiber while also being readily and inexpensively manufacturable in existing textile PAN plants. Successful completion of this project will result in defining the precursor formulation and preliminary manufacturing

methods to produce carbon fiber. A follow-on step may be necessary to optimize the properties, optimize the manufacturability in high volume and transfer the technology to a carbon fiber manufacturer. Deliverables include spools of fully carbonized and sized carbon fiber and composites made from that carbon fiber. This project is on the critical path for the development of lower cost carbon fiber.

Approach

The first step to developing a new precursor is to define and analyze candidate precursor formulations. Those are then down-selected and multiple candidate polymer formulations are produced. In this case, Fibras Acricas Portugese (FISIPE) down-selected to 11 candidate formulations. Those polymer formulations were sent to ORNL for evaluation from which three polymer formulations were selected to be spun into precursor fiber for attempted conversion into carbon fiber. FISIPE worked to determine how to spin each of those three formulations into precursor fiber tows and send them to ORNL for conversion trials. Developing uniformly round fibers and maintaining fiber consistency from fiber to fiber and along the length of each fiber were critical parameters.

Upon receipt of the precursor spools, ORNL began the thermal evaluations to pinpoint conversion temperatures of the precursor, particularly the temperatures to be used for oxidative stabilization. The next step was to determine the limits of fiber stretching that can be achieved in each of the oxidative stabilization stages. As a general rule, higher levels of tension (i.e. percentage of stretching) will promote better polymer chain alignment along the axis of the fiber and will result in higher breaking strengths of the fiber. It is therefore necessary to apply the maximum tension to the fiber, especially during the early stages of oxidative stabilization, without breaking the filaments.

The amount of stretching in each stage of conversion, the optimum temperatures for conversion and the time that the precursor is exposed to those conditions must be developed for each of the seven stages (Prestretching, Oxidation 1, Oxidation 2, Oxidation 3, Oxidation 4, Low-Temperature Carbonization and High-Temperature Carbonization) of processing. These must be done sequentially completing each processing step before proceeding to the next. Only after completing all of these steps can the final properties of the fiber be determined. The plan is to evaluate the three formulations, pinpointing processing parameters in approximate ranges and then down-select to one final formulation. For that formulation, all spinning and conversion parameters will then be optimized.

Results

The down-selection of chemical compositions and formulation started in April of 2011. The main issue related

to achieving the proper formulation was the generation of the PAN-polymer with a higher acrylonitrile (AN) content. Dealing with AN co-monomered polymer required some changes to FISIFE's equipment and standard practices which required three months. They were able to generate 11 candidate compositions. Three compositions were down-selected and sent to ORNL for evaluations. Differential scanning calorimetry (DSC) curves and other technical data for those compositions were generated for comparison to each other and to known aerospace and industrial grade precursors.

Upon receipt of the precursor spools, ORNL began the thermal evaluations to pinpoint conversion temperatures of the precursor, particularly the temperatures to be used for oxidative stabilization. Two features are prominent and were expected from the thermal evaluations: (1) The onset of the exotherm occurs at a slightly different temperature from traditional precursors indicating a different starting temperature for oxidative stabilization; (2) The exothermic curve is steeper than the PAN-vinyl acetate (VA) precursors indicating a slower temperature ramp up being necessary during oxidative stabilization.

Figure 2 shows the DSC curves for one of the new precursors at various stages of oxidation. Each "stage" in the legend corresponds to the resulting material property after exposure to a different temperature and gives a strong indication of the temperatures necessary in the oxidative stabilization ovens during conversion of the precursor. From these curves, we derive the first indication of both the times and temperatures necessary in each of the later three stages of oxidative stabilization. The profile is very similar to typical aerospace grade precursors with the only surprise being how far the stabilization process has progressed after stage 3. Similar curves were generated

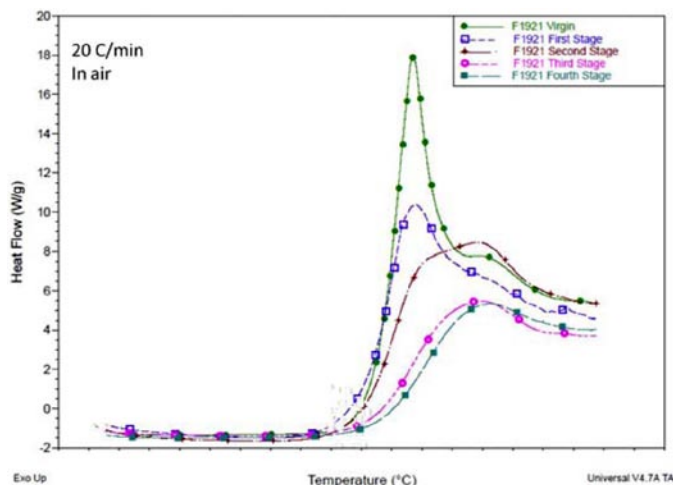


FIGURE 2. DSC curves for F1921 precursor after subsequent Oxidative Stabilization Treatments

comparing this new precursor to a typical 3,000 filament aerospace grade precursor after four each of the four stages of oxidative stabilization. That data indicated that we may need to proceed with a slightly higher temperature during oxidative stabilization in the final stage. The data collected in these types of evaluations gives a strong indication of the temperatures necessary for processing and a beginning understanding of the exposure times. After completion of the thermal analysis, ORNL then began the process of determining the optimum conversion protocol (combination of time, temperature and tension).

The next step was to determine the limits of fiber stretching that can be achieved in each of the stages during oxidative stabilization. As a general rule, higher levels of tension (i.e. percentage of stretching) will promote better polymer chain alignment along the axis of the fiber and will result in high breaking strength of the fiber. It is therefore necessary to apply the maximum tension to the fiber, especially during the early stages of oxidative stabilization, without breaking the filaments. Figure 3 shows the tension and percent stretching for fibers after exposure to the temperatures determined in the previous step. Of particular interest are the points marked with a triangle which indicate the upper tension limit of the processing window for these precursors. Export control restrictions require that all tension loads, stretching percentages, oven temperatures and residence times not be publicly disclosed, therefore axis values are intentionally left off of these charts. Filament diameters for the new precursor were measured at 11.7 microns which is within the desired range for an oxidized precursor. Normal ranges are 11-12 micron to produce a 7-micron diameter carbonized fiber.

The amount of stretching in each stage of conversion, the optimum temperatures for conversion and the time that the precursor is exposed to those conditions must be developed for each of the seven stages (Pre-stretching, Oxidation 1, Oxidation 2, Oxidation 3, Oxidation 4, Low-Temperature Carbonization and High-Temperature Carbonization) of processing. We have completed determination of the baseline conversion protocol for two of the precursors.

One issue that had to be dealt with for these precursors was "fuzzing" of the fiber tow during processing. Figure 4 shows an example of this. Fiber fuzzing is typically due to small, not fully developed "baby" fibers present in the precursor. Upon tensioning, these fibers see a higher than average stress, exceed their strength and break. This issue has been resolved.

The first carbonization trials were held in January with the first precursor. In the initial trials, a strength of 282 KSI and modulus of 27 MSI were achieved. Two weeks later, with further refinement, fibers were produced with strengths of 383 KSI and modulus of 36 MSI. The gate milestone for the end of March was to achieve 300 KSI and 30 MSI. This

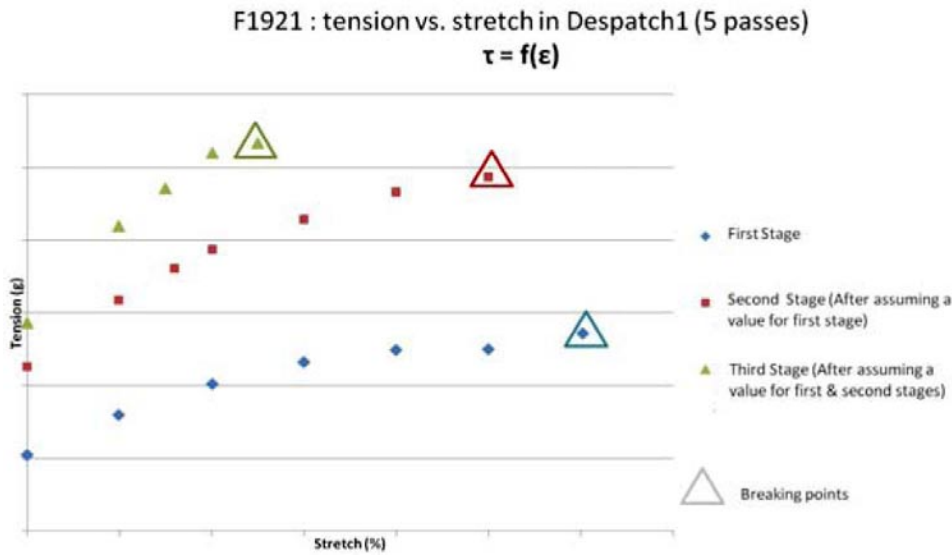


FIGURE 3. Tension vs. Percentage Stretching for the F1921 Precursor after various Oxidative Stabilization Treatments to Determine the Tension Limits during Processing

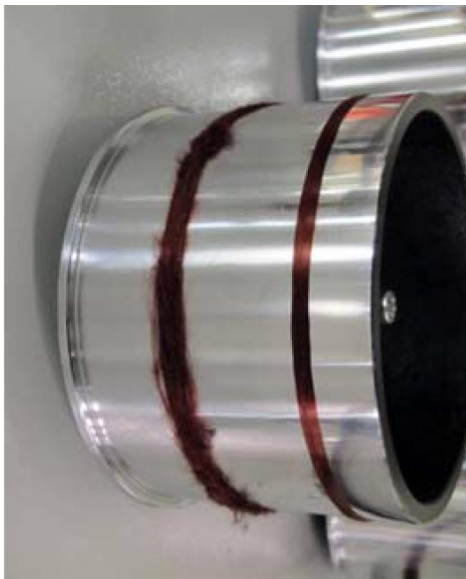


FIGURE 4. Left: “Fuzzing” of Filament Tow during Oxidative Stabilization; Right: Tow not Exhibiting “Fuzzing”

milestone was completed. Figures 5 and 6 are the property as a function of time charts for tracking precursor progress. Each data point is the average of 18 tests.

Next we turned our attention to developing the conversion protocol for the second precursor. Initial values for this precursor were low but with further refinement have been demonstrated at an acceptable level for us to still consider this precursor a viable option. By reviewing some

Tensile Strength (KSI)

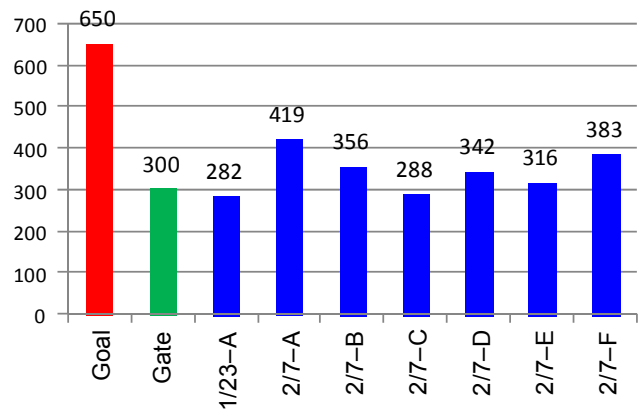


FIGURE 5. Tensile Strength as a Function of Time for the F1921 Precursor

of the oxidation data, we will be revising some conversion parameters which should allow us to reach significantly higher values with this precursor. Figures 7 and 8, are the property as a function of time charts for tracking precursor progress. Each data point is the average of 18 tests.

We have recently received precursor spools from the other selected material F2027. Those are being evaluated and preliminary processing parameters being determined.

Conclusions and Future Directions

Both precursor evaluated meet our minimum screening criteria for properties. The gate milestone for project continuation has been met. We will be completing screening

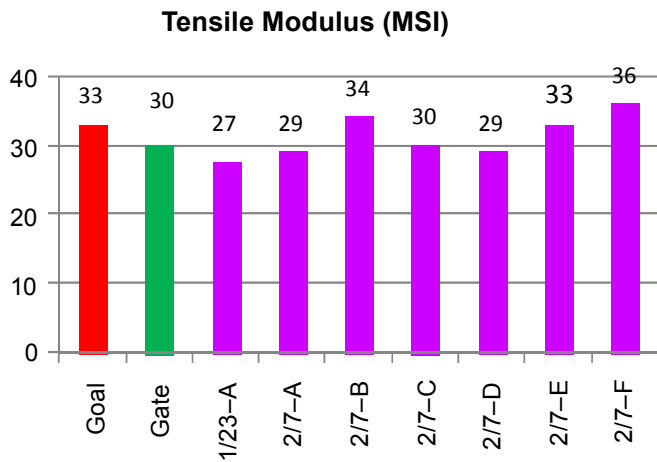


FIGURE 6. Tensile Modulus as a Function of Time for the F1921 Precursor

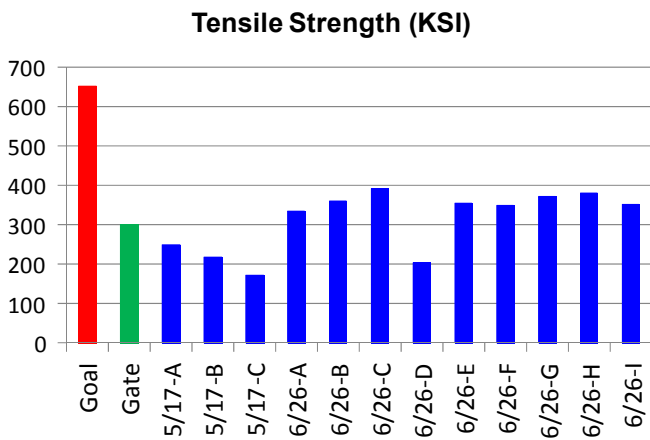


FIGURE 7. Tensile Strength as a Function of Time for the F1999/2000 Precursor

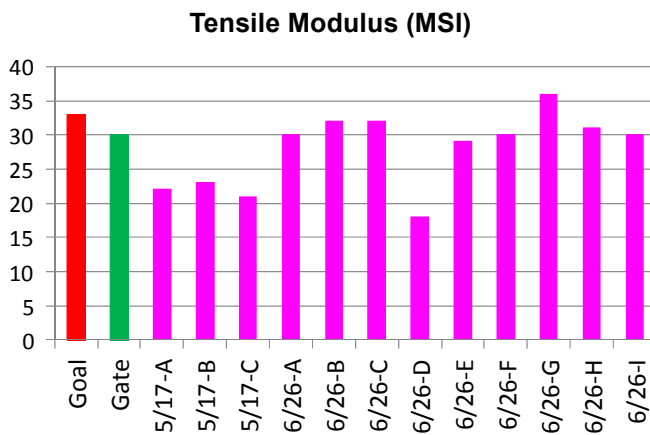


FIGURE 8. Tensile Modulus as a Function of Time for the F1999/2000 Precursor

of the third precursor and then will make a decision as to which formulation to pursue for property optimization. Some work in fiber to fiber consistency during precursor spinning will also be part of the work plan for the next year. The final carbon fiber achieved will be incorporated in a fiber plaque and tested in an epoxy resin system. If minimal fiber properties of 650 KSI strength and 35 MSI modulus are achieved, then closer work with a carbon fiber manufacturer will be warranted to incorporate this precursor into a production facility and optimize surface treatment and sizing protocols.

Special Recognitions

- 1. Dr. Felix Paulauskas won the 2012 DOE Vehicle Technologies Program R&D Award for carbon fiber research

FY 2012 Publications/Presentations

- 1. Warren, C.D. “Lower Cost Carbon Fiber in High Volumes for 21st Century Industries”, Presented at and published in the proceedings of the SPE Automotive Composites Conference & Exhibition, Detroit, MI, 13–15 September, 2011.

IV.F.4 Synergistically Enhanced Materials and Design Parameters for Reducing the Cost of Hydrogen Storage Tanks

Kevin L. Simmons (Primary Contact),
Kenneth Johnson, and Kyle Alvine
Pacific Northwest National Laboratory (PNNL)
902 Battelle Blvd
Richland, WA 99352
Phone: (509) 375-3651
Email: Kevin.Simmons@pnnl.gov
Norman Newhouse (Lincoln Composites, Inc.),
Mike Veenstra (Ford Motor Company),
Anand V. Rau (TORAY Carbon Fibers America) and
Thomas Steinhausler (AOC, L.L.C.)

DOE Managers

HQ: Ned Stetson
Phone: (202) 586-9995
Email: Ned.Stetson@ee.doe.gov
GO: Jesse Adams
Phone: (720) 356-1421
Email: Jesse.Adams@go.doe.gov

Contract Number: DE-AC05-76RL01830

Project Start Date: January 1, 2012
Project End Date: March 31, 2015

General to All Storage Approaches

- (A) System Weight and Volume
- (B) System Cost
- (D) Durability/Operability
- (G) Materials of Construction
- (H) Balance of Plant (BOP) Components

Technical Targets

Combining new tank design at enhanced operating conditions and more efficient use of CF through new materials and lower cost materials is estimated to save 37% of overall tank cost compared to a standard Type-IV, 700-bar tank. These cost savings, combined with future reductions in CF costs, should result in the 50% DOE target. Specifically the approaches are (A) enhanced operating conditions to improve energy density/pressure ratios; (B) load translational efficiency improvements through CF surface modification and resin matrix modifications and resin alternatives; and (C) improved CF use efficiency through advanced fiber placement and the use of alternate fibers. We expect the cost savings to be generated by offsetting CF usage as follows: (A) 25%, (B) 20%, (C) 10%, for a combined savings (assuming multiplicative) of ~46% of the CF cost or a savings of ~37% of the overall tank cost.

Fiscal Year (FY) 2012 Objectives

Our objective is to reduce carbon fiber (CF) usage and associated tank cost through a series of combined material and design synergistic approaches whose total contribution is estimated to be nearly 37% in overall cost savings. It is probable that these cost savings, combined with future reductions in CF cost could lead to the 50% DOE target. The project will take a holistic approach to improve performance by modifying the operating envelope down to the composite constituent level. As such, the project team includes industry experts in each of the following focus areas of improvement: enhanced operating conditions to improve energy density/pressure ratios, load translational efficiency improvements by CF surface modification, resin matrix modifications and alternatives, and alternate fiber placement and materials. We expect these savings approaches to be compatible and additive.

Technical Barriers

This project addresses the following technical barriers from the Storage section of the Fuel Cell Technologies Program Multi-Year Research, Development and Demonstration Plan:

FY 2012 Accomplishments

- Developed baseline cost model of 350- and 700-bar 5.6-kg hydrogen pressure vessel
- Developed fiber surface treatments for testing with low-cost resin systems
- Identified three low-cost resin systems for testing composite performance
- Identified initial temperature and pressure operating conditions for tank design
- Established test protocol for comparing material property improvements



Introduction

The goal of this research is to reduce the cost of 350- and 700-bar compressed gas hydrogen storage vessels by at least 50% from the current high volume projections of \$15.4/kWh to \$6/kWh for commercialization in early market and light-duty hydrogen fuel cell vehicles. This will be

done by developing enhanced materials and manufacturing methods to reduce the cost of hydrogen storage tanks. The baselines for cost and performance comparisons are the current 350- and 700-bar, high-pressure storage vessels primarily constructed of standard-modulus, high-strength CF in an epoxy matrix that is overwrapped on a metallic or polymeric liner, which are classified as Type-III and Type-IV tanks, respectively. The use of high-strength CF composite accounts for nearly 80% of the overall tank costs.

Our objective is to reduce CF usage and associated tank cost through a series of combined material and design synergistic approaches whose total contribution is estimated to be nearly 37% in overall cost savings. It is probable that these cost savings, combined with future reductions in CF cost could lead to the 50% DOE target. The project will take a holistic approach to improve performance by modifying the operating envelope down to the composite constituent level. As such, the project team includes industry experts in each of the following focus areas of improvement: (A) enhanced operating conditions to improve energy density/pressure ratios, led by Ford Motor Company (Ford); (B.1) load translational efficiency improvements by CF surface modification, led by Toray and (B.2) resin matrix modifications and alternatives, led by Pacific Northwest National Laboratory (PNNL) and AOC; and (C) alternate fiber placement and materials, led by Lincoln Composites (Lincoln). We expect the cost savings to be generated by offsetting CF usage as follows: (A) 25%, (B) 20%, and (C) 10%, for a combined savings (assuming multiplicative combination) of ~46% of the CF cost or a savings of ~37% of the overall tank cost. We expect these savings approaches to be compatible and additive.

Improvements in CF composites and other fiber/resin systems gained in this project will have synergistic benefits for other industries and applications beyond high-pressure hydrogen storage tanks. Applications of high-strength fiber/resin composites in other industries include advanced turbine blades for wind energy, aerospace composites, light-weight automobile components, and other pressure-vessel applications. Each of these industries will benefit from advances in the areas of lower-cost and higher-strength composites. Other benefits may include the expansion of the low-cost or higher-strength resin to glass or other alternative fiber applications and a broader market for higher-strength CF through surface modification.

Approach

The project consists of improving specific important properties of the constituent materials to synergistically improve the overall performance of the composite. This will reduce the material needed and optimize the use of alternate lower cost materials. The initial phase focuses on each key property in the tank materials, starting with specifying

the operating conditions of the tank that can maximize energy storage down to the specific critical properties where improvements can have the greatest gain in tank performance. The second phase will progressively combine the individual material improvements into lamina structures that can be used to optimize the tank structure design. Upon successful demonstration of improvements in each task, the modeling of the new improved property will be compared to the initial modeling effort to demonstrate how the effect changes the overall cost and performance. The project will then integrate the new materials and material systems into a sub-scale prototype that will be designed and constructed at Lincoln.

At the conclusion of the project, PNNL and its partners will have built and tested a sub-scale prototype pressure vessel. A second prototype will be delivered to DOE for independent testing and verification of its performance and improvement. A final report detailing the unique improvements in performance and the outcome of the cost analysis will be completed.

Results

Enhanced Operating Conditions

The enhanced operating conditions task within this quarter conducted a literature search of previous concepts that have considered cold gas (200 K) as an onboard hydrogen storage option. In addition, well-to-wheels analyses for the cold gas concept were examined based on prior studies using the DOE models such as H2A and the Hydrogen Delivery Scenario Analysis Model. The tank requirement document was discussed but needs to be further developed based on the baseline cost analysis and projections.

Low-Cost Resins and Resin Matrix Modifications

AOC has identified three resin systems for the team to initiate their research. The resin properties were selected based on typical epoxy properties and with variations of high and low elongations for toughness. The data from these studies will further guide AOC with additional resin changes that will be optimal for fiber and filler materials.

Two materials have been received for modifying the resin. The first material is a nanoclay with amine surface modifications and the second is a silicate nanofiber that has just become commercially available. Safety protocols are being developed for handling the materials.

CF Surface Modifications

Toray has developed several surface treatments for T700 that are being tested with the AOC resin sources. Short-beam shear tests specimens are being fabricated and prepped for testing.

Cost Analysis

The Argonne National Laboratory/TIAX baseline 350-bar, 258 L, L/D=3 Type-IV tank provides a good baseline to what was done before. It also corresponds to 5.6 kg of usable hydrogen, which is the DOE standard of comparison. Another consideration is a standard Lincoln Composites product that is a 350-bar, 200 L tank with outside diameter of 16 inches.

A spreadsheet was developed for comparing tanks at different operating conditions. The spreadsheet estimates the tank volume, weight, and cost of tank materials based on netting analysis and the reported lamina strength for T700S fibers. The spreadsheet is improved over the simple netting analysis formula for the thick-walled geometry effect and the difference in elastic modulus inline and transverse to the fibers. The spreadsheet calculates those effects to estimate the translation factor and increase the hoop strain at the inside wall, which increases the lamina stresses in the hoop and helical fibers at the inside surface. With user input for the desired inside radius and length of the cylindrical section, the lamina strength, fiber and matrix moduli, safety factor, coefficient of variation, etc. The user can then modify the layer thicknesses and angles (two helical plus hoop layers) in the model until the thick-wall stresses are slightly less than the allowable lamina stress. Currently it assumes spherical dome ends, but a solution for the iso-tensoid dome shape is under consideration to improve the model for additional variations. Other factors could be applied to account for the extra composite needed to pass drop, ballistic, and fire tests.

Conclusions and Future Directions

- New vinylester resin compounds to replace more expensive epoxy systems.
- Development of new sizing on carbon fiber for vinylester resin systems.
- Enhanced vinylester resin properties utilizing nanoclays and silicate nanofibers for improved load transfer in through thickness of the composite.

- Cost analysis:
 - Complete baseline model.
 - Compare material property changes and their effects on tank costs.
- Cost analysis being combined with vessel design models.

Future work for FY 2013:

- Combining new improvements to resin and combining with surface treated carbon fiber for filament winding and tank testing.
- Development of tank fiber placement.
- Cost analysis:
 - Update analysis with new material properties and design.

FY 2012 Publications/Presentations

Presentations

1. Simmons K., M Veenstra, D Houston, N Newhouse, M Dettre, T Steinhausler, K Johnson, K Alvine 2012. “Project Kickoff for Low Cost Manufacturing of Hydrogen Storage Pressure Vessels.” Presented by Kevin Simmons and team members (Invited Speaker) Golden, CO on February 1, 2012.

2. Simmons K., M Veenstra, D Houston, N Newhouse, M Dettre, T Steinhausler, K Johnson, K Alvine 2012. “Annual Merit Review for Low Cost Manufacturing of Hydrogen Storage Pressure Vessels.” Poster Presented by Kevin Simmons and team members Arlington, VA on April 16, 2012.

IV.G.1 HGMS: Glasses and Nanocomposites for Hydrogen Storage*

Kris Lipinska (Primary Contact), Oliver Hemmers
Harry Reid Center, University of Nevada Las Vegas (UNLV)
4505 Maryland Parkway, Box 454009
Las Vegas, NV 89154-4009
Phones: (702) 895-4450, (702) 895-3742
Emails: kristina.lipinska@unlv.edu,
oliver.hemmers@unlv.edu

DOE Managers

HQ: Grace Ordaz
Phone: (202) 586-8350
Email: Grace.Ordaz@ee.doe.gov
GO: Jesse Adams
Phone: (720) 356-1421
Email: Jesse.Adams@go.doe.gov

Contract Number: DE-EE0000269

Project Start Date: November 25, 2009

Project End Date: October 31, 2012

*Congressionally directed project

Technical Targets

In this project basic studies are being conducted aimed to answer fundamental questions essential for considering glasses and glass-based materials as H-storage media. As such, this project does not address any H-storage technical targets. In particular, H-sorption and desorption tests or kinetics measurements are not part of the project scope. Though, results of these studies could contribute toward the design and synthesis of new hydrogen storage materials that could potentially be applied towards the following DOE hydrogen storage technical targets:

- Weight and Volume: 0.045 kg H₂/kg system; 0.028 kg H₂/L system
- Energy density: 0.9 kWh/L

FY 2012 Accomplishments

- Demonstrated fabrication of glass materials and nanocrystalline composites with potential interest in H-storage.
- Performed microstructural studies using a multi-technique experimental approach.
- Demonstrated tunability of size and density of nanocrystals in glass matrices.
- Improved UNLV research infrastructure through state-of-the-art experimental instrumentation acquisition.
- Established two new research laboratories and jump-started glass and glass-ceramic composites research on campus.



Fiscal Year (FY) 2012 Objectives

- Fabricate glasses and nanocrystalline composites: improve materials composition by introducing functional dopants
- Demonstrate controlled nucleation of nanocrystals
- Quantify the nanocrystallization processes
- Identify best glass systems, compositions and nanocomposites with interest in H-storage

Technical Barriers

This is a fundamental research project in physics and chemistry of glasses and glass-based nano-crystalline composite materials with potential interest in H-storage. As such, this project does not directly address any H-storage technical barriers. However, the insights gained from these studies could help to answer fundamental questions necessary for considering glass-based materials as H-storage media and could be of interest for the following technical barriers from the Storage section of the Fuel Cell Technologies Program Multi-Year Research, Development and Demonstration Plan:

- (A) System Weight and Volume
- (B) System Cost
- (D) Durability/Operability

Introduction

Proposed previously, but never practically implemented, one of promising concepts for storing hydrogen are micro-containers built of glass and shaped into hollow microspheres. Drawing inspiration from that concept we have expanded it to the exploration of bulk glass materials and glass-derived nanocrystalline composites as inert H-storage media. It is commonly accepted that the most desirable materials for H-storage do not interact chemically with hydrogen and possess a high surface area to host substantial amounts of hydrogen. Glasses are built of disordered networks with ample void spaces that make them permeable to hydrogen even at room temperature. Glass-derived nanocrystalline composites, hybrids of glass and nanocrystals, appear to be promising candidates for H-storage. Key advantages of glasses include simplicity of

preparation, flexibility of composition, chemical durability, non-toxicity and mechanical strength, as well as low production costs and environmental friendliness.

Our goal is to propose glass systems and glass-derived nanocrystalline composites with potential interest in H-storage. These materials with flexible void spaces are able to precipitate functional nanocrystals capable to attract hydrogen. However, for the concept of glass-based materials to be practically implementable as H-storage media, a substantial amount of basic research is still required into physics and chemistry of bulk glasses.

Approach

The research was focused on synthesis of previously pre-selected oxide glass systems and glass compositions with emphasis on their fabrication route and characterization using a multi-technique experimental approach. These studies were directed at the nucleation of nanocrystals in glass matrices and qualitative evaluation of the kinetics of the crystal growth. The use of dopants was essential for effective progress of nanocrystallization.

Results

Research on optimization of glass compositions was continued. New glasses were synthesized and these add to the pool of those previously synthesized (2010) based on titanium- and tantalum-doped silica. To test the effect of dopants and molecular ratios of glass formers to glass modifiers that result in different glass micro-structures (voids, bridging/non-bridging oxygens), several silica-based glass compositions doped by IIIB oxides were investigated. Research on these glasses has been reported [1]. Microstructural characterization of glasses was performed using micro-Raman spectroscopy, synchrotron radiation-based X-ray absorption fine structure (XAFS), transmission electron microscopy and X-ray diffraction.

The glass systems optimal for the project were identified. These are based on silicate glasses variably doped by IIIB oxides. Only some compositions showed formation of desired - from hydrogen storage point of view - functional nanocrystals. From those compositions a number of glass-crystal hybrids (complex nanocrystalline composites) were fabricated and their microstructure was determined using a multi-technique experimental approach. Glass ability to nucleate nanocrystals was monitored using differential scanning calorimetry and Raman spectroscopy, complemented by X-ray diffraction. Local structural environment around atoms of dopants in glass matrices was evaluated using synchrotron radiation-based XAFS spectroscopy.

Analysis has shown that nucleation of nanocrystals is preceded by, and also governed by, a change of local structural environment in the vicinity of the atoms of dopants. The change of coordination number of dopant atoms (from 4 to 6) precedes the structural transition from as-quenched glass to nano-crystalline composite and it occurs prior to nucleation of nanocrystals.

Finally, it was concluded that the use of IIIB oxides as glass dopants results in enhancing overall glass ability to nucleate nanocrystals. These dopants are critical in the progress of crystallization processes that rule nuclei formation and growth within host glass matrices. Also the presence of IIIB oxides as silicate glass dopants is essential in formation of glass-crystal composites with nanocrystals virtually capable to attract hydrogen.

Conclusions and Future Directions

- Complete the synthesis and microstructural characterization of glasses: determine the best glass compositions for nanocrystallization.
- Complete synthesis and microstructural characterization of glass-derived nanocrystalline composites: determine the best nanocomposites compositions.
- Select the most promising materials for further exploration in the H-storage field.
- Even though H-sorption and desorption tests or kinetics measurements were not part of the project, if time permits additional work is being planned in terms of H-sorption measurements on selected glass materials at a collaborator's facility.

FY 2012 Publications/Presentations

1. Kris Lipinska: "Glasses and Nanocomposites for Hydrogen Storage", Presentation at 2012 DOE Annual Merit Review & Peer Evaluation Meeting, Washington, D.C., May 2012.

IV.H.1 From Fundamental Understanding to Predicting New Nanomaterials for High-Capacity Hydrogen/Methane Storage and Carbon Capture

Taner Yildirim^{1,2}

¹Department of Materials Science and Eng.
University of Pennsylvania
Philadelphia, PA 19104

²National Institute of Standards and Technology, NCNR
Gaithersburg, MD 20899
Phone: (301) 975-6228
Email: taner@seas.upenn.edu

DOE Program Manager: Dr. Thiyaga P. Thiyagarajan
Phone: (301) 903-9706
Email: P.Thiyagarajan@science.doe.gov

Objectives

- Use neutron scattering methods along with first-principles computation to achieve fundamental understanding of the chemical and structural interactions governing the storage and release of hydrogen/methane and carbon capture in a wide spectrum of candidate materials.
- Study the effect of scaffolding, nanosizing, doping of the candidate materials on their hydrogen storage and dynamics properties.
- Provide timely feedback and guidance from theory to de novo materials design and targeted syntheses throughout the DOE programs.

Technical Barriers

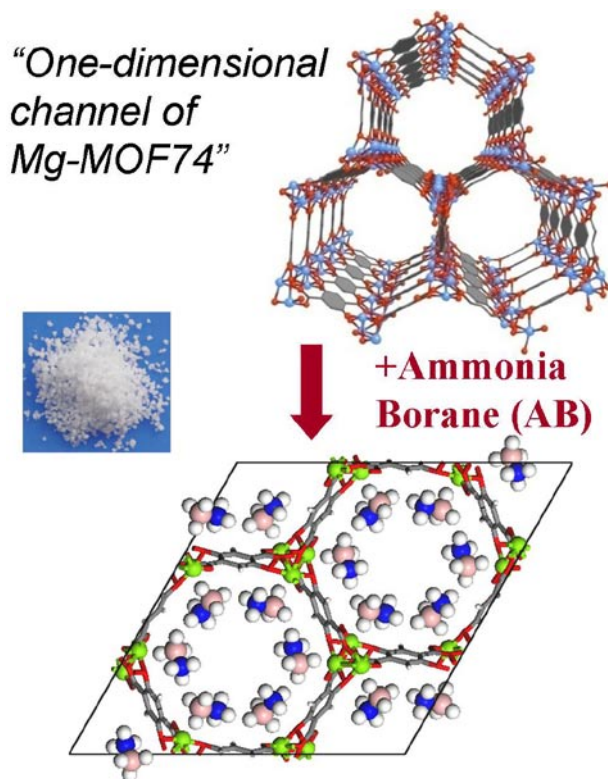
- Currently there is no hydrogen storage materials which can be produced economically perform reversibly and reliably, and meet long-term storage targets e.g. reversible gravimetric capacity 6 wt% or better at practical temperatures and pressures.
- The main obstacles in hydrogen storage are slow kinetics, poor reversibility and high dehydrogenation temperatures for the chemical hydrides; and very low desorption temperatures/energies for the physisorption materials (metal-organic frameworks [MOFs], porous carbons).
- Carbon capture suffers from similar problems where the current technology is based on absorption in amine-based solvents which has limited reversibility and high regeneration cost. The solid-absorbers such as MOFs are either not stable against real flue-gas conditions and/or do not have large enough CO₂ capture (i.e. working) capacity to be practical and cost effective.

Abstract

Onboard hydrogen storage in fuel cell-powered vehicles is a major component of the national need to achieve energy independence and protect the environment. Fundamental breakthrough discoveries in materials science will be required to achieve light-weight, low-volume, safe, economical and recyclable storage technology. The goals of this proposal are a) to achieve fundamental microscopic understanding of how molecular hydrogen interacts chemically, structurally and energetically with novel storage materials; then b) use this understanding to predict and create nanoscale entities with precisely tuned hydrogen binding energies, which can c) be embedded as guests in nanoscale host scaffolds with large surface area to optimize hydrogen capacity, charge and discharge kinetics. This will be achieved by combining broad-based *ab initio* theory and computer modeling with novel materials synthesis and wide-ranging neutron scattering experimental studies.

Progress Report

We are currently working on many research avenues along the lines discussed in our original proposal. Below we briefly discuss some selected recent results.



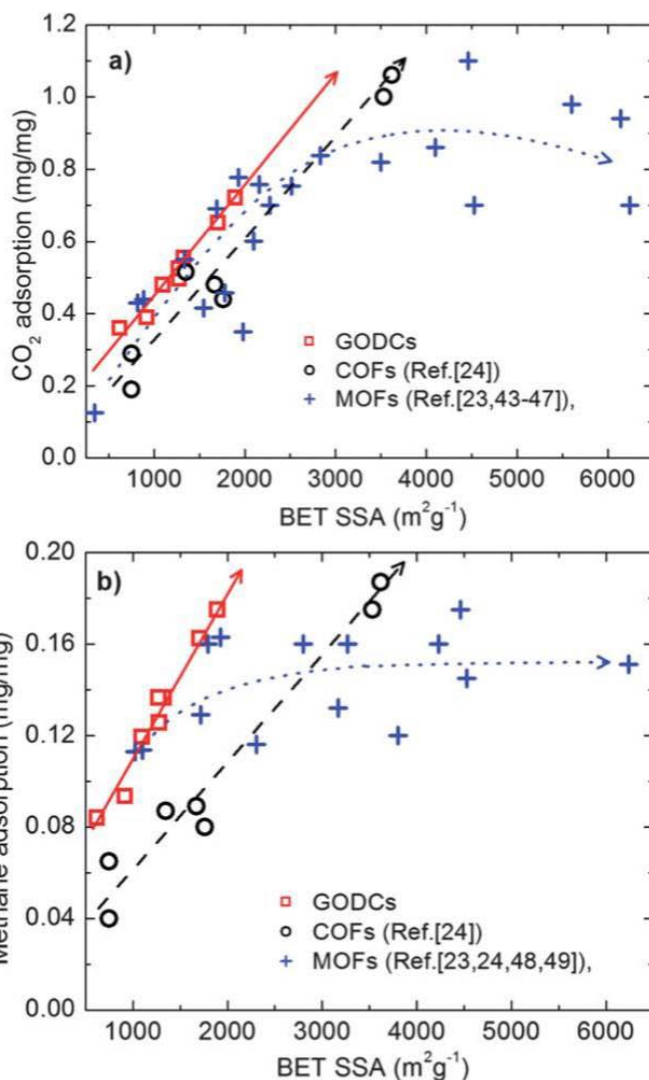
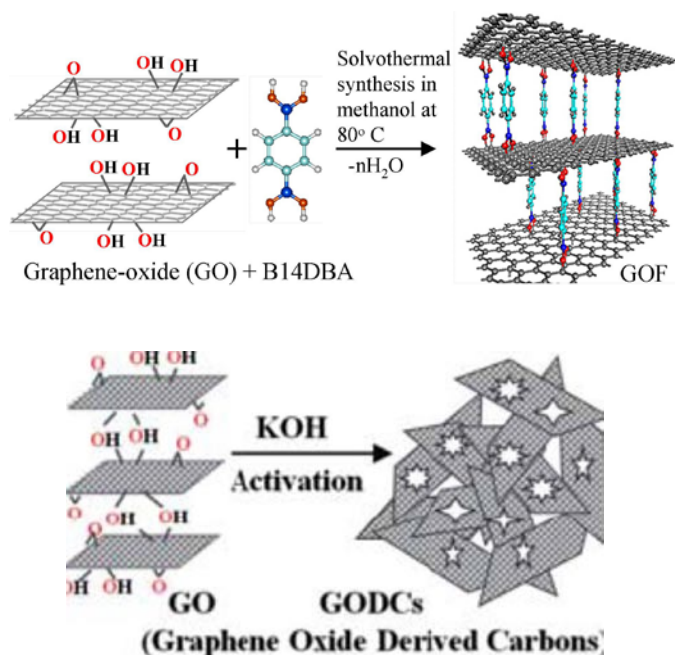
Clean and Fast Hydrogen Release from Nano-Confined AB-MOF Hybrid System

Ammonia borane (AB) has recently received much attention because of its satisfactory air stability, relatively low molecular mass and remarkably high energy storage densities (19.6 wt% and 140 g/L, respectively). However, the direct use of pristine AB as a hydrogen energy carrier in onboard/fuel cell applications is prevented by its very slow dehydrogenation kinetics below 100°C and the concurrent release of detrimental volatile by-products such as ammonia, borazine and diborane. In this study [8,9], we find that the nanoconfinement of AB molecules within the one-dimensional pores of Mg-MOF-74 could be an ideal system for delivering fast and clean hydrogen for fuel cell applications. We show that nanoconfined AB/MOF system improves the dehydrogenation kinetics significantly at temperatures <100°C. More importantly, the AB-Mg-MOF-74 system offers clean hydrogen delivery by suppressing the detrimental byproducts of ammonia, borazine, and diborane, thus putting us one step closer for using AB as hydrogen carrier for fuel cell applications.

Graphene Oxide Derived Carbons (GODCs): High-Surface Area NanoPorous Materials for Hydrogen Storage and Carbon Capture

Even though there has been extensive research on gas adsorption properties of various carbon materials based on activated carbon and nanotubes, there has been little work done on the gas adsorption properties of graphite oxide (GO). In this study, we show that one-and-a-half-century-old graphite oxide can be easily turned into a potentially

useful gas storage material. In order to create high-surface nanoporous materials from GO, we used two different approaches. In the first approach [10,5], we have successfully synthesized graphene-oxide framework materials (GOFs) by interlinking GO layers by diboronic acids. The resulting GOF materials have well defined pore size and Brunauer-Emmett-Teller surface area up to 500 m²/g with twice larger heat of adsorption of H₂ and CO₂ than those found in other physisorption materials such as MOF5. In the second approach [3], we synthesized a range of high surface area GO derived carbons (GODC) by chemical activation with potassium hydroxide and studied their applications toward H₂, CO₂, and CH₄ gas storage. We obtain largely increased surface areas up to nearly 1,900 m²/g for GODC samples from 10 m²/g for initial GO. A detailed experimental study of high pressure excess sorption isotherms on GODCs reveal an increase in both CO₂ and CH₄ storage capacities compared to other systems such as MOFs, zeolitic imidazolate frameworks, and COFs (see figure). On comparing with respect to the surface area below 2,000 m²/g, it is clear that



none of the MOFs surpass CO₂ and methane adsorption capacities of the GODCs. It is important for the potential adsorbents to be stable in the presence of flue gases in which the most of MOFs do not survive. In this regard, the new GODC materials with the rigid pores, good chemical resistance, high surface areas and tuneable pore volume could play a promising role as high pressure adsorbents. These results clearly demonstrate that GODCs are very promising solid adsorbents for gas adsorption applications due to their easy synthesis, tunable pore size/volume, high chemical stability and low cost production.

Efficient Carbon Capture in Metal-Organics Frameworks

Investigations of the application of MOFs to adsorptive carbon capture have focused on their appreciable storage capacities but fail to address the more pertinent issue of how MOFs perform under common industrial separation processes that are at the heart of carbon capture. Typical processes rely on swing adsorption and are limited to relatively low CO₂ partial pressures such that the total pore volume and the surface area are under-utilized. Here, we investigate the performance of a number of MOFs with particular focus on their behavior at the low pressures commonly used in swing adsorption. This comparison clearly shows that it is the process that determines which MOF is optimal rather than there being one best MOF, though MOFs that possess enhanced binding at open metal sites generally perform better than those with high surface area. In particular, using neutron scattering we unveiled the mechanism of carbon capture and found that MOFs that possess coordinatively unsaturated metal centers offer as much as 9 mmol g⁻¹ swing capacity under certain conditions. This work [4] will be an important guideline for deciding the best pair of carbon capture process and MOF material for optimum carbon capture.

Future Directions

We will focus our efforts on AB-hybrid systems and try to regenerate MOFs after AB is decomposed, which will make the hydrogen storage reversible. We will perform more work on nanoporous carbon materials derived from GO and MOFs, functionalize them such as B and N doping to tune their hydrogen storage and carbon capture properties.

Recent Publications acknowledging the DOE BES grant

1. *Direct Observation of Activated Hydrogen Binding to a Supported Organometallic Compound at Room Temperature*, J.M. Simmons, T. Yildirim, A. Hamaed, D.M. Antonelli, M.I. Webb, and C.J. Walsby, *Chem. Eur. J.* **18**, 4170 (2012).
2. *Metal hydrazinoborane LiN₂H₃BH₃ and LiN₂H₃BH₃•2N₂H₃BH₃: Crystal structures and high-extent dehydrogenation*, H. Wu, W. Zhou, F. Pinkerton, T. Udovic, T. Yildirim and J. Rush, *Energy Environ. Sci.*, DOI: 10.1039/C2EE21508J, Communication (2012)
3. *Graphene oxide derived carbons (GODCs): synthesis and gas adsorption properties*, G. Srinivas, J. Burress and T. Yildirim, *Energy Environ. Sci.* **5**, 6453-6459 (2012, commun.)
4. *Carbon capture in metal-organic frameworks—a comparative study*, J.M. Simmons, H. Wu, W. Zhou and T. Yildirim, *Energy Environ. Sci.* **4**, 2177-2185 (2011).
5. *Porous graphene oxide frameworks: Synthesis and gas sorption properties*, G. Srinivas, J.W. Burress, J. Ford and T. Yildirim, *J. Mater. Chem.* **21**, 11323-11329 (2011).
6. *Sodium magnesium amidoborane: the first mixed-metal amidoborane*, H. Wu, W. Zhou, F.E. Pinkerton, M.S. Meyer, Q. Yao, S. Gadipelli, T.J. Udovic, T. Yildirim and J.J. Rush, *Chem. Commun.* **47**, 4102-4104 (2011).
7. *“A highly practical route for large-area, single layer graphene from liquid carbon sources such as benzene and methanol”*, G. Srinivas, I. Calizo, J. Ford, G. Cheng, A.H. Walker, and Taner Yildirim, *J. Mater. Chem.* **21**, 16057-16065 (2011).
8. *Zn-MOF assisted dehydrogenation of ammonia borane: Enhanced kinetics and clean hydrogen generation*, G. Srinivas, J. Ford, Wei Zhou, and Taner Yildirim, *Int. Journal of Hydrogen Energy*, doi:10.1016/j.ijhydene.2011.04.008 (2011).
9. *Nanoconfinement and catalytic dehydrogenation of ammonia borane by magnesium-metal-organic-framework-74*, G. Srinivas, J. Ford, W. Zhou, H. Wu, T.J. Udovic, and Taner Yildirim, *Chem. Eur. J.* **17**, doi:10.1002/chem.201100090 (2011)
10. *Graphene-Oxide-Framework (GOF) Materials; Theoretical Predictions and Experimental Results*, J. Burress, G. Srinivas, J.M. Simmons, J. Ford, W. Zhou, Taner Yildirim, *Angew. Chem. Int. Ed.*, **49**, 8902-8904 (2010).
11. *Structural stability and elastic properties of prototypical covalent organic frameworks*, W. Zhou, H. Wu, Taner Yildirim, *Chem. Phys. Lett.* **499**, 103-107 (2010).
12. *A new family of metal borohydride ammonia borane complexes: Synthesis, structures, and hydrogen storage properties*, H. Wu, W. Zhou, F.E. Pinkerton, M.S. Meyer, G. Srinivas, Taner Yildirim, T.J. Udovic, *J. Mat. Chem.* **20**, 6550 (2010).
13. *Adsorption Sites and Binding Nature of CO₂ in Prototypical Metal-Organic Frameworks: A Combined Neutron Diffraction and First-Principles Study*, H. Wu, J. M. Simmons, G. Srinivas, W. Zhou, and Taner Yildirim *J. Phys. Chem. Lett.* **1**, 1946 (2010).
14. *Metal-Organic Frameworks with Exceptionally High Methane Uptake: Where and How is Methane Stored?*, H. Wu, J.M. Simmons, Y. Liu, C.M. Brown, X.-S. Wang, S. Ma, V.K. Peterson, P.D. Southon, C.J. Kepert, H.-C. Zhou, T. Yildirim, and W. Zhou, *Chem. Eur. J.*, **16**, 5205–5214 (2010).
15. *Alkali and alkaline-earth metal dodecahydro-closo-dodecaborates: Probing structural variations via neutron vibrational spectroscopy*, N. Verdal, W. Zhou, V. Stavila, J.-H. Her, M. Yousufuddin, T. Yildirim, and T.J. Udovic, *J. Alloys Comp.* (2010).
16. *Metal Amidoboranes*, Hui Wu, Wei Zhou, and Taner Yildirim, in *“Boron Hydrides, High Potential Hydrogen Storage Materials*, edited by Umit B. Demirci and Philippe Miele, Nova Publishers (2010).

IV.H.2 Novel Theoretical and Experimental Approaches for Understanding and Optimizing Hydrogen-Sorbent Interactions in Metal Organic Framework Materials

Yves. J. Chabal (Primary Contact), Jing Li,
Timo Thonhauser
UT Dallas – Department of Materials Science and Engineering
800 W. Campbell Road, RL 10
Richardson, TX 75080
Phone: (972) 883-5751
Email: chabal@utdallas.edu

DOE Program Officer: Dr. Bonnie Gersten
Phone: (301) 903-0002
Email: Bonnie.Gersten@science.doe.gov

Subcontractors:

- Jing Li (Rutgers University)
- Timo Thonhauser (Wake Forest University)

Objectives

- Develop a comprehensive understanding of how small molecules (e.g. H₂) bind inside metal organic framework (MOF) materials, using experimental methods (infrared [IR] and Raman spectroscopy) and theoretical tools (first-principles density functional theory).
- Develop an accurate model for the kinetics and diffusion of molecular hydrogen and gas mixtures through MOF materials.
- Devise approaches to increase the binding energy and uptake of molecular hydrogen in MOF materials to the required 20 kJ/mol by designing new MOFs with tailored, unsaturated metal clusters or catalytic centers.

Technical Barriers

- MOFs of very high surface area have been developed by making use of long ligands and suitable metal nodes, but great challenges remain in achieving sufficiently high hydrogen binding energies (the highest Q_{st} values are still below 15 kJ/mol and low porosity is usually associated with high Q_{st}) that will lead to high H₂ uptake at room temperature.
- The microscopic nature of the interaction between gas molecules and the MOF network is difficult to extract from spectroscopy alone (without theoretical modeling), although much information on the adsorption sites and relaxation of the MOF network is reflected in both IR and Raman spectra. Many MOFs are also sensitive to

water vapor, which may complicate adsorption studies, requiring in some cases H₂O co-adsorption studies.

- First-principles spin-polarized simulations of interesting MOFs with magnetic atoms (Fe, Ni, Co) and the effective inclusion of temperature and dynamical effects are not yet possible in our simulations, as van der Waals density functional (vdW-DF) has not been extended for such cases.

Abstract

Hydrogen storage is a key challenge and the largest barrier to a hydrogen economy. Many hydrogen-storage materials have been investigated, e.g. transition-metal hydrides or light-element hydrides. MOF materials—metal-oxide clusters connected by organic ligands (e.g. linkers or pillars)—use a different approach. These structures are porous and have a huge effective surface area, making them ideal for H₂ storage through physisorption. Possible combinations of clusters and ligands are literally limitless and give hope that desired properties can be obtained by designing the “right” combination. MOF properties of interest are the hydrogen-storage capacity and the thermodynamics of the hydrogen adsorption/desorption. At high pressures or low temperatures, MOFs typically have a hydrogen-storage capacity of up to 5 wt% and a hydrogen binding energy of up to 10 kJ/mol. The overall aim is to increase both, as required for on-board applications, by designing improved metal clusters and linkers. To this end, it is necessary to understand how the hydrogen interacts with clusters and linkers. Our specific aim is to develop a fundamental mechanistic understanding of the interaction of H₂ in MOFs, using a combination of novel synthesis, theoretical analysis, and characterization. We combine high-pressure and low-temperature IR absorption and Raman measurements, adsorption isotherms, and isosteric heat of adsorption measurements with first-principles calculations based on vdW-DF. This provides insight into the role of unsaturated metal centers in enhancing molecular uptake, selective adsorption, and diffusion. The short-term impact of this work is that the control and understanding of common MOF systems makes it possible to determine the theoretical loading limits and stability of a specific class of materials. The long-term impact includes the development of (i) theoretical and experimental methods to gain a fundamental understanding of molecular interactions within these systems, and (ii) new classes of microporous MOFs with enhanced molecular binding.

Progress Report

Synthesis, structure characterization, and modification of MOFs: We have functionalized a bdc ligand in $\text{Zn}(\text{bdc})(\text{ted})_{0.5}$ by introducing hydroxyl and amino groups that lead to two related structures, $\text{Zn}(\text{bdc}-\text{OH})(\text{ted})_{0.5}$ and $\text{Zn}(\text{bdc}-\text{NH}_2)(\text{ted})_{0.5}$ (bdc = terephthalate, ted = tryethylenediamine, bdc-OH = 2-hydroxyterephthalate, bdc-NH₂ = 2-aminoterephthalate). $\text{Zn}(\text{bdc})(\text{ted})_{0.5}$ can be considered a three-dimensional (3D) porous structure having three interlacing one-dimensional (1D) channels, while both $\text{Zn}(\text{bdc}-\text{OH})(\text{ted})_{0.5}$ and $\text{Zn}(\text{bdc}-\text{NH}_2)(\text{ted})_{0.5}$ contain only 1D open channels as a result of ligand functionalization. A notable decrease in surface area and pore size is observed in both compounds. Consequently, $\text{Zn}(\text{bdc})(\text{ted})_{0.5}$ takes up the highest amount of H₂ at low temperatures. However, the isosteric heats of hydrogen adsorption is higher in $\text{Zn}(\text{bdc}-\text{OH})(\text{ted})_{0.5}$ than in $\text{Zn}(\text{bdc})(\text{ted})_{0.5}$, suggesting a stronger H₂-framework interaction in the former.

Calculation of IR intensities of adsorbed H₂ in MOFs: Knowledge of the strengths and frequencies of the IR bands resulting from molecules adsorbed at varying adsorption sites is crucial for the correct interpretation of IR data. The calculation of frequencies is fairly straightforward, but the intensities have proved difficult or impossible to calculate for an IR inactive molecule like H₂ adsorbed in a large structure such as MOFs. This is because the dipole moments are only induced and small, and occupy a large volume. This is exacerbated by the fact that vibrations, rotations, and translations contribute strongly to the spectra. We have developed theoretical methods to tackle this problem and successfully applied them to the IR spectra of an important MOF (MOF-74). Our ability to do this substantially enhances our ability to use our now more powerful experimental/theoretical combination to unravel the complexities of H₂ adsorption in less understood structures.

H₂-H₂ interactions in MOF-74: We have identified H₂-H₂ interactions between near neighboring sites and next-near neighboring sites in MOF-74. Using our vdW-DF approach, we have shown that H₂ dipole moments and IR shifts are greatly affected by these interactions. We were able to detect these effects using IR absorption measurements of H₂ in MOF-74-M (M= Zn, Mg), as a function of temperature and pressure. A small shift (~ -30 cm⁻¹ with respect to the unperturbed H₂ molecule) is observed for the internal stretch frequency of H₂ adsorbed on the metal site at low loading. This contrasts the much larger shifts (~ -70 cm⁻¹) observed in previous studies of MOFs with unsaturated metal centers (including MOF-74) and the general assumption that the H₂ stretch shifts depend on adsorption energies. We show that larger shifts (~-70 cm⁻¹) do occur, but only when the next available site (“oxygen” site) is occupied. This larger shift originates from H₂-H₂ interactions on near neighboring sites, consistent with the short distance between H₂ in these two sites ~2.6 Å.

Improving computational tools: The original exchange-correlation functional vdW-DF showed slightly overestimated binding distances and underestimated binding energies. Before his untimely passing, Langreth and his group had refined this functional and developed a successor, i.e. vdW-DF2. We adapted this functional and tested it for gas adsorption in MOFs under the current DOE grant. We now use it to calculate nuclear positions, molecular binding sites, and IR spectra for gases adsorbed in MOFs; it is more accurate for calculations of gas adsorption in MOFs than vdW-DF. We implemented vdW-DF and vdW-DF2 in PWscf (part of QUANTUM-ESPRESSO), which is faster by a factor of 2–3 compared to our original implementation in ABINIT, resulting in much increased productivity. We also derived a formalism to calculate the vdW-DF stress tensor, allowing for a much more efficient structural optimization. With these new computational tools, we performed a purely theoretical study of the hydrogen-storage capacity of (H₂)₄CH₄ in MOFs and carbon nanotubes. While we find that MOFs cannot provide sufficient pressure to stabilize this extraordinary hydrogen-storage material at room temperature, we do find that carbon nanotubes have the potential to do so, with storage capacities of up to 20 wt%.

Future Directions

From a structure designing point of view, our future focus will be to incorporate a high density of functional groups (e.g. -OH, -Cl, -F, -NR₂) and metal clusters (e.g. Mg, Li) in MOF structures that have strong binding interactions with hydrogen and other targeted small molecules, while keeping the high porosity of the MOF framework.

Future theoretical work will focus on: (i) Our DFT calculations are performed with our vdW-DF exchange-correlation functional, including van der Waals forces—which are crucial for the description of H₂ physisorbed in MOF structure—seamlessly. Currently, vdW-DF cannot describe spin-polarized systems, excluding many interesting MOFs. We will work on finding suitable approximations for such systems, with applications to MOF74-Fe, MOF74-Co, and MOF74-Ni. (ii) For hydrogen storage in MOFs, not only the binding energy is important, but also the kinetics of hydrogen diffusion through the network. We plan to investigate H₂ diffusion barriers in MOFs from first-principles, using nudged-elastic-band calculations. These barriers will reveal previously inaccessible information about hydrogen kinetics and migration in MOFs. (iii) Currently, all simulations are strictly speaking performed at zero K. The effect of temperature can be included by performing first-principles molecular dynamics simulations. To this end, we will incorporate vdW-DF into a molecular dynamics code.

The methods and approaches developed here are directly applicable to study the interaction of many other small molecules such as CO, CO₂, N₂, H₂O, and CH₄ with

MOFs. We plan to apply our successful experiment/theory framework to study co-adsorption of CO₂, H₂O, and H₂ in MOFs with unsaturated metal centers for the purpose of gas sequestration of these molecules.

Publications acknowledging the grant or contract

1. “vdW-DF stress tensor: Structural evolution of amino acids under stress,” R. Sabatini, E. Küçükbenli, B. Kolb, T. Thonhauser, and S. de Gironcoli, *J. Phys.: Cond. Matter*, submitted March (2012).
2. “Tuning the gate opening pressure of MOFs for the selective separation of C₂ isomers,” N. Nijem, H. Wu, P. Canepa, A. Marti, K. Balkus Jr., T. Thonhauser, J. Li, and Y.J. Chabal, *Ang. Chem. Int. Ed.*, submitted Feb. (2012).
3. “Spectroscopic characterization of van der Waals interactions of adsorbates in porous materials,” N. Nijem, P. Canepa, L. Kong, H. Wu, J. Li, T. Thonhauser, and Y. J. Chabal, *J. Phys.: Cond. Matter*, submitted Feb. (2012).
4. “A theoretical study of the hydrogen-storage potential of (H₂)₄CH₄ in metal organic framework materials and carbon nanotubes,” Q. Li and T. Thonhauser, *J. Phys.: Cond. Matter*, in press (2012).
5. “Analyzing the frequency shift of physisorbed CO₂ in metal-organic framework materials,” Y. Yao, N. Nijem, J. Li, Y.J. Chabal, D. C. Langreth, and T. Thonhauser, *Phys. Rev. B* 85, 064302 (2012).
6. “Dual functionalization leads to significantly enhanced binding affinity, remarkable selectivity and high capacity of CO₂ in a new rht-type MOF based on hexacarboxylate ligand with N-rich imino triazine backbone,” B. Li et al., *Ang. Chem. Int. Ed.* 51, 1412 (2012).
7. “Effects of the chemical environment on the vibrational modes of adsorbed CO₂ in MOFs,” N. Nijem, H. Wu, Y. Zhao, J. Li, and Y.J. Chabal, *Prepr. Pap.-Am. Chem. Soc., Div. Fuel Chem.*, submitted Nov. (2011).
8. “Experimental and theoretical investigations on the MMOF Selectivity for CO₂ vs N₂ in flue gas mixtures,” Z.J. Zhang, J.C. Liu, Z. Li, and J. Li, *Dalton Transac.* 41, 4232 (2012).
9. “Raman spectroscopy for probing guest-host interactions in metal organic frameworks,” N. Nijem, K. Roodenko, Y. Zhao, J. Li, and Y. J. Chabal, 2011 MRS Spring Meeting Proceedings 1334.
10. “Understanding the preferential adsorption of CO₂ over N₂ in a flexible Metal Organic Framework,” N. Nijem et al., *J. Am. Chem. Soc.* 133, 12849 (2011).
11. “The effect of methyl functionalization on microporous metal-organic frameworks’ capacity and binding energy for carbon dioxide adsorption,” H. Liu, Y. Zhao, Z. Zhang, N. Nijem, Y.J. Chabal, H. Zeng, and J. Li, *Adv. Funct. Mater.* 21, 4754 (2011).
12. “First-principles approach to rotational-vibrational frequencies and infrared intensity for H₂ adsorbed in nanoporous materials,” L. Kong, Y.J. Chabal, and D.C. Langreth, *Phys. Rev. B* 83, 121402 (2011).
13. “Spectroscopic evidence for the influence of the benzene sites on tightly bound H₂ in Metal Organic Frameworks with Unsaturated Metal Centers: MOF-74-Cobalt,” N. Nijem, L. Kong, Y. Zhao, H. Wu, J. Li, D.C. Langreth, and Y.J. Chabal, *J. Am. Chem. Soc. (Communication)* 133, 4782 (2011).
14. “Enhancing gas adsorption and separation capacity through ligand functionalization of microporous metal-organic frameworks,” Y.G. Zhao et al., *Chem. Eur. J.* 17, 5101 (2011).
15. “The effect of methyl functionalization on MMOFs’ capacity and binding energy for carbon dioxide adsorption,” H. Liu, Y.G. Zhao, Z.J. Zhang, N. Nijem, Y.J. Chabal, H.P. Zeng, and J. Li, *J. Adv. Func. Mater.* 21, 4754 (2011).
16. “Molecular hydrogen ‘pairing’ interaction in a metal organic framework system with unsaturated metal centers (MOF-74),” N. Nijem, J. Veyan, L. Kong, H. Wu, Y. Zhao, J. Li, D.C. Langreth, and Y.J. Chabal, *J. Am. Chem. Soc.* 132, 14834 (2010).
17. “Highly selective CO₂ capture by a flexible microporous MOF Material,” H.H. Wu, S.R. Randall, D.A. Smith, M.T. Trachtenberg, and J. Li, *Chem. A. Euro. J.* 16, 13951 (2010).
18. “Commensurate adsorption of hydrocarbons in microporous metal-organic frameworks,” K.H. Li, D.H. Olson, and J. Li, *Trends Inorg. Chem.* 12, 13 (2010).
19. “Interaction of molecular hydrogen with microporous metal organic framework materials at room temperature,” N. Nijem, J. Veyan, L. Kong, K. Li, S. Pramanik, Y. Zhao, J. Li, D. Langreth, and Y.J. Chabal, *J. Am. Chem. Soc.* 132, 1654 (2009).
20. “Theoretical and experimental analysis of H₂ binding in a prototype metal-organic framework material,” L. Kong, V. R. Cooper, N. Nijem, K. Li, Jing Li, Y. J. Chabal, and D. C. Langreth, *Phys. Rev. B* 79, 081407 (2009).
21. “RPM3: A multifunctional microporous MOF with recyclable framework and high H₂ binding energy,” A. Lan et al., *Inorg. Chem.* 48, 7165 (2009).

IV.H.3 SISGR: Design and Synthesis of Chemically and Electronically Tunable Nanoporous Organic Polymers for Use in Hydrogen Storage Applications

Hani M. El-Kaderi (Primary Contact),
Mohammad G. Rabbani, Thomas E. Reich,
Karl T. Jackson, Refaie M. Kassab
Virginia Commonwealth University
Department of Chemistry
1001 West Main St
Richmond, VA 23284-2006
Phone: (804) 828-7505
Email: helkaderi@vcu.edu

DOE Program Officer: Michael Sennett
Phone: (301) 903-6051
Email: Michael.Sennett@science.doe.gov

of amine-borane or amine-borontrihalide adducts in non-polar solvent mixtures. The textural properties and hydrogen storage capacity of these polymers were carried out using conventional low- and high-pressure gas sorption experiments. Additionally, porous BILPs featuring high imidazole linkage density were synthesized and tested for hydrogen storage. Among the most attractive properties of this class of polymers are their chemical and physical stabilities, amphoteric pore walls, and their high gas storage capabilities. BLPs can store up to 4.25 wt% of hydrogen at 77 K and 40 bar whereas BILPs can store 2.3 wt% of hydrogen at 77 K and only 1 bar. Both types of these purely organic polymers exhibit relatively moderate hydrogen isosteric heats of adsorption (6.0 to 8.3 kJ mol⁻¹). An advantageous feature of these polymers is their functionalizable channels/pores that alter their affinity for small gases.

Objectives

- Design and synthesis of new classes of low density nanoporous organic polymers that are linked by strong covalent bonds and composed of chemically and electronically tunable building blocks.
- Use gas sorption experiments to investigate porosity and determine hydrogen storage at variable temperature and pressure ranges.
- Investigate the impact of pore functionalization on hydrogen storage and binding affinity and predict gas binding sites by computational studies.

Technical Barriers

This project addresses the following technical barriers for on-board hydrogen storage:

- Gravimetric and volumetric storage
- Fueling/defueling rates
- Chemical stability of sorbents

Abstract

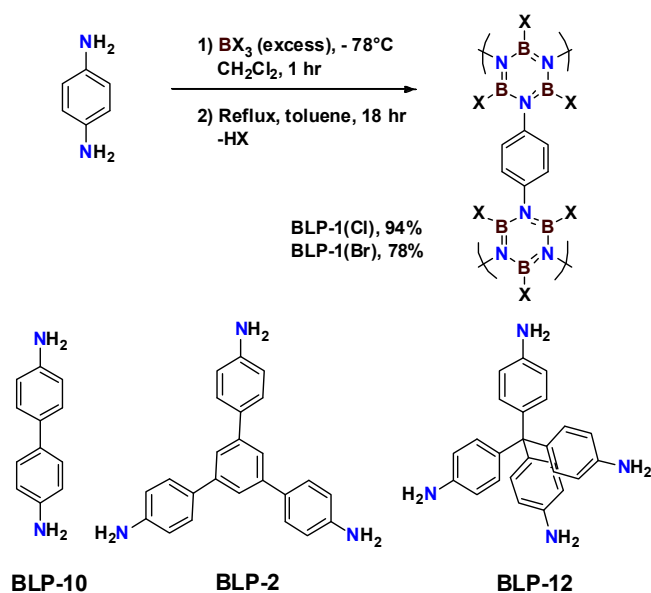
The designed synthesis of two novel classes of porous organic polymers, borazine-linked polymers (BLPs) and benzimidazole-linked-polymers (BILPs), that are composed of chemically and electronically tunable building blocks have been performed and their use in hydrogen and other small gas storage has been investigated. Highly porous BLPs were prepared by employing thermal decomposition

Progress Report

This project is aimed at the synthesis and characterization of two new classes of porous organic polymers: BLPs and BILPs. In these polymers the resulting chemical connectivity between building units can potentially lead to structures analogous to those of covalent-organic frameworks (COFs) linked by B-O bonds [1,2]. BLPs and BILPs feature functionalized pore walls and moderate surface areas. One significant motivation for pursuing isolated B₃N₃ rings in porous materials was the potential of the borazine rings to undergo hydrogenation by molecular dihydrogen in the presence of a catalyst. Thereby BLPs would store hydrogen by both chemical (B-H and N-H) and physical (physisorption within the pores) means.

Borazine-Linked Polymers (BLPs)

We have described for the first time the incorporation of borazine units bearing three different B-substituents (H, Cl, Br) as building blocks for the construction of porous networks to assess the impact of pore decoration on hydrogen storage and selective gas binding. In halogen-decorated BLPs, treatment of arylamines with the corresponding boron trihalide followed by thermolysis in toluene under refluxing conditions produced the desired polymer (Scheme 1). We have extended this approach to prepare seven polymers in good yields using various amine building units. The chemical composition and structural aspects of these polymers were investigated by spectral (Fourier transform infrared, ¹¹B and



SCHEME 1. Representative synthesis for halogen-decorated BLPs

^{13}C solid-state nuclear magnetic resonance, scanning electron microscopy) and analytical methods (elemental analysis) while porosity was examined by N_2 porosity measurements. Unlike COFs, all BLPs are amorphous which precluded their investigation by X-ray diffraction techniques. From their porosity measurements, halogen-decorated BLPs exhibit moderate surface areas and relatively high gas uptakes in comparison to porous organic polymers (Table 1). The highest gas uptake was reported for BLP-12(Cl) which has the highest surface area and pore volume values; it stores 1.75 wt% of hydrogen with an isosteric heat of adsorption of 7.08 kJ/mol which is considerably somewhat higher than those reported for two-dimensional and three-dimensional COFs as a result of the narrower halogen decorated pores.

We have expanded the field of BLPs by the synthesis of halogen-free polymers following the same thermolysis approach described above to produce several borazine-rich polymers with very high surface areas. All BLPs

were isolated as white powders in good yields and subjected to a battery of characterization methods: powder X-ray diffraction, scanning electron microscopy, thermogravimetric analysis, Fourier transform infrared, and Ar porosity measurements. Halogen-free BLPs are thermally stable up to $\sim 420^\circ C$ and were subjected to hydrogen storage experiments under low- and high-pressure conditions. Our studies indicate that halogen-free BLPs can store significant amounts of hydrogen under high pressure settings as in the case of BLP-12(H) which stores 4.25 wt% at 77 K and 40 bar.

Benzimidazole-Linked-Polymers (BILPs)

In addition to our work on BLPs, we have developed a simple synthetic route for several organic polymers by using condensation reactions between a variety of aryl-o-diamine and aryl-aldehyde building units to form BILPs. BILPs have remarkable chemical and thermal stabilities and considerable H_2 uptakes as well as high CO_2 selectivity over N_2 and CH_4 . The notable enhanced CO_2 capture and selectivity of BILPs compared to other purely organic or organic-inorganic hybrid materials such as MOFs, for example, were attributed to their subnano pore dimensions and imidazole-functionalized pore walls that facilitate selective CO_2 capture and storage. Similarly, these textural properties of BILPs resulted in high H_2 uptakes and binding affinities at low pressure and cryogenic conditions as shown in Figure 1 and summarized in Table 2.

All BILPs exhibit excellent chemical stability that allow for their handling and purification under ambient conditions. They remain intact upon washing with a 2M aqueous solution of HCl or NaOH. BILPs also exhibit high thermal stability according to thermogravimetric analysis which showed decomposition only after $\sim 420^\circ C$. Porosity and gas storage measurements (Table 2) reveal that BILPs are some of the most attractive purely organic materials for gas storage applications. BILPs with high surface area in particular exhibit noteworthy hydrogen storage capabilities (1.9-2.3 wt% at 77 K and 1 bar). In addition, these polymers in general can store significant amounts of CO_2 (up to

TABLE 1. Porous properties and H_2 uptakes of BLPs. SA_{Lang} : calculated by the Langmuir method. P_{vol} : calculated from nitrogen adsorption at $P/P_0 = 0.9$. PSD: calculated using non-local density functional theory (NLDFT).

| Polymer | SA_{Lang} ($m^2 g^{-1}$) | P_{vol} ($cm^3 g^{-1}$) | PSD (nm) | H_2 , 77 K (wt%) | $H_2 Q_{st}$ ($kJ mol^{-1}$) |
|------------|------------------------------|-----------------------------|----------|----------------------|--------------------------------|
| BLP-1(Cl) | 1,828 | 0.746 | 1.33 | 1.00 | 7.06 |
| BLP-1(Br) | 730 | 0.303 | 1.27 | 0.68 | 7.14 |
| BLP-2(Cl) | 1,699 | 0.649 | 1.27 | 1.30 | 7.19 |
| BLP-2(Br) | 1,221 | 0.571 | 1.27 | 0.98 | 7.49 |
| BLP-12(Cl) | 2,091 | 0.853 | 1.13 | 1.75 | 7.08 |
| BLP-1(H) | 1,360 | 0.69 | 1.27 | 1.33; (3.97, 40 bar) | 6.8 |
| BLP-2(H) | 1,178 | 0.59 | 1.13 | 1.43; (2.48, 40 bar) | 6.8 |
| BLP-12(H) | 2,866 | 1.08 | 1.27 | 1.93; (4.25, 40 bar) | 6.0 |

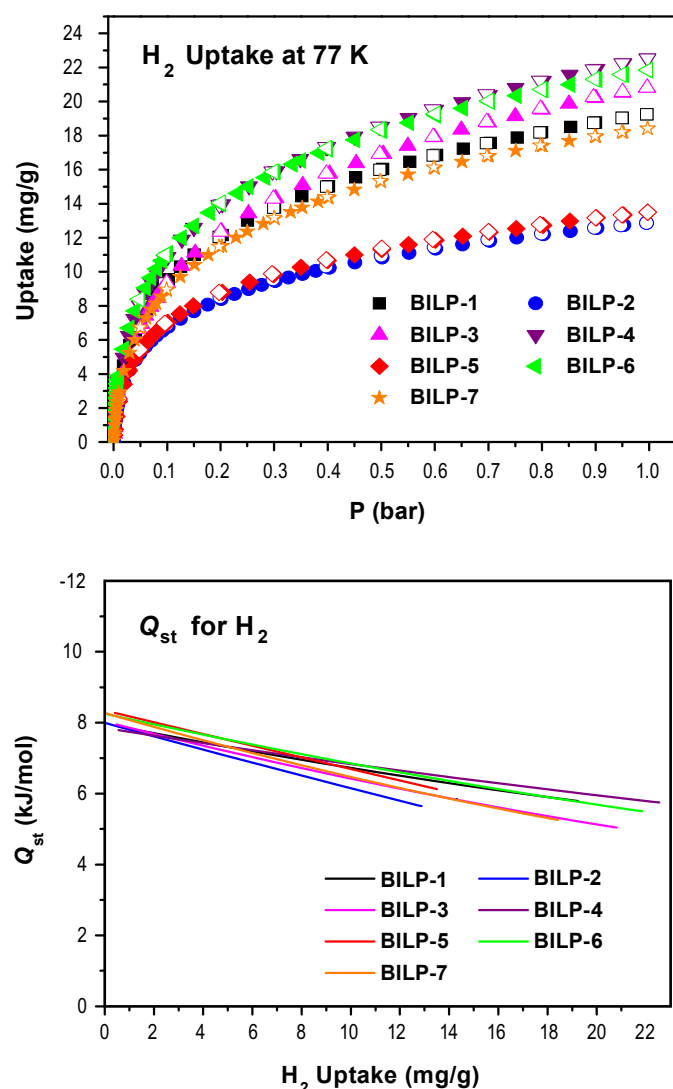


FIGURE 1. Hydrogen uptake isotherms and isosteric heats of adsorption for H₂. Adsorption (filled) and desorption (empty).

TABLE 2. H₂ Storage Capacity for BILPs

| polymer | Surface Area (m ² g ⁻¹) ^a | | Pore Size ^b nm | Pore Volume ^c cm ³ g ⁻¹ | H ₂ uptake at 1 bar (wt%) | | Q _{st} for H ₂ kJ mol ⁻¹ |
|---------|---|----------|------------------------------|---|--------------------------------------|------|--|
| | BET | Langmuir | | | 77 K | 87 K | |
| BILP-1 | 1,172 | 1,563 | 6.8 | 0.70 | 1.9 | 1.4 | 7.9 |
| BILP-2 | 708 | 942 | 6.8 | 0.49 | 1.3 | 1.0 | 8.0 |
| BILP-3 | 1,306 | 1,715 | 7.2 | 0.65 | 2.1 | 1.5 | 8.0 |
| BILP-4 | 1,135 | 1,486 | 6.8 | 0.65 | 2.3 | 1.6 | 7.8 |
| BILP-5 | 599 | 799 | 6.8 | 0.36 | 1.4 | 1.0 | 8.3 |
| BILP-6 | 1,261 | 1,654 | 6.2 | 0.66 | 2.2 | 1.6 | 8.2 |
| BILP-7 | 1,122 | 1,489 | 6.8 | 0.74 | 1.8 | 1.4 | 8.3 |

^aSurface area was calculated from Ar isotherm. ^bPore size distribution was calculated by NLDFT. ^cPore volume was calculated at $P/P_0 = 0.95$. BET = Brunauer-Emmett-Teller

5.3 mmol g⁻¹ at 273 K and 1 bar) with very high selectivities. The presence of amphoteric building units in the pore walls of BILPs can allow for post-synthesis modification with light metal ions (Li⁺, Na⁺, etc.) for enhanced hydrogen storage capacities which will be addressed in future work.

Future Directions

Our future research goals will focus on developing new synthetic methods to enhance the crystallinity and porosity of BLPs and BILPs to attain higher hydrogen storage capacities in these polymers especially under elevated pressure conditions. Additionally, pore surface modification by post-synthesis processes or by the use of pre-functionalized building blocks will also be explored to enhanced H₂ isosteric heat of adsorption. Future studies will also address the potential of borazine-rich BLPs in chemical hydrogen storage.

References

1. El-Kaderi, H.M.; Hunt, J.R.; Mendoza-Cortés, J.L.; Côté, A.P.; Taylor, R.E.; O’Keeffe, M.; Yaghi, O.M. *Science* **2007**, *316*, 268-272.
2. Côté, A.P.; El-Kaderi, H.M., Furukawa, H.; Hunt, J.R.; Yaghi, O.M. *J. Am. Chem. Soc.* **2007**, *129*, 12914-12915.

Publications and patents acknowledging the grant or contract

1. “Synthesis and Characterization of Porous Benzimidazole-Linked Polymers and Their Performance in Small Gas Storage and Selective Uptake,” Rabbani, M.G.; El-Kaderi, H. M. *Chem. Mater.* **2012** (DOI: <http://dx.doi.org/10.1021/cm300407h>).
2. “High CO₂ uptake and selectivity by triptycene-derived benzimidazole-linked polymers,” Rabbani, M.G.; Reich, T.E.; Jackson, K.T.; Kassab, R.M.; El-Kaderi, H. M. *Chem. Commun.* **2012**, *48*, 1411.

3. "Impact of tailored chemical and textural properties on the performance of nanoporous borazine-linked polymers in small gas uptake and selective binding," Reich, T.E.; El-Kaderi, H.M. *J. Nanopart. Re.* **2012** (submitted)
4. "Synthesis of highly porous borazine-linked polymers and their application to H₂, CO₂, and CH₄ storage," Jackson, K.T.; Rabbani, M.G.; Reich, T.E.; El-Kaderi, H.M. *Polym. Chem.* **2011**, *2*, 2775.
5. "Design, Synthesis, and Characterization of Halogen-Decorated Porous Borazine-Linked Polymers and their performance in hydrogen storage application," Reich, T.E, Jackson, K.T.; Li, S.; Jena. P.; El-Kaderi, H.M. *J. Mater. Chem.*, **2011**, *21*, 10629.
6. "Template-Free Synthesis of a Highly Porous Benzimidazole-Linked Polymer for CO₂ Capture and H₂ Storage," Rabbani, M.G.; El-Kaderi, H.M. *Chem. Mater.*, **2011**, *23*, 1650.
7. "Nickel-Catalyzed Synthesis of Soft Nanoporous Organic Frameworks and Their Potential Use in Gas Storage Applications" Kassab, R.M.; Jackson, K.T.; El-Kaderi, O.M.; El-Kaderi, H.M. *Res. Chem. Intermed.* **2011**, *7*, 747.
8. "Synthesis and Characterization of Highly Porous Borazine-Linked Polymers via Dehydrogenation/Dehydrocoupling of Borane-Amine Adducts and their Applications to Gas Storage," Jackson, K.T. Virginia Commonwealth University, Richmond, VA, December **2011**, Ph.D. thesis.
9. "Designed Synthesis and Characterization of Halogenated Borazine-Linked Polymers and their Application to Gas Storage," Reich, T.E. Virginia Commonwealth University, Richmond, VA, December **2011**. Ph.D. thesis.
10. "Highly Porous Benzimidazole-Linked Polymers for Use in Gas storage and Separation Applications," Rabbani, M.G.; El-Kaderi, H.M. Provisional Patent (Issued on Jan 14th, **2011** by Virginia Commonwealth University).

IV.H.4 Atomistic Mechanisms of Metal-Assisted Hydrogen Storage in Nanostructured Carbons

Nidia C. Gallego (Primary Contact),
Cristian I. Contescu, James R. Morris,
Stephen J. Pennycook, Takeshi Egami
Oak Ridge National Laboratory (ORNL)
Materials Science and Technology Division
Oak Ridge, TN 37831-6087
Phone: (865) 241-9459
Email: gallegonc@ornl.gov

DOE Program Manager: Dr. Jane Zhu
Phone: (301) 903-3811
Email: Jane.Zhu@science.doe.gov

Objectives

- Establish scientific bases for designing the “building blocks” of nanoporous carbons and metal-doped carbons that enable synergistic interactions leading to enhanced hydrogen uptake at near-ambient temperatures.
- Identify local atomic structures in disordered carbons and metal-doped carbons, explore the nature of hydrogen binding in such sites and the role of metal particles, and understand the mechanism of hydrogen adsorption and the properties of adsorbed hydrogen.
- Characterize and model medium-range order of carbon in the partially amorphous-partially graphitic structure of nanoporous carbons.
- Understand the mechanism of molecular activation of H₂ by metal catalyst particles and of the transfer of hydrogen across the metal-carbon interface.
- Characterize the energetics and dynamics of hydrogen species confined in pure- and metal-doped carbons.

Abstract

Hydrogen storage by adsorption on materials with high surface area and a wide range of molecular-scale porosity comes close to the some of the DOE target levels, but only at cryogenic temperatures. None of porous adsorbents known today allow reaching satisfactory uptake levels at near ambient temperatures. When adsorption is based on van der Waals interactions only, enhancing the uptake levels for hydrogen at temperatures far from its critical point (33 K) is a great challenge. Key to enhanced adsorption is local structure of the adsorbent. The simple picture is that H₂ molecules need sufficient neighbors to bind them, while also allowing sufficient pore volume for storage and for cyclic charging/

discharging. This picture neglects, however, the details of local atomic arrangements. Optimizing local structures for adsorption is difficult even for ordered carbon materials (nanotube bundles, carbon nanofibers etc), and is a more daunting task for disordered carbon materials.

It was empirically observed that adding metal promoters to porous carbon materials could enhance hydrogen uptake at near-room temperatures beyond the limited capacity of pure carbon supports. At least three mechanisms have been proposed to explain this behavior: (1) multiple covalent binding of H₂ molecules to isolated transition metal atoms stabilized by carbon (the Kubas mechanism); (2) dissociation of H₂ on metal catalyst particles and migration of H atoms on the carbon surface to new storage sites (the spillover mechanism); and (3) enhanced physisorption through polarization of H₂ molecules by discrete charges on metal ions (Li⁺, K⁺ etc). The Kubas mechanism is based on theoretical predictions but has not been verified experimentally because of difficulty of stabilizing single atoms of transition metals on carbons. The spillover mechanism is well established in heterogeneous catalysis, and has been often used to explain enhanced H₂ uptake on metal-doped nanoporous carbons compared with the uptake on metal-free carbons. However, spillover remains elusive and escapes direct proof with analytical methods. The third mechanism received only marginal attention.

In this project we focused on developing realistic models of nanoporous carbons that allow understanding the role of local atomic structure, composition, and order on the mechanisms of H₂ adsorption. The task is challenging because of the lack of clear atomic picture of nanoporous carbon materials. We have addressed this challenge using existing expertise at ORNL, including strengths in materials synthesis, advanced X-ray and neutron scattering techniques for characterization of disordered materials, electron microscopy with sub-Ångstrom resolution, and atomistic modeling of structure, dynamics, and adsorption in carbon nanostructures. Our specific goals include (1) identification of atomic structures in disordered carbons and metal-doped carbons; (2) exploration of the nature of hydrogen binding on such sites and of the role of metal particles and modifiers; (3) identification of H₂ adsorption mechanisms and characterization of energetics and dynamics of adsorbed hydrogen.

Progress Report

We made the experimental observation that H₂ uptake by Pd-modified activated carbon fibers (Pd-ACF) is about 30% higher than on metal-free activated carbon fibers (ACF) even

after subtracting the amount of H_2 needed to convert all Pd to Pd hydride (Figure 1c). Using in situ X-ray diffraction and inelastic neutron spectroscopy, we obtained evidence of two elementary steps of the spillover process: (i) destabilization of saturated Pd-hydride by the carbon support and easier release of H atoms to carbon [1]; and (ii) formation of new C-H bonds by chemisorption of mobile H to unsaturated C atoms [2].

Furthermore, examination of Pd-ACF by high resolution scanning transmission electron microscopy (HR-STEM) confirmed that single Pd atoms are stable in the nanoporous carbon matrix (Figure 1a,b) and their concentration was determined [3]. This fact led us to examine whether the Kubas mechanism is energetically favorable for Pd atoms on graphenes (Figure 1d). First principles calculations showed that, in the pressure and temperature conditions of H_2 adsorption measurements, each Pd atom can bind up to four H_2 molecules. Comparison with the experimental uptake (Figure 1c) showed that, although enhanced Kubas binding is a viable route, it cannot substitute for the spillover mechanism. It follows that the enhanced uptake at 300 K is the result of physisorption on carbon support, Kubas-type binding of H_2 to single Pd atoms, conversion of Pd nanoparticles to Pd hydride, and spillover by release of H from destabilized $PdH_{0.6}$ followed by H diffusion on carbon surface and remote storage by either chemisorption or physisorption [4]. Of all these mechanisms, physisorption to

the nanoporous carbon support remains the most important (and limiting) mechanism; spillover may play a lesser role than what has been previously thought.

Doping nanoporous carbon with alkali metals can also promote enhanced H_2 uptake through the mechanism of polarization-induced physisorption. We found out that a high surface area wood-derived ultramicroporous carbon (UMC) has very high H_2 uptake (0.8 wt% at 300 K and 20 bar) compared with ACF and other activated carbons at the same conditions. This atypical behavior cannot be attributed solely to its particular pore structure. However, this carbon has traces of K and Na (residual from chemical activation) which may explain both the large uptake and the hysteretic behavior based on the concept of polarization-induced physisorption of H_2 on alkali ion sites [5].

To confirm this mechanism, we doped a polymer-derived carbon (PFAC) with 0.2 wt% K and observed enhanced uptake at 298 K compared with the pure carbon. Adding K to PFAC also increased the isosteric heat of adsorption by 35% at low coverage (from 16 to 23 kJ/mol at 0.125 mmol H_2 /g) and by 8% at high coverage (from 14 to 15 kJ/mol at 0.5 mmol H_2 /g). These values of heat of adsorption measured at near room temperatures are in the range considered optimal for practical adsorptive hydrogen storage. However, the amounts adsorbed are still very low, limited by the small volume of narrow nanopores available for adsorption.

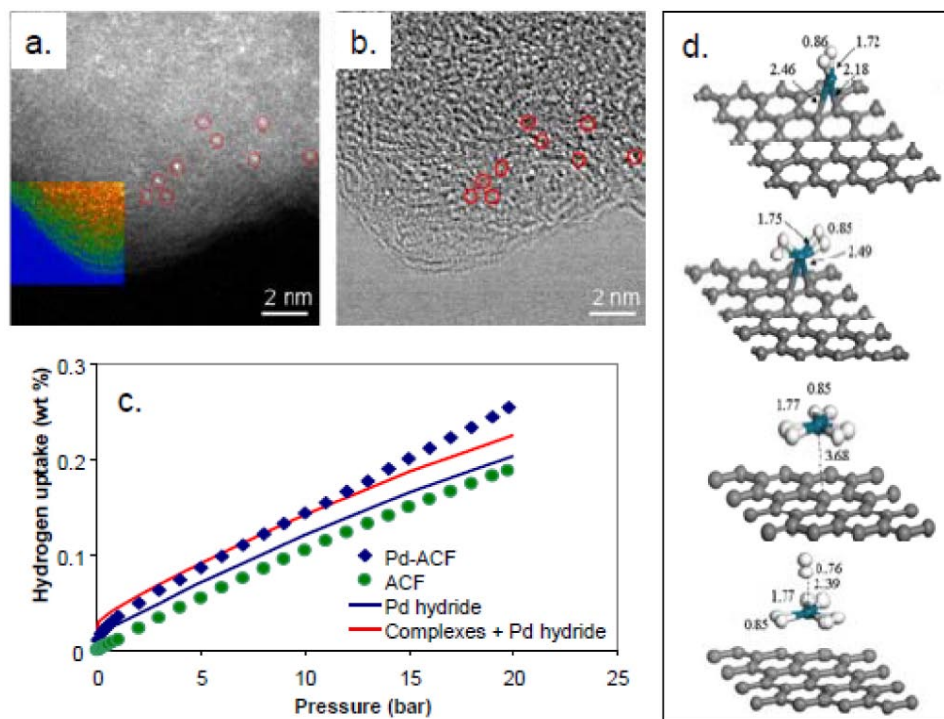


FIGURE 1. (a) Single Pd atoms and (b) carbon structures identified by HR-STEM; (c) experimental H_2 adsorption on ACF and Pd-ACF compared with behavior expected if all Pd is converted to Pd hydride and based on Kubas mechanism hypothesis; and (d) predicted Kubas structures for multiple bonding of H_2 to single Pd atoms.

Adsorption on UMC, although higher than on ACF and PFAC, is remarkably slower, and desorption shows a strong hysteresis. We explored the effect of physically mixing UMC with Pd black (10 wt%) on the amounts adsorbed and the adsorption kinetics. Figure 2a,b shows that the amounts adsorbed on Pd-UMC mixtures (after subtracting the amounts needed to convert Pd into Pd hydride) did not increase significantly at the temperatures studied. However, physically mixing Pd black with UMC has a significantly accelerating effect on the rates of adsorption (Figure 2c) but did not affect the rates of desorption [6]. This behavior indicates again that Pd initiates H spillover to carbon particles with which it is in close contact, and therefore adsorption is faster. However, spillover cannot further increase the (already large) storage capacity of UMC, which is limited by its pore structure, surface area, and concentration of residual alkali ions. Desorption from Pd-UMC mixture is not faster because

hydrogen molecules adsorbed on UMC are not in direct contact with the Pd powder (which is a separate phase) and therefore the inverse spillover process cannot be initiated.

The data presented above suggest that narrow nanopores in carbons are strong adsorption sites for H₂. Because of the large heat of adsorption (15-20 kJ/mol) these sites should afford high densities of adsorbed hydrogen. Knowledge of the density of hydrogen adsorbed in pores is critical for designing better adsorption systems. However this information has not been reported before, because of numerous experimental complications. We used in situ high-pressure small angle neutron scattering (SANS) experiments at room temperature and an improved high-pressure cell with modified geometry and obtained for the first time direct estimates of the density of H₂ trapped in carbon nanopores (Figure 3a) [7]. The data show clearly that, *at room temperature* and for any given external pressure, the density of confined H₂ is much higher

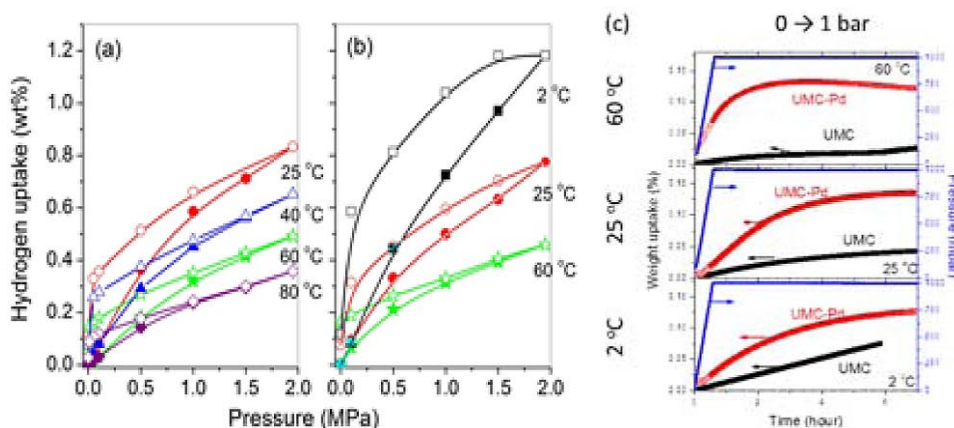


FIGURE 2. Effect of temperature on hydrogen adsorption-desorption isotherms on UMC (a) and Pd-UMC physical mixture with 10 wt% Pd (b) and on the rates of adsorption (c) at equal pressure increments. The additional amount of hydrogen needed to convert all Pd into saturated Pd hydride in physical mixtures has been subtracted.

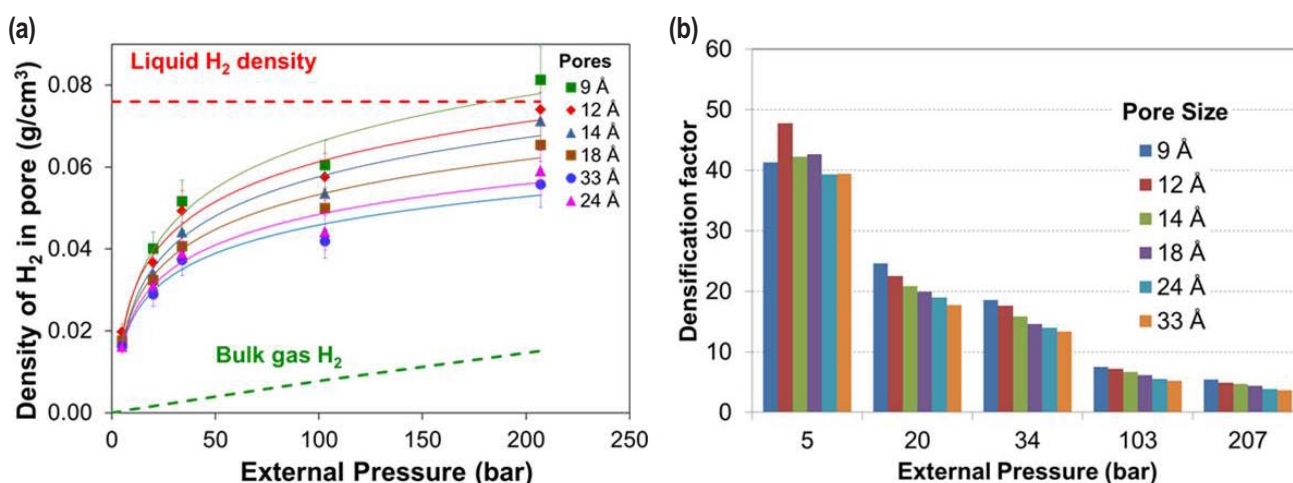


FIGURE 3. (a) Estimated densities of H₂ trapped in PFAC nanopores as a function of pore size and external H₂ pressure, and (b) the densification factors showing the large increase in density at low pressures and the gradually weaker effect at higher pressures.

than that of the bulk H_2 gas and approaches the density of liquid H_2 at the highest pressure (207 bar) in the narrowest pores (9 Å) accessed in our experiment. At low pressures, H_2 confined in the narrowest pores experiences densities some 40-50 times larger than the bulk gas; the densification factor decreases with the increase of pressure (Figure 3b). Furthermore, using the equation of state for H_2 , we calculated the corresponding pressure experienced by the confined fluid. The fluid confined in pores has much larger pressures than the external bulk gas. The adsorption energy calculated from the simple relationship between internal and external pressure, $P_{int} = P_{ext} \exp(-E_{ads}/RT)$, is about -10 kJ/mol in the 9 Å pores saturated at 5 bar external pressure, and probably larger at lower saturation levels. With increase in external pressure, as more H_2 is compressed in pores, adsorption becomes weaker, especially in large pores.

Small angle neutron and X-ray scattering patterns show that the porous carbons investigated have a dominant two-dimensional (2-D) character consistent with sp^2 hybridization on C atoms, but with limited (ACF, PFAC) or extremely weak (UMC) interlayer coherent stacking of graphene sheets perpendicular to their main orientation. More information on the local atomic arrangement was obtained by X-ray and neutron atomic pair distribution function (PDF) methods [8]. They allow for studying both local and medium range structures of disordered materials in real space (Figure 4). It was found that in-plane coherence is limited to about 13-14 Å (8-9 hexagon units) and that graphene sheets are likely to have local folds and cusps that limit the extent of flat areas. Depending on the particular carbon's origin (ACF, UMC) the micro-texture defined by graphene stacking in the perpendicular direction is different, which results in different adsorption characteristics.

Theoretical modeling of hydrogen adsorption in nanoporous carbons provided similar results. We used the method of tight binding molecular dynamics (TBMD)

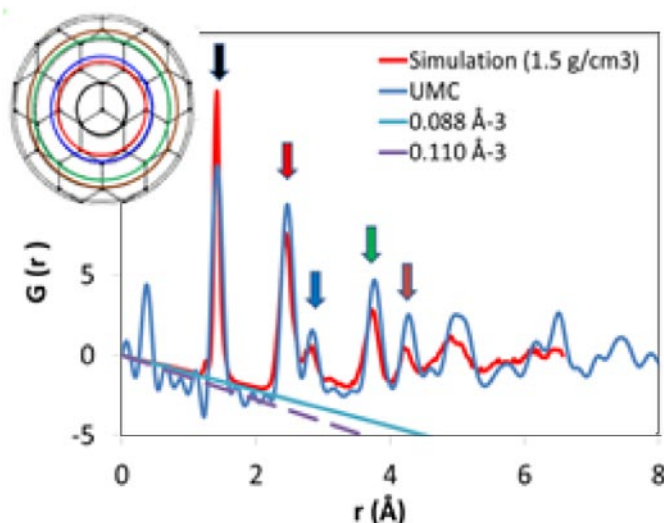


FIGURE 4. Experimental PDF for UMC versus 1.5 g/cm³ simulated structure. The straight line slope scales with atomic density of scattering atoms: 0.088 Å⁻³ (UMC; blue) and 0.11 Å⁻³ (graphite, purple). Insert: origin of PDF peaks graphite structure.

to generate carbon structures with various densities and calculated the amounts of adsorbed H_2 as a function of pressure [9,10]. With increasing carbon density, the structures develop domains of hexagonal symmetry of carbon atoms, interrupted by 5- and 7-atom rings. Hydrogen adsorption calculations identified pockets in the porous structure with favorable adsorption energy (Figure 5a). The heat of adsorption increases with carbon density, but the available volume drops, so that carbon density is an important structural factor that controls practical uptake capacity. These calculations demonstrate that small pores in denser carbon materials adsorb very strongly, with isosteric heat of adsorption at zero coverage limit ranging from 12 to 22 kJ/mol. This range overlaps the range considered suitable

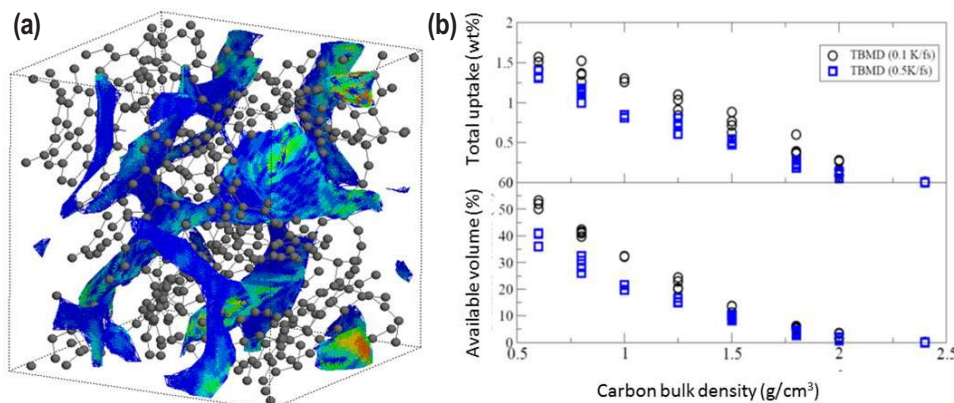


FIGURE 5. (a) Simulated carbon structure (1.25 g/cm³) showing pockets for H_2 adsorption with favorable adsorption energy (< -10 kJ/mol), with blue indicating weaker, and red stronger adsorption sites; (b) Correlation between total H_2 uptake (298 K at 50 bar), available volume, and bulk carbon density. Data show reproducibility between structures obtained in repeated simulations with two quenching rates (black - 0.1 K/fs; blue - 0.5 K/fs).

for hydrogen storage and delivery (15-40 kJ/mol), but the scarcity of these pores that leads to poor uptake. In contrast, although carbons simulated at low densities demonstrate lower heat of adsorption (due to weaker interactions in larger pores), the available pore volume is larger, and the overall effect is an increase in uptake. Figure 5b shows the competition between optimizing the available adsorption volume and optimizing the adsorption potential in narrow pores for high gas uptake.

We emphasize that the results obtained for simulated carbon structures is consistent with the information from in situ SANS experiments which were presented above. The density of adsorbed H₂ in the metal-free carbon is much higher than the bulk-phase density and approaches the density of liquid H₂ even though the ambient temperature is close to 300 K. SANS experiments showed that the density of adsorbed H₂ was larger in narrower pores, in perfect agreement with the image obtained from simulations (e.g. the bottom-right corner of the image in Figure 5a shows high adsorption energy in a narrow pore). Moreover, while the heat of adsorption calculated from SANS experiments (5-10 kJ/mol) corresponds to H₂ adsorbed in high concentrations from compressed gas (5-200 bar), the heat of adsorption obtained from simulations (12-22 kJ/mol) corresponds to strong H₂ – carbon interactions in the limit of zero coverage. The two ranges complement each other, as it is well known that the heat of adsorption decreases with the increase of adsorbed molecules concentration.

Future Directions

Our goal in the few next years is to better understand the relationship between local atomic structure and large scale architecture of nanoporous carbons, and their impact on the nature of interactions with the surrounding gaseous environment, including the phase behavior and properties of molecular species confined in carbon's nanopores.

We will use advanced characterization tools available on the ORNL campus and in other DOE facilities, such as neutron and X-ray scattering, diffraction, spectroscopy; atomic resolution electron microscopy; and powerful computing resources to advance our understanding of fundamental interactions at the atomic and molecular scale between carbon atoms, electronic spins, topological defects, and defectively stacked graphenes; of the interaction with the gaseous environment surrounding nanoporous carbons, of which a large fraction of constituent carbon atoms is exposed at interfaces in porosity. The results acquired during the course of this research will materialize in fundamental understanding of how to design and construct better materials for energy storage and conversion, and the development of new techniques, methods, and procedures that will be transferable to other porous materials of

comparable properties or to other applications operating on corresponding principles.

References

1. VV Bhat, CI Contescu, and NC Gallego, *Nanotechnology*, 20 (2009) 204011 [10 pages].
2. CI Contescu, CM Brown, Y Liu, VV Bhat, and NC Gallego, *J Phys Chem C*, 113 (2009) 5886-5890.
3. K. van Benthem, C.S. Bonifacio, C.I. Contescu, N.C. Gallego, S.J. Pennycook, *Carbon* 49 (2011): 4059-4073.
4. C I Contescu, K van Benthem, S Li, CS Bonifacio, SJ Pennycook, P Jena, NC Gallego, *Carbon* 49 (2011): 4050-4058.
5. VV Bhat, CI Contescu, NC Gallego, FS Baker: *Carbon*, 48 (2010) 1331-1340
6. VV Bhat, CI Contescu, NC Gallego, *Carbon*, 48 (2010): 2361-2364.
7. NC Gallego, L He, D Saha, CI Contescu, YB Melnichenko, *JACS* 133, 13794-13797 (2011).
8. W Dmowski, CI Contescu, A Llobet, NC Gallego, T Egami, *J Phys Chem C* 116 (2012) 2946-2951.
9. L Peng, JR Morris: *J Phys Chem C*, 114 (2010) 15522-15529.
10. LJ Peng, JR Morris, *Carbon* 50 (2012) 1394-1406.

Publication list (selected) acknowledging the DOE grant or contract

1. D Saha, CI Contescu, NC Gallego, "Tetrahydrofuran-induced K and Li doping onto poly(furfuryl alcohol)-derived activated carbon (PFAC): Influence on microstructure and H₂ sorption properties", *Langmuir* (published on line 2012); dx.doi.org/10.1021/la3002948.
2. W Dmowski, CI Contescu, A Llobet, NC Gallego, T Egami, "Local atomic density of microporous carbons", *J Phys Chem C* 116 (2012) 2946-2951.
3. CI Contescu, D Saha, NC Gallego, E Mamontov, AI Kolesnikov, VV Bhat, "Restricted dynamics of molecular hydrogen confined in activated carbon nanopores", *Carbon* 50 (2012) 1071-1082.
4. LJ Peng, JR Morris, "Structure and hydrogen adsorption properties of low density nanoporous carbons from simulations", *Carbon* 50 (2012) 1394-1406.
5. NC Gallego, L He, D Saha, CI Contescu, YB Melnichenko, "Hydrogen confinement in carbon nanopores: Extreme densification at ambient temperature", *JACS* 133, (2011) 13794-13797.
6. J Jagiello, J Kevin, JP Olivier, AR Lupini, CI Contescu, "Using a finite slit pore model for NLDFT analysis of carbon pore structure", *Adsorption Sci Technol*, 29 (2011) 769-780.
7. K. van Benthem, C.S. Bonifacio, C.I. Contescu, N.C. Gallego, S.J. Pennycook, "STEM imaging of single Pd atoms in activated carbon fibers considered for hydrogen storage", *Carbon* 49 (2011) 4059-4073.
8. CI Contescu, K van Benthem, S Li, CS Bonifacio, SJ Pennycook, P Jena, NC Gallego, "Single Pd atoms in activated carbon fiber and their contribution to hydrogen storage", *Carbon* 49 (2011) 4050-4058.

9. FW Averill, JR Morris. “Graphene/graphene interface energy and implications for defects”, *Phys Rev B* 84, (2011) 035411 [7 pages].
10. L Peng, JR Morris: “Hydrogen adsorption calculations in expanded graphite and amorphous carbons”, *Mater Res Symp Proc* Vol. 1216 © 2010 Materials Research Society, 1216-W01-08.
11. L Peng, JR Morris: “Prediction of hydrogen adsorption properties in expanded graphite model and in nanoporous carbon”, *J Phys Chem C*, 114 (2010) 15522-15529.
12. VV Bhat, CI Contescu, NC Gallego: “Kinetic effect of Pd addition on the hydrogen uptake of chemically-activated ultramicroporous carbon”, *Carbon*, 48 (2010) 2361-2364.
13. VV Bhat, CI Contescu, NC Gallego, FS Baker: “Atypical hydrogen uptake on chemically-activated, ultramicroporous carbon”, *Carbon*, 48 (2010) 1331-1340.
14. CI Contescu, CM Brown, Y Liu, VV Bhat, and NC Gallego, “Detection of hydrogen spillover in palladium-modified activated carbon fibers during hydrogen adsorption”, *J Phys Chem C*, 113 (2009) 5886-5890.
15. VV Bhat, CI Contescu, and NC Gallego, “The role of destabilization of palladium hydride on the hydrogen uptake of Pd-containing activated carbons”, *Nanotechnology*, 20 (2009) 204011 [10 pages].
16. FW Averill, JR Morris, VR Cooper, “Calculated properties of hydrogenated single layers of BN, BC₂N, and graphene: Graphane and its BN-containing analogues”, *Phys Rev B* 80 (2009), 195411 [8 pages].

IV.H.5 Elucidation of Hydride Interaction Mechanisms with Carbon Nanostructures and the Formation of Novel Nanocomposites

Ragaiy Zidan (Primary Contact),
Joseph A. Teprovich Jr., Douglas A Knight,
Robert Lascola, Lucile C. Teague
Savannah River National Laboratory
Building 999-2W, Aiken, SC 29808
Phone: (803) 646-8876
Email: ragaiy.zidan@srl.doe.gov

Collaborators:

- Prof. Puru Jena – Department of Physics – Virginia Commonwealth University
- Prof. Mark Conradi – Department of Physics – Washington University of St. Louis
- Prof. Sonjong Hwang – Chemistry and Chemical Engineering Division – California Institute of Technology

Objectives

- Continue to support the office of Basic Energy Sciences mission through the development of a basic understanding of the formation and the physiochemical properties of carbon nanostructures, formed by the interaction of carbon nanomaterials with hydrides and/or hydrogen gas.
- Obtain knowledge that allows us to control material properties at the electronic, molecular, and atomic level which will serve as the foundation of new energy technologies that can support other aspects of DOE missions.
- Utilize a simple solvent-assisted method, developed during previous work, to intercalate carbon nanomaterials with metal using metal hydrides to form a desired metallo-fullerides (M_x-C_{60}) with specific stoichiometries.
- Based on preliminary results from previous work, these novel materials can have unique hydrogen storage, electronic properties and high ionic mobility.
- The proposed work is aimed at examining how the presence or absence of hydrogen in these materials can affect its physical and chemical properties which will allow us to “fine-tuning” the properties of the material.

Technical Barriers

- The ability to disperse metal atoms uniformly in a carbon nanostructure is necessary in order to reliably synthesize composites with uniform properties on small and large scales.

- Little experimental information about the mechanism of hydrogen interaction with un/doped carbon nanostructures is available.
- Initial studies on the hydrogenation of carbon nanostructures have shown that the physical and chemical properties of the material can be significantly altered and controlled.
- Advances in atomic scale imaging (i.e. scanning tunneling microscopy [STM], transmission electron microscopy [TEM]) have shown that morphological changes at the atomic scale can affect the properties of the bulk material.

Abstract

This program will continue to support the office of Basic Energy Sciences mission. A simple method, relying on metastasis reaction between hydrides and carbon nanostructures to precisely achieve desired stoichiometries will be employed to form novel metal-fulleride nanocomposites with unprecedented properties. Our preliminary results indicated that these metal-fulleride nanocomposites interact with hydrogen reversibly at temperatures well below the precursor components used in forming the nanocomposites. The preliminary data showed a tremendous *enhancement of mobility* of species such as hydrogen and alkali metals in a solid electrolyte made of $LiBH_4$ and C_{60} [1]. The hydrogen binding energy in the hydride allows the exchange of elemental metal to form homogenous structures. Commonly used material characterizations techniques (e.g. TEM, SEM/energy dispersive X-ray, X-ray diffraction [XRD], neutron scattering, raman spectroscopy [NMR]) will provide information on morphology, composition, crystal structure, vibration spectra, ionic mobility and nature of bonding. Thermodynamic measurements will be used to obtain basic understanding of the formation of these nanocomposites and their interaction with hydrogen. Computer controlled thermogravimetric, volumetric analyzers, and DSC will also be used in this study.

Our study is aimed at attempting to predict and control material properties at the electronic, atomic, and molecular level that can be the foundation of new energy technologies and can support other aspects of DOE missions.

The proposed research is performed as ONE TASK organized around the following four integrated activities:

- Activity 1: Synthesis and Characterization of M_x -Fullerene Materials

- Activity 2: Investigation of Ionic Mobility Enhancement and Alteration of Electronic Properties
- Activity 3: Investigation of the Properties of Carbon Nanostructures Modified With Non Metallic Elements
- Activity 4: Atomistic Modeling of Metal Doped Carbon Nanostructures

Progress Report

This research work is aimed at obtaining a fundamental understanding of the nanoscale level of hydrogen sorption behavior of metal-doped carbon nanostructures. It is well established that the doping or intercalation of carbon nanomaterials with metal atoms has a significant impact on the chemical and physical properties of the resulting material. Furthermore, the physical and chemical properties of these materials are extremely sensitive to the identity of the added metal(s) as well as its molar ratio with the carbon nanomaterial. The experimental work is closely linked to relevant modeling studies of these materials [2]. Advances in hydrogen storage technology based on pure carbon nanostructures and particularly metal-doped carbon nanostructures require the development of a basic understanding of their physicochemical properties and the manner in which these properties influence the hydrogen bonding. Our effort is focused on the understanding of the hydrogen interaction mechanisms such as physisorption, weak covalent bonding, and chemisorption in these nanocarbon systems.

Our recent efforts have focused on the synthesis and characterization of a lithium doped C_{60} material that can reversibly store and release hydrogen via a chemisorption mechanism. Through a systematic series of experiments it was determined that a material synthesized with a 6:1 ($Li:C_{60}$) mole ratio can absorb the highest weight percent of hydrogen (~5 wt %). Spectroscopic characterization of the material revealed that it resembles a hydrogenated fullerene (i.e. *fullerane*), however, the material can store and release hydrogen at much milder conditions than an undoped C_{60} sample.

NMR characterization demonstrated that hydrogen atoms are associated with both Li and C and indicates that the presence of Li in the material dictates the hydrogen absorption sites. Interestingly, there is a reversible phase change observed for C_{60} doped with lithium in the XRD measurements. When the material is hydrogenated at 350°C and 105 bar H_2 , a phase change from face-centered cubic (*fcc*) to body-centered cubic (*bcc*) is observed in the material. Upon dehydrogenation the material returns to its original *fcc* structure. The 7Li MAS NMR also suggests that upon rehydrogenation a Li atom may actually go inside the fullerene cage as indicated by the upfield resonance (~10 ppm).

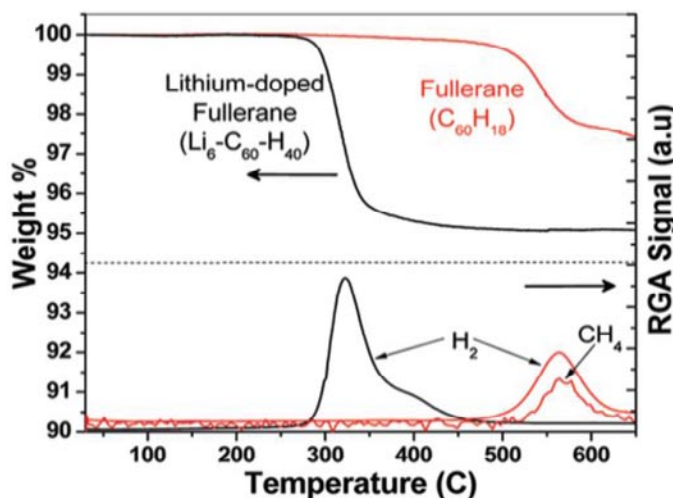


FIGURE 1. Thermogravimetric analysis (TGA)- residual gas analysis (RGA) comparison of the fourth desorption of the $LiH:C_{60}$ (6:1) sample (black) and hydrofullerene (red). The materials were hydrogenated at 350°C under 105 bar H_2 for 11 h. The colors of the RGA signals correspond to the TGA signal.

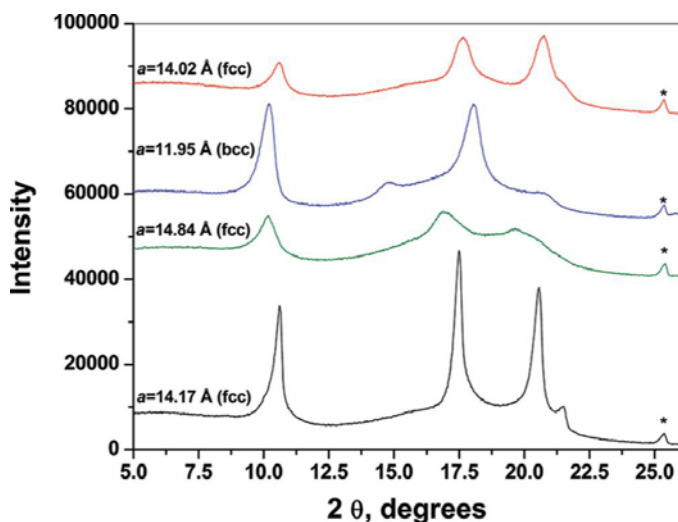


FIGURE 2. XRD stack plot of $LiH:C_{60}$ (6:1) during the hydrogen desorption/absorption experiments. Black, as prepared; green, after third rehydrogenation (250°C, 105 bar H_2); blue, after third rehydrogenation (350°C, 105 bar H_2); and red, after third dehydrogenation. The (*) is a peak from the Al_2O_3 internal standard.

We have also demonstrated that the intercalation of C_{60} with sodium (via NaH) results in almost identical hydrogen storage behavior, via a similar mechanism. The material was subject to 10 desorption/absorption cycles and demonstrated a reversible capacity of ~2.5 wt% H_2 through the reversible formation of a sodium doped fullerene.

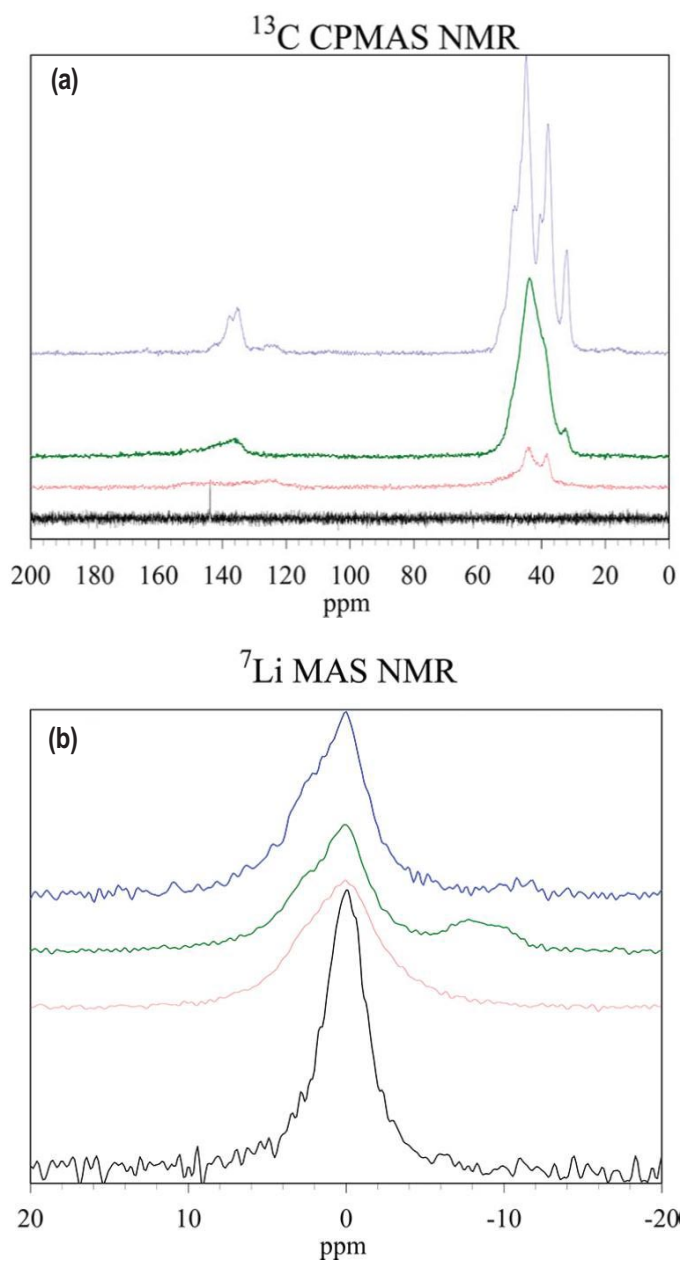


FIGURE 3. All of the samples are of the LiH:C60 (6:1) material: black, as prepared; red, third dehydrogenation; green, third rehydrogenation (250°C, 105 bar H₂), and blue, third rehydrogenation (350°C, 105 bar H₂). (a) ^{13}C MAS NMR; (b) ^7Li MAS NMR. Samples were spun at 15 kHz under dry N₂ gas.

Future Directions

Our current interests include atomic scale imaging utilizing the scanning probe microscopy facility at the Center for Nanoscale Materials to get atomic scale imaging of the material at various states of hydrogenation. Utilizing the facility's ultra-high vacuum atomic force microscopy/ scanning tunneling microscopy, we will gain a fundamental understanding of the physical and chemical properties of carbon nanostructures or composites. We have been allotted two weeks of instrument time to perform our experiments in Fiscal Year 2012. We are also collaborating with Prof. Rosario Cantelli of Sapienza University of Rome to perform anelastic spectroscopy of Li and Na intercalated C₆₀ materials at different states of hydrogenation. This technique can be used to quantitatively determine the dynamics and the diffusion parameters of mobile species in solids and the occurrence of phase transitions, including chemical reactions. We are currently preparing samples for neutron diffraction experiments. This will allow us to determine the structure of the metal intercalated C₆₀ as well as the preferential binding sites for hydrogen in the material.

References

1. D.T. Shane, R. Corey, L. Rayhel, M. Wellons, J.A. Teprovich Jr., R. Zidan, S. Hwang, R. Bowman, Jr., M.S. Conradi. *J. Phys. Chem. C.*, 2010, *114*, 19862-79866.
2. P.A. Berseth, A.G. Harter, R. Zidan, A. Blomqvist, C.M. Araujo, R.H. Scheicher, R. Ahuja, P. Jena, *Nano Letters*, **2009**, *9*, 1501-1505.

Publications (including patents) acknowledging the grant or contract

1. J.A. Teprovich Jr., D. Knight, M.S. Wellons, R. Zidan, *J. Alloys Compd.* **2011**, *509*, S562-S566.
2. A.C., Stowe, J.A. Teprovich Jr., D.A. Knight, M.S. Wellons, R. Zidan, *J. SC Acad. Sci.* **2011**, *9*, 13-19.
3. J.A. Teprovich Jr., M. Wellons, R. Lascola, S. Hwang, P. Ward, R. Compton, R. Zidan. *Nano Letters*, **2012**, *12*, 582-589.

Patents

1. R. Zidan, M.S. Wellons High Capacity Hydrogen Storage Nanocomposite Materials patent application filed
2. R. Zidan, J.A. Teprovich, H. Colon-Mercado, Novel Nano-Composite Electrodes for Hybrid Lithium-Ion Battery patent application filed

IV.H.6 Synthetic Design of New Metal-Organic Framework Materials for Hydrogen Storage

Pingyun Feng (Primary Contact), Qipu Lin,
Xiang Zhao

Department of Chemistry
University of California
Riverside, CA 92521
Phone: (951) 827-2042
Email: pingyun.feng@ucr.edu

DOE Program Officer: Dr. Michael Sennett
Phone: (301) 903-6051
Email: Michael.Sennett@science.doe.gov

Objectives

- Design and synthesize new metal-organic framework materials using lightweight chemical elements to help improve gravimetric hydrogen storage capacity.
- Develop new synthetic strategies to generate novel active binding sites on metal ions and ligands to enhance solid-gas interactions for increased uptake near ambient conditions.
- Develop synthetic methods to create porous frameworks with novel architectural features such as partitioned pore space for the optimum size match with hydrogen molecule.

Technical Barriers

- Lithium ion usually has a low coordination number of 4 and the generation of open metal sites in the absence of cluster or chain formation would reduce its connectivity and may also destabilize the framework.
- Lithium ion has strong solvation energy in many polar solvents. The identification of best solvents that promote crystallization and generation of reversible solvent binding sites is challenging.
- To achieve pore space partition often requires the co-assembly of multiple components of inorganic building blocks, which are formed in situ and difficult to control.

Abstract

Crystalline porous materials such as zeolites have played an important role in energy-related applications due to the unique coupling between their geometrical features and chemical functionalities. The overall objective of this project is to develop synthetic strategies to synthesize new

porous materials with new geometrical features and chemical functionalities useful for hydrogen storage applications.

The project places a strong emphasis on the use of lightweight elements (lithium in particular) as the structural building block. Lithium is the lightest metallic element and also possesses desirable binding affinity for dihydrogen molecule if active binding sites can be created. Compared with other metallic ions used for the construction of porous materials, lithium is unique in its synthetic and structural chemistry, because of its small ionic radius, low oxidation state, and high solvation enthalpy. Therefore, innovative synthetic methods need to be developed to realize lithium based porous materials. In this work, synthetic strategies are being developed that aim to match the unique characteristics of lithium with proper charge and coordination geometry of organic ligands. One method seeks to create zeolite-type porous materials by using charge-complementary polyhedral nodes (e.g., through the integration between Li^+ and a higher valent element such as Mg^{2+} and B^{3+}). Another method uses lithium ions as the sole polyhedral node, but integrates charge-complementary ligands to create porous zeolite-like frameworks. Other strategies being studied for enhancing hydrogen storage capacity include a comparative study of the related lightweight ion Mg^{2+} , the creation of high-density binding sites on ligands, and partition of pore-space for better size match with hydrogen molecules.

Progress Report

A highly stable porous material constructed from lithium aryloxide clusters.

In order to further enhance the adsorption property, an emergent and promising strategy is to introduce lightweight elements into the framework, which may lead to an increase in the gravimetric uptake capacity. A new porous material based on Li_4O_4 cubane cluster has been realized. While $\text{Li}_4(\text{OPh})_4$ type clusters linked by neutral ligands are well-known in the literature, none is porous, mainly because phenol-type ligands used for the formation of lithium clusters also block the pore space. Our success was through the use of a very unique ditopic ligand 4-pyridinol (also called 4-hydroxypyridine). Because 4-pyridinol serves dual roles (i.e., cluster formation and intercluster crosslinking), this strategy eliminates the pore-blocking effect of the aryloxide ligand, leading to the accessible porosity. The synthesized material exhibits a zeolite topology and possesses large pore channels (Figure 1). Considering that it is based on low-valent lithium framework, this material has an unbelievably high

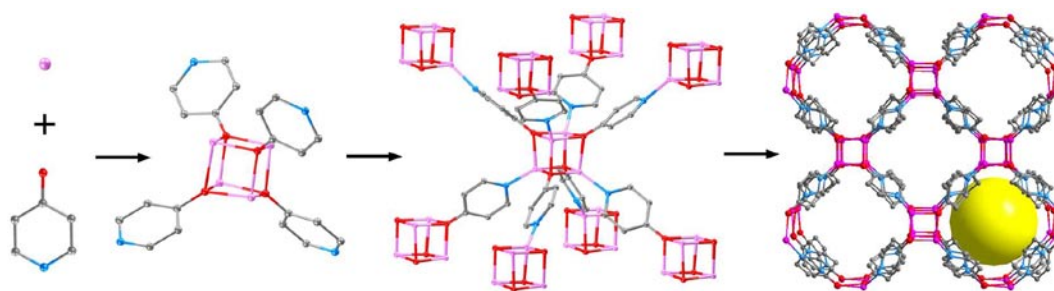


FIGURE 1. Illustration of the self-assembly process from molecular species Li^+ and 4-pyridinol to Li_4O_4 cubane clusters, and finally to three-dimensional (3-D) framework. (purple: Li; red: O; blue: N; grey: C)

thermal stability up to at least 500°C . Its Brunauer-Emmett-Teller and Langmuir surface areas reach $440.3\text{ m}^2/\text{g}$ and $632.5\text{ m}^2/\text{g}$, respectively and its hydrogen storage capacity is $1.4\text{ wt}\% \text{ H}_2$ at 77 K-1 atm . While these numbers are modest compared to the best metal-organic framework materials (MOFs) based on some other metal ions, they are nevertheless the highest among lithium-based MOFs, demonstrating the significant potential of this system [1].

Lithium zeolitic imidazolate frameworks (Li-ZIF) constructed with charge-complementary ligands

A versatile synthetic method capable of generating a large family of Li-based porous materials has been developed. This method is based on the use of mixed charge-complementary ligands (mono-negative L^- and neutral L^0 , L = ligand) specifically chosen to mimic SiO_2 composition and to create $\text{Li}^+\text{L}^-\text{L}^0$ -type lithium-based zeolitic imidazolate frameworks. We have so far synthesized four types of 3-D framework materials with the general SiO_2 -type framework composition of LiL^0L^- .

A porous tetragonal magnesium-carboxylate framework with nanotubular channels

Because highly negative tetraanionic ligands can increase the metal-to-ligand ratio (for the simple reason of charge balance), which has the potential to increase the density of active metal sites and gas uptake capacity as shown by MOF-74 [2], the use of tetraanionic ligands should have a great potential for developing high-capacity porous materials. In this work, we sought to mimic the tetraanionic ligand used in MOF-74 ($\text{Mg}_2(\text{dobdc})$, $\text{H}_4\text{dobdc} = 2,5\text{-dihydroxyterephthalic acid}$) by investigating the reaction of Mg^{2+} with a tetracarboxylate (biphenyl-3,3',5,5'-tetracarboxylic acid or H_4bptc) (Figure 2) and were able to synthesize a new Mg-MOF (denoted CPF-1) from a solvent mixture of *N-ethylformamide* (NEF) and water.

CPF-1 is built from 4_1 -helical inorganic chains (space group: $I4_122$), connected to each other with a tetracarboxylate to form one-dimensional (1-D) cylindrical nanotubular channels with tetragonal symmetry, in contrast with the 1-D

hexagonal channels in MOF-74 (Figure 2). We were able to achieve a higher density of solvent sites on Mg^{2+} sites with each Mg^{2+} bonded to two solvent molecules. However, solvent sites on two adjacent Mg^{2+} sites are oriented toward each other, which leads to the bridging mode for the coordinated solvent molecules. This apparently complicates the sample activation due to the more difficult removal of coordinated solvent molecules. The present measurement data show that its storage capacity ($1.3\text{ wt}\% \text{ H}_2$ at 77 K-1 atm , $84\text{ cm}^3/\text{g}$ of CO_2 at 273 K-1 atm) is lower than that of MOF-74-Mg, and is the second highest among known Mg-MOFs [2,3], demonstrating the potential of the synthesis strategy for further advancing the hydrogen uptake capacity.

Single-walled metal-organic channels with high density of open nitrogen-donor sites and gas uptake

In addition to uncoordinated metal sites, unused functional groups of the organic ligands can play a key role in gas adsorption of MOF materials. Thus, having available the largest number of exposed functional sites (on either metals or non-metals) would likely contribute to the enhanced gas sorption properties.

Of particular interest are functional groups such as aromatic $-\text{N}(\text{H})-$ donors found in metal azolate frameworks. Despite the fact that the use of triazoles and tetrazoles has led to some MOF compounds, it is still an ongoing challenge to create porous frameworks in which the largest possible number of N-donor sites are left uncoordinated to metals (called open donor sites, in analogy with open metal sites).

For the purpose of increasing the percentage of open donor sites, individual triazole or tetrazole ligands are less effective, because at least two N-donor sites will be needed for the framework connectivity, and the maximum percentage of open donor sites would be only 33% for a triazole and 50% for a tetrazole framework. Hence, we are especially interested in ligands containing multiple triazole and tetrazole groups (i.e., polytriazole or polytetrazole such as 1,3,5-tris(2*H*-tetrazol-5-yl)benzene or H_3BTT in short), and such a ligand can achieve a high connectivity if they only use one N-donor site (per triazole or tetrazole group) for

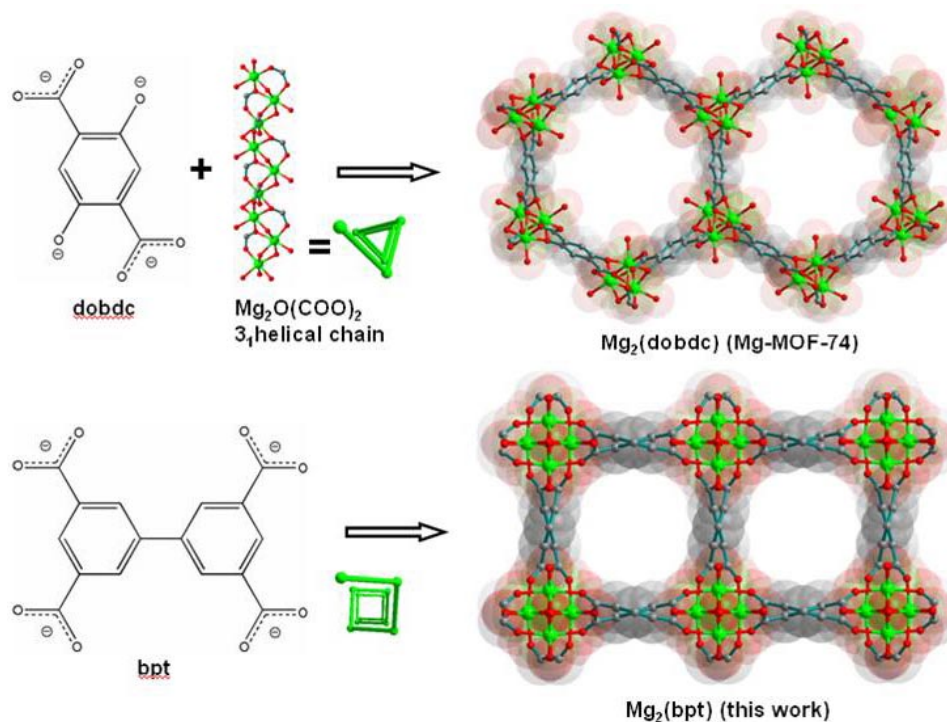


FIGURE 2. A comparison between two MOFs based on tetraanionic ligands. (top) $\text{Mg}_2(\text{dobdc})$ (Mg-MOF-74) and (bottom) CPF-1.

bonding with metals. The highest percentage of open donor sites would be 67% for a triazole and 75% for a tetrazole, assuming each ligand uses just one N-donor site for the framework formation. However, such a high percentage of open donor sites have not yet been achieved.

In this work, by using a urea derivative (1,3-dimethylpropyleneurea) as the co-solvent in *N,N*-dimethylacetamide (DMA), an interesting porous framework (denoted CPF-6) with 1-D square single-atom-walled channel system has been prepared (Figure 3). This material has a highly porous 3-D framework with a large percentage (67%) of N-donor sites unused for bonding with metals. Even though it does not have any open metal sites, it exhibits high gas storage capacity (ca. 1.9 wt% H_2 at 77 K-1 atm, 98 cm^3/g CO_2 at 273 K-1 atm). The high percentage of open N-donor sites, coupled with the low-framework density resulting from single-walled channels is believed to contribute to the high gas uptake capacity.

Future Directions

To develop high-capacity hydrogen storage materials, we will need to further develop synthetic methods to synthesize porous materials that combine multiple features including lightweight building block, active binding sites, and high stability. A systematic study of solvent systems that can bind reversibly to metal ions such as Li^+ without adversely

affecting the crystallization process is important. Also important is to create a stable support system for Li^+ with active binding sites. The application of the pore partition strategy to the lightweight building units would make it possible to integrate advanced architectural features with desirable chemical compositions and functionality.

References

1. Abrahams, B.F.; Grannas, M.J.; Hudson, T.A.; Robson, R. "A Simple Lithium(I) Salt with a Microporous Structure and Its Gas Sorption Properties." *Angew. Chem. Int. Ed.* 2010, 49, 1.
2. Caskey, S.R.; Wong-Foy, A.G.; Matzger, A.J. "Dramatic Tuning of Carbon Dioxide Uptake via Metal Substitution in a Coordination Polymer with Cylindrical Pores." *J. Am. Chem. Soc.* 2008, 130, 10870-10871
3. Dinca, M.; Long, J.R. "Strong H_2 Binding and Selective Gas Adsorption with the Microporous Coordination Solid $\text{Mg}_3(\text{O}2\text{C}-\text{C}10\text{H}_6-\text{CO}_2)_3$ ". *J. Am. Chem. Soc.* 2005, 127, 9376.

Publications (selected) acknowledging the DOE

1. Zheng, S.; Wu, T.; Zhang, J.; Chow, M.; Nieto, R.; Feng, P.; Bu, X. "Porous Metal Carboxylate Boron Imidazolate Frameworks", *Angew. Chem. Int. Ed.* 2010, 49, 5362-5366.
2. Zheng, S.; Li, Y.; Wu, T.; Nieto, R.; Feng, P.; Bu, X. "Porous Lithium Imidazolate Frameworks Constructed with Charge-Complementary Ligands", *Chem. Eur. J.* 2010, 16, 13035-13040

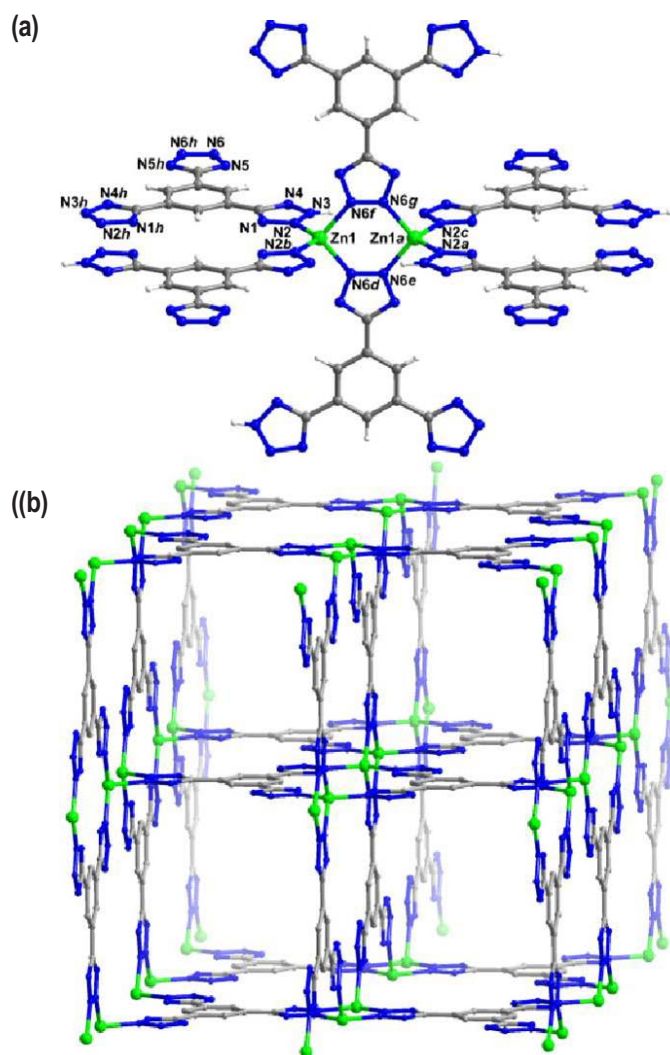


FIGURE 3. (a) View of the zinc dimer bridged by two tetrazolate groups (in bidentate fashion) and completed by four other tetrazolate groups (in unidentate fashion), (b) the 3-D extended network showing large channels.

3. Zhang, J.; Bu, J.; Chen, S.; Wu, T.; Zheng, S.; Chen, Y.; Nieto, R., Feng, P.; Bu, X. "Urothermal Synthesis of Crystalline Porous Materials", *Angew. Chem. Int. Ed.* **2010**, 49, 8876-8879.

4. Zheng, S.; Bu, J.T.; Li, Y.; Wu, T.; Zuo, F.; Feng, P.; Bu, X. "Pore Space Partition and Charge Separation in Cage-within-Cage Indium-Organic Frameworks with High CO₂ Uptake", *J. Am. Chem. Soc.* **2010**, 132, 17062-17064.

5. Zheng, S.; Zuo, F.; Wu, T.; Irfanoglu, B.; Chou, C.; Nieto, R.A.; Feng, P.; Bu, X. "Cooperative Assembly of 3-Ring-Based Zeolite-Type Metal-Organic Frameworks and Johnson-Type Dodecahedra", *Angew. Chem. Int. Ed.* **2011**, 50, 1849-1852.

6. Zhao, X.; Wu, T.; Zheng, S-T.; Wang, L.; Bu, X., Feng, P. "Zeolitic Porous Lithium Organic Framework Constructed from Cubane Clusters", *Chem. Commun.* **2011**, 47, 5536-5538.

7. Zheng, S.; Wu, T.; Irfanoglu, B.; Zuo, F.; Feng, P.; Bu, X. "Multi-Component Self-Assembly of A Nested Co₂₄@Co₄₈ Metal Organic Polyhedral Framework", *Angew. Chem. Int. Ed.* **2011**, 50, 8034-8037.

8. Zhao, X.; Wu, T.; Bu, X.; Feng, P. "A Mixed Ligand Route for Construction of Tetrahedrally Coordinated Porous Lithium Frameworks", *Dalton Trans.* **2011**, 40, 8072-8074.

9. Zheng, S.; Bu, J.J.; Wu, T.; Chou, C.; Feng, P.; Bu, X. "Porous Indium-Organic Frameworks and Systematization of Structural Building Blocks", *Angew. Chem. Int. Ed.* **2011**, 50, 8858-8862.

10. Jiang, G.; Wu, T.; Zheng, S-T.; Zhao, X.; Lin, Q.; Bu, X.; Feng, P. "A nine-connected mixed-ligand nickel-organic framework and its gas sorption properties", *Crystal Growth & Design* **2011**, 11, 3713-3716.

11. Lin, Q.; Wu, T.; Zheng, S.; Bu, X.; Feng, P. "A Chiral Tetragonal Magnesium-Carboxylate Framework with Nanotubular Channels", *Chem. Commun.* **2011**, 47, 11852-11854.

12. Zhao, X.; Wu, T.; Bu, X.; Feng, P. "Lithium Cubane Clusters as Tetrahedral, Square Planar, and Linear Nodes for Supramolecular Assemblies", *Dalton Trans.* **2012**, 41, 3902-3905.

13. Lin, Q.; Wu, T.; Zheng, S-T.; Bu, X.; Feng, P. "Single-Walled Polytetrazolate Metal-Organic Channels with High Density of Open Nitrogen-Donor Sites and Gas Uptake", *J. Am. Chem. Soc.* **2012**, 134, 784-787.

14. Zheng, S.; Wu, T.; Zuo, F.; Chou, C-T; Feng, P.; Bu, X. "Mimicking Zeolite to Its Core: Porous Sodalite Cages as Hanger for Pendent Trimeric M₃(OH) Clusters (M = Mg, Mn, Co, Ni, Cd)", *J. Am. Chem. Soc.* **2012**, 134, 1934-1937.

15. Zhai, Q.; Lin, Q.; Wu, T.; Zheng, S-T; Bu, X.; Feng, P. "Induction of Trimeric [Mg₃(OH)(COO)₆] in a Porous Framework by a Desymmetrized Tritopic Ligand", *Dalton Trans.* **2012**, 41, 2866-2868.

16. Zheng, S.; Wu, T.; Chou, C-T; Fuhr, A.; Feng, P.; Bu, X. "Development of Composite Inorganic Building Blocks for Metal-Organic Frameworks", *J. Am. Chem. Soc.* **2012**, 134, 4517-4520.

IV.H.7 New Pathways and Metrics for Enhanced, Reversible Hydrogen Storage in Boron-Doped Carbon Nanospaces

Peter Pfeifer, Ph.D (Primary Contact),
Carlos Wexler, Ph., M. Frederick Hawthorne, Ph.D.,
Mark W. Lee, Ph.D., Satish S. Jalistegi, Ph.D.

The Curators of the University of Missouri
Office of Sponsored Program Administration
University of Missouri
310 Jesse Hall
Columbia, MO 65211
Phone: (573) 882-2335
Email: PfeiferP@missouri.edu

DOE Program Officer: Bonnie Gersten
Phone: (301) 903-0002
Email: Bonnie.Gersten@science.doe.gov

Subcontractors:

- Ping Yu, Ph.D., University of Missouri
- Haskell Taub, Ph.D., University of Missouri
- Anupam Sing, Ph.D., University of Missouri
- Jan Ilavsky, Ph.D., Argonne National Laboratory
- Bogdan Kuchta, Ph.D., Univ. Aix-Marseille, France
- Lucyna Firlej, Ph.D., Univ. Montpellier 2, France
- Raina Olsen, Ph.D., Oak Ridge National Laboratory

Objectives

- An integrated synthesis/characterization/computational effort to develop novel materials: monolithic boron-doped carbon made from polymeric precursors, crisscrossed by networks of nanopores.
- To develop a fundamental understanding of the mechanisms by which boron, through its electron-deficient electronic structure and long-range effect on distant carbon atoms, combined with appropriate pore geometries, creates deep potential wells which can hold films of physisorbed molecular hydrogen at densities much higher than undoped carbon.
- Such high-density films and their understanding at the molecular, statistical mechanical, and macroscopic thermodynamic level are critical for the rational design of high-performance materials with controlled reversible storage characteristics at low pressure and room temperature.

Abstract, Progress Report and Future Directions

Carbon-based materials have recently shown promise for hydrogen storage at moderate pressures. Our group

has focused on the development of materials derived from synthetic precursors in order to optimize, measure and control pore geometries at the sub-nm scale; and to enhance the adsorption of H₂ (particularly at low pressure, high temperature) by increasing the depth of the H₂-carbon potential by chemically functionalizing the adsorbent's surface. Our group has spearheaded the effort to improve these materials and in previous grant periods have reported: (i) record-breaking H₂ storage in very high-surface area activated carbons; (ii) *ab initio* theoretical predictions that boron doping of carbon at 5-10% B:C concentration raises the H₂ binding energy from ~5 kJ/mol to 10-14 kJ/mol; (iii) Grand Canonical Monte Carlo (GCMC) simulations that successfully reproduce the experimental adsorption of H₂ in heterogeneous pore structures, and that demonstrated enhanced H₂ storage in B-doped carbon; (iv) demonstrated experimentally the existence of B-C bonds in B-doped carbon; (v) demonstrated experimentally that in B-doped carbons the isosteric heat of adsorption nearly doubles from 5-7 kJ/mol to 9-12 kJ/mol, this is accompanied by an enhancement of the H₂ sorption at cryogenic and room temperature; (vi) demonstrated that activated carbon from synthetic precursors have a nearly monodisperse network of narrow pores; (vii) developed pore characterization methods based on small-angle X-ray scattering (SAXS); and (viii) developed the theoretical background to utilize incoherent inelastic neutron scattering (IINS) off adsorbed H₂ to characterize the interaction potentials as seen by molecular H₂ in sub-nm pores. In what follows we present the most relevant results attained in the current reporting period.

a) Observation of anomalous adsorption of H₂ in synthetic carbon: significantly higher excess adsorptions normalized per Brunauer-Emmett-Teller (BET) surface area at both cryogenic and room temperature (e.g., at room temperature synthetic sample HS:0B has more than doubles the performance of our best lignocellulose carbon, sample 3K). This indicates higher binding energies (consistent with a narrower pores). In addition, synthetic carbons show anomalous excess adsorption isotherms, with the maximum of the excess adsorption occurring at higher than normal pressures. See Figure 1.

b) Determination of adsorbed film characteristics: we succeeded in measuring important adsorbed film characteristics (excess and absolute adsorption, isosteric heat of adsorption, film thickness and volume, saturation density) by using an integrated combination of experimental methods (N₂ characterization, He "picnometry", H₂ adsorption isotherms at cryogenic and room temperature up to 200 bar, SAXS), data processing (extrapolation to calculate saturated

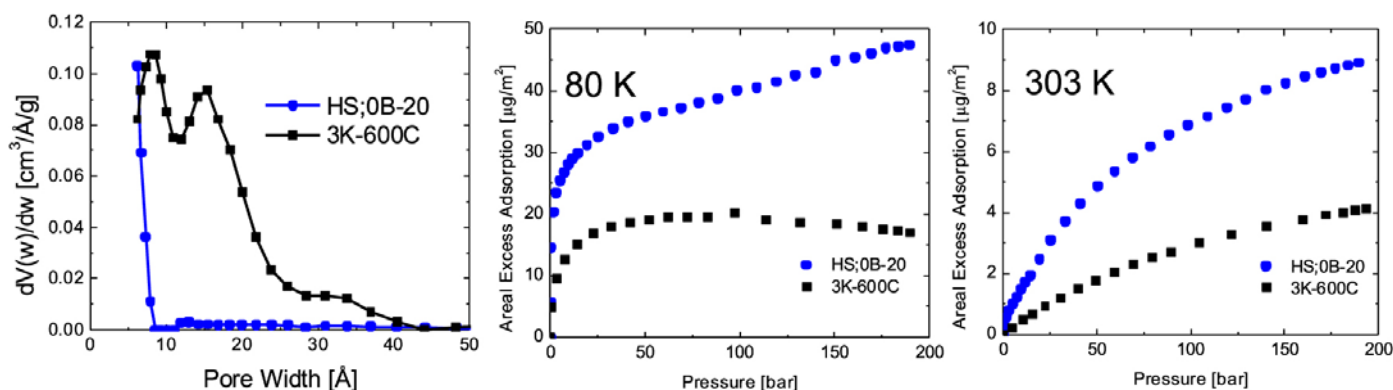


FIGURE 1. Pore size distribution (left), and H₂ excess adsorption per unit area at 80 K (center) and 303 K (right) for synthetic carbon HS;0B ($\Sigma_{\text{BET}} = 900 \text{ m}^2/\text{g}$) and lignocellulose carbon 3K ($\Sigma_{\text{BET}} = 2,600 \text{ m}^2/\text{g}$).

film density), theoretical modeling (isosteric heats from Clausius-Clapeyron eq., absolute adsorption, film thickness from monotonicity of isosteric heat), and computational efforts (GCMC). Film densities are significantly in excess of the density of liquid H₂. See Figure 2.

c) Design and construction of sub- and super-critical H₂ Sievert instrument: we have built a Sievert sorption instrument to be used for sub-critical and super-critical H₂ adsorption (temperature range: 4-300+ K). This will permit determination of BET surface areas, and pore and skeletal volumes using H₂ rather than N₂; and permit a more precise determination of adsorbed film densities, especially in synthetic precursors that have maximum of the excess adsorption at anomalously high pressures.

d) High resolution transmission electron microscopy: Aberration corrected scanning transmission electron microscopy performed at the Oak Ridge National Laboratory (ORNL) Center for Nanophase Materials Sciences show detailed atomic structure of synthetic carbon: these have

regions of graphitic and amorphous carbon consistent with $700 \text{ m}^2/\text{g}$ BET surface areas. See Figure 2.

e) IINS: we conducted experiments at ORNL over an unprecedented broad range of energy and momentum transfer. We developed a novel theoretical methodology that permitted the classification of the H₂ excitations into localized and mobile states. This provides a measure of the planarity of the adsorption surface on the >1 nm scale, and gives insight on the quantum states of adsorbed H₂.

f) Pore conformability: we have performed a mechanical analysis of the stability of pores in carbon, this indicates that pores with lateral (in plane) dimensions larger than 2-4 nm would naturally collapse and close, consistent with our SAXS experiments. More interestingly, we observe that pores that are above this “critical length” may be partially opened by H₂ at $P > 20\text{-}30$ bar. Interestingly, this model results in excess adsorption isotherms that do not show a clear maximum at low and moderate pressures.

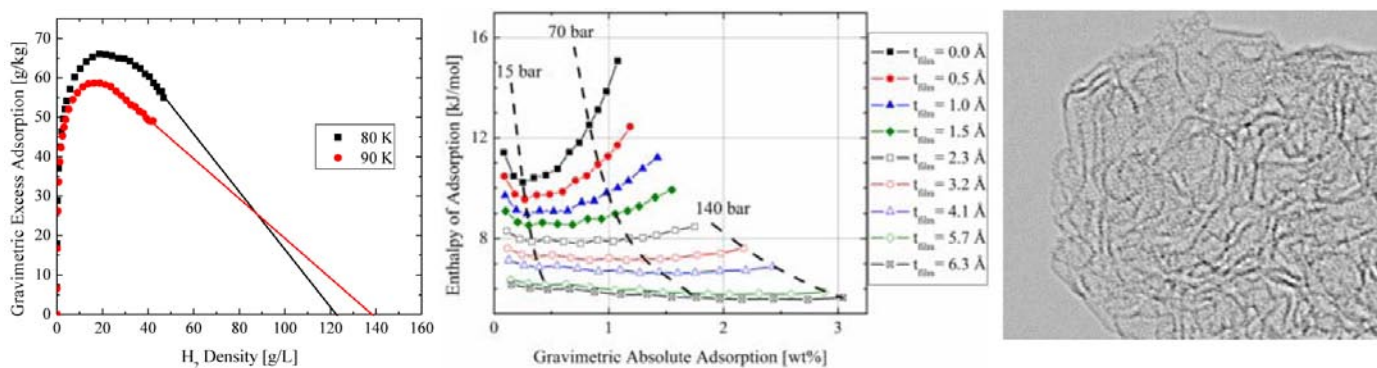


FIGURE 2. Determination of saturated film densities from extrapolation of the excess adsorption (left). Determination of film thicknesses (and volume) from the thermodynamic requirement that the isosteric heat of adsorption is a monotonically decreasing function of coverage (center). At the lower bound for film thickness, $t_{\text{film}} = 4.1 \text{ Å}$, these results are consistent with the adsorption values (Figure 1). High resolution transmission electron microscopy of synthetic carbon HS;0B (right).

Publications (including patents) acknowledging the grant or contract

Publications Acknowledging DOE-BES Support during FY 2012

1. *The Quantum Excitation Spectrum of Adsorbed Hydrogen*, R. Olsen, M. Beckner, P. Pfeifer, C. Wexler, and H. Taub, Phys. Rev. Lett. (under review).
2. *Functional B-C Bonds in Nanoporous Boron Carbide and Boron Doped Carbon Materials*, J. Romanos, D. Stalla, M. Beckner, A. Tekeci, G. Suppes, S. Jalisatgi, M. Lee, F. Hawthorne, D. Robertson, L. Firlej, B. Kuchta, C. Wexler, P. Yu, P. Pfeifer, Carbon (under review).
3. *Elastic Pore Structure of Activated Carbon*, M.J. Connolly and C. Wexler, Phys. Rev. B (in preparation).
4. *Infrared Study of Boron-Carbon Chemical Bonds in Boron Doped Activated Carbon*, J. Romanos, M. Beckner, D. Stalla, A. Tekeci, G. Suppes, S. Jalisatgi, M. Lee, F. Hawthorne, J.D. Robertson, L. Firlej, B. Kuchta, C. Wexler, P. Yu, and P. Pfeifer (in preparation).
5. *Hydrogen Adsorption Studies of Engineered and Chemically Modified Activated Carbons*, M. Beckner, Ph.D. Thesis (University of Missouri, 2012, director: P. Pfeifer).
6. *Nanospace Engineering of Porous Carbon For Gas Storage*, J. Romanos, Ph.D. Thesis (University of Missouri, 2012, director: P. Pfeifer).
7. *Numerical Analysis of Hydrogen Storage in Carbon Nanopores*, C. Wexler, R. Olsen, P. Pfeifer, B. Kuchta, L. Firlej, Sz. Roszak, in *Condensed Matter Theories* Vol. 25, Eds. E.V. Ludeña, R.F. Bishop, & P. Iza (Nova Science Publishers, 2011).
8. Sub-nanometer characterization of activated carbon by inelastic neutron scattering, R. Olsen, L. Firlej, B. Kuchta, H. Taub, P. Pfeifer, and C. Wexler, Carbon **49**, 1663-1671 (2011).

Presentations Acknowledging DOE-BES Support during FY 2012

1. *Conformability of Pores in Activated Carbon*, M. Connolly and C. Wexler, 1st Iberoamerican Symposium on Adsorption, Recife, Brasil, May, 2012.
2. *Elastic Pore Structure of Activated Carbon*, M. Connolly and C. Wexler, The 6th International Workshop on Characterization of Porous Materials—from Angstroms to Millimeters (CPM-6), Delray Beach, FL, April, 2012.

3. *Recoiling and Bound Quantum Excitations of Adsorbed Hydrogen As An Assessment of Planarity*, R. Olsen, H. Taub and C. Wexler, The 6th International Workshop on Characterization of Porous Materials—from Angstroms to Millimeters (CPM-6), Delray Beach, FL, April, 2012.
4. *Reversible Storage of Hydrogen and Natural Gas in Nanospace-Engineered Activated Carbons*, J. Romanos, M. Beckner, T. Rash, P. Yu, G. Suppes, and P. Pfeifer, *March 2012 Meeting of the American Physical Society (Bull. Am. Phys. Soc. 57, W33.05 (2012))*, Boston, MA, March 2012.
5. *Measured Enthalpies of Adsorption of Boron-Doped Activated Carbons*, M. Beckner, J. Romanos, E. Dohnke, A. Singh, J. Schaeperkoetter, D. Stalla, J. Burress, S. Jalisatgi, G. Suppes, M. F. Hawthorne, P. Yu, C. Wexler, and P. Pfeifer, *March 2012 Meeting of the American Physical Society (Bull. Am. Phys. Soc. 57, W33.07 (2012))*, Boston, MA, March 2012.
6. *Performance of Carbon Hydrogen Storage Materials as a Function of Post-Production Thermal Treatment*, E. Dohnke, J. Romanos, M. Beckner, J. Burress, P. Yu, and P. Pfeifer, *March 2012 Meeting of the American Physical Society (Bull. Am. Phys. Soc. 57, W33.08 (2012))*, Boston, MA, March 2012.
7. *The Stationary States of Adsorbed Hydrogen*, R. Olsen, H. Taub, and C. Wexler, *March 2012 Meeting of the American Physical Society (Bull. Am. Phys. Soc. 57, W33.06 (2012))*, Boston, MA, March 2012.
8. *Measured Enthalpies of Adsorption of Boron-Doped Activated Carbons*, M. Beckner, J. Romanos, E. Dohnke, A. Singh, J. Schaeperkoetter, D. Stalla, J. Burress, S. Jalisatgi, G. Suppes, M.F. Hawthorne, P. Yu, C. Wexler, and P. Pfeifer, *March 2012 Meeting of the American Physical Society (Bull. Am. Phys. Soc. 57, W33.07 (2012))*, Boston, MA, March 2012.
9. *Adsorption-induced Pore Expansion and Contraction in Activated Carbon*, M. Connolly and C. Wexler, *March 2012 Meeting of the American Physical Society (Bull. Am. Phys. Soc. 57, X11.11 (2012))*, Boston, MA, March 2012.
10. *Nanoporous Carbon for Reversible Storage of Hydrogen*, C. Wexler, Low Carbon Earth Summit-2011 (LCES-2011), Dalian, China, October 2011.

IV.H.8 Novel Molecular Materials for Hydrogen Storage Applications

Maddury Somayazulu (Primary Contact),
Timothy Strobel, Robert Potter, Raja Chellappa,
Viktor Struzhkin, Russell J Hemley

Geophysical Laboratory
Carnegie Institution of Washington
5251 Broad Branch Rd NW
Washington, D.C. 20015
Phone: (202) 478-8911
Email: zulu@gl.ciw.edu

DOE Program Manager: Dr. P. Thiyagarajan
Phone: (301) 903-9706
Email: P.Thiyagarajan@science.doe.gov

Objectives

- Discover, identify and characterize novel hydrogen-rich compounds that can be used for hydrogen storage or as agents for rehydrogenation of hydrogen storage materials at high pressures.
- Investigate high pressure routes to rehydrogenating ammonia borane and polymeric complexes of ammonia borane.
- Investigate interaction of hydrogen with metallo-organic polymers at high pressures and high temperatures to identify new *Kubas complexes* capable of high potential for hydrogen retention.

Technical Barriers

- Understanding the structural basis of the high pressure interaction of molecular hydrogen requires using a combination of Raman and infrared spectroscopies and preferably neutron diffraction of small sub-mm³ samples in high pressure diamond anvil cells.
- Developing new strategies to extract information about reaction kinetics and thermodynamics of chemical reactivities at elevated pressure-temperature conditions needs development of appropriate spectroscopy protocols as well as diamond cells that allow introduction of reactants, extraction of products and capability to initiate/arrest the chemical reaction.
- Developing strategies to metastably recover materials synthesized at high pressure – high temperature conditions.

Abstract

The technology of using hydrogen as an environmentally clean and efficient fuel is an active research area worldwide [1-3]. The key to emergence of a viable global hydrogen economy is the availability of light weight transport and safe storage of hydrogen as a fuel. Major factors that dictate this include high volumetric and gravimetric density of the storage media, optimal thermodynamics and kinetics of hydrogenation and re-hydrogenation, ease of handling, and small environmental footprint. The effort to develop new materials and investigate their thermo-physical tunability is outpaced by the growing world energy consumption [4]. There are currently four leading methods to store hydrogen: physical means, sorbents, metal hydrides (classical and complex), and so-called chemical hydrides. At the heart of the issue is the fact that hydrogen is a gas at standard pressure and temperature and therefore low volumetric density.

On other hand, hydrogen molecules can bind to the surface of any material either through weak dispersive interactions (physisorption) or through stronger chemical bonding (chemisorption). Storage via physisorption in metal-organic or covalent-organic frameworks and activated carbons is a field that has received a lot of experimental and theoretical attention [5-9]. While both these routes to hydrogen storage show a high degree of reversibility (rehydrogenation), they suffer from poor retention and low gravimetric capacity limiting their storage capability to low temperatures (typically below 77 K) and off-board applications.

Hydrogen clathrates and molecular (van der Waal) compounds of H₂ and other simple molecules such as CH₄, NH₃, CO₂, N₂ have been known to form under high pressures and some of them can be recovered at ambient pressure and low temperatures [10-11]. The hydrogen storage potential of such clathrates and molecular compounds has received much attention not only because of their superior gravimetric capacity (the compound CH₄(H₂)₄ has 33.4 wt% of stored hydrogen and is found stable at ambient pressure and 77 K), but potentially small environmental footprint and high degree of reversibility [12].

Progress Report

We have discovered a new structure type in the H₂-H₂O system at low pressure-temperature conditions. The structure of the new phase is consistent with a water framework similar to α -quartz; the structure could also be related to the tetragonal clathrate phase reported previously for nitrogen and argon guests.

Raman spectroscopy and synchrotron X-ray diffraction are used to examine the high-pressure behavior of tetramethylammonium borohydride (TMAB) to 40 GPa at room temperature. The measurements reveal weak pressure-induced structural transitions around 5 and 20 GPa. Rietveld analysis and Le Bail fits of the powder diffraction data based on known structures of tetramethylammonium salts indicate that the transitions are mediated by orientational ordering of the BH_4^- tetrahedra followed by tilting of the $(\text{CH}_3)_4\text{N}^+$ groups.

Hydrogen sulfide (H_2S) and hydrogen (H_2) crystallize into a ‘guest-host’ structure at 3.5 GPa and, at the initial formation pressure, the rotationally disordered component molecules exhibit weak van der Waals type interactions. With increasing pressure, hydrogen bonding develops and strengthens between neighboring H_2S molecules, reflected in a pronounced drop in S-H vibrational stretching frequency and also observed in first-principles calculations. At 17 GPa, an ordering process occurs where H_2S molecules orient themselves to maximize hydrogen bonding and H_2 molecules simultaneously occupy a chemically distinct lattice site. Intermolecular forces in the $\text{H}_2\text{S}+\text{H}_2$ system may be tuned with pressure from the weak hydrogen-bonding limit to the ordered hydrogen-bonding regime, resulting in a novel clathrate structure stabilized by cooperative interactions.

Previous efforts had focused on the $\text{NH}_3\text{BH}_3/\text{H}_2$ system and its polymeric analogs which were found to form van der Waals compounds at elevated pressures. In order to address questions regarding rehydrogenation of spent BN materials, compounds of the series $\text{NR}_x\text{H}_{(3-x)}\text{BH}_3$ were analyzed using gas phase G3MP2 calculations previously shown to reproduce BN and BH bond forming reactions to within 1.0 and 1.8 kcal/mol, respectively. Me_2NHBH_3 was down selected from the series due to the inability of the compound to lose multiple equivalents of H_2 and the modest enthalpy associated with the hydrogen release reaction as compared to other compounds of the series. $\text{Me}_2\text{NHBH}_3/\text{H}_2$ mixtures were found to hydrogenate ethylene and carbon dioxide at room temperature and pressures above 0.5 GPa. Control cells with no Me_2NHBH_3 showed no reaction after several weeks. The reaction with CO_2 was found to consistently produce CH_4 as the only product, but due to the multiple phases present, rates of the reaction have difficult to measure.

As a continuation of our high pressure studies of metal-rich hydrides, we continued to pursue synthesis, characterization and high pressure studies on this unique class of hydrides. The structural behavior of Na_2ReH_9 and K_2ReH_9 at high pressure was studied using in situ Raman spectroscopic and X-ray diffraction studies at high-pressure. The measurements reveal new phase transformation above 9 GPa and 18 GPa for both Na_2ReH_9 and K_2ReH_9 due to compression. The deuterated analogues have been synthesized and characterized. These samples were used to

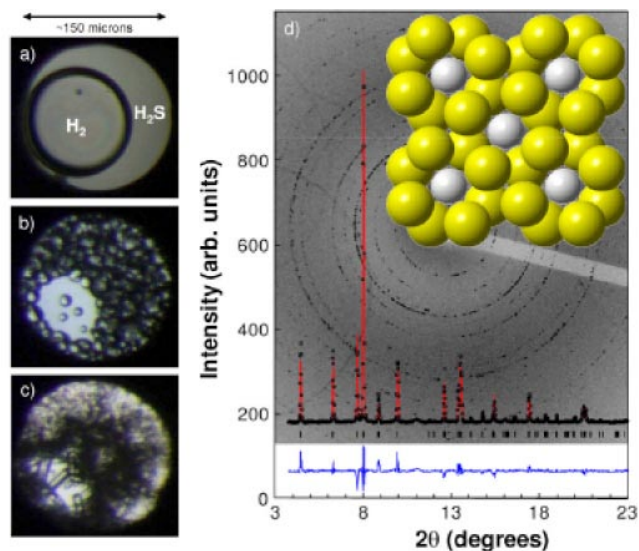


FIGURE 1 (color online). Photomicrographs of $\text{H}_2 + \text{H}_2\text{S}$ mixtures at room temperature: (a) 0.2 GPa: fluid H_2 and liquid H_2S ; (b) 1.0 GPa; fluid H_2 and solid H_2S phase I; (c) 3.5 GPa: fluid H_2 and compound. Dark areas result from light scattering off grain boundaries and dissipated with time. (d) Experimental diffraction pattern ($\lambda = 0.40548 \text{ \AA}$) at 4.5 GPa (points) and Rietveld profile refinement (red line). Difference is shown as lower blue trace, $R_{wp} = 3.52\%$. The background shows the two-dimensional diffraction image, and the crystal structure, normal to the c -axis, is provided as the inset; yellow and white spheres represent disordered H_2S and H_2 molecules, respectively.

obtain in situ diffraction patterns at high pressures using the Paris-Edinburgh cell at SNS.

The solid phase that occurs at 4.2 GPa and 300 K in the Xe- H_2 system has been identified as $\text{Xe}(\text{H}_2)_{24}$. The stoichiometry has been deduced from a determination of the overall xenon stoichiometry based on direct method solution of the crystal structure. The volume of the unit cell and the known molar volume of xenon at this pressure is then used to determine the lower bound on the hydrogen stoichiometry. Refinement of crystal structure indicates higher hydrogen content based on the fact that the xenon site occupancy is lower than unity for one of the three sites. Raman spectroscopy and X-ray diffraction studies show that this phase can be retrieved at 90 K and at atmospheric pressure.

References

1. Graetz, J., *New Approaches to hydrogen storage*. Chem. Soc. Rev., 2009. **38**: p. 73-82.
2. Tromp, T.K., et al., *Potential Environmental Impact of a Hydrogen Economy on the Stratosphere*. Science, 2003. **300**(5626): p. 1740-1742.
3. Dresselhaus, M.S. and I.L. Thomas, *Alternative energy technologies*. Nature, 2001. **414**: p. 332 - 337.

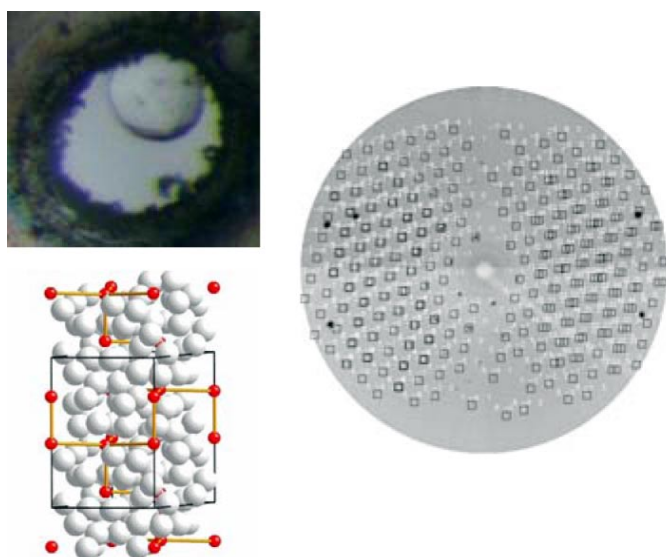


FIGURE 2. Photomicrograph of $\text{Xe}(\text{H}_2)_{24}$ in a diamond cell. The diffraction pattern could be indexed to a hexagonal unit cell and the structure of the xenon sublattice is shown in red. The hydrogen molecules are shown in gray.

4. *Basic Research Needs for Electrical Energy Storage - a report of Basic Energy Sciences Workshop on Electrical Energy Storage*, U.S.D.o. Energy, Editor. 2007.

5. Murray, L.J., M. Dinca, and J.R. Long, *Hydrogen storage in metal-organic frameworks*. Chem. Soc. Rev., 2009. **38**: p. 1294-1314.

6. Rosi, N.L., et al., *Hydrogen Storage in Microporous Metal-Organic Frameworks*. Science, 2003. **300**(5622): p. 1127-1129.

7. Ward, M.D., *MATERIALS SCIENCE: Enhanced: Molecular Fuel Tanks*. Science, 2003. **300**(5622): p. 1104-1105.

8. Yang, Z., Y. Xia, and R. Mokaya, *Enhanced Hydrogen Storage Capacity of High Surface Area Zeolite-like Carbon Materials*. Journal of the American Chemical Society, 2007. **129**(6): p. 1673-1679.

9. Yaghi, O.M., *Organic Molecular Solids: Properties and Applications Edited by William Jones*. CRC Press: Boca Raton, FL. 1998. 441 pp. \$145.00. ISBN 0-8493-9428-7. Journal of the American Chemical Society, 1999. **121**(51): p. 12214-12215.

10. Vos, W.L., et al., *Novel H_2 - H_2O clathrates at high pressures*. Phys. Rev. Lett., 1993. **71**: p. 3150-3153.

11. Somayazulu, M.S., et al., *New high-pressure compounds in methane-hydrogen mixtures*. Science, 1996. **271**: p. 1400-1402.

12. Mao, W.L. and H.K. Mao, *Hydrogen storage in molecular compounds*. Proc. Nat. Acad. Sci., 2004. **101**: p. 708-710.

Publication list (selected) acknowledging the DOE grant or contract

1. "Novel Cooperative interactions and structural ordering in $\text{H}_2\text{S}-\text{H}_2$ " Timothy Strobel, P. Ganesh, Maddury Somayazulu, P.R.C. Kent and Russell J Hemley, Phys. Rev. Lett. **107**, 255503 (2011)
2. "Static Compression of Tetramethylammonium Borohydride" Douglas Allen Dalton, M. Somayazulu, Alexander F. Goncharov, and Russell J. Hemley. JI. Phys. Chem A, **115**, 11033 (2011)
3. "High-pressure study of silane to 150 GPa" Timothy A. Strobel, Alexander F. Goncharov, Christopher T. Seagle, Zhenxian Liu, M. Somayazulu, Viktor V. Struzhkin, and Russell J. Hemley, Phys. Rev **B83**, 144102 (2011).
4. "Phase Behavior of H_2 - H_2O at High Pressures and Low Temperatures" Timothy A. Strobel, Maddury Somayazulu, and Russell J. Hemley, J. Phys. Chem. C, **115**, 4898-4903 (2011).
5. "High-Pressure Hydrogen interactions with polyaminoborane and polyiminoborane" Raja. S. Chellappa, Thomas Autrey, M. Somayazulu, V.V. Struzhki and R.J. Hemley, ChemPhysChem, **11**, 93 (2010)
6. "Vibrational dynamics, intermolecular interactions, and compound formation in GeH_4 - H_2 under pressure" Timothy A Strobel, X-J Chen, M. Somayazulu and R.J. Hemley, J. Chem. Phys., **133**, 164512 (2010)
7. "Pressure-induced bonding and compound formation in xenon-hydrogen solids" M. Somayazulu, P. Dera, A.F. Goncharov, S.A. Gramsch, P. Liermann, W. Yang, Z. Liu, H.K. Mao and R.J. Hemley, Nature Chemistry, **2**, 50 (2009)

IV.H.9 Metastability of Clathrate Hydrates for Energy Storage

Carolyn A. Koh (Primary Contact), Amadeu K. Sum,
R. Gary Grim, Matthew R. Walsh, Prasad B. Kerkar
Center for Hydrate Research
Colorado School of Mines
1600 Illinois Street
Golden, CO 80401
Phone: (303) 273-3237
Email: ckoh@mines.edu

DOE Program Officer: Bonnie Gersten
Phone: (303) 903-0002
Email: Bonnie.Gersten@science.doe.gov

Objectives

The current project aims to probe key questions surrounding the metastability of hydrates relating to synthesis, structure, and composition. The questions on metastability are crucial in all energy applications of clathrate hydrates including energy storage, energy transportation, and energy recovery. Specifically, this project addresses:

1. Self-preservation metastability – hydrates preserved outside equilibrium conditions.
2. Structure/phase metastability – coexistence/transitions of metastable phases.
3. Metastable cage composition/occupancy – variable cage occupancy and dynamics.

Abstract

Clathrate hydrates or ‘gas hydrates’ are a class of inclusion compounds that form when water and suitably sized guest gas species come into contact at favorable temperature and pressure conditions. A network of hydrogen bonds between water molecules stabilizes these polyhedral cages and depending on the size of the trapped molecule and the thermodynamic environment, different cages types/sizes or ‘structures’ may be formed. Clathrate hydrates can concentrate gases by a factor of approximately 160 times the hydrate volume at ambient conditions [1], thereby offering a potential solution for many energy-related issues including storage, transportation, and recovery.

Although thermodynamically stable clathrate hydrate structures are well known, the phenomenon known as metastability of clathrate hydrates is poorly understood. One major challenge to unraveling the complex behavior of clathrate hydrates in all energy applications is to understand

guest-host interactions and metastability in terms of structure and composition. Specifically, some of the remaining challenges lie in understanding: (a) how guests can readily fill small cages, yet experience resistance in large cages, (b) how guest molecules can distort the cavities and/or form clusters, and (c) how synthesis pathways play a prominent role in guest molecule enclathration and preferential small/large cage occupancy. These synthesis-structure-stability relations of clathrate hydrates are severely under-explored, yet hold the key to successful application and control of clathrate hydrates in all energy applications.

Our most recent advances are providing new insight into synthesis and structure (objective 2) and cage dynamics (objective 3); specifically: identifying the formation mechanisms and elementary building blocks of clathrate hydrates during nucleation/growth; increasing H₂ storage capacity (3.4 wt%) with a breakthrough synthesis method of solid-solid mixing; rapid growth and novel templating of new hydrate structures. Highlights of these recent advances are described below.

Progress Report

Expanding upon the discoveries in the previous update (July 2011), we have continued to explore synthesis and structure relationships (objective 2) as well as metastable cage dynamics during hydrate nucleation (objective 3).

Synthesis Pathway for Novel Small and Large Cage Occupancy of H₂ in Structure I

In contrast to the traditional clathrate synthesis method of simply mixing water with an appropriate hydrate former and then implementing a thermodynamic driving force for nucleation by pressurizing/cooling, a new synthesis method involving the addition of preformed hydrates was studied. Using this new technique that we refer to as the “repressurization/templating method”, we prepare a preformed hydrate and then repressurize the sample to very high (>700 bar) pressures with H₂ in an attempt to force H₂ to occupy new environments. Therefore, by simply changing the initial hydrate structure (*e.g.* the structure of the preformed hydrate), we can control the final structure, and to some degree, the metastable composition of hydrogen in the system. A conceptual picture and description of this process is shown in Figure 1.

Raman spectroscopic results using the aforementioned synthesis pathway are provided in Figure 2-I. These results show that after pressurizing the sI CH₄ hydrate with H₂ we observe three distinct H₂ environments. We show for the first time that these environments are not the normally observed

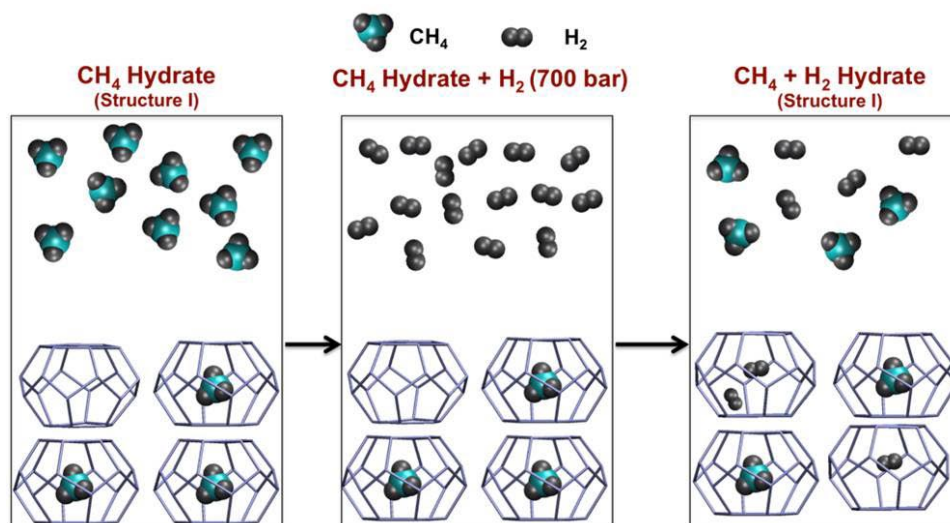


FIGURE 1. Repressurization method for clathrate hydrate synthesis. (Left) Initial sI hydrate is in equilibrium with gas phase. (Middle) The sI gas is vented and replaced with H_2 at high pressures. (Right) To establish a new equilibrium between the gas and hydrate phase, H_2 enters the preformed hydrate.

sII environments, but rather can be characterized as singly and doubly occupied sI cages. This key result shows that by altering our synthesis procedure, we were able to observe both small and large cage enclathration in sI and not the thermodynamically preferred structure for H_2 (sII). This work serves as a proof-of-concept for the synthesis technique to facilitate novel large cage filling through a potential metastable pathway.

Preservation of sVI Hydrates with H_2

Structure VI (sVI) is the only known hydrate structure which has the potential to store the amount of H_2 needed to meet the revised DOE goal of 5.5 wt%. However, previous attempts to synthesize this structure have found that upon introduction of H_2 , the structure rapidly decomposes into sII. Using the same “repressurization method” as described above, we demonstrate the first experimental evidence of binary H_2 + *tert*-butylamine (tBA) sVI hydrate. This

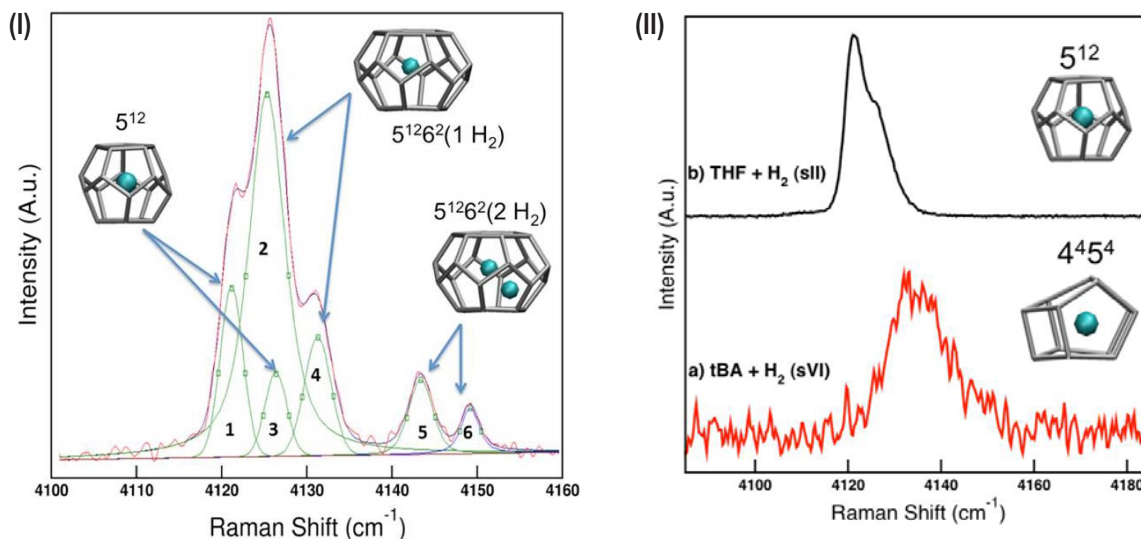


FIGURE 2. (I) Results of the repressurization method using a preformed sI hydrate showing three novel H_2 environments in sI. Peaks 1 & 3 (4,121 – 4,126 cm^{-1}) correspond to singly occupied 5^{12} cage. Peaks 2 & 4 (4,125 – 4,131 cm^{-1}) correspond to singly occupied $5^{12}6^2$ cage. Peaks 5 & 6 (4,143 – 4,149 cm^{-1}) correspond to doubly occupied $5^{12}6^2$ cage. (II) sVI H_2 peaks (a) are blue-shifted from known sII positions (b), indicating a more constrained environment.

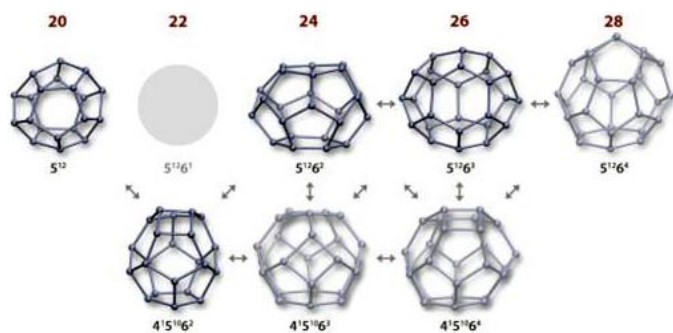


FIGURE 3. Seven dominant cages in sl hydrate nucleation

result was confirmed with both Raman and powder X-ray diffraction. Raman spectroscopic results are presented in Figure 2-II.

Discovery of Key Clathrate Hydrate Building Blocks – Metastable Pathways

Direct molecular dynamics simulations investigating nucleation and growth of sI methane hydrate identified seven common cages during hydrate nucleation (Figure 3). It was also discovered that these seven elementary cage types comprise 95% of all cages present in the nucleating trajectories. Interestingly, only two of these cages, the 5^{12} and 5^{126^2} , are present in ‘normal’ sI on experimental time scales.

This observation of seven cages (two stable, five metastable) leads to two important discoveries [3]: (i) the initial nucleated hydrate is a kinetic product of metastable cage clusters (Figure 4-I), (ii) after nucleation the metastable clathrate hydrate cages must undergo dynamic transitions to reach their equilibrium cage orientation. To undergo this type of solid-solid rearrangement (*cf.* solid-solid synthesis pathways), recent simulations have shown several different pathways of metastable cage insertions, deletions, or rotations as illustrated in Figure 4-II.

Future Directions

In the future stages of the project we will build upon our recent discoveries and continue to explore the synthesis-structure-stability relationships of hydrates on the molecular level. Specifically we plan to extend the new synthesis pathway described above to different, more promising, structures such as structure VI (sVI) and structure T (sT). Not only do these structures offer a potentially higher capacity for energy storage, but also present a unique opportunity to study new cage environments and dynamics.

References

1. “Clathrate Hydrates of Natural Gases”, 3rd Ed., E.D. Sloan and C.A. Koh, CRC/Taylor & Francis, Boca Raton, FL (2008)

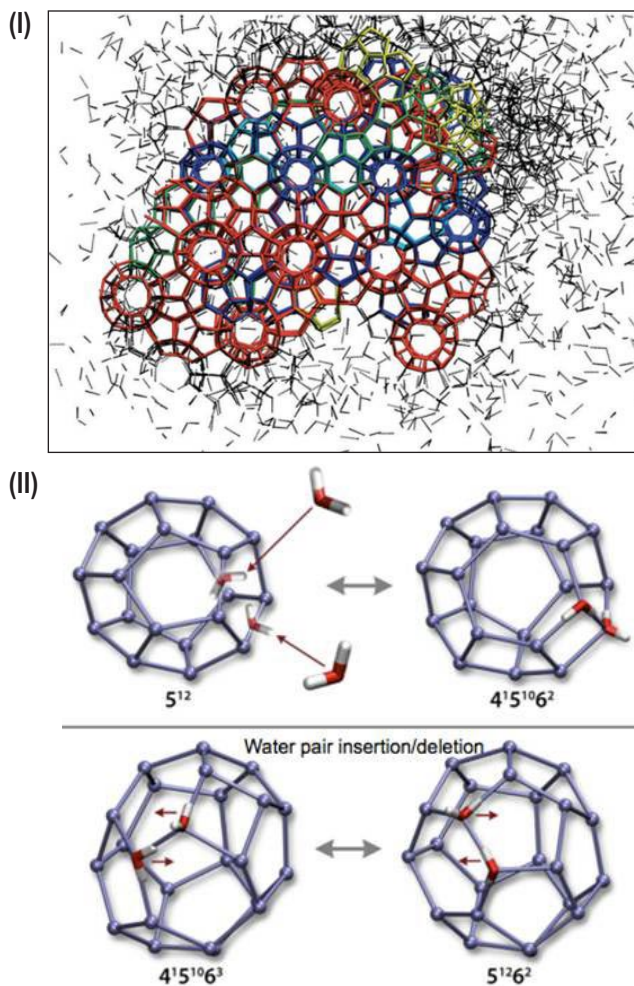


FIGURE 4. Metastable hydrate cluster after nucleation (I); insertion, deletion, and rotational cage dynamic pathways (II).

2. “Hydrogen Storage Properties of Clathrate Hydrate Materials” T.A. Strobel, C.A. Koh, E.D. Sloan, *Fluid Phase Equilibria* 261, 382 (2007).

3. “The Cages, Dynamics, and Structuring of Incipient Methane Clathrate Hydrates” M.R. Walsh, J.D. Rainey, P.G. Lafond, D.-H. Park, G.T. Beckham, M.D. Jones, K.-H. Lee, C.A. Koh, E.D. Sloan, D.T. Wu, A.K. Sum, *Phys. Chem. Chem. Phys.* 13, 19951 (2011).

Publications (including patents) acknowledging the grant or contract

1. “Microsecond Simulations of Spontaneous Methane Hydrate Nucleation and Growth” M.R. Walsh, C.A. Koh, E.D. Sloan, A.K. Sum, D.T. Wu, *Science* 326, 1095 (2009).

2. “Increasing Hydrogen Storage Capacity Using Tetrahydrofuran” T. Sugahara, J.C. Haag, P.S.R. Prasad, A.A. Warntjes, E.D. Sloan, A.K. Sum, and C.A. Koh, *J. Am. Chem. Soc.* 131, 14616 (2009).

3. “Large-Cage Occupancies of Hydrogen in Binary Clathrate Hydrates Dependent on Pressures and Guest Concentrations”

T. Sugahara, J.C. Haag, A.A. Warntjes, P.S.R. Prasad, E.D. Sloan, C.A. Koh, and A.K. Sum, *J. Phys. Chem. C* 15218 (2010).

4. “The Cages, Dynamics, and Structuring of Incipient Methane Clathrate Hydrates” M.R. Walsh, J.D. Rainey, P.G. Lafond, D.-H. Park, G.T. Beckham, M.D. Jones, K.-H. Lee, C.A. Koh, E.D. Sloan, D.T. Wu, A.K. Sum, *Phys. Chem. Chem. Phys.* 13, 19951 (2011).

5. “Methane Hydrate Nucleation Rates from Molecular Dynamics Simulations: Effects of Aqueous Methane Concentration, Interfacial Curvature, and System Size” M.R. Walsh, G.T. Beckham, C.A. Koh, E.D. Sloan, D.T. Wu, A.K. Sum, *J. Phys. Chem. C* 115, 21241 (2011).

6. “Interfacial mechanisms governing cyclopentane clathrate hydrate adhesion/cohesion” Z.M. Aman, E.P. Brown, E.D. Sloan, A.K. Sum, C.A. Koh, *Phys. Chem. Chem. Phys.*, 44, 19796 (2011).

IV.H.10 Exploration of Novel Carbon-Hydrogen Interactions

Angela D. Lueking (Primary Contact),
Xiao Ming Liu, En Shi Xu, Thomas C. Fitzgibbons,
Paramita Ray, Greg Larsen, Youjian Tang,
Humberto R. Gutierrez, John V. Badding,
Vincent H. Crespi

The Pennsylvania State University
120 Hosler
University Park, PA 16802
Phone: (814) 862-6256
Email: lueking@psu.edu

DOE Program Officer: Bonnie Gersten
Phone: (301) 903-0002
Email: Bonnie.Gersten@science.doe.gov

Objectives

Hydrogen trapped in a carbon cage, captured through *repulsive* interactions, is a novel concept in hydrogen storage which borrows an idea from macroscale hydrogen storage (i.e. compressed gas storage tanks) and reapplies these concepts on the nanoscale in specially designed molecular containers. Under extreme conditions of pressure, hydrogen solubility in carbon materials is expected to increase and carbon is expected to restructure to minimize volume via a mixed sp^2/sp^3 hydrogenated state. Our approach to form hydrogen caged in carbon relies on unique chemical reaction conditions provided by mechanochemistry, including dynamic shearing/compression via mechanical milling and static high-pressure chemistry in a diamond anvil cell. Materials are currently being characterized via multiwavelength in situ Raman spectroscopy to probe carbon-hydrogen interactions and structural changes in the carbon backbone. Complementary first-principles materials theory is being used to examine candidate carbon-cage structures to predict the characteristic Raman signatures of hydrogen held in place by either repulsive interactions (caged hydrogen) or attachment to the carbon backbone in mixed sp^2/sp^3 states.

Abstract, Progress Report and Future Directions

1. Transformation of Hydrogenated Bucky-Balls at High pressure

Thermodynamics dictate that pre-formed C-H structures will rearrange with increased pressure, yet the final carbon-hydrogen interactions may be dependent upon the mechanism by which hydrogen is introduced. Molecular

dynamics with reactive force fields (ReaxFF) have been implemented in modeling compressed hydrocarbons and hydrogenated C_{60} (mainly $C_{60}H_{36}$ and $C_{60}H_{18}$, systems also being investigated experimentally). The cage structure of C_{60} and the interplay between inter-ball polymerization into sp^3 geometries and on-ball sp^3 sites of H attachment could be beneficial for loading hydrogen into local traps. Compression of two initial crystal structures of $C_{60}H_{36}$ was simulated by ReaxFF under a series of high pressures up to 30 GPa. Polymerization of hydrogenated C_{60} is not achieved under hydrostatic compression, but under shock compression it can be induced, with hydrogen released. A simple theoretical model for understanding the propensity for H release during compression of various hydrocarbon systems has been designed in which a volume is associated with each bond type (C-H, etc.). The model shows consistency with simple alkane molecules. The model needs more delicate tweaks to accommodate complex hydrocarbons such as hydrogenated C_{60} with the simulation support of first principle theory and ReaxFF.

Experimentally, $C_{60}H_{14}$ has been synthesized to validate the ReaxFF models. A hydrogen transfer reaction between C_{60} and a complex amine, diethylene triamine, was used to synthesize the hydrogenated C_{60} . Synthesis and storage under inert atmosphere with no exposure to light ensured resistance to oxidation and cleavage of C-H bonds respectively. Hydrogenation of C_{60} and minimization of oxidation has been confirmed with solid state ^{13}C nuclear magnetic resonance and Fourier transform infrared spectroscopy (FTIR). Matrix-assisted laser desorption/ionization mass spectrometry shows a broad distribution of ions from 728 to 740, and an intense peaks at 734 confirm the formation of $C_{60}H_{14}$. An FTIR experiment at static high pressure indicates no change in the C-H stretching region, consistent with the theoretical predictions. Ongoing Raman spectroscopy studies are being performed to analyze changes in the lattice modes and C-C bonding in the hydrogenated C_{60} . A combination of FTIR and Raman spectroscopy will be utilized to determine if H_2 is evolved during the high pressure compression. Future work includes compression under non hydrostatic and shear conditions.

Compression of other hydrocarbons with the potential for release of H_2 upon carbon polymerization are on-going. For example, compression of triptycene in the diamond anvil cell under non-hydrostatic conditions at room temperature led to polymerization at 25.4GPa. Future work will include compression of the same under hydrostatic conditions (H_2 at 23,000psi) with resistive heating methods. The main goal is to find conditions for polymerization of triptycene under hydrostatic pressure and study the interaction of molecular H_2 with the polymerized caged product. We are also studying

the diffusion and potential trapping of H₂ in pre-formed carbon materials such as glassy carbons and carbon onions. Parallel modeling studies include nanocage formation upon compression of triptycene and anthracene in the presence and absence of molecular H₂.

2. In Situ Micro Raman Detection of Reversible Basal Plane Hydrogenation in Pt-doped Activated Carbon

Development of in situ spectroscopic measurement techniques capable of combined high-pressure and variable temperature measurements has allowed us to explore carbon-hydrogen interactions that are unresolved and debated in the literature. One such carbon-hydrogen interaction of particular interest is the binding mechanism between hydrogen and a carbonaceous support in the presence of a noble-metal dissociation catalyst, i.e. the hydrogen spillover mechanism [1]. Incorporation of a catalyst into nanoporous materials has led to several reports of particularly high hydrogen uptake at room temperature and pressures less than 100 bar [2], but the results are contested [3,4], reproducible by only a fraction of laboratories [5-7], and the active sites on the nanoporous support that bind reversibly with spilled over atomic hydrogen remains unclear [8,9]. We have investigated the local interaction between atomic H and the graphite basal plane adjacent to a Pt dissociation catalyst with in situ Raman spectroscopy and complementary density functional theory calculations. These results demonstrate spectroscopic evidence for hydrogenation of the carbon basal plane via the spillover mechanism; the feature is reversible for spillover to curved and defected oxidized activated carbon and irreversible to graphene and non-oxidized activated carbon. Poisoning of the catalyst eliminates the reversibility, showing desorption is through a reverse spillover mechanism. These results clarify whether H is chemisorbed or physisorbed, how reversibility is achieved, and how carbon structure and metal-carbon contact dictate the degree of reversibility.

References

1. Conner, W.C.; Falconer, J.L., Spillover in Heterogeneous Catalysis. *Chem Rev* **1995**, *95* (3), 759-788.
2. Wang, L.; Yang, R.T., New sorbents for hydrogen storage by hydrogen spillover - a review. *Energy & Environmental Science* **2008**, *1* (2), 268-279.
3. Stadie, N.P.; Purewal, J.J.; Ahn, C.C.; Fultz, B., Measurements of Hydrogen Spillover in Platinum Doped Superactivated Carbon. *Langmuir* **2010**, *In Press*.
4. Campesi, R.; Cuevas, F.; Latroche, M.; Hirscher, M., Hydrogen spillover measurements of unbridged and bridged metal-organic frameworks-revisited. *Phys Chem Chem Phys* **2010**, *12* (35), 10457-10459.
5. Tsao, C.S.; Yu, M.S.; Chung, T.Y.; Wu, H.C.; Wang, C.Y.; Chang, K.S.; Chent, H.L., Characterization of pore structure in metal-organic framework by small-angle X-ray scattering. *J Am Chem Soc* **2007**, *129* (51), 15997-16004.
6. Tsao, C.S.; Yu, M.S.; Wang, C.Y.; Liao, P.Y.; Chen, H.L.; Jeng, U.S.; Tzeng, Y.R.; Chung, T.Y.; Wut, H.C., Nanostructure and Hydrogen Spillover of Bridged Metal-Organic Frameworks. *J Am Chem Soc* **2009**, *131* (4), 1404-+.
7. Froudakis, G.E.; Psfogiannakis, G.M.; Steriotis, T.A.; Bourlinos, A.B.; Kouvelos, E.P.; Charalambopoulou, G.C.; Stubos, A.K., Enhanced hydrogen storage by spillover on metal-doped carbon foam: an experimental and computational study. *Nanoscale* **2011**, *3* (3), 933-936.
8. Froudakis, G.E.; Psfogiannakis, G.M., DFT Study of Hydrogen Storage by Spillover on Graphite with Oxygen Surface Groups. *J Am Chem Soc* **2009**, *131* (42), 15133-+.
9. Froudakis, G.E.; Psfogiannakis, G.M., DFT Study of the Hydrogen Spillover Mechanism on Pt-Doped Graphite. *Journal of Physical Chemistry C* **2009**, *113* (33), 14908-14915.

Publications (including patents) acknowledging the grant or contract

1. Liu, X.M.; Rather, S.; Li, Q.; Lueking, A.D.; Zhao, Y.; Li, J., Hydrogenation of CuBTC framework with the introduction of a PtC hydrogen spillover catalyst. *J Phys. Chem. C*, *116* (5), 3477-3485, 2012.

IV.H.11 Complex Hydrides – A New Frontier for Future Energy

Vitalij K. Pecharsky,¹ Marek Pruski,²
L. Scott Chumbley,³ Duane D. Johnson,⁴
Takeshi Kobayashi⁵

¹FWP Leader: Ames Laboratory,
253 Spedding Hall, Ames, IA 50011,
Email: vitkp@ameslab.gov, Phone: (515) 294-8220

²PI: Ames Laboratory, 230 Spedding Hall, Ames, IA 50011,
Email: mpruski@iastate.edu, Phone: (515) 294-2017

³PI: Ames Laboratory, 214 Wilhelm Hall, Ames, IA 50011,
Email: chumbley@iastate.edu, Tel.: 515-2947903;

⁴PI: Ames Laboratory, 311 TASF, Ames, IA 50011,
Email: ddj@ameslab.gov, Phone: (515) 2949649

⁵Ames Laboratory, 229 Spedding Hall, Ames, IA 50011,
Email: takeshi@iastate.edu, Phone: (515)-294-6823

DOE Program Officer: Dr. Refik Kortan
Phone: (301) 903-3308
Email: Refik.Kortan@science.doe.gov

Objectives

- Examine and compare mechanical and thermal energy-driven phase transformations in model complex hydrides at and away from thermodynamic equilibrium to enable their future use.
- Establish the nature and structure of the products and intermediaries using high resolution solid-state nuclear magnetic resonance (NMR), electron microscopy, as well as first principles theory and modeling.
- Provide a fundamental understanding of the nature of hydrogen bonding and formation, structure, and stability of the model systems, the effects of mechanical energy, temperature, and pressure in controlling the nature of hydrogen-metal bonds.
- Identify events critical to achieving reversibility of hydrogen in model systems under mild conditions.

Technical Barriers

- Substantial progress is required to reduce the energy cost associated with reversible and safe hydrogen storage using metal hydrides.
- Current understanding of the mechanisms of solid-state transformations must be extended from a few known hydrides to complex hydride-hydrogen systems.
- Predictive tools should be developed to guide the discovery of materials at the atomic scale and the processing strategies for controlling the nano-, meso- and microscopic structures.

Abstract

Limited reserves of fossil fuels and the environmental impacts of their consumption drive the demand for alternative sources of energy. Although hydrogen has the highest gravimetric energy density of all fuels, its energy-related applications require safe and efficient storage media. Significant progress in relevant materials science is needed to enable the use of hydrogen in mobile applications, especially in transportation. We seek solids mimicking the structure of methane and ammonia, where several hydrogen atoms encapsulate a single carbon or nitrogen atom forming neutral CH_4 and NH_3 molecules, as opposed to conventional metal hydrides where a single hydrogen atom is encapsulated by several metal atoms. Mechanochemistry and thermochemistry coupled with advanced characterization, theory, modeling, and simulations are utilized to understand composition-structure-processing-property relationships in complex materials consisting of various light-metal hydride compounds and their derivatives.

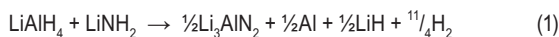
Our approach is to: (1) use different forms of energy (mechanical and thermal) to activate complex hydride materials, examine (non)equilibrium thermodynamics involved, study kinetics of (de)hydrogenation, and prepare new solid systems with hydrogen contents exceeding 10 wt%; (2) carry out state-of-the-art characterization of the structure, chemical, thermodynamic, and physical properties of the prepared complex hydrides in amorphous, nanocrystalline and crystalline forms to expand our current understanding of the mechanisms of solid-state hydrogenation-dehydrogenation, and (3) couple the experiments with the first principles theory.

Progress Report

In recent studies, we built upon our early experiments, in which we pioneered the idea of destabilizing TiCl_4 - LiAlH_4 [1-3] and alanate-amide systems [8] using mechanochemical processing (ball milling), to study the mechanisms of dehydrogenation in $M\text{NH}_2$ - CaH_2 ($M=\text{Li}$ or Na) [9] and $2M\text{NH}_2$ - 3MgH_2 ($M=\text{Li}$ or Na) [10,11]. Moreover, we demonstrated that mechanisms of mechanochemical transformations in some of these systems are different from those induced by temperature [11,12], carried out exploratory studies of direct mechanochemical hydrogenation of Al and magnesium diboride as well as dehydrogenation of ammonia borane [13], and showed that solid-state NMR is an invaluable tool in characterization of both the mechanochemical [3,8,11,14] and thermochemical [12,13,15] processes that occur in complex hydrides. As a result, we established that mechanochemistry adds a new dimension

to well-known destabilization by chemical substitutions. From density functional theory (DFT) methods, including simulated annealing and nudge-elastic band techniques, we are currently investigating the thermodynamics and kinetic barriers for materials directly relevant to our experiments, namely, (1) vacancy-mediated formation of alane (AlH_3) complexes, which may interact with other metallic elements, e.g., Li, and (2) the effects of particle size on (de)hydrogenation of MgH_2 , relevant to ball-milling [16]. In previous work, theory has detailed the issues with reversibility of H-storage reactions [4-6], e.g., LiBH_4 and $M(\text{BH}_4)_2$ with $M=\text{Ca}, \text{Mg}$, especially avoiding thermodynamically very stable $\text{MB}_{12}\text{H}_{12}$ intermediates. A brief, selected summary of our progress is given below.

Transformations of the LiAlH_4 - LiNH_2 and MNH_2 - MgH_2 ($M=\text{Li}$ or Na) Systems. To establish differences between the mechanochemical and thermochemical events occurring in the same system, we carried out a detailed study of the mechanism of thermal decomposition of (1:1) LiAlH_4 - LiNH_2 system using pressure-composition-temperature analysis, solid-state NMR, X-ray diffraction (XRD), and residual gas analysis [12]. Figure 1 illustrates the evolution of hydrogen during heating of the 1:1 mixture of LiAlH_4 and LiNH_2 from 25 to 390°C. Rapid desorption initiates at ~140°C and a total of ~9 wt% of pure hydrogen is released. To obtain insights into the chemical transformations occurring during the thermal treatment, the mixture was held at selected temperatures (see open circles in Figure 1) until the hydrogen release ceased. Subsequently, the samples were analyzed by XRD and solid-state NMR (Figure 2) providing coherent information about the intermediates and products. The major transformations detailed in this study result in the following overall reaction:



The final products in Eq. 1 are different than in the mechanochemical process, where LiAlH_4 and LiNH_2 react with one another [8]. Thermochemical transformation of the LiAlH_4 - LiNH_2 system is initiated by the decomposition of LiAlH_4 , and further release of hydrogen is determined by the presence and the concentration of LiNH_2 [12].

In other studies, several mixed systems containing Mg have been investigated. Examination of thermochemical transformations in (2:3) MNH_2 - MgH_2 system ($M = \text{Li}$ or Na) indicated the following overall reactions [10]:



The 2NaNH_2 - 3MgH_2 system can be partially rehydrogenated in 190 bar hydrogen at 395°C with formation of the MgNH imide. Similarly, mechanochemical transformations during ball milling of sodium amide (NaNH_2) with MgH_2 in 2:3 and 2:1 molar ratios have

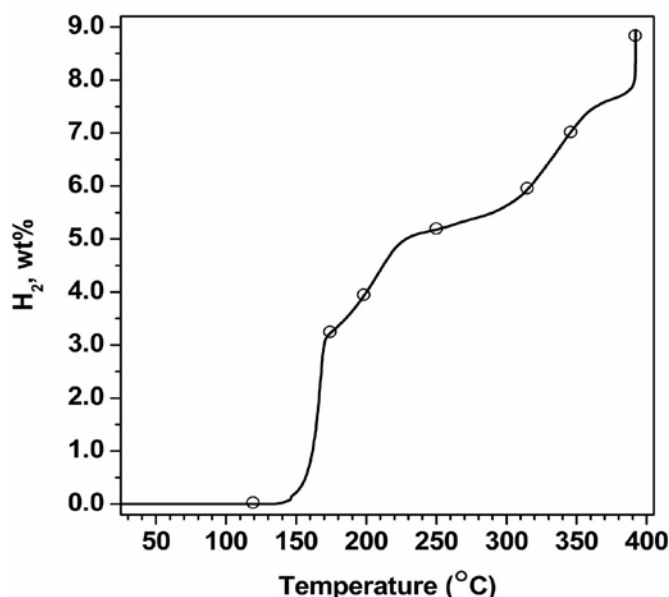
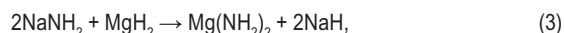


FIGURE 1. Temperature programmed decomposition of the 1:1 LiAlH_4 - LiNH_2 mixture with a heating rate of 1°C/min

been studied using XRD and solid-state NMR [11]. The mechanochemical processing of the 2NaNH_2 - 3MgH_2 system yields the same final products as the thermochemical reaction (see Eq. 2 with $M=\text{Na}$) via a different pathway, which involves the formation of MgNH [11]. However, the mechanochemical transformation of the 2NaNH_2 - MgH_2 system proceeds without any hydrogen release:



Our studies also revealed a possibility that some mechanochemical reactions, which appear to be solid-state processes, may occur in a liquid phase via the formation of low-melting eutectics [14].

Ammonia Borane-Based Materials. The mechanism of thermochemical dehydrogenation of the 1:3 mixture of Li_3AlH_6 and NH_3BH_3 (AB) has been studied by the extensive use of solid-state NMR and theoretical calculations. The activation energy for the dehydrogenation is lower than for pristine AB (110 kJ mol^{-1} vs. 184 kJ mol^{-1}) [13]. The major hydrogen release from the mixture occurs at 60°C and 72°C, which compares favorably with pristine AB and related hydrogen storage materials, such as lithium amidoborane (LiNH_2BH_3 , LiAB). Based on the reported chemical reaction between lithium hydride (LiH) and AB [7], we expected the thermal treatment of Li_3AlH_6 -3AB to proceed via the formation of lithium amidoborane (LiNH_2BH_3 ; LiAB) through the reaction $\text{Li}_3\text{AlH}_6 + 3\text{AB} = 3\text{LiAB} + \text{Al} + 9/2 \text{H}_2$. However, the solid-state NMR measurements and calculations showed that the mixture decomposes via the formation of a different intermediate phase with improved dehydrogenation properties as compared to pristine AB.

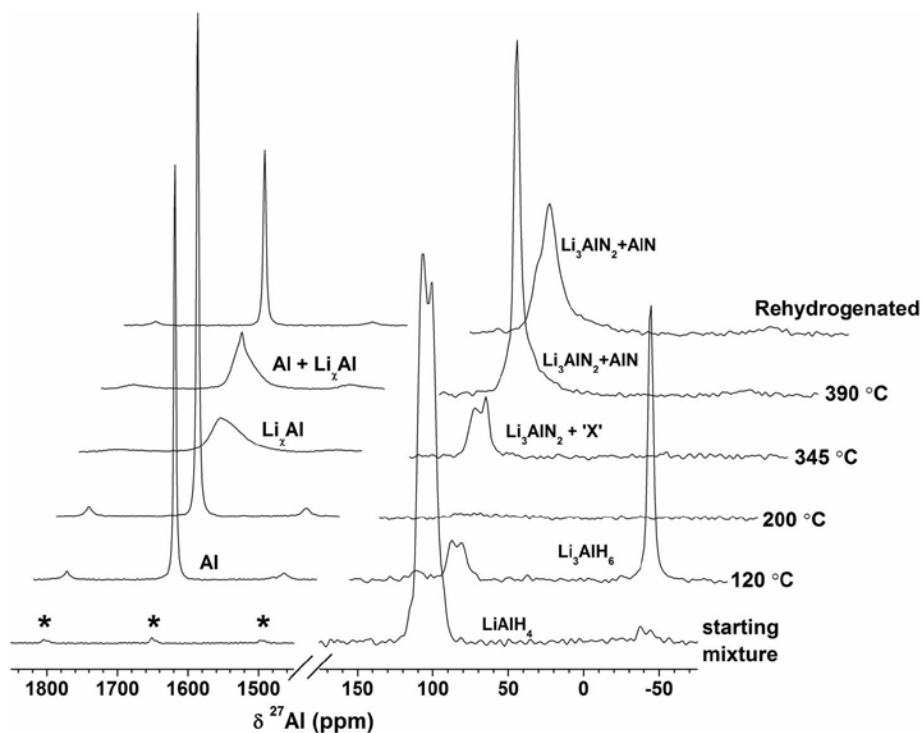


FIGURE 2. ^{27}Al magic angle spinning NMR spectra of LiAlH_4 - LiNH_2 mixture treated at various temperatures. Asterisks indicate spinning sidebands.

DFT Study of H-Desorption in Doped MgH_2 (110)

Surfaces. Using DFT nudged-elastic bands, H_2 desorption barrier with Ti-doping (Figure 3) drops by 0.41 eV (–22% change), agreeing with 0.46 eV from experiment [16]. In addition, we find that particle size alone does not affect desorption enthalpies [17], so it is a combination of dopant and non-equilibrium processing.

Vacancy-Mediated Formation of Alane. Using DFT-based molecular dynamics, we have shown that vacancy (as created by ball-milling) stabilizes alane formation on Al(111), whereas Ti-doping helps dissociate H_2 , making alane formation exothermic only with defect-dopant interactions. These results are being prepared for publication.

Future Directions

More work at fundamental level is needed to understand the structure – hydrogen storage activity relationships among promising complex hydrides and the role of nonequilibrium states in dehydrogenation and hydrogenation. Reaching our goals requires basic understanding of the mechanisms of processes occurring in a ball mill, and differences between the mechanically- and thermally-induced transformations. We will continue to rely upon integrating innovative transformations with state-of-the-art characterization and modeling that directly addresses processing effects, especially those dictated by defect-mediated mechanisms

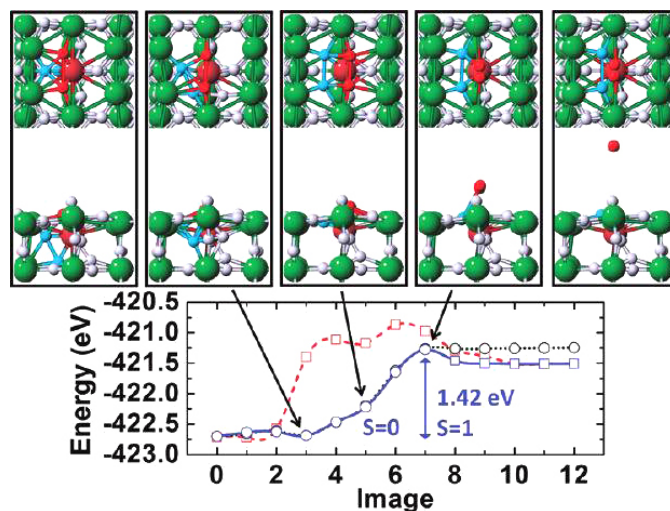


FIGURE 3. H_2 desorption path for Ti-doped MgH_2 (110) rutile surface. With Ti spin state S changes from 0 (circles) to 1 (squares) during desorption. Fixed S results are given as dashed (dotted) line.

inherent in mechanical processing. Our general objectives and strategy will remain similar as in the previous funding period while pursuing new research directions, including: (1) understanding of the direct mechanochemical synthesis of AlH_3 with high yields; (2) mechano- and thermo-chemical studies of magnesium borohydride- and aminoborane-based systems; (3) development and testing

of hybrid materials composed of complex hydrides and conventional intermetallic hydrogen absorbers; (4) use of mechanical energy to create nonequilibrium rehydrogenation pathways under low temperatures and hydrogen pressures; (5) development of improved characterization methods, such as in situ solid-state NMR spectroscopy; and (6) integration of experiments with theoretical modeling providing better understanding of thermodynamics and kinetics of (de)hydrogenation in selected model systems and guidance toward the discovery of hydrogen-containing solids that would be unattainable using synthetic and processing methods alone.

References

1. “Rapid Solid-State Transformation of Tetrahedral $[\text{AlH}_4]^-$ into Octahedral $[\text{AlH}_6]^{3-}$ in Lithium Aluminohydride,” V.P. Balema, K.W. Dennis, and V.K. Pecharsky, *Chem. Comm.* **2000**, 17, 1665.
2. “Solid State Phase Transformations in LiAlH_4 during High Energy Ball-Milling,” V.P. Balema, V.K. Pecharsky, and K.W. Dennis, *J. Alloys Comp.* **2000**, 313, 69.
3. “Titanium Catalyzed Solid-State Transformations in LiAlH_4 during High-Energy Ball-Milling,” V.P. Balema, J.W. Wiench, K.W. Dennis, M. Pruski, and V.K. Pecharsky, *J. Alloys Comp.* **2001**, 329, 108.
4. “Predicting Enthalpies of Molecular Substances: Exemplified via LiBH_4 ,” N.A. Zarkevich, D.D. Johnson, *Phys. Rev. Letts.*, **2008**, 100, 040602.
5. “On the Reversibility of H-storage Reactions in $\text{Ca}(\text{BH}_4)_2$: Experiment and Theory,” L.-L. Wang, D. Graham, I.M. Robertson, D.D. Johnson, *J. Phys. Chem. C*, **2009**, 113, 20088.
6. “First-Principles Characterization of Amorphous Phases of $\text{MB}_{12}\text{H}_{12}$, $\text{M}=\text{Mg}, \text{Ca}$,” A.D. Kulkarni, L.-L. Wang, D.D. Johnson, D. Sholl, K. Johnson, *J. Phys. Chem. C*, **2010**, 114, 14601.
7. “Ammonia Borane Destabilized by Lithium Hydride: An Advanced On-Board Hydrogen Storage Material,” X.D. Kang, Z.Z. Fang, L.Y. Kong, H.M. Cheng, X.D. Yao, G.Q. Lu, P. Wang, *Adv. Mater.*, **2008**, 20, 2756.
8. “Mechanochemical Transformations in $\text{Li}(\text{Na})\text{AlH}_4 - \text{Li}(\text{Na})\text{NH}_2$ Systems,” O. Dolotko, H. Zhang, O. Ugurlu, J.W. Wiench, M. Pruski, L.S. Chumbley, and V.K. Pecharsky, *Acta Mater.* **2007**, 55, 3121.
9. “Mechanochemically Driven Nonequilibrium Processes in $\text{MNH}_2\text{-CaH}_2$ Systems ($\text{M}=\text{Li}$ or Na),” O. Dolotko, H. Zhang, Sa Li, P. Jena, and V.K. Pecharsky, *J. Alloys Comps.* **2010**, 506, 224.
10. “Thermochemical Transformations in $2\text{MNH}_2\text{-3MgH}_2$ Systems ($\text{M} = \text{Li}$ or Na),” O. Dolotko, N. Paulson, and V.K. Pecharsky, *Int. J. Hydrogen Energy* **2010**, 35, 4562.
11. “Mechanochemical Transformations in $\text{NaNH}_2/\text{MgH}_2$ Mixtures,” N.K. Singh, T. Kobayashi, O. Dolotko, J.W. Wiench, M. Pruski, and V.K. Pecharsky, *J. Alloys Comps.*, **2012**, 513, 324.
12. “Investigation of the Thermochemical Transformations in the $\text{LiAlH}_4 - \text{LiNH}_2$ System,” O. Dolotko, T. Kobayashi, J.W. Wiench, M. Pruski, and V.K. Pecharsky, *Int. J. Hydrogen Energy* **2011**, 36, 10626.
13. “A Solid-State NMR Study of Li-assisted Dehydrogenation of Ammonia Borane,” T. Kobayashi, I.Z. Hlova, N.K. Singh, V.K. Pecharsky, and M. Pruski, *Inorg. Chem.*, **2012**, <http://dx.doi.org/10.1021/ic202368a>.
14. “Mechanically Induced Reactions in Organic Solids: Liquid Eutectics or Solid-State Processes?,” O. Dolotko, J. Wiench, K.W. Dennis, V.K. Pecharsky, and V.P. Balema, *New J. Chem.* **2010**, 34, 25.
15. “Solid State ^{27}Al NMR Investigation of Thermal Decomposition of LiAlH_4 ,” J. W. Wiench, V.P. Balema, V.K. Pecharsky, and M. Pruski, *J. Solid State Chem.* **2004**, 177, 648.
16. “Hydrogen Desorption from Ti-doped $\text{MgH}_2(110)$ Surfaces: Catalytic Effect on Reaction Pathways and Kinetic Barriers,” L.-L. Wang D.D. Johnson, *J. Phys. Chem. C*, **2012**. <http://dx.doi.org/10.1021/jp300794x>.
17. “Hydrogen Desorption from Catalyst-Doped Rutile MgH_2 : Surface and Particle-Size Effects,” J. M. Reich, L.-L. Wang, D.D. Johnson, (2012), in preparation.

Publications acknowledging the contract

8. “Mechanochemical Transformations in $\text{Li}(\text{Na})\text{AlH}_4 - \text{Li}(\text{Na})\text{NH}_2$ Systems,” O. Dolotko, H. Zhang, O. Ugurlu, J.W. Wiench, M. Pruski, L.S. Chumbley, and V.K. Pecharsky, *Acta Mater.* **2007**, 55, 3121.
9. “Mechanochemically Driven Nonequilibrium Processes in $\text{MNH}_2\text{-CaH}_2$ Systems ($\text{M}=\text{Li}$ or Na),” O. Dolotko, H. Zhang, Sa Li, P. Jena, and V.K. Pecharsky, *J. Alloys Comps.* **2010**, 506, 224.
10. “Thermochemical Transformations in $2\text{MNH}_2\text{-3MgH}_2$ Systems ($\text{M} = \text{Li}$ or Na),” O. Dolotko, N. Paulson, and V.K. Pecharsky, *Int. J. Hydrogen Energy* **2010**, 35, 4562.
11. “Mechanochemical Transformations in $\text{NaNH}_2/\text{MgH}_2$ Mixtures,” N.K. Singh, T. Kobayashi, O. Dolotko, J.W. Wiench, M. Pruski, and V.K. Pecharsky, *J. Alloys Comps.*, **2012**, 513, 324.
12. “Investigation of the Thermochemical Transformations in the $\text{LiAlH}_4 - \text{LiNH}_2$ System,” O. Dolotko, T. Kobayashi, J.W. Wiench, M. Pruski, and V.K. Pecharsky, *Int. J. Hydrogen Energy* **2011**, 36, 10626.
13. “A Solid-State NMR Study of Li-assisted Dehydrogenation of Ammonia Borane,” T. Kobayashi, I.Z. Hlova, N.K. Singh, V.K. Pecharsky, and M. Pruski, *Inorg. Chem.*, **2012**, <http://dx.doi.org/10.1021/ic202368a>.
14. “Mechanically Induced Reactions in Organic Solids: Liquid Eutectics or Solid-State Processes?,” O. Dolotko, J. Wiench, K.W. Dennis, V.K. Pecharsky, and V.P. Balema, *New J. Chem.* **2010**, 34, 25.
15. “Solid State ^{27}Al NMR Investigation of Thermal Decomposition of LiAlH_4 ,” J. W. Wiench, V.P. Balema, V.K. Pecharsky, and M. Pruski, *J. Solid State Chem.* **2004**, 177, 648.
16. “Hydrogen Desorption from Ti-doped $\text{MgH}_2(110)$ Surfaces: Catalytic Effect on Reaction Pathways and Kinetic Barriers,” L.-L. Wang D.D. Johnson, *J. Phys. Chem. C*, **2012**. <http://dx.doi.org/10.1021/jp300794x>.
17. “Hydrogen Desorption from Catalyst-Doped Rutile MgH_2 : Surface and Particle-Size Effects,” J. M. Reich, L.-L. Wang, D.D. Johnson, (2012), in preparation.

IV.H.12 Atomistic Transport Mechanisms in Aluminum-Based Hydrides

Jason Graetz (Primary Contact), Peter Sutter,
James Muckerman
Brookhaven National Laboratory
Upton, NY 11973
Phone: (631) 344-3242
Email: graetz@bnl.gov

DOE Program Officer: John Vetrano
Phone: (301) 903-5976
Email: John.Vetrano@science.doe.gov

Subcontractor:
Yves Chabal, University of Texas at Dallas

Objectives

Complementary high-resolution microscopy and spectroscopy in close connection with theory will be used to address the following scientific areas: (i) atomic processes associated with hydrogen uptake and release kinetics; (ii) the role of surface structures and chemistry in affecting hydrogen-materials interactions; (iii) the effect of dopants; the formation of alanes; and (iv) the structure and bonding of alane and alane amine adducts. The objective is to provide a comprehensive understanding of the role of dopants and complex reaction environments in facilitating the hydrogenation and dehydrogenation of Al-based hydrogen storage materials.

Technical Barriers

Al-based hydrides (e.g., AlH_3 , LiAlH_4) exhibit high hydrogen densities and low desorption temperatures, but these materials are often difficult to form by direct hydrogenation at low pressure. The development of new routes for the formation of aluminum-based hydrides requires a better understanding of hydrogen-metal interactions, hydrogenation and the role of catalysts near technologically relevant conditions. In addition, new regeneration routes being proposed to reform aluminum-based hydrides using stabilizing ligands (e.g., ethers, amines) will require new insights into alane chemistry, Al-O and Al-N bonding in alane adducts (e.g., $\text{AlH}_3\text{-NR}_3$), and new methods of separating these adducts at low temperatures.

Abstract

Hydrogen fuel cell vehicles will reduce greenhouse gas emissions faster than any other technology (e.g., batteries) and a system based on solid-state hydrogen storage (e.g.,

metal hydrides) remains the most promising method of achieving high hydrogen storage densities at low pressure. The Al-based kinetically stabilized hydrides (e.g. AlH_3 , LiAlH_4 , $\text{Mg}(\text{AlH}_4)_2$) represent a class of materials that have received little attention due to poor reversibility, but may offer some advantages over the more stable on-board reversible materials, such as high hydrogen density, low reaction enthalpy (<30 kJ/mol) and the ability to supply hydrogen at high pressures >>1 bar and rapid rates at low temperature (<100°C). However, these hydrides cannot easily be formed by direct hydrogenation at low pressure and therefore, their use as hydrogen storage compounds has been limited. This research program is focused on understanding the atomic-scale effects of hydrogen with catalyzed light metals (e.g., Al) and to exploring how complex reaction environments affect and control these fundamental interactions. These results will be used to develop new procedures for the formation of metastable aluminum-based hydrides.

Progress Report

Model systems for Al-based hydrogen storage:

Doping catalytically inactive materials with dispersed atoms of an active species is a promising route toward realizing ultra-dilute binary catalyst systems. Beyond heterogeneous catalysis, strategically placed metal atoms can accelerate a wide range of solid-state reactions, particularly in hydrogen storage processes. We used in situ scanning tunneling microscopy experiments on a Ti:Al(111) model system in a controlled ultrahigh vacuum environment, combined with ab-initio calculations, to analyze the role of atomic Ti catalysts in the hydrogenation of aluminum-based hydrogen storage materials.

Our results show that Ti atoms near the Al surface activate gas phase H_2 , a key step toward hydrogenation. Controlling the placement of Ti we find that the overall reaction – comprising H_2 dissociation and H spillover onto the Al surface – is governed by a pronounced tradeoff between lowering the H_2 dissociation barrier and trapping of the products near the active site. Ti existing as adatoms on the surface or embedded in the Al surface layer efficiently dissociates H_2 , but the products (H) cannot be transferred to the Al surface due to a deep potential well trapping H near the active site. As a result, the Ti catalyst becomes rapidly poisoned, and no significant amounts of atomic H are made available for Al hydrogenation. H spillover can be enabled by burying Ti in subsurface Al layers, an effect which we explored by controlling the placement of Ti with atomic-layer precision. Experiments and calculations show a sharp maximum in the overall activity for Ti in the first subsurface layer. Ti incorporation into deeper subsurface layers causes

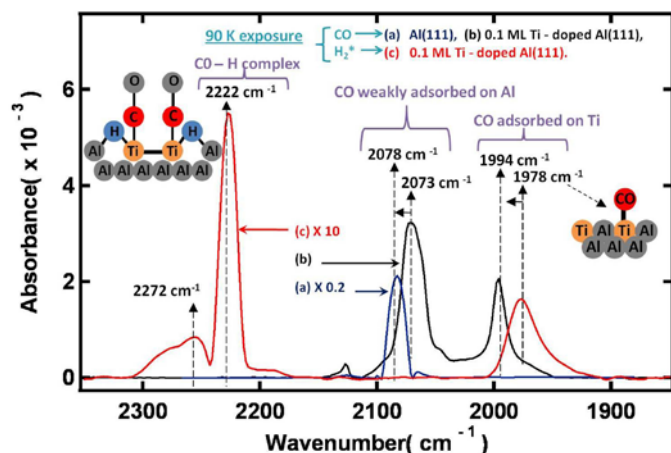


FIGURE 1. Infrared reflection-absorption spectra of CO molecules adsorbed on Al(111) surfaces at 90 K. Pure CO gas (7 L exposure) on (a) clean Al, (b) Al with 0.1 ML Ti and (c) H_2^* on Al with 0.1 ML Ti, where H_2^* is H_2 titrated with CO ($1.2 \times 10^{20} H_2/cm^2$ with $\sim 0.0001\%$ CO). The band at $1,994\text{ cm}^{-1}$ is associated with CO adsorbed at Ti sites (spectrum b); a new feature at $2,222\text{ cm}^{-1}$ (and $\sim 2,272\text{ cm}^{-1}$) is due to CO on Ti complexed with hydrogen.

the H_2 dissociation barrier to rapidly approach the high value ($>1\text{ eV}$) for clean Al(111). Our findings demonstrate the importance of controlling the placement of the active species for optimizing the activity in dilute binary systems, and provide important insight into the atomic-scale mechanisms of transition metal catalyzed hydrogenation of Al-based hydrogen storage materials.

Molecular hydrogen activation: Using in situ infrared spectroscopy the first direct experimental evidence for the activation of molecular hydrogen on Ti doped Al(111) was observed. For these experiments CO was used as a probe molecule to investigate the chemical nature of the surface. The changes in the frequency of the CO stretch were shown to be a sensitive probe of the electronic states of surface Ti atoms. Ti arrangement was shown to be a critical parameter for hydrogen activation. Only Ti present in the nearest neighbor or next nearest neighbor configuration was shown to be catalytically active for hydrogen activation with the next nearest sites being more active. The catalytic activity also depends on the Ti concentration/coverage with the highest catalytic activity observed for 0.1 ML Ti coverage. Above 0.1 ML, the additional Ti atoms are inactive. Once dissociated, the hydrogen spills over from these catalytic sites on Al and prevents further CO adsorption on Al. It is interesting to note that CO molecules, selectively adsorbed on catalytically active sites, form a complex with activated hydrogen that is removed at remarkably low temperatures (115 K). These results provide the first direct evidence that Ti-doped Al can carry out the essential first step of molecular hydrogen activation under nearly barrierless conditions, thereby challenging the monopoly of noble metals in hydrogen activation.

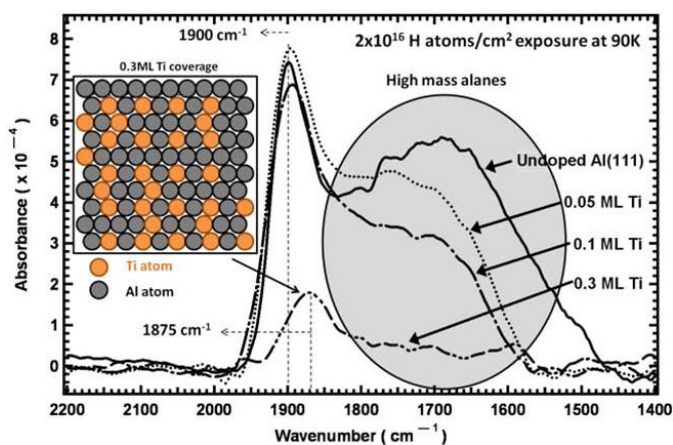


FIGURE 2. Infrared absorbance spectra obtained after saturating four different Al(111) surfaces at 90 K with alanes, using atomic H exposures of $\sim 2 \times 10^{16} H\text{ atoms/cm}^2$: clean (undoped) Al(111) surfaces; 0.05 ML Ti, 0.1 ML Ti, 0.3 ML Ti. The broad band at $1,600\text{ cm}^{-1}$ is associated with bridge hydrogen of high mass alanes formed by oligomerization and the intensity is reduced with increasing Ti.

Effect of Ti on alane mobility and formation: Alanes are critical intermediates in hydrogen storage reactions for mass transport during the formation of complex metal hydrides. The initiation of alane formation occurs through the saturation of steps on the Al surface by H atoms followed by diffusion of small, weakly adsorbed alane clusters on the Al surface, leading to subsequent oligomerization (formation of larger alanes). For Ti doped Al(111) surfaces the diffusion dynamics and oligomerization rates are severely altered as indicated by a marked decrease of higher mass alane concentrations. The mobility of chemisorbed H on Ti-doped Al surfaces at 90 K is substantially lowered by small Ti coverages compared to undoped Al surfaces. Lower mobility leads to a lower diffusion of H to steps, and therefore slows the replenishment of H as AlH_3 , which is eventually released as a mobile, physisorbed species. Titanium also stabilizes Al surface atoms (higher cohesive energy). As a result, fewer Al adatoms (particularly step Al atoms) are available for the formation of AlH_3 , further lowering the rate of alane production.

The location of Ti atoms can also influence alane mobility. When Ti atoms are deposited at 90 K, they remain mostly on the surface, substituting for surface Al atoms. In contrast, when Ti is deposited at 300 K most Ti atoms are thermodynamically expected to go subsurface and therefore there are fewer surface Ti atoms than when deposited at 90 K. Since surface Ti hinders kinetics by trapping H atoms, the Ti deposited at 300 K does not reduce alane formation as much as Ti deposited at 90 K. The incorporation of Ti also lowers the alane desorption temperature primarily due to induced Al-H bond breaking and lower partitioning of thermal energy in translational modes (with Ti doping the diffusing alane clusters are trapped thereby losing

translational modes and thus the rotational modes are populated leading to lower temperatures of desorption).

Surface and solution phase calculation: many alane-amine adducts can be formed at low temperature and pressures from a reaction between H_2 and Ti-doped aluminum suspended in ether solutions of tertiary amines. However, the triethylamine (TEA)-alane cannot be formed by a direct reaction of TEA with AlH_3 formed on the doped aluminum powder. Surface calculations indicate that stabilizing amine molecules can interact with AlH_3 and pull it off the aluminum surface. Since a weak electron donor such as TEA cannot compete with the strong binding energy (27.8 kcal/mol) between AlH_3 and Al(111) surface, the AlH_3 -TEA adduct is not obtained in such an experiment.

Figure 3 shows the optimized structures of different adsorbates on Al(111) surface. A TEA molecule next to AlH_3 does not affect the bonding between AlH_3 and the surface (Figure 3b), which is 2.31 Å and is similar with that of an isolated AlH_3 on Al(111) (Figure 3a). The Al-N distance is 2.43 Å, which is much longer than in the isolated AlH_3 -TEA cluster in gas phase (2.10 Å), indicating weak interaction between AlH_3 and amine. When a dimethylethylamine (DMEA) (Figure 3c) approaches the surface, a strong interaction between Al and N drags AlH_3 away, resulting in a longer distance between Al and the surface. The calculations suggest that removing AlH_3 from the Ti-doped Al(111) surface is the crucial step in alane-amine formation. If it is not removed, the AlH_3 blocks the surface sites and shuts down the surface reaction in which the AlH_3 is formed. The calculations suggest that two properties of the amine are important for promoting alane-amine formation: a strong electron donor with minimal steric hindrance for binding to AlH_3 .

The stabilized alane complexes need to be decomposed to regenerate AlH_3 . An important requirement is that the complex must be sufficiently unstable that the stabilizing molecule is removed before hydrogen is lost from AlH_3 . We have examined five amines [DMEA, $N(CH_3)(C_4H_8)$

(N-methyl-pyrrolidine), DEMA (diethylmethylamine), $N(CH_3)(C_5H_{10})$ (N-methyl-piperidine), TEA] and one ether (Me_2O) which are potential candidates for successful thermal decomposition of alane adducts. Monomer, bis, and dimer complex geometries were all considered. The most stable structures of each complex are shown in Figure 3d. The binding Gibbs free energies were calculated and the overall order of alane adducts stability is $DMEA-AlH_3 > N(CH_3)(C_5H_{10})-AlH_3 > DEMA-AlH_3 > Me_2O-AlH_3 > N(CH_3)(C_4H_8)-AlH_3 > TEA-AlH_3$. This trend is able to provide guidance for thermal decomposition strategies.

Future Work

1. Investigate the formation of alane amine and alanate amine adducts by low pressure hydrogenation and identify routes for adduct separation either directly or through transamination (amine exchange).
2. The formation of alane amine and alanate amine complexes will be investigated using in situ infrared and Raman spectroscopy.
3. Spectroscopy experiments will be performed on Al(100) and Al(111) surfaces to study the effect of crystal morphology on alane formation using a variety of different catalysts (TiO₂, Zr, Co, Pd). The nature of the catalyst sites, activity, and arrangements will be investigated.
4. We will explore the effect of solvation on the hydrogenation process and investigate the interaction between the adsorbed surface species and the solute/solvent.

Publications (selected) acknowledging the grant or contract

1. "Site-Dependent Activity of Atomic Ti Catalysts in Al-Based Hydrogen Storage Materials", A. Al-Mahboob, E. Muller, A. Karim, J.T. Muckerman, C.V. Ciobanu, and P. Sutter, *Angewandte Chemie Int. Ed.*, submitted (2012).

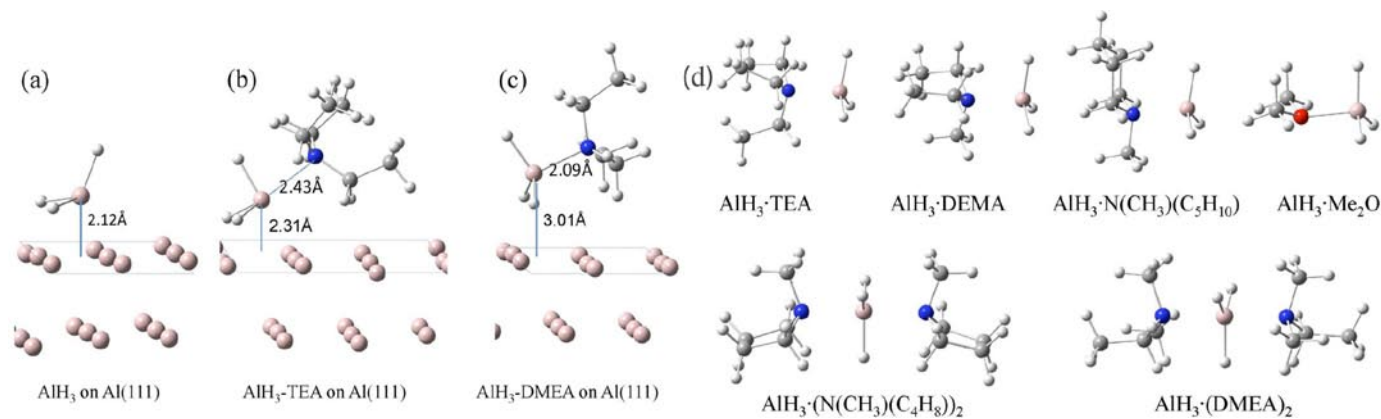


FIGURE 3. Optimized structures of (a) AlH_3 , (b) AlH_3 -TEA, (c) AlH_3 -DMEA on Al(111) surface. (d) Optimized geometries of the most stable configuration of different alane complexes in Et_2O .

2. "Investigation of LiAlH₄-THF formation by direct hydrogenation of catalyzed Al and LiH" D. Lacinca, L. Yang, I. Chopra, J. Muckerman, Y. Chabal, J. Graetz, *Phys. Chem. Chem. Phys.* DOI: 10.1039/c2cp40493a (2012).
3. "Effect of Titanium doping of Al(111) Surfaces on Alane Formation, Mobility, and Desorption" S. Chopra, S. Chaudhuri, J.-F. Veyan, J. Graetz, and Y. J. Chabal, *J. Phys. Chem. C*, **115** 16701 (2011).
4. "Turning aluminium into a noble-metal-like catalyst for low-temperature activation of molecular hydrogen" I.S. Chopra, S. Chaudhuri, J.-F. Veyan, and Y.J. Chabal, *Nat. Mat.*, **10** 884 (2011).
5. "Regeneration of Aluminum Hydride using Trimethylamine" D. Lacinca, J. Wegrzyn, J. Reilly, J. Johnson, Y. Celebi and J. Graetz, *J. Phys. Chem. C*, **115** 3789 (2011).

IV.H.13 Theory of Hydrogen Storage in Complex Hydrides

Christopher Wolverton

Department of Materials Science & Engineering,
Northwestern University
2220 Campus Drive, Room 2036
Evanston, IL 60208-3108
Phone: (734) 678-6319
Email: c-wolverton@northwestern.edu

Vidvuds Ozolins

Department of Materials Science & Engineering,
University of California, Los Angeles

DOE Program Officer: James Davenport

Program Manager

Theoretical Condensed Matter Physics

Office of Basic Energy Sciences

Email: James.Davenport@science.doe.gov

Phone: (301) 903-0035

Objectives

Using first-principles methods, determine the atomic-level processes that are rate limiting in hydrogen storage reactions involving complex hydrides. The energetics of point defects are calculated in order to find those that form in the largest concentrations and the mobility of these defects is obtained from stochastic Kinetic Monte Carlo methods. The activation energy from these calculations is used to determine whether mass transport may be rate-limiting in various storage reactions, both during dehydrogenation and rehydrogenation. Methods are also being developed to study nucleation and to determine its role in the kinetics of hydrogen storage reactions.

Technical Barriers

The slow kinetics observed during absorption and desorption of hydrogen in complex hydrides limits their applicability in real system. However, it is not clear in many cases what the rate-limiting processes are in these reactions. Identification of these rate-limiting processes will aid the improvement of reaction rates and the design of new catalysts.

Abstract

Complex metal hydrides are attractive as potential storage media due to the large volumetric and gravimetric hydrogen densities. However, the absorption and desorption of hydrogen is generally too slow for practical applications

under the conditions that exist in systems using proton exchange membrane fuel cells. It is therefore important that an understanding of the kinetic processes in these reactions be developed in order to guide further improvement of reaction rates. Experimental evidence has shown that mass transport may be rate limiting in some hydrogen storage reactions. In particular, metal-containing point defects have been identified as a potential mechanism for this transport in the sodium alanate system [1,2]. Methods have been developed to study the role of point defects during mass transport at the atomic level using properties obtained from ab-initio density functional theory (DFT) calculations. In this model, chemical potential gradients that are developed in a system that is out of equilibrium (that is, at temperatures other than the equilibrium temperature for the reaction) drive diffusion of defects between regions of different phases. These differences in chemical potentials are manifested as concentration gradients of defects, which are obtained after calculating the associated formation energies. Where necessary, the mobility of these defects is studied using Kinetic Monte Carlo simulations that are parameterized using DFT calculations. Together, these provide the necessary parameters to find the flux of defects through the phases involved in a particular reaction. The activation energy of this flux is compared to experimentally determined activation energy for the reaction in order to determine if mass transport may be rate limiting. In systems for which there is no experimentally measured activation energy, the calculated value can be used to screen for those reactions that may be kinetically limited, assuming that bulk diffusion is a requisite for the reaction.

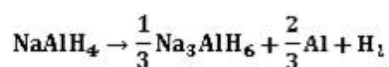
Progress Report

We have developed a model that describes mass transport via the diffusion of point defects during hydrogen storage reactions using properties from first-principles calculations. In this model, chemical potentials are set by local equilibrium conditions. At temperatures other than the equilibrium temperature for the reaction, this leads to gradients in the chemical potentials between interfaces of different phases, which drives mass transport. Using DFT, we calculate the formation energies of native point defects in all of the phases involved in a reaction and use Kinetic Monte Carlo simulations to determine their diffusivities. From this we calculate the flux of defects as $J = -D\nabla C$, where D is the diffusivity and ∇C is the concentration gradient between interfaces. Comparing then to the Arrhenius equation, the activation energy is equal to

$$E_{\text{act}} = -k_{\text{B}} \frac{\partial \ln J}{\partial (1/T)}$$

We have applied this model to the storage reactions involving NaAlH_4 , Li_3AlH_6 and $\text{B}_{20}\text{H}_{16}$.

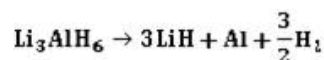
The first step in the dehydrogenation of sodium alanate follows



where there is experimental evidence that mass transport may be rate limiting when doped with small amounts of Ti [1,2]. We have calculated the formation energies of native defects in all three solid phases. From this, we identify neutral AlH_3 vacancies, negatively charged Na vacancies, and positively charged AlH_4 vacancies as the metal-containing defects that form in the largest concentrations in NaAlH_4 . In Na_3AlH_6 , the metal defect with the largest concentration is negatively charged Na vacancies, which are balanced by positively charged H vacancies. We have calculated the diffusivities of these defects and the resulting fluxes are shown as a function of temperature in Figure 1. Of these defects, the one with the largest flux is the Na vacancy in Na_3AlH_6 (a product phase of the reaction), which we identify as the defect that facilitates

mass transport during this reaction. The calculated activation energy for the formation and migration of this defect is 70 kJ/mol, near to the experimentally obtained activation energy for the reaction of 80 kJ/mol in Ti-doped systems [3]. From this we conclude that mass transport is the rate-limiting step in the dehydrogenation of Ti-doped sodium alanate.

The second step in the dehydrogenation of lithium alanate is



where the measured activation energy is 100 kJ/mol [4]. In this system, the relevant mass flux is through the initial phase, Li_3AlH_6 . Four defects have been found to have large concentration gradients in this system: positively charged H vacancies and Li interstitials, negative Li vacancies, and neutral LiH vacancies. Of these, the two Li defects have the largest gradients and are therefore expected to dominate mass transport. The calculated formation enthalpy for both of these defects is equal to 86 kJ/mol. With the addition of the diffusion barrier (the calculation of which is ongoing),

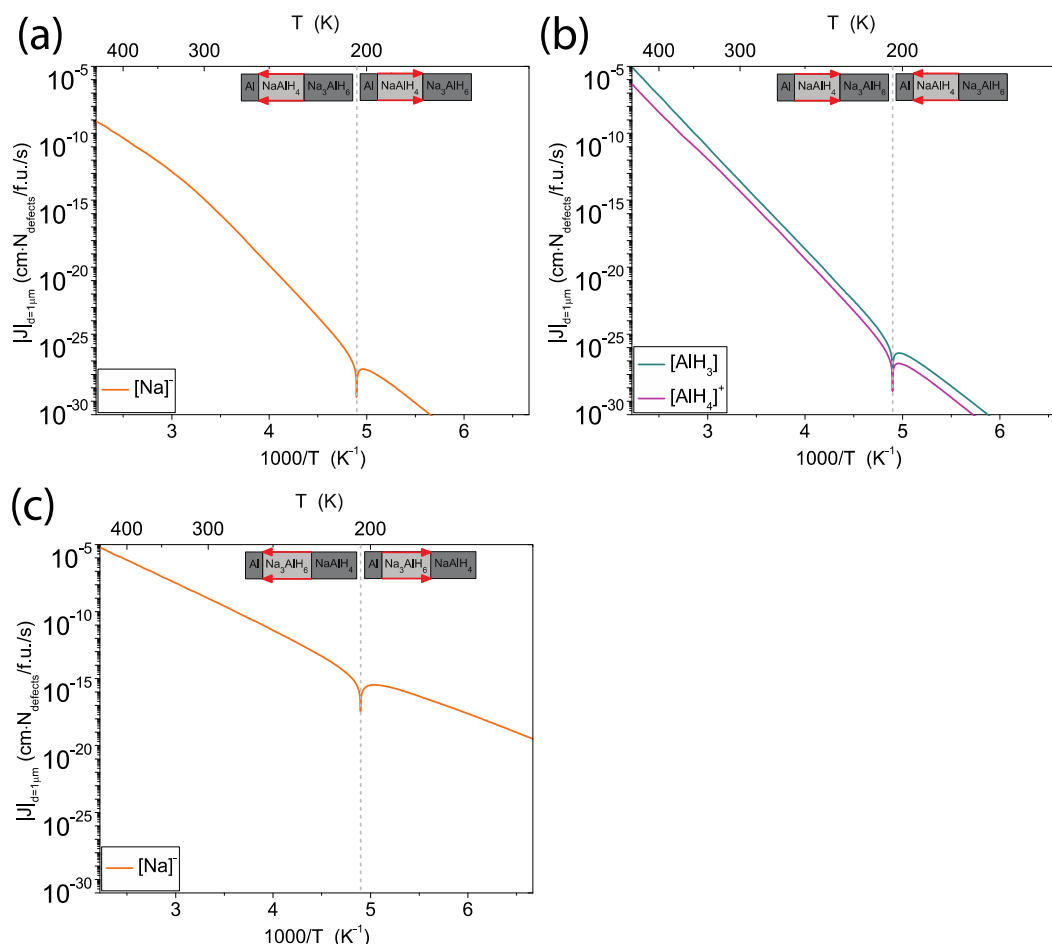


FIGURE 1. Calculated flux of defects in NaAlH_4 (a, b) and Na_3AlH_6 (c).

the activation energy for this flux will likely be near to the measured activation energy for the reaction. It is therefore likely that mass transport is also rate limiting in this reaction.

Finally, we have calculated the formation energies of native defects in the dehydrogenation of $B_{20}H_{16}$ into pure boron and hydrogen gas. We find that the formation energy of atomic hydrogen in boron is much larger than the defect formation energies in $B_{20}H_{16}$ so that diffusion through this phase does not facilitate mass transport. Of the defects in $B_{20}H_{16}$, the lowest formation energy is of interstitial H_2 in a neutral charge state and all other defects are predicted to occur in negligible concentrations compared to it. The formation enthalpy for this defect is equal to 51 kJ/mol under dehydrogenation conditions. Even with the addition of the diffusion barrier, this likely represents a relatively low activation energy. Therefore, if mass transport is rate limiting in this reaction, it should proceed relatively rapidly compared to other storage reactions. However, it is still possible that some other process besides bulk diffusion is limiting the reaction.

Future Work

Having examined mass transport in a number of reactions, we will begin to study nucleation as another possible kinetically limiting process. There is experimental evidence that nucleation may be rate limiting in the $MgH_2 + 2LiNH_2$ system where seeding with the product phase, $Li_2Mg(NH)_2$, has been shown to lower the activation energy [5]. We are in the process of developing a stochastic model to study such systems. In particular, a seed of the product phase is modeled in the host and a search is performed for the ground-state configuration. We plan to use classical potentials to model the energetics that are fit to each system individually using properties from first-principles calculations. The goal is to search for additional reactions that may be kinetically limited by nucleation.

References

1. O. Kircher and M. Fichtner, *J. Appl. Phys.* 95, **2004**, 7748.
2. W. Lohstroh and M. Fichtner, *Phys. Rev. B* 75, **2007**, 184106.
3. K.J. Gross, G.J. Thomas, and C.M. Jensen, *J. Alloy. Compd.* 330, **2002**, 683.
4. R.A. Varin and L. Zbronic, *J. Alloy. Compd.* 509, **2010**, S736.
5. A. Sudik, J. Yang, D. Halliday, and C. Wolverton, *J. Phys. Chem C*, 111, **2007**, 6568.

Publications acknowledging grant

1. G. Grimvall, B. Magyari-Köpe, V. Ozolins, and K. Persson, "Lattice instabilities in metallic elements," *Reviews of Modern Physics* (submitted, 2011).
2. Y. Zhang and C. Wolverton, "Predicted crystal structures, phase stabilities, and hydrogen storage properties of metal amidoboranes", *Phys. Rev. B* (submitted, 2011).
3. D. Farrell and C. Wolverton, "First-Principles Study of Vacancies and Hydrogen Interstitials Under Varied Chemical Conditions in $Li_4BN_3H_{10}$ ", *Phys. Rev. B* (submitted, 2012).
4. D. Farrell and C. Wolverton, "Structure and Diffusion in Liquid Complex Hydrides via Ab-Initio Molecular Dynamics", *Phys. Rev. B* (submitted, 2012).
5. B. Meredig and C. Wolverton, "An Automatic Symmetry-Leveraging Approach for Solving Incomplete Many-Atom Crystal Structures", in preparation (2012).
6. Y. Zhang, T. Autrey, and C. Wolverton, "First-principles prediction of intermediate products in the decomposition of metal amidoboranes", in preparation (2012).
7. K. Michel and V. Ozolins, "Theory of Mass Transport in Sodium Alanate", in preparation (2012).
8. K. Michel, Y. Zhang, and C. Wolverton, "The Role of Point Defects in the Formation and Decomposition of $B_{20}H_{16}$ ", in preparation (2012).
9. B. Rolih, H. Gunaydin, X. Zhao, and V. Ozolins, "Metal diffusion pathways during hydrogen release from $LiNH_2/LiH$ ", in preparation (2011).

IV.H.14 Computational Studies of Hydrogen Interactions with Storage Materials

Chris G. Van de Walle (Primary Contact),
Lars Ismer, Anindya Roy, and Anderson Janotti
Materials Department, University of California
Santa Barbara, CA 93106-5050
Phone: (805) 893-7144
Email: vandewalle@mrl.ucsb.edu

DOE Program Officer: James Davenport
Phone: (301) 903-0035
Email: James.Davenport@science.doe.gov

Objectives

Building on our accumulated knowledge of hydrogen interactions with semiconductors and insulators we have been conducting computational studies with the goal of developing new insights for hydrogen interactions with hydrogen storage materials. Using state-of-the-art density functional calculations, our research addresses the energetics and electronic structure of hydrogen atoms interacting with potential storage materials. In contrast to previous computational studies of bulk quantities, our investigations explicitly address the behavior and interactions of individual hydrogen atoms with the host material. Our **overall goal** is twofold: (1) to provide direct insight into the processes of hydrogen uptake and release, and help in developing guidelines for designing storage media with improved storage capacity; and (2) to generate new fundamental knowledge, for instance, about mechanisms that govern ionic transport, the shape of reaction curves, or reaction rates as a function of particle size.

Abstract

Our studies comprise two classes of materials: metal hydrides and complex hydrides. **Metal hydrides** can store large amounts of hydrogen, but due to the high atomic mass of the host element(s) the weight-percent efficiency is typically low. We are focusing on materials in which the atomic mass of the metal is low, such as MgH_2 and AlH_3 . Comprehensive studies of point defects and migration enable us to identify the dominant diffusion mechanisms. We are also performing Kinetic Monte Carlo simulations of the dehydrogenation process. For **complex hydrides**, a major result of our studies is that the point defects that are relevant for transport are all *charged*. Their formation energy (and hence the kinetics of diffusion and decomposition) thus depends on the electron chemical potential, which in turn

is affected by the presence of additives. This explains, for instance, the effect of transition metal impurities on the kinetics. Our recent work has focused on LiBH_4 , LiAlH_4 , and $\text{Li}_2\text{NH/LiNH}_2$. For the latter, we have been able to explain the particle-size dependence of the activation energy for decomposition.

Progress Report

We investigate the kinetics of hydrogen uptake and release in high-capacity hydrogen storage materials using first-principles calculations based on density functional theory. Our approach takes into account that defects and impurities in non-metallic systems can occur in charge states other than the neutral state; this important aspect of the problem had not been addressed in previous computational studies performed by other groups. Our investigations showed that this has extremely important consequences for defect concentration and diffusion, and other groups have now started to apply this methodology as well.

We are constantly expanding our methodology. To more accurately model the electronic structure of materials with a band gap, we have employed the screened hybrid functional of Heyd, Scuseria, and Ernzerhof [1], an approach we successfully applied to AlH_3 [2]. We have also implemented a multiscale approach that combines *ab initio* calculations with Kinetic Monte Carlo simulations, enabling us to model the complete dehydrogenation reaction. Both of these developments go beyond the current state-of-the-art methodology.

1. Dehydrogenation of AlH_3 via Vacancy Clustering Mechanism

Aluminum hydride (AlH_3) has emerged as a prime candidate for hydrogen storage applications [3,4]. We have performed density functional calculations as well as Kinetic Monte Carlo simulations in order to develop a systematic understanding of the hydrogen uptake and release in this material. Though thermodynamically unstable at room temperature, AlH_3 does not decompose and remains stable on a timescale of years [5]. Above 150°C , however, it rapidly decomposes into Al and H_2 [3,6]. The origin of the kinetic barriers responsible for the metastability of AlH_3 has been widely debated [7-9].

We have first used density functional theory calculations to investigate the role played by point defects in the dehydrogenation of AlH_3 . We used a hybrid functional [1], which provides an accurate description of the electronic

structure. Positively charged hydrogen vacancies (V_{H}^+) turn out to play the dominant role in the dehydrogenation of the hydride. We also found that the hydrogen vacancy defects have a strong tendency towards clustering, with binding energies of 0.5 to 1.6 eV. Vacancy clusters of sizes ranging from 2 to 12 were analyzed. The clusters establish the nuclei of a local Al phase which forms inside the hydride during dehydrogenation.

We subsequently performed Kinetic Monte Carlo simulations to model the overall dehydrogenation process, using parameters obtained from first principles. Our results allow us to identify the contributions of the various microscopic mechanisms that govern the dehydrogenation reaction. The overall activation energy for the dehydrogenation process, $E_a = 1.62$ eV, is dominated by the activation energy for self-diffusion of the positively charged hydrogen vacancies, 1.21 eV; this accounts for mass transport and growth of the Al phase cores which drive the AlH_3/Al phase transformation. A second, smaller contribution to the activation energy is related to the nucleation of the Al phase cores. These results clearly indicate that the reaction is diffusion limited, and produce reaction curves that agree well with the experimental observations.

Our research has also produced insights that go well beyond the specific case of dehydrogenation of AlH_3 . Systematic and general classifications of solid-state reactions were presented by Avrami [10] and later by Sharp *et al.* [11], who derived nine different equations for the reaction kinetics, i.e., the fraction of decomposed material as a function of time. Sharp *et al.* classified these as either diffusion controlled (identified by a “square-root-like” onset of the reaction curve) or phase-boundary controlled (“S-shape-like” onset). These classifications have subsequently been widely used in the literature. In the case of dehydrogenation of AlH_3 , an S-shape-like onset is observed, and on this basis it was previously reported that the kinetics must be phase-boundary controlled and that diffusion can be ruled out as a rate-limiting factor (e.g., [12]). Our study, however, clearly demonstrates that the self-diffusion of point defects is the rate-limiting step—and still the reaction curves have an S-shape! This example illustrates that the classification proposed by Sharp *et al.* [11] is too restrictive and can be misleading when used to infer conclusions about microscopic mechanisms.

The Kinetic Monte Carlo simulations and results about shapes of reaction curves have been submitted to the *Journal of Chemical Physics*.

2. Particle-Size Dependence of the Activation Energy for Decomposition of Lithium Amide

Lithium amide (LiNH_2) is a promising material for reversible hydrogen storage [13], yet atomistic mechanisms behind the dehydrogenation process are unknown. The

activation energy for LiNH_2 decomposition has been observed to strongly vary with ball milling [14-16], suggesting a dependence of the thermodynamics and kinetics of the decomposition on the particle size. We have examined these mechanisms based on first-principles calculations for native point defects and defect complexes in LiNH_2 .

Our results show that the decomposition of LiNH_2 into lithium imide (Li_2NH) and ammonia (NH_3) occurs through two competing mechanisms, one involving the formation of native defects in the interior of the material and the other at the surface. As a result, the prevailing mechanism and hence the activation energy depend on the surface-to-volume ratio, or the specific surface area, which changes with the particle size. These insights allow us to explain the observed variations of activation energy.

The results were published in *Angewandte Chemie* and in *Physical Review B*.

Once again this study has implications that go beyond the case of the specific material studied (LiNH_2), but sheds light on kinetics of reactions in bulk *versus* nanoscale systems in general, i.e., not just in hydrogen storage materials. A dependence on particle size has often been observed but a rigorous explanation has been lacking. Our model attributes the differences to the formation of native defects (which are always necessary for diffusion and reactions) in the *bulk* as opposed to on the *surface*. This leads to specific, verifiable differences in activation energies.

3. Decomposition Mechanisms of LiBH_4 and LiAlH_4

Lithium borohydride (LiBH_4) has a high hydrogen density (18.4 wt%) [17] but its high decomposition temperature and slow hydrogen desorption kinetics prevent practical use [18]. Incorporation of certain metal additives has been reported to lower the decomposition temperature and enhance the kinetics [17,19,20], but the mechanisms are poorly understood. Our first-principles calculations show that Li vacancies and interstitials have low formation energies and are highly mobile. These defects can participate in Li-ion conduction, and act as accompanying defects in H and B mass transport. We propose a specific mechanism for the decomposition: LiBH_4 releases borane (BH_3) at the surface or interface, leaving negatively charged H interstitials in the material, which then act as nucleation sites for LiH formation. The diffusion of H interstitials in the bulk is the rate-limiting step in the decomposition kinetics. Li vacancies and interstitials have low formation energies and are highly mobile, and are responsible for maintaining local charge neutrality as other charged defects migrate along the material, as well as assisting in the formation of LiH. Based on this mechanism, the effects of metal additives on hydrogen desorption kinetics can also be explained. This research has been published in the *International Journal of Hydrogen Energy*.

Lithium alanate (LiAlH_4) has a relatively low decomposition temperature [21]. We find that the compound is prone to Frenkel disorder on the Li sublattice: lithium interstitials and vacancies have low formation energies and are highly mobile. They can participate in lithium-ion conduction, and act as accompanying defects in hydrogen mass transport. We have proposed a specific mechanism for the decomposition of LiAlH_4 that involves the formation and migration of negatively charged hydrogen interstitials, Li Frenkel pairs, and AlH_4 vacancies, with the latter constituting the rate-limiting step. Our results also suggest that it is the structure of the negatively charged hydrogen interstitial that determines the hydride phase (Li_3AlH_6 or LiH) in the decomposition products, a relationship that should be further explored in other complex hydrides.

Future Directions

a) Role of hydrogen-related Frenkel pairs for the dehydrogenation kinetics

The aim is to compile the results that we have already obtained for Frenkel pairs in a variety of systems, and carry out calculations for additional materials. The materials include NaAlH_4 , LiBH_4 , $\text{Li}_4\text{BN}_3\text{H}_{10}$, LiNH_2 , Li_2NH , MgH_2 , Mg_2Fe -hydride, Mg_2Ni -hydride, Na_3AlH_6 , LiAlH_4 , and Li_3AlH_6 . The hypothesis is that Frenkel-pair formation may be the rate-limiting step to dehydrogenation and/or mass transport in some cases, while in other cases Frenkel pairs play the role of enabling local charge neutrality. Systematic studies will elucidate the physics.

b) Role of transition metal doping in MgH_2

We are investigating two prominent and effective transition-metal additives, Ni and Fe. The effects on formation energies and migration barriers of point defects will be studied.

References

1. J. Heyd, G.E. Scuseria, M. Ernzerhof, *J. Chem. Phys.* **118**, 8207 (2003); *ibid.* **124**, 219906 (2006).
2. L. Ismer, A. Janotti, and C.G. Van de Walle, *Appl. Phys. Lett.* **97**, 201902 (2010).
3. J. Graetz, *Chem. Soc. Rev.* **38**, 73 (2009).
4. R. Zidan *et al.*, *Chem. Commun.*, 3717 (2009).
5. J. Graetz and J.J. Reilly, *J. Alloys and Compd.* **424**, 262 (2006).
6. H. Saitoh, A. Machida, Y. Katayama, and K. Aoki, *Appl. Phys. Lett.* **93**, 151918 (2008).

7. G. Sandrock *et al.*, *J. Alloys Compd.* **421**, 185 (2006).
8. S. Kato *et al.*, *Appl. Phys. Lett.* **96**, 051912 (2010).
9. L. Senadheera *et al.*, *J. Alloys and Compd.* **463**, 1 (2008).
10. M.J. Avrami, *Chem. Phys.* **7**, 1103 (1939); *ibid.* **8**, 212 (1940).
11. J.H. Sharp, W. Brindley, and B.J. Narahari Achar, *Chem. Phys.* **8**, 212 (1940).
12. J. Graetz, and J.J. Reilly, *J. Phys. Chem. B* **109**, 22181 (2005).
13. P. Chen, Z.T. Xiong, J.Z. Luo, J.Y. Lin, K.L. Tan, *Nature* **420**, 302 (2002).
14. T. Markmaitree, R. Ren, L.L. Shaw, *J. Phys. Chem. B* **110**, 20710 (2006).
15. L.L. Shaw, R. Ren, T. Markmaitree, W. Osborn, *J. Alloys Compds.* **448**, 263 (2008).
16. R.A. Varin, M. Jang, M. Polanski, *J. Alloys Compds.* **491**, 658 (2010).
17. A. Züttel *et al.*, *J. Power Sources* **118**, 1 (2003).
18. P. Mauron *et al.*, *J. Phys. Chem. B* **112**, 906 (2008).
19. H.W. Li, Y. Yan, S.I. Orimo, A. Züttel, and C.M. Jensen, *Energies* **4**, 185 (2011).
20. C. Li, P. Peng, D.W. Zhou, and L. Wan, *Int. J. Hydrogen Energy* **36**, 14512 (2011).
21. S. Orimo *et al.*, *Chem. Rev.* **107**, 4111 (2007).

Publications acknowledging the grant (since August 2010)

1. “Point-defect-mediated dehydrogenation of AlH_3 ”, L. Ismer, A. Janotti, and C.G. Van de Walle, *Appl. Phys. Lett.* **97**, 201902 (2010).
2. “Stability and mobility of native point defects in AlH_3 ”, L. Ismer, A. Janotti, and C.G. Van de Walle, *J. Alloys Compd.* **509S**, S658 (2011).
3. “The particle-size dependence of the activation energy for decomposition of lithium amide”, K. Hoang, A. Janotti, and C.G. Van de Walle, *Angew. Chem. Int. Ed.* **123**, 10352 (2011).
4. “Mechanisms for the decomposition and dehydrogenation of Li amide/imide”, K. Hoang, A. Janotti, and C.G. Van de Walle, *Phys. Rev. B* **85**, 064115 (2012).
5. “Mechanism for the decomposition of lithium borohydride”, K. Hoang and C.G. Van de Walle, *Int. J. Hydrogen Energy* **37**, 5825 (2012).
6. “Decomposition mechanism and the effects of metal additives on the kinetics of lithium alanate”, K. Hoang, A. Janotti, and C.G. Van de Walle, *Phys. Chem. Chem. Phys.* **14**, 2840 (2012).
7. “Dehydrogenation of AlH_3 via vacancy clustering mechanism”, L. Ismer, A. Janotti, and C.G. Van de Walle, submitted to *J. Phys. Chem.*

IV.H.15 In Situ NMR to Understand Hydrogen Storage Chemistry

Mark Conradi (Primary Contact), Eric Sorte,
Tim Ivancic, David Shane, Laura Rayhel, Bob Corey
Washington University
Department of Physics
St. Louis, MO 63130
Phone: (314) 935-6292
Email: msc@wustl.edu

DOE Program Manager: Dr. Refik Kortan
Email: refik.kortan@science.doe.gov

Objectives

- To understand the hydrogen chemistry of hydrogen storage solids.
- To develop nuclear magnetic resonance (NMR) techniques for in situ probing of these systems.

Technical Barriers

- Reaction intermediate species may have very low concentrations and/or short lifetimes.
- Intermediate may be difficult to study by an array of analytical techniques.

Abstract

We have used in situ NMR of 27-aluminum to discover a new mobile species in the hydrogen chemistry of NaAlH₄. This species is identified by its aluminum chemical shift of 105 ppm, S105. It appears that this is a defect-ridden form of NaAlH₄ itself. This species is likely the long-sought mechanism by which metal atoms are transported in the dehydriding and rehydriding reactions of the alanate. Structure searching has identified a new structure of NaAlH₄ that has a chemical shift in good agreement with S105. It is not yet clear what makes the defect concentration unusually large in this structure. We have developed a new method of measuring the rate of exchange between metal-hydrides and the surrounding gas phase. The H nuclear spins in the hydride have two paths for relaxation: (1) intrinsic (and usually slow) relaxation in the hydride, and (2) exchange with H from the very rapidly relaxing gas phase. In this technique, the observed effective relaxation rate in the hydride is a good estimate of the rate of exchange from the hydride to the gas phase. We have applied the method to PdH_x and PdD_x and find overall exchange activation energies of 0.32 eV in both.

The gamma phase of Mg(BH₄)₂ has 33% open space, suggesting that BH₄ diffusion may be substantially enhanced

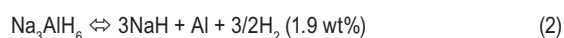
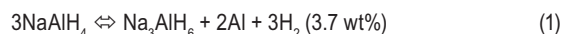
in this phase. However, our hydrogen NMR lineshapes and T_{1D} (slow-motion) measurements show no evidence of diffusion (to 100 s⁻¹) at temperatures to 150°C. The borohydride group reorientations in this phase have a large barrier energy, much like the alpha phase, as measured through the hydrogen T₁ relaxation. At and above 175°C, the gamma phase transforms to something equal or very similar to the beta phase, as demonstrated by the hydrogen T₁ and X-ray diffraction.

Sodium hydride is one of the simplest hydrides, yet little is known about its H and Na diffusion. We report H and ²³Na lineshapes and T₁, as well as hydrogen T_{1p} for commercial samples of NaH and a sample of pure and ball-milled NaH from Jensen in Hawaii. For the commercial material, there is an increasing fraction of mobile H as the temperature is increased. The remainder of the H line narrows between 250 and 300°C. By 300°C, the sodium line is only narrowed by a factor of 2, showing that Na-Na interactions are not being averaged (the Na are not yet diffusing). The UH sample of ball-milled NaH displays line narrowing of the hydrogen at a remarkably lower temperature (about 130°C).

Progress Report

NaAlH₄

NaAlH₄ is a complex hydride, having covalently bonded AlH₄⁻ anions ionically bonded with the Na⁺ counterions. While the (complex) LiBH₄ and Mg(BH₄)₂ systems have larger theoretical reversible hydrogen mass fractions (18.4 and 14.9%), NaAlH₄ (5.6 wt%) remains the archetypal complex storage system when doped with titanium or other metals. Its status reflects the early discovery of the catalysis effect, the large amount of subsequent NaAlH₄ research, and the prospect of operation near 100°C, using waste heat from a polymer electrolyte membrane hydrogen fuel cell. The decomposition of this system occurs in two generally distinct steps, each releasing H₂ gas and Al metal:



Despite years of intense study, the mechanism of the above reactions and the role of the catalyst remain uncertain. Good reviews of the current knowledge on NaAlH₄ have appeared.

In the rehydriding direction, spent NaH + Al metal under excess H₂ gas pressure combine to form NaAlH₄. Therefore, spatially separated Na and Al atoms are somehow brought into intimate (stoichiometric) contact. This transport of metal atoms has been identified as the likely reaction

bottleneck, according to H-D isotopic scrambling and other measurements. Therefore, we and others have hypothesized the existence of a mobile, Al- or Na-bearing species that is a key intermediate in the reaction(s).

We report here the discovery by in situ ^{27}Al NMR spectroscopy of just such a mobile, Al-bearing species. Crucially, the new species (i.e. not one of the well-known species of reactions 1 and 2), formed at elevated temperature and pressure, can be retained for further study at ambient pressure and temperature.

Taken together, the results suggest that S105 is a highly mobile, Al- and H-bearing entity with an ^{27}Al chemical shift very near that of NaAlH_4 itself. S105 accounts for $\sim 10\%$ of the aluminum spins for undoped NaAlH_4 melted under excess H_2 pressure. We propose that S105 is a highly defective form of NaAlH_4 . In particular, following the calculations of Guyadin et al, the defects are AlH_3 vacancies. Such vacancies were calculated to diffuse on the several picosecond time scale; this would lead to rapid motion of a much larger number of Al and H atoms. This proposal provides natural explanations for the ^{27}Al shift of S105 being close to that of NaAlH_4 , motionally narrowed resonances of S105 in ^{27}Al and hydrogen (but not ^{23}Na) NMR, the large number of Al spins in the S105 line, and the disorder apparent in X-ray diffraction. Crucially, such AlH_3 vacancies would promote the aluminum atom transport needed for rehydriding in reaction 1.

The NMR of S105 shows, for the first time, direct spectroscopic evidence of a mobile chemical intermediate in the hydrogen reactions of NaAlH_4 . Importantly, the new species can be harvested under ambient conditions for further study.

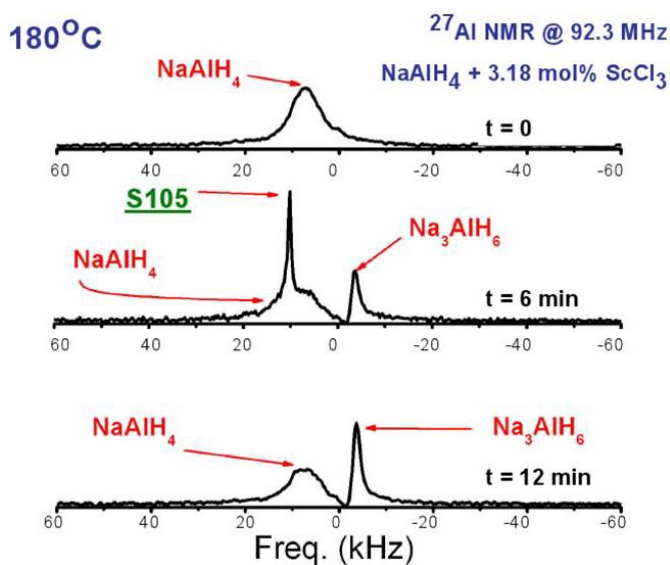


FIGURE 1.

Hydride to Gas Exchange

At thermal equilibrium, many metal-hydrides and deuterides are surrounded by H_2 or D_2 gas at a considerable pressure. Exchange of H or D between the solid and gas phases provides a new pathway for nuclear spin relaxation, beyond the processes that are intrinsic to the solid phase, because of the extremely rapid spin relaxation of the gas at typical conditions. A crucial requirement is that the number of spins in the gas phase must be of the same order as the number of spins in the solid. Thus, the solid powder particles (where H or D is at high density compared to the gas) should be spread out in space, supported on a substrate in dilute fashion.

This effect, an increase in the apparent relaxation rate by exchange with the surrounding gas, has been observed. More recently, it was used to determine the exchange rate K_{pg} (from palladium to gas) of H in PdH_x in equilibrium with H_2 gas. The probability of successful crossing of the surface barrier (from palladium to gas) was estimated as 2.8×10^{-7} at 20°C , in agreement with earlier work based on H,D exchange.

The PdD_x/D_2 system has a larger ratio of the intrinsic relaxation rate of the gas to the intrinsic relaxation rate of the solid, compared to the PdH_x/H_2 system. Thus, the exchange rate of D atoms from the solid metallic phase to the gas phase, K_{pg} , can be followed over a wider range of temperatures and rates. This allows a more accurate determination of the activation energy for the exchange

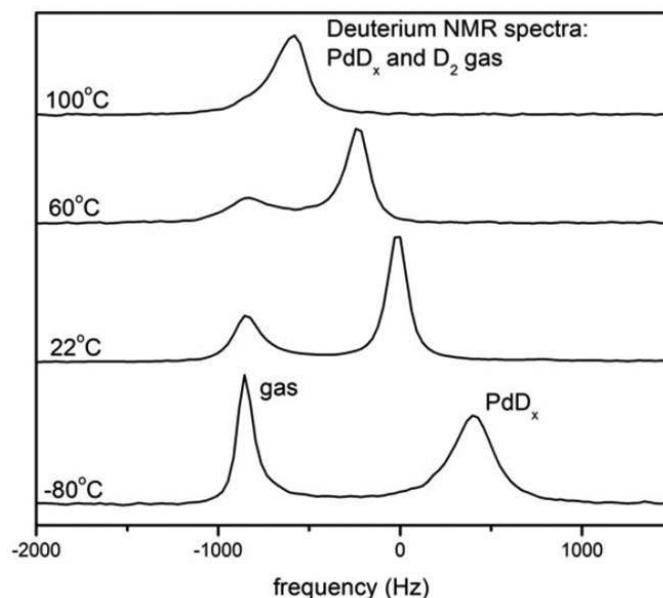


FIGURE 2. Deuterium NMR spectra of PdD_x and the surrounding D_2 gas at several temperatures. The 22°C spectrum shows that there are about half as many D nuclear spins in the gas as in the deuteride. At -80°C , PdD_x broadens due to the slowing of the internal motions. At 60°C , the gas resonance is broadened by gas-deuteride exchange; by 100°C , the resonances are partially merged.

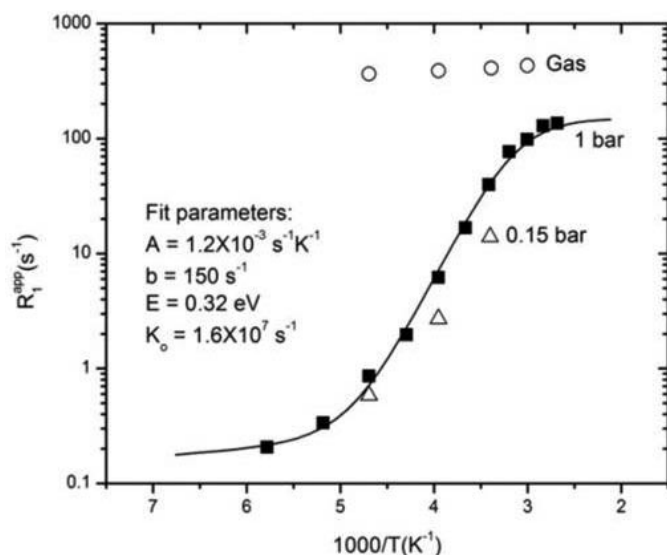


FIGURE 3.

process. Here in PdD_x/D_2 , we follow K_{pg} over about three decades and find (Figure 3) K_{pg} to have $E = 0.32 \text{ eV} \pm 10\%$. A re-analysis of the relaxation data from the PdH_x/H_2 system (Figure 4) shows very similar exchange rates and activation energy, compared to the deuterium system.

$\gamma\text{-Mg}(\text{BH}_4)_2$

Metal borohydrides are attractive candidates for hydrogen storage for transportation and other applications, due to their typically large mass fractions of hydrogen. The utilization of metal borohydrides is often hampered by slow hydrogen release and uptake kinetics, which call for fundamental studies of mobility and dynamics of hydrogen and the complex tetrahydridoborate anions, BH_4^- , in this class of materials.

Magnesium borohydride has an extreme structural flexibility (several polymorphs have been observed) and high gravimetric hydrogen storage density of $\rho_{\text{m}} = 14.9 \text{ wt}\% \text{ H}_2$, and it stores hydrogen reversibly. It is therefore considered one of the most interesting hydrogen storage materials. However, hydrogen uptake (from the dehydrided state) has up to now only been realized at relatively harsh conditions (400°C and 950 bar).

A new nanoporous polymorph of magnesium borohydride denoted $\gamma\text{-Mg}(\text{BH}_4)_2$ was recently discovered. This polymorph crystallizes with space group symmetry $I\bar{d}\text{-}3a$ and has a remarkably low material density of $\rho = 0.55 \text{ g/cm}^3$ due to a three-dimensional net of interpenetrating channels of $\sim 8 \text{ \AA}$ diameter giving $\sim 33\%$ empty void space.

The large void space in the γ -phase crystal structure suggests that rapid diffusion of BH_4 units, as observed in LiBH_4 but not in α or $\beta\text{-Mg}(\text{BH}_4)_2$, may occur at an enhanced

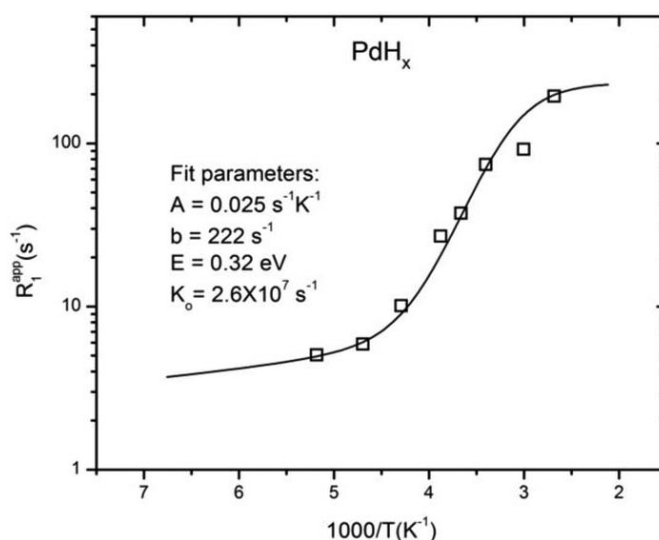


FIGURE 4. Nuclear spin-lattice relaxation data for PdH_x surrounded by 0.9 bar H_2 (at 20°C). The points are data from reference 3; the solid curve is a fit using equations (5) and (6) with the listed parameters.

rate in the γ -phase. Rapid diffusion of BH_4 could have a positive effect on the kinetics of dehydriding and rehydriding of this material. This has prompted our present investigation of hydrogen NMR lineshape and T_{1D} (T_{1D} is sensitive to motions which are too slow to narrow the line). Hydrogen T_1 is also reported, because it is determined by and can report upon reorientations of the BH_4 units.

Hydrogen NMR lineshapes reveal no motional narrowing due to translational self-diffusion in the main part of the resonance, up to 175°C. “Slow” motion measurements by means of the hydrogen T_{1D} indicate the absence of translational motions faster than 10^2 s^{-1} up to this temperature. Thus, despite the large amount (33%) of open volume in $\gamma\text{-Mg}(\text{BH}_4)_2$, we find no evidence for rapid diffusion.

The hydrogen T_1 is controlled by the rate of BH_4 reorientation. Observation of a deep minimum in T_1 at 50°C demonstrates that the mean rate of reorientation is about 10^9 s^{-1} at 50°C. The T_1 behavior of γ -phase is similar to that reported in α -phase, where activation energies for BH_4 reorientation were found to be 0.12, 0.20, and 0.36 eV. By comparison, in β -phase $\text{Mg}(\text{BH}_4)_2$, a T_1 minimum occurs at -135°C and is described by an 0.12 eV activation energy. Thus, the mean activation energy for BH_4 reorientation in γ -phase is high, as in α -phase. The ^{11}B T_1 shows a minimum at 50°C, as well. This is as expected, because the intramolecular B-H dipole interaction, modulated by BH_4 reorientations, drives (in part) both the hydrogen and ^{11}B spin-lattice relaxations.

Our γ -phase material transformed to another phase upon standing at 175°C for 2 h in one case. Subsequent heating to 225°C completed the transformation. A second sample

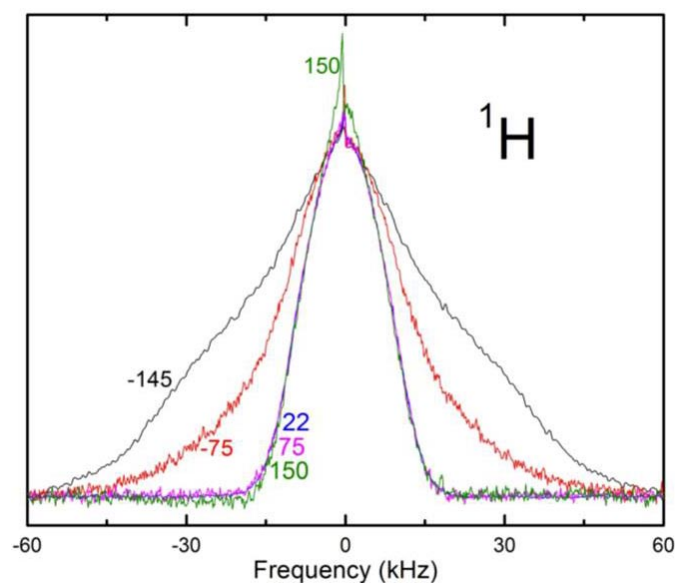


FIGURE 5. Hydrogen NMR spectra of γ -Mg(BH₄)₂ at several temperatures. At -75 and -145°C, pronounced broadening is due to slowing of the BH₄ reorientations. At and above 22°C, no further narrowing of the main resonance occurs, ruling out rapid BH₄ translational diffusion. At the highest temperature, a narrow component appears, reflecting a small fraction of mobile spins, probably from residual solvent.

of γ -phase Mg(BH₄)₂ transformed during 1 h at 250 °C. T₁ of the transformation products down to -125°C were found to be similar but not equal to T₁ of β -Mg(BH₄)₂. The data suggest that the transformation products are largely β -phase. Boron-11 magic-angle spinning NMR of the recovered transformation product demonstrates the transformed material is not significantly dehydrided; essentially all the boron atoms remain as BH₄. Powder X-ray diffraction shows that material TP2 has a crystallographic structure equal to that of the β -polymorph; an amorphous component can not be ruled out.

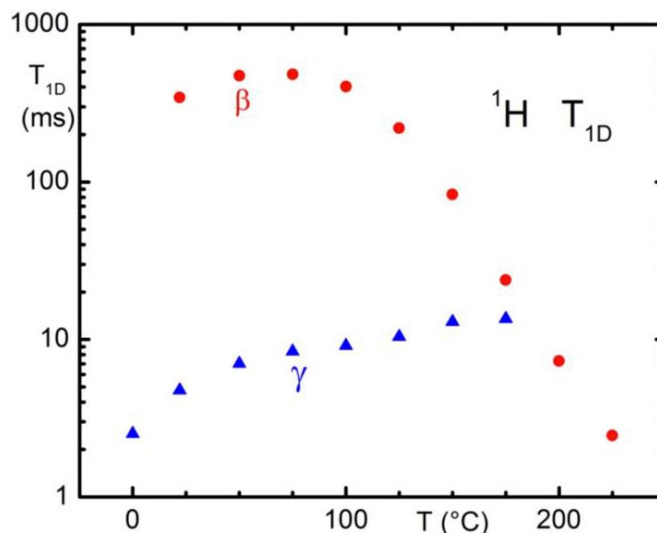


FIGURE 6. Hydrogen NMR measurements of T_{1D} in γ -Mg(BH₄)₂, together with β -polymorph data from reference 14 for comparison. In γ -phase, there is no sharp decrease in T_{1D} at elevated temperatures that would signal thermally activated diffusive hopping with rates 10² s⁻¹ or faster.

Future Directions

Our program is focusing on the complex hydrides. We will look first for systematics in the formation of S105 in NaAlH₄. We will make measurements on pure Na₃AlH₆, with the aim of excluding the hexahydride as the source of S105. Potassium alanate will be examined next, as it is the alanate most similar to sodium alanate. We will extend this work to include Li and Mg borohydrides, because of the large interest generated by those high capacity materials. In each case, the program is aimed at finding mobile intermediate species that are keys to understanding the hydrogen reactions of these storage solids.

IV.H.16 Activation of Small Molecules with Bi-Functional Ambiphilic Catalyst Complexes

Tom Autrey (Primary Contact), Greg Schenter,
Don Camaioni, Abhi Karkamkar, Herman Cho,
Bojana Ginovska-Pangovska

Pacific Northwest National Laboratory
P.O. Box 999 MS#K2-57
Richland, WA 99352
Phone: (509) 375-3792
Email: tom.autrey@pnnl.gov

DOE Program Officer: Raul Miranda

Objectives

The objective of our research is to develop fundamental insight into small molecule activation in molecular complexes that will provide the basis for developing rational approaches in new catalysis design. Our focus is bi-functional – ambiphilic catalyst centers – molecular complexes comprised of both electron-rich and electron-poor sites. We are interested in the development of catalyst structures capable of multiply reactions ranging from the heterolytic activation of hydrogen, important for obtaining high selectivity's in the reduction of molecular structures found in biomass, to the direct activation of CO and CO₂ for conversion to energy storage materials.

Technical Barriers

- Tuning thermodynamics and kinetics of ambiphilic molecular complexes to enhance catalytic efficiency.
- Controlling structure and reactivity to enable catalysis of a wide range of substrates in a wide range on environments.

Abstract

Five years ago few chemists would have predicted that molecular hydrogen could be activated at ambient temperature and pressure using a combination of an amine or phosphine Lewis base with a borane Lewis acid. The accepted view had been that metals and d-electrons are required to activate hydrogen [1]. However, a paradigm shift in our appreciation of hydrogen activation and catalysis was initiated by the reports from the Stephan group [2] that a *frustrated Lewis pair* (FLP) – that is, an ambiphilic complex of a Lewis acid and Lewis base that cannot form a formal Donor – Acceptor dative bond provides a *vacancy* of latent reactivity, between the D and A to heterolytically activate

molecular hydrogen – at room temperature. Recently the collaborative efforts by Stephan & Erker [3,4] and Soós & Papai [5] have demonstrated the use of FLP's in catalytic hydrogenation of polar functional groups. The novel reactivity afforded by a bi-functional catalyst, illustrated in Figure 1, demonstrates that there are new approaches to catalysis and small molecule activation that do not require metals [6].

Recent computational studies suggested a few intriguing proposals to describe the unique reactivity of FLPs; Pápai and co-workers suggested that a *reactive pocket* is formed in loosely organized frustrated pair at an optimal acid-base distance providing bifunctional cooperativity for a synergistic interaction with molecular hydrogen [7]. Wang and co-workers suggest that *geometrical constraints* are important and optimal alignment of the Lewis acid and Lewis base can lower the activation barrier [8]. Pyykko describes an energy decomposition analysis (EDA) of H₂ activation by a FLP suggesting the attraction between the protonic and hydridic hydrogen in the products compensates for the energy required to split H₂ homolytic [9]. Finally, Grimme has put forth a provocative hypothesis – that the molecular or chemical nature of the FLP is not as important as the strong electrostatic attraction induced by the FLP [10]. He notes that the *electric field strength* in FLPs approaches the magnitude required to split H₂ in a vacuum without a barrier and that

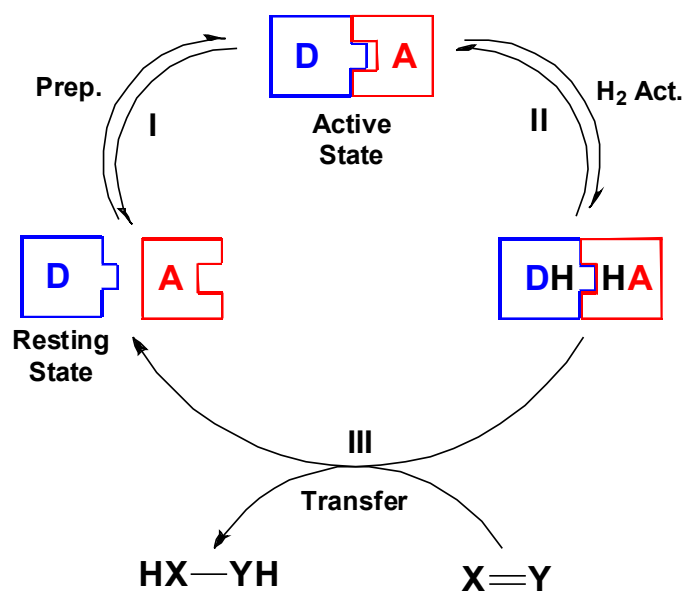


FIGURE 1. Illustration of the catalytic reduction cycle; step I, catalyst preparation; step II, H₂ activation; step III, H₂ transfer.

the rate limiting step for H₂ activation is diffusion into a *prepared Lewis pair* (PLP).

This recent computational work provides some thought-provoking propositions to explain the latent reactivity afforded by bringing together an electron-rich Lewis base and an electron-deficient Lewis acid species – this creates a new reactive *vacancy*. However, there is little experimental insight into either the thermodynamics or kinetics of FLP formation, H₂ activation by FLPs or H₂ transfer from FLPs to unsaturated substrates. **A central theme to our catalysis research program is to minimize the heights of the hills and the depths of the valleys along the reaction pathway.** To this end, we use methods to determine reaction thermodynamics to understand the factors that control the depth of the valleys and measure activation barriers to understand the factors that control the height of the hills in the catalytic reaction cycle. Further to this understanding there are a number of fundamental scientific questions that we will address in our research to maximize the potential of the catalytic cycle outlined in Figure 1:

- Is a sufficient electric field all that is necessary for H₂ activation or are bonding and other environmental factors just as important? Are there geometrical constraints, e.g., specific angles and distances between the Lewis acid and Lewis base to enhance reactivity, both H₂ activation and catalytic H₂ transfer?
- How does the reactivity of a bidentate Lewis acid or base differ from the reactivity of an intramolecular Lewis acid-base complex?
- What parameters best describe the reactivity created in the vacancy, {}, between the Lewis base, D and Lewis acid, A, pair, i.e., D{}A? What is the rate limiting step in the catalytic reduction of polar molecules; hydride transfer, proton transfer, a concerted H⁺/H⁻ transfer?
- How does this distinctive property, i.e., a quasi-open coordination site, {}, formed between an electron rich and electron poor site, correlate with vacancies and defects in heterogeneous catalysis structures and surfaces composed of Lewis acid and Lewis base sites? What properties in these molecular structures are

essential to understand to enable the building of parallel properties in heterogeneous structures?

- What can we learn from fundamental studies of molecular complexes of FLPs combined with transition metals, i.e., ‘tri-functional’ sites to build new catalysts complexes, heterogeneous and homogeneous complexes for small molecule activation and catalysis?
- How general is this phenomena of small molecule activation without metals? How can these *reactive pockets* be optimized for the catalytic reduction of CO₂ or biomass functions, e.g., carbonyls?

Fundamental understanding of novel approaches to catalysis and small molecule activation are of direct relevance to research missions supported by the U.S. Department of Energy to enable basic research science to predict and control matter and energy at the electronic, atomic and molecular levels in order to provide foundations for new energy technologies critical to energy, environment and national security.

Progress Report

In previous research we investigated the heterolytic activation of hydrogen in the *non-frustrated* Lewis acid-base pair, i.e., the pedagogical Lewis acid-base pair, ammonia borane and ammonium borohydride.



In this work we made significant progress on understanding the interaction of protonic and hydridic hydrogen bonding interactions (publishing more than 40 papers in the past 6 years). We focused on ammonium borohydride and ammonia borane because of their relevance to hydrogen storage, which seeks to maximize hydrogen content. However, with our new directions towards catalytic activation of hydrogen, other small molecules, e.g., CO₂, N₂, a wide range of new Lewis acid/base catalyst complexes are now open to study.

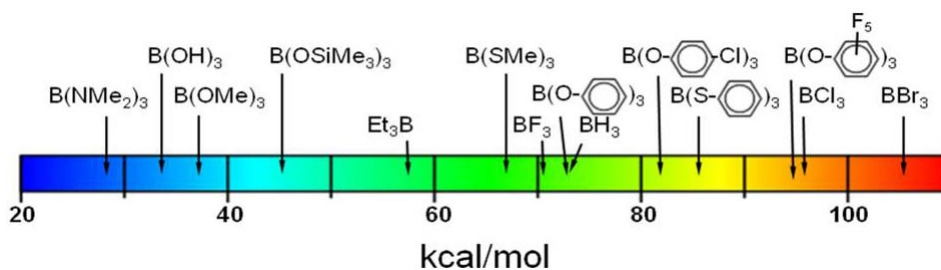


FIGURE 2. Calculated gas phase hydride affinities, ΔH_{HA} , for a series of organic borate esters and BX_3 compounds. Large thermodynamic range, ~90 kcal/mol, suggests high degree of tunability for heterolytic hydrogen activation.

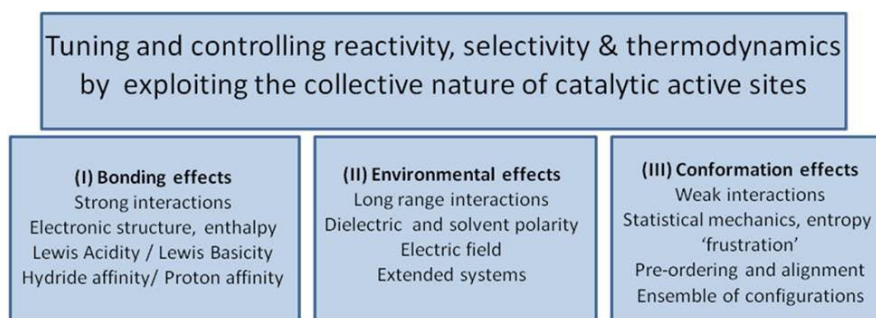


FIGURE 3. Partitioning the effects that give rise to the collective nature of catalysis: (1) bonding, (2) environmental, and (3) conformational factors to determine the reactivity and thermodynamics within an active site. Understand the balance of these factors is a critical bridge between homogeneous and heterogeneous catalysis.

Of direct relevance is the work we performed towards regenerating ammonia borane in which we developed structure reactivity relationships for a series of Lewis acidic borate esters, [11] shown in Scheme 1. This work shows how modification of the structure of the borate ester profoundly affects the hydride affinity of the Lewis acid, a critical parameter that can be tuned to optimize reactivity and thermochemistry of FLPs [12]. Therefore, it is a natural transition for our group to expand the research to investigate small molecule activation within Lewis acid/base pairs using skills and methodologies that we have previously developed.

Future Directions

We are developing a new research task to obtain fundamental insight into the unique reactivity of FLP catalysts. Our proposed research and expertise in thermodynamics and kinetics perfectly complements the ongoing international research in FLP catalysis.

The ultimate goal of our research is to develop predictive models for the rational design of new and novel catalysis systems relevant to DOE missions. Specifically, to develop descriptive models that permits the tuning and control of reactivity of multi-functional catalysis complexes. This will require an in-depth understanding of the factors that control chemical reactivity and thermodynamics in a catalytic active site by characterizing the collective nature of the reacting system, Figure 3. Specifically, a model that describes *bonding, environmental, and conformational factors* in an active site is required to control reactivity and tune thermodynamics. Understanding the balance of these factors can potentially provide a rational bridge between homogeneous and heterogeneous catalysis.

References

1. G Kubas. *Science* **2006**, 314, 1096.
2. GC Welch, RRS Juan, JD Masuda, DW Stephan, *Science* **2006**, 314, 1124.

3. PA Chase, GC Welch, T. Junea, G Erker, DW Stephan, D.W. *Angew. Chem. Int. Ed.* **2007**, 46, 8050.
4. Stephan, D.W.; Erker, G. *Angew. Chem. Int. Ed.* **2010**, 49, 46.
5. G Erős, H Mehdi, I Pápai, TA Rokob, P Király, G Tárkányi, T Soós, *Angew. Chem. Int. Ed.* **2010**, 49.
6. PP Power, *Nature* **2010**, 463.
7. Rokob, T. A.; Hamza, A.; Stirling, A.; Soós, T.; Pápai, I. *Angew. Chem.* **2008**, 120, 2469.
8. Lu, G; Li, L.; Zhao, L.; Huang, F.; Wang, Z-X. *Inorg. Chem.* **2010**, 49, 295.
9. Pyykko, P.; Wang, C. *Phys Chem. Chem. Phys.* **2010**, 12, 149.
10. Grimme, S.; Kruse, H.; Goerigk, L.; Erker, G. *Angew. Chem. Int. Ed.* **2010**, 49, 1402.
11. MT Mock, RG Potter, DM Camaioni, J Li, WG Dougherty, WS Kassel, B Twamley, DL DuBois. *J. Am. Chem. Soc.*, **2009**, 131, 14454
12. GC Welch, L Cabrera, PA Chase, E Hollink, JD Masuda, P Wei, DW Stephan. *Dalton* **2007**, 3407.

Publications (selected) acknowledging the grant or contract

1. Shawn M. Kathmann, Christopher J. Mundy, Gregory K. Schenter, Tom Autrey, Philippe Aeberhard, Bill David, Martin O. Jones, Timmy Ramirez-Cuesta. Understanding Vibrational Anharmonicity and Phonon Dispersion in Solid Ammonia Borane. *J. Phys Chem A*, **2012**, ASAP.
2. Tom Autrey, Mark Bowden, Abhi Karkamkar. Control of hydrogen release and uptake in amine borane molecular complexes: Thermodynamics of ammonia borane, ammonium borohydride, and the diammoniate of diborane. *Faraday Disc.*, **2011**, 151, 157.
3. Mark Bowden and Tom Autrey. Characterization and Mechanistic Studies of the Dehydrogenation of NHxBHx Materials. *Current Opinion in Solid State & Materials Science.* **2011**, 15, 73.
4. Mark Bowden, David J. Heldebrant, Abhi Karkamkar, Thomas Proffen, Gregory K. Schenter, Tom Autrey. The diammoniate of diborane: Crystal structure and hydrogen release. Invited paper for Chem Comm. **2010**, 46, 8564.

5. Abhijeet Karkamkar, Shawn M. Kathmann, Gregory K. Schenter, David J. Heldebrant, Nancy Hess, Maciej Gutowski and Tom Autrey. Thermodynamic and Structural Investigations of Ammonium Borohydride a Solid with a Highest Content of Thermodynamically and Kinetically Accessible Hydrogen. *Chem Materials*, **2009**, 21, 4356.
6. Hyunjeong Kim, Abhi Karkamkar, Tom Autrey, Peter Chupas, Thomas Proffen. Determination of structure and phase transition of light element nanocomposites in mesoporous silica: case study of NH_3BH_3 in MCM-41. *J. Am. Chem. Soc.* **2009**, 131, 13749.
7. Roger Rousseau, Greg Schenter, John Fulton, John Linehan, Tom Autrey. Defining the Active Catalyst Structure and Reaction Pathways from *Ab initio* Molecular Dynamics and *Operando* XAFS: Dehydrogenation of Dimethylaminoborane by Rhodium Clusters. *J. Am. Chem. Soc.* **2009** 131, 10516.
8. Nancy J. Hess, Gregory K. Schenter, Michael R. Hartman, Luc L. Daemen, Thomas Proffen, Shawn M. Kathmann, Christopher J. Mundy, David J. Heldebrant, Ashley C. Stowe and Tom Autrey. Neutron Powder Diffraction and Molecular Simulation Study of the Structural Evolution of Ammonia Borane from 15 to 340 K. *J. Phys Chem. A.* **2009** DOI: 10.1021/jp900839c.
9. Shawn M. Kathmann, Vencislav Parvanov, Gregory K. Schenter, Ashley C. Stowe, Luc L. Daemen, Monika Hartl, John Linehan, Nancy J. Hess, Abhi Karkamkar and Tom Autrey. Experimental and Computational Studies on Collective Hydrogen Dynamics in Ammonia Borane: Incoherent Inelastic Neutron Scattering. *J. Chem Phys*, **2009**, 130, 024507.

IV.H.17 Heavy Cycloadditions: Reactions of Digallene with Cyclic Polyolefins

Philip P. Power (Primary Contact),
Christine A. Caputo, Jing-Dong Guo,
Shigeru Nagase, James C. Fettinger
University of California at Davis
1 Shields Ave.
Davis, CA 95616
Phone: (530) 752-6913
Email: pppower@ucdavis.edu

Objectives

- We are interested in investigating the interactions of low-valent Group 13 heavy alkene analogues with a variety of small molecules.
- To investigate uncatalysed, room temperature cyclization reactions of digallene with a variety of cyclic polyolefins.

Technical Barriers

Facile activation of cyclic polyolefins has not been investigated with terphenyl-stabilized digallene prior to this work.

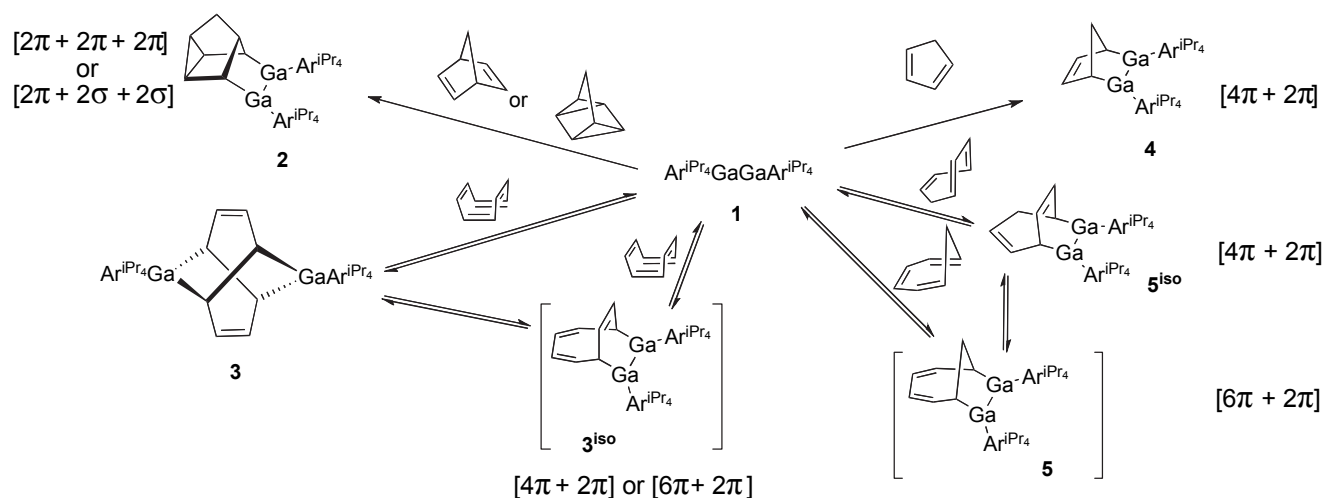
Abstract

The heavier group 13 element alkene analogue, digallene $\text{Ar}^{\text{iPr}_4}\text{GaGaAr}^{\text{iPr}_4}$ (**1**, $\text{Ar}^{\text{iPr}_4} = \text{C}_6\text{H}_3\text{-}2,6\text{-}(\text{C}_6\text{H}_3\text{-}2,6\text{-}$

$\text{iPr}_2)_2$), was shown to react readily in an $[n + 2]$ (where $n = 6, 4, 2+2$) cycloaddition reaction with norbornadiene (NBD), quadricyclane, 1,3,5,7-cyclooctatetraene (COT), 1,3-cyclopentadiene (CpH) and 1,3,5-cycloheptatriene (CHT) to afford the heavier element deltacyclane species $\text{Ar}^{\text{iPr}_4}\text{Ga}(\text{C}_7\text{H}_8)\text{GaAr}^{\text{iPr}_4}$ (**2**), pseudo-inverse sandwich $\text{Ar}^{\text{iPr}_4}\text{Ga}(\text{C}_8\text{H}_8)\text{GaAr}^{\text{iPr}_4}$ (**3**, **3^{iso}**) and polycyclic compounds $\text{Ar}^{\text{iPr}_4}\text{Ga}(\text{C}_5\text{H}_6)\text{GaAr}^{\text{iPr}_4}$ (**4**) and $\text{Ar}^{\text{iPr}_4}\text{Ga}(\text{C}_7\text{H}_8)\text{GaAr}^{\text{iPr}_4}$ (**5**, **5^{iso}**) under ambient conditions. These reactions are facile, and may be contrasted with other all-carbon versions which require transition metal catalysis or forcing conditions (temperature, pressure) or with the corresponding heavier group 14 species $\text{Ar}^{\text{iPr}_4}\text{EEAr}^{\text{iPr}_4}$ ($\text{E} = \text{Ge}, \text{Sn}$) which gave very different product structures. We discuss several mechanistic possibilities including radical and non-radical mediated cyclization pathways. These mechanisms are consistent with the improved energetic accessibility of the lowest unoccupied molecular orbital of the heavier group 13 element multiple bond in comparison to that of a simple alkene or alkyne. We show that the calculated frontier molecular orbitals of $\text{Ar}^{\text{iPr}_4}\text{GaGaAr}^{\text{iPr}_4}$, are of $\pi\text{-}\pi$ symmetry which allows its engagement in a wider range of reactions than that of the usual $\pi\text{-}\pi^*$ frontier orbitals of C-C π -bonds or the $\pi\text{-}n^+$ frontier orbitals of heavier group 14 alkyne analogues.

Progress Report

We have shown that the double bonded digallene, $\text{Ar}^{\text{iPr}_4}\text{GaGaAr}^{\text{iPr}_4}$, behaves as a highly reactive heavy alkene analogue in cyclization reactions with polyolefins including i) the $[4\pi + 2\pi]$ reaction with cyclopentadiene



SCHEME 1. Cycloaddition of various polyolefins with $\text{Ar}^{\text{iPr}_4}\text{GaGaAr}^{\text{iPr}_4}$, **1**.

and cycloheptatriene ii) $[6\pi + 2\pi]$ cyclization reaction with cycloheptatriene and cyclooctatetraene and iii) $[2\pi + 2\sigma + 2\sigma]$ and $[2\pi + 2\pi + 2\pi]$ quadricyclane and norbornadiene respectively to furnish digalladeltacyclane. The higher-order ring structures obtained are only achievable under catalytic conditions in the all-carbon system or with highly electron deficient alkenes. The increased reactivity is attributed to the smaller highest occupied molecular orbital-lowest unoccupied molecular orbital gap and the π - π symmetry of the frontier molecular orbitals of $\text{Ar}^{\text{iPr}^4}\text{GaGaAr}^{\text{iPr}^4}$ which is in sharp contrast to the frontier orbitals of alkenes, alkynes and their heavier group 14 element analogues. The increased electrophilicity and nucleophilicity of these species and their propensity to undergo non-radical cyclization pathways make them closer analogues to the all-carbon system than the heavier group 14 analogues which behave in a manner more consistent with significant diradicaloid character [1].

Future Directions

Singlet carbenes have been shown to react with 2 π equivalents to form stable cyclopropanes [2] and singlet silylenes [3] and germynes [4] have both been shown to undergo preferential $[2 + 1]$ and $[4 + 1]$ cyclizations. We see no evidence for $[n + 1]$ (where $n = 2, 4, 6$) cyclization products, which would arise from the reaction of a $\text{Ar}^{\text{iPr}^4}\text{Ga}$: monomer with an alkene, diene or triene, though a mechanism involving a multi-step reaction of between a cyclic polyolefins and two equivalents of $\text{Ar}^{\text{iPr}^4}\text{Ga}$: monomer remains a possibility. We also highlight that all structures obtained possess two ' $\text{Ar}^{\text{iPr}^4}\text{Ga}$ ' fragments, and compounds **2**, **4**, and **5**^{iso} maintain an intact Ga-Ga bond. We believe this is convincing evidence for the formulation and reactivity of these dimetallene species as heavier group 13 alkene analogues rather than weakly associated monomers. Further investigations regarding the mechanistic details of these cycloaddition reactions are underway.

References

- (a) Hurni, K.; Baines, K.M., *Chem. Commun.* **2011**, 47, 8382; (b) Dixon, C.R.; Baines, K.M., *Phosphorus, Sulfur Silicon Relat. Elem.* **1997**, 124 & 125, 123; (c) Jung, Y.; Brynda, M.; Power, P.P.; Head-Gordon, M., *J. Am. Chem. Soc.* **2006**, 128, 7185.
- (a) Doering, W.v.E.; Hoffman, A.K., *J. Am. Chem. Soc.* **1954**, 76, 6162; (b) Jefford, C.W.; Kabengele, n.; Kovacs, J.; Burger, U., *Helv. Chim. Acta* **1974**, 57, 104; (c) Jefford, C.W.; Kabengele, n.; Kovacs, J.; Burger, U., *Tetrahedron Lett.* **1974**, 257; (d) Jefford, C.W.; Mareda, J.; Gehret, J.-C.E.; Kabengele, n.; Graham, W.D.; Burger, U., *J. Am. Chem. Soc.* **1976**, 98 (9), 2585; (e) Jefford, C.W.; Huy, P.T., *Tetrahedron Lett.* **1980**, 21, 755; (f) Misslitz, U.; Jones, M.J., *Tetrahedron Lett.* **1985**, 26, 5403.
- (a) Barton, T.J.; Juvet, M., *Tetrahedron Lett.* **1975**, 45, 3892; (b) Kroke, E.; Will, P.; Weidenbruch, M., Silylene and Disilene Additions to the Double Bonds of Alkenes, 1,3-Dienes, and Hetero-1,3-dienes. In *Organosilicon Chemistry II: From Molecules to Materials*, Auner, N.; Weis, J., Eds. VCH: Weinheim, Germany, 1996; pp 309; (c) Haaf, M.; Schmedake, T.A.; West, R., *Acc. Chem. Res.* **2000**, 33 (10), 704.
- (a) Schriewer, M.; Neumann, W.P., *J. Am. Chem. Soc.* **1983**, 105, 897; (b) Huck, L.A.; Leigh, W.J., *Organometallics* **2009**, 28, 6777.

Publications (including patents) acknowledging the grant or contract

- Peng, Y.; Guo, J.-D.; Ellis, B.D.; Zhu, Z.; Fettinger, J.C.; Nagase, S.; Power, P.P. Reaction of Hydrogen or Ammonia with Unsaturated Germanium or Tin Molecules under Ambient Conditions: Oxidative Addition versus Arene Elimination. *Journal of the American Chemical Society*, **2009**, 131, 16272-16282.
- Sutton, A.D.; Davis, B.L.; Bhattacharyya, K.X.; Ellis, B.D.; Power, P.P.; Gordon, J.C. . Recycle of Tin Thiolate Compounds relevant to Ammonia-Borane Regeneration. *Chemical Communications*. **2010**, 148-149.
- Peng, Y.; Wang, X.; Fettinger, J.C.; Power, P.P. Reversible Complexation of Isocyanides by the Distannyne $\text{Ar}'\text{SnSnAr}'$ ($\text{Ar}' = \text{C}_6\text{H}_3\text{-2,6}(\text{C}_6\text{H}_3\text{-2,6-}^{\text{iPr}}\text{Pr}_2)_2$). *Chemical Communications*. **2010**, 943-945.
- Summerscales, O.T.; Wang, X.; Power, P.P. Cleavage of the Sn-Sn Multiple Bond in a Distannyne by Cyclooctatetraene: Formation of the π -Bound Inverse Sandwich Complex ($\text{Ar}'\text{Sn}_2(\mu^2\text{-}\eta^2\text{-}\eta^3\text{-COT})$) ($\text{Ar}' = \text{C}_6\text{H}_3\text{-2,6}(\text{C}_6\text{H}_3\text{-2,6-}^{\text{iPr}}\text{Pr}_2)_2$). *Angew. Chem. Int. Ed.* **2010**, 49, 4788-4790.
- Ellis, B.D.; Atkins, T.M.; Peng, Y.; Sutton, A.D.; Gordon, J.C.; Power, P.P. Synthesis and Thermolytic Behavior of Tin(IV) Formates: In Search of Recyclable Metal-Hydride Systems. *Dalton Transactions*. **2010**, 39, 10664-10670.
- Summerscales, O.T.; Jimenez-Galla, J.O.; Merino, G.; Power, P.P. Unusual Electrocyclic Rearrangements with Group 14 Element Compounds: Formation and Isomerization of a π -Aromatic Digermyl Complex with Carbon-Carbon and Germanium-Germanium Multiple Bond Cleavage. *Journal of the American Chemical Society*. **2011**, 133, 180-182.
- Caputo, C.A.; Zhu, Z.; Fettinger, J.C.; Power, P.P. Activation of Simple Olefins with Low Valent Gallium Compounds under Ambient Conditions. *Chemical Communications*. **2011**, 47, 7506-7508.
- Summerscales, O.T.; Olmstead, M.M.; Power, P.P. Tethered Heavy Dicarbene Analogues: Synthesis and Structure of Ditetryldiyl Ethers ($\text{Ar}'\text{E}_2(\mu\text{-O})$) ($\text{E} = \text{Ge}, \text{Sn}$; $\text{Ar}' = \text{C}_6\text{H}_3\text{-2,6}(\text{C}_6\text{H}_3\text{-2,6-}^{\text{iPr}}\text{Pr}_2)_2$). *Organometallics*. **2011**, 30, 3468-3471.
- Summerscales, O.T.; Fettinger, J.C.; Power, P.P. C-H Activation of Cycloalkenes by p -Block Compounds under Ambient Conditions. *Journal of the American Chemical Society*. **2011**, 133, 11960-11963.
- Power, P.P. Interaction of Multiple Bonded and Unsaturated Heavier Main Group Compounds with Hydrogen, Ammonia, Olefins and Related Molecules. *Accounts of Chemical Research*. **2011**, 44, 627-637.
- Brown, Z.D.; Vasco, P.; Fettinger, J.C.; Tuononen, H.M.; Power, P. P. A Germanium Isocyanide Complex Featuring ($n \rightarrow \pi^*$) Back-

Bonding and Its Conversion to a Hydride/Cyanide Produce via C-H Bond Activation Under Mild Conditions. *Journal of the American Chemical Society*. **2012**, *134*, 4045-4048.

12. Power, P.P. Reactions of Heavier Main Group Compounds with Hydrogen, Ammonia, Ethylene and Related Small Molecules. *Chemical Record*. **2012**.

13. Caputo, C.A.; Guo, J-D.; Nagase, S.; Fettinger, J.C.; Power, P.P. Reversible and Irreversible Higher-Order Cycloaddition Reactions of Polyolefins with a Multiple Bonded Higher-Order Group 13 Alkene Analogue: Contrasting Behavior of a System with π - π , π - π^* , and π - n Frontier Molecular Orbitals. *Journal of the American Chemical Society*. DOI: 10.1021/ja301247h.

14. Rekken, B.; Brown, T.; Fettinger, J.; Tuononen, H.; Power, P.P. Isolation of a Stable Acyclic, Two-Coordinate Silylene. *Journal of the American Chemical Society*. DOI: 10.1021/ja301091v.

15. Brown, Z.D.; Guo, J-D.; Nagase, S.; Power, P.P. Experimental and Computational Study of Auxiliary Molecular Effects in the Addition of Hydrazines to a Low-Valent Germanium Complex. Manuscript submitted.

IV.H.18 Mechanistic Studies of Activated Hydrogen Release from Ammonia-Borane

Larry G. Sneddon (Primary Contact),
Martin Bluhm, Dan Himmelberger, William Ewing,
Laif Alden, Emily Berkeley, Chang Won Yoon and
Allegra Marchione

University of Pennsylvania
Department of Chemistry
231 S. 34th Street
Philadelphia, PA 19104-6323
Phone: (215) 898-8632
Email: lsneddon@sas.upenn.edu

DOE Program Officer: Larry Rahn

Phone: (301) 903-2508
Email: Larry.Rahn@science.doe.gov

Subcontractors:

R. Tom Baker, Richard Burchell, Felix Gaertner,
Hassan Kalviri, Morgane Le Fur, Larena Menant,
Giovanni Rachiero Matthew Rankin, Johannes Thomas,
and William Wright

University of Ottawa
Department of Chemistry and Centre for Catalysis Research
and Innovation
30 Marie Curie, Ottawa
ON K1N 6N5 Canada
Phone: (613) 562-5698
Email: rbaker@uottawa.ca

Objectives

- Develop a fundamental understanding of the various thermolytic hydrogen release mechanisms (using acid and base initiators, ionic liquid activators, or metal complex catalysts) for ammonia-borane (AB) and to elucidate the important controlling factors for each type of reaction.
- Apply this understanding to achieve rapid, controlled release of pure hydrogen from an AB-based liquid fuel formulation.

Technical Barriers

- While thermolytic hydrogen release from AB can afford >10 wt% hydrogen, the dehydro-oligomerization process is complicated, with different products being obtained depending on the phase (solid vs. solution), initiator (acid or base), activator (ionic liquids) or catalyst (metal complex or supported metal/metal boride) employed.

- Demonstrated engineering solutions for controlled hydrogen release involve passing a liquid fuel (with concomitant reduced gravimetric storage) over a heterogeneous catalyst bed.
- Volatile impurities in the hydrogen stream need to be less than ppm levels to ensure long fuel cell catalyst lifetime.

Abstract

Significant advances have been made in our understanding of various hydrogen release mechanisms from AB in glycol methyl ether and ionic liquid [1,2] solutions. In previous work, we demonstrated that addition of 5 mol% bis(dimethylamino)naphthalene base (proton sponge) to a solution of AB accelerated the release of the second equivalent of hydrogen at 85°C affording >5 material wt% in 40 min [3]. Using Verkade's base, P[N(i-Bu)CH₂CH₂]₃N, we have now demonstrated that stepwise anionic chain growth produces both linear and branched borane-capped oligomers, with the 'trimer' analogs isolated and fully characterized by multinuclear magnetic resonance spectroscopy and single crystal X-ray diffraction [4]. Further thermal dehydrogenation of these oligomers affords a mixture of BN analogs of benzene (borazine) and polyaromatic hydrocarbons (known collectively as polyborazylene [5]). In another study combining the activation effects of ionic liquids (ILs) [1,2] with catalytically active Ru complexes, we showed that AB dehydrogenation can be selectivity 'tuned' by altering the donor strength of the IL anion [6]. Remarkably, nearly 2 equiv. of hydrogen are obtained even in tetraalkylphosphonium chloride ILs where the Cl⁻/Ru ratio is >100! Whereas metal complex catalysts that effect rapid (minutes) AB dehydrogenation are usually limited in extent of hydrogen release (1 equiv.) due to formation of insoluble poly(aminoborane) [7,8] we showed that most selective catalysts produce initially a mixture of the BN cyclohexane and ethylcyclobutane isomers [9]. In a more detailed investigation of the second equivalent of hydrogen release, we have now identified catalysts that dehydrogenate *both isomers* to borazine and polyborazylene. Turning our attention to inexpensive, earth-abundant catalysts, we have now discovered that FeH₂(depe)₂ [depe = 1,2-bis(diethylphosphino)-ethane] is an efficient catalyst for poly(amino-borane) formation while mixtures of AB and FeCl₂ afford nanoparticle iron boride catalysts that release >2 equiv. hydrogen and can be reused for multiple cycles in glycol methyl ether or ionic liquid solutions without loss of activity or selectivity.

Progress Report

Introduction: Effective storage of hydrogen presents one of the most significant technical gaps to successful implementation of the hydrogen economy, particularly for transportation applications [10]. AB, H_3NBH_3 , has been identified as a promising, high-capacity chemical hydrogen storage medium containing potentially readily released protic (N-H) and hydridic (B-H) hydrogens [11-13]. The dehydro-oligomerization process, however, is complicated, with different products being obtained under different reaction conditions. At the outset of our studies in 2005, AB dehydrogenation had been studied primarily in the solid state, but our work clearly demonstrated that ionic liquids, acid and base initiators, and metal complex-catalysts can each significantly increase both the rate and extent of hydrogen release from AB under moderate conditions. Our studies have also shown that depending on the activation method, hydrogen release from amine-boranes can occur by very different mechanistic pathways and yield different types of spent-fuel materials. The goal of the current project was to develop a fundamental understanding and to elucidate the important controlling factors for each type of reaction. This information is vital to the continued refinement and optimization of chemical-hydride based hydrogen release systems.

Base Initiators: In previous work, we demonstrated the efficiency of non-nucleophilic strong bases such as proton sponge (PS) in promoting the rate and extent of hydrogen release from AB [3]. In addition, reactions of the triethylborane-capped model compound $[\text{Et}_3\text{BNH}_2\text{BH}_3]^- \text{Li}^+$ with AB showed evidence of chain-growth, providing support for a PS-promoted anionic dehydro-polymerization of AB. In our most recent study, use of Verkade's base, $\text{P}[\text{N}(\text{i-Bu})\text{CH}_2\text{CH}_2]_3\text{N}$, demonstrated that stepwise anionic chain growth occurs by a mechanism involving both linear and branched borane-capped oligomers (Figure 1), with the 'trimer' analogs isolated and fully characterized by multi-nuclear NMR spectroscopy and single crystal X-ray diffraction [4] (Figure 2).

Metal Complex Catalysts in Ionic Liquids: In previous work combining the activation effects of ionic liquids [1,2] with catalytically active Ru complexes, we showed that AB dehydrogenation can be selectively 'tuned' to avoid formation of insoluble poly(aminoborane) (Figure 3) by altering the donor strength of the IL anion [6]. In more recent studies, IL cation effects were also noted, which could be partially correlated with the IL viscosity that greatly affects the rates of intermolecular aminoborane oligomerization. Remarkably, the Ru catalyst retained its activity even in phosphonium halide ILs and hydrogen release approaching 5 wt% was achieved, albeit at impractical rates. Further studies suggested that a fast initial rate of AB dehydrogenation could raise the reaction temperature sufficiently to allow for

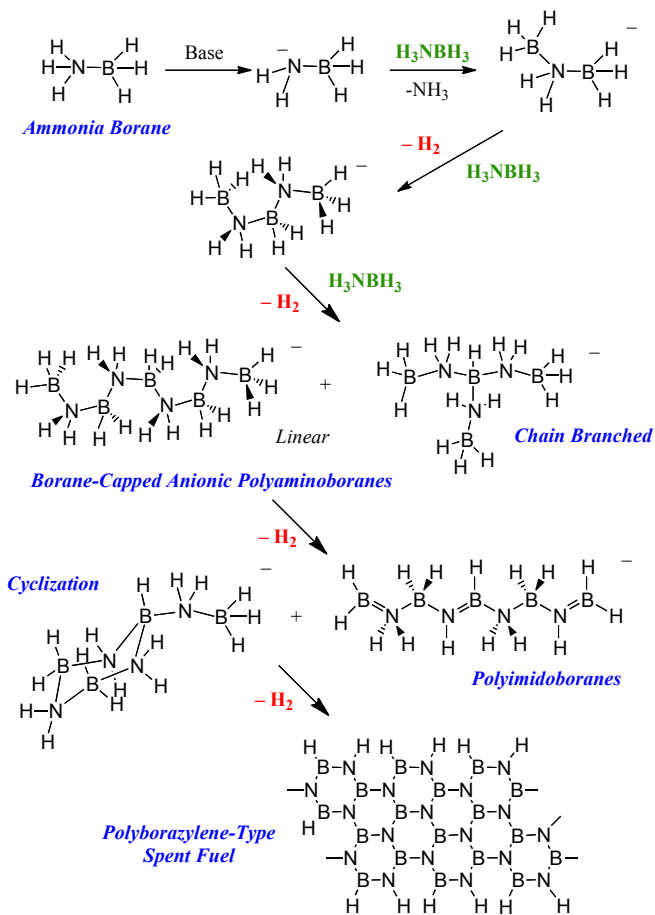


FIGURE 1. Anionic AB polymerization mechanism

efficient activation of the subsequent H_2 release steps by the ionic liquid solvent.

Investigating the Second Equivalent of H_2 Release: Over the last seven years, a multitude of papers have appeared describing metal complex catalysts for AB dehydrogenation, including some with rapid rates and excellent selectivity to poly(aminoborane) [14-16] (1 equiv. H_2), and others that form exclusively borazine and polyborazylene [17,18] (>2 equiv. H_2). The reaction pathways traversed by the latter selective catalysts involve cyclic aminoborane intermediates such as the BN cyclohexane analog, cyclotriborazane (CTB) and its BN ethylcyclobutane (ECB) isomer that we reported previously (Figure 3) [9]. While CTB is easily prepared from borazine, all synthetic routes to ECB that we developed led to significant contamination from Ni or Fe metal. After significant effort, we finally discovered that use of Schwartz's reagent, Cp_2ZrHCl , affords ECB in 40% yield contaminated only by ca. 10-20% of its CTB isomer. With samples of ECB in hand we were able to show first that thermolysis of ECB leads primarily to CTB, but a competing pathway affords borazine and AB via a hydrogen redistribution reaction [19].

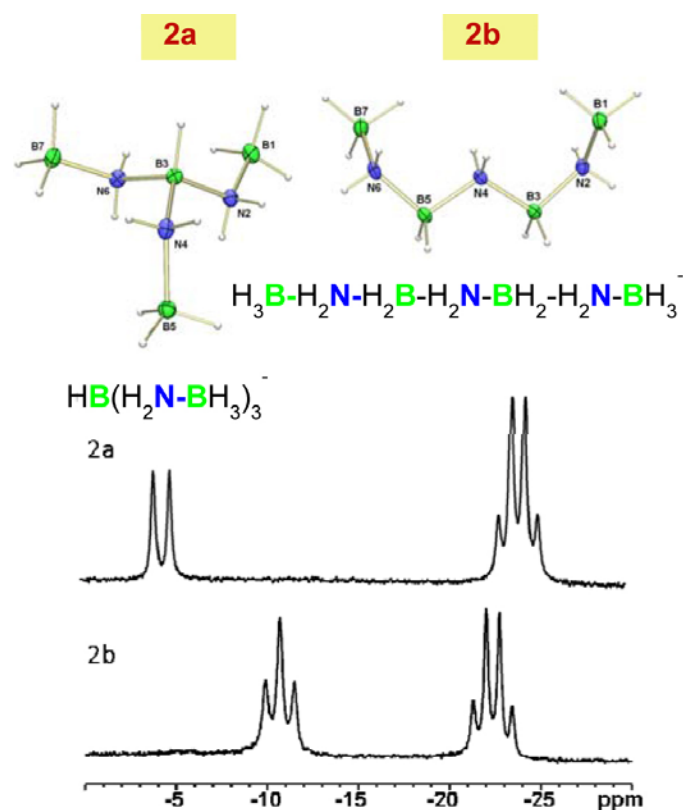


FIGURE 2. ^{11}B nuclear magnetic resonance spectra and molecular structures of borane-capped aminoborane oligomers

Secondly, we found that some metal catalysts converted ECB cleanly to borazine and polyborazylene, leaving CTB untouched, while others effectively dehydro-genated both isomers.

Iron Catalysts for AB Dehydrogenation: In previous work on iron amido phosphine bifunctional catalysts, we discovered the most active base metal AB dehydrogenation catalyst that was selective for poly(aminoborane) formation, but it exhibited limited lifetime due to unwanted reactivity of the diamido ligand [20]. Using less bulky bis(phosphine) ligands, we have now identified stable Fe catalysts, $\text{FeH}_2(\text{P-P})_2$, where P-P is depe or dmpe, that react with a variety of primary amine-boranes to afford the poly(aminoborane)s exclusively. Further work is underway with chiral bis(phosphine) ligands to assess tacticity and concomitant microstructure control in the resulting BN polymers. Finally, in extended studies of AB dehydrogenation catalyzed by metal-containing Lewis acids, we recently found that mixtures of AB and FeCl_2 afford nanoparticle iron-on-iron-boride catalysts that release >2 equiv. hydrogen. These are the most promising heterogeneous catalysts yet reported for AB dehydrogenation and can be reused for multiple cycles in glycol methyl ether or ionic liquid solutions without loss of activity or selectivity. Further work in this area involves detailed investigations of hydrogen purity and use of oxygen-

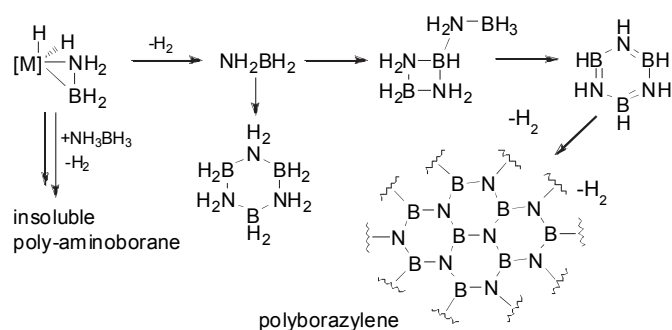


FIGURE 3. Observed dehydrogenation products from metal complex-catalyzed AB dehydrogenation

free BN supports to prepare practical heterogeneous catalysts for use with ionic liquid/AB fuels.

Future Directions

Although this Basic Energy Sciences project has been completed, the PIs are working with Los Alamos National Lab and DOE's Engineering Hydrogen Storage Center of Excellence to develop a working ammonia-borane-based liquid-fuel/spent-fuel combination working in concert with an iron-based heterogeneous catalyst to achieve rapid, controlled release of pure hydrogen streams.

References

1. Bluhm, M.E.; Bradley, M.G.; Butterick, R.; Kusari, U.; Sneddon, L.G. *J. Am. Chem. Soc.* **2006**, *128*, 7748-9.
2. Himmelberger, D.; Yoon, C.W.; Bluhm, M. E.; Carroll, P.J.; Sneddon, L.G. *J. Am. Chem. Soc.* **2009**, *131*, 14101-14110.
3. Himmelberger, D.W.; Alden, L.R.; Bluhm, M.E.; Carroll, P.J.; Sneddon, L.G. *Inorg. Chem.* **2009**, *48*, 9883-9889.
4. Ewing, W.C.; Marchione, A.; Himmelberger, D.W.; Carroll, P.J.; Sneddon, L.G. *J. Am. Chem. Soc.* **2011**, *133*, 17093-17099.
5. Fazen, P.J.; Remsen, E.E.; Beck, J.S.; Carroll, P.J.; McGhie, A.R.; Sneddon, L.G. *Chem. Mater.* **1995**, *7*, 1942-1956.
6. Wright, W.H.R.; Berkeley, E.; Baker, R.T.; Sneddon, L.G. *Chem. Commun.*, **2011**, *47*, 3177-3179.
7. Staubitz, A.; Presa Soto, A.; Manners, I. *Angew. Chem., Int. Ed.* **2008**, *47*, 6212-6215.
8. Staubitz, A.; Sloan, M.E.; Robertson, A.P.M.; Friedrich, A.; Schneider, S.; Gates, P.J.; Günne, J.S. a. d.; Manners, I. *J. Am. Chem. Soc.*, **2010**, *132*, 13332-13345.
9. Pons, V.; Baker, R.T.; Linehan, J.; Matus, M.H.; Dixon, D.A., *Chem. Commun.* **2008**, 6597-6599.
10. Satyapal, S.; Petrovic, J.; Read, C.; Thomas, G.; Ordaz, G. *Catal. Today* **2007**, *120*, 246-256.
11. Stephens, F.H.; Pons, V.; Baker, R.T. *Dalton Trans.*, **2007**, 2613-2626.

12. Hamilton, C.W.; Baker, R.T.; Staubitz, A.; Manners, I. *Chem. Soc. Rev.*, **2009**, *38*, 279-293.
13. Staubitz, A.; Sloan, M.E.; Robertson, A.P.M.; Manners, I. *Chem. Rev.* **2010**, *110*, 4079-4124.
14. Denney, M.C.; Pons, V.; Hebden, T.J.; Heinekey, D.M.; Goldberg, K.I. *J. Am. Chem. Soc.* **2006**, *128*, 12048-12049.
15. Blaquiere, N.; Diallo-Garcia, S.; Gorelsky, S.I.; Black, D.A.; Fagnou, K. *J. Am. Chem. Soc.* **2008**, *130*, 14034-14035.
16. Käß, M.; Friedrich, A.; Drees, M.; Schneider, S. *Angew. Chem., Int. Ed.* **2009**, *121*, 922-924.
17. Keaton, R.J.; Blacquiere, J.M.; Baker, R.T. *J. Am. Chem. Soc.*, **2007**, *129*, 1844-1845.
18. Conley, B.L.; Guess, D.; Williams, T.J. *J. Am. Chem. Soc.*, **2011**, *133*, 14212-14215.
19. A paper on hydrogen redistribution from AB to bulky aminoborane monomers appeared recently: Robertson, A.P.M.; Leitao, E.M.; Manners, I. *J. Am. Chem. Soc.* **2011**, *133*, 19322-19325.
20. Baker, R.T.; Gordon, J.G.; Hamilton, C.W.; Henson, N.J.; Lin, P.-H.; Maguire, S. *J. Am. Chem. Soc.* **2012**, *134*, 5598-5609.
- Recent Publications (including patents) acknowledging the grant or contract**
1. "Tuning the Selectivity of Transition Metal-Catalyzed Ammonia-Borane Dehydrogenation in Ionic Liquids," Wright, W.R.H.; Menant, C.L.; Baker, R.T., submitted to *Inorganic Chemistry*, 2012.
2. "Synthesis, Characterization and Reactivity Study of B-(cyclo-diborazanyl)aminoborohydride: the Second Dehydrogenation Step in Ammonia-Borane Dehydrogenation," Gaertner, F.; Kalviri, H.; Baker, R.T., submitted to *Chemical Science*, 2012.
3. "Iron Complex-Catalyzed Ammonia-Borane Dehydrogenation. A Potential Route Towards B-N Containing Polymer Motifs Using Earth Abundant Metal Catalysts," Baker, R.T.; Gordon, J.G.; Hamilton, C.W.; Henson, N.J.; Lin, P.-H.; Maguire, S. *J. Am. Chem. Soc.* 2012, *134*, 5598-5609.
4. "Syntheses and Structural Characterizations of Anionic Borane-Capped Ammonia-Borane Oligomers: Evidence for Ammonia Borane H₂-Release via a Base-Promoted Anionic Polymerization Mechanism," Ewing, W.C.; Marchione, A.; Himmelberger, D.W.; Carroll, P.J.; Sneddon, L.G. *J. Am. Chem. Soc.* 2011, *133*, 17093-17099.
5. "Transition Metal-Catalysed Ammonia-Borane Dehydrogenation in Ionic Liquids," Wright, W.H.R.; Berkeley, E.; Baker, R.T.; Sneddon, L.G. *Chem. Commun.*, **2011**, *47*, 3177-3179 (Invited for special Hydrogen issue).
6. "Ammonia Triborane: A New Synthesis, Structural Determinations and Hydrolytic Hydrogen-Release Properties," Yoon, C.W.; Carroll, P.J.; Sneddon, L.G. *J. Am. Chem. Soc.* **2009**, *131*, 855-864.
7. "Base Promoted Ammonia Borane Hydrogen Release," Himmelberger, D.W.; Yoon, C.W.; Bluhm, M.E.; Carroll, P.J.; Sneddon, L.G. *J. Am. Chem. Soc.* **2009**, *131*, 14101-14110.
8. "Ammonia Borane Hydrogen Release in Ionic Liquids," Himmelberger, D.W.; Alden, L.R.; Bluhm, M.E.; Carroll, P.J.; Sneddon, L.G. *Inorg. Chem.* **2009**, *48*, 9883-9889.
9. "B-N Compounds for Chemical Hydrogen Storage," Hamilton, C.W.; Baker, R.T.; Staubitz, A.; Manners, I. *Chem. Soc. Rev.*, **2009**, *38*, 279-293. (invited review for thematic issue on Renewable Energy).
10. "Mechanistic Studies of Metal-Catalyzed Amine-Borane Dehydrogenation: Selectivity Dictates Extent of Hydrogen Release from Ammonia-Borane," Pons, V.; Baker, R.T.; Linehan, J.; Matus, M.H.; Dixon, D.A. *Chem. Commun.* **2008**, 6597-6599.
11. "Soluble Boron-Nitrogen High Polymers from Metal Complex-Catalyzed Amine Borane Dehydrogenation," Pons, V.; Baker, R.T. *Angew. Chem. Int. Ed.*, **2008**, *47*, 9600-9602.

IV.H.19 Influence of Pressure on Physical Property of Ammonia Borane and its Re-Hydrogenation

Jiuhua Chen (Primary Contact), Shah Najiba,
Yongzhou Sun, Jennifer Girard, Vadym Drozd
Center for the Study of Matters at Extreme Conditions
Department of Mechanical and Materials Engineering
Florida International University
11200 SW 8th Street
Miami, FL 33199
Phone: (305) 348-3140
Email: chenj@fiu.edu

DOE Program Officer: Dr. Lane Wilson
Phone: (301) 903-5877
Email: Lane.Wilson@science.doe.gov

Subcontractor:
Wendy Mao, Stanford University

Objectives

- Understand pressure influence on the structure, phase stability, dehydrogenation of ammonia borane and its derivative through in situ study using X-ray diffraction and Raman spectroscopy.
- Study pressure influence on the rehydrogenation after thermolysis of ammonia borane and its derivative to explore the possibility of pressure induced rehydrogenation.

Technical Barriers

Ammonia borane-based chemical hydrogen storage materials have high hydrogen density (gravimetric and volumetric) with slow discharge rate and nearly irreversibility. Characterizing the materials under high pressure so that we can understand the stability of the materials and reversibility of their discharge process is not trivial.

Abstract

Behavior of ammonia borane under high pressure up to 20 GPa and temperature from 80–350 K has been studied using Raman spectroscopy/X-ray diffraction and diamond anvil cell. Abundant phases are found in this molecular crystal at this pressure and temperature range. More changes in the feature of Raman spectroscopy are observed than the crystal structure changes identified by X-ray diffraction, indicating Raman spectroscopy may identify bonding changes in addition to crystal structural transitions. Based

on Raman spectra of ammonia borane, four new phases are observed for the first time at high pressure and low temperature. Confining the sample into mesopores of nano-scaffold (SBA-15 with 1:1 ratio to sample) shifts the pressure induced phase transitions at ~ 0.9 GPa and ~ 10.2 GPa to ~ 0.5 GPa and ~ 9.7 GPa respectively, and the temperature induced transformation from 217 K to 195 K in ammonia borane. Raman spectroscopy study has also been conducted on lithium amidoborane at high pressures up to 19 GPa and room temperature. Two new high pressure phases are observed.

Progress Report

Improved in situ X-ray diffraction patterns of ammonia borane have been collected at high pressure up to 15 GPa and room temperature. These data are of much higher quality with respect to our earlier diffraction study, and confirm two structural phase transitions at pressures about 1 GPa ($I4mm$ to $Cmc2_1$) and 12 GPa ($Cmc2_1$ to $P2_1$) respectively (Figure 1) (Lin et al. 2012). All other phase changes (e.g. at 5 GPa and 8 GPa) (Lin et al. 2008; Xie et al. 2009) observed in Raman spectroscopy are apparently of second order transition.

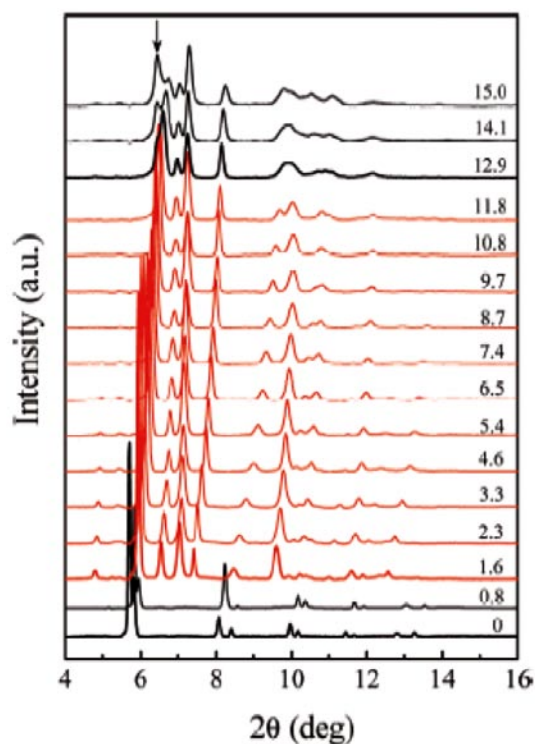


FIGURE 1. X-ray diffraction of ammonia borane at high pressures collected at APS (Lin et al. 2012)

In situ Raman spectra of ammonia borane have been collected at high pressure up to 12 GPa and temperature from 80 K to 350 K. Figure 2 and Figure 3 show the phase relation above and below room temperature respectively. Within the orthorhombic ($Cmc2_1$) structure stability field, there are two possible second order phase transitions above room temperature (Figure 2). At low temperature, four new phases are observed in the Raman scattering (Figure 3). The phase boundary between the room temperature tetragonal ($I4mm$) phase and low temperature orthorhombic ($Pmn2_1$) phase is determined having a positive Clapeyron slope ($dP/dT = 25.7$ MPa/K), indicating that the transition is exothermic.

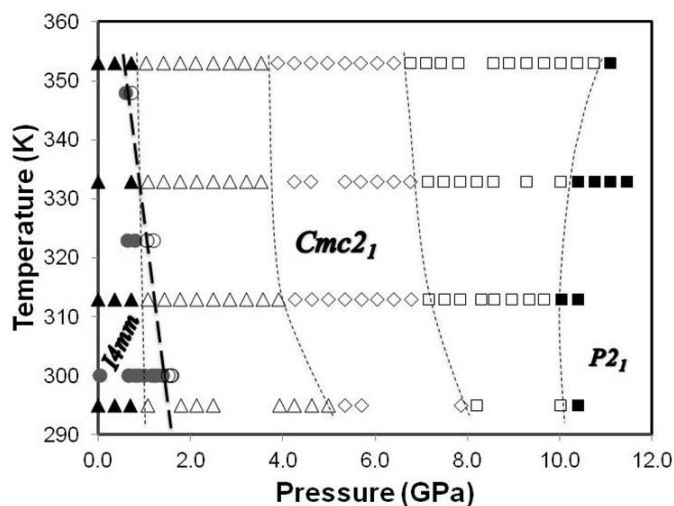


FIGURE 2. Phase boundary of ammonia borane at high pressure and elevated temperature. Solid and open circles represent $I4mm$ and $Cmc2_1$ phases respectively, determined by X-ray diffraction. Solid triangles and squares represent $I4mm$ and $P2_1$ phases respectively, determined by Raman spectroscopy. Open symbols between $I4mm$ and $P2_1$ phases represent $Cmc2_1$ phase.

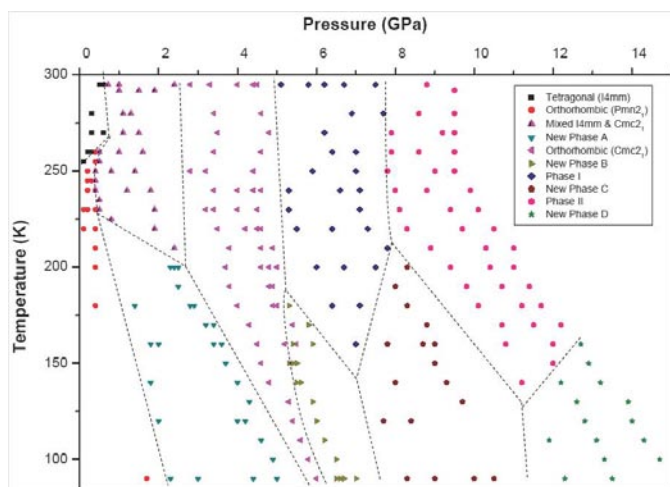


FIGURE 3. Phase boundary of ammonia borane at high pressure and low temperature determined by Raman spectroscopy

Influence of confining ammonia borane in mesoporous confinement (i.e. SBA15 silica nanoscaffold) on behavior of ammonia borane has also been studied. Not only does the nanoconfinement change the dehydrogenation temperature and kinetics of ammonia borane (Xiong et al. 2008) but also it influences phase equilibrium. Comparative study using Raman spectroscopy indicates that the temperature induced body-centered-tetragonal ($I4mm$) structure to orthorhombic ($Pmn2_1$) structure transition is suppressed from 217 K to 195 K when the sample is confined in SBA15. Compared to the result with MCM-41 (Kim et al. 2009), this result demonstrates a size effect on the influence of nanoconfinement. When the pore size is reduced from 7-9 nm to 3-4 nm, the tetragonal to orthorhombic structural transition is totally suppressed in the temperature down to 80 K. A similar influence of the nanoconfinement on pressure induced phase transitions is also observed using Raman spectroscopy. The phase boundary between the phase and high pressure $Cmc2_1$ phase at ambient temperature shifts from 0.9 GPa to 0.5 GPa; and that between the $Cmc2_1$ phase and higher pressure $P2_1$ phase shifts from 10.2 GPa to 9.7 GPa.

Remarkably, confining ammonia borane makes it possible to reverse its thermolysis process by applying high pressure to the system. The result is more promising for the case of lithium amidoborane (to be published). In situ Raman spectroscopy study on lithium amidoborane indicates that the sample experiences two phase transition at high pressure up to 19 GPa (Figure 4). The first transition is observed about 3 GPa for peak splitting at $2,175$ cm^{-1} and peak merging at $2,300$ cm^{-1} , and the second phase transition is observed at about 12 GPa for peak splitting at $3,375$ cm^{-1} and 3450 cm^{-1} (Figure 5).

Future Directions

Expand the in situ high pressure study of the ammonia borane derivative, lithium amidoborane, from ambient temperature to both elevated temperature and low temperature.

Study pressure influence on dehydrogenation and rehydrogenation of lithium amidoborane. Apply the same experimental protocol used in ammonia borane system to lithium amidoborane system to explore reversibility of its thermolysis process through pressure.

Synthesize and characterize aluminum amidoborane.

References

- Kim, H., A. Karkamkar, T. Autrey, P. Chupas and T. Proffen (2009). "Determination of Structure and Phase Transition of Light Element Nanocomposites in Mesoporous Silica: Case study of NH_3BH_3 in MCM-41." *Journal of the American Chemical Society* **131**(38): 13749-13755.

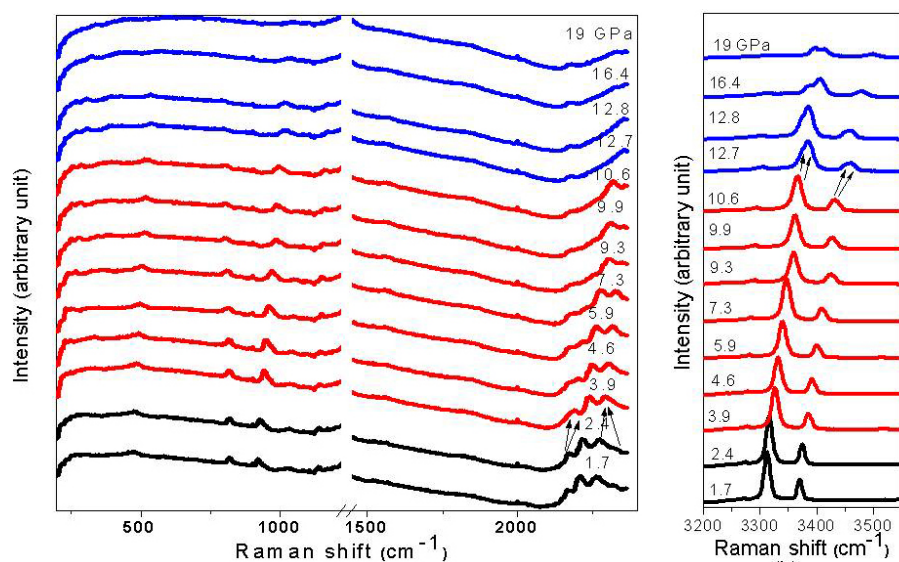


FIGURE 4. High Pressure Raman Spectra of lithium amidoborane. Numbers next to the spectra indicate the pressure in GPa.

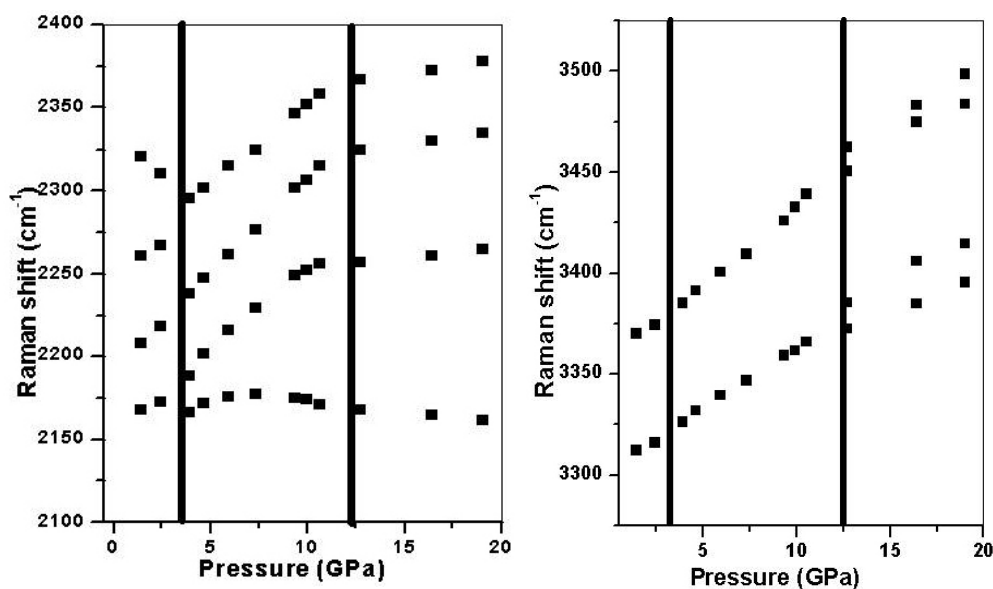


FIGURE 5. Pressure dependence of Raman peaks of lithium amidoborane. Bold lines indicate the phase boundaries where change of slope, merging or splitting of peaks occurs.

2. Lin, Y., H. Ma, C.W. Matthews, B. Kolb, S. Sinogeikin, T. Thonhauser and W.L. Mao (2012). "Experimental and Theoretical Studies on a High Pressure Monoclinic Phase of Ammonia Borane," *Journal of Physical Chemistry C* **116**: 2172-2178

3. Lin, Y., W.L. Mao, V. Drozd, J. Chen and L.L. Daemen (2008). "Raman spectroscopy study of ammonia borane at high pressure." *Journal of Chemical Physics* **129**: 234509, DOI: 10.1063/1.3040276.

4. Xie, S., Y. Song and Z. Liu (2009). "In Situ High-Pressure Study of Ammonia Borane by Raman and IR Spectroscopy." *Can. J. Chem./Rev. Can. Chim.* **87**(9): 1235-1247.

5. Xiong, Z., C.K. Yong, G. Wu, P. Chen, W. Shaw, A. Karkamkar, T. Autrey, M.O. Jones, S.R. Johnson, P.P. Edwards and W.I.F. David (2008). "High-capacity hydrogen storage in lithium and sodium amidoboranes." *Nat. Mater.* **7**(2): 138-141.

Publications (including patents) acknowledging the grant or contract

1. Jihua Chen, Helene Couvy, Haozhe Liu, Vadym Drozd, Luke L. Daemen, Yusheng Zhao and Chi-Chang Kao, In situ x-ray study of ammonia borane at high pressures, *International Journal of*

Hydrogen Energy, 35 (20), October 2010,11064-11070, doi:10.1016/j.ijhydene.2010.07.085.

2. Shah Najiba, Jihua Chen, Vadym Drozd, Andriy Durygin, Yongzhou Sun, Tetragonal to orthorhombic phase transition of ammonia borane at low temperature and high pressure, *Journal of Applied Physics*, 2012 in print.

3. Shah Najiba, Jihua Chen, Vadym Drozd, Andriy Durygin, Yongzhou Sun, Raman spectroscopy study of ammonia borane at low temperature and high pressure, in *Energy Technology 2012: Carbon Dioxide Management and Other Technologies*, Edited by Maria D. Salazar-Villalpando, Neale R Neelameggham, Donna Post Guillen, Soobhankar Pati, and Gregory K. Krumdick, TMS (The Minerals, Metals & Materials Society), 2012, pp 339-346

4. Ali Hadjikhani, J. Chen, S. Das, W. Choi, Raman spectroscopy of graphene and plasma treated graphene under high pressure, 2012 TMS Proceedings: Volume 2: Materials Properties, Characterization, and Modeling, TMS (The Minerals, Metals & Materials Society), 2012, pp 75-79

5. Yu Lin, Hongwei Ma, Charles Wesley Matthews, Brian Kolb, Stanislav Sinogeikin, Timo Thonhauser, and Wendy L. Mao, Experimental and Theoretical Studies on a High Pressure Monoclinic Phase of Ammonia Borane, *Journal of Physical Chemistry C*, 116, 2172–2178 (2012).

V. FUEL CELLS

V.0 Fuel Cells Sub-Program Overview

INTRODUCTION

The Fuel Cells sub-program supports research, development, and demonstration of fuel cell technologies for a variety of stationary, transportation, and portable applications, with a primary focus on reducing cost and improving durability. These efforts include research and development (R&D) of fuel cell stack components, system balance-of-plant (BOP) components and subsystems, as well as system integration. The sub-program seeks a balanced, comprehensive approach to fuel cells for near-, mid-, and longer-term applications. Existing early markets and near-term markets include portable power, backup power, auxiliary power units, and specialty applications such as material handling equipment. In the mid- to long-term, development of fuel cells for transportation applications is a primary goal, due to the significant reduction in the nation's energy and petroleum requirements that would result from market availability of high-efficiency fuel cell electric vehicles. Development of fuel cells for distributed power generation (e.g., combined heat and power [CHP] for residential and commercial applications) is also underway. The sub-program's portfolio of projects covers a broad range of technologies, including polymer electrolyte membrane fuel cells, direct methanol fuel cells, alkaline fuel cells, and solid oxide fuel cells.

The Fuel Cells sub-program's tasks in the *Fuel Cell Technologies Program Multi-Year Research, Development and Demonstration Plan* are organized around development of components, stacks, sub-systems, and systems; supporting analysis; and testing, technical assessment, and characterization activities. Task areas for fuel cell system and fuel processor sub-system development for stationary power generation applications are included, as are those for early market fuel cell applications, such as portable power, and for the development of innovative concepts for fuel cell systems.

GOAL

The sub-program's goal is to advance fuel cell technologies for transportation, portable, and stationary applications to make them competitive in the marketplace in terms of cost, durability, and performance, while ensuring maximum environmental and energy-security benefits.

OBJECTIVES¹

The sub-program's key objectives include:

- By 2015, develop a fuel cell system for portable power (<250 W) with an energy density of 900 Wh/L.
- By 2017, develop a 60% peak-efficient, direct-hydrogen fuel cell power system for transportation, with 5,000-hour durability, that can be mass-produced at a cost of \$30/kW.
- By 2020, develop distributed generation and micro-CHP fuel cell systems (5 kW) operating on natural gas or liquefied petroleum gas that achieve 45% electrical efficiency and 60,000-hour durability at an equipment cost of \$1,500/kW.
- By 2020, develop medium-scale CHP fuel cell systems (100 kW–3 MW) that achieve 50% electrical efficiency, 90% CHP efficiency, and 80,000-hour durability at a cost of \$1,500/kW for operation on natural gas and \$2,100/kW when configured for operation on biogas.
- By 2020, develop a fuel cell system for auxiliary power units (1–10 kW) with a specific power of 45 W/kg and a power density of 40 W/L at a cost of \$1,000/kW.

¹Note: Targets and milestones were recently revised; therefore, individual project progress reports may reference prior targets. Some targets are still currently under revision, with updates to be published in Fiscal Year 2013.

FISCAL YEAR (FY) 2012 STATUS AND PROGRESS

Cost reductions and improvements in durability continue to be the key challenges facing fuel cell technologies. In addition, advances in air, thermal, and water management are necessary for improving fuel cell performance; some stationary applications would benefit from increased fuel flexibility; and, while fuel cells are approaching their targets for power density and specific power, further progress is required to achieve system packaging requirements necessary for commercialization.

One of the most important metrics is the projected high-volume manufacturing cost for automotive fuel cells, which the Program tracks on an annual basis. The 2012 estimate of this cost is \$47/kW, which represents a 36% decrease since 2008 and an 83% decrease since 2002, as depicted in Figure 1. The 36% decrease in projected cost since 2008 stems in part from a reduction in platinum group metal (PGM) loading and an increase in cell power density, allowing the design of smaller and less expensive stacks. The 2012 cost analysis estimated the cost of the fuel cell stack to be \$20/kW. BOP cost has also been reduced during this time. Major sources of the reduction in BOP cost include modification of the ejector system based on stakeholder input, improved design of the system controller, and reduction of the radiator size. The reduced radiator size was enabled by improvements in stack components, allowing a higher stack operating temperature.

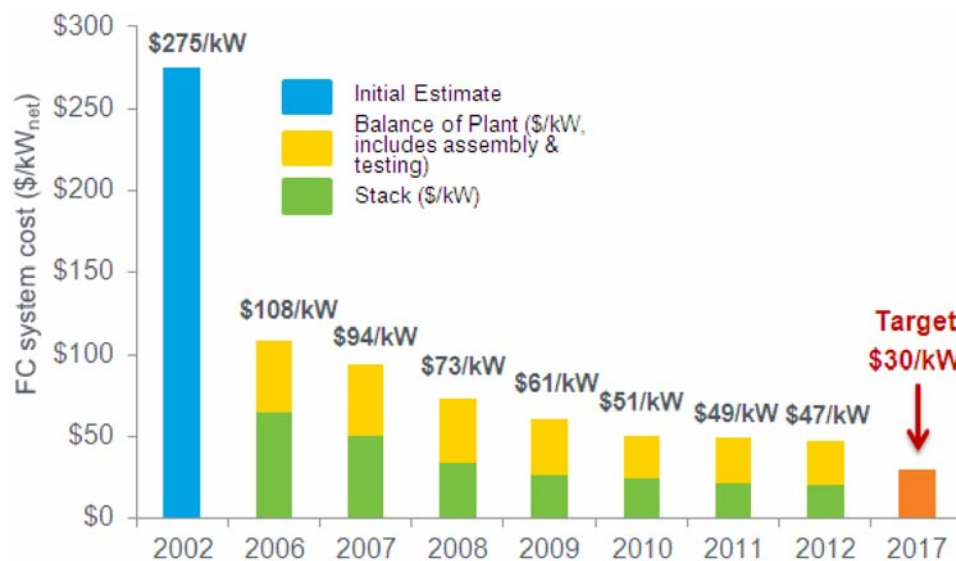


FIGURE 1. Current modeled cost of an 80-kW automotive fuel cell system based on projection to high-volume manufacturing (500,000 units/year)²

High durability is also a requirement for commercial fuel cell systems. Average durability (time to 10% voltage degradation) of fuel cell stacks and systems in laboratory testing was 4,000 hours as of April 2012, which represents a doubling in durability since 2006.³ These durability improvements are all the more impressive given the reduction in PGM loading over the years, with typical PGM content decreasing from 0.6 g/kW in 2007 to <0.18 g/kW in 2012.

²DOE Hydrogen and Fuel Cells Program Record #12020, http://hydrogen.energy.gov/pdfs/12020_fuel_cell_system_cost_2012.pdf.

³DOE Hydrogen and Fuel Cells Program Record #11003, http://hydrogen.energy.gov/pdfs/11003_fuel_cell_stack_durability.pdf.

Catalysts

Developed dealloyed catalysts that meet mass activity target and show high performance in high current fuel cell testing (General Motors): Dealloyed PtNi and PtCo catalysts developed in a project led by General Motors have high mass activity, 0.46 A/mg_{PGM} for PtCo and 0.52 A/mg_{PGM} for PtNi, exceeding the 2017 mass activity target of 0.44 A/mg_{PGM}. The PtCo catalyst also meets durability targets, with only a 28% loss in mass activity during 30,000 voltage cycles (target <40%). To date, the PtNi dealloyed catalyst does not meet the durability target, but based on analysis of the chemical properties of Co and Ni, GM anticipates that PtNi catalysts with durability similar to that of PtCo will be developed. In addition to their high mass activity, the General Motors dealloyed PtNi catalyst has demonstrated high performance operation in membrane electrode assemblies (MEAs), with performance of a dealloyed PtNi₃ cathode at 0.1 mg_{PGM}/cm² matching that of a conventional 0.4 mg_{PGM}/cm² Pt/C cathode at testing up to 1.5 A/cm² (Figure 2). At 1.5 A/cm², the PtNi₃ cell yielded up to 0.63 V, exceeding the 0.56 V project milestone.

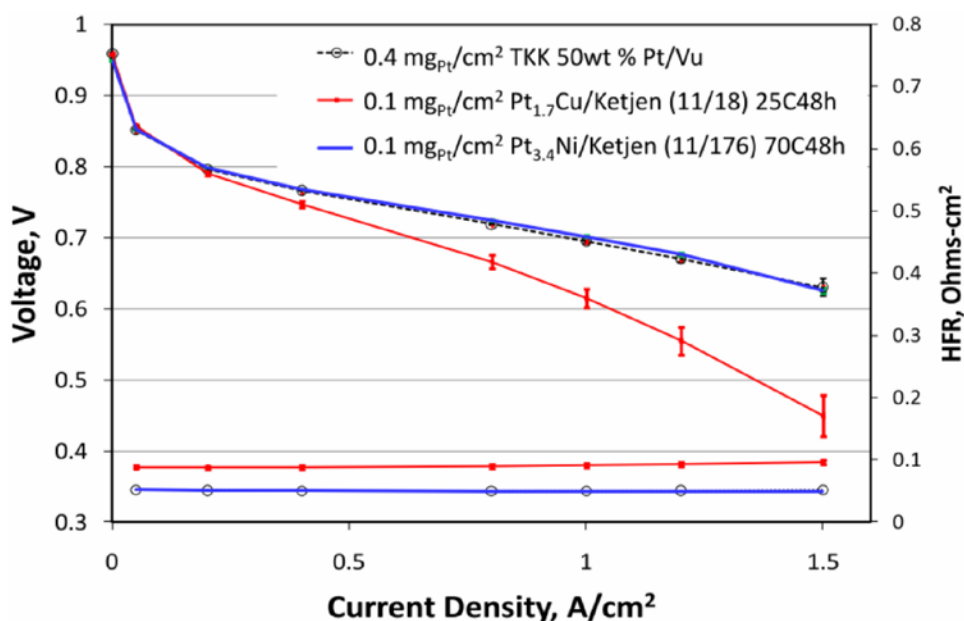


FIGURE 2. MEA performance of PtNi dealloyed catalyst

Reduced PGM total content to 0.14-0.18 g/kW (3M): Improvements in PtNi nanostructured thin film (NSTF) catalysts have enabled performance improvement at high current densities, resulting in PGM total content levels as low as 0.14–0.18 g/kW, depending on operating pressure, at an areal loading of 0.15 mg/cm² in MEA testing (Figure 3). This result represents a 15% reduction in PGM total content when compared to the previous generation PtCoMn NSTF catalyst. The operating voltage and temperature at which these results were obtained (approximately 0.6 V and 80°C, respectively) still need to be increased to enable achievement of the MEA heat rejection requirement. Further development is also required to achieve the 2017 target level of 0.125 g/kW.

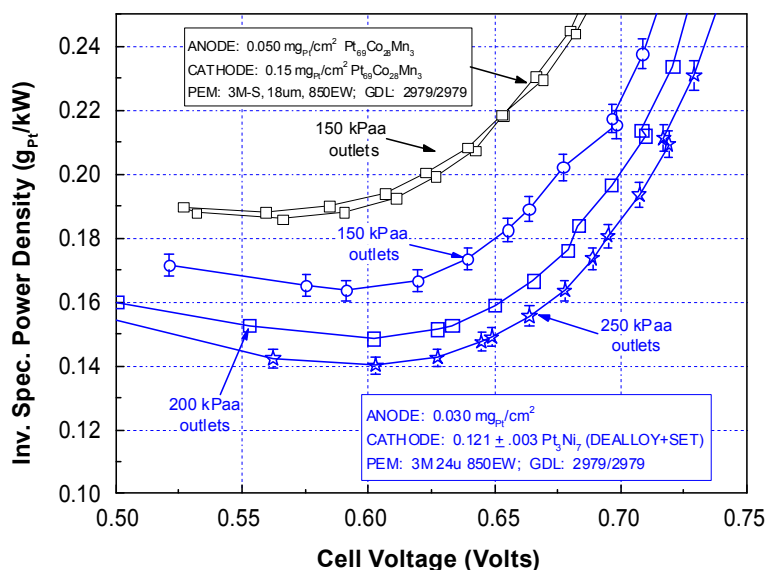


FIGURE 3. PGM total content of NSTF catalysts

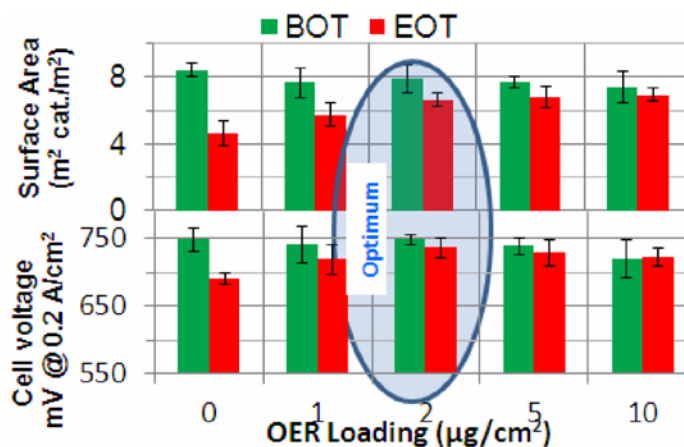
Durability

Modified anode and cathode catalysts meet performance milestones with total PGM loading $<0.135 \text{ mg}/\text{cm}^2$ (3M): Modified NSTF catalysts that include a highly active and durable oxygen evolution catalyst, based on Ru and Ir, are under development at 3M for deposition on both the anode and the cathode. By enhancing oxygen evolution capability, these catalysts suppress excursions to high voltage, and thus mitigate corrosion of catalysts and supports that otherwise may occur under startup, shutdown, and fuel starvation conditions. In 2012, these modified catalysts met all performance milestones with a total PGM loading of $0.135 \text{ mg}/\text{cm}^2$, including demonstration of 5,000 startup/shutdown cycles with a maximum cathode voltage of 1.48 V (target: $<1.6 \text{ V}$), 200 cell reversals with a maximum anode voltage of 1.65 V (target: $<1.8 \text{ V}$), and a tenfold suppression of the anode oxygen reduction reaction activity in the kinetic region (Figure 4).

Portable Power

Improved direct dimethyl ether fuel cell performance by 60% (Los Alamos National Laboratory [LANL]): Direct dimethyl ether (DME) fuel cells developed by LANL have demonstrated a 60% increase in power density at 0.5 V since 2011, with performance rivaling that of direct methanol fuel cells (DMFCs) at low current. Direct DME fuel cells benefit from low fuel crossover, eliminating one of the major sources of loss present in DMFCs. The improved DME performance in 2012 is due in part to a new ternary PtRuPd anode

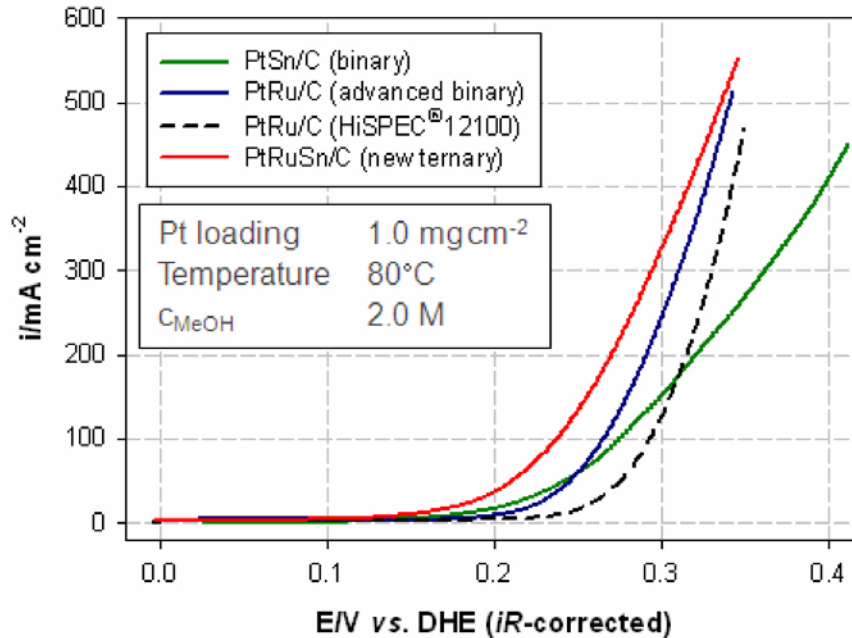
Start up/Shut down: 5,000 cycles; $< 90 \mu\text{g}/\text{cm}^2$ PGM



BOT – beginning of test; EOT – end of test; OER – oxygen evolution reaction

FIGURE 4. Effect of cathode oxygen evolution catalyst loading on durability during startup/shutdown

catalyst, which outperforms earlier PtRu catalysts in MEA as well as half-cell testing. Progress was also made in DMFC development (Johnson Matthey Fuel Cells), with a new PtRuSn catalyst that combines the low-current performance of PtSn with the high-current performance of PtRu (Figure 5). DMFCs based on the new anode catalyst have demonstrated mass activity of 500 mA/mg_{Pt} at 0.35 V, 150% higher than the FY 2012 milestone.



DHE – dynamic hydrogen electrode

FIGURE 5. A new ternary methanol oxidation catalyst outperforms conventional binary catalysts

Balance of Plant

New humidifier projected to meet \$100 cost target (Gore): A humidifier containing a novel composite membrane developed by Gore and an integrated module developed by DPoint is projected to meet the \$100 cost target when manufactured at high volume. The module uses a membrane pocket over plate assembly concept, in which the membrane contains a very thin, highly permeable ionomer sandwiched between two microporous polymer supports. Further work is required to improve durability, with current modules showing a 20-30% drop in water transfer rate during 5,500 hours of testing (target: <10% drop over 5,000 hours).

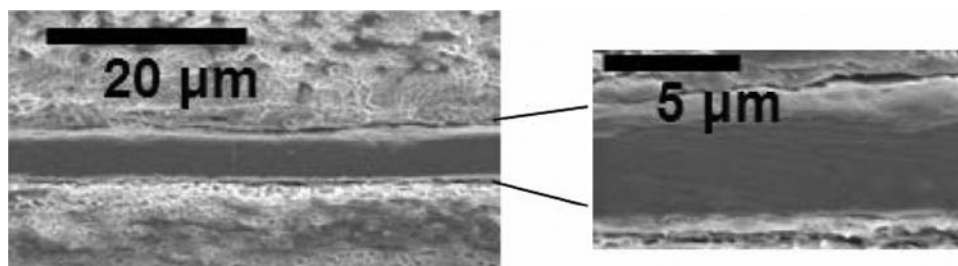
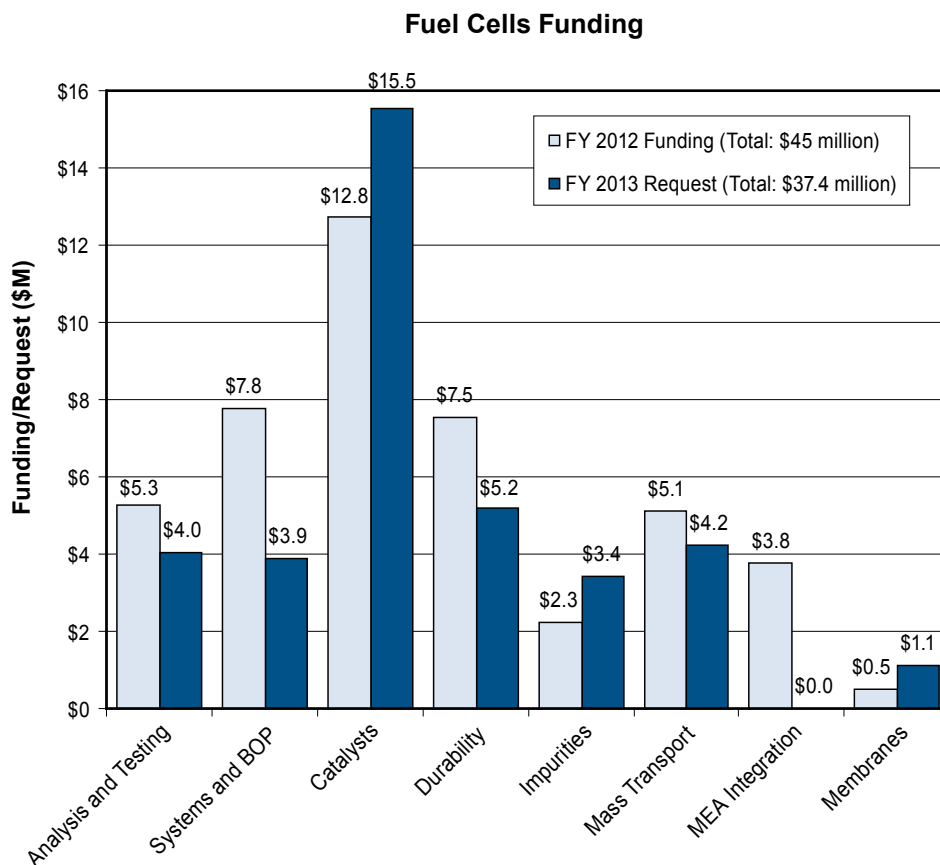


FIGURE 6. The Gore humidifier membrane contains a dense ionomer layer sandwiched between two microporous layers.

BUDGET

The President's FY 2013 budget request calls for approximately \$38 million for the Fuel Cell sub-program. The figure below shows the budget breakdown by R&D area for the FY 2012 congressional appropriation of \$44 million and the FY 2013 budget request. The sub-program continues to focus on reducing costs and improving durability with an emphasis on fuel cell stack components. In the budget breakdown, Systems and BOP includes projects related to portable and stationary power. New projects were awarded in FY 2012 for BOP and MEA integration. In accordance with reprogramming requirements included in the 2012 House and Senate Appropriation, new projects in FY 2012 were fully funded.



FY 2013 PLANS

In FY 2013, the Fuel Cells sub-program will continue R&D efforts on fuel cells and fuel cell systems for diverse applications, using a variety of technologies (including PEM, solid oxide, and alkaline fuel cells) and a range of fuels (including hydrogen, diesel, natural gas, and bio-derived renewable fuels). Support will continue for R&D that addresses critical issues with electrolytes, catalysts, electrodes, and modes of operation. The sub-program will also continue its emphasis on science and engineering with a focus on component integration at the cell and stack level, as well as on integration and component interactions at the system level. Emphasis will continue to be placed on BOP component R&D, such as air compressors that can lead to lower cost and lower parasitic losses. Ongoing support of modeling will guide component R&D, benchmarking complete systems before they are built and enabling exploration of alternate system components and configurations. Cost analysis efforts have been expanded beyond transportation applications to also include distributed power generation

systems (including CHP) and systems for emerging markets for a variety of fuel cell technologies; further detailed results of these analyses are expected in FY 2013.

Dr. Dimitrios Papageorgopoulos
Fuel Cells Team Lead
Fuel Cell Technologies Program
Department of Energy
1000 Independence Ave., SW
Washington, D.C. 20585-0121
Phone: (202) 586-5463
Email: Dimitrios.Papageorgopoulos@ee.doe.gov

V.A.1 Analysis of Laboratory Fuel Cell Technology Status – Voltage Degradation

Jennifer Kurtz (Primary Contact), Keith Wipke, Sam Sprik, Genevieve Saur, Huyen Dinh
National Renewable Energy Laboratory (NREL)
15013 Denver West Parkway
Golden, CO 80401-3305
Phone: (303) 275-4061
Email: jennifer.kurtz@nrel.gov

DOE Manager
HQ: Kathi Epping Martin
Phone: (202) 586-7425
Email: Kathi.Epping@ee.dog.gov

Project Start Date: July 1, 2009
Project End Date: Project continuation and direction determined annually by DOE

- Published eight composite data products (CDPs) on:
 - Operation time and projected operation time to 10% voltage drop
 - Projected operation time sensitivity to voltage drop levels
 - Comparison of automotive and material handling equipment (MHE) lab and field durability projections
 - Power capability
 - Data sets operated beyond 10% voltage drop
 - Durability projections by configuration and test condition.
- Projected operation time to 10% voltage drop summary by application:
 - Backup
 - Average projected operation hours to 10% voltage drop ~2,400 hours
 - Maximum projected operation hours to 10% voltage drop ~7,000 hours
 - Automotive
 - Average projected operation hours to 10% voltage drop ~4,000 hours
 - Maximum projected operation hours to 10% voltage drop ~12,200 hours
 - Forklift
 - Average projected operation hours to 10% voltage drop ~14,600 hours
 - Maximum projected operation hours to 10% voltage drop ~21,800 hours
 - Stationary
 - Average projected operation hours to 10% voltage drop ~11,200 hours
 - Maximum projected operation hours to 10% voltage drop ~40,600 hours.
- Included data on proton exchange membrane fuel cell (PEMFC) and solid oxide fuel cell (SOFC) of full active area short stacks and full stacks with systems
- Shared all detailed data analysis results with data providers.



Fiscal Year (FY) 2012 Objectives

- Conduct an independent assessment to benchmark state-of-the-art fuel cell durability in a non-proprietary method
- Leverage analysis experience from the Fuel Cell Electric Vehicle Learning Demonstration project
- Collaborate with key fuel cell developers on the analysis

Technical Barriers

This project addresses the following technical barrier from the Fuel Cells section (3.4) of the Fuel Cell Technologies Program Multi-Year Research, Development and Demonstration Plan:

(A) Durability

Technical Targets

This project is conducting an independent assessment of the durability of current laboratory fuel cell stacks and systems. The analysis, applied uniformly on all data sets, studies the projected operation time to 10% voltage drop. All results are aggregated to protect proprietary information and reported on by expected application.

FY 2012 Accomplishments

- Analyzed fuel cell stack and system data in four application categories (backup, automotive, forklift, and stationary) and from 10 fuel cell developers

Introduction

The DOE has funded significant research and development activity with universities, national laboratories,

and the fuel cell industry to improve the market competitiveness of fuel cells. Most of the validation tests to confirm improved fuel cell stack performance and durability (indicators of market competitiveness) are completed by the research organizations themselves. Although this allows the tests to be conducted by the developers most familiar with their specific technology, it also presents a number of challenges in sharing progress publicly because test conditions and data analysis take many forms and data collected during testing are often considered proprietary.

NREL is benchmarking the state-of-the-art fuel cell performance, specifically focusing on durability, through independent assessment of current laboratory data sets. NREL’s data processing, analysis, and reporting capitalize on capabilities developed in DOE’s Fuel Cell Electric Vehicle Learning Demonstration. Fuel cell stack durability status is reported annually and includes a breakdown of status for different applications. A key component of this project is the collaborative effort with key fuel cell developers to understand what is being tested in the lab, study analysis results, and expand the included data sets.

Approach

The project involves voluntary submission of data from relevant fuel cell developers. We are contacting fuel cell developers, for multiple fuel cell types, to either continue or begin a data sharing collaboration. A continuing effort is to include more data sets, types of fuel cells, and developers.

Raw and processed data are stored in NREL’s Hydrogen Secure Data Center. Processing capabilities are developed or modified for new data sets and then included in the analytical processing of NREL’s Fleet Analysis Toolkit (NRELFAT). The incoming raw data may be new stack test data or they may be a continuation of data that have already been supplied to NREL. After the raw data are processed, the results are analyzed with particular attention to durability and operating conditions. Each individual data set has a set of data figures that are shared with the data provider and used to create the CDPs. CDPs are designed to report on the technology status without revealing proprietary information.

Results

This fuel cell stack durability analysis expanded in the number of data sets analyzed, applications and fuel cell types studied, and amount of details published. Results published in April 2012 were the fourth update for this analysis effort, and the next analysis update is scheduled for February 2013. The annual voltage degradation analysis of state-of-the-art lab durability was completed in advance of the milestone in order to provide an update that could be presented at the DOE’s Annual Merit Review. In the last published data set, four applications were covered, 10 fuel cell developers supplied data (more than one data set in many cases), and the data sets covered PEMFC and SOFC stack testing. A total of 82 data sets have been analyzed, including 39 new data sets added over the last 12 months. Note that a data set represents a short stack, full stack, or system test data. Of the total data sets, 78% have been retired (Figure 1), meaning the system

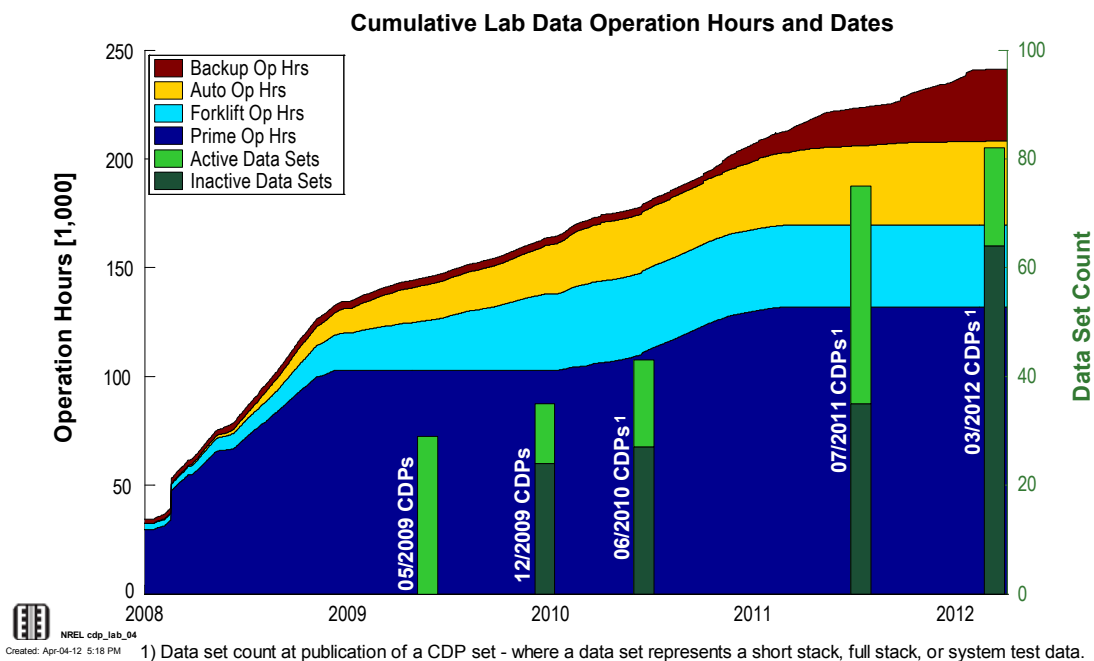


FIGURE 1. Cumulative lab data operation hours and dates

or stack is not accumulating any new operation hours either because of test completion, technology upgrades, or failures. The published data results include eight CDPs. The power capability illustrates the range of fuel cell power for the data sets by application from <2 kW to >50 kW. Most of the analyzed data sets are lab systems at less than 14 kW power.

The analyzed data sets are from lab testing of full active area short stacks (e.g., stacks with fewer cells than the expected full power stack) and test systems with full power stacks. The data sets also vary from one to the other in how the stack/system was tested. Data were generated between 2004 and late 2011 from different testing methods that included constant load, transient load, and accelerated testing. The variability in test conditions and test setups created a group of data that can be difficult to compare. Additional breakdown of the data sets is an important aspect of future work and is dependent on the accumulation of more data sets in order to not reveal an individual data supplier’s contribution to the results or proprietary data.

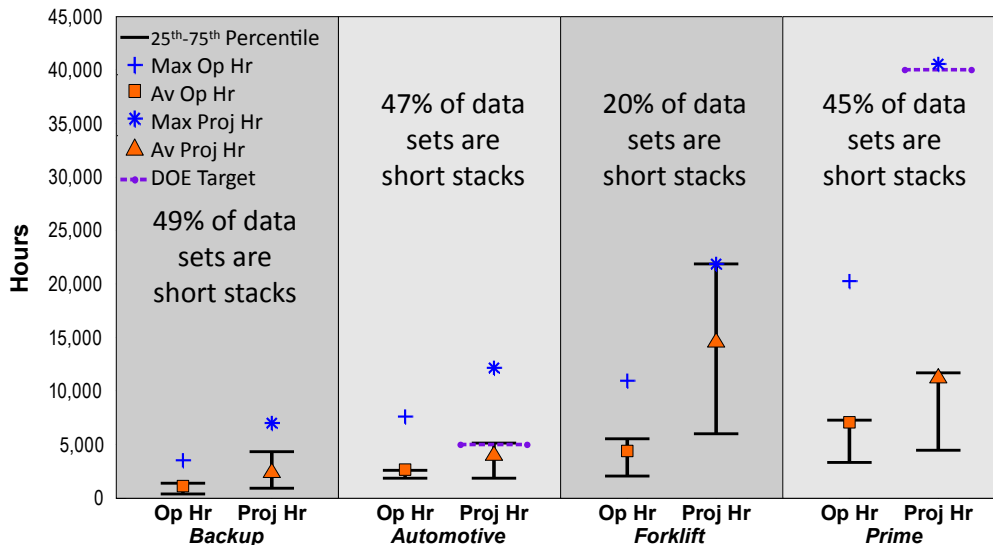
Fuel cell durability is studied at a design-specific current point and measured against a target of 10% voltage drop from beginning of life. The 10% voltage drop metric is used for assessing voltage degradation with a common measurement, but the metric may not be the same as end-of-life criteria and does not address catastrophic failure modes. Figure 2 is an aggregated set of results separated by application and identifies the percentage of short stacks. Each application has the average, maximum, and 25th and 75th percentile values

identified for the operation hours and the projected hours to 10% voltage drop. Table 1 summarizes the average values highlighted in Figure 2.

TABLE 1. Summary of Average Operation Hours and Average Projected Hours to 10% Voltage Drop by Application

| Application | Average Operation Hours | ~Average Projected Hours to 10% Voltage Drop |
|-------------|-------------------------|--|
| Backup | 1,100 | 2,400 |
| Automotive | 2,700 | 4,000 |
| Forklift | 4,400 | 14,600 |
| Stationary | 7,100 | 11,200 |

The 10% voltage drop level is not necessarily a measurement for end-of-life or even significant reduction in performance. Many data sets have not passed (or did not pass) the metric of 10% voltage degradation. The reason data sets operated beyond 10% voltage degradation could be because end-of-life criteria may be greater than 10% voltage degradation or because the test was designed to operate until a failure. The stack configuration and test conditions can have a significant impact on the projected time to 10% voltage degradation within an application. In general, the average projection decreases with more aggressive test conditions and full systems (Figure 3). Not all applications have data sets in each configuration or test condition group. The test condition groups include:



(1) At least 9 fuel cell developers supplied data. Analysis will be updated periodically.
 (2) PEM & SOFC data from lab tested, full active area short stacks and systems with full stacks. Data generated from constant load, transient load, and accelerated testing between 2004 and early 2011.
 (3) The DOE 10% voltage degradation metric is used for assessing voltage degradation; it may not be the same as end-of-life criteria and does not address catastrophic failure modes.
 (4) DOE targets are for real-world applications; refer to Hydrogen, Fuel Cells, & Infrastructure Technologies Program Plan.

FIGURE 2. Operation hours and projected hours to 10% voltage drop by application category

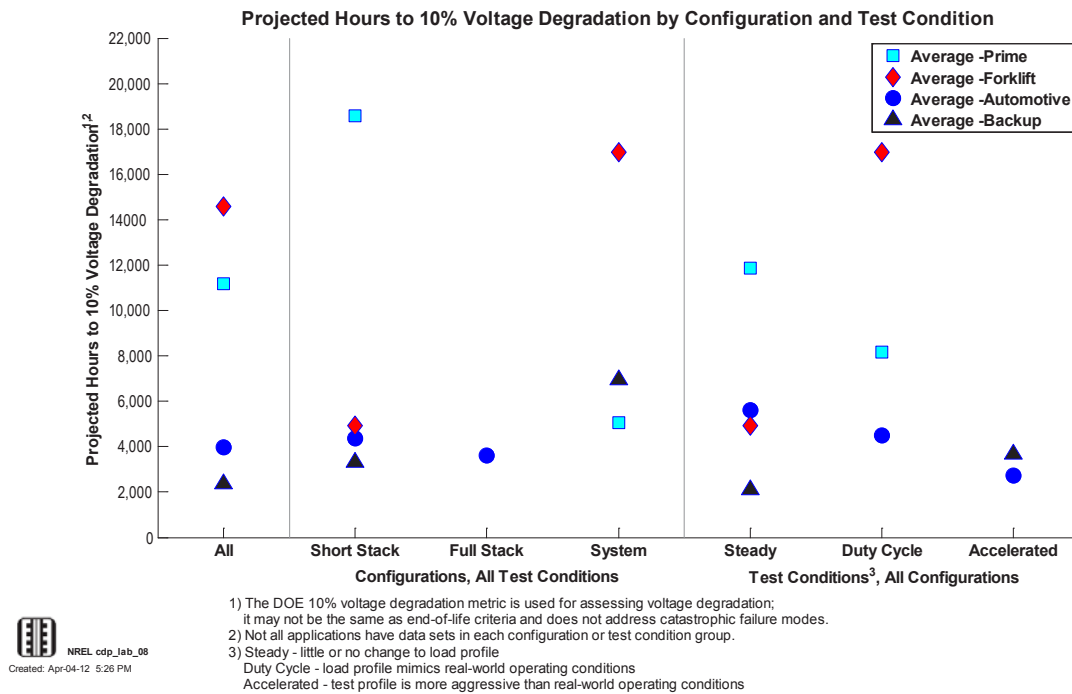


FIGURE 3. Projected hours to 10% voltage drop by configuration and test condition

- Steady – little or no change to load profile
- Duty Cycle – load profile mimics real-world operating conditions
- Accelerated – test profile is more aggressive than real-world operating conditions

Comparisons in the automotive and material handling applications indicate there are gaps between field and lab voltage durability performance (Figure 4). Possible reasons include different data providers, technology generations, operating conditions, and test procedures. Additional comparisons to investigate are projections by configuration and test conditions with field performance.

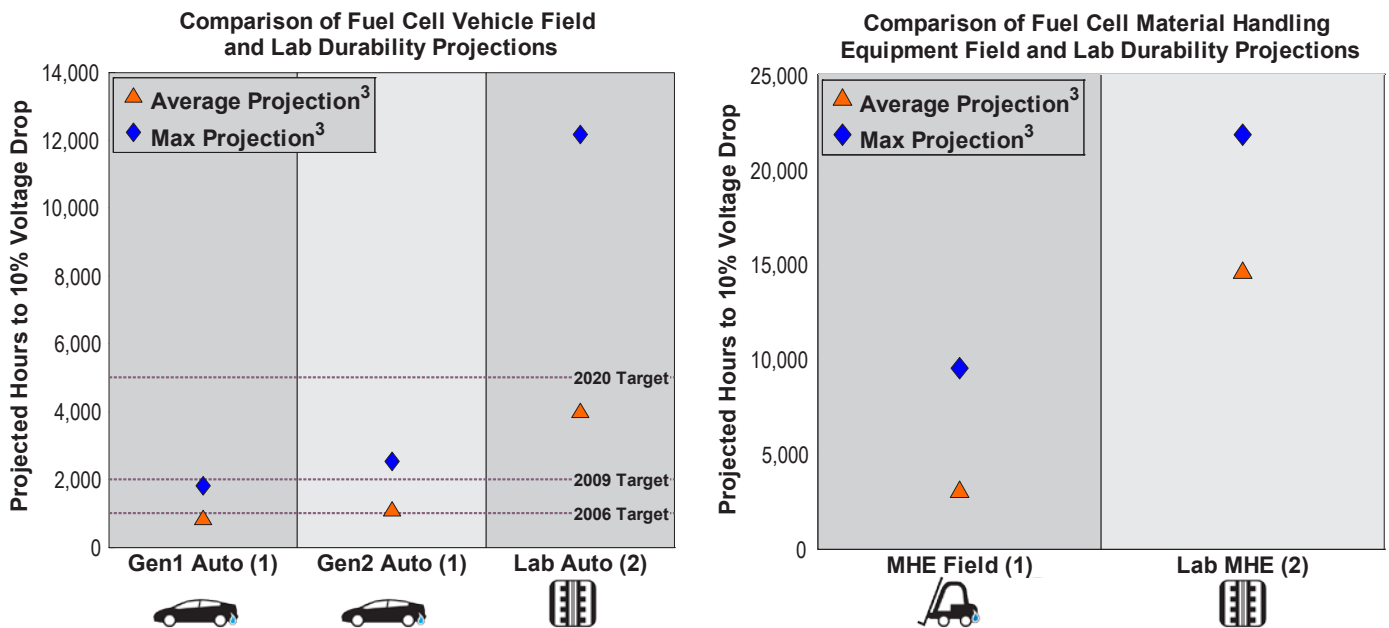


FIGURE 4. Comparison of field and lab durability projections for automotive and MHE application categories

A new website was created for this Fuel Cell Technology Status project at http://www.nrel.gov/hydrogen/proj_fc_analysis.html. The website, located with NREL's technology validation website, provides the following information:

- A project overview
- Links to more information about the Hydrogen Secure Data Center
- A contact link for developers interested in participating
- Links to all of the CDPs, publications, and reports.

Conclusions and Future Directions

This project has leveraged other Technology Validation projects and existing industry relationships to steadily increase the quantity and depth of reporting on the state-of-the-art fuel cell durability status with a relatively low investment from DOE. Half of the 20 fuel cell developers contacted have voluntarily supplied at least one data set, and it is an ongoing effort to include new data sets, update data sets already included (if applicable), and include new fuel cell developers, applications, and types. The voluntary participation of leading fuel cell developers showcases the fuel cell durability improvements with the current technology and provides an overall technology benchmark (with the published aggregated data) and an individual developer benchmark (with the detailed data products). The data are fully integrated into NRELFAT and an online interface provides information on the project, contact information for interested collaborators, and all publications. The published results from April 2012 are the fourth update and were completed ahead of the milestone requirement with many

new data sets and results. An annual update is planned for February 2013 and the future work includes the following:

- Continue cultivating existing collaboration and developing new collaborations with fuel cell developers
- Expand the type of testing to include single cell or short stack testing that is early in the development stage and may not have a clear path to a commercial product
- Identify results from DOE accelerated stress test protocols
- Investigate the difference between field and lab projections and data sets
- Expand results aimed at improving data comparability and statistical confidence
- Investigate other aging parameters for fuel cell durability (e.g., start/stops, soak time)
- Include other applications such as portable.

FY 2012 Publications/Presentations

1. Kurtz, J., Wipke, K., Sprik, S., Saur, G., "Fuel Cell Technology Status – Voltage Degradation," Presented at the 2012 Annual Merit Review and Peer Evaluation Meeting, Washington, D.C. (May 2012)
2. Kurtz, J., Sprik, S., Saur, G., "State-of-the-Art Fuel Cell Voltage Durability Status, 2012 Composite Data Products," Composite data products produced by the NREL Hydrogen and Fuel Cells Research team. (April 2012)
3. Kurtz, J., Wipke, K., Sprik, S., Saur, G., "Analysis of Laboratory Fuel Cell Technology Status – Voltage Degradation," Excerpt from the 2011 Annual Progress Report. (November 2011)

V.A.2 Mass-Production Cost Estimation for Automotive Fuel Cell Systems

Brian D. James (Primary Contact), Kevin Baum,
Andrew B. Spisak, Whitney G. Colella
Strategic Analysis, Inc.
4075 Wilson Blvd. Suite 200
Arlington VA 22203
Phone: (703) 778-7114
Email: bjames@sainc.com

DOE Managers

HQ: Jason Marcinkoski,
Phone: (202) 586-7466
Email: Jason.Marcinkoski@ee.doe.gov
GO: Gregory Kleen
Phone: (720) 356-1672
Email: Gregory.Kleen@go.doe.gov

Contract Number: DE-EE0005236

Project Start Date: September 30, 2011

Project End Date: September 30, 2016

FY 2012 Accomplishments

- Updated automotive FCS cost analysis to include the most up-to-date fuel cell stack performance data provided by Argonne National Laboratory (ANL) and 12 additional significant innovations to FCS performance and manufacture.
- Projected the FCS cost for a 80-kW light-duty vehicle application using a Design for Manufacturing and Assembly (DFMA[®]) methodology at an annual production rate of 500,000 FCSs per year to be \$48.47/kWe.
- Initiated cost analysis of a 150-kWe FCS for bus application based on automotive proton exchange membrane (PEM) stacks.



Introduction

This project represents an update to the ongoing PEM FCS cost model for 80-kWe systems. New technologies, materials data, and optimization modeling were incorporated to give an up-to-date value for system cost. In addition, a new system was modeled based upon the existing automotive system; preliminary costs of a PEM FCS for 150-kWe bus applications were computed.

FCSs for transportation applications are a longstanding area of fuel cell product development. Numerous prototype vehicles exist for a variety of transportation applications and research continues into improving the competitiveness of fuel cells as compared to the internal combustion engine. To better assess the potential usefulness and market-worthiness of fuel cells for transportation applications, this work describes a DFMA[®]-style [1] analysis of the cost to manufacture two different transportation FCSs. The systems analyzed are low-temperature (LT) PEM FCSs with peak electrical capacities of 80 kWe for light-duty vehicle (automobile) applications and 150 kWe for bus applications. The FCSs consume a hydrogen gas fuel stream from an onboard compressed hydrogen storage system. The impact of annual production rate on the cost of both systems is examined to assess the difference between a nascent and a mature product manufacturing base. The annual production rates analyzed are 1,000, 10,000, 30,000, 80,000, 130,000, and 500,000 FCSs per year.

This work focuses primarily on the efforts to update the existing DFMA[®] cost model of the automobile FCS as well as new efforts to design and cost-model the bus FCS. These systems' stack and balance-of-plant (BOP) designs and performance parameters are discussed and the methods

Fiscal Year (FY) 2012 Objectives

- Update 2011 automotive fuel cell cost model to include latest performance data and system design information.
- Examine costs of fuel cell systems (FCSs) for light-duty vehicle and bus applications.

Technical Barriers

This project addresses the following technical barriers from the Fuel Cells section of the Fuel Cell Technologies Program Multi-Year Research, Development and Demonstration Plan:

(B) System Cost

- Realistic, process-based system costs
- Need for realistic values for current and future cost targets

Technical Targets

This project conducts cost modeling to attain realistic, process-based system costs estimates for integrated transportation FCSs operating on direct hydrogen. These values can help inform future technical targets:

- DOE fuel cell system cost target: 30 \$/kilowatts-electric (kWe)

of cost-modeling each explained. Cost trends are evaluated in terms of the capital costs per unit of installed electrical capacity (\$/kWe) and system annual production rate.

Approach

A DFMA[®]-style analysis is conducted to attain cost estimates of PEM FCSs for automobiles and buses at low to high manufacturing production rates. Important fuel cell stack parameters are optimized by ANL and included in the PEM FCS performance and cost model. In addition, industry partners provide feedback on the design, materials, and manufacturing and assembly of FCS components and overall system. Fuel cell stack polarization data was updated for 2012 based on modeling results [2] from ANL, in turn based on data from 3M for their nano-structured, thin-film membrane electrode assemblies (MEAs). The FCS is sized based on rated power operating parameters. System performance is based on performance estimates of individual components, built up into an overall system energy budget. Overall system and component performance are cross checked against estimates made by the Argonne detailed models [2]. DFMA[®] process-based cost estimation techniques are applied to the major system components (and other specialty components) such as the fuel cell stack, membrane humidifier, air compressor/expander/motor unit, and hydrogen recirculation ejectors. For each of these, a manufacturing process train detailed the specific manufacturing and assembly machinery, and processing conditions is identified and used to assess component cost. For lesser components such as valves, heat exchangers, sensors, and piping, a less detailed method of cost estimate is applied. These methods include simplified DFMA[®]-style techniques or price quotation from vendors. Frequent communication with vendors to obtain price quotes, discuss component design and characteristics, and manufacturing methods is used to ensure the validity of the assumptions used in the cost estimates.

The analysis explicitly includes fixed factory expenses such as equipment depreciation, tooling amortization, utilities, and maintenance as well as variable direct costs such as materials and labor. However, because this analysis is intended to model manufacturing costs, a number of components that usually contribute to the original equipment manufacturer price are explicitly not included in the modeling. The following costs are not included in this analysis: profit and markup, one-time costs such as non-recurring research/design/engineering, and general expenses such as general and administrative costs, warranties, advertising, and sales taxes.

Results

The automotive cost model update included several changes that altered the final predicted cost relative to the results from 2011. Table 1 summarizes the main design and

TABLE 1. PEM FCV system design assumptions (light-duty vehicle applications)

| | 2012 Auto System Technology System |
|--|---|
| Power Density (mW/cm ²) | 984 |
| Total Pt loading (mgPt/cm ²) | 0.196 |
| Gross Power (kW gross) | 88.24 |
| Operating Pressure (atm) | 2.50 |
| Peak Stack Temp. (°C) | 87 |
| Active Cells | 369 |
| Membrane Material | Nafion [®] on 25-micron ePTFE |
| Radiator/Cooling System | Aluminum Radiator, Water/Glycol Coolant, DI Filter, Air Precooler |
| Bipolar Plates | Stamped SS 316L with TreadStone Coating |
| Air Compression | Centrifugal Compressor, Radial-Inflow Expander |
| Gas Diffusion Layers | Carbon Paper Macroporous Layer with Microporous Layer |
| Catalyst Application | Nanostructured Thin Film (NSTF) |
| Air Humidification | Tubular Membrane Humidifier |
| Hydrogen Humidification | None |
| Exhaust Water Recovery | None |
| MEA Containment | Injection-Molded LIM Hydrocarbon MEA Frame/Gasket around Hot-Pressed M&E |
| Coolant & End Gaskets | Laser Welding/ Screen-Printed Adhesive Resin |
| Freeze Protection | Drain Water at Shutdown |
| Hydrogen Sensors | 2 for FC System 1 for Passenger Cabin (not in cost estimate) 1 for Fuel System (not in cost estimate) |
| End Plates/ Compression System | Composite Molded End Plates with Compression Bands |
| Stack Conditioning (hrs) | 5 |

DI - deionized; SS - stainless steel; M&E - membrane and electrode

manufacturing features of the 2012 automotive system. Table 2 summarized the changes and their cost impacts that occurred between 2011 and 2012. System and cost parameters for the 2012 bus application are not yet available.

The cost analysis yields results detailing the final estimated capital cost of the entire system at different manufacturing rates. As shown in Figure 1, the capital cost of both the fuel cell stack and the overall FCS per unit of electric output (\$/kWe) is seen to decrease with increasing system annual production rate for automobile FCSs. The steepest reduction in cost that is plotted is between 1,000 and 10,000 systems per year. In comparing these curves to each other, one also can see that the proportion of the capital cost that is attributable to production of the stack itself represents 45% of the total FCS cost at the highest manufacturing rates, with the rest of the cost attributable to BOP and FCS assembly.

To help probe the primary cost drivers of the automobile FCS, a sensitivity analysis was conducted for a variety of stack and system parameters. Parameter ranges were chosen

TABLE 2. Summary of major changes between 2011 and 2012 (light-duty vehicle applications)

| Change | Reason | Change from previous value | Cost (500k systems/year, \$/kW) |
|--|--|----------------------------|---------------------------------|
| 2011 AMR Preliminary Cost Value | | N/A | \$47.81 |
| Press force calculations & capital cost parameters for bipolar plate stamping | Analysis altered to account for swaging of material, as opposed to simple bending. | \$0.06 | \$47.87 |
| Gasket injection molding calculations | Model refined and molding cavity count re-optimized | \$0.31 | \$48.18 |
| GDL Thickness reduced from 300 μm to 150 μm | | -\$0.25 | \$47.93 |
| Final system assembly calculations refined and expanded | Response to industry review | -\$0.16 | \$47.78 |
| Piping configuration/costing updated and expanded | Response to industry review | \$0.66 | \$48.43 |
| Air temperature sensor added to system to monitor coolant exit conditions | Response to industry review | \$0.06 | \$48.49 |
| Purge valve upgraded to multi-function model | Response to industry review | \$0.33 | \$48.82 |
| Hot pressing process removed and replaced with crimping roller process prior to cutting and slitting | Hot pressing incompatible with NSTF catalyst deposition, new method required for combining membrane & GDL layers | -\$0.06 | \$48.76 |
| Ionomer cost curve reduction | Ionomer cost curve changed to reflect industry estimated value at high production | -\$0.23 | \$48.53 |
| Pressure, platinum loading, power density, and temperature updated to 2012 ANL optimization values | New release of ANL optimization curves for performance parameters | \$1.83 | \$50.36 |
| Membrane air humidifier design change | Air humidifier changed to tubular design (effect offset by ionomer cost reduction) | \$0.25 | \$50.61 |
| Gaskets changed from frame gaskets to sub-gaskets with screen-printed seals | New manufacturing process modeled in response to industry discussions | -\$2.14 | \$48.47 |
| Final 2012 Value | | \$0.66 | \$48.47 |

NSTF - nanostructured thin film; GDL - gas diffusion layer

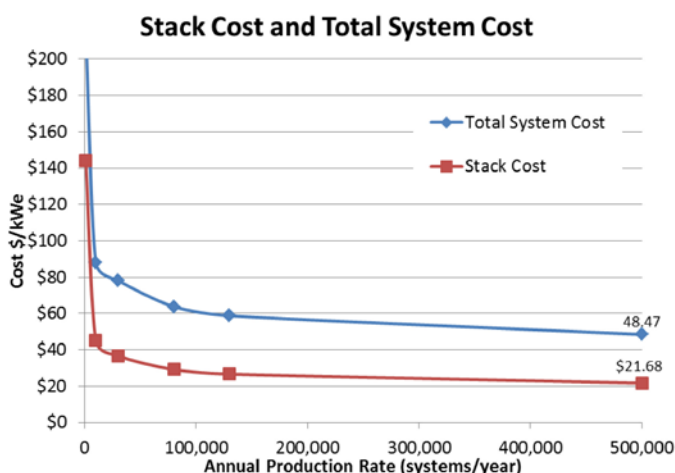


FIGURE 1. PEM fuel cell system and stack cost as a function of production rate (light-duty vehicle applications)

based on a 90%/10% confidence interval for expected variation in each parameter. Power density is determined to be the dominant cost parameter. The air compressor cost and the platinum loading are the top second and third most important cost parameters, respectively. Building on this single variable sensitivity analysis, a Monte Carlo simulation was conducted to show the likely range of systems costs. Figure 2 shows that middle 90% band ranges from \$46.86/kWe to \$55.83/kWe.

Finally, the cost results of the current iteration of transportation modeling are compared to previous years' results in Figure 3. In every year except for the current, predicted manufacturing costs for automobile FCSs have trended steadily downward. This is due to improvements in technology, modeling of new manufacturing and assembly methods, and improved level of detail within the cost model itself. However, the most recent results show a modest cost increase of \$0.66/kWe in modeled cost at the highest manufacturing rates.

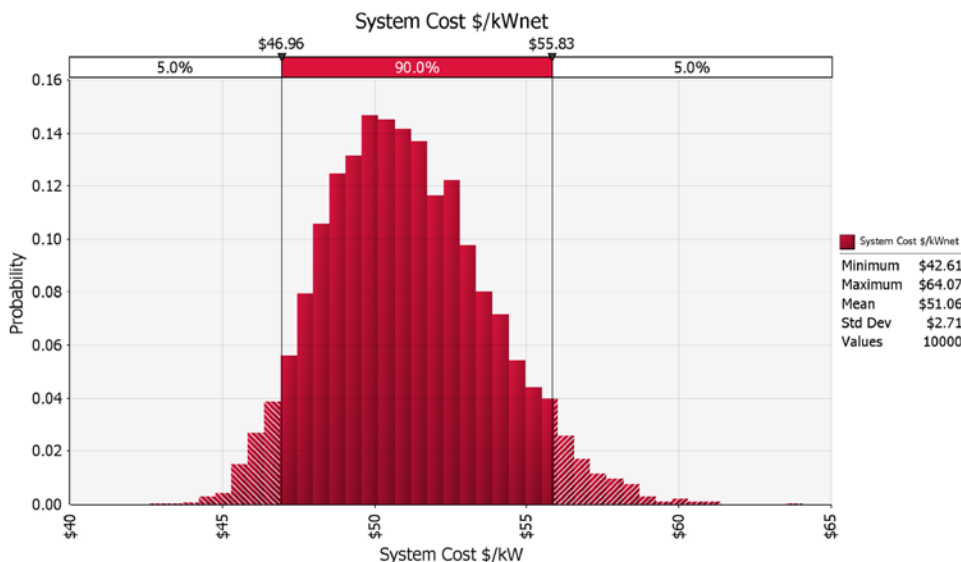


FIGURE 2. Monte Carlo simulation results for 80-kW FCS at 500,000 systems/year (light-duty vehicle applications)

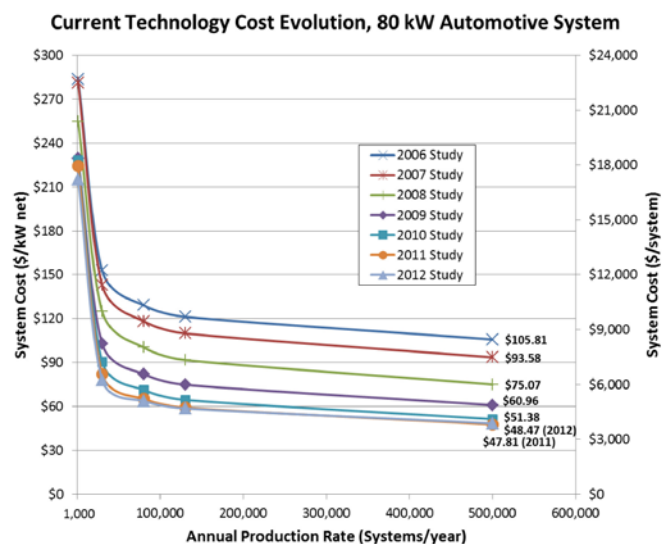


FIGURE 3. Evolution of FCS costs

Conclusions and Future Directions

The primary findings of this analysis of transportation FCSs relate to the key cost drivers of the automobile systems. Based on the analysis presented here, automobile FCS cost decreases dramatically between production rates of 1,000 and 10,000 systems per year, and then continues to decrease in a gentle curve for manufacturing rates through 500,000 systems per year. Additional results quantify that the relative cost contribution of the fuel cell stack is about 45% of the total FCS capital cost at high production volumes. The remaining contributors to system capital cost are from

the BOP and assembly. The nominal 2012 fuel cell system cost for light-duty vehicle applications at 500,000 systems per year manufacturing rate is \$48.47/kWe with an expected range of \$46.96 to \$55.83/kWe for the middle 90% confidence band (as predicted by Monte Carlo simulation). Finally, in every year except for the current, model results indicate that the expected capital costs for automobile FCSs trend steadily downward.

FY 2012 Publications/Presentations

1. James, Brian D., Spisak, Andrew, “Mass Production Cost Estimation for Direct Hydrogen PEM Fuel Cell Systems for Automotive Applications,” Presentation to the Fuel Cell Tech Team, Southfield MI. July 18, 2012.
2. James, Brian, “Fuel Cell Transportation Cost Analysis, Preliminary Results,” *Department of Energy (DOE) Fuel Cell Technology (FCT) Program Annual Merit Review*, Washington, D.C., May 14–18, 2012.
3. James, Brian D., Perez, Julie, Baum, Kevin N., Spisak, Andrew, Sanders, Matt. “Low Temperature PEM Stationary Fuel Cell System Cost Analysis,” *2011 Fuel Cell Seminar*, Orlando, Florida, 1 November 2011.

References

1. Boothroyd, G., P. Dewhurst, and W. Knight. “Product Design for Manufacture and Assembly, Second Edition,” 2002.
2. Ahuwalia, R. “Fuel Cell Systems Analysis,” Argonne National Laboratory, Presentation to DOE Fuel Cell Tech Team, 18 July 2012, Southfield MI.

V.A.3 Stationary Fuel Cell System Cost Analysis

Brian D. James (Primary Contact),
Andrew B. Spisak, Whitney G. Colella
Strategic Analysis, Inc.
4075 Wilson Blvd. Suite 200
Arlington, VA 22203
Phone: (703) 778-7114
Email: bjames@sainc.com

DOE Managers

HQ: Jason Marcinkoski
Phone: (202) 586-7466
Email: Jason.Marcinkoski@ee.doe.gov
GO: Gregory Kleen
Phone: (720) 356-1672
Email: Gregory.Kleen@go.doe.gov

Technical Advisor

Bryan Pivovar
Phone: (303) 275-3809
Email: bryan.pivovar@nrel.gov

Sub-Contract Number No: AGB-0-40628-01 under
Prime Contract No. DE-AC36-08G028308

Project Start Date: July 8, 2010
Project End Date: September 7, 2012

Fiscal Year (FY) 2012 Objectives

- Perform Design for Manufacturing and Assembly (DFMA[®]) cost analysis for low-temperature (LT) proton exchange membrane (PEM), high-temperature (HT) PEM, and solid oxide fuel cell (SOFC) systems at manufacturing rates of 100, 1,000, 10,000, and 50,000 systems per year for 1-kilowatt-electric (kWe), 5-kWe, 25-kWe, and 100-kWe systems.
- Explore sensitivity of DFMA[®] cost to design parameters.
- Validate cost results and sensitivities against industry partner costs.

Technical Barriers

This project addresses the following technical barriers from the Hydrogen Storage section of the Fuel Cell Technologies Program Multi-Year Research, Development and Demonstration Plan:

(B) System Cost

- Realistic, process-based system costs
- Need for realistic values for current and future cost targets

- Demonstrates impact of technical targets and barriers on system cost:
 - Balance of plant
 - Materials of construction
 - System size and capacity (weight and volume)

(H) Balance-of-Plant (BOP) Components

Technical Targets

This project conducts cost modeling to attain realistic, process-based system costs for a variety of stationary fuel cell systems. These values can help inform future technical targets for stationary fuel cell system cost.

FY 2012 Accomplishments

- Completed preliminary DFMA[®] cost analysis for LT PEM, HT PEM, and SOFC systems at manufacturing rates of 100, 1,000, 10,000, and 50,000 systems per year for 1-kWe, 5-kWe, 25-kWe, and 100-kWe systems.
- Identified primary capital cost drivers for all systems, with roughly ~40% of capital costs stemming from the fuel processing sub-system and ~40% of capital costs from the fuel cell sub-system, depending on the production rate, system size, and fuel cell type.
- Quantified the marginal increase in capital cost for grid-independent operation (5% to 10% of total capital costs) and for combined heat and power (CHP) operation (2% to 5% of total capital costs).
- Calculated the decrease in fuel cell system (FCS) capital cost with increased FCS size (for example, 100-kWe SOFC systems are 18% of the cost of 1-kWe systems at a global installed capacity of 10,000 kWe in one year; 5-kWe SOFC systems are 43% of the cost of 1-kWe systems for a 50,000 kWe global installed capacity in one year.)



Introduction

To better assess the potential usefulness and market-worthiness of stationary FCSs, this work describes a DFMA[®]-style [1] analysis of the cost to manufacture a series of stationary FCSs. The manufacturing costs of stationary FCSs based on three different fuel cell technologies are studied: LT PEM, HT PEM, and SOFC. The FCS's fuel processing subsystem includes a steam reforming reactor external to the fuel cell stack that converts natural gas into a hydrogen-rich gas for the fuel cells. Systems are cost-

modeled with peak electrical capacities of 1 kWe, 5 kWe, 25 kWe, and 100 kWe across annual production rates of 100, 1,000, 10,000, and 50,000 systems per year. In addition, this analysis assesses the marginal cost increase from enhancing an electricity-only FCS (base design) to one that can serve CHP applications [2] and/or grid-independent conditions.

This work focuses primarily on efforts to design and cost-model LT PEM, HT PEM, and SOFC stationary systems. Each system's stack, fuel processor, and BOP design and performance parameters are discussed and the methods of cost-modeling are explained. Cost trends are evaluated in terms of the capital costs per unit (\$/kWe) as a function of system installed capacity, system annual production rate, and individual system capacity for the same global installed capacity. Finally, LT PEM, HT PEM, and SOFC system costs are compared.

Approach

The cost model relies upon a DFMA[®]-style methodology to determine the cost to manufacture several stationary system designs at varied rates of production. The methodology consists of three major steps: (1) System Conceptual Design, (2) System Physical Design, and (3) Cost Modeling.

(1) System Conceptual Design

A main purpose of the system conceptual design phase is to develop a conceptual model of a fully functional FCS with defined thermodynamic performance. In this phase, design requirements are identified and performance parameters are determined. Design requirements include considerations such as system technology (LT PEM, HT PEM, SOFC), system-rated electrical output (1, 5, 25, and 100 kWe for each technology), whether to allow for CHP operation or grid-independent operation, input fuel composition, water neutrality, and so forth. Once these design requirements are identified, a conceptual system can be laid out which satisfies the requirements. Detailed designs are developed for the four main fuel cell subsystems: the fuel cell subsystem, the fuel processing subsystem, the electrical management subsystem, and the thermal management subsystem. The entire FCS is modeled within Aspen HYSYS[®] process modeling software to determine performance parameters such as net system electrical efficiency, flow rates, temperatures, and pressures. Table 1 indicates several of the key design assumptions made for the SOFC system. Reference to existing FCSs is made to assure the performance parameters are consistent with expected values for systems with similar performance and operational goals. The system conceptual design also facilitates the next stage, system physical design, by identifying all required system components and their physical constraints, for example mass flow quantities, operating temperatures, and heat exchanger area.

TABLE 1. SOFC System Design Assumptions

| Assumption | Value |
|---|---|
| Design Stack Power Density | 291 mW/cm ² (0.8 volts/cell at 364 mA/cm ²) |
| Stack Geometry | Planar SOFC geometry |
| Electrolyte Manufacturing Method | Tape casting |
| System Net Electrical Efficiency | 49% (Net Alternating Current Electrical Out/Natural Gas Higher Heating Value Input) |
| Operating Pressure | 1 atm |
| Reactants | Fuel: reformat gas from the stream reformer, oxidant: air |
| Electrode Material | Yttria-Stabilized Zirconia (YSZ) |
| Cathode Catalyst Material and Application Method | Lanthanum strontium cobalt ferrite, screen-printing |
| Anode Catalyst Material and Application Method | Nickel cobalt, spray deposition |

(2) System Physical Design

A main purpose of the system physical design phase is to develop detailed bills of materials for each major system and subsystem component. The system physical design is based on the system conceptual design. For standardized components such as compressors, blowers, sensors, heat exchangers, piping, etc. (common in the BOP), it is sufficient to use the required performance parameters to obtain an appropriate price quote for each piece of equipment. For integral components for which a full DFMA[®]-style analysis will be performed, the system physical design step involves determining the full physical embodiment of the system, including materials, geometry, and manufacturing methods. Design for this step is supplemented by assistance from industry partners and previous design work. For example, the fuel processor subsystem design is based upon an integrated reactor designed by Tokyo Gas [3,4]. For the LT and HT PEM FCSs, fuel cell subsystem designs are based upon prior work on automotive PEM subsystems, adapted for the new requirements identified in the previous step [5,6]. The physical design for the SOFC stack was based upon the FlexCell SOFC system by NexTech [7].

(3) Cost Modeling

Once the physical embodiment has been determined, costs can be modeled. There are two levels of detail in cost modeling: (A) detailed DFMA[®]-style cost modeling of the core system components, and (B) less detailed quote-based cost estimates of standardized components common in the system BOP. For (A), a full physical, manufacturing process train is specified. For (B), mass-produced cost estimates are obtained for all subcomponents via industry quotes.

Iteration

To reduce costs and optimize system performance, changes at all stages of the modeling and design process are constantly considered as the system conceptual design, system physical design, and manufacturing cost models are developed. Additionally, feedback from industry is continuously incorporated into this work. Thus, the three-step methodology is constantly iterated upon. New design approaches and physical system embodiments are continually examined, and the cost model refined, with the primary aim of identifying the design and manufacturing processes that result in the lowest system cost.

Results

The cost analysis yields preliminary results detailing the final estimated capital cost of the entire stationary FCS, at different annual manufacturing rates and installed capacities. As shown in Figure 1, the capital cost per unit of electric output (\$/kWe) is seen to decrease dramatically both with increasing system size and increasing system annual production rate. Example results shown are for SOFC systems.

Results also indicate the proportion of capital cost attributable to each subsystem and subsystem component. Figure 2 (for an SOFC system) shows that the marginal increase in cost between producing a basic system which is not capable of CHP or grid-independent operation and producing a more advanced FCS that is capable of both CHP and grid-independent operation is in fact relatively small, with grid-independent operation capital costs representing 5% to 10% and CHP operation capital costs representing only 2% to 5% of the overall capital cost of such a system.

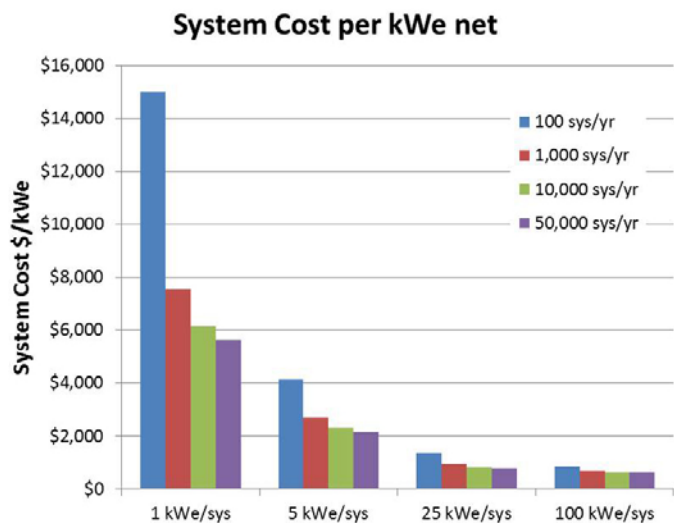


FIGURE 1. Total SOFC system cost results across all system sizes and production rates

Figure 3 breaks down total system capital costs for the baseline 5-kWe SOFC system (i.e. no CHP or grid independent operation) into six different categories. These categories are exhaust gas heat exchanger/condenser, housing and final assembly, power electronics subsystem, cost margin, fuel processing subsystem, and fuel cell stack subsystem. As evident from the figure, the greatest contributors to the capital cost are the fuel processing subsystem and the fuel cell subsystem, together representing 2/3rds to 3/4ths of the total system capital cost. Model results also tabulate the capital cost breakdowns for the fuel

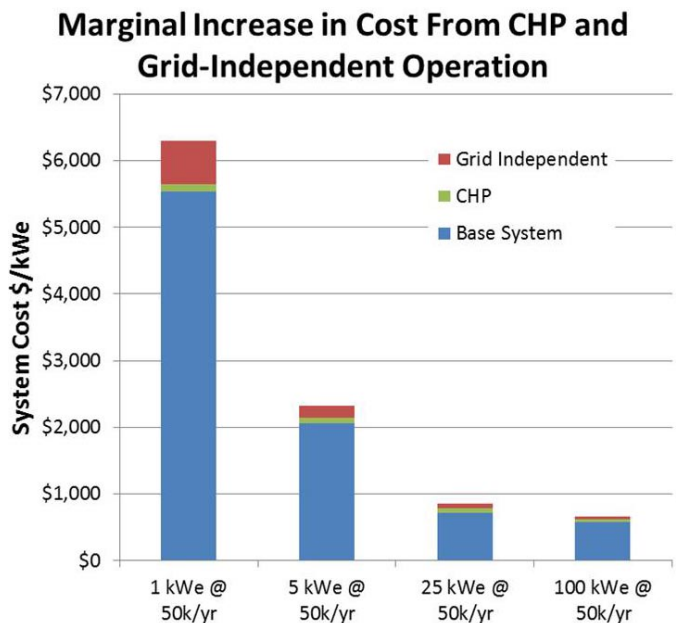


FIGURE 2. Marginal increase in cost with CHP and with grid-independent operation

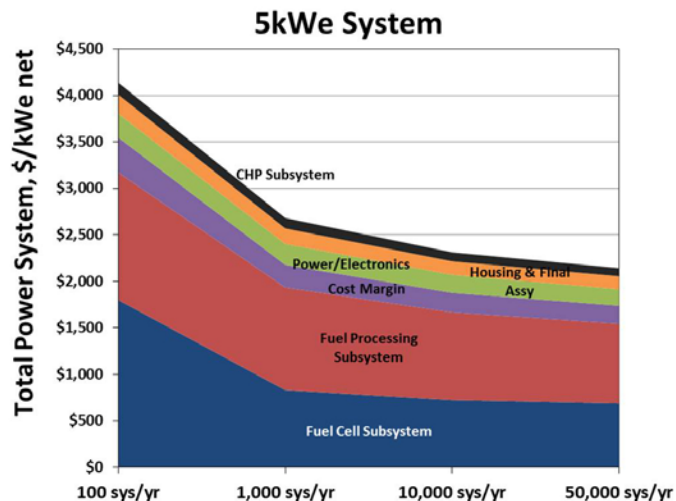


FIGURE 3. SOFC subsystem cost breakdown for a 5-kWe system

processing subsystem's BOP. For example, within the fuel processor BOP of the 5-kWe SOFC system, the natural gas compressor and the condenser are identified as large cost contributors and thus are prime candidates for cost reduction efforts.

Model results indicate that, at the same cumulative global installed capacity, higher power FCSs are expected to have lower per unit capital costs (\$/kWe) than lower power FCSs. For the same cumulative global installed capacity in a given year, FCSs with a higher electrical power output are several times more economical per kilowatt of electric power than systems with a lower power output. For example, for a 10,000 kWe global installed capacity in one year, 100-kWe SOFC systems are 13% of the cost of 1-kWe systems (\$836/kWe vs. \$6,157/kWe). For a 50,000 kWe global installed capacity in one year, 5-kWe SOFC systems are 41% of the cost of 1-kWe systems (\$2,312/kWe vs. \$5,651/kWe). For a 250,000 kWe global installed capacity in one year, 25-kWe SOFC systems are 39% of the cost of 5-kWe systems (\$828/kWe vs. \$2,142/kWe). This analysis implicitly assumes that the FCS electricity and heat will be used with 100% utilization in the buildings that they serve, regardless of system size. In practice, lower power FCSs may experience higher utilizations than higher power systems [8,9]. Also, the total market volume for lower power FCSs may be larger, allowing for higher production rates.

Additional results include the comparison of fuel cell stack cost to fuel cell subsystem BOP at different system sizes. Results indicate that for a 1-kWe SOFCs, at the highest production rates evaluated (50,000 units/year), the BOP is the largest contributor to fuel cell subsystem capital costs. At this fuel cell size and production rate, BOP costs are higher than stack costs. By contrast, for higher power SOFCs, stack costs dominate subsystem costs. Results further indicate that, in the larger 5-kWe SOFC systems, the stack costs are the largest contributor to the fuel cell subsystem capital costs. For comparison, at the same 5-kWe level, fuel processor BOP costs dominate fuel processing subsystem capital costs. The fuel processing reactor itself did not contribute greatly to the cost. Model results indicate that fuel processor BOP costs are the largest contributor to fuel processing subsystem capital costs for all SOFC sizes and production rates.

Model results indicate that LT PEM stacks are less expensive than SOFC and HT PEM stacks. Based on a series of parallel analyses conducted for HT PEM [10] and LT PEM FCSs [11], for a 100-kWe stack at a production volume of 10,000 units per year, stack costs are \$129/kWe for LT PEM, \$352/kWe for HT PEM, and \$318/kWe for SOFC. (Stack power densities assumed in these analyses are 408 mW/cm², 240 mW/cm², and 291 mW/cm², respectively.) According to these data, SOFC stack capital costs are about 10% lower than HT PEM stack capital costs but 2.5 times higher than LT PEM stack capital costs. These results are preliminary and analysis is still underway. Further, the PEM cost models

used in this comparison have been fine-tuned over the past 15 years [12,13] whereas the SOFC models have only been recently developed. Consequently, the cost estimates may shift as the analysis is refined. Computation of the total system costs for LT PEM, HT PEM, and SOFC are not yet complete, thus preventing a total system cost comparison at this time.

It is further noted that the cost comparisons between fuel cell technologies in this analysis apply only to initial capital cost rather than to life-cycle cost. The projected net system electrical efficiency based on higher heating value of natural gas of the SOFC FCS (49%) is substantially higher than that of LT PEM (32%) or HT PEM (27%). While a life-cycle analysis has not been conducted, it is expected that the higher net electrical efficiency of the SOFC system could substantially off-set the higher initial stack capital cost.

Conclusions and Future Directions

The primary findings of this analysis of stationary LT PEM, HT PEM, and SOFC systems relate to the key cost drivers across the range of analysis, from the low power (1-kWe) FCSs to the large (100-kWe) FCSs and from low production (100 systems/year) to higher production rates (50,000 systems/year). Based on the analysis presented here, it was found that for a given cumulative global installed quantity, FCS capital costs are lower if manufacturers produce fewer very large systems as compared to a large number of lower power systems. Thus, while both production quantity and system size drove cost down, capital cost was found to be more sensitive to system size than to production rate. At the same time, this analysis does not consider other important economic factors, including life-cycle costs, market accessibility, and FCS in-use heat recovery and electrical efficiency within buildings. Additional results quantify the relative cost contribution of various subsystems. The greatest contributors to the FCS capital cost are the fuel processing subsystem and the fuel cell subsystem, together representing 2/3^{rds} to 3/4^{ths} of the total system capital cost. Furthermore, model results indicate that the addition of CHP and grid-independent operation adds only about 10% to total system capital costs, compared with the base case design involving no CHP or grid-independent operation. Finally, model results indicate that SOFC stack capital costs are about 10% lower than HT PEM stack capital costs, and SOFC stack capital costs are about 2.5 times higher than LT PEM stack capital costs.

FY 2012 Publications/Presentations

1. James, Brian D., Spisak, Andrew, Colella, Whitney G. "Combined heat and power (CHP) and Grid-Independent Stationary Fuel Cell Systems (FCSs) -- Conceptual and Physical Design and Capital Cost Estimates," American Society of Mechanical

Engineers (ASME) 2012 International Mechanical Engineering Congress and Exposition, Houston, Texas, November 9th-15th, 2012.

2. James, Brian D., Spisak, Andrew, Colella, Whitney G. “Design for Manufacturing and Assembly (DFMA) Cost Estimates of Stationary Fuel Cell Systems,” Fuel Cell Seminar, November 5th-8th, 2012.

3. James, Brian., “Fuel Cell Transportation Cost Analysis, Preliminary Results,” *Department of Energy (DOE) Fuel Cell Technology (FCT) Program Annual Merit Review*, Washington, D.C., May 14-18th, 2012.

4. James, Brian D., Perez, Julie., Baum, Kevin N., Spisak, Andrew, Sanders, Matt. “Low Temperature PEM Stationary Fuel Cell System Cost Analysis,” *2011 Fuel Cell Seminar*, Orlando, Florida, 1 November 2011.

References

1. Boothroyd, G., P. Dewhurst, and W. Knight. “Product Design for Manufacture and Assembly, Second Edition,” 2002.

2. Colella, W.G., Niemoth, C., Lim, C., Hein, A. “Evaluation of the Financial and Environmental Feasibility of a Network of Distributed 200 kWe Cogenerative Fuel Cell Systems on the Stanford University Campus,” *Fuel Cells – From Fundamentals to Systems*, 1, 148-166, Feb. 2005.

3. Komiya, J., et al., “Single-Pipe Cylinder-Type Reformer.” US Patent 7,037,472, issued May 2, 2006.

4. Miura, T., et al., “Cylindrical Steam Reforming Unit.” US Patent 7,182,921, issued February 27, 2007.

5. James, B., J. Kalinoski, and K. Baum, “Mass Production Cost Estimation for Direct H₂ PEM Fuel Cell Systems for Automotive Applications: 2010 Update,” September 30, 2010.

6. James, B., “Fuel Cell Transportation Cost Analysis, Preliminary Results,” *United States (U.S.) Department of Energy (DOE) Fuel Cell Technology (FCT) Program Annual Merit Review*, Washington, D.C., May 17th, 2012.

7. NexTech Materials, Ltd., *Validation of Novel Planar Cell Design for MW-Scale SOFC Power Systems: Final Technical Report*, December 31, 2011.

8. Colella, W.G. and Srivastava, V., 2012, “Examining the Integration of Fuel Cell Systems Into Buildings Through Simulation,” *Proceedings of the ASME 2012 10th Fuel Cell Science, Engineering and Technology Conference*, July 23-26, 2012, San Diego, CA, USA. ESFuelCell2012-91474. PNNL-SA-87066.

9. Colella, W.G. and Pilli, S.P., 2012, “Independent Evaluation of Micro-Cogenerative Fuel Cell Systems For Commercial Buildings,” *Proceedings of the ASME 2012 10th Fuel Cell Science, Engineering and Technology Conference*, July 23-26, 2012, San Diego, CA, USA. ESFuelCell2012-91479. PNNL-SA-84709.

10. James, B., Perez, J., Baum, K., Spisak, A., Sanders, M., *High Temperature PEM Stationary Fuel Cell System Cost Analysis*, U.S. Department of Energy, Office of Energy Efficiency and Renewable Energy (EERE), Fuel Cell Technologies (FCT) Program, Forrestal Building, Washington, D.C., Nov. 11th, 2011.

11. James, B., Perez, J., Baum, K., Spisak, A., Sanders, M., “Low Temperature PEM Stationary Fuel Cell System Cost Analysis,” *2011 Fuel Cell Seminar*, Orlando, FL, Nov. 1st, 2011.

12. James, B., Lomax, F., Thomas, S. and Colella, W.G., *PEM Fuel Cell Power System Cost Estimates: Sulfur-Free Gasoline Partial Oxidation and Compressed Direct Hydrogen*, report for the U.S. Department of Energy, 1997.

13. Kuhn, I., Thomas, S., Lomax, F., James, B. and Colella, W.G., *Fuel Processing Systems for Fuel Cell Vehicles*, report for the U.S. Department of Energy, 1997.

V.A.4 Performance of Automotive Fuel Cell Systems with Low-Pt Nanostructured Thin Film Catalysts at High Power Densities

Rajesh K. Ahluwalia (Primary Contact),
Xiaohua Wang, Romesh Kumar
Argonne National Laboratory
9700 South Cass Avenue
Argonne, IL 60439
Phone: (630) 252-5979
Email: walia@anl.gov

DOE Manager
HQ: Nancy Garland
Phone: (202) 586-5673
Email: Nancy.Garland@ee.doe.gov

Project Start Date: October 1, 2003
Project End Date: Project continuation and direction
determined annually by DOE

- Specific power: 650 W/kg for system, 2,000 W/kg for stack
- Transient response: 1 s from 10% to 90% of rated power
- Start-up time: 30 s from -20°C and 5 s from $+20^{\circ}\text{C}$ ambient temperature
- Precious metal content: 0.2 g/kW

FY 2012 Accomplishments

- Collaborated with 3M in taking cell data to validate the model for nanostructured thin-film catalyst-based membrane electrode assembly (MEA) and stacks.
- Formulated a hybrid model combining theory for reversible potentials and electrode kinetics and neural network for mass transfer overpotentials.
- Conducted a single-variable optimization study to determine the optimum stack temperatures and inlet relative humidities (RHs) for different stack inlet pressures, cathode stoichiometry, Pt loading in cathode, and system efficiency.
- Conducted a multi-variable optimization study to determine the optimum stack temperatures, inlet RHs, cathode stoichiometry and Pt loading for specified stack inlet pressure and system efficiency.



Fiscal Year (FY) 2012 Objectives

- Develop a validated model for automotive fuel cell systems, and use it to assess the status of the technology.
- Conduct studies to improve performance and packaging, to reduce cost, and to identify key research and development (R&D) issues.
- Compare and assess alternative configurations and systems for transportation and stationary applications.
- Support DOE/United States Driving Research and Innovation for Vehicle efficiency and Energy sustainability automotive fuel cell development efforts.

Technical Barriers

This project addresses the following technical barriers from the Fuel Cells section of the Fuel Cell Technologies Program Multi-Year Research, Development and Demonstration Plan:

- (B) Cost
- (C) Performance

Technical Targets

This project is conducting system level analyses to address the following DOE 2015 technical targets for automotive fuel cell power systems operating on direct hydrogen:

- Energy efficiency: 50%-60% (55%-65% for stack) at 100%-25% of rated power
- Power density: 650 W/L for system, 2,000 W/L for stack

Introduction

While different developers are addressing improvements in individual components and subsystems in automotive fuel cell propulsion systems (i.e., cells, stacks, balance-of-plant components), we are using modeling and analysis to address issues of thermal and water management, design-point and part-load operation, and component-, system-, and vehicle-level efficiencies and fuel economies. Such analyses are essential for effective system integration.

Approach

Two sets of models are being developed. The GCtool software is a stand-alone code with capabilities for design, off-design, steady-state, transient, and constrained optimization analyses of fuel cell systems (FCSs). A companion code, GCtool-ENG, has an alternative set of models with a built-in procedure for translation to the MATLAB®/SIMULINK platform commonly used in vehicle simulation codes, such as Autonomie.

Results

In FY 2012, we collaborated with 3M to obtain reference performance data on eight 50-cm² active area single-cell fixtures from Fuel Cell Technologies with serpentine flow fields. The MEAs consisted of 3M 24- μ m membrane (850 equivalent weight), ternary Pt_{0.68}Co_{0.3}Mn_{0.02} nanostructured thin-film catalyst (NSTFC), and 3M gas diffusion layers made by applying a hydrophobic treatment to a backing paper and a micro-porous layer [1]. All cells had a Pt loading of 0.050 mg-cm⁻² in the anode. Two of the eight cells had a Pt loading of 0.103 mg-cm⁻² in the cathode. The Pt loading in the cathode in the other cells (two each) was 0.054, 0.146 and 0.186 mg-cm⁻². All cells were first conditioned using a “thermal cycling” process, described in detail in Steinbach et al. [2], which consisted of repeated temperature and voltage cycles over a period of 2-3 days until stable performance was reached. The polarization curves were obtained on these cells for different temperatures (30-90°C), inlet pressures (1-2.5 atm), inlet RHs (25-100%), and stoichiometries for the cathode (1.5-10) and the anode (1.2-5) by running galvanodynamic scans at cell current densities varying from 0.02 to 2 A-cm⁻². The cell was held for 120 s at each current step and the cell voltage and the high-frequency resistance (from alternating current impedance measurements) were recorded every 5 s. Prior to the start of the experiments, for each cell, the electrochemical surface area (ECSA) was determined by cyclic voltammetry, the hydrogen crossover current density and cell short resistance were determined by measuring the plateau currents, and the mass activity of Pt was measured in H₂/O₂ at 80°C, 1-atm reactant H₂ and O₂ pressures, and 100% RH.

We used the measured polarization curves, high-frequency resistances, mass activities, ECSAs, and H₂ crossover current density to develop, train, and validate a multi-nodal hybrid fuel cell model combining the theory for reversible potentials and kinetic overpotentials for the oxygen reduction reaction (ORR) with an artificial neural network for mass transfer and ohmic overpotentials. The Nernst equation was used to determine the reversible potential as a function of the cell temperature and the partial pressures of H₂, O₂, and water vapor in the anode and cathode flow fields. The polarization data at low current densities (<0.4 A-cm⁻²) were analyzed to develop a Tafel equation for ORR kinetic overpotential as a function of the current density, temperature, O₂ partial pressure, and relative humidity [3]. Figure 1 shows good agreement between the modeled and measured polarization curves for one series of tests conducted by varying the operating conditions from their reference values: 1.5 atm, 80°C, 100% RH at cell exit, SR_c=SR_a=2, and 0.050(a) and 0.103(c) mg-cm⁻² Pt loading. Similar good agreement was also obtained for other series of tests and the model accuracy was within the reproducibility of the polarization data.

The hybrid cell model was used to evaluate the performance of an NSTFC stack in an 80-kW_{net} fuel cell system (see Refs. [4,5] for system configuration). As discussed elsewhere [5], the cells are identical to the ones described above except for the flow fields that are assumed to be stamped from thermally nitrided Fe-20Cr-4V alloy foils. The air management subsystem consists of a compressor-expander module (CEM) with an air and liquid-cooled motor, mixed axial and radial flow compressor, variable-nozzle radial inflow turbine, and airfoil bearings [6]. The fuel management subsystem includes a hybrid ejector-hydrogen pump to recirculate the spent anode gas. The water management subsystem includes a membrane humidifier for the cathode air and an air pre-cooler. The system is designed to be water balanced, i.e., only the water produced in the stack is used for humidifying the feed gases. The dual-loop heat rejection subsystem has a high-temperature circuit for supplying coolant to the stack, and a low-temperature circuit for supplying coolant to the vehicle traction motor, CEM motor and air pre-cooler. The coolant in both circuits is aqueous ethylene glycol solution.

Figure 2 compares the modeled performance of the NSTFC stack in systems S2 and S1 with 1.5 atm and 2.5 atm stack inlet pressures, respectively. Some of the important stack and system parameters are: 47.5% net system efficiency on lower heating value basis, Pt loading (L_{Pt}) of 0.050 mg-cm⁻² in the anode catalyst and 0.100 mg-cm⁻² in the cathode catalyst, 10°C rise in coolant temperature across the stack (ΔT_c), anode and cathode stoichiometries of 2, and 71% CEM compressor and 73% CEM expander efficiencies. Figure 2 indicates that there is an optimum stack temperature (assumed to be 5°C higher than the coolant exit temperature) and inlet RH_c (not shown) at which the Pt content (g.kW⁻¹) and the system cost are the lowest. Here, the system cost has been estimated using the correlations presented in Ref. [7]. The optimum stack temperature depends on the operating pressure, increasing from 75°C at 1.5-atm stack inlet pressure to 82°C at 2.5-atm stack inlet pressure. The Pt content is ~13% lower in S1 in spite of the higher CEM parasitic power, 9.6 kW vs. 5.1 kW for S2. Thus, the stack in S1 has to produce an additional 4.5 kW for the fixed 80 kW net power, and to operate at 34 mV higher cell voltage to achieve the specified 47.5% net system efficiency. The model indicates that the power density at the design point is ~19% higher for the stack in S1, 837 mW-cm⁻² at 679 mV, compared to 705 mW-cm⁻² at 645 mV for the stack in S2. At high-volume manufacturing, the estimated cost is \$53.1 kW⁻¹ for system S2 and \$49.7 kW⁻¹ for system S1; see Refs. [7,8] for all assumptions used in estimating these costs.

Figure 3 quantifies the effect of Pt loading in the cathode catalyst layer on Pt content and system cost for systems S1 and S2. Our results indicate that the stack power density increases less than linearly (668 to 979 mW-cm⁻² in S1 and 620 to 760 W-cm⁻² in S2) with the increase in

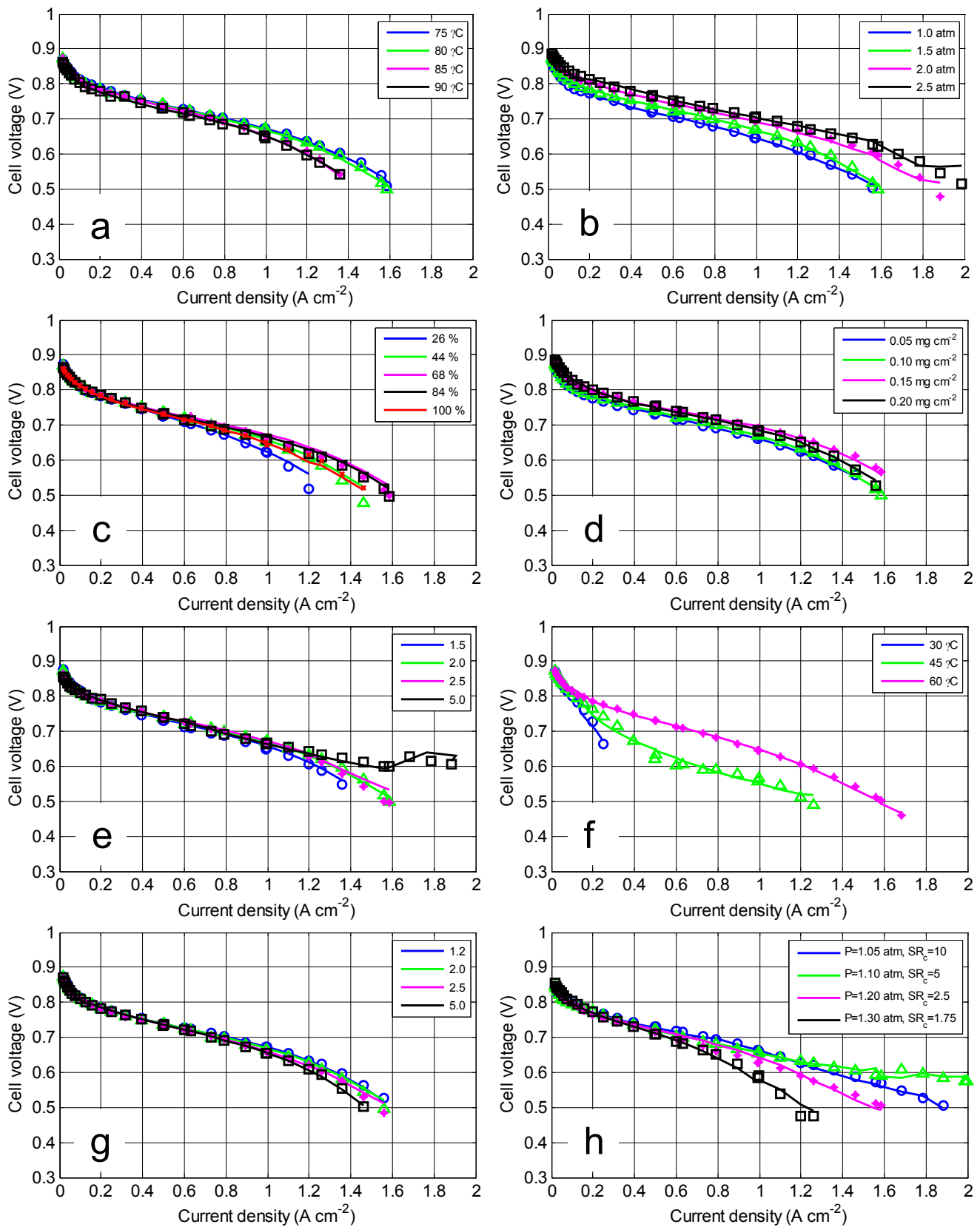


FIGURE 1. Validation of the hybrid fuel cell model using polarization curves for the cell with 0.1 mg.cm⁻² Pt in the cathode catalyst. The variables are: a) cell temperature; b) inlet pressure; c) inlet relative humidity; d) cathode Pt loading; e) cathode stoichiometry; f) low temperature, g) anode stoichiometry; and h) low pressure and high cathode stoichiometry

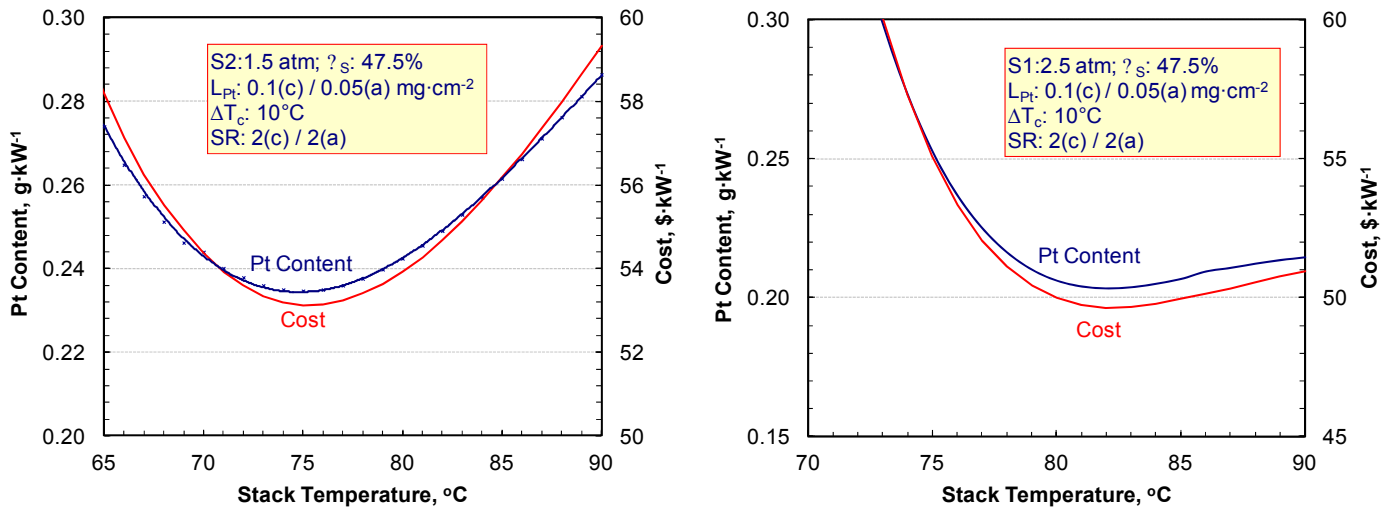


FIGURE 2. Effect of operating conditions on Pt content and system cost, 47.5% system efficiency

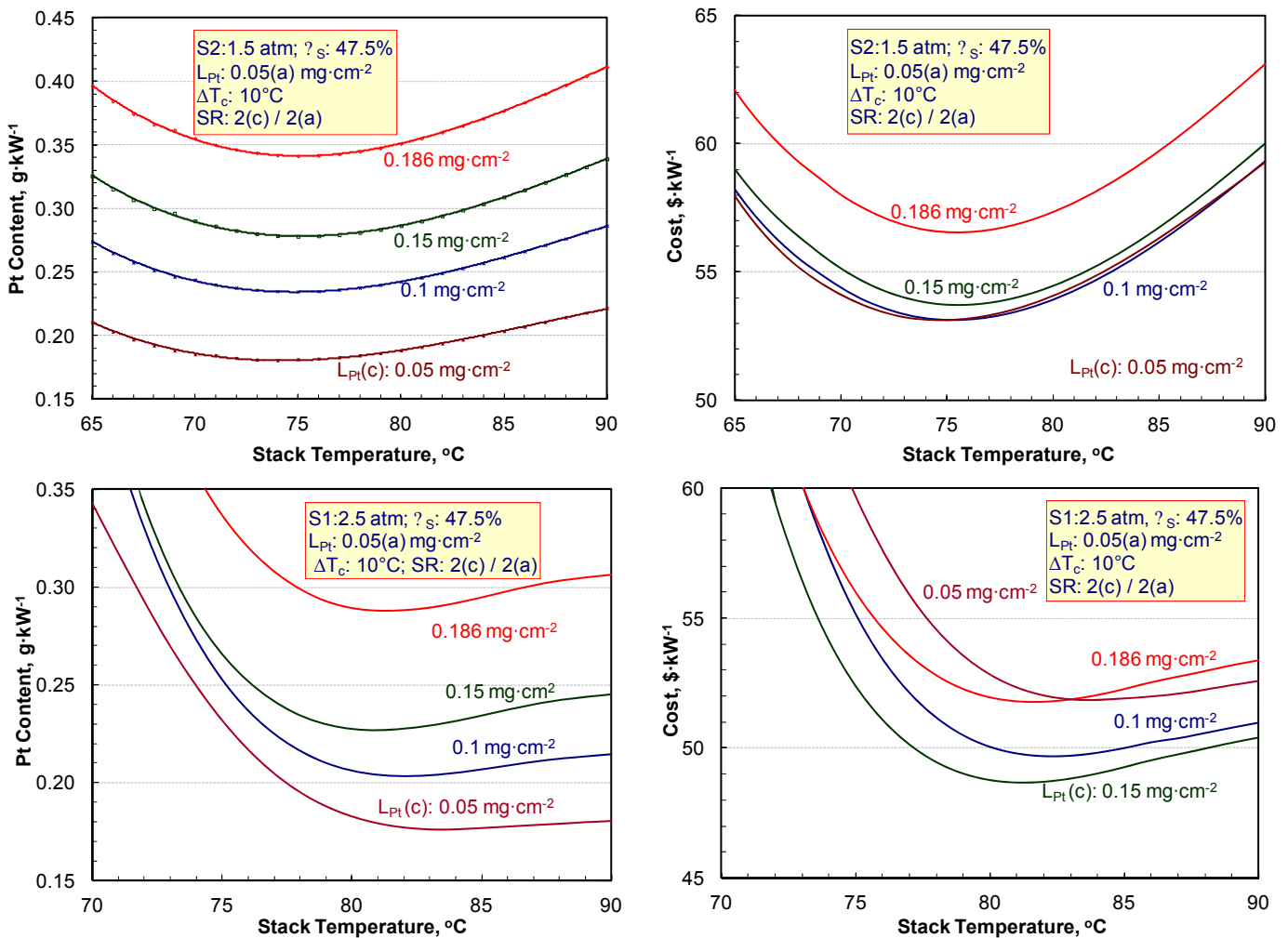


FIGURE 3. Effect of Pt loading in cathode catalyst on Pt content and system cost, 47.5% system efficiency

cathode Pt loading from 0.050 to 0.150 mg·cm⁻², and that it actually decreases if the Pt loading is increased beyond 0.150 mg·cm⁻². The optimum stack temperature shows a small increase as the Pt loading is reduced because of the temperature dependence of ORR activity. The lowest Pt loading (0.050 mg·cm⁻²) in the cathode catalyst layer results in the smallest Pt content, in spite of the lowest stack power density. The stack and system costs are lowest for 0.150 mg·cm⁻² Pt loading in cathode for system S1 and 0.050-0.100 mg·cm⁻² Pt loading in cathode for system S2. At the optimum operating conditions and Pt loadings, the lowest system cost is \$48.8 kW⁻¹ for system S1 and \$53.1 kW⁻¹ for system S2, divided nearly equally between the stack (51.4% for system S1, 54.7-55.3% for system S2) and the balance-of-plant components (44.7-49.6%). Pt accounts for 16.5% of the system cost and 32.1% of the stack cost in system S1 and 12.1-15.6% of the system cost and 22.1-28.5% of the stack cost in system S2.

Figure 4 shows the effect of CEM performance on Pt content and system cost for system S1. The label “CEM-Map” in Figure 4 refers to 71% compressor, 73% expander, and 80% combined motor and controller efficiencies, as measured in laboratory tests, with additional losses due to air-foil bearings and motor cooling air. The label “CEM-Status” refers to the same component efficiencies but it is assumed that instead of venting the motor cooling air, it is combined with the compressed and humidified air before entering the stack. The label “CEM-Target” refers to 75% compressor, 80% expander and 85% combined motor and controller efficiencies, and a 10% allowance for other losses. The estimated CEM parasitic power is 11.1 kW_e for CEM-Map, 9.6 kW_e for CEM-Status and 7.9 kW_e for CEM-Target. Figure 4 shows that, for fixed 47.5% system efficiency, a 1.7 kW_e reduction in parasitic power (CEM-Status vs. CEM-Target)

translates to ~8.6% reduction in Pt content and ~3.8% saving in system cost.

Figure 5 summarizes results from a parametric study on the effect of cathode stoichiometry ratio (SR_c) on the performance of systems S2 and S1 for fixed system efficiency. The lower-pressure system S2 shows only a small benefit in lowering SR_c from 2 to 1.5, implying that the benefit of reduced parasitic power is offset by the resulting decrease in stack power density. The higher-pressure system S1 shows a greater sensitivity of Pt content and system cost to SR_c. Figure 5 indicates that as SR_c is lowered in system S1, the optimum stack temperature increases to prevent flooding of the cathode catalyst layer. At 2.5 atm stack inlet pressure, the advantage of reduced parasitic power at SR_c of 1.5 more than compensates for the decrease in the stack power density.

Finally, we conducted an optimization study, in which the system cost was minimized by simultaneously varying the stack temperature (70-90°C), coolant ΔT (5-25°C), cathode Pt loading (0.1-0.2 mg·cm⁻²), and inlet RH for specified stack inlet pressure (1.5-2.5 atm) and system efficiency (35-50%). The FCS net power (80 kW_e), cathode stoichiometry (1.5) and Pt loading in the anode catalyst (0.050 mg·cm⁻²) were held constant. We found that the optimum Pt loading in the cathode is a function of stack inlet pressure and system efficiency, and it decreases as the value of either parameter is reduced. Both the Pt content and system cost decrease as the stack inlet pressure is increased. At 2.5 atm, the required cell voltage decreases by 43 mV (from 689 mV to 646 mV) if the target system efficiency is lowered from 50% to 45% with a resulting 29% reduction in Pt content and \$3.1 kW⁻¹ saving in system cost. The lower the system efficiency, the cheaper is the stack, but more expensive are the BOP components. Thus, the cost saving is quite marginal and may be negative in system S1 if the

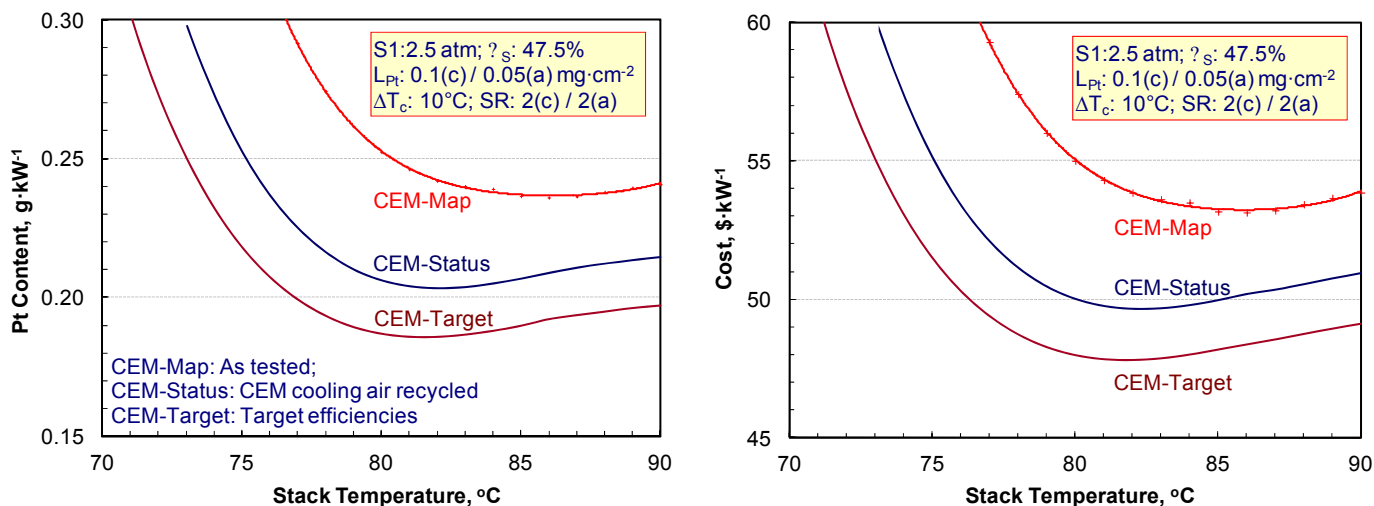


FIGURE 4. Effect of CEM performance on Pt content and system cost, 47.5% system efficiency

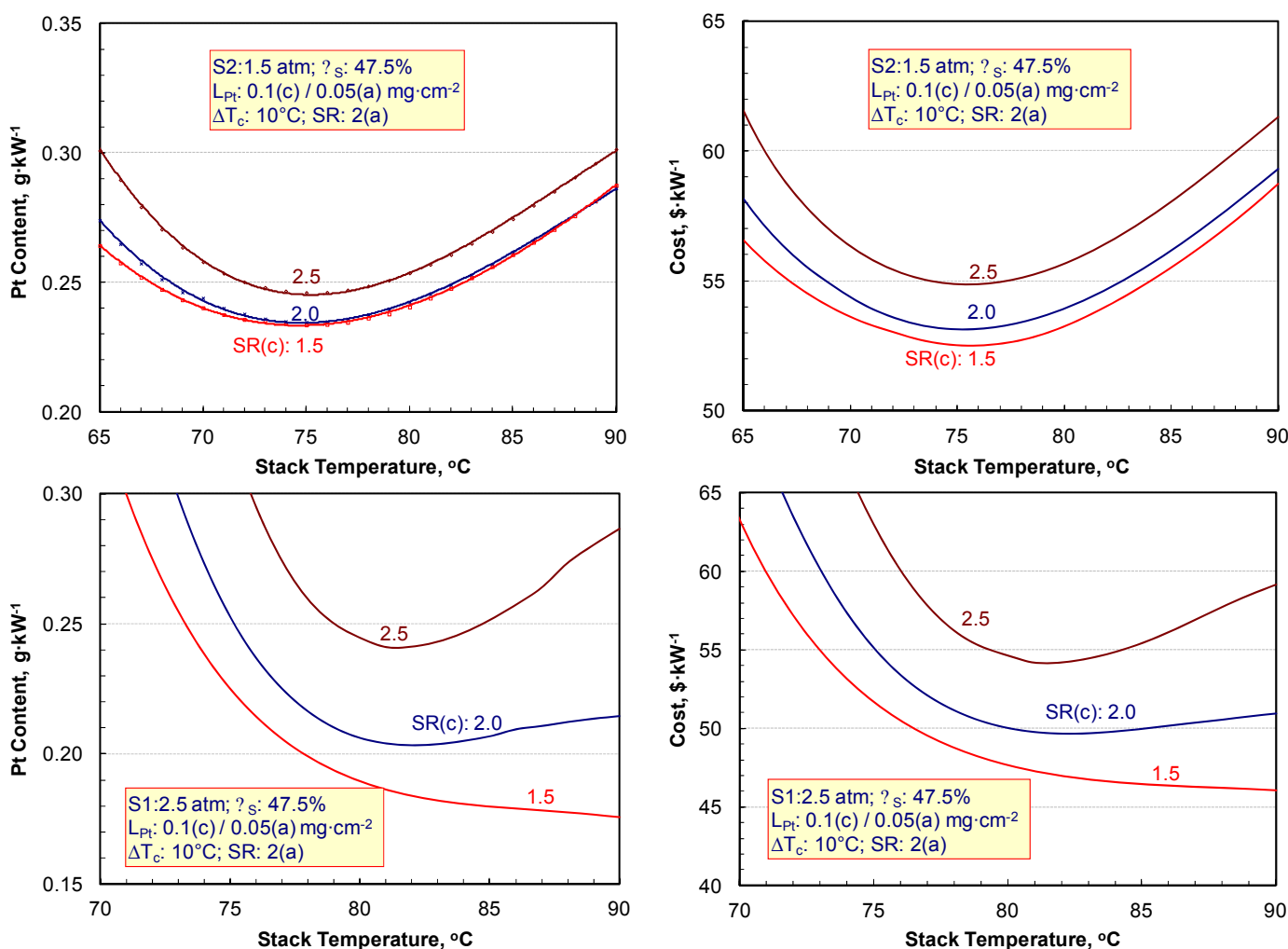


FIGURE 5. Effect of cathode stoichiometry on Pt content and system cost, 47.5% system efficiency

system efficiency (η_s) at rated power is further reduced to 40% from 45%. Also, the radiator heat load is proportional to $(1-\eta_s)/\eta_s$, so that heat rejection becomes more difficult at lower system efficiencies.

Conclusions and Future Directions

- Experimental data on 50-cm² single cells has been used to develop, train, and validate a multi-nodal hybrid model for fuel cells with NSTFC-based MEAs.
- Single-variable optimization studies using the hybrid model showed the dependence of the Pt content and fuel cell system cost on cell operating conditions. The optimum stack temperature was found to depend on the stack inlet pressure, increasing from 75°C at 1.5-atm stack inlet pressure to 82°C at 2.5-atm stack inlet pressure ($SR_c = 2$). The Pt content and system cost decreased as the cathode stoichiometry was reduced from 2.5 to 1.5, with the advantage of lower parasitic

power more than compensating for the decrease in the stack power density at 2.5-atm stack inlet pressure.

- A multi-variable optimization study showed that the optimum Pt loading in the cathode catalyst decreased with decreasing stack inlet pressure or system efficiency. Over a range of 47.5–50% system efficiency, it was 0.100 mg·cm⁻² at 1.5 atm and 0.150 mg·cm⁻² at 2.5-atm stack inlet pressure.
- Under optimum operating conditions at 2.5-atm stack inlet pressure, the projected Pt content and system cost varied from 0.21 g·kW⁻¹ and \$46.1 kW⁻¹ for 47.5% system efficiency to 0.23 g·kW⁻¹ and \$48 kW⁻¹ for 50% system efficiency. At 1.5-atm stack inlet pressure, the projected Pt content and system increased to 0.23 g·kW⁻¹ and \$52.4 kW⁻¹ for 47.5% system efficiency and to 0.25 g·kW⁻¹ and \$54.3 kW⁻¹ for 50% system efficiency.
- In FY 2013, we will investigate the effects of alternative NSTFCs and air management system on system performance and cost.

FY 2012 Publications/Presentations

1. R.K. Ahluwalia, X. Wang, A. Lajunen, A.J. Steinbach, S.M. Hendricks, M.J. Kurkowski, and M.K. Debe, "Kinetics of Oxygen Reduction Reaction on Nanostructured Thin-Film Platinum Alloy Catalyst," *J. Power Sources*, 215, 77-88, 2012.
2. R.K. Ahluwalia and X. Wang, "Dynamic Performance of Automotive Fuel Cell Systems with Low Platinum Loadings," *ECS Transactions*, 41 (1), 293-305, 2011.
3. X. Wang, R.K. Ahluwalia, A.J. Steinbach, and M.K. Debe, "Dynamic Performance of Automotive Fuel Cell Systems with Low Platinum Loadings," 220th ECS Meeting and Electrochemical Energy Summit, Boston, MA, October 9–14, 2011.
4. Lajunen, X. Wang, and R.K. Ahluwalia, "Artificial Neural Network-Based Model for Polymer Electrolyte Fuel Cells," 5th International Conference on Polymer Batteries and Fuel Cells, Argonne, IL, August 1–5, 2011.
5. X. Wang, X. Wang, and R.K. Ahluwalia, "Effect of Air Contaminants on Performance of Polymer Electrolyte Fuel Cells," 5th International Conference on Polymer Batteries and Fuel Cells, Argonne, IL, August 1–5, 2011.
6. J. Kwon, X. Wang, R.K. Ahluwalia, and A. Rousseau, "Impact of Fuel Cell System Design used in Series Fuel Cell HEV on Net Present Value," IEEE Vehicle Power and Propulsion Conference, Chicago, IL, September 6–9, 2011.
7. R.K. Ahluwalia, X. Wang, J. Kwon, and A. Rousseau, "Drive-Cycle Performance and Life-Cycle Costs of Automotive Fuel Cell Systems," 2011 Fuel Cell Seminar & Exposition, Orlando, FL, October 31 – November 2, 2011.

References

1. M.K. Debe, "Advanced Cathode Catalysts and Supports for PEM Fuel Cells," Grant No. DE-FG36-07GO17007, FreedomCAR Technical Team Review, Detroit, MI, March 10, 2010.
2. A.J. Steinbach, C.V. Hamilton, and M.K. Debe, "Impact of Micromolar Concentrations of Externally-Provided Chloride and Sulfide Contaminants on PEMFC Reversible Stability," *ECS Transactions* 11(1), 889-897, 2007.
3. R.K. Ahluwalia, X. Wang, A. Lajunen, A.J. Steinbach, S.M. Hendricks, M.J. Kurkowski, and M.K. Debe, "Kinetics of Oxygen Reduction Reaction on Nanostructured Thin-Film Platinum Alloy Catalyst," *J. Power Sources*, 215, 77-88, 2012.
4. R.K. Ahluwalia, X. Wang, J. Kwon, and A. Rousseau, "Drive-Cycle Performance and Life-Cycle Costs of Automotive Fuel Cell Systems," 2011 Fuel Cell Seminar & Exposition, Orlando, FL, October 31 – November 2, 2011.
5. R.K. Ahluwalia, X. Wang, J. Kwon, A. Rousseau, J. Kalinoski, B. James, and J. Marcinkoski, "Performance and Cost of Automotive Fuel Cell Systems with Ultra-Low Platinum Loadings," *J. Power Sources*, 196, 4619, 2011.
6. M.K. Gee, "Cost and Performance Enhancement for a PEM Fuel Cell System Turbocompressor," FY 2005 Annual Progress Report, DOE Hydrogen Program, 985, 2005.
7. B.D. James, J.A. Kalinoski, and K.N. Baum, "Mass-production cost estimation for automotive fuel cell systems," DOE Hydrogen Program, Washington, DC, 2010.
8. B.D. James, J.A. Kalinoski, and K.N. Baum, "Mass Production Cost Estimation for Direct H₂ PEM Fuel Cell Systems for Automotive Applications: 2009 Update," DTI Report GS-10F-0099J, January 2010.

V.A.5 Characterization of Fuel Cell Materials

Karren L. More

Oak Ridge National Laboratory (ORNL)

1 Bethel Valley Rd.

Oak Ridge, TN 37831-6064

Phone: (865) 574-7788

Email: morekl1@ornl.gov

DOE Manager

HQ: Donna Ho

Phone: (202) 586-8000

Email: Donna.Ho@ee.doe.gov

Contributors:

- David Cullen (ORNL)
- Miaofang Chi (ORNL)
- Kelly Perry (ORNL)

Project Start Date: Fiscal Year (FY) Year 1999

Project End Date: Project continuation and direction determined annually by DOE

complementary microstructural/compositional analysis techniques, and provide feedback for materials (and MEA) optimization.

Technical Barriers

This project addresses the following technical barriers from the Fuel Cells section of the Fuel Cell Technologies Program Multi-Year Research, Development, and Demonstration Plan:

- (A) Durability
- (C) Performance

Technical Targets

This project is focused on conducting fundamental characterization studies on the stability of individual material constituents comprising fuel cell MEAs. Of primary importance is relating MEA microstructural changes during aging to fuel cell durability and performance. Insights gained through these extensive microstructural studies will be applied toward the design and manufacture of MEAs that meet the following DOE 2015 MEA targets:

- Cost: \leq \$5/kW
- Durability with cycling: 5,000 hours
- Operating temperatures: \leq 120°C
- Total catalyst loading (for both electrodes): 0.2 g/kW (rated)
- Extent of performance degradation over lifetime: 5%

Fiscal Year (FY) 2012 Objectives

- Develop and/or apply novel preparation, imaging, and analytical methods to characterize fuel cell materials and architectures in the as-processed (fresh) state, during operation (in situ), and after electrochemical testing (post-mortem). Fuel cell materials of particular interest include novel electrocatalysts (especially related to low catalyst loadings, alloy electrocatalysts, and non-Pt-group metal catalysts), catalyst support structures (carbon and non-carbon supports), ionomer layers, gas diffusion layers (GDLs), and microporous layers (MPLs).
- Elucidate membrane electrode assembly (MEA) degradation and/or failure mechanisms by conducting extensive microstructural characterization using advanced electron microscopy techniques, with a specific focus on distinguishing the structural and chemical contributions from the material constituents contributing to fuel cell performance loss.
- Develop the critical correlations between MEA microstructure, composition, and architecture and MEA durability.
- Compare microstructural changes resulting from accelerated stress testing (AST) with microstructures observed after field aging.
- Collaborate with polymer electrolyte membrane fuel cell (PEMFC) component developers and manufacturers, university researchers, and other national laboratories, to evaluate MEAs using electron microscopy and

FY 2012 Accomplishments

- Continued effort to characterize a series of MEAs subjected to various ASTs at Los Alamos National Laboratory (LANL) designed to accelerate either carbon corrosion or catalyst degradation. These studies focused on evaluating “material-specific” Å-scale structural and compositional changes contributing to measured performance loss.
- Completed study with Nissan Technical Center North America to characterize a series of Pt/C with varying Pt loadings and carbon supports. This study focused on establishing a correlation between Pt nanoparticle morphology, dispersion, and size distribution with carbon support structure. Recently, aged MEAs with the same cathode Pt/C materials were sent to ORNL to quantify the material’s structural degradation.
- Initiated study with General Motors (GM) to characterize ionomer layers deposited on Pt surfaces, which has evolved to include ionomer layers deposited

in several model single-crystal surfaces. The goal of this study is to establish critical bonding characteristics of ionomer layers of varying thickness on relevant surfaces.

- Initiated study with Ballard to study the effect of catalyst and ionomer loading on MEA architecture and correlate structural observations with performance.
- Collaborated with Naval Research Laboratory researchers to characterize the nature of Pt nanoparticle interactions (anchoring) with tantalum phosphate films deposited on Vulcan carbon supports.
- Established method(s) to quantify the amount of Pt loss due to dissolution and migration from cathode – this work was done in collaboration with Nuvera and LANL and focused on establishing differences in Pt migration/loss as a function of Pt loading, carbon support, and AST, and results were correlated with catalyst degradation in cathode due to coalescence.
- Collaborated with Proton OnSite to characterize manufacturing defects in catalyst layers.



Introduction

PEMFCs are being developed for future use as efficient, zero-emission power sources. However, the performance of PEMFCs degrades with time at elevated temperature and relative humidity (RH) during electrochemical aging in automotive and stationary applications. Performance degradation can be directly attributed to the durability of individual material constituents comprising the MEA, including the electrocatalyst, catalyst support, ionomer, polymer membrane, and GDL/MPL. Unfortunately, the structural and chemical degradation mechanisms contributing to performance loss have not been fully quantified. During the past several years, the Microstructural Characterization Program at ORNL has been focused on forming collaborative relationships with numerous industrial PEMFC developers/manufacturers, universities, and national laboratories, to apply ORNL's advanced electron microscopy techniques and expertise to characterize as-fabricated (fresh) fuel cell materials (individual constituents and/or materials incorporated in fresh MEAs), MEAs subjected to ASTs designed to degrade specific MEA components, and field-aged MEAs. These studies are used to establish critical processing-microstructure-performance correlations and to elucidate the individual materials changes contributing to measured MEA degradation, performance loss, and failure. Understanding the structural and compositional changes of the materials comprising the MEA during electrochemical aging will allow for the implementation of processing changes and critical materials development that are required for optimizing PEMFC durability and performance.

Approach

The microstructural characterization task utilizes advanced electron microscopy analysis techniques to characterize the individual material components comprising PEMFCs, before and after incorporation into an MEA, and after electrochemical aging. Our approach is focused on identifying and optimizing novel high-resolution imaging and compositional/chemical analysis techniques, and developing unique specimen preparation methodologies, for the μm - to \AA -scale characterization of the material constituents of fuel cells (electrocatalyst, catalyst support, ionomer, membrane, etc.). ORNL applies these advanced analytical and imaging techniques for the evaluation of the microstructural and microchemical changes of each material constituent and correlates these observations with fuel cell performance (aging studies are conducted at the collaborator's laboratories). These studies are designed to elucidate the microstructure-related degradation mechanisms contributing to fuel cell performance loss. Most importantly, ORNL is making the techniques and expertise available to fuel cell researchers outside of ORNL via several mechanisms – (1) work for others (proprietary) research, (2) ORNL User Facilities (e.g., Shared Research Equipment User Facility), and (3) collaborative non-proprietary research projects via the Microstructural Characterization Project that are consistent with ORNL's "baseline project" research activities.

Results

In addition to extensive microstructural characterization of a wide range of starting/fresh materials used in PEMFC MEAs, previous annual reports have summarized observations for the structural and compositional degradation of MEA constituents, primarily the electrocatalyst and carbon catalyst supports. ORNL's FY 2011 report focused on initial attempts to characterize the structure and chemistry of the ionomer, studies which continued in FY 2012 as part of new collaborations initiated with GM, 3M, and Ballard. These new collaborations are specifically focused on characterizing ionomer films of varying thicknesses (1-10 nm) deposited on specific model surfaces (e.g., Pt on 3M's nanostructured thin films [NSTF] or on low surface area carbon [LSAC] surfaces) and loading variations within electrode structures. These new studies will take advantage of ORNL's new aberration-corrected low-voltage scanning transmission electron microscope (STEM), the Nion UltraSTEM 60-100. These studies are ongoing.

A major research focus in FY 2012, which was initiated as a result of requests from two major partners (3M and Nuvera), has been to *quantify* the amount of catalyst (Pt) loss specifically due to migration out of the cathode into the membrane following various aging protocols. The fact that Pt migrates into the membrane is well known; [1,2]

however, quantifying differences in migration profiles resulting from specific aging conditions or specific materials used in the cathode, have not been conducted successfully. Many techniques have been used to try and fully quantify the Pt loss in the membrane, including scanning electron microscopy (SEM), electron probe microanalysis (EPMA), X-ray photoelectron spectroscopy (XPS), etc., [3] but none have accurately captured the extent of Pt migration out of the cathode. We have focused our effort on using transmission electron microscopy (TEM) imaging to establish particle size distributions across intact MEAs as a viable method for quantifying the amount of Pt loss.

MEAs subjected to different AST protocols were prepared in cross-section via microtomy such that the entire 3-layer MEA could be imaged in the TEM (cathode-membrane-anode). A series of high-magnification images were acquired from the cathode-membrane interface across the entire membrane to the anode-membrane interface. Particle size distributions were measured across the membrane thickness (within sequential areas $\sim 1 \mu\text{m} \times 5 \mu\text{m}$) to compare Pt migration profiles from the different MEAs and ASTs, and to calculate the amount of Pt present within each membrane particle. Examples of MEA cross-sections with different Pt particle distributions in the membrane are shown in Figure 1. The baseline Pt (number of atoms) present in the same cathode area was established for fresh MEA cathodes. For example, the Pt dispersion/morphology in a $1 \mu\text{m} \times 5 \mu\text{m}$ area of a cathode containing 0.2 mg/cm^2 Pt supported on high surface area carbon (HSAC), Figure 2a, is quite different from 0.2 mg/cm^2 Pt supported on LSAC,

Figure 2b. This comparison is especially noteworthy since the resulting cathode thickness ($25 \mu\text{m}$ and $15 \mu\text{m}$) and porosity are significantly different for the Pt/HSAC and Pt/LSAC, respectively, which impacts the Pt morphology and dispersion even for the same Pt loading (0.2 mg/cm^2). The particular MEAs described here were supplied and tested by collaborators at LANL; additional MEAs were provided by Nuvera and 3M. All MEAs characterized thus far were prepared with reinforced (3-layer) membranes.

An example of the Pt migration profiles resulting from an AST for carbon corrosion (1.2 V hold in H_2/N_2) for the Pt/HSAC and Pt/LSAC after 100 h and 400 h, respectively, are compared in Figure 3 (particles present in the cathode side of the 3-layer membrane are shown for simplicity). Most notable is the number of Pt particles observed in the membrane for the Pt/HSAC cathode after only 100 h (144 particles), Figure 3a, compared to the significantly lower number of Pt particles present in the membrane for the Pt/LSAC cathode after a longer hold time of 400 h (23 particles), Figure 3b. The amount of Pt loss from the cathode can be directly related to the starting microstructures of the Pt/HSAC vs. Pt/LSAC (shown in Figure 2) and is calculated as 9.5% and 1.3% Pt loss into the membrane, respectively, from the starting Pt loading in the cathode. Clearly, the Pt/LSAC is significantly more stable than Pt/HSAC and exhibits much less (by $\sim 8\text{X}$) Pt loss (as well as less Pt coalescence and carbon corrosion (not shown)) for 4X longer hold times compared with Pt/LSAC. Similar measurements are being made for other ASTs and cathode materials (alloy electrocatalysts, Pt/NSTF, Pt loadings, etc.).

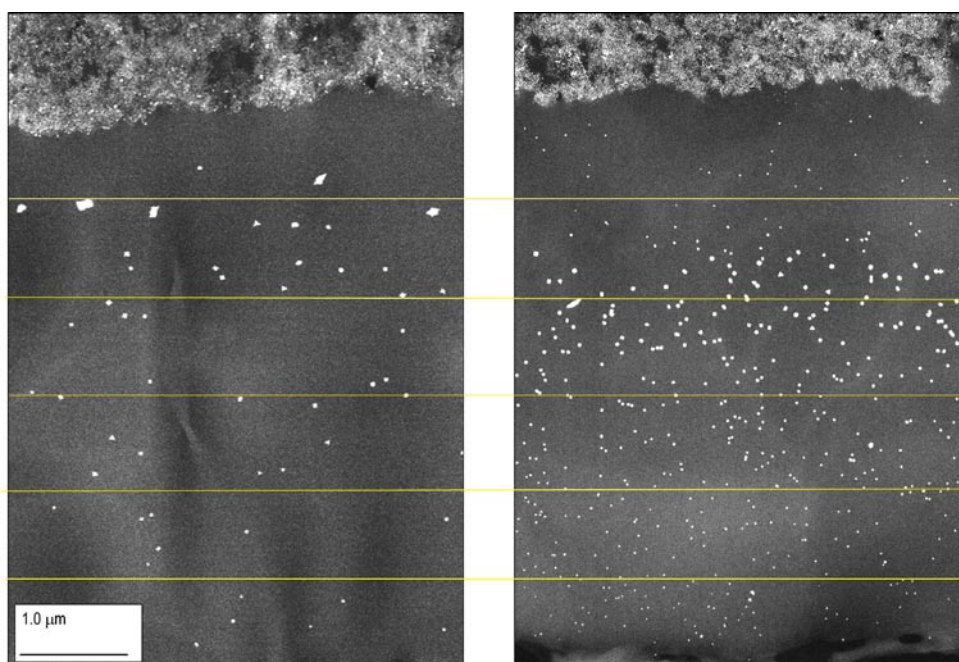


FIGURE 1. Example Pt particle distributions in the membrane (cathode side) following aging under different AST protocols

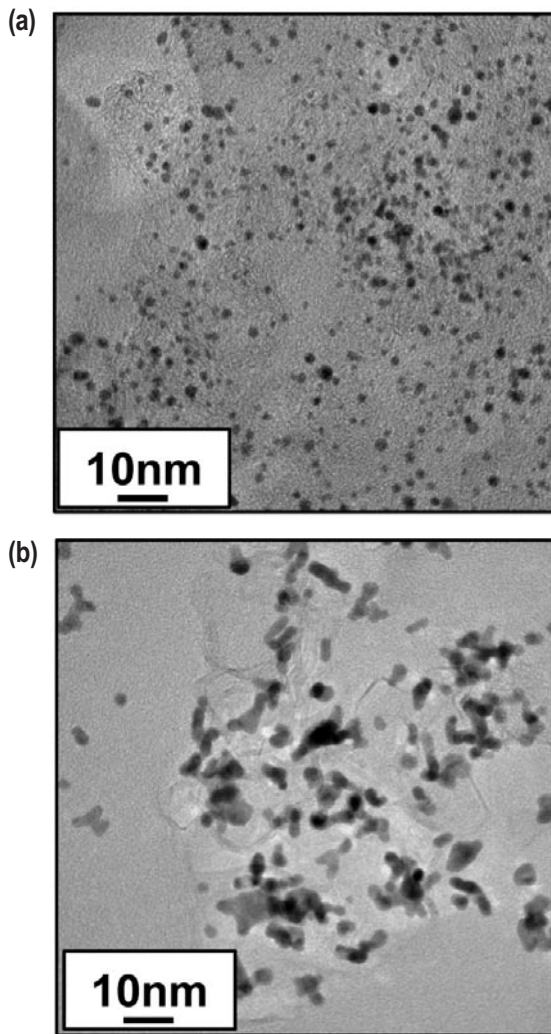


FIGURE 2. TEM images of (a) 0.2 mg/cm² Pt supported on HSAC (25- μ m thick cathode) and (b) 0.2 mg/cm² Pt supported on LSAC (15- μ m thick cathode)

Conclusions and Future Directions

- ORNL continues to focus on relevant materials degradation studies that provide insight regarding fuel cell material’s durability and stability. Specifically, ORNL research has focused on characterizing the microstructural- and microchemical-related mechanisms that contribute to materials degradation and performance loss.
- Correlate microstructural/compositional observations with AST protocols (automotive and stationary), especially related to catalyst dissolution, coarsening, and migration, carbon corrosion, membrane degradation – these studies continue to be a priority of this research program and have been part of ongoing and proposed “future” research each year.
- Expand on ionomer studies with GM to include interactions with carbons(s) using the low-voltage imaging/electron energy loss spectroscopy capabilities of ORNL’s Nion UltraSTEM microscope.
- Develop in situ liquid TEM/STEM as a priority for ORNL’s baseline characterization project – this has emerged as a future work topic because of community-wide interest and the fact that we have successfully demonstrated such capabilities for battery research.
- Continue to establish collaborations with industries, universities, and national laboratories (including access via ORNL User Facilities) to facilitate “transfer” of unique capabilities. This will include supporting new DOE projects with microstructural characterization and developing/applying advanced characterization techniques.

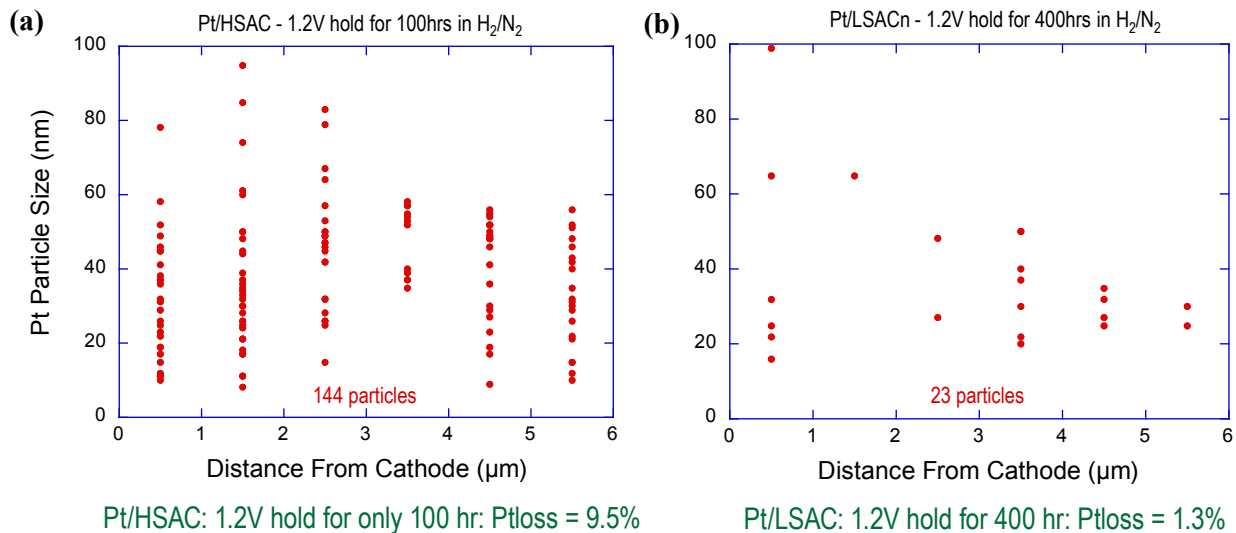


FIGURE 3. Pt particle migration profiles for AST of 1.2 V hold in H₂/N₂ for (a) Pt/HSAC after 100 h and (b) Pt/LSAC after 400 h

FY 2012 Publications/Presentations

1. Y. Liu, M. Chi, V. Mazumder, K.L. More, S. Soled, J.D. Henao, and S.H. Sun, "Composition-controlled Synthesis of Bimetallic PdPt Nanoparticles and Their Electro-oxidation of Methanol," *Chemistry of Materials* 23[18] 4199-4203.
2. C. Wang, M. Chi, D. Li, D. van der Vliet, G. Wang, Q. Lin, J. Mitchell, K.L. More, N.M. Markovic, and V.R. Stamenkovic, "Synthesis of Homogeneous Pt-Bimetallic Nanoparticles as Highly Efficient Electrocatalysts," *ACS Catalysis* 1[10] 1355-1359 (2011).
3. Z. Zhang, K.L. More, K. Sun, Z. Wu, and W. Li, "Preparation and Characterization of PdFe Nanoleaves as Electrocatalysts for Oxygen Reduction Reaction," *Chemistry of Materials* 23[6] 1570-1577 (2011).
4. C. Wang, M. Chi, D. Li, D. Strmcnik, D. van der Vliet, G. Wang, V. Komanicky, K.C. Chang, A.P. Paulikas, D. Tripkovic, J. Pearson, K.L. More, N.M. Markovic, and V.R. Stamenkovic, "Design and Synthesis of Bimetallic Electrocatalyst with Multilayered Pt-Skin Surfaces," *Journal of the American Chemical Society* 133[36] 14396-14403 (2011).
5. D.A. Cullen, K.L. More, K.S. Reeves, G.D. Vernstrom, L.L. Atanasoska, G.M. Haugen, and R.T. Atanasoski, "Characterization of Durable Nanostructured Thin Film Catalysts Tested Under Transient Conditions Using Analytical Aberration-corrected Electron Microscopy," *ECS Transactions* 41[1] 1099-1103 (2011).
6. G. Wu, C.M. Johnston, N.H. Mack, K. Artyushkova, M. Ferrandon, M. Nelson, J.S. Lezama, S.D. Conradson, K.L. More, D.J. Myers, and P. Zelenay, "Synthesis-Structure-Performance Correlation for Polyaniline-Me-C Non-precious Metal Cathode Catalysts for Oxygen Reduction in Fuel Cells," *Journal of Materials Chemistry* 21[30] 11392-11405 (2011).
7. K.J. Blackmore, L. Elbaz, E. Bauer, E.L. Brosha, K.L. More, T.M. McCleskey, and A.K. Burrell, "High Surface Area Molybdenum Nitride Support for Fuel Cell Electrodes," *Journal of the Electrochemical Society* 158[10] B1255-B1259 (2011).
8. V. Mazumder, M. Chi, M.N. Mankin, Y. Liu, O. Metin, D.H. Sun, K.L. More, and S.H. Sun, "A Facile Synthesis of MPd (M=Co, Cu) Nanoparticles and Their Catalysis for Formic Acid Oxidation," *Nano Letters* 12[2] 1102-1106 (2012).
9. C. Wang, D.G. Li, M. Chi, J. Pearson, R.B. Rankin, J. Greeley, Z.Y. Duan, G.F. Wang, D. van der Vliet, K.L. More, N.M. Markovic, and V.R. Stamenkovic, "Rational Development of Ternary Alloy Electrocatalysts," *Journal of Physical Chemistry Letters* 3[12] 1668-1673 (2012).
10. *Keynote Presentation*: M.P. Brady, K.L. More, T.J. Toops, H.M. Meyer, P.F. Tortorelli, M. Abd Elhamid, G. Dadheech, J. Bradley, H. Wang, and J.A. Turner, "PEM Fuel Cell Metallic Bipolar Plates: Technical Status and Nitridation Surface Modification for Improved Performance," *Technoport 2012*, Trondheim, Norway – April 16, 2012.
11. *Short Course*: K.L. More, "Advanced Microscopy Methods for Studying PEM Fuel Cell Materials" *221st Meeting of the Electrochemical Society*, Seattle, WA – May 6, 2012.
12. *Invited Presentation/Tutorial*: K.L. More, D.A. Cullen, M. Chi, and J.-C. Idrobo, "Advanced Microscopy Methods for Studying PEM Fuel Cell Materials," *221st Meeting of the Electrochemical Society*, Seattle, WA – May 8, 2012.
13. *Keynote Presentation*: K.L. More, "Application of Advanced Microscopy Methods to Understand MEA Materials Degradation," *International Workshop on the Characterization and Quantification of MEA Degradation Processes*, Grenoble, France – September 26, 2012.

References

1. P. Ferreira, G.J. la O', Y. Shao-Horn, D. Morgan, R. Makharia, S. Kocha, and H.A. Gasteiger, "Instability of Pt/C Electrocatalysts in Proton Exchange Membrane Fuel Cells," *Journal of the Electrochemical Society* 152[11] A2256-A2271 (2005).
2. S.F. Burlatsky, M. Gummalla, V.V. trazhev, D.V. Dmitriev, N.Y. Kuzminykh, and N.S. Erikman, "The Dynamics of Platinum Precipitation in an Ion Exchange Membrane," *Journal of the Electrochemical Society* 158[3] B322-B330 (2011).
3. W. Bi, G.E. Gray, and T.F. Fuller, "PEM Fuel Cell Pt/C Dissolution and Deposition in Nafion Electrolyte," *Electrochemical and Solid State Letters* 10[5] B101-B104 (2007).

V.A.6 Neutron Imaging Study of the Water Transport in Operating Fuel Cells

Muhammad Arif (Primary Contact),
David L. Jacobson, Daniel S. Hussey
National Institute of Standards and Technology (NIST)
100 Bureau Drive
Gaithersburg, MD 20899
Phone: (301) 975-6303
Email: arif@nist.gov

DOE Manager
HQ: Nancy L. Garland
Phone: (202) 586-5673
Email: Nancy.Garland@ee.doe.gov

Contract Number: DE-AI-01-01EE50660

Project Start Date: Fiscal Year (FY) 2001
Project End Date: Project continuation and direction
determined annually by DOE

- Unassisted start from low temperature: -40°C .
- Durability with cycling at operating temperature of $\leq 80^{\circ}\text{C}$: 5,000 h.
- System Energy density: 650 W/L.
- System Specific power: 650 W/kg.
- Energy efficiency: 65% at 25% rated power, 55% at 100% rated power.
- Cost: $\$35/\text{kW}_e$.
- Start-up time to 50% power: 30 seconds from -20°C , 5 seconds from 20°C .
- Durability with cycling: 5,000 hrs.

FY 2012 Accomplishments

- Revealed that a microporous layer (MPL) on the anode and cathode drives product water into the anode gas diffusion layer (GDL), whereas without a MPL, product water exits only through the cathode GDL.
- Showed that on increasing hydration, the conductivity of Nafion[®] increases faster than expected based on steady-state correlations.
- Submitted for publication a study of systematic effects and required corrections in measuring the membrane water content with neutron imaging.



Fiscal Year (FY) 2012 Objectives

- Provide state-of-the-art research and testing infrastructure to enable the fuel cell industry to design, test, and optimize prototype-to-commercial grade fuel cells using in situ neutron imaging techniques.
- Provide a secure facility for proprietary research by industry. Provide beam time at no cost to non-proprietary research through a competitive proposal process. Make open research data available for beneficial use by the general fuel cell community.
- Continually improve and develop methods and technology to accommodate rapidly changing industry/academia needs.

Technical Barriers

This project addresses the following technical barriers from the Fuel Cells section of the Fuel Cell Technologies Program Multi-Year Research, Development and Demonstration Plan:

- (A) Durability
- (B) Cost
- (C) Performance

This project is conducting fundamental studies of water transport in the fuel cell. Insights gained from these studies will be applied toward the design of components and operation strategies of polymer electrolyte membrane fuel cells that meet the following DOE fuel cell targets:

Introduction

At NIST, we maintain the premier fuel cell neutron imaging facility in the world and continually seek to improve its capabilities to meet the changing needs of the fuel cell community. This facility provides researchers with a powerful and effective tool to visualize and quantify water transport inside operating fuel cells. Imaging the water dynamics of a polymer electrolyte membrane fuel cell (PEMFC) is carried out in real time with the required spatial resolution needed for fuel cells that are being developed today. From these images, with freely available NIST-developed image analysis routines, PEMFC industry personnel and researchers can obtain in situ, non-destructive, quantitative measurements of the water content of an operating PEMFC. Neutron imaging is the only in situ method for visualizing the water distribution in a “real-world” PEMFC. Unlike X-rays, whose interaction with materials increases with the number density of electrons, neutrons interact via the nuclear force, which varies somewhat randomly across the periodic table, and is isotopically sensitive. For instance, a neutron’s interaction with hydrogen is approximately 100 times greater than

that with aluminum, and 10 times greater than that with deuterium. It is this sensitivity to hydrogen (and insensitivity to many other materials) that is exploited in neutron imaging studies of water transport in operating fuel cells.

Approach

The typical length scales of interest in a PEMFC are: channels approximately 1 mm wide and 1 mm deep, the diffusion media are 0.1 mm to 0.3 mm thick, the membrane is 0.01 mm to 0.02 mm thick, and the active area of test sections can range from 2 cm² to 500 cm². Though the study of water transport within these length scales is technically very challenging, the unique capabilities of neutron imaging have already successfully addressed many of the questions. However, as fuel cell research matures, the water transport questions become increasingly more demanding, requiring for instance resolving the water content in catalyst layers. To meet these demands, based on fuel cell community feedback and need, we continue to develop new facilities and improve existing capabilities for obtaining higher spatial and temporal resolution neutron images. These improvements will enable users to perform even more detailed, nondestructive, and in situ studies of the water and hydrogen transport in PEM fuel cells to meet DOE goals. In addition, employing mathematical models of neutron scattering, we will develop a software suite that enables users to obtain reliable, accurate, quantitative measurements of the water content in an operating PEMFC. Due to the complexity of PEMFCs and the large number of remaining open questions regarding water transport in PEMFCs, we will develop partnerships with industry, academia, and national laboratories to train them in the use of the facility, seek their feedback, and collaborate with them on research projects, to seek measurement breakthroughs that will facilitate the rapid, efficient, and robust development of fuel cells.

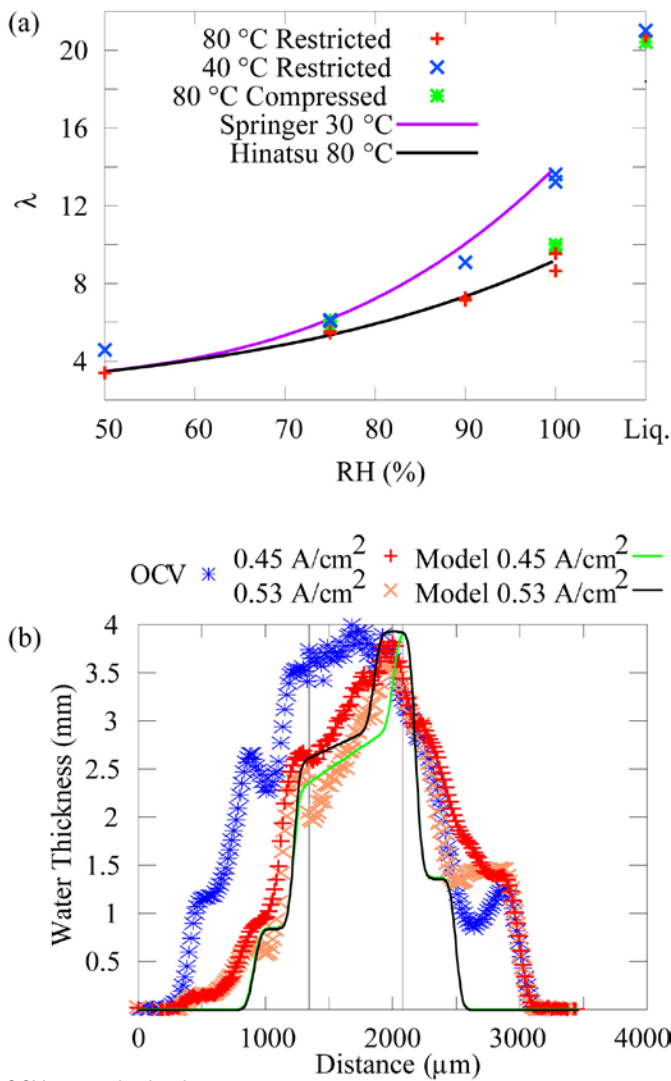
Results

The NIST Center for Neutron Research has been completing work under a five year expansion project, which required that the neutron source be shut down from April 2011 until April 2012. After this successful neutron source upgrade the imaging facility is back online and providing fuel cell researchers access to beam time. During the shutdown period, the project focus was on completing analysis of prior data and conducting facility improvements that might have interrupted the fuel cell user program. Numerous updates of the small-scale fuel cell test stand have been carried out, including adding dual liquid coolant temperature control and absolute pressure control. In addition, a large-scale test stand was acquired for running small stacks or automotive scale single cell test sections. In collaboration with one of our testing partners, General Motors, a standard fuel cell and test fixture for high resolution imaging was designed and built

and will be available for all facility users. This new fixture allows fuel cell researchers that are new to neutron imaging to quickly start an experiment as the fixture requires only a membrane electrode assembly and diffusion media for testing. The fixture can also accommodate custom flow field designs. To further improve the quantification of water in the fuel cell a neutron energy selector was designed, installed and tested. This device will allow examination of the energy dependent neutron scattering of water, sometimes referred to as beam hardening, and is critical to obtain accurate values of the water content in the membrane in through-plane water measurements of fuel cells.

A full length journal article has been submitted that provides a thorough analysis of systematic effects and required corrections in using neutron imaging to measure the water content in membranes. This work will be the basis for all future analysis of water content in membranes [1] and was a collaborative work involving NIST, Los Alamos National Laboratory and Lawrence Berkeley National Laboratory. To obtain an accurate measurement of the membrane water content from neutron imaging, two critical effects must be accounted for in the image analysis: under typical test section compression the membrane is essentially in a free swelling state [2] and the membrane retains water even after long dry gas purges. If one ignores these effects, neutron radiography measurements will report systematically lower water content in the membrane by 40% to 50%. Shown in Figure 1a is the excellent agreement in the membrane water sorption vs. water activity between historic gravimetric data and the corrected neutron radiography data, including the existence of Schroeder's paradox for Nafion[®] 117. In addition to steady water sorption measurements, the through-plane water content in a test section with a 1-mm thick membrane, during hydrogen pump mode was measured and compared with a literature-based model [3]. A thick membrane was used to overcome any limitations due to the spatial resolution. Hydrogen pump mode reduced the model complexity as one can neglect product water. In Figure 1b, the maximum measured water content is in good agreement with that predicted from modeling. However, there is disagreement on the effect of Schroeder's paradox on the through-plane membrane water content during operation. The model contains a sharp transition in the water content due to a switching function used to account for Schroeder's paradox, which is not supported by the neutron radiography data. Future studies are planned to investigate the effects of relative humidity (RH) and saturation gradients across the membrane to provide this water transport data to models. The corrections of the systematic effects will also be necessary in the measurement of the water content across commercially competitive membranes as the neutron spatial resolution improves.

Researchers at the University of Tennessee explored the role of the microporous layer in distributing product water throughout the fuel cell [4]. To do this a cell running



OCV - open circuit voltage

FIGURE 1. (a) Comparison of different methods of measuring water sorption measurements as a function of hydration. (b) Comparison of data and model of hydrogen pump data of a thick membrane.

on hydrogen was switched to deuterium, which allowed the redistribution of product water to be followed throughout the fuel cell. Since deuterium has a factor of 10 smaller neutron scattering cross-section than hydrogen the resulting water signal was reduced when hydrogen was replaced by deuterium. Two test sections were studied, one with a MPL on both the anode and cathode and one with no MPL. The test section was operated for 15 minutes with air, hydrogen and light water for humidification. After steady operation was established, the anode fuel stream was changed from hydrogen to deuterium, while maintaining all other operating conditions. As a result, the product water will be heavy water and will manifest as regions of higher neutron transmission or lower observed light water content. As Figure 2 shows, with a MPL on both the anode and cathode, the product heavy water is distributed both in the cathode and anode

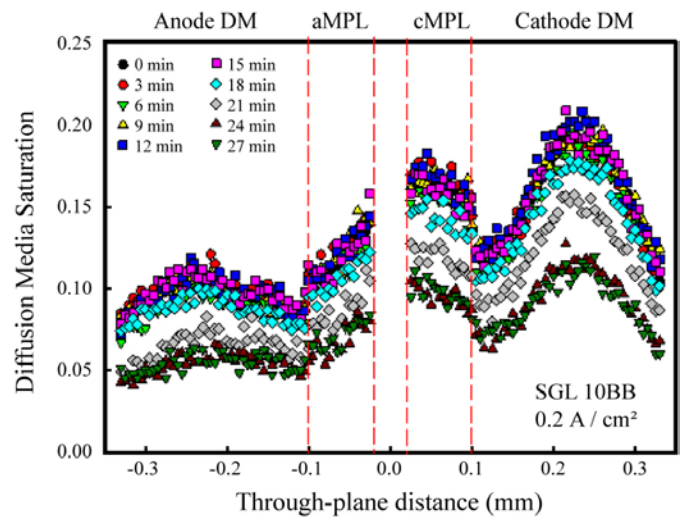


FIGURE 2. Influence of the MPL on the product water revealed by switching the anode gas stream to deuterium.

GDL substrates, while with no MPL, the product heavy water is primarily in the cathode. From these images it can be seen that the MPL is affecting at least two facets of water transport. First, it is promoting back diffusion through the membrane and into the anode GDL, which could be beneficial for low humidity operation. Second, the overall water content in the GDL substrate is less with a MPL, which will reduce the energy required to purge the cell on shutdown.

In a collaborative study with the University of South Carolina, the membrane conductivity was measured while the RH of the inlet gas was cycled between humidified and dry [5]. The primary finding is that the conductivity increased more rapidly during hydration than one would predict from steady-state correlations. In the test, a Nafion[®] 117 membrane was placed in a Bekktech 4-point conductivity cell flowing 200 sccm of nitrogen that was either dry or humidified at 50% RH. Thinner membranes were also investigated, as well as different flow rates and humidity levels. All cases followed the general trend shown in Figure 3, where the membrane conductivity is shown in the initially hydrated state (50% RH inlet gases). A switch is made to dry inlet gas at 120 s and the conductivity and water content decrease proportionally as expected from steady-state correlations [6]. After drying for about 120 s, the inlet gas is humidified and one can see that the conductivity rapidly increases compared to the water content, which is an indication that the startup of a cell will result in more efficient operation before the membrane has reached a given hydration state.

There is a continued effort to measure water transport phenomena in automotive-competitive membranes and standard carbon-supported Pt catalysts, for instance to investigate the role of water in carbon corrosion of the catalyst support with neutron imaging. To do this it is necessary to improve the spatial resolution to 1 μm , which

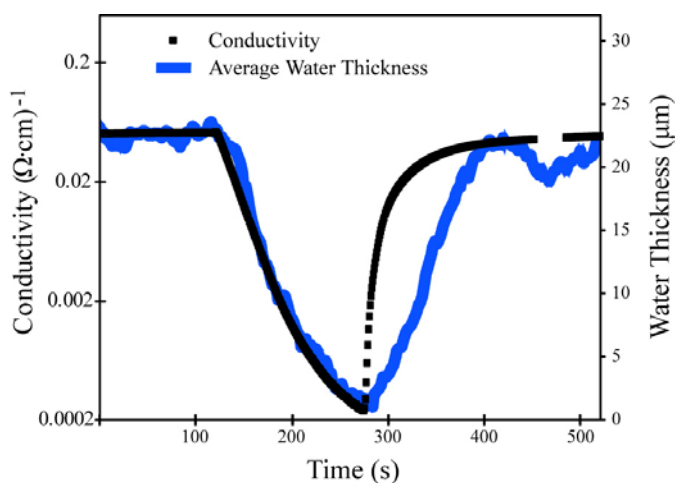


FIGURE 3. Nafion® 117 conductivity during a drying/hydration transient showing that on rehydration the conductivity increases more rapidly than expected based on correlations measured at steady state.

represents a factor of 10 improvement over the state of the art in neutron imaging detector technology. Two paths toward achieving this goal have been identified: the first is using structured illumination to limit the exposed area of the test section to about 1 μm ; the second is using a neutron focusing optic that enables magnification of up to 10X. The structured illumination approach requires fabricating an absorbing neutron grating that has neutron transparent sections that are 1 μm wide and are sufficiently separated to be resolved by a detector, or about 50 μm . Full field of view images are obtained by stepping the grating through one period and acquiring images at each step and then stitching the images together. This process will require integration times of several hours and thus the test section must be operated under steady state conditions. The grating fabrication is being carried out at the NIST nanofabrication facility. The primary challenge in the grating manufacture is obtaining a sufficiently thick, stable coating of Gd, the neutron absorber. A neutron focusing optic represents a major shift in neutron imaging facility design in that collimating the neutron beam is not required enabling a much higher (factor of about 100) neutron flux to be used. This will reduce the time to obtain an image of the through-plane water content from the current 20 minutes to about 10 s, allowing a much broader range of fuel cell operating conditions to be investigated. In addition to the increased flux, image magnification is also possible so that the image resolution can be improved over the intrinsic detector resolution; a magnification of 10 is possible which will enable direct measurements of the water content in commercially competitive membranes and standard catalyst layers. A feasibility experiment using an optic with a magnification of 4 is scheduled for the first two weeks in July 2012.

Conclusions and Future Directions

- Neutron imaging is a powerful probe to reveal the liquid water transport phenomena in PEMFCs.
 - The effect of the MPL on distributing product water in the fuel cell was investigated using the neutron scattering contrast between hydrogen and deuterium.
 - Combining in situ water sorption and conductivity measurements revealed that the membrane conductivity increases much more rapidly on hydration than expected from correlation derived at steady state conditions.
- Collaborate with the fuel cell research community to provide needed measurements of the water content in operating fuel cells.
 - Accurate measurements of the membrane water content are obtained after applying corrections for all systematic measurement effects.
 - Provide training to fuel cell researchers on how to employ NIST image analysis code that provides water content and uncertainty analysis.
 - The fuel cell test stands have been upgraded and a new fixture for through-plane water content measurements will be available to all facility users.
- Develop methods capable of resolving the liquid water content in commercial membranes and catalyst layers for durability studies by improving the neutron spatial resolution and sensitivity to hydrogen.
 - Image the water in a commercial cathode catalyst layer in a small-scale fuel cell with resolution approaching 1-2 micrometers in order to study degradation mechanisms that are induced by liquid water.
 - Utilize gratings at the thermal neutron imaging facility to improve the spatial resolution by a factor of 10 over the intrinsic resolution of 10 micrometers.
 - Conduct feasibility tests to magnify images of fuel cells by a factor of 10 to thereby improve the spatial resolution using a novel neutron imaging optic to obtain magnified images of an operating fuel cell.
 - Enable higher spatial and temporal resolution images of water transport phenomena during accelerated stress tests of PEMFCs.
 - A factor of 2 or more can be achieved in sensitivity to liquid water by utilizing cold neutrons instead of thermal neutrons.
 - Begin studies of degradation during accelerated stress tests of PEMFCs by completing the design and installation of a cold neutron imaging facility at NIST.

FY 2012 Publications/Presentations

1. D.S. Hussey, D. Spornjak, J. Fairweather, J. Spindelov, R. Mukundan, A.Z. Weber, D.L. Jacobson, and R. Borup (2012) Measuring the through-plane water content of membranes in PEMFCs with neutron radiography. *Journal of Applied Physics*, submitted.
2. Fairweather, J., Spornjak, D., Mukundan, R., Hussey, D.S., Weber, A.Z., Wessel, S., and Borup, R., 2011a, "Effects of carbon corrosion on the through-plane water transport in PEMFCs", in preparation.
3. Fairweather, J.D., Spornjak, D., Mukundan, R., Spindelov, J., Artyushkova, K., Atanassov, P., Hussey, D.S., Jacobson, D.L., and Borup, R., 2011b, Interaction of Heat Generation, MPL, and Water Retention in Corroded PEMFCs: *ECS Transactions*, v. 41, p. 337-348.
4. Hussey, D.S., Baltic, E., Coakley, K.J., and Jacobson, D.L., 2011, Improving quantitative neutron radiography through image restoration: Submitted to NIMA.
5. Hussey, D.S., Jacobson, D.L., and Baltic, E., 2011, Changing optical axis due to reactor operation: *Nuclear Instruments & Methods in Physics Research Section a-Accelerators Spectrometers Detectors and Associated Equipment*, v. 651, p. 73-76.
6. Kusoglu, A., Kienitz, B.L., and Weber, A.Z., 2011, Understanding the Effects of Compression and Constraints on Water Uptake of Fuel-Cell Membranes: *Journal of the Electrochemical Society*, v. 158, p. B1504-B1514.
7. Mishler, J., Wang, Y., Mukherjee, P.P., Mukundan, R., and Borup, R.L., 2012, Subfreezing operation of polymer electrolyte fuel cells: Ice formation and cell performance loss: *Electrochimica Acta*, v. 65, p. 127-133.
8. Mishler, J., Wang, Y., Mukundan, R., Spindelov, J., Hussey, D.S., Jacobson, D.L., and Borup, R., 2011, Probing the Water Content in Polymer Electrolyte Fuel Cells Using Neutron Radiography: *Energy & Environmental Science*, v. Submitted.
9. Owejan, J.P., Gagliardo, J.J., Reid, R.C., and Trabold, T.A., 2012, Proton transport resistance correlated to liquid water content of gas diffusion layers: *Journal of Power Sources*, v. 209, p. 147-151.
10. Preston, J.S., Fu, R.S., Pasaogullari, U., Hussey, D.S., and Jacobson, D.L., 2011a, Consideration of the Role of Micro-Porous Layer on Liquid Water Distribution in Polymer Electrolyte Fuel Cells: *Journal of the Electrochemical Society*, v. 158, p. B239-B246.
11. Preston, J.S., Pasaogullari, U., Hussey, D.S., and Jacobson, D.L., 2011b, High Resolution Neutron Radiography Imaging of Microporous Layers in PEFCs: *ECS Transactions*, v. 41, p. 319-328.
12. Rigdon, W.A., Huang, X., Hussey, D.S., and Jacobson, D.L., 2011, Proton Conductivity of Polymer Electrolyte Membranes during Transient Hydration and Dehydration Cycles: *ECS Transactions*, v. 41, p. 1381-1392.
13. Selamet, O.F., Pasaogullari, U., Spornjak, D., Hussey, D.S., Jacobson, D.L., and Mat, M., 2011, In Situ Two-Phase Flow Investigation of Proton Exchange Membrane (PEM) Electrolyzer by Simultaneous Optical and Neutron Imaging: *ECS Transactions*, v. 41, p. 349-362.
14. Spornjak, D., Hussey, D.S., Weber, A.Z., Mukundan, R., Fairweather, J., Brosha, E.L., Davey, J., Spindelov, J., Jacobson, D.L., and Borup, R., 2012, Environmental effects on PEM water content.: *Journal of the Electrochemical Society*, v. Submitted.
15. Spornjak, D., Wu, G., Fairweather, J., Hussey, D., Mukundan, R., Borup, R., and Zelenay, P., 2011, In situ measurement of flooding in thick Pt and PANI-derived catalyst layers in PEM fuel cells: *Journal of the Electrochemical Society*, v. In preparation.
16. Wood, B.M., Ham, K., Hussey, D.S., Jacobson, D.L., Faridani, A., Kaestner, A., Vajo, J.J., Liu, P., Dobbins, T.A., and Butler, L.G., 2011, Real-Time Observation of Hydrogen Absorption by LaNi₅ with Dynamic Neutron Tomography: Establishing Time-Windows, Projection Weighting, and Image Processing.: *Journal of Physical Chemistry*, v. In preparation.
17. "Isolation of Transport Mechanisms in PEFCs with High Resolution Neutron Imaging", J. LaManna, S. Chakraborty, F. Zhang, M. Mench, J. Gagliardo, and J.P. Owejan, 220th ECS Meeting, Boston, MA, October, 2011.
18. "Interaction of Heat Generation, MPL and Water Retention in Corroded PEMFCs", J.D. Fairweather, D. Spornjak, R. Mukundan, J. Spindelov, K. Artyushkova, P. Atanassov, D.S. Hussey, D.L. Jacobson, and R. Borup, 220th ECS Meeting, Boston, MA, October, 2011.
19. "In Situ Two-Phase Flow Investigation of Proton Exchange Membrane (PEM) Electrolyzer by Simultaneous Optical and Neutron Imaging", O.F. Selamet, U. Pasaogullari, D. Spornjak, D.S. Hussey, D.L. Jacobson, and M. Mat, 220th ECS Meeting, Boston, MA, October, 2011.
20. "High Resolution Neutron Imaging of PEMFCs with Scintillator-Based Detectors", D.S. Hussey and D.L. Jacobson, 220th ECS Meeting, Boston, MA, October, 2011.
21. "Proton Conductivity of Polymer Electrolyte Membrane during Transient Hydration and Dehydration Cycles", W.A. Rigdon, X. Huang, D.S. Hussey, and D.L. Jacobson, 220th ECS Meeting, Boston, MA, October, 2011.
22. "Validation and Characterization Database Supporting Two-Phase 1+1D PEMFC Model Development", J.P. Owejan, W. Gu, J. Gagliardo, P. Nicotera, A. Kongkanand, R. Reid, M. Mench, J. LaManna, S. Chakraborty, F. Zhang, M. Hickner, S. Petrina, S.G. Kandlikar, T. Trabold, G. Zhang, J. Sergi, and M. Daino, 220th ECS Meeting, Boston, MA, October, 2011.
23. "Characterization of Heat & Water Transport in Gas Diffusion Layers and Associated Interfaces", Matthew M. Mench, 220th ECS Meeting, Boston, MA, October, 2011.
24. "Investigation of Micro-Porous Layer effect in the Water Distribution in the Polymer Electrolyte Membrane Fuel Cell by Hydrogen-Deuterium Contrast Neutron Radiography", K. Cho, A. Turhan, and M. Mench, 220th ECS Meeting, Boston, MA, October, 2011.
25. "Neutron Imaging for Electrochemistry", D.S. Hussey, D.L. Jacobson, E. Baltic, and M. Arif, ESS, Seminar, Lund, Sweden, 12 DEC 2011.
26. "Neutron Imaging for Electrochemistry", D.S. Hussey, D.L. Jacobson, E. Baltic, and M. Arif, RISO Seminar, Roskilde, Denmark, 13 DEC 2011.

References

1. D.S. Hussey, D. Spornjak, J. Fairweather, J. Spendelow, R. Mukundan, A.Z. Weber, D.L. Jacobson and R. Borup, "Accurate Measurement of the Through-Plane Water Content of Proton-Exchange Membranes Using Neutron Radiography", *Journal of Applied Physics*, submitted (2012).
2. A. Kusoglu, B.L. Kienitz, and A.Z. Weber, "Understanding the Effects of Compression and Constraints on Water Uptake of Fuel-Cell Membranes", *Journal of the Electrochemical Society*, **158**, B1504 (2011).
3. A.Z. Weber and M.A. Hickner, *Electrochim. Acta*, **53**, 7668 (2008); A.Z. Weber and J. Newman, *J. Electrochem. Soc.*, **151**, 311 (2004); A.Z. Weber and J. Newman, *J. Electrochem. Soc.*, **151**, A326 (2004).
4. K-T. Cho and M.M. Mench, "Investigation of the role of the micro-porous layer in polymer electrolyte fuel cells with hydrogen deuterium contrast neutron radiography", *Physical Chemistry Chemical Physics*, **14**, 4296 (2012).
5. W.A. Rigdon, X. Huang, D.S. Hussey, and D.L. Jacobson, *ECS Trans.* **41**, 1381 (2011).
6. T.A. Zawodzinski, Jr., M. Neeman, L.O. Sillerud, and S. Gottesfeld, "Determination of Water Diffusion Coefficients in Perfluorosulfonate Ionomeric Membranes", *Journal of Physical Chemistry*, **95**, 6040 (1991).

V.A.7 Technical Assistance to Developers

T. Rockward and R.L. Borup (Primary Contacts),
F. Garzon, R. Mukundan, and D. Spornjak
Los Alamos National Laboratory (LANL)
P.O. Box 1663
Los Alamos, NM 87545
Phone: (505) 667-9587 and (505) 667-2823
Emails: trock@lanl.gov, borup@lanl.gov

DOE Manager

HQ: Nancy Garland
Phone: (202) 586-5673
Email: Nancy.Garland@ee.doe.gov

Project Start Date: October 2003

Project End Date: Project continuation and direction determined annually by DOE

FY 2012 Accomplishments

- Evaluation of novel MPL materials showing improvements in mass transport and durability after hydrophilic treatment including the addition of C-nanotubes into the MPL.
- Successful protocol development and completion of startup/shutdown protocol tests.
- Testing of graphite bipolar plate hydrophobic treatment showing better performance than an untreated graphite plate at low current densities (i.e. $<500 \text{ mA/cm}^2$).
- Application of several different diagnostics tools to study the titania-coated stainless steel bipolar plates corrosion resistance including fuel cell testing using a drive cycle protocol, alternating current (AC) impedance spectroscopy, and X-ray fluorescence (XRF) elemental imaging. Participation in the DOE Fuel Cell Technical Team, co-chairing DOE Working Group meetings on Durability and Transport Modeling Working; presenting data and leading discussions on protocol development.



Objectives

- Support technically, as directed by DOE, fuel cell component and system developers
- Assess fuel cell materials and components and give feedback to developers
- Assist the DOE Durability Working Group with the development of various new material durability testing protocols
- Provide support to the U.S. Council for Automotive Research (USCAR) and the USCAR/DOE Fuel Cell Technology Team
- Fiscal Year (FY) 2012 Specific Technical Objectives:
 - Evaluate novel micro-porous layer (MPL) materials
 - Develop of startup/shutdown protocol
 - Test the impact of hydrophobic treatment on graphite bipolar plates
 - Perform complete diagnostics on metal bipolar plates for corrosion
 - Participate and lead efforts in the DOE Working Groups

Technical Barriers

This project addresses the following technical barriers from the Fuel Cells section (3.4.4.2) of the Fuel Technologies Program Multi-Year Research, Development and Demonstration Plan:

- (A) Durability
- (B) Cost
- (C) Performance

Introduction

This task supports the allowance of technical assistance to fuel cell component and system developers as directed by the DOE. This task includes testing of novel materials and participation in the further development and validation of single-cell test protocols. This task also covers technical assistance to DOE Working Groups, USCAR and the USCAR/DOE Driving Research and Innovation for Vehicle efficiency and Energy sustainability (U.S. DRIVE) Fuel Cell Technology Team. Assistance includes technical validation of new fuel cell materials and methods, single-cell fuel cell testing to support the development of targets and test protocols, and regular advisory participation in other working groups and reviews. This assistance is made available to polymer electrolyte membrane (PEM) fuel cell developers by request and DOE approval.

Approach

The LANL fuel cell team has extensive knowledge and in-house analytical capabilities. These capabilities along with the personnel uniquely allow us to conduct thorough diagnostics and confirm results of existing and novel materials. In FY 2012, several requests were approved by the DOE to be completed under this task. Requests granted were the testing of novel MPL materials, development and testing a new startup/shutdown protocol, investigation of the

impact of the hydrophilic treatment of a graphite bipolar plate material, and validation of enhanced corrosion protection of titania-coated stainless steel bipolar plate materials. Detailed highlights of these projects will be further discussed in the following.

Results

In FY 2012, we completed testing, analysis provided feedback to both the collaborator and our DOE managers in four major component areas. Some selected findings were as follows:

- Novel MPL materials were evaluated in a 50-cm² fuel cell operating at 80°C, 100% relative humidity (RH), 50% air utilization and 28.4 psig back pressure. We tested three different cathode gas diffusion layers (GDLs) with varying MPL amounts and different carbon-fiber substrates. In particular, the GDLs were a standard MPL with carbon/Teflon®/binder (25BC), a standard MPL with a hydrophilic treatment (25BL), and a standard MPL with carbon nanotubes (25BN). The findings indicated that GDLs 25BL and 25BN both improved in the mass transport region compared to 25BC, but only 25BN resolved durability issues that surfaced in the others.
- The startup/shutdown protocol was developed in collaboration with Ballard Power and initial tests were conducted. A graphical representation of the start up/shut down protocol is shown in Figure 1.
- Figure 2 shows pictures of a plain bipolar plate (top) and a hydrophobic-treated bipolar plate (bottom). Water

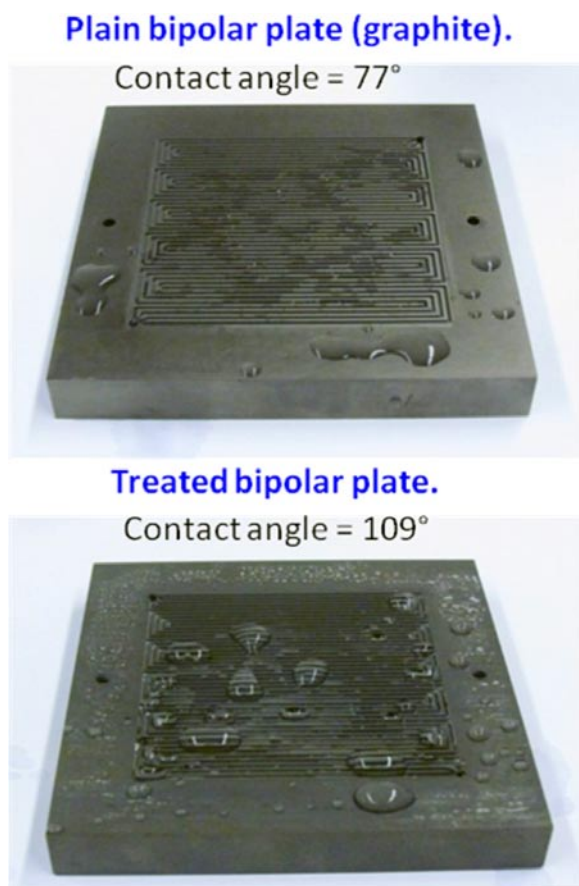


FIGURE 2. Illustration comparing the contact angles of graphite bipolar plates: plain vs. treated

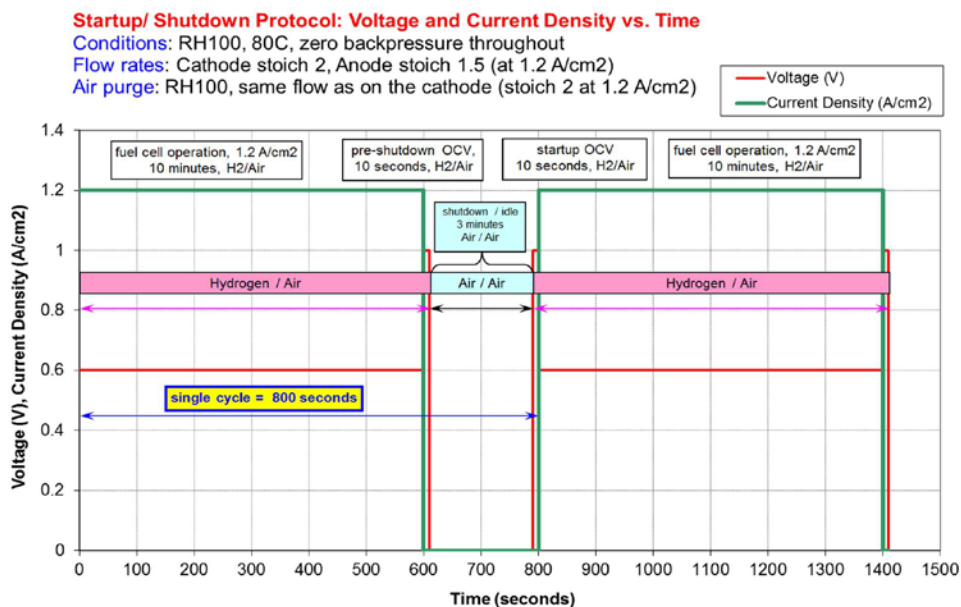


FIGURE 1. Test results using newly developed startup/shutdown protocol

droplet contact angle measurements clearly demonstrated that the treated plate is more hydrophobic. Here we focus on their impact on PEM fuel cell performance when the treated bipolar plates were used on the cathodes. We used identical test materials, varying cathode plate types only, to allow for a direct comparison between the plates. An identical test protocol was performed on both plates. The test protocol included a 2 hr break-in period, voltage-current tests (V-Is), and several full impedance spectra at various current densities using 100 and 25% RH (Figure 3). The V-Is showed at low currents densities ($<500 \text{ mA/cm}^2$) the hydrophobic plate performs slightly better, while extensive flooding was observed at the higher currents. In order to further investigate this phenomenon, impedance spectra in the different regions of the V-I were probed. At low current densities ($<20 \text{ mA/cm}^2$), the hydrophobic plate keeps the cathode catalyst layer and MEA more hydrated. This results in improvement in high-frequency resistance and decreased catalyst sheet resistance. Product water keeps the catalyst layer hydrated especially at drier inlet RH operation. At higher current densities ($>1 \text{ A/cm}^2$), the use of a hydrophobic flow field became a detriment since it led to increased mass transport resistance due to less efficient water removal from the cathode catalyst layer and GDL.

- We conducted a systematic study using several different diagnostics to test coated metal bipolar plates for enhanced corrosion protection. This task was requested after the observation of small discolorations in the metal bipolar plates after they were manufactured and coated and fuel cell tested. Initial speculation was that they were due to galvanic corrosion; however, our X-ray elemental mapping results did not indicate materials losses from corrosion. In fact, no significant change in the elemental composition of the titanium oxide coating or the underlying stainless steel was observed.

The long-term corrosion resistance of the treated plates still needs confirmation. Laboratory corrosion tests were developed to further characterize the corrosion resistance of the treated plates. However, the uncertainty of this material after being subjected to an aggressive drive cycle conditions in an actual fuel cell remained. There are currently no accelerated stress tests for corrosion testing bipolar plates; however an existing DOE drive-cycle was modified and used in this task. The drive cycle called for 30K cycles going from 1 A to 60 A with a 30 seconds settling time at each current for a total of 500 hours. The fuel cell operates with hydrogen and air fixed flows (669 and 1,773 sccm) at 80°C and slightly oversaturated humidification conditions and ambient back pressure. We performed beginning-of-test and end-of-test diagnostics for comparisons, which included digital imaging, XRF elemental mapping of plates and MEA, initial and final voltage-current-resistance tests (VIRs), AC impedance and contact

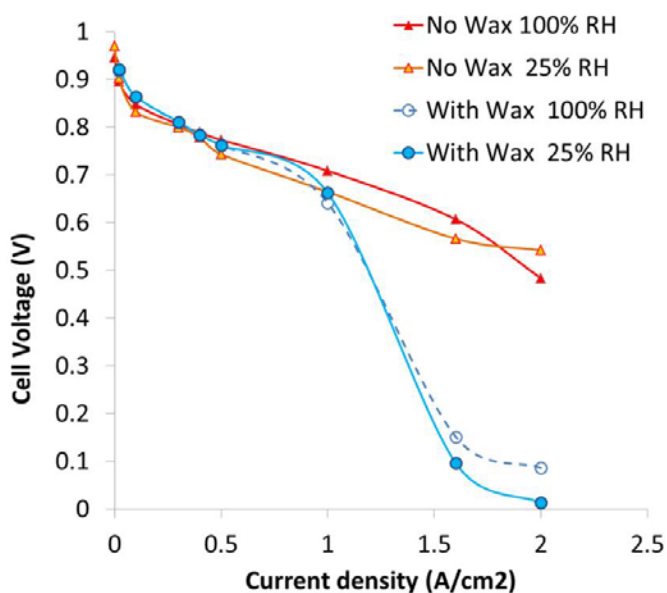


FIGURE 3. Polarization curves measurements from a plain vs. treated bipolar plate operating at 100 and 25% RH

resistance measurements. The VIRs behaved similarly for the metal and graph plates. The digital imaging showed visible discoloration for the metal plates, more significant at the anode outlets. These changes were compared with the neutron imaging of a similar plate tested under similar conditions. The location of liquid water imaged by neutron scattering coincided with the regions of discoloration observed on the metal plates. Elemental mapping at the anode outlet show titanium loss from the outer layer. This is depicted in Figure 4. Analyses of bipolar plates (post test) indicates corrosion present on anode plate, typically where large amounts of liquid water were present and minimal corrosion present on cathode plate (but not zero). Analysis of MEAs shows small levels of metal contamination of GDL/MEA which correlates to approximately $\sim 5\%$ to $\sim 14\%$ of the sulfonic acid sites if all of the cations reside inside the membrane; the cationic concentration was also higher where liquid water was present. In addition the contact resistance increased of the cathode plate.

Conclusions and Future Directions

In FY 2012 LANL:

- Completed testing of new novel MPL layers with hydrophilic fibers to analyze the changes in mass transport.
- Interacted with various organizations to discuss the proper protocols for start up/shut down in terms of durability testing (with results presented from the University of Nancy at the AMR).

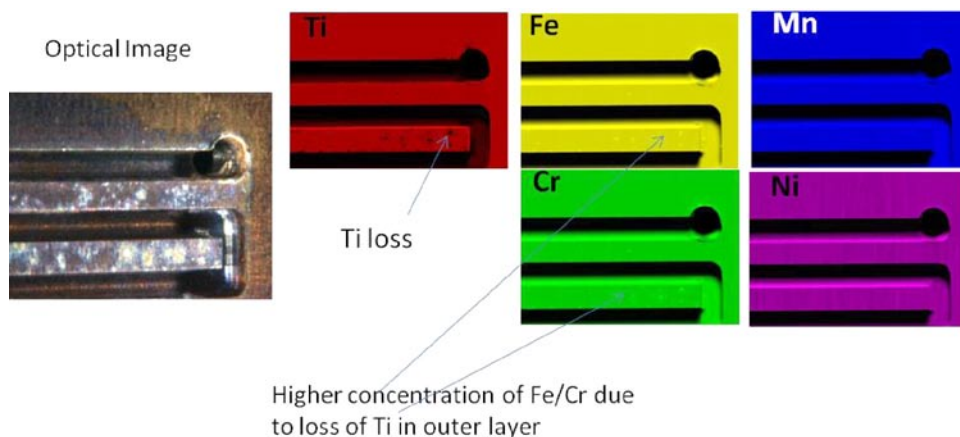


FIGURE 4. Elemental mapping images of metal bipolar plates taken after completing a DOE drive cycle protocol

- Measure the performance of novel hydrophobic bipolar plate flow field coatings.
- Performed characterization on tested metal bipolar plates, and performed in situ testing of metal bipolar and presented these results to DOE and the U.S. DRIVE Fuel Cell Tech Team.
- Provided support for program interaction with DOE; such as the support for the co-chair of the DOE Fuel Cell Technologies Durability Working Group and the co-chair of the DOE Transport Modeling Working Group, and permanent representative to the DOE Fuel Cell Technical Team.

For FY 2013, we will continue to support fuel cell developers as directed by DOE to provide capabilities that exist at LANL not readily available to many developers.

V.A.8 Enlarging the Potential Market for Stationary Fuel Cells Through System Design Optimization

Chris Ainscough (Primary Contact), Sam Sprik, Michael Penev

National Renewable Energy Laboratory (NREL)
15013 Denver West Parkway
Golden, CO 80401-3305
Phone: (303) 275-3781
Email: chris.ainscough@nrel.gov

DOE Manager

HQ: Kathi Epping Martin
Phone: (202) 586-7425
Email: Kathi.Epping@ee.doe.gov

Subcontractor:

University of California Irvine, Irvine, CA (planned)

Project Start Date: January 1, 2011

Project End Date: Project continuation and direction determined annually by DOE

- Characterize building control systems and include in the tool advanced control strategies for integrating fuel cell systems and building control systems.
- Validate the model outputs against real-world data from stationary fuel cell installations.

Technical Barriers

This project addresses the following technical barriers from Fuel Cells section (3.4) of the Fuel Cell Technologies Program Multi-Year Research, Development and Demonstration Plan:

- (C) Performance
- (B) Costs

Technical Targets

TABLE 1. Technical Targets that Will Be Evaluated as Parameters in the Stationary Fuel Cell Model

| Excerpted from the 2011 Multi-Year Research, Development and Demonstration Plan, Table 3.4.6 Technical targets: 100 kW–3 MW Combined Heat and Power (CHP) and Distributed Generation Fuel Cell Systems Operating on Natural Gas. | | | | |
|--|---------------------|-------------|--------------|--------------|
| Characteristic | Units | 2011 Status | 2015 Targets | 2020 Targets |
| Electrical efficiency @ rated power | % LHV of input fuel | 42–47 | 45 | >50 |
| CHP energy efficiency | % | 70–90 | 87.5 | 90 |
| Installed cost, natural gas | \$/kW | 3,500–5,000 | 3,000 | 1,500 |
| Number of planned/forced outages over lifetime | Count | 50 | 50 | 40 |
| Operating lifetime | Thousand hours | 40–80 | 50 | 80 |

LHV – lower heating value

Fiscal Year (FY) 2012 Objectives

- Develop a complete stationary fuel cell model user’s guide including:
 - Operational details on the model with guidance on appropriate inputs.
 - Documentation of control strategy algorithms.
 - Instructions on operating and configuring each of the model’s component modules.
 - Documentation of energy equations used.
 - Distributed generation system specifications.
- Develop a detailed plan and prioritized list of proposed additional features and enhancements to the model, in concert with stakeholders at DOE, industry, and academia.
- Build a tool for optimizing fuel cell attributes, including control parameters, and system and component sizes for unique individual building characteristics. The tool is flexible for adding user-defined building, fuel cell, financial, control characteristics.
- Use the tool to minimize lifecycle cost, lifetime greenhouse gas (GHG) emissions, or installed capital costs of fuel cell installations.
- Characterize the largest segments of the U.S. building inventory for use in the tool, leveraging the Commercial Building Energy Consumption Survey building survey.

FY 2012 Accomplishments

- Implemented the model in a scalable, flexible, modular framework that allows for easy customization in the future by non-programmers.
- Developed a stable graphical user interface (GUI).
- Completed a detailed user guide for the model and incorporated it into the GUI.
- Developed a detailed plan and prioritized list of additional features and enhancements.

- Incorporated model building profiles for 16 different building types in 16 climate zones for three different vintages (768 total), which represent 67% of the U.S. commercial building inventory.
- Synchronized with other DOE-funded projects at Lawrence Berkeley National Laboratory, Strategic Analysis, Inc., and Battelle in order to lay the groundwork for incorporating their cost models.



Introduction

According to DOE, 80% of the current U.S. building stock will still be in use in the year 2050. For fuel cells to penetrate the stationary market in significant numbers, retrofitting existing buildings with stationary fuel cells must be an important part of the U.S. strategy. This means that systems must be appropriately sized for today's heat and power loads, with some consideration for the energy demands of future construction.

The objective of this project is to construct a software model including proton exchange membrane (PEM), high temperature PEM, molten carbonate, phosphoric acid, and solid oxide fuel cells to optimize sizing and control strategies for particular building types and sizes and geographic locations. This model will be further enhanced with more fuel cell types, more control strategies, optimization capabilities, and further refinements to the user interface and post-processing capability.

Approach

The model is implemented in a scalable, flexible modular MATLAB[®] framework. The model includes modules for the model buildings (768 so far), control strategies, fuel cell systems, economic inputs, manufacturing cost models, and feedstock costs (electricity and natural gas).

In order to synchronize with other work in industry, the project team is building strong links to other DOE projects that will provide the manufacturing volume models for 1, 5, 25, and 100 kW systems in manufacturing rates of 100, 1,000, 10,000, and 50,000 annually. In addition, NREL is working with stationary fuel cell original equipment manufacturers to incorporate their feedback on the model and allow them the opportunity to test a beta version.

Results

The project team has created a detailed fuel cell model that includes a number of user-customizable modules, which will enable the use of the model for large-scale analysis and simulations, and highly detailed planning and engineering of proposed installation sites.

The Stationary Fuel Cell Model is designed to allow the operator to assess the economics of installing stationary fuel cell systems in a variety of building types in the United States. The model allows the user to select from among four different dispatch strategies to attain different goals: cost minimization, GHG minimization, load following, and peak shaving.

The model contains 16 reference building load profiles, both electric and heat, in 16 different climate zones, with three different vintages. Combined, this allows the user to select from up to 768 different building scenarios.

The user can also control hour-by-hour summer and winter electric grid pricing scenarios, economic factors, and manufacturing costs, along with natural gas prices.

The main screen of the model allows the user to add and configure modules, and explore different views of the building heat and electricity loads. This is shown in Figure 1.

The fuel cell modules in the model are designed to allow the user to easily update, change, and copy in order to add new and different types of fuel cells and other non-fuel cell CHP systems (see Figure 2).

Figure 3 shows an example of the manufacturing cost models NREL will incorporate from other DOE projects. These models include cost as a function of system size and annual manufacturing volume.

Figure 4 shows the main output screen from the model. This allows the user to quickly compare the lifetime fuel and electricity costs of the building with and without the fuel cell system. Often the fuel cell will result in significantly higher fuel costs, but reduced electricity costs often result in a net savings on energy consumption.

Conclusions and Future Directions

NREL has created a flexible software model that will help fuel cell developers and DOE assess the ability of stationary fuel cell systems to penetrate the existing commercial building market in the United States.

For future work, NREL will expand the available fuel cell types, implement design of experiments and optimization capability, improve the execution speed, work with other DOE projects to continue including cost models, and provide input to the Commercial Building Energy Consumption Survey 2012 survey.

FY 2012 Publications/Presentations

1. *Enlarging the Potential Market for Stationary Fuel Cells Through System Design Optimization*, presented at DOE Annual Merit Review, May 14–18, 2012, Washington, D.C.

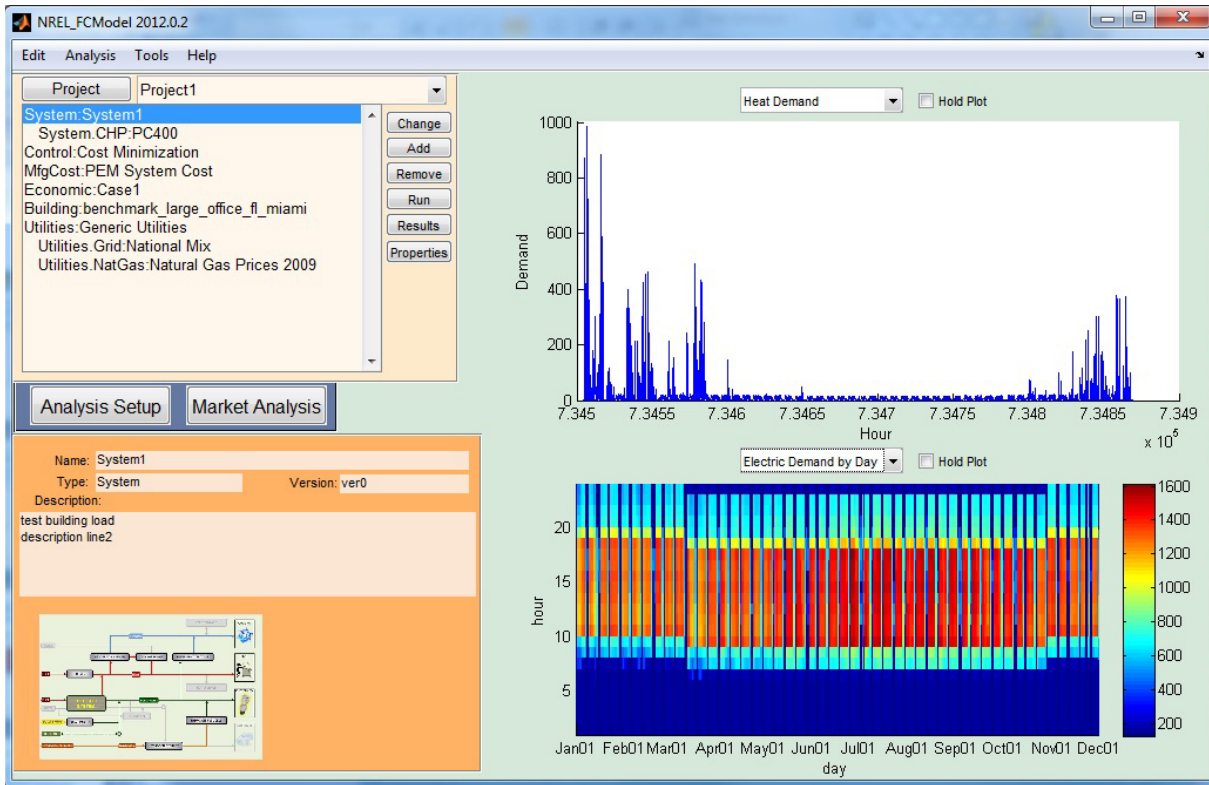


FIGURE 1. The main model screen, which consists of four panels that allow users to specify modules, see building profiles, and see component data

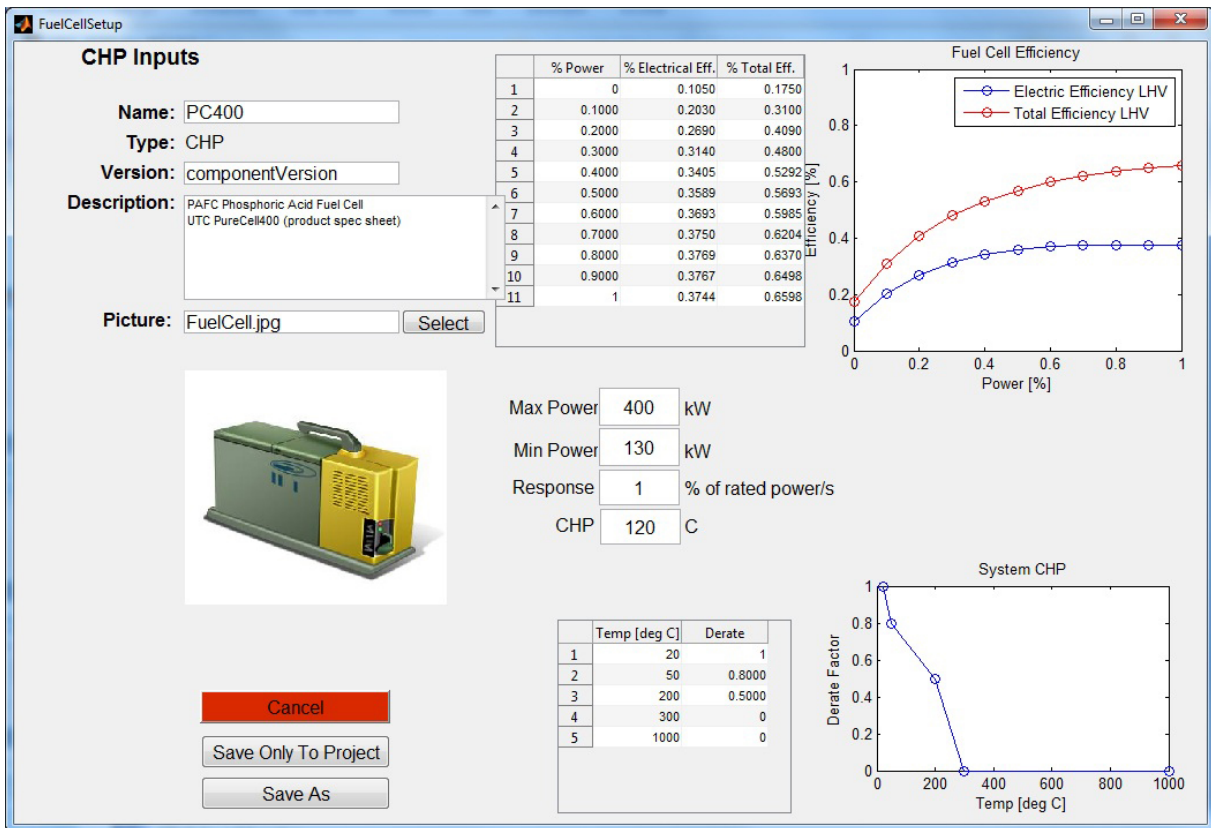


FIGURE 2. The fuel cell module allows users to quickly modify the fuel cell (or other CHP system) behavior and performance

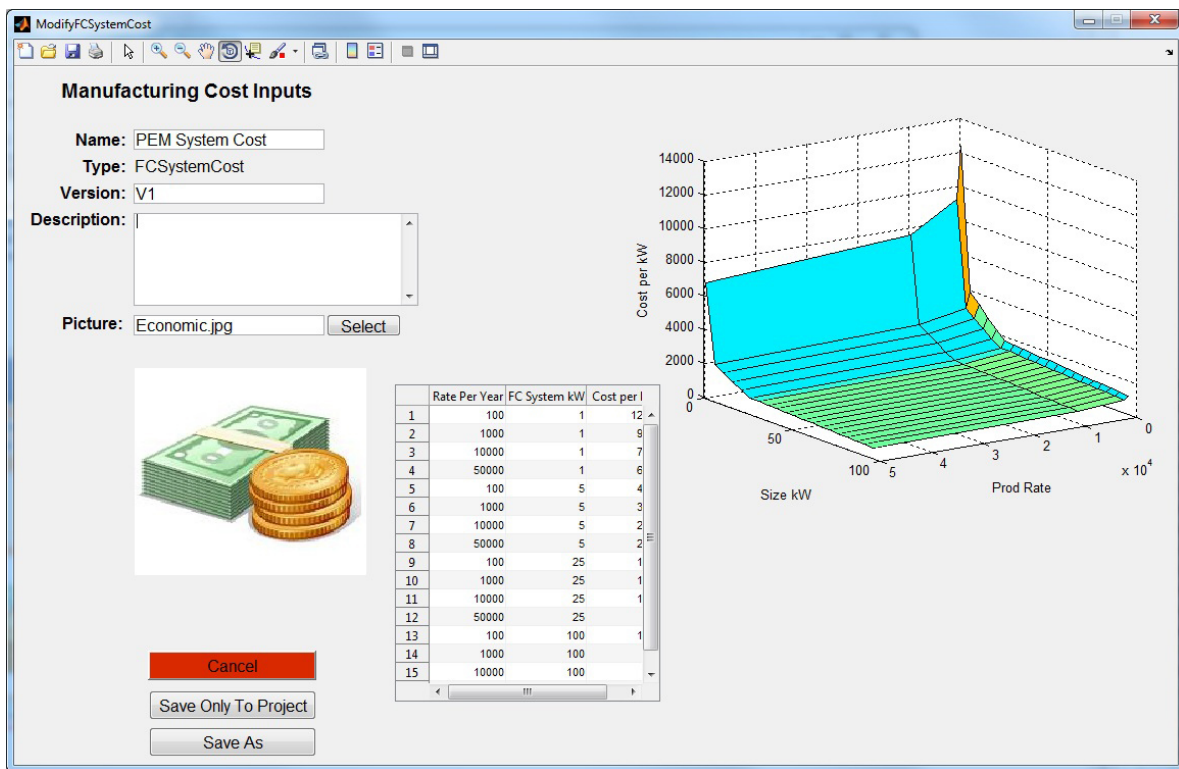


FIGURE 3. Manufacturing cost surfaces will be imported from other DOE projects performing detailed cost analysis

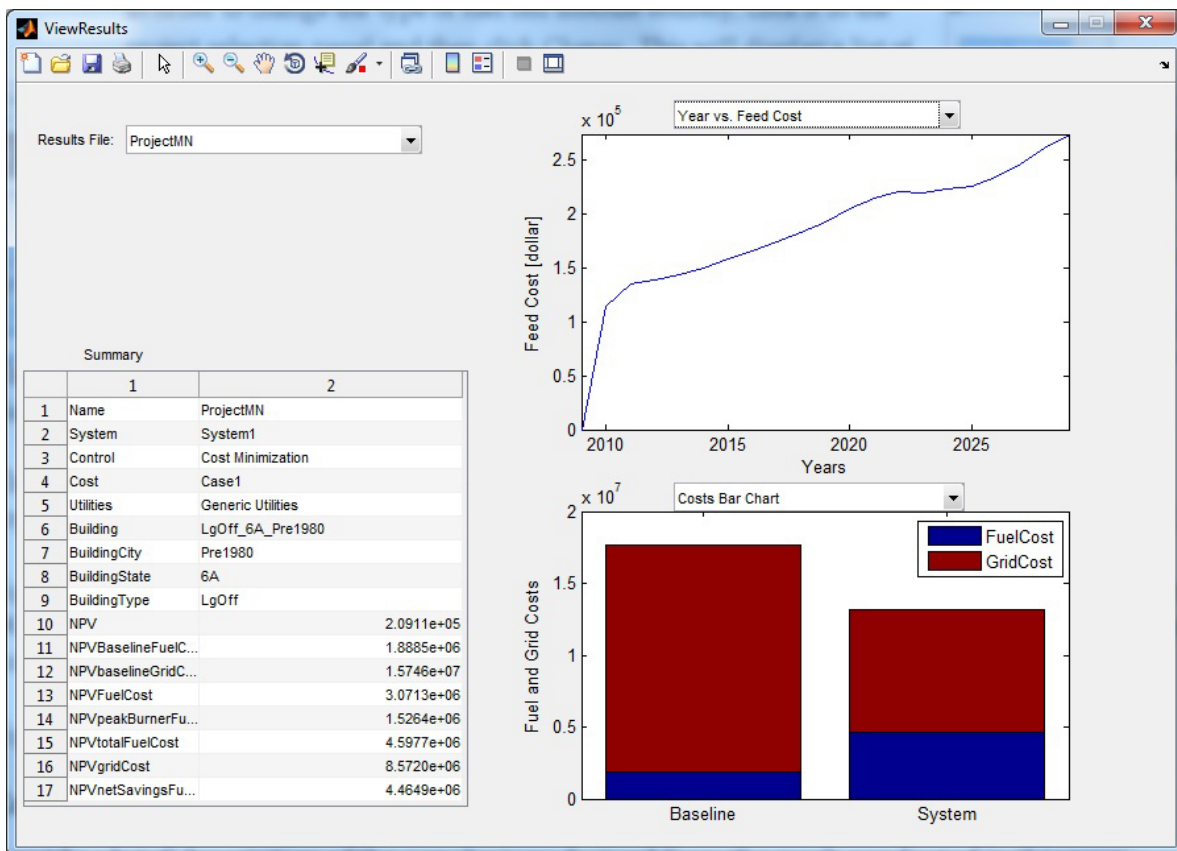


FIGURE 4. The model output screen allows users to quickly evaluate the viability of a fuel cell installation relative to the existing building baseline

V.A.9 Stationary and Emerging Market Fuel Cell System Cost Analysis

Kathya Mahadevan (Primary Contact),
VinceContini, Matt Goshe, and Fritz Eubanks
Battelle
505 King Avenue
Columbus, OH 43201
Phone: (614) 424-3197
Email: mahadevank@battelle.org

DOE Managers

HQ: Jason Marcinkoski
Phone: (202) 586-7466
Email: Jason.Marcinkoski@ee.doe.gov
GO: Reg Tyler
Phone: (720) 356-1805
Email: Reginald.Tyler@go.doe.gov

Contract Number: DE-EE0005250/001

Project Start Date: September 30, 2011
Project End Date: Project continuation and direction
determined annually by DOE

Technical Targets

To widely deploy fuel cells significant strides must be made in lowering the cost of components and systems without compromising reliability and durability. This cost analysis will identify the fundamental drivers of component and system cost and the sensitivity of the cost to various component and system parameters. The cost analyses will provide the DOE information on the impact of production volumes on lowering costs of fuel cells and the types of high volume manufacturing processes that must be developed to enable the widespread commercialization. The study will also provide insights into the optimization needed for use of off-the-shelf components in fuel cell systems to drive down system costs. Finally, the study will analyze the lifecycle costs of owning and operating a fuel cell to estimate primary costs drivers to the end user in applicable markets.



Approach

Battelle will apply the established methodology used successfully on the previous fuel cell cost analysis study for the DOE [1-3]. The technical approach consists of four steps – market assessment, system design, cost modeling, and sensitivity analysis (Figure 1). The first step characterizes the potential market and defines the requirements for system design. The second step involves developing a viable system design and associated manufacturing process vetted by industry. The third step involves building the cost models and gathering inputs to estimate manufacturing costs. Manufacturing costs will be derived using the Boothroyd-Dewhurst Design for Manufacture Assembly Software (DFMA[®]). Custom manufacturing process models will be defined where necessary and parametrically modeled based on knowledge of the machine, energy and labor requirements for individual steps that comprise the custom process. The fourth step will evaluate the sensitivity of stack and system costs to various design parameters. Both single factor sensitivity analysis and Monte Carlo analysis will be performed. Single factor sensitivity analysis helps determine the impact of individual parameters on system costs. The Monte Carlo analysis will help determine the impacts of cost variability. In addition to the sensitivity analysis, we will conduct a lifecycle cost analysis to estimate total cost of ownership for the target application and markets.

Fiscal Year (FY) 2012 Objectives

To assist the DOE in developing fuel cell systems for stationary and emerging markets by developing independent cost models and costs estimates for manufacture and ownership. In FY 2012, the project will estimate costs of:

- 10-kW and 25-kW polymer electrolyte membrane fuel cell (PEMFC) for material handling equipment applications at annual production volumes of 100 units, 1,000 units, and 10,000 units.
- 1- and 5-kW solid oxide fuel cells (SOFC) and high-temperature polymer electrolyte membrane (HTPEM) fuel cells for auxiliary power unit applications at annual production volumes of 100 units, 1,000 units, and 10,000 units.

Technical Barriers

This project addresses the following technical barriers from the Fuel Cell section of the Fuel Cell Technologies Program Multi-Year Research, Development and Demonstration Plan:

(B) Cost

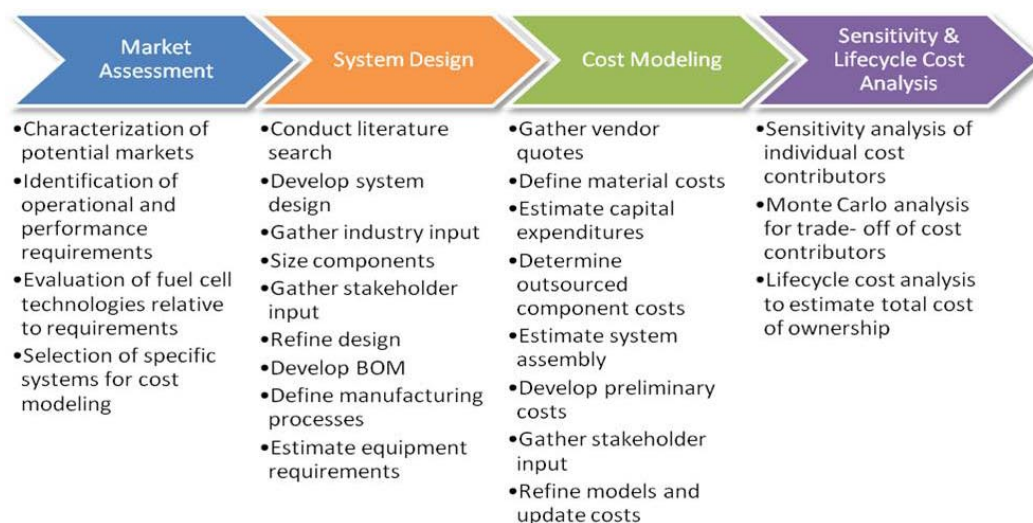


FIGURE 1. Battelle's Cost Analysis Methodology

FY 2012 Accomplishments

- Completed the market assessment for the material handling equipment and auxiliary power unit markets:
 - Defined the application requirements.
 - Selected appropriate fuel cell technologies and system sizes to meet requirements.
- Detailed performance specifications and system requirements and completed preliminary system design of:
 - 10-kW and 25-kW PEMFCs for material handling equipment specifically forklifts.
 - 1-kW and 5-kW SOFCs for auxiliary power units.

Next Steps

In FY 2012, Battelle will:

- Finalize design of the PEM and SOFC systems.
- Initiate and finalize design of the high temperature PEM system for auxiliary power applications.
- Complete full cost assessment of 10-kW and 25-kW PEMFC systems for material handling applications.
- Complete full cost assessment of 1-kW and 5-kW SOFC and HTPM systems for auxiliary power applications.

References

1. Battelle. 2011. The High Volume Manufacture Cost Analysis of 5 kW Direct Hydrogen Polymer Electrolyte Membrane (PEM) Fuel Cell for Backup Power Applications. Contract No. DE-FC36GO13110.
2. K. Mahadevan, K. Judd, H. Stone, J. Zewatsky, A. Thomas, H. Mahy, and D. Paul. 2007. Identification and characterization of near-term direct hydrogen proton exchange membrane fuel cell markets. Contract No. DE-FC36GO13110. Available at http://www1.eere.energy.gov/hydrogenandfuelcells/pdfs/pemfc_econ_2006_report_final_0407.pdf.
3. H. Stone, K. Mahadevan, K. Judd, H. Stein, V. Contini, J. Myers, J. Sanford, J. Amaya, and D. Paul. 2006. Economics of Stationary Proton Exchange Membrane Fuel Cells, Interim Report. Contract No. DE-FC36GO13110.

V.A.10 Total Cost of Ownership Model for Design and Manufacturing Optimization of Fuel Cells in Stationary and Emerging Market Applications

Max Wei (Primary Contact), Tom McKone, Tim Lipman¹, David Dornfeld², Josh Chien², Chris Marnay, Adam Weber, Paul Beattie³, Patricia Chong³

Lawrence Berkeley National Laboratory (LBNL)
1 Cyclotron Road
MS 90R-4000
Berkeley, CA 94706
Phone: (510) 486-5220
Email: mwei@lbl.gov

DOE Manager

HQ: Jason Marcinkoski
Phone: (202) 586-7466
Email: Jason.Marcinkoski@ee.doe.gov

Subcontractors:

¹ University of California, Berkeley, Transportation Sustainability Research Center and DOE Pacific Region Clean Energy Application Center, Berkeley, CA

² University of California, Berkeley, Laboratory for Manufacturing and Sustainability, Department of Mechanical Engineering, Berkeley, CA

³ Ballard Power Systems, Burnaby, British Columbia

Project Start Date: October 1, 2011

Project End Date: September 31, 2016

Development and Demonstration Plan (<http://www1.eere.energy.gov/hydrogenandfuelcells/mypp/>):

- (A) Lack of High-Volume Membrane Electrode Assembly Processes
- (B) Lack of High-Speed Bipolar Plate Manufacturing Processes

Technical Targets

This project develops total cost of ownership models for stationary fuel cell applications in emerging markets. The objectives are to include direct manufacturing costs and life cycle costs and to extend existing cost models to include possible ancillary financial benefits such as carbon credits, end of life recycling, and reduced costs for building equipment operations. This work will quantify more fully the benefits of fuel cell systems taking into account life cycle assessment, air pollutant impacts and policy interactions.

A key output of this project will be a publicly available total cost of ownership modeling tool for the design and manufacturing optimization of fuel cell systems for stationary and emerging market applications with the ability to do sensitivity analysis toward meeting 2015 and 2020 DOE cost targets.

TABLE 1. DOE multiyear plan system equipment cost targets for fuel cell combined heat and power (CHP) systems

| Characteristic | 2015 Target | 2020 Target |
|-------------------|-------------|-------------|
| 10 kW CHP System | \$1,900/kW | \$1,700/kW |
| 100 kW CHP System | \$2,300/kW | \$1,000/kW |

Fiscal Year (FY) 2012 Objectives

- Literature review including review of fuel cell design and manufacturing patents
- Technical and performance specifications defined for technology/application anchor points
- Detailed design plans and technology bill of materials for low-temperature (LT) polymer electrolyte membrane (PEM) systems
- Ballard and other industry partners engaged

Technical Barriers

- High capital and installation costs
- Potential policy and incentive programs may not value fuel cell total benefits

This project addresses the following technical barriers from the Manufacturing R&D section (Chapter 3.5.5) of the Fuel Cell Technologies Program Multi-Year Research,

FY 2012 Accomplishments

- Literature review completed for fuel cell system cost studies, market studies, and patent review for LT PEM stack components.
- CHP functional requirements characterized in the LBNL DER-CAM model (Distributed Energy Resource Customer Adoption Model) to model fuel cell system market penetration and operating capacity parameters for power and heat.
- Functional specifications for combined heat and power applications defined for LT PEM fuel cell systems.



Introduction

The DOE has supported cost analysis studies in the past for fuel cell systems, notably automotive systems [1]. This work extends cost analysis studies to stationary applications and emerging market applications such as combined heat and power and back-up power systems. Detailed cost studies can develop cost sensitivities to stack components, materials, and balance-of-plant components and identify key cost component limiters such as platinum loading. Manufacturing cost sensitivities as a function of system size and annual manufacturing volume are another key output. Such studies can help to validate DOE cost targets or highlight key requirements for DOE targets to be met.

This work extends existing cost models to include possible ancillary financial benefits such as carbon credits, end of life recycling, and reduced costs for building equipment operations. Thus a more comprehensive picture of fuel cell system benefits is provided, consistent with a policy and incentive environment that increasingly values these ancillary benefits. We plan to develop optimized system designs for the lowest manufacturing cost and total cost of ownership as a function of application/functional targets, capacity, and production volume. Three fuel cell technologies will be included (low- and high-temperature [HT] PEM and solid-oxide) and initial stationary applications to be studied are combined heat and power and back-up power.

Approach

The overarching approach is to utilize Design for Manufacturing and Assembly (DFMA[®]) techniques to optimize system design, materials and manufacturing flow for lowest manufacturing cost and total cost of ownership. System designs will be developed and refined based on the following: (1) existing cost studies where applicable; (2) literature and patent sources; (3) industry and national laboratory advisors. The total cost of ownership model will be implemented in Analytica and include manufacturing costs, operations and end of life disposition, life cycle impacts and policy incentives and benefits. Other software tools employed include commercially available Boothroyd Dewhurst DFMA[®] software, existing life-cycle analysis database tools, and LBNL exposure and health impact models. The overall research and modeling approach is shown in Figure 1.

Results

In this start-up phase of work, the team has completed literature review of existing fuel cell system cost studies [1,2,3], market studies [4,5], and patent review for LT PEM stack components. Literature review of cost studies were focused on capturing the scope, key learning, and key assumptions of each study. The MEA followed by the

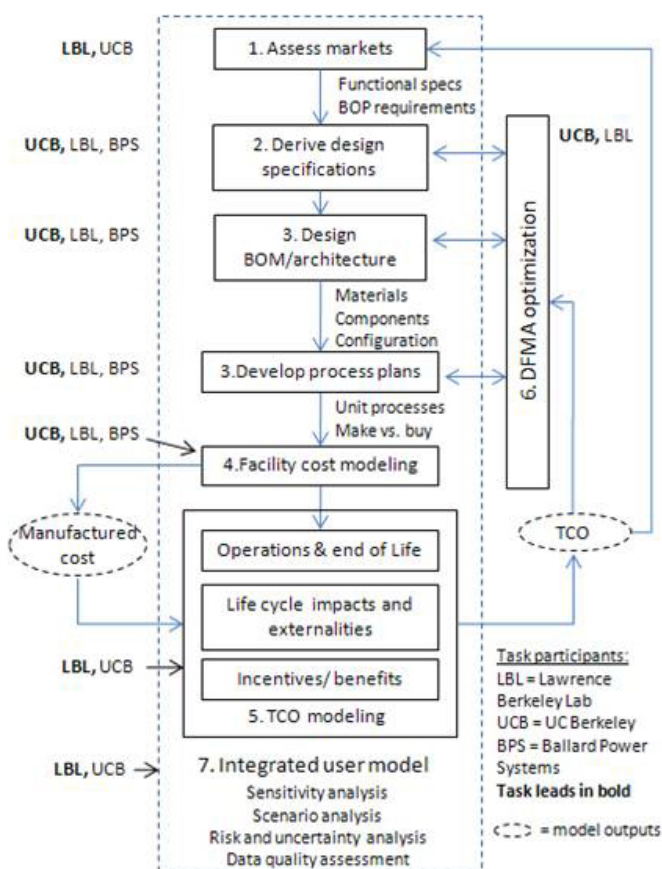


FIGURE 1. Research and Modeling Approach

bipolar plates dominate stack costs and the studies primarily focus on direct manufacturing with vertical integration. General market studies identify fuel cell cost, durability and utilization as key drivers. Forklift/material handling systems and backup power systems were highlighted as key market opportunities with some opportunity for micro-CHP in colder climates.

CHP functional requirements and an initial characterization of realistic operational parameters were modeled using LBNL's DER-CAM [6]. Operational parameters such as duty cycles will be an input to the total cost of ownership model and will vary as a function of building type and climate zone. DER-CAM is a cost optimization tool for the deployment of distributed energy supply sources such as combustion engines, solar photovoltaic, and fuel cell systems in addition to utility-provided power. Currently DER-CAM utilizes the California Commercial End-Use Survey database of commercial building electrical and thermal demand profiles in California but will be expanded to include building profiles from other regions. DOE cost targets for 2020 were utilized to model fuel cell system penetration and operating capacity parameters for power and heat. Figure 2 shows the DER-CAM output for a large office building in San Diego showing

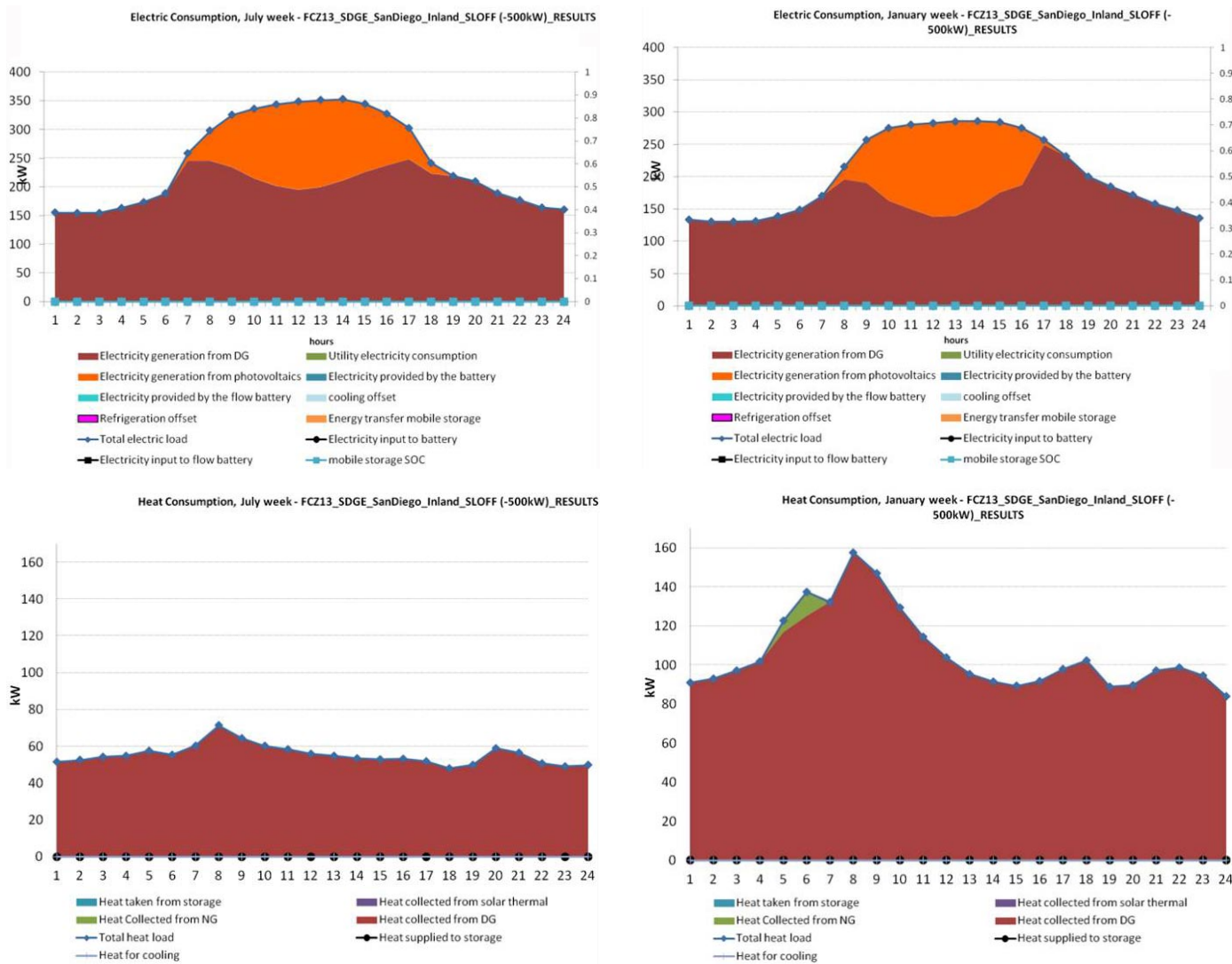


FIGURE 2. Large office building load profiles in San Diego and build-out of distributed energy resources including 250 kW HT PEM fuel cell system for electricity (top) and heating (bottom)

that a HT PEM fuel cell system provides a fairly steady supply of power and virtually all the thermal load for this building.

Based on literature review of company specifications sheets, engineering judgment, and consultation with Ballard Power Systems, initial functional specifications have been defined for combined heat and power applications for LT PEM systems. This includes the cell stack and system sizing, and estimates for parasitic and system efficiencies. This will be the basis for system design and costing activities.

Conclusions and Future Directions

- This project provides more comprehensive cost analysis for fuel cell systems in emerging markets including ancillary financial benefits.

- The approach employs DFMA[®] analysis cost modeling including mass flow and energy balance for integrated lifecycle cost analysis impacts.
- Future work will focus on system designs, balance-of-plant definition and material/component bill of materials and costing.

References

1. James, Brian, J. Kalinoski, J., and K. Baum. Mass-Production Cost Estimation for Automotive Fuel Cell Systems. 2010 Annual Merit Review Proceedings, Department of Energy, Hydrogen and Fuel Cells Program. Washington, D.C. June 2010.
2. Sinha, Jayanti and Y. Yang. *Direct Hydrogen PEMFC Manufacturing Cost Estimation* for Automotive Applications. 2010 Annual Merit Review Proceedings, Department of Energy, Hydrogen and Fuel Cells Program. Washington, D.C. June 2010.

3. Mahadevan, Kathya, V. Contini, M. Goshe, J. Price, F. Eubanks, and F. Griesemer. Economic Analysis of Stationary PEM Fuel Cell Systems. 2010 Annual Merit Review Proceedings, Department of Energy, Hydrogen and Fuel Cells Program. Washington, D.C. June 2010.

4. Mahadevan, Kathya, K. Judd, H. Stone, J. Zewatsky, A. Thomas, H. Mahy, and D. Paul. *Identification and Characterization of Near-Term Direct Hydrogen Proton Exchange Membrane Fuel Cell Markets*. U.S. Department of Energy, Golden Field Office, Golden, Colorado. April 2007. DOE Contract No. DE-FC36-03GO13110.

5. Greene, D.L, K.G. Duleep, G. Upreti. *Status and Outlook for the U.S. Non-Automotive Fuel Cell Industry: Impacts of Government Policies and Assessment of Future Opportunities*. Oak Ridge National Laboratory, Oak Ridge, Tennessee, May 2011. DOE Contract No. DE-AC05-00OR22725.

6. Stadler, Michael, Chris Marnay, Gonçalo Cardoso, Timothy Lipman, Olivier Mégel, Srirupa Ganguly, Afzal Siddiqui, and Judy Lai. *The Carbon Dioxide Abatement Potential of California's Mid-Sized Commercial Buildings*. California Energy Commission, PIER Program. 2011. CEC-500-2010-050.

V.B.1 Effect of System Contaminants on PEMFC Performance and Durability

Huyen N. Dinh (Primary Contact), Clay Macomber, Heli Wang, Guido Bender, Kevin O'Neill, Bryan Pivovar

National Renewable Energy Laboratory (NREL)
15013 Denver West Parkway
Golden, CO 80401-3305
Phone: (303) 275-3605
Email: Huyen.Dinh@nrel.gov

DOE Manager

HQ: Kathi Epping Martin
Phone: (202) 586-7425
Email: Kathi.Epping@ee.doe.gov

Subcontractors:

- Kelly O'Leary, Balsu Lakshmanan, Rob Reid, General Motors LLC (GM), Honeoye Falls, NY
- John Van Zee and Masato Ohashi, University of South Carolina (USC), Columbia, SC
- Tommy Rockward, Los Alamos National Laboratory (LANL), Los Alamos, NM
- Jean St-Pierre, University of Hawaii, Honolulu, HI
- Ryan Richards and Jason Christ, Colorado School of Mines (CSM), Golden CO
- Steve Hamrock (in kind partner), 3M, St. Paul, MN

Project Start Date: July 20, 2009

Project End Date: 2013

Technologies Program's Multi-Year Research, Development and Demonstration Plan:

- (A) Durability
- (B) Cost

Technical Targets

This project focuses on quantifying the impact of system contaminants on fuel cell performance and durability. Insights gained from these studies will increase performance and durability by limiting contamination-related losses and decrease overall fuel cell system costs by lowering balance-of-plant (BOP) material costs. Proper selection of BOP materials will help meet the following DOE 2020 targets:

- Cost: \$30/kW for transportation; \$1,000–1,700/kW for stationary
- Lifetime: 5,000 hours for transportation; 60,000 hours for stationary

FY 2012 Accomplishments

- Screened 55 relevant BOP materials for fuel cell contamination.
- Completed preliminary assessment of studied BOP materials on fuel cell performance.
- Identified leached species for all structural materials and assembly aids.
- Determined that leached species come from the hydrolysis and degradation of the polymer resins and additives.
- Selected model organic compounds and leachant extracts for in-depth parametric studies.
- Performed initial ex situ and in situ studies on selected model compounds.



Fiscal Year (FY) 2012 Objectives

Our overall objective is to decrease the cost associated with system components without compromising function, fuel cell performance, or durability. Our specific project objectives are:

- Identify and quantify system derived contaminants.
- Develop ex situ and in situ test methods to study system components.
- Identify severity of system contaminants and impact of operating conditions.
- Identify contamination mechanisms.
- Develop models/predictive capability.
- Guide system developers on future material selection.
- Disseminate knowledge gained to the community.

Technical Barriers

This project addresses the following technical barriers from the Fuel Cells section (3.4.4) of the Fuel Cell

Introduction

Cost and durability issues of polymer electrolyte membrane fuel cell (PEMFC) systems have been challenging in the fuel cell industry. The cost of the BOP system (\$49/kW in 2012 [1]) has risen in importance as fuel cell stack cost has decreased (\$22/kW in 2012 [1] compared to \$65/kW in 2006 [2]). Lowering the cost of PEMFC system components requires understanding of the materials used in the system components and the contaminants that are derived from them, which have been shown to affect the performance and durability of fuel cell systems. Unfortunately, there are many possible contamination sources from system

components [3-5]. Currently-deployed, high-cost, limited-production systems are using expensive materials for system components. In order to make fuel cell systems commercially competitive, the cost of the BOP components needs to be lowered without sacrificing performance and durability. Fuel cell durability requirements limit the performance loss attributable to contaminants to at most a few mV over required lifetimes (thousands of hours), which means system contaminants must have close to zero impact.

As catalyst loadings decrease and membranes are made thinner (both are current trends in automotive fuel cell R&D), operation of fuel cells becomes even more susceptible to contaminants. In consumer automotive markets, low-cost materials are typically required, but lower cost typically implies higher contamination potential. The results of this project will provide the information necessary to help the fuel cell industry make informed decisions regarding the cost of specific materials versus the potential contaminant impact on fuel cell performance and durability.

Approach

Our goal is to provide an increased understanding of fuel cell system contaminants and help provide guidance in the implementation and, where necessary, development of system materials that will help enable fuel cell commercialization. While much attention has been paid to air and fuel contaminants, system contaminants have received limited public attention and very little research has been publicly reported [6-9]. Our approach is to perform parametric studies to characterize the effects of system contaminants on fuel cell performance and durability, as well as to identify the severity of contamination, identify contamination mechanisms, develop predictive modeling, and disseminate information about material contamination potential that would benefit the fuel cell industry in making cost-benefit analyses of system components. We are identifying and quantifying potential contaminants derived from stack or component fabrication materials and quickly screening the impact of the leachants on the fuel cell catalyst and membrane via *ex situ* tests. Model compounds capable of replicating the deleterious impact of system-based contaminants are also being studied. The majority of our effort is focused on the liquid-based contaminants derived from structural plastics and assembly aid materials (lubricant, grease, adhesive, seal). A minor part of our efforts is focused on an *in situ* durability study of gas-based contaminants (siloxane focus) and an *ex situ* electrochemical study of the effect of membrane degradation by-products on catalysis.

Our prioritization and selection of system materials is based on properties such as exposed surface area, total mass or volume in a system, fluid contact, function, cost, and performance implications. Material selection is also based on the materials' physical properties (i.e., stable in

fuel cell operating conditions: 0% – 100% relative humidity, -40° – 90°C), cost, commercial availability, and input from original equipment manufacturers and fuel cell system manufacturers. These commercially available commodity materials are generally developed for other applications for which common additives/processing aids may not be a concern, but they may present problems for fuel cells.

Results

We completed screening of 55 BOP materials (Table 1)—from 10 different manufacturers, comprising different chemistries, and used for different functions—using multiple screening methods, totaling more than 660 experiments. The screening techniques included leaching tests to extract water-based contaminants, solution conductivity, pH, total organic carbon (TOC), cyclic voltammetry, membrane conductivity, *in situ* 50 cm² fuel cell test, and advanced analytical characterization (gas and liquid chromatography mass spectrometry [GCMS, LCMS], inductively coupled plasma – optical emission spectroscopy [ICP-OES], ion chromatography, and Fourier transform infrared spectroscopy).

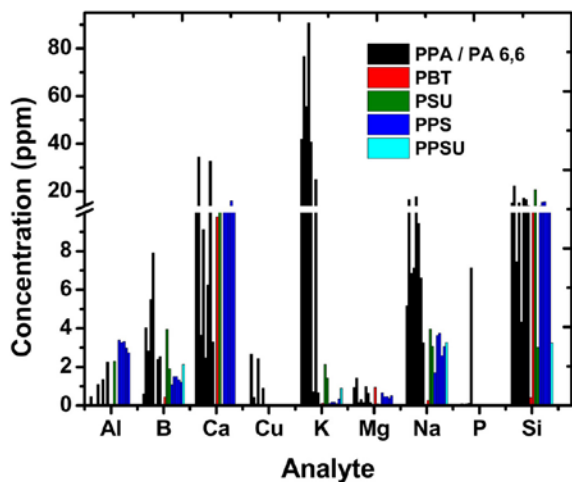
A wide range of TOC and solution conductivity values were measured for the 55 BOP materials screened. The low-cost Nylon™ family (polyamide and polyphthalamide) showed the greatest variety with grades, as expected by design. Higher-cost, non-commodity materials (perfluoroalkylether/polytetrafluoroethylene [PFAE/PTFE], polyphenylene sulfide, polybutylene terephthalate, polysulfone, polyphenylsulfone) were cleaner, leaching out less ionic and organic contaminants. Elemental analyses were performed by ICP-OES to identify and quantify the species present in the leachant solutions. The elements with the highest concentrations, via ICP screening of the six-week leached structural material extracts and the one-week leached urethane material extracts, are identified in Figure 1. Based on knowledge of the plastic type, common additives in these types of plastics, and information from material datasheets, the identified elements were linked to fillers and additives. For example, Al, B, Si, and Ca are commonly found in glass fiber reinforcement additives (alumino-borosilicates and soda lime) for structural automotive thermoplastics. Common additives in urethane adhesive/seal materials include fillers and flame retardants (alumina trihydrate, talc, dolomite), hence Al, Ca, Mg, and Si were found in the urethane extracts. If it is found that these species adversely affect the fuel cell performance and that the additive is not needed for a material's function in fuel cell applications, then perhaps the manufacturers can remove the additive. If an additive is required for function, then perhaps a different, non-contaminating additive can be used. This type of information is valuable for properly selecting BOP materials and can help DOE meet its durability and cost targets.

TABLE 1. Summary table of the 55 BOP materials studied (structural materials, adhesives, sealants, greases), grouped by chemical description

| Function Description | Chemical Description | Manufacturer | Trade Name | Total Grades |
|----------------------|--|----------------------------|---|--------------|
| Structural Plastic | Polyamide (PA), polyphthalamide (PPA) (Nylon™) | DuPont, EMS, BASF, Solvay, | Zytel®, Grivory®, Grilon®, Grilamid® Ultramid®, Amodel® | 26 |
| Structural Plastic | Polyphenylene sulfide (PPS) | Chevron Phillips | Ryton® | 4 |
| Structural Plastic | Polysulfone (PSU) | Solvay | UDEL® | 2 |
| Structural Plastic | Polyphenylsulfone (PPSU) | Solvay | RADEL® | 1 |
| Structural Plastic | Polybutylene terephthalate (PBT) | DuPont | Crastin® | 2 |
| Lubricant/Grease | Perfluoroalkylether/ polytetrafluoroethylene (PFAE/PTFE) | DuPont | Krytox® | 4 |
| Adhesive/Seal | Urethane | 3M, Bostik, Henkel | Marine®, Loctite® | 6 |
| Adhesive/Seal | Silicone | 3M | Super silicone | 2 |
| Adhesive | Epoxy | 3M, Reltek® | Scotch Weld®, Bond-IT® | 3 |
| Adhesive | Acrylic acrylate | LORD® | LORD® | 1 |
| Thread Lock/Seal | Polyglycol dimethacrylate (PGDMA) | Henkel | Loctite® | 4 |
| Total | | | | 55 |

↓
Assembly Aids

ICP Results for Structural Materials



ICP Results Urethanes

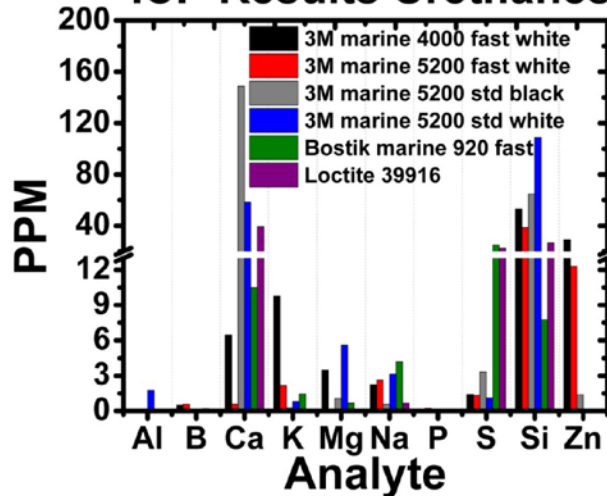


FIGURE 1. Elements with the highest concentrations identified by ICP-OES for all structural materials (left) and urethane materials (right)

Liquid GCMS analysis identified a large number of organic species in the material extracts. Using the same approach as described above, we determined that the organic compounds come from the hydrolysis and degradation of the polymer resins, additives (water scavenger, cross-linking agent, solvent), and by-products of incomplete polymerization. A few organic model compounds from structural materials and assembly aids were selected for further fundamental/mechanistic studies. Their chemical structures are shown in Figure 2. The identified organic compounds consist of aromatics and aliphatics with a variety of functional groups. These compounds have not

been studied before in in situ, parametric, or recoverability experiments and are part of our future work. Identifying and quantifying specific model compounds and/or functional groups that adversely affect fuel cell performance can provide valuable understanding of the impact of organic compounds and can help determine the “bad actor” in the leachant extract mixture.

In situ infusion screening of the BOP materials showed that system contaminants can have an adverse effect on fuel cell performance, but the effect is complex. Figure 3 shows the in situ infusion results for three groups of assembly

Structural Materials and Assembly Aids:

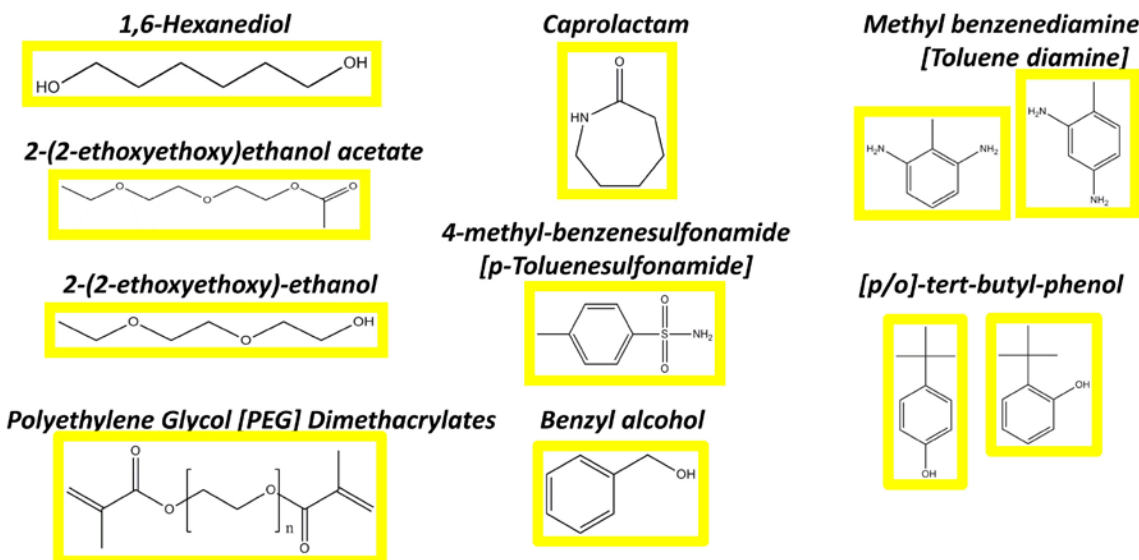


FIGURE 2. Chemical structure of organic model compounds selected for further in-depth studies. The organic species were identified by liquid GCMS and came from structural materials and assembly aids.

aids material. These examples were selected to show the different types of effects system contaminants have on fuel cell performance. The more expensive PFAE/PTFE materials (different grades of Krytox[®]) showed essentially no effect on the fuel cell performance (voltage response at 0.2 A/cm² is similar to the deionized (DI) water baseline) and were classified as “clean”. The two urethane Marine[®] adhesive/seal materials showed a voltage drop of 100–150 mV and the effect was partially reversed when DI water was infused instead of the leachant solutions. These materials were classified as “contaminating but partially recovers”. The two epoxy materials (different grades of Bond-It[®]) showed a very large voltage drop (ca. 550 mV) and the effect was not reversible with DI water infusion. These materials were classified as “contaminating and does not recover”. The high frequency resistances were essentially constant for all materials over the 15–20 h of contaminant infusion, indicating that membrane conductivity was not affected during this short duration of infusion. Concentration, species, and operating condition effects will be studied further to understand the mechanism of contamination.

Conclusions and Future Directions

- We determined that structural materials and assembly aids can leach contaminants that adversely impact fuel cell performance.
- We identified and quantified the elements, anions, and organic species in the leached solutions for all of the structural materials and assembly aids.
- We selected organic species and extracts for further studies.

- We determined that leached species come from the hydrolysis and degradation of the polymer resins, additives, and by-products of incomplete polymerization.
- We will establish statistical relationships and capabilities for correlating ex situ characteristics to in situ performance loss.
- We will perform parametric in situ studies on selected leachate solutions.
- We will perform fundamental/mechanistic studies on selected model compounds.
- We will model the effects of operating conditions on fuel cell performance for specific contaminating species and model compounds.
- We will perform durability testing of selected contaminants.

FY 2012 Publications/Presentations

1. H.-S. Cho, M. Ohashi, and J. W. Van Zee, “The Effect on PEMFC Contamination of Functional Groups of Some Organic Contaminants,” *ECS Trans.*, Vol. 41(1), Polymer Electrolyte Fuel Cells 11- Diagnostics and Phenomena: Porous Transport Layers, The Electrochemical Society, pp. 1487-1499 (2011).
2. J. St-Pierre, “PEMFC contaminant tolerance limit - Foreign cations in ionomers,” *Int. J. Hydrogen Energy*, Vol. 36, pp. 5527-5535 (2011).
3. J. St-Pierre, “PEMFC contamination model: Foreign cation exchange with ionomer protons,” *J. Power Sources*, Vol. 196, pp. 6274-6283 (2011).

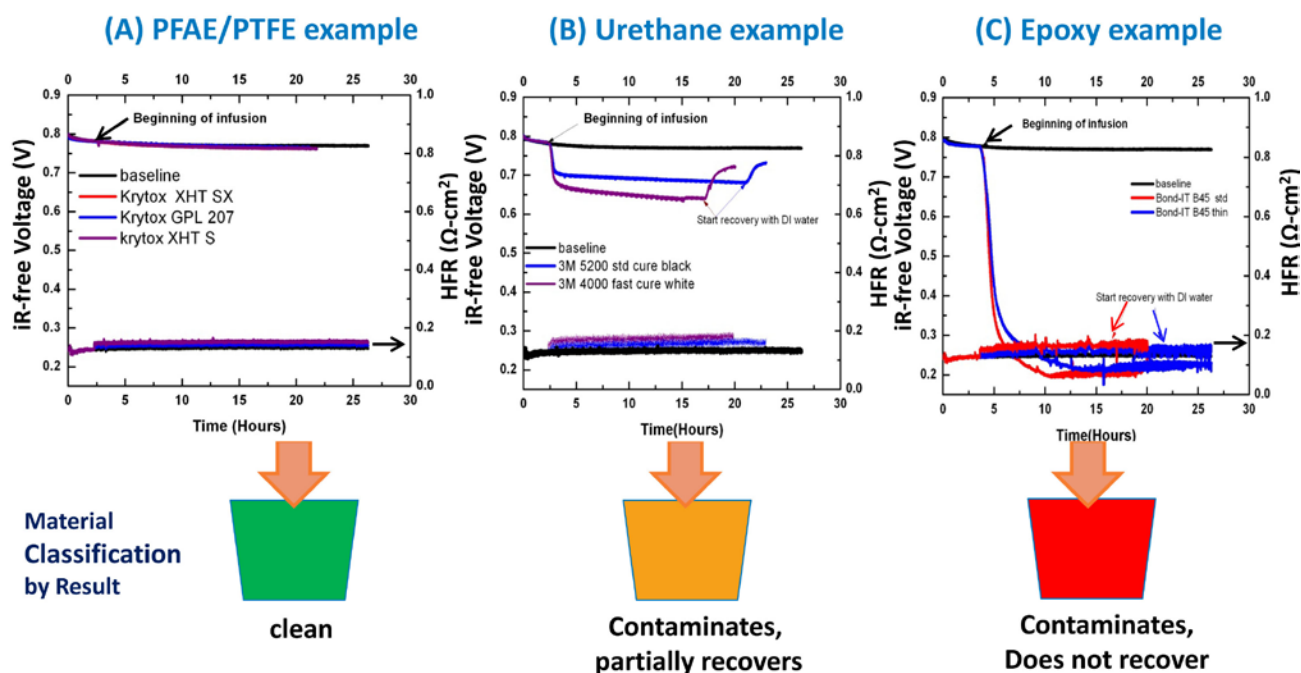


FIGURE 3. Voltage and high frequency resistance responses at 0.2 A/cm^2 during the infusion of DI water (black, baseline) and leachant solutions from different assembly aids materials. (A) three PFAE/PTFE materials (6 week soak): Krytox[®] XHT SX (red), Krytox[®] GPL 207 (blue), Krytox[®] XHT S (purple); (B) two urethane materials (1 week soak): 3M 5200 standard cure black (blue), 3M 4000 fast cure white (purple); (C) two epoxy materials (1 week soak): Bond-IT[®] B45 (blue), Bond-IT[®] B45TH (red). (cell temperature = 80°C , relative humidity = 32%/32%, H_2 and air stoich = 2/2, back pressure = 150 kPa)

4. K.A. O'Leary, R. Reid, and B. Lakshmanan, "A Systematic Comparison of Screening Techniques to Evaluate Fuel Cell System Contamination," 220th Meeting of the Electrochemical Society, Boston, MA, October 9–14, 2011.
5. M.S. Opu, M. Ohashi, K.A. O'Leary, B. Lakshmanan, R. Reid, C.S. Macomber, H. Wang, H. Dinh, and J. Van Zee, "In Situ Experiments for Understanding the Effects of Contaminants from Balance of Plant Materials on PEMFCs," 220th Meeting of the Electrochemical Society, Boston, MA, October 9–14, 2011.
6. M. Das, M. Ohashi, C.S. Macomber, H. Wang, H. Dinh, K.A. O'Leary, R. Reid, B. Lakshmanan, and J. Van Zee, "Ex Situ Experiments for Understanding the Effect of Contaminants from Balance of Plant Materials on PEMFCs," 220th Meeting of the Electrochemical Society, Boston, MA, October 9–14, 2011.
7. C.S. Macomber, H. Wang, K. O'Neill, J. Christ, M. Das, J.W. Van Zee, K.A. O'Leary, and H.N. Dinh, "Leachant Contaminants and Degradation Schemes of PEM Fuel Cell System Components," 220th Meeting of the Electrochemical Society, Boston, MA, October 9–14, 2011.
8. J. Christ, H. Wang, G. Bender, R. Richards, and H.N. Dinh, "Impact of Proton Exchange Membrane Degradation Products on the Activity of the Oxygen Reduction Reaction in PEM Fuel Cells," 220th Meeting of the Electrochemical Society, Boston, MA, October 9–14, 2011.
9. H. Cho, M. Ohashi, C.S. Macomber, H. Wang, H. Dinh, and J.W. Van Zee, "The Effect on PEMFC Contamination of Functional Groups of Some Organic Contaminants," 220th Meeting of the Electrochemical Society, Boston, MA, October 9–14, 2011.
10. C.S. Macomber, H. Wang, K. O'Neill, J. Christ, G. Bender, B. Pivovar, H.N. Dinh, "Identifying leachant contaminants and degradation schemes of PEM fuel cell system components, leading to effects on performance," 2011 Fall ACS Meeting, Denver, CO, August 28–September 1, 2011.
11. H. Wang, C.S. Macomber, K. O'Neill, G. Bender, B. Pivovar, R. Reid, B. Lakshmanan, K. O'Leary, M. Das, M. Ohashi, J.W. Van Zee, H.N. Dinh, "Effect of PEMFC system contaminants on the performance of catalyst," 2011 Fall ACS Meeting, Denver, CO, August 28–September 1, 2011.
12. H.N. Dinh and K. O'Leary, "Effect of System Contaminants on PEMFC Performance and Durability," Fuel Cell Tech Team Meeting, Southfield, MI, December 14, 2011.
13. H.N. Dinh, C.S. Macomber, H. Wang, J. Christ, "Effect of System and Air Contaminants on PEMFC Performance and Durability," DOE Mid-Year Review, Denver, CO, February 7, 2012.
14. J. Christ, K.C. Neyerlin, H. Wang, R. Richards, H.N. Dinh, "Impact of Proton Exchange Membrane Degradation Products on Platinum Catalyst Performance," Western States Catalysis Club Conference, Boulder, CO, March 9, 2012.
15. H. Wang, J. Christ, C.S. Macomber, K. O'Neill, K.C. Neyerlin, K.A. O'Leary, R. Reid, B. Lakshmanan, M. Das, M. Ohashi, J.W. Van Zee, and H.N. Dinh, "Effect of fuel cell system contaminants on the Pt catalyst," 243rd ACS Meeting in San Diego, CA, March 25–29, 2012.
16. H.N. Dinh, "Effect of System Contaminants on PEMFC Performance and Durability," DOE Fuel Cell Technologies Program Annual Merit Review, Washington, D.C., May 14–18, 2012.

References

1. B. James, "Fuel Cell Transportation Cost Analysis, Preliminary Results," 2012 U.S. DOE Annual Merit Review and Peer Evaluation Meeting, FC018, Washington, D.C., May 17, 2012.
2. R. Farmer, Presentation on Fuel Cell Technologies: FY 2011 Budget Request Briefing, February 12, 2010.
3. D. Gerard, "Powertrain Plastic Materials," SAE Mid Michigan Conference, February 11, 2008.
4. D. Gerard, "Materials and Materials Challenges for Advanced Automotive Technologies being Developed to Reduce Global Petroleum Consumption" (Invited). 2007 Materials Science and Technology, Detroit, MI, September 16–20, 2007.
5. D.A. Masten, A.B. Bosco, *Handbook of Fuel Cells* (eds.: W. Vielstich, A. Lamm, H.A. Gasteiger), Wiley (2003): Vol. 4, Chapter 53, p. 714.
6. Q. Guo, R. Pollard, J. Ruby, T. Bendon, P. Graney, and J. Elter, *ECS Trans.*, Vol. 5(1), p. 187 (2007).
7. G.A. James, et. al., "Prevention of membrane contamination in electrochemical fuel cells," U.S. Patent Application US2005089746A.
8. R. Moses, "Materials Effects on Fuel Cell Performance," National Research Council Canada Institute for Fuel Cell Innovation, International Fuel Cell Testing Workshop, September 20–21, 2006.
9. K. O'Leary, B. Lakshmanan, and M. Budinski, "Methodologies for Evaluating Automotive PEM Fuel Cell System Contaminants," 2009 Canada-USA PEM Network Research Workshop, February 16, 2009.

V.B.2 The Effect of Airborne Contaminants on Fuel Cell Performance and Durability

Jean St-Pierre (Primary Contact), Yunfeng Zhai, Michael Angelo, Trent Molter, Leonard Bonville, Ugur Pasaogullari, Mark Aindow, William Collins, Silvia Wessel

Hawaii Natural Energy Institute
1680 East-West Road
Honolulu, HI 96822
Phone: (808) 956-3909
Email: jsp7@hawaii.edu

DOE Managers

HQ: Nancy Garland
Phone: (202) 586-5673
Email: Nancy.Garland@ee.doe.gov

GO: Reginald Tyler
Phone: (720) 356-1805
Email: Reginald.Tyler@go.doe.gov

Technical Advisor

Walt Podolski
Phone: (630) 252-7558
Email: podolski@anl.gov

Contract Number: DE-EE0000467

Subcontractors:

- University of Connecticut, Storrs, CT
- UTC Power, South Windsor, CT
- Ballard Power Systems, Burnaby, BC, Canada

Project Start Date: April 1, 2010
Project End Date: March 31, 2014

Fiscal Year (FY) 2012 Objectives

- Quantify performance loss for at least four different contaminants under various operating conditions.
- Initiate and partly complete activities to identify principal poisoning mechanisms for the same four contaminants.

Technical Barriers

This project addresses the following technical barriers from the Fuel Cells section of the Fuel Cell Technologies Program Multi-Year Research, Development and Demonstration Plan:

- (A) Durability
- (C) Performance

Technical Targets

The following 2017 transportation technical targets are considered:

- Durability: 5,000 h in automotive drive cycle
- Performance: 60% energy efficiency at 25% of rated power

Airborne contaminants are studied and the information will be used to impact both preventive measures and recovery procedures:

- Filtering system component specification input derived from contaminant tolerance limits leading to negligible performance losses.
- Fuel cell stack material, design, operation or maintenance changes to recover performance losses derived using contamination mechanisms.

FY 2012 Accomplishments

- The 19 airborne contaminants derived from the overall validated list of more than 260 species using first tier qualitative down selection criteria (first tier airborne contaminants) were tested with both wet and dry reactant streams and ranked using two quantitative, empirical selection criteria.
- Seven second tier airborne contaminants are organic and representative of different functionalities: acetonitrile (nitrile), acetylene (alkyne), bromomethane (halocarbon), iso-propanol (alcohol), methyl methacrylate (ester), naphthalene (aromatic), propene (alkene).
- The effect of the operating conditions impacting contamination more severely, contaminant concentration, current density and temperature, was investigated using second tier contaminants:
 - Tests for six of the seven second tier contaminants were completed.
- Impedance spectroscopy data indicate that all seven second tier airborne contaminants lead to kinetic and mass transport losses whereas only acetonitrile leads to additional ohmic losses.
- Tests with first tier ionic contaminants (K^+ , Ca^{+2} , Ba^{+2} , Al^{+3} , Cl^- , OH^- , ClO_4^-) indicated that water management related operating conditions and membrane electrode assembly design significantly impact contamination, and suggested new avenues for mitigation strategy development.



Introduction

The composition of atmospheric air cannot be controlled and typically includes contaminants, volatile compounds as well as ions entrained by liquid water drops in the form of rain, mist, etc. Proton exchange membrane fuel cells operated with ambient air are therefore susceptible to deleterious effects which include decreased cell performance and durability [1]. Numerous air contaminants have not yet been tested in fuel cells and consequently their effects are unknown. This increases the risk of failure for fuel cell systems and thus jeopardizes their introduction into the market.

A significant amount of resources is required to characterize the effect of each species on fuel cell performance. Therefore, a method for species down-selection is essential to keep the research scope within feasible limits. In this project, airborne contaminants were down-selected to manageable yet representative groups (first tier and second tier). Screening tests were completed on the first tier contaminants to determine their effects on performance and the ability of the fuel cell to self recover after contaminant exposure. These factors were accounted for with two quantitative cell performance ranking criteria which were used for a second tier down-selection. Fuel cells are used under a wide range of operating conditions. It is therefore important to determine the contamination effect under many operating conditions including temperature and relative humidity (startup and shutdown periods), current density (power demand during drive cycle) and local atmosphere composition variations. The contaminant concentration effect is particularly important because it provides guidance on contaminant threshold concentrations and invaluable information to define air filtering system tolerances (prevention). Also, during the screening and operating condition tests (first and second tier contaminants), impedance spectroscopy diagnostic tests were also completed for mechanism determination clues. This information will also be invaluable to design more effective recovery procedures (maintenance).

Approach

Two methods were considered for contaminant ranking and rely on four time/voltage pairs (denoted by subscripts a to d in equations 1 and 2) that define steady-state changes in cell performance during contamination and recovery periods and associated time scales. These four parameters are general and were observed with all tested contaminants. Method 1 relies on the combination of steady-state contamination and irrecoverable performance losses, corresponding time scales and contaminant concentration. Method 2 relies on the

combination of the energy lost to contamination and regained during self-recovery:

$$SC_1 = \frac{(V_a - V_b)^2 (V_a - V_d)(t_d - t_c)}{c_{\text{contaminant}} (V_d - V_c)(t_b - t_a)} \quad (1)$$

$$SC_2 = \int_a^b (V_a - V) dt / \int_c^d (V - V_c) dt \quad (2)$$

where SC represents a selection criteria ($V^2 \text{ ppm}^{-1}$ or dimensionless), V_i the cell voltage at point i (V), t_i the time at point i (h), $c_{\text{contaminant}}$ the contaminant concentration in the dry reactant stream (ppm), and V the cell voltage (V). Larger SC_1 and SC_2 values generally mean more significant performance losses.

A partial factorial design was used to limit the number of tests. Even with this restriction the number of tests is equal to 49 (seven contaminants, three operating conditions and three levels with a central point) and each generally requires at least a week for completion. The contaminant concentration is the first operating condition to be investigated. Subsequent tests at other current densities and temperatures are generally completed using the contaminant concentration that led to a loss in cell performance equal to or near 20%. For acetylene, experiments are currently being repeated with higher concentrations to ensure a 20% performance loss. For bromomethane, a performance loss higher than 20% was tolerated because tests would otherwise take too long to complete. For iso-propanol, higher gas phase concentrations were not possible and would lead to condensation.

Mechanistic information was collected during screening and operating condition tests (first and second tier contaminants). This information was obtained using impedance spectroscopy allowing separation in the frequency domain of the different processes. An equivalent circuit model was used to fit experimental data and extract key parameters including the different processes' resistances.

Results

Table 1 shows the resulting contaminant rankings for the 19 first tier airborne contaminants. The largest five selection criteria values in each column are highlighted in red. Generally, the selection criteria values are not too sensitive to relative humidity. Two contaminants, highlighted in green, led to a cell performance after the recovery period exceeding the initial value. The SC_2 selection criterion is able to pinpoint such contaminants (propene). For this reason and also because SC_2 is less sensitive to the change in operating conditions, it was used to create the second tier list. As a result, all contaminants with highlighted SC_2 values were selected with the exception of acetone. Rather, acetonitrile was added to the list because it was the only contaminant that led to ohmic losses.

TABLE 1. Gaseous Airborne Contaminant Rankings (Red highlight indicates the highest values in any given column. Green highlight indicates contaminants that led to a cell performance after recovery exceeding the initial value.)

| Contaminant ^a | SC ₁ (V ² ppm ⁻¹) | | SC ₂ | |
|---|---|--------------------------|---------------------|------------------|
| | 100/50 ^b | 0/0 ^b | 100/50 ^b | 0/0 ^b |
| 1,1-difluoroethane ^c | 7.23 x 10 ⁻⁴ | 3.74 x 10 ⁻⁴ | 0.0259 | 0.0682 |
| 1,1,1,2-tetrafluoroethane ^d | 2.16 x 10 ⁻⁴ | 1.88 x 10 ⁻⁴ | 0.0414 | 0.00532 |
| 2,2-bis(4-hydroxyphenyl) propane ^e | No effect | No effect | No effect | No effect |
| Acetaldehyde | -2.35 x 10 ⁻⁴ | -1.03 x 10 ⁻⁴ | 0.214 | 0.409 |
| Acetone | -2.86 x 10 ⁻⁷ | 1.24 x 10 ⁻⁶ | 6.75 | 6.59 |
| Acetonitrile | 5.78 x 10 ⁻³ | 9.51 x 10 ⁻³ | 0.0575 | 0.0410 |
| Acetylene | 3.13 x 10 ⁻⁶ | 3.86 x 10 ⁻⁶ | 30.6 | 16.5 |
| Bromomethane | 4.04 x 10 ⁻³ | 7.37 x 10 ⁻³ | 7.57 | 8.03 |
| Chlorobenzene | 1.57 x 10 ⁻² | 4.09 x 10 ⁻² | 0.165 | 0.0978 |
| Dichloromethane | No effect | No effect | No effect | No effect |
| Iso-propanol | -2.55 x 10 ⁻⁷ | 1.54 x 10 ⁻⁴ | 17.8 | 0.100 |
| Methyl methacrylate | 1.44 x 10 ⁻⁵ | 1.32 x 10 ⁻⁴ | 4.86 | 3.94 |
| Methyl tert-butyl ether | 6.69 x 10 ⁻⁶ | 4.62 x 10 ⁻⁴ | 2.05 | 0.260 |
| Naphthalene | ∞ | ∞ | ∞ | ∞ |
| Ozone | 5.38 x 10 ⁻⁴ | 4.68 x 10 ⁻⁴ | 0.149 | 0.188 |
| Propene | -3.08 x 10 ⁻⁵ | -6.55 x 10 ⁻⁵ | 32.1 | 1.05 |
| Toluene | 5.38 x 10 ⁻⁴ | 1.34 x 10 ⁻³ | 0.349 | 0.247 |
| Trichlorofluoromethane ^f | No effect | 8.76 x 10 ⁻⁴ | No effect | 0.277 |
| Vinyl acetate | -4.42 x 10 ⁻⁵ | -1.16 x 10 ⁻⁴ | 1.19 | 0.879 |

^a 20 ppm contaminant concentration with the exception of bromomethane (50 ppm for wet conditions), bisphenol A (0.1 ppm) and ozone (95/83 ppm for wet/dry conditions).

^b anode/cathode relative humidity (%).

^c also referred to as HFC-152a.

^d also referred to as HFC-134a.

^e also referred to as bisphenol A.

^f also referred to as CFC-11.

Figure 1 illustrates the effect of acetonitrile concentration on cell performance for a temporary contaminant injection, which shows that the steady-state cell performance loss increases with acetonitrile concentration. Such a data set for all second tier airborne contaminants will be used to set tolerance limits which in turn will determine filtering system performance and design. Table 2 summarizes completed and planned operating condition tests for second tier airborne contaminants. Only a few bromomethane tests (highlighted in red) remain to be completed.

Figure 2 depicts the effect of 100 ppm of acetonitrile on cell performance. In addition, Figure 2 also shows several resistance values derived from the equivalent circuit model. Three resistances show increases in values during the temporary contaminant injection period. These increases are ascribed to kinetic, ohmic and mass transport losses. More specifically, acetonitrile impacts the cathode catalyst

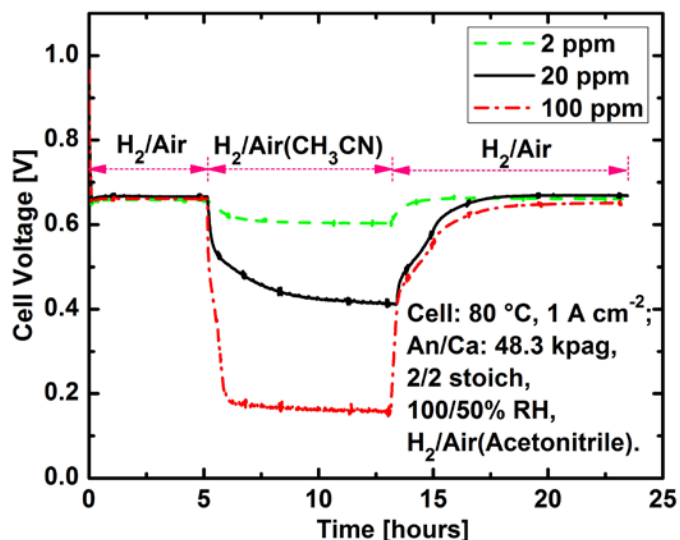


FIGURE 1. Fuel cell response resulting from a temporary acetonitrile injection in the air stream. Gore M715 membrane electrode assembly, 25 BC SGL Technologies gas diffusion layer, 50 cm² active area, 80°C, 1 A cm⁻², anode/cathode, H₂/air, 48.3/48.3 kPag, 100/50% relative humidity, 2/2 stoichiometry.

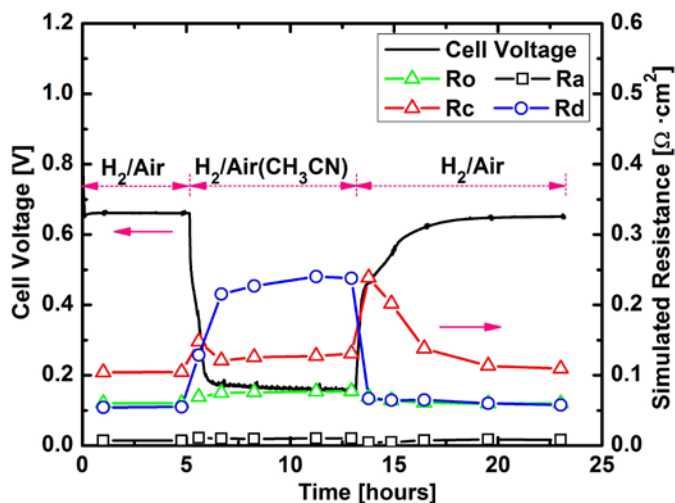


FIGURE 2. Fuel cell response resulting from a temporary acetonitrile injection in the air stream and associated changes in ohmic (R_o), anode (R_a), cathode (R_c) and diffusion (R_x) resistances. Gore M715 membrane electrode assembly, 25 BC SGL Technologies gas diffusion layer, 50 cm² active area, 80°C, 1 A cm⁻², anode/cathode, H₂/air+100 ppm acetonitrile, 48.3/48.3 kPag, 100/50% relative humidity, 2/2 stoichiometry.

(surface coverage, change in oxygen reduction mechanism, etc), the membrane (absorption increases swelling, decreases the distance between ion exchange groups and reduces conductivity) and water transport (acetonitrile adsorption on the catalyst carbon support and gas diffusion layer carbon surface affects hydrophobicity). The presence of different cell performance losses likely requires multi-step recovery procedures, either sequential or in parallel.

TABLE 2. Summary of the contaminant concentrations and steady-state cell performance loss for the different contaminants and operating condition tests. Red highlight indicates tests that have not yet been completed.

| Contaminant | Operating conditions ^a | | | | | | |
|---------------------|-----------------------------------|----------------------------|----------------------------|------------------------------|------------------------------|---------------------------------------|---------------------------------|
| | 80°C, 1 A cm ⁻² | 80°C, 1 A cm ⁻² | 80°C, 1 A cm ⁻² | 80°C, 0.6 A cm ⁻² | 80°C, 0.2 A cm ⁻² | 45°C, 1 A cm ⁻² | 10°C, 1 A cm ⁻² |
| Acetonitrile | 100 ppm (75%) | 20 ppm (38%) | 2 ppm (9%) | 20 ppm (35%) | 20 ppm (33%) | 20 ppm (68%) | 20 ppm (78%) |
| Acetylene | 20 ppm (0%) | 50 ppm (1%) | 100/500 ppm (1/92%) | 100 ppm (1%) | 100 ppm (1%) | 5/20/100 ppm (1/77/85%) | 100 ppm (90%) |
| Bromomethane | 20 ppm | 5 ppm (43%) | 2 ppm (38%) | 5 ppm | 5 ppm | 5 /20/50 ppm (?/48%) | 5 ppm |
| Iso-propanol | 250/700 ppm (2/2%) | 5.2k ppm (7%) | 8.6k ppm (9%) | 8.6k ppm (8%) | 8.6k ppm (6%) | 8.6k ppm (23%) | 8.6k ppm (>80%) ^c |
| Methyl methacrylate | 100 ppm (34%) | 20 ppm (11%) | 2 ppm (3%) | 20 ppm (8%) | 20 ppm (5%) | 20 ppm (73%) | 20 ppm (>80%) ^c |
| Naphthalene | 2.4 ppm (>80%) ^d | 1.4 ppm (26%) | 0.5 ppm (9%) | 1.4 ppm (14%) | 1.4 ppm (8%) | 1.4/3.1/17 ppm (>80%) ^d | 1.4 ppm (>80%) ^d |
| Propene | 100 ppm (18%) | 20 ppm (6%) | 2 ppm (1%) | 100 ppm (14%) | 100 ppm (8%) | 100/20 ppm (77/30%) | 100 ppm (>80%) ^c |

^a Other operating conditions: H₂/air+contaminant, 2/2 stoichiometry, 100/50% relative humidity, 48.3/48.3 (for 80°C), 10/10 (for 45°C) or 5/5 (for 10°C) kPag.

^b Injection stopped before the steady state was reached. The time required to reach a steady state was greater than the planned test duration.

^c Test stopped because the cell voltage was below the 0.1 V value triggering a contaminant injection interruption. At this particular time, the cell performance was still decreasing.

^d Cell voltage oscillations appeared before a steady state was reached. These oscillations prevent a clear identification of the steady-state cell performance loss. Before these oscillations appeared, the cell performance loss was >80%.

Conclusions and Future Directions

- Complete operating condition tests with second tier airborne contaminants and define tolerance limits that can be applied to filtering system component specifications.
- Collect other ex situ and in situ information to facilitate the determination of contamination mechanisms using methods such as rotating ring/disc electrode (catalyst effect), conductivity cell (membrane effect), residence time distribution (gas diffusion electrode and flow field channel liquid water content effect), gas chromatography (contaminant decomposition effect), segmented cell (current/voltage distribution effect) and fingerprinting using a mathematical model library (mechanism identification).
- Consider use of multi-step recovery procedures in view of the multiple and different contaminant effects observed with all second tier airborne contaminants.

FY 2012 Publications/Presentations

1. J. St-Pierre, M.S. Angelo, Y. Zhai, 'Effect of Selected Airborne Contaminants on PEMFC Performance', *J. Electrochem. Soc.*, submitted.
2. J. St-Pierre, Y. Zhai, M. Angelo, 'Quantitative Ranking Criteria for PEMFC Contaminants', *Int. J. Hydrogen Energy*, **37** (2012) 6784-6789.
3. Y. Zhai, J. St-Pierre, M. Angelo, 'The Impact of Operating Conditions on the Performance Effect of Selected Airborne PEMFC Contaminants', *Electrochem. Soc. Trans.*, accepted.

4. B. Wetton, J. St-Pierre, 'Liquid Water Scavenging of PEMFC Contaminants', *Electrochem. Soc. Trans.*, accepted.
5. J. St-Pierre, 'PEMFC Contamination Model: Neutral Species Sorption by Ionomer', *Electrochem. Soc. Trans.*, **41** (1) (2011) 307-315.
6. J. St-Pierre, M.S. Angelo, Y. Zhai, 'Focusing Research by Developing Performance Related Selection Criteria for PEMFC Contaminants', *Electrochem. Soc. Trans.*, **41** (1) (2011) 279-286.
7. B. Wetton, J. St-Pierre, 'Liquid Water Scavenging of PEMFC Contaminants', in *Meeting Abstracts*, Electrochemical Society volume 2012-2, The Electrochemical Society, Pennington, NJ, 2012, abstract 1296 (forthcoming 222th Electrochemical Society meeting oral presentation).
8. Y. Zhai, M. Angelo, J. St-Pierre, 'The Impact of Operating Conditions on the Performance Effect of Selected Airborne PEMFC Contaminants', in *Meeting Abstracts*, Electrochemical Society volume 2012-2, The Electrochemical Society, Pennington, NJ, 2012, abstract 1294 (forthcoming 222th Electrochemical Society meeting oral presentation).
9. K.A. O'Leary, B. Lakshmanan, J. St-Pierre, 'Impact of Ethylene Glycol Contamination on Proton Exchange Membrane (PEM) Fuel Cells', in *Meeting Abstracts*, Electrochemical Society volume 2012-1, The Electrochemical Society, Pennington, NJ, 2012, abstract 1101 (221th Electrochemical Society meeting oral presentation).
10. J. St-Pierre, 'The Effect of Airborne Contaminants on Fuel Cell Performance and Durability', United States Department of Energy 2012 Annual Merit Review meeting, Washington, DC, May 16, 2012.
11. J. St-Pierre, 'The Effect of Airborne Contaminants on Fuel Cell Performance and Durability', US DRIVE Fuel Cell Tech Team meeting, Southfield, MI, December 14, 2011.

References

1. J. St-Pierre, 'Air Impurities', in *Polymer Electrolyte Fuel Cell Durability*, Edited by F.N. Büchi, M. Inaba, T.J. Schmidt, Springer, 2009, pp. 289-321.

V.C.1 Lead Research and Development Activity for DOE's High Temperature, Low Relative Humidity Membrane Program

James Fenton (Primary Contact), Darlene Slattery
Florida Solar Energy Center (FSEC)
1679 Clearlake Road
Cocoa, FL 32922
Phone: (321) 638-1002
Email: JFenton@fsec.ucf.edu

DOE Managers

HQ: Kathi Epping Martin
Phone: (202) 586-7425
Email: Kathi.Epping@ee.doe.gov
GO: Greg Kleen
Phone: (720) 356-1672
Email: Gregory.Kleen@go.doe.gov

Technical Advisor

John Kopasz
Phone: (630) 252-7531
Email: kopasz@anl.gov

Contract Number: DE-FG36-06GO16028

Subcontractor:

Scribner Associates, Inc., Southern Pines, NC

Project Start Date: April 1, 2006
Project End Date: May 31, 2012

low relative humidity membrane for polymer electrolyte membrane fuel cells (PEMFCs). FSEC has developed standardized experimental methodologies to: (1) measure conductivity (in-plane and through-plane); (2) characterize mechanical, mass transport and surface properties of the membranes as working membrane electrode assemblies; and (3) predict durability of the membranes and their MEAs.

This project manufactures, tests and evaluates MEAs for performance and stability. Test results were evaluated against DOE's 2010 membrane targets:

- Oxygen cross-over: $<2 \text{ mA/cm}^2$
- Hydrogen cross-over: $<2 \text{ mA/cm}^2$
- Membrane conductivity at 120°C : 0.10 Siemens/cm

FY 2012 Accomplishments

- FuelCell Energy (FCE) electrode composition (with FCE ionomer) optimized through FSEC/FCE collaboration.
- Prepared and tested Case Western Reserve (CWR) University 25 cm^2 MEA using FSEC's membrane catalyzing, cell assembly, and cell test procedures.



Introduction

Generally, two regimes of PEMFC operation exist: the typical operating temperatures between $60\text{--}80^\circ\text{C}$, and elevated temperatures higher than 100°C . The ability for current automotive radiators to reject heat is insufficient at continuous full power waste heat loads for $60\text{--}80^\circ\text{C}$ fuel cell stack temperatures. Running the stack at 120°C under full load would allow the use of radiators similar to those available in automobiles today. This has driven the need for development of high-temperature membranes and MEAs that could operate at temperatures of up to 120°C , low RH and near atmospheric pressure.

The objective of this phase of the project is to fabricate and test MEAs from fuel cell membrane materials that meet the goals outlined by the DOE in the multi-year plan. Specific goals are: operation at elevated temperatures (up to 120°C) with unhumidified inlet streams, with a demonstrated conductivity of $>0.1 \text{ S/cm}$ at 120°C . Calculations indicate that with unhumidified inlets, the water produced in the MEA at rated power will result in water partial pressures of about 40 kPa.

Fiscal Year (FY) 2012 Objectives

- Fabricate membrane electrode assemblies (MEAs) from team membranes.
- Test team MEAs for fuel cell performance.

Technical Barriers

This project addresses the following technical barriers from the Fuel Cells section of the Fuel Cell Technologies Program Multi-Year Research, Development and Demonstration Plan:

- (A) Durability: Membrane and MEA durability
- (C) Performance: High MEA performance at low relative humidity (RH) and high temperature

Technical Targets

FSEC plays a supporting role to the six teams who are tasked with developing an improved high temperature,

Approach

The High Temperature, Low Relative Humidity Membrane project for the last three years, encompassed six teams, each of which is skilled in producing novel membranes expected to meet the goals of the Fuel Cell Technologies sub-program. Some of these teams are not necessarily skilled in the ability to produce an MEA, or to test the MEAs in a fuel cell. FSEC's objective is to provide the expertise to test the membranes under fuel cell conditions. FSEC worked closely with the membrane manufacturers to develop appropriate methods for manufacture of the MEA and to test the MEAs according to a procedure that has been developed at FSEC. This approach involved a detailed logic flow chart that itemized each step of the manufacture, fuel cell testing and post-test analysis of the MEA. Each membrane manufacturer approved the steps of the logic flow chart in advance of the process. Furthermore, FSEC iterated with the teams to optimize the results.

Results

The preparation of MEAs requires a certain amount of optimization in order to determine the full performance capability of a particular membrane. In the majority of the MEAs fabricated under this project, a 3M ionomer was used in the catalyst layer. However, FuelCell Energy chose to have its own ionomer used in order to achieve a better interface between the membrane and the catalyst layer. As a result, it was necessary to run a number of experiments with varying amounts of ionomer to determine the level for highest performance. As can be seen from the data in Table 1, the optimization of one parameter often leads to a decrease

in another. In the case of the FuelCell Energy membranes, a decrease in fluoride emission rate (an increase in durability) led to an increase in resistance.

The FuelCell Energy B5 MEA exceeded the 2017 DOE target for performance and was found to be very durable. Additional work would need to be done to balance these improvements with the higher than desired area specific proton resistance.

Most of the membranes that were developed under this project were fluorocarbons and, therefore, the preparation of the MEAs was accomplished using a procedure based upon use of Nafion[®] membranes. However, the membranes developed by CWR were hydrocarbons and required alternative procedures. Early in the project, the CWR membranes were found to be highly conductive at low RH and high temperature but there were issues involved with the membranes cracking and crumbling during attempts at MEA manufacture. It had not been possible to obtain a large enough piece of membrane with the integrity to prepare a standard 25 cm² MEA. This year, we were able to recast and crosslink a piece of CWR membrane that was large enough to manufacture a standard size MEA (Figure 1). Because of concerns about the membrane withstanding the spraying process typically used to apply the electrode to the membrane, it was decided that a gas diffusion electrode (GDE) would be prepared and hot pressed onto the membrane. The procedure was successful and the resulting MEA was tested under the agreed to protocol conditions, i.e. 35% RH for all temperatures at the request of CWR. For comparison purposes, an NRE211 membrane was also prepared with a GDE and tested under the same conditions. As can be seen in Figure 2, the CWR membrane,

TABLE 1. Optimization of Ionomer Content in FuelCell Energy Membranes

| Characteristic | Units | Target 2017 | B5 Opt. | B9 Opt. | NRE211 CCM ¹ |
|---|---------------------|-------------|--------------------|--------------------|-------------------------|
| Area specific proton resistance at: | | | | | |
| 120°C and 40-80 kPa H ₂ O partial pressure | Ohm cm ² | ≤0.02 | 0.064 ² | 0.110 ² | 0.144 ² |
| 80°C and 25-45 kPa H ₂ O partial pressure | Ohm cm ² | ≤0.02 | 0.016 ³ | 0.045 ³ | 0.020 ³ |
| Contact Resistance (Interrupt – ASR ⁴) | | | | | |
| 120°C and 70 kPa water partial pressure | Ohm cm ² | | 0.042 | 0.039 | 0.036 |
| 80°C and 38 kPa water partial pressure | Ohm cm ² | | 0.030 | 0.009 | 0.037 |
| Maximum hydrogen cross-over | mA/cm ² | 2 | 1.6 | <0.4 | 1.08 |
| Minimum electrical resistance | Ohm cm ² | 1,000 | 417 | 855 | 526 |
| Performance @ 0.8V | mA/cm ² | 300 | 209 | 137 | 158 |
| Performance @ rated power | mW/cm ² | 1,000 | 1,239 | 577 | 936 |
| Total fluoride emission during stability test | mmol | - | 89 | 62 | |

¹ Catalyst-coated membrane

² Measured at 120°C and 70 kPa water partial pressure

³ Measured at 80°C and 38 kPa water partial pressure

⁴ Area-specific resistance



FIGURE 1. CWR membrane after recasting and crosslinking

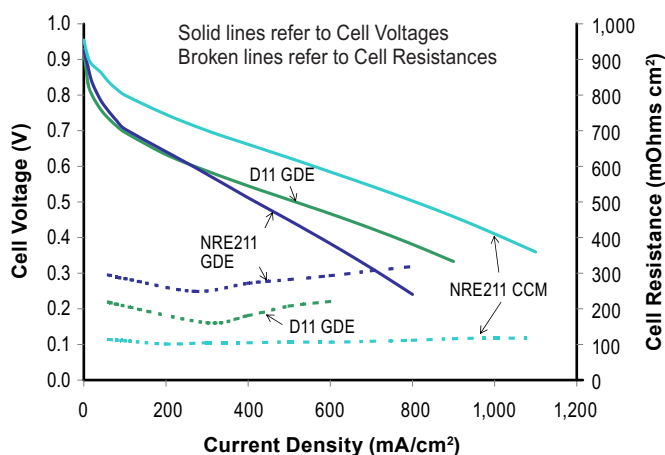


FIGURE 2. Comparison of performance of CWR and Nafion® MEAs GDE versus Nafion® CCM

D11, performed better than the NRE211 with a GDE. For comparison, the NRE211 with a standard CCM is also shown. Based upon subsequent preliminary data, a D11 prepared with a CCM outperforms the NRE211 CCM.

Conclusions and Future Directions

Project is complete and no additional work is anticipated. However, open issues include:

Examination of membrane /electrode interface:

- Study interfacial resistance:
 - Examine CWR MEAs by scanning electron microscope to determine degree of contact between membrane and GDE.
 - Decrease interfacial resistance of CWR MEAs by alternative electrode application methods.
 - Focus on interfacial resistance for MEAs made with FCE ionomers. Understand interfacial resistance for MEAs made with 3M ionomer and with Team member's ionomer.
- Determine differences in swelling rates between team member membranes and Nafion®.

Investigate mechanical properties as a function of degradation.

FY 2012 Publications/Presentations

- M.P. Rodgers, L.J. Bonville, H.R. Kunz, D.K. Slattery, J.M. Fenton, "Defining the correlation between membrane/MEA degradation rate from accelerated testing and lifetime", accepted in *Chemical Reviews*, 2012.
- M.P. Rodgers, P.B. Brooker, N. Mohajeri, L.J. Bonville, H.R. Kunz, D.K. Slattery, J.M. Fenton, "Verification of the correlation between membrane/MEA degradation rate from accelerated and lifetime testing", accepted in *Journal of the Electrochemical Society*, 2012.
- M.P. Rodgers, L.J. Bonville, H.R. Kunz, D.K. Slattery, J.M. Fenton, Defining the correlation between membrane/MEA degradation rate from accelerated testing and lifetime, Fuel Cell Seminar, Orlando, Florida, USA. November 2011 Presentation #LRD42-3.

V.C.2 Dimensionally Stable High Performance Membrane (SBIR Phase III)

Cortney Mittelsteadt (Primary Contact),
Avni A. Argun, Castro Laicer
Giner, Inc. / Giner Electrochemical Systems (GES), LLC
89 Rumford Avenue
Newton, MA 02466
Phone: (781) 529-0529
Email: cmittelsteadt@ginerinc.com

DOE Manager
HQ: Donna Ho
Phone: (202) 586-8000
Email: Donna.Ho@ee.doe.gov

Contract Number: DE-EE0004533

Project Start Date: October 1, 2010
Project End Date: Project continuation and direction
determined annually by DOE

and Demonstration Plan. Table 1 lists the DOE's technical targets and where our research and development efforts stand to date.

TABLE 1. DOE Technical Targets and GINER/GES Status

| Characteristic | Unit | 2017 Target | DSM™ Status |
|--|---------------------|-------------|--------------------|
| Oxygen crossover | mA/cm ² | 2 | 1.5 ^a |
| Hydrogen crossover | mA/cm ² | 2 | 1.8 ^a |
| Membrane Conductivity | S/cm | | |
| Operating Temperature | | 0.10 | 0.093 ^b |
| 20°C | | 0.07 | 0.083 |
| -20°C | | 0.01 | Not tested |
| Operating temperature | °C | ≤120 | 95 |
| Area resistance | Ohm*cm ² | 0.02 | 0.03 |
| Cost | \$/m ² | 20 | ~\$100 |
| Lifetime | hours | 5,000 | Untested |
| Durability with cycling <80°C | cycles | 20,000 | 20,000 |
| Unassisted start from low temperature | °C | -40 | Untested |
| Thermal cyclability in presence of condensed water | | Yes | Yes |

^aCrossover measured for 1 atm of *pure H₂ and pure O₂ at 95°C and 50% relative humidity.*

^b*For 18 μm DSM operating at 95°C with H₂/Air at 20 psi. H₂/Air stoichiometry = 1.1/2.0*

Fiscal Year (FY) 2012 Objectives

- Develop a process to fabricate microporous DSM™ support films with 50% pore density.
- Optimize DSM™ support materials to yield high tensile strength and negligible dimensional changes in water at 80°C.
- Qualify the resulting fuel cell membranes by freeze/thaw and wet/dry testing.
- Develop and characterize membrane electrode assemblies (MEAs) based on the DSM™ technology.
- Demonstrate a cost-effective, roll-to-roll adaptable MEA fabrication method.

Technical Barriers

This project addresses the following technical barriers from the 3.4.5 (Fuel Cells)¹ and 3.5.5 (Manufacturing R&D)² sections of the Fuel Cell Technologies Program Multi-Year Research, Development and Demonstration Plan:

- (A) Durability¹
- (B) Cost¹
- (C) Performance¹
- (A) Lack of High-Volume Membrane Electrode Assembly Processes²

Technical Targets

Progress has been made in achieving the DOE targets listed in the Multi-Year Research, Development

This project is pursuing three DSM™ fabrication processes based on the criteria of performance optimization and cost reduction. As described later in this report, all three processes (ultraviolet microreplication, mechanical deformation, and inversion casting) are based on the use of molding technology and are favorably scalable for high-volume production. Upon completion of their evaluation, the selected process will yield fuel cell membranes that meet the following DOE targets:

- Area resistance: <0.02 Ω.cm²
- Cost: <20 \$/m²
- Lifetime: >5,000 hours
- Durability at 80°C: >20,000 cycles

FY 2012 Accomplishments

- Using a thermal microreplication process, fabricated 4" diameter round high modulus polymer molds with low surface energy to allow rapid release of DSM™ supports. These molds consisted of closely packed vertical pillars with 20 μm diameter and 10 μm height.
- Designed and executed a material matrix that includes a series of photo-crosslinkable polymers such as acrylates,

thiol-enes, epoxies, and urethanes towards selection of a DSM™ support that has high mechanical stability at 80°C in water.

- In collaboration with UMass, utilized a state-of-the-art imprinter to obtain 10- μm -thick thiol-ene DSM™ support with 50% porosity. Demonstrated the versatility of this process by fabricating both standalone and substrate-bound films. Upon incorporation of the ionomer layers, the resulting DSM™ will be $\sim 25\ \mu\text{m}$ thick to yield very low ($<0.02\ \Omega\cdot\text{cm}^2$) area resistance.
- Using a mold-assisted mechanical deformation method, generated highly porous ($\sim 35\%$) polysulfone DSM™ supports at $\$50/\text{m}^2$. This method is projected to yield $<\$20/\text{m}^2$ when adapted to a roll-good process.
- Investigated the phase inversion solvent casting method from Phase II using high-modulus, fluorinated molds to eliminate residual layers.



Introduction

In proton exchange membrane fuel cells, attaining and maintaining high membrane conductivity at various operating conditions is crucial for the fuel cell performance and efficiency. Lowering the equivalent weight (EW) of perfluorinated ionomers is one of the few options available to improve membrane conductivity, especially in the low relative humidity (RH) regime. However, excessive changes in membrane dimensions upon application of wet/dry or freeze/thaw cycles yield catastrophic losses in membrane integrity, hindering their long-term durability. This is especially of concern when low-EW ionomers are used in thin membrane configurations to minimize resistive losses. Incorporating perfluorinated ionomers of low EW within highly porous, dimensionally stable support materials is an optimal method to achieve the DOE membrane metrics for conductivity and durability. A scalable, cost-effective method to fabricate these composite membranes is also necessary to achieve the DOE target of $<\$20/\text{m}^2$. Giner/GES has developed DSM™ technology to provide mechanical support for the conductive ionomer. These composite membranes include a highly conductive and high-acid-content ionomer within a thin and durable polymer support with well-defined pores and high (50%) porosity. Utilizing high-strength engineering polymers, the DSM™ approach has completely restrained in-plane swelling. Providing a non-tortuous, through-plane path for ionic transport minimizes the conductivity penalty due to the support structure. Additionally, when filled with low-EW perfluorinated sulfonic acid (PFSA) ionomers, they meet nearly all of the Department of Energy's 2017 durability and performance targets, including those for freeze/thaw cycling and wet/dry cycling operation.

As currently manufactured, DSM™ is far too expensive ($\sim 1,000/\text{m}^2$) for automotive or even stationary applications. A scalable, continuous fabrication method is needed to reduce the DSM™ cost down to or below the DOE's 2017 cost target of $\$20/\text{m}^2$. This project is directed toward the commercialization of DSM™ for highly reliable fuel cell systems operated under harsh environments. The overall objective of this project is to develop a scaled-up fabrication process geared towards roll-to-roll manufacturing of DSM™.

Approach

A major milestone for this project is to develop a cost-effective route to fabricate a composite DSM™ that includes a low-EW PFSA ionomer embedded in a 10- to 12- μm -thick microporous support film with 20 μm pore diameter and 50% pore density. Currently, three types of micromold-based fabrication techniques are being actively pursued by Giner/GES to achieve the DOE's 2017 targets for cost, performance, and durability. Figure 1 shows scanning electron micrographs of a micromold with 10 μm pillar heights and 50% area coverage that has been generated earlier in the project to utilize the scalability of these micromolding approaches.

"*UV Microreplication*" method is a soft lithography approach that involves the deposition of low-viscosity formulations on a micromold followed by ultraviolet-assisted polymerization to yield highly porous DSM™ substrates. This is a highly scalable process that generates materials at low cost and high volume, and current research is on increasing the mechanical stability of ultraviolet-cured polymers to qualify them as fuel cell components. "*Mechanical Deformation*" method relies on puncturing softened thermoplastics using an array of micropillars. This process is also readily scalable to generate a proven DSM™ support material at low cost, and current research is directed towards the use of fluorinated thermoplastics for effortless release from the micromold. "*Inversion Casting*" method is a solvent-based approach based on the deposition of a solution-processable polymer on a micromold followed by its precipitation using a non-solvent. This process already demonstrated roll-to-roll adaptability in Phase II of this project, and the current research is towards reduction of environmental impact and improvement of mechanical properties. Table 2 ranks each method based on their cost advantages and future prospects as well as the results obtained to date.

Results

UV Microreplication. This process flow involves the use of a low-viscosity, ultraviolet-crosslinkable formulation (precursor) placed between a low-surface-energy mold (Figure 1) and a suitable backing layer such as Nafion® or poly(vinyl alcohol) followed by removal of the crosslinked polymer to yield a DSM™ support with well-defined

TABLE 2. Three DSM™ fabrication techniques compared side-by-side based on several criteria including scalability, materials, and development/final DSM™ cost. (1-Fair, 2-Good, 3- Proven)

| Technique | Scalability | Materials | Development cost | Final Cost |
|------------------------|-------------|-----------|------------------|------------|
| UV Microreplication | 3 | 1 | 1 | 3 |
| Mechanical Deformation | 3 | 3 | 2 | 3 |
| Inversion Casting | 2 | 2 | 2 | 2 |

cylindrical pores. The resulting 10- μm -thick free-standing films have high tensile strength, and they are sufficiently flexible for roll-to-roll adaption. However, they often fail to yield the desired mechanical properties at elevated ($\sim 80^\circ\text{C}$) temperatures. To overcome this issue, Giner/GES prepared and tested a number of polymers to achieve a suitable formulation that will give high tensile strength (>10 MPa), elastic modulus (>100 MPa), and elongation at break ($>5\%$) while retaining dimensional stability and resistance to acid hydrolysis. Table 3 shows a selected list of formulations along with their relevant mechanical properties at 80°C in water. The mechanical properties of a Nafion® 112 film are also given for comparison. Based on the numerous formulations tested to date, a diphenol acrylate polymer (SR348, Sartomer) yielded the most promising properties. Figure 2 shows the chemical structure and stress-strain curves of this polymer in water at 25°C and 80°C as compared to Nafion® 112.

Mechanical Deformation. This is a direct perforation route that involves puncturing softened thermoplastics with tapered micromolds to fabricate porous films. This method can utilize commodity thermoplastics with very fast processing times allowing for roll-to-roll production. Preliminary perforation trials were conducted with polysulfone and yielded 10- to 15- μm -wide pores with less than the targeted 50% porosity as shown in Figure 3. This

TABLE 3. Mechanical Properties of Ultraviolet Crosslinked Polymers Tested at 80°C in Water

| Polymer | Family | Tensile Strength (MPa) | Modulus (MPa) | Elongation at Break (%) |
|------------------|-------------------------|------------------------|---------------|-------------------------|
| Nafion® 112 | Perfluoro sulfonic acid | 6.08 | 21.36 | 3 |
| NOA86 (Norland) | Thiol-enes | 0.52 | 15.5 | 3.32 |
| EB3300 (Cytec) | Epoxy Acrylate | 1.04 | 48.65 | 4.97 |
| SR348 (Sartomer) | Phenol Acrylate | 9.65 | 227.1 | 7.44 |
| EB264 (Cytec) | Urethane Acrylate | 2.04 | 14.07 | 6.86 |

was mainly due to excessive tearing of polysulfone during the mold release step. To circumvent this issue, Giner/GES is currently pursuing a high modulus thermoplastic film with high tear-resistance that can be easily released due to the film's low surface energy.

Inversion Casting. First used during Phase II of this project, this method aims to fabricate DSM™ support materials using a solution-processable polymer such as polysulfone. The process involves roll-casting a 30 wt% polysulfone solution from N-methylpyrrolidone on the same polymer micromold shown in Figure 1 followed by rapid precipitation of the polymer in water. Figure 4 shows top-down and cross-sectional views of a 6.8- μm -thick free-standing polysulfone film released from the micromold. It is important to note that the film is free of residual layers to yield the 50% targeted porosity. Since the phase inversion process generates a sponge-like film, it will require further annealing (such as heating above the T_g) to increase the mechanical strength of the films.

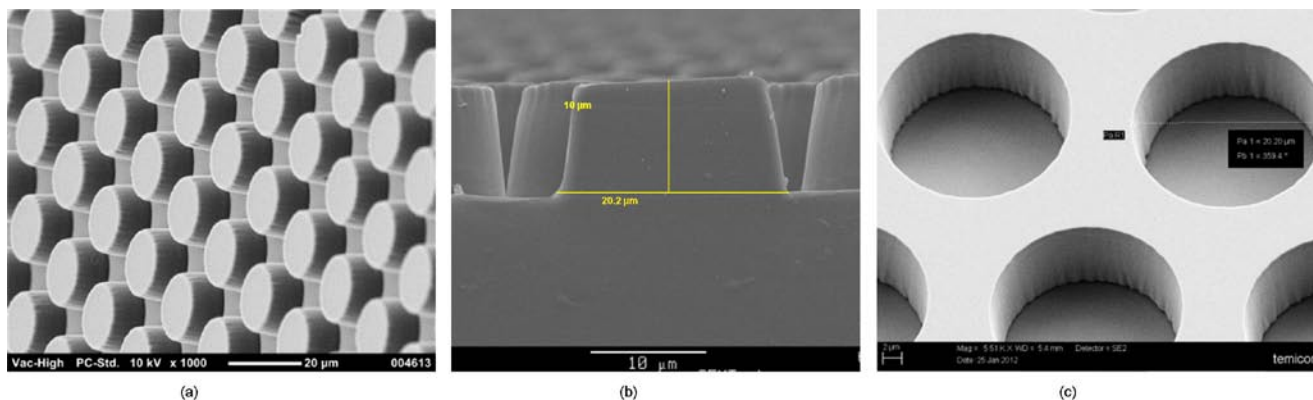


FIGURE 1. Scanning electron micrographs of high modulus, low surface energy polymer micromold pillars (a and b) replicated from an electroplated nickel hole pattern (c)

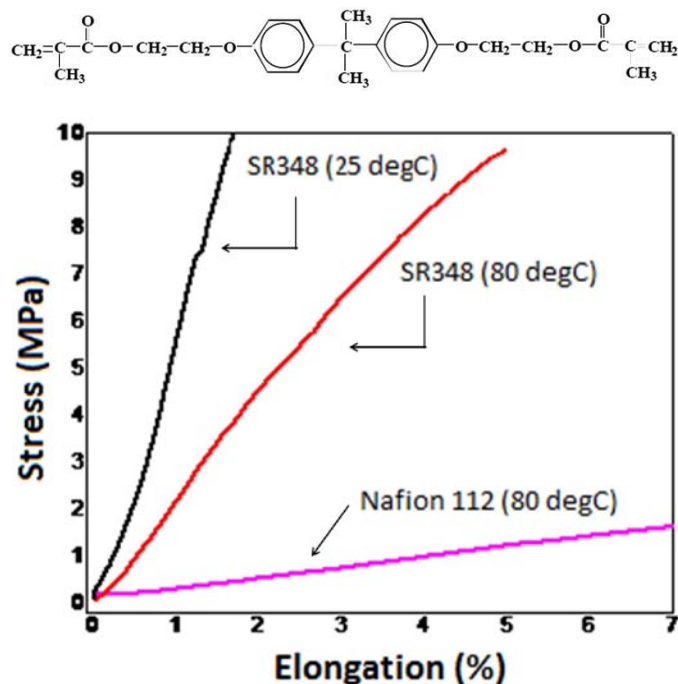


FIGURE 2. Chemical structure of an ethoxylated bisphenol A dimethacrylate polymer (SR348, Sartomer) shown with its stress-strain curves in water at 25°C and 80°C. Also shown is Nafion®’s behavior at 80°C for comparison.

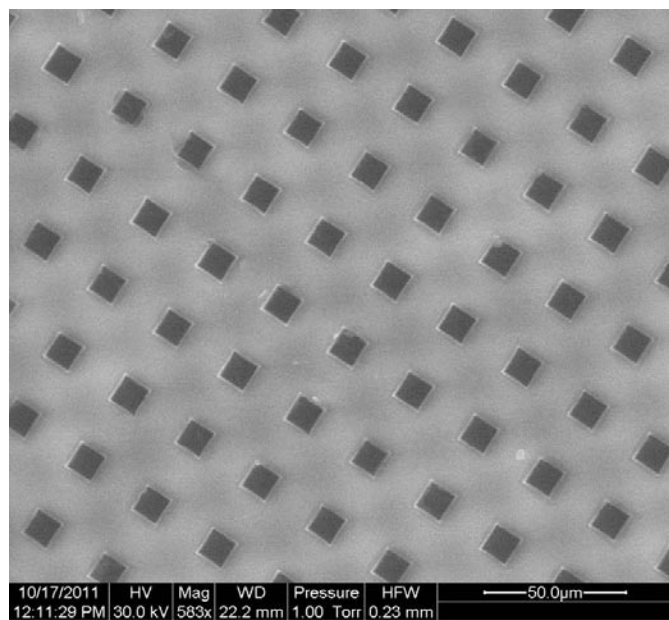


FIGURE 3. Top-down scanning electron micrograph of a perforated polysulfone film with ~30% porosity

Conclusions and Future Directions

The goal by the end of FY 2012 was to demonstrate a scalable process for cost-effective manufacturing of DSMs™

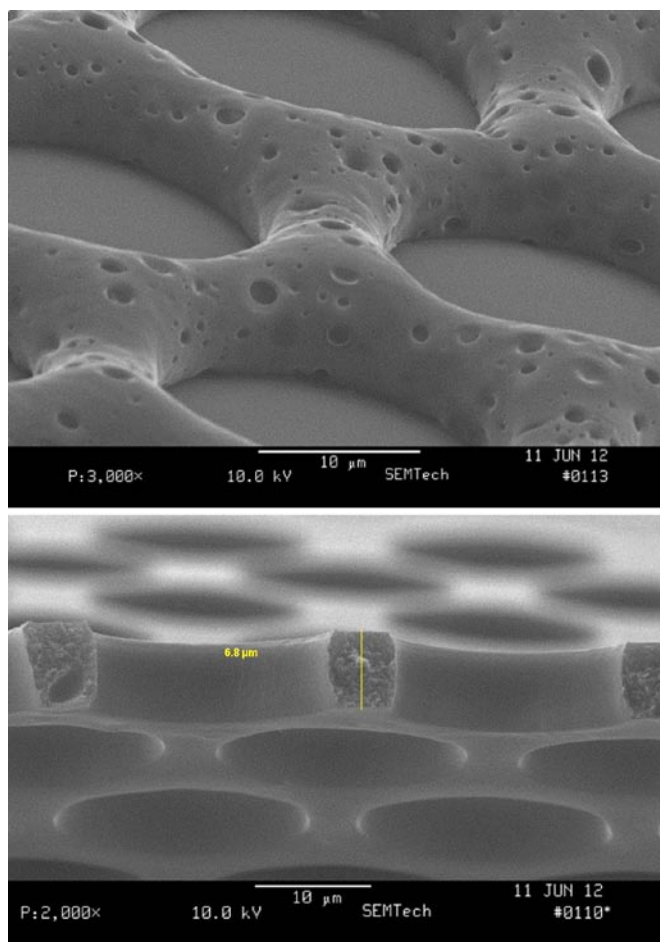


FIGURE 4. Top-down and cross-sectional scanning electron micrographs of a polysulfone film inversion-cast on a micromold from a 30 wt% N-methylpyrrolidone solution

for fuel cells. We believe that we have shown three scalable micromolding methods that are capable of performing this goal. Upon further validation of mechanical properties obtained by the ultraviolet microreplication method, we will start using the roll-to-roll apparatus at University of Massachusetts – Amherst through an ongoing research agreement. The roll-to-roll setup at UMass is specifically tailored for processing of ultraviolet-curable formulations with micromolding (imprint lithography) and will be a valuable asset to the development of this project. The DSM™ supports generated by the mechanical deformation and inversion casting methods will gain traction pending the optimization of process conditions to obtain closely packed micropores to meet the 50% porosity. Their validation as a DSM™ component will be attempted by integrating a low-EW ionomer followed by applying the DSM™ testing protocols that include the measurement of conductivity and freeze-thaw and wet/dry cycling durability.

FY 2012 Publications/Presentations

1. Mittelsteadt, C.K., A. Argun, C. Laicer “4th Quarterly Report” Oct. 2011.
2. Mittelsteadt, C.K., A. Argun, C. Laicer “Annual Progress Report” Dec. 2011
3. Mittelsteadt, C.K., A. Argun, C. Laicer “5th Quarterly Report” Jan. 2012.
4. Mittelsteadt, C.K., A. Argun, C. Laicer “6th Quarterly Report” Apr. 2012.
5. Mittelsteadt, C.K., A. Argun, C. Laicer, J. Willey, P. Maxwell. “2012 Annual Merit Review Proceedings– Fuel Cells ” May, 2012

V.C.3 High-Temperature Membrane with Humidification-Independent Cluster Structure

Ludwig Lipp (Primary Contact), Pinakin Patel,
Ray Kopp

FuelCell Energy (FCE), Inc.
3 Great Pasture Road
Danbury, CT 06813
Phone: (203) 205-2492
Email: llipp@fce.com

DOE Managers

HQ: Donna Ho
Phone: (202) 586-8000
Email: Donna.Ho@ee.doe.gov

GO: Greg Kleen
Phone: (720) 356-1672
Email: Gregory.Kleen@go.doe.gov

Technical Advisor

Thomas Benjamin
Phone: (630) 252-1632
Email: benjamin@anl.gov

Contract Number: 36-06GO16033

Start Date: June 1, 2006

Projected End Date: August 31, 2012

Technical Targets

This project is developing a multi-component composite (mC^2) membrane to meet the following DOE 2015 technical targets for membranes:

- Membrane Conductivity: At $\leq 120^\circ C$: 0.1 S/cm; at room temperature: 0.07 S/cm; at $-20^\circ C$: 0.01 S/cm
- Membrane ASR: $0.02 \Omega cm^2$

FY 2012 Accomplishments

- Protonic Conductivity: Met DOE protonic conductivity target: achieved 0.113 S/cm (DOE Target >0.1 S/cm)

The membrane electrode assembly (MEA) was re-optimized for mC^2 in collaboration with the University of Central Florida (UCF), resulting in the following performance improvements:

- Electrical Conductivity: Met DOE electrical conductivity target: achieved $2,860 \Omega cm^2$ (DOE Target: $>1,000 \Omega cm^2$)
- Cross-Over: Met DOE hydrogen cross-over target: achieved $0.3 mA/cm^2$ (DOE Target $<2 mA/cm^2$)
- Cell Performance: Met DOE power density target: achieved $1,247 mW/cm^2$ at rated power (DOE Target: $>1,000 mW/cm^2$)
- Additive Development: Developed process to stabilize protonic conductivity enhancer in mC^2



Fiscal Year (FY) 2012 Objectives

- Develop humidity-independent, thermally stable, low equivalent weight composite membranes with controlled ion-cluster morphology, to provide high proton-conductivity at up to $120^\circ C$ (overall goal: meet DOE 2015 targets).
- Improve mechanical properties to significantly increase the durability and reduce the gas cross-over.
- Reduce the membrane area specific resistance (ASR) to increase cell performance and lower the capital and operating costs.

Technical Barriers

This project addresses the following technical barriers from the Fuel Cells section of the Multi-Year Research, Development and Demonstration Plan [1] of the DOE Fuel Cell Technologies Program:

- (A) Durability
- (B) Cost
- (C) Performance

Introduction

This project is focused on the development of composite proton exchange membranes (PEMs) that can operate at low relative humidity (RH) and over a wide temperature range (-20 to $120^\circ C$). Their main application is in transportation fuel cells. In addition, FCE is considering use of these membranes for co-production of hydrogen from high-temperature fuel cells. The higher operating temperature imparts improved tolerance to impurities, such as carbon monoxide, thereby increasing the co-production efficiency and simplifying the system.

The goal is to develop a structure in which ion-conducting clusters remain intact at low RH. A major challenge is that current proton conducting polymers cannot sufficiently hold on to water under these conditions. Since the conduction mechanism relies on movement of hydrated species, the conducting path is compromised, resulting in

low performance. Membranes that can operate at lower RH at elevated temperatures up to 120°C will reduce the fuel cell system complexity and cost. This project is developing a composite membrane, in which both the ionic conductivity and mechanical properties are enhanced to meet DOE's 2015 and 2017 goals for transportation fuel cells.

Approach

The approach to address the DOE target parameters is summarized in Table 1. The emphasis in the past year has been to fabricate MEAs that can meet DOE's cell performance targets.

TABLE 1. Approach for the Composite Membrane

| Target Parameter | DOE Target (2017) | Approach |
|--|-------------------------------|--|
| Area specific proton resistance at: 120°C and 40-80 kPa water partial pressure | 0.02 Ω cm ² | Multi-component composite structure, lower equivalent weight, additives with highly mobile protons |
| 80°C and 25-45 kPa water partial pressure | 0.02 Ω cm ² | Higher number of functional groups |
| Hydrogen and oxygen cross-over at 1 atm | 2 mA/cm ² | Higher molecular weight polymer for stronger membrane structure |
| Minimum electrical resistance | 1000 Ω cm ² | Improved membrane thickness tolerance and additive dispersion |
| Cost | 20 \$/m ² | Simplify polymer processing |
| Performance @ 0.8 V (¼ rated power) | 300 mA/cm ² | MEA with matching polymer in membrane and electrodes |
| Performance @ rated power | 1,000 mW/cm ² | Optimized ionomer content in electrodes |

Results

This year's efforts were focused on improving the MEA fabrication process with the mC² membrane. Cell performance analysis carried out by UCF in the previous year [2] suggested that electrode improvements would be necessary to realize the full potential of the mC² membrane. In particular, analysis results showed that the biggest losses while operating on H₂/air occur on the cathode electrode. Hence, the anode was kept the same and changes were made to the cathode. The changes were focused on the ionomer content. It was studied in a range from 15 to 32% by weight. Figure 1 shows cell performance results for each of four different ionomer contents in the cathode. Because of membrane fabrication-related differences in the average membrane thickness between MEA samples, the data are presented with an internal resistance-free voltage. This allows elimination of the effect of membrane thickness on the cell resistance and therefore cell voltage. Moreover, the data were corrected for crossover hydrogen resulting from the variations in membrane thickness. This was done by deducting the limiting current density in the linear sweep voltammogram from the measured current densities in the polarization curves to isolate the effect of ionomer content in the cathode. Record performance was observed. The actual voltages measured were as follows:

- At 120°C and 35% RH: 510 mV at 1 A/cm²
- At 95°C and 83% RH: 585 mV at 2 A/cm²

Data at 120°C and 35% RH suggests that 29 wt% ionomer gives the highest performance in a current density range up to 1,000 mA/cm². From 1,000 to 2,000 mA/cm²,

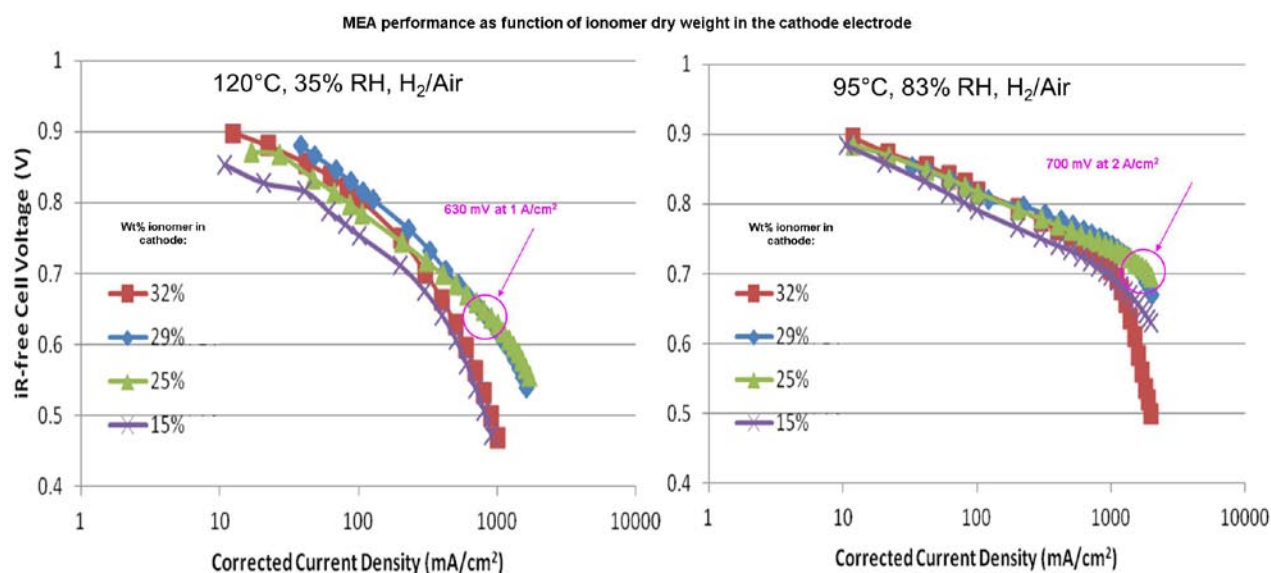


FIGURE 1. Re-optimization of MEA for mC² led to significantly improved performance

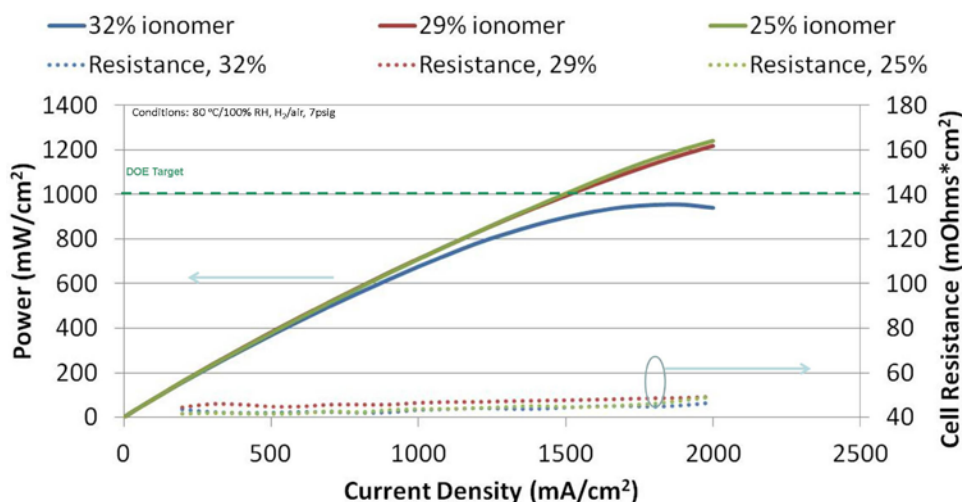


FIGURE 2. Electrode improvements led to higher power density

Relatively homogeneous dispersion of aggregated particles are observed in the membrane (#82) with a higher loading. The aggregated particles may have achieved a continuous 3-dimensional network.

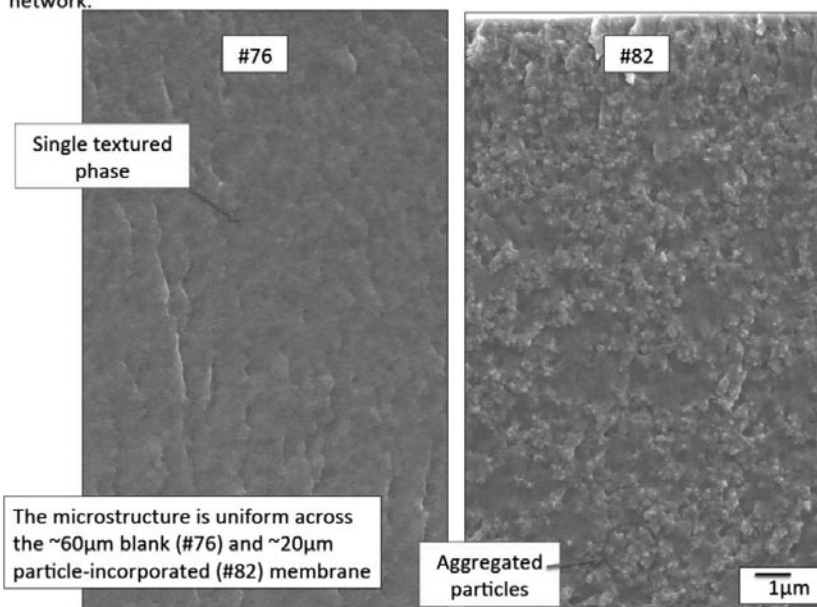


FIGURE 3. Achieved uniform distribution of additives in mC²

25 wt% ionomer gives slightly higher performance than 29 wt%. Testing at 95°C gave similar results.

The three highest performing MEAs were then used to determine performance at rated power. As can be seen in Figure 2, the MEA with 25% ionomer in the cathode gave the highest power density, reaching 1,247 mW/cm² at 2,000 mA/cm². This result exceeds the DOE target by almost 25%.

The MEAs made by UCF using the improved mC² membrane survived UCF's 11-day test protocol (approved by

DOE) without failures. This was enabled by improvements to the additive fabrication process. The superacid additive, which is designed to enhance the protonic conductivity of mC², was deposited onto the zeolite additive, which retains water in the membrane even at elevated temperature. This ensures immobilization of the superacid on the surface of the zeolite, where it is in direct contact with the ionomer, resulting in faster proton transfer and therefore enhanced membrane conductivity. Processing improvements led to uniform distribution of the additives throughout the mC², as can be seen in the scanning electron images in Figure 3. These

images were obtained by Dr. Kelly Perry and Dr. Karren More at the Oak Ridge National Laboratory. The left image shows the texture of the membrane without additives. The right image is that of an mC². It shows the additives in the form of nanometer-size aggregates, which may have achieved a continuous three-dimensional network. X-ray diffraction analysis showed that the nano-zeolite structure remained intact after superacid deposition.

The project's achievements to date are summarized in Table 2. A comparison of major DOE 2017 target parameters to the values measured by the project team and independently verified by UCF show that most performance targets have been met (indicated by a green check mark) and the remaining ones are approaching the target values.

Conclusions and Future Direction

An mC² membrane design for high temperature and low RH operation has been implemented to fabricate membranes and MEAs with enhanced performance at the DOE target conditions (Table 1). Accomplishments include:

- Re-optimized MEA for mC² with improved cathode electrodes incorporating advanced ionomer; incorporated in DOE high temperature membrane validation protocol implemented by UCF.
- Obtained record performance, especially at high current density, with the improved MEAs: 510 mV at 1 A/cm² at 120°C, 35% RH (Figure 1).
- Achieved high power density of 1,247 mW/cm² at rated power with the improved MEAs (Figure 2).
- Also met ASR, hydrogen cross-over and electrical resistance targets (Table 2).

TABLE 2. MEA Test Results Compared to DOE 2017 Targets

| Characteristic | Units | DOE 2017 Target | FY11-12 Result |
|--|---------------------|-----------------|----------------|
| Area specific proton resistance ^c at: | | | |
| 120°C and 40-80 kPa water partial pressure | Ohm cm ² | ≤0.02 | 0.025 |
| 80°C and 25-45 kPa water partial pressure | Ohm cm ² | ≤0.02 | 0.016 ✓ |
| Maximum Hydrogen cross-over ^a | mA/cm ² | 2 | 0.3 ✓ |
| Minimum electrical resistance ^b | Ohm cm ² | 1,000 | 2,860 ✓ |
| Performance @ 0.8 V (¼ Power) | mA/cm ² | 300 | 209 |
| Performance @ rated power | mW/cm ² | 1,000 | 1,247 ✓ |

* Values are at 80°C unless otherwise noted

^a Measure in humidified H₂/N₂ at 25°C

^b Measure in humidified H₂/N₂ using LSV curve from 0.4 to 0.6 V at 80°C

^c Determined by subtracting contact resistances from cell current interrupt values

Future efforts should be directed towards more comprehensive characterization and improvement of mC² durability. These include mechanical and chemical stability to withstand continuous operation at elevated temperature and low relative humidity, as well as automotive cycling conditions. An intermediate temperature of 95°C has been suggested by car companies for the near-term.

FY 2012 Publications/Presentations

1. L. Lipp, "High Temperature Membrane With Humidification-Independent Cluster Structure", 2012 DOE Hydrogen Program and Vehicle Technologies Program Annual Merit Review and Peer Evaluation Meeting, Washington, D.C., May 14–18, 2012.

References

1. DOE Multi-Year Research, Development and Demonstration Plan, Section 3.4 "Fuel Cells", http://www1.eere.energy.gov/hydrogenandfuelcells/mypp/pdfs/fuel_cells.pdf.
2. L. Lipp, "High Temperature Membrane With Humidification-Independent Cluster Structure", FY 2011 DOE Hydrogen and Fuel Cells Program Annual Progress Report, pages 688-691 (2011).

V.C.4 Corrugated Membrane Fuel Cell Structures

Stephen Grot

Ion Power Incorporated
720 Governor Lea Rd
New Castle, DE 19720-5501
Phone: (302) 832 9550
Email: s.grot@ion-power.com

DOE Managers

HQ: Donna Ho
Phone: (202) 586-8000
Email: Donna.Ho@ee.doe.gov

GO: Reginald Tyler
Phone: (720) 356-1805
Email: Reginald.Tyler@go.doe.gov

Technical Advisor

Thomas Benjamin
Phone: (630) 252-1632
Email: benjamin@anl.gov

Subcontractors:

- Graftech International Holdings Inc., Parma, OH
- General Motors Corporation, Flint, MI

Contract Number: DE-EE0000462

Project Start Date: September 1, 2010

Project End Date: February 28, 2014

Fiscal Year (FY) 2012 Objectives

The following objectives characterize the project goals for FY 2012:

- Develop the forming fixture required for corrugating gas diffusion layer (GDL) materials.
- Develop a GDL material that can meet or exceed the baseline performance in a flat configuration. This material must then have the ability to be formable for corrugation.
- Demonstrate the target properties of <10 mOhm-cm² electrical resistance at >20 psi compressive strength over the active area, in combination with offering at least 80% of the power density that can be achieved by using the same membrane electrode assembly (MEA) in a flat plate structure (This is the next DOE Go/No-Go decision point).

Technical Barriers

This project addresses the following technical barriers from the Fuel Cells section of the Fuel Cell Technologies

Program Multi-Year Research, Development and Demonstration Plan:

- (B) System Cost (GDL, lower plate/GDL manufacturing costs)
- (C) Performance (high power density with low Pt-loaded MEAs)

Technical Targets

In this project, corrugated membrane fuel cell structures are being constructed to assist the Fuel Cell Technologies Program in meeting the important objectives of power density (1 W/cm²) and platinum utilization (0.2 g/kW). In order to meet these technical targets, Ion Power has tested several GDLs with varying pore sizes, to determine the configuration with the greatest ability to meet power density needs when used in a corrugated structure. Table 1 illustrates Ion Power's findings:

In summary, Ion Power has identified GDL material that meets or exceeds the baseline without micro-porous layer (MPL) for the GKD Woven Wire Screen (Gold Screen 10BC) – when using the Ti Metal Screen, MPL is required.

FY 2012 Accomplishments

The following is a list of accomplishments achieved to date in FY 2012:

- Completed the development and production of cell fixture and sub gasket forming tools for the single-cell 50-cm² fuel cell test jig.
- Designed and manufactured the tooling fixture to allow for corrugation of the GDL screen.
- Initiated a new method for the manufacture of a catalyst-coated membrane, that directly applies the catalyst and membrane onto the GDL surface using coating operations.
- Identified a suitable, formable, metal-based GDL material that meets or exceeds baseline performance in a flat cell configuration (the GKD woven wire screens).



Introduction

The DOE supports research to overcome critical technical barriers in fuel cell technology. Corrugated membrane fuel cell structures possess the potential to meet the targeted demands of the DOE by 2015. These targets consist of meeting both the power density objective

TABLE 1. Comparison of GDL Polarization Curves Impacted by Openings/cm²

| Comparison of GDL Polarization Curves Impacted by Pore Size | | | | | | | |
|---|---------------------|---------|-------------------|-------------------|-----------------------|---------------------|---------------------|
| GDL Data | | | | | | | |
| Fuel Cell # | FC45 | FC65 | * | * | FC56 | FC29 | FC55-1 |
| Membrane | XL100 (Baseline) | NR212 | XL100 | XL100 | XL100 | XL100 | NR212 |
| MPL | Yes | No | No | Yes | Yes | No | Yes |
| Gas Diffusion Layer | 10BC | 10AA | 10BC Ti Screen | 10BC Ti Screen | GrafTech 28.49% OA | GrafTech FFP 300 | Gold screen 10BC |
| Openings/cm ² | ~10,000 | ~10,000 | 2,500 | 2,500 | 200 | 300 | 10,000 |
| Current (A) at Voltage (V) of 0.8 | 3 | 5 | 5 | 7.5 | 7.5 | 2.5 | 5 |
| Current (A) at Voltage (V) of 0.4 | 39.5 | 26 | 27 | 50 | 32 | 5 | 75 |

Sources: Annual report Feb 6, 2012 without FC Number

of 1 W/cm² and platinum utilization of (0.2 gPt/kW) simultaneously.

For the past 40 years the traditional proton exchange membrane (PEM) fuel cell stack has been the dominant method of construction of multi-kW fuel cells. These stacks featured grooved bipolar plates, with flat MEAs and GDLs, seals and heavy compression end-plates. Some smaller sub-watt and portable applications featured the “jelly roll” concept cell design variation. However, these design concepts were never able to achieve the power density of the traditional stack construction due to inefficient collection of currents and inefficient distribution of reactant flows.

In order to meet the DOE’s goal of reducing the use of platinum in fuel cell cathodes [1], Ion Power has demonstrated the novel concept of a corrugated membrane fuel cell structure. The target is a fuel cell single cell (50 cm²) with a two-fold increase in the membrane active area over the geometric area of the cell by corrugating the MEA structure.

Approach

Achieving the platinum catalyst utilization target of 0.2 g Pt/kWe set forth by the DOE [2,3] is one of the most challenging aspects of traditional PEM fuel cell stacks. For the development of the corrugated membrane electrode structure, Ion Power’s approach will consist of compressing additional membrane area into the same geometric plate footprint. A fuel cell consisting of a 50-cm² single-cell test jig will be designed and fabricated such that it will allow testing of both conventional, flat MEAs possessing standard flow fields and the corrugated single cell assemblies. This test jig will also allow the hand assembly of each of the individual components. Inserts will be created to generate both straight through flow and serpentine flow in both the flat and corrugated MEAs. Water, thermal and gas flow management issues will be investigated.

Results

The forming fixture for corrugating GDL materials has been designed and built (Figure 1). The first set of tests using the newly built forming fixture revealed a minor challenge; the blades forming the individual convolutions were dragging prematurely on the membrane, causing resistance for an accurate sliding motion and resulting in the improper forming of the corrugation. In order to resolve this issue, modification slides were designed and added to the fixture to hold the blades off of the membrane. A release mechanism was implemented to release the blades at the appropriate location on the membrane. A second set of tests will be conducted.

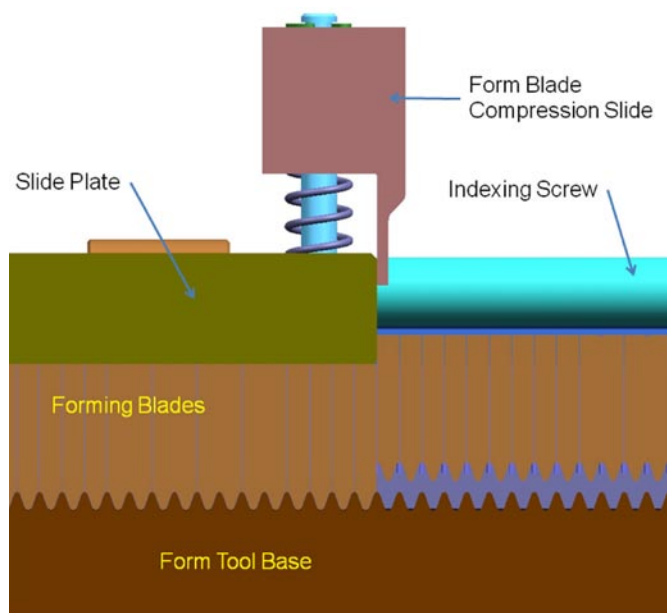


FIGURE 1. Forming Fixture for Corrugating GDL Materials

Ion Power has made significant progress in the sourcing of metal screen diffusion media. Research has shown that for non-traditional gas diffusion media, small pore sizes are extremely beneficial. Small pore sizes on the order of 70 microns, or roughly 10,000 openings/cm² outperformed Graftech’s 300 openings/cm² material. They also outperformed an expanded titanium screen with 2,500 openings/cm² as shown in Figure 2. The results clearly indicate that the finer the pore size, the higher the performance. Thus, moving forward Ion Power will seek materials consistent with this research.

Performance tests have been completed to analyze the GKD woven wire screens. For these performance tests, test conditions were standardized to 1 atm dry air/hydrogen at 65°C with 60 cm² of cell hardware. Ion Power is quite pleased with the improved performance of the GKD woven wire screen over the baseline, however when the GDK screen was applied to both sides of the fuel cell, the performance was quite low (Figure 3). When the GKD wire screen is used as an anode or a cathode the performance is above the baseline, however when used as both anode and cathode together the performance is far below the baseline. Ion Power does not understand this phenomenon but is aggressively investigating its cause.

Additional developments have occurred on the manufacturing process for the catalyst-coated membrane. Although the MEA forming fixture is designed to allow the introduction of a flat catalyst-coated membrane sheet into the corrugated structure, this approach has inherent risks and challenges associated with it. The ultimate in manufacturing cost savings would be to form in place the catalyst layer and the membrane layer via a two-step spray coating process on the corrugated GDL-plate subassembly (Figure 4). Thus the process will allow for a spray coating

of the corrugated GDL-plate subassembly with a catalyst coating, followed by an ionomer coating. When these two halves are brought together the two membrane halves form a reliable membrane separator between anode and cathode. The large manufacturing cost savings comes about since no membrane needs to be purchased, and furthermore, no membrane insertion fixture would be required. In order to demonstrate the process in the flat geometry, Ion Power used a SIGRACET™ 34BC gas diffusion layer, roll-coated the catalyst ink on the top surface, and cured it. Next, Ion Power re-coated the catalyzed SIGRACET 34BC with a 13-micron thick ionomer layer. Then we took two pieces of the two-step coated SIGRACET™ and bonded them face to face through a 2-mil thick KAPTON™ perimeter frame. This MEA, sized at 900 cm² active area, was submitted to a customer for

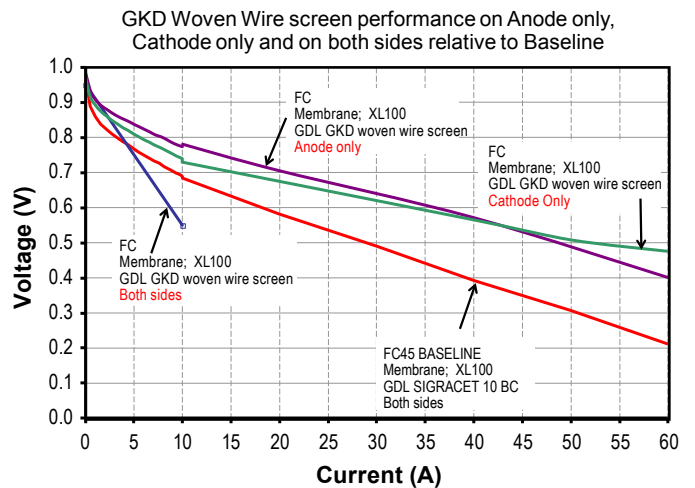


FIGURE 3. GDK Woven Wire Screen Performance

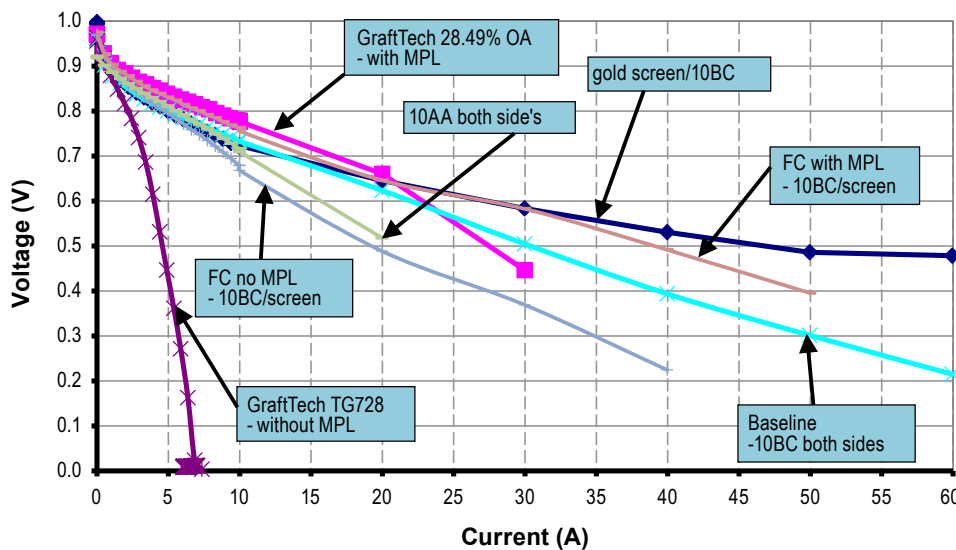


FIGURE 2. Impact of Gas Diffusion Layer Openings/cm²

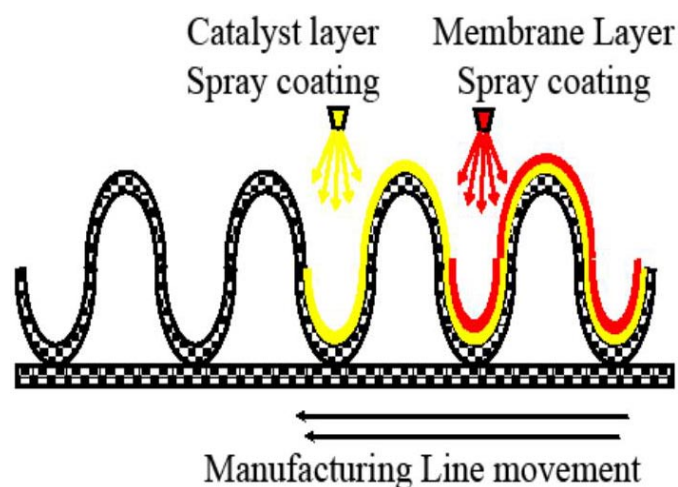


FIGURE 4. Continuous Spray Coating of Corrugated GDL Plate Subassembly

evaluation and testing. The first testing conducted will be the leak test, followed by the performance testing.

Ion Power has further identified Sono-tek, a company that specializes in the application of the catalyst-coated membrane via ultrasonic spray nozzles, as a well suited vendor for the spray coating approach. Ion Power is in the process of negotiating a trial at Sono-tek's facility, using Ion Power's coating materials and substrates.

Conclusions and Future Directions

Over the past year, Ion Power has reached the following conclusions:

- Ion Power has completed a significant amount of work in the design and manufacture of tooling fixtures.
- Ion Power has performed extended research to determine the most effective materials for use in the corrugation design process. Ion Power has concluded that the GKD

woven wire screen with 10,000 openings/cm², provides the highest and best value.

Future Directions for the project include:

- Ion Power will pursue the corrugation of metal screens to metal plates and begin actual fuel cell testing of authentic corrugated fuel cell structures.
- Ion Power will further work with Sono-tek to implement a spray coating manufacturing process for the MEA.

FY 2012 Publications/Presentations

2012 Hydrogen and Fuel Cells Program Annual Merit Review Presentation

References

1. United States. U.S. Department of Energy. Energy Efficiency and Renewable Energy. "Parts of a Fuel Cell" Web. <<http://www1.eere.energy.gov/hydrogenandfuelcells/>>.
2. HFCIT Program "Multi-Year Research, Development and Demonstration Plan", U.S. DOE Office of Energy Efficiency and Renewable Energy, February 2005, <www.eere.energy.gov/hydrogenandfuelcells/mypp/>.
3. M.F Mathias, et al "Two Fuel Cell Cars in Every Garage?" The ECS Interface Fall 2005, pg 24.

V.D.1 Advanced Cathode Catalysts and Supports for PEM Fuel Cells

Mark K. Debe (Primary Contact),
Andrew J. Steinbach, Susan M. Hendricks,
Michael J. Kurkowski, George D. Vernstrom,
Amy E. Hester, Eric Iverson, Sean Luopa,
Paul Kadera, and Radoslav T. Atanasoski

Fuel Cell Components Program, 3M Company
3M Center, Building 201-2N-19
St. Paul, MN 55144-1000
Phone: (651) 736-9563
Email: mkdebe1@mmm.com

DOE Managers

HQ: Kathi Epping Martin
Phone: (202) 586-7425
Email: Kathi.Epping@ee.doe.gov

GO: David Peterson
Phone: (303) 275-4956
Email: David.Peterson@go.doe.gov

Technical Advisor

Thomas Benjamin
Phone: (630) 252-1632
Email: Benjamin@cmt.anl.gov

Contract Number: DE-FG36-07GO17007

Subcontractors and Federally Funded Research and Development Centers:

- Dalhousie University, Halifax, Nova Scotia, Canada (Jeff Dahn, David Stevens)
- Argonne National Laboratory (ANL), Argonne, IL (V. Stamenkovic, Dennis van der Vliet, Nenad Markovic)
- Jet Propulsion Laboratory (JPL), Pasadena, CA (Charles Hays)
- GM Global Research and Development, Honeoye Falls, NY (E. Thompson, stack testing)

Project Start Date: April 1, 2007

Project End Date: June 30, 2012

- Durability sufficient to operate at $>80^{\circ}\text{C}$ for 2,000 hours, $\leq 80^{\circ}\text{C}$ for 5,000 hours, with cycling for transportation applications
- High prospects for 40,000 hours durability under operating conditions for stationary applications
- High volume manufacturability

Technical Barriers

This project addresses the following technical barriers from the Fuel Cells section of the Fuel Cell Technologies Program Multi-Year Research, Development and Demonstration Plan:

- (A) Durability
- (B) Cost
- (C) Performance

Technical Targets

This project is focused on improving the performance and durability of the 3M nanostructured thin film (NSTF) roll-to-roll fabricated electrocatalysts and MEAs. Table 1 compares the NSTF catalysts/MEA status as of the second quarter, 2012, with DOE electrocatalyst targets for 2017 updated from Table 3.4.12 of the Fuel Cell Technologies Program Multi-Year Research, Development and Demonstration Plan. Changes from last year's annual report reflect recent gains in mass activity and performance with post-processed NSTF- Pt_3Ni_7 alloys (quotation marks " Pt_3Ni_7 " imply the exact composition is changed from as-deposited), and accelerated durability test results with NSTF- $\text{Pt}_{68}(\text{CoMn})_{32}$. The MEAs used for the inverse specific power density values listed in the first row, PGM total content, had catalyst loadings of $0.03/0.12 \text{ mg}_{\text{Pt}}/\text{cm}^2$ on the anode and cathode respectively with NSTF- PtNi cathodes fabricated by improved roll-to-roll deposition, de-alloying and annealing processes. These same materials exhibited the improved mass and specific activities listed in Table 1 as measured at General Motors (GM) using both 3M and GM oxygen reduction reaction (ORR) test protocols. The improved 30,000 cycle durability results were obtained with PtCoMn catalysts containing $0.05 \text{ mg}_{\text{Pt}}/\text{cm}^2$ on the anode and $0.15 \text{ mg}_{\text{Pt}}/\text{cm}^2$ on the cathode that were fabricated for full size short stack testing.

Fiscal Year (FY) 2012 Objectives

The objectives of this project continue to be development of a durable, low-cost (both precious group metal [PGM] content and manufacturability), high-performance cathode electrode (catalyst and support), which is fully integrated into a proton exchange membrane electrode assembly (MEA) characterized by:

- Total PGM loading per MEA of $\leq 0.25 \text{ mg}/\text{cm}^2$
- Short-stack specific power density of $\leq 0.3 \text{ g}/\text{kW}$ at rated power

TABLE 1. Progress towards Meeting Technical Targets for Electrocatalysts and MEAs for Transportation Applications
(Values in blue are new targets/results this year)

| Characteristic | Units | Targets 2017 | Status: Values for roll-good CCM w/ 0.15mg _{Pt} /cm ² per MEA or as stated |
|---|---|--------------------------|---|
| PGM Total Content | g _{Pt} /kW _e rated in stack | 0.125 | 0.14 - 0.18 g _{Pt} /kW for cell 0.6 < V < 0.65 at 80 °C and 150kPaa to 250 kPaa outlet. Pt ₃ Ni ₇ , 50 cm ² cell w/ 0.15 mg/cm ² total Pt. |
| PGM Total Loading | mg PGM / cm ² total | 0.125 | 0.15 to 0.20, A+C with PtCoMn alloy 0.15 A+C with Pt/Pt ₃ Ni ₇ |
| Mass Activity (150kPa H ₂ /O ₂ , 80°C, 100% RH, 1050 sec) | A/mg-Pt @ 900 mV, 150kPa O ₂ | 0.44 | 0.24 A/mg in 50 cm ² w/ PtCoMn 0.47 – 0.67 A/mg in 50 cm ² with Pt ₃ Ni ₇ |
| Specific Activity (150 kPa H ₂ /O ₂ at 80°C, 100% RH) | mA/cm ² -Pt @ 900 mV | 0.720 | 2.1 for PtCoMn, 0.1mg _{Pt} /cm ² 2.7-3.0 for R2R Pt ₃ Ni ₇ , 0.125 mg _{Pt} /cm ² |
| Durability: 30,000 cycles 0.6 -1.0V, 50mV/sec, 80/80/80°C, 100kPa, H ₂ /N ₂ | - mV at 0.8 A/cm ² - % ECSA loss - % Mass activity | < 30mV < 40% < 40% | 10±7mV loss at 0.8 A/cm ² 16±2% loss ECSA, PtCoMn 37±2% loss mass activity |
| Durability: 1.2 V for 400 hrs. at 80°C, H ₂ /N ₂ , 150kPa, 100% RH | - mV at 1.5 A/cm ² % ECSA loss % Mass activity | < 30mV < 40% < 40% | 10 mV loss at 1.5 A/cm ² 10% loss ECSA 10 % loss mass activity |
| Durability: OCV hold for 500 hrs. 250/200 kPa H ₂ /air, 90°C, 30%RH | H ₂ X-over mA/cm ² % OCV loss | < 20 < 20 % | 13 ± 4 mA/cm ² at 500 hrs (5 MEAs) 12 ± 5 % OCV loss in 500 hrs |
| Durability under Load Cycling (membrane lifetime test) | Hours, T ≤ 80°C Hours, T > 80°C | 5000 5000 | 9000 hrs, 3M PEM (20µm, 850 EW w/ stabilizers), 50cm ² , 80/64/64 °C 2000 hrs (OEM short stack, 0.1/0.15) |

CCM – catalyst-coated membrane; RH – relative humidity; OEM - original equipment manufacturer

FY 2012 Accomplishments

New catalyst activity and understanding; annealing and process scale up (Task 1.3)

- Extended the enhanced catalyst deposition process improvement (P1) from pure Pt and PtCoMn to Pt₃Ni₇, obtaining same dramatic gains in Pt(hkl) grain size with a simpler, more cost-effective coating process.
- Screened over 100 different ex situ de-alloying conditions in batch processes for impact on fuel cell performance. Down-selected to one de-alloying condition that is 240 times faster than initial nitric acid bath conditions.
- Successfully transferred faster ex situ dealloy process to a roll-to-roll pilot-scale process that maintained the 240-fold increased dealloying rate:
 - Applied 240x roll-to-roll dealloying and surface energy treatment (SET, annealing) processes to 0.12 mg-Pt/cm² loaded as-made Pt₃Ni₇ that generated cathode mass activities in 50-cm² cells at GM ranging from 0.47 A/mg to 0.67 A/mg depending on 3M's MEA membrane cleaning process and ORR protocol used by GM.
 - Achieved 0.14–0.18 g_{Pt}/kW over 0.6 to 0.65 V, at 80°C and 150–250 kPa using 0.15 mg/cm² total Pt in the MEA.

Met 2017 cyclic voltammetry (CV) cycling and open circuit voltage (OCV) targets with MEA type used in short-stack testing (Task 2)

- 30,000 CV cycle test: Demonstrated 10±7 mV loss at 0.8 A/cm², 16±2% loss of electrochemical surface area, and 37±2% loss of mass activity w/MEA used in the second short-stack tests.
- Met 3M OCV hold test: 570 hours with OCV loss = 13% under 50 kPa H₂ overpressure.

Membrane-electrode integration and catalyst-coated membrane (CCM) scale up (Task 5.1)

- Produced over 60,000 linear ft combined of NSTF substrate, coated-catalyst supports, and catalyst-coated membrane for process development, short stack and customer use.

Short-stack testing with PtCoMn-based NSTF electrodes (Task 5.3)

- Completed first 29-cell rainbow short stack performance testing at GM to down-select the MEA configuration from 6 to 1 configuration for a final second durability short-stack test.

- Initiated durability cycling tests with second short stack (20 cells with one type of 3M MEA), however tests were not completed before end of project.



Introduction

State-of-the-art proton exchange membrane (PEM) fuel cell electrocatalyst technology utilized in today's prototype fuel cell vehicles reveals limitations with respect to general durability and robustness under start-stop cycling, adequate performance with low PGM loadings, and low-cost manufacturability. To a large degree, these deficiencies are traceable to properties of the conventional carbon supported dispersed Pt catalysts in use today and issues with membrane integration. The research and development of this project are focused on overcoming these three most critical barriers for fuel cell MEA automotive deployment by using an alternative catalyst support and deposition method.

Approach

The approach to achieve the above objectives builds on a fifteen-year DOE/3M-funded development of the 3M NSTF catalyst and MEA technology. The NSTF catalyst fundamentally has higher specific activity for oxygen reduction [1-11], removes all durability issues with carbon supports, demonstrates much lower losses due to Pt dissolution and membrane chemical attack [12-15], and has significant high volume all-dry roll-good manufacturing advantages [16].

The scope of work in the initial three-year budget period included extensive work at 3M to increase the NSTF catalyst support film surface area, fabrication and screening of new alloys in 50-cm² single cells, and evaluation of multiple deposition parameters to obtain increased catalyst surface area and utilization. Complementary to this work at 3M, collaborative work included high throughput fabrication and characterization of new multi-element Pt alloys (ternaries and quaternaries) with Dalhousie University, fundamental catalyst characterization studies with ANL, and development and evaluation of a pseudo-rotating disk electrode (RDE) catalyst evaluation technique with JPL. Research last year (the fourth year) focused at 3M on continued studies of water management improvements for cool/wet operation via optimization of materials, electrode structure and operating conditions; catalyst fabrication process improvements for increased catalyst performance and production efficiency; in-depth MEA component screening to down-select final configurations for the final short-stack testing; continued accelerated testing to benchmark the NSTF-MEA durability with each generation of MEA components; and initial fabrication of roll-good materials for initial stack testing by the GM fuel cell laboratory.

This final year the focus was on a) completing the first year short stack testing to down-select a final MEA type for a second (durability) stack; b) resolving specific production and MEA integration issues related to the final stack MEAs; c) second stack durability protocol development and initial testing; d) extension of the improved, more cost effective P1 deposition process to the as-made NSTF-Pt₃Ni₇ catalysts; and e) development of fast roll-to-roll capable de-alloying and annealing processes for the NSTF "Pt₃Ni₇" catalysts.

Results

The technical accomplishments for the fifth and final year fall roughly into three areas of research and development corresponding to project tasks 1, 2, and 5.3. We briefly summarize the main results from each of these areas.

Task 1

The NSTF-Pt₆₈Co₂₉Mn₃ catalyst has been the workhorse cathode and anode of choice for a number of years. As indicated last year, with it we have been able to exceed the previous DOE 2015 target of 0.2 g-Pt/kW in a full-size short stack with 0.05 mg/cm² of PGM on the anode and 0.1 mg/cm² on the cathode [17]. More recent work has focused on improving the NSTF-catalyst roll-to-roll process so that the support whiskers and sputter deposited catalyst alloy can be applied simultaneously on the moving substrate web in a single step. This new process, called P1, offers greater simplicity and more cost-effective coating than the standard process called P4. In last year's report we showed the positive impact on PtCoMn crystallite size and surface smoothness for loadings between 0.054 and 0.184 mg_{Pt}/cm² produced by using the improved P1 process, as well as small fuel cell performance benefits. As indicated in our 2011 annual report, to reach the new more rigorous DOE 2017 target for cathode catalyst inverse mass specific power density of 0.125 g-Pt/kW, a new catalyst alloy will be required, and the NSTF-Pt₃Ni₇ as-made alloy [18] was the best candidate. We also pointed out the important effects of two post-processes, ex situ dealloying and SET "annealing", that when applied to the as-made NSTF-Pt₃Ni₇ significantly improved the mass activity and helped with the limiting current density issue that comes with excess Ni going into the PEM. This past year we have applied the P1 process to the as-made NSTF-Pt₃Ni₇ with similar benefits as seen with the PtCoMn (see slide 30, in reference 19), and put significant effort into developing and scaling up the dealloying and SET post-processes.

A broad series of batch process experiments were completed to investigate the effects of both electrochemical and passive chemical dealloying, with acid bath composition, concentrations, time and temperature as parameters. These were applied to various catalyst material factors, including Pt₃Ni₇ loading (0.075 to 0.15 mg-Pt/cm²), alloy homogeneity (P1 vs. P4), and the SET annealing process. The objective was

to try and optimize the process both to improve the limiting current density without loss of ORR activity, and to find conditions suitable for roll-to-roll processing at reasonable web speeds. Over 100 different combinations of the acid bath conditions, catalyst fabrication and process parameters were screened and tested in 50-cm² fuel cells in duplicate. Conditions were found that allowed speeding up the rate of dealloying by a factor of 240 over the baseline nitric acid bath soak. Using existing facilities at 3M, full-width roll-to-roll dealloying was developed with the faster process conditions. Sixteen ORR relevant kinetic and performance metrics were extracted from the fuel cell potentiodynamic and galvanodynamic polarization curves and correlated with materials and proprietary process parameters. Without disclosing proprietary process information, a total of 38 global scatter-plots can be generated to illustrate how critical metrics vary with two basic catalyst properties, surface area and loading. Figure 1(A) shows one such global metric plot of ORR absolute activity at 900 mV under 150 kPa saturated oxygen, versus the surface area enhancement factor in cm² of Pt per cm² of planar surface area. The inset graph in Figure 1(A) illustrates the conditions and protocol used for the ORR measurement; for the MEA ORR activity measurement the total current density is recorded 1,050 seconds after setting the potential at 900 mV. The current density, in mA/cm²_{planar} is decreasing as the Pt is oxidizing, so the ORR activity is measured on an oxidized surface in contrast to most RDE measurements [9]. The slope of the scatter plot in Figure 1(A) gives an indication of the high specific activity of the Pt₃Ni₇ derived catalysts, ~3.6 mA/cm²-Pt, which is somewhat higher than an average of the actual values measured for each sample. Figure 1(B) is a similar scatter plot showing that roll-to-roll dealloying and annealing conditions were found which generated mass activities of 0.44 A/mg-Pt using the 3M ORR protocol above, equivalent to the DOE 2017 target. These were obtained at higher loadings than demonstrated in last year's report for SET batch treated as-made Pt₃Ni₇ catalysts with loadings below 0.09 mg/cm² that did not give high absolute fuel cell performance at either low or high current densities. Other such plots (see slides 21 and 23 in reference 19) show that mass specific surface areas of 15 to 20 m²/g were common for the dealloyed/SET annealed catalysts with the highest mass activities. The increased surface area and specific activity both contributed to the improved mass activity.

CCMs made with P1 fabricated, roll-to-roll dealloyed and SET treated Pt₃Ni₇ alloy cathodes at loadings of 0.121±0.003 mg-Pt/cm² were tested at GM using both their own and 3M's ORR mass activity protocols. These CCMs were made at 3M with 3M membranes that were either as-made or cleaned using both nitric acid and peroxide baths. Table 2 summarizes the results from the GM measurements in which the standard treatment refers to the usual NSTF thermal cycling for break-in conditioning. The last column in Table 2 shows that a proprietary GM additional pretreatment

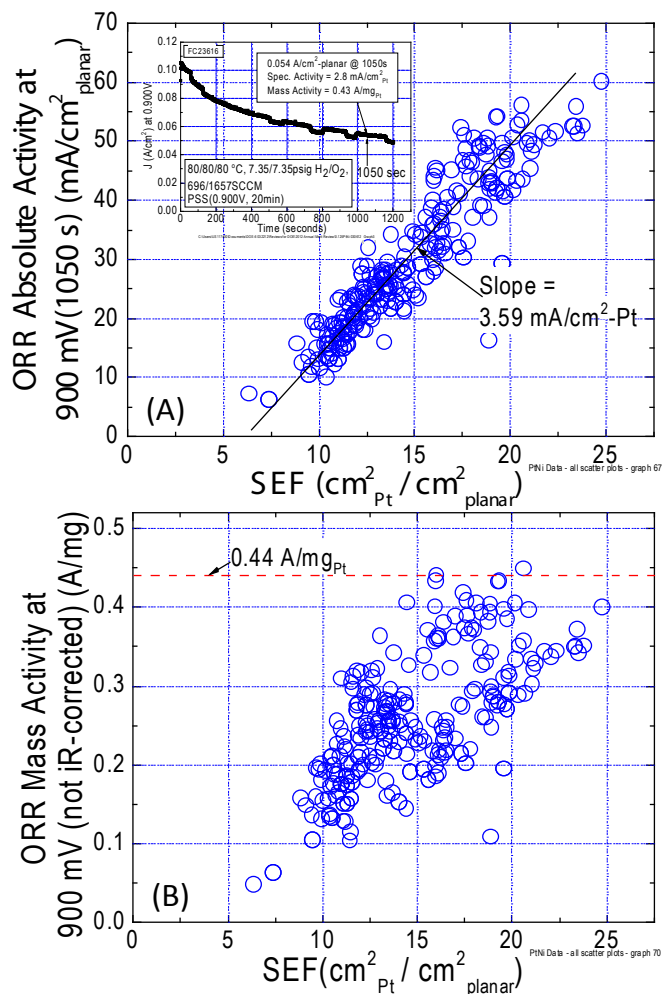


FIGURE 1. (A) ORR absolute activity as a function of surface area enhancement factor for over 100 different NSTF-PtNi cathodes derived from the as-deposited Pt₃Ni₇ catalysts for various loading, dealloying and SET post-process parameters. (B) Mass activity as a function of surface area enhancement factor for the same MEA cathodes as in (A).

TABLE 2. Mass activities measured at GM of 3M CCMs having NSTF Pt₃Ni₇ roll-to-roll dealloyed and SET treated cathodes laminated to either cleaned or as-made 3M PEMs. Cathode loadings were 0.121±0.003 mg-Pt/cm².

| Sample membrane used in CCM | Protocol used for measurement | Standard Treatment (A/mg) | With Additional Pretreatment (A/mg) |
|-----------------------------|-------------------------------|---------------------------|-------------------------------------|
| As-made PEM | GM | 0.45 | 0.47 |
| As-made PEM | 3M | 0.52 | 0.67 |
| Cleaned PEM #1 | GM | 0.41 | 0.54 |
| Cleaned PEM #1 | 3M | 0.23 | 0.65 |
| Cleaned PEM #2 | GM | 0.41 | 0.58 |
| Cleaned PEM #2 | 3M | 0.21 | 0.62 |

process can further substantially increase the apparent mass activities over the standard treatment, which now cover the ranges of 0.47 to 0.58 A/mg by the GM ORR protocol and 0.62 to 0.67 A/mg using the 3M protocol.

To test the best overall performance possible with these roll-to-roll dealloyed/annealed Pt/Ni cathode catalysts, 50-cm² CCMs were prepared with Pt₃Ni₇ cathode loadings of 0.121±0.003 mg-Pt/cm², pure NSTF-Pt anodes with 0.030 mg/cm², and 3M 24 micron, 850 equivalent weight non-supported membrane, as-made. GDLs were the 3M standard 2979, and testing was done with quad-serpentine flow fields. Figure 2(A) shows galvanodynamic scan (GDS) polarization curves at three pressures and the conditions indicated in the legend. The inset graph shows that the higher kinetic performance expected from the high mass activity is realized in the MEAs at 0.8 V (quarter peak power point), with 0.21 to 0.31 A/cm² at 0.8 V obtained over a 150 to 250 kPa outlet pressure range. Even though the limiting current densities are still not as high as they should be, there is a substantial improvement over that obtained with the as-made Pt₃Ni₇ catalysts (about 0.8 A/cm², as shown in [17] and reasonable current densities are being realized at 650 mV. Figure 2(B) shows the inverse specific power density plots for the three polarization curves shown in Figure 2(A). These advanced PtNi cathodes with the lower anode loading on a 24-micron thick membrane exhibit values of 0.14 to 0.18 g-Pt/kW over 0.6 to 0.65 V and the 150 to 250 kPa operating range at 80°C. There is little temperature sensitivity over the 80 to 95°C range (see slide 34 in reference 19). Further improvements in understanding and controlling the dealloying and SET treatment processes are required to take advantage of thinner membranes which should further improve their performance towards the 0.125 g-Pt/kW target for 2017.

Task 5.3 – stack 1

The other major effort over the past year has been to prepare for, fabricate roll-good CCMs and execute independent short-stack testing of MEAs comprising catalysts and process advancements developed under this project through early 2011. The stack testing has been provided by GM's fuel cell facilities at Honeoye Falls, NY. Last year's annual report summarized work done in 2010/2011 towards MEA component down-selection for initial and final stack testing. Two stack tests were planned. The first was a 29-cell "Rainbow" stack, one "color" for each MEA type, for initial beginning of life operation under various automotive relevant test protocols. This first stack was to enable down-selecting to the final MEA type to be tested in a second stack under an accelerated durability protocol. The first stack compared the six MEA configurations shown in Table 3.

The stack 1 performance was a surprise in that it significantly underperformed what we expected based on 50-cm² single cells. Figure 3(A) compares polarization curves from the four configuration-1 MEAs in stack 1 with what we and GM had previously measured in 50-cm² single cells for similar MEAs under similar conditions.

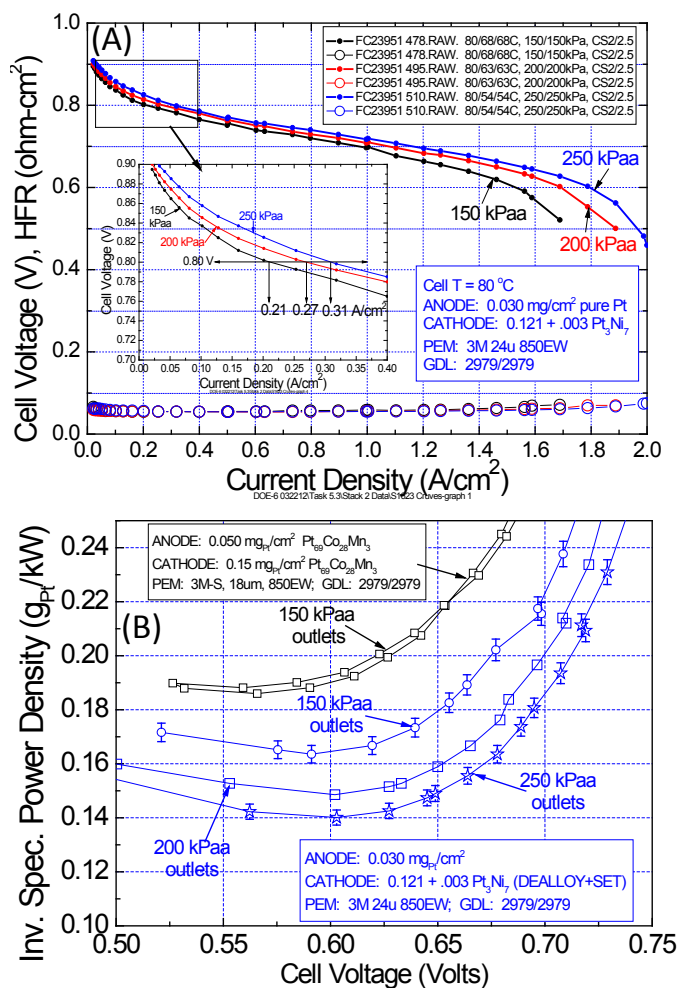


FIGURE 2. (A) GDS polarization curve performances for the 2012 "best of class" MEA based on the roll-to-roll dealloyed and SET "annealed" NSTF-Pt₃Ni₇ cathodes. The MEA contained a total PGM loading of 0.15 mg-Pt/cm². (B) Inverse specific power density versus cell voltage for the three GDS polarization curves shown in (A).

Significant effort was spent by both 3M and GM to "debug" the low performance over a 2.5-month period. A number of confounding issues contributed, including test station water purity, properties or contamination of the ionomer used for the membrane lots used to fabricate the CCMs, and more effective break-in conditioning that is possible with single cells versus large area stacks. Further tests revealed the catalyst ORR metrics and surface areas were as expected, stack compression was nominal, but 50-cm² CCMs made in the lab with the same membrane lots as used in roll-to-roll fabrication of the CCM for stack 1 also underperformed what was expected. CCMs from the same roll-to-roll lots were also tested in a 3M short stack (5 cell, 312 cm²) and found to underperform the single cell results at ambient pressure but give similar results at 22 psig, and slightly better than the GM stack at a similar pressure (see slide 8 in reference 19). Still the GM stack 1 tests were successful in clearly being

TABLE 3. Definition of six MEA configurations evaluated in Stack 1, a 29-cell “rainbow” stack

| CCM ID | PEM | Anode | Cathode | S1622 Cells |
|-----------|--------------------|----------------|----------------------|-------------|
| Config. 1 | 3M-24um (w/add. 2) | 0.05 P1 PtCoMn | 0.15 P4 PtCoMn + SET | 9-12 |
| | 3M-24um (w/add. 1) | 0.05 P1 PtCoMn | | |
| Config. 2 | 3M-24um (w/add. 2) | 0.05 P1 PtCoMn | 0.10 P1 PtCoMn | 5-8, 22-25 |
| Config. 3 | 3M-S | 0.05 P1 PtCoMn | 0.15 P1 PtCoMn | 13-16 |
| | | 0.05 P1 PtCoMn | | |
| Config. 6 | 3M-X | 0.05 P1 PtCoMn | 0.15 P1 PtCoMn | 17,18 |
| Config. 7 | | 0.05 P1 PtCoMn | 0.10 P1 PtCoMn | 19-21 |
| Config. 8 | 3M-24um (w/add. 1) | 0.05 P1 PtCoMn | 0.15 P1 PtCoMn | 1-4, 26-29 |

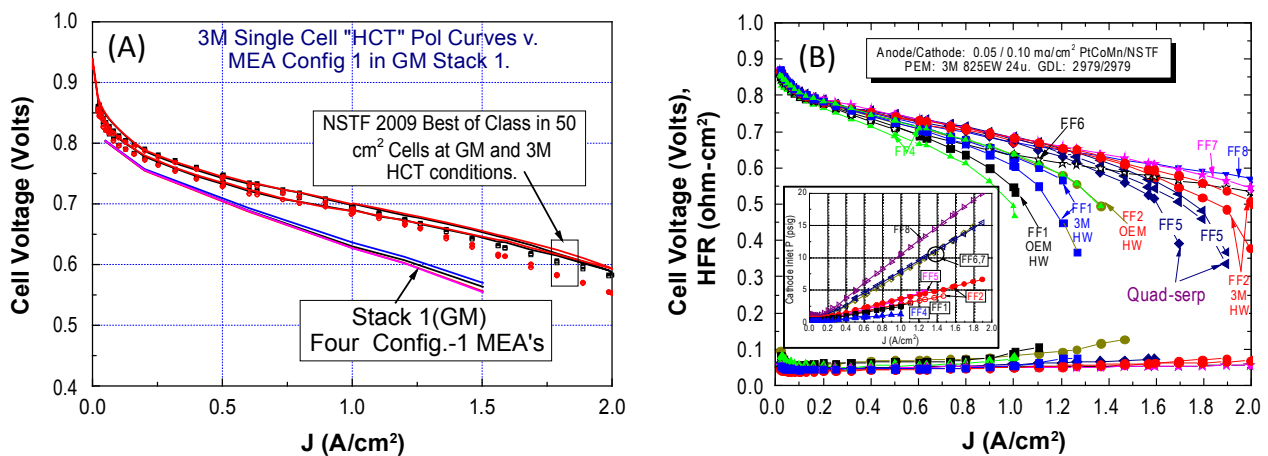


FIGURE 3. (A) Comparison of the polarization curves obtained from the four configuration 1 MEAs in stack 1, with the expected performance based on 50-cm² single-cell tests measured both at 3M and GM. (B) Comparison of single cell (50 cm²) GDS polarization curves from the standard quad serpentine flow field (FF5) with six alternative flow fields: FF1 = 6 serpentine channels, 2 loops, 2 mm channel width, 2 mm land width, ~0.3 mm channel depth; FF2 = 24 serpentine channels, 2 loops, 0.5 mm channel width, 0.5 mm land width, ~0.25 mm channel depth; FF4 = 9 serpentine channels, 4 loops, 1 mm channel width, 0.6 mm land width, 1 mm channel depth; FF5 (quad-serpentine) = 4 serpentine channels, 10 loops, 0.8 mm channel width, 0.8 mm land width, 1 mm channel depth; FF6 = single channel 3M Zig-Zag (21); FF7 = 2 serpentine channels, 21 loops, 1 mm channel width, 1 mm land width, 1 mm channel depth; FF8 = single serpentine, 43 loops, 0.8 mm channel width, 1.0 mm land width, 1.5 mm channel depth.

able to delineate the performance order of the six MEA configuration types, with MEA configuration 1 being the best and down-selected MEA for the eventual stack 2 durability testing (see slide 7 in reference 19). Figure 4 shows a pressure-series of polarization curves, comparing the 4-cell average stack performance of the configuration-1 MEAs with six, 50-cm² single-cell tests (done at 3M) having the identical type MEA. (The test conditions used for the data in Figure 4 were those supplied by the systems modeling group at ANL, Ahluwalia et al., and used by 3M for generating other MEA data requested by that group.) Performance improves with

pressure similarly in single cells and the stack, consistent with mass transport issues. The stack 1, MEA type 1 performance average underperforms the single-cell tests at all conditions, but not by too much as long as the current density is below ~1.5 A/cm². At higher current densities the stack 1 performance falls considerably short of the small single cells.

There is still a question of the possible impact of flow field differences between the quad-serpentine 50-cm² cells used at 3M and the flow field of the GM stack. Flow fields

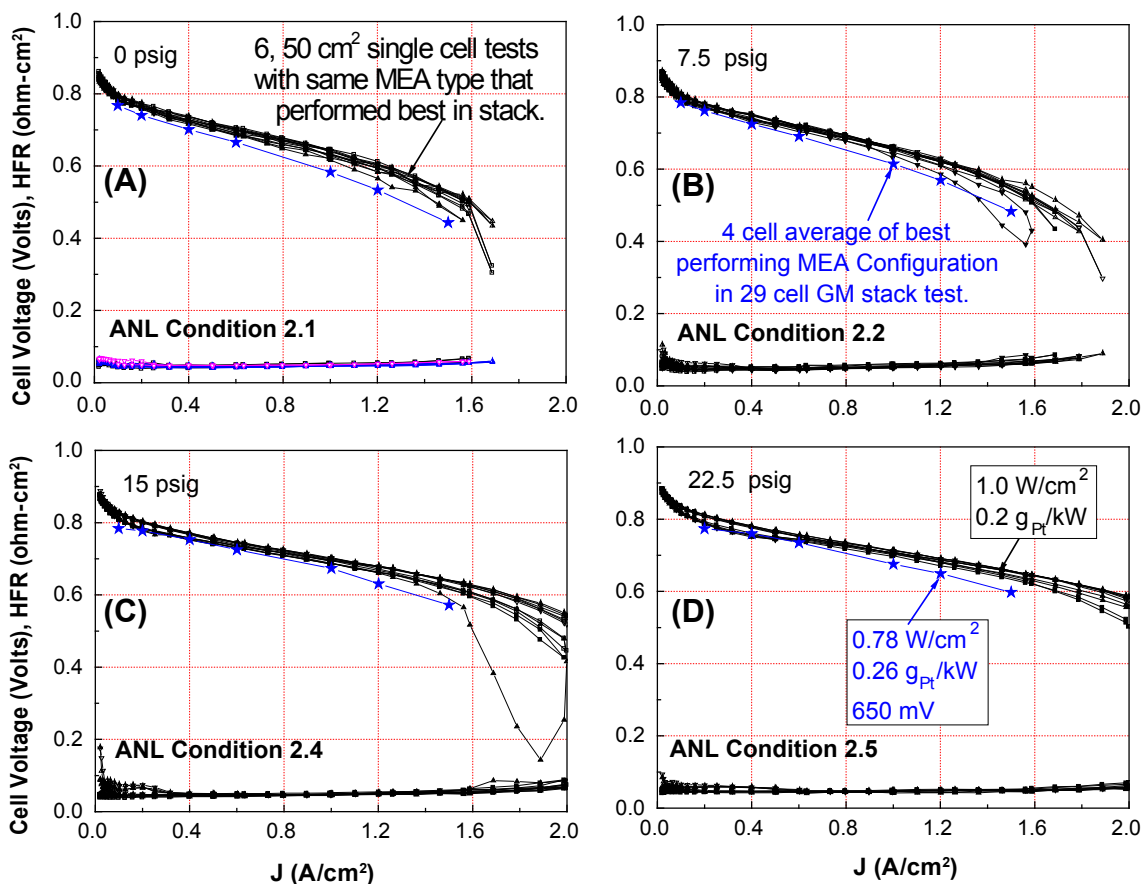


FIGURE 4. (a) GDS polarization curve comparisons at four pressures, of the 4-cell average GM stack 1 performance (configuration-1 MEAs) with six, 50-cm² single-cell tests (at 3M) having the identical type MEA. GDS polarization scan: 0.02->2->0.02 A/cm², 10 steps/decade, 120 s/pt, 0.4 V limit, 0.1 max current density step. The test conditions used for the data in Figure 4 were those supplied by the systems modeling group at ANL (Ahluwalia et al.) and used by 3M for generating other MEA data requested by that group:

ANL Condition 2.1 = 80/73/73°C, 1/1 atm H₂/Air, CS(2,100)/CS(2.0, 200)

ANL Condition 2.2 = 80/70/70°C, 1.25/1.25 atm H₂/Air, CS(2,100)/CS(2.0, 200)

ANL Condition 2.4 = 80/56/56°C, 2.0/2.0 atm H₂/Air, CS(2,100)/CS(2.0, 200)

ANL Condition 2.5 = 80/40/40°C, 2.5/2.5 atm H₂/Air, CS(2,100)/CS(2.0, 200)

have never been systematically optimized for the NSTF type ultra-thin electrodes yet can clearly have a strong effect that might not be considered an issue with conventional thick layer electrodes. To establish a baseline of these effects we initiated tests of NSTF MEAs having a similar construction as MEA configuration 1 (but nominally non-contaminated PEM lot) in a series of nine alternative flow field designs. The 50-cm² flow field graphite blocks were all tested in one set of 3M cell hardware or one set of OEM cell hardware (OEM HW). Figure 3(B) compares the GDS polarization curves from six alternative flow fields with the standard quad-serpentine (FF5), completed at the end of this project. As shown there is a huge impact of the flow field type on the limiting current density, and several that perform better than our standard quad serpentine. The HFR differences are small and not responsible for the differences when the graphite blocks are all in the same set of 3M Al cell hardware (3M HW). Cathode pressure drop was also measured for

the different flow fields, and can explain the high current density performance gain with the single channel flow fields FF7 and FF8 relative to the standard FF5. However, the FF2 flow field blocks used in the 3M Hardware significantly out-performed the standard with similar or slightly lower pressure drops. This suggests that the smaller (0.5 mm) channel and land width dimensions of the FF2 are key to improved performance and a guide to optimizing the flow field for NSTF MEAs.

Task 5.3 – stack 2

The down-selected MEA configuration type 1 in Table 3 from the stack 1 tests was intended to be the sole MEA type used in the second stack, slated for accelerated durability testing. Due to various issues, this exact MEA configuration 1 did not end up being the final MEA type used in stack 2, as a different membrane was ultimately

used. Factoring into the decision were NSTF CCM-production issues with available standard, non-supported PEM lots, which made it attractive to move to the newer generation membrane. This gave the opportunity to switch the membrane type from a standard, non-supported membrane to a new, 3M experimental supported membrane, which previous data had indicated helped improve certain accelerated MEA durability tests. There was risk associated with this decision as these were still experimental PEMs and optimized integration with the NSTF had not been completed. Work related to resolving these issues required an additional 9 month no-cost extension of the project. The final MEA stack 2 catalysts used were the same as that used in configuration 1 in Table 3. We subsequently discovered that performance in 50-cm² single cells was again much worse than expected. Once the final CCM roll-goods were fabricated, and shortly after shipment to GM, the reason for the underperformance was tracked to the inadvertent production release of an experimental PEM lot to make the CCMs that had been put on hold due to suspected contamination of its ionomer. Due to lack of time and funding to make further MEAs, the decision was made to continue with the stack 2 testing with these CCMs. Figure 5(A) compares 50-cm² single-cell beginning of life performances at 7.5 psig H₂/air from MEAs using the same CCM lots as used in stack 2, with that from MEAs using CCMs made with the same catalyst lots but with normally performing experimental 3M-supported membrane (best 3M-S) at 7.5 and 22 psig H₂/air. In addition to the dramatic loss of limiting current density with the contaminated PEM, the ORR activities were slightly depressed, while the catalyst electrochemical surface areas and MEA HFR were normal. Surprisingly however, as the stack 2 type MEA was tested in a single 50-cm² cell using the same cycling durability protocol discussed below for stack 2, but with periodic recovery, the MEA performance continuously improved for nearly 400 hours and approached that of the best 3M-S curves shown in Figure 5(A).

Despite these issues with beginning of life performance, Figures 5(B) and 5(C) show that the MEAs using CCMs from the same lots as in the stack 2 MEAs, passed both the DOE OCV hold tests and the CV cycling tests. The objective of the OCV hold test is assessment of the whole MEA/membrane durability at OCV at 90°C under 30% RH, 250/200 kPa H₂/air. The target is 500 hours with less than 20% loss of OCV. This MEA went 570 hours with a 13% loss under the 50 kPa H₂ overpressure. The CV cycling accelerated stress test characterizes the resistance of the catalyst to dissolution, agglomeration or loss of activity due to high voltage cycling. The protocol involves cycling the cathode between 0.6 and 1.0 volts and back again at 50 mV/sec under 100/100 kPa H₂/N₂ at 80°C cell and dew points. The target is to have after 30,000 cycles, less than 40% loss of surface area and ORR mass activity and a polarization curve loss of less than 30 mV at 0.8 A/cm².

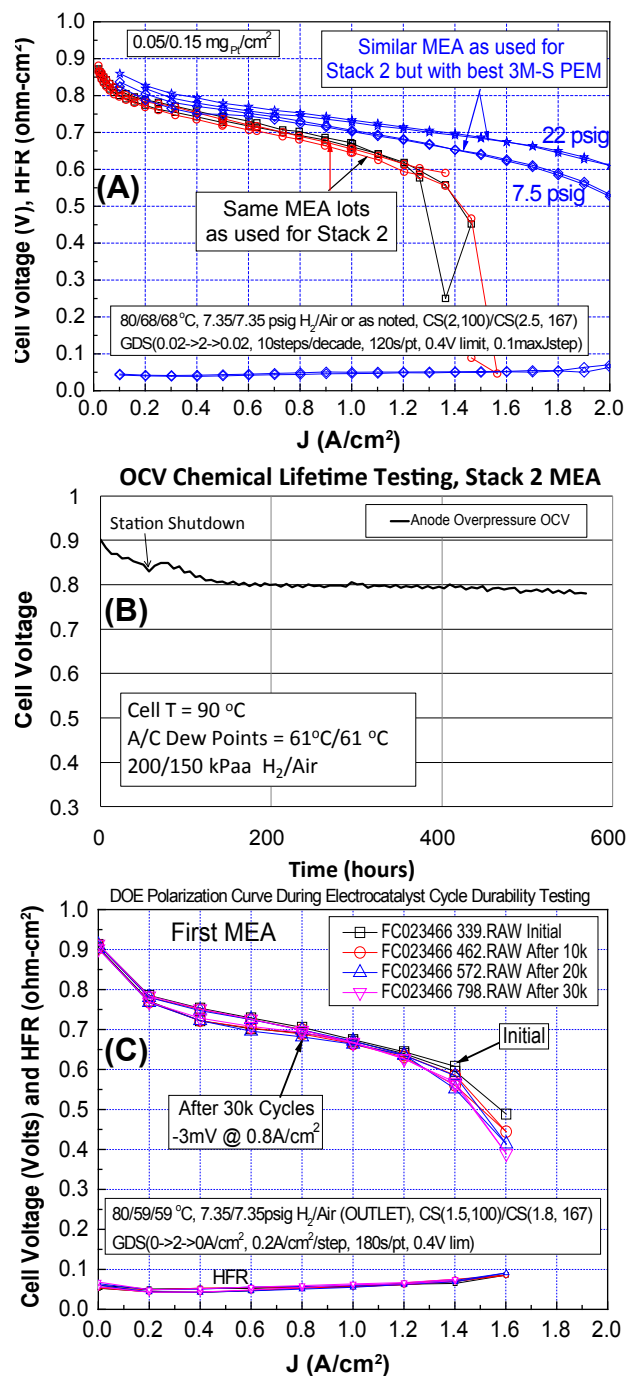


FIGURE 5. (A) Single-cell 50-cm² GDS polarization curves at 7.5 psig from MEAs taken from the same lot as used for stack 2, compared with a similar MEA that used a known non-contaminated 3M-S membrane, at both 7.5 and 22 psig. (B) OCV hold versus time durability test for an MEA identical to that used for stack 2. (C) GDS polarization curve and HFR impedance for an MEA identical to that used for stack 2 before, during and after 30,000 CV cycles from 0.6 to 1 volt.

The stack 2 lot of MEAs (two were tested) demonstrated a 10±7 mV loss at 0.8 A/cm², 16±2% loss of surface area, and 37±2% loss of mass activity. This is the first time we have

TABLE 4. Conditions used for beginning of life tests of stack 2

| Stack Cond. | T (°C) | An/Ca St. | An RH in (%) | Can RH out (%) | Pressure |
|-------------|--------|-----------|--------------|----------------|----------|
| 1 | ~ 82 | ~1.5/1.8 | 25 | 82 | Variable |
| 2 | ~ 75 | ~1.5/1.8 | 30 | 85 | Variable |
| 3 | ~ 65 | ~2 /1.8 | 30 | ≥100 | Variable |
| 4 | ~ 78 | ~1.5/1.8 | 20 | 65 | Variable |
| 5 | ~ 78 | ~2.0/1.8 | ≥100 | ≥100 | Variable |

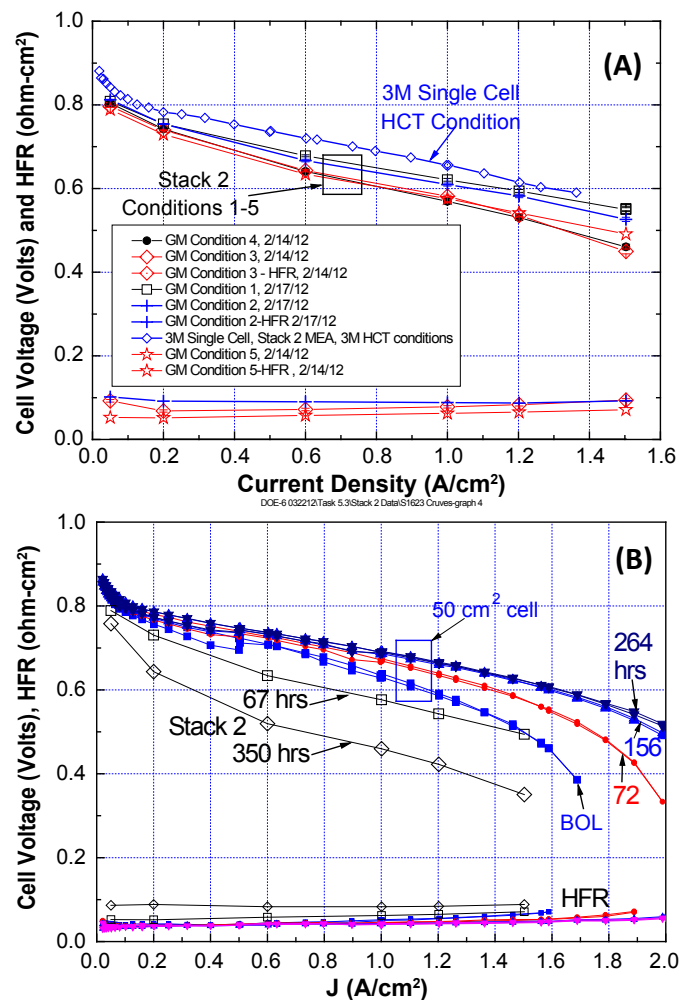


FIGURE 6. (A) Average MEA beginning-of-life performance in stack 2 at the five conditions shown in Table 3, compared to the 50-cm² single-cell test under GDS high current test conditions of: 80/68/68°C cell temperature/anode/cathode dew points; 150 kPa H₂/air; and anode/cathode stoichiometric flows of 2/2.5. GDS polarization curve conditions are same as in Figure 3. (B) Comparison of stack 2 performance change after 4 sets of 1,500 load cycles (~300 hours) with the performance change of the same MEA type in a 50-cm² single-cell (at 3M) after 200 hours of a similar load cycle, interspersed with periodic recovery shutdowns every 12 or 24 hours. Procedure Loop: 1) 5 thermal cycles, 2) polarization curves, 3) 12- or 24-hr cycling under following procedure - 3a) 80/83/83°C, H₂+N₂/Air, 0/0psig, PSS(x,30s); x=0.85, 0.60 V - 3b) 80/53/53°C, H₂+N₂/Air, 0/0psig, GSS(x,30s); x=0.02, 0.10 A/cm.

been able to demonstrate meeting all the targets with this accelerated stress test.

The stack 2 beginning of life performance was evaluated under five different sets of operating conditions as in Table 4. Consistent with the single-cell tests, the beginning of life stack 2 MEA performances were much lower than expected and lower than single-cell tests with the same MEA lot, but did not vary significantly from the driest to the wettest conditions, see Figure 6(A). Average cathode surface areas were approximately normal at 8.2 m²/g, while in-stack shorting resistances were lower than the standard GM baseline MEAs used as end-cells in the 29-cell short stack.

The objective of stack 2 was to conduct a load-cycling protocol representative of an accelerated stress test for lifetime durability. The protocol chosen was close to that recommended by the U.S. Drive Fuel Cell Tech Team with some modifications to adapt it to the under-performing MEA and the slower cool-wet transient behavior of the thin-layer NSTF electrodes with the GDLs used (see reference 20 for impact of anode GDL type on this behavior). Higher pressure, controlled current ramp rate, and minimum voltage control were the main modifications to the protocol. After four sets of 1,500 cycles, ~350 hours of operation, the following observations were made: two point (beginning and end) performance decay rates were much higher than expected (by factors of 3x to 8x); cross-over leak rates and hydrogen take-over in the cells were high; high frequency resistance increased with time but could not account for the lost performance; there were significant fluctuations in performance between each of the 4-cycle sets. Figure 6(B) shows the beginning-of-life performance (67 hours, open squares) of the stack and that after 350 hours (open diamonds) of cycling, showing extreme decay. Also shown in 6(B) are the performances of the same stack 2 type MEA tested in a 50-cm² single cell at 3M at beginning of life and after 72 hours (red circles), 156 hours (up triangles) and 264 hours (down triangles) with nominally the same load cycling protocol. One key difference in the single cell tests and the stack tests is that the single cell was recovered periodically (12- or 24-hour period) by stopping the load cycling and doing five thermal cycles before resuming the load cycling. Thermal cycling is the typical break-in conditioning protocol used for NSTF MEAs and the large improvement in performance of the single-cell MEA seen with the load cycling is consistent with removal of impurities in the vicinity of the electrodes. The performance of the single-cell MEA in Figure 6(B) continued to improve or stabilized depending on current density for nearly 400 hours, after which its performance started to decay and by 580 hours it had failed due to edge failure of the CCM. This MEA did not have subgasket edge-protection which would be expected to improve lifetime significantly. Low performing cells in the stack 2 prevented going to high current densities and necessitated replacing MEAs and rebuilding the stack on two occasions. It was observed that the shorting resistance

for every cell, including the GM baseline cells, would significantly worsen (drop in value) after each such rebuild. It was eventually determined that further work with the stack would not be instructive and testing was discontinued just prior to the 6/30/12 end of this project.

Conclusions and Future Directions

The encouraging work with the NSTF Pt₃Ni₇ dealloying, annealing and membrane integration development will be continued in part in a follow-up DOE/3M project “High Performance, Durable, Low Cost Membrane Electrode Assemblies for Transportation Applications,” that is just beginning. Stack testing and GDL/MEA component integration will be a significant part of that effort and will hopefully identify the sources for some of the impedance, shorting, and contamination issues plaguing the stack testing in this project, as well as further understand the importance of the flow field design for optimum performance with ultra-thin electrodes.

FY 2012 Publications/Presentations

Publications

1. M.K. Debe, R.T. Atanasoski, and A.J. Steinbach, “Nanostructured Thin Film Electrocatalysts – Current Status and Future Potential,” *ECS Trans*, **41**(1) 937-954 (2011).
2. A. Steinbach, M. Debe, M. Pejsa, D. Peppin, A. Haug, M. Kurkowski and S. Maier-Hendricks, “Influence of Anode GDL on PEMFC Ultra-thin Electrode Water Management at Low Temperatures,” *ECS Trans*, **41**(1) 449-457 (2011).
3. Dennis van der Vliet, Chao Wang, Mark Debe, Radoslav Atanasoski, Nenad M. Markovic and Vojislav R. Stamenkovic, “Platinum-alloy Nanostructured Thin Film Catalysts for the Oxygen Reduction Reaction,” *Electrochim. Acta*, **56** 8695-8699 (2011).
4. Mark K. Debe, “Effect of Electrode Structure Surface Area Distribution on High Current Density Performance of PEM Fuel Cells,” *J. Electrochem. Soc* **159**(1) B54-B67 (2011).
5. Mark K. Debe, “Electrocatalyst Approaches and Challenges for Automotive Fuel Cells,” invited review article, *Nature*, **486**(9401) 43-51(2012).
6. Mark K. Debe, “Nanostructured Thin Film Electrocatalysts for PEM Fuel Cells – A Tutorial on the Fundamental Characteristics and Practical Properties of NSTF Catalysts,” *ECS Transactions* **45**, (2) 47-68 (2012).
7. M.K. Debe, S.M. Hendricks, G.D. Vernstrom, M. Meyers, M. Brostrom, M. Stephens, and Q. Chan, Jason Willey, Monjid Hamden, and Cortney K. Mittelsteadt, Christopher B. Capuano, Katherine Ayers and Everett Anderson, “Initial Performance and Durability of Ultra-low Loaded NSTF Electrodes for PEM Electrolyzers,” *J. Electrochem. Soc.*, **159**(6) K165-K176 (2012).
8. R.K. Ahluwalia, X. Wang, A. Lajunen, A.J. Steinbach, S.M. Hendricks, M.J. Kurkowski, and M.K. Debe, “Kinetics of Oxygen Reduction Reaction on Nanostructured Thin-Film Platinum Alloy Catalyst,” *Journal of Power Sources* **215** (2012) 77-88.
9. Dennis van der Vliet, Chao Wang, Dusan Tripkovic, Dusan Strmcnik, Xiaofeng Zhang, Mark Debe, Radoslav Atanasoski, Nenad M. Markovic and Vojislav R. Stamenkovic, “Metallic Nanotubes with Tunable Composition and Structure as Advanced Electrocatalysts,” submitted to *Nature Materials*, (2012).
10. J.E. Harlow, D.A. Steven, R.J. Sanderson G. C-K Liu, L.B. Lohstreter, G.D. Vernstrom, R.T. Atanasoski, M.K. Debe, and J.R. Dahn, “The oxygen reduction reaction activity of a Pt Mn binary composition spread,” *J. Electrochem. Soc.* **159** (6)¹ B670-B676 (2012).
11. Mark K. Debe et al., “Advanced Cathode Catalysts and Supports for PEM Fuel Cells,” DOE Hydrogen and Fuel Cells Program, FY 2011 Annual Progress Report, page 697-705.

Presentations

1. M. Debe, S.M. Hendricks, G. Vernstrom, J. Wiley, M. Hamden, C. Mittelsteadt, C. Capuano, K. Ayers and E. Anderson, “Initial Performance and Durability of Ultra-low Loaded NSTF Electrodes for PEM Electrolyzers,” Abs. #694, 220th ECS Meeting, Boston, MA, Oct., 2011.
2. M.K. Debe, Project review at the DOE Hydrogen Program 2012 Annual Merit Review, Washington, D.C., May 15, 2012, presentation FC001.
3. M.K. Debe (Invited), R.T. Atanasoski, and A.J. Steinbach, “Nanostructured Thin Film Electrocatalysts – Current Status and Future Potential,” 220th ECS Meeting, Boston, MA, Oct. 2011.
4. A. Steinbach, M. Debe, M. Pejsa, D. Peppin, A. Haug, M. Kurkowski and S.M. Hendricks, “Influence of Anode GDL on PEMFC Ultra-thin Electrode Water Management at Low Temperatures,” Abs. #781, 220th ECS Meeting, Boston, MA, Oct. 2011.
5. M. Debe, S.M. Hendricks, G. Vernstrom, J. Wiley, M. Hamden, C. Mittelsteadt, C. Capuano, K. Ayers and E. Anderson, “Initial Performance and Durability of Ultra-low Loaded NSTF Electrodes for PEM Electrolyzers,” 220th ECS Meeting, Boston, MA, Oct. 2011.
6. Mark K. Debe, (Invited), “Designing Electrocatalysts for Fuel Cell Vehicles-It’s going to Take More than Just High Activity,” Cornell University Annual Energy Materials Symposium, August 12, 2011.
7. X. Wang, R.K. Ahluwalia, A.J. Steinbach, and M.K. Debe, “Dynamic Performance of Automotive Fuel Cell Systems with Low Platinum Loadings,” 220th ECS Meeting, Boston, MA, Oct. 2011.
8. M.K. Debe (Invited plenary), “PEM Fuel Cell Performance Factors Determined by Electrocatalyst Structure Characteristics,” Zing International Hydrogen and Fuel Cell Conference, Riviera Maya, Mexico, Dec. 1, 2011.
9. Mark K. Debe, (Invited), “A New Generation of Catalysts and Electrode Designs for PEM Water Electrolysis: Fundamentals and Practical Examples,” Hydrogen Production and Water Electrolysis Short Course, North-West University, Potchefstroom, South Africa, April 18–19, 2012.

10. Mark K. Debe, (Invited), "Nanostructured Thin Film Electrocatalysts for PEM Fuel Cells – A Tutorial on the Fundamental Characteristics and Practical Properties of NSTF Catalysts," 221st ECS Meeting, Seattle, Washington, May 8, 2012.

12. R.K. Ahluwalia, X. Wang, A. Lajunen, A.J. Steinbach, S.M. Hendricks, M.J. Kurkowski and M.K. Debe, "Performance of PEFC Stacks with Low-Pt Nanostructured Thin Film Catalysts at High Power Densities," submitted 2012 Grove Conference.

13. Mark K. Debe, (Invited), "Looking to the Future and Assuming Success – Are current approaches for MEA electrocatalyst and membrane integration on a path to meet cost and high volume manufacturing requirements for automotive PEM fuel cells?," 6th International Fuel Cell Workshop - 2012, Kofu, Yamanashi, Japan, August 2-3, 2012.

References

1. Arman Bonakdarpour, Krystal Stevens, George D. Vernstrom, Radoslav Atanasoski, Alison K. Schmoeckel, Mark K. Debe, and Jeff R. Dahn, "Oxygen Reduction Activity of Pt and Pt-Mn-Co Electrocatalysts Sputtered on Nanostructured Thin Film Support," *Electrochimica Acta* **53** (2007) 688-694.
2. D. Van der Vliet, D. Strmcnik, C. Wang, R. Atanasoski, M. Debe, N. Markovic and V. Stamenkovic, "Multimetallic Catalysts for Oxygen Reduction Reaction," 216th ECS Meeting, Vienna, Austria, Oct. 4–9, 2009.
3. K.J.J. Mayrhofer, D. Strmcnik, B.B. Blizanac, V. Stamenkovic, M. Arenz, N.M. Markovic, "Measurement of oxygen reduction activities via the rotating disc electrode method: From Pt model surfaces to carbon-supported high surface area catalysts," *Electrochimica Acta* **53** (2008) 3181-3188.
4. Liu, Gary C-K.; Sanderson, R.J.; Vernstrom, G; Stevens, D.A.; Atanasoski, R.T.; Debe, M.K.; Dahn, J.R., "RDE Measurements of ORR Activity of Pt_{1-x}Ir_x (0<x<0.3) on High Surface Area NSTF-Coated Glassy Carbon Disks," *J. Electrochem. Soc.* (2010), **157**(2), B207-B214.
5. Gary Chih-Kang, D.A. Stevens, J.C. Burns, R.J. Sanderson, G.D. Vernstrom, R.T. Atanasoski, M.K. Debe and J.R. Dahn, "Oxygen reduction activity of dealloyed Pt_{1-x}Ni_x catalysts." *J. Electrochem. Soc.* **158**(8) B919-B26 (2011).
6. Dennis van der Vliet, Chao Wang, Mark Debe, Radoslav Atanasoski, Nenad M. Markovic and Vojislav R. Stamenkovic, "Platinum-alloy Nanostructured Thin Film Catalysts for the Oxygen Reduction Reaction," *Electrochimica Acta.* **56** 8695-8699 (2011).
7. A.K. Schmoeckel, G.D. Vernstrom, A.J. Steinbach, S.M. Hendricks, R.T. Atanasoski and M. K. Debe, "Nanostructured Thin Film Ternary Catalyst Activities for Oxygen Reduction," 2006 Fuel Cell Seminar, Honolulu, Hawaii, Nov. 13–17, 2006.
8. M. Debe, A. Steinbach, G. Vernstrom, S.M. Hendricks, M.J. Kurkowski, R.T. Atanasoski, P. Kadera, D.A. Stevens, R.J. Sanderson, E. Marvel and J.R. Dahn, "Extraordinary oxygen reduction activity of Pt₃Ni₇," *J. Electrochem. Soc.* **158**(8) B910-B918 (2011).
9. Mark K. Debe, "Electrocatalyst Approaches and Challenges for Automotive Fuel Cells," invited review article, *Nature*, **486**(9401) 43-51(2012).
10. Mark K. Debe, "Nanostructured Thin Film Electrocatalysts for PEM Fuel Cells – A Tutorial on the Fundamental Characteristics and Practical Properties of NSTF Catalysts," *ECS Transactions* **45**, (2) 47-68 (2012).
11. R.K. Ahluwalia, X. Wang, A. Lajunen, A.J. Steinbach, S.M. Hendricks, M.J. Kurkowski, and M.K. Debe, "Kinetics of Oxygen Reduction Reaction on Nanostructured Thin-Film Platinum Alloy Catalyst," *Journal of Power Sources* **215** (2012) 77-88.
12. Debe, M.K.; Schmoeckel, A.; Hendricks, S.; Vernstrom, G.; Haugen, G.; Atanasoski, R., *ECS Transactions* **1**(1), 51 (2006).
13. Debe, M.K.; Schmoeckel, A.K.; Vernstrom, G.D.; Atanasoski, R., *Journal of Power Sources* **161**, 1002 (2006).
14. Steinbach, A.J.; Noda, K.; Debe, M. K., *ECS Transactions* **3**(1) 835 (2006).
15. Bonakdarpour, A.; Lobel, R.; Atanasoski, R.T.; Vernstrom, G.D.; Schmoeckel, A.K.; Debe, M.K.; Dahn, J.R., *Journal of The Electrochemical Society* **153**, A1835 (2006).
16. M. Debe, A. Hester, G. Vernstrom, A. Steinbach, S. Hendricks, A. Schmoeckel, R. Atanasoski, D. McClure and P. Turner, in proceedings of the 50th Annual Technical Conference of the Society of Vacuum Coaters, p. 658, Louisville, KY, May 1, 2007.
17. Mark K. Debe, Project review at the DOE 2011 Vehicle Technologies and Hydrogen Programs Annual Merit Review, May 10, 2011, Washington, D.C., number FC 001.
18. M.K. Debe, A.J. Steinbach, G.D. Vernstrom, S.M. Hendricks, M.J. Kurkowski, R.T. Atanasoski, P. Kadera, D.A. Stevens, R.J. Sanderson, E. Marvel and J.R. Dahn, "Extraordinary oxygen reduction activity of Pt₃Ni₇," *J. Electrochem. Soc.* **158**(8) B910-B918 (2011), and *ECS Trans.*, **33** 143 (2010).
19. Mark K. Debe, Project review at the DOE 2012 Vehicle Technologies and Hydrogen Programs Annual Merit Review, May 15, 2012, Washington, D.C., number FC 001.
20. A. Steinbach, M. Debe, M. Pejisa, D. Peppin, A. Haug, M. Kurkowski and S. Maier-Hendricks, "Influence of Anode GDL on PEMFC Ultra-thin Electrode Water Management at Low Temperatures," *ECS Transactions*, **41**(1) 449-457 (2011).
21. Mark K. Debe and Thomas Herdtle, "Design and development of a novel flow field for PEM fuel cells to obtain uniform flow distribution," *ECS Transactions*, **1**(6) 581-604 (2006).

V.D.2 Highly Dispersed Alloy Catalyst for Durability

Vivek S. Murthi (Primary Contact), Elise Izzo,
Wu Bi, Sandra Guerrero and Lesia Protsailo

UTC Power Corporation
195 Governor's Highway
South Windsor, CT 06042
Phone: (860) 727-2126
Email: vivek.srinivasamurthi@utcpower.com

DOE Managers

HQ: Kathi Epping Martin
Phone: (202) 586-7425
Email: Kathi.Epping@ee.doe.gov
GO: Reginald Tyler
Phone: (720) 356-1805
Email: Reginald.Tyler@go.doe.gov

Technical Advisor

Thomas Benjamin
Phone: (630) 252-1632
Email: Benjamin@anl.gov

Contract Number: DE-FG36-07GO17019

Subcontractors:

- Johnson-Matthey Fuel Cells, Sonning Commons, UK
- Texas A&M University, College Station, TX
- Brookhaven National Laboratory, Upton, NY

Project Start Date: May 1, 2007
Project End Date: June 30, 2012

Fiscal Year (FY) 2012 Objectives

- Develop structurally and compositionally advanced supported alloy catalyst system with loading ≤ 0.3 mg platinum group metal (PGM)/cm².
- Optimize catalyst performance and decay parameters through quantitative models.
- Demonstrate 5,000 cyclic hours below 80°C with less than 40% loss of electrochemical surface area and catalyst mass activity.

Technical Barriers

This project addresses the following technical barriers from the Fuel Cells section (3.4.4) of the Fuel Cell Technologies Program Multi-Year Research, Development and Demonstration Plan:

- (A) Durability
- (B) Cost

(C) Performance

Technical Targets

TABLE 1. DOE technical targets for electrocatalysts and the current status of this project

| Electrocatalyst Targets | Units | Current Status | DOE 2010 Target | DOE 2017 Target |
|--|---|--|-----------------|-----------------|
| PGM (total content) | g/kW | 0.50 | 0.3 | 0.125 |
| PGM (total loading) | mg/cm ² | 0.40 ^a | 0.3 | 0.125 |
| Mass activity @ 900 mV | A/mg _{PGM} at 900 mV (iR-free) | 0.20 (in MEA) 0.30 (in liquid cell) | 0.44 | 0.44 |
| Specific activity | μA/cm ² at 900 mV (iR-free) | 940 (in MEA) 612 (in liquid cell) | 720 | 720 |
| Cyclic durability At T $\leq 80^\circ\text{C}$ | h | 2,050 ^{b,c} | 5,000 | 5,000 |
| At T $> 80^\circ\text{C}$ | h | | 2,000 | 5,000 |
| ECA Loss | percent | 30 ^d | <40 | <40 |
| Cost | \$/kW at \$51.55/g | ~26 ^e | 5 | 3 |
| Electrocatalyst Support mV after 400 hours @ 1.2 V | mV | 92 ^f | <30 | <10 |

iR – internal resistance; MEA – membrane electrode assembly; ECA – electrochemical area

^a Based on current scaled-up 30% Pt₂IrCr/C MEA; anode/cathode loading – 0.1/0.3 mg/cm² (PGM).

^b Under an accelerated vehicle drive cycle protocol in a short stack; 40% mass activity loss under UTC-defined accelerated single-cell test after 270 hours at 70°C and 120 hours at 80°C.

^c Primary degradation mechanism in the alloy catalyst due to transition metal alloy dissolution.

^d Durability data measured after 30,000 cycles under UTC-defined accelerated test protocol.

^e 5-year average PGM price \$51.55/g (Pt = \$1,234.33/troy oz.; Ir = \$369.06/troy oz.); costs not projected to high volume production.

^f 40 mV iR-free O₂ performance loss at 1.5 A/cm² after 360 hours at 1.2 V.

FY 2012 Accomplishments

- Completed the scale up and MEA optimization of down-selected dispersed catalyst, 30% Pt₂IrCr/C for performance at high current densities in a full-size fuel cell. A mass activity of 0.17 A/mg (PGM) was achieved compared to the previous status of 0.14 A/mg (PGM) with a 53 mV improvement in performance at 1 A/cm² in H₂/air.
- Completed the durability testing of 30% Pt₂IrCr/C in a short stack under an accelerated vehicle drive cycle protocol. The stack accumulated 2,050 hours of uninterrupted operation at 70°C in H₂/Air. Completed

stack teardown to understand degradation mechanism for Pt₂IrCr alloy: primary durability loss in the alloy catalyst was due to transition metal dissolution.



Introduction

For the proton exchange membrane fuel cell (PEMFC) technology to become commercially viable, the production cost of the components in a fuel cell must be reduced and, more importantly, the durability of the MEA must be improved. This project focuses on two distinct approaches to the DOE 2010 durability and performance targets. The first approach is the development of conventional but high performance highly dispersed Pt alloy electrocatalyst on a carbon support. The second system utilizes a novel “Pt monolayer core-shell” approach capable of achieving very high Pt mass activities [1-3]. Under the former concept, the main objectives are to improve the high current density performance and durability towards cycling of the cathode catalyst by optimizing the MEA fabrication methods.

Approach

To achieve the objectives on this project, UTC Power (UTCP) has teamed with Brookhaven National Laboratory (BNL), Texas A&M University (TAMU) and Johnson Matthey Fuel Cells (JMFC). The research focus and the role of all partners were reported previously [4]. BNL's role on the project focuses on the development of Pt monolayer “core-shell” systems on various cores including ideal surfaces such as single crystals. In addition, BNL leads our efforts to understand the effect of electronic properties, crystal structure and particle size on activity and durability of this class of electrocatalysts. TAMU focuses on development of computational atomistic models to study parameters that influence the activity and durability of core shell and dispersed catalyst systems. The overall scope of JMFC activities in the project encompasses development of (i) dispersed Pt alloy catalysts including scale up on conventional and advanced carbon supports, (ii) novel synthesis methodologies to scale up Pt monolayer core-shell catalysts and (iii) MEA optimization and fabrication. Apart from overall project management, UTCP primarily focuses on the development of advanced dispersed Pt-based binary and ternary alloy catalysts. UTCP activities also include electrode modeling for MEA optimization, carbon support corrosion studies, fuel cell testing on full-size (410 cm²) MEAs, and fabrication and testing of a 20-cell short stack for verification.

Results

Dispersed Pt Alloy Catalyst

Many factors such as structure, particle dispersion, particle size, type of carbon support, etc, influence the electro-catalytic activity of Pt and Pt alloy nanoparticles. Previously, within this project, a 30 wt% Pt₂IrCr cathode (0.3 mg_{PGM}/cm² loading) showed higher durability in both active electrochemical area (ECA) and mass activity (MA) under potential cycling. This catalyst showed much lower loss (~30% ECA and MA) compared to the standard Gore Pt/C (0.4 mg_{PGM}/cm² loading) which showed ~50% loss and was down-selected for further development and scale up into full size MEAs [4]. In the past year, a significant amount of effort was focused towards development and optimization of the cathode catalyst layer in an MEA with 30% Pt₂IrCr alloy catalyst to improve the catalyst utilization in electrodes keeping low PGM loading and enabling good performance at high current densities. This involved an elaborate investigation to identify key parameters such as catalyst ink formulations, ionomer equivalent weight and content, to produce an optimum cathode electrode capable of achieving good fuel cell performance in wide range of current densities.

Figure 1 shows the sub-scale (25 cm²) solid plate fuel cell performance curves in H₂/O₂ and H₂/air at 80°C for the 30% Pt₂IrCr/C MEA with two different ionomer equivalent weights during the optimization process compared to a baseline Gore 5710 Pt/C MEA. The performance at 100 mA/cm² is 0.87 V for the electrode with 1000 equivalent weight (EW) (cell 11-74) compared to 0.84 V for the electrode with 1100 EW (cell 11-67) for a loading of 0.3 mg_{PGM}/cm². Figures 2a and 2b show the

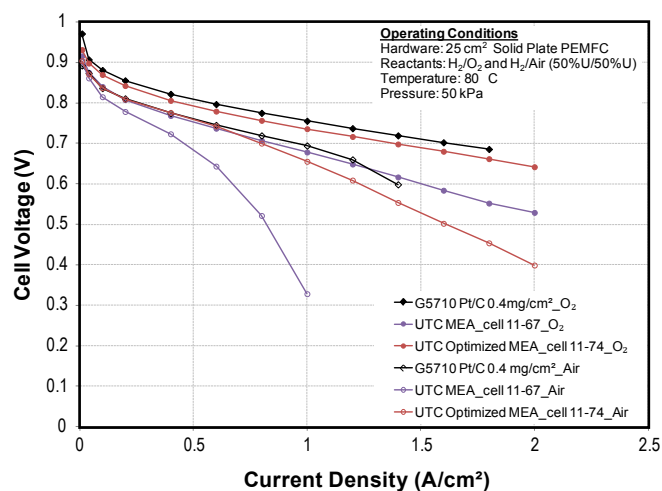


FIGURE 1. Polarization curves of H₂/O₂ and H₂/air performance for the preliminary optimization of JM 10-112 (30% Pt₂IrCr/C_{KB}) MEAs compared to the Gore Pt (0.4mg/cm²) MEA in sub-scale solid plate cells at 80°C, 50 kPa backpressure operation

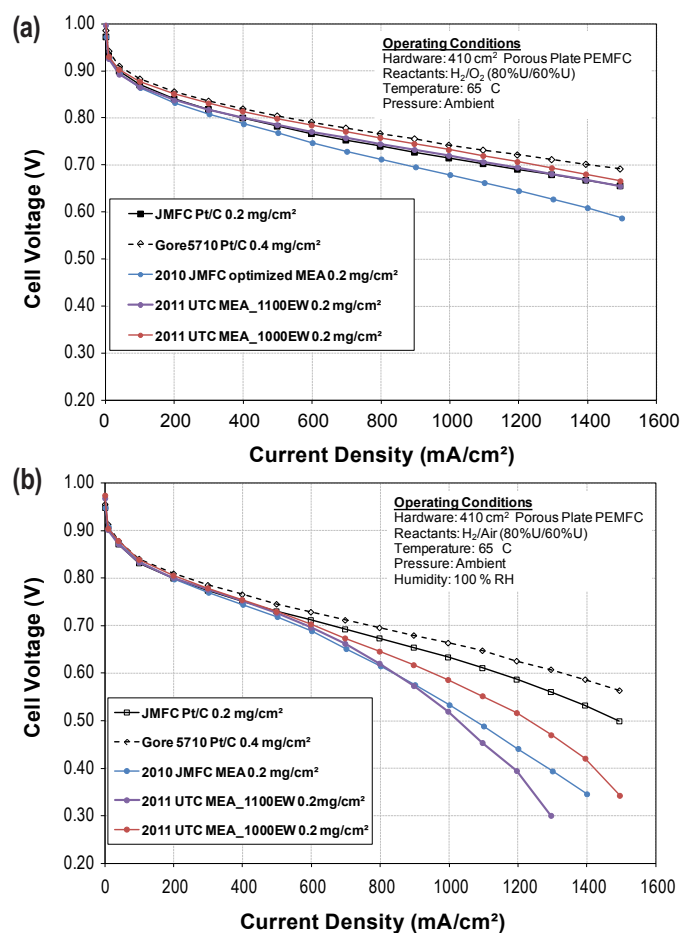


FIGURE 2. Polarization curves of (a) H_2/O_2 and (b) H_2/air performance for the optimization of JM 10-112 (30% Pt_2IrCr/C_{KB}) MEAs compared to JMFC Pt ($0.2\text{ mg}/\text{cm}^2$) MEA in full-size porous plate cells at 65°C , 0 kPa backpressure operation

performance in H_2/O_2 and H_2/air , respectively, for the (30% Pt_2IrCr/C_{KB}) in a porous plate cell at 65°C using various EW Nafion[®] ionomer solutions in the cathode catalyst layer after optimizing the MEA for suitable solvents, ionomer/carbon ratio and fabrication methods. The performance curves for a baseline JM Pt/C and the 2010 JMFC optimized 30% Pt_2IrCr/C_{KB} MEA is also included for comparison. Table 2 summarizes the performance of all the MEAs. As shown in Figure 2, the MEAs using different ionomer solutions in the catalyst layer of the cathode electrode results in higher performance than the 2010 JMFC optimized MEA in both oxygen and air at low current density regions. Moreover, the electrode with 1000 EW shows significant improvement in the mass activity ($0.17\text{ A}/\text{mg}_{\text{PGM}}$) and the corresponding H_2/air performance for the 2011 UTC-optimized MEA shows a 53 mV improvement at $1\text{ A}/\text{cm}^2$ compared to the 2010 JMFC-optimized MEA. This improvement in activity and performance is primarily due to the better utilization of the catalyst and improved mass transport resistance in the MEA.

TABLE 2. Summary of H_2/O_2 and H_2/air performance of the 30% Pt_2IrCr/C alloy catalyst MEAs compared to a commercial Gore Pt/C ($0.4\text{ mg}_{\text{PGM}}/\text{cm}^2$) and JMFC Pt/C ($0.2\text{ mg}_{\text{PGM}}/\text{cm}^2$) MEA

| Cell | Voltage at $0.1\text{ A}/\text{cm}^2$ in H_2/O_2 (V) | Voltage at $1\text{ A}/\text{cm}^2$ in H_2/Air (V) | iR at $1\text{ A}/\text{cm}^2$ in H_2/Air (V) |
|---------------------|--|--|---|
| JM Pt/C (0.2) | 0.871 | 0.634 | 0.079 |
| Gore5710 Pt/C (0.4) | 0.883 | 0.664 | 0.062 |
| JMFC MEA | 0.864 | 0.533 | 0.093 |
| UTC MEA 1100EW | 0.866 | 0.520 | 0.076 |
| UTC MEA 1000EW | 0.886 | 0.586 | 0.084 |

20-Cell Stack Validation

In FY 2011, a 20-cell short stack built at UTC containing the 30% Pt_2IrCr/C_{KB} MEAs completed 2,000 hours of cycling using the accelerated lifetime test conditions developed under a DOE-funded project at UTC Power titled “Improved Accelerated Stress Tests Based on Fuel Cell Vehicle Data”. The short stack contained four Pt MEAs as references and sixteen alloy catalyst 30% Pt_2IrCr/C_{KB} MEAs. All MEAs were manufactured by JMFC with a cathode Pt loading of $0.2\text{ mg}_{\text{PGM}}/\text{cm}^2$ and anode Pt loading of $0.1\text{ mg}_{\text{PGM}}/\text{cm}^2$. After conditioning, beginning-of-life (BOL) performance was tested in both oxygen and air. Cell resistance was measured by the H_2 -pump method.

The average performance of the cells in O_2 and air with the alloy catalyst was lower than the Pt catalyst cells as shown in Figure 3. The resistance of $79\pm 5\text{ m}\Omega\cdot\text{cm}^2$ in the alloy catalyst cells was similar to that of Pt catalyst cells ($73\pm 3\text{ m}\Omega\cdot\text{cm}^2$). In general, the Pt catalyst outperformed the alloy catalyst by 100 mV in air at $1\text{ A}/\text{cm}^2$. This performance gap is ascribed to oxygen permeability and proton concentration losses in the cathode due to Cr ion contamination in the 30% Pt_2IrCr/C_{KB} MEA. Figure 4a shows the average voltage at $800\text{ mA}/\text{cm}^2$ in air for both Pt/C and the alloy catalysts decrease with load cycles at an average voltage decay rate of $20\text{ }\mu\text{V}/\text{h}$ and $19\text{ }\mu\text{V}/\text{h}$ (or $\mu\text{V}/\text{cycle}$) respectively. Previously, a higher rate of activity and performance loss was observed for the Pt-alloy compared to the pure Pt under a load cycling test in the full-scale water transport plate cells ($85\text{ }\mu\text{V}/\text{h}$ compared to $36\text{ }\mu\text{V}/\text{h}$). In terms of the catalyst activity, no current density steps lower than $100\text{ mA}/\text{cm}^2$ were measured during the polarization curve measurement and hence mass activity cannot be determined from the 20-cell stack data. Although from the BOL oxygen curves in Figure 3, the Pt/C cells show slightly higher average voltage than the alloy catalyst cells at $100\text{ mA}/\text{cm}^2$,

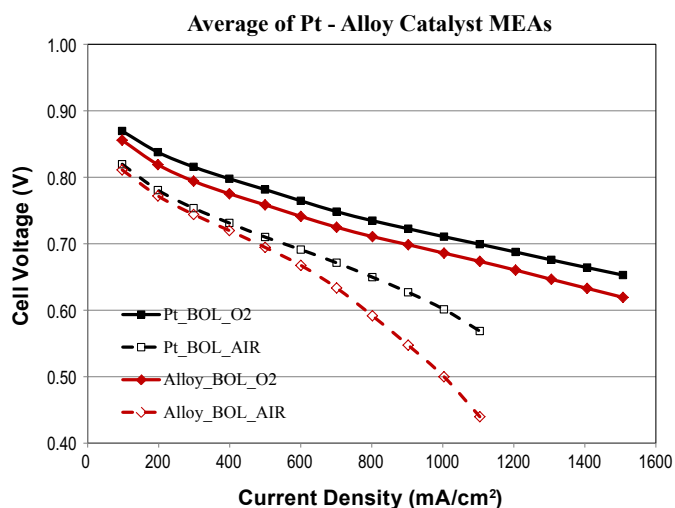


FIGURE 3. BOL performance of Pt/C and the alloy catalyst (30% Pt₂IrCr/KB) in the 20-cell stack

during the load cycling, the alloy catalyst shows a higher performance compared to the Pt/C at a lower current density of 16 mA/cm² (Figure 4b). After periodic diagnostic tests, both Pt and Pt alloys show partial performance recovery. This was mostly due to the removal of Pt oxides on catalyst surfaces at high current density. During subsequent load cycles following the diagnostic tests, it's noticeable that the alloy catalyst had initial lower voltage or activity decay than Pt/C, which was mostly due to the slower surface Pt oxidation. However, with continued load cycling, the alloy performance decreases slowly while the Pt/C catalyst quickly reaches a steady-state voltage. This difference is attributed to alloy catalyst compositional changes with the loss of Cr as discussed below.

Post-test observations including catalyst composition and electrode structure were conducted on the degraded MEAs after the stack tear down. Figure 5 shows the presence of Pt, Ir, and Cr in the MEA as measured by electron microprobe analysis (EMPA) from one of the cells from the 20-cell stack after 2,000 hours of cycling. The EMPA image shows a significant amount of Cr in the membrane and the anode electrode after durability cycling. Table 3 shows the ratio of Pt, Ir and Cr in the cathode electrode before and after cycling as determined by energy dispersive spectroscopy. A significant reduction (~50%) in Cr concentration in the electrode is comparable to the EMPA elemental analysis shown in Figure 5. Transmission electron microscope image analysis of the cathode catalyst particles did not show significant increase in particle size for the alloy catalyst before (5 nm) and after cycling (5.6 nm). However, a pure Pt catalyst from a baseline MEA with Pt/C in the cathode electrode showed a significant increase in particle size before (~2 nm) and after (5.6 nm) cycling for 2,000 hours in the 20-cell stack. Based on the post-test analysis shown

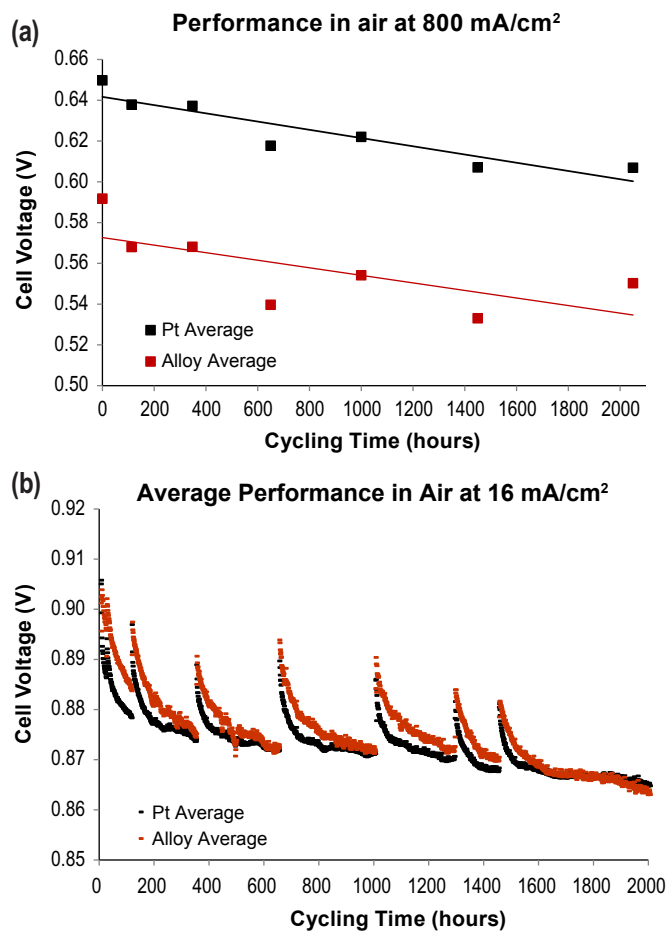


FIGURE 4. 20-cell short-stack performance decay during load cycles for Pt/C and the alloy catalyst (30% Pt₂IrCr/C_{KB}) in air at (a) 800 mA/cm² and (b) 16 mA/cm²

TABLE 3. Ratio of Pt, Ir and Cr in the cathode electrode before and after durability cycling in the 20-cell stack as determined by energy dispersive spectroscopy

| 30% Pt ₂ IrCr alloy composition | Pt | Ir | Cr |
|--|------|------|------|
| Initial wt.% | 61.4 | 30.4 | 8.2 |
| Initial atomic ratio | 1.0 | 0.50 | 0.50 |
| Final wt.% | 71.0 | 24.2 | 4.8 |
| Final atomic ratio | 1.0 | 0.35 | 0.25 |

above, it is concluded that the primary durability loss in the 30% Pt₂IrCr/C alloy catalyst is due to the transition metal dissolution (~50% loss) from the alloy catalyst.

Conclusions and Future Directions

The effects of MEA compositions were studied for the scaled-up 30% Pt₂IrCr/C in full-size water transport plate fuel cells. The electrode optimization studies clearly

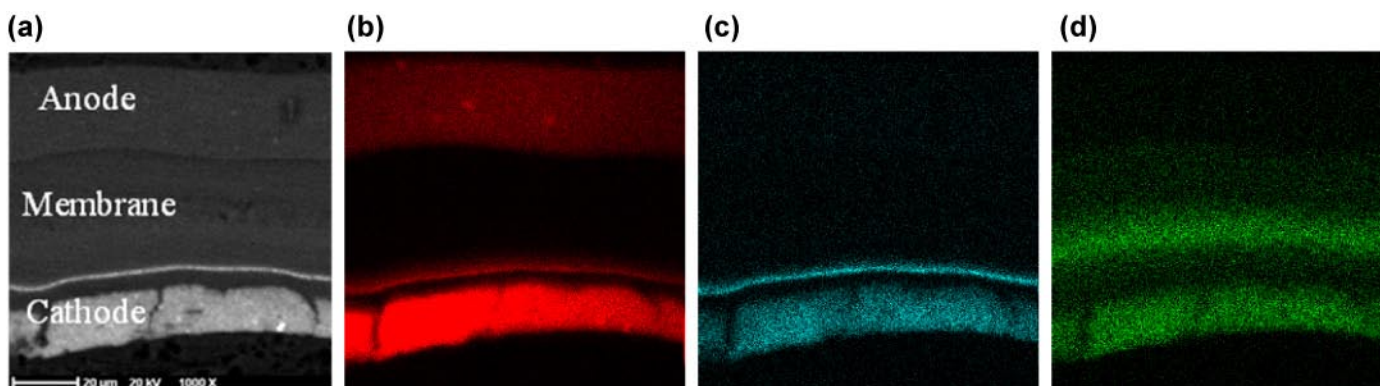


FIGURE 5. (a) Representative electron microscopy image of the MEA cross section and EMPA elemental map in the MEA after 2,000 hours of accelerated cycling in the 20-cell stack (b) Pt, (c) Ir and (d) Cr

show that MEA ink formulations and processing methods significantly impact the electrode structure in an MEA and their performance under high current density operations. A short stack containing the Pt-alloy was built and the durability of 30% Pt₂IrCr/C alloy catalysts under an accelerated vehicle drive cycle protocol showed that the durability loss was primarily due to the transition metal dissolution (~50% loss) from the alloy catalyst. Although some progress was made to overcome key barriers for the incorporation of the 30% Pt₂IrCr in an MEA such as low catalyst utilization in electrodes, the transition metal stability under operating conditions remains a concern. It is now recognized that a focus on MEA optimization during the early stages of catalyst development is essential to identify

and understand the limits of alloy catalysts and their impact on the high current density performance.

References

1. J. Zhang, M.B. Vukmirovic, K. Sasaki, F. Uribe and R.R. Adzic, *J. Serb. Chem. Soc.*, **70**, 513 (2005).
2. M.B. Vukmirovic, J. Zhang, K. Sasaki, A.U. Nilekar, F. Uribe, M. Mavrikakis and R.R. Adzic, *Electrochim. Acta*, **52**, 2257 (2007).
3. M. Shao, K. Sasaki, N.S. Marinkovic, L. Zhang and R.R. Adzic, *Electrochem. Comm.*, **9** 2848, (2007).
4. V.S. Murthi, DOE Hydrogen Program Annual Progress Report (2011).

V.D.3 Durable Catalysts for Fuel Cell Protection during Transient Conditions

Radoslav T. Atanasoski (Primary Contact),
George D. Vernstrom, Gregory M. Haugen,
Jimmy Wong, Theresa M. Watschke,
Ljiljana L. Atanasoska, Amy E. Hester
Fuel Cell Components Program, 3M Company
3M Center, Building 201-2N-05
St. Paul, MN 55144-1000
Phone: (651) 733-9441
Email: rtatanasoski@mmm.com

Timothy C. Crowtz, Jessie E. Harlow,
Robbie J. Sanderson, David A. Stevens, Jeff R. Dahn
Dalhousie University, Halifax, Nova Scotia, Canada

David A. Cullen, Karren L. More, Shawn Reeves
Oak Ridge National Laboratory, Oak Ridge, TN

Deborah J. Myers, Xiaoping Wang,
Ramachandran Subbaraman,
Vojislav R. Stamenkovic, Nenad M. Markovic
Argonne National Laboratory, LeMont, IL

Sumit Kundu, Wendy Lee
AFCC Automotive Fuel Cell Cooperation, Burnaby,
BC, Canada

DOE Managers

HQ: Kathi Epping Martin
Phone: (202) 586-7425
Email: Kathi.Epping@ee.doe.gov

GO: David Peterson
Phone: (720) 356-1747
Email: David.Peterson@go.doe.gov

Technical Advisors

Thomas Benjamin
Phone: (630) 252-1632
Email: Benjamin@cmt.anl.gov

John P. Kopasz
Phone: (630) 252-7531
Email: kopasz@anl.gov

Contract Number: DE-EE0000456

Subcontractors and Federally Funded Research and Development Centers:

- Dalhousie University, Halifax, Nova Scotia, Canada
- Oak Ridge National Laboratory, Oak Ridge, TN
- AFCC Automotive Fuel Cell Cooperation, Burnaby, BC, Canada

Project Start Date: August 1, 2009

Projected End Date: December 31, 2013

Fiscal Year (FY) 2012 Objectives

- Develop catalysts that will enable proton exchange membrane (PEM) fuel cell systems to weather the damaging conditions in the fuel cell at voltages beyond the thermodynamic stability of water during the transient periods of fuel starvation.
- Demonstrate that these catalysts will not substantially interfere with the performance of nor add much to the cost of the existing catalysts.

Technical Barriers

This project addresses the following technical barriers from the Fuel Cells section of the Fuel Cell Technologies Program Multi-Year Research, Development and Demonstration Plan:

(A) Durability

Technical Targets

While the number of start-up and shut-down (SU/SD) cycles for an automotive fuel cell has been projected to be over 30,000, the number of these events when the cathode electrochemical potential exceeds 1.23 V has been estimated at ~5,000. The number of complete fuel starvation events when a cell experiences a voltage reversal has been anticipated at ~200 [1].

Upon the Tech Team and the Durability Working Group recommendations, DOE approved the third year and the Go/No-Go technical targets of the project. In Table 1 these targets are listed along with the dates when they were accomplished. Also included are the 2013 targets.

Details of the evaluation procedures will be presented under the Results section.

FY 2012 Accomplishments

- Efficient oxygen evolution reaction (OER) catalysts were developed and successfully tested for SU/SD and cell reversal with a total precious group metal (PGM) content of 0.132 mg/cm²: 0.122 mg/cm² Pt + 0.009 mg/cm² IrRu.
- 5,000 startup/shutdown cycles were achieved with the addition of only 2 μg/cm² PGM on the cathode: 0.085 mg/cm² Pt + 0.002 mg/cm² IrRu.
- 200 high current density pulses of 200 mA/cm² for cell reversal were achieved while maintaining cell voltage <1.8 V with the addition of only 8 μg/cm² PGM on the anode: 0.037 mg/cm² Pt + 0.008 mg/cm² IrRu.

TABLE 1. The Technical Targets

| Task 1: OER Active Catalyst | | # of Cycles | PGM (mg/cm ²) | End Voltage | ECSA Loss | Status/Comments |
|------------------------------------|----------|--|---------------------------|-------------|-----------|-----------------------------------|
| SU/SD (Cathode) | | (>) | (<) | (<) | (<) | |
| | 2011 | 5,000 | 0.095 | 1.60 V | 12% | Achieved 09/2011 |
| | Go/No-Go | 5,000 | 0.090 | 1.60 V | 10% | Achieved 01/2012 |
| | 2013 | 5,000 | 0.088 | 1.45 V | 10% | 03/2013 |
| Cell Reversal (Anode) | | | | | | |
| | 2011 | 200 | 0.050 | 2.00 V | 10% | Achieved 09/2011 |
| | Go/No-Go | 200 | 0.045 | 1.80 V | 10% | Achieved 01/2012 |
| | 2013 | 200 | 0.037 | 1.75 V | 10% | 03/2013 |
| Task 2: Suppression of ORR (Anode) | | | | | | |
| | Go/No-Go | Factor of 10 in the kinetic region | | | | 01/2012 |
| | 2013 | Factor of 100 in the kinetic region | | | | 03/2013 |
| Task 3: Scale-up | | | | | | |
| | 2013 | Scale up to full size cells and Independent evaluation | | | | 2011: >10 full scale short stacks |
| | 2013 | 'Real life' evaluation readiness | | | | 12/2013; ~11 stacks |

ECSA – electrochemical surface area; ORR – oxygen reduction reaction

- The added OER catalyst satisfactorily maintained platinum stability and performance at both the anode and the cathode; Pt dissolution rate was constrained to <10%.
- The fundamentals of the added OER catalysts were revisited; Ru and Ir mass activity of 4 A/mg at 1.45 V and 3.9 A/mg at 1.55 V respectively were reached [2].
- High resolution scanning transmission electron microscopy combined with core level X-ray photoelectron spectroscopy data analysis provided insight into the observed OER catalyst activity and durability [2].
- Chemically and physically modified Pt/nano-structured thin-film (NSTF) anode exhibited very low ORR without inhibiting the hydrogen oxidation reaction (HOR), thus diminishing the impact of SU/SD.
- Scale-up and independent evaluation further confirmed the 3M lab results: In over 10 short stacks and over 80 MEAs utilizing 3M anodes tested in full-scale architecture by AFCC, the *OER-Pt/NSTF anode consistently outperformed* dispersed baselines with higher loadings.



Introduction

The project addresses a key issue of importance for successful transition of PEM fuel cell technology from development to pre-commercial phase (2010-2015). This issue is the failure of the catalyst and the other thermodynamically unstable membrane electrode assembly (MEA) components during SU/SD and local fuel starvation at the anode, commonly

referred to as transient conditions. During these periods the electrodes can reach potentials up to 2 V. One way to minimize the damage from such transient events is to lower the potential seen by the electrodes. At lower positive potentials, increased stability of the catalysts themselves and reduced degradation of the other MEA components is expected.

Approach

This project will try to alleviate the damaging effects during transient conditions from within the fuel cells via improvements to the existing catalyst materials. We are modifying both the anode and the cathode catalysts to favor the oxidation of water over carbon corrosion by maintaining the cathode potential close to the onset potential for water oxidation. The presence of a highly active OER catalyst on the cathode reduces the overpotential for a given current demand thus reducing the driving force for carbon and platinum dissolution. In addition, inhibition of the ORR on the anode side lowers the ORR current through reduced proton demand which in turn decreases the OER current on the cathode resulting in reduced cathode potential.

Key requirements for both concepts are to implement the added catalyst with negligible inhibition of the fuel cell performance and with minimal additional PGM.

Results

Efficient Oxygen Evolution Reaction Catalysts

The activity during the third year of the project continued to revolve around making a more efficient and

durable model catalyst containing ruthenium and iridium [3]. At the same time, the effort was focused on decreasing the total PGM content towards the 2017 DOE target of 0.125 mg/cm^2 . Most of the OER catalysts tested during this reporting period were nominally 90% at. Ir and 10% at. Ru. All the catalysts were tested in a 50-cm^2 PEM fuel cell, with the working electrode under nitrogen and the reference/counter electrode under either 1% or 100% hydrogen.

SU/SD Test

During the third year of the project, the generic electrochemical test mimicking the real SU/SD events was modified upon the recommendation the Tech Team and the Durability Working Group [4]. The test consisted of the following main steps (the modifications from the previous year are in *italics*):

- *100 mV/s* ramp from 0.9 V mimicking the H_2 front
- *1.6 V upper limit* or 5 mA/cm^2 , mimicking the equivalent amount of O_2 to be reacted off for the H_2/H^+ electrode potential to be established
- *650 mV every 10 cycles/pulses* mimicking the cell voltage during normal operation
- ECSA evaluation every 1,000 cycles

A schematic representation of the 2011 test protocol along with the 2012 modifications can be found in [4].

To fulfill the targets/milestones in Table 1, a systematic study was performed on a series of samples with 0.085 mg/cm^2 of Pt/NSTF. The added OER catalyst was varied from $1\text{--}10 \text{ }\mu\text{g/cm}^2$ of IrRu. The results of this study are presented in Figures 1 and 2. In Figure 1 a comparison between the Pt/NSTF substrate and OER-added catalyst is presented. In the upper panels the voltage cycles and the current responses of unmodified Pt/NSTF and Pt/NSTF with $2 \text{ }\mu\text{g/cm}^2$ of IrRu are presented. The voltage was allowed to reach 1.6 V unless sufficient current to react all of the remaining oxygen in the cathode compartment was reached (in this test 20 mA/cm^2). As expected, bare platinum is not able to produce the required current and therefore it always reaches the 1.6 V test limit. On the other hand, only $2 \text{ }\mu\text{g/cm}^2$ of IrRu is needed to reach the OER current of 20 mA/cm^2 at 1.48 V. The logical consequence of the lower voltage should be a reduced Pt dissolution. In the middle panel, the current responses for characteristic cycles of the test procedure are presented: the cycle before the potential is lowered to 0.65 V (cycle n10) and the two cycles following the 0.65 V step (cycles nn1 and nn2). First of all, the figure illustrates the effectiveness of the IrRu catalyst as demonstrated by the much higher OER current at lower voltage. Secondly, the drop to 0.65 V regenerates the current response on the following voltage sweep for both Pt and for IrRu. As was presented last year [5], in the case of Pt, this is due to the oxide formation on the reduced surface of Pt after being exposed to 0.65 V, while in the case of IrRu, it is due to the

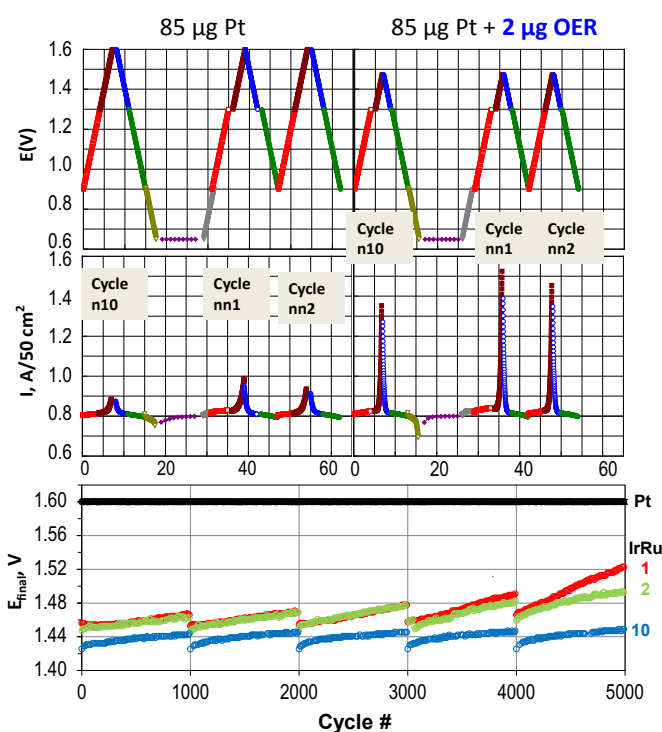


FIGURE 1. Comparison between the Pt/NSTF substrate and OER added catalyst loading under 2012 SU/SD test protocol (see text); 0.085 mg/cm^2 of Pt/NSTF; OER catalyst loading $1\text{--}10 \text{ }\mu\text{g/cm}^2$ of IrRu. 50-cm^2 MEA under nitrogen/1% hydrogen, 70°C , fully saturated. (upper) Voltage response for characteristic cycles for Pt/NSTF (left) and $2 \text{ }\mu\text{g/cm}^2$ of IrRu on Pt/NSTF (right). Voltage allowed to reach 1.6 V unless current surpasses 20 mA/cm^2 . (middle) Current responses for the same cycles as in (upper). (lower) The end voltage at the upper going potential sweep until current reaches 20 mA/cm^2 during the 5,000 SU/SD cycles; IrRu loading indicated on the graph.

regeneration of the OER catalyst itself. The lower panel in Figure 1 presents the change in the OER activity during the 5,000 SU/SD cycles by following the voltage at the end of positive going step from 0.9 V until the current surpasses the 20 mA/cm^2 or until the upper voltage limit of 1.6 V is reached. As we already pointed out, unmodified Pt always reaches the upper voltage limit of 1.6 V since its activity towards OER is very small. The activity of the three samples with 1, 2, and $10 \text{ }\mu\text{g/cm}^2$ of IrRu follow the anticipated trend, with the $10 \text{ }\mu\text{g/cm}^2$ of IrRu having the lowest peak voltage. During the first 2,000 cycles, the three IrRu loadings follow each other very closely, indicating that no noticeable changes/dissolution in the OER catalysts take place. However, with further cycling the differences between the three samples becomes more obvious, indicating clearly the superior stability of the highest IrRu sample.

In Figure 2 the surface area changes during the SU/SD testing is presented along with the impact of the presence of the IrRu on the fuel cell performance. A large number of MEAs (45) were tested in order to compensate for the inevitable glitches during these very long procedures. The upper panel presents the Pt surface area changes before

and after the 5,000 cycles measured via Hupd (ECSA). The loss of Pt ECSA is clearly correlated with the OER catalyst loading, since the Pt is exposed to lower cell voltages with higher IrRu loading. The lower panel follows the relative changes of Pt ECSA during the 5,000 SU/SD cycles. Here again the difference between bare Pt/NSTF and IrRu modified samples is quite obvious. From the point of view of the project targets, change in Pt ECSA of <10%, the samples with 2 and 5 $\mu\text{g}/\text{cm}^2$ of IrRu are both within the target range and are within the total Go/No-Go PGM requirement of 90 $\mu\text{g}/\text{cm}^2$.

For completeness, in the middle panel the fuel cell performance of the samples is presented. Looking at the fuel cell performance before and after the SU/SD test, it seems that the samples with 2 $\mu\text{g}/\text{cm}^2$ of IrRu show the optimal performance, which means that the project target can be fulfilled with a total of only 87 $\mu\text{g}/\text{cm}^2$ of total PGM, 85 $\mu\text{g}/\text{cm}^2$ of Pt with only 2 $\mu\text{g}/\text{cm}^2$ of IrRu.

Cell Reversal Test

In electrochemical terms, the cell reversal test procedure remained the same as in the previous year [5]. However, the total PGM loading target was decreased to 45 $\mu\text{g}/\text{cm}^2$. The upper voltage limit requirements were 2 V for the 2011 FY and was lowered by 0.2 V, to 1.8 V for

the Go/No-Go decision. In Figure 3 the number of 15 sec. 200 mA/cm^2 cycles up to the two voltage limits, 2 V and 1.8 V, are presented for catalysts with 40 $\mu\text{g}/\text{cm}^2$ Pt/NSTF as a substrate, with 1–10 $\mu\text{g}/\text{cm}^2$ added IrRu. There is a linear relationship between the OER catalyst loading and the number of cycles to ‘failure’, i.e. until the voltage limit was reached. Only some of the 5 $\mu\text{g}/\text{cm}^2$ IrRu samples fulfilled the 2 V required and none achieved the Go/No-Go 1.8 V. Only the samples with 10 $\mu\text{g}/\text{cm}^2$ IrRu completed the 200 pulses without surpassing the 2 V limit (not presented) and 1.8 V limit. Therefore, additional samples were made with the Go/No-Go target total PGM loading of 45 $\mu\text{g}/\text{cm}^2$: 37 $\mu\text{g}/\text{cm}^2$ Pt/NSTF with 8 $\mu\text{g}/\text{cm}^2$ IrRu. As presented in Figure 3, these samples reached the 200th 200 mA/cm^2 pulse without going over the limit of 1.8 V. As a matter of fact, the voltage at the end of the test was more than 0.15 V lower than the Go/No-Go target. In the lower panel of Figure 3, the evolution of the end voltages of all 200 pulses for three different combinations of Pt and IrRu loadings are presented. An interesting observation from this figure is that both the IrRu loading and the Pt loading influence durability and OER activity. This could be important in designing the future catalyst, where an obvious optimization between the amount of Pt, a necessary component for the HOR activity, and the added IrRu, the key to the cell reversal performance, has to be attained.

Scale Up and Independent Evaluation

The scale up and the full size stack evaluation could be considered as the most important achievement of the project. While within the scope of the statement of project objectives, the whole effort was entirely financed by 3M and AFCC.

3M produced many hundreds of lineal meters of fully integrated OER catalyst on Pt/NSTF that were subsequently converted into full-size CCMs. The CCMs were evaluated in Short Stacks by AFCC for Cell Reversal and SU/SD. The next section is the AFCC report (modified based on AMR presentation slides 14 and 15) [4].

AFCC Overview of OER/NSTF Evaluation

The NSTF anode + OER concept has been evaluated at AFCC during the last two years. Significant effort using both subscale and full-scale testing has been done following AFCC’s demanding technology development process using anodes tailored for AFCC requirements. Over 10 short stacks and over 80 MEAs using OER-Pt/NSTF anodes have been tested in full-scale architecture. Promising results demonstrating performance, CO tolerance, freeze tolerance, SU/SD benefits, and reversal tolerance were obtained.

Overall, the OER-modified NSTF anode is a promising MEA vehicle component. In stacks, as in AFCC’s subscale configuration (reported at the 2011 AMR), the OER-Pt/NSTF anode consistently outperformed dispersed baselines with

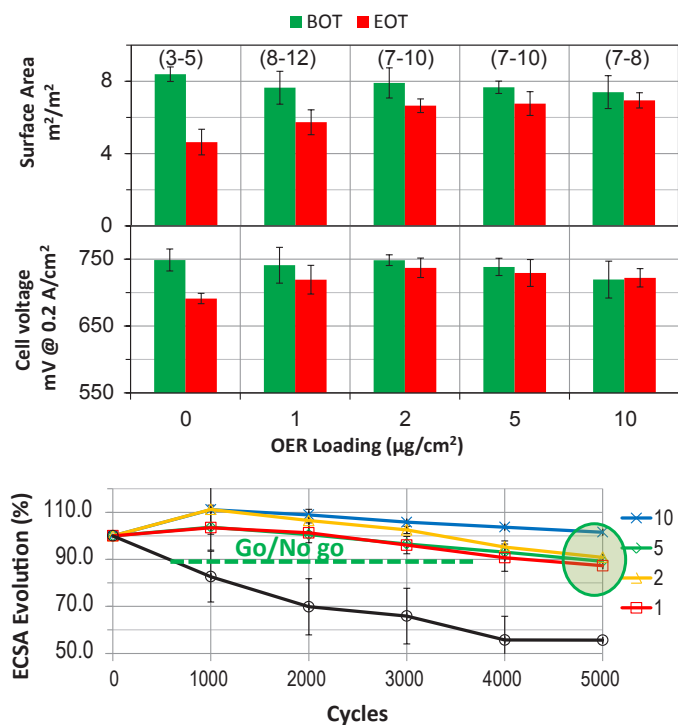


FIGURE 2. (upper) Surface area and (middle) fuel cell performance changes before and after the 5,000 SU/SD cycles; In parenthesis: number of MEAs tested; (lower) Surface area evolution during the SU/SD test. Samples and testing same as in Figure 1.

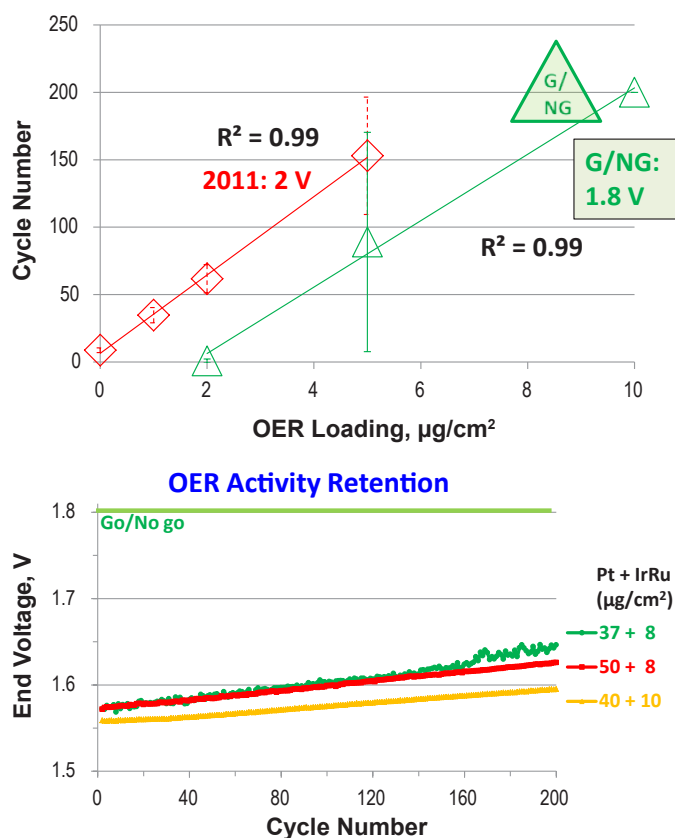


FIGURE 3. (upper) Cell reversal testing of OER catalyst with RuIr loading 1–10 $\mu\text{g}/\text{cm}^2$ on 40 $\mu\text{g}/\text{cm}^2$ Pt/NSTF. Number of cell reversal pulses of 200 mA/cm² up to the target voltage are presented. The big triangle represents the sample with 8 $\mu\text{g}/\text{cm}^2$ on 37 $\mu\text{g}/\text{cm}^2$ Pt/NSTF. (lower) Cell voltage at the end of each of the 200 mA/cm² pulses for different Pt and IrRu loadings.

higher loadings. As presented in Figure 4 (upper panel), despite lower tolerance than in subscale hardware, the NSTF anode concept still has a very good reversal tolerance for the given loadings.

As presented in Figure 4 (lower panel), OER-Pt/NSTF anode has a positive impact on SU/SD durability in a gas switching SU/SD accelerated stress test. The NSTF anode with OER catalyst is very selective since it inhibits ORR as shown by fuel cell polarization results (see inset: the anode was tested as a cathode, under air). This finding by AFCC is a direct confirmation of the alternative, Task 2 approach in mitigating SU/SD negative impact based on inhibiting the ORR on the anode. Smaller, secondary effects contributing to the OER-Pt/NSTF anode positive impact on SU/SD may be due to some Ir migration to the cathode that could produce an OER-enhancing cathode effect. The low Ru content leads to lower Ru crossover-related degradation.

AFCC listed the following as Future Challenges:

- OER/NSTF performance should have no negative impact compared to a conventional dispersed anode

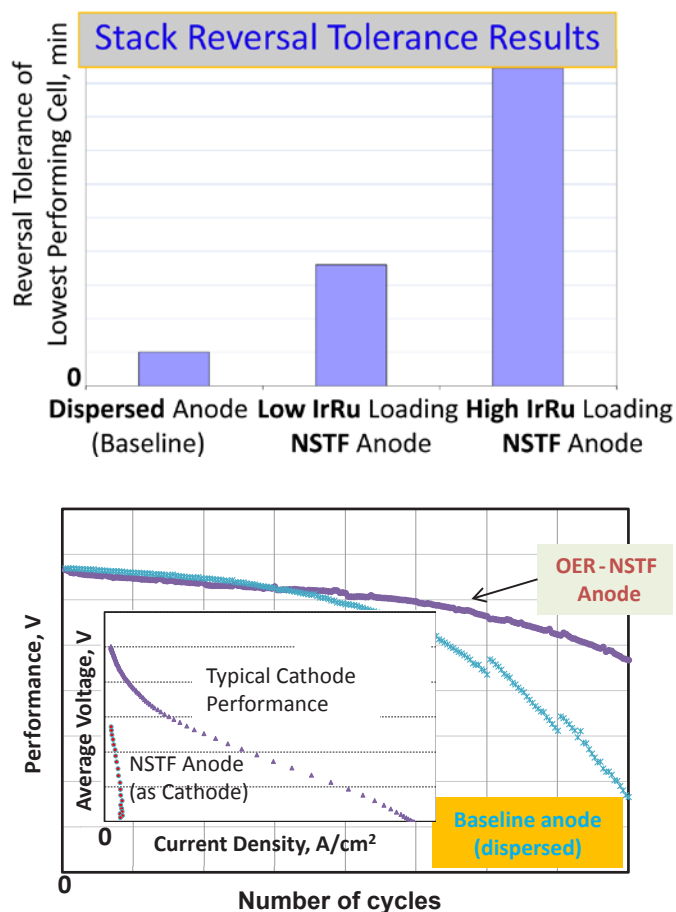


FIGURE 4. Short stacks full cell architecture evaluation of OER modified Pt/NSTF substrate by AFCC. (upper) Cell reversal tolerance of two IrRu loadings in comparison with baseline dispersed Pt/C with higher loading OER catalyst. (lower) Stack SU/SD tolerance with OER-Pt/NSTF in a gas switching SU/SD accelerated stress test. Inset: FC polarization curves in typical configuration and with IrRu on Pt/NSTF as a cathode.

- Show stability of the OER layer under extended drive cycles (2,000 hours) and after SU/SD testing
- Tolerance for anode contaminants (in addition to CO)
- 3M and AFCC should drive the fundamental understanding of engineering issues related to interfaces and compatibility of OER/NSTF with other MEA components and anode layer design.

Conclusions and Future Directions

In conclusion, besides completing all the Go/No-Go milestones, the project has accomplished the following:

- Achieved unprecedented OER mass activity
- NSTF delivered a new level for OER activity as it has previously done for ORR/NSTF
- Performance proved in short stacks at AFCC

- OER/NSTF brought NSTF catalyst concept very close to “real”/stack application
- Most of the work proposed and outcomes envisaged have been realized and/or accomplished by 3M, AFCC and their partners/collaborators

Future Work

Further research and development of the OER catalyst with respect to PGM loading and durability:

- Attempt to reach new milestones with total PGM loadings aligned with the DOE targets of 0.125 mg/cm²
- Assess the limits of PGM cathode – anode distribution while preserving the required cathode (ORR) and anode (HOR) performance
- Proceed with fundamental materials studies aimed at understanding the extraordinary activity and stability of the OER-Pt/NSTF catalysts
- Conduct fundamental engineering studies of the OER-Pt/NSTF catalysts aimed at understanding the processing, integration and interaction with other MEA components
- Evaluate OER-Pt NSTF catalysts’ readiness for “real life” automotive applications.

Special Recognitions

1. 2012 DOE Hydrogen and Fuel Cells Program R&D Award in Recognition of Outstanding Achievements in Low Platinum Group Metal Catalyst Performance and Durability.

FY 2012 Publications/Presentations

Papers

1. L.L. Atanasoska, G.D. Vernstrom, G.M. Haugen, and R.T. Atanasoski: *Catalyst Durability for Fuel Cells under Start-up and Shutdown Conditions: Evaluation of Ru and Ir Sputter-Deposited Films on Platinum in PEM Environment*, *ECS Transactions*, 41 (1) 785-795 (2011).
2. M.K. Debe, R.T. Atanasoski and A.J. Steinbach, *Invited presentation* “Nanostructured Thin Film Electrocatalysts – Current Status and Future Potential,” *ECS Transactions*, 41 (1) 937-954 (2011).
3. D.A. Cullen, K.L. More, K.S. Reeves, G.D. Vernstrom, L.L. Atanasoska, G.M. Haugen, and R.T. Atanasoski: *Characterization of durable nanostructured thin film catalysts tested under transient conditions using analytical aberration-corrected electron microscopy*, *ECS Transactions*, 41 (1) 1099-1103 (2011).
4. David A. Cullen, Karren L. More, Radoslav T. Atanasoski, Sumit Kundu, and Wendy Lee: “Comparison of quantitative electron microscopy methods for determining Pt-loss in PEM fuel cells”, Fuel Cell Seminar, Orlando, Nov. 2011.

5. R.T. Atanasoski, L.L. Atanasoska, D.A. Cullen, G.M. Haugen, K.L. More, G.D. Vernstrom: “*Fuel Cells Catalyst for Start-up and Shutdown Conditions: Electrochemical, XPS, and TEM Evaluation of Sputter-Deposited Ru, Ir, and Ti on Pt-Nano-Structured Thin Film (NSTF) Support*”, *Electrocatalysis* DOI 10.1007/s12678-012-0092-3.

6. R. Atanasoski: “Durable Catalysts for Fuel Cell Protection during Transient Conditions” http://www.hydrogen.energy.gov/pdfs/review11/fc006_atanasoski_2011_o.pdf.

7. D.A. Cullen, K.L. More, R.T. Atanasoski: “Towards Quantifying Catalyst Losses from Fuel Cell Electrodes: An Electron Microscopy Study”, *Microscopy and Microanalysis 2012*, Phoenix, AZ, Jul. 2012.

Invited Presentations

1. R. Atanasoski: “Catalyst Degradation during Transient Conditions focused on Durable Catalysts for Fuel Cell Protection during Transient Conditions” 2nd INTERNATIONAL WORKSHOP on DEGRADATION ISSUES OF FUEL CELLS, 21–23 SEPTEMBER, 2011, Thessaloniki, Greece (by DOE invitation).
2. R. Atanasoski: “Catalysts Durability in PEM Fuel Cells focused on Durable Catalysts for Fuel Cell Protection during Transient Conditions”, *Twin Cities Electrochemistry Symposium 2012*, April 12, 2012.
3. D.A. Cullen, K. Perry, K.L. More: “Electron Microscopy Applied to Understanding Stability of Fuel Cell Materials”, 2012 *Electrochemical Energy Storage and Conversion Forum*, Knoxville, TN, April 19–20, 2012.
4. R.T. Atanasoski, L.L. Atanasoska, D.A. Cullen, G.M. Haugen, G.D. Vernstrom: “Catalyst Materials for Fuel Cell Voltages beyond 1.23 V”, *ILED 2012*, Rome, May 30 – June 01, 2012.

Presentations to DOE

1. Go/No go review: “Durable Catalysts for Fuel Cell Protection during Transient Conditions” Project progress Review, presented to DOE, Feb., 2012, Golden, Colorado.
2. “Durable Catalysts for Fuel Cell Protection during Transient Conditions” presented at the FC Tech Team, Detroit, April, 2012.
3. “Durable Catalysts for Fuel Cell Protection during Transient Conditions” presented at the DOE 2010 AMR, May, 2012, Washington, D.C.

References

1. A. Nelson, Presentation at the 12th *Ulm ElectroChemical Talks*, Ulm, Germany, June 15–17, 2010.
2. R.T. Atanasoski, L.L. Atanasoska, D.A. Cullen, G.M. Haugen, K.L. More, G.D. Vernstrom: “*Fuel Cells Catalyst for Start-up and Shutdown Conditions: Electrochemical, XPS, and TEM Evaluation of Sputter-Deposited Ru, Ir, and Ti on Pt-Nano-Structured Thin Film (NSTF) Support*”, *Electrocatalysis* DOI 10.1007/s12678-012-0092-3.

3. R.T. Atanasoski, Project review at the DOE 2010 Vehicle Technologies and Hydrogen Programs Annual Merit Review, June 2010, Washington, D.C., FC# 006.

4. R.T. Atanasoski, Project review at the DOE 2010 Vehicle Technologies and Hydrogen Programs Annual Merit Review, May 2012, Washington, D.C., FC# 003.

5. R.T. Atanasoski, Project review at the DOE 2010 Vehicle Technologies and Hydrogen Programs Annual Merit Review, May 2011, Washington, D.C., FC# 006.

V.D.4 Extended, Continuous Pt Nanostructures in Thick, Dispersed Electrodes

Bryan Pivovar (Primary Contact), Shyam Kocha, KC Neyerlin, Jason Zack, Shaun Alia, Arrelaine Dameron, Tim Olson, Svitlana Pylypenko, Justin Bult, Brian Larsen, Jeremy Leong, Niccolo Aieta, Guido Bender

National Renewable Energy Laboratory (NREL)
15013 Denver West Parkway
Golden, CO 80401
Phone: (303) 275-3809
Email: Bryan.Pivovar@nrel.gov

DOE Manager

HQ: Kathi Epping Martin
Phone: (202) 586-7425
Email: Kathi.Epping@ee.doe.gov

Subcontractors:

- Kelly Perry, Oak Ridge National Laboratory (ORNL), Oak Ridge, TN
- Rod Borup, Los Alamos National Laboratory (LANL), Los Alamos, NM
- Yushan Yan, University of Delaware, Newark, DE
- Eric Eisenbraun, State University of New York – Albany, Albany, NY
- Stacey Bent and Han-Bo-Ram Lee, Stanford University, Stanford, CA
- Tom Zawodzinski and Alex Papendrew, University of Tennessee, Knoxville, TN
- Jeremy Meyers, University of Texas – Austin, Austin, TX
- Kev Adjemian (in-kind), Nissan Technical Center North America, Farmington Hills, MI
- Paolina Atanassova (in-kind), Cabot Fuel Cells, Albuquerque, NM
- Fumiaki Ogura (in-kind), Tanaka Kikinzoku Kogyo, Hiratsuka, Japan

Project Start Date: July 20, 2009

Project End Date: September 30, 2013

mass and specific activity and electrochemical surface area for best performing, high-yield ETFECS.

Technical Barriers

This project addresses the following technical barriers from the Fuel Cells section (3.4.4) of the Fuel Cell Technologies Program's Multi-Year Research, Development and Demonstration Plan:

- Durability (of catalysts and membrane electrode assemblies)
- Cost (of catalysts and membrane electrode assemblies)
- Performance (of catalysts and membrane electrode assemblies)

Technical Targets

This project synthesizes novel ETFECS and incorporates these catalysts into electrodes with and without carbon for further study. The project has targets outlined in the Multi-Year Research, Development and Demonstration Plan for both electrocatalysts for transportation applications (Table 3.4.13) and membrane electrode assemblies (MEAs) (Table 3.4.14). The specific targets and status of highest relevance are presented in Table 1.

TABLE 1. Technical Targets for Electrocatalysts for Transportation Applications

| Characteristic | Units | 2017/2020 Targets | Status |
|---|----------------------|-------------------|------------------|
| Mass Activity (150 kPa H ₂ /O ₂ 80°C 100% RH ^a) | A/mg-Pt @ 900 mV | 0.44/0.44 | 0.45 |
| Electro catalyst support stability | % mass activity loss | <10/<10 | <10 ^b |
| Loss in initial catalytic activity | % mass activity loss | <40/<40 | <10 ^b |

^a relative humidity

^b measured in rotating disk electrode (RDE), following 30,000 cycles between 0.6 and 1 V.

Fiscal Year (FY) 2012 Objectives

- Produce novel extended thin film electrocatalyst structures (ETFECs) with increased activity and durability, moving towards meeting all 2020 DOE catalyst targets.
- Further increase electrochemically available surface area (ECA) and mass activity of extended surface catalysts.
- Scale up novel ETFECs synthesis to gram quantities.
- Quantify impact in rotating disc electrode of potential cycling, and carbon and ionomer content on observed

FY 2012 Accomplishments

- Joule Milestone - Maintained greater than 30 m²/g Pt and 720 micro amps/cm² (at 900 mV internal resistance-free) - DOE 2015 target, in scale up of ETFECs synthesis to gram quantity.
- Quantified impact in RDE of potential cycling, and carbon and ionomer content on observed mass and specific activity and ECA for best performing, high yield ETFECs.

- Demonstrated mass activities of ETFECS as high as 450 mA/mg-Pt @ 900 mV.
- Demonstrated high durability of ETFECS in potential cycling between 0.6 and 1 V for 30,000 cycles.
- Screened >5 substrates and/or adhesion layers for their applicability to yield fast nucleation rates and form thin continuous films by atomic layer deposition (ALD).
- Screened carbon blacks for inclusion in electrode compositions containing extended surface Pt nanostructures based on ability to produce dispersed electrodes and electrochemical stability up to 1.5 V.



Introduction

Conventional nanoparticle Pt/C electrocatalysts (2–5 nm) used in automotive fuel cells appear to have plateaued in terms of electrochemical area and catalytic activity. ETFECS offer the possibility of higher specific activities comparable to that of bulk poly-Pt. ETFECS typically exhibit lower ECAs and consequently lower mass activities. By investigating a number of alternative synthesis techniques, we expect to raise the ECA to deliver the benefits of both a high specific and mass activity. An additional benefit of ETFECS is that larger Pt structures are less susceptible to oxidation and dissolution thus leading to a highly active, durable and low-cost electrocatalyst system.

Approach

Our overall approach towards developing extended surface Pt catalysts for their high mass activity and durability, and incorporating these structures into robust, high efficiency MEAs is multipronged and includes: i) Synthesis of novel ETFECS—Pt nanoparticles with continuity over 10s of nm or more have demonstrated enhanced specific activity and exceptional durability (3M [1], others [2]). In our work we examine vapor deposition including sputtering, chemical vapor deposition (CVD) and ALD as well as wet chemistry methods that include spontaneous galvanic displacement (SGD); ii) focus on increased Pt mass activity—low Pt ECAs have (~10 m²/gPt) resulted in limited mass activity in the past; iii) electrode studies involving ETFECS—effective incorporation of extended Pt catalysts into electrodes. Studies with Pt Black as an unsupported surrogate, expanded to ETFECS, including carbon incorporation; and iv) modeling—of catalyst particles, electrode structure and electrode performance.

Results

Moving beyond template synthesis development, our current year's work focused on Pt deposition and scale up of

high performing materials. We have continued our focus on ALD, and SGD, have added CVD as a technique and have de-emphasized sputtering. While sputtering is still deemed to be of merit (including for commercial processes), sputtering is not being currently pursued within the project due to cost of implementation for roll to roll processes, specialty equipment, and time - as well as promise of other approaches.

ALD work largely led by Stanford has focused on lower temperature deposition processes and the use of ultraviolet exposure to samples and the use of ozone as a more powerful oxidant in the reaction process. The use of ozone in particular has shown major improvements in lowering the reaction temperature and allowing thinner (single nm) continuous Pt coatings to be obtained. CVD work implemented at the University of Tennessee in the past year has resulted in free-standing Pt nanotubes from deposition into, followed by dissolution of, anodized aluminum oxide templates. The resultant catalyst structures have shown specific activities approaching that of polycrystalline Pt and far higher than other pure Pt nanostructures. These materials are limited in terms of low ECAs, and current focus is being spent exploring increasing ECA and exploring Pt alloys.

SGD continues to be a route that shows high promise and that we are pursuing with significant efforts. The work at UC-Riverside has stopped and has transitioned to the University of Delaware with the relocation of project co-PI, Yushan Yan. Based on the high performance of these materials, we performed scaled up synthesis to produce gram quantities for expanded studies in electrodes. Table 2 show the result of four batch synthesis where each batch consisted of between 250 and 400 mg of catalyst. We also distributed these samples to ORNL and LANL for advanced characterization to supplement and compare to measurements made at NREL. Table 1 summarizes the properties obtained for scaled up ETFECS. Most notably the ECAs for these materials are unusually high for extended surface catalysts and retain high specific activities, resulting in mass activities at or near DOE 2020 Targets.

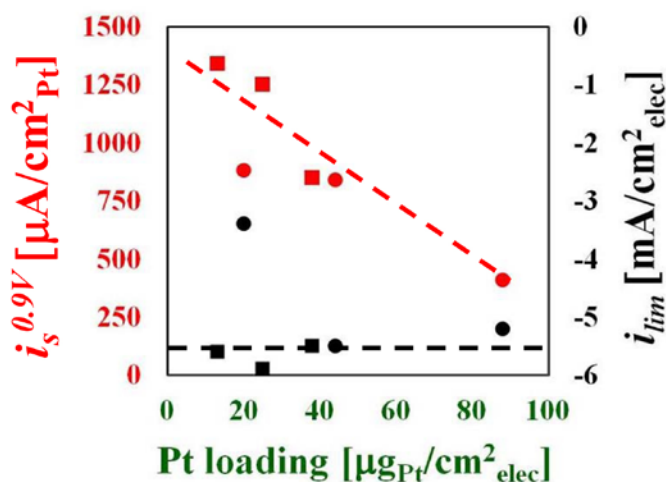
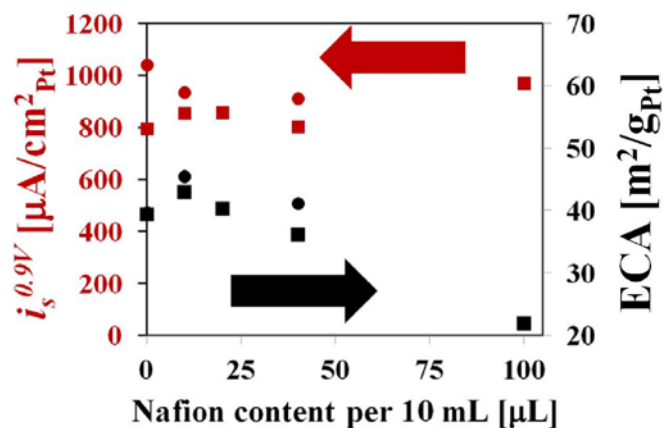
In the area of electrochemical characterization and electrode studies, we focused at first on Pt black as a surrogate for advanced ETFECS. The focus on Pt black allowed us to study catalyst dispersions and performance with and without carbon inclusion. Figure 1 shows the impact of carbon inclusion (squares) on specific activity (i_s) and limiting current as a function of RDE loading. These results demonstrate the importance of carbon in obtaining good dispersions to achieve high specific activity.

The role of carbon inclusion and the dependence of Nafion[®] on observed properties of ETFECS were also probed. Figure 2 shows examples of increasing Nafion[®] content in RDE studies with (circles) and without (squares) carbon. The role of both carbon and Nafion[®] in improving dispersion can be seen at low levels of Nafion[®] content. However, high Nafion[®] contents led to a systematic trend of decreasing ECA. Carbon incorporation always had a positive or neutral effect.

TABLE 1. Characterization of Scaled Up ETFECS Synthesis

| | ECA (m ² /g _{Pt}) | $i_s^{0.9V}$ ($\mu\text{A}/\text{cm}^2_{\text{Pt}}$) | $i_m^{0.9V}$ (mA/mg _{Pt}) | Pt Wt% | | | |
|---------|---|---|--|---------------|---------------|---------------|---------------|
| | | | | XRF (NREL) | XRF (LANL) | EDS (NREL) | EDS (ORNL) |
| Batch 1 | 38.6 | 1050 | 400 | 82 | 77.5 | 80-86 | 87-91 |
| Batch 2 | 53.0 | 630 | 340 | 95 | 95 | 96-99 | 98-100 |
| Batch 3 | 45.6 | 980 | 450 | 94 | 90 | 94-96 | 94-97 |
| Batch 4 | 51.0 | 640 | 330 | 96 | 92 | 95-97 | 93-95 |
| Average | 47.0 | 820 | 390 | | | | |

XRF - X-ray fluorescence spectroscopy; EDS - energy-dispersive X-ray spectroscopy

**FIGURE 1.** Specific activity and limiting current of Pt black as a function of RDE loading with (squares) and without carbon (circles)**FIGURE 2.** Specific activity and ECA of ETFECS as a function of Nafion® content with (circles) and without carbon (squares)

Durability of the samples was also tested and showed high promise for the ETFECS approach. Data are presented in Table 2 for 30,000 cycles between 0.6 and 1.0 V for ETFECS samples with and without carbon. ECA decreased

TABLE 2. Durability Cycling of ETFECS With and Without Carbon Inclusion

| | ECA | NECA | $i_s^{0.9V}$ | $N i_s^{0.9V}$ | $i_m^{0.9V}$ | $N i_m^{0.9V}$ |
|----------------|---------------------------------|---------------------------------|---------------------------------------|----------------|---------------------|----------------|
| | m ² /g _{Pt} | m ² /g _{Pt} | $\mu\text{A}/\text{cm}^2_{\text{Pt}}$ | | mA/mg _{Pt} | |
| Pt only (pre) | 41 | | 964 | | 393 | |
| Pt only (post) | 33 | 81 | 1071 | 111 | 355 | 90 |
| Pt + C (pre) | 39 | | 1078 | | 420 | |
| Pt + C (post) | 30 | 78 | 1330 | 123 | 405 | 96 |

NECA - normalized electrochemical surface area

by approximately 20% in both cases, but was accompanied by a modest (11 to 23%) increase in specific activity. The resulting mass activity was 90 to 96% of the initial activity, a remarkably high result, much better than that of conventional Pt/C and highly supportive of our approach to improved cost, durability and performance of fuel cell catalysts. The reported mass activities approach DOE 2020 targets and show exceptionally good durability.

Conclusions and Future Directions

The project has synthesized many novel catalysts using materials, geometries, and approaches not previously demonstrated. We have reached poly crystalline Pt specific activity in nanostructures using CVD, and have demonstrated continuous ALD Pt coatings down to single nm thickness. We have met the 2020 DOE mass activity target without alloying advantages and commonly produce extended surface catalysts with >40 m²/g ECA. We have shown good cyclic durability, and elucidated the role of carbon in RDE studies of unsupported catalysts. Future work, broken down by topical area, includes:

- Pt deposition
 - CVD (Tennessee): Systematic studies involving wall thickness, annealing T, co-deposition of metals with potential alloy benefits (Ni, Co).
 - ALD (Stanford, Center for Nanoscience and Engineering, NREL): Further studies involving ozone with a focus on low-temperature ALD, application of developed techniques to nanostructured substrates and removable RDE

- tips (highly-ordered pyrolytic graphite, edge-plane pyrolytic graphite, gas chromatograph).
- SGD (NREL, Delaware): further process optimization focusing on reproducibility and characterization of initial samples.
- Electrode studies (NREL)
 - Incorporation of highest performing catalyst into MEA electrodes.
 - Expanded MEA fabrication and fuel cell testing of ETFECS.
- Modeling
 - Colloidal interactions to probe dispersions and inks of ETFECS (Tennessee).
 - RDE models to investigate specific activity, limiting current and electrochemical surface area (Texas).

Special Recognitions & Awards/Patents Issued

1. Principal Investigator, Bryan Pivovar, has been awarded the 2012 Charles Tobias Young Investigator Award (Electrochemical Society).

FY 2012 Publications/Presentations

1. Han-Bo-Ram Lee and Stacey F. Bent, “Microstructure-Dependent Nucleation in Atomic Layer Deposition of Pt on TiO₂,” *Chem. Mater.* 2012, 24, 279–286.
2. Arrelaine A. Dameron, Svitlana Pylypenko, Justin B. Bult, K.C. Neyerlin, Chaiwat Engtrakul, Christopher Bochert, G. Jeremy Leong, Sarah L. Frisco, Lin Simpson, Huyen N. Dinh, Bryan Pivovar, “Aligned Carbon Nanotube Array Functionalization for Enhanced Atomic Layer Deposition of Platinum Electrocatalysts,” *Applied Surface Science*, 258 (13), 2012, 5212–5221.
3. Shaun M. Alia, Kurt O. Jensen, Bryan S. Pivovar, and Yushan Yan, “Platinum Monolayered Palladium Nanotubes as Oxygen Reduction Reaction Electrocatalysts,” *ACS Catal.*, 2012, 2 (5), pp 858–863.
4. Brian A. Larsen, K. C. Neyerlin, Justin Bult, Christopher Bochert, Jeffrey L. Blackburn, Shyam Kocha, Bryan Pivovar, “Platinum nanoplates as novel oxygen reduction reaction electrocatalysts” accepted *JECs* July, 2012.

5. Bryan Pivovar, “Extended Surface Catalysts,” Johns Hopkins University, December 13, 2011.
6. Bryan Pivovar, “ETFECs Development at NREL,” ACS Colorado Section, January 23, 2012.
7. Bryan Pivovar, “NREL’s Fuel Cell R&D/Extended Surface Catalysts”, GM, Honeoye Falls, NY June 13, 2011.
8. Bryan Pivovar, “3-D Catalyst Structures for PEM Fuel Cell Electrocatalysts,” Meet. Abstr. - Electrochem. Soc. 1201 558 (2012).
9. Brian A. Larsen, Christopher Chang, Svitlana Pylypenko, and Bryan Pivovar, “Spontaneous Galvanic Displacement Reactions: Effects of Template and Surface Ligand Interaction,” Meet. Abstr. - Electrochem. Soc. 1101 83 (2011).
10. K. Neyerlin, B. Larsen, J. Zack, S. Kocha, and B. Pivovar, “Incorporation of Carbon with Unsupported Pt Electrocatalysts,” 220th ECS Meeting - Boston, MA October 9 – October 14, 2011, Abstract No. 807.
11. K. Neyerlin, B. Larsen, T. Olson, S. Pylypenko, J. Zack, S. Kocha, and B. Pivovar, “Electrochemically Available Surface Area and Mass and Specific Activities of Extended Surface Pt Nanostructures,” 220th ECS Meeting - Boston, MA October 9 – October 14, 2011, Abstract No. 808.
12. S.M. Alia and Y. Yan, “Platinum Monolayered Palladium Nanotubes for the Oxygen Reduction Reaction,” 220th ECS Meeting - Boston, MA October 9 – October 14, 2011, Abstract No. 1059.
13. Brian A Larsen, K. C. Neyerlin, Justin Bult, Christopher Bochert, Jeffrey Blackburn, Shyam Kocha, Bryan Pivovar, “Platinum nanoplates as novel oxygen reduction reaction electrocatalysts,” 242nd ACS National Meeting, Fall 2011, Denver, Colorado, August 28 – September 1, Abstract No. 403.
14. Han-Bo-Ram Lee and Stacey F. Bent, “The Effects of TiO₂ Crystallinity on Nucleation in Atomic Layer Deposition of Platinum,” ALD 2011.

References

1. http://www.hydrogen.energy.gov/pdfs/review08/fc_1_debe.pdf.
2. Z. Chen, W. Li, M. Waje, Y.S. Yan, *Angew. Chem. Int. Ed.* 2007, 46:4060-4063.

V.D.5 Nanosegregated Cathode Alloy Catalysts with Ultra-Low Platinum Loading

Nenad M. Markovic (Primary Contact) and
Vojislav R. Stamenkovic

Argonne National Laboratory (ANL)
Argonne, IL 60439
Phone: (630) 252-5181
Email: nmmarkovic@anl.gov

DOE Manager

HQ: Nancy Garland
Phone: (202) 586-5673
Email: Nancy.Garland@ee.doe.gov

Subcontractors:

- Karren More, Oak Ridge National Laboratory, Oak Ridge, TN
- Charles Hays, Jet Propulsion Laboratory, Pasadena, CA
- Shuoheng Sun, Brown University, Providence, RI
- Guofeng Wang, University of Pittsburgh, Pittsburgh, PA
- Radoslav Atanasoski, 3M Company, Saint Paul, MN

Project Start Date: September, 2009
Project End Date: September, 2013

Fiscal Year (FY) 2012 Objectives

- Fundamental understanding of the oxygen reduction reaction on multimetallic PtM (M = Co, Ni, Fe, Mn, Cr, V, and Ti) and PtM₁N₂ (M₁ = Co or Ni; N₂ = Fe, Mn, Cr, V, and Ti) materials.
- Develop highly-efficient, durable, nanosegregated Pt-skin PtM and PtM₁N₂ catalysts with ultra-low Pt content.
- Develop highly-active and durable Au/PtM₃ nanoparticles with ultra-low Pt content.
- Find relationships between activity/stability of well-characterized bulk alloys and real nanoparticles.
- Develop novel chemical and physical methods for synthesis of monodispersed PtM and PtM₁N₂ alloy nanoparticles and thin metal films.
- Resolve electronic/atomic structure and segregation profile of PtM and PtM₁N₂ systems.
- Resolve composition effects of PtM and PtM₁N₂ systems.
- Demonstrate mass activity and stability improvement of PtM and PtM₁N₂ alloy nanoparticles in rotating disk electrode (RDE) and membrane electrode assembly (MEA).
- Use computational methods as the basis to form any predictive ability in tailor making binary and ternary systems to have desirable reactivity and durability properties.

Technical Barriers

This project addresses the following technical barriers from Fuel Cells section of the Fuel Cells Technologies Program Multi-Year Research, Development and Demonstration Plan:

- (A) Durability
- (B) Cost
- (C) Performance

Technical Targets

ANL is conducting fundamental studies of the oxygen reduction reaction on Pt-based PtM (M= Ni, Co, Fe, Cr, V, and Ti) binary and PtM₁N₂ (NM = Fe, Co, and/or Ni) catalysts as well as on Au/Pt₃M ternary nanoparticles. Insights gained from these studies will be applied toward the design and synthesis of highly-efficient, durable, nanosegregated Pt-skin catalysts with ultra-low Pt content that meet or exceed the following DOE 2015 targets:

| | |
|---|--|
| • Specific activity @ 0.9 V iR-free: 720 mA/cm ² | • Platinum group metal total content: 0.2 g/kW |
| • Mass activity @ 0.9 V: 0.44 A/mg _{Pt} | • Total loading: 0.2 mg/cm ² |
| • Catalyst support loss: <30% | • Durability w/cycling (80°C): 5,000 hrs |

iR - internal resistance

FY 2012 Accomplishments

- Synthesized wide range of bi/multi metallic nanoparticles with controlled size and composition by colloidal organic solvo-thermal approach.
- Developed vapor deposition/annealing methods to make stable and active Pt thin metal film (1-7 atomic layers) on Pt₃Ni substrate.
- Established relationships between the morphology/thickness of Pt atoms in skeleton structure and stability/activity of the catalysts: Pt film can both effectively protect Ni from dissolution and provide superior catalytic activity (x6 vs. Pt).
- Developed experimental protocol to synthesize PtNi/C nanoparticles with Pt multilayered "skin" (2-3 ML) that are mimicking stability/activity of thin metal film systems.
- In MEA, for PtNi/C multilayered skin confirmed:
 - (i) three times higher specific (surface area ~0.8 mA/cm²) than benchmark Pt/C catalysts and mass

activity of $\sim 0.35 \text{ A/mg}_{\text{Pt}}$; (ii) high durability, e.g., after 20,000 cycles activity, surface area loss was only 12% compared to $\sim 40\%$ for Pt/C.

- Established accurate surface area determination for the nanoscale catalyst with Pt-skin surfaces.
- Performed extended X-ray absorption fine structure analysis characterization in an MEA on PtNi multilayered skin catalysts, which revealed that catalyst did not suffer structural/composition changes after 20,000 cycles in the MEA.
- Developed magnetron sputtering deposition methods and annealing protocol to make reproducible ternary Pt-alloy thin metal films.
- Performed composition optimization of ternary $\text{Pt}_3\text{M}_1\text{N}_2$ catalysts.
- Developed synthetic routes and characterized monodisperse, highly homogeneous ternary alloy nanoparticles.
- Performed modeling related to the existence of Pt-skin structure in ternary alloy catalysts for extended and nanoscale systems.
- Establish activity trend for ternary Pt_3MN nanoparticles.
- Synthesis and characterization of the core/shell Au/CoPt₃ nanoparticles
- Demonstrated that ternary alloys could provide additional activity gain vs. binaries (4-fold vs. Pt-poly).



Introduction

In the quest to make the polymer electrolyte membrane fuel cell a competitive force, one of the major limitations is to reduce the significant overpotential for the oxygen reduction reaction (ORR) and minimize dissolution of the cathode catalysts. Here, we report a progress for FY 2012 in experimental and theoretical studies to addressing the importance of alloying Pt with 3d elements (M= Ni, Co, Fe etc.) and making a novel tailored nanostructure of Au/Pt₃M in order to form catalytically active materials with so-called *nanosegregated profile* [1]. In our previous work we have identified that the nanosegregated surfaces are superior in both: exceptional catalytic activity for the ORR and improved stability of Pt surface atoms.

Approach

In order to address the challenges that are listed as the DOE targets for the Fuel Cell Technologies Program we rely on our materials-by-design approach [1-9]. This involves four major steps: (i) synthesis of novel nanoscale materials, with controlled size, structure and composition; (ii) establishing atomic and electronic properties by utilizing ex situ and

in situ surface characterization techniques and theoretical methods; (iii) resolving the surface electronic and crystal structures at atomic/molecular level that govern efficient kinetics of the ORR; and (iv) synthesis/fabrication (scale up) of the highly efficient nanoscale materials.

Results

Real surface area of the catalysts with Pt-skin surfaces. The term Pt-skin has been used to describe unique arrangement of Pt surface atoms that is formed after thermal-induced segregation profile of bimetallic Pt₃M alloys. An oscillatory concentration profile with 100% Pt in the first layer is counterbalanced by depletion of Pt in the second layer, which is followed by enrichment of Pt in the third layer. Alloys with such segregation profile in near surface region we term nanosegregated systems, and they have been found to have superior catalytic properties [1]. For the extended Pt₃M electrodes we found that the Pt-skin surfaces are more active for the ORR than the corresponding Pt-skeleton structures [8]. In the FY 2011 report, we emphasized the feasibility to form Pt-skin-like surfaces at the nanoscale. In addition to numerous characterization techniques to confirm Pt-skin surface profile, we developed strategy for fast electrochemical screening of Pt-alloy catalysts in order to reveal the existence of Pt-skin formation on the catalyst surface. In the case of Pt₃Ni(111)-skin, we found that the formation of H_{upd} adlayer is substantially suppressed (up to 50%) when compared to Pt(111) with the same geometric surface area. In turn, for the Pt-skin type catalysts, it is not possible to establish electrochemically active surface area (ECSA) solely on the surface coverage by H_{upd}. For that reason, it is important to use the CO stripping methodology because we found that surface coverage of adsorbed CO is the same on Pt and Pt-skin surfaces. The latter approach, therefore, eliminates errors originated by underestimation of ECSA, and hence, overestimation of specific activity. Moreover, the observed discrepancy between surface area estimations based on H_{upd} and CO stripping can serve as descriptor for the formation of a skin-type nanocatalyst alloy, as acid leached skeleton-type surfaces and nanoparticles do not show such behavior. Specifically, the ECSA of the multilayered PtNi-skin catalyst [9] obtained from integrated H_{upd} region was over 30% lower than that from CO stripping, which confirms the formation of Pt-skin type of surface in the nanocatalyst. All of results related to PtNi catalysts include surface area revealed from CO stripping experiments.

Formation of Pt-skin surfaces in ternary alloys. Since the last report our focus has been placed on possibility to form Pt-Skin surfaces over ternary alloys. We first studied the ternary systems on extended surfaces of polycrystalline thin films to establish the trend of electrocatalytic activities, and then applied this knowledge to synthesize ternary alloy nanocatalysts prepared by solvo thermal approach. Polycrystalline 50-nm thick ternary films were prepared

by confocal magnetron sputtering. Different targets of pure metals were used for sputtering over mirror polished glassy carbon substrate with 6 mm in diameter. The obtained films were subjected to annealing to induce homogeneous elemental distribution and subsequent surface analyses in order to explore existence of Pt-skin formation in ternary systems (see the Methods). Figure 1 summarizes the results of electrochemical studies for these thin films acquired by RDE. Compared to polycrystalline Pt (Pt-poly), cyclic voltammetry (CV, Figure 1A) of the as-sputtered films have similar features for underpotentially deposited hydrogen (H_{upd}) regions ($E < 0.4$ V) with slightly suppressed peaks. In the ORR-relevant regions ($E > 0.6$ V), the ternary alloy surfaces exhibit positive shifts for the onset of Pt-OH_{ad} formation, which occurs at ~ 0.9 V on the alloys, compared to Pt-poly, indicating weaker chemisorptions of oxygenated species on these surfaces. After annealing at 400°C the H_{upd} peaks of ternary systems are additionally suppressed, while the onset of Pt-OH_{ad} formation is shifted to even more positive potentials. Even though both effects could be mistaken by altered surface morphology upon thermal annealing, we proved by applying CO stripping methodology that they are associated with the formation of Pt-skin structure due to Pt segregation, see models in Figure 1. Compared to the Pt-poly surface, the as-sputtered and annealed $\text{Pt}_3(\text{CoNi})_1$ surfaces show positive shifts of half-wave potentials by 12 and 22 mV, respectively. The specific activity at 0.95 V of the annealed surface reaches 1.75 mA/cm^2 , whereas the as-sputtered surface achieves 1.12 mA/cm^2 (Figure 1C). These values correspond to improvement factors of 4 and 2.5 compared to Pt-poly (0.45 mA/cm^2), respectively. The same strategy

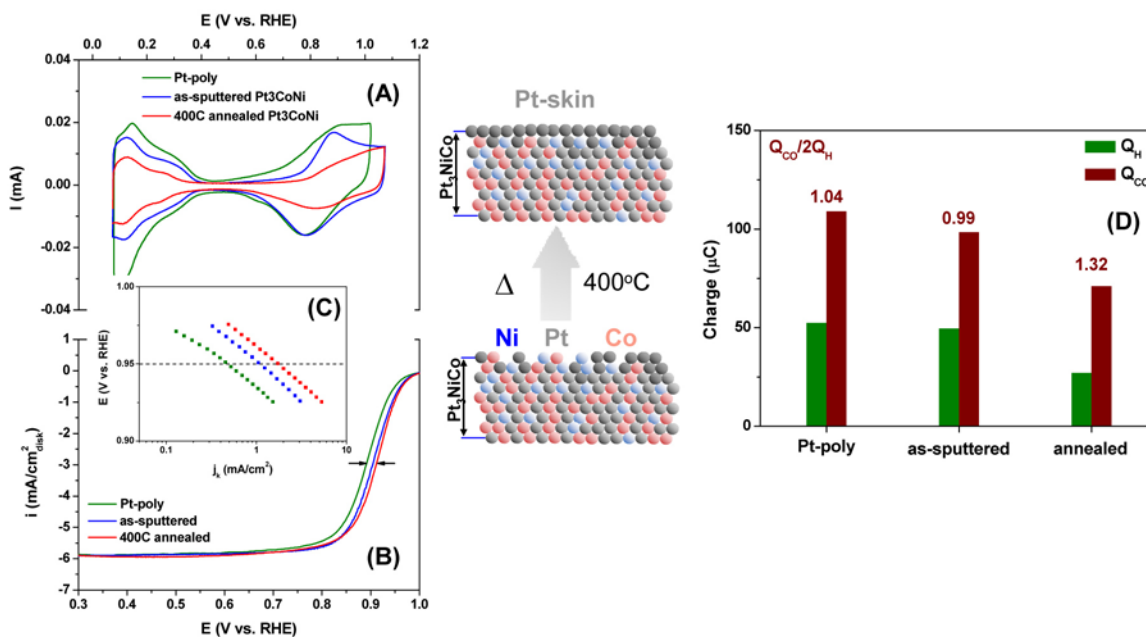


FIGURE 1. Electrochemical characterization of the extended $\text{Pt}_3(\text{CoNi})_1$ thin-film surfaces. (A) Cyclic voltammograms, (B) polarization curves and (C) Tafel plots. Specific activities for the ternary systems were presented as kinetic currents normalized by ECSAs obtained from CO_{ad} stripping curves. (D) H_{upd} (Q_{H}) and CO stripping (Q_{CO}) integrated charges assessed under the hydrogen adsorption/desorption peaks and a CO stripping peak.

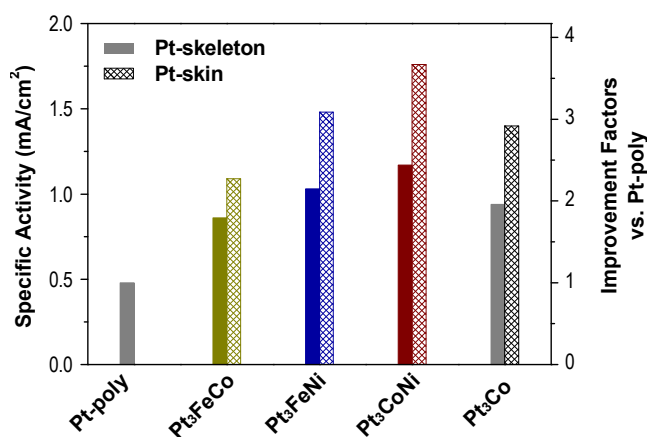


FIGURE 2. Summary of the ORR catalytic activities for the Pt-bimetallic and Pt-ternary alloy thin films compared to Pt-poly. Activities of both as-sputtered (Pt-skeleton) and annealed (Pt-skin) surfaces are presented.

was employed to investigate other ternary alloys, and hence a trend in the ORR activity has been established. Figure 2 shows a summary of the catalytic activities of the ternary alloys for the ORR in comparison with Pt-poly and Pt_3Co . All the as-sputtered alloy surfaces show higher activity than Pt-poly, with the improvement factors ranging from 1.7 to 2.5. Further improvement was consistently achieved by thermal annealing for each alloy. For the annealed surfaces, $\text{Pt}_3(\text{CoNi})_1$ shows an improvement factor of ~ 4 vs. Pt-poly, vs. ~ 2.2 and ~ 3.0 for $\text{Pt}_3(\text{FeCo})_1$ and $\text{Pt}_3(\text{FeNi})_1$, respectively. We used these findings to approach corresponding nanoscale

systems. As reported previously we used a solvo-thermal approach to obtain monodisperse and highly homogeneous Pt₃MN nanoparticles. In addition to the previous year activities our focus lately has been focused on ability to form Pt-skin surfaces on ternary alloy NPs. Figure 3 summarizes results from electrochemical measurements of ternary alloys and confirms formation of Pt-skin. In accordance to extended surfaces results, the improvement factors show better performance when compared to Pt-bimetallic alloys. Our future efforts will be dedicated to increasing the content of non-precious metals, since our initial attempts were not successful. The main obstacle is different nucleation growth of Pt, which is much faster than Co, Ni and Fe and that induces formation of separate Pt NPs, Pt-rich core and inhomogeneous distribution elements across the nanoparticle.

MEA durability studies. For the most promising catalyst we performed detailed MEA characterization. Catalytic activity and stability of Pt-skin PtNi/C NPs were tested by the electrochemical potential cycling in 50-cm² fuel cells at General Motors. The electrodes were prepared by GM via a decal method. First, a catalyst ink with a targeted ionomer/carbon mass ratio of 0.8-1.0 was drawn down across an oversized (100-cm² frame) to coat the decal substrate. After drying, the decal was die-cut to 50 cm² and the electrode was laminated to a DuPont (25 μm) NRE 211 membrane in a hot press. The loadings on the cathodes were 0.13 mg_{Pt}/cm². X-ray absorption spectra were collected for the PtNi/C MEAs before and after the prolonged potential cycling. Figure 4 presents the normalized X-ray absorption near-edge spectroscopy (XANES) spectra at Ni K and Pt L₃

edges for the “fresh” and “cycled” PtNi/C catalysts overlaid with the appropriate Ni and Pt foil standards. No shift in the absorption edge energies (E_0) was detected against the standards in either case, indicating that the bulk oxidation states of Ni and Pt are zero in the catalysts. The line shapes of the PtNi/C catalysts at the Ni K edge deviate from the Ni foil standard. In particular, the pre-edge features (-4 to +4 eV relative to E_0) are slightly muted, and the magnitudes of the white line features (+5 to +25 relative to E_0) are considerably larger than the bulk Ni foil, but neither signal approaches that of NiO. Both the pre-edge and white line features should arise from dipole-forbidden 1s to p and d transitions and are indicative of the oxidation and change of local symmetry of the Ni atoms in vicinity to Pt. At the Pt L₃ edge, the catalysts show a bulk Pt oxidation state of zero and an increase in the white line intensity compared to the Pt foil standard. This feature, and also the dampened post-edge oscillations (in comparison to the Pt foil), can be ascribed to the nanoscale nature of the catalysts. From both Ni and Pt edges it can be seen that negligible changes occurred to the PtNi/C catalyst after the extensive (but mild) potential cycling, suggesting that the outer Pt layers protected the subsurface Ni. That this catalyst is capable of preserving the nanostructure during electrochemical reactions is consistent with the findings from electrochemical studies. Therefore, in addition to high specific activity, multilayered PtNi-skin catalyst also exhibits high durability that is verified by high-resolution transmission electron microscopy, RDE [9], MEA, and XANES.

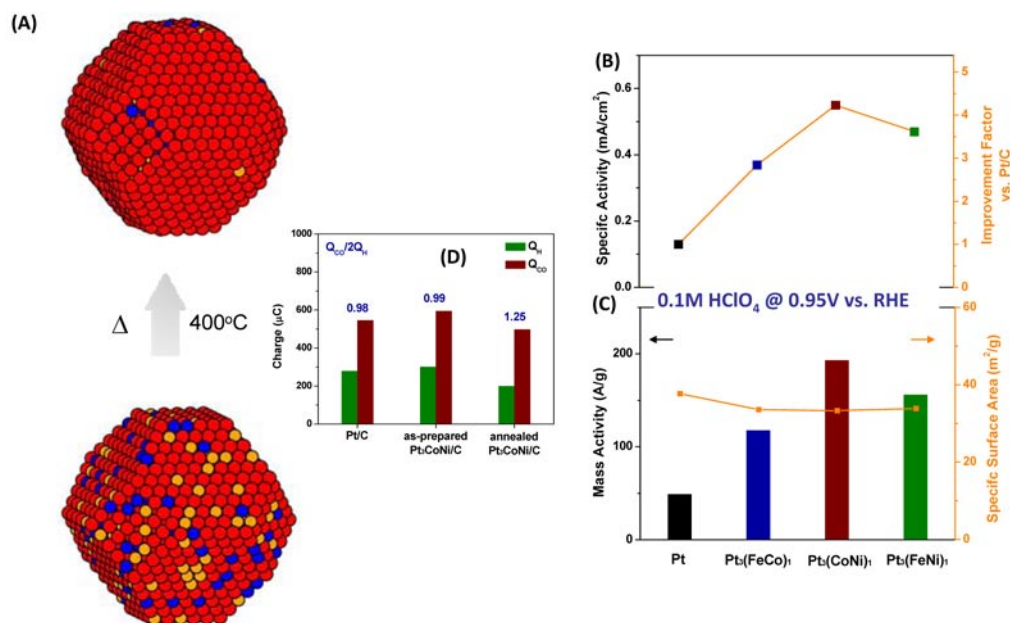


FIGURE 3. Pt₃MN NPs (A) Monte Carlo simulation confirms Pt-skin formation (B) Specific activity and improvement factor vs. Pt/C (C) Mass activity and specific surface area (D) (Q_{H_2}) and CO stripping (Q_{CO}) integrated charges assessed under the hydrogen adsorption/desorption peaks and a CO stripping peak.

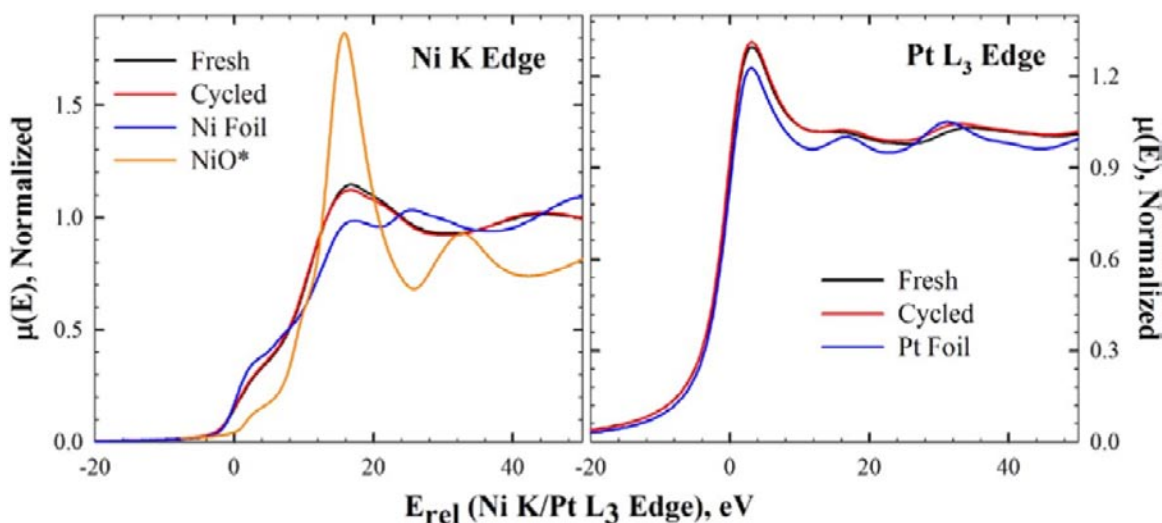


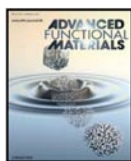
FIGURE 4. Ni K (left) and Pt L_3 (right) edge XANES spectra of the fresh and cycled electrocatalyst cathode-side MEAs with the appropriate reference foils overlaid.

Conclusions and Future Directions

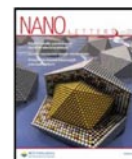
- PtM and $Pt_3M_1N_2$ NPs cathode catalysts obtained from the organic solvo-thermal synthesis exhibit superior activity and stability than those prepared by the conventional methods. The method to synthesize Pt_3MN NPs with highly active Pt-skin morphology is established.
- Specific and mass activity improvements are obtained for Pt-skin Pt_3MN/C NPs in RDE measurements. Advanced theoretical modeling (density functional theory, Monte Carlo) methods predicted and confirmed Pt-skin type of nanosegregated structures in ternary alloys.
- Ternary systems operate through the same mode of action of improving the catalytic properties of the topmost Pt atoms as binary alloys.
- Ex situ characterization in MEA of the most promising nanoscale catalyst confirmed that the structure and composition of the catalyst were not changed after 20,000 cycles.
- Future effort will be dedicated to the scale-up synthesis of the most promising catalysts and MEA evaluation.
- Further increase of the non precious metal content will be pursued for ternary systems.

FY 2012 Publications/Presentations

1. C. Wang, M. Chi, G. Wang, D. van der Vliet, D. Li, K.L. More, H. Wang, J.A. Schluter, N.M. Markovic and V.R. Stamenkovic, *Relationship between Surface Chemistry and Electrocatalytic Properties of Monodisperse Pt_xNi_{1-x} Nanoparticles*, *Advanced Functional Materials*, 21 (2011) 147, Cover Article.



2. C. Wang, D. van der Vliet, K.L. More, N.J. Zaluzec, S. Peng, S. Sun, H. Daimon, G. Wang, J. Greeley, J. Pearson, A.P. Paulikas, G. Karapetrov, D. Strmcnik, N.M. Markovic and V.R. Stamenkovic, *Multimetallic Au/FePt₃ Nanoparticles as Highly Durable Electrocatalysts*, *Nano Letters*, 11 (2011) 919-928, Cover Article.



3. C. Wang, M. Chi, D. Li, D. Strmcnik, D. van der Vliet, G. Wang, V. Komanicky, K.-C. Chang, A.P. Paulikas, D. Tripkovic, J. Pearson, K.L. More, N.M. Markovic and V.R. Stamenkovic, *Design and Synthesis of Bimetallic Electrocatalyst with Multilayered Pt-Skin Surfaces*, *Journal of American Chemical Society*, 133 (2011) 14396.

4. D. van der Vliet, C. Wang, M.K. Debe, R.T. Atanasoski, N.M. Markovic, V.R. Stamenkovic, *Platinum Alloy Nanostructured Thin Film Catalysts for the Oxygen Reduction Reaction*, *Electrochimica Acta*, 56, 24 (2011) 8695.

5. C. Wang, M. Chi, D. Li, D. van der Vliet, G. Wang, Q. Lin, J.F. Mitchell, K.L. More, N.M. Markovic, V.R. Stamenkovic, *Synthesis of Homogeneous Pt-Bimetallic Nanoparticles as Highly Efficient Electrocatalysts*, *ACS Catalysis*, 1 (2011) 1355.

References

1. V. Stamenkovic, B. Fowler, B.S. Mun, G. Wang, P.N. Ross, C. Lucas, and N.M. Markovic, "Improved Oxygen Reduction Activity on $Pt_3Ni(111)$ via Increased Surface Site Availability", *Science*, **315** (2007) 493-497.
2. N.M. Markovic and P.N. Ross, "Surface Science Studies of Model Fuel Cell Electrocatalysts", *Surface Science Report*, **45** (2002) 121-229.
3. V. Stamenkovic and N.M. Markovic, "Electrocatalysis on Model Metallic and Bimetallic Single Crystal Surfaces, Model Systems in Catalysis: From Single Crystals and Size Selected Clusters", Editor: Robert M. Rioux, Harvard University, USA,; Publisher: Elsevier Science, Amsterdam, The Netherlands, 2009.

4. K.J.J. Mayrhofer, B.B. Blizanac, M. Arenz, V. Stamenkovic, P.N. Ross and N.M. Markovic, "The Impact of Geometric and Surface Electronic Properties of Pt-catalysts on the Particle Size Effect in Electrocatalysis", *J. Phys. Chem. B*, **109** (2005) 14433-14440.
5. C. Wang, D. van der Vliet, K.C. Chang, H. You, D. Strmcnik, J.A. Schlueter, N.M. Markovic, V.R. Stamenkovic, "Monodisperse Pt₃Co Nanoparticles as a Catalyst for the Oxygen Reduction Reaction: Size Dependent Activity", *J. Phys. Chem. C.*, **113**(2009)19365.
6. C. Wang, D. van der Vliet, K.C. Chang, N.M. Markovic, V.R. Stamenkovic, "Monodisperse Pt₃Co Nanoparticles as Electrocatalyst: the Effect of Particle Size and Pretreatment on Electrocatalytic Reduction of Oxygen", *Phys.Chem.Chem.Phys.*, **12**(2010)6933-6939; *COVER Article*.
7. N.M. Markovic, V. Radmilovic, P.N. Ross, "Physical and Electrochemical Characterization of Bimetallic Nanoparticle Electrocatalysis", in *Catalysis and Electrocatalysis at Nanoparticle Surfaces*, Edited by A. Wieckowski, E. Savinova and C. Vayenas, Marcel Dekker, Inc., Chapter 9, (2003) 311-342.
8. V. Stamenkovic, B.S. Mun, M. Arenz, K.J.J. Mayrhofer, C. Lucas, G. Wang, P.N. Ross, and N.M. Markovic, " Trends in Electrocatalysis on Extended and Nanoscale Pt-bimetallic Alloy Surfaces", *Nature Materials.*, **6** (2007) 241-247.
9. C. Wang, M. Chi, D. Li, D. Strmcnik, D. van der Vliet, G. Wang, V. Komanicky, K.-C. Chang, A.P. Paulikas, D. Tripkovic, J. Pearson, K.L. More, N.M. Markovic and V.R. Stamenkovic, *Design and Synthesis of Bimetallic Electrocatalyst with Multilayered Pt-Skin Surfaces*, *Journal of American Chemical Society*, **133**(2011)14396.

V.D.6 Contiguous Platinum Monolayer Oxygen Reduction Electrocatalysts on High-Stability Low-Cost Supports

Radoslav Adzic (Primary Contact),
Miomir Vukmirovic, Kotaro Sasaki, Jia Wang,
Yang Shao-Horn¹, Rachel O'Malley²
Brookhaven National Laboratory (BNL), Bldg. 555
Upton, NY 11973-5000
Phone: (631) 344-4522
Email: adzic@bnl.gov

DOE Manager

HQ: Nancy Garland
Phone: (202) 586-5673
Email: Nancy.Garland@ee.doe.gov

Subcontractors:

- ¹ Massachusetts Institute of Technology (MIT),
Cambridge MA
- ² Johnson Matthey Fuel Cells (JMFC), London, England

Project Start Date: July 1, 2009
Project End Date: September 30, 2013

content of Pt-group metal (PGM) and more simple membrane electrode assemblies (MEAs) formation.

TABLE 1. Progress toward Meeting DOE Fuel Cell Electrocatalysts Technical Targets

| Characteristic | Units | Target | Achieved |
|-------------------|---------------------------------------|--------|---|
| | | 2015 | 2011 |
| PGM Total Loading | mg PGM/cm ² electrode area | 0.2 | 0.12 |
| Mass Activity | A/mg Pt @ 900 mV iR-free | 0.44 | 2.8 (Pd nanowires) |
| Specific Activity | μA/cm ² @ 900 mV iR-free | 720 | 1,100 (Pd rods) |
| PGM Mass Activity | | 0.44 | 0.57 (hollow PdAu alloy) |
| Durability | | | Some loss in activity in 20,000 cycles to 1.4 V Pt/Pd(Au) |

iR – internal resistance

Fiscal Year (FY) 2012 Objectives

Developing high-performance fuel cell electrocatalysts for the oxygen reduction reaction (ORR) comprising contiguous Pt monolayer (ML) on stable, inexpensive metal or alloy:

- Nanoparticles
- Nanowires
- Hollow nanostructures
- Carbon nanotubes

Technical Barriers

This project addresses the following technical barriers from the Fuel Cells section of the Fuel Cell Technologies Program Multi-Year Research, Development and Demonstration Plan:

- (A) Performance
- (B) Cost
- (C) Durability

Technical Targets

We are focusing on simplifying synthetic processes to obtain better catalysts' activity, higher Pt utilization, lower

FY 2012 Accomplishments

- Demonstrated the stability of Pt_{ML}/Pd₉Au/C and Pt_{ML}/Pd/C electrocatalysts under potential cycling to 1.4 V is high. Self-healing-mechanism confirmed in this test.
- Four patents on their technology have been licensed to N.E. ChemCat Co. by BNL.
- Demonstrated synthesis of Pd alloys with refractory metals to provide stable and inexpensive cores, reduced PGM content.
- Developed an electrochemical method for Pt_{ML} electrocatalysts syntheses involving electrochemical deposition on gas diffusion layers (GDLs). High-activity, high-stability electrocatalysts are obtained, Pt utilization close to 100%; scale up is simple.
- Synthesis of ultra-thin Pd alloy nanowires using simple surfactant has been developed to provide an excellent support for a Pt_{ML}.
- An efficient method for Pt_{ML} deposition on Pd nanoparticles using ethanol as a medium and reactant has been developed.
- Further development of synthesis of hollow Pd nanoparticle catalysts with hollow-induced lattice contraction enhancing the ORR activity of a Pt ML.



Introduction

Further developments of oxygen reduction electrocatalysts to lessen the remaining technological difficulties that used to hamper the automotive applications of fuel cells still have to focus on reducing Pt, or PGM contents, increasing their stability and activity. The understanding of the properties of Pt ML electrocatalysts, and of a broader class of core-shell electrocatalysts, has grown up considerably. Thus, the complex influence of the nanoparticle core's composition, size and shape on the catalyst's activity make it possible to optimize the properties of certain classes making them ready for application.

Approach

Based on our understanding of the role of OH_{ads} on Pt on the ORR our recent finding of significant weakening of binding energy of oxygen (BE-O) on the (111) facet compared to the extended surface due to nanoscale induced in-plane lattice contraction, our approach focuses on having surfaces with the high coordination (111) facets. These surfaces are most conducive to the ORR on nanoparticles. In addition, they are less prone to dissolution than low-coordinated edges, defects, and less close-packed facets. Thus, we will study the electrocatalysts comprising Pt monolayer deposited on selected shapes of nanoparticles (hollow cores), nanorods and nanowires. These nano-shapes have surface structures and the average atom coordination close to surfaces on bulk materials. Several synthetic approaches, including the electrodeposition to make Pd nanorods or nanowires on C nanoparticles and carbon fibers in GDL (5 cm^2 and 25 cm^2), using simple surfactants to form ultra-thin bimetallic nanowires, using ethanol as a dispersion medium and reducing agent to make a Pt ML on Pd and hollow Pd nanoparticles.

Results

Decreasing the content of Pd in cores: Ru, and PdW and NiW alloys as cores

A highly useful feature of PtML core-shell catalysts is a possibility of a simple and efficient tuning the ML shell-core interaction and consequently the catalytic activity. This feature also allows decreasing the catalysts' PGM contents. We showed that Ru nanoparticles can serve as a convenient, inexpensive cores if two Pt MLs are deposited, which is an optimal thickness positioned at the top of volcano plot of activity vs. Pt thickness. Pt mass activity is 0.81 A/mg ; specific activity = 0.58 mA/cm^2 and PGM activity is 0.50 A/mg .

In order to make inexpensive and stable cores, Pd can be alloyed with suitable refractory metal, which, if exposed to

electrolyte, will passivate. A 1:1 PdW alloy was obtained in H_2 , 600°C . Pt mass activity is 0.81 A/mg ; specific activity = 0.58 mA/cm^2 and PGM activity is 0.22 A/mg .

Another very promising approach to decrease PGM content that we developed involves electrochemical co-deposition of W and Ni (deposition of W alone is not possible in aqueous solutions) to make W-Ni alloy cores. The 50:50 NiW alloy was deposited at carbon constituting a GDL, confirmed using energy dispersive X-ray spectroscopy (EDS). Two features of these nanoparticles are important: 1st they have no PGM content, their costs are negligible. Dissolution of Ni from these nanoparticles can take place from the top 1-2 layers and then it stops because W atoms dominating now in the surface layer will not dissolve. They will passivate above certain potential. We displace Ni in the surface layer by about 2 monolayers of Pd and then place a Pt monolayer on such nanoparticles. Figure 1 shows polarization curve for the ORR on the electrode having only $40 \mu\text{g PGM/cm}^2$.

Electrochemical deposition for a 100% Pt utilization

Electrodeposition of $\text{Pd}_{0.9}\text{Au}_{0.1}$ alloy core for the $\text{Pt}_{\text{ML}}/\text{Pd}_{0.9}\text{Au}_{0.1}/\text{GDL}$ catalyst

Electrochemical deposition of Pt monolayer electrocatalysts has a great potential for syntheses of the low-Pt content electrocatalysts since it facilitates 100% utilization of Pt. The first step involves the electrodeposition of core nanoparticles on GDL. Subsequent deposition of a Pt monolayer, using the Cu underpotential deposition displacement method, will take place only on the nanocores surface that is in contact with electrolyte. This surface, upon

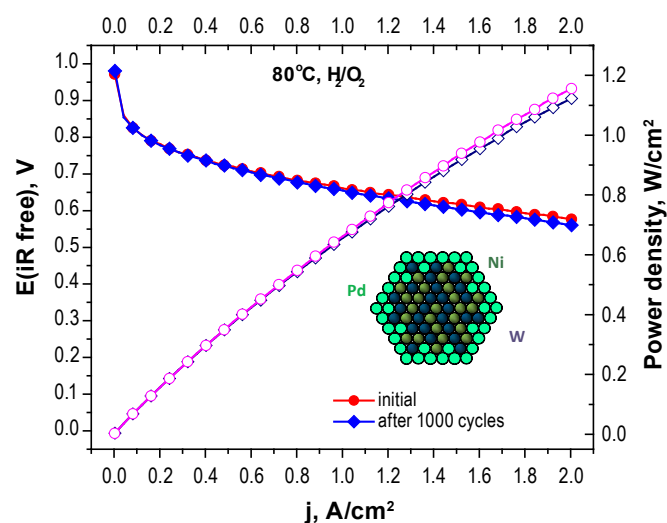


FIGURE 1. Pt ML on a NiW core obtained by codeposition. The ORR kinetics on $\text{PtML}/\text{Pd}/\text{W}/\text{C}$. Pt content is less than $40 \mu\text{g/cm}^2$. Insert: Model of NiW core with a partially displaced Ni by Pd.

formation of the MEA, will be accessible to O_2 and will be in contact with the membrane. None of Pt atoms will be blocked by contact with carbon or occluded by Nafion[®] having no contact with the current collecting carbon as commonly occurs with the catalyst ink or spraying used in MEAs preparation. Figure 2 shows polarization curves of Pt ML catalyst on electrodeposited PdAu alloy core.

Stability of Pt ML electrocatalysts under potential cycling to 1.4 V

To verify stability of Pt ML catalysts at extreme potential excursions the test with potential cycling to 1.4 V has been carried out. Figure 3 shows a decrease in activity after 20,000 potential cycles and formation of a Pd band in the membrane, but no Pt or Au loss.

Pt Monolayer on Hollow Pd Nanoparticles Electrocatalysts

We fabricated Pt monolayer catalysts on Pd and Pd-Au hollow cores that were made using Ni nanoparticles as sacrificial templates. The hollow architecture of the Pd-Au particles achieved is stemmed from the synergistic action of both galvanic replacement and Kirkendall effect in controlling reaction kinetics. The electrocatalyst has total-metal mass activities for the ORR up to 0.57 A mg^{-1} , which is 2.2 times that of 0.25 A mg^{-1} for a Pt monolayer on solid Pd cores, and 3.5 times that of 0.16 A mg^{-1} for solid Pt nanoparticles made by pulse electrodeposition. The cores' hollow structures enhance catalyst's properties and thus are promising for fuel cell applications.

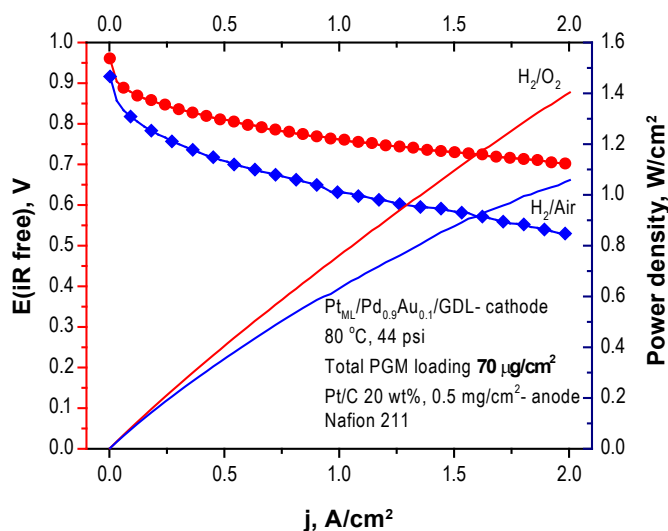


FIGURE 2. Polarization curve for electrodeposited PtML on Pd_{0.9}Au_{0.1} alloy. Comparison of performance with oxygen and air. The PGM content is approximately $70 \mu\text{g}/\text{cm}^2$.

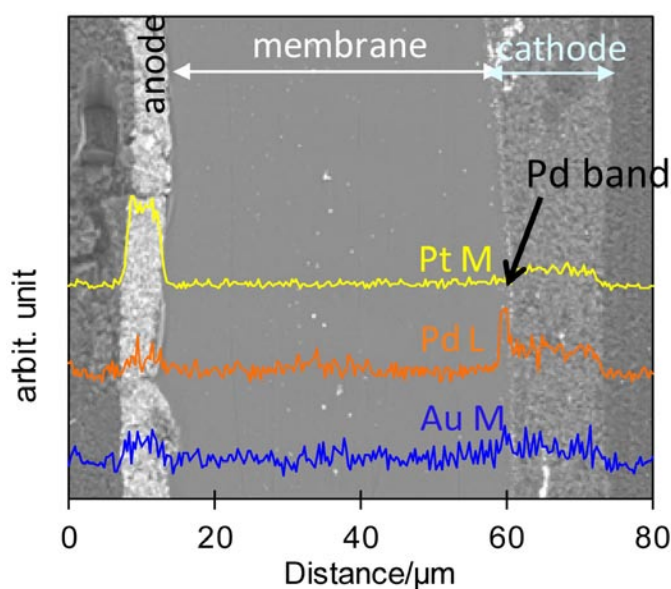
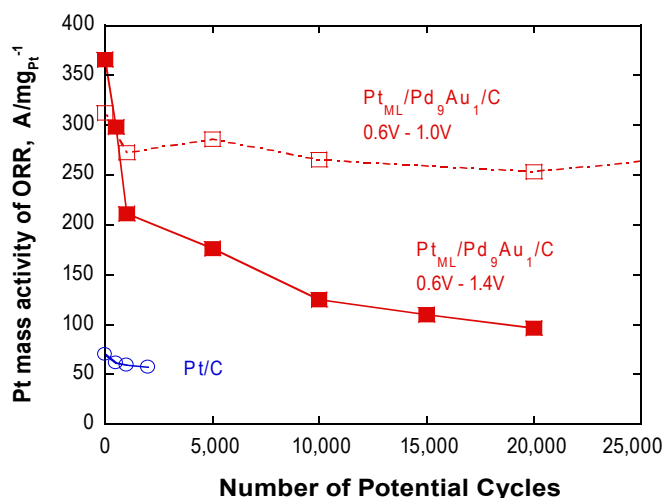


FIGURE 3. Stability of PtML/PdAu/C catalysts under potential cycling to 1.4 V. Top panel: polarization curves after 20,000 potential cycles from 0.6 to 1.4 V. For comparison, data for commercial Pt/C electrocatalyst are given and the cycling test 0.6-1. Bottom panel: scanning electron microscope image of the MEA cross-section and EDS distribution of catalyst constituents. A Pd band is formed from dissolved Pd; no dissolution of Pt and Au is observed. (With H. Naohara, Toyota Motor Co.).

Conclusions and Future Directions

- Pt_{ML}/Pd₉Au/C and Pt_{ML}/Pd/C are practical electrocatalysts. Stability under potential cycling to 1.4 V.
- Four patents on their technology have been licensed to N.E. ChemCat Co. by BNL.
- Pd alloys with refractory metals provide stable and inexpensive cores, reduced PGM content.
- An efficient method for Pt_{ML} electrocatalysts synthesis involving electrochemical deposition on GDLs has been

developed. High activity, high stability electrocatalysts are obtained, Pt utilization close to 100%; scale up is simple.

- Synthesis of ultra-thin Pd alloy nanowires using simple surfactant has been developed to provide an excellent support for a Pt_{ML}.
- The mechanism of stability of core-shell electrocatalysts, in which shell is protected by the core, and the self-healing mechanism have been verified in tests involving potential cycling to 1.4 V.

Future studies will focus on:

1. Scale up synthesis of Pd alloy nanowires by electrodeposition electrodes of 25 and 300 cm².
2. Scale up of synthesis to produce 20 grams of ultra-thin nanowires using weak surfactants.
3. Developing the microemulsion method to synthesize hollow Pd nanoparticles.
4. Further work on the Pd-refractory metal alloy cores.
5. MEA fabrication and tests.

Special Recognitions & Awards/Patents Issued

1. R. Adzic was named 2012 Inventor of the Year by the New York Intellectual Property Law Association (NYIPLA).
2. R. Adzic received The 2012 DOE Hydrogen and Fuel Cells Program Annual Award.
3. R. Adzic, J. Wang, M. Vukmirovic, K. Sasaki received an R&D100 Award.

Patents

Electrocatalyst for oxygen reduction with reduced platinum oxidation and dissolution rates Radoslav Adzic, Junliang Zhang, Miomir Vukmirovic. U.S. Patent No. 8,062,552, issued November 22, 2011.

Three patent applications have been submitted.

Four patents on Pt monolayer electrocatalysts have been licensed by BNL to N.E. ChemCat Corp., Japan.

FY 2012 Publications/Presentations

1. Carbon-supported IrNi core-shell nanoparticles: synthesis, characterization, and catalytic activity / Kotaro Sasaki, Kurian A. Kuttiyiel, Laura Barrio, Dong Su, Anatoly I. Frenkel, Nebojsa Marinkovic, Devinder Mahajan, Radoslav R. Adzic // *Journal of Physical Chemistry C*. 20 (2011) 9894-9902.
2. Electrodeposition of metals in catalyst synthesis: the case of platinum monolayer electrocatalysts / Miomir B. Vukmirovic, Stoyan T. Bliznakov, Kotaro Sasaki, Jia X. Wang, Radoslav R. Adzic // *Electrochemical Society Interface*. 2 (2011) 33-40.
3. Electrodeposition of Pd nanowires and nanorods on carbon nanoparticles / Stoyan Bliznakov, Miomir Vukmirovic, Eli Sutter, Radoslav Adzic // *Macedonian Journal of Chemistry and Chemical Engineering*. ISSN 1857-5552. 30 : 1 (2011) 19-27.
4. Enhanced electrocatalytic performance of processed, ultrathin, supported Pd-Pt core-shell nanowire catalysts for the oxygen reduction reaction / Christopher Koenigsmann, Alexander C. Santulli, Kuanping Gong, Miomir B. Vukmirovic, Wei-ping Zhou, Eli Sutter, Stanislaus S. Wong, Radoslav R. Adzic // *Journal of the American Chemical Society*. 25 (2011) 9783-9795.
5. Kirkendall effect and lattice contraction in nanocatalysts : a new strategy to enhance sustainable activity / Jia X. Wang, Chao Ma, YongMan Choi, Dong Su, Yimei Zhu, Ping Liu, Rui Si, Miomir B. Vukmirovic, Yu Zhang, Radoslav R. Adzic // *Journal of the American Chemical Society*. 34 (2011) 13551-13557.
6. Low-coordination sites in oxygen-reduction electrocatalysis: their roles and methods for removal / Yun Cai, Chao Ma, Yimei Zhu, Jia X. Wang, Radoslav R. Adzic // *Langmuir*. 13 (2011) 8540-8547.
7. Platinum monolayer electrocatalysts for the oxygen reduction reaction: improvements induced by surface and subsurface modifications of cores : [review article] / Yun Cai, Radoslav R. Adzic // *Advances in Physical Chemistry*. (2011) Special issue: *Advances in Electrocatalysis*; article ID 530397 (16 p.).
8. Platinum monolayer on IrFe core-shell nanoparticle electrocatalysts for the oxygen reduction reaction / Kotaro Sasaki, Kurian A. Kuttiyiel, Dong Su, Radoslav R. Adzic // *Electrocatalysis*. 2 (2011) 134-140.
9. Hollow core supported Pt monolayer catalysts for oxygen reduction/ Zhang, Y., Ma, C., Zhu, Y., Si, R., Cai, Y., Wang, J.X., Adzic, R.R., *Catalysis today*, in press.

V.D.7 The Science and Engineering of Durable Ultralow PGM Catalysts

Fernando H. Garzon (Primary Contact),
Jose-Maria Sansiñena, Mahlon Wilson,
Jerzy Chlistunoff, Ivana Matanovic, Neil Henson
and Eric L. Brosha

Los Alamos National Laboratory
MPA-11, MS. D429
Los Alamos, NM 87545
Phone: (505) 667-6643
Email: garzon@lanl.gov

DOE Manager

HQ: Nancy Garland,
Phone: (202) 586-5673
Email: Nancy.Garland@ee.doe.gov

Subcontractors:

- Yushan Yan, University of California Riverside, CA/
University of Delaware, Newark, DE
- Abhaya Datye and S. Michael Stewart, University of New
Mexico, Albuquerque, NM
- Siyu Ye and David Harvey, Ballard Fuel Cells, Burnaby,
BC, Canada

Project Start Date: October, 2009
Project End Date: October, 2014

Fiscal Year (FY) 2012 Objectives

- Development of durable, high mass activity platinum group metal (PGM) cathode catalysts enabling lower cost fuel cells.
- Elucidation of the fundamental relationships between PGM catalyst shape, particle size and activity to help design better catalysts.
- Optimization of the cathode electrode layer to maximize the performance of PGM catalysts improving fuel cell performance and lowering cost.
- Understanding the performance degradation mechanisms of high mass activity cathode catalysts—provide insights to better catalyst design.
- Development and testing of fuel cells using ultralow loading high activity PGM catalysts—validation of advanced concepts.

Technical Barriers

- PGM catalysts are difficult to synthesize in configurations other than quasi-spherical particles.
- PGM area specific activity may decrease with decreasing particle size.

- Durability may decrease with greater PGM surface area to volume ratios.

TABLE 1. Technical Targets: Electrocatalysts for Transportation Applications (Extracted from Table 3.4.12. Technical Plan April 27, 2007) Technical Targets

| Characteristic | Units | 2005 Status | | Stack Targets | |
|-------------------------------------|---------------------------------------|-------------|-------|---------------|------|
| | | Cell | Stack | 2010 | 2015 |
| PGM total content (both electrodes) | g/kW (rated) | 0.6 | 1.1 | 0.3 | 0.2 |
| PGM total loading | mg PGM/cm ² electrode area | 0.45 | 0.8 | 0.3 | 0.2 |

The technical targets for catalyst loading are indicated in Table 1. These targets were formulated with the assumption that fuel cell durability and impurity tolerance would not be impacted by the decreased Pt loadings used in the fuel cells

FY 2012 Accomplishments

- New Pt/carbon-ceria catalysts were developed and characterized by X-ray diffraction (XRD), high-resolution transmission electron microscopy (HRTEM), cyclic and rotating disc electrode (RDE) voltammetry, and thermogravimetry and they exhibit enhanced oxygen reduction reaction (ORR) activity over Pt-C.
- New Pt-Y and Pt-Sc alloy catalysts were developed and characterized by transmission electron microscopy (TEM) and cyclic and RDE voltammetry which show greater ORR activity than Pt-C.
- Pt on pyrolyzed polypyrrole synthesized and characterized by TEM and cyclic and RDE voltammetry exhibits high activity for ORR and good stability.
- New theoretical models developed for Pt nanotubes and new predictions made for the stability of these active catalysts.
- X-ray absorption spectroscopy experiments on a variety of carbons and using different Pt solution precursors revealed the mechanism of Pt catalyst nucleation and growth.
- The chemical reduction of Pt IV to Pt II by the carbon was shown to be an essential step in the formation of Pt nanoparticles.



Introduction

Minimizing the quantity of Pt group metals used in polymer electrolyte membrane fuel cells (PEMFCs) is one of the remaining grand challenges for fuel cell

commercialization. Tremendous progress has been achieved over the last two decades in decreasing the Pt loading required for efficient fuel cell performance. Unfortunately, the fluctuations in the price of Pt represent a substantial barrier to the economics of widespread fuel cell use. Durability and impurity tolerance are also challenges that are tightly coupled to fuel cell Pt electrode loading. Traditional approaches to decreasing the amount of Pt required for good performance include:

- Increasing mass activity by decreasing Pt particle size by supporting on carbon.
- Alloy formulation Pt-Co, Pt-Cr alloys to improve mass activity.
- Increasing Pt utilization by optimization of electronic and ionic contact of the Pt particles.
- Improving conductivity of the electronic and ionic conducting constituents of the membrane electrode assembly.
- Improving reactant to and product mass transport away from the electroactive sites.

Recent novel approaches include the nanoengineering of core shell catalysts and Pt particles of unusual geometries such as nanowires/whiskers.

The success of the aforementioned approaches has been great; however further advances using such approaches have been hampered by a lack of underlining scientific understanding of the catalyst activity, particle growth mechanisms, and optimization strategies for designing composite electrodes.

Approach

Our approach to new PGM catalyst design is multi-tiered. We are designing new low platinum loading catalysts on novel support materials to improve fuel cell performance. Novel PGM shapes; nanoparticles, nanotubes and nanowires are being synthesized in a variety of sizes. We are using contemporary theoretical modeling and advanced computational methods to understand and engineer the new catalysts. We are also modeling and designing appropriate catalyst architectures to maximize the performance of our novel catalysts. Catalyst-support interactions and their effects on durability and mass activity are also investigated. We study and test the performance of the catalysts in electrochemical cells, single-cell fuel cells and fuel cell stacks. The new catalysts are extensively characterized before and after fuel cell operation.

Results

We have improved our theoretical understanding of the stability and reactivity of Pt nanotubes and nanowires. We used density functional theory to study the difference

in the structure, stability and catalytic reactivity between ultrathin, 0.5-1.0 nm diameter, platinum nanotubes and nanowires. Inserting an inner chain of platinum atoms in the corresponding nanotubes formed model nanowires. In this way more stable, non-hollow structures were formed. The difference in the electronic structure of platinum nanotubes and nanowires was examined by inspecting the density of surface states and band structure. Furthermore, reactivity towards the oxygen reduction reaction of platinum nanowires was addressed by studying the change in the chemisorption energies of oxygen and hydroxyl groups, induced by inserting the inner chain of platinum atoms into the hollow nanotubes. Ultrathin platinum nanotubes and nanowires both have very different chemical reactivity than bulk platinum. We found that adsorption energies of oxygen and hydroxyl in general decrease as the diameter of the nanotube or a nanowire increases. However, the reactivity towards oxygen and hydroxyl varies considerably with the chirality and structure of the nanotube.

All the studied platinum nanotubes and nanowires with diameters less than approximate 1 nm bind oxygen and hydroxyl stronger than bulk surface and dissolve at very low cell potentials. The best candidates for fuel cell applications were found among single-wall nanotubes with approximately 1-nm diameter and $n=m$ chiralities. However, these tubes still have lower dissolution properties than the bulk platinum by up to 100 meV. Both double-wall nanotubes and nanowires with approximately 1-nm diameter have shown to have favorable interaction with oxygen but bind hydroxyl too strongly which would lead to the poisoning of the catalytic surface with hydroxyl during the ORR cycles.

Optimizing the reactivity of platinum nanotubes and nanowires for fuel cell applications might be challenging due to the complexity of factors that govern their reactivity and due to the inadequacies of simple descriptors, like d -band theory, to predict their reactivity; however, we believe it is still plausible. Future studies would require the evaluation of more chiralities than we have studied in order to find multi-wall nanotubes and nanowires that have smaller affinity for hydroxyl and dissolutions properties superior to those of bulk. However, we believe that this work presents an important first step towards that goal.

We are developing new conductive nanostructured materials based on pyrolyzed polypyrrole (PPy) nanowires that can be used as conductive support for metal catalysts. With this new approach we seek to produce a high surface area metal catalyst that can be easily incorporated into the fuel cell assembly and lead to a higher ORR catalytic activity by enhancing both electronic conductivity and transport properties. Figure 1 shows the typical structure of the Pt coated PPy/starch nanowires electrochemically deposited on the glassy carbon disk electrode. PPy/starch preserved structural integrity during pyrolysis and nanowires were uniformly deposited on the electrode with a narrow

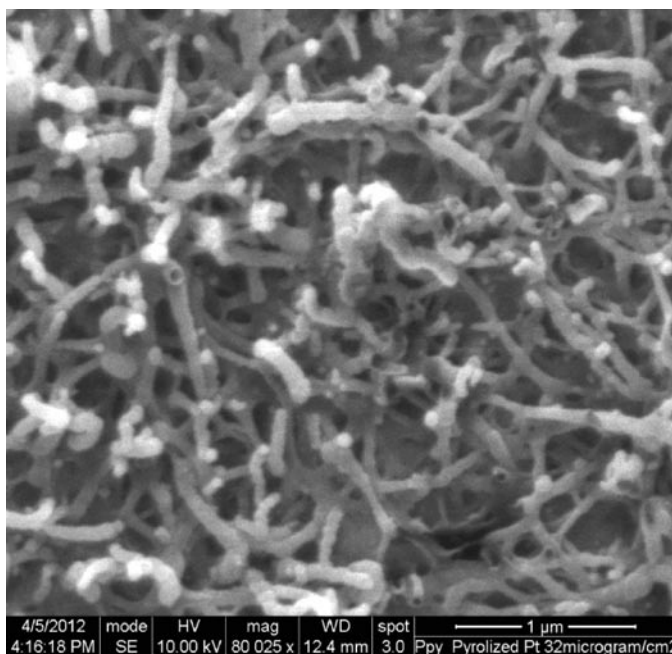


FIGURE 1. Electron micrograph of pyrolyzed polypyrrole nanowires

diameter distribution, which is directly dependent on the polymerization time. Moreover, we proved it was possible to deposit the PPy/starch nanowires on a carbon paper gas diffusion layer, which can be easily incorporated into the MEA structure as a gas diffusion electrode once coated with platinum. The new materials provided very good rotating ring disc electrode results as supports for low Pt load metal catalysts when compared with 46% Pt/C TKK catalyst, which was used as a reference. They demonstrate great potential to increase ORR catalytic activity by enhancing both electronic conductivity and transport properties. The specific surface area for the pyrolyzed PPy/starch nanowires coated with impregnated Pt ($83 \text{ m}^2 \text{ g}^{-1}$) was higher than the one obtained for 46% Pt/C TKK ($72 \text{ m}^2 \text{ g}^{-1}$), while the catalyst based on pyrolyzed PPy/starch nanowires coated with sputtered Pt was much lower ($29 \text{ m}^2 \text{ g}^{-1}$). The higher Pt surface area obtained using the Pt impregnation compared with the sputtering method suggests a smaller Pt particle size. This is consistent with the lower surface activity observed since smaller particles are intrinsically less active than bulk-like larger particles. However, the higher surface area of the impregnated Pt overcomes the deficiency and the apparent (mass) activity becomes comparable with the one obtained for the 46% Pt/C TKK used as a reference. Ultimately, PPy-Pt nanowires based catalysts may facilitate the preparation a fuel cell membrane electrode assembly by incorporating them as part of a GDE when PPy is directly electrodeposited onto a gas diffusion layer.

New alloy formulations may also improve Pt mass activity. In 2011-2012 we synthesized nanoparticles of platinum-scandium and platinum-yttrium using novel

organometallic precursors and synthesis conditions. These methods yielded alloys in the 4-7 nm particle size range as measured by transmission electron microscopy. The nanomaterials show significant improvement in oxygen reduction behavior over commercial catalysts as measured by rotating disk electrode techniques. Figure 2 shows the relative mass activities and area specific activities of these new catalysts compared to conventional nanocrystalline Pt-C and Pt-Pd alloys. The specific activity approaches that of bulk platinum, behavior not observed in nanocatalysts.

The formation of Pt catalysts on active oxide supports may also improve activity and fuel cell durability. Ceria has been shown to effectively eliminate destructive oxygen free radicals. The activity of the ceria is predominately due to the presence of Ce(III) in the oxide lattice. The Ce (III)/Ce(IV) ratio increases with decreasing particle size yet active surface area increases. Highly crystalline ceria nanoparticles were previously formed in porous carbon matrices by the simple pyrolysis of cerium loaded ion-exchange resins. Incorporating Gd or Pr dopants with Ce in the resins provided uniform dispersions and equally small ceria crystallites upon pyrolysis, typically 1–2 nm. Highly active particles were obtained, as demonstrated by fast peroxide decomposition rates. The combination of the high pyrolysis temperature ($1,000^\circ\text{C}$) and the controlled dispersion and stable environment provided by the ion-exchange resin precursors are key to provide highly crystalline and extremely small ceria particles in a conductive carbon matrix. We have incorporated mixtures of Pt-C and ceria nanoparticles to decrease free radical attack on the fuel cell components and are currently testing them in fuel cells as illustrated by HRTEM in Figure 3.

One of the outstanding challenges in the wider deployment of PEMFCs is improving the utilization of Pt in

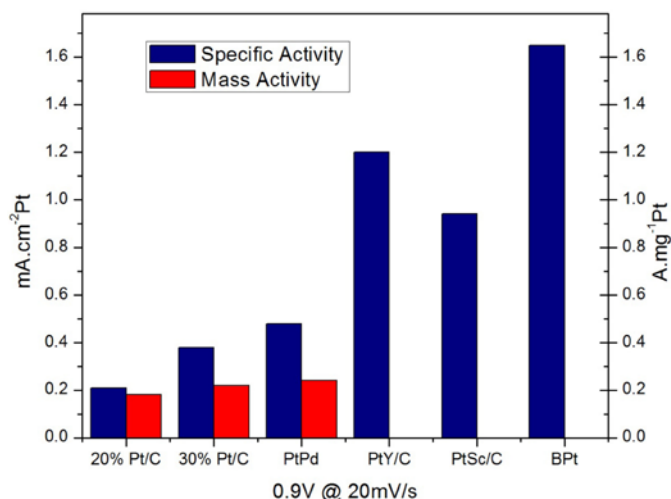


FIGURE 2. Mass activity and area specific activity of various Pt catalysts, Pt alloys and bulk Pt

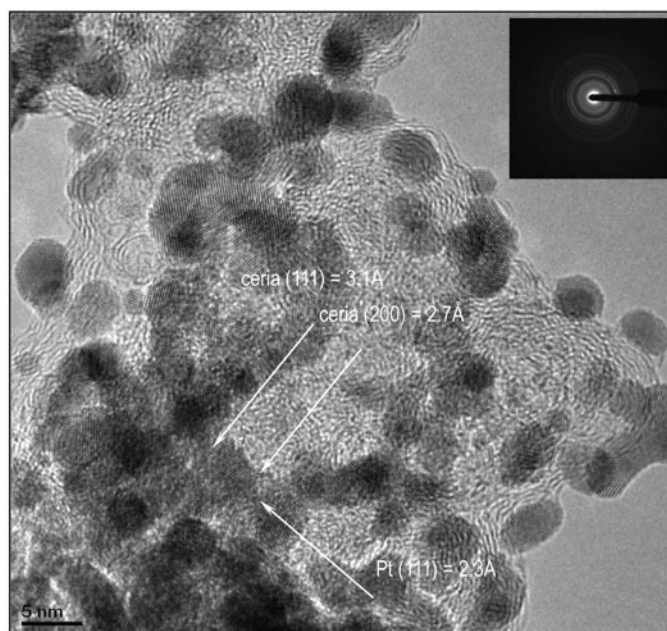


FIGURE 3. TEM and electron diffraction pattern of Pt-C/Ceria composite catalyst

carbon supported Pt nanocatalysts. While decreasing particle size improves accessibility of the Pt, it also destabilizes the Pt particles and leads to dissolution/re-precipitation and rapid grain growth. A parameter that is as yet poorly characterized is the number of nucleation sites on the carbon support. Increased nucleation site density could provide a valuable approach to improve Pt utilization. We have designed and performed X-ray absorption spectroscopy (XAS) experiments at Argonne National Laboratory that directly studied the formation of the Pt particles from an ionic solution precursor. The XAS experiments are powerful probes of the valence of the species and X-ray absorption fine structure region probes the local near neighbor environment of the nanoclusters of Pt as they nucleate and grow. We observed that the reduction of Pt (IV) chloride precursors to Pt (II) by the carbon surface governed the nucleation and growth of the Pt nanoparticles illustrated in Figure 4. Both types of carbon, high surface area Norit (red) and Vulcan XC-72 (green) show the rapid formation of Pt (II) as indicated by the figure; Pt metal (purple) and Pt(IV) chloride (blue) are plotted for comparison. The reduction site density varied with the types of carbon high surface area activated carbons having the most followed by partially graphitic carbon. No nucleation was observed on vitreous (glassy carbons).

Conclusions and Future Directions

- Pt/Ceria/C catalyst research:
 - Pt-C/Ceria catalyst optimization—improve Pt dispersion
 - Pt/Ceria/catalyst neutron scattering

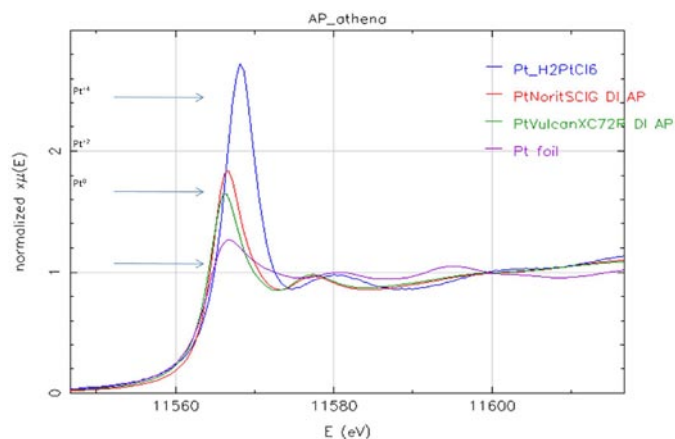


FIGURE 4. XAS spectrum of Pt after exposure to Norit (red) or Vulcan (green) carbon surfaces. Pt foil (blue) and Pt(IV)Chloroplatinic acid (blue) shown for reference

- Scale up for fuel cell testing
- Incorporation into catalyst layers and MEA optimization
- Fuel cell performance and durability testing
- Pt/Polypyrrole catalyst research:
 - Large batch synthesis and fuel cell testing
 - Calculate and synthesize optimal MEA geometries
- Pt/Y,Sc nanoplate research:
 - Decrease nanocrystal size
 - TEM and XRD characterization
 - Scale up for fuel cell testing
 - Incorporation into catalyst layers and MEA optimization
 - Fuel cell performance and durability testing
- Development of models and theory:
 - Density functional theory model extension to catalyst coated nanotube and nanowires
 - Microstructural model application to novel catalysts
 - Model validation

FY 2012 Publications

1. Matanovic, I.; Garzon, F.H.; Kent, P.R.; Henson, N.J., Density Functional Theory Study of Oxygen Reduction Activity on Ultrathin Platinum Nanotubes, submitted to *Journal of Physical Chemistry C*.
2. Matanovic, I.; Garzon, F.H.; Kent, P.R.; Henson, N.J., Theoretical Study of the Structure, Stability and Oxygen Reduction Activity of Ultrathin Platinum Nanotubes. Accepted for publication *ECS Transactions* 2012.
3. Sansinena, J.-M.; Wilson, M.S.; Garzon, F.H., Conductive Nanostructured Materials for Supported Metal Catalysts. Accepted for publication *ECS Transactions* 2012.

4. Sansinena, J.-M.; Nelson, M.; Wilson, M.S.; Garzon, F.H., Electrochemical Synthesis of Oxygen Reduction Catalysts Based on Pt Coated Polypyrrole Nanowires Using Starch as Template Molecule. *ECS Transactions* 2011, 33 (27), 13-19.
5. Wilson, M.S.; Delariva, A.; Garzon, F.H., Synthesis of sub-2 nm ceria crystallites in carbon matrixes by simple pyrolysis of ion-exchange resins. *Journal of Materials Chemistry* **2011**, 21 (20), 7418-7424.
6. Matanovic, I.; Henson, N.J.; Garzon; F.H. Theoretical Study of Electrochemical Processes on Pt-Ni Alloys, *Journal of Physical Chemistry C*. 2011, (2011) Vol.115, iss.21, p.10640-10650.

FY 2012 Presentations

1. Matanovic, I.; Garzon, F.H.; Kent, P.R.; Henson, N.J., Theoretical Study of the Structure, Stability and Oxygen Reduction Activity of Ultrathin Platinum Nanotubes. *ECS Meeting Abstracts 2012, 1202* (13), 1563-1563.
2. Sansinena, J.-M.; Wilson, M.S.; Garzon, F.H., Conductive Nanostructured Materials for Supported Metal Catalysts. *ECS Meeting Abstracts 2012, 1202* (13), 1688-1688.
3. Matanovic, I.; Garzon, F.; Henson, N., Theoretical Study of Electrochemical Processes on Novel Platinum Group Metal Catalysts. *ECS Meeting Abstracts 2011, 1101* (41), 1894-1894.

V.D.8 Molecular-Scale, Three-Dimensional Non-Platinum Group Metal Electrodes for Catalysis of Fuel Cell Reactions

John B. Kerr¹ (Primary Contact), Piotr Zelenay²,
Steve Hamrock³

¹Lawrence Berkeley National Laboratory (LBNL)
MS 62R0203, 1 Cyclotron Road
Berkeley, CA 94720
Phone: (510) 486-6279
Email: jbkerr@lbl.gov

²Los Alamos National Laboratory (LANL)
³3M Fuel Cell Components Program

DOE Manager

HQ: Donna Ho
Phone: (202) 586-8000
Email: Donna.Ho@ee.doe.gov

Collaborators:

- Adam Weber, John Arnold Jeff Reimer, Martin Head-Gordon, Robert Kostecki (LBNL)
- James Boncella, Yu Sueng Kim, Jerzy Chlistunoff, Neil Henson (LANL)
- Radoslav Atanasoski (3M)

Project Start Date: August 31, 2009

Project End Date: September 30, 2012

- (C) Performance (better electrode efficiency)
- (B) Cost
- (A) Durability

Technical Targets

- Non-Pt catalyst activity per volume of supported catalyst: 300 A/cm³
- Cost: <\$3/kW
- Durability: >5,000 hours (>120°C)
- Electrochemical support loss: <30 mV after 100 hrs @ 1.2 V

FY 2012 Accomplishments

- Completed Objective #1) to demonstrate that non-PGM catalysts can be used for oxygen reduction in polymer-coated electrode structures based on polyelectrolyte membranes.
- Completed Objective #2). Non-PGM catalysts have been incorporated into the polymer binders of composite electrodes used in MEAs and have been shown to support high current densities (up to 1.2 A/cm²).
- Completed Objective #3). Achievement and maintenance of high current densities (>250 A/cm³) has demonstrated that the 3-D matrix is capable of supporting high current densities. However, calculation of turnover frequencies (TOFs) based on the catalyst loading indicates that the catalysts possess activity at least as great as platinum and that the assumption of low activity for these catalysts does not hold. The 3-D matrix is able to make up for low loading of the catalysts due to the larger size of the catalyst centers. Use of redox mediators within the catalyst layers has been shown to be an effective method to reduce the overpotential of the ORR and to increase electron conduction within the catalyst layers. It has been demonstrated by theoretical calculation and by experimental results that the morphology of the 3-D matrix polymer array is particularly important in the promotion of the mediation effect.
- Completed Objective #4). MEAs containing the catalysts and mediators have been operated under high current conditions and appear to be stable after initial break-in for up to 50 hours of operation. The MEAs underwent temperature, humidity and voltage cycling. Impedance measurements were taken at a variety of current densities (up to 250 mA/cm², 125 A/cm³) prior to and after steady state operation which showed very little change in the various impedances within the cell. The

Fiscal Year (FY) 2012 Objectives

- 1) Demonstrate that non-platinum group metal (non-PGM) catalysts can be used for oxygen reduction reactions (ORRs) in polymer-coated electrode structures based on polyelectrolyte membranes. (Year 1)
- 2) Incorporate catalysts into polymer binders of composite electrodes for the construction of membrane electrode assemblies (MEAs) to demonstrate that this is an effective matrix for testing of new catalysts. (Year 2)
- 3) Demonstrate that the three-dimensional (3-D) structure of polymer-coated electrocatalyst layers can offset slower kinetics of the catalyst centers when compared with two-dimensional platinum or non-platinum catalysts. (Year 3)
- 4) Demonstrate that significant stability of the matrix is possible. (Year 3)

Technical Barriers

This project addresses the following technical barriers from the Fuel Cells section (3.4.5) of the Fuel Cell Technologies Program Multi-Year Research, Development and Demonstration Plan:

results confirmed that the 3-D matrix is stable enough in an MEA to warrant further investigation of such matrices as catalyst supports.

- The project achieved all the goals and milestones set out in the original proposal save one, which is to achieve a current density of 100 A/cm³ of catalyst layer volume for greater than 10 hours at a voltage of 800 mV_{ir-free}. Both the current density and lifetime criteria were met but the voltage was not met. Since this was a Go/No-Go criterion, the project is now in close-out due to failure to meet this milestone. However, the results have provided a clear, science-based path to how the voltage criterion may be achieved:
 - Methods for mechanistic determination have been developed that provide intrinsic catalyst activity. Combination of these methods with molecular modeling and targeted catalyst synthesis provides well defined pathways to lower overpotentials and achieve higher TOFs. The use of electron transfer mediators with high TOF catalysts mimics the action of enzyme catalysts known to outperform platinum and provides a route to achieve The DOE long-term goals for non-PGM catalysts.
 - Modeling procedures have been developed and validated for prediction of MEA performance using non-PGM catalyst layers. The model predicts that the catalyst layer morphology is critical for achievement of the electron mediation and this has been experimentally confirmed.



Introduction

Proton exchange membrane (PEM) fuel cells are not particularly efficient energy conversion devices (~50% fuel efficiency) and there is considerable interest in improving the performance while reducing the cost. One approach is to develop alternative catalysts that are more efficient than the traditional PGM catalysts and which also might be less expensive. Gasteiger and co-workers [1] have provided a very thorough review of the benchmark activities required for Pt, Pt-alloy and non-Pt catalysts for oxygen reduction and which describes in detail different approaches to catalysis of this important reaction. Methods have been reported to prepare non-PGM catalysts that involve a curious procedure whereby a rather complicated molecule such as a metal porphyrin or a complex such as iron phenanthroline is adsorbed on carbon and then heated to over 800°C to form the catalyst [2-5]. In some cases the carbon support is treated with nitrogenous compounds at high temperature followed by addition of metal ions such as Fe or Co. The pyrolysis process introduces considerable uncertainty as to the actual identity of the catalytic center but the reported results imply that new

physics of considerable complexity must be occurring. By contrast, the approach taken in this project involves electrode structures which can allow incorporation of catalytic species of known structure into MEAs, which increase the density of the electrocatalysts in the catalyst layer and which allow the known homogeneous activity of the catalyst to be retained. No “new physics” is required.

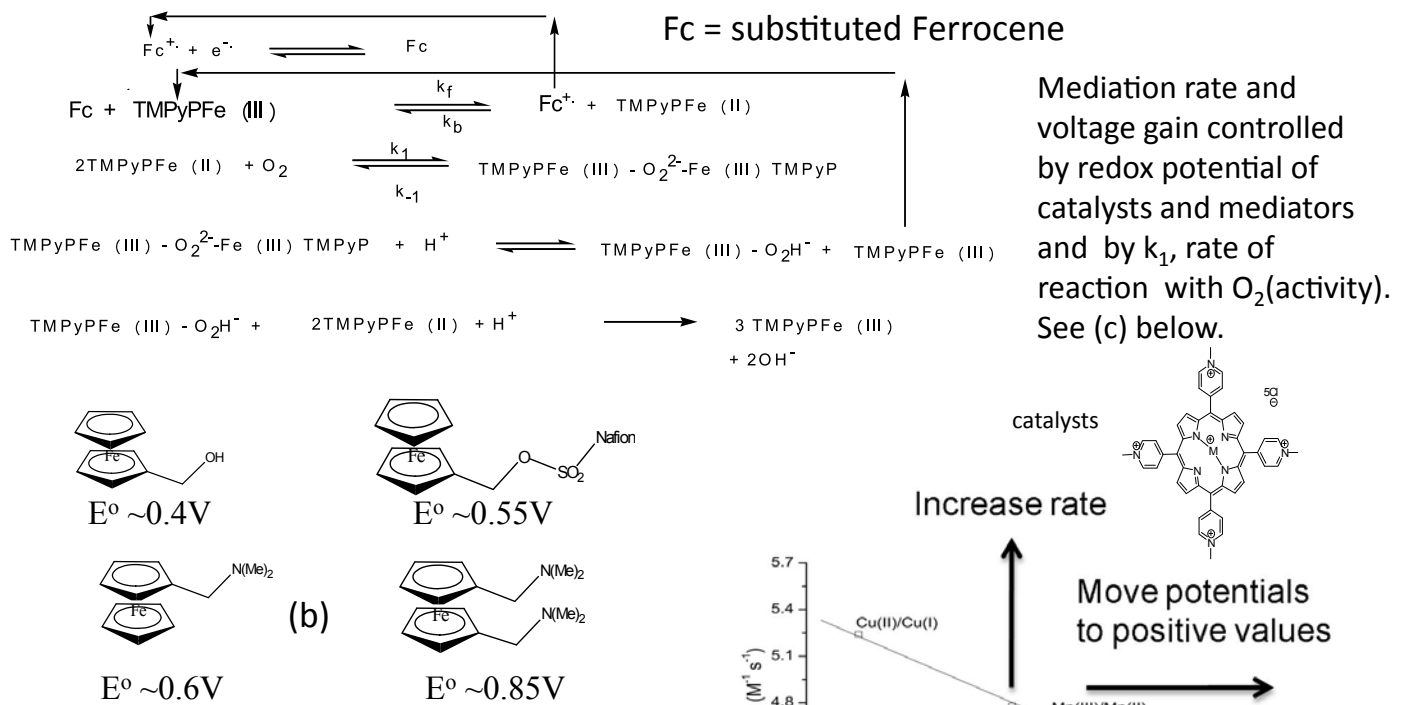
Approach

Homogeneous redox catalysis has been the center of considerable academic attention for several decades and a review by Saveant [6] provides an extensive overview of the topic and includes methods of tethering catalysts close to the electrode surface. These methods suggest ways to incorporate into fuel cell MEAs electrocatalysts that mimic very efficient enzyme catalyst centers and may lead to better performance at reduced cost. The principles, advantages and drawbacks behind the approach were explained at greater length in the FY 2010 and 2011 annual reports. The most important advantage of the approach is that the catalyst functions essentially as a homogeneous catalyst that can be thoroughly characterized in solution. This makes design and synthesis of the catalysts straight forward since they can be studied without resort to surface analysis techniques and to the invocation of surface effects that are poorly understood. The catalysts are then incorporated into polymers for coating on electrode surfaces and again the behavior can be characterized by simple electrochemical methods prior to incorporation of the polymer-bound catalysts into composite electrodes for MEAs. This last step is critical for the project and represented the Go/No-Go decision point that allows the flow of more efficient catalysts into the PEM fuel cell platform for practical use. This report outlines the experiments that have been carried out that demonstrate the validity of the approach. Although the project failed to achieve the required voltage it demonstrated that the catalyst matrix can achieve high current densities for extended periods of operation and also provided clear indications of how to achieve the voltage through appropriate catalyst design and control of the electrode layer structure.

Results

Figure 1 illustrates the concept of the 3-D electrode structure and the dynamics of the transport processes that deliver electrons and substrate to the catalytic centers. Examples of a catalyst and an electron mediator are shown. Since the objective is to keep the catalyst and mediator off the surface of the carbon to achieve the 3-D effect they both contain solubilizing groups (hydroxymethyl for the ferrocene and quaternized pyridines for the catalysts). The flow of the electrons is shown in Figure 1(c) where one can observe that the process is precisely the same as in a homogeneous system. Figure 1(d) shows the progress that has been

Mediator Approach - (a) Catalyst reacts with O₂ in a quasi-redox inner-sphere mechanism



- Mediator impacts onset potential – supplies electrons to the 3D matrix in outer-sphere mechanism. Change mediator type and can gain up to a maximum of 0.5 V theoretically

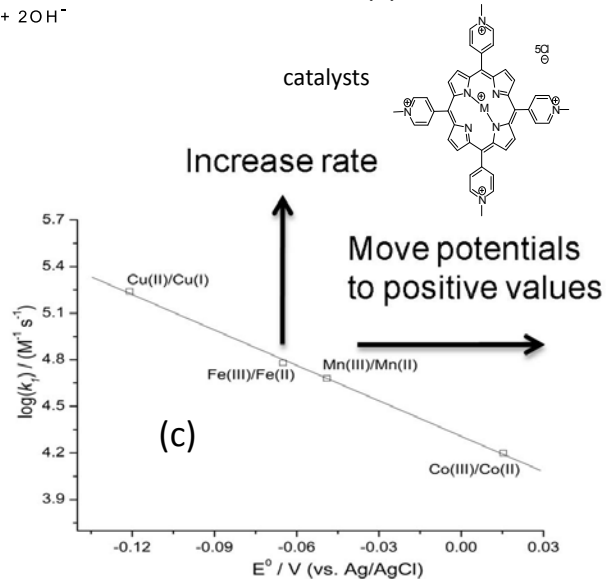


FIGURE 2. (a) Postulated mechanism of the reaction of the catalyst with oxygen through an inner-sphere route where the catalyst is activated by reduction by the ferrocene mediator. (b) shows the structures and potentials of candidate mediators that progress towards the desired potential. (c) is a plot of the measured rate constant of reaction of metal catalysts with oxygen as a function of potential, add 0.2 V to convert from the Ag/AgCl reference to the normal hydrogen electrode.

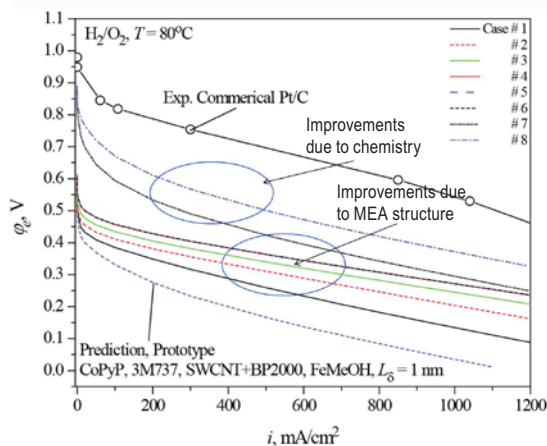
close to the target voltage of 0.9 V. These mediators will only function if the voltage of the catalyst is sufficiently positive and still with a high rate of reaction with oxygen as is shown in Figure 2(c).

Modification of the catalyst structure is one approach to provide higher voltage. This may be accomplished by means of electron withdrawing substituents on the pyridine rings or by direct substitution of the porphyrin rings with electron withdrawing groups such as fluoride, chloride, CF₃ or amino groups. These groups alter the electron density on the metal which leads to a shift in potential. The change in the metal electron density also leads to a difference in the rate of the reaction with oxygen which is equally important. Unfortunately as shown in Figure 2(c) a shift in the potential to more positive values tends to lead to lower activity. To approach this problem a combination of molecular modeling, synthesis and measurement has been undertaken to provide data on how substituents may affect the potentials and the

rate constants. The former are relatively easy to obtain for substituents on the porphyrin ring but more difficult for the pyridines due to the greater complexity of the molecules. Even more difficult is calculation of the rates of reaction with oxygen but both are necessary to provide complete understanding of the chemistry. As was mentioned in the FY 2011 report, deformed rings such as corrin or corrole rings can lead to faster rates due to extra strain in the molecules. This work is ongoing and will be pursued under alternative funding to support such fundamental research.

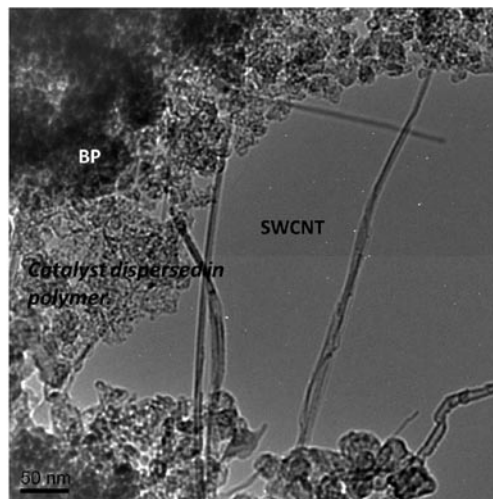
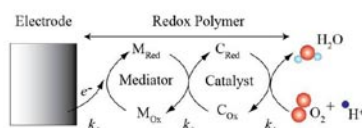
Figure 3(a) shows the results on modeling of the transport properties within the electrode layer. The prototype prediction has been validated by experiment and a number of parameters have been varied such as the loading of catalyst/mediator, nature of the carbon support, the equivalent weight of the ionomer used and the solvent used for the electrode inks. Variation of these properties leads to variations in the polymer thickness, the surface area/volume ratio, for

(a) Eight design improvements towards commercial Pt/C catalyst performance.



Prototype 20µm CL thickness.

- #1: 10 x L thickness
- #2: 10 x σ_{H^+}
- #3: 10 x k_1
- #4: 100 x k_1
- #5: 100 x k_1 ; 10 x D_{O_2}
- #6: 100 x k_1 ; 10 x D_{O_2}
- #7: 10 X k_1 ; $E_m^o = 0.8V$
- #8: 100 X k_1 ; $E_m^o = 0.8V$



(b) TEM picture of MEA electrode showing black pearl (BP) carbon and Single wall carbon nanotube (SWCNT) support and PFSA polymer with catalyst.

FIGURE 3. (a) Results of modeling of the catalyst layer using the schematic in Figure 1 where various parameters are modified to observe the predicted effect on the performance. (b) TEM picture of an MEA electrode showing the carbon support and the polymer morphology. This electrode had not been hot-pressed.

example, which allows the overall rate to be increased as well as the transport of electrons and oxygen to be varied. Curves 1-6 show the effects of modification of the layer structure which represent optimization strategies. Curves 7 and 8 show the effects of using mediators with better voltages and catalysts with better kinetics although the intrinsic potential of the catalyst is not changed. The intrinsic potential of the catalyst is thought to be the cause of the low open circuit voltage, which can be improved with catalysts with more positive voltages and higher activity. Thus two regimes are identified where optimization of the structure can achieve some improvement but major improvements are realized by changes in the chemistry of the mediator and the catalyst structures. It is important to realize that the improvements that accrue from the chemistry changes are only effective if the electrode structure changes are also made. This can be illustrated by Figure 3(b) which is a transmission electron microscope (TEM) picture of an MEA electrode prepared with the mediators and catalysts. It can be immediately seen that the polymer possesses a morphology that is derived from the shapes of the dispersed particles in the electrode inks. Such morphologies clearly affect the transport pathways of the electrons and oxygen and also the dispersion of the catalyst through the layer. The morphology observed here indicates that the catalysts are distributed on the outside of the polymer particles and that this limits the catalyst loading that can be achieved. It is anticipated that changing the morphology by use of different solvents to disperse the polymer will lead to better catalyst and mediator distribution.

Clearly there remains much work to do to understand the effect of morphology and to optimize the electrode structures. One striking feature of the TEM picture is that the polymer thickness is quite small, of the order of 50 nm. This is consistent with the modeling which also indicated that the film thicknesses were rather small and that under these circumstances the efficiency of the mediation would be impaired.

Figure 4(a) shows polarization curves for some of the catalysts whose potentials and kinetics are shown in Figure 2(c), as well as cobalamin (vitamin B₁₂). The cobalamin is an example of the use of a catalyst obtained from nature. It is quite striking that the performances in the MEAs track the behavior in the voltammetry experiments almost exactly. This was one of the goals of the project and is very gratifying that the correlation is so strong. Figure 4(b) shows the performance of MEAs with catalyst that includes some that are not water soluble. The excellent performance in the kinetic region of the CoTPP shows that it is not necessary to provide solubilizing groups and that smaller catalyst can be used that will allow for higher loadings. It appears that these water insoluble catalysts are partitioned into some of the hydrophobic phases of the ionomer and hence held off the electrode surface but are still available to mediators, protons and oxygen. The DiCop catalyst did not perform well in this set of experiments but since its structure is rather different some optimization needed. This material was obtained from Professor Love at the University of Edinburgh, Scotland

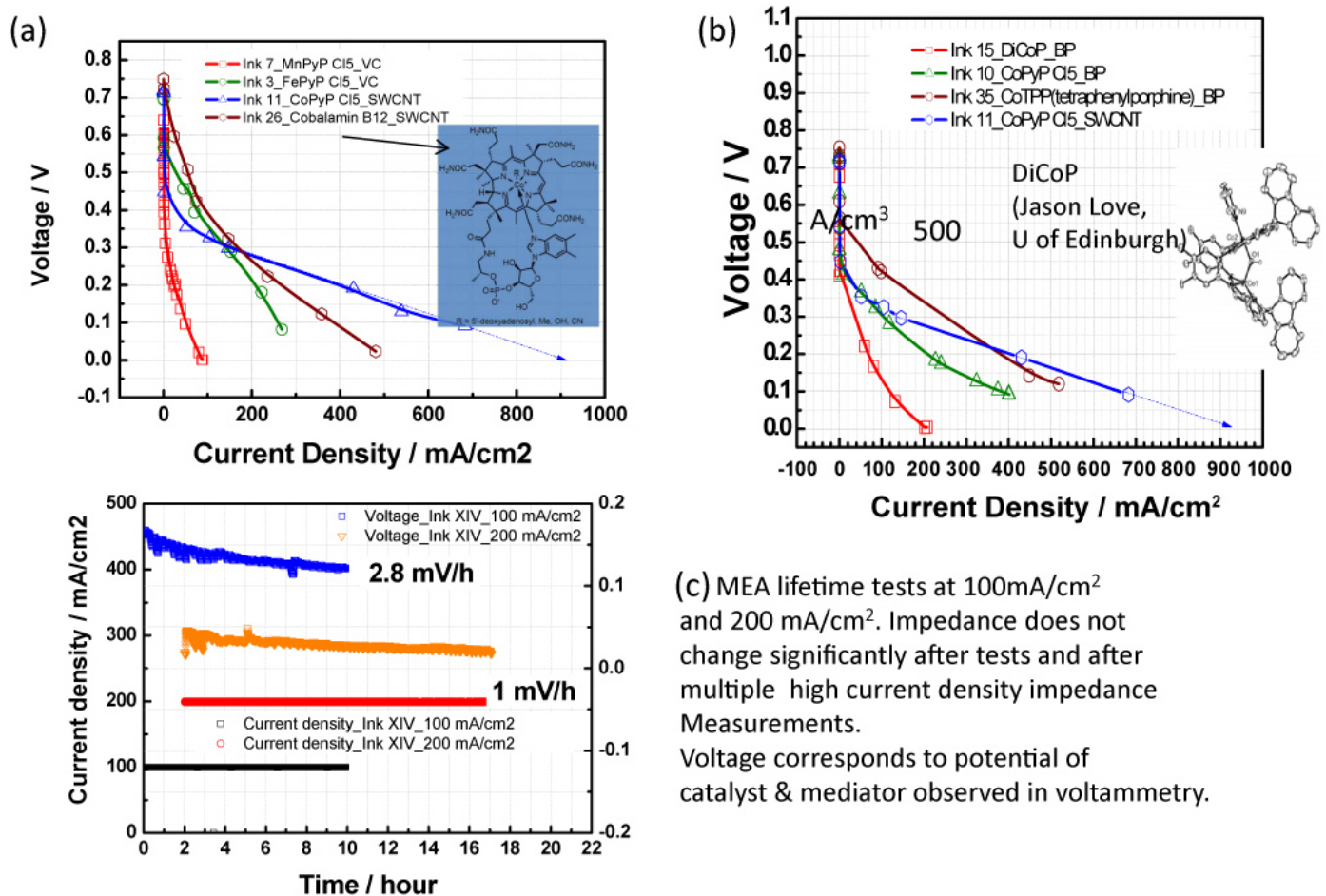


FIGURE 4. (a) Polarization curves of MEAs with different catalysts including cobalamin (vitamin B12). (b) Polarization curves of MEAs with different catalysts including two which are not soluble in water (CoTPP and DiCoP), (b) had not which are apparently supported by the polymer matrix. (c) Steady-state potentials for an MEA under two different current densities.

and this provides an excellent example of the how this MEA system can be used to evaluate catalysts from many different sources.

Finally Figure 4(c) shows the evolution of potential of an MEA under steady-state current conditions that clearly demonstrate stable performance. Although the delivered potential is very low it is stable and quite reproducible after the initial break-in. Similar behavior was observed for many MEAs which were run at various current densities to obtain impedance values. The impedance measurements showed no significant changes after multiple voltage, temperature and humidity cycles. These observations lead to the conclusion that the electrodes are surprisingly stable as are the catalysts under these conditions. This therefore refutes a frequent criticism of this approach that the catalyst will not be stable under “real” fuel cell conditions.

(c) MEA lifetime tests at 100mA/cm² and 200 mA/cm². Impedance does not change significantly after tests and after multiple high current density impedance Measurements. Voltage corresponds to potential of catalyst & mediator observed in voltammetry.

Conclusions and Future Directions

Conclusions

- The results from the MEA experiments reported here represent a proof-of-principle of the concept of polymer supported 3-D catalyst arrays for MEA. The correspondence of the modeling with the experimental results indicates that the correct parameters are being considered.
- The correspondence of the MEA results with the electroanalytical results indicates that a practical method catalyst screening exists that is rapid, inexpensive and relevant to MEA operation. Quantitative electroanalytical results are applicable to MEA operation through the electrode modeling.
- Better catalysts can be obtained through fundamental understanding of the factors that influence redox potential and rate of reaction with oxygen. Molecular modeling can address these problems.

- Somewhat surprisingly, the MEAs exhibit stable performance after break-in that indicate the catalysts and the supporting electrode matrix are stable for extended periods and are able to support high current densities.

Future Directions

- Optimization of MEA fabrication to improve performance through modification of electrode inks, coating procedures and initial break-in treatments.
- Use of electrochemical techniques including impedance to determine rate limiting phenomena in the MEAs and correlation with electroanalytical measurements made using conventional cell systems.
- Development of a coordinated molecular modeling/ synthesis/ electrochemical screening process that will provide understanding of the catalyst structural features that yield better performance. Better performance requires more positive intrinsic potentials and higher activities.

FY 2012 Publications/Presentations

1. “Molecular-scale, Three-dimensional Non-Platinum Group Metal Electrodes for Catalysis of Fuel Cell Reactions,” John Kerr, DOE Fuel Cells Technologies Program Review Meeting, May 15, 2012, Arlington, VA, poster presentation FC 11.
2. Ward, A.L., Elbaz, L., Kerr, J.B. & Arnold, J. Nonprecious Metal Catalysts for Fuel Cell Applications: Electrochemical Dioxygen Activation by a Series of First Row Transition Metal Tris(2-pyridylmethyl)amine Complexes. *Inorg Chem* 51, 4694-4706, (2012).
3. He, Q. et al. Molecular catalysis of the oxygen reduction reaction by iron porphyrin catalysts tethered into Nafion layers: An electrochemical study in solution and a membrane-electrode-assembly study in fuel cells. *J Power Sources* 216, 67-75, (2012).
4. Zhu, X. et al. Bridge to Fuel Cell Molecular Catalysis: 3D Non-Platinum Group Metal Catalyst in MEAs. *ECS Transactions* 45, 143-152 (2012).
5. Electroreduction of Molecular Oxygen by Water-Soluble Metal Porphyrins in Trifluoromethane Sulfonic Acid Solution, Qinggang He, Gi Suk Hwang, Adam Z. Weber, Robert Kostecki and John B. Kerr, Abstract 1154 ECS Fall Meeting, Boston MA, October 13, 2011.

References

1. Gasteiger, H.A., Kocha, S.S., Sompalli, B. & Wagner, F.T. Activity benchmarks and requirements for Pt, Pt-alloy, and non-Pt oxygen reduction catalysts for PEMFCs. *Applied Catalysis B-Environmental* 56, 9-35 (2005).
2. Gojkovic, S.L., Gupta, S. & Savinell, R.F. Heat-treated iron(III) tetramethoxyphenyl porphyrin supported on high-area carbon as an electrocatalyst for oxygen reduction - I. Characterization of the electrocatalyst. *Journal of the Electrochemical Society* 145, 3493-3499 (1998).
3. Gojkovic, S.L., Gupta, S. & Savinell, R. F. Heat-treated iron(III) tetramethoxyphenyl porphyrin chloride supported on high-area carbon as an electrocatalyst for oxygen reduction - Part II. Kinetics of oxygen reduction. *Journal of Electroanalytical Chemistry* 462, 63-72 (1999).
4. Gouerec, P. & Savy, M. Oxygen reduction electrocatalysis: ageing of pyrolyzed cobalt macrocycles dispersed on an active carbon. *Electrochimica Acta* 44, 2653-2661 (1999).
5. Sun, G.Q., Wang, J.T. & Savinell, R.F. Iron(III) tetramethoxyphenylporphyrin (FeTMPP) as methanol tolerant electrocatalyst for oxygen reduction in direct methanol fuel cells. *J Appl Electrochem* 28, 1087-1093 (1998).
6. Saveant, J.M. Molecular catalysis of electrochemical reactions. Mechanistic aspects. *Chemical Reviews* 108, 2348-2378 (2008).
7. Wu, G., More, K.L., Johnston, C.M. & Zelenay, P. High-Performance Electrocatalysts for Oxygen Reduction Derived from Polyaniline, Iron, and Cobalt. *Science* 332, 443-447, doi:10.1126/science.1200832 (2011).

V.D.9 Tungsten Oxide and Heteropoly Acid Based System for Ultra-High Activity and Stability of Pt Catalysts in PEM Fuel Cell Cathodes

John Turner (Primary Contact), Jason Zack, Katherine Hurst, Kelly Mason, Virginia Anderson, KC Neyerlin, Anne Dillon, Bryan Pivovar and Shyam Kocha.

National Renewable Energy Laboratory (NREL)
15013 Denver West Pkwy
Golden, CO 80401
Phone: (303) 275-4270
Email: John.Turner@nrel.gov

DOE Manager

HQ: Kathi Epping Martin
Phone: (202) 586-7425
Email: Kathi.Epping@ee.doe.gov

Subcontractors:

- UC Boulder, Boulder, CO
- Colorado School of Mines, Golden, CO

Project Start Date: May 2010

Project End Date: April 2014

- (A) Durability
- (B) Cost
- (C) Performance

Technical Targets

This project addresses the precipitous corrosion and electrode degradation that takes place when using carbon-supported Pt catalysts (Pt/C) in automotive applications during start-up and shut-down operations. Alternative supports such as WO_x as well as HPA-functionalized carbon blacks are being synthesized and evaluated for improved corrosion resistance while maintaining or improving on the activity in comparison to conventional Pt/C. Studies are first being conducted in rotating disk electrode (RDE) setups due to the small quantity of materials synthesized and will be followed by testing in fuel cells. The following targets are being addressed:

- Mass activity: $>275 \text{ mA/mg}_{Pt}$
- Durability under start-up/shut-down cycling: ECA loss $<40\%$

Fiscal Year (FY) 2012 Objectives

Improve Pt electrocatalyst and membrane electrode assembly (MEA) durability and activity through the use of tungsten oxide (Pt/ WO_x) and heteropoly acid (HPA) catalyst support modifications to approach DOE targets for activity (0.44 mA/mg Pt) and durability (5,000 hours/10 years) for automotive polymer electrolyte membrane fuel cells.

- Enhance Pt anchoring to support:
 - Suppress loss in Pt electrochemical area (ECA) under load cycling operations.
 - Enhance electrocatalytic activity.
- Lower support corrosion:
 - Increase durability under automotive startup/shutdown operation. Suppress Pt agglomeration and electrode degradation.

Technical Barriers

This project addresses the following technical barriers from the Fuel Cells section of the Fuel Cell Technologies Program Multi-Year Research, Development and Demonstration Plan:

FY 2012 Accomplishments

- Synthesized well-distributed and high wt% Pt/ WO_x using atomic layer deposition (ALD) for Pt and hot-wire chemical vapor deposition (HWCVD) for tungsten oxide.
- Synthesized Pt nanoparticles using a colloidal technique and deposited onto carbon functionalized with HPA.
- Established protocols to evaluate and benchmark the durability of alternative supports.
- Measured the electronic conductivity of WO_x and WO_x mixed with carbon powders.
- Measured the electrochemical activity of Pt black- WO_x mixtures and determined the amount of carbon black required to meet the activity of baseline Pt/C.
- Determined the most accurate and relevant method of determining the surface area of Pt/ WO_x catalysts.
- Obtained electrochemical areas for Pt/ WO_x that exceeded $25 \text{ m}^2/\text{g}$.
- Synthesized and evaluated Pt/ WO_x in RDE with a mass activity of 175 mA/mg_{Pt} .
- Synthesized and evaluated Pt/C-HPA with a mass activity of 300 mA/mg_{Pt} .
- Demonstrated improved durability of Pt/C-HPA over Pt/C.
- Demonstrated activity of Pt/ SnO_2 to meet that of Pt/C and durability exceeding that of Pt/C.



Introduction

Conventional nanoparticle Pt/C electrocatalysts used in automotive fuel cells suffer significant degradation during start-up and shut-down operations. Under these conditions the potential at the cathode approaches ~1.6 V for short bursts of time, leading to carbon corrosion. In this project we evaluate alternative supports for Pt that might be more stable and corrosion resistant than conventional carbon blacks. Developing such a support will allow the fuel cell system to be simplified, lowering the costs and simultaneously increasing the durability.

Approach

Oxide supports such as WO_x are grown using a HWCVD method and then ALD or wet-chemistry is used to deposit Pt nanoparticles on the support. These oxide supports are inherently more stable than carbon black but have drawbacks in terms of lower surface area and lower electronic conductivity as compared to the carbon blacks. Therefore the electronic conductivity and the electrochemical activity as a function of adding small quantities of highly graphitized carbon blacks/fibers are being studied. The added graphitized carbon is not susceptible to corrosion because the Pt nanoparticles have a closer interaction with the WO_x or C-HPA. Durability cycling protocols that simulate start-up/shut-down were developed to quantify the suppression of degradation with the alternative corrosion resistant supports.

Results

Synthesis: Tungsten oxide nanostructures were prepared using HWCVD. Material synthesis employing sequential depositions at room temperature led to rod-like nanostructured growth as shown in Figure 1 (a,b). The stoichiometry and crystalline structure of WO_x nanoparticles can be controlled by subsequent annealing in air, as demonstrated by the X-ray diffraction spectra (not shown). Near edge X-Ray absorption fine structure spectroscopy data were obtained from the Stanford Linear Accelerator Center to provide insight into oxygen bonding on tungsten oxide. Our initial ALD work resulted in a high Pt loading with large particle sizes and agglomeration. By increasing the precursor temperature, a higher flux of Pt enabled more uniform nucleation, leading to smaller particles throughout the sample. Figure 1 (c) depicts the Pt nanoparticles on tungsten oxide rods with a fairly uniform distribution for a 25 wt% Pt material. Recent work has resulted in materials with up to 50–60 wt% Pt loadings. At this high loading, the particles almost reach full coverage of the WO_x surface, as shown in Figure 1 (d). This has been achieved by performing ALD in a stop flow configuration with increased dosing time of the

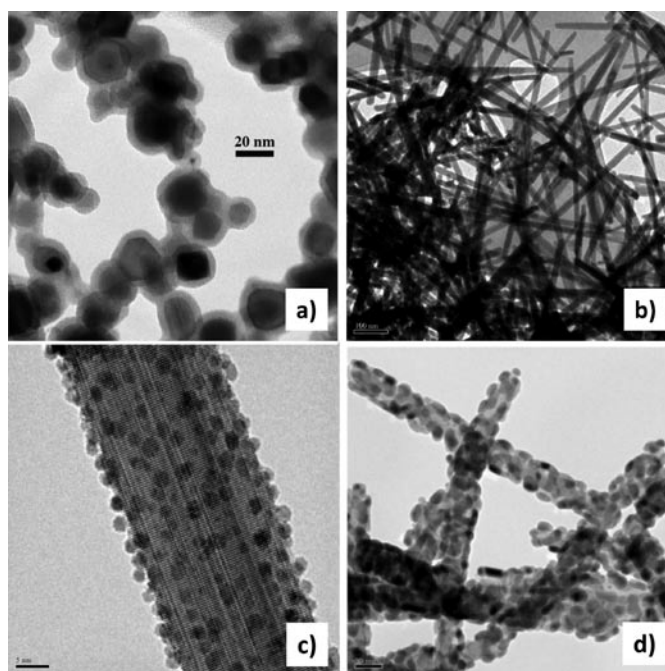


FIGURE 1. TEM micrographs (a, b) for WO_x after a few and after 60 cycles showing nanorods; (c) Pt/ WO_x at 25 wt% Pt; and (d) Pt/ WO_x at 50 wt% Pt

platinum precursor as well as increased soak times during deposition.

HPA functionalization of carbon was carried out to: i) shield carbon against corrosion; ii) stabilize nano-metallic particles; iii) decompose peroxide; iv) alter electrochemistry on Pt surface; and v) conduct protons. These functionalized carbons were used as supports for depositing Pt nanoparticles that were synthesized using a colloidal preparation. A literature recipe [1] was modified significantly to synthesize small controlled Pt nanoparticles by decreasing the temperature to 80°C; bubbling dilute CO into solution; and gradually adding 0.25 M NaOH over 3 h. Figure 2 (a) illustrates the transmission electron microscope (TEM) image and particle size distribution of the synthesized colloids. The Pt colloids were deposited onto the HPA-functionalized carbon, Figure 2 (b), by the following process: i) dispersion of HPA-C material in water via 20 min ultrasonication; ii) addition of Pt colloid followed by ultrasonication for an additional 20 min; iii) catalyst separation via Buchner filtration; and iv) drying at 200°C for 2 h.

Conductivity: Conductivity measurements were carried out in an in-house experimental setup that consisted of Au-coated Cu plates. The density and conductivity of WO_3 and WO_2 as well as WO_x mixed with various amounts of a graphitized carbon were determined at various loads and are reported in Figure 3 at 500 N/cm². The bulk conductivity of the WO_x materials was also investigated by four-point probe measurement in the Van der Pauw geometry. The as-produced materials were pressed into a pellet and the

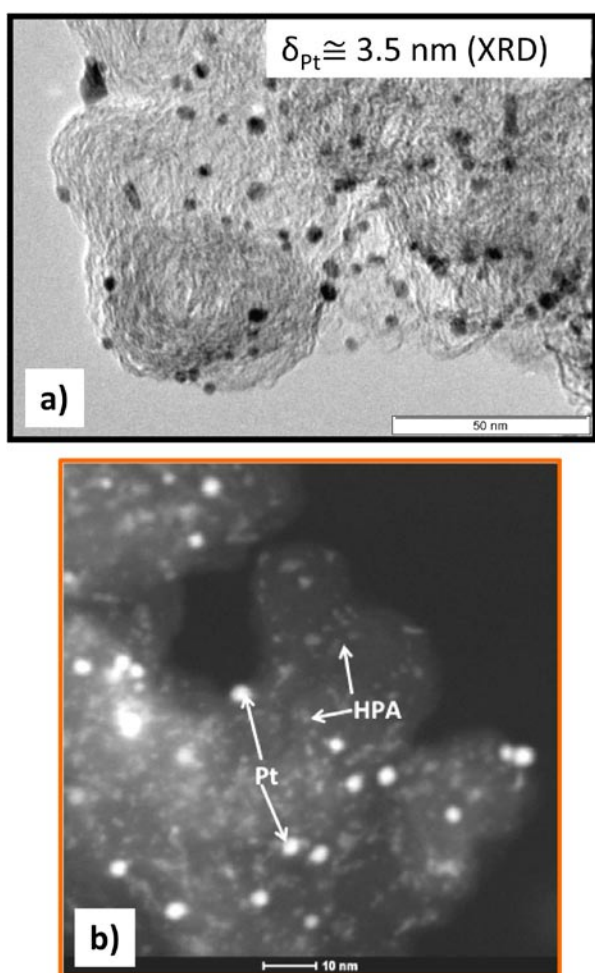


FIGURE 2. TEM micrograph showing Pt colloids (a); dark field image showing Pt and HPA on carbon support (b)

conductivity was measured over a range of pellet pressing pressures. The average conductivity was ~ 0.25 (ohm cm^{-1}).

Electrochemical Area Measurements: Because of the formation of tungsten bronzes that produces a peak in the same voltage domain as the hydrogen underpotential deposition, the accurate determination of the ECA of Pt/ WO_x becomes difficult. We have used CO stripping as well as Cu underpotential deposition to determine the Pt area for these electrocatalysts. Cu underpotential deposition is preferred because CO appears to get oxidized and shows an anodic peak that complicates the determination of a good baseline for the CO stripping area.

Durability Protocols: Durability protocols were established for evaluating the corrosion resistance of alternate supports in collaboration with the DOE Durability Working Group [2]. The measurements are designed to be conducted at room temperature in RDE setups.

Mass Activity Measurements, Pt black- WO_x Mixtures: To support the conductivity studies and verify the necessity

of carbon black addition to achieve high mass activities, we conducted a study that evaluated Pt black mixed with various amounts of carbon black. For very thin films (low loadings) with the addition of carbon black, it was possible to meet the baseline Pt/C oxygen reduction reaction activity values. The results verify that electronic conductivity issues will be encountered when WO_x or other corrosion-resistant oxide supports are used as a support due to their low conductivity.

Pt/ WO_x and Pt/HPA-C: The mass activity of Pt/ WO_x was found to be ~ 100 mA/mg by both wet-chemistry and ALD deposition methods, Figure 4 (a,b). More recently, the 50 wt% Pt/ WO_x has shown a higher activity of about 175 mA/mg_{Pt} (not shown). This is a significant improvement but falls short of the activity of baseline Pt/C. Pt/HPA-C was found to have comparable mass activity to Pt/C of more than 300 mA/mg_{Pt}.

Pt/ SnO_2 : Since the mass activity of Pt/ WO_x has not yet met the benchmark values for commercial Pt/C in RDE studies, we investigated the performance of a Pt/ SnO_2 electrocatalyst produced by a commercial catalyst manufacturer (TKK). For these catalysts, with the addition of a graphitized carbon black to enhance conductivity, values close to the benchmark Pt/C of 275 mA/mg_{Pt} were achieved. Figure 4 (c) shows the activity of these catalysts in comparison to baseline Pt/C.

Conclusions and Future Directions

Tungsten oxides provide durable supports for Pt catalysts, and while their lower conductivity limits the activity, the activity can be restored by adding a conductive matrix.

Future work will include the following:

- Complete a systematic conductivity analysis of WO_x films with and without conductive matrices to guide catalyst ink formulations.
- Improve wet-chemistry Pt deposition and ALD Pt deposition on WO_x and characterize electrochemically, with and without a conductive matrix, to obtain mass activities comparable to Pt/C.
- Make decision on using ALD Pt/ WO_x versus wet-chemistry Pt/ WO_x for meeting project goals. (December 2012)
- Evaluate alternative catalysts such as Pt-alloys (on WO_x + conductive matrix) in RDE for higher activities. (2013)
- Scale up the selected electrocatalyst system synthesis process to prepare Pt/ WO_x + conductive matrix in gram quantities for MEA preparation. (2013, 2014)
- Evaluate HPA incorporation into catalyst layers of MEA to ascertain proton conduction and durability impacts. (2013, 2014)
- Optimize catalyst inks for MEA preparation and evaluation in subscale cells. (2013, 2014)

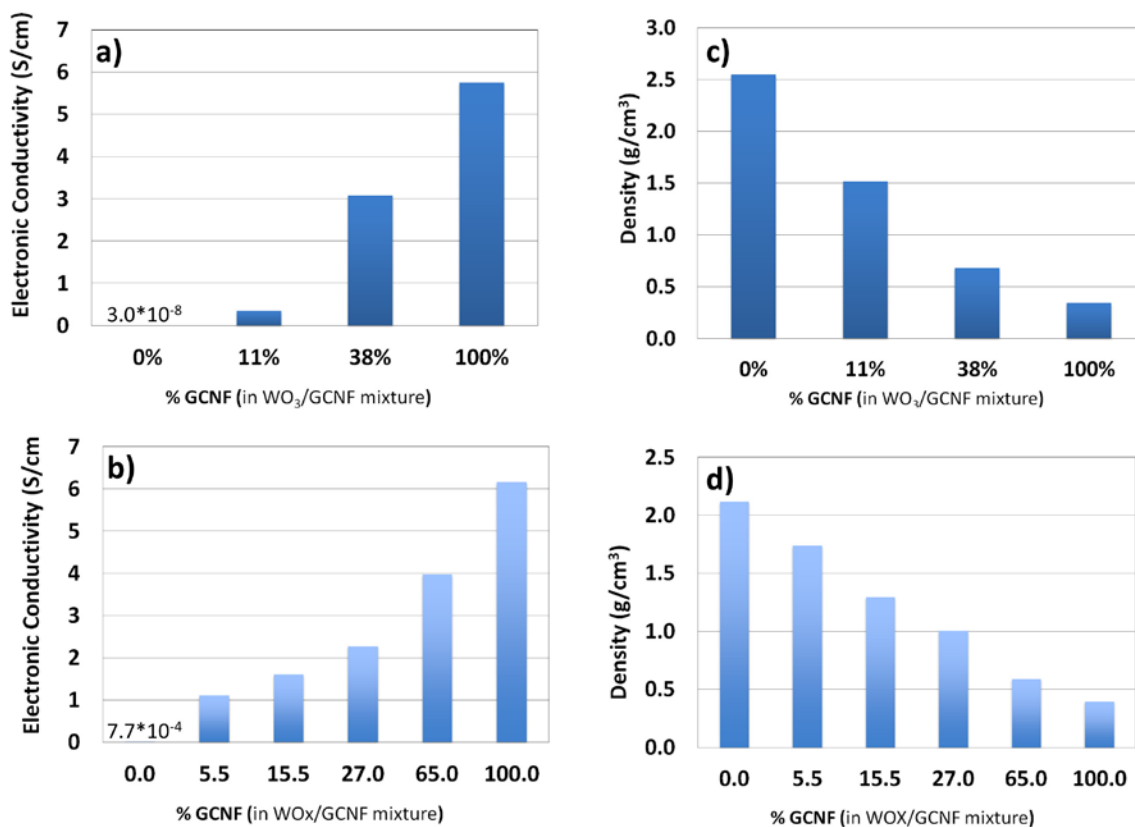


FIGURE 3. Electronic conductivity of WO_3 (a) and WO_x (b) with various additions of graphitized carbon nano-fibers (GCNF). Corresponding density of each mixture is shown in (c) and (d) respectively.

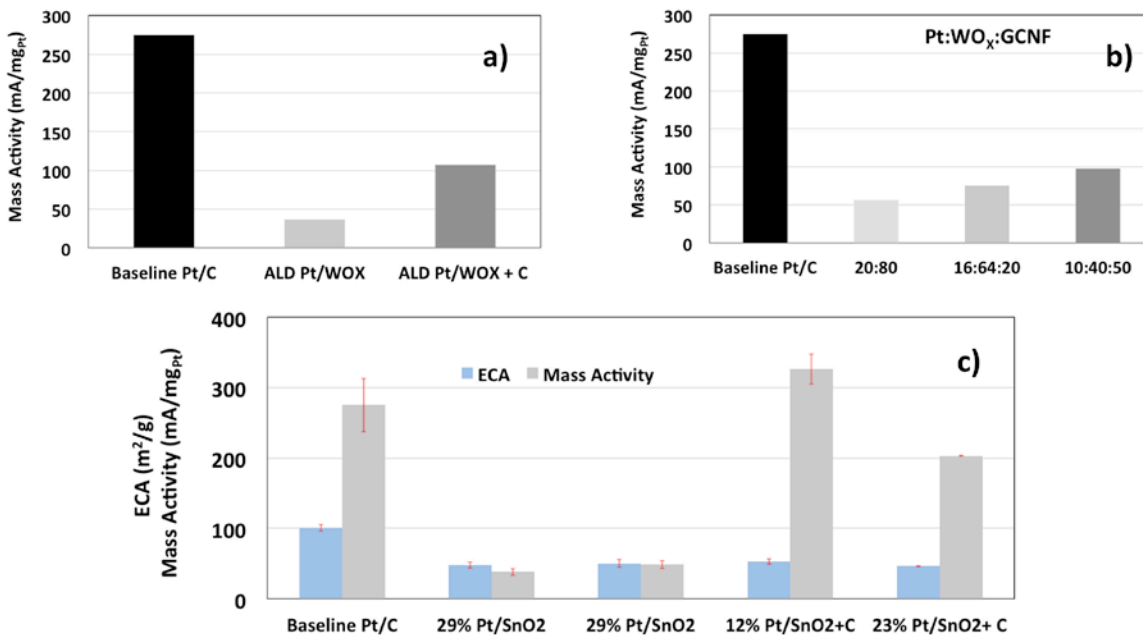


FIGURE 4. Mass activity (a) of various ALD Pt/ WO_x with and without carbon addition; (b) based on samples from wet-chemistry Pt colloid deposition; and (c) for Pt/SnO₂ with and without carbon addition.

FY 2012 Publications/Presentations

1. “Nano-Pt and Tungsten Oxides as a Novel PEM Cathode Catalyst,” Katherine E. Hurst, Virginia R. Anderson, Steve Christensen, Shyam Kocha, K.C. Neyerlin, Jason Zack, Kim Jones, Steven George, John Turner, and Anne Dillon. Talk given at the American Chemical Society Fall Meeting, Denver, Colorado, August 31, 2011.
2. “Atomic Layer Deposition of Platinum on Tungsten Oxide as a Novel PEM Cathode Catalyst,” Katherine E. Hurst, Virginia R. Anderson, Steven T. Christensen, Arrelaine A. Dameron, Shyam S. Kocha, K.C. Neyerlin, Jason Zack, Steven M. George, John Turner, and Anne C. Dillon. Talk given at ALD2012, Dresden, Germany, June 18, 2012.
3. “Effect of Silicotungstate Functionalization on Carbon Black Supported Platinum Electrocatalysts”, K. Mason, M. Kuo, S. Kocha, K. Neyerlin, J. Turner, and A. Herring, Abstract 66, 221st Meeting of the Electrochemical Society, May 6–10, 2012, Washington State Convention Center, Seattle, Washington.

4. “Investigation of a Silicotungstic Acid Functionalized Carbon on Pt Activity and Durability for the Oxygen Reduction Reaction”, K. Mason, M. Kuo, K. Horning, K. Neyerlin, and A. Herring, *Journal of the Electrochemical Society* (Submitted June 2012).
5. “Durability Enhancement of Pt/C Catalysts via Support Functionalization with Silicotungstic Acid”, K. Mason, K. Neyerlin, M. Kuo, K. Horning, S. Kocha, J. Turner, and A. Herring, Abstract 1418, 222nd Meeting of the Electrochemical Society, October 7–12, 2012, Hawaii Convention Center, Honolulu, Hawaii.

References

1. Wang, Y.; Ren, J.; Deng, K.; Gui, L.; Tang, Y. *Chem. Mater.* **2000**, *12*, 1622.
2. Kocha, S.; Myers, D.; Borup, R. *Accelerated stress tests for oxide supports*, DOE-EERE Durability Working Group Meeting, Boston, MA, 2011.

V.D.10 Synthesis and Characterization of Mixed-Conducting Corrosion Resistant Oxide Supports

Vijay K. Ramani (Primary Contact), Jai Prakash
Illinois Institute of Technology (IIT)
10 W 33rd Street 127 PH
Chicago, IL 60616
Phone: (312) 567-3064
Email: ramani@iit.edu

DOE Managers

HQ: Kathi Epping Martin
Phone: (202) 586-7425
Email: Kathi.Epping@ee.doe.gov

GO: Katie Randolph
Phone: (720) 356-1759
Email: Katie.Randolph@go.doe.gov

Contract Number: DE-EE0000461

Subcontractor:

Nissan Technical Center, North America (NTCNA)
Farmington Hills, MI

Project Start Date: September 1, 2010

Project End Date: August 31, 2013

Technical Targets

This project addresses the following technical targets:

- <40% electrochemical area (ECA) loss in electrocatalysts using the synthesized supports tested per the General Motors (GM) protocol.
- <30 mV electrocatalyst support loss in the synthesized supports after 100 hrs at 1.2 mV; tested per the GM protocol.
- These targets are taken from Table 3.14.12, Multi-Year Research, Development and Demonstration Plan.

FY 2012 Accomplishments

- Demonstrated that the synthesized RuO₂-TiO₂ (TRO) catalyst supports possessed the following properties: a) excellent electrical conductivity (~22 S/cm), b) excellent electrochemical stability, and c) comparable fuel cell performance with Pt/C baseline. Start-stop stability tests for stand alone supports and membrane electrode assemblies (MEAs) were performed by potential cycling of the cell between 1 V to 1.5 V vs. the normal hydrogen electrode (NHE) for 10,000 cycles. Tests performed both at IIT and Nissan Technical Center, North America (NTCNA) and have confirmed support durability.
- Tests at NTCNA have confirmed that using the ruthenium-titanium oxide (RTO) supports synthesized and catalyzed at IIT, the beginning of life performance is exactly equal to end of life performance in an MEA that has been subjected to severe start-stop cycling (1-1.5 V, 10,000 cycles). This is in sharp contrast to baseline Pt/C catalyst that shows significant performance deterioration.
- Indium tin oxide (ITO) aerogels with high surface area (283±2 m²/g) have been synthesized using a supercritical drying technique. The annealed ITO possessed higher stability than carbon.
- Functionalized silica aerogel with different levels of sulfonic acid functionalization were synthesized. These materials have demonstrated varying degrees of proton conductivity and thermal stability proportional to the loading of sulfonic acid functional group.

Fiscal Year (FY) 2012 Objectives

- To develop and optimize innovative non-carbon mixed conducting materials that will serve as corrosion resistant, high surface area supports for anode and cathode electrocatalysts.
- Concomitantly facilitate the lowering of ionomer loading in the electrode (by virtue of surface proton conductivity of the electrocatalyst support), thereby enhancing performance.

Technical Barriers

This project addresses the following technical barriers from the Fuel Cell section of the Fuel Cell Technologies Program Multi-Year Research, Development and Demonstration Plan:

(A) Durability



Introduction

While Pt supported on carbon is the most commonly used electrocatalyst for polymer electrolyte fuel cells (PEFCs), the

carbon support has limitations with respect to its durability during excursions to high electrode potentials that arise during startup and shutdown sequences and during fuel starvation. The issue of carbon corrosion is a major technical barrier. Carbon corrosion facilitates the agglomeration of Pt particles and dissolution of Pt from the support, which leads to a loss in the ECSA of the electrode [1]. To address this issue, the development of non-carbon mixed-conducting catalyst support materials is explored. Desirable properties of these alternative materials include (i) high electrical conductivity; (ii) high surface area; and (iii) high electrochemical stability. In addition, it is hypothesized that fuel cell performance can be enhanced by utilizing non-carbon catalyst supports that conduct protons on their surface. The addition of sulfonic acid functionalities on the support surface should permit lowering the ionomer content in the electrode, thereby enhancing gas transport to the catalyst site without compromising on the efficacy of ion transport.

Approach

To achieve the objectives discussed above, two classes of non-carbon support have been synthesized. The first class of support involves the development of a RuO₂-TiO₂ structure. TiO₂ was used as core matrix and was further functionalized with a layer of RuO₂ to introduce electronic conductivity. A similar approach was also pursued in parallel, using silica or functionalized silica as the high surface area matrix. The second class of support involved the synthesis of conductive metal oxides by doping. The metal oxide aerogels with high surface area such as ITO, and metal-doped TiO₂ were prepared using the supercritical drying technique. The electrochemical stability of non-carbon support and Pt/non-carbon support were measured under accelerated start-stop and load cycling test protocols and compared with that of commercial XC-72R carbon and baseline Pt/C (TKK TEC10E50E).

Results

The non-carbon supports and catalysts were prepared using a wet-chemical synthesis procedure. These materials were characterized by X-ray diffraction, transmission electron microscopy, and Brunauer-Emmett-Teller (BET) surface area analysis. Their electrical conductivity and electrochemical properties such as stability, ECSA, electrocatalytic activity, and fuel cell performance were also determined.

The stability of the non-carbon supports and catalysts was evaluated in rotating disk electrode (RDE) and single-cell MEA as a function of cycle number using accelerated start-stop and load cycling durability protocols provided by NTCNA. The start-stop cycling test was conducted by cycling the electrode potential between 1.0 V to 1.5 V vs. NHE (triangular wave form) at a scan rate of 500 mV/s to simulate the startup-shutdown transients in an operating

PEFC. Load cycling was conducted by cycling the electrode potential between 0.6 V to 0.95 V vs. NHE (rectangle wave form) with 3 seconds hold at each potential to simulate full load-no load transients in an automotive drive cycle. The stability of the support was quantified by measuring the change in capacitance (including double layer and pseudo capacitance) calculated at 0.4 V with potential cycling. The stability of the catalyzed support was evaluated by monitoring the change in ECSA, and performance.

RuO₂-TiO₂ (TRO)

TRO powders in hydrous (TRO-a) and anhydrous (TRO-h), ITO, and SO₄²⁻/SnO₂ were prepared. The electrical conductivity and BET surface area are summarized in Table 1, with Vulcan XC-72 as the baseline. The amorphous ITO with high surface area (283±2 m²/g) was successfully prepared with supercritical drying technique. To increase the electrical conductivity, the ITO was further annealed at 820°C.

TABLE 1. Properties of Supports

| | Vulcan XC-72 | TRO-a | TRO-h | ITO | SO ₄ ²⁻ /SnO ₂ |
|--------------------------------|--------------|-------|-------|-------------------|---|
| BET (m ² /g) | 207±4 | 33±4 | 97±8 | 41±1 ^a | 91±5 |
| Electrical conductivity (S/cm) | 31±5 | 21±5 | 10±3 | 1.9±0.1 | ~10 ⁻⁵ |

^aannealed at 820°C

RDE Characterization

The stability data obtained using the TRO-a, TRO-h, ITO, and SO₄²⁻/SnO₂ and XC-72R carbon samples upon performing the start-stop stability protocol in RDE are shown in Figure 1. All non-carbon supports exhibited excellent stability in contrast to carbon. Carbon showed a 220% change in capacitance after 10,000 cycles due to the hydroquinone–quinone (HQ–Q) redox couple of carbon. TRO-h showed less stability, where Ru is mixed III/IV valent and therefore Ru^{III} can be further oxidized to Ru^{IV} during the potential cycling.

The various TRO powders were then catalyzed by depositing platinum nanoparticles by an impregnation-reduction method to yield Pt/TRO electrocatalysts. The Pt/TRO-a electrocatalysts possessed a mass activity of 220 mA/mg_{Pt} and a specific activity of 580 μA/cm_{Pt}² for the oxygen reduction reaction.

MEA Characterization of Pt/TRO-a

In situ durability of TRO-a MEAs was evaluated using NTCNA's accelerated start-stop and load cycling test protocols. Change in ECA and cell potential at 1 A/cm² were employed as parameters to study the effect of the durability tests on TRO-a MEAs.

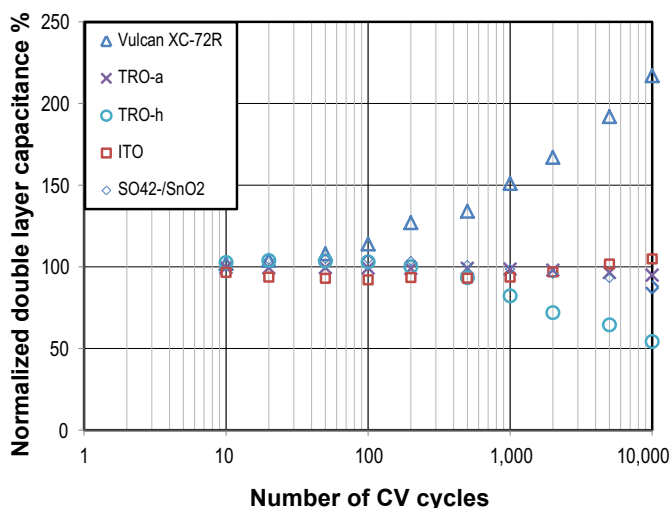
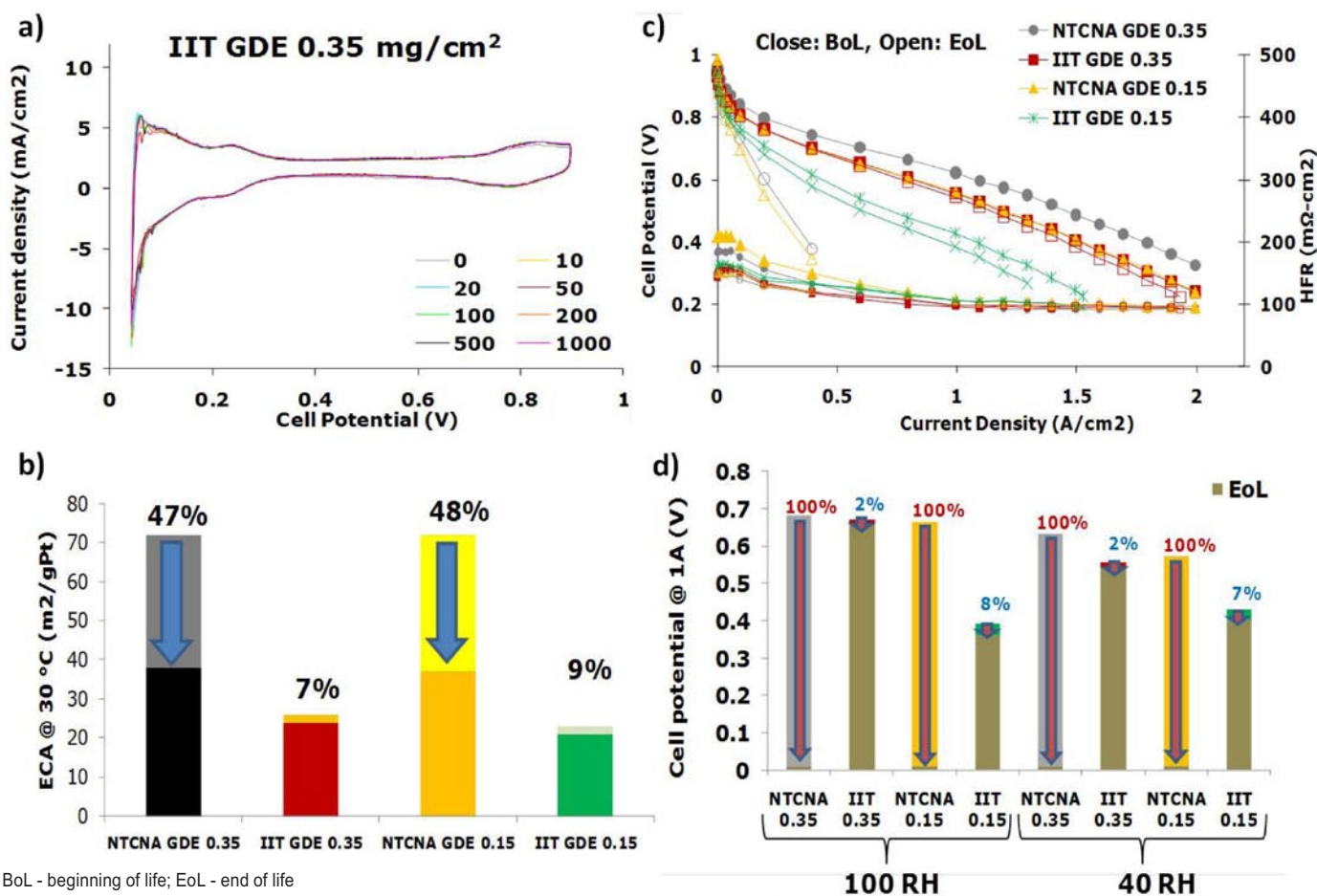


FIGURE 1. Change of double layer capacitance of catalyst supports as a function of cycling numbers. The cycling experiments were conducted in a N_2 saturated 0.1M $HClO_4$ solution at room temperature.

Effect of Start-Stop Cycling

The RuO_2 - TiO_2 support showed excellent support durability compared to high surface area carbon (HSAC). Minimal change in cyclic voltammetry (CV) pattern for $0.35\text{ mg}_{Pt}/\text{cm}^2$ TRO-a MEA (IIT MEA) was observed after 1,000 cycles as shown in Figure 2(a). Similar results were also observed for $0.15\text{ mg}_{Pt}/\text{cm}^2$ loaded MEA. Change in ECSA due to start-stop cycling at the beginning and at the end is shown in Figure 2(b). This study proves the excellent stability of RuO_2 - TiO_2 support ($\sim 7\sim 9\%$ ECSA change) over conventional carbon support ($\sim 47\%\sim 48\%$ ECSA change) under this accelerated stress test.

Effect of this stability test on current-voltage (iV) performance is shown in Figure 2(c) under 40% relative humidity (RH) condition. Similar measurements were also performed under 100% RH condition. As shown, minimal loss in performance was observed for the Pt/TRO support (IIT MEA) compared to Pt/carbon support (NTCNA gas diffusion electrode) that showed substantial loss in performance due to support loss, loss in electronic conductivity and flooding. Similar behavior is also evident



BoL - beginning of life; EoL - end of life

FIGURE 2. In situ durability of TRO-a MEAs was evaluated using NTCNA accelerated start-stop cycling protocol. Change in a) CV b) ECSA as a function of cycle number c) iV performance under H_2/Air , $80^\circ C$, 40% RH and d) loss in cell potential at $1\text{ A}/\text{cm}^2$ under both 100 and 40% RH.

in the results of cell potential loss at 1 A/cm² as shown in Figure 2 (d). Under both RH conditions, the carbon supported catalyst demonstrated significant loss in activity, while the TRO supported catalyst showed minimal loss in performance, exhibiting its superior stability.

Effect of Load Cycling

Catalyst stability under load cycling was tested using Nissan’s accelerated protocol test. Less ECSA loss than Pt/HSAC catalyst was observed for TRO catalyst as an effect of this durability test as shown in Figure 3(a) for 0.35 mg_{Pt}/cm² loading. Similar loss in iV performance was

observed for both the catalyst as shown in Figure 3(b). Cell potential at 1 A/cm² is compared in Figure 3(c) shows similar loss for both the carbon and non-carbon supported catalyst under this durability test. This was consistent with expectation as the load cycling protocol tests electrocatalyst durability and not support durability.

Sulfonic Acid Functionalized Silica Aerogel

In FY 2011, sulfonic acid functionalized silica with high proton conductivity was prepared. However, it was not thermally stable and decomposed around 100°C. In FY 2012, a different synthesis procedure for preparing functionalized silica was employed to improve stability and proton conductivity. The properties of the functionalized silica aerogels are summarized in Table 2. Even though the ion exchange capacity (IEC) of the functionalized silica aerogels increased from 1.4 to 2.1 mmol/g, very small change was observed in the ionic conductivities of the silica with extent of functionalization (33, 50 and 67 mol%). This was because that the increase of IEC and carrier groups was offset by the concomitant decrease of internal surface, leading to a constant value for ionic conductivity. The conductivity at each extent of sulfonation was measured three times at four temperatures (60, 80, 100 and 120°C) and four RHs (25, 50, 75 and 100%). The conductivity variations between the samples with different extents of functionalization were within the measured experimental error at all conditions; the values obtained are shown in Figure 4.

Conclusions and Future Directions

- Non-carbon supports including RuO₂-TiO₂ (hydrous and anhydrous), ITO, and SO₄²⁻/SnO₂ were synthesized and had higher stability over baseline Vulcan carbon.
- The performance of MEA with Pt/RTO-a was comparable with a commercial Pt/C MEA.
- The MEA with Pt/RTO-a demonstrated superior stability in comparison to carbon catalyst supports under start-stop cycling test.
- The MEA with Pt/RTO-a showed similar Pt dissolution stability to that with Pt on HSAC under load cycling test.

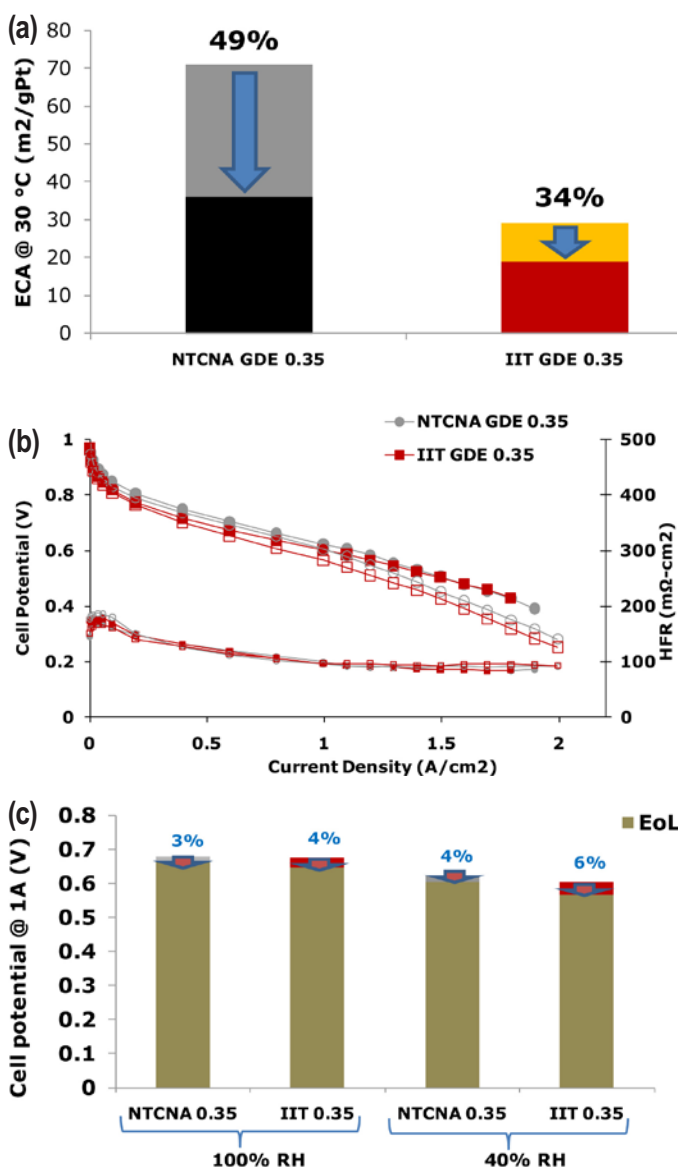


FIGURE 3. In situ durability of TRO-a MEAs was evaluated using NTCNA accelerated load cycling protocol. Change in a) ECSA as a function of cycle number c) iV performance under H₂/Air, 80°C, 40% RH and d) loss in cell potential at 1 A/cm² under both 100 and 40% RH.

TABLE 2. Properties of the Functionalized Silica Aerogels

| Functionalization degree, % | Ion exchange capacity, mmol/g | BET surface area, m ² /g | Pore volume, cm ³ /g | Average pore diameter, nm |
|-----------------------------|-------------------------------|-------------------------------------|---------------------------------|---------------------------|
| 0 | 0 | 944±63 | 2.4 | 10.1 |
| 33 | 1.4 | 499±8 | 1.0 | 8.4 |
| 50 | 1.7 | 233±2 | 0.6 | 9.6 |
| 67 | 2.1 | 116±3 | 0.2 | 8.3 |

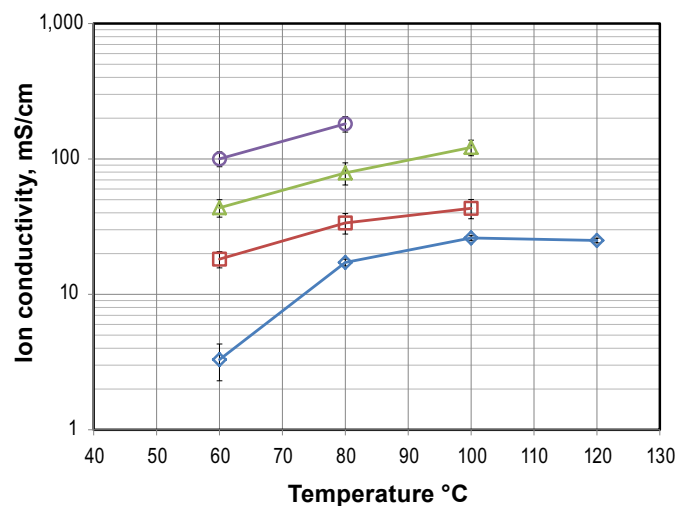


FIGURE 4. Proton conductivity of sulfonic acid functionalized silica aerogel at various temperatures at (●) 25% RH, (○) 50% RH, (▼) 75% RH and (△) 100% RH.

- Several samples of sulfonic acid functionalized silica aerogel with high thermal stability have been prepared and demonstrate excellent proton conductivity.
- In phase two, the initial focus will be on enhancing mass activity of the catalysts prepared with RTO supports as well as to incorporate proton conducting functionalities onto the support. Studies on ITO and sulfonated tin oxide supports will continue.

References

1. Landsman, D.A., Luczak, F.J., In Handbook of Fuel Cells Fundamentals, Technology, and Applications; Vielstich, W., Gasteiger, H.A., Lamm, A., Eds.; John Wiley and Sons Ltd.: West Sussex, England, 2003; Vol. 4.

V.D.11 Development of Novel Non-PGM Electrocatalysts for Proton Exchange Membrane Fuel Cell Applications

Sanjeev Mukerjee

Department of Chemistry and Chemical Biology,
Northeastern University (NEU)
Boston, MA 02115
Phone: (617) 373-2382
Email: S.mukerjee@neu.edu

DOE Managers

HQ: Kathi Epping Martin
Phone: (202) 586 7425
Email: Kathi.Epping@ee.doe.gov

GO: David Peterson
Phone: (720) 356-1747
Email: David.Peterson@go.doe.gov

Contract Number: DE-EE0000459

Subcontractors:

- University of New Mexico, Albuquerque, NM (UNM) (Prof. Plamen Atanassov)
- Michigan State University, East Lansing, MI (MSU) (Prof. Scott Barton)
- University of Tennessee, Knoxville, TN (UTK) (Prof. Thomas Zawodzinski)
- Nissan Technical Center, North America (NTCNA), Detroit, MI (Dr. Kev Adjemian)
- BASF Fuel Cells, Somerset, NJ (BASF) (Dr. Emory De Castro)
- Los Alamos National Laboratory, Los Alamos, NM (LANL) (Dr. Piotr Zelenay)

Project Start Date: August 1, 2010

Project End Date: August 1, 2014

Fiscal Year (FY) 2012 Objectives

The objective of this project is to design non platinum group metal (PGM)-based materials and supporting gas transport layer, both in the interfacial reaction layer between the electrode and membrane as well as in the underlying gas diffusion medium, for meeting and exceeding DOE goals for application in solid polymer electrolyte fuel cells. This project is focused on materials development and is assisted by advanced analytical tools, computation, and testing for improving the design via critical understanding of electrocatalysis in these novel structures.

Technical Barriers

This project addresses the following technical barriers from the Fuel Cells section of the Fuel Cell Technologies Program Multi-Year Research, Development and Demonstration Plan:

- (B) Cost (eliminate precious metal loading of catalysts)
- (C) Performance (increase the specific and mass activities of catalysts)
- (A) Durability (increase the durability/stability of catalysts with cycling)

Technical Targets

TABLE 1. Progress towards Meeting Technical Targets for Non-PGM Electrocatalysts for Transportation Applications

| Characteristic | Units | 2017 Target | NEU 2012 status |
|---|--|---|---|
| Specific Activity @ 80°C, 150 kPa, H ₂ /O ₂ , 100% relative humidity (RH) | A/cm ³ A/cm ² | 300 A/cm ³ (internal resistance free) 100 mA/cm ² (internal resistance free) | 130 A/cm ³ 105 mA/cm ² |
| Durability at 80°C Cycling: Catalyst Durability | % loss of activity | 5% | <1% |
| Durability at 80°C Cycling: Carbon Corrosion Durability | % loss of activity | 10% | <50% Partially recoverable |

FY 2012 Accomplishments

- Cross laboratory measurement of a wide variety of samples emanating from diverse choice of polymer precursors at MSU, NEU, UNM indicate a confluence in terms of performance; these are very close (within the errors inherent in these measurements) to the current state-of-the-art materials recently reported by our partners at LANL [1]. One of the most recent samples reported by LANL under the label LANL-2 however shows a ~49 mV lower overpotential loss as compared to the other materials.
- Wide variety of polymeric precursors indicating such confluence of inherent oxidation reduction reaction (ORR) activity strongly suggests, at least qualitatively, evolution of a common active site as a result of pyrolysis conditions.
- Extrapolation of fuel cell derived internal resistance (iR) corrected data currently indicates volumetric performance in the range of 160-175 A/cm³. Geometric area activity (iR-free) is currently 105 mA/cm².

- Durability measurements conducted in one of such samples derived from Melamine polymeric precursor and iron acetate followed with plasma pyrolysis shows excellent tolerance to catalysts stability tests (based on Nissan protocol, similar to DOE protocol). Carbon corrosion tests which involves load cycling to 1.5 V vs. the reference hydrogen electrode (RHE) however indicated significant losses; this however was recoverable over 1,600 cycles beyond which irreversible losses occurred.
- Understanding of the nature of the active site was significantly advanced in this reporting period with identification of a dual site mechanism wherein the N_{2+2} site was responsible for the initial adsorption and reduction of oxygen to peroxide moieties followed with a second cascade step of further reduction of the peroxide in closely surrounding Fe- N_2 sites. Such formulation of the mechanism was supported with in situ X-ray absorption spectroscopy (XAS) and targeted electrochemical probe measurements.



Introduction

Recent reports [1-2] have clearly demonstrated the significant advancements made in enabling good oxygen reduction activity by Fe-based non-PGM catalysts. These so called Fe- N_x based systems have evolved over several decades of intense work leading up to the current state of the art, reported recently in references [1-2]. This report provides for the first time a comprehensive view of (a) confluence of ORR activity derived from materials prepared using a variety of polymeric precursor materials viz. the current state of the art [1-2] by three different university groups (b) excellent durability in terms of catalyst stability (via DOE and Nissan protocols) and recovery of losses incurred during carbon corrosion measurement when placed under load (c) detailed understanding of nature of active site and electrocatalytic pathway as distinct from the parallel pathway in alkaline electrolytes.

Approach

The approach adopted in this reporting period involved (a) material preparation using of a wide variety of polymer precursor materials in conjunction with Fe-containing salts pyrolyzed up to temperatures of 700-800°C under inert atmosphere followed with repeated steps (up to three) of etching (in acid) and repyrolysis. Rotating ring disc electrode (RRDE) and fuel cell tests using well established protocols for cross laboratory performance comparison and extrapolation of volumetric activity (from iR-corrected fuel cell data). Durability measurements using two well

established protocols (catalyst durability) and carbon corrosion tests (both DOE protocols) and investigation on the nature of active site and ORR electrocatalysis steps as measured using in situ synchrotron spectroscopy at the Fe K edge under actual cell operational conditions.

Results

Figure 1 shows three different polymer precursor starting materials, namely poly aniline (LANL), poly vinyl guanidine (NEU) and 1 amino anti-pyrene (UNM). These were polymerized on either Ketjen black 600 (LANL and NEU) or templated on high surface area silica moieties. All of the polymerizations were initiated using well known procedures reported in our July interim report. Extent of polymerization has been previously calibrated using reference molecular weight measurements conducted with the aid of mass spectrometry. All the polymerization steps were conducted in the presence of Fe salts (typically acetate) and in one case also with Co salt (also acetate). Following polymerization with simultaneous incorporation of the metal salt, each sample was pyrolyzed under inert gas (Ar) in a temperature range of (700 to 800°C); this was followed by a series of acid leach (0.5 M H_2SO_4) and repyrolysis steps (up to three times) before final formation of the catalyst material. In the case of the Si template materials from UNM, the initial pyrolysis step was followed with an acid etch step using dilute HF (0.05 M). This provided for an in situ open framework carbon structure to form along with the evolution of the Fe- N_x structure as was the goal of the LANL and NEU samples albeit without the Si template. In the MSU sample case shown in Figure 3, a single high-pressure pyrolysis step was adopted using nitrogen precursor (Melamine), carbon (Ketjen black or Vulcan XC-72) and the metal salt Fe^{2+} acetate. Figure 2, shows a cross laboratory ORR measurement using a glassy carbon-based RRDE experiment with high loading of catalysts mentioned above (600 $\mu g/cm^2$). Also shown are the results of samples obtained from LANL, namely the new sample referred to as LANL-2 and the previously reported material [1] referred to as PANI-Fe-Co derived using preparation conditions mentioned above. As can be seen from Figure 2, measured using 0.1 M $HClO_4$ (900 rpm) under oxygen saturation conditions, room temperature, all samples with the exception of a new hitherto unreported material from LANL labeled as LANL-2 performed similarly. The LANL-2 material showed a ~ 40 mV initial lower ORR overpotential. In addition to the materials mentioned above, Figure 2 also shows the performance of an earlier reported material referred to as PEIbFe from NEU, which constitutes the poly ethylene imine polymer in conjunction with Fe acetate prepared in exactly similar conditions as reported above. Such close performance levels observed for a wide variety of samples prepared using different procedures, LANL, NEU vs. UNM and MSU samples strongly indicates possible evolution of common active site as a result of such

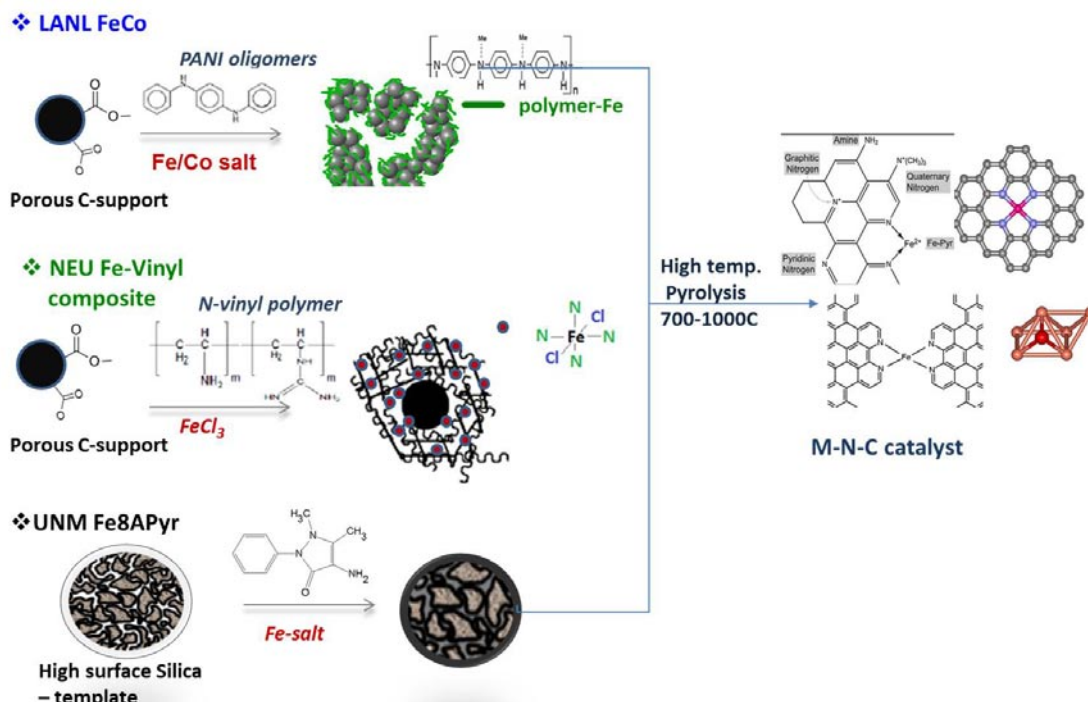


Figure 1. Representation of chemistry and pyrolysis conditions used by cross laboratory partners, UNM, LANL, and NEU

Cross Laboratory Materials Characterization

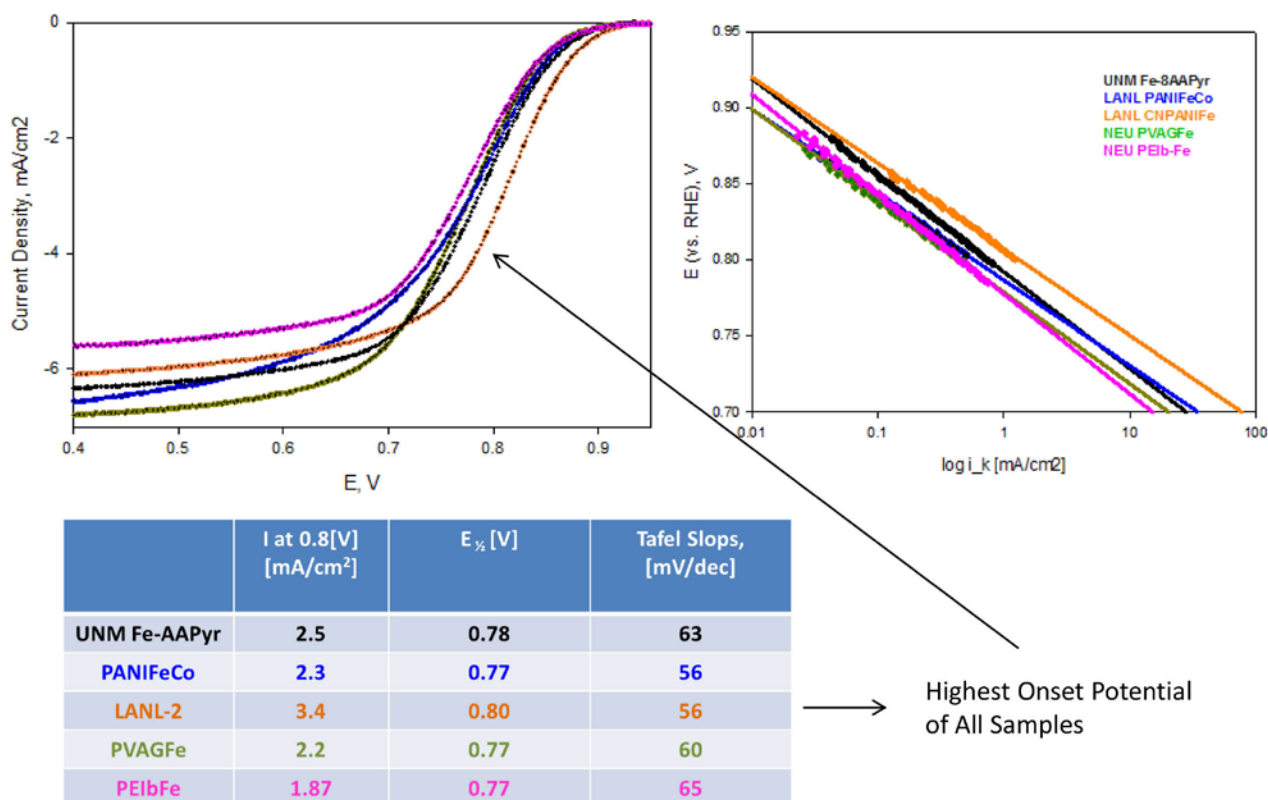
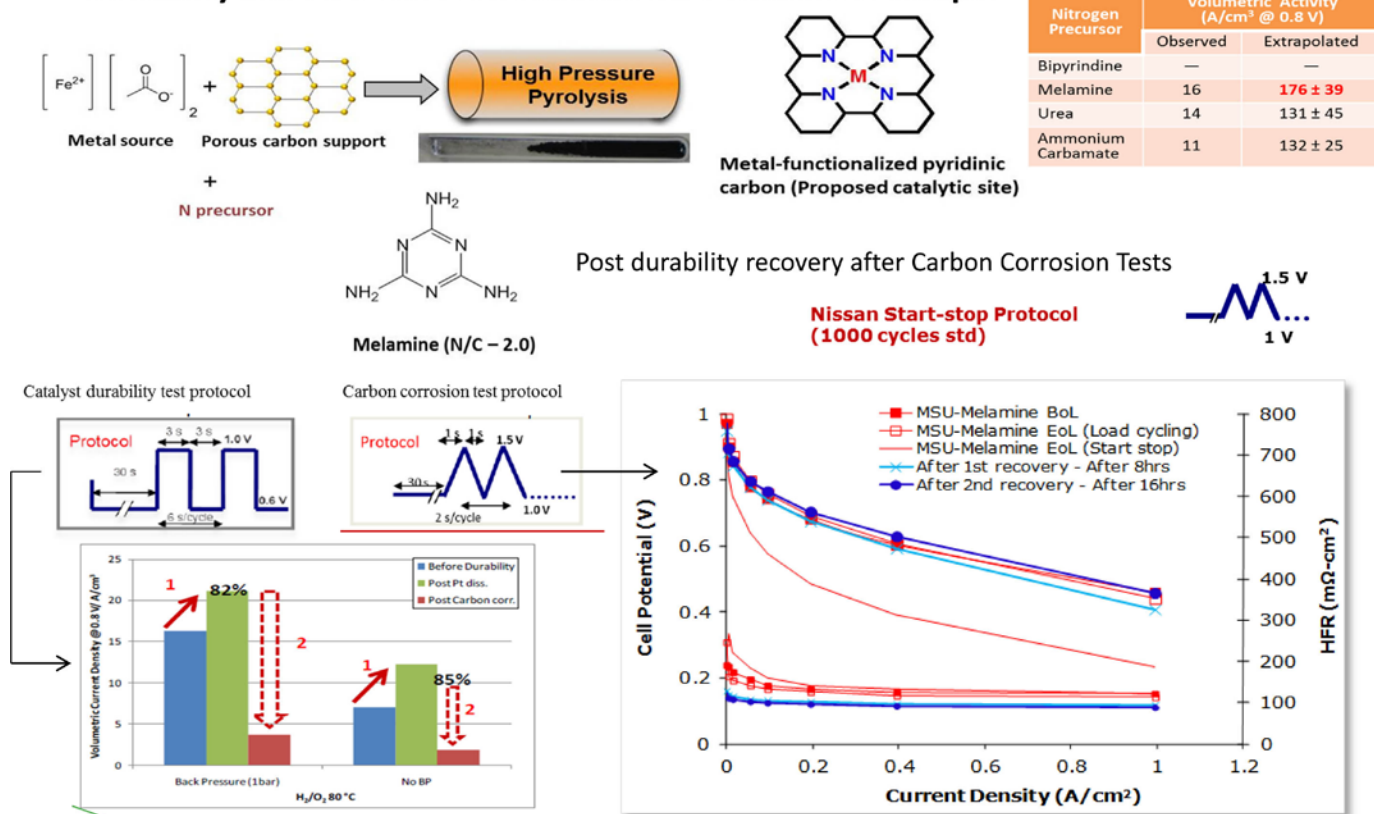


Figure 2. Cross laboratory comparison of ORR activity measured using rotating ring disk electrode technique, performance comparison shown at 900 rpm. Electrolyte is 0.1 M HClO₄, room temperature with standard catalyst loading of ~600 μg/cm². Corresponding Tafel slopes and kinetic activity are shown in associated plot and table.

pyrolysis. It should be noted that attempts to prepare such Fe-based (most likely Fe-N_x) type materials have a three decade history of evolution in activity. One important distinction between the current materials and the wealth of data reported earlier is the use of starting materials. Most of the earlier work used metal heme type macrocycles such as Fe or Co containing phthalocyanines or porphyrins. In the current evolution of materials showing true enhancement of both onset of ORR as well as inherent activity emanate from slow evolution of Fe-N_x structures via pyrolysis of polymeric precursors with no existing Fe-N structures. This is an important distinction to make as this will be later used to explain the reason for enhanced performance of such metal polymer composite pyrolysis derived materials as opposed to previous attempts involving heme-containing macrocycles. Figure 3 provides a snapshot of durability and fuel cell performance reported via MSU prepared sample, wherein the extrapolated volumetric activity (A/cm³) shows values in the range of 160-170 A/cm³. While not stellar this is within the DOE mandated target of 300 A/cm³. More importantly

however the catalyst degradation measurements conducted using Nissan protocols (square waves with 3 second on and 3 sec off periods between a potential range of 0.6 and 1.0 V) indicated no degradation; in fact over the short range of time (1,600 cycles) there was a slight improvement of performance (Figure 3). Subjecting the same membrane electrode assembly (MEA) to carbon corrosion test using DOE protocols (1.0 to 1.5 V load cycling tests) showed immediate lowering of performance, an occurrence not surprising considering the most likely active site formation involving a local graphene structure. Most surprising observation however was the recovery observed when the MEA was left under load at 400 mA/cm². This recovery lasted through till 1,600 cycles after which irrecoverable losses were observed. Figure 4 represents a proposed mechanism drawing distinction between the observed activity differences observed between the two extreme ends of the pH scale, at high pH ORR activity (900 rpm) is always better with a ~150-200 mV lower overpotential (see lower left hand plot). This is clearly observed in the rotating disk electrode profiles

Durability and Fuel Cell Performance: MSU Melamine Sample



Data from tests conducted at Nissan Technical Center North America (NTCNA)

Figure 3. Preparation conditions for sample prepared by MSU using high pressure pyrolysis of nitrogen precursor Melamine in conjunction with carbon support (Ketjen black 300) and Fe salt (acetate), iR-free fuel cell performance projections to 0.8 V is also made for obtaining volumetric activity (Table 1). Durability measurements are shown for this sample measured at the Nissan technical center North America using DOE protocols for both catalyst stability and carbon corrosion. As shown, this sample showed excellent durability for catalyst stability test; carbon corrosion test however exhibited losses which however were recoverable till 1,600 cycles.

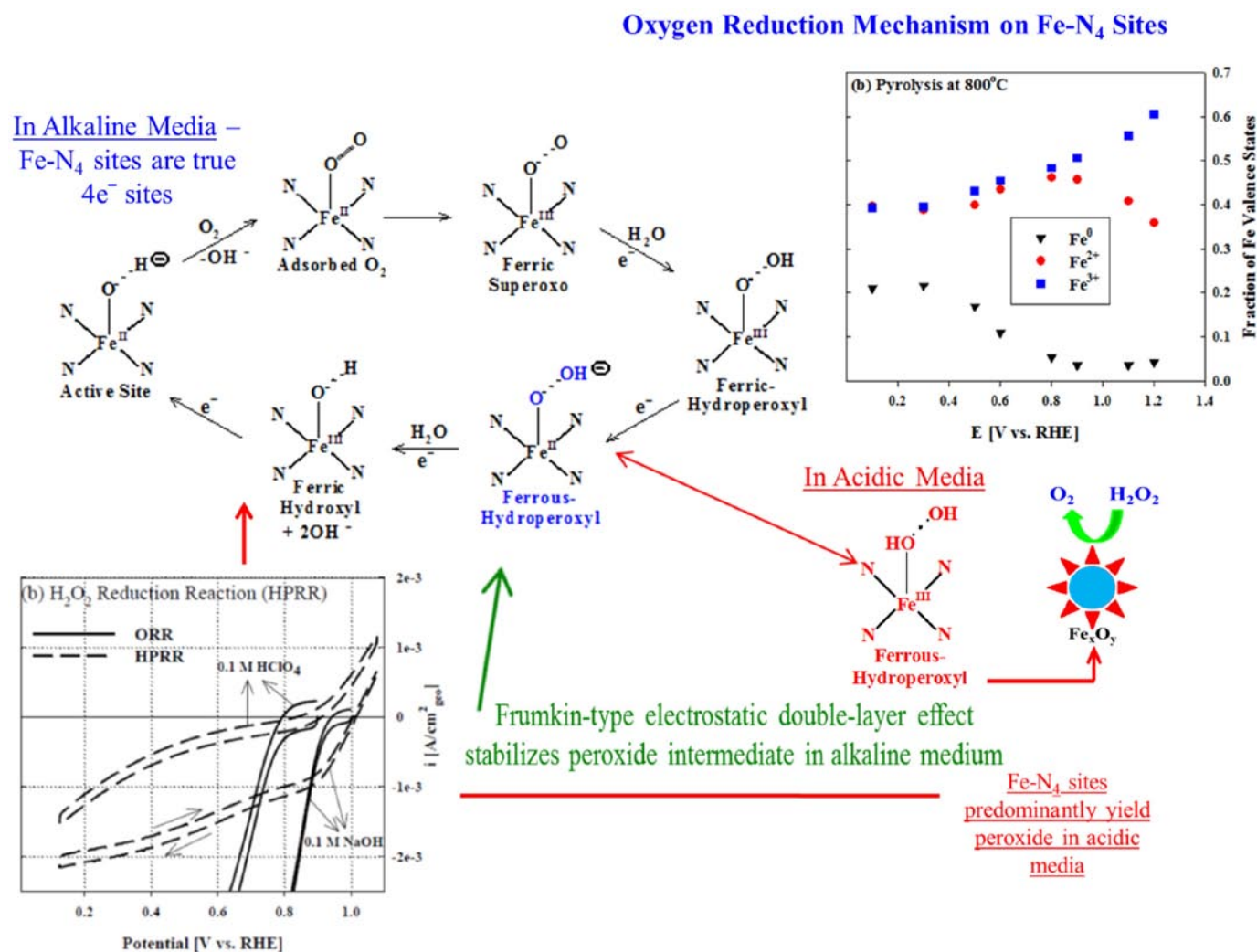


Figure 4. Mechanistic interpretation of the active site based on RDE measurements at acid and alkaline pH with O₂ and peroxide and in situ and *operando* synchrotron measurements conducted at Fe K edge (not shown) which explains the important distinction of observed activities at the two pH scales and need for a dual site mechanism in the acidic environment.

of a representative Fe-TPP (tetraphenyl porphyrin) sample pyrolyzed at 800°C on Ketjen black (600) support. When the electrolyte is instead dosed with 0.1 M H₂O₂, the higher pH response is better than O₂. Corresponding behavior at lower pH scale represents only initial decomposition of the peroxide. Detailed XAS measurements (not shown) support the mechanism shown in Figure 4, wherein this difference in activity over the pH scale is explained on the basis of the fact that the initial turnover number for the adsorption of molecular oxygen on F-N₂₊₂ is extremely fast both in acid and alkaline pH; however it is only in the alkaline pH that the peroxy-anion is stabilized and allows for the further reduction to water. In the acid pH the inability of such stabilization therefore requires an additional site where peroxy-anion can be further reduced.

Conclusions and Future Directions

Conclusions

- Cross-laboratory studies of materials emanating from the pyrolysis of diverse polymer precursors in conjunction of Fe and Co salts indicate a common evolution of active sites for ORR reduction.
- Detailed durability studies indicate excellent tolerance to catalyst stability tests, and relatively poor resistance to carbon corrosion test protocols, the latter however is recoverable over several cycles.
- Mechanism for an active site is proposed which is supported by activity observations at both ends of the spectrum.

Future Directions

- Principal focus of the group will include meeting and exceeding DOE targets for ORR activity in terms of both volumetric and geometric areas (see Table 1).
- Meet and exceed DOE durability milestones for more diverse materials.
- Further test the validity of the proposed mechanism using final set of in situ and *operando* synchrotron XAS data in conjunction with density functional theory calculations.

FY 2012 Publications/Presentations

1. 'Fundamental Mechanistic Understanding of Electrocatalysis of Oxygen Reduction on Pt and Non Pt Surfaces: Acid vs. Alkaline Medium', N. Ramaswamy and S. Mukerjee, *Advances in Physical Chemistry*, Vol. 2012, Article ID 491604, (2012).

References

1. Wu, G.; More, K.L.; Johnston, C.M.; Zelenay, P. *Science* **2011**, *332*, 443.
2. Lefevre, M.; Proietti, E.; Jaouen, F.; Dodelet, J.P. *Science* **2009**, *324*, 71.

V.D.12 High-Activity Dealloyed Catalysts

Frederick T. Wagner (Primary Contact),
Anusorn Kongkanand
General Motors, LLC (GM)
10 Carriage St.
Honeoye Falls, NY 14472
Phone: (585) 624-6726
Email: frederick.t.wagner@gm.com

DOE Managers

HQ: Dimitrios Papageorgopoulos
Phone: (202) 586-5463
Email: Dimitrios.Papageorgopoulos@ee.doe.gov
GO: Gregory Kleen
Phone: (720) 356-1672
Email: Gregory.Kleen@go.doe.gov

Contract Number: DE-EE0000458

Subcontractors:

- George Washington University (GWU), Washington, D.C.
- Johnson Matthey Fuel Cells (JMFC),
Sonning Common, UK
- Massachusetts Institute of Technology (MIT),
Cambridge, MA
- Northeastern University (NEU), Boston, MA
- Technical University Berlin (TUB), Berlin, Germany

Project Start Date: August 1, 2010

Project End Date: November 30, 2013

Technical Barriers

This project addresses the following technical barriers from the Technical Plan--Fuel Cells section of the Fuel Cell Technologies Program Multi-Year Research, Development and Demonstration Plan:

- (B) Cost
- (A) Durability
- (C) Performance

Technical Targets

TABLE 1. Progress towards Meeting Technical Targets for Electrocatalysts for Transportation Applications (first 4) or for MEAs (last 2)

| Characteristic | Units | 2017 DOE StackTargets | Project 2012 Status (50 cm ² at GM) |
|-----------------------------------|---|-----------------------|---|
| Mass activity | A/mg _{PtGM} @ 900 mV _{IR-free} | ≥0.44 | 0.52 (PtNi ₃) 0.46 (PtCo ₃) |
| Loss in catalytic (mass) activity | % lost after 30k cycles 0.6-1.0 V | ≤40% | 28%(PtCo ₃) 69% (PtNi ₃) |
| PGM Total Content | g _{PGM} /kW _{rated} | ≤0.125 | 0.16 (PtNi ₃) @1.5 A/cm ² in H ₂ /air |
| PGM Total Loading | mg _{PGM} /cm ² _{geo} | ≤0.125 | 0.15 (0.05 on anode) |
| Performance @ rated power | mW/cm ² | 1,000 | 940 |
| Performance @ 0.8 V | mA/cm ² | 300 | 200 |

PGM - Platinum group metal

Fiscal Year (FY) 2012 Objectives

- Demonstrate, in 50-cm² membrane electrode assemblies (MEAs) in fuel cells, a dealloyed catalyst both (1) giving an initial oxygen reduction activity ≥0.44 A/mg_{PGM} and (2) losing less than 40% of that activity after 30,000 voltage cycles from 0.6 to 1.0 V.
- Optimize manufacturable procedures for precursor synthesis and dealloying of the catalyst powders.
- Demonstrate electrodes made from dealloyed catalysts that give good high current density performance using air as the oxidant: >570 mV at 1.5 A/cm² when tested with the DOE-targeted cathode loadings ≤0.1 mg_{PGM}/cm².
- Improve understanding of where alloying-element atoms should reside with respect to the surface of the catalyst particle for simultaneously good activity, durability, and high-current-density performance in air.

FY 2012 Accomplishments

- Developed catalysts achieving initial mass activities of 0.52 (dealloyed PtNi₃) and 0.46 A/mg_{PGM} (D-PtCo₃), exceeding the target of ≥0.44, with better durability and high-current-density performance than the D-PtCu₃ reported last year.
- The small-batch GM D-PtCo₃ lost only 38% percent of its initial activity after 30,000 cycles 0.6-1.0 V, bettering the target of <40% loss and giving more than a 2-fold improvement vs. last year's D-PtCu₃. The durability of the dealloyed large-batch JMFC PtNi₃ tested to date, while better than that of D-PtCu₃, still needs improvement.
- MEAs made with large-batch D-PtNi₃ at 0.1 mg_{PGM}/cm² matched or bettered, at all current densities on H₂/air, the initial performance of those made with baseline Pt/carbon at 0.4 mg_{PGM}/cm². They thereby demonstrate a pathway to the Pt-cost reduction needed for mass

production of fuel cells, if the durability limitations seen to date with this material can be overcome.



Introduction

The amount of expensive platinum used as the oxygen reduction catalyst in fuel cells must be reduced about 4-fold to make proton exchange membrane fuel cells (PEMFCs) cost-competitive with other power sources. Pt-alloy catalysts, typically prepared with a composition of Pt_3M (M being a non-precious metal) have historically provided about half of the necessary activity gain vs. state-of-the-art pure-Pt/carbon catalysts. Prior to this project, team member Peter Strasser's group had shown, in small-scale laboratory experiments, that additional activity gains could be obtained by first synthesizing alloys with excess M and then removing most of the M by an electrochemical treatment [1]. They hypothesized that this treatment leaves the surface Pt atoms closer to one another than they are in pure Pt, causing electronic structure changes that accelerate the reduction of oxygen [2]. This project has developed manufacturable means of scaling up these dealloyed catalysts, confirming that most of the activity gains seen in ex situ laboratory experiments can also be achieved in practical fuel cells at GM which satisfy the DOE catalyst activity target. However, we identified severe problems: (1) lack of durability and (2) poor performance in hydrogen/air fuel cells at high current density, associated with the use of the alloying element, copper, which had seemed most attractive in ex situ experiments. In FY 2012 we have successfully shifted to other alloying elements, cobalt and nickel, which avoid one of the mechanisms whereby copper caused problems. Made in small batches, several dealloyed PtCo catalysts satisfied DOE catalyst targets for both activity and durability in GM fuel cells. Larger-scale dealloyed $PtNi_3$ catalysts have to date satisfied the DOE activity target and the project milestone for high current density performance in GM fuel cells. We continue to pursue ideas to solve the durability shortfall that we have seen to date for the large-scale dealloyed $PtNi_3$ materials.

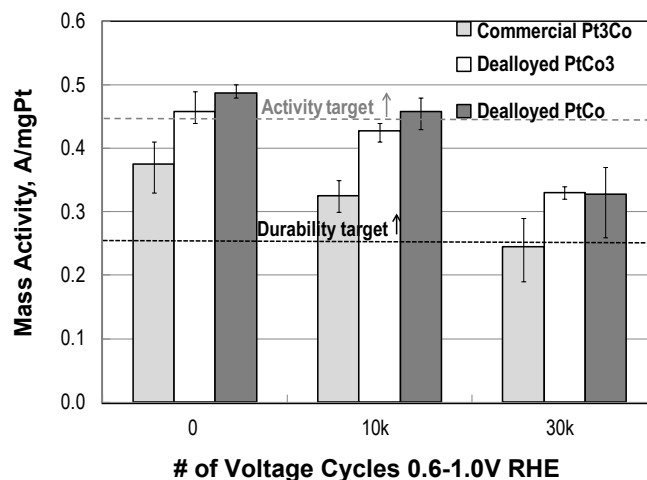
Approach

Project member Peter Strasser's group had demonstrated, in ex situ experiments prior to this project, that electrochemical removal of most of the non-noble alloying element M from Pt-alloy precursors with initial composition of PtM_3 could give higher oxygen reduction activities than the ~2-3-fold improvement vs. Pt alone that had historically been seen for Pt-alloy catalysts directly prepared at a composition of Pt_3M . Last year, this project demonstrated that this improved activity could be achieved in MEAs tested in fuel cells with $PtCu_3$, dealloyed as a catalyst powder using manufacturable chemical methods. However, GM

found the durability of the D- $PtCu_3$ to be very poor. Also, amounts of Cu (remaining after dealloying) sufficient to give good initial kinetic activity gave very poor performance in H_2 /air fuel cells at high current density. The latter effect was due in part to Cu^{2+} crossing from the cathode through the membrane to the anode, where it plated out as Cu metal and blocked the H_2 oxidation reaction. This year extensive work was done, optimizing manufacturable methods, to generate dealloyed catalysts and cathode electrodes using two alloying elements, Co and Ni, which do not plate out as the metals at the hydrogen potential in the acidic electrolyte of a PEMFC. Advanced electron microscopy and synchrotron X-ray techniques were applied to aged electrodes to correlate atomic-scale structure and composition with differences in activity and durability between individual catalysts, thereby guiding the further development of durably active catalysts.

Results

Figure 1 shows that GM-made small-batch D- $PtCo_3$ and D- $PtCo$ catalysts met, in 50-cm² fuel cells at GM, both the initial activity and the durability DOE 2017 targets shown in Table 1, as well as outperforming a commercial Pt_3Co catalyst subjected to the same test procedures. These results show that a dealloyed catalyst can simultaneously meet the DOE numerical targets for kinetic activity and durability. However, insufficient quantities of these catalysts could be prepared to allow testing in multiple laboratories and at different loadings. The intention of this project is for JMFC, as an established catalyst manufacturer, to generate the primary materials for investigation so as to facilitate eventual commercial availability of the advanced catalysts developed.



RHE - reference hydrogen electrode

FIGURE 1. ORR Pt mass activities measured in GM 50-cm² H_2/O_2 fuel cells at standard conditions for three catalysts, at 0.2 mg_{Pt}/cm² loadings, as a function of the number of 0.6-1.0 V triangle-wave potential cycles at 50 mV/s in fully-humidified H_2/N_2 at 80°C. "Activity target" (see Table 1) is judged at 0 cycles; "Durability target" is judged at 30,000 cycles. Error bars show range of 3 MEAs/point.

Based on some preliminary data from TUB suggesting that the Pt-Ni system could be superior to the Pt-Co, JMFC generated several large (~100 g) batches of PtNi₃ precursors. GM chemically dealloyed this material in 1 M HNO₃ for different times and temperatures, yielding catalyst powders with the compositions labeled for individual sets of points in Figure 2. GM fabricated 50-cm² MEAs from these powders, giving the initial (after break-in) activities shown in Figure 2. While the initial oxygen reduction reaction (ORR) activity dropped as more Ni was removed from the precursor with more aggressive dealloying, the activity remained above the DOE target for a wide range of final catalyst compositions. This provides us with the freedom to optimize for other properties such as durability and high-current-density performance.

Figure 3 shows that the durability against voltage cycling of the large-batch D-PtNi₃ catalyst dealloyed for 1 day at 70°C did not meet the DOE target. Transmission electron microscopy of the fresh and cycled MEAs showed that this catalyst had a spongy, hole-riddled structure in all sizes of particles, and extended X-ray absorption fine structure (EXAFS) of these electrodes showed little evidence of Pt-Ni bonding, though a fair amount of Ni remained in the catalyst. In contrast, the more durable small-batch D-PtCo₃ catalyst had shown much more Pt-M binding in EXAFS, and detailed atomic-scale elemental mapping with electron energy loss spectroscopy had shown Pt-Co cores within Pt shells, as well as some pores, in all particle sizes [3]. We hypothesize that the alloy cores of this D-PtCo₃ catalyst improved its durability vs. the more porous, percolated structure of this

Acid leaching conditions on mass activity

95% CI for the Mean

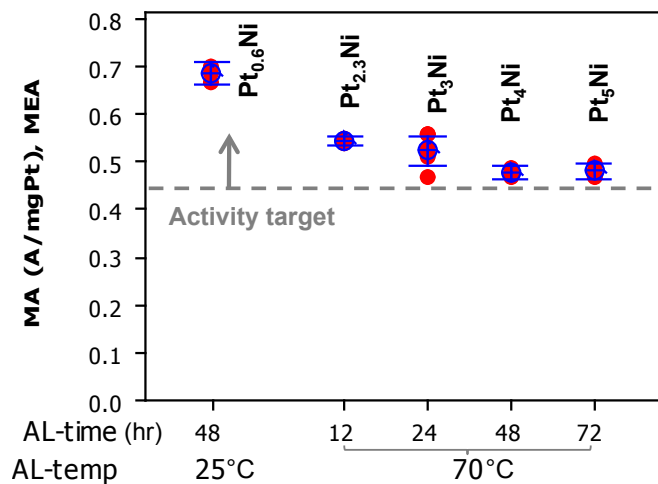


FIGURE 2. Initial ORR Pt mass activities measured in GM 50-cm² H₂/O₂ fuel cells at standard conditions for JMFC large-batch PtNi₃/Ketjen dealloyed (in the powder form) by GM in 1 M HNO₃ for the temperatures and times shown. Error bars are 95% confidence intervals for 4-7 MEAs for each type. Compositions shown are for the dealloyed catalyst powders prior to fabrication of the MEAs.

D-PtNi₃ (Ni and Co have similar corrosion chemistry); and we are trying a range of different dealloying conditions to promote more of a core-shell structure as a means of improving durability in the PtNi system.

While the durability of the kinetic activity of the large-batch D-PtNi₃ has so far been disappointing, its initial performance at high current density in air has been quite good, particularly in light of the lack of optimization of cathode electrode structure to date. Figure 4 shows that the 50-cm² MEA performance in H₂/air of 0.1 mg_{PGM}/cm² D-PtNi₃,

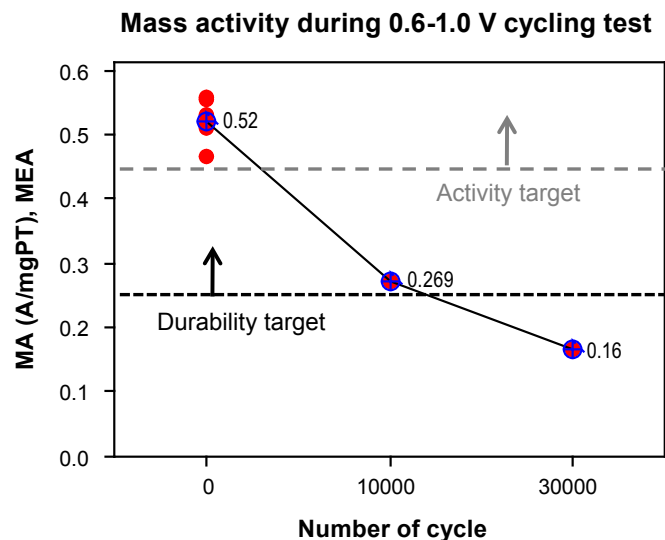


FIGURE 3. ORR Pt mass activities for JMFC large-batch PtNi₃/Ketjen dealloyed by GM for 24 h at 70°C as a function of the number of H₂/N₂ voltage cycles 0.6-1.0 V at the conditions of Figure 1.

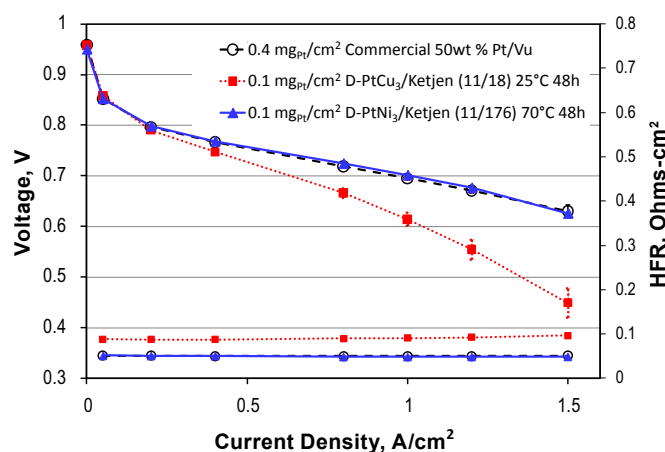


FIGURE 4. Comparison of GM 50-cm² H₂/air polarization curves for 0.4 mg_{Pt}/cm² loadings of commercial Pt/V and for 0.1 mg_{Pt}/cm² loadings of JMFC PtCu₃/Ketjen and JMFC PtNi₃/Ketjen dealloyed by GM to give initial activities >0.44 A/mg_{Pt}. 80°C, 170 kPa_{abs}, relative humidity 100%/100%, stoichiometries 1.5/2. High-Frequency Resistances measured at 1 kHz. Error bars show the standard errors of 3-4 MEAs of each type.

dealloyed to a point that still satisfies the initial activity target, matches or exceeds that of MEAs with a $0.4 \text{ mg}_{\text{PGM}}/\text{cm}^2$ loading of a conventional Pt/Vulcan carbon catalyst at all points of the polarization curve. In contrast, D-PtCu₃ with enough Cu left to give good kinetic activity gave very poor performance in air at high current density. The benefits of the shift from Cu to a less-noble alloying element are clear. Detailed alternating-current impedance studies have shown that the higher high-frequency resistance values for the PtCu electrode were due to an additional impedance loop caused by the poisoning of most of the anode surface with metallic copper. The D-PtNi₃ data in Figure 4 satisfy the project milestone for the initial high-current-density performance, but we still need to further optimize the electrodes to fully comply with the more recent DOE electrode performance targets shown in the last two lines of Table 1.

Conclusions and Future Directions

- D-PtNi₃ is looking good for initial kinetic activity and high-current-density performance.
- Working to improve durability of D-PtNi₃ by:
 - Modifying dealloying conditions to promote core/shell vs. percolated structure.
 - JMFC is running diverse precursor preparation techniques to improve particle-size uniformity.
 - Adding third components to control dealloying process.
 - TUB is controlling facet exposure, adding third components to limit activity loss.
- MIT is investigating how relative positions in electrochemical series and metal-Pt binding strengths influence dealloying.
- Once durability of kinetic activity is under control, will scale up to full-active-area fuel cells to test durability of high-current-density performance.

FY 2012 Publications/Presentations

1. Liu, Z.Y.; Xin, H.L.; Yu, Z.Q.; Zhu, Y.; Zhang, J.L.; Mundy, J.A.; Muller, D. and Wagner, F.T., “Atomic-Scale Compositional Mapping and 3-Dimensional Electron Microscopy of Dealloyed PtCo₃ Catalyst Nanoparticles with Spongy Multi-Core/Shell Structures”, *J. Electrochem. Soc.*, in press (likely V. 159, no. 9, 2012).
2. Jia, Q.; Halder, A.; Ramaker, D.E.; Ziegelbauer, J.M. and Mukerjee, S., “Investigation of Cathodic Underpotential Deposition of Cu onto Pt/C Electrocatalysts and its Influence on the Oxygen Reduction Reaction”, *The Electrochemical Society*, 9–14 October 2011, Boston, MA.; Abstract # 930, manuscript in preparation.
3. Jia, J.Q.; Trahan, M.; Ramaker, D.E.; Ziegelbauer, J.M. and S. Mukerjee, “X-ray Absorption Spectroscopy Investigations on the Activity and Durability of a Dealloyed PtCo₃ Electrocatalyst”, *The Electrochemical Society*, 9–14 October 2011, Boston, MA.; Abstract #770, manuscript in preparation.

4. Caldwell, K.; Mukerjee, S.; Qingying, J.; Ziegelbauer, J.M. and Ramaker, D.E., “X-ray Absorption Spectroscopy Investigation on a High Activity Dealloyed PtCo₃ Cathodic Catalyst”, *The Electrochemical Society*, 9–14 October 2011, Boston, MA.; Abstract #860, manuscript in preparation.
5. Wagner, F.T.; Lakshmanan, B.; Gu, W.; Greszler, T.A. and Mathias, M.F., “Electrons to Go: Electrochemistry and the Future of the Automobile”, invited plenary-session talk at the 220th national meeting of The Electrochemical Society, Boston, MA, October 9–14, 2011. Included short section on dealloyed catalysts. Abstract #770 and *Electrochemical Society Transactions* 41 (2011) 13-26.
6. Wagner, F.T., “Reduction of Platinum Usage in Automotive Fuel Cells, *Acta Materiala Materials and Society Award Forum: Vehicle Electrification Honoring Dr. Alan Taub*, Boston, MA, November 27, 2011. Section on dealloyed catalysts.
7. Wagner, F.T., “Near-Surface Science and Oxygen Reduction Electrocatalysis”, *Fuel Cell Seminar at Yamanashi Univ., Kofu, Japan*, December 9, 2011. Section on dealloyed catalysts.
8. Wagner, F.T. “Surface Science towards the Electrification of the Automobile”, *International Symposium on Surface Science and Nanotechnology*, Tokyo, Japan, December 14, 2011. Section on dealloyed catalysts.
9. Strasser, P., “Materials for Fuel Cell Catalysts”, *American Chemical Society*, San Diego, CA, March 26, 2012.
10. Strasser, P., “Core-Shell Nanoparticle Catalyst Concepts for High Performance Polymer Electrolyte Membrane Fuel Cells”, keynote presentation at the *Grove Fuel Cells 2012 Science & Technology Conference*, Berlin, Germany, April 11, 2012.
11. Kongkanand, A.; Gu, W. and Wagner, F.T., “Electrocatalyst Design in Proton Exchange Membrane Fuel Cells for Automotive Application”. In “*Heterogeneous Catalysis at the Nanoscale for Energy Applications.*”; Tao, F.; Schneider, W. and Kamat, P. eds.; Wiley-VCH (2012) submitted. Section on dealloyed catalysts.
12. Ramaker, D.E.; Caldwell, K.; Mukerjee, S.; Jia, Q. and Ziegelbauer, J.M. “Investigations on High Activity De-alloyed Pt₃Co Cathodic Catalysts using XAS”, *63rd Annual Meeting of the International Society of Electrochemistry*, Aug. 19–20, 2012, Prague, Cz; ISE#120638; manuscript in preparation.

References

1. Koh, S.; Strasser, P., “Electrocatalysis on Bimetallic Surfaces: Modifying Catalytic Reactivity for Oxygen Reduction by Voltammetric Surface Dealloying”, *J. Am. Chem. Soc.*, Vol. 129, pp. 12624-12625, 2007.
2. Strasser, P.; Koh, S.; Anniyev, T.; Greeley, J.; More, K.; Yu, C.; Liu, Z., Kaya, S.; Nordlund, D.; Ogasawara, H.; Toney, M.F. and Nilsson, A., “Lattice-Strain Control of the Activity in Dealloyed Core-Shell Fuel Cell Catalysts”, *Nature Chemistry*, Vol. 2, pp. 454-460, 2010.
3. Liu, Z.Y.; Xin, H.L.; Yu, Z.Q.; Zhu, Y.; Zhang, J.L.; Mundy, J.A.; Muller, D. and Wagner, F.T., “Atomic-Scale Compositional Mapping and 3-Dimensional Electron Microscopy of Dealloyed PtCo₃ Catalyst Nanoparticles with Spongy Multi-Core/Shell Structures”, *J. Electrochem. Soc.*, in press (likely V. 159, no. 9, 2012).

V.D.13 Development of Ultra-Low Platinum Alloy Cathode Catalysts for PEM Fuel Cells

Branko N. Popov

University of South Carolina (USC)
301 Main Street
Columbia, SC 29208
Phone: (803) 777-7314
Email: popov@cec.sc.edu

DOE Managers

HQ: Donna Lee Ho
Phone: (202) 586-8000
Email: Donna.Ho@ee.doe.gov

GO: David Peterson
Phone: (720) 356-1747
Email: David.Peterson@go.doe.gov

Technical Advisor

Thomas Benjamin
Phone: (630) 252-1632
Email: benjamin@anl.gov

Contract Number: DE-EE0000460

Subcontractor:

Dr. Hansung Kim (Co-PI) Yonsei University, S. Korea.

Project Start Date: September 1, 2010

Project End Date: May 31, 2014

Objectives

- Develop low-cost and durable hybrid cathode catalyst (HCC).
- Develop Pt alloy/activated graphitic carbon catalyst.
- Develop corrosion resistant supports.
- Develop facile scale-up catalyst synthesis procedure (at least 100 g).
- Optimize the parameters which control the number of catalytic sites on carbon composite catalyst (CCC).
- Optimize the procedure for the formation of more active Pt alloy catalysts.
- Demonstrate kinetic mass activity in H_2/O_2 fuel cell higher than DOE target of $0.44 \text{ A mg}_{\text{PGM}}^{-1}$ and durability of the mass activity.
- Demonstrate high current performance in H_2 /air fuel cell to meet DOE targets.
- Construct short stack (50 cm^2 up to 10 cells) and evaluate the performance under simulated automotive conditions.

Specific Objectives for Fiscal Year (FY) 2012

- Evaluate the oxygen reduction reaction (ORR) kinetics of the CCC support.
- Evaluate the synergistic effect of CCC support and Pt or Pt-alloy catalysts.
- Evaluation of different strategies for the optimization of HCC and Pt-alloy/carbon nanocage (CNC) catalysts with total loadings of $0.2 \text{ mg}_{\text{Pt}} \text{ cm}^{-2}$ /membrane electrode assembly (MEA).
 - Initial and durability of kinetic mass activities.
 - Initial high current density performance in H_2 -air.

Technical Barriers

This project addresses the following technical barriers from the Fuel Cells section of the Fuel Cell Technologies Program Multi-Year Research, Development and Demonstration Plan:

- (A) Durability
- (B) Cost
- (C) Performance

Technical Targets

The technical targets for the year FY 2012 are to: (i) study the effect of various surface modifications on USC CCC, (ii) evaluate the oxygen reduction reaction (ORR) kinetics of the CCC support, and (iii) evaluate the synergistic effect of CCC support, Pt and Pt alloy catalyst.

To increase the catalyst performance and durability, the following new procedures were developed during the reporting period.

- A new low temperature method was developed to synthesize partially graphitized carbon composite catalyst (support) based on catalyzed pyrolysis in presence of transition metals.
- 1-pyrene carboxylic acid was used to modify and functionalize the partially graphitized CCC and CNC supports.
- A high temperature alloying process was developed to synthesize uniformly distributed platinum alloy particles with an average particle of 3.3 nm deposited on functionalized partially graphitized CCC and CNC supports.

TABLE1. Progress towards Meeting Technical Targets for Electrocatalysts

| Characteristic | Units | 2017 Targets | Status |
|---|--|---------------------|---|
| Power Density | g/kW | 0.125 | |
| Precious group metal (PGM) total loading | mg/cm ² | 0.125 | 0.1-0.2 mg _{metal} cm ⁻² with HCC and 0.1 mg _{metal} cm ⁻² with Pt ₂ Ni ₁ /CNC catalysts |
| Mass activity (80°C, 100% relative humidity (RH), 150 kPa _{abs}) | A mg _{Pt} ⁻¹ @ 0.9 V _{IR-free} | 0.44 | 0.45 A mg _{Pt} ⁻¹ for Pt ₂ Ni ₁ /CCC ^(A) (0.1 mg cm ⁻²) 0.33 A mg _{Pt} ⁻¹ for Pt ₂ Ni ₁ /CCC ^(B) (0.15 mg cm ⁻²) 0.37 A mg _{Pt} ⁻¹ for Pt ₁ Co ₁ /CCC ^(C) (0.2 mg cm ⁻²) 0.41 A mg _{Pt} ⁻¹ for Pt _{1.3} Co ₁ /CCC ^(D) (0.1 mg cm ⁻²) 0.44 A mg _{Pt} ⁻¹ for Pt ₂ Ni ₁ /CNC (0.1 mg _{metal} cm ⁻²) |
| Catalyst durability (30,000 cycles, 0.6-1.0 V, 50 mV/s, 80/80/80, 100 kPa _{abs} , H ₂ /N ₂) | % Mass activity loss % ECSA loss mV loss @ 0.8 A/cm ² | ≤40% ≤40% ≤30 | 30.3% mass activity loss (Pt ₂ Ni ₁ /CCC ^(B)) 46-49.3% mass activity loss and 27.8% ECSA loss (Pt ₁ Co ₁ /CCC ^(C)) 31.8% mass activity loss and 26.3% ECSA loss (Pt ₂ Ni ₁ /CNC) |
| Support durability (1.2 V for 400 h at 80°C, H ₂ -N ₂ , 150 kPa _{abs} , 100% RH) | % Mass activity loss | <10% | 47.7% mass activity loss for Pt ₂ Ni ₁ /CNC. |
| High current density performance [H ₂ /air (1.5/1.8), 80°C, 40% RH, 150 kPa _{abs}] | A cm ⁻² @ 0.58 V _{IR-free} | - | 1.25 (1.5/1.8) and 1.4 (1.5/2.0) for Pt ₂ Ni ₁ /CCC ^(A) (0.1 mg cm ⁻²) |

CCC^(A) – Brunauer-Emmett-Teller (BET) surface area higher than 600 m² g⁻¹; CCC^(B) – BET surface area = 250 m² g⁻¹; CCC^(C) – BET surface area = 380 m² g⁻¹;
CCC^(D) – BET surface area = 350 m² g⁻¹.

FY 2012 Accomplishments

- Accomplished onset potential for oxygen reduction reaction close to 0.9 V_{RHE} and <2.5% H₂O₂ production for the CCC support.
- Accomplished initial mass activities of 0.45, 0.33, 0.37, and 0.41 A mg_{Pt}⁻¹ for Pt₂Ni₁/CCC^(A), Pt₂Ni₁/CCC^(B) (0.15 mg_{Pt} cm⁻²), Pt₁Co₁/CCC^(C) (0.2 mg_{Pt} cm⁻²) and Pt_{1.3}Co₁/CCC^(D) catalysts, respectively.
- Accomplished mass activity loss of 30.3% and 46-49.3% for Pt₂Ni₁/CCC^(B), Pt₁Co₁/CCC^(C) catalysts, respectively.
- Accomplished ECSA loss of 27.8% for the Pt₁Co₁/CCC^(C) catalyst.
- Accomplished mass activity of 0.44 A mg_{Pt}⁻¹ for Pt₂Ni₁/CNC catalyst.
- Achieved 0.3 A mg_{Pt}⁻¹ after 30 k cycles for Pt₂Ni₁/CNC catalyst.
- Achieved 1.25 A cm⁻² and 1.4 A cm⁻² at 0.58 V_{IR-free} for the Pt₂Ni₁/CCC^(A) catalyst at 1.5/1.8 and 1.5/2.0 stoichiometry, respectively under H₂-air operating conditions (80 °C, 40% RH, 150 kPa_{abs}).



Introduction

Stable and highly active HCC was developed which shows higher performance than the commercial Pt/C at low loadings (between 0.04 and 0.4 mg cm⁻²). The hybrid cathode catalyst is a combination of nitrogen-containing CCC and platinum for oxygen reduction reaction [1-12]. Pt-alloy catalyst deposited on activated graphitic carbon support with

high activity towards oxygen reduction was synthesized and its catalytic activity was evaluated [13-15].

Approach

Currently, the main strategies to decrease the platinum loading in cathode electrodes are based on the optimization of electrode structures and implementation of more active Pt alloy catalysts. The new approach used in this work consists of development of a HCC through a patented process. The goal of our second strategy is the synthesis of Pt-alloy catalysts deposited on activated graphitic carbon support.

Results

In this reporting period, procedures for CCC synthesis were optimized and the synergistic effect of CCC support and low Pt (5%) was studied. Furthermore, HCCs using various CCC with different BET surface areas as supports and Pt₂Ni₁/CNC catalysts were synthesized. The performance of the synthesized catalysts including ECSA, kinetic mass activity, catalyst durability after 30 k cycles, specific activity and initial high current performance were evaluated in a 25 cm² polymer electrolyte membrane fuel cell (PEMFC) under DOE suggested fuel cell operating conditions.

Carbon composite catalysts were prepared according to the procedures developed previously and used as catalyst supports. The ORR kinetics of as-received carbon (Ketjen black) and Ketjen black subjected to various surface modification steps is compared in Figure 1(a). The onset potential for ORR increases when the as-received carbon is subjected to various surface modifications including oxidation in HNO₃ and incorporation of nitrogen and

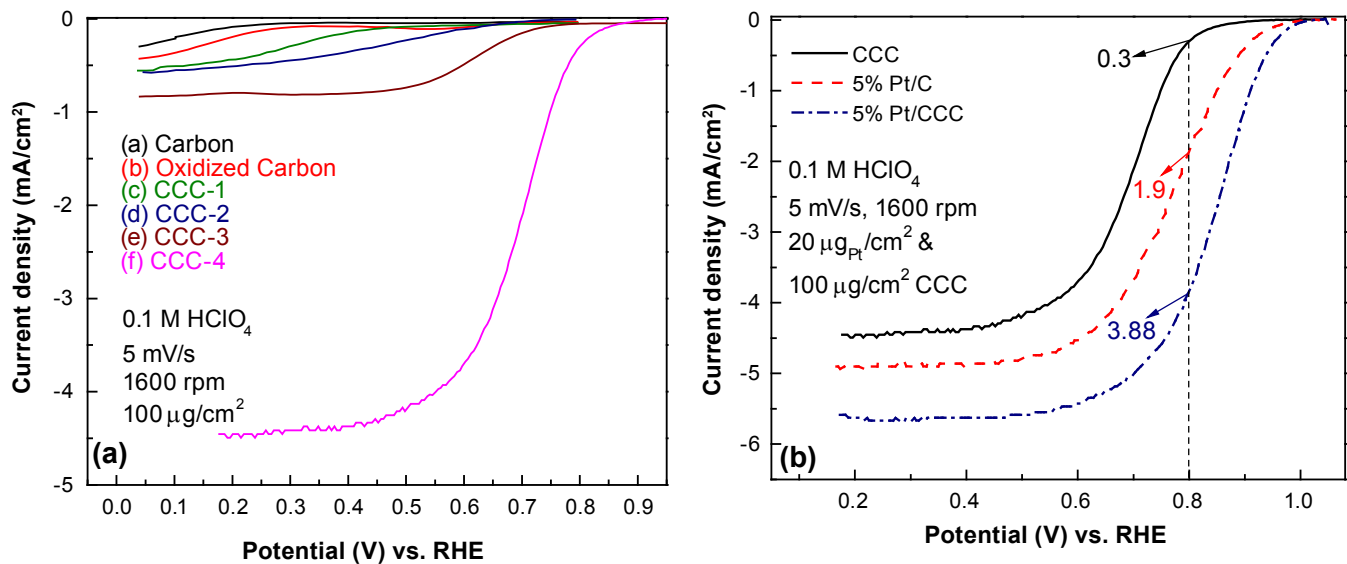


FIGURE 1(A). Comparison of ORR performances of carbon (Ketjen black) and surface modified carbons. Polarization curves: (a) as received Ketjen black carbon, (b) HNO₃-oxidized carbon, (c) oxidized carbon with nitrogen and transition metal (CCC-1), (d) oxidized carbon with nitrogen and transition metal (CCC-2), (e) oxidized carbon with nitrogen and transition metal (CCC-3) and (f) low temperature graphitized oxidized carbon with nitrogen and transition metal (CCC-4). **FIGURE 1(B).** Comparison of ORR activities of carbon composite catalyst, 5% Pt/C and 5% Pt/CCC in rotating ring disk electrode (RRDE).

transition metals. The carbon composite catalyst (curve f in Figure 1a) showed an onset potential of 0.9 V_{RHE} and well-defined kinetic and mass transfer regions in 0.1 M HClO₄ electrolyte at room temperature. The H₂O₂ production for CCC was in the range between 2-3% (figure not shown).

The synergistic effect of CCC carbon composite catalyst used as the catalyst support and Pt catalyst was evaluated by depositing 5 wt% Pt on CCC and Ketjen black supports. The results are compared in Figure 1(b). As can be seen from the figure, the onset potential for ORR for CCC, 5% Pt/C and 5% Pt/CCC are 0.97 V, and 1.01 V, respectively. The current density at 0.8 V (vs. the reversible hydrogen electrode, RHE) for the CCC, 5% Pt/C and 5% Pt/CCC catalysts are 0.3, 1.9 and 3.88 mA cm⁻², respectively. The highest open circuit potential of 1.01 V and current density measured at 0.8 V of 5% Pt/CCC clearly indicated the presence of the synergistic effect between CCC and Pt. The diffusion currents of CCC, 5% Pt/C and 5% Pt/CCC catalysts are 4.5, 4.9 and 5.6 mA cm⁻², respectively.

During the reporting period, we developed a new methodology to functionalize partially graphitized CCC and CNC supports through non-covalent π-π interaction using a bifunctional molecule, 1-pyrenecarboxylic acid (1-PCA). The functionalization resulted in an average Pt particle size of 2.5 ± 0.2 nm as measured by the X-ray diffraction studies using the Scherrer equation. A new coating and impregnation method was also developed to inhibit the Pt-alloy particle sintering during high temperature alloying process. The normal heat-treatment procedure resulted in an average Pt-alloy particle size of 10.8 nm while the new protective

coating methodology resulted in 3.4 nm particles. The aggregation of Pt particles was restrained by the protective film used in this study.

Comparison of mass activities of various HCC catalysts (Pt-alloy deposited on CCC support) and conventional Pt/C catalyst is shown in Figure 2. As shown in the figure, the mass activities of HCC Pt/C catalyst, are nearly 3-4 times higher than that of conventional Pt/C, which confirms our initial studies for presence of a synergistic effect between

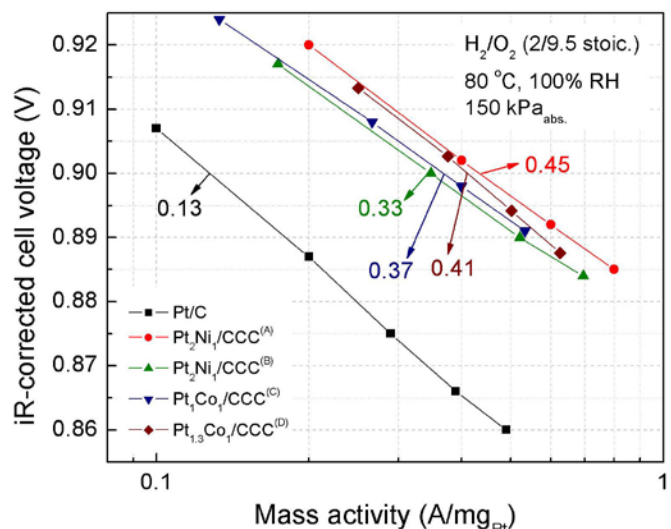


FIGURE 2. Comparison of mass activities of conventional Pt/C and various HCC (Pt-alloy deposited on CCC support) catalysts.

CCC and Pt or Pt-alloy in the USC developed Hybrid Cathode Catalyst. $\text{Pt}_2\text{Ni}_1/\text{CCC}^{(A)}$ catalyst showed mass activities of $0.45 \text{ A mg}_{\text{Pt}}^{-1}$. The mass activities of Pt/C, $\text{Pt}_2\text{Ni}_1/\text{CCC}^{(B)}$, $\text{Pt}_1\text{Co}_1/\text{CCC}^{(C)}$ and $\text{Pt}_{1.3}\text{Co}_1/\text{CCC}^{(D)}$ are 0.13, 0.33, 0.37 and $0.41 \text{ A mg}_{\text{Pt}}^{-1}$, respectively.)

One of the primary challenges facing the development of PEMFCs for automotive and stationary power applications is the durability of the fuel cell catalyst and support. The DOE cycling protocol to evaluate the durability of the $\text{Pt}_2\text{Ni}_1/\text{CCC}^{(B)}$ and $\text{Pt}_1\text{Co}_1/\text{CCC}^{(C)}$ catalysts indicated mass activity loss of 46–49.3% and 30.3% after 30 k cycles, respectively. Furthermore, the $\text{Pt}_1\text{Co}_1/\text{CCC}^{(C)}$ catalysts showed ECSA loss of only 27.8% after 30 k cycles which is lower than the DOE target (40%) (Table 1). DOE cycling protocol was also performed to evaluate the durability of 50% $\text{Pt}_2\text{Ni}_1/\text{CNC-NA}$ (NA-no acid treatment) catalysts. The ECSA, ORR mass activity, and H_2 -air polarization curves were performed

after 5,000, 10,000, 20,000, and 30,000 cycles. As shown in Figures 3 (a) and (b), the mass activity loss of 50% $\text{Pt}_2\text{Ni}_1/\text{CNC-NA}$ is 31% and the ECSA loss of the $\text{Pt}_2\text{Ni}_1/\text{CNC-NA}$ after 30 k cycles is only 26% which are lower than the 2017 DOE targets for mass activity and ECSA activity after 30 k cycles (40% loss).

The H_2 -air fuel cell performance of Pt/C and HCC catalysts (Pt-alloy deposited on CCC support) is shown in Figure 4. The fuel cell operating conditions are given in the figure caption. The observed current densities are: 0.9 A cm^{-2} for 46% Pt/C, 0.95 A cm^{-2} for 30% $\text{Pt}_3\text{Co}_1/\text{CCC}^{(D)}$, and 1.25 A cm^{-2} for 46% $\text{Pt}_2\text{Ni}_1/\text{CCC}^{(A)}$ at 1.5/1.8 stoichiometry. The $\text{Pt}_2\text{Ni}_1/\text{CCC}^{(A)}$ catalyst exhibited 1.4 A cm^{-2} with an increased cathodic stoichiometry of 2.0.

Conclusions and Future Directions

Conclusions

- Accomplished onset potential for oxygen reduction reaction close to $0.9 \text{ V}_{\text{RHE}}$ and $<2.5\%$ H_2O_2 production for the CCC support.
- Accomplished initial mass activities of 0.45, 0.33, 0.37, and $0.41 \text{ A mg}_{\text{Pt}}^{-1}$ for $\text{Pt}_2\text{Ni}_1/\text{CCC}^{(A)}$, $\text{Pt}_2\text{Ni}_1/\text{CCC}^{(B)}$, $\text{Pt}_1\text{Co}_1/\text{CCC}^{(C)}$ and $\text{Pt}_{1.3}\text{Co}_1/\text{CCC}^{(D)}$ catalysts, respectively.
- Accomplished initial mass activity of $0.44 \text{ A mg}_{\text{Pt}}^{-1}$ for the $\text{Pt}_2\text{Ni}_1/\text{CNC}$ catalyst.
- Accomplished mass activity loss of 30.3% and 46–49.3% after 30 k cycles for $\text{Pt}_2\text{Ni}_1/\text{CCC}^{(B)}$, $\text{Pt}_1\text{Co}_1/\text{CCC}^{(C)}$ catalysts, respectively.

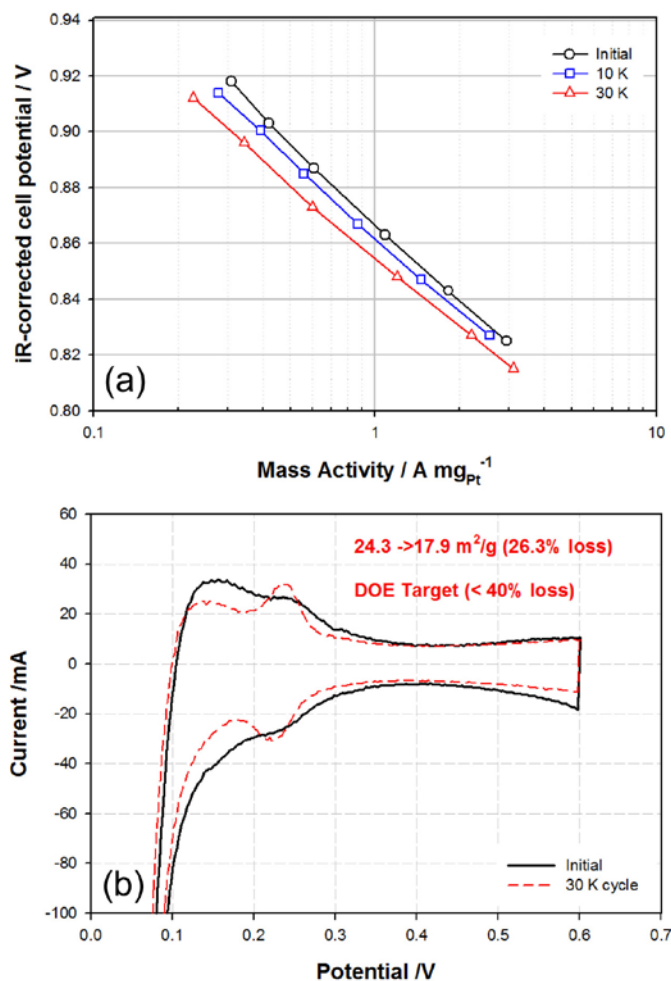


FIGURE 3(A). Catalytic oxygen reduction activities of the 50 wt% $\text{Pt}_2\text{Ni}_1/\text{CNC-NA}$ catalysts ($0.1 \text{ mg}_{\text{metal}} \text{ cm}^{-2}$) during accelerated stress test (AST) by cycling protocol.

FIGURE 3(B). Cyclic voltammogram of the 50wt% $\text{Pt}_2\text{Ni}_1/\text{CNC-NA}$ catalyst ($0.1 \text{ mg}_{\text{metal}} \text{ cm}^{-2}$) before and after the accelerated stress test.

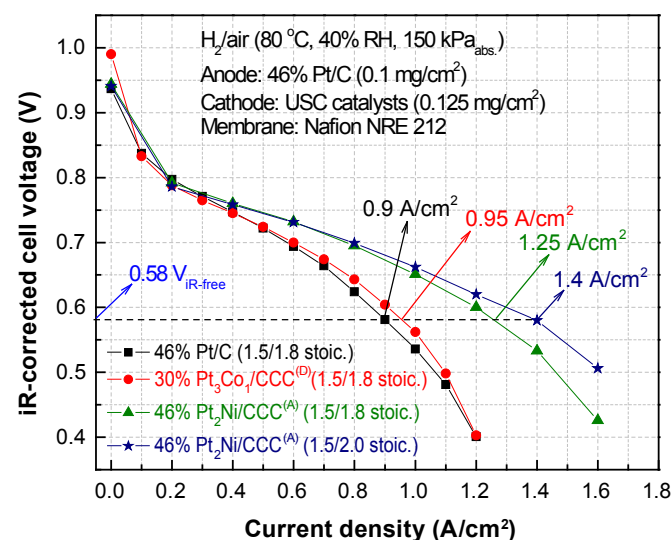


FIGURE 4. Comparison of H_2 -air fuel cell performances of Pt/C and HCC catalysts (Pt-alloy deposited on CCC support). The fuel cell was operated at 80°C , 40% RH, $150 \text{ kPa}_{\text{abs}}$ back pressure and 1.5/1.8 H_2/air stoichiometry. The anode and cathode Pt loadings were 0.1 and 0.125 mg cm^{-2} , respectively, and Nafion® 212 membrane was used as the electrolyte.

- Accomplished ECSA loss of 27.8% for the Pt₁Co₁/CCC^(C) catalyst.
- Accomplished 0.3 A mg_{Pt}⁻¹ after 30 k cycles for the Pt₂Ni₁/CNC catalyst.
- Achieved 1.25 A cm⁻² and 1.4 A cm⁻² at 0.58 V_{iR-free} for the Pt₂Ni/CCC^(A) catalyst at 1.5/1.8 and 1.5/2.0 stoichiometry, respectively, under H₂-air operating conditions (80°C, 40% RH, 150 kP_{abs.} outlet pressure).

Future anticipated accomplishments are to:

- Confirm durability of kinetic mass activity of at least 0.24 A mg_{Pt}⁻¹ after 30 k cycles or less than 40% loss of mass activity at 0.9 V_{iR-free} and ECSA loss less than 40% for the HCC catalysts.
- Accomplish durability of catalyst support according to DOE target of less than 40% loss of mass activity at 0.9 V_{iR-free} and less than 40% loss of ECSA.
- Accomplish high current density performance and durability in H₂/air fuel cells (80°C, 40% RH, 150 kP_{abs.} 1.5/1.8 stoichiometry).
- Reproducibility of catalyst performance evaluation in at least three MEAs in two laboratories using 25 and 50 cm² cells.
- Demonstrate facile scale-up synthesis of the catalysts.

Special Recognitions & Awards/Patents Issued

1. Carbon-based composite electrocatalysts for low temperature fuel cells, *US 7,629,285*, 2009.
2. Composite catalysts supported on modified carbon substrates and methods of making the same, *US 7,618,915*, 2009.

FY 2012 Publications/Presentations

Publications

1. Sheng-Yang Huang, Prabhu Ganesan, and Branko N. Popov, "Electrocatalytic Activity and Stability of Titania Supported Platinum-Palladium Catalysts for Polymer Electrolyte Membrane Fuel Cell" *ACS Catalysis*, 2 (2012) 825-831.
2. Sheng-Yang Huang, Prabhu Ganesan, Ho-Young Jung and Branko N. Popov, "Development of supported bifunctional oxygen electrocatalysts and corrosion-resistant gas diffusion layer for unitized regenerative fuel cell applications", *J. Power Sources*, 198 (2012) 23-29.
3. Sehkyu Park, Branko N. Popov, Effect of a GDL based on carbon paper or carbon cloth on PEM fuel cell performance, *Fuel*, 90, (2011) 436-440.
4. Xuguang Li, Branko N. Popov, Takeo Kawahara, Hiroyuki Yanagi, Non-precious metal catalysts synthesized from precursors of carbon, nitrogen, and transition metal for oxygen reduction in alkaline fuel cells, *Journal of Power Sources*, 196 (2011), 1717-1722.

5. Gang Liu, Xuguang Li, Jong-Won Lee and Branko Popov, A Review of the Development of Nitrogen Modified Carbo-based catalyst for Oxygen Reduction at USC, *Catalysis Science & Technology*, 1, (2011) 207-217.
6. Sheng-Yang Huang, Prabhu Ganesan, Branko N. Popov, Titania supported platinum catalyst with high electrocatalytic activity and stability for polymer electrolyte membrane fuel cell, *Appl. Catal. B: Environmental*, 102 (2011) 71-77.
7. Xuguang Li, Gang Liu, Prabhu Ganesan, Hansung Kim, Bumwook Roh, and Inchul Hwang, Development of Ultra-Low Pt Alloy Cathode Catalyst for PEM Fuel Cells, Branko N. Popov, *ECS Transactions*, 2011, 41 (1), 955-969.
8. S.Y. Huang, P. Ganesan, and B.N. Popov, Titanium dioxide-supported platinum catalysts, *ECS Transactions*, 41, 2255-2268 (2011).

Presentations

1. Branko N. Popov, Tae-keun Kim, Xie Tianyuan, Prabhu Ganesan, and Hansung Kim, Development of ultra-low platinum alloy cathode catalyst for PEM fuel cells, *220th ECS Meeting*, Boston, MA, October 9–14, 2011.
2. S. Huang, P. Ganesan, and B.N. Popov, Titanium Dioxide-Supported Platinum Catalysts, *220th ECS Meeting*, Boston, MA, October 9–14, 2011.
3. X. Li, G. Liu, T. Kim, S. Ganesan, P. Ganesan, and B.N. Popov, Development of Non-Precious Metal Catalysts for Oxygen Reduction Reaction in Fuel Cells with High Activity and Stability, *220th ECS Meeting*, Boston, MA, October 9–14, 2011.

References

1. N.P. Subramanian, S.P. Kumaraguru, H.R. Colon-Mercado, H.Kim, B.N. Popov, T. Black and D.A. Chen, "Studies on Co-Based Catalysts Supported on Modified Carbon Substrates for PEMFC Cathodes", *J. Power Sources*, 157 (2006) 56-63.
2. R.A. Sidik, A.B. Anderson, N.P. Subramanian, S.P. Kumaraguru and B.N. Popov, "O₂ Reduction on Graphite and Nitrogen-Doped Graphite: Experiment and Theory", *J. Phys. Chem. B*, 110 (2006) 1787-1793.
3. X. Li, H.R. Colon-Mercado, G. Wu, J.-W. Lee, B.N. Popov, "Development of Method for Synthesis of Pt-Co Cathode Catalysts for PEM Fuel Cells," *Electrochem. Solid-State Lett.*, 10 (2007) B201-B205.
4. Nallathambi, Vijayadurga; Lee, Jong-Won; Kumaraguru, Swaminatha P, Wu, Gang; Popov, Branko N, "Development of high performance carbon composite catalyst for oxygen reduction reaction in PEM Proton Exchange Membrane fuel cells", *J Power Sources*, 183 (2008) 34-42.
5. Subramanian, Nalini P, Li, Xuguang, Nallathambi, Vijayadurda, Kumaraguru, Swaminatha P, Colon-Mercado, Hector, Wu, Gang, Lee, Jong-Won, Popov, Branko N, "Nitrogen-modified carbon-based catalysts for oxygen reduction reaction in polymer electrolyte membrane fuel cells", *J Power Sources*, 188 (2009) 38-44.

6. Liu, Gang, Li, Xuguang, Ganesan, Prabhu, Popov, Branko N, Development of non-precious metal oxygen-reduction catalysts for PEM fuel cells based on N-doped, *Appl. Catal. B: Environmental*, **93** (2009) 156-165.
7. Liu, Gang, Li, Xuguang, Ganesan, Prabhu, Popov, Branko N, “Studies of oxygen reduction reaction active sites and stability of nitrogen-modified carbon composite catalysts for PEM fuel cells”, *Electrochim. Acta*, **55** (2010) 2853-2858.
8. Li, Xuguang, Park, Sehkyu, Popov, Branko N, “Highly stable Pt and PtPd hybrid catalysts supported on a nitrogen-modified carbon composite for fuel cell application”, *J Power Sources*, **195** (2010) 445-452.
9. Xuguang Li, Gang Liu, Branko N. Popov, “Activity and stability of non-precious metal catalysts for oxygen reduction in acid and alkaline electrolytes”, *J. Power Sources*, **195** (2010) 6373-6378.
10. B.N. Popov, X. Li and J.W. Lee, “Power source research at USC: Development of advanced electrocatalysts for polymer electrolyte membrane fuel cells”, *Int. J. Hyd. Energy*, **36** (2011) 1794-1802.
11. Xuguang Li, Branko N. Popov, Takeo Kawahara, Hiroyuki Yanagi, Non-precious metal catalysts synthesized from precursors of carbon, nitrogen, and transition metal for oxygen reduction in alkaline fuel cells, *Journal of Power Sources*, 196 (2011), 1717-1722.
12. Gang Liu, Xuguang Li, Jong-Won Lee and Branko Popov, A Review of the Development of Nitrogen Modified Carbon-based catalyst for Oxygen Reduction at USC, *Catalysis Science & Technology*, 1, (2011) 207-217.
13. K.H Lim, H-S Oh, H. Kim, Use of a carbon nanocage as a catalyst support in polymer electrolyte membrane fuel cells *Electrochem. Commun.*, **11** (2009) 1131-1134.
14. K.H Lim, H-S Oh, S-E Jang, Y-J Ko, H-J Kim, H. Kim, Effect of operating conditions on carbon corrosion in polymer electrolyte membrane fuel cells, *J. Power Sources*, **193** (2009) 575-579.
15. H-S Oh, K.H. Lim, B. Roh, I. Hwang, H. Kim, Corrosion resistance and sintering effect of carbon supports in polymer electrolyte membrane fuel cells, *Electrochim. Acta*, **54** (2009) 6515-6521.

V.D.14 High Aspect Ratio Nano-Structured Pt-Based PEM Fuel Cell Catalysts

Brian A. Larsen
 National Renewable Energy Lab
 1617 Cole Blvd
 Golden, CO 80401
 Phone: (303) 803-6989
 Email: brian.a.larsen@nrel.gov

DOE Manager
 HQ: Kathi Epping Martin
 Phone: (202) 586-7425
 Email: Kathi.Epping@ee.doe.gov

Project Start Date: December 5, 2011
 Project End Date: December 4, 2013

Technical Targets

This project will provide a pathway towards successfully achieve the electrocatalyst DOE technical targets for Pt mass activity. The Pt-based materials developed in this project will support the cost and performance targets in Table 1 by significantly improving the Pt utilization in Pt-based electrocatalyst, thus lowering the primary cost of polymer electron membrane fuel cell systems.

Approach

Fabrication of Pt-based fuel cell electrocatalysts that will exceed U.S. DOE mass activity targets by synthesizing nanostructured Pt and Pt-alloy materials with high aspect ratios. This approach has been developed to leverage two proven strategies for improving electrocatalyst activity: 1) alloying Pt with other metals, such as Fe, Co, and Ni, and 2) creating high-aspect ratio materials that exhibit “extended surface” enhancement of their electrocatalytic activity. Both of these strategies, forming Pt alloys and extended surfaces, will increase the specific activity of the high aspect ratio, extended surface Pt-based (HES-Pt) catalyst materials that will be developed in this project. In addition, methods will be developed to create high surface areas for the HES-Pt catalysts, and the combination of the enhanced specific activity and high surface areas will result in mass activities that will surpass the DOE mass activity targets. This approach is depicted in Figure 1.

Fiscal Year (FY) 2012 Objectives

- Demonstrate the synthesis of shape-controlled Pt-alloy fuel cell catalysts
- Quantify the enhanced activity of these fuel cell catalysts

Technical Barriers

This project addresses the following technical barriers from the Fuel Cell section of the Fuel Cell Technologies Program Multi-Year Research, Development and Demonstration Plan:

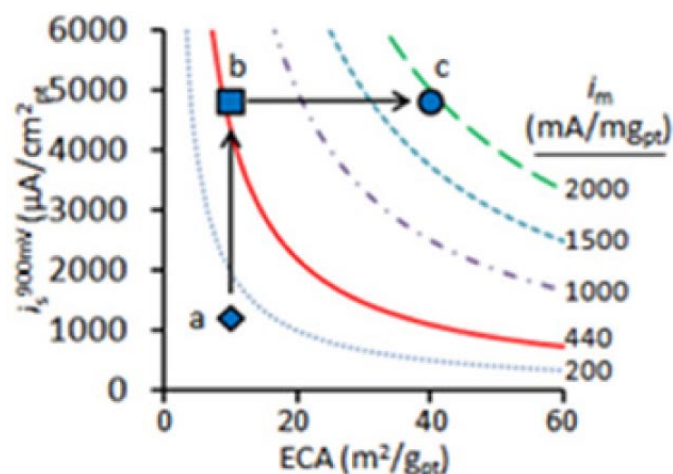
- (B) Cost
- (C) Performance

FY 2012 consists of the following main tasks:

- Fabricate base metal (Ni, Co, Fe) nanowires or nanoplates – Ni, Co, and Fe have been selected as

TABLE 1. Technical Targets for Electrocatalysts for Transportation Applications

| Table 3.4.13 Technical Targets: Electrocatalysts for Transportation Applications | | | | |
|--|---|---|---------|-------|
| Characteristic | Units | 2011 Status | Targets | |
| | | | 2017 | 2020 |
| Platinum group metal total content (both electrodes) | g/kw (rated) | 0.19 | 0.125 | 0.125 |
| Platinum group metal (PGM) total loading | Mg PGM/cm ² electrode area | 0.15 | 0.125 | 0.125 |
| Loss in initial catalytic activity | % mass activity loss | 48 | <40 | <40 |
| Electro catalyst support stability | % mass activity loss | <10 | <10 | <10 |
| Mass activity | A/mg Pt @ 900 mV _{iR-free} | 0.24 | 0.44 | 0.44 |
| Non-Pt catalyst activity per volume of supported catalyst | A/cm ³ @ 800 mV _{iR-free} | 60 (measured at 0.8 V) 165 (extrapolated from >0.85 V) | 300 | 300 |



ECA - electrochemical area

FIGURE 1. Electrocatalyst mass activity may be increased by separate strategies to increase specific activity (A → B) and ECA (B → C). The colored lines are constant mass activities corresponding to the i_m labels on the right of the plot.

the best candidates to create high activity HES-Pt alloy catalyst materials based on previous studies of activity enhancement in nanoparticle-based Pt alloys with these metals. The nanowire and nanoplate shapes were selected to yield the extended surface activity enhancement that has been previously observed in Pt nanowires at NREL.

- Create a Pt-alloy using a base metal nanoplate/nanowire – The base metals may be used to create Pt-alloys by the galvanic displacement method, which displaces the base metal atoms with Pt. This has been proven to be an effective method to create alloys with base metals while preserving the base metal shape.
- Characterize the electrochemical performance of the Pt-alloy nanoplate/nanowire by rotating disc electrode (RDE) – Electrochemical characterization of the materials by RDE provides a preliminary means to evaluate the activity of the HES Pt-alloy material to determine the materials best suited for implementation in fuel cells.

FY 2012 Accomplishments

- Task 1 - Synthesized both nanowires and nanoplates of Ni and Co (Figures 2 and 3)
 - Successfully developed methods to fabricate four different base metal materials for HES Pt-alloy catalysts
- Task 2 – Synthesized nanowire HES Pt-Co catalyst (Figure 4)
 - Successfully fabricated the HES Pt-Co nanowire by galvanic displacement of Co nanowires synthesized from Task 1

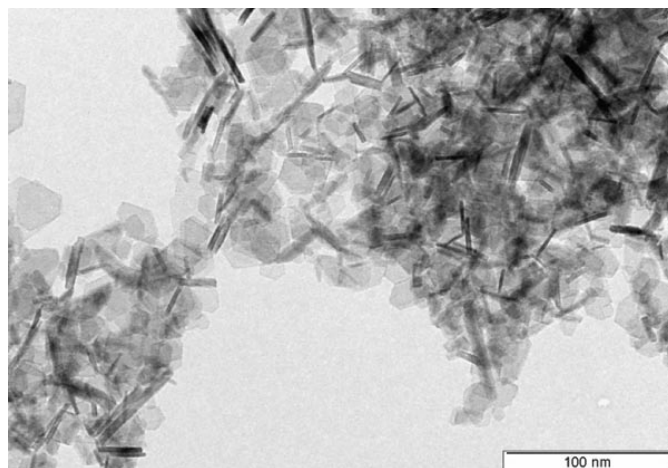


FIGURE 2. Transmission electron microscopy of Ni nanoplates

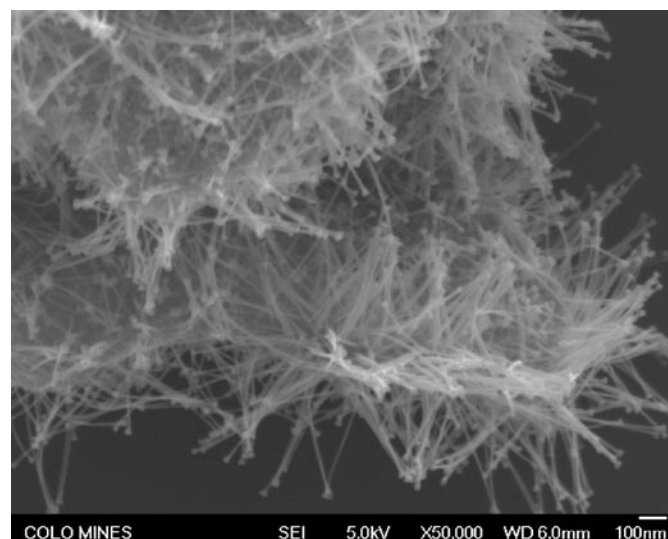


FIGURE 3. Scanning electron microscopy of Co nanowires

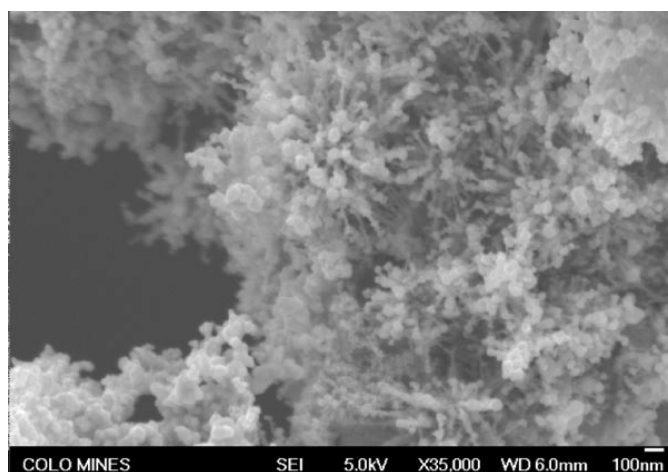


FIGURE 4. Scanning electron microscopy of nanowire-based HES Pt-Co catalyst materials

- Task 3 – Attempted electrochemical characterization of HES Pt-Co catalyst material
 - Results were inconclusive, further development of the HES Pt-Co preparation is needed before electrochemical characterization.



FY 2012 Publications/Presentations

1. “Enhanced activity fuel cell electrocatalysts achieved by shape control of platinum nanostructures,” Presented at the 2012 World Tech Connect, Larsen BA, Neyerlin KC, Bult JB, Bochert C, Blackburn JL, Kocha SS, Pivovar BS.

Future Directions

In FY 2013, the following tasks will be performed:

- Synthesize HES Pt-alloys from another base metal or shape: To fully explore the activity enhancement of HES-Pt alloys, fabricate a Ni nanowire or nanoplate-based HES-Pt alloy material or a Co nanoplate-based HES-Pt alloy material.
- Continue development of existing HES Pt-Co catalyst preparation methods to enable electrochemical characterization.
- Develop methods to create high surface areas for HES-Pt alloy catalysts.

FY 2013 Planned Milestones

- Characterize the compositional dependence of Pt in HES-Pt alloy materials.
- Complete the synthesis and characterization of three separate HES-Pt alloy materials.
- Fabricate and evaluate the highest performing HES-Pt alloy in fuel cells.

V.D.15 Development of Alternative and Durable High Performance Cathode Supports for PEM Fuel Cells

Yong Wang (Primary Contact),
 Vilayanur Viswanathan, Jun Liu, Yuehe Lin,
 Sehkyu Park, Yuyan Shao
 Pacific Northwest National Laboratory
 902 Battelle Boulevard, PO Box 999
 MS K2-12
 Richland, WA 99352
 Phone: (509) 371-6273
 Email: yongwang@pnl.gov

DOE Manager
 HQ: Nancy Garland
 Phone: (202) 586-5673
 Email: Nancy.Garland@ee.doe.gov

Subcontractors:
 AFCC Automotive Fuel Cell Cooperation Corp.,
 Burnaby, BC: Stephen Campbell

Project Start Date: January, 2007
 Project End Date: December, 2012

Fiscal Year (FY) 2012 Objectives

Develop new classes of alternative support materials that meet the 2010 DOE performance targets by achieving the following specific objectives:

- Understand structural and compositional requirements of conductive metal oxides (CMO) for improved activity and durability over standard Pt/Vulcan XC-72.
- Demonstrate durability and performance advantages of alternative cathode supports such as carbon nanotubes (CNTs), ordered graphitic mesoporous carbon (OGMC), graphene and graphitized carbon nanotubes (GCNT).
- Demonstrate durability and performance of non-carbon CMO supports such as tin-doped indium oxide (ITO).

Technical Barriers

This project addresses the following technical barriers from Fuel Cells section (3.4) of the Fuel Cell Technologies Program Multi-Year Research for Fuel Cells, Development and Demonstration Plan:

- (A) Durability (cathode catalyst supports)
- (C) Performance (supported cathode catalyst)

Technical Targets

This project is directed at conducting durability and activity studies of Pt on various supports, with the objective of meeting the DOE life time criteria. Membrane electrode assembly (MEA) tests have been performed for lead supports using CMO modification of novel carbon supports, and have shown 3-4X improvement in stability over baseline Vulcan XC-72 carbon supports (Table 1). Rotating disc electrode (RDE) tests have also shown significant improvement in durability over baseline. Promising results have been obtained for carbon-free supports, with ex situ results showing similar electrochemical surface area (ESA) values and excellent durability. Electrode architecture optimization is ongoing to improve in situ performance of these supported catalysts.

TABLE 1. Progress towards Meeting Technical Targets for Electrocatalysts for Transportation Applications

| Parameter | Units | 2015 Stack Target | PNNL 2011 Status |
|--|-------------------|-------------------|---|
| Accelerated test loss, 200 h @ 1.2 V at 80°C | mV at rated power | <30 | 10% retention for baseline after 100 hours |
| | % ESA loss | <40 | 42% retention of ESA for baseline after 100 hours |
| Durability with cycling at 80°C | Hours | 5,000 | To be determined |

FY 2012 Accomplishments

Throughout the course of the project, we achieved the following:

- Thermodynamic stability of Pt-CMO-carbon triple junction using periodic density functional theory (DFT) calculations.
- Verification of formation of Pt-CMO-carbon triple junction by microscopy and its high stability by ex situ and in situ electrochemical tests.
- Identification of contribution of catalyst layer ohmic and ionic resistances to MEA performance and degradation, providing insights into electrode architecture optimization.
- High durability of carbon-free CMO support of various aspect ratios, mesoporosity and Pt loading.

For FY 2012 specifically, we achieved the following:

- Synthesized TiO₂ nanorod supported catalyst with continuous Pt nanowire networks.

- Determined effect of ITO mesopore size on ex situ performance, with ESA equal to vulcan carbon baseline.
- Developed accelerated stress test (AST) protocol to increase throughput by 4X.
- Obtained promising in situ trends for Pt-ITO by optimizing electrode architecture and platinum loading.
- Methodology developed to estimate ionic resistance and concentration polarization in the supported catalyst layer for various carbon supports, and their degradation during AST, which can guide electrode architecture optimization for various supports.
- Higher durability of CNT, OGMC and GCNT over Vulcan XC-72 carbon baseline provides potential for >4X improvement over baseline in durability with metal oxide modification.
- Carbon free metal oxides (ITO) with tailored conductivity and mesoporosity show positive trend in terms of activity and performance.
- Metal oxides with optimized aspect ratio and Pt wt% in the support provide pathway for enhanced durability and performance.
- Identification of catalyst layer ohmic and mass transfer resistance contribution to MEA performance and degradation provides opportunity to tailor electrode architecture for electrodes with various supports.



Introduction

Conventional cathode catalyst supports are susceptible to corrosion during high potential excursions, high temperature and under start-stop conditions [1]. Hence lack of cathode support durability is a major technical barrier with respect to commercialization of fuel cells for transportation [2]. Oxidation of support leads to detachment of Pt from support, while repeated oxidation and reduction of catalyst leads to dissolution and reprecipitation [3]. The dissolution of platinum is accompanied by penetration of Pt into the membrane or gas diffusion layer, while reprecipitation leads to agglomeration of Pt in the catalyst layer. These lead to an overall decrease in ESA along with non-uniform current density distribution, leading to sintering of Pt catalysts caused by localized heating.

In order to overcome these barriers and meet the DOE technical targets for durability and performance, we have developed new classes of alternative and durable cathode supports, based on modifying the carbon surface by conductive metal oxides [4] such as tin-doped ITO, TiO₂ and SnO₂. Alternate supports such as CNT, graphene sheets, OGMC and GCNT were also investigated to take advantage of their superior properties [5-7]. In addition, conductive metal oxides were also used as an alternative to carbon-based supports. The durability and performance have been enhanced due to the following advantages for our cathode supports [8]:

- Thermodynamic stability of Pt-CMO-carbon triple junction, as shown by ex situ and in situ electrochemical tests and periodic DFT calculations, prevents Pt agglomeration.
- Preference of metal oxide nanoparticles to stay at the carbon defect sites lowers carbon corrosion.
- More uniform dispersion of Pt, allowing better performance at equivalent loading.
- Direct contact of Pt with carbon allows use of low cost conductive and non-conductive stable oxides.

Approach

New classes of carbon supports modified by CMOs have been developed to improve durability and performance of the cathode catalysts. In order to prevent alloy formation, electrocatalysts were synthesized by the chemical reduction method using ethylene glycol [9]. Durability of various carbon supports such as Vulcan XC-72 carbon, multiwalled CNT (referred to as CNT in this report), GCNT, OGMC and graphene were compared. DFT calculations performed in FY 2010 on Pt-ITO-graphene were leveraged to study benefits of CMO-modified GCNT support. Conductivity studies were performed in FY 2011 on hybrid support-Nafion[®] layers to verify electronic percolation through the catalyst layer. Measurements were also done with ITO/Nafion[®] layers to explore pathways for improvement of performance. Various diameters of CNTs were modified with ITO to get a more uniform coating. The effect of functionalization of the nanotubes on activity and stability was also studied.

Non-carbon support synthesis was modified to reflect the need for higher conductivity and higher triple phase boundary length. In FY 2010, for CMO supports, a doubling in performance with no loss in stability was obtained using cetyl trimethyl ammonium bromide (CTAB) surfactant assisted CMO synthesis. In FY 2011, in order to improve electronic conductivity and tailor particle crystallinity and mesoporosity, both hard template and solvothermal annealing methods were used to synthesize ITO support. In FY 2012, further optimization was conducted for ITO synthesis, with increase in mesopore size by 50% to 12 nm to facilitate Nafion[®] electrolyte and gas access to the catalyst site. TiO₂ supports of various shapes were synthesized, and a continuous Pt nanowire network was successfully deposited on TiO₂ nanorod supports, with ESA equivalent to baseline.

As described in earlier reports, the durability was investigated ex situ using an internally developed accelerated test protocol, with voltage stepped from 1.4-0.85 V vs. normal hydrogen electrode. An investigation of the effect of CMO modification of GCNT was conducted. MEA tests were

performed on various supports with and without metal oxide modification, with the fuel cell held at 1.2 V at 80°C, and measurement of ESA, oxygen reduction reaction activity at 0.9 V and polarization curves performed every 20 hours.

Results

In FY 2011, ITO-modified GCNT was found to have 3-4X higher durability than baseline. In FY 2012, various functional groups on CNTs and GCNTs were investigated. No major effect of functional groups on ex situ performance was found. In order to allow use of more cost-effective supports, CNTs of various diameters were modified with ITO to get a more uniform coating. A uniform coating was obtained on 30-50 nm CNTs. Ex situ tests however, did not show significant improvement in activity over prior ITO modified GCNT and CNT. Hence in situ tests were not done for these supported catalysts.

In FY 2011, using hard template synthesis of ITO, the ESA was increased by 12% from 40 to 45 m²/g. However, the activity was low, hence further optimization was done related to ITO synthesis in FY 2012. Using hard-template synthesis, the mesopore size was increased by 50% to 12 nm in order

to facilitate Nafion[®] and reactant access to the catalyst site. Figure 1 a-f show transmission electron microscope (TEM) and scanning transmission electron microscope (STEM) images of 20 wt% Pt loaded onto mesoporous ITO. An ordered ITO structure is obtained, with mesopores in the 10-12 nm range. Ex situ tests showed significant improvement over previous results obtained on ITO supports, with an ESA of 55 m²/g and mass activity of 55 A/g (Figure 1 g, h). Durability tests (ex situ) also showed extremely stable results.

In FY 2012, we also investigated the effect of metal oxide support aspect ratio on performance and durability. TiO₂ nanorods were synthesized by hydrolysis/hydrothermal method. The effect of Pt loading on the TiO₂ support was studied. As seen in Figure 2a, for 20 wt% Pt, Pt nanoparticles were mostly isolated from each other, thus relying on the conductivity of the TiO₂ nanorod support, associated with low ESA. 50% Pt corresponded to a continuous Pt nanowire network around the nanorod (Figure 2b), and led to higher ESA of 55 m²/g. (Figure 2c). However, the mass activity of both samples was low. TiO₂ nanoparticles were subsequently synthesized by surfactant assisted method using CTAB surfactant, with Pt loading at 50 wt%. Figure 3a shows TEM images for these supported catalysts, while Figure 3b

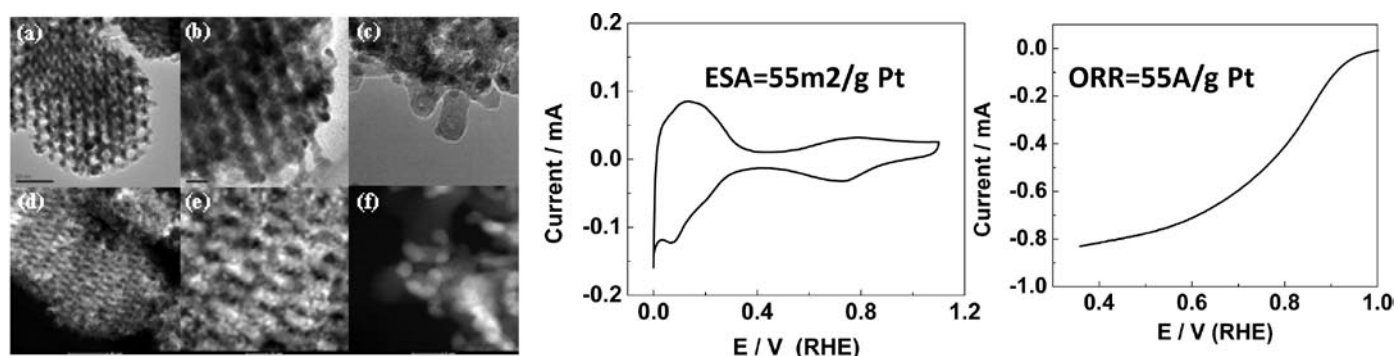


FIGURE 1. TEM and STEM data for Pt/mesoporous ITO: a, b and c) low and high magnification of TEM images; d, e and f) low and high magnification of STEM images; g) ESA, h) oxygen reduction reaction

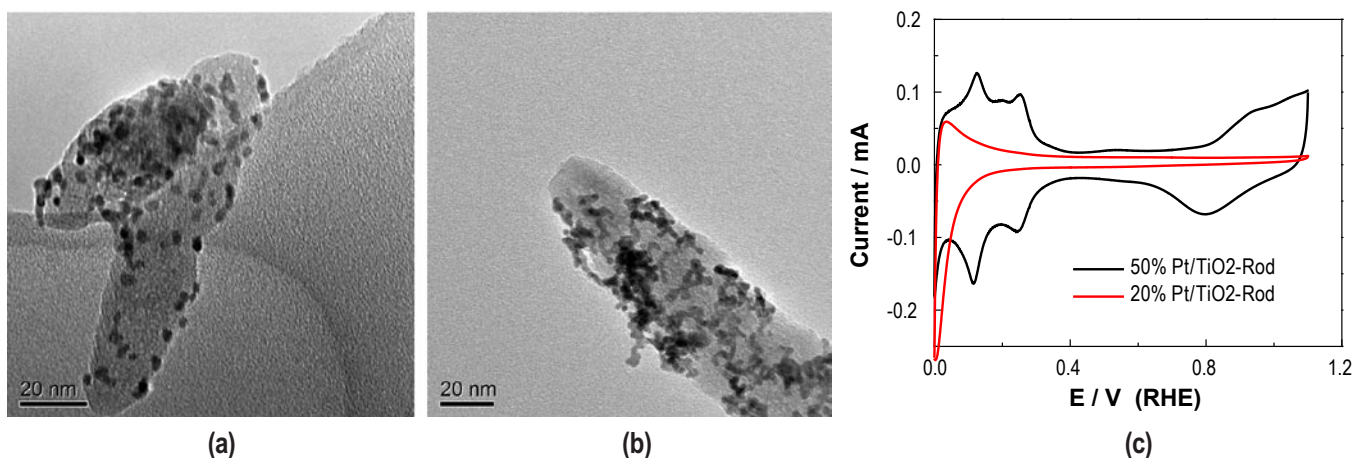


FIGURE 2. Effect of % Pt on TiO₂ nanorod support. (a) 20 wt% Pt, (b) 50 wt% Pt, (c) ESA for 20 wt% and 50 wt% Pt

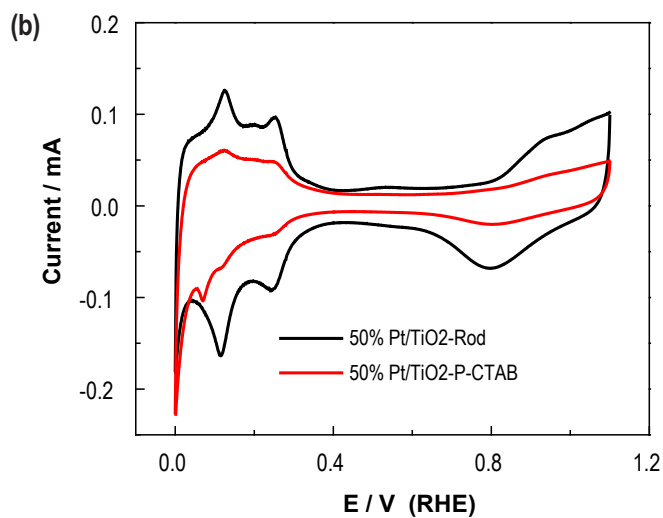
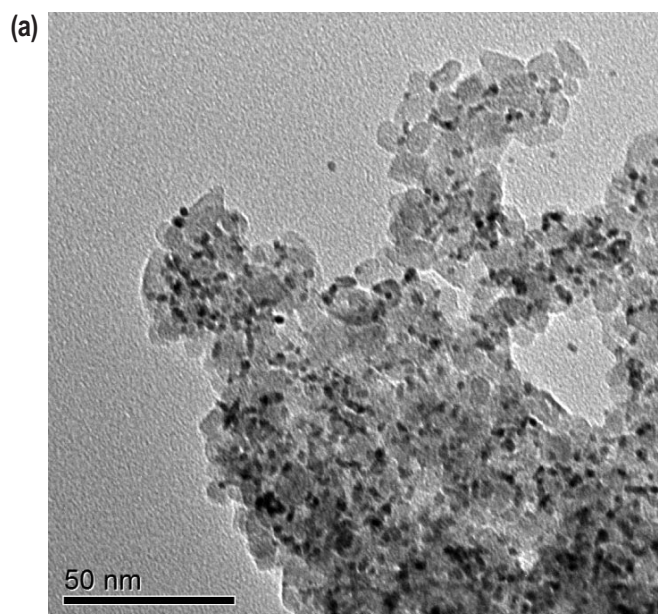


FIGURE 3. Pt supported on CTAB assisted TiO_2 nanoparticles. (a) TEM Pt/ TiO_2 (CTAB), (b) ESA comparison of Pt/ TiO_2 (CTAB) with Pt/ TiO_2 nanorods

shows the performance comparison with 50 wt% Pt on TiO_2 nanorods. The ESA for Pt supported on CTAB assisted TiO_2 was much lower, indicating the influence of synthesis method and morphology on performance.

In FY 2011, Pt/ITO-GCNT was found to be the most durable low carbon support during in situ tests, with >3-4X more stability than the vulcan carbon baseline. In FY 2012, a protocol was successfully developed to increase testing throughput by 5X by increasing the hold potential to 1.4 V.

In situ tests were done on 20 wt% Pt/mesoporous ITO, which yielded 55 m^2/g ESA and 55 mA/g mass activity in ex situ tests as mentioned earlier. For a loading of 0.2 $\text{mg Pt}/\text{cm}^2$ the performance was quite poor, with a high ohmic resistance adversely affecting performance. This was hypothesized as

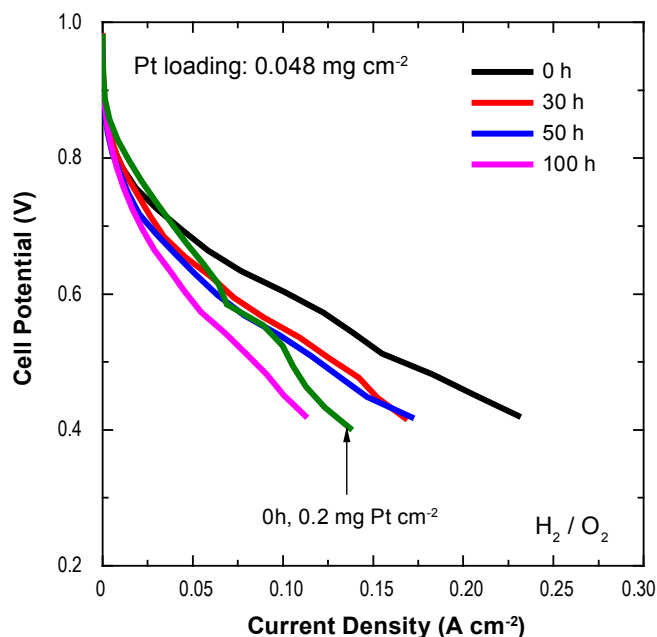


FIGURE 4. Polarization curves at various AST durations for 50 wt% Pt/mesoporous ITO at 0.048 $\text{mg Pt}/\text{cm}^2$, compared with initial polarization curve for 0.2 $\text{mg Pt}/\text{cm}^2$

being due to the catalyst layer being too thick, leading to high electronic resistance of ITO, with the hydrophilicity of the electrode potentially adversely impacting ionic conductivity in the catalyst layer. Adding Teflon[®] to counter ITO hydrophilicity did not help, possibly due to decrease in electronic conductivity. Decreasing Nafion[®] content also lowered performance, thus showing ionic conductivity in the catalyst layer also plays an important role. The Pt loading was decreased by 4X, with significantly improved results as shown in Figure 4. Increasing the Pt wt% in the Pt/ITO is expected to enable thinner catalyst layers and higher electronic conductivity, while increasing ITO conductivity would lower electronic resistance. These options are being investigated to provide an anticipated 4X improvement in performance over the current Pt/ITO results.

Since electrode architecture is clearly important, in FY 2012, fundamental studies on MEA catalyst layer degradation were carried out on Pt/OGMC and Pt/baseline vulcan carbon support. Using a transmission layer model, the catalyst layer ohmic resistance was determined from alternating current (AC) impedance data, flowing N_2 at the cathode [10]. The high frequency resistance was quite stable, indicating absence of membrane degradation from attack by hydroxyl radicals formed by decomposition of hydrogen peroxide in the presence of trace metal contaminants. This was confirmed by the stability of the hydrogen crossover current data over the AST duration. The catalyst layer ionic resistance, while increasing slowly initially, increased at a much higher rate after 100 hours of the AST, accompanied

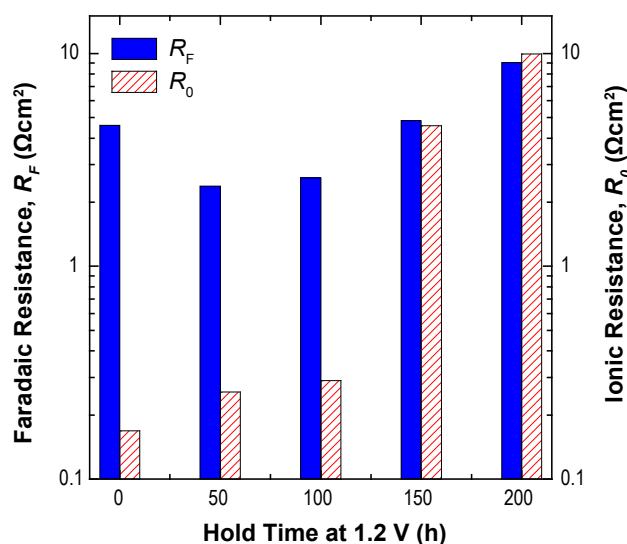


FIGURE 5. Comparison of Faradaic resistance R_F and ionic resistance in the Pt/OGMC cathode catalyst layer R_0 as a function of hold time at 1.2 V.

by an increase in faradaic resistance from AC impedance using air at the cathode at 0.9 V (Figure 5). This indicates that the increase in catalyst layer ohmic resistance plays a major role in the increase of Faradic resistance. The increase in catalyst layer resistance was probably caused by support corrosion and associated increase in contact resistance at the membrane/supported catalyst and supported catalyst/gaseous diffusion layer (GDL) interfaces.

Experiments repeated with vulcan carbon showed a similar increase in catalyst layer resistance with AST duration [11]. With increasing potential hold time, the internal resistance-corrected polarization curves showed a single Tafel slope of 51 mV/decade initially in the 0.001-0.1 A/cm² region, with a second slope of 110-118 mV/decade in the 0.01-0.1 A/cm² region, at higher hold times, with this slope increasing with AST duration. This appears to indicate a mixed kinetic and mass transfer controlled process at high hold times, attributed to increasing presence of oxygen containing functional groups in the support leading to higher hydrophilicity and greater support corrosion. The kinetic overpotential, concentration overpotential in the catalyst layer and concentration overpotential in the GDL microporous layer were extracted from the polarization curves. As seen in Figure 6a, the kinetic overpotential increased very slowly with AST duration, while the concentration overpotential in the catalyst layer and non-catalyst layers jumped at 50 hours and 100 hours respectively. The charge transfer resistance obtained for fresh electrodes from AC impedance at various potentials showed charge transfer resistance (R_{ct}) decreasing with decrease in potential, thus showing no limitations from mass transfer. At 100 hours hold, R_{ct} showed a minimum at 0.75 V and started increasing, due to mass transfer limitations both in the

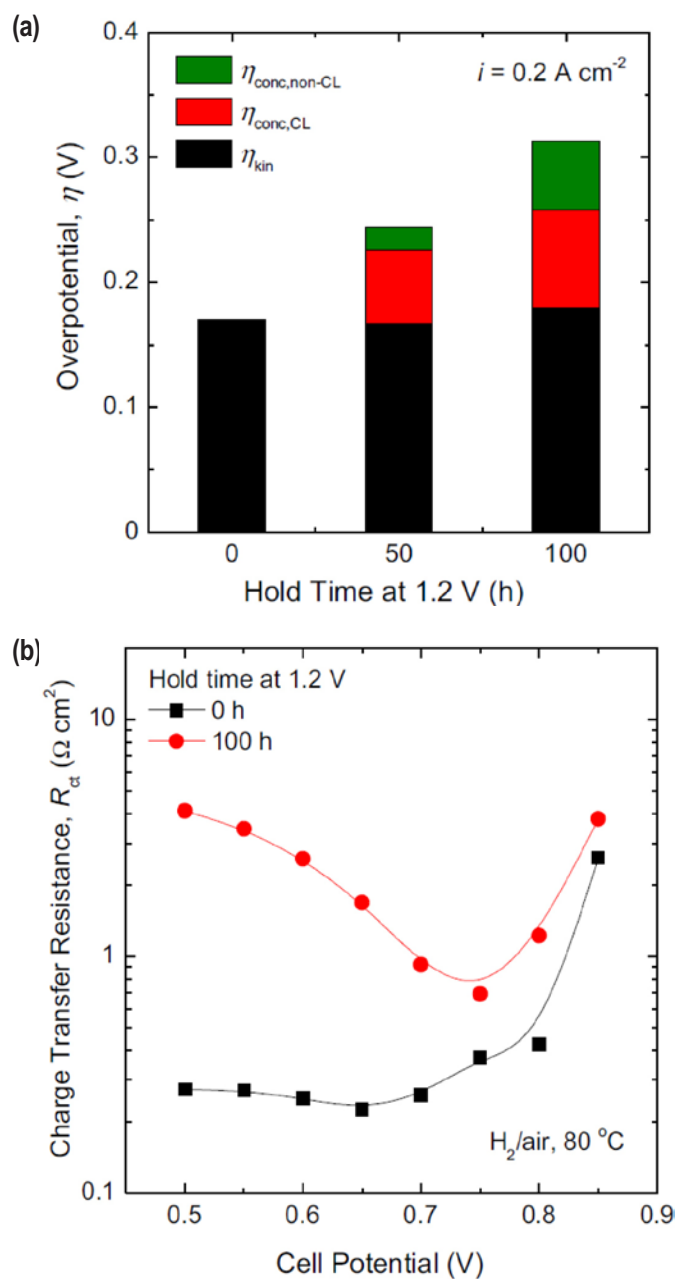


FIGURE 6. Pt/Vulcan carbon AST results (a) kinetic and concentration overpotentials at 0.2 A/cm², (b) R_{ct} from AC impedance using H₂/air at various potentials before and after AST

catalyst layer and in the non-catalyst layer (Figure 6b). Since at 100 hours, mass transport in the non-catalyst layer also is significant, this work shows the importance of tailoring the architecture of the microporous layer to avoid flooding at the catalyst GDL interface. The catalyst layer contribution to increased charge transfer resistance arises from both the increase in catalyst layer ionic resistance and catalyst layer mass transport resistance, thus providing a pathway for MEA architecture optimization for various catalyst supports.

Conclusions and Future Directions

Significant progress has been made in improving supported cathode performance and durability.

- A stable Pt-CMO-carbon triple junction was predicted using periodic DFT calculations and verified experimentally.
- Optimum CMO content was determined for both ex situ and in situ tests to adequately cover the carbon support defect sites and for maximum activity and performance.
- High durability of carbon free CMO support of various aspect ratios, mesoporosity and Pt wt% in support was obtained with ESA similar to vulcan carbon baseline in ex situ tests.
- Pathway was established for improving in situ performance of carbon free support by increasing Pt wt% in the supported catalyst, decreasing catalyst layer thickness and increasing support conductivity.
- Identification of significant contribution of catalyst layer ohmic and ionic resistances to MEA performance and degradation, thus providing insights into electrode architecture optimization.

Ongoing work will involve improving the performance of non-carbon CMO supports by increasing support electronic conductivity, further optimization of mesoporosity within the supports, controlling Pt wt% in the support, and improving MEA formulation for these novel supports by decreasing catalyst layer thickness and adjusting Nafion[®] content. Electrode architecture optimization will also be performed of low carbon CMO modified supports. The completion of these tasks would position this project well for continuation of this work, focusing on:

- CMO modification of inter-connected carbon network with subsequent deposition of a thin continuous Pt film either between CMO particles or on the CMO particles.
- Pt deposition on oriented TiO₂ nanorods with varying Pt/TiO₂ ratio.
- Investigation of other oxides such as SiO₂ nanoparticles and nanowires, CeO₂ and sulfonated ZrO₂.
- Optimization of electrode architecture focusing on thin catalyst layers, catalyst layer porosity and pore size distribution, low Pt loading and Nafion[®] content.

FY 2012 Publications/Presentations

1. S. Park, Y. Shao, H. Wan, V.V. Viswanathan, S. Towne, P.C. Rieke, J. Liu, Y. Wang, “Degradation of the Ionic Pathway in a PEM Fuel Cell Cathode”, *J. Phys. Chem. C* 115 (45) (2011) 22633-22639.
2. S. Park, Y. Shao, V.V. Viswanathan, J. Liu, and Y. Wang, “Non-Kinetic Losses Caused by Electrochemical Carbon Corrosion in PEM Fuel Cells”, *Int. J. Hydrogen. Energy* 37 (2012) 8451-8458.

3. Kou R, Y Shao, D Mei, Z Nie, D Wang, CM Wang, VV Viswanathan, SK Park, IA Aksay, Y Lin, Y Wang, and J Liu. 2011. “Stabilization of Electrocatalytic Metal Nanoparticles at Metal-Metal Oxide-Graphene Triple Junction Points.” *Journal of the American Chemical Society* 133(8):2541-2547. doi:10.1021/ja107719u.
4. S. Park, Y. Shao, V.V. Viswanathan, J. Liu, and Y. Wang, “Irreversible Losses in a PEM Fuel Cell during Accelerated Stress Test of Catalyst Support”, 221st Meeting of The Electrochemical Society, 6–10 May, Seattle, WA, USA.
5. S. Park, Y. Shao, H. Wan, V.V. Viswanathan, J. Liu, and Y. Wang, “Development of novel electrocatalyst support in proton exchange membrane fuel cells for automotive applications”, 2011 AIChE annual meeting, 16–21 October 2011, Minneapolis, MN, USA.

References

1. K.H. Kangasniemi, D.A. Condit, and T.D. Jarvi, “Characterization of Vulcan Electrochemically Oxidized under Simulated PEM Fuel Cell Conditions”, *J. Electrochem. Soc.*, **151** (4) E125-E132 (2004).
2. R. Borup *et al.*, “Scientific Aspects of Polymer Electrolyte Fuel Cell Durability and Degradation”, *Chem. Rev.* **107** 3904-3951 (2007).
3. Y. Shao, G. Yin, and Y. Gao, “Understanding and Approaches for the Durability Issues of Pt-based Catalysts for PEM Fuel Cell”, *J. Power Sources* **171** 558-566 (2007).
4. G. Chen, S.R. Bare, and T.E. Mallouk, “Development of Supported Bifunctional Electrocatalysts for Unitized Regenerative Fuel Cells”, *J. Electrochem. Soc.*, **149** (8) A1092-A1099 (2002).
5. Y. Shao, J. Liu, Y. Wang and Y. Lin, “Novel catalyst support materials for PEM fuel cells: current status and future prospects” *J. Mat. Chem.*, **19** 46-59 (2009).
6. R. Kou, Y. Shao *et al.*, Enhanced activity and stability of Pt catalysts on functionalized graphene sheets for electrocatalytic oxygen reduction”, **11** 954-957 (2009).
7. S. Park, Y. Shao, H. Wan, P.C. Rieke, V.V. Viswanathan, S.A. Towne, L.V. Saraf, J. Liu, Y. Lin, Y. Wang, “Design of graphene sheets-supported Pt catalyst layer in PEM fuel cells”, *Electrochem. Commun.* **13** (2011) 258-261.
8. Kou R, Y Shao, D Mei, Z Nie, D Wang, CM Wang, VV Viswanathan, SK Park, IA Aksay, Y Lin, Y Wang, and J Liu. 2011. “Stabilization of Electrocatalytic Metal Nanoparticles at Metal-Metal Oxide-Graphene Triple Junction Points.” *Journal of the American Chemical Society* 133(8):2541-2547. doi:10.1021/ja107719u .
9. W.Z. Li, C.H. Liang, W.J. Zhou *et al.*, Preparation and characterization of multiwalled carbon nanotube-supported platinum for cathode catalysts of direct methanol fuel cells”, *J. Phys. Chem. B*, **107** (26) 6292-6299 (2003).
10. S. Park, Y. Shao, H. Wan, V.V. Viswanathan, S. Towne, P.C. Rieke, J. Liu, Y. Wang, “Degradation of the Ionic Pathway in a PEM Fuel Cell Cathode”, *J. Phys. Chem. C* 115 (45) (2011) 22633-22639.
11. S. Park, Y. Shao, V.V. Viswanathan, J. Liu, and Y. Wang, “Non-Kinetic Losses Caused by Electrochemical Carbon Corrosion in PEM Fuel Cells”, *Int. J. Hydrogen. Energy* 37 (2012) 8451-8458.

V.E.1 Polymer Electrolyte Fuel Cell Lifetime Limitations: The Role of Electrocatalyst Degradation

Deborah J. Myers (Primary Contact),
Xiaoping Wang, Nancy Kariuki, Tammi Nowicki,
Stacy DeCrane, Ram Subbaraman, Rajesh
Ahluwalia, and Srikanth Arisetty

Argonne National Laboratory (ANL)
9700 S. Cass Avenue
Lemont, IL 60439
Phone: (630) 252-4261
Email: dmyers@anl.gov

DOE Manager

HQ: Nancy Garland
Phone: (202) 586-5673
Email: Nancy.Garland@ee.doe.gov

Subcontractors:

- Johnson Matthey Fuel Cells, Sonning Commons, United Kingdom
Sarah Ball, Jonathan Sharman, Brian Theobald, Stephen Thorpe, Alex Martinez, Elvis Christian, and Graham Hards
- United Technologies Research Center, East Hartford, CT
Mallika Gummalla, Zhiwei Yang, and Steve Zhitnik
- Massachusetts Institute of Technology, Boston, MA
Yang Shao-Horn and B.H. Han
- University of Texas at Austin, Austin, TX
Paulo Ferreira, Shreyas Rajasekhara, Daniel Groom, Stephanie Matyas, Somaye Rasouli, and Kang Yu; Jeremy Meyers, Preethi Mathew, and Seok Koo Kim
- University of Wisconsin-Madison, Madison, WI
Dane Morgan, James Gilbert, and Brian Puchala

Project Start Date: October 1, 2009

Project End Date: September 30, 2012

Fiscal Year (FY) 2012 Objectives

- Quantify and understand the role of Pt-Co alloy composition and acid leaching of these alloys in the degradation of polymer electrolyte membrane fuel cell (PEMFC) performance,
- Establish dominant catalyst and cathode degradation mechanisms for Pt, Pt-Co alloys, and Pt₃Sc,
- Identify key properties of catalysts and catalyst supports that influence and determine their degradation rates,
- Quantify the effect of cell operating conditions, load profiles, and type of electrocatalyst on the performance degradation,

- Determine operating conditions and catalyst types/structures that will mitigate performance loss and allow PEMFC systems to achieve the DOE lifetime targets.

Technical Barriers

This project addresses the following technical barriers from the Fuel Cells section of the Fuel Cell Technologies Program Multi-Year Research, Development and Demonstration Plan:

- (A) Durability
- (B) Cost
- (C) Performance

Technical Targets

The Argonne-led team is conducting fundamental studies of platinum-based PEMFC cathode electrocatalyst degradation mechanisms. Insights gained from these studies can be applied toward the definition of operating conditions to extend PEMFC lifetimes and to the development of cathode electrocatalyst materials that meet the following DOE 2015 electrocatalyst durability targets with voltage cycling:

- 5,000 hours ($\leq 80^\circ\text{C}$) and 5,000 hours ($> 80^\circ\text{C}$)
- $\leq 40\%$ loss of initial catalytic mass activity after 30,000 cycles between 0.6 and 1.0 V
- < 30 mV loss at 0.8 A/cm² after 30,000 cycles between 0.6 and 1.0 V

FY 2012 Accomplishments

- Prepared Pt/alternative carbons, Pt/C with different levels of Cl impurities. Fabricated and tested membrane electrode assemblies (MEAs) of Pt_xCo_(1-x), acid-leached Pt_xCo_(1-x), Pt₃Sc, and various Pt/C.
- Established relationship between loss of electrochemically-active surface area (ECA), mass activity, and particle size for Pt and Pt alloys.
- Determined that the operating parameters of upper potential limit and anodic sweep rate have the most significant impact on cell degradation.
- Established most significant factors governing cycling-induced changes in catalyst particle size distribution (PSD) and ECA loss.



Introduction

One of the primary challenges facing the development of PEMFCs for automotive and stationary power applications is the durability of the fuel cell materials, especially the Pt-based cathode catalyst. The project's primary focus is elucidation of the effects of cathode catalyst and support physicochemical properties and cell operating conditions on the rates and mechanisms of cathode catalyst degradation. The results of this project will define the operating conditions and catalyst types/structures that will mitigate performance loss and allow PEMFC systems to achieve the DOE lifetime targets.

Approach

The project approach is to identify the degradation modes and factors contributing to cathode catalyst degradation by utilizing: (1) systematic cell degradation tests, (2) in situ and ex situ structural characterization of the catalysts, (3) fundamental out-of-cell studies, and (4) theoretical atomistic and macroscopic kinetic and transport modeling. The catalysts studied are benchmark Pt on carbon supports with varying properties, Pt alloys, acid-leached Pt alloys, and 3M's Pt-based nano-structured thin film catalysts. In the experimental aspects of the project, we utilize accelerated stress tests of membrane-electrode assemblies (MEAs) containing various catalysts and supports and in situ and ex situ dissolution, microscopic, structural, and chemical characterization of these catalysts, which are input into the catalyst and cell models. These measurements provide complementary information and, in the case of the aqueous studies, information such as catalyst component dissolution rates, that are not accessible in the MEA environment.

The goal of the project is to elucidate the effects of catalyst physicochemical properties on catalyst and cell performance degradation by systematically varying these properties (particle size, catalyst oxophilicity, catalyst type, surface area of carbon support, and effect of catalyst impurity). The effects of the various properties are decoupled by either controlling or carefully determining the catalyst particle size and particle size distributions.

Results

The focus of this year's effort has been on determining the effects of potential profile on Pt catalysts, compositional studies of Pt-Co alloy catalysts, cell studies of Pt₃Sc, effects of acid leaching and dissolution studies of Pt-Co alloys, dissolution studies of 3M's Pt NSTF catalyst, Kinetic Monte Carlo-based modeling of Pt-Co alloys, and modeling of PSD and ECA evolution.

Four cycling profiles sweeping between 0.6 and 1.0 V with 16 s periods were applied to MEAs containing a 3.2 nm

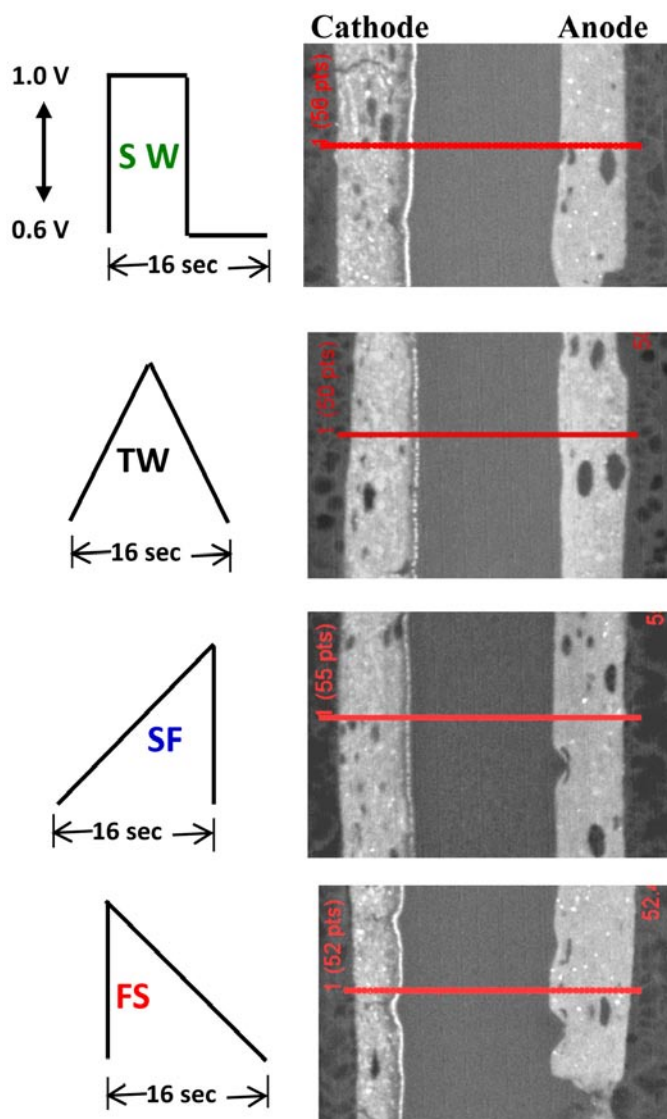


FIGURE 1. Potential profiles applied to MEAs containing the 3.2 nm mean diameter Pt cathode catalyst and SEMs of cross-sections of the MEAs after application of 10,000 of the respective cycles. These images show that the amount of Pt in the membrane (bright vertical band near the cathode) is highest for the SW and FS profiles.

mean diameter Pt catalyst. These profiles, illustrated in Figure 1, were square wave (SW), triangle wave (TW), 25 mV/s anodic sweep and a cathodic step to 0.6 V denoted slow/fast (SF), and a step to 1.0 V and a 25 mV/s sweep back to 0.6 V denoted fast/slow (FS). After 10,000 cycles, these four MEAs were cross-sectioned and analyzed for Pt content in the membrane using scanning electron microscopy (SEM) and electron microprobe analysis. The trends of performance loss on air, ECA loss, oxygen reduction reaction (ORR) mass activity (MA) loss, and amount of Pt in the membrane were found to be $SW \cong FS \gg TW \cong SF$. The anodic sweep rate had the most impact on the rates of performance, ECA, and MA loss and on the amount of Pt found in the membrane (Figure 1).

Catalysts were prepared containing 40 wt% Pt₃Co nanoparticles with a mean diameter of 5.6 nm and 35 wt% PtCo with a mean diameter of 4.1 nm on high-surface-area Ketjen black carbon support (Pt₃Co/C and PtCo/C). These materials were acid treated by soaking in 80°C 0.5 M H₂SO₄ for two days. The resulting catalysts are designated AL Pt₃Co and AL PtCo and were found to have Pt:Co atomic ratios of 80:20 and 71:29, respectively. These catalysts were incorporated into the cathodes of MEAs and subjected to the DOE cycling protocol (0.6 to 1.0 V, 50 mV/s). Following fabrication, an MEA containing the non-acid-leached Pt₃Co was also acid-treated (AT Pt₃Co) for comparison with both the as-prepared Pt₃Co MEA and the MEA prepared from AL Pt₃Co. Cell diagnostics of cathode catalyst ECA, ORR MA, and air and oxygen polarization curves were performed after 1,000, 3,000, 5,000, 10,000, and 30,000 voltage cycles. Studies were also performed on the effect of various fuel cell operating parameters (relative humidity [RH]), temperature, cycling profile, and upper potential limit) on the degradation of the cathode electrocatalyst performance with MEAs containing the AL Pt₃Co and AL PtCo and an AT Pt₃Co MEA.

The initial low current density oxygen and high current density air performances of MEAs containing all the catalysts studied in this project are summarized in Figure 2. Specific to the studies performed this year, this figure shows that: (1) AL PtCo has lower initial ORR activity than AL Pt₃Co, but comparable initial performance on air at high current densities, (2) catalyst leaching and MEA acid treatment decrease the ORR activity of the Pt₃Co catalyst, resulting in ~10 mV lower MEA O₂ performance (at 0.8 A/cm²), and (3) acid leaching of Pt₃Co and acid treatment of the Pt₃Co MEA increases the H₂/Air performance at high currents (~25-30 mV at 1.5 A/cm²) due to a decrease in the resistance to proton transport in the cathode. Figure 2 also summarizes the effect of potential cycling using the DOE protocol. It was found that ECA, MA, ORR specific activity (SA, activity per square centimeter of ECA), and O₂ performance decay trends are the same for Pt₃Co, AL Pt₃Co, and AT Pt₃Co. Acid-leached PtCo shows the highest loss of both ORR activity and air performance. Parametric studies on these catalysts showed that Pt₃Co, as compared to AT Pt₃Co and AL Pt₃Co, has a greater decay in high current density performance when subjected to 0.4 V to 0.95 V SW cycling. This was attributed to a higher increase in resistance to proton transport in the cathode. However, acid leaching of Pt₃Co did not affect the decay trends of ECA, MA, SA, and performance with cycling. For all catalysts, cycling to 1.05 V, rather than 0.95 V, had the most detrimental impact on ORR activity and air performance of all cell operating conditions tested. Lower RH on the cathode (30% RH versus 100% RH) decreased this degradation.

A summary of the ECA and ORR MA losses of all the cathode catalysts studied in this project when subjected to 10,000 cycles of the DOE protocol (0.6 to 1.0 V, 50 mV/s

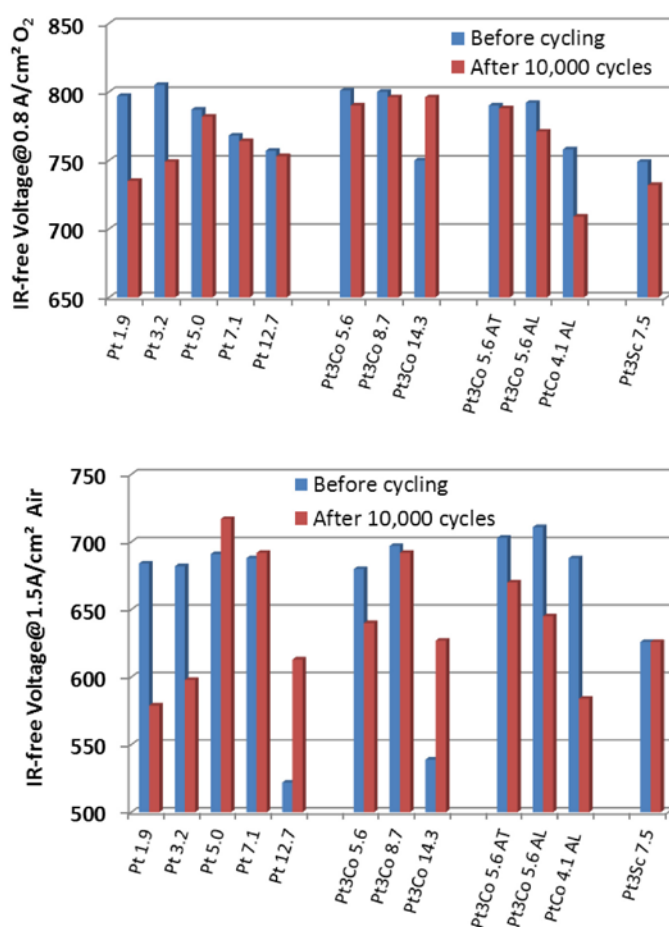


FIGURE 2. Initial and post-cycling low current density oxygen and high current density air performances of MEAs containing all the catalysts studied in this project. Cycling profile: 0.6 to 1.0 V, 50 mV/s triangle.

triangle) in the MEA environment is shown in Figure 3. This plot shows that all catalysts fall along the same trendline of loss versus initial particle size, irrespective of the catalyst composition, indicating that this is the dominant factor controlling cycling-induced catalyst losses.

This year's effort in the ex situ characterization tasks included TEM and anomalous small-angle X-ray scattering (ASAXS) analyses of the Pt₃Co MEAs after 30,000 DOE protocol cycles. These analyses, summarized in Figure 4, showed that cycling decreases the fraction of smaller particles in the PSDs and increases the fraction of larger particles, which increases the tailing of the PSDs toward larger particle sizes. The extent of growth in the mean particle size and the extent of changes in the PSDs increased with decreasing initial Pt₃Co particle size, as was reported last year for the Pt catalysts.

The in situ characterization task included a study of the 3.2 nm Pt in an MEA using ASAXS. This catalyst was subjected to 1,500 square wave cycles between 0.4 to 1.05 V (20 s period). The ASAXS-derived Pt PSDs (Figure 5)

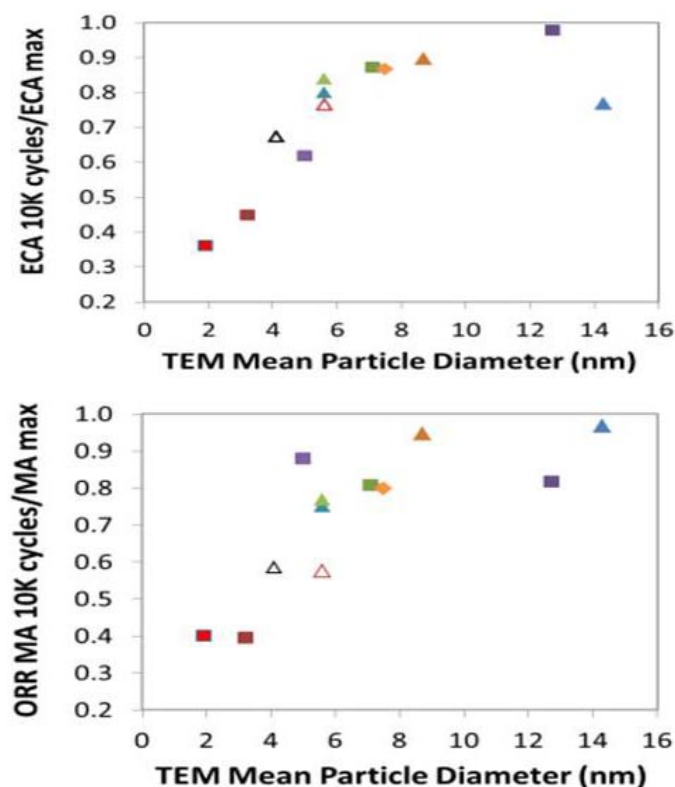


FIGURE 3. Fraction of ECA (top) and ORR MA (bottom) remaining after 10,000 DOE protocol cycles as a function of initial mean diameter of the catalysts. Squares: Pt, Triangles: Pt₃Co, Hollow triangles: Acid-leached Pt₃Co, Hollow black triangle: Acid-leached PtCo, Diamond: Pt₃Sc.

illustrate that the main impact of cycling on the PSD in the MEA environment is loss of particles <3.7 nm in diameter, with a minor contribution from an increase in the number of particles >3.7 nm. Comparison of ECA losses to the changes in geometric surface area calculated from the SAXS data illustrate that the catalyst lost geometric surface area even while the ECA was increasing during the initial cycling (i.e., during the well-known MEA conditioning period).

In the fundamental out-of-cell studies task, the effect of potential and particle size on the steady-state dissolved concentration of Pt and Co in perchloric acid electrolyte was determined for the Pt₃Co catalysts (5.6, 8.7, and 14.3 nm). These studies, illustrated in Figure 6, showed that: (1) the steady-state dissolved Pt concentration increases with decreasing mean particle size, as was observed for Pt catalysts, (2) the loss of cobalt from catalyst is potential independent at potentials >0.85 V and <~1.0 V corresponding with the potential region with decreased platinum dissolution, (3) the fraction of total cobalt leached from catalyst decreases with increasing particle size corresponding with decreased fraction of total cobalt on the surface and in the sub-surface layer of the particle, and (4) the largest loss of cobalt is observed during electrode preparation and wet-up.

In the theoretical task of the project, the model for Pt cyclic voltammetry and Pt dissolution under steady-state and cycling conditions was further refined using additional Pt dissolution data and oxide coverage as a function of Pt particle size. The model assumes formation of a non-ideal solid solution between Pt and Pt oxide and that this oxide decreases the surface activity of Pt and thus the concentration of dissolved Pt. The kinetics for oxide formation were determined using cyclic voltammetry experiments and were utilized to model the effects of potential cycling rates, upper potential limits, and lower potential limits on the loss of Pt due to dissolution and on Pt re-deposition. The resulting model was utilized to calculate the evolution of the PSD and ECA with number of DOE protocol potential cycles (shown in Figure 7 for the 3.2 nm Pt catalyst). It was determined that the experimental ECA losses cannot be explained solely on the basis of Pt dissolution or change in PSD due to preferential dissolution of smaller particles and re-deposition on larger particles. It was necessary to include particle coalescence due to Pt re-deposition between particles and not particle migration to accurately model the ECA loss data.

In the atomistic modeling tasks of the project, a Kinetic Monte Carlo model was further developed to determine the effect of initial alloy composition, particle size, and potential on the extent of Pt and base metal loss from the particles and the effect on particle size and shape. The Kinetic Monte Carlo model predicts rapid de-alloying of Pt_{1-x}Co_x nanoparticles at $x > 0.35$ and that the maximum retention of Co in the particles, and thus maximum retention of ORR activity, is achieved with initial Co concentrations near this value.

Conclusions and Future Directions

The major conclusions from this work are:

- The predominant catalyst physicochemical property in defining the extent of ECA and ORR activity loss of Pt and Pt alloy nanoparticle catalysts induced by potential cycling is the initial size of the catalyst particles.
- The operating parameters of upper potential limit and anodic sweep rate have the most significant impact on cathode performance degradation.
- Acid leaching of Pt-Co alloys decreases the initial ORR activity, but increases high current density fuel cell performance due to loss of Co and increase in proton conductivity in cathode, respectively.
- The best overall cathode catalyst performance and performance durability with cycling of all catalysts studied in this project was achieved for the Pt₃Co catalyst with initial mean particle size of ~8.5 nm. This catalyst achieves the DOE cathode catalyst durability targets of ≤40% loss of initial catalytic mass activity and <30 mV loss at 0.8 A/cm² after 30,000 cycles between 0.6 and 1.0 V (24% and 14 mV, respectively).

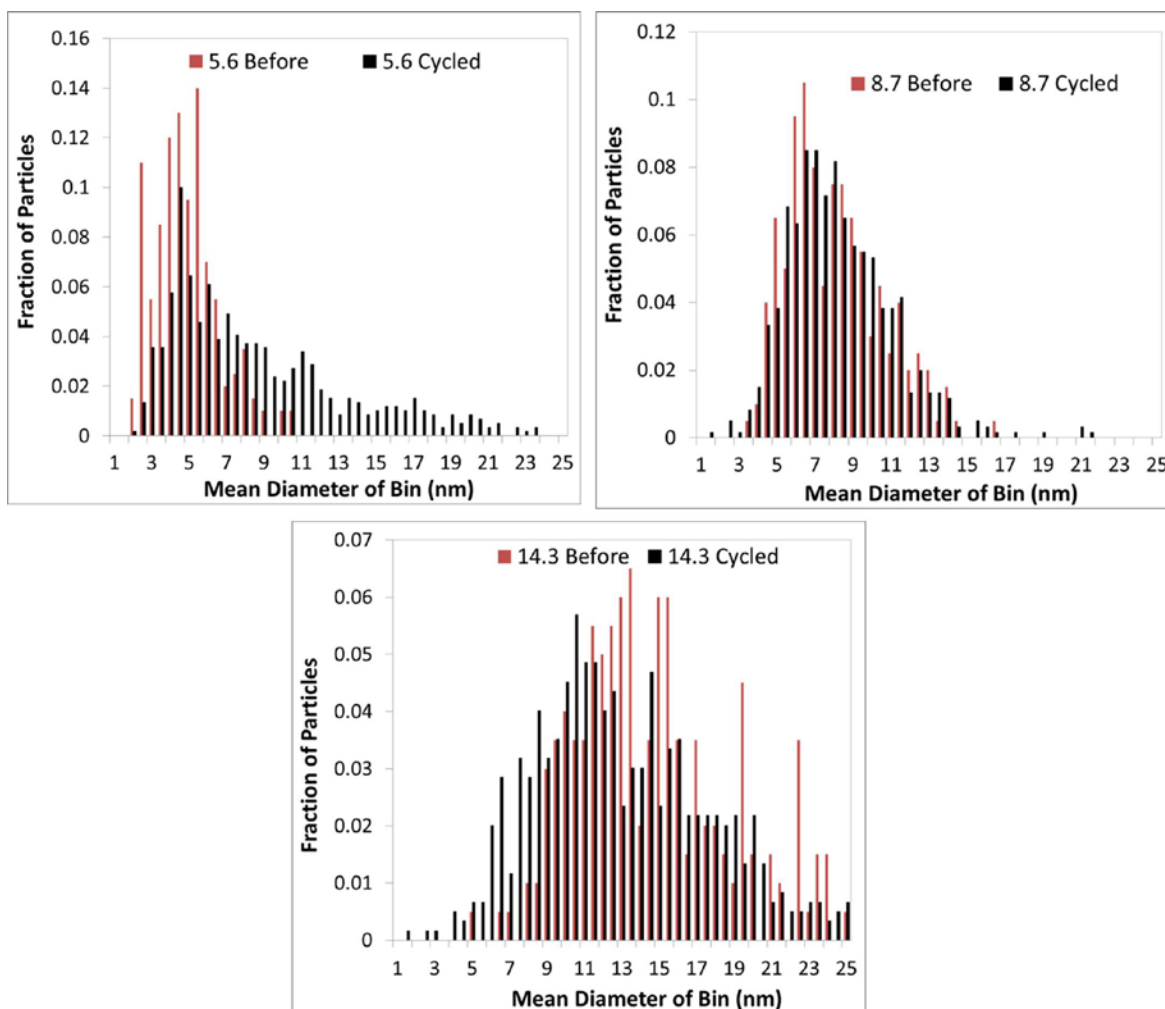


FIGURE 4. PSDs, determined using TEM characterization, of the three Pt_3Co catalysts with initial mean diameters of 5.6, 8.7, and 14.3 nm before and after 30,000 DOE protocol cycles.

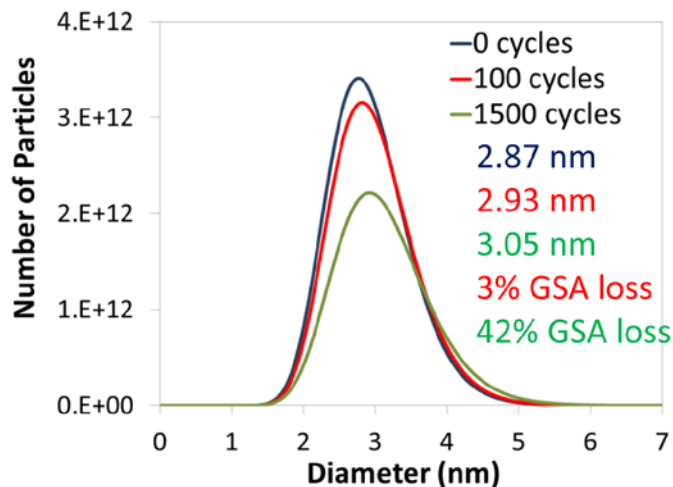


FIGURE 5. PSDs, determined using ASAXS, of a Pt catalyst with nominal initial mean diameter of 3.2 nm, during DOE protocol cycling in an MEA.

- The most significant factors governing cycling-induced change in PSD and ECA loss are competition between Pt dissolution and oxide formation and coalescence of particles via Pt re-deposition.
- Kinetic Monte Carlo modeling indicates that the maximum retention of Co in $\text{Pt}_{1-x}\text{Co}_x$ nanoparticles, and thus maximum retention of ORR activity upon exposure to the MEA environment, is achieved with initial Co concentrations (x) near 0.35.

Future plans for the remainder of this project are:

- Prepare, characterize, and test MEAs containing Pt-Ni catalysts; characterize and test MEAs containing Pt/alternative carbons and Pt/Ketjen carbon with Cl impurities.
- Complete analysis of ASAXS and XAFS data for Pt and Pt_3Co MEAs.

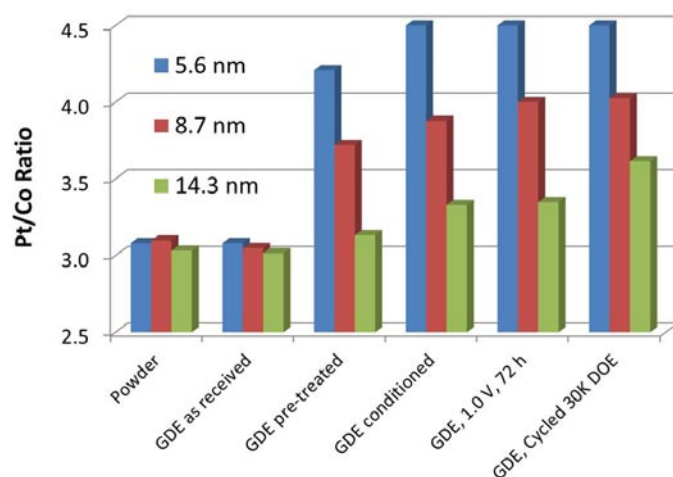
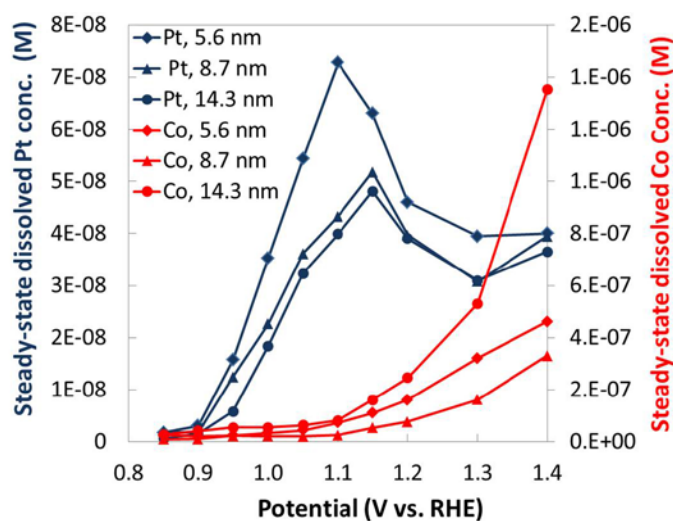


FIGURE 6. Potential dependence of the steady-state dissolved Pt and Co concentrations in perchloric acid electrolyte for the three Pt₃Co catalysts. Evolution of the Pt to Co atomic ratio with electrode preparation stages. GDE pre-treated: soaking in room temperature water; Conditioning: potential cycling from 0.05 to 1.1 V, 15-20 cycles; 1.1 V, 72 h: held for 72 h in room temperature perchloric acid electrolyte.

- Study the effect of temperature on extent of oxide formation and on dissolution.

FY 2012 Publications/Presentations

Publications

1. Z. Yang, S. Ball, D. Condit, M. Gummalla, "Systematic Study on the Impact of Pt Particle Size and Operating Conditions on PEMFC Cathode Catalyst Durability", *J. Electrochem. Soc.*, 158 (11), B1439-B1445 (2011).
2. D.J. Groom, S. Rajasekhara, S. Matyas, Z. Yang, M. Gummalla, S. Ball, P.J. Ferreira, "Influence of Pt Catalyst Nanoparticle Size on the Electrochemical Performance of PEM Fuel Cells", *Electrochem. Soc. Trans.*, 41 (1) 933-936 (2011).

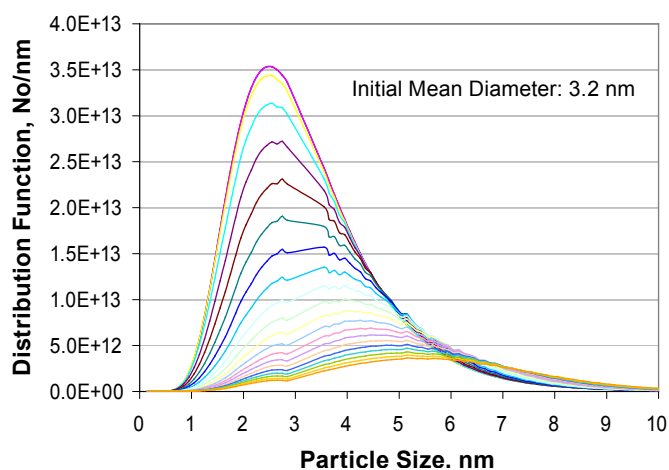


FIGURE 7. Modeled evolution of the PSD of 3.2 nm mean diameter Pt with DOE protocol cycling.

3. D. Myers, J. Gilbert, X. Wang, N. Kariuki, S. Niyogi, A.J. Kropf, D. Morgan, S. Ball, J. Sharman, B. Theobald, and G. Hards, "In situ X-ray absorption and scattering studies of PEMFC cathode electrocatalysts", *Prep. Pap.-Am. Chem. Soc., Div. Fuel Chem.*, 57 (1), 414-416, (2012).
4. J.A. Gilbert, N.N. Kariuki, R. Subbaraman, A.J. Kropf, M.C. Smith, E.F. Holby, D. Morgan, and D.J. Myers, "In-situ Anomalous Small Angle X-Ray Scattering Studies of Platinum Nanoparticle Fuel Cell Electrocatalyst Degradation", *J. Am. Chem. Soc.*, 134, 14823-14833 (2012).
5. B. Puchala, S.-K. Lin, L. Wang, D. Morgan, "PEMFC Nanoparticle Dealloying from Kinetic Monte Carlo Simulations", *Electrochem. Soc. Trans.*, accepted.
6. J. Gilbert, N. Kariuki, A.J. Kropf, D. Morgan, D. Myers, S. Ball, J. Sharman, B. Theobald, G. Hards, "In Situ Anomalous Small-Angle X-ray Scattering Study of Fuel Cell Catalyst Degradation in Aqueous and Membrane Electrode Assembly Environments", *Electrochem. Soc. Trans.*, accepted.

Presentations

1. R. Subbaraman, X. Wang, X. Wang, N.Kariuki, D.Myers, and R.K. Ahluwalia, "Ex-situ Potentiostatic and Potentiodynamic Durability of Low Pt Loading fuel cell MEAs", 220th Electrochemical Society Meeting, Boston, MA, Oct. 9 -14, 2011.
2. D.J. Groom, S. Rajasekhara, S. Matyas, Z. Yang, M. Gummalla, S. Ball, P.J. Ferreira, "Influence of Pt Catalyst Nanoparticle Size on the Electrochemical Performance of PEM Fuel Cells", 220th Electrochemical Society Meeting, Boston, MA, Oct. 9-14, 2011.
3. E. Holby, S.-K. Lin, B. Puchala, L. Wang, D. Morgan, "Modeling Pt and Pt-alloy Degradation in PEMFC Cathodes", DOE Fuel Cell Technologies Program Durability Working Group Meeting", Boston, MA, Oct. 13, 2011. [Invited]
4. X. Wang, D. Myers, and N. Kariuki, "Investigation of PEMFC Electrocatalyst Degradation", IEA-AFC Annex 22 Fall 2011 Workshop, Jülich, Germany, December 12-13, 2011.

- 5.** D. Myers, J. Gilbert, X. Wang, N. Kariuki, S. Niyogi, A.J. Kropf, Dane Morgan, Sarah Ball, Jonathan Sharman, Brian Theobald, and Graham Hards, “In situ X-ray absorption and scattering studies of PEFC cathode electrocatalysts”, 243rd American Chemical Society National Meeting and Exposition, San Diego, CA, March 25–29, 2012. [Invited]
- 6.** D.J. Myers, J.A. Gilbert, N.N. Kariuki, X. Wang, A.J. Kropf, S. Niyogi, M.C. Smith, and D. Morgan, S.C. Ball, J. Sharman, B. Theobald, E. Christian, and G. Hards, “In Situ Anomalous Small Angle X-ray Scattering and X-ray Absorption Studies of Fuel Cell Catalysts”, 221st Electrochemical Society Meeting, Seattle, WA, May 6–10, 2012. [Invited]
- 7.** P.J. Ferreira, “Seeing Small: Enabling new discoveries in Li-ion batteries and Fuel Cells Through Advanced Transmission Electron Microscopy”, G-COE Special Lecture, Kyushu University, Japan, June 12, 2012.
- 8.** X. Wang, D. Myers, N. Kariuki, S. DeCrane, T. Nowicki, S. Arisetty, and R. Ahluwalia, “Polymer Electrolyte Fuel Cell Lifetime Limitations: The Role of Electrocatalyst Degradation”, IEA-AFC Annex 22 Spring 2012 Workshop, Daejeon, Korea, June 21–22, 2012.
- 9.** P.J. Ferreira, “Seeing Small: Enabling new discoveries in Energy Materials Through Advanced Transmission Electron Microscopy”, HVEM Seminar, Kyushu University, Japan, June 24, 2012.
- 10.** D. Morgan, Y.-L. Lee, B. Puchala, L. Wang, and S.-K. Lin, “Atomistic-Based Approaches For Modeling Activity and Degradation in Fuel Cell Catalysts”, 244th American Chemical Society National Meeting and Exposition, Philadelphia, PA, August 19–23, 2012. [Invited]
- 11.** D. Morgan, B. Puchala, E. Holby, Y. Shao-Horn, L. Wang, S.-K. Lin, J. Gilbert, and D. Myers, “Computational Studies of Fuel Cell Electrocatalysts”, Gordon Research Conference on Fuel Cells, Smithfield, RI, August 5–10, 2012. [Invited]
- 12.** D. Morgan, B. Puchala, E. Holby, Y. Shao-Horn, L. Wang, S.-K. Lin, J. Gilbert, and D. Myers, “Evolution of Pt and Pt-Alloy Nanoparticles under PEMFC Conditions: Insights from Modeling”, Energy Materials Center at Cornell Annual Energy Materials Symposium, Ithaca, NY, USA, August 10, 2012. [Invited]

V.E.2. Durability Improvements through Degradation Mechanism Studies

Rod Borup¹ (Primary Contact),
Rangachary Mukundan¹, Yu Seung Kim¹,
Christina Johnston¹, Dusan Spornjak¹,
Joe Fairweather¹, John Davey¹, Roger Lujan¹,
David Langlois¹, Nathan Mack¹, Bo Li¹,
Rajesh Ahluwalia², Xiaohua Wang²,
Adam Weber³, Ahmet Kusoglu³,
Karren More⁴, Mike Brady⁴, Sylvia Wessel⁵,
Paul Beattie⁵, Greg James⁵, Daniel Ramrus⁵,
Svetlana Loif⁶, Warren Williams⁵, Steve Grot⁶,
Kateryna Artyushkova⁷, Plamen Atanasov⁷,
Anant Patel⁷, Dan Hussey⁸, David Jacobson⁸,
Gaël Maranzana⁹, Adrien Lamibrac⁹, Jérôme Dillet⁹,
Sophie Didierjean⁹, Olivier Lottin⁹

¹Los Alamos National Laboratory (LANL)
MS D429, P.O. Box 1663
Los Alamos, NM 87545
Phone: (505) 667-2823
Email: Borup@lanl.gov

DOE Manager

HQ: Nancy Garland
Phone: (202) 586-5673
Email: Nancy.Garland@ee.doe.gov

Subcontractors and Collaborators:

- ² Argonne National Lab, Argonne, IL
- ³ Lawrence Berkeley National Lab, Berkeley, CA
- ⁴ Oak Ridge National Laboratory, Oak Ridge, TN
- ⁵ Ballard Power Systems, Burnaby, BC, Canada
- ⁶ Ion Power, New Castle, DE
- ⁷ University of New Mexico, Albuquerque, NM
- ⁸ National Institute of Standards and Technology, Gaithersburg, MD
- ⁹ Nancy-Université, Lorraine, France

Start Date: October 2009
Project End Date: 2013

Fiscal Year (FY) 2012 Objectives

- Identify and Quantify Degradation Mechanisms
 - Degradation measurements of components and component interfaces
 - Elucidation of component interactions, interfaces, operation leading to degradation
 - Development of advanced in situ and ex situ characterization techniques
 - Quantify the influence of inter-relational operation between different components

- Identification and delineation of individual component degradation mechanisms
- Understand Electrode Structure Impact - Applied Science Subtask
 - Better understand the electrode structural and chemical effects on durability
 - Understand impact of electrode structure on durability and performance
 - Correlate different electrode structures to fuel cell performance and durability
 - Define different fabrication effects (esp. solvents) for high durability electrode structures
- Develop Models Relating Components and Operating Conditions to Fuel Cell Durability
 - Development of individual degradation models of individual fuel cell components
 - Development and dissemination of an integrated comprehensive model of cell degradation
- Methods to Mitigate Degradation of Components
 - New components/properties, designs, operating conditions

Technical Barriers

This project addresses the following technical barriers from the Fuel Cells section of the Fuel Cell Technologies Program Multi-Year Research, Development and Demonstration Plan:

- (A) Durability
- (B) Cost

Technical Targets

- Transportation Durability: 5,000 hours (with cycling)
 - Estimated Start/Stop cycles: 17,000
 - Estimated Frozen cycles: 1,650
 - Estimated Load cycles: 1,200,000
- Stationary Durability: 40,000 hours
 - Survivability: Stationary -35°C to 40°C
 - Cost (25 \$/kW_e)

FY 2012 Accomplishments

- Detailed the catalyst degradation mechanism and dependency on loading
- Examined electrode structural changes for different electrode structures and processing techniques for low-loaded cathodes

- Measured chemical changes in catalyst layer ionomer and detailed differences between different types of ionomer
- Quantified carbon corrosion for different types of carbon and different operating parameters
- Modeled the parametric effects on carbon corrosion
- Identified carbon structural changes and localized corrosion
- Measured and modeled hydrogen crossover effect due to Pt particle migration into the membrane
- Measured and quantified surface chemistry changes of carbon bipolar plates
- Conducted parametric studies on metal bipolar plates and examined corrosion rates and increases in contact resistance



Introduction

The durability of polymer electrolyte membrane (PEM) fuel cells is a major barrier to the commercialization of these systems for stationary and transportation power applications [1]. By investigating component and cell degradation modes, defining the fundamental degradation mechanisms of components and component interactions, new materials can be designed to improve durability. To achieve a deeper understanding of PEM fuel cell durability and component degradation mechanisms, we have assembled a multi-institutional and multi-disciplinary team with significant experience investigating these phenomena.

Approach

Our approach to understanding durability and degradation mechanisms within fuel cells is structured in three areas: fuel cell testing (life testing, accelerated stress tests [ASTs], ex situ aging), characterization of component properties as a function of aging time, and modeling (component aging and integrated degradation modeling). The modeling studies tie together what is learned during component characterization and allow better interpretation of the fuel cell studies. This approach and our team give us the greatest chance to increase the understanding of fuel cell degradation and to develop and employ materials that will overcome durability limitations in fuel cell systems. This work is also being coordinated with other funded projects examining durability through a DOE Durability Working Group.

Results

Correlating Electrode Structure to Durability

We have demonstrated that the solvents used can have a dramatic effect on the performance/durability of fuel cell electrodes, although the catalyst durability is unaffected. Examining the effect of loading on performance from membrane electrode assemblies (MEAs) made via decal process using a more traditional water/alcohol/glycerol mixture in the ink shows that the loading has a significant impact. Figure 1 shows the polarization performance during the potential cycling AST for Pt loadings of 0.25, 0.11 and 0.05 mg/cm². The electrochemical surface area (ECSA) change was similar for the different catalyst loadings at -55%, -56% and -74%, respectively. However, the performance change is substantially different. During potential cycling:

- The ultra-low loading cathode (0.05 mg/cm²) increased in performance
- The “*high*” loading (0.25 mg/cm²) decreased in performance
- The “*low*” loading (0.11 mg/cm²) stayed the same

The fact that the ECSA shows similar decreases during the potential cycling indicates that other changes in performance are occurring. Further measurements show that the mass transport resistance is decreasing during the potential cycling. Enhanced performance and impedance behavior of ultra-low loading cathode with potential cycling have similarity with performance improvement with HelOx (or air flow increase). Thus, electrode structural changes occur during potential cycling which favor oxygen diffusion, and lower mass transport resistance.

Noble Metal Loading Effect on Degradation Mechanism

Figure 2 shows how platinum particle size changes during accelerated testing of the catalyst and catalyst support for two different catalyst loadings. The MEAs for the two different ASTs (potential cycling from 0.6–1.0 V in Figure 2a, carbon corrosion AST hold at 1.2 V in Figure 2b) had identical loadings of 0.2 mg/cm² (20 wt% Pt) and 0.4 mg/cm² (40 wt% Pt). The Pt particle size distribution (PSD) growth is identical for the potential cycling AST from ~1.8 nm to ~2.2 nm (Figure 2a). This indicates that dissolution/re-precipitation particle-growth kinetics is unaffected by Pt particle concentration. However after a carbon support AST, greater Pt coarsening for the cathode with higher Pt loading is observed, showing that an increased concentration of Pt particles led to higher degree of agglomeration (Figure 2b). This demonstrates that rate of platinum agglomeration depends upon the relative loading; more particle agglomeration occurs at high Pt loadings.

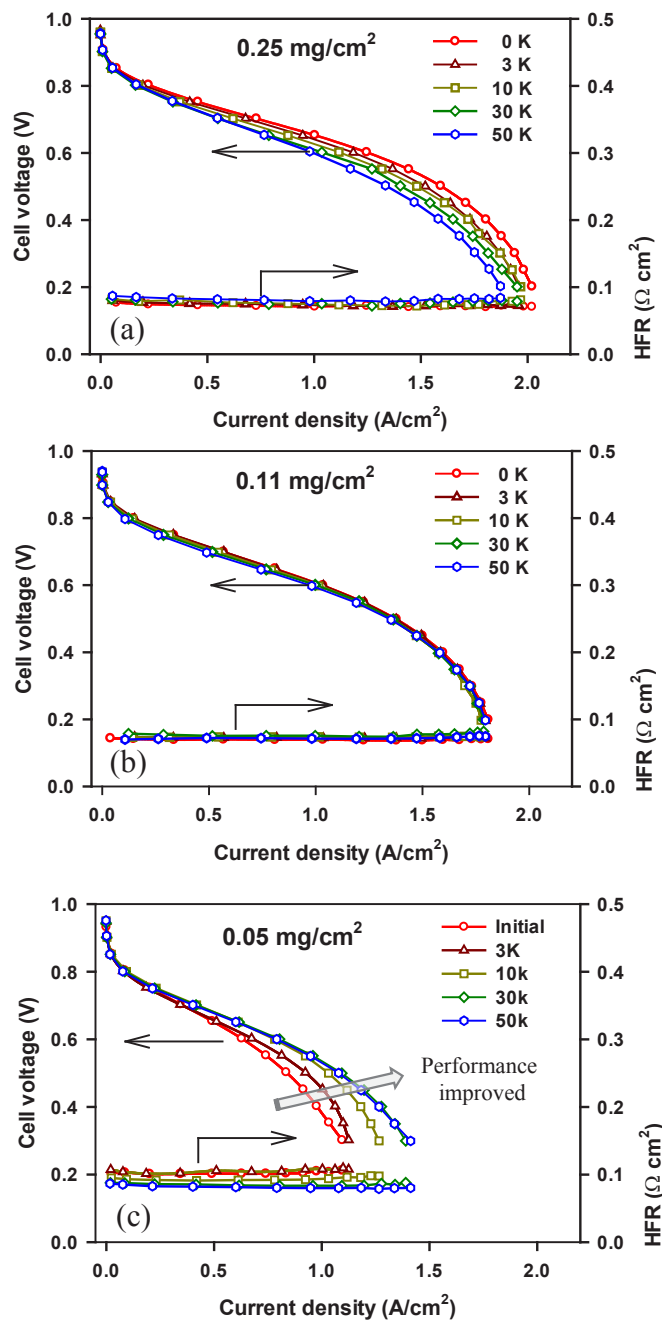


FIGURE 1. The polarization performance during potential cycling from 0.6–1.0 V for (a) 0.25 (b) 0.11 and (c) 0.05 mg-Pt/cm² cathode loadings. Anode: 0.2 mg-Pt/cm². Membrane: Nafion® 212; Cell: 80°C, 30 psig backpressure. Typical LANL decal process using water/alcohol/glycerol mixture in the ink.

Kinetics of Carbon Corrosion: Experimental Measurements and Model Development

Support corrosion leads to detachment and agglomeration of catalyst particles, while weakening of the carbon structure allows collapse of electrode pores and severely limits gas transport [1]. This report includes a summary of ongoing experimental work to improve existing

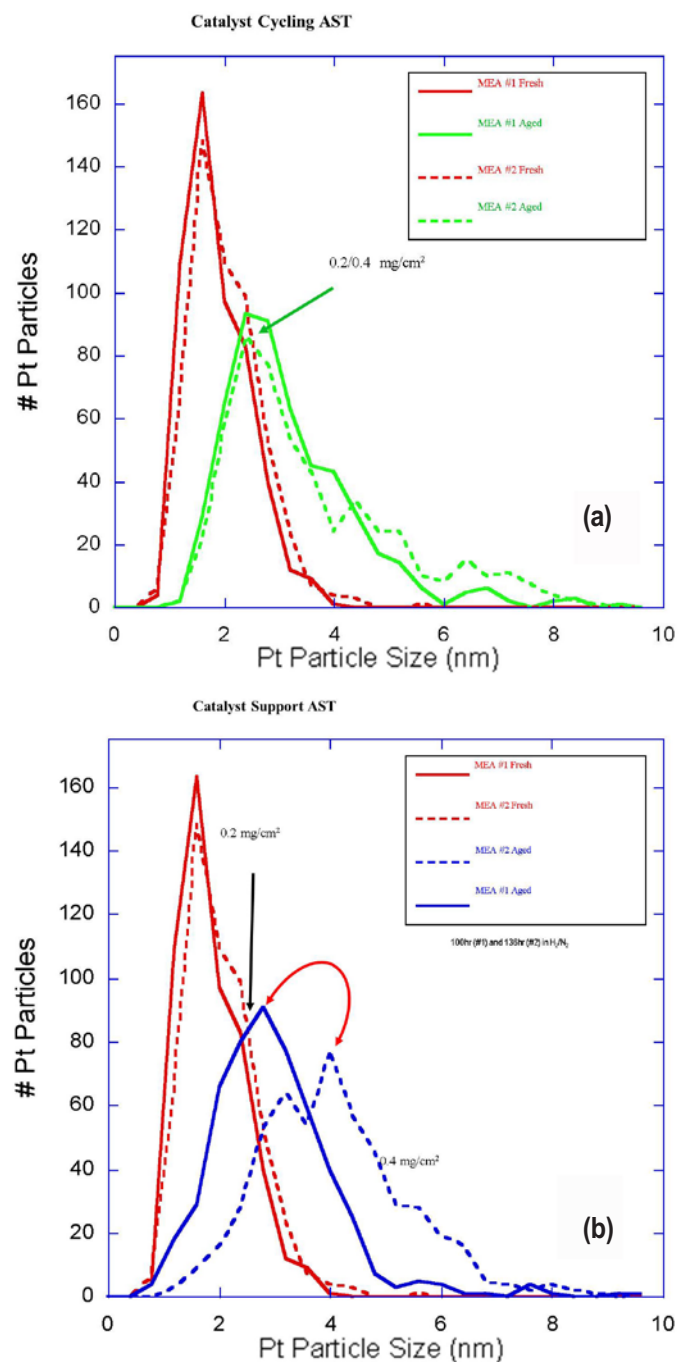


FIGURE 2. Platinum particle size distribution. (A) Pt PSD before and after 30,000 0.6-1.0 V cycles (B) Pt PSD before/after 1.2 V hold. Loadings of 0.2 mg/cm² (20 wt% Pt) and 0.4 mg/cm² (40 wt% Pt).

models through inclusion of electrode aging effects. Some clarification will also be offered on the decay of corrosion rates over time under potentiodynamic conditions.

To illustrate typical observed oxidation patterns, potentiodynamic corrosion rates of two different electrodes are shown in Figure 3. Several features for the high surface area support are labeled: we use the peak naming convention

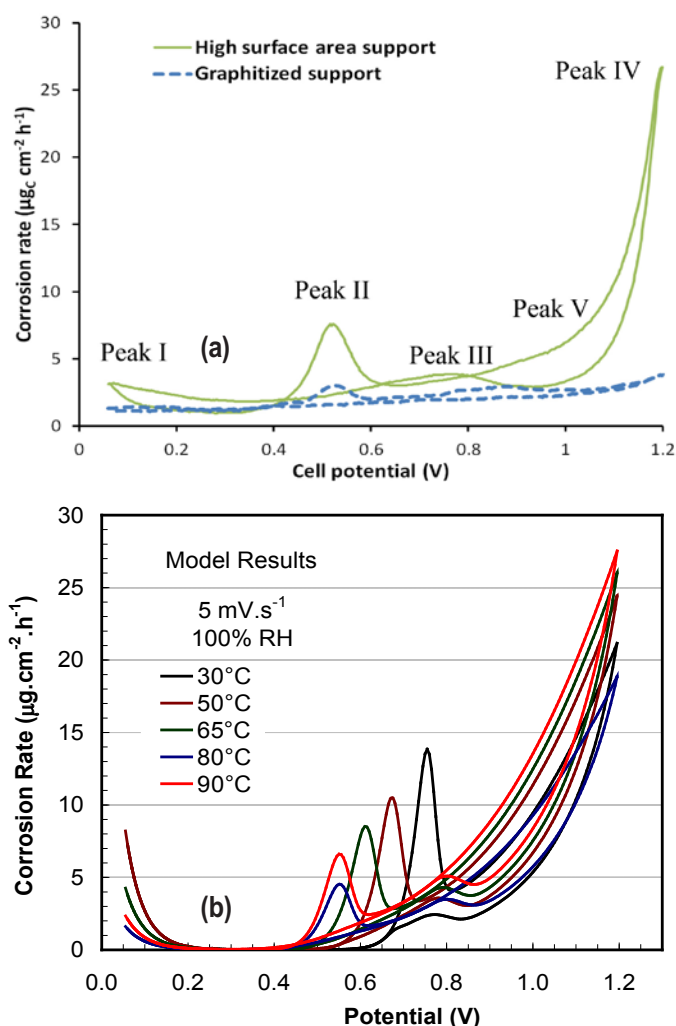
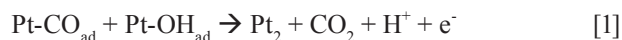
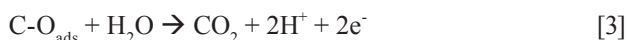
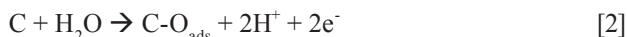


FIGURE 3. (a) Corrosion behavior during potential cycling for two different electrodes, calculated from CO₂ emissions. The mechanisms for peaks I-V are explained in the text. Cycle: 0.06 to 1.2 V vs. reference hydrogen electrode @ 5 mV/s. (b) model results predicting the effect of temperature on the carbon corrosion.

of Maass et al. [2] to describe such plots. Starting with the anodic sweep, peak II is closely related to CO stripping from Pt, or at least CO-like surface species oxidizing in close proximity to Pt.



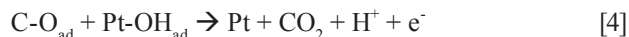
Peak IV is the Tafel-region electrochemical oxidation of carbon, increasing exponentially with overpotential.



Peak V, which initially appears as a shoulder to Peak IV and becomes prominent for aged electrodes (2), is thought to represent the oxidation of accumulated surface oxides, or

equation 3 alone. Switching to the cathodic sweep, Peak III is similarly associated with surface oxides, likely catalyzed by the reduction of Pt oxides below 0.9 V. Peak I is thought to be due to the formation of hydrogen peroxide from trace oxygen, and subsequent chemical attack on carbon.

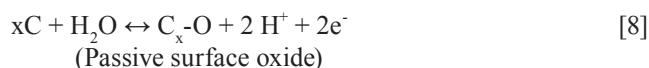
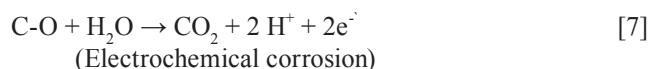
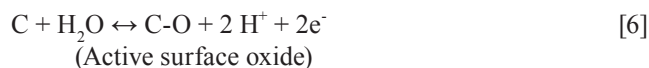
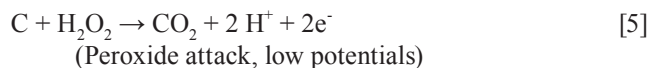
The role of Pt in corrosion rates has been of special interest. CO₂ release at high potentials is generally faster in the presence of Pt [2-4], and this is thought to be due to the catalyzing role of Pt surface oxides:



However, most of the evidence for corrosion catalysis is under potentiodynamic conditions. For long holds at constant high potential, the effect may be much smaller [5]. Peaks II and III only appear on catalyzed electrodes [3], and definitely involve Pt in the CO₂ release. Peak I, meanwhile, is much smaller when Pt is present [2], likely due to accelerated chemical decomposition of peroxide.

Figure 3a shows the durability advantage of using a graphitized carbon support vs. a high surface area carbon. The corrosion rate in all potential ranges is reduced, most crucially in the exponential range (Peak IV). The penalty from using a graphitized support comes from increased materials cost (from the additional high temperature treatments required), and lower initial performance due to lower Pt electrochemical surface area. Experimental measurements have examined different parameters on the carbon corrosion reaction including cell temperature, scan rate and relative humidity.

The Initial Model for Corrosion of High Surface Area Carbon considers:



The model development predicts the effect of cell temperature, showing at higher temperatures, Peak I shifts to lower potentials and decreases in magnitude; Peak IV corrosion rate also increases. Modeling results of the effect of temperature on the carbon corrosion are shown in Figure 3b. At higher scan rates, the corrosion rates are generally higher and the curves lose their fine structure (Peaks II and III disappear). In agreement with equations 5-8, the corrosion rates are higher for higher relative humidity.

Carbon Corrosion shows Localized Structure Changes

Corrosion of catalyst-support carbon leads to numerous changes in the catalyst layer (CL): pore space collapse (lower porosity of the CL), lower electro-active surface area, lower catalyst connectivity, and less hydrophobic pore surface (2). Ex situ characterizations were performed to evaluate morphological changes in the catalyst layer and the gas diffusion layer (GDL) after operation. A surprising result observed by transmission electron microscopy (shown in Figure 4a) is the distinct interface between Pt/high surface area carbon cathode and micro-porous layer (MPL); the MPL carbon retains its meso-graphitic structure and porous network (even adjacent to the cathode surface) whereas the high surface area carbon directly at the interface is fully oxidized and loses its meso-graphitic structure.

In the absence of an MPL, the Pt/C cathode catalyst layer degrades faster due to higher water content during potential holds [5], exhibiting higher kinetic losses, faster Pt particle growth, and faster decrease of the active surface area. In the presence of an MPL, performance degradation is slower, however some cells suffered from mass-transport issues.

Influence of the cathode MPL on the cell degradation rate was investigated by aging cells in situ at 1.3 V (H_2/N_2) with GDL materials with and without an MPL, where two cathode CL materials were compared using (i) commercial carbon-supported Pt MEA supplied by W. L. Gore, and (ii) carbon-free MEA (Pt black). The X-ray tomography shown in Figure 4b illustrates a dramatic non-uniform cathode thinning due to the GDL fibers and water content of the structure, which is not observed for similar measurements for GDLs with MPLs.

Conclusions

Catalyst, support and electrode durability remain primary degradation modes. Measurements show that the degradation is dependent upon the electrode structure, which changes during durability tests, at least in some cases improving transport faster than the kinetics degrade. In other cases, the loading changes the Pt degradation mechanism from primarily dissolution/re-precipitation to include Pt particle agglomeration during support corrosion.

The structure of the support itself changes and is dependent upon the local environment. Loss of meso-graphitic structure of carbon is observed inside the catalyst layer, but not immediately adjacent in the GDL/MPL. The rates of degradation are dependent on many operating parameters including temperature and water content. Some of these were examined by parametric studies, and degradation modeling has modeled the various parameters in different sub-component models. These sub-component models are being integrated to develop an overall model to predict the

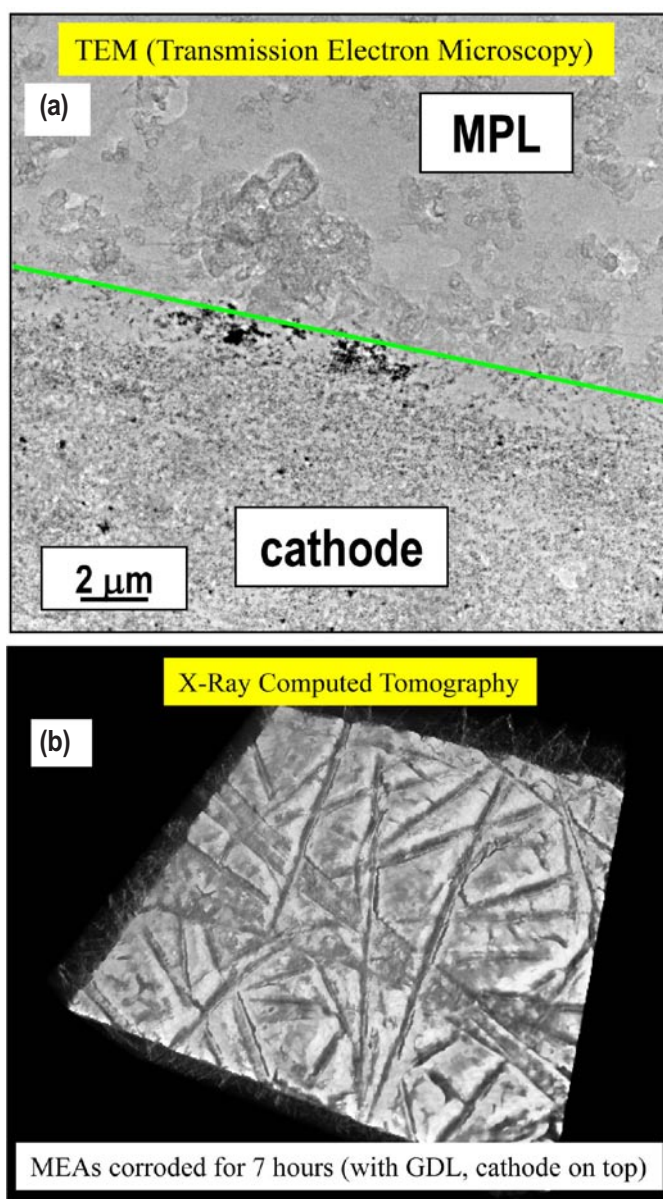


FIGURE 4. (a) Transmission electron micrograph of the MEA/GDL interface after fuel cell testing (b) X-ray tomography of the cathode surface of an MEA tested with a GDL with no MPL layer by a constant 1.3 V AST.

performance degradation of fuel cells with various materials and operating parameters.

Future Directions

Identify and Quantify Degradation Mechanisms

- Continue examination of MEA materials to better define degradation mechanisms
 - Expand mixed hydrocarbon and PFSA materials for unambiguous chemical analysis

Electrode Structure

- Identify structural change of electrodes during potential cycling and operation
- Identify causes behind ionomer and solvent impact on MEA durability
 - Establish correlation of electrode structure durability to mechanical strength

Start-Up/Shut-Down (SU/SD)

- Series segmented cell SU/SD measurements comparing catalyst support materials
- Compare CO₂ during SU/SD to 1.2 V AST holds
- Compare the degradation mechanisms from the SU/SD to the ASTs

Carbon Corrosion

- Characterize corrosion rates of carbon supports with higher degree of graphitization during the aging process
- Measure and model the effect of aging on carbon corrosion rates:
 - Initial observations: high surface area carbon dropped by ~90%, carbon mass decreased by ~47%, yet the cell capacitance increased and the carbon corrosion rate did not slow down
- Measure and model the effects of carbon corrosion on growth of Pt particles, loss in ECSA and mass transfer overpotentials
- Define the hysteresis and age effect on carbon degradation (i.e. degradation rates: new vs. aged samples)

Component Interactions

- Metal bipolar plate evaluation and evaluation of interactions with MEA/GDL
 - Fuel cell testing of metal materials to correlate corrosion rate to metal cation contamination of membrane and proton conduction
- Composite (graphite) bipolar plate evaluation
 - Standardize surface evaluation improving data consistency to evaluate surface properties

Modeling

- Incorporate parametric studies of components into integrated model
- Water profile modeling during carbon corrosion comparing overpotential and hydrophobicity changes to water transport

FY 2012 Publications/Presentations

Journal Publications

1. Arisetty, S.; Wang, X.; Ahluwalia, R.K.; Mukundan, R.; Borup, R.; Davey, J.; Langlois, D.; Gambini, F.; Polevaya, O.; Blanchet, S., **Catalyst Durability in PEM Fuel Cells with Low Platinum Loading**, Journal of the Electrochemical Society (2012), 159(5), B455-B462.
2. Arisetty S., X. Wang, R. Ahluwalia, R. Mukundan, R. Borup, J. Davey, D. Langlois, F. Gambini, O.Y. Polevaya, and S. Blanchet, **Effect of Platinum Loading on Catalyst Stability under Cyclic Potentials**, ECS Trans. 41 (1), 797 (2011).
3. Fairweather J.D., D. Spornjak, R. Mukundan, J. Spendelow, K. Artyushkova, P. Atanassov, D.S. Hussey, D.L. Jacobson, and R. Borup, **Interaction of Heat Generation, MPL, and Water Retention in Corroded PEMFCs**, ECS Trans. 41 (1), 337 (2011).
4. Mishler, Jeffrey; Wang, Yun; Mukherjee, Partha P.; Mukundan, Rangachary; Borup, Rodney L., **Subfreezing operation of polymer electrolyte fuel cells: Ice formation and cell performance loss**, Electrochimica Acta (2012), 65, 127-133.
5. Mishler, Jeffrey, Yun Wang, Rangachary Mukundan, Jacob Spendelow, Daniel S. Hussey, David L. Jacobson, Rodney Borup, **Probing the Water Content in Polymer Electrolyte Fuel Cells Using Neutron Radiography** Electrochimica Acta, 75 (2012) 1-10.
6. Spornjak, Dusan, Joseph Fairweather, Rangachary Mukundan, Tommy Rockward, Rodney L. Borup, **Influence of the microporous layer on carbon corrosion in the catalyst layer of a polymer electrolyte membrane fuel cell**, Journal of Power Sources 214 (2012) 1-13.
7. Spornjak D., J.D. Fairweather, T. Rockward, R. Mukundan, and R. Borup, **Characterization of Carbon Corrosion in a Segmented PEM Fuel Cell**, ECS Trans. 41 (1), 741 (2011).
8. Chlistunoff J., J.R. Davey, K.C. Rau, R. Mukundan, and R.L. Borup, **PEMFC Gas Diffusion Media Degradation Determined by Acid-Base Titrations**, Submitted to ECS.
9. Dillet J., A. Lamibrac, G. Maranzana, S. Didierjean, O. Lottin, J. Durst, F. Maillard, L. Dubau, M. Chatenet D. Spornjak, J. Fairweather, R. Mukundan, R.L. Borup **Internal Currents, CO₂ Emissions and Decrease of the Pt Electrochemical Surface Area during Fuel Cell Start-Up and Shut-Down**, Submitted to ECS.
10. Fairweather J.D., D. Spornjak, R. Mukundan, R.K. Ahluwalia, S. Arisetty, R.L. Borup, **Time Resolved Corrosion of Electrode Supports in PEM Fuel Cells**, Submitted to ECS.
11. Mukundan, Rangachary, Greg James, Dana Ayotte, John Davey, David Langlois, Dusan Spornjak, Dennis Torracco, Sivagaminathan Balasubramanian, Adam Z Weber, Karren More, and Rodney L. Borup **Accelerated testing of carbon corrosion and membrane degradation in PEM fuel cells**, Submitted to ECS.
12. Hussey, D.S., D. Spornjak, A.Z. Weber, R. Mukundan, J. Fairweather, E.L. Brosha, J. Davey, J.S. Spendelow, D.L. Jacobson, R.L. Borup, **Accurate Measurement of the Through-Plane Water Content of Proton-Exchange Membranes Using Neutron Radiography**, Submitted to Journal of Applied Physics.

Invited Presentations

1. Borup, Rod & Nancy Garland, **LANL Fuel Cell Program**, International Hydrogen Energy Development Forum 2012, Kyushu University, Fukuoka, Japan / January 29 – February 3, 2012.
2. Borup, Rod et al., **Electrode Degradation Mechanisms in PEM Fuel Cells**, 2nd INTERNATIONAL WORKSHOP ON DEGRADATION ISSUES OF FUEL CELLS, Thessaloniki, Greece 21–23 SEPTEMBER, 2011.
3. Borup, Rod et al., **Effects of Fuel and Air Impurities on PEM Fuel Performance**, 2nd INTERNATIONAL WORKSHOP ON DEGRADATION ISSUES OF FUEL CELLS, Thessaloniki, Greece 21–23 SEPTEMBER, 2011.
4. Borup, Rod et al., **Durability Improvements Through Degradation Mechanism Studies**, FC Tech Team, Detroit MI, September 14, 2011.
5. Borup, Rod et al., **Durability Improvements Through Degradation Mechanism Studies**, DOE Fuel Cell Technologies Annual Merit Review, Arlington, Va, May 9–13, 2012.
6. Borup, Rod et al., **LANL Fuel Cell Activities and Electrode Degradation Mechanisms in PEM Fuel Cells, Invited Seminar**, Nancy-Université, Lorraine, France, Nov 7, 2011.
7. Borup, Rod et al., **LANL Fuel Cell Activities and Electrode Degradation Mechanisms in PEM Fuel Cells, Invited Seminar**, CEA (Commissariat à l'énergie atomique), Grenoble, France Nov 9, 2011.

Contributed Presentations

1. Fairweather J.D., D. Spornjak, R. Mukundan, J. Spendelow, K. Artyushkova, P., D.S. Hussey, D.L. Jacobson, and R. Borup, **Interaction of Heat Generation, MPL and Water Retention in Corroded PEMFCs**, 220th ECS Meeting - Boston, MA, Oct. 9 – Oct. 14, 2011.
2. Mukundan R., G. James, J. Davey, D. Langlois, D. Torracco, W. Yoon, A.Z. Weber, and R. Borup, **Accelerated Testing Validation**, 220th ECS Meeting - Boston, MA, Oct. 9 – Oct. 14, 2011.
3. Spornjak D., J.D. Fairweather, T. Rockward, R. Mukundan, and R. Borup, **Characterization of Carbon Corrosion in a Segmented PEM Fuel Cell**, 220th ECS Meeting - Boston, MA, Oct. 9 – Oct. 14, 2011.
4. Gambini F., O.Y. Plevaya, S. Blanchet, R. Mukundan, R. Borup, J. Davey, D. Langlois, S. Arisetty, and R. Ahluwalia, **Durability of Fuel Cells under High Power Density Operation**, 220th ECS Meeting - Boston, MA, Oct. 9 – Oct. 14, 2011.

5. Arisetty S., X. Wang, R. Ahluwalia, R. Mukundan, R. Borup, J. Davey, D. Langlois, F. Gambini, O.Y. Plevaya, and S. Blanchet, **Effect of Platinum Loading on Catalyst Stability under Cyclic Potentials**, 220th ECS Meeting - Boston, MA, Oct. 9 – Oct. 14, 2011.
6. Li B., R. Mukundan, C. Welch, K.L. More, K. Artyushkova, P. Atanassov, J. Fenton, and R. Borup, **Characterization of Catalyst Layer Ionomer Degradation in PEM Fuel Cells**, 220th ECS Meeting - Boston, MA, Oct. 9 – Oct. 14, 2011.
7. Kusoglu A., W. Yoon, R. Mukundan, R. Borup, and A.Z. Weber, **Combined Chemical-Mechanical Degradation of Fuel-Cell Membranes**, 220th ECS Meeting - Boston, MA, Oct. 9 – Oct. 14, 2011.
8. Choi B., C.M. Johnston, N. Mack, and Y. Kim, **Effect of Electrode Structure on PFSA Membrane Degradation**, 220th ECS Meeting - Boston, MA, Oct. 9 – Oct. 14, 2011.
9. Borup R., Rangachary Mukundan, Christina Johnston, Yu Seung Kim, Karren, Kateryna Artyushkova, Plamen Atanassov, James Fenton, Bo Li, Adam Weber, Ahmet Kusoglu, **Characterization of Catalyst Layer Ionomer Degradation in PEM Fuel Cells, 2011 Fuel Cell Seminar & Exposition**, 31 Oct. – 4 Nov. 2011, Orlando, Florida.
10. Borup R., Christina Johnston, Yu Seung Kim, Baeck Choi, Dae Sik Kim, Bo Li, Joe Fairweather, Dusan Spornjak, Rangachary Mukundan, Wonseok Yoon, Adam Weber, Cindi Welch, Bruce Orlor, Rex Hjelm, John Davey, David Langlois, Dennis Torracco, Zhongfen Ding, David Jacobson, Daniel Hussey, Greg James, **Degradation Mechanisms and Accelerated Testing in PEM Fuel Cells, 2011 Fuel Cell Seminar & Exposition**, 31 Oct. – 4 Nov. 2011, Orlando, Florida.

References

1. Borup, R., J. Meyers, B. Pivovar, et al., *Chemical Reviews*; **107(10)**, 3904 (2007).
2. S. Maass, et al., *J. Power Sources*, **176(2)**: p. 444-451 (2008).
3. L.M. Roen, C.H. Paik, and T.D. Jarvic, *Electrochem. Solid-State Lett.*, **7(1)**: p. A19-A22 (2004).
4. K.G. Gallagher, D.T. Wong, and T.F. Fuller, *J. Electrochem. Soc.*, **155(5)**: p. B488-B493 (2008).
5. J. Fairweather, et al., *ECS Transactions*, **41 (1)**, pp. 337-348 (2011).

V.E.3 Durability of Low Platinum Fuel Cells Operating at High Power Density

Scott Blanchet (Primary Contact), Olga Polevaya,
May Tan

Nuvera Fuel Cells Inc.
Building 1, 129 Concord Rd.
Billerica, MA 01821
Phone: (617) 245-7667
Email: blanchet.s@nuvera.com

DOE Managers

HQ: Kathi Epping Martin
Phone: (202) 586-7425
Email: Kathi.Epping@ee.doe.gov

GO: Gregory Kleen
Phone: (720) 356-1672
Email: Gregory.Kleen@go.doe.gov

Technical Advisor

Thomas G. Benjamin
Phone: (630) 252-1632
Email: Benjamin@anl.gov

Contract Number: DE-EE0000469

Subcontractors:

- Los Alamos National Laboratory, Los Alamos, NM
- Argonne National Laboratory, Argonne, IL

Project Start Date: September 1, 2009
Project End Date: August 31, 2013

Fiscal Year (FY) 2012 Objectives

- The objective of this project is to study and identify strategies to assure durability of fuel cells designed to meet DOE 2015 cost targets.
- Develop a practical understanding of the degradation mechanisms impacting durability of fuel cells with low platinum loading ($\leq 0.2 \text{ mg/cm}^2$) operating at high power density ($\geq 1.0 \text{ W/cm}^2$)
- Develop approaches for improving the durability of low-loaded, high-power stack designs.

Technical Barriers

This project addresses the following technical barriers from the Fuel Cells section of the Fuel Cell Technologies Program Multi-Year Research, Development and Demonstration Plan:

- (A) Durability
- (B) Cost

Technical Targets

TABLE 1. Progress toward Meeting Technical Targets for Transportation Fuel Cell Stacks Operating on Direct Hydrogen for the Transportation Applications

| Characteristics | Units | 2010/2015 Stack Targets | Nuvera 2012 Status |
|----------------------------|--------------------|-------------------------|--|
| Cost | \$/kWe | 25/15 | ~22 estimated ¹ |
| Durability with cycling | Hours | 5,000 | 12,000 hrs ² 5,500 hrs in automotive cycle conditions ³ |
| Performance at rated power | mW/cm ² | 1,000 | 1,145 ⁴ and 1,200 ⁵ |

¹ Cost assessment of Nuvera's architecture by Directed Technologies Inc. based on their DOE-sponsored Design for Manufacturing and Assembly model [1]. 0.572 V/cell @ 2.0 A/cm² was obtained at 0.2 mg/cm² platinum loading on Orion stack by Nuvera.

² Demonstrated under power profile specific-to-fork truck applications in material handling market at total platinum loading of 0.5 mg/cm².

³ Demonstrated in 20-cell stack of 360-cm² cell active area by Nuvera customer under automotive load profile, at the total platinum loading of 0.50 mg/cm².

⁴ Demonstrated in 250-cm² Orion stack by Nuvera at platinum loading of 0.2 mg/cm².

⁵ Demonstrated in 50-cm² single cell with open flowfield (SCOF) by Nuvera at platinum loading of 0.2 mg/cm².

FY 2012 Accomplishments

- The third project milestone, completed on schedule, benchmarked the serpentine land-channel cell with the open flowfield cell (SCOF) developed by Nuvera and validated at Los Alamos National Laboratory (LANL). Results were reported under selected accelerated stress test (AST) protocols on the MEAs with 0.4 mg_p/cm² and 0.15 mg_p/cm² cathode loadings. The data analysis indicated ohmic, diffusion, and pressure drop benefits of SCOF over the land-channel architecture at the beginning of life (BOL) at low pressure conditions. Similar voltage degradation was observed at the current densities below 1 A/cm² in both cell architectures.
- Go/No-Go project review by the DOE resulted in a Go decision to continue with the project as scheduled. Durability testing of MEAs with 0.4 mg_p/cm² and 0.15 mg_p/cm² cathode loadings in both SCOF and stack cells concluded that subscale SCOF adequately represents full-area Orion stack for performance and durability under automotive load protocols.
- Argonne National Laboratory (ANL) completed development of platinum dissolution and cell performance models, representing the building blocks of the fuel cell durability model and establishing relations between changes in overpotentials, electrocatalyst surface area (ECSA) and oxygen mass transport, and moved to modeling of the platinum transport.

- Durability testing under the new stress test (NST) representing combined power cycle protocols has been completed on Orion short stacks and will continue in SCOF at Nuvera and in the General Motors/Rochester Institute of Technology 50-cm² cell at LANL.



Introduction

Understanding and improving the durability of cost-competitive fuel cell stacks is imperative to successful deployment of the technology. Stacks will need to operate well beyond today's state-of-the-art rated power density with very low platinum loading in order to achieve the cost targets set forth by DOE (\$15/kW) and ultimately be competitive with incumbent technologies. Little to no study of durability factors has been carried out in this area of design and operation. The industry today is focusing mostly on reduced platinum loading as it heads for the DOE target point of 0.2 mg/cm² platinum and 1.0 W/cm² power density. As demonstrated through DOE-sponsored cost modeling, this point falls short of the corresponding \$15/kW stack cost target for 2015.

Approach

Nuvera proposes an accelerated cost-reduction path focused on substantially increasing power density to address non-PGM material costs as well as platinum. Understanding the largely unstudied factors affecting stack durability under these high power conditions is the focus of the present program. Of specific interest is the impact of combining low platinum loading with high power density operation, as this offers the best chance of achieving long-term cost targets. The team effort is divided into two activities: modeling and experimentation.

Results

Durability testing in 50-cm² SCOF cells and 250-cm² Orion stacks was conducted in order to prove consistency in the degradation mechanisms between the two test articles in support of the Go/No-Go project milestone. Testing was conducted under load cycling NST protocol N1A, at two levels of temperature and cathode humidification on 0.45 mg_{Pt}/cm² and 0.2 mg_{Pt}/cm² MEAs. N1A test was designed to mimic catalyst cycling AST B1 protocol, defined by the DOE, with the addition of the current draw, cycled between 0.025 and 2 A/cm². The upper potential in N1A is lower than in the B1 AST, and consistent with the simulated driving cycle N3 previously tested on Orion short stacks. Aggregated assessment of the performance metrics for N1A durability testing concluded qualitative and quantitative similarity in the degradation patterns and mechanisms

between both test articles. Voltage degradation as a function of tested current densities under N1A protocols is shown in Figure 1. Low platinum MEAs exhibited increasing decay as current increased while decay for the higher-loaded MEAs remained relatively constant with change in current. This result was reproduced at different test conditions. The differences between SCOF and Orion were small, thereby proving results from SCOF to be representative for durability model development at ANL – the final deliverable of this project.

Over the past year, SCOF, developed by Nuvera under DOE funding, was validated at LANL under AST catalyst cycling protocols, by comparison to the serpentine land-channel cell, previously tested with the same platinum loading MEAs. Low resistivity and pressure drop of the open flow fields resulted in measurable performance benefits of lower Pt loading MEAs at the BOL over the quad serpentine cell at low pressure conditions as shown in Figure 2. In both cell architectures cathode ECSA and mass activity decreased similarly during 30,000 potential cycles and resulted in similar cathode thinning and Pt particle growth, confirmed by scanning electron microscopy and X-ray diffraction measurements. The analysis of cell impedance showed equal increase in charge transport resistance with ageing at low current density. At current densities higher than 1 A/cm² the voltage decays in SCOF were higher than the land-channel cell. This is attributed to the lower pressure drop and, therefore, lower average cathode operating pressure in SCOF, given the same value of the back pressure was maintained in both tests.

Durability testing in short stacks under simulated combined city and highway driving cycle NST N3 protocol continued at the rated current density (RCD) of 2 and

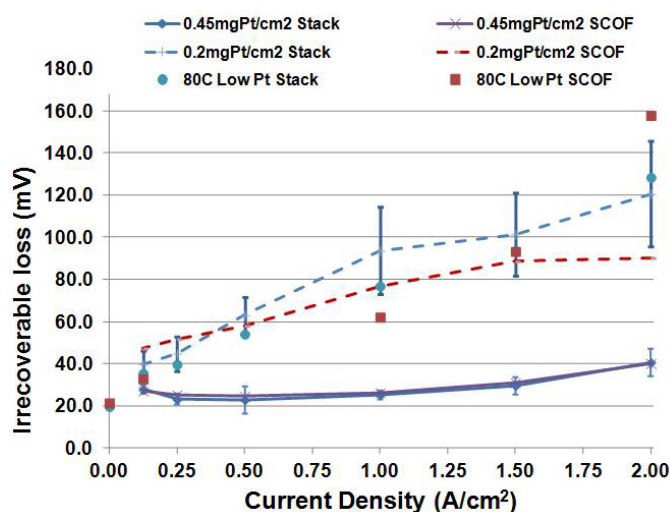


FIGURE 1. Cell voltage decay in SCOF and Orion stack cells past 30,000 load cycles, data from 60°C and 80°C N1A NSTs. Total MEAs loading 0.45 and 0.2 mg_{Pt}/cm².

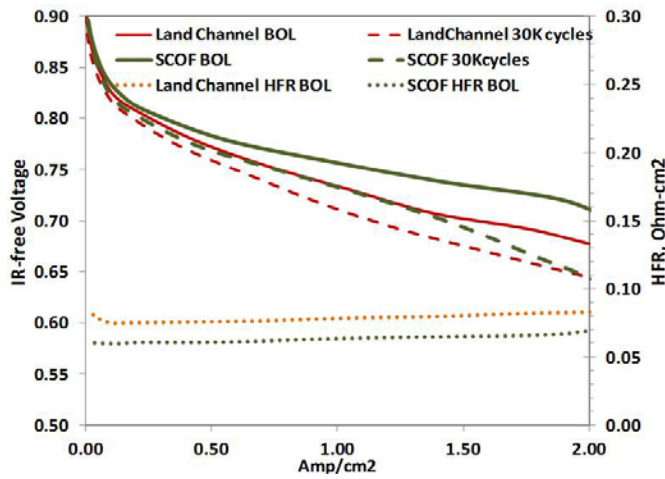


FIGURE 2. BOL and end-of-test polarization curves of 0.2 mg_{Pt}/cm² MEAs in SCOF and quad-serpentine land-channel cell, aged under catalyst cycling AST (30,000 triangle potential cycles 0.582-0.883 V). 100% relative humidity inlets, 80°C cell, 3.4 ata.

were affected by the decreased Pt loading as shown in the upper graphs in Figure 3.

The cell voltage degradation of the low loaded Pt MEAs was two times higher at 2 A/cm² than at 1 A/cm², attributed to the near zero oxygen partial pressure at the electrode with the increased operating current. At current densities lower than 1 A/cm², the cell voltage degradation was not influenced by the current density, which was in agreement with the levels of oxygen partial pressure and consistent with the AST results reported last year.

In 0.45 mg_{Pt}/cm² MEAs the irrecoverable voltage losses in the representative stack cells during NST N3 have been estimated by subtracting the measured voltage recovery, following test restarts and concluding that operation at the RCD of 3 A/cm² did not accelerate degradation compared with operation at the rated current density RCD of 2 A/cm² as shown in the lower graphs in Figure 3.

Post-NST diagnostics of the MEAs included evaluation of platinum loss to the membrane, using transmission electron microscopy imaging and direct particle counting methods developed at the Oak Ridge National Laboratory. Platinum migration out of the cathode and re-deposition in the membrane, occurring with ageing MEAs under load cycle protocols, was quantified for particle size and mass distribution. Results are summarized in Figure 4 for the

3 A/cm² on 0.2- and 0.45 mg_{Pt}/cm² MEAs respectively. In this NST the cathode pressure and flow conditions vary with the current density, following the operating map of the air compressor in the automotive system. Both activation and mass transfer overpotentials and their increase with aging

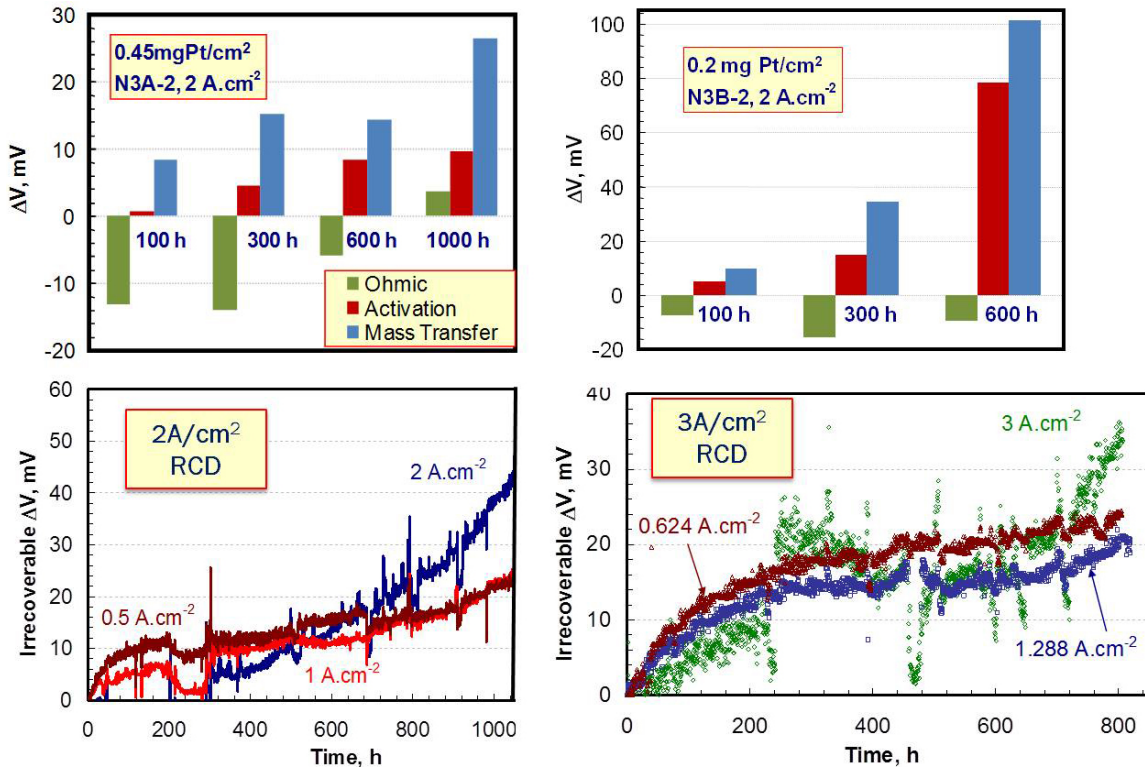


FIGURE 3. Effect of Platinum cathode loading (upper graphs) and RCD (lower graphs, MEAs with the total loading 0.45 mg_{Pt}/cm²) on durability of stack cells in the simulated drive cycle tests N3.

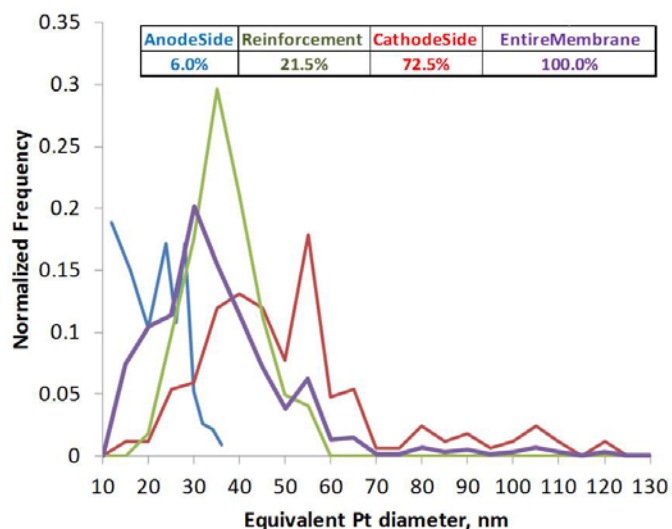


FIGURE 4. Platinum particle size and platinum mass distribution in the membrane after N3 NST at 3 A/cm² RCD.

MEA sectioned after completing the N3 driving cycle test at 3 A/cm² RCD for 820 hours. While platinum mass balance will provide the direct input to the durability modeling studies, the presence of multiple platinum particles early in cell testing, as well as the consistency of the cathode-membrane interface throughout the test provided innovative insights on the mechanism of platinum loss to the membrane.

Development of the durability model by ANL continued with the completion of thermodynamically independent platinum dissolution studies and material-specific kinetics. The team demonstrated good progress on the analysis of the cell transport properties with ageing and moved to defining the platinum ion transport – the final step in composing the full picture of fuel cell ageing. The model, independent of the cell architecture, will utilize inputs from catalyst cycle ASTs, BOL properties of the studied material set, and prescribed use cycles to output cathode ECSA, particle size distribution, overpotentials and cell voltage as a function of cycle time and the current density.

Conclusions and Future Direction

- Durability study of 0.45 and 0.2 mg_{Pt}/cm² MEAs in SCOF and stack cells concluded similarity in the degradation patterns and mechanisms between both test articles. Therefore, the data from SCOF, adequately representing full-area Orion stack for the performance and durability under automotive load protocols, proved the quality inputs to the durability model development at ANL – the final deliverable of the Spire project.

- The NST campaign will be moved from SCOF to General Motors/Rochester Institute of Technology herringbone cell architecture for durability benchmarking at LANL and will continue in SCOF at Nuvera, refocusing efforts towards the next project milestone: validating results of the durability model.
- Development of the durability model will be completed by the addition of the platinum transport block, and the model results will be validated against the fuel cell tests in support of 2013 project milestones #4 and #5. (Milestone #4 - Model correlations to full-area test results; milestone #5 - Validated model and data set published.)
- Post-test analysis of platinum in the membrane using transmission electron microscopy will continue in support of platinum ion transport model development by ANL.
- Operation at high power densities enabled by the open flowfield architecture and proven at the low platinum loading provided the ground work for accelerated cost-reduction path to the cost targets set by the DOE.

FY 2012 Publications/Presentations

1. O. Plevaya, Durability of Low Pt Fuel Cells Operating at High Power Density, 2012 DOE Annual Merit Review, Washington, D.C., May 16, 2012.
2. S. Arisetty et. al., Catalyst Durability in PEM Fuel Cells with Low Platinum Loading, JECS, 159(5) B1-B8 (2012) .
3. S. Arisetty, Effect of platinum loading on catalyst stability under cycling potentials, 220th Meeting of ECS, 2011, Boston, MA.
4. O. Plevaya, Spire Project Review with Freedom Car Technical Team, January 11, 2012, Southfield, MI.
5. F. Gambini et. al., Durability of fuel cells under high power density operation, 220th Meeting of ECS, 2011, Boston, MA.
6. S. Arisetty et. al, Effect of platinum loading on catalyst stability under cycling potentials, ECS Transactions, 41 (1), 797 (2011) .
7. S. Arisetty et al, Effect of load cycles on fuel cell durability, Poster, 5th International conference on polymer batteries and fuel cells, ANL, Argonne, July 2011.
8. R.K. Ahluwalia, Dissolution of Platinum from ORR catalysts in polymer electrolyte fuel cells, 2nd International Workshop on Degradation Issues in Fuel Cells, Thessaloniki, Greece, September 21–23, 2011.
9. R. Subbaraman, Ex-situ Potentiostatic and Potentiodynamic Durability of Low Pt Loading fuel cell MEAs, 220th Meeting of ECS, 2011, Boston, MA.

V.E.4 Improved Accelerated Stress Tests Based on Fuel Cell Vehicle Data

Timothy Patterson (Primary Contact),
V. Srinivasamurthi, T. Skiba

UTC Power Corp.
195 Governor's Highway
South Windsor, CT 06074
Phone: (860) 727-2274
Email: timothy.patterson@utcpower.com

DOE Managers

HQ: Kathi Epping Martin
Phone: (202) 586-7425
Email: Kathi.Epping@ee.doe.gov

GO: David Peterson
Phone: (720) 356-1747
Email: David.Peterson@go.doe.gov

Contract Number: DE-EE0000468

Subcontractors:

- United Technologies Research Center, East Hartford, CT
- Los Alamos National Laboratory, Los Alamos, NM
- Oak Ridge National Laboratory, Oak Ridge, TN

Project Start Date: December 1, 2009

Project End Date: November 30, 2011

Approach

UTC lead a top-tier team of industry and national laboratory participants to update and improve DOE's ASTs for hydrogen fuel cells. This in-depth investigation focused on critical fuel cell components (e.g. membrane electrode assemblies [MEAs]) whose durability represents barriers for widespread commercialization of hydrogen fuel cell technology. UTC has access to MEA materials that have accrued significant load time under real-world conditions in PureMotion[®] 120 power plant used in transit buses. These materials are referred to as end-of-life (EOL) components in the rest of this document. Advanced characterization techniques were used to evaluate degradation mode progress using these critical cell components extracted from both bus power plants and corresponding materials tested using the DOE ASTs. These techniques were also applied to samples at beginning of life (BOL) to serve as a baseline. These comparisons will advise the progress of the various failure modes that these critical components are subjected to, such as membrane degradation, catalyst support corrosion, platinum group metal dissolution, and others. Gaps in the existing ASTs to predict the degradation observed in the field in terms of these modes were outlined. Using these gaps, new ASTs were recommended and tested to better reflect the degradation modes seen in field operation. Also, BOL components were degraded in a test vehicle at UTC designed to accelerate the bus field operation.

Fiscal Year (FY) 2012 Objectives

Validate the use of post test fatigue cycling in a dynamic mechanical analyzer (DMA) as a method to estimate "remaining life" of a tested membrane.

Technical Barriers

- >5,000 hours stack durability (including cycling and all materials, e.g. membrane, seals).
- <10% overall performance decay (including start/stop and transient operation).
- Current DOE accelerated stress tests (ASTs) not calibrated with real-world degradation.

FY 2012 Accomplishments

- Accelerated life test (ALT) complete.
- Validation of post-test fatigue tool for predicting remaining life of membrane complete.



Results

An update on the durability progression of the UTC bus fleet is shown in Figure 1. The UTC fleet leader has achieved over 12,000 hours operation in the field. This corresponds to over four years in service. Three previous models had failed in the field prior to 12,000 hours. All of the failures have been verified using ASTs. These results have been reported previously, but a summary is provided here. The 2006 and 2007 fleet leaders failed due to oxidation of the carbon in the cathode microporous layer. The failure mechanism was replicated using the carbon corrosion AST. The microporous layer used in the 2008 fleet leader and beyond was determined to be 2-3 times more durable. This was borne out in the improvement of the UTC fleet from ~1,000 hours to over 2,800 hours. The 2008 fleet leader failed due to failure of the membrane at the air inlet caused in turn by hydration/dehydration cycling. A more durable membrane was implemented in the 2012 fleet leader. Both membranes were tested in a combined membrane mechanical-chemical AST. The 2012 fleet leader membrane lasted over 15 times longer than the 2008 fleet leader in the AST. Based on AST testing, the membrane in the 2012 fleet leader is expected to last longer than 30,000 hours.

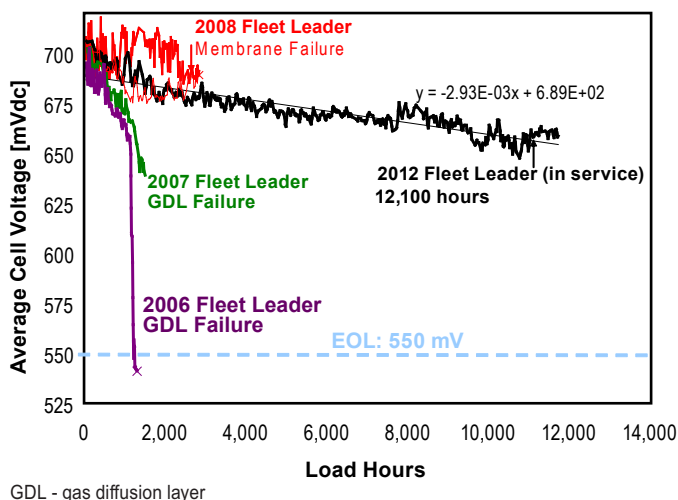


FIGURE 1. UTC Power fleet data

For FY 2012, one of the remaining tasks was to validate the use of post test fatigue cycling in a DMA as a method to estimate “remaining life” of a tested membrane. One of the advantages of this tool would be that degradation of a membrane can be detected prior to failure, reducing time consuming and expensive testing. Another advantage would be that areas with highly localized degradation could be identified, such as different areas within a cell or different cells within a cell stack assembly. This gives fuel cell developers early insight about the durability of materials in a realistic operating environment as well as the impact of cell design on durability. This is becoming more important as some market requirements, such as the bus, range from 35,000 to 50,000 hours.

In order to verify the tool, an MEA was run to failure using the combined membrane mechanical-chemical degradation AST, described in Table 1. The MEA was removed from test after 218 hours after it had failed. A second MEA was subjected to same AST protocol, but was intentionally removed from test before failure had occurred, at 70 hours. A third sample was an as-received MEA. The open-circuit voltage (OCV) voltage response to fuel pressure sweep of both test samples is shown in Figure 2.

After test, small dog-bone shaped samples were excised from the used MEAs and subjected to fatigue cycling in a DMA. The fatigue cycling was performed in an environmental chamber to control the temperature and humidity. The stress was cycled from maximum stress of 5 MPa to minimum stress of 1 MPa. A minimum stress of 20% maximum stress was used to prevent buckling of the sample. The fatigue cycling frequency was 10 Hz. The parameters for the fatigue cycling are summarized in Table 2.

Figure 3 shows the normal probability distribution function, which was fit to the fatigue test data of each MEA. (To interpret Figure 3, each line represents the frequency at

TABLE 1. Membrane Flow/Load Cycling AST Protocol

| | | |
|---------------------|---|-------------------------|
| Coolant temperature | 80°C | |
| Cycle | Square wave galvanostatic | |
| | 20 sec | 0.015 A/cm ² |
| | 15 sec | 1.5 A/cm ² |
| Anode | H ₂ ; 80% utilization(S.R. = 1.25) | |
| Cathode | Air; 60% utilization(S.R. = 1.66) | |

S.R. – stoichiometry ratio

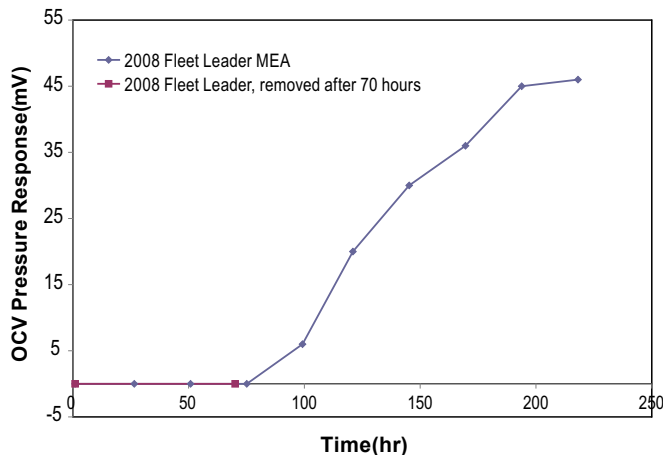


FIGURE 2. OCV pressure response during membrane combined chemical-mechanical AST

TABLE 2. Parameters used in Fatigue Cycling

| | | |
|--------------------------|---------|-------|
| Sample temperature | 50°C | |
| Sample relative humidity | 50% | |
| Stress | Minimum | 1 MPa |
| | Maximum | 5 MPa |
| Frequency | 10 Hz | |

which the MEA failed at a given number of fatigue cycles.) Figure 4 shows the same data in a slightly different way. The cumulative normal distribution function is shown for each MEA, along with the raw data. Also shown is the 90% confidence interval for each MEA (To interpret Figure 4, the line represents the fraction of the distribution that has failed at or before a given number of fatigue cycles. The confidence interval represents the uncertainty in the data.) For the as-received MEA, the average cycles to failure (CTF) was 193,000 cycles. The standard deviation was 13,000 cycles. For the MEA tested to 218 hours, the mean CTF decreased to 83,000 cycles, which is a 57% reduction in CTF from the as-received MEA. The standard deviation also increased to 29,000 cycles. This indicates that the membrane degradation is highly localized. For the MEA which was intentionally removed from test before failure at 70 hours, the mean

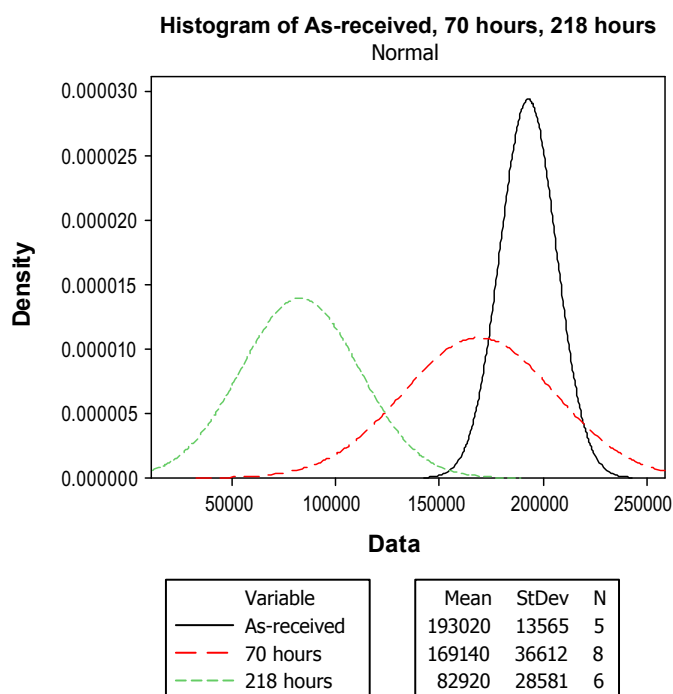


FIGURE 3. Probability distribution of cycles to failure (as-received MEA; cell run for 70 hours in membrane combined chemical-mechanical AST, and cell run for 218 hours in membrane combined chemical-mechanical AST)

time to failure decreased to 163,000 cycles, which is only 16% reduction compared to the as-received MEA. There was a large increase in the variability of CTF, as indicated by the increase in the standard deviation to 36,000 cycles, which is almost three times the variability compared to the as-received sample. A difference between the as-received sample and a sample that had not yet exhibited any sign of failure in cell testing was detected using this method. This indicates that the technique is useful for detecting localized degradation much earlier than any other method. Further work would need to be completed to investigate the limits of the sensitivity of this method.

UTC has facilitated the development of a test vehicle for accelerated evaluation of stack components under this program. The main motivation for this exercise results from the relatively slow rate of load-hour accrual for buses in the field. Because UTC Power is currently targeting >18,000 hours stack durability for bus fleet applications, a more rapid test vehicle is necessary to increase product maturity on new stack configurations. The test vehicle for accelerated stack component evaluation is termed the accelerated life test (ALT). This small power plant has the identical piping and instrumentation configuration as the bus power plant, but operates on a 5-kW short stack. The key operating modes of the bus that have been linked to stack component degradation have been reflected in the protocol. The 2008 fleet leader MEA was tested in the ALT rig and run until membrane failure was observed. Failure was observed after 1,400 load

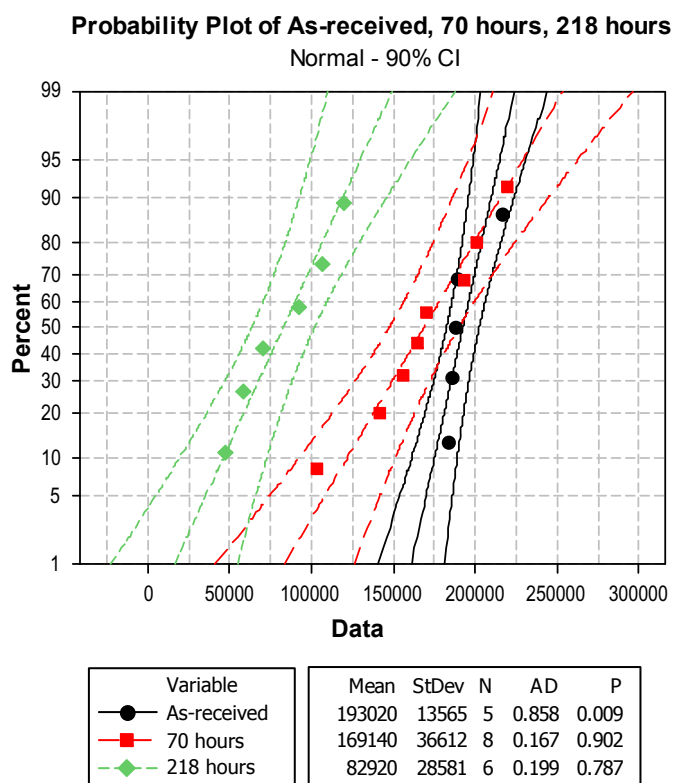


FIGURE 4. Comparison of cumulative probability distribution of the cycles to failure (as-received MEA; cell run for 70 hours in membrane combined chemical-mechanical AST, and cell run for 218 hours in membrane combined chemical-mechanical AST)

hours, which is 50% faster than observed in the fleet (due to higher operating temperature). Just as important, the ALT rig was run 90% of the time, whereas the fleet typically operates at 34-66% of the time. Therefore, time to failure can be achieved in less than 17-34% of the time, on a calendar basis.

A summary of the ASTs for each failure mode is shown in Table 3. The table shows the time to failure in the AST and in the fleet, as well as an AST acceleration factor, for each failure mode. In some cases, an improved component was also tested in the AST. In these cases, an “AST improvement factor”, which is the ratio of time to failure of a component with improved durability to the time to failure of a baseline component, is shown. Finally, where an improved component was also tested in the fleet, a “fleet improvement factor” is shown. There is good agreement for the GDL. For other failure modes, there is not yet enough fleet data to make comparisons.

Conclusions and Future Directions

- Fleet/Real-World: UTC fleet performance and operating cycle analyses have been completed and reported. Teardown analyses of the real-world degraded components have been completed and reported.

TABLE 3. Summary of ASTs for each of the Four Failure Modes

| Mechanism | AST | Baseline | | Acceleration Factor | Improved Component | | AST Improvement Factor | Fleet Improvement Factor |
|--------------------------------------|--------------------------|-------------------|----------------------|---------------------|--------------------|---------|------------------------|--------------------------|
| | | AST | Fleet | | AST | Fleet | | |
| GDL carbon corrosion | Air-air cycling | 150 | 1,250 | 8X | >550 | >12,000 | >3.6X | >9.6 X |
| Catalyst layer carbon corrosion | DOE Carbon Corrosion AST | 10 | >12,000 | >1,200X | 20 | TBD | 2X | TBD |
| Membrane chemical/mechanical failure | 80°C flow/load cycling | 140 | 2,800 | 20X | 2,500 | >12,000 | 18X | >4.3 |
| Platinum loss | PGM AST | 7 mV in 200 hours | 15 mV in 2,800 hours | 6.5X | - | - | N/A | N/A |

TBD – to be determined; PGM – platinum-grade metal

- Lab-World: ASTs for platinum group metal decay, carbon support corrosion, membrane mechanical decay, and membrane chemical decay have been completed. Teardown analyses of the lab-world degraded components have been completed and reported.
- Acceleration factors for each AST have been determined. Wherever available, an “AST improvement factor” and “Fleet improvement factor” has been calculated and compared.
- ALT: Testing has been completed. A reduction in test time, on a calendar basis, of 17-34% has been demonstrated for the 2008 fleet leader.
- DMA has been used to determine remaining life of a membrane that was removed from test prior to any evidence of failure. Differences were observed between samples that were tested to 70 hours and 220 hours. Further investigation is recommended to determine limits of the sensitivity of the method.

FY 2012 Publications/Presentations

1. “Use of Mechanical Tests to Predict PEMFC Membrane Durability under Humidity Cycling”, Journal of Power Sources, 196 (2011) 3851–3854.
2. “Improved AST’s based on FCV data” presentation to Freedom CAR & Fuel Partnership, Fuel Cell Tech Team Review January 13, 2011.
3. “Improved AST’s based on FCV data” presentation to DOE Annual Merit Review meeting May 12, 2011.
4. “A model of membrane mechanical stress in PEMFC during load cycling”, to be submitted.

V.E.5 Accelerated Testing Validation

Rangachary Mukundan¹ (Primary Contact),
Rod Borup¹, John Davey¹, Roger Lujan¹,
Dennis Torrace¹, David Langlois¹, Fernando Garzon¹,
Dusan Spornjak¹, Joe Fairweather¹,
Sivagaminathan Balasubramanian², Adam Weber²,
Mike Brady³, Karren More³, Greg James⁴,
Dana Ayotte⁴, and Steve Grot⁵

¹Los Alamos National Laboratory
MS D429, P.O. Box 1663
Los Alamos, NM 87545
Phone: (505) 665-8523
Email: Mukundan@lanl.gov

DOE Manager

HQ: Nancy Garland
Phone: (202) 586-5673
Email: Nancy.Garland@ee.doe.gov

Subcontractors:

²Lawrence Berkeley National Lab, Berkeley, CA

³Oak Ridge National Laboratory, Oak Ridge TN

⁴Ballard Power Systems, Burnaby, BC V5J 5J8 Canada

⁵Ion Power, New Castle, DE

Project Start Date: Oct 2009

Project End Date: 2013

Fiscal Year (FY) 2012 Objectives

- Correlation of the component lifetimes measured in an accelerated stress test (AST) to “real-world” behavior of that component.
- Validation of existing component specific ASTs for electrocatalysts, catalyst supports and membranes (mechanical and chemical degradation).
- Development of new ASTs for gas diffusion layers (GDLs) and bipolar plates.
- Co-ordinate effort with the Durability Working Group.

Technical Barriers

This project addresses the following technical barriers from Fuel Cells section (3.4.5) of the Fuel Cell Technologies Program Multi-Year Research, Development and Demonstration Plan:

- (A) Durability
- (B) Cost

Technical Targets

Cost and durability are the major challenges to fuel cell commercialization. ASTs enable rapid screening of fuel cell materials and are critical in meeting the long life times required for stationary and automotive environments. Moreover these ASTs can also help predict the lifetime of the various components in “real-world” applications.

- Transportation Durability: 5,000 hours (with cycling)
 - Estimated start/stop cycles: 17,000
 - Estimated Frozen cycles: 1,650
 - Estimated Load cycles: 1,200,000
- Stationary Durability: 40,000 hours (2015); 60,000 hours (2020)
 - Survivability: Stationary -35°C to 40°C
- Cost: (30 \$/kW)

FY 2012 Accomplishments

- Performed the electrocatalyst and catalyst-support ASTs on three different catalyst types based on different carbon support materials.
- Performed the membrane chemical and mechanical ASTs on four different membranes and proposed a new combined mechanical/chemical membrane AST.
- Performed failure analysis of MEAs and correlation between AST and real world data.
- Modeling of voltage loss breakdown and assigning voltage losses to specific degradation mechanisms.
- Proposed GDL AST based on ex situ aging in H₂O₂ and evaluated mass transport losses after aging.



Introduction

The durability of polymer electrolyte membrane (PEM) fuel cells is a major barrier to the commercialization of these systems for stationary and transportation power applications [1]. Commercial viability depends on improving the durability of fuel cell components to increase the system reliability and to reduce system lifetime costs by reducing the stack replacement frequency. The need for ASTs can be quickly understood given the target lives for fuel cell systems: 5,000 hours (~7 months) for automotive, and 40,000 hrs (~4.6 years) for stationary systems. Thus testing methods that enable more rapid screening of individual components to determine their durability characteristics, such as off-line environmental testing, are needed for

evaluating new component durability with a rapid turn-around time. This allows proposed improvements in a component to be evaluated rapidly and independently, subsequently allowing rapid advancement in PEM fuel cell durability. These tests are also crucial to developers in order to verify that durability is not sacrificed while making improvements in costs (e.g. lower platinum group metal [PGM] loading) and performance (e.g., thinner membrane or a GDL with better water management properties).

DOE has suggested AST protocols for use in evaluating materials, but only for the catalyst layer components (electrocatalyst and support), and for the membrane [2,3]. The US Fuel Cell Council has also suggested AST protocols for the same materials [4]. While these protocols have concentrated on the catalyst, catalyst support and membrane materials, to date, no accelerated degradation protocols have been suggested for GDL materials or micro-porous layers, bipolar plates or seals. In spite of recent advances in AST development, a main portion, which is deficient, is the quantitative correlation between the results of a given fuel cell AST, and the degradation rate or life in an operating fuel cell.

Approach

A main desired outcome of this task is the correlation of the component lifetimes measured in an AST to in situ behavior of that component in “real-world” situations. This requires testing of components via ASTs and in operating fuel cells, and delineating the various component contributions to the overall cell degradation. This will primarily be performed by using a simplified one-dimensional model that takes into account the different component contributions like membrane ionic conductivity, cathode catalyst layer kinetic losses and mass transport losses (catalyst layer and GDL) to the overall losses observed in operating cells [5]. This project will then attempt to correlate the performance losses observed due to a particular component in “real-world” situations with

the degradation in AST metrics of that component. The correlation between AST and life data if state-of-the-art materials are used, in essence, gives one data point. Thus, for a reasonable correlation to be made, materials with different life spans are utilized in this project. Providing the variable material durability relies on the expertise of the suppliers as partners in this project. This work is also being coordinated with other funded projects examining durability through a DOE Durability Working Group.

Results

Carbon Corrosion

The DOE Fuel Cell Technical Team-recommended AST [6] for carbon corrosion was performed on three different MEAs, each with a different catalyst supplied by Tanaka Kikinoku Kogyo K.K., and designated TEC10E20E, TEC10V40E and TEC10EA40E. The carbon supports included a high surface area carbon (E-carbon), a vulcan carbon (V-carbon) and a highly graphitized carbon (EA-carbon). The MEAs with these three carbons had nominal cathode Pt loadings of 0.15 mg-Pt/cm² (E-carbon), 0.17 mg-Pt/cm² (V-carbon), and 0.25 mg-Pt/cm² (EA-carbon). Figure 1a illustrates the performance of these three MEAs after various periods of the 1.2 V AST. The initial performance of all three MEAs is comparable while their degradation rate is distinctly different. After only 20 hours of the AST, the E-carbon shows significant loss in performance, the V-carbon a slight loss in performance, and the EA carbon a slight improvement in performance. After 400 hours of this AST, only the MEA based on the EA-carbon had reasonable fuel cell performance with a loss of <40 mV @ 1.5 A/cm². The DOE target of 30 mV loss @ 1.5 A/cm² was exceeded after 4 hours, 32.5 hours and 240 hours for the E-carbon, V-carbon and EA-carbon respectively.

The electrochemical surface area (ECSA) and mass activity (MA) obtained before and after the high potential

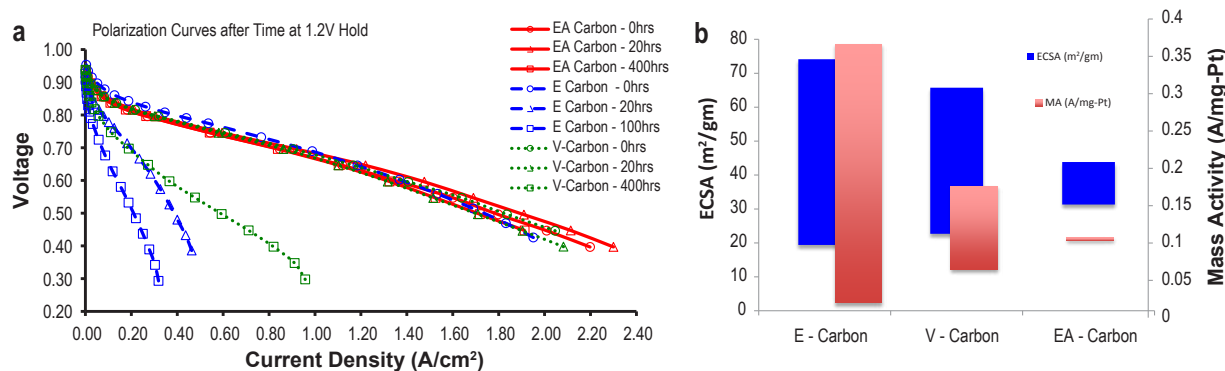


FIGURE 1. a) Polarization curves of three different catalysts using different carbon types before and after carbon corrosion AST of 1.2 V potential hold. b) Initial performance (electrochemical surface area and mass activity) characteristics of three different catalysts and degradation (bar length) using different carbon types.

hold (1.2 V) AST is illustrated in Figure 1b (the bar length represents the loss in performance). The performance characteristics of the three different carbon types used in this experiment are significantly different, with the E-carbon having the highest initial ECSA ($74 \text{ m}^2/\text{gm-Pt}$) and MA (0.37 A/mg-Pt) and the EA-carbon having the lowest initial ECSA ($44 \text{ m}^2/\text{gm-Pt}$) and MA (0.1 A/mg-Pt). However, the degradation rates of these three carbons are dependent on the degree of graphitization with the EA-carbon showing the most resistance to corrosion. As a result, after the 400-hour hold (only 100 hours for the E-carbon) the EA-carbon exhibited the best performance characteristics (ECSA = $31 \text{ m}^2/\text{gm-Pt}$; MA = 0.1 A/mg-Pt) and the E-carbon the lowest (ECSA = $19 \text{ m}^2/\text{gm-Pt}$; MA = 0.02 A/mg-Pt). Scanning electron microscopy studies revealed that the E-carbon and V-carbon corroded significantly and lost $\geq 60\%$ of their electrode thickness, in contrast to the EA-carbon that exhibited little ($<15\%$ loss in catalyst layer thickness) corrosion. Transmission electron microscopy studies showed that the catalyst based on the EA-carbon retained its structure while the E-carbon and V-carbon based electrodes exhibit significant densification and loss of porosity due to carbon becoming more amorphous.

Correlation of AST and Field Data

The AST (performed at LANL) and field data (obtained by Ballard) from two different bus module configurations were presented in our FY 2011 report. The two bus modules were labeled P5 and HD6 and operated in the field in Hamburg, Germany and on an Orange County Transportation Authority drive cycle in the laboratory respectively. In FY 2012 the ex situ analysis was completed and the correlations between the AST data and field data established.

Catalyst Degradation: The coarsening of Pt observed in the AST and field data is plotted in Figure 2 and illustrates significant Pt particle agglomeration variations in field samples from inlet to outlet. The HD6 AST showed a 58% increase in Pt crystallite size with respect to the beginning of life while the HD6 module sample showed similar Pt crystallite growth (average from inlet to outlet) at around 1,900 hours of operation (Figure 2a). The P5 AST showed a 102% increase in Pt crystallite size with respect to the beginning of life while P5 field samples at 2,600 hours showed a larger average Pt crystallite size growth of 157%. These results indicate that 30,000 AST potential cycles correspond to $\approx 2,000$ hours of field operation under high relative humidity (RH) conditions. Carbon corrosion AST samples also showed excellent agreement with field data with the HD6 catalyst layer exhibiting no thinning while the P5 data showed 60% thinning in the AST and 30–70% thinning in the field.

Membrane Degradation: The open circuit voltage (OCV-hold) AST resulted in failure of the P5 and HD6 MEAs after approximately 100 hours. This test also resulted in significant

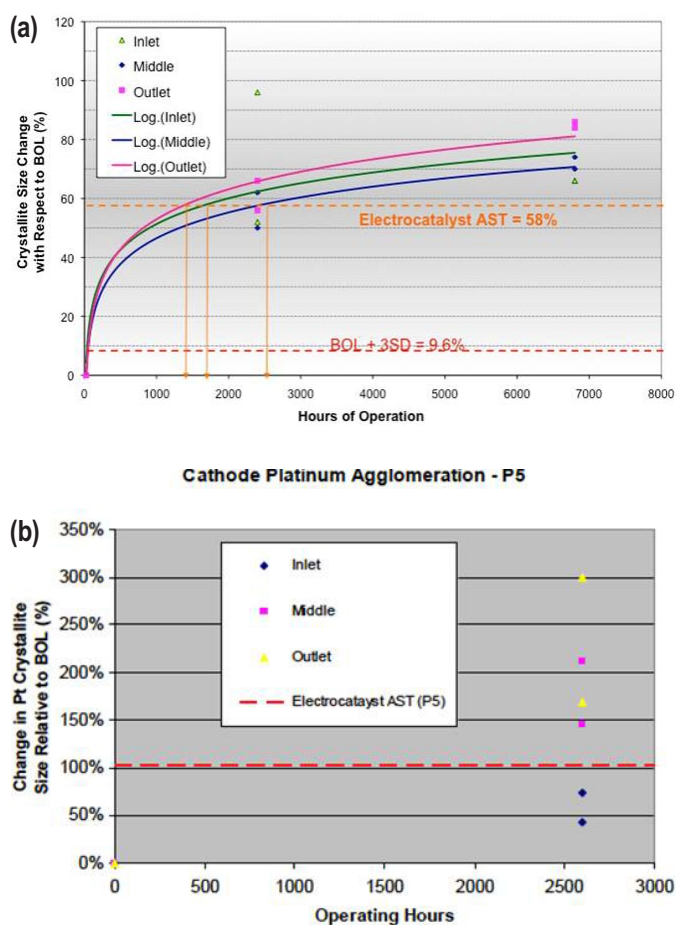


FIGURE 2. Platinum crystallite growth in AST and field samples: a) HD6 bus module operated in OCTA drive cycle, b) P5 bus modules operated in the field

thinning of the P5 and HD6 membranes before failure. The thickness change for the P5 MEA after the AST and bus operation is illustrated in Figure 3a. The P5 MEA shows no thinning after $>2,500$ hours of field operation (left 2 bars of Figure 3a) whereas the AST resulted in 28% and 48% thinning after 104 and 168 hours at OCV respectively (right two bars in Figure 3a). Similar results were obtained for the HD6 MEA (not shown) where no thinning was observed after $>6,500$ hours of operation in a bus module, while the AST resulted in 20% thinning after 144 hours. This clearly illustrates that the chemical degradation AST that has been designed for drier automotive applications is too severe and does not capture the membrane degradation occurring in the wetter bus module environment.

The RH cycling AST resulted in no observable increase in crossover in either the P5 or the HD6 MEAs over the life of the test, which was 20,000 cycles or 1,333 hours (open symbols in Figure 3b). However, this test did result in a partial tearing of the MEA near the cathode side and the formation of divots, with the catalyst layer detached from the MEA. Similar failure was observed in the field for both

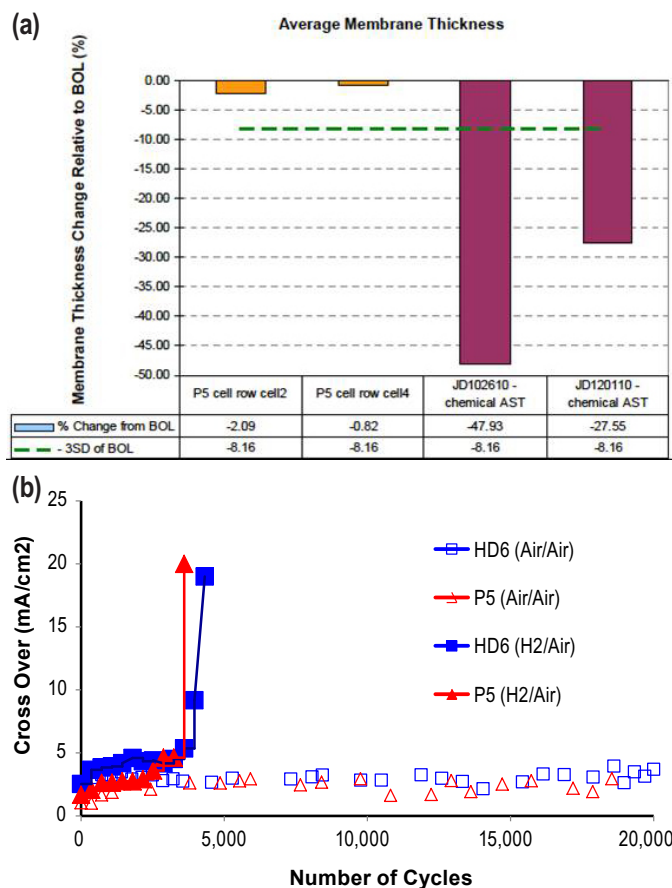


FIGURE 3. a) Change in membrane thickness of the P5 MEA after field test and after AST. Field test data from cell 2 and cell 4 are shown (orange bars) and AST data after 168 and 104 hours from two different cells are shown (maroon bars). b) Crossover of P5 and HD6 MEAs subjected to RH cycling in air/air and RH cycling in H₂/Air.

P5 and HD6 modules especially near the inlets and outlets. These results indicate that while the chemical degradation AST greatly overestimates the membrane degradation rate, the RH cycling greatly underestimates it. Therefore to better capture the failure modes observed in the field a combined chemical/mechanical AST was performed. As illustrated by the solid symbols in Figure 3b this combined chemical/mechanical AST (replacing the air on one side of the MEA in the RH cycling test with H₂) resulted in the failure of the P5 MEA after 3,500 cycles (233 hours) and the HD6 MEA after 4000 cycles (267 hours). Failure analysis of these MEAs and repeat experiments are in progress to verify the degradation mechanisms under operation during this combined membrane degradation test.

GDL AST

Different GDL materials were subjected to ex situ aging protocols in H₂O₂, and in situ tested with fresh commercial Gore MEAs to illustrate the effect of GDL aging on fuel cell performance. The simulated aging of GDLs was achieved by

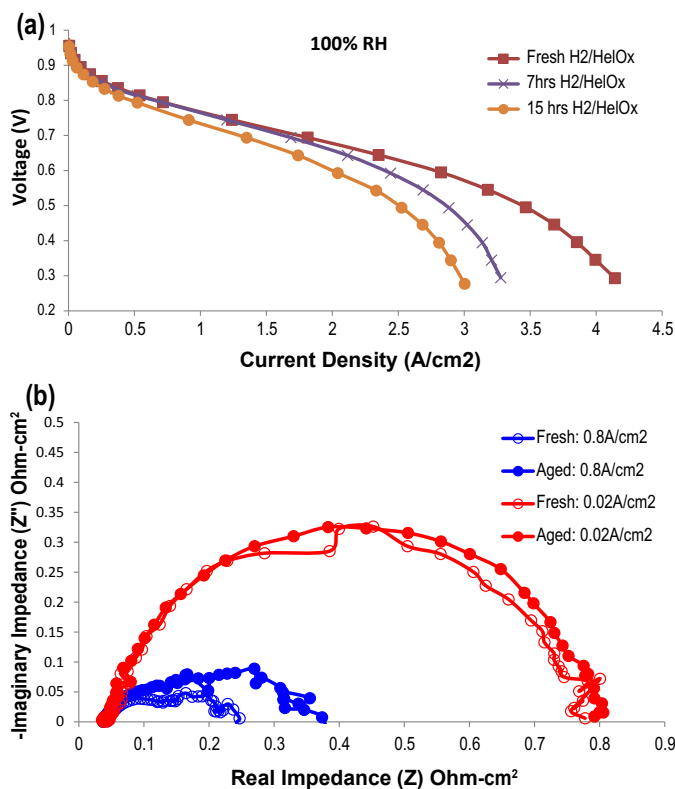


FIGURE 4. a) Performance of fresh and ex situ AST aged 25BC GDL materials and b) impedance of fresh and ex situ AST aged 25BC GDL materials

boiling them in 30% hydrogen peroxide at 95°C, contained in a reaction vessel equipped with a coil reflux condenser (based on previously developed AST by SGL). GDLs were removed periodically at different time intervals to examine rate of aging. Figure 4a illustrates the effect of aging on performance losses of an SGL Sigracet® 25BC GDL under high RH, 21% oxygen/79% helium gas mixture operation while the dry performance is identical to the fresh GDL (not shown). Figure 4b shows that both fresh and aged GDLs have identical cell resistances in the kinetic region (0.2 A/cm²), while the resistance of the aged cells in the mass transport region (low frequency arc of 0.8 A/cm²) is significantly increased. Contact angle measurements revealed that the hydrophobicity of these GDLs decreased over time consistent with in situ fuel cell GDL degradation reported previously [7].

Conclusions and Future Directions

High surface area carbon exhibited the best initial performance but also the fastest degradation rate. Highly graphitized carbon on the other hand, had the lowest initial performance while also exhibiting the slowest degradation rate. Transmission electron microscopy analysis of the MEAs after corrosion indicated Pt particle size growth in all the catalyst layers in addition to significant thinning of the high surface area carbon-based catalyst layers. While Pt sintering

due to coalescence led to performance losses up to 40 mV, the greatest performance loss (up to 360 mV) was associated with mass transport losses resulting from a compaction of the catalyst layer porosity due to the formation of amorphous oxidized carbon. The carbon corrosion and electrocatalyst ASTs were able to accurately capture the field data with 30,000 AST potential cycles corresponding to \approx 2,000 hours of bus operation. The membrane/chemical degradation AST resulted in significant membrane thinning not observed in the field. The membrane mechanical degradation AST was able to reproduce the degradation phenomenon observed in the field but had little ability to distinguish between various membranes each operating for over 1,300 hours without observable performance degradation. A combined mechanical/chemical AST was successful at accelerating the degradation rates observed in the field and failure analysis is in progress to correlate this AST to field data. A new GDL AST was designed and this AST resulted in performance losses due to hydrophobicity loss of GDL consistent with previously reported in situ fuel cell data. The following specific work will be carried out in the next year of this project in order to validate existing ASTs and recommend new ASTs.

- AST testing:
 - Develop ASTs for metal bipolar plate materials
 - Correlate degradation in newly proposed GDL AST with Fuel Cell testing
- “Real-world” testing:
 - Complete simulated automotive drive cycle testing on selected materials with differing durability
 - Continue studying effect of operating conditions (stressors) like temperature, pressure and RH on drive cycle testing
- Characterization of materials:
 - Complete ex situ characterization of catalyst particle size distribution, layer thickness, membrane thickness, and GDL hydrophobicity as a function of AST, drive cycle, and “real-world” testing
- Correlation of AST to “real-world” data:
 - Statistical correlation of performance degradation with physical properties in both AST and “real-world” data

FY 2012 Publications/Presentations

1. R. Mukundan, Invited talk, 2nd International Workshop on Degradation Issues of Fuel Cells, Thessaloniki, Greece, September 2011.
2. R. Mukundan, Invited talk, 220th ECS meeting, Boston, MA, October, 2011.
3. R. Mukundan, G. James, J. Davey, D. Langlois, D. Torrace, W. Yoon, A.Z. Weber, and R. Borup, “Accelerated Testing Validation” ECS Trans. 41 (1), 613 (2011).
4. R. Mukundan, G. James, D. Ayotte, J. Davey, D. Langlois, D. Spornkaj, D. Torrace, S. Balasubramanian, A. Weber, K. More, and R. Borup, Accelerated testing of carbon corrosion and membrane degradation in PEM fuel cells, Abstract accepted, 222th ECS meeting, Honolulu, HI.

References

1. R. Borup, J. Meyers, B. Pivovar, et al., *Chemical Reviews*; **107(10)**, 3904 (2007).
2. T.G. Benjamin, Abstracts of the International Workshop On Degradation Issues in Fuel Cells, Hersonessos, Crete, Greece, (2007).
3. N.L. Garland, T.G. Benjamin, J.P. Kopasz, *ECS Trans.*, **V. 11 No. 1**, 923 (2007).
4. S. Knights, G. Escobedo, *Meeting Abstracts of 2006 Fuel Cell Seminar*, Honolulu, HI (2006).
5. A.Z. Weber, J. Newman, “Modeling Transport in Polymer-Electrolyte Fuel cells” *Chemical Reviews*, **V. 104**, 4679-4726 (2004).
6. FreedomCAR Fuel Cell Tech Team Cell Component AST and polarization curve Protocols for PEM Fuel Cells (Electrocatalysts, Supports, Membranes and MEAs), Revised December 16, 2010.
7. D. Wood, Ph.D. Thesis, “Fundamental Material Degradation Studies During Long Term Operation of Hydrogen/Air PEMFCs”, University of New Mexico, (2007).

V.E.6 Development of Micro-Structural Mitigation Strategies for PEM Fuel Cells: Morphological Simulations and Experimental Approaches

Dr. Silvia Wessel (Primary Contact), David Harvey,
Dr. Vesna Colbow

Ballard Power Systems
9000 Glenlyon Parkway
Burnaby, B.C. V5J 5J8
Phone: (604) 453-3668
Email: silvia.wessel@ballard.com

DOE Managers

HQ: Kathi Epping Martin
Phone: (202) 586-7425
Email: Kathi.Epping@ee.doe.gov

GO: David Peterson
Phone: (720) 356-1747
Email: David.Peterson@go.doe.gov

Technical Advisor

John Kopasz
Phone: (630) 252-7531
Email: kopasz@anl.gov

Contract Number: DE-EE0000466

Subcontractors:

- Georgia Institute of Technology, Atlanta, GA (Dr. S.S. Yang)
- Los Alamos National Laboratory, Los Alamos, NM (Dr. R. Borup)
- Michigan Technological University, Houghton, MI (Dr. J. Allen)
- Queen's University, Kingston, Ontario (Drs. K. Karan, J. Pharoah)
- University of New Mexico, Albuquerque, NM (Dr. P. Atanassov)

Project Start Date: January 1, 2010

Project End Date: March 31, 2013

Fiscal Year (FY) 2012 Objectives

- Completion of the molecular dynamics model of the catalyst 3-phase interface.
- Implementation of 2-phase flow in the micro-structural catalyst model and simulation of effective properties and performance with liquid water.
- Validation of the one-dimensional (1D)-statistical membrane electrode assembly (MEA) model as a function of catalyst layer composition and operational conditions, including an investigation of low loaded

catalyst layers using both the 1D-statistical MEA model and micro-structural catalyst model.

- Evaluation of the effect of cathode catalyst layer composition (Pt loading, Pt/C ratio, ionomer equivalent weight) and operational conditions (relative humidity [RH], dwell time at 1.4 V upper potential limit) on degradation mechanisms, performance degradation, and structural changes of the cathode catalyst layer.

Technical Barriers

This project addresses the following technical barriers of the Fuel Cells section of the Fuel Cell Technologies Program Multi-Year Research, Development, and Demonstration Plan [1].

- (A) Durability
Pt catalyst and Pt catalyst layers degradation:
 - Effect of cathode structure and composition
 - Effect of operational conditions
- (B) Performance
 - Effect of cathode catalyst structure and composition
- (C) Cost (in-direct)

Technical Targets

In this project fundamental studies of the Pt/carbon catalyst degradation mechanisms and degradation rates are conducted and correlated with unit cell operational conditions and catalyst layer structure and composition. Furthermore, forward predictive micro- and macro-models for cathode performance and degradation are being developed. Design curves, generated both through model simulations and experimental work, will enable MEA designers to optimize performance, durability, and cost towards the 2020 targets for fuel cell commercialization [1]:

- System Durability (10% performance loss)
 - Transportation applications: 5,000 hours
 - Stationary applications (1-10 kW_e): 60,000 hours
- Electrocatalyst (transportation applications)
 - Support Stability: <10% mass activity loss after 400 hrs @ 1.2 V in H₂/N₂
 - Electrochemically active catalyst surface area (ECSA) loss <40%
 - Precious group metal (PGM) total loading: 0.125 mg/cm²

FY 2012 Accomplishments

- Completed the molecular dynamics-based description of the carbon supported-Pt and ionomer system and evaluated the platinum surface coverage of a variety of moieties.
- Extended validation of the 1D-statistical Unit Cell Performance model over the compositional ranges of interest.
- Model predictions suggest higher water content in low-loaded catalyst layers as a partial cause of low performance and increased oxygen sensitivity.
- Correlated the cathode catalyst layer structure and composition (Pt/C ratio, Pt loading) and operational conditions (RH, temperature) with durability.
- Developed a semi-empirical carbon corrosion model.



Introduction

Catalyst/catalyst layer degradation has been identified as a substantial contributor to fuel cell performance degradation and this contribution will most likely increase as MEAs are driven to lower Pt loadings in order to meet the cost targets for full-scale commercialization. Over the past few years significant progress has been made in identifying catalyst degradation mechanisms [2,3] and several key parameters that greatly influence the degradation rates, including electrode potentials, potential cycling, temperature, humidity, and reactant gas composition [2,4,5,6]. Despite these advancements, many gaps with respect to catalyst layer degradation and an understanding of its driving mechanisms still exist. In particular, acceleration of the mechanisms under different fuel cell operating conditions, due to different structural compositions, and as a function of the drive to lower Pt loadings remains an area not well understood. In order to close these gaps an understanding of the effect of operating conditions and the layer structure and composition on catalyst layer degradation mechanisms and degradation rates is needed.

The project focus is to develop forward predictive models and to conduct systematic cell degradation studies that enable quantification of the cathode catalyst layer degradation mechanisms and rates and correlation of materials properties to key operational and structural parameters.

Approach

Models will be developed at the molecular, micro-structural, and macro-homogeneous scales that include degradation effects related to platinum dissolution, transport and plating, carbon surface oxidation and corrosion, and ionomer thinning/conductivity loss. The models will

provide the ability to study the effects of composition, the morphological design, and the operational window on catalyst degradation via simulated accelerated stress testing (AST). The design curves generated in each scale of the modeling work will enable the development of mitigation strategies through trade-off analysis.

Accelerated stress testing coupled with ‘state-of-the-art’ in situ/ex situ characterization techniques will be used to correlate MEA performance loss with structural changes measured within the Pt cathode; as well as to develop key operational and catalyst/catalyst layer structural degradation design curves. The experimental results will also serve to provide model validation.

Results

Model Development

During this year the modeling efforts continued to focus on advancing capabilities on each of the three length scales. For the molecular dynamics, the focus was on completion of the Pt/ionomer/carbon interface model, with species interactions and estimates of the Pt surface coverage by a variety of moieties. On the micro-structural scale, attention was directed to completing a refinement of the performance solvers with water saturation and the prediction of a capillary pressure relationship for the catalyst morphologies. The unit cell performance model was expanded to transient operation, with the inclusion of a multi-step oxygen reduction reaction description, and integration of a profilometry-based contact resistance model (gas diffusion layer [GDL]/catalyst, GDL/plate).

Molecular dynamics simulations investigated interactions between a bare and oxygen covered Pt particle anchored at graphene sheet dislocations and H_2O , H_3O^+ , O_2 , RSO_3 , and polymer species. The simulations were run at different time scales to probe the state of relaxation of the interface structure. Figure 1A shows the oxygen covered Pt particle and coverage by the various species. An estimation of the concentration of these surface moieties reveals that O_2 molecules appear to prefer the ionomer phase over water and that RSO_3 species interact strongly with the Pt/PtO surface. The interaction and occupation of the various species at the Pt and PtO surfaces (Figure 1B) are important factors in fundamentally understanding the mechanism of Pt dissolution.

The 1D-MEA model which allows for statistical variation of the structural, operational, and physico-chemical parameters was used to study the effect of cathode platinum loadings from 0.05 to 0.5 mg/cm^2 on beginning of test (BOT) performance. The catalyst layer thickness varied linearly from 2.5 μm to 18 μm and ECSA values ranged from 25 to 250; the ECSA values indicated that utilization

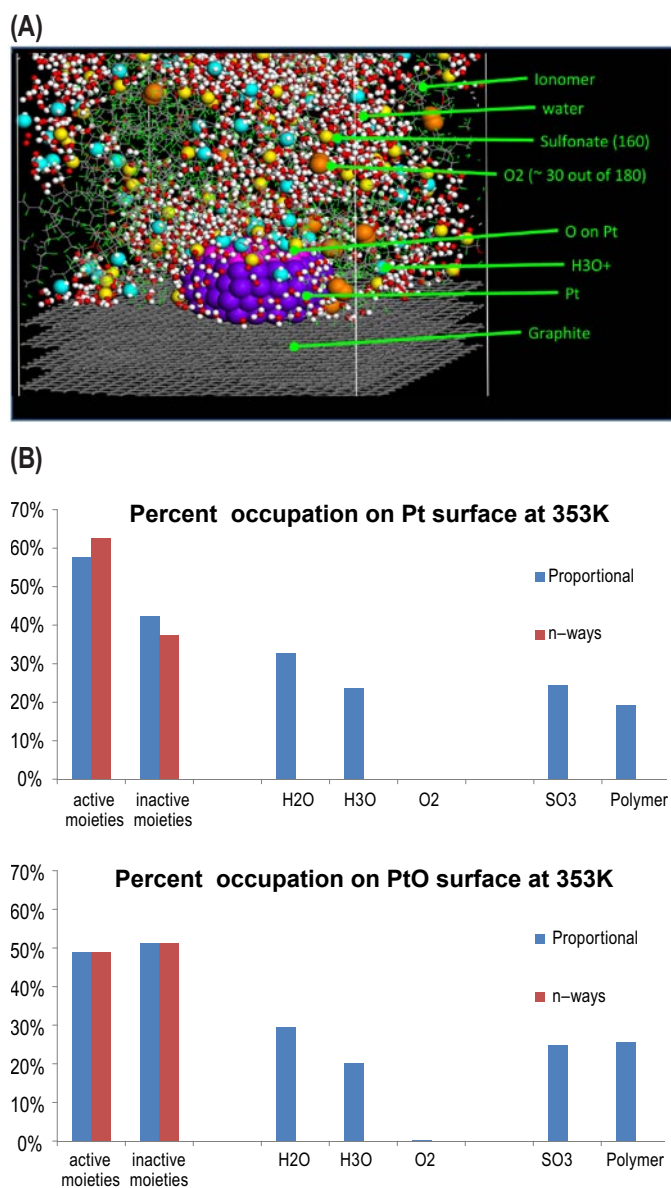


FIGURE 1. (A) Molecular Dynamics Model simulation of PtO anchored on graphene sheets interacting with H_2O , H_3O^+ , O_2 , SO_3 , and polymer species, (B) % occupation of Pt and PtO sites by the moieties.

was nearly constant for the beginning of life (BOL) MEAs across the loading range. As shown in Figure 2A, the model demonstrates the ability to capture the changes in performance between a high and low platinum-loaded cathode under various O_2 partial pressures; specifically the model captures the effect of changes in surface area and reaction penetration within the catalyst layer as a result of proton penetration, oxygen transport, liquid water content. The model results shown in Figure 2B suggest that the increased sensitivity to lower oxygen partial pressures for low loaded catalyst structures was, at least in part, due to higher liquid water saturation levels within the MEA, particularly within the electrode itself.

Experimental Parametric Studies

Efforts within this FY were focused on correlating the cathode catalyst layer structure and composition for a range of platinum loadings and Pt/C ratios with the AST degradation rates. Further, the effect of ionic equivalent weight was studied in order to identify its role on the degradation mechanisms (platinum dissolution and carbon corrosion). A semi-empirical carbon oxidation/corrosion model was developed to assist in understanding and enabling the separation of the effects of oxidation and corrosion as a function of several key variables (operation/structural). The in-house MEAs (low surface area carbon supported Pt catalyst coated on Nafion[®] 211 membrane and sandwiched between Ballard Materials Product GDLs) were subjected to AST cycling using a square wave cycle (30 s at 0.6 V to 60 s at 1.2 V) under baseline operational conditions (air/ H_2 , 80°C, 100% RH). The MEAs used a catalyst with a Pt/C ratio of 50 wt% and a anode/cathode Pt loading of 0.1/0.4 mg/cm² unless stated otherwise. Cell characterization was performed at 0 (BOT), 50, 700, 1,400, 2,100, and 4,700 (end of test [EOT]) cycles with a post mortem failure analysis performed at EOT.

The effect of Pt loading on BOT performance and degradation is shown in Figure 3. For loadings larger than 0.3 mg/cm² (ECSA >75), the performance at 1 A/cm² is relatively constant; however, for low loadings <0.2 mg/cm² (ECSA <50), the BOT performance is severely impacted. As discussed above; this is believed to be due, at least in part, to the increased water content in thin catalyst layers. Figure 3A shows that the performance correlates well with ECSA with the relationship holding as the structure changes and the ECSA is reduced due to Pt dissolution and agglomeration. Moreover, the degradation rate and ECSA loss follow the same trend with Pt loading, as seen in Figure 3B. There is an ~8-fold increase in voltage degradation rate when the Pt loading is reduced from 0.3 to 0.1 mg/cm².

The effect of the Pt/C ratio on the catalyst layer structure (BOT) was primarily through a change in the catalyst layer thickness which ranged from 9 μ m to 31 μ m and the ECSA which varied from ~100 to 200 for Pt/C ratios from 60 to 30 wt%. It was observed that the porosity of the catalyst layer effectively remained unchanged at ~70%; further, the higher Pt/C ratios demonstrated low ECSA primarily due to the presence of substantially larger Pt crystallites. The BOL performance was found to be very similar for all Pt/C ratios while the larger crystallites seen at higher Pt/C ratios were observed to affect the Pt dissolution and agglomeration rates. At EOT (4,700 cycles at 1.2 V upper potential limit [UPL]) the catalyst layer containing 60% Pt/C showed the lowest degradation and the 30% Pt/C showing the highest. ECSA results revealed an ECSA loss at EOL of ~50% independent of the Pt/C ratio. Voltage loss analysis showed that the voltage degradation was predominantly a result of catalyst layer ionic

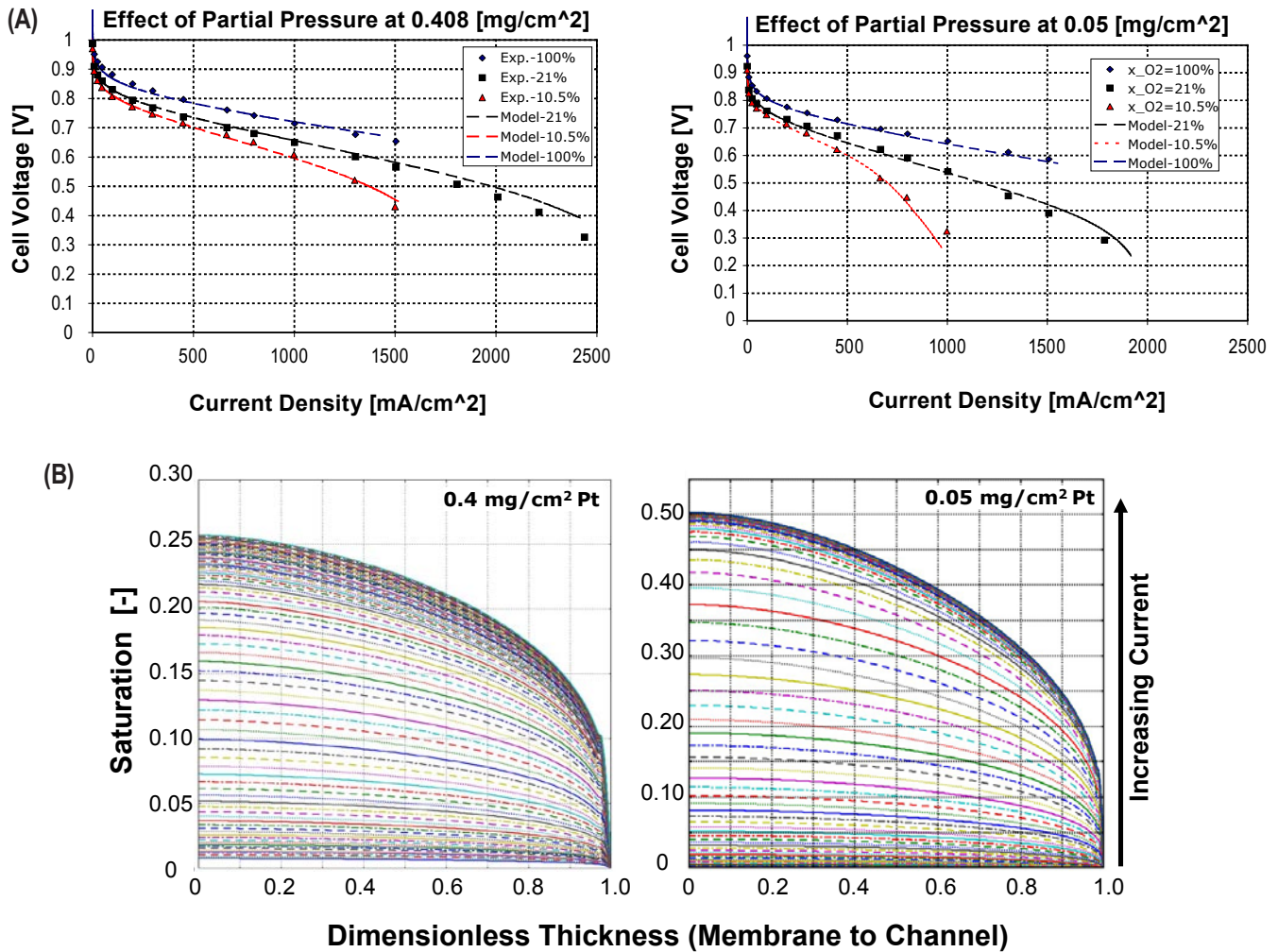


FIGURE 2. (A) 1D-statistical Unit Cell Model BOT performance simulations of 0.4 and 0.05 mg/cm² Pt loaded catalyst layers at different O₂ concentrations, (B) Modeled water saturation characteristics of the 0.4 and 0.05 mg/cm² Pt loaded catalyst layers.

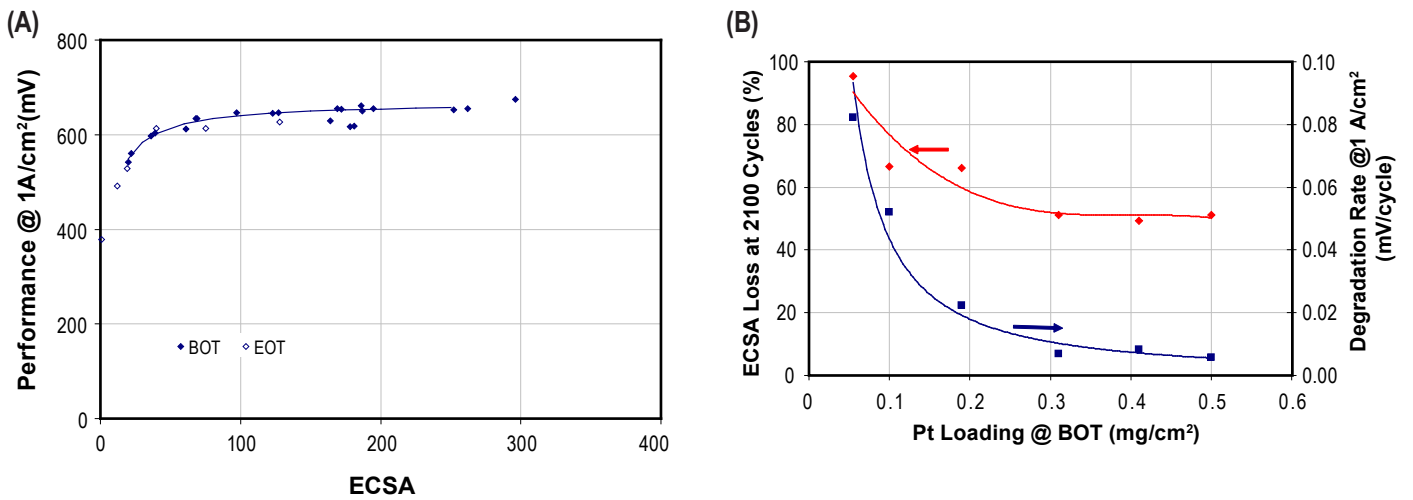


FIGURE 3. (A) BOT and EOT performance characteristics as a function of ECSA, (B) ECSA loss and degradation rate behaviour as a function of cathode catalyst layer loading.

resistance changes due to the reaction penetration pushing further into the catalyst layer as a result of the low ECSA.

Semi-Empirical Carbon Corrosion Model

In order to understand carbon catalyst support degradation, the performance of MEAs subjected to AST cycling at an upper potential limit ranging from 0.9 to 1.4 V was analyzed for changes in double layer capacitance (Cdl). Carbon support corrosion can be separated into two reaction steps: (1) oxidation of the carbon surface forming surface oxide species and (2) corrosion of the carbon sites causing evolution of carbon dioxide/monoxide. The carbon surface oxidation and carbon corrosion reactions have opposing effects on Cdl which enables separation of the two reaction rate constants. Surface oxidation increases the Cdl due to a larger specific capacitance for a carbon surface with carbon-oxygen groups, while the corrosion reaction evolving carbon dioxide/monoxide causes a decrease in the carbon surface area and Cdl. The reaction rate constants, after accounting for the effect of changing platinum surface area due to Pt dissolution/agglomeration on the Cdl, showed a clear trend in increasing reaction rate with UPL for both steps of the corrosion mechanism. A comparison of two carbons with different corrosion resistance (low surface area carbon [LSAC] and medium surface area carbon [MSAC]) showed a distinct difference in the surface oxidation reaction, while the corrosion reaction and the specific capacitances (at BOT and EOT) were similar. Further, to understand the effects of cycling versus potential hold stress tests, i.e. transient vs. pseudo steady-state behaviour, the effect of dwell time at 1.4 V UPL was evaluated between 5 to 600 seconds; no significant differences as a result of increased dwell time were found. Figure 4A shows that the onset of corrosion (performance loss) is dependent on the total time spent at the upper potential rather than the number of AST cycles. Furthermore, as shown in Figure 4B, the onset of corrosion (observed performance loss) decreases logarithmically with increasing upper potential limit. For example, a total time of ~4 hours at a UPL of 1.4 V is equivalent to ~160 hours at a UPL of 1.2 V for the LSAC catalyst, while ~1 hour and ~80 hours were observed for the MSAC catalyst, respectively.

Conclusions and Future Directions

The interim conclusions are:

- Molecular modeling of the carbon/Pt/ionomer and interaction with different moieties showed that the RSO_3^- species of the ionomer side chain strongly interacts with Pt and/or PtO.
- 1D-statistical Unit Cell model predictions of BOT performance for a variety of different catalyst layer structures and operating conditions show good agreement with experimental results over the full range of current densities.

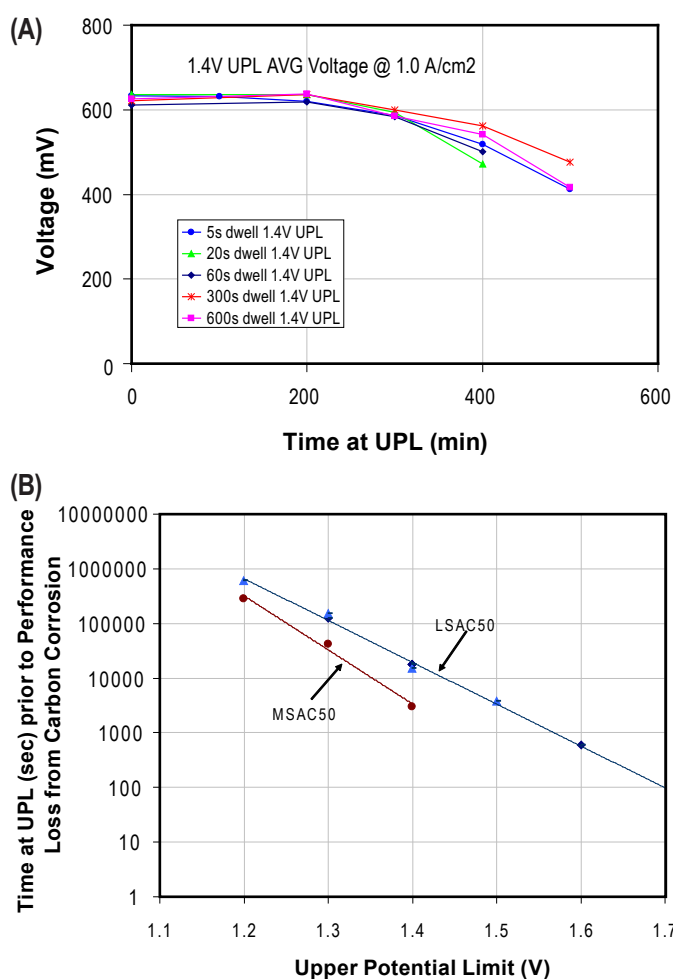


FIGURE 4. (A) Voltage characteristics as a function of dwell time at an upper potential limit of 1.4 V, (B) Onset of carbon corrosion (performance loss) as a function of upper potential limit for two different Pt catalysts (Pt catalyst supported on graphitized carbon [LSAC] and MSAC).

- Cathodes with Pt loadings $<0.2 \text{ mg/cm}^2$ (ECSA <50) exhibit BOT performance that is severely impacted due at least in part, to the increased water content in thin catalyst layers. Degraded catalyst layers that reach ECSA values <50 indicate the same performance impact.
- The catalyst Pt/C ratio (30 to 60 wt%) affects the thickness and ECSA of the catalyst layer. While the BOT performance was not impacted by the Pt/C ratio, the degradation was found to be higher for the lower Pt/C ratios.
- A semi-empirical carbon oxidation/corrosion model was used to separate the carbon oxidation and carbon corrosion reaction rates for different catalyst supports.

Future directions include:

- Complete the Pt dissolution molecular dynamics model

- Expand and refine the Micro-structural catalyst and 1D-statistical Unit Cell Degradation Models and validate with experimental AST cycle data.
- Correlate catalyst materials and structural properties with performance and degradation.

FY 2012 Publications/Presentations

1. A. Patel, K. Artyushkova, P. Atanassov, D. Harvey, M. Dutta, V. Colbow, and S. Wessel, “Effect of Graphitic Content on Carbon Supported Catalyst Performance”, presented at 220th ECS Meeting & Electrochemical Energy Summit in Boston, Massachusetts (October 9-14, 2011).
2. A. Patel, K. Artyushkova, P. Atanassov, D. Harvey, M. Dutta, V. Colbow, S. Wessel, “Effect of Graphitic Content on Carbon Supported Catalyst Performance”, ECS Transactions 41 (1), 845-852, 2011.
3. D.B. Harvey, M. Khakbzbaboli, B. Jayasankar, C.C. Chueh, C.A. Bellemare-Davis, J.G. Pharoah, and K. Karan, “Multi-scale Modelling of the PEMFC Catalyst Layer: Coupling Microstructure to Performance”, presented at 220th ECS Meeting & Electrochemical Energy Summit in Boston, Massachusetts (October 9-14, 2011).
4. J. Pharoah, H-W. Choi, C-C Chueh, D. Harvey, “Effective Transport Properties Accounting for Electrochemical Reactions of Proton-Exchange Membrane Fuel Cell Catalyst Layers”, ECS Transactions 41 (1), 221-227, 2011.
5. Silvia Wessel, David Harvey, Vesna Colbow, “Considering the Role of Component Structure on PEM Fuel Cell Durability”, Presented at Zing Hydrogen and Fuel Cells Conference 2011, Xcaret Mexico, December 1 to 5, 2011.
6. S. Wessel, V. Colbow, D. Harvey, S. Knights, “The Effect of Cathode catalyst structure on PEM Fuel cell Durability”, presented at Grove Fuel Cells Conference 2012, Berlin, April 11–12, 2012.

7. A. Patel, K. Artyushkova, P. Atanassov, V. Colbow, M. Dutta, D. Harvey, S. Wessel, “Investigating the Effects of PEMFC Conditions on Carbon Supported Platinum Electrocatalyst Composition and Performance”, J. Vac Sci & Tech, A: Vacuum, Surfaces, and Films 30 (4), 04D107 – 04D107-7, 2012.

References

1. Hydrogen, Fuel Cells & Infrastructure Technologies Program: Multi-Year Research, Development and Demonstration Plan, U.S. Department of Energy, Energy Efficiency and Renewable Energy, 2011 revision. <http://www.eere.energy.gov/hydrogenandfuelcells/mypp/>
2. J. Wu, X.Z. Yuan, J.J. Martin, H. Wang, J. Zhang, J. Shen, S. Wu, W. Merida, A Review of PEM Fuel Cell Durability: Degradation Mechanisms and Mitigation Strategies. Journal of Power Sources 184, 104-119.
3. R. Borup, J.P. Meyers, B. Pivovar, Y.S. Kim, R. Mukundan, N. Garland, D. Myers, M. Wilson, F. Garzon, D. Wood, P. Zelenay, K. More, K. Stroh, T. Zawodinski, J. Boncella, J.E. McGarth, M. Inaba, K. Miyatake, M. Hori, K. Ota, Z. Ogumi, S. Miyata, A. Nishikata, Z. Siroma, Y. Uchimoto, K. Yasuda, K. Kimijima, N. Iwashita, Scientific Aspects of Polymer Electrolyte Fuel Cell Durability and Degradation. Chemical Reviews 2007, 107, 3904-3951.
4. Y. Shao, G. Yin, Y. Gao, Understanding and Approaches for the Durability Issues of Pt-Based Catalysts for PEM Fuel Cell. Journal of Power Sources 2007, 171, 558-566.
5. M.S. Wilson, F. Garzon, K.E. Sickafus, S. Gottesfeld, Surface Area Loss of Supported Platinum in Polymer Electrolyte Fuel Cells. Journal of the Electrochemical Society 1993, 140, 2872-2876.
6. P.J. Ferreira, G.J. Ia O', Y. Shao-Horn, D. Morgan, R. Makharia, S. Kocha, H. Gasteiger, Instability of Pt/C Electrocatalysts Membrane Fuel Cells A Mechanistic Investigation. Journal of the Electrochemical Society 2005, 152, A2256-A2271.

V.E.7 Analysis of Durability of MEAs in Automotive PEMFC Applications

Randal L. Perry
E.I. du Pont de Nemours and Company
Chestnut Run Plaza, 701/209
4417 Lancaster Pike
Wilmington, DE 19805
Phone: (302) 999-6545
Email: randal.l.perry @usa.dupont.com

DOE Managers

HQ: Kathi Epping Martin
Phone: (202) 586-7425
Email: Kathi.Epping@ee.doe.gov

GO: David Peterson
Phone: (720) 356-1747
Email: David.Peterson@go.doe.gov

Technical Advisor

Thomas Benjamin
Phone: (630) 252-1632
Email: Benjamin@anl.gov

Contract Number: DE-EE0003772

Subcontractors:

- Nissan Technical Center North America, Farmington Hills, MI
- Illinois Institute of Technology (IIT), Chicago, IL

Project Start Date: September 1, 2010

Project End Date: February 28, 2014

target of 5,000 hours with <7% degradation and that show a clear path towards meeting the DOE 2015 technical targets. Actual MEA development is not part of the scope of the funded project. However, development is performed concurrently by DuPont, and some mitigation strategies from the project are included, and the developmental materials tested.

Technical Barriers

This project addresses the following technical barriers from the Fuel Cells section (3.4.5) of the Fuel Cell Technologies Program Multi-Year Research, Development and Demonstration Plan:

- (A) Durability
- (C) Performance

The first is the primary focus, with the second being important to continue to stack testing.

Technical Targets

The technical targets are in terms of timelines and advancement of the modeling and mechanism studies. Performance targets are based on work done by DuPont outside the DOE project, but incorporating mitigation strategies developed in the project. Business changes at DuPont have changed the fuel cell focus from MEAs to membranes and dispersions. With the reduced resources in the MEA areas, we do not expect to meet durability or performance targets for MEAs, only for membranes. The primary project targets are:

- Select and confirm ASTs to be used for modeling work. Timing: 3/31/2012.

Current Status: Complete 4/30/2012

- Select SSC PFSA membrane:
 - Membrane design must meet accelerated durability targets.
 - Results verified in repeated lab testing. Timing: 8/31/2012.

Current Status: Mechanical Durability: 25,000 of 30,000 required cycles completed and still in progress using new reinforcement, vs <10,000 cycles with initial reinforcement.

- Chemical durability: Failure at ~400 of required 500 hrs.
- Define MEA design for stack test:
 - MEA based on durable materials as determined in the lab testing.

Fiscal Year (FY) 2012 Objectives

- Select and confirm accelerated stress tests (ASTs) designed to separate individual degradation mechanisms. The selected tests must ensure that degradation mechanisms seen in membrane electrode assemblies (MEAs) tested in the project match Nissan's automotive experience. The membrane portion of this work is focused on membranes made from short side-chain (SSC) perfluorosulfonic acid (PFSA) polymers.
- Modify selected tests to generate necessary data for developing an overall degradation model. This model will correlate stack operating conditions to degradation of the MEA.
- Define a material set based on initial tests to be used to develop the model and make it applicable to a range of MEA designs.
- Begin defining mitigation strategies for the mechanisms identified in the testing and modeling. These strategies will be used to develop MEAs with a design lifetime

- MEA must meet minimum performance and durability goals. Timing: 9/30/2012.

Current Status: Catalysts limited to a class of commercially available materials. To date, catalysts attain about 80% of required life and 75% of performance.

- MEA design must meet performance and accelerated durability targets with results verified in lab testing in order to proceed to fabrication and testing of a full-scale short stack:

1. Attain 5,000 hr lifetime in durability in automotive cycling protocol.
2. Attain 1 kW/cm² performance @ rated power at beginning-of-life in sub-scale testing.
3. Attain extent of performance decline over lifetime (as in #1 above) of $\leq 7\%$.

Note: Criteria 1 and 3 above will be evaluated using projections based on accelerated testing results, e.g., #1 will be extrapolated from 30,000 cycles. Timing: 9/30/2012.

Current Status: With the emphasis on membranes and dispersions rather than MEAs in DuPont, we do not expect to attain this target.

- Repeatability of AST data is verified to enable confidence in data for modeling work. Timing 9/30/2012.

Current Status: Verified by ex situ testing. Not enough data have been developed for statistical confirmation.

- Stack test: Timing: 3/1/2013.

Current Status: Not anticipated to be carried out.

- Model finalized and ready for publication. Timing: 3/31/2014.

Current Status: Model framework complete, but still early in data acquisition stage.

FY 2012 Accomplishments

- Completed contractual agreements among DuPont, Nissan and IIT.
- Completed multiple repeats of ASTs and analyses for baseline materials.
- Evaluated results and selected ASTs to carry forward.
- Modified testing methods and equipment at Nissan and DuPont to generate more detailed modeling data from the ASTs.
- Illinois Institute of Technology completed project to automate analysis of polarization curves.
- Developed electrochemical impedance spectroscopy methodology to improve understanding of degradation properties.
- Increased mechanical durability of membranes from 8,000 to 16,000 cycles using membrane post-treatment methods.

- Further increased mechanical durability to greater than 25,000 cycles of the 30,000 cycle goal without loss of performance.



Introduction

The components of an automotive fuel cell undergo significant stresses due to the variability of operating conditions: starting and stopping, idling, hill-climbing, cruising and so forth. This project involves the study of the effects of these stresses on the components of an automotive fuel cell stack operating under real-world driving conditions. In terms of the fuel cell stack, these driving conditions can be translated into conditions within the stack itself. For instance, at high temperature ($>80^{\circ}\text{C}$) and low relative humidity (RH) conditions, the conductivity of many membranes become low, resulting in the failure of fuel cell operation [1]. Moreover, membrane mechanical properties also deteriorate under prolonged humidity cycling, leading to membrane failure [2]. The DOE considers the durability of fuel cell components to be among the major technical barriers for successful implementation of fuel cell systems. The minimum required life expectancy for automotive fuel cell stacks is 5,000 hours.

This project is aimed at a better understanding of the degradation mechanisms in the fuel cell stack, and to develop a model to quantify the rate of degradation. Further, the project intends to use the knowledge gained from these and other degradation studies to determine mitigation methods for those mechanisms. Although this project does not include materials development, it is expected that a parallel program, unfunded by the DOE, will develop improved materials based on these mitigation strategies, especially for the membrane and electrode ionomers. These materials will be tested for durability as part of the project.

Approach

The general approach involves testing various components in several ASTs and using both in situ and ex situ methods to analyze the degradation and postulate the degradation mechanisms. These proposed mechanisms are tested by making modifications to the MEAs and further testing in the ASTs. The actual implementation is performed in an iterative fashion.

These studies on materials both before and after the accelerated tests are used first to compare with Nissan stack results and define the best set of accelerated tests to use in this project. The testing and analyses are then extended to a wider range of components, so that a quantitative model of stack degradation is developed. Next, the results of

degradation mechanism work are used to develop methods to mitigate some of these mechanisms in order to increase the durability of the membrane electrode assemblies. These mitigation methods are incorporated into the next phase of testing, and the process continues.

Results

While the contractual agreements were being negotiated, the work focused on testing baseline materials of SSC PFSA membranes with commercially available catalysts and gas diffusion layers (GDLs). Numerous samples were tested using AST protocols from Nissan and the Fuel Cell Tech Team (FCTT). The protocols used are designed to separate four well-known MEA degradation mechanisms:

- Dissolution and re-deposition of the platinum catalyst
- Corrosion of the carbon catalyst support by oxidation
- Chemical degradation of the membrane
- Mechanical failure of the membrane due to mechanical stresses.

Nissan performed tests using their own protocols. DuPont ran the US Fuel Cell Council AST and rebuilt test stations to run the FCTT ASTs. These AST protocols are summarized and compared in Table 1.

From an efficiency perspective, there was a bias toward the Nissan protocols for the catalyst layer due to their significantly shorter test time. After multiple tests were run using all the ASTs, the results of both in situ and ex situ testing were compared. The in situ testing included polarization curves, electrochemically active surface area, hydrogen crossover, and shorting resistance. The ex situ tests included scanning electrode microscope and transmission electron microscope studies, chemical analysis for membrane composition, and fluoride in the cell effluent. Table 2 summarizes the comparison of the methods.

The detailed data were reviewed internally and with the Fuel Cell Tech Team. The conclusions of the project team are that:

- Baseline material set and test protocols show reasonable consistency and behave (in most ways) as expected.
- Nissan ASTs for catalyst degradation appear to demonstrate the same degradation mechanisms as the FCTT ASTs. The FCTT ASTs cause more degradation over the duration of the test, as expected.
- Nissan catalyst ASTs are advantageous for data generation due to much shorter test duration. Supplemental FCTT catalyst ASTs will be run to generate data more representative of end-of-life.
- Nissan and FCTT ASTs results for chemical durability were surprising due to the small differences. Nissan AST was expected to be harsher due to the use of oxygen over air. The differences between the US Fuel Cell Council

TABLE 1. Comparison of AST Protocols used for Baseline Samples

| Test Protocol | Voltage Profile | Test Time | Temp/RH | Notes |
|---|---|----------------------------|----------------|----------------------|
| Carbon Corrosion (Nissan Start-Stop B) | Triangle sweep. 1.0-1.5 V 2 s/cycle | 1,000 cycles <1 hr | 80°C 100% | Significantly faster |
| Carbon Corrosion (FCTT AST) | Hold at 1.2 V | 400 hr | 80°C 100% | |
| Test Protocol | Voltage Profile | Test Time | RH | Notes |
| Pt Dissolution (Nissan Load Cycle) | 3 s @ 0.95 V 3 s @ 0.6 V | 10,000 cycles 17 hr | 80°C 100% | Significantly faster |
| Pt Dissolution (FCTT AST) | Triangle sweep. 0.6-1.0 V 16 s/cycle | 30,000 cycles 134 hr | 80°C 100% | |
| Test Protocol | Voltage Profile | Test Time | RH | Notes |
| Chemical Stability (Nissan OCV hold) | Open Circuit | 500 hr | 90°C 30% | Oxygen on cathode |
| Chemical Stability (FCTT AST) | Open Circuit | 500 hr | 90°C 30% | Air on cathode |
| Chemical Stability (US Fuel Cell Council AST) | Open Circuit | 72 hr | 90°C 30% | Oxygen on cathode |
| Test Protocol | Voltage Profile | Test Time | RH | Notes |
| Mechanical Durability (Nissan) | (varies) | 30,000 cycles ~1,500 hr | 0% to >100% | at 80°C |
| Mechanical Durability (FCTT AST) | N/A | 20,000 cycles 1334 hr | 0% to >100% | at 80°C |

AST and the others agree with data previously released by General Motors.

- Differences in the post mortem results of the FCTT and Nissan membrane durability tests were surprising. We will continue some of both tests until the reasons for the differences are understood.

Going forward, Nissan ASTs will be used as the primary protocols for catalyst degradation, and the FCTT ASTs will be the primary protocols for membrane degradation.

The data generated during the baseline testing was evaluated for use in model development. A number of shortcomings were discovered, and the protocols were refined to provide better data and analysis tools.

TABLE 2. Summary of Comparison of Test Results from ASTs Used in the Project

| Test Protocol | Test Time | ECA Loss | IV Loss | Comments |
|---|------------|--------------|--------------|---|
| Carbon Corrosion (Nissan Start-Stop B) | 8 hrs | 29-35% | 30-35% | Cathode thinned ~15% |
| Carbon Corrosion (FCTT AST) | >400 hrs | >35% | 30-35% | Cathode thinning ~25% |
| Test Protocol | Test Time | ECA Loss | IV Loss | Comments |
| Pt Dissolution (Nissan Load Cycle) | <24 hrs | 35-45% | 4-10% | Pt growth 5-10 nm; Pt migration (including large crystals) |
| Pt Dissolution (FCTT AST) | >135 hrs | >40% | 14-25% | Similar to Nissan. Some larger Pt in cathode. |
| Test Protocol | Test Time | Time to fail | FER | Comments |
| Chemical Stability (Nissan OCV hold) | 500 hrs | 450-500 hrs | 3-4 | 1 - OCV fail, 1 - no fail. Different microscopy results than FCTT AST |
| Chemical Stability (FCTT AST) | 500 hrs | 400 hrs | 0.4-0.7 | Hydrogen crossover fail |
| Chemical Stability (US Fuel Cell Council AST) | 72 hrs | N/A (72 hr) | 0.05 | FER is 60% of Nafion® XL; But, FER >> Nafion® XL in long-term test. |
| Test Protocol | Test Time | Time to fail | Cycles | Comments |
| Mechanical Durability (Nissan) | ~1,500 hrs | 100 hrs | 12k cycles | OCV Failure |
| Mechanical Durability (DOE - DuPont) | >1,350 hrs | 400 hrs | 8,000 cycles | Shorting Resistance Failure |

OCV – open circuit voltage; FER – fluoride emission rate

- The polarization curves were extended so that they include at least five points each over four decades of current.
- Polarization curves are performed for four different cathode gasses: air, oxygen, 21% oxygen in helium, and 4% oxygen in nitrogen.
- Due to the time required to measure four extended polarization curves, the frequency of testing was reduced. At least four sets of curves are measured on each sample in the carbon corrosion and platinum dissolution ASTs. These are beginning of life (BOL), end of life, and at least two intermediate measurements. In all, this allows discrimination of various kinetic and mass-transfer effects at several stages of electrode degradation.
- IIT developed a computer program developed for rapid data organization and analysis.
- Additional membranes and catalysts were defined for the next set of tests.

Modifications to the test stations at Nissan and DuPont were required to perform these tests. These modifications are complete, and testing is underway.

The poor mechanical performance of the baseline membranes led to several variations of the membrane, and some additional needs in testing. First, the baseline membrane, which is reinforced with expanded polytetrafluoroethylene (ePTFE) was treated after manufacture to improve the integrity of the PFSA phase. By varying the conditions of the treatment, the membrane was able to achieve about 16,000 cycles in duplicate tests, compared to 8,000 before the treatment. There was little

change in BOL performance, though there was some loss in chemical durability. The cause of this loss is under study.

In order to more fully understand this mechanism, a set of materials is being tested that use different reinforcements and both SSC and long side-chain polymers. Use of a mechanically weaker reinforcement (in terms of tensile modulus and tear) that reduces swell has been shown to significantly increase lifetime in the mechanical durability test, currently achieving 25,000 cycles and still under test as of this writing. The results are preliminary, but we expect to see significant effects of polymer type and reinforcement type on the membrane durability, and are beginning to explore chemical mechanisms.

Conclusions and Future Directions

- Despite differences in the electrical potential used in the tests, and the additional acceleration factor involved, the Nissan and FCTT catalyst durability tests exhibit similar degradation mechanisms.
- The testing strategy going forward appears to be a reasonable balance of gathering important data and improving sample throughput.
- Further interactions between mechanical and chemical durability were noted, though not understood.

In the next quarter (until the Go/No-Go decisions):

- Complete extended data acquisition and multiple gas testing for modeling of catalyst layer with three different catalysts.

- Continue generating data for modeling, using variants of baseline MEA and GDL.
- Test a matrix of SSC and long side-chain PFSA polymers and mechanically different reinforcements (ePTFE and others) to continue analysis of mechanical/chemical durability interaction.
- Include new ionomers and alternative reinforcements in durability testing.
- Complete ex situ analysis of new test samples.
- Analyze in situ and ex situ data to ensure that results have statistical significance to model building.
- Revise preliminary model as need.

FY 2013

- Continue above items in the iterative method described in the approach.
- Develop mitigation strategies based on analysis of new membrane material sets.
- Test proposed model against data from modified material sets in lab cells.

FY 2012 Publications/Presentations

1. 2012 AMR presentation, May 16, 2012.
2. Poster at Spring 2012 ECS meeting, based in part on work in this project. **Investigating the effect of accelerated catalyst durability tests on PEM fuel cell performance using electrochemical impedance spectroscopy.** Gregory DiLeo, Ramesh Yadav, Nilesh Dale, Kev Adjemian (Nissan)
3. A.V. Anantaraman, C.L. Gardner, “Studies on ion-exchange membranes. Part 1. Effect of humidity on the conductivity of Nafion[®]”, *Journal of Electroanalytical Chemistry*, **1996**, 414, 115-120.
4. F. Bauer, S. Denneler, M. Willert-Porada, “Influence of temperature and humidity on the mechanical properties of Nafion[®] 117 polymer electrolyte membrane” *Journal of Polymer Science: Part B*, **2005**, 43, 786-795.

V.F.1 Air-Cooled Stack Freeze Tolerance

Dave Hancock
 Plug Power Inc.
 968 Albany Shaker Rd
 Latham, NY 12110
 Phone: (518) 782-7700
 Email: david_hancock@plugpower.com

DOE Managers
 HQ: Donna Ho
 Phone: (202) 586-8000
 Email: Donna.Ho@ee.doe.gov
 GO: Reginald Tyler
 Phone: (720) 356-1805
 Email: Reginald.Tyler@go.doe.gov

Technical Advisor
 Walt Podolski
 Phone: (630) 252-7558
 Email: podolski@anl.gov

Contract Number: DE-EE0000473

Subcontractor:
 Ballard Power Systems, Burnaby, British Columbia, Canada

Project Start Date: June 1, 2009
 Project End Date: November 15, 2011

Fiscal Year (FY) 2012 Objectives

- Advance the state of the art in technology for air-cooled proton exchange membrane (PEM) fuel cell stacks and related GenDrive™ material handling application fuel cell systems.
- Demonstrate FCvelocity™ 1020ACS stack durability of 5,000 hours (2.5x nominal durability) through enhanced system operational strategies or utilization of advanced fuel cell stack materials.
- Determine a stack/system concept that is suitable for sub-zero operation down to -30°C.
- Determine a stack/system concept that achieves a total cost that is competitive with incumbent materials handling fuel cell technology solutions.
- Develop, evaluate and trade-off the stack and system to meet materials handling requirements for freeze and cost.
- Develop an understanding around integrating air-cooled stack technology into a dynamic materials handling system.

- Perform life-cycle cost analyses for freeze tolerance strategies.

Technical Barriers

This project addresses the following technical barriers from the Fuel Cells section of the Fuel Cell Technologies Program Multi-Year Research, Development and Demonstration Plan. This plan can be accessed at <http://www.eere.energy.gov/hydrogenandfuelcells/mypp/>).

- (A) Durability (with respect to start-up, freezing and low relative humidity operation)
- (B) Cost (with respect to stack and balance of plant [BOP] trade-off)
- (C) Performance (with respect to voltage degradation, low relative humidity and sub-zero performance)

Technical Targets

| Characteristic (DOE Barrier) | Project Target | Project Results |
|------------------------------|---|---|
| Cost | ≥25% cost reduction compared to liquid cooled stack solution (simultaneously meeting durability and performance targets) | Projected 57% initial product cost reduction and projected 32% product life cycle cost reduction |
| Durability | 5,000 hour stack life with >0.54 volts/cell at 51.7 amps | Validated 5,000 hour durability on 6 air-cooled fuel cell stacks (average durability 5,700 hours) |
| Performance | Sustained operation in -30°C ambient temperature with stack inlet air temperature >0°C and stack temperature gradient <10°C | Designed and validated sustained operation at -30°C ambient temperature; stack inlet temperature >2°C and stack temperature gradient <6°C |

FY 2012 Accomplishments

- Completed testing of next generation membrane electrode assembly (MEA) designs with operating strategies with advanced system operating strategies. The operating strategies focus on reducing cathode catalyst dissolution and corrosion and chemical and mechanical stress on the membrane.
- Developed mitigation strategies for issues found in the prototype system testing.
- Built a system with all mitigation designs and performed system level high and low ambient temperature testing.

Test results demonstrate all issues were successfully mitigated.



Introduction

Plug Power's objective was to advance the state-of-the-art fork-lift technology by use of air-cooled fuel cell stacks and to improve related GenDrive™ material handling systems to improve function and reduce cost. This was accomplished through a collaborative work plan to reduce overall system cost by simplification of the system balance of plant through the use of an air-cooled stack as well as to improve the freeze tolerance and mitigate freeze-thaw failure modes through innovative fuel cell system design.

The fuel cell system was derived from Plug Power's commercially available GenDrive™ platforms, which were used to provide battery replacement for equipment in the material handling industry. The fuel cell stacks were Ballard's commercially available FCvelocity™ 9SSL (9SSL) liquid-cooled PEM fuel cell stack and FCvelocity™ 1020ACS air-cooled PEM fuel cell stack. Plug Power lead the design-build-test and design-of-experiment efforts for the GenDrive™ systems with the support of Ballard Power Systems for the fuel cell stack and stack integration.

Approach

In this project the fuel cell stack, system and fuel cell stack operation were designed together in order to trade off stack durability and freeze function with overall stack-system cost. Both stack and system level mitigation of freeze failure modes were explored. The project developed an understanding of market needs, system requirements, and stack-system limitations and used historical data, models and small-scale testing to define stack/system operating strategies that achieved the required freeze function and durability.

Multiple design, build, test cycles were employed at both the stack and system level to increase the learning through each iteration. Analytical models for durability and freeze were developed and verified on stacks and system modules. Accelerated testing was used to reduce the test duration

where it was possible. Stacks and systems were operated under material handling freezer conditions, failure analysis was performed to understand the root cause of failures, stacks and systems were designed to mitigate the failure modes, then built and tested. Trade-off analysis was used to determine the design solutions that were built and tested.

Results

Durability tests for the current design (V2) MEA and an advanced concept (V2-A) MEA were completed and are compared against the prior test results of the original (V1) MEA. The V2 MEA has a catalyst which is more resistant to carbon corrosion than the V1. The V2-A MEA has the additional feature of a membrane that is more resistant to transfer leaks (cross leaks from anode to cathode). System operating strategies were developed in collaboration with Ballard to mitigate stressors linked to cell and stack failure modes. The following stressors were identified: A) Air-air starts degrade the catalyst and cause voltage degradation; B) Time at open-circuit voltage (OCV) degrades the membrane and causes transfer leaks; C) High currents and stack temperatures stress the membrane; D) Mixed potentials (at start-up and shutdown) degrade the catalyst. Table 1 identifies the MEA type and system strategy and also summarizes the test results.

The stacks were tested using a simulated material handling load profile; the stack load was modeled analytically for the stack durability tests. Figure 1 shows the average cell voltage over time for the stacks and system strategies tested. Figure 2 illustrates when a transfer leak (cross leak from anode to cathode) occurs in the stack at one or more cells. A pressure decay measurement is taken with the anode loop closed. Stack SN 8135 which operated with a system control strategy to reduce the time at OCV ran over 6,400 hours and did not develop a transfer leak. Stack SN 13086, which incorporates a membrane more resistant to transfer leaks, operated over 5,200 hours without a transfer leak. Note that for stack SN 13086, large leaks were measured several times between 2,200 and 2,800 hours that were due to test stand issues; once these leaks were repaired the stack leakage rate returned to normal. Stack SN 8134, 13077 and 13078 all show transfer leak initiation started around 4,200 hours. This was expected for the V2 MEA (13077 and 13078) compared

TABLE 1. Summary of Stack Test Results

| Stack | Cells | MEA | Strategy | Hours | Cycles | Deg Rate at 51.7A (µV/hr) | Transfer Leak | Completed |
|---------|-------|------|----------|-------|--------|---------------------------|---------------|-----------|
| SN8134 | 36 | V1 | A, C, D | 6253 | 2163 | -16.2 | Yes | 2010 |
| SN8135 | 36 | V1 | B, C | 6456 | 3275 | -27.1 | No | 2010 |
| SN13077 | 36 | V2 | A, C, D | 5785 | 1119 | -16.8 | Yes | 2011 |
| SN13078 | 36 | V2 | A, C, D | 7054 | 1354 | -15.6 | Yes | 2011 |
| SN13086 | 36 | V2-A | A, C, D | 5261 | 1019 | -13.3 | No | 2011 |

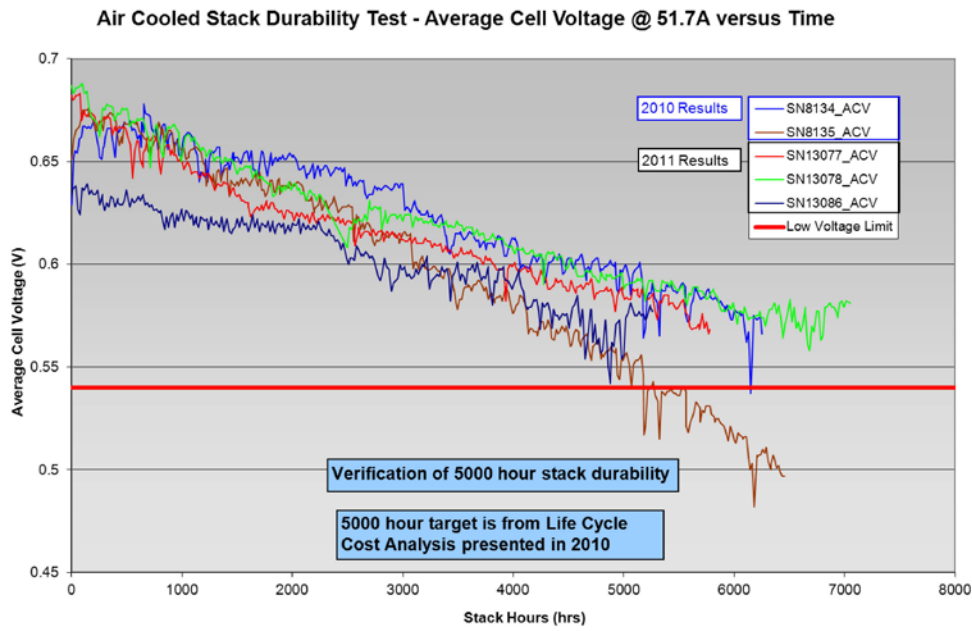


FIGURE 1. Average Cell Voltage versus Time

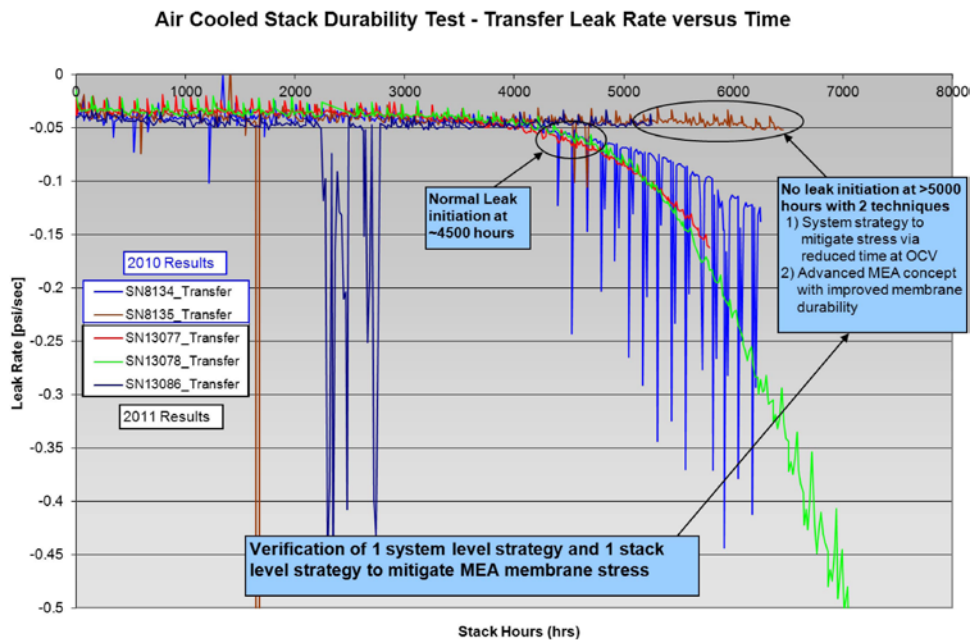


FIGURE 2. Stack Transfer Leak Rate versus Time

to the V1 MEA (8134) because the membrane durability was not addressed in the V2 design. Specific membrane improvements were made on the V2-A MEA (13086) and the test results demonstrate the effectiveness of those improvements.

The final system built with freeze mitigation strategies was tested at both low and high ambient temperatures. All

issues found during the initial test phase were addressed and mitigation strategies selected are as follows.

Initial testing at high ambient temperature indicated the system pressure drop was too high on the cathode to properly cool the stack at a +40°C ambient temperature. A lower pressure drop filter was developed during the design mitigation phase. System level high ambient temperature

testing proved the fan was able to maintain the target stack temperatures at a +40°C ambient temperature.

Initial testing indicated a high inlet air temperature gradient across the stack and that moisture was condensing and freezing in some areas. Computational fluid dynamics (CFD) modeling was used to improve the inlet air temperature gradient. It proved so effective that auxiliary heaters were not required to obtain target air inlet temperatures even while operating in a -30°C ambient temperature environment. CFD models were validated by module level testing in an environmental test chamber. Additional duct work refinements plus manufacturing

changes to allow simpler duct fabrication were again tested at the module level to verify the final design configuration. In addition to not needing auxiliary heaters, the ducting improvements also demonstrated that no moisture was condensing or freezing in the recirculation loop. In a low ambient temperature environment, warm stack exhaust air is efficiently moved to the stack inlet and then mixed with the cold ambient air. Target stack inlet temperatures as well as temperature gradients are maintained over the entire operating regime.

Additionally, air-cooled stack durability was investigated in more detail because even though initial stack testing proved the 5,000 hour life target could be met; any gains in durability only stand to improve the product life cycle cost. The startup controls and idle time were modified to create a 46% reduction in the number of air-air starts (strategy A improvement). Additionally a cathode air starve technique was developed to minimize oxide layer growth on the catalyst; this improves cell performance because it allows the MEA to operate at a higher potential. If an oxide layer builds on the catalyst the performance is suppressed and the stack will reach end of life sooner. The strategy to minimize mixed potentials on shutdown was optimized to minimize carbon corrosion (strategy D optimization).

Final system verification testing at a low ambient temperature of -30°C was performed in the environmental testing chamber at Plug Power. Figure 3 shows the test set up and Figure 4 shows the test results. The system was operated at both high and low loads over an 8-hour period.



FIGURE 3. Final System Shown in Plug Power Environmental Testing Chamber

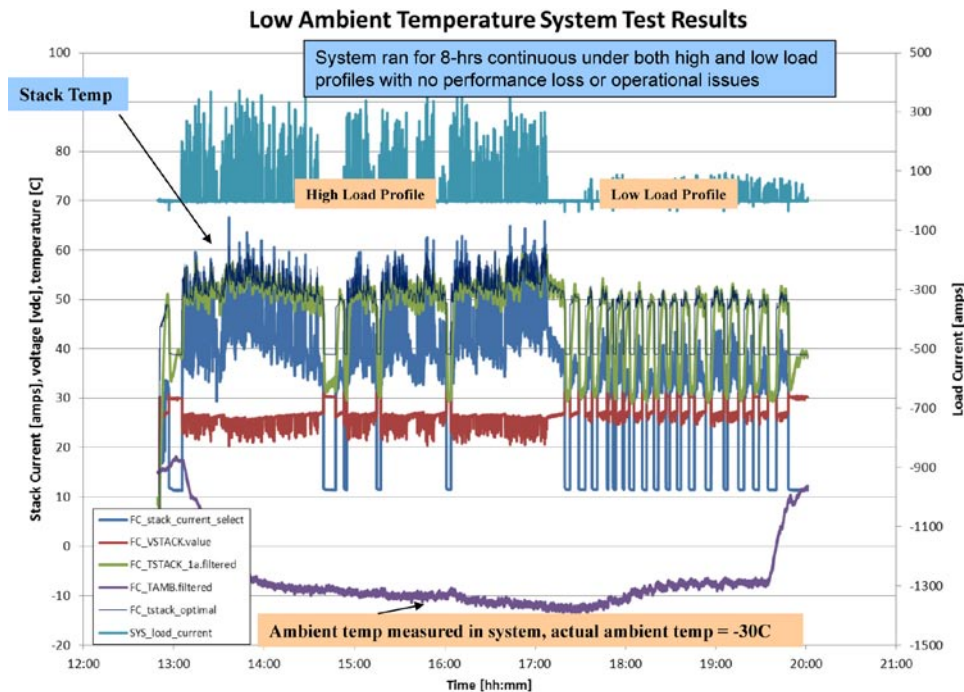


FIGURE 4. System Test Results from -30°C Ambient Temperature Testing

No performance or operation issues were observed and the system was able to maintain the optimal stack temperature. This test data is the culmination of all the freeze tolerance operation strategies developed and optimized over the course of this project.

The Air-Cooled Stack Freeze Tolerance project with DOE support was a success for Plug Power on multiple fronts. First, several technical achievements were realized through the work of this project; from proving 5,000 hour durability with an air-cooled stack, to understanding and addressing failure modes for both durability and freeze tolerance to the operation of an air-cooled stack in a -30°C ambient temperature environment without the use of heaters. And second, Plug Power demonstrated commercial success by releasing a new, 30% lower cost, fuel cell product that incorporated the learning from this project. The new GenDrive Class 3 fuel cell would not have been able to drive a step change in the cost structure without all the achievements from the Air-Cooled Stack Freeze Tolerance project. This project was able to translate research and development into commercial success.

Conclusions and Future Directions

- 5,000 hour durability target met with advanced MEA designs developed to improve corrosion resistance and membrane durability operating with system strategies developed to reduce air-air starts, OCV time and mixed potentials at shut down.
- Sustained operation at -30°C possible with system mitigation strategies employed and without the use of heaters.
- Product cost and life cycle cost analysis demonstrates significant lower cost utilizing ACS technology for material handling order picker applications.

This project is complete. Plug Power would like to express thanks to the DOE and Ballard Power Systems for the work and contributions that helped make this project a success.

FY 2012 Publications/Presentations

- 1. PEM Cathode Catalyst Layer Degradation with Ambient and Freeze-Thaw Cycling;** Joanna Kolodziej P.Eng and Cara Startek; Ballard Power Systems, ASME Conference – August 2011.
- 2. PEMFC MEA and System Design Considerations;** S. Knights, R. Bashyam, P. He, M. Lauritzen, C. Startek, V. Colbow, T. T. H. Cheng, J. Kolodziej, and S. Wessel, meeting abstract, Electrochemical Society 1102, 774 (2011).
- 3. Durability Approach for Air Cooled Stack Integration in a Materials Handling Application;** Cara Startek and Shanna Knights, Ballard Power Systems, Small Fuel Cells Conference 2011.

V.F.2 Fuel Cell Fundamentals at Low and Subzero Temperatures

Adam Z. Weber

Lawrence Berkeley National Laboratory (LBNL)
1 Cyclotron Rd, MS 70-108B
Berkeley, CA 94720
Phone: (510) 486-6308
Email: azweber@lbl.gov

DOE Manager

HQ: Donna Ho
Phone: (202) 586-8000
Email: Donna.Ho@ee.doe.gov

Subcontractors:

- Los Alamos National Laboratory, Los Alamos, NM
- United Technologies Research Center, East Hartford, CT
- 3M Company, St Paul, MN
- The Pennsylvania State University, State College, PA

Project Start Date: September 21, 2009

Project End Date: September 30, 2013

Technical Targets

This project is conducting fundamental investigations into fuel cell operation at low and subzero temperatures. The knowledge gained will enable various metrics to be met or exceeding. These include those related to durability, performance, and cost. Specially:

- Durability
 - 5,000 hr (automotive) and 40,000 hr (stationary)
 - Thermal cycling ability with liquid water
- Performance
 - Unassisted start from -40°C
 - Cold start to 50% power in 30 seconds and with 5 MJ or less energy
 - Efficiency of 65% and 55% for 25% and 100% rated power, respectively
 - Stack power density of 2 kW/kg
 - Precious group metal loading of 0.2 g/kW
- Cost: \$15/kW_e

Fiscal Year (FY) 2012 Objectives

- Fundamentally understand transport phenomena and water and thermal management at low and subzero temperatures
- Examine water (liquid and ice) management with nano-structured thin-film (NSTF) catalyst layers
- Develop diagnostic methods for critical properties for operation with liquid water
- Elucidate the associated degradation mechanisms due to subzero operation and enable mitigation strategies to be developed

Technical Barriers

This project addresses the following technical barriers from the Fuel Cells section of the Fuel Cell Technologies Program Multi-Year Research, Development and Demonstration Plan:

(A) Durability

(C) Performance

- Cell Issues
- Stack Water Management
- System Thermal and Water Management
- System Start-Up and Shut-Down Time and Energy/Transient Operation

FY 2012 Accomplishments

- Site baseline data converged and systematic cell testing was initiated which showed possible ohmic-limitations with NSTF at lower temperatures.
- Measured adhesion forces accurately and representatively for droplets on the gas diffusion layer (GDL) surface.
- Isothermal data demonstrated low ice capacity of NSTF but superb durability.
- Examined in-depth the underlying membrane structure/function relationships.
- Examined water uptake in traditional catalyst layers:
 - Low uptake in ionomer due to interfacial character and morphology
 - Slow freeze kinetics
 - Some hydrophilicity which depends strongly on existence of cracks



Introduction

Polymer-electrolyte fuel cells experience a range of different operating conditions. As part of that range, they are expected to be able to survive and start at low and subzero temperatures. Under these conditions, there is a large amount of liquid and perhaps frozen water due to the low vapor

pressure of water. Thus, water and thermal management become critical to understanding and eventually optimizing operation at these conditions. Similarly, durability aspects due to freeze and low temperatures are somewhat unknown and need further study to identify mechanisms and mitigation strategies. In addition, it is known that thin-film catalyst layers such as the NSTF developed by 3M have issues with large amounts of liquid water due to their thinness. These layers provide routes towards meeting the DOE cost targets due to their high catalytic activities. This project directly focuses on the above aspects of operation at lower temperatures with both NSTF and traditional catalyst layers with the goal that improved understanding will allow for the DOE targets to be met with regard to cold start, survivability, performance, and cost.

Approach

The overall approach is to use a synergistic combination of cell, stack, and component diagnostic studies with advanced mathematical modeling at various locations (national laboratories, industry, and academia). Ex situ diagnostics are used to quantify transport properties and to delineate phenomena that are used in the modeling. The one plus two-dimensional cell model is developed and validated by comparison of measured in situ cell performance in single cells under a variety of cell assemblies and architectures to highlight specific controlling phenomena. Durability is probed by doing cycling and other stress tests as well as taking failed cells from the in situ testing and duplicating their failure ex situ. To understand controlling phenomena and the impact of various layers, a systematic investigation at the component scale is accomplished including the development of a suite of ex situ diagnostics that measure and evaluate the various critical material properties and transport-related phenomena.

Results

As fuel cells operate at low and subzero conditions, liquid water and water management become more important. Thus, there is a need to study properties of the porous fuel cell layers in the presence of liquid water. It is also expected that this probably is exacerbated in thin-film catalyst layers such as NSTF. To test the limitations in NSTF cells, baseline cells (3M 2009 “Best in Class”) were studied using polarization-curve analysis at different temperatures. First, the cells must be properly broken-in using thermal cycling, which consists of fixed-flow polarization curves at 70°C (for 40 min), followed by open-circuit cool down by liquid-water injection (for 40 min). These cycles help remove contaminants and establish water pathways through the system. Once conditioned, hydrogen-pump experiments were carried out at different temperatures and the results compared to those obtained using traditional Pt/C catalyst layers. To

analyze the results, the change in polarization at different temperatures and humidities are plotted as shown in Figure 1. The analysis follows that of Perry and coworkers where the sharp increase at the lower humidity is seemingly due to mass-transport and probably ionic-transport limitations, which agrees with similar oxygen-reaction-order analysis (not shown). Also, at lower temperatures, the NSTF cell shows a kinetic loss indicative of the slow change in potential after dropping temperature. These simple characterization measurements can help to delineate what is limiting in the cell, and focus optimization and further diagnostic efforts.

While understanding performance is important, durability issues are also critical for the eventual use in applications. To study and compare different catalyst layers in terms of durability issues related to low temperatures, freeze/thaw experiments were conducted. These experiments were done both within a cell as well as in an environmental scanning electron microscope (ESEM). For the former, Figure 2(a,c) shows that the NSTF demonstrated negligible decay in polarization performance after 10 freeze/thaw cycles, whereas the traditional catalyst layer did exhibit a performance decrease. These results can be explained by Figure 2(b,d), where freeze/thaw cycling in the ESEM demonstrated that the traditional catalyst layer develops substantially more cracks than the NSTF one. The reason for this is that the traditional catalyst layer has ice that forms in between the catalyst particles which forces the layer apart, whereas for the NSTF, the water forms mainly on the surface. In addition, the NSTF itself is a stronger layer due to the underpinning of the substrate and the existence of the Pt-extended surface.

A key issue in operating at lower temperatures is water removal from the cell. This removal is most often accomplished by liquid droplets entering the gas channels in the flowfield. The way in which the droplets detach has been modeled previously using a force balance. However, the

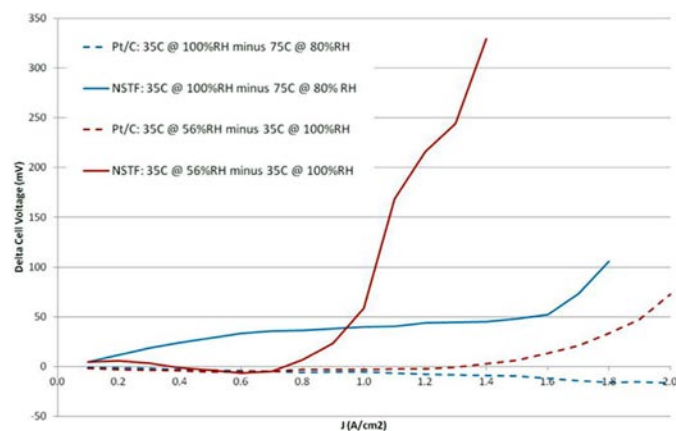


FIGURE 1. Polarization-performance changes for both traditional and NSTF catalyst layers at different temperatures or relative humidities

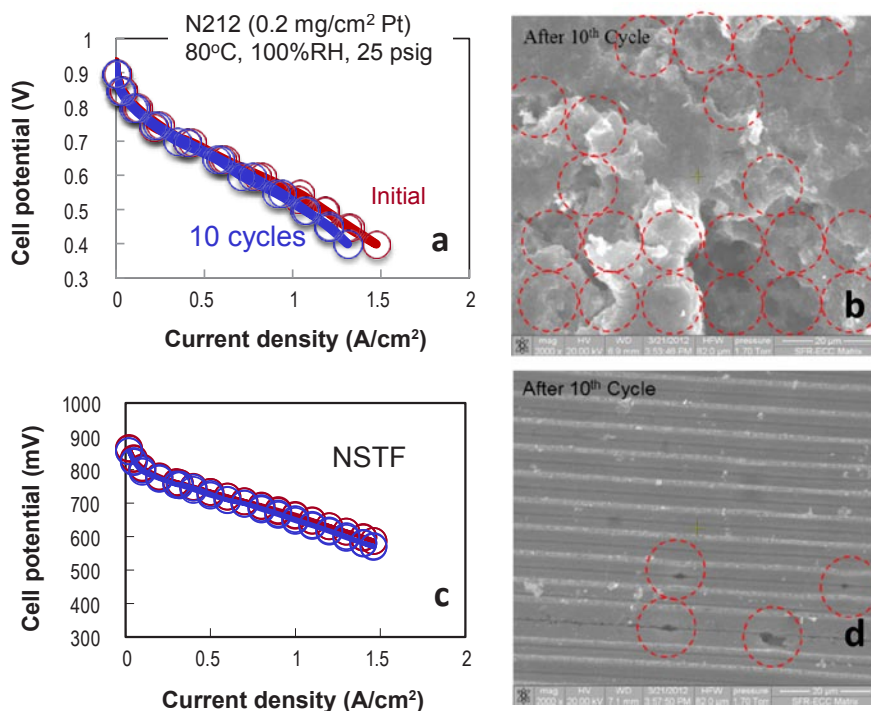


FIGURE 2. Polarization performance both initial and after 10 freeze/thaw cycles for a traditional (a) and NSTF (c) catalyst layer; and the resulting ESEM profiles after 10 freeze/thaw cycles in the ESEM for traditional (b) and NSTF (d) catalyst layers, where the circles denote existence of cracks

droplet adhesion force or force to remove the droplet from the surface was taken either from experiments of droplets placed on the surface or through ancillary studies like droplet contact-angle hysteresis. In the last year, we utilized a custom-built goniometer to calculate directly the adhesion force of droplet injected through the GDL. The apparatus functions by injecting a droplet of a given volume through the GDL, and then rotating the whole apparatus and measuring the angle at which the droplet falls off as shown in Figure 3 (a and b). This angle is then used to calculate the gravity force to remove the droplet, which, when normalized for the wetted diameter of the droplet on the surface, is the adhesion force. Resulting measurements are shown in Figure 3 (c and d) for the top placement and bottom injection. As shown, the adhesion force is a function of poly-tetrafluoroethylene (PTFE) content, where some minimal content is required to lower it (i.e., make it easier to remove the droplets). Also, the bottom injection demonstrates a much higher adhesion force due to the underlying water column attached to the droplet, something that has been ignored in previous analyses. This test and these forces will allow for a more complete picture of water-droplet removal to emerge and better modeling and understanding of low-temperature fuel cell operation.

Other diagnostics are aimed at determining what happens when water freezes in the various fuel cell layers. Last year, we developed a rate expression for freeze kinetics and data using nucleation theory and dynamic scanning

calorimetry. This year we adapted this to catalyst layers with the results that catalyst layers freeze slower than GDLs at the same subcooling, which we believe is due to nucleation on a small spherical particle instead of a long fiber. Also, this year we examined water uptake in traditional catalyst layers in more detail showing that the capillary properties of the catalyst layer are similar but slightly more hydrophilic than GDLs. However, this behavior depends strongly on cracking where cracked samples are more hydrophilic. In addition, we also confirmed and expanded the study of water uptake into catalyst-layer ionomer, showing that it is not a diffusive process but dominated probably by polymer relaxation, and also results in much lower water uptake than in bulk ionomer.

In terms of the last point, a lot of work was done to understand better the structure/function relationships of ionomer membranes. To this end, we developed a relatively straightforward energy-balance approach for predicting membrane water uptake. This approach is based on equating the chemical energy of solvation with that of the mechanical energy on the polymer (either external or internal) to keep it from dissolving. The multiscale model relies on information from both the macroscale (i.e., water uptake and λ , moles of water per sulfonic acid group) and the nanoscale (i.e., distance between ionomer domains or d-spacing). To understand the latter, small-angle X-ray scattering (SAXS) studies were done using the Advanced Light Source at LBNL. These studies revealed a figure of merit as shown

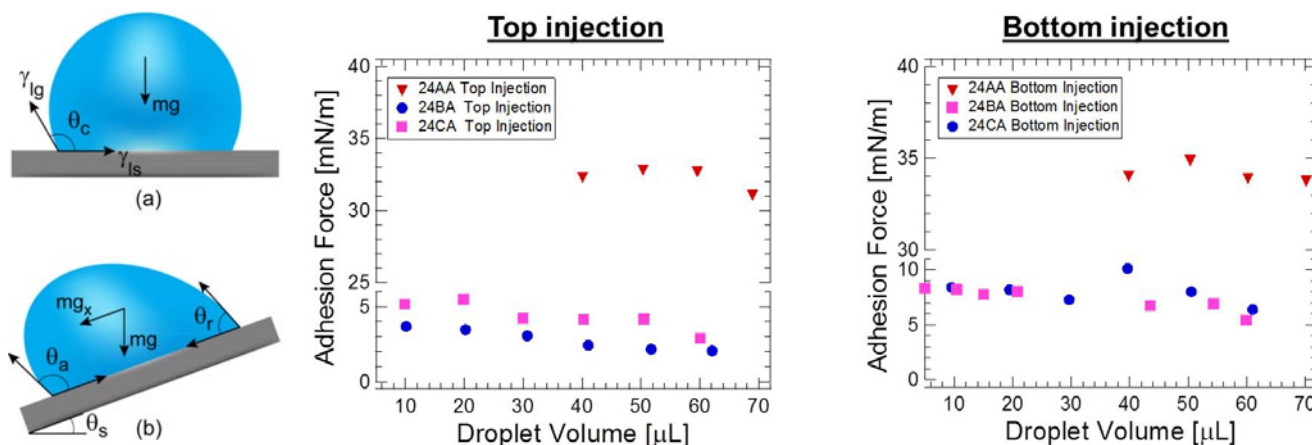


FIGURE 3. Schematic of a droplet on a GDL surface both sessile (a) and at the critical sliding angle (b); and droplet adhesion force as a function of droplet volume for three GDLs of different PTFE content (A=0, B = 5%, C = 10%) for both a top placement (c) and bottom injection (b) of the droplet

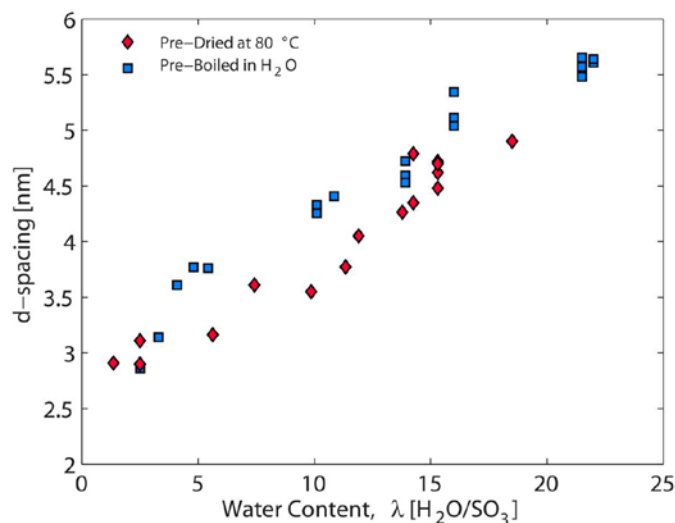


FIGURE 4. Hydrophilic domain spacing as a function of water content for a preboiled and pre-dried or as-received Nafion® 212 membrane

in Figure 4, which demonstrates a linear correlation in terms of the d-spacing and λ . Furthermore, as also shown, while the swelling changes with water content are similar for both an as-received or pre-dried membrane and a pre-boiled membrane, the actual values are different which demonstrates that the morphology and underlying structure/function relationship are also different. We have also shown that this difference can probably be attributed to a change in the structure of the ionic domains with more cylindrical domains existing for the preboiled sample. In addition, other SAXS studies explored how the drying or annealing of the membrane results in backbone crystallinity and this changes the mechanical energy which results in lower uptake. Throughout, the model and the studies underline the importance in reporting membrane conditions and any pretreatment when reporting experimental data.

Conclusions and Future Directions

The project focus this year was on developing and utilizing diagnostic methods for fuel cell components at low temperatures. To this end, several novel methods were developed and measurements for both traditional and NSTF catalyst layers made. The results allow for a better understanding of liquid and ice formation and movement within the cell. In addition, single-cell testing of NSTF cells was accomplished and site-to-site agreement obtained, where the latter is dependent on the way in which the cells are thermally cycled or conditioned before testing. In terms of modeling, both component-level models (e.g., membrane) and multidimensional models were developed and examined, with the latter showing that a two-dimensional framework is sufficient for modeling the critical transport-related phenomena. In terms of future work, this can be summarized as:

- Cell Performance
 - Testing of non-baseline assemblies
 - Examine low-temperature behavior and conditioning for NSTF Pt_3Ni_7
 - Impact of anode GDLs
 - Adiabatic starts including NSTF and low-loaded traditional membrane electrode assemblies
 - Temperature and power transients including neutron-imaging analysis
- Component Characterization
 - Catalyst Layers
 - More data on water-related properties including ionomer morphology, freeze, water uptake, and gas diffusion
 - Study proton migration along NSTF whiskers
 - Diffusion Media

- Measure effective gas-diffusion coefficient as a function of saturation
- Determine how liquid water gets out of the GDL (boundary condition)
- Membrane
 - Structure/function relationships, especially with reinforced membranes and impact of environment
- Modeling
 - Use data from all partners and understand the anode GDL and water-out-the-anode scheme for NSTF
 - Develop transient model and examine catalyst layer water capacity versus water removal fluxes or resistances as a function of catalyst layer thickness
 - Mechanical stress model and its impacts on performance
- Examine failed membrane electrode assemblies and cyclical isothermal cold starts for durability concerns
- Understand and increase the operating window for thin-film catalyst layers

Awards

1. The PI of this project was awarded the Supramaniam Srinivasan Young Investigator Award of the Energy Technology Division of the Electrochemical Society.
2. Work on the catalyst-layer diagnostics was awarded a Best Poster Paper at the 2012 Grove Fuel Cell Science and Technology Conference in Berlin.

FY 2012 Publications

1. Ahmet Kusoglu and Adam Z. Weber, 'Water Transport in Nafion Membranes,' in *Polymers for Energy Storage and Delivery: Polyelectrolytes for Batteries and Fuel Cells*, Kirt A. Page, Christopher L. Soles, and James Runt, Editors, ACS Symposium Series, 175-199 (2012).
2. Daniel S. Hussey, Dusan Spornjak, Adam Z. Weber, Rangachary Mukundan, Joseph Fairweather, Eric L. Brosha, John Davey, Jacob S. Spendelow, David L. Jacobson, and Rodney L. Borup, 'Accurate measurement of the through-plane water content of proton-exchange membranes using neutron radiography,' *J. Appl. Phys.*, submitted (2012).
3. Ahmet Kusoglu, Alexander Hexemer, Ruichun Jiang, Craig S Gittleman, and Adam Z. Weber, 'Effect of Compression on Conductivity and Morphology of PFSA Ionomers,' *J. Membrane Science*, in press (2012).
4. Miguel A. Modestino, Ahmet Kusoglu, Alexander Hexemer, Adam Z. Weber, and Rachel A. Segalman, 'Controlling Nafion Structure and Properties via Wetting Interactions,' *Macromolecules*, **45** (11), 4681-4688 (2012).
5. Prodip K. Das, Adam Grippin, Anthony Kwong, and Adam Z. Weber, 'Liquid-Water-Droplet Adhesion-Force

Measurements on Fresh and Aged Fuel-Cell Gas-Diffusion Layers,' *Journal of The Electrochemical Society*, **159** (5), B489-B496 (2012).

6. Thomas J. Dursch, Monica A. Ciontea, Clayton J. Radke, and Adam Z. Weber, 'Isothermal Ice-Crystallization Kinetics in the Gas-Diffusion Layer of a Proton-Exchange-Membrane Fuel Cell,' *Langmuir*, **28** (2), 1222-1234 (2012).
7. Ahmet Kusoglu, Miguel A. Modestino, Alexander Hexemer, Rachel A. Segalman, and Adam Z. Weber, 'Subsecond Morphological Changes in Nafion during Water Uptake Detected by Small-Angle X-Ray Scattering,' *ACS Macro Letters*, **1**, 33-36 (2012).
8. Ahmet Kusoglu, Brian L. Kienitz, and Adam Z. Weber, 'Understanding the Effects of Compression and Constraint on Water Uptake of Fuel-Cell Membranes,' *J. Electrochem. Soc.*, **158** (12), B1504-B1514 (2011).
9. Gi Suk Hwang, Massoud Kaviani, Jeffrey T. Gostick, Brian Kientiz, Adam Z. Weber, and Moo Hwan Kim, 'Role of Water States on Water Uptake and Proton Transport in Nafion using Molecular Simulations and Bimodal Network,' *Polymer*, **52**, 2584-2593 (2011).
10. Haluna P. Gunterman, Anthony Kwong, Jeff T. Gostick, Ahmet Kusoglu, and Adam Z. Weber, 'Water Uptake in PEMFC Catalyst Layers,' *ECS Transactions*, **41** (1), 647 (2011).
11. Prodip K. Das, Adam Grippin, and Adam Z. Weber, 'Detachment of Liquid-Water Droplets from Gas-Diffusion Layers,' *ECS Transactions*, **41** (1), 459 (2011).
12. Adam Z. Weber, 'Macroscopic Modeling of the Proton-Exchange-Membrane Fuel-Cell Catalyst Layer' *ECS Transactions*, **42** (1), 71-84 (2012).

FY 2012 Presentations

1. Adam Z. Weber, 'Macroscopic Modeling of the Proton-Exchange-Membrane Fuel-Cell Catalyst Layer,' *221st Meeting of the Electrochemical Society*, Seattle, Washington, May 2012. (invited talk)
2. Ahmet Kusoglu and Adam Z. Weber, 'Modeling Water Uptake in Fuel-Cell Membranes,' ModVal 9, Sursee, Switzerland, April 2012.
3. Ahmet Kusoglu, Anthony Kwong, Kyle Clark, Haluna Gunterman, and Adam Z. Weber, 'Water Uptake in Fuel-Cell Catalyst Layers,' *Fuel Cells 2012 Science & Technology*, Berlin, Germany, April 2012.
4. Ahmet Kusoglu and Adam Z. Weber, 'Understanding Schroeder's Paradox,' *March APS Meeting*, Boston, Massachusetts, March 2012.
5. Ahmet Kusoglu and Adam Z. Weber, 'Water Sorption and Related Structure-Function Properties of Nafion at Multiple Time- and Length-Scales,' *220th Meeting of the Electrochemical Society*, Boston, Massachusetts, October 2011 (invited talk).
6. Prodip K. Das and Adam Z. Weber, 'Detachment of Liquid-Water Droplets from Gas-Diffusion Layers,' *220th Meeting of the Electrochemical Society*, Boston, Massachusetts, October 2011.
7. Ahmet Kusoglu, Ruichun Jiang, Craig S Gittleman, and Adam Z. Weber, 'Effect of Compression on Conductivity and Morphology of PFSA Membranes,' *242nd ACS National Meeting & Exposition*, Denver, Colorado, August 2011.

8. Prodip Das, Haluna Gunterman, and Adam Z. Weber, 'Understanding Water Removal from Fuel-Cell Gas-Diffusion Layers,' *European Fuel Cell Forum 2011*, Lucerne, Switzerland, June 2011.

9. Adam Z. Weber, Wonseok Yoon, and Prodip Das, 'Continuum Modeling of Fuel-Cell Transport Phenomena,' *219th Meeting of the Electrochemical Society*, Montreal, May 2011 (invited talk).

10. Ahmet Kusoglu and Adam Z. Weber, 'Dynamic Water Sorption Behavior of PFSA Membranes,' *241st American Chemical Society Meeting*, Anaheim, April 2011.

11. Adam Z. Weber, Prodip K. Das, Haluna P. Gunterman, Anthony Kwong, Gisuk Hwang, Kyle T. Clark, and Ahmet Kusoglu, 'Liquid-Water Uptake and Removal in PEM Fuel-Cell Components,' *2011 Fuel Cell Seminar*, Orlando, November 2011.

V.F.3 Development and Validation of a Two-Phase, Three-Dimensional Model for PEM Fuel Cells

Ken S. Chen¹ (Primary Contact), Brian Carnes¹,
Chao-Yang Wang², Rod Borup³, David Harvey⁴,
Yuichiro Tabuchi⁵

¹Sandia National Laboratories (SNL)
Org. 8237, MS 9154, P.O. Box 969
Livermore, CA 94551-0969
Phone: (925) 294-6818
Email: kschen@sandia.gov

DOE Manager

HQ: Donna Ho
Phone: (202) 586-8000
Email: Donna.Ho@ee.doe.gov

Subcontractors:

² The Pennsylvania State University (PSU),
University Park, PA

³ Los Alamos National Laboratory (LANL),
Los Alamos, NM

⁴ Ballard Power Systems (Ballard), Burnaby BC, Canada

⁵ Nissan Motor Co. Ltd. (Nissan), Kanagawa, Japan
(in-kind or no-fee participant)

Project Start Date: October, 2009

Project End Date: October, 2012

Fiscal Year (FY) 2012 Objectives

- Perform the validation of the three-dimensional (3-D), partially two-phase, single-cell polymer electrolyte membrane (PEM) fuel cell model.
- Validate model under real-world conditions and architectures using data from Ballard and Nissan for non-automotive and automotive applications.
- Validate fully two-phase, 3-D cell model with micro-porous layer effect using neutron imaging data.
- Generate test suite for PEM fuel cell model and create user manual.

Technical Barriers

This project addresses the following technical barriers from the Fuel Cells section of the Fuel Cell Technologies Program Multi-Year Research, Development and Demonstration Plan:

- (B) Cost
- (C) Performance

Technical Targets

Since the validated PEM fuel cell model developed in this project can be employed to improve and optimize the design and operation of PEM fuel cells, insights gained from applying the model will help meet the following technical targets:

- Cost: \$15/kW for transportation fuel cell stacks.
- Performance: 2,250 W/L or 65% energy efficiency for transportation fuel cell stacks.

FY 2012 Accomplishments

- Model validation using polarization and current distribution data obtained by LANL using a 10x10 segmented cell was performed. At 80°C model current distribution prediction error was <15% root mean square (RMS) error and +/-30% local error. At 60°C errors were <20% RMS and between -40/+60% local error.
- Nissan collaboration resulted in new sub-models for low Pt loading. A model for micro-resistance was applied for performance prediction of low-Pt loaded catalyst layers, with excellent performance agreement up to 2.2 A/cm².
- Single-channel models for Ballard stack and single-cell architecture have been built. Models are being used for validation of down-the-channel current, temperature and liquid water distribution.
- Demonstration of the two-phase model for predicting liquid water in a form comparable to neutron imaging studies of liquid water for in situ fuel cells. Qualitative validation against experimental through-plane liquid water profiles.
- Channel liquid water predictions were demonstrated using the fully two-phase model on the LANL 10x10 segmented cell flow field.
- Water saturation convergence at both anode and cathode sides is greatly improved for the latest code with simulation time to convergence reduced by 60%.
- A user manual has been documented for the two-phase code developed and demonstrated in this project.



Introduction

As PEM fuel cell (FC) technology matures and enters the stage of commercialization such that the industry strives to achieve desired performance and durability and reduce costs, process design and optimization become increasingly

important and indeed critical. Modeling and simulation can provide guidance in PEMFC design and optimization and thus help accelerate the commercialization of PEMFC technology. Despite tremendous research efforts and a large number of models published in the literature (see Chen and others [1] and references therein), a comprehensive, multi-physics computer model suitable for practical use by PEMFC engineers and designers, particularly in transportation and stationary applications, is still lacking.

The objectives of this project are twofold: 1) to develop and validate a two-phase, three-dimensional transport model for simulating PEMFC performance under a wide range of operating conditions; and 2) to apply the validated PEMFC model to identify performance-limiting phenomena or processes and develop recommendations for improvements so as to accelerate the commercialization of fuel cell technology. To achieve these two objectives, a multi-institutional and interdisciplinary team with significant experience in modeling PEMFCs and in measuring model-input parameters and model-validation data has been assembled. This team is led by SNL, and it includes another national laboratory (LANL), a university (PSU), and two PEMFC manufacturers (Nissan and Ballard). In addition to developing and validating a two-phase, 3-D PEMFC model, we are also coupling the PEMFC model with Design Analysis Kit for Optimization and Terascale Applications (DAKOTA) [2] (a toolkit for design, optimization, and uncertainty quantification developed by Sandia National Labs) in order to create a computational capability that can be employed for PEMFC design and optimization. This report documents technical progress made in the project during FY 2012.

Approach

Our approach is both computational and experimental. We first develop a two-phase, 3-D, transport model for simulating PEMFC performance under a wide range of operating conditions by integrating the detailed component sub-models; FLUENT (a commercial computational fluid dynamics code) is employed as the basic computational platform. We then validate our PEMFC model in a staged approach using experimental data available from the literature and those generated by team members. Lastly, we plan to apply the validated PEMFC model to identify performance-limiting phenomena or processes and develop recommendations for improvements.

Results

A validation milestone of local current distribution was successfully completed in the first quarter. We compared local current distribution from the model to experimentally measured current distributions (obtained by LANL) from a 10x10 segmented current collector plate on the cathode of a 50-cm² cell with serpentine flow field. Agreement with

experimental data for cell voltage was within 15 mV for all cases (80°C and 50/100 relative humidity, RH). At 80°C, local current distribution agreed with measurements to within 15% RMS and with min/max local errors of -30/30%. However, at 60°C, RMS error increased to 20% and min/max local errors were -30/60%, indicating overestimation of local current (see Figure 1). A novel feature of our validation approach was the quantification of experimental and model uncertainty and inclusion of this uncertainty into the validation metrics [publications 1-3,6].

The model for local current distribution was used to assess the effect of the fully two-phase model on channel liquid water (the partially two-phase model reported previously assumes only water vapor in gas channels). While the liquid water did not significantly impact the cell performance (polarization curve), a large difference in liquid water *distribution* was seen, as shown in Figure 2. Here we see that in the partially two-phase model, at the cathode gas diffusion layer (GDL)/channel interface liquid water can only appear under the lands (areas not in contact with channels). In contrast, the fully two-phase model predicts a more even distribution of liquid water over the entire lower portion of the cell, with maximum liquid water saturation under the land areas. In addition, a parametric study indicated that liquid water accumulation in the cathode gas channel would increase with increasing RH and decreasing temperature [publications 6,7,15].

Neutron imaging experiments were performed by LANL at the National Institute of Standards and Technology (NIST) facility in order to measure distribution of liquid water in an operating fuel cell. These were done using a special 2.5-cm² area cell with a single serpentine channel. A PEMFC model was built for this geometry and a special postprocessing script was used to convert computed

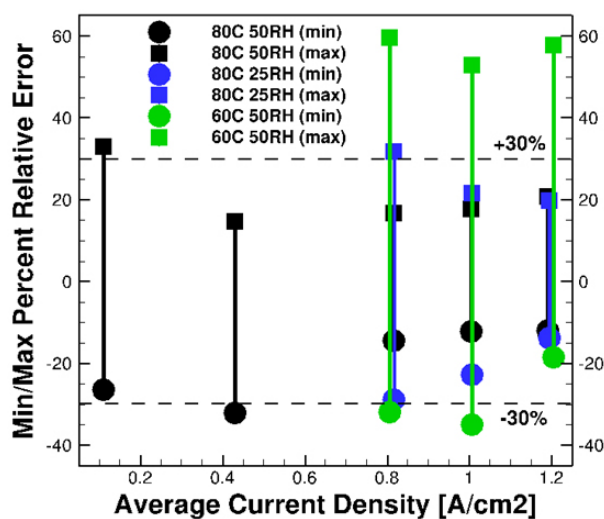


FIGURE 1. Validation of local current distribution (min/max errors) under various temperature, current and RH conditions

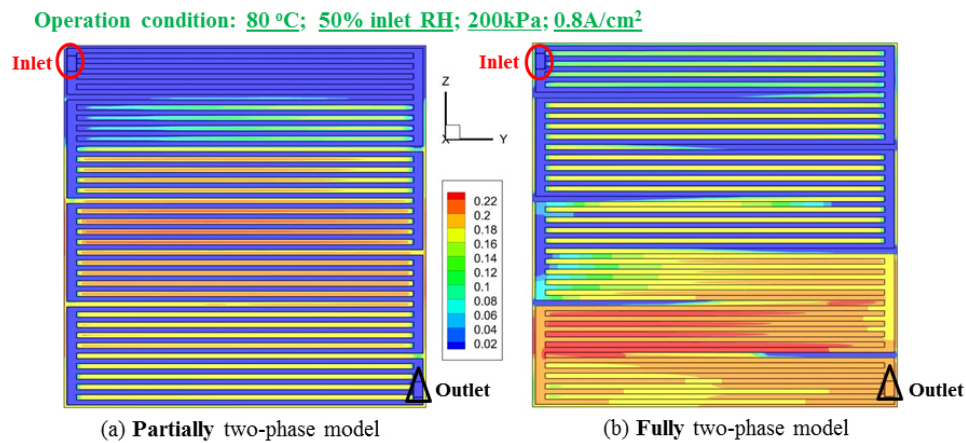


FIGURE 2. Comparison of partially/fully two-phase model using 50-cm² flow field used for current distribution validation. Two-dimensional plots of liquid water saturation at the cathode GDL/channel interface.

liquid water in the porous layers (GDL/microporous layer/catalyst layer/membrane) into an equivalent water thickness comparable to the water thickness measured in the neutron beam path. Results from the model compared favorably with the experimental water profiles, at least qualitatively (see Figure 3). However, it is uncertain whether quantitative comparisons of liquid water distribution are currently possible. This question will be pursued in the remainder of this project. [publications 4,5,11]

The code was applied to model two different Ballard fuel cell architectures: 1) a single channel from a full stack and 2) a single channel from a single cell used for parametric studies and neutron imaging of liquid water. The stack

model is being used to compare distributions of current and temperature from inlet to outlet. The single-cell model will be used to predict distributions of current, temperature, and liquid water. These models are also being used to identify performance-limiting phenomena or processes.

An engineer from Nissan worked onsite at PSU and helped to develop and implement a new resistance sub-model to improve prediction of cell performance of low Pt loaded catalyst layers. In Figure 4 we show a comparison of model prediction both with and without the new sub-model along with Nissan performance data. The improved predictive

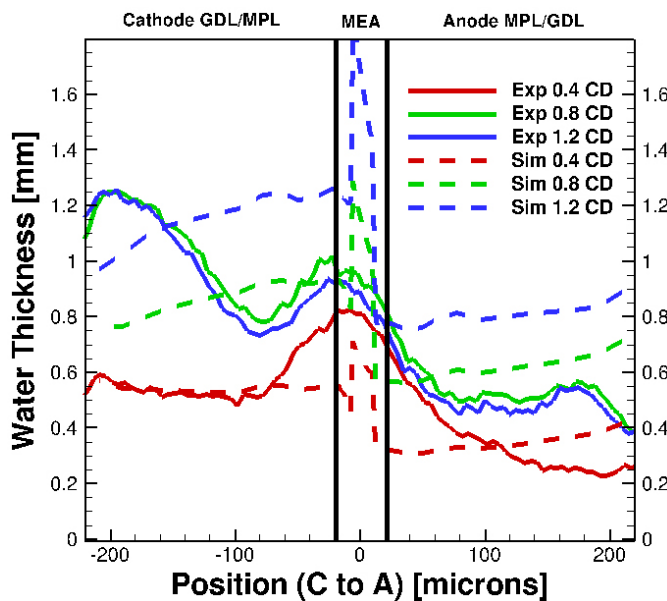


FIGURE 3. Validation of through-plane liquid water distribution model prediction by comparison with LANL/NIST neutron imaging experimental data at 100% RH

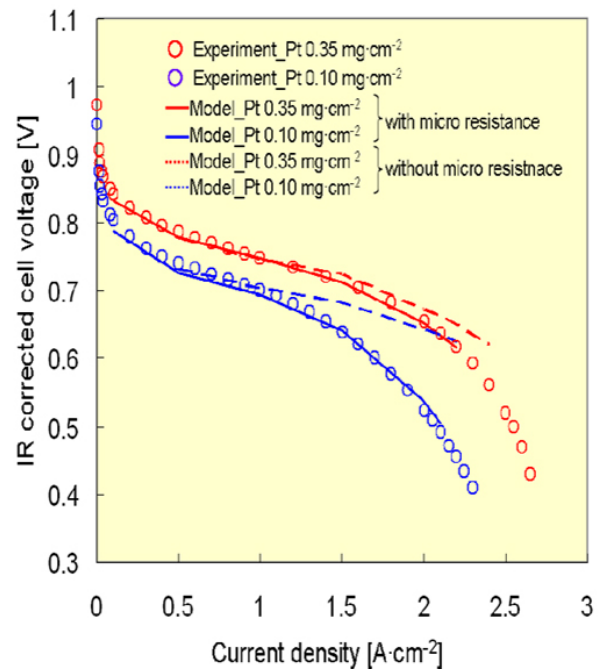


FIGURE 4. Validation of new resistance model for low Pt-loaded catalyst layers using data from Nissan

capability is clear, especially for current density greater than 1 A/cm².

The performance of the computer model was improved, so that simulation time is reduced by up to 60%. This was done by improving the implementation of the liquid water transport in the model. In addition, the user manual has been revised and test problems created to facilitate new users of the model. Finally, the scripts used to couple the model with the DAKOTA optimization toolbox [2] were documented and will be supported by Brian Carnes (bcarnes@sandia.gov) at SNL. Requests for information about running the code should be directed to Dr. Chao-Yang Wang (cxw31@psu.edu) at PSU.

Conclusions

- The model can produce current distributions that have quantitative predictive capability, within about 30% local relative error at 80°C.
- The model's predictive capability for liquid water predictions in porous layers is still only qualitative. Quantitative prediction of liquid water distribution is not yet proven.
- The model is suitable for studies to identify performance-limiting phenomena or processes.

Future Directions

- Complete model validation of liquid water distribution using neutron imaging data.
- Complete validation studies using test data from Nissan and Ballard.

FY 2012 Publications/Presentations

1. B. Carnes, K.S. Chen, D. Spornjak, G. Luo, "Validation of PEMFC computer models using segmented current and temperature data", *Polymer Electrolyte Fuel Cells 11, ECS Transactions 41 (1) 287-292 (2011)*.
2. B. Carnes, D. Spornjak, G. Luo, L. Hao, K.S. Chen, C.-Y. Wang, "Validation of a two-phase multidimensional PEMFC computational model using high-resolution current distribution data", submitted to *Journal of Power Sources*.
3. B. Carnes, "Development and validation of a three-dimensional, two-phase, PEM fuel cell model", presentation at the *2012 DOE Hydrogen Program Annual Merit Review and Peer Evaluation Meeting*, Washington, DC, May 15, 2012, paper #FC027.
4. B. Carnes, K.S. Chen, D. Spornjak, L. Hao, G. Luo, C.-Y. Wang, "Simulation and validation of liquid water transport in fuel cells from neutron imaging experiments", in *ASME Proceedings of FuelCell2012*, paper #91130.
5. B. Carnes, D. Spornjak, G. Luo, L. Hao, K.S. Chen, C.-Y. Wang, "Validation of a two-phase multidimensional PEMFC computational model using high-resolution neutron imaging data", in preparation.
6. K.S. Chen, B. Carnes, L. Hao, Y. Ji, G. Luo, C.-Y. Wang, Y. Wang, "Toward the development and validation of a comprehensive PEM fuel cell model", in *ASME Proceedings of FuelCell2011*, paper #54693.
7. K.S. Chen, B. Carnes, L. Hao, G. Luo, C.-Y. Wang, "A three-dimensional two-phase model for simulating PEM fuel cell performance", accepted for publication in the *ASME Proceedings of ESFuelCell2012*, paper #91302.
8. S.C. Cho, Y. Wang, and K.S. Chen, "Droplet dynamics in a polymer electrolyte fuel cell gas flow channel: deformation and detachment. II: comparisons of analytical solution with numerical and experimental results", *Journal of Power Sources* (in press).
9. S.C. Cho, Y. Wang, and K.S. Chen, "Droplet dynamics in a polymer electrolyte fuel cell gas flow channel: forces, deformation, and detachment. I: theoretical and numerical analyses", *Journal of Power Sources* (in press).
10. J.D. Fairweather, D. Spornjak, R. Mukundan, J. Spindelov, K. Artyushkova, P. Atanassov, D.S. Hussey, D. Jacobson, and R. Borup, "Interaction of heat generation, MPL and water retention in corroded PEMFCs", *Polymer Electrolyte Fuel Cells 11, ECS Transactions 41 (1) 337-348 (2011)*.
11. D.D. Hussey, D. Spornjak, A.Z. Weber, R. Mukundan, J. Fairweather, E.L. Brosha, J. Davey, J.S. Spindelov, D.L. Jacobson, R. Borup, "Accurate measurement of the through-plane water content of proton-exchange membranes with neutron radiography", in review, *Journal of Physical Chemistry B*.
12. K.S. Chen, B. Carnes, L. Hao, G. Luo, C.-Y. Wang, "A three-dimensional two-phase model for simulating PEM fuel cell performance", in *ASME Proceedings of ESFuelCell2012*, paper #91302 (2012).
13. D. Spornjak, J.D. Fairweather, R. Mukundan, T. Rockward, and R. Borup, "Influence of the microporous layer on carbon corrosion in the catalyst layer of a PEM fuel cell", in review, *Journal of Power Sources*.
14. Y. Wang and K.S. Chen, "Effect of spatially-varying GDL properties and land compression on water distribution in PEM fuel cells", *Journal of The Electrochemical Society*, 158 (11) B1292-B1299 (2011).
15. Y. Wang and K.S. Chen, "Modeling two-phase transport in PEM fuel cell channels", in *ECS Transactions*, 41 (1) 189-199 (2011).
16. Y. Wang, and K.S. Chen, "Modeling of polymer electrolyte membrane fuel cells and stacks", in *Fuel Cells Science and Engineering: Materials, Systems, Processes and technologies*, First Edition, Edited by Detlef Stolten and Bernd Emonts, Chapter 31, in press (2012).
17. Y. Wang, and K.S. Chen, "Modeling of polymer electrolyte membrane components", in *Fuel Cells Science and Engineering: Materials, Systems, Processes and technologies*, First Edition, Edited by Detlef Stolten and Bernd Emonts, Chapter 30, in press (2012).

References

1. K.S. Chen, B. Carnes, L. Hao, Y. Ji, G. Luo, C.-Y. Wang, and Y. Wang, “Toward the development and validation of a comprehensive PEM fuel cell model,” in *ASME Proceedings of ESFuelCell2011*, paper #54693 (2011).
2. <http://www.cs.sandia.gov/dakota/index.html>

V.F.4 Transport Studies Enabling Efficiency Optimization of Cost-Competitive Fuel Cell Stacks

Amedeo Conti (Primary Contact), Robert Dross

Nuvera Fuel Cells
129 Concord Road
Billerica, MA 01821
Phone: (617) 245-7605
Email: aconti@nuvera.com
Email: rdross@nuvera.com

DOE Managers

HQ: Kathi Epping Martin
Phone: (202) 586-7425
Email: Kathi.Epping@ee.doe.gov
GO: Gregory Kleen
Phone: (720) 356-1672
Email: Gregory.Kleen@go.doe.gov

Technical Advisors

Thomas Benjamin
Phone: (630) 252-1632
Email: benjamin@anl.gov
John Kopasz
Phone: (630) 252-7531
Email: kopasz@anl.gov

Contract Number: DE-EE0000472

Subcontractors:

- Johnson Matthey Fuel Cell Ltd., UK
- Lawrence Berkeley Laboratory, Berkeley, CA
- Pennsylvania State University, State College, PA

Project Start Date: September 1, 2009

Project End Date: August 31, 2012

Program Multi-Year Research, Development and Demonstration Plan:

- (B) Cost
- (C) Performance

Technical Targets

This project is primarily focused on reducing stack cost and improving efficiency by modeling and optimizing transport properties of the membrane electrode assembly (MEA). Stack cost is reduced through a combination of increased power density and decreased noble metal content. The performance target of 7.5 W/mg-Pt @ 500 mV was selected based on cost modeling results, as the performance required to achieve the 2015 DOE cost target of \$15/kW_e. Efficiency (electric potential at rated current) of the stack technology will be optimized with the ultimate goal of approaching the DOE efficiency target for stack efficiency at 25% rated power of 65% and a project target of 55% efficiency at rated power.

FY 2012 Accomplishments

- Achieved the technical target for the project by demonstrating stable and repeatable performance above 7.5 W/mg-Pt @ 500 mV on a full-format stack.
- Developed and tested several MEAs optimized for ultra-high current densities with Pt loadings <0.2 mg-Pt/cm².
- Tuned and validated a two-dimensional plus one mathematical model, capable of predicting ultra-high current density operation in different architectures, under a wide range of conditions.
- Demonstrated stable performance at high temperatures (90°C), with both single cells and full-format automotive stacks.



Fiscal Year (FY) 2012 Objectives

- Develop and validate a predictive transport model that enables efficiency maximization at conditions that meet DOE cost targets.
- Demonstrate stable and repeatable high performance on a full-format fuel cell stack, namely 7.5 W/mg-Pt.
- Optimize the efficiency (electric potential at rated current) of a stack technology that meets DOE cost targets.

Technical Barriers

This project addresses the following technical barriers from the Fuel Cells section of the Fuel Cell Technologies

Introduction

Hydrogen fuel cells are recognized as one of the most viable solutions for mobility in the 21st century; however, there are technical challenges that must be addressed before the technology can become available for mass production. One of the most demanding aspects is the cost of present-day fuel cells which is prohibitively high for the majority of envisioned markets. The fuel cell community recognizes two major drivers to an effective cost reduction: (1) decreasing

the noble metals content, and (2) increasing the power density in order to reduce the number of cells needed to achieve a specified power level. Nuvera's technology exhibits great promise for increasing power density on account of its proven ability to operate stably at high current densities ($>1.5 \text{ A/cm}^2$). However doing so compromises efficiency, increases the heat rejection duty, and is thus more demanding on the cooling system. These competing aspects are being assessed in order to identify the proper tradeoffs, and ensure the modeling and experimental activities of the Area Use and Reactant Optimized at Rated Amperage Program respect system-level constraints for automotive applications. This project will develop a predictive transport model to identify and help us reduce losses and increase efficiency for high current density operation.

Approach

Nuvera structured the activities in the scope of the project to orbit around a focal point consisting of the fuel cell predictive model. Cost and system analyses were performed in order to define the boundaries of the design space that the model should represent. This analytical work will inform the experimental tests on a new single-cell fixture to illuminate the physics and the parameters composing the backbone of the fuel cell model. The predictions generated by the model drive both the process of optimization of the fuel cell operating conditions and the material development. The combined results of these two activities are verified on single-cell fixtures as well as on full active area hardware, and the experimental data obtained is used to validate and calibrate the model through multiple iterations.

Results

In FY 2012 Johnson Matthey Fuel Cells (JM) continued to develop and deliver MEAs optimized for performance at ultra-high current densities. Following the MEA development roadmap established at the beginning of the project JM continued working to reduce the MEA ionic resistivity. Two MEA designs were developed and delivered with a new low resistivity membrane (MEM3). Significant performance and durability improvements were demonstrated for this new membrane at JM on a cell with a channel/land architecture, however when Nuvera tested the MEAs there was no performance improvement measured. The improved performance measured by JM is now believed to be specific to the conditions and architecture tested, and do not translate to the open flowfield architecture and Nuvera automotive conditions.

As part of the MEA development roadmap JM also continued working to reduce Pt loading of the electrodes. While the original development plan for the project specified average total Pt loadings between 0.2 and 0.5 mg/cm^2 , JM and Nuvera agreed that decreasing the Pt loading even

further was the best option to maximize the specific power and reach the technical target for the project ($7.5 \text{ W/mg-Pt @ } 500 \text{ mV}$). Several MEAs were developed and delivered with reduced Pt loading of both anode and cathode electrodes. These MEAs were evaluated by Nuvera, and the results of the best performing MEA (#29) are reported here. As shown in Figure 1 MEA #29, with an average total Pt loading of 0.131 mg/cm^2 , was tested in a 4-cell, full-format automotive stack. The results at 2 A/cm^2 (yellow) demonstrate a cell potential of 552 mV and specific power of 8.43 W/mg Pt , exceeding the specific power target for the program by almost 1 W/mg Pt and the voltage target by over 50 mV ! A second stack was built with the same MEA which also exceeded the project targets and demonstrated stability during a 100-hour stability test, thus satisfying the technical target requirement to demonstrate stable and repeatable performance of the MEA.

In order to address concerns about the heat rejection capability of the stack Nuvera conducted a temperature sensitivity study on a 64-cell full-format automotive stack. As shown in Figure 2 four sets of conditions were tested, two with no cathode humidification and two with a membrane humidifier connected to the cathode side of the stack. For each condition the coolant temperature was increased until performance became unstable. As shown with the dark blue line, humidifying the cathode and reducing cathode stoichiometry allowed the stack to achieve stable performance above 90°C . This elevated temperature will significantly improve the heat rejection capability of an automotive style system.

The University of Tennessee, Knoxville (UTK) completed extensive validation of the predictive transport model across a wide range of test conditions and operating temperatures up to 90°C . Model predictions were compared

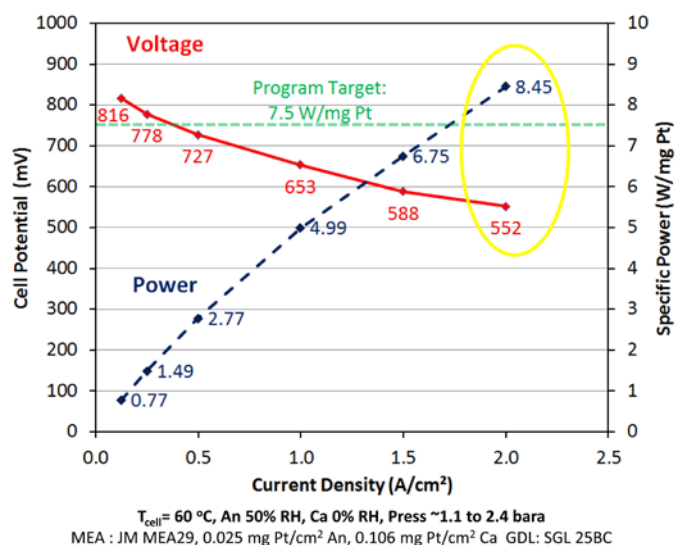


FIGURE 1. Polarization Curve for JM MEA#29

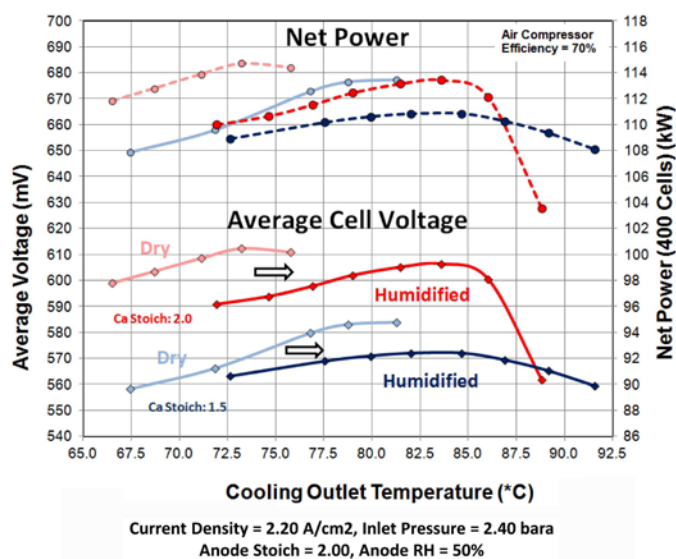


FIGURE 2. Temperature Sensitivity Test for a 64-Cell Full-Format Orion Stack

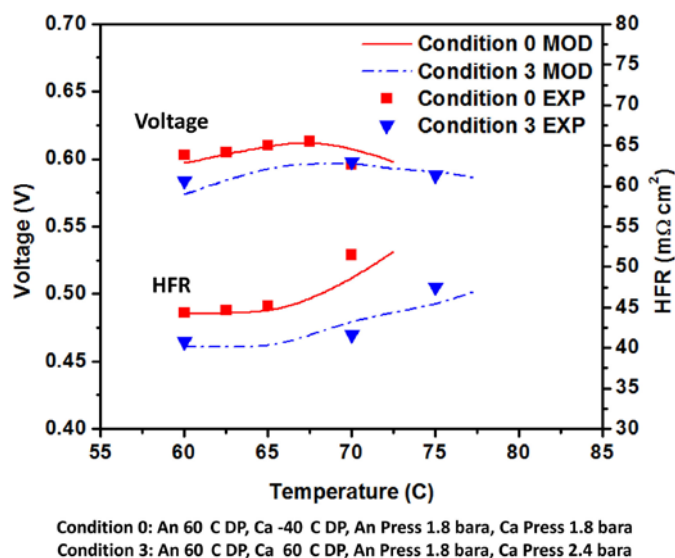
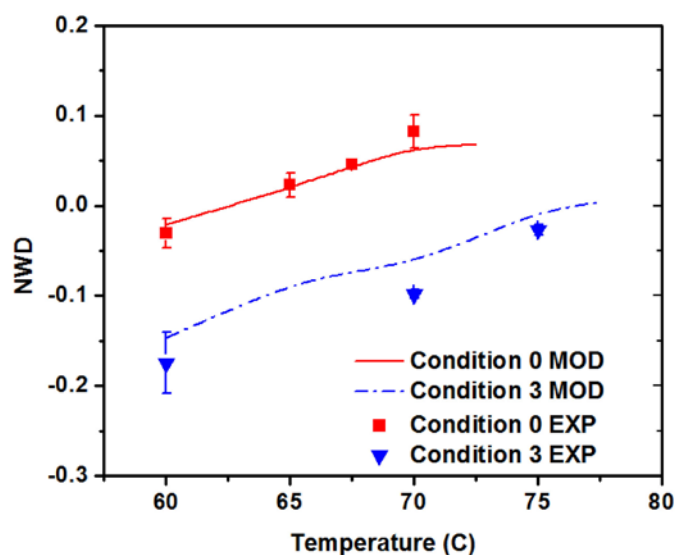


FIGURE 3. Predictive Model Validation Study for Voltage and HFR

with experimental results in terms of cell voltage, high frequency resistance (HFR), and net water drag across a wide range of operating conditions. As an example of the model validation conducted in this project, Figures 3 and 4 show a temperature sensitivity study for two conditions with varied reactant humidification and pressure. Condition 0 (red) has a cathode inlet dewpoint of -40°C at 1.8 bara, and condition 3 (blue) has a cathode inlet dewpoint of 60°C at 2.4 bara. Figure 3 shows close agreement between modeling predictions and experimental results for cell voltage and HFR, specifically trends and inflection points measured experimentally are predicted well with the model. Figure 4 again shows close agreement between the model and data in



Condition 0: An 60 C DP, Ca -40 C DP, An Press 1.8 bara, Ca Press 1.8 bara
Condition 3: An 60 C DP, Ca 60 C DP, An Press 1.8 bara, Ca Press 2.4 bara

FIGURE 4. Predictive Model Validation Study for Net Water Drag

terms of net water drag throughout the temperature range studied. The model validation studies conducted by UTK provide a high level of confidence that the model is valid through a wide range of reactant and cell conditions.

Conclusions and Future Directions

- Finish model validation studies
- Publish the predictive model in format agreed to by the DOE

FY 2012 Publications/Presentations

1. Dross, R. 2012. "Ultra-High Power Density Fuel Cell Stacks Enabling Commercialization Through Cost Reduction". Plenary Talk presented at the Electrochemical Energy Storage and Conversion Forum, Knoxville, Tennessee.
2. Dross, R. 2012. "Transport Studies Enabling Efficiency Optimization of Cost-Competitive Fuel Cell Stacks" Paper presented at the DOE Hydrogen Program Annual Merit Review, Washington, D.C.
3. Dross, R. 2012. "Transport Studies Enabling Efficiency Optimization of Cost-Competitive Fuel Cell Stacks" Presented at the Fuel Cell Tech Team Review, Detroit, Michigan.
4. Mench, M.M. 2011. "Characterization of Heat & Water Transport in Gas Diffusion Layers and Associated Interfaces". Plenary Talk presented at the Fall meeting of the Electrochemical Society, Boston, Massachusetts.
5. Srouji, A., and M. M. Mench. 2011. "A Comparison of Open Flow Field and Conventional PEFC Architecture Limitations at Ultra-High Current Density". Paper #292 presented at the Spring meeting of the Electrochemical Society, Montreal, Quebec.

6. Srouji, A., L. Zheng, R. Dross, A. Turhan, and M.M. Mench. 2012. "Performance and Mass Transport in Open Metallic Element Architecture Fuel Cells at Ultra-high Current Density." *Journal of Power Sources*. doi:10.1016/j.jpowsour.2012.06.075.
7. Zheng, L., A. Srouji, F. Gambini, and M.M. Mench. 2011. "Exploration of Ultra-High Current Operation in PEFC Using a Validated Model." In *Electrochemical Society Transactions*, 41(1):229–240. Boston, Massachusetts.
8. Zheng, L., A. Srouji, F. Gambini, and M.M. Mench. 2011. "Exploration of Ultra-High Current Operation in PEFC Using a Validated Model". Paper #1032 presented at the Fall meeting of the Electrochemical Society, Boston, Massachusetts.
9. Zheng, L., A. Srouji, A. Turhan, and M.M. Mench. 2012. "Computational Exploration of Ultra-high Current PEFC Operation with Porous Flow Field." *Journal of the Electrochemical Society* 159 (7): D1–D11.

V.F.5 Water Transport in PEM Fuel Cells: Advanced Modeling, Material Selection, Testing, and Design Optimization

J. Vernon Cole
CFD Research Corporation
215 Wynn Drive
Huntsville, AL 35805
Phone: (256)-726-4852
Email: jvc@cfdr.com

DOE Managers

HQ: Donna Ho
Phone: (202) 586-8000
Email: Donna.Ho@ee.doe.gov

GO: David Peterson
Phone: (720) 356-1747
Email: David.Peterson@go.doe.gov

Technical Advisor

Walt Podolski
Phone: (630) 252-7558
Email: podolski@cmt.anl.gov

Contract Number: DE-FG36-07GO17010

Subcontractors:

- Ballard Power Systems, Burnaby, BC, Canada
- BCS Fuel Cells, Bryan, TX
- ESI US R&D, Huntsville, AL
- Techverse, Cary, NC
- SGL Carbon, Meitingen, Germany
- University of Victoria, Victoria, BC, Canada

Project Start Date: June 1, 2007

Project End Date: May 31, 2012

Fiscal Year (FY) 2012 Objectives

- Complete cell-scale model testing and validation against steady state and transient operational cell data.
- Complete fuel cell water transport model improvements and code package development to include two phase flow.
- Complete validation of water transport model based on data gathered during optimization studies, and make recommendations for water management improvement including operating strategies and gas diffusion layer (GDL) materials modification.

Technical Barriers

This project addresses the following technical barriers from the Fuel Cells section of the Fuel Cell Technologies

Program Multi-Year Research, Development and Demonstration Plan:

(C) Performance

Technical Targets

This project addresses fundamental issues in water transport within the fuel cell stack. The resulting understanding will be applied toward the design of stack components and operating strategies that enable meeting the 2017 targets for transportation fuel cell stacks operating on direct hydrogen:

- Stack power density: 2,250 W/L
- Cold start-up time to 50% rated power @ 20°C: 5 secs
- Unassisted start from low temperature: -30°C

FY 2012 Accomplishments

Specific accomplishments for the past year include:

- Validation of key two-phase (liquid and vapor) flow effects against relevant benchmarks such as channel flow over a porous slab, impinging flow on porous media, and transient flows resulting from local injection of the secondary phase.
- Demonstration of improved agreement with measured polarization curves in the mass transfer limited regime, and significant improvement in the qualitative nature of the predicted liquid water distribution due to several numerical algorithm improvements.
- Completion of the software package development, including: transfer and integration of the model solver software code; addition of model options and parameter inputs to the graphical user interface for model setup; and outputs for post-processing results.



Introduction

Water management in polymer electrolyte membrane (PEM) fuel cells is challenging because of the inherent conflicts between: supplying adequate water to establish and maintain the membrane electrical conductivity, removing the water produced by the electrochemical reactions at the cathode, and uniformly distributing the gaseous reactants at catalyst surfaces near the membrane to effectively utilize these costly catalysts. As power density of the cells increases,

more water will be generated within the same cell volume. Therefore, increasing power density requirements will drive a greater need for design tools incorporating an improved understanding of how liquid water is transported within fuel cells. An additional barrier to widespread use of fuel cells for automotive power is the performance degradation caused when liquid water freezes within the cells. Optimizing water management to influence where the liquid water remains at shutdown is a promising path to improving cold starting capabilities and freeze-thaw reliability.

This project is intended to improve fundamental understanding of water transport within a PEM fuel cell, and capture that knowledge in design tools capable of assisting the industry to meet targets for increased power densities and improved cold-start performance. To achieve these objectives, the project is focused on developing predictive models for water transport in GDL materials, characterizing materials for model inputs and verification, implementing the resulting understanding in engineering design tools, and validating the resulting design tools against fuel cell performance data and in situ diagnostics of water distribution within operating fuel cells.

Approach

To meet the high level objectives of improving fundamental understanding of water transport in PEM fuel cells and demonstrating improved performance, the team will integrate experimental characterization with model development and application. The initial focus of the experimental characterization was on measuring relevant physical and transport properties of the GDL materials typically placed between the catalyst and reactant flow channels. Diagnostic and characterization studies have transitioned to water and two-phase (water and air) fluid transport properties of GDL materials and analysis of water transport across material interfaces and in fuel cell channels. The related modeling studies follow a similar progression, with initial emphasis on microscale simulations of single fluid and two-phase transport within GDL materials. The simulations allow us to analyze key effects such as the impact of the microstructure and surface treatment of the solids within porous GDL materials on the two-phase water and gas transport. The knowledge gained from the materials characterization and microscale simulations is being used to develop models suitable for incorporation into an engineering design tool for fuel cell scale analysis of reactant and water transport coupled with power generation. The verification of these models and the resulting design tool will be accomplished by comparing predicted and measured effects of material and operating conditions on cell performance and water distribution within the cell. Applying our models to screen and improve water management strategies, then testing the resulting concepts in prototype fuel cells,

will further demonstrate our improved fundamental understanding and validate the resulting design tools.

Results

In this final year of research, the emphasis has been on validation of the developed simulation tools and models for fuel cell performance and water transport during operation, and on inserting the developed capabilities into the commercially available version of the multiphysics software utilized in this work.

The model solution approaches for two-phase flow of liquid water and gases were further improved to better address flow across the interfaces between the porous GDLs and the gas channels. The treatment of those interfaces was modified to enforce the pressure and stress matching condition suggested by Beavers and Joseph [1], and by Betchen et al. [2]. In this form, a part of the normal stresses is absorbed by the porous solid, not the fluid in the porous media. A benchmark case relevant to fuel cell operation, the Beavers-Joseph problem with flow in a channel that is segregated into an open and porous region, was used to validate the implementation. As seen in Figure 1, the improved boundary condition treatment results in excellent agreement for the velocity profile as a function of vertical position in the channel and porous layer, without spurious velocity oscillations. The two-phase results are equivalent to the single-phase results after scaling the superficial velocity for the phase fractions. This improvement removed velocity oscillations at the interface which were introducing numerical noise and slowing overall convergence of the models.

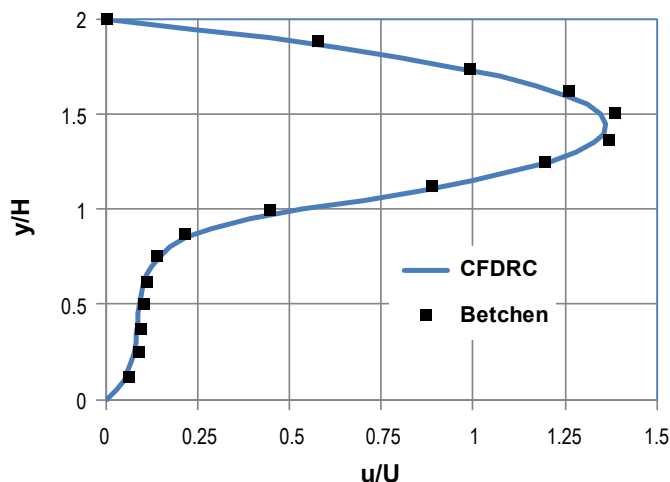


FIGURE 1. Comparison of velocity profile as a function of vertical position between benchmark simulations (symbols) [2] and CFD Research Corporation results (curve) for Beavers-Joseph problem. Porous region is below $y/H=1$, open channel above.

Model testing against operational fuel cell data has continued to show quantitative and qualitative improvement in the predictions. Ballard experiments for characterization of the membrane electrode assembly (MEA) used in current and next-generation cells have been utilized for some of these model evaluations. The experiments are performed in a small test cell designed to have minimal resistance losses outside the MEA, and operated under high stoichiometry conditions to reduce the effects of reactant depletion on the measured performance. An example measured polarization curve is shown in Figure 2, along with simulation results for the full two-phase model and a simpler single-phase model with no liquid water formation. The cell performance was obtained during 60°C operation with a 100% relative humidity cathode feed, and model parameters for the catalyst kinetics were extracted from a reduced model that only considers the cathode GDL and catalyst layers in detail [3]. The developed two-phase flow models for liquid water transport reduce the cell performance at higher current densities, and bring the predicted polarization curve closer to the experimental values.

The predicted liquid water distribution in the cathode GDL for an 85% relative humidity cathode feed, Figure 3, has a similar range to earlier predictions but is qualitatively improved with much less numerical noise. The liquid water is preferentially formed under the landings, and in the downstream portion of the cathode, due to the temperature and water vapor distributions. Model improvements causing the reduction in numerical noise relative to earlier results include the reformulation of the channel-GDL interface condition described above, a more detailed numerical treatment of the liquid water fraction effect on the phase change rate, and extending the capillary pressure functions to capture both hydrophobic and hydrophilic regimes for materials with a non-zero residual water saturation.

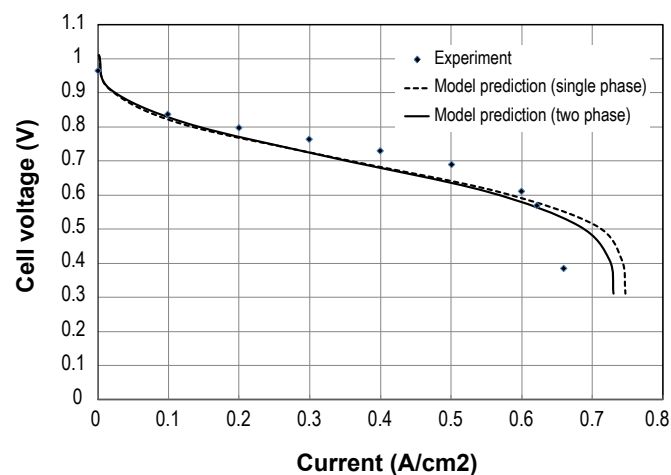


FIGURE 2. Comparison of experimental polarization curve, detailed model with single-phase flow, and detailed two-phase model prediction at 60°C, 100% relative humidity operation.

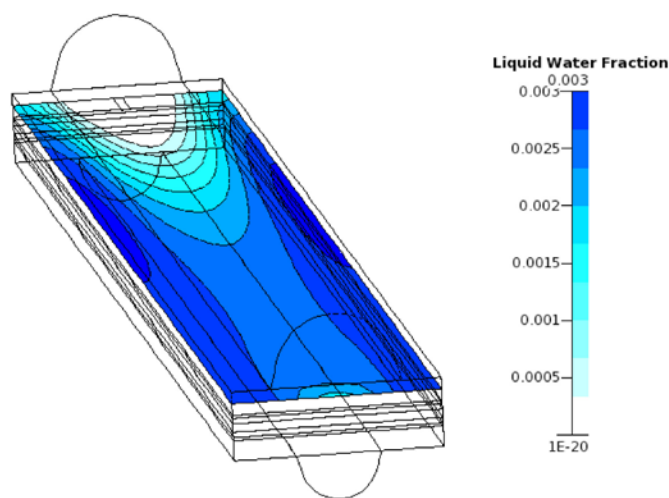


FIGURE 3. Predicted liquid water distribution in cathode GDL mid-plane for 70°C, 85% relative humidity, 1 A/cm² operation.

The capabilities for predicting liquid water transport effects developed in this work have been inserted into the commercially available version of the computational fluid dynamics-ACE+ multiphysics software that has served as the development framework. In addition to incorporating the model capabilities, ESI Group and CFD Research Corporation have designed and implemented the appropriate changes to the user interface and property databases. The graphical user interface used to define the models now includes inputs for key properties such as capillary pressure models, relative permeability functions, and models for calculating evaporation/condensation phase change. Printed and graphical results have also been extended to allow detailed analysis of the results.

Conclusions and Future Directions

During the past year, we have further improved and validated the developed models for predicting liquid water and two-phase flow effects in fuel cells. Fundamental capabilities of the models have been validated, and numerical algorithm changes have resulted in improved robustness and convergence. Specific accomplishments for the past year include:

- Validation of key two-phase (liquid and vapor) flow effects against relevant benchmarks such as channel flow over a porous slab, impinging flow on porous media, and transient flows resulting from local injection of the secondary phase.
- Demonstration of improved agreement with measured polarization curves in the mass transfer limited regime, and significant improvement in the qualitative nature of the predicted liquid water distribution due to several numerical algorithm improvements.

- Completion of the software package development, including: transfer and integration of the model solver software code; addition of model options and parameter inputs to the graphical user interface for model setup; and outputs for post-processing results.

The most significant open issue remaining from this project is thorough evaluation of the GDL treatment approach developed by our partner Techverse during the latter stages of this project.

FY 2012 Publications/Presentations

1. J. Vernon Cole, “Water Transport in PEM Fuel Cells: Advanced Modeling, Material Selection, Testing, and Design Optimization,” Proceedings of the DOE Hydrogen and Fuel Cells Program Annual Merit Review, Crystal City, Virginia, 2012, http://www.hydrogen.energy.gov/pdfs/review12/fc030_cole_2012_p.pdf.

References

1. G.S. Beavers, D.D. Joseph, Boundary conditions at a naturally permeable wall, *Journal of Fluid Mechanics* **30**, 197-207 (2006).
2. L. Betchen, A. Straatman, B. Thompson, A Nonequilibrium Finite-Volume Model for Conjugate Fluid/Porous/Solid Domains, *Numerical Heat Transfer: Part A: Applications* **49**, 543-565 (2006).
3. Andrew J. Desouza, Radu Bradean, Virginia Branzea, Stephen Hamada, Joerg Kleemann, Herwig Haas, Joy Roberts, and Emerson Gallagher, in *214th ECS Meeting, Volume 16, Issue 2, Proton Exchange Membrane Fuel Cells 8*, edited by Thomas F. Fuller, K. Shinohara, V. Ramani, P. Shirvanian, H. Uchida, S. Cleghorn, M. Inaba, S. Mitsushima, P. Strasser, H. Nakagawa, H. Gasteiger, T. Zawodzinski, and C. Lamy (ECS, Honolulu, HI, 2008), pp. 35-44.

V.F.6 Transport in PEMFC Stacks

Cortney Mittelsteadt (Primary Contact),
Hui Xu, Junqing Ma (GES); John Van Zee,
Sirivatch Shimpalee, Visarn Lilavivat (USC);
James E. McGrath Myoungbae Lee, Nobuo Hara,
Kwan-Soo Lee, Chnng Hyun (VT); Don Conners,
Guy Ebbrell (Ballard); Kevin Russell (Tech Etch)

Giner Electrochemical Systems, LLC
89 Rumford Ave.
Newton, MA 02466
Phone: (781) 529-0529
Email: cmittelsteadt@ginerinc.com

DOE Managers

HQ: Donna Ho
Phone: (202) 586-8000
Email: Donna.Ho@ee.doe.gov

GO: Gregory Kleen
Phone: (720) 356-1672
Email: Gregory.Kleen@go.doe.gov

Contract Number: DE-EE0000471

Subcontractors:

- Tech-Etch, Plymouth, MA
- Ballard Material Products, Inc., Lowell, MA
- Virginia Polytechnic and State University, Blacksburg, VA
- University of South Carolina (USC), Columbia, SC

Project Start Date: November 9, 2009

Project End Date: August 31, 2013

Fiscal Year (FY) 2012 Objectives

- Design of fuel cell components targeting specific transport properties:
 - Synthesis of block copolymers
 - Design of flow fields and gas diffusion layers (GDLs)
- Determination of bulk membrane properties:
 - Water uptake and diffusivity
 - Gas permeability
 - Electro-osmotic drag
- Transient, three-dimensional modeling of fuel cell operation.

Technical Barriers

This project addresses the following technical barriers from the Fuel Cells section of the Fuel Cell Technologies

Program Multi-Year Research, Development and Demonstration Plan:

(C) Performance

Technical Targets

The goal of this project is to improve the understanding of water transport through a combination of experiment and modelling. The ultimate goal of the project is to create a model that takes the most common variables utilized in fuel cell engineering and predict fuel cell performance. Once established, the model will be used to link improvements in fuel cell components to improvements in fuel cell performance, and thereby focusing future research efforts. This will be accomplished by generating fuel cell components with specific properties, developing new methods to characterize their transport properties, then testing and modelling their performance.

FY 2012 Accomplishments

- Completed the synthesis of a full list of hydroquinone-based hydrophilic-hydrophobic block copolymers (hydroquinone sulfone-hexafluoro bisphenol a benzonitrile [HQSH-6FPAEB]) with lower equivalent weight, structure, chemistry and phase separation.
- Successfully casted copolymer powders to membranes varying in size from 4"x4" (for standard fuel cell technology plates) to 12"x5" (for General Motors [GM] plates).
- Automated dynamic water uptake/diffusivity test system and completed diffusivity measurements of VA Tech HQSH-6FPAEB membranes.
- Developed an open-ended hydrogen pump apparatus to characterize electro-osmotic drag coefficient (EODC) and measured EODC for Nafion® membrane and HQSH-6FPAEB hydrocarbon membranes.
- Designed new GDLs and completed pore size distribution measurements with fuel cell performance tests.
- Simulated cell performance and current distribution at various values of the water uptake, membrane diffusivity, and EODC.
- Compared modeling results with segmented-cell data for both serpentine and parallel flow-fields.
- Completed simulation of GM down-the-channel fuel cell and compared with available data and validated modeling result with water balance experiment.



Introduction

Many fuel cell component properties that influence water transport and thermal management are not well-understood [1,2]. A better understanding of how water transport and thermal management can be controlled would represent a significant step forward in meeting the DOE's stated 2015 targets. This project aims for a better understanding of water transport and thermal management by tailoring fuel cell components to exhibit specific measurable transport properties. These transport properties are then used in a model, which enables the prediction of the effect of changing component parameters on transport properties.

Approach

This project seeks to develop a transport model and test the model by developing fuel cell components possessing specific transport properties. Membranes will be developed to achieve different ratios of water transport and conductivity. Bulk membrane properties (i.e., diffusivity, water uptake, conductivity) will be evaluated and modeled. Also, GDLs, bipolar plates, and flow fields will be developed and tailored to illustrate specific differences in porosity, tortuosity and hydrophobicity. The fuel cell performance will be evaluated using these components and compared with the model. The model will be used to predict the effect of changing component parameters (i.e., changing membrane type and thickness, changing flow field configuration) on component transport properties and fuel cell performance.

Results

Membrane work on 6FPAEB-HQS100 as well as on previous 6FPAEB-biphenyl sulfone (BPS100) provides design guidelines for polymer electrolyte membranes (PEMs) beyond Nafion® membranes, as the structure, chemistry,

and phase separation of copolymer blocks largely impact the transport properties in PEM fuel cells. Block copolymer HQS100-6FPAEB based on 6FPAEB and HQS100 oligomers have been successfully synthesized. The obtained block copolymers vary in molecular weights (from 6K-6K, 9K-9K, to 11K-11K), ion exchange capacity, and proton conductivity. Giner used polymer powders delivered from VA Tech to cast membranes and subsequently measure water uptake, conductivity, diffusivity, and EODC, as well as fabricate these into MEAs. The properties of these membranes are used in modeling work at USC to investigate the fuel cell performance, water distribution, and current distribution. VA Tech first synthesizes a variety of copolymer powders. These block copolymer powders are then cast into films (from 25 to 50 μm) at Giner. Giner then measures the transport properties which are provided to USC for their modeling work. Also at Giner, catalyst inks are deposited onto the membranes to make MEAs. These MEAs are shipped to USC for fuel cell performance evaluation (See Figure 1).

A dead-end hydrogen pump has been developed for characterizing the EODC of Nafion® membranes and hydrocarbon membranes (see Figure 2). The EODC characterization system consists of two cells: a membrane saturator cell and a hydrogen pump cell. Liquid water is fed with a micro-flow meter to one side of the membrane saturator cell while hydrogen flows into the other side of the saturator cell that was pre-evacuated and shown in Figure 2a. Water vapor pressure is controlled by the saturator oven temperature and total pressure is controlled by the hydrogen mass flow meter/pressure controller. By varying these two pressures we can control the water: hydrogen ($\text{H}_2\text{O}:\text{H}$) feed ratio. Protons generated by hydrogen oxidation at the anode travel across the membrane and then are reduced to hydrogen at the cathode. The voltage of the hydrogen pump cell can be monitored and its stability depends on how close the feed ratio is to the EODC. The ratio corresponding to the most stable voltage can approximate 2^*EODC . The most

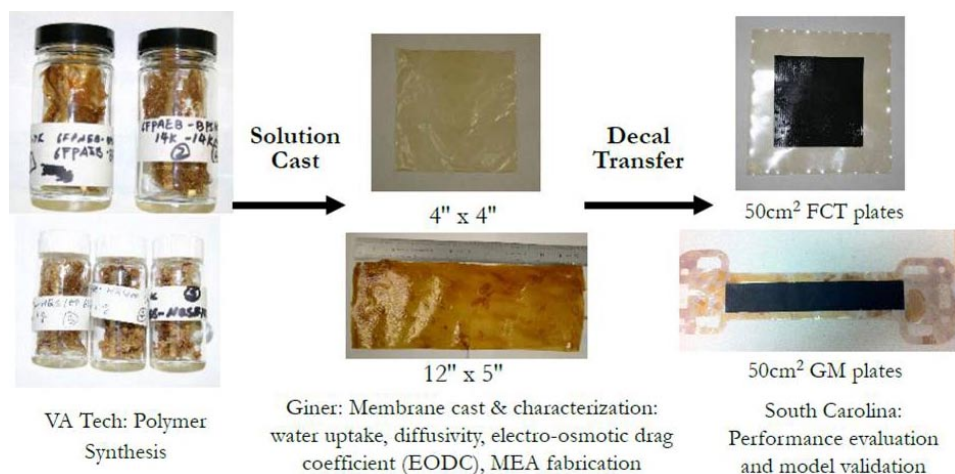


FIGURE 1. Schematic of hydrocarbon membrane development and MEA fabrication

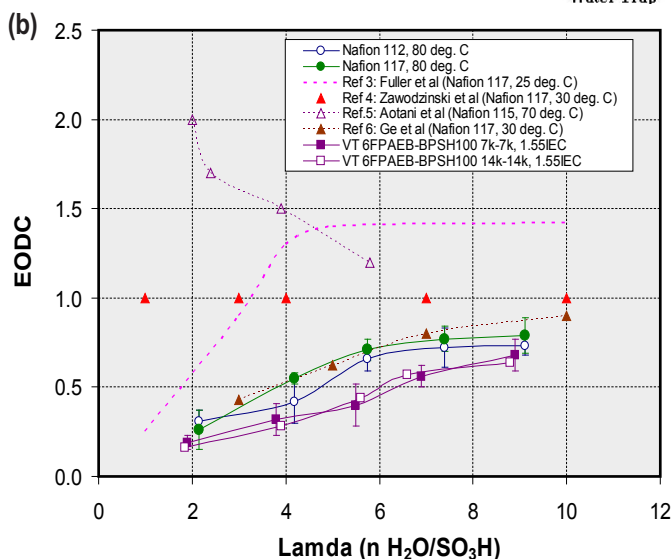
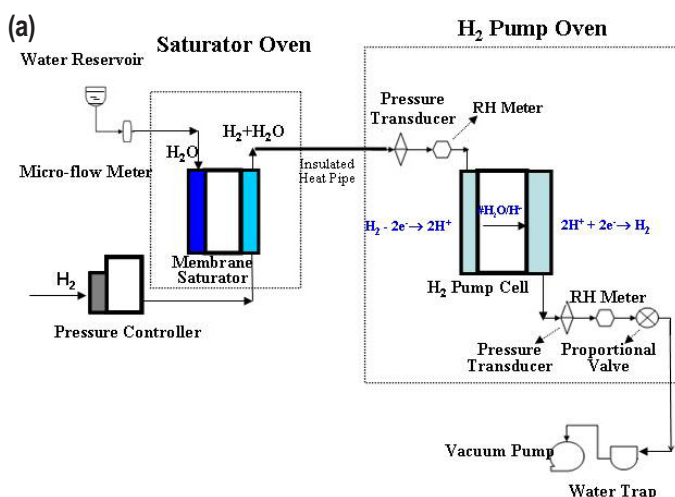


FIGURE 2. Dead-end hydrogen pump for EODC measurements: (a) dead-end hydrogen pump system; (b) EODC measurements for various membranes and from different researchers

distinctive features of the system are that gas/gas diffusion is eliminated prior to the membrane surface, and there is a minimal relative humidity (RH) difference between the inlet and outlet of the hydrogen pump cell (<1%). The other advantages include precisely-controlled water vapor (no condensation) and flexibility in RH and temperature variations. Figure 2b shows the measured EODC of a variety of membranes using this system, as well as a comparison of previous work from several groups. For both the Nafion® membranes (112 and 117) and hydrocarbon membranes (VA Tech 6FPAEB-BPSH100 7k-7k and 14k-14k), the EODC increases as lambda (nH₂O/SO₃H) increases with slightly lower numbers for hydrocarbon membranes. The EODC numbers from this work follow those by Ge et al. However, this figure also reflects significant disagreement between different investigators [3-6].

A total of twelve gas diffusion layers (GDLs) were designed for the purpose of varying transport properties. The newly designed GDLs were modified from three standard Ballard substrates P50, EP40 and P75 by adding two micro-porous layers (MP1 and MP2) with small or large carbon particles either close to or away from the catalysts layer. Each set was treated to provide two different values of diffusivity (See Table 1).

TABLE 1. Principles for designing GDLs

| Substrate | Diffusivity Modification | MP1/MP2 (Carbon Particle Size) |
|-----------|--------------------------|--------------------------------|
| P50 | Low and High | Small/Large and Large/Small |
| EP40 | Low and High | Small/Large and Large/Small |
| P75 | Low and High | Small/Large and Large/Small |

Mercury pore size distributions of newly-designed GDLs were obtained. The baseline of a treated EP40 (i.e., EP40T) has the most pore volume compared to P75T and P50T. All three GDLs have the maximum peak of differential distribution at a pore diameter of 50 μm. Modification of the GDL greatly reduces the volume of large pores. The effect of different GDLs on PEMFC performance was also demonstrated. P75T shows the highest performance at lower humidity whereas EP40T shows the highest performance at higher humidity. Therefore, P75T will be used in the anode and EP40T will be used in the cathode in baseline testing. The MacMullin Number, which is a function of tortuosity and porosity, is often found to follow the equation below [7],

$$N_M = f(\tau, \varepsilon) = \frac{\tau^n}{\varepsilon^m}$$

This relationship has been previously used to characterize the GDLs. The MacMullin Number of these substrates does not appear to follow previous relationships (see Figure 3). The GDLs with micro porous layers have lowered the MacMullin Numbers, a trend which was observed with treatments of Toray TGP-H-060 paper.

Current distributions with a USC-designed parallel flow-field at two conditions were measured using a current distribution board and simulated with the CFD model (see Figure 4): (a) for high RH operation at 1,200 mA/cm² and (b) for low RH operation 294 mA/cm². First, the CFD model predicts experimental current distribution well. This is reflected in the bar charts where for most segments the two current densities, experimental and CFD-based, are very close. At the wet condition (a), the segment current density decreases from Segment 1 to 5 and from Segment 6 to 10; this is because Segment 1 and 6 are near the inlet, and Segment 5 and 10 are near the outlet. The current decreases for this wet condition because there is sufficient membrane conductivity and because the partial pressure of oxygen decreases as the partial pressure of water increases. The trend at low RH condition (b) is almost opposite from (a) because the dry inlet yields a low membrane conductivity

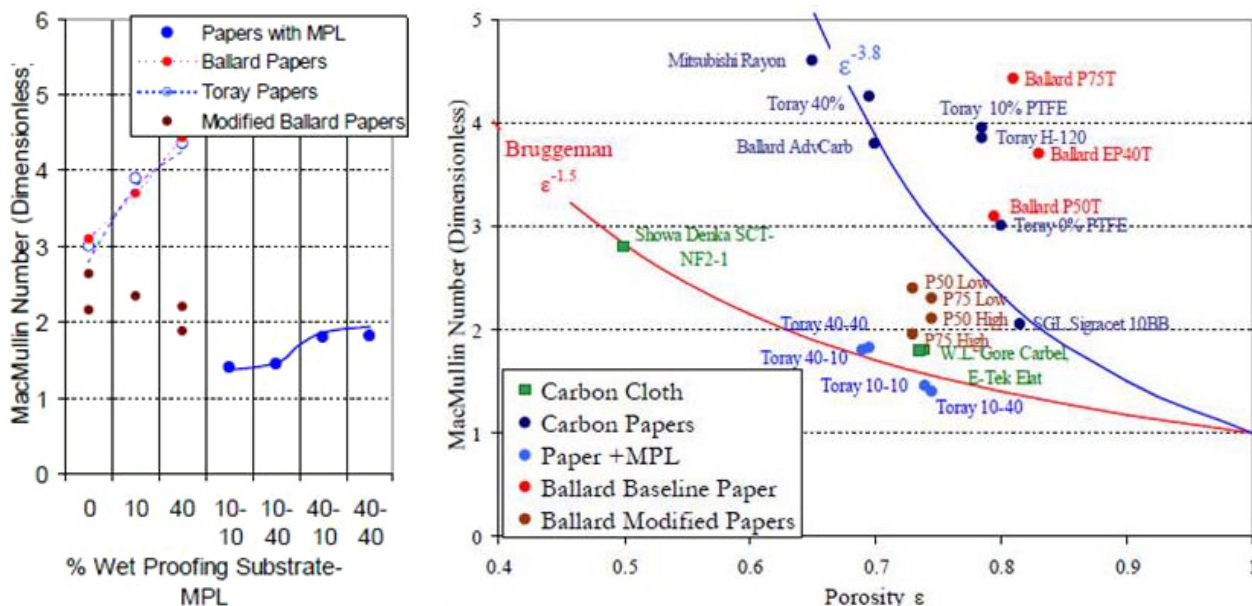


FIGURE 3. MacMullin number for GDL characterization: (left) MacMullin number as function of wet proofing in substrate and MPL (right) MacMullin number as function of porosity.

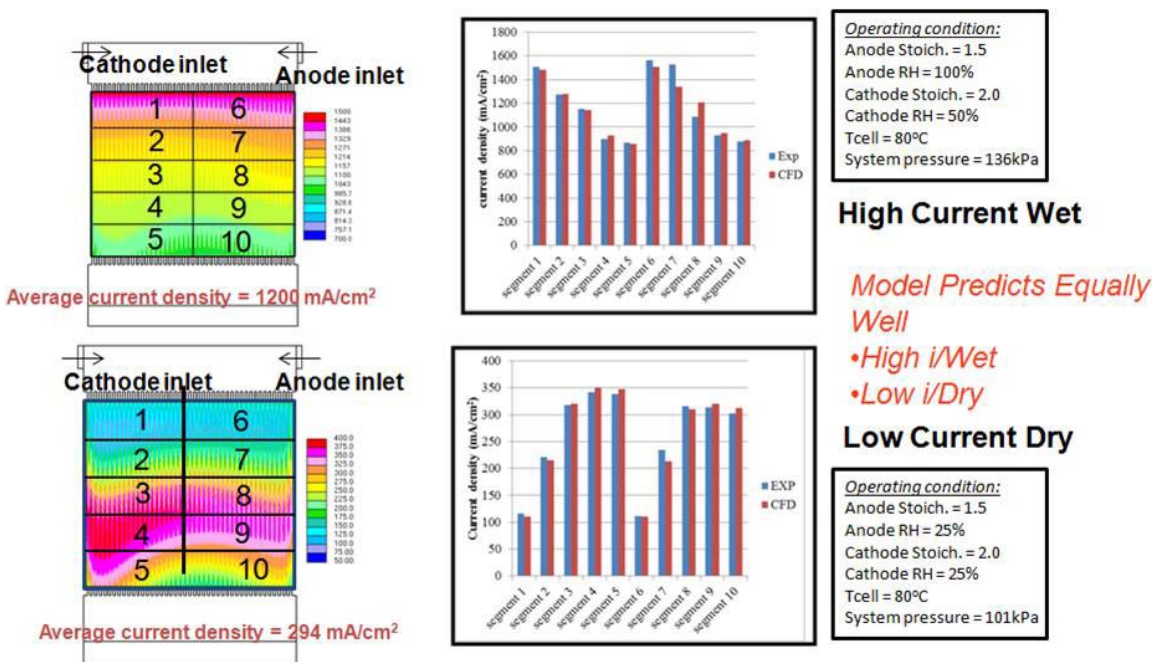


FIGURE 4. Experimental and CFD model-based current distribution on USC parallel metallic plates at two operation conditions: (left) high RH operation at 1,200 mA/cm² and (right) low RH operation 294 mA/cm².

until sufficient water is produced and accumulated down the channel at sections 3-4 and 8-9 where the current density is a maximum. The current density decreases in sections 5 and 10 because the partial pressure of oxygen decreases. The non-uniformity between sections 4 and 9 is due to the higher velocity in the parallel channel on the cathode side

of the cell; that is because the flow-field was designed for 1.0 A/cm² rather than the low flowrates associated with the 0.3 A/cm². The modeling results for the GM flow-field were also compared with experimental results from GM (www.pemfcd.org), including temperature distributions, and they demonstrate excellent consistency (data not shown).

Conclusions and Future Directions

- Widely varied PEMs and diffusion media will allow us to model the important parameters of each.
- Diffusivity measurement systems have been automated for precise control and a variety of hydrocarbon membranes characterized using the advanced system:
 - No interfacial resistance found
 - Techniques widely available to community
- Dead-end hydrogen pump system has been developed for EODC measurements for Nafion® membranes and hydrocarbon membranes:
 - No water condensation found
 - Water diffusion eliminated
- Gas diffusion media with different structure and properties have been designed and characterized and performance compared.
- Experimental and CFD results have been obtained for various flow channels (USC and GM plates) and two results are highly consistent.
- Extend testing and model predictions to additional automotive conditions.
- Down-select alternative polymers and generate larger, consistent materials.
- Confirm model with performance, current distribution and water collection results.
- Use model to determine performance sensitivity to build materials, suggest focus areas.

FY 2012 Publications/Presentations

1. “Transport Studies and Modeling in PEM Fuel Cells,” DOE Annual Merit Review, oral FC054, May 13–18, 2012.
2. “Simultaneous Water Uptake, Diffusivity and Permeability Measurement of Perfluorinated Sulfonic Acid Polymer Electrolyte Membranes,” *ECS Transactions*, 41 (1) 101-121 (2011).
3. “Novel Current Distribution Board for PEM Devices,” *ECS Transactions*, 41 (1) 549-559 (2011).
4. “Effect of Microporous Layer on MacMullin Number of Carbon Paper Gas Diffusion Layer,” *J. Power Sources*, 207 (1) 91-100 (2012).
5. “Assessing Porosity of PEM Fuel Cell Gas Diffusion Layers by SEM Image Analysis” , *J. Power Sources*, 197, 1-11 (2012).
6. “Understanding the Effect of Channel Tolerances on Performance of PEMFCs,” *International J. Hydrogen Energy*, 36 (19) 12512-12523 (2011).

References

1. T.A. Zawodzinski, C. Derouin, S. Radzinski, R.J. Sherman, V.T. Smith, T.E. Springer and S. Gottesfeld, *J. Electrochem. Soc.*, **140**, 1041 (1993).
2. T.V. Nguyen and R.E. White, *J. Electrochem. Soc.*, **140**, 2178 (1993).
3. T. Fuller and J. Newman, *J. Electrochem. Soc.*, **139**, 1332 (1992).
4. T.A. Zawodzinski, J. Davey, J. Valerio, and S. Gottesfeld, *Electrochimica Acta*, **40**, 297 (1995).
5. K. Aotani, S. Miyazaki, N. Kubo, and M. Katsuta, *ECS Transactions*, **16**, 341 (2008).
6. S. Ge, B. Yi and P. Ming, *J. Electrochem. Soc.*, 153, A1443 (2006).
7. M.J. Martinez, S. Shimpalee, and J.W. Van Zee *J. of the Electrochem. Soc.*, **156 (1)** B80-B85 (2009).

V.F.7 Investigation of Micro- and Macro-Scale Transport Processes for Improved Fuel Cell Performance

Jon P. Owejan (Primary Contact), Matthew Mench, Michael Hickner, Satish Kandlikar, Thomas Trabold, Jeffrey Gagliardo, Anusorn Kongkanand, Wenbin Gu, Paul Nicotera

General Motors
10 Carriage Street
Honeoye Falls, NY 14472
Phone: (585) 953-5558
Email: jon.owejan@gm.com

DOE Managers
HQ: Donna Ho
Phone: (202) 586-8000
Email: Donna.Ho@ee.doe.gov
GO: David Peterson
Phone: (720) 356-1747
Email: David.Peterson@go.doe.gov

Technical Advisor
John Kopasz
Phone: (630) 252-7531
Email: kopasz@anl.gov

Contract Number: DE-EE0000470

Subcontractors:

- Penn State University, University Park, PA
- University of Tennessee, Knoxville, TN
- Rochester Institute of Technology, Rochester, NY
- University of Rochester, Rochester, NY

Project Start Date: June 1, 2010
Project End Date: May 31, 2013

Fiscal Year (FY) 2012 Objectives

- Characterize saturated relationships in state-of-the-art fuel cell materials.
- Obtain a comprehensive down-the-channel validation dataset for a baseline and auto-competitive material set.
- Develop multidimensional component models to output bulk and interfacial transport resistances.
- Demonstrate integrated transport resistances with a one plus one-dimensional (1+1D) fuel cell model solved along a straight gas flow path.
- Identify critical parameters for low-cost material development.

Technical Barriers

This project addresses the following technical barriers from the Fuel Cells section of the Fuel Cell Technologies Program Multi-Year Research, Development and Demonstration Plan:

- (B) Cost
- (C) Performance

Technical Targets

This project supports fundamental studies of fluid, proton and electron transport with a focus on saturated operating conditions. Insights gained from these studies are being used to develop modeling tools that capture fundamental transport physics under single- and two-phase conditions. The primary deliverables are:

- Validated cell model including all component physical and chemical properties.
- Public dissemination of the model and instructions for exercise of the model.
- Compilation of the data generated in the course of model development and validation.
- Identification of rate-limiting steps and recommendations for improvements to the plate-to-plate fuel cell package.

FY 2012 Accomplishments

- Baseline validation data set is complete with 95% confidence intervals.
- Several 1-D relationships have been established or refined based on parametric and characterization methods developed within the project.
- Demonstrated improved down-the-channel 1+1D model prediction with new relationships integrated.
- Developed novel material solutions to improve key transport limitations.
- Published validation, parametric studies, and characterization data to a project website at: www.pemfcddata.org.



Introduction

The transport physics associated with fuel cell operation are widely debated amongst researchers because

comprehensive micro/nano-scale process validation is very difficult. Furthermore, fuel cell operation has a strong interdependence between components making it difficult to separate the key relationships required for predictive models with ex situ methods. Generally, a validated model that predicts operation based on known design parameters for fuel cell hardware and materials is highly desired by developers. Such a model has been proposed by many research groups for dry (less than 100% relative humidity [RH] exhaust) operation with moderate success; however, these modelers unanimously assert that their ability to predict wet operation is limited by two-phase component-level understanding of transport processes. Additionally, as two-phase models continue to be refined, benchmarking progress is difficult due to incomplete validation datasets.

In the current work, our team is developing characterization tools for saturated relationships based on the evolution of a dry 1+1D model for accurate wet prediction [1]. To complement this work we are also developing a comprehensive validation dataset based on a wide proton exchange membrane fuel cell (PEMFC) operating space. As data and modeling reach a final form, these are uploaded to a project website at www.pemfcdata.org. All characterization and validation work is conducted with common material sets that represent current and next generations of PEMFC design.

Approach

This project is organized around baseline and next-generation material sets. These materials define parametric bounds for component and integrated down-the-channel modeling efforts. The baseline material set was chosen based on the commercial state of the art that exists today. The next-generation material set consists of transport impacting parametric changes that are in-line with the DOE 2015 targets for reduced cost while improving durability and performance. For characterization and validation experiments, a standard protocol was also developed to enable the team to conduct experiments with the same boundary conditions.

The first phase of this project was experimentally focused on characterization work that is organized by transport domain, comprising thin film ionomers, bulk membranes, porous electrodes, gas diffusion layers (GDLs) and flow distribution channels. The specifics of these relationships were outlined previously [2]. In anticipation of this integrated model, validation data sets are being collected in parallel with small-scale hardware specifically designed to include automotive stack constrains [3]. Currently with these experimental methods established, work in the second phase of the project is more modeling focused as the physical mechanisms that govern the observed transport phenomenon are described multi-dimensionally at the component level and evaluated with a 1+1D fully integrated model. This work continuously guides parametric studies with novel material changes.

Results

Validation Data

The project protocol varies outlet temperature, inlet RH, outlet pressures, and current density [4]. With three replicate experiments, the baseline validation campaign resulted in 333 data points for analysis of single parameter (potential, differential pressure, water balance, etc.) and distributed measurements (temperature, current, ohmic resistance, liquid water content). Using three replicates for each test point, 95% confidence intervals were calculated. The majority of these data have upper or lower confidence intervals less than 10 mV centered on the mean and only 5% have upper or lower confidence intervals greater than 30 mV centered on the mean. This level of experimental certainty, resulting from rigorous material preparation and advanced instrumentation, is a significant accomplishment as this enables a higher level of model precision. All baseline data and analyses have been uploaded to the project website and the second phase of validation work with the next generation material set is underway.

Membrane Permeability

By first characterizing the sources of water transport resistance that do not originate in the membrane, experimental methods for measuring water permeability of fuel cell membranes as a function of temperature and RH have been refined. Results show that there is no discernible dependence of the permeability on membrane thickness, suggesting that any localized transport resistance that may exist at the membrane surface is undetectable by this method. It is possible to fit the data to a simple 3-constant empirical expression for the membrane permeability as a function of temperature and RH. Proper accounting of the device resistance turns out to be very important when measuring the membrane water transport properties. At high degrees of membrane saturation, the device resistance can be more than three times larger than that of the membrane itself. Combined with a published expression for the Nafion[®] water uptake as a function of temperature and RH [5], the measurements of membrane permeability can be used to calculate corresponding results for the membrane water diffusion coefficient. The diffusion coefficient increases monotonically with membrane hydration, with little or no change occurring above 50% RH. The current result is compared to literature in Figure 1 [6-10].

Transport in Thin Ionomer Films

Performance loss at high current density gets progressively worse as Pt loading is decreased in dispersed catalysts. This apparent transport loss has been shown to occur at or near the Pt surface. Measurement of coverage

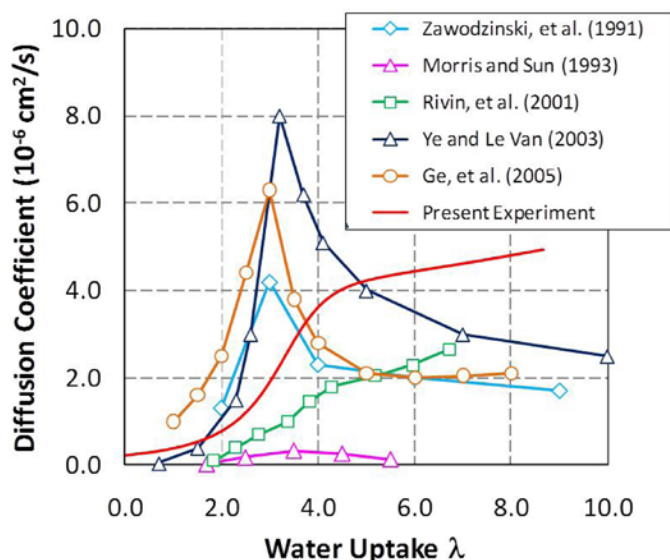


FIGURE 1. Water diffusion coefficient for a Nafion® membrane at 30°C determined in the present experiment compared with corresponding results from five previous experiments [6-10] at temperatures from 25-32°C, all plotted as a function of the water uptake.

dependent kinetics have further isolated the magnitude of this residual loss [11]. Recent fuel cell experiments from this project with varied Pt dispersions at a given loading (Figure 2) along with modeling of limiting current at an individual Pt particle based on oxygen transport through the ionomer demonstrate that the trends observed in pressure independent transport resistance are only resolved if a substantial interfacial resistance is occurring at both the gas and Pt interfaces. This transport theory is being further investigated using a model system with a well-defined flat Pt surface that is coated with thin ionomer films. This project is also investigating the behavior of thin ionomer films with ex situ methods.

Because of the small oxygen transport resistance in thin ionomer films (10-1,000 nm), if any oxygen-transport resistance not associated with transport through the ionomer film (i.e. the device resistance) was comparable to the resistance of the ionomer film, the film transport measurement would be compromised. The device resistance is originated mainly from the oxygen transport in the gas phase; therefore it can be measured by varying the gas pressure. The device resistance was quantified using a 1- μm thick Nafion® film. The resistance was less than 3 s/m when measured at 80°C and the effect of gas RH was also found to be negligible. This resistance is equivalent to ~10-nm thick ionomer film and by assuming the same oxygen transport properties as those of bulk membranes; the ionomer film measurement should be reliable down to ~100-nm with less than 10% uncertainty. The measured oxygen diffusivities (2×10^{-7} and 6×10^{-7} cm^2/s at 40°C and 80°C, respectively) in this 1- μm thick film were consistent with that measured

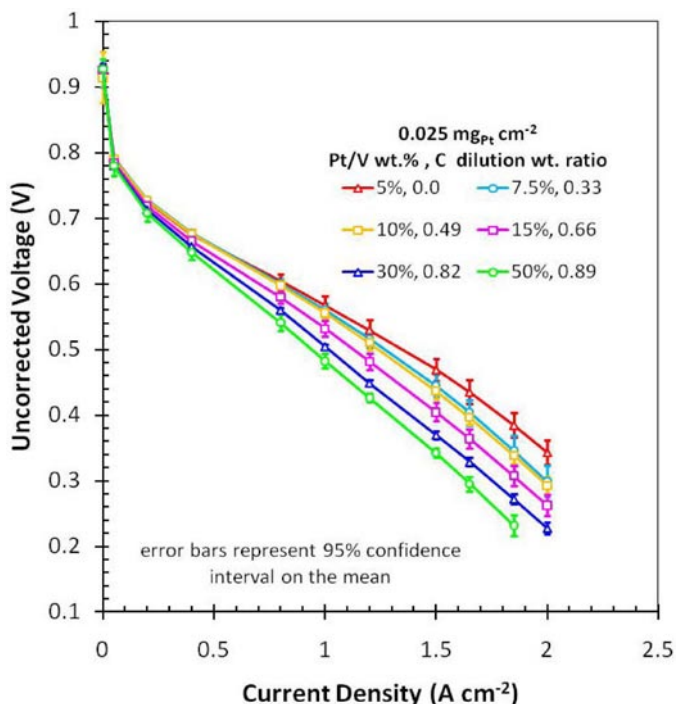


FIGURE 2. Performance of varied Pt dispersions at $0.025 \text{ mg}_{\text{Pt}} \text{ cm}^{-2}$ with electrode thickness kept constant using bare carbon dilution at H_2/air , 65% RH, 80°C, 150 kPa operating conditions.

previously for bulk membranes. This investigation is currently ongoing with thinner film thicknesses.

Using ex situ methods we have measured significant differences in the proton dynamics of membranes and thin Nafion® films using fluorescence. A more proton accepting environment in bulk membranes relative to thin films was observed. The origin of the suppressed deprotonation is likely due to the different morphologies in the membrane and thin film. A less interconnected structure in the thin film would lead to lower deprotonation due to the isolated water-filled ionic domains in the material. We have also measured the thickness swelling as a function of RH by ellipsometry and the hydration number as a function of RH by quartz crystal microbalance (QCM). On SiO_2 , thinner Nafion® films swell more than thicker films. This trend is consistent for both adsorbed films (from Queen's University) and spin-coated films (from Penn State) of Nafion® on SiO_2 . The thickness swelling results were confirmed with QCM hydration number measurements that show more water being absorbed into thin films than thick films.

Transport in Diffusion Materials

Several in situ and ex situ measurements have been developed to measure transport in the porous components that include the electrode, microporous layer and carbon fiber macroporous substrate. In situ neutron imaging, infrared

imaging and acoustic microscopy were used to map through-plane liquid water distributions within the anode vs. cathode diffusion layers. These data were combined with limiting current experiments that measure the increase in transport resistance associated with liquid water accumulation.

Additional ex situ measurements of thermal conductivity and mass diffusivity as a function of water saturation and capillary pressure relationships for the baseline GDL and catalyst layer were also completed. These data are being used to support the model development by isolating specific parameters in component validation data. These key transport relationships are now included in the model.

Based on results from the baseline experiments and modeling it was determined that within practical constraints the only material-based mechanism to adjust the overall water balance was with changes to the macroporous diffusion substrate. An experimental GDL with significantly increased tortuosity has been designed and fabricated using a simplified and lower energy process [12]. The advanced material set for fuel cell testing includes the high tortuosity GDL on the anode side, while the baseline GDL continues to be used on the cathode side. By increasing the anode GDL tortuosity

to greater than 7 while maintaining all other properties approximately constant, comparable average performance is observed along with a reduced sensitivity to RH, as well as 11% to 44% more product water being removed on the cathode side (depending on operating conditions). Fast reaction kinetics and hydrogen gas transport enable the fuel cell to tolerate decreased effective diffusivity on the anode side. Due to the lower cost fabrication process and reduced carbon fiber content, the current anode GDL is more compressible than desired. Thus, a mixture design study is ongoing to determine a formulation that maintains high tortuosity and reduces compressibility.

Transport in Flow Distributor Channels

Interfacial oxygen transport resistance in the presence of liquid water causes a significant concentration drop across the channel-GDL interface. The effect of liquid water was numerically studied and expressed with the Sherwood number (Sh). The numerical model was validated against the theoretically predicted fully developed Sherwood number for a dry channel ($Sh = 3.36$). The Sherwood number was numerically calculated by introducing experimentally obtained droplet and film shaped obstructions. Figure 3 shows the Sherwood number down the channel length for two consecutive droplets 2 mm apart and for a single 5-mm long film. The Sherwood number over the dry regions was also reported to further characterize the local oxygen mass transport near water obstructions. The small increase in Sherwood number in the vicinity of the first droplet was due to increased gas mixing, while the significant increase near the second droplet was due to the impinging developing flow of the wake region behind the first droplet. The effect of water contact area was non-negligible for the film simulation as shown in Figure 3. The Sherwood number in the dry region along the film was greater than the fully developed value but a significant reduction was observed for the effective Sherwood number. These case studies of channel water obstructions show that a simple scaling of the fully developed Sherwood number is insufficient to accurately describe the local Sherwood number. This novel approach will be further used to obtain a statistical description of the effective Sherwood number by utilizing experimentally obtained liquid coverage in the operating space of the standard test protocol.

Transport resistance associated with two-phase flow in the flow distribution system beyond the active area is also being characterized. This project activity focused on understanding the relationship between fuel cell operating conditions and water accumulation at the channel-to-manifold interface, and correlating these in situ data to ex situ two-phase pressure drop measurements. At relatively low temperature conditions for which product water will be present in the liquid phase, it was found that accumulated water within the active area is a strong function of both

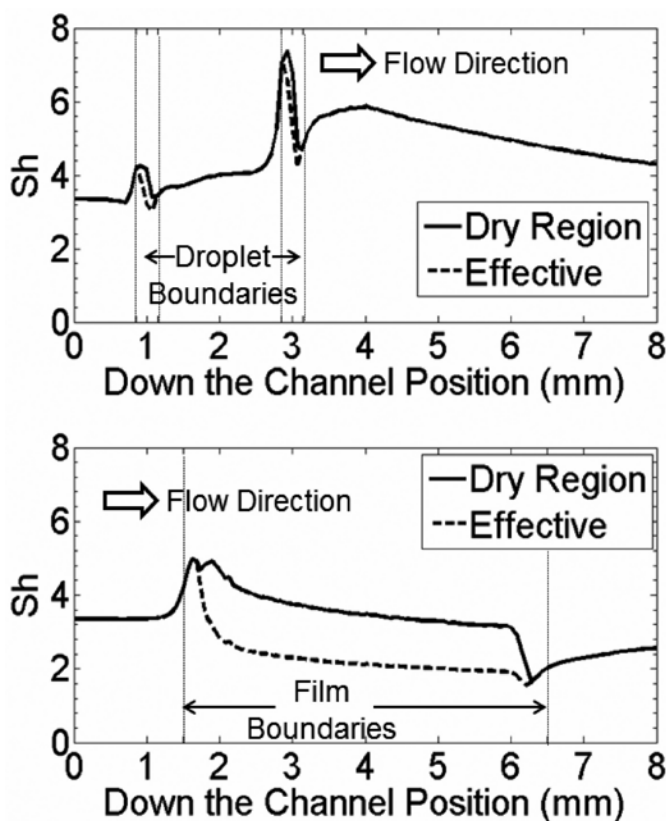


FIGURE 3. The dry region and effective Sherwood number in the presence of two consecutive droplets and a 5-mm long film. The channel-GDL oxygen interfacial transport resistance is highly dependent on local water obstructions and is insufficiently described by a simple scaling of the fully developed Sherwood number.

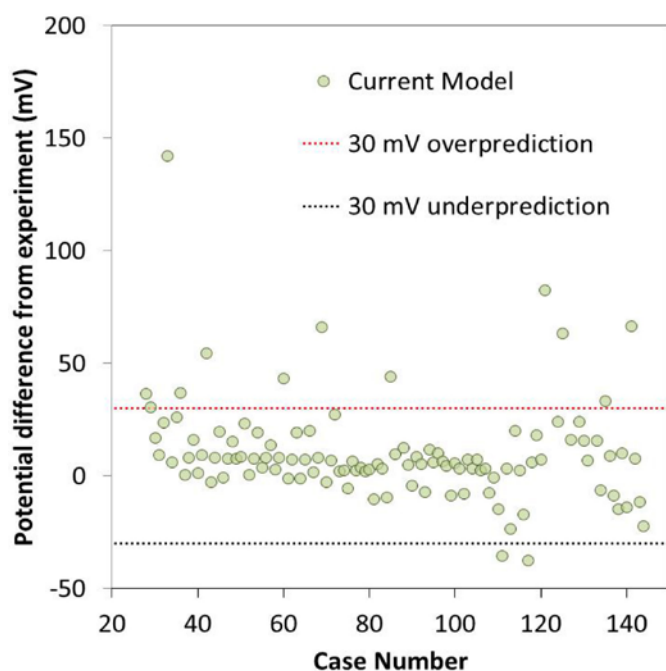


FIGURE 4. Down-the-channel model predictions for all test cases in the project protocol [4] with maximum experimental error indicated.

current density and anode/cathode pressure, whereas water in the anode exit is nearly independent of these operating variables. These in situ two-phase flow dynamics were simulated in an ex situ apparatus in which water and air flow rates can be independently controlled to produce conditions of interest at the channel-to-manifold transition region. It was found that water present downstream of the active area can have a significant impact on the overall system pressure drop. These data were used to formulate a generalized expression for the system pressure drop with channel-level water present only downstream of the active area.

Modeling

The relationships described above for the various components are summarized with a down-the-channel 1+1D model. More accurately accounting for the transport relationships elucidated in this project has improved predictions of the performance and water balance response to key changes in material and operating parameters. Considering the baseline material set with the current model, Figure 4 shows the prediction for the 111 validation test points. Since the majority of the validation data points have a 30 mV or less 95% confidence intervals, Figure 4 demonstrates that the current performance prediction is accurate within uncertainty across most of the experimental space. As the model is finalized during the next phase of the project with liquid/vapor fronts in the porous components (uniform saturation is currently used) we expect to reduce the number of outlying predictions.

Conclusions and Future Directions

A well-organized characterization, modeling and validation framework was developed early in this project. The first phase (FY 2011) of execution was largely focused on experimental development. During the second phase of the project (FY 2012), results from these methods were described with multidimensional component models and summarized in a down-the-channel model that is compared to a comprehensive validation database. Specific highlights from FY 2012:

- Comprehensive baseline validation dataset with 95% confidence intervals established.
- New steady membrane permeability relationship results in a higher water flux at high RH.
- For a constant Pt loading, pressure independent transport resistance was shown to increase with the ratio of Pt to C surface area, thus indicating that increased ionomer surface area relative to the Pt particles is preferred.
- Coverage-dependent kinetic relationship improves overpotential prediction at less than 750 mV.
- GDL transport resistance transition from dry to wet is refined with a critical saturation value and thermal conductivity as a function of saturation.
- Sherwood number based on statistical representations of measured two-phase flow in channels improves 1D prediction of transport loss in channels.
- Dry entrance and two-phase exit relationships identify residual loss and isolate active area pressure drop.
- Performance and water balance prediction improved based on a comparison to baseline validation data.

The final phase of this project is focused on refining the component and down-the-channel models while completing characterization and validation work for the next-generation material set. The model will be finalized by adding nonuniform saturation relationships in the porous layers and it will be validated with data from the next generation material set that varies key parameters of interest in new materials. Using this model as a guide, the project will be completed with parametric studies focused on rate limiting material constraints for transport within a PEMFC.

Patents

1. Nicotera, P., Owejan, J.P., Evans, R., Mench, M.M., “Low Cost Fuel Cell Diffusion Layer Configuration for Optimized Anode Water Management,” US Patent Application, filed 2012.

FY 2012 Publications/Presentations

1. LaManna, J.M., Chakraborty, S., Zhang, F.Y., Gagliardo, J.J., Owejan, J.P., and Mench, M.M., “Isolation of Transport Mechanisms in PEFCs with High Resolution Neutron Imaging,” *ECS Transactions*, 41 (1) 329-336 (2011).

2. Daino, M.M., and Kandlikar S.G., “3D Phase-Differentiated GDL Microstructure Generation with Binder and PTFE Distributions,” *International Journal of Hydrogen Energy*, 37(6), pp. 5180-5189 (2012).
3. LaManna, J.M., and Kandlikar S.G., “Determination of effective water vapor diffusion coefficient in pemfc gas diffusion layers,” *International Journal of Hydrogen Energy*, 36(8), pp. 5021-5029 (2011).
4. Daino, M.M., and Kandlikar, S.G., “Advances in Digital Microstructure Generation of a PEMFC GDL with Localized Binder and PTFE Distributions,” EFC11275, *Proceedings of the 4th European Fuel Cell Piero Lunghi Conference & Exhibition*, December 14–16, Rome, Italy, pp. 405-406 (2011).
5. Lu Z., Rath C., Zhang G., and Kandlikar S.G., “Water management studies in PEM fuel cells, part IV: Effects of channel surface wettability, geometry and orientation on the two-phase flow in parallel gas channels,” *International Journal of Hydrogen Energy*, 36(16), pp. 9864-9875 (2011).
6. Rath, C.D., and Kandlikar, S.G., “Liquid filling in a corner with a fibrous wall—An application to two-phase flow in PEM fuel cell gas channels,” *Colloids and Surfaces A: Physicochemical and Engineering Aspects*, 384(1-3), pp. 653-660 (2011).
7. Sergi, J.M., and Kandlikar, S.G., “Quantification and characterization of water coverage in PEMFC gas channels using simultaneous anode and cathode visualization and image processing,” *International Journal of Hydrogen Energy*, 36(19), pp. 12381-12392 (2011).
8. Zhang, G., and Kandlikar, S.G., “A critical review of cooling techniques in proton exchange membrane fuel cell stacks,” *International Journal of Hydrogen Energy*, 37(3), pp. 2412-2429 (2012).
9. Subramanian, N.P., Greszler, T.A., Zhang, J., Gu, W., Makharia, R., “Pt-Oxide Coverage-Dependent Oxygen Reduction Reaction (ORR) Kinetics,” *J. Electrochem. Soc.* 159, B531 (2012).
10. Owejan, J.P., Gagliardo, J.J., Reid, R.C., Trabold, T.A., “Proton transport resistance correlated to liquid water content of gas diffusion layers,” *J. Power Sources*, 209, pp.147-151 (2012).
11. See, E.J., Banerjee, R., Daino, M.M., Sergi, J.M., Koz, M., Owejan, J.P., Gagliardo, J.J., and Kandlikar, S.G., “Thermal Management Considerations in the Design of an Experimental Fuel cell with Material Evaluation,” EFC11237, *Proceedings of the 4th European Fuel Cell - Piero Lunghi Conference & Exhibition*, December 14–16, Rome, Italy, pp. 363-364 (2011).
12. Dishari, S.K., M.A. Hickner, “Anti-plasticization and Water Uptake of NAFION® Thin Films,” *ACS Macro Lett.*, 1, 291–295 (2011).
13. Banerjee, R., and Kandlikar, S.G., “Effect of Temperature on In-Plane Permeability of Water Vapor in the Gas Diffusion Layer of PEM Fuel Cells,” *ECS Transactions*, 41(1), pp. 489-497 (2011).
14. Gopalan, P., and Kandlikar, S.G., “Investigation of Water Droplet Interaction with the Side Wall of the Gas Channel in the PEM Fuel Cell in the Presence of Gas Flow,” *ECS Transactions*, 41(1), pp.479-488 (2011).
15. Dishari, S.K., M.A. Hickner, “Anti-plasticization and Water Uptake of NAFION® Thin Films,” *ACS Macro Lett.*, 1, 291–295 (2011).
16. Rath, C.D., and Kandlikar, S.G., “Effect of Channel Geometry on Two-Phase Flow Structure in Fuel Cell Gas Channels,” ICNMM2011-58252, *Proceedings of the ASME 2011 9th International Conference on Nanochannels, Microchannels, and Minichannels*, June 19–22, Edmonton, AB, Canada, 2011.
17. LaManna, J.M., Chakraborty, S., Zhang, F.Y., Gagliardo, J.J., Owejan, J.P., and Mench, M.M., “Isolation of Transport Mechanisms in PEFCs with High Resolution Neutron Imaging,” The 4th Annual Global Conference on Energy: International Forum on Multidisciplinary Education and Research for Energy Science. Honolulu Hawaii, Dec. 2011.
18. Mench, M.M., “Characterization of Heat & Water Transport in Gas Diffusion Layers and Associated Interfaces,” Plenary Talk, ECS Fall 2011 meeting.
19. LaManna, J.M., Chakraborty, S., Zhang, F.Y., Gagliardo, J.J., Owejan, J.P., and Mench, M.M., “Isolation of Transport Mechanisms in PEFCs with High Resolution Neutron Imaging,” Paper #976, Presented at Fall meeting of the Electrochemical Society, Boston, Massachusetts, 2011.
20. Subramanian, N.P., Greszler, T.A., Zhang, J., Gu, W., Makharia, R., “Pt-Oxide Coverage-Dependent Oxygen Reduction Reaction (ORR) Kinetics,” Presented at Fall meeting of the Electrochemical Society, Boston, Massachusetts, 2011.
21. Gagliardo, J.J., Owejan, J.P., Trabold, T.A., “Liquid Water Measurement in an Operating Planar PEMFC 4-cell Stack,” ASME Fuel Cell Conf., Washington, DC, July 2011.

References

1. Gu, W., Baker, D.R., Liu, Y., Gasteiger, H.A., “Proton exchange membrane fuel cell (PEMFC) down-the-channel performance model,” *Handbook of Fuel Cells* - Volume 5, Prof. Dr. W. Vielstich *et al.* (Eds.), John Wiley & Sons Ltd., (2009).
2. Owejan, J.P., 2011 Annual Progress Report for the DOE Hydrogen and Fuel Cells Program, (2011).
3. Owejan, J.P., Gagliardo, J.J., Sergi, J.M., Kandlikar, S.G., Trabold, T.A., “Water management studies in PEM fuel cells, Part I: Fuel cell design and in situ water distributions,” *International Journal of Hydrogen Energy*, 34 (8), pp. 3436-3444, (2009).
4. http://www.pemfcdata.org/data/Standard_Protocol.xls
5. Mittelstaedt, C.K., and Liu, H., “Conductivity, permeability, and ohmic shorting of ionomeric membranes,” Chapter 23 of *Handbook of Fuel Cells*, Vol. 5, W. Vielstich, H. Yokokawa, H. A. Gasteiger, eds., John Wiley & Sons, 2009.
6. Ye, X., and Le Van, M.D., “Water transport properties of Nafion membranes Part II. Multi-tube membrane module for air drying,” *Journal of Membrane Science*, 221, pp. 163-173 (2003).
7. Zawodzinski, T.A., Neeman, M., Sillerud, L.O., Gottesfeld, S., “Determination of Water Diffusion Coefficients in Perfluorosulfonate Ionomeric Membranes,” *Journal of Physical Chemistry*, 95, pp. 6040-6044 (1991).
8. Morris, D.R., and Sun, X., “Water Sorption and Transport Properties of Nafion 117 H” *J. Appl. Polym. Sci.*, 50, pp. 1445-1452 (1993).

9. Ge, S., Li, X., Yi, B., Hsing, I.M., “Absorption, Desorption, and Transport of Water in Polymer Electrolyte Membranes for Fuel Cells,” *Journal of the Electrochemical Society*, 152, pp. A1149-A1157 (2005).

10. Rivin, D., Kendrick, C.E., Gibson, P.W., Schneider, N.S., “Solubility and transport behavior of water and alcohols in Nafion,” *Polymer*, 42, pp. 623-635 (2001).

11. Subramanian, N.P., Greszler, T.A., Zhang, J., Gu, W., Makharia, R., “Pt-Oxide Coverage-Dependent Oxygen Reduction Reaction (ORR) Kinetics,” *J. Electrochem. Soc.* 159, B531 (2012).

12. Nicotera, P., Owejan, J.P., Evans, R., Mench, M.M., “Low Cost Fuel Cell Diffusion Layer Configuration for Optimized Anode Water Management,” US Patent Application, filed 2012.

V.G.1 Novel Materials for High Efficiency Direct Methanol Fuel Cells

Chris Roger (Primary Contact), David Mountz,
Wensheng He, and Tao Zhang

Arkema Inc.
900 First Ave
King of Prussia, PA 19406
Phone: (610) 878-6707
Email: chris.roger@arkema.com

DOE Managers

HQ: Donna Ho
Phone: (202) 586-8000
Email: Donna.Ho@ee.doe.gov

GO: Reg Tyler
Phone: (303) 275-4929
Email: Reginald.Tyler@go.doe.gov

Technical Advisor

John Kopasz
Phone: (630) 252-7531
Email: kopasz@anl.gov

Contract Number: DE-EE0000474

Subcontractor:

Illinois Institute of Technology (IIT), Chicago, IL

Project Start Date: May 1, 2010
Project End Date: June 30, 2013

- Develop a second generation membrane with an areal resistance $\leq 0.0375 \Omega\text{cm}^2$ and a methanol permeation coefficient $\leq 1 \times 10^{-7} \text{ cm}^2/\text{s}$ (deliverable – September 2012).
- Demonstrate an MEA performance of $135 \text{ mW}/\text{cm}^2$ @ 0.4 V with a composite membrane in 1M methanol (Go/No-Go decision – September 2012).

Technical Barriers

This project addresses the following technical barriers from the portable power section of the Fuel Cell Technologies Program Multi-Year Research, Development, and Demonstration Plan:

- (A) Durability
- (B) Cost
- (C) Performance

Technical Targets

This project is conducting focused research on next generation membrane and cathode catalyst materials for direct methanol fuel cells. Insights gained from these studies will be applied toward the design of a MEA for portable power devices that meet the DOE 2013 targets:

- Performance: specific power (30 W/kg), power density (35 W/L), specific energy (430 Wh/kg), and energy density (500 Wh/L)
- Cost: \$10/W
- Lifetime: 3,000 hours

In translating DOE targets, the following goals for the membrane and MEA performance were defined (Table 1). The progress towards meeting these goals is also summarized.

Fiscal Year (FY) 2012 Objectives

- Demonstrate membrane electrode assembly (MEA) performance of $120 \text{ mW}/\text{cm}^2$ at 0.4 V with an Arkema membrane in 1M methanol (Go/No-Go decision - January 2012).
- Obtain a specific power $\geq 50 \text{ mW}/\text{mg}$ precious group metal (PGM) in an MEA with 50% Pt reduction.

TABLE 1. Progress toward Meeting the Project Technical Targets for Portable Power Applications

| Characteristic ¹ | Units | Industry Benchmark | Project Target | Status |
|----------------------------------|-----------------------------|----------------------------------|--------------------|--------------------|
| Methanol Permeability | cm^2/s | $1\text{-}3 \cdot 10^{-6}$ | 1×10^{-7} | 1×10^{-7} |
| Areal Resistance, 70°C | Ωcm^2 | 0.120 (7 mil PFSA ²) | 0.0375 | 0.080 |
| MEA Cathode Catalyst Loading | mg/cm^2 PGM | 2.5 | 2 | ~1.3 |
| MEA I-V Cell Performance (0.4 V) | mW/cm^2 | 90 | 150 | 120 ³ |
| MEA Lifetime | Hours | >3,000 | 5,000 | In progress |

¹ Targets based on a methanol concentration of 1M.

² Perfluorinated sulfonic acid

³ Measured with commercial gas diffusion electrode (GDE) with $1.5 \text{ mg}/\text{cm}^2$ Pt on the cathode. The anode contains a Pt loading of $3.0 \text{ mg}/\text{cm}^2$ and a Ru loading of $1.5 \text{ mg}/\text{cm}^2$. This is intended to be reference for MEA development work.

FY 2012 Accomplishments

- Met the January 2012 Go/No-Go MEA performance target using an Arkema membrane and either a commercial GDE or a lab-made cathode.
- Obtained a specific power of 80-100 mW/mg PGM in a MEA with a cathode Pt loading in the range of 1.0-1.3 mg/cm².
- Demonstrated a technique to deconvolute performance loss from individual components and sources in direct methanol fuel cell (DMFC) operation.
- Started durability test in 2M methanol. MEAs failed earlier than expected and major performance loss came from degradation in both electrodes.
- Synthesized 23 different polyelectrolytes to develop a second generation DMFC membrane. The membrane is being designed to have higher performance and a lower cost than the first generation. All second generation membranes have unacceptably high polyelectrolyte loss after a brief immersion in water. Strategies to reduce the polyelectrolyte loss are being explored.
- Evaluated composite membranes containing sulfonated silica and rare-earth triflates. The most promising candidates are showing higher conductivity than the ones prepared last year.



Introduction

There is a tremendous need for small, efficient portable power sources. The explosive growth of the lithium-ion batteries market is fueled by the ever-growing demand for portable power used in consumer electronics. For the direct methanol fuel cell industry to emerge as an alternative to batteries, very difficult technical hurdles have to be overcome in terms of reduced methanol cross-over in the membrane and improved catalyst efficiencies.

Approach

Arkema and IIT are developing new DMFC membranes with lower fuel cross-over and high conductivity. The membranes are formed from blends of poly(vinylidene fluoride) with a variety of highly sulfonated polyelectrolytes. A number of variables can be easily adjusted in the blending process to tailor properties such as conductivity and methanol permeation. The key to obtaining the desired properties resides in control of composition, architecture, and morphology of the membrane components. These are controlled on a practical level through polyelectrolyte chemistry, processing, and use of inorganic materials, which are being systematically investigated.

Arkema completed the development of the first generation of polyelectrolytes this past year and began work on a new generation of polyelectrolyte technology that can be used in membranes to form different microstructures than the ones used in the current technology. These microstructures may be potent factor to increase membrane performance. The new technology may also have a potentially lower cost stemming from the use of less expensive, commercially available monomers and reducing the number of steps in the membrane fabrication process. IIT continued work on the addition of sulfonated silica and rare-earth triflate additives to Arkema's membranes, which have been shown to lower methanol permeability. IIT's efforts are now focused on improving membrane conductivity while keeping the methanol permeability low.

Results

Go/No-Go Decision

After the down-selection of membranes that have met the first year milestone requirements in July 2011, efforts focused on the development and testing of MEAs from these membranes to meet the Go/No-Go decision in January 2012. The membranes down-selected produced lower than expected MEA performance, and we identified that conductivity has a higher contribution on performance than methanol permeation in 1-2M methanol. The Go/No-Go milestone was met using a membrane composition containing slightly more polyelectrolyte than a down-selected candidate from the milestone and either a commercial GDE or a lab-made cathode¹. Data collected using the lab-made cathode and Arkema membrane in 2M methanol is shown in Figure 1 with a specific power of 92 mW/mg PGM.

The use of palladium-based cathode co-catalysts being developed in the project reduced MEA performance when it was added to the cathode ink formulations. The cause of the lower performance is, at least, partially attributed to the palladium catalyst agglomerating, causing poor catalyst distribution. Various strategies were explored (e.g. ink mixing method), but none of them were effective. The work on the Pd based co-catalyst was stopped after the Go/No-Go project review.

MEA Diagnostics

Electrochemical diagnostic techniques were employed to understand how the electrocatalyst, electrode, and MEA properties affect performance and durability. These diagnostic techniques are currently used in the membrane

¹ Lab-made cathode made with JM Hispec™ 9100 Pt/C catalyst with a loading between 1.0-1.5 mg/cm². Anode was a commercial material from Johnson Matthey (same as described in in Table 1 - note #3).

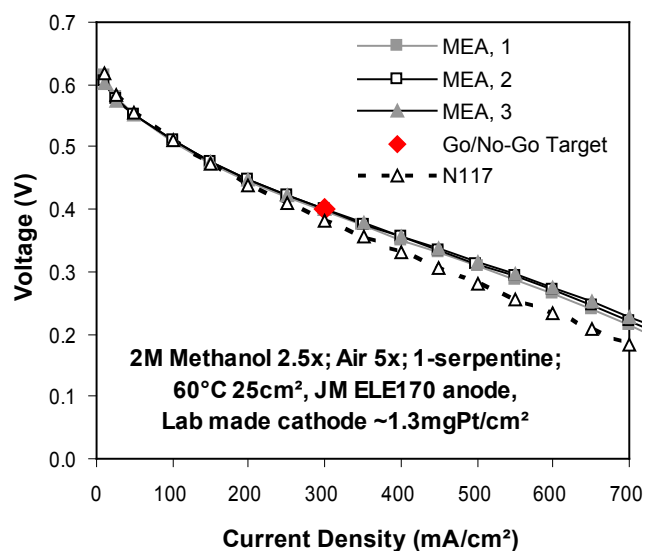


FIGURE 1. Polarization curves of Arkema membranes and lab-made cathodes in 2M methanol at 60°C. Each curve shown represents a sample replicate. This data also shows that MEA exhibited a specific power of 92 mW/mg PGM.

and MEA developments in both Arkema and IIT facilities. IIT can also perform in situ alternating current impedance spectroscopy and that can be used to gain further insights into MEA performance analysis by using an in-cell reference electrode.

IIT has recently demonstrated a useful technique based on the procedure described by Williams and coworkers to enable detailed breakdown of all the major contributions in MEA performance losses. One example of voltage loss breakdown of an MEA with Johnson Matthey standard electrodes and M43 membrane is shown in Figure 2. This technique does not account for methanol crossover on cathode performance in its current form. However, work is planned to account for this effect in coming year.

MEA Durability Testing

Several samples of the membrane developed for the Go/No-Go work were tested and most failed within 500-1,000 hours due to overall performance degradation (>20% voltage loss at 0.2 A/cm²). During the life testing, significant losses at the anode and cathode were also observed. An example of the distribution of voltage losses over the lifetime of an MEA using the Go/No-Go membrane, Johnson Matthey anode and Arkema cathode is shown in Figure 3. This data shows that the majority of the performance loss stems from the electrodes, especially the cathode. The MEAs also developed much higher (~50%) resistance and lower methanol crossover current over the cell lifetime. It is worth noted that despite the significant resistance increase, the resultant performance loss is still

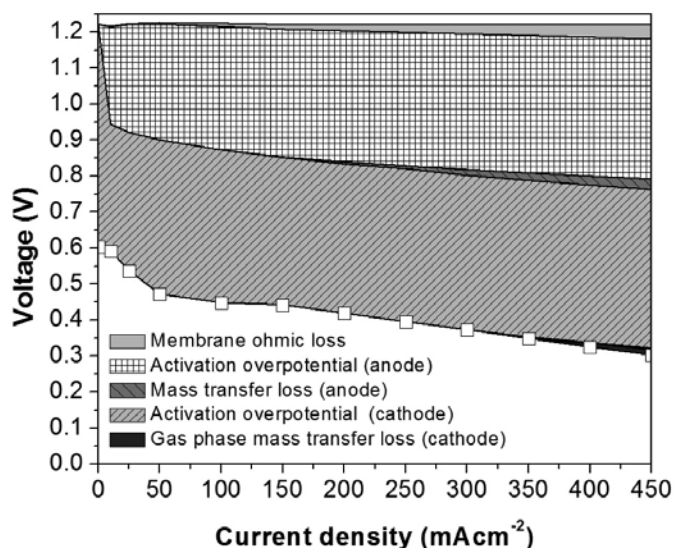


FIGURE 2. Contribution of the different losses in the actual performance of a 25 cm² MEA fabricated using Arkema M43 membrane and Johnson Matthey commercial electrodes. The polarization curve was acquired at 60°C using 3M methanol (2 stoichiometry) as fuel and air, oxygen, and helox as oxidants (3.5 stoichiometry). Cathode contributions from the electrode ohmic loss and binder-liquid phase mass transfer loss are negligible compared to the other losses plotted.

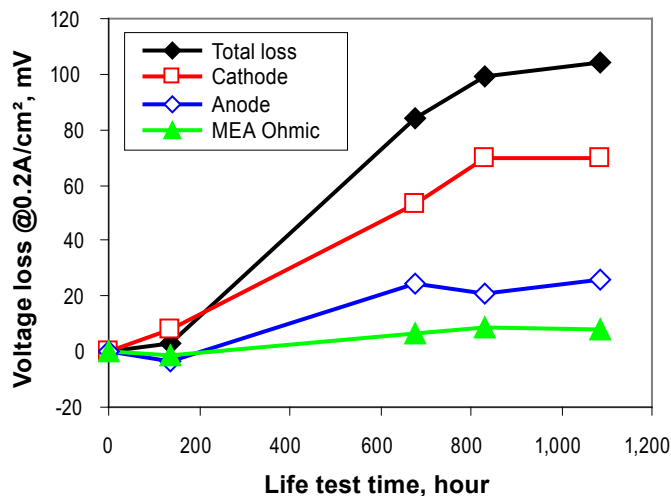


FIGURE 3. Distribution of voltage losses (relative to beginning of life) during life test of a MEA using Arkema Go/No-Go membrane and Johnson Matthey ELE170 anode and Arkema lab-made cathode. Life test conditions are 60°C, 2M methanol 3 stoichiometry, air 3.5 stoichiometry, at constant current of 0.2 A/cm².

smaller than the contribution by both electrodes. Detailed diagnostics and more controlled durability experiments will be conducted next year to understand why and how electrode degradation occurs.

Generation 2 Membrane Development

Twenty-three different polyelectrolytes were synthesized this past year to develop the current membrane generation. All membranes showed >30% sulfur loss and low conductivity after a short period of immersion in water, which is originating from polyelectrolyte leaching from the membrane. The leaching was traced back to inadequate crosslinking/tethering of the polyelectrolyte in the membrane. Without adequate crosslinking, the polyelectrolytes are quickly removed from the membrane since they are water soluble. Various strategies to improve crosslinking and limit polyelectrolyte water solubility are being explored.

Composite Membrane Development

Most inorganic additives screened reduced both methanol permeability and conductivity, as shown in Figure 4. There is a correlation between conductivity and permeability with most materials prepared with lower additive loadings (highlighted area of Figure 4) showing

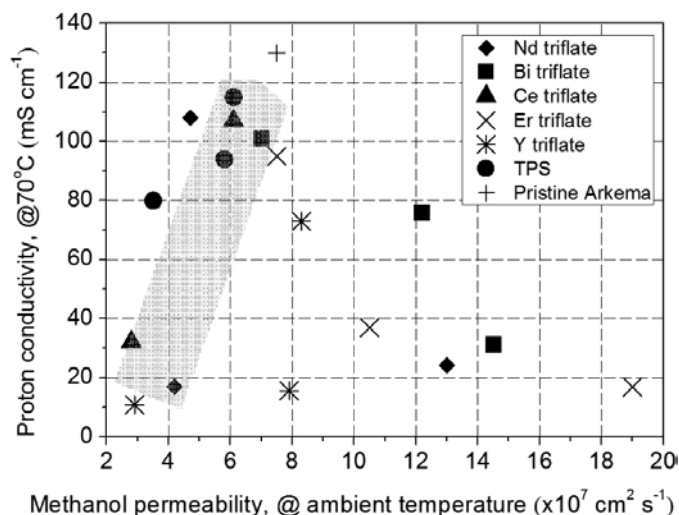


FIGURE 4. Relationship between proton conductivity and methanol permeability for composite membranes prepared with several inorganic fillers and loadings between 5-30 wt%.

only slight changes in selectivity. The most promising candidates were prepared with 5 wt% 3-(trihydroxysilyl)-1-propane-sulfonic acid (TPS) or neodymium triflate, which showed more selectivity than the unfilled Arkema membrane reference and have higher conductivity than the composites prepared last year (conductivity of composites last year was 58-75 mS/cm). The higher selectivity has not yield better performance in MEA testing thus far. Work is continuing on developing membrane composites with higher conductivity.

Conclusions and Future Directions

- Met the January Go/No-Go MEA performance target using an Arkema membrane and either a commercial GDE or a lab-made cathode in 1-2M methanol. Work on the cathode co-catalyst was stopped at this point due to low performance.
- Demonstrated a technique to deconvolute performance loss from individual components and sources in DMFC operation.
- Initiated durability testing. MEAs have failed earlier than expected; major performance losses have come from degradation in the electrodes.
- Continued development of membrane composites at IIT. Initiated the work on the second membrane generation at Arkema.
- Future work includes continuing the investigation of the failure modes in DMFC durability testing; understanding the effect of key factors such as membrane chemistry, methanol concentration, and catalyst loading, on durability; and continuing development of the second generation Arkema membrane and membrane composite materials.

FY 2012 Publications/Presentations

1. "Novel Materials for High Efficiency Direct Methanol Fuel Cells," David Mountz, Wensheng He, Tao Zhang, and Chris Roger. Presentation at the 2012 DOE Hydrogen Program and Vehicle Technologies Program Annual Merit Review and Peer Evaluation Meeting, May 16.

V.G.2 New MEA Materials for Improved Direct Methanol Fuel Cell (DMFC) Performance, Durability, and Cost

James Fletcher (Primary Contact), Philip Cox
 University of North Florida (UNF)
 1 UNF Drive
 Jacksonville, FL 32224
 Phone: (904) 620-1844
 Email: jfletche@UNF.edu

DOE Managers

HQ: Donna Ho
 Phone: (202) 586-8000
 Email: Donna.Ho@ee.doe.gov

GO: Katie Randolph
 Phone: (720) 356-1759
 Email: Katie.Randolph@go.doe.gov

Contract Number: DE-EE0000475

Subcontractors:

- University of Florida, Gainesville, FL
- Northeastern University, Boston, MA
- Johnson Matthey Fuel Cells, Swindon, UK

Project Start Date: January 1, 2010

Project End Date: June 30, 2012

Technical Barriers

This project addresses the following technical barriers for consumer based electronic applications of less than 50 Watt from the Fuel Cells section of the Fuel Cell Technologies Program Multi-Year Research, Development and Demonstration Plan:

- (A) Durability
- (B) Cost
- (C) Performance

Technical Targets

TABLE 1. Comparison of the status of the UNF 25-W DMFC power supply based on the passive water recovery MEAs optimized in this project versus the DOE technical targets for portable fuel cell power supplies

| Technical Targets: Portable Power Fuel Cell Systems (10-50 Watts) | | | | |
|---|-----------|----------------------------------|--------------|----------------------------------|
| Characteristic | Units | UNF 2011 (25 W Net) ¹ | 2013 Targets | UNF 2013 (25 W Net) ² |
| Operational Time | Hours | 10.0 | - | 14.3 |
| Specific Power | W/kg | 26.3 | 30 | 30.1 |
| Power Density | W/L | 28.0 | 35 | 30.6 |
| Specific Energy | (W-hr)/kg | 263 | 430 | 430 |
| Energy Density | (W-hr)/L | 280 | 500 | 437 |

¹ System data include weight and volume of hybrid battery and fuel as defined by the DOE.

² Calculation assumes reduction in weight and volume based on component and brassboard (unpackaged) test results. Current MEA performance is used.

Fiscal Year (FY) 2012 Objectives

The primary objective of this project is to optimize the functionality and internal water recovery features of the UNF passive water recovery membrane electrode assembly (MEA) to facilitate overall system simplicity, thereby increasing power and energy density and lowering the cost at the system level to address DOE's fuel cell target goals for consumer electronics applications.

- Optimize the UNF MEA design:
 - Improve durability and reliability
 - Increase power and energy density
 - Lower cost
- Develop commercial production capabilities:
 - Scale up the process to commercial batch operation level
 - Improve performance and increase reproducibility
 - Lower cost
- Increase catalyst stability and lower loading:
 - Increase the anode catalyst stability
 - Lower MEA cost

FY 2012 Accomplishments

- Optimized the membrane properties to minimize methanol cross-over and improve overall MEA performance.
- Continued optimization and characterization of the properties of the liquid barrier layer integrated into the passive water recovery MEA.
- Integrated the new Johnson Matthey anode, the optimized membrane, and improved cathode into the passive water recovery MEA which resulted in >20% increase in efficiency.
- Minimized the off-state degradation through change in wetting agents used in the cathode electrode.
- Continued optimization of rest/rejuvenation profile to minimize on-state degradation and achieved nearly 10,000 hours of durable MEA operation.

- In collaboration with Johnson Matthey, continued development of commercially viable processes for production of the passive–water recovery MEA technology.



Introduction

Typical DMFC systems use bulky condensers and other components to recover water at the system level. These system components occupy a large volume and weight within the system design and have a significant impact on the system power and energy density. The UNF passive water recovery MEA (Figure 1) has been designed to incorporate novel passive water recycling features within the MEA to provide water recovery and management. This approach enables a significant simplification and miniaturization of the DMFC at the system level and facilitates substantial progress towards the DOE goals for power and energy density in small portable power systems as shown in Table 1.

Approach

The approach was to optimize the performance of the UNF passive water recovery MEA and to transition the technology to commercially viable processes, thereby lowering the cost and increasing the durability of the MEA. The MEA performance was improved through better anode catalysts, improved membrane properties, and optimization of the liquid barrier layer in the cathode--specifically the

water retention capability. By improving the anode catalyst structure to enhance the stability of the ruthenium, the MEA durability will be significantly enhanced. Optimizing the membrane physical properties, such as thickness, can improve overall efficiency by minimizing methanol cross-over. Optimizing the cathode barrier layer parameters will maximize the oxygen content at the cathode catalyst and thus improve the MEA performance.

Scale up of the manufacturing process for the different MEA layers is expected to enhance the performance and reliability as well as reduce the overall cost. Optimizing the manufacturing process will move beyond the prototype operation by developing batch manufacturing processes that will minimize the MEA-to-MEA variability. The methodology also includes evaluation of the MEA both on the test stand as well as integrated into the lightweight, compact DMFC system developed in a related project at UNF.

Results

The overall efficiency of the UNF passive water recovery MEA was improved by more than 20%, as shown in Figure 2. The efficiency improvement was achieved through improvements in the membrane properties and in the liquid barrier layer characteristics of the cathode. The UNF DM1 membrane was extensively tested to optimize the passive water recovery MEA performance. Increasing the membrane thickness to 45 micron from 20 micron reduced the methanol cross-over by more than 50% with minimal increase in the membrane resistance. Extensive effort was undertaken to

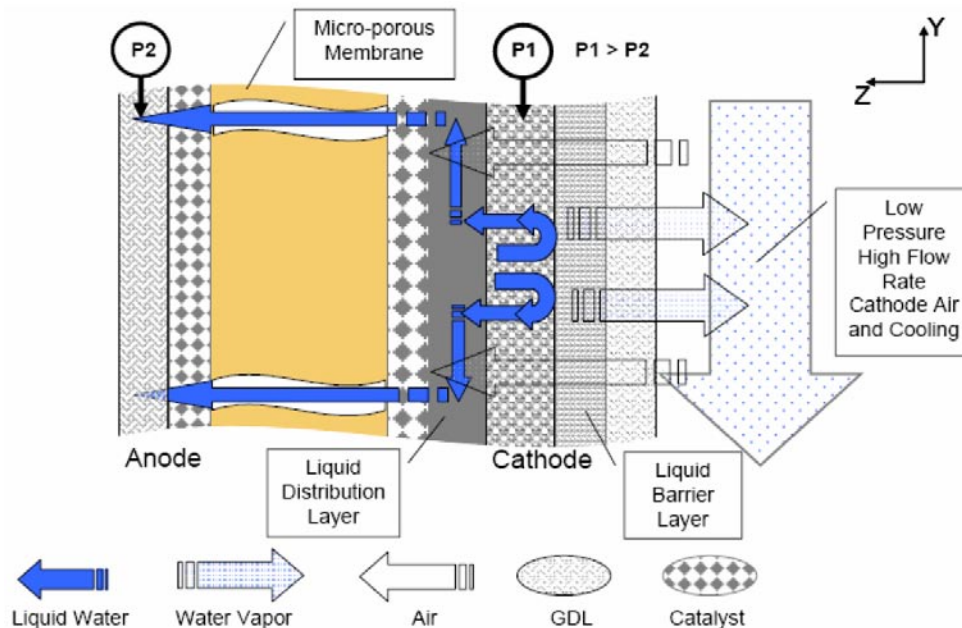


FIGURE 1. Water Transport characteristics optimized to internally recycle water to anode compartment

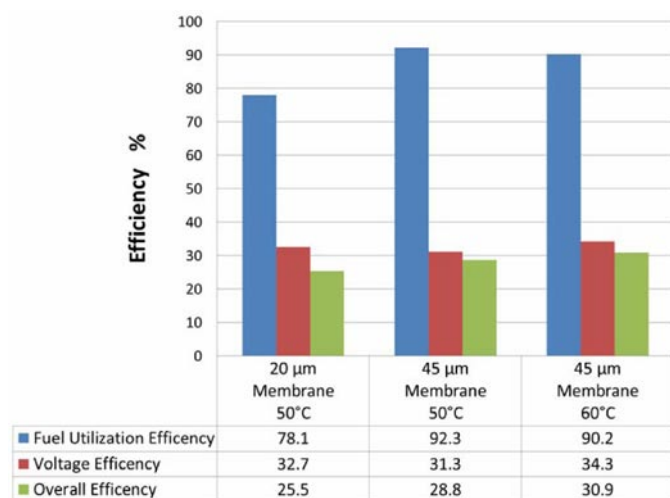


FIGURE 2. Improvement in overall MEA efficiency

evaluate the performance of the liquid barrier layer, while focusing on the trade-off between retaining water within the MEA versus ensuring adequate oxygen access to the cathode catalyst reaction zone. Through careful material selection and thorough investigation of manufacturing processes and physical properties of the barrier layer such as thickness, the MEA operating temperature at which water balance is achieved was increased from approximately 45°C to 55°C.

MEA durability is a critical factor in system durability. In addition to investigating the MEA and its sub-components to improve MEA performance characteristics, extensive optimization was undertaken to remove impurities and improve the durability both in the on-state, as well as the off-state. The current MEA design continued to exhibit excellent durability in continuous operation, with MEAs achieving nearly 10,000 hours of operation (Figure 3). The off-state degradation was significantly improved through changes in wetting agents used during the manufacturing process, which led to a significant reduction of the quantity and influence of organic impurities. Testing has now shown a substantial reduction in the off-state degradation to acceptable levels for system operation and life. Investigation continued into optimizing the rest/rejuvenation cycle, specifically into the air starve step which is particularly challenging in an open-cathode MEA. Changes to the voltage during the air-starve has resulted in more thorough reduction in oxides on the cathode catalyst and lowered on-state degradation.

Anode stability is a particular concern for long-term durability due to the loss of ruthenium from the anode. To address this issue, new Johnson Matthey anode electrodes were studied with testing indicating reduced degradation and improved lifetime. In addition, new ultra-stable ternary anode catalyst inks, developed by project partners, which incorporates a third metal in order to both stabilize the ruthenium and enhance the catalyst activity were

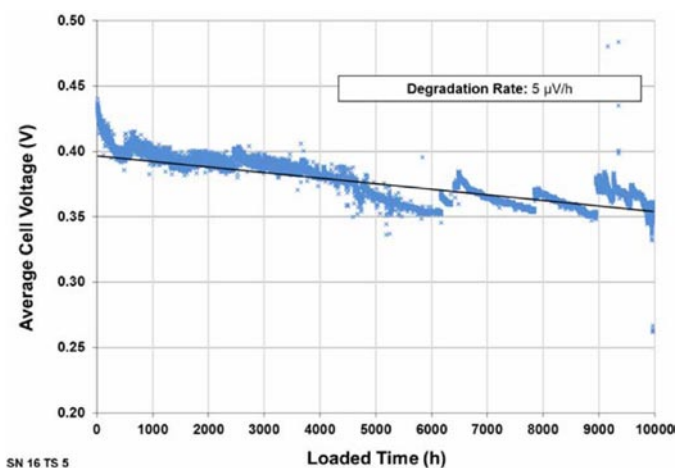


FIGURE 3. Passive water recovery MEAs show excellent durability under continuous operation (eight-cell stack operating at 120 mA/cm², 50°C, and at 0.8M methanol).

investigated. Project personnel scaled up the production process of these catalysts and MEA testing is underway.

During the past year, the UNF and Johnson Matthey have continued to optimize the formulation and mixing process to enhance the barrier layer reproducibility, as well as improve control of the key barrier layer properties of capillary pressure and permeability. By utilizing dual centrifuge mixing, a commercially applicable, scalable batch mixing processes, the project team has optimized the formulation. We have applied it to a knife coating process to provide a commercially scalable manufacturing process for the liquid barrier layer. Additionally, Johnson Matthey has developed a scalable coating process for the deposition of the cathode catalyst layer ink onto the liquid barrier layer to produce a well adhered, high performing cathode catalyst layer.

Conclusions and Future Directions

Research conducted during the past year has:

- Improved the overall efficiency of the UNF passive water recovery MEA by more than 20% by improving the membrane properties and the performance of the liquid barrier layer within the cathode electrode.
- Increased the MEA operating temperature at which water balance is achieved from approximately 45°C to 55°C, primarily through improved manufacturing techniques.
- Improved the durability of MEA in both the on-state and off-state. Continuous testing showed acceptable performance for nearly 10,000 hours.

Future efforts include:

- Continue to optimize the manufacturing techniques and formulations for the liquid barrier layer to maximize performance and durability.
- Improve the MEA performance by increasing the operating temperature and improving the oxygen access to the cathode catalyst.
 - Optimize the cathode structures for water management and power density.
 - Optimize the anode for durability and performance in the passive water recovery MEA.
- Continue the investigation of the rest/rejuvenation cycle and optimize for the open cathode structure of the passive water recovery MEA.

V.G.3 Advanced Materials and Concepts for Portable Power Fuel Cells

P. Zelenay (Primary Contact), H. Chung,
C.M. Johnston, Y.S. Kim, Q. Li, D. Langlois,
D. Spornjak, P. Turner, G. Wu

Materials Physics and Applications Division
Los Alamos National Laboratory (LANL)
Los Alamos, NM 87545
Phone: (505) 667-0197
Email: zelenay@lanl.gov

DOE Manager

HQ: Nancy Garland
Phone: (202) 586-5673
Email: Nancy.Garland@ee.doe.gov

Subcontractors:

- R.R. Adzic (PI), S. Bliznakov, M. Li, P. Liu, K. Sasaki, M.-P. Zhou
Brookhaven National Laboratory, Upton, NY
- Y. Yan (PI), S. Alia, J. Zheng
University of Delaware, Newark, DE
- J. McGrath (PI), Y. Chen, C. H. Lee, M. Lee
Virginia Polytechnic and State University, Blacksburg, VA
- N. Cabello-Moreno (PI), G. Hards, G. Spikes
Johnson Matthey Fuel Cells, Swindon, United Kingdom
- C. Böhm (PI), V. Graf, P. Hassell
SFC Energy, Brunenthal, Germany
- K. More (PI), D. Cullen
Oak Ridge National Laboratory, Oak Ridge, TN (no-cost partner)

Project Start Date: September 2010

Project End Date: August 2014

- Design and implement innovative electrode structures with better activity and durability in portable power fuel cell systems.
- Develop new hydrocarbon membranes based on (i) multiblock copolymers and (ii) copolymers with cross-linkable end-groups to assure lower MEA cost and enhanced fuel cell performance.
- Develop and demonstrate new oxidation electrocatalysts for two alternative fuels: ethanol (EtOH) and dimethyl ether (DME); evaluate viability of portable power systems based on alternative fuels to methanol.

Technical Barriers

This project addresses the following technical barriers in the Fuel Cells section 3.4.5 of the Fuel Cell Technologies Multi-Year Research, Development and Demonstration Plan [1]:

- (A) Durability (catalysts, membranes, electrode layers)
- (B) Cost (catalysts, MEAs)
- (C) Performance (catalysts, membranes, electrodes, MEAs)

Technical Targets

Portable fuel cell research in this project focuses on the DOE technical targets specified in Tables 3.4.7a, 3.4.7b, and 3.4.7c in Section 3.4.4 (Technical Challenges) of the Multi-Year Research, Development and Demonstration Plan [1]. Table 1 summarizes the latest DOE performance targets for portable power fuel cell systems in three power ranges.

Using DOE's Table 3.4.7 as guidance relevant to portable power systems, the following specific project targets have been devised:

- System cost target: \$5/W
- Performance target: Overall fuel conversion efficiency (η_{Σ}) of 2.0-2.5 kWh/L (per liter of fuel)
- In the specific case of a DMFC, the above assumption translates into a total fuel conversion efficiency (η_{Σ}) of 0.42-0.52, corresponding to a 1.6-to-2.0-fold improvement over the state of the art (*ca.* 1.250 kWh/L). Assuming fuel utilization (η_{fuel}) and balance-of-plant efficiency (η_{BOP}) of 0.96 and 0.90, respectively (efficiency numbers based on information obtained from DMFC systems developers), and using theoretical voltage (V_{th}) of 1.21 V at 25°C, the cell voltage (V_{cell}) targeted in this project can be calculated as: $V_{\text{cell}} = V_{\text{th}} [\eta_{\Sigma} (\eta_{\text{fuel}} \eta_{\text{BOP}})^{-1}] = 0.6-0.7$ V

Objectives

The main objective of this project is to:

- Develop advanced materials, catalysts, membranes, electrode structures, membrane-electrode assemblies (MEAs), and operating concepts for fuel cells that would help meet cost, performance, and durability requirements established by DOE for portable fuel cell systems; assure path to large-scale fabrication of successful materials.

Fiscal Year (FY) 2012 Objectives

- Develop direct methanol fuel cell (DMFC) anode catalysts with enhanced activity, improved durability, and reduced cost.

TABLE 1. DOE Performance Targets for Portable Power Fuel Cell Systems in Three Power Ranges

| Technical Targets: Portable Power Fuel Cell Systems (< 2 W; 10-50 W; 100-250 W) | | | | |
|---|-------|---------------------|---------------------|---------------------|
| Characteristics | Units | 2011 Status | 2013 Targets | 2015 Targets |
| Specific power | W/kg | 5; 15; 25 | 8; 30; 40 | 10; 45; 50 |
| Power Density | W/L | 7; 20; 30 | 10; 35; 50 | 13; 55; 70 |
| Specific energy | Wh/kg | 110; 150; 250 | 200; 430; 440 | 230; 650; 640 |
| Energy density | Wh/L | 150; 200; 300 | 250; 500; 550 | 300; 800; 900 |
| Cost | \$/W | 150; 15; 15 | 130; 10; 10 | 70; 7; 5 |
| Durability | Hours | 1,500; 1,500; 2,000 | 3,000; 3,000; 3,000 | 5,000; 5,000; 5,000 |
| Mean time between failures | Hours | 500; 500; 500 | 1,500; 1,500; 1,500 | 5,000; 5,000; 5,000 |

Thus, the ultimate target of the materials development effort in the DMFC part of this project is to assure an operating single fuel cell voltage of at least 0.6 V. Very similar voltage targets have been calculated for fuel cells operating on two other fuels, EtOH and DME.

- A new ternary PtRuPd catalyst of DME oxidation synthesized and shown to perform better than a “standard” binary PtRu catalyst in electrochemical-cell testing.



FY 2012 Accomplishments

- PtRu “advanced anode catalyst” of methanol oxidation demonstrated with performance exceeding that of the HiSPEC[®] 12100 benchmark by 40 mV; the catalyst synthesis successfully scaled up to 100 g.
- A ternary PtRuSn/C catalyst synthesized with methanol oxidation combining unique activity of PtSn/C at low overpotentials with superior performance of PtRu/C at high overpotentials; mass activity exceeding 500 mA/mg_{Pt} at 0.35 V (higher than that of the most active thrifted PtRu catalysts).
- Onset potential of methanol oxidation improved by 30 mV with PtRu/CuNWs relative to the HiSPEC[®] 12100 benchmark durability on par with the benchmark catalyst.
- DMFC fuel utilization milestone of ≥95% at peak power achieved with 6F25BP75PAEB-BPS100 copolymer.
- DMFC accelerated performance degradation with increasing feed concentration of methanol shown to be associated with significant formation of cracks in the anode and cathode catalyst layers.
- Several carbon-supported Pt_{ML}/Au and Pt_{ML}/Pd catalysts demonstrated with the onset potential of ethanol oxidation in an electrochemical cell near 0.20 V vs. reference hydrogen electrode (RHE) at room temperature.
- Excellent DEFC anode activity shown with two ternary catalysts with the onset potential of ethanol oxidation very close to the thermodynamic value of ca. 0.04 V at 80°C.
- 250 mA cm⁻² at 0.40 V achieved in the DME fuel cell, exceeding the FY 2011 performance at 0.50 V by ca. 65%.

Introduction

This multitask, multi-partner project targets advancements to portable fuel cell technology through the development and implementation of novel materials and concepts for (i) enhancing performance, (ii) lowering cost, (iii) minimizing size, and (iv) improving durability of fuel cell power systems for consumer electronics and other mobile and off-grid applications. The primary focus of the materials research in this project is on electrocatalysts for the oxidation of methanol, EtOH, and DME; on innovative nanostructures for fuel cell electrodes; and on hydrocarbon membranes for lower MEA cost and enhanced fuel cell performance (fuel crossover, proton conductivity). In parallel with new materials, this project targets development of various operational and materials-treatment concepts, concentrating among others on improvements to the long-term performance of individual components and the complete MEA.

Approach

The two primary research goals of this project are (i) the development of binary and ternary catalysts for the oxidation of methanol, ethanol, and DME, and (ii) synthesis of hydrocarbon polymers (multiblock copolymers, copolymers with cross-linkable functional groups) for lower cost and better fuel cell performance through reduced fuel crossover and increased protonic conductivity. Better understanding of the key factors impacting the performance of both catalysts and polymers is also pursued through a major characterization effort including X-ray absorption spectroscopy, X-ray photoelectron spectroscopy, nuclear magnetic resonance, and transmission electron microscopy.

Development of new catalysts and polymers is closely tied to novel electrode nanostructures tailored to minimize precious metal content, maximize mass activity, and enhance durability. The electrode-structure component of the effort concentrates on two groups of materials: (i) solid-metal nanostructures (e.g., nanowires and nanotubes) and (ii) carbon-based nanostructures acting as supports for metal catalysts.

In addition to short-term testing and initial performance assessment, the catalysts, membranes, supports, electrode structures, and MEAs developed in this project are subject to long-term performance (durability) testing. Performance-limiting factors and degradation mechanisms are being identified and, if possible, addressed. Fabrication and scale up of viable catalysts, membranes, and supports is also being tackled through collaboration between partners in this project.

Results

DMFC Catalysts — Development of new methanol oxidation catalysts continued in FY 2012 through “thrifting” of both precious metals, Pt and Ru, in the binary PtRu catalysts. A Variation 4 advanced anode catalyst (AAC) was synthesized and tested in the DMFC anode at 80°C, showing ca. 40 mV activity improvement relative to the benchmark HiSPEC® 12100 catalyst. The synthesis of the Variation 4 AAC was successfully scaled up to a 100-gram batch without a performance loss, in spite of a slightly lower specific surface area of the catalyst from the large batch. The DMFC anode research is on track to reaching the target of improved activity of thrifted PtRu catalysts without a durability loss and to achieving the project catalyst activity goal of 150 mA/cm² at 0.60 V (the DMFC voltage target).

An activity advantage of PtSn/C catalysts, PtSn catalyst with an atomic Pt-to-Sn ratio of 3:1 in particular, relative to PtRu/C was confirmed in the kinetic region (at current densities up to 150 mA/cm²). At the same time, the PtSn/C catalyst activity was found to be limited at potentials higher than 0.2 V due to the formation of a surface SnO₂, resulting in a decrease in the OH availability for the oxidation of surface CO. This drawback of the PtSn catalyst was the reason of a “no-go” decision for further research on binary PtSn catalysts.

However, in an attempt to combine the unique activity of the PtSn catalyst at low methanol oxidation overpotentials with the superior performance of PtRu binary catalysts at high current densities, the effort shifted to the development of a PtRuSn/C ternary catalyst. Four different synthesis approaches were used, of which one proved particularly successful yielding a catalyst with significantly higher methanol oxidation activity in the entire range of the DMFC anode potentials than that of the most active “thrifty” PtRu catalysts and the benchmark HiSPEC® 12100 catalyst

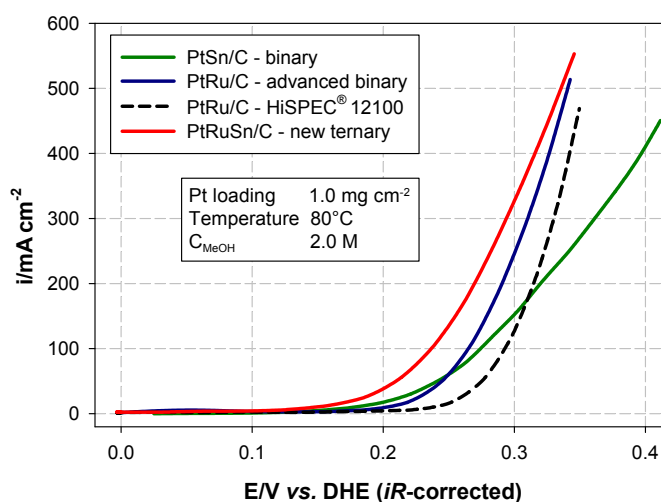


FIGURE 1. DMFC anode polarization plots recorded with a new ternary PtRuSn/C catalyst. Polarization plots for an advanced binary PtRu/C, a binary PtSn/C and a benchmark HiSPEC® 12100 PtRu catalyst shown for reference.

(Figure 1, red curve). The mass activity of 500 mA/mg_{Pt} at 0.35 V was reached with the new ternary catalyst, exceeding by 150% the interim mass-activity target of 200 mA/mg_{Pt} at 0.35 V. Future research will focus on further improvements in the PtRuSn/C catalyst activity and on assuring its durability under the operating conditions of a DMFC.

Innovative Electrode Structures — PtRu and PtSn nanowire catalysts for methanol oxidation were obtained using Cu nanowire (CuNWs) supports. The onset potential of methanol oxidation in an electrochemical cell at a room temperature was improved by 20 and 30 mV with PtSn/CuNWs and PtRu/CuNWs relative to the benchmark PtRu/C catalyst (HiSPEC® 12100), respectively. Performance stability of both catalysts was demonstrated to be on par with the benchmark catalyst.

Multiblock Copolymers for Reduced MeOH Crossover — Highly conductive multiblock copolymers were prepared using telechelic block polysulfone ether polymer (BPSH)-100 oligomers. The block size of these polymers varied between 7,000 and 15,000 g. The copolymers showed much reduced methanol permeability relative to previous-generation multiblock materials (no more than 10-15% higher than that of the reference Nafion® perfluorosulfonic acid polymer). Thanks to their high protonic conductivity the multiblock copolymer membranes were found to outperform Nafion® 212 in DMFC testing. DMFC current densities in excess of 0.28 A/cm² at 0.5 V (a membrane performance milestone) were demonstrated with three out of 11 multiblock copolymers synthesized.

In order to further reduce methanol permeability of the copolymers, biphenyl (BP) groups were introduced into the polymer backbone and ratio of BP to 6F-BPA was varied. Small angle X-ray scattering profiles obtained with different

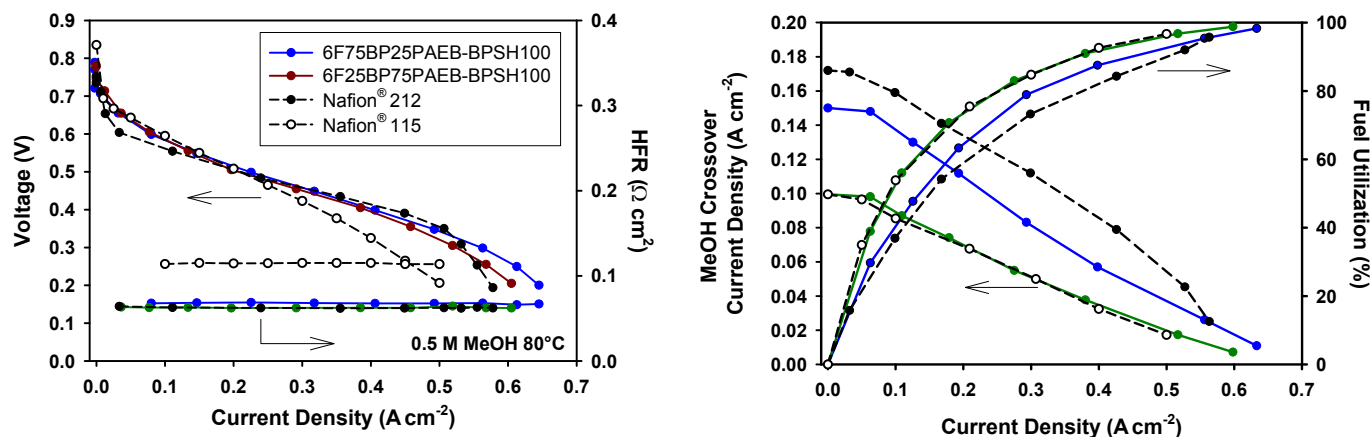


FIGURE 2. DMFC polarization plots (left) and methanol crossover and fuel utilization plots (right) for two multiblock copolymers and reference Nafion® 212 and 115 membranes; $c_{\text{MeOH}} = 0.5 \text{ M}$; cell temperature 80°C .

copolymers indicated an increase in the interdomain distance with a decrease in the 6F-BPA content, accompanied by the formation of a less ordered structure of copolymers and drop in methanol permeability. A 55% reduction in methanol crossover relative to Nafion® was measured with the least permeable copolymer, containing 25% of 6F-BPA groups (versus 75% of BP groups).

Fuel cell test data attested to improved MEA performance of multiblock-copolymer membranes relative to Nafion® at DMFC voltages higher than ca. 0.55 V (Figure 2, left), with similar resistance of the hydrocarbon and Nafion® membranes maintained across the entire range of fuel voltages. A fuel utilization of 95% was achieved with a multiblock copolymer at the peak DMFC power point (Figure 2, right).

DMFC Performance Degradation— The impact of the feed concentration of methanol on the rate of DMFC performance degradation was studied at four MeOH concentrations, 0.5, 1.0, 2.0, and 4.0 M. The unrecoverable DMFC performance loss was found to significantly increase with methanol concentration. At the same time, the fraction of the overall performance loss that could be recovered noticeably decreased. A relatively small unrecoverable performance loss of 3% after a 100-hour test at 0.40 V was measured only with 0.5 M MeOH.

Post-mortem X-ray tomography of MEAs revealed cracking of both the anode and cathode catalyst layers that substantially increased with the feed concentration of methanol. The cathode was found more vulnerable to cracking at high methanol concentrations, with more than 9% of the surface covered by the cracks after a 100-hour life test with 4.0 M methanol. Once (and if) unequivocally correlated to DMFC performance loss crack formation may require development of an effective mitigation strategy.

EtOH Oxidation Catalysts— In the part of research involving well-defined surfaces, the lattice expansion in Pt_{ML} supported on Au(111) was found to result in significantly enhanced EtOH oxidation current relative to Pt(111), with indications of improved selectivity in CO₂ generation. “Engineering” of the Pt_{ML}/Au(111) surface led to an additional shift in the onset EtOH oxidation potential to below 0.2 V vs. RHE at the Sn(OH)_x/(Pt₃Ir₁)_{ML}/Au(111) catalyst. While these effects pave the road for further improvements in ethanol-oxidation electrocatalysis they also highlight the need for cost-effective core materials.

In the part of research focusing on highly DEFC-relevant carbon-supported catalysts, very promising activity was demonstrated using a Pt_{ML}/AuNi_{0.5}Fe/C catalyst with reduced noble metal loading in the nanoparticle core (Figure 3, left). A SnO₂/Pt_{ML}/Pd₉Au₁/C catalyst (Figure 3, right) was found to exhibit the lowest onset potential of EtOH oxidation among carbon-supported catalysts, comparable to that measured with the most active single-crystal catalysts (high CO₂ yields are also likely). In situ infrared reflection-absorption spectroscopy (IRRAS) and on-line differential electrochemical mass spectroscopy (DEMS) are close to being completed for the study of substrate-induced change in Pt_{ML}'s selectivity for the oxidation of EtOH.

Finally, excellent activity was demonstrated with two ternary catalysts developed in FY 2011. The onset potential of EtOH oxidation measured in a DEFC at 80°C with the PtIrSnO₂ and PtRhSnO₂/C anode catalysts was very close to the thermodynamic value of ca. 0.04 V (Figure 4). However, the DEFC performance was significantly below that expected based on the activity of both anodes due to the cathodes contamination by crossover anode species. Reduction in the non-noble metal migration from the anode is required.

DME Fuel Cell Research— It was determined that the DME-to-H₂O ratio of 1.4:1 used previously for in the DME fuel cell (with anode humidifier at 85°C) was much

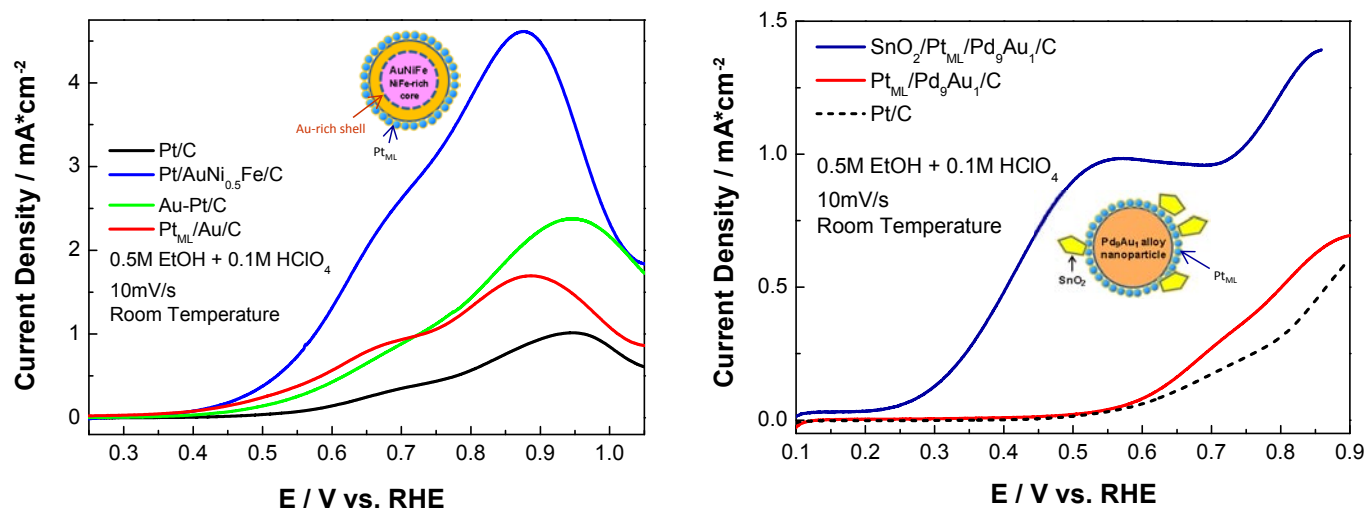


FIGURE 3. Ethanol oxidation plots on carbon-supported Pt_{ML}/Au (left) and Pt_{ML}/Pd catalysts (right) in an aqueous 0.1 M HClO₄ electrolyte electrochemical cell at room temperature; $c_{\text{EtOH}} = 0.5$ M. Catalysts structures shown in the insets.

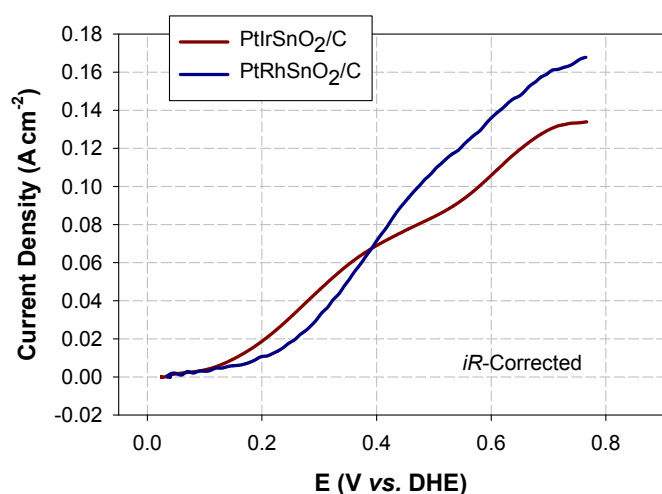


FIGURE 4. Direct EtOH fuel cell anode polarization plots recorded with two carbon-supported ternary catalysts, PtIrSnO₂/C and PtRhSnO₂/C at 80°C. Anode: 1.0 mg/cm²_{metal} 12 wt% PtIrSnO₂/C or 13% PtRhSnO₂/C, 0.5 M EtOH, 1.8 ml/min; cathode: 4.0 mg/cm² Pt black, 200 sccm H₂; membrane: a triple Nafion® 212 sandwich.

larger than required by the reaction stoichiometry (1:3) and possibly resulted in a water deficiency at the anode. DME fuel cell performed better with the molar DME-to-H₂O ratio closer to stoichiometric. As a result, a gas-fed DDMFC with the anode humidifier maintained at 110°C was found to outperform the liquid-fed DME fuel cell. Unlike DMFC performance, the internal resistance-corrected direct DME fuel cell performance was found to be independent of the membrane thickness, attesting to a relatively low fuel crossover and/or lower activity of the Pt cathode in DME than MeOH oxidation at high potentials.

The direct DME fuel cell performance reached current density of more than 250 mA/cm² at 0.40 V, exceeding previous-year performance by ca. 65%. At voltages higher than 0.49 V, the direct DME fuel cell performance was found superior to that of a corresponding DMFC, mainly due to reduced effect of DME crossover on the cathode activity compared to that of methanol crossover (Figure 5). Based on those results a “go” decision was made for further DME research.

Finally, a new ternary PtRuPd catalyst was synthesized, with Pd added to aid in the C-O bond cleavage during DME oxidation. The catalyst, which exhibited significant activity in testing performed in an electrochemical cell, will be next optimized for maximum activity and stability under DME fuel cell operating conditions.

Conclusions

- The latest PtRu “advanced anode catalyst” exceeded performance of the HiSPEC® 12100 benchmark by 40 mV; the catalyst synthesis was successfully scaled up to 100 g; a “no-go” decision was made for further PtSn catalyst research; the effort was redirected towards PtRuSn catalysts that already showed very promising activity in methanol oxidation.
- PtRu/CuNW catalyst was synthesized with a ca. 30 mV improvement in the onset potential of methanol oxidation relative to the HiSPEC® 12100 benchmark.
- Multiblock copolymers, e.g. 6F25BP75PAEB-BPS100, allowed for up to 55% reduction in methanol crossover relative to the Nafion® 212 benchmark; fuel utilization up to 95% was reached with 0.5 M methanol feed near the peak-power point.

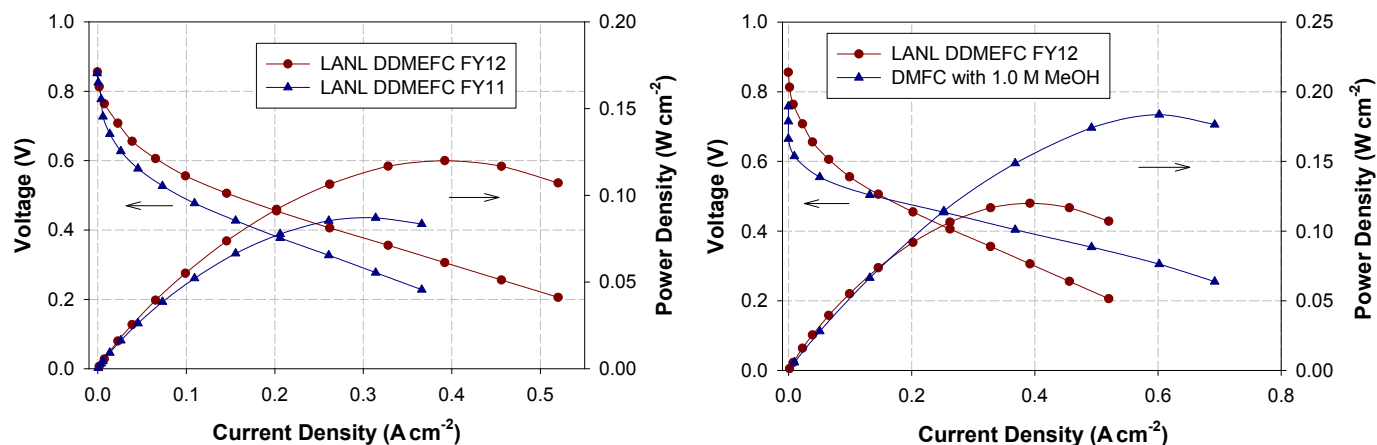


FIGURE 5. Polarization and power-density plots depicting progress in direct DME fuel cell performance at LANL (left) and performance comparison between direct DME fuel cell and DMFC at 80°C (right). Anode: 6 mg/cm² Pt₅₀Ru₅₀ black, 40 sccm DME gas (direct DME fuel cell), 30 psig or 1.0 M MeOH (DMFC); cathode: 4 mg/cm² Pt black, 20 psig (direct DME fuel cell) or 0 psig (DMFC), 500 sccm air; membrane: Nafion® 212.

- High feed concentration of methanol was found to accelerate DMFC performance degradation strongly and lead to significant cracking of both the anode and the cathode.
- Pt_{ML} catalysts with expanded lattice and “engineered” catalysts were found capable of delivering the onset potential of EtOH oxidation of ca. 0.2 V vs. reference hydrogen electrode (room temperature).
- Both PtIrSnO₂/C and PtRhSnO₂/C ternary catalysts showed capability of oxidizing EtOH in an MEA at 80°C at potentials close to the thermodynamic value of 0.04 V.
- DME performance was improved by 65% relative to the previous year, resulting in a “go” decision for further DME research; a new PtRuPd/C catalyst showed promise in aiding the C-O bond cleavage.

Future Directions

- Methanol oxidation catalysis: Further develop PtRuSn ternary catalysts to improve the kinetic performance at low Pt loadings; develop protocols for stack testing under 75-80°C, 0.5 M methanol conditions; evaluate stability and durability of new methanol oxidation catalysts; meet durability milestone (durability of thrifed PtRu catalyst matching that of HiSPEC® 12100 without activity loss); carry out breakdown of performance losses in DMFCs and initiate development of mitigation strategies; optimize accelerated corrosion test to mimic decay mechanisms in long-term stack testing.
- Innovative membranes and electrode structures: Continue reducing methanol crossover by introducing hydroquinone into multiblock copolymers; improve durability of alternative membranes in the presence of higher concentrations of MeOH; develop PtSn/CuNW

structure to achieve the onset potential of methanol oxidation of 0.29 V and 20% improvement in platinum group metal mass activity of innovative nanostructure catalysts.

- EtOH oxidation catalysis: Establish methodology for the synthesis of Pt_{ML}-nanoparticle catalysts with cost-effective core materials for the deposition of Pt_{ML} and active promoters (SnO_x, SnO₂, Ru, etc.); scale up the synthesis; implement in situ IRRAS and on-line DEMS to determine substrate-induced selectivity of Pt_{ML}s in EtOH (and methanol) oxidation and EtOH oxidation at ternary PtRhSnO₂/C and PtIrSnO₂/C catalysts; determine the mechanism of cathode performance loss in direct ethanol fuel cells operating with ternary anode catalysts; develop a mitigation strategy.
- DME research: Develop a model of DME oxidation and catalyst requirements; optimize the ternary PtRuPd catalyst for maximum activity and stability at the DME fuel cell anode.

References

1. *Multi-Year Research, Development and Demonstration Plan: Section 3.4 Fuel Cells*, Fuel Cell Technologies Program, 2011. http://www1.eere.energy.gov/hydrogenandfuelcells/mypp/pdfs/fuel_cells.pdf

FY 2012 Publications

1. M. Li, N.S. Marinkovic, K. Sasaki, “In situ Characterization of Ternary Pt-Rh-SnO₂/C Catalysts for Ethanol Electrooxidation”, *Electrocatalysis*, in press.
2. Y.J. Kang, L. Qi, M. Li, R. Diaz Rivas, R.R. Adzic, E. Stach, J. Li, C.B. Murray, “Highly active Pt₃Pb and core-shell Pt₃Pb-Pt electrocatalysts for formic acid oxidation”, *ACS Nano*, in press.

3. Q. Li, G. Wu, C. M. Johnston, P. Zelenay, "Anode Catalysts for the Direct Dimethyl Ether Fuel Cell," *ECS Trans.* **41**, 1969 (2011).
4. W.P. Zhou, M. Li, C. Koenigsmann, C. Ma, S.S. Wong, R.R. Adzic, "Morphology-dependent activity of Pt nanocatalysts for ethanol oxidation in acidic media: nanowires versus nanoparticles," *Electrochim. Acta* **56**, 9824 (2011).
5. D. Konopka, M. Li, K. Artyushkova, N.S. Marinkovic, K. Sasaki, R.R. Adzic, T. Ward, P. Atanassov, "Platinum Supported on NbRu_yO_z as Electrocatalyst for Ethanol Oxidation in Acid and Alkaline Fuel Cells," *J. Phys. Chem. C* **115**, 3043 (2011).
6. C.M. Johnston, D. Cao, P. Zelenay, "Se-modified Ru nanoparticles as ORR catalysts. Part 2: Evaluation for use as DMFC cathodes;" J.-H. Choi, *J. Electroanal. Chem.* **662**, 267 (2011).

FY 2012 Presentations

1. J.E. McGrath, Y. Chen, A. Roy, X. Yu, R. Van Houten, H.S. Lee, R. Guo, K.S. Lee, M. Lee, C.H. Lee, Y.S. Kim, P. Zelenay, "Disulfonated Poly(arylene ether) Copolymers as Proton Exchange Membranes for H₂/Air and DMFC Fuel Cells," 2011 MRS Fall Meeting & Exhibit, November 28 – December 2, 2011, Boston, MA, USA (invited lecture).
2. C.M. Johnston, A. Trendewicz, Q. Li, G. Wu, H. Chung, N. Mack, F. Garzón, P. Zelenay, "Impact of Catalyst Structure and Operating Conditions on Ruthenium Crossover in Direct Methanol Fuel Cells;" 220th Meeting of the Electrochemical Society, Boston, Massachusetts, October 9–14, 2011.
3. Q. Li, G. Wu, C. Johnston, P. Zelenay, "Anode Catalysts for the Direct Dimethyl Ether Fuel Cell," 220th Meeting of the Electrochemical Society, Boston, Massachusetts, October 9–14, 2011.
4. S.M. Alia, Y. Yan, "Ruthenium Nanotubes as Methanol Oxidation Reaction Catalysts," 220th Meeting of the Electrochemical Society, Boston, Massachusetts, October 9–14, 2011.

V.H.1 Low-Cost PEM Fuel Cell Metal Bipolar Plates

Conghua “CH” Wang

TreadStone Technologies, Inc.
201 Washington Rd.
Princeton, NJ 08543
Phone: (609) 734-3071
Email: cwang@TreadStone-Technologies.com

DOE Managers

HQ: Jason Marcinkoski
Phone: (202) 586-7466
Email: Jason.Marcinkoski@ee.doe.gov

GO: David Peterson
Phone: (720) 356-1747
Email: David.Peterson@go.doe.gov

Technical Advisor

Thomas Benjamin
Phone: (630) 252-1632
Email: benjamin@anl.gov

Contract Number: 09EE0000463

Subcontractors:

- Ford Motor Company, Dearborn, MI
- Gas Technology Institute, Des Plaines, IL
- The State University of New York, Stony Brook, Stony Brook, NY
- IBIS Associates, Inc., Waltham, MA

Project Start Date: September 1, 2009

Project End Date: October 31, 2012

Program Multi-Year Research, Development and Demonstration Plan:

- (A) Durability
- (B) Cost
- (C) Performance

Technical Targets

The focus of this project is to further develop TreadStone’s proprietary corrosion-resistant metal plate technology reducing the metal plate cost to <\$3/kw, while still meet the performance requirements. There are a number of performance requirements for PEM fuel cell bipolar plates. The most challenging requirements for metal bipolar plates are summarized in Table 1. The status of TreadStone’s low-cost metal plates is summarized in the table as well.

TABLE 1. TreadStone's Metal Plate Status and DOE's Targets

| Parameter | Unit | TreadStone 2010 Status | DOE Targets | |
|--------------------------------|---------------------|------------------------|-------------|-------|
| | | | 2010 | 2015 |
| Plate Cost ^a | \$/kW | \$3.82 | 5 | 3 |
| Plate Weight ^b | kg/kW | <0.4 | <0.4 | <0.4 |
| Corrosion Anode ^c | μA/cm ² | n/a | <1 | <1 |
| Corrosion Cathode ^d | μA/cm ² | <0.01 | <1 | <1 |
| Resistance ^e | Ohm cm ² | <0.01 | <0.02 | <0.02 |

^a Based on 50% utilization of active area on the whole plate surface, stainless steel foil cost at historical average of \$2/lb, 1 W/cm² power density and projected 500,000 stacks per year production.

^b based on the 0.1-mm thick stainless steel foil.

^c pH 3, 0.1 ppm hydrofluorhydric acid, 80°C, peak active current <1x10⁻⁶ A/cm² (potentiodynamic test at 0.1 mV/s, -0.4 V to +0.6 V (Ag/AgCl)) de-aerated with Ar purge.

^d pH 3, 0.1 ppm hydrofluorhydric acid, 80°C, passive current <5x10⁻⁸ A/cm² (potentiostatic test at +0.6 V (Ag/AgCl)) for at least 24 hours, aerated solution.

^e Includes contact resistance (on as-received and after potentiostatic experiment) measured.

Fiscal Year (FY) 2012 Objectives

- Reduce or eliminate the small amount of gold used in TreadStone’s current corrosion-resistant metal plate technology for proton exchange membrane (PEM) fuel cell applications.
- Develop low-cost metal bipolar plates using commercially available low-cost carbon steel or aluminum as the substrate materials.
- Optimize the fabrication process for large-scale manufacture.
- Demonstrate TreadStone’s low-cost metal plate technology in the applications of portable, stationary and automobile fuel cell systems.

Technical Barriers

This project addresses the following technical barriers from the Fuel Cell section of the Fuel Cell Technologies

FY 2012 Accomplishments

- Modified the spray system for small-scale commercial production of metal plates.
- Optimized the processing condition for the quality consistency of metal bipolar plate production.
- Conducted accelerated corrosion test of metal plates with Los Alamos National Laboratory.
- Finished 40 bipolar plates for the second stack demonstration at Ford Motor Company.
- Demonstrated the application of the technology in a PEM electrolyzer, anion exchange membrane (AEM) fuel cells and flow battery applications.



Introduction

It has been reported that using metal bipolar separate plates can reduce the PEM fuel cell stack weight and volume by 40-50%, comparing with current graphite-based bipolar plates [1]. The major barrier to use metal bipolar plates in PEM fuel cell is the severe corrosion condition during stack operation. Most metals do not have the adequate corrosion resistance in PEM fuel cell environment, which results in rapid performance degradation due to the formation of the electrically resistive surface oxide scale, and potential contamination of the MEA by the dissolved ions from the metal plates. Various corrosion protection techniques have been investigated to prevent the metal plate corrosion in PEM fuel cell environments [2-7]. Some of these technologies have developed corrosion-resistant metal plates that can meet the performance requirements. However, it is still a challenge to have the metal bipolar plate that can meet both the performance and cost requirements. The focus of TreadStone's project is to develop the corrosion-resistant metal bipolar plates at low cost to meet DOE's 2015 targets.

Approach

Most researches on metal bipolar plates have been focused on covering the entire plate surface with an electronically conductive and corrosion-resistant material that protects the metal from corrosion and maintain the electrical conductance of the metal. The challenge of this approach is that there are only limited number of low-cost materials that can meet electrically conductive and corrosion resistive requirements for PEM fuel cell applications. In addition, the processing required to apply these materials on the metal substrate are either difficult or high cost.

TreadStone takes a different approach to develop the metal bipolar plates for PEM fuel cell applications. It was found that it is unnecessary to have the entire surface electrically conductive to ensure low interfacial contact resistance ($<10 \text{ m}\Omega\cdot\text{cm}^2$) between the bipolar plate and the gas diffusion layer (GDL). TreadStone's approach is based on this principle, as shown in Figure 1.

The majority of the metal surface area is covered with the low-cost corrosion resistant but non-(or poor) conductive material (purple layer in Figure 1). A corrosion resistant and highly electrically conductive material (such as Au) forms a path for electron transport, in the form of small conductive vias (yellow bars) penetrating through the non-conductive layer. Electrons generated from the anode reaction will flow through the GDL to the conductive vias (illustrated as red arrows) passing through the metal plate to the other side for the cathode reaction on the cathode of the adjacent cell. The conductive vias, having a dimension as small as several

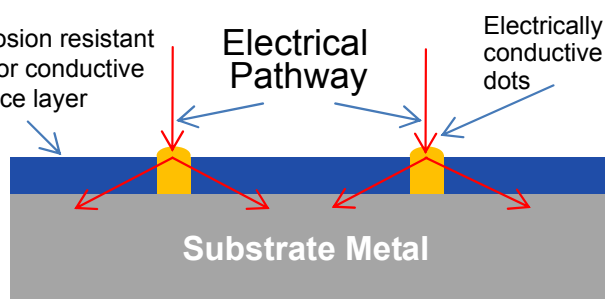


FIGURE 1. Schematic drawing of TreadStone's corrosion resistant metal plate design

micrometers, are distributed on the metal surface. The average distance between the conductive vias is 20-70 μm . The dense distribution of conductive vias ensures a uniform current distribution between the GDL and metal bipolar plate.

TreadStone's approach is unique because it uses only a small portion ($<1-2\%$) of the plate surface for electrical contact. It was found that more than 500,000 via/in² cover the metal plate surface as the electrical contact point of metal plate with GDL, when small ($<5 \mu\text{m}$) conductive vias are used. It is because of the high amount of the contact points that enable the low contact resistance of metal plates.

Results

The focus of this year's project is the scale up and optimization of TreadStone's current metal bipolar plate using small amount of gold (gold dots technology) that was demonstrated in a 1,000-hour durability test by Ford Motor Company in a full-size 10-cell stack testing under dynamic driving condition in 2010. The objective is to scale up the process for small scale commercial production with good processing consistency across the large size plates and between batches.

As reported in last years' annual report, there was a small increase of through plate voltage (TPV) drop (TPV increased from 15 mV to 18 mV) of TreadStone's metal bipolar plate after the 1,000-hour test at Ford. The post-test evaluation of the plate was conducted to identify the cause of the TPV increase. It was found that some gold splats on Ford's bipolar plates were lost after the test. Scanning electron microscope (SEM) observation of the plate indicates that a large amount of gold splats on Ford's bipolar plates are in spherical shape and can be removed by rubbing of the plate with a tissue (or GDL). The hypothesis is that the spherical gold splats, that have small bonding area with the stainless steel (SS) substrate as shown in Figure 1A, were rubbed off the SS substrate surface during stack assembly and testing leading to the higher TPV after the stack testing. Therefore, optimization of the process is focused on the process controls

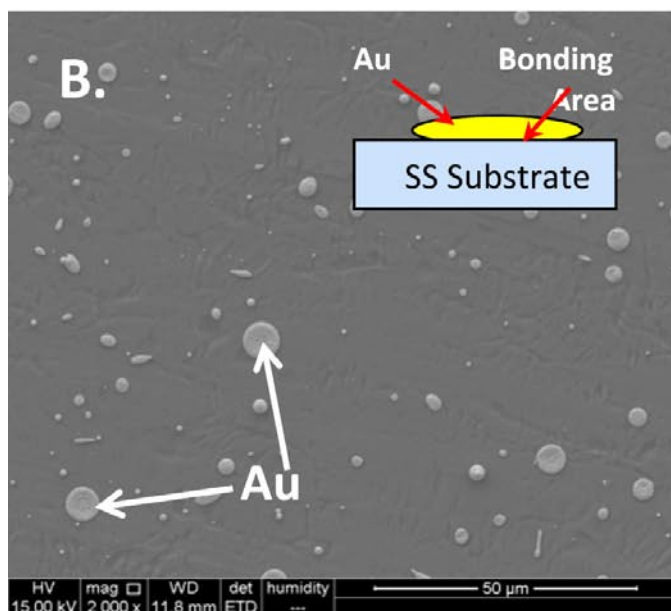
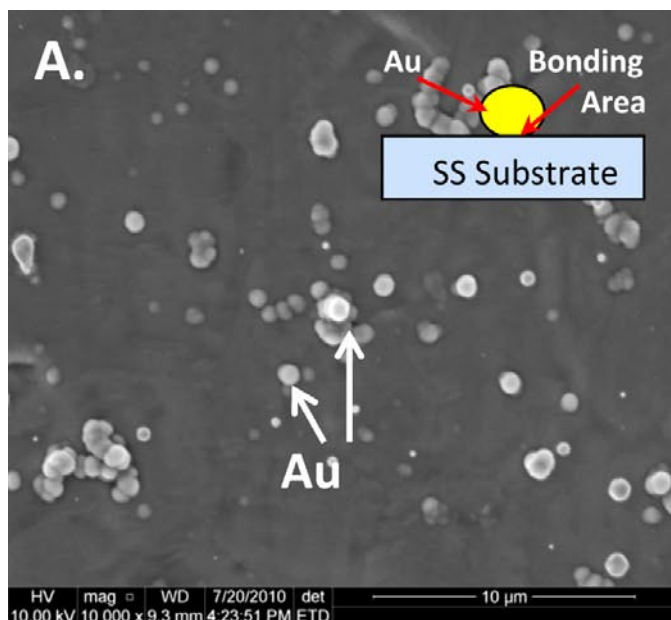
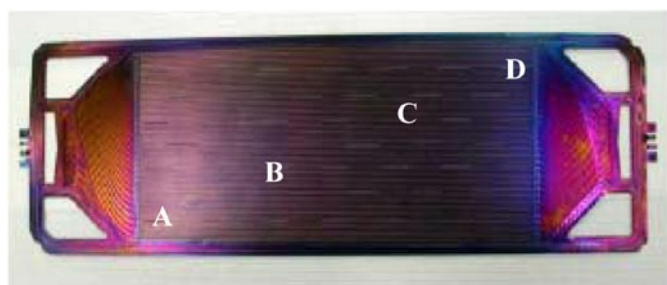


FIGURE 2. SEM pictures and schematic drawings of gold splats on SS substrate. A: spherical gold splats that have small bonding area with SS substrate, and B: flat gold splats that have large bonding area with SS substrate.

to obtain the flat gold splats that have much large bonding area with SS substrate, as shown in Figure 2B.

In conjunction with the process optimization, we have modified the spray system for small volume commercial production. We have finished the system modification and processing optimization to produce metal plates with consistent quality. Using this modified system, we processed 40 bipolar plates with the optimized processing condition, for the second 20-cell stack demonstration at Ford. The picture of the plate and comparison of TPV of five plates at four spots



| Plate # | TPV mV (@ 1A/cm ²) | | | | Average |
|---------|--------------------------------|------|------|------|---------|
| | A | B | C | D | |
| #1 | 6.75 | 6.14 | 6.64 | 6.45 | 6.50 |
| #2 | 5.36 | 6.25 | 6.95 | 6.60 | 6.29 |
| #3 | 7.60 | 7.12 | 7.00 | 6.40 | 7.03 |
| #4 | 7.00 | 6.40 | 6.00 | 7.40 | 6.70 |
| #5 | 7.60 | 6.90 | 7.50 | 7.50 | 7.38 |

FIGURE 3. Picture of the SS bipolar plate and the comparison of TPV at four spots of the plate for five plates

on each plate is shown in Figure 3. It shows that all plates have very low TPV and is uniform across the plate.

We have conducted the accelerated corrosion of TreadStone's metal plates at Los Alamos National Laboratory. The experiment is conducted with 30,000 cycles of the cell current between 0 A (open circuit voltage) and 1.2 A/cm². It was found the performance of the cell using TreadStone's metal plates is similar as the cell using standard graphite plates. The post-test analysis indicates that TreadStone's metal plates are stable in normal PEM fuel cell operational conditions.

The development of metal bipolar plate using carbon steel and aluminum substrates using TreadStone's metal plate design focused on the coating process development to protect the metal substrate from corrosion in PEM operational conditions. Different from other technologies, the only requirement of the coating for TreadStone's metal design is corrosion resistance. The electrical contact resistance can be reduced using gold (or other conductive materials) dots as demonstrated in the SS substrate. We treated the carbon steel and aluminum substrates using anodizing, phosphate treatment and chromium plating. It was found that anodizing and phosphate treatment could provide a stable surface in alkaline conditions, but not in low pH (pH 2-3) PEM fuel cell conditions. Chromium plate surface can meet the corrosion resistance requirements for PEM fuel cells, but it is difficult to obtain defect-free coating. There were pin-holes in a thin chromium coating layer, and micro-cracks in thick chromium coating layer.

In addition to PEM fuel cells, we have demonstrated the application of this technology in similar applications, including PEM electrolyzer, AEM fuel cells and some flow battery systems. These demonstrations have shown

that TreadStone's metal plate technology can meet the requirements of high corrosion resistance and low electrical contact resistance of metal plates at low cost. We will continue the technology development in these areas.

Conclusions and Future Directions

TreadStone's unique corrosion resistant metal bipolar plates have demonstrated stable operation for PEM fuel cell applications in portable, stationary and automobile applications. The process has been optimized for small-scale commercial production. In addition to the PEM fuel cell applications, we have demonstrated the application of this technology in other similar application, such as electrolyzer, AEM fuel cells and flow batteries. Further development will be focused on:

- Identify a manufacturing partner for large-scale commercial fabrication of the metal plates.
- Further evaluation with more industrial partners.
- Extend the application into electrolyzer and flow battery markets.

References

1. A.S. Woodman, E.B. Anderson, K.D. Jayne, and M.C. Kimble, AESF SUR/FIN '99 Proceedings, 6/21-24, 1999.
2. M.P. Brady, B. Yang, H. Wang, J.A. Tuner, K.L. More, M. Wilson, and F. Garzon, JOM, 2006, 58, 50.
3. H. Wang, M.P. Brady, K.L. More, H.M. Meyer and J.A. Turner, J. Power Sources, 2004, 138, 75.
4. Y. Wang, D.O. Northwood, Int. J. Hydrogen Energy 2007, 32, 895.
5. C.Y. Chung, S.K. Chen, P.J. Chiu, M.H. Chang, T.T. Hung, T.H. Ko, J. Power Sources 2008, 176, 276.
6. M.A.L. Garcia, M.A. Smith, J. Power Sources 2006, 158, 397.
7. D.G. Nam, H.C. Lee, J. Power Sources 2007, 170, 268.

V.I.1 Materials and Modules for Low-Cost, High-Performance Fuel Cell Humidifiers

William B. Johnson

W.L. Gore and Associates, Inc. (Gore)
201 Airport Road
P O Box 1488
Elkton, MD 21922-1488
Phone: (410) 506 7567
Email: wjohnson@wlgore.com

DOE Managers

HQ: Jason Marcinkowski
Phone: (202) 586-7466
Email: Jason.Marcinkoski@ee.doe.gov
GO: Reg Tyler
Phone: (720) 356-1805
Email: Reginald.Tyler@go.doe.gov

Contract Number: DEEE0000465

Subcontractor:

dPoint Technologies, Inc.
Vancouver, British Columbia, CANADA

Start Date: April 1, 2010

Projected End Date: September 30, 2012

FY 2012 Accomplishments

- Humidifier operating conditions for stationary, automotive and portable fuel cells have been established using input from original equipment manufacturers (OEMs) and other stakeholders.
- A range of humidifier membrane materials have been prepared and characterized.
- Permeance, air permeability and membrane durability testing for a range of humidifier membranes have been performed. One class of membranes, GORE™ M311.05^{1*}, has been identified as particularly promising.
- A room temperature static water vapor transport test protocol has been developed for rapid permeance testing and/or quality control of humidifier membranes.
- Performance and durability testing of the GORE™ M311.05 membrane indicate that it has acceptable performance for automotive humidifier modules, with a projected loss in performance of 20-25% in 5,000 hours.
- Humidifier membrane and module cost modeling have shown that the humidifier module using the preferred Gore humidifier membrane has projected a module cost at a volume level of 500,000 vehicles per year of less than \$150 per module.
- A high-performance humidifier module has been designed and sub-scale prototypes indicate that all automotive specifications can be met with the full-scale module. The initial full-scale modules are under construction, and will be tested in the final stages of the program, prior to delivery of a prototype to DOE.



Fiscal Year (FY) 2012 Objectives

- Demonstrate a durable, high-performance water transport membrane.
- Build and test a compact, low-cost, membrane-based module utilizing that membrane for use in an automotive stationary and/or portable fuel cell water transport exchangers.
- Model and show high volume costs associated with membrane and module.

Technical Barriers

This project addresses the following technical barriers from the Fuel Cells section (3.4) of the Fuel Cell Technologies Program Multi-Year Research, Development and Demonstration Plan in Task 7, “Develop balance of plant components”:

- (A) Durability
- (B) Cost
- (C) Performance

Introduction

Today it is essential to humidify the gases supplied to the fuel cell inlets for automotive and many stationary fuel cell stack designs. In this work, we are providing a new, inexpensive, composite membrane capable of very high water vapor transport and low air cross-over. The composite structure has been designed to allow lower total cost while still meeting automotive and stationary humidifier water transport and durability targets.

Because the transport rates of these new materials are so high, current planar membrane humidifier designs are not capable of fully utilizing the high rates. Therefore, the project is using an innovative, low-cost humidifier module with customized channel geometries that can take advantage

^{1*}GORE and designs are trademarks of W.L. Gore and Associates, Inc.

of the high water transport rates. By having a materials development effort integrated with a humidifier module-system design and build project, we will be able to effectively exploit the improved material properties in an actual device.

Approach

Perfluorosulfonic acid (PFSA) membranes fulfill most of the requirements for the water transport media at the heart of the planar membrane water exchanger. They fall short primarily on cost, and secondarily on durability, especially when they are made thin to increase performance and lower cost. Gore has developed a composite water vapor transport membrane that has overcome both of these limitations [1]. The basic composite structure consists of a very thin ionomer layer sandwiched between two microporous polymer layers. The ionomer layer provides the active water transport and provides an impermeable layer to prevent gas cross-over. The water transport rate can be engineered to be very high either through the use of a material that has very high inherent water transport rates (e.g., PFSA polymers), or by making it extremely thin (e.g., $<5\ \mu\text{m}$). The microporous layer provides three critical features: first it protects the thin ionomer layer from mechanical damage during handling; second, it confers strength to the thin layer allowing it to be more durable during use. Third, it offers a strong, protective support layer for placement of a macroporous gas diffusion layer.

Our subcontractor, dPoint Technologies, has developed an innovative pleated planar membrane humidifier that is able to achieve automotive OEM water transport and pressure drop requirements. The pleated design utilizes existing low-cost, high-volume pleating equipment that is used to manufacture air filters for automotive and heating, ventilation and air conditioning applications. The pleated humidifier is a proven technology that dPoint has been developing in cooperation with several major automotive OEMs. Further improvement in humidifier size, cost and performance is possible through the use of the Gore membrane and optimizing the flow field channel design to take full advantage of this new membrane.

Results

During the past year, the membrane focus of the work has been on developing and testing a polymer composite structure of a thin PFSA polymer sandwiched between two expanded polytetrafluoroethylene layers. This membrane was selected for further work after an extensive selection process of various composite materials prepared by Gore [2]. The ability to prepare very thin layers of an ionomer allows very high permeances to be achieved with these materials. For example, by using an ~ 5 micron PFSA layer in this sandwich structure, described as GORE™ M311.05, permeances of close to two times a 25-micron homogeneous PFSA membrane are achieved. The work in this project year

has been aimed at characterizing this membrane for the key properties for use in a humidifier module in automotive or stationary fuel cell systems. These properties include performance durability after extended high temperature soaks, performance after relative humidity (RH) cycling, and performance after freeze-thaw cycling. A high-temperature test for water transport has been developed to allow rapid testing of water transport characterization [3], and has been used exclusively during testing in this project year. This test is a modified version of International Organization for Standardization standard 15496 for room moisture transport measurement of fabrics [3].

Initial studies of the durability of the sandwich M311.05 composite microstructures, e.g., showed virtually no performance degradation with time at 65°C [2]. We have now extended these studies to 80°C , where a degradation of ~ 20 - 25% in water transfer capability is observed after a $\sim 4,200$ hour hold in a module (Figure 1). There appears to be two major causes of this degradation: contamination by ionic species, and the thermally driven reaction of the PFSA polymer to cross-link at high temperature with the loss of water and the formation of a sulfonic anhydride [3,4]. The former mechanism can be minimized in operation by maintaining a clean system. The anhydride formation on PFSA polymers has been confirmed by infrared spectroscopy (Figure 2) and nuclear magnetic resonance [4], and is driven by thermodynamics so occurs faster in drier conditions and at higher temperatures [3]. The anhydride has lower water sorption, and lower water transport than the acid form of the polymer. Thus, the loss of performance of the M311 membrane after extended holds at high temperature arises from these chemical changes in the PFSA polymer. The anhydride formation of PFSA polymers is reversible by treatment with acid [3,4], or under active fuel cell operation [5].

Durability under freeze-thaw cycling and RH cycling has also been performed. The former shows no effect on performance [2]. When RH cycling is performed at 80°C there is no effect on performance beyond that expected from temperature holds at 80°C (Figure 3). The water transport loss is driven by anhydride formation just as it is with high-temperature holds [3]. The gas cross-over does not change after 20,000 cycles, the equivalent of $\sim 5,500$ hours of automotive use [3].

In summary, the testing results of the M311 membrane show some degradation of performance that arises from the chemical formation of anhydrides with the concomitant water loss. The performance loss is significant, but the magnitude should not prevent the use of this membrane in automotive humidifier applications since it is on the order of only 20% over the expected fuel cell system lifetime. In stationary applications, which operate at lower temperatures, there is much less degradation so the membrane should be acceptable for use in those applications as well.

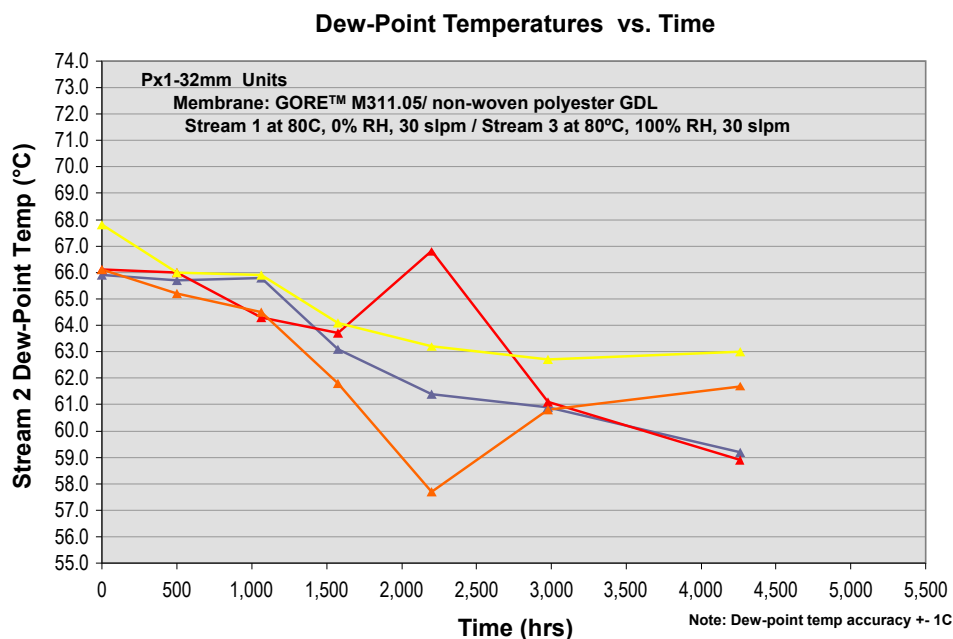


FIGURE 1. The performance of the M311 humidifier membranes made in this project degrade with time at 80°C in the conditions shown in the figure. (The Stream 2 dew point temperature is the dew point of the dry outlet.) The water transport degradation, on the order of 25% over the >4,000 hours, is likely acceptable for automotive fuel cell life times

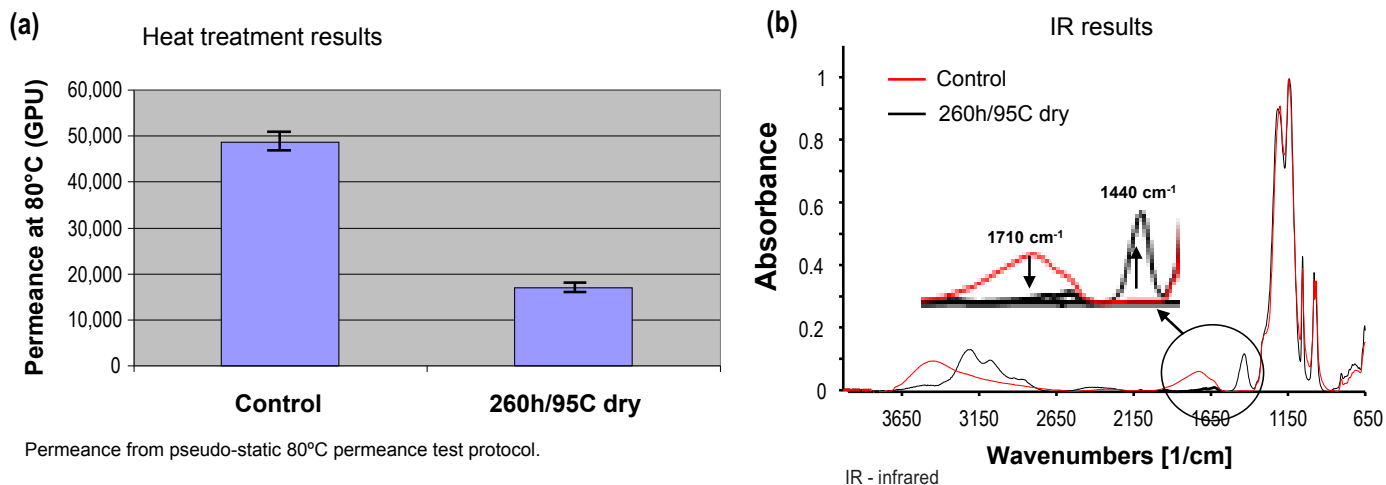


FIGURE 2. (a) An ex situ dry soak at elevated temperatures of 95°C leads to accelerated water transport degradation compared to testing at 80°C shown in Figure 1. (b) The degradation in both wet and dry conditions is driven by the loss of water and the concomitant formation of anhydride, which has lower water sorption and lower water transport. The formation of the anhydride is confirmed by infrared spectroscopy.

The design and prototyping of humidifier modules by dPoint Technologies is proceeding according to plan. Using a finite element model, the module flow field and other design parameters have been optimized, and a housing design has been chosen (Figure 4a and 4b). Several subscale modules, have been built using the designs identified by the modeling. The initial results from these subscale modules indicate that the high permeance Gore composite materials will allow modules to be built that have the requisite size and water

transport characteristics required in demanding fuel cell automotive humidifier module applications.

A high-volume cost model for module production has been completed [3]. At volumes of 500,000 units per year, the projected module cost is less than \$100. Further reductions are possible depending on final module design, system performance and size. This easily meets the automotive targets for humidifier modules.

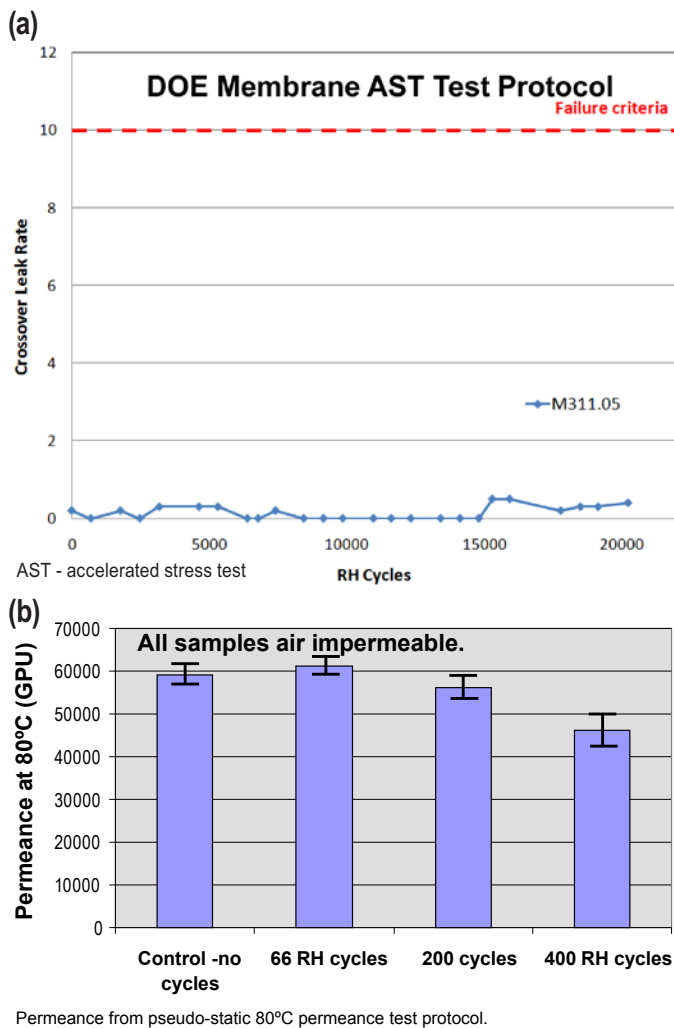


FIGURE 3. (a) RH cycling using a standard DOE test protocol shows the membrane does not leak after 20,000 cycles (data courtesy of General Motors Company). (b). Ex situ RH cycling shows there is no performance loss beyond that expected by holding at the 80°C test temperature. (Ex situ RH cycle is 80°C/88% RH to 20% RH/80°C over 3 hours; samples are restrained during testing.)

Conclusions and Future Directions

- Water transport rates through GORE™ M311 humidification membranes are high.
- Durability testing after extended high temperature soaks, after RH cycling, and after freeze-thaw cycling indicate the M311 membrane has acceptable properties for automotive and stationary application in humidifier modules.
- A high-volume cost model has demonstrated that demonstrates automotive cost targets can be met using the most promising Gore composite membranes.
- Humidifier module modeling and sub-scale module prototypes show that using the high-performance Gore composite humidifier membrane will enable an automotive humidifier module that meets the cost, durability and performance automotive targets.
- In the remaining time in the program, a full-scale humidifier module using the M311 membrane will be assembled and tested.

References

1. Yamakawa, Keiichi; Johnson, William B.; Murthy, Mahesh; Berta, Thomas; “Composite Membrane and Moisture Adjustment Module Using Same”, US 2009/0324929 A1, 12/31/2009.
2. William. B. Johnson, “Materials and Modules for Low-Cost, High Performance Fuel Cell Humidifiers”, DOE Annual Review, Crystal City, VA, May 12, 2011, Oral Presentation fc067, available from www.doe.gov.
3. William. B. Johnson, “Materials and Modules for Low-Cost, High Performance Fuel Cell Humidifiers”, DOE Annual Review, Crystal City, VA, May 17, 2012, Oral Presentation fc067, available from www.doe.gov.
4. Collette, Floraine M.; Lorentz, Chantal; Gebel, Gerard; Thominet, Francette, “Hygrothermal aging of Nafion”, Journal of Membrane Science, 330(1-2), 21-29(2009).

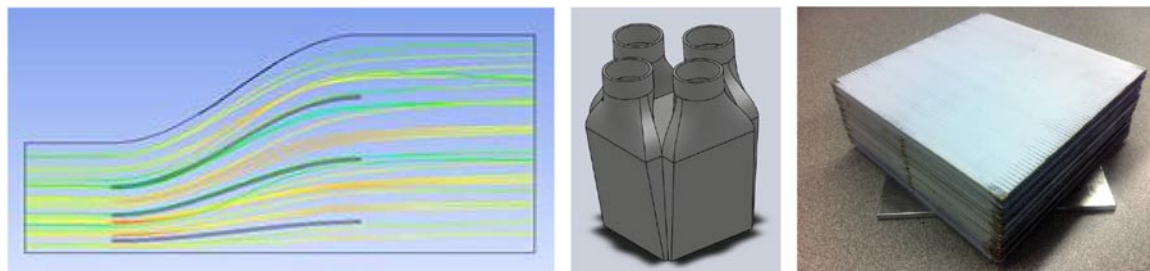


FIGURE 4. Using a finite element model of potential flow field geometries, the velocity contours, (a) have been used to optimize the housing design, (b) several subscale stacks have been built, and the final design leads to a very compact unit, and (c) the initial results from sub-scale modules indicate that the high permeance Gore composite materials will allow modules to be built that have the requisite automotive humidifier size and water transport characteristics

5. Collette, Floraine M.; Thominet, Francette; Escibano, Sylvie; Ravachol, Angèle; Morin, Arnaud; Gebel, G., "Fuel cell rejuvenation of hygrothermally aged Nafion", Journal of Power Sources, 202, 126-133(2012).

FY 2012 Publications/Presentations

1. Materials and Modules for Low-Cost, High Performance Fuel Cell Humidifiers, DOE Annual Review, May 17, 2012, Oral Presentation fc067.

2. Materials and Modules for Low-Cost, High Performance Fuel Cell Humidifiers, DOE Annual Review, May 12, 2011, Oral Presentation fc067.

V.I.2 Large Scale Testing, Demonstration and Commercialization of the Nanoparticle-Based Fuel Cell Coolant (SBIR Phase III)

Satish Mohapatra (Primary Contact), Sreya Dutta and Patrick McMullen

Dynalene Inc.
5250 W. Coplay Rd.
Whitehall, PA 18052
Phone: (610) 262-9686
Email: satishm@dynalene.com

DOE Manager

HQ: Kathi Epping Martin
Phone: (202) 586-5463
Email: Kathi.Epping@ee.doe.gov

Contract Number: EE00004532

Subcontractors:

University of Tennessee, Knoxville, TN
Protonex Inc., MA

Project Start Date: October 1, 2010

Project End Date: September 30, 2013

Technical Barriers

This project addresses the following technical barriers from the Fuel Cells section (3.4.4) of the Fuel Cell Technologies Program Multi-Year Research, Development and Demonstration Plan:

- (A) Durability
- (B) Cost

Technical Targets

Dynalene's fuel cell coolant (Dynalene FC) is expected to help the fuel cell industry achieve its durability and cost targets to some degree. First of all, the coolant itself is being designed to have a life of 5,000 hrs. It is also expected to have excellent compatibility with the system materials and inhibit corrosion in the coolant loop. This will help in extending the durability of the fuel cell system components such as the pump, the radiator, valves, seals/gaskets and any other components coming in contact with the coolant. The coolant is also designed to work at -40°C, which will assist both transportation and stationary fuel cells to quickly warm up during cold starts.

The cost target for the coolant (in plant-scale production) is about \$10/gallon, which is very close to the retail price of current automotive coolants. This coolant will also eliminate the de-ionizing filter and other hardware associated with it (i.e. fittings, valves). It is also being designed to work with cheaper, lighter and thermally efficient components such as aluminum radiators (instead of stainless steel) and brass heat exchangers.

Fiscal Year (FY) 2012 Objectives

The overall objective of this Phase III Small Business Innovation Research project is to demonstrate the 5,000 hr durability of the nanoparticle-based coolant fluid developed in Phase I and II, and perform further research into how durability is affected and how to improve it. The specific objectives in 2012 are listed below:

- Build, install and validate two fuel cell coolant test systems: one at University of Tennessee, Knoxville and the other, a Protonex fuel cell system, at Dynalene location.
- Study the effect of nanoparticle properties on its durability under severe conditions such as high temperature (up to 120°C), thermal cycling, high electric field and presence of contaminants.
- Determine the efficiency of corrosion inhibitors in long-term tests under severe conditions as well as electrochemical tests.
- Increase the nanoparticle surface charge to >500 µeq/g for both cationic and anionic particles.
- Perform testing of the coolant samples by fuel cell companies and begin commercialization.

FY 2012 Accomplishments

Following are the accomplishments from October 1, 2011 to June 30, 2012:

- Scale up and Optimization:
 - Scaled up the nanoparticle production to 100 L
 - Developed quality assurance/quality control methods for the coolant
 - Reduced final fluid cost
- Completed design and fabrication of two separate fuel cell systems:
 - University of Tennessee, Knoxville (UTK) fuel cell being tested at its facility
 - Protonex fuel cell being tested at Dynalene

- Dynalene has performed short-term immersion testing (pH and electrical conductivity) of the coolants at temperatures between 80-100°C to demonstrate preliminary fluid-material compatibility.
- Electrochemical Corrosion Study:
 - Corrosion rate of aluminum decreased when exposed to Dynalene LC (low conductivity, without nano-particles) and FC (with nano-particles) as compared to ultra-pure distilled water (UP-DW) and 65% bio-glycol-35% distilled water (BG-DW). Dynalene LC was formulated with glycol, water and corrosion inhibitors.
 - Dynalene FC and LC showed better corrosion protection for shorter immersion time (1 hr) as well as improved corrosion resistance for longer immersion times (4 days) as compared to the base fluids.



Introduction

This project addresses the goals of the Fuel Cell Technologies Program of the DOE to have a better thermal management system for fuel cells. Proper thermal management is crucial to the reliable and safe operation of fuel cells. A coolant with excellent thermo-physical properties, non-toxicity, and low electrical conductivity is desired for this application.

An ideal coolant must be durable for >5,000 hr of operation, and therefore, the coolant must be tested for such duration. Electrical conductivity of the coolant should be less than 10 $\mu\text{S}/\text{cm}$ throughout the testing period and the coolant must be compatible with all the materials (metals, plastics, rubbers and composites) at the highest operating temperature (up to 120°C). Current automotive coolants do not satisfy the electrical conductivity criteria due to the presence of ionic corrosion inhibitors in them. Water/glycol solutions without inhibitors can have low starting electrical conductivity, but it can increase rapidly due to corrosion of metal components leading to build-up of ions in the coolant. Fuel cell developers are using water or water/glycol mixtures with a de-ionizing filter in the coolant loop. The filter needs to be replaced frequently to maintain the low electrical conductivity of the coolant. This method significantly increases the operating cost and also adds extra weight/volume to the system.

Dynalene Inc. has developed and patented a fuel cell coolant with the help of DOE Small Business Innovation Research Phase I and Phase II funding. This technology has been patented in the U.S., Canada and Europe. The technical feasibility of this coolant was demonstrated in short-term tests using a dynamic re-circulating loop. The nanoparticles used in the coolant were optimized for size and surface charge density.

Approach

In this Phase III project, Dynalene's plan is to validate the durability of the coolant fluid by developing long-term test plans in-house as well as in subcontractor locations. Two test systems were built (one at University of Tennessee, Knoxville and the other at Dynalene) and are currently being used for testing various coolant compositions. Direct current corrosion testing (open circuit potential, potentiodynamic and polarization resistance experiments) was performed on the Al 3003 alloy in different coolants using a Gamry Potentiostat. A range of metals and polymers were immersed in UP-DW, BG-DW and the two Dynalene coolants (LC and FC) at temperatures between 80-120°C for up to three weeks. Dynalene performed measurements of electrical conductivity in these fluids as well as base fluids. Scanning electron microscopy and energy dispersive X-ray spectroscopy were used to characterize the metal surfaces and the inhibitive layers.

Results

UTK researchers performed elevated temperature (70°C) testing for 100 hrs with Dynalene LC and FC coolants in chamber-integrated and insulated fuel cell system (Figure 1). FC and LC showed a slight increase in average conductivity rate @ 0.005 $\mu\text{S}/\text{cm}\cdot\text{h}$. Dynalene conducted short-term testing with one of the Protonex fuel cells in-house (Figure 2). While the coolants were circulated in the fuel cell loop, it was observed that the FC attained steady state faster compared to the other fluids and also demonstrated lowest conductivity change. Dynalene will also start 5,000 hour testing on selected coolant formulations shortly. The other fuel cell will be tested at the Protonex facility for 2,000 to 3,000 hours.

Change in the electrical conductivity of the fluids in presence of metals and polymers, is an important deciding

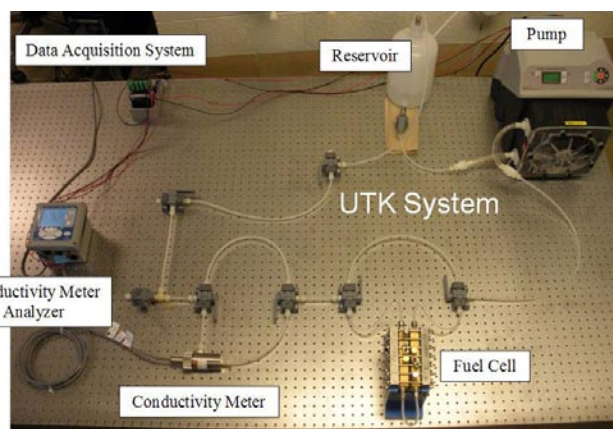
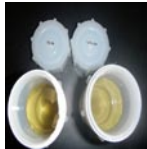


FIGURE 1. Fuel Cell Set-Up at UTK

factor for materials selection for fuel cells, as a considerable increase in the conductivity might indicate that ions might be leaching from the immersed materials and contaminating the fluids. Metals (brass and aluminum) and polymers (high-density polyethylene and silicone) showed smaller change in the electrical conductivity in the Dynalene coolants LC and FC when compared to UP-DW and BG-DW, as shown in Figure 3. All the base fluids/coolants were also heated up to 120°C for a period of two weeks to study their degradation behavior. The coolants showed discoloration and a significant change in the pH and electrical conductivity due to break down of the glycol at higher temperature. The data is tabulated in Table 1.

Corrosion Rate was derived from the potentiodynamic/Tafel plots. Aluminum exposed to FC and LC after short immersion time (1 hr) demonstrated a lower corrosion rate compared to UP-DW and BG-DW, and after longer

TABLE 1. Base Fluid Properties after Two weeks at 120°C

| Appearance of Fluids | Initial pH | Final pH | Initial Conductivity (μS) | Final Conductivity (μS) |
|--|------------|----------|---------------------------|-------------------------|
| UP-DW  | 5.87 | 6.12 | 1.11 | 2.50 |
| BG-DW  | 4.56 | 3.91 | 1.85 | 10.23 |
| LC  | 4.59 | 3.87 | 1.85 | 10.69 |
| FC  | 6.22 | 3.9 | 0.75 | 13.6 |

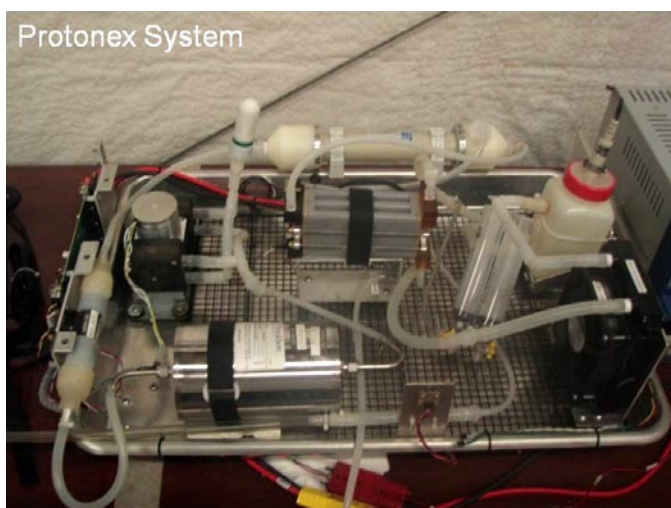


FIGURE 2. Protonex Fuel Cell System at Dynalene

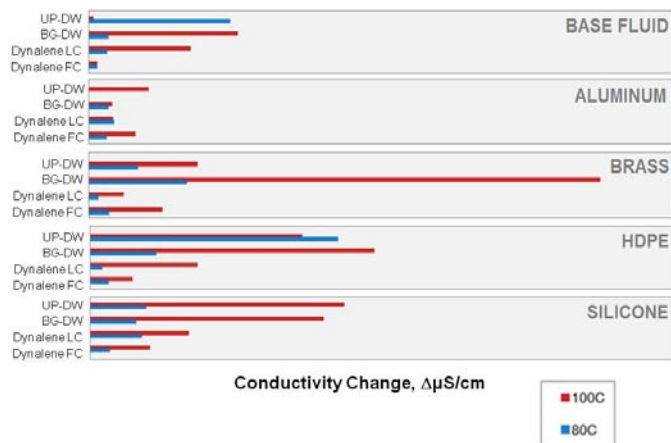


FIGURE 3. Electrical conductivity of materials in various fluids after 250 hour tests at 80°C and 100°C in Teflon® jars

immersion times (4 days), FC and LC showed marked improvement in the corrosion protection behavior of aluminum (Figure 4).

Scanning electron microscopy and energy dispersive X-ray spectroscopy characterization on the metal coupons

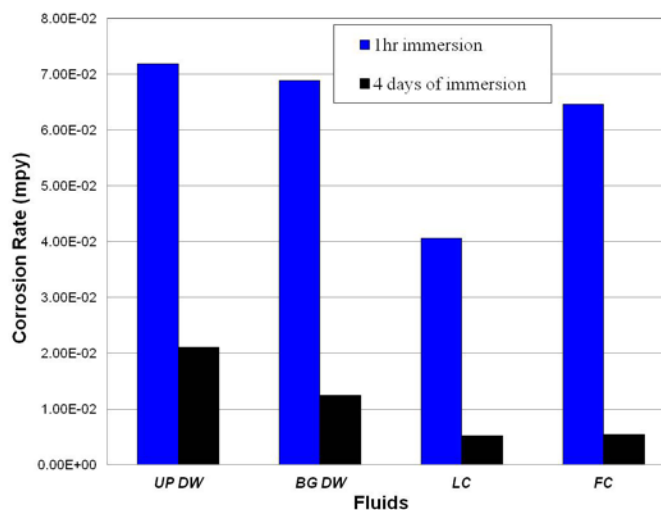


FIGURE 4. Corrosion Rate of 3003 Al immersed for different times in the fluids, derived from the potentiodynamic experiments

exposed to BG-DW, LC and FC at 88°C for two weeks showed oxide rich corrosion layer in presence of BG-DW, organic inhibiting layer (rich in nitrogen and carbon) when exposed to LC, and a much cleaner metal surface when exposed to FC. The coolants are playing a role in inhibiting corrosion in the metals but further studies are needed to confirm their contribution.

Conclusions and Future Directions

Summary of the work done so far this year:

- The fuel cell coolant optimization and scale up has been completed and Dynalene is capable of producing Dynalene FC coolant in large quantities.
- The fuel cell coolant testing skids at Dynalene and the University of Tennessee, Knoxville have been completed, performed successful short-term testing and are ready for long-term testing.
- The corrosion inhibitors were validated in short-term testing using immersion and electrochemical methods.

Future work planned for rest of the FY:

- Validate corrosion inhibitors in 5,000 hour tests.
- Increase of anionic particle surface charge to match cationic at 500 $\mu\text{eq/g}$.
- Perform compatibility and thermal degradation studies at temperature exceeding 100°C.
- Perform 5,000 hour testing of final coolant formulation in two fuel cell systems.
- Characterize samples after immersion testing with scanning electron microscopy and energy dispersive X-ray spectroscopy to understand the inhibitive effect of the coolant.

FY 2012 Publications/Presentations

1. S. Mohapatra, P. McMullen, S. Dutta and K. Coscia, “Fuel Cell Coolant Optimization and Scale-up”, Presented at the Annual DOE Hydrogen Program Review Meeting, May 2012, Washington, D.C.
2. Y. Garsany, S. Dutta and K. E. Swider-Lyons, “Effect of Glycol-based Coolants on the Suppression and Recovery of Platinum Fuel Cell Electrocatalysts” *J. Power Sources*, 2012, 216, 515-525.
3. Y. Garsany, S. Dutta and K. E. Swider-Lyons, “The Poisoning and Recovery of Pt/VC Electrocatalysts Contaminated with Glycol-Based Coolant Formulations” oral presentation at Pacific RIM Meeting, Honolulu, Hawaii, Oct. 7–12th 2012.
4. K. Coscia, S. Dutta, S. Mohapatra and P. McMullen, “Materials Compatibility and Corrosion in Glycol-Based Fuel Cell Coolants for Automotive Applications” manuscript accepted for Fuel Cell Seminar & Exposition 2012, Uncasville, CT.

V.I.3 New High Performance Water Vapor Membranes to Improve Fuel Cell Balance of Plant Efficiency and Lower Costs (SBIR Phase I)

Earl H. Wagener (Primary Contact), Brad P. Morgan,
Jeffrey R. DiMaio

Tetramer Technologies L.L.C.
657 S. Mechanic St.
Pendleton, SC 29670
Phone: (864) 646-6282
Email: earl.wagener@tetramertechnologies.com

DOE Manager

HQ: Nancy Garland
Phone: (202) 586-5673
Email: Nancy.Garland@ee.doe.gov

Contract Number: DE-SC0006172

Project Start Date: June 17, 2011
Project End Date: March 16, 2012

Fiscal Year (FY) 2012 Objectives

- Demonstrate water vapor transport membrane with >18,000 gas permeation units (GPU)
- Water vapor membrane with less than 20% loss in performance after stress tests
- Crossover leak rate: <150 GPU
- Temperature Durability of 90°C with excursions to 100°C
- Cost of <\$10/m² at volumes of 2,500 kg/yr

Technical Barriers

- Ionomer membrane performance optimization through improvements in molecular architecture
- Durability improvement
- Scale up of high performance materials to lower cost

This project addresses the following technical barriers from the Fuel Cell section of the Fuel Cell Technologies Program Multi-Year Research, Development and Demonstration Plan:

- (A) Durability
- (B) Cost
- (C) Performance

Technical Targets

The design and development of high performance low cost water vapor membranes for cathode humidification through unique polymer structures was explored. The commercially available 25- μm (N111) and 50- μm (N112) Nafion[®] membranes do not meet the 18,000 GPU performance target herein, and neither does a Perma Pure[™] device made with Nafion[®] hollow tube membranes. The water transfer permeance target of 18,000 GPU (1 GPU=1x10⁻⁶ cm³(standard temperature and pressure)/(cm²·s·cmHg) is a 50% increase over the 25 μm Nafion[®] N111. Once the performance is met, the need for minimal crossover, loss in performance, highest durability temperatures and lowest cost will be addressed as outlined in our Phase II proposal. The current status for water permeance is highlighted in Figure 1, in which the 18,000 GPU target was achieved.

TABLE 1. Technical Targets for Water Vapor Transport Membranes

| Characteristic | Units | 2012 SBIR Targets | Status |
|---------------------|----------------------|-------------------|--------------------|
| Water Permeance | GPU | >18,000 | 18,319 |
| Crossover leak rate | GPU | <150 | <50 |
| Loss in performance | % after stress test | <20 | 11 after 500 hours |
| Durability | °C for 20,000 cycles | 90 | 85 |
| Cost | \$/m ² | <10 | ~20 |

SBIR – Small Business Innovation Research



Approach

Tetramer's basic ionomer technology has been developed for hydrogen ion transport in polymer electrolyte membrane (PEM) fuel cells. Currently Tetramer's semifluorinated ionomer, whose identity will be released after intellectual property is established, has equaled or exceeded the incumbent perfluorosulfonic acid with significant (>50%) cost and processing advantages.

These ionomers have come surprisingly close to meeting the initial target of 18,000 GPU for water vapor permeance in water vapor transport application, but have mechanical deficiencies, which will inhibit making thinner membranes. Higher permeance is always desirable and considering that initially the materials were not at all optimized for water vapor transport, we are optimistic the newly tailored

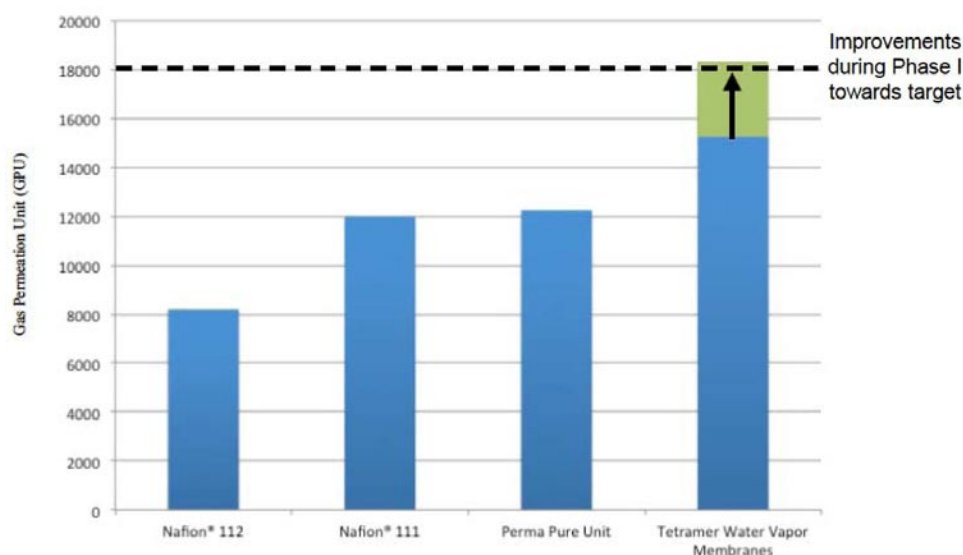


FIGURE 1. Performance of Water Vapor Membranes

versions of ionomers described below will produce improved permeance and durability.

Accomplishments

- Demonstrated that from the 20 new proprietary structures, we were able to exceed the original goal of >18,000 GPU.
- Determined that current polymer structures would not reach the target water vapor permeation or mechanical stability goals.
- Demonstrated the ability to improve structures towards long-term stability through various means.
- Consistently met the target goal of 150 GPU crossover leak rate.
- Passed the 20,000-cycle hours durability test.
- Scaled up the down-selected polymer to the 100 g scale to verify cost projections.

Future Directions

- Increase water vapor transport from 18,000 GPU to 30,000 GPU.
- Utilize initial results to optimize membrane durability to less than 20% loss in performance after 20,000 cycle hours in humidity cycle testing from 0 to 100% relative humidity with 2-minute hold times.
- Use these new molecular architectures to increase Temperature durability from 80°C to 90°C with excursions of 100°C.
- Automotive prototype membrane performance testing in FY 2013.
- Down-selected membranes will be then tested for non-automotive prototype membrane performance using module prototype production.

V.J.1 Development and Demonstration of a New-Generation High Efficiency 10-kW Stationary Fuel Cell System

Kevin Tock (Primary Contact), Russ Howell
 Intelligent Energy (IE)
 2955 Redondo Ave.
 Long Beach, CA 90806
 Phone: (562) 304-7683
 Email: kevin.tock@intelligent-energy.com

DOE Managers
 HQ: Kathi Epping Martin
 Phone: (202) 586-7425
 Email: Kathi.Epping@ee.doe.gov
 GO: David Peterson
 Phone: (720) 356-1747
 Email: David.Peterson@go.doe.gov

Contract Number: DE-FG36-07GO17013

Project Start Date: July 28, 2007
 Project End Date: January 31, 2013

Technical Targets

Work under the project is aimed at developing novel fuel processing, polymer electrolyte membrane (PEM) fuel cell technologies and integration strategies in order to make progress toward achieving DOE targets for stationary PEM fuel cell power systems for year 2012. These targets and project progress are shown in Table 1.

TABLE 1. DOE Targets vs. Project Achievements

| Metric | 2011 Project Status | 2012 Project Achievement | 2015 DOE Target ¹ |
|---|---|---|------------------------------|
| Electrical efficiency at rated power | 32.6%-prototype | 29% -demonstration unit testing underway | 42.5% |
| Combined heat and power (CHP) energy efficiency | 60.8%-prototype | 73%-demonstration unit testing underway | 87.5% |
| Operating lifetime | 3,425 hours on hydrogen generator (Phase 1 & 2) | 2,439 hours on Phase 2-only hydrogen generator ² | 40,000 hours |

¹Complete DOE table 3.4.5 found at http://www1.eere.energy.gov/hydrogenandfuelcells/mypp/pdfs/fuel_cells.pdf

²Accumulated on prototype, new retrofit hydrogen generator integrated into demonstration CHP unit now under test through February 2012.

Fiscal Year (FY) 2012 Objectives

- To identify core technology improvements, methodologies and engineered solutions to overcome challenges facing the development of fuel cells (FCs) for use in combined heat and power (CHP) applications.
- To design an integrated system based on the most promising down-selected fuel cell and fuel processor building blocks.
- To build and test a prototype unit in a laboratory setting and collect 300 hours of operating data.
- To optimize, redesign and retrofit a pressure swing adsorption (PSA) unit using lessons learned from prototype to develop a field demonstrator.
- Conduct a six-month demonstration in a International Partnership for the Hydrogen Economy country.

Technical Barriers

This project addresses the following technical barriers from the Fuel Cells section of the Fuel Cell Technologies Program Multi-Year Research, Development and Demonstration Plan:

- (A) Durability
- (B) Cost
- (C) Performance

Other challenges being addressed under the project are:

- Reduced startup time by improved thermal management design
- Reduced size by improved subassembly integration and packaging

Accomplishments

IE built two CHP prototypes and sent them to Loughborough, England, UK to do initial commissioning at the BSI testing Laboratories and later to IE-CHP in Bellshill, Scotland, UK for grid-tied demonstration.

- Conformité Européenne (“European Conformity”) compliant design of demonstration unit resulting in:
 - Grid tie enabled using commercial solar photovoltaic inverter
 - Integrated feed gas compressor, water system and gas quality monitoring
 - Onboard safety and emissions management
 - System health monitor with remote data acquisition and analysis for predictive maintenance

- Twin-stack fuel cell system developed for CHP application to improve system efficiency
- Combined heat and power efficiency is expected to increase to 78%¹
- End-to-end electrical efficiency is expected to increase to 33%²
- Construction of field demonstration unit
- Prove-out of the feasibility of adsorption enhanced reforming (AER) as a potential lower cost fuel processor option (eliminates expensive alloys and PSA required by steam methane reformer [SMR] technology)

2,439 hours of total hot hours of operation of which over 150 hours of grid-tied operation has been accomplished in the two CHP prototypes in the U.S. and UK operation.



Introduction

The development of highly efficient and cost effective clean energy solutions is not without challenge. Hydrogen fuel cell technologies are expected to become a significant player in reducing our dependence on imported fossil fuels and curb the further accumulation of green house gases and criteria pollutants.

This project is focused on the design, fabrication and field demonstration of a stationary CHP system that will provide multi-dwelling residential and light commercial end-users with on-site generated electrical and heating needs.

Approach

The approach to achieving this project's 40% electrical efficiency target is incremental and based on (1) optimization of the SMR+FC architecture and (2) the development of an 80% or greater thermally efficient AER hydrogen generator that can "plug and play" into the same SMR+FC hydrogen feed interface. The SMR+FC optimization relies on allowing slightly less than 100% hydrogen to enter the FC (99% H₂, balance methane [inert to FC]) which has a negligible impact on the FC performance, but allows for increased hydrogen recovery from the processor whereby its thermal efficiency can be boosted from 70% up to as much as 73%. Process simulations indicate that this method when combined with the benefits of a twin-stack FC configuration can increase the overall CHP system electrical efficiency from its current status of 29% to approximately 33% (demonstration unit now under test).

¹ Expected performance based on updated system model developed during retrofit redesign and new optimization approach: actual validation testing planned for the fourth quarter of FY 2011 through the second quarter of FY 2012.

² See above footnote: prototype achieved 29% electrical efficiency-increase to 33% predicted by new model.

An AER hydrogen generator produces a feed stream similar to what the optimized SMR+FC system would receive but operates at 500°C versus 900°C. This means less external energy is needed for AER making it more thermally efficient than SMR. Predictive models developed for us by Sandia National Laboratories during Year 1 of the project indicate that an efficiency of up to 85% can be achieved with the AER compared to only 70%-73% which is the maximum one can obtain with SMR. The product of the AER hydrogen generator and the fuel cell efficiencies, less 12% (assumed value) for the parasitic power requirements to run the CHP system ($[0.85 \times 0.55] - 0.12$), would result in a total system electrical efficiency of approximately 41%. Furthermore, with AER, carbon dioxide removal and reforming occur simultaneously thereby eliminating the need to have an additional purification step (such as a PSA) ultimately leading to lower cost and smaller system. Our work on AER culminated in Year 2 as further development and funding is required to mature the technology the point of a "plug-and-play" swap of SMR.

At the beginning of this last year of the project, a twin-stack FC configuration was chosen for integration into the CHP demonstrator. Since each of the two stacks can run at a lower output and be combined to produce 10 kW, the efficiency of each stack will be at its maximum point thereby synergistically operating together to achieve an improvement of efficiency from 53% (single stack) to 59%. The result of using two stacks together in terms of total performance can be seen the Results section.

Results

Over the course of FY 2012, our project team focused on (1) twin-stack fuel cell system development and testing, (2) two demonstrator units were built, debugged and shipped to UK for completing Conformité Européenne certification and field demonstration, (3) the demonstrator CHP units with shorter PSAs for the purpose of optimization through relaxing the hydrogen purity requirement all while achieving a system size reduction performed well producing power at 4-, 8- and 12-kW levels, feeding the power to the grid both in Long Beach, CA and Bellshill, Scotland UK.

Two demonstration units shown in Figure 1 and Figure 2, were built after subjecting to IE's normal four-stage gated design review process which facilitated being able to reduce the number of subsystems from 23 (on prototype) down to just nine. Key component suppliers were also engaged early on to provide a purpose-built PSA that is 1.5' shorter than the previous generation, and natural gas compressor suitable for integration within the main frame by being less than one third in size compared to its equivalent standard model.

The field unit of course must meet all safety and environmental regulations as mandated by the European Union, and as such been implemented with an emissions

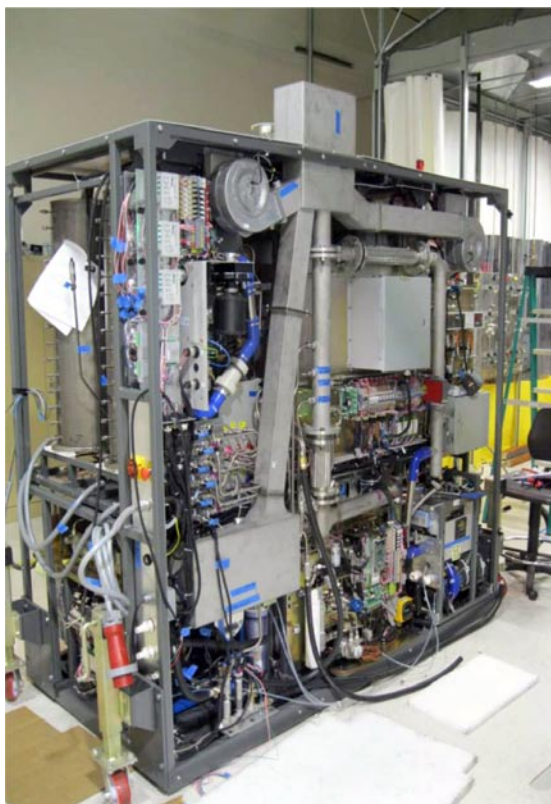


FIGURE 1. Retrofitted Demonstration Unit

monitoring and redundant, hard-wired safety shut down subsystem that constantly watches over the main system controller and software. The unit was also designed for ease of installation requiring that the site connections comprise nothing more than city water and gas, drain, heating water inlet and outlet, network connection, and flue. Components that will demand periodic maintenance while under field trial are located in areas of the machine that provide quick and easy access (e.g. water filters, sulfur adsorbent, etc.).

While on site, the system will show real-time status and performance data on a local user interface while also being stream back to IE headquarters. Startup and shutdowns will normally occur based on those commands the unit receives from the site’s own energy management system.

In addition to designing and building the demonstration unit this last year, the planned site received National Environmental Protection Act determination as required by the project and federal law. A six-month field trial was planned at Chalvey, 40 miles southwest of London, England at a multi-residential housing development called Greenwatt Way. This site is owned by Scottish and Southern Energy with who IE has formed a joint venture and will serve to showcase green technologies and provide housing for up to eight families.

As the CHP unit readiness and the Chalvey site availability did not match in timing, IE and IE CHP decided to stage some of the Conformité Européenne certification related work at BSI laboratories in Loughborough, England, UK and the initial field testing at the facilities of IE CHP in Bellshill, Sctoland, UK.

Table 2 shows run-time hours of the prototype between those reported last year versus additional time logged since then (for FY 2012). The mode of particular importance is that for pure hydrogen production; the increase in hours without loss of mechanical integrity and/or notable deterioration in fuel conversion is indicative of a fundamentally sound reformer design.

TABLE 2. Accumulated Hours on Prototypes

| CHP Unit | I (UK+US) | II (UK+US) |
|-----------------|---------------------|----------------------|
| Hot Hours | 1,370 | 1,069 |
| Reforming Hours | 531 | 625 |
| Fuel cell Hours | 25 | 62 |
| Cold Starts | 70 | 48 |
| Warm Starts | 107 | 172 |
| AC to grid | 48 in US 0 in UK | 48 in US 54 in UK |

Preliminary performance measurements are given in Tables 3 and 4 and also in Figure 3.



FIGURE 2. Packaged Demonstration Unit Installed

TABLE 3. Efficiency Calculations

| | Expected Initial Performance @ 10kW | Achieved with Prototype @ 11kW | Projected Performance of Demonstrator (Task 4) |
|--|-------------------------------------|--------------------------------|--|
| Pure Hydrogen Produced (SLPM) | | 117 | |
| Natural Gas Fed to Reformer (SLPM) | | 54 | |
| Natural Gas Fed to Combustor (SLPM) | | 1.5 | |
| Fraction of Natural Gas Power Converted to Pure Hydrogen | 72% | 66% | 72% (inc. ref. temp) |
| Fuel cell Gross power (W) | | 11,109 | |
| Hydrogen Consumed by Fuel Cell (SLPM) | | 117 | |
| Gross Efficiency of Fuel Cell | 53% | 49% | 59% (optimize) |
| Fuel cell parasitic power (W) | 720 | 722 | 620 |
| Hydrogen production parasitic power (W) | 850 | 1050 | 610 |
| Percentage of DC Power Available to Customer | | 84% | 86% |
| End-to-End Electrical Efficiency (Electricity Out / LHV Fuels In)* | 33% | 29% | 33% (optimize) |
| Thermal Power Recovered from Hydrogen Generator (W) | 4200 | 6983 | 6983 |
| Thermal Power Recovered from Fuel Cell (W)** | 4200 | 6640 | 6640 |
| End-to-End Thermal Efficiency | | 44% | 44% |
| Overall Combined Heat and Power Efficiency | 61% | 73% | 77% |

TABLE 4. Preliminary Performance Measurements

| | |
|--|--------------|
| Methane conversion | ~82% |
| PSA H2 recovery | ~67% |
| H2 generated/methane feed | ~3 |
| Lower heating value (LHV) efficiency for hydrogen generation | ~66% |
| Fuel cell gross efficiency (FC net efficiency) | ~54% ~49% |
| Overall electrical efficiency | ~29% |

Figure 4 shows the operation of the CHP with electricity feeding to the grid at 8- and 12-kw levels where as the hydrogen generator (reformer plus PSA) producing 116.9 slpm hydrogen for steady-state 11-kW operation. There was a hydrogen buffer tank which was used to store the excess hydrogen during 8-kW operation and the stored hydrogen is used subsequently during 12-kW operation. This illustrates a method with which the CHP can operate to meet different electric loads.

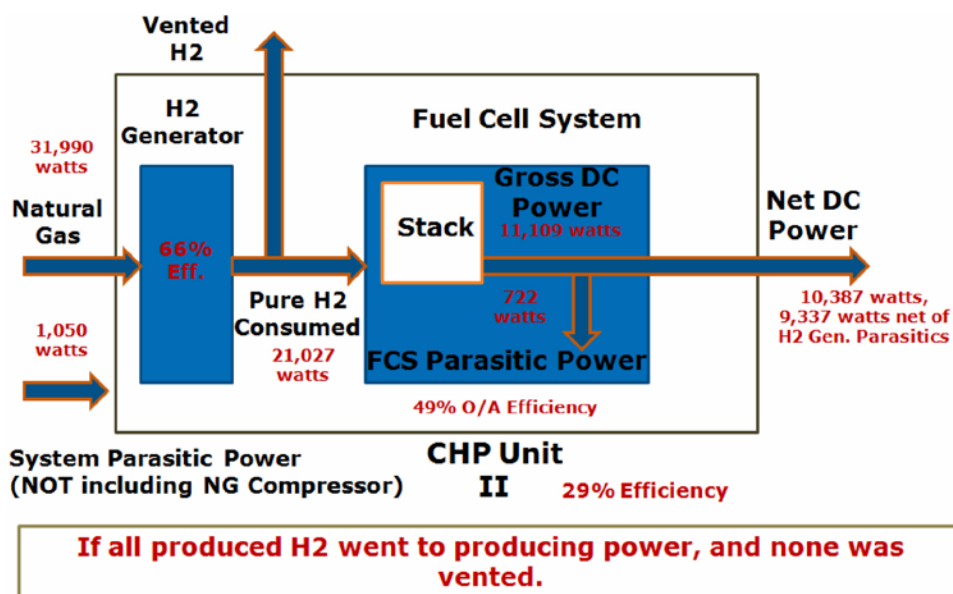


FIGURE 3. Electrical Power Diagram

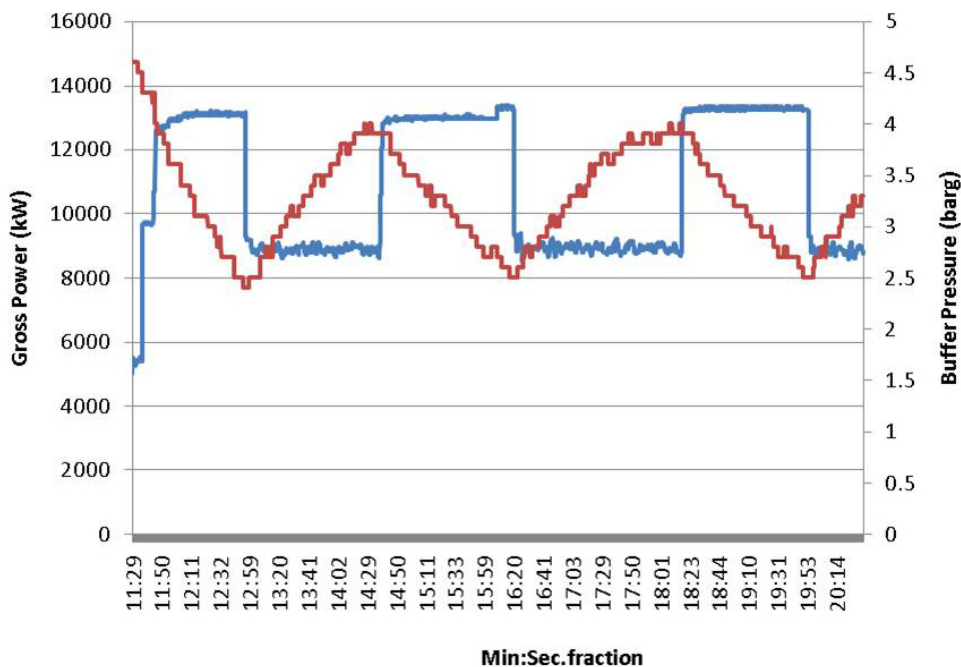


FIGURE 4. Nominal 8- and 12-kW operation of CHP feeding to alternating current to electric grid

Conclusions and Future Direction

- 2012 - Two Conformité Européenne compliant field demonstrators designed and built:
 - Approximately 30% smaller than prototype
 - Projected system electrical efficiency increased to 33%
 - Added functionality
- 2012 - Testing of fuel cell stacks with 99+% hydrogen produced by the demonstrators 1 and 2 showing no adverse impact.
- 2012-13 – Six-month field demonstration and project closure:
 - A third party company (UPS Systems PLC, Berkshire, UK) provides installation and system maintenance support.
 - SHM system relays real-time data back to the IE Knowledge Center.

Special Recognitions & Awards/Patents Issued

Patent Pending:

1. K. Duraiswamy, A. Chellappa and Mack Knobbe; Hydrogen Generation Utilizing Integrated CO₂ Removal With Steam Reforming, WO/2011/075490.

V.J.2 Development of a Low-Cost 3-10 kW Tubular SOFC Power System

Norman Bessette
 Acumentrics Corporation
 20 Southwest Park
 Westwood, MA 02090
 Phone: (781) 461-8251;
 Email: nbessette@acumentrics.com

DOE Managers
 HQ: Dimitrios Papageorgopoulos
 Phone: (202) 586-5463
 Email: Dimitrios.Papageorgopoulos@ee.doe.gov
 GO: Reginald Tyler
 Phone: (720) 356-1805
 Email: Reginald.Tyler@go.doe.gov

Contract Number: DE-FC36-03NT41838

Project Start Date: April 1, 2008
 Project End Date: March 31, 2013

project will work on cost reduction of the desired product while also demonstrating required life and efficiency targets through multi-level testing.

TABLE 1. Progress towards Meeting Technical Targets for Stationary Fuel Cell Power Generators

| Characteristic | Units | 2011 Goal | 2011 Status |
|--|---------|-----------|----------------------------|
| Electrical Efficiency | % | 40 | 40 |
| CHP Efficiency | % | 80 | 85 |
| Durability @<10% Rated Power Degradation | hours | 40,000 | 12,000 |
| Start-Up Time | minutes | <30 | <20 |
| Transient Response (from 10-90%) | seconds | <3 | <10 |
| Cost | \$/kWe | \$750 | \$729 (estimate on volume) |

Fiscal Year (FY) 2012 Objectives

The goal of the project is to develop a low-cost 3-10 kW solid oxide fuel cell (SOFC) power generator capable of meeting multiple market applications. This is accomplished by:

- Improving cell power and stability
- Cost reduction of cell manufacturing
- Increase stack and system efficiency
- Prototype testing to meet system efficiency and stability goals
- Integration to remote and micro-combined heat and power (mCHP) platforms to allow short and longer term market penetrations

Technical Barriers

This project addresses the following technical barriers from the Fuel Cells section of the Fuel Cell Technologies Program Multi-Year Research, Development and Demonstration Plan:

- (A) Durability
- (B) Cost
- (C) Performance

Technical Targets

This project is directed toward achieving the stationary generation goals of the DOE fuel cell power systems. This

FY 2012 Accomplishments

- Improved cell stability and increased current density and therefore increased power per cell.
- Demonstrated acceptable thermal cycle stability for entire systems.
- Reduced the overall parasitic load on the generator by nearly 20% enhancing overall system efficiency.
- Reduced part count per system by 48% in the past year to reduce cost and ease the manufacture of initial commercial systems.



Introduction

Achieving combined heat and power goals of over 40% net electrical efficiency and over 85% total energy efficiency are goals of the DOE and present administration to reduce our dependence on foreign energy and reduce the emission of greenhouse gases. SOFCs, with their ability to use the present U.S. fuel infrastructure and high grade waste heat are ideal candidates for this challenge. To date, the limitation on making this goal a reality has been the reliability and cost of such systems.

This project is designed to address these limitations and bring this promising technology to the market place. This is being achieved by working on all aspects of the SOFC power generator including: (1) improving cell power and stability, (2) cost reducing cell manufacture, (3) increasing stack and system efficiency, (4) prototype system testing, (5) and integration into a mCHP platform. This phase of the project

will make a major drive toward the DOE’s goals set forth for 2012 stationary power generators.

Approach

To achieve the project objectives, the approach has been to perfect the individual system pieces followed by optimizing their integration through:

- **Cell Technology:** Improving power and stability of the cell building block.
- **Cell Manufacturing:** Improving processing yield and productivity while decreasing material consumption.
- **Stack Technology:** Refining stack assembly and improve heat removal and integrity while cost reducing individual component costs.
- **System Performance:** Developing simplified controls and balance-of-plant (BOP) components to allow for a reliable, highly efficient unit.

Results

In the past years review, increases in efficiency and current density were demonstrated showing the overall goals of the DOE Hydrogen and Fuel Cells Program could be met. It was stated in last year’s summary that further work would be performed into durability and also sub-assembly and overall system cost reduction to allow for the introduction of a commercial product. All of these goals were met in the research performed under this project in 2011.

In the 2011 write-up, it was demonstrated that the current density could be increased from 150 mA/cm² to 250 mA/cm² for thousands of hours. Figure 1 shows that the current density was further increased from 250 mA/cm² to 350 mA/cm². During this period, it was shown that the voltage actually slightly increased with the increase in current density. This is most likely due to some sintering of the electrical connections between cells. Cells are now repeatable tested at a minimum of 250 mA/cm² and over 350 mA/cm². As such, a machine capable of 500 W for remote power now only requires 10 cells where in the past it could require as many as 45 cells.

To demonstrate stability of overall systems, one of Acumentrics’ commercial entry machines was tested under thermal cycle conditions. Figure 2 shows the voltage and current density traces of a remote power machine operational on line natural gas and connected to a remote direct current (DC) load. The unit operated autonomously over approximately a two week period and completed over 20 thermal cycles to room temperature. In this period, the unit had a voltage decrease of less than 2% over those cycles. During subsequent steady-state operation, some of this 2% was recovered. Based on these results, it is believed that the thermal cycle stability of the present technology is sufficient

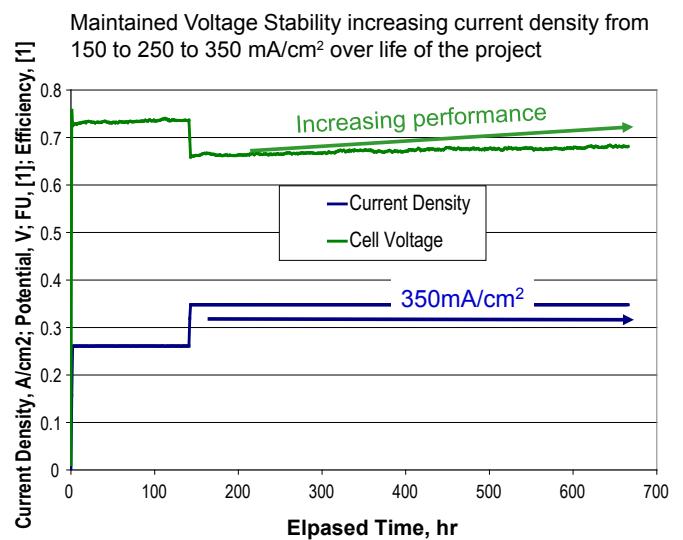


FIGURE 1. Cell Stability at Increased Current Density

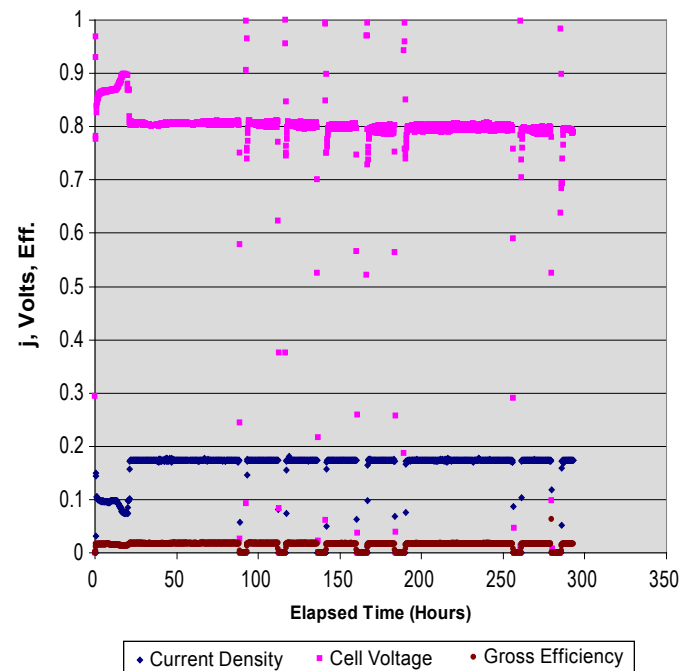


FIGURE 2. Performance Stability during Thermal Cycles

for continuous remote power operations as well as mCHP devices which probably would only cycle one or two times per winter heating season.

In additions to gains in cell power and stability, enhancements were made in reducing the overall parasitic consumption of the unit. Last report period it was noted that with improvements in cell performance and reforming technology that the overall DC efficiency had exceeded 40%, even at power levels at or below 1 kW. To assure that the overall system could also exceed 40%, work was done in

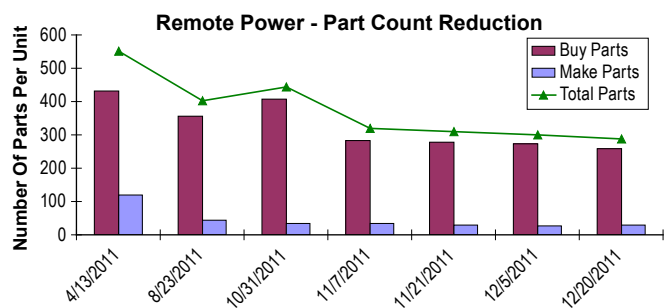


FIGURE 3. BOP Power Consumption Reductions

reducing from two blowers to one blower on partial oxidation machines. Figure 3 shows the comparison of blower power, the largest single parasitic consumer, for both two blower and one blower machines. Over 33% of the overall blower power, and approximately 20% of the overall parasitic consumption, were recovered with this advancement. The total parasitic power is now below 100 W and is capable of supporting machines up to ~3 kW output.

To simplify the overall system, effort has been made into manufacturing scale up with both reductions in labor and materials. For an initial product offering in the remote power market, systems between 500 W and 1,500 W have been designed and tested. These systems are proving to be the platform upon which mCHP systems are being developed. For the remote market, and especially the mCHP market, significant focus is needed in cost reduction. Figure 4 shows the significant part count reduction made for each system during the 2011 period. The year started with each system requiring 551 parts and ended at 287 parts for a reduction of

48%. Likewise, the amount of parts internally manufactured was reduced through effective use of local vendors more suited at mass production of strategic components. Through this focus and emphasis on labor reduction, Acumentrics has developed a system capable of commercial sales in the remote power market. For penetration of the mCHP market, significantly more funding will be required to further enhance performance and durability as well as continue cost reduction.

Conclusions and Future Directions

Significant strides have been made in achieving the goals set forth for stationary fuel cell generators under the DOE multi-year plan.

- Improved cell stability and increased current density and therefore increased power per cell.
- Demonstrated acceptable thermal cycle stability for entire systems.
- Reduced the overall parasitic load on the generator by nearly 20% enhancing overall system efficiency.
- Reduced part count per system by 48% in the past year to reduce cost and ease the manufacture of initial commercial systems.

Moving forward, further testing to achieve all of the DOE multi-year goals will be performed as well as cost reduction of the cell and all major sub-systems. Work will continue on market introduction of the technology into remote markets for short term introduction as well as mCHP for longer term market penetration.

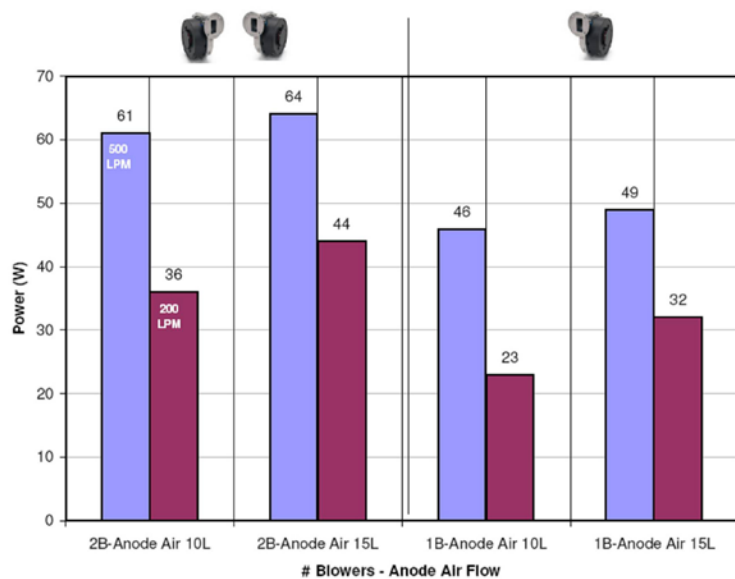
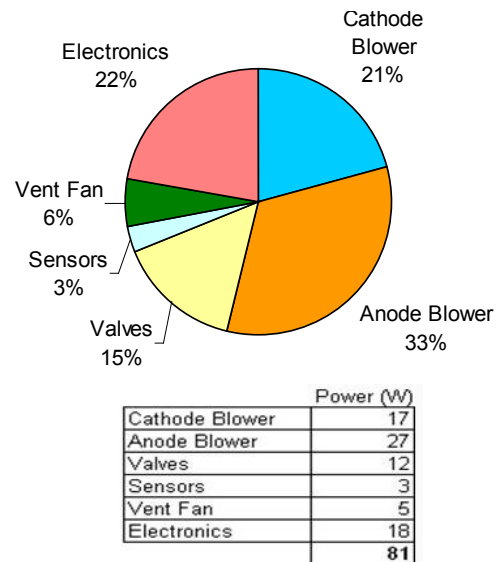


FIGURE 4. Product Part Cost Reductions



FY 2012 Publications/Presentations

1. 2011 Fuel Cell Seminar, “Progress in Acumentrics’ Fuel Cell Program”, Orlando, FL, October, 2011.
2. 2012 DOE Hydrogen Program Review. Washington, D.C., May 16, 2012.

V.J.3 Advanced Materials for Reversible Solid Oxide Fuel Cell (RSOFC), Dual-Mode Operation with Low Degradation

Eric Tang, Tony Wood, Sofiane Benhaddad,
Casey Brown, Hongpeng He, Jeff Nelson,
Oliver Grande, Ben Nuttall, Mark Richard,
Randy Petri (Primary Contact)

Versa Power Systems
10720 Bradford Road #110
Littleton, CO 80127
Phone: (303) 226-0762
Email: randy.petri@versa-power.com

DOE Managers

HQ: Kathi Epping Martin
Phone: (202) 586-7425
Email: Kathi.Epping@ee.doe.gov

GO: David Peterson
Phone: (720) 356-1747
Email: David.Peterson@go.doe.gov

Contract Number: DE-EE0000464

Project Start Date: October 1, 2009
Project End Date: September 30, 2012

- RSOFC dual-mode operation of 1,500 hours with more than 10 SOFC/solid oxide electrolysis cell (SOEC) transitions.
- Operating current density of more than 300 mA/cm² in both SOFC and SOEC modes.
- Overall decay rate of less than 4% per 1,000 hours of operation.

Meeting those performance and endurance technical targets will be the key RSOFC cell stack technology development step towards meeting DOE's technical targets for distributed water electrolysis hydrogen production by an RSOFC system.

FY 2012 Accomplishments

- Over 20 types of RSOFC cells were developed in the project. Many of those exceeded the performance (area-specific resistance <0.3 Ω-cm²) and the endurance (degradation rate less than 4% per 1,000 hours) targets—in both, fuel cell and electrolysis modes.
- Down-selected and demonstrated RSOFC-7 in a single-cell Go/No-Go milestone test which included:
 - Steady-state electrolysis with a degradation rate of about 1.5% per 1,000 hours.
 - Ultra-high current electrolysis over 3 A/cm² at 75% water electrolysis efficiency voltage of 1.67 V.
 - Daily SOFC/SOEC cyclic test of 500 days, that is 1.37 years, with a similar degradation rate of 1.5% per 1,000 hours
- Validated cell material systems via a dual metric—fuel cell/electrolysis—cyclic metric. Over 6,000 SOFC/SOEC cycles were demonstrated in accelerated cycling. The degradation obtained was less than 3% per 1,000 cycles.
- Completed stack design and component down-select, and conducted a number of kW-class RSOFC stack development tests to demonstrate:
 - Steady-state electrolysis operation of over 5,000 hours.
 - Daily SOFC/SOEC cyclic test of 100 cycles.
 - Scale up capability of using large area cells with 550 cm² active area.



Fiscal Year (FY) 2012 Objectives

The objective of project is to advance RSOFC cell stack technology in the areas of endurance and performance.

Technical Barriers

This project addresses the following technical barriers from the Production section of the Fuel Cell Technologies Program Multi-Year Research, Development and Demonstration Plan [1]:

- (G) Capital Cost
- (H) System Efficiency
- (I) Grid Electricity Emissions (for distributed power)
- (J) Renewable Electricity Generation Integration (for central power)

Technical Targets

This project includes RSOFC materials development, and reversible stack design, and demonstration. The project objectives include meeting the following performance and endurance targets in a kW-class RSOFC stack demonstration:

Introduction

RSOFCs are devices which enable the energy conversion, storage, and re-conversion to power. They are capable of operating in both power generation mode (SOFC) and electrolysis modes (SOEC). RSOFC can integrate renewable production of electricity and hydrogen when power generation and steam electrolysis are coupled in a system, which can turn intermittent solar and wind energy into “firm power.” In order to address the technical and cost barriers, DOE funded a number of research projects over the past ten years [2]. Although significant progress was made in those projects, it was concluded that further development was required, especially in the areas of RSOFC performance and endurance. In this project, Versa Power Systems Inc. (VPS) is addressing those performance and endurance issues for RSOFC cells and stacks.

Approach

VPS has identified four task areas in an effort to improve the performance and endurance of RSOFC systems: degradation mechanism study, cell material development, interconnect material development, and stack design and demonstration. A stage-gate project management process is employed with a quantitative Go/No-Go decision point. The scope of the work has been carried out by:

1. Building on VPS’ strong SOFC cell and stack baseline, and leveraging cell and stack advancements from the DOE State Energy Conversion Alliance (SECA) program.
2. Carrying out parallel materials development activities and integrating them with cell production technology development.
3. Developing RSOFC stack and process designs to address durability, performance, and cost in both fuel cell and electrolysis operating modes.

Results

The development path for RSOFC cell technology at VPS can be summarized in Figure 1. More than 20 material systems have been developed in the project. At the project Go/No-Go milestone test, one of the best cell material system—RSOFC-7—demonstrated 223 and 224 $\text{m}\Omega\text{-cm}^2$ ASR values in electrolysis and fuel cell modes, respectively, at 750°C compared with the target of less than 300 $\text{m}\Omega\text{-cm}^2$. The same materials system also demonstrated ~1.5% per 1,000 hours degradation rate as compare with the target of 4% per 1,000 hours. To further explore the performance capability in electrolysis mode, a single stack repeat unit with one RSOFC-7 cell was tested to ultra-high electrolysis current. The DOE’s water electrolysis FY 2017 efficiency target of 75% was used to establish the electrolysis operating voltage of 1.67 V. As shown in Figure 2, the cell demonstrated excellent performance of exceeding 3 A/cm^2 at 75% water electrolysis efficiency, with an operating voltage of 1.67 V.

The project initially focused on performance improvement; then the emphasis for RSOFC materials system development switched to endurance—for both SOEC steady-state and SOFC/SOEC cyclic, transient conditions. Twelve material systems, highlighted in yellow in Figure 1, were developed based on the RSOFC-7 cell. RSOFC cell material systems have been further validated in fuel cell/electrolysis cyclic operation. A cyclic test profile was designed to simulate an integrated reversible SOFCEL/solar power system. The test runs a 24-hour cycle with 10.5 hours in electrolysis, 12.5 hours in fuel cell operation, and the balance in transitions. One SOFCEL daily cyclic test of an RSOFC cell completed over 11,900 hours (~500 days) as shown in Figure 3; the degradation in fuel cell mode is about 0.6% per 1,000 hours. The SOEL mode testing was conducted at twice the current density in as that in SOFC; the SOEC degradation is slightly more than double—at about 1.5% per 1,000 hours. This is similar to the steady-state SOEC degradation rate at

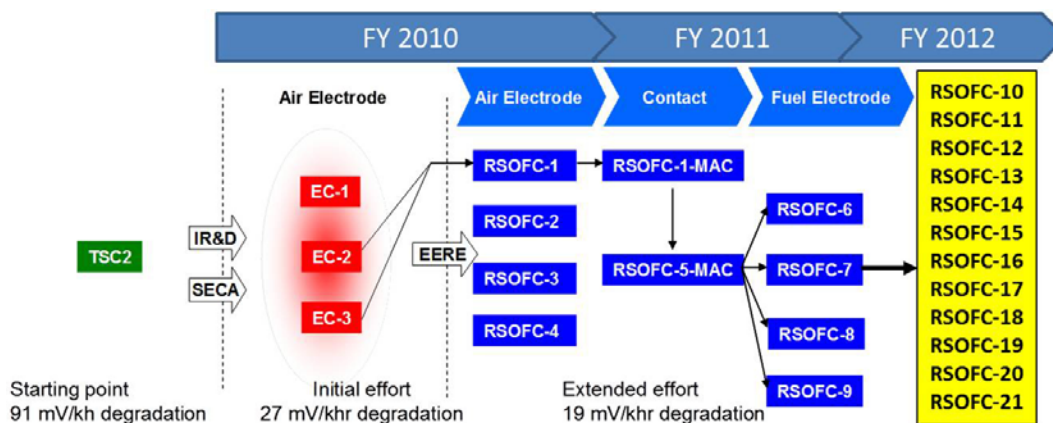


FIGURE 1. RSOFC cell development path at VPS

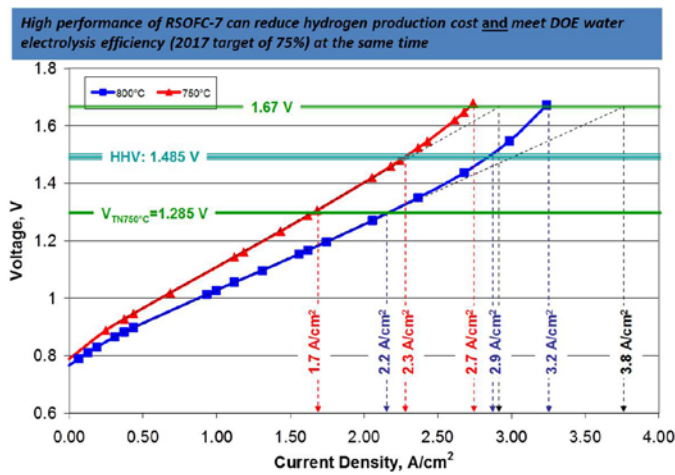


FIGURE 2. Single-cell test of a RSOFC-7 cell performance at ultra-high electrolysis current density of over 3 A/cm²

the same current density. In both cases, the degradation rate of the RSOFC-7 bettered the project target of less than 4% per 1,000 hours for over 1,000 hours. To further validate the SOFC/SOEC cyclic capability of the VPS materials systems, a single-cell stack repeat unit with one RSOFC-7 cell was tested in an accelerated cycling test—to more than 6,000 SOFC/SOEC cycles. This is equivalent to daily cycles for more than 15 years. Most of the transients in this accelerated

test were conducted over a 20 minute duration (8 minutes in SOFC, 8 minutes in SOEC, and 4 minutes in transient). The cyclic degradation rate is identical to that of daily cycle, at 3 mV/100 cycles.

Finally, in FY 2011, the improvement in steady-state SOEC degradation was verified in a long-term steady-state electrolysis test of a kW-class stack for over 5,000 hours—with less than 4% per 1,000 hours degradation rate. Last, in FY 2012, the project team has focused on the cyclic operation capability and scale up potential of the RSOFC stack. A kW-class stack with 20 RSOFC-7 cells (Figure 4) demonstrated over 100 SOFC/SOEC cyclic operations. The cyclic degradation in SOFC and SOEC were 13 mV and 64 mV per 100 cycles, respectively. This degradation rate is substantially higher than the degradation rate from the single stack repeat unit test. It was identified that the gap is mainly due to thermal management issues in an RSOFC stack. Improving thermal management in RSOFC stacks for SOFC/SOEC transient will be the main focus in the remaining of the project.

In addition, one scaled up kW-class stack with large area 25 cm x 25 cm cells (550-cm² active area) developed under the DOE SECA program, was built and tested in both steady-state electrolysis and cyclic SOFC/SOEC modes for over 1,500 hours. The results demonstrated the potential for large-scale RSOFC stack development in the future.

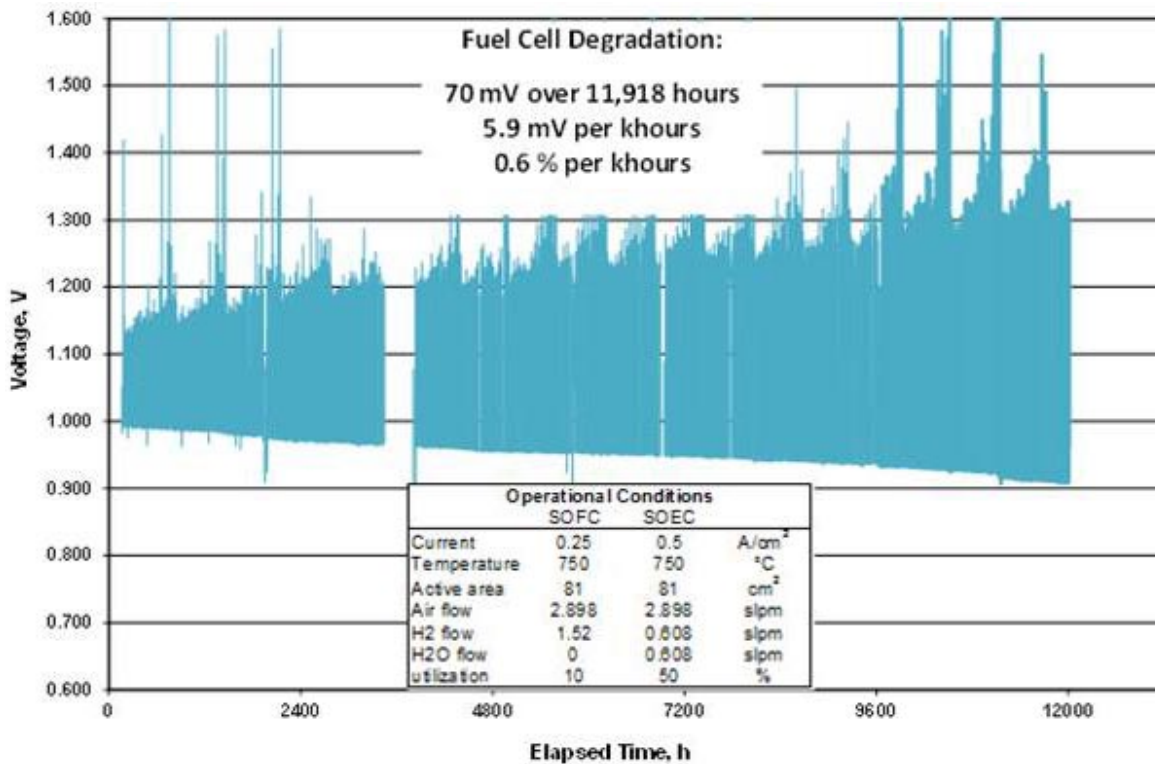


FIGURE 3. Daily cyclic operation of a RSOFC-7 in a single-cell test for ~500 days

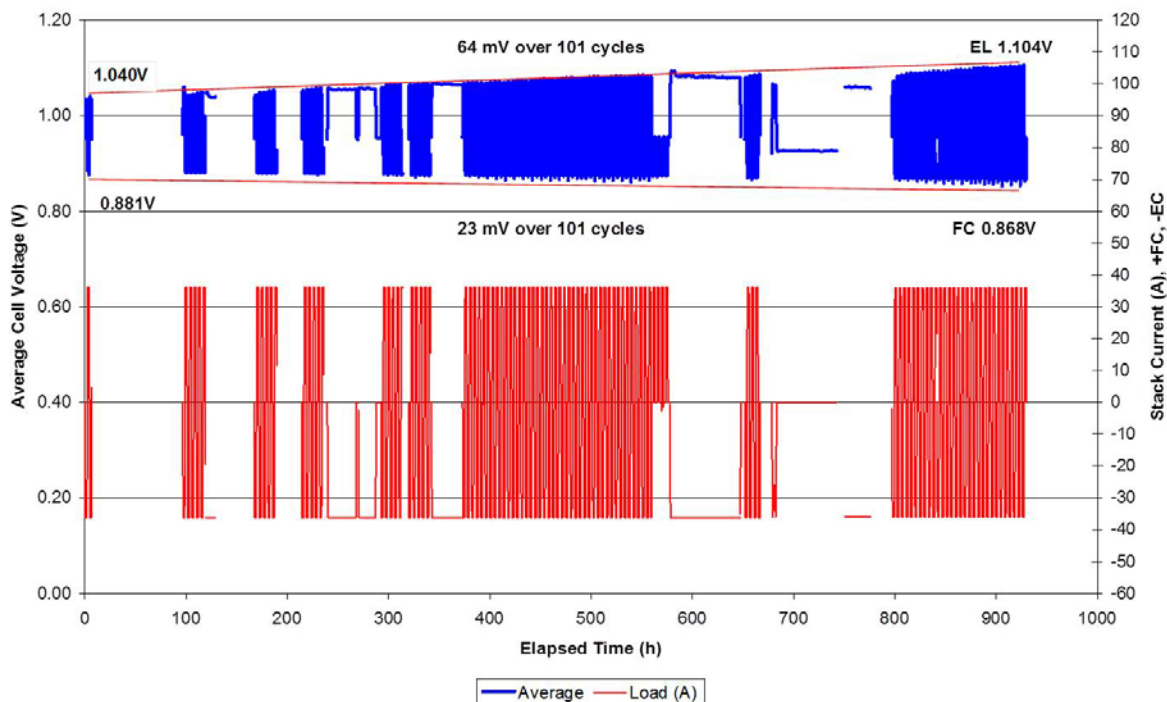


FIGURE 4. SOFC/SOEC cyclic test of a kW-class stack with RSOFC-7 cells

Conclusions and Future Directions

The project team will continue on the current development path. This includes:

1. Continuation of the RSOFC cell and stack development and testing
2. Complete the end-of-the-project kW-class RSOFC stack metric test

FY 2012 Publications/Presentations

1. An oral presentation for this effort was made at the 2012 DOE Hydrogen and Vehicle Technologies Programs Annual Merit Review and Peer Evaluation Meeting.

References

1. DOE EERE Multi-Year Research, Development and Demonstration Plan, Page 3.1-7 (2007).
2. J. Guan et al., High Performance Flexible Reversible Solid Oxide Fuel Cell, Final Technical Report, DOE DE-FC36-04G014351.

V.J.4 Power Generation from an Integrated Biomass Reformer and Solid Oxide Fuel Cell (SBIR Phase III)

Quentin Ming (Primary Contact), Patricia Irving
 InnovaTek, Inc.
 3100 George Washington Way, Suite 108
 Richland, WA 99354
 Phone: (509) 375-1093
 Email: ming@innovatek.com

DOE Managers

HQ: Charles Russomanno
 Phone: (202) 586-7543
 Email: Charles.Russomanno@ee.doe.gov
 HQ: Kathi Epping Martin
 Phone: (202) 586-7425
 Email: Kathi.Epping@ee.doe.gov

Contract Number: DE-EE0004535

Project Start Date: October 1, 2010
 Project End Date: September 30, 2013

Technical Targets

InnovaTek's research plan addresses several DOE technical targets for stationary applications for fuel cell power systems. DOE has also established technical targets for integrated stationary fuel cell power systems operating on natural gas [1]. Progress in meeting DOE's technical targets is provided in Table 1. Although the InnovaTek system was developed for use with multiple fuel types including liquid bio-fuels as well as natural gas, our research plan is addressing the same characteristics for energy efficiency and cost identified in DOE's targets.

TABLE 1. Progress toward Meeting Technical Targets for Integrated Stationary Fuel Cell Power Systems Operating on Reformate^a

| Characteristic | Units | 2015 Target ^c | InnovaTek 2012 Status ^d |
|---|--------------------|--------------------------|------------------------------------|
| Electrical Energy Efficiency ^b @ rated power | % | 42.5 | 40 |
| Equipment Cost, 5-kW system | \$/kW _e | 1,700 | 3,500 |

^a Includes fuel processor, stack, and all ancillaries

^b Regulated alternating current net/lower heating value of fuel

^c For a fuel cell system using natural gas as fuel

^d For a solid oxide fuel cell and fuel reformer system using bio-kerosene as fuel

Fiscal Year (FY) 2012 Objectives

- Establish the requirements and design for an integrated fuel cell and fuel processor that will meet the technical and operational needs for distributed energy production.
- Develop and integrate key system components – including the fuel cell stack, fuel processor, water management, thermal management, burner, air handling, control system and software.
- Demonstrate that component and mechanical design for the proposed energy system proves the technical and commercial potential of the technology for energy production, emissions, and process economics.

Technical Barriers

This project addresses the following technical barriers from the Distributed Hydrogen Production section of the Fuel Cell Technologies Program Multi-Year Research, Development and Demonstration Plan:

- Reformer Capital Costs
- Reformer Manufacturing
- Operation and Maintenance
- Feedstock Issues
- Greenhouse Gas Emissions
- Control and Safety

FY 2012 Accomplishments

- Developed system design to meet safety codes and standards for a fuel cell distributed energy system.
- Completed simulation and modeling studies to develop superior component/system designs.
- Developed optimized catalysts for liquid biofuel reforming.
- Fabricated and integrated proprietary system hardware, software, and catalysts.
- Demonstrated 1.2 kW power production from bio-kerosene and sent power to grid.
- Began Design for Manufacturing and Assembly (DFMA[®]) analyses to reduce system complexity and costs.
- Supported five students and developed partnerships with the Pacific Northwest National Laboratory, Washington State University, Boeing, City of Richland, Impact Washington, and the Mid-Columbia Energy Initiative.



Introduction

Alternative energy sources must be sought to meet energy demand for our growing economy and to improve energy security while reducing environmental impacts. Power generation from biomass, along with solar energy, wind energy, nuclear energy, geothermal energy, and others will inevitably be the ingredients of our future energy mix [2]. In addition to facilitating the use of a renewable fuel source, cost and durability are among the most significant challenges to achieving clean, reliable, cost-effective fuel cell systems. Therefore this project is focusing on lowering the cost and increasing the durability of a fuel cell distributed renewable energy system, while also assuring that its performance meets or exceeds that of competing technologies. Work was performed to develop proprietary steam reforming technology that will make it possible to use multiple fuel types, including renewable liquid bio-fuels, with a solid oxide fuel cell (SOFC). A highly efficient integrated system design with an SOFC was developed that reduces the loss of heat through an effective thermal design and the use of micro-channel heat exchangers. Modeling and simulations were completed to produce designs for prototype components and to analyze process flow for alternative system configurations. Design alternatives were compared and an integrated system design was fabricated and tested during this period. A major effort to reduce system complexity and cost was initiated using DFMA (design for manufacturing and assembly) software tools.

Approach

The technological approach utilizes a steam reforming reactor to convert bio-fuel derived from residual biomass to hydrogen-rich reformat that fuels an integrated SOFC for power generation. The project will evolve through three developmental stages. Meeting DOE targets for system performance, cost, and durability will be emphasized at each stage.

- Optimization of SOFC and fuel processor integration – is completed using process simulation and analysis to optimize system design and produce a complete mass and energy balance for individual components of the system. Process flow and piping and instrumentation diagrams are prepared to analyze possible system configurations using MathCAD® and FEMLAB® models to simulate the process flow paths in the system.
- Design for manufacturing and field operation – requires continued modeling and analysis such as failure modes and effects analysis, DFMA® and several iterations of component builds and tests to compare design options. The dimensions, geometries and flow patterns defined from optimization modeling work completed in stage 1 are translated into three-dimensional computer-aided design (CAD) images and drawings.

- System demonstration and validation for commercial applications – takes place after down-selection of the final design. Several complete systems will be built to meet the required codes and standards for demonstration at a field site to gain performance data necessary to validate the design and operation of the system. Requirements validation and routine tests will be performed before and during the demonstration, and system durability will be assessed.

Results

System Design and Fabrication

Our design objective for the integrated fuel processing and fuel cell system is to optimize the product design with the production system which includes suppliers, material handling systems, manufacturing processes, labor force capabilities and distribution systems. Design alternatives were evaluated and design tools were used to develop a more mature and producible design before final design selection. Manufacturability and integrated product development concepts were used to achieve cost and performance targets for a pre-commercial fuel cell energy system design. During the design process there was also a primary focus on addressing safety issues, in particular the potential fire hazards from leaking liquid fuel and hydrogen-rich gas.

Various design concept alternatives were evaluated against design for manufacturing objectives to help reduce both capital equipment costs and maintenance cost while increasing lifetime and robustness. CAD was used to aid in cost effectively developing and analyzing design alternatives. All drawings, specifications, and price quotes were consolidated for subsystem components along with the specifications developed. This information formed the detailed design package for building a prototype system. A list was prepared for all fabricated parts and components supplied by vendors. Critical specifications, including materials, welds, and tolerances, were described for each part.

The component list was used to prepare a bill of materials for all subsystems of the fuel cell power plant. The bill of materials was used to obtain cost estimates from potential vendors and fabricators. Requests for quotations were sent for all fabricated parts such as the reformer, heat exchangers, burner, and condenser, while pricing comparisons were made for manufacturer items. Suppliers were down-selected based on pricing and quality of products.

Significant cost reductions were realized for many of the fuel processor components compared to previous designs that were completed during Phase II. For example, the design for the catalytic reforming reactor was simplified, resulting in lower materials and fabrication costs. A total cost reduction of 47% was achieved (Figure 1). The cost of the air recuperator was reduced by about half because we found an

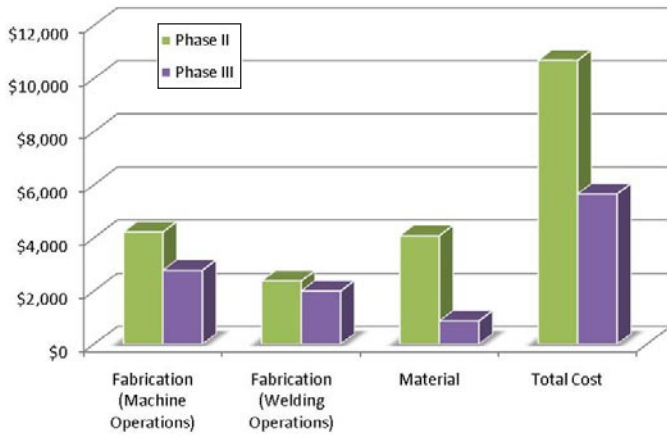


FIGURE 1. Phase III fuel processor reformer costs for materials and fabrication compared to Phase II



FIGURE 2. InnovaTek proprietary hydrogen burner components

original equipment manufacturer substitute for one that had previously been fabricated by InnovaTek.

Purchase orders were prepared for all materials and components required for the system, and fabrication of proprietary components was completed. A photo of the burner components is provided in Figure 2 and the catalytic reforming reactor in Figure 3. In addition to the hardware, the catalysts for the system were manufactured at InnovaTek’s catalyst development lab. All subcomponents, including the SOFC manufactured by Topsoe, were assembled into an integrated system using the CAD model we developed for an optimized integration scheme (Figure 4).

System Test

Initial testing of the integrated fuel cell system successfully achieved 1.2 kW net power production and a



FIGURE 3. InnovaTek proprietary catalytic steam reforming reactor



FIGURE 4. Fully integrated InnovaGen Power System that produces 1-3 kW power from liquid bio-fuel

major milestone was achieved when full water neutrality was demonstrated during operation on bio-kerosene. The important goal of optimized thermal management was also achieved when the heat requirement for the reformer was fully met by recycling anode off-gas from the fuel cell to the burner in the reformer.

Conclusions and Future Directions

- Test results from InnovaTek's prototype technology indicate that a fuel cell distributed energy system that operates on renewable, non-food bio-kerosene is possible through integration of InnovaTek's steam reforming technology and a SOFC.
- On the basis of careful systems modeling and component integration using CAD and thermal systems design with micro-channel heat exchangers, an overall system electrical efficiency of 40% is possible.
- Results from prototype testing will be used to optimize the design for field-ready systems to be constructed and demonstrated in the City of Richland Renewable Energy Park where they will be tied to the electric utility grid.
- DFMA[®] analyses and demonstration results will be used to determine whether system cost, performance, and durability targets for a commercially viable system can be met.

FY 2012 Publications/Presentations

1. Irving, P.M., Q. Ming, and P. Griffin; Distributed Power Generation from a Bio-Oil Reformer and Solid Oxide Fuel Cell; oral presentation, Fuel Cell Seminar, November 2011.
2. Griffin, P. Design Optimization and Validation of Fuel Processing Systems Using CFD and FEA Simulators; poster presentation, Fuel Cell Seminar, November 2011.

References

1. Fuel Cell Technologies Program Multi-Year Research, Development and Demonstration Plan, U.S. Department of Energy, 2011. <http://www1.eere.energy.gov/hydrogenandfuelcells/mypp/>
2. Duane B. Myers, Gregory D. Ariff, Reed C. Kuhn, and Brian D. James; Hydrogen from Renewable energy sources: Pathway to 10 quads for transportation uses in 2030 to 2050. Hydrogen, Fuel Cells, and Infrastructure Technologies, 2003 DOE Hydrogen, Fuel Cells, and Infrastructure Technologies Progress Report.

V.J.5 Research and Development for Off-Road Fuel Cell Applications

Michael T. Hicks
IdaTech, LLC
63065 NE 18th Street
Bend, OR 97701
Phone: (541) 322-1040
Email: mhicks@idatech.com

DOE Managers
HQ: Kathi Epping Martin
Phone: (202) 586-7425
Email: Kathi.Epping@ee.doe.gov
GO: David Peterson
Phone: (720) 356-1747
Email: David.Peterson@go.doe.gov

Technical Advisor
Walt Podolski
Phone: (630) 252-7558
Email: podolski@anl.gov

Contract Number: DE-FC36-04G014303

Subcontractors:

- The Toro Company, Bloomington, MN
- University of California, Davis, CA (UC Davis)

Project Start Date: August, 2007
Project End Date: September 30, 2012

the design and synthesis of air filters that meet the DOE transportation requirements for:

- Stack durability: 5,000 hours
- Humidifier durability: 5,000 hours

FY 2012 Accomplishments

- Gathered information on the air contaminants that may have an effect on fuel cell operation.
- Built exterior test facility to house air filtration test stand.
- Built test stand for evaluating air filters. Test stand has the ability to control contaminant level, humidity, temperature and flow rate.
- Completed standalone application for data acquisition.
- Verified control loops are functioning properly.



Introduction

Air filters are a critical part of a fuel cell system. They remove harmful contaminants (oxides of nitrogen and sulfur) from the oxidant stream before they reach and damage the fuel cell stack. However, filter suppliers routinely characterize air filters according to standard test procedures that are not suitable for fuel cell systems. These test methods evaluate contaminants at ppm levels when ppb levels are more representative; they only test one contaminant at a time when multiple contaminants exist in ambient air; and they do not evaluate the impact of ambient air conditions (temperature and humidity) on air filter performance. These shortcomings make it impossible to extrapolate the results from the standard test conditions to fuel cell test conditions. As a result, IdaTech proposes to evaluate air filters under “real-life” conditions.

Approach

- Determine reasonable air contaminant levels.
- Perform ex situ testing of air filters to evaluate breakthrough and filter capacitance at different contaminant levels, gas flow rates, temperatures and relative humidity.
- Utilize statistical design of experiments to plan and analyze experimental data.

Fiscal Year (FY) 2012 Objectives

- Build test stand for evaluation of commercial air filters for off-road applications.
- Evaluate air-filtration technologies for off-road applications.

Technical Barriers

This project addresses the following technical barriers from the Fuel Cells section (3.4.4) of the Fuel Cell Technologies Program Multi-Year Research, Development and Demonstration Plan:

(A) Durability

Technical Targets

This project is evaluating the efficiency at which air filter remove compounds that are known contaminants to low temperature polymer electrolyte membrane fuel cells. Insights gained from these evaluations will be applied toward

Results

Completed building outdoor test stand for air filtration. Initial shakedown testing revealed several significant issues in both hardware and controls. First, it was determined that all check valves leaked under backpressure, and they were replaced. Second, the gas-sampling solenoid valves failed to seal and were rebuilt. Lastly, the control loops for temperature and humidity were not functioning as designed and were re-written. After implementing the hardware and software changes, the system ran successfully for two weeks under a preliminary test condition (no air contaminants) in order to verify the correct regulation of the test parameters and the new data acquisition system.

Future Directions

- Calibrate Horiba gas analyzers for oxides of nitrogen and sulfur.
- Start air contamination tests and data collection.

V.J.6 150 kW PEM Stationary Power Plant Operating on Natural Gas

Shriram Ramanathan

UTC Power

195 Governors Hwy,
South Windsor, CT 06042

Phone: (860) 727-2036

Email: shriram.ramanathan@utcpower.com

DOE Managers

HQ: Kathi Epping Martin

Phone: (202) 586-1747

Email: Kathi.Epping@ee.doe.gov

GO: David Peterson

Phone: (720) 356-1747

Email: David.Peterson@go.doe.gov

Contract Number: DE-FC36-04GO14053

Project Start Date: January 2004

Project End Date: Go/No-Go Decision milestone

December 2012

HT PEM stationary fuel cell operating on natural gas reformat. Insights gained from these studies will be applied towards designing a power plant, such as described above, that meets the following 2015 DOE targets:

- Operating lifetime: 50,000 hrs
- Installed cost, natural gas: \$3,000/kW
- Electrical efficiency at rated power: 45% electrical efficiency

FY 2012 Accomplishments

- Completed cell stack assembly (CSA) and systems analysis to arrive at a power plant baseline design capable of producing steam for reforming and achieving 40% electrical efficiency, with path to 45% electrical efficiency.
- Completed membrane durability testing on current generation membranes; used projections to evaluate lifetime for next generation membranes to be anywhere between 44,000 and 220,000 hrs.
- Prepared detailed technical/project plan for design and demonstration of advanced fuel processing breadboard system capable of delivering H₂ rich low-CO (<10 ppm) reactant stream to PEM stack (currently in progress).
- Completed methanation catalyst down-selection and durability testing.
- Completed preliminary sizing and design of methanator reactor.



Fiscal Year (FY) 2012 Objectives

- Investigate feasibility and value proposition of a 150-kW high-temperature (HT) proton exchange membrane (PEM) stationary fuel cell operating on natural gas (NG) reformat.
- Evaluate durability and reliability of PEM fuel cell components.
- Preliminary systems analysis of PEM powerplant with path to achieving >45% electrical efficiency.
- Demonstrate advanced fuel processing breadboard system capable of delivering H₂-rich, low-CO (<10 ppm), reactant stream to the PEM stack.

Technical Barriers

This project addresses the following technical barriers from the Fuel Cells section of the Fuel Cell Technologies Program Multi-Year Research, Development and Demonstration Plan:

- (A) Durability
- (B) Cost
- (C) Performance

Technical Targets

This project involves conducting various studies to investigate the feasibility and value proposition of a 150-kW

Introduction

DOE is supporting development of distributed generation stationary fuel cell power plants using natural gas as fuel. The primary considerations in developing such a power plant include efficiency, cost and durability. Previously, technologies based on phosphoric acid, solid oxide and molten carbonate technologies have been used to design stationary fuel cell power plants operating on natural gas. However, PEM-based technology was not considered that promising an alternative because of the poor durability of previous generation membranes and the inability to operate them at high enough temperatures to produce steam for reforming natural gas. Because of the low operating temperatures, PEM catalyst layers are also very intolerant to even ppm levels of CO present in the natural gas reformat. Recent advances in membrane technology have not only made them more durable but also allow higher temperature operation. We believe that these new generation membranes,

in combination with UTC's experience in developing state-of-the-art reformer technology, will allow us to develop a natural gas-based PEM stationary power plants that meet DOE requirements/targets.

To date, we have conducted a CSA and systems level analysis to show that a power plant capable of achieving 45% electrical efficiency is indeed feasible. Using cell testing, we have obtained lifetime projections for the next generation membranes and shown that these membranes are indeed capable of attaining the DOE specified durability goals. We are currently working on designing and demonstrating an advanced fuel processing system that is capable of reforming natural gas to produce a H₂-rich stream with less than 10 ppm of CO, as required for operating PEM NG-based power plants.

Approach

Cell performance data along with a three-dimensional CSA model and a system model was used to evaluate different CSA and power plant configurations and to down-select the most promising design. Cell testing was conducted at the conditions listed in Table 1 to determine the durability of current generation membranes.

Briefly, the cell was operated at constant current density and the fluoride emission rate measured at regular intervals to determine the membrane life. This data was then used in conjunction with vendor data to obtain a life projection for next generation membranes. Currently, an advanced fuel processing system is being designed that is capable of reforming NG to a H₂-rich stream with less than 10 ppm of CO. Tests are being conducted to evaluate the kinetics and durability of reformer and methanation catalysts and detailed reactor designs are in progress.

Results

Steam for the reformer can be generated either inside the CSA coolers or, alternatively, outside the CSA by passing through the coolant through an expansion device under vacuum and then using a separator to separate the steam from liquid water. Table 2 summarizes the three different concepts with different steam generation approaches that were analyzed as a part of the system down-selection process. Tables 3 and 4 summarize the CSA operating conditions obtained using the three-dimensional CSA model.

TABLE 2. Summary of different concepts analyzed

| Concept | Description |
|-----------|--|
| Concept 1 | Ambient operation with steam generation outside CSA |
| Concept 2 | Ambient operation with steam generation within CSA |
| Concept 3 | Pressurized operation with steam generation within CSA |

TABLE 3. Coolant operating conditions from CSA model

| Concept | Flow rate per cooler (g/s) | Product water per cooler (g/s) | Coolant | | | |
|---------|----------------------------|--------------------------------|-----------|--------------|-----------|--------------|
| | | | Inlet | | Exit | |
| | | | Temp (°C) | Press (kPag) | Temp (°C) | Press (kPag) |
| 1 | 1.9 | 3.71e-3 | 47.0 | -12.0 | 82.0 | -6.5 |
| 2 | 0.7 | -5.49e-2 | 67.0 | -54.0 | 80.0 | -48.5 |
| 3 | 0.9 | -9.45e-3 | 47.0 | -41.2 | 86.0 | -35.7 |

Note: Negative values of product water added per cooler indicate removal of water from cooler.

Higher operating temperatures are much more conducive for steam generation. However, the CSA model indicates that it is difficult to achieve steam temperatures above 86°C with the existing flow configuration and low to moderate operating pressures. Therefore, a concept with steam generation outside the stack was down-selected, the schematic for which system is shown in Figure 1 along with flows, operating pressures and component level power consumptions. Efficiencies and parasitic power for this baseline configuration are shown in Table 5. Higher efficiency can be traded for cost by increasing the number of cells. Figure 2 shows how variations in the parasitic power affect the required active area for a fixed electrical efficiency of 40%.

Figure 3 shows the fluoride emission vs. time for a current generation membrane as measured using the technique described earlier. Based on this data, the life of the current generation membrane was estimated to be around 23,000 hours. By extrapolating vendor data for next generation membranes, we have estimated that next generation membranes should last anywhere between 44,000 to 220,000 hours.

Conclusions and Future Directions

Our work to date has indicated that a 150-kW PEM stationary power plant based on NG is indeed feasible and can meet DOE requirements for efficiency and durability.

TABLE 1. Conditions for CSA analysis and membrane durability testing; 1% air bleed was used on the anode-side to mitigate CO contamination effects

| Coolant | | | Cathode | | | | Anode | | | | | | |
|-----------------|------------------|--------|------------------|------------------|------|----------------|------------------|------------------|------|----------------|-----------------|-------|----------------|
| T _{in} | T _{out} | Flow | T _{out} | P _{out} | Util | O ₂ | T _{out} | P _{out} | Util | H ₂ | CO ₂ | CO | O ₂ |
| °C | °C | cc/min | °C | kPag | % | % | °C | kPag | % | % | % | % | % |
| 60 | 90 | 315 | 80 | 50 | 60 | 21 | 60 | 50 | 80 | 79.8 | 20 | 0.001 | 0.2 |

TABLE 4. Reactant operating conditions and cell temperatures from the CSA model

| Concept # | Avg cell temp (°C) | Hot spot temp (°C) | Cathode | | | | Anode | | | |
|-----------|--------------------|--------------------|-----------|--------------|-----------|--------------|-----------|--------------|-----------|--------------|
| | | | Inlet | | Exit | | Inlet | | Exit | |
| | | | Temp (°C) | Press (kPag) |
| 1 | 75.9 | 84.1 | 37.0 | 13.3 | 68.2 | 0.0 | 71.0 | 7.3 | 60.7 | 0.0 |
| 2 | 78.1 | 82.6 | 37.0 | 13.3 | 79.3 | 0.0 | 71.0 | 7.3 | 77.4 | 0.0 |
| 3 | 83.7 | 88.9 | 37.0 | 56.3 | 78.8 | 50.0 | 71.0 | 52.3 | 76.9 | 50.0 |

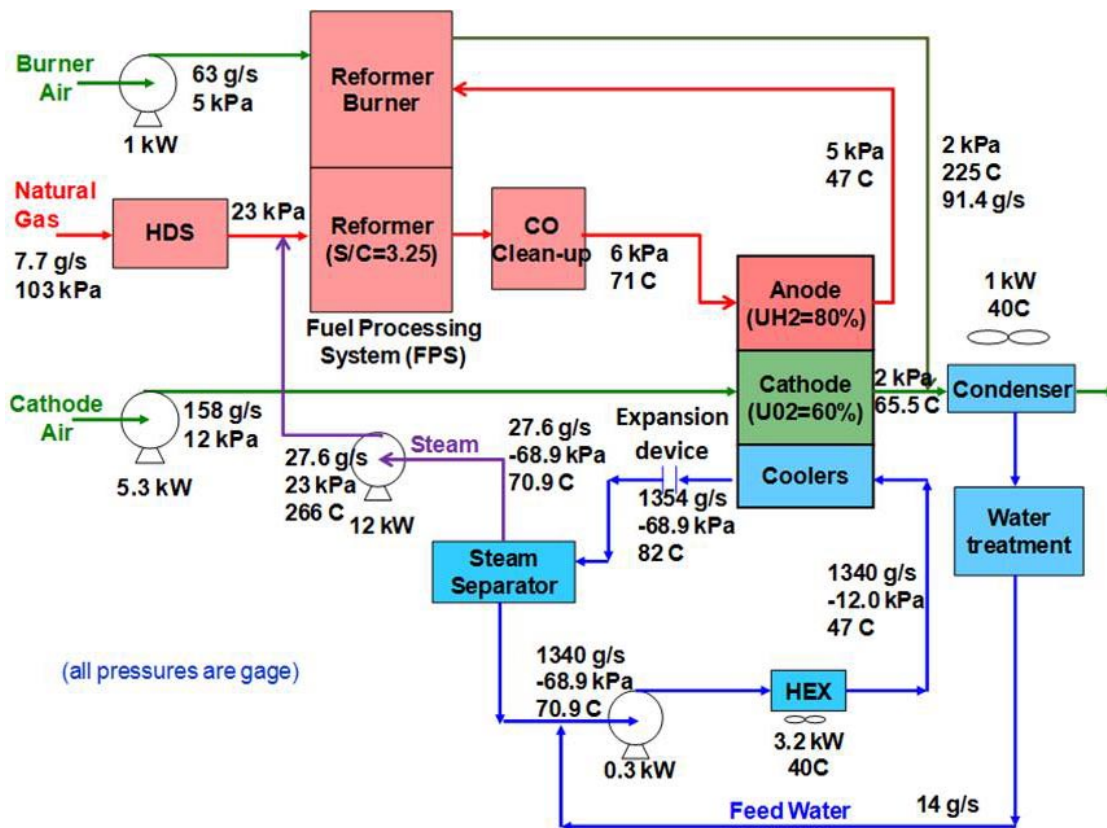


FIGURE 1. Schematic for down-selected baseline 150 kW PEM system based on concept 1

TABLE 5. Summary of operating efficiencies and parasitic power

| | |
|-----------------------|-------|
| Cell efficiency | 54.4% |
| FPS efficiency | 88.5% |
| PCS efficiency | 97.0% |
| Mech. efficiency | 85.7% |
| Electrical efficiency | 40.0% |
| Gross kW | 180 |
| Parasite power (kW) | 25.0 |

FPS – fuel processing system; PCS – power conditioning system

Preliminary systems analysis demonstrates that a 40% electrical efficiency can be achieved easily and that there

is a path to achieving 45% efficiency by trading efficiency for cost by increasing the number of cells in the stack. The remainder of FY 2012 will focus on the following tasks:

- Develop and demonstrate an advanced fuel processing system (reformer plus methanator) capable of reforming NG to a H₂-rich stream with less than 10 ppm CO. (Go/No-Go decision: CO ppm levels cannot be reduced to less than 10 ppm.)
- Develop a high-level mass-energy balance model for the system.
- Conduct single-cell tests to evaluate performance and durability of next generation membranes and catalyst layers. (Go/No-Go decision: membrane durability cannot meet 50,000 hr requirement.)

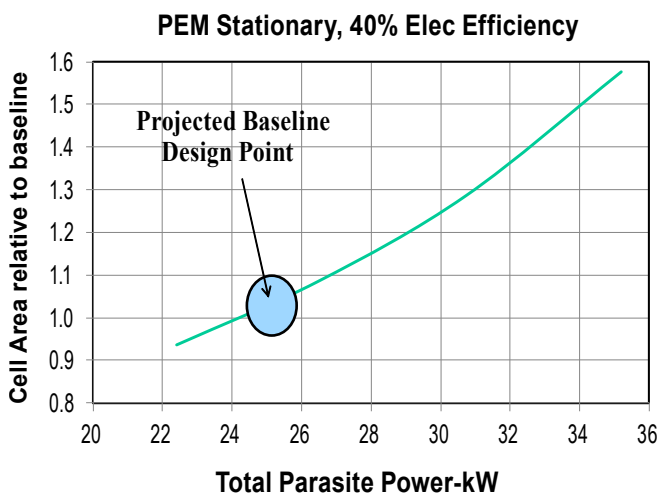


FIGURE 2. Effect of variation in total parasitic power on total active area required for 40% electrical efficiency

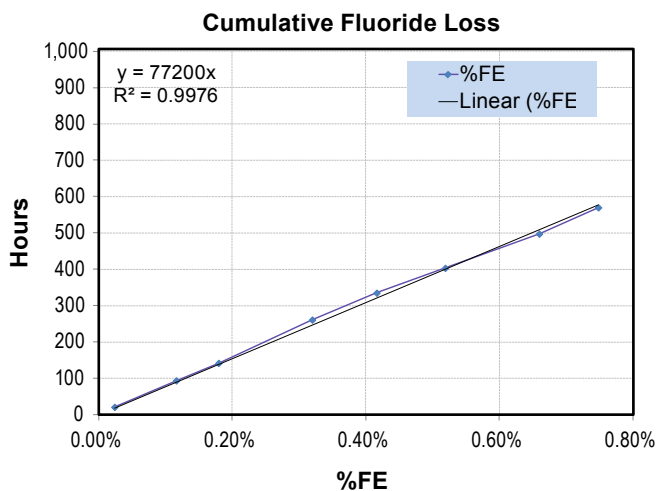


FIGURE 3. Cumulative fluoride loss vs. testing time for current generation membrane

FY 2012 Publications/Presentations

1. “Quarterly Research Performance Progress Report on 150 kw PEM fuel cell power plant verification”, Jan 2012.
2. “PEM Stationary Power Plant”, DOE Gate Review, Golden, CO, Feb 2012.
3. “Quarterly Research Performance Progress Report on 150 kw PEM fuel cell power plant verification”, Apr 2012.

V.K.1 Development of a Kilowatt-Scale Coal Fuel Cell Technology*

Steven S.C. Chuang (Primary Contact),
Tritti Siengchum, Jelvehnaz Mirzababaei,
Azadeh Rismanchian, and Seyed Ali Modjtahedi
The University of Akron
302 Buchtel Common
Akron, OH 44310-3906
Phone: (330) 972-6993
Email: schuang@uakron.edu

DOE Managers

HQ: Dimitrios Papageorgopoulos
Phone: (202) 586-5463
Email: Dimitrios.Papageorgopoulos@ee.doe.gov
GO: Reg Tyler
Phone: (720) 356-1805
Email: Reginald.Tyler@go.doe.gov

Contract Number: DE-FC36-08GO0881114

Project Start Date: June 1, 2008

Project End Date: May 31, 2012

*Congressionally directed project

(B) Cost

(C) Performance

Technical Targets

This project will develop a technological basis for the scale up of power generation capability of a kilowatt SOFC to megawatt scale. A current density of 100 mA/cm² at 0.4 V was the initial target for demonstration of a coal-based SOFC.

FY 2012 Accomplishments

- The source contributing to polarization loss is the capacitance of the Ni/YSZ anode, which suggests the necessity of improving anode and anode current collector conductivity.
- The exposure of the carbon SOFC to 7 mol% H₂O increases the maximum power density of the carbon fuel cell by 1.7 times during the continuous operation.
- The integration of individual fuel cells in series and parallel stacks achieved an open circuit voltage close to the expected Nernst potential.
- The efficiency of carbon SOFC operated with coconut coke was evaluated and the products were quantified.

Fiscal Year (FY) 2012 Objectives

To develop a kilowatt-scale coal-based solid oxide fuel cell (SOFC) technology. The outcome of this research effort will form the technological basis for developing a megawatt-scale coal-based SOFC technology. Objectives for 2012 included the following:

- Identifying the sources contributing to polarization loss which limit the activity of the Ni/yttria-stabilized zirconia (YSZ) anode electrode.
- Demonstrating continuous operation of SOFC in solid carbon with additional H₂O.
- Integrating individual fuel cells in series and parallel stack.
- Evaluating the effect of fuel cell load on the formation of CO and CO₂, and the fuel cell efficiency on the SOFC operated in solid carbon.

Technical Barriers

This project addresses the following technical barriers from the Fuel Cells section described in the Fuel Cell Technologies Multi-Year Research, Development and Demonstration Plan:

(A) Durability



Introduction

The direct use of coal in the SOFC to generate electricity is an innovative concept for electric power generation. The coal-based SOFC could offer significant advantages: (i) minimization of oxides of nitrogen emissions due to the operating temperature range of 700-1,000°C, (ii) high overall efficiency because of the direct conversion of coal to CO₂, (iii) production of a nearly pure CO₂ exhaust stream for the direct CO₂ sequestration, and (iv) low investment and maintenance costs due to the simplicity of the process. This technology also promises to provide low-cost electricity by expanding the utilization of U.S. coal supplies and relieving our dependence on foreign oil.

A small-scale coal SOFC system including coal injection and fly ash removal parts will be fabricated. The main objectives of this project are (i) improving the anode catalyst structure, and the interface between electrodes and electrolyte, (ii) developing and refining the coal-based SOFC fabrication techniques, and (iii) testing a small-scale coal SOFC system. Successful development of this novel coal fuel cell technology will significantly enhance the energy security

of the U.S. and bridge the gap between a fossil fuel-based economy and the future hydrogen-based economy.

Approach

An experimental campaign was designed and implemented with the objectives of: (i) measuring electrochemical impedance spectra of carbon SOFC at different direct current bias, (ii) evaluating the fuel cell performance characteristics in the presence of H₂O streams, (iii) quantifying the amount of CO and CO₂ produced from operation of carbon SOFCs at different operating current densities, and (iv) evaluating the efficiency of the carbon fuel cell in flowing He and CO/He. A procedure was developed for the large-scale fabrication of anode-supported SOFCs using tape casting and screen-printing techniques. Tape casting formulations containing NiO and YSZ powders, organic additives, and different amounts of pore formers (i.e., organic fillers that can be burned completely without leaving ash residues) were prepared and tested. Fuel cells fabricated by this approach were characterized by X-ray fluorescence, scanning electron microscopy, and electrochemical impedance spectroscopy. The effect of H₂O on the performance of the fuel cell was studied by recording the steady-state voltage–current polarization plots (i.e., V-I curves) in H₂ and carbonaceous fuels, and analyzing the composition of gases at the exhaust of the cell. Low ash carbon fuels, i.e., coconut coke, were tested during continuous operation of the fuel cell at a constant load. Quantification of CO and CO₂ was achieved by means of a calibration factor obtained from gas chromatography and mass spectrometry calibrations.

Results

Identifying the Sources Contributing to Polarization Loss

A Ni/YSZ fuel cell was tested in a spring-loaded reactor comprising an alumina tube, a steel plate serving as cathode current collector, and a Cu tube serving as anode current collector. Pellets of pyrolyzed Ohio #5 coal were loaded between the Ni/YSZ anode and Cu tube anode current collector. The fuel cell was tested at 750°C and 1 atm in flowing 100 sccm He. Electrochemical impedance spectra of the fuel cell was recorded with a potentiostat unit (1,400 cell test Solartron) from 1 MHz to 0.01 Hz with signal amplitude of 10 mV at various direct current density biases, shown in Figure 1(a). A direct current density bias of 0 A/cm² exhibits two overlapping arcs. Increasing the direct current density bias caused a significant growth in the high frequency arc until eventually concealed the low frequency arc, as observed in the spectrum at 0.09 A/cm². Changing the direct current bias did not cause significant variations in the intercept of the high frequency arc (160-250 Hz) with the X-axis, indicating that the total ohmic losses remained constant. The rise in

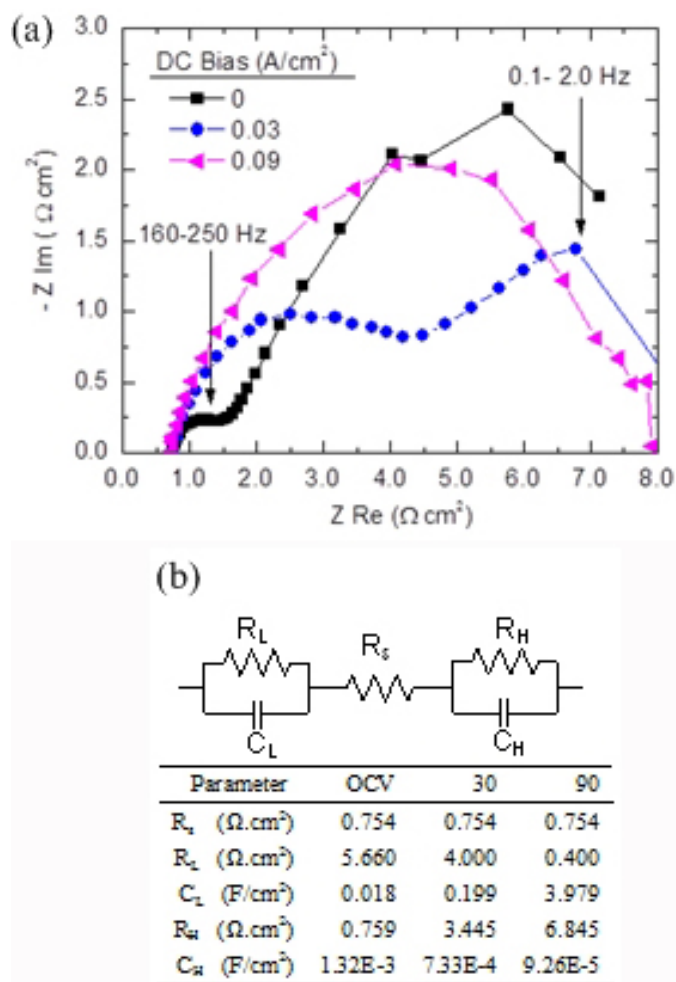


FIGURE 1. (a) Impedance spectra collected at a direct current density of 0.09, 0.03, and 0 A/cm²; (b) Parameters calculated from the equivalent circuit and the experimental impedance spectra of fuel cell with Ohio #5 coke fuel

the height of the high frequency arc can be attributed to the larger contributions of the anode electrode to the electrode polarization.

Modeling of the electrode polarization was conducted by fitting the impedance spectra to an equivalent circuit comprising a resistor and two parallel resistance-capacitance (RC) circuits, shown in Figure 1(b). The inset table in Figure 2(b) shows that increasing the direct current density bias from 0.03 to 0.09 A/cm² increased the capacitance at low frequencies C_L from 0.0176 F/cm² to 3.979 F/cm². The increase in the anode capacitance of the equivalent circuit suggests accumulation of charges at the anode electrode. Results from these studies revealed that operation of the fuel cell in Ohio #5 coke at high current densities results in large anode overpotentials that can be ascribed to an increased capacitance of the Ni/YSZ anode. Development of a highly active anode catalyst would require tailoring the morphology and composition of the anode electrode, with the purpose of

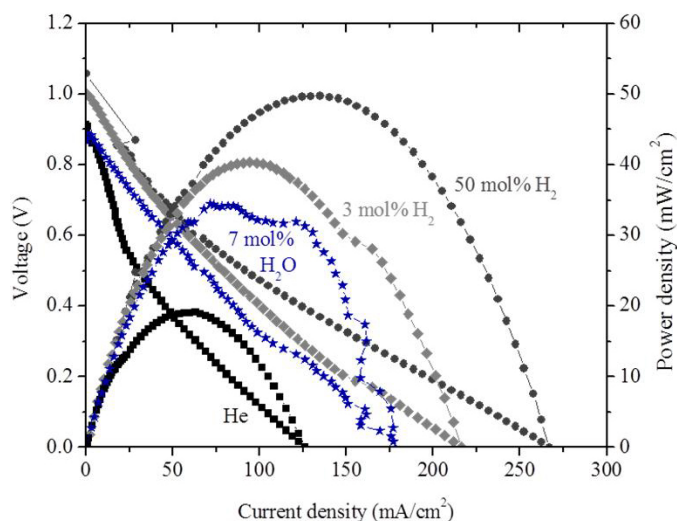


FIGURE 2. V-I curve of the fuel cell recorded at 800°C in 4 g of coconut carbon and H₂/He (100 sccm, 3 and 50 mol% H₂), He/H₂O (100 sccm, 17 mol% H₂O) and pure He (100 sccm)

reducing the accumulation of charges at the anode surface and improving the anode electronic conductivity.

Demonstrating the Operation of the Carbon SOFC with Addition of H₂O

Figure 2 shows V-I curves recorded from the carbon fuel cell operated in flowing H₂/He, He, and H₂O/He.

The fuel cell produced maximum power density as high as 50.4 mW/cm² in flowing 50 mol% H₂, and 19 mW/cm² in flowing He. Reducing the concentration of H₂ from 50 mol% to 3 mol% decrease the maximum power density to 40.0 mW/cm² indicating that the concentration of H₂ as low as 3 mol% can maintain the Ni particle in the anode structure in reduced state. Replacing the H₂-containing feed by H₂O/He (100 sccm, 7 mol% H₂O) produced a maximum power density of 34 mW/cm², 1.7 times higher than the power density obtained in pure He and only 15% lower than the performance in 3 mol% H₂/He. The relatively high fuel cell performance in H₂O/He feed could result from formation of H₂ at the anode electrode due to reactions involving carbon from coconut coke, and H₂O (reaction 1), and subsequent electrochemical oxidation of H₂ by O⁻² diffused from the cathode electrode (reaction 2).



Integration of Individual Fuel Cells in Series and Parallel Stacks

Testing two fuel cells in series configuration using H₂ fuel produced an open-circuit voltage (OCV) of 2.0 V, closely resembling the expected Nernst potential in H₂ at 750°C, and a maximum current of 180 mA, as shown in Figure 3(a). Changing the gas feed from H₂/He to He allowed operating the stack in petcoke, producing an OCV of 1.2 V. The observed fuel cell OCV was found 30-35%

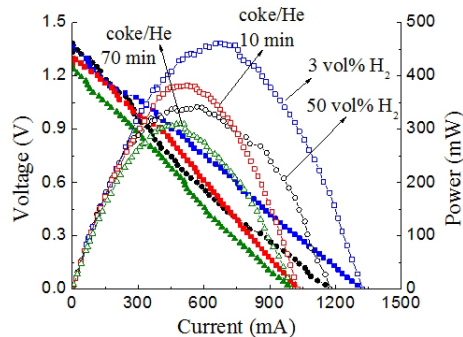
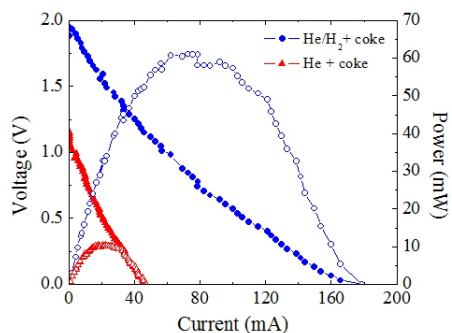
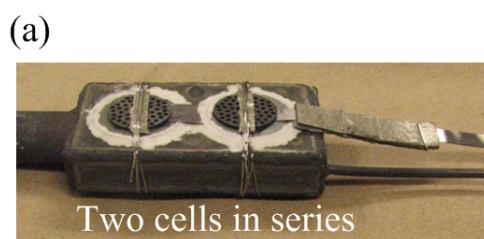


FIGURE 3. Effluent molar concentration profile during fuel cell testing at 800°C in 4 g of coconut carbon and H₂/He (100 sccm, 3 vol.% H₂), pure He (100 sccm), and H₂O/He (100 sccm, 17 mol% H₂O)

lower than the Nernst potential expected from two cells connected in series and operating in carbon fuel at 750°C. The lower performance of the fuel cell in petcoke reflects the limited contact area between the anode and the carbon fuel. Figure 3(b) shows a picture of a two fuel cell parallel stacks connected in series, designed with the purpose of producing (i) high current due to the parallel configuration of each fuel-cell-parallel-stack, and (ii) high voltage due to their integration in series. Testing of the stack in H₂ and coconut carbon produced an OCV of 1.3 V and maximum current of 1,200 mA. Replacing the gas feed from 50 to 3 vol% H₂ only decreased the fuel cell maximum current from 1,200 to 1,050 mA, indicating that electrochemical oxidation of coconut carbon has a significant contribution to the generation of electric current. Replacing the gas feed from 3 vol% H₂ to pure He did not cause major changes in the voltage and current characteristic of the fuel cell stack. The high performance of the two fuel cell parallel stacks reflects the advantages of the series and parallel configuration as well as the high reactivity of the coconut carbon.

Evaluating the Effect of Fuel Cell Load on the Formation of CO and CO₂ and the Fuel Cell Efficiency

The evolution of gases from direct utilization of carbon in SOFC was studied by potentiostatic/galvanostatic discharge of a fuel cell operated with coconut coke, a carbonaceous material with low ash and sulfur content. Operation of the carbon SOFC at 750°C produced less CO and more CO₂ than those predicted by thermodynamic calculation using total Gibbs-free energy minimization method. The addition of CO₂ to the anode chamber increased the CO formation and the maximum power density from 0.09 to 0.13 W/cm², indicating the occurrence of Boudouard reaction ($\text{CO}_2 + \text{C} \rightleftharpoons 2\text{CO}$) coupling with CO electrochemical oxidation on the fuel cell. Analysis of CO and CO₂ concentration as a function of current and voltage revealed that electricity was mainly produced from the electrochemical oxidation of carbon at low current density and produced from the electrochemical oxidation of CO at high current density. The results suggest the electrochemical oxidation of solid carbon has more mass transfer limitations than the electrochemical oxidation of CO.

Figure 4 shows the CO and CO₂ equilibrium molar flow rates as a function of temperature for the carbon SOFC with He feed at a current density of 0.50 and 1.0 A/cm². The equilibrium calculation indicates that elevating the SOFC operating temperature from 500 to 750°C increases the CO flow rate. At temperatures above 750°C, CO becomes the dominant product while CO₂ flow rates decrease to 0.01 μmol/s. As a result the operation of the carbon SOFC at lower temperatures can increase the CO₂/CO molar flow rate ratio. The operation at high current densities (i.e., 1 A/cm²) can also result in higher CO₂/CO ratio as shown in Figure 4(b), and as suggested by previous thermodynamic studies of carbon

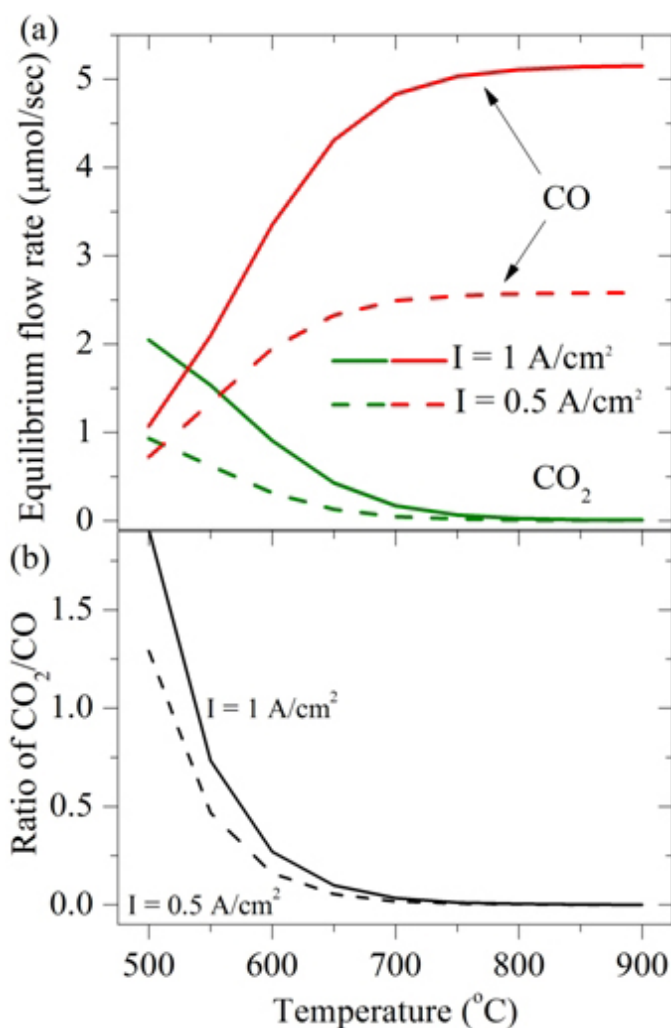


FIGURE 4. Plot of (a) CO and CO₂ equilibrium flow rates and (b) ratio of the equilibrium CO₂/CO flow rates as a function of temperature for the carbon SOFC operated at 0.5 and 1 A/cm² on carbon with He feed (200 sccm)

fuel cells [1]. Evolution of high CO₂/CO molar flow rate ratios benefits the carbon SOFC energy conversion efficiency, since electrochemical oxidation of carbon producing CO₂ is a four-electron process and that of CO is a two-electron process [2].

Table 1 summarizes the efficiencies of the carbon fuel cell under various fuels. The thermodynamic efficiency was calculated by relating the electric power produced by the fuel cell at the operating voltage (0.4 V) and the enthalpy change of the carbon oxidation reaction. The net efficiency represents the theoretical limiting efficiency of the fuel cell at 0.40 V and 750°C. The thermodynamic efficiency of fuel cell operating on carbon was higher than that of carbon with flowing of CO. This result indicates that the presence of CO in the anode compartment decreases the efficiency of the fuel cell, despite the improvement in energy generation. The decrease in thermodynamic efficiency in presence of CO is also in agreement with the decrease of net efficiency.

The efficiency of carbon fuel cell with flowing of CO was estimated to be between the net efficiency of the fuel cell operated with CO up to that operated with carbon.

TABLE 1. Summary of the Carbon Fuel Cell Efficiencies

| Fuel | Thermodynamic Efficiency | Net Efficiency |
|-----------|--------------------------|----------------|
| Carbon | 49.4% | 52.8% |
| Carbon+CO | 40.7% | 33.1-52.8% |
| CO | N/A | 33.1% |

Conclusions and Future Directions

Studies conducted during FY 2012 documented that the anode charge separation majorly contributes to polarization loss, which limits the performance of the fuel cell. Demonstration of the improvement in the carbon fuel cell power generation with addition of H₂O, and evaluation of the efficiency of the carbon SOFC operated in coconut carbon were also reported.

Future studies will be focus:

- Investigation of the change in coal structure and properties resulting from coal pyrolysis process which will be integrated to the carbon fuel cell.
- Demonstration the long-term operation of the carbon fuel cell stack in series and parallel configuration.
- Evaluation the efficiency of the carbon fuel cell operation with coal and coke.

FY 2012 Publications/Presentations

1. Tritti Siengchum, Felipe Guzman, Steven S.C. Chuang, Analysis of Gas Products from Direct Utilization of Carbon in a Solid Oxide Fuel Cell. *Journal of Power Sources* **2012**, 213 (0), 375-381.

References

1. J.-H. Koh, B.-S. Kang, H.C. Lim, Y.-S. Yoo, Thermodynamic analysis of carbon deposition and electrochemical oxidation of methane for SOFC anodes, *Electrochemical and Solid-State Letters*, 4 (2001) A12-A15.
2. S. Nurnberger, Bu, P. Desclaux, B. Franke, M. Rzepka, U. Stimming, Direct carbon conversion in a SOFC-system with a non-porous anode, *Energy & Environmental Science*, 3 (2010) 150-153.

V.K.2 Alternate Fuel Cell Membranes for Energy Independence*

Robson F. Storey (Primary Contact),
Daniel A. Savin, Derek L. Patton
The University of Southern Mississippi
118 College Drive #5050
Hattiesburg, MS 30406
Phone: (601) 266-4879
Email: Robson.Storey@usm.edu

DOE Managers

HQ: Dimitrios Papageorgopoulos
Phone: (202) 586-5463
Email: Dimitrios.Papageorgopoulos@ee.doe.gov
GO: David Peterson
Phone: (720) 356-1747
Email: David.Peterson@go.doe.gov

Contract Number: DE-FG36-08GO88106

Project Start Date: August 1, 2009

Project End Date: May 31, 2012

*Congressionally directed project

blocks composed of *N,N*-diisopropylethylammonium 2,2-bis(*p*-hydroxyphenyl)pentafluoropropanesulfonate (HPPS) and 3,3'-disulfonate-4,4'-dichlorodiphenylsulfone (sDCDPS).

- Introduce amphiprotic 1-H-1,2,3-triazole moieties onto side chains into poly(arylene ether sulfone) (PAES) to provide PEMs that can operate at high temperatures and low humidity.
- Prepare poly(perfluorinated propylene oxide) (PFPO)-sPAES block copolymers to serve as strongly segregated model systems to explore morphology-proton conductivity relationships.
- Prepare membranes from selected polymers above and measure water uptake, conductivity, mechanical properties, accelerated degradation, and fuel cell in situ properties. Compare properties to performance standards established by the DOE.

FY 2012 Accomplishments

- Two sPAES multi-block copolymers were prepared, with hydrophilic blocks consisting of HPPS and sDCDPS monomer units and hydrophobic blocks consisting of 4,4'-biphenol (BP) and 4,4'-dichlorodiphenylsulfone (DCDPS) monomer units, designated MB-1 and MB-2.
- 4-Fluorophenylsulfonyl-terminated PFPO was prepared and successfully chain coupled in a model reaction with hydrophobic PAES blocks.
- Comparison of fuel cell performance and mechanical properties, under fuel cell operating conditions, of PAES-based multiblock membranes showed improvement in variables affecting mechanical durability and performance, relative to baseline materials.



Fiscal Year (FY) 2012 Objectives

- Synthesize novel, low-cost hydrocarbon fuel cell membrane polymers with high-temperature performance and long-term chemical/mechanical durability.
- Investigate fundamental structure-property relationships of these polymers.
- Identify superior membrane materials and optimize membrane electrode assembly (MEA) processing.
- Investigate the nature and mechanisms of coupled chemical and mechanical degradation during accelerated ex situ chemical degradation and in situ proton exchange membrane (PEM) fuel cell testing.

Technical Barriers

This project addresses the following technical barriers from the Fuel Cells section of the Fuel Cell Technologies Program Multi-Year Research, Development and Demonstration Plan:

- (B) Cost
- (C) Performance

Technical Targets

- Develop sulfonated poly(arylene ether sulfone) (sPAES)-based multi-block copolymers possessing hydrophilic

Introduction

Ours is a vertically-integrated project of synthesis, characterization, and evaluation of novel hydrocarbon fuel cell membranes for high temperature performance with excellent durability. The synthetic effort seeks to produce PEMs based on aromatic hydrocarbon polymers of the PAES type, containing ion exchange groups, which in some cases are tethered to the backbone via perfluorinated alkylene linkages. Both protic (sulfonic acid-based) and amphiprotic (nitrogen-containing heterocyclic-based) resin types are being explored. In addition, we are exploring block copolymers, created via coupling reactions between PFPO and a proton-conducting block, including any of the aromatic hydrocarbon polymers discussed above and optionally

other polymers that are ionic or polar. Some synthesized membranes have been inorganically modified using domain-targeted sol-gel polymerization schemes to impart greater hydration, increased mechanical durability and reduced fuel crossover.

The synthesized materials have been characterized within the context of proton conductivity and mechanical/chemical/thermal stability over a broad temperature and humidity range using a variety of spectroscopic, dielectric, microscopic, and viscoelastic methods, and evaluated for proton conductivity and performance in operating fuel cells.

Approach

In the past year, much of the synthetic effort was phased out in favor of polymer characterization, ex situ properties measurements, and MEA fabrication and testing. The exception was sPAES-based multi-block copolymers containing HPPS and sDCDPS.

Results

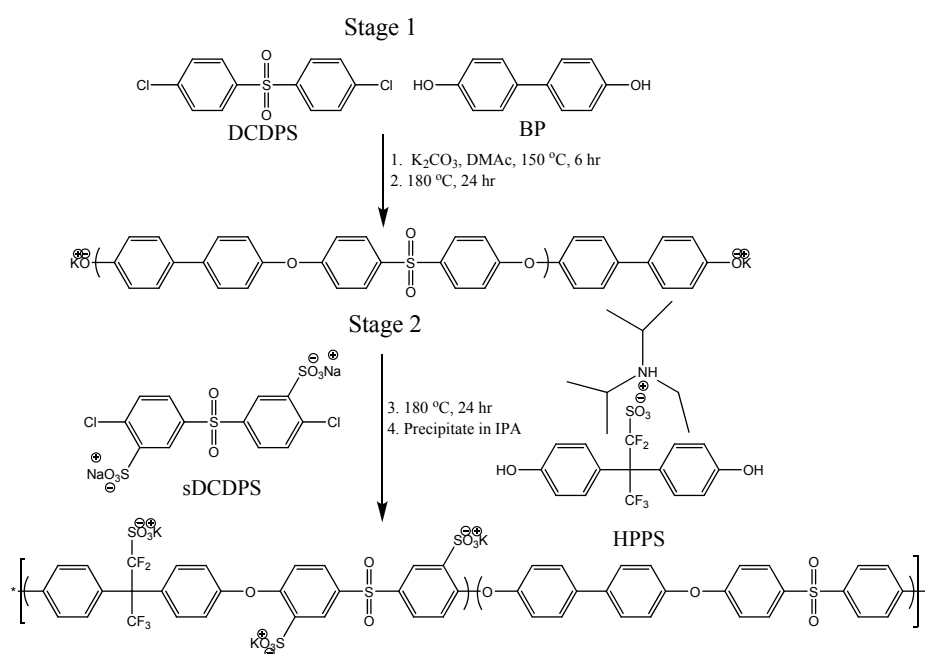
PAES polymers based on HPPS and sDCDPS. We synthesized PAES multi-block copolymers with hydrophilic block composed of HPPS and sDCDPS, using a two stage reaction sequence (one-prepolymer method). The monomers BP and DCDPS were used to synthesize phenoxide-terminated hydrophobic prepolymers in the range of 5,000 -15,000 g/mol. HPPS and sDCDPS were then added to the reaction to increase the molecular weight and incorporate hydrophilic sequences in the polymer (Scheme 1).

Two block copolymers of this type were prepared, designated MB-1 and MB-2. Table 1 lists ion exchange capacity (IEC), conductivity, molecular weight (gel permeation chromatography, GPC), and composition of these two materials. As reported below, we observed improved water uptake and conductivity performance in these PAES-based block copolymers compared to recently published block copolymers [1], which contained HPPS but not the combination of HPPS and sDCDPS.

TABLE 1. Characterization Data for Multi-Block sPAES Copolymers MB-1 and MB-2

| Multi-block sPAES | IEC (meq/g) | Conductivity mS/cm | M _n (g/mol) | M _w (g/mol) | wt% hydrophilic block |
|-------------------|-------------|--------------------|------------------------|------------------------|-----------------------|
| MB-1 | 1.68 | 49.9 | 18,550 | 27,330 | 23 |
| MB-2 | 1.08 | 2.2 | 25,120 | 35,170 | 49 |

We also explored an alternate, two-prepolymer synthetic method toward PAES-based block copolymers with hydrophilic blocks composed of HPPS and sDCDPS. Early efforts to couple the blocks by reaction of a terminal phenoxide with a terminal aromatic chloride were unsuccessful. We attributed this to the low reactivity of the aromatic chloride, since coupling reactions involving an aromatic fluoride have proven successful [1,2]. Therefore, we adopted a strategy that would allow coupling to take place using an aromatic fluoride. First, hydrophilic prepolymers carrying phenoxide end groups were synthesized from sDCDPS and HPPS. Then, hydrophobic prepolymers carrying aromatic fluoride functions were prepared in a



SCHEME 1. Synthesis of PAES based multi-block copolymers

two-step procedure. First, DCDPS and BP were reacted to produce prepolymers carrying phenoxide end groups. Then these prepolymers were reacted with hexafluorobenzene to create the desired aromatic fluoride-terminated hydrophobic prepolymers. The number average molecular weight of the product was measured using GPC and exhibited a slight increase from 17,530 to 19,310 g/mol. However, ^1H NMR analysis of the product indicated that phenoxide end groups were present and that full conversion of end groups to aromatic fluoride was not achieved. We believe this was due to the volatility of hexafluorobenzene, which led to its evaporation during the course of the reaction. We are currently attempting the analogous reaction with difluorodiphenyl sulfone (DFDPS), which is non-volatile under these reaction conditions.

Synthesis of Pendant *N*-heterocycle Aromatic Main-chain Polymers. We have continued to explore the introduction of 1-*H*-1,2,3-triazole moieties into PAES to provide PEMs that can operate at high temperatures and low humidity. Results reported last year suggested that proton conduction could be improved by spacing the triazole moieties away from the PAES backbone. This was done by polymerizing 1-*H*-1,2,3-triazole functionalized methacrylate from chloromethylated PAES using atom transfer radical polymerization.

Chloromethylated PAES with degrees of chloromethylation ranging from 0.25-1.9 chloromethyl groups per repeat unit was produced according to a literature procedure [3] by varying the time of the reaction. As a model reaction, we successfully grafted methyl methacrylate from PAES; however the degree of polymerization was less than desired. Once the conditions are optimized, substitution of the methyl methacrylate with a triazole functionalized methacrylate will allow for a high weight percent of the triazoles in the material to allow for better phase separation and wider channels for proton transport to occur. PAES with methacrylate-based triazole grafts were successfully prepared; however, preliminary proton conductivity measurements under low humidity environments showed poor performance.

Synthesis and Phase Behavior of PFPO-Based Block Copolymers. We synthesized block copolymers containing a proton-conducting block and PFPO blocks, to serve as strongly segregated model systems to explore morphology-proton conductivity relationships. PFPO-COOH was modified to afford terminal benzimidazole functionality through imidization with 3,4-diaminobromobenzene. Post reaction with 4-fluorobenzenesulfonyl chloride yielded 4-fluorophenylsulfonyl end groups, which are better suited for nucleophilic aromatic substitution. Reaction of the 4-fluorophenylsulfonyl-terminated PFPO with hydrophobic (non-acid containing) PAES blocks in hexafluoroisopropanol at 120°C for 24 h was successful. However, in the case of sPAES, we obtained only black, insoluble materials that we were unable to characterize.

Membrane Characterization and MEA Fabrication.

Free standing films of the PAES-based block copolymers shown earlier in Scheme 1 were obtained by solution casting in polytetrafluoroethylene dishes using a 10% (w/v) solution of polymer in dimethylacetamide. After acidification the films were titrated to determine their IEC, followed by water activity and conductivity measurements. The water activity of the new films (MB-1 and MB-2) was determined by isothermal desorption at 80°C and compared to PAES-based block copolymers (MB-3 and MB-4) in which HPPS is the only sulfonated monomer (Figure 1).

Samples MB -1 and MB-2 were synthesized via the method shown in Scheme 1, and had IEC values of 1.68 and 1.08 meq/g, respectively. Samples MB-3 and MB-4 were synthesized via a coupling reaction between hydrophobic and hydrophilic prepolymers in which the hydrophilic block was composed of HPPS and DCDPS, and had IEC values of 1.17 and 1.35 meq/g, respectively. The water activity data show that the acid groups of MB-1 and MB-2 absorbed fewer moles of water at a given humidity, than MB-3 or MB-4. Early results from conductivity measurements suggest block copolymers incorporating both HPPS and sDCDPS in the hydrophobic block will display improved conductivity without increased water uptake. More testing is being conducted to confirm our results; however MB-1 exhibited a conductivity of 49.9 mS/cm at 80°C and 100% relative humidity (RH). Conductivity values of MB-3 and MB-4 at 80°C and 100% RH were reported to be 34 and 14 mS/cm, respectively [1].

The data obtained from water activity and conductivity measurements, for samples with similar IEC values, suggest that improved performance of the new copolymers is due to a change in morphology, resulting from a difference in composition of the hydrophilic block. The sulfonic acid groups of MB-1 and MB-2 are spaced more closely together along the backbone of the chain than MB-3 and MB-4. The

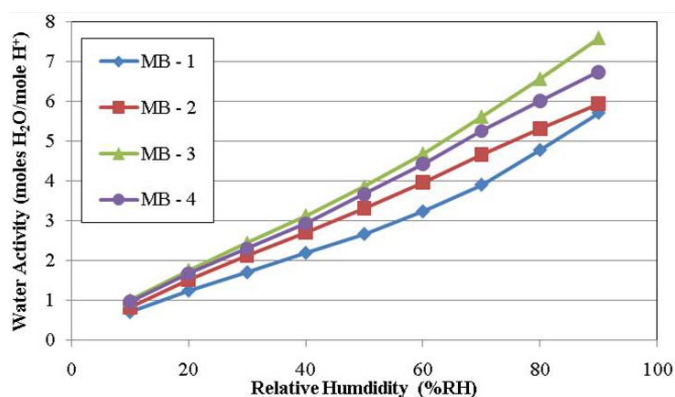


FIGURE 1. Water activity (moles H₂O/ mole H⁺) versus %RH at 80°C. Samples MB-3 and MB-4 above are the same as samples MB-2 and MB-3, respectively, in Ref. 1.

increase in hydrophilicity of these chain segments results in an increase in phase separation leading to fewer isolated sulfonic acid groups and the formation of less tortuous channels for proton conduction. The improvement in morphology allows better conductivity at lesser hydration levels, which is beneficial from a swelling/durability standpoint.

Membrane Ex Situ Durability Characterization - Mechanical Durability: We performed several tests to compare the mechanical durability of sPAES multiblock copolymer MB-1 vs. Nafion[®] 112 membrane at operating fuel cells conditions. Tensile properties were measured using an MTS Alliance RT/10 tensile setup equipped with a 100 N load cell. A custom-design environmental chamber and a sparger were built to control chamber temperature and humidity. Samples, 13 mm wide, were punched from the membrane for all of the mechanical experiments. The membranes, after being clamped in the chamber, were conditioned for 2 h with a 100% RH nitrogen stream at a flow rate of 300 cc/min and a temperature of 80°C. Samples were then strained at a rate of 10 mm/min, as shown in Figure 2. An expansion of the initial strain region of Figure 2 (not shown) showed that the curve for Nafion[®] is displaced rightward along the strain axis because of dimensional increase due to water uptake; this is not the case for sPAES. This indicates low water uptake and higher dimensional stability for sPAES compared to Nafion[®]. After this stress lag, however, the curves for both samples are “typical” and a modulus can be computed from the initial, displaced linear regions. The failure of sPAES at low strain shows reduced ductility compared to Nafion[®]. sPAES shows much higher stress-at-break compared to Nafion[®], 47 MPa vs. 22.4 MPa, respectively. sPAES also showed a very high modulus (897 MPa) compared to that for Nafion[®] (41.5 MPa). The lower modulus for the Nafion[®] membrane suggests that it can

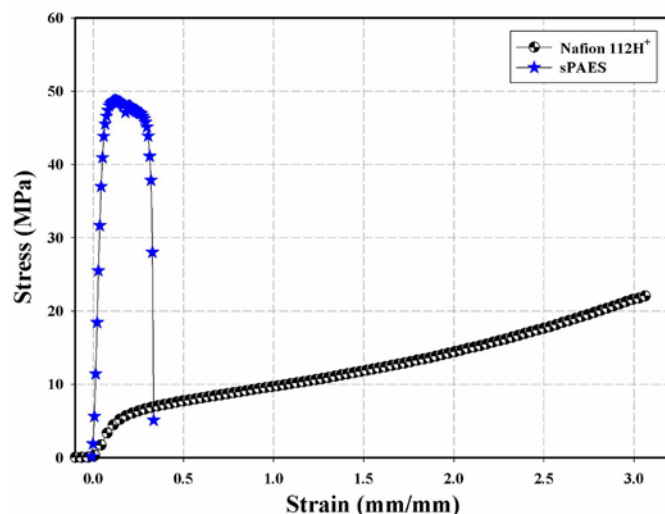


FIGURE 2. Stress-strain curves for sPAES vs. Nafion[®] at 100% RH and 80°C

easily deform when subjected to stresses and rupture due to reduced stress-at-break, thereby promoting pathways for fuel crossover and membrane failure.

Membrane Ex Situ Durability Characterization - Contractile Stress Test: Contractile stresses generated by the membranes as they attempted to shrink when subjected to a drop in RH were monitored under the same conditions used in the tensile studies. Samples were held at their extended swollen length by zeroing the load cell and slowly adjusting the crosshead position until a tension of 0.4 N was reached. The crosshead position was then locked, and the 100% RH nitrogen stream was switched to dry nitrogen at the same flow rate while maintaining the temperature of the dry stream and chamber at 80°C. The ensuing contractile force was monitored as a function of time. The stress levels developed are diagnostic of the ability of the membrane to resist dimensional changes associated with drying and related to mechanical durability. The stress–time profiles for the membranes showed peaks at different times with the sPAES exhibiting higher stress than Nafion[®] (Figure 3).

In the sPAES sample, stress initially drops below zero due to drying of the chamber. During the experiment it was observed that the load increased as the chamber was humidified, even though the sample was not yet extended. The excess load was attributed to condensation on the clamps and the load cell was zeroed before extending the swollen sample. Evaporation of water from the clamps occurred before the sample began to dry and contract, resulting in a decrease in the load below the point at which it was zeroed. Neither of the membranes could withstand the induced contractile stress and eventually yielded, most likely due to macromolecular chain slippage through entanglements. Previously it was determined that the second stress

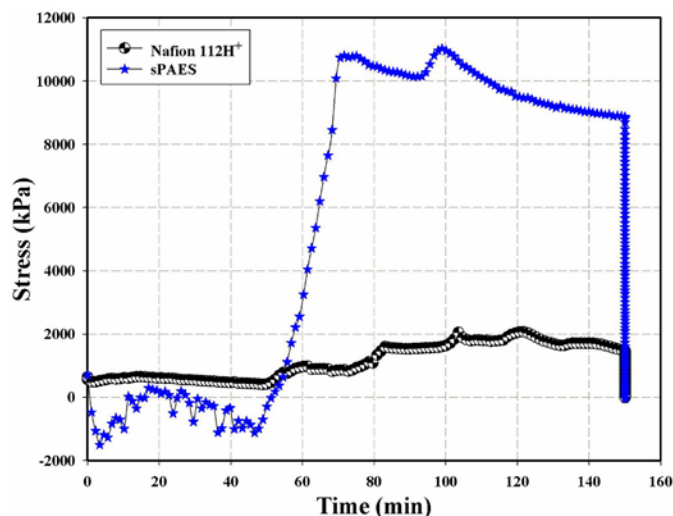


FIGURE 3. Contractile stress response to humidity decrease from 100 to 0% RH at 80°C for Nafion[®] 112 and sPAES

increase in Nafion[®] must be due to a longer range structural reorganization and that the series of peaks on the curve are not due to measurement error, but to a sequence of non-catastrophic crazes spanned by fibrils that prevent further damage growth in the region [4]. The absence of numerous peaks and relaxations in the sPAES curve indicates that the sample did not experience non-catastrophic deformations which would result in decreased fuel cell performance. These results agree with the stress-strain test and indicate that sPAES has a greater resistance to mechanical deformation at high temperature and humidity.

Conclusions and Future Directions

Conclusions

- The synthetic routes used in this work allow for a broad range of polymer compositions.
- The synthesized PAES-based multiblocks exhibit an increase in phase separation leading to fewer isolated sulfonic acid groups and the formation of less tortuous channels for proton conduction, improving water management and conductivity.
- sPAES membranes in this work have greater resistance to mechanical deformation at fuel cell operating conditions, providing improved mechanical durability compared to Nafion[®].

Future Directions

- Produce additional quantities of sPAES material to fabricate MEAs.
- Demonstrate that critical membrane properties, fuel cell performance, and accelerated degradation (both mechanical and chemical durability) are improved for MEAs fabricated from PAES-based multiblocks, relative to baseline materials.

FY 2012 Publications/Presentations

Publications

1. Mauritz, K.A.; Nalawade, A.; Hassan, M.K. "Proton Exchange Membranes for H₂ Fuel Cells Applications," In *Sol-Gel Processing for Conventional and Alternative Energy*; Aparicio, M., Jitianu, A., Klein, L.C., Eds.; Springer: New York, 2012; Chap. 5, pp 73-98.
2. Hassan, M.K.; Abukmail, A.; Mauritz, K.A. "Broadband Dielectric Spectroscopy Studies of Molecular Motions in a Nafion Membrane vs. Annealing Time and Temperature" *Eur. Polym. J.* **2012**, *48*(4), 789-802.
3. Nalawade, A.; Hassan, M.K.; Jarrett, W.A.; Mauritz, K.A.; Litt, M.H. "Broadband Dielectric Spectroscopy Studies of Glassy State Relaxations in Annealed Poly (2,5-benzimidazole)" *Polym. Int.* **2012**, *61*(1), 55-64.
4. Li, H.; Kirk, N.J.; Mauritz, K.A.; Storey, R.F. "Poly(arylene ether sulfone) Multi-Block Copolymers Bearing Perfluoroalkylsulfonic Acid Groups" *Polymer*, **2011**, *52*(16), 3550-3559.

Presentations

1. Baranek, A.; Suggs, S.; Patton, D. "Synthesis of Tethered Triazole Poly(arylether sulfones) toward High Temperature, Low Humidity Proton Exchange Membranes" Poster, American Chemical Society, Fuel Division, Denver, CO August 2012.

References

1. Li, H.; Kirk, N.J.; Mauritz, K.A.; Storey, R.F. *Polymer* **2011**, *52*(16), 3550-3559.
2. Lee, H.; Roy, A.; Lane, O.; Dunn, S.; McGrath, J. *Polymer* **2008**, *49*, 715-723.
3. Avram, E.; Butu, E.; Luca, C. *J.M.S.-Pure Appl. Chem.* **1997**, *A34*, 1701-1714.
4. Patil, Y.P.; Jarrett, W.L.; Mauritz, K.A. *J. Membrane Sci.* **2010**, *356*, 7-13.

V.K.3 Biomass Fuel Cell Systems*

Neal Sullivan (Primary Contact), Robert Braun,
Anthony Dean, Robert Kee, Ryan O'Hayre,
Tyrone Vincent

Colorado School of Mines
1500 Illinois Street
Golden, CO 80401
Phone: (303) 273-3656
Email: nsulliva@mines.edu

DOE Managers
HQ: Kathi Epping Martin
Phone: (202) 586-7425
Email: Kathi.Epping@ee.doe.gov

GO: Reginald Tyler
Phone: (720) 356-1805
Email: Reginald.Tyler@go.doe.gov

Contract Number: DE-EE0000260

Project Start Date: October 1, 2009
Project End Date: September 30, 2012

*Congressionally directed project

This project addresses the following technical barriers from the Fuel Cells section of the Fuel Cell Technologies Program Multi-Year Research, Development and Demonstration Plan:

- (A) Durability
- (C) Performance

Technical Targets

In this project, we conduct a range of studies to improve the durability, efficiency, and transient operation of SOFC systems. Fuel streams for these systems include anaerobic digester-derived biogas. Insights gained from these studies will be applied toward the design and synthesis of SOFC materials and systems to meet the DOE 2015 technical target for durability (40,000 hours), start-up time (30 minutes), and degradation with cycling (0.5%/1,000 h). Targets are taken from the Fuel Cell Technologies Program Multi-Year Research, Development and Demonstration Plan, Table 3.4.5 Technical Targets: 1–10 kWe Residential Combined Heat and Power and Distributed Generation Fuel Cell Systems Operating on Natural Gas.

FY 2012 Accomplishments

- Demonstrated steam-methane reforming in ceramic microchannel reactor with greater than 90% conversion and 70% hydrogen selectivity at 10,000 hr⁻¹ space velocity.
- Utilized state-of-the-art hybrid computational fluid dynamics (FLUENT)/chemical kinetics (CHEMKIN) models of steam-methane reforming (SMR) in ceramic microchannel reactor.
- Utilized system-level models to understand inefficiencies in MW-scale SOFC systems for use in wastewater treatment facilities.
- Developed model-predictive controller for dynamic load following in a SOFC system.



Introduction

The objective of this project is to advance the current state of technology of SOFC systems to improve performance when operating on biomass-derived fuel streams. The target fuel stream is “biogas” (~65% CH₄/35% CO₂) generated by the anaerobic digesters that are widely used for treatment of sludge in municipal wastewater treatment facilities. In this project, we are developing new SOFC materials and

Fiscal Year (FY) 2012 Objectives

- Utilize ceramic microchannel reactor technology for reforming of natural gas and biogas fuels for subsequent electrochemical oxidation within a solid-oxide fuel cell (SOFC).
- Employ system modeling to optimize SOFC system configurations for biogas systems.
- Extend model-predictive control strategies to integrate system hardware for improved load following and dynamic response in biogas-fueled SOFC systems.

Technical Barriers

- Durability: Broaden SOFC operating windows under hydrocarbon and bio-derived fuel streams.
- Balance-of-plant costs: Integrate fuel reforming and heat recuperation hardware into a single low-cost ceramic micro-channel reactive heat exchanger.
- Performance: Increase efficiency and decrease costs through system optimization and balance-of-plant component development and integration.
- Transient operation: Develop model-predictive control algorithms for use in dynamic control.

architectures to improve the robustness of systems operating under biogas. Additionally, modeling and experimentation is being conducted to examine performance tradeoffs across numerous fuel-processing strategies for this fuel. Fuel-reforming processes are being integrated with exhaust-gas recuperation processes through development of a single low-cost ceramic microchannel reactive heat exchanger, created in collaboration with industrial partner CoorsTek, Inc. System-level models are being used to predict SOFC system efficiencies under biogas fuels utilizing the fuel-reforming microchannel-reactor integration strategies under development. Model-predictive control strategies are being developed and applied to improving the dynamic response of the biogas-fueled system, with particular focus placed on reforming components.

Approach

The Colorado School of Mines has assembled a strong and diverse team of scientists and researchers with broad skill sets applicable to fuel cell development. Coordinated through the Colorado Fuel Cell Center, this team examines both the fundamental underpinnings and the key technical problems facing SOFC operation under biomass-derived fuel streams. We develop new SOFC materials and architectures to address the technical challenges and operating windows associated with SOFC operation on biomass-derived fuels. Through development of low-cost ceramic microchannel reactive heat exchangers with industrial partner CoorsTek, Inc., we

create system-integration strategies to combine balance-of-plant processes into single hardware units, reducing system complexity and decreasing cost. A range of computational models are developed to examine the physical processes underway during SOFC and fuel-reformer operation. Model-predictive control strategies are created and applied to fuel-reforming hardware in an effort to improve the dynamic response of SOFC systems.

Results

Ceramic Microchannel Reactors for Biogas Fuel Processing

Ceramic microchannel reactors are being developed to convert biogas into syngas for subsequent electrochemical oxidation within SOFCs. A schematic and photograph of this reactor is shown in Figure 1. The reactor is fabricated by industrial partner CoorsTek, Inc. using low-cost ceramic materials (Al_2O_3) that are joined in a single high-temperature sintering process. After sintering, rhodium catalysts are wash-coated over ceria-alumina catalyst supports within the microchannels; a scanning electron micrograph of the catalyst support is shown in the inset of Figure 1. In the exploded image, hot inlet gases generated by a tail-gas combustor are fed to the inert layers of the reactor and used to drive endothermic steam reforming reactions on the catalytically active side of the reactor. These ceramic microchannel reactors offer great cost and performance advantages over

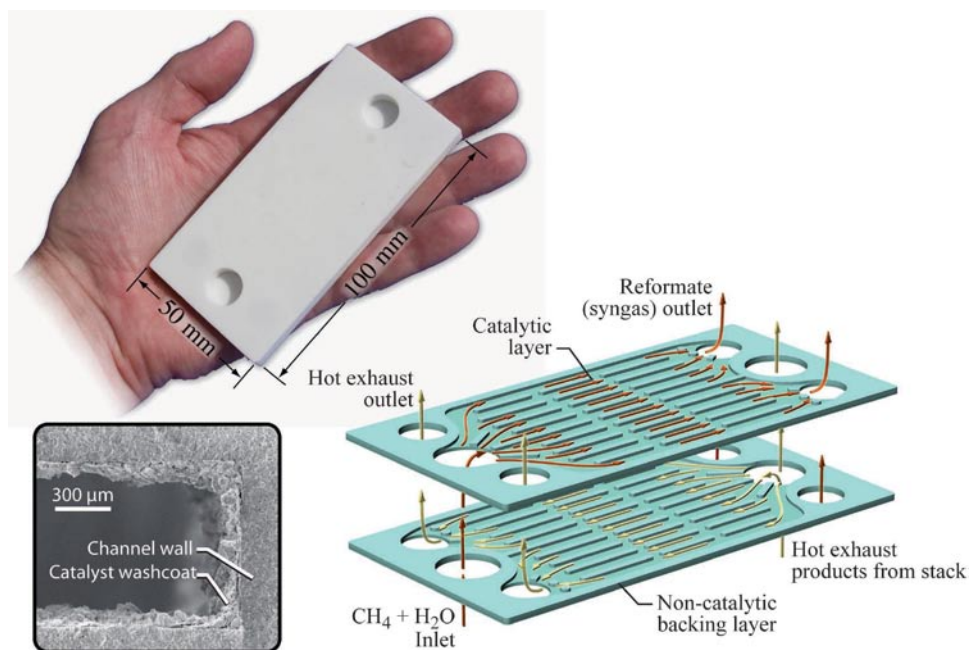


FIGURE 1. Photograph and exploded view of ceramic microchannel reactor, including inert and reactive gas streams. Inset shows high-resolution electron micrograph of ceria-alumina catalyst support wash-coated onto walls of microchannels.

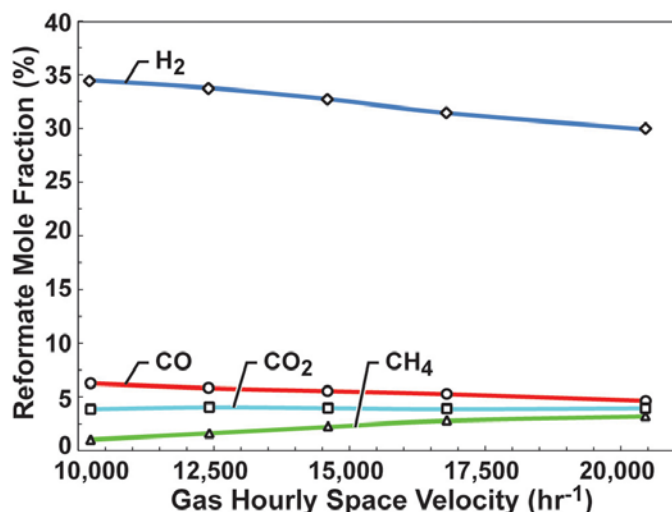


FIGURE 2. Reformate composition as a function of GHSV (reactant flow rate) for steam-methane reforming within the ceramic microchannel reactor.

conventional shell-and-tube reactors through improved heat transfer and thermal regulation of reforming processes.

During the past FY, methane steam reforming was demonstrated within this microchannel reactor over a range of operating conditions. Results are shown in Figure 2; reformate composition is shown as a function of reactive inlet gas hourly space velocity (GHSV, flow rate between 1 and 4 slpm). The inert layers are fed with nitrogen at a constant flow rate of 40 slpm and inlet temperature of 750°C. High methane conversion and reasonable hydrogen selectivity is observed at GHSV of ~10,000 hr⁻¹. Excellent methane conversion is observed at GHSV of <10,000, with some CH₄ slip observed at higher GHSVs. Hydrogen formation is also quite high, but drops off as more methane slips through unreacted. Carbon dioxide formation is higher than desirable, possibly due to the relatively low reforming temperatures used in this series of experiments. These steam-reforming results are an important milestone for the microchannel-reactor efforts. Reactor design is currently being modified to improve performance through the application of FLUENT computational fluid dynamics software.

SOFC System Modeling under Biogas Fuels

The potential of SOFC systems for enhancing the prospects of biogas utilization via co-production (or tri-generation) of heat, fuel, and power is being examined using system-level computational models. This effort involves a techno-economic performance evaluation of ‘mature’ SOFC combined-heat-and-power (CHP) systems fueled with biogas generated in small- (300 kW), medium- (1.5 MW), and large-scale (>5 MW) wastewater treatment plants. Representative biogas feedstock is established from compositional data for a large wastewater reclamation facility in Denver, Colorado.

A steady-state SOFC-CHP system model is developed with Aspen Plus[®] for the integration with small (640 kW-lower heating value, LHV), medium (3 MW-LHV) and large (12 MW-LHV) biogas sources.

The proposed SOFC system concept includes anode-gas recirculation equipped with a biogas-pretreatment system and a waste-heat recovery unit. The system performance is evaluated at near atmospheric pressure with a 725°C nominal stack operating temperature and system fuel utilization of 80%. The SOFC-CHP system employs 80% internal reforming at a steam-to-carbon (S/C) ratio of 1.2.

During the past FY, modeling efforts have been used to show that the system concept is estimated to offer a net electrical efficiency of 51.6% LHV and a net CHP efficiency of 87.5% LHV. A characteristic result is shown in Figure 3, where the exergy destruction (inefficiency creation) is shown for each of the system components. The afterburner, waste-heat recovery unit, and air preheater present significant sources of inefficiency.

Additionally, the effect of operating parameters on system efficiency has been investigated with a parametric study. The economic performance is evaluated using a levelized cost of electricity (LCOE) and a levelized cost of heat. The results are compared with the LCOE from reciprocating internal-combustion engines, microturbines, gas turbines, and molten carbonate fuel cell technologies and grid electricity prices. The influence of economic parameters including biogas feedstock cost, system first cost, and stack operating parameters on the LCOE was also investigated.

The proposed SOFC-based cogeneration system concept for waste water treatment facilities offer a net electrical efficiency approaching 52% (LHV) even for small-scale facility applications. This efficiency is significantly higher compared with efficiencies offered by competing cogeneration technologies (with the exception of molten

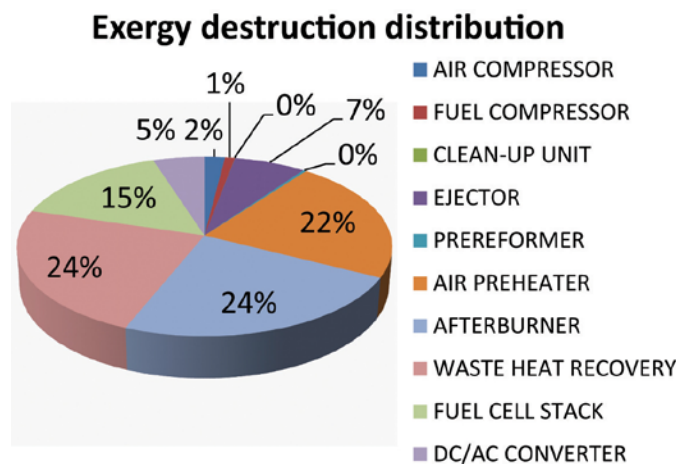


FIGURE 3. System-model predictions of exergy destruction and inefficiency creation from the multiple components making up the biogas SOFC system.

carbonate fuel cells). Moreover, the net electrical efficiency of the proposed SOFC system concept could be further increased by a few percentage points by optimizing the operating conditions (i.e. decreasing the steam-to-carbon ratio). The economic analysis based on the cost of electricity indicates that only medium- and large-scale SOFC systems could successfully compete against the grid electricity price without incentives. This is caused by a high unit capital cost of small SOFC units and the cost of the required biogas pretreatment system.

Model-Predictive Control of Biogas-Fueled SOFC System

The aim of this work is to develop a model-based controller that is capable of achieving variable current output while ensuring all operating constraints of the system are met, such as the required stack and reformer temperatures, fuel utilization, etc. To this end, a high-fidelity, non-linear model of an SOFC system was designed, consisting of two blowers, a fuel reformer, the SOFC stack, tail-gas burner, and a heat exchanger. This non-linear model is too complex and slow for model-predictive control. For controller development, a rapid, linear model is identified that accurately captures the dynamics found in the non-linear model. The comparative simplicity of the linear model enables rapid response to variations in electrical load, and is used to implement model-predictive control.

The low-order linear model takes the form of a four-input, five-output state-space model. Inputs are taken as the power provided to the stack and reformer blowers, mass flow of biogas fuel to the reformer, and the stack voltage.

Outputs are taken as stack and reformer temperature, stack H_2 -exhaust concentration, current, and the proximity of the reformate composition from the thermodynamic carbon-deposition barrier. The results for the linear model fit over a variety of current set points are shown in Figure 4. Reasonable agreement with the high-fidelity model is observed. The risk of carbon formation has proven to be a significant constraint to the response time. Rapid changes in fuel flow rate cannot be stoichiometrically matched by air blowers, so more modest response times are expected.

In the case of an operating change from very high mass flow to low mass flow, the discrepancy in transient response of the fuel and air flow rates can result in the current dropping suddenly before recovering to a nominal value. In the case of a rapid increase, the stack is fed almost pure biogas, causing a spike in the distance from the carbon deposition barrier. Both the non-linear and the identified linear model predict this transient mismatch, and thus the model-predictive controller can be designed to compensate.

The effect of this compensation is an increase in the time the current takes to reach a given set point, and an overall decrease in the rapidity of the controller dynamic response. It is exactly this kind of response that is interesting to analyze, as it provides a direct method to determine what kind of load sharing will be needed based off of the transient response desired. That is, if the SOFC system needs to provide extremely rapid current changes, the controller shows what is possible for the blowers and the fuel reformers to provide, the deficit indicating what is required of any battery that may supplement the SOFC system.

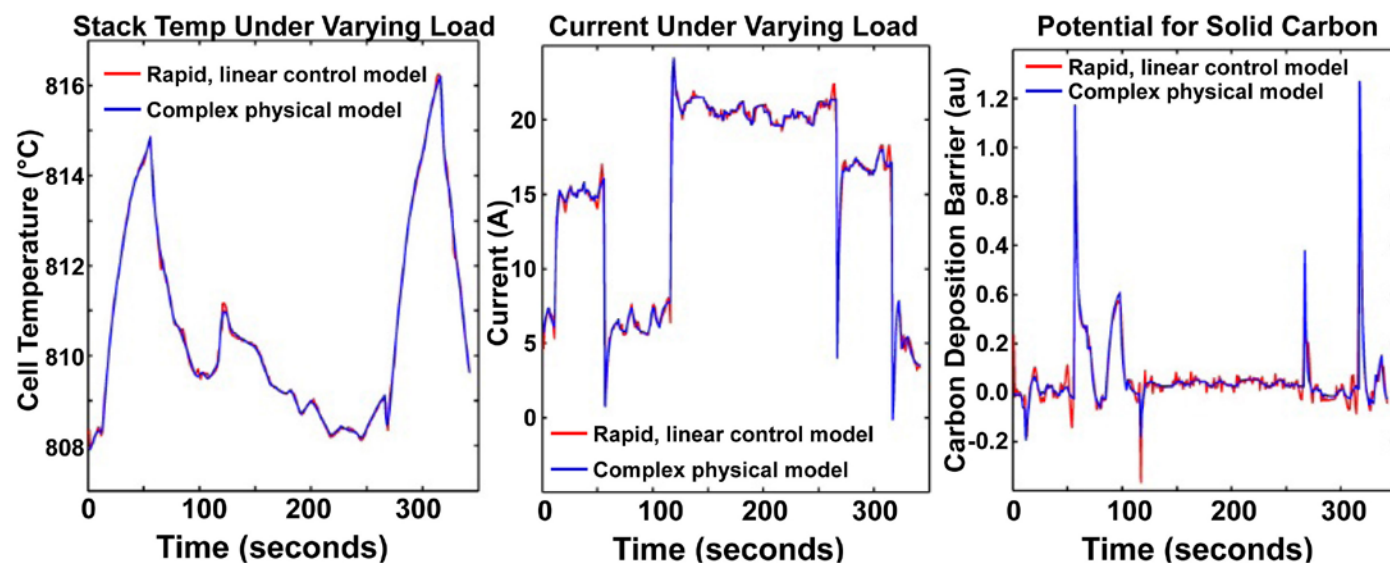


FIGURE 4. Comparison of model outputs from the multi-dimensional high-fidelity model with the rapid, lower-order linear model. Positive values for the carbon-deposition barrier (far right) indicate deposit-free operating conditions.

Conclusions and Future Directions

Ceramic Microchannel Reactors for Biogas Fuel Processing

Building on the important milestone of demonstrating steam methane reforming within the ceramic microchannel reactor, goals for the upcoming year include:

- Explore effects of ceramic microchannel reactor design on increasing throughput for SMR conversion and hydrogen selectivity.
- Utilize computational modeling to guide reactor design for improved performance.
- Disseminate results in peer-reviewed journal publications.

SOFC System Modeling Under Biogas Fuels

System modeling efforts indicate:

- Net electrical efficiency approaches 52% (LHV) even for small-scale facility applications. This efficiency is significantly higher compared with efficiencies offered by competing cogeneration technologies (with the exception of molten-carbonate fuel cells).
- The economic analysis based on the cost of electricity indicates that only medium- and large-scale SOFC systems could successfully compete against the grid electricity price without incentives. This is caused by a high unit capital cost of small SOFC units and the cost of the required biogas pretreatment system.
- The sensitivity analysis of the cost of electricity from an SOFC system indicates high sensitivity to the biogas cost and the system-first cost.

Future goals for the system-level modeling work include dissemination of results in a peer-reviewed journal.

Model-Predictive Control of Biogas-Fueled SOFC System

The linear model accurately captures the dynamics found in the high-fidelity, multi-dimensional model. In the coming FY, this linear model will be used in numerical simulations to control the complete SOFC system.

FY 2012 Publications/Presentations

1. D.M. Murphy, A.E. Richards, A. Colclasure, W.A. Rosensteel, N.P. Sullivan, "Biogas fuel reforming for solid oxide fuel cells," *Journal of Renewable and Sustainable Energy* **4** (2012) <http://dx.doi.org/10.1063/1.3697857>.
2. R.J. Kee, B.B. Almand, J.M. Blasi, B.L. Rosen, M. Hartmann, N.P. Sullivan, H. Zhu, A.R. Manerbino, S. Menzer, W.G. Coors, J.L. Martin, "The design, fabrication, and evaluation of a ceramic counter-flow microchannel heat exchanger," *Applied Thermal Engineering* **31** (2011) 2004-2012.
3. D.M. Murphy, M. Parker, J. Blasi, A. Manerbino, R.J. Kee, H. Zhu, and N.P. Sullivan, "Fuel processing in ceramic microchannel reactors for SOFC applications," *European Fuel Cell Forum*, June 26 – June 29, 2012.
4. D.M. Murphy, M. Parker, J. Blasi, A. Manerbino, R.J. Kee, H. Zhu, N.P. Sullivan, "Fuel processing in ceramic microchannel heat exchanger reactors," *IMRET12 - The International Conference on Microreaction Technology*, Lyon, France, February 20-22, 2012.
5. A.E. Richards, M.G. McNeeley, R.J. Kee, N.P. Sullivan, "Gas transport and internal-reforming chemistry in Ni-YSZ and ferritic-steel supports for solid-oxide fuel cells," *Journal of Power Sources* **196** (2011) 10010–10018.
6. W.A. Rosensteel, S.M. Babiniec, D.D. Storjohann, J. Persky, N.P. Sullivan, "Use of anode barrier layers in tubular solid-oxide fuel cells for robust operation on hydrocarbon fuels," *Journal Power Sources* **205** (2012) 108–113.
7. S. Babiniec, B. Gorman, and N.P. Sullivan, "Processing of lanthanum-doped strontium titanate anode supports in tubular solid oxide fuel cells," *European Fuel Cell Forum*, Lucerne, Switzerland, June 26 – 29, 2012.
8. K.J. Kattke, R.J. Braun, "Characterization of a novel, highly integrated tubular solid oxide fuel cell system using high-fidelity simulation tools," *Journal of Power Sources* **196** (2011) 6347–6355.
9. K.J. Kattke, R.J. Braun, A. Colclasure, G. Goldin, "High-fidelity stack and system modeling for tubular SOFC system design and thermal management," *Journal of Power Sources* **196** (2011) 3790–3802.
10. M.J. Kupilik, T.L. Vincent, "Estimation of biogas composition in a catalytic reactor via an extended Kalman filter," *2011 IEEE International Conference on Control Applications* (2011) 768–773.
11. M.J. Kupilik, T.L. Vincent, "Model Predictive Control of Reformate Composition for use in Solid Oxide Fuel Cells," *ASME 2012 Dynamic Systems and Control Conference*, Ft. Lauderdale, FL, USA, October 17–19 2012.

V.K.4 Improving Reliability and Durability of Efficient and Clean Energy Systems*

Prabhakar Singh

Center for Clean Energy Engineering
University of Connecticut (UConn)
44 Weaver Road, Unit 5233
Storrs, CT 06268-5233
Phone: (860) 486-8379
Email: singh@enr.uconn.edu

DOE Managers

HQ: Dimitrios Papageorgopoulos
Phone: (202) 586-5463
Email: Dimitrios.Papageorgopoulos@ee.doe.gov
GO: Reginald Tyler
Phone: (720) 356-1805
Email: Reginald.Tyler@go.doe.gov

Technical Advisor

Thomas Benjamin
Phone: (720) 356-1805
Email: benjamin@anl.gov

Contract Number: DE-EE00003226

Project Start Date: August 1, 2010
Project End Date: July 31, 2013

*Congressionally directed project

Fiscal Year (FY) 2012 Objectives

- Develop an understanding of the degradation processes in advanced electrochemical energy conversion systems.
 - Advance fuel cell-based power generation systems architecture, including renewable hybridized energy conversion and storage.
 - Develop novel cell and stack structural and functional materials and validate their performance under the nominal and transient operational conditions for the evaluation of long-term bulk, interfacial and surface stability.
 - Gain fundamental understanding of chemical, mechanical, electrochemical and electrical processes related to:
 - Utilization of fuels ranging from bio-derived fuels to liquid petroleum to hydrogen.
 - The role of fuel impurities on degradation and processes for removal from feedstock.
 - Surface and interface phenomena related to surface adsorption, interfacial compound

formation, and electron/ion generation and transport.

- Electrode and electrochemistry.
- Novel membranes, heterogeneous catalyst materials and structures will be developed and subsequently validated.

- Develop collaborative research projects with industry to improve the performance stability and long-term reliability of advanced fuel cells and other power generations systems.

Technical Barriers

This project addresses the following technical barriers from the Fuel Cells section of the Fuel Cell Technologies Program Multi-Year Research, Development and Demonstration Plan:

- (A) Durability
- (B) Cost
- (C) Performance

Technical Targets

The projects associated with this project address technical aspects of stationary fuel cells and stationary fuel processors. DOE 2011 targets are as follows:

Stationary polymer electrolyte membrane (PEM) fuel cell stack systems (5-250 kW) operating on reformat:

- Cost: \$530/kWe
- Durability: 40,000 hours

Stationary fuel processors (equivalent to 5-250 kW) to generate hydrogen-containing fuel gas:

- Cost: \$220/kWe
- Durability: 40,000 hours
- H₂S content in product stream: <4 ppbv (dry)

FY 2012 Accomplishments

- The Center for Clean Energy Engineering has successfully developed in total 18 industrially sponsored research, development and engineering projects in the field of clean and sustainable energy, eight of these projects were added in FY 2012.
- These collaborative projects have leveraged DOE funds with industrial financial support to accelerate

the development of advanced materials, cell and stack components, catalysts and fuel cleanup, and balance-of-plant sub-systems.

- The industrial projects support the DOE mission through the development of reliable and cost-effective advanced clean and efficient fuel cell power generation systems.



Introduction

The scope of this energy systems and technology research and development initiative will focus on the development and validation of the mechanistic understanding and subsequent creation of novel cost-effective materials to mitigate degradation processes. Through a unique collaborative project with industry we will solve technology gaps through joint industry/university projects. These relationships will accelerate the development and deployment of clean and efficient multi-fuel power generation systems.

The scope of the research projects will include identification and prioritization of the technology gaps and research needs along with the development of enabling technologies that meet the overall stack and balance-of-plant improvements from a durability, cost and performance perspective. Specifically the performance stability and reliability of the power generation systems will be improved through the implementation of advanced materials and fabrication processes. Technical areas of interest, to be addressed by the industry/university collaborations will include: a) performance stability and reliability of fuel cell systems, b) fuels, fuel processing and catalysis, c) advanced functional and structural materials, processes and systems, d) hydrogen storage and power management and e) renewable energy and resources.

Approach

The approach used for this project was to develop collaborative industry/university research projects aimed specifically at accelerating the development and deployment of clean and efficient multi-fuel power generation systems. Through a competitive process faculty developed relationships with industry that provided additional amounts of cash and in-kind support thus leveraging funding available through this project. By requiring a financial commitment from industry this methodology ensured that technology problems of commercialization relevance would be addressed. Industry collaborative projects have been developed with UTC Power, FuelCell Energy, UTC Research Center, nzymSys, NanoCell Systems, APSI, Oasys Water, Nissan, Corning, Proton OnSite, BC Hydro, Sci-Tech and WR Grace & Company. The project topics have addressed issues ranging from performance stability and reliability

of fuel cell systems to fuels, fuel processing and catalysis and finally including advanced functional and structural materials, processes and systems.

Results

1. Role of Multi-Scale Water Transport in Dynamic Performance of Polymer Electrolyte Fuel Cells (Project PI: Prof. Ugur Pasaogullari, industry partner – Nissan): The collaboration between Nissan and UConn focuses on understanding the transport phenomena at very high current density operation of PEM fuel cells (PEMFCs). Our work in the last year resulted in detailed understanding of the micro-structure of the gas diffusion layers (GDL) in PEMFCs. GDLs are responsible from ~50% of the oxygen transport losses in PEMFCs, and high current density operation requires very effective oxygen transport to active reaction sites. We have also developed numerical models that describe the multi-phase transport phenomena at very high current density conditions, and the results are being compared with neutron radiography results obtained at the National Institute of Standards and Technology Center for Neutron Radiography.
2. Modeling Resin Flow in Phosphoric Acid Fuel Cell (PAFC) GDLs (Project PI: Prof. Rajeswari Kasi, industry partner – UTC Power): UTC Power was interested in attaining stable graphitized GDLs that are used in PAFCs. This project successfully evaluated ways to improve GDL stability by 1) modeling the resin flow during GDL impregnation and lamination, 2) investigating the properties of GDLs at each experimental step, and 3) improving substrate manufacturing efficiency based on the model developed and properties of the GDLs.
3. High Performance Phosphoric Acid Fuel Cell Electrodes for Soluble Polymers and Alternate: Fabrication Methods (Project PI: Prof. Ned Cipollini, industrial partner – UTC Power): As none of the common perfluoropolymers form stable solutions at room temperature we have been able to produce viable electrodes by heating mixtures of perfluoroalkoxy (PFA) solid, cathode catalyst and solvent to 25°C above the melting point of PFA, where it is soluble, and allowing the PFA to coat the catalyst as the PFA comes out of solution while cooling to room temperature. Catalyst layers were formed by doctor-blade techniques on carbon paper. Subscale fuel cell testing shows the performance of these electrodes is poorer than present state-of-the-art PAFC cathodes. The poorer performance has been attributed to low Pt loading and non-uniformity on the macro-scale of the uniform PFA coating on the catalyst. These both can be addressed by modifying processing conditions of the cathodes.

4. Mechanistic Understanding of Matrix Stability in Molten Carbonate Fuel Cells (MCFCs) (Project PI: Prof. Prabhakar Singh, industry partner – FuelCell Energy): The electrolyte matrix of the MCFC, commonly fabricated from lithium aluminate, have shown coarsening during long-term exposure. Experiments conducted in our laboratory have reproduced the in-cell observations on coarsening of the matrix. Role of additives and electrolyte chemistry has been examined. Faceted crystals grow during the exposure to the molten salt. Particle size distribution, phase identification have been performed.
5. Waste to Energy: Biogas Cleanup (Desulfurization) for Energy Generation (Project PI: Prof. Steven Suib, industry partner - FuelCell Energy): The hypothesis of this project is that development of novel adsorbents, catalysts, and mixed adsorbents will lead to more efficient cleanup of anaerobic digester gas (ADG). Mixed adsorbents are likely to be needed to efficiently get all sulfur species in ADG. This project has focused on the optimization of adsorbents that can get sulfur-containing species. Our results show that some of the adsorbents are 40 times better in terms of breakthrough times and adsorbed amounts than commercial activated carbon adsorbents. We are studying the mechanism of adsorption over these materials. Characterization studies are being done in order to optimize the performance of these materials.
6. Fuel Reforming Catalysts for Efficient Energy Usage (Project PI: Prof. Steven Suib, industry partner – APSI): The hypothesis of this project is that the development of next generation high surface area fuel reforming catalysts and determination of mechanisms of reaction will lead to enhanced efficiency, activity, and stability of these materials. Over the past year the focus has been on 1) the preparation of thin film reforming catalysts made with a novel process, and 2) the study of the mechanism of the fuel reforming process with an emphasis on mass spectrometry detection.
7. Evaluation of Enzyme-Based Sulfur Removal Technology for Gas Cleanup (Project PI: Prof. Ashish Mhadshwar, industrial partner – nzymSys): The overall goal of this project is to test and demonstrate a novel enzymatic way to reduce the sulfur content in biogas, with a primary focus on hydrogen sulfide (H_2S) removal. The application of the novel enzymatic technology (nzymSys, Inc.) for (simulated) biogas desulfurization was investigated in a lab-scale semi-batch reactor. We observed that even dilute enzyme solutions (4-5 wt%) are effective in removing up to 100% of the feed H_2S , during 8-hour tests. The enzyme is also selective to H_2S , and does not show any adverse effect on the other dominant components in biogas, such as methane and carbon dioxide. Experiments with enzyme replenishment indicated that the biogas desulfurization process could be potentially operated continuously for consistent removal of H_2S . Long-term studies performed at higher enzyme concentration (20 wt%) demonstrated formation of sulfur precipitate, which could be recovered as a valuable product.
8. Structure-Activity Correlations in Soot Oxidation (Project PI: Prof. Ashish Mhadshwar, industrial partner – Corning): The overall research objective of this project is to develop structure-activity correlations for non-catalytic oxidation of soot to understand the dependence of oxidation kinetics on nature of soot. This work focuses on a comprehensive investigation of structure-activity relationships for 13 commercially available carbon blacks and two diesel engine soot samples (Corning). Various structural parameters, such as the average particle size, specific surface area, degree of organization, and average crystallite stacking height, are correlated with the thermogravimetric oxidation activity data. Our analysis for a large number of samples with multiple techniques has indicated unique and previously unknown correlations between soot structure and reactivity.
9. High Reliability, Low Cost Thermally Integrated Water-Gas Shift System Design Development Support (Project PI: Prof. Ashish Mhadshwar, industrial partner – FuelCell Energy): The overall goal of this project is to support FuelCell Energy, Inc. (FCE) in the design, development and scale up of a thermally integrated water-gas shift system to efficiently process reformat gas, such as from FCE's DFC[®] power plant anode exhaust. This task involves evaluation and analysis of the proprietary catalyst samples provided by FCE. Catalyst performance has been evaluated for CO oxidation, CO methanation, and water-gas shift reaction.
10. Stannate-Based Semiconductor Nanocomposites for Solar Energy Utilization (Project PI: Prof. Puxian Gao, industry partner - UTC Research Center): Zinc hydroxystannate nanocubes have been achieved in the forms of both free-standing particle in solution, and continuous thin film on substrates via hydrothermal synthetic strategy. Gradient stannate nanostructures have been successfully fabricated using non-equilibrium fast thermal annealing processes. Amongst various stannate-based nanostructures through thermal annealing, the amorphous zinc stannate nanocubes were found to be highly active in organic dye degradation under both ultraviolet and visible lights.
11. Optimization of Fluid Catalytic Cracking (FCC) Selectivity Through detailed Modeling of Catalyst Evaluation Experiments and the Contributions of Catalyst Components (Project PI: Prof. George Bollas, industry partner – W.R. Grace & Co.): Models of state-of-the-art catalyst evaluation procedures for the FCC process have been developed, incorporating key characteristics of different catalyst testing reactors. Model predictions (in good agreement with experimental

data) have provided metrics for comparison and analysis of data from different reactors and for the study of the performance of catalyst decay functions on the same basis, and are providing theoretical insights to decoupling the effect of matrix type and zeolite diffusional properties on catalysts, as well as to the analysis of several different reaction kinetic networks.

12. Evaluation of the Performance of Rapidly Quenched Yttria-Stabilized Zirconia (YSZ) Electrolytes in a Solid Oxide Fuel Cell and its Comparison with Conventional Solid Oxide Fuel Cell Architecture (Project PI: Prof. Radenka Maric, industrial partner – NanoCell Systems): The electrical conductivity and microstructure of $\text{La}_{0.65}\text{Sr}_{0.3}\text{MnO}_3$ (LSM)–8 mol% YSZ cathode composite were investigated from room temperature to 1,000°C in air conditions. The results of half-cell the charge transfer resistance and ohmic resistance for LSM/YSZ samples using plasma-sprayed powder show that resistance of YSZ electrolyte remained very low with reducing temperature from 750-550°C while the resistance of cathode significantly increased. The activation energy of YSZ for the conduction above 550°C is 93 and 103 kJ mol^{-1} below 550°C, respectively. The higher activation energy at low temperatures for conduction is due to the association of the point defects ($\text{Y}'_{\text{Zr}}\text{V}_{\text{O}}\dots$). The reason for the lower activation energy for conduction at temperatures higher than 550°C is due to the migration of $\text{V}_{\text{O}}\dots$. The electrode and electrolyte microstructures have not yet been fully optimized; thus, substantial performance improvement is envisioned.
13. Nanostructured Catalyst Support Systems for Next Generation Electrolyzers (Project PI: Prof. William Mustain, industry partner – Proton OnSite): During this project, the UConn/Proton team has made significant progress in the identification of a new anode hydrogen evolution reaction catalyst with commercial potential. The team has identified a Pt/WC electrocatalyst that allows for only 20% of the Pt loading that is in the Proton commercial catalyst with 96% activity retention during ageing. This far exceeded the performance of other supported Pt commercial catalysts. In addition, the team has demonstrated high activity oxygen evolution catalysts using a new flame based synthesis approach that reduces the number of processing steps for membrane electrode assembly fabrication.
14. Reliability Evaluation and Enhancement of Synchronized Phasor Network (Project PI: Prof. Peng Zhang, industrial partner – BC Hydro): Over the past 12 months this project has resulted in an invention disclosure and several innovations that enable reliable integration of renewable resources into power systems. A new Monte Carlo-based method was proposed for reliability evaluation of active distribution systems with

multiple microgrids. A combined statistical and fuzzy Markov method was devised for reliability evaluation of phasor measurement unit. An accurate high-resolution and robust method called S-LMS (subspace-least mean square) was invented for reliable estimation of power system phasor, harmonics, and interharmonics. An enhanced version of S-LMS was developed to speed up S-LMS more than 150 times by taking advantage of sparsity of power system signal. A precise method was derived to increase the accuracy of power system measurement by eliminating decaying dc components which expose during fault occurrence.

15. Plasmonic Nanostructures for Solar Energy Harvesting (Project PI: Prof Brian Willis, Industry Partner – SciTech): Tunnel diodes have successfully been nano-fabricated and converged to nano-dimensions using our atomic layer deposition processes. Particulate contamination has been found to limit our progress due to the susceptibility of the devices to short circuiting via particulates landing on the devices. A new series of experiments is in the planning stages to overcome these difficulties.

Conclusions and Future Directions

Of the 15 projects listed above 11 of them will continue into FY 2013. At this time the list of projects is stable and we do not anticipate additional ones. We do, however continue to expect the following achievements to continue from the above list of activities:

1. Advanced functional and structural materials research and development will continue to address long-term surface, interface and bulk instabilities at engineered systems level. Research will continue in areas related to solid-liquid-gas interactions as they relate to surface corrosion, electrochemical poisoning, agglomeration and coarsening of porous aggregates, and catalytic degradation.
2. UConn and its partners will continue to develop advanced fuel cleanup and processing technologies to enable multi-fuel capabilities of advanced fuel cell systems. Cost-effective technologies for the removal of contaminants from gas phase will be developed and validated.
3. Developed technologies will be transferred to industries to accelerate the development and deployment of advanced fuel cell systems.
4. Research findings will be presented and published in technical meetings and peer reviewed journals. Intellectual property will be disclosed through invention disclosures and review by the university's center for science and technology commercialization.

Special Recognitions & Awards/Patents Issued

1. P.X. Gao, and C.H. Liu, Method of making gradient composite nanostructures through thermal engineering, UConn Invention Disclosure, in preparation, Fall 2011.
2. P.X. Gao, and C.H. Liu, Methods for making continuous stannate nanofilms, UConn invention disclosure, in preparation, 2012.
3. Peng Zhang, Robust high resolution spectrum estimation method for accurate phasor, harmonic and interharmonic measurement in power systems, Invention Disclosure, UConn #11-033.

FY 2012 Publications/Presentations

1. M. Dragan, R. Maric, P. Strutt, "Morphological and sintering properties of rapidly-quenched nanostructured YSZ powders synthesized by plasma solution spray", submitted to *Journal of Material Science* in April 2012.
2. Monica Navarro, Dariusz Orlicki, George M. Bollas, "Detailed modeling of FCC selectivity in catalyst evaluation experiments," Spring *ACS National Meeting*, March 2012, San Diego CA USA.
3. C.H. Liu, G. Wrobel, P.X. Gao, "Thermal Decomposition of Hydroxystannate Cubes into Stannate-based Semiconductor Nanocomposites for Energy Harvesting and Utilization," *MRS Fall meeting 2011*, Boston, Nov., 2011. (oral)
4. K.T. Liao, P. Shimpi, P.X. Gao, "Scale-up Synthesis of nanostructured copper hydroxystannates and Cu-Sn dendrite alloys on selected substrates," *MRS Fall meeting 2011*, Boston, Nov., 2011. (poster)
5. G. Wrobel, C.H. Liu, M. Piech, S. Dardona, P.X. Gao, "Synthesis and Fire Retardant Property of Zinc Hydroxystannate coated microfibers," *Sci. Adv. Mater.*, 2012, in press.
6. C.H. Liu, H.Y. Chen, G. Wrobel, Y.B. Guo, S. Dardona, M. Piech, J.M. Bai, M.H. Shao, Z.H. Zhang, H.Y. Gao, P.X. Gao, "Controlled synthesis and structure tunability of photocatalytically active mesoporous zinc-based stannate nanostructures," to be submitted, 2012.
7. Lakshitha Pahalagedera, Hom N. Sharma, Chung-Hao Kuo, Saminda Dharmarathna, Ameya V. Joshi, Steven L. Suib, and Ashish B. Mhadeshwar, "How Does the Oxidation Activity of Carbon Blacks and Diesel Soot Correlate with the Structure?" in preparation for submission to *Carbon*, 2012.
8. Hom N. Sharma, Lakshitha Pahalagedera, Ameya Joshi, Steven L. Suib, and Ashish B. Mhadeshwar, "Non-catalytic Oxidation Kinetics of Carbon Black and Diesel Engine Soot Samples by Thermogravimetric Analysis," submitted to *Energy & Fuels*, 2012.
9. Lakshitha Pahalagedera, Chung-Hao Kuo, Saminda Dharmarathna, Hom N. Sharma, Ameya V. Joshi, Steven L. Suib, and Ashish B. Mhadeshwar, "Comparative Analysis of the Structure and Chemical Nature of Carbon Blacks and Diesel Soot," accepted, *AIChE Annual Meeting*, 2012.
10. Lakshitha Pahalagedera, Hom N. Sharma, Chung-Hao Kuo, Saminda Dharmarathna, Ameya V. Joshi, Steven L. Suib, and Ashish B. Mhadeshwar, "Influence of Particle Size and Microstructure on the Oxidation Behavior of Carbon Blacks and Diesel Soot," accepted, *AIChE Annual Meeting*, 2012.
11. Hom N. Sharma, Lakshitha Pahalagedera, Ameya Joshi, Steven L. Suib, and Ashish B. Mhadeshwar, "Non-catalytic Oxidation of Carbon Black and Diesel Engine Soot Samples - Kinetics and Structure-activity Relationships," accepted, *AIChE Annual Meeting*, 2012.
12. Y. Liu, and W.E. Mustain, "Evaluation of Tungsten Carbide as the Electrocatalyst Support for Platinum Hydrogen Evolution/Oxidation Catalysts," *Int. J. Hydrogen Energy*, 37 (2012) 8929.
13. Z. Bie, P. Zhang, G. Li, B. Hua, M. Meehan, and X. Wang, "Reliability evaluation of active distribution system including microgrids," *IEEE Trans. Power Systems*, Accepted for publication.
14. Y. Wang, W. Li, P. Zhang and B. Wang, "Reliability analysis of Phasor Measurement Unit considering data uncertainty," *IEEE Trans. Power Delivery*, Accepted for publication.
15. H. Xue and P. Zhang, "Subspace-Least Mean Square Method for accurate harmonic and interharmonic measurement in power systems," *IEEE Trans. Power Delivery*, vol. 27, no. 3, Jul. 2012.
16. A. Abdollahi, P. Zhang and H. Xue, "Enhanced Subspace Least Mean Square for fast and accurate power system measurement," Submitted to *IEEE Trans. Power Delivery*, 2012.
17. A. Abdollahi and P. Zhang, "Precise removal of decaying DC in DFT algorithm for power system measurement", *Proceeding of IEEE Power & Energy Society General Meeting*, San Diego, Jul. 2012.
18. Brian Willis, "Nanoscale Devices for Rectification of High Frequency Radiation from the Infrared through the Visible: A New Approach," *Journal of Nanotechnology*, vol. 2012, Article ID 512379, 19 pages, 2012.

VI. MANUFACTURING R&D

VI.0 Manufacturing R&D Sub-Program Overview

INTRODUCTION

The Manufacturing R&D sub-program supports research and development (R&D) needed to reduce the cost of manufacturing hydrogen and fuel cell systems and components. Manufacturing R&D will enable the mass production of components (in parallel with technology development) and will foster a strong domestic supplier base. R&D activities address the challenges of moving today's laboratory-produced technologies to high-volume, pre-commercial manufacturing to drive down the cost of hydrogen and fuel cell systems. This sub-program focuses on the manufacture of components and systems that will be needed in the early stages of commercialization. Research investments are focused on reducing the cost of components currently used (or planned for use) in existing technologies, as well as reducing the cycle times of the processes being developed. Progress toward goals is measured in terms of reductions in the cost of producing fuel cells, increased manufacturing processing rates, and growth of manufacturing capacity.

In Fiscal Year (FY) 2012, manufacturing projects continued in the following areas: novel electrode deposition processes for membrane electrode assembly (MEA) fabrication, reduction in the number of assembly steps for MEAs, flow field plate manufacturing variability and its impact on performance, and fabrication technologies for high-pressure composite storage tanks.

GOAL

Research and develop innovative technologies and processes that reduce the cost of manufacturing fuel cell systems and systems for hydrogen production, delivery, and storage.

OBJECTIVES¹

Key objectives for Manufacturing R&D include:

- Develop manufacturing techniques to reduce the cost of automotive fuel cell stack assembly and testing at high volume (500,000 units/year) from the 2008 value of \$38/kW to \$21/kW by 2017.
- Develop processes that will reduce the fabrication and assembly costs for compressed-hydrogen storage systems by 12% from the current high-volume costs of \$18/kWh—to enable widespread commercialization of fuel cell electric vehicles across most light-duty vehicle platforms by 2017.
- Support efforts to reduce the cost of manufacturing components and systems to produce hydrogen at \$2-4/gge (2007 dollars) (untaxed, delivered, and dispensed) in 2020.

FY 2012 TECHNOLOGY STATUS

Presently, fuel cell systems are fabricated in small quantities. The cost of 5-kW, low-temperature polymer electrolyte membrane (PEM) fuel cell systems for stationary applications is projected to be ~\$3,100/kW_{net} at a volume of 1,000 systems per year.² For automotive applications using today's technology, the cost of an 80-kW PEM fuel cell system is projected to be \$47/kW for high-volume manufacturing (500,000 systems/year) and

¹ Note: Targets and milestones were recently revised; therefore, individual project progress reports may reference prior targets. Some targets are still currently under revision, with updates to be published in FY 2013.

² James, B. D., et al., "Low Temperature PEM Stationary Fuel Cell System Cost Analysis: Preliminary Results", NREL Subcontract Report, Subcontract number AGB-0-40628-01, May 2011.

about \$220/kW at manufacturing volumes of 1,000 systems/year.³ Projected costs include labor, materials, and related expenditures, but do not account for manufacturing R&D investment.

FY 2012 KEY ACCOMPLISHMENTS

FY 2012 saw a number of advancements in the manufacture of fuel cells and hydrogen storage systems, including:

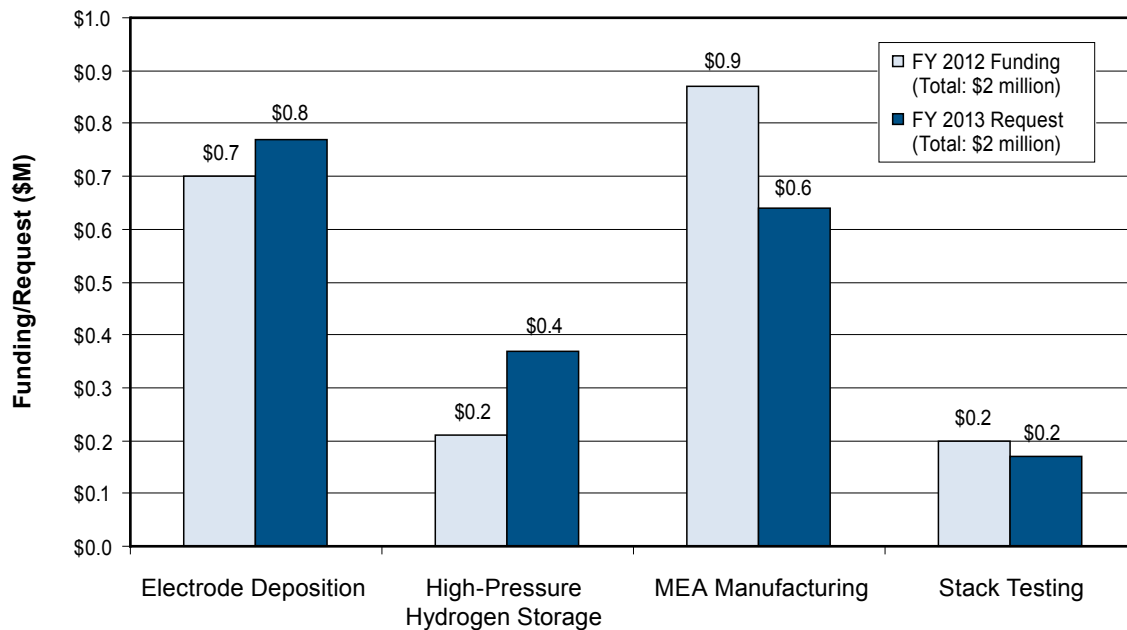
- **Electrode Deposition:** W.L. Gore improved the performance of an MEA containing a direct-coated cathode to be comparable to an MEA containing a non-direct coated cathode by adjusting the ink formulations. Using direct coating, Gore projects a 25% reduction in MEA cost.
- **High-Pressure Storage:** Quantum used lower-strength and higher-modulus fiber on the outer layers of the hydrogen storage vessel, where the vessel experiences lower stress; this allows those layers to take the load earlier before the inner layers fail. The result is a greater than 5% cost savings with less than 2% increase in weight over the 2011 vessel.
- **MEA Manufacturing:** By modifying additive and processes, BASF reduced the cost of the microporous layer by 37% compared with the benchmark and increased the capacity 3x against the benchmark.
- **Component and Stack Measurement:** Using optical diagnostics on a full-scale webline, NREL detected defects on the order of ~10–100 μ in membranes at standard web speeds of 30 feet per minute.
- **Ultrasound Sealing of High Temperature MEAs:** Besides the time and energy savings provided by the ultrasound method, Rensselaer Polytechnic Institute found that performance is slightly higher for MEAs bonded with the ultrasound method, increasing from an average of 0.64 ± 0.13 V at 0.2 A/cm² to 0.65 ± 0.01 V at 0.2 A/cm².
- **Bipolar Plate Metrology:** The National Institute of Standards and Technology (NIST) developed a technique using laser spot triangulation probes to measure channel height and width on fuel cell bipolar plates, with errors of less 2 μ . Compared with traditional coordinate measuring machines, this rapid dimensional measurement technique developed by NIST is nearly as accurate, yet significantly faster. As a result, this technique offers the potential for 100% part inspection on an assembly line, compared with traditional techniques that take hours to complete measurements on a single part.
- **Manufacturing Workshop:** The report from the National Renewable Energy Laboratory/DOE Hydrogen and Fuel Cell Manufacturing R&D Workshop was published. The workshop identified strategies and R&D needs for lowering the cost of manufacturing hydrogen production, delivery, and storage systems and fuel cell systems and components. The top priorities identified at the workshop, and outlined in the report, are:
 - Facilitate a manufacturing group for DOE to expand the supply chain for PEM fuel cells/electrolyzer balance of plant.
 - Develop dual-direct coating of catalyst coated membranes.
 - Develop high-volume stack assembly processes—improving automation and reducing labor costs.
 - Develop methods of identifying coating defects on a moving web, then rejecting single pieces downstream.
 - Develop methods for defect detection after MEA assembly when defects may no longer be visible.
 - Develop manufacturing processes to enable multi-layer/component sintering of solid oxide fuel cells.

BUDGET

The President's FY 2013 budget request for the Fuel Cell Technologies Program includes \$2 million for Manufacturing R&D. The FY 2012 appropriation for Manufacturing R&D was \$2 million.

³ Hydrogen and Fuel Cells Program Record #12020, "Fuel Cell System Cost – 2012," http://hydrogen.energy.gov/pdfs/12020_fuel_cell_system_cost_2012.pdf

Manufacturing R&D Funding



FY 2013 PLANS

In FY 2013, activities in the Manufacturing R&D sub-program will:

- Continue to refine the configuration and optimize the performance of diagnostics on weblines as well as assess industry needs and begin to evaluate other diagnostic techniques.
- Initiate work on MEA conditioning and low-cost MEA process scale up.
- Continue to investigate applicability of optical scatterfield microscopy for online inspection of catalyst coated membranes.
- Demonstrate a non-woven microporous layer platform reducing total cost by an additional 30% (materials and labor) over the best woven scenario.
- Complete a final cost model analysis of new hydrogen storage vessel designs.

The input from the Hydrogen and Fuel Cell Manufacturing R&D workshop will be used to identify topics for a funding opportunity planned to be released in FY 2013, with awards subject to appropriation and announced later in the fiscal year. The sub-program will also coordinate with other agency activities (including DOD and NIST) and with Energy Efficiency and Renewable Energy's Advanced Manufacturing Office to identify synergies and leverage efforts.

Nancy Garland
 Manufacturing R&D Team Lead (Acting)
 Fuel Cell Technologies Program
 Department of Energy
 1000 Independence Ave., SW
 Washington, D.C. 20585-0121
 Phone: (202) 586-5673
 Email: Nancy.Garland@ee.doe.gov

VI.1 Fuel Cell Membrane Electrode Assembly Manufacturing R&D

Michael Ulsh (Primary Contact), Guido Bender,
Niccolo Aieta, Huyen Dinh
National Renewable Energy Laboratory
15013 Denver West Parkway
Golden, CO 80401
Phone: (303) 275-3842
Email: michael.ulsh@nrel.gov

DOE Manager

HQ: Nancy Garland
Phone: (202) 586-5673
Email: Nancy.Garland@ee.doe.gov

Partners:

- Lawrence Berkeley National Laboratory (LBNL), Berkeley, CA
- Colorado School of Mines, Golden, CO
- University of Hawaii, Hawaii Natural Energy Institute, Honolulu, HI
- Rensselaer Polytechnic Institute, Troy, NY
- 3M, St. Paul, MN
- Acumentrics, Westwood, MA
- Ballard Material Products, Lowell, MA
- BASF Fuel Cells, Somerset, NJ
- Delphi, Fenton, MI
- General Motors, Honeoye Falls, NY
- Proton OnSite, Wallingford, CT
- Ultra Electronics – Adaptive Materials Inc., Ann Arbor, MI
- W.L. Gore and Associates, Elkton, MD

Project Start Date: July 16, 2007

Project End Date: Project continuation and direction determined annually by DOE

Fiscal Year (FY) 2012 Objectives

NREL and its collaborators are developing capabilities and acquiring knowledge for in-line quality control during fuel cell manufacturing. We are focusing on membrane electrode assemblies (MEAs) and MEA components (membranes, coated electrodes, and gas diffusion media) of polymer electrolyte membrane (PEM) fuel cells, as well as on cast tapes and fired cells of solid oxide fuel cells (SOFCs), in the transition to high-volume manufacturing methods. Our main tasks are to:

- Evaluate and develop in-line diagnostics for cell and component quality control and validate diagnostics in-line.
- Investigate the effects of MEA component manufacturing defects on MEA performance and

durability to understand the required performance of diagnostic systems and contribute to the basis of knowledge available to functionally determine manufacturing tolerances for these materials.

- Use established models to predict the effects of local variations in MEA component properties, and integrate modeling of the operational and design characteristics of diagnostic techniques into the design and configuration of in-line measurement systems.

These objectives have strong support from the industry. Specifically, the outcomes of the 2011 NREL/DOE Hydrogen and Fuel Cell Manufacturing R&D Workshop and the Office of Naval Research-funded Manufacturing Fuel Cell Manhattan Project confirmed the importance of continued development of in-line quality control techniques for cell manufacturing. Our specific development activities have been and will continue to be fully informed by direct input from industry. As new technologies emerge and as the needs of the industry change, the directions of this project will be adjusted.

Technical Barriers

This project addresses the following technical barriers from the Manufacturing R&D section (3.5) of the Fuel Cell Technologies Program's Multi-Year Research, Development and Demonstration Plan:

- (A) Lack of High-Volume Membrane Electrode Assembly (MEA) Processes
- (F) Low Levels of Quality Control and Inflexible Processes.

Contribution to Achievement of DOE Manufacturing Milestones

This project contributes to the achievement of the following DOE milestones from the Manufacturing R&D section (3.5) of the Fuel Cell Technologies Program Multi-Year Research, Development and Demonstration Plan:

- Milestone 2: Develop continuous in-line measurement for MEA fabrication (4Q, 2012)
- Milestone 3: Demonstrate sensors in pilot-scale applications for manufacturing MEAs (4Q, 2013)
- Milestone 4: Establish models to predict the effect of manufacturing variations on MEA performance (4Q, 2013).

FY 2012 Accomplishments

- Demonstrated the detection of defects in gas diffusion media (GDM) roll materials at 30 foot per minute (fpm) line speed on NREL's research web-line using our in-plane infrared/direct-current excitation (IR/DC) technique.
- Demonstrated the detection of defects in catalyst-coated membrane (CCM) sheet materials at 30 fpm line speed on NREL's research web-line using our in-plane IR/DC technique.
- Demonstrated the detection of defects in membrane sheet materials at 30 fpm line speed on NREL's research web-line using our optical reflectometry technique.
- Demonstrated the detection of shorting defects in full MEAs at 30 fpm roller speed on NREL's bench-top roller system using our through-plane IR/DC technique.
- Demonstrated detection of surface defects in planar fired SOFC cells on our bench-top motion stage using our optical reflectometry technique.
- Proved the feasibility of using our infrared/reactive flow-through (IR/RFT) technique to detect coating defects in in-house fabricated gas diffusion electrodes (GDEs).
- Performed modeling of IR/RFT process variables and GDE defect size, and integrated modeling results into further improvement of the technique.
- Used segmented cell testing to understand how variability in GDM polytetrafluoroethylene (PTFE) content and defects in CCM catalyst layers affects local (spatially resolved) and total cell performance.
- Continued collaboration with our industry partners, including three of DOE's competitively awarded Manufacturing R&D projects, in accordance with our project charter.



Introduction

In FY 2005–2007, NREL provided technical support to DOE in developing a new key program activity: Manufacturing R&D for hydrogen and fuel cell technologies. This work included a workshop on manufacturing R&D, which gathered inputs on technical challenges and barriers from the fuel cell industry, and subsequent development of a roadmap for manufacturing R&D. In late FY 2007, NREL initiated a project to assist the fuel cell industry in addressing these barriers, initially focusing on in-line quality control of MEA components. The project is utilizing the unique and well-established capabilities of NREL's National Center for Photovoltaics for developing and transferring diagnostic and process technology to the manufacturing industry.

Defects in MEA components differ in type and extent depending on the fabrication process used. The effects of these defects also differ, depending on their size, location in the cell relative to the reactant flow-field, cell operating conditions, and which component contains the defect. Understanding the effects of these different kinds of defects is necessary to be able to specify and/or develop diagnostic systems with the accuracy and data acquisition/processing rates required for the speed and size scales of high-volume continuous manufacturing methods. Furthermore, predictive capabilities for manufacturers are critical to assist in the development of transfer functions and to enable assessment of the effects of material and process changes.

Approach

NREL and its partners are addressing the DOE manufacturing milestones listed above by evaluating, developing, and validating (in-line) diagnostics that will support the use of high-volume manufacturing processes for the production of MEAs and MEA component materials. Prioritization of this work is based on inputs from our industry partners on their critical manufacturing quality control needs. We are focusing on diagnostic capabilities not addressed by commercially available in-line systems; in particular we are evaluating methods to make areal rather than point measurements such that discrete defects can be identified. We are also developing test methodologies to study the effects of the size and/or extent of each important type of variability or defect. These results will assist our industry partners in validating manufacturing tolerances for these materials, ultimately reducing scrap rates and cost, and improving supply chain efficiency. Finally, predictive models are being used at Lawrence Berkeley National Laboratory to understand the operational and design characteristics of diagnostic techniques by simulating the behavior of MEA components in different excitation modes. These results are being fed back to our design effort in configuring the diagnostics for in-line implementation. MEA models are also being utilized to understand the in situ behavior of defect MEAs to guide and further elucidate experiments.

Results

A strong focus of our efforts this year was demonstration of diagnostics on our research web-line. We demonstrated use of the in-plane IR/DC technique for the detection of defects in both GDM (with and without micro-porous layer, MPL) materials and CCM catalyst layers on the web-line. In both cases, we manually created defects using roll and sheet materials provided to us by our industry partners. The defects consisted of a series of scratches from 0.04 to 2.0 cm² and a series of surface cuts from 0.5 to 2.0 cm long. Detection was demonstrated at 30 fpm line speed, which is consistent with current manufacturing rates for MEA materials. Figure 1

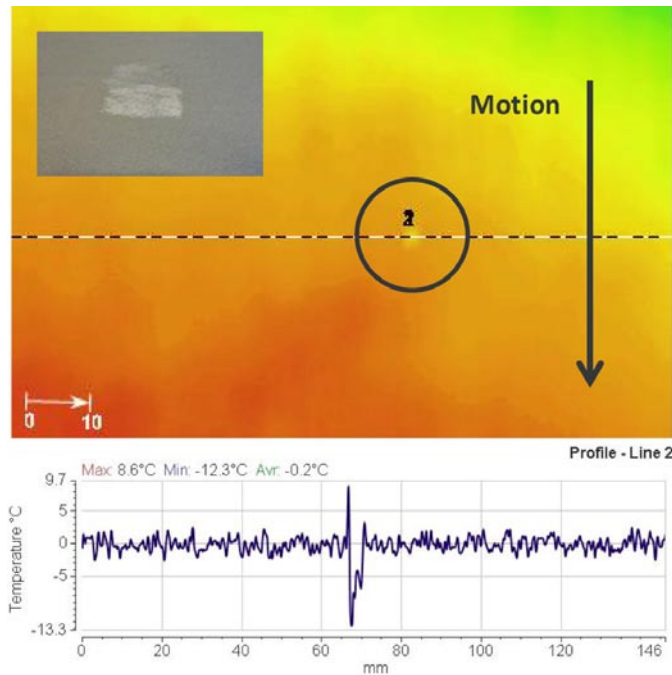


FIGURE 1. Infrared image of a 0.04 cm² surface scratch in an MPL (optical micrograph of defect shown in inset) moving at 30 fpm on the web-line, obtained using NREL's in-plane IR/DC technique (top); filtered line data (bottom)

is an infrared image showing detection of a small square scratch (top) and the filtered line data along the dotted line in the image (bottom). An optical photograph of the defect is shown in the inset. We also demonstrated use of our optical reflectometry technique to detect membrane defects from 10 to 100 μm. This validation was also performed at 30 fpm line speed.

In more developmental work, we demonstrated that a through-plane, spatially resolved resistivity measurement indicating potential shorting of an MEA can be made on a moving MEA using our bench-top roller system and the IR/DC technique. Figure 2 is an infrared image of an MEA fabricated to have GDM fibers protruding into the membrane. The regions of higher temperature indicate locations of high conductivity through the membrane. In another close industry interaction, we demonstrated that the optical reflectometry technique could be used to identify defects in the electrolyte surface of a planar SOFC cell. Defects as small as 10 μm were detected using our bench-top motion stage. Figure 3 shows a 98 x 154 mm fired half-cell and the zoomed reflectance image of a known defect. We also made progress in the development of our IR/RFT technique. Both experimental and numerical studies improved our understanding of how process variables, GDE materials, and defect size affect the sensitivity of the technique. Finally, various in situ studies were completed or are ongoing exploring the local and overall effects of as-manufactured defects on MEA performance.

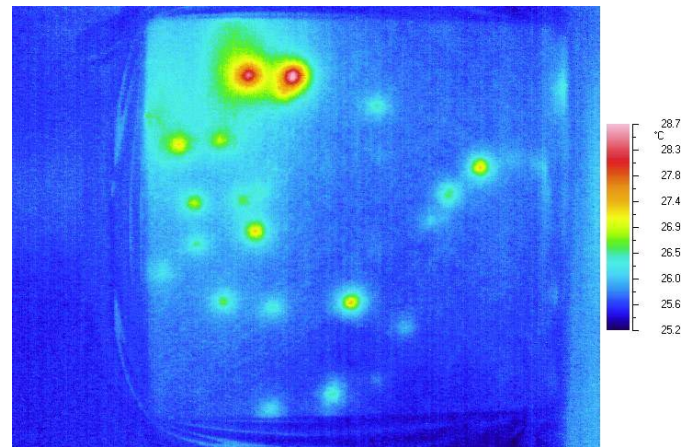


FIGURE 2. Infrared image of an MEA with GDM fibers protruding into the membrane, obtained using NREL's through-plane IR/DC excitation technique. The sample is moving through the roller system at 30 fpm.

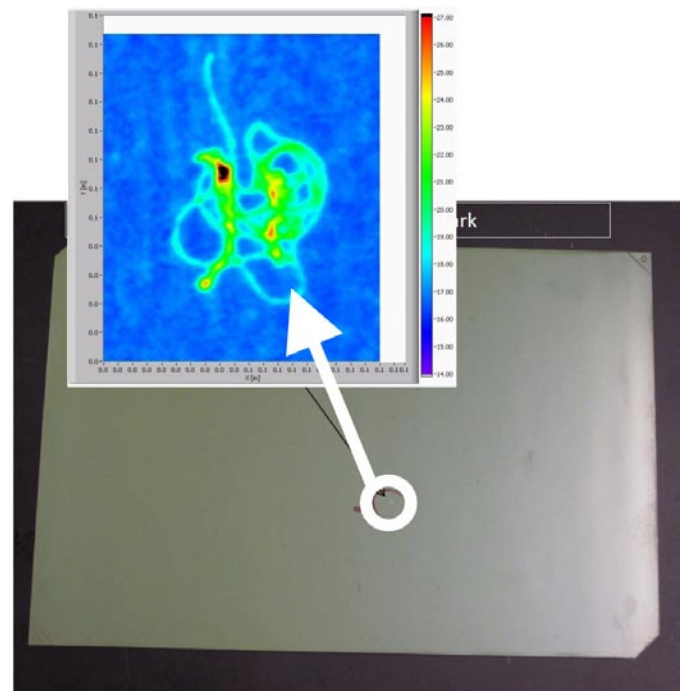


FIGURE 3. SOFC half-cell (bottom) and reflectance image of electrolyte surface defect (top)

Future Directions

- Demonstrate the through-plane IR/DC technique on our bench-top roller system using MEA sheet material provided by our industry partner.
- Determine the feasibility of using the IR/RFT technique in a configuration enabling in-line measurement.
- Determine the feasibility of using optical reflectometry to detect surface defects in SOFC tube cells.

- Continue to use predictive modeling and single and segmented cell test methods to feed requirement and configuration information back to diagnostic development, device design, and detection algorithm assessment.
- Study the effect of as-manufactured defects on MEA lifetime using standard or modified accelerated stress tests.
- Continue to work with our industry partners to ensure the relevance of our studies to their evolving needs and directions, including exploration of new diagnostic techniques.

FY 2012 Publications and Presentations

1. “Fuel Cell MEA Manufacturing R&D,” DOE Fuel Cell Technologies Program Annual Merit Review; Washington, D.C.; May 2012.
2. “Applying Infrared Thermography as a Quality-Control Tool for the Rapid Detection of Polymer-Electrolyte-Membrane-Fuel-Cell Catalyst-Layer-Thickness Variations,” N.V. Aieta, P. Das, A. Perdue, G. Bender, A. Herring, A. Weber, M. Ulsh; *J. Power Sources*, **211** (2012), p. 4.
3. “2011 NREL/DOE Hydrogen and Fuel Cell Manufacturing R&D Workshop Report,” Washington, D.C.; February 2012.
4. “2010 Manufacturing Readiness Assessment of PEM Fuel Cell Systems and Stacks for the Material Handling Equipment and Backup Power Markets,” M. Ulsh, D. Wheeler; Fuel Cell Seminar & Exposition; Orlando, FL; November 2011.
5. “Identification of gas diffusion layer PTFE content local anomalies using a segmented cell system,” T. Reshetenko, J. St-Pierre, K. Bethune, R. Rocheleau; *ECS Trans.* **41** (1) (2011), p. 539-548.
6. “Spatial performance impact of electrode defects in PEMFC,” G. Bender, A. Tsang, N.V. Aieta, A. Perdue, M. Ulsh; National Meeting of the American Chemical Society; Denver, CO; August 2011.
7. “Detecting loading variation in Pt PEMFC electrodes using IR thermography,” N.V. Aieta, A. Perdue, P. Das, A. Weber, M. Ulsh; National Meeting of the American Chemical Society; Denver, CO; August 2011.
8. “State of Automation in the Manufacturing of Combined Heat and Power Fuel Cell Systems in the U.S.,” M. Ulsh, D. Wheeler, P. Protopappas, N. Garland; 9th ASME Fuel Cell Science, Technology, and Engineering Conference; Washington, DC; August 2011.

VI.2 Manufacturing of Low-Cost, Durable Membrane Electrode Assemblies Engineered for Rapid Conditioning

F. Colin Busby

W.L. Gore & Associates, Inc (Gore)
Gore Electrochemical Technologies Team
201 Airport Road
Elkton, MD 21921
Phone: (410) 392-3200
Email: CBusby@WLGore.com

DOE Managers

HQ: Nancy Garland
Phone: (202) 586-5673
Email: Nancy.Garland@ee.doe.gov
GO: Jesse Adams
Phone: (720) 356-1421
Email: Jesse.Adams@go.doe.gov

Contract Number: DE-FC36-08G018052

Subcontractors:

- UTC Power, South Windsor, CT
- University of Delaware, Newark, DE (UD)
- University of Tennessee, Knoxville, TN (UTK)

Project Start Date: October 1, 2008

Project End Date: June 30, 2014

Fiscal Year (FY) 2012 Objectives

The overall objective of this project is to develop a unique, high-volume manufacturing process that will produce low-cost, durable, high-power density 5-layer membrane electrode assemblies (MEAs) that minimize stack conditioning:

- Manufacturing process scalable to fuel cell industry MEA volumes of at least 500k systems/year.
- Manufacturing process consistent with achieving \$9/kW_e DOE 2017 transportation MEA cost target.
- The product made in the manufacturing process should be at least as durable as the MEA made in the current process for relevant automotive-duty cycling test protocols.
- The product developed using the new process must demonstrate power density greater or equal to that of the MEA made by the current process for relevant automotive operating conditions.
- Product form is designed to be compatible with high-volume stack assembly processes: 3-layer MEA roll-good (anode electrode + membrane + cathode electrode) with separate rolls of gas diffusion media.

- The stack break-in time should be reduced to 4 hours or less.

Phase 2 Objectives

- Low-Cost MEA Research and Development (R&D)
 - New 3-Layer (3-L) MEA Process Exploration
 - Investigate equipment configuration for low-cost MEA production
 - Investigate raw material formulations
 - Map out process windows for each layer of the MEA
 - Mechanical Modeling of Reinforced 3-L MEA
 - Use model to optimize membrane reinforcement for 5,000+ hour durability and maximum performance
 - Develop a deeper understanding of MEA failure mechanisms
 - 5-Layer (5-L) Heat and Water Management Modeling
 - Optimization of gas diffusion media (GDM) thermal, thickness, and transport properties to enhance the performance of thin, reinforced membranes and unique properties of direct-coated electrodes using a validated model
 - Optimization
 - Execute designed experiments which fully utilize UD and UTK modeling results to improve the new MEA process and achieve the highest possible performance and durability
 - MEA Conditioning
 - Evaluate potential for new process to achieve DOE cost targets prior to process scale-up (Go/No-Go decision)
- Scale-Up and Process Qualification
- Stack Validation

Technical Barriers

This project addresses the following technical barriers from the Manufacturing R&D section of the Fuel Cell Technologies Program Multi-Year Research, Development and Demonstration Plan:

- (A) Lack of High-Volume Membrane Electrode Assembly Processes

Contribution to Achievement of DOE Manufacturing R&D Milestones

This project will contribute to achievement of the following DOE milestones from the Manufacturing R&D section of the Fuel Cell Technologies Program Multi-Year Research, Development and Demonstration Plan:

- RD&D Plan Section 3.4, Task 10.1: Test and evaluate fuel cell systems and components such as MEAs, short stacks, bipolar plates, catalysts, membranes, etc. and compare to targets. (3Q, 2011 thru 3Q, 2020)
- RD&D Plan Section 3.4, Task 10.2: Update fuel cell technology cost estimate for 80 kW transportation systems and compare it to targeted values. (3Q, 2011 thru 3Q, 2020)

FY 2012 Accomplishments

- Direct Coating Process Development
 - The primary path for the new 3-L MEA process has succeeded in incorporating the previously modeled process improvements which indicated potential for a 25% reduction in high-volume 3-L MEA cost.
 - Lab-scale development of the new 3-L MEA process is nearing completion:
 - Each layer in the primary path process has been sheet coated on control substrate materials.
 - Gore identified a replacement for a discontinued backer which satisfied the criteria for:
 - Thickness uniformity
 - Mechanical stability up to max drying and piece-part conversion temperatures
 - Chemical stability
 - Cleanliness
 - Electrode release
 - Supply chain reliability
 - Cost
 - Cathode electrode coating on the new backer has been demonstrated on a roll-to-roll coating line and is equivalent to or better than the current commercial electrode in Gore's beginning-of-life test, start/stop accelerated stress test (AST), and voltage cycling AST.
- Gore has demonstrated mechanical durability of a 10-micron expanded polytetrafluoroethylene (ePTFE)-reinforced membrane. In previous testing, GORE™ MEAs exceeded 2,000 hours of accelerated mechanical durability testing, which has been equated to achieving 9,000 hours of membrane durability in an 80°C automotive duty cycle. This exceeds the DOE 2015 membrane durability target of 5,000 hours. Gore's 10-micron ePTFE reinforced membrane technology has

been successfully incorporated into the lab-scale new 3-L MEA process.

- A quasi-static elastic/plastic layered structure MEA mechanical model has been modified to include visco-elastic/plastic behavior. Mechanical property experiments which are required to calculate model input parameters are complete and modeling of different membrane reinforcement geometries is underway. The final model will be used to predict reinforced MEA mechanical lifetime for a variety of temperature and relative humidity cycling scenarios. The model will also be used to explore different reinforcement strategies and optimize mechanical durability of the MEA structure targeted by the new low-cost process.
- 5-Layer Heat & Water Management Model development at UTK is complete.



Introduction

Over the past 20 years, great technical progress has been made in the area of improving power density and durability of fuel cell stacks, so much so that most of the requisite technical targets are now within reach. Yet, three major technical challenges remain. First and foremost is meeting the cost targets. The second challenge is producing components that are amenable for use in a high-speed, automotive assembly line. One impediment to this latter goal is that stack components must currently go through a long and tedious conditioning procedure before they produce optimal power. This so-called “break-in” can take many hours, and can involve quite complex voltage, temperature and/or pressure steps. These break-in procedures must be simplified and the time required reduced, if fuel cells are to become a viable power source. The third challenge is to achieve the durability targets in real-world operation. This project addresses all three challenges: cost, break-in time, and durability for the key component of fuel cell stacks: MEAs.

Approach

The overall objective of this project is to develop unique, high-volume manufacturing processes for low-cost, durable, high-power density 3-Layer MEAs that require little or no stack conditioning. In order to reduce MEA and stack costs, a new process will be engineered to reduce the cost of intermediate backer materials, reduce the number and cost of coating passes, improve safety and reduce process cost by minimizing solvent use, and reduce required conditioning time and costs. MEA mechanical durability will be studied and optimized using a combination of ex situ mechanical property testing, non-linear mechanical model optimization,

and in situ accelerated mechanical durability testing. Fuel cell heat and water management will be modeled to optimize electrode and GDM thermal, geometric, and transport properties and interactions. Unique enabling technologies that will be employed in new process development include:

- Direct coating which will be used to form at least one membrane–electrode interface.
- Gore’s advanced ePTFE membrane reinforcement and advanced perfluorinated sulfonic acid ionomers which enable durable high-performance MEAs.
- Advanced fuel cell testing and diagnostics.

Results

Low-Cost MEA Process Development

Primary path

- Process step 1: Coat bottom electrode on low-cost, non-porous backer
- Process step 2: Direct coat reinforced membrane on top of the bottom electrode

- Process step 3: Direct coat top-side electrode on top of the reinforced membrane

The alternate path is to directly coat the anode electrode onto a backer-supported reinforced half-membrane to make an anode-side 1.5-layer intermediate rolled-good. The cathode electrode is then directly coated onto a backer-supported reinforced half-membrane in a similar process. In the final step, the backers are removed from the anode-side and cathode-side 1.5-layers intermediates and the webs are laminated together to form the 3-layer product.

Electrodes made using lab-scale versions of the current primary path process equipment have demonstrated performance equivalent to or better than the current commercial electrodes across a broad range of operating conditions. Figures 1 and 2 show performance of direct coated electrodes paired with opposing control electrodes in a range of operating conditions which can be used to assess the viability of an MEA for different applications (automotive, stationary, portable, etc.), or for dynamic operation within a single application.

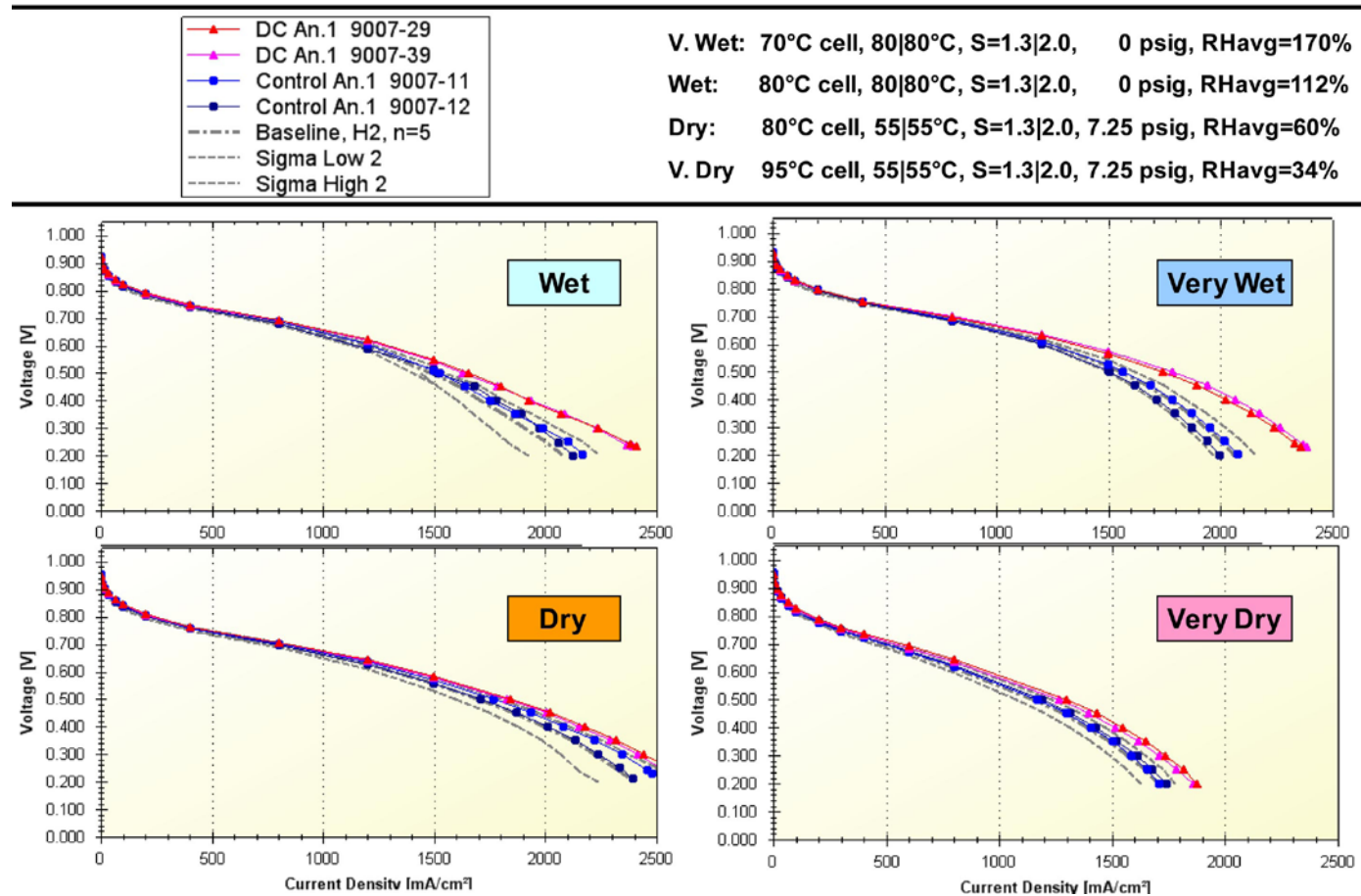
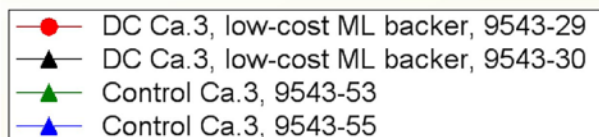


FIGURE 1. Direct-Coated Anode Performance (DC = direct coated)



V. Wet: 70°C cell, 80|80°C, S=1.3|2.0, 0 psig, RHavg=170%
 Wet: 80°C cell, 80|80°C, S=1.3|2.0, 0 psig, RHavg=112%
 Dry: 80°C cell, 55|55°C, S=1.3|2.0, 7.25 psig, RHavg=60%
 V. Dry 95°C cell, 55|55°C, S=1.3|2.0, 7.25 psig, RHavg=34%

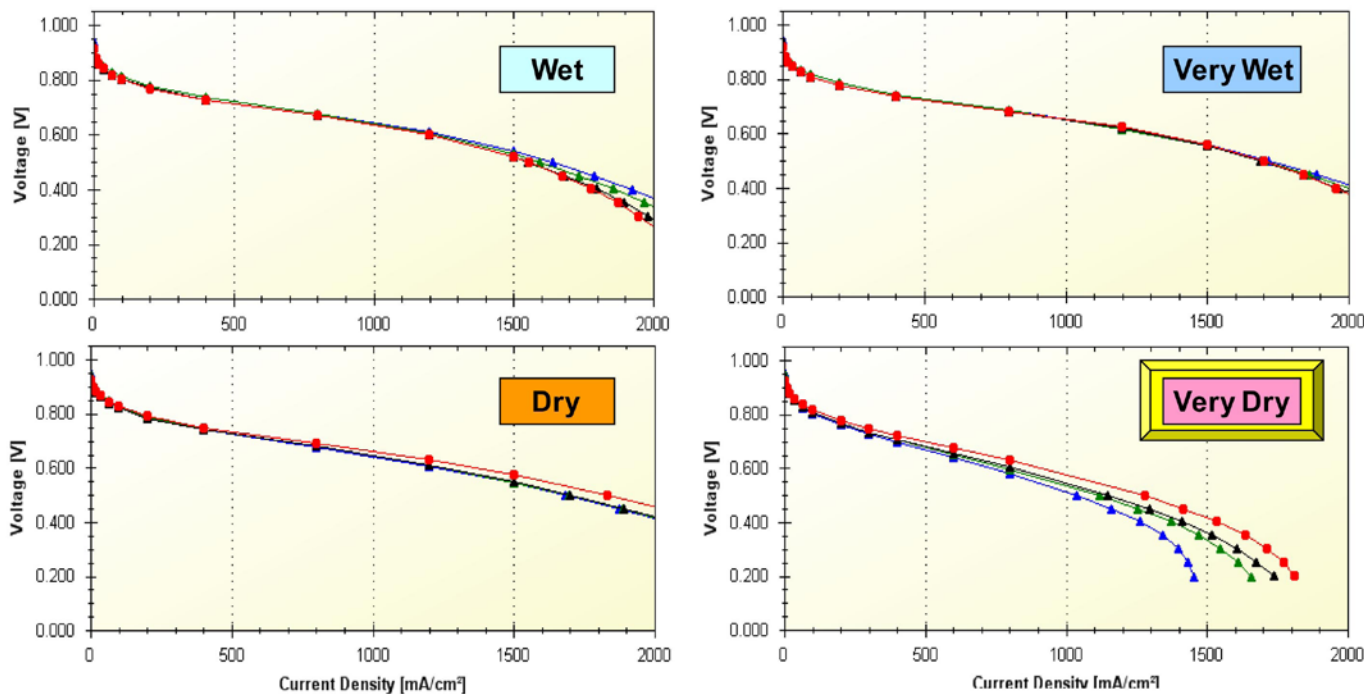


FIGURE 2. Direct-Coated Cathode Performance

Coating research during the past year focused on backer development and demonstration of cathode-on-backer coating on a roll-to-roll pilot line. Future experiments will combine direct-coated anodes and direct-coated cathodes and test the durability of direct-coated MEA.

Mechanically Durable 10-µm Reinforced Membrane

Gore has successfully incorporated a mechanically durable 10-µm reinforced membrane into the current primary path process. The 10-µm membrane construction has demonstrated high performance due to reduced resistance and increased water back-diffusion (see Figure 3). In previous testing, GORE™ MEAs exceeded 2,000 hours of accelerated mechanical durability testing, which has been equated to achieving 9,000 hours of membrane durability in an 80°C automotive-duty cycle. This exceeds the DOE 2015 membrane durability target of 5,000 hours. The accelerated mechanical durability testing protocol is summarized in Table 1.:

For further protocol information, see: W. Liu, M. Crum, ECS Transactions 3, 531-540 (2007).

TABLE 1. Accelerated Mechanical Durability Testing Protocol

| Tcell (°C) | Pressure (kPa) | Flow (Anode/Cathode, cc/min) |
|------------|----------------|------------------------------|
| 80 | 270 | 500 N2/1,000 N2 |

Cycle between dry feed gas and humidified feed gas (sparger bottle temp = 94°C)
 Dry feed gas hold time: 15 seconds
 Humidified feed gas hold time: 5 seconds

Mechanical Modeling of Reinforced 3-L MEA (UD)

A quasi-static elastic/plastic layered structure MEA mechanical model has been modified to include visco-elastic/plastic behavior. Mechanical property experiments which are required to calculate model input parameters are complete and modeling of different membrane reinforcement geometries is underway.

Nafion® 211 membrane is used for the model membrane and the temperature, relative humidity (RH), and time dependent properties are calculated from the ongoing experimental results. The viscous properties are modeled

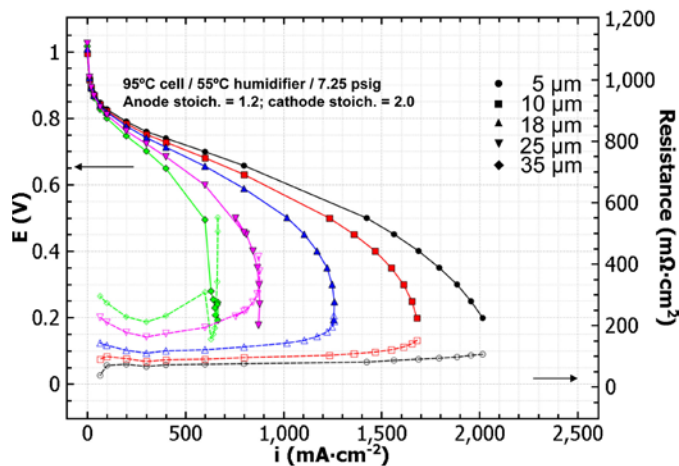


FIGURE 3. Performance of Thin, Mechanically Durable Reinforced Membranes

using a 2-layer viscoplastic constitutive model. This material model consists of an elastoplastic “arm” that is in parallel with an elastoviscous “arm.” The elastoplastic arm consists of an elastic spring (stiffness K_p) and a plastic component (yield stress, σ_y and hardening H'). Yielding according to the Mises criterion is used here. The elastoviscous arm has two

elements, one spring (stiffness K_v) and one dashpot (using a time hardening law $\dot{\epsilon}_v = A\sigma_v^n$). Thus, the instantaneous elastic stiffness of the material is the sum of the elastic elements, $K_p + K_v$. In summary, the parameters that are required for this model are K_p , σ_y , H' , K_v , A and n . These properties are determined from the experimental results. Tensile testing was conducted for a range of displacement rates to investigate the influence of this parameter on the mechanical response. The rates were selected so that the full visco-elastic-plastic constitutive equations can be determined. The relationships obtained from the MEA testing are “composite properties,” combining the properties of the membrane with the electrodes. The constitutive equations for the electrodes will be obtained via reverse analysis. The experimental results have shown that the mechanical response of Nafion® 211 membrane and the MEA is dependent on temperature and humidity as well as displacement rate. Figure 4 shows the dynamic response of modeled membrane stress as a function of RH in the flow channels. Peak stress after dehydration decreases by about 25% with a reduction of humidity transition time from 1 s to 50 s, indicating that an abrupt change in hydration is a more severe case than a gradual change in hydration. Results also indicate that lower

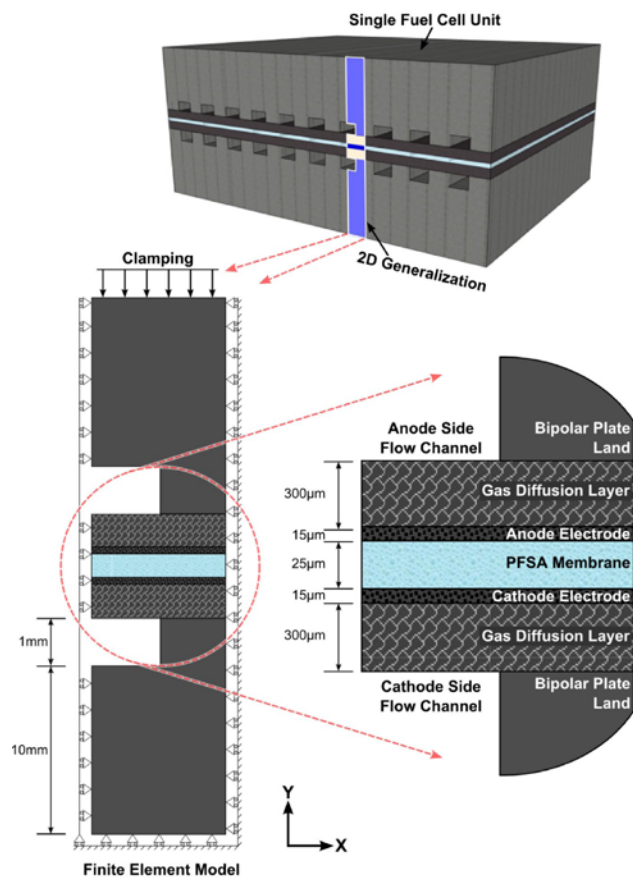
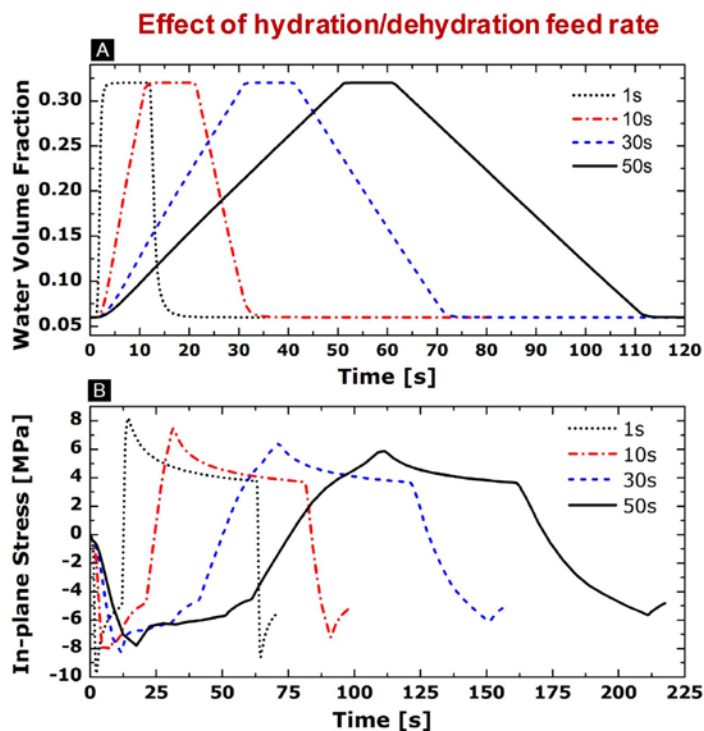


FIGURE 4. Two-Dimensional Plane Strain Finite Element Model for a Single Cell under RH Cycling

| Water Volume Fraction | Swelling Strain | Thermal Strain |
|--|--|---|
| $\phi_w = \frac{18\lambda}{EW/\rho_p + 18\lambda}$ | $\epsilon^{sw} = \left(\frac{\theta + 273}{\theta_0 + 273} \right) \ln(1 - \phi_w)$ | $\epsilon^{th} = \alpha(\theta - \theta_0)$ |



temperature, lower humidity or faster displacement rate result in a larger stress for a given strain.

5-L Heat & Water Management Modeling (UTK)

Membrane electrode assemblies and diffusion media materials were selected and experimental testing was initiated. Computationally, an initial first round of two-dimensional single-phase computational model simulation was completed to simulate the impact of diffusion media and membrane thickness and thermal properties. This analysis has enabled some understanding of the consequences of the various micro/macro diffusion media designs. The thermal properties of the diffusion media and microporous layer were shown to be critical to facilitate proper water management and are critical engineering parameters.

Conclusions and Future Directions

The combination of Gore's advanced materials, expertise in MEA manufacturing, and fuel cell testing with the mechanical modeling experience of University of Delaware and the heat and water management experience of University of Tennessee enables a robust approach to development of a new low-cost MEA manufacturing process.

- Electrodes made using lab-scale versions of the current primary path process equipment have demonstrated performance equivalent to or better than the current commercial electrodes across a broad range of operating conditions. Cathode coating on the new low-cost backer has been demonstrated on a roll-to-roll process. Future work will focus on combining direct coated anodes

and cathodes as well as accelerated stress testing to ensure that durability of the new, direct-coated MEAs is equivalent to or better than the current commercial control MEA.

- Fuel cell heat and water management modeling will be used to efficiently optimize electrode and GDM thermal, geometric, and transport properties and interactions. Direct-coated electrodes will be paired with the most appropriate GDM materials identified in this study. In this way, GDM will enable maximum performance and durability of the low-cost 3-layer MEA.
- A quasi-static elastic/plastic layered structure MEA mechanical model has been modified to include visco-elastic/plastic behavior. Mechanical property experiments which are required to calculate model input parameters are complete and modeling of different membrane reinforcement geometries is underway. The model will be validated with MEA accelerated durability testing. The final model will then be used to predict reinforced MEA lifetime for a variety of temperature and relative humidity cycling scenarios. The model will also be used to optimize mechanical durability of the MEA structure targeted by the new low-cost process.

Nafion is a registered trademark of E. I. DuPont de Nemours & Company

GORE and designs are trademarks of W. L. Gore & Associates, Inc.

FY 2012 Publications/Presentations

1. 2012 Hydrogen Program Annual Merit Review: mn004_busby_2012_o.pdf

VI.3 Adaptive Process Controls and Ultrasonics for High-Temperature PEM MEA Manufacture

Daniel F. Walczyk (Primary Contact),
Stephen J. Rock
Center for Automation Technologies and Systems
Rensselaer Polytechnic Institute (RPI)
Suite CII 8015
110 8th Street
Troy, NY 12180-3590
Phone: (518) 276-2397
Email: walczd@rpi.edu

DOE Managers
HQ: Nancy Garland
Phone: (202) 586-5673
Email: Nancy.Garland@ee.doe.gov
HQ: Jesse Adams
Phone: (720) 356-1421
Email: Jesse.Adams@do.doe.gov

Contract Number: DE-FG36-08GO18053

Subcontractors:
Arizona State University, Tempe, AZ

Project Start Date: September 1, 2008
Project End Date: September 30, 2013

Fiscal Year (FY) 2012 Objectives

- Conduct experiments to determine the feasibility and benefits of using ultrasonics for bonding low-temperature (Nafion[®]) membrane electrode assemblies (MEAs).
- Test and evaluate the performance of ultrasonically and thermally bonded high-temperature polymer electrolyte membrane fuel cell (PEMFC) MEAs (160-180°C) in 5- and 10-cell short stacks to (1) investigate the compatibility of the bonding process with cell stacks and (2) increase testing throughput to support simultaneous testing of cells fabricated with similar conditions.
- Test and evaluate the performance of ultrasonically and thermally bonded MEAs with larger active area (140 cm²) and compare with the 'standard' MEA size (45 cm²).
- Investigate the causes of excessive variation in ultrasonically and thermally bonded high-temperature MEAs using more diagnostics applied during the entire fabrication and cell build process.
- Perform a cost analysis that compares roll-to-roll manufacturing and discrete manufacturing (current) approaches for high-temperature MEAs.

- Develop guidelines and analytical models that allow manufacturing engineers to design/specify tooling and determine optimal process parameters for bonding high-temperature PEM MEAs using ultrasonics.

Technical Barriers

This project addresses the following Manufacturing R&D technical barriers in the Manufacturing R&D section (3.5.5) of the Fuel Cell Technologies Program Multi-Year Research, Development and Demonstration Plan:

- (A) Lack of High-Volume Membrane Electrode Assembly (MEA) Processes
- (F) Low Levels of Quality Control and Inflexible Processes.

Contribution to Achievement of DOE Manufacturing R&D Milestones

This project will contribute to achievement of the following DOE milestones from the Manufacturing R&D section (3.5.7) of the Fuel Cell Technologies Program Multi-Year Research, Development and Demonstration Plan:

- Milestone 2: Develop continuous in-line measurement for MEA fabrication. (4Q, 2012)
- Milestone 3: Demonstrate sensors in pilot scale applications for manufacturing MEAs. (4Q, 2013)
- Milestone 4: Establish models to predict the effect of manufacturing variations on MEA performance. (4Q, 2013)

FY 2012 Accomplishments

- Found that performance of ultrasonically bonded low-temperature MEAs is sensitive to electrode composition and structure.
- Optimized the thermal and ultrasonic bonding processes for low-temperature MEAs, i.e., consisting of Nafion[®] 115 and commercial (Fuel Cell Earth) electrodes, using designed experiments and analysis of variance (ANOVA) to estimate main effects of the bonding process.
- Characterized performance loss of low-temperature MEAs between ultrasonic and thermal bonding, high and low catalyst loading gas diffusion electrodes (GDEs), and conditioned and dry membrane conditions.
- Stack for high-temperature MEAs with composite bipolar plates was developed and qualified as having insignificant impact on cell performance.

- Stack utilized for high-throughput, simultaneous high-temperature MEA cell testing.
- Demonstrated consistent cell performance for thermally and ultrasonically bonded high-temperature MEAs in stack and single-cell testing.
- Completed dynamic modeling of ultrasonic bonding process with mixed results related to model versus experimental temperature measurement of membrane/electrode interfaces.
- Polarization (voltage/current, V/I) curves for larger high-temperature MEAs (140 cm²) that were ultrasonically and thermally bonded showed similar performance, but both types initially performed below the BASF fuel cell specification for MEAs with 45 cm² active area.
- Redesigned MEA flow field plate made from composite material instead of graphite helped improve V/I performance, and new polarization curves were obtained.
- Demonstrated that the performance of MEAs bonded in 2 seconds using an ultrasonic bonding method is the same as MEAs bonded in 30 seconds using the traditional thermal bonding method.
- Developed cyclic voltammetry-based quality control methods to detect shorted MEAs and the degree of bonding between the electrodes and the membrane. The methods can be applied during manufacturing prior to cell build.
- Demonstrated using X-ray diffraction that ultrasonic bonding does not induce catalyst coarsening.
- Implemented a suite of diagnostic tests to detect variations in catalyst loading, catalyst crystallite size, MEA fabrication, cell performance, and specific processes within operating cells.
- Obtained data suggesting the possibility of a 6X reduction in MEA thermal bonding and annealing cycle times to increase manufacturing throughput on existing production equipment.
- By using ultrasonic bonding instead of thermal bonding, experimentally demonstrated 96% energy and 93% cycle time reductions with 45-cm² high-temperature MEAs, and 98% energy and 94% cycle time reductions with 10-cm² low-temperature MEAs.



Introduction

To realize the tremendous potential of fuel cell technology, high-volume, high-quality manufacturing technologies must be developed in parallel with the materials and designs for MEAs, stacks, and the other stack components, which is currently not the case. There are currently three main barriers to the development of high

volume fuel cell manufacturing. First, the current practice involving extensive testing and burn-in of components and stacks will not allow the industry to achieve the necessary cost targets and throughput for stacks, components, and systems. Second, for the current process used to press low-temperature (e.g. Nafion[®]) MEAs for both PEMFCs and direct methanol fuel cells, it is common to thermally press for as long as 1½ -5 minutes. Even the pressing process for high-temperature (polybenzimidazole, or PBI) MEAs, although much shorter than for Nafion[®]-based MEAs at about one minute, is still too long for high-volume manufacture. Third is the variability of MEA performance. The component materials, including gas diffusion layer (GDL) or GDE membranes or catalyst-coated membranes, and gasketing materials all exhibit variations in key properties such as thickness, porosity, catalyst loading, and water or acid content and concentration. Yet, it is common practice to employ a fixed combination of pressing process parameter values (time, temperature and pressure), regardless of these component variations, which leads to MEAs that exhibit different physical and performance-related properties.

The research being conducted in this project will help reduce all three of these barriers by reducing the unit process cycle time for MEA pressing by the use of ultrasonic bonding, and by minimizing the variability in performance of MEAs produced using advanced diagnostics to gain insight into how process conditions and variables affect performance. This will in turn help lead to the reduction or elimination of the practice of burn-in testing of fuel cell stacks. All of these benefits will contribute to a reduction in manufacturing costs for MEAs. The specific research tasks addressed during FY 2012 include applying ultrasonic bonding to low-temperature MEAs, demonstrating the performance of ultrasonically and thermally bonded high-temperature MEAs in 10-cell stacks, continued development of an ultrasonic bonding process model, demonstrating ultrasonic bonding process scale up from 45 to 140 cm² active area MEAs, and using advanced diagnostics to fully understand and improve the high-temperature MEA ultrasonic bonding process.

Approach

Low-Temperature MEA Bonding – Through extensive R&D efforts, commercially available low-temperature PEMFC electrodes have been optimized by their manufacturers for thermal pressing, but not for ultrasonic pressing. Hence, four different GDEs (two commercially available and two custom made) were compared using conditioned and unconditioned Nafion[®] membrane for both ultrasonic and thermal bonding. A pilot study determined the ranges of energy and pressure required for ultrasonic bonding. Two-way ANOVA estimated main effects and interaction of process parameters for ultrasonic and thermal process optimization based on performance data collected

from fuel cell testing. Finally, additional diagnostic techniques including impedance spectroscopy, cyclic voltammetry and flow sensitivity were used to compare performance losses between optimized ultrasonic and thermally bonded MEAs. Electrode catalyst loading and membrane preconditioning were also studied. A duplicate array of MEAs was sent to the National Renewable Energy Laboratory (NREL) for third party testing to verify results and conduct additional performance characterization incapable at RPI.

High-Temperature MEA Stack Testing – A new stack architecture was developed in computer-aided design software, prototyped at the 5-cell scale, and then expanded to 10 cells. Each cell was monitored for performance versus current, temperature, reactant composition and time. The cell-to-cell variation was then analyzed and compared to variation observed when testing individual cells to determine if the ultrasonic bonding process had an adverse effect on performance in stacks, and to validate the stack architecture for simultaneous testing of cells. Thermal management was performed through a combination of end plate heaters and one cooling plate (with internal air cooling manifold) located between cells 5 and 6. The end plate heaters were used to bring the stack up to operating temperature and the cooling plate was used in conjunction with natural convection to maintain operating temperature once reasonable currents were drawn.

Ultrasonic Bonding Modeling – Work on modeling of the ultrasonic bonding process continued with a different approach to solving the system of ordinary differential equations (ODEs) necessary to describe the system behavior. Solving eight simultaneous ODEs, especially with terms several orders-of-magnitude apart in value, proved to be too computationally intensive to complete. Instead, a method for solving the system of ODEs symbolically was found, which allowed the resultant output to be computed directly. Additionally, the model now contains eight degrees of freedom (previously six). The two additional degrees are used to mimic present sinusoidal displacement input from the ultrasonic welder.

Testing of Scaled-Up MEAs – Not knowing if ultrasonic bonding would produce functional scaled-up MEAs, ultrasonically and thermally pressed MEAs with 140 cm² active area were produced for comparison. These MEAs were produced using larger tooling, but with parameters used for the 45-cm² MEAs scaled proportionally. Likewise, the ultrasonically bonded MEAs were produced with proportionally scaled energy flux and force. All scaled-up MEAs underwent V/I curve testing using similar test conditions as before. Because the overall performance was worse than the manufacturer specifications, the flow field plates were redesigned to minimize losses. V/I curves were also taken using these flow field plates and results were compared to that of the smaller MEAs.

Applying Advanced Diagnostics to PBI MEA Ultrasonic Bonding – Ultrasonic bonding of PBI MEAs was studied to reduce the cycle time required for bonding MEAs and increase manufacturing throughput. The fuel cell performance of MEAs fabricated using ultrasonic bonding was compared to thermally bonded MEAs. Measuring properties of the incoming electrodes such as catalyst loading and crystallite size and also defining variance in critical parameters associated with MEA fabrication and cell testing helped eliminate sources of noise in cell performance caused by the MEA fabrication and testing after initial cell performance results exhibited variation. Diagnostic test techniques were developed to detect electronic shorts and measure the degree of electrode/membrane bonding. These methods were applied at various stages of cell production including post bonding, annealing, and cell build. The diagnostic testing allowed fabrication issues to be isolated prior to cell assembly and improved the understanding of changes in performance related attributes of the MEAs during fabrication. The assembled cells were tested through a protocol of V/I curves and electrochemical diagnostic tests to allow performance differences to be ascribed to specific physical processes within the cells. A complete suite of test capabilities was developed for critical parameters related to characteristics of the catalyst, MEA fabrication cell assembly, and cell performance. This suite of tests will allow the effect of changes in manufacturing parameters, MEAs components, and cell hardware design to be accessed in the future.

Results

Low-Temperature MEA Bonding – Composition of the GDE is a major factor in performance of ultrasonically bonded MEAs. Different GDL materials are adversely affected by the ultrasonic vibrations resulting in irreversible mechanical deformation of the structure. Both lower catalyst-loaded, custom-made RPI GDEs (0.16 and 0.33 mg Pt/cm²) outperformed commercial Fuel Cell Earth GDE (0.5 mg Pt/cm² reported loading) in ultrasonic MEAs. Performance of thermally bonded MEAs was much more consistent across the various GDEs.

The ultrasonic optimization study tested two factors (energy level and sealing pressure) with three and two levels, respectively. Performance data at three operating current densities (0.4, 0.6, and 0.8 A/cm²) are used for the ANOVA. Two-way ANOVA estimates no main effects of energy flux or sealing pressure in ultrasonic bonding, and there is no statistically significant interaction effect either. This suggests that the ultrasonic bonding process is robust as the variance in performance cannot be explained by variation in the manufacturing process parameters. Optimized ultrasonic bonding conditions are found to be 9.0 J/mm² energy fluence and 3.0 MPa bonding pressure. The thermal press optimization study used two factors (temperature and sealing pressure) of three levels each. Hold time and all

other manufacturing parameters were kept constant. Two-way ANOVA estimates temperature to be a main effect on performance, with performance improving with increasing bonding temperature. No main effect of sealing pressure and no interaction effect are estimated from the statistical analysis. Optimized thermal pressing parameters of 170°C and 2.0 N/mm² produced the best MEA performance.

Ultrasonic MEA performance was comparable to thermal at all current densities operating on H₂/O₂ and low current densities on H₂/Air but quickly degraded at higher current densities on air due to increased diffusion resistance. Figure 1 compares V/I curves of optimized ultrasonic and thermally bonded MEAs made using conditioned membrane and high (0.36 mg Pt/cm²) loaded electrodes. Infrared correction of the performance voltages show that the 7 mV improvement measured on ultrasonic MEAs is attributable to decreased membrane impedance as a result of thinner final MEA thicknesses seen from ultrasonics. Studies in the literature show that membrane preconditioning improves ionic conductivity and performance [1,2]. Conditioned Nafion[®] measured nearly 20% reduced membrane impedance and increased performance by 35 and 16 mV at 0.6 A/cm² operating conditioned for ultrasonically bonded high- and low-loaded (0.16 mg Pt/cm²) MEAs, respectively. Doubling the catalyst loading from 0.16 to 0.33 mg Pt/cm² for ultrasonic MEAs resulted in a performance improvement of 26 mV for dry, unconditioned membrane and 12 mV for conditioned membrane while increasing electrochemical surface area by 65%.

High-Temperature MEA Stack Testing – The stack architecture was proven as an effective tool by validating the temperature distribution and cell voltage distribution at various operating points. Temperature distribution data for a 5-cell stack operating at 0.2 A/cm² showed less than 5°C variation in temperature between MEAs.

A separate test of cell performance versus temperature was performed for a single cell running at multiple constant

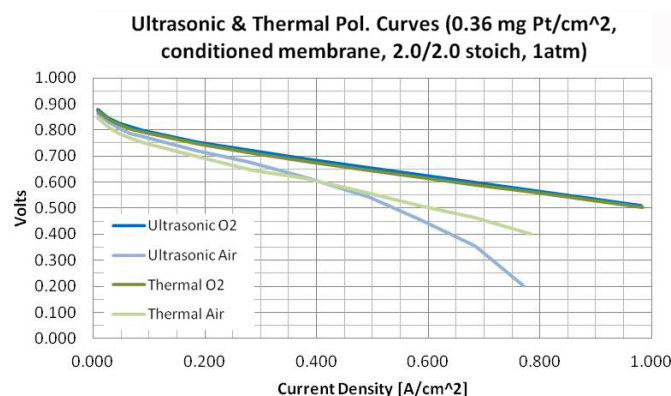


FIGURE 1. Optimized ultrasonic and thermally bonded low-temperature MEAs tested on both H₂/O₂ and H₂/Air

currents and varying temperatures. It was found that the voltage sensitivity to temperature was in the range of 0.9–1.3 mV/°C. This implies a stack temperature distribution induced voltage distribution as high as 6.5 mV. Further, each cell in the stack is monitored for voltage and temperature and temperature induced voltage variation can be accounted for during analysis.

Once the stack architecture and hardware was proven to have a minimal and predictable impact on individual cell performance, testing of ultrasonically and thermally bonded cells was performed. Ultrasonically bonded and thermally bonded MEAs were built in groups of 10 and run through similar testing routines. The difference in performance was found to be negligible, as shown in Figure 2.

Ultrasonic Bonding Modeling – The model was able to predict the bonding temperatures of 45-cm² MEAs within about 10°C at the top membrane/electrode interface (i.e. closest to vibrating horn) but significantly over predicted the bottom interface. Validity of the finite element analysis model thermal boundary conditions between the stationary anvil and bottom electrode needs to be investigated.

Testing of Scaled-Up MEAs – The larger 140-cm² MEAs were manufactured by hand and V/I curves were taken. A comparison of V/I curves (see Figure 3) shows that the thermally bonded and ultrasonically bonded MEAs were matched in performance; however neither one matched the performance of the BASF specification [3]. We suspect that this is due to a sub-optimal flowfield plate design and other potential performance losses that are currently being investigated.

Applying Advanced Diagnostics to PBI MEA Ultrasonic Bonding – The overall cell performance measured while testing 45-cm² single cells was not impacted by the MEA bonding method; however, the MEA bonding method did influence specific performance characteristics of the cells. At a standard operating current density of 0.2 A/cm², the

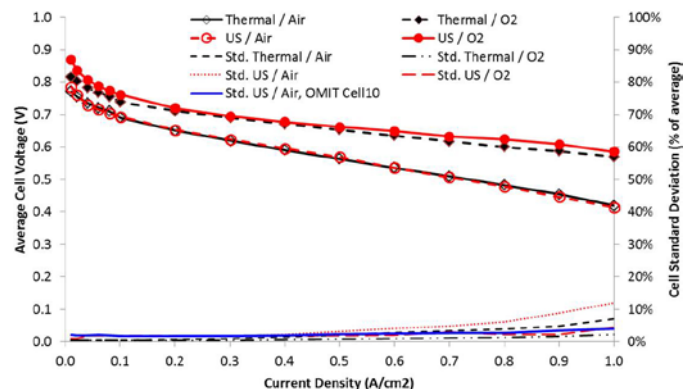


FIGURE 2. Average and standard deviation ("std") of 10-cell stack performance for ultrasonically and thermally bonded MEAs in a 10-cell stack (1.2 stoichiometry H₂/2 stoichiometry O₂ and air).

BASF Specification as Compared to V/I Curves of Ultrasonically Bonded Cells at 160°C, 1.2/2.0 stoich Hydrogen/Air, New Flow Fields

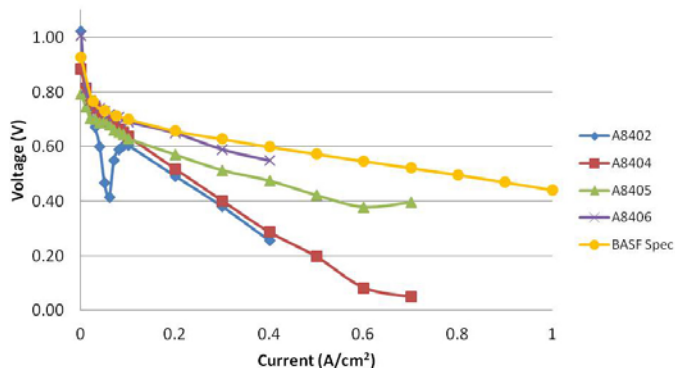


FIGURE 3. V/I curves of ultrasonically bonded cells at 160°C, 1.2/2.0 stoichiometry hydrogen/air and new flow field plates as compared to BASF specification

average cell voltage for ultrasonically bonded and thermally bonded MEAs was 0.668 V and 0.671 V, respectively. The average cell voltages at 0.2 A/cm² were based on five replicates with standard deviations of 0.004 mV for ultrasonically bonded cells and 0.005 mV for thermally bonded cells. Although the cell voltage at 0.2 A/cm² was independent of bonding process, specific performance attributes may be affected by the bonding process. The oxygen gain at 0.6 A/cm², which is used as a metric of transport losses at higher current densities, was 0.88 mV for ultrasonically bonded cells and 0.127 mV for thermally bonded cells. The catalytic current measured on oxygen at 0.85 volts was 0.13 mA for ultrasonically bonded cells and 0.15 mA for thermally bonded cells. Further testing would be required to truly link the deviations in specific performance attributes to bonding method.

A diagnostic test method based on cyclic voltammetry (CV) was developed to detect MEA quality control issues during MEA manufacturing. The method allows rejected MEAs to be detected prior to assembling the MEAs into stacks and cells and provides insight into the effect of manufacturing processes on the MEAs. One quality control issue detected with the technique was the presence of electronically shorted cells. Evaluating CV data plot of current as a function of voltage for an electronically shorted and a normal cell following cell build, the presence of an electronic short is indicated by a high slope on the plot of current as a function of voltage. In other words, a cell showing a higher slope failed to operate properly during fuel cell testing.

A parameter related to the electrochemically active catalyst area can be extracted from the cyclic voltammetry data. The width of the CV plots or current at zero volts provides a measurement of the electrochemical capacitance

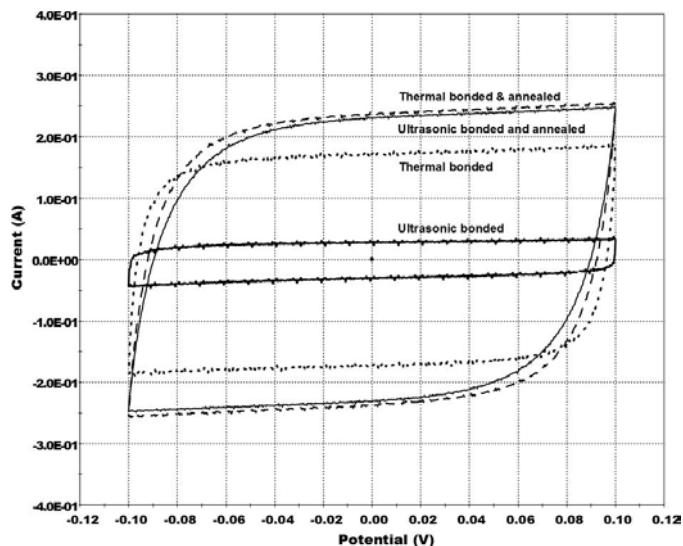


FIGURE 4. CV measurements of electrochemical capacitance following various MEA fabrication processes

which is proportional to the catalyst area wetted with electrolyte. Figure 4 plots the cyclic voltammetry data for ultrasonic and thermally bonded cells following bonding and annealing. It can be seen that the capacitance following ultrasonic bonding is significantly lower following thermal bonding of MEAs. However, the capacitance values following annealing are independent of the bonding process. This suggests that area of contact between electrolyte and catalyst (i.e. degree of bonding) is lower follow ultrasonic bonding than thermal bonding but that after annealing the degree of bonding is normalized. As previously mentioned, the cell performance was the same for ultrasonic and thermally bonded MEAs.

As a result of the apparent wide latitude in the degree of MEA bonding which ultimately produced a normal functioning cell, it was hypothesized that the thermal bonding time could be reduced without negatively affecting cell performance provided the cells were annealed. The annealing time was also varied. A single combination of reduced thermal bonding and annealing times is highlighted to suggest the possibility to increase manufacturing throughput by shortening the cycle times of the existing processes. Average V/I curves for cells bonded for 30 seconds and annealed for 30 minutes (standard conditions) and cells bonded for 5 seconds and annealed for 5 minutes (6X reduction in cycle time) were plotted. Each curve V/I curve is the average of five cells tested simultaneously in a 10-cell stack. The positions of the MEAs manufactured with normal and reduced cycle time manufacturing parameters were alternated up the length of the 10-cell stack to remove cell positioning bias from the data set. The performance was the same at the standard operating current density of 0.2 A/cm² but the faster cycle time conditions performed better at

higher current densities. These results indicate the possibility of improving manufacturing throughput with existing equipment and processes.

The platinum catalyst crystallite size was estimated before and after electrodes were ultrasonically bonded to see if ultrasonic bonding caused coarsening of platinum crystallites. The Scherrer formula was used to calculate the platinum crystallite size from the full width at half maximum of the platinum (111) peak. The data indicate that the platinum crystallite size did not increase during ultrasonic bonding.

Conclusions and Future Directions

- Low-Temperature MEA Bonding – GDL structure and mechanical properties are sensitive to ultrasonic vibrations resulting in performance effects. After ultrasonic and thermal bonding processes were optimized, no main or interaction effects were estimated in ultrasonics, while bonding temperature is estimated to be a main effect for thermal pressing. Ultrasonically bonded MEA performance was equal to thermally pressed MEAs at all H₂/O₂ and low H₂/Air operating current densities. However, ultrasonics increases diffusion resistance compared to thermal bonding resulting in poor performance for H₂/Air. No future work is planned for DOE regarding ultrasonic bonding of low-temperature MEAs. Performance testing results will be compiled from NREL and used to support and/or improve conclusions made about ultrasonic bonding.
- High-Temperature MEA Stack Testing – The stack hardware will be utilized to increase the rate at which testing of high-temperature MEAs can be performed. Future testing will focus on optimization of the bonding and treatment conditions and also determining why cell performance in a stack is better than that of a single cell.
- Ultrasonic Bonding Modeling – The model does not predict temperatures exactly, especially for the membrane/electrode interface farthest from the vibrating horn. The validity of thermal boundary conditions used in the model will need to be investigated.
- Testing of Scaled-Up MEAs – Since ultrasonic and thermally bonded MEAs are matched in performance, it can be concluded that the ultrasonic bonding process is effective in producing functional MEAs. However, since the performance of either using the new flow field plates does not match the BASF Fuel Cell specification and testing conditions are identical to those used for the 45-cm² MEAs, the testing protocol and hardware needs to be investigated to determine if other causes of performance error can be determined. A hardware redesign may be necessary.

- Applying Advanced Diagnostics to PBI MEA Ultrasonic Bonding
 - The performance of PBI-phosphoric fuel cells is not strongly affected by the degree ultrasonic and thermal bonding of the MEA assuming an annealing step is preformed following bonding.
 - The wide manufacturing latitude during bonding of PBI/phosphoric acid MEAs supports the possible implementation of a variety of new bonding methods such as ultrasonic bonding and significant reductions in thermal bonding time.
 - CV-based quality control methods are a valuable tool for accessing MEA bond formation and detecting electronic shorts in MEAs.
 - Ultrasonic bonding times on the order of 1-2 seconds can adequately bond MEAs prior to annealing.
 - Early data indicate that anneal times can be reduced from 30 to 5 minutes and traditional thermal pressing times can be reduced from 30 seconds to 5 seconds without negatively impacting performance.
- Diagnostic testing will be used to understand the dependence of MEA bond formation of time during hot pressing and annealing steps.
- The effect of faster cycle time annealing processes on anode performance needs to be defined.
- The applicability of ultrasonic bonding to paper GDLs and larger active areas will be studied.

Special Recognitions & Awards/Patents Issued

1. Snelson, T., Puffer, R., Pyzza, J., Walczyk, D. and Krishnan, L., "Method for the production of an electrochemical cell," *U.S. and International Patents Pending*, 2011. (Licensed to BASF Fuel Cell, Somerset, NJ)

FY 2012 Publications/Presentations

1. Beck, J., Walczyk, D., Buelte, S., Hoffman, C., "Comparison of Performance Losses between Ultrasonic and Thermal Bonding of Membrane Electrode Assemblies in PEMFC," submitted to the *Journal of Fuel Cell Science and Technology* (in review).
2. Beck, J., Walczyk, D., Hoffman, C., Buelte, S., "Ultrasonic Bonding of Membrane Electrode Assemblies for Low Temperature PEM Fuel Cells," *Journal of Fuel Cell Science and Technology*, Paper # FC-12-1022 (in press).
3. Walczyk, D., "Adaptive Process Controls and Ultrasonics for High Temperature PEM MEA Manufacture," DOE 2012 Annual Merit Review, Arlington, VA, May 16, 2012.
4. Hoffman, C. and Walczyk, D. "Non-Contact Spraying of PEM-FC Electrodes: Effects on Production and Performance" *Proceedings of the 2012 World Hydrogen Energy Conference*. Toronto, Canada June 3–8, 2012.

5. Hoffman, C., Walczyk, D. and Cichetti C. “Ultrasonic Spraying of PEM-FC Electrodes,” *European Fuel Cell Forum 2011*, Lucerne, Switzerland. June 28–July 1, 2011.

6. Hoffman, C. and Walczyk, D. “Non-Contact Spraying of PEM-FC Electrodes: Effects on Production and Performance” *Proceedings of the 2012 World Hydrogen Energy Conference*. Toronto, Canada June 3–8, 2012.

References

1. Barrio, A., Paddondo, J., Mijangos, F., and Lombrana, J.I. “Influence of Proton Exchange Membrane Preconditioning Methods on the PEM Fuel Cell Performance.” *Journal of New Materials for Electrochemical Systems*, Vol. 12, 2009: 87-91.
2. Gavach, C., Pamboutzoglou, G., Nedyalkov, M., and Pourcelly, G. “AC Impedance Investigation of the Kinetics of Ion Transport in Nafion Perfluorosulfonic Membranes.” *Journal of Membrane Science*, Vol. 45, 1989: 37-53.
3. BASF. (n.d.). *Celtec-P MEA*. Retrieved July 9, 2012, from BASF Fuel Cell: http://www.fuel-cell.basf.com/ca/internet/Fuel_Cell/en_GB/function/conversions:/publish/content/Microsite/Fuel_Cell/6546_Produktblatt_CeltecMEAs_2_Ansicht.pdf.

VI.4 Non-Contact Sensor Evaluation for Bipolar Plate Manufacturing Process Control and Smart Assembly of Fuel Cell Stacks

Eric Stanfield

National Institute of Standards and Technology
100 Bureau Dr., MS 8211-8211
Gaithersburg, MD 20899
Phone: (301) 975-4882
Email: eric.stanfield@nist.gov

DOE Managers

HQ: Nancy Garland
Phone: (202) 586-5673
Email: Nancy.Garland@ee.doe.gov
GO: Jesse Adams
Phone: (720) 356-1421
Email: Jesse.Adams@go.doe.gov

Contract Number: DE-EE0001047

Project Start Date: October 1, 2009
Project End Date: September 30, 2013

Fiscal Year (FY) 2012 Objectives

- Expand the capabilities of the measurement system to include measurement of plate thickness and variation-in-thickness.
- Identify and quantify all measurement system error sources in the form of an uncertainty budget.
- Optimize the measurement uncertainty of the system by either physically modifying the system design or application of unique and/or improved calibration methods and physical standards.
- Evaluate the uncertainty of the measurement system as a function of scan speed.

Technical Barriers

This project will address the following technical barriers from the Manufacturing R&D — Fuel Cells section of the Fuel Cell Technologies Program Multi-Year Research, Development and Demonstration Plan:

- (B) Lack of High-Speed Bipolar Plate Manufacturing Processes
- (F) Low Levels of Quality Control and Inflexible Processes

Contribution to Achievement of DOE Manufacturing R&D Analysis Milestones

This project will contribute to achievement of the following DOE milestones from the Manufacturing R&D section of the Fuel Cell Technologies Program Multi-Year Research, Development and Demonstration Plan:

- Milestone 2.2 Develop rapid prototyping and flexible tooling specifically for the manufacture of bipolar plates. (4Q, 2012),
- Milestone 2.3: Develop manufacturing processes for PEM bipolar plates that cost <\$3/kW while meeting all technical targets. (1Q, 2018).

FY 2012 Accomplishments

- In FY 2012, we designed and fabricated a fixture to perform opposed point thickness measurements on fuel cell plates (one probe looking down on the plate while the second probe is positioned below the plate looking up). Thickness and parallelism measurements on plates are critical for ‘smart assembly’.
 - Studied error sources in the measurement of thickness using opposed point probing.
 - Developed uncertainty budget for such measurements and validated the budget using thickness measurements on gage blocks of known width.



Introduction

The objective of this project is to enable cost reduction in the manufacture of fuel cell plates by providing a rapid non-contact measurement system that can be used for in-line process control. Manufacturers currently either visually inspect plates or use machine vision systems for verifying tolerances. Such methods do not provide the sub-10 μm accuracy that manufacturers are targeting. In this context, we have studied available non-contact sensors in the market for their suitability to be used for fuel cell plate metrology. From our studies, we have short-listed laser spot triangulation probes as one of the promising candidates for further exploration. We have since incorporated these probes in a unique two-probe system to develop a rapid yet high accuracy non-contact system that manufacturers can adopt towards process control and metrology. We reported the

results of this work in the 2011 DOE Hydrogen and Fuel Cells Program Annual Progress Report and in References 2 and 3. In FY 2012, we have modified the fuel cell measurement system by designing and fabricating a fixture so as to measure thickness of fuel cell plates using an opposed probe configuration (Figure 1). Plate thickness information is critical in ensuring that the stack parallelism and thickness uniformity is within stated tolerances. We have studied error sources in the measurement and developed an uncertainty budget for thickness measurements.

Approach

To achieve the objectives of this project we surveyed both the fuel cell plate manufacturing industry and the measurement equipment manufacturing industry. With regards to the fuel cell plate manufacturing industry, we identified the current measurement inspection technologies being employed, the dimensional parameters of interest, and the applicable tolerance levels encountered. Using this information we researched commercially available high-speed non-contact measurement technologies that might be suitable based on published literature. With potentially suitable measurement technologies identified, we evaluated their suitability more rigorously using a set of tests designed to determine their sensitivity to material characteristics (i.e., surface reflectivity) and ability to measure dimensions representing common plate parameters of interest. The bounds of the material sensitivity testing were chosen so that sensors deemed suitable would be able to measure both highly reflective and highly diffuse materials, representative of metallic and carbon based plates currently being manufactured.

The measurement technology most suitable (laser spot triangulation probes) was assembled into a measurement system (test bed) capable of performing detailed single-sided vertical and lateral channel dimensional inspection. This was followed by the expansion of the system to achieve the ultimate goal of dual-sided evaluation enabling thickness and

variation-in-thickness measurement capability. To achieve this dual-sided capability we were able to adopt the same non-contact probing technology in an alternative configuration versus incorporating another independent non-contact measurement technology. At both design iteration stages, the uncertainty capability of the measurement system developed was rigorously evaluated and optimized, for accuracy and accuracy as a function of speed, through the measurement of reference artifacts and comparison measurements against reference measurements made on sample fuel cell plates using an alternative higher-accuracy method. The sample plates used were representative of plate materials and fabrication methods commonly found in the fuel cell industry. Throughout this process we developed documented testing protocols to enable replication by the industry user in the evaluation of their own systems.

Results

This section describes our results from our opposed-probe thickness measurement.

There are several possible sources of error in our measurement. We consider the following sources of error in thickness measurements:

1. X , Y , Z offsets for both top and bottom probes.
2. Tilt angles in YZ plane for both top and bottom probes.
3. Tilt angles in XZ plane for both top and bottom probes

The offset error occurs when the two probes do not read zero at the same point in space. This separation may be resolved along the X , Y , and Z directions. We compensate the measured data for the X and Z offsets as discussed below. We also present a method to estimate the Y offset; this is later used in the uncertainty budget. While we estimate the tilt angles of the probes, we do not compensate the measured data; we simply used the estimates in the uncertainty budget for thickness.

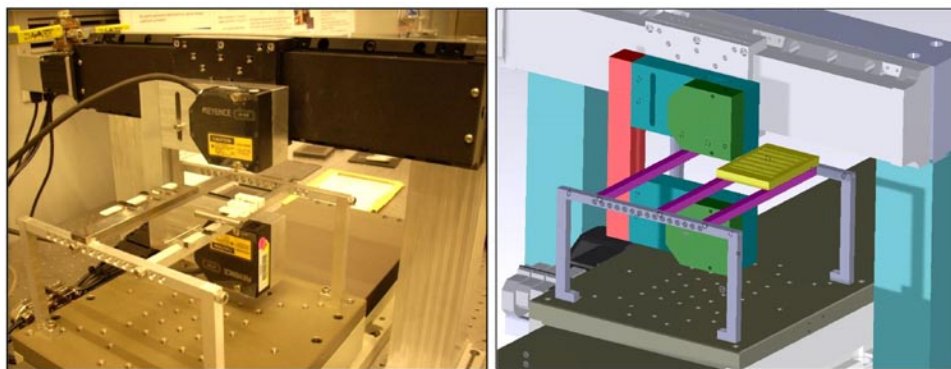


FIGURE 1. Photo and schematic of opposed probe configuration for thickness measurements

Probe Z Offset

Since the thickness measurement is the sum of the readings of the two probes, a Z offset error will directly affect thickness measurements. While measuring the thickness of a single calibrated gage block (and comparing against its known thickness) will provide an estimate of this offset, we measured thicknesses of multiple blocks to determine an average offset.

Probe X and Y Offset

The X offset calibration is performed by mounting a cylinder so that its axis is parallel to the Y axis. The two probes then scan a profile across this cylinder. Best fit circles are constructed on the data and the shift along the X axis is used as the estimate for the X offset. In order to estimate the Y offset, a disk with sharp edges is placed on the table and scans are performed on chords away from the largest diameter (all scans are along X axis). From the measured chord lengths for the two probes (L_1 and L_2), and the known disk radius R , we estimate the Y offset. Refer to Figures 2(a) and 2(b).

Tilt Angles

The probes can be tilted in both the XZ and the YZ planes. We estimate the magnitude of the tilts by measuring the thickness of several gage blocks of known thickness. Tilted probes will produce a larger measured thickness. This produces an upper bound on the tilt angle for the probes. We manually adjust the tilt to obtain an upper bound of $\pm 3^\circ$ on the probe tilt and use this value in the uncertainty budget for thickness measurements.

Opposed Probe Thickness Measurement Uncertainty Budget (using 4-mm nominal thickness gage block)

Laser triangulation probes are sensitive to material/optical properties of the test artifact and suffer from linearity errors. Assuming the Z offset calibration suffers from a $\pm 5 \mu\text{m}$ error due to the difference in material properties between the calibration artifact and the test artifact, and assuming a rectangular distribution, the standard uncertainty in the offset calibration will be $5/\sqrt{3} = 3 \mu\text{m}$. The manufacturer's specification for probe linearity is also $\pm 5 \mu\text{m}$, and therefore assuming a rectangular distribution, the standard uncertainty in thickness measurements will be $5/\sqrt{3} = 3 \mu\text{m}$.

The X and Y offsets will not introduce an error when measuring perfectly flat/parallel gage blocks if the block is aligned to have no tilt. On the other hand, if the block is tilted (we are assuming a bound of $\pm 3^\circ$ for the tilt and a rectangular distribution), and assuming a 50- μm error in the calibration of the X and Y offset, we estimate a standard uncertainty of $5 \mu\text{m}$ in thickness due to these offsets.

Assuming a bound of $\pm 3^\circ$ for the probe tilt in the XZ and YZ planes, we estimate a standard uncertainty of $3.5 \mu\text{m}$ for thickness of the 4-mm thick gage block due to probe tilt.

It is not clear yet how the stage motion errors will contribute to thickness measurement errors. Z straightness errors have a negligible effect on the thickness errors since it affects both probes in the same way. The rigidity of the plate fixture will perhaps contribute to thickness measurement errors, but we have not yet determined its precise quantitative influence. We are currently operating the stage at 30 mm/sec. Increasing the speed will deteriorate measurement accuracy unless a more rigid fixture is designed.

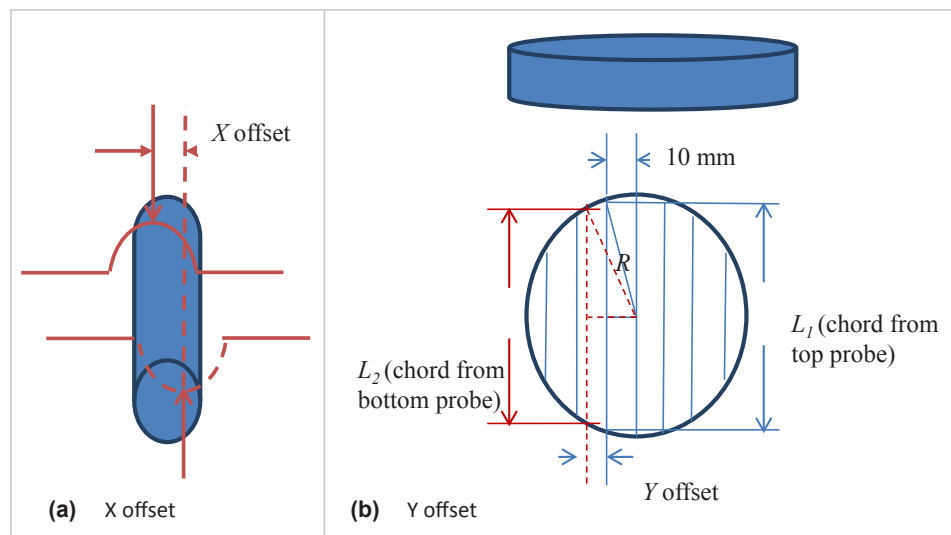


FIGURE 2. Estimating the X and Y offsets

Combining the terms above, we estimate a combined standard uncertainty of 10 μm , or an expanded uncertainty of 20 μm ($k = 2$) on the thickness values.

TABLE 1. Results from measurements on gage blocks

| Gage Block Manufacturer | Nominal (mm) | Deviation from Nominal (mm) |
|-------------------------|--------------|-----------------------------|
| Webber | 3.302 | -0.0067 |
| Webber | 6.350 | -0.0051 |
| Mitutoyo | 4.318 | -0.0014 |
| European | 4.000 | -0.0020 |

Conclusions and Future Directions

- Designed and fabricated a fixture to measure opposed point thickness of fuel cell plates.
- Studied error sources in the measurement, developed procedures to calibrate the system parameters (offsets and tilts), and developed an uncertainty budget for thickness measurements.
- Validated the system by measuring gage blocks of known width.
- Future work includes measurement of fuel cell plate thickness and comparing the measured values against measurements from other techniques (using a coordinate measuring machine to measure the thickness).
- Refine the uncertainty budget by further studying the error sources.

Disclaimer

Certain commercial equipment, instruments, or materials are identified in this paper in order to specify the experimental procedure adequately. Such identification is not intended to imply recommendation or endorsement by the National Institute of Standards and Technology, nor is it intended to imply that the materials or equipment identified are necessarily the best available for the purpose.

Acknowledgements

The work detailed in this report would not have been possible without the contributions of the following; all are NIST employees unless designated otherwise: Wei Ren, Bala Muralikrishnan, Eric Stanfield, and Ted Doiron.

FY 2012 Publications/Presentations

1. B. Muralikrishnan, W. Ren, D. Everett, E. Stanfield, T. Doiron, Performance evaluation experiments on a laser spot triangulation probe, *Measurement: Journal of the IMEKO*, 45(3) 2012, 333-343.

References

1. E. Stanfield, "Non-Contact Sensor Evaluation for Bipolar Plate Manufacturing Process Control and Smart Assembly of Fuel Cell Stacks," 2011 DOE Hydrogen and Fuel Cells Program Annual Progress Report, November 2011, http://www.hydrogen.energy.gov/pdfs/progress11/vi_10_stanfield_2011.pdf
2. B. Muralikrishnan, W. Ren, D. Everett, E. Stanfield, T. Doiron, Dimensional Metrology of Bipolar Fuel Cell Plates Using Laser Spot Triangulation Probes, *Measurement Science and Technology*, 22(7), July 2011.
3. B. Muralikrishnan, W. Ren, D. Everett, E. Stanfield, T. Doiron, Performance evaluation experiments on a laser spot triangulation probe, *Measurement: Journal of the IMEKO*, 45(3) 2012, 333-343.

VI.5 High Speed, Low Cost Fabrication of Gas Diffusion Electrodes for Membrane Electrode Assemblies

Emory S. De Castro
BASF Fuel Cell, Inc.
39 Veronica Avenue
Somerset, NJ 08873
Phone: (732) 545-5100 ext 4114
Email: Emory.DeCastro@BASF.com

DOE Managers
HQ: Nancy Garland
Phone: (202) 586-5673
Email: Nancy.Garland@ee.doe.gov
GO: Jesse Adams
Phone: (720) 356-1421
Email: Jesse.Adams@go.doe.gov

Contract Number: DE-EE0000384

Subcontractor:
Dr. Vladimir Gurau
Case Western Reserve University, Cleveland, Ohio

Project Start Date: July 1, 2009
Project End Date: June 30, 2013

Contribution to Achievement of DOE Manufacturing R&D Milestones

This project will contribute to achievement of the following DOE milestones from the Manufacturing R&D section of the Fuel Cell Technologies Program Multi-Year Research, Development and Demonstration Plan (Section 3.5.7):

- Develop continuous in-line measurement for MEA fabrication. (4Q, 2012)
- Establish models to predict the effect of manufacturing variations on MEA performance. (4Q, 2013)

This project addresses coating speed and uniformity of gas diffusion electrodes (GDEs), a critical component for MEA fabrication. One sub-task is to develop a continuous X-ray fluorescence (XRF) analyzer that directly measures catalyst deposition level and distribution on rolled goods, ultimately guiding improvements in through-put and uniformity. This sub-task directly contributes to the fourth quarter 2012 goal for in-line measurement. Another sub-task is to develop models that predict the effect of manufacturing variations in catalyst distribution and porosity in GDEs, and relate these variations as six-sigma limits for a component specification. The establishment of a model that predicts MEA performance based on manufacturing variations in GDEs contributes to improving the quality of the component as well as achieving the fourth quarter 2013 DOE milestone above.

FY 2012 Accomplishments

- Reduced labor cost to manufacture GDE further from last year's 50% to 75%.
- Scaled up all ink preparations >10-fold.
- Exceeded project goal of three-fold increase of throughput for cloth-based GDEs at production scale.
- Demonstrated path to further cost reductions for GDEs on a lower cost non-woven web.



Introduction

The basis of this project is to create gas diffusion electrodes at a far lower cost than those currently available. GDEs are critical components of membrane electrode assemblies and represent the highest cost subcomponent

Fiscal Year (FY) 2012 Objectives

- Reduce cost in fabricating gas diffusion electrodes through the introduction of high speed coating technology, with a focus on materials used for the high-temperature membrane electrode assemblies (MEAs) that are used in combined heat and power generation (CHP).
- Relate manufacturing variations to actual fuel cell performance in order to establish a cost-effective product specification.
- Use advanced quality control methods previously developed to guide realization of these two objectives.

Technical Barriers

This project addresses the following technical barriers from the Manufacturing R&D section of the Fuel Cell Technologies Program Multi-Year Research, Development and Demonstration Plan (Section 3.5):

- (A) Lack of High Volume Membrane Electrode Assembly (MEA) Processes
- (F) Low Levels of Quality Control and Inflexible Processes

of the MEA. Cost reduction will be accomplished through development of a higher throughput coating process, modeling the impact of defects due to the higher speed process, and overcoming these limitations and providing a six-sigma manufacturing specification that relates performance to defects. The main focus of the effort is creating next-generation inks through advanced additives and processing methodologies. As part of our approach, we will also develop on-line quality control methods such as determination of platinum concentration and distribution during the coating process. The on-line mapping of platinum will guide the ink development process and provide feedback on uniformity.

For this reporting period we applied last year's understanding to scale up our approach to preparing stable inks of carbon black or catalyzed carbon black and hydrophobic binder. The use of a hydrophobic binder is critical to create GDEs for high temperature MEAs. In this period we significantly scaled up and further improved the inks. We demonstrated that these more concentrated inks are able to reduce the number of applications needed per pass. The improvements noted last year (increase of throughput, superior catalyst utilization, improved surface quality) were maintained in this period's scale up efforts. We also continued our efforts at ink development for the even lower cost non-woven carbon substrates.

Approach

GDEs are comprised of a gas diffusion layer coated with catalyst. The gas diffusion layer is simply carbon cloth or a non-woven carbon that has been coated with carbon black and serves as a current collector for the catalyst. For both the carbon black and catalyst, a hydrophobic binder is added to achieve critical porosity and hydrophobicity in the final structure. Of the carbon black, catalyst, or hydrophobic binder none are soluble in aqueous solutions. Aqueous solutions must be used as solvents since the use of organic solvents with a highly active catalyst is too dangerous in a production environment. Also, the hydrophobic binder is shear-sensitive, meaning it becomes less stable when pumped or subjected to shear forces in the coating applicator. Thus, the challenge in this project is overcoming the inherent physical limitations in these materials through advanced formulations and processing.

Our approach to solving this challenge begins with identifying key quality GDE metrics that relate directly to ink performance, develop an understanding of the forces behind ink stability, and introduce solution measurement methods that relate ink performance to the quality metrics. With more stable ink formulations, we anticipate being able to coat longer and wider webs at higher speeds. If an ink can be made more concentrated and remain stable we can use less application passes and save cost. The ink development

process is supplemented by two other activities that ultimately lead to lower cost GDEs. We developed a model that will predict the impact of manufacturing variations on MEA performance, and used this model to determine the level of coating quality needed to maintain consistent current and voltage. Also, we created on-line instruments to lead development of more precise coating processes.

Results

Ink Scale Up

Last year we reported on a combination of additives and processing that allowed us to create a superior carbon-binder ink for the microporous layer (MPL). We were able to reduce the number of passes needed to form the MPL and created an improved surface. Upon scaling this preparation to support our final goal of coating cloth widths >1 meter and lengths ~300 linear meters, we developed new methods to safely introduce high volumes of carbon that led to severe bubble formation. This increase in bubbles led to variations in viscosity as the bubbles slowly degassed. We identified a defoaming approach that solved this issue and thus increased the preparation scale. Table 1 summarizes our efforts on ink scale up.

TABLE 1. Ink Scale-Up Metrics

| | Cost Decrease vs. benchmark | Capacity increase vs. benchmark |
|---------|-----------------------------|---------------------------------|
| MPL | 37% | 3.0X |
| Anode | 31% | 2.1X |
| Cathode | 40% | 2.4X |

In Table 1, "Cost Decrease" represents the reduction of labor-hours to make the ink. "Capacity increase" indicates the total time saved to create a batch of ink now using larger scale preparation equipment.

Cathode and Anode Electrode Layers

Last year we reported on improvements for both the anode and cathode ink preparations. At that time, these improvements had not been evaluated at a full length of carbon cloth nor a full width. These two conditions place the maximum challenge on ink stability. Also, materials made under this project were sent as MEAs to a major supplier of micro-combined heat and power (μ -CHP) stationary power systems. From this evaluation we confirmed with large-scale format MEAs the performance and quality gains shown in our lab, but also learned the overall thickness was less than the commercially accepted product. We modified the MPL architecture based on this feedback to move the average thickness within range. Table 2 provides an overview of key metrics achieved at the full length-width scale. These metrics

were also achieved with a 4-fold increase in throughput due to: increase in solids content of inks and reduction in number of coating passes, more than doubling the width of the carbon cloth, and increasing the speed of some of the application steps.

TABLE 2. Performance Metrics at >300 Linear Meter Length and >1 Meter Width Carbon Cloth

| | Benchmark at Start | This Project |
|---|-------------------------------|------------------------------|
| Agglomerates (avg. over roll) | 18/m ² | 1.6/m ² |
| Pt variation (via on-line XRF, roll average) | +/- 2.0 gm Pt/ m ² | +/-0.4 gm Pt/ m ² |
| Performance | | |
| 0.2 A/cm ² H ₂ /air, 45 cm ² test cell, 160°C | 0.657 V | 0.683 V |
| 0.5 A/cm ² H ₂ /air, 45 cm ² test cell, 160°C | 0.573 V | 0.598 V |
| 0.2 A/cm ² , 1.4/5 Reformate (71% H ₂ , 27% CO ₂ , 2% CO)/Air, 45 cm ² test cell, 180°C | 0.668 V | 0.689 V |
| 0.5 A/cm ² , 1.4/5 Reformate (71% H ₂ , 27% CO ₂ , 2% CO)/Air, 45 cm ² test cell, 180°C | 0.571 V | 0.589 V |

Conversion of Lower Cost Substrates

A second major focus of this project is to develop lower cost substrates into gas diffusion electrodes. Non-woven carbon fiber materials (“carbon paper”) are believed to be ~30% lower in cost compared to the carbon cloth at higher volumes. The porosity, hydrophobicity, and absorption properties of the carbon papers are totally different than carbon cloth, and we had to develop an entirely new class of inks for MPL, anode electrode layer, and cathode electrode layer. We continue our work in this area with a goal of further increasing the solid content beyond that of the carbon cloth inks and subsequently reducing again the number of application passes.

Conclusions and Future Directions

We have successfully exceeded the project’s target for carbon cloth substrates by gaining a four-fold increase in material throughput and a labor savings of ~75%. Advances from this project are being transitioned to our current production with a direct immediate impact on component cost and a release of a new product. Future directions for the remaining time will be on the non-woven substrates and a further reduction in cost.

Upcoming Focus

1. Demonstrate on the pilot scale a further 30% reduction in total cost of gas diffusion electrodes when using non-woven substrates.

VI.6 Development of Advanced Manufacturing Technologies for Low Cost Hydrogen Storage Vessels

Mark Leavitt

Quantum Fuel Systems Technologies Worldwide, Inc.
25242 Arctic Ocean Drive
Lake Forest, CA 92630
Phone: (949) 399-4584
Email: mleavitt@qtww.com

DOE Managers

HQ: Nancy Garland
Phone: (202) 586-5673
Email: Nancy.Garland@ee.doe.gov
GO: Jesse Adams
Phone: (720) 356-1421
Email: Jesse.Adams@go.doe.gov

Contract Number: DE-FG36-08GO18055

Subcontractors:

- Boeing Research and Technology, Seattle, WA
- Pacific Northwest National Laboratory (PNNL), Richland, WA

Project Start Date: September 1, 2008

Project End Date: March 31, 2013

Fiscal Year (FY) 2012 Objectives

Develop new methods for manufacturing Type IV pressure vessels for hydrogen storage with the objective of lowering the overall product cost by:

- Optimizing composite usage through combining traditional filament winding (FW) and advanced fiber placement (AFP) techniques.
- Exploring the usage of lower-strength, higher-modulus fibers on the outer layers of FW.
- Building economic and analytical models capable of evaluating FW and AFP processes including manufacturing process variables and their impact on vessel mass savings, material cost savings, processing time, manufacturing energy consumption, labor and structural benefits.
- Studying polymer material degradation under high-pressure hydrogen environment to optimize storage volume.

Technical Barriers

The project addresses the following technical barriers from the Manufacturing R&D section (3.5) of the Fuel Cell Technologies Program Multi-Year Research, Development and Demonstration Plan:

- (G) High-Cost Carbon Fiber
- (H) Lack of Carbon Fiber Fabrication Techniques for Storage Tanks

Contribution to Achievement of DOE Manufacturing R&D Milestones

This project will contribute to achievement of the following DOE milestone from the Manufacturing R&D section of the Fuel Cell Technologies Program Multi-Year Research, Development and Demonstration Plan:

- Milestone 6.2: Develop fabrication and assembly processes for high pressure hydrogen storage technologies that can achieve a cost of \$6/kWh. (4Q, 2015)

FY 2012 Accomplishments

- Modified the current in-house computer program (KWind) for generating a finite element analysis (FEA) model of the composite shell using the filament winding process to mWind, which allows more composite shell layer options using AFP methods.
- Completed the next vessel design with mWind to incorporate lower-cost fiber in addition to AFP dome caps and baseline fiber.
- Implemented infrared (IR) heater to reduce cutter jamming and improve precision of heated area for manufacturing AFP dome caps.
- Re-engineered the tensioning system, which utilizes low-cost active control (passive feedback controls) allowing consistent tension, and avoids slack during head and arm movements.
- Conducted process improvements to reduce marcelling or wrinkling in AFP end dome plies.
- Built and tested an in situ tensile rig for high-pressure hydrogen to test polymer materials.



Introduction

The goal of this project is to develop an innovative manufacturing process for Type IV high-pressure hydrogen storage vessels, with the intent to significantly lower manufacturing costs. Part of the development is to integrate the features of high precision AFP and commercial FW. Evaluation of an alternative fiber to replace a portion of the baseline fiber will help to reduce costs further.

Approach

The hybrid vessel designs were based on FEA results to optimize strain distribution and achieve uniform displacement in the domes of the vessel. The in-house software for generating a FEA model of the composite shell based on the filament winding process was modified to allow more composite shell layer options using the AFP methods. AFP dome caps were manufactured by Boeing according to FEA results. A series of testing to national standards will be conducted to validate the hybrid designs.

Results

Vessel Designs

Vessel 8: In the 2011 annual report, it was reported that Vessel 8, which was an identical build to Vessel 7 (passed burst test at 22,925 psi; requirement is 22,843 psi), did not pass the ambient cycle test at Quantum. It completed 13,500 out of the required 15,000 cycles.

After cutting the forward dome off the vessel, it was found that the liner was bonded to the composite at two different locations. One was near the forward boss, and the other was along the entire circumference of the transition area between AFP and FW on the forward dome. The bonding was caused by curing the vessel at a temperature that was too close to the softening temperature of the liner material. On the vessels for ambient cycle tests in the future, a plastic film with higher melting temperature than the desired curing temperature will be applied between the liner and composite to prevent bonding. Previous experience with this film assures that this failure mode will not repeat in the future.

Vessel 9: With the failure mode of Vessel 8 understood, Vessel 9 was designed to utilize lower-cost fiber to further reduce vessel cost. The identified lower-cost fiber has lower strength but higher modulus than the baseline fiber. The rationale is that the outer layers experience a lesser load than the inner layers; therefore, usage of baseline fiber on the outside is not necessary. Meanwhile, the higher modulus property distributes the load onto the outer layers without overloading the inner baseline fiber layers.

To satisfy the design criteria established by Vessel 7 in the FEA, two additional helical patterns were added to

maintain the same strains. Overall 37% of the baseline fiber in Vessel 7 was replaced with lower-cost fiber in Vessel 9. Although an additional fiber type was introduced in the design, the resin system remained the same for the entire FW process. The cost savings and weight increase are detailed out in the Cost Model section of this report.

The result was 5.2 MPa (760 psi) short of the burst requirement. The failure location was at the tangent between the cylinder section and the aft dome. Since the result was very close to the requirement and the vessel was wound over two days (due to winding pattern development), it was determined to repeat the Vessel 9 build. Experience shows a 10% performance gain when a vessel is wound in just one day.

Vessel 10: Vessel 10 only improved by 2.1 MPa (305 psi) from Vessel 9 in burst pressure. The improvement was negligible. The failure location was again at the tangent between the cylinder section and the aft dome. The result indicated that it was not a manufacturing issue of winding over two days.

Vessel 11: The allowable strains of Vessels 9 and 10 were based on the successful results of Vessel 7, which passed the burst test by 0.56 MPa (82 psi). Both Vessels 9 and 10 results showed that the design criteria used in the previous analyses were too aggressive to ensure successful burst tests. Therefore, all but seven of the lower-cost fiber layers were replaced back with the baseline fiber. Although this design would make the vessel heavier and more expensive than Vessel 7, it would verify whether the failure was caused by using the wrong fiber material properties or other design issues.

Surprisingly the burst test result was lower in Vessel 11 than those of Vessels 9 and 10. It only achieved 138.1 MPa (20,026 psi), although the allowable fiber strains from analysis were even lower than those of Vessel 7. This vessel also failed at the tangent between the cylinder section and the aft end. While the vessel was designed with the highest strain in the cylinder section, the burst location was at the tangent. It shows the analysis method needs to be modified to accommodate the hybrid (AFP + FW) design.

FEA Model Generation Software Upgrade

The current in-house computer program (KWind) generates a FEA model of the composite shell using the filament winding process. KWind was originally written for only filament wound pressure vessels and was rewritten (called mWind) to allow more composite shell layer options using AFP methods.

KWind only models the ending points of a composite layer created during filament winding, but it does not allow a composite layer to have a starting point which can be generated using the AFP process. Up to this point in time, models generated with KWind were hand modified to account

for different start and stop points in the middle of a layer. These modifications left unused elements in the layers that did not model the composite structure correctly. The overlap areas where plies started and stopped in the middle of the layer were also not modeled correctly to provide accurate results.

The basic methodology of KWind was to build the composite shell one layer at a time. mWind took the approach of taking a small section of the composite shell and building up each layer in the section. This allows the model to add and subtract layers through the model with start and stop points for each layer. mWind starts by building a base model from the geometry, material properties and composite layup information. The base model and loading conditions are used to write an input file for a two-dimensional (2-D) axisymmetric shell model, a three-dimensional shell model, or the traditional 2-D axisymmetric continuum model similar to KWind. Currently mWind writes shell models to the FEA program ABAQUS.

KWind contains a subroutine to read the results of finite element solution and calculate fiber strains for selected layers in the composite structure. mWind also has incorporated this subroutine to calculate and plot fiber strains. For plotting, the graphics calls of KWind were not translated. Instead the graphics functions of Excel are used. mWind also reads the base finite element results into Excel and allows users to create other calculations and plots using Excel commands and other user written subroutines. mWind also has subroutines to read and store analysis results into an Excel worksheet without the base model information. This latest software was used to design Vessel 12 to incorporate AFP with baseline and lower-cost fibers. The build was just completed at the time of writing this report.

New Six-Tow Quarter-Inch Head Integration (AFP)

Boeing has built and implemented the next-generation fiber placement head, specifically designed for the fiber placement of pressure vessels. Laying towpreg (resin-impregnated tow) on the vessel or liner demands a very narrow head that can pass as close to the polar bosses as possible to allow many design options for optimal vessel performance. The new fiber placement head assembly has been integrated into Boeing's AFP KUKA KR240 long arm robotic cell. The integration also includes the kinematic linking between the robot and the head stock (rotation axis) to which the dome tool is fixed. This allows the translation and rotation between the motions of the robot and the tool to be linked to one another. Tests were conducted to verify that no slipping or misalignment was present in the layup that would be caused by the kinematics between the robot and the head stock.

Advanced Tensioning System

Boeing has also incorporated a new dynamic spool tension system, capable of accurately controlling the tension

of each spool as material is both pulled off and rewound back onto the spool. The underlying goal of a tensioning system is a low-cost, highly-reliable system that can be packaged on the arm of a medium-sized robot without overloading its payload capacity. The advanced design improves upon reducing slack in the system when tow is needed to be "taken up" or back spooled, as well as creating a consistent desired level of tension throughout the entire layup process. This is created by adding dancer arms to pick up the excess slack in the system caused by the response rate of the motor as it changes both direction and torque/velocity levels. The new tensioning system reduces the amount of high-level tension seen during the starts and directional change, giving it a more consistent level of tension throughout the course layup. A closed-loop, feed-back control system reduces the excessive spike levels of tension in the system during layup, increasing the overall quality of the layup.

Newly Designed Infrared Heating System

At Boeing, a newly designed infrared heating system was incorporated into the head to overcome limitations with the previous hot-gas heater. Previous issues included hot gas pockets, hot air entering cutter region, frequent cutter jams associated with excessive heating, inability to control heated area efficiently, and noise level. Figure 1 shows the IR heating system in use on our first Phase III forward dome cap. The new heating system has increased the reliability and productivity by eliminating excessive heating of the cutter blade. The heated zone of the IR heating system is better controlled, allowing for a more efficient and effective system.

Cost Model

The estimated cost of Vessel 9 was compared with Vessel 7 by PNNL. A cost savings of more than 5% was

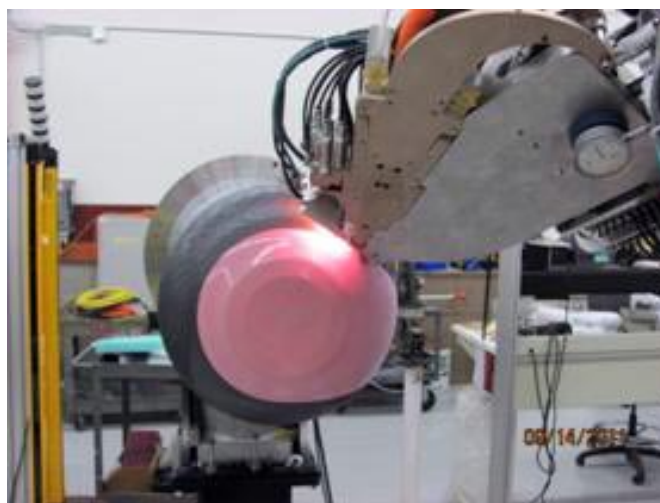


FIGURE 1. Implemented New Infrared Heating System, which Reduces the Frequency of Cutter Jams due to Excessive Heating in the Cutter Region

estimated (based on low volume price of \$13/lb for low-cost fiber vs. the \$16/lb for baseline fiber) with a weight increase of less than 2%. During the year, the cost models were also used to provide information on the possible cost savings of advanced vessel manufacturing methods to the National Academies of Sciences review of the U.S. DRIVE Program.

Polymer Materials Characterization

At PNNL, the in situ tensile test frame (Figure 2) was further refined and used to quantify the effects of high-pressure hydrogen on polymer vessel liner materials. The miniature tensile frame (28 cm in height, 12 cm in diameter) fits inside the high-pressure autoclave and is actuated by a solenoid. High density poly-ethylene (HDPE) samples were pulled in air and in 100% hydrogen at 4,000 psi hydrogen. Figure 3 shows that hydrogen in the polymer structure (the blue curve) lowers both the elastic modulus and the yield strength. Additional tests of different HDPE materials are being analyzed for documentation in the final technical report and a peer-reviewed publication. While the test frame has been used exclusively for polymer testing to date, metal foils could also be tested if the sample cross-sectional area was matched to the maximum load of the system. The system has been shown to work reliably in pure hydrogen.

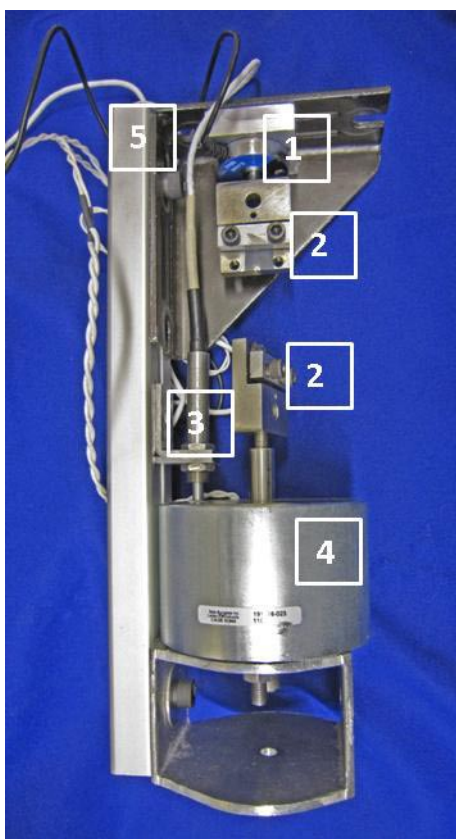


FIGURE 2. Side View of the In Situ Tensile Tester showing the (1) Load Cell, (2) Sample Grips, (3) LVDT, (4) Solenoid, and (5) Support Frame

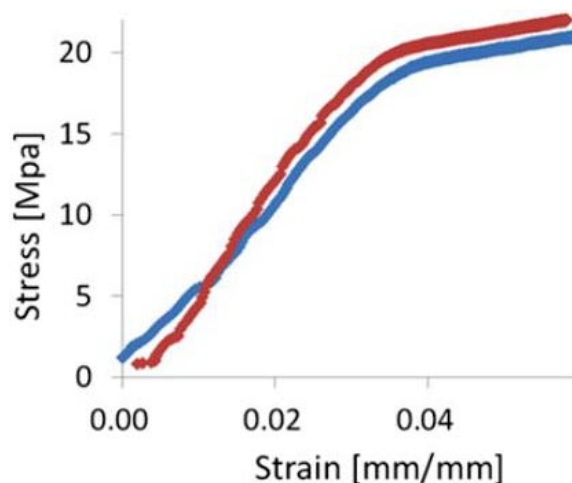


FIGURE 3. Difference in Modulus between the HDPE Pulled in Air (Blue) and the HDPE Pulled in High-Pressure Hydrogen (Red)

Conclusions and Future Directions

- Test results in 2011 showed that this hybrid process is a promising method to reduce vessel cost. 22.9% of composite was saved while equipment and factory costs for the process are small relative to the composite savings.
- In-house software has been modified to generate more accurate FEA models of the composite shell specifically for AFP.
- Lower-cost fiber has been incorporated with baseline fiber and AFP to further reduce vessel cost by 5% while keeping weight increase to less than 2%.
- AFP manufacturing tooling and method have been improved to deliver higher quality dome caps.
- Boeing is working on the next revision of the tension controls, further refining the tensioning, allowing faster response in directional change, and enabling active feedback controls.
- For further understanding of polymer material behaviors in high-pressure hydrogen, PNNL has built and tested an in situ tensile rig that operates at 4,000 psi.
- Perform burst test, ambient temperature cycle test, extreme temperature cycle test and accelerated stress rupture test to validate process and material changes critical to the hybrid vessel design.
- Update cost model with the cost and amount of lower-cost fiber used in the final hybrid design.
- Complete in situ testing of HDPE in hydrogen at pressure.

FY 2012 Publications/Presentations

1. Development of Advanced Manufacturing Technologies for Low Cost Hydrogen Storage Vessels, Annual Merit Review, Department of Energy, May 14–18, 2012, Arlington, VA.

2. Development of Advanced Manufacturing Technologies for Low Cost Hydrogen Storage Vessels, Hydrogen Storage Tech Team, June 21, 2012, Oak Ridge National Lab, Oak Ridge, Tennessee.

VI.7 Cause and Effect: Flow Field Plate Manufacturing Variability and its Impact on Performance

Eric Stanfield

National Institute of Standards and Technology (NIST)
100 Bureau Drive, MS 8211
Gaithersburg, MD 20899-8211
Phone: (301) 975-4882
Email: eric.stanfield@nist.gov

DOE Managers

HQ: Nancy Garland
Phone: (202) 586-5673
Email: Nancy.Garland@ee.doe.gov
GO: Jesse Adams
Phone: (720) 356-1421
Email: Jesse.Adams@go.doe.gov

Contract Number: DE-EE0001047

Subcontractor:

Los Alamos National Laboratory (LANL), Los Alamos, NM

Project Start Date: October 1, 2007

Project End Date: September 30, 2012

Contribution to Achievement of DOE Technology Manufacturing R&D Milestones

This project will contribute to achievement of the following DOE milestones from the Manufacturing R&D section of the Fuel Cell Technologies Program Multi-Year Research, Development and Demonstration Plan:

- Milestone 2.3: Develop manufacturing processes for polymer electrolyte membrane bipolar plates that cost <\$3/kW while meeting all technical targets. (1Q, 2018).

FY 2012 Accomplishments

- Completed a statistical analysis of LANL's polarization measurements obtained from each of the ten experimental plates.
- Submitted and received approval for a NIST NCNR beam experiment to visualize the water content within the channels for a subset of the experimental plates representing the best, worst, and nominal designs.
- Fabricated and dimensionally verified the replacement experimental plate 5C to enable completion of the backpressure sensitivity experiment.
- Fabricated and dimensionally verified all experimental plates and end plate hardware to facilitate the NCNR beam experiment (material substitutions were required for optimal imaging).
- Acquired the assistance of Dr. Jeffery Allen from Michigan Technological University who is an expert in two-phase flow with specific application to fuel cells to help in the understanding of the underlying physics and to provide guidance in the development of the imaging experiment objectives.



Fiscal Year (FY) 2012 Objectives

- Fabricate and verify replacement experimental plate 5C in order to conclude back pressure sensitivity experiment.
- Complete statistical analysis of polarization curve measurements for each of the 10 experimental cathode plates.
- Incorporate NIST Neutron Center for Neutron Research (NCNR) imaging experiment to visually quantify differences in water management between poor and optimal performing experimental plates, as well as, the nominal design plates made with minimal dimensional variations.

Technical Barriers

This project addresses the following technical barriers from the Manufacturing R&D section of the Fuel Cell Technologies Program Multi-Year Research, Development and Demonstration Plan:

- (B) Lack of High-Speed Bipolar Plate Manufacturing Processes
- (F) Low Levels of Quality Control and Inflexible Processes

Introduction

This project originated conceptually as a result of a workshop organized by the Center of Automobile Research and NIST in December of 2004, where industry bipolar plate manufacturers identified a need for engineering data that relate geometric bipolar plate tolerances to fuel cell performance. This need is in response to pressure from fuel cell designers to produce lower cost plates that potentially require quality related trade-offs, by plate manufacturers, to achieve desired cost targets. Manufacturers questioned the relevance of stated tolerances on dimensional features of bipolar plates and expressed a desire for published

engineering data relating performance and dimensional quality of the plates. This project was proposed to address this need and was partially funded through the NIST Advanced Technology Program Intramural Competition for a period of three years (FY 2005-FY 2007). The Advanced Technology Program funding was also intended to aid NIST with the development and validation of a single-cell testing laboratory. In 2008, DOE recognized the potential value in the outcome of this project, subsequently adding it to their portfolio of fuel cell manufacturing related projects and provided funding in an attempt to ensure successful completion.

This experiment focuses on introducing very precisely controlled dimensional variations within the flow field channels of the cathode side flow field plate where reaction-generated water often interferes with the supply of oxygen (via air). Through the fabrication of multiple cathode plates with specific dimensional variations with different magnitudes and through substitution of these plates in a fuel cell, we hope to observe measureable differences in the output (performance) of the fuel cell. Using these differences, we then hope to statistically determine which single factors or two-factor interactions are most important. The most challenging aspect of this experiment comes from choosing the proper factors to vary and their corresponding magnitudes along with controlling and limiting all other sources of variability, such as those related to materials or the experimental testing procedure

Approach

Using a statistically based design-of-experiments (Figure 1), NIST fabricated experimental “cathode” side flow field plates with various well-defined combinations of flow

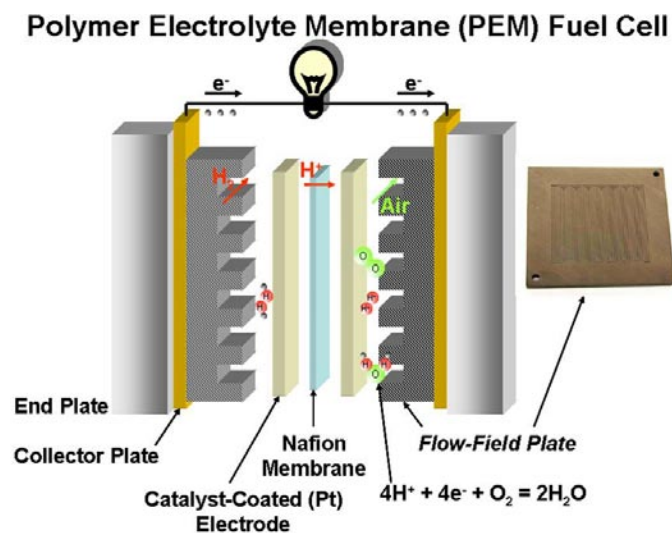


FIGURE 1. Concept - Reference Single Cell and NIST Fabricated Cathode Flow-Field Plates

field channel dimensional variations (Table 1). Then through single-cell fuel cell performance testing, using a well-defined protocol, NIST quantified any performance effects and correlated these results into required dimensional fabrication tolerance levels.

Results

Prior work included several performance testing protocol revisions necessary to achieve improved repeatability and to highlight the mass transport differences between the experimental cathode plates. Protocol optimization was validated through repeatability testing and results were commensurate with our benchmarks. LANL evaluated the performance of all the experimental plates by integrating each one in the reference single cell full cell then running multiple polarization curves. The DOE Annual Merit Review process combined with industry interactions have been invaluable with regards to the incorporation of additional experiments that validate the results over a broader range of applicability (back pressure sensitivity experiment) and the addition of alternative means to ensure intended channel perturbations are indeed the cause of the observed variability (neutron imaging experiment). All of the above work is described in detail in references [1-3] with the exception of the neutron imaging experiment, which is discussed in the following section.

In 2011 and 2012 we have focused on concluding the back pressure sensitivity test by fabricating and dimensionally verifying a replacement plate 5C and finalizing the project outcome with a rigorous statistical analysis of all the measurement results. During this time we received feedback from our peers regarding potential causes for operational differences that could be unrelated to the intended variations and that a lack of verification could limit the usefulness of the results. In response, we decided to explore the opportunity to perform neutron imaging on a subset of these experimental plates that represent the largest dispersion in output so that we can better understand the water management dynamics within the flow field channels. The submitted proposal was awarded beam time allotment in January 2012 and is currently scheduled for mid-September 2012. In preparation for this experiment, several material substitutions were required to optimize imaging; these included fabrication of the endplates from 6061 aluminum to replace the current stainless steel plates and fabrication of the experimental plate subset from a pure carbon material (POCO AXF-5Q) versus the same material but with a hydrocarbon material impregnation (POCO AXF-5QCF). The plate material substitution added additional processing and expense caused by the porosity of the plates needing to be sealed to prevent water uptake. Following the flow field fabrication at NIST, we are having POCO post-process the plates using their proprietary purifying and pyrosealing process. This process does not introduce any new materials

TABLE 1. Design of Experiment 2⁴⁻¹ Fractional Factorial Design...4 Parameters, 2 Levels, and Replicate Center Point

| 2 ⁴⁻¹ Fractional Factorial Design with replicated center point (k=4,n=10) | | | | | | | | | |
|--|-----------------------|-----------------------|---------------------|----------------|-----------|-----------|---------------|---------------|-----|
| | Sidewall Straightness | Sidewall Straightness | Bottom Straightness | Sidewall Taper | | | | | |
| | Amplitude | Phase | Amplitude | | Sequence | | | Drawing | |
| Part | X1 | X2 | X3 | X4 | Machining | Measuring | Perf. Testing | Cross-Section | Top |
| 9 | 0(25µm) | 0(90) | 0(25µm) | 0(5) | 1 | 1 | 1 | | |
| 3 | -1(0) | +1(180) | -1(0) | +1(10) | 2 | 2 | 2 | | |
| 2 | +1(50µm) | -1(0) | -1(0) | +1(10) | 3 | 3 | 3 | | |
| 4 | +1(50µm) | +1(180) | -1(0) | -1(0) | 4 | 4 | 4 | | |
| 8 | +1(50µm) | +1(180) | +1(50µm) | +1(10) | 5 | 5 | 5 | | |
| 5 | -1(0) | -1(0) | +1(50µm) | +1(10) | 6 | 6 | 6 | | |
| 7 | -1(0) | +1(180) | +1(50µm) | -1(0) | 7 | 7 | 7 | | |
| 10 | 0(25µm) | 0(90) | 0(25µm) | 0(5) | 8 | 8 | 8 | | |
| 6 | +1(50µm) | -1(0) | +1(50µm) | -1(0) | 9 | 9 | 9 | | |
| 1 | -1(0) | -1(0) | -1(0) | -1(0) | 10 | 10 | 10 | | |

to the composition matrix. All end plates and experimental plates have been fabricated, verified, and are awaiting pyrosealing scheduled for July 2012. We decided that fabrication of only one 5C plate made from the alternative POCO AXF-5Q material, rather than two plates one from each material, would be necessary to meet all our objectives. With this decision, we intend to use this plate to confirm that the material substitution still produces the same polarization curve results at 25 psig as the original 5C plate. Then, assuming successful correlation of results, we will then use this plate to complete the back pressure sensitivity testing and for the neutron beam imaging experiment.

Though statistical analysis of the data did not yield significant conclusions, our statisticians classified them as strongly suggestive. To be statistically conclusive the F-distribution cumulative density function or probability needed to be 95% or greater for a main factor. Unfortunately, due to the fractional-factorial nature of the experiment this statistic could not be determined for the two-factor interactions because of their “confounded” nature. The fractional-factorial design-of-experiments alternative was chosen because it reduced the number of experimental plates needed and the associated testing. A further implication of this decision is that if a two-factor interaction is significant, there are not enough data to determine if the most important interaction, in the case of our experiment, is 1 & 2 or 3 & 4 or a combination of 1 & 2 and 3 & 4. The ranked order of significant factors and interactions is shown in Table 2 below. It is important to point out that (1) 3 and 4 factor interactions were not tested and (2) The “effect” in the table and subsequent plots represents the voltage difference multiplied by 100 for visualization purposes.

TABLE 2. Statistical Analysis Summary - Single Factors and Two-Factor Interaction Ranked by Order of Importance

| Ranked Order | | | |
|--------------|----------------|------------|-------------|
| Factor | Effect (V*100) | Rel. Eff % | Fcdf Stat % |
| 12 + 34 | 18.59 | | * |
| 3 | 16.17 | 106 | 82.4 ** |
| 1 | 15.28 | 101 | 79.4 ** |
| 4 | 6.02 | 40 | 36.1 |
| 14 + 23 | -5.67 | | |
| 2 | -3.71 | 24 | 22.6 |
| 13 + 24 | -2.74 | | |

Although the first three results were not statistically significant, the main factors were not far off and thus can be classified as of strongly suggestive. Figures 2a and 2b show different graphical representations of the statistical results. In Figure 2a each factor and interaction has a corresponding box plot: the greater the slope, the more significant the factor or interaction is. The confounding for the two-factor interactions can be seen by identical plots for three different two-factor interactions. Figure 2b is more intuitive and clearly shows the experiment included a center

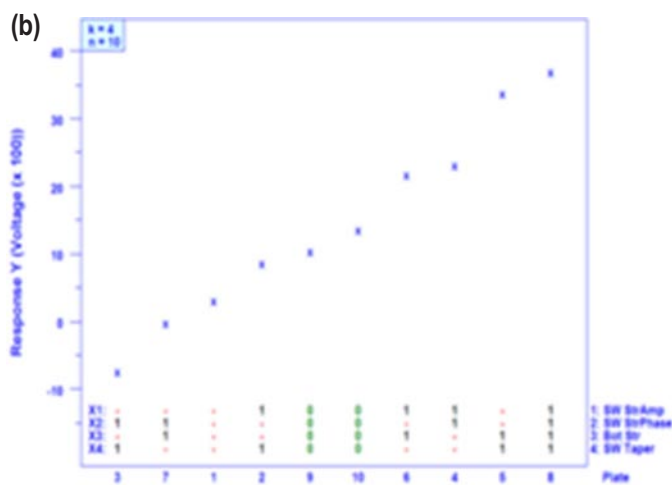
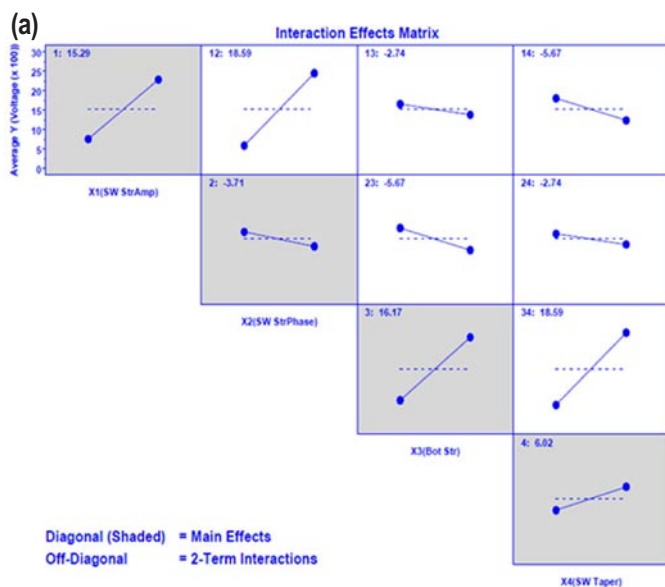


FIGURE 2. Statistical Plots

replication point to test for consistency, one of the intended characteristics of the design of experiments. Plates 9 and 10 were identical with all factors set mid-range, performing as expected, with both producing nearly the same output, with an output ranking near the mean relative to the other plates.

We consider the statistical analysis described as initial and we will continue to find new published methods to analyze the data to create more definitive conclusions.

Conclusions

- The duration of this project has been longer than anticipated but the modifications that have been adopted, experiments added, and the care that has been taken to ensure every detail has been considered will hopefully go a long way towards ensuring confidence in the conclusions.

- Although not statistically conclusive, the analysis of the results based on the design of experiments strongly suggests that precisely controlled complex dimensional variability improves water management and yields improved performance. This is evident from the most important single factor and two factor interactions being side wall straightness, bottom straightness, and the interaction of sidewall straightness and phase of the side wall straight (variation in width). Applying intuition to unravel the confounded two-factor interactions might suggest the interaction of factors 1 and 2 being more important than 3 and 4; however it does not eliminate the possibility of three- and four-factor interactions.
- The preliminary statistical analysis dictated the need for a microfluidic two-phase flow expert; however, in hindsight, the project would have benefited greatly with this addition during the design stage of this project.

Future Directions

- Complete all preparations for the imaging experiment, verify that with the substitute plate material the experimental results correlate with those initially obtained, and with the assistance of Dr. Allen finalize the imaging protocol.
- Complete the back pressure sensitivity experiment through testing at LANL using the replacement experiment cathode plate 5C.
- Continue working with Dr. Allen to obtain a better understanding of the physics that explain the results obtained.
- With the assistance of the NIST Statistical Engineering Division continue researching the application of different statistical analysis based data exploration techniques in an attempt to reveal the most rigorous conclusions. Incorporate, if possible, the physics based understanding in the statistical evaluation of the results as prior information.
- Deliver a detailed publication to disseminate our results to the fuel cell industry.

Disclaimer

Certain commercial equipment, instruments, or materials are identified in this paper in order to specify the experimental procedure adequately. Such identification is not intended to imply recommendation or endorsement by the National Institute of Standards and Technology, nor is it intended to imply that the materials or equipment identified are necessarily the best available for the purpose.

Acknowledgements

The work detailed in this report would not have been possible without the contributions of the following, all are NIST employees

unless designated otherwise: Tommy Rockward (LANL), Jeffery Allen (Michigan Technical University), James Filliben, Ted Doiron, Daniel Hussey, David Jacobson, Brian Pries.

FY 2012 Publications/Presentations

1. E. Stanfield, “Cause and Effect: Flow Field Plate Manufacturing Variability and its Impact on Performance,” DOE Annual Merit Review Proceedings, MN011, May 16, 2012, http://www.hydrogen.energy.gov/pdfs/review12/mn011_stanfield_2012_p.pdf
2. E. Stanfield, “Cause and Effect: Flow Field Plate Manufacturing Variability and its Impact on Performance,” 2011 DOE Hydrogen and Fuel Cells Program Annual Progress Report, November 2011, http://www.hydrogen.energy.gov/pdfs/progress11/vi_6_stanfield_2011.pdf

References

1. E. Stanfield, “Metrology for Fuel Cell Manufacturing,” 2008 DOE Hydrogen and Fuel Cells Program Annual Progress Report, November 2008. http://www.hydrogen.energy.gov/pdfs/progress08/vi_3_stanfield.pdf
2. E. Stanfield, “Cause and Effect: Flow Field Plate Manufacturing Variability and its Impact on Performance,” 2010 DOE Hydrogen and Fuel Cells Program Annual Progress Report, February 2011. http://www.hydrogen.energy.gov/pdfs/progress10/vi_6_stanfield.pdf
3. E. Stanfield, “Cause and Effect: Flow Field Plate Manufacturing Variability and its Impact on Performance,” 2011 DOE Hydrogen and Fuel Cells Program Annual Progress Report, November 2011. http://www.hydrogen.energy.gov/pdfs/progress11/vi_6_stanfield_2011.pdf

VI.8 Optical Scatterfield Metrology for Online Catalyst Coating Inspection of PEM (Fuel Cell) Soft Goods

Eric Stanfield (Primary Contact), Michael Stocker
National Institute of Standards and Technology (NIST)
100 Bureau Drive, MS 8211
Gaithersburg, MD 20899-8211
Phone: (301) 975-5102
Email: eric.stanfield@nist.gov, michael.stocker@nist.gov

DOE Managers

HQ: Nancy Garland
Phone: (202) 586-5673
Email: Nancy.Garland@ee.doe.gov
GO: Jesse Adams
Phone: (720) 356-1421
Email: Jesse.Adams@ee.doe.gov

Contract Number: DE-EE0001047

Project Start Date: October 1, 2009

Project End Date: October 1, 2012

Fiscal Year (FY) 2012 Objectives

- Collect crucial optical property data for catalyst-coated membrane (CCM) constituent materials.
- Improve theory to experiment agreement of CCM structures.
- Explore suitability of optical scatterfield microscopy (OSM) to CCM defect detection.
- Investigate other optics based measurement approaches as in situ process control fuel cell manufacturing metrology solutions.

Technical Barriers

This project addresses the following technical barriers from the Manufacturing R&D section of the Fuel Cell Technologies Program Multi-Year Research, Development and Demonstration Plan:

(F) Low Levels of Quality Control and Inflexible Processes

Contribution to Achievement of DOE Manufacturing R&D Milestones

This project will contribute to achievement of the following DOE milestones from the Manufacturing R&D section of the Fuel Cell Technologies Program Multi-Year Research, Development and Demonstration Plan:

- Milestone 1. Demonstrate sensors in pilot scale applications for manufacturing MEAs. (4Q, 2012)
- Milestone 2. Develop continuous in-line measurement for MEA fabrication (4Q, 2014)
- Milestone 3. Complete development of standards for metrology of production systems. (4Q, 2014)

FY 2012 Accomplishments

- Performed spectroscopic ellipsometry (SE) measurements on both the annealed and unannealed sample sets. Analyzed SE data and extracted meaningful numbers for the real (n) and imaginary (k) parts of the complex index of refraction for bulk perylene PR149.
- Demonstrated good qualitative agreement between a two-dimensional (2D) finite element model (FEM) and a 2D rigorous coupled waveguide analysis (RCWA) simulation of a 0.250- μm catalyst layer on top of a 20- μm finite ionomer substrate.
- Incorporating the new perylene PR149 n & k data, demonstrated good qualitative theory to experiment agreement for a 0.1 mg Pt/cm² 3M nano-structured thin film (NSTF) CCM.
- Built and tested a varying height and cross-section pillar modeling structure to allow for the quantifying of surface roughness in CCM simulations.
- Devised a new scatterometry approach that has promising application to fuel cell process control metrology. This scatterometry approach is called large aperture scatterometry (LAS). Completed a design study of a LAS device.
- Completed initial computer simulations demonstrating:
1) sensitivity of OSM to detecting pinhole defects and
2) utility in identifying optimal measurement parameters for ensuring simultaneous independent single-sided measurements of a double-coated CCM.



Introduction

Industry has identified the need for high-speed, in situ process control measurement techniques for controlling the quantity of the platinum in the catalyst layer and for the rapid identification of critical defects. Online X-ray fluorescence (XRF) is the current in situ technique for controlling the various parameters of interest, most commonly catalyst loading; however this technique provides the total through

sample platinum loading thus must be implemented prior to the transfer of the anode and cathode catalyst layer to the membrane in the production of a CCM. The ideal solution would provide in-line process control of the finished product (CCM) by way of dual-side simultaneous but independent measurement of catalyst loading. The solution would eliminate concerns related to platinum lost and not accounted for during the decal transfer step and it would ultimately enable real-time loading process control when dual-side direct catalyst layer application becomes the standard approach. The Semiconductor and Dimensional Metrology Division within the Physical Measurement Laboratory has years of expertise with a technology identified as OSM [1], specifically its development as a process control tool for the semiconductor industry. This technique is a combination of the best attributes of traditional bright-field optical microscopy and scatterometry. This technique focuses on the complex optical signatures of subwavelength size features, where the response can be optimized by varying the illumination angle, varying the illumination source wavelength, and application of various image analysis algorithms. The overall objective of this project is to demonstrate the applicability of the OSM technique to this application with the hope that it will provide proton exchange membrane (PEM) CCM manufacturers with an automated high-throughput approach for process control inspection of Pt loading with sensitivity equal to or better than that currently provided by XRF and simultaneous identification/quantification of other parameters of interest, such as critical defects. Model-based simulations will be developed concurrently as they are critical to the study and optimization of this technique for this application and will ultimately give manufacturers insight that will enable them to tune their measurement equipment to the parameter(s) of interest as design changes are made.

Approach

The initial focus, driven by industry input, is to demonstrate that the OSM tool is sensitive to differences in catalyst loading. To reach this Go/No-Go point this project has relied heavily on support from CCM manufacturers, specifically in the supply of samples by which sensitivity studies could be performed. CCM manufacturers were also helpful in establishing a benchmark catalyst loading sensitivity of 0.01 mg/cm^2 which is equivalent to that of the online XRF tool currently used. At this juncture, we now know that the tool is indeed sensitive to changes in catalyst loading at the benchmark level based on a sample set of 3M Pt alloy NSTF-type CCMs. With sensitivity successfully demonstrated, the remainder of the project is dedicated to developing accurate analytical models for each type of CCM tested then to use these models for simulations aimed at understanding and optimizing the tool's sensitivity to catalyst loading based on variation of the adjustable parameters of

the tool and to further extend the study of the applicability of the tool to other critical catalyst layer parameters identified by the manufacturers. In the development of these models, we will again rely heavily on CCM manufacturers to supply specialized samples so that we can experimentally obtain optical constants for the constituent materials which are critical to ensuring accuracy. Lastly, to claim that a thorough investigation has been performed we aim to demonstrate the tool's capabilities on many of the common types of CCMs being manufactured, these include 3M's NSTF CCM with Pt and Pt alloy catalysts and the different conventional Pt on carbon-based CCMs made by several manufacturers.

Results

Having demonstrated relevant sensitivities on industrial collaborator provided samples in the year before, the research direction this year focused largely on improving modeling accuracy and better theory to experiment agreement. The ability to perform accurate simulations facilitates developing accuracy when making optical measurements that require small uncertainties. It also provides a flexible and efficient platform to evaluate and optimize measurement parameters even before samples are available and measured.

In working towards accurate CCM electromagnetic scattering models, we collaborated with 3M to generate samples that would allow us to measure the optical properties of CCM constituent materials. The first sample set included six 4-inch perylene PR149-coated Si wafers. Three were coated with $1,500 \text{ \AA}$ and three with $1,800 \text{ \AA}$ of perylene and then annealed. The whiskers created a surface texture that made SE measurements extremely difficult. A second set of samples were made identical to the first, however, this time the wafers were coated, but not annealed. This created a smoother surface, relative to wavelengths of light we were using, allowing us to make useful SE measurements and extract an n & k for perylene PR149. We realize these optical constants are for bulk perylene, which is not the same crystal structure as the perylene whiskers, but these values provide valuable initial information in the modeling. The n & k data for bulk perylene PR149 are shown in Figure 1.

With these new n & k data, we performed two modeling tests. The first was a model-to-model comparison. We compared a 2D RCWA model to a 2D FEM model. The simulation was of a 0.250 \mu m effective medium approximation (EMA) catalyst coating on a top of a 20 \mu m finite ionomer substrate. This set of simulations was run as angle-resolved scans. Both polarizations trended the same direction with similar reflectivity values as a function of angle. The second test was a theory to experiment comparison. The experimental data were acquired from a 3M 0.1 mg Pt/cm^2 NSTF CCM sample. For the simulation, a wavelength scan was performed on a 2D model of this structure built in the FEM code. There is promising

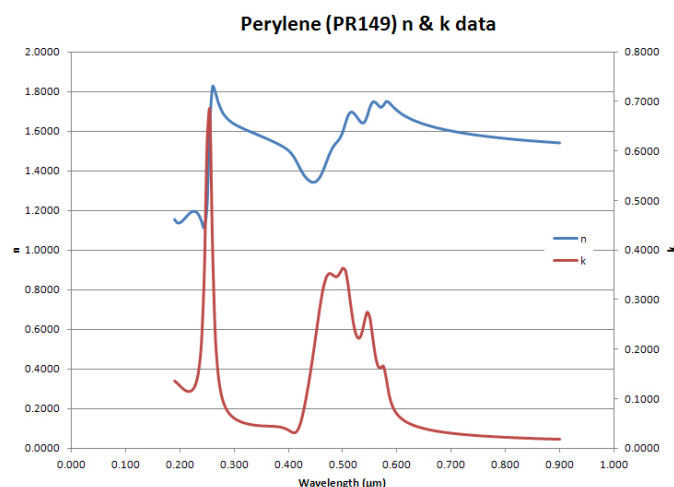


FIGURE 1. Perylene PR149 n & k data as function of wavelength

qualitative agreement with both the theory and experiment trending the same as a function of wavelength at an illumination angle of 70 degrees. Other angles of incidence give very different values of reflectivity.

The modeling of CCMs presents a challenge for several different reasons, one of them being the randomness and magnitude of the surface roughness. To study this problem, we built a structure in the FEM model consisting of pillars with varying heights and cross-sections. This was designed to represent both: 1) the surface texture created from hot pressed Pt-coated perylene whiskers in the 3M NSTF CCM as well as 2) the surface texture from 50 nm to 100 nm carbon grains in a carbon-Pt nanoparticle CCM. Some initial simulations were run to see the effects of roughness on reflectivity as a function of grain size and illumination angle of incidence. This pillar modeling structure can be seen in Figure 2. The model consists of air (in gold) between pillars atop an EMA catalyst layer (in purple), which contains Pt, perylene, air, and ionomer.

For Pt loading measurement, we devised a new scatterometric approach (no high magnification) we call LAS, allowing for averaging over a large sample area. A design study was completed in which four LAS configurations were considered. We decided a multiple source and multiple detector configuration showed the most promise, factoring in cost, simplicity of design, and failure modes. A schematic of this design can be seen in Figure 3. We have completed an optical design for this configuration and have ordered prototype parts. Assembly and testing of this LAS is currently underway.

Lastly, some initial simulation demonstrations were performed. The first was a pinhole defect simulation. We ran simulations of a 300 nm and a 500 nm pinhole as a function of wavelength, polarization, and illumination angle of incidence. Sensitivity to the change in diameter of the

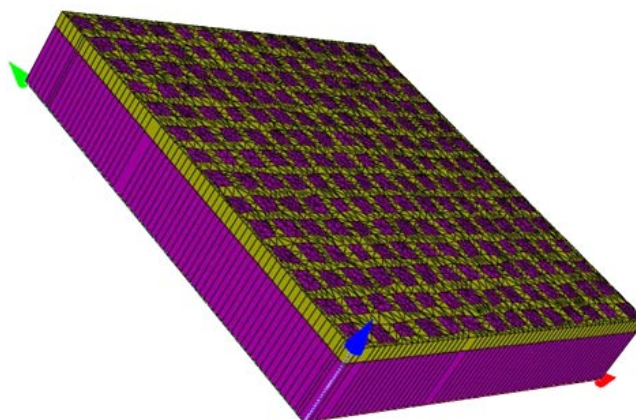


FIGURE 2. FEM-based roughness modeling structure

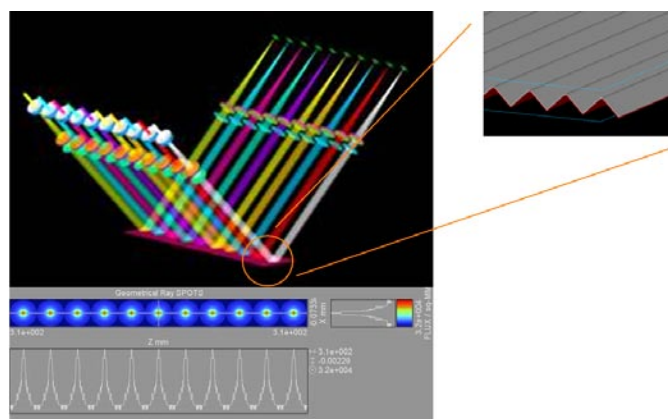


FIGURE 3. Multiple source, multiple detector LAS configuration design

pinhole was observed. We are working with collaborators to obtain actual samples with intentional defects (pinholes, hotspots, etc.) created in the CCM. The second simulation was a demonstration of the capability of OSM to perform simultaneous independent single-sided measurements of a double-coated CCM. In this simulation, we compared results from: 1) a 20- μm PEM layer coated with 0.06 mg Pt/cm² on one side and nothing on the other side to 2) a 20- μm PEM layer coated with 0.06 mg Pt/cm² on one side and 0.03 mg Pt/cm² on the other. We were able to observe that an optimal set of simulation measurement parameters (wavelength, polarization, illumination angle of incidence, etc.) existed that minimized the influence of the 0.03 mg Pt/cm² side on the measurement of the 0.06 mg Pt/cm² side. This observation shows the flexibility to tune an optical system to a given measurement task.

Conclusions

We turned our attention to the time consuming task of developing accuracy and achieving quantitative theory to

experiment agreement. We successfully obtained index of refraction data for bulk perylene PR149 and subsequently used them in performing various simulations that indicate improvement in accuracy and progress towards theory to experiment quantitative agreement. Surface roughness remains a difficult issue to address in our CCM modeling although measurable progress was made in our ability to quantify the effect. There is still much work to be done in these areas. We investigated the applicability of LAS as a process control solution for fuel cell manufacturing metrology. It is our belief that OSM, LAS, or the combination of the two remains a viable in situ process control solution for Pt loading and defect detection.

Future Directions

- Continue working with industrial collaborators to create samples that allow optical property measurements of CCM constituent materials. The next materials to characterize are the actual proton exchange membrane (Nafion[®] and 3M membrane) and amorphous carbon. Continue optical index of refraction measurements of CCM constituent materials.
- Demonstrate quantitative theory-to-experiment agreement on traditional carbon/Pt nanoparticle and 3M NSTF CCMs.
- Finish design and optimization of LAS sensor. Collect data on various CCMs as a function of web speed, illumination angle of incidence, wavelength, and polarization.
- Continue to investigate applicability of OSM to fuel cell defect detection. Solicit industry input as to the types of defects that cause real performance losses.
- Pursue testing of OSM and LAS approaches on the NREL weblane after completion of feasibility studies at NIST.
- Publish OSM fuel cell results in refereed journal.

Disclaimer

Certain commercial equipment, instruments, or materials are identified in this paper in order to specify the experimental procedure adequately. Such identification is not intended to imply recommendation or endorsement by the National Institute of Standards and Technology, nor is it intended to imply that the materials or equipment identified are necessarily the best available for the purpose.

Acknowledgements

The work detailed in this report would not have been possible without the contributions of the following. All are NIST personnel and guest researchers unless otherwise noted: Mark Debe (3M), Judy Rudolf and Colin Busby (W.L. Gore), Mike Ulsh (National Renewable Energy Laboratory, NREL), Richard Silver, Francois Goasmat, Jing Qin, Bryan Barnes, John Kramar, Bin Ming, Brad Damazo, Hui Zhou, Prem Kavuri, Yeung-Joon Sohn.

FY 2012 Publications/Presentations

1. Stocker M, Goasmat F, Qin J, Silver R, Barnes B, Stanfield E. Optical Scatterfield Microscopy for PEMFC Catalyst Coating Manufacturing Process Control. Poster session presented at: Fuel Cell Seminar and Exposition 2011; 2011 Oct 31 – Nov 3; Orlando, FL.

References

1. E. Stanfield and M. Stocker, "Metrology for Fuel Cell Manufacturing," DOE Annual Merit Review Proceedings, MN006, May 12, 2011, http://www.hydrogen.energy.gov/pdfs/review11/mn006_stanfield_2011_o.pdf.
2. E. Stanfield, M. Stocker, and B. Muralikrishnan, "Metrology for Fuel Cell Manufacturing." Invited Presentation Given to the FreedomCAR Tech Team, USCAR, Southfield, MI, March 16, 2011.
3. E. Stanfield, "Optical Scatterfield Metrology for Online Catalyst Coating Inspection of PEM Soft Goods," FY 2010 Annual Progress Report, DOE Hydrogen and Fuel Cells Program, February 2011, http://www.hydrogen.energy.gov/pdfs/progress10/vi_8_stanfield.pdf.

VII. TECHNOLOGY VALIDATION

VII.0 Technology Validation Sub-Program Overview

INTRODUCTION

The Technology Validation sub-program demonstrates, tests, and validates hydrogen and fuel cell technologies and uses the results to provide feedback to the Program's research and development (R&D) activities. This year, the sub-program concluded the National Fuel Cell Electric Vehicle Learning Demonstration, the principal emphasis of the sub-program over the past decade, which encompassed the co-development and integration of hydrogen infrastructure with hydrogen fuel cell-powered vehicles, allowing industry to assess progress toward technology readiness. In addition, the Technology Validation sub-program completed a project on combined hydrogen, heat, and power (tri-generation or CHHP). Continuing efforts include the real-world evaluation of fuel cell bus technologies at various transit authorities, and monitoring performance of fuel cells in stationary power, backup power, and material handling applications. The sub-program solicited proposals for a new data collection effort, which will continue to track technological progress in the performance, durability, and reliability of refueling stations, advanced refueling components, and fuel cell electric vehicles (FCEVs).

GOAL

Validate the state of the art of fuel cell systems in transportation and stationary applications as well as hydrogen production, delivery, and storage systems. Assess technology status and progress to determine when technologies should be moved to the market transformation phase.

OBJECTIVES¹

- By 2012, publish the final report on the National Hydrogen Fuel Cell Electric Vehicle and Infrastructure Learning Demonstration.
- By 2014, validate durability and efficiency of stationary fuel cell systems against fuel cell targets (40,000-hour durability, 40% efficiency).
- By 2017, complete the validation of commercial fuel cell combined heat and power systems target (50,000-hour durability).
- By 2017, validate durability of auxiliary power units against fuel cell systems target (15,000-hour durability).
- By 2019, validate hydrogen FCEVs with greater than 300-mile range and 5,000-hour fuel cell durability. Validate a hydrogen fueling station capable of producing and dispensing 200 kg H₂ per day to cars and/or buses.
- By 2020, validate large-scale systems for grid energy storage that integrate renewable hydrogen generation and storage with fuel cell power generation—operating for more than 10,000 hours, with a round-trip efficiency of 40%.

FY 2012 TECHNOLOGY STATUS

National Fuel Cell Electric Vehicle Learning Demonstration

In 2012, the National Fuel Cell Electric Vehicle Learning Demonstration—a government-industry cost-shared project initiated in 2004 with four automobile and energy company teams—continued to provide data for evaluating the status of the technologies, including key metrics such as fuel cell durability, driving range,

¹Note: Targets and milestones were recently revised; therefore, individual project progress reports may reference prior targets. Some targets are still currently under revision, with updates to be published in Fiscal Year (FY) 2013.

and efficiency. The project is now complete and the final report has been published. Data has been collected on a total of 183 fuel cell vehicles and 25 hydrogen fueling stations during the learning demonstration, with 13 stations still in operation as of 9/30/2011. FCEVs in the project traveled 3.6 million miles, and 151,000 kg of hydrogen was either produced or dispensed (with some of this hydrogen being used in vehicles outside the Learning Demonstration). Durability results indicate fuel cell durability exceeded 2,500 hours (~75,000 miles). FCEVs met or exceeded the 250-mile driving-range goal, and fuel cell system efficiency at 25% net power was 53–59%, which is close to the DOE target of 60%. Table 1 shows all of the key performance metrics that have been reported in the Learning Demonstration.

TABLE 1. Summary of key performance metrics for the Learning Demonstration. Outside of this project, DOE independent panels estimated that producing hydrogen from distributed reforming of natural gas would cost approximately \$2.75-\$3.50/kg H₂ (2006 study) and producing hydrogen from distributed electrolysis would cost approximately \$4.90-\$5.70/kg H₂ (2009 study)—both analyses assume a build-out rate of 500 stations/year, with stations producing 1,500 kg of H₂/day.¹

| Vehicle Performance Metrics | Gen 1 Vehicle | Gen 2 Vehicle | 2009 Target | 2010 – 2011 Results |
|---|---------------|---------------|-------------|---------------------|
| Fuel Cell Stack Durability | | | 2,000 hours | |
| Maximum Team Projected Hours to 10% Voltage Degradation | 1,807 hours | 2,521 hours | | -- |
| Average Fuel Cell Durability Projection | 821 hours | 1,062 hours | | 1,748 hours |
| Maximum Hours of Operation by a Single FC Stack to Date | 2,375 hours | 1,261 hours | | 1,582 hours |
| Driving Range | | | 250 miles | |
| Adjusted Dynamometer (Window Sticker) Range | 103-190 miles | 196-254 miles | | -- |
| Median On-Road Distance Between Fuelings | 56 miles | 81 miles | | 98 miles |
| <i>Fuel Economy (Window Sticker)</i> | 42 – 57 mi/kg | 43 – 58 mi/kg | no target | -- |
| <i>Fuel Cell Efficiency at ¼ Power</i> | 51 – 58% | 53 – 59% | 60% | -- |
| <i>Fuel Cell Efficiency at Full Power</i> | 30 – 54% | 42 – 53% | 50% | -- |

¹ Distributed Hydrogen Production from Natural Gas: Independent Review, NREL, October 2006, <http://hydrogen.energy.gov/pdfs/40382.pdf>; and Current (2009) State-of-the-Art Hydrogen Production Cost Estimate Using Water Electrolysis: Independent Review, NREL, 2009, <http://hydrogen.energy.gov/pdfs/46676.pdf>.

FY 2012 KEY ACCOMPLISHMENTS

National Fuel Cell Electric Vehicle Learning Demonstration

The National Renewable Energy Laboratory (NREL) completed the data collection and analysis portion of the Learning Demonstration project and published a comprehensive Final Report in July 2012. Throughout the project, over 500,000 individual vehicle trips were analyzed, and 99 different composite data products (CDPs) were produced by NREL to validate the current status of FCEV technology (see Table 1 for the status of specific performance metrics). The Final Report represents the last of a number of significant and groundbreaking accomplishments by NREL during the project, including the establishment of the Hydrogen Secure Data Center (HSDC), the methodology of securely aggregating business sensitive

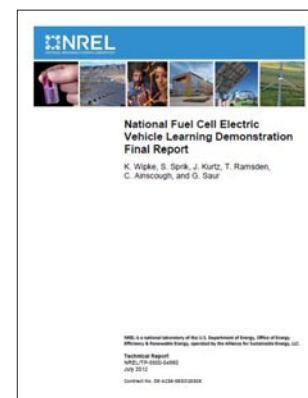


FIGURE 1. The final report of the Fuel Cell Electric Vehicle Learning Demonstration (<http://www.nrel.gov/hydrogen/pdfs/54860.pdf>)

performance data into useful public data, and the development of many unique and innovative data products for FCEVs and hydrogen fueling stations.

Fuel Cell Bus Evaluation

NREL began collecting and analyzing data from 17 second-generation fuel cell buses from three transit agencies (SunLine, AC Transit, and CTTRANSIT) in 2010. Transit agencies are increasing the number of scheduled miles per day: buses are operating as many as 19 hours per day and over 1,500 hours per month, with some weekend service. The second-generation bus designs have twice the fuel economy (7.78 miles per diesel gallon equivalent) of diesel buses, and the latest data show an increase in availability—9 of 17 buses are over 70% available and overall availability is 62%. NREL categorizes the reasons for unavailability and has found that the unavailability is not typically due to fuel cell issues, but relate to accident repair, air conditioning problems, and materials compatibility. Hybrid system issues were primarily software related, and battery issues have diminished in comparison to previous designs. The mean time between road calls (MBRC) for the fuel cell system (8,158 miles) improved 38% compared to first-generation systems. The target MBRC for the propulsion system is 10,000 miles. The fuel cell powerplant with the most hours of operation exceeded 12,000 hours of operation by August, 2012. Three of the powerplants exceeded 6,000 hours of operation without repair. Fuel cell bus targets vs. status are list in Table 2.

TABLE 2. Performance, Cost, and Durability Targets for Fuel Cell Transit Buses

| | Units | 2012 Status | 2016 Target | Ultimate Target |
|---|------------------------------------|------------------------|--------------|-----------------|
| Bus Lifetime | years/miles | 5/100,000 ¹ | 12/500,000 | 12/500,000 |
| Power Plant Lifetime | hours | 12,000 | 18,000 | 25,000 |
| Bus Availability | % | 60 | 85 | 90 |
| Fuel Fills | per day | 1 | 1 (<10 min) | 1 (<10 min) |
| Bus Cost | \$ | 2,000,000 | 1,000,000 | 600,000 |
| Road Call Frequency (Bus/Fuel Cell System) | miles between road calls | 2,500/10,000 | 3,500/15,000 | 4,000/20,000 |
| Operation Time | hours per day/days per week | 19/7 | 20/7 | 20/7 |
| Scheduled and Unscheduled Maintenance Cost | \$/mile | 1.20 | 0.75 | 0.40 |
| Range | miles | 270 | 300 | 300 |
| Fuel Economy | miles per gallon diesel equivalent | 7 | 8 | 8 |

¹ Status represents data from NREL fuel cell bus evaluations. New buses are currently projected to have 8 year/300,000 mile lifetime.



FIGURE 2. The bus pictured, which is in service at CTTRANSIT in Hartford, Connecticut, is a fuel cell dominant Van Hool 40-foot bus with a UTC Power Fuel Cell System, Seimens ELFA hybrid system using lithium-based batteries

California Hydrogen Infrastructure Project (CHIP)

The California Hydrogen Infrastructure project, a congressionally directed project from 2005, concluded in December 2011. The project developed, constructed, and operated three permanent hydrogen stations in California, described below in more detail. In addition, Air Products completed temporary deployments of HF-150 mobile refuelers at the district office of the U.S. Forest Service in Placerville, California, and at a City of Long Beach facility in Long Beach, California. The Air Products HF-150 maintains about 150 kg of gaseous hydrogen at 6,600 psig. It can dispense approximately 80 to 90 kg before needing to be refilled. It is ideal for small fleet fueling and offers the advantage of being an automated, highly reliable, cost-effective fueling system that can be easily installed.

The University of California, Irvine station is supplied with liquid hydrogen and operates at 350 or 700 bar, has 25 kg/day capacity with actual demand approaching 50 kg/day and is to be expanded to 100 kg/day. The station has completed over 8,000 fills since starting up in August 2006.

The Torrance Pipeline Station, developed by Shell Hydrogen and shown in Figure 3, uses an Air Products industrial-grade hydrogen pipeline, and the station can dispense 350- or 700-bar hydrogen for \$4.50 to \$5.00 per kg. It has a 48-kg/day capacity (enough to fill 12 cars per day) and is expandable to 96 kg/day with additional compression. When starting with full storage, six cars can be filled in succession. It has completed over 2,000 fills since April 2011. The station includes a 4-kg/hour compressor skid, along with storage for 100 kg of hydrogen at 7,777 psig and 20 kg of hydrogen at 15,000 psig. The station can dispense hydrogen according to SAE TIR-J2601, and it includes the first example of hydrogen purification technology for production of an ultra-pure hydrogen stream from an industrial-grade pipeline supply.



FIGURE 3. The dispenser area at Shell's Torrance, California, fueling station, which is supplied by an Air Products pipeline

The Fountain Valley Renewable Hydrogen Station² also supplies hydrogen at 350 and 700 bar. This installation, located at the Orange County Sanitation District (OCSA) in Southern California, is the world's first tri-generation energy station and hydrogen refueling station, producing hydrogen and electric power from wastewater treatment gas, using a molten carbonate fuel cell, with a capacity of 100 kg H₂ per day. The Integrated Hydrogen Energy Station will continue to be operated on anaerobic digester gas from the wastewater treatment facility until May 31, 2014, under sponsorship of the California Air Resources Board and South Coast Air Quality Management District.

- The first co-production of hydrogen (using natural gas) at the Hydrogen Energy Station in OCSA took place in October 2010.
- In February 2011, the first hydrogen from the Hydrogen Energy Station at OCSA was sent to the hydrogen fueling station. Initial test fills of FCEVs at the hydrogen fueling station were completed in March 2011.
- In May 2011, operation on biogas from the wastewater treatment facility began.
- Over 1,000 hours of operation in power and power-and-hydrogen modes have been completed during the performance period. The hydrogen produced has met all quality standards.

²This station is based on a technology that co-produces power, heat, and hydrogen. This type of system is referred to as a CHHP (Combined Heat, Hydrogen, and Power or Tri-generation) system. The station uses a high-temperature fuel cell to co-generate heat, hydrogen and power. The fuel cell can use a diversity of hydrogen-rich fuels, including digester gas, natural gas, landfill gas, and syngas. This technology is expected to provide a source of cost-competitive hydrogen, which can be renewable when digester gas or landfill gas is used as the feedstock.

- Over 5 million standard cubic feet of digester gas has been processed to produce over 5,000 kg of hydrogen and over 1 million kWh of power.
- The unit has achieved nominal 54% efficiency (power + hydrogen) when operating in hydrogen co-production mode.

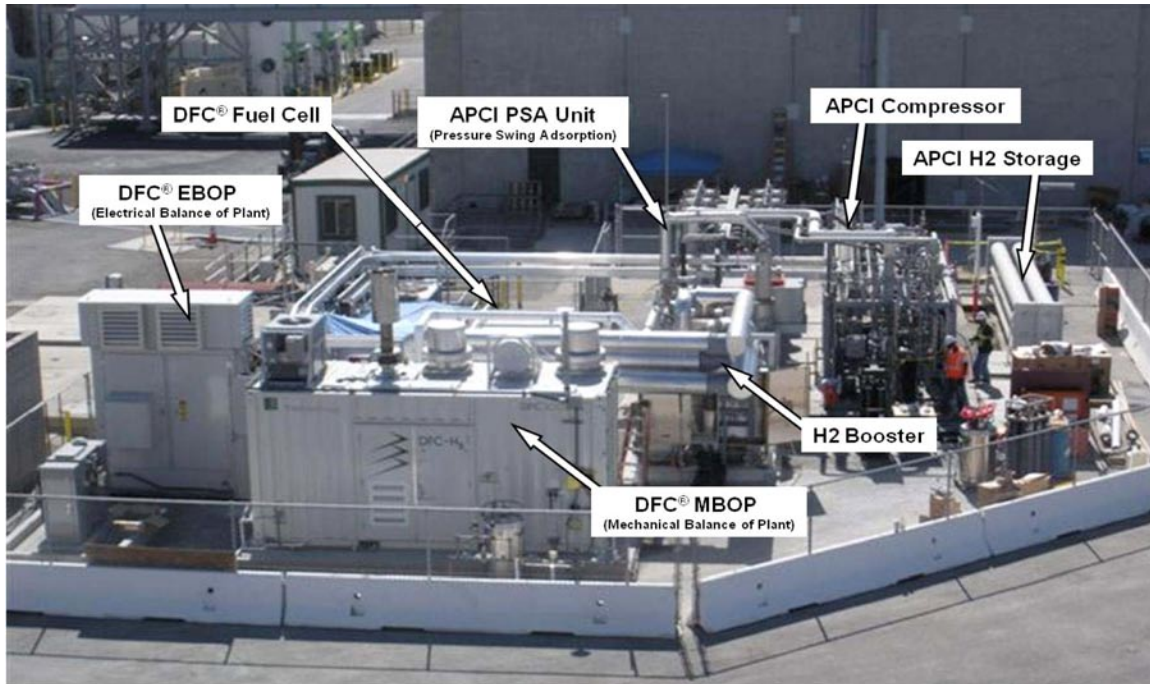


FIGURE 4. The Energy Station at Fountain Valley, California (dispensing area not shown)

Next Generation Hydrogen Station Analysis

The objective of the Next Generation Hydrogen Station Analysis project is to collect data from state-of-the-art hydrogen fueling facilities, such as those funded by the California Air Resources Board, to enrich the analyses and CDPs on hydrogen fueling originally established by the Learning Demonstration project. NREL's analyses provide valuable feedback on sensitive data from hydrogen infrastructure for industry and DOE. NREL works with facility owners/operators to benchmark performance of the fueling events relative to current SAE International procedures. Data templates were updated and the Fleet Analysis Toolkit code was updated to accept data from stations in the new templates for processing and analysis leading to CDPs. A set of 12 CDPs was created from data reported from four stations in early 2012. NREL continues to maintain an accurate database (location and status) of all online hydrogen stations in the United States, providing periodic updates to other online resources, specifically NREL's Alternative Fuels Data Center station locator, the Fuel Cell and Hydrogen Energy Association, the California Fuel Cell Partnership, and FuelCells.org.

Stationary Fuel Cell Evaluation

The analysis of stationary fuel cell operation includes systems providing primary power to a site. Operation, maintenance, and safety data are collected on site by project partners for fuel cell systems and infrastructure. NREL receives the data quarterly and stores, processes, and analyzes the data in the Hydrogen Secure Data Center. A key step in this project is the identification of locations and end users operating stationary fuel cells, as well as stationary fuel cell developers. The California Stationary Fuel Cell

Collaborative provides a strong partnership for NREL, because it involves multiple developers, end users, fuel cell technologies, and fuel cell system sizes.

Sustainable Hydrogen Fueling Station

The College of Engineering, Computer Science, & Technology at California State University, Los Angeles, as part of its energy curriculum, is building a sustainable hydrogen station to teach and demonstrate the production and application of hydrogen as the next generation of fully renewable fuel for transportation. In FY 2012, installation of all station equipment was completed and the station was commissioned, capable of fills at both 350 and 700 bar. The project was completed.

Hawaii Hydrogen Power Park

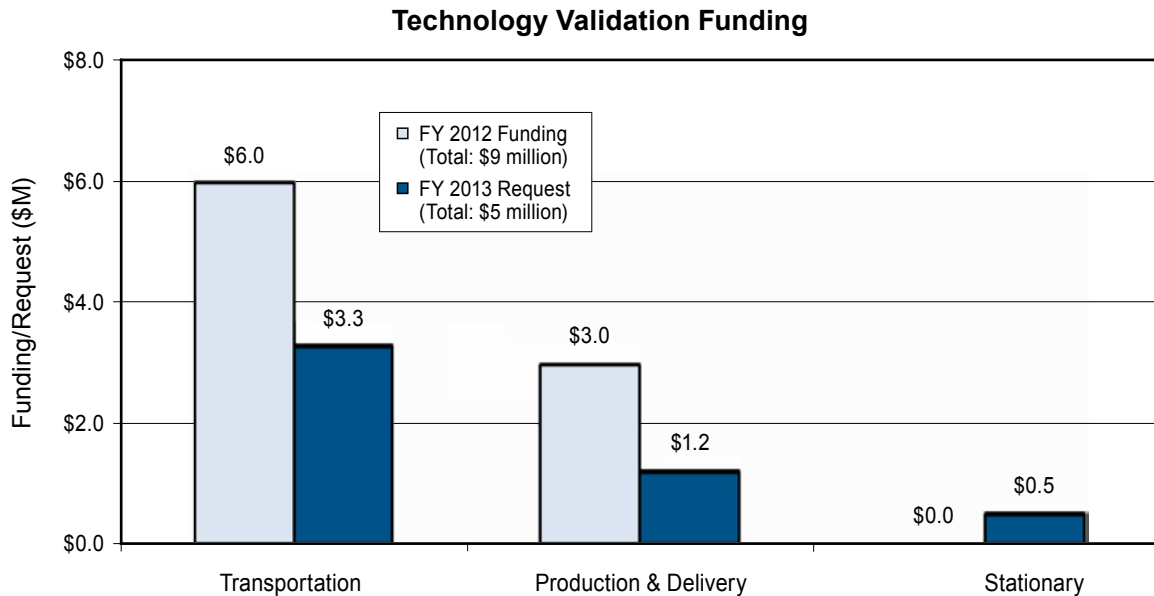
The Hawaii Hydrogen Power Park integrates a broad scope of technologies and activities funded by DOE as well as the State of Hawaii, the National Park Service, and the Office of Naval Research. The project addresses barriers to the widespread deployment of hydrogen vehicles in Hawaii and includes the deployment of hydrogen infrastructure, including 700-bar fast-fill and novel cascade non-compressor fueling systems, the installation of hydrogen fueling infrastructure at Hawaii Volcanoes National Park, and the operation, education and outreach, and economic and operational analysis of Hawaii Volcanoes National Park hydrogen shuttle bus service. The station supports the General Motors Equinox FCEV demonstration on Oahu and leverages the DOE and Naval Research Laboratory 60 kg/day geothermal-to-hydrogen grid management project to produce hydrogen.

Wind-to-Hydrogen Project, NREL/Excel Energy

NREL is demonstrating commercially available low-temperature electrolyzer technologies (proton exchange membrane and alkaline electrolyzers) to evaluate their response to commands to increase and decrease stack power (which enable them to shorten frequency disturbances on an alternating current microgrid). Results show that both the proton exchange membrane and alkaline electrolyzers are capable of adding or removing stack power to provide sub-second response that reduced the duration of grid frequency disturbances. The integrated renewable electrolysis system brings together wind turbines, solar panels, electrolyzers, compressors, storage, fuel cells, and power control components. The quick response and precise control offered by variable electrolyzer stack operation has been shown to be superior to the control capabilities of many conventional generators. NREL is demonstrating that electrolyzers can perform repeated high cyclic power variations (20–100% of rated stack power) to model performance with wind and solar power. To date, NREL has completed 7,000 hours of operation to help quantify performance differences between constant and variable stack power operation.

BUDGET

The funding portfolio for Technology Validation addresses the need to validate integrated hydrogen and fuel cell technologies for transportation, under real-world operating conditions. In Fiscal Year (FY) 2012, \$9 million in funding was appropriated for the Technology Validation sub-program, and \$5 million was requested for FY 2013.



FY 2013 PLANS

In FY 2013, the Technology Validation sub-program will continue its detailed evaluations of hydrogen and fuel cell technologies in transit buses, next generation hydrogen fueling stations, and stationary power applications. The sub-program will also award several new projects resulting from its funding opportunities issued in February and March 2012. The light-duty FCEV validation projects will supply dynamometer and real-world vehicle data to the HSDC at NREL for analysis and aggregation into CDPs for a minimum of five vehicles of the same model. Projects validating hydrogen refueling station performance will also supply data to the HSDC for analysis and aggregation into CDPs. A high-pressure electrolyzer and high-capacity hydrogen tanks will be installed at one or more refueling station for validation of performance and durability improvements in these advanced station components. Further funding opportunities will also be developed in FY 2013, subject to appropriations.

Jason Marcinkoski
 Acting Technology Validation Team Lead
 Fuel Cell Technologies Program
 Department of Energy
 1000 Independence Ave., SW
 Washington, D.C. 20585-0121
 Phone: (202) 586-7466
 Email: Jason.Marcinkoski@ee.doe.gov

VII.1 Controlled Hydrogen Fleet and Infrastructure Analysis

Keith Wipke (Primary Contact), Sam Sprik,
Jennifer Kurtz, Todd Ramsden, Chris Ainscough,
Genevieve Saur

National Renewable Energy Laboratory (NREL)
15013 Denver West Pkwy.
Golden, CO 80401-3305
Phone: (303) 275-4451
Email: keith.wipke@nrel.gov

DOE Manager

HQ: Jason Marcinkoski
Phone: (202) 586-7466
Email: Jason.Marcinkoski@ee.doe.gov

Start Date: October 2003

Projected End Date: September 2012

Fuel Cell Technologies Program's Multi-Year Research, Development, and Demonstration Plan:

- (A) Lack of Fuel Cell Electric Vehicle and Fuel Cell Bus Performance and Durability Data
- (C) Hydrogen Storage
- (D) Lack of Hydrogen Refueling Infrastructure Performance and Availability Data
- (E) Codes and Standards
- (H) Hydrogen and Electricity Co-Production

Contribution to Achieving DOE Technology Validation Milestones

Throughout this project, researchers are gathering data and providing technical analysis that contributes to achieving the following DOE technology validation milestones from the Fuel Cell Technologies Program's Multi-Year Research, Development, and Demonstration Plan that was in place when the project commenced:

Objectives

- By 2008, validate that hydrogen vehicles have a greater than 250-mile range without impacting passenger or cargo compartments.
 - By 2009, validate 2,000-hour fuel cell durability in vehicles, and validate hydrogen infrastructure that results in a hydrogen production cost of less than \$3.00/gallon of gasoline equivalent (gge) (untaxed) delivered and safe and convenient fueling by drivers (with training).
 - Help DOE demonstrate the use of fuel cell electric vehicles (FCEVs) and hydrogen infrastructure under real-world conditions, using multiple sites, varying climates, and a variety of hydrogen sources.
 - Analyze detailed fuel cell and hydrogen data from vehicles and infrastructure to obtain maximum value for DOE and industry from this "learning demonstration."
 - Identify the current status of the technology and its evolution over the project duration.
 - Provide feedback and recommendations to DOE to promote hydrogen and fuel cell research and development (R&D) activities and assess technical progress.
 - Publish results for key stakeholder use and investment decisions by generating composite data products (CDPs) for public dissemination.
- Milestone 2: Demonstrate FCEVs that achieve 50% higher fuel economy than gasoline vehicles (Q3, FY 2005). This milestone was achieved.
 - Milestone 3: Decision for purchase of additional vehicles based on projected vehicle performance and durability and hydrogen cost criteria (Q4, FY 2006). This milestone was achieved.
 - Milestone 4: Operate fuel cell vehicle fleets to determine if 1,000 hour fuel cell durability, using fuel cell degradation data, was achieved by industry (Q4, FY 2006). This milestone was achieved.
 - Milestone 5: Validate vehicle refueling time of 5 minutes or less for a 5 kg tank [1 kg/min] (Q4, FY 2006). At the time of the milestone, we had analyzed more than 2,000 vehicle fueling events and had calculated an average rate of 0.69 kg/min and a median rate of 0.72 kg/min, with 18% of the events exceeding the 1 kg/min target. At the end of the project, from a total of 33,000 fueling events we found that the fueling rate was 0.77 kg/min from the first five years (23% greater than 1 kg/min) and 0.65 kg/min from the last two years of the project (7% greater than 1 kg/min). This milestone was achieved.
 - Milestone 7: Validate refueling time of five minutes or less for 5 kg of hydrogen (1 kg/min) at 5,000 psi through the use of advanced communication technology (Q4, FY 2007). The first five years of data show that communication fills can fuel at a higher rate (up to 1.8 kg/min) and have an average fill rate 30% higher than that of non-communication fills (0.86 kg/min versus 0.66 kg/min). This milestone was achieved.

Technical Barriers

This project addresses the following technical barriers from the Technology Validation section (3.6.4) of the

- Milestone 8: Fuel cell vehicles demonstrate the ability to achieve a 250-mile range without impacting passenger cargo compartment (Q4, FY 2008). This milestone was achieved in 2008 using data from the Learning Demonstration results, with a demonstrated range of 196–254 miles. In June 2009, an on-road driving range evaluation was performed in collaboration with Toyota and Savannah River National Laboratory (SRNL). The results indicated up to a 431-mile on-road range was possible in southern California using Toyota's FCHV-adv fuel cell vehicle [1]. This milestone was achieved.
- Milestone 10: Validate FCEVs' 2,000-hour fuel cell durability using fuel cell degradation data (Q4, FY 2009). On-road fuel cell voltage data from second-generation fuel cell systems were analyzed and published in the Fall 2009 CDP results. Results indicate that the highest projected team average to 10% voltage degradation for second-generation systems was 2,521 hours, with a four-team average of 1,020 hours. The Spring 2010 results only slightly increased the four-team average (to 1,062 hours) and the highest team average remained the same at 2,521 hours. This milestone was achieved.
- Milestone 12: Validate cold-start capability at -20°C (2Q, 2011). This milestone was achieved and published in the Fall 2008 CDPs, demonstrating freeze starts between -9 and -20 degrees C and documenting both time to drive away and time to maximum fuel cell power. This milestone was achieved.
- Milestone 23: Total of 10 stations constructed with advanced sensor systems and operating procedures (Q1, FY 2008). This milestone was achieved.
- Milestone 24: Validate a hydrogen cost of \$3.00/gge (based on volume production) (Q4, FY 2009). Cost estimates from the Learning Demonstration energy company partners were used as input to an H2A analysis to project the hydrogen cost for 1,500 kg/day early market fueling stations. Results indicate that on-site natural gas reformation would lead to \$8–\$10/kg hydrogen cost and on-site electrolysis would lead to \$10–\$13/kg hydrogen cost. Although these results do not meet the \$3/gge cost target, two external independent panels concluded that distributed natural gas reformation could lead to a cost of \$2.75–\$3.50/kg hydrogen [2] and distributed electrolysis could lead to a cost of \$4.90–\$5.70/kg hydrogen [3]. This milestone was achieved outside of the Learning Demonstration project.
- Additional milestone in FY 2011: Validate up to 40 advanced technology FCEVs with up to 600 hours operation. At the end of the project, 51 advanced technology FCEVs were providing data to NREL and achieved a maximum operation time of 1,582 hours. This milestone was achieved.

Accomplishments

- Published the “National Fuel Cell Electric Vehicle Learning Demonstration Final Report,” summarizing all of the analysis results from the seven-year project. The report is 102 pages long, includes 126 figures, and is the most comprehensive report published on the project.
- Received and processed data quarterly from a total of 500,000 individual vehicle trips, amounting to more than 122 giga-byte of on-road data, since project inception.
- Created and published a total of 99 CDPs, with the Winter 2011 CDP results including 14 new CDPs since last year and updates to 26 previously published CDPs. The results emphasize the changes observed over the last two years and include data from two Learning Demonstration original equipment manufacturers (OEMs) plus Air Products' California Hydrogen Infrastructure Project.
- Documented and archived each quarter's analysis results in the NREL Fleet Analysis Toolkit (FAT) graphical user interface, and executed NREL FAT to produce detailed data results and CDPs in parallel for convenient industry and internal review.
- Presented project results publicly at the Fuel Cell Seminar, EVS-26, and the 2012 DOE Hydrogen and Fuel Cells Program Annual Merit Review meeting.
- Maintained NREL's Web page at http://www.nrel.gov/hydrogen/proj_learning_demo.html to allow direct public access to the latest CDPs organized by topic, date, and CDP number, including adding a new “sunburst,” a graphical way to preview and select CDPs for viewing.
- Provided presentations of results to key stakeholders, including two FreedomCAR and Fuel technical teams (storage and fuel cells).
- Continued to leverage key NREL analysis tools and capabilities to enable results to be quickly generated from fuel cell forklifts and other early market fuel cell applications. This year we added new analyses on FCEVs and fueling stations that were developed originally for fuel cell forklifts and their infrastructure.



Introduction

The primary goal of this project is to validate vehicle/infrastructure systems using hydrogen as a transportation fuel for light-duty vehicles. This means validating the use of FCEVs and hydrogen fueling infrastructure under real-world conditions using multiple sites, varying climates, and a variety of sources for hydrogen. Specific targets for 2009 were hydrogen vehicles with a range greater than 250 miles, 2,000-hour fuel cell durability, and \$3.00/gge hydrogen production cost (based on modeling for volume production).

We are identifying the current status of the technology and tracking its evolution over the project duration, particularly between the first- and second-generation fuel cell vehicles, and tracking further improvements to the second-generation vehicles demonstrated in the final two years. NREL's role in this project is to provide maximum value for DOE and industry from the data produced by this "learning demonstration." We seek to understand the progress toward the technical targets and provide information to help move the Fuel Cell Technologies (FCT) Program's R&D activities more quickly toward cost-effective, reliable hydrogen FCEVs and supporting hydrogen fueling infrastructure.

Approach

Our approach to accomplishing the project's objectives has been structured around a highly collaborative relationship with each industry team including Chevron/Hyundai-Kia, Daimler/BP, Ford/BP, GM/Shell, and Air Products (through the DOE California Hydrogen Infrastructure Project). We are receiving raw technical data from the hydrogen vehicles and from the fueling infrastructure that enable us to perform unique and valuable analyses across all teams. Our primary objectives are to feed the current technical challenges and opportunities back into the DOE FCT R&D Program and assess the current status and progress toward targets.

To protect the commercial value of these data for each company, we established the Hydrogen Secure Data Center at NREL to house the data and perform our analysis. To ensure value is fed back to the hydrogen community, we publish CDPs twice a year at technical conferences and on NREL's

website to report on the progress of the technology and the project, focusing on the most significant results. Additional CDPs are being conceived as additional trends and results of interest are identified, and as we receive requests from DOE, industry, and the codes and standards community. We also provide each individual company with our detailed analytical results (not public) of that company's data to maximize the industry benefit of NREL's analysis work and to obtain feedback on our methodologies.

Results

The results in FY 2012 came from analyzing an additional 9 months of data (January–September 2011), creating 14 new and 26 updated CDPs, and presenting these results at several technical conferences. This brings the total number of CDPs published to 99. To accomplish this, we continued to improve and revise our in-house analysis tool, NREL FAT. In 2007 NREL launched a Web page at http://www.nrel.gov/hydrogen/proj_learning_demo.html to provide stakeholders and the public with direct access to the results. Two distinct sets of results (labeled "Fall 2011" and "Winter 2011") have also been presented publicly at conferences in the last year. All 99 of the CDPs are documented in the "National Fuel Cell Electric Vehicle Learning Demonstration Final Report" and available on the website, so this report will include only a few highlights from the last year.

- Status of Vehicle Deployment: Figure 1 shows the cumulative number of vehicles that have been deployed by quarter and hydrogen storage system type since project inception. A total of 183 vehicles were deployed

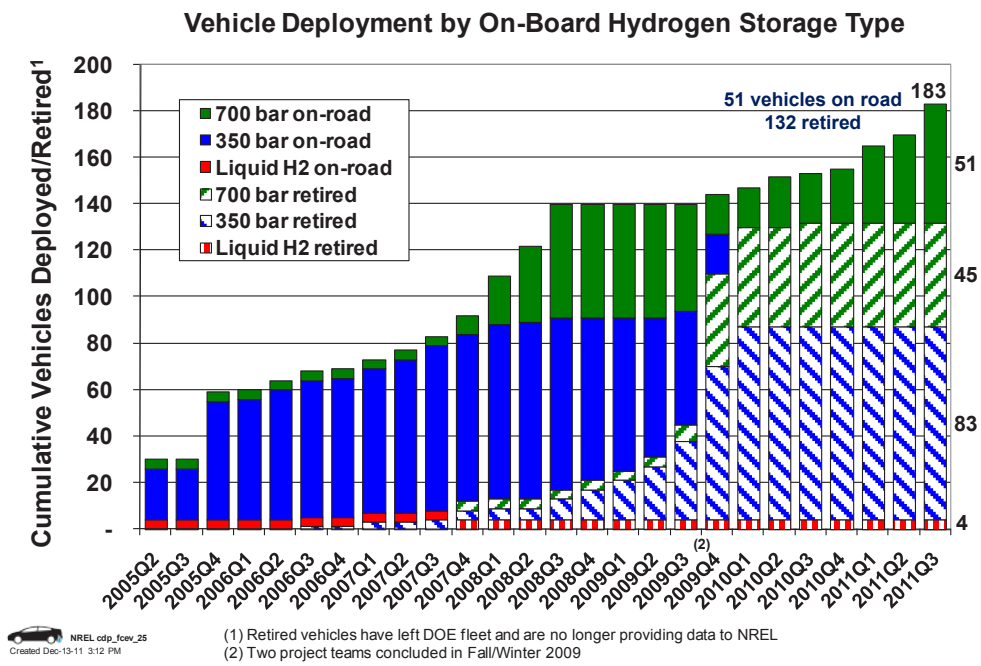


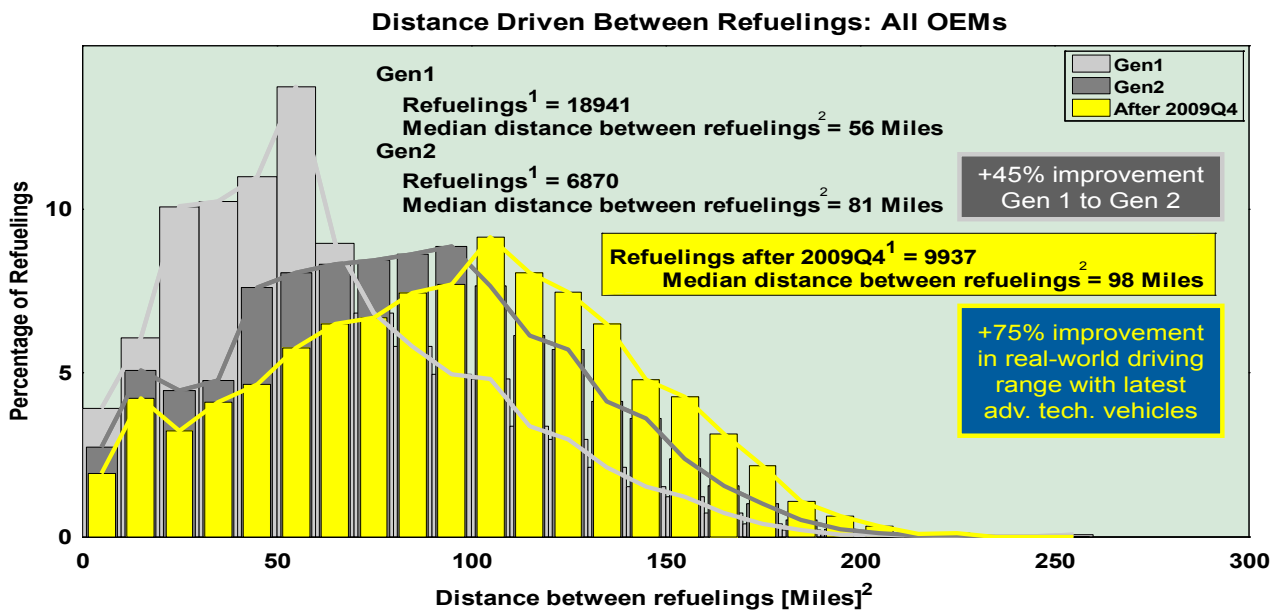
FIGURE 1. Cumulative Vehicles Deployed by Quarter and by Storage Type

through September 2011; 132 have been retired from the project and 51 vehicles were still on the road at project conclusion.

- Real-World Vehicle Driving Range:** In FY 2008, the driving range of the project’s FCEVs was evaluated based on fuel economy from dynamometer testing and onboard hydrogen storage amounts and compared to the 250-mile target. Additional on-road data were obtained from second- and first-generation vehicles in 2009, as well as from improved second-generation vehicles in 2010 and 2011. This enabled us to evaluate the distribution of real-world driving ranges of all the vehicles in the project. The data show (Figure 2) a 45% improvement in the median real-world driving range of second-generation vehicles (81 miles) compared to first-generation vehicles (56 miles), based on distances driven between more than 25,000 fueling events. In 2011, with continued operation of some second-generation vehicles and the introduction of some second-generation vehicles with improved performance, we have seen an increase in the median distance traveled between fuelings to 98 miles. This reflects a 75% improvement in real-world driving range with the latest advanced technology vehicles compared to the first-generation vehicles first introduced in 2005. As previously discussed, all the vehicles are capable of two to three times greater range than this when pushed to their full capabilities with sufficient fueling infrastructure, but the median distance traveled between fuelings is one way to measure the improvement in the vehicles’ capability as well as the

way in which they are actually being driven. We believe the reason for the increase in median driving distance between fuelings is due to slight improvements in the vehicle capabilities (better efficiency) and to more widespread infrastructure, which enables the vehicle storage tanks to be drawn down closer to empty because drivers are confident they can obtain fuel close by.

- Fuel Cell Durability:** The Spring 2010 results indicated that the highest average projected team time to 10% voltage degradation for second-generation systems was 2,521 hours, with a multi-team average projection of 1,062 hours. Therefore, the 2,000-hour target for durability was achieved. Since that time, two automotive teams concluded their participation in the project and additional data were acquired on some second-generation vehicles. Improved second-generation vehicles were also introduced to the project. Only two companies now provide durability data, and some vehicles have limited hours on the road, but we evaluated the average of all teams’ fleet projections to 10% voltage degradation and found the first-generation systems had an average projection of 821 hours, the second-generation systems had an average projection of 1,062 hours, and the fuel cell systems operated after 2009 Q4 (two OEMs) had an average projection of 1,748 hours. This shows dramatic improvement in durability over the seven-year project.
- Vehicle Fueling Rates:** Because of the change in makeup of the automotive and energy teams for the final two years of the project, we analyzed the fueling rates for the five years up through 2009 Q4 separately from



1. Some refueling events are not detected/reported due to data noise or incompleteness.
 2. Distance driven between refuelings is indicative of driver behavior and does not represent the full range of the vehicle.

FIGURE 2. Real-World Improvement in Driving Range Between Gen 1, Gen 2, and Latest Advanced Technology Learning Demonstration Vehicles

the fueling rates for the year after 2009 Q4. Figure 3 shows the distribution of the fueling rates for each of the seven years of the project, with a red arrow showing the shift each year in the average fueling rate, tabulated in the inset table. We found that in the first five years of the project, from more than 25,000 fueling events, the average fill rate was 0.77 kg/min with 23% of the events exceeding DOE’s target of 1 kg/min, representing a 5 kg fill in 5 minutes. Over the last two years, from a set of 8,050 fills, we observed an average fill rate of 0.65 kg/min with 7% of the fills exceeding the 1 kg/min target. Several factors explain this 16% drop in fueling rate. The average hydrogen dispensed per fill increased by 24%, but the average fueling time increased by 38%. The root cause is that the hydrogen community is migrating toward 700-bar-pressure fueling as the new standard, but the state-of-the-art stations that can achieve a fast and complete fill at this pressure with precooling are just now coming online, and minimal data were received from those stations through September 2011. Additionally, some 350-bar stations and vehicles that demonstrated fast fill times have been decommissioned. So this reduction in reported fill rate should be a temporary phenomenon until the new 700-bar station data are included in a new hydrogen infrastructure project being launched by DOE. With the new data

and analysis results, NREL will be able to document the significant progress that has been made relative to 700-bar infrastructure.

- Hydrogen Fueling Infrastructure Usage Patterns: The final technical result to highlight is the usage patterns of the hydrogen fueling stations within the project over the last two years. Note that at this point in the deployment of FCEVs, station coverage is much more important than throughput is to enable the automotive companies to launch early commercial vehicles. Figure 4 shows the percentage of hydrogen dispensed by day of the week (bars with left-axis labels) along with the average amount of hydrogen dispensed by day for each of the eight stations included in this dataset (curves with right-axis labels). The data show that weekday fueling is still more common than weekend fueling, which had been shown in a previous CDP from the first five years of the project. The graph also shows that two stations have relatively high average throughput (15–27 kg/day), one has moderate throughput (6 kg/day), and the other five are only lightly used, dispensing 3 kg/day or less on average. This type of result will be useful as a baseline to track future throughput of each station individually and by specific geographic region to better coordinate and advise stakeholders on optimal future vehicle deployments and new station placement.

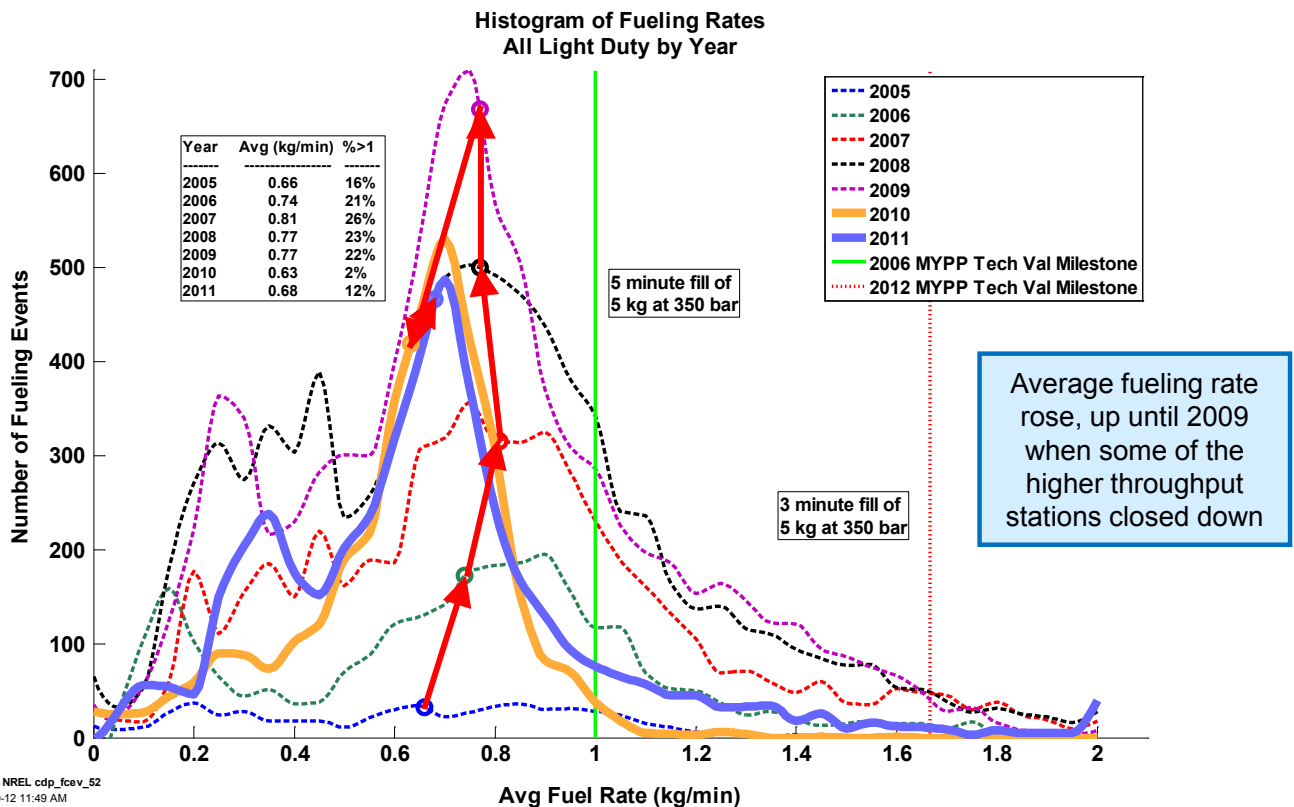


FIGURE 3. Fueling Rate Trends Are Monitored as Industry Moves to 700-bar Pressure as Standard

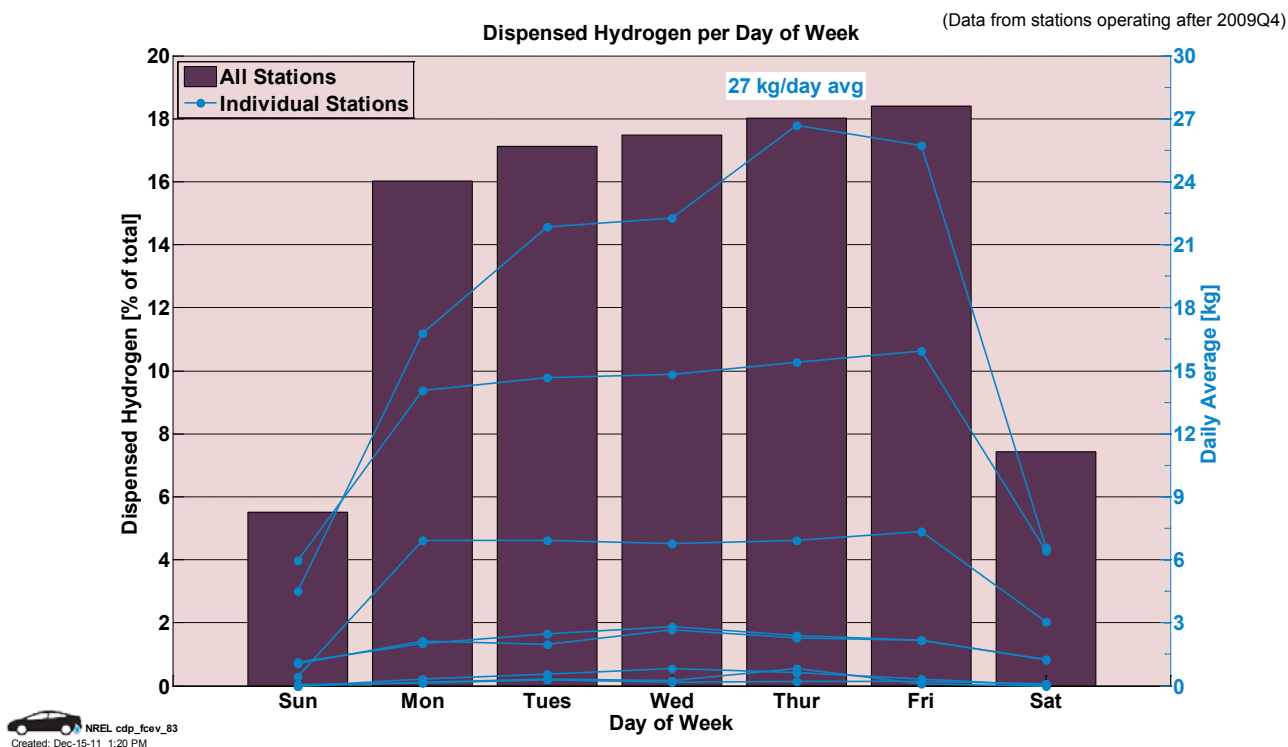


FIGURE 4. New Infrastructure CDP Provides Insight Into Specific Fueling Usage Patterns

Conclusions and Future Direction

- We successfully completed the largest single fuel cell vehicle and hydrogen infrastructure demonstration in the world to date; this project is the first time such comprehensive data were collected by an independent third party and consolidated and analyzed for public dissemination.
- The project addressed the critical need for technology validation to bridge the gap between R&D and commercial readiness of the vehicle and station technologies.
- NREL published 99 CDPs to communicate the technical results to a broad audience of stakeholders.
- Through seven years of real-world validation the project deployed 183 vehicles travelling 3.6 million miles through 500,000 trips, resulting in 154,000 hours of second-by-second data delivered to NREL. The project also deployed 25 hydrogen fueling stations that produced or dispensed 152,000 kg of hydrogen through more than 33,000 fueling events.
- The technical results from this project have exceeded the DOE expectations established in 2003. Two of DOE's key interim technical targets for 2009 were achieved—demonstrating >250 mile range and >2,000 hour fuel cell stack durability. The third target of \$3/gge on-site hydrogen production cost was met outside of this project through results from an independent review panel of experts.
- Infrastructure utilization has improved in the last two years but is still in a mode focused on geographic coverage rather than capacity utilization.
- Hydrogen fueling rates have dropped slightly in the last two years because some higher throughput stations were decommissioned and some of the latest technology stations (700 bar) were gradually being brought up to full speed.
- This project fulfilled a key objective of providing lessons learned to guide and inform research and development activities within DOE.
- NREL will be analyzing and publishing CDPs from future hydrogen vehicle and infrastructure projects supported by DOE.
- From all of the project results that NREL has generated, it is our conclusion that FCEVs have advanced rapidly in the last seven years. As the automotive OEMs and other researchers worldwide continue to focus on the remaining challenges of balancing durability, cost, and high-throughput manufacturability, we are optimistic that improvements will result in a manageable incremental cost for fuel cell technology. We therefore expect continued progress to lead to several vehicle manufacturers introducing thousands of vehicles to the market in the 2014–2016 timeframe, at which time the hydrogen community will have its first true test of whether the technology will be embraced by the public.

FY 2012 Publications/Presentations

1. Wipke, K., Sprik, S., Kurtz, T., Ramsden, T., Ainscough, C., Saur, G., “National Fuel Cell Electric Vehicle Learning Demonstration Final Report,” NREL/TP-5600-54860, Golden, CO, July 2012. (paper)
2. Wipke, K., Sprik, S., Kurtz, T., Ramsden, T., Ainscough, C., Saur, G., “Controlled Hydrogen Fleet and Infrastructure Analysis,” 2012 U.S. DOE Hydrogen and Fuel Cells Program and Vehicle Technologies Program Annual Merit Review and Peer Evaluation Meeting, Washington, D.C., May 2012. (presentation)
3. Wipke, K., Sprik, S., Kurtz, J., Ramsden, T., Ainscough, C., Saur, G., “Final Results from U.S. FCEV Learning Demonstration,” 26th International Battery, Hybrid and Fuel Cell Electric Vehicle Symposium (EVS-26), Los Angeles, CA, May 2012. (paper and presentation)
4. Kurtz, J., Wipke, K., Eudy, L., Sprik, S., Ramsden, T., “Fuel Cell Technology Demonstrations and Data Analysis,” Chapter in Hydrogen Energy and Vehicle Systems, Green Chemistry and Chemical Engineering, CRC Press, April 2012. (book chapter)
5. Wipke, K., Sprik, S., Kurtz, J., Ramsden, T., Ainscough, C., Saur, G., “National Hydrogen Learning Demonstration Status,” DOE’s Informational Webinar Series, February 2012. (presentation and webinar recording)
6. Wipke, K., Sprik, S., Kurtz, J., Ramsden, T., Ainscough, C., Saur, G., “Winter 2011 – All Composite Data Products: National FCEV Learning Demonstration, with Updates through January 18, 2012,” Golden, CO: National Renewable Energy Laboratory, published January 2012. (presentation)
7. Wipke, K., Sprik, S., Kurtz, J., Ramsden, T., Ainscough, C., Saur, G., 2011 Annual Progress Report for NREL’s “Controlled Hydrogen Fleet and Infrastructure Analysis Project,” November 2011. (paper)
8. Wipke, K., Sprik, S., Kurtz, J., Ramsden, T., Ainscough, C., Saur, G., “Conclusion of the National FCEV Learning Demonstration Project,” presented at the Fuel Cell Seminar, Orlando, Florida in November 2011. (presentation)
9. Wipke, K., Sprik, S., Kurtz, J., Ramsden, T., Ainscough, C., Saur, G., “Fall 2011 – All Composite Data Products with Updates through October 5, 2011: National FCEV Learning Demonstration,” Golden, CO: National Renewable Energy Laboratory, published October 2011. (presentation)
10. Sprik, S., Kurtz, J., Wipke, K., Ramsden, T., Ainscough, C., Eudy, L., and Saur, G., “Real-World Hydrogen Technology Validation,” International Conference on Hydrogen Safety (ICHS 2011), September 2011. (presentation and paper)

References

1. Wipke, K., Anton, D., Sprik, S., “Evaluation of Range Estimates for Toyota FCHV-adv Under Open Road Driving Conditions,” prepared under SRNL CRADA number CR-04-003, August 2009.
2. Fletcher, J., Callaghan, V., “Evaluation Cost of Distributed Production of Hydrogen from Natural Gas – Independent Review,” NREL/BK-150-40382, October 2006.
3. Genovese, J., Harg, K., Paster, M., Turner, J., “Current (2009) State-of-the-Art Hydrogen Production Cost Estimate Using Water Electrolysis – Independent Review,” NREL/BK-6A1-46676, September 2009.

VII.2 Validation of an Integrated Hydrogen Energy Station

Edward C. Heydorn
Air Products and Chemicals, Inc.
7201 Hamilton Blvd
Allentown, PA 18195
Phone: (610) 481-7099
Email: heydorec@airproducts.com

DOE Managers
HQ: Jason Marcinkoski
Phone: (202) 586-7466
Email: Jason.Marcinkoski@ee.doe.gov
GO: Jim Alkire
Phone: (720) 356-1426
Email: James.Alkire@go.doe.gov

Contract Number: DE-FC36-01GO11087

Subcontractor:
FuelCell Energy, Danbury, CT

Project Start Date: September 30, 2001
Project End Date: December 31, 2011

Technical Barriers

This project addresses the following technical barriers from the Technology Validation section (3.5.4) of the Fuel Cell Technologies Program Multi-Year Research, Development and Demonstration Plan:

- (C) Hydrogen Refueling Infrastructure
- (I) Hydrogen and Electricity Co-Production

Contribution to Achievement of DOE Technology Validation Milestones

This project will contribute to achievement of the following DOE milestones from the Technology Validation section of the Fuel Cell Technologies Program Multi-Year Research, Development and Demonstration Plan:

- Milestone 37: Demonstrate prototype energy station for 6 months; projected durability >20,000 hours; electrical energy efficiency >40%; availability >0.80. (4Q, 2008)
- Milestone 38: Validate prototype energy station for 12 months; projected durability >40,000 hours; electrical energy efficiency >40%; availability >0.85. (1Q, 2014)

Fiscal Year (FY) 2012 Objectives

Demonstrate the technical and economic viability of a hydrogen energy station using a high-temperature fuel cell designed to produce power and hydrogen.

- Complete a technical assessment and economic analysis on the use of high-temperature fuel cells, including solid oxide and molten carbonate, for the co-production of power and hydrogen (energy park concept).
- Build on the experience gained at the Las Vegas H₂ Energy Station and compare/contrast the two approaches for co-production.
- Determine the applicability of co-production from a high-temperature fuel cell for the existing merchant hydrogen market and for the emerging hydrogen economy.
- Demonstrate the concept at a suitable site with demand for both hydrogen and electricity.
- Maintain safety as the top priority in the system design and operation.
- Obtain adequate operational data to provide the basis for future commercial activities, including hydrogen fueling stations.

FY 2012 Accomplishments

- On 25 May 2011, the clean-up system for anaerobic digester gas (ADG) was commissioned, and renewable hydrogen was produced for the first time from the Hydrogen Energy Station. System efficiency of 53.5% exceeds the goal of 50%.
- The formal opening of the Hydrogen Energy Station and hydrogen fueling station at Orange County Sanitation District (OCS D) was held on 16 August 2011.
- Hydrogen coproduction economics based on the installation and operation at OCS D were prepared, with costs of \$3 to \$5 per kilogram achievable with next-generation hydrogen purification technology.
- The DOE Cooperative Agreement was extended to December 31, 2011.



Introduction

One of the immediate challenges in the development of hydrogen as a transportation fuel is finding the optimal means to roll out a hydrogen-fueling infrastructure concurrent with the deployment of hydrogen vehicles. The low-volume hydrogen requirements in the early years of

fuel cell vehicle deployment make the economic viability of stand-alone, distributed hydrogen generators challenging. A potential solution to this “stranded asset” problem is the use of hydrogen energy stations that produce electricity in addition to hydrogen. To validate this hypothesis, a four-phase project was undertaken to design, fabricate and demonstrate a high-temperature fuel cell co-production concept. The basis of the demonstration was a FuelCell Energy DFC[®]-300 molten carbonate fuel cell modified to allow for the recovery and purification of hydrogen from the fuel cell anode exhaust using an Air Products-designed hydrogen purification system.

The DFC[®] technology is based on internal reforming of hydrocarbon fuels inside the fuel cell, integrating the synergistic benefits of the endothermic reforming reaction with the exothermic fuel cell reaction. The internal reforming of methane is driven by the heat generated in the fuel cell and simultaneously provides efficient cooling of the stack, which is needed for continuous operation. The steam produced in the anode reaction helps to drive the reforming reaction forward. The hydrogen produced in the reforming reaction is used directly in the anode reaction, which further enhances the reforming reaction. Overall, the synergistic reformer-fuel cell integration leads to high (~50%) electrical efficiency.

The baseline DFC[®] power plant (electricity only) is designed to operate at 75% fuel utilization in the stack. The remaining 25% of fuel from the anode presents a unique opportunity for low-cost hydrogen, if it can be efficiently recovered from the dilute anode effluent gases. The recovery and purification of hydrogen from the anode presents several challenges: (1) the anode off-gas is a low-pressure, high-temperature gas stream that contains ~10% hydrogen by volume; (2) the anode exhaust stream must be heat integrated with the fuel cell to ensure high overall system efficiency; and (3) the parasitic power used for purification must be optimized with the hydrogen recovery and capital cost to enable an economically viable solution.

Approach

A hydrogen energy station that uses a high-temperature fuel cell to co-produce electricity and hydrogen was evaluated and demonstrated in a four-phase project. In Phase 1, Air Products completed a feasibility study on the technical and economic potential of high-temperature fuel cells for distributed hydrogen and power generation. As part of this analysis, three different high-temperature fuel cells were evaluated to determine the technology most suitable for a near-term demonstration. FuelCell Energy’s DFC[®]-300 technology was selected for concept development. In Phase 2, a process design and cost estimate were completed for the hydrogen energy station that integrated the fuel cell with a pressure swing adsorption (PSA) system selected and designed by Air Products. Economics were developed

based on actual equipment, fabrication, and installation quotes as well as new operating cost estimates. High-level risks were identified and addressed by critical component testing. In Phase 3, a detailed design for the co-production system was initiated. The system was fabricated and, prior to shipping to the field, the entire system was installed at FuelCell Energy’s facility in Danbury, CT for complete system check-out and validation. In Phase 4, the system was operated on municipal waste water-derived biogas at OCS D, Fountain Valley, California, under a 3-year program with the California Air Resources Board (CARB), with co-funding by the South Coast Air Quality Management District (AQMD). DOE received 6 months of data from the initial operating phase to validate the system versus DOE’s economic performance targets.

Results

Figure 1 shows the process flow diagram for the Hydrogen Energy Station. Methane is internally reformed at the fuel cell anode to hydrogen and carbon dioxide. The fuel cell operates near 600°C and uses molten carbonate electrolyte as the charge carrier. Heated air is combined with the waste gas from the hydrogen purification system and oxidized. These resultant waste gases are fed to the cathode. The fuel cell cathode converts waste gas carbon dioxide to the carbonate charge carrier to complete the fuel cell circuit. The fuel cell stack generates a direct current voltage, which is then converted to alternating current by an inverter in the electrical balance of plant. The system produces 480 VAC, 60 HZ, and a nominal 300 kW without hydrogen co-production. Excess carbon dioxide and water leave the cathode as exhaust, and heat can be recovered from these exhaust gases.

About 70 to 80% of the hydrogen is converted to power, and some hydrogen remains available for recovery. The anode exhaust gas is cooled and sent to a water-gas shift catalytic reactor to convert most of the carbon monoxide present in the stream to hydrogen and carbon dioxide. After an additional cooling step, this gas stream is then compressed and sent to the PSA system. The PSA uses adsorbents to remove carbon monoxide, carbon dioxide, and water to produce a high-purity hydrogen stream. The waste gas from the PSA is catalytically oxidized and returned to the cathode. The PSA system can also be placed in stand-by mode to stop hydrogen production and allow for maximum power production by the DFC[®] system, thereby improving the system efficiency and economics.

In late 2008, the Hydrogen Energy Station was installed at FuelCell Energy’s facilities in Danbury, CT for a system check-out and validation of performance on natural gas and simulated digester gas. In June 2010, the Hydrogen Energy Station was disassembled and prepared for shipment from Danbury, CT to the OCS D wastewater treatment plant in

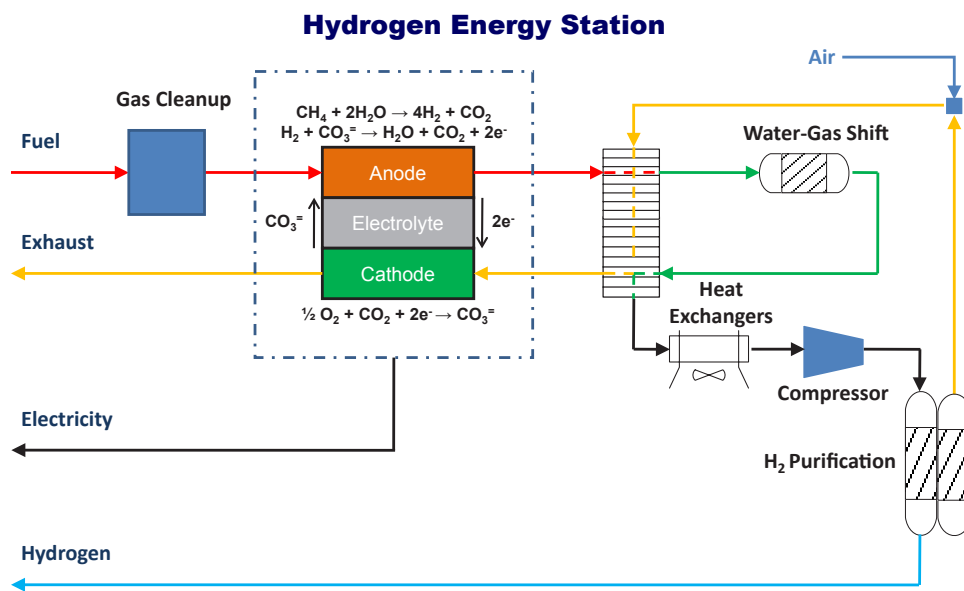


FIGURE 1. Hydrogen Energy Station Process Flow Diagram

Fountain Valley, CA. The system was delivered in early July, and full-load operation on natural gas was achieved on September 20, 2010. Initial co-production of hydrogen from the Hydrogen Energy Station on natural gas at OCSD occurred on 20 October 2010. Figure 2 shows the installation of the Hydrogen Energy Station at OCSD.

On 25 May 2011, the clean-up system for ADG was commissioned, and renewable hydrogen was produced for the first time from the Hydrogen Energy Station. This system was deployed under a second DOE project. June 1, 2012 marked the beginning of a three-year operating project under sponsorship of CARB and AQMD. One of the improvements made to the system was the addition of capability to direct hydrogen from the gas storage system to the ADG clean-up system to assist in the removal of sulfur species. In addition, hydrogen not used to replenish the storage system can now be routed to the fuel cell instead of vented to atmosphere as was the case during initial operation in 2010.

The formal opening of the Hydrogen Energy Station and hydrogen fueling station at OCSD was held on August 16, 2011. A total of 140 guests were in attendance. Speakers included representatives from project sponsors/participants Air Products, FuelCell Energy, the University of California, Irvine, AQMD, CARB, and the DOE, and also included U.S. Representative Dana Rohrabacher (CA 46th District).

During operation on ADG, a detailed heat and material balance was performed to determine the overall efficiency of the Hydrogen Energy Station. The calculated efficiency of 53.3% exceeded the target of 50%. During the 6 months of operation on ADG, the fuel cell continued to experience power quality issues at OCSD. A total of 115 trips (excluding trips less than 15 minutes apart) took place during the

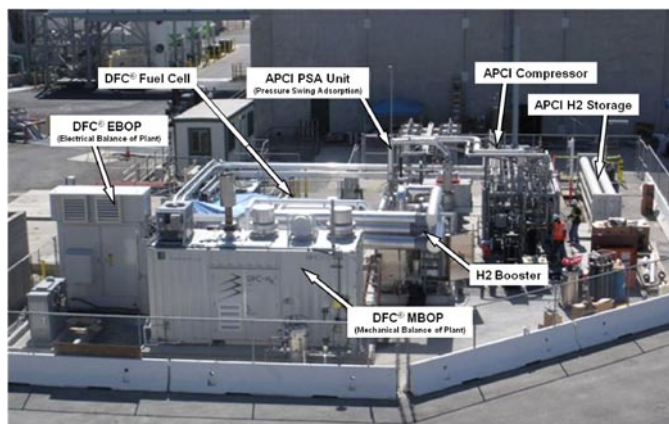


FIGURE 2. Hydrogen Energy Station Installation at Orange County Sanitation District

last quarter of calendar year 2011. These trips limited hydrogen production, as the system was programmed to de-integrate the hydrogen purification system each time the fuel cell power production is interrupted. Changes are being considered to this logic, especially to short-duration outages through which it may be feasible for the hydrogen purifier to continue operation. As a result of modifications within the power grid at OCSD, no trips related to power quality have occurred since January 31, 2012.

An overall operations summary (through April 2012) of performance of the Hydrogen Energy Station at OCSD is provided in Figure 3. Over 5 million standard cubic feet of ADG was processed, and over 1 million kWh of power was exported to the power grid at OCSD.

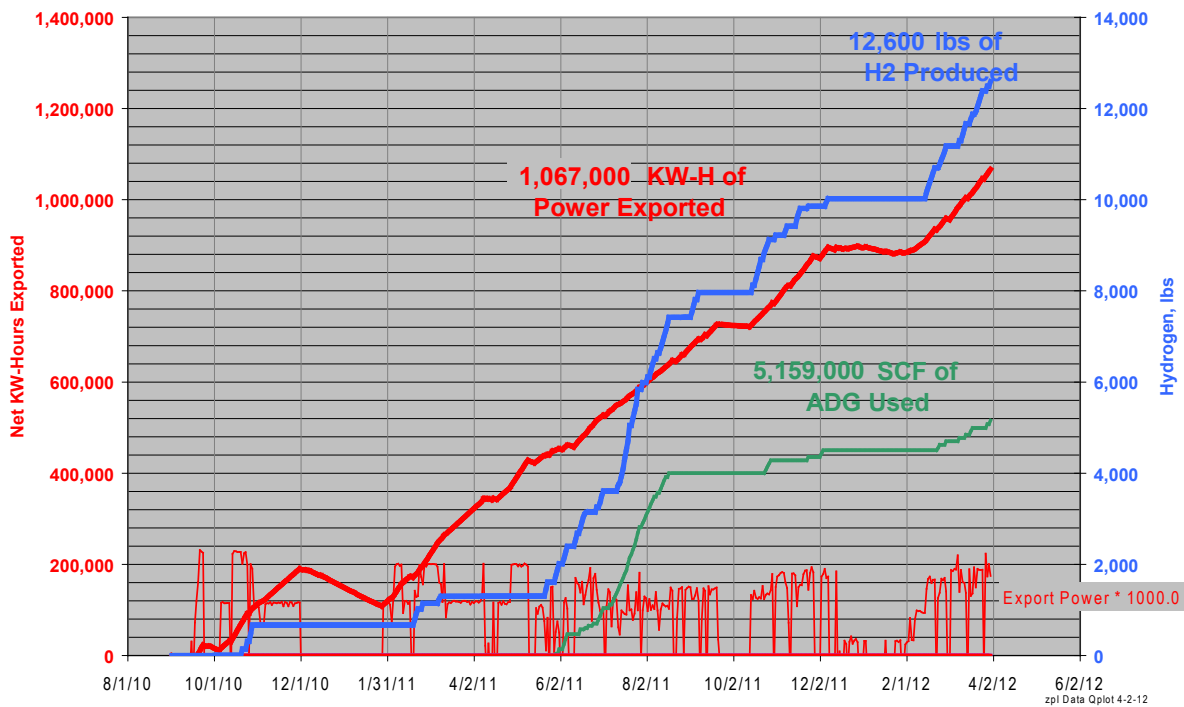


FIGURE 3. Hydrogen Energy Station Overall Operations Summary at OCSD

Based on the learnings from the design, installation, and initial operation at OCSD, an economic analysis on the cost of hydrogen from a Hydrogen Energy Station was performed. Hydrogen production rates up to 6,000 kilograms per day were considered, and Figure 4 shows two cases, (1) near-term pricing of \$6 to \$8 per kilogram utilizing PSA for hydrogen purification and (2) longer-term estimates of \$3 to \$5 per kilogram using next generation, electrochemical separation processes.

Conclusions and Future Direction

- The Hydrogen Energy Station began operation on ADG at OCSD’s wastewater treatment facility. System efficiency of 53.5% exceeded program targets. Over 1 million kWh of power was exported to the OCSD power grid. Hydrogen coproduction economics were updated.
- The DOE Cooperative Agreement has ended, but operation will continue at OCSD until May 31, 2014 under continuing sponsorship of CARB and AQMD.

FY 2012 Publications/Presentations

1. Presentation at the DOE Annual Merit Review Meeting, Washington, D.C., May 2012.

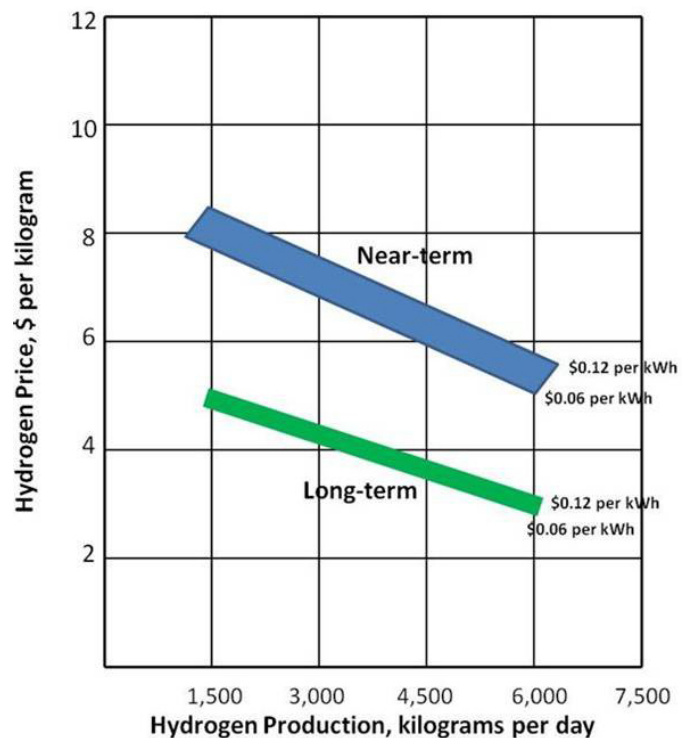


FIGURE 4. Hydrogen Energy Station Economics (updated December 2012)

VII.3 Technology Validation: Fuel Cell Bus Evaluations

Leslie Eudy
National Renewable Energy Laboratory
15013 Denver West Parkway
Golden, CO 80401
Phone: (303) 275-4412
Email: leslie.eudy@nrel.gov

DOE Manager
HQ: Jason Marcinkoski
Phone: (202) 586-7466
Email: Jason.Marcinkoski@ee.doe.gov

Subcontractor:
Kevin Chandler, Battelle, Columbus, Ohio

Project Start Date: March 2001
Project End Date: Project continuation and direction determined annually by DOE

Milestone 2.3: Validate fuel cell electric vehicles achieving 5,000-hour durability (service life of vehicle) and a driving range of 300 miles between fuelings. (4Q, 2019) By the end of April 2012, NREL had documented three FCEB fuel cell systems with operation in excess of 7,000 hours with no major repairs. One of these systems has logged more than 12,000 hours in service. Bus fuel economy is dependent on duty-cycle. Based on in-service fuel economies between 5 and 7 miles per kilogram, the hybrid FCEBs currently in service can achieve a range between 200 and 280 miles per fill.

FY 2012 Accomplishments

- Published reports on 2nd-generation performance and operational data on 13 full-size FCEBs in revenue service in the United States.
- Began data collection on FCEBs in revenue service at two additional transit agencies.

Fiscal Year (FY) 2012 Objectives

- Determine the status of fuel cell electric bus (FCEB) technologies in transit applications by evaluating them in real-world service.
- Coordinate with the Department of Transportation's Federal Transit Administration (FTA) on the data collection for the National Fuel Cell Bus Program (NFCBP) and with international work groups to harmonize data-collection methods and enable the comparison of a wider set of vehicles.

Technical Barriers

This project addresses the following technical barriers from the Technology Validation section of the Fuel Cell Technologies Program's Multi-Year Research, Development, and Demonstration Plan:

- (A) Lack of Fuel Cell Electric Vehicle and Fuel Cell Bus Performance and Durability Data
- (C) Lack of H₂ Fueling Infrastructure Performance and Availability Data

Contribution to Achievement of DOE Technology Validation Milestones

This project has contributed to achievement of the following DOE milestone from the Technology Validation section of the Fuel Cell Technologies Program Multi-Year Research, Development and Demonstration Plan:



Introduction

Transit agencies continue to aid the FCEB industry in developing and optimizing advanced transportation technologies. These in-service demonstrations are necessary to validate the performance of the current generation of fuel cell systems and to determine issues that require resolution. The evaluations conducted to date have included two generations of FCEB design. Using fuel cells in a transit application can help accelerate the learning curve for the technology because of the high mileage accumulated in short periods of time. During the last year, major progress was made in improving fuel cell durability; however, more work is needed to improve reliability, increase durability to meet the needs of transit agencies, lower capital and operating costs, and transition the maintenance to transit staff.

Approach

NREL uses a standard evaluation protocol to provide:

- Comprehensive, unbiased evaluation results of advanced technology vehicle development and operations.
- Evaluations of hydrogen infrastructure development and operation.
- Descriptions of facility modifications required for the safe operation of FCEBs.
- Detailed performance and durability results of FCEBs to validate status against technical targets, educate key stakeholders, and further DOE goals.

The evaluation protocol includes two levels of data: operation and maintenance data on the bus and infrastructure, and more detailed data on the fuel cell, system, and components. The first set of data is considered non-sensitive and is obtained mainly from the transit fleet. The analysis, which consists of economic, technical, and safety factors, focuses on performance and use, including progress over time and experience with vehicle systems and supporting infrastructure.

The detailed data are collected with cooperation from the bus and fuel cell system manufacturers and are considered highly sensitive. Results include aggregate data products that protect each manufacturer’s specific data. To date, NREL has collected this type of data from two fuel cell manufacturers. Aggregate results will be published if and when enough data are available to protect each company’s identity and source data.

Results

During FY 2012, NREL collected and analyzed data on several 2nd-generation FCEB demonstrations at three transit agencies in the United States: SunLine Transit Agency in Thousand Palms, California; AC Transit in Oakland, California; and Connecticut Transit (CTTRANSIT) in Hartford, Connecticut. The first two of these evaluations were funded by DOE, and the third evaluation was covered by funding from FTA. NREL published results from each of these demonstrations. A summary of selected results is included in this report, followed by an overview of the newest FCEBs being evaluated. Under FTA funding, NREL began collecting data on two additional FCEBs, one at SunLine and one at Capital Metro in Austin, Texas.

In the demonstrations reported here, the 2nd-generation FCEBs are fuel cell dominant hybrid buses:

- Zero Emission Bay Area (ZEBA) Demonstration – five Bay Area transit agencies led by AC Transit are demonstrating twelve 40-foot Van Hool buses with UTC Power fuel cells in a Siemens hybrid system. The hybrid system was integrated by Van Hool and uses lithium ion batteries from EnerDel.
- ‘Nutmeg’ Fuel Cell Electric Bus Demonstration – named for Connecticut’s state nickname, the Nutmeg project is part of FTA’s NFCBP. The four buses, which are identical to the 12 ZEBA buses, were operated by CTTRANSIT in Hartford, Connecticut.
- Advanced Technology FCEB Project – SunLine is operating one New Flyer 40-foot bus with a Bluways hybrid system and Ballard fuel cell. This bus was the pilot bus from a fleet of 20 buses operating in Whistler, British Columbia, Canada.

NREL completed reports on operational and performance data on these FCEBs and conventional baseline buses at each agency. Table 1 provides a summary of the reported results from the operation at each agency, including data from the baseline buses.

One of the performance targets for FCEBs is to demonstrate fuel economy that is two times that of conventional bus technology. The 1st-generation FCEBs showed fuel economy improvements ranging from 48% to nearly 150% compared to conventional buses, depending on duty-cycle. Figure 1 shows the fuel economy of the 2nd-generation buses at each of the three transit agencies in miles per diesel gallon equivalent. (Note that the baseline buses at SunLine are CNG buses.) These data show that the 2nd-generation FCEBs are demonstrating fuel economies about two times that of the baseline buses, thus meeting the target.

Comparing FCEBs to competing technologies is valuable if the data are available. One such competing technology is

TABLE 1. Summary Data Results for 2nd-Generation FCEBs

| Vehicle data | AC Transit | | CTTRANSIT | | SunLine | |
|----------------------------------|-----------------|-----------------|-----------------|-----------------|-----------------|-----------------|
| | FCEB | Diesel | FCEB | Diesel | FCEB | CNG1 |
| Number of buses | 12 | 3 | 4 | 3 | 1 | 5 |
| Data period (year, month) | Sep 11 – Apr 12 | Sep 11 – Apr 12 | Oct 10 – May 12 | Oct 10 – May 12 | May 10 – Jan 12 | May 10 – Jan 12 |
| Number of months | 8 | 8 | 20 | 20 | 21 | 21 |
| Total fleet miles | 147,007 | 83,599 | 100,390 | 183,497 | 31,857 | 483,237 |
| Average miles per month | 1,598 | 3,635 | 1,385 | 3,219 | 1,517 | 4,602 |
| Total fuel cell hours | 17,619 | | 7,305 | | 2,591 | |
| Fuel economy (mi/kg) | 6.68 | | 6.89 | | 5.75 | 2.98 |
| Fuel economy (mi/diesel gal eq.) | 7.55 | 4.00 | 7.78 | 3.93 | 6.5 | 3.49 |
| Average speed (mph) | 9.4 | N/A | 13.8 | N/A | 13.1 | 13.9 |
| Availability (%) | 56 | 77 | 52 | 85 | 62 | 88 |

¹ CNG = compressed natural gas

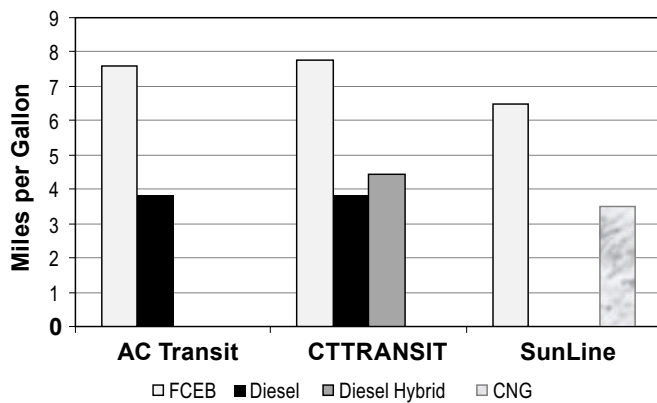


FIGURE 1. Fuel economy comparison by fleet (diesel equivalent)

diesel hybrid buses. The primary challenge for adding these data to the evaluations is the fact that few of the agencies demonstrating FCEBs also operate similar diesel hybrid buses. Fuel economy is highly variable based on duty-cycle—the most accurate comparisons require similarly sized buses operated in the same service. Over the past year, NREL has begun to collect data on new hybrid buses at CTTRANSIT (included in Figure 1); however the hybrids of similar size to the FCEBs operate out of a different division. The hybrid buses have a more challenging duty-cycle than that of the FCEBs, characterized by more stops (buses operated out of this division typically have a 2% to 3% lower fuel economy). This fact should be noted when comparing the results presented in the table; however, this indicates that the duty-cycles are reasonably similar enough to compare.

One key challenge for the fuel cell bus industry is increasing the durability and reliability of the fuel cell system to meet FTA life cycle requirements for a full-size bus—12 years or 500,000 miles. Because transit agencies typically rebuild the diesel engines at approximately mid-life, a fuel cell power plant (FCPP) should be able to operate for at least half the life of the bus. DOE and FTA have set an early FCPP performance target of 4–6 years (or 25,000 hours) durability for the fuel cell propulsion system. Since NREL first began collecting data on the technology in 2002, FCEBs are now demonstrating some of the highest hours in service. These high-hour FCPPs are operating in the new ZEBAs at AC Transit. At the time the first new bus bodies were delivered, three FCPPs from the 1st-generation demonstration were reaching very high hours without significant degradation. To further test this FCPP version, the manufacturers installed the three older FCPPs into the new ZEBAs being delivered. Those three FCPPs continue to operate and accumulate hours in service. The top FCPP has now achieved more than 12,000 hours without major repair or cell replacements. The second FCPP is nearing 10,000 hours and the third is just under 8,000 hours. The manufacturer (UTC Power) reports that these FCPPs continue to provide the rated power of 120 kW. This is a significant achievement toward

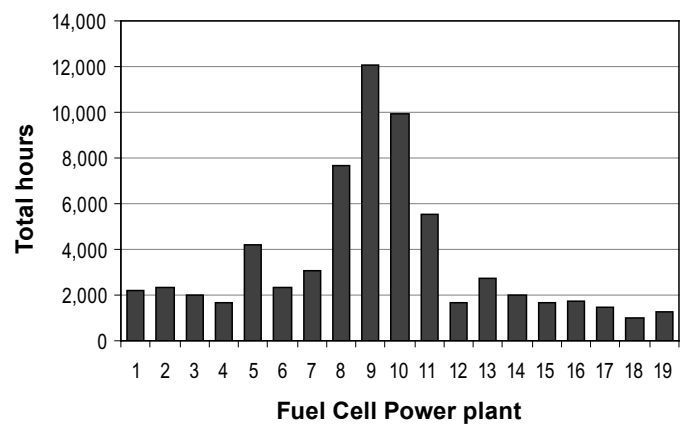


FIGURE 2. Hours accumulated on each fuel cell power plant

meeting the 25,000 hour target. The FCPPs in the Nutmeg buses are of the same version and are also expected to reach in excess of 10,000 hours in service. Figure 2 shows the total hours accumulated on each of the 2nd-generation buses.

NREL began collecting data on other types of fuel cell buses at the following transit agencies:

- City of Burbank – one battery dominant, plug-in hybrid FCEB developed by Proterra using Hydrogenics fuel cells and lithium titanate batteries.
- Capital Metro, Austin, Texas – one battery dominant, plug-in hybrid FCEB developed by Proterra using Hydrogenics fuel cells and lithium titanate batteries. This is the prototype bus to the Burbank bus and is funded under the NFCBP.
- SunLine, American Fuel Cell Bus – one fuel cell dominant EIDorado 40-foot bus with a BAE Systems hybrid drive using Ballard fuel cells and lithium ion batteries. This project is also part of the NFCBP.

Conclusions and Future Direction

Fuel cell propulsion systems in buses have continued to show progress in increasing the durability and reliability of FCEBs and the primary components. The current technology already meets fuel economy targets and is showing promise to exceed the fuel cell durability target. There are still challenges to overcome before fuel cell buses can match the current standard of diesel bus performance. These include:

- Continue operation to validate durability and reliability of the fuel cell systems and other components to match transit needs.
- Optimizing the propulsion system to maximize operation and resolve integration issues.
- Lowering the costs of purchasing, operating, and maintaining buses and infrastructure
- Transferring all maintenance work to transit personnel.

Future work by NREL includes:

- Continuing data collection, analysis, and reporting on performance data for FCEBs in service at the following sites:
 - ZEBA FCEB demonstration led by AC Transit
 - SunLine
 - City of Burbank
 - Additional sites as funding allows
- Investigating reliability, durability, and life cycle of FCEBs as a part of ongoing evaluations.
- Coordinating with FTA to collect data on the demonstrations funded under the NFCBP.
- Coordinating with national and international FCEB demonstration sites.

FY 2012 Publications/Presentations

1. L. Eudy, K. Chandler. (2012). *SunLine Transit Agency Advanced Technology Fuel Cell Bus Evaluation: Third Results Report*. NREL/TP-5600-54427. National Renewable Energy Laboratory, Golden, CO, May.
2. K. Chandler, L. Eudy. (2012). *FTA Fuel Cell Bus Program: Research Accomplishments through 2011*. FTA Report No. 0014. Federal Transit Administration, Washington, DC, March.
3. L. Eudy. (2012). *American Fuel Cell Bus Project: Developing and Demonstrating the Next-Generation Fuel Cell Bus Made in America*. Fact Sheet: NFCBP-FS4-Feb12. Federal Transit Administration, Washington, DC, March.
4. L. Eudy. (2011). *Monitoring Ionic Compressor at AC Transit, Emeryville Station*. Presentation to the Hydrogen Delivery Tech Team, January.
5. L. Eudy, K. Chandler, C. Gikakis. (2011). *Fuel Cell Buses in U.S. Transit Fleets: Current Status 2011*. NREL/TP-5600-52927. National Renewable Energy Laboratory, Golden, CO, November.
6. L. Eudy. (2011). *Fuel Cell Electric Bus Evaluations: Recent Results*. Presentation at the California Transit Assoc. Annual Conference, San Jose, CA, November.
7. L. Eudy, K. Chandler. (2011). *SunLine Transit Agency Advanced Technology Fuel Cell Bus Evaluation: Second Results Report and Appendices*. NREL/TP-5600-52349-1 and NREL/TP-5600-52349-2. National Renewable Energy Laboratory, Golden, CO, October.
8. L. Eudy. (2011). *2011 Status of Fuel Cell Electric Buses in U.S. Transit*. Presentation at the National Fuel Cell Bus Workshop, New Orleans, LA, October.
9. L. Eudy, K. Chandler. (2011). *National Fuel Cell Bus Program: Proterra Fuel Cell Hybrid Bus Report, Columbia Demonstration*. FTA Report No. 0003. Federal Transit Administration, Washington, DC, October.
10. K. Chandler, L. Eudy. (2011). *Zero Emission Bay Area (ZEBA) Fuel Cell Bus Demonstration: First Results Report*. NREL/TP-5600-52015. National Renewable Energy Laboratory, Golden, CO, August.
11. L. Eudy. (2011). *Connecticut Nutmeg Fuel Cell Bus Project: Demonstrating Advanced-Design Hybrid Fuel Cell Buses in Connecticut*. Fact Sheet: NFCBP-FS3-Jul11. Federal Transit Administration, Washington, DC, July.
12. L. Eudy. (2011). *Compound Fuel Cell Hybrid Bus Hits the Streets of San Francisco: San Francisco Hosts National Fuel Cell Bus Program Demonstration*. Fact Sheet: NFCBP-FS2-Jul11. Federal Transit Administration, Washington, DC, July.
13. L. Eudy. (2011). *Fuel Cell Electric Buses Demonstrate Early Market Progress*. Presentation at the APTA Bus Conference, Memphis, TN, May.
14. L. Eudy. (2011). *Technology Validation: Fuel Cell Bus Evaluations*. Presentation at the DOE Hydrogen Program Annual Merit Review, Arlington, VA, May.

VII.4 California Hydrogen Infrastructure Project

Edward C. Heydorn
Air Products and Chemicals, Inc.
7201 Hamilton Boulevard
Allentown, PA 18195
Phone: (610) 481-7099
Email: heydorec@airproducts.com

DOE Managers
HQ: Jason Marcinkoski
Phone: (202) 586-7466
Email: Jason.Marcinkoski@ee.doe.gov
GO: Jim Alkire
Phone: (720) 356-1426
Email: James.Alkire@go.doe.gov

Contract Number: DE-FC36-05G085026

Working Partners/Subcontractors:

- University of California Irvine (UCI), Irvine, CA
- National Fuel Cell Research Center (NFCRC), Irvine, CA

Project Start Date: August 1, 2005

Project End Date: December 31, 2011

Contribution to Achievement of DOE Technology Validation Milestones

This project will contribute to achievement of the following milestones from the Technology Validation section of the Fuel Cell Technologies Program Multi-Year Research, Development and Demonstration Plan:

- Milestone 23: Total of 10 stations constructed with advanced sensor systems and operating procedures. (1Q, 2008).

FY 2012 Accomplishments

- Began operation of the hydrogen pipeline fueling station (350 and 700 bar) in Torrance, CA.
- Installed, commissioned and began operation of a renewable hydrogen fueling station and a gas clean-up system for anaerobic digester gas in Fountain Valley, CA.
- Continued high-reliability operation of the hydrogen fueling station in Irvine, CA.



Fiscal Year (FY) 2012 Objectives

Demonstrate a cost-effective infrastructure model in California for possible nationwide implementation:

- Design, construct and operate seven hydrogen fueling stations
- Collect and report infrastructure data
- Document permitting requirements and experiences
- Validate expected performance, cost, reliability, maintenance, and environmental impacts

Implement a variety of new technologies with the objective of lowering costs of delivered H₂:

- New Delivery Concept
- High pressure/high purity clean up equipment

Technical Barriers

This project addresses the following technical barriers from the Technology Validation section (3.6.4) of the Fuel Cell Technologies Program Multi-Year Research, Development and Demonstration Plan:

(C) Hydrogen Refueling Infrastructure

Introduction

Air Products and Chemicals, Inc. is leading a comprehensive, multiyear project to demonstrate a hydrogen infrastructure in California. The specific primary objective of the project is to demonstrate a model of a “real-world” retail hydrogen infrastructure and acquire sufficient data within the project to assess the feasibility of achieving the nation’s hydrogen infrastructure goals. The project will help to advance hydrogen station technology, including the vehicle-to-station fueling interface, through consumer experiences and feedback. By encompassing a variety of fuel cell vehicles, customer profiles and fueling experiences, this project is obtaining a complete portrait of *real market needs*. The project is also opening its stations to other qualified vehicle providers at the appropriate time to promote widespread use and gain even broader public understanding of a hydrogen infrastructure. The project is engaging major energy companies to provide a fueling experience similar to traditional gasoline station sites to foster public acceptance of hydrogen.

Approach

Work over the course of the project was focused in multiple areas. With respect to the equipment needed, technical design specifications were written, reviewed, and

finalized. Both safety and operational considerations were a part of this review. After finalizing individual equipment designs, complete station designs were started including process flow diagrams and systems safety reviews. Material quotes were obtained, and in some cases, depending on the project status and the lead time, equipment was placed on order and fabrication was started. Consideration was given for expected vehicle usage and station capacity, standard features needed, and the ability to upgrade the station at a later date.

In parallel with work on the equipment, discussions were started with various vehicle manufacturers to identify vehicle demand (short- and long-term needs). Discussions included identifying potential areas most suited for hydrogen fueling stations, with focus on safe, convenient, fast-fills. These potential areas were then compared and overlaid with suitable sites from various energy companies and other potential station operators. Work continues to match vehicle needs with suitable fueling station locations. Once a specific site has been identified, the necessary agreements can be completed with the station operator and expected station users. Detailed work can begin on the site drawings, permits, safety procedures and training needs. Once stations are brought online, infrastructure data will be collected and reported to DOE using Air Products’ Enterprise Remote Access Monitoring system. Feedback from station operators will be incorporated to improve the station user’s fueling experience.

Results

The first of the hydrogen fueling stations within the California Hydrogen Infrastructure Project continued operation at the NFCRC at UCI. The capability for fueling vehicles with gaseous hydrogen at 350 bar, involving the installation of a 1,500 gallon horizontal liquid hydrogen tank, 2 kg/hr compressor skid, storage for 50 kg of hydrogen, and a dual dispenser for both 350- and 700-bar hydrogen was brought onstream in August of 2006. The 700-bar system, including the installation of a booster compressor, was commissioned in February of 2007. Based on a 50% compressor on-stream factor, the station has the capacity to dispense 24 kg/day or approximately 6 cars per day. The station continues to see high usage, with daily throughput often reaching 50 kg/day. Table 1 shows the growth in usage of the station over time.

A proposal by Air Products to expand the station to 100 kg/day capacity was selected for support by the California Energy Commission. A photograph of the dispensing system is provided in Figure 1.

The world’s first fueling station supplied by a hydrogen pipeline completed construction in early 2011 to demonstrate a low-cost, reliable supply of hydrogen. A site in the Torrance, CA area in proximity to an existing Air Products

TABLE 1. UCI 350/700 Bar Hydrogen Fueling Station Usage Growth over Time

| Period | # of Fills | Period | # of Fills | Period | # of Fills |
|-----------|------------|-----------|------------|-----------|------------|
| Q1 FY2007 | 88 | Q1 FY2009 | 326 | Q1 FY2011 | 544 |
| Q2 FY2007 | 60 | Q2 FY2009 | 368 | Q2 FY2011 | 605 |
| Q3 FY2007 | 111 | Q3 FY2009 | 450 | Q3 FY2011 | 608 |
| Q4 FY2007 | 107 | Q4 FY2009 | 507 | Q4 FY2011 | 616 |
| Q1 FY2008 | 257 | Q1 FY2010 | 527 | Q1 FY2012 | 643 |
| Q2 FY2008 | 198 | Q2 FY2010 | 455 | | |
| Q3 FY2008 | 313 | Q3 FY2010 | 531 | | |
| Q4 FY2008 | 385 | Q4 FY2010 | 549 | | |

Q - quarter



FIGURE 1. UCI 350/700 Bar Hydrogen Fueling Station

hydrogen pipeline was developed by Shell Hydrogen. A 4 kg/hr compressor skid and a total of 100 kg of 7,777 psig storage and 20 kg of 15,000 psig storage have been provided. This station dispenses hydrogen according to SAE International specification TIR-J2601. Hydrogen purification technology has been deployed for the first time in this application to demonstrate the production of an ultra-pure hydrogen stream from the industrial-grade pipeline supply. Two dual dispensers for both 350- and 700-bar hydrogen have been installed, and 4 vehicles can be filled simultaneously. Based on a 50% compressor on-stream factor, the station will have the capacity to dispense 48 kg/day or approximately 12 cars per day. When starting with full storage, 6 cars can be filled in succession. An opening ceremony was held on 10 May 2011. Station usage has been high since start-up, with

daily throughput often exceeding the station's nameplate capacity. Table 2 shows the increase in activity over time.

TABLE 2. Torrance, CA Hydrogen Pipeline Fueling Station Increase in Activity over Time

| Period | # of Fills | Period | # of Fills |
|-------------|------------|----------------|------------|
| April 2011 | 163 | September 2011 | 261 |
| May 2011 | 193 | October 2011 | 270 |
| June 2011 | 261 | November 2011 | 298 |
| July 2011 | 247 | December 2011 | 284 |
| August 2011 | 203 | | |

A photograph of the dispenser area is provided in Figure 2.

Air Products was selected under a 2006 California Air Resources Board solicitation with additional funding from South Coast Air Quality Management District to install a renewable-based hydrogen fueling station and cleanup system for anaerobic digester gas (ADG) at Orange County Sanitation District (OCSD) in Fountain Valley, CA. Hydrogen was produced utilizing the Hydrogen Energy Station concept being developed under a second DOE project. The statement of work for this project was modified to include procurement and installation of a hydrogen fueling station (sized at 100 kilograms per day) and of a gas cleanup skid to remove contaminant species such as sulfur from the ADG that will be fed to the Hydrogen Energy Station. The fueling station includes compression, storage, and dispensing of hydrogen at 350 and 700 bar according to SAE TIR-J2601. Hydrogen use at the fueling station was limited as automakers continued



FIGURE 2. Torrance, CA Hydrogen Pipeline Fueling Station



FIGURE 3. Fountain Valley Renewable Hydrogen Station

to negotiate access and payment agreements related to station use. As of December 31, 2011, three automakers have executed the access agreement and were in discussions with UCI (who was managing operation of the hydrogen fueling station) regarding the payment agreement. A photograph of the fueling station area, with the dispenser in the foreground and the balance of fueling station equipment in the background, is provided in Figure 3.

The ADG clean-up system was delivered to the site in May of 2011, and initial performance of the system has been excellent. One of the features of this system was the use of hydrogen from the Hydrogen Energy Station to assist in the removal of sulfur species. As shown in Figure 4, performance of the ADG clean-up system has met the requirements for supply to the fuel cell.

The formal opening of the Hydrogen Energy Station and hydrogen fueling station at OCSD was held on August 16, 2011.

Conclusions and Future Directions

This project has ended, but operation will continue at Irvine, Torrance and Fountain Valley under a variety of funding mechanisms.

FY 2012 Publications/Presentations

1. A presentation regarding the overall project status was given at the DOE Annual Merit Review Meeting (May 2012).

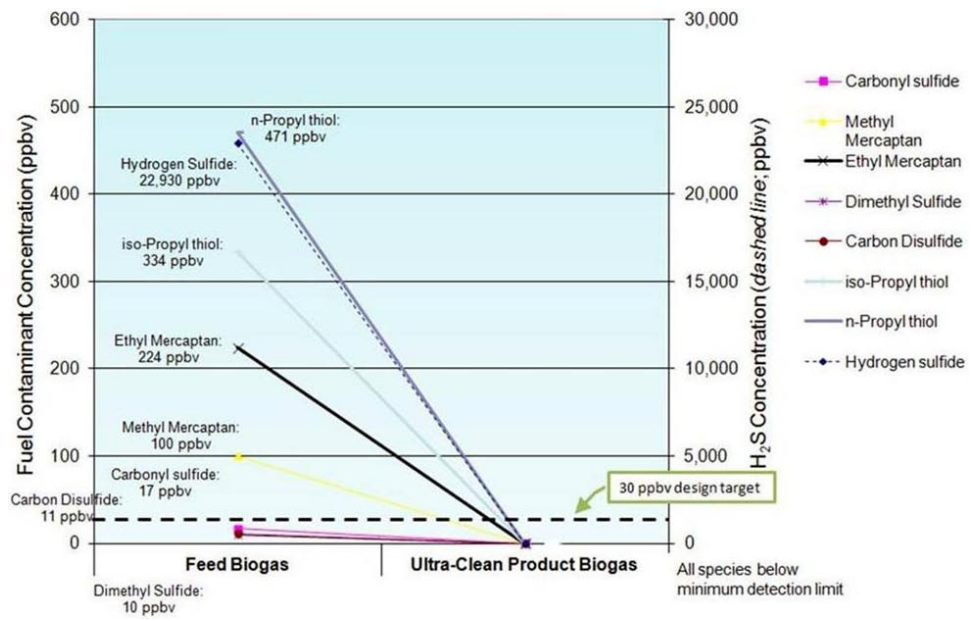


FIGURE 4. Performance of ADG Clean-Up System, Fountain Valley (2/23/12)

VII.5 Hawaii Hydrogen Power Park

Richard (Rick) E. Rocheleau (Primary Contact),
Mitch Ewan

Hawaii Natural Energy Institute
School of Ocean and Earth Science and Technology
University of Hawaii at Manoa
1680 East-West Road, POST 109
Honolulu, HI 96822
Phone: (808) 956-8346
Email: rochelea@hawaii.edu

DOE Managers

HQ: Jason Marcinkoski
Phone: (202) 586-7466
Email: Jason.Marcinkoski@ee.doe.gov
GO: Reginald Tyler
Phone: (720) 356-1805;
Email: Reginald.Tyler@go.doe.gov

Contract Number: DE-FC51-02R021399 A008

Project Start Date: June 29, 2009

Project End Date: December 31, 2014

Fiscal Year (FY) 2012 Objectives

Island of Hawaii (Big Island)

- Install hydrogen fueling station infrastructure at Hawaii Volcanoes (HAVO) National Park on the Big Island of Hawaii
- Support the operations of the HAVO hydrogen fuel cell electric vehicle (FCEV) shuttle buses through December 2014
- Conduct engineering and economic analysis of HAVO bus operations on different routes, grades, elevations and climatic conditions
- Validate fuel cell system performance in harsh environments including high SO₂ concentrations
- Position HAVO as an alternative fuel vehicle test bed for the National Park Service (NPS)
- Attract new partners and applications for the Big Island hydrogen infrastructure
- Conduct outreach to local authorities and the general public regarding hydrogen infrastructure

Oahu

- Support operations of the General Motors Equinox FCEV Hawaii demonstration project in partnership with Office of Naval Research (ONR)

- Install a 350-bar Powertech fast-fill hydrogen production, storage, and dispensing system at Marine Corps Base Hawaii (MCB Hawaii)
- Upgrade the Powertech fueling system to support fast-fill fueling at 700 bar (ONR funded)
- Procure and operate a lightweight hydrogen delivery trailer to support fueling requirements
- Conduct engineering and economic analysis of GM FCEV fueling operations

Barriers

This project addresses non-technical issues that prevent full commercialization of fuel cells and hydrogen infrastructure as indicated in the following sections of the April 2009 edition (amended in 2011) of the Fuel Cell Technologies (FCT) Program Multi-Year Research, Development and Demonstration Plan:

Technology Validation, Section 3.6.5

- (A) Lack of Fuel Cell Vehicle Performance and Durability Data
- (C) Hydrogen Storage
- (D) Lack of Hydrogen Refueling Infrastructure Performance and Availability Data
- (E) Codes and Standards
- (G) Hydrogen from Renewable Resources

Hydrogen Safety, Section 3.8.4

- (A) Limited Historical Database
- (D) Liability Issues
- (F) Safety is Not Always Treated as a Continuous Process
- (G) Expense of Data Collection and Maintenance
- (H) Lack of Hydrogen Knowledge by Authorities Having Jurisdiction
- (I) Lack of Hydrogen Training Facilities for Emergency Responders

Technical Targets

No specific technical targets have been set.

FY 2012 Accomplishments

- Re-scoped project to support the GM Hawaii Equinox FCEV rollout at MCB Hawaii
- Developed several legal agreements among project partners to address liability issues:

- HAVO
- Kilauea Military Camp
- MCB Hawaii
- Initiated actions to relocate Powertech integrated hydrogen production and dispensing system to MCB Hawaii on Oahu
- Initiated actions to upgrade Powertech station to 700-bar fast-fill to support GM Equinox FCEV fueling requirements
- Developed infrastructure design for MCB Hawaii hydrogen fueling station
- Selected contractor to install fueling infrastructure at MCB Hawaii
- Secured additional \$400k in state funding for MCB Hawaii infrastructure
- Purchased hydrogen delivery tube trailer for use on Oahu



Introduction

This project addresses barriers to the widespread deployment of hydrogen vehicles through the deployment of hydrogen infrastructure including 700-bar “fast-fill” and novel cascade non-compressor fueling systems. The Power Park project scope was expanded in 2011 to support collaboration between DOE and the Department of Defense that includes installation of higher capacity hydrogen infrastructure at the Puna Geothermal facility on the Island of Hawaii (see Hydrogen Systems as a Grid Management Tool) and Office of Naval Research/General Motors FCEV demonstration project at Marine Corps Base Hawaii on Oahu. The project will support the operations of the HAVO hydrogen FCEV shuttle buses through to December 2014 and in particular validate fuel cell system performance in a harsh environment including high SO₂ levels.

Approach

- Leverage DOE/Naval Research Laboratory 65-kg/day geothermal-to-hydrogen grid management project to supply HAVO hydrogen requirements
- Leverage ONR investment (\$1.8 million) in GM vehicles to be operated from MCB Hawaii and other Department of Defense sites on Oahu
- Leverage National Park Service, State of Hawaii investment, ONR in FCEV shuttle buses (NPS \$1 million + State of Hawaii \$300k + ONR \$500k) at HAVO
- Develop and demonstrate SO₂ mitigation technologies and operational techniques to manage impact of high SO₂ on proton exchange membrane fuel cell performance and durability at HAVO

- Install Powertech fueling station at MCB Hawaii on Oahu to support GM Equinox FCEV project
- Use hydrogen produced at Puna Geothermal under DOE/NRL hydrogen grid management project to fuel HAVO buses using high pressure tube trailers and cascade non-compressor dispensing technology
- Collaborate with existing data analysis groups to compare system data under different operating conditions (fueling stations and vehicles)
- Evaluate the effect of different grades, climatic zones, air quality conditions including SO₂ on vehicle performance
- Engage the DOE Hydrogen Safety Panel to support hydrogen safety including equipment installation, project hydrogen safety plans, outreach to the authorities having jurisdiction, and first responder training
- Transfer results to industry and government agencies

Results

- Re-scoped project to support the GM Hawaii Equinox FCEV rollout at MCB Hawaii
- Developing several MOAs among project partners:
 - HAVO
 - Kilauea Military Camp
 - MCB
- Issued purchase order to upgrade Powertech station to 700-bar fast-fill
- Developed infrastructure design for MCB Hawaii
- Selected contractor to install infrastructure at MCB Hawaii
- Secured additional \$400k in state funding and \$600k in ONR funding for MCB Hawaii infrastructure and station upgrades
- Purchased hydrogen delivery tube trailer for use on Oahu
- Installing dual 350/700 bar hydrogen dispenser at MCB Hawaii

Conclusions and Future Directions

Oahu

- Execute remaining memorandums of agreement with project partners
- Install Powertech 350-bar system at MCB Hawaii
- Install Powertech 700-bar “fast-fill” system at MCB Hawaii

Island of Hawaii

- Install hydrogen 350-bar non-compressor dispensing system at HAVO

- Purchase tube trailer to deliver hydrogen from Puna Geothermal to HAVO - deliver geothermal hydrogen to HAVO with tube trailer;
- Support HAVO FCEV bus operations
- Collect and analyze fueling station and vehicle data
- Seek opportunities for expansion of fleets and/or additional hydrogen infrastructure

A major project challenge to the timely deployment of hydrogen infrastructure and equipment necessary to conduct operations has been the amount of time required to develop legal agreements to address liability issues. This is approaching two years in this project. This in turn has required our requesting no-cost extensions to extend the project to meet operational test duration requirements. This represents a large investment in outreach and education of all parties concerned including the legal profession, risk managers, first responders, and authorities having jurisdiction. Hopefully follow-on projects will not take so long.

FY 2012 Publications/Presentations

1. R. Rocheleau and M. Ewan, "The Hawaii Hydrogen Power Park," *US DOE Annual Merit Review*, Washington, D.C., May 2012.

VII.6 Florida Hydrogen Initiative*

David L. Block, Director Emeritus
Florida Solar Energy Center/University of Central Florida
1679 Clearlake Road
Cocoa, FL 32922
Phone: (321) 638-1001
Email: block@fsec.ucf.edu

DOE Managers

HQ: Jason Marcinkoski
Phone: (202) 586-7466
Email: Jason.Marcinkoski@ee.doe.gov

GO: Greg Kleen
Phone: (720) 356-1672
Email: Greg.Kleen@go.doe.gov

Contract Number: DE-FC36-04GO14225

Subcontractors:

- EnerFuels, Inc., West Palm Beach, FL
- Florida Atlantic University, Boca Raton, FL
- Florida Solar Energy Center, Cocoa, FL
- SRT Group, Inc., Miami, FL
- Electrolytic Technologies Corporation, Miami, FL
- Florida State University, Tallahassee, FL
- Bing Energy, Inc., Tallahassee, FL
- Florida Institute of Technology, Melbourne, FL
- University of South Florida, Tampa, FL

Project Start Date: October 1, 2004
Project End Date: December 31, 2012

*Congressionally directed project

Fiscal Year (FY) 2012 Objectives

Develop Florida's hydrogen and fuel cell infrastructure and to assist the U.S. Department of Energy in its hydrogen and fuel cell programs and goals by:

- Developing hydrogen and fuel cell infrastructure
- Creating partnerships
- Sponsoring fuel cell and hydrogen research and development
- Facilitating technology transfer
- Developing industry support
- Developing unique hydrogen/fuel cell university level education programs

Technical Barriers

This project addresses technical barriers from the Technology Validation section of the Fuel Cell Technologies

Program Multi-Year Research, Development and Demonstration Plan as follows:

- (A) Lack of Fuel Cell Vehicle Performance Data and Durability Plan
- (C) Hydrogen Storage
- (D) Lack of Hydrogen Refueling Infrastructure Performance and Availability Data
- (G) Hydrogen from Renewable Resources
- (H) Hydrogen and Electricity Co-Production

Contribution to Achievement of DOE Technology Validation Milestones

This project will contribute to achievement of the DOE Technology Validation milestones 6, 11, and 24 from the Fuel Cell Technologies Program Multi-Year Research, Development and Demonstration Plan.

- Validate onboard cryo-compressed storage system on a technology development vehicle achieving 1.5 kWh/kg and 1.0 kWh/L. (2Q, 2007)
- Decision to proceed with Phase 2 of the learning demonstration. (2Q, 2010)
- Validate a hydrogen cost of \$3.00/gasoline gallon equivalent (based on volume production). (4Q, 2009)

FY 2012 Accomplishments

- Project solicited proposals to conduct work.
- Project composed of 12 projects with three projects completed.
- Four projects scheduled for completion on June 30, 2012.
- Five projects scheduled for completion on December 31, 2012.



Introduction and Approach

The Florida Hydrogen Initiative (FHI) is a hydrogen and fuel cell project funded for the purpose of developing a hydrogen and fuel cell infrastructure. The FHI project has operated by funding individual projects which conduct the research, development and demonstration activities. Each of the individual projects have been approved by DOE and each project is then issued a subcontract with tasks, deliverables and a budget. At the present time, there are nine active projects with four in fuel cells, three in hydrogen and two in hydrogen and fuel cells.

Individual Project Descriptions

The nine active projects are briefly described as project tasks in the remaining sections.

Task 2. Methanol Fuel Cell Vehicle Charging Station
(Old Title – Hydrogen Technology Rest Area), Michel Fuchs, EnerFuel, Inc., (561) 868-6720 x239

This project is the oldest active project beginning in 2006. The project objectives are to design, construct, and demonstrate a 10 kW net polymer electrolyte membrane (PEM) fuel cell stationary power plant operating on methanol, to achieve an electrical energy efficiency of 32% and to demonstrate transient response time <3 ms. The project activities have completed the installation of the fuel cell at an electric vehicle charging station located at Florida Atlantic University in Boca Raton, FL. The system is undergoing testing and operation data is being collected. EnerFuel intends to finish the project by June 30, 2012. During a project visit, M. Fuchs stated that there would be dollars left over from the project and that EnerFuel would like to apply these remaining dollars to the bipolar plate project. Action on the change is awaiting further information from EnerFuel.

Task 7. Chemochromic Hydrogen Leak Detectors for Safety Monitoring – Dr. N. Mohajeri and Dr. N. Muradov, FSEC, (321) 638-1525

The objective of this project is to develop and demonstrate a cost-effective, high specific chemochromic (visual) hydrogen leak detector for safety monitoring at any facility engaged in handling and use of hydrogen. The work will lead to a new generation of versatile chemochromic hydrogen detectors that employ “smart” materials that cost less, possess fast discoloration kinetics, are user-friendly, are reliable and have superior field worthiness. Project scheduled for completion on June 30, 2012. The yearly results are summarized as follows:

Irreversible Sensor

- TiO_2 is the original material and the one that Japanese have patented. New material has been formulated with TiO_2 and Pt. (Dr. N. Mohajeri formulation.) Results show five times quicker response time than original material.
- Barium sulfate (BaSO_4) is a new pigment developed by N. Mohajeri. This material replaces the material in Japanese patent and is undergoing environmental testing by FSEC. Two provisional patents on material have been submitted.
- Outlook for project is very promising assuming that a manufacturing company is found for production and marketing (3M has expressed interest).

Reversible Sensor

- Synthesized and tested more than 20 novel molybdenum-, tungsten- and vanadium-based chemochromic formulations. Determined the effect of co-catalyst/activator on the rate of coloration in presence of H_2 .
- Evaluated the performance (sensitivity) of the sensors at different H_2 concentrations in air (from 1 to 100 vol.%).
- Determined the extent of interference with other reducing gases (CO , NH_3 , CH_4 , H_2S). Found no interference.
- Main work on tungsten- and molybdenum-based materials. FSEC has already received patent on reversible hydrogen sensing materials developed by Dr. N. Muradov.
- Outdoor and ultraviolet exposure for three months has shown slow degradation. Materials, particularly, Mo-based pigments, are ultraviolet sensitive. Materials work indoor.

Task 8. Development of High Efficiency Low Cost Electrocatalysts for Hydrogen Production and PEM Fuel Cell Applications – Dr. M. Rodgers, FSEC, (321) 638-1709

The objectives of this project are to develop highly active metal alloys with low Pt loading and metal-metal oxide-based electrocatalysts having nanosized grains. The new catalysts will be evaluated for their activity toward oxygen reduction applications for PEM fuel cells. The relevance of this project is that Pt and its alloys are the most effective PEM fuel cell catalysts, but their use is impeded by costs and the efficiency of the oxygen reduction reaction.

The main results is the development of a process of applying Pt to gas diffusion layer (GDL) using Pt nano particle (2 nm) seeds. The nano-particles are applied by sonication in a colloid solution and the Pt is applied by electrodeposition using rotating disk electrodes (400 rpm) in Pt solution. The results show the same performance as a commercial catalyst, but at one fifth the amount of Pt. These results assume that Pt is evenly distributed.

Future activities are to complete testing and to scale up size from 1 cm^2 to 5 cm^2 . Work has shown the need to develop a new process for the scale-up application. Present plans are to have a stationary GDL with fluid flow around the GDL. The work will also examine the use of other electrode materials.

Task 9. Understanding Mechanical and Chemical Durability of Fuel Cell Membrane Electrode Assemblies – Dr. D. Slattery, FSEC, (321) 638-1449

The objective of this project is to increase the knowledge base of the degradation mechanisms for membranes used

in PEM fuel cells. The approaches to mitigate membrane degradation can be classified into three areas: membrane composition changes; radical quenching; and platinum band formation mitigation. To meet the project objectives, four tasks are being conducted: (1) chemical mitigation of membrane degradation, (2) evaluation of platinum band formation, (3) development of Pt band formation mitigation strategy, (4) combination of chemical mitigation and Pt band reduction.

The results show that the addition of ceria (cerium oxide) has given durability improvements by reducing fluoride emission by an order of magnitude during an accelerated durability test (fluoride emission is measure of membrane degradation). Ceria has also shown two-fold decrease in open circuit voltage decay (taken from accelerated durability test). Ceria is radical scavenging additive to Nafion[®] membrane and has shown 5-fold reductions in fluoride emissions during liquid Fenton tests (commonly used to determine stability ex situ to fuel cell).

Other results show that PtCo/C is better than Pt/C (Cobalt and Pt are deposited on carbon support material) and that the incorporation of a heteropolyacid sublayer reduces fluoride emission by 2-3 factor. However, the sublayer is detrimental to cell performance and the process needs to include heteropolyacid as part of Pt layer to avoid performance degradation.

Project work is continuing by Benny Pearman, a UCF Ph.D. student, who is conducting research (oxidation state, Fenton testing) on ceria materials. He is currently focused on chemical behavior during fuel cell operation. He has also submitted proposal to the Oak Ridge National Laboratory (proposal accepted) to use their scientific instruments to assist in ceria and Pt band evaluation. The final report is in preparation.

Task 10. Production of Low-Cost Hydrogen from Biowaste (HyBrTec™) – Mr. R. Parker, SRT Group, Inc., (305) 321-3677

This project solves some of the problems associated with conventional biowaste-to-fuel processing using anaerobic digester by exploiting two thermochemical advantages that reduce both the cost and energy of converting waste-to-fuel. First, at moderate temperatures and pressures the chemical reactions are fast, the product yields are high, and significant thermal energy is released. This minimizes the size of equipment and use of the co-produced heat. Second, the intermediate hydrogen carrier chemical bond is weak, requiring less energy to free hydrogen than the hydrogen will produce as a fuel when burned with oxygen from air.

The project approach is a process which produces hydrogen bromide from wet-cellulosic waste and co-produces carbon dioxide. Next, electrolysis dissociates hydrogen bromide ($E^{\circ} = 0.555$ V) producing recyclable bromine and

hydrogen (endothermic). The hydrogen can then be used for combustion or in a fuel cell for power.

A bench-scale unit has completed testing and the results are being compiled. The unit is a reactor surrounded by a heating coil. Two ¼" diameter rods are immersed in the reactor and serve as cathode and anode of the electrolyzer. Results show that more cathode surface area is needed for electrolyzer and that the process can operate at 180°C. The initial analysis believed that the temperature would be higher at 225°C. Future plans are to separate reactor and electrolyzer and to get a glass lined reactor from De Dietrich (NJ) and an electrolyzer stack from Electrolytic Technologies Corporation of N. Miami Beach, FL.

Task 11. Development of a Low-Cost and High-Efficiency 500 W Portable PEMFC System – Drs. J. Zheng, R. Liang, and W. Zhu, Florida State University, Mr. H. Chen, Bing Energy, Inc., (850) 410-6464

The project research objectives are to develop a new catalyst structures comprised of high conducting buckpaper and Pt catalyst nanoparticles coated at or near the surface of buckpaper and to demonstrate fuel cell efficiency, durability improvements and cost reductions by using buckpaper based electrodes.

Project results are that Dr. Zheng has been working with Bing Energy, Inc. on the optimized single cells with buckpaper supported catalyst. Bing Energy has focused on the stack design, modeling, fixture, and tooling to accomplish the manufacture of membrane electrode assemblies (MEAs), components, and stack. The project has tested the performance and durability of the single cell per DOE's testing protocols to optimize the design. A table showing 2017 DOE Targets and current results achieved at Florida State University for electrocatalyst and MEAs has been presented. These results show the meeting of selected DOE performance goals and expectation of meeting all DOE goals.

Task 12. Interdisciplinary Hydrogen and Fuel Cell Technology Academic Program – Florida Institute of Technology, John Politano, Carolyn R. Lockyer, Mary Helen McCay, (321) 674-8960

This project has the objective to develop a hydrogen and fuel cell technology (HFCT) academic program at the Florida Institute of Technology (FIT) in Melbourne, FL. The FIT HFCT program will allow students to follow hydrogen technology from introduction to long-term applications, to obtain a basic understanding of the fundamentals of the field, to redirect their current technology focus as a means for new career options, to measure students' gains in knowledge of hydrogen as a fuel source, to interact with outside industries and to satisfy the need for hydrogen technology graduates.

The project results are the development of hydrogen- and fuel cell-related modules that have been implemented

into courses in the General Chemistry laboratory, MAE and Sustainability Engineering. A new hydrogen technology course will be implemented in both CHE and MAE as part of the new MSME and MSChE specializations in hydrogen technology. Projects were identified for consideration as junior/senior design projects. Surveys have been administered in courses in both the College of Engineering and College of Science to determine how the new hydrogen curriculum impacts student' knowledge and opinions of hydrogen and fuel technology.

New courses developed were: MAE 5330, Principles of Fuel Cells, CHE 5240, Electrochemical Engineering, and CHE 5250, Hydrogen Technology. The program specializations and new courses have been approved by the Florida Tech College of Engineering Council and the Florida Tech Graduate Council.

Task 13. Design and Development of an Advanced Hydrogen Storage System using Novel Materials – Drs. E. Stefanakos, D. Goswami, and A. Kumar, University of South Florida. (813) 974-4413

The project goal is to design and develop novel conducting polymeric nanomaterials for onboard hydrogen storage with a system gravimetric capacity of 5.5 wt% or greater and completed reversible hydrogen storage characteristics at moderate temperature (<100°C). The proposed approach was to conduct synthesis of polyaniline (PANI), a solid state hydrogen storage material and to modify the synthesis parameters for optimized storage capabilities. The major challenge is to develop polymer nanostructures that can store hydrogen at room temperature, and be reversible for many cycles.

Results show that the PANI storage figures originally reported by other researchers could not be duplicated at USF. As reported the results in the first two references were obtained from polymer samples provided to USF by a center in Italy. Later on USF tried to reproduce the results with samples obtained from the same individual or produced by us following similar manufacturing methods, but we were unable to duplicate the results. After going back and forth between the University of South Florida and Tuskegee University, we have come to the conclusion that our pressure-concentration-temperature instrument may not have been working correctly at the time we obtained the initial results indicated in the first two publications. Presently the gravimetric densities we are able to measure are less than 1%. The present approach is to modify the polymers in an effort to increase the gravimetric density.

Task 14. Advanced HiFoil™ Bipolar Plates – Mr. J. Braun, EnerFuel, Inc., (561) 868-6720

The project relevance is to address cost and durability barriers for high-temperature proton exchange membrane

fuel cells by providing a low cost, easy to form, corrosion-resistant laminate bipolar plate having high thermal conductivity and improved mechanical strength/crack resistance. The expected results will lead to longer life, high power density fuel cell stacks and better thermal management/cell heat transfer.

The project results showed that embossing could not be accomplished because the graphite was too rigid and brittle. The new concept is to replace interior metal sheet with sheet of graphite and to make the sheet continuous except for holes for ports. Outer sheets are made of graphite composite materials with the flow channels done by a molding process. The flow channels are presently machined. EnerFuel has operated a 4-cell stack (130 W) and a 36-cell stack (1.2 kW) that demonstrated the bipolar plates resistance to the electrochemical and acid MEA environment within the fuel cell. In a 36-cell test, the results showed that the heat transfer characteristics of the bipolar plate produced low cell-to-cell temperature and voltage variations. Based on these positive results, the company plans to demonstrate scalability by building a 132-cell stack (4.6 kW) that could be used for stationary fuel cell applications, such as telecommunication backup and micro-CHP, and transportation applications such as truck auxiliary power units and electric vehicle range extenders.

Conclusions and Future Directions

The FHI project is on schedule to be completed by December 31, 2012. Of the nine active projects, four are scheduled for completion by June 30, 2012. The future work will continue the project monitoring, review of the final reports and continuation of five projects. There are no open issues.

Patents Submitted/Issued

1. P. Brooker, N. Mohajeri "Chromochromic membranes for membrane defect detection", UCF 10390P (submitted).
2. N. Mohajeri "Doped palladium containing oxidation catalysts", UCF-10380P (submitted).
3. J.P. Zheng, Z.Y. Liang, B. Wang, C. Zhang, and W. Zhu, "Catalytic electrode with gradient porosity and catalyst density for fuel cells", US Patent Pub. No. US2011/0008705.

FY 2012 Publications/Presentations

1. R. Brooker, L. Bonville and D. Slattery. "Decreasing Membrane Degradation through Heteropolyacid Sub-layers." *Journal of the Electrochemical Society*, under review.
2. R. Brooker, D. Slattery, L. Bonville, and J. Fenton. "Mechanism of Platinum-band Formation Mitigation with Heteropolyacid Electrodes." Abstract # 1208, 220th ECS Meeting, October 9-14, 2011, Boston MA.

3. R. Brooker, D. Slattery, L. Bonville and J. Fenton. "Platinum Band Formation Mitigation through Heteropolyacid Sublayers." Abstract # LRD42-1, Fuel Cell Seminar, October 31-November 3, 2011, Orlando FL.
4. N. Muradov, A. T-Raissi, G. Bokerman, E. Hinkamp, Passive Chemochromic Hydrogen Leak Detectors for Safety Monitoring. Proceedings of XIX World Hydrogen Energy Conf., Toronto, Canada.
5. M. Rodgers, N. Mohajeri, L. Bonville, D. Slattery, "Accelerated testing of polymer electrolyte membranes in fuel cells containing Pt/C and PtCo/C catalysts", *Journal of the Electrochemical Society*, 159, B564, 2012.
6. M. Rodgers, L. Bonville, D. Slattery, Evaluation of the Durability of Polymer Electrolyte Membranes in Fuel Cells Containing Pt/C and Pt-Co/C Catalysts under Accelerated Testing, *Electrochemical Society Transactions*, 41(1) 1461, 2011.
7. W. Zhu, C. Zeng, J. Zheng, R. Liang, C. Zhang, and B. Wang, "Preparation of Buckypaper Supported Pt Catalyst for PEMFC Using Supercritical Fluid Method", *Electrochem. and Solid-State Lett.* **14**, B81 (2011).
8. W. Zhu, R. Liang, and J. Zheng, "A 3-D Catalytic Electrode Structure for Ultra-low Platinum Loading and High Performance PEMFCs", submitted to *Electrochem. Soc. Trans.*, presented at the 221st Electrochemical Society Meeting, Seattle, WA, May 6-10, 2012.
9. Invited Talk: J.P. Zheng, "A 3-D Catalytic Electrode Structure for High Performance and Low Cost PEMFCs", the 243rd American Chemical Society National Meeting, San Diego, California, March 27, 2012.
10. Invited Talk: J.P. Zheng, "A 3-D Catalytic Electrode Structure for Ultra-low Platinum Loading and High Performance PEMFCs", the 2012 Villa Conference on Energy and Environmental Research, Orlando, Florida, April 17, 2012.

VII.7 Sustainable Hydrogen Fueling Station, California State University Los Angeles*

David Blekhman
California State University Los Angeles
Los Angeles, CA 90032
Phone: (323) 343-4569
Email: blekhman@calstatela.edu

DOE Managers
HQ: Jason Marcinkoski
Phone: (202) 586-7466
Email: Jason.Marcinkoski@ee.doe.gov
GO: Gregory Kleen
Phone: (720) 356-1672
Email: Gregory.Kleen@go.doe.gov

Contract Number: DE-EE0000443

Subcontractors:
• General Physics Corporation, Elkridge, MD
• Weaver Construction, Anaheim, CA

Project Start Date: January, 2009
Project End Date: December, 2012

*Congressionally directed project

- **Milestone 26.** Validate refueling site stationary storage technology provided by the delivery team. (4Q, 2012)
- **Milestone 28.** Validate the cost of compression, storage and dispensing at refueling stations and stationary power facilities to be <\$.80/gge of hydrogen. (4Q, 2013)

FY 2012 Accomplishments

- Installed all the core equipment under DOE funding.
- Installed all the equipment beyond DOE funding for station operation.
- Completed station building construction.
- Initiated commissioning phase in preparation for opening.



Introduction

The College of Engineering, Computer Science, & Technology at CSULA as part of its energy curriculum and research efforts is building a sustainable hydrogen station to teach and demonstrate the production and application of hydrogen as the next generation of fully renewable fuel for transportation. The DOE funding is applied toward the acquisition of the core hydrogen station equipment: electrolyzer (partial), three compressors and hydrogen storage tanks.

Approach

The CSULA hydrogen station deploys the latest technologies with the capacity to produce and dispense 60 kg/day, sufficient to fuel 15-20 vehicles. The station is utilizing a Hydrogenics electrolyzer, first and second stage compressors capable of fast filling at 10,000 psi (700 bar), 60 kg of hydrogen storage, water purification and equipment cooling system. The station will be grid-tied and powered by 100% renewable power.

The station will also be used as an applied research facility for equipment testing and verification, testing of hydrogen purity and dispensing accuracy. Another primary function of the station is to be a living laboratory for CSULA students and to introduce hydrogen as a safe transportation fuel through public education and local partnerships.

Fiscal Year (FY) 2012 Objectives

- Procure core equipment for the California State University Los Angeles (CSULA) hydrogen station
- Install/integrate the core equipment

Technical Barriers

This project addresses the following technical barriers from the Technology Validation section of the Fuel Cell Technologies Program Multi-Year Research, Development and Demonstration Plan:

- (C) Lack of Hydrogen Refueling Infrastructure Performance and Availability Data
- (D) Maintenance and Training Facilities
- (E) Codes and Standards

Contribution to Achievement of DOE Technology Validation Milestones

This project will contribute to achievement of the following DOE milestones from the Technology Validation section of the Fuel Cell Technologies Program Multi-Year Research, Development and Demonstration Plan:

Results

The station construction has been completed and it is currently in the commissioning stage, see Figure 1. The equipment under the DOE funding was delivered by General Physics. The equipment integration and station construction was through Weaver Construction. Quantum Corp. provided the hydrogen chiller and dispenser.

The grant provided funding for acquisition of the core hydrogen station equipment: compressors, hydrogen storage and partially electrolyzer. The balance-of-plant equipment was installed including the compressor cooling, air compressor, hydrogen chiller, dispenser, etc. Figure 2 provides a panoramic view inside of the station.

As part of commissioning, purity testing was conducted with the initial test showing slightly higher quantity of nitrogen present in the stream most likely from flushing the storage tanks with it. The follow-up test, after the tanks were emptied and refilled, showed the compliance with SAE J2719. In addition, initial fill tests have been performed with 5,000 psi internal combustion engine vehicles and 10,000 psi fuel cell vehicles, see Figure 3.



FIGURE 1. CSULA Hydrogen Fueling Facility



FIGURE 2. CSULA Hydrogen Fueling Facility, from left to right: storage tanks, PDC 350-bar bar compressor, two Hydro Pac 700-bar compressors, and Quantum chiller



FIGURE 3. Test fueling with General Motors vehicles during commissioning

Conclusions and Future Directions

The station construction has been completed and is currently in commissioning. Future research into station/ vehicle performance is planned.

VII.8 Renewable Electrolysis Integrated Systems Development and Testing

Kevin Harrison

National Renewable Energy Laboratory (NREL)
15013 Denver West Parkway
Golden, CO 80401
Phone: (303) 384-7091
Email: Kevin.Harrison@nrel.gov

DOE Manager

HQ: Jason Marcinkoski
Phone: (202) 586-7466
Email: Jason.Marcinkoski@ee.doe.gov

Contributors:

Chris Ainscough and Michael Peters

Subcontractor:

Marc Mann, Spectrum Automation Controls, Arvada, CO

Project Start Date: October 1, 2011

Project End Date: Project continuation and direction determined annually by DOE

Technical Targets

This project is focused on validation efforts to better integrate renewable hydrogen systems and measure their ability to deliver low-cost hydrogen. The project work scope includes quantifying system performance, operation and maintenance, durability, and reliability under real-world operating conditions. Innovation and insights gained from this work benefit the hydrogen-based industry and relevant stakeholders as the market for this equipment and products expands.

One of the project's primary goals is to validate hydrogen production and compression systems as they are applied to hydrogen as an energy storage medium for varying renewable electricity sources like wind and solar. The project includes optimization of the electrical pathway (power conversion) between renewable sources and the electrolyzer and storage of hydrogen at various pressures. Finally, this project supports the validation of water electrolysis systems from the DOE Hydrogen Production and Delivery sub-program RD&D plan by testing DOE-awarded electrolyzer stack and system performance to help meet the following DOE hydrogen Technology Validation targets:

- Task 3.3 – By 2nd quarter 2014, validate large-scale (>100 kg/day) integrated wind-to-hydrogen production system.
- Task 3.9 – By 4th quarter 2020, validate large-scale systems for grid energy storage that integrate renewable hydrogen generation and storage with fuel cell power generation by operating for more than 10,000 hours with a round-trip efficiency of 40%.
- Validate full-size hydrogen and fuel cell components and systems using NREL's Wind-to-Hydrogen facility and their new state-of-the-art test facility, the Energy Systems Integration Facility, scheduled for completion in October 2012.

Fiscal Year (FY) 2012 Objectives

- Collaborate with hydrogen production, delivery, storage, and fuel cell industries to test, demonstrate, and track performance of unique integration opportunities for renewable hydrogen systems compared with baseline (incumbent) technologies.
- Validate and work to increase equipment reliability, efficiency, and relevant sub-system performance of state-of-the-art DOE-awarded, prototype and pre-commercial systems.
- Operate, maintain, track durability of, and perform strategic experimentation on the fully-functional integrated renewable hydrogen demonstration project to support industry innovation and DOE Technology Validation goals.

Technical Barriers

This project addresses the following technical barriers from the Technology Validation section of the 2011 Fuel Cell Technologies Program's Multi-Year Research, Development and Demonstration (RD&D) Plan:

- (G) Hydrogen from Renewable Resources
- (H) Hydrogen and Electricity Co-Production

FY 2012 Accomplishments

- Completed frequency mitigation testing of alkaline and polymer electrolyte membrane (PEM) electrolyzers on an alternating current (AC) microgrid:
 - Both commercially available technologies provided sub-second response to significantly reduce the magnitude and duration of disturbance.
- Designed, built, and began testing a volumetrically-based mass flow system for high-accuracy determination of electrolyzer hydrogen production.
- Reported detailed reliability metrics for the station relative to other hydrogen stations operating at 350 bar.



Introduction

Management of distributed power systems is expected to become more commonplace as grids and devices become “smarter” and distributed renewable resources become a larger proportion of our energy supply. A critical element for the advancement of smart-grid technologies is managing distributed resources, which includes renewable electricity generation, distributed energy storage, and taking advantage of active (or controllable) loads to provide grid support services like frequency and voltage regulation. Large-scale hydrogen production using renewable electricity is well positioned to produce near-zero greenhouse-gas emission vehicle fuel in the coming years as hydrogen-powered electric vehicles are introduced into the marketplace. An integrated system with advanced sensing and communications will enable grid operators to take advantage of the controllable nature of distributed and central water electrolysis systems to maintain grid stability.

Distributed water electrolysis allows hydrogen to be produced from renewable wind, solar, and geothermal energy sources as well as nuclear power. Additionally, the electrolyzers can be used to produce and subsequently store hydrogen from grid electricity during off-peak periods or from otherwise curtailed wind energy. Electrolyzers and hydrogen storage may be sited with renewable sources; however, with appropriate communication, the electrolyzer does not need to be located in the immediate vicinity of the renewable resource to effectively use it. Electrolyzers may be controlled remotely to use inexpensive electricity that is produced when intermittent renewable sources are available, but demand is not.

Approach

The Xcel Energy/NREL Wind-to-Hydrogen (Wind2H2) demonstration project is advancing the integration of renewable electricity sources with state-of-the-art hydrogen production, compression, storage, and dispensing systems. This project provides independent testing and verification of the technical readiness of these advanced integrated systems by operating them from the grid and renewable electricity sources.

Real-world data from daily system operation are revealing opportunities for improved system design and unique hardware configurations to advance the commercialization of this technology. Lessons learned and data-driven results provide feedback to industry and to the analytical and modeling components of this project.

Results

NREL operated both of the commercially available low-temperature electrolyzer technologies, PEM and alkaline,

on an AC microgrid (shown in Figure 1) to evaluate their response to commands to increase and decrease stack power to shorten frequency disturbances. Results show that both the PEM and alkaline electrolyzers are capable of adding or removing stack power to provide sub-second response that reduced the duration of frequency disturbances.

Figure 2 compares a control test where electrolyzers are not triggered to shed load and the separate alkaline and PEM response tests where the electrolyzers are commanded to reduce stack power by 10 kW. In each of these three tests from Figure 2, the load simulator instantly applies 10 kW of resistive load to initiate a frequency disturbance on the grid. High-resolution monitoring of the AC microgrid frequency (nominally 60 Hertz) generates a control signal for the electrolyzer when the frequency exceeds ± 0.2 Hertz.

Similar tests were performed by removing load from the AC microgrid and commanding the electrolyzers to add 25 kW of stack power to mitigate an over-frequency disturbance (Figure 3). Both the alkaline and PEM electrolyzers reduced the magnitude and the duration of the frequency disturbance compared with the control test where the electrolyzers were not providing load support.

Accurately measuring hydrogen mass flow from an electrolyzer, fuel cell, compressor, and hydrogen dispenser is challenging. Commercially available mass flow sensors are expensive and their accuracy can vary significantly depending on the type of transducer employed. This project, under its role as the DOE test and validation facility for advanced electrolyzer systems, designed, built, and began testing a volumetrically based mass flow device.



FIGURE 1. Frequency regulation experimental system where electrolyzers are powered by diesel generators on an AC microgrid

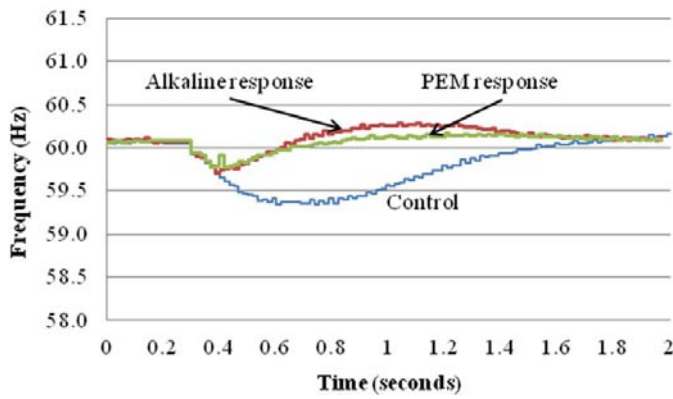


FIGURE 2. Resulting mitigation effects using electrolyzers to shed 10 kW of stack power during an under frequency disturbance on an AC microgrid

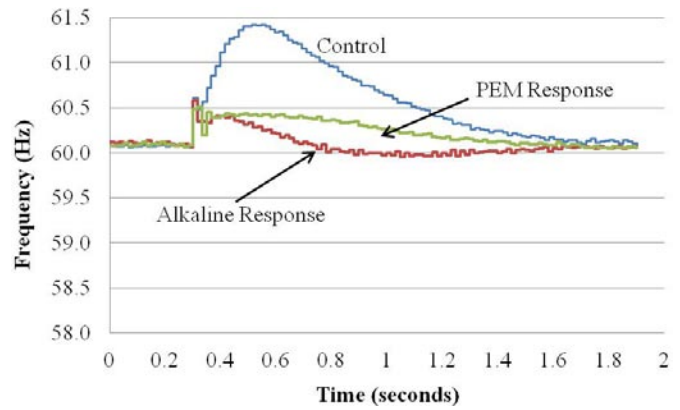
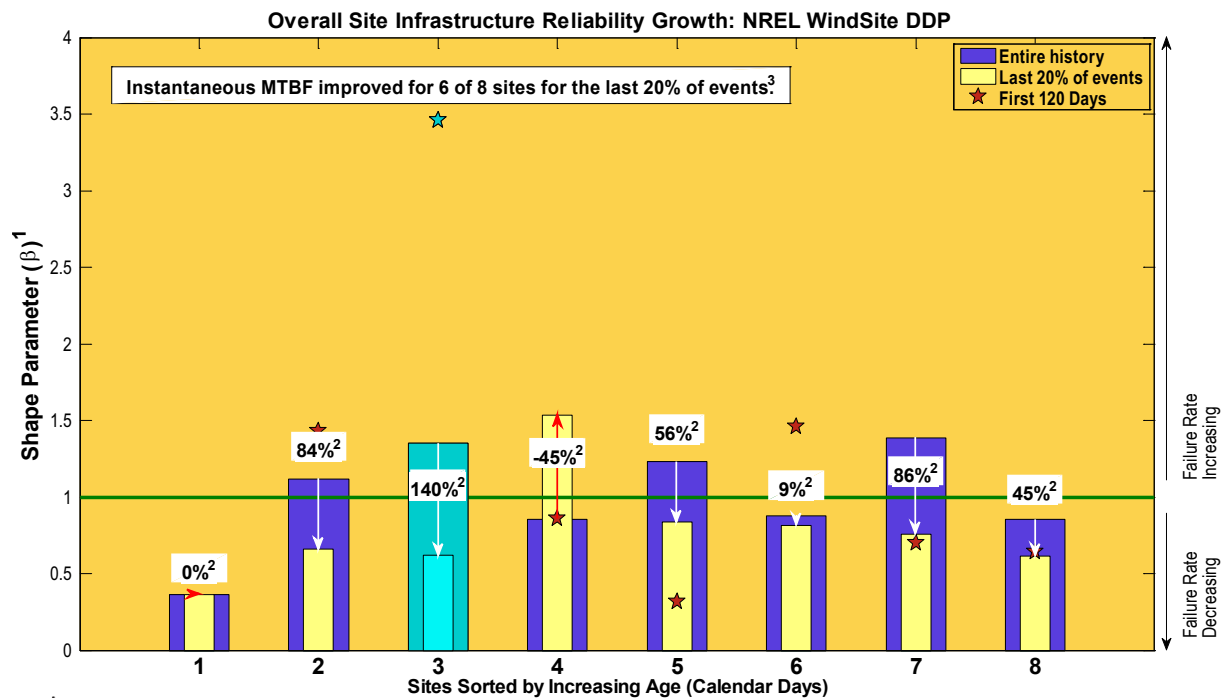


FIGURE 3. Resulting mitigation effects using electrolyzers to add 25 kW of stack power during an over frequency disturbance on an AC microgrid



NREL cdp_mhe_45b
Created: Mar-16-12 8:41 AM
NREL WindSite DDP

1. IEC 61164:2004(E), Reliability Growth - Statistical Test and Evaluation Methods, IEC. 2004.
2. % change in instantaneous MTBF
3. Some sites are no longer active. Final results are shown for those sites.

FIGURE 4. Reliability growth, as determined by the Beta shape parameter from a Crow-AMSAA analysis, indicates that reliability growth at Wind to Hydrogen is in line with other similar sites

The design of the mobile mass flow device took advantage of industry partner feedback. The device calculates the mass flow from (or to) a piece of equipment by accurately measuring the pressure and temperature and by knowing the water volume of the composite overwrapped pressure vessel and interconnecting tubing. Using the National Institute of Standards and Technology equations-of-state for hydrogen, the onboard controller determines the mass flow by subtracting the initial from the final mass of hydrogen in the pressure vessel and how long it took to reach

the final mass. Preliminary data from the mass flow device for 30+ samples are promising and have resulted in standard deviations of 0.002–0.004 kg per hour while sampling an electrolyzer with a nominal flow rate of 0.5 kg per hour.

NREL compared the reliability growth rate of this project relative to other 350-bar refueling stations for which NREL collects data. The analysis showed good improvement in reliability growth in the most recent 20% of reliability events. The beta parameter of 0.6 shown on Figure 4 indicates

that reliability at the Wind-to-Hydrogen site is improving, and is improving on pace with other, similar stations.

Conclusions and Future Direction

By testing the response of these commercially available electrolyzer systems NREL has shown that distributed and central electrolysis systems have another potential (economic) value stream because of their ability to quickly increase or decrease stack power, which could be used to improve grid stability. Finally, the volumetric mass flow device has shown low variability (2–4 g/hour) during initial testing of a 0.5 kg/hour electrolyzer. NREL compared the reliability growth rate of this project relative to other 350-bar refueling

stations for which NREL collects data. The analysis showed good improvement in reliability growth in the most recent 20% of reliability events.

In the coming year the team will complete the following;

- Install, commission, and perform 2,500 hours of testing of a pneumatically-driven hydrogen gas booster:
 - Reliability and performance will be monitored and reported
- Substantiate volumetric mass flow measurements by conducting variance and error analysis and integrating a master meter or gravimetric measurement approach.

VII.9 Stationary Fuel Cell Evaluation

Jennifer Kurtz (Primary Contact), Keith Wipke,
Sam Sprik, Todd Ramsden, Chris Ainscough

National Renewable Energy Laboratory
15013 Denver West Parkway
Golden, CO 80401-3305
Phone: (303) 275-4061
Email: jennifer.kurtz@nrel.gov

DOE Manager

HQ: Jason Marcinkoski
Phone: (202) 586-7466
Email: Jason.Marcinkoski@ee.doe.gov

Project Start Date: October 1, 2012
Project End Date: Project continuation and direction
determined annually by DOE

- Validate stationary fuel cell operation of multiple fuel cell technologies such as polymer electrolyte membrane, solid-oxide, molten carbonate, and phosphoric acid
- Assess stationary fuel cell performance domestically and internationally



Approach

The analysis of stationary fuel cell operation includes systems providing prime, continuous, or regular power to a site. Without a separately-funded stationary fuel cell deployment in technology validation, a key step in this project is the identification of locations and end users operating stationary fuel cells, as well as stationary fuel cell developers. The leading stationary fuel cell developers cover multiple fuel cell technologies and power plant sizes. Building relationships with these developers is based on past experience, industry meetings, and individual communications. The highest concentration of stationary fuel cell end users is in a few states; some of these states have dedicated collaboratives for fuel cell installation and operation. An organization such as the California Stationary Fuel Cell Collaborative (CaSFCC) provides a strong partnership for NREL because it involves multiple developers, end users, fuel cell technologies, and fuel cell system sizes.

The data collection plan builds on other technology validation activities. Data (operation, maintenance, and safety) are collected on-site by the project partners for the fuel cell system(s) and infrastructure. NREL receives the data quarterly and stores, processes, and analyzes the data in NREL's HSDC (Figure 1). The HSDC is an off-network room with access for a small set of approved users. An internal analysis of all available data is completed quarterly and a set of technical Composite Data Products (CDPs) is published every six months. The CDPs present aggregated data across multiple systems, sites, and teams in order to protect proprietary data and summarize the performance of hundreds of fuel cell systems and thousands of data records. A review cycle is completed before the publication of CDPs. The review cycle includes providing Detailed Data Products (DDPs) of individual system and site performance results to the individual data provider. DDPs also identify the individual contribution to CDPs to provide context of system performance back to the developer. The NREL Fleet Analysis Toolkit (NRELFAT) is an internally developed tool for data processing and analysis structured for flexibility, growth, and simple addition of new applications. Analyses are created for general performance studies as well as application- or technology-specific studies.

Fiscal Year (FY) 2012 Objectives

- Establish partnership(s) within the stationary fuel cell industry and with end users
- Create data templates for stationary fuel cell data collection
- Leverage the Hydrogen Secure Data Center (HSDC), analysis experience, and tools from other fuel cell technology validation activities

Technical Barriers

This project addresses the following technical barriers from the Technology Validation section (3.6) of the Fuel Cell Technologies Program Multi-Year Research, Development and Demonstration Plan:

- (B) Lack of Data on Stationary Fuel Cells in Real-World Operation
- (E) Codes and Standards
- (H) Hydrogen and Electricity Co-Production

Technical Targets

This project is in the initial set-up stage, establishing partnerships, data templates, and methods to analyze operation data from stationary fuel cell systems operating under real-world conditions. These analyses will:

- Validate stationary fuel cell durability and efficiency against targets of 40,000 hours and 40% efficiency lower heating value (2014)



FIGURE 1. HSDC Data Flow Diagram

FY 2012 Accomplishments

- NREL/FAT was expanded to include stationary fuel cell processing and analysis capabilities for preparation of the first data analysis cycle. (New work)
- Data templates were created for consistent and complete data sharing. The data templates include site overview, operation, maintenance, and summary. Key targets that will be validated with these data include durability and efficiency. (New work)
- A partnership has been established with the National Fuel Cell Research Center (NFCRC) and the CaSFCC. This partnership includes validation of stationary fuel cell systems using different technologies and approximately 40 MW installed capacity. (New work)
- On-going communications have occurred with several organizations, including state and regional fuel cell organizations and developers, to establish agreements for sharing data. (New work)

Future Directions

- Establish partnerships with end users, state collaborations, and fuel cell developers to create data sets of stationary fuel cell systems operating in real-world conditions
- Receive first delivery of data from NFCRC and CaSFCC
- Publish first set of CDPs for stationary fuel cell operation in Fall 2012

VII.10 Next Generation H2 Station Analysis

Sam Sprik (Primary Contact), Keith Wipke,
Todd Ramsden, Chris Ainscough, Jen Kurtz
National Renewable Energy Laboratory (NREL)
15013 Denver West Parkway
Golden, CO 80401-3305
Phone: (303) 275-4431
Email: sam.sprik@nrel.gov

DOE Manager

HQ: Jason Marcinkoski
Phone: (202) 586-7466
Email: Jason.Marcinkoski@ee.doe.gov

Project Start Date: October 1, 2011
Project End Date: Project continuation and direction
determined annually by DOE

Fiscal Year (FY) 2012 Objectives

- Collect data from state-of-the-art hydrogen (H2) fueling facilities, such as those funded by the California Air Resources Board (CARB), to enrich the analyses and composite data products (CDPs) on H2 fueling originally established by the Learning Demonstration project.
- Work with codes and standards activities and fueling facility owners/operators to benchmark performance of the fueling events relative to current SAE International procedures.
- Perform analysis and provide feedback on sensitive data from hydrogen infrastructure for industry and DOE. Aggregate these results for publication.
- Participate in technical review meetings and site visits with industry partners to discuss results from NREL's analysis in an interactive manner.
- Maintain an accurate database (location and status) of all online hydrogen stations in the United States, and provide periodic updates to other online resources, specifically NREL's Alternative Fuels Data Center (AFDC) station locator, the Fuel Cell and Hydrogen Energy Association, the California Fuel Cell Partnership (CaFCP), and FuelCells.org.

Technical Barriers

This project addresses the following technical barrier from the Technology Validation section of the Fuel Cell Technologies Program Multi-Year Research, Development and Demonstration Plan:

- (D) Lack of Hydrogen Refueling Infrastructure Performance and Availability Data

Contribution to Achievement of DOE Technology Validation Milestones

This project contributes to achievement of the following DOE milestones from the Technology Validation section of the Fuel Cell Technologies Program Multi-Year Research, Development and Demonstration Plan:

- Verifying shorter fueling times for 700-bar fills using pre-cooling.

FY 2012 Accomplishments

- Created a set of 12 Spring 2012 CDPs from four stations reporting data.
- Updated NREL's internal database of stations and their locations and submitted updates to the AFDC.
- Presented station CDPs and metrics for station performance to the CaFCP working group.
- Participated in a CaFCP station implementation team and provided performance metrics for stations.
- Internally processed and analyzed quarterly infrastructure data in the Hydrogen Secure Data Center (HSDC) for later inclusion in CDPs.
- Created templates for infrastructure data collection.
- Updated NREL Fleet Analysis Toolkit (NRELFAT) code to accept data from stations in the new templates form for processing and analysis leading to CDPs.
- Participated with the California Energy Commission (CEC) in workshops and other discussions regarding hydrogen station funding.



Introduction

In the past decade, approximately 60 hydrogen fueling stations supported a few hundred fuel cell electric vehicles (FCEVs) in the United States. Of these stations, 25 supported the 183 DOE Learning Demonstration vehicles. As original equipment manufacturers are ramping up FCEV bus, forklift, and car production, there is an effort to build additional stations, increase individual station fueling output, and cluster stations to cover the area where vehicles are located.

California has been a leader in supporting additional hydrogen infrastructure through multiple state agencies, including CARB and the CEC. Two separate actions by

CARB funded seven stations of which several are online with the remainder soon to be open in 2012. CEC is also working on funding stations, moving the state toward the CaFCP goal of 68 stations by 2015 when FCEVs will be introduced in larger numbers. These stations are expected to be included in subsequent evaluations.

Keys to success for improving hydrogen fueling availability are selecting the fueling location, ensuring public access, and providing adequate output to support the vehicles. Developing multi-use facilities that can serve cars, buses, and/or forklifts may help the economics and capacity utilization. Hydrogen output from existing and upcoming facilities varies from 12 to 140 kg/day, with most new fueling facilities being in the 100-kg/day range. There is an effort to focus on clusters of stations near population centers in the Los Angeles area. Using available hydrogen energy from landfills and wastewater treatment plants is one way to make use of a renewable feedstock and to lower greenhouse gas emissions. As more vehicles come online, all fueling facilities will need to be accessible to anyone with a hydrogen vehicle. Long construction lead times need to be accounted for when planning for the upcoming vehicles. As these optimized fueling facilities are developed, there is a need to continue data collection and analysis to track the progress and determine future technology development needs.

Approach

The emphasis of this project is documenting the innovations in hydrogen fueling and how it will meet vehicle customer needs. This includes analysis that captures the technology capability (such as back-to-back filling capability, impact of pre-cooling temperature, and radio-frequency identification of vehicles to allow unique fueling profiles) as well as the customer perspective (such as fueling times and rates, safety, and availability). Individual components such as compressors will be evaluated with the available data to establish current status and research needs. Station locations will be evaluated within the context of both available vehicles and future vehicles and their fueling patterns. NREL will also use the analysis results to support DOE in identifying trends from the data that will help guide DOE's research and development (R&D) activities.

Data analysis will be performed on sensitive industry hydrogen fueling data in NREL's HSDC and recommendations will be provided to DOE on opportunities to refocus or supplement R&D activities. Aggregation of the analyzed data allows for creation of composite results for public dissemination and presentation. Some existing CDPs from the previous learning demonstration will be updated with new data, as appropriate. All this involves working with industry partners to create and publish CDPs that show the current technology status without revealing proprietary data. Feedback to industry takes form in detailed data products

(protected results) and provides direct benefit to them from the NREL analysis performed on their data. We will continue exercising the fueling analysis functionality of the NRELFAT to preserve and archive a snapshot of the analysis results from each quarter. This allows a deeper level of results to be stored in an easy-to-access form within the HSDC.

Using unique analysis capabilities and tools developed at NREL, researchers are providing valuable technical recommendations to DOE based on real-world experiences with the technology. NREL will continue to provide multiple outputs in the form of CDPs and presentations and papers at technical conferences.

Results

The results presented in this section are from the Spring 2012 CDPs and pertain to four stations that reported data. The location of these hydrogen stations can be seen in Figure 1 along with locations of the other U.S. stations that are kept in the hydrogen station database. As stations are built or retired, updates are made to the database and shared with others including the AFDC. The stations reporting data included one where hydrogen was delivered to the station as a liquid, one with hydrogen pipeline delivery, and two that reformed natural gas or methane.

The total amount of fueling reported was 4,600 kg. Fueling times from the stations varied and on average took 4.72 minutes. More than half (61%) of the fuelings took less than 5 minutes, while 22% took less than 3 minutes. The average amount fueled at the stations was 2.95 kg. As can be seen in Figure 2, the average fueling rate was 0.72 kg/min with 20% of fills faster than 1 kg/min and 3% of fills faster than 1.67 kg/min. The 1.67 kg/min reference comes from a 2012 milestone of a 3-minute fill of 5 kg.

For comparison, fuelings at 350 bar and 700 bar were analyzed and their average rates were 0.77 kg/min and 0.71 kg/min, respectively. Final pressures in the vehicle tanks were also compared and found on average to be 376 bar for the nominally 350-bar fills and 707 bar for the nominally 700-bar fills.

The amount of hydrogen dispensed by each station was analyzed by day of the week and can be seen in Figure 3. The highest average for a station was 30 kg/day and occurred on Thursday. The highest average for the combined stations was dispensed on Fridays.

A new analysis was created to start to quantify time between fills and provide some insight into how long a customer may have had to wait for a back-to-back fill. Figure 4 shows a histogram of the times between fills. For times less than 5 minutes, it is assumed that the customer had to wait for the previous customer. From the data, 6% of the fills were within 0 to 5 minutes of each other, and these were considered back-to-back fills. The final pressures are

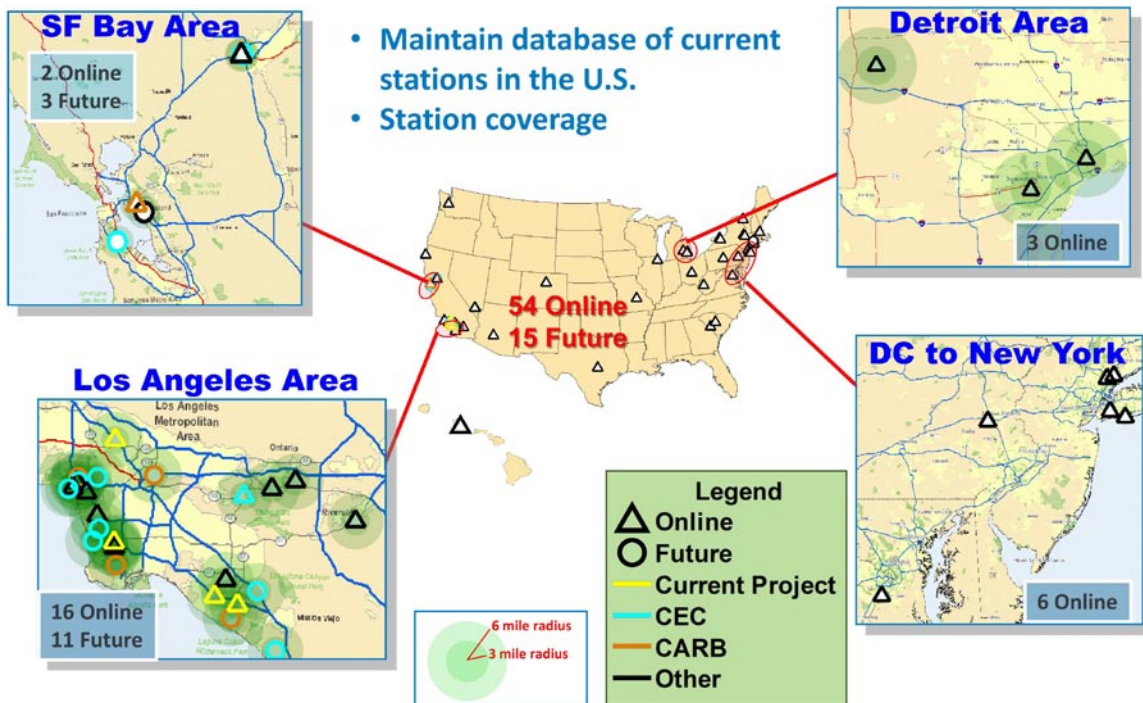


FIGURE 1. Hydrogen station locations

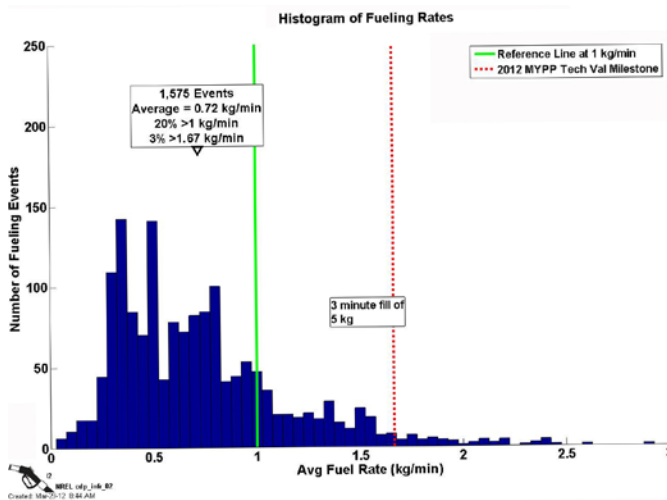


FIGURE 2. Histogram of fueling rates

also shown in a histogram comparing the previous fill final pressure to the next fill final pressure as a check to see if the equipment would have trouble performing a full fill in a back-to-back filling scenario. From the small set of data, no obvious trends were identified in that regard.

Conclusions and Future Directions

As new stations come online or are updated, their performance and availability will affect how successfully

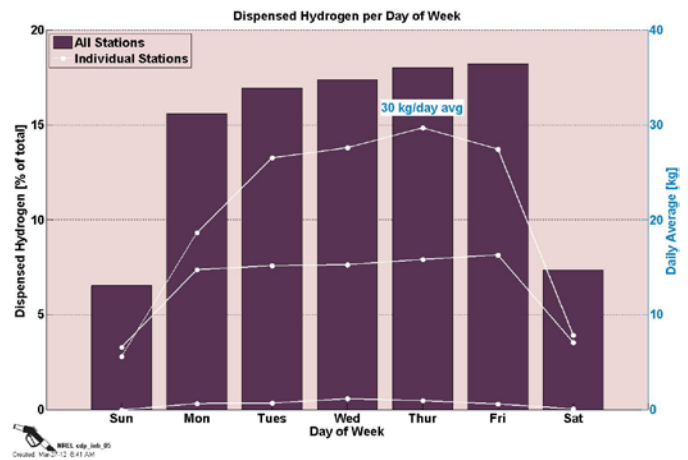
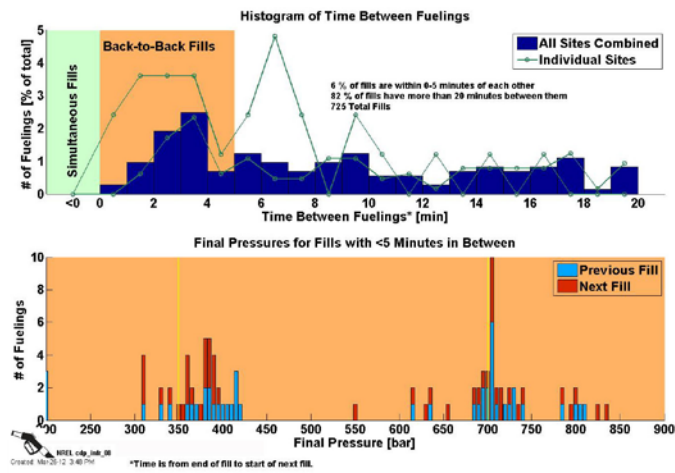


FIGURE 3. Dispensed hydrogen per day of week

they support the current and upcoming fleet of fuel cell vehicles. Continual data collection, analysis, and feedback will provide DOE and the hydrogen and fuel cell community with awareness of the technology readiness and identify research areas for improvement. With so few stations providing data at the present, it is difficult to aggregate the data without revealing individual station identity, and to identify general trends in the industry. As more data become available from more stations, there will be an increase in data analysis possibilities to validate the technology for hydrogen infrastructure.



FY 2012 Publications/Presentations

1. “Next Generation H2 Station Analysis,” poster presented at the 2012 DOE Annual Merit Review and Peer Evaluation Meeting, May 14–18, 2012, Washington, D.C.
2. CDPs and other publications available on the Hydrogen Infrastructure section of NREL’s Technology Validation website, http://www.nrel.gov/hydrogen/proj_tech_validation.html.

FIGURE 4. Time between fueling

VIII. SAFETY, CODES & STANDARDS

VIII.0 Safety, Codes & Standards Sub-Program Overview

INTRODUCTION

The Safety, Codes and Standards sub-program supports research and development (R&D) to provide an experimentally validated fundamental understanding of the relevant physics, critical data, and safety information needed to define the requirements for technically sound and defensible codes and standards. This information is used to help facilitate and enable the widespread deployment and commercialization of hydrogen and fuel cell technologies. In Fiscal Year (FY) 2012, the sub-program continued to identify and evaluate safety and risk management measures that can be used to define the requirements and close the gaps in codes and standards in a timely manner.

The sub-program promotes collaboration among government, industry, codes and standards development organizations, universities, and national laboratories in an effort to harmonize regulations, codes, and standards (RCS), both internationally and domestically. Communication and collaboration among codes and standards stakeholders is emphasized in order to maximize the impact of the sub-program's efforts and activities in international RCS. The sub-program is leading a round-robin testing effort by the Regulations, Codes and Standards Working Group of the International Partnership for Hydrogen and Fuel Cells in the Economy, which aims to harmonize high-pressure tank-testing measurement protocols required for tank certification. In addition, in December 2011, a Global Technical Regulation on hydrogen-fueled vehicles was submitted to the United Nations Economic Commission for Europe Working Party 29 (UN ECE WP.29). This regulation will serve as the technical underpinning for the United States Federal Motor Vehicle Safety Standard.

The sub-program utilizes the expertise of the Hydrogen Safety Panel to disseminate relevant information and implement safe practices pertaining to the operation, handling, and use of hydrogen and fuel cell technologies in Program-funded projects. The Safety Panel provides recommendations on the safe conduct of project work as well as lessons-learned and best practices that can be of broad benefit to the Program. The sub-program continues to share current safety information and knowledge with the community.

In addition, extensive external stakeholder input—from the fire-protection community, academia, automobile manufacturers, and energy, insurance, and aerospace sectors—is used to create and enhance safety knowledge tools for emergency responders and authorities having jurisdiction. The sub-program has renewed its emphasis on ensuring the continual availability of safety knowledge tools, distributed via an array of media outlets to reach the largest number of safety personnel possible.

GOALS

The sub-program's key goals are to provide the validated scientific and technical basis required for the development of codes and standards, to promulgate safety practices and procedures to allow for the safe deployment of hydrogen and fuel cell technologies, and to ensure that best safety practices are followed in Hydrogen and Fuel Cells Program activities.

OBJECTIVES

The sub-program's key objectives are to:

- Facilitate the development and promulgation of essential codes and standards by 2015 to enable widespread deployment and market entry of hydrogen and fuel cell technologies and completion of all essential domestic and international RCS by 2020:

- Conduct R&D to provide critical data and information needed to define requirements in developing codes and standards.
- Develop and validate test-measurement protocols and methods to support and facilitate international harmonization of codes and standards for high-pressure tanks by 2013.
- Conduct materials R&D to provide the technical underpinning to enable fault-tolerant system designs in time to enable their use in the anticipated rollout of hydrogen fueling infrastructure in 2015.
- Conduct a quantitative risk assessment study to address indoor refueling requirements to be adopted by code developing organizations (e.g., National Fire Protection Association and International Code Council) by 2015.
- Develop safety-related information resources and lessons-learned and share these resources with first responders, authorities having jurisdiction, and other key stakeholders.
- Ensure that best safety practices are followed in all research, technology development, and market deployment activities supported by the Hydrogen and Fuel Cells Program.

FY 2012 STATUS

The sub-program continues to support R&D to provide the technical basis for codes and standards development, with projects in a wide range of areas, including fuel specification, separation distances, materials and components compatibility, and hydrogen sensor technologies. Utilizing the results from these R&D activities, the sub-program continues to actively participate in discussions with standards development organizations such as the National Fire Protection Association, International Code Council, SAE International, CSA Group, and the International Organization for Standardization to promote domestic and international collaboration and harmonization of RCS.

The following websites provide additional, up-to-date information relevant to the status of the sub-program's activities:

- Technical Reference for Hydrogen Compatibility of Materials (www.ca.sandia.gov/matlsTechRef/)
- Hydrogen Incident Reporting and Lessons Learned Database (www.h2incidents.org/)
- Hydrogen Bibliographic Database (www.hydrogen.energy.gov/biblio_database.html)
- Hydrogen Safety Best Practices Manual (www.h2bestpractices.org/)
- Hydrogen Safety Training for Researchers (<https://www-training.llnl.gov/training/hc/HS5094DOEW/index.html>)
- Introduction to Hydrogen for Code Officials (www.hydrogen.energy.gov/training/code_official_training/)
- Hydrogen Safety for First Responders (www.hydrogen.energy.gov/firstresponders.html)

FY 2012 KEY ACCOMPLISHMENTS

The sub-program continued to make progress in several areas, including the following:

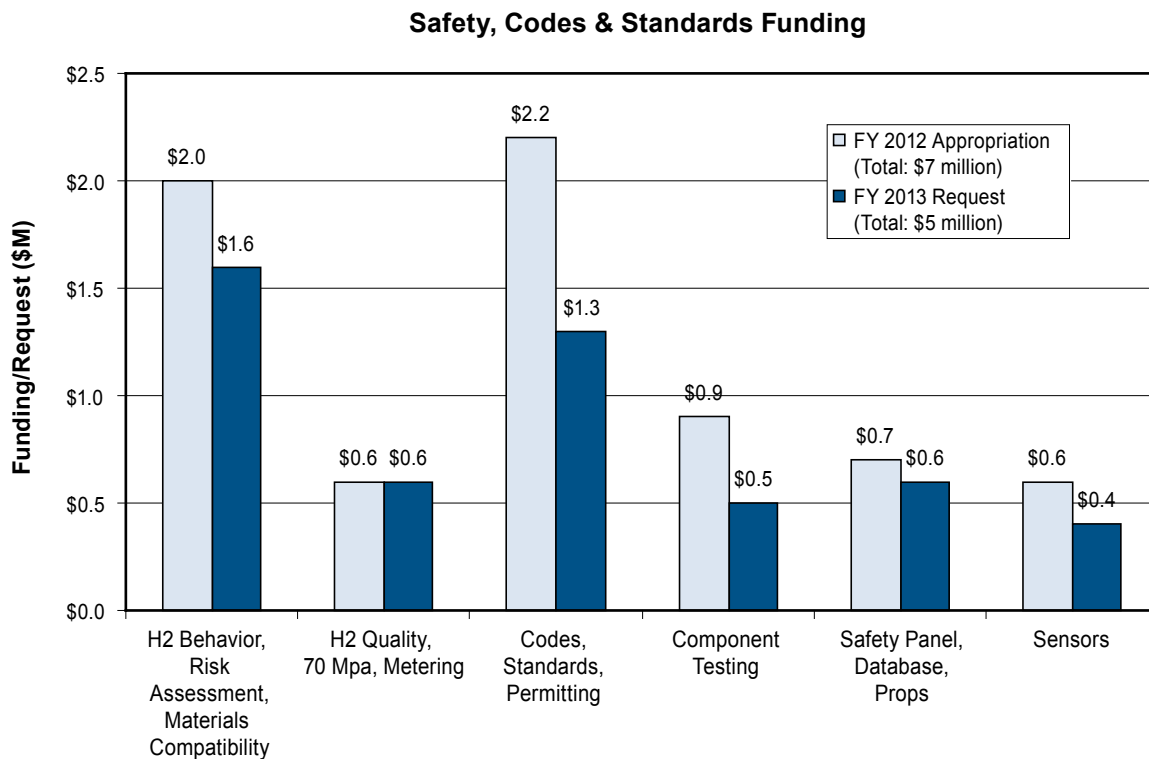
- *Hydrogen Behavior, Risk Assessment, and Materials Compatibility* (Sandia National Laboratories):
 - Published compressed-hydrogen materials compatibility (CHMC) testing and data application standard, CSA CHMC 1 Part 1, in May 2012.
 - Developed accelerated test methods for measurement of hydrogen-assisted fatigue crack growth; this accelerated test greatly reduces the cost barriers that prevent qualification of new materials in hydrogen service.
 - Compressed Hydrogen Powered Industrial Truck (HPIT) component standard, CSA HPIT 1, completed in September 2011; this standard will be the first to allow the development of design criteria for components for hydrogen storage systems.

- Developed test methods for evaluating the effectiveness of stainless steel welds in a hydrogen environment; this test methodology leverages past test methods and identifies methods for evaluating the hydrogen resistance of materials under actual use conditions, such as welding.
- Developed a method to measure flame light-up probability, which will be used to determine the overall hazard classification of a hydrogen release.
- *Hydrogen Quality* (Los Alamos National Laboratory):
 - Determined that an anode loading of 0.05 mg Pt/cm² can tolerate a CO concentration of at least 75 ppb and 100 ppb at 60°C and 80°C respectively.
 - Completed the validation of ASTM D7653-10-*Determination of Trace Gaseous Contaminants in Hydrogen Fuel by Fourier Transform Infrared (FTIR) Spectroscopy* for both ammonia (NH₃) and water (H₂O).
- *Coordination of Codes and Standards Development, Domestic and International* (National Renewable Energy Laboratory, NREL):
 - Developed a permit template for hydrogen dispensing stations, which will be used in California as the permitting template for hydrogen dispensing stations and will contain the basic codes and standards requirements, including those related to the California Risk Management Plan requirements.
 - Developed a fact sheet summarizing the requirements for siting stationary fuel cells and the associated hydrogen storage systems.
 - Developed and began implementing a plan for identifying and supporting the development of the codes and standards required for a wider deployment of hydrogen and fuel cell technologies, with a particular emphasis on fuel cell electric vehicles, by the year 2020.
- *Component Testing* (NREL):
 - Completed the validation testing of Hydrogen Pressure Relief Device 1 phase 1. Results were utilized to modify test protocols in order to provide a more representative set of worst case conditions during cycle testing.
- *Hydrogen Safety Panel, Databases, Props, and First Responders* (Pacific Northwest National Laboratory):
 - The Hydrogen Safety Panel reviewed 11 safety plans for projects in fuel cell and hydrogen storage R&D—results of these safety evaluations indicate that over 90% of report recommendations have been accepted.
 - Added 12 new safety event records from national laboratories, universities, and private-sector firms in the U.S. and other countries since the 2011 Annual Merit Review and Peer Evaluation Meeting, for a total of 206 records currently in the database.
 - Added 30 new links between safety event records and best practices databases.
 - Conducted two fire training classes at the Los Angeles City and County Fire Department, with approximately 300 first responders attending.
 - Received 200–300 unique visits per month through the Web-based first responders’ training awareness course; the course is registered on the TRAIN (Training-finder Real-time Affiliate Integrated Network) website, for broader dissemination to first responders (TRAIN is a central repository for public health training courses, and nearly 30,000 TRAIN users identify themselves as emergency responders.)
- *Hydrogen Sensors*:
 - Measured sensor long-term durability over a one-year period using 2% hydrogen exposures in a newly built long-term exposure chamber with environmental controls (NREL).

- Developed a more advanced sensor platform, with input from an industrial partner, to provide temperature-control capabilities for a low-cost, durable, and reliable hydrogen safety sensor (Los Alamos National Laboratory and Lawrence Livermore National Laboratory).

BUDGET

The sub-program received an appropriation of \$7.0 million in FY 2012. This allowed for sustained progress in key R&D and codes and standards development work. The President's FY 2013 budget request includes \$5.0 million for Safety, Codes and Standards, which will ensure continuity in key R&D and focus areas as shown below.



FY 2013 PLANS

The Safety, Codes and Standards sub-program will continue to work with codes and standards organizations to identify and address needs for the development of new hydrogen-specific codes and standards. To address these needs, the sub-program will continue to support its rigorous technical R&D program—including assessment of materials compatibility for component designs and high-pressure tank cycle testing—and continue to promote a quantitative risk assessment approach to ensure the development of technically sound codes and standards. The sub-program will also continue to promote the domestic and international harmonization of RCS by working with the appropriate domestic and international organizations such as the National Fire Protection Agency, International Code Council, SAE International, CSA Standards, and the International Standards Organization. The sub-program will continue to participate in International Partnership for Hydrogen and Fuel Cells in the Economy's Regulations, Codes and Standards Working Group and the IEA's Hydrogen Implementing Agreement, both of which are engaged in hydrogen safety work.

Antonio Ruiz

Safety, Codes & Standards Team Lead

Fuel Cell Technologies Program

Department of Energy

1000 Independence Ave., SW

Washington, D.C. 20585-0121

Phone: (202) 586-0729

Email: Antonio.Ruiz@ee.doe.gov

VIII.1 Hydrogen Safety, Codes and Standards R&D – Release Behavior

Aaron Harris (Primary Contact), Isaac Ekoto,
Adam Ruggles, Terry Johnson
Sandia National Laboratories (SNL)
P.O. Box 969
Livermore, CA 94551-0969
Phone: (925) 294-4530
Email: apharri@sandia.gov

DOE Manager
HQ: Antonio Ruiz
Phone: (202) 586-0729
Email: Antonio.Ruiz@ee.doe.gov

Project Start Date: October 1, 2003
Project End Date: Project continuation and direction
determined annually by DOE

- Milestone 2.1: Provide critical understanding of hydrogen behavior relevant to unintended releases in enclosures. (4Q, 2013)
- Milestone 2.2: Understand flame acceleration leading to transition to detonation (4Q, 2014)
- Milestone 2.3: Develop and validate simplified predictive engineering models of hydrogen dispersion and ignition (4Q 2015)
- Milestone 2.5: Develop holistic design strategies (4Q, 2017)
- Milestone 2.6: Validate inherently safe design for hydrogen fueling infrastructure (4Q, 2019)
- Milestone 4.1: Identify and evaluate failure modes (3Q, 2013)
- Milestone 4.2: Develop supporting research programs (round robins) to provide data and technologies (2Q, 2012)
- Milestone 4.3: Complete determination of safe refueling protocols for high pressure systems (1Q, 2015)
- Milestone 4.4: Complete risk mitigation analysis for advanced transportation infrastructure systems (1Q, 2015)
- Milestone 4.5: Revision of National Fire Protection Association 2 to incorporate advanced fueling and storage systems and specific requirements for infrastructure elements such as garages and vehicle maintenance facilities (3Q, 2016)

Fiscal Year (FY) 2012 Objectives

- Present results of reduce order model development efforts to the Hydrogen Industry Panel on Codes (HIPOC)
- Development and publication of new and validated source models for dispersion from high-source pressure releases
- Map ignition and light-up boundaries for multiple nozzle diameters and pressure ratios using laser spark apparatus

This project addresses the following technical barriers from section 3.8 of the Fuel Cell Technologies Program Multi-Year Research, Development and Demonstration Plan:

- (A) Safety Data and Information: Limited Access and Availability
- (F) Enabling national and international markets requires consistent RCS
- (G) Insufficient Technical Data to Revise Standards
- (L) Usage and Access Restrictions – parking structures, tunnels and other usage areas

Contribution to Achievement of DOE Safety, Codes & Standards Milestones

This project will contribute to achievement of the following DOE milestones from the Safety Codes and Standards section of the 2011 Fuel Cell Technologies Program Multi-Year Research, Development and Demonstration Plan:

FY 2012 Accomplishments

- Created benchmark data set to evaluate the optimum distribution functions used to model mixture ignitability in support of milestones 2.1, 2.3, 2.5, 2.6, and 4.4.
- Performed comprehensive review of notional nozzle models for compressed hydrogen releases in support of milestones 2.1, 2.2, 2.3, 2.5, 2.6, 4.1, 4.2, and 4.4.
- Developed measurement apparatus necessary to experimentally investigate flame light-up probability, which is the probability that an incipient ignition kernel will lead to a sustained flame. The probability of flame light up is integral to determining the overall hazard of a release (no flame is less hazardous). This accomplishment is critical to milestones 2.1, 2.2, 2.3 and provides validated simulation support for milestones 2.5, 2.6, 4.1, 4.2, 4.3, 4.4.
- Applied flame radiation models and experimental results to industry partner collected data set for large hydrogen flame releases. This collaborative effort supports ongoing advancement of milestones 2.1 and 2.3 while contributing to milestones 2.5, 2.6, 4.1, 4.2, and 4.4.

- Completed phase 1 of composite overwrapped pressure vessel (COPV) testing in support of milestones 2.3, 2.5, 2.6, 4.2 and 4.3. Data collected from laboratory testing used to validate three-dimensional, dynamic finite element model of COPV during fill process. This validation effort is part of an international ‘round robin’ effort by the International Partnership on Hydrogen Energy. Dynamic modeling of tank response to various fill protocol scenarios is critical to improving hydrogen fill protocols and tank construction.



Introduction

Safety is critical to enabling the use of hydrogen as an energy carrier. While hydrogen has been used for industrial purposes for many years bringing industrial technology to a retail setting such as a refueling station involves many unknowns with regard to safety. Understanding release behavior of hydrogen is fundamental to performing quantitative risk assessments (QRA) – the use of past failures to predict the likelihood of future failures and thereby estimate the risk of harm from an accident. The hydrogen specific QRA approach is incorporated in the development of model codes and standards to appropriately regulate the retail/commercial use of hydrogen.

Simulations and models, validated with experimental data, are the cornerstone of the hydrogen specific QRA. These simulations and models provide critical input to the overall risk evaluation. While risk is classically defined as the product of frequency and consequences, a more detailed definition specific to hydrogen hazards is shown in Equation 1. For hydrogen systems, analysis has identified the major hazard surrounds the release of hydrogen gas with subsequent ignition. Equation 1 characterizes the various factors of risk for ignition of a hydrogen release as a function of probability of a release, probability of ignition given the release type, probability of a hazard given a specific release and ignition type and finally the probability of harm given the associated hazard. Release behavior models and experiments provide insight to factors (shown in red in Equation 1) for predicting risk.

The goal of the Fast Fill project is to develop a set of high quality experimental results for rapid filling and venting of Type-III and Type-IV hydrogen storage tanks that can be used for model validation and the development of refueling protocols for 35 MPa and 70 MPa hydrogen refueling stations and consumption during aggressive driving cycles.

Material temperature is the primary barrier for hydrogen fueling. Extreme material temperatures are achieved through interactions between the tank (at a given “soaked temperature” at the start of fueling (hot and cold) and the gas flow rate and gas temperature.

Approach

Isaac Ekoto, Bill Houf, and Daniel Dedrick, developed a five-year roadmap with the explicit goal of addressing short-, medium-, and long-term hydrogen behavior safety research needs. The plan was based on an analysis of the current knowledge base, key SNL contributions to this knowledge base, and critical outstanding gaps that serve as barriers to the creation of future standards but can be informed by leveraging unique SNL capabilities. Research topics were divided into five main areas:

- General release behavior (relevant release geometries, storage states, jet dynamics)
- Ignition mechanisms (diffusion ignition, electrostatic discharge, conduction)
- Necessary ignition conditions (minimum ignition energy, mixture ignitability)
- Necessary flame light-up conditions (ignition characteristics, flow strain rates)
- Light-up consequences (flame radiation, pressure, flame impingement).

Development of a comprehensive risk assessment tool that couples arbitrary system failure mode analysis with quantifiable consequence modeling obtained from improved hydrogen behavior understanding remains the overarching goal. Ultimately this tool would be used to inform standards creation processes. Highlights from the research roadmap were condensed into a presentation to be given at the International Energy Agency (IEA) Task 31 Subtask A Coordination Meeting held in Oslo, Norway, on January 10 by Daniel Dedrick. As a result of this presentation, Sandia will be coordinating with the IEA task 31 Subtask to develop and disseminate models developed. A workshop with H2CAN collaborators (Pierre Bernard, et al. of Université du Québec à Trois-Rivières) was held April 11 and 12 in Livermore, CA to identify common research areas. Collaborative research topics ranging from risk assessment methodologies, flow dispersion, ignition mechanisms, and flame radiation characterization and modeling were identified, with ongoing data sharing occurring between both entities. User input and institutional expertise has likewise

$$Risk \propto \sum_{i,j,k} P(\text{Release}_i)P(\text{Ignition}_j|\text{Release}_i)P(\text{Hazard}_k|\text{Ignition}_j \cap \text{Release}_i)P(\text{Harm}|\text{Hazard}_k)$$

EQUATION 1. Risk as a function of probability of a release, probability of ignition given a release, probability of a hazard given a release and ignition and finally the probability of harm given the hazard.

been solicited from relevant industrial and regulatory partners (HIPOC, National Fire Protection Association, etc.).

Regarding COPV safety Sandia started the first phase of this project using a Type-IV 39-L 70 MPa tank provided by Lincoln Composites. Sandia then instrumented the tank with thermocouples fully characterize the gas and composite tank wall temperatures during dynamic H₂ filling and vent. Five thermocouples spaced along the tank axis are used to measure the gas temperature in the tank. At four locations on the wall of the tank there are sets of four thermocouples that measure, from inside to outside, the liner temperature, the composite/liner interface temperature, a mid-wall composite temperature, and an outer composite temperature. Three of the locations are spaced along a parallel to the tank axis. The fourth location is centered along the tank axis and clocked 90 degrees around the tank circumference from the other three. That provides a total of 21 temperature measurements. The tank is mounted and attached to a H₂ manifold in one of Sandia's high pressure hydrogen labs. The manifold is currently limited to 2,000 psi (14 MPa) hydrogen pressure, but future plans will increase the pressure capacity to 70 MPa. Although the maximum pressure is limited, the computer controlled manifold allows for significant experimental flexibility. For hydrogen filling, the tank pressure can be linearly ramped from 20 psi to 2,000 psi or any pressure combination in between. The ramp time can be varied from tens of seconds to tens of minutes. The hydrogen flow rate is measured by a high accuracy Coreolis mass flow meter and the pressure is measured at the inlet to the tank as well as at the opposite dead-ended fitting. We use an infrared camera to capture tank surface temperature gradients and compare to thermocouple measurements.

Results

Improved Accuracy of Turbulent Jets

To accurately assess the ignitability of given hydrogen releases the simulation must be accurate. Current computational fluid dynamics simulations treat intermittency (the presence of a concentration at a particular location) as linearly proportional to the ratio of the first and second order statistical moments. High fidelity experiments conducted at Sandia National Laboratories, however, demonstrate that this relationship is in fact non-linear, which contradicts current modeling approaches. The collection of these data provide new benchmarks for the evaluation of optimum distribution functions used to model mixture ignitability (Figure 1).

High Source Pressure Hydrogen Release Behavior

Turbulent hydrogen releases, both ignited and unignited, are typically treated and canonical expanded free-jets using similarity arguments based on the jet exit diameter. For underexpanded jets with choked flow releases and

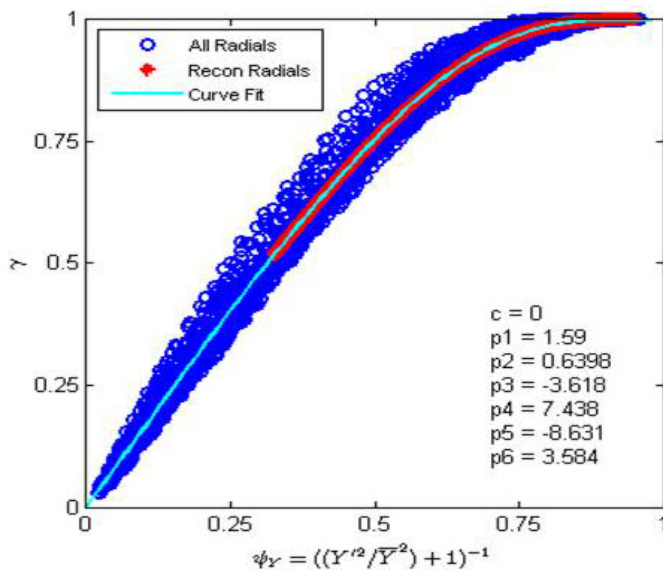


FIGURE 1. Intermittency plotted against the ratio of the first and second turbulent concentration moments. Commonly used intermittency models assume a linear fit between the first and second statistical moments of the scalar concentration field, but these data indicate a highly non-linear correlation, particularly for intermittency values (γ) greater than ~0.75.

complex jet-exit structure past the release point a notional nozzle, modeled from thermodynamic variables, is used to create a pseudo source jet exit diameter, and the dispersion characteristics of the downstream flow is solved for with the use of the incompressible jet-similarity relations. These release types are important, since most hydrogen is stored at a compressed state that is above the critical pressure ratio. The optimum method to model the pseudo source term, however, had not yet been determined for hydrogen. A schlieren image of the underexpanded jet is provided at the left in Figure 2. Using the planar laser Raleigh scatter technique to measure statistical dispersion fields of mole fraction, a comprehensive comparison of measured data to model results using six separate notional nozzle formulations was performed. For each notional nozzle model, both ideal and non-ideal equations of state were analyzed. The evaluation showed poor correlation for all existing models, with the most comprehensive model (Harstad & Bellan) substantially and unexpectedly overpredicting the size of the mass weighted effective diameter (d^*). Nonetheless, the measurements indicate better ways to more accurately model these release types; refined model development is ongoing.

Applied Flame Radiation Evaluation

Previous radiation experiments conducted by Sandia National Laboratories provided a universal correlation for small and mid-size flames regardless of fuel gas type. Recent experiments, conducted by Air Products and Chemicals has revealed larger than expected radiative emission values from larger flames. The results of this work are still pending,

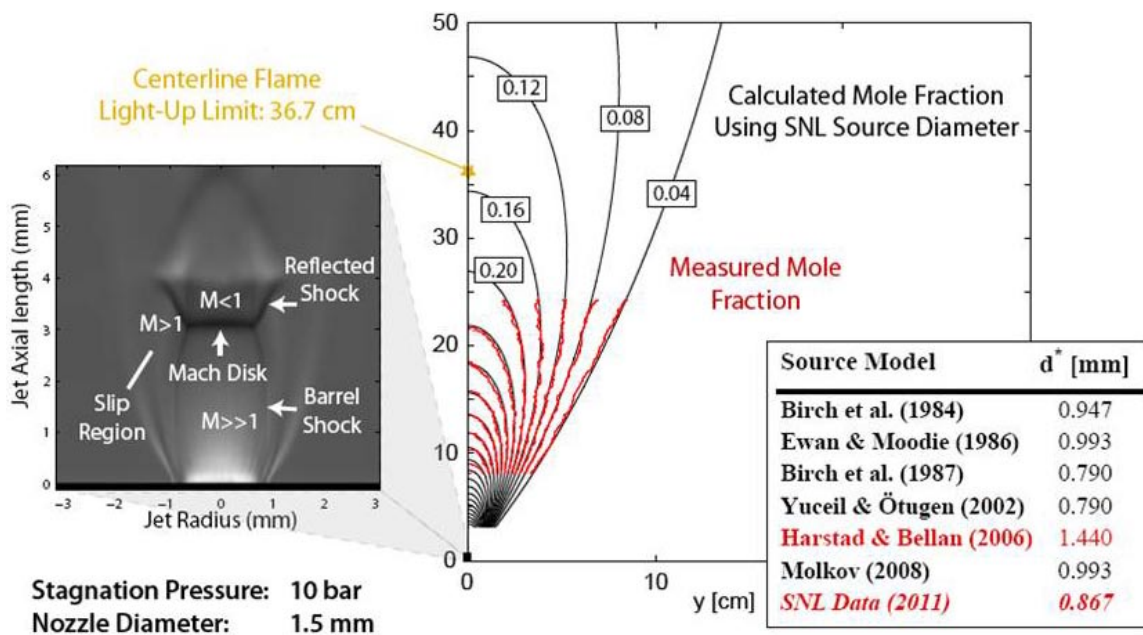


FIGURE 2. Left, schlieren image of hydrogen under-expanded jet. Center, calculated mole fraction in black using the measured effective nozzle diameter compared to the measured mole fraction in red; the centerline light-up limit is also shown for comparison. Right, table comparing the predicted mass weighted effective diameter based on various notional nozzle models relative to the 'true' measured result.

however, several hypothesis have been tested using Sandia National Laboratories using the high source pressure flame capabilities previously developed to analyze notional nozzle models from choked flow releases. Figure 3 shows images of the flames used in the experiment, which are reproduced with the permission of the industry collaborator.

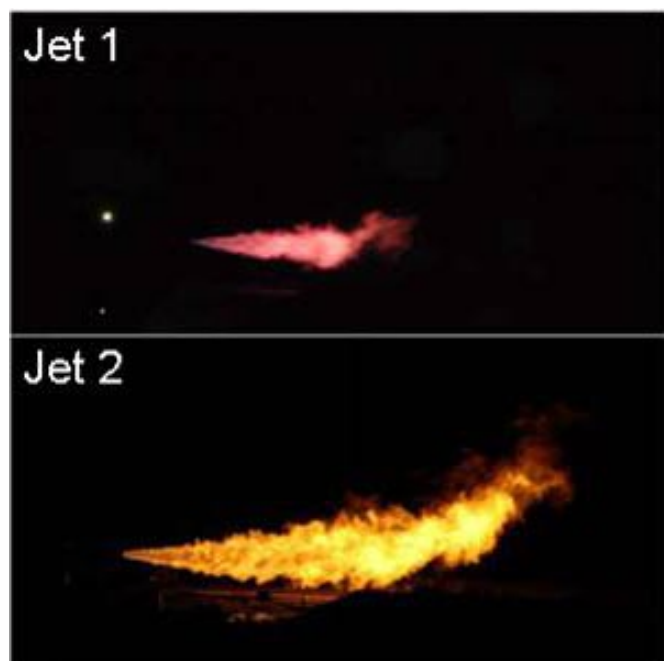


FIGURE 3. Images of Large-Scale Hydrogen Flames

COPV Testing and Characterization

The experimental results met the target accuracy (<1% error, mass balanced). In addition the qualitative information gained in the thermography reinforced the choice of temperature measurement locations. Images from thermography are shown in Figure 4.

The models developed and validated by this experiment are part of an international collaboration. Professor Jinyang Zheng conducts hydrogen storage research at Zhejiang University of China. Dr. Jianjun Ye, a member of the Zhejiang University team, arrived at Sandia in November 2011. Dr. Ye completed the development of the three-dimensional model geometry and has optimized the finite element mesh for accuracy and minimum computational time. The model is running and several of the experimental conditions are being simulated.

In addition to Dr. Ye's work Sandia is developing a one-dimensional simulation of hydrogen dispensers using the Sandia-developed, multi-species compressible-flow, simulation program, Netflow.

Netflow calculations have been carried out for several of the H2 filling experiments conducted during the last two quarters and the comparison between simulation results and experimental data is currently being analyzed. These simulations are comparable to simulations currently underway by automotive original equipment manufacturers in support of hydrogen fueling protocol standard, SAE J2601.

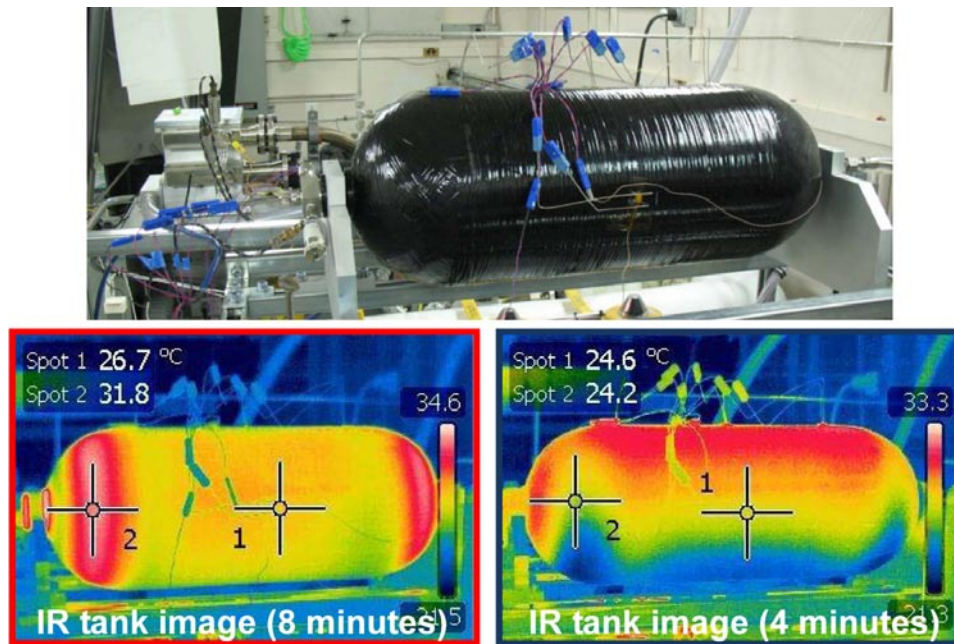


FIGURE 4. Above, instrumented tank in test facility, below left, thermal image of tank during fill – screen capture of video taken 8 minutes for a 90 sec, 13 MPa fill, below right, thermal image of tank during vent – screen capture of video taken at 4 minutes for a 1.9 g/sec vent from 9 MPa.

Conclusions and Future Directions

- Computational fluid dynamics models for hydrogen ignitability should be evaluated against benchmark data.
- Characteristics of predictive choked flow dispersion models were examined against Sandia generated validation datasets:
 - Deficiencies identified and from the measurements, more accurate modeling methods have been proposed.
- Qualitative high-speed ignition imaging elucidated potential sustained flame light-up mechanisms:
 - Light-up boundaries for choked flow releases were experimentally mapped for several different source pressure ratios and nozzle diameters.
 - Enhanced flamelet models can be used to predict light-up boundaries—experimental apparatus needed to measure relevant flow and combustion variables was constructed.
- Measured radiative heat fluxes from large-scale H₂ flames were compared against model predictions:
 - Deficiencies identified and improved modeling methods have been proposed.
- Future Direction – develop simplified model for overpressure transient releases. A simplified model is necessary for risk assessment of deflagrations created from delayed ignition of hydrogen releases.

- Future Direction – Develop improved models of choked flow dispersion including notional nozzle deficiencies.
- Future Direction – Evaluate jet elongation due to surface effects for horizontal releases.
- Future Direction – Develop models to predict the reflection due to surfaces for various hydrogen flame scenarios.

Sandia National Laboratories is a multi-program laboratory managed and operated by Sandia Corporation, a wholly owned subsidiary of Lockheed Martin Corporation, for the U.S. Department of Energy's National Nuclear Security Administration under contract DE-AC04-94AL85000.

FY 2012 Publications/Presentations

1. Ruggles, A.J., and Ekoto, I.W., "Ignitability and mixing of underexpanded hydrogen jets," 4th International Conference on Hydrogen Safety, San Francisco, CA, Sept. 12–14, 2011. (Accepted for publication in IA-HySafe special edition of *Int. J. Hydrogen Ener.*)
2. Houf, W.G., Evans, G.H., Ekoto, I., Merilo, E. and Groethe, M., "Hydrogen Releases and Ignition from Fuel-Cell Forklift Vehicles in Enclosed Spaces," 4th International Conference on Hydrogen Safety, San Francisco, CA, Sept. 12–14, 2011. (IA-HySafe special edition of *Int. J. Hydrogen Ener.*)
3. Houf, W.G. and Winters, W.S., "Simulation of High Pressure Liquid Hydrogen Releases," 4th International Conference on Hydrogen Safety, San Francisco, CA, Sept. 12–14, 2011. (IA-HySafe special edition of *Int. J. Hydrogen Ener.*)

4. Ekoto, I.W., Merilo, E.G., Houf, W.G., Evans, G.H., Groethe, M.A., “Hydrogen Fuel-Cell Forklift Vehicle Releases in Enclosed Spaces,” 4th International Conference on Hydrogen Safety, San Francisco, CA, Sept. 12–14, 2011. (IA-HySafe special edition of *Int. J. Hydrogen Ener.*)
5. Merilo, E., Groethe, M., Adamo, R., Schefer, R., Houf, W., Dedrick, D., “Self-Ignition of Hydrogen Jet Fires by Electrification of Entrained Particulates,” 4th International Conference on Hydrogen Safety, San Francisco, CA, Sept. 12–14, 2011. (IA-HySafe special edition of *Int. J. Hydrogen Ener.*)
6. Ekoto, I.W., Dedrick, D. E., Merilo, E., Groethe, M., “Performance-Based Testing for Hydrogen Leakage into Passenger Compartments,” *International Journal of Hydrogen Energy* Vol. 36, Issue 16, 2011.
7. Dedrick, D.E., “Approach to establishing technical basis for Codes and Standards,” IEA Task 31 Subtask A Coordination Meeting: Hydrogen Behavior Research, Oslo, Norway, Jan. 10, 2012.
8. Ekoto, I.W. “General Release Behavior R&D for H2 Safety, Codes & Standards,” H2CAN/Sandia Workshop April 11, 2012.
9. Ruggles, A.J. “Summary of Hydrogen Release and Ignition Behavior at Sandia National Labs,” H2CAN/Sandia Workshop April 11, 2012.
10. Ekoto, I.W. “Summary of Hydrogen Release and Ignition Behavior at Sandia National Labs IEA Task 31 Subtask A Coordination Meeting: Hydrogen Behavior Research, Oslo, Norway, April, 2012.
11. Ekoto, I.W., Houf, W.G., Ruggles, A.J., Crietz, L.W., Li, J.X., “Large-Scale Hydrogen Jet Flame Radiant Fraction Measurements and Modeling,” 19th World Hydrogen Energy Conf., Toronto, Canada, June 16–21, 2012.
12. Ekoto, I.W., Houf, W.G., Ruggles, A.J., Crietz, L.W., Li, J.X., “Large-Scale Hydrogen Jet Flame Radiant Fraction Measurements and Modeling,” International Pipeline Conference, Calgary, Canada, September 24–28, 2012 (Accepted).

VIII.2 Risk-Informed Safety Requirements for H2 Codes and Standards Development

Aaron Harris (Primary Contact), Jeffrey LaChance,
Katrina Groth

Sandia National Laboratories
P.O. Box 969
Livermore, CA 94551-0969
Phone: (925) 294-4530
Email: apharri@sandia.gov

DOE Manager

HQ: Antonio Ruiz
Phone: (202) 586-0729
Email: Antonio.Ruiz@ee.doe.gov

Project Start Date: October 1, 2003

Project End Date: Project continuation and direction
determined annually by DOE

Contribution to Achievement of DOE Safety, Codes & Standards Milestones

This project will contribute to achievement of the following DOE milestones from the Safety Codes and Standards section of the Fuel Cell Technologies Program Multi-Year Research, Development and Demonstration Plan:

- Milestone 2.4: Publish national indoor hydrogen fueling standard. (4Q, 2015)
- Milestone 2.5: Develop holistic design strategies. (4Q, 2017)
- Milestone 2.6: Validate inherently safe design for hydrogen fueling infrastructure. (4Q 2019)
- Milestone 2.9: Publish protocols for identifying potential failure modes (2Q, 2013)
- Milestone 2.10: Publish risk mitigation approaches (2Q, 2014)
- Milestone 2.11: Publish draft protocol for identifying potential failure modes and risk mitigation (4Q, 2014)
- Milestone 2.12: Publish a system for classifying accident types (2Q, 2013)
- Milestone 2.13: Publish a methodology for estimating accident likelihood (2Q, 2013)
- Milestone 2.14: Release a report of the most common accident scenarios (4Q, 2013)

Fiscal Year (FY) 2012 Objectives

- Present results of indoor refueling risk assessment to the National Fire Protection Association (NFPA) 2 Fueling Working Group.
- Perform and document required risk assessment (with input from NFPA 2 and others) for developing science-based risk-informed codes and standards for indoor refueling of hydrogen lift trucks or other vehicles.
- Perform scoping risk assessment for accident mitigation features for refueling stations and indoor refueling applications including development of any required data and new methodologies.

This project addresses the following technical barriers from the Safety Codes and Standards section (3.8) of the 2011 Fuel Cell Technologies Program Multi-Year Research, Development and Demonstration Plan:

- (A) Safety Data and Information: Limited Access and Availability
- (F) Enabling National and International Markets Requires Consistent Regulations, Codes and Standards
- (G) Insufficient Technical Data to Revise Standards
- (L) Usage and Access Restrictions – parking structures, tunnels and other usage areas

FY 2012 Accomplishments

- Presented results of risk assessment for indoor fueling to NFPA 2 Fueling Working Group. While code development is an iterative discussion among the committee members, this accomplishment is in direct support of milestone 2.4 and continues progress toward milestones 2.5, 2.6, 2.9, 2.10, 2.11, 2.12, 2.13 and 2.14.
- Provided leadership for code development activities associated with indoor hydrogen fueling, NFPA 2 Fueling Working Group. Leadership in code development activities signifies a commitment to a continuous improvement process for the risk assessment methods developed under this project. This directly supports the achievement of milestone 2.10 and ensures that the publication of this approach leverages industry and peer research input. All other milestones (2.4, 2.5, 2.6, 2.9, 2.11, 2.10, 2.12, 2.13, 2.14) benefit from a continuous feedback loop rather than uni-directional communication.
 - Facilitated discussion with industry and research collaborators to identify safety data, specifically

necessary data information for improved quantitative risk assessment (QRA) fidelity.

- Developed generic hydrogen fueling system plumbing and instrumentation drawings to facilitate the discussion surrounding NFPA 2 chapter 10 for both indoor and outdoor refueling. This holistic approach to refueling leverages information from indoor fueling experience to inform the revision of codes for outdoor systems.



Introduction

Safety is critical to enabling the hydrogen as an energy carrier. While hydrogen has been used for industrial purposes for many years, bringing industrial technology to a retail setting such as a refueling station involves many unknowns with regard to safety. QRA has been used in several high-consequence industries in recent years including nuclear power and oil/gas production. QRA utilizes data from previous failure events to model postulated accidents and estimate the associated risk from operation of a facility. Risk considerations are incorporated in to the development of model codes and standards to appropriately regulate the retail/commercial use of hydrogen.

The overarching goal of applying QRA to the hydrogen industry is to ensure that the use of hydrogen is ‘as safe or safer’ than existing fuel technologies. The quantitative approach allows engineers to identify the main risk contributors and develop targeted improvements that have the greatest potential to reduce risk.

Approach

Sandia National Laboratories uses QRA to establish a common understanding of the safety level of the hydrogen industry. This process provides a basis for risk-informed decision-making with regard to implementing hydrogen systems in a variety of applications. Application of the risk-informed approach began with establishing separation distances for stationary bulk hydrogen storage as covered in NFPA 55 and adopted into NFPA 2. The work continues by addressing the indoor refueling requirements in chapter 10 of NFPA 2.

The goal of QRA is to establish that the risk is “As Low As Reasonably Practicable” or ALARP. Embedded in the ALARP approach is the understanding that there is no zero risk situation, but that there is an unacceptably high level of risk. This unacceptable risk threshold varies based on activity—the approach balances the fatality risk with the personal or societal benefit of the technology. For hydrogen applications, the unacceptable level of risk was determined

to be a fatality rate greater than $1 e^{-4}$ /year for an individual worker or a fatality rate greater than $1 e^{-5}$ /yr for a member of the public. Once it is determined that a risk is below the unacceptable threshold, the best practice is to continue to allocate reasonable resources to further reduce the risk (i.e., continuously target improvements to the major remaining risk drivers in a cost-effective manner).

Results

Preliminary results from the risk assessment of indoor hydrogen fueling indicate that the risk of fatalities from indoor refueling in a generic, representative warehouse is not unacceptable. Based on the available information, the risk of fatality for any given individual, called the average individual risk (AIR) is $4.0 e^{-6}$ fatalities/exposed worker or 1 in 24,900. Note that this value is below the unacceptable threshold of $1 e^{-4}$ /year for workers identified previously. The result is also lower than the AIR for freight, stock and material movers, which is $7.0 e^{-5}$ fatalities/person (Bureau of Labor Statistics, 2007).

A ‘generic’ plumbing and instrumentation diagram was created to facilitate discussion and represent the hardware requirements of NFPA 2 for indoor refueling activities; shown in Figure 1. This activity also uncovered gaps in current code language.

Conclusions and Future Directions

Based on the current analysis, the risk of fatality resulting from indoor hydrogen refueling is less than the activities that it supports (operating forklifts in a warehouse).

Future efforts will leverage the methods refined in this analysis to develop a hydrogen specific quantitative risk assessment tool kit for use in a variety of applications by a variety of users. The planned efforts will:

- Incorporate data from industry collaborators into the next iteration of risk assessments.
- Continue facilitating discussion and eliminating discussion barriers through working group leadership.
- Develop academic and research partnerships to improve broad focus feedback loop:
 - Incorporate National Renewable Energy Laboratory composite data product outputs into hydrogen-specific QRA toolkit.
 - Incorporate hydrogen-specific QRA toolkit results into infrastructure analysis tools such as Spatially & Temporally Resolved Energy & Environment Tool.
- Host workshop of QRA practitioners and potential end-users to identify hydrogen specific QRA toolkit needs.
- Scope the activity to produce and disseminate a hydrogen specific QRA toolkit.

Indoor
Non-Public
Fast Fill*
Dispenser
P&ID
Code
Compliant

*Note – Fast Fill Doesn't exist in IFC; limits H2 flow to 12 SCFM (0.027kg/min) IFC 2309.3.1.2 (3)

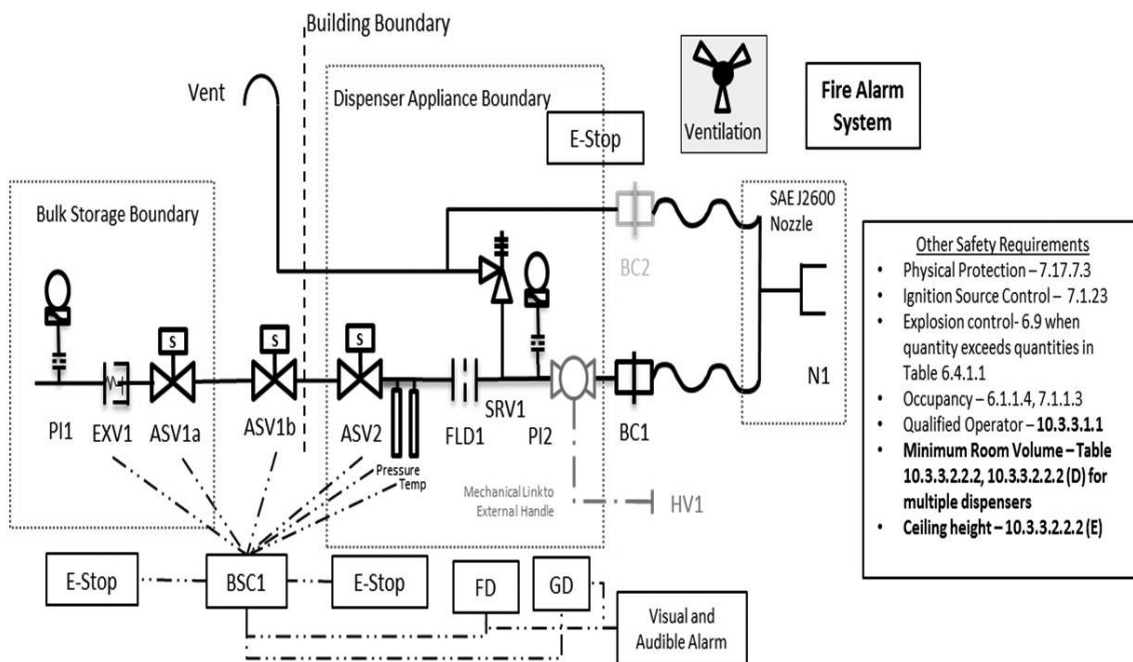


FIGURE 1. Plumbing and Instrumentation Diagram for Generic Code-Compliant Indoor Non-Public Fast-Fill Dispenser with references to NFPA 2

Sandia National Laboratories is a multi-program laboratory managed and operated by Sandia Corporation, a wholly owned subsidiary of Lockheed Martin Corporation, for the U.S. Department of Energy’s National Nuclear Security Administration under contract DE-AC04-94AL85000.

FY 2012 Publications/Presentations

1. J. LaChance, A. Tchouvelev, Angunn Engebo, “Development of Uniform Harm Criteria for Use in Quantitative Risk Analysis of the Hydrogen Infrastructure,” International Journal of Hydrogen Energy 36 (2011) pgs. 2381-2388.
2. Groth, K. M. & LaChance, J. L. “Risks associated with hydrogen indoor refueling.” World Hydrogen Energy Conference, 2012.
3. J. LaChance, “Progress in the Use of Quantitative Risk Assessment in Hydrogen Safety,” H2Can 3rd AGM and Annual conference, Niagara Falls Ontario, June 9, 2012.

4. J. LaChance, “QRA Data Analysis,” IEA Task 31 hydrogen safety meeting in Paris (March 16–18, 2012) on US progress in Activities C1, C2, and C.
5. J. LaChance and K. Groth. “Progress in QRA for Indoor Refueling of Forklifts,” IEA Task 31 hydrogen safety meeting in Paris (March 16–18, 2012) on US progress in Activities C1, C2, and C.
6. J. LaChance “QRA Quality,” IEA Task 31 hydrogen safety meeting in Paris (March 16–18, 2012) on US progress in Activities C1, C2, and C.
7. LaChance, J.L.; Middleton, B. & Groth, K.M. “Comparison of NFPA and ISO approaches for evaluating separation distances.” International Journal of Hydrogen Energy, In Press. Corrected Proof published 29 June 2012. Doi: 10.1016/j.ijhydene.2012.05.144.

VIII.3 Component Standard Research and Development

Robert Burgess (Primary Contact), William Buttner, Matthew Post, Carl Rivkin, Chad Blake
National Renewable Energy Laboratory (NREL)
15013 Denver West Parkway
Golden, CO 80401
Phone: (303) 275-3823
Email: robert.burgess@nrel.gov

DOE Manager
HQ: Antonio Ruiz
Phone: (202) 586-0729
Email: Antonio.Ruiz@ee.doe.gov

Subcontractor:
SAE International, Troy, MI

Project Start Date: Fiscal Year (FY) 2008
Project End Date: Project continuation and direction determined annually by DOE

- (G) **Insufficient Technical Data to Revise Standards**
The role of DOE/NREL is focused on the need to provide sound technical data in the form of test data and analysis for the purpose of revising relevant hydrogen codes and standards.
- (H) **Insufficient Synchronization of National Codes and Standards**
Harmonization of national codes and standards is a top priority of the RCS efforts within the DOE Hydrogen and Fuel Cells Program.
- (K) **No Consistent Codification Plan and Process for Synchronization of Research and Development (R&D) and Code Development**
Planning and prioritization is needed to guarantee that resources are well placed for the expeditious development of new and existing documents and to assure that codification activities are synchronized with the needs of the relevant technical committees.

Contribution to Achievement of DOE Safety, Codes & Standards Milestones

This project contributes to achievement of the following DOE milestones from the Hydrogen Codes and Standards section of the Fuel Cell Technologies Program's Multi-Year Research, Development and Demonstration Plan:

- Milestones: Completion of necessary codes and standards needed for the early commercialization and market entry of hydrogen energy technologies in support of the 2015 model year release planned for hydrogen fuel cell vehicles.

FY 2012 Accomplishments

- Completed oxygen dependence evaluation of multiple sensor platforms. This work was presented at the International Conference on Hydrogen Safety in San Francisco California and is being published in the International Journal of Hydrogen Energy. This work was identified as a need through multiple sensor users with needs for robust sensors capable of operation in reduced oxygen environments.
- Completed sensor test laboratory objective, for a fifth sensor platform as part of the NREL/Joint Research Centre (JRC) round robin inter-laboratory comparison, under a formal Memorandum of Understanding with the JRC laboratory (a European Commission funded laboratory). Round robin test result comparison provided validation of test methods.
- Collaboration with JRC's Cleaner Energy Unit and the Université du Québec at Trois-Rivières has led to an

Fiscal Year (FY) 2012 Objectives

- Support development of new codes and standards required for commercialization of hydrogen technologies.
- Create code language that is based on the latest scientific knowledge by providing analytical, technical and contractual support.
- Participate directly on codes and standards committees to identify technology gaps, then work to define research and development needs required to close those gaps.
- Conduct laboratory testing to provide a basis for improved code language.
- Collaborate with industry, university and government researchers to develop improved analytical and experimental capabilities.

Technical Barriers

This project addresses the following technical barriers identified in the Hydrogen Codes and Standards section of the 2012 Fuel Cell Technologies Program's Multi-Year Research, Development and Demonstration Plan:

- (F) **Enabling National and International Markets Requires Consistent Regulations Codes and Standards (RCS)**
Standards being developed at the component level need to be harmonized across national and international jurisdictions, requiring technical expertise at the technical committee level to monitor and inform on issues of consistent requirements.

evaluation of numerous miniaturized hydrogen sensor platforms (e.g., micro-fabricated, micro-machined, thin-film) and an assessment of the resulting improvements in certain performance metrics as well as degradations in others. These results were presented at the World Hydrogen Energy Conference by our collaboration partners from the Université du Québec.

- Partnering with Lawrence Livermore and Los Alamos National Laboratory has led to results being presented at the 221st Electrochemical Society meeting on the subject "Humidity Tolerance of Electrochemical Hydrogen Safety Sensors Based on Yttria-Stabilized Zirconia (YSZ) and Tin-doped Indium Oxide (ITO)".
- Conducted Hydrogen Safety Sensor Workshop in Chicago Illinois leading to summary document with sensor application specific targets and recommendations. Follow up webinars are being held quarterly for continued communications with key stakeholders in the sensor industry.
- Support of hydrogen fuel cell electric vehicle crash test leakage measurements. Sensors were evaluated for crash test survivability, leading to a successful field deployment of a sensor platform at the Transportation Research Facility. The sensor is capable of measuring hydrogen or helium leakage during pre and post crash. Helium was selected as a surrogate test fluid during full vehicle crash testing.
- Designed and built multiple long-term exposure chambers with environmental controls for extended life testing of hydrogen safety sensors as part of the NREL/JRC Memorandum of Understanding. Accumulated data over a one year time period has been collected for 2% hydrogen exposures at two week intervals.
- NREL maintains a Memorandum of Understanding with Element One for the purposes of hydrogen safety sensor development. This work has led to Element One being awarded the Next Top Energy Innovator runner up award.
- NREL is working with the BAM laboratory in Germany (Federal Institute for Materials Research and Testing) to develop an outline for a hydrogen safety sensor textbook. A publisher has been contacted and work is moving forward to defining market needs.
- Component test validation work on Hydrogen Pressure Relief Device 1 (HPRD1) phase 1 has been completed. Results were utilized to modify test protocols in order to provide a more representative set of worst case conditions during cycle testing.
- Component validation testing needs are being identified through NREL subcontract efforts for the purpose of prioritizing for future resource allocation. In addition, NREL has organized a meeting, to be held at the end of the fourth quarter FY 2012 to bring together component

manufacturers for open discussion relative to component development needs.



Introduction

Development of codes and standards has been identified in the 2012 Fuel Cell Technologies Program's Multi-Year Research, Development and Demonstration Plan as a key area needing support for the commercialization and growth of hydrogen technologies. NREL is providing research and development support to these codes and standards organizations through validation testing, analytical modeling, and product commercialization efforts. NREL has been tasked with these responsibilities as defined in the 2012 Fuel Cell Technologies Program's Multi-Year Research, Development and Demonstration Plan.

Approach

NREL is participating on relevant codes and standards committees to help identify gaps and define research and development needs to close those gaps. Working at the committee level allows us to quickly identify areas that need R&D support and to work directly with the technical experts in planning a path forward. This process is instrumental in avoiding delays and setbacks in the development of new codes and standards and in the revision of existing codes and standards. By providing support from a national lab we are able to help establish codes and standards language with solid technical basis.

Hydrogen safety sensors are a key component for the safe commercialization of hydrogen technologies. NREL is tasked with being a national resource for testing sensors designed to meet the needs of this growing market. By developing standard test methods and measuring sensor performance of a wide range of sensors of different designs and from a many different manufacturers, NREL is characterizing sensor performance and identifying gaps relative to DOE performance targets. With this information we work closely with sensor manufacturers so that they can better understand the performance of their sensor relative to the needs of hydrogen stationary applications. This work is directed toward sensor R&D, such that sensor manufacturers, utilizing the resources of a national lab, can expedite their product development life cycle. In addition, the sensor market expertise gained by NREL will be used to support commercialization through development of representative codes and standards for safety sensor certification. Commercialization support includes collaboration with key stakeholders as well as direct participation on the relevant codes and standards committees.

Results

NREL has been working toward identifying gaps and supporting R&D efforts for developing new and improved hydrogen codes and standards. Results reported here are for efforts specifically directed at component level standards. Results are organized in the following three sections; Hydrogen Safety Sensors, Component R&D and Codes and Standards Support.

Hydrogen Safety Sensors

DOE published performance targets for hydrogen safety sensors in the multi-year RD&D plan. NREL's has identified more than 150 commercially available sensors and near-term developmental sensors from six sensor categories. Test data is being compiled in a generic format as a resource for end users. This format will allow for publishing a characterization study of the sensor market, while keeping individual results proprietary.

NREL completed validation testing of the sensor test apparatus that was built in FY 2010. Validation testing consisted of systems level testing to characterize the repeatability and reproducibility of the apparatus, showing capabilities surpassing requirements in certification standards. Capabilities were further validated through round robin testing completed with the JRC Institute for Energy laboratory in Petten Netherlands. NREL is now leveraging accomplishments in hydrogen safety sensor testing through our collaboration with the JRC laboratory.

NREL is currently working directly with more than 20 sensor developers to support commercialization as their products move from prototype designs to full-scale production. This effort is directed at providing independent evaluation and testing of sensor platforms. This work has been completed in conjunction with other DOE supported projects in developing new technologies that have shown promise in meeting the identified DOE sensor targets.

Component R&D

Compressing, storing and dispensing gaseous hydrogen at 70 MPa can be a challenging application for hardware that is available on the market today. As hydrogen fuel cell market penetration grows, component suppliers will be able to use increased sales volume to support development of product improvements. At the demonstration phase, the limited number of suppliers can benefit from National Laboratory research and development support. This is aimed at increasing the understanding of the fuel cell market needs then developing product that meet performance targets required by this new service. NREL is holding a meeting of component suppliers at the end of FY 2012 to discuss the merits of the Energy Systems and Integration facility and potential for product testing support. NREL also has a

subcontract in place to help identify and prioritize codes and standards validation test needs. These needs will be used for defining resources required for support of codes and standards development.

Codes and Standards Support

Through direct participation on the hydrogen components codes and standards committees, NREL has identified R&D gaps, including further HPRD testing, localized fire testing, tank level stress rupture testing and radio-frequency identification fill protocol validation. NREL has developed statements of work required to close these gaps and finalize these components requirements.

Conclusions and Future Direction

NREL made significant contributions in supporting commercialization of hydrogen sensor technologies. This includes collaborative work with domestic and international partners. NREL hosted a hydrogen sensor workshop in June 2011 and is following up with quarterly webinars to identify hydrogen sensor research and development gaps and to help define future sensor test laboratory direction. We continue to work closely with codes and standards development organizations to close gaps and promulgate codes and standards that are based on the latest technical knowledge. In addition to continuing to support component level codes and standards development, NREL will undertake a number of initiatives including:

- Identifying gaps to hydrogen technology commercialization.
- Providing national laboratory support needed to provide a sound basis for component level codes and standards content.
- Working directly with sensor manufacturers in order to reach performance targets defined in the 2012 Fuel Cell Technologies Program's Multi-Year Research, Development and Demonstration Plan.
- Executing sensor test laboratory testing over a wider range of environmental conditions and finalizing long-term exposure and response time testing methodologies.
- Leveraging our efforts with national and international collaborations to provide a path toward commercialization of hydrogen components that are designed to meet the latest safety standards.

FY 2012 Publications/Presentations

1. "Use of Hydrogen Safety Sensors Under Anaerobic Conditions – Impact of Oxygen Content on Sensor Performance", W.J. Buttner, R. Burgess, C. Rivkin, M.B. Post, L. Boon-Brett, G. Black, F. Harskamp, P. Moretto, International Conference on Hydrogen Safety (ICHS), Presented San Francisco, September, 2011 and submitted for publication in conference proceedings.

2. “Validation Testing in Support of Hydrogen Codes and Standards Development”, R.M. Burgess, M. McDougall, N.L. Newhouse, C. Rivkin, W.J. Buttner, M.B. Post, International Conference on Hydrogen Safety (ICHS), Presented San Francisco, September, 2011 and submitted for publication in conference proceedings.

3. “On-Board Storage (SAE J2579 rational for performance based criteria for on board hydrogen storage systems)” at the HySafe Hydrogen Safety Workshop, San Francisco CA, September 2011.

4. “FY2011 Year End Safety Sensor Testing Laboratory Accomplishments”, DOE Report, FY11 Annual Operating Plan, September 2011.

5. “NREL/DOE Hydrogen Safety Sensor Workshop Summary”, Document review completed December 2011, Submitted for publication as NREL technical report (Note: workshop held in Chicago, IL, June 2011).

VIII.4 Hydrogen Materials and Components Compatibility

Aaron Harris (Primary Contact), Brian Somerday,
Chris San Marchi

Sandia National Laboratories
P.O. Box 969
Livermore, CA 94551-0969
Phone: (925) 294-4530
Email: apharri@sandia.gov

DOE Manager

HQ: Antonio Ruiz
Phone: (202) 586-0729
Email: Antonio.Ruiz@ee.doe.gov

Project Start Date: October, 2003

Project End Date: Project continuation and direction
determined annually by DOE

- Milestone 2.5: Develop holistic design strategies. (4Q, 2017)
- Milestone 2.6: Validate inherently safe design for hydrogen fueling infrastructure. (4Q, 2019)
- Milestone 2.16: Publish technical bases for optimized design methodologies of hydrogen containment vessels to account appropriately for hydrogen attack. (Q4, 2014)
- Milestone 2.17: Implement validated mechanism-based models for hydrogen attack in material. (Q4, 2018)
- Milestone 2.18: Demonstrate the use of new high performance materials for hydrogen applications that are cost-competitive with aluminum alloys. (4Q, 2017)
- Milestone 4.1: Identify and evaluate failure modes. (3Q, 2013)

FY 2012 Accomplishments

- Materials compatibility testing and data application standard, CSA CHMC1 Part 1 published May 2012.
- Developed accelerated test methods for measurement of hydrogen assisted fatigue crack growth in Cr-Mo pressure vessel steels. This accelerated test greatly reduces the cost barriers that challenge qualification of new materials in hydrogen service. This directly supports milestone 2.16.
- Developed test methods for evaluating the effectiveness of stainless steel welds in hydrogen. This activity leverages past test methods and identifies methods for evaluating the hydrogen resistance of material under actual use conditions such as welding. This activity directly supports milestones 2.16 and 4.1
- Continued development of international collaborations:
 - Hosted research collaborators from HYDROGENIUS/Japanese National Institute of Advanced Industrial Science and Technology (AIST) at Sandia in February 2012
 - Visited researchers at AIST in June 2012
 - Developing collaborative research goals for FY 2013
 - Developing collaborative research concepts with German industrial partners for FY 2013



Fiscal Year (FY) 2012 Objectives

- Complete Canadian Standards Association (CSA) Test Method for Evaluating Material Compatibility for Compressed Hydrogen Applications – Phase I - Metals (CHMC1) document
- Issue Sandia report reflecting updated content from Technical Reference website
- Present progress on optimizing fatigue crack growth testing in H₂ gas to American Society of Mechanical Engineers (ASME) Project Team on Hydrogen Tanks
- Develop detailed materials testing program on austenitic stainless steel welds with industrial partner

This project addresses the following technical barriers from the Safety, Codes and Standards section (3.7) of the Fuel Cell Technologies Program Multi-Year Research, Development and Demonstration Plan:

- (A) Safety Data and Information: Limited Access and Availability
- (F) Enabling National and International Markets Requires Consistent Regulations, Codes and Standards
- (G) Insufficient Technical Data to Revise Standards

Contribution to Achievement of DOE Safety, Codes and Standards Milestones

This project will contribute to achievement of the following DOE milestones from the Safety Codes and Standards section of the Fuel Cell Technologies Program Multi-Year Research, Development and Demonstration Plan:

Introduction

Lack of validated safety testing methods in safety standards and insufficient technical data to revise these standards are major barriers to the deployment of hydrogen technologies. The purpose of this project is twofold,

1) provide the technical basis for assessing the safety of hydrogen-based systems with the accumulation of knowledge feeding into the development or modification of relevant codes and standards and, 2) using the development of these test methods to support a broader understanding of material compatibility and thus stimulate technical innovation.

Approach

The focus of the Materials and Components Compatibility project is to optimize materials characterization methodologies, generate critical hydrogen compatibility data for materials to enable technology deployment, and compose the Technical Reference on Hydrogen Compatibility of Materials. Two activities proceed in parallel: generating new data and understanding through materials testing, and identifying and summarizing existing data from technical documents. The high-priority structural materials featured in these activities are low-alloy and carbon steels, austenitic stainless steels, and aluminum alloys. The materials testing activity emphasizes high hydrogen gas pressures (>100 MPa), fatigue crack initiation and propagation test methods, and technology-critical material fabrication (e.g. welds) and service variables (e.g., temperature). The data from materials testing are rigorously reviewed to identify pathways to improve the test methods and to ensure the data are suitable for implementation in structural design.

As part of codes and standards advocacy, Sandia personnel provide leadership in the codes and standards development process through direct participation in organizations such as ASME, CSA, and SAE International. This participation ensures that the standards development organizations have the most current technical information on structural materials compatibility. Sandia personnel provide leadership in the development of both component design standards as well as materials testing standards.

Specific objectives for FY 2012 include:

- Optimize fatigue crack growth rate measurements for pressure vessel steels in H₂ and report results to ASME
- Evaluate effects of load-cycle frequency on fatigue crack growth rates for 7000 series aluminum alloys in high-pressure H₂
- Measure H₂-affected fracture properties of technologically relevant welds in collaboration with industry partner
- Enable completion of standards through committee leadership and data evaluation
- Develop capability for variable-temperature testing in high-pressure H₂ gas

Results

The accomplishments summarized below are directly related to the objectives and milestones featured in FY 2012: The Materials Compatibility Task accomplished many of the milestones with several more expected for completion by the end of FY 2012.

- The results of optimized fatigue crack growth rate measurements for pressure vessel steels in hydrogen were presented to ASME at their quarterly meeting Nov. 2011. This optimized measurement procedure (illustrated in Figure 1) greatly accelerates the time required to test and validate new pressure vessel steels.
- The results of the evaluation of load cycle frequency effects on fatigue crack growth rates for 7000 series aluminum alloys in high-pressure hydrogen demonstrates that these alloys are resistant to hydrogen embrittlement, enabling qualification of this high-strength aluminum alloy as an alternative to 6061 aluminum.
- Welded tubes were tested after high-pressure hydrogen exposure to produce an initial data set. This work was particularly interesting as the tubing was supplied by an industrial partner and is a representative sample of tubing and welds commonly found in the commercial hydrogen applications. Preliminary testing showed no effect of hydrogen on fracture resistance of the weld (Figure 2). Fatigue testing protocol is under development.
- Several standards have been updated or revised with data generated from this project and through leadership of Sandia personnel in guiding committee experts to appropriately apply the experimental analysis. The new standards are: CSA CHMC1, CSA HPIT1 and the revised standards are: SAE J2579, ASME KD-10.
- Development of the Technical Reference has identified a gap in material properties at temperatures above and

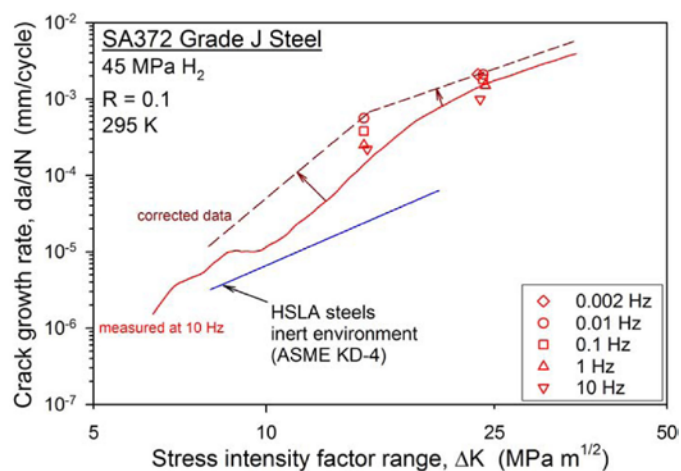


FIGURE 1. Evaluation of various load cycle frequencies for use in developing accelerated test protocol

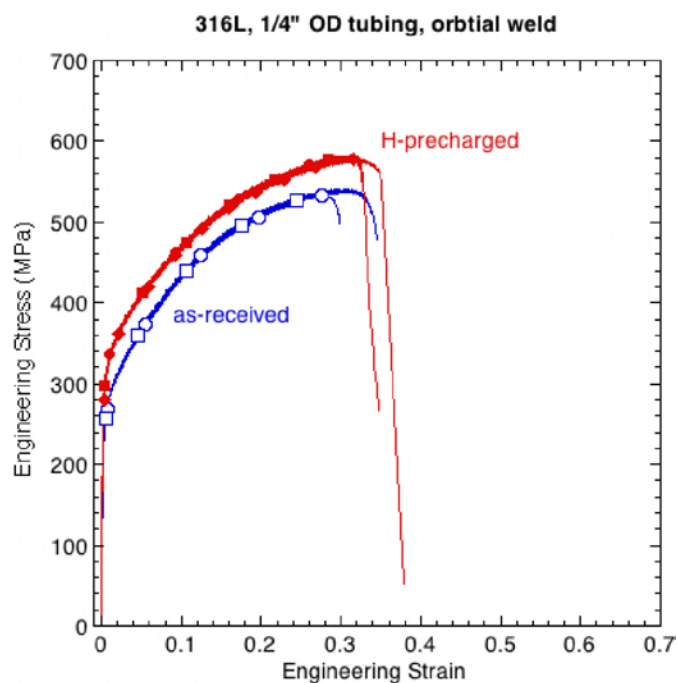


FIGURE 2. Preliminary results of welded tube tensile testing

below ambient. Construction of a new automated gas manifold that will support a future capability for variable temperature testing is nearly complete. This future capability will increase testing throughput at ambient temperatures and provide a new testing capability at sub-ambient and elevated temperatures.

Conclusions and Future Directions

FY 2012 brought about the conclusion of several multi-year efforts in the publication and revision of several standards. These publications represent hundreds of testing hours and hundreds of hours dedicated to standards development meetings and communication regarding the appropriate application of testing results to the standards development

FY 2013

- Measure fatigue crack initiation resistance of H₂-exposed stainless steel tube welds.
- Develop validated methodology to account for fatigue crack initiation life in steel H₂ pressure vessels for consideration in ASME Article KD-10.
- Develop research and development project with industry partner to improve resistance of high-strength pressure vessel steel to H₂-assisted fatigue crack growth.
- Procure pressure vessel to complete variable-temperature testing in H₂ gas system.

- Leverage results on fatigue crack growth of steels in H₂ to advance international coordination with AIST and International Institute on Carbon-Neutral Energy Research on materials testing and basic science.
- Develop a Hydrogen Materials Collaboration Database as a resource for the broader hydrogen community. It will include discussion forums, archives of open-source content and reports from conferences or meetings, and new results on hydrogen compatibility testing that have not yet gone through peer review for incorporation into the Technical Reference. The Hydrogen Materials Collaboration Database will enable global harmonization of test methods, facilitate research coordination, and lead to accelerated deployment of hydrogen systems.

Sandia National Laboratories is a multi-program laboratory managed and operated by Sandia Corporation, a wholly owned subsidiary of Lockheed Martin Corporation, for the U.S. Department of Energy's National Nuclear Security Administration under contract DE-AC04-94AL85000.

FY 2012 Publications/Presentations

1. R. Gangloff and B. Somerday, Eds., *Gaseous Hydrogen Embrittlement of Materials in Energy Technologies*, Woodhead Publishing, Cambridge, UK, 2012.
2. C. San Marchi, "Hydrogen Embrittlement of Austenitic Stainless Steels and Their Welds", in *Gaseous Hydrogen Embrittlement of Materials in Energy Technologies*, R. Gangloff and B. Somerday, Eds., Woodhead Publishing, Cambridge, UK, 2012, pp. 592-623.
3. K. Nibur and B. Somerday, "Fracture and Fatigue Test Methods in Hydrogen Gas", in *Gaseous Hydrogen Embrittlement of Materials in Energy Technologies*, R. Gangloff and B. Somerday, Eds., Woodhead Publishing, Cambridge, UK, 2012, pp. 195-236.
4. K. Nibur, B. Somerday, C. San Marchi, J. Foulk, M. Dadfarnia, P. Sofronis, "The Relationship Between Crack-Tip Strain and Subcritical Cracking Thresholds for Steels in High-Pressure Hydrogen Gas", *Metallurgical and Materials Transactions A*, 2012, accepted for publication.
5. C. San Marchi, A. Harris, M. Yip, B. Somerday, K. Nibur, "Pressure Cycling of Steel Pressure Vessels with Gaseous Hydrogen", Proceedings of the ASME 2012 Pressure Vessels and Piping Division Conference, July 15–19, 2012, Toronto, Canada, PVP2012-78709.
6. K. Nibur, B. Somerday, C. San Marchi, J. Foulk, M. Dadfarnia, P. Sofronis, "The Relationship Between Crack-Tip Strain and Subcritical Cracking Thresholds for Steels in High-Pressure Hydrogen Gas", Joint HYDROGENIUS and I²CNER International Workshop on Hydrogen-Materials Interactions, Fukuoka, Japan, February 2012.
7. K. Nibur and B. Somerday, "Effect of Crack Tip Strain on the Subcritical Cracking Thresholds for Steels in High-Pressure Gaseous Hydrogen", MS&T Conference 2011, Columbus OH, October 2011.

VIII.5 Component Testing for Industrial Trucks and Early Market Applications

Aaron Harris (Primary Contact), Brian Somerday,
Chris San Marchi

Sandia National Laboratories
P.O. Box 969
Livermore, CA 94551-0969
Phone: (925) 294-4530
Email: apharri@sandia.gov

DOE Manager

HQ: Antonio Ruiz
Phone: (202) 586-0729
Email: Antonio.Ruiz@ee.doe.gov

Project Start Date: January 2010

Project End Date: May 2011 (carryover from Fiscal
Year [FY] 2011 extended objectives into FY 2012)

Fiscal Year (FY) 2012 Objectives

- (1) Provide technical basis for the development of standards defining the use of steel (Type 1) storage pressure vessels for gaseous hydrogen:
 - Compare fracture mechanics based design approach for fatigue assessment of pressure vessels for gaseous hydrogen to full-scale performance tests.
 - Generate performance test methods and data for fatigue assessment of full-scale pressure vessels with gaseous hydrogen.
- (2) Codes and Standards Advocacy:
 - Participate in the standards development activities for gaseous hydrogen storage in pressure vessels, in particular Canadian Standards Association (CSA) and SAE International activities.

This project addresses the following technical barriers from the Safety Codes & Standards section (3.8) of the 2011 Fuel Cell Technologies Program Multi-Year Research, Development and Demonstration Plan:

- (A) Safety Data and Information: Limited Access and Availability
- (F) Enabling National and International Markets Requires Consistent Regulations, Codes & Standards
- (G) Insufficient Technical Data to Revise Standards

Contribution to Achievement of DOE Safety, Codes & Standards Milestones

This project will contribute to achievement of the following DOE milestones from the Safety Codes & Standards section of the Fuel Cell Technologies Program Multi-Year Research, Development and Demonstration Plan:

- Milestone 2.5: Develop holistic design strategies. (4Q, 2017)
- Milestone 2.6: Validate inherently safe design for hydrogen fueling infrastructure. (4Q, 2019)
- Milestone 2.16: Publish technical bases for optimized design methodologies of hydrogen containment vessels to account appropriately for hydrogen attack. (Q4, 2014)
- Milestone 2.17: Implement validated mechanism-based models for hydrogen attack in material. (Q4, 2018)
- Milestone 2.18: Demonstrate the use of new high performance materials for hydrogen applications that are cost-competitive with aluminum alloys. (4Q, 2017)
- Milestone 4.1: Identify and evaluate failure modes. (3Q, 2013)

FY 2012 Accomplishments

- Hydrogen Powered Industrial Truck (HPIT) component standard, CSA HPIT1 completed September 2011. Publication is delayed by CSA pending harmonization with other hydrogen component standards (e.g., CSA HPRD1, CSA HGV 3.1, etc.). This will be the first standard to allow use of design criteria for qualifying hydrogen storage system. Milestone 2.16 is directly impacted by this work and further understanding is gained toward achieving milestones 2.5, 2.6, 2.18 and 4.1.
- Presentation to American Society of Mechanical Engineers (ASME) project team for revision of ASME Boiler and Pressure Vessel Code (BPVC) Article KD-10. Based on results of testing Type-1 pressure vessels the design approach considered in KD-10 may be revised. This is in direct support of Milestone 2.16 and 2.17. This work also contributes toward achieving milestones 2.5, 2.6, 2.18 and 4.1.



Introduction

Fatigue cracks can nucleate and grow in metals subjected to cyclic stress. The increment of crack growth per load cycle (da/dN) is a function of the driving force for fatigue cracking, which is called the applied stress intensity factor range (ΔK).

Under conditions of stable fatigue crack growth, a simple empirical relationship can be used to describe fatigue crack growth in terms of the driving force: $da/dN = C(\Delta K)^m$, where C and m are experimentally determined constants.

Fatigue crack growth of a pressure vessel subjected to pressure cycling is enabled by the presence of manufacturing defects in the steel and accelerated by exposure to gaseous hydrogen. The latter characteristic is often referred to as “hydrogen embrittlement” and depends on the partial pressure of the gaseous hydrogen and the kinetics of hydrogen uptake into the steel. Consequently, the fatigue crack growth relationship is affected by variables such as hydrogen pressure, pressure-cycle frequency, pressure-time relationship (wave form), and temperature.

Although steel pressure vessels may be vulnerable to fatigue crack growth aided by hydrogen embrittlement, the industrial gas companies have used such pressure vessels for hydrogen transport and storage for decades. Typically, these pressure vessels are subjected to less than one pressure cycle per day (and in many cases less than one cycle per month), thus fatigue crack growth is generally not a concern. Pressure vessels for hydrogen storage in new applications such as those for lift trucks are anticipated to experience up to six pressure cycles per day, approaching an order of magnitude greater than the duty cycle of typical transportable industry gas pressure vessels.

Since the duty cycle for lift truck pressure vessels is outside the window of current experience, a methodology for determining the cycle life must be established. A deterministic engineering analysis for quantifying the progression of fatigue cracks is provided in the ASME BPVC (Section VIII, Division 3, Article KD-4) and extended to the specific case of high-pressure gaseous hydrogen in Article KD-10. This framework provides a method for conservatively estimating the fatigue cycle life of pressure vessels based on assessment of existing flaws in the pressure vessel. An alternate method has been proposed based on the measured performance of manufactured pressure vessels subjected to pressure cycling coupled with statistical assessment of the quality of the pressure vessels and desired cycle life. These two methods have been referred to as engineering analysis method and performance evaluation method respectively.

Approach

During this project, pressure vessels were pressure cycled with gaseous hydrogen; the pressure vessels were identical to those in service for fuel cell forklift applications with gaseous hydrogen, with the exception that defects were engineered in some pressure vessels. The engineered defects were designed to simulate manufacturing flaws in the pressure vessels. Engineering analysis methods were used employed to compare the engineering analysis predictions

with experimental results from the performance evaluation of full-scale pressure vessels. These efforts have required collaborations with fuel cell system integrators and pressure vessel manufacturers to obtain as-manufactured pressure vessels and produce pressure vessels with engineered defects for cycle testing, as well as development of a testing plan that reflects relevant engineering conditions, including pressure vessel designs, manufacturing flaws, and pressurization schedules. Additionally, direct participation in standards development activities has been a cornerstone of this effort, in particular with the technical advisory group for CSA's Hydrogen-Powered Industrial Trucks (HPIT1) and the subgroup drafting the language for the pressure vessel appendix in SAE J2579.

Results

Materials Testing

Sandia National Labs measured the rate of fatigue crack growth for three heats of 4130 steels in high-pressure gaseous hydrogen; testing coupons were extracted from pressure vessels supplied by the industrial partners (each heat of material came from a different vendor). ASME BPVC (VIII-3) Article KD-10 requires the testing of three heats of a given steel to demonstrate that the effects of hydrogen are not sensitive to variations in the material's microstructure or processing history. These measured fatigue crack growth rates are used to predict cycle life using engineering analysis methodologies that quantify crack growth through the vessel wall from manufacturing flaws in the pressure vessel.

Full-Scale Tank Testing

A system was designed and constructed to pressure cycle up to 10 full-scale tanks in parallel at a rate of approximately 250 discrete pressure cycles per day (approximately 5-minute pressure cycle time). The pressure vessels are cycled between 3.4 and 43.8 MPa, with an approximately 2-minute pressure ramp rate, 2-minute hold time at maximum pressure, 30-second depressurization rate, and 30-second hold at minimum pressure. Pressure vessels cycled for 47,000 cycles without failure, although not all pressure vessels experienced this number of cycles. Pressure vessels with engineered defects were subjected to fewer cycles and four vessels failed after as few as 8,000 cycles. Generally, there are two components to fatigue life, crack initiation and crack propagation. The engineering predictions are based on crack propagation only, since there is no broadly accepted method to account for crack initiation.

Leak-before-burst was observed for each of the four pressure vessel failures. This is an important observation because larger safety factors are generally applied when burst is a probable failure mode. Additionally, post-mortem

analysis suggests that the engineered defects form cracks that propagate with a semi-circular profile, although as the crack depth reaches the full thickness of the vessel the shape again changes. This is also an important observation if shown to be generally true. Cracks with larger aspect ratios (such as the aspect ratio of the engineered defects) propagate at higher rates because the driving force is greater for a “long” crack compared to a “short” crack of the same depth.

These results were incorporated into the standard CSA HPIT1. The testing procedures are also under development in SAE J2579.

The conclusion of the testing revealed that ASME BPVC calculations were conservative by a factor of 4 or more, with the safety factor for small initial defects approaching 10. Figure 1 shows the number of cycles experienced by the cylinder as a function of the depth of the initial crack. Symbols with arrows indicate cylinders that had not yet failed and were still capable of achieving more cycles. The solid lines represent the predictions based on the ASME BPVC Article KD-10 approach.

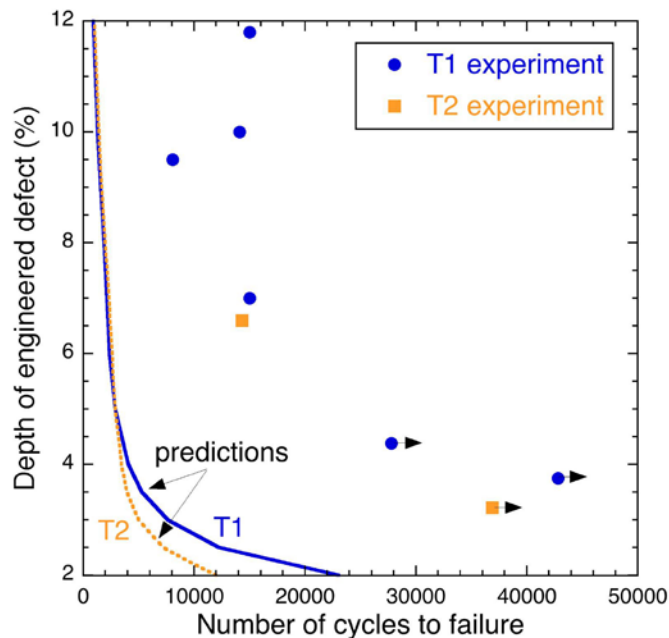


FIGURE 1. Number of cycles vs. depth of engineered defect for various cylinders in the ‘full tank’ testing. Symbols with arrows represent tanks which had not yet failed and were capable of further cycles. Solid lines represent the predicted failure from ASME BPVC Article KD-10.

Conclusions and Future Directions

Previous Conclusions:

- Commercial pressure vessels being used for hydrogen storage on forklifts have been subjected to more than 47,000 pressure cycles with gaseous hydrogen (between pressure of 3.4 and 43.8 MPa):
 - Primary aim of the remainder of project is to cycle tanks until they fail or reach 50,000 cycles.
- Fatigue crack growth assessment of engineered defects in these pressure vessels using engineering analysis appears to be conservative:
 - Post-mortem analysis is being used to refine predictions and interpret failure process.
- Code language based on the test methods developed in this study are being drafted as part of CSA HPIT1 and SAE J2579 for performance based tests:
 - Results are being shared with committees as they are generated.
- Leak-before-burst was observed in all failures.

Additional conclusions gained in FY 2012:

- Revision of ASME BPVC Article KD-10 is necessary based on the results of the full tank cycling.

Sandia National Laboratories is a multi-program laboratory managed and operated by Sandia Corporation, a wholly owned subsidiary of Lockheed Martin Corporation, for the U.S. Department of Energy’s National Nuclear Security Administration under contract DE-AC04-94AL85000.

FY 2012 Publications/Presentations

- B. Somerday and C. Sloane, “Addressing Hydrogen Embrittlement in the SAE J2579 Fuel Cell Vehicle Tank Standard”, International Conference on Hydrogen Safety ICHS 2011, San Francisco CA, September 2011, Paper No. 130.
- C. San Marchi, D. Dedrick, P. Van Blarigan, B. Somerday, K. Nibur, “Pressure Cycling of Type 1 Pressure Vessels with Gaseous Hydrogen”, International Conference on Hydrogen Safety ICHS 2011, San Francisco CA, September 2011, Paper No. 215.
- C. San Marchi and B. Somerday, “Fatigue Crack Growth of Structural Metals for Hydrogen Service”, ASME Pressure Vessels & Piping Division Conference (PVP 2011), Baltimore MD, July 2011, Paper No. PVP2011-57701.

VIII.6 National Codes and Standards Coordination

Carl Rivkin, (Primary Contact), Chad Blake,
Robert Burgess, William Buttner, and Matthew Post
National Renewable Energy Laboratory (NREL)
1617 Cole Boulevard
Golden, CO 80401
Phone: (303) 275-3839
Email: carl.rivkin@nrel.gov

DOE Manager

Antonio Ruiz
Phone: (202) 586-0729
Email: Antonio.Ruiz@ee.doe.gov

Subcontractors:

- CSA, Standards, Cleveland, OH
- FP2 Fire Protection Engineering, Golden, CO
- GWS Solutions, Tolland, CT
- Kelvin Hecht, Avon, CT
- MorEvents, Englewood, CO
- SAE International (SAE), Warrendale, PA
- Sloane Solutions, Oxford, MI
- Steele Consulting, Cypress, CA

Project Start Date: 1995

Project End Date: Project continuation and direction determined annually by DOE

Fiscal Year (FY) 2012 Objectives

- Support the safe deployment of hydrogen and fuel cell technologies.
- Identify the codes and standards required to deploy hydrogen and fuel cell technologies.
- Identify the research and validation testing required to support the development of the needed codes and standards.
- Advance hydrogen and fuel cell technologies safety, code development, and technology deployment through collaborations with appropriate stakeholders.

Technical Barriers

This project addresses the following technical barriers from the Safety, Codes and Standards section (3.7) of the Fuel Cell Technologies Program's Multi-Year Research, Development and Demonstration Plan:

- A. **Limited Government Influence on Model Codes**
The code development process is voluntary, so the government can affect its progression, but ultimately it is up to the CDOs.

B. **Competition among standards development organizations (SDOs) and code development organizations (CDOs)**

The competition between various organizations may hinder the creation of consistent vehicle codes and standards.

D. **Large Number of Local Government Jurisdictions (approximately 44,000)**

The large number of jurisdictions hinders the universal adoption of codes and standards.

E. **Lack of Consistency in Training of Officials**

The training of code officials is not mandated and varies significantly. The large number of jurisdictions leads to variation in training facilities and requirements.

F. **Limited DOE Role in the Development of International Standards**

Governments can participate and influence the development of codes and standards, but they cannot direct the development of international standards.

G. **Inadequate Representation at International Forums**

Participation in international forums and meetings is voluntary and, to date has been limited by budgetary constraints.

H. **International Competitiveness**

Economic competition complicates the development of international standards.

I. **Conflicts between Domestic and International Standards**

National positions can complicate the harmonization of domestic and international standards.

J. **Lack of National Consensus on Codes and Standards**
Competitive issues hinder consensus.

K. **Lack of Sustained Domestic Industry Support at International Technical Committees**

Cost, time and availability of domestic experts have limited consistent support of the activities conducted within the international technical committees.

Q. **Parking and Other Access Restrictions**

Complete access to parking, tunnels and other travel areas has not yet been secured. Appropriate Codes and Standards need to be developed to provide safe access to these areas.

Technical Targets

The set of key tasks shown below are taken from the draft Safety, Codes and Standards Multi-Year Plan.

The tasks shown are supported by the work done in the NREL coordination task, with a major focus on the National Codes and Standards Chronological Development Plan

(which includes several other tasks) and the fueling station codes template. Both of these activities will be complete by the planned dates.

| Task 4: Development and Harmonization of Regulations, Codes and Standards |
|--|
| Identify and evaluate failure modes. (3Q, 2013) |
| Develop supporting research programs (round robins) to provide data and technologies. (2Q, 2012) |
| Complete determination of safe refueling protocols for high pressure systems. (1Q, 2012) |
| Complete risk mitigation analysis for advanced transportation infrastructure systems. (1Q, 2015) |
| Revision of National Fire Protection Association (NFPA) 2 to incorporate advanced fueling and storage systems and specific requirements for infrastructure elements such as garages and vehicle maintenance facilities. (3Q, 2016) |
| Complete National Codes and Standards Chronological Development Plan. (4Q, 2014) |
| Complete fueling station codes and template. (4Q, 2014) |
| Completion of standards for critical infrastructure components and systems. (4Q, 2014) |
| Completion of Global Technical Regulation Phase 2. (1Q, 2017) |

Table 1 shows the NREL support for achieving DOE technical targets, specifically supporting the development of the codes and standards required to deploy hydrogen and fuel cell technologies. This technical target is described on page 3.7-1 and 2 of the Codes and Standards –Technical Plan.

FY 2012 Accomplishments

NREL accomplished the following in support of section 3.7 of the DOE Fuel Cell Technologies Program Multi-Year Research, Development and Demonstration Plan:

- NREL has produced the DOE 2020 Codes and Standards Plan for the Deployment of Hydrogen Fuel Cell Vehicles. This plan (the 2020 Plan) defines the codes and standard work required for commercial deployment of hydrogen fuel cell vehicles by 2020.
- NREL supported the development of NFPA 2 Hydrogen Technologies Code that was published as a final document January 2011. NREL staff acted as a principal member of the NFPA Hydrogen Technology Technical Committee and acted as task group leader with the planning task group that will produce the 2014 edition *NFPA 2 Hydrogen Technologies Code*.
- Sensor Laboratory: NREL conducted a Sensor Workshop in June 2011. The final report from the workshop was published in 2012 and it defines sensor needs including the need for auto-calibration to decrease maintenance costs.
- Component testing: Compressed natural gas (CNG) nozzle failure study that was initiated in 2011 was completed in 2012. The report describes potential

problems and solutions to CNG nozzle failures that could be applied to hydrogen nozzles.

- Fuel quality specification: Continued to support the promulgation of ASTM International standards required to test contaminants to show compliance with the ISO standard through funding the production of calibration gases required to verify the ASTM test methods. Additionally, NREL supported the work of Michael Steele, Chairman of the SAE Fuel Cells technical Committee that has produced the final SAE J2719 standard.
- Codes and standards coordination: NREL continued to support the coordination of codes and standards development through software that identified the SDOs and CDOs involved in hydrogen and fuel cell technologies codes and standards development. NREL has updated this software to include current project information. This software is shown in Figure 2.
- Subcontract Management: NREL assumed responsibility for several additional subcontracts. NREL staff developed new statements of work for these subcontracts that reflected DOE priorities and budget constraints. NREL has in 2012 developed subcontract tracking process that shows the progress made under each subcontract and the funding status.



Introduction

It is essential to develop and promulgate codes and standards in order to provide for the safe use of hydrogen and fuel cell technologies. With the help of key stakeholders, the DOE Fuel Cell Technologies (FCT) Program and NREL are coordinating a collaborative national effort to prepare, review, and promulgate codes and standards for all hydrogen and fuel cell technologies.

Approach

The FCT Program recognizes that domestic and international codes and standards must be established to enable the timely commercialization and safe use of hydrogen and fuel cell technologies. The lack of codes and standards applicable to hydrogen and fuel cell technologies is an institutional barrier to deploying these technologies. It is in the national interest to eliminate this potential barrier. As such, the sub-program works with domestic and international SDOs to facilitate the development of performance-based and prescriptive codes and standards. These standards are then referenced by building and other codes to expedite regulatory approval of hydrogen and fuel cell technologies. This approach ensures that U.S. consumers can purchase products that are safe and reliable, regardless of their country of

TABLE 1. Progress towards Meeting Technical Targets for Safety Codes and Standards

| DOE Accomplishments in Support of the Development of Regulations, Codes and Standards for the Deployment of Hydrogen and Fuel Cell Technologies | | | |
|--|--|---|--|
| Regulation, Code, or Standard | NREL Support | Status | Time Saved Producing Document (resulting from DOE support) |
| 1. Global Technical Regulation (GTR) for fuel cell vehicles | Tank testing data, SAE International standard that provided basis for document, expert technical support from Dr. Sloane and Glenn Scheffler | Phase 1 work complete in 2011 | 5 years |
| 2. NFPA 2 Hydrogen Technologies Code 2011 edition | Extensive technical analysis to develop Risk informed requirements for siting hydrogen storage systems. Extensive logistical support including support committee chair and consultant producing draft code document | Final document promulgated 2011 | 3 years |
| NFPA 2 Hydrogen Technologies Code 2014 edition | Extensive support of NFPA 2 task groups including task groups that address fueling and vehicle infrastructure | Final document to be issued 2014 | 1 year |
| 3. International Fire Code (IFC) Section 2209 Hydrogen Motor-Fuel Dispensing and Generation Facilities | Supported Hydrogen Ad Hoc Working Group that wrote section 2209 | Final document promulgated 2003 | 6 years |
| 4. SAE J2579 Technical Information Report for Fuel Systems in Fuel Cell and Other Hydrogen Vehicles The Fuel Cell Standards Committee has the next edition of J2579 listed as a Work in Progress | Performed validation testing through subcontractor. Provided logistical support for SAE Fuel Cell Technical Committee NREL supports this project through committee participation | Technical Information Report published 2009 | 3 years |
| 5. SAE J2601 Fueling Protocols for Light Duty Gaseous Hydrogen Surface Vehicles The Fuel Cell Standards Committee is actively working on revising this document to incorporate the latest information vehicle fueling protocols | Performed validation testing for fueling algorithm in standard. Provided logistical support for SAE Fuel Cell Standards Technical Committee NREL supports this project through committee participation | Standard published 2010 | 3 years |
| 6. International Organization for Standardization (ISO) 14687 Hydrogen fuel -- Product specification -- Part 2: Proton exchange membrane (PEM) fuel cell applications for road vehicles/SAE J2719 Development of a Hydrogen Quality Guideline for Fuel Cell Vehicles | Extensive test data, logistical support, and coordination of ISO/SAE standard development activities. | SAE J2719 issued as final document in 2011 and ISO 14687 achieved final vote stage in 2011. | 5 years |
| 7. CSA Standards H series of component standards for hydrogen dispensing operations and onboard vehicle safety | Extensive logistical support as well as validation testing of Hydrogen pressure relief device standard | | 6 years |
| 8. ASME B31.12 Hydrogen Piping and Pipelines | Provided test data and logistical support. | Final document 2008 | 3 years |
| 9. Compressed Gas Association Hydrogen Documents including G-5 through G5-8 | Provided logistical support | Documents issued 2004 through 2007 | 3 years |

origin, and that U.S. companies can compete internationally by having coordinated consistent requirements.

Results

The Safety Codes and Standards work is divided into three major areas:

- Codes and Standards Coordination
- Codes and Standards Research
- Codes and Standards Training and Outreach

This report addresses the Codes and Standards Coordination work.

Codes and Standards Coordination

Figure 1, Hierarchy of Codes and Standards Implementation, shows both the hierarchy for enforcing codes and standards and some of the progress made in promulgating the codes and standards required to implement hydrogen and fuel cell technologies. Figure 2 shows the front page of the coordinating software NREL has developed to track codes and standards development activities.

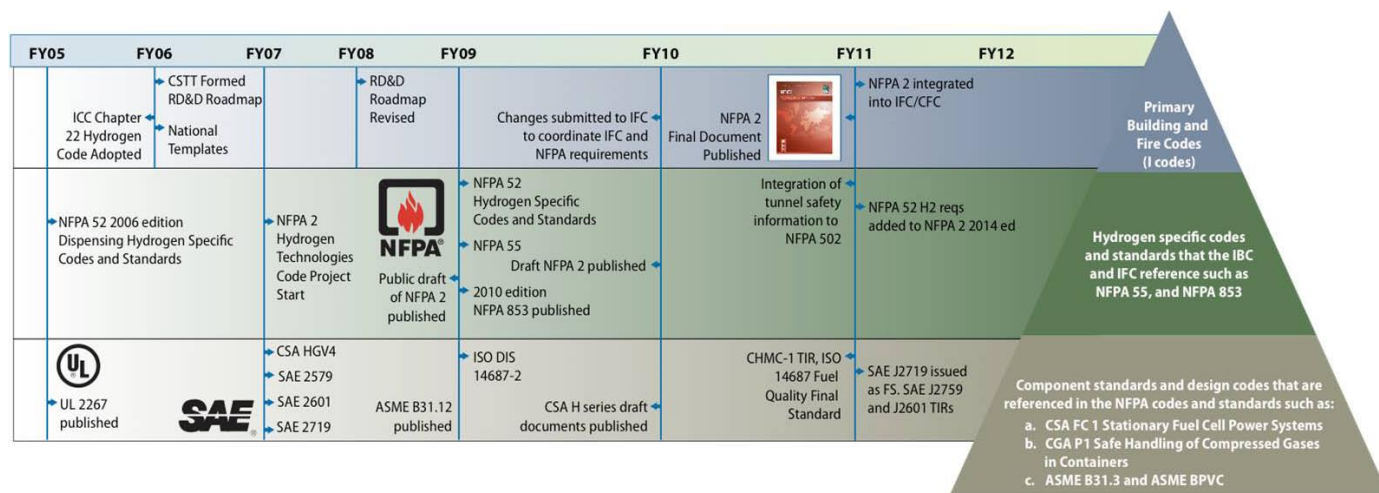


FIGURE 1. Hierarchy of Codes and Standards Implementation

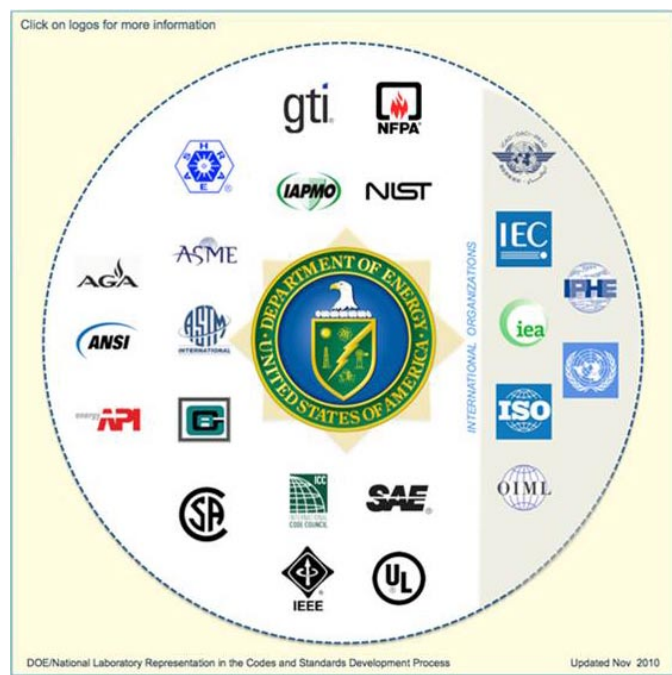


FIGURE 2. NREL Codes and Standards Coordinating Software

In FY 2012 good progress was made in this implementation effort. NFPA 2 Hydrogen Technologies Code was published as final document in January 2011. NREL is working on coordinating the requirements of NFPA 2 with the hydrogen requirements in the IFC through a proposal to reference NFPA 2 in the 2015 edition of the IFC. NREL supported the development of NFPA 2 in several ways including:

- Principal membership of the technical committee
- Funding subcontractors actively participating in the development of the document such as FP2 Fire Protection Engineering

- Reviewed status of key infrastructure that could restrict the deployment of hydrogen fuel cell vehicles such as tunnels and public parking garages

Another key codes and standards development area is the development of hydrogen fueling station component and system standards being performed by Canadian Standards Association (CSA) Standards. These H-4 series of documents consists of nine component standards and one system standard that address hydrogen dispensing. An NREL staff member participated as a member of the CSA technical committee drafting these documents. Several of these standards were issued as final documents in 2012.

NREL supported the Fuel Cell and Hydrogen Energy Codes and Standards Coordinating Committee. This effort, which is coordinated and directed by NREL, held monthly meetings where SDOs, DOE laboratories, industry representatives, DOE and other interested parties are given topical information on codes and standards development activities. In the first quarter of 2012 NREL ran and administered all aspects of this task.

NREL also supported the Hydrogen Industry Panel on Codes which has as its primary objective the coordination of hydrogen safety requirements in the IFC and other key International Code Council codes such as the International Building Code and the NFPA hydrogen safety requirements that reside primarily in NFPA 2. In May 2012 Hydrogen Industry Panel on Codes successfully concluded their key work in coordinating the IFC and NFPA codes. They voted to end the Hydrogen Industry Panel on Codes organization. This action reflects the progress made in hydrogen technologies code development.

NREL supported both the development of fuel quality standards through acquiring test data and coordinating the activities of the ISO Technical Committee 197 and the SAE

Fuel Cell Technical Committee. These efforts resulted in the promulgation of SAE J2719 Hydrogen Fuel Quality for Fuel Cell Vehicles.

Conclusions and Future Direction

NREL will continue to support the development of codes and standards by:

- Working with DOE to implement a plan for identifying and supporting the development of the codes and standards required to deploy hydrogen and fuel cell technologies with a particular emphasis on road vehicles by the year 2020 (the 2020 Deployment Plan).
- Continuing research and development at the NREL Sensor Laboratory to support the development of sensors required to deploy hydrogen and fuel cell technologies.
- Developing a plan to address hydrogen dispensing component safety issues, performing work to address these issues, and making codes and standards proposals to address any codes and standards issues associated with component safety.

- Managing subcontracts required to support the 2020 Deployment Plan.
- Performing outreach work to distribute information on hydrogen and fuel cell technologies to code officials, project developers, and other interested parties.
- Coordinating Domestic codes and standards and International standards to ensure consistent requirements.

FY 2012 Publications/Presentations

1. Codes and Standards Requirements for Deployment of Emerging Fuel Cell Technologies. R. Burgess, W. Buttner, C. Rivkin 2011. NREL Technical Report TP-5600-52641.

VIII.7 Codes and Standards Outreach for Emerging Fuel Cell Technologies

Carl Rivkin, (Primary Contact), Chad Blake,
Robert Burgess, William Buttner, and Matthew Post
National Renewable Energy Laboratory
1617 Cole Boulevard
Golden, CO 80401
Phone: (303) 275-3839
Email: carl.rivkin@nrel.gov

DOE Manager
HQ: Antonio Ruiz
Phone: (202) 586-0729
Email: Antonio.Ruiz@ee.doe.gov

Subcontractor:
MorEvents, Englewood, CO

Project Start Date: 1995
Project End Date: Project continuation and direction
determined annually by DOE

Fiscal Year (FY) 2012 Objectives

- Facilitate the safe deployment of hydrogen and fuel cell technologies.
- Provide information on hydrogen and fuel cell technologies codes and standards to code officials, project developers, and other interested parties.
- Present workshops and other outreach activities such as webinars on hydrogen and fuel cell technologies codes and standards to code officials, project developers, and other interested parties in geographic areas where these technologies are being deployed.
- Develop tools to streamline the permitting process for fuel cell and hydrogen technology projects.
- Perform site visits to fuel cell and hydrogen technology project sites to obtain safety, codes and standards information for publication in technical reports and incorporation into codes and standards.
- Present safety, codes and standards information on DOE websites and through webinars.

Technical Barriers

This project addresses the following technical barriers from section 3.7 of the Fuel Cell Technologies Program's Multi-Year Research, Development and Demonstration Plan:

- (D) **Large Number of Local Government Jurisdictions (approximately 44,000).**

The large number of jurisdictions hinders the universal adoption of codes and standards.

- (E) **Lack of Consistency in Training of Officials**

The training of code officials is not mandated and varies significantly. The large number of jurisdictions leads to variation in training facilities and requirements.

- (F) **Limited DOE Role in the Development of International Standards**

Governments can participate and influence the development of codes and standards, but they cannot direct the development of international standards.

- (G) **Inadequate Representation at International Forums**

Participation in international forums and meetings is voluntary and, to date has been limited by budgetary constraints.

- (H) **International Competitiveness**

Economic competition complicates the development of international standards.

- (I) **Conflicts between Domestic and International Standards**

National positions can complicate the harmonization of domestic and international standards.

- (J) **Lack of National Consensus on Codes and Standards**

Competitive issues hinder consensus.

Technical Targets

Table 1 shows the NREL support for achieving DOE technical targets, specifically supporting the development of the codes and standards required to deploy hydrogen and fuel cell technologies. This technical target is described on page 3.7-1 and 2 of the Codes and Standards – Technical Plan.

FY 2012 Accomplishments

NREL accomplished the following in support of section 3.7 of the DOE Fuel Cell Technologies Program's Multi-Year Research, Development and Demonstration Plan:

- **Sensor Workshop:** Issuance of NREL Technical Report summarizing 2011 Sensor Workshop. NREL conducted a Sensor Workshop in June 2011. The purpose of the workshop was to review the performance benchmarks set at the 2007 DOE Sensor Workshop and refine them based on defining performance criteria for specific applications. These applications include indoor hydrogen fueling, hydrogen storage, and residential fuel cells and fuel dispensing.
- **Support of Hydrogen Fuel Cell Vehicle Deployment in California:** NREL has actively participated on the

TABLE 1. Progress towards Meeting Technical Targets for Safety Codes and Standards

| DOE/NREL Project Work Areas Supporting the Development of Regulations, Codes and Standards (RCS) for the Deployment of Hydrogen and Fuel Cell Technologies Outreach Activities | | |
|--|--|--|
| Activity | Primary Impacted Groups | Progress Towards Meeting DOE Targets |
| Safety Codes and Standards Workshops | Code officials, project developers, and other interested parties | Workshops make information available to expedite process for developing and permitting fuel cell and hydrogen technology projects. NREL has moved from larger workshop to a more targeted approach in FY 2012. |
| Sensor Workshop and Webinars | Sensor developers, project managers, | Improve performance of sensors to increase project safety |
| Updating codes and standards citations on DOE websites | Code officials, project developers, and other interested parties | Web information make information available to expedite process for developing and permitting fuel cell and hydrogen technology projects |
| Permitting template for hydrogen dispensing stations | Code officials and project developers | Standardized permitting will streamline permitting for fuel cell and hydrogen technology projects |
| Hydrogen dispensing station site visit and technical report | Project developers | Improve fuel cell and hydrogen codes and standards by identifying safety issues that can be addressed by codes and standards modifications |

California Fuel Cell Partnership Station Implementation team Working Group.

- Codes and Standards Workshops: NREL conducted a Codes and Standards workshop on October 26, 2011 in collaboration with the Society of Automotive Engineers. NREL has also met directly with code officials in areas where key projects are to be located such as Santa Monica, CA.
- Permit Template for Hydrogen Dispensing Stations. NREL developed a California specific permitting template for hydrogen dispensing stations that contains the basic codes and standards requirements as well as California specific requirements such as the California Risk Management plan requirements.
- Hydrogen Dispensing Station Site Visit. NREL performed a site visit to a hydrogen dispensing station (AC Transit facility located in Emeryville, CA) to evaluate code compliance and safety issues. The results of the visit will be used in evaluating the hydrogen dispensing system component safety issues.

- Support of Stationary Fuel Cell Deployment. NREL developed a fact sheet summarizing the requirements for siting stationary fuel cells and the associated hydrogen storage systems required to power the fuel cell.
- NREL webinars and other information outreach. NREL has conducted webinars and other information outreach to share information on sensors for deployment of hydrogen and fuel cell technologies.



Introduction

It is essential to develop and promulgate codes and standards in order to provide for the safe use of hydrogen and fuel cell technologies. With the help of key stakeholders, the DOE Fuel Cell Technologies Program and NREL are coordinating a collaborative national effort to prepare, review, and promulgate codes and standards for all hydrogen and fuel cell technologies. To complement this codes and standards development effort, NREL is conducting outreach activities to inform code officials, project developers, and other interested parties of these codes and standards requirements.

Approach

Domestic and international codes and standards must be established to enable the timely commercialization and safe use of hydrogen and fuel cell technologies. The lack of codes and standards applicable to hydrogen and fuel cell technologies is an institutional barrier to deploying these technologies. It is in the national interest to eliminate this potential barrier. As such, the sub-program works with domestic and international standards development organizations to facilitate the development of performance-based and prescriptive codes and standards. These standards are then referenced by building and other codes to expedite regulatory approval of hydrogen and fuel cell technologies. This approach ensures that U.S. consumers can purchase products that are safe and reliable, regardless of their country of origin, and that U.S. companies can compete internationally by having coordinated consistent requirements.

Results

The Safety Codes and Standards work is divided into three major areas:

- Codes and Standards Coordination
- Codes and Standards Research
- Codes and Standards Training and Outreach

This report addresses the Outreach activities.

Codes and Standards Outreach

In FY 2012 NREL continued outreach work in both in-person workshops, site visits, in-person meetings with code officials and project developers, and permitting tool development. These activities consisted of the following:

- Codes and Standards Workshop presented October 26, 2011 in collaboration with the Society of Automotive Engineers.
- Sensor Workshop report issued as NREL technical report July, 2012.
- California Environmental Quality Act summary document.
- Codes and Standards citations were updated for the DOE website.
- Codes and Standards permit template for hydrogen fueling stations completed (shown in Figure 1).



Regulations, Codes, and Standards (RCS) Template for Hydrogen Dispensing Stations To be Located in California

April 2012

Background and Purpose

Building hydrogen dispensing stations for hydrogen fuel cell vehicles is a critical piece of the infrastructure required to support the deployment of hydrogen fuel cell vehicles on a commercial scale. There are fewer than one hundred hydrogen dispensing stations in the US as of April 2012 and all of these stations are prototype or developmental stations. They are dissimilar to the common commercial gasoline retail dispensing stations that often contain convenience stores and other products sales such as propane as well as multiple dispensers and multiple dispenser islands. They also differ from existing retail station in the relatively low number of vehicles they fuel.

The US Department of Energy (DOE) Office of Energy Efficiency and Renewable Energy (EERE) Fuel Cell Technology Safety, Codes and Standards (SCS) Project has as one of its objectives the accelerated deployment of hydrogen and fuel cell technologies. To achieve this objective The National Renewable Energy Laboratory (NREL) through direction and funding from EERE has developed a template for a commercial hydrogen dispensing station to streamline the project development and permitting process for widespread deployment of hydrogen dispensing stations.

This template will define a hydrogen dispensing station regulatory requirements that more closely approximates a commercial hydrogen station than the prototype or developmental stations that account for most of the station projects.

FIGURE 1. NREL Template for California Hydrogen Dispensing Stations, CA

Conclusions and Future Direction

NREL will continue to support outreach activities associated with the development and deployment of codes and standards by:

- Working with DOE to implement the DOE 2020 Deployment Plan for Hydrogen Fuel Cell Vehicles (the 2020 Deployment Plan).
- Performing outreach work to distribute information on hydrogen and fuel cell technologies to code officials, project developers, and other interested parties using in-person meetings, site visits, webinars, and other effective venues for distributing information.
- Collecting information from outreach activities to help identify gaps in codes and standards and research and testing projects that could fill these gaps.
- Performing site visits at fuel cell and hydrogen technology project sites to collect information to assist in the code development process and project permitting process.
- Developing information tools such as technical summary documents for code officials and project developers.

FY 2012 Publications/Presentations

1. Codes and Standards Workshop October 27, 2011 Troy, MI.
2. NREL Technical Report on Sensor Workshop held June 8, 2011 Rosemont, IL (report issued July 2012).

VIII.8 Leak Detection and H₂ Sensor Development for Hydrogen Applications

Eric L. Brosha¹ (Primary Contact), Fernando H. Garzon¹, Robert S. Glass², Cortney Kreller¹, Rangachary Mukundan¹, Catherine G. Padro¹, and Leta Woo²

¹Los Alamos National Laboratory (LANL)
MS D429, P.O. Box 1663
Los Alamos, NM 87545
Phone: (505) 665 4008
Email: Brosha@lanl.gov

²Lawrence Livermore National Laboratory (LLNL)

DOE Manager

HQ: Antonio Ruiz
Phone: (202) 586-0729
Email: Antonio.Ruiz@ee.doe.gov

Project Start Date: Fiscal Year (FY) 2008

Project End Date: FY 2014

- Sensitivity: 1-4 vol% range in air
- Accuracy: $\pm 1\%$ full scale in the range of 0.04-4 vol%
- Response Time: <1 min at 1% and <1 sec at 4%; recovery <1 min
- Temperature operating range: -40°C to 60°C
- Durability: minimal calibration or no calibration required for over sensor lifetime (as defined by particular application)
- Cross-Sensitivity: minimal interference to humidity, H₂S, CH₄, CO, and volatile organic carbons

FY 2012 Accomplishments

- Designed, built, and tested high-impedance buffer (HIB) circuit boards to isolate sensor element from outside voltage and current influences; added baseline offset and gain control.
- Tested more advanced sensor substrates incorporating onboard temperature control and completed initial calibration procedures for advanced prototypes.
- Designed, built, and tested sensor power supply and heater control electronics.
- Made additional refinements to effective packaging scheme adopted for advanced prototypes.
- Fabrication of multiple advanced prototype devices with HIB circuits for Round 2 of National Renewable Energy Laboratory (NREL) testing; six devices prepared with high level of reproducibility.
- Conducted Round 2 NREL testing. Results of Round 2 successful: isolation electronics developed in FY 2012 successfully resolved issues identified in Round 1 FY 2011 NREL testing. Sensor protected from leakage currents present in data acquisition electronics; baseline and hydrogen response nominal with minimal humidity interference and response to variations in barometric pressure, exceptional low-level H₂ sensitivity, high signal-to-noise, and minimal influence from methane, ammonia, carbon dioxide, and carbon monoxide.

FY 2012 Objectives

- Develop a low-cost, low-power, durable, and reliable hydrogen safety sensor for a wide range of vehicle and infrastructure applications.
- Continually advance test prototypes guided by materials selection, sensor design, electrochemical research and development (R&D) investigation, fabrication, and rigorous life testing.
- Disseminate packaged sensor prototypes and control systems to DOE laboratories and commercial parties interested in testing and fielding advanced prototypes for cross-validation.
- Evaluate manufacturing approaches for commercialization.
- Engage an industrial partner and execute technology transfer.

This project addresses the following technical barriers from the Hydrogen Safety section (3.8) of the Fuel Cell Technologies Program Multi-Year Research, Development and Demonstration Plan:

- (A) Limited Historical Database
- (F) Safety is Not Always Treated as a Continuous Process

Technical Targets

Technical targets vary depending on the application [1,2], but in general include:



Introduction

Recent developments in the search for sustainable and renewable energy coupled with the advancements in fuel cell-powered vehicles have augmented the demand for hydrogen safety sensors [2]. There are several sensor technologies that have been developed to detect hydrogen, including deployed systems to detect leaks in manned space systems and hydrogen safety sensors for laboratory and industrial usage.

Among the several sensing methods electrochemical devices [3-9] that utilize high temperature-based ceramic electrolytes are largely unaffected by changes in humidity and are more resilient to electrode or electrolyte poisoning. The desired sensing technique should meet a detection threshold of 1% (10,000 ppm) H₂ and response time of ≤1 min [10], which is a target for infrastructure and vehicular uses. Further, a review of electrochemical hydrogen sensors by Korotcenkov *et.al* [11] and the report by Glass and others [10,12] suggest the need for inexpensive, low power, and compact sensors with long-term stability, minimal cross-sensitivity, and fast response. This view has been largely validated and supported by the fuel cell and hydrogen infrastructure industries by the NREL/DOE Hydrogen Sensor Workshop held on June 8, 2011 [13]. Many of the issues preventing widespread adoption of best-available hydrogen sensing technologies available today outside of cost, derive from excessive false positives and false negatives arising from signal drift and unstable sensor baseline; both of these problems necessitate the need for unacceptable frequent calibration [13].

As part of the Hydrogen Codes and Standards sub-program, LANL and LLNL are working together to develop and test inexpensive, zirconia-based, electrochemical (mixed potential) sensors for H₂ detection in air. Previous work conducted at LLNL showed [9] that indium tin oxide (ITO) electrodes produced a stable mixed potential response in the presence of up to 5% of H₂ in air with very low response to CO₂ and water vapor. The sensor also showed desirable characteristics with respect to response time and resistance to aging, and degradation due to thermal cycling.

In this investigation, the development and testing of an electrochemical hydrogen (H₂) sensor prototype based on 'ITO/yttria-stabilized zirconia (YSZ)/platinum (Pt)' configuration is detailed. The device fabricated using commercial ceramic sensor manufacturing methods on an alumina substrate with an integrated Pt resistance heater to achieve precise control of operating temperature while minimizing heterogeneous catalysis and loss of hydrogen sensitivity. Targeting fuel cell-powered automotive applications, the safety sensor was subjected to interference studies, temperature cycling, operating temperature variations, and long-term testing now exceeding over 6,000 hrs for some sensor configurations. In FY 2012, the mixed potential electrochemical technology was independently validated at the hydrogen safety sensor-testing lab at NREL; two packaged pre-commercial prototypes were tested against a standard testing protocol including sensor resistance to cross-interferences such as CO, CO₂, CH₄, and NH₃. In general, NREL testing showed a fast response to H₂ with exceptional low-level sensitivity and high signal-to-noise, very little deviation in sensor response to changes in ambient conditions such as humidity and barometric pressure, and minimal response to some common interference gases.

The salient features of the H₂ sensor prototype developed by LANL and LLNL are (a) low power consumption, (b) compactness to fit into critical areas for some applications, (c) simple operation, (d) fast response, (e) a direct voltage read-out circumventing the need for complicated signal processing, and (f) a low cost sensor platform conducive to commercialization using common ceramic manufacturing methods.

Approach

Two alternative sensor measurement approaches were used to develop devices with superior performance.

Controlled Electrode\Electrolyte\Gas Interface for Potentiometric Sensors

In the first approach, electrochemical potentiometric modality is utilized for designing the sensors. Mixed potential sensors are a class of electrochemical devices that develop an open-circuit electromotive force due to the difference in the kinetics of the redox reactions of various gaseous species at each electrode/electrolyte/gas interface, referred to as the triple phase boundary [14]. Therefore these sensors have been considered for the sensing of various reducible or oxidizable gas species in the presence of oxygen. Based on this principle, a unique sensor design was developed. The uniqueness these sensors, originally developed at LANL [15], derive from minimizing heterogeneous catalysis (detrimental to sensor response) by avoiding gas diffusion through a catalytically active material and minimizing diffusion path to the 3-phase interface (electrode/electrolyte/gas referred to as triple phase boundary). Unlike the conventional design of these devices that use a dense solid electrolyte and porous thin film electrodes (similar to the current state-of-the-art zirconia-based sensors and fuel cells), this design uses dense (either metal wires, oxide pellets or thin film) electrodes and porous electrolytes (bulk or thin film). Such a sensor design facilitates a stable and reproducible device response, since dense electrode morphologies are easy to reproduce and are significantly more stable than the conventional porous morphologies. Moreover, these sensors develop higher mixed potentials since the gas diffusion is through the less catalytically active electrolyte than the electrode. Further, the choice of electrodes is primarily based on their O₂ reduction kinetics. Sensors will typically involve one electrode with fast (Pt) and another with slow (Au or LaCrO₃) O₂ reduction kinetics aimed at improving the sensitivity.

Impedance Metric

In the second design, a new impedance-based measurement technique, originally developed at LLNL for electrochemical oxides of nitrogen (NO_x) sensors, was shown

to generate more stable sensor responses and may be able to offer a way to compensate for cross-sensitivity effects. The technique is based on the measurement of parameters related to the complex impedance of the sensor in the frequency range of 1 Hz to 10 kHz. Measurements are typically made at a single frequency selected to maximize the desired sensitivity, although measurements performed at additional frequencies have been shown to be useful for correcting the response to interfering gases. It has been found in the NO_x sensor studies that it may be possible to use a wider variety of electrodes for the sensor in impedance-based sensing. Additional possible advantages included better tolerance to mechanical defects (such as delamination) and better longer-term stability.

Results

(a) Development of high impedance buffer board and testing with pre-commercial prototype

FY 2011 testing at NREL uncovered an unanticipated interaction of the sensor element with the data acquisition system used in the hydrogen sensor testing system. The first sensor testing and validation experiments showed data with an anomalously high baseline (when no H_2 was present) and poor sensitivity to H_2 (when H_2 was present). These behaviors were never seen in LANL or LLNL laboratory sensor development work and could only be explained if there was insufficient input impedance on the data acquisition

system. As a result, an HIB circuit board was designed and built to isolate the naked electrochemical sensor from stray electric currents that would generate a high baseline voltage which, depending on the direction of the current flow, would induce an offset voltage that would reduce the sensor voltage generated in response to H_2 exposure. The HIB is designed around a Burr Brown INA116 electrometer amplifier integrated circuit and is designed to minimize leakage between the electrodes, and from the sensor itself to the electrometer circuit. The circuit was designed with built in offset and span adjustment. Figure 1 shows that implementation of the HIB board did not appreciably alter the characteristics of the sensor response when using a laboratory Keithley 2400 source-meter, which employ very high input impedance measurement circuitry, to record voltage vs. time.

(b) Transfer of packaged, pre-commercial H_2 safety sensors to NREL for Round 2 testing

Multiple packaged advanced prototype sensors and two sets of HIB boards were prepared and used for Round 2 testing at the NREL sensor evaluation facility. In the first experiment, one of the sensors was placed into the NREL test chamber and connected directly to the data acquisition system and a simple on/off response to 2% H_2 was performed in air. The unusual and undesirable response characteristics reported in FY 2011 were immediately reproduced (bottom curve in Figure 2a). The HIB board was then connected to this sensor and placed alongside the sensor element within

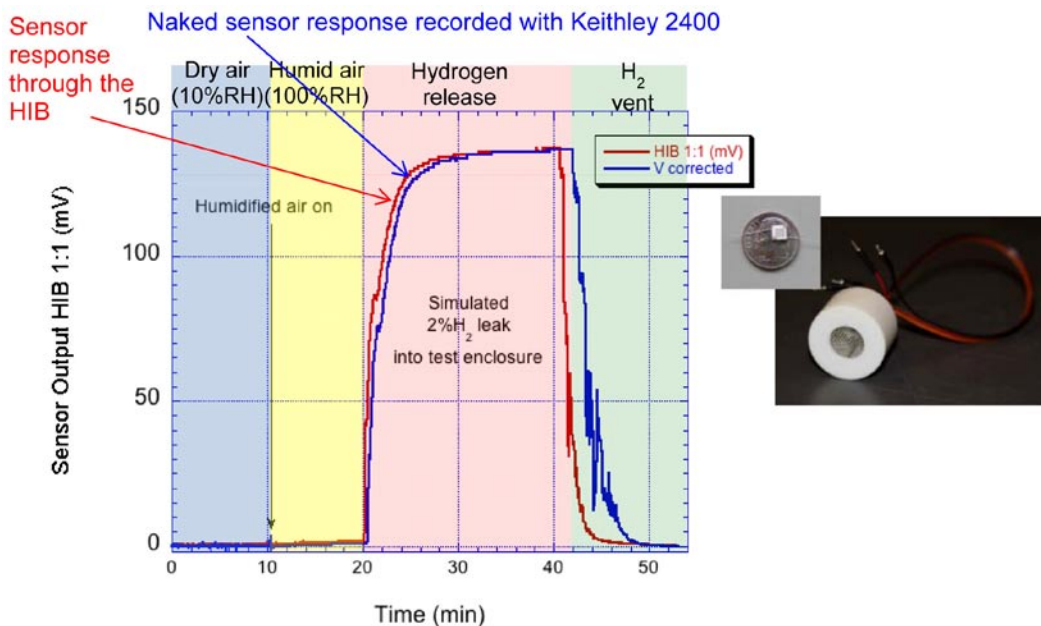


FIGURE 1. Testing of LANL/LLNL mixed-potential, electrochemical H_2 safety sensor with HIB board. Results show that the HIB isolates the electrochemical sensor from the measuring electronics without appreciably altering the response characteristics of the device. A photograph of the packaged prototype and naked sensor element is shown in the inset.

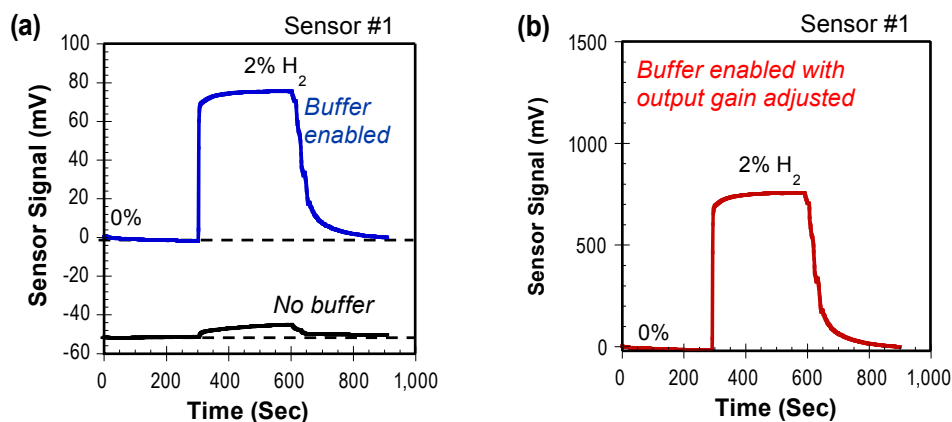


FIGURE 2. Data obtained at NREL of the mixed potential sensor performance of the packaged LANL/LLNL ITO/YSZ/Pt advanced prototype showing (a) use of HIB board to remove an anomalous baseline and recover sensitivity and (b) use of HIB board to magnify the output gain. The data in (a) clearly show the magnitude of the influence that the external data acquisition circuitry can impart on the measured sensor response.

the test chamber. A second H₂ sensor and HIB board was installed into the test chamber so that response data could be obtained from two devices simultaneously throughout the testing. The implementation of the isolation electronics immediately resolved the anomalous behavior and proves that the anomalous results obtained in Round 1 testing were introduced by undesirable influences imparted on the sensor from the NREL data acquisition system (Figure 2a).

The gain on the HIB board was increased to amplify the signal from the device (Figure 2b). The large voltage signal produced by the sensor, high signal-to-noise, and fast response time are both very desirable qualities that will be easily exploited during subsequent stages of development and ultimate commercialization.

(c) Validation testing of the packaged LANL/LLNL pre-commercial prototype sensor and HIB electronics using NREL protocols: Round 2

Given the exception high H₂ sensitivity that the LANL/LLNL electrochemical devices exhibited, the standard NREL protocol to test device response and reproducibility to H₂ in air was modified. H₂ levels at 0.05%, 0.1%, and 0.5% were also tested, in addition to the standard NREL testing protocol using 0.2%, 1%, and 2% H₂ concentrations. While the overall results have been summarized in the FY 2012 Accomplishments section above, one particular test – effect of relative humidity (RH) changes – is highlighted below. The effects of changes in RH can have a dramatic effect on rates of false positives; for example, metal oxide-based semiconducting explosimeter sensors will easily trigger a false positive response to the moisture in human breath.

Two LANL/LLNL H₂ sensors were placed into the NREL H₂ sensor test chamber and were subsequently tested using the standard NREL protocols used for other H₂ sensor

technologies [1]. Standard tests included: H₂ sensitivity, H₂ response reproducibility, humidity response, effects of changes in ambient conditions such as temperature and barometric pressure, effect of likely interference gases such as CO₂, CO, ammonia, and methane, and an extreme anaerobic durability test where the sensor is subjected to hours of operation in pure H₂. Figure 3 is an example of how well the LANL/LLNL H₂ safety sensor responded to a comprehensive NREL humidity test. The lack of intrinsic response to changes in humidity for the prototype sensors was shown in Figure 1. In this quick test of the sensor/HIB boards, the air base gas was switched from very dry 10% water content to a humidified air stream (100% RH at 25°C). The data in Figure 1 show no change in sensor baseline despite the abrupt change in RH. Figures 3a and 3b show the mixed potential sensor performance in more rigorous RH testing, with two sensors (Sensor #1 and Sensor #2) tested side-by-side in the NREL test stand using separate HIB boards with the output gain adjusted. To monitor system environmental variability from nominal set parameters, a humidity sensor and thermocouple continuously monitored water and temperature in the chamber (Figures 3c and 3d). In Figures 3a and 3b, the mixed potential sensors show good and reproducible response to hydrogen in the concentration range of 0.01-1% in both dry conditions and in the presence of water up to 2%.

In follow-on, Round 3 testing, emphasis will be placed expanding the tests to include additional interference gases, including those that are potentially corrosive in nature.

Conclusions

- All FY 2012 milestones were completed this year.
- A viable H₂ safety sensor technology has been developed on an advanced sensor platform that continues to

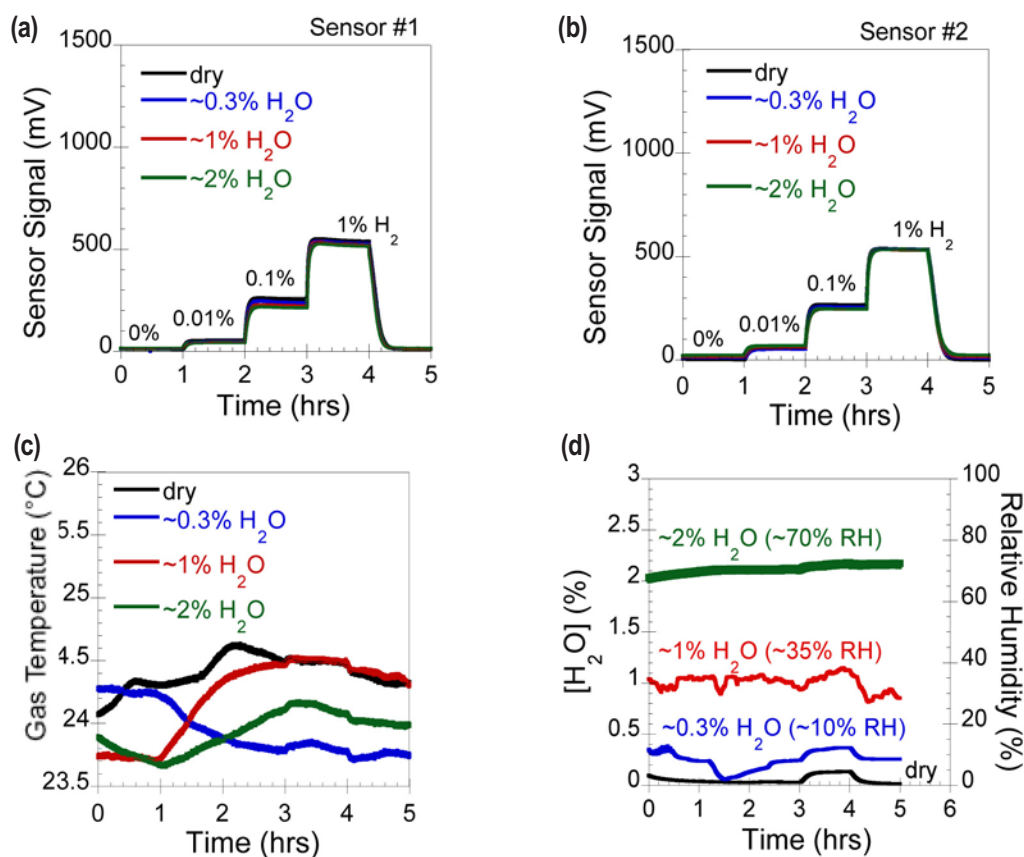


FIGURE 3. Mixed potential sensor performance of packaged LANL/LLNL ITO/YSZ/Pt advanced prototype, (a) Sensor #1 and (b) Sensor #2, with corresponding (c) gas temperature and (d) water concentration measurements under dry conditions and in the presence of ~0.3, ~1, and ~2% water.

improve. An advanced H₂ sensor prototype was fabricated on an alumina substrate with ITO and Pt electrodes and YSZ electrolyte with an integrated Pt heater to achieve precise operating temperature and minimize heterogeneous catalysis.

- Multiple sensors were prepared and packaged that exhibited excellent response and device-to-device reproducibility.
- Sensors and electronic packages were prepared and underwent cross-validation Round 2 testing at the NREL sensor test facility.
- Anomalous sensor behavior observed in Round 1 NREL testing in FY 2011 was reproduced and attributed to the presence of stray leakage currents in the data acquisition system, which introduced an undesired voltage between the sensor electrodes. HIB board electronics were designed, constructed, and tested in FY 2012, and they effectively eliminated these anomalies.
- NREL Round 2 testing show excellent sensitivity to H₂, reproducible device response with high signal-to-noise, minimal interferences to changes in relative humidity

and barometric pressure, and good rejection of potential interference gases CO₂, CO, NH₃, and CH₄.

Future Directions

- Assemble complete sensor systems for field trial experiments in fuel cell laboratories and refueling facilities (e.g. power supply, HIB board, wireless internet protocol transmission of sensor signal, and data recording, display, and alerting algorithms).
- Identify commercialization partners and plan for a path forward.
- Improve power supply electronics to use single input control point.
- Reduce size and power consumption of the sensor element.
- Work with NREL partners to develop testing protocols for mixed potential type, electrochemical gas sensors.
- Provide new sensors and optimized electronics for Round 3 testing at NREL.

Collaboration and Coordination with Other Institutions

- Los Alamos National Laboratory
- Lawrence Livermore National Laboratory
- National Renewable Energy Laboratory
- ESL ElectroScience, Inc.
- BJR Sensors, LLC.
- Custom Sensor Solutions, Inc.

FY 2012 Publications and Presentation

1. L.Y. Woo, R.S. Glass, E.L. Brosha, R. Mukundan, F.H. Garzon, W.J. Buttner, M.B. Post, C. Rivkin, and R. Burgess, "Humidity Tolerance of Electrochemical Hydrogen Safety Sensors Based on Yttria-Stabilized Zirconia (YSZ) and Tin-doped Indium Oxide (ITO)," submitted ECS Transactions, Summer 2012.
2. L.Y. Woo, R.S. Glass, E.L. Brosha, R. Mukundan, F.H. Garzon, W.J. Buttner, M.B. Post, C. Rivkin, and R. Burgess, "Humidity Tolerance of Electrochemical Hydrogen Safety Sensors Based on Yttria-Stabilized Zirconia (YSZ) and Tin-doped Indium Oxide (ITO)," 221st Meeting of the ECS, Seattle, WA May 9, 2012.
3. P.K. Sekhar, E.L. Brosha, R. Mukundan, H. Mekonen, B. Farber, C. Kreller, and F.H. Garzon, "Packaging and Testing of a Hydrogen Safety Sensor Prototype," in preparation summer 2012.
4. P.K. Sekhar and E.L. Brosha, "Electrochemical Gas Sensor based Detection and Discrimination of Trace Explosives and Energetic Materials," 221st Meeting of the ECS, Seattle, WA May 9, 2012.

References

1. W.J. Buttner, M.B. Post, R. Burgess, C. Rivkin, *Int. J. Hydrogen Energy*, **36**, 2462 (2011).
2. L. Boon-Brett, J. Bousek, G. Black, P. Moretto, P. Castello, T. Hübert, and U. Banach, Identifying performance gaps in hydrogen safety sensor technology for automotive and stationary applications, *International Journal of Hydrogen Energy*, **35** (2010), 373-384.
3. H. Iwahara, H. Uchida, K. Ogaki and H. Nagato, Nernstian Hydrogen Sensor Using BaCeO₃-Based, Proton-Conducting Ceramics Operative at 200-900^o C, *Journal of The Electrochemical Society*, **138** (1991), 295-299.
4. Y. Tan and T.C. Tan, Characteristics and Modeling of a Solid State Hydrogen Sensor, *The Journal of Electrochemical Society*, **141** (1994), 461-466.
5. Z. Samec, F. Opekar, and G.J.E.F. Crijns, Solid-state Hydrogen Sensor Based on a Solid-Polymer Electrolyte, *Electroanalysis*, **7** (1995), 1054-1058.
6. Y.-C. Liu, B.-J. Hwang, and I.J. Tzeng, Solid-State Amperometric Hydrogen Sensor Using Pt/C/Nafion Composite Electrodes Prepared by a Hot-Pressed Method, *Journal of The Electrochemical Society*, **149** (2002), H173-H178.
7. L.B. Kriksunov, and D.D. Macdonald, Amperometric hydrogen sensor for high-temperature water, *Sensors and Actuators B*, **32** (1996), 57-60.
8. G. Lu, N. Miura, and N. Yamazoe, High-temperature hydrogen sensor based on stabilized zirconia and a metal oxide electrode, *Sensors and Actuators B*, **35-36** (1996), 130-135.
9. L.P. Martin and R.S. Glass, Hydrogen Sensor Based on Yttria-Stabilized Zirconia Electrolyte and Tin-Doped Indium Oxide Electrode, *Journal of The Electrochemical Society*, **152** (2005), H43-H47.
10. R.S. Glass, J. Milliken, K. Howden, R. Sullivan (Eds.), *Sensor Needs and Requirements for Proton-Exchange Membrane Fuel Cell Systems and Direct-Injection Engines*, 2000, pp. 7 – 15. DOE, UCRL-ID-137767.
11. G. Korotcenkov, S.D. Han and J.R. Stetter, Review of Electrochemical Hydrogen Sensors, *Chemical Review*, **109** (2009), 1402-1433.
12. L.P. Martin and R.S. Glass, Electrochemical Sensors for PEMFC Vehicles, presented at The 2004 DOE Hydrogen, Fuel Cells, and Infrastructure Technologies Program Review, Philadelphia, PA (May 27, 2004).
13. NREL/DOE Hydrogen Sensor Workshop, June 8, 2011, Chicago IL. http://www.hydrogen.energy.gov/pdfs/progress11/viii_3_burgess_2011.pdf
14. F.H. Garzon, R. Mukundan, and E.L. Brosha, Solid state mixed potential gas sensors: theory, experiments and challenges, *Solid State Ionics*, **136-137** (2000), 633-638.
15. P.K. Sekhar, E.L. Brosha, R. Mukundan, M.A. Nelson and F.H. Garzon, Application of Commercial Automotive Sensor Manufacturing Methods for NO_x/NH₃ Mixed Potential Sensors for Emission Control, *ECS Transactions*. **19** (2009), 45-49.

VIII.9 Hydrogen Fuel Quality Research and Development

Tommy Rockward (Primary Contact), C. Quesada, K. Rau, E. Brosha, F. Garzon, R. Mukundan, and C. Padró

Los Alamos National Laboratory (LANL)
P.O. Box 1663
Los Alamos, NM 87545
Phone: (505) 667-9587
Email: trock@lanl.gov

DOE Manager
HQ: Antonio Ruiz
Phone: (202) 586-0729
Email: Antonio.Ruiz@ee.doe.gov

Project Start Date: October 1, 2011
Project End Date: September 30, 2015

- Milestone 26 - Revised (Society of Automotive Engineers/ISO) hydrogen quality guidelines adopted. (4Q, 2010)

FY 2012 Accomplishments

- Performed baseline tests with 2010 and 2015 DOE target platinum loadings for fuel cell anodes.
- Completed test to determine CO tolerance using 0.05 mg Pt/cm² anode loadings.
- Measured the impact of hydrogen sulfide and ammonia at the levels in the ISO hydrogen fuel specification in an operating fuel cell.
- Validated newly developed ASTM method using Fourier transform infrared (FTIR) to measure trace contaminants in hydrogen.



Fiscal Year (FY) 2012 Objectives

- Determine the allowable levels of hydrogen fuel contaminants in support of the development of science-based international standards for hydrogen fuel quality (International Organization for Standardization [ISO] TC197 WG-12).
- Validate the ASTM International test method for determining low levels of non-hydrogen constituents.

Technical Barriers

This project addresses the following technical barriers from the Hydrogen Codes and Standards section (3.7) of the Fuel Technologies Program Multi-Year Research, Development and Demonstration Plan:

- (F) Enabling National and International Markets Requires Consistent Regulations Codes and Standards
- (G) Insufficient Technical Data to Revise Standards

Contribution to Achievement of DOE Safety, Codes & Standards Milestones

This project will contribute to achievement of the following DOE milestones from the Codes and Standards sub-program section of the Fuel Cell Technologies Program Multi-Year Research, Development and Demonstration Plan:

- Milestone 21 - Completion of necessary codes and standards needed for the early commercialization and market entry of hydrogen energy technologies. (4Q, 2012)

Introduction

For the past six years, open discussions and/or meetings have been held and are still on-going with manufacturers, hydrogen suppliers, other test facilities from the north America team and international collaborators regarding experimental results, fuel clean-up cost, modeling, and analytical techniques to help determine levels of constituents for the development of an international standard for hydrogen fuel quality (ISO TC197 WG-12). Significant progress has been made. The process for the fuel standard is entering final stages as a result of the technical accomplishments.

Approach

Our approach utilizes our expertise in ultra-low impurity measurement and analysis for single-cell testing and methodology development for data collection and analysis. This work is in support of the development of consensus standards for fuel quality with the ISO TC197 WG-12 international team. We also provide technical feedback and guidance to collaborators on selection of materials, calibration techniques, test methods, and data analysis.

Results

In FY 2012, tests using a common membrane electrode assembly (MEA) containing 0.1/0.4 mg Pt/cm² at the anode and cathode, respectively were completed. These results while providing valuable insights for understanding mechanisms, are not in line with the DOE targets. The 2010 and 2015 target loadings have 0.05 mg Pt/cm² at the

anode. We identified a commercial supplier to provide us with samples at the target loadings. The initial tests results indicated that these low-loaded MEAs had durability and performance comparable to the common MEA and therefore further tests using these MEAs were initiated. The CO tolerance of the low-loaded anode varied with temperature as shown in Figure 1. At 80°C, the MEA could tolerate >100 ppb CO, while the tolerance was 75 ppb at 60°C and <500 ppb at 45°C. We also observed a lower tolerance limit for NH₃ and H₂S. The common MEA tolerated 4 ppb H₂S and 100 ppb NH₃ for 100 h with <1% (<7 mV decay) performance decay. At 100% relative humidity with an anode loading of 0.05 mg Pt/cm², there is an ≈11 mV decay, while at 25% relative humidity this increases to 20 mV (clearly more sensitive than common MEA). The losses increased as the relative humidity was lowered and with NH₃, the life test showed approximately 50 mV loss within the first 100 hours. The voltage-current-resistance indicated similar findings and the impedance suggested the ionomer was mostly responsible for this voltage loss.

A significant portion of FY 2012 effort included participation in the validation of an ASTM test method using FTIR to measure trace contaminants in gaseous hydrogen. This technique can identify unknown materials, determine the quality or consistency of a sample and quantify the components in a mixture, since no two molecular structures have the same infrared spectra. This method was chosen for multiple reasons such as it being a powerful tool to quantify multiple gaseous species without the need for chromatography to separate contaminants. In addition, hydrogen is not infrared active, so there is no interference when probing other constituents. This method is also precise with a short analysis time and sensitivity can be increased

by running multiple scans. We focused on NH₃ and H₂O in these measurements and obtained several spectra at various concentrations. A calibration curve was built by diluting down a known contaminant standard and obtaining the spectra. Figures 2 and 3 are examples of these findings. The calibration curves allowed the detection limits to be determined and verified.

Conclusions and Future Directions

In FY 2012, baseline tests on MEAs with DOE target loadings (i.e. anode = 0.05 mg Pt/cm²) were performed in order to qualify these materials before introducing contaminants at the fuel specification levels. In addition, various tests using CO, H₂S and NH₃ were performed. The CO tolerance increased with increasing temperature while the H₂S tolerance decreased with decreasing relative humidity.

Our future work plans will focus on testing the existing hydrogen fuel specifications on ultra-low platinum loading as well as state-of-the-art materials including nano-structured thin film-based MEAs. Uncertainty in the fuel tolerance of state-of-the-art materials can potentially be a detriment to fuel cell systems and their viability. We plan to address this issue by:

1. Focusing on coupling the tolerance to fuel impurities as a function of platinum loading and/or state-of-the-art materials.
2. Actively participating in other ASTM methods development.
3. Contributing to other working groups such as:

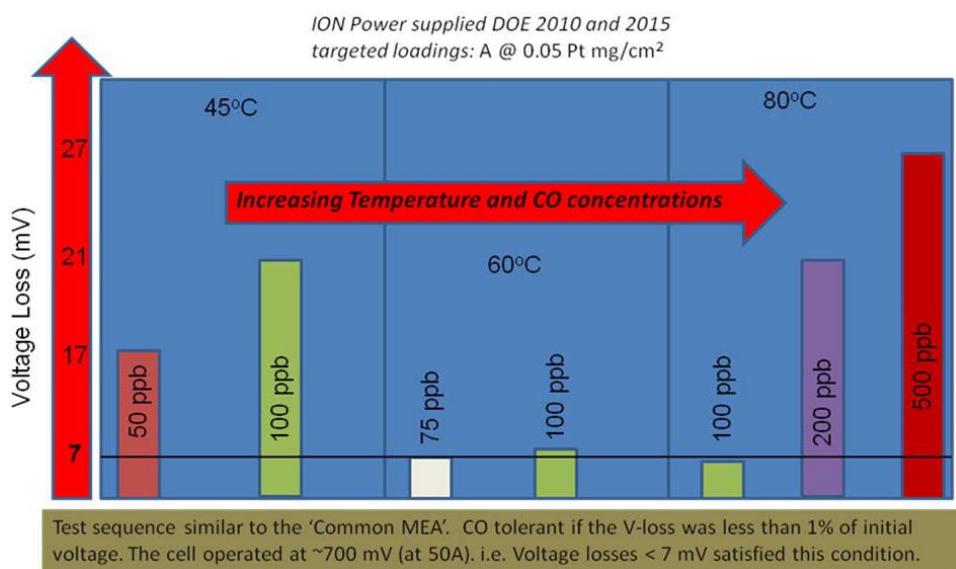


FIGURE 1. Voltage loss due to CO impurity in fuel at various temperatures using an anode loading of 0.05 mg Pt/cm²

**0.625ppm, 2.5ppm, 5ppm and 20ppm NH₃
 10m Cell @ 70°C, Gain 1, Resolution 0.5cm⁻¹
 LN Cooled MCT Detector, 128 Scans**

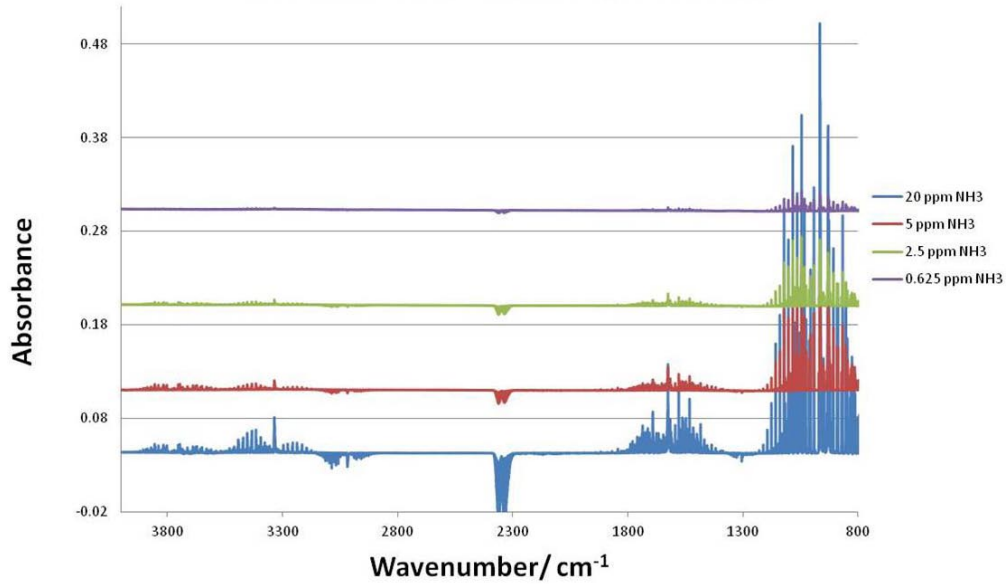


FIGURE 2. FTIR measurements of spectra for multiple H₂O concentrations

**NH₃ Peak 3334, 10M Cell heated 70°C
 Gain 1, Resolution 0.5cm⁻¹
 LN Cooled MCT Detector, 128 scans**

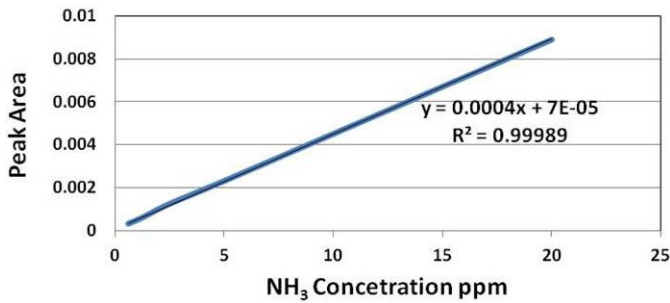


FIGURE 3. A calibration curve produced from different NH₃ concentrations

- TC 197/WG 13 – Hydrogen detection apparatus - Stationary applications
- TC 197/WG 14 – Hydrogen fuel - Product Specification - Proton exchange membrane (PEM) fuel cell applications for stationary appliances

FY 2012 Publications/Presentations

1. PEMFC Poisoning with CO: Measuring Tolerance vs. Temperature and Low Platinum Loadings, Tommy Rockward, Calita Quesada, Karen Rau, and Fernando Garzon, 220th Electrochemical Society Meeting, Boston, MA.

VIII.10 Hydrogen Safety Panel

Steven C. Weiner

Pacific Northwest National Laboratory (PNNL)
901 D Street SW, Suite 900
Washington, D.C. 20024-2115
Phone: (202) 646-7870
Email: sc.weiner@pnnl.gov

DOE Manager

HQ: Antonio Ruiz
Phone: (202) 586-0729
Email: Antonio.Ruiz@ee.doe.gov

Subcontractors:

- Addison Bain, NASA (ret), Melbourne, FL
- David J. Farese, Air Products and Chemicals, Inc., Allentown, PA
- William C. Fort, Shell Global Solutions (ret), Houston, TX
- Don Frikken, Becht Engineering, St. Louis, MO
- Richard A. Kallman, City of Santa Fe Springs, CA
- Glenn W. Scheffler, GWS Solutions of Tolland, LLC, Tolland, CT
- Andrew J. Sherman, Powdermet Inc., Euclid, OH
- Ian Sutherland, General Motors, Warren, MI
- Edward G. Skolnik, Energetics, Inc. Columbia, MD
- Robert G. Zalosh, Firexplo, Worcester, MA

Project Start Date: 2004

Project End Date: Project continuation and direction determined annually by DOE

Fiscal Year (FY) 2012 Objectives

- Provide expertise and recommendations to DOE and assist with identifying safety-related technical data gaps, best practices and lessons learned.
- Help DOE integrate safety planning into funded projects to ensure that all projects address and incorporate hydrogen and related safety practices.

Technical Barriers

This project addresses the following technical barriers from the Hydrogen Safety section of the Fuel Cell Technologies Program Multi-Year Research, Development and Demonstration Plan:

- (A) Safety Data and Information: Limited Access and Availability
- (C) Safety is Not Always Treated as a Continuous Process
- (G) Insufficient Technical Data to Revise Standards

Contribution to Achievement of DOE Hydrogen Safety Milestones

This project contributes to achievement of the following DOE milestones from the Hydrogen Safety section (3.8) of the Fuel Cell Technologies Program Multi-Year Research, Development and Demonstration Plan:

- Milestone 8: Complete investigation of safe refueling protocols for high pressure systems. (1Q, 2012)
- Milestone 20: Update peer-reviewed Best Practices Handbook (4Q, 2008/ongoing)

Related milestones in Task 3 (Failure Modes), Task 5 (Safety of DOE R&D Projects), Task 6 (Hydrogen Safety and Incidents), Task 7 (Best Practices Handbook) and Task 8 (Hydrogen Safety Props) of the above reference have all been achieved with support from the Hydrogen Safety Panel.

FY 2012 Accomplishments

- Conducted the 16th Hydrogen Safety Panel meeting in San Francisco, CA, September 11, 2011 in conjunction with the International Conference on Hydrogen Safety; conducted the 17th Hydrogen Safety Panel meeting in Washington, D.C., March 28-29, 2012.
- Reviewed 11 safety plans since July 1, 2011 for projects in fuel cell and hydrogen storage research and development (R&D).
- Conducted safety review site visits; completed and submitted safety evaluation reports; conducted follow-up teleconferences for previously issued safety evaluation reports and submitted interview reports.
- Provided technical guidance, source material and review for the Hydrogen Incident Reporting and Lessons Learned database (www.h2incidents.org) and Hydrogen Safety Best Practices (www.h2bestpractices.org).
- Examined the longer-term role of the Hydrogen Safety Panel through brainstorming, discussion and recommendations to DOE.



Introduction

Safety is an essential element for realizing the “hydrogen economy” – safe operation in all of its aspects from hydrogen production through storage, distribution and use; from research, development and demonstration to deployment and commercialization. As such, safety is given paramount importance in all facets of the research, development,

demonstration and deployment work of the DOE Fuel Cell Technologies (FCT) Program Office.

Recognizing the nature of the DOE FCT Program and the importance of safety planning, the Hydrogen Safety Panel was formed in December 2003 to bring a broad cross-section of expertise from the industrial, government and academic sectors to help ensure the success of the program as a whole. The experience of the Panel resides in industrial hydrogen production and supply, hydrogen R&D and applications, process safety and engineering, materials technology, risk analysis, accident investigation and fire protection. The Panel provides expertise and recommendations on safety-related issues and technical data gaps, reviews individual DOE-supported projects and their safety plans and explores ways to bring best practices and lessons learned to broadly benefit the FCT Program.

Approach

The Panel strives to raise safety consciousness most directly at the project level. Safety should be driven at the project level by organizational policies and procedures, safety culture and priority. Project safety plans are reviewed in order to encourage thorough and continuous attention to safety aspects of the specific work being conducted. Panel-conducted safety reviews focus on engagement, learning, knowledge-sharing and active discussion of safety practices and lessons learned, rather than as audits or regulatory exercises. Through this approach, DOE and the Hydrogen Safety Panel are trying to achieve safe operation, handling and use of hydrogen and hydrogen systems for all DOE projects.

Results

The Hydrogen Safety Panel was formed in FY 2004 and the first meeting was held in Washington, D.C., December 11-12, 2003. The 16th Panel meeting was held in San Francisco, CA, September 11, 2011 in conjunction with the International Conference on Hydrogen Safety and focused principally on brainstorming new ideas to support the Safety, Codes & Standards sub-program vision and goals. The Panel was joined by stakeholders and other subject matter experts. In all 75 ideas were generated, collated and ranked and Table 1 emphasizes the initiatives which got the highest number of votes and were, therefore, worthy of further consideration.

The 17th meeting was held in Washington, D.C., March 28-29, 2012 and included the following topics: (1) an “incident owner” discussing the events and learnings from a hydrogen tube trailer fire; (2) brainstorming of ideas for a safety checklist to be utilized for assessing the installation of hydrogen systems with an outdoor supply system providing for an indoor use; (3) discussion of Panel work and results to be presented at the 2012 Annual Merit Review meeting.

TABLE 1. Strategically Examining the Hydrogen Safety Panel's Work

| Current Initiatives | New Initiative Ideas |
|---|---|
| Safety Planning and Evaluation | |
| Continue safety planning work, safety plan reviews, site visits | Evaluate long-term implementation of site visit recommendations |
| | Conduct non-DOE project site visits upon request including Department of Defense, National Aeronautic and Space Administration facilities |
| Safety Events, Best Practices and New Tools | |
| Publish safety event learnings and best practices in technical journals | Establish a mechanism for the Panel to access all reported incidents and near-misses |
| Panel as technical contributors for international workshops and initiatives | Expand role of investigating H ₂ incidents beyond DOE |
| | New web-based tools: leak/detection sensors, quantitative risk assessment, maintenance practices, hydrogen properties |
| Other | |
| | Tie to codes and standards work; evaluate and propose code changes |
| | Support authorities having jurisdiction with reviewing hydrogen applications and additional training |

Current Panel membership is noted in Table 2.

TABLE 2. Hydrogen Safety Panel

| | |
|-----------------------------------|----------------------------------|
| Steven C. Weiner, Program Manager | PNNL |
| Richard A. Kallman, Chair | City of Santa Fe Springs, CA |
| Addison Bain | NASA (ret) |
| Nicholas F. Barilo | PNNL |
| David J. Farese | Air Products and Chemicals, Inc. |
| William C. Fort | Shell Global Solutions (ret) |
| Don Frikken | Becht Engineering |
| Aaron Harris | Sandia National Laboratories |
| Miguel J. Maes | NASA White Sands Test Facility |
| Glenn W. Scheffler | GWS Solutions of Tolland, LLC |
| Andrew J. Sherman | Powdermet Inc. |
| Edward G. Skolnik | Energetics, Inc. |
| Ian Sutherland | General Motors |
| Robert G. Zalosh | Firexplo |

The Panel conducted safety reviews for projects as noted in Table 3 since the last reporting (safety reviews have been conducted for 47 projects since March 2004). Final reports issued to DOE with recommendations are also noted [1,2].

In FY 2010, the Panel first established a follow-up protocol to interview project teams in order to identify

TABLE 3. Project Safety Reviews and Reports since July 1, 2011

| Program Area | Project Title | Contractor |
|--------------|--|---|
| ARRA | # Accelerating Acceptance of Fuel Cell Backup Power Systems [1,3] | Plug Power/Robins Air Force Base, Warner Robins, GA |
| ARRA | Fuel Cell-Powered Lift Truck Fleet Deployment [2] | Coca-Cola Bottling Co. Consolidated, Charlotte, NC |
| Storage | # New Carbon-Based Materials with Increased Heats of Adsorption for Hydrogen Storage [4] | Northwestern University, Evanston, IL |
| Storage | # Design of Novel Multi-Component Metal Hydride-Based Mixtures for Hydrogen Storage [5] | Northwestern University, Evanston, IL |
| ARRA | # Fuel Cell-Powered Lift Truck Fleet Deployment [6] | Sysco Food Services, Houston, TX |

Follow-up interview and report for previously conducted site visit
ARRA – American Recovery and Reinvestment Act

actions, findings and conclusions regarding safety review recommendations as one means for measuring the value of this work. Action on report recommendations represents a rich source of safety knowledge that can have broader benefits to others. Table 3 identifies the follow-up interviews that were conducted since the last reporting [4-6] and Table 4 summarizes the conclusions for all follow-up interviews conducted to date.

The Panel concluded that all interviewees have improved the safety aspects of the work they are conducting. Overall, over 90% of the recommendations – 119 in number – have been implemented in some manner or are in progress for the 14 follow-up interviews conducted. The Panel has concluded that the mechanism used by the Panel for seamless discussion and knowledge sharing at the project level has helped augment the prime responsibility of any organization to ensure the safe conduct of work [7,8].

The Hydrogen Safety Panel has been engaged in discussing how hydrogen and fuel cell safety event and

equipment failure information and data can serve as a rich and valuable resource if it is systematically collected, analyzed and used to enhance our knowledge. The Panel issued a unanimously endorsed statement to DOE to identify appropriate mechanisms for such information sharing and to facilitate the necessary interactions for such discussion with project teams that would fully recognize and respect confidentiality and contractual obligations [9].

Leadership has been provided to the International Energy Agency Hydrogen Implementing Agreement Task 31 (Hydrogen Safety) for the work under Subtask D, Knowledge Analysis, Dissemination and Use. Under this task, collaborations in safety event databases continued between member countries. Online tools were demonstrated at the International Conference on Hydrogen Safety [10].

Collaborations to share and disseminate safety information and knowledge continue to be an important aspect of Hydrogen Safety Panel work. For example, the Panel contributed to the University of California Center for Laboratory Safety Workshop, Irvine, CA, March 15-16, 2012. The workshop examined new, more effective ways to make certain that research is performed safely. Work on incidents, lessons learned and best practices was shared with attendees [11].

Conclusions and Future Directions

The work and approaches taken by the Panel will continue to focus on how safety knowledge, best practices and lessons learned can be brought to bear on the safe conduct of project work and the deployment of hydrogen technologies and systems in applications of interest and priority in the DOE FCT Program.

The Panel will undertake a number of initiatives over the next year including:

- Safety plan reviews, safety review site visits and a final report for ARRA fuel cell deployment projects in specialty vehicle, auxiliary and back-up power, portable and combined heat and power applications.

TABLE 4. Categorizing Actions Taken on Report Recommendations - 14 Interviews

| Category | Recommendations Implemented | In Progress | No Action | Total Recommendations |
|---|-----------------------------|-------------|-----------|-----------------------|
| Safety Vulnerability/ Mitigation Analysis | 23 | 4 | 6 | 33 |
| System/Facility Design Modifications | 8 | 5 | 1 | 14 |
| Equipment/Hardware Installation and O&M | 15 | 6 | 1 | 22 |
| Safety Documentation | 14 | 7 | 0 | 21 |
| Training | 3 | 3 | 0 | 6 |
| Housekeeping | 14 | 6 | 1 | 21 |
| Emergency Response | 8 | 3 | 2 | 13 |
| Total | 85 | 34 | 11 | 130 |

- Follow-up teleconferences with all project teams for which safety review site visit reports have been issued in order to identify actions taken, findings, conclusions and other learnings.
- Completion of a safety checklist for an outdoor supply system providing hydrogen for an indoor application to be utilized as a resource for hazard analysis.
- Additional topics for study and knowledge dissemination that utilize the new initiative ideas discussed previously and consistent with the Hydrogen Safety Panel's charter to identify safety-related data and knowledge gaps.

FY 2012 Publications/Presentations

1. Elmore, M.R., Fassbender, L.L., Hamilton, J.J. and Weiner, S.C., "Hydrogen Emergency Response Training for First Responders," PNNL-SA-79009, International Journal of Hydrogen Energy (manuscript HE-D-11-03656 submitted December 2011).
2. Weiner, S.C., Fassbender, L.L., Blake, C., Aceves, S., Somerday, B.P. and Ruiz, A., "Web-based Resources Enhance Hydrogen Safety Knowledge," PNNL-SA-82812/83988, HYPOTHESIS IX, San José, Costa Rica, December 12-15, 2011.
3. Weiner, S.C., "Safety, Codes and Standards – An Overview," U.S. Department of Energy, HYPOTHESIS IX, San José, Costa Rica, December 12-15, 2011.
4. Weiner, S.C. and Fassbender L.L., "Lessons Learned from Safety Events," PNNL-SA-86551, International Journal of Hydrogen Energy (manuscript HE9746, <http://dx.doi.org/10.1016/j.ijhydene.2012.03.152>, published online April 28, 2012).
5. Kallman, R.A., Barilo, N.F. and Murphy, W.F., "Permitting of a Project Involving Hydrogen – A Code Official's Perspective," PNNL-SA-87780, World Hydrogen Energy Conference, Toronto, Ontario, Canada, June 3-7, 2012.
6. Weiner, S.C., Fassbender, L.L., Blake, C., Aceves, S., Somerday, B.P. and Ruiz, A., "Web-Based Resources Enhance Hydrogen Safety Knowledge," PNNL-SA-82812, International Journal of Hydrogen Energy (manuscript HE10236, <http://dx.doi.org/10.1016/j.ijhydene.2012.07.028>, published online August 2, 2012).

References

1. Barilo, N.F., D. Frikken, S.C. Weiner and R.G. Zalosh, "Safety Evaluation Report: Accelerating Acceptance of Fuel Cell Backup Power Systems, Robins Air Force Base, Warner Robins, GA," PNNL-21078, January 17, 2012.
2. Barilo, N.F., D. Frikken, S.C. Weiner and R.G. Zalosh, "Safety Evaluation Report: Fuel Cell Powered Lift Truck Fleet Deployment, Coca-Cola Bottling Co. Consolidated, Charlotte, NC," PNNL-21079, January 18, 2012.
3. Weiner, S.C., Safety Evaluation Follow-up Report for "Safety Evaluation Report: Accelerating Acceptance of Fuel Cell Backup Power Systems, Robins Air Force Base, Warner Robins, GA," June 28, 2012.
4. Skolnik, E.G., Safety Evaluation Follow-up Report for "Safety Evaluation Report: New Carbon-Based Materials with Increased Heats of Adsorption for Hydrogen Storage, Northwestern University, Evanston, IL," January 27, 2012.
5. Skolnik, E.G., Safety Evaluation Follow-up Report for "Safety Evaluation Report: Design of Novel Multi-Component Metal Hydride-Based Mixtures for Hydrogen Storage, Northwestern University, Evanston, IL," February 6, 2012.
6. Skolnik, E.G., Safety Evaluation Follow-up Report for "Safety Evaluation Report: Fuel Cell-Powered Lift Truck Fleet Deployment, Sysco Food Services of Houston, Inc., Houston, TX," March 20, 2012.
7. Weiner, S.C., R.A. Kallman and E.G. Skolnik, "Speaking of Safety: Learning from Safety Reviews," PNNL-SA-71062, 18th World Hydrogen Energy Conference, Essen, Germany, May 18, 2010.
8. Weiner, S.C., "Hydrogen Safety Panel," PNNL-SA-86512, DOE Hydrogen and Fuel Cells Program Annual Merit Review and Peer Evaluation Meeting, Arlington, VA, May 15, 2012.
9. Weiner, S.C., "Learning from Safety Events – A Statement from the Hydrogen Safety Panel," PNNL-SA-85153, January 17, 2012.
10. On-line demonstrations of *Hydrogen Incident Reporting and Lessons Learned* (<http://H2incidents.org>) and *Hydrogen Incident and Accident Database* (HIAD – http://www.hysafe.org/HIAD_DAM/HIAD.php) at the International Conference on Hydrogen Safety, San Francisco, CA, September 12–15, 2011.
11. Gibson, J.H. and N.L. Wayne, "Proceedings of the 2012 University of California Center for Laboratory Safety Workshop," University of California Center for Laboratory Safety, UCLA, Los Angeles, CA, May 5, 2012 (draft).

VIII.11 Hydrogen Safety Knowledge Tools

Linda Fassbender
Pacific Northwest National Laboratory
P.O. Box 999
Richland, WA 99352
Phone: (509) 372-4351
Email: Linda.Fassbender@pnnl.gov

DOE Manager
HQ: Antonio Ruiz
Phone: (202) 586-0729
Email: Antonio.Ruiz@ee.doe.gov

Project Start Date: March 2003
Project End Date: Project continuation and direction determined annually by DOE

Fiscal Year (FY) 2012 Objectives

- Hydrogen Incident Reporting and Lessons Learned
 - Collect information and share lessons learned from hydrogen incidents and near-misses, with a goal of preventing similar safety events from occurring in the future.
 - Increase number of records in database by encouraging “incident owners” to share lessons learned with the hydrogen community.
 - Analyze and summarize lessons learned from incidents and near-misses.
- Hydrogen Safety Best Practices
 - Capture vast and growing knowledge base of hydrogen experience and make it publicly available.
 - Update existing content and develop relevant new content utilizing the Hydrogen Safety Panel and other subject matter experts.

Technical Barriers

This project addresses the following technical barriers from the Hydrogen Safety, Codes & Standards section of the Fuel Cell Technologies Program Multi-Year Research, Development and Demonstration Plan:

- (A) Safety Data and Information: Limited Access and Availability
- (C) Safety is Not Always Treated as a Continuous Process
- (D) Lack of Hydrogen Knowledge by AHJs

Contribution to Achievement of DOE Safety, Codes & Standards Milestones

This project contributes to meeting the following DOE milestones from the Hydrogen Safety, Codes & Standards section of the Fuel Cell Technologies Program Multi-Year Research, Development and Demonstration Plan:

- Milestone 1.3: Publish final Best Practices Manual for Hydrogen Safety. (3Q, 2013)
- Milestone 5.1: Update safety bibliography and incidents databases. (4Q, 2011-2020)

FY 2012 Accomplishments

- Hydrogen Incident Reporting and Lessons Learned
 - Added 12 new safety event records from national laboratories, universities, and private-sector firms in the U.S. and other countries since the 2011 Annual Merit Review and Peer Evaluation Meeting, for a total of 206 records currently in the database.
 - Created three postings of the Lessons Learned Corner (LLC) to analyze hydrogen safety themes illustrated with database content.
 - Collaborated with IA HySafe on sharing safety event records between “H₂incidents.org” and the Hydrogen Incidents and Accidents Database (HIAD) and made joint presentations at the International Conference on Hydrogen Safety in September 2011.
 - Participated in the national dialogue on laboratory safety after the Texas Tech University laboratory explosion (which was not a hydrogen incident). “H₂incidents.org” was recognized by the U.S. Chemical Safety and Hazard Investigation Board as “an example of an online near-miss database that should be emulated by laboratories to foster learning from incidents and near-misses”.
 - Added 30 new links between safety event records and best practices.
- Hydrogen Safety Best Practices
 - Two issues of *H₂ Safety Snapshot* added to website as references:
 - Handling Compressed Hydrogen Gas Cylinders [1]
 - Identifying Safety Vulnerabilities [2]



Introduction

The Pacific Northwest National Laboratory (PNNL) has developed and continues to improve two software tools to support the DOE Hydrogen and Fuel Cell Program's Safety, Codes & Standards Sub-Program. This report covers the Hydrogen Incident Reporting and Lessons Learned database (<http://h2incidents.org>) and the Hydrogen Safety Best Practices online manual (<http://h2bestpractices.org>). We believe that these web-based resources play a key role in reaching, educating, and informing stakeholders whose contributions will help enable the deployment of new hydrogen and fuel cell technologies. Based on all the positive feedback we have received, we are confident that our tools are well respected in the U.S. and within the international hydrogen safety community.

Approach

Hydrogen Incident Reporting and Lessons Learned – The purpose of “h2incidents.org” is to facilitate open sharing of lessons learned from hydrogen safety events to help avoid similar events from occurring in the future. Our approach includes encouraging DOE-funded project teams and others to voluntarily submit records of incidents and near-misses, along with specific lessons learned. We continue to pursue the addition of new records by actively seeking news reports on hydrogen events and searching existing databases and other sources for hydrogen-related safety event records. We contact private-sector companies and universities who experience hydrogen-related safety events to solicit their permission to publish such records. We continue to maintain a mechanism for online submission of records. Specific safety event records are linked to best practices online manual content to emphasize safe practices for working with hydrogen and avoiding future incidents. Expert review of all safety event records and lessons learned is provided by PNNL subject matter experts and Hydrogen Safety Panel members.

Hydrogen Safety Best Practices – Best practices are compiled from learnings and observations from Hydrogen Safety Panel site visits, safety plan reviews, and other work, and available reference materials tailored specifically to working with hydrogen. There are many references and resources that deal with the safe use of hydrogen, and our intent is to organize and compile relevant information in an easy-to-use web-based manual without duplicating existing resources. PNNL teams with the Hydrogen Safety Panel, other national laboratory staff, and other subject matter experts to compile hydrogen-specific best practices from a variety of references. Links to web-based resources and actual files are provided on the website. PNNL staff members, with assistance from the Hydrogen Safety Panel, respond to user questions and comments submitted through the website.

Results

We have collaborated with three other national laboratories on our two websites over the years (Los Alamos National Laboratory, Sandia National Laboratories, and the National Renewable Energy Laboratory), as well as the Hydrogen Safety Panel, the National Aeronautics and Space Administration, two task groups under the International Energy Agency (IEA) Hydrogen Implementing Agreement, and IA HySafe's Hydrogen Incident and Accident Database. The IEA task groups provided a number of safety event records to “h2incidents.org” in past years, and also developed best practices for Hydride Storage and Handling for “h2bestpractices.org”.

Linking our two websites enhances the value of both. Links from best practices to relevant safety event records illustrate what can go wrong if best practices are not followed. Likewise, the lessons learned from safety events are enhanced by links to relevant best practices that should have been followed in order to avoid the occurrence of the events in the first place.

This year, our rate of progress has declined due to significant budget reductions. There are currently 206 safety event records in the database, and we are working on a backlog of about 55 safety events. There are now eight LLCs posted and 30 new links were added from safety event records to LLCs and/or best practices. Past issues of *H₂ Safety Snapshot* were posted on “h2bestpractices.org”.

We are pleased to report that the total number of unique visitors to “h2incidents.org” increased by a factor of six between 2006 and 2011. Unique visits are tracked by PNNL on a monthly basis. Regardless of how many times a particular individual may access a website during a particular month, they are counted as one unique visitor. The LLC is the most popular website feature and the following three themes were the most popular of the archives: 1) burst disk failures, 2) battery charging facility ventilation, and 3) the importance of purging. Although the total number of unique visitors to “h2bestpractices.org” doubled between 2008 and 2011, the traffic is still an order of magnitude below what is achieved for “h2incidents.org”. Visitors to the Laboratory Safety section of the website have been steadily increasing over the past four years, but we are seeking ways to increase the volume of traffic.

Conclusions and Future Directions

Our hydrogen safety knowledge tools help remove barriers to the deployment and commercialization of hydrogen and fuel cell technologies. Feedback on both of our websites has been extremely positive. But in order to remain vital and useful, databases and websites require a concerted effort beyond just general maintenance. The content must

be current, relevant to the community being served, and valuable to the users.

Some of the work we have planned for the future includes:

- Continue to encourage DOE projects and private-sector incident owners to submit records of incidents and near-misses to share their lessons learned with the hydrogen community.
- Continue to analyze and summarize hydrogen safety themes in the LLC.
- Conduct a best practices gap analysis with the Hydrogen Safety Panel.
- Continue collaborations with IA HySafe by sharing records between “H₂incidents.org” and HIAD for the benefit of both databases.
- Conduct a stakeholder survey to obtain feedback on the utility of the two websites and suggestions for improvement.
- Brainstorm ideas to increase visitors to “H₂bestpractices.org”.

FY 2012 Publications/Presentations

1. Weiner, S.C. and Fassbender L.L., “Lessons Learned from Safety Events,” PNNL-SA-86551, International Journal of Hydrogen Energy (manuscript HE9746, <http://dx.doi.org/10.1016/j.ijhydene.2012.03.152>, published online April 28, 2012).
2. Weiner, S.C., Fassbender, L.L., Blake, C., Aceves, S., Somerday, B.P. and Ruiz, A., “Web-based Resources Enhance Hydrogen Safety Knowledge,” PNNL-SA-82812, International Journal of Hydrogen Energy (manuscript HE-D-12-00823 submitted March 22, 2012).
3. Weiner, S.C., Fassbender, L.L., Blake, C., Aceves, S.M., Somerday, B.P., and Ruiz, A. PNNL-SA-82812. “Web-Based Resources Enhance Hydrogen Safety Knowledge,” HYPOTHESIS IX, San José, Costa Rica, December 12-15, 2011.
4. Weiner, S.C. and Fassbender, L.L. “Lessons Learned from Safety Events,” PNNL-SA-78868, International Conference on Hydrogen Safety, San Francisco, CA, September 12-14, 2011.

References

1. Barilo, N.F. and Fassbender, L.L., “Handling Compressed Hydrogen Gas Cylinders,” *H2 Safety Snapshot*, Volume 2, Issue 1, PNNL-SA-75299, November 2010.
2. Barilo, N.F. and Fassbender, L.L., “Identifying Safety Vulnerabilities,” *H2 Safety Snapshot*, Volume 2, Issue 2, PNNL-SA-77099, July 2011.

VIII.12 Hydrogen Emergency Response Training for First Responders

Monte R. Elmore
Pacific Northwest National Laboratory (PNNL)
902 Battelle Blvd.
Richland, WA 99352
Phone: (509) 372-6158
Email: monte.elmore@pnnl.gov

DOE Manager
HQ: Antonio Ruiz
Phone: (202) 586-0729
Email: Antonio.Ruiz@ee.doe.gov

Subcontractors:

- Jennifer Hamilton, California Fuel Cell Partnership (CaFCP), Sacramento, CA
- Hanford Fire Department, Richland, WA
- Hazardous Materials Management and Emergency Response (HAMMER) training center, Richland, WA

Project Start Date: October 2004

Project End Date: Project continuation and direction determined annually by DOE

Contribution to Achievement of DOE Hydrogen Safety Milestones

This project will contribute to achievement of the following DOE milestone from the Safety Codes and Standards section of the Fuel Cell Technologies Multi-Year Research, Development and Demonstration Plan:

- Enhance hydrogen safety training props and deliver classroom curriculum for emergency response training. (4Q, 2012)

In addition, the following milestones were met in previous years:

- Milestone 1 (ED): Develop “Awareness-Level” information package for first responders. (4Q, 2006)
- Milestone 3 (ED): Develop “prop-course” using hands-on training devices for first responders. (4Q, 2008)
- Milestone 4 (ED): Update “Awareness-Level” information package for first responders. (4Q, 2009).
- Milestone 21 (SAF): Conduct first hydrogen safety class (non-prop) offered at HAMMER. (3Q, 2005)
- Milestone 22 (SAF): Complete first life-size prop for hands-on training of emergency responders. (1Q, 2008).

Fiscal Year (FY) 2012 Objectives

- Support the successful demonstration and deployment of hydrogen and fuel cell technologies by providing technically accurate hydrogen safety and emergency response information to first responders.
- Provide a one-day first responder training course, “Hydrogen Emergency Response Training for First Responders,” that integrates the use of DOE’s mobile hydrogen fuel cell vehicle (FCV) prop.
- Continue to support the web-based awareness-level course, “Introduction to Hydrogen Safety for First Responders.” www.hydrogen.energy.gov/firstresponders
- Disseminate first responder hydrogen safety educational materials at appropriate fire fighter conferences to raise awareness.

Technical Barriers

This project addresses the following technical barriers from the Safety Codes and Standards section of the Fuel Cell Technologies Multi-Year Research, Development and Demonstration Plan:

- (H) Lack of Hydrogen Knowledge by Authorities Having Jurisdiction (AHJs)
- (I) Lack of Hydrogen Training Materials and Facilities for Emergency Responders

FY 2012 Accomplishments

- **Prop-Based Course:** This operations-level course was presented at two fire training centers in the Los Angeles area of California in the past year. Three consecutive one-day training classes were held at each of the following locations:
 - Los Angeles City Fire Department, Los Angeles, CA (Jan 2012)
 - Los Angeles County Fire Department, San Dimas, CA (Mar 2012)

Approximately 300 first responders from the above sites received this training. Extremely positive feedback from each of the sites continues to reinforce the value of this course to first responder organizations.

- **Awareness-Level Course:** After almost six years, our website continues to receive ~200-300 unique visits per month from almost every state and some foreign countries. The course is registered on the TRAIN (TrainingFinder Realtime Affiliate Network) website for broader dissemination to first responders. TRAIN is a central repository for public health training courses. Almost 30,000 TRAIN users identify themselves as emergency responders.

- **Outreach:** CDs of the awareness-level course were distributed through the DOE Energy Efficiency and Renewable Energy Information Center.



Introduction

Safety in all aspects of a future hydrogen infrastructure is a top priority, and safety concerns influence all DOE hydrogen and fuel cell projects. Despite the most concerted effort, however, no energy system can be made 100% risk-free. Therefore, for any fuel and energy system, a suitably trained emergency response force is an essential component of a viable infrastructure. The Fuel Cell Technologies Program has identified training of emergency response personnel as a high priority, not only because these personnel need to understand how to respond to a hydrogen incident, but also because firefighters and other emergency responders are influential in their communities and can be a positive force in the introduction of hydrogen and fuel cells into local markets.

This project employs the Occupational Safety and Health Administration and National Fire Protection Association frameworks for hazardous materials emergency response training to provide a tiered hydrogen safety education program for emergency responders. The effort started with development and distribution of the awareness-level web-based course in FY 2006-2007. A more advanced course and materials to facilitate education were developed in FY 2008-2009, complementing the design, construction, and operation of a fuel cell vehicle prop (developed under PNNL's Hydrogen Safety project). The overall first-responder education project will continue to be updated. In addition, PNNL has implemented outreach efforts to key stakeholder groups to facilitate delivery of the training to a broad audience.

Approach

PNNL works with subject matter experts in hydrogen safety and first responder training to develop hydrogen safety course materials. Draft materials undergo considerable review and revision before being released. The PNNL team works with DOE to make stakeholder groups aware of training opportunities and to provide “live” training when appropriate. The web-based awareness-level course is available “online” or on CDs and provides the student with a basic understanding of hydrogen properties, uses, and appropriate emergency response actions. The prop-based course, a more advanced operations-level course, was initially presented at the HAMMER training facility in Richland, WA. Subsequently, the mobile prop has enabled the course to be delivered at several offsite fire training

centers (in California during 2010-12) in order to reach larger audiences in areas where hydrogen and fuel cell technologies are being deployed.

Results

Prop-based course: The focus of the curriculum is on teaching first responders what is the same and what is different about hydrogen and FCVs as compared to conventional fuels and vehicles. Course evaluation forms are distributed and feedback obtained at each class to help us improve the course content and delivery. Based on feedback from all the training sessions held this past year (January and March 2012), we conclude that following the training, first responders are more familiar with the properties and behavior of hydrogen, and are prepared to operate in a safe and effective manner if a hydrogen incident should occur in their jurisdiction.

The FCV prop has been integrated into the “Hydrogen Emergency Response Training for First Responders” course. The prop demonstrates potential conditions that could be encountered during the control and suppression of a FCV fire.

Conclusions and Future Directions

The introductory web-based course has been highly successful, based on the usage recorded and feedback received. The course is fulfilling a need expressed by the first responder community to receive more information about hydrogen and fuel cells so they will be prepared in the rare event of a hydrogen incident. The in-depth prop-based course builds on that success and is very useful in giving first responders a hands-on experience with simulated FCV incidents that integrates well with classroom training. PNNL will continue to update both courses as needed to reflect current applications and markets for hydrogen and fuel cells.

There is an identified need for the prop course curriculum to achieve a better balance between the vehicles (including industrial lift trucks) and stationary facilities modules, through the development of some type of prop for stationary applications of fuel cells. An interactive video training tool of virtual hydrogen incident scenarios and responses to simulate both outdoor fueling of passenger FCVs and indoor fueling of hydrogen forklifts could address that need. We propose to develop a virtual model by first demonstrating the concept with a simplified model, and subsequently adding additional features and capabilities.

The prop course will be offered at additional first responder training facilities in FY 2013. As additional hydrogen fueling stations are commissioned and more FCVs appear on the road, more first responder organizations are inquiring about this training. As with the previous training classes, the prop will be transported to each site for about a week. Multiple classes will be offered at each site. In future

years, the prop will be transported to other locations across the country for use in delivery of this course at training centers in areas that have emerging deployments of hydrogen and fuel cell technologies. PNNL will also work with DOE and other stakeholders to determine what, if any, additional types of educational courses and materials are warranted, and to develop and implement plans to provide education to specific groups.

FY 2012 Publications/Presentations

1. Elmore, M.R., Fassbender, L.L., Hamilton, J.J., and Weiner, S.C. "Hydrogen Emergency Response Training for First Responders." International Journal of Hydrogen Energy. (Manuscript submitted December 2011).

IX. EDUCATION

IX.0 Education Sub-Program Overview

INTRODUCTION

The Education sub-program facilitates early market hydrogen and fuel cell deployments and supports future commercialization by providing technically accurate and objective information to key target audiences that can help transform the market (see Table 1).

TABLE 1. Key Target Audiences for the Education Sub-Program

| Target Audience | Rationale |
|--|---|
| Code Officials | Code officials must be familiar with hydrogen to facilitate the permitting process and local project approval. |
| First Responders | Firefighters, as well as law enforcement and emergency medical personnel, must know how to handle potential incidents; their understanding can also facilitate local project approval. |
| Local Communities/General Public | Local communities will be more likely to welcome hydrogen and fuel cell projects if they are familiar with hydrogen. |
| Potential End-Users | Potential early adopters need information about commercially available hydrogen and fuel cell products and the opportunities for incorporating the technologies into their operations. |
| State and Local Government Representatives | A broad understanding of hydrogen encourages favorable decision-making regarding opportunities for near-term deployment and lays the foundation for long-term change. |
| Middle School and High School Teachers and Students | Teachers need technically accurate information and usable classroom activities to educate the next generation of potential researchers, engineers, policy-makers, and end-users about the technologies. |
| University Faculty and Students | Graduates are needed for research and development in government, industry, and academia. |

The Education sub-program develops and disseminates information resources and conducts training. It strives to communicate a balanced message to help target audiences become familiar with hydrogen and fuel cell technologies and how they fit in the portfolio of renewable energy and energy-efficiency options. To aid with market introduction, the sub-program helps target audiences develop an accurate understanding of hydrogen safety, recognize opportunities for deployment in near-term markets, and understand the role of early markets in facilitating the use of hydrogen and fuel cells.

GOALS

The goal of the Education sub-program is to educate key audiences about hydrogen and fuel cell technologies to facilitate near-term deployment, broad commercialization, and long-term market acceptance.

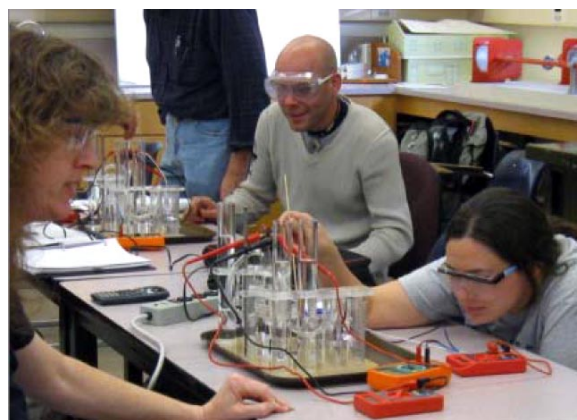
OBJECTIVES

The Education sub-program is closely coordinated with the Program's activities in technology demonstration and validation; safety, codes and standards; and early market deployment and associated market transformation activities, as well as state and regional-based hydrogen and fuel cell outreach programs as part of a comprehensive strategy to transform success in demonstrating and deploying technologies into success in the broader marketplace. These integrated efforts form a comprehensive strategy to transform success in demonstrating and deploying technologies into success in the broader marketplace. Specific objectives for the Education sub-program include the following:

- Increase the acceptance and inclusion of hydrogen and fuel cell technologies as a part of a clean energy portfolio of energy efficiency and renewable energy technologies in federal, state, and local government and private sector activities.
- Reduce the “soft costs” associated with the deployment and early adoption of hydrogen and fuel cell technologies in multiple applications (e.g., insurance, permitting, uniform codes and standards) through education, outreach, and training of “second generation” clean energy professionals.
- Increase general knowledge and awareness of the benefits of the use of hydrogen and fuel cell technologies in multiple applications among key target audiences.
- Increase awareness of the broad range of applications for fuel cells and hydrogen—beyond light-duty vehicles and buses.

FISCAL YEAR (FY) 2012 STATUS

The Education sub-program continued to conduct activities based on prior-year funds. These activities include supporting state and regional outreach efforts by providing consistent messages and readily available information resources, along with other activities, as appropriate. The sub-program’s outreach projects are focused on states with an active hydrogen and fuel cell presence, and they are working to develop case studies, best practices, and technical assistance resources to help decision-makers identify and assess opportunities for future deployment. In the area of academics, the sub-program also continued to support university, high-school, and middle-school education, including dissemination of lesson plans, curricula, and laboratory materials.



FY 2012 KEY ACCOMPLISHMENTS

- Organized an event to “match” suppliers and manufacturers.
- Initiated Northeast cluster group for collaboration between states and developed roadmaps for seven states in the cluster.
- Completed PBS Motorweek Series with Virginia Clean Cities by developing an episode focused on a vehicles and infrastructure update that began airing in October 2011.
- Webinar series included over 1,500 attendees in FY 2011. Topics included Federal Facilities Guide to Fuel Cells in May, America’s Next Top Energy Innovator Runner Up in April, National Hydrogen Learning Demonstration Status in February. Based on the success of the 2011 series, the webinars have been continued into 2012 and are now coordinated by the Program.
- Published more than 70 news articles in FY 2011 to continue communication of Program accomplishments. Publicity and media activities are continuing to gain momentum in 2012.
- Launched a monthly *Fuel Cell Technologies Program Newsletter*, which recaps news and events and previews upcoming activities, reaching more than 7,500 subscribers.
- Trained more than 9,700 middle school and high school teachers (cumulative total) in 35 states, through “H2 Educate!”— 90% felt that resources increased effectiveness of lesson plans.

- 2012 Hydrogen Student Design Contest included 20 universities from nine countries. The winning team presented their design during a keynote session at the Young Scientist Symposium of the World Hydrogen Energy Conference 2012 in Toronto, Canada. At the awards ceremony, the theme for the next contest was announced as well. The 2013 contest will ask students for their plans for the development of hydrogen fueling infrastructure in the Northeast.

BUDGET

The Education sub-program's FY 2012 budget and FY 2013 request are zero. New projects that were competitively awarded in FY 2004 and FY 2008 were fully funded in FY 2010. The remaining projects are scheduled to be completed in FY 2012. Given budget constraints and the need for including hydrogen and fuel cells within the broader Energy Efficiency and Renewable Energy portfolio, Education activities will be coordinated with other DOE-wide efforts. Target audiences have been prioritized according to their near-term relevance and the effect on the use of hydrogen and fuel cell technologies today.

FY 2013 PLANS

In FY 2013, the Education sub-program will complete expenditures of prior-year appropriations in relevant areas and focus on facilitating the introduction of hydrogen and fuel cell technologies into early markets. Future efforts will coordinate with other DOE-wide efforts to leverage recent project successes through the development of educational materials and webinars to highlight the benefits of hydrogen and fuel cell technologies.

Gregory J. Kleen
Education Team Lead (Acting)
Fuel Cell Technologies Program
Department of Energy Golden Field Office
1617 Cole Blvd.
Golden, CO 80401
Phone: (720) 356-1672
Email: Gregory.Kleen@go.doe.gov

IX.1 Development of Hydrogen Education Programs for Government Officials

Shannon Baxter-Clemmons
South Carolina Hydrogen and Fuel Cell Alliance (SCHFCA)
P.O. Box 12302
Columbia, SC 29211
Phone: (803) 545-0189
Email: baxterclemmons@schydrogen.org

DOE Manager
GO: Gregory Kleen
Phone: (720) 356-1672
Email: Gregory.Kleen@go.doe.gov

Technical Advisor
Kim Cierpik
Phone: (720) 356-1266
Email: kim.cierpik@go.doe.gov

Contract Number: DE-FG36-08GO18113

Subcontractors:
• Greenway Energy, Aiken, SC
• Advanced Technology International, Charleston, SC

Project Start Date: October 1, 2008
Project End Date: January 31, 2013

Fiscal Year (FY) 2012 Objectives

- Further develop relationships with government consortium groups and associations.
- Further establish direct lines of communication with individual city, county and state officials to disseminate important hydrogen and fuel cell information through project partners existing communication resources.
- Further institute recurring statewide events to provide public officials with opportunities to view the latest hydrogen and fuel cell technologies.
- Continue to raise public awareness and acceptance of the benefits of hydrogen and fuel cell technologies in order to increase interest in the adoption of hydrogen and fuel cells.
- Synthesize objective and technically accurate information that will be made available to a wide audience through the internet, a national meeting, and smaller personal meetings.

Technical Barriers

This project addresses the following technical barriers from the Education section (3.8.5) of the Fuel Cell Technologies Program Multi-Year Research, Development and Demonstration Plan:

- (A) Lack of Readily Available, Objective, and Technically Accurate Information
- (B) Mixed Messages
- (C) Disconnect Between Hydrogen Information and Dissemination Networks
- (D) Lack of Educated Trainers and Training Opportunities
- (E) Regional Differences
- (F) Difficulty of Measuring Success

Technical Targets

This project will contribute to achievement of the following DOE milestones from the Education (3.8) section of the Fuel Cell Technologies Program Multi-Year Research, Development and Demonstration Plan:

- Milestone 11: Develop set of introductory materials suitable for a non-technical audience. (4Q, 2006)
- Milestone 13: Develop materials for community seminars. (4Q, 2008)
- Milestone 14: Hold community seminars to introduce local residents to hydrogen. (4Q, 2008 through 4Q, 2012)
- Milestone 17: Hold “Hydrogen 101” seminars. (4Q, 2008 through 4Q, 2012)
- Milestone 29: Evaluate knowledge and opinion of hydrogen technology of key target audiences and progress toward meeting objectives. (4Q, 2009)

Progress for the Hydrogen 101: State and Local Government Education

FY 2012 Accomplishments

- In person presentations to over 45 groups of targeted South Carolina decision makers.
- Featured presenter in a DOE webinar: Where the Jobs Are: Hydrogen and Fuel Cells in South Carolina.
- Reached 21,672 targeted additional state and local government officials and decision makers.
- Webinar presentations can be viewed through a SlideShare channel.

- Videos of educational information on hydrogen are available on the SCHFCA YouTube and Greenway Energy YouTube channels.
- Developed market value proposition case studies on material handling equipment (MHE) early markets for hydrogen and fuel cell technologies.
- Presentations to groups including: national congressional candidates, staff of national presidential candidates, state house and senate members and staff, Leaders at the SC Department of Commerce, and the Coastal Conservation League.
- Hydrogen 101 materials were utilized in wider public education efforts that reached additional non-decision makers.
- Educational efforts with SC House and Senate members to demonstrate the effect of state level incentives for fuel cells and renewable technologies on creating viable markets.
- Hosted the DOE Secretary Chu visit in South Carolina, which included briefing Congressman James Clyburn.

Facilitate Cooperation and Best Practices with Southeastern States

The SCHFCA is working with state stakeholders to pinpoint resources in other southeastern states that could potentially be the start of a neighboring state's Hydrogen and Fuel Cell Economic Cluster. The SCHFCA intends to survey economic developers in southeastern states regarding opportunities to use the Market Value Proposition case study to promote fuel cell use in fork lifts.

1. Compile and document the “best practices” that have benefited the development of the South Carolina Hydrogen and Fuel Cell Economic Cluster.
2. Identify stakeholders (i.e., State Department of Commerce, State Energy Office, Clean Cities office, DOE award staff) that are knowledgeable about the industry, research facilities and projects in neighboring southeastern states.
3. Work with state stakeholders to pinpoint resources in other southeastern states that could potentially be the start of a neighboring state's Hydrogen and Fuel Cell Economic Cluster.
4. Survey economic developers in southeastern states regarding opportunities to use market value proposition case studies to promote fuel cells for forklifts, combined heat and power (CHP) and cell tower back up power.
5. Document and report the state's resources that make a case for a hydrogen and fuel cell economic cluster.
6. Travel to meet with state leaders (potential champions) to discuss and present our findings regarding resources already in their state that potentially make up an

economic cluster and some best practices that they could adopt or modify to fit their needs.

7. Meet and present market value proposition case studies to potential customers and regional economic developers in southeastern states.
8. Follow up with invitations to travel to South Carolina to see what we are doing and continue discussions on how we can work together.



Introduction

This project exists to develop and distribute educational material focusing on hydrogen and fuel cell technology to be presented to state and local government officials. These officials range from legislators at the state level to the planners at the local level. The activities associated with this project are based on a fundamental understanding of our diverse target audience and what issues and topics are of greatest interest to them.

The SCHFCA has been building relationships with key government and industry groups to promote the creation of a hydrogen economy throughout South Carolina and the southeast. Educational efforts have been key to the success of the SCHFCA in gaining acceptance of hydrogen energy technologies among government officials. Greenway Energy has worked with Aiken Technical College, the Applied Research Center: Hydrogen and Savannah River National Laboratory on hydrogen workforce education and public outreach. Efforts on this project will leverage existing materials and expertise and create materials for government officials.

Hydrogen and fuel cell technologies are moving out of the laboratory and into economically competitive niche markets such as cell phone tower back-up power and forklift operations. As hydrogen technologies become competitive in these early markets, communities will need to be educated about the opportunities afforded by hydrogen technologies and about safety concerns associated with them. The Hydrogen 101 program led by the SCHFCA seeks to raise awareness about hydrogen and fuel cells to community leaders within South Carolina and the Southeast.

South Carolina is among a small, but growing, number of states that have a hydrogen implementation strategy and is on the leading edge of fuel cell research and adoption. The state has been recognized as one of the top five leaders in hydrogen and fuel cells, but a significant lack of information on hydrogen still exists among state and local leaders. In order to maximize the resources existing in the state and surrounding region, it is imperative that an effective outreach and education program be conducted so that the decision

to accept hydrogen technologies in the local community is informed and wise.

Approach

The project team is composed of South Carolina-based hydrogen experts with connections to technically accurate information and civic organizations and associations that have already established communication networks and events with our target audience. The entire team works together to identify specific messaging that the local audience and sub audiences are interested in. Based on the feedback we gather from the civic organizations and other community opinion leaders, education materials and demonstrations are developed.

The marketing of the program is conducted through the existing websites, email distribution lists and communication networks. The distribution of the material is primarily conducted at events associated with each of the civic associations partnered on the project; however, several stand-alone events and webinars are planned.

Results

Building on the educational successes that assisted in the passage of the South Carolina Hydrogen Permitting Act, the SCHFCA has focused on decision makers in FY 2012 and reaching out to new candidates to state and national political offices, economic developers and business leaders. These efforts have been focused on discussing the success of hydrogen and fuel cell technologies in early markets and methods to increase adoption of hydrogen technologies within the state and region.

The Hydrogen 101 program in 2012 expanded its audience again to include business leaders and economic development officials based on input gathered from stakeholders. The focus of interactions with decision makers has been to emphasize the business case for fuel cells in early markets. This education focuses on helping them understand where fuel cells can provide a value proposition for their organizations. The program performed outreach through group presentations, webinars, and small group or individual meetings. Presentation materials were updated and expanded depending on the audience and brochures were printed to summarize key messages.

The development of early market hydrogen technology case studies included: H₂ Lift Truck Case Study, Telecom Backup Case Study, CHP Case Study

The MHE Market Value Proposition Case study hand-out was developed, printed and distributed at meetings and to specific decision makers in government and business.

The direct number of stakeholders reached was 21,339 and the wider educational efforts that leveraged Hydrogen

101 materials reached over 1 million people. In addition to education of leadership groups, the SCHFCA reached out to candidates for political offices and has continued discussions with newly elected leaders. The educational efforts focused on helping them understand how the hydrogen and fuel cell industry is growing the state economy, creating high paying jobs, and saving businesses money.

Groups have been overwhelmingly supportive of hydrogen and fuel cell technologies as a result of the presentations and view the technologies as having the potential to foster economic development within the state. Work has been started to collaborate with other states including Tennessee, North Carolina, and Florida to help educate regional leaders about opportunities for hydrogen technologies in their state and the potential to grow an interconnected regional hydrogen economy.

Conclusions and Future Directions

The SCHFCA Hydrogen 101 program has met all of its goals and its efforts are having an impact in creating wider support for hydrogen. Education about the effect of state level incentives on the market for fuel cell and other renewable technologies has started to show how states can grow their hydrogen economy. In 2012, SCHFCA will focus on working with other southeastern states to start more hydrogen and fuel cell activities.

Special Recognitions

1. Hosted the DOE Secretary Chu visit to South Carolina. There was national press pickup of the successful visit.

FY 2012 Publications/Presentations

1. The “Hydrogen and Fuel Cells: Lift Trucks, A Practical Application” brochure was revised, printed and distributed at the 2011 Fuel Cell Seminar & Exposition to over 800 attendees. It is given out at every meeting held with Dr. Shannon Baxter-Clemmons, and will be distributed at the 2012 Fuel Cell Seminar & Exposition to an expected attendance of 1,000.
2. Dr. Baxter-Clemmons co-authored an article titled, Staying the Course with Hydrogen, which was published in the Columbia Regional Business Report in September-October 2011 issue.
3. SCHFCA participated in the 2011 SC Renewable Energy Forum as a host sponsor with nearly 300 registrants.
4. Exhibited at the 2011 Green is Good for Business Conference and the 2011 Green Tie Event.
5. Dr. Baxter-Clemmons presented at the Charleston Energy Conference in 2011.
6. Dr. Baxter-Clemmons presented at the Hydrogen and Fuel Cell Technical Advisory Committee (HTAC) in Washington, DC, in November 2011.

7. Dr. Baxter-Clemmons presented on Hydrogen Fueling and conducted an End-User Educational Program at the 2011 Fuel Cell Seminar & Exposition in Orlando, Florida.

8. Dr. Baxter-Clemmons presented at the 91st Transportation and Research Board Annual Meeting held in Washington, DC in January 2012.

9. Dr. Baxter-Clemmons was guest speaker at the SC Society of Professional Engineers and the American Council of Engineering Companies of SC Winter Meeting in February 2012 to 93 attendees.

10. Dr. Baxter-Clemmons presented on the updates of the BMW Landfill Gas-to-Hydrogen project and the Development of Hydrogen Education Programs for Government Officials project at the Annual Merit Review conference held in Washington, DC in May 2012.

11. Dr. Baxter-Clemmons presented on Permitting Hydrogen and Fuel Cells in SC, held a poster presentation on Hydrogen Fuel Cell lift trucks and was a speaker at a Hydrogen and Fuel Cells Municipalities session at the World Hydrogen Energy Conference held in Toronto, Canada in June 2012.

12. SCHFCA was a sponsor of the SC Clean Energy Summit and conducted a four speaker session in July 2012 with an attendance of 240 high level energy stakeholders.

13. Dr. Baxter-Clemmons spoke at the Senate Fuel Cell and Hydrogen Caucus briefing in Washington, DC in July 2012.

IX.2 Raising H2 and Fuel Cell Awareness in Ohio

Patrick Valente
Ohio Fuel Cell Coalition
151 Innovation Drive, Suite 240D
Elyria, OH 44035
Phone: (614) 542-7308
Email: Pat.valente@fuelcellcorridor.com

DOE Manager
GO: Gregory Kleen
Phone: (720) 356-1672
Email: Gregory.Kleen@go.doe.gov

Contract Number: DE-FC36-08GO18117

Subcontractor:
Edison Material Technology Center, Dayton, OH

Project Start Date: March 2009
Project End Date: June 30, 2012

Fiscal Year (FY) 2012 Objectives

- Increase understanding of hydrogen and fuel cell technologies among state and local governments by 10% compared to 2004 baseline.
- Increase knowledge of hydrogen and fuel cell technologies among key target populations (state and local governments) by 20 percent compared to 2004 baseline.

Technical Barriers

This project addresses the following technical barriers from the Education section of the Fuel Cell Technologies Program Multiyear Research Development and Demonstration Plan:

- (A) Lack of Readily Available, Objective and Technical Accurate Information
- (B) Mixed Messages
- (C) Disconnect Between Hydrogen Information and Dissemination Networks
- (D) Lack of Educated Trainers and Training Opportunities
- (E) Regional Differences
- (F) Difficulty of Measuring Success

Contribution to Achievement of DOE Education Milestones

This project will contribute to the following DOE Milestones from the Education section of the Fuel Cell Technologies Program Multiyear Research Development and Demonstration Plan.

- Milestone 11: Develop set of introductory materials suitable for a non-technical audience (3Q, 2009)
- Milestone 13: Develop material for community seminars (ongoing)
- Milestone 16: Develop database of state activities (ongoing)
- Milestone 17: Hold "Hydrogen 101" seminars (3Q, 2009 through 3Q, 2012)

FY 2012 Accomplishments

- August 12, 2011 – Lorain County Community College, Elyria, OH - 20 people
- September 14 – 15, 2011 - NorTech B2B Conference, Cleveland, OH - 70 people
- September 19, 2011 - Global Business Forward, Gahanna, OH - 30 people
- September 22, 2011- Community Leaders Forum, Dayton, OH - 60 people
- October 3, 2011 - Manufacturing Educational Council, Akron, OH - 25 people
- November 2, 2011 - Ohio Reception at Fuel Cell Seminar, Orlando, FL - 100 people
- November 15, 2011 - Community Leaders Forum, Athens, OH - 40 people
- May 1, 2012 - Supply Chain Exchange at Ohio Fuel Cell Coalition Symposium, Elyria, OH - 100 people
- May 1-2, 2012 – Ohio Fuel Cell Coalition Symposium, Elyria, OH - 200 people
- June 7, 2012 – TechSolve, Cincinnati, OH – 10 people
- June 12, 2012 – Lima Editorial Board, Lima, OH – 15 people

The Ohio Fuel Cell Coalition was tasked with raising the awareness and understanding of fuel cells and the hydrogen economy to Ohio Community Leaders. In 2011 through 2012 the Ohio Fuel Cell Coalition held 11 community leaders forums. On May 1 and 2 over 200 people gathered at the Lorain County Community College Campus for the 2012 Ohio Fuel Cell Symposium, the theme this year was Fuel Cell Collaborations, Trends & Applications. The Symposium presented by the Coalition began with the first ever Members'

Only Meeting where participants had an opportunity to be engaged in a strategic planning process. This was followed by a Supply Chain Exchange event where eight integrators were matched up with 30 suppliers from throughout the United States. On day 2 of the symposium we had a series of speakers opening with Dr. Roy Church, President, Lorain County Community College followed by Dr. Roger Saillant, Case Western Reserve University. The speakers also included David Mustine, JobsOhio; Ed Cohen, Honda; Morry Markowitz, Fuel Cell Hydrogen Energy Association; Greg Kleen, Department of Energy; and Julie Cairns, CSA Group. This event allowed the Coalition to educate over 200 individuals on fuel cells and the hydrogen economy which certainly exceeded our expectations.



Approach

The approach we used for all the Community Leaders Forums were presentations by the Ohio Fuel Cell Coalition in conjunction with regional leaders. The presentations were followed by question and answers periods followed up by informal discussions on fuel cells and the hydrogen economy.

Results

In summary, as you see the Community Leader Forums have been very successful in the last two years with over 1,585 people being drawn to them. As always we followed up the forums with a survey and the survey results were very positive in that the participants had a significant increase in knowledge and awareness of fuel cells and the hydrogen economy.

IX.3 Hydrogen Technology and Energy Curriculum (HyTEC)

Barbara Nagle
University of California, Berkeley
Lawrence Hall of Science #5200
1 Centennial Drive
Berkeley, CA 94720-5200
Phone: (510) 642-8718
Email: bnagle@berkeley.edu

DOE Manager
GO: Gregory Kleen
Phone: (720) 356-1672
Email: Gregory.Kleen@go.doe.gov

Contract Number: DE-FG36-04-GO14277

Subcontractor:
• Schatz Energy Research Center, Humboldt State University, Arcata, CA

Project Start Date: September 1, 2004
Project End Date: August 31, 2012

Contribution to Achievement of DOE Education Milestones

This project will contribute to achievement of the following DOE milestones from the Education section of the Fuel Cell Technologies Program Multi-Year Research, Development and Demonstration Plan:

- Milestone 26: Develop modules for high schools. (4Q, 2007)
- Milestone 27: Launch high school teacher professional development. (4Q, 2008 through 3Q, 2011)

FY 2012 Accomplishments

- Completion of the website, including seven video segments for teacher professional development.
- Dissemination of the program through seven workshops at state, national, and regional science education conferences.
- A partnership was developed with the Connecticut Science Center, where a two-day workshop for teacher professional development was delivered in May 2012.
- Collaborated with the publisher to train teacher-trainers who provide professional development to adopters of the curriculum.



Fiscal Year (FY) 2012 Objectives

- Complete website materials and video for teacher professional development and support
- Collaborate with the publisher to disseminate the program through science teacher conferences
- Collaborate with the publisher to conduct professional development for new implementation sites and teacher leaders
- Develop partners for dissemination in areas with fuel cell projects

Technical Barriers

This project addresses the following technical barriers from the Education section (3.9.5) of the Fuel Cell Technologies Program Multi-Year Research, Development and Demonstration Plan:

- (A) Lack of Readily Available, Objective, and Technically Accurate Information
- (C) Disconnect Between Hydrogen Information and Dissemination Networks
- (D) Lack of Educated Trainers and Training Opportunities
- (E) Regional Differences

Introduction

This project has produced a two-week curriculum module about hydrogen and fuel cells for high school students. A group of experienced science curriculum developers, teacher professional developers, leaders in the field of hydrogen and fuel cell technology and its application to transportation, and publishers of instructional materials collaborated to develop and produce this curriculum as a commercial educational module. The module includes a teacher's guide, student handouts, an equipment kit, and support materials such as a compact disk (CD) and website. It is intended to fit into high school courses such as physical science, chemistry, environmental science, and physics. In order to ensure that it can be used in these courses, the module addresses topics teachers usually teach and correlates to the National Science Education Standards and/or state and local standards. The project has developed professional development workshops and videos to prepare teachers to teach the curriculum and develop teacher leaders. Project evaluation focuses on evaluating the classroom usability of the curriculum module, students' progress toward

the intended learning goals, and the effectiveness of the professional development workshops. The past years' work focused on completing the web support for the curriculum and on disseminating the curriculum module along with an equipment kit and support materials such as a CD and website.

Approach

The curriculum materials were developed and revised through a close collaboration between curriculum developers at the Lawrence Hall of Science (LHS), scientists and engineers at the Schatz Energy Research Center (SERC), experienced teacher associates, local and national field test teachers, and LAB-AIDS, Inc., an established publisher of kit-based science curriculum materials. The materials were developed by LHS with input from SERC, and classroom-tested by the developers, then by expert teachers, and finally by a broader group of teachers from local and national sites.

The module uses an issue-oriented approach to teaching concepts related to chemistry and energy topics. This approach teaches about hydrogen and fuel cells in the context of energy issues and current and future options for powering vehicles. This approach also demonstrates to students both the relevance of their science education to their lives and the role of scientists and engineers in conducting research and development to solve practical problems.

Teachers who field-test the curriculum receive two to three days of professional development prior to using the curriculum and have access to additional support as needed during the field test. The professional development workshops prepare the teachers with content background and hands-on experience for teaching the curriculum and for providing thorough feedback on the curriculum. In addition, these early professional development workshops for field-test teachers help to identify teacher leaders who will assist with dissemination and implementation of the published curriculum.

Dissemination is conducted by presentations and displays of the materials at science teacher education conferences and through the extensive networks of both LHS and LAB-AIDS, Inc.

Results

The curriculum module addresses Education technical barriers A (Lack of Readily Available, Objective, and Technically Accurate Information) by providing information about hydrogen and fuel cells in a curriculum format that is usable by teachers and students in typical classrooms. This module was developed during previous years of the grant through four rounds of classroom testing and revision to ensure that it works well in a wide variety of high school settings, thus addressing barrier E (Regional Differences).

Work during the past year focused on completing videos to support teachers' use of the module, building a partnership in Connecticut and providing professional development to Connecticut teachers, and disseminating the materials nationally.

The videos for teachers are complete and available on the project website and on YouTube. These videos provide general information helpful in disseminating the materials, as well as teacher professional development and support for using the curriculum with students. The videos address Education technical barriers A (Lack of Readily Available, Objective, and Technically Accurate Information) and C (Disconnect Between Hydrogen Information and Dissemination Networks) by providing teachers with an additional form of support, in addition to the teacher support materials embedded within the curriculum guide. The videos include:

1. An introduction to the curriculum.
2. How to set up and run the student electrolyzer and produce hydrogen (Curriculum Activity 2).
3. How to identify the gases produced by the electrolyzer (Curriculum Activity 2).
4. How to operate the fuel cell (Curriculum Activity 3).
5. Modeling the fuel cell reaction (Curriculum Activity 4).
6. Measuring the energy efficiency of the fuel cell (Curriculum Activity 5).
7. Safety and care of the equipment.

To view these videos, visit <http://sepuplhs.org/high/hydrogen/videos.html> and click on "Teacher Support Videos."

The professional development and dissemination work address Education technical barriers C (Disconnect Between Hydrogen Information and Dissemination Networks) and D (Lack of Educated Trainers and Training Opportunities) by building on the dissemination networks of the LHS and partners and preparing teachers who will be able to provide professional development in their regions. Presentations at science teacher conferences reached approximately 200 teachers during the past year. In these one- to two-hour presentations, teachers were introduced to the module and information about fuel cells in the U.S. and their state or region, and conducted an activity on the fuel cell reaction that they were then given to take back to their classrooms and try out.

A two-day professional development conference led by a project staff member and hosted by the Connecticut Science Center prepared 17 teachers to implement the module in their classrooms. The Lab-Aids sales representative from the northeast helped to recruit participants and attended the workshop to enhance her knowledge and ability to promote the module. Two science educators from the Connecticut

Science Center attended the conference, and a scientist from UTC power contributed a one-hour presentation. In addition to training the teacher participants, this event helped to build our relationships with potential partners in Connecticut.

Conclusions and Future Directions

Conclusions:

- The project is now nearly complete. In the past year, we have continued dissemination and professional development activities and have developed a relationship with the Connecticut Science Center around fuel cell education.

Future Directions:

- SEPUP and our publisher, Lab-Aids, Inc., will continue to promote the product, conduct awareness workshops, identify partners, and provide professional development to districts that purchase the curriculum.

FY 2012 Publications/Presentations

1. Willcox, M. "Alternative Energy for Transportation: Hydrogen and Fuel Cells." California Science Teachers Association Regional Conference. October 21, 2011. Pasadena, California.
2. Nagle, B. "Alternative Energy for Transportation: Hydrogen and Fuel Cells." National Science Teachers Association Regional Conference. October 29, 2011. Hartford, Connecticut.
3. Willcox, M. "Teaching about Hydrogen Fuel Cells." National Science Teachers Association Regional Conference. December 10, 2011. Seattle, Washington.

4. Willcox, M. "Investigating Alternative Energy: Hydrogen and Fuel Cells." Georgia Science Teachers Association Conference. February 17, 2012. Atlanta, Georgia.
5. Willcox, M. "Teaching Chemistry with Hydrogen and Fuel Cells." Wisconsin Science Teachers Association Conference. March 9, 2012. Madison, Wisconsin.
6. Lenz, L. "Fuel for the Next Generation." Michigan Science Teachers Association Conference. March 9, 2012. Lansing, Michigan.
7. Nagle, B. "Fuel for the Next Generation." National Science Teachers Association Conference. March 30, 2012. Indianapolis, Indiana.
8. Keller, C. "HyTEC." Two-day professional development session. May 30-31, 2012. Connecticut Science Center, Hartford, Connecticut.
9. Nagle, B. "HyTEC." Workshop presentation for teacher leaders. Scheduled for July 26, 2012. Elkhart, Indiana.

IX.4 State and Local Government Partnership

Joel M. Rinebold
Connecticut Center for Advanced Technology (CCAT), Inc.
222 Pitkin Street, Suite 101
East Hartford, CT 06108
Phone: (860) 291-8832
Email: Jrinebold@ccat.us

DOE Managers
HQ: Connie Bezanson
Phone: (202) 586-8055
Email: Connie.Bezanson@ee.doe.gov
GO: Gregory Kleen
Phone: (720) 356-1672
Email: Gregory.Kleen@go.doe.gov

Contract Number: DE-FC36-08GO18116 / 003

Project Start Date: September 1, 2008
Project End Date: December 31, 2011

Project Objectives

- Foster strong relationships among federal, state, and local government officials, industry, and appropriate stakeholders.
- Serve as a conduit between the DOE and state and local government decision makers.
- Provide technically accurate and objective information to government decision-makers and identified stakeholders to improve/enhance decision making.
- Increase the knowledge base and improve awareness regarding hydrogen and fuel cells.
- Provide support for hydrogen and fuel cells in early market applications, consistent with DOE's market transformation efforts.

Technical Barriers

This project addressed the following technical barriers from the Education section of the Fuel Cell Technologies Program Multi-Year Research, Development and Demonstration Plan:

- (A) Lack of Readily Available, Objective, and Technically Accurate Information
- (C) Disconnect Between Hydrogen Information and Dissemination Networks
- (D) Lack of Educated Trainers and Training Opportunities

Contribution to Achievement of DOE Hydrogen Education Milestones

This project contributed to the achievement of the following DOE milestones from the Hydrogen Education section of the Fuel Cell Technologies Program Multi-Year Research, Development and Demonstration Plan:

- Milestone 17: Hold "Hydrogen 101" seminars (4Q, 2008 through 4Q, 2012).
- Milestone 30: Evaluate knowledge and opinion of hydrogen technology of key target audience and progress toward meeting objectives. (4Q, 2012).

Related milestones in *Task 3* (Educate State and Local Government Representatives) and *Task 7* (Assess Knowledge and Opinions of Hydrogen Technologies) of the above reference have both been achieved with support from the State and Local Government Partnership.

Project Accomplishments

- *Identify Key Stakeholders* - Developed a database of local and state decision-makers and key stakeholders.
- *Develop Resources for Hydrogen and Fuel Cell Deployment* – Developed modeling, "Roadmap" documents and a database detailing criteria for the deployment of hydrogen and fuel cell technologies for transportation, stationary and portable power applications, as well as, potential sites for the deployment of hydrogen and fuel cell technology including: commercial and public buildings and transit, public and private fleet vehicle locations.
- *Develop Online Information, Models and Tools for User Analysis* - Developed an inventory of appropriate models and tools to assess environmental value, energy management, renewable energy, cost and economics, and a comparison of competing technologies. Developed a website and Regional Resource Center with appropriate information, models and tools.
- *Educate State and Local Decision Makers* – Organized and held over 120 project partner meetings, and approximately 20 regional and/or Connecticut state collaborative meetings/workshops, including assistance provided to municipalities regarding the development of fuel cell projects, grant applications, and transportation initiatives.
- *Integrate Local Energy Plans with State Plans* – Developed a "Connecticut Hydrogen and Fuel Cell Deployment Transportation Strategy" plan for the Connecticut Department of Transportation to develop

hydrogen fueling and vehicle deployment strategies and local municipalities to integrate energy plans with state plans and energy goals.

- *Identify Financial and Investment Opportunities* - Developed “Roadmap” documents incorporating incentives, funding, and investment opportunities for hydrogen and fuel cell technologies.
- *Organize and Hold Regional Briefing* - Developed a database of DOE contacts and key stakeholders in northeast states for regional briefing.
- *Pre- and Post-Program Survey* - Developed surveys to assess level of knowledge of local and state decision makers and key stakeholders for the beginning of the project.
- *Developed Market Assessment* - Undertook economic modeling and use of an IMPLAN economic model to assess the economic impact of the hydrogen and fuel cell industry (H₂/FC) in an 8-state region consisting of NJ, NY, CT, MA, RI, NH, VT, and ME in terms of its direct, indirect, and induced economic effects. Identified and Mapped target locations for fuel cell deployment in the Northeast region.
- *Develop a Toolbox for Roadmap Construction* - Developed an inventory of models and tools to assess environmental value, energy management, renewable energy, cost and economics, and a comparison of competing technologies.
- *Train Individuals on Models* – Held at least nine regional briefings and workshops including webinars.
- *Educate and Assist State and Local Officials and State Organizations* – Held roughly ten state and local briefings to build upon existing partnerships while creating new opportunities.
- *Develop a Basic “Roadmap” to provide Guidance for Technology Deployment* - A “Roadmap” has been developed for each state making up the 8-state region. These development plans include information on the economic value of the region’s hydrogen and fuel cell industry identified through a multi-state economic impact model, deployment opportunities including mapping of potential end users, and a summary of supporting policies/incentives.
- *Outreach and Reporting* - Provided “Roadmaps”, white papers, and supporting educational materials to strengthen the level of knowledge of local and state decision makers and key stakeholders.



Introduction

This project assisted with the building of partnerships between the DOE, states and municipalities. CCAT

developed a structure with an approach that provides an opportunity for federal, regional, state, and local involvement to encourage and promote the use of hydrogen and fuel cell technologies. The structure included leadership by the DOE; the establishment of collaborative meetings, workshops, and briefings to provide information to municipal and state decision makers; the provision of resources for potential developers to assess opportunity for deployment; support for state stakeholder groups to implement initiatives in support of state and federal policies; identification and assessment of economic benefits of the hydrogen and fuel cell industry; and development of “Roadmap” documents with implementation of strategies to facilitate the deployment of hydrogen and fuel cell systems in each Northeast regional state.

The structure also included a virtual Regional Resource Center developed by CCAT that provides online information, models, and other tools to assist decision makers and end users to quantify the costs and benefits of hydrogen and fuel cell technology at potential sites. The Regional Resource Center provides tools for implementation to assist local and state planners and decision-makers in identifying potential opportunities for the deployment of hydrogen and fuel cell technologies. The models available through the Regional Resource Center are used to assess environmental value, energy management, renewable energy, cost and economics, and comparisons of competing technologies.

CCAT published the Hydrogen and Fuel Cell Development Plans (“Roadmaps”) for New York, New Jersey and each of the states in New England. These development plans provide links to relevant information to help assess, plan, and initiate hydrogen or fuel cell projects to help meet the energy, economic, and environmental goals in the region. The plans identify policies and incentives that support hydrogen and fuel cell technology to increase deployment at sites that would benefit from on-site generation. The “Roadmaps” show the relationship between increased demand for hydrogen and fuel cell technologies, increased production, and job creation throughout the supply chain. The development plans show how policies and incentives can be coordinated regionally to maintain the regional economic cluster as a global exporter for long-term growth and economic development.

Approach

CCAT’s approach has been to develop resources for hydrogen and fuel cell deployment to aid in the education of state and local decision makers. These resources include online information, models, and tools for potential users to analyze the costs and benefits of hydrogen and fuel cell technology. Coordination and cooperation is sought by both local and state decision-makers in order to introduce hydrogen and fuel cell technology in early market applications. The project uses local “bottoms up”

decisions guided by state/regional “tops down” assistance to help reduce conflict, improve state/regional and municipal relations, and provide better solutions to community-based energy problems. Because of the high risk and high capital cost of implementing new technologies, CCAT also coordinates with local, state, and regional decision makers to identify innovative funding and procurement mechanisms, such as group purchases and corporate tax credits, to encourage market growth, reduce costs, and increase public acceptance.

Results

Informational Tools

CCAT has developed and refined resources to analyze development of hydrogen and fuel cell facilities throughout the region. These models make available information for non-technical and technical audiences, including state and local decision makers and potential end users. The Regional Resource Center models are described in Table 1.

TABLE 1. Regional Resource Center Models and Descriptions

| Model Type | Description |
|---|---|
| Environmental | Assesses the environmental benefits of hydrogen and fuel cell applications compared with other conventional technologies. The model can be used to assess potential emissions reductions, including greenhouse gases, using hydrogen and fuel cell technology. |
| Economic / Cost | Assesses potential yearly heating and electricity cost savings when using a commercially available fuel cell for baseload power. The model allows users to assess the economic viability of a fuel cell system. |
| Energy Management | Assesses the efficiency benefits of stationary fuel cell applications. The model can be used to assess the potential energy savings using a fuel cell to replace conventional electricity generating technologies. |
| Distributed Technology Comparison | Allows a user to compare fuel cells with other distributed energy technologies including microturbines, combustion turbines, reciprocating engines, photovoltaic systems, and wind turbines, based on certain criteria such as installation cost, efficiency, emissions, heat rate, etc . |
| Hydrogen Generation From Renewable Technology | Assesses wind, photovoltaic and hydroelectric power generation technologies to identify hydrogen production capacities and average cost per kilogram of generated hydrogen from these renewable technologies. |

Economic Impact

A regional economic impact was conducted for each state of the Northeast Region to examine the overall economic values of the industry in state and the collective region. The economic impact was defined as the direct output, employment, and labor income associated with the

25 hydrogen and fuel cell manufacturers located in CT, MA, and NY, as well as the region-wide multiplier effects supported by the purchases of businesses and workers related to the industry. A summary for each state as well as the region as a whole is illustrated in Table 2.

TABLE 2. Economic Impact Summary

| | CT | NY | MA | VT | NH | RI | VT | NJ | Regional |
|---|-------|-------|--------|-------|-------|-------|-------|--------|----------|
| Total Employment | 2,529 | 1,728 | 964 | 18 | 45 | 32 | 16 | 111 | 5,443 |
| Total Revenue/ Investment (\$ million) | \$496 | \$292 | \$171 | \$2.9 | \$8.7 | \$6.9 | \$3.3 | \$26.5 | \$1,009 |
| Manufacturer Revenue/ Investment (\$ million) | \$254 | \$119 | \$59.6 | 0 | 0 | 0 | 0 | 0 | \$433 |
| Total Supply Chain Companies | 599 | 183 | 322 | 28 | 25 | 19 | 5 | 8 | 1189 |
| Total Manufacturers | 8 | 9 | 8 | 0 | 0 | 0 | 0 | 0 | 25 |

Currently, approximately 1,180 companies make up the growing hydrogen and fuel cell industry supply chain in the Northeast region. These companies making up the region are estimated to have realized over \$1 billion in revenue and investment, contributed more than \$51 million in state and local tax revenue, and approximately \$650 million in gross state product from their participation in this regional energy cluster. The manufacturers consist of 25 companies responsible for supplying 2,228 direct jobs and \$433.15 million in direct revenue and investment.

Collaborations

CCAT continues to build upon existing relationships while creating new opportunities. Table 3 lists significant businesses and organizations of which CCAT was successful in growing relationships and/or developing new bonds with through interactions, as a result of the project.

Conclusions and Future Directions

This partnership effort has successfully identified a process with stakeholder participants; created models and tools that will allow potential adapters to assess opportunities for deployment of hydrogen and fuel cell technologies in early market applications; and has been expanded to replicate the stakeholder process and tools to develop guideline “Roadmap” documents in each of the New England States, NY and NJ. The process models and tools and guideline documents have been created to facilitate the education of decision makers/end users and to analyze potential sites for hydrogen and fuel cell technologies. Final copies of these documents are currently available through the CCAT,

TABLE 3. Collaborations

| Type | Organization | | |
|---|---|---|---|
| Hydrogen and Fuel Cell Industry | - FuelCell Energy - UTC Power - Proton Onsite - Nuvera Fuel Cells - Plug Power | - Avalence - General Motors - Infinity Fuel Cell - Ballard - Acumentrics | - Electrochem - Nanoptek - Watt Fuel Cell - Protonex - SiEnergy Systems |
| Federal Partners | - Department of Energy - Small Business Administration | - Department of Defense - Department of Commerce | |
| State Partners | - CT Department of Public Utility Control - CT Department of Economic and Community Development - Department of Transportation - CT Siting Council | - CT Clean Energy Finance and Investment Authority - New York State Energy Research and Development Authority - Massachusetts Clean Energy Center | |
| Regional Organizational Partners | - CT Power and Energy Society - Northeast Energy and Commerce Association - Clean Energy States Alliance | - New Energy New York - Massachusetts Hydrogen Coalition | - Hydrogen Energy Center - Northeast Electrochemical Energy Storage Cluster |
| Local Partners | - Mayors - First Selectmen | - Public Works Officials - Council of Governments | |
| Utilities | - Northeast Utilities | - United Illuminating | |

Northeast Electrochemical Energy Storage Cluster, and Connecticut Hydrogen Fuel Cell Coalition websites.

Next steps: On behalf of CCAT, the Connecticut Innovations/Connecticut Small Business Innovation Research Office and the Department of Commerce will bring two workshops specifically focused on the clean energy/hydrogen and fuel cell sector to the Small Business Innovation Research and Global Trade Summit, taking place on July 24-26 at Mohegan Sun in Connecticut. Topics of these two workshops include 1) Opportunities for the Clean Energy Sector: Hydrogen and Fuel Cells and 2) Clean Energy Opportunities in Canada. In addition, the Fuel Cell Seminar & Exposition, a premier meeting for the fuel cell industry, taking place at Mohegan Sun on November 5-8, is plotted to host the 2012 Regional Supply Chain Exchange for the hydrogen and fuel cell industry.

CCAT will continue to educate and train state and local official, organizations, and decision makers on a limited basis by leveraging resources from other projects. CCAT will continue to disseminate “roadmap” documents amongst state and regional agencies and coordinate the development of supportive state policies.

CCAT has recently proposed a project that incorporates replication of the “Roadmap” process with the focus of promoting the coordinated development of hydrogen refueling infrastructure and deployment of fuel cell electric vehicles in the Northeast region. The Northeast Corridor Hydrogen Infrastructure Development Initiative would address the four critical areas that provide significant obstacles to alternative fuel and vehicle use: 1) Policies, 2) Barrier Reduction, 3) Safety and Training, and 4) Market Development Outreach.

Special Recognition & Awards/Patents Issued

2011 Annual Merit Review Awards. On May 11, 2011, the DOE recognized CCAT for work on the advancement of fuel cell and hydrogen technologies for Connecticut and the Northeast. The award highlighted CCAT’s collaborative educational outreach efforts that span the Northeast with groups such as the Northeast Energy Commerce Association and the Northeast Sustainable Energy Association; the analysis of job growth and economic development impacts attributable to the fuel cell industry and its supply chain; and the development of models to help potential fuel cell customers evaluate the life-cycle costs and benefits of deploying fuel cells.

FY 2012 Publications/Presentations

1. Rinebold, J.M., “Hydrogen and Fuel Cell Development “Roadmap” Plans (CT, MA, NY, VT, NH, ME, NJ, RI)”, U.S. DOE, and SBA, Final Reports, April 10, 2012.
2. Rinebold, J.M., “Connecticut Hydrogen Fuel Cell Industry Status and Direction: 2012”, CHFCC, April 2012.
3. Rinebold, J.M., “Northeast Hydrogen Fuel Cell Industry Status and Direction: 2012”, NEESC, April 2012.
4. Rinebold, J.M., “State and Local Government Partnership”, presentation at the 2012 DOE Annual Merit Review and Peer Evaluation Meeting, Washington, D.C., May 17, 2012
5. Rinebold, J.M., “Fuel Cell CHP, Jobs, Economic Development, Clean Energy”, presentation at NECHPI 2012, January 31, 2012.
6. Rinebold, J.M., “Assessing the Economic Impact of the Northeast Electrochemical Energy Storage Industry”, presentation at 2011 Fuel Cell Seminar and Exposition, November 3, 2011.

X. MARKET TRANSFORMATION

X.0 Market Transformation Sub-Program Overview

INTRODUCTION

The Market Transformation sub-program is conducting activities to help promote and implement commercial and pre-commercial hydrogen and fuel cell systems in real-world operating environments and to provide feedback to research programs, U.S. industry manufacturers, and potential technology users. One of the sub-program's goals is to achieve sufficient manufacturing volumes in emerging commercial applications that will enable cost reductions through economies of scale, which will help address the current high cost of fuel cells (currently the capital and installation costs of fuel cells are from five to six times higher than incumbent technologies).¹ These early market deployments will also address other market acceptance factors, resulting in further expansion of market opportunities.

Current key objectives of the Market Transformation sub-program are to build on past successes in material handling equipment (e.g., lift trucks) and emergency backup power applications that were part of the Recovery Act, by exploring other emerging applications for market viability. Fiscal Year (FY) 2012 activities were primarily focused on completing projects using FY 2010 appropriations and preparing for a new solicitation using FY 2012 appropriations. These projects are highly leveraged, with an average of more than half of the projects' funds being provided by DOE's partners. Partners providing resources to these projects have shown a high level of interest in exploring these applications and markets, and this level of industry interest is very promising for the potential growth of the domestic fuel cell industry.

GOALS

Market Transformation activities provide financial and technical assistance for the use of hydrogen and fuel cell systems in early market applications, with the key goals of: achieving sales volumes that will enable cost reductions through economies of scale, supporting the development of a domestic industry, and providing feedback to testing programs, manufacturers, and potential technology users.

OBJECTIVES²

- Advance understanding of the use of fuel cells for waste-to-energy systems, shipboard auxiliary power units, and aviation applications through testing and evaluation efforts coordinated with the Technology Validation sub-program and in partnership with the Department of Defense (DOD), the Department of Agriculture, the Federal Aviation Administration, and others; evaluate design requirements for aircraft auxiliary power units by 2012 and waste-to-energy fuel cells by 2014.
- By 2014, establish baseline energy efficiency and reliability performance metrics for commercially available emergency backup power, material handling, and light commercial/residential fuel cell systems and provide feedback to component suppliers regarding cost reduction opportunities.
- By 2015, in coordination with the DOE Office of Electricity Delivery and Energy Reliability, test emerging approaches to grid management using fuel cell systems and renewably produced hydrogen.
- By 2016, develop and launch energy efficiency and reliability certification programs for fuel cells.
- By 2017, identify lessons learned from existing policies and regulations and promote the development of effective and applicable incentives for hydrogen and fuel cell technologies.

¹ Catalog of CHP Technologies, U.S. Environmental Protection Agency, December 2008, www.epa.gov/chp/basic/catalog.html.

² Note: Targets and milestones were recently revised; therefore, individual project progress reports may reference prior targets. Some targets are still currently under revision, with updates to be published in FY 2013.

FY 2012 STATUS

Fuel cells have been enjoying growing success in key early markets, particularly in material handling (e.g., forklift) and backup power applications. The Program's early market deployment efforts—including Market Transformation funding and Recovery Act funding—have successfully catalyzed a significant level of market activity in these areas, which has been accompanied by substantial reductions in the price of fuel cells. The sub-program is actively pursuing additional opportunities for effective stimulation of market activity. Ongoing activities and additional areas of interest include the following:

- **Material Handling Equipment (MHE):** As a complement to the hydrogen fuel cell forklift deployments currently underway, the sub-program is investigating the use of direct methanol fuel cell (DMFC) technologies. DMFC MHE will provide the same operational benefits as hydrogen-powered fuel cell MHE, with significant additional benefits from the use of a liquid fuel, including reduced infrastructure costs, high energy density, and lower overall fueling costs.
- **Mobile Lighting:** The sub-program is exploring the potential for expanded use of fuel cells for mobile lighting, which is commonly used for road maintenance, general construction, and large outdoor events. Unlike conventional diesel-based systems, fuel cells offer the benefits of nearly silent operation, with no harmful exhaust emissions. Working with manufacturers of fuel cells and mobile lighting equipment, the Program has supported the design, construction, and testing of fuel cell power mobile lighting prototypes (Sandia National Laboratories). Demonstration and testing was conducted at a Boeing Manufacturing Plant, NASA Kennedy Space Center, Caltrans, Paramount Pictures/Saunders Electric, and the San Francisco International Airport.
- **Market Analysis and Deployment Tools:** The sub-program continues to pursue opportunities for collaboration through the DOE-DOD memorandum of understanding, including two projects that have analyzed the technical feasibility of using fuel cells for auxiliary power onboard commercial passenger airliners, addressing both low-temperature polymer electrolyte membrane fuel cells (Sandia National Laboratories), and high-temperature ceramic-type fuel cells (Pacific Northwest National Laboratory).
- **Micro-CHP (Combined Heat and Power):** To document the market viability of fuel cells for small facilities, the sub-program is working with fuel cell developers and system users to demonstrate micro-CHP systems at five commercial facilities. ClearEdge Power is providing 15 fuel cells. A key objective of this work is to obtain performance data on these systems over the course of several years.
- **Big Island of Hawaii Hydrogen Energy Storage Project:** In partnership with the Naval Research Laboratory and the University of Hawaii's Hawaii Natural Energy Institute, the sub-program is supporting the demonstration of a hydrogen energy storage system as a grid management tool. While hydrogen produced from the system could be used in a variety of value-added applications, the initial phase of the project will use the hydrogen in two fuel cell buses operated by the County of Hawaii Mass Transportation Agency.
- **South Carolina Landfill Gas Purification Project:** The sub-program is demonstrating the business case and technical viability of using landfill gas (LFG) as a source of renewable hydrogen production, using BMW's assembly plant in South Carolina as the host site. Should such a scale-up operation prove viable, it would represent a first-of-its-kind LFG-to-hydrogen production project in the nation, and it would serve as a model for future adoption of renewable biogas as a feedstock for hydrogen production.

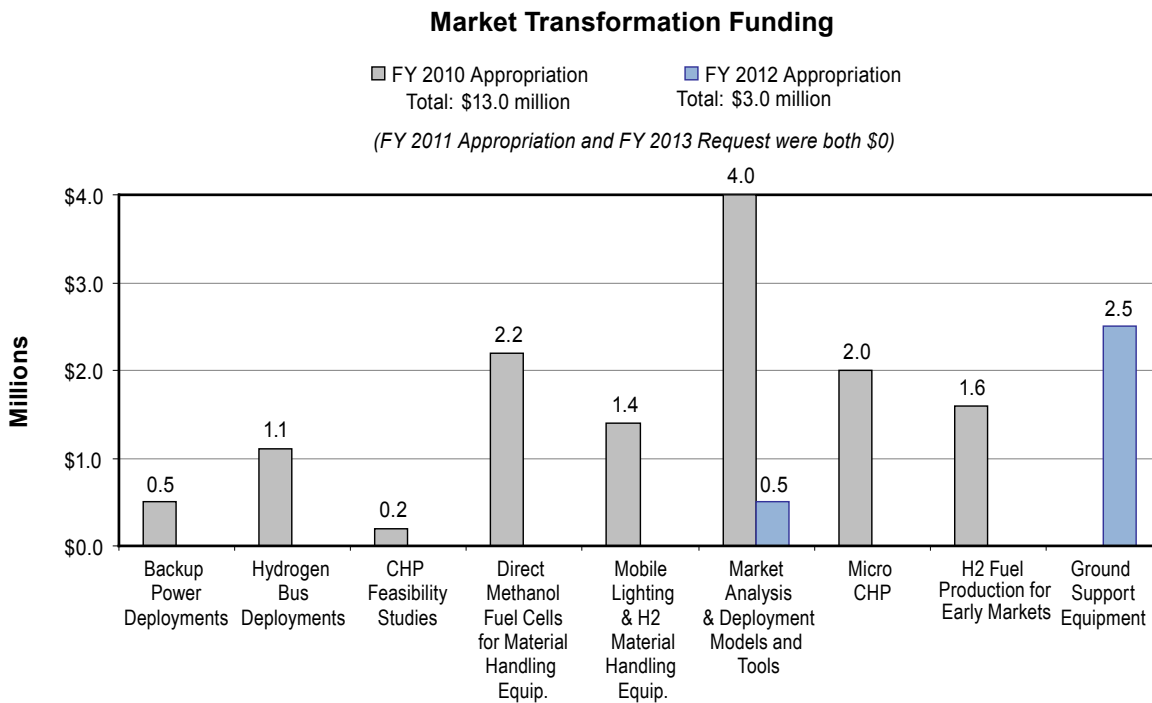
FY 2012 KEY ACCOMPLISHMENTS

In FY 2012, the sub-program developed deployment tools and business cases for various fuel cell applications, conducted public outreach activities, and analyzed and tested potential new early markets in mobile lighting, DMFC-powered lift trucks, and auxiliary power. The following are some of the key milestones the sub-program achieved in FY 2012:

- Demonstrated and validated a fuel cell mobile lighting system that combines high-pressure (5,000-psi) hydrogen storage, efficient lighting, and a 5-kW PEM fuel cell; field tested the system at industry and government installations; and expanded public awareness of the technology by using fuel cell mobile lighting at various entertainment-industry award events, including the Oscars, the Golden Globe Awards, and the Screen Actors Guild Awards.
- Developed and published guidelines for federal facilities managers to procure energy from stationary fuel cell power systems, including the use of innovative financing mechanisms that require little or no capital investment.
- Demonstrated 75 DMFC lift trucks at four food distribution sites.
- Initiated a competitive funding opportunity to deploy fuel-cell powered ground support equipment at airports or air freight distribution centers.
- Conducted modeling and simulation for evaluating onboard fuel cell rechargers for battery-electric road vehicles.
- Initiated demonstration and deployment of fuel cell auxiliary power systems for refrigerated trucks.

BUDGET

FY 2012 appropriation was \$3 million and no funding was requested in FY 2013.



FY 2013 PLANS

In FY 2013, the sub-program will continue to document lessons-learned associated with previously funded projects, including the strategies developed for market entry and for risk management with respect to safety, environmental, and siting requirements. Business analysis and case studies will be initiated. Collection and evaluation of data from these projects will provide the basis for verifying the business cases for various early market fuel cell systems, as well as providing an assessment of the performance of these integrated systems. Data will be made publicly available so that more customers will become aware of the benefits of integrated hydrogen and fuel cell systems. In addition, a near-term priority will be to continue collaborating with other federal agencies—in accordance with existing interagency cooperative agreements such as the DOE-DOD memorandum of understanding—to increase the use of fuel cells in market-ready applications and to increase awareness of the benefits of these deployments. Competitive award(s) will be made and deployment of fuel cell powered ground support equipment will begin.

Pete Devlin

Market Transformation and Interagency Coordination Manager

Fuel Cell Technologies Program

Department of Energy

1000 Independence Ave., SW

Washington, D.C. 20585-0121

Phone: (202) 586-4905

Email: Peter.Devlin@ee.doe.gov

X.1 Hydrogen Energy Systems as a Grid Management Tool

Richard (Rick) E. Rocheleau (Primary Contact),
Mitch Ewan

Hawaii Natural Energy Institute
School of Ocean and Earth Science and Technology
University of Hawaii at Manoa
1680 East-West Road, POST 109
Honolulu, HI 96822
Phone: (808) 956-8346
Email: rochelea@hawaii.edu

DOE Manager

HQ: Pete Devlin
Phone: (202) 586-4905
Email: Peter.Devlin@ee.doe.gov

Technical Advisor

Karen Swider-Lyons
Naval Research Laboratory
Phone: (202) 404-3314
Email: karen.lyons@nrl.navy.mil

Project Start Date: September 30, 2010

Project End Date: September 29, 2012

- Install a 350-bar hydrogen fuel dispenser at the MTA base yard in Hilo.
- Purchase an El Dorado 2012 ENC AeroElite 290, 19-seat shuttle bus.
- Contract the Hawaii Center for Advanced Transportation Technologies to convert the El Dorado bus to a fuel cell electric vehicle (FCEV) utilizing a Hydrogenics fuel cell power system.
- Supply hydrogen for a FCEV shuttle bus for local community bus service operated by the County of Hawaii MTA.
- Demonstrate the use of the Proton polymer electrolyte membrane (PEM) electrolyzers as a grid management tool to mitigate the impacts of intermittent renewable energy on the grid.
- Characterize performance/durability of the Proton PEM electrolyzer under dynamic load conditions.
- Conduct performance/cost analysis to identify benefits of integrated systems including grid services and off-grid revenue streams.

Barriers

This project addresses non-technical issues that prevent full commercialization of fuel cells and hydrogen infrastructure as indicated in the following sections of the April 2009 edition (amended in 2011) of the Fuel Cell Technologies Program Multi-Year Research, Development and Demonstration Plan:

Hydrogen Production, Technical Challenges Section 3.1.4

- (I) Grid Electricity Emissions (for distributed)
- (J) Renewable Energy Generation Integration (for central)
- (Q) Testing & Analysis

Technology Validation, Section 3.6.5

- (A) Lack of Fuel Cell Vehicle Performance and Durability Data
- (C) Hydrogen Storage
- (D) Lack of Hydrogen Refueling Infrastructure Performance and Availability Data
- (E) Codes and Standards
- (G) Hydrogen from Renewable Resources

Hydrogen Safety, Section 3.8.4

- (A) Limited Historical Database
- (D) Liability Issues
- (F) Safety is Not Always Treated as a Continuous Process

Fiscal Year (FY) 2012 Objectives

- Conduct an environmental assessment for the installation of a hydrogen system at the Puna Geothermal Ventures (PGV) geothermal plant on the Island of Hawaii.
- Purchase a Proton 65 kg/day electrolyzer hydrogen production and compression system from Powertech. The system includes an autonomous data acquisition and control system to operate the hydrogen system.
- Install site improvements and utilities at the PGV geothermal plant to support the operation of the hydrogen system.
- Hire an operations and maintenance company to operate and maintain the hydrogen system.
- Develop a project hydrogen safety plan.
- Engage the DOE Hydrogen Safety Panel to support hydrogen safety including equipment installation, project hydrogen safety plans, outreach to the authorities having jurisdiction, and first responder training.
- Install and commission the hydrogen system at PGV.
- Procure two Powertech 450-bar tube trailers to transport hydrogen from PGV to the County of Hawaii Mass Transportation Agency (MTA) bus yard in the town of Hilo.
- Purchase a Ford 450 diesel pickup truck to tow the tube trailer.

- (G) Expense of Data Collection and Maintenance
- (H) Lack of Hydrogen Knowledge by Authorities Having Jurisdiction
- (I) Lack of Hydrogen Training Facilities for Emergency Responders

Technical Targets

No specific technical targets have been set.

FY 2012 Accomplishments

- Developed system requirements and specification
- Awarded contract to Powertech to supply “turn-key” hydrogen system
- Started environmental assessment
- Developed memorandum of agreement with PGV
- Developed memorandum of agreement with MTA
- Awarded contract to Powertech for additional hydrogen delivery trailers
- Developing site design with infrastructure contractor
- Procured additional \$500k funding from State of Hawaii to purchase and convert the El Dorado bus to a FCEV bus
- Procured additional \$1 million from the State of Hawaii H2 Fund for site infrastructure
- Procured additional \$600k from Office of Naval Research for overall project support including purchase of additional hydrogen delivery trailers
- Engaged DOE Hydrogen Safety Team to support hydrogen safety
- Developed operations and maintenance contract to support daily operation of the hydrogen systems



Introduction

While solar and wind resources offer a major opportunity for supplying energy for electrical grid electricity production and delivery systems, their variability and intermittency can raise challenges for the cost-effective and high-reliability integration of these renewable sources on electrical grids. Curtailment and grid management-related costs experienced by these renewable sources are a challenge at today’s level of generation capacity, and these costs will hinder the substantive additional penetration of electricity generation supplied by these renewable resources. Hydrogen production through electrolysis may provide an energy storage opportunity to mitigate curtailment and grid management costs by serving as a controllable load that produces a storable energy product during time periods

where the electricity generation capacity is not required by the system operators. Energy storage via hydrogen production can provide the power producer or systems operator with increased options for coordinating system loads. The renewable hydrogen product can also create new and incremental revenue streams to the power producers through the sale of hydrogen products to customers outside of the electricity delivery system. Accordingly, hydrogen energy storage at a utility scale offers the potential for increasing the levels of variable renewable energy that can be harnessed by the power producers or systems operators.

Approach

A four-step process is required to evolve energy systems:

1. Develop and validate rigorous analytic models for electricity and transportation.
2. Develop and model scenarios for the deployment of new energy systems including additional renewables.
3. Identify and analyze mitigating technologies (demand side management, storage, Smart Grid, advanced controls, forecasting, future gen) to address systems integration (grid stability) and institutional issues.
4. Conduct testing and evaluation to validate potential solutions to facilitate utility acceptance.

General Electric (GE) was our subcontractor under a separate DOE funded project and we used the results of that for this project. However, GE is not a subcontractor under this specific project. GE developed two models of the Big Island grid utilizing GE’s proprietary modeling technology. Transient performance was modeled using the GE Power Systems Load Flow software model:

- Full network model incorporating generator governors and automatic generator control
- Transient stability simulation looks at challenging times with fluctuating renewables to check transient stabilities
- Long-term dynamic simulation

A production cost model was developed using the GE Multi Area Production Simulation software model:

- Representation of dispatch and unit commitment rules.
- Hour-by-hour simulation of grid operations for a full year taking into account ramp rates and dispatch rules. For example minimum percentage load for baseload units.
- Yields cumulative fuel usage, emissions, and variable cost.

Frequency variability due to wind fluctuation of the Big Island grid was used as the initial test of the model. The Big Island grid has the following characteristics:

- 100 to 200 MW with early evening peak
- 30 MW wind
- 30 MW unregulated geothermal
- Significant and growing photovoltaics

To explore the potential of the hydrogen energy storage opportunity, this project will evaluate the value proposition of using utility-scale electrolyzers to both regulate the grid and use excess electricity from renewables to make hydrogen for various products. In this initial phase of the project, an electrolyzer will be installed at the PGV geothermal plant on the Big Island. In this first phase, it will not be connected to the grid. The electrolyzer will be operated in a dynamic mode designed to simulate future operation as a grid-connected variable load that can be quickly ramped up and down to provide frequency regulation. Data will be collected to analyze the ability of the electrolyzer to ramp up and down, and to determine its durability and performance under dynamic operating conditions. The hydrogen produced by the system will be used to fuel one hydrogen-fueled bus to be operated by the County of Hawaii bus company - MTA.

Results

- Progressed legal agreements among project participants (PGV, MTA) including resolution of liability, indemnification, and insurance issues and requirements.
- Procured \$1.5 million of additional funding from the State of Hawaii to augment DOE funding to support the installation of infrastructure and procurement of a 19-passenger FCEV shuttle bus.
- Awarded contract to Powertech for the supply of a “turn key” hydrogen system.
- Initiated an environmental assessment.

Conclusions and Future Directions

- The project is underway but equipment and infrastructure need to be installed and operated before any results can be evaluated.

- Future work involves the procurement, installation, and operation of the following:
 - Installing hydrogen production systems and infrastructure at the PGV geothermal site.
 - Installing hydrogen dispensing systems and infrastructure at the MTA bus depot site in Hilo.
 - Procuring and operating a FCEV shuttle bus.
 - Operating the electrolyzer and hydrogen systems at the PGV and MTA sites.
 - Collecting and analyzing system performance data.
 - Preparing performance reports and sharing it with project sponsors and industry.
- If Phase 1 results show positive results, apply for a Phase 2 follow-on project that increases the size of the electrolyzer.

A major project challenge to the timely deployment of hydrogen infrastructure and equipment necessary to conduct operations has been the amount of time required to develop legal agreements to address liability issues. This is approaching two years in this project. This in turn has required our requesting a no-cost extension to extend the project to meet operational test duration requirements. This represents a large investment in outreach and education of all parties concerned including the legal profession, risk managers, first responders, and authorities having jurisdiction. Hopefully follow-on projects will not take so long.

FY 2012 Publications/Presentations

1. R. Rocheleau and M. Ewan, “*Hawaii Energy Systems as a Grid Management Tool*”, *US DOE Annual Merit Review*, Washington, D.C., May 2012.
2. R. Rocheleau and M. Ewan, “*Hawaii Energy Systems as a Grid Management Tool*”, *World Hydrogen Energy Conference*, Toronto, Canada. June 2012.

X.2 Fuel Cell Combined Heat and Power Industrial Demonstration

Kriston P. Brooks (Primary Contact), Siva P. Pilli,
Dale A. King

Pacific Northwest National Laboratory
P.O. Box 999
Richland, WA 99352
Phone: (509) 372-4343
Email: kriston.brooks@pnnl.gov

DOE Manager

HQ: Peter Devlin
Phone: (202) 586-4905
Email: Peter.Devlin@ee.doe.gov

Contract Number: DE-AC05-76RL01830

Subcontractor:

ClearEdge Power, Portland, OR

Project Start Date: May 2010

Project End Date: September 2012

Technical Targets

No specific technical targets have been set.

FY 2012 Accomplishments

- Established baseline models to evaluate the cost and technical performance of FCSs.
- ClearEdge Power provided 15 CHP FCSs that were installed at four different deployment sites (refer to the results section for location list).
- Have been remotely monitoring several parameters (see Approach for the list) at one-second intervals for all 15 operating units.
- Established several new performance definitions and characterized baseline system performance for ongoing data analysis.
- Engaged and informed stakeholders in different industry venues:
 - Presented initial data analysis results to more than 13 conferences and trade groups.
 - Submitted three peer-reviewed journal articles (two accepted, one in review) for publication.

Fiscal Year (FY) 2012 Objectives

The overall objective of this project is to:

- Demonstrate combined heat and power (CHP) fuel cell systems (FCS) in small commercial buildings.
- Analyze engineering, economic, and environmental performance data from the demonstration systems to reveal barriers to commercialization that should be emphasized - identify where industry needs to spend the greatest effort to achieve high market penetration and reveal issues that may expedite its commercialization.
- In the longer term, document market viability (a business case) of this class of fuel cells for small commercial buildings.

Technical Barriers

This project addresses technical and economic issues preventing the full commercialization of CHP FCSs. This includes the lack of long-term validated performance data for 5 kilowatt-electric (kWe) to 100 kWe FCSs such as:

- Energy production performance, durability, and reliability.
- Installation, operations, and maintenance costs.



Introduction

The objective of this project is to demonstrate CHP FCSs in small commercial facilities and assess their performance to help determine and document market viability. This information is important for the DOE, the fuel cell community, and most importantly for small commercial facilities that have operational power and heat requirements. The FCSs for this demonstration were acquired through an open competition in which ClearEdge Power won the award. Between September 2011 and March 2012, ClearEdge Power installed 15 of their CHP FCSs for application and demonstration at four small industrial facilities. Pacific Northwest National Laboratory (PNNL) began obtaining performance data of these systems as they were commissioned, and will continue with this objective over the course of the next few years. This project provides “real-world” data from units “in the customer’s hands” to validate performance, durability, and reliability; installation, operations, and maintenance costs; and identifies remaining barriers to widespread commercialization.

Approach

First, we established a baseline method for cost and technical performance of the FCSs to assure a common basis in which to evaluate the systems that were eventually to be deployed. Next we set out to acquire the FCSs for demonstration. The acquisition process was described in detail in the previous year's progress report [1]. ClearEdge Power was selected as the fuel cell manufacturer, and four different industrial partners, including retail, education, food provision, and recreation/community buildings, were selected for these deployments. Deployments occurred between September 2011 and March 2012. We are currently remotely monitoring several parameters at one-second intervals for these 15 operating units: (1) natural gas mass inlet flow rate to burner; (2) natural gas mass inlet flow rate to reactor; (3) current exported from FCS to the building's electrical grid; (4) grid voltage measured by FCS inverter; (5) estimated FCS heat generated; (6) net electrical power generated; (7) system electrical power setpoint; and (8) temperature of heat delivered by FCS to site. We began to analyze and document the performance data collected over the last few months of each FCS deployed. We will continue to analyze the performance data collected over at least a two-year period for each FCS deployed and document the overall market viability of this class of FCSs for small commercial buildings. These ongoing analyses will include overall technical, economic, and environmental performance.

Results

ClearEdge Power provided 15 CHP FCSs that were installed at four different deployment sites: two sites in Northern California, one site in Southern California, one site in Oregon (for a sample deployment see Figure 1). Independent evaluation of manufacturer-stated economic, engineering, and environmental performance of the CHP FCSs was performed. The analysis data presented here is for five FCS units that were commissioned early in the deployment. Analysis of the other units is in progress.

Economic Performance: This analysis is based on the rated performance data (5 kWe and 5.5 kilowatt-thermal [kWt]) provided by the manufacturer (i.e., not independently measured data). The average electrical and thermal demand values were calculated using all the 10 deployment sites, which includes the four sites mentioned above, that were initially down selected (see Figure 2). Using both a standard and a management accounting approach, an economic analysis was performed to calculate (1) the average per-unit cost of the CHP FCSs per unit of power (electricity only); and (2) the average per-unit cost of the CHP FCSs per unit of energy. The average per-unit cost of electrical power for these systems ranged from \$15,000–19,000/kWe (depending on site-specific installation, fuel, and other costs), while the average per-unit cost of combined electrical and heat recovery power ranged from



FIGURE 1. Two FCS units tested for this study in Portland, Oregon

\$7,000–\$9,000/kW. From the energy perspective, the average per-unit cost of electrical energy was estimated to range from \$0.38 to \$0.46/kilowatt-hour-electric (kWh_e), while the average per-unit cost per unit of electrical and heat recovery energy varied from \$0.18 to \$0.23/kWh (Figure 2). The breakdown of the total cost per unit of installed electrical and heat recovery energy capacity is also illustrated in Figure 2 (DOE shows the portion that is provided/paid by the project, Partner shows the portion that is paid by the installation partner, and Federal/State shows the portion paid by federal and state incentives). In addition, Figure 2 compares the CHP FCSs' costs with the average electricity and heating prices for California and Oregon [2,3,4]. The combination of federal and state incentives reduces CHP FCS costs in several cases to be within ~25% of being economically competitive with existing average commercial electricity prices in California. When federal and state incentives are accounted for, the CHP FCS price drops to within a range of \$0.14/kWh to \$0.23/kWh with an average of \$0.17/kWh. Tax incentives help CHP FCSs compete more closely with statewide average commercial electricity and heating prices in California and Oregon.

Engineering Performance: Engineering performance parameters are independently evaluated. Based on an

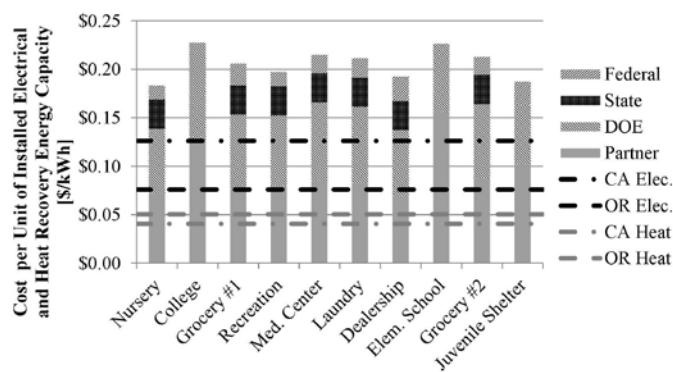


FIGURE 2. Breakdown of cost per unit of electrical and heat recovery energy capacity [2,3,4]

analysis of the first few months (October 2011 to April 2012) of measured operating data of the five FCS units, FCS performance is consistent with manufacturer-stated performance. Initial data indicate that the FCSs have relatively stable performance and a long-term average production of about 4.57 kWe of power. This value is consistent with, but slightly below, the manufacturer’s stated rated electric power output of 5 kWe. The measured system net electric efficiency has averaged 33.7%, based on the higher heating value of natural gas fuel. This value also is consistent with, but slightly below, the manufacturer’s stated rated electric efficiency of 36%. The FCSs provide low-grade hot water to the building at a measured average temperature of about 48.4°C, lower than the manufacturer’s stated maximum hot water delivery temperature of 65°C. A summary of the results for five CHP FCSs is shown in Table 1. The uptime of the systems is also evaluated. System availability (A_o) can be defined as the quotient of total operating time compared to time since commissioning. The average values for system availability vary between 96.1% and 97.3%, depending on the FCS evaluated in the field.

For FCS Unit 130, a maximum decline in electric power output of approximately 18% was observed over a 500-hour period in January 2012, as shown in Figure 3.

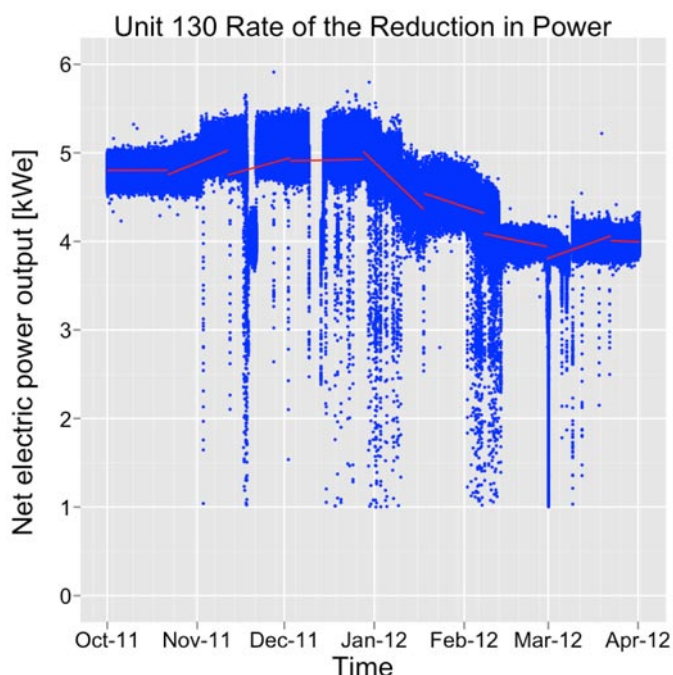


FIGURE 3. Decline in Power Output (Unit 130). A maximum decline in electric power output of approximately 18% over 500 hours was observed.

Power output declined from approximately 5 kWe to 4.3 kWe over this time period due in part to ClearEdge Power reducing the system setpoint (from 5 KWe to 4 KWe). The rate of change was calculated by fitting a simple linear regression (red solid lines) of the power output data. Power output data below 1 kW was not included in the regression analysis. Although 1,000-hour periods are more standard in industry, the system downtime for some of the units made it difficult to calculate 1,000-hour rates, so periods of 500 hours were considered in this work and the rates have been converted to the more standard unit. Table 2 indicates that the rate of decline averaged over the fuel cells evaluated is near 0.16 kW per 1,000 hours. The decline represents a maximum degradation rate during the observation period. This decline could be partly a result of high-temperature

TABLE 1. FCS Performance Summary. Downtime events (power output less than 1 kWe) and startup were not included in the calculated averages. The average heat recovery values are calculated by the manufacturer, and do not represent a measured value.

| Unit | Average Net Electric Power Output (kWe) | Average Net Heat Recovery for External Heating (kWth) | Average Temp of Water Sent to Site (°C) | Average Net System Electrical Efficiency (%) | Average Net Heat Recovery Efficiency (%) | A_o (%) |
|------------------|---|---|---|--|--|-------------|
| 129 | 4.58±0.5 | 5.19±0.5 | 46.1±3 | 33.5 | 38 | 96.3 |
| 130 | 4.53±0.5 | 5.14±0.5 | 45.7±3 | 32.8 | 37.2 | 96.2 |
| 131 | 4.58±0.4 | 5.19±0.5 | 51.5±6 | 33.7 | 38.2 | 96.1 |
| 132 | 4.64±0.4 | 5.26±0.4 | 50±6 | 33.5 | 37.9 | 96.7 |
| 133 | 4.50±0.4 | 5.1±0.5 | 48.7±7 | 34.8 | 39.4 | 97.3 |
| All Units | 4.57 | 5.18 | 48.4 | 33.7 | 38.1 | 96.5 |

proton exchange membrane degradation and/or fuel cell stack degradation. Other units show a similar downward trend prior to maintenance performed in March, which may include a partial stack replacement or regeneration. It is also possible that a portion of the decline in power output may be attributable to changes in setpoint that are unrelated to degradation. The rate of decline when corrected for the system setpoint is an order of magnitude lower (right hand column of Table 2). The degradation rate most likely lies somewhere between these values.

TABLE 2. Decline in Power Output. Maximum power output rate of decline based on the power output and the normalized power output ΔW_E (difference between the control setpoint and the power output).

| Unit | Power Output Maximum Rate of Decline (kW per 1,000 hrs) | Normalized Power Output Maximum Rate of Decline from ΔW_E (kW per 1,000 hrs) |
|------------------|---|--|
| 129 | -0.24 | -0.007 |
| 130 | -0.18 | -0.014 |
| 131 | -0.08 | -0.004 |
| 132 | -0.05 | -0.004 |
| 133 | -0.25 | -0.004 |
| All Units | -0.16 | -0.007 |

Environmental Performance: Preliminary environmental analyses (not reported at this time, analysis is underway) were shown to decrease the greenhouse gas (GHG) emissions by one-third by shifting from a conventional energy system to a CHP FCS system. The GHG mitigation costs also were proportional to the changes in the GHG gas emissions. Human health costs were estimated to decrease significantly with a switch from a conventional system to a CHP FCS system.

Conclusions and Future Directions

The real-time monitoring of five FCSs over a five-month period has provided a variety of insights about the system performance.

- CHP FCS costs in several cases are found to be within ~25% of being economically competitive with existing average commercial electricity prices. Federal and/or state incentives further improve this competitiveness.
- FCS engineering performance is consistent with manufacturer-stated performance, but slightly below the manufacturer's stated rated electric power.
- The rate of decline in electric power output averaged over the five fuel cells evaluated is near 0.16 kW per 1,000 hours.

Future directions:

- Continue analyzing engineering, economic, and environmental performance data from all the demonstration systems.

- In the next FY, develop a business case documenting the market viability of this class of fuel cells for small buildings. This business case will include estimates of the projected costs would be at various production levels and the process of power that would make the system cost competitive both with and without government incentives.

Special Recognitions & Awards/Patents Issued

1. Whitney G. Colella, Siva P. Pilli, "Analysis of Combined Heat and Power (CHP) High Temperature Proton Exchange Membrane (HTPEM) Fuel Cell Systems (FCSs) for Light Commercial Buildings," ASME 2012 10th Fuel Cell Science, Engineering & Technology Conference, San Diego, CA, July 23rd-26th, 2012. *Nominated for the Best Paper Award.*

FY 2012 Publications/Presentations

Peer-Reviewed Journal Articles and Conference Proceedings

1. Whitney G. Colella, Siva Pilli, "Analysis of Combined Heat and Power (CHP) High Temperature Proton Exchange Membrane (HTPEM) Fuel Cell Systems (FCSs) for Light Commercial Buildings," ASME 2012 10th Fuel Cell Science, Engineering & Technology Conference, San Diego, CA, July. 23rd-26th, 2012.
2. Whitney G. Colella, Heather E. Dillon, "Independent Evaluation of Real-Time Measured Performance Data From Micro-Combined Heat and Power Fuel Cell Systems Installed in the Field," ASME 2012 10th Fuel Cell Science, Engineering & Technology Conference, San Diego, CA, July. 23rd-26th, 2012.
3. Whitney G. Colella, Viraj Srivatsava, "System Integration of Combined Heat and Power Fuel Cells within Commercial Buildings Using Advanced Computer Models," ASME 2012 10th Fuel Cell Science, Engineering & Technology Conference, San Diego, CA, July. 23rd-26th, 2012.
4. Whitney G. Colella, Siva Pilli, "Analysis of Combined Heat and Power (CHP) High Temperature Proton Exchange Membrane (HTPEM) Fuel Cell Systems (FCSs) for Light Commercial Buildings,," Accepted to Journal of Fuel Cell Science & Technology.
5. Whitney G. Colella, Heather E. Dillon, "Independent Evaluation of Real-Time Measured Performance Data From Micro-Combined Heat and Power Fuel Cell Systems Installed in the Field," Accepted to Journal of Fuel Cell Science & Technology.
6. Whitney G. Colella, Viraj Srivatsava, "System Integration of Combined Heat and Power Fuel Cells within Commercial Buildings Using Advanced Computer Models," Submitted to Journal of Fuel Cell Science & Technology.
7. W.G. Colella, "Initial Deployment and Independent Testing of Micro-Combined Heat and Power Fuel Cell Systems in Light Commercial Buildings," EFC11178, Proceedings of the European Fuel Cell - Piero Lunghi Conference & Exhibition (EFC2011), Rome, Italy, Dec. 14-16th, 2011 (in press).

Oral Conference Presentations

1. W.G. Colella, H Dillon, S Pilli, V Srivastava, 2011, “Fuel Cell Combined Heat and Power Industrial Demonstration,” U.S. DOE Hydrogen and Fuel Cells Program and Vehicle Technologies Program Annual Merit Review and Peer Evaluation Meeting, May 16th, 2012.
2. Thomas Benjamin, Dimitrios Papageorgopoulos, “DOE Efforts for Development and Deployment of Small-Scale Systems for Stationary Power,” 1st International Expert Workshop - High Temperature Fuel Cells, March 27-28, 2012, Duisburg, Germany (PNNL contribution: Slides 15 to 19).
3. Colella, W.G., Advances in Distributed, Grid-Connected Energy Generation and Storage, Korea Institute of Energy Research Seminar, Korea Institute of Energy Research, Daejeon, Republic of Korea, Feb. 17th, 2012.
4. Colella, W.G. “The Next Generation, Low Carbon Electricity Grid,” The International Workshop on Energy, Environment, Water and Sustainability (EWS) at the Korea Advanced Institute of Science and Technology (KAIST), Seoul, Republic of Korea, Feb. 16th, 2012.
5. Colella, W.G. “Addressing Increased Variability on the U.S. Electric Grid from Higher Renewables Penetration using Generation and Storage in the Balancing Market,” Korea Advanced Institute of Science and Technology (KAIST), Seoul, Republic of Korea, Feb. 16th, 2012.
6. Colella, W.G. “Independent Analysis of Real-Time Performance Data from Multiple Co-Generative Fuel Cell Systems Installed in Buildings,” Korea Advanced Institute of Science and Technology (KAIST), Seoul, Republic of Korea, Feb. 16th, 2012.
7. Colella, W.G., Innovative Power Generation, Storage, and Control, Seoul National University Seminar, Seoul National University (SNU), Seoul, Republic of Korea, Feb. 15th, 2012.
8. Colella, W.G., Independent Analysis of High Temperature Proton Exchange Membrane Combined Heat and Power Fuel Cell Systems Deployed in Light Commercial Buildings, Korea Institute of Science and Technology (KIST) Seminar, Fuel Cell Research Center, KIST, Seoul, Korea, Feb. 14th, 2012.
9. Colella, W.G. Stationary Cogenerative and Polygenerative Fuel Cells, Korea Institute of Science and Technology (KIST), Seoul, Republic of Korea, Feb 14th, 2012.
10. Colella, W.G., Advanced Distributed Generation for Buildings using Co-generative and Poly-generative Fuel Cells. Green Manufacturing Research Center (GMRC) at Korea University, Seoul, Republic of Korea, Feb. 13th, 2012.
11. Colella, W.G., Next Generation Building Energy Technologies: Independent Testing of Micro Co-generative Fuel Cell Systems for Light Commercial Buildings, Pacific Northwest National Laboratory (PNNL) Building Energy Systems and Technologies (BEST) Seminar, Richland, WA, Jan. 25th, 2012.
12. Colella, W.G., Cutting-Edge Electricity Generation and Storage for Future Electricity Grids, Pacific Northwest National Laboratory (PNNL) Seminar, PNNL-Seattle Office, Seattle, WA, Jan. 5th, 2012.
13. Colella, W.G., Dillon, H. “Initial Deployment and Independent Testing of Micro-Combined Heat and Power Fuel Cell Systems in Light Commercial Buildings,” American Society of Mechanical Engineers (ASME) Journal of Fuel Cell Science and Technology -- Proceedings of the European Fuel Cell - Piero Lunghi Conference & Exhibition (EFC2011), Rome, Italy, Dec. 14–16th, 2011 (delivered remotely by video file).
14. Colella, W.G., Dillon, H. “Independent Analysis of the Engineering, Economic, and Environmental Performance of Micro Combined Heat and Power High Temperature Proton Exchange Membrane Fuel Cell Systems in Buildings,” Zing Conference -- 1st Annual International Hydrogen & Fuel Cells Conference: Hydrogen production, storage, and utilisation, Xcaret, Mexico, Dec. 1st–5th, 2011 (delivered remotely by video file).
15. Colella, W.G., “Independent Evaluation of Measured Performance Data from Stationary Combined Heat and Power (CHP) Fuel Cell Systems (FCSS) Installed in Light Commercial Buildings,” Fuel Cell Seminar, Orlando, FL, Nov. 2nd, 2011.
17. Colella, W.G., Advanced On-Site Power Generation, Storage, and Control for Residential and Commercial Buildings, Pacific Northwest National Laboratory (PNNL) Seminar, PNNL-Portland Office, Portland, OR, Dec. 16th, 2011.
18. Colella, W.G., Independent Analysis of High Temperature Proton Exchange Membrane Fuel Cells for Micro-CHP, International Energy Agency (IEA) Advanced Fuel Cells Bi-Annual Meeting, Orlando, FL, Oct. 31st, 2011.

References

1. Rinker MW, Colella WG, and Timme RJ; “Fuel Cell Combined Heat and Power Industrial Demonstration” FY 2011 Annual Progress Report, DOE Hydrogen and Fuel Cells Program.
2. U.S. Energy Information Administration, 2011, “Electrical Power Monthly, April 2011,” DOE/EIA-0226 (2011/04), Washington, DC, USA.
3. U.S. Energy Information Administration, 2011, “Electric Power Annual, 2009,” DOE/EIA-0348 (2009), Washington, DC, USA.
4. U.S. Energy Information Administration, 2011, “Natural Gas Monthly, April 2011,” DOE/EIA-0130 (2011/04), Washington, DC, USA.

X.3 Direct Methanol Fuel Cell Material Handling Equipment Demonstration

Todd Ramsden
National Renewable Energy Laboratory
15013 Denver West Parkway
Golden, CO 80401
Phone: (303) 275-3704
Email: todd.ramsden@nrel.gov

DOE Manager
HQ: Peter Devlin
Phone: (202) 586-4905
Email: Peter.Devlin@ee.doe.gov

Subcontractor:
Oorja Protonics, Inc., Fremont, CA

Project Start Date: June 1, 2010
Project End Date: March 31, 2013

- DMFC operational data for more than 6,000 methanol fueling events were collected and analyzed. Analysis determined that DMFC MHE average ~10 hours of operation between fills, allowing a full labor shift to be completed without refueling.
- Product improvements were developed and implemented, enabling better performance and reliability of DMFC systems operating in cold-temperature environments (refrigerated warehouses). Upgraded DMFC systems had 40% lower unscheduled maintenance events compared to original systems.



Introduction

The National Renewable Energy Laboratory (NREL) and the U.S. Department of Energy (DOE) are interested in supporting the development of early market applications for fuel cell technologies. A study by Battelle Memorial Institute, “Identification and Characterization of Near-term Direct Hydrogen Proton Exchange Membrane Fuel Cell Markets,” showed that fuel cells have the potential to power material handling equipment (also known generically as forklifts) at a lower overall cost than lead-acid batteries for certain types of operations [1]. Battery-powered forklifts typically use lead-acid batteries that can only provide enough power for one 8-hour shift. Multi-shift operations therefore generally require additional battery packs and battery change-outs, which reduces productivity and increases costs of operation.

NREL and DOE are currently evaluating the benefits of hydrogen-fueled polymer electrolyte membrane (PEM) fuel cells for MHE and have found that PEM fuel-cell-powered MHE can have a lower total cost of ownership compared to battery-powered forklifts [2,3]. As a supplement to the hydrogen-fueled PEM fuel-cell-powered forklift deployment testing, NREL is investigating the use of DMFC technologies in material handling applications. DMFCs, which use a liquid methanol fuel, hold promise to deliver many of the same operational benefits of hydrogen-powered fuel cell MHE, including long run times, short fueling times, and increased productivity. Liquid alcohol fuels such as methanol offer reduced infrastructure costs, high energy density, and low overall fueling costs.

Approach

NREL has partnered with Oorja Protonics on a project to demonstrate and evaluate DMFCs to provide power for material handling equipment in four commercial wholesale

Fiscal Year (FY) 2012 Objectives

- Operate and maintain fuel-cell-powered material handling equipment (MHE) using direct methanol fuel cell (DMFC) technology.
- Compile operational data of DMFCs and validate their performance under real-world operating conditions.
- Provide an independent technology assessment that focuses on DMFC system performance, operation, and safety.
- Evaluate the market viability of using DMFCs in material handling applications.

Barriers

This project addresses non-technical issues that prevent full commercialization of fuel cells.

Technical Targets

No specific technical targets have been set.

FY 2012 Accomplishments

- 75 DMFC systems and their supporting methanol fueling infrastructure were operated and maintained at four customer warehouse sites for real-world use and testing in Class III MHE.
- DMFC MHE accumulated 6 to 12 months of operations per lift, totaling more than 160,000 hours of operation (as of December 2011).

distribution centers. In total, 75 DMFC-powered Class III pallet jacks have been deployed in warehouses operated by Unified Grocers, Testa Produce, and Earp Distribution. DMFC lifts are being operated two shifts per day for a 15-month deployment, with 3,500 to 5,000 total operational hours expected on each unit.

As part of the project, Oorja built, tested, and deployed its OorjaPac Model 3 DMFC power pack into Class III pallet jacks. The DMFC system delivers an output power of approximately 1.5 kW and includes a 3-gallon methanol storage tank expected to provide approximately 12 hours of autonomy between fuelings. Methanol fuel is being dispensed to the DMFC MHE using the OorjaRig methanol dispenser, which is designed to meet all relevant fire and safety codes for indoor methanol dispensing. Oorja is collecting data on both the DMFC systems and the supporting methanol fueling infrastructure. NREL is compiling and analyzing these data and is providing a third-party assessment on the performance of DMFCs used in material handling applications.

Results

During the first six months of 2011, 75 DMFC systems and their supporting methanol fueling infrastructure were deployed at end-user warehouse sites for real-world use and testing in Class III MHE. The DMFC MHE fleets continue to be operated and maintained, and detailed system-level data have been collected by Oorja and provided to NREL for analysis. The data include dozens of system parameters captured 10 times per minute, characterizing a wide variety

of DMFC performance metrics. Detailed data analysis is performed every six months, with the latest evaluation completed in March 2012.

In total, the combined DMFC MHE fleet had more than 160,000 hours of operation as of December 2011. DMFC systems had significant usage, with over half of the units logging more than 1,500 hours of operation, and nearly 25% of the systems reaching more than 2,170 hours (see Figure 1). Overall, the three fleets operated by Unified Grocers, Testa Produce, and Earp Distribution had fleet averages of 750 hours, 1,500 hours, and 1,800 hours per DMFC system.

The OorjaPac Model 3 DMFC power packs used in this deployment project act in concert with traditional MHE battery systems. Unlike traditional battery systems that have limited run time and require frequent battery changes and charging from the electricity grid, the OorjaPac DMFC system acts as an onboard battery charger, maintaining the battery pack state-of-charge and eliminating electric-grid-based battery charging. Under this configuration, actual DMFC operation time depends on the battery state-of-charge. With a high charge level, the DMFC system may turn off while the pallet jack continues to be used. Hence, the operation hours noted above reflect actual run-time of the DMFC systems but may underestimate actual MHE hours of operation.

The DMFC Class III pallet jacks are deployed in warehouses operating two shifts per day. Data provided indicate that DMFC systems are typically operated 7 to 12 hours per day (with actual MHE operation hours potentially

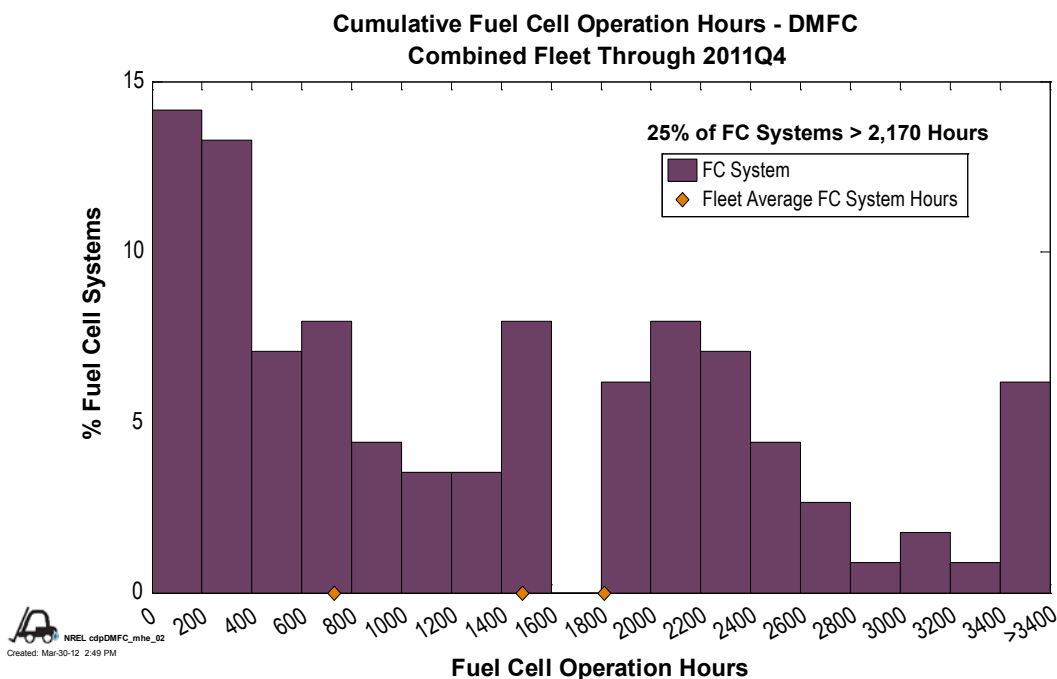


FIGURE 1. Operation Hours for DMFC Systems

higher). Based on an analysis of more than 6,000 methanol fueling events, NREL found that DMFC systems operate for an average of 9.8 hours between methanol fuelings (see Figure 2). Thus, the DMFC systems can easily operate for a full shift on a single methanol fill, and given their typical use pattern, they can often operate for a complete two-shift day on a single fill. Reflecting this, analysis of the methanol fueling data shows that the DMFC systems are filled one time per day on average.

This demonstration project provided the opportunity to deploy DMFC MHE in cold-temperature, refrigerated environments. Initial DMFC system designs were not optimized for cold-temperature operation, leading to a variety of unscheduled maintenance events and, in some cases, early DMFC stack failures. Oorja conducted a fault analysis of systems exhibiting problems and found common failure modes. Based on their analysis, Oorja developed system and technology improvements to DMFC methanol concentration control, electronics control, and fuel fittings, and incorporated those into the DMFC fleet. An analysis of unscheduled maintenance events before system upgrades and after fleet-wide electronics control and fuel fitting upgrades (and an initial rollout of upgrades to methanol concentration control) showed that unscheduled maintenance events were reduced by 40% (see Figure 3).

NREL analyzed individual DMFC systems to characterize system voltage, current, and power; maximum

voltage and power over time; and stack voltage decay. DMFC systems typically operate at high current and power levels (with power generally above 1 kW) and within a tight voltage range of 30–36 volts (see Figure 4). The DMFC systems that exhibited problems and early stack failures prior to the rollout of system upgrades and technology improvements operated below 30 volts and across a wide range of power levels, and showed more significant overall stack voltage degradation.

Detailed analysis of the upgraded DMFC fleet following technology improvements will continue, but initial analyses indicate significant performance improvement in the upgraded fleet. The DMFC fleet also has demonstrated long run-times and autonomy between methanol fuelings, enabling increased productivity by avoiding the need for multiple and time-consuming battery changes during the workday. In FY 2013, a total cost of ownership analysis will be conducted for DMFC MHE that will incorporate data analyses of system performance, maintenance, and methanol fueling.

Conclusions and Future Direction

- 75 OorjaPac DMFC systems and their associated methanol fueling infrastructure were operated and maintained at customer warehouse sites for real-world use and testing.

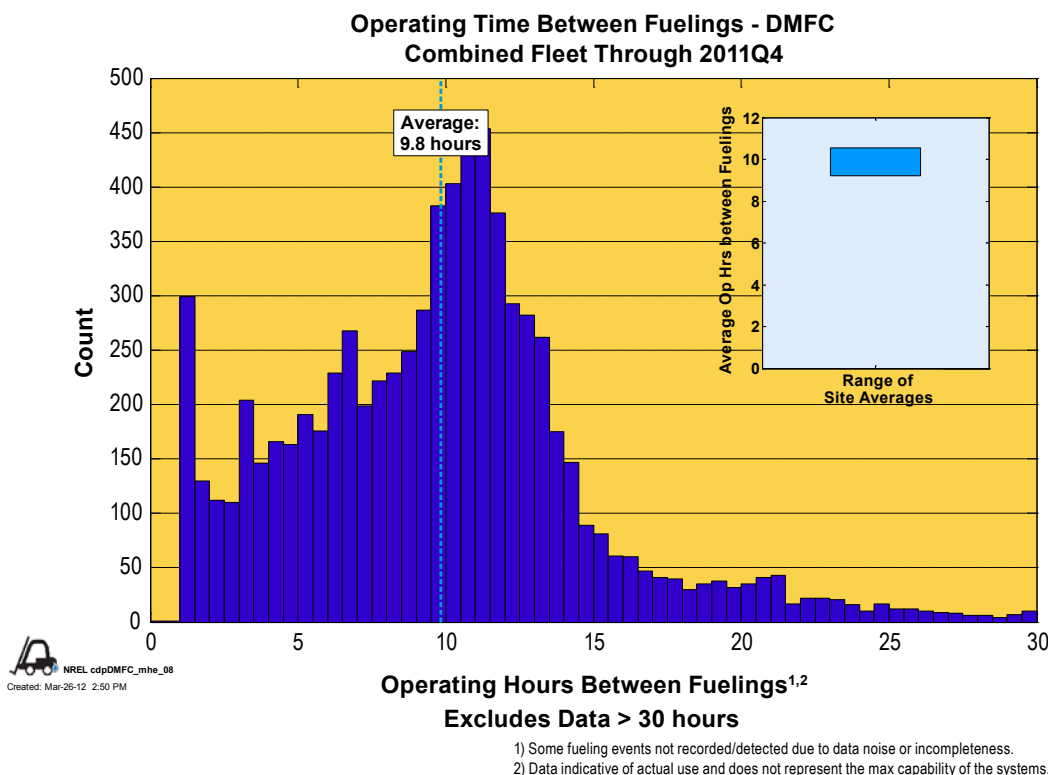


FIGURE 2. DMFC Operation Hours between Fuelings

Note: Data is not available in Excel form

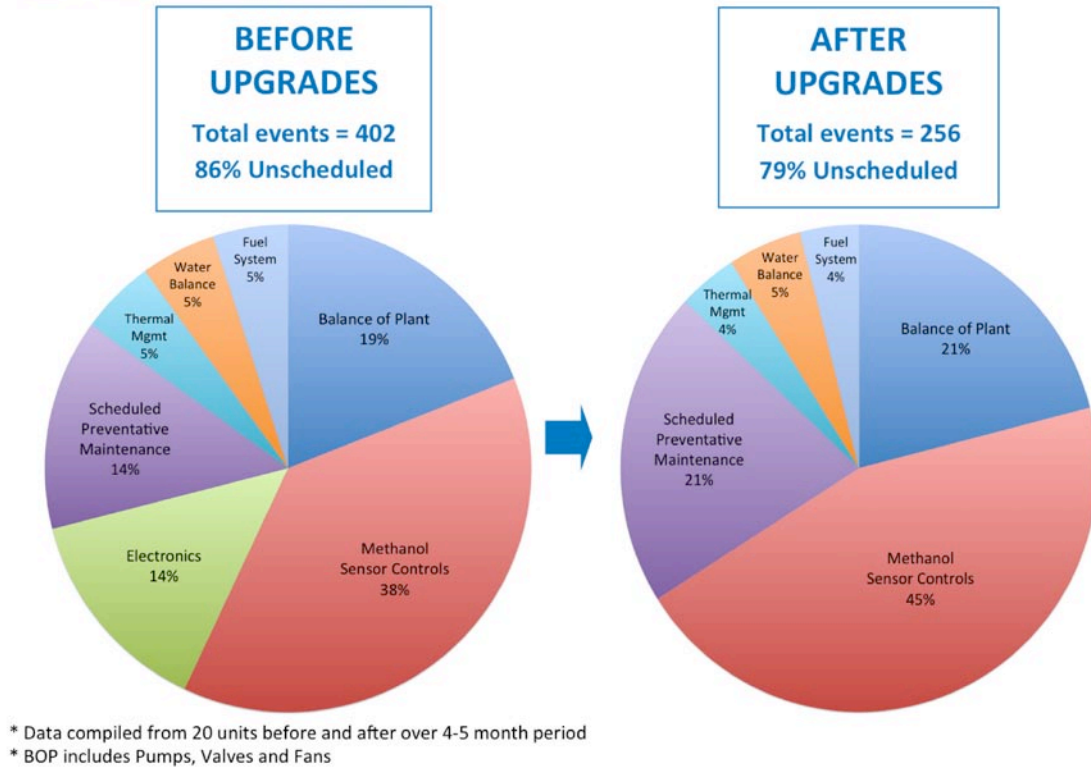


FIGURE 3. Maintenance Events Before and After DMFC System Changes

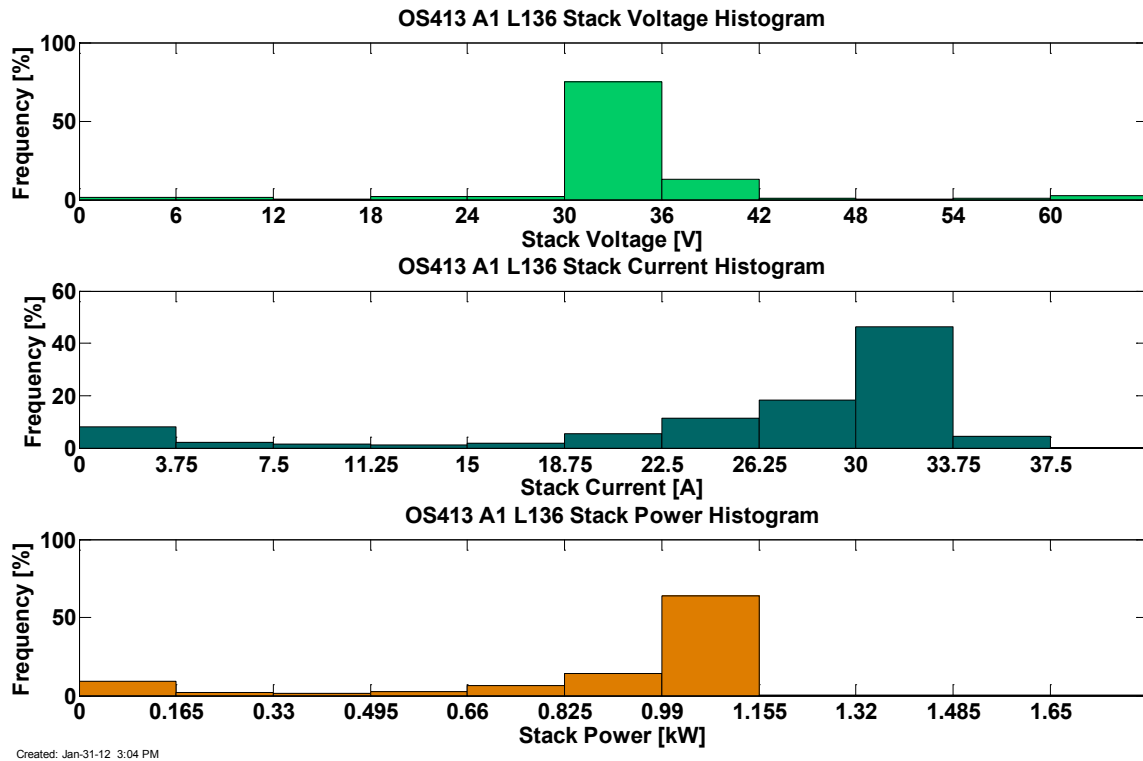


FIGURE 4. Typical DMFC Voltage, Current, and Power Levels during Use

- DMFC systems in the demonstration operate an average of 9.2 hours per day. These DMFCs average 9.8 hours of operation between fueling, and the systems average one fueling per day.
- Initial DMFC system designs showed reliability issues, particularly related to operation in cold-temperature environments. Initial analyses of the maintenance and performance of upgraded DMFC systems show significant improvement.

In the next year, NREL will use real-world operating data to characterize the performance of DMFC systems used in material handling applications, including evaluation of:

- Performance, reliability, and maintenance of deployed DMFC systems, particularly the performance of DMFC systems incorporating the latest technology improvements.
- Business case analysis of DMFC systems compared to typical battery-only systems for Class III MHE, including an assessment of equipment costs, maintenance costs, productivity and labor costs, and costs of fuel and fueling infrastructure.

FY 2012 Publications/Presentations

1. Todd Ramsden, “Direct Methanol Fuel Cell Material Handling Equipment Deployment,” DOE Hydrogen and Fuel Cells Program Annual Merit Review, May 16, 2012, Washington, D.C.

References

1. K. Mahadevan et al., “Identification and Characterization of Near-Term Direct Hydrogen Proton Exchange Membrane Fuel Cell Markets,” Battelle. April 2007.
2. National Renewable Energy Laboratory, “Hydrogen and Fuel Cells Research: Early Fuel Cell Market Demonstrations.” http://www.nrel.gov/hydrogen/proj_fc_market_demo.html.
3. National Renewable Energy Laboratory, Hydrogen Technologies and Systems Center’s Technology Validation Program, “Total Cost of Ownership for Class I, II, & III Forklifts,” March 2012. http://www.nrel.gov/hydrogen/cfm/images/cdp_mhe_58_totalcostofownership.jpg.

X.4 Landfill Gas-to-Hydrogen

Shannon Baxter-Clemmons (Primary Contact),
Russ Keller¹

South Carolina Hydrogen Fuel Cell Alliance
P.O. Box 12302
Columbia, SC 29211
Phone: (803) 727-2897
Emails: baxterclemmons@schydrogen.org;
russ.keller@ati.org

DOE Managers

HQ: Pete Devlin
Phone: (202) 586-4905
Email: Peter.Devlin@ee.doe.gov

GO: Gregory Kleen
Phone: (720) 356-1672
Email: Gregory.Kleen@go.doe.gov

Contract Number: DE-FG36-08GO18113

Subcontractor:

¹ Advanced Technology International, Charleston, SC

Project Start Date: March 1, 2011

Project End Date: January 31, 2013

Fiscal Year (FY) 2012 Objectives

- Validate that a financially viable business case exists for a full-scale deployment of commercially available equipment capable of taking landfill gas (LFG) to hydrogen under the specific BMW operating environment,
- Validate that commercially available clean-up and reformation equipment can convert BMW's LFG to hydrogen at purity levels consistent with fuel cell industry standards.
- Conduct a side-by-side operational verification of fuel cell material handling equipment (MHE) performance and durability between a test group operating on LFG-supplied hydrogen and a control group operating on delivered hydrogen supplied by an industrial gas provider.

Technical Targets

There are no specific technical targets associated with this particular project. Rather, the LFG-to-hydrogen project will focus on validating that integrated systems comprised of commercially available equipment can deliver low-cost hydrogen, which includes system performance, operation and maintenance, durability, and reliability under real-

world operating conditions. This initiative to convert LFG to hydrogen, in this geography (South Carolina) provides an excellent "fit" for advancing DOE's fuel cell market transformation efforts. Several South Carolina manufacturers already use LFG energy for heat/power; several already have elected to convert their MHE inventory to fuel cells; marrying the two could foster a significant increase in fuel cell MHE market penetration goals within the private sector.

FY 2012 Accomplishments

- Completed feasibility study October 26, 2011.
- Received BMW approval of feasibility study and "Go" decision to proceed to the second phase of the project November 21, 2011.
- Identified clean-up equipment requirements specific to BMW LFG stream.
- Determined equipment pad sizes and locations.
- Initiated and completed fabrication of LFG clean-up skid.
- Initiated and completed preparation of mobile hydrogen unit (MHU, reformer/storage/controls).
- Determined connections necessary to existing LFG, natural gas and power services.
- Commenced site prep for landing LFG clean-up skid and MHU.
- Commenced testing of LFG clean-up skid and MHU at the subcontractor's site (prior to delivery to the BMW site).



Introduction

BMW Manufacturing Company has incorporated more than 100 pieces of fuel cell-powered MHE into a new assembly line that became operational 2010. While BMW is prepared in the short term to purchase hydrogen services from an established industrial gas supplier, they strongly desire a future option where they could produce their own hydrogen, preferably from a renewable source -- and ideally as a follow-on effort from their nationally acclaimed 2002 landfill methane project. BMW's original LFG project was implemented in December 2002, and the initial infrastructure allowed for collecting and cleaning methane gas from the Palmetto Landfill near Spartanburg, SC, transporting it through a 9.5-mile pipeline to the BMW plant, compressing and then using it to power four gas turbine generators. BMW recently expanded its on-site electrical generation capacity fueled from LFG, and integrated a new specialized

treatment system to remove siloxanes from the methane gas. The project proposes to leverage the considerable capital investments to date that make pressurized, pre-treated LFG available on-site, thus providing significantly lower cost than would be the case if the LFG were uncleaned, unfiltered and 9.5 miles away from the intended MHE deployment site.

Assessments by BMW of the available quantity of LFG beyond that currently devoted to electrical power generation confirm that, should the LFG-to-hydrogen production initiative prove viable, there would be sufficient LFG available to fuel the entire BMW MHE fleet in both their existing and new facilities. This would enable BMW to fuel nearly 300 additional pieces of fuel cell-powered MHE in their existing production lines. LFG is probably the most challenging waste stream from which hydrogen could be recovered. Should this initiative prove economically and technically viable, less-daunting hydrocarbon waste streams could be considered (such as agriculture waste, wastewater treatment effluent, etc.). South Carolina has many “candidate” landfill sites in the state where this solution may be viable. Additionally, South Carolina has a high concentration of large manufacturing facilities (BMW, Boeing, Michelin, Bridgestone-Firestone, etc.) and major warehousing and distribution facilities with large inventories of MHE, many of which are within 20 miles of an active landfill.

Approach

The over-arching objective is to validate there is a viable business case for full-scale operation should the proposed LFG-to-hydrogen conversion technology prove viable. The basic components required for a fully functional LFG-to-hydrogen system at the host facility are the existing LFG supply, further gas clean-up equipment, steam-methane reformer (SMR) and hydrogen purification equipment, and the existing hydrogen delivery and dispensing equipment.

Meeting the project objectives will give BMW leadership the confidence to move forward with scale up should they choose. Additionally, this effort will lay the groundwork for proving the business case for future adopters. Validating that the technical solution proposed will work in a “real-world” LFG to hydrogen environment is critical to addressing key DOE technology validation barriers. None of the individual technology pieces are “new science;” however, no one has assembled these proven pieces into this particular solution.

Results

The project commenced officially on June 17, 2011 with the first phase of an anticipated three phase program of work. This initial phase was an economic feasibility study and business case analysis designed to assess whether a capital equipment investment in on-site LFG clean-up and methane

conversion to hydrogen would enable production of hydrogen at or below the cost of having hydrogen delivered to the host site by an industrial gas company. This study completed on October 26, 2011 and was delivered to BMW management. BMW approved the study’s conclusions on November 21 2011, and authorized the project team to proceed to the second phase of the project.

The business case analysis had a BMW requirement to investigate only commercially available equipment. This would allow for a quicker transition to full-scale production should the LFG testing phase of the project prove viable. The team executed two separate data calls to industry seeking quotes for gas clean-up equipment and SMR equipment. This equipment was evaluated for two hydrogen production capacities – 50 kg per day and 500 kg per day.

The feasibility study concluded that technologies exist and are commercially available to achieve the expected level of clean-up required to meet specifications of hydrogen generation system provides and that these technologies are very mature. Additionally, large-scale industrial hydrogen production by SMR in the oil refining and petrochemical industry is very mature; though applications for smaller scale SMR equipment (<800 kg/day) are less mature. Future SMR equipment may benefit from lower pricing from increased competition within the market, more efficient heat reclaim strategies within the SMR process, improved catalyst efficiency and the ability to withstand hydrocarbon feedstocks with higher concentrations of undesirable constituents. Small-scale SMR hydrogen production equipment is available, but is designed for use with pipeline quality natural gas. Although more expensive, the cost of SMR and clean-up equipment does not increase in cost as quickly as capacity rises. Therefore, the study concluded that it probably is not economically viable for installations at the 50 kg/day level while a viable business case may be made at the 500 kg/day level.

The conclusions presented from the feasibility study are based on a 10-year analysis; however, longer analysis periods most likely would result in a lower cost per kilogram of hydrogen produced because of the benefit of the initial utility infrastructure and installation costs being amortized over a longer evaluation period. The “bottom line” conclusion is that at the 500 kg/day level, with the existing LFG supply and equipment at the host facility, onsite production of hydrogen using LFG as the hydrocarbon feedstock appears to be cost competitive, if not advantageous, over hydrogen sourced from vendors, produced offsite and transported to the facility.

Implication for DOE Fuel Cell Technologies Program: Although the analysis presented within the feasibility study are specific to the LFG equipment and constituents at the host facility, the basic principles of hydrocarbon feedstock clean-up and reformation to hydrogen should apply to agricultural waste streams, wastewater systems, digester gases and other process off-gases.

Since the November 21, 2011 approval of the feasibility study by BMW and their authorization to proceed forward with the second phase of work, the team has been working toward the preparation of equipment and site work necessary to begin LFG-to-hydrogen production. This second phase of the project will construct a pilot-scale LFG-to-hydrogen production facility on the grounds of the BMW host site, commission and place it into operation, and monitor the quality and purity of the hydrogen that is produced.

The team has identified the clean-up requirements for the particular LFG stream at the BMW site necessary to produce sufficiently pure hydrogen quality for use in fuel cell-powered MHEs. Work also has begun on preparing the MHU. This is a trailer-mounted hydrogen production and fueling system that will receive the cleaned up LFG and produce purified hydrogen. This unit contains an onboard fuel processor, purification, compression and storage components, and can produce 10-15 kg/day of hydrogen, sufficient for executing the planned side-by-side testing (third phase). The unit also contains onboard controls, diagnostics and hydrogen, flame and carbon monoxide detection. The team has replaced the catalyst and reconditioned the reformer, reconfigured and replaced gas quality instruments and overhauled the pressure swing absorption unit for reinstallation into the MHU. The MHU currently is being tested prior to shipment to the BMW site for installation. Long-lead equipment for the gas clean-up skid has been ordered, the gas clean-up skid has been fabricated and the skid currently is undergoing final testing. A picture of the clean-up skid and MHU is presented in Figure 1.

Additionally, the team has identified the equipment pad size and location, and has provided a full site layout including placement of the clean-up skid, the MHU and necessary piping and electrical runs. All utilities requirements have been determined and site-prep work is nearly complete.



FIGURE 1. Gas clean-up skid and mobile hydrogen unit

Conclusions and Future Directions

The completed and approved feasibility study provided the “Go” decision to proceed to Phase 2 – LFG-to-hydrogen production and testing. We are in the final weeks of this stage with only equipment delivery, installation, start-up, testing and commissioning remaining. Additional work in this year is indicated in the following.

- Complete testing of LFG clean-up skid prior to delivery to site.
- Finalize in-house testing of mobile hydrogen unit prior to delivery to site.
- Finalize and extend utilities to equipment pad at BMW site.
- Complete equipment installation at BMW site (clean-up skid and MHU).
- Start up, test and commission equipment.

Once the equipment is up and running we will initiate a testing period of approximately six to eight weeks to determine if the purity of the hydrogen (relative to purchased hydrogen) is adequate for use in the fuel cell-powered MHEs. If the hydrogen proves to be of sufficient purity, a “Go/No-Go” decision will be made to proceed to the third phase of the project – the side-by-side trial.

This final phase of the project would take the hydrogen produced from the purified LFG source, and then compress, store, and distribute it to a single site within the host site manufacturing facility that would permit a “side-by-side” performance evaluation using actual fuel cell-powered MHE. Hydrogen already available on-site from an industrial gas provider (contracted outside the scope of this project) would fuel the “control group” of MHE; hydrogen produced from the pilot scale LFG-to-hydrogen project would fuel the “test group” of MHE.

Notionally, the test would employ 3-5 pieces of MHE in each site that have nearly identical operating requirements and profiles. Data would be gathered monthly to determine whether there is a discernible difference in fuel cell performance or reliability that can be attributed to the LFG source of hydrogen.

FY 2012 Publications/Presentations

1. Feasibility Study Report – 25 October 2011.
2. DOE Annual Merit Review – 16 May 2012.
3. NDIA Environment, Energy Security & Sustainability (E2S2) Symposium & Exhibition – 24 May 2012.

XI. SYSTEMS ANALYSIS

XI.0 Systems Analysis Sub-Program Overview

INTRODUCTION

The Systems Analysis sub-program supports decision-making by providing a greater understanding of technology gaps, options and risks, and the interaction of individual technologies and components and their contributions to the performance of larger systems—e.g., the entire hydrogen fuel system, from production to utilization. The sub-program also analyzes cross-cutting issues, such as the integration of hydrogen and fuel cell systems with the electrical sector and the use of renewable fuels. Particular emphasis is given to assessing stationary fuel cell applications, the impacts of fuel quality on fuel cell performance, and the implications of various approaches to establishing hydrogen infrastructure.

The Systems Analysis sub-program made several significant contributions to the Hydrogen and Fuel Cells Program (the Program) during Fiscal Year (FY) 2012. Hydrogen infrastructure costs were compared with similar costs for other advanced fuels, and opportunities for reducing these infrastructure costs were examined by utilizing stakeholder input and exploring synergies with other fuels such as natural gas. The JOBS FC model was developed by Argonne National Laboratory (ANL) and RCF Economic and Financial Consulting, and it was issued to the public domain to enable employment and revenue generation to be estimated from fuel cell and hydrogen deployment. Infrastructure and early market analyses were conducted to better understand supply and demand issues, and the Greenhouse Gases, Regulated Emissions, and Energy Use in Transportation (GREET) model was modified to enable greenhouse gas emissions to be evaluated on a well-to-wheels basis for hydrogen generation from natural gas extracted by hydraulic fracturing.

GOAL

Provide system-level analysis to support the development of hydrogen and fuel cell technologies, including: evaluating individual technologies and technology pathways to assess issues such as resource needs and infrastructure challenges; providing insight and guidance for balancing the Program's research, development and demonstration (RD&D) portfolio; and estimating the potential value of various RD&D approaches.

OBJECTIVES

- By 2012, complete an evaluation of the use of hydrogen for energy storage and as an energy carrier to supplement energy and electrical infrastructure.
- By 2012, complete an evaluation of fueling station costs for early vehicle penetration to determine the cost of fueling pathways for low and moderate fueling demand rates.
- By 2014, complete environmental studies that should be done in advance of widespread commercialization.
- By 2017, complete analysis of Program performance, cost status, and the potential benefits of using fuel cells for a portfolio of commercial applications.
- By 2019, complete analysis of the market potential for hydrogen, stationary fuel cells, fuel cell electric vehicles and other fuel cell applications such as material handling equipment; the analysis will address the various needs for commercialization of these applications, including: hydrogen production, transportation infrastructure, and required performance of stationary fuel cells and vehicles. It will also assess the impact of the growth of fuel cell market shares on various sectors of the economy.
- Provide milestone-based analysis, including risk analysis, independent reviews, financial evaluations, and environmental analysis, to identify other needs the Program should address as fuel cells achieve technology readiness for various applications.

- Periodically update analyses of the life-cycle energy, petroleum use, greenhouse gas emissions, and criteria pollutant emissions from various fuel cell technologies and hydrogen fuel pathways—including updates based on technological advances or other changes.

FY 2012 STATUS

The Systems Analysis sub-program focuses on examining the economics, benefits, opportunities, and impacts of fuel cells and renewable fuels with a consistent, comprehensive analytical framework. Activities in FY 2012 included: assessing socio-economic impacts, such as increased employment from fuel cell deployment; coordinating with the DOE Vehicle Technologies Program to assess the life-cycle cost of various vehicle platforms, including fuel cell electric vehicles; identifying early markets for fuel cells and opportunities to reduce cost; and exploring various approaches to reducing the cost of hydrogen infrastructure. The Systems Analysis sub-program has transitioned from activities focused on developing key models, to the application of those models in order to complete critical program analyses. As evidenced by the completed and ongoing analysis activities in the “FY 2012 Key Accomplishments” section, the initial strategy of the Systems Analysis sub-program has been effective in enabling the completion of a diverse portfolio of analytical projects.

FY 2012 KEY ACCOMPLISHMENTS

Develop and Maintain Models and Systems Integration

ANL, with assistance from RCF Economic and Financial Consulting, developed the JOBS FC model to estimate the employment and revenue impacts of fuel cell manufacturing and deployment. The model was used to estimate the impact of American Recovery and Reinvestment Act (ARRA) deployments of fuel cells (this analysis was supplemented with calculations that capture economic impacts from expenditures unique to the ARRA program that are not modeled in JOBS FC)—preliminary results indicate that nearly 700 net jobs were created in 2011 as a result of ARRA funding for fuel cell deployments (Figure 1). The JOBS FC model uses input-output methodology to estimate changes in industry expenditures as a result of fuel cell

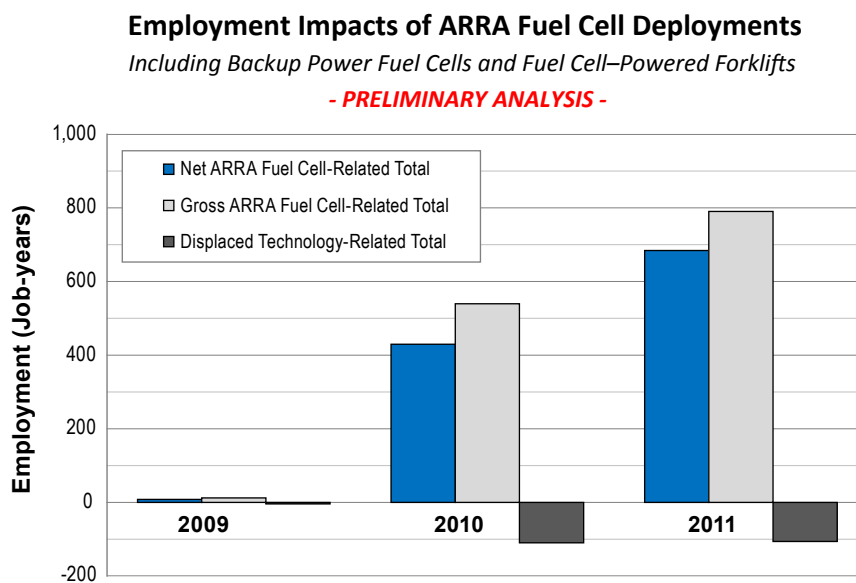


FIGURE 1. Preliminary analysis of employment impacts from ARRA fuel cell deployments, using the JOBS FC model (supplemented with calculations that capture economic impacts from expenditures unique to the ARRA program that are not modeled in JOBS FC) (source: ANL).

deployments and calculates the effects of those changes throughout the economy. Version 1.0 of the model was released for public use in May 2012 and includes forklift and backup power applications of polymer electrolyte membrane fuel cells and stationary power applications of phosphoric acid and molten carbonate fuel cells for user-specified analyses at the state, regional or national level. The model, a user’s guide, and other background material are available for download at <http://jobsfc.es.anl.gov>.

Studies and Analysis

Market Analysis

- Pike Research completed a global and domestic market analysis of the fuel cell markets for portable, stationary power, and transportation applications—identifying increased growth in the fuel cell market and showing that the market remains strong, with over 20,000 systems shipped in 2011, an increase of more than 35% over 2010 (Figure 2).

Infrastructure Analysis

- Analysis of infrastructure costs for hydrogen fueling and electric vehicle charging, conducted by the National Renewable Energy Laboratory (NREL), show that the capital intensities of the two infrastructure systems are roughly comparable, as illustrated in Figure 3. The analysis also indicates that the cost of fuel for fuel cell electric vehicles, battery electric vehicles, and plug-in hybrid-electric vehicles would be comparable to the cost of gasoline for hybrid electric vehicles, on a cents-per mile basis. Advanced light-duty vehicles fueled by hydrogen and electricity offer significant benefits by reducing greenhouse gas emissions, improving energy security, and improving air quality. A complete report based on this analysis will be issued by the end of 2012.
- NREL, along with a diverse group of stakeholders, examined opportunities for reducing the cost of hydrogen infrastructure. Using their infrastructure cost calculator, NREL evaluated potential cost reductions for early market fueling stations. Using stakeholder input, NREL analysis indicated that station cost could be reduced by >70% through standardization and modular station design in the early commercial phases; analysis also indicated that additional station cost reductions of >40% could be realized through economies of scale (Figure 4). Results from the stakeholder input to the cost calculator are shown below and will be published at the end of 2012.

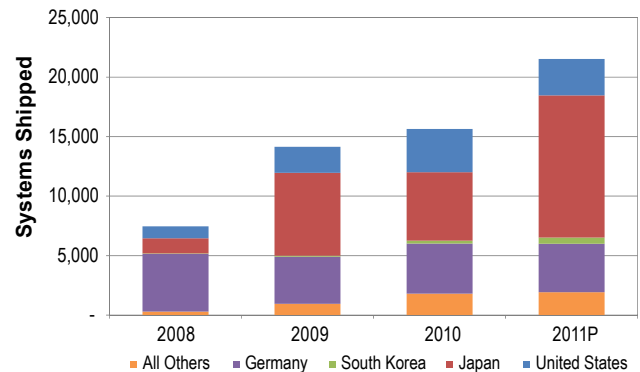
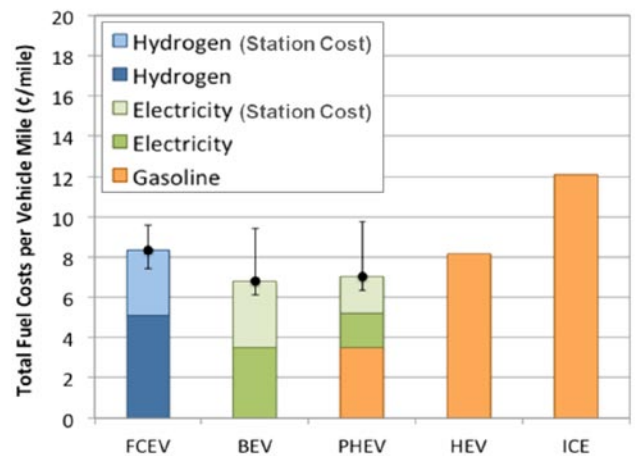


FIGURE 2. Global shipments of fuel cell systems, by key countries, including stationary, portable, and transportation fuel cell systems (source: Pike Research).

Fuel Costs (preliminary analysis)



FCEV – fuel cell electric vehicle; BEV – battery electric vehicle; PHEV – plug-in hybrid electric vehicle; HEV – hybrid electric vehicle; ICE – internal combustion engine (vehicle)

FIGURE 3. Preliminary analysis of the total fuel costs (on a cents-per-mile basis) for various vehicles, including the costs of refueling stations or charging stations (Error bars shown represent variations in retail infrastructure capital costs, source: NREL)

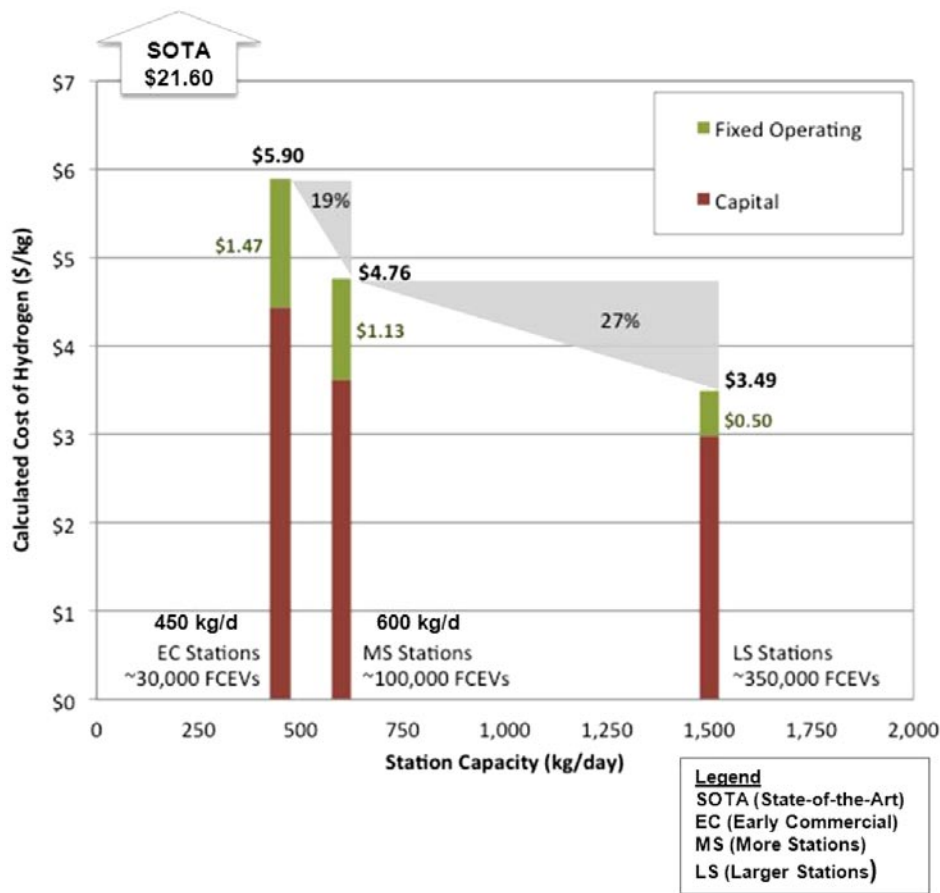


FIGURE 4. Results of stakeholder input to NREL's cost calculator show the potential for substantial reductions in the impact of station cost on the overall cost of hydrogen (source: NREL).

- DOE and ANL held a natural gas workshop with multiple stakeholders to gain valuable insight for potential synergies between hydrogen and natural gas. The objectives were to identify the current status of natural gas and hydrogen infrastructure, identify key challenges preventing or delaying widespread deployment of natural gas and hydrogen infrastructure, and identify opportunities for addressing challenges and for government and industry stakeholders. The results of the workshop highlighted that natural gas and hydrogen have similar storage and regulatory concerns; clusters of refueling centers are required to support a critical mass of both types of vehicles; by types of infrastructure should be developed along major commercial corridors; and consistent, long-term energy policies are required for natural gas and hydrogen fuel applications. A summary report was published by ANL and is available at: www.transportation.anl.gov/pdfs/AF/812.PDF

Environmental Analysis

- ANL revised the GREET model to include hydraulic fracturing for natural gas to assess the impact of various pathways utilizing natural gas as a feedstock or an energy source. As shown in Figure 5, the greenhouse gas emissions would be ~10% lower for a natural-gas-to-hydrogen pathway that used natural gas from hydraulic fracturing. Hydraulic fracturing and horizontal drilling require fewer wells to be drilled to produce the same amount of natural gas as the conventional production method, resulting in less methane leakage.

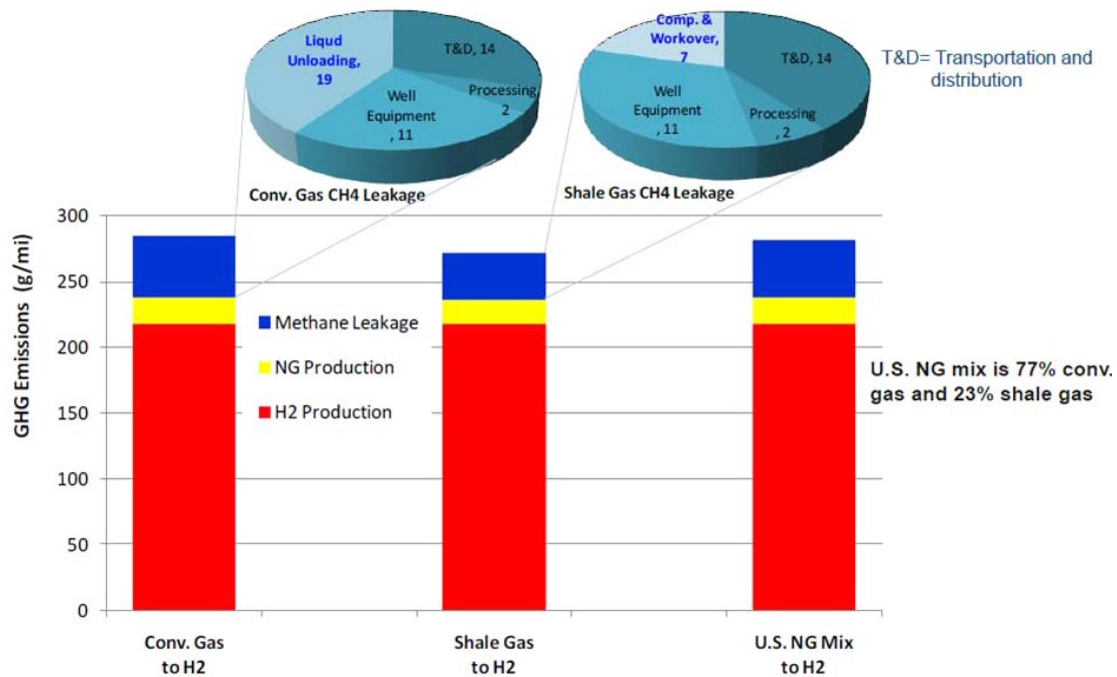


FIGURE 5. Results of analysis, using the GREET model, of life-cycle emissions from fuel cell electric vehicles using hydrogen produced from natural gas (source: ANL).

- ANL enhanced the life-cycle analysis capabilities of the GREET model by adding the greenhouse gas emissions associated with the plant cycle. Plant cycle emissions include those associated with the building, operation, and decommissioning of the power plants and steam methane reforming plants. The stages included in this life-cycle analysis include raw material acquisition, transportation and processing, product manufacturing and distribution, and disposal and recycling. With the addition of the plant cycle, the model indicates that the plant cycle would generally be a minor contributor to the total life cycle greenhouse gas emissions of various pathways (Figure 6). The key reason for this is that the emissions associated with a plant will be amortized over its lifetime.

Programmatic Analysis

- Pacific Northwest National Laboratory (PNNL) updated the commercial benefits of the Fuel Cell Technologies Program. Every year, PNNL's analysis tracks the commercial products and technologies and patents developed from Fuel Cell Technologies Program funding. This year, their analysis showed that the benefits of DOE funding continue to grow (as illustrated in Figures 7 and 8), with a total of 363 patents awarded and 36 products commercialized by 2012. Full results of PNNL's analysis are documented in *2012 Pathways to Commercial Success* (www.hydrogenandfuelcells.energy.gov/pdfs/pathways_2012.pdf).

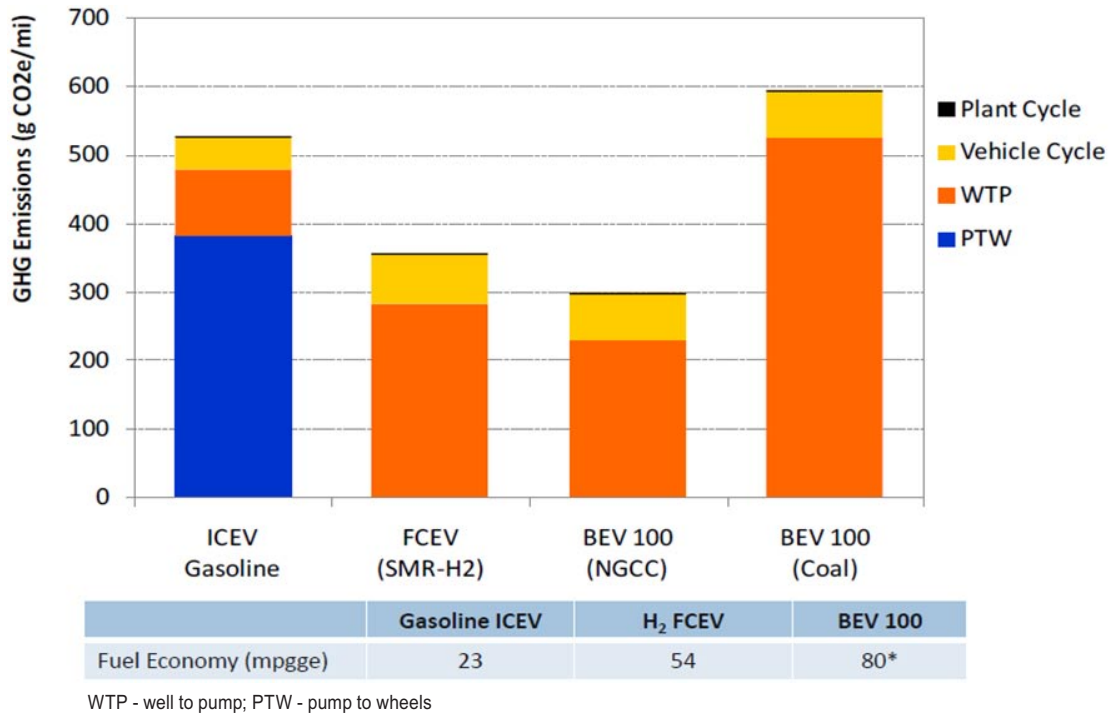


FIGURE 6. Life-cycle greenhouse gas emissions from various vehicle-fuel pathways, including plant-cycle emissions (source: ANL).

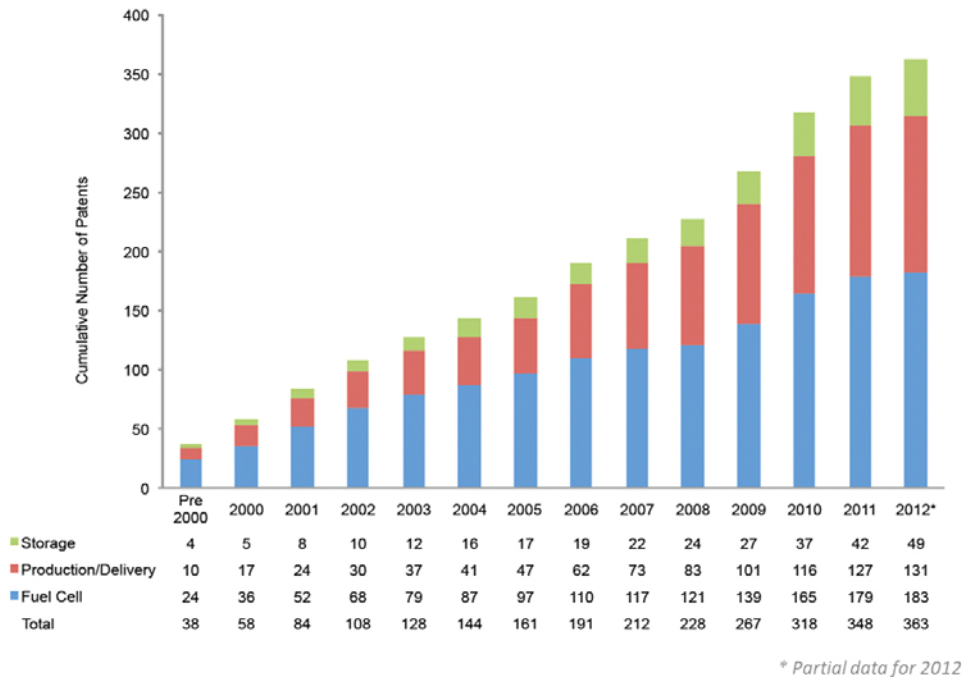


FIGURE 7. Cumulative number of patents awarded as a result of funding by the DOE Fuel Cell Technologies Program (source: Pacific Northwest National Laboratory).

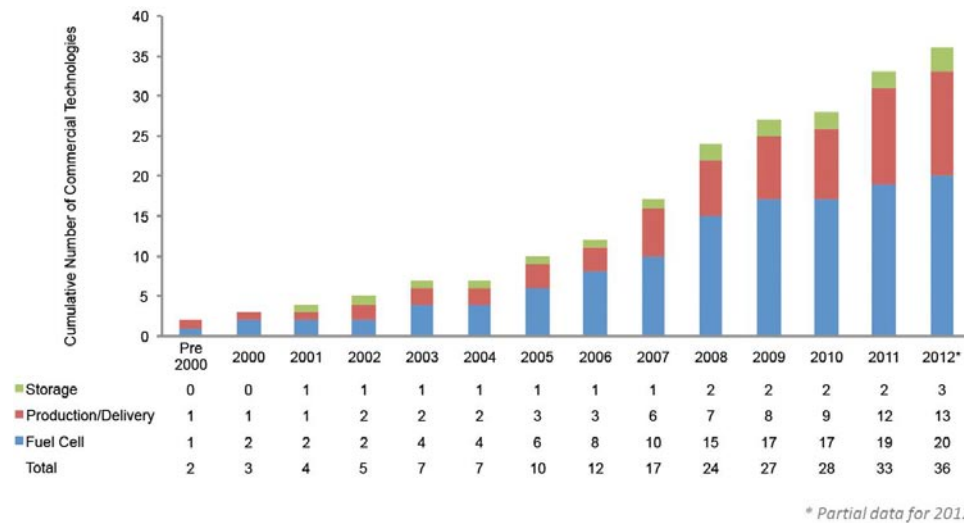
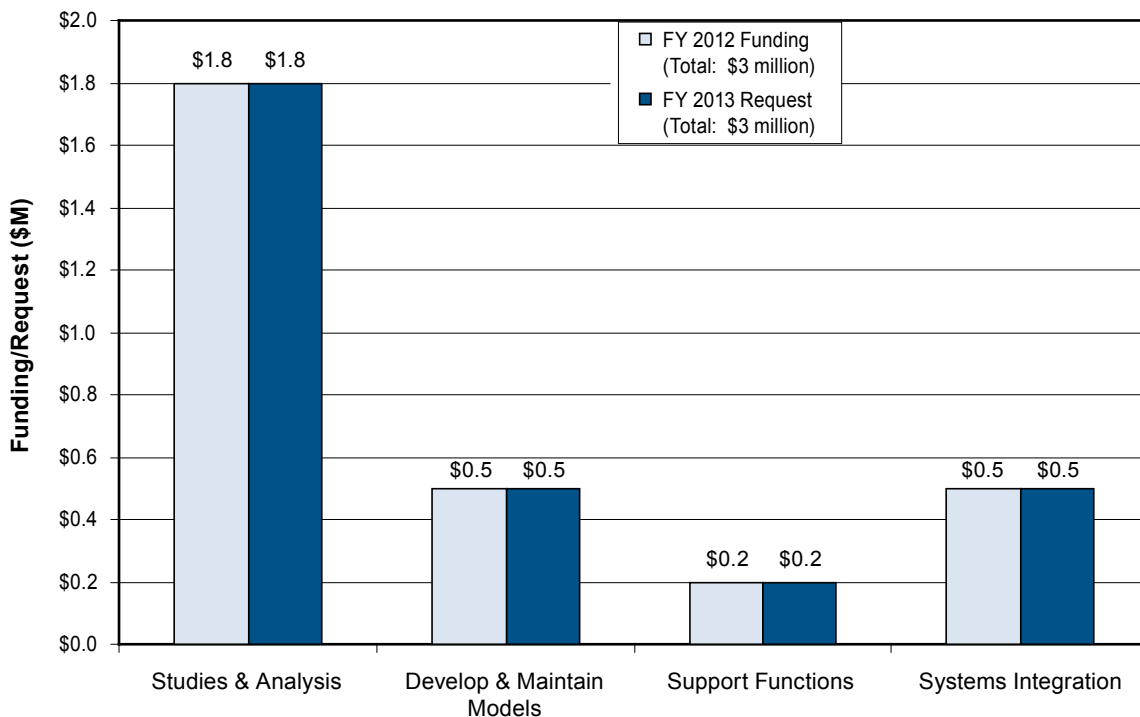


FIGURE 8. Cumulative number of commercial products on the market as a result of funding by the DOE Fuel Cell Technologies Program (source: Pacific Northwest National Laboratory).

BUDGET

The FY 2013 budget request for the Systems Analysis sub-program is consistent with the goals and objectives of the sub-program and is will enable the sub-program to continue to assess the viability and benefits of fuel cells for a wide range of applications, including stationary power generation, energy storage, specialty applications, and light-duty transportation.

Systems Analysis Funding



FY 2013 PLANS

In FY 2013, the Systems Analysis sub-program will conduct analysis of: early fuel cell and hydrogen markets, hydrogen infrastructure, the impacts and tradeoffs of fuel quality requirements, and environmental and socio-economic impacts of fuel cell and hydrogen market growth. The sub-program will continue its systems integration efforts, analysis of Program impacts, and work on developing and improving models. The sub-program will also continue to assess new opportunities for using fuel cells and hydrogen in energy storage systems, explore potential synergies of linking stationary fuel cell power generation with other renewable technologies such as biofuel production, and assess opportunities for integrating the distribution of hydrogen with existing natural gas pipeline networks.

Fred Joseck

Systems Analysis Team Lead
Fuel Cell Technologies Program
Department of Energy
1000 Independence Ave., SW
Washington, D.C. 20585-0121
Phone: (202) 586-7932
Email: Fred.Joseck@ee.doe.gov

XI.1 Infrastructure Analysis of Early Market Transition of Fuel Cell Vehicles

Brian Bush (Primary Contact), Marc Melaina,
Olga Sozinova, Michael Penev
National Renewable Energy Laboratory
15013 Denver West Parkway, Mail Stop RSF300
Golden, CO 80401
Phone: (303) 384-7472
Email: brian.bush@nrel.gov

DOE Manager
HQ: Fred Joseck
Phone: (202) 586-7932
Email: Fred.Joseck@ee.doe.gov

Subcontractor:
Brent Daniel, Los Alamos National Laboratory,
Los Alamos, NM

Project Start Date: May 1, 2011
Project End Date: Project continuation and direction
determined annually by DOE

Fiscal Year (FY) 2012 Objectives

In order to analyze the infrastructure requirements and infrastructure-cost implications of early market transitions to fuel cell vehicles (FCEVs), we use the Scenario Evaluation, Regionalization and Analysis (SERA) model, which is a geospatially and temporally oriented analysis model that determines the optimal production and delivery scenarios for hydrogen, given resource availability and technology cost. The objectives of this analysis-oriented project are:

- Improve interoperability of SERA with other models and with data sources:
 - Synchronize SERA costs with those from more detailed cost models such as H2A
 - Collaboration with MA3T model developers
- Enhance integration of a variety of infrastructure models into SERA:
 - Develop cost submodels representing a variety of alternative infrastructure development pathways
- Perform scenario analysis using SERA:
 - Region-specific early market scenarios
 - Niches and synergies for FCEVs and refueling stations in the early adoption period
 - Minimizing delivery cost of renewable hydrogen
 - Implications of stakeholder behavior and consumer preferences

Technical Barriers

This project addresses the following technical barriers from the Systems Analysis section (4.5) of the Fuel Cell Technologies Program's Multi-Year Research, Development and Demonstration Plan:

- (B) Stove-Piped/Siloed Analytical Capability
- (D) Suite of Models and Tools
- (E) Unplanned Studies and Analysis

Contribution to Achievement of DOE Systems Analysis Milestones

This project is contributing to achievement of the following DOE milestones from the Systems Analysis section of the Fuel Cell Technologies Program's Multi-Year Research, Development and Demonstration Plan:

- Milestone 3. Begin a coordinated study of market transformation analysis with H2A and Delivery models.
- Milestone 5. Complete analysis and studies of resource/feedstock, production/delivery and existing infrastructure for various hydrogen scenarios.
- Milestone 24. Complete the linear optimization model (HyDS) to analyze the optimum production facilities and infrastructure for hydrogen demand scenarios.
- Milestone 26. Annual model update and validation.

FY 2012 Accomplishments

- Early market scenarios were constructed from published plans for FCEV introductions in California, and then these early market estimates were generalized to create a National Academy of Sciences (NAS)-compatible nationwide scenario.
- In order to study clustering effects in those scenarios, refueling stations and FCEV garaging locations were estimated, nationwide, at the ZIP code level.
- The optimal choice of production technology was computed as a function of feedstock prices and demand conditions. Similarly, the optimal choice of transmission infrastructure is based on calculations sensitive to the nearness of production centers and demand conditions.
- By calculating cash flows, we determined that, for these scenarios, long-term levelized delivered costs for hydrogen tend towards \$6.00/kg nationally and zero cumulative cash flow is achieved between 2018 and 2025 if hydrogen is priced at \$11.00/kg or \$6.75/kg, respectively.



Introduction

The SERA model fills a unique and important niche in the temporal and geospatial analysis of hydrogen infrastructure build-out for production and delivery. It nicely complements other hydrogen analysis tools and is well suited to contribute to scenario analysis involving the temporally specific geospatial deployment of hydrogen production and transmission infrastructure. Its key capabilities are (i) an optimization of the physical build-out of hydrogen infrastructure; (ii) the unified treatment of production, transmission, and distribution; (iii) the ease with which new technologies can be added to an analysis; (iv) the consistent physical and economic computations; (v) the ability to estimate costs and cash flows; (vi) the spatial and temporal resolution of hydrogen infrastructure networks, including refueling stations; (vii) regional specificity; and (viii) the allowance for exogenously specified urban hydrogen demands. Its internal architecture is flexible, and it is compatible with geographic information systems and the H2A models [1,2,3]. SERA is designed to answer questions such as: Which pathways will provide least-cost hydrogen for a specified demand? What network economies can be achieved by linking production facilities to multiple demand centers? How will particular technologies compete with one another? How does clustering of refueling stations and FCEV garaging affect infrastructure requirements and costs?

Approach

In order to answer such questions, SERA supports analyses aimed at identifying optimal infrastructure to meet specified annual urban hydrogen demands, perhaps coupled to other multiple objectives and constraints. Cash flows are computed, detailed by infrastructure component, city, and region, and these provide insights into components of hydrogen costs, which are determined by year, volume, and locality. Four methods of long distance hydrogen transport are considered: pipeline, gaseous truck, liquid truck, and railroad. The major use of SERA is for studying potential turning points in infrastructure choice via sensitivity analysis on infrastructure, feedstock, and fuel cost inputs in the context of the complex transient and transitional interactions between increasing hydrogen demand and hydrogen infrastructure construction. With carefully constructed input data sets, SERA can also weigh tradeoffs between investments in various infrastructure types, given policy constraints (e.g., green house gas). Figure 1 shows the interrelationship between the input data for SERA and the algorithms applied to them in order to compute the delivered cost of hydrogen. The infrastructure networks are optimized using a simulated-annealing algorithm that explores the large set of potential build-out plans that meet the input requirements for hydrogen delivery at cities over time. The hydrogen transport computations are based on graph-theoretic algorithms for determining optimal flows in networks. The cash flow computations rely on standard discounting approaches.

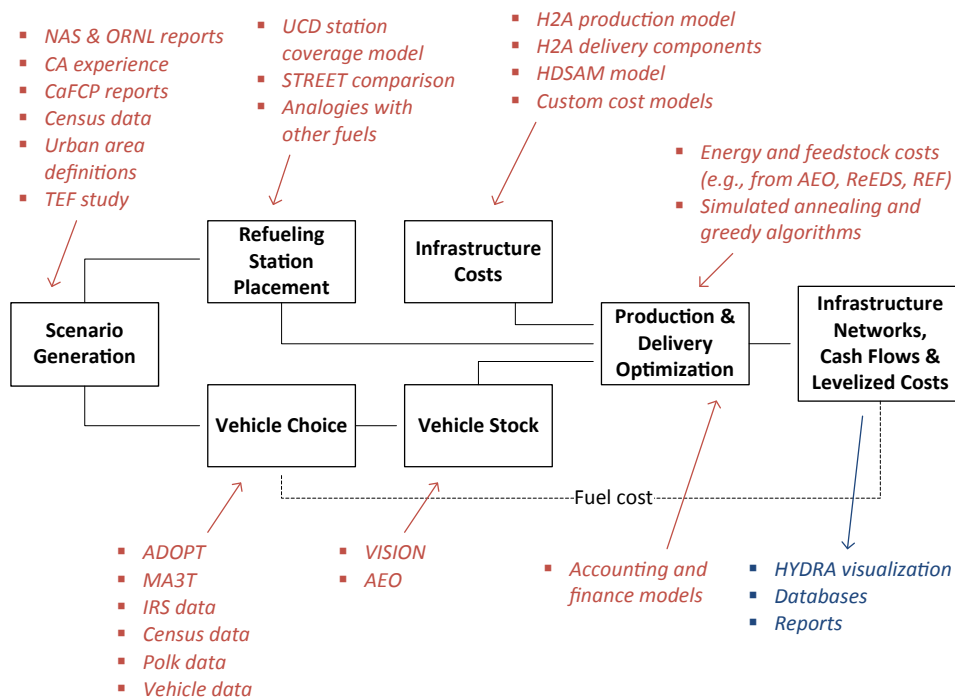


FIGURE 1. SERA input and output data and algorithms

We developed detailed temporal and spatial scenarios for early market infrastructure clustering and vehicle rollout for use in SERA by tuning nationwide scenarios to observations and lessons learned in California early market evolution and planning. In order to examine the regional implications of these nationwide scenarios, we refined our methodology for locating and sizing stations within urban areas and developed a new methodology for locating FCEVs at households within urban areas. We next refined our methodology for optimizing the choice of hydrogen production and delivery infrastructure in SERA and applied that optimization in order to understand the cash-flow implications of the detailed temporal and spatial scenarios for early market infrastructure clustering and vehicle rollout. This allowed us to gain insight into the nuances of cash flows within FCEV-rollout scenarios. As part of this work, a repeatable process for developing and refining detailed temporal and spatial scenarios for early market infrastructure clustering and vehicle rollout has been incorporated into SERA.

Results

The resulting scenarios, which partially account for early-market intra-urban clustering effects, are characterized by their more aggressive FCEV roll-outs than the standard NAS scenarios: These scenarios were calibrated to the early market adoption rates anticipated by stakeholder within the California Fuel Cell Partnership, and comparable (but later) infrastructure rollout patterns are extended to all major U.S. urban areas. In the middle and long term, these scenarios approach the standard NAS scenarios (“accelerated”, “success”, and “partial success” scenarios).

Analyses of these scenarios focused on understanding the infrastructure build-out and the cash-flow implications in temporal and spatial detail, by optimizing the choice of hydrogen production and delivery infrastructure. Figures 2 and 3 summarize the properties of the optimal hydrogen infrastructure for the early-market “hydrogen success” scenario. Note particularly that the average refueling station capacity grows from small early-market conditions (~250 kg/day) to larger mature-market conditions (~1,500 kg/day) that resemble the H2A design cases [3].

These early-market clustering analyses highlighted the following insights:

- Low natural gas costs in most regions and the favorable economies of scale for large coal plants lead to the predominance of central natural gas reforming and coal gasification.
- Central grid electrolysis has niches in areas of low electricity prices.
- Onsite natural gas reforming is optimal in low-demand conditions.

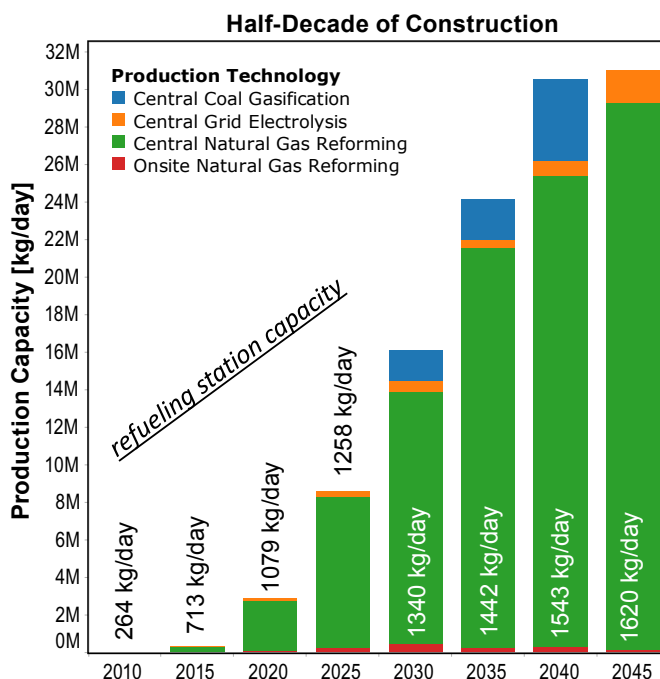


FIGURE 2. Production infrastructure build-out under the early-market “hydrogen success” scenario

- Gaseous hydrogen pipelines are favorable for high flow conditions and moderate distances.
- Truck delivery predominates at lower flow (i.e., for gaseous transport) or longer distance (i.e., for liquid transport).
- Long-term levelized delivered costs for hydrogen tend towards \$6.00/kg nationally.
- Zero cumulative cash flow is achieved between 2018 and 2025 if hydrogen is priced at \$11.00/kg or \$6.75/kg, respectively. (See Figure 4 for an example.) However, the use of alternative accounting methods for cash flow or different financing assumptions would alter this conclusion.
- Underutilization of infrastructure in the first couple of years after its construction raises the overall proportion of capital costs.

Conclusions and Future Direction

In summary, SERA is an effective, integrated, cross-cutting model for optimization-analysis studies of hydrogen infrastructure build-out compatible with the H2A models. It will be applied to more complex deployment scenarios such as (i) identifying regional niches for production technologies and delivery infrastructure and (ii) assessing the influence of feedback from computed delivered costs of hydrogen to consumer and stakeholder decisions. In particular, we plan to compare scenarios involving three different types of



FIGURE 3. Transmission infrastructure build-out under the early-market “hydrogen success” scenario

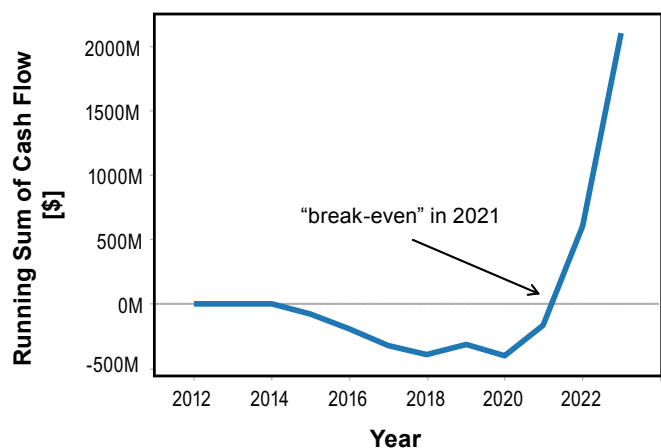


FIGURE 4. Cumulative cash flow, nationwide, if hydrogen is priced at \$8.00/kg in the early-market “hydrogen success” scenario

subsidies: (1) vehicles only (e.g. \$7,500/vehicle); (2) vehicles and fuels; versus (3) vehicles and fuels and stations. The results will be analyzed in terms of metrics such as fuel cost per mile for FCEVs vs. plug-in hybrid electric vehicles/ battery electric vehicles, investments for FCEV stations and electric vehicle supply equipment, utilization ratios, extent of station coverage, economies of scale, penetration rates, and charger ratios.

FY 2012 Publications/Presentations

1. B. Bush, O. Antonia, M. Melaina, D. Steward, J. Svede, K. Webster, “Summary of SERA Capabilities”, Management Report, 18 October 2011.
2. B. Bush, M. Melaina, “Cash Flows in SERA Scenarios for Early Market Clustering”, Presentation to FFPIT, 20 March 2012.
3. B. Bush, M. Melaina, “SERA Overview and Recent Scenario Analyses”, Presentation to UC Davis STEPS Team, 23 March 2012.
4. B. Bush, M. Melaina, K. Webster, “SERA Scenarios for Early Market Clustering”, Management Report, 31 July 2011.
5. B. Bush, M. Melaina, K. Webster, “Cash Flows in SERA Scenarios for Early Market Clustering”, Management Report, 15 October 2011.

References

1. “H2A Production Models and Case Studies.” Version 2.1.2. *DOE H2A Production Analysis*. http://www.hydrogen.energy.gov/h2a_production.html. Accessed 17 Jan 2009.
2. “H2A Delivery Scenario Model.” Version 2.0. *DOE H2A Delivery Analysis*. http://www.hydrogen.energy.gov/h2a_delivery.html. Accessed 17 Jan 2009.
3. “H2A Delivery Components Model.” Version 2.0. *DOE H2A Delivery Analysis*. http://www.hydrogen.energy.gov/h2a_delivery.html. Accessed 17 Jan 2009.

XI.2 Life-Cycle Analysis of Vehicle and Fuel Systems with the GREET Model

Michael Wang (Primary Contact),
Amgad Elgowainy, Jeongwoo Han and Hao Cai
Argonne National Laboratory (ANL)
ESD362
9700 South Cass Avenue
Argonne, IL 60439
Phone: (630) 252-2819
Email: mqwang@anl.gov

DOE Manager
HQ: Fred Joseck
Phone: (202) 586-7932
Email: Fred.Joseck@ee.doe.gov

Project Start Date: October 2009

Project End Date: Project continuation and direction determined annually by DOE

Technical Targets

This project contributes to achievement of the following DOE milestone from the Systems Analysis section of the Fuel Cell Technologies Program Multi-Year Research, Development, and Demonstration Plan:

- Milestone 13: Complete environmental analysis of the technology environmental impacts for hydrogen and fuel cell scenarios and technology readiness. (4Q, 2015)

FY 2012 Accomplishments

- Updated conventional natural gas to hydrogen production pathway with the inclusion of shale gas (SG) pathway and updated methane (CH₄) emissions of natural gas to hydrogen pathways.
- Evaluated the well-to-wheels (WTW) energy use and emissions benefits of FCEVs powered by hydrogen from renewable sources such as biomass gasification and renewable natural gas (RNG) from sources such as landfill gas and animal manure.
- Evaluated vehicle-cycle energy use and emissions of baseline gasoline internal combustion engine vehicles (ICEVs), FCEVs with updated platinum loading of fuel cells, battery electric vehicles (BEVs) with updated battery manufacturing analysis, and light weighting materials for future vehicle designs.
- Evaluated the life-cycle energy use and emissions associated with the construction of petroleum refineries, hydrogen plants, and electric power plants.



Fiscal Year (FY) 2012 Objectives

- Evaluate environmental benefits of hydrogen fuel cell electric vehicles (FCEVs) with various renewable hydrogen production pathways relative to baseline gasoline pathways.
- Conduct vehicle-cycle analysis of hydrogen FCEVs.
- Conduct life-cycle analysis of hydrogen and petroleum infrastructure build up.
- Provide life-cycle results for DOE's Fuel Cell Technologies (FCT) Program activities such as the Multi-Year Research, Development, and Demonstration Plan.
- Engage in discussions and dissemination of energy and environmental benefits of fuel cell systems and applications.

Technical Barriers

This project addresses the following technical barriers from the Systems Analysis section of the Fuel Cell Technologies Program Multi-Year Research, Development, and Demonstration Plan:

- (C) Inconsistent Data, Assumptions and Guidelines
- (D) Suite of Models and Tools
- (E) Unplanned Studies and Analysis

Introduction

The stages included in life-cycle analysis (LCA) are raw material acquisition, transportation and processing, as well as product manufacturing, distribution, use and disposal or recycling. LCA of a fuel is known as fuel-cycle analysis or WTW analysis (if the fuel is used for transportation applications), while LCA of vehicle manufacturing is known as vehicle-cycle analysis. Combining WTW with the vehicle-cycle facilitates the comparison of alternative fuel/vehicle systems on a common (life-cycle) basis. More recently, there has been significant interest in expanding the system boundary of life-cycle analysis of transportation fuels to include the impact of fuel infrastructure build up. Argonne examined fuel-cycle energy use and emissions associated with the production of shale gas for hydrogen production and updated the renewable pathways for hydrogen production. It

also conducted vehicle cycle analysis of hydrogen FCEVs, including impacts of reduced platinum loading and vehicle light weighting for improved fuel economy. To complete the LCA of hydrogen FCEVs relative to baseline ICEVs and BEVs, Argonne evaluated the life-cycle energy use and emissions associated with the construction of steam methane reforming (SMR) plants for hydrogen production, the construction of petroleum refineries for gasoline production and of power plants for electricity generation.

Argonne updated the methane emissions associated with well field infrastructure and well completion for conventional natural gas (NG) pathway. Argonne also developed a new SG pathway in GREET. Currently, SG contributes to about 23% of the total U.S. natural gas supply, which is the main source for current hydrogen production. RNG from landfill gas or from anaerobic digestion of animal manure produces substantially less greenhouse gas (GHG) emissions than conventional NG and SG [1], and can be employed as feedstock sources to produce renewable hydrogen for FCEVs via SMR. This is especially important in places such as California where regulations require 33% of the hydrogen produced for use as a transportation fuel to come from renewable sources [2]. Vehicle manufacturing and recycling contribute fewer emissions compared to the fuel cycle but still constitute a significant portion of the total life-cycle GHG emissions. Argonne evaluated the impacts of critical materials on vehicle-cycle energy use and GHG emissions, including the platinum loading for FCEVs, battery manufacturing for BEVs, and light weight materials for future vehicle designs that target improved fuel economy. Energy use and GHG emissions associated with infrastructure and plant construction for baseline petroleum fuels and alternative fuels such as hydrogen for FCEVs and electricity for BEVs have long been expected to be much smaller compared to both fuel cycle and vehicle cycle. However, there have been recommendations from National Research Council [3] to quantify the impact of such infrastructure build up on the LCA of the baseline and alternative transportation fuels. Argonne examined in details the energy use and emissions associated with gasoline production in refineries, hydrogen production in SMR plants, and electricity production in various power plants. The energy use and GHG emissions associated with the construction of these plants were evaluated and added to the energy and emissions from the related fuel and vehicle cycles.

Approach

This analysis relied on GHG emissions data developed by the U.S. Environmental Protection Agency for different sectors to estimate the CH₄ emissions sources and amounts for conventional gas and SG [4]. These sectors include production, processing, transmission and distribution of natural gas. Within the production sector, the most important sources of CH₄ emissions are the well equipment, the liquid

unloading, and the well completion and workover. Argonne examined in detail the key parameters affecting the life cycle energy use and emissions of conventional gas and SG and their implications on the current hydrogen production from the mix of these two NG sources.

Argonne also examined the parameters influencing the life cycle energy use and emissions associated with the production of RNG from landfill gas (LFG) and animal manure, and the subsequent conversion of RNG to hydrogen fuel for use in FCEVs. These parameters include the process efficiency and fuel yield, CH₄ leakage, and current practices with purging and flaring of LFG as well as the current manure management practices and anaerobic digestion residue applications. The net emissions associated with RNG production are calculated by subtracting emissions associated with current practices from those emitted in the conversion process to RNG. To assess the impact of the construction of fuel production plants, Argonne obtained data from a demolished refinery (that processed 120,000 BBL/day) and for a large SMR hydrogen plant (that produced 19 mmSCF/day). The refinery and SMR plant materials were compiled and then used as building blocks to estimate the environmental impacts of constructing gasoline and hydrogen production facilities. Vehicle component specifications and fuel economy are provided by the Autonomie modeling group at Argonne based on guidance from the DOE's FCT and Vehicle Technologies Programs. The fuel cell platinum loading reduction data is extracted from the DOE Hydrogen Program Record [5]. The material compositions by component for each vehicle are ported to the Greenhouse gases, Regulated Emissions and Energy use in Transportation (GREET2) vehicle cycle model to evaluate the environmental impacts of vehicle manufacturing and recycling or disposal.

Results

The WTW GHG emissions for hydrogen production from conventional gas, SG, and the U.S. mix of NG are shown in Figure 1. The figure shows that CH₄ leakage is a major GHG emissions source for the hydrogen production pathway via SMR of NG. The major CH₄ emission source for conventional gas is the liquid unloading followed by the transmission and distribution of NG and the well equipment, while the major source for CH₄ emissions for SG is the transmission and distribution of NG, followed by the well equipment and the well completion and workover.

Figure 2 shows the WTW GHG emissions of various conventional and renewable hydrogen production pathways, including the hydrogen use by FCEV. The fuel economy values for the baseline gasoline ICEV and the alternative fuel/vehicle systems considered in this analysis are provided in Table 1. The figure shows that FCEVs with hydrogen produced from fossil NG reduce GHG emissions by over

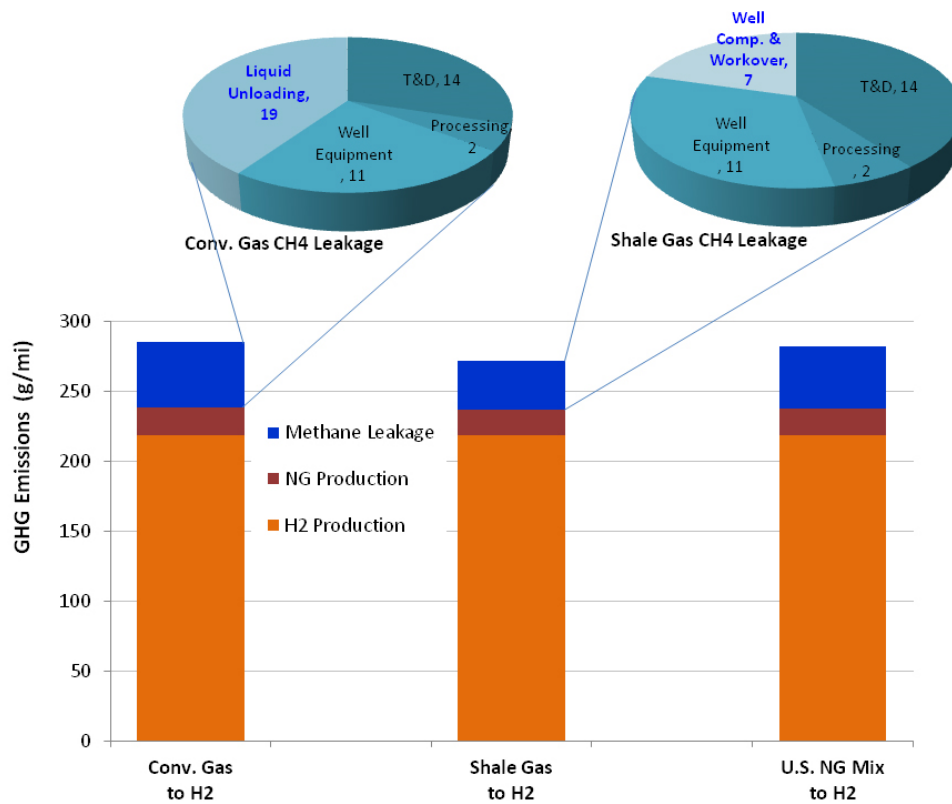
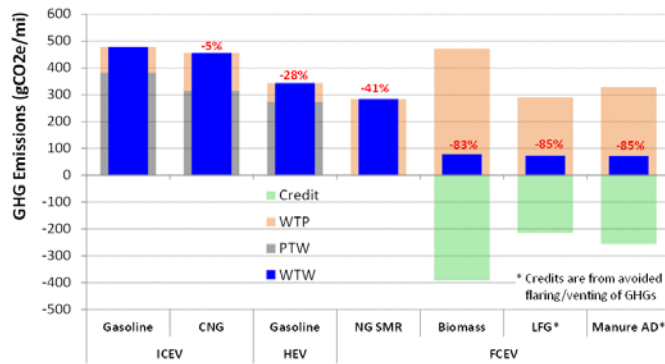


FIGURE 1. WTW GHG emissions of hydrogen production from conventional and shale gas for use in FCEVs



WTP - well to pump; PTW - pump to wheels; HEV - hybrid electric vehicle; LPG - liquefied petroleum gas; AD - anaerobic digestion

FIGURE 2. WTW GHG emissions of hydrogen FCEVs compared to conventional ICEVs and HEVs

40% relative to gasoline ICEVs, which compares to a 5% reduction if NG is used directly in compressed natural gas (CNG) vehicles. Hydrogen produced from renewable sources such as cellulosic biomass and RNG provides a substantial (83-85%) reduction in GHG emissions relative to gasoline ICEVs. To compare FCEVs with the baseline gasoline ICEVs and with BEVs on a life-cycle basis, we evaluated the vehicle cycle energy use and emissions associated with the manufacturing of these vehicles as well as the construction

TABLE 1. Fuel Economy Assumptions for Alternative Fuel/Vehicle Systems

| Fuel/Vehicle System | Fuel Economy [mpgge*] |
|----------------------------|-----------------------|
| Conventional gasoline ICEV | 23 |
| CNG Vehicle | 22 |
| Gasoline HEV | 33 |
| Hydrogen FCEV | 54 |
| BEV | 79** |

* mpgge = miles per gallon of gasoline equivalent
 ** from wall outlet (assuming 85% charging efficiency)

of their associated fuel production plants. Platinum loading is critical for the performance of fuel cell stacks in FCEVs. Each gram of platinum contributes approximately 12 kg of life-cycle GHG emissions. Based on a 70-kW fuel cell stack and platinum loading reduction from 1.1 g/kW in 2005 to 0.125 g/kW in 2015, GHG emissions of FCEVs are reduced by 5 g_{CO_{2e}}/mi or 7% of the vehicle cycle GHG emissions. The GHG emissions per million Btu (mmBtu) of gasoline produced in a petroleum refinery are evaluated and compared with those of a SMR plant for hydrogen production, and NG combined cycle (NGCC) and coal power plants for electricity generated as shown in Figure 3. The figure shows that the emission profiles for refineries and hydrogen SMR plants are much smaller compared to NGCC and coal power plants.

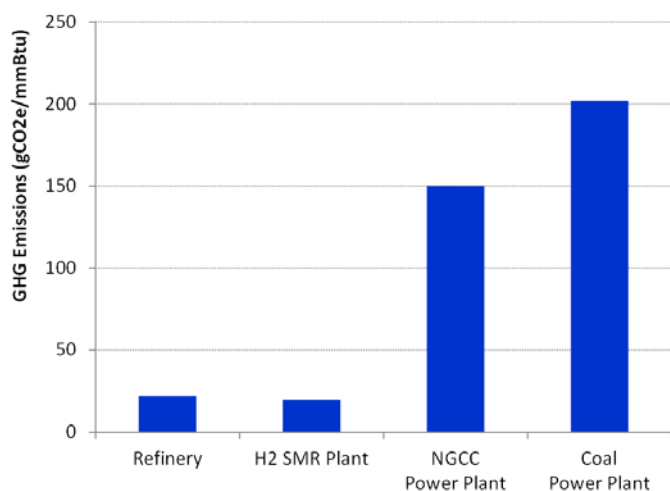


FIGURE 3. Plant construction GHG emissions for petroleum refineries, hydrogen SMR plants, and NGCC and coal power plants (per mmBtu of fuel produced)

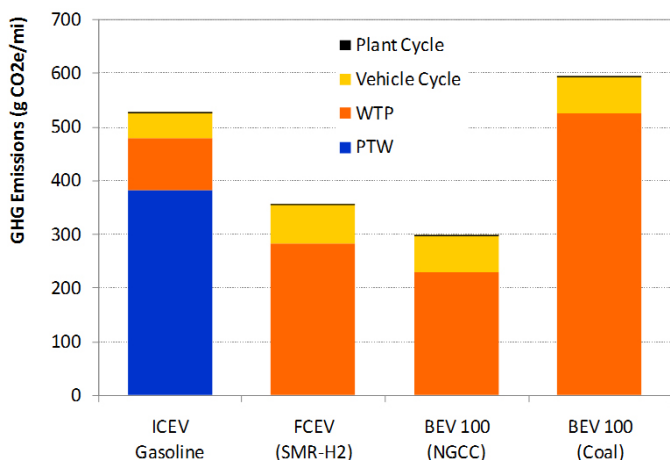


FIGURE 4. Comparison of life cycle GHG emissions of hydrogen FCEVs with gasoline ICEVs and BEVs

However, when these emissions are evaluated on a per-mile basis using fuel economies of the vehicles employing these fuels, the plant construction impact becomes negligible (<1% of the combined fuel and vehicle cycle emissions) compared to the fuel and vehicle cycles for all fuel/vehicle systems as shown in Figure 4.

Conclusions

- CH₄ leakage is a major GHG emissions source for production of hydrogen from conventional gas and shale gas.
- FCEVs with fossil and renewable hydrogen production pathways could have significant GHG reductions relative to gasoline ICEVs (by 41% when hydrogen is produced

from fossil NG/SG and by 83-85% when hydrogen is produced from RNG or biomass).

- FCEV vehicle-cycle GHG emissions are reduced by 7% with platinum loading reduction.
- Emissions of fuel plant construction are negligible compared to fuel- and vehicle-cycle emissions.

Future Work

- WTW analysis of range extender FCVs.
- Complete and update upstream plant construction activities for the baseline petroleum-derived fuels and hydrogen plant construction.
- Expand the electricity module and develop stationary fuel cell systems in GREET.

Special Recognitions

1. DOE Fuel Cells Program R&D Award “In Recognition of Outstanding Contribution to Analysis and Modeling of Hydrogen Delivery.” Awarded to Amgad Elgowainy at the DOE’s Hydrogen Program Annual Merit Review (2012).

References

1. Han, J., Mintz, M., Wang, M., 2011, “Waste-to-Wheel Analysis of Anaerobic-Digestion-Based Renewable Natural Gas Pathways with the GREET Model,” Center for Transportation Research, Argonne National Laboratory, Argonne, IL.
2. California Senate Bill 1505: Environmental Performance Standards for Hydrogen Fuel.
3. FreedomCAR and Fuel Partnership Phase 3 Review Report, 2010 — Recommendation 2-14.
4. Burnham, A., Han, J., Clark, C., Wang, M., Dunn, J., Palou-Rivera, I., 2012, “Life-Cycle Greenhouse Gas Emissions of Shale Gas, Natural Gas, Coal and Petroleum,” Environ. Sci. Technol., 46 (2), pp 619–627.
5. DOE Hydrogen Program Record, June 1, 2010, Record # 9018.

FY 2012 Publications/Presentations

1. Burnham, A., Han, J., Clark, C., Wang, M., Dunn, J., Palou-Rivera, I., 2012, “Life-Cycle Greenhouse Gas Emissions of Shale Gas, Natural Gas, Coal and Petroleum,” Environ. Sci. Technol., 46 (2), pp 619–627.
2. Han, J., Mintz, M., Wang, M., 2011, “Waste-to-Wheel Analysis of Anaerobic-Digestion-Based Renewable Natural Gas Pathways with the GREET Model,” Center for Transportation Research, Argonne National Laboratory, AN/ESD/11-06, Argonne, IL.

XI.3 Hydrogen Refueling Infrastructure Cost Analysis

Marc W. Melaina (Primary Contact), Michael Penev and Darlene Steward

National Renewable Energy Laboratory (NREL)
15013 Denver West Parkway
Golden, CO 80401
Phone: (303) 275-3836
Email: Marc.Melaina@nrel.gov

DOE Manager

HQ: Fred Joseck
Phone: (202) 586-7932
Email: Fred.Joseck@hq.doe.gov

Subcontractor:

IDC Energy Insights, Framingham, MA

Project Start Date: October 1, 2010

Project End Date: September 28, 2012

FY 2012 Accomplishments

- Responses from the Hydrogen Station Cost Calculator (HSCC) were weighted and aggregated to develop a generic representation of hydrogen station costs and rollout timeframes.
- Received HSCC responses from 11 stakeholders, representing a variety of stakeholder groups.
- HSCC responses were collected by IDC Energy Insights and were conveyed in a weighted, aggregated form to NREL staff, with the highest detail possible while still maintaining respondent anonymity.
- Identified priorities for research, development, demonstration and deployment across an array of component options.
- Quantification of station sizes (kg/day), capital costs, lifetime average utilization rates, and deployment time periods for 4 distinct station types: State-of-the-Art (SOTA), Early Commercial (EC), More Stations (MS), and Larger Stations (LS).

Fiscal Year (FY) 2012 Objectives

- Identify the capacity (kg/day) and capital costs associated with “Early Commercial” hydrogen stations (defined below)
- Identify cost metrics for larger numbers of stations and larger capacities

Technical Barriers

This project addresses the following technical barriers from the Systems Analysis section of the Fuel Cell Technologies Program Multi-Year Research, Development and Demonstration Plan:

- (A) Future Market Behavior
- (C) Inconsistent Data, Assumptions and Guidelines
- (E) Unplanned Studies and Analysis

Contribution to Achievement of DOE Systems Analysis Milestones

This project will contribute to achievement of the following DOE milestone from the Systems Analysis section of the Fuel Cell Technologies Program Multi-Year Research, Development and Demonstration Plan:

- Milestone 1.4 (Systems Analysis Task 1: Perform Studies and Analysis): Complete evaluation of fueling station costs for early vehicle penetration to determine the cost of fueling pathways for low and moderate fueling demand rates. (4Q, 2012)



Introduction

The early introduction of fuel cell electric vehicles (FCEVs) will prove to be dependent upon the successful deployment of hydrogen refueling stations (HRS). Deployment of HRS will depend, in part, upon cost reductions over time due to learning, mass production, and economies of scale achieved with increasing station capacities (measured in kg/day). This project builds upon many past HRS cost studies and data sources [1-4] by conveying quantitative, near-term HRS cost estimates provided by multiple key stakeholders through the HSCC. This work builds upon the qualitative feedback received from the Market Readiness workshop held in February 2011 [5]. The quantitative results from the HSCC provide insight into how the qualitative cost reductions opportunities discussed at the Market Readiness workshop might be realized within the 2014-2016 timeframe. These results are relevant to a wide range of stakeholders, including public-private partnerships developing plans for the early introduction of FCEVs.

Approach

Based upon feedback from Market Readiness workshop participants, four station types were defined within the HSCC. These definitions are provided in Table 1 as they were presented within the HSCC. The most relevant station type is EC, which provides a baseline from which additional cost

reductions might be attained through deployment of multiple stations, MS, and production of similar stations at larger capacities, LS. Stations being installed today are defined as SOTA stations. The HSCC was distributed to a select list of organizations with direct experience with hydrogen station projects. Responses were received from 11 stakeholders, shown by type in Figure 1. IDC Energy Insights administered collection of feedback from these stakeholders, and conveyed aggregated, weighted, anonymous results to NREL staff. IDC Energy Insights weighted responses based upon the historical experience of each respondent with the installation of hydrogen stations, thereby giving greater weight to respondents with more extensive experience. These results underwent several reviews, including reviews by HSCC respondents, and were revised as a result to best articulate costs associated with each station type defined in Table 1.

The HSCC was designed to allow respondents to provide a significant amount of detail, or to provide relatively sparse detail, and to place multiple types of responses on a consistent basis. Within the HSCC respondents could calculate the cost of hydrogen (\$/kg), based upon discounted cash flow calculations used in the Hydrogen Analysis (H2A) models [1], and then revise inputs in response to the resulting \$/kg cost. However, due to the variety of approaches in which the HSCC was completed, and the limited number of respondents, costs could only be reported for a limited number of cost factors while maintaining the anonymity of respondents. In additional, station costs could not be

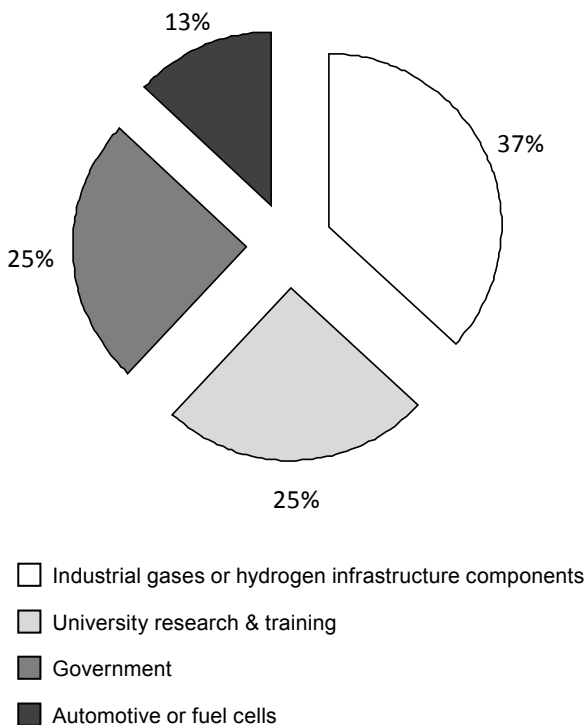


FIGURE 1. HSCC respondents by stakeholder type

associated with specific station configurations, such as onsite production vs. truck delivery. The estimates are therefore general representations of HRS costs as stations are deployed in certain volumes and over a specified timeframe. Additional information on the HSCC is provided in [5].

Results

The cost, size, and timeframe results by station type are summarized in Table 2. Given that SOTA stations are being installed today, these results suggest that significant cost reductions will be achieved before the 2014-2016 timeframe when EC stations with an estimated average capacity of

TABLE 1. Definitions of station types, as presented within the HSCC

| |
|--|
| <p>1. State-of-the-Art Stations (SOTA). Newly installed hydrogen stations with the following attributes:</p> <ul style="list-style-type: none"> The stations would be installed and operational within the 2011-2012 timeframe. The stations would include the most recent generations of major components, but would not necessarily include novel or "demonstration" components that have not been previously tested in the field. The stations would be sized to meet hydrogen demands in a geographic region with promising future market demand. |
| <p>2. Early Commercial Stations (EC). Based upon your organization's understanding of the growth in demand for hydrogen in the near future (next 5-20 years from the fuel cell electric vehicle, transit bus and material handling equipment markets), consider hydrogen stations to be "Early Commercial" stations if they have the following attributes:</p> <ul style="list-style-type: none"> The stations are financially viable with little government support. Based on financial criteria, such as return on investment, and requiring far less financial support or subsidy than the average support offered to all previous hydrogen stations in the same area or region (70-90% less). Disregard ongoing support offered to all types of alternative or low carbon fuels, such as low carbon fuel standard fuels, alternative fuel credits or carbon credits. The stations are sized to support growing demand in a promising market region, and to ensure adequate return on investment. This size could vary from station to station and neighborhood to neighborhood, but consider what might be a typical size for new EC stations. The station design enables cost reductions because it is replicable. The same station design may be used for other stations, reducing the cost of subsequent stations through standardization and economies of production. |
| <p>3. More Stations (MS). Identical to EC stations, but deployed in larger numbers. Default value is 10 times more stations being deployed than anticipated in the time period identified for EC stations. Additional cost reductions are achieved through standardization, mass production, streamlining of installation processes and learning by doing.</p> |
| <p>4. Larger Stations (LS). Identical to EC stations, but designed for higher volume output. The number deployed is assumed to be similar to EC stations, but growth in market demand warrants larger station sizes. Default value is a 1.5 increase in size over the EC stations, with 2,000 kg/day as an upper limit.</p> |

TABLE 2. Early station sizes, timeframes and capital costs

| Station Attribute | Units | Station Type | | | |
|---------------------------|------------------|------------------|------------------|---------------|-----------------|
| | | State-of-the-Art | Early Commercial | More Stations | Larger Stations |
| Introduction timeframe | years | 2011-2012 | 2014-2016 | after 2016 | after 2016 |
| Capacity | kg/day | 160 | 450 | 600 | 1,500 |
| Utilization | % | 57% | 74% | 76% | 80% |
| Average output | kg/day | 91 | 333 | 456 | 1,200 |
| Total Capital | \$M | \$2.65 | \$2.80 | \$3.09 | \$5.05 |
| Capital Cost per capacity | \$1,000 per kg/d | \$16.57 | \$6.22 | \$5.15 | \$3.37 |
| Reduction from SOTA | % | na | 62% | 69% | 80% |

450 kg/day are expected to be installed at a capital cost of \$2.8 million per station. On a capacity basis, EC capital costs represent a 62% reduction from the capital intensity of SOTA stations. Additional capital cost reductions are achieved with MS and LS station types, with LS stations reaching a capacity of 1,500 kg/day after 2016 and an 80% reduction in capital per capacity. Examples of opportunities that would likely contribute to these cost reductions include the following [5]:

- Develop “Standard” station designs
- Harmonize/Standardize dispensing equipment specifications
- Develop “Type Approvals” for use in permitting
- Encourage station buyers to design request for proposals that incentivize standard, scalable designs or networks of stations (rather than one-off, custom-built projects)

These weighted, aggregate results were re-entered into the HSCC to calculate costs per kg of hydrogen delivered from each station type. Unfortunately, a consistent view of variable costs (feedstock costs and variable operating costs such as compression) could not be included in these general \$/kg estimates. The resulting costs are therefore only part of the total costs that must be recovered at the pump (e.g., from consumers or fuel subsidies). For example, in the case of a truck delivery station, these costs would not include the cost of the hydrogen delivered to the station—though they do include some upstream capital cost components directly associated with truck delivery stations. The \$/kg costs associated with fixed operating and capital costs are indicated in Figure 2, along with the approximate number of FCEVs that would be served when each station type becomes viable. As indicated, significant reductions are anticipated between SOTA and EC stations, and then an additional 19%

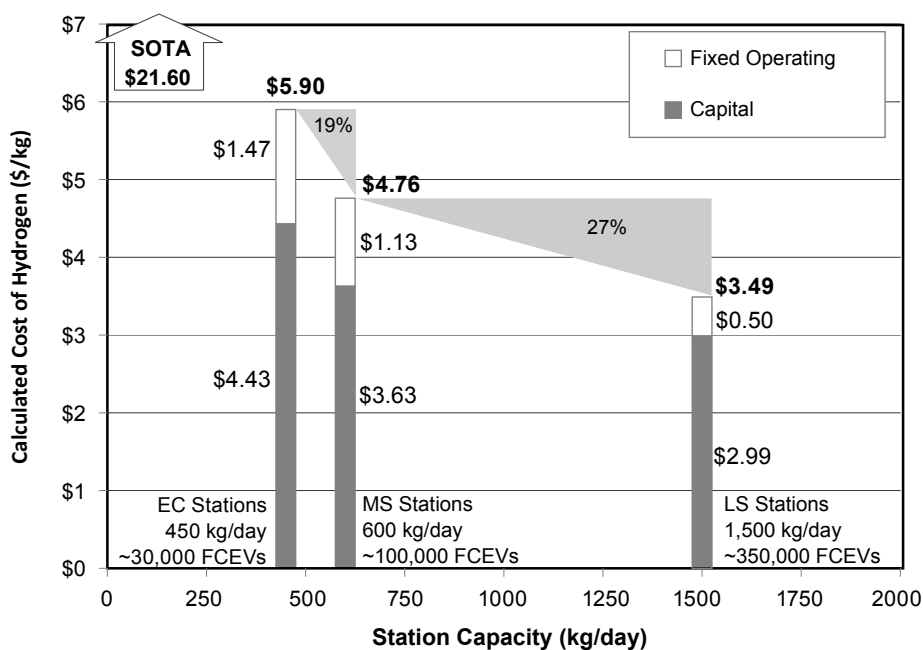


FIGURE 2. Capital and fixed operating costs by station type and capacity. Station capacities and total FCEVs supported at the time of introduction are indicated for each station type.

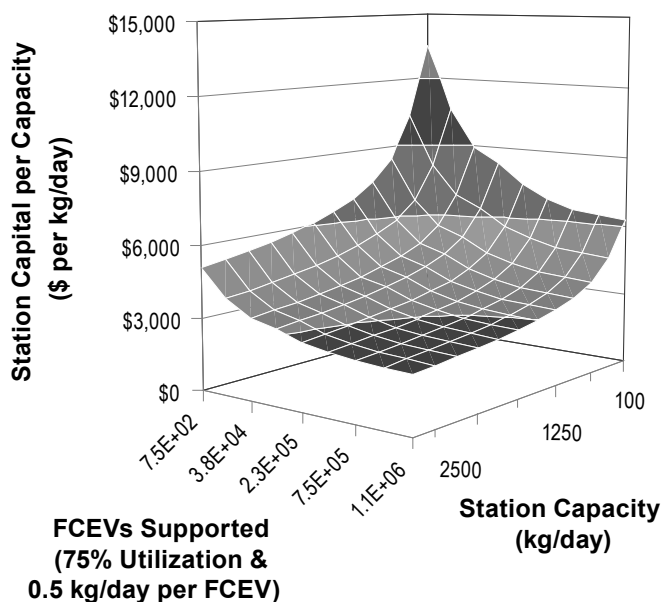


FIGURE 3. Surface plot of general function for capital cost per capacity

reduction moving from EC to MS stations, and an additional 27% reduction moving from MS to LS stations. Research, development, demonstration and deployment priorities from the HSCC are reviewed in [5].

Capital cost results from the HSCC can be articulated as a function of station size and the total capacity of stations installed over time, which itself can be expressed as the total number of FCEVs supported. This capital cost function, shown in Figure 3, is the following:

$$C' = C^o \left(\frac{Q'}{Q^o} \right)^\alpha \left(\frac{V'}{V^o} \right)^\beta$$

Where,

- C' = Station Capital Cost (\$/station)
- C^o = Base Station Capital Cost (\$/station) (C_{EC}^o = \$2.65M)
- Q' = Station Capacity (kg/d)
- Q^o = Base Station Capacity (kg/day) (Q_{HSCC}^o = 450 kg/day)
- V' = Cumulative Capacity (kg/day)
- V^o = Cumulative Capacity at Cost Status of Base Station (kg/day) (V_{HSCC}^o = 25,000 kg/d)
- α = Scaling Factor (α_{HSCC} = 0.707)
- β = Learning Factor (β_{HSCC} = -0.106)

The numerical values for base station capital cost, scaling factor, and learning factor result from a functional fit to the data shown in Table 1.

Conclusions and Future Directions

Additional information on HRS costs in the near term (2012 to 2016+) has been quantified on a consistent basis for general hydrogen stations, as expected by a select group of expert stakeholders for four types of hydrogen stations. Each station type represents a distinct level of technology development: SOTA stations represent HRS being deployed today, EC stations have a unique market-based definition (Table 1), MS stations reflect EC stations deployed in larger numbers, and LS stations represent EC stations deployed with higher capacities. Cost reductions associated with each station type have been quantified on a weighted, aggregated basis, reflecting input provided from 11 stakeholders by way of the HSCC. Significant reductions in HRS capital costs are anticipated in the 2014-2016 timeframe; capital cost per capacity (\$ per kg/day) is expected to be reduced by 62% between SOTA and EC stations, and by 80% between SOTA and LS stations (Table 2). Additional items that must be taken into consideration to develop more realistic analytic representations of future HRS network rollout costs are:

- Improving the representation of station size distributions, especially with respect to infrastructure rollout requirements for station coverage (stations per area) and capacity (with larger stations having more favorable return on investment).
- More realistic business case metrics to inform investment decisions and rollout strategies. The dynamic interaction between station rollout over time and vehicle adoption rates will determine station utilization rates across a given network of stations. Moreover, multi-party agreements will likely include different sources of capital with different risk tolerance levels, and subsidies may be applied selectively to best leverage public funds.

References

1. DOE (2012). H2A Analysis website, U.S. Department of Energy, Hydrogen and Fuel Cells Program, available at http://www.hydrogen.energy.gov/h2a_analysis.html.
2. Weinert, J. (2005). A Near-Term Economic Analysis of Hydrogen Fueling Stations. University of California at Davis, Institute of Transportation Studies, Davis, CA. UCD-ITS-RR-05-04.
3. Ogden, J. and M. Nicholas (2011). “Analysis of a “cluster” strategy for introducing hydrogen vehicles in Southern California.” Energy Policy 39(4): 1923-1938.
4. CARB (2011). Advanced Clean Cars, Staff Report: Initial Statement of Reasons, California Air Resources Board, December, available at <http://www.arb.ca.gov>.
5. Melaina, M.W., D. Steward, M. Penev, S. McQueen, S. Jaffe, C. Talon (2012). Hydrogen Infrastructure Market Readiness: Opportunities and Potential for Near-term Cost Reductions, National Renewable Energy Laboratory, Technical Report NREL/BK-5600-55961, August.

XI.4 Comparing Infrastructure Costs for Hydrogen and Electricity

Marc W. Melaina (Primary Contact), Michael Penev and Darlene Steward

National Renewable Energy Laboratory (NREL)
15013 Denver West Parkway
Golden, CO 80401
Phone: (303) 275-3836
Email: Marc.Melaina@nrel.gov

DOE Manager

HQ: Fred Joseck
Phone: (202) 586-7932
Email: Fred.Joseck@hq.doe.gov

Subcontractor:

TIAX, LLC. Lexington, MA.

Project Start Date: October 1, 2010

Project End Date: December 31, 2012

- Milestone 1.4 (Systems Analysis Task 1: Perform Studies and Analysis): Complete evaluation of fueling station costs for early vehicle penetration to determine the cost of fueling pathways for low and moderate fueling demand rates. (4Q, 2012)

FY 2012 Accomplishments

- The analysis framework provides a side-by-side comparison of HRS and EVSE retail infrastructure costs in 2025 when 10% of light-duty vehicles (LDVs) in a city with 1.5 million persons (equal to 120,000 LDVs) are either plug-in electric vehicles (PEVs, including battery electric vehicles [BEVs] and plug-in hybrid electric vehicles [PHEVs]) or hydrogen fuel cell electric vehicles (FCEVs).
- Annual levelized capital costs for HRS and EVSE are essentially indistinguishable given the uncertainty and variability around input assumptions. These costs fall within the range of 2.5–6.0 cents per mile, with central values of 3.0–3.2 cents per mile.
- Comparisons of two distinct EVSE scenarios suggest that, given optimistic assumptions about utilization rates, a *Robust Public* EVSE infrastructure with significant Level 2 work and public fast charging can be as capital intensive as a *Home Dominant* EVSE infrastructure with most electricity provided by charging at home.
- When including a consistent representation of vehicle performance and costs [1], total vehicle and fuel costs per mile range from 21 to 34 cents per mile. Within this range, PHEVs and hybrid electric vehicles (HEVs) have slightly lower costs per mile than conventional internal combustion engine (ICE) gasoline vehicles (Figure 4). Costs for FCEVs and BEVs are 2–6 cents per mile higher than those for PHEVs and HEVs.
- Cost differentials are reduced significantly when including a cost penalty of \$150 per tonne of CO₂ equivalent (tCO₂e) greenhouse gas emissions, assuming hydrogen from natural gas, electricity from a business-as-usual grid [2], and conventional gasoline.



Fiscal Year (FY) 2012 Objectives

- Develop consistent retail infrastructure cost estimates for hydrogen refueling stations (HRS) and electric vehicle supply equipment (EVSE)
- Compare retail costs on a common transportation energy service basis: per vehicle mile traveled
- Compare retail costs on a common early market adoption basis: fuel service to 10% of all light-duty vehicles in a typical 1.5 million person city in 2025
- Establish an analysis basis that can be extended to a dynamic and regional representation of retail costs across all major U.S. urban areas

Technical Barriers

This project addresses the following technical barriers from the Systems Analysis section of the Fuel Cell Technologies Program Multi-Year Research, Development and Demonstration Plan:

(A) Future Market Behavior

(E) Unplanned Studies and Analysis

Contribution to Achievement of DOE Systems Analysis Milestones

This project will contribute to achievement of the following DOE milestones from the Systems Analysis section of the Fuel Cell Technologies Program Multi-Year Research, Development and Demonstration Plan:

Introduction

Advanced LDVs fueled by either hydrogen or electricity offer significant social benefits, including reductions in greenhouse gas (GHG) emissions, improved energy security, and improved air quality. Both fuel types have zero tailpipe emissions and can be produced from a diversity of domestic energy resources. One of the key barriers to introducing

hydrogen and electric vehicles is the upfront capital cost of retail fuel supply equipment. We develop a simple apples-to-apples framework to compare capital costs for HRS and EVSE for early market introduction scenarios in 2025. Results are highly dependent upon a number of uncertain and variable input assumptions, including units required per vehicle, utilization rates, and cost reductions due to experience. Our findings suggest that HRS and EVSE capital costs are similar on a per-vehicle-mile-traveled basis. When accounting for total vehicle and fuel costs, hydrogen and electric vehicles are slightly more expensive than HEVs running on gasoline. Additional benefits of hydrogen and electricity, such as reduced GHG emissions or improved energy security, would likely need to be taken into account to reach cost parity with gasoline HEVs.

Approach

The simple cost estimation framework incorporates key variables that influence costs per mile driven and per equivalent early market share. The fueling service provided by EVSE and HRS is fundamentally different; while HRS may provide a level of convenience comparable to gasoline refueling stations various types of EVSE have distinct levels of convenience and accessibility. In an attempt to compare these services on a consistent cost basis, optimistic assumptions were made about the utilization of each HRS or EVSE unit. These assumptions correspond to very high, but feasible, utilization rates, which translate into relatively low capital costs per vehicle mile traveled. A mismatch in the joint deployment of vehicles and refueling equipment would result in higher costs per mile than those estimated in this study. Due to the variety of EVSE options and the uncertainty of how EVSE infrastructure will evolve to meet consumer needs, two EVSE deployment scenarios were developed: *Home Dominant* and *Robust Public*. A greater quantity of electricity is delivered to vehicles through Level 2 work and public fast charging stations in the *Robust Public* scenario compared to the *Home Dominant* scenario. Of all PEVs, 20% are BEVs in the *Home Dominant* scenario and 30% are BEVs in the *Robust Public* scenario.

Because both HRS and EVSE will undergo cost reductions in the near-term as the number of units deployed increases, our analysis framework assumes provision of fuel for 10% of LDVs in a city of 1.5 million persons in the year 2025. This early market adoption phase includes 120,000 LDVs fueled either by hydrogen as FCEVs or, in another case, by electricity as a mix of BEVs and FCEVs. We estimate the number of HRS and EVSE units required per FCEV or PEV, which provides a basis for the utilization rates discussed below. Unit costs for EVSE are based primarily upon near-term costs [3], with reference to some long-term cost estimates, and applying a 15% capital and installation cost reduction due to experience and economies of scale. Unit

costs for HRS are based upon results from recent input from industry on near-term station costs [4].

The EVSE and HRS infrastructure required to support 120,000 PEVs or FCEVs depends upon assumptions about refueling convenience, vehicle miles traveled (VMT) per year, and utilization rates. Hydrogen is used in FCEVs and electricity is used in PEVs, including BEVs and PHEVs, with the latter fueled with both electricity and a liquid fuel such as gasoline or biofuel. A key assumption unique to this study is the VMT on electricity per year for PEVs. We assume that early adopters within the first 10% of the LDV market will attain significant utility from vehicle electrification, driving more electric miles per year than would be driven in typical households. This assumption, indicated in Figure 1, results in a reduction in the cost per mile driven for PEVs. In addition, we assume that some additional electric VMT are induced in the *Public Robust* scenario. For HRS we assume an average station utilization rate of 75% and VMT per year equivalent to gasoline vehicles, which is optimistic given the changes in supply and demand that are likely to occur during early market growth.

Results

Because the majority of PEVs are assumed to be PHEVs, and because PHEVs are partially fueled by gasoline (Figure 1), the total VMT on electricity is less than the VMT on hydrogen for the same 120,000 LDVs deployed as either PEVs or FCEVs. This difference is reconciled by dividing total capital costs for HRS and EVSE by the number of miles driven on hydrogen or electricity, respectively. Results are summarized in Figure 2 with annual VMT shown on the left-hand vertical axis and with stacked bars, and with leveled retail capital costs per mile shown on the right-hand axis and with dots. Gasoline fuel costs, for the gasoline miles driven by PHEVs, are indicated for the two PEV scenarios. Fewer gasoline miles are driven in the *Robust Public* scenario due to induced electric miles (Figure 1) and the larger market share for BEVs. Capital costs per mile are nearly identical for hydrogen and electricity retail infrastructure.

For electricity and hydrogen we distinguish between capital costs associated with retail infrastructure and other costs associated with upstream fuel supply. These “Station” and “Fuel” costs are summarized in Figure 3 for the *Home Dominant* scenario and are compared with gasoline fuel costs for PHEVs, HEVs, and ICEs on a per-mile-driven basis. Key assumptions underlying these cost results are provided in [3], and include fuel costs from the Annual Energy Outlook (AEO) for 2025 and vehicle fuel economies from [1]. We assume that hydrogen is delivered to the HRS at a cost of \$3.00/kg. As indicated, BEV and PHEV costs per mile are 16%–19% lower than FCEV fuel costs, while ICE fuel costs are ~\$0.04 per mile higher (50%) than FCEV or HEV fuel costs. The error bars indicated in Figure 3 are only for the

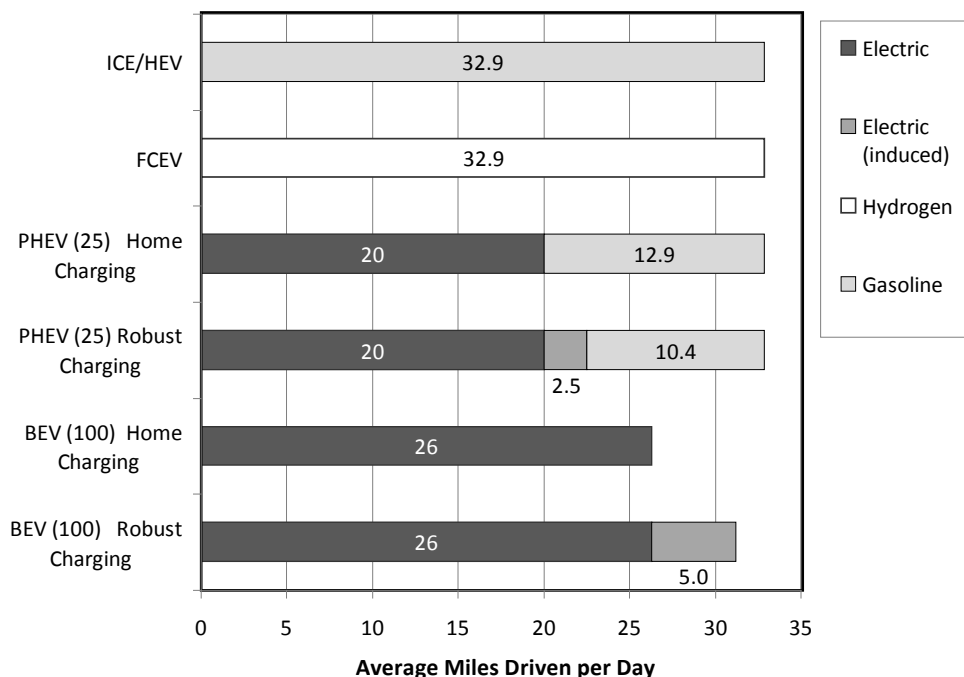


FIGURE 1. Average miles driven per day for LDVs, assuming a high percentage of electric miles for ideal PEV households within the early 10% of the LDV market

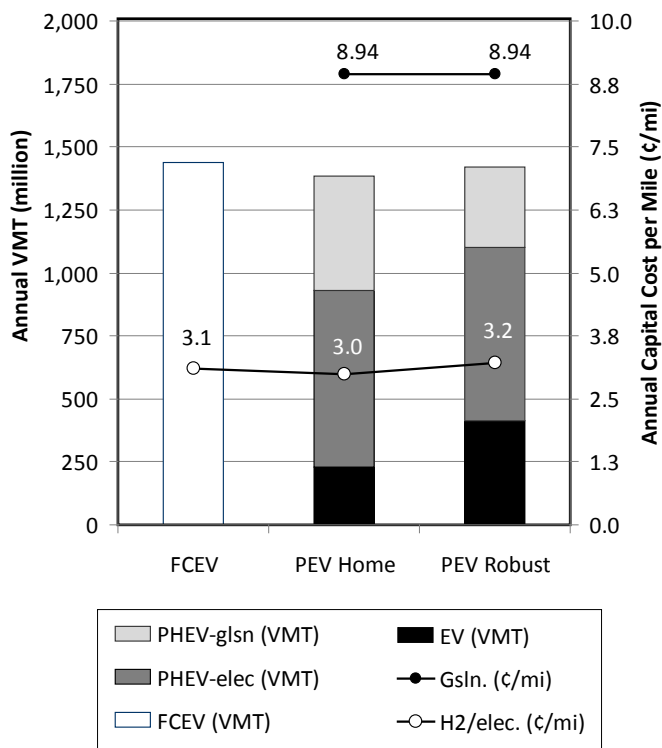


FIGURE 2. Annual vehicle miles traveled for all FCEVs or PEVs in three scenarios, gasoline costs per mile for PHEVs, and levelized capital costs per mile for corresponding HRS and EVSE retail infrastructure

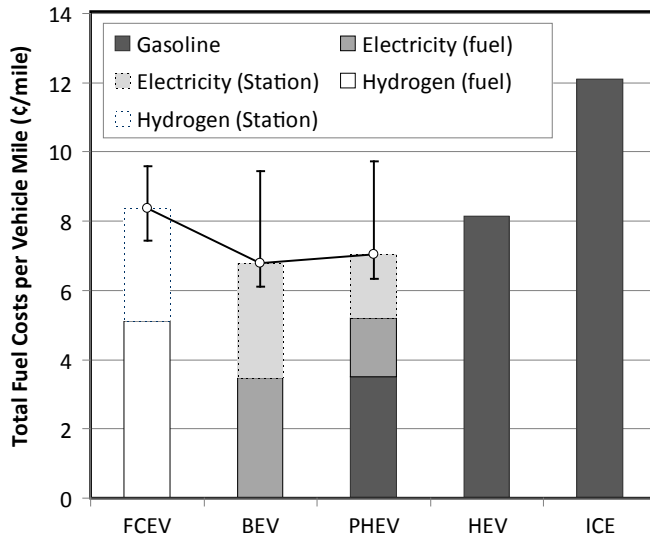


FIGURE 3. Total fuel costs per mile for hydrogen, electricity, and gasoline by vehicle type. “Station” costs refer to retail infrastructure, and “fuel” costs are additional upstream production and delivery costs.

capital cost estimates associated with HRS and EVSE, not for uncertainty or variation in upstream fuel costs. EVSE costs only include the equipment installed onsite and do not include any upstream investments.

Fuel costs can be combined with levelized vehicle costs per mile in 2025 by averaging vehicle cost estimates from

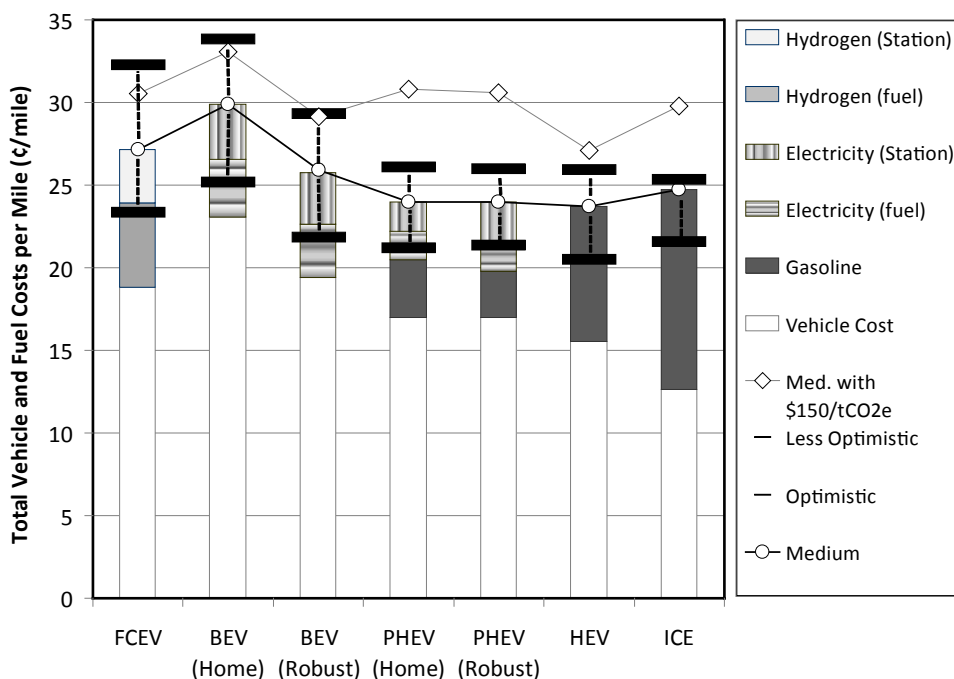


FIGURE 4. Total vehicle and fuel costs, with sensitivities for vehicle cost and fuel economy. GHG price signal result is based upon business-as-usual electricity (from AEO), hydrogen from natural gas, and a conventional gasoline blend.

DOE for years 2020 and 2030 [1]. These costs are shown in Figure 4, with error bars representing ranges associated with high and low vehicle cost estimates as well as high and low vehicle fuel economies [1]. As shown, vehicle and fuel costs per mile are slightly higher for FCEVs and BEVs, with higher BEV utilization (VMT per year) reducing levelized costs in the *Robust Public* scenario. Introducing a hypothetical \$150/tCO₂e price signal greatly reduces cost differentials between vehicle types, though HEVs running on gasoline retain a 6%-22% cost advantage over other vehicle types.

- Extend the comparison framework to incorporate variability of inputs across U.S. geographies, including fuel costs, consumer preferences, resource availability, and spatial dynamics associated with retail equipment deployment.
- Explore how fueling behavior and the premium consumers place upon convenience might influence the dynamic rollout of retail infrastructure and vehicle deployment.
- Develop more in-depth analysis of business decisions to invest in retail infrastructure.

Conclusions and Future Directions

A simple apples-to-apples comparison of HRS and EVSE capital costs on a per-vehicle-mile-traveled basis suggests that the capital intensity of hydrogen and electricity retail infrastructure is comparable in the context of an early market adoption scenario where 10% of LDVs are either FCEVs or PEVs in 2025. Results suggest that HRS and EVSE capital costs are similar on a per-vehicle-mile-traveled basis, and when total vehicle and fuel costs are accounted for hydrogen and electric vehicles are slightly more expensive than HEVs running on gasoline. These results are based upon optimistic assumptions about electric miles driven per year per PEV (Figure 1), assuming that the first 10% of the LDV market includes households demanding high electric VMT per year. Future work will include the following:

References

1. DOE (2012). Total Costs of Ownership of Future Light-Duty Vehicles. U.S. Department of Energy, DE-FOA-0000592. Retrieved February 17, 2012, from <https://www.fedconnect.net/fedconnect/?doc=DE-FOA-0000592&agency=DOE>.
2. EIA (2012). Annual Energy Outlook 2012. U.S. Energy Information Administration, Report Number DOE/EIA-0383(2012), available at <http://www.eia.gov/forecasts/aeo/>.
3. Melaina, M.W. (2012). Comparing Infrastructure Costs for Hydrogen and Electricity, DOE Annual Merit Review, available at http://www.hydrogen.energy.gov/annual_review12_analysis.html.
4. Melaina, M.W. (2012). Hydrogen Refueling Infrastructure Cost Analysis, DOE Annual Merit Review, available at http://www.hydrogen.energy.gov/annual_review12_analysis.html.

XI.5 Infrastructure Costs Associated with Central Hydrogen Production from Biomass and Coal

Darlene Steward (Primary Contact), Billy Roberts,
Karen Webster

National Renewable Energy Laboratory (NREL)
15013 Denver West Parkway
Golden, CO 80401-3305
Phone: (303) 275-3837
Email: Darlene.Steward@nrel.gov

DOE Manager

HQ: Fred Joseck
Phone: (202) 586-7932
Email: Fred.Joseck@hq.doe.gov

Project Start Date: Fiscal Year (FY) 2010
Project End Date: Project continuation and direction
determined annually by DOE

FY 2012 Objectives

- Elucidate the location-dependent variability of infrastructure costs for biomass- and coal-based central hydrogen production and delivery and the tradeoffs inherent in plant-location choices
- Provide modeling output and correlations for use in other integrated analyses and tools
- Publish results so they are available to relevant decision makers and analysts

Technical Barriers

This project addresses the following technical barriers from the Systems Analysis section of the Fuel Cell Technologies Program Multi-Year Research, Development and Demonstration Plan:

- (B) Stove-piped/Siloed Analytical Capability
- (D) Insufficient Suite of Models and Tools
- (E) Unplanned Studies and Analysis

Contribution to Achievement of DOE Systems Analysis Milestones

This project will contribute to achievement of the following DOE milestones from the Systems Analysis section of the Fuel Cell Technologies Program Multi-Year Research, Development and Demonstration Plan:

- Milestone 1.9: Complete analysis and studies of resource/feedstock, production/delivery, and existing infrastructure for technology readiness. (4Q, 2014)

FY 2012 Accomplishments

- Calculated costs of pipeline-based delivery of hydrogen from hypothetical hydrogen-production plant locations throughout the entire United States to nearest demand centers, ranging from about \$0.20 to \$2.70 per kilogram of hydrogen.
- Identified viable biomass-based hydrogen-production plant locations based on adequacy of woody biomass resources within a 100-mile radius for enabling full-capacity plant operation (about 730,000 dry metric tons per year required for 155,200 kg H₂/year plant), concluding that biomass resource availability determines where plants can be built.
- Calculated costs of truck-based delivery of biomass to the viable plant locations, ranging from \$0.11 to \$0.26 per kilogram of hydrogen.
- Calculated total biomass-based hydrogen infrastructure costs for plants located near select cities, ranging from \$0.35 per kilogram (for a plant 25 miles from Houston) to \$0.58 per kilogram (for a plant 50 miles from Detroit).
- Identified carbon-sequestration sites with storage potential equivalent to 40 years of carbon storage from coal-based hydrogen-production plants.
- Calculated costs of transporting carbon dioxide (CO₂) from potential coal-based hydrogen-production plant locations to carbon-sequestration sites. Pipeline and well infrastructure needed to transport and sequester CO₂ adds approximately \$0.20 to \$0.70 per kilogram to the cost of hydrogen.
- Calculated costs of building railroad spurs for coal delivery from primary rail lines to potential hydrogen-production plant locations, ranging from \$0.01 to approximately \$0.40 per kilogram of hydrogen.
- Concluded that distance from adequate carbon-sequestration sites limits coal-based hydrogen-production plant locations or increases infrastructure costs (for pipeline delivery of CO₂ to sequestration sites) substantially.
- Calculated total coal-based hydrogen infrastructure costs for plants located near select cities, ranging from \$0.42 per kilogram (for a plant 25 miles from Detroit) to \$0.96 per kilogram (for a plant 25 miles from Boston).

- Produced geographic information system (GIS) maps illustrating infrastructure costs for biomass- and coal-based hydrogen production.



Introduction

The United States has abundant biomass and coal resources, which could be used to produce substantial amounts of hydrogen in support of a national hydrogen economy. Further, the environmental impact of producing hydrogen from both types of resources could be manageable. Biomass captures CO₂ as part of its natural growth, so biomass-based hydrogen could produce near-zero net greenhouse gas emissions. The CO₂ emitted during coal-based hydrogen production could be sequestered, thus reducing the associated environmental impact.

As with all hydrogen technologies, reducing cost is a key challenge related to biomass- and coal-based hydrogen production. Cost-reduction opportunities exist for growing biomass feedstocks and for producing hydrogen from coal and biomass. However, few studies have addressed the location-dependent cost of the distribution infrastructure required to transport biomass and coal to centralized hydrogen-production plants, transport hydrogen from the plants to demand centers, and transport CO₂ (from coal-based plants) to carbon-sequestration sites. This project takes a first step toward filling this gap by quantifying national infrastructure requirements and costs related to centralized hydrogen production plants based on woody biomass resources (this project focuses on forest residues and primary mill residues) and coal. Project partners include the U.S. DRIVE Fuel Pathways Integrated Tech Team, DOE Biomass Program researchers, Pacific Northwest National Laboratory, and the National Energy Technology Laboratory (NETL).

Approach

The project's approach combines GIS data and tools with DOE's Hydrogen Analysis (H2A) models—the H2A Production and Delivery Components models—following three general steps: 1) Map resources, existing infrastructure, land features that impact infrastructure construction, and demand centers; 2) Construct infrastructure cost correlations in H2A models based on distance, terrain, and land use; and 3) Determine infrastructure costs for hypothetical plants in each square kilometer across the United States.

Hypothetical plant configurations were selected, including characteristics such as hydrogen-production capacity and flow of biomass or coal required to operate at full capacity. For biomass-based plants, a maximum distance of 100 miles from the plants to biomass-collection areas

was defined by assuming that 100 miles is the maximum distance that could be served economically via truck transport of biomass to plants. National woody biomass resources were quantified, and potential plant locations were identified wherever a plant could obtain enough biomass within a 100-mile radius to operate at full capacity (approximately 155,200 kg of hydrogen per year). The cost of trucking biomass (including harvest, pre-processing, grower payments, and trucking of biomass on existing roads) to the potential plant locations was calculated and mapped. Next, the pipelines required to transport hydrogen from potential plant locations to the nearest hydrogen-demand centers were identified and their costs calculated and mapped. Finally, the biomass trucking costs and hydrogen pipeline costs were combined and mapped to show the total infrastructure costs of potential biomass-based hydrogen-production plants.

For coal-based plants, similar assumptions about piping hydrogen to nearest demand centers were used. However, instead of truck delivery of biomass, rail delivery of coal to hydrogen-production plants was assumed, and the cost of building spurs from existing rail lines to plants was calculated and mapped (accounting for distance, land use, and terrain). In addition, carbon-sequestration sites with storage potential equivalent to 40 years of carbon storage from coal-based plants were identified—using NETL's National Carbon Sequestration Database and Geographic Information System—and the cost of piping CO₂ from the plants to the sites was calculated and mapped. Finally, the rail, hydrogen-pipeline, and carbon-sequestration costs were combined and mapped to show the total infrastructure costs of potential coal-based plants.

Results

Figure 1 shows the map of viable biomass-based plant locations based on the adequacy of woody biomass resources within a 100-mile radius for enabling full-capacity plant operation. Based on this analysis, the cost of truck-based delivery of biomass to the viable plant locations ranges from \$0.11 to \$0.26 per kilogram of hydrogen. Figure 2 maps costs for delivering hydrogen via pipeline from hypothetical hydrogen-production plant locations (all potential U.S. locations, not just viable biomass-based plant locations) to nearest demand centers, ranging from about \$0.20 to \$2.70 per kilogram of hydrogen; note that terrain and federally protected land restrictions impact costs in the western United States. For biomass-based plants, hydrogen pipeline cost dominates the total cost, and biomass resource availability determines where plants can be built. Table 1 shows the infrastructure-cost variations for biomass-based hydrogen-production plants near select cities. Note that Boston's low hydrogen-delivery cost gives the city the lowest overall infrastructure cost even though its biomass-delivery cost is higher than for Houston or Seattle.

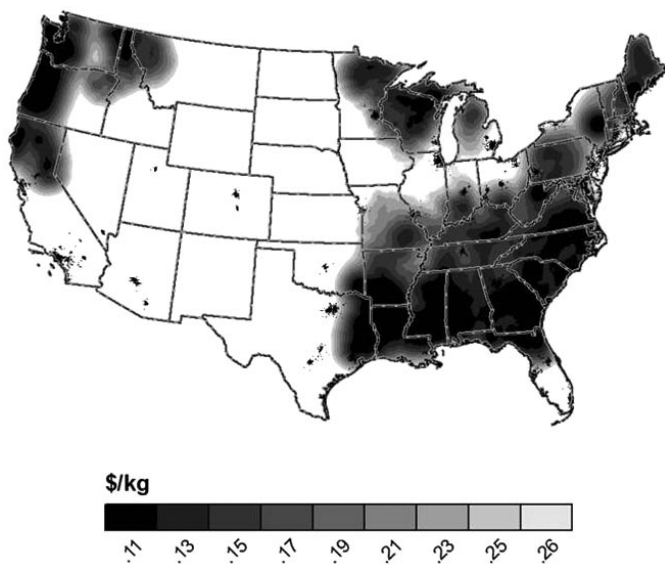


FIGURE 1. Total estimated cost of delivering woody biomass to hydrogen plants via truck (100-mile maximum transport distance). White denotes areas in which the hypothetical biomass plants are not viable because full-capacity operation cannot be supported with the woody biomass resources available within the 100-mile transport distance. Billy Roberts, NREL, July 2012.

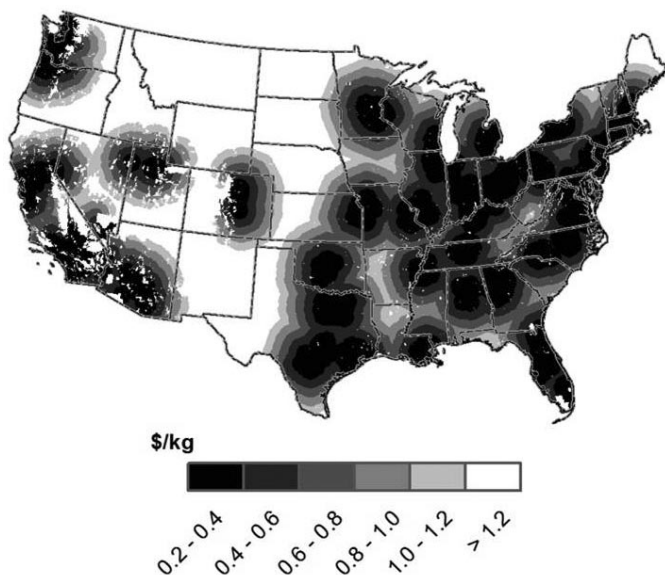


FIGURE 2. Total estimated cost of delivering hydrogen to demand centers via pipeline. Billy Roberts, NREL, July 2012.

Figure 3 shows carbon-sequestration sites with storage potential equivalent to 40 years of carbon storage from coal-based hydrogen-production plants. Costs of CO₂ pipelines account for restrictions on sequestration site access based on proximity, pipeline route availability (e.g., avoiding restricted areas such as national parks), and the impact of terrain characteristics on installation cost. Total infrastructure

TABLE 1. Biomass-based hydrogen infrastructure costs for plants near select cities

| City (plant distance to city outskirts - miles) | Biomass Truck Delivery (¢/kg) | H ₂ Pipeline Delivery (¢/kg) | Total Infrastructure Cost (¢/kg) |
|---|-------------------------------|---|----------------------------------|
| Boston (25, W) | 19 | 21 | 40 |
| Boston (50, W) | 17 | 24 | 40 |
| Houston (25, N) | 11 | 25 | 35 |
| Houston (50, N) | 11 | 37 | 48 |
| Seattle (25, S) | 11 | 32 | 43 |
| Seattle (50, S) | 10 | 34 | 44 |
| San Francisco (25, N) | 23 | 26 | 48 |
| San Francisco (50, N) | 21 | 35 | 55 |
| Detroit (25, W) | 24 | 22 | 46 |
| Detroit (50, W) | 23 | 35 | 58 |

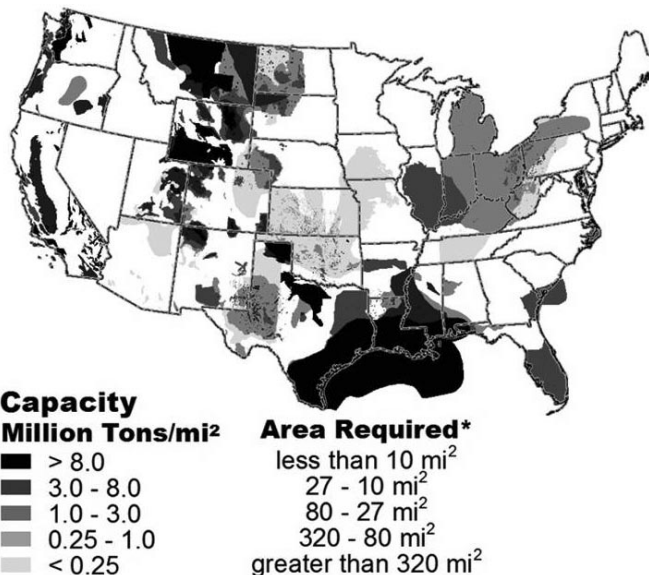


FIGURE 3. Total estimated U.S. CO₂ sequestration capacity from un-mineable coal seams, saline formations, and depleted oil and gas reservoirs with adequate storage for 40 years. Reservoir data: National Energy Technology Laboratory (www.natcarb.org). Billy Roberts, NREL, July 2012. *Approximate surface area of reservoir required for 40 years of CO₂ storage from a single hydrogen-production plant.

costs were calculated based on CO₂ pipeline/well costs (about \$0.20 to \$0.70 per kilogram of hydrogen) the cost of building railroad spurs for coal delivery from primary rail lines to potential hydrogen-production plant locations (about \$0.01 to \$0.40 per kilogram of hydrogen), and the cost of piping hydrogen to demand centers (about \$0.20 to \$2.70 per kilogram of hydrogen, Figure 2). The distance from adequate carbon-sequestration sites limits hydrogen-production plant

locations or increases infrastructure costs substantially. Table 2 shows the infrastructure-cost variations for coal-based plants near select cities. Boston has high infrastructure costs because suitable carbon sequestration sites are far from the city.

TABLE 2. Coal-based hydrogen infrastructure costs for plants near select cities

| City (plant distance to city outskirts - miles) | CO ₂ Pipeline (¢/kg) | Rail Spur (¢/kg) | H ₂ Pipeline Delivery (¢/kg) | Total Infrastructure Cost (¢/kg) |
|---|---------------------------------|------------------|---|----------------------------------|
| Boston (25, W) | 72 | 3 | 21 | 96 |
| Boston (50, W) | 60 | 0 | 24 | 84 |
| Houston (25, N) | 17 | 5 | 25 | 47 |
| Houston (50, N) | 17 | 2 | 37 | 56 |
| Seattle (25, S) | 17 | 3 | 32 | 52 |
| Seattle (50, S) | 17 | 14 | 34 | 65 |
| San Francisco (25, N) | 24 | 0 | 26 | 50 |
| San Francisco (50, N) | 23 | 11 | 35 | 69 |
| Detroit (25, W) | 17 | 3 | 22 | 42 |
| Detroit (50, W) | 17 | 1 | 35 | 53 |

Figure 4 compares total infrastructure costs for biomass-based (top) and coal-based (bottom) hydrogen-production plants, with plant locations limited to those with infrastructure costs of \$1 per kilogram of hydrogen or less. As the figure shows, infrastructure for coal-based hydrogen plants is usually more expensive than infrastructure for biomass-based hydrogen plants. However, coal-based plants are viable in some metropolitan areas where biomass-based plants are not because of inadequate biomass resources within the assumed 100-mile truck-delivery radius.

Conclusions and Future Directions

This analysis shows the benefit of using GIS data and tools in conjunction with established DOE models to explore the location-dependent variability of infrastructure costs for hydrogen production and delivery from various feedstocks as well as the tradeoffs inherent in plant-location choices. The modeling output and correlations will be made available for other integrated analyses and tools, and the results will be published so they are available to relevant decision makers and analysts.

Although work in the remainder of FY 2012 will focus on publishing results of the work done to date, various strategies could refine and/or reduce hydrogen infrastructure costs. For example, performing the analysis assuming

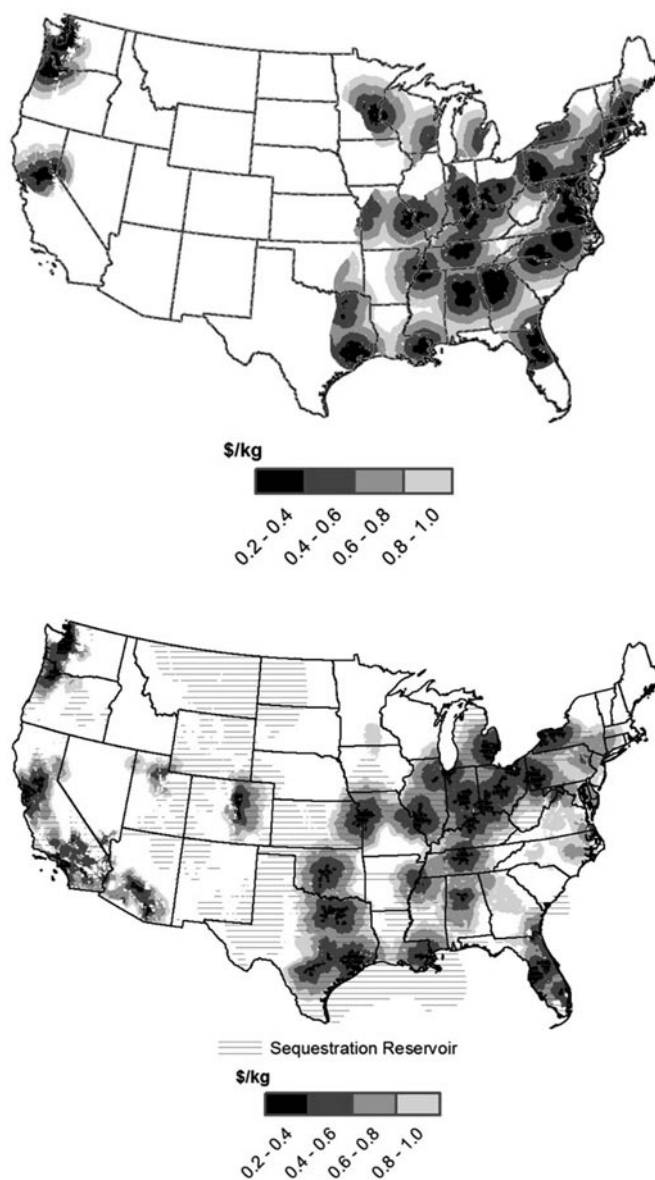


FIGURE 4. Total estimated infrastructure cost of producing and delivering hydrogen from woody biomass-based (top) and coal-based (bottom) plants. Billy Roberts, NREL, July 2012.

rail delivery of biomass, smaller biomass-based hydrogen plants, or both could show increased geographic availability of this technology. For coal-based hydrogen plants, CO₂ sequestration costs could be refined by accounting for differences in carbon reservoir permeability and size. For both hydrogen-production technologies, infrastructure cost/supply curves could be developed. Finally, the National Renewable Energy Laboratory’s Scenario Evaluation, Regionalization & Analysis model could be used to optimize hydrogen infrastructure locations.

XI.6 Sensitivity Analysis of H2-Vehicles' Market Prospects, Costs and Benefits

David L. Greene (Primary Contact), Zhenhong Lin, Jing Dong

Oak Ridge National Laboratory
National Transportation Research Center
2360 Cherahala Boulevard
Knoxville, TN 37932
Phone: (865) 946-1310
Email: dlgreene@ornl.gov

DOE Manager

HQ: Fred Joseck
Phone: (202) 586-7932
Email: Fred.Joseck@hq.doe.gov

Subcontractor:

Department of Industrial Engineering,
University of Tennessee, Knoxville, TN

Project Start Date: October, 2010

Project End Date: Project continuation and direction determined annually by DOE

of the Fuel Cell Technologies Program Multi-Year Research, Development and Demonstration Plan:

- 1.15 Complete analysis of program milestones and technology readiness goals – including risk analysis, independent reviews, financial evaluations, and environmental analysis – to identify technology and risk mitigation strategies. (4Q, 2015)
- 1.16 Complete analysis of program performance, cost status, and potential use of fuel cells for a portfolio of commercial applications. (4Q, 2018)
- 2.2 Annual model update and validation. (4Q 2011 through 4Q, 2020)

FY 2012 Accomplishments

- Produced 48 scenarios with alternative assumptions about technological progress and market conditions.
- Tested sensitivity of scenario results to alternative assumptions about consumers' preferences and behavior.
- Published refereed journal article describing FY 2011 research on markets for non-automotive fuel cells.

Fiscal Year (FY) 2012 Objectives

- Project market shares of hydrogen fuel cell vehicles (FCVs) under varying market conditions using the Market Acceptance of Advanced Automotive Technologies (MA3T) model.
- Analyze the sensitivity of projected market shares of hydrogen FCVs to alternative assumptions about consumers' preferences and behavior.

Technical Barriers

This project addresses the following technical barriers from the Systems Analysis section of the Fuel Cell Technologies Program Multi-Year Research, Development and Demonstration Plan:

- (A) Future Market Behavior
- (B) Stove-piped/Siloed Analytical Capability
- (D) Insufficient Suite of Models and Tools
- (E) Unplanned Studies and Analysis

Contribution to Achievement of DOE Systems Analysis Milestones

This project will contribute to achievement of the following DOE milestones from the Systems Analysis section



Introduction

The future market potential of hydrogen vehicles and the challenges to achieving market success depend partly on technological factors and partly on market behavior. The Hydrogen and Fuel Cells Program has formulated program goals for hydrogen production, storage and fuel cell technologies that are a function of the theoretical potential of the technologies and what is believed to be necessary for success in the market place. There is uncertainty both with respect to what can be achieved technologically and how the market is likely to respond.

As hydrogen and fuel cell technologies progress and more is learned about the cost and performance that is achievable, it is important to re-evaluate the likelihood of market success and the resulting impacts on economic, energy security and environmental benefits. But there is also substantial uncertainty about how markets will respond to novel automotive technologies and how hydrogen and fuels cells may compete in the market with other advanced automotive technologies. This study makes use of a state-of-the-art market penetration model, the MA3T model, to assess the sensitivity of the market success of hydrogen FCVs to alternative scenarios of technological progress and alternative assumptions about consumer behavior.

Approach

Scenarios of technological progress for FCVs and competitive/synergistic advanced technologies were constructed based on simulations developed by the Argonne National Laboratory's Autonomie model. The Autonomie model simulations are generally consistent with DOE's program goals for advanced vehicle technologies. These were combined with projections of energy prices and light-duty vehicle sales from the 2011 Annual Energy Outlook (AEO). The scenarios were input to the Department of Energy's MA3T model. The MA3T model is a nested discrete choice model that estimates future market shares of 20 powertrain technologies, separately for automobiles and light trucks, and produces projections to the year 2050. The technology sets include plug-in versions of both internal combustion engine and fuel cell-powered vehicles. MA3T includes a detailed market segmentation to better represent heterogeneity in consumer demand. Its 1,458 segments account for differences among regions, degree of urbanization, housing types, risk preferences, and distributions of daily vehicle use.

Variants to a baseline scenario were developed to reflect uncertainties along the following four dimensions:

- Technology status
- Energy prices
- Consumers' preferences
- Policies

The baseline scenario assumed automotive fuel cell systems would cost \$60/kW and onboard hydrogen storage would cost \$10/kWh; it assumed batteries for battery electric vehicles would cost \$450/kWh. More successful technology scenarios were constructed, including fuel cell system costs down to \$25/kW and on-board storage at \$5/kWh; battery success scenarios included costs down to \$150/kWh and accelerated progress. Three energy price scenarios were used, based on the AEO 2011 High, Reference and Low oil price cases. Alternative policies focused on early infrastructure provision and subsidies for fuels and vehicles. Sensitivity to four key aspects of consumer behavior were explored: 1) sensitivity of choices to price, 2) cost of limited refueling availability, 3) cost of limited vehicle range and long refueling time, 4) the extent to which consumers factor future fuel costs into their new vehicle purchase decisions.

Results

The results of the sensitivity analysis suggest that the market success of hydrogen vehicles (H2Vs), given appropriate policies, is relatively robust to both the evolution of fuel cells and competing/synergistic technologies and to consumers' preferences. Figure 1 illustrates the outcomes of scenarios in which the key factors varied were technological success and the provision of infrastructure (the dip in shares

around 2015 is due to the expiration of tax credits). Given adequate provision of early infrastructure, the ultimate market success depends most strongly on the progress of automotive fuel cell technology. The effects of the progress of other advanced technologies are reflected in the dispersion among curves of the same color (green, blue and red). Assuming successful development of fuel cell technology, it appears that fuel cells could achieve market shares in the range of 60-70% of new light-duty vehicle sales by 2050. Interestingly, lower battery costs produce a slight increase in the estimated FCV market share because the benefits of lower battery costs to FCVs appear to outweigh the effect of greater competition from lower-cost plug-in electric vehicles (PEVs).

Given technological success, H2Vs appear to be competitive under a range of prices for hydrogen and petroleum. DOE program goals are aimed at hydrogen prices between \$2 and \$4 per kilogram, in the long run. As Figure 2 illustrates, hydrogen prices do affect sales but raising the long-run, high-volume delivered hydrogen price from \$2.50 to \$4.00 reduces sales of hydrogen vehicles by less than 15%. The price of petroleum will also have an impact: the range from the Low to High Oil Price cases is about +/-20% of the Reference Case estimate if fuel cell technology is successful but +/- 50% if the base assumptions are used.

The sensitivity of the market success of hydrogen vehicles to consumers' preferences was also tested. Figure 3 illustrates the effect of greater or lesser sensitivity of consumers' choices to price (Beta). In discrete choice models, such as the MA3T, sensitivity to price reflects the degree to which consumers consider the alternatives to be close substitutes for one another. Insensitivity to price indicates that there are many attributes of the vehicles about which consumers have widely different evaluations. At low levels of market penetration less price sensitivity favors hydrogen vehicles. However, in the technology success case in later years greater price sensitivity increases H2V sales. This result is not seen in the Base case; less price sensitivity uniformly favors H2V's market share. In the Technology Success case FCVs eventually become less expensive to own than alternatives and so greater sensitivity to price favors them.

Other consumer preference factors that had similar impacts (approximately +/-20%) on hydrogen vehicles' market success were the degree to which consumers consider future fuel costs in new car purchase decisions and the perceived cost of limited fuel availability. Consumers' perception of the value of fuel availability matters greatly when the market shares of hydrogen vehicles are small but has only a small effect as market shares approach 50%. The cost of limited range and long refueling times affects PEVs more than H2Vs and has a very minor impact on the market success of H2Vs. Based on this result and the beneficial effect of lower battery costs on FCVs' market share, it appears that there is little competition between PEVs and FCVs for market share.

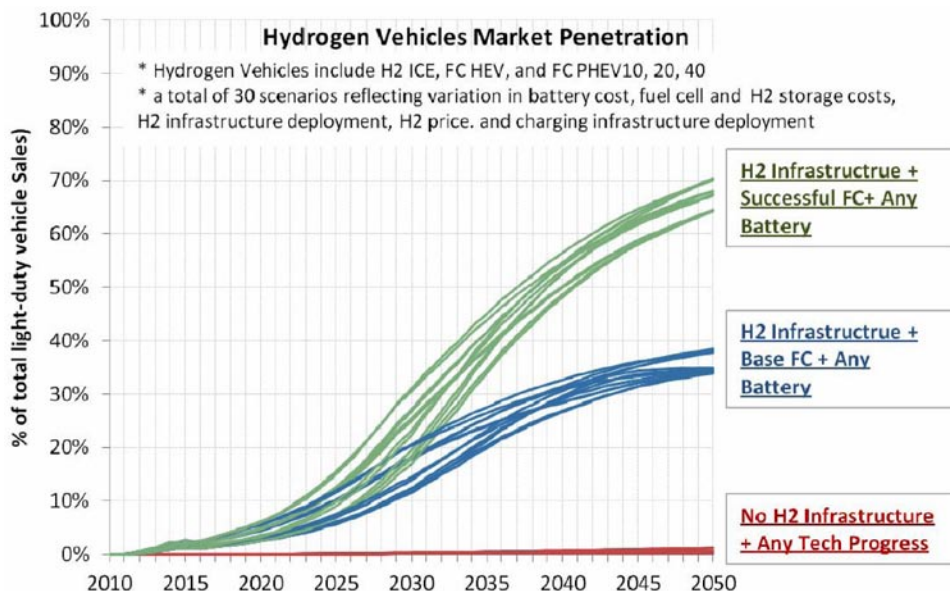


FIGURE 1. Hydrogen Vehicles Market Penetration: Sensitivity to Technological Progress

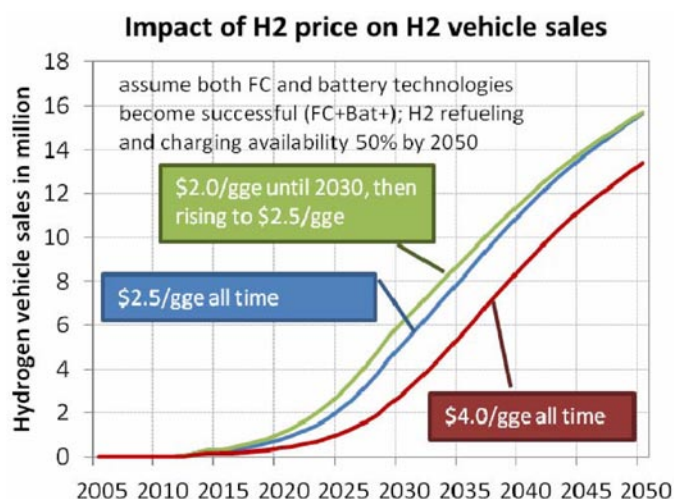


FIGURE 2. Impact of Hydrogen Price on Hydrogen Vehicle Sales

Conclusions and Future Directions

This analysis suggests that, given appropriate transition policies, particularly the early provision of refueling infrastructure, FCVs are likely to achieve substantial market success. If the technology goals for FCVs are achieved, the market share of H2Vs could well be in the range of 60% to 70% by 2050. Furthermore, given technology success, the market acceptance of H2Vs seems to be robust to a range of external market conditions and assumptions about consumers’ preferences. However, this analysis represents a first attempt to comprehensively analyze the sensitivity of hydrogen vehicle market success to a wide range of uncertainties. Not all relevant uncertainties have been

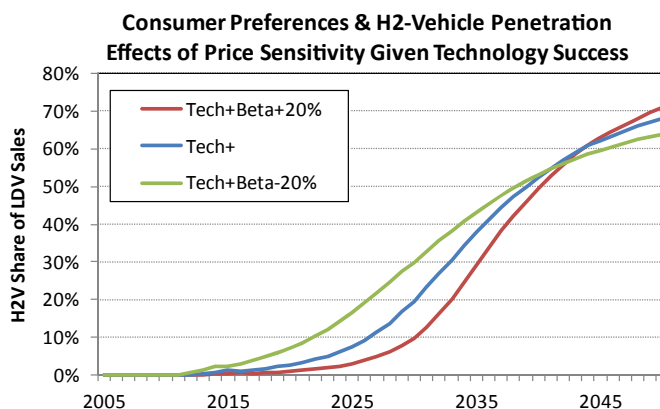


FIGURE 3. Effect of Consumer Price Sensitivity on Hydrogen Vehicle Sales

included in the analysis and a full experimental design has not been carried out due to the complexity of the MA3T model and limited time and resources to execute potentially thousands of model runs. Future research may address these issues depending on the evaluation of this initial analysis, availability of funding and program priorities.

The analysis will be documented in the form of an article that will be submitted for consideration for publication in an appropriate refereed journal. Based on the referees’ comments the analysis may be revised.

FY 2012 Publications/Presentations

1. Upreti, G., D.L. Greene, K.G. Duleep and R. Sawhney, 2012. “Fuel cells for non-automotive uses: Status and prospects”, *International Journal of Hydrogen Energy*, vol. 37, no. 8, pp. 6339-6348.

References

1. Lin, Z., 2012. MA3T Model: Modeling the Market Acceptance of Advanced Automotive Technologies, Center for Transportation Analysis, Oak Ridge National Laboratory, <http://cta.ornl.gov/ma3t/>.
2. Energy Information Administration, 2011. *Annual Energy Outlook 2011*, DOE/EIA-0484(2011), U.S. Department of Energy, Washington, D.C.

XI.7 Effects of Technology Cost Parameters on Hydrogen Pathway Succession

Mark F. Ruth* (Primary Contact), Victor Diakov*, Brian James†, Julie Perez‡, Andrew Spisak†

*National Renewable Energy Laboratory

15013 Denver West Pkwy.

Golden, CO 80401

Phone: (303) 817-6160

Email: Mark.Ruth@nrel.gov and Victor.Diakov@nrel.gov

† Strategic Analysis, Inc.

‡ New West Technologies

DOE Manager

HQ: Fred Joseck

Phone: (202) 586-7932

Email: Fred.Joseck@ee.doe.gov

Subcontractor:

Strategic Analysis, Inc., Arlington, VA

Project Start Date: February 1, 2009

Project End Date: October 31, 2011

Contribution to Achievement of DOE Systems Analysis Milestones

This project will contribute to achievement of the following DOE milestones from the Systems Analysis section of the Fuel Cell Technologies Program Multi-Year Research, Development and Demonstration Plan:

- Milestone 1.1: Complete an analysis of the hydrogen infrastructure and technical target progress for hydrogen fuel and vehicles. (2Q, 2011)
- Milestone 2.1: Complete the 2nd version of the Macro-System Model to include the analytical capabilities to evaluate the electrical infrastructure. (2Q, 2011)
- Milestone 2.2: Annual model update and validation. (4Q, 2011 through 4Q, 2020)

FY 2012 Accomplishments

- Linked the HyPro pathway progression model to the MSM framework.
- Performed numerous MSM-HyPro runs utilizing up-to-date production and delivery data from H2A and the Hydrogen Delivery Scenario Analysis Model (HDSAM).
- Performed an analysis on effects of technology cost parameters on hydrogen pathway succession.



Fiscal Year (FY) 2012 Objectives

- Develop a macro-system model (MSM):
 - Aimed at performing rapid cross-cutting analysis
 - Utilizing and linking other models
 - Improving consistency between models
- Improve understanding of options and tradeoffs in the evolution of hydrogen production and delivery infrastructure for transportation with a specific focus on:
 - What is a likely succession of hydrogen pathways?
 - What factors influence the sequence most?

Technical Barriers

This project addresses the following technical barriers from the Systems Analysis section of the Fuel Cell Technologies Program Multi-Year Research, Development and Demonstration Plan:

- (B) Stove-piped/Siloed Analytical Capability
- (C) Inconsistent Data, Assumptions and Guidelines
- (D) Insufficient Suite of Models and Tools

Introduction

At the DOE Hydrogen Program's behest, we are developing an MSM to analyze cross-cutting issues because no existing model sufficiently simulates the entire system, including feedstock, conversion, infrastructure, and vehicles, with the necessary level of technical detail. In addition, development of the MSM exposes inconsistencies in methodologies and assumptions between different component models so that they can be identified and corrected when necessary. Version 1.0 of the MSM was developed previously and is available to the hydrogen analysis community. It links H2A Production, HDSAM, the Greenhouse gases, Regulated Emissions and Energy use in Transportation (GREET) model, and physical property information from the Hydrogen Analysis Resource Center to estimate the economics, primary energy source requirements, and emissions of multiple hydrogen production/delivery pathways.

Version 2.0 of the MSM links the HyPro [1] model that is a MatLab®-based computer model developed by

Directed Technologies Inc. under contract to the DOE for calculation of the expected “pump price” of hydrogen (i.e. the profited cost of hydrogen ready to be dispensed into a customer’s vehicle at the dispensing station) for a variety of production/delivery/dispensing pathways in an area of uniform demand density over a span of years. By postulating the yearly hydrogen demand and calculating which supply infrastructure pathway is expected to provide the least expensive hydrogen in any given year, the model projects infrastructure build-out over time. This build-out projection takes into consideration potential advances in technology, underutilization of facilities in the early years of a station coming on line, potential stranded assets, feedstock cost differences, economies of scale for the production equipment, and “learning curve” capital cost reductions due to repetitious fabrication of multiple systems. The build-out projection allows for only one “winner” each year and all the pathways built that year will have the same combination of technologies. In reality, there is likely to be a diversity of opinion regarding demand level and price projections that will lead to more than one technology being built out each year.

Approach

The MSM is being developed as a tool that links or federates existing models across multiple platforms. This approach was chosen because the task of building a single monolithic model incorporating all of the relevant information in the existing models would have been overwhelming because the necessary expertise to do so was spread among half a dozen DOE laboratories and a dozen or more universities and private contractors. Linking models allows model users that depend on data from component models to continue using their models while retrieving data

from component models in a less labor-intensive manner. In addition, it provides a common platform for data exchange necessary to update integrated models when the component models have been updated.

The MSM is being built on a framework inspired by an example of a federated object model (FOM). The MSM uses a common interlingua that is extensible (accommodates new models with a minimum of difficulty), distributable (can be used by multiple people in different areas of the country), and scalable (to a larger number of participating models) using exogenous data. FOMs are exemplified by the Department of Defense high-level architecture [2]. Version 2.0 of the MSM uses Ruby and Ruby interfaces to Microsoft Excel and other platforms to collect, transfer, and calculate data.

Results

All runs include an exogenous demand curve based on the form recommended by the National Academy of Sciences [3] adapted for Los Angeles and 50% penetration of fuel cell electric vehicles (FCEVs). The fuel economy assumed for the FCEVs is 45 miles per gallon gasoline equivalent (mpgge).

The base case scenario uses default inputs from H₂ production and delivery models and its results are shown in Figure 1. The analysis shows the forecourt steam methane reforming (FCSMR) production option as the most cost-effective (by a large margin of >\$1/kgH₂) in the early years of hydrogen FCEV market development. This option is replaced by central coal gasification with pipeline delivery when the market matures and advanced technology options (both production and delivery) are available. The base case is associated with significant greenhouse gas emissions (GHGs) brought about by coal gasification (not shown).

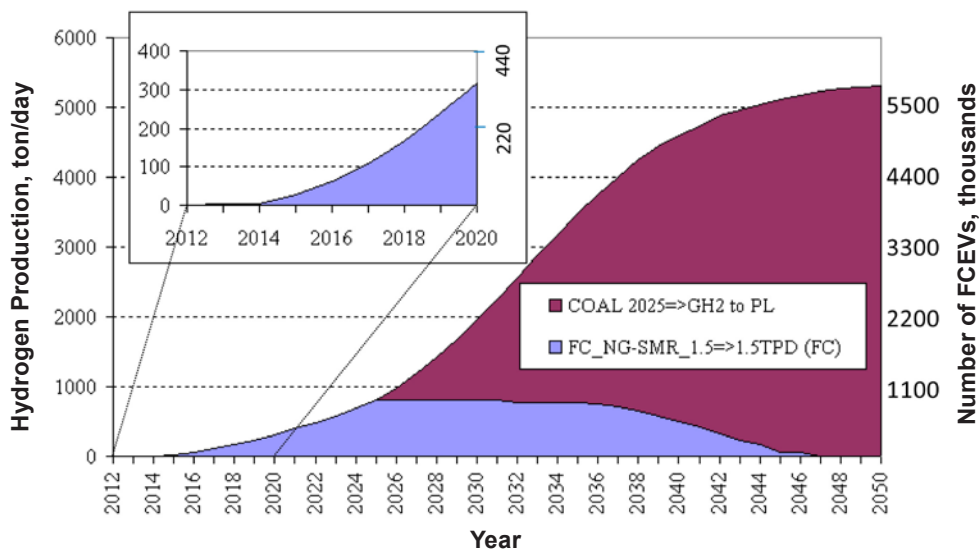


FIGURE 1. Hydrogen production for the base case hydrogen pathway evolution scenario

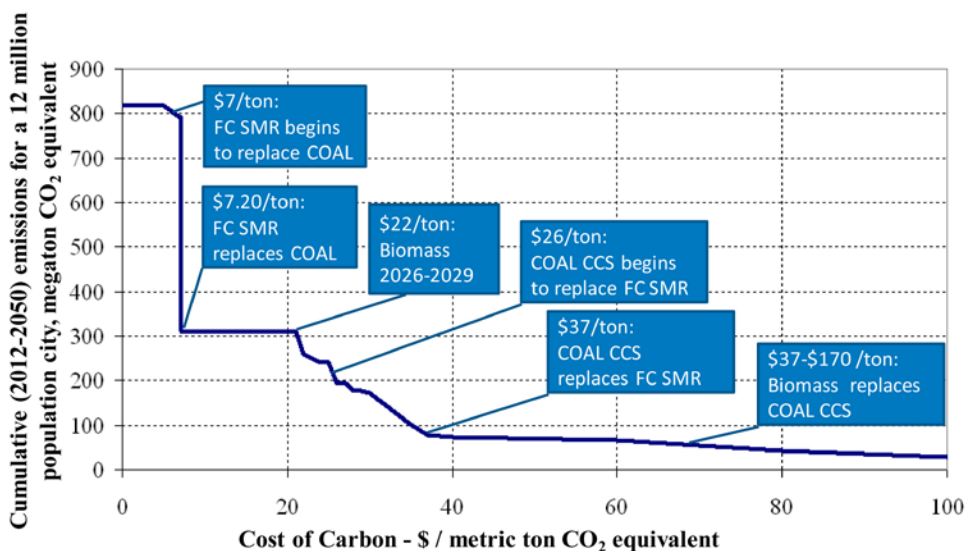


FIGURE 2. Cumulative GHG emissions from hydrogen production facilities as affected by a cost of carbon

Figure 2 shows the effects of a cost of carbon on technology selection. Low costs of carbon do not affect the technology mix or the GHG emissions. Then, at moderate levels (7-7.14 \$/metric ton CO₂ equivalent), FCSMR becomes more economical than coal gasification and results in a large (62%) reduction in the overall amount of GHGs. Further increases in carbon costs up to about 21\$/metric ton) does not induce any technology changes: between \$7.14/ton and \$21/ton the cost optimal scenario involves only FCSMR hydrogen production for any year under consideration (2012-2050). Biomass gasification becomes competitive for several years at carbon cost level of \$22/ton. (Biomass feedstock projected price is gradually increasing so there is no sharp takeover as in the COAL–FCSMR case at ~\$7/ton cost of carbon.) Between \$26/ton and \$37/ton carbon cost, coal gasification with carbon capture and sequestration (COAL CCS) replaces FCSMR as the preferred advanced technology option (for years 2027-2050).

As shown in Figure 2, increased costs of carbon open the markets for more expensive but cleaner technologies. Thus, consumer costs (levelized cost plus cost of carbon) go up and the carbon footprint goes down. However, the amount paid for carbon emissions is limited by the incremental cost of related technologies. Figure 3 shows this effect by reporting both the average levelized cost of hydrogen and the portion of that cost that pays for carbon emissions in 2050. Irregularities observed on the hydrogen cost and GHG tax curves are inflicted by technology breakthrough points that cause one technology to replace others.

In scenarios where coal without CCS is not allowed, distributed SMR is the only technology selected. The increase in SMR capital cost to make other technologies competitive was analyzed. The results are shown in

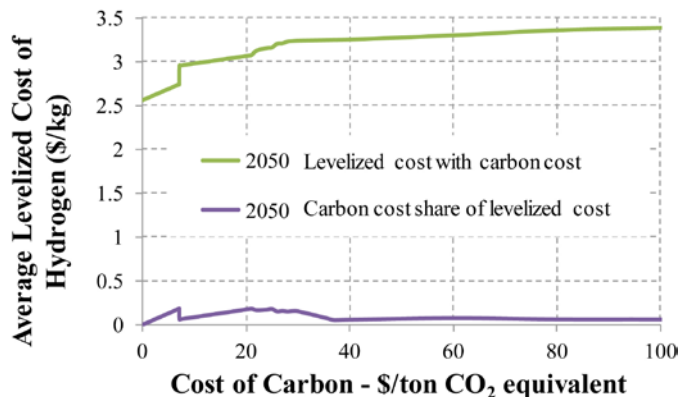


FIGURE 3. Effects of a cost of carbon on the average levelized cost of hydrogen and the portion paid for carbon emissions

Figure 4 and indicate that other technologies do not become cost competitive until capital cost of distributed SMR is increased by over 70%. Increased forecourt natural gas SMR capital costs would result in replacing it with even more capital intensive central production technologies, biomass gasification and coal gasification with carbon capture and sequestration. The replacement with higher capital cost technologies becomes possible only because of relatively low biomass and coal feedstock prices.

Conclusions and Future Directions

- Based on current cost projections and a required 10% internal rate of return, distributed SMR is the most cost-effective technology to roll out in the early commercial stage.

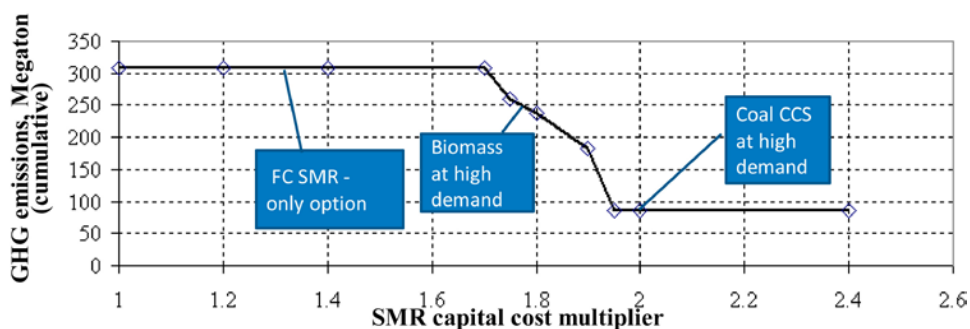


FIGURE 4. Effects of increased SMR capital costs on GHG emissions due to technology selection

- Central coal (without CCS) is the most cost-effective technology at higher demand growth if carbon emissions are not limited.
- The cost of carbon limits coal without CCS. It is replaced by distributed SMR, biomass, and coal with CCS as the cost increases.
- Distributed SMR is the most cost-competitive technology when central coal without CCS is not allowed. Other technologies need large capital or feedstock cost reductions to become competitive.

No additional funding is planned for this analysis. If we had additional funding, we would like to:

- Update the analysis using new versions of H2A, HDSAM, and GREET.
- Update the analysis with 200 kg/day stations, tube trailer delivery, and tri-generation options.
- Spread out technology improvement (potentially using learning curves).
- Use supply curves instead of single values
- Add unforeseen randomness to the demand function.

Within ongoing projects, the MSM is being updated. An analysis of the parameters used in estimating levelized cost and energy use and emissions is underway.

FY 2012 Publications/Presentations

1. Diakov, V; Ruth, M.F.; James, B.; Perez, J.; Spisak, A. “Technical Breakthrough Points and Opportunities in Transition Scenarios for Hydrogen as Vehicular Fuel,” NREL Report No. 53489 (2011) <http://www.nrel.gov/docs/fy12osti/53489.pdf>.
2. Diakov V., Ruth, M., James, B., Perez, J. and Spisak, A. “Technical breakthrough points and opportunities in transition scenarios for hydrogen as vehicular fuel.” Presentation at the Fuel Cell Seminar, Washington, D.C., October 2011.

3. Diakov, V., Ruth, M., Goldsby, M., Sa, T. (2011) “Macro-System Model for Hydrogen Energy Systems Analysis in Transportation.” In the International Mechanical Engineering Conference and Exhibit, Paper 63815, Denver, CO, November 2011.
4. Diakov, V; Ruth, M.F.; Sa, T.J., Goldsby, M.E. “WREF 2012: Macro-Systems Model for Hydrogen Energy Systems Analysis in Transportation,” World Renewable Energy Conference Presentation. May 15, 2012.
5. Diakov, V; Ruth, M.F.; Sa, T.J., Goldsby, M.E. “WREF 2012: Macro-Systems Model for Hydrogen Energy Systems Analysis in Transportation,” World Renewable Energy Conference Proceedings. In Press.

References

1. James, B. D., P. O. Schmidt, J. Perez. 2008. Using HyPro to evaluate competing hydrogen pathways. Report on DOE contract DE-FG36-05GO15019. Available via http://www.hydrogen.energy.gov/pdfs/progress07/viii_1_james.pdf [Accessed May 20, 2011].
2. Judith S. Dahmann, Richard Fujimoto, and Richard M. Weatherly. “The Department of Defense high level architecture.” In Winter Simulation Conference, pages 142–149, 1997.
3. National Academy of Sciences. 2004. The Hydrogen Economy: Opportunities, Costs, Barriers, and R&D Needs, National Academy Press, Washington, D.C.

XI.8 Impact of DOE Program Goals on Hydrogen Vehicles: Market Prospect, Costs, and Benefits

Zhenhong Lin (Primary Contact), David Greene,
Jing Dong
Oak Ridge National Laboratory (ORNL)
National Transportation Research Center
2360 Cherahala Boulevard
Knoxville, TN 37932
Phone: (865) 946-1308
Email: linz@ornl.gov

DOE Manager
HQ: Fred Joseck
Phone: (202) 586-7932
Email: Fred.Joseck@hq.doe.gov

Project Start Date: October 2011
Project End Date: September 2012

Fiscal Year (FY) 2012 Objectives

- Project market penetrations of hydrogen vehicles under varied assumptions on processes of achieving the DOE program goals for fuel cells, hydrogen storage, batteries, motors, and hydrogen supply.
- Estimate social benefits and public costs under different program goals scenarios, including petroleum use reduction, greenhouse gas (GHG) reduction, zero-emission vehicle population, grid-connected vehicle population, public expenditure for infrastructure, and public expenditure for vehicle purchase subsidy.
- Compare cost-effectiveness of public expenditure among scenarios.
- Conduct market analysis by integrating output of various DOE-sponsored and other federal projects, including ORNL's Market Acceptance of Advanced Automotive Technologies (MA3T) model, Argonne National Laboratory's Autonomie model, National Renewable Energy Laboratory's H2A model, Energy Information Administration's Annual Energy Outlook projection, Department of Transportation's National Highway Traffic Safety database, and the Environmental Protection Agency's technology assessment.

Technical Barriers

This project addresses the following technical barriers from the Systems Analysis section of the Fuel Cell Technologies Program Multi-Year Research, Development and Demonstration Plan:

- (A) Future Market Behavior
- (B) Stove-piped/Siloed Analytical Capability
- (D) Insufficient Suite of Models and Tools
- (E) Unplanned Studies and Analysis

Contribution to Achievement of DOE Systems Analysis Milestones

This project will contribute to achievement of the following DOE milestones from the Systems Analysis section of the Fuel Cell Technologies Program Multi-Year Research, Development and Demonstration Plan:

- Milestone 4: Complete evaluation of fueling station costs for early vehicle penetration to determine the cost of fueling pathways for low and moderate fueling demand rates. (4Q, 2012)
- Milestone 8: Determine economies of scale required for government ramp down of funding for RD&D. (4Q, 2013)
- Milestone 12: Complete an analysis of the hydrogen infrastructure and technical target progress for technology readiness. (4Q, 2015)

FY 2012 Accomplishments

- Constructed 42 different exogenous projections of technology status relative to program goals and projected corresponding sales of hydrogen vehicles using the MA3T model.
- Evaluated the social benefits of promoting hydrogen vehicle market in terms of petroleum use reduction, GHG emission reduction, and the stock penetration of zero-emission vehicles (for air quality) and grid-connected vehicles (for oil demand elasticity).
- Compared the cost-effectiveness of public expenditure among scenarios of program goal progresses.



Introduction

The Department of Energy's Hydrogen and Fuel Cell Program has established ambitious goals for hydrogen technologies, from production to delivery and end use [1]. Over the years, program goals have been modified in light of new information and using more advanced methods for establishing goals for an uncertain future. Very substantial progress had been made in recent years toward the

achievement of the DOE’s hydrogen and fuel cell technology program goals, as illustrated by successive annual estimates of the cost of high-volume production of automotive fuel cells [2]. These estimates show that projected, high-volume fuel cell costs are very close to meeting program goals. Progress toward meeting goals for power density and stack energy efficiency has also been impressive [3].

This study aims at a better understanding of the hydrogen vehicle market prospect, the social benefits and the required public expenditure resulting from different level of progress in achieving the DOE’s program goals on fuel cells, batteries, motors, hydrogen storage and hydrogen infrastructure.

Approach

To examine the impact of program goals on hydrogen vehicle market penetration, as well as the associated costs and benefits, the MA3T model, developed by ORNL, is adopted to project U.S. consumer demand for hydrogen vehicles, including hydrogen internal combustion engine vehicles, fuel cell electric vehicles, and fuel cell plug-in hybrid electric vehicles, in competition with other automotive powertrain technologies, including conventional gasoline and diesel vehicles, hybrid electric vehicles, plug-in hybrid electric vehicles, and battery electric vehicles. Using the MA3T model, 42 scenarios were designed to estimate the impact of program goals on market prospect, social benefits, required government support, and cost-effectiveness of light-duty vehicle market transition. These scenarios can be grouped

into: 1) the Base case (with MA3T default assumptions); 2) all program goals met on time; 3) all goals met on time except one goal is delayed by 10 years; 4) all goals delayed by 10 years except one goal met on time; 5) all goals delayed to the Base case except one goal met on time.

Results

Program goals are important for hydrogen vehicle market success. In particular, the hydrogen delivered cost and the fuel cell system cost have the biggest impact in the long-term market and that infrastructure deployment is the key for the early market. The key findings of this study include:

- By achieving all or some of the program goals, hydrogen vehicle penetration will range from 20% to 70% by 2050 (see Figure 1).
- There appears to be a minimum level of infrastructure deployment to enable the emergence of the hydrogen vehicle market. With 5% hydrogen availability at local levels, hydrogen vehicles can reach 2%-7% of the total light-duty vehicle sales, depending on progresses on reaching other program goals (see Figure 1).
- The goals on fuel cell costs and hydrogen costs have the biggest impacts on the hydrogen vehicle market. With the 5% hydrogen availability at local levels by 2025, achieving only the fuel cell cost goal or only the hydrogen cost goal increases the hydrogen vehicle share by 2025 from 1.88% to 5.09% and 3.55%, respectively, assuming all other technologies following the baseline progresses (see Figure 1).

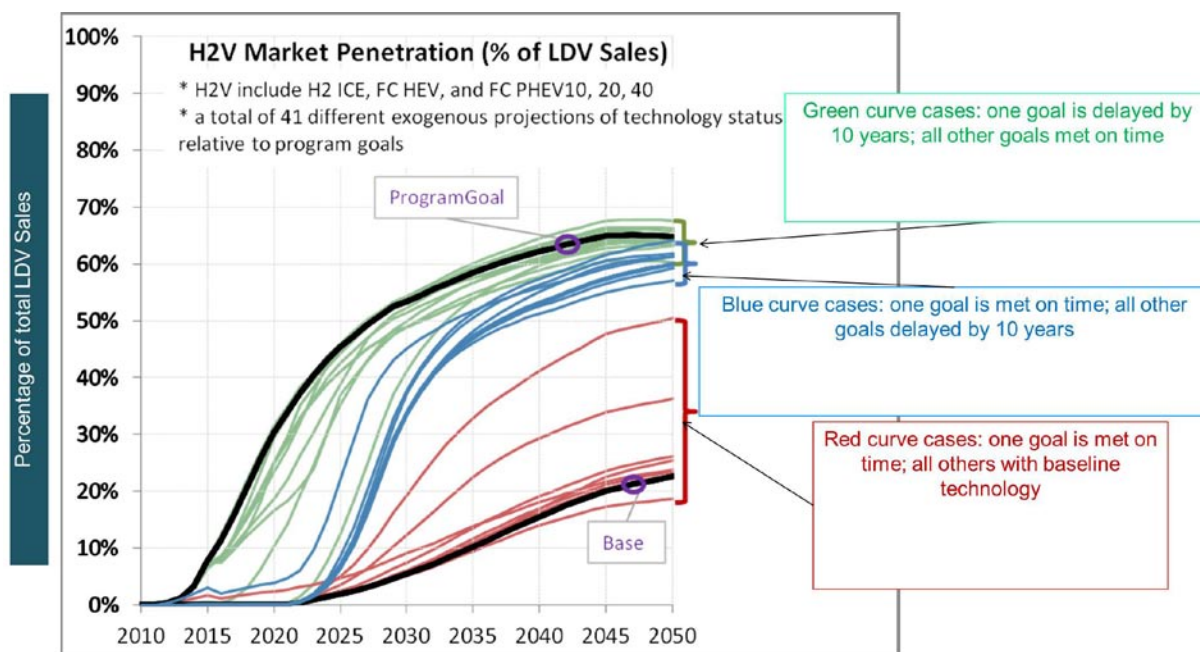


FIGURE 1. Hydrogen vehicle penetrations under varied technology progress, infrastructure and hydrogen price

- If all goals met, both hydrogen vehicles and plug-in hybrid electric vehicles could dominate the market. Fuel cell plug-in hybrid electric vehicles appear to have significant market potential (see Figure 2).
- The sooner the program goals are met, the larger the oil/GHG reduction benefits. Figure 3 shows that meeting all goals allow ~80% cut in petroleum use and ~60% cut in GHG by 2050. These cuts are robust against one goal being missed or delayed.
- The success of hydrogen technologies does not require all DOE program goals goals (fuel cells, batteries,

motors, hydrogen storage and hydrogen infrastructure) to be met on time, but key goals need to be met without major delay, including fuel cell costs, delivered hydrogen costs, and the deployment of a basic hydrogen supply infrastructure.

- If most goals met on time, the transition requires 30-50 billion dollars of hydrogen subsidy and 10-20 billion dollars of vehicle subsidy through 2050 (see Figure 4).

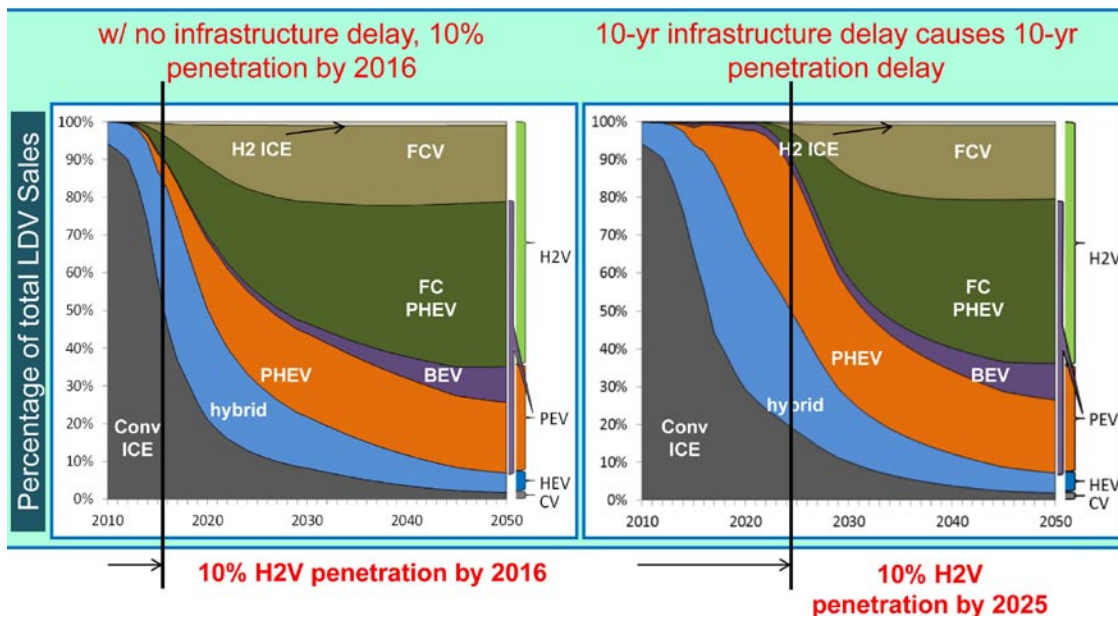


FIGURE 2. Hydrogen vehicle penetration when all program goals are met on time

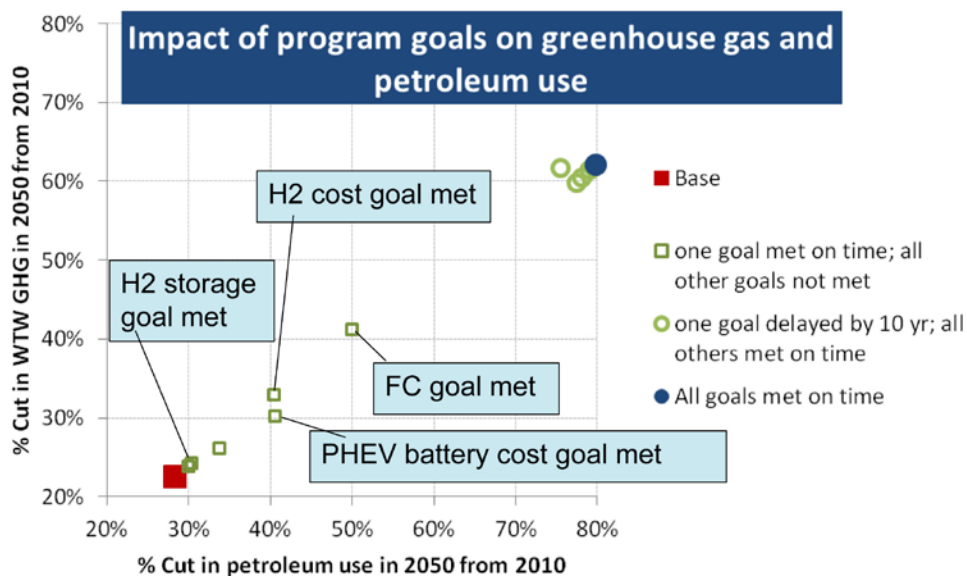


FIGURE 3. Impact of program goals on GHG emissions and petroleum use

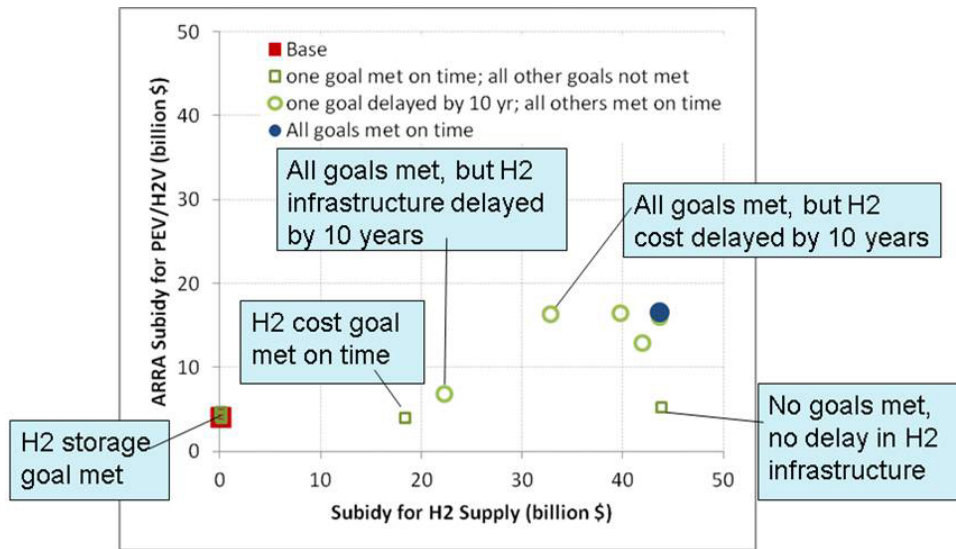


FIGURE 4. Required public support

Conclusions and Future Directions

ORNL has studied and quantified the importance of program goals for hydrogen vehicle market success and the resulting social benefits. The results suggest that a fast deployment of a basic refueling infrastructure (about 5% hydrogen availability at local levels) is required for hydrogen vehicles to penetrate the market noticeably. With such basic infrastructure and its continued expansion, hydrogen vehicles can reach 20%-70% of the market by 2050, depending on other progresses on other components. To bring more hydrogen vehicles to the road by 2050, low fuel cell costs and low hydrogen costs are the key drivers. With just A conference paper/journal publication will be prepared, as well as a final report summarizing all the results and research findings.

References

1. U.S. Department of Energy, Hydrogen and Fuel Cells Program (DOE/HFC), 2009. Fuel Cell Technologies Program Multi-Year Research, Development and Demonstration Plan.
2. (DTI) James, B.D., Kalinoski, J. and Baum, K. (2011). Manufacturing Cost Analysis Of Fuel Cell Systems, Directed Technologies Inc.
3. National Research Council, 2008b. Transitions to Alternative Transportation Technologies: A Focus on Hydrogen, National Academies Press, Washington, D.C.

XI.9 Resource Analysis for Hydrogen Production

Marc W. Melaina (Primary Contact), Michael Penev and Donna Heimiller

National Renewable Energy Laboratory
15013 Denver West Parkway
Golden, CO 80401
Phone: (303) 275-3836
Email: Marc.Melaina@nrel.gov

DOE Manager

HQ: Fred Joseck
Phone: (202) 586-7932
Email: Fred.Joseck@hq.doe.gov

Project Start Date: October 1, 2009

Project End Date: September 28, 2012

FY 2012 Accomplishments

- Incorporated updated renewable energy resource potential data used for hydrogen production potential estimates [1].
- Updated conversion efficiencies based upon revised Hydrogen Analysis (H2A) production case studies.
- Revised demand scenario to meet an illustrative FCEV market share projection by 2040.
- Incorporated new resource data on fossil and uranium resources from the Energy Information Administration (EIA).
- Incorporated new energy consumption projections based upon EIA forecasts.
- Updated resource maps for biomass, wind and solar energy hydrogen production potential.

Fiscal Year (FY) 2012 Objectives

- Understand the hydrogen production requirements for a future demand scenario
- Estimate low-carbon energy resources required to meet the future scenario demand
- Compare resource requirements to current consumption and projected future consumption
- Determine resource availability geographically and on a per kg hydrogen basis
- Estimate fuel cell electric vehicle (FCEV) miles traveled per quad of resource

Technical Barriers

This project addresses the following technical barrier from the Systems Analysis section of the Fuel Cell Technologies Program Multi-Year Research, Development and Demonstration Plan:

(C) Inconsistent Data, Assumptions and Guidelines

Contribution to Achievement of DOE Systems Analysis Milestones

This project will contribute to achievement of the following DOE milestone from the Systems Analysis section of the Fuel Cell Technologies Program Multi-Year Research, Development and Demonstration Plan:

- Milestone 1.9 (Systems Analysis Task 1: Perform Studies and Analysis): Complete analysis and studies of resource/feedstock, production/delivery, and existing infrastructure for technology readiness. (4Q, 2014)



Introduction

The widespread adoption of hydrogen vehicles would result in a shift in reliance on fuels produced from petroleum to reliance on other primary energy resources. The present study examines the degree to which these other resources would be consumed with respect to: (1) the existing resource base, and (2) projections of future consumption by FCEVs in 2040. Hydrogen can be produced from any primary energy resource. Rather than predicting the mix of resources that may be relied upon given future policy, technology, and market dynamics, this study examines a series of simple scenarios in which 50% of a future hydrogen demand level is derived from any one of six primary energy resources: natural gas, coal, nuclear (uranium), biomass, wind and solar (photovoltaic [PV] with electrolysis). In addition to estimating total resources required in 2040, resource maps of production potential by county have been updated to match new resource assessment results for biomass, wind and solar [1] as well as updated H2A production conversion efficiencies [2]. The projected increase in consumption of each resource in 2040 is determined as a percentage of projected consumption in the 2012 Annual Energy Outlook (AEO) Reference Case for future energy consumption [3].

Approach

A demand scenario is developed in which 100 million FCEVs have been deployed by 2040. We assume that these FCEVs travel, on average, 12,000 miles per year and achieve an on-road fuel economy of 60 miles per kg of hydrogen, which is roughly equivalent to 60 miles per gallon of gasoline

[c.f., 4]. This results in a demand of 20 million metric tonnes (MMT) of hydrogen in the year 2040. For our resource consumption scenarios, we examine requirements for each resource to provide 50% of this total demand, or 10 MMT of hydrogen per year by 2040. Table 1 lists the resources examined, conversion processes, resource required per kg of hydrogen produced (in physical units), production efficiency and the number of FCEVs that would be supported by conversion of one quad of each resource. In all calculations we only consider production efficiencies and do not account for additional conversion losses or energy inputs required for storage and delivery of the hydrogen between the point of production and dispensing at the hydrogen refueling station. The influence of conversion losses from these additional supply chain phases on resource requirements will vary between resource types; this influence is omitted here for the sake of simplicity [5,6,7].

To place resource requirements in context, we compare them with estimates of energy resources available today (e.g., reserves or annual potential) and projected consumption in 2040. Resource availability estimates are taken from

TABLE 1. Primary energy resource, conversion process, physical units per kg hydrogen, production efficiency and FCEVs supported per quad

| Resource | Conversion Process | Resource per kg hydrogen produced (physical units) | | Production Eff. (E_{out}/E_{in} , HHV) | Million FCEVs per quad |
|-------------|--------------------|--|---------------|---|------------------------|
| Natural gas | SMR | 143 | scf | 86% | 37 |
| Coal | Gasification | 9.8 | kg | 61% | 26 |
| Uranium | Nuclear fission | 0.35 | mmBtu | 35% | 15 |
| Biomass | Gasification | 13 | kg (bone-dry) | 60% | 26 |
| Wind | Electrolysis | 46 | kWh | 86% | 37 |
| Solar | PV or ThChem | 46 | kWh | 86% | 37 |

Notes: SMR = steam methane reforming; PV = photovoltaic; Production efficiency is the energy of the hydrogen produced (E_{out}) divided by the energy of the primary resource input to the production process (E_{in}) on a higher heating value (HHV) basis; Uranium efficiency refers to the heat energy input used in a turbine; million FCEVs supported per quad of energy resource converted assumes 12,000 vehicle miles traveled/year and 60 miles per kg hydrogen.

TABLE 2. Hydrogen production resource potential for non-renewable resources

| Carbon Neutral Resource | Availability ^a | Current Consumption (2012) ^b | Projected Consumption (2040) ^a | Needed to Produce 50% of all Hydrogen | Increase in Projected Consumption |
|---------------------------|--|---|---|---------------------------------------|-----------------------------------|
| Natural Gas | 2,543 trillion cubic feet (total technically recoverable resources) | 25 trillion cubic feet | 27 trillion cubic feet | 1.4 trillion cubic feet | 1.05 |
| Coal (with sequestration) | 441 billion tonnes (demonstrated reserve base) | 870 million metric tonnes/year (all grades) | 992 million metric tonnes/year (all grades) | 98 million metric tonnes/year | 1.10 |
| Nuclear | 6,077 million pounds at <\$50/lb (reserves and estimated additional resources) | 102 GWe | 120 GWe | 53 GWe | 1.44 |

Notes: (a) availability values are from Annual Energy Review 2010, (b) current and projected consumption values are from AEO 2012 Early Release, Reference Case.

multiple sources. Resource estimates for natural gas, coal and uranium are from the Energy Information Administration’s Annual Energy Review 2012 [8], and biomass, wind and solar resource potentials are from a recent update of renewable resource potential [1]. Projected consumption is determined based upon a linear extrapolation of demand trends between 2025 and 2035 reported from the AEO 2012 Reference Case. Hydrogen production conversion efficiencies, shown in Table 1, are taken from the updated H2A Production Case Studies [2,9].

Results

Analysis results for non-renewable resources are summarized in Table 2 and results for renewable resources are summarized in Table 3. The tables show total resource availability, current consumption in 2012, projected consumption in 2040, and the quantity of resource needed to produce 50% of projected hydrogen demand in 2040. The increase in projected consumption is indicated in the last column, shown as a factor calculated using the following equation:

$$\text{Increase Factor} = \frac{\text{Projected} + \text{Needed for 50\%}}{\text{Projected}}$$

This factor result can also be read as a percentage. The additional hydrogen required to produce 50% of projected demand in 2040 would require the following percentage increases in projected consumption: 5% increase in natural gas, 10% increase in coal, 44% increase in nuclear, 33% increase in biomass, 153% increase in wind, and a 575% increase in solar. Figure 1 places current and projected consumption values on an equivalent energy basis to further highlight relative reliance of each resource to meet 50% of projected demand in 2040. Additional resources needed for hydrogen production are shown as a stacked bar on top of projected AEO consumption in 2040. It should be noted that these projected consumption values are based upon business-as-usual policy and technology input assumptions. Arguably, any scenario resulting in 100 million FCEVs by 2040 would include policy and market factors that would likely also

TABLE 3. Hydrogen production resource potential for renewable resources

| Carbon Neutral Resource | Availability ^a | Current Consumption (2012) ^b | Projected Consumption (2040) ^b | Needed to Produce 50% of all Hydrogen | Increase in Projected Consumption |
|-------------------------|--|---|---|---------------------------------------|-----------------------------------|
| Biomass | Between 0.4-1.1 billion dry tonnes/year | 160 million metric tonnes/year | 389 million metric tonnes/year | 130 million metric tonnes/year | 1.33 |
| Wind | 3,750 GWe (nameplate capacity, not power output) | 130 billion kWh | 300 billion kWh | 460 billion kWh | 2.53 |
| Solar (PV) | 32,300 GWe (capacity, full U.S.) | 2.15 billion kWh | 80 billion kWh | 460 billion kWh | 6.75 |

Notes: (a) availability values are from a forthcoming NREL report [1], and high biomass estimate is based upon the recent Billion Ton Study, (b) current and projected consumption values are from AEO 2012 Early Release, Reference Case.

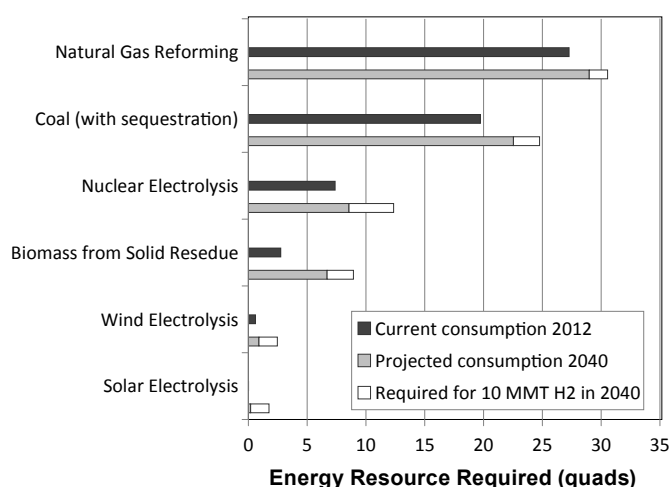


FIGURE 1. Current and projected resource consumption compared to resource requirements to provide 50% of hydrogen demand in 2040.

influence consumption of these resources for other end uses. For example, if a high penetration of FCEVs arises within a carbon-constrained future, it might be expected that all resource consumption values would be lower due to energy efficiency measures and that lower-carbon resources (e.g., nuclear and renewables) would increase in relative use due to greater market pull.

Renewable hydrogen production potential estimates at the county level, previously reported by Milbrandt and Mann [10], have been updated based upon updated conversion efficiencies and resource estimates for biomass, wind and solar resources. Updated resource estimates for biomass, wind and solar are based upon a consistent basis for technical potential, rather than market, economic or theoretical physical potential [1]. This spatial representation of production potential provides insight into which regions may rely upon different hydrogen supply pathways, especially in carbon-constrained scenarios or market conditions that result in a premium on low-carbon hydrogen.

Several important factors must be considered to better understand the spatial aspects of this resource production potential:

- Biomass resources will evolve over time in response to various market forces and policy constraints. Technical availability may increase significantly beyond what has been estimated for “current” potential today. Market availability may prove to be more of an issue than technical availability, in part due to competition among end uses.
- A more detailed time series model would capture plant production efficiency increasing over time and with economies of scale. This may result in slightly higher resource requirements due to inefficiencies of older vintage plants.
- Previous studies suggest that wind farms that generate both electricity (for baseload transmission) and hydrogen (during peak supply) may prove economically favorable. This may also alter our technical resource potential estimates.
- Fuel economy of FCEVs is a critical input, especially when comparing resource requirements among multiple vehicle types and fuel pathways.

Conclusions and Future Directions

Hydrogen production requirements for a future demand scenario to 2040 have been estimated with respect to natural gas, coal, nuclear (uranium), biomass, wind and solar resources. Providing 50% of hydrogen demand in 2040 would require relatively small increases in projected consumption of natural gas (5%) or coal (10%) resources, and more significant increases in projected consumption of nuclear (44%), biomass (33%), wind (153%), and solar (575%) resources. Future work would consist of the following:

- Compare resource use across multiple fuel types (e.g., biofuels or electricity).
- Assess regional variations in resource potential with respect to regional demand.

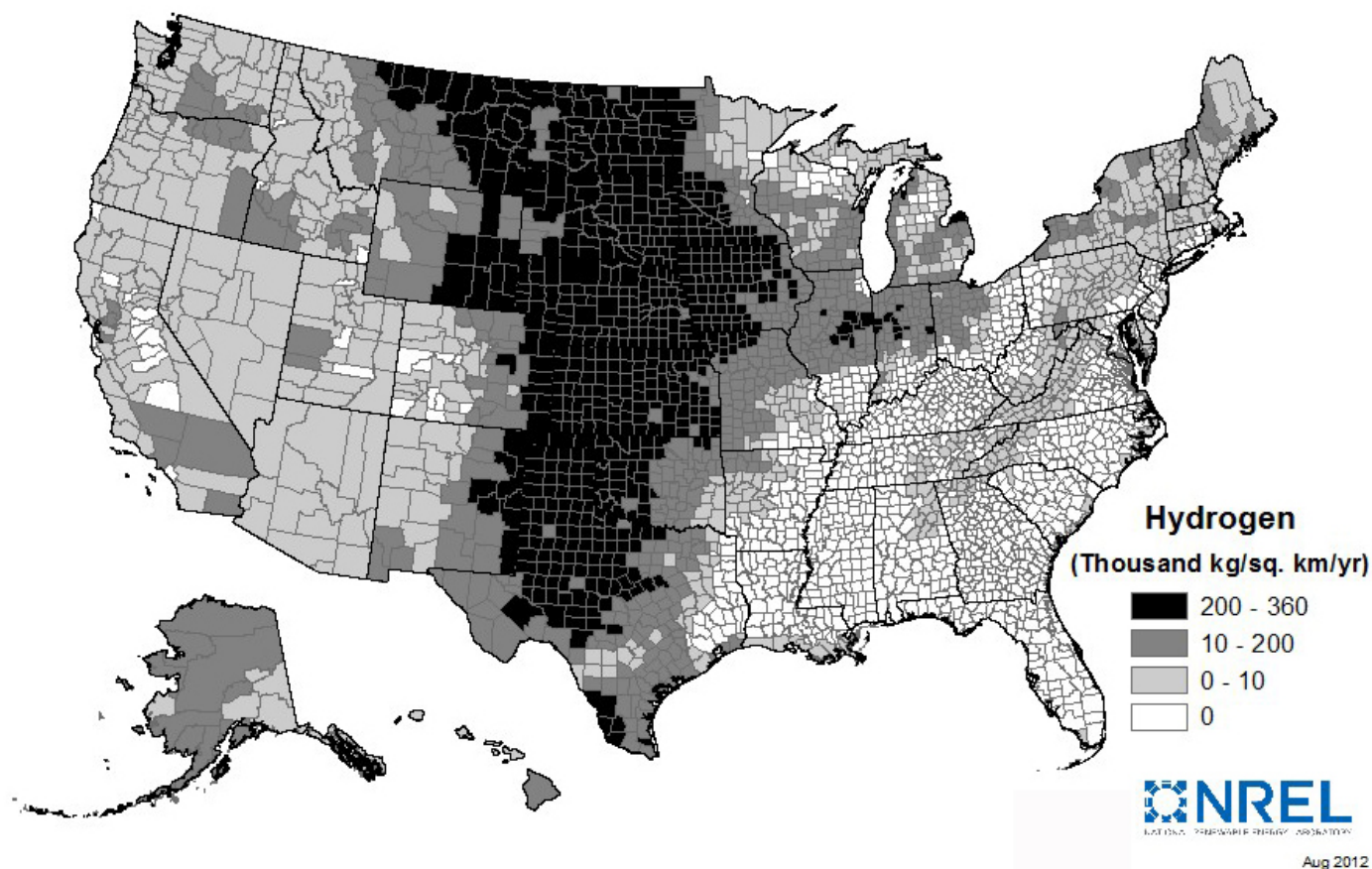


FIGURE 2. Hydrogen potential from onshore wind resources. This analysis represents potential generation from onshore wind turbines at 80 m height above ground, with a power density of 5 MW/sq. km. It excludes environmental and land use areas, and areas with slope greater than 20%.

- Contribute to resource-constrained scenarios of transportation energy use.
- Incorporate estimates of non-light-duty vehicle fuel demands, such as aviation biofuels.
- Contribute to supply curve calculations for low-carbon scenarios.

References

1. Lopez, A., B. Roberts, D. Heimiller, N. Blair and G. Porro (2012). U.S. Renewable Energy Technical Potentials: A GIS-Based Analysis. National Renewable Energy Laboratory, Technical Report number NREL/TP-6A20-51946, available at http://www.nrel.gov/gis/re_potential.html.

2. Steward, D (2012). H2A Hydrogen Production Analysis Model Version 3. Presented at the 2012 U.S. Department of Energy Hydrogen and Fuel Cells Program Review, Washington, DC, May 15, available at http://www.hydrogen.energy.gov/pdfs/review12/pd089_steward_2012_p.pdf.

3. EIA (2012). Annual Energy Outlook 2012. U.S. Energy Information Administration, Report Number DOE/EIA-0383(2012), available at <http://www.eia.gov/forecasts/aeo/>.

4. Ruth, M., F. Joseck (2012). Hydrogen Threshold Cost Calculation. Program Record, U.S. Department of Energy’s Fuel Cell Technologies Program, Record #11007, available at http://www.hydrogen.energy.gov/pdfs/11007_h2_threshold_costs.pdf.

5. DOE (2012). Department of Energy, Hydrogen and Fuel Cells Program, DOE H2A Delivery Analysis website, available at http://www.hydrogen.energy.gov/h2a_delivery.html.

6. OpenEI (2012). Scenario Evaluation, Regionalization & Analysis (SERA), model website, available at <http://en.openei.org/wiki/>.

7. GREET (2012). Greenhouse Gases, Regulated Emissions, and Energy Use in Transportation Model, Argonne National Laboratory, GREET website, available at <http://greet.es.anl.gov/>.

8. EIA. (2011). Annual Energy Review 2010, DOE/EIA-0384(2010). Energy Information Administration, available at <http://www.eia.gov/aer>.

9. DOE (2012). H2A Analysis website, U.S. Department of Energy, Hydrogen and Fuel Cells Program, available at http://www.hydrogen.energy.gov/h2a_analysis.html.

10. Milbrandt, A.; Mann, M. (2006). Potential for Producing Hydrogen from Key Renewable Resources in the United States. 32 pp.; NREL Report No. TP-640-41134 <http://www.nrel.gov/docs/fy07osti/41134.pdf>.

XI.10 Cost, Energy Use, and Emissions of Tri-Generation Systems

Mark F. Ruth* (Primary Contact),
Michael E. Goldsby†, Timothy J. Sa†, Victor Diakov*

*National Renewable Energy Laboratory
15013 Denver West Pkwy.
Golden, CO 80401
Phone: (303) 817-6160
Email: Mark.Ruth@nrel.gov

† Sandia National Laboratories

DOE Manager

HQ: Fred Joseck
Phone: (202) 586-7932
Email: Fred.Joseck@ee.doe.gov

Project Start Date: December 1, 2010

Project End Date: October 31, 2011

Fiscal Year (FY) 2012 Objectives

- Develop a macro-system model (MSM):
 - Aimed at performing rapid cross-cutting analysis
 - Utilizing and linking other models
 - Improving consistency between models
- Incorporate tri-generation systems into the MSM and develop a methodology for MSM users to analyze optimized tri-generation (also known as combined hydrogen, heat, and power – CHHP) scenarios easily.
- Support decisions regarding programmatic investments through MSM analyses and sensitivity runs on tri-generation systems focusing on quantification of levelized cost and greenhouse gas (GHG) emissions for various fuel cell types, building types, and building locations.

Technical Barriers

This project addresses the following technical barriers from the Systems Analysis section of the Fuel Technologies Program Multi-Year Research, Development and Demonstration Plan:

- (B) Stove-piped/Siloed Analytical Capability
- (C) Inconsistent Data, Assumptions and Guidelines
- (D) Insufficient Suite of Models and Tools

Contribution to Achievement of DOE Systems Analysis Milestones

This project will contribute to achievement of the following DOE milestones from the Systems Analysis section

of the Fuel Cell Technologies Program Multi-Year Research, Development and Demonstration Plan:

- Milestone 1.1: Complete an analysis of the hydrogen infrastructure and technical target progress for hydrogen fuel and vehicles. (2Q, 2011)
- Milestone 1.4: Complete evaluation of fueling station costs for early vehicle penetration to determine the cost of fueling pathways for low and moderate fueling demand rates. (4Q, 2012)
- Milestone 2.1: Complete the 2nd version of the Macro-System Model to include the analytical capabilities to evaluate the electrical infrastructure. (2Q, 2011)
- Milestone 2.2: Annual model update and validation. (4Q, 2011 through 4Q, 2020)

FY 2012 Accomplishments

- Linked the Fuel Cell Power Model (FC Power) in the MSM framework.
- Performed an analysis on tri-generation systems focusing on quantification of levelized cost and GHG emissions for various fuel cell types, building types, and building locations.



Introduction

At the DOE Hydrogen Program's behest, we are developing an MSM to analyze cross-cutting issues because no existing model sufficiently simulates the entire system, including feedstock, conversion, infrastructure, and vehicles, with the necessary level of technical detail. In addition, development of the MSM exposes inconsistencies in methodologies and assumptions between different component models so that they can be identified and corrected when necessary. Version 1.0 of the MSM was developed previously and is available to the hydrogen analysis community. It links H2A Production, HDSAM, the Greenhouse gases, Regulated Emissions and Energy use in Transportation (GREET) model, and physical property information from the Hydrogen Analysis Resource Center to estimate the economics, primary energy source requirements, and emissions of multiple hydrogen production/delivery pathways.

Version 2.0 of the MSM links the H2A Power [1] model that simulates reformers and fuel cells providing heat and power for buildings and hydrogen for transportation. Version 2.0 also links Hydrogen Demand and Resource Analysis [2] data to incorporate county-specific grid mixes and natural gas costs. Utilizing the updated MSM, an analysis

was performed on CHHP for various building types, in various locations, and with two different types of fuel cells.

Approach

The MSM is being developed as a tool that links or federates existing models across multiple platforms. This approach was chosen because the task of building a single monolithic model incorporating all of the relevant information in the existing models would have been overwhelming because the necessary expertise to do so was spread among half a dozen DOE laboratories and a dozen or more universities and private contractors. Linking models allows model users that depend on data from component models to continue using their models while retrieving data from component models in a less labor-intensive manner. In addition, it provides a common platform for data exchange necessary to update integrated models when the component models have been updated.

The MSM is being built on a framework inspired by an example of a federated object model (FOM). The MSM uses a common interlingua that is extensible (accommodates new models with a minimum of difficulty), distributable (can be used by multiple people in different areas of the country), and scalable (to a larger number of participating models) using exogenous data. FOMs are exemplified by the Department of Defense high-level architecture [3]. Version 2.0 of the MSM uses Ruby and Ruby interfaces to Microsoft Excel and other platforms to collect, transfer, and calculate data.

Results

To run FC Power, the user defines the size of the fuel cell (kW capacity) and the hydrogen demand. Using the MSM, multiple fuel cell sizes are tested. For each size, the maximum hydrogen production level is determined. A range of hydrogen production levels up to the maximum were run to determine the levelized hydrogen cost of each production level. The production level with the minimum levelized cost was defined as the optimum for that fuel cell size. As seen on the Figure 1, for any given fuel cell size, the levelized hydrogen cost in both molten carbonate fuel cell (MCFC) and phosphoric acid fuel cell (PAFC) reaches its minimum at high hydrogen production levels; this trend holds for all cases considered within this study. Additionally, the fuel cell size is a strong factor affecting the hydrogen costs; consequently, in the following sections the size of the fuel cell is optimized for each location and building type.

The MCFC fuel cell energy output for a large office building in Los Angeles is shown in Figure 2a and the PAFC energy output is shown in Figure 2c. For the MCFC, the two largest constituents are electricity supplied and hydrogen produced with heat supplied to the building and electricity sold to the grid as other energy uses. The overall building energy loads are met by electricity and heat generated from

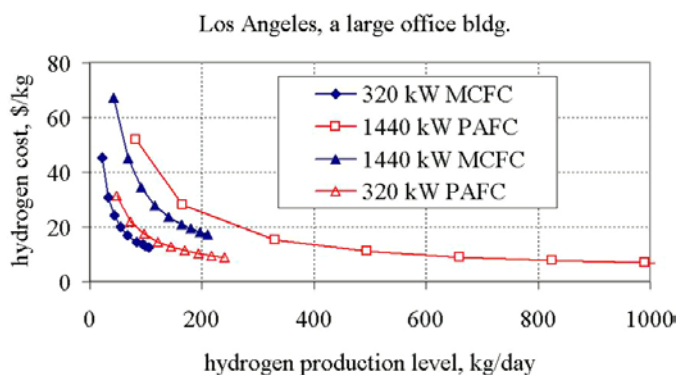


FIGURE 1. Hydrogen cost for various fuel cell types (MCFC and PAFC), sizes (320 and 1,440 kW maximal alternating current rating) depending on hydrogen production level. Each curve (except for 1,440 kW PAFC) is shown as limited by the maximum hydrogen production level allowed for the correspondent fuel cell size (maximum allowed H₂ production level for 1,440 kW PAFC is 1,630 kg/day and falls beyond the figure limits)

natural gas supplied to the fuel cell, natural gas supplied to the peak burner, and supplemental electricity from the grid as shown in Figure 2b. In the case shown in Figure 2b, the fuel cell capacity (320 kW) is sufficient for supplying most of the electric load to the building while consuming only a small fraction from the grid. For the MCFC, the main contributors to the hydrogen levelized costs are capital costs and variable expenses. Byproduct credits offset an insignificant portion of the hydrogen levelized cost (Figure 3a). In addition to fuel cell system, compression, storage and dispensing (CSD) are the major contributors to the overall capital costs (Figure 3b).

If the building had a large (1,440 kW) electricity load-following PAFC the results would be different. Hydrogen becomes the dominant product (Figure 2c); the fuel cell provides almost all necessary electricity so there is virtually no electricity bought from the grid (Figure 2d); and capital costs account for as much as half of the hydrogen cost at the pump (Figure 3c) with fuel cost being the second major contributor. The capital costs distribution (Figure 3d) is similar to the MCFC case shown above. For both MCFC (Figure 3a) and PAFC (Figure 3c), capital costs are the leading contributor to the levelized hydrogen cost. This is the reason why lower hydrogen cost is achieved at the maximal (for a given fuel cell size) hydrogen production level.

As stated, the objective was to not only investigate CHHP for a large office building in Los Angeles but to investigate the opportunity for different building types in various locations. The procedure described above was used to select CHHP configurations for the analysis. Levelized cost and GHG emissions results are reported in Table 1 and Table 2, respectively.

For both MCFC and PAFC, a large office building in Los Angeles presents the lowest H₂ cost option (Table 1). The same location (when compared to Seattle, Chicago and Baltimore) is favorable for any building type with an MCFC

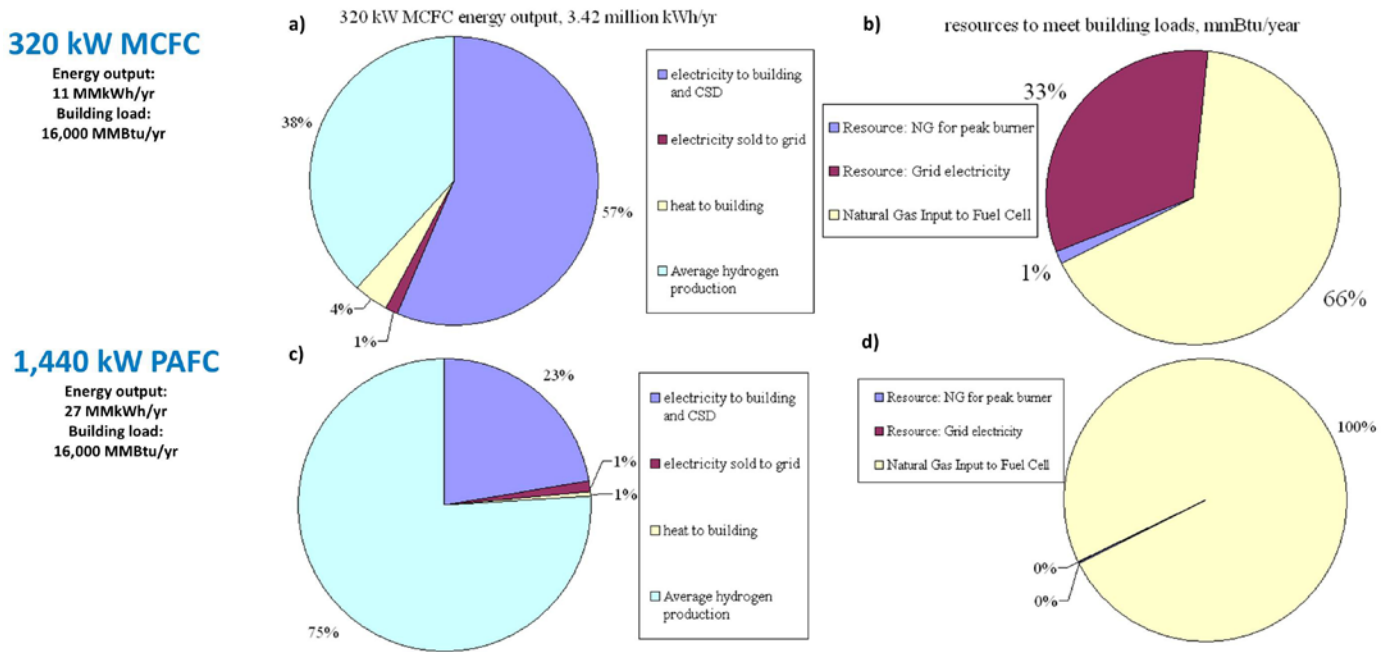


FIGURE 2. CHHP system energy output distribution for a large office building in Los Angeles, CA using 320 kW MCFC (a,b) and 1,440 kW PAFC (c,d) system: energy output distribution (a,c) and resources used to meet the building's energy loads (b, c).

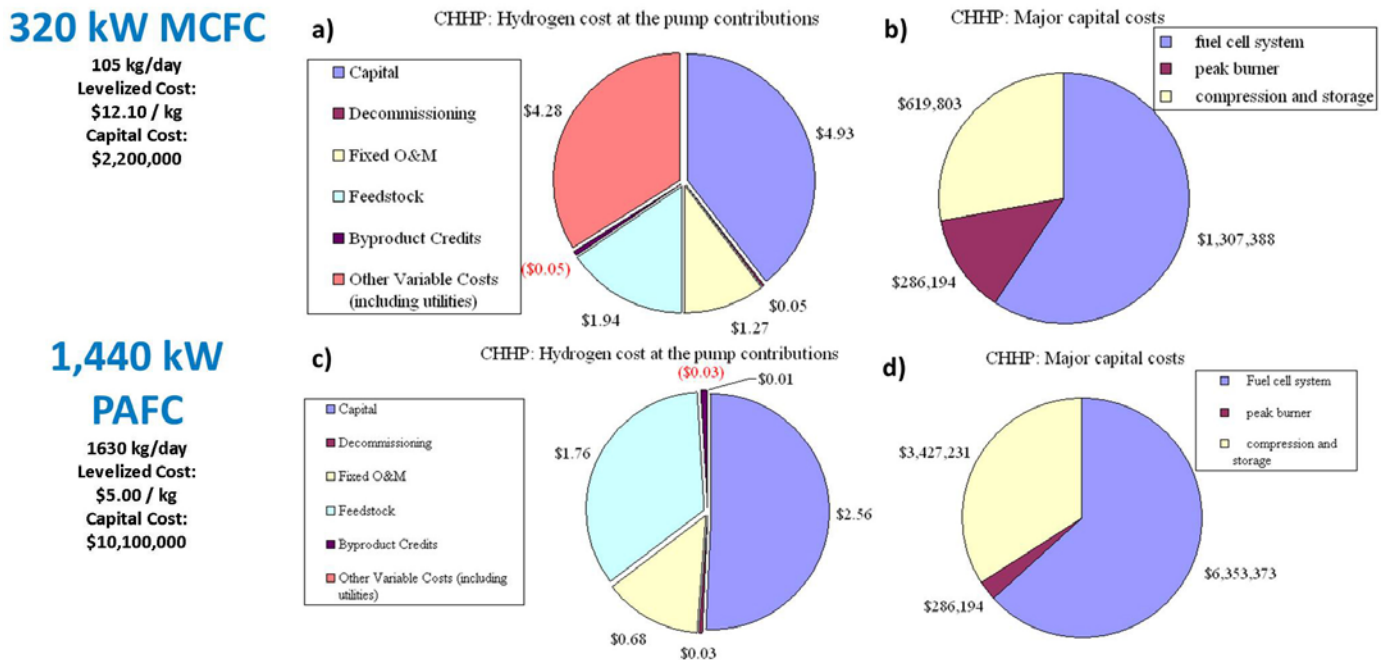


FIGURE 3. CHHP system energy output distribution for a large office building in Los Angeles, CA using 320 kW MCFC (a,b) and 1,440 kW PAFC (c,d) system: hydrogen cost breakdown (a, c), and capital costs (b, d).

system because of lower feedstock natural gas price (\$9.48/mmBtu in Los Angeles vs. \$10.58 in Seattle, \$10.70 in Chicago and \$12.10 in Baltimore).

Most hydrogen costs for MCFC in each column of the upper half of Table 1 are close, with exception of a supermarket and a small hotel in Chicago. There are several

reasons why those differ so much from the others. First, for a MCFC, the feedstock cost does not represent a large fraction of the hydrogen cost (Figure 3a). Second, a comparison between Chicago large and small hotel cases (not shown) indicates that the CHHP model's optimization routine chooses to produce excess electricity rather than produce

TABLE 1. CHHP levelized hydrogen cost for various building types and locations

| MCFC: H₂ cost, \$/kg (and % change to the baseline system¹) | | | | |
|--|--------------------|-----------------------|--------------------|--------------------|
| | Large Hotel | Large Office | Supermarket | Small Hotel |
| Seattle, WA | \$15.88 (+52%) | \$14.34 (+66%) | \$16.59 (+59%) | \$27.70 (+79%) |
| Los Angeles, CA | \$12.17 (+28%) | \$12.10 (+38%) | \$13.27 (+36%) | \$23.48 (+61%) |
| Chicago, IL | \$16.17 (+57%) | \$14.54 (+71%) | \$47.76(+231%) | \$58.00(+198%) |
| Baltimore, MD | \$14.73 (+41%) | \$13.36 (+53%) | \$15.74 (+49%) | \$25.31 (+67%) |
| PAFC: H₂ cost, \$/kg (and % change to the baseline system) | | | | |
| | Large Hotel | Large Office | Supermarket | Small Hotel |
| Seattle, WA | \$5.73 (+31%) | \$5.36 (+51%) | \$6.95 (+28%) | \$9.66 (+30%) |
| Los Angeles, CA | \$6.21 (+20%) | \$5.00 (+40%) | \$7.43 (+23%) | \$10.93 (+29%) |
| Chicago, IL | \$6.02 (+34%) | \$5.60 (+55%) | \$6.13 (+22%) | \$8.66 (+23%) |
| Baltimore, MD | \$6.15 (+30%) | \$5.71 (+48%) | \$7.37 (+28%) | \$10.12 (+28%) |

¹For consistency, hydrogen costs are compared for CHHP vs. baseline systems at equal production levels.

TABLE 2. GHG emissions reduction as compared to a baseline system

| MCFC: GHG emissions reduction, % | | | | |
|---|--------------------|---------------------|--------------------|--------------------|
| | Large Hotel | Large Office | Supermarket | Small Hotel |
| Seattle, WA | 20.5% | 23.6% | 20.9% | 17.8% |
| Los Angeles, CA | 20.2% | 8.3% | 11.1% | 4.3% |
| Chicago, IL | 39.6% | 38.8% | -2.8% | 12.4% |
| Baltimore, MD | 32.0% | 25.0% | 34.0% | 33.0% |
| % = (emissions change/baseline emissions); negative = increase in emissions | | | | |
| PAFC: GHG emissions reduction, % | | | | |
| | Large Hotel | Large Office | Supermarket | Small Hotel |
| Seattle, WA | -2.0% | -8.7% | -3.5% | -6.2% |
| Los Angeles, CA | -2.0% | -15.0% | -13.3% | -17.1% |
| Chicago, IL | 11.2% | 6.7% | -7.9% | -2.4% |
| Baltimore, MD | 4.3% | -2.1% | 3.2% | 1.4% |

hydrogen. Lower hydrogen production levels result in higher H₂ production costs due to a lack of economies of scale for hydrogen compression, storage, and dispensing.

The MCFC, when compared to the PAFC, is more efficient in reducing the GHG emissions (Table 2) due to overall energy efficiency. For regions with cleaner electricity generation mix (California, Washington), the emission reductions by MCFC (top part of the table) are smaller; the two cases showing unusually high hydrogen costs (Table 1, MCFC, a supermarket and a small hotel in Chicago) also have smaller reduction in GHG emissions. It is not clear at this point what has the largest impact on GHG emissions reduction: is it just the overall load (and system size), or the shape of load profile (that also depends on building type and location).

The GHG emissions reduction for large hotel and large office buildings in Chicago (Table 2) compare well with 38% GHG emissions reduction expected for a hospital building in Chicago. The decrease in GHG emissions reduction for a supermarket or small hotel in Chicago, as compared to large buildings at same location, is likely induced by suboptimal fuel cell sizing discussed above.

Conclusions and Future Directions

Conclusions

- Hydrogen cost is minimized at the highest hydrogen production rate due to economies of scale for the costs of dispensing.
- But those resulting levelized costs may not be the most competitive with conventional technologies.
- Levelized costs of hydrogen can compete with steam methane reforming at low production capacities (<70 kg/day) providing the cost-of-rent scales.
- GHG emissions from tri-generation systems are lower than the conventional option when the system size matches the building load.

No additional funding is planned for this analysis. If we had additional funding, we would like to:

- Test other options for setting CHHP parameters in the MSM.
- Update GREET and H2A FC Power models.
- Analyze tri-generation systems to balance the grid where variable (or intermittent) generation is in place.
- Additional review of parameters and gap analysis.

As ongoing projects, the MSM is being updated and an analysis of the parameters used in estimating levelized cost and energy use and emissions is underway.

FY 2012 Publications/Presentations

1. Ruth, M.; Diakov, V.; Evans, T. “Cost, Energy Use, and Emissions of Combined Hydrogen, Heat, and Power Tri-Generation Systems.” NREL Report, in press.

References

1. Steward, D.; M. Penev, G. Saur, J. Zuboy. Fuel Cell Power Model: Startup Guide, System Designs, and Case Studies. Modeling Electricity, Heat, and Hydrogen Generation from Fuel Cell–Based Distributed Energy Systems.

Draft. November 2010. http://www.hydrogen.energy.gov/pdfs/fuel_cell_power_model_user_guide_version1.pdf.

2. Levene, J.; W. Sparks, D. Getman. “HyDRA: Hydrogen Demand and Resource Analysis Tool.” 2010 DOE Hydrogen Program Annual Progress Report. Pp 1240-1243. November 2010.

3. Judith S. Dahmann, Richard Fujimoto, and Richard M. Weatherly. “The Department of Defense high level architecture.” In Winter Simulation Conference, pages 142–149, 1997.

XI.11 Employment Impacts of Early Markets for Hydrogen and Fuel Cell Technologies

Marianne Mintz
Argonne National Laboratory
9700 S. Cass Ave.
Argonne, IL 60439
Phone: (630) 252-5627
Email: mmintz@anl.gov

DOE Managers
HQ: Fred Joseck
Phone: (202) 586-7932
Email: Fred.Joseck@ee.doe.gov

GO: Greg Kleen
Phone: (720) 356-1672
Email: Gregory.Kleen@go.doe.gov

Subcontractor:
RCF Economic and Financial Consulting, Inc.

Project Start Date: October 2010
Project End Date: Project continuation and direction determined annually by DOE

Technical Targets

The project is using a computer model to estimate the impact of deploying fuel cells in early markets. Insights from the model will assist the Fuel Cell Technologies Program and its stakeholders in estimating employment and other economic impacts from DOE technology development and in identifying fuel cell markets and regions that are most likely to generate jobs and economic activity.

FY 2012 Accomplishments

- Initiated close collaboration with stakeholders, fuel cell market participants and other researchers via a series of meetings, teleconferences and webinars. Demonstrated beta versions of the JOBS and economic impacts of Fuel Cells (JOBS FC) model to this group to validate data and obtain feedback on desired functionality, granularity, and outputs.
- Completed characterization of supply chains (in terms of the dollar purchases from individual industrial sectors per fuel cell kW) for low-temperature polymer electrolyte membrane (PEM) fuel cells, phosphoric acid fuel cells (PAFCs) and molten carbonate fuel cells (MCFCs), and launched version 1.0 of the JOBS FC model. Launch required development of:
 - A user's guide.
 - A dedicated website for users to register and download the model and User's Guide.
 - A webinar introducing JOBS FC 1.0.
- Completed an initial analysis of employment impacts of select PEM fuel cell projects funded under the American Recovery and Reinvestment Act (ARRA).



Fiscal Year (FY) 2012 Objectives

- Facilitate early market deployment of fuel cells by developing a downloadable, user-friendly tool to estimate economic impacts.
- Identify opportunities for enhancing the economic impact of fuel cell production and deployment by better understanding where and how impacts occur.
- Meet stakeholder needs for estimating impacts of fuel cell production and deployment on state, regional and national employment, earnings, and economic output.

Technical Barriers

This project addresses the following technical barriers from the Education section of the Fuel Cell Technologies Program Multi-Year Research, Development and Demonstration Plan:

- (A) Lack of Readily Available, Objective, and Technically Accurate Information
- (E) Regional Differences
- (F) Difficulty of Measuring Success

Introduction

Section 1820 of the Energy Policy Act of 2005 (Public Law 109-58) directed DOE to assess the impact of a large-scale transition to hydrogen on U.S. employment. In response to that directive, RCF Economic and Financial Consulting, Inc., Argonne National Laboratory, and other partners undertook an in-depth analysis of the economic impacts of hydrogen deployment in the transportation sector. That study relied on input-output (I-O) analysis to estimate net employment changes at the national level and produced a final report which was submitted to Congress in July 2008. But the study did not address initial fuel cell

(FC) applications or issues associated with early markets. Neither did it develop a method to examine alternative deployment scenarios and their employment impacts. Now, however, it is increasingly important to understand and expand employment impacts associated with early FC market development. Developing that capability is the focus of this project.

Results

In FY 2011, Argonne National Laboratory and RCF Economic and Financial Consulting began work on the design and implementation of a spreadsheet tool to calculate the economic impact of fuel cell production, installation, and utilization in early markets (i.e., 2015–2020) at the state, regional, and national levels. Known as JOBS FC the tool is designed as a user-friendly, spreadsheet-based model. In FY 2012, development culminated in a series of beta tests, the May 2012 launch of JOBS FC 1.0, and the application of the model to examine employment impacts of ARRA-funded fuel cell projects.

Model Development and Stakeholder Collaboration

A considerable portion of FY 2012 was devoted to model development and quality assurance — including data validation, development of the user interface, and outreach. In order to provide users with unlimited, free access to the JOBS FC tool, the underlying I-O multipliers had to come from publicly available, unrestricted sources. Thus, Regional Input-Output Modeling System II multipliers – developed by the U.S. Department of Commerce – were secured and embedded in the model. Supply chains were characterized using information from the literature, fuel cell suppliers and stakeholders. Default values for fuel cell costs and operating parameters were obtained from these sources as well as through basic engineering design calculations.

For each FC application and technology in JOBS FC 1.0 default parameters include unit size (kW), capital and operating cost (\$/kW), production location (domestic/import), installation location (domestic/import), utilization, fuel use, etc. The user can replace these values, thus defining a unique scenario, or use the default values embedded in the model.

For each of 60 geographies — 50 states, nine census regions, and the nation as a whole — JOBS FC estimates the effect of fuel cell deployments on employment, earnings and economic output. It does so by adjusting the dollar flows among economic sectors within the relevant geography. As FC systems are deployed, the purchases send dollars up the supply chain for PEMFC, PAFC, or MCFC technologies as well as to the relevant supply chains for FC system integrators, installers, fuel suppliers and businesses providing operation and maintenance services. These incremental purchases flow to other sectors which represent purchases

from their supply chains. In the aggregate, the resulting web of transactions represents a nascent fuel cell industrial sector. Purchases include not only the fuel cell itself, but all transactions required to install, fuel and operate the fuel cell system. To illustrate, a set of base or “reference scenarios” (Table 1) were postulated and used to generate an initial set of results. Results for the forklift reference scenario are shown in Figure 1.

TABLE 1. “Reference Scenario” Input Assumptions

| Reference Scenario Parameter | Forklifts | | Backup Power | Prime Power | |
|------------------------------|------------|-----------|--------------|-------------|------|
| | Class I/II | Class III | | PAFC | MCFC |
| Capacity (kW) | 10 | 2 | 5 | 400 | 1400 |
| Installations: | | | | | |
| 2015 | 1,500 | 1,500 | 3,000 | 100 | 50 |
| 2016 | 3,000 | 3,000 | 6,000 | 125 | 60 |
| 2017 | 4,500 | 4,500 | 9,000 | 150 | 70 |
| 2018 | 6,000 | 6,000 | 12,000 | 175 | 80 |
| 2019 | 7,500 | 7,500 | 15,000 | 200 | 90 |
| 2020 | 9,000 | 9,000 | 18,000 | 225 | 100 |

Reference scenarios were also used to investigate model sensitivities to various input parameters. Figure 2 shows the effect of FC capacity, the cost of delivered hydrogen, the number of FC units deployed and annual operating hours on cumulative employment over the period 2015–2020. Figure 2 is limited to forklifts. Similar results were obtained for backup power and prime power applications. Note that job-years are defined as employment for one person for one year.

Figure 2 suggests that JOBS FC results are relatively sensitive to the number of units deployed and insensitive to annual utilization. Thus, scenarios with greater numbers of FCs deployed may be expected to yield larger increases

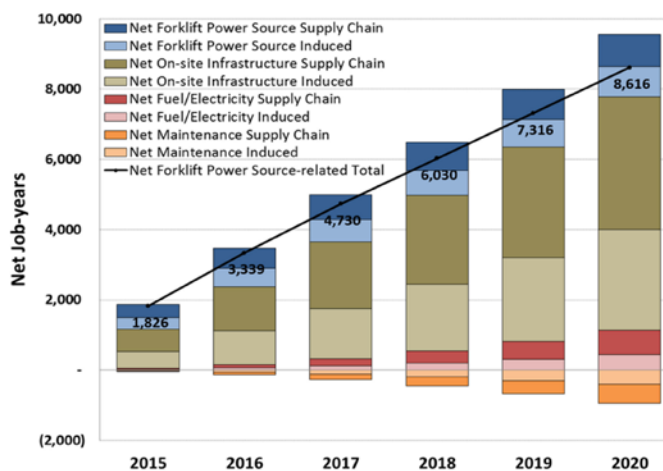


FIGURE 1. Employment Impact of Forklift “Reference Scenario”

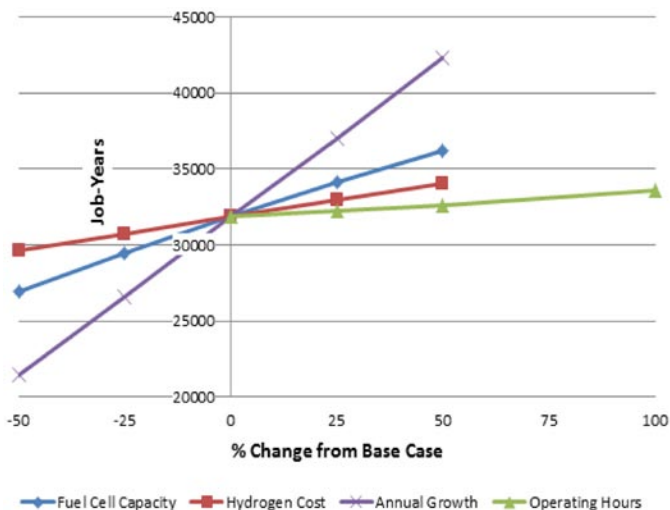


FIGURE 2. Sensitivity Analysis of Forklift Net Employment

in employment than those with increased operating hours or capacity.

Employment Impacts of ARRA-Funded Fuel Cell Projects

In FY 2012, JOBSFC 1.0 was used to develop an initial estimate of the employment impact of select ARRA-funded FC projects. Using data compiled for Fuel Cell Technologies Program market transformation sub-program, model inputs were developed for forklift and cell tower backup power systems placed in service under the ARRA program from 2009 through the end of 2011 (Table 2).

TABLE 2. Fuel Cells Deployed in Forklift and Cell Tower Backup Power, 2009–2011

| ARRA Deployments, 2009-2011 | Forklifts | | Cell Tower Backup Power |
|-----------------------------|------------|-----------|-------------------------|
| | Class I/II | Class III | |
| Units: 2009 | 14 | 0 | 24 |
| 2010 | 122 | 172 | 166 |
| 2011 | 124 | 72 | 417 |
| Total | 260 | 244 | 607 |
| Ave. capacity (kW) | 8 | 2 | 2.1 |
| Annual operating hrs | 2,500 | 2,500 | 24 |
| Fuel type | LH2/GH2 | LH2/GH2 | GH2 |
| Operating hrs/fueling | 4 | 4 | 72 |

LH2 - liquefied hydrogen; GH2 - gaseous hydrogen
 Source: Kurtz, J., K. Wipke, S. Sprik, T. Ramsden and C. Ainscough, Early Fuel Cell Market Deployments: ARRA and Combined (IAA, DLA, ARRA) NREL Composite Data Products, March 8, 2012.

Results are shown in Figure 3 [1]. For both applications, H₂ infrastructure supply accounts for a large share of employment gains (note that the category “supply chain” = direct + indirect employment) because a relatively large number of job-years are associated with storage tank fabrication, installation and shipping. Note also that gross results are nearly equal to net results because a significant portion of FCs will displace imported batteries and diesel generators, and/or installation, fueling and operation and maintenance for the incumbent technologies (batteries and engines) are not very labor intensive.

¹ Since ARRA-funded projects are assumed to have been “shovel ready” initial numbers of FCs may be assumed to have come from inventory. Thus, shadows have been applied to the bars associated with FC production in Figure 3. By 2011 it may be argued that few (if any) FCs would still come from 2009 inventories.

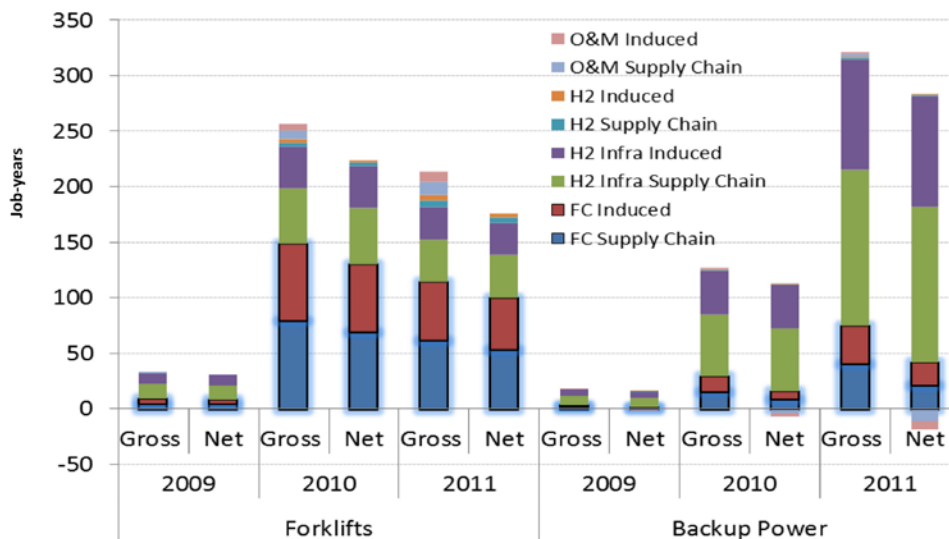


FIGURE 3. Preliminary Estimate of Employment Impact of ARRA Projects Deploying Fuel Cells in Forklift and Cell Tower Backup Power Applications

Conclusions and Future Directions

FY 2012 work focused on completion of the JOBS FC model to estimate gross and net economic impacts from the manufacture, installation, fueling, and operation of fuel cells in distributed prime power, backup power, and material handling (e.g. forklift) applications. That work included outreach to industry and stakeholders to develop and validate input and refine the user interface; model testing and quality assurance via a series of webinars, beta tests and sensitivity analyses; and model launch. The initial application of the model — to analyze the employment impact of fuel cell deployments under the ARRA — produced a set of preliminary “bottom-up” estimates which are being compared with “top-down” estimates based on total expenditures. FY 2013 work will build on these efforts, incorporating stakeholder recommendations for enhancements to the functionality and scope of the model, as well as developing estimates of employment impacts to support ongoing FC deployment programs.

Potential future model enhancements include adding SOFC and high-temperature PEM technologies for prime power applications, distributed hydrogen production and biologically-derived hydrogen as options for fueling FCs in forklift or prime power applications, and retail hydrogen fuel stations to serve emerging vehicle markets.

FY 2012 Publications

1. Mintz, M., J. Molburg, C. Mertes and E. Stewart, *Impacts of Non-Automotive Fuel Cells and Natural Gas Vehicles*, presented at the 91st Annual Meeting of the Transportation Research Board, Washington, DC, Jan. 23, 2012.
2. Mintz, M. *Employment Impacts of Early Markets for Hydrogen and Fuel Cell Technologies*, presented to the California Stationary Fuel Cell Collaborative, Sacramento, June 1, 2011.
3. *Job and Output Benefits of Stationary Fuel Cells (JOBS FC): An Economic Impact Tool Developed for USDOE*, Technology Transitions Corporation webinar *Where the Jobs Are: Hydrogen and Fuel Cells in Your Area*, July 19, 2011.
4. *Jobs and Output Benefits of Stationary Fuel Cells (JOBS FC): User Reference Guide for Beta Release 2.0*, draft report, Feb. 28, 2012.
5. *Jobs and Output Benefits of Stationary Fuel Cells (JOBS FC): User Reference Guide for Beta Release 1.0*, draft report, Dec. 15, 2011.

XII. AMERICAN RECOVERY AND REINVESTMENT ACT ACTIVITIES

XII.0 American Recovery and Reinvestment Act Activities

INTRODUCTION

In April 2009, the U.S. Department of Energy (DOE) announced the investment of \$41.6 million in American Recovery and Reinvestment Act (Recovery Act) funding for fuel cell technologies. These investments were made to accelerate the commercialization and deployment of fuel cells and to spur the growth of a robust fuel cell manufacturing industry in the United States, with accompanying jobs in fuel cell manufacturing, installation, maintenance, and support services. Twelve grants were awarded to develop and deploy a variety of fuel cell technologies, including polymer electrolyte membrane, solid oxide, and direct-methanol fuel cells in auxiliary power, backup power, combined heat and power (CHP), material handling equipment, and portable-power applications. The cost share provided by the project teams is about \$54 million, more than 56% of the total cost of the projects.

All Recovery Act project teams submit quarterly reports, which are available to the public through the Recovery.gov website. These reports include technology and deployment status as well as data on jobs created and funds spent. Collection and analysis of operational data from the fuel cell deployments are being performed by the National Renewable Energy Laboratory's (NREL's) Hydrogen Secure Data Center (HSDC) to assess the performance and commercial readiness of the fuel cell technologies. Data are aggregated across multiple systems, sites, and teams, and are made available on a quarterly basis through composite data products (CDPs), published on NREL's website. Fifteen presentations containing all CDPs have been published thus far, with the latest CDPs including performance, reliability, maintenance, and safety data for material handling equipment and backup power.

GOALS & OBJECTIVES

The Recovery Act fuel cell projects are addressing the objectives stated above as well as the overall Recovery Act goals of creating new jobs and saving existing ones, spurring economic activity, and investing in long-term economic growth. These deployments have also required project teams to address key challenges, including siting and permitting, fueling infrastructure, and fuel cell lifetime and reliability (Figure 1). These deployments have also attracted significant attention, with media events taking place at three of the Recovery Act deployment sites.

FISCAL YEAR (FY) 2012 STATUS AND PROGRESS

As of October 2012, more than 500 fuel cell lift trucks and more than 690 fuel cell backup power systems for cellular communications towers and stationary backup power systems had been deployed—surpassing the original deployment goal of up to 1,000 fuel cells—and over 90% of the Recovery Act project funds had been spent by the projects. NREL's HSDC has established data reporting protocols with each of the project teams. CDPs and detailed data products showing progress to date have been prepared. The CDPs are available on the NREL HSDC website, http://www.nrel.gov/hydrogen/proj_fc_market_demo.html. Of the original 12 projects, four have been successfully completed.

The Hydrogen Safety Panel has made four deployment site visits with at least one more planned and has reviewed the safety plans for each project. In addition, Sandia National Laboratories (funded through the Safety, Codes and Standards sub-program) continues to perform testing and analysis on the material handling equipment hydrogen tanks to facilitate market entry for fuel cell powered lift trucks.¹ Results from these tasks

¹“R&D for Safety Codes and Standards: Materials and Components Compatibility,” Brian Somerday, Safety, Codes and Standards Chapter of this volume.

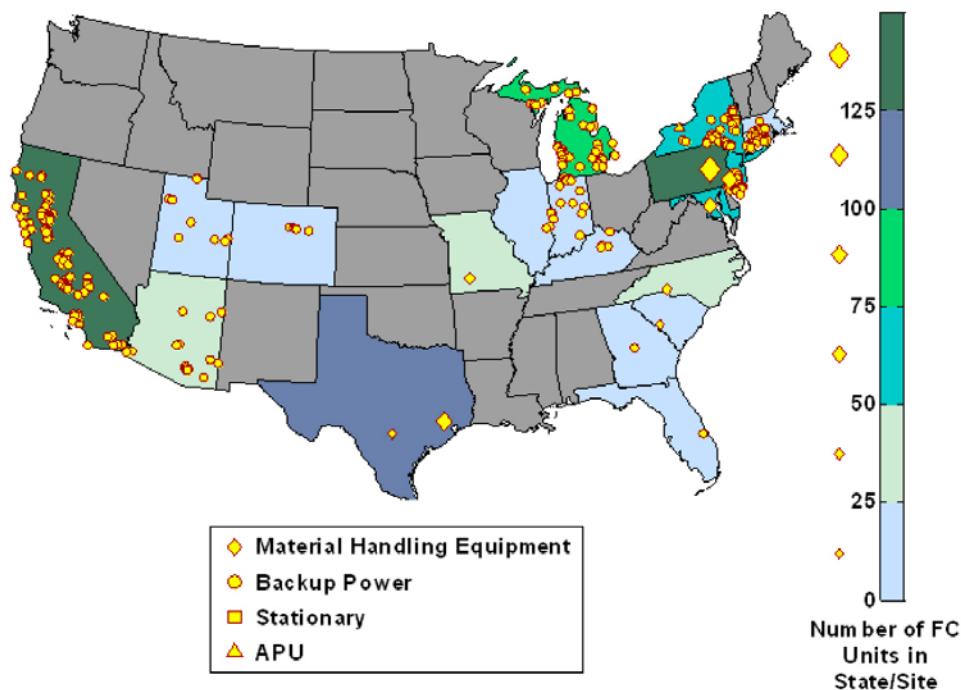


FIGURE 1. DOE Recovery Act-funded fuel cell deployment locations.

are being used to inform the Canadian Standards Association HPIT1 and SAE J2579 working documents for performance testing.

Auxiliary Power

Delphi Automotive (Troy, Michigan and Rochester, New York): Delphi is developing a 3- to 5-kW solid oxide fuel cell (SOFC) auxiliary power unit (APU) for heavy-duty commercial Class-8 trucks at their laboratory in Rochester, New York. Delphi will test and demonstrate the diesel APU in a high visibility fleet vehicle that will provide power for vehicle hotel loads and other vehicle needs under real-world operating conditions. The primary focus will be accelerating the development and acceptance of the APU by the Class-8 heavy-duty truck market. Delphi Automotive Systems has initiated the system and subsystem vibration analysis and has completed over 20% of their planned thermal cycle testing on their A-Level SOFC APU. They have also conducted initial road testing, driving >3,000 miles with the unit mounted on a Peterbilt Class-8 truck. A new stack with improved system efficiency and new endothermic reformer with improved heat transfer and lower cost have been integrated into the B-Level, next-generation system. Over the next year Delphi will begin monitoring the SOFC APU performance in an on-road, real-world demonstration.

Backup Power

Sprint Nextel Inc. (Reston, Virginia): Sprint is demonstrating the technical and economic viability of deploying 1- to 10-kW polymer electrolyte membrane (PEM) hydrogen fuel cells with 72 hours of on-site fuel storage (using a new Medium Pressure Hydrogen Storage Solution with on-site refueling) to provide backup power for critical code division multiple access cell sites on the Sprint Wireless network. Over 250 new hydrogen fuel cell systems will be deployed at sites in California, Connecticut, New Jersey, and New York. Sprint has completed over 670 site surveys at potential deployment sites for their fuel cell backup-power systems. They had installed and commissioned more than 310 new PEM backup-power fuel cells at 172 sites as of June 2012, with an additional 88 sites expecting fuel cells over the next year.

Plug Power Inc. (Latham, New York): Plug Power has been demonstrating the market viability of low-temperature, 6-kW PEM GenCore[®] fuel cells fueled by liquid petroleum gas to provide clean and reliable primary power and emergency backup power (72 hours or more). They will install and operate 20 fuel cell systems at Fort Irwin in Barstow, California, and Warner Robins Air Force Base (WRAFB) in Warner Robins, Georgia. These units will run continuously on liquid petroleum gas, providing power to the grid and will switch to emergency backup power during a grid failure. A small battery pack will be used to accommodate spikes in power demand. As of June 2012, the 10 GenCore[®] fuel cells installed at the Warner Robins Air Logistics Center at WRAFB have generated about 39 MWh of power at an average efficiency of approximately 24%. The units are providing backup power for lighting within the building. Plug Power plans to install 10 additional fuel cells at an engineering building at Fort Irwin in Barstow, California, in FY 2012.

Combined Heat and Power

Plug Power Inc. (Latham, New York): Plug Power has been evaluating the performance of high-temperature, natural gas-fueled, 5-kW micro-CHP fuel cell units (GenSys Blue[®]). The objective of the project is to validate the durability of the fuel cell system and verify its commercial readiness. Six units have undergone internal Plug Power testing to estimate failure rates, and three units were installed and tested in a real-world environment at the National Fuel Cell Research Center at the University of California, Irvine. These systems have logged over 34,000 hours in two years and have met their 30% electrical efficiency and 99% heat availability targets. Due to membrane electrode assembly supply and quality issues, Plug Power did not meet the durability target of >8,700 hours per unit. Plug Power has since transferred the role of deploying units at customer sites in California to ClearEdge Power, Inc. Over the next year, two additional fuel cell systems will be deployed.

Fuel Cell Powered Lift Trucks

FedEx Freight East (Harrison, Arkansas): FedEx deployed 35 Class-1 fuel cell systems as battery replacements for a complete fleet of electric lift trucks at FedEx's service center in Springfield, Missouri. Success at this service center may lead to further fleet conversions at some or all of FedEx's other 470 service centers. FedEx deployed their fleet of lift trucks in June 2010, at their 53,000-square-foot distribution center in Springfield, Missouri. Due to the favorable operational results, they purchased an additional five fuel cell lift trucks, *without any additional DOE funding*. As of June 2012, the lift trucks had accumulated over 90,000 hours of operation and used over 29,200 kilograms of hydrogen. FedEx has seen 125% more operating hours in between repairs for fuel cell lift trucks than for propane-powered internal combustion engine lift trucks. Over the next year FedEx will continue to monitor the performance of their fuel cell lift truck fleet.

GENCO (Pittsburgh, Pennsylvania): GENCO deployed 357 Class-1, Class-2, and Class-3 fuel cell systems as battery replacements for fleets of electric lift trucks at five existing distribution centers (Coca Cola in Charlotte, North Carolina; Kimberly Clark in Graniteville, South Carolina; Sysco Foods in Philadelphia, Pennsylvania; Wegmans in Pottsville, Pennsylvania; and Whole Foods Market in Landover, Maryland). Success at these distribution centers may lead to further fleet conversions at some or all of GENCO's other 109 distribution centers. Some of the fuel cell units at the Wegmans site have already accumulated over 9,000 hours of operation.

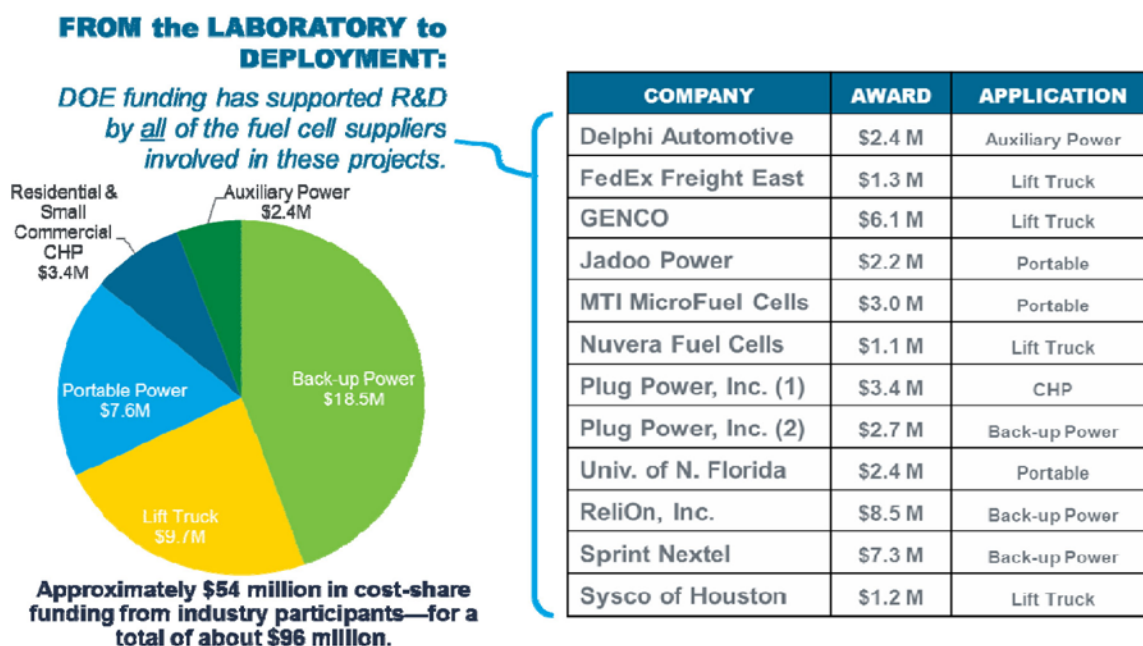
Sysco Houston (West Houston, Texas): Sysco Houston deployed 98 Class-2 and Class-3 fuel cell systems as battery replacements for a fleet of lift trucks at Sysco's new 585,000 square foot food distribution center in Houston, Texas, opened in March 2010. This installation was the first-ever greenfield installation without prior battery infrastructure for a pallet truck fleet. Success at this distribution center has led to further fleet conversions at some of Sysco's other 169 distribution centers. By the end of FY 2012, the lift trucks had accumulated over 790,000 hours of operation, and refueling operations had supplied the lift trucks with more than 66,000 kilograms of hydrogen. While Sysco Houston is currently not experiencing any difference in cost between charging batteries and fueling with hydrogen, they are saving nearly \$100,000 annually in fewer

man-hours spent refueling lift trucks compared with swapping batteries. Based in part on the success of this deployment site, Sysco Corporate is planning to replace about 1,800 batteries with 900 or more fuel cells at seven sites over the next 24 months—with no additional DOE funding.

Data Collection & Analysis

National Renewable Energy Laboratory (Golden, Colorado): NREL is analyzing operational data (operation, maintenance, and safety) from the Recovery Act fuel cell deployments to better understand and highlight the business case for fuel cell technologies. Data collected by the project partners is being stored, processed, and analyzed in NREL’s HSDC. Reports on the technology status are generated on a quarterly basis, while technical composite data products are published every six months. NREL has published nine deployment-focused CDPs and four cycles of technical CDPs—currently composed of 63 CDPs for material handling equipment and 13 CDPs for backup power. In addition, they have provided hundreds of detailed data results to the individual projects. NREL has created a website to host these published results and presentations. Over the next year, they plan to continue collecting and analyzing Recovery Act deployment data and publishing the results on their website.

BUDGET



FY 2013 PLANS

Continued data collection on performance and productivity at the various deployment sites is a priority for FY 2013. In FY 2013, deployment of over 100 additional fuel cell systems for APUs, backup power installations, and CHP applications is anticipated. All projects will conclude by the end of FY 2013.

Finally, in FY 2013, DOE will continue to document the lessons learned associated with the Recovery Act projects, including strategies developed for market entry and management of risks relating to safety, environmental, and siting requirements. EERE will finalize its evaluation of early-stage “market change” impacts (for the period of 2010 through the end of 2012) of the Recovery Act fuel cell deployments.

Jim Alkire

Project Officer and Lead for Recovery Act Activities

U.S. Department of Energy

EERE Fuel Cell Technologies Program

Phone: (720) 356-1426

Email: James.Alkire@go.doe.gov

Sara Dillich

U.S. Department of Energy

EERE Fuel Cell Technologies Program

Phone: (202) 586-7925

Email: Sara.Dillich@ee.doe.gov

XII.1 Solid Oxide Fuel Cell Diesel Auxiliary Power Unit Demonstration

Dan Hennessy (Primary Contact), Jim Banna
Delphi Automotive Systems, LLC
300 University Drive
m/c 480-300-385
Auburn Hills, MI 48326
Phone: (248) 732-0656
Email: daniel.t.hennessy@delphi.com

DOE Managers

HQ: Dimitrios Papageorgopoulos
Phone: (202) 586-5463
Email: Dimitrios.Papageorgopoulos@ee.doe.gov
GO: David Peterson
Phone: (720) 356-1747
Email: David.Peterson@go.doe.gov

Contract Number: DE-EE0000478

Subcontractors:

- Electricore, Inc., Valencia, CA
- PACCAR, Inc., Bellevue, WA
- TDA Research, Inc., Wheat Ridge, CO

Project Start Date: August 1, 2009

Project End Date: April 30, 2013

- Utilize Delphi's next generation SOFC system as the core power plant and prove the viability of the market opportunity for a 3-5 kW diesel SOFC APU system.
- Test and demonstrate the diesel SOFC APU system in a high visibility fleet customer vehicle application that will support hotel loads and other real world operating conditions.

Relevance to the American Recovery and Reinvestment Act (ARRA) of 2009 Goals

- During this phase of the project, a total of eight jobs were created/maintained;
 - Delphi 6 jobs
 - PACCAR 1 job
 - TDA 1 job
- As a result of this project, Delphi will be able to install its SOFC APU on a high visibility fleet truck. This will provide Delphi, and its fleet customer, with real world use experience as well as the associated fuel consumption and emission data. This demonstration should increase the overall awareness of SOFC APUs and provide positive momentum in preparing to commercialize this product.

Objectives

- Design, develop, and demonstrate a 3-5 kW solid oxide fuel cell (SOFC) auxiliary power unit (APU) for heavy-duty commercial Class-8 trucks (Figure 1).

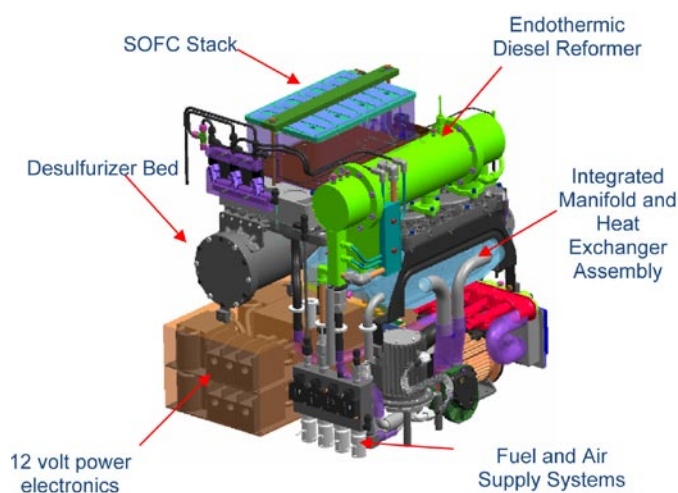


FIGURE 1. Delphi SOFC APU (A-Level Prototype) Schematic

Technical Barriers

- As a result of the successful execution of this project, Delphi will have addressed:
 - System vibration robustness
 - Overall system packaging
 - System weight
 - System cost
 - System manufacturability
 - System durability/reliability
- During a recent SOFC APU system test, we discovered a significant issue with the desulfurizer during repeated thermal cycles. This issue needs to be resolved before the unit could begin fleet testing.

Technical Targets and Milestones

- Deliver the next-generation prototype (B-Level) SOFC APU for installation on fleet customer truck during the third quarter of 2012. Begin on-road, real-world application demonstration.
- Provide 3-5 kW of power during idle periods allowing for reduced fuel consumption and harmful emissions.
- Specific power: $\geq 15\text{w/kg}$

- Power density: $\geq 10\text{w/l}$
- Net system efficiency: $\geq 35\%$
- $\geq 2,000$ hours of operation

Accomplishments

- B-Level SOFC APU mounted on Peterbilt Class-8 truck and driven on a local demonstration loop to gain durability and performance data. Current unit has more than 100 miles and 200 hours of demonstration (Figure 2). A second unit has compiled more than 1,500 miles and 200 hours of testing.
- B-Level SOFC APU completed more than 3,800 hours of lab testing on seven systems across typical start-up, power, and shut-down cycles. This testing includes 195 thermal cycles, start up, shut-down cycles.
- B-Level SOFC APU system validation testing:
 - Completed 19 thermal cycles of 416 planned on an accelerated thermal cycle test.
 - System and subsystem vibration testing completed.
 - System tested to the equivalent of 500,000 highway miles on a single axis vibration test.
 - Stack tested to the equivalent of 3.5 million miles on a vibration table with no measurable stack degradation noted.
- This testing has resulted in many improvements to the system calibration, reformer, stack, power electronics and air and fuel control systems.
- Integrated a sorbent bed for removal of hydrogen sulfide (H_2S) from the reformat. Above mentioned issue needs to be addressed.
 - Requirement is to remove H_2S to <0.010 ppm at a specified sorbent capacity.



FIGURE 2. Delphi SOFC APU (B-Level Prototype) Installed on PACCAR Truck

- Delphi continues to investigate an alternative, non-sorbent based solution.
- Launched the next generation endothermic reformer. Provides improved durability, heat transfer, and reduced manufacturing complexity.
- System level performance demonstrated to date:
 - 28% efficiency at 1.6 kW.
 - Less than 0.085 gallons per hour idle fuel consumption.
 - 2 kW of power for truck hotel loads, working towards a 3 kW system for production.



Introduction

Delphi's SOFC power system, installed on heavy-duty commercial trucks as an APU, addresses the growing concerns about emissions, fuel consumption, and noise. In the United States today, there are more than one million long-haul heavy-duty commercial trucks with sleeper cabs on the road. When drivers stop for their mandatory rest periods or loading/unloading, they often leave their engines idling in order to heat/cool their sleeping areas and operate other vehicle systems. This idling practice is costly to the driver, the fleet owner, and harmful to the environment. The Environmental Protection Agency's SmartWay Transport Partnership estimates that each year, long duration idling of truck engines consumes approximately 960 million gallons of diesel fuel and emits 11 million tons of carbon dioxide, 180 thousand tons of nitrogen oxides, and 5 thousand tons of particulate matter into the air. In addition to the consumed fuel and emissions, idling trucks create elevated noise levels. The SOFC APU has the potential to decrease idling fuel consumption by up to 85%, reduce exhaust emissions below federal regulation emission standards, and decrease radiated noise levels to less than 60 dBA when compared to the truck's main engine.

As a result of the on-road demonstration under this project, Delphi will be able to present user profile data from its fleet customer. This data will reinforce the lab-generated data showing that use of a SOFC APU as an anti-idling solution will provide drivers and fleets with reduced fuel consumption as well as reduced emissions and noise. This demonstration should increase the overall awareness of SOFC APUs and provide positive momentum in preparing to commercialize this product.

Approach

Under this project, Delphi is pursuing a 3-phased approach to conduct its research. During Phase 1, Delphi, working with its partner PACCAR, will establish the

applications specifications and commercial requirements for a SOFC APU. Phase 2 work will focus on design verification and system testing (bench top and on-vehicle). Phase 3 will include the demonstration of the SOFC APU on a heavy-duty Class-8 vehicle. The data collected during this phase will be analyzed and reported will respect to fuel consumption, emissions, and noise.

All Delphi facilities involved with this project are required to meet Delphi's stringent safety requirements which are aligned with the Safety Planning Guidance documentation specified by DOE. Additionally, there are no changes to the National Environmental Policy Act information submitted.

Results

During this report period, Delphi has completed several of the tasks necessary to provide a road ready SOFC APU to our fleet customer.

- Updated our requirements document.
- Completed SOFC APU B-Level system builds.
- Completed SOFC APU system integration into the truck including mounting the APU controls in the sleeper and adding data logging systems to the vehicle.
- Developed a user's manual and service procedures.
- Continued in-house subcomponent and system testing.
- Completed numerous small scale and full scale desulfurizer materials evaluations.
- Completed system level testing with US07 diesel fuel with no desulfurizer system.
- Completed system testing at elevated ambient temperatures.
- Evaluated and integrated anode protection and fire suppression systems.
- SOFC APU system installed on the vehicle is scheduled to be delivered to our fleet partner during the third quarter of 2012.

Specific subcomponent and system development achievements are described in the Accomplishment section above.

Conclusions and Future Directions

Delphi continues to make significant progress towards introducing a production-intent SOFC APU for use by heavy-duty truck manufacturers, fleets, and drivers. This leading-edge technology will provide users with the ability to run their hotel electrical loads during idling without the need to run their main truck engine or a diesel generator. As a result of using a SOFC APU, they will see reduced fuel consumption, reduced harmful emissions, and reduced noise.

Under this specific project, Delphi will next deliver its B-Level prototype SOFC APU to its fleet partner. After vehicle delivery and fleet/driver user training, the unit will be deployed in a real-world application. During this demonstration period, Delphi will be able to monitor the SOFC APU performance real time through a dedicated telematic connection.

Design direction has changed to reduce maintenance requirements by eliminating the desulfurizer in the near term. This requires delivering a 2-kW APU. We are redesigning the system to deliver 3 kW by taking advantage of the space available.

FY 2012 Publications/Presentations

1. May 2012 DOE Hydrogen Program Peer Review Presentation: "Solid Oxide Fuel Cell Diesel Auxiliary Power Unit Demonstration", Dan Hennessy.

XII.2 Demonstrating Economic and Operational Viability of 72-Hour Hydrogen PEM Fuel Cell Systems to Support Emergency Communications on the Sprint Nextel Network

Kevin Kenny
Sprint Nextel
12000 Sunrise Valley Drive
MS: VARES0401-E4064
Reston, VA 20191
Phone: (703) 592-8272
Email: kevin.p.kenny@sprint.com

DOE Managers
HQ: Sara Dillich
Phone: (202) 586-7925
Email: Sara.Dillich@ee.doe.gov
GO: James Alkire
Phone: (720) 356-1426
Email: James.Alkire@go.doe.gov

Contract Number: EE-0000486

Project Partners:

- Air Products & Chemicals, Inc., Allentown, PA (Fuel Project Partner)
- Alteryx Systems, Folsom, CA (PEM Fuel Cell Project Partner)
- Black & Veatch Corporation, Overland Park, KS (A&E Project Partner)
- Burns & McDonnell Engineering Co., Inc., Kansas City, MO (A&E Project Partner)
- Ericsson Services, Inc., Overland Park, KS (Deployment Management Project Partner)
- ReliOn, Inc., Spokane, WA (PEM Fuel Cell/A&E Project Partner)

Project Start Date: March 18, 2010
Project End Date: December 31, 2012

Objectives

- Eliminate barriers to siting and permitting 72 hours of hydrogen fuel storage
- Eliminate barriers to re-fueling sites at the required level of performance
- Collect and analyze data sample to evaluate economic and operational metrics

Relevance to the American Recovery and Reinvestment Act (ARRA) of 2009 Goals

Sprint, through this deployment effort, seeks to:

- Support the creation of new jobs.
- Maintain existing jobs.
- Bring proton exchange membrane (PEM) technology into the market which will foster job training opportunities:
 - Installation
 - Service
 - Repair

Relevance to the DOE-Fuel Cell Technologies' ARRA Project Goals

Through the successful deployment of this technology, it is expected that the following goals shall be achieved:

- Demonstrate the operational acceptance and financial viability of using PEM technology to support critical emergency power requirements:
 - Telecommunications
 - Health care/life support systems
 - Critical government operations
- Expanded user community offers many positive market opportunities:
 - Increased demand prompts greater production volume – lowers unit cost.
 - Cross industry adoption spurs “services” growth (construction, maintenance, ancillary support) as more units are deployed – lower costs due to competition.
 - Fueling infrastructure is “pulled” into the market by true demand rather than being “pushed” into the market to support speculative potential.

Technical Barriers

Major barriers being addressed under our project are summarized as follows:

- Higher costs: initial capital cost, as well as increased site lease costs to support code mandated hydrogen setbacks than incumbent technology (diesel generator).

- Siting and permitting: due to variations in the applicable code requirements and versions recognized by the authorities having jurisdiction, each market launch requires time with the local officials (building, fire) to help them understand the referenced codes and how Sprint interprets/complies with code requirements.
- Fueling infrastructure: this project deploys a new model for stationary hydrogen fuel cells, relying upon an on-site refillable medium pressure storage solution rather than the low-pressure hydrogen cylinder exchange model. Our Project Partner, Air Products, has invested in a small fleet of transport vehicles to deliver bulk compressed hydrogen to small, geographically diverse, remote cell sites.

Technical Targets and Milestones

The following performance targets and associated milestones have been set for this project.

- Install 260 additional PEM fuel cells for backup power by end of December, 2012.
 - California – 100 units
 - Connecticut – 30 units
 - New Jersey – 65 units
 - New York – 65 units

(These were the original state/quantity targets. See “Accomplishments” for updated allocation targets.)

- Retrofit a total of 70 existing low-pressure hydrogen storage systems with the new medium-pressure on-site refillable hydrogen storage solution in the following states:
 - California
 - Louisiana
 - Texas

Accomplishments

To date, our team has:

- As of June 30, 2012, we have successfully commissioned a total of 172 PEM hydrogen fuel cells of the 260 total new units slated to be completed under this grant award. These units have been deployed as shown in Table 1.
- As of June 30, 2012, 21 sites have been successfully retrofit with the medium-pressure on-site refillable hydrogen storage solution.
- Our team has conducted site surveys at 676 candidate sites to support new PEM deployments at 260 locations.
- A total of 389 of the 676 candidates were removed from consideration for a variety of reasons during Phase 1 (site survey, entitlement review):

TABLE 1. PEM Fuel Cells Deployed as of June 30, 2012

| State | Original Target QTY | Revised Target QTY | Total # of Systems In Service |
|----------------|---------------------|--------------------|-------------------------------|
| California | 100 | 76 | 74 |
| Connecticut | 30 | 30 | 27 |
| New Jersey | 65 | 42 | 27 |
| New York | 65 | 59 | 44 |
| Louisiana | 0 | 10 | 0 |
| Texas | 0 | 40 | 0 |
| Mississippi | 0 | 1 | 0 |
| North Carolina | 0 | 2 | 0 |
| Grand Total | 260 | 260 | 172 |

- Space constraints within the cell site compound (real estate and setbacks).
- Access restrictions for hydrogen fueling vehicle.
- An additional 63 candidates “fell out” during Phase 2 (site acquisition) due to:
 - Cost
 - Landlord issues
 - Zoning issues
- Expect to have 260 new PEM fuel cells commissioned by the end of 2012.
- Project modifications may be required to reduce the number of retrofit target sites (70) down to a number at or near to the 21 completed to date as we have encountered similar site fallout rate/reasons.



Introduction

The relevance of this project to the goals of the American Recovery and Reinvestment Act (ARRA) of 2009 is threefold. First, Sprint seeks to support the creation of new jobs, as well as maintain existing jobs, to successfully complete this deployment effort. Second, Sprint intends to spur economic activity through the positive impact to various industries and service providers at all levels of the supply chain. And finally, Sprint is confident that this investment in PEM hydrogen fuel cells, to provide emergency power to our critical wireless network facilities, will truly benefit our nation’s long-term economic growth.

Approach

After reviewing the Code Division Multiple Access Network Site Inventory, a master candidate site list was created based upon the restoration priority of the facility,

and whether or not the site was equipped with a fixed generator. Sprint focused on specific markets to exploit the site’s proximity to the hydrogen distribution facility (within 200 miles), as well as to concentrate on market clusters to minimize site acquisition, siting/permitting, installation, commissioning, and training expenditures. In addition, this cluster approach helps to minimize costs associated with the maintenance of a PEM spare parts inventory. Finally, this concentration permits a consistent presentation to the local building officials, which in turn helps to clarify applicable code (Uniform Building Code, National Fire Protection Association, etc.) interpretations. In theory, all of these efforts should help to facilitate a rapid, safe, and successful deployment in the market.

A Hydrogen Safety Plan (HSP) was submitted to DOE on July 13, 2010. On January 18, 2011, feedback from the Safety Panel team at DOE was received. Additional work is required on the HSP to ensure that the issues identified by DOE are satisfactorily addressed prior to resubmission. In reality, modifications to the HSP were put on the “back burner” as efforts to demonstrate progress on new PEM deployments required the team’s full time and attention – now targeting delivery of the revised HSP to DOE by August 10, 2012. This will enable the Hydrogen Safety Panel to have the HSP in hand when they conduct site visits in mid-August.

A National Environmental Policy Act comprehensive Categorical Exclusion was secured on May 12, 2011.

Results

Since the initial installation under this DOE/ARRA-funded project on May 11, 2011, a total of 172 systems have been brought into service (as of June 30, 2012). These installations, coupled with our original stand-alone deployment effort (243 systems in the 2005–2007 timeframe), provide a grand total of 415 PEM fuel cells providing backup power for critical cell site locations on the Sprint Network. When the planned 260 new and 70 retrofits (fuel storage converted from low-pressure tanks to the medium-pressure refillable solution) are completed, we will have more than doubled the number of sites in our Network with emergency power provided by PEMs! Figure 1 provides the deployment schedule for this project.

To date, a total of 676 sites have been evaluated to determine if the cell site location is suitable for new PEM fuel cell deployment. Figure 2 provides a summary of the various reasons 389 sites were dropped from consideration following the completion of Phase 1 activities.

Once the candidate site makes it through Phase 1, sites can be dropped from consideration during Phase 2. Figure 3 provides a summary of the various reasons a site can be dropped at this stage of deployment. Interestingly, it appears that the education of property owners (landlords, tower aggregators), municipal officials, and/or the zoning board might permit more sites to remain in consideration.

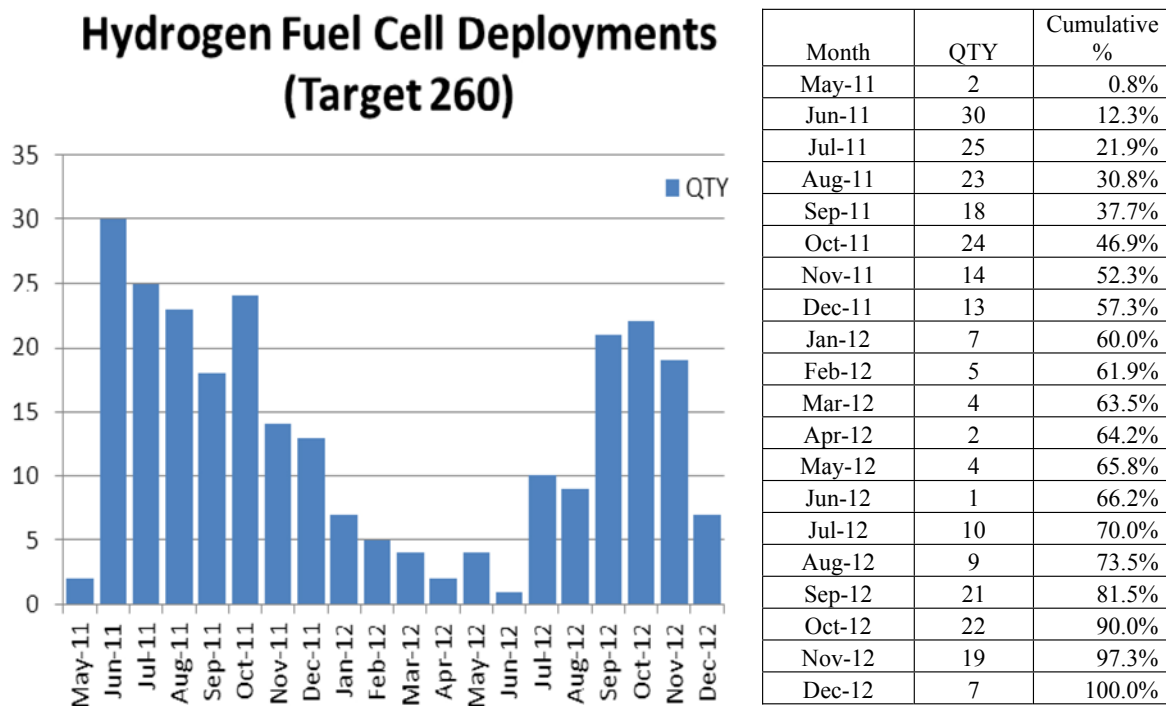


FIGURE 1. Deployment Schedule

PH1 Fallout

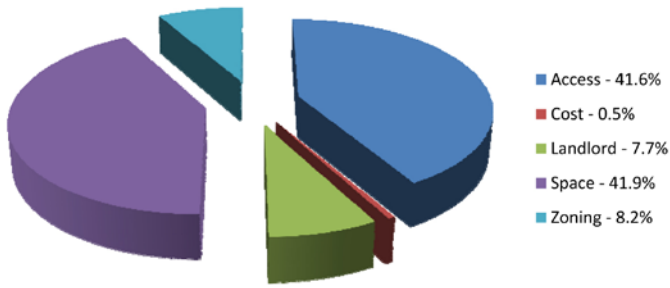


FIGURE 2. Phase 1 (Site Survey/Entitlement Review) Fallout Summary

Conclusions and Future Directions

We recognized going into this project that the fallout rate for candidate sites would be in the 40% range due to the limited amount of space available in the cell site compound. Limited real estate, in the case of PEM fuel cell deployment, can be a double edged sword. There may be physical space to permit the placement of the equipment on-site, however, code-mandated setback distances may or may not be able to be supported at the facility. Without uniform authorities having jurisdiction-recognized hydrogen/fire codes, it appears that PEM fuel cell deployment will continue to require more time/effort/money to deploy versus the incumbent diesel generator solution.

Phase 2 Fallout

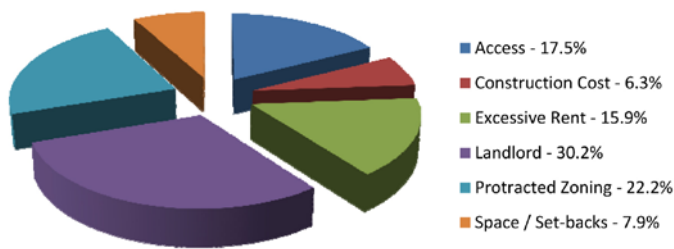


FIGURE 3. Phase 2 (Site Acquisition/Zoning) Fallout Summary

XII.3 Analysis Results for ARRA Projects: Enabling Fuel Cell Market Transformation

Jennifer Kurtz (Primary Contact), Keith Wipke, Sam Sprik, Todd Ramsden, Genevieve Saur, and Chris Ainscough

National Renewable Energy Laboratory
15013 Denver West Parkway
Golden, CO 80401-3305
Phone: (303) 275-4061
Email: jennifer.kurtz@nrel.gov

DOE Manager

HQ: Sara Dillich
Phone: (202) 586-7925
Email: Sara.Dillich@ee.doe.gov

Subcontractors:

Pacific Northwest National Laboratory, Richland, WA

Project Start Date: August 2009

Project End Date: December 2012, with future evaluations covered under DOE's Technology Validation sub-program

reported publically in aggregated data sets to inform and educate hydrogen and fuel cell stakeholders as well as current and potential end users. Individual, detailed results are shared with each project partner for deep dive performance status (down to individual systems) and technology benchmarking. This project studies and tracks 1,111 fuel cell systems in operation.

Technical Barriers

This project addresses the technical barrier of commercialization of fuel cells in key early markets and the associated performance capabilities and benefits. Specific areas of hydrogen fuel cell systems in material handling and backup power applications include:

- Technology status
- Value proposition
- Durability and reliability
- Safety

Technical Targets and Milestones

Deployment of up to 1,000 fuel cell systems: Successfully achieved with 1,111 systems in operation by December 2011.

Accomplishments

- By December 2011, 1,111 fuel cell systems were in operation throughout the United States, more than double the number of systems that were in operation at the end of 2010. All of the MHE sites are fully operational, and in backup power, the number of installed sites increased from 5 to 292 in just 18 months.
- The technical results published in April 2012 include 13 backup power composite data products (CDPs) and 63 MHE CDPs. The results are categorized as deployment, fuel cell operation, infrastructure operation, fuel cell safety, infrastructure safety, fuel cell durability, fuel cell maintenance, infrastructure maintenance, fuel cell reliability, infrastructure reliability, and cost of ownership. There were 24 new CDPs created in the past year.
- Deployment CDPs were updated to depict the number of systems delivered and in operation by application, the system/site locations, and the number of systems deployed with ARRA funds by state.
- The number of successful backup power starts was validated at 99.7%, or 1,187 good starts from 1,191 attempted starts.

Objectives

- Perform an independent assessment of technology in real-world operation conditions, focusing on fuel cell systems and hydrogen infrastructure
- Leverage data processing and analysis capabilities developed under the Fuel Cell Vehicle Learning Demonstration
- Support market growth through reporting on technology status to key stakeholders and performing analyses relevant to the markets' value proposition
- Study fuel cell systems operating in material handling equipment (MHE), backup power, portable power, and stationary power applications; the project includes approximately 1,000 deployed fuel cell systems.

Relevance to the American Recovery and Reinvestment Act (ARRA) of 2009 Goals

This technology validation project supports the ARRA project goals of accelerating the commercialization and deployment of fuel cells and fuel cell manufacturing, installation, maintenance, and support services through the independent technology assessments and reports. The analyses focus on performance areas such as durability, safety, and reliability that are critical to the successful implementation and continued operation. The analyses are

- A continuous run time of 29 hours was demonstrated for at least one backup power system.
- The average fill time for 504 MHE units was 2.2 minutes per fill, providing a significant operating savings for the facilities.
- A detailed cost of ownership analysis of MHE, comparing battery and hydrogen fuel cell lifts, showed an annual savings of \$1,900 dollars per lift in high-use facilities.



Introduction

The DOE has designated more than \$40 million in ARRA funds for the deployment of up to 1,000 fuel cell systems. This investment is enabling fuel cell market transformation through development of fuel cell technology, manufacturing, and operation in strategic markets where fuel cells can compete with conventional technologies. The strategic markets include MHE, backup power, stationary power, and portable power, and the majority of the deployed systems are in the MHE and backup power markets. NREL is analyzing operational data from these key deployments to better understand and highlight the business case for fuel cell technologies and report on the technology status.

Approach

The project’s data collection plan builds on other technology validation activities. Data (operation,

maintenance, and safety) are collected on-site by the project partners for the fuel cell system(s) and infrastructure. NREL receives the data quarterly and stores, processes, and analyzes the data in NREL’s Hydrogen Secure Data Center (HSDC). The HSDC is an off-network room with access for a small set of approved users. An internal analysis of all available data is completed quarterly and a set of technical CDPs is published every six months. The CDPs present aggregated data across multiple systems, sites, and teams in order to protect proprietary data and summarize the performance of hundreds of fuel cell systems and thousands of data records. A review cycle is completed before the publication of CDPs. The review cycle includes providing detailed data products (DDPs) of individual system and site performance results to the individual data provider. DDPs also identify the individual contribution to CDPs. The NREL Fleet Analysis Toolkit (NRELFAT) is an internally developed tool for data processing and analysis structured for flexibility, growth, and simple addition of new applications. Analyses are created for general performance studies as well as application- or technology-specific studies.

Results

An objective of the ARRA fuel cell project—to deploy up to 1,000 fuel cell systems in key early markets—was met within two years from the first deployments. Early market end users are operating 1,111 fuel cell units at 301 sites in 20 states (Figure 1). By the end of 2011, 504 MHE fuel cell units were operating at eight facilities, and 607 backup power fuel cell units were operating at 293 sites. The results have

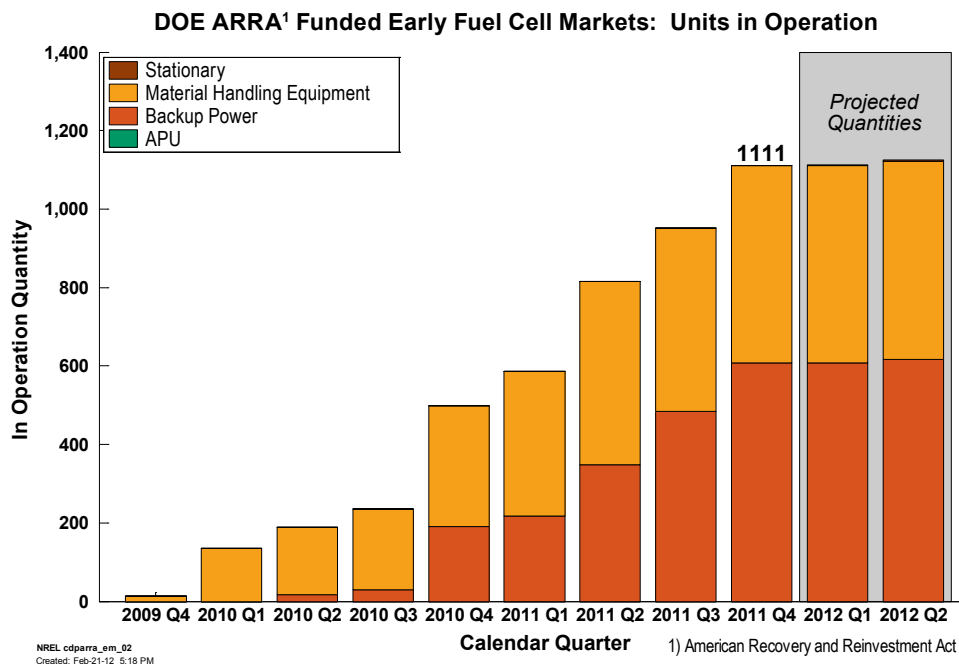


FIGURE 1. DOE ARRA-funded early fuel cell markets: units in operation

shown that MHE and backup power are two markets where fuel cells are capable of meeting the operating demands, and deployments can be leveraged to accelerate fuel cell commercialization.

In 1.5 years the number of backup power fuel cell sites has increased from 5 to 292. The project partners have identified many challenges with installation, such as determining the correct site and permitting, but these systems can be installed and in operation quickly. Backup power fuel cell systems can also be installed just about anywhere, as long as hydrogen can be delivered, and the deployments include urban and remote sites. Backup power fuel cell systems have demonstrated high reliability for successful starts, at 99.7%, and more than half of the starts are because of grid outages or site demands (see Figure 2). These reliable backup power fuel cell systems are operating in many different U.S. regions and are capable of long continuous run times with little or no emissions. At least one system has demonstrated a continuous operation of more than 29 hours due to an unscheduled outage.

The MHE fuel cell systems accumulated 959,887 hours by the end of 2011 and are estimated to have accumulated 1 million operation hours in early 2012. High operation hours on the 504 systems indicate these systems are successfully performing and making an impact at the high-productivity facilities. These end-user facilities have had experience with battery and propane lifts and expected the fuel cell systems to meet and exceed performance expectations in a few key areas for both the retrofit and greenfield sites. These key

performance areas include fill amount, operation per fill, operation per day (and year), mean time between failure, and voltage degradation (or fuel cell operation durability). These areas were studied in detail for each system, fleet, and lift classification. A difference in operating conditions exists between lift classes and is observed in the reliability and durability results; Class 3 lifts demonstrated higher reliability and durability than Class 1 and Class 2 lifts (see Figure 3). These differences warrant additional investigation, but two potential reasons for the higher performance observed in Class 3 lifts are that they use a smaller system and have less demanding operation than the other lift classes studied. Operation time accumulates quickly in MHE facilities, providing a large set of data to study fuel cell durability and system reliability. The average projected time to 10% fuel cell voltage degradation is 5,500 hours, and only 15% of the fuel cell stacks have actually seen 10% voltage degradation. System reliability is also analyzed to provide a more complete picture of the fuel cell MHE performance. The average system availability is high at approximately 98%, but more than a third of the systems have a mean time between failure of less than 250 hours.

Fuel cell MHEs can have a lower annual operating cost than battery MHEs at high-use facilities. The cost of ownership analysis shows that, for a facility with 58 Class 1 and 2 fuel cell MHEs that average 2,100 operation hours per year, a fuel cell MHE costs approximately \$2,000 less to operate annually than a battery MHE (Figure 4). The primary, positive factors for the lower cost are decreased maintenance, fast fill times, and decreased interior space for

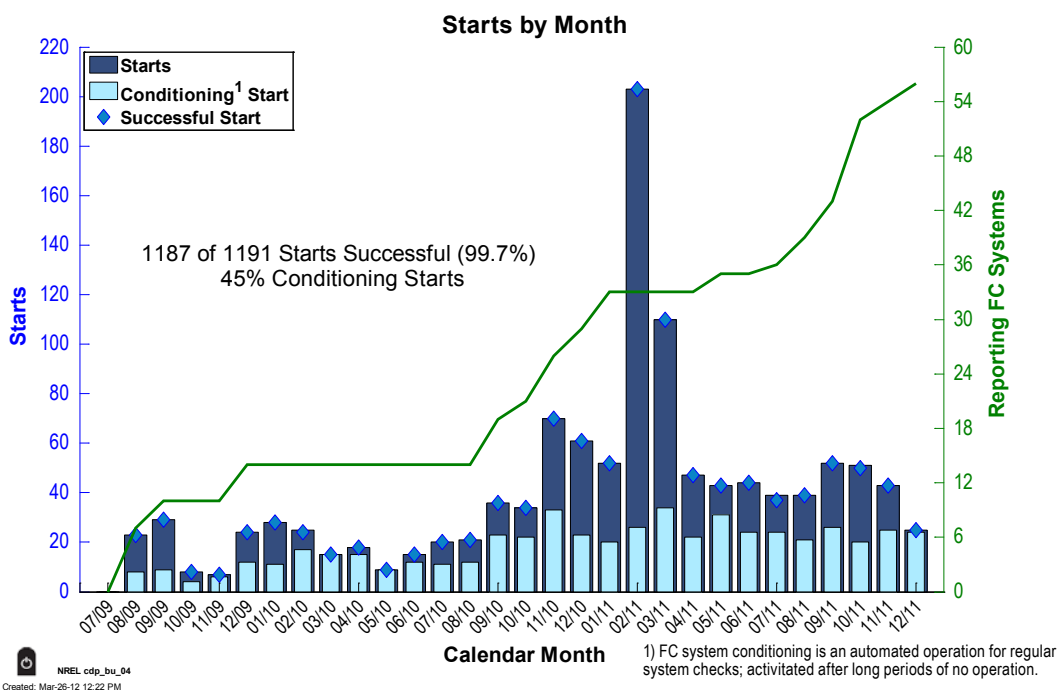
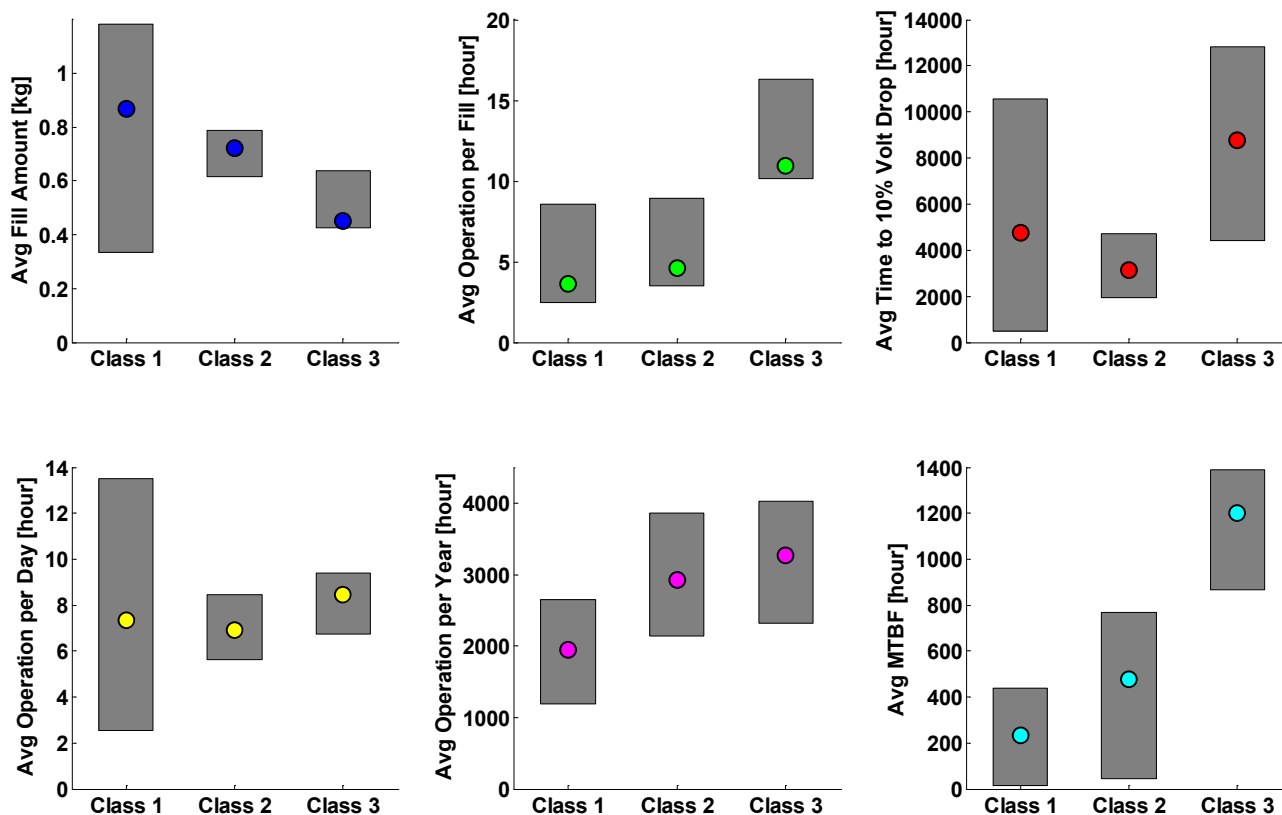


FIGURE 2. Backup power fuel cell system starts by month

Material Handling Equipment Performance By Class



 NREL cdp_mhe_63
Created: Mar-28-12 3:37 PM

FIGURE 3. Material handling equipment performance by class

infrastructure. Even though fuel cell MHEs have a lower annual operating cost than battery MHEs, there are still cost categories where the fuel cell MHEs are more expensive than battery MHEs. Advancements that lower infrastructure capital costs, fuel cell capital costs, and hydrogen fuel costs will open up the possibility for low-fleet-size facilities to see the cost benefits of fuel cell MHEs.

Conclusions and Future Directions

The deployment of 1,111 fuel cell units has established a significant data set of successful and safe operation in the hands of end users, has increased fuel cell manufacturing and support capabilities, and has translated lessons learned from the field into improved fuel cell systems for future operation. The aggregated data showcase the significant use and performance status at end user sites over the last two years in MHE and backup power applications. The CDPs address a need for published results on the technology status that can be utilized by industry, developers, and end users. The analyses have evolved as the accumulated time and hydrogen dispensed have increased, providing an insight into

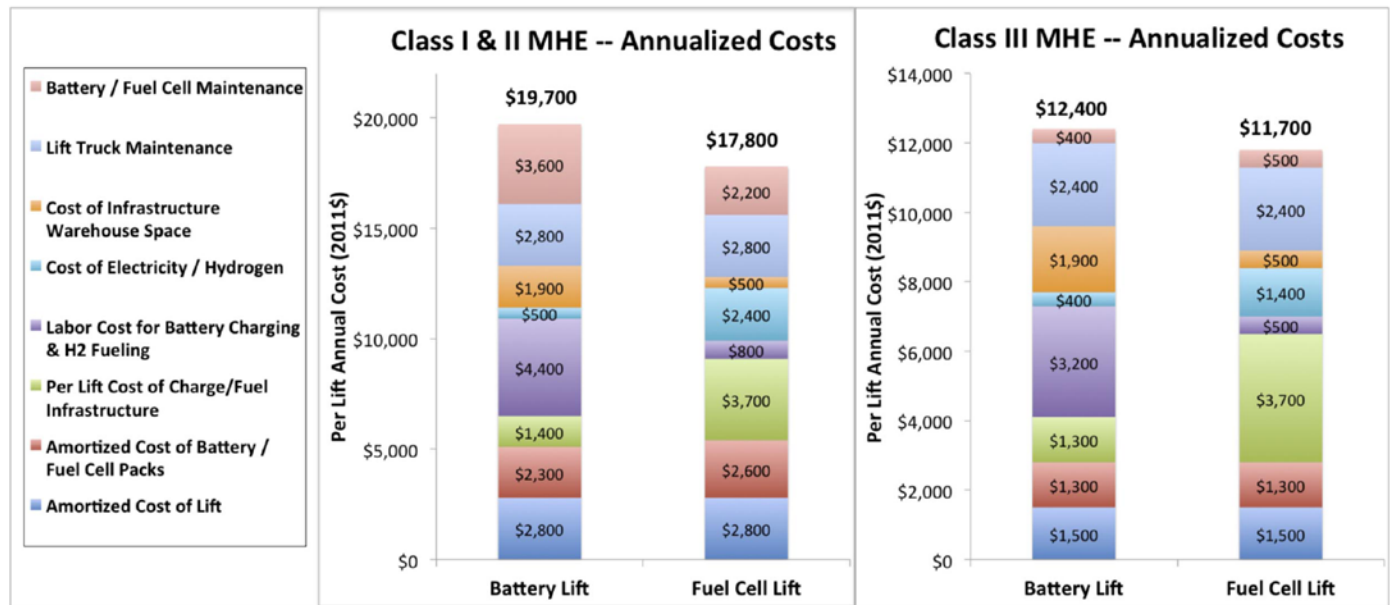
market behaviors and expectations. Continued analyses will be covered under the Technology Validation sub-program and include:

- Quarterly analysis of operation data for MHE and backup power systems
- Publication of bi-annual technical CDPs
- Demonstration of a 72-hour continuous run time for a backup power fuel cell system
- Analysis of backup power value proposition.

FY 2012 Publications/Presentations

1. Kurtz, J., Wipke, K., Sprik, S., Ramsden, T., Ainscough, C., Saur, G., “Analysis Results for ARRA Projects: Enabling Fuel Cell Market Transformation” NREL Presentation 2011 DOE Hydrogen and Fuel Cells Program, and Vehicle Technologies Program Annual Merit Review and Peer Evaluation. 5/12/2011
2. Kurtz, J., Wipke, K., Sprik, S., Ramsden, T., Ainscough, C., Saur, G., “ARRA Fuel Cell Deployments: Operation Data Overview” presented at the Hydrogen Safety Panel Meeting in Washington, D.C. 4/7/2011

Total Cost of Ownership for Class I, II & III Forklifts¹



(1) Total cost represents the annualized cost of ownership of Class I, II, and III forklifts on a net present value basis, accounting for capital, operating, and maintenance costs of forklifts, power packs, and infrastructure (labor costs for maintenance and for charging or fueling are included, but labor costs of forklift material handling operations are excluded). Costs are calculated assuming that the material handling operations are ongoing, with equipment replacements made as necessary. Capital, operating, and maintenance costs are assumed to remain constant in real-dollar terms, and capital purchases are discounted using a discount rate representing the time value of money. Fuel cell system costs reflect the current fuel cell tax credit of \$3,000/kW or 30% of purchase price. Analysis does not consider the potential productivity increases resulting from the constant power output of fuel cell systems, which may be significant. Costs of ownership of Class II forklifts are expected to be similar for Class I forklifts, though the cost of the lift itself is expected to be higher.



Costs are based on information provided by deployment host partners (end-users) based on a questionnaire developed by NREL, supplemented with data provided by project partners, and are reflective of the material handling operations of these deployments. Where appropriate, fuel cell deployment data were used in place of end-user questionnaire data; in particular, data from CDPs 1, 6, 8, 14, and 22 were used. Cost assessment will be further refined as additional data are available.

FIGURE 4. Total cost of ownership for Class 1, 2, and 3 forklifts

3. Kurtz, J., Wipke, K., Sprik, S., Ramsden, T., Ainscough, C., Saur, G., “ARRA MHE Composite Data Products for Data Through 2011 Q4” Composite data products produced by the NREL Hydrogen & Fuel Cells Research early fuel cell market demonstrations team. 4/4/2012

4. Kurtz, J., Wipke, K., Sprik, S., Ramsden, T., Ainscough, C., Saur, G., “Spring 2012 Composite Data Products - Backup Power” Composite data products produced by the NREL Hydrogen & Fuel Cells Research early fuel cell market demonstrations team. 4/3/2012

4. Kurtz, J., Wipke, K., Sprik, S., Ramsden, T., Ainscough, C., Saur, G., “Early Fuel Cell Market Deployments: ARRA and Combined (IAA, DLA, ARRA), Quarter 1 2012, Composite Data Products – Deployment” Composite data products produced by the NREL Hydrogen & Fuel Cells Research early fuel cell market demonstrations team. 3/8/2012

6. Kurtz, J., Wipke, K., Sprik, S., Ramsden, T., Ainscough, C., Saur, G., “Early Fuel Cell Market Deployments: ARRA and Combined (IAA, DLA, ARRA), November 2011, Composite Data Products – Deployment” Composite data products produced by the NREL Hydrogen & Fuel Cells Research early fuel cell market demonstrations team. 11/30/2011

7. Kurtz, J., Wipke, K., Sprik, S., Ramsden, T., Ainscough, C., Saur, G., “Fall 2011 Composite Data Products: ARRA Material Handling Equipment” Composite data products produced by the NREL Hydrogen & Fuel Cells Research early fuel cell market demonstrations team. 9/30/2011

8. Kurtz, J., Wipke, K., Sprik, S., Ramsden, T., Ainscough, C., Saur, G., “Fall 2011 Composite Data Products: Backup Power” Composite data products produced by the NREL Hydrogen & Fuel Cells Research early fuel cell market demonstrations team. 9/30/2011

9. Kurtz, J., Wipke, K., Sprik, S., Ramsden, T., Ainscough, C., Saur, G., “2011 Early Fuel Cell Market Deployments: ARRA and Combined (IAA, DLA, ARRA)” Composite data products produced by the NREL Hydrogen & Fuel Cells Research early fuel cell market demonstrations team. 9/30/2011

XII.4 Fuel Cell-Powered Lift Truck FedEx Freight Fleet Deployment

Jonathan King

FedEx Freight
2200 Forward Drive
Harrison, AR 72601
Phone: (870) 704-5358
Email: jonathan.king@fedex.com

DOE Managers

HQ: Dimitrios Papageorgopoulos
Phone: (202) 586-5463
Email: Dimitrios.Papageorgopoulos@ee.doe.gov

GO: David Peterson
Phone: (720) 356-1747
Email: David.Peterson@go.doe.gov

Contract Number: DE-EE0000482

Suppliers:

- Plug Power Inc., Latham, NY
- Air Products, Allentown, PA

Project Start Date: October 1, 2009
Project End Date: September 30, 2013

Objectives

The objectives of this project are to:

- Convert an entire fleet of 35 class-1 electric lift trucks to hydrogen fuel cells at the FedEx Freight facility in Springfield, MO.
- Demonstrate the safe and reliable operation of hydrogen-fueled material handling equipment (MHE).
- Demonstrate the economic benefits of conversion to hydrogen fuel cell-powered MHE.
- Demonstrate operator acceptance of hydrogen fuel cell-powered MHE.
- Provide a cost-effective and reliable hydrogen fuel supply.
- Spur further lift truck fleet conversions to hydrogen fuel cells.
- Establish a proving ground for hydrogen fuel cell-powered MHE.

Relevance to the American Recovery and Reinvestment Act (ARRA) of 2009 Goals

This project advances the goals of the American Recovery and Reinvestment Act (ARRA) of 2009 to create

new jobs, save existing jobs, and spur economic activity and investment in long-term economic growth by:

- Creating jobs at Plug Power to design, build and commission the fuel cell power units.
- Creating jobs at Air Products to design, install and commission hydrogen storage and fueling equipment.
- Creating jobs at Air Products to deliver hydrogen to the FedEx Freight Springfield, MO facility.
- Training FedEx Freight lift truck operators in hydrogen safety, fueling procedures, and fuel cell operation.
- Training FedEx Freight lift truck maintenance personnel to service fuel cells.
- Improving the overall economic efficiency of material handling operations.

This project advances the DOE Fuel Cell Technologies' ARRA project goals of accelerating the commercialization and deployment of fuel cells and fuel cell manufacturing, installation, maintenance, and support services by demonstrating:

- Safe and reliable operation of hydrogen storage and fueling equipment and fuel delivery.
- Reliable and efficient operation of hydrogen fuel cells.
- Economic and environmental advantages of fuel cells over batteries.
- Practical operation and maintenance of fuel cells.

Technical Barriers

This project addresses the following technical barriers to the use of fuel cell-powered lift trucks:

- Repair frequency of hydrogen fuel cells
- Cold weather operation of hydrogen fuel cells.
- Cold weather operation of hydrogen storage and fueling equipment.

Technical Targets and Milestones

The technical targets and milestones of this project include:

- Installing hydrogen storage and fueling equipment by May 2010.
- Developing a hydrogen safety plan by May 2010.
- Commissioning 35 class-1 power units by December 2009.
- Completing startup and training by June 2010.
- Starting operation and evaluation by July 2010.

Accomplishments

The accomplishments of this project include:

- Commissioning 35 GenDrive class-1 power units by December 2009.
- Commissioning hydrogen storage and fueling equipment by June 2010.
- Completing all fueling, operation, and maintenance training by June 2010.
- Purchasing and commissioning an additional five GenDrive class-1 power units in December 2010 (without DOE funding).
- Determining that problems with air-actuated valves during cold-weather operation of the hydrogen storage and fueling system were caused by excessive moisture in the air supply and rectifying these problems.
- Modifying lift trucks to prevent drive-offs that damaged the hydrogen fueling hose.
- Logging over 90,000 hours of fuel cell operation by June 30, 2012.
- Purchasing 29,240 kilograms of hydrogen by June 30, 2012.
- Monitoring operating costs and reliability of 40 GenDrive power units (ongoing).
- Demonstrating 125% more operating hours per repair for fuel cells compared to propane lift trucks between July 2010 and February 2012.



Introduction

The purpose of this project is to demonstrate that hydrogen fuel cells are a safe and economical alternative to batteries for powering electric lift trucks. The primary barriers to widespread use of hydrogen fuel cells for material handling equipment are concerns about the safety of hydrogen storage and fueling equipment, operating costs for fuel and maintenance, and the long-term reliability of fuel cells.

Approach

This project is evaluating the safety and economics of using hydrogen fuel cells to power a fleet of 35 class-1 electric lift trucks at the FedEx Freight facility in Springfield, MO. FedEx Freight is supplying the lift trucks, Plug Power is supplying the GenDrive fuel cell power units and Air Products is supplying the hydrogen fuel and the hydrogen storage and fueling equipment. The fuel cell equipment is maintained by FedEx Freight personnel with assistance from Plug Power and Air Products personnel when necessary. Plug

Power and Air Products will also assist FedEx Freight in developing a comprehensive hydrogen safety plan.

Previous FedEx Freight field trials with a limited number of GenDrive power units demonstrated productivity gains and improved performance compared to battery-powered lift trucks. The lift truck fleet conversion in Springfield is expected to demonstrate improved operational efficiencies and help the environment by reducing greenhouse gas emissions and the use of toxic battery materials. A successful demonstration of these advantages at the Springfield facility could lead to additional fleet conversions at other FedEx Freight facilities.

Results

Based on the favorable operational results with the initial 35 power units, FedEx Freight purchased an additional five power units in December 2010 without DOE funding.

To date, this project has successfully demonstrated the safe and economical operation of 40 GenDrive class-1 power units and associated hydrogen storage and fueling equipment. The power units have accumulated over 90,000 hours of operation and consumed 29,240 kilograms of hydrogen.

Cold-weather operational problems experienced last year with air-operated fueling station valves were solved by reducing moisture in the air supply. Cold-weather operation of the power units was also improved by installing heaters and updating software in the units.

No damage to the fueling station hoses has occurred since the lift trucks were modified to prevent them being driven while the fueling hoses were attached.

Between July 2010 and February 2012, FedEx Freight found the fuel cell-powered lift trucks at the Springfield facility had 125% more hours of operation per repair (144 hours/repair) compared to similar propane-powered lift trucks at the Whittier California facility (64 hours/repair).

Figure 1 shows that the average mean time between repairs (MTBR) during cold-weather operation from December 2010 to March 2011 was only 90 hours compared to 310 hours before and 245 hours after that period, including cold-weather operation during the first quarter of 2012. Between February and June 2012 the average MTBR improved significantly to 590 hours. Figure 2 and Figure 3 show the MTBR distribution and repair time distribution for all power units since start-up.

Conclusions and Future Directions

Based on our operational experience to date, hydrogen fuel cells appear to be a safe alternative to batteries for electric lift trucks. We will continue to monitor the long term costs and reliability of hydrogen fuel cells by:

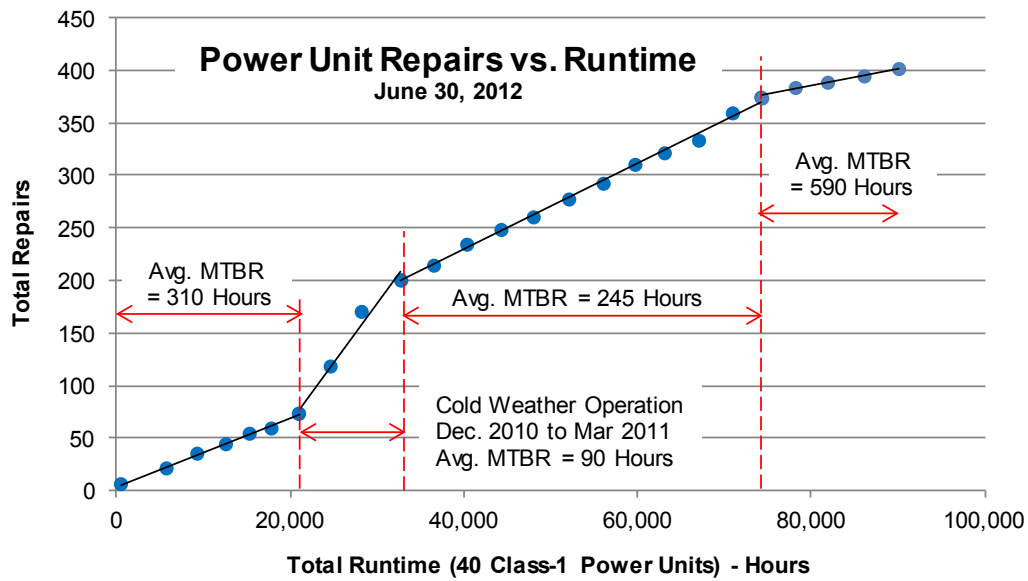


FIGURE 1. Power Unit Repairs vs. Runtime

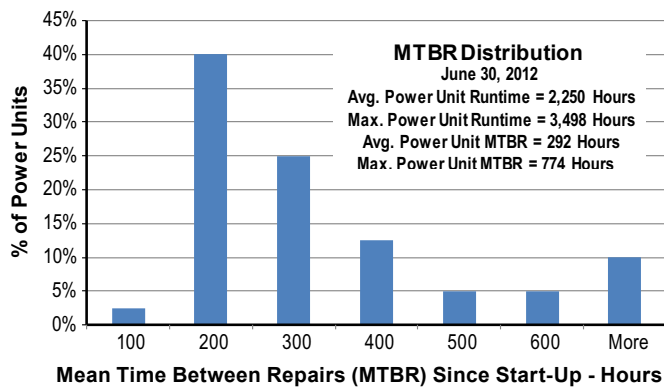


FIGURE 2. Mean Time between Repair (MTBR) Distribution

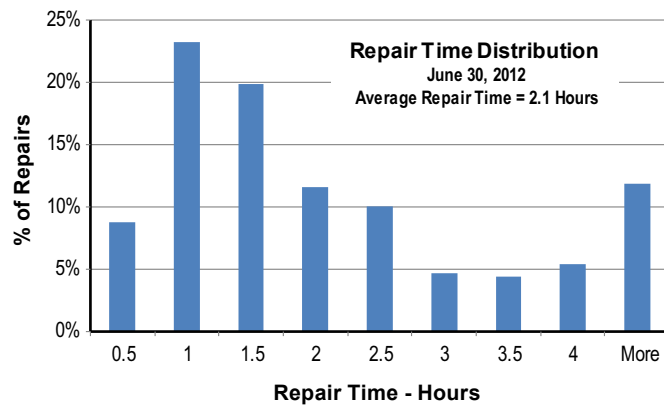


FIGURE 3. Repair Time Distribution

- Providing ongoing operational and maintenance support for the GenDrive power units and the hydrogen storage and fueling equipment.
- Collecting data from the power units to evaluate performance, operability and safety.
- Collecting data from the hydrogen storage and fueling equipment to evaluate performance, operability, and safety.

FY 2012 Publications/Presentations

1. Hosted a visit from Toyota to see the fuel cell-powered lift truck operation in December 2011.
2. Delivered an American Recovery and Reinvestment Act merit review presentation in Washington, D.C. in May 2012.

XII.5 Fuel Cell-Powered Lift Truck Sysco Houston Fleet Deployment

Scott Kliever
Sysco Houston
10710 Greens Crossing Boulevard
Houston, TX 77038
Phone: (713) 679-5574
Email: kliever.scott@hou.sysco.com

DOE Managers

HQ: Dimitrios Papageorgopoulos
Phone: (202) 586-5463;
Email: Dimitrios.Papageorgopoulos@ee.doe.gov
GO: David Peterson
Phone: (720) 356-1747
Email: David.Peterson@go.doe.gov

Contract Number: DE-EE0000485

Subcontractors:

- Plug Power Inc., Latham, NY
- Air Products, Allentown, PA
- Big-D Construction, Salt Lake City, UT

Project Start Date: October 1, 2009
Project End Date: September 30, 2013

Relevance to the American Recovery and Reinvestment Act (ARRA) of 2009 Goals

This project advances the goals of the American Recovery and Reinvestment Act (ARRA) of 2009 to create new jobs, save existing jobs, and spur economic activity and investment in long-term economic growth by:

- Creating jobs at Plug Power to design, build and commission the fuel cell power units.
- Creating jobs at Air Products and Big-D Construction to design, install and commission hydrogen storage and fueling equipment.
- Creating jobs at Air Products to deliver hydrogen to the Sysco Houston facility.
- Training Sysco Houston lift truck operators in hydrogen safety, fueling procedures and fuel cell operation.
- Training Sysco Houston lift truck maintenance personnel to service fuel cells.
- Improving the overall economic efficiency of material handling operations.

This project advances the DOE Fuel Cell Technologies' ARRA project goals of accelerating the commercialization and deployment of fuel cells and fuel cell manufacturing, installation, maintenance, and support services by demonstrating:

- Safe and reliable operation of hydrogen storage and fueling equipment and fuel delivery.
- Reliable and efficient operation of hydrogen fuel cells.
- Economic and environmental advantages of fuel cells over batteries.
- Practical operation and maintenance of fuel cells.

Technical Barriers

This project addresses the following technical barriers to the use of fuel cell powered lift trucks:

- Safe and reliable hydrogen use in a high-throughput distribution center.
- Fuel cell use in sub-zero temperatures.
- Fuel cell lifetime and reliability.

Technical Targets and Milestones

The technical targets and milestones of this project include:

- Installing hydrogen storage and fueling equipment by December 2009.
- Developing a hydrogen safety plan by May 2010.

Objectives

The objectives of this project are to:

- Convert a fleet of 79 class-3 electric lift trucks to hydrogen fuel cells at the Sysco Houston facility (including seven temporary rental units and 25 sub-zero temperature units).
- Demonstrate the safe and reliable operation of hydrogen-fueled material handling equipment (MHE).
- Demonstrate the economic benefits of conversion to hydrogen fuel cell-powered MHE.
- Demonstrate operator acceptance of hydrogen fuel cell-powered MHE.
- Demonstrate the operation of hydrogen fuel cells in sub-zero temperatures.
- Provide a cost effective and reliable hydrogen fuel supply.
- Spur further lift truck fleet conversions to hydrogen fuel cells.
- Establish a proving ground for hydrogen fuel cell-powered MHE.

- Commissioning 79 class-3 power units by February 2010.
- Completing startup and training by February 2010.
- Starting operation and evaluation by March 2010.

Accomplishments

The accomplishments of this project include:

- Commissioning hydrogen storage and fueling equipment by December 2009.
- Commissioning 79 GenDrive class-3 power units by February 2010.
- Completing all fueling, operation and maintenance training by February 2010.
- Training over 100 Sysco personnel in the safe use and fueling of hydrogen fuel cells.
- Commissioning 26 GenDrive class-2 power units by April 2010 (these power units are not included in the scope of this project).
- Demonstrating the successful operation of 25 class-3 power units in sub-zero temperatures.
- Logging 25 months and over 647,000 hours of fuel cell operation by March 2012.
- Consuming 60,350 kilograms of hydrogen by June 2012.
- Monitoring operating costs and reliability of all GenDrive power units (ongoing).



Introduction

The purpose of this project is to demonstrate that hydrogen fuel cells are a safe and economical alternative to batteries for powering electric pallet jacks and lift trucks. The primary barriers to widespread use of hydrogen fuel cells for material handling equipment are concerns about the safety of hydrogen storage and fueling equipment, operating costs for fuel and maintenance, and the long-term reliability of fuel cells.

Approach

This project is evaluating the safety and economics of using hydrogen fuel cells to power a fleet of 26 class-2 and 79 class-3 electric lift trucks at the Sysco Houston facility. Sysco Houston will supply the lift trucks, Plug Power is supplying the GenDrive fuel cell power units, Air Products and Big-D Construction are supplying the hydrogen storage and fueling equipment, and Air Products is supplying the hydrogen fuel. The equipment will be maintained by Sysco Houston personnel with assistance from Plug Power and Air Products personnel when necessary. Plug Power and

Air Products also assist Sysco Houston in developing a comprehensive hydrogen safety plan.

Sysco Houston and Plug Power monitor the operation and maintenance of the power units and the hydrogen storage and fueling equipment over the duration of the project. This information is reported to the DOE and the National Renewable Energy Laboratory quarterly and summarized annually.

Results

This project has successfully demonstrated the safe and economical operation of 26 class-2 and 72 class-3 power units and associated hydrogen storage and fueling equipment. The class-2 power units were not included in the funding for this project. Seven of the original 79 power units were rentals and have been returned to Plug Power. Twenty-five of the class-3 power units were modified to operate in sub-zero temperatures.

The current cost of hydrogen fuel is approximately the same as the cost of electricity to charge lead-acid batteries but Sysco is saving nearly \$100,000 per year in fewer man-hours spent refueling fuel cells compared to swapping batteries. The lift truck operators also appreciate the improved performance of fuel cells compared to lead-acid batteries.

Sysco and Plug Power have been monitoring the type and frequency of fuel cell repairs. Figure 1 shows the mean time between repairs (MTBR) vs. run-time for each class of power unit. Figure 2 shows the MTBR distribution by class and Figure 3 show the repair time distribution by class. To date, no conclusions have been drawn to explain the differences in repair statistics between the class-2 and class-3 power units. However, Sysco has changed the way they maintain pallet jack and lift truck power sources from reactive maintenance

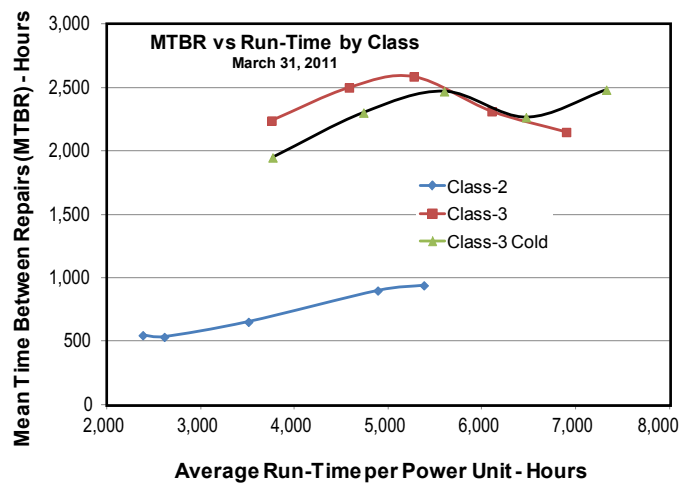


FIGURE 1. MTBR vs Run-Time by Class

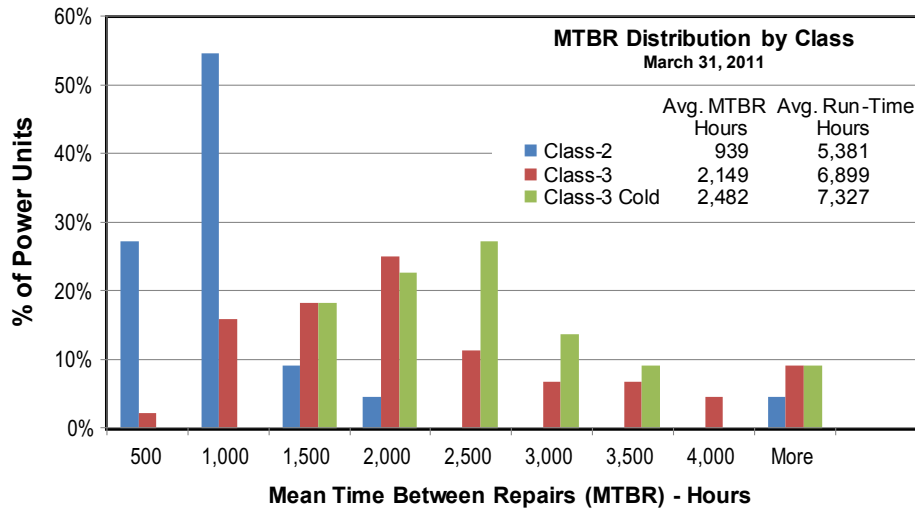


FIGURE 2. MTBR Distribution by Class

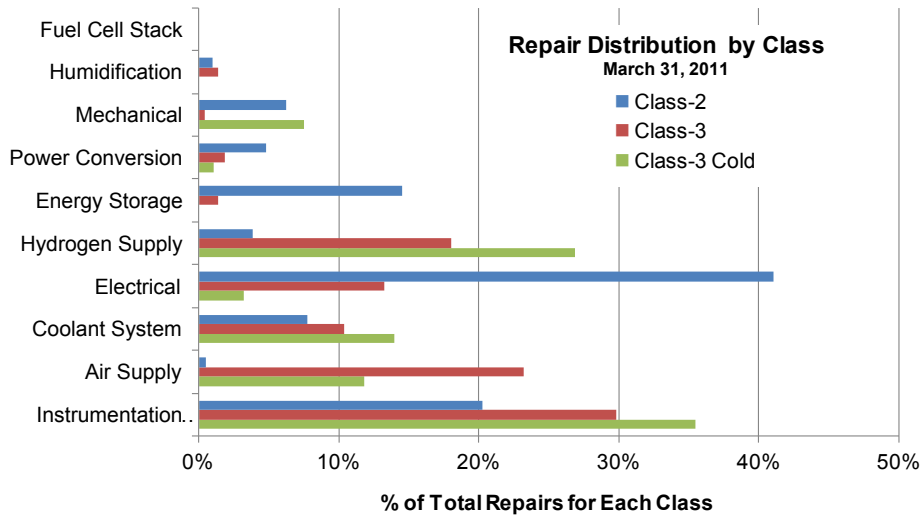


FIGURE 3. Repair Distribution by Class

with lead-acid batteries to preventative maintenance with the hydrogen fuel cells.

Since we have seen less unplanned disruptions in our operations of hydrogen fuel cells and with the ease that Sysco Houston was able to introduce them into our fleet of pallet jacks and forklifts, this helped Sysco to expand the use of hydrogen fuel cells at more of our 70+ operating companies across North America.

Conclusions and Future Directions

Based on the proven reliability and safety of current hydrogen fuel cell operations at Sysco Houston, Sysco’s future directions include:

- Ongoing operational and maintenance support for power units and hydrogen storage and fueling equipment.
- Ongoing data collection from power units and hydrogen storage and fueling equipment.
- Finish implementing fuel cell fleet conversions at Philadelphia, San Antonio, Long Island and Northeast regional distribution center facilities by mid-2012; this is part of Sysco’s overall capital investment project of replacing approximately 1,000 lead-acid batteries with 500+ fuel cells at seven additional sites over the next 24 months.
- Planning to add five new class-3 power units to the Houston lift truck fleet at a cost of approximately \$65,000 over the next year.

- Committed to additional fuel cell fleet conversions at Boston, Riverside and Los Angeles facilities.
- Supporting the conversion to fuel cells to help reduce the overall costs of fuel cell power units and hydrogen fuel.
- Helping other Sysco facilities develop hydrogen safety plans.

FY 2012 Publications/Presentations

1. Scott Kliever participated in the Update on Fuel Cell Technologies workshop session at the IFDA 2011 Distribution Solutions Conference in Fort Worth, TX on October 24, 2011.
2. Scott Kliever delivered an American Recovery and Reinvestment Act merit review presentation in Washington, D.C. in May 2012.

XII.6 GENCO Fuel Cell-Powered Lift Truck Fleet Deployment

Jim Klingler

GENCO Infrastructure Solutions
100 Papercraft Park
Pittsburgh, PA 15238
Phone: (412) 820-3718
Email: klinge@genco.com

DOE Managers

HQ: Sara Dillich
Phone: (202) 586-7925
Email: Sara.Dillich@ee.doe.gov

GO: James Alkire
Phone: (720) 356-1426
Email: James.Alkire@go.doe.gov

Contract Number: DE-EE0000483

Subcontractors:

- Plug Power Inc., Latham, NY
- Air Products, Allentown, PA
- Linde North America, Murray Hill, NJ

Project Start Date: October 1, 2009
Project End Date: September 30, 2013

Objectives

The objectives of this project are to:

- Convert 357 electric-drive fork lift trucks from batteries to fuel cell power units in five large distribution centers and manufacturing facilities.
- Demonstrate the safe and reliable operation of hydrogen-fueled material handling equipment (MHE).
- Demonstrate the economic benefits of conversion to hydrogen fuel cell-powered MHE.
- Demonstrate operator acceptance of hydrogen fuel cell-powered MHE.
- Provide a cost effective and reliable hydrogen fuel supply.
- Spur further lift truck fleet conversions to hydrogen fuel cells.
- Establish a proving ground for hydrogen fuel cell-powered MHE.

Relevance to the American Recovery and Reinvestment Act (ARRA) of 2009 Goals

This project advances the goals of the American Recovery and Reinvestment Act (ARRA) of 2009 to create

new jobs, save existing jobs, and spur economic activity and investment in long-term economic growth by:

- Creating jobs at Plug Power to design, build and commission the fuel cell power units.
- Creating jobs at Air Products and Linde to design, install and commission hydrogen storage and fueling equipment.
- Creating jobs at Air Products and Linde to deliver hydrogen to GENCO facilities.
- Training lift truck operators in hydrogen safety, fueling procedures and fuel cell operation.
- Training lift truck maintenance personnel to service fuel cells.
- Improving the overall economic efficiency of material handling operations.

This project advances the DOE Fuel Cell Technologies' ARRA project goals of accelerating the commercialization and deployment of fuel cells and fuel cell manufacturing, installation, maintenance, and support services by demonstrating:

- Safe and reliable operation of hydrogen storage and fueling equipment and fuel delivery.
- Reliable and efficient operation of hydrogen fuel cells.
- Economic and environmental advantages of fuel cells over batteries.
- Practical operation and maintenance of fuel cells.

Technical Barriers

This project addresses the following technical barriers to the use of fuel cell-powered lift trucks:

- Represents a change in technology, which is often met with reluctance.
- Uncertain power unit reliability due to lack of widespread performance data.
- Safety and expense of hydrogen and fueling equipment.
- Difficulty in obtaining permits and approvals for hydrogen fueling stations.

Technical Targets and Milestones

The class and number of power units and the hydrogen supplier for five GENCO locations are shown in Table 1. All power units were installed and operating by September 2011.

TABLE 1. Summary of Power Units at Five GENCO Locations

| | Wegmans | Whole Foods | Coca-Cola | Sysco Phil. | Kimberly-Clark | TOTAL |
|-------------------|--------------|-------------|-----------|--------------|----------------|------------|
| Class 1 GenDrive | 0 | 45 | 40 | 0 | 25 | 110 |
| Class 2 GenDrive | 36 | 14 | 0 | 25 | 0 | 75 |
| Class 3 GenDrive | 100 | 2 | 0 | 70 | 0 | 172 |
| TOTAL | 136 | 61 | 40 | 95 | 25 | 357 |
| Hydrogen Supplier | Air Products | Linde | Linde | Air Products | Air Products | |

Accomplishments

The accomplishments of this project include:

- Commissioning hydrogen storage and fueling equipment at all sites (see Table 2 for completion dates).
- Commissioning power units at all sites by September 2011.
- Completing fueling, operation and maintenance training at all sites.
- Operating power units at all sites (ongoing).
- Some power units at Wegmans have accumulated over 9,000 hours of operation.



Introduction

The purpose of this project is to demonstrate that hydrogen fuel cells are a safe and economical alternative to lead-acid batteries for powering electric-drive lift trucks. The primary barriers to widespread use of hydrogen fuel cells for material handling equipment are concerns about the safety of hydrogen storage and fueling equipment, operating costs for fuel and maintenance, and the long-term reliability of fuel cells.

Approach

This project will evaluate the safety and economics of using hydrogen fuel cells to power over 350 lift trucks at five GENCO facilities. GENCO will supply the lift trucks, Plug Power will supply the GenDrive fuel cell power units, Air Products and Linde will supply the hydrogen storage and fueling equipment and the hydrogen fuel. The equipment will be maintained by GENCO personnel with assistance from Plug Power, Air Products and Linde personnel when necessary.

TABLE 2. Summary of Power Unit Operating Data at Five GENCO Locations (to March 31, 2012)

| | Wegmans | Whole Foods | Coca-Cola | Sysco Phil. | Kimberly-Clark |
|--|---------|-------------|-----------|-------------|----------------|
| Average operating hours per unit | 5,300 | 3,800 | n/a | n/a | n/a |
| Total operating hours | 721,000 | 231,000 | n/a | n/a | n/a |
| Total hydrogen dispensed (kg) | 60,816 | 19,306 | 25,806 | 21,942 | 23,001 |
| Average hydrogen dispensed per fill (kg) | n/a | 0.89 | 1.28 | n/a | n/a |

Note: Some operating data not available at this time due to problems with data collection equipment

GENCO and the subcontractors will monitor the operation and maintenance of the power units and the hydrogen storage and fueling equipment over the duration of the project. This information will be reported to the DOE and NREL quarterly and summarized annually.

Results

This project has successfully demonstrated the safe and economical operation of 357 class-1, 2 and 3 fuel cell power units and associated hydrogen storage and fueling equipment at five GENCO facilities. Table 2 shows a summary of operating data collected for the power units and fueling equipment at these locations.

Conclusions and Future Directions

Based on the proven reliability and safety of current hydrogen fuel cell operations at GENCO facilities to date, future directions include:

- Ongoing operational and maintenance support for power units and hydrogen storage and fueling equipment.
- Ongoing data collection from power units and hydrogen storage and fueling equipment.
- Helping to reduce the overall costs of fuel cell power units and hydrogen fuel by supporting the conversion to fuel cells at other locations.

FY 2012 Publications/Presentations

1. GENCO delivered an American Recovery and Reinvestment Act merit review presentation in Washington, D.C. in May 2012.

XII.7 Highly Efficient, 5-kW CHP Fuel Cells Demonstrating Durability and Economic Value in Residential and Light Commercial Applications

James Petrecky
Plug Power
968 Albany Shaker Road
Latham, NY 12110
Phone: (518) 782-7700 ext: 1977
Email: james_petrecky@plugpower.com

DOE Managers
HQ: Jason Marcinkoski
Phone: (202) 586-7466
Email: Jason.Marcinkoski@ee.doe.gov
GO: Reg Tyler
Phone: (720) 356-1805
Email: Reginald.Tyler@go.doe.gov

Vendor:
ClearEdge Power, Hillsboro, OR

Project Start Date: October 1, 2009
Project End Date: September 15, 2013

- Long-term: Advances were made to prove the durability and efficiency of fuel cell technologies for CHP that will help power and fuel the long-term economic health of our nation.
- This project used six fuel cell-powered CHP systems that were built, installed and maintained by commercial entities. The fuel cell manufacturer gained valuable reliability data/experience that will advance their ability to meet customer expectations in order to be a viable competitor to traditional technologies.

Technical Barriers

- Ability to match the durability and reliability of traditional energy sources.
- Produce adequate heat to meet consumer comfort requirements.
- Prove supply vendors can deliver the quality and timely delivery of sub-components.

Technical Targets and Milestones

- Met heat availability target of >99%
- Met electricity efficiency target of >30%
- Did not meet the target of 8,760 hours per year. Performance was 3,000 hours.

Accomplishments

- Installation of six systems in Latham, NY and three systems and the University of California Irvine.
- Logged system performance for over two years resulting in over 34,000 run hours that produced:
 - 57,000 kWh of electricity and 780,000 kWh of thermal.
 - A startup reliability level of 56% and a thermal availability of 100%.
- Manufacturing build time reduced from >120 to <50 hr
- Direct material cost reduction: ~\$90k to \$53k in volumes <20



Introduction

The partners of this project operated or leased a total of 11 fuel cell-powered CHP systems in order to prove the

Objectives

- Quantify the durability of proton exchange membrane (PEM) fuel cell systems in residential and light commercial combined heat and power (CHP) applications in California.
- Optimize system performance through testing of multiple high-temperature units through collection of field data.
- Demonstrate that GenSys Blue product is a technology that is commercially ready for the marketplace.
- The goal of the project is to demonstrate in the real-world that high-temperature PEM technology can offer reliable heat without additional equipment and to refine the product design and subcomponent performance related to polybenzimidazole (PBI) technology, stacks, advanced controls and fuel reforming.

Relevance to the American Recovery and Reinvestment Act (ARRA) of 2009 Goals

- Near-term: The expenses of the project sustained jobs for the companies involved through work on the installation of the fuel cell-powered systems, the engineering work to sustain system performance, and all third parties involved in building sub-components, shipping parts to on-site locations and managing/coordinating the project.

durability and reliability of fuel cell-powered CHP systems. The CHP systems operated for over two years and were operational for over 34,000 hours, as shown in Table 1. Each system was installed, operated, repaired and analyzed by technical staff with the results reported to the DOE.

The fuel cell CHP systems were high-temperature and the project achieved 100% availability for heat production. This is a significant achievement for advancing fuel cells to become competitive or advantaged over traditional technologies. Through development of fuel cell products that run on hydrogen and can meet or exceed customer expectations, fuel cells will enable a hydrogen economy.

Approach

To collect the necessary data that would prove our goals around availability, reliability and durability, we needed to keep the systems running. We trained technical staff available to trouble-shoot and fix the system or sub-component issues. Several engineers, along with the trained technical staff, reviewed the system performance through site visits or through the transfer of data, to determine the corrective actions.

There was extensive documentation of failures and corrections that allowed us to replace the responsible failed components. All site preparation and grid interconnection was performed with a safety first attitude. During site visits and trouble-shooting/find and fix events, safety was a primary concern.

Results

The high-temperature systems that were in service met a major piece of our objectives but not all. Issues with our membrane electrode assembly (MEA) supply and quality

led the majority of systems to run in heat-only mode, significantly decreasing the availability performance metrics of the CHP system as a whole. A significant amount of time was spent diagnosing the CHP sub-component issues and communicating them with the supplier, to resolve the issue. See Table 1 for quantitative support.

In addition to the uneven performance of the power versus the heat, we have seen a decrease in reliability of the power output (Figure 1). The main cause of this decrease in reliability has been the MEA quality and performance. We experienced a significant degree of variation in beginning of life stacks and unfortunately, the decision to switch to a previous version of the MEA that has a thinner cross-section took much time. The deliberation and engineering review pushed us further back in our supplier’s production queue.

Our service calls were reduced by running in heat-only mode, which is prone to less failure and downtime. Recent calls relate to our combustion monitors, oil pump failures and control board diagnostics. See Figure 2 for a breakdown of our failures and service calls over the project.

See Figure 3 for a breakdown of our failure-modes as of June 1, 2012.

Conclusions and Future Directions

A contract with ClearEdge was executed on June 15, 2012. Two ClearEdge units that are being leased will run for one year as part of this demonstration. One unit will run in the laboratory at the University of California at Irvine. The second unit is part of a commercial demonstration and will run at a Taco Bell in San Juan Capistrano, California. The electricity will be used to power a portion of the power needs while the heat will be used for steam in food preparation and storage.

TABLE 1. Cumulative Run-Time by Operational Mode

| HT GenSys Reliability Fleet Stats Through | | | | | | | | | |
|---|-------------------|------------------------|-----------------------|----------------|----------------|-------------|---------------------|-----------------------|----------------------|
| 6/1/2012 0:00 | | | | | | | | | |
| System S/N | Commissioned Date | System Runtime (Hours) | Current Stack Runtime | Burner Runtime | Electrical kWh | Thermal kWh | Startup Reliability | Heat Operational A(t) | CHP Operational A(t) |
| EpsilonPlus8 | 1/8/2010 14:50 | 7823 | 6058 | 14401 | 15247 | 141427 | 0.56 | 1.00 | 0.60 |
| EpsilonPlus9 | 1/11/2010 15:14 | 4381 | 3802 | 12400 | 7349 | 123059 | 0.68 | 1.00 | 0.34 |
| EpsilonPlus10 | 4/9/2010 8:55 | 1777 | 1777 | 11695 | 2520 | 124008 | 0.56 | 0.99 | 0.44 |
| Foxtrot2 | 1/8/2010 14:59 | 11884 | 4558 | 10883 | 19072 | 151272 | 0.59 | 1.00 | 0.73 |
| Foxtrot3 | 3/2/2010 10:47 | 5011 | 3098 | 13549 | 6679 | 140065 | 0.53 | 1.00 | 0.45 |
| Foxtrot4 | 6/11/2010 14:45 | 3249 | 3249 | 10368 | 6002 | 98676 | 0.47 | 0.99 | 0.40 |
| Totals | - | 34126 | 22542 | 73295 | 56868 | 778506 | - | - | - |
| Average | - | 5688 | 3757 | 12216 | 9478 | 129751 | 0.56 | 1.00 | 0.49 |

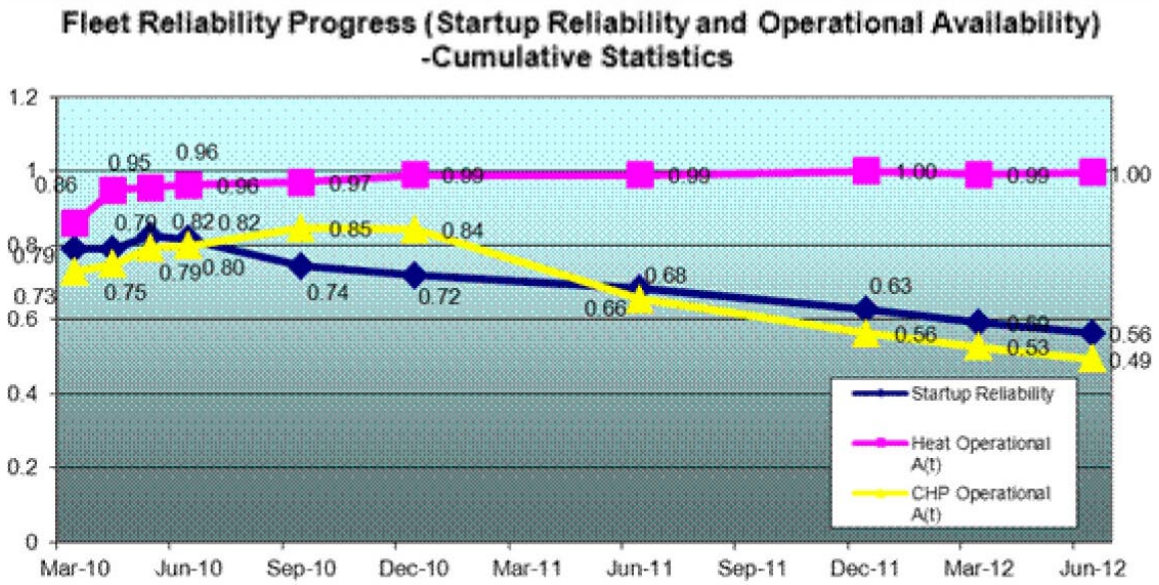
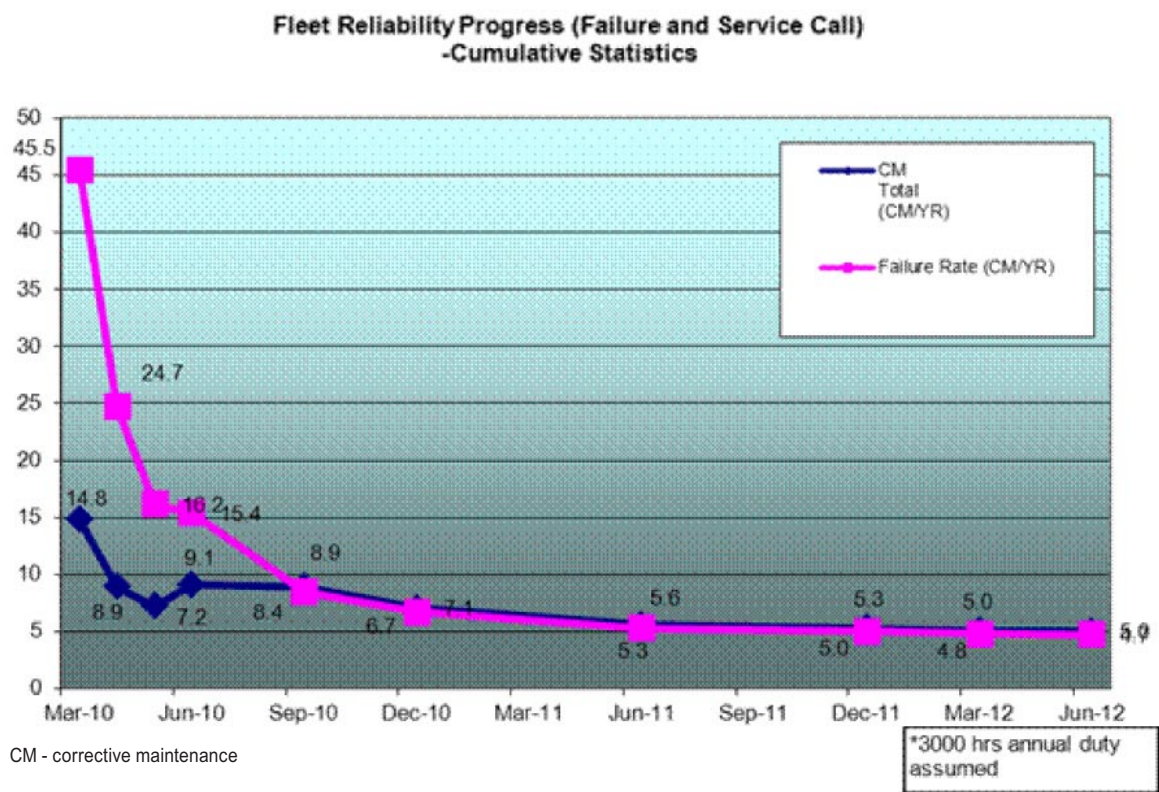


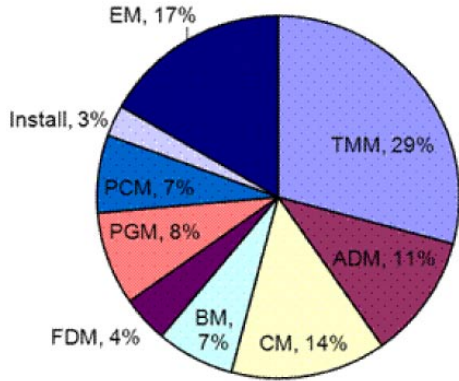
FIGURE 1. CHP Reliability by Mode



CM - corrective maintenance

FIGURE 2. Service Calls and Failures

Reliability Fleet Failure-Module Allocation (34125 cumulative system hours & 73294 burner hours) as of 06/01/12



TMM - Thermal Management Module; ADM - Air Delivery Module;
 CM - Control Module; BM - Burner Module; FDM - Fuel Delivery Module;
 PGM - Power Generation Module; PCM - Power Control Module;
 Install - Installation; EM - Electronics Module

FIGURE 3. Failure Mode Breakdown

XII.8 Accelerating Acceptance of Fuel Cell Backup Power Systems

James Petrecky
Plug Power
968 Albany Shaker Road
Latham, NY 12110
Phone: (518) 782-7700 ext: 1799
Email: james_petrecky@plugpower.com

DOE Managers
HQ: Jason Marcinkoski
Phone: (202) 586-7466
Email: Jason.Marcinkoski@ee.doe.gov
GO: Reg Tyler
Phone: (720) 356-1805
Email: Reginald.Tyler@go.doe.gov

Subcontractor:
IdaTech LLC, Bend, OR

Project Start Date: October 1, 2009
Project End Date: September 15, 2013

Objectives

- Quantify the performance of 20 low-temperature fuel cell systems at two locations
- Optimize the maintenance of the systems and data collection practices
- The project is intended to increase distributed power generation, improve reliability and efficiency of mission critical backup power and decrease fossil fuel dependencies for power generation

Relevance to the American Recovery and Reinvestment Act (ARRA) of 2009 Goals

- This project sustained jobs for the companies involved through the work required during the installation of the fuel cell-powered systems, the engineering work to sustain system performance, and all third parties involved in building sub-components, shipping parts to on-site locations and managing/coordinating the project.
- Long-term: Advances were made to prove the durability and efficiency of fuel cell technologies for critical backup applications that will help power and fuel the long-term economic health of our nation.
- This project used 20 fuel cell-powered low-temperature systems that were built, installed, maintained and analyzed. The fuel cell manufacturer gained valuable reliability data/experience that will advance their ability

to meet customer expectations in order to be a viable competitor to traditional technologies.

Technical Barriers

- The siting, installation and operation of 20 low-temperature fuel cell systems
- Eliminate the hydrogen start requirement

Technical Targets and Milestones

- Build 20 low-temperature fuel cell systems
- Operate the fuel cell systems for one year at two locations

Accomplishments

- Built 20 low-temperature fuel cell systems
- Sited and installed of 10 low-temperature fuel cell systems at Robins Air Force Base Georgia
- Sited and installed 10 low-temperature fuel cell systems at Ft. Irwin in California
- Implemented eight safety-related improvement recommended by the Hydrogen Safety Panel at Robins Air Force Base



Introduction

The project uses low-temperature GenSys fuel cell systems to provide power in remote, off-grid systems or primary power where grid power is unreliable or nonexistent. Coupled with high-efficiency performance, low-temperature GenSys reduces operating costs making it an economical solution for prime power requirements.

Currently, field trials at telecommunication and industrial sites across the globe are proving the advantages of fuel cells—lower maintenance, fuel costs and emissions, as well as longer life—compared with traditional solutions. This project will enhance the experience and knowledge of all partners involved bringing another hydrogen-powered fuel cell product into commercialization.

Approach

The 20 low-temperature systems were built for use at two distinct locations with each location having an installation plan. The siting of the fuel cells at Robins Air

Force Base had to be undertaken while keeping disruption to compound operations and future fuel cell maintenance to a minimum.

In the process of gaining sign-off of the National Environmental Policy Act form, we experienced some minor site engineering changes. Ultimately, the National Environmental Policy Act forms were approved and submitted to the DOE.

Results

Tables 1-3 summarize the unit performance at Robins Air Force Base. Table 1 contains 2012 statistics, Table 2 summarizes the totalized statistics, and Table 3 illustrates the total MW-hrs of power generated by each system. As can be seen in each table, units 7, 8 and 9 are the poorest performers while units 2, 3, 4, 6, and 10 are collecting more operational hours.

For these systems, we have a total of 13,500 cumulative operating hours, 13,370 cumulative hours of stack operation and have generated about 39 MW-hrs of power. The average efficiency is ~23.7%.

Table 3 summarizes our top problem list for the Robins Air Force Base systems. The top three problems based on occurrence are anode tailgas oxidizer (ATO) ignition timeout, scanner communication loss, and loss of fuel flow. The ATO timeout problem occurs when the ATO does not light off fast enough. Scanner communication loss happens either in the disruption of the signal through the cable or through a

scanner board issue. Loss of fuel flow seems to be caused by a software bug where the fuel control valve momentarily closes.

The amount of operating hours we have on our systems demonstrates our ability to increase distributed power generation, improve reliability and efficiency of mission critical backup power and decrease fossil fuel dependencies for power generation through the use of low-temperature fuel cell systems.

Plug Power continues advance the deployment of fuel cells in their material handling “GenDrive” product line. We have sold over, and installed close to, 3,000 fuel cells across the United States that continues to advance the commercialization of fuel cells.

Conclusions and Future Directions

- Continue to monitor, maintain and repair systems.
- Prepare and log service and maintenance records for the low temperature fuel cell systems.
- Continue open communication with all partners on the performance of the systems and continue analyzing the field data.
- The fleet at Robins Air Force Base will continue to run and collect data until the end of October 2012. Fort Irwin will continue to run and collect data until mid-September 2013. A final report will coincide with the decommissioning of the Ft. Irwin site.

TABLE 1. 2012 Unit Statistics at Robins Air Force Base

| | WRAFB #1 | WRAFB #2 | WRAFB #3 | WRAFB #4 | WRAFB #5 | WRAFB #6 | WRAFB #7 | WRAFB #8 | WRAFB #9 | WRAFB #10 |
|----------------------------------|----------|----------|----------|----------|----------|----------|----------|----------|----------|-----------|
| Serial Number>> | 1028 | 1022 | 1033 | 1009 | 0005 | 1001 | 1019 | 1016 | 1002 | 1006 |
| Cumulative System Hours | 275 | 659 | 474 | 743 | 624 | 626 | 58 | 427 | 45 | 969 |
| System Uptime | 25.2% | 30.2% | 21.7% | 34.0% | 28.6% | 28.6% | 2.6% | 19.6% | 4.3% | 44.4% |
| System kW-hrs produced | 840 | 1770 | 1467 | 2298 | 1931 | 1931 | 141 | 929 | 131 | 2865 |
| System Electrical Efficiency@3kW | 23.3% | 23.2% | 24.0% | 23.6% | 22.4% | 21.7% | 26.2% | 22.2% | 20.9% | 23.7% |
| Cum Stack Hours | 275 | 659 | 474 | 743 | 624 | 626 | 58 | 427 | 45 | 969 |
| Degradation Rate(μV/hr) @3kW | 47.81 | -38.88 | 23.17 | 24.22 | 2.61 | -3.89 | N/A | N/A | -29.26 | 22.22 |
| Estimated Hrs to 48v | N/A | 2578 | N/A | N/A | N/A | 31626 | N/A | N/A | 4583 | N/A |

TABLE 2. Exported Power Performance

| | WRAFB #1 | WRAFB #2 | WRAFB #3 | WRAFB #4 | WRAFB #5 | WRAFB #6 | WRAFB #7 | WRAFB #8 | WRAFB #9 | WRAFB #10 | Totals |
|-----------------------------------|----------|----------|----------|----------|----------|----------|----------|----------|----------|-----------|--------|
| Serial Number>> | 1028 | 1022 | 1033 | 1009 | 0005 | 1001 | 1019 | 1016 | 1002 | 1006 | |
| Cumulative System Hours | 934 | 1573 | 1754 | 1665 | 875 | 2136 | 555 | 920 | 520 | 2576 | 13506 |
| System Uptime | 33.8% | 42.0% | 45.4% | 43.4% | 19.9% | 55.6% | 14.6% | 28.2% | 19.5% | 66.7% | 36.9% |
| System MW-hrs produced | 2.86 | 4.40 | 5.41 | 5.12 | 2.26 | 6.56 | 1.07 | 2.00 | 1.57 | 7.81 | 39.07 |
| System Electrical Efficiency@3kW* | 24.4% | 24.4% | 24.6% | 23.9% | 22.9% | 22.9% | 24.6% | 21.9% | 24.2% | 24.8% | 23.9% |
| Cum Stack Hours | 936 | 1571 | 1750 | 1661 | 752 | 2131 | 554 | 919 | 519 | 2577 | 13369 |
| * Hourly Weighted Average | | | | | | | | | | | |

TABLE 3. Failure Modes

| Summary of Top Failures | | |
|--------------------------------|------------------|--|
| Failure | # of occurrences | Description |
| ATO Preheat Timeout | 15 | ATO did not reach ignition temperature before a hard coded timer expired. |
| Scanner Comm Loss | 26 | Communication link between cell scanner and controller is lost |
| Loss of Fuel Flow | 22 | A bug in the control system causes a momentary cycling of the fuel inlet solenoid valve, fuel flow decreases to 0 and the system shuts down |
| Coolant Leak | 4 | Coolant level decreasing over time |
| Anode Air Pump failed to start | 13 | The anode air pump fails to start during system startup - the electrical connection to the pump needs to be physically disconnected and reconnected; or the system needs to be manually shut down and the controller rebooted. |
| Gas Leak | 13 | All leaks were detected during system startups and corrected prior to commissioning. No leaks were detected during normal operation |
| Unknown | 7 | |
| Fuel Flow Too High | 5 | Fuel flow meter failures or fuel proportional valve failures cause increased fuel flow readings inducing a system shutdown |
| Max Low Cell Trips | 5 | Usually a result of high CO levels in the reformat stream |
| FAD desulf cond timeout | 4 | During system startup, a hard coded timer expires when fuel flow is not detected |
| Firmware Update, Boot failure | 4 | |
| Anode Air Pump | 2 | Anode Air Pump failed and was replaced |
| ATO Can | 2 | ATO Can failed and was replaced |
| ATO MCB | 2 | ATO Blower Motor Control Board failed and was replaced |
| ATR In Temp High | 1 | Steam Temp did not rise during system startup causing a system shut down; caused by ATO Preheat timeout |
| Cathode Blower | 2 | Cathode Blower failed and was replaced |
| EIB Reset | 3 | |
| EIB/Sphere | 3 | EIB and/or Sphere Controller failed and was replaced |
| Exhaust Rad Fan | 2 | Exhaust Radiator Fan failed and was replaced |
| Float Cup | 3 | Float Cup failed and was repaired |
| Fuel Prop Valve | 3 | Fuel Proportional Valve failed and was replaced |

ATO – anode tailgas oxidizer; FAD – fuel/air delivery; MCB – motor control board; EIB – electronic interface board

**XIII. SMALL BUSINESS INNOVATION
RESEARCH (SBIR) HYDROGEN PROGRAM
NEW PROJECTS AWARDED IN FY 2012**

XIII.0 Small Business Innovation Research (SBIR) Hydrogen Program New Projects Awarded in FY 2012

The Small Business Innovation Research (SBIR) program provides small businesses with opportunities to participate in DOE research activities by exploring new and innovative approaches to achieve research and development (R&D) objectives. The funds set aside for SBIR projects are used to support an annual competition for Phase I awards of up to \$150,000 each for about nine months to explore the feasibility of innovative concepts. Phase II R&D efforts further demonstrate the technologies to move them into the marketplace, and these awards are up to \$1,000,000 over a two-year period. Small Business Technology Transfer (STTR) projects include substantial (at least 30%) cooperative research collaboration between the small business and a non-profit research institution.

Tables 1 and 2 list the Phase-I and Phase-II (respectively) SBIR projects awarded in FY 2012 related to the Hydrogen and Fuel Cells Program. Brief descriptions of each project follow.

TABLE 1. FY 2012 Phase-I SBIR Projects Related to the Hydrogen and Fuel Cells Program

| Title | Company | City, State |
|---|-------------------------------|-----------------|
| XIII.1 Using ARB Biotech for H2 Generation and Efficient Commercial Wastewater Treatment | Arbsource, LLC | Tempe, AZ |
| XIII.2 Low-Noble-Metal-Content Catalysts/Electrodes for Hydrogen Production by Water Electrolysis | Proton OnSite | Wallingford, CT |
| XIII.3 Low-cost Integrated Nanoreinforcement for Composite Tanks | Nextgen Aeronautics, Inc. | Torrance, CA |
| XIII.4 Novel Structured Metal Bipolar Plates for Low Cost Manufacturing | Treadstone Technologies, Inc. | Princeton, NJ |

TABLE 2. FY 2012 Phase-II SBIR Projects Related to the Hydrogen and Fuel Cells Program

| Title | Company | City, State |
|---|----------------------------|---------------|
| XIII.5 Ultra-Lightweight High Pressure Hydrogen Fuel Tanks Reinforced with Carbon Nanotubes (Phase II Project) | Applied Nanotech, Inc. | Austin, TX |
| XIII.6 New High Performance Water Vapor Membranes to Improve Fuel Cell Balance of Plant Efficiency and Lower Costs (Phase II Project) | Tetramer Technologies, LLC | Pendleton, SC |

PHASE I PROJECTS

XIII.1 Using ARB Biotech for H2 Generation and Efficient Commercial Wastewater Treatment

Arbsource, LLC
 1235 W Laird Street
 Tempe, AZ 85281-5312

Food and beverage processors are burdened with the high cost of managing wastewater, totaling six or seven figures per year just in operations. This project will cut this cost in half by supplying low-energy high-quality wastewater treatment for customers, and it is expected to deliver a two year payback period.

XIII.2 Low-Noble-Metal-Content Catalysts/Electrodes for Hydrogen Production by Water Electrolysis

Proton OnSite
10 Technology Drive
Wallingford, CT 06492

Proton OnSite manufactures hydrogen generation systems that can be integrated with renewable energy sources to generate hydrogen fuel, while producing a minimal carbon footprint. This project aims to reduce the cost of this technology through development of improved electrode materials designed to reduce use of expensive raw materials and overall system capital cost.

XIII.3 Low-Cost Integrated Nanoreinforcement for Composite Tanks

Nextgen Aeronautics, Inc.
2780 Skypark Drive, Suite 400
Torrance, CA 90505

This project will incorporate a low-cost nanoreinforcement into high-pressure all-composite tank designs to further increase pressure and lower costs. NextGen proposes the development of a Low-cost Integrated Nanoreinforcement design for composite tanks. Partners are Precision Nanotechnologies and Lincoln Composites. NextGen will electrodeposit polyacrylonitrile nanofibers to Lincoln's 240-bar and 700-bar Type IV tanks. Early results have shown significant improvement in the fracture toughness of Toray fiber composite with no measurable increase in mass. They are targeting 10% improvement in burst strength and 30% improvement to the burst after impact strength, which could reduce the amount of carbon fiber needed and reduce the overall cost of the tank.

XIII.4 Novel Structured Metal Bipolar Plates for Low-Cost Manufacturing

Treadstone Technologies, Inc.
201 Washington Road
Princeton, NJ 08540

This project will develop a low-cost novel-structured metal bipolar plate technology for low-temperature polymer electrolyte membrane fuel cells for transportation applications.

PHASE II PROJECTS

XIII.5 Ultra-Lightweight High Pressure Hydrogen Fuel Tanks Reinforced with Carbon Nanotubes

Applied Nanotech, Inc.
3006 Longhorn Blvd.
Austin, TX 78758

Carbon fiber is very expensive, ranging from \$20-\$50 per kilogram. This work will develop technologies that will reduce the dependence on carbon fiber material needed in carbon fiber reinforced plastic (CFRP) tanks through carbon nanotube reinforcement. Using nano-reinforcement upon the composite resin matrix will result in a reduced amount of required carbon fiber for CFRP tanks while making them more lightweight and efficient.

XIII.6 New High Performance Water Vapor Membranes to Improve Fuel Cell Balance of Plant Efficiency and Lower Costs

Tetramer Technologies, LLC
657 South Mechanic Street
Pendleton, SC 29670-1808

This project's new water vapor membrane technology will create 20 high paying jobs in South Carolina while helping the U.S. lower its dependence on foreign oil. Already growing modestly in the U.S., the fuel cell commercial enterprise will be accelerated with the higher performance and lower costs targeted in Phase II.

XIV. Acronyms, Abbreviations and Definitions

| | | | |
|----------------------------|---|--------------------------------|---|
| α -AlH ₃ | Alpha polymorph of aluminum hydride | 6FPAEB-BPS100 | Hexafluoro bisphenol A benzonitrile-biphenyl sulfone |
| ~ | Approximately | 8YSZ | 8 mol% yttria-stabilized zirconia |
| @ | At | a.k.a. | Also known as |
| °C | Degrees Celsius | A | Ampere, amps |
| °F | Degrees Fahrenheit | Å | Angstrom |
| Δ | Change, delta | AB | Ammonia-borane, NH ₃ BH ₃ |
| ΔG | Gibbs free energy of reaction | ABH ₂ | Ammonium borohydride, NH ₄ BH ₄ |
| ΔH | Enthalpy of reaction, Enthalpy of hydrogenation | AC | Alternating current |
| ΔH_f° | Standard heat of formation | ACC | Advanced anode catalyst |
| ΔK | Stress intensity factor | ACF | Activated carbon fibers |
| ΔP | Pressure drop, pressure change | A/cm ² | Amps per square centimeter |
| ≈ | Equals approximately | ACN | Acetonitrile |
| > | Greater than | ACNT | Aligned carbon nanotube |
| ≥ | Greater than or equal to | AC Transit | Alameda Contra Costa Transit |
| < | Less than | AD | Anaerobic digestion; Anode dew point |
| ≤ | Less than or equal to | ADG | Anaerobic digester gas |
| μ CHP | Micro-combined heat and power | AEM | Anion exchange membrane; Analytical electron microscopy |
| μ CHX | Microscale combustor/heat exchanger | AEO | Annual Energy Outlook |
| μ c-Si | Microcrystalline silicon | AER | Absorption-enhanced reforming; All-electric range |
| μ m | Micrometer(s), micron(s) | AFDC | Alternative Fuels Data Center |
| η | Viscosity | AFM | Atomic force microscopy; Anti-ferromagnetic |
| # | Number | AFP | Automated fiber placement |
| Ω | Ohm(s) | AFV | Alternative fuel vehicle |
| Ω /cm ² | Ohm(s) per square centimeter | Ag | Silver |
| Ω -cm ² | Ohm-square centimeter | AGC | Activated graphitic carbon |
| % | Percent | AgCl | Silver chloride |
| ® | Registered trademark | A-h | Amp-hour |
| \$ | United States dollars | AHJ | Authorities having jurisdiction |
| ¹¹ B-NMR | Boron 11 nuclear magnetic resonance | AIR | Average individual risk |
| 1-D, 1D | One-dimensional | AISI | American Iron & Steel Institute |
| 1Q | First quarter of the fiscal year | AIST | Japanese National Institute of Advanced Industrial Science and Technology |
| 2-D, 2D | Two-dimensional | AK | Alkali |
| 2Q | Second quarter of the fiscal year | Al | Aluminum |
| 3-D, 3D | Three-dimensional | Al ₂ O ₃ | Aluminum oxide |
| 3DSM | Dimensionally stable membrane with 3-dimensional porous support | ALARP | As low as reasonably practicable |
| 3Q | Third quarter of the fiscal year | Al-AB | Aluminum-ammonia-borane |
| 3-L | Three-layer | AlCl ₃ | Aluminum chloride |
| 4Q | Fourth quarter of the fiscal year | | |
| 5-L | Five-layer | | |

XIV. Acronyms, Abbreviations and Definitions

| | | | |
|------------------|--|-------------------------------|---|
| ALD | Atomic layer deposition | ATR | Autothermal reformer; Autothermal reforming; Attenuated total reflection |
| AlH ₃ | Aluminum hydride; Alane | ATR-FTIR | Attenuated total reflectance Fourier transform infrared |
| ALS | Advanced Light Source at Lawrence Berkeley National Laboratory | a.u. | Arbitrary units |
| ALT | Accelerated life test | Au | Gold |
| AM | Air mass | AuS | Gold sulfide |
| AM 1.5 | Air Mass 1.5 solar illumination | AuSnO _x | Gold supported on hydrous tin oxide |
| AM1.5G | Air Mass 1.5 Global (solar spectrum) | AuTiO _x | Gold supported on titanium oxide |
| AMBH | Amminine metal borohydride | Autonomie | Plug-and-Play Powertrain and Vehicle Model Architecture and Development Environment software model by Argonne National Laboratory to support the rapid evaluation of new powertrain/propulsion technologies for improving fuel economy through virtual design and analysis in a math-based simulation environment |
| AMC | Aminomethyl-cyclohexane | | |
| AMR | Annual Merit Review | | |
| AMR | Active magnetic regenerator | | |
| AMRL | Active magnetic regenerative liquefier | | |
| AMRR | Active magnetic regenerative refrigerator | | |
| AN | Acrylonitrile | | |
| ANL | Argonne National Laboratory | | |
| ANOVA | Analysis of variance | Avg | Average |
| ANSI | American National Standards Institute | AZO | Aluminum zinc oxide |
| A _o | Arrhenius constant, ml/[cm ² -min-atm ^{1/2}]; Availability | ¹¹ B-NMR | Boron 11 nuclear magnetic resonance |
| APCI, APCi | Air Products and Chemicals, Inc. | B | Boron |
| APD | 3-aminopropane-1,2-diol | B ₂ O ₃ | Boron oxide; Diboron trioxide |
| APR | Aqueous-phase reforming | Ba | Barium |
| APU | Auxiliary power unit | Bara | Bar absolute |
| AQMD | Air Quality Management District | barg | Bar gauge |
| Ar | Argon | BBC | 4,4',4''-(benzene-1,3,5-triyl-tris(benzene-4,1-diyl))tribenzoate |
| ARRA | American Recovery and Reinvestment Act | BCC | Body-centered cubic |
| As | Arsenic | BCN | Boron carbon nitride |
| ASAXS | Anomalous small-angle X-ray scattering | Be | Beryllium |
| a-Si | Amorphous silicon | BES | Basic Energy Sciences office within the DOE Office of Science |
| a-SiC | Amorphous silicon carbide | BET | Brunauer-Emmett-Teller surface area analysis method |
| a-SiGe | Amorphous silicon germanium | BEV | Battery electric vehicle |
| a-SiN | Amorphous silicon nitride | BFZ0 | BaFe _{0.975} Zr _{0.025} O ₃ |
| ASME | American Society of Mechanical Engineers | BFZ1 | BaFe _{0.90} Zr _{0.10} O ₃ |
| ASPEN | Modeling software, computer code for process analysis | BG-DW | 65% bio-glycol-35% distilled water |
| ASR | Area-specific resistance | B-G | Boron doped graphitic material |
| AST | Accelerated stress test | B-H | Boron/hydrogen bond |
| ASTM | ASTM International, originally known as the American Society for Testing and Materials | B-H, BH, BH ₄ | Borohydride |
| AT | Ammonia tritorane | Bi | Bismuth |
| at% | Atomic percent | BILI | Bio-derived liquid fuels |
| atm | Atmosphere | BILP | Benzimidazole-linked-polymers |
| ATP | Adenosine triphosphate; Advanced Technology Program | BisSF | Bisphenol-sulfone |
| ATPase | Adenosine triphosphatase | BLP | Borazine-linked polymers |

| | | | |
|---------------------|--|-------------------------------------|---|
| bmimBF ₄ | 1-butyl-3-methyl-imidazolium tetrafluoroborate | BTC | 1,3,5-benzenetricarboxylate |
| bmimCl | 1-butyl-3-methyl-imidazolium chloride | BTE | 4,4',4''-(benzene-1,3,5-triyltris(ethyne-2,1-diyl))tribenzoate |
| BmimOTf | 1-butyl-3-methyl-imidazolium triflate | BTT | Benzene tris-tetrazole |
| bmimPF ₆ | 1-butyl-3-methyl-imidazolium hexafluorophosphate | BTTCD | Octa-carboxylate ligand |
| BMPFFP | 1-butyl-1-methyl-pyrrolidinium tris(pentafluoroethyl)trifluorophosphate | BTU, Btu | British thermal unit(s) |
| BN | Boron-nitrogen | Bu ₃ SnCl | Tributyltin chloride |
| BNH | Boron-nitrogen-hydrogen | Bu ₃ SnSnBu ₃ | Hexabutyl-distannane |
| BNHx | Dehydrogenated ammonia-borane | BV | Benzyl viologen |
| BNL | Brookhaven National Laboratory | BxHy | Polyhedral boranes |
| BNNT | Boron nitride nanotubes | BZYC | BaZr _{0.1} Ce _{0.7} Y _{0.1} Yb _{0.1} O _{3-δ} |
| B-O | Any oxidized boron species, borate | C | Carbon |
| Boc | Tert-butoxycarbonyl | C | Coulomb |
| B(OH) ₃ | Boric acid | C ₂ H ₄ | Ethylene |
| BOL | Beginning of life | C ₂ H ₆ | Ethane |
| BOP, BoP | Balance of plant | C ₃ H ₈ | Propane |
| BOT | Beginning of test | Ca | Calcium |
| BP | Bisphenol; Biphenyl | CA | Carbon aerogel |
| bpe | Bis(4-pyridyl)ethane | CA | Chronoamperometry |
| BPEE | 1,2-bipyridylethene | CaBr ₂ | Calcium bromide |
| BPDC | Biphenyl-4,4'-dicarboxylate | CaCO ₃ | Calcium carbonate |
| BPP | Bipolar plate | CAD | Computer-aided design |
| BPPPO | Biphenol-based phenyl phosphine oxide | CAE | Computer-assisted engineering |
| BPPPO-35 | Biphenol-based phenyl phosphine oxide copolymer, 35% molar fraction of disulfonic acid unit (35% level of sulfonation) | CAER | Center for Applied Energy Research |
| BPS | Ballard Power Systems | CaFCP | California Fuel Cell Partnership |
| BPS | Bi Phenyl Sulfone | CaI | <i>Clostridium acetobutylicum</i> hydrogenase |
| BPS100 | Fully disulfonated poly(arylene ether sulfone) | CaO | Calcium oxide |
| BPSH | Block polysulfone ether polymer | CARB | California Air Resources Board |
| BPSH | Bi Phenyl Sulfone: H Form | CaS | Calcium sulfide |
| BPSH-30 | Biphenyl sulfone H form, 30% molar fraction of disulfonic acid unit (30% level of sulfonation) | CaSFCC | California Stationary Fuel Cell Collaborative |
| BPSH-x | BiPhenyl based disulfonated polySulfone (H+ form) (x denotes degree of sulfonation) | CbHS | Carbon-based hydrogen storage |
| BPVC | Boiler and Pressure Vessel Code | CB | Conduction band |
| BPVE | Perfluorocyclobutane-biphenyl vinyl ether | CBM | Conduction band minimum |
| BPVE-6F | Perfluorocyclobutane-biphenyl vinyl ether hexafluoroisopropylidene | CBN | Carbon-boron-nitrogen |
| BPY | 2,2'-bipyridine | CBS | Casa Bonita strain; Complete basis set |
| BPY | 4,4'-bipyridine | cc | Cubic centimeter(s) |
| Br | Bromine | CCC | Carbon composite catalyst |
| Br ₂ | Diatomic bromine | CCD | Charge-coupled device |
| BTB | 1,3,5-benzenetribenzoate | CCF | Complex coolant fluid |
| | | cc/g cat/hr | Cubic centimeter(s) per gram catalyst per hour |
| | | CcH2 | Cryo-compressed hydrogen |
| | | CCHSS | Complex Compound Hydrogen Storage System |
| | | CCM | Catalyst-coated membrane; Coordinate measuring machine |

XIV. Acronyms, Abbreviations and Definitions

| | | | |
|-------------------|---|--------------------|---|
| Cc/min, ccm | Cubic centimeters per minute | CHSCoE | Chemical Hydrogen Storage Center of Excellence |
| ccp | Cubic close-packing | CI | Compression ignition |
| CCS | Carbon capture and storage | CIGSe ₂ | Copper indium gallium diselenide |
| CC&S | Carbon capture and sequestration | CIGS | Copper indium gallium diselenide |
| CCVJ | 9-([E]-2-carboxy-2-cyanovinyl)julolidine | CIRRUS | Cell Ice Regulation & Removal Upon Start-up |
| Cd | Cadmium | Cl | Chlorine |
| CD | Compact disk; Charge depleting; Cathode dewpoint | CL | Catalyst layer; ε-caprolactone |
| Cdl | Double layer capacitance | cm | Centimeter |
| cDNA | Complementary DNA | CM | Controls module |
| CDO | Code development organization | cm ² | Square centimeter |
| CDP | Composite data product | CMO | Conductive metal oxides |
| CdS | Cadmium sulfide | CMWNT | Carbon multi-walled nanotube |
| C-DSM™ | Chemically etched dimensionally stable membrane | CN | Carbon-nitrogen |
| Ce | Cerium | CNC | Carbon nanocage |
| CEA | Commissariat à l'Énergie Atomique | CNF | Carbon nano-fiber |
| CEC | California Energy Commission | CNG | Compressed natural gas |
| CEM | Compressor/expander motor (module) | CNT | Carbon nanotube |
| CeO ₂ | Ceric oxide | Co | Cobalt |
| CF | Carbon fiber; Carbon foam | CO | Carbon monoxide |
| CFC | Chlorofluorocarbon | CO ₂ | Carbon dioxide |
| CFD | Computational fluid dynamics | COD | Chemical oxygen demand |
| CFF | Complex coolant fluid | COE | Cost of electricity |
| cfm | Cubic feet per minute | COF | Covalent-organic framework |
| CGA | Compressed Gas Association | COF ₂ | Carbonyl fluoride |
| CGH2 | Compressed gaseous hydrogen | COGS | Cost of goods sold |
| CGM | Charge-generating material | COMSOL | Multiphysics modeling and engineering simulation software |
| CGO | Cerium gadolinium oxide, Gd-doped CeO ₂ | COPV | Composite overwrapped pressure vessel |
| CGS | Copper gallium diselenide, CuGaSe ₂ | COS | Carbon oxysulfide; Carbonyl sulfide |
| CGSe ₂ | Copper gallium diselenide | COx | Oxides of carbon |
| CH | Hydrogenated graphene | c _p | Specific heat |
| cH ₂ | Compressed hydrogen gas | cp | Commercial purity |
| CH ₄ | Methane | cP | Centipoise |
| CHARGEH2 | GTI hydrogen cylinder filling model | CpI | <i>Clostridium pasteurianum</i> [FeFe]- hydrogenase |
| CHARM | Cost-effective High-efficiency Advanced Reforming Module | CPMAS | Cross polarization magic angle spinning |
| CHEX | Continuous catalytic heat exchanger | CPO, CPOX | Catalytic partial oxidation |
| CHHP | Combined heat, hydrogen, and power | c.p.s. | Counts per second |
| Chl | Chlorophyll | CPU | Computer processing unit |
| CHMCI | Test Method for Evaluating Material Compatibility for Compressed Hydrogen Applications – Phase I - Metals | CPV | Composite pressure vessel |
| CHP | Combined heat and power | Cr | Chromium |
| CHPFC | Combined heat and power fuel cell | CRADA | Cooperative Research and Development Agreement |
| CHS | Chemical hydrogen storage | Cs | Cesium |
| | | C&S | Codes and standards |

| | | | |
|-------------------|---|-----------------------|--|
| CSA | Canadian Standards Association | DEGDBE | Diethylene glycol dibutyl ether |
| CSA | Cell stack assembly | DEMS | Differential electrochemical mass spectroscopy |
| CSMP | Cabot Superior MicroPowders | ΔB_a | The difference in magnetic induction at high and low applied magnetic fields |
| CSTT | Codes and Standards Tech Team | ΔG | Gibbs free energy of reaction |
| CSU | California State University | ΔH | Enthalpy of reaction; Enthalpy of hydrogenation |
| CSULA | California State University Los Angeles | ΔH_f° | Standard heat of formation |
| CTA | Charge transfer agent | ΔK | Stress intensity factor |
| CTAB | Cetyl trimethyl ammonium bromide | ΔP | Pressure drop; Pressure change |
| CTB | Cyclotriborazane | DFM | Design for manufacturing |
| CTE | Coefficient of thermal expansion | DFMA [®] | Design for Manufacturing and Assembly |
| CTTRANSIT | Connecticut Transit | DFT | Density functional theory |
| Cu | Copper | DGDE | Di-ethylene glycol di-butyl ether |
| CU | University of Colorado | DHBC | 2,5-dihydroxybenzene dicarboxylate |
| Cu ₂ O | Cuprous oxide | DI | Deionized; De-ionized water |
| cu in. | Cubic inch | DLC | Diamondlike carbon |
| CuNW | Copper nanowire | dL/g | Deciliters per gram |
| CuO | Cupric oxide; Copper(II) oxide | DM | Diffusion media |
| cu.yd. | Cubic yard(s) | DMA | Dynamic mechanical analysis |
| CV | Cyclic voltammetry; Cyclic voltammogram | DMA | Dimethylacetamide |
| CVD | Chemical vapor deposition | DMAc | Dimethyl acetamide |
| CVS | Chemical vapor synthesis | DMC | Diffusion Monte Carlo; Direct manufactured cost |
| CWRU | Case Western Reserve University | DMDF | 2,5-dimethoxy 2,5-dihydrofuran |
| CY | Calendar year | DMDS | Dimethyldisulfide |
| CZO | Ceria-zirconia | DME | Dimethyl ether; Dimethoxyethane |
| d | Day(s) | DMEA | Dimethylethylamine |
| D ₂ | Deuterium | DMEAA | Dimethylethylamine alane |
| D-A | Dubinin-Astakhov | DMF | n, n-di-methyl formamide |
| DAC | Diamond anvil cell | DMFC | Direct methanol fuel cell |
| DADB | Diammoniate of diborane, [(NH ₃) ₂ BH ₂][BH ₄] | dmimMeSO ₄ | 1,3-dimethyl-imidazolium methylsulfate |
| DAKOTA | Design Analysis Kit for Optimization and Terascale Applications | dmpe | Dimethylphosphinoethane |
| DB | Diborane (B ₂ H ₆) | DMPO | 5,5-Dimethylpyrroline-N-oxide |
| dB(A) | Decibel(s) A scale | DMSO | Dimethyl sulfoxide |
| DBBPDSA | 4, 4'-dibromobiphenyl 3, 3'-disulfonic acid, monomer | DMT | Dimethyltrityl |
| DBPDSA | 1, 4-dibromo phenylene 2, 5-disulfonic acid | DMTHF | Dimethyltetrahydrofuran |
| DC | Direct current | DNA | Deoxyribonucleic acid |
| DCTDD | 1,8-diazacyclotetradecane-2,7-dione | DNG | Desulfurized natural gas |
| DDMEFC | Direct dimethyl ether fuel cell | DNI | Direct normal insolation |
| DDP | Detailed Data Product | DOD | Depth of discharge |
| d_{DR} | Dubini-Radushkevich average micropore diameter | DOD | Department of Defense |
| DDR | A zeolite structure code | DOE | Department of Energy |
| DEF | Diethylformamide | DOT | Department of Transportation |
| Deg | Degree | | |

XIV. Acronyms, Abbreviations and Definitions

| | | | |
|--------------------------------|--|-------------------|---|
| DP | Dew point | EDX | Energy dispersive X-ray |
| DRIFTS | Diffuse reflectance infrared Fourier transform spectroscopy | EELS | Electron energy loss spectroscopy |
| DSC | Differential scanning calorimetry; Dynamic scanning calorimetry | EERE | U.S. DOE Office of Energy Efficiency and Renewable Energy |
| DSM TM | Dimensionally stable membrane | EFR-AHJ | Emergency first responder-authorities having jurisdiction |
| DSM-MC | Distance scaling method Monte Carlo | EFTE | Ethylene-tetrafluoroethylene |
| DVBPC | Divinyl aryl ether monomer | e.g. | <i>Exempli gratia</i> : for example |
| DVD | Digital video disk | EGR | Exhaust gas recirculation |
| DVMT | Daily vehicle miles traveled | EHC | Electrochemical hydrogen compressor |
| e ⁻ | Electron | EHS | Environmental Health and Safety |
| E | Activation energy, kJ/mol | EIA | Energy Information Administration of the U.S. Department of Energy |
| E85 | 85%-15% blend of ethanol with gasoline | EIGA IGC | European Industrial Gases Association/ Industrial Gases Council |
| E ₀ xE ₁ | Utilization efficiency of incident solar light energy | EIHP | European Integrated Hydrogen Project |
| E _{1/2} | Half-wave potential | EIS | Electrochemical impedance spectroscopy |
| E _a | Activation energy | EISF | Elastic incoherent structure factor |
| E _{ad} | Hydrogen adsorption heat | ELAT [®] | Registered Trademark of De Nora North America, Inc., covers GDLs and GDEs |
| EAN | Ethylammonium nitrate | EMA | Effective medium approximation |
| EASA | Electrochemically active surface area | EMF | Electromagnetic field |
| E-BOP | Electrical balance of plant | EMI | Electro magnetic interference |
| EBSD | Electron backscatter diffraction | EMPA | Electron microprobe analysis |
| EC | European Commission; Electro-chemical | ENG | Expanded natural graphite |
| EC | Evaporative-cooled; Efficiency of conversion | eNMR | Electrochemical nuclear magnetic resonance |
| EC | Electrochemical capacitance | EODC | Electro-osmotic drag coefficient |
| EC | Early commercial | EOL | End of life |
| ECA | Electrochemical area | EOT | End of test |
| ECA | Estimated surface area | EPA | Environmental Protection Agency |
| ECB | Ethylcyclobutane | EPDM | Ethylene propylene diene monomer |
| ECC | Electrochemical compressor; Engineered cementitious composite | EPHC | Ethylperhydrocarbazole |
| ECE | Economic Commission for Europe | ePTFE | Expanded polytetrafluoroethylene |
| ECS | Equilibrium crystal shape | ER | Emergency responder |
| ECSA | Electrochemically active surface area; Electrochemical surface area; Effective catalyst surface area | ERW | Electric resistance weld |
| ED | Ethylenediamine | ES | Energy storage |
| EDA | Ethylene diamine; Energy decomposition analysis | ESA | Electrochemical surface area |
| EDAX | Manufacturer of energy dispersive X-ray hardware and software | ESEM | Environmental scanning electron microscope |
| EDBB | Ethylenediamine bisborane | et al. | <i>Et Alii</i> : and others |
| EDC | Energy distribution curve | ETA | Event tree analysis |
| edmimCl | 2-ethyl-1,3-dimethyl-imidazolium ethylsulfate | etc. | <i>Et cetera</i> : and so on |
| EDS | Energy dispersive X-ray spectroscopy; Energy dispersive spectrum | E-TEK | Division of De Nora North America, Inc. |
| EDTA | Ethylenediamine tetraacetic acid | ETFE | Ethylene-tetrafluoroethylene |
| | | ETFECS | Extended thin film electrocatalyst structures |
| | | EtOH | Ethanol |
| | | EU | European Union |

| | | | |
|--------------------------------|---|--------------------|---|
| eV | Electron volt | FLP | Frustrated Lewis pair |
| EVD | Extreme value distributions | FLUENT | Computer code for computational fluid dynamics |
| EVOH | Ethylene vinyl alcohol | FMEA | Failure modes and effects analysis |
| EVSE | Electric vehicle supply equipment | ¹⁹ FNMR | ¹⁹ Fluorine nuclear magnetic resonance |
| EW | Equivalent weight | FNR | Ferredoxin NADP+ oxidoreductase |
| EXAFS | Extended X-ray absorption fine structure analysis | FOM | Federated object model |
| F | Fluorine | FOM | Figure of merit |
| F | Faraday constant, the amount of electric charge in one mole of electrons (96,485.3383 coulomb/mole) | FPA | Fluoroalkyl phosphonic and phosphinic acids |
| F ⁻ | Fluorine ion | fpi | Fins per inch |
| FA | Furfyl alcohol | fpm | Feet per minute |
| FANS | Filter analyzer neutron spectroscopy | FPS | Bis(4-fluorophenyl)sulfone; Fuel processing system |
| FAT | Fleet Analysis Toolkit; Factory acceptance test | FRP | Fiber-reinforced composite piping; Fiber-reinforced polymer; Full rate production |
| FBMR | Fluidized bed membrane reactor | FRR | Fluoride release rate |
| FC | Fuel cell | F-SPEEK | Fluorosulfonic acid of polyetheretherketone |
| FCB | Fuel cell bus | FSW | Friction stir welding |
| FCC | Face-centered cubic; Fuel Cell Catalyst; Fluid catalytic cracking | ft | Feet |
| FCEB | Fuel cell electric bus | FT | Fault tree |
| FCEV | Fuel cell electric vehicle | ft ² | Square feet |
| FC POWER | Fuel Cell Power Model | ft ³ | Cubic feet |
| FCPP | Fuel cell power plant | FTA | Federal Transit Administration |
| FCS | Fuel cell system | FTA | Fault tree analysis |
| FCSMR | Forecourt steam methane reformer (ing) | FT-IR, FTIR | Fourier transform infrared |
| FCT | Fuel Cell Technologies | FTIR-ATR | Fourier transform infrared attenuated total reflection |
| FCTES ^{QA} | Fuel Cell Testing, Safety and Quality Assurance (an international effort to harmonize fuel cell testing procedures) | FTO | Fluorine-doped tin oxide |
| FCTT | Fuel Cell Technical Team | FTP, FTP-75 | Federal Test Procedure |
| FCV | Fuel cell vehicle | FW | Formula weight |
| Fd | Ferredoxin | FW | Filament winding |
| Fe | Iron | FWHM | Full width at half maximum |
| FE | U.S. DOE Office of Fossil Energy | FY | Fiscal year |
| Fe ₂ O ₃ | Ferric oxide | g | Gram; acceleration of gravity |
| FEA | Finite element analysis | G | Graphite |
| FEM | Finite element model | Ga | Gallium |
| FEP | Fluorinated ethylene propylene; Teflon [®] | GaAs | Gallium arsenic |
| FESEM | Field emission scanning electron microscope | GADDS | General area diffraction system |
| fg-ELAT | Fine gradient ELAT | gal | Gallon |
| FIB | Focused ion beam | GaP | Gallium phosphide |
| FISIPE | Fibras Acrilicas Portugese | GB | Gigabyte |
| FIT | Florida Institute of Technology | GC | Gas chromatograph; General computational |
| FLiNaK | LiF-NaF-KF eutectic salt | GC | Glassy, or vitreous carbon; a pure carbon that is amorphous (non-crystalline) |
| | | g/cc | Grams per cubic centimeter |
| | | GCLP | Grand-canonical linear programming |

XIV. Acronyms, Abbreviations and Definitions

| | | | |
|-----------------|--|--------------------------------|--|
| GCMC | Grand Canonical Monte Carlo | GREET2 | Greenhouse gases, Regulated Emissions and Energy use in Transportation model |
| GCMS | Gas chromatograph-mass spectroscopy | GRPE | Working Party on Pollution and Energy |
| GCNF | Graphitized carbon nano-fiber | g/s | Grams per second |
| GCNT | Graphitized carbon nanotubes | GTI | Gas Technology Institute |
| GCTool | Software package developed at ANL for analysis of fuel cells and other power systems | GTR | Global Technical Regulations |
| Gd | Gadolinium | GUI | Graphical user interface |
| GDC | Gadolinium-doped ceria | GV | Gasoline vehicle |
| GDE | Gas diffusion electrode | GW | An approximation permitting practical calculation of excitation energies in metals, semi-conductors and insulators |
| GDL | Gas diffusion layer | GWe, GW _e | Gigawatt(s) electric |
| GDM | Gas diffusion media | h | Hour(s) |
| GDS | Galvanodynamic scan | H | Hydrogen |
| Ge | Germanium | H ⁺ | Proton |
| GES | Giner Electrochemical Systems, LLC | H ⁻ | Hydride |
| GF | Glass fiber | H ₂ | Diatomic hydrogen |
| GFC | Gas flow channel | H2A | Hydrogen Analysis project sponsored by DOE |
| GGA | Generalized gradient approximation | H ₂ BPYDC | 2,2'-bipyridine-5,5'-dicarboxylic acid |
| GGE, gge | Gasoline gallon equivalent | H ₂ cat | Catechol, 1,2 dihydroxybenzene |
| GH ₂ | Gaseous hydrogen | H ₂ -FCS | Stationary fuel cell system designs that co-produce hydrogen |
| GHG | Greenhouse gas | H ₂ (hfipbb) | 4,4'-(hexafluoroisopropylidene)bis(benzoic acid) |
| GHSV | Gas hourly space velocity | H2-ICE, H ₂ ICE | Hydrogen internal combustion engine |
| GIS | Geographic information system | H ₂ Lib | Library of H ₂ component models in Simulink |
| GJ | Gigajoule(s) | H ₂ O | Water |
| g/kW | Gram(s) per kilowatt | H ₂ O ₂ | Hydrogen peroxide |
| GLACD | Glancing angle co-deposition | H ₂ oba | 4,4'-oxybis-benzoic acid |
| GLAD | Glancing angle deposition | H2QWG | DOE Hydrogen Quality Working Group |
| GLS | Gas-liquid separator | H ₂ S | Hydrogen sulfide |
| GLY | Glycerol | H ₂ SO ₄ | Sulfuric acid |
| Glyme | Dimethoxyethane | H2V | Hydrogen vehicle |
| gm | Gram(s) | H ₃ BBC | 1,3,5-tris(4'-carboxy[1,1'-biphenyl]-4-yl-)benzene |
| GM | General Motors | H ₃ BTB | 4,4',4''-benzene-1,3,5-triyl-tribenzoic acid |
| gm/day | Gram(s) per day | H ₃ PO ₄ | Phosphoric acid |
| g/min | Gram(s) per minute | HAADF | High-angle annular dark-field |
| GNF | Graphite nanofiber | HAADF-STEM | High angle annular dark field scanning transmission electron microscopy |
| GO | Graphene oxide | HAMMER | Hazardous Materials Management and Emergency Response |
| GODC | Graphene oxide derived carbon | HATCI | Hyundai-KIA America Technical Center Inc. |
| GOF | Graphene-oxide framework | HAVO | Hawaii Volcanoes National Park |
| GPa | Gigapascal(s) | HAZ | Heat affected zone |
| GPC | Gel permeation chromatography | HAZID | Hazard Identification Analysis |
| GPS | Global positioning system | | |
| GPU | Gas permeation units | | |
| GRC | Glass-reinforced concrete | | |
| GREC | Graphite reinforced epoxy composite (IM6 continuously wound) | | |

| | | | |
|-------------------------------|---|------------------|---|
| HAZOP | Hazards and Operational Safety Analysis; Hazards and operability analysis | HGM | Hydrogen Generation Module |
| HB | Hydrazine borane | HGMs | Hollow glass microspheres |
| HBr | Hydrogen bromide | HGV | Hydrogen gaseous vehicle |
| HBTU | o-Benzotriazol-1-yl-N,N,N',N'-tetramethyluronium hexafluorophosphate | HHV | Higher heating value |
| HC | High concentration | HI | Hydrogen iodide, hydriodic acid |
| HCC | Hybrid cathode catalyst | HIA | Hydrogen-induced amorphization; Hydrogen Implementing Agreement |
| HCl, HCL | Hydrochloric acid; Hydrogen chloride | HIAD | Hydrogen Incidents and Accidents Database |
| HClO ₄ | Perchloric acid | HIB | High-impedance buffer |
| HCN | Hydrogen coordination number | HIC | Hydrogen-induced cracking |
| HCNG | Hydrogen-compressed natural gas | HICE | Hydrogen internal combustion engine |
| HCO ₃ ⁻ | Bicarbonate | HiPCO, HiPCo | High-pressure carbon monoxide |
| hcp | Hexagonal close-packing | HIPOC | Hydrogen Industry Panel on Codes |
| HC&S | Hawaiian Commercial and Sugar Company | HIx | Blend of hydrogen iodide, iodine, and water |
| HD | Deuterium hydride | HKUST | 1 Cu ₃ (1,3,5-benzenetricarboxylate) ₂ |
| HDF | Hydrogen dispensing facility | HLA | High level architecture |
| HDPE | High-density polyethylene | HMC | Hyundai Motor Company |
| HDS | Hydrogen desulfurization | HNEI | Hawaii Natural Energy Institute |
| HDSAM | Hydrogen Delivery Scenario Analysis Model | HNO ₃ | Nitric acid |
| He | Helium | HOMO | Highest occupied molecular orbital |
| HE | Hydrogen embrittlement | HOPG | Highly-ordered pyrolytic graphite |
| HEMA | 2-hydroxyethyl methacrylate | HOR | Hydrogen oxidation reaction |
| HEN | Heat exchange network | hp | Horsepower |
| HEPA | High efficiency particulate air filter | HP | High pressure |
| HER | Hydrogen evolution reaction | HPA | Heteropoly acid |
| HES | Hydrogen energy station | HPC | Highly porous carbon |
| HEV | Hybrid electric vehicle | HPIT | Hydrogen-powered industrial truck |
| HEX | Heat exchanger | HPLC | High performance liquid chromatography |
| Hf | Hafnium | HPPH | 1,6-di(4-hydroxyl)phenylperfluorohexane |
| HF | Hydrogen Fueler | HPPS | N,N-diisopropylethylammonium 2,2-bis(p-hydroxyphenyl) pentafluoropropanesulfonate |
| HF | Hydrofluorhydric acid; Hydrogen fluoride; Hartree Fock | HPRD | Hydrogen pressure relief device |
| HFB | Hexafluorobenzene | HQS100 | Hydroquinone sulfone |
| HFC | Hydrogen fuel cell | hr | Hour(s) |
| HFCTF | Hawaii Fuel Cell Test Facility | HRA | Home refueling appliance |
| HFCV | Hydrogen fuel cell vehicle | HRS | Hydrogen refueling stations |
| HFI | Hydrogen Fuel Initiative | HRT | Hydraulic retention time |
| HFP | Hexafluoropropylene | HRTEM | High-resolution transmission electron microscopy |
| HFP | 1,1,1,3,3,3 hexafluoro-2-propanol | HRS | Hydrogen refueling stations |
| HFR | High-frequency resistance | HR-STEM | High resolution scanning transmission electron microscopy |
| HFS | Hydrogen fueling station | HRXRT | High-resolution X-ray tomography |
| HFSS | High-flux solar simulator | HS | Hydrogen sorption |
| HFV | Hydrogen-fueled vehicle | HSAC | High surface area carbon |
| HGEF | Hawaii Gateway Energy Center | | |

XIV. Acronyms, Abbreviations and Definitions

| | | | |
|------------------|--|----------------|---|
| HSC | Database name derived from the letters for enthalpy, entropy and heat capacity | HyTRANS | DOE's market simulation model for the transition to hydrogen vehicles |
| HSCC | Hydrogen Station Cost Calculator | Hz | Hertz |
| HSCoE | Hydrogen Sorption Center of Excellence | HZM | Hot zone module |
| HSDC | Hydrogen Secure Data Center | i | Current density (mA/cm ²) |
| HSE | High surface area electrode | I | Current |
| HSECoE | Hydrogen Storage Engineering Center of Excellence | I ₂ | Diatomic iodine |
| HSMCoE | Hydrogen Storage Material Center of Excellence | IBAD | Ion beam assisted deposition |
| HSO ₄ | Bisulfate anion | IBS | Ion beam sputtering |
| HSP | Hydrogen safety plan | IC | Internal combustion |
| HSRP | Hydrogen Safety Review Panel | ICC | International Code Council |
| HSSIM | Hydrogen Storage SIMulator | ICE | Internal combustion engine |
| HSU | Hydrogen separation unit | ICEV | Internal combustion engine vehicle |
| HT | High temperature | ICMS | Integrated ceramic membrane system |
| HTAC | Hydrogen and Fuel Cell Technical Advisory Committee | ICP | Inductively coupled plasma |
| HTFC | High-temperature fuel cell | ICPAE | Inductively coupled plasma atomic emission |
| HTFSA | Trifluomethylsulfonic acid | ICP-AES | Inductively coupled plasma atomic emission spectroscopy |
| HTGR | High-temperature gas-cooled reactor | ICP-MS | Inductively coupled plasma mass spectrometry |
| HTHX | High-temperature heat exchanger | ICP-OES | Inductively coupled plasma optical emission spectroscopy |
| HTM | High-temperature membrane | ICR | Interfacial contact resistance |
| HTM | Hydrogen transport membrane | ID | Inside diameter |
| HTMWG | High Temperature Membrane Working Group | i.e. | <i>id est</i> : that is |
| HTPEM | High-temperature polymer electrolyte membrane | IE | Intelligent Energy |
| HTWGS | High-temperature water-gas shift | IEA | International Energy Agency |
| HTXRD | High-temperature X-ray diffraction | IEA-HIA | International Energy Agency Hydrogen Implementing Agreement |
| HVAC | Heating, ventilation and cooling | IEC | International Electrotechnical Commission |
| HWCVD | Hot-wire chemical vapor deposition | IEC | Ion exchange capacity, milliequivalents of acid groups per gram of material |
| HWD | Hot wire deposition | IECV | Integrated end cap vessel |
| HWFET | Highway Fuel Economy Test | IEEE | Institute of Electrical and Electronics Engineers, Inc. |
| HX | Heat exchanger | IFC | International Fire Code |
| HyARC | Hydrogen Analysis Resource Center | IGBT | Insulated-gate bipolar transistor |
| Hydrofill™ | GTI hydrogen dispenser filling control algorithm | IGCC | Integrated gasification combined cycle |
| HyDRA | Hydrogen Demand and Resource Analysis | IGCC-CMR | Integrated gasification combined cycle-catalytic membrane reactor |
| HyPro, HYPRO | Analysis tool | IGCC-MR | Integrated gasification combined cycle-membrane reactor |
| HyQRA | Hydrogen quantitative risk assessment | IGCC-PBR | Integrated gasification combined cycle-paladium-based reactor |
| HyS | Hybrid sulfur | IGT | Institute of Gas Technology |
| HYSYS® | Process simulation software by AspenTech, computer code for flowsheet analysis | IINS | Inelastic incoherent neutron scattering |
| HyTEC | Hydrogen Technology and Energy Curriculum | IIT | Illinois Institute of Technology |
| HyTEx | Hydrogen Technical Experimental (database) | | |

| | | | |
|------------------|--|-------------------|---|
| IL | Ionic liquid | JHQTF | Joint Hydrogen Quality Task Force (U.S. Fuel Cell Council) |
| In | Indium | JM | Johnson Matthey |
| In., in | Inch | JMFC | Johnson-Matthey Fuel Cells, Inc. |
| in ² | Square inch | JNAIST | Japanese National Institute of Advanced Industrial Science and Technology |
| INER | Institute of Nuclear Energy Research | JOBS FC | JOBS and economic impacts of Fuel Cells |
| INERI | International Nuclear Energy Research Initiative | JPL | Jet Propulsion Laboratory |
| InP | Indium phosphorus | JRC | Joint Research Centre |
| INS | Inelastic neutron scattering | J-V | Current density-voltage |
| I-O | Input-output | K | Sievert's constant, ml/[cm ² -min-atm ^{1/2}] |
| IOS | Intelligent Optical Systems, Inc. | K | Kelvin, absolute temperature |
| IP | Induction period | K | Potassium |
| IP | Intellectual property | kÅ | 1000 angstroms |
| IPA | Isophthalate | KAERI | Korea Atomic Energy Research Institute |
| IPA | Isopropyl alcohol | KAIST | Korea Advanced Institute of Science and Technology |
| IPCC | Intergovernmental Panel on Climate Change | kA/m ² | Kilo-ampere(s) per square meter |
| IPCE | Incident photon conversion to electrons; Incident photon conversion efficiency | kb | Kilo-base pair, a unit of measurement used in genetics equal to 1,000 nucleotides |
| IPE | Integrated photovoltaic electrolysis | KBr | Potassium bromide |
| IPES | Inverse photoemission spectroscopy | kcal | Kilocalorie(s) |
| IPHE | International Partnership for the Hydrogen Economy | kcal/mol | Kilocalorie(s) per mole |
| IPNS | Intense Pulse Neutron Scattering Facility at Argonne National Laboratory | KeV | Kilo electron volt(s) |
| IQE | Internal quantum efficiency | kg | Kilogram(s) |
| IR | Infrared | kg/d | Kilogram(s) per day |
| iR | Internal resistance | kg/hr | Kilogram(s) per hour |
| Ir | Iridium | kg/m ³ | Kilogram(s) per cubic meter |
| IRMOF | Isorecticular metal organic framework | KH | Potassium hydride |
| IrO _x | Iridium oxide | KHTC | Hydrotalcites |
| IRR | Internal rate of return | KHTC | Potassium-promoted hydrotalcite |
| IRRAS | Infrared reflection-absorption spectroscopy | kHz | Kilohertz |
| ISIS | World's leading pulsed neutron and muon source located at the UK Rutherford Appleton Laboratory near Oxford. | KIA | Kia Motor Company |
| ISO | International Organization for Standardization | KIC | Key industrial collaborators |
| ISO TC197 | International Standards Organization Technical Committee | K _{IH} | Fracture toughness measured in hydrogen gas |
| ISS | Ion scattering spectroscopy | kJ | Kilojoule(s) |
| ITM | Ion transport membrane | K _{JIC} | Fracture toughness |
| ITO | Indium tin oxide | kJ/mol | Kilojoule(s) per mole |
| ITP | Indium tin phosphate | km | Kilometer(s) |
| IV | Current-voltage | KMC | Kinetic Monte Carlo; Kilauea Military Camp; Kia Motors Corporation |
| J | Current | KOH | Potassium hydroxide |
| J | Joule(s) | kPa | Kilopascal(s) |
| | | kph | Kilometer(s) per hour |
| | | ksi | 1,000 pound-force per square inch |

XIV. Acronyms, Abbreviations and Definitions

| | | | |
|----------------------|--|--------------|---|
| kT/y | Kiloton(s) per year | LHC | Light-harvesting chlorophyll |
| Kth, K_{th} | Fracture toughness threshold | LHS | Lawrence Hall of Science |
| K_{TH} | Hydrogen-assisted crack growth threshold | LHSV | Liquid hourly space velocity, h^{-1} |
| kVA | Kilovolt-amp (units of apparent power) | LHV | Lower heating value |
| kW | Kilowatt(s) | Li | Lithium |
| kWe, kW_e | Kilowatt(s) electric | Li_3N | Lithium nitride |
| kWh | Kilowatt-hour(s) | Li-AB | Lithium amidoborane, $Li-NH_2-BH_3$ |
| kWh/kg | Kilowatt-hour(s) per kilogram | $LiBH_4$ | Lithium borohydride |
| kWh/L | Kilowatt-hour(s) per liter | LIBS | Laser-induced breakdown spectroscopy |
| kW/kg | Kilowatt(s) per kilogram | LiH | Lithium hydride |
| kWt | Kilowatt(s) thermal | LLC | Limited Liability Company |
| L, l | Liter(s) | LLC | Lessons Learned Corner |
| La | Lanthanum | LLNL | Lawrence Livermore National Laboratory |
| LAGP | Lithium aluminum germanium phosphate | L/min, l/min | Liter(s) per minute |
| LAH | Lithium aluminum hydride ($LiAlH_4$) | LMWO | Lanthanum molybdenum tungsten oxide (<i>e.g.</i> , $La_2Mo_{1.8}W_{0.2}O_{9-x}$) |
| λ | Lambda, hydration number | LN_2 | Liquid nitrogen |
| LAMH | Lithium amide and magnesium hydride | LNG | Liquefied natural gas |
| LAMOX | Lanthanum molybdenum oxide (<i>e.g.</i> , $La_2Mo_2O_9$) | LOC | Liquid organic carrier |
| LANL | Los Alamos National Laboratory | LOHC | Liquid organic hydrogen carrier |
| LAO | Lanthanum-modified alumina | LP | Lattice parameter |
| LAS | Large aperture scatterometry | LPG | Liquefied petroleum gas |
| lb | Pound(s) | LPM | Liters per minute |
| LBM | Lattice Boltzmann method | LPR | Liquid-phase reforming |
| lbmol | Pound-mole(s) | LQ* | Dehydrogenated liquid carrier |
| LBL | Lawrence Berkeley National Laboratory | LQ*H2 | Hydrogenated liquid carrier |
| LC | Liquid carrier; Low concentration | LRIP | Low rate initial production |
| LCA | Life cycle assessment; Life-cycle analysis | LRS | Laser raman spectroscopy |
| LCC | Life cycle cost | LS | Larger Stations |
| LCC | $La_{0.7}Ca_{0.3}CrO_{3-\delta}$ | LSAC | Low surface area carbon |
| LCH ₂ | Hydrogenated liquid carrier; Compressed hydrogen produced from liquid hydrogen | LSC | Lanthanum strontium cobalt oxide, (La, Sr) $CoO_{3\delta}$, strontium-doped lanthanum cobaltite, $La_{0.8}Sr_{0.2}CoO_{3+\delta}$ |
| LCHPP | Low Cost Hydrogen Production Platform (DOE Program Title) | LSCF | Lanthanum strontium cobalt iron oxide, (La, Sr)(Co, Fe)O ₃ |
| LCMS | Liquid chromatography-mass spectroscopy | LSCF7328 | La-Sr-Cu-Fe-O |
| LCOE | Levelized cost of electricity | LSCM | Lanthanum strontium chromium manganese oxide, (La, Sr)(Cr, Mn)O ₃ |
| L/D | Length to diameter ratio | LSCr | Lanthanum strontium chromium oxide, (La, Sr)CrO ₃ |
| LDV | Light-duty vehicle | LSM | Lanthanum strontium manganese |
| LED | Light emitting diode | LSMO | Lanthanum strontium manganese oxide, (La, Sr)MnO ₃ , strontium-doped lanthanum manganite, $La_{0.8}Sr_{0.2}MnO_{3+\delta}$ |
| LEED | Low-energy electron diffraction | LST | Lanthanum strontium titanium oxide, (La, Sr) TiO ₃ |
| LEL | Lower explosion limit | | |
| LFG | Landfill gas | | |
| LFL | Lower flammability limit | | |
| L/h, l/h | Liter(s) per hour | | |
| LH2, LH ₂ | Liquid hydrogen | | |

| | | | |
|-------------------------|---|----------------------|--|
| LSV | Lanthanum strontium vanadate; Linear sweep voltammetry | MBMS | Molecular beam mass spectrometry |
| LT | Low-temperature | M-BOP | Mechanical balance of plant |
| LTDMS | Laser induced thermal desorption mass spectrometry | MBRC | Miles between roadcall |
| LUMO | Lowest unoccupied molecular orbital | MBWR | Modified Benedict Webb Rubin |
| m | Meter(s) | MC | Monte Carlo |
| M | Mole, molar | MC | Methyl cellulose |
| M | Million | mC ² | Multi-component composite (membrane) |
| m ² | Square meter(s) | MCB | Marine Corps Base |
| m ² /g | Square meter(s) per gram | mC-cm ⁻² | MilliCoulomb(s) per square centimeter |
| m ² /s | Square meter(s) per second | MCEL | Millenium Cell, Inc. |
| m ³ | Cubic meter(s) | MCFC | Molten carbonate fuel cell |
| M31 | Arkema's first-generation membrane candidate | mCHP | Micro-combined heat and power |
| M41 | Arkema's second-generation membrane candidate | μc-Si | Microcrystalline silicon |
| M43 | Arkema's third-generation membrane candidate | MDES | Methyl-diethoxy silane |
| M51, M52, M53 | Arkema's membanes incorporating phosphonic acid | mdip | 5,5'-methylene-di-isophthalate |
| M70 | Arkema's fourth-generation membrane candidate | MEA | Membrane electrode assembly |
| MA | Mass activity; methyl acrylate | MeAB | Methylamine borane |
| MA3T | Market Acceptance of Advanced Automotive Technologies | MEAM | Modified embedded atom method |
| μA | Micro ampere(s) | MEC | Microbial electrolysis cell; Minimum explosive concentration |
| mA | MilliAmps (s) | MeCN | Acetonitrile |
| MA | Mass activity | MEIC | Mixed electronic and ionic conducting (membranes) |
| M-AB | Metal ammonia-borane | MEMS | Micro-electro-mechanical systems |
| MAB, M-AB | Metal amidoboranes | MeOH | Methanol |
| μA/cm ² | Micro ampere(s) per square centimeter | meq | Milliequivalents |
| mA/cm ² | Milliamp(s) per square centimeter | meq/g | Milliequivalents/gram |
| MARKAL | Market Allocation Model - A generic, multi-sector energy model developed by the Energy Technology Systems Analysis Program of the International Energy Agency | MeV | Mega electron volt |
| MAS | Magic angle spinning | mf | Mass fraction |
| MAS ¹¹ B-NMR | Magic angle spinning boron-11 nuclear magnetic resonance spectroscopy | Mg | Megagram(s) |
| MAS-NMR | Magic angle spinning nuclear magnetic resonance | μg | Microgram(s) |
| MATI | Modular Adsorption Tank Insert | mg | Milligram(s) |
| MAWP | Maximum allowable working pressure | MgCl ₂ | Magnesium chloride |
| MB | Megabyte | mg/cm ² | Milligram(s) per square centimeter |
| MBE | Molecular beam epitaxy | MgH ₂ | Magnesium hydride |
| | | MgH ₂ @C | MgH ₂ incorporated in carbon scaffold |
| | | MgO | Magnesium oxide |
| | | Mg(OH) ₂ | Magnesium hydroxide |
| | | mgPt/cm ² | Milligram (s) of platinum per square centimeter |
| | | MH, M-H | Metal hydride |
| | | MHC | Metal hydride-based compressor |
| | | MHCoE | Metal Hydride Center of Excellence |
| | | MHE | Material handling equipment |
| | | MHz | Megahertz |

XIV. Acronyms, Abbreviations and Definitions

| | | | |
|--------------------------------|---|--------------------|--|
| mi | Mile(s) | MPHI | Methylperhydroindole |
| μCHP | Micro-combined heat and power | MPL | Microporous layer |
| μCHX | Microscale combustor/heat exchanger | MPMC | Massively Parallel Monte Carlo |
| MIE | Minimum ignition energy | mpy | Mils per year |
| MIEC | Mixed ionic and electronic conduction | MQMAS | Multiple quantum magic angle spinning |
| mi/kg | Mile(s) per kilogram | MR | Membrane reactor |
| mil | Millimeter(s) | MRCAT | Materials Research Collaborative Access Team |
| min | Minute(s) | MREC | Microbial reverse-electrodialysis electrolysis cell |
| MIT | Massachusetts Institute of Technology | MRI | Magnetic resonance imaging |
| MiTi® | Mohawk Innovative Technologies Inc. | MRL | Manufacturing readiness level |
| MJ | Megajoule(s) | ms | Millisecond(s) |
| mL, ml | Milliliter(s) | MS | Mass spectroscopy; Mass spectrometry; More Stations |
| ML | Monolayer | MSAC | Mid-range carbon support; Medium surface area carbon |
| μCHP | Micro-combined heat and power | mS/cm | Milli-Siemen(s) per centimeter |
| μm | Micrometer(s); micron(s) | MS-H ₂ | Hydrogen mass spectrometry |
| μM | Micromolar | MSM | Macro-System Model |
| mM | Millimolar | MSR | Membrane steam reformer |
| mm | Millimeter(s) | MSRI | Materials and Systems Research, Inc. |
| MMBtu | Million British thermal units | MTA | Metric tonne per annum; Mass Transportation Agency |
| MM-FSW | Multi-pass, multi-layer friction stir welding | MTBF | Mean time between failure |
| MMOF | Microporous metal-organic framework | MTBR | Mean time between repairs |
| mmol | Millimole(s) | M/TC | Metal-doped templated carbon |
| μmol | Micromole(s) | M-TCPP | M = Fe, Mn, Co, Ni, Cu, Zn, H ₂ , tetrakis(4-carboxyphenyl)porphyrin |
| MMSCFD | Million standard cubic feet/day | mtorr | Millitorr |
| MMT | Million metric tonnes | μV | Microvolt(s) |
| Mn | Manganese | mV | Millivolt(s) |
| Mn ₂ O ₃ | Manganese oxide | MV | Methyl viologen |
| M-N-H | Amide/imide | mW | Milliwatt(s) |
| MnO | Manganese oxide | MW | Megawatt(s) |
| mΩ | Milli-ohm(s) | MW | Molecular weight |
| MΩ | Mega-ohm(s) | mW/cm ² | Milliwatt(s) per square centimeter |
| mΩ/cm ² | Milli-ohm(s) per square centimeter | MWCNT | Multiple-wall carbon nanotube |
| μΩ-cm ² | Micro-ohm(s) - square centimeter | MWe | Megawatt(s) electric |
| Mo | Molybdenum | MWh | Megawatt-hour(s) |
| MO | Molecular orbital; metal oxide | MWNT | Multi-wall carbon nanotube |
| MOF | Metal-organic framework | MWOE | Midwest Optoelectronics, LLC |
| mol | Mole(s) | MWth | Megawatt(s) thermal |
| mol% | Mole percent | MYPP | Multi-Year Program Plan (the Fuel Cell Technologies Program's Multi-Year Research, Development and Demonstration Plan) |
| mol/min | Mole(s) per minute | | |
| MoPc | Molybdenum phthalocyanine | | |
| MOR | Methanol oxidation reaction | | |
| MPa | Megapascal (s) | | |
| MPG, mpg | Mile(s) per gallon | | |
| MPGGE | Miles per gasoline gallon equivalent | | |
| mph | Mile(s) per hour | | |

| | | | |
|----------------------------------|--|-----------------|---|
| MYRDD, MYRD&DP | Multi-Year Research, Development and Demonstration Plan | NEED | National Energy Education Development Project |
| N | Normal (e.g., 1N H ₃ PO ₄ is 1 normal solution of phosphoric acid) | NEF | N-ethylformamide |
| N | Nitrogen atom | NEMS | National Energy Modeling System |
| N | Newton (unit of force) | NEPA | National Environmental Policy Act |
| N112 | Nafion [®] 1100 equivalent weight, 2 millimeter thick membrane | NETL | National Energy Technology Laboratory |
| N ₂ | Diatomic nitrogen | NEU | Northeastern University |
| N ₂ O | Nitrous oxide | NEXAFS | Near edge X-ray absorption fine structure |
| Na | Sodium | NFCBP | National Fuel Cell Bus Program |
| NA | North American | NFCRC | National Fuel Cell Research Center |
| Na ₂ S | Sodium sulfide | NFM | Nanoporous framework material |
| Na ₃ AlH ₆ | Trisodium hexahydroaluminate | Nfn-Pt/C | Nafion [®] -loaded Pt/C |
| NaAlH ₄ | Sodium aluminum hydride; Sodium tetrahydroaluminate; Sodium alanate | NFPA | National Fire Protection Association |
| NaBH ₄ | Sodium borohydride | ng | Nanogram |
| NaBO ₂ | Sodium metaborate | NG | Natural gas |
| NACE | National Association of Corrosion Engineers | NGCC | Natural gas combined cycle |
| NaCl | Sodium chloride | NGV | Natural gas vehicle |
| NACS | North American Catalysis Society | NH ₃ | Ammonia |
| NADH | (reduced) Nicotinamide adenine dinucleotide | NHA | National Hydrogen Association |
| NADP | Nicotinamide adenine dinucleotide phosphate | NHE | Normal hydrogen electrode |
| NADPH | Nicotinamide adenine dinucleotide phosphate | NHFC4 | National Hydrogen and Fuel Cells Codes and Standards Coordinating Committee |
| Nafion [®] | Registered Trademark of E.I. DuPont de Nemours | NHI | Nuclear Hydrogen Initiative |
| NaH | Sodium hydride | NHTSA | National Highway Traffic Safety Administration of the U.S. Department of Transportation |
| NA NG | North American natural gas | Ni | Nickel |
| NaOH | Sodium hydroxide | NICC | Natural gas Infrastructure Component Cost model |
| NAS | National Academy of Sciences | NILS | Normal interstitial lattice sites |
| NASA | National Aeronautics and Space Administration | NiMH | Nickel metal hydride |
| Nb | Niobium | NIR | Near infra-red |
| N/cm ² | Newton(s) per square centimeter | NIST | National Institute of Standards and Technology |
| Ncc | Normal cubic centimeters | NL | Normal liter(s) |
| NCNR | NIST Center for Neutron Research | NLDFT | Non-local density functional theory |
| ND | Not determined at this time | nm | Nanometer(s) |
| NDC | New delivery concept, Naphthalene-2,6-dicarboxylate | NM | Noble metal |
| nDDB | N-dodecyl benzene | Nm ³ | Normal cubic meter(s) |
| NDE | Non-destructive examination | NMHC | Non-methane hydrocarbons |
| NE | U.S. DOE Office of Nuclear Energy, Science and Technology | nmol | Nanomole(s) |
| NEB | Nudged elastic band | NMP | N-methylpyrrolidone |
| NEC | National Electrical Code | NMR | Nuclear magnetic resonance |
| | | NMSU | New Mexico State University |
| | | NMT | New Mexico Tech |
| | | NNA | Non-North American |

XIV. Acronyms, Abbreviations and Definitions

| | | | |
|-----------------------------------|--|-----------------|---|
| NNA NG | Non-North American natural gas | OCP | Open circuit potential |
| NNIF | NIST neutron imaging facility | OCSD | Orange County Sanitation District |
| NNSA | National Nuclear Security Administration | OCV | Open-circuit voltage |
| NMOC | Non-methane organic carbons | o.d.,OD | Outer diameter |
| NO ₂ | Nitric oxide | ODA | Oxygenated form of diamine |
| NO _x , NO _x | Oxides of nitrogen | ODE | Ordinary differential equation |
| NOA | Norland Optical Adhesive | OEC | Oxygen evolving complex |
| nOB | N-octyl benzene | OEM | Original equipment manufacturer |
| NP | Nanoparticle | OER | Oxygen evolution reaction |
| NPB | Neopentyl benzene | OGMC | Ordered graphitic mesoporous carbon |
| NPC | Nanoporous carbon; Normalized photocurrent | OH ⁻ | Hydroxyl radical |
| NPGM | Non-precious metal group | O&M | Operation and maintenance |
| NPMC | Non-precious metal catalyst | OMC | Ordered mesoporous carbon |
| NPD | Neutron powder diffraction | ONR | Office of Naval Research |
| NPDF | Neutron powder diffraction | ORNL | Oak Ridge National Laboratory |
| NPM | Nanostructured polymeric materials | ORNL-HTML | Oak Ridge National Laboratory High Temperature Materials Laboratory |
| NPM | Non-precious metal | ORR | Oxygen reduction reaction |
| NPPD | n-phenyl-phenylenediamine | OSC | Oxygen storage capability |
| NPS | National Park Service | OSHA | Occupational Safety and Health Administration |
| NPT | Normal pressure and temperature | OSM | Optical scatterfield microscopy |
| NPV | Net present value | o-SWNH | Oxidized single-walled nanohorn |
| NR | Nanorod | OSU | Ohio State University |
| NR ₃ | Tertiary amine | OSU | Oregon State University (Microproducts Breakthrough Institute) |
| NRC | National Research Council | OTM | Oxygen transport membrane |
| NREL | National Renewable Energy Laboratory | P | Phosphorus |
| NRELFAT | NREL Fleet Analysis Toolkit | P | Pressure |
| NSF | National Science Foundation | Pa | Pascal(s) |
| NSTF | Nano-structured thin-film | PA | Phenylacetylene; Polyamide |
| NSTFC | Nano-structured thin film catalyst | PAA | Poly(acrylic acid) |
| NT | Nanotube | PADD | Petroleum Administration for Defense District |
| NTCNA | Nissan Technical Center, North America | PAES | Poly(arylene-ether-sulfone) |
| NTE | Negative thermal-expansion | PAFC | Phosphoric acid fuel cell |
| NV | Neutron vibrational | PAN | Peroxyacetyl nitrate; Polyacrylonitrile |
| NVS | Neutron vibrational spectroscopy | PANI | Polyaniline |
| NWM | “Natural Water Management”, UTC Power’s system and cell stack design which utilizes evaporative cooling in the cell stack assembly | PAN-MA | Polyacrylonitrile with methyl acrylate |
| NYSERDA | New York State Energy Research and Development Authority | PAN-VA | Polyacrylonitrile with vinyl acetate |
| NZVI | Nano zerovalent iron | PA/PBI | Phosphoric-acid-doped polybenzimidazole |
| Ω | Ohm(s) | PAR | Photosynthetically-active radiation |
| Ωcm ² | Ohm(s) - square centimeter | PAS | Photoactive semiconductor; Photo acoustic |
| O | Oxygen | Pb | Lead |
| O ₂ | Diatomic oxygen | PB | Polyborazylene |
| O/C | Oxygen-to-carbon ratio | | |

XIV. Acronyms, Abbreviations and Definitions

| | | | |
|-------------------------------------|--|--------------------|---|
| Ph ₃ SnCl | Triphenyltin chloride | PPI | Pore(s) per inch |
| Ph ₃ SnSnPh ₃ | Hexaphenyldistannane | ppm, PPM | Part(s) per million |
| PHA | Process hazard analysis; Preliminary hazard analysis | ppmv | Part(s) per million by volume |
| PHEC | Perhydro-ethylcarbazole | ppmw | Part(s) per million by weight |
| PHEV | Plug-in hybrid electric vehicle | PPN | Porous polymer network |
| PHI | Perhydro-indolizidine | PPO | Phenyl phosphine oxide |
| PHIP | Para-hydrogen induced polarization | PPOR | Metalloporphyrin porous organic polymer |
| PHMI | Perhydro-methylindole | P-POSS | Phosphonic acid polyhedral oligomeric silsesquioxane |
| PhOH | Phenol | PPS | Polyphenylene sulfide |
| PI | Principal investigator | PPSA | Poly (p-phenylene sulfonic acid) |
| PI | Polyimide | PPSA | Partial pressure swing adsorption |
| P&ID | Piping and instrumentation diagram; Process and instrumentation diagram | PPSU | Polyphenylsulfone |
| PIL, pIL | Protic ionic liquid | PPy | Polypyrrole |
| PIM, pIM | Protic ionic membrane | Pr | Praseodymium |
| pK _a | Acid dissociation constant | PR | Pressure ratio |
| PLC | Programmable logic controller | PRA | Probabilistic risk assessment |
| PLLA | Poly-L-lactic acid | PRD | Pressure relief device |
| PLP | prepared Lewis pair | PrOx | Preferential oxidation |
| PLRS | Planar laser Raleigh scatter | PRSV | Peng-Robinson Stryjek-Vera |
| PLS | Polymer-layered silicate | PS | Proton sponge (bis- (dimethylamino) naphthalene) |
| PM | Precious metal such as platinum | PS | Polysiloxane |
| PM | Particulate matter | PSA | Pressure swing adsorption, adsorber |
| PMG | Glycidyl methacrylate-type copolymer | PSAT | Powertrain Systems Analysis Toolkit, a vehicle simulation software package developed at Argonne National Laboratory |
| PMMA | Poly(methyl methacrylate) | PSD | Particle size distribution, pore size distribution |
| PND | Polymerized nitrogen donor | PSEPVE | Perfluoro (4-methyl-3,6-dioxaoct-7-ene) sulfonyl fluoride |
| PNNL | Pacific Northwest National Laboratory | PSf | Poly(arylene ether sulfone) |
| pO ₂ | Oxygen partial pressure | psi, PSI | Pound(s) per square inch |
| POC | Proof of concept | PSI | Photosystem I |
| POCOP | <i>P,P</i> -bis(1,1-dimethylethyl)-3-[[<i>bis</i> (1,1-dimethylethyl)phosphino]oxy]phenyl ester | psia | Pound(s) per square inch absolute |
| POF | Polymeric-organic framework; Porous organic framework | psid | Pound(s) per square inch differential |
| POM | Polyoxometallate | psig, PSIG | Pound(s) per square inch gauge |
| POP | Porous organic polymers | PSOFC | Planar solid oxide fuel cell |
| POSS | Polyhedral oligomeric silsesquioxane | PSS | Porous stainless steel; Potentiostatic scan |
| POX | Partial oxidation | PSU | Polysulfone |
| PP | Polyphosphazene; Polypropylene; Poly(phenylene) | PSU | Pennsylvania State University |
| PPA | Polyphosphoric acid; Polyphthalamide | Pt | Platinum |
| ppb | Part(s) per billion | PT | Phosphazene trimer |
| ppbv | Part(s) per billion by volume | P-T | Pressure-temperature |
| PPDSA | Poly (p-phenylene disulfonic acid) | Pt ₃ Co | Platinum-cobalt alloy |
| PPE | Porous polyethylene | Pt ₃ Fe | Platinum-iron alloy |
| PPI | Plug Power, Inc. | | |

| | | | |
|--------------------|--|----------------------|---|
| Pt ₃ Ni | Platinum-nickel alloy | QRA | Quantitative risk assessment |
| PTA | Phosphotungstic acid | Qst | Isosteric heats of adsorption |
| Pt/AC/BC/IRMOF-8 | Isorecticular metal organic framework (MOF) doped with platinum supported on activated carbon, and further coupled to MOF with a bridging compound | R | Universal or ideal gas constant, 8.314472 J · K ⁻¹ · mol ⁻¹ |
| Pt/AX-21 | Pt-doped microporous carbon AX-21 | RAMAN | A spectroscopic technique |
| Pt/C | Platinum/carbon | RAS | Russian Academy of Sciences |
| PTC | Production tax credit | RBS | Rutherford back scattering |
| PTFE | Teflon [®] – poly-tetrafluoroethylene | RC | Resistance-capacitance; Research cluster |
| Pt-FePO | Platinum iron phosphate | RCD | Rated current density |
| PTM | Proton transport membrane | RCS | Regulations codes and standards |
| PtML | Platinum monolayer | Rct | Charge transfer resistance |
| Pt-MM | Platinum group mixed metal | RCWA | Rigorous couples waveguide analysis |
| Pt-NH | Platinum decorated carbon nano-horns | R&D | Research and development |
| PtO | Platinum oxide | RD&D, R,D&D | Research, development & demonstration |
| PtO ₂ | Platinum dioxide | RDE | Rotating disk electrode |
| PtRu | Platinum ruthenium | Re | Rhenium |
| Pt-SWNH | Platinum decorated single-walled nanohorns | ReaxFF | Reactive force field large-scale molecular dynamic calculations |
| Pt-TaPO | Platinum tantalum phosphate | REC | Renewable energy credit |
| PTTPP | Poly-tetrakis(3,5-dithiophen-2-ylphenyl)-porphyrin | RED | Reverse electro dialysis |
| PTW | Pump to wheels | REWP | Renewable Energy Working Party |
| PV | Photovoltaic; Present value | Rf | Generic fluoroalkyl group |
| PVA | Polyvinyl alcohol | RF, rf | Radio frequency |
| PVC | Polyvinyl chloride | RFC | Regenerative fuel cell |
| PVD | Physical vapor deposition | RFP | Request for proposals |
| PVDC | Poly-vinylidene chloride | RFT | Reactive flow-through |
| PVDF | Polyvinylidene fluoride | RGA | Residual gas analyzer (analysis) |
| PVP | Polyvinylpyrrolidone | Rh | Rhodium |
| PVPP | Polyvinyl pyridinium phosphate | RH | Relative humidity |
| PVT, P-V-T | Pressure-Volume-Temperature | RHE | Reference hydrogen electrode; Reversible hydrogen electrode |
| PXRD | Powder X-ray diffraction | RHLC | Relative humidity/load cycle test |
| PyC | 4-pyrazole carboxylate | ρ_a | Apparent density of activated carbon |
| PzDC | 2,8-pyrazabole dicarboxylate | \tilde{n}_{ad,H_2} | Adsorbate hydrogen density in micropores |
| Q | Neutron momentum transfer | RIXS | Resonant inelastic X-ray scattering spectra |
| Q1, Q2, Q3, Q4 | Quarters of the fiscal year | RMS | Root mean square |
| QC | Quality control | RNA | Ribo nucleic acid |
| QCM | Quartz crystal microbalance | RNG | Renewable natural gas |
| QE | Quantum efficiency | ROI | Return on investment |
| QENS | Quasielastic neutron scattering | ROM | Rough order of magnitude |
| QLRA | Qualitative risk analysis | ROMP | Ring-opening metathesis polymerization |
| QMC | Quantum Monte Carlo | ROW | Right of way |
| QNS | Quasielastic neutron scattering | RPC | Ruthenium-polypridyl complex |
| | | RPI | Rensselaer Polytechnic Institute |
| | | rpm | Revolution(s) per minute |

XIV. Acronyms, Abbreviations and Definitions

| | | | |
|------------------|--|--------------------------------|---|
| RPN | Risk priority number | SD | Standard deviation; System dynamics |
| RPS | Renewable portfolio standard | SDAPP | Sulfonated Diels-Alder polyphenylene |
| RPSA | Rapic pressure swing adsorption | SDAPPe | Sulfonated Diels-Alder polyphenylene ether |
| RRDE | Rotating ring disc electrode | SDC | Samarium-doped ceria |
| RSOFC | Reversible solid oxide fuel cell | sDCDPS | 3,3'-disulfonate-4,4'-dichlorodiphenylsulfone |
| RT | Room temperature | SDE | SO ₂ -depolarized electrolyzer |
| RTIL | Room temperature ionic liquid | SDO | Standards development organization |
| RTO | Ruthenium-titanium oxide | Se | Selenium |
| Ru | Ruthenium | SE | Secondary electron; spectroscopic ellipsometry |
| s | Second(s) | sec | Second(s) |
| S | Siemen(s) | SECA | Solid State Energy Conversion Alliance |
| S | Sulfur | SECM | Scanning electrochemical microscope |
| -S | Sulfur-deprived | SEM | Scanning electron microscopy; Scanning electron microscope |
| SA | Specific amperage | SEOS | Simple equation of state |
| SA | Surface area | SERA | Scenario Evaluation, Regionalization and Analysis |
| SA | Sulfur-ammonia thermochemical water-splitting cycle; System Architect | SERC | Schatz Energy Research Center |
| SAE | SAE International, originally known as the Society of Automotive Engineers | SET | Surface energy treatment |
| SAFC | Solid acid fuel cell | SF | Safety factor; Polystyrene-b-PFPO |
| SAH | Sodium aluminum hydride | SF ₆ | Sulfur hexafluoride |
| SAM | Scanning Auger microscopy | SFA | Sulfonic acid |
| SAMPE | Society for the Advancement of Material and Process Engineering | SFC2 | SrFeCo _{0.5} O _x |
| SANS | Small angle neutron scattering | SFM | Sr ₂ Fe _{1.5} Mo _{0.5} O _{6.8} |
| SAS | Styrene-acrylonitrile-vinylsulfate | SFT | Sr-Fe-Ti oxide |
| SASSP | Solvent assisted solid state processing | SFTI | Sr _{0.1} Fe _{0.9} Ti _{0.10} O _x |
| SAXS | Small angle X-ray scattering | SG | Shale gas |
| SBAB | Sec-butylamineborane | SGD | Spontaneous galvanic displacement; System gravimetric density |
| S _{BET} | BET specific surface area | SHE | Standard hydrogen electrode |
| SBH | Sodium borohydride | Si | Silicon |
| SBIR | Small Business Innovation Research | S-I | Sulfur-iodine |
| Sc | Scandium | SI | Sulfur-iodine cycle; Spectrum image |
| S/C | Steam to carbon ratio | Si ³ N ⁴ | Silicon nitride |
| SCC | Stress corrosion cracking | SiC | Silicon carbide |
| sccm, SCCM | Standard cubic centimeter(s) per minute | SiCN | Silicon carbonitride |
| SCE | Saturated calomel electrode | SIMS | Secondary ion emission spectroscopy |
| SCF, scf | Standard cubic feet; Supercritical fluid | Si-NS | Silica nanosprings |
| scfd | Standard cubic feet per day | SiO ₂ | Silicon dioxide |
| SCFH, scfh | Standard cubic feet per hour | SIU | Southern Illinois University |
| SCFM | Standard cubic feet per minute | sL | Standard liter (0°C, 1 atm) |
| S/cm | Siemen(s) per centimeter | slpm, slm, sL/min | Standard liter(s) per minute |
| SCOF | Single cell with open flowfield | SMART | Specific, measurable, attainable, relevant, timely |
| SCR | Selective catalytic reduction; Semi-conductor rectifier | | |
| ScSZ | Scandia-stabilized zirconia | | |

| | | | |
|------------------|--|--------------------|---|
| SMR | Steam methane reformer; Steam methane reforming | SR | Steam reformer; Steam reforming; Salinity ratio; Stoichiometric ratio |
| SMR-ECM | Steam methane reformer with electrochemical purifier | SRNL | Savannah River National Laboratory |
| SMR-PSA | Steam methane reformer with pressure swing adsorption | SrO | Strontium oxide |
| SMT | Single-molecule trap | SrTiO ₃ | Strontium titanate |
| Sn | Tin | SS | Stainless steel |
| SNG | Substitute natural gas | SSA | Specific surface area |
| SNL | Sandia National Laboratories | SSAWG | Storage System Analysis Working Group |
| SNLL | Sandia National Laboratory Livermore | SSC | Short side-chain; Structure, system, and component |
| SNR | Signal-to-noise ratio | SSNMR | Solid-state nuclear magnetic resonance |
| SNS | Spallation neutron source | SSRL | Stanford Synchrotron Radiation Laboratory |
| SNTT | Spiral notch torsion test | SSWAG | Storage System Working Analysis Group |
| SLAC | Stanford Linear Accelerator Center | STEM | Scanning transmission electron microscopy |
| SLPH | Standard liter(s) per hour | STEM | Science, technology, engineering, and mathematics |
| SLPM | Standards liter(s) per minute | STH | Solar-to-hydrogen |
| SLT | Strontium-doped lanthanum titanate | STM | Scanning tunneling microscopy |
| SnO | Tin oxide | STMBMS | Simultaneous thermogravimetric modulated beam mass spectrometer |
| SnO ₂ | Tin oxide | STP | Standard temperature and pressure |
| SO ₂ | Sulfur dioxide | STS | Scanning tunneling spectroscopy |
| SO ₃ | Sulfur trioxide | STTP | Shared Technology Transfer Project |
| SOC | State-of-charge | STTR | Small Business Technology Transfer |
| SOEC | Solid oxide electrolysis cell; Solid oxide electrolyzer cell | S _u | Ultimate tensile strength |
| SOFC | Solid oxide fuel cell | SU/SD | Start-up and shut-down |
| SOFEC | Solid oxide fuel-assisted electrolysis cell | SUNY-ESF | State University New York Environmental Science Forestry |
| SOM | Solid-oxide oxygen-ion-conducting membrane | SV | Space velocity |
| SORFC | Solid oxide regenerative fuel cell | SVD | System volumetric density |
| SOTA | State of the art | SW | Square wave |
| SOW | Statement of work | SWCNH | Single-wall carbon nanohorn |
| SOx | Oxides of sulfur | SWCNT | Single-walled carbon nanotube |
| sPAES | Sulfonated poly(arylene ether sulfone) | SWNH | Single-walled nanohorn |
| SPE | Solid phase epitaxial | SWNT | Single-wall nanotube |
| SPEEK | Sulfonated poly(ether ether ketone) | SwRI® | Southwest Research Institute® |
| SPEK | Sulfonated poly-etherketone-ketone | S _y | Yield strength |
| SPEKK | Sulfonated polyether(ether ketone ketone) | SYT | Yttrium-doped strontium titanate |
| SPEX | Type of milling machine | T | Temperature |
| SPM | Scanning probe microscope | T, t | Ton, tonne |
| sPOSS | Sulfonated octaphenyl polyhedral oligomeric silsesquioxanes | T | Tesla (unit of magnetic induction) |
| S-PPSU | Sulfonated polyphenylsulfone | t | Time |
| SPS | Spark plasma sintering | T _{1bar} | Temperature at which equilibrium pressure of hydrogen is 1 bar for a hydrogen exchange reaction |
| sq. in. | Square inch(es) | Ta | Tantalum |
| Sr | Strontium | | |

XIV. Acronyms, Abbreviations and Definitions

| | | | |
|--|--|---------------------------------|---|
| TA | Terephthalic acid | tf-Si | Thin-film silicon |
| TAG | Technical Advisory Group | TFSI | bis(Trifluoromethylsulfonyl)imide |
| TAMU | Texas A&M University | TFVE | Trifluorovinyl ether |
| TaON | Tantalum oxynitride | T _g , T _g | Glass transition temperature |
| TaPO | Tantalum phosphate | TG | Thermogravimetric; Theory Group |
| TBAB | Tetra- <i>n</i> -butylammonium bromide | TGA | Thermal gravimetric analysis; Thermogravimetric analysis; Thermogravimetric analyzer |
| TBA ₂ B ₁₂ H ₁₂ | Tetra- <i>n</i> -butylammonium dodecahydrododecaborate | TGA-DSC | Thermo-gravimetric analysis-differential scanning calorimetry |
| TBABh | Tetra- <i>n</i> -butylammonium borohydride | TGA-MS | Thermogravimetric analysis-mass spectrometer |
| TBA-PF ₆ | Tetra- <i>n</i> -butylammonium hexafluorophosphate | TG-DTA | Thermo-gravimetric/differential thermal analyzer |
| TBD | To be determined | THF | Tetrahydrofuran |
| TBMD | Tight-binding molecular dynamic | Ti | Titanium |
| TC | Templated carbon | TiCl ₃ | Titanium trichloride |
| TC | Thermocouple | TiF ₃ | Titanium trifluoride |
| TCCR | Transparent, conducting and corrosion resistant | TiH ₂ | Titanium hydride |
| TCD | Thermal conductivity detector | Ti-IRMOF-16 | Titanium (Ti) intercalated IRMOF-16 |
| TCNE | Tetracyanoethylene | TiO ₂ | Titanium dioxide (anatase) |
| TCO | Transparent conductive oxide | TIVM | Toroidal intersecting vane machine |
| TDDFT | Time-dependent density functional theory | TKK | Tanaka Kikinzoku Kogyo K. K. |
| TDLAS | Tunable diode laser absorption spectroscopy | <i>Tla</i> | Truncated light-harvesting chlorophyll antenna |
| TDS | Transitional demand scenario | <i>tla1</i> | Mutant of the Tla1 gene (GenBank Assession No. AF534570) |
| Te | Tellurium | <i>tlaR</i> | Mutant of unknown gene with a truncated light-harvesting chlorophyll antenna |
| te | Metric ton or tonne (1,000 kg) | <i>tlaX</i> | Mutant of unknown gene with a truncated light-harvesting chlorophyll antenna |
| TEA | Triethylamine | TM | Transition metal |
| TEA ₂ B ₁₂ H ₁₂ | Triethylammonium dodecahydrododecaborate | TMA | Trimethylamine; Trimethylaluminum |
| TEAA | Triethylamine alane adduct | TMA | Thermal mechanical analyzer |
| TEAB | Tetraethyl ammonium borohydride | TMAA | Trimethylamine alane adduct |
| TEAH | Tetraethylammonium hydroxide | TMAB | Tetramethylammonium borohydride |
| TEAMS | tetraethylammonium methane sulfonic | TMAH | Tetramethylammonium hydroxide |
| TED | Triethylene-diamine | TMB | Trimethylborate |
| TEDA | Triethylenediamine | TMEDA | Tetramethylethane-1,2-diamine; <i>N</i> ¹ , <i>N</i> ¹ , <i>N</i> ² , <i>N</i> ² - tetramethylethane-1,2-diamine |
| TEM | Transmission electron microscopy | TMG | Tetramethyl guanidine |
| TEOA | Triethanolamine | TMOS | Tetramethoxy silane |
| TEOM | Tapered element oscillating microbalance | TMPP | Tetramethoxyphenyl porphyrins |
| TEOS | Tetra-ethoxy silane | TMPS | Trimethoxyl phenyl silane |
| tf | Thin film | TMPyP | Tetramethylpyridylporphine |
| Tf | Trifluoromethane sulfonate, or triflate anion (CF ₃ SO ₃ ⁻) | TNA | Titania nanotube array |
| TFA | Trifluoromethanesulfonic acid | TNT | Trinitrotoluene |
| TFAc | Trifluoroacetate | | |
| TFE | Tetrafluoroethylene | | |
| TFMPA | Trifluoromethylphosphonic acid | | |
| TFMSA | Trifluoromethane sulfonic acid | | |
| TF-RDE | Thin film rotating disk electrode | | |

| | | | |
|----------|--|-------------|--|
| TOC | Total organic content | um | Micrometer(s) |
| TOF | Turnover frequency | UM | University of Michigan |
| ToF-SIMS | Time-of-flight secondary ion spectroscopy | UMC | Unsaturated metal centers |
| TPA | Tripropylamine; Temperature-programmed adsorption | UMC | Ultramicroporous carbon |
| TPAH | Tetra-n-propylammonium hydroxide | UMCP | University of Maryland College Park |
| TPB | Triple phase boundary | UMSL | University of Missouri – St. Louis |
| TPD | Tonne(s) per day | UN | United Nations |
| TPD | Thermally programmed desorption; Temperature-programmed desorption | UNB | University of New Brunswick |
| TPDMS | Temperature-programmed desorption mass spectrometry | UNCC | University of North Carolina at Charlotte |
| TPPS | 5,10,15,20-tetrakis(4-sulfonatophenyl) porphyrin | UNECE | United Nations Economic Commission for Europe |
| TPO | Temperature-programmed oxidation | UNLV | University of Nevada, Las Vegas |
| TPP | Tetraphenyl porphyrin | UNLVRF | UNLV Research Foundation |
| TPR | Temperature-programmed reduction | UNM | University of New Mexico |
| TPRD | Thermally-activated pressure relief device | UNR | University of Nevada, Reno |
| TPS | 3-(trihydroxysilyl)-1-propane-sulfonic acid | UP-DW | Ultra-pure distilled water |
| TPV | Through plate voltage | UPE | Ultra-high molecular weight polyethylene |
| TRA | Technology Readiness Assessment | UPL | Upper potential limit |
| TRAIN | TrainingFinder Realtime Affiliate Network | UPS | Ultraviolet photoelectron spectroscopy |
| TRL | Technology readiness level | U.S. | United States |
| TRO | $\text{RuO}_2\text{-TiO}_2$ | US06 | Environmental Protection Agency vehicle driving cycle |
| Trityl | Chemical blocking group used to protect amines | USA | United States of America |
| tr. oz. | Troy ounce | USANS | Ultra-small angle neutron scattering |
| TW | Triangel wave | USB | Universal serial bus |
| UC | University of California | USC | University of South Carolina |
| UCB | University of California, Berkeley | USC | University of Southern California |
| UCF | University of Central Florida | USCAR | United States Council for Automotive Research, U.S. Cooperative Automotive Research |
| UCI | University of California, Irvine | U.S. DRIVE | United States Driving Research and Innovation for Vehicle efficiency and Energy sustainability |
| UCLA | University of California, Los Angeles | USFCC | United States Fuel Cell Council |
| UCONN | University of Connecticut | USM | University of Southern Mississippi |
| UCSB | University of California, Santa Barbara | USTAG | U.S. Technical Advisory Group |
| UDDS | Urban Dynamometer Driving Schedule | UT | University of Toledo |
| UEL | Upper explosive limit | UT | University of Tennessee |
| UFL | Upper flammability limit | UTC, UTC FC | United Technologies Corporation Fuel Cells |
| UGA | University of Georgia, Athens | UTC | University of Tennessee, Chattanooga |
| UH | University of Hawaii | UTCP | UTC Power |
| UHP | Ultra-high purity | UTRC | United Technologies Research Center |
| UHV | Ultra-high vacuum | UV | Ultraviolet |
| UIUC | University of Illinois, Urbana-Champaign | UV-vis | Ultraviolet-visual |
| UL | Underwriters Laboratory | UW | University of Washington |
| ULAM | Ultra-low-angle microtomy | V | Vanadium |
| ULSD | Ultra-low sulfur diesel | | |

XIV. Acronyms, Abbreviations and Definitions

| | | | |
|--------------------|---|-----------------------|---|
| V | Volt | W/cm ² | Watt(s) per square centimeter |
| VA | Vinyl acetate | WDD | Water displacement desorption |
| VAC | Volts alternating current | We, W _e | Watt(s) electric |
| VACNTs | Vertically aligned carbon nanotubes | WG | Working group |
| VANTA | Vertically aligned nanotube arrays | WG-12 | Working Group 12 |
| VASP | Vienna ab initio simulation package | WGS | Water-gas shift |
| VaTech | Virginia Polytechnic Institute and State University | WGSMR | Water-gas shift membrane reactor |
| VB | Valence band | WGSR | Water-gas shift reactor |
| VBM | Valence band minimum | Wh | Watt-hour(s) |
| VBM | Valence band maximum | W(H ₂) | Gravimetric hydrogen storage capacity |
| VC | Vanadium carbide | W-h/kg | Watt-hour(s) per kilogram |
| VC | Vulcan carbon | W-h/L, Wh/liter, Wh/L | Watt-hour(s) per liter |
| VDC | Volts direct current | WHSV | Weight hourly space velocity |
| VDF | Vinylidene fluoride | Wind2H2 | Wind to hydrogen demonstration project |
| VDOS | Vibrational density of states | W/kg | Watt(s) per kilogram |
| vdW | van der Waals | W/L, W/l | Watt(s) per liter |
| vdW-DF | van der Waals density function | W/m-K, W/m.K, W/mK | Watt(s) per meter-Kelvin (unit of thermal conductivity) |
| VFA | Volatile fatty acid | WMO | World Meteorological Organization |
| VFS | Vehicle fueling station | WO ₃ | Tungsten trioxide |
| V(H ₂) | Volumetric hydrogen adsorption capacity | WP.29 | Working Party 29 - World Forum for Harmonization of Vehicle Regulations |
| V(H ₂) | Volumetric hydrogen storage capacity | Wppm | Weight part(s) per million |
| VHSV | Volumetric hourly space velocity | WSTF | White Sands Test Facility |
| VHTR | Very high temperature gas-cooled nuclear reactor | wt | Weight |
| VHTS | Virtual high-throughput screening | Wt | Watt(s) thermal |
| VI | Venter Institute | wt%, wt.% | Weight percent (percent by weight) |
| V-I, V/I | Voltage – current | WTP | Well to pump |
| VIM/VAR | Vacuum induction melting/vacuum arc remelting | WTP | Water transport plate |
| VIR | Voltage-current-resistance | WTPP | Well-to-power plant |
| VIS | Visible light at 400-700 nm | WTT | Well-to-tank |
| V _{mp} | Micropore volume | w/v | Weight by volume |
| VMT | Vehicle miles traveled | WTW | Well-to-wheels |
| VOC | Volatile organic compound | X- | an anionic ligand such as chloride |
| VOC | Voltage open circuit | XAFS | X-ray absorption fine structure |
| Vol., vol. | Volume | XANES | X-ray absorption near-edge spectroscopy |
| vol% | Volume percent | XAS | X-ray absorption spectroscopy |
| V _{pore} | Total pore volume | XC72 | High-surface-area carbon support made by Cabot |
| VT | Virginia Tech | XES | X-ray emission spectroscopy |
| W | Tungsten | XPS | X-ray photoelectron spectroscopy, X-ray photon spectroscopy, X-ray photoemission spectroscopy, X-ray photoluminescence spectroscopy |
| W | Watt(s) | | |
| WAXD | Wide-angle X-ray diffraction | | |
| WAXS | Wide angle X-ray scattering | | |
| WBS | Work breakdown schedule | | |
| WC | Tungsten carbon; Tungsten carbide | | |

XIV. Acronyms, Abbreviations and Definitions

| | | | |
|---------|--|------------------|--|
| XPS-UPS | X-ray photoelectron-ultraviolet photoelectron spectroscopy | ZIF | Zeolitic imidazolate framework |
| XRD | X-ray diffraction | ZMOF | Zeolite(-type) metal-organic framework |
| XRF | X-ray fluorescence | Zn | Zinc |
| Y | Yttrium | ZnO | Zinc oxide |
| yr, YR | Year | ZPE | Zero point energy |
| YSZ | Ytria-stablized zirconia | zpp | Zirconium phenyl phosphonate |
| Z | Atomic number | Zr | Zirconium |
| ZEBA | Zero Emission Bay Area | ZrO ₂ | Zirconium dioxide |
| ZEV | Zero emission vehicle | ZrSPP | Zirconium phosphate sulfophenylphosphonate |
| ZHS | Zinc hydroxystannate | ZVI | Zerovalent iron |

XV. Primary Contacts Index

| | |
|------------------------------------|--------------------------------|
| A | |
| Aceves, Salvador | .III.11 |
| Adzic, Radoslav | V.D.6 |
| Ahluwalia, Rajesh | IV.E.1, V.A.4 |
| Ainscough, Chris | V.A.8 |
| Anton, Don | IV.D.1 |
| Arif, Muhammad | V.A.6 |
| Atanasoski, Radoslav | V.D.3 |
| Autrey, Tom | IV.H.16 |
| Ayers, Katherine | II.D.2, II.D.5 |
| B | |
| Baxter-Clemmons, Shannon | IX.1, X.4 |
| Bessette, Norman | V.J.2 |
| Blanchet, Scott | V.E.3 |
| Blekhman, David | VII.7 |
| Block, David | VII.6 |
| Borup, Rod | V.E.2 |
| Brooks, Kriston | X.2 |
| Brosha, Eric | VIII.8 |
| Burgess, Robert | VIII.3 |
| Busby, Colin | VI.2 |
| Bush, Brian | XI.1 |
| C | |
| Cai, Mei | IV.D.7 |
| Chabal, Yves | IV.H.2 |
| Chen, Jihua | IV.H.19 |
| Chen, Ken | V.F.3 |
| Chuang, Steven | V.K.1 |
| Cole, Vernon | V.F.5 |
| Conradi, Mark | IV.H.15 |
| Conti, Amedeo | V.F.4 |
| Czernik, Stefan | II.A.2 |
| D | |
| Dalton, Luke | II.H.2 |
| Davis, Benjamin | IV.B.2 |
| De Castro, Emory | VI.5 |
| Debe, Mark | V.D.1 |
| Dedrick, Danial | III.1 |
| Di Bella, Frank | III.7 |
| Dinh, Huyen | V.B.1 |
| Drost, Kevin | IV.D.9 |
| E | |
| Eisman, Glenn | II.C.2 |
| Elgowainy, Amgad | III.2 |
| El-Kaderi, Hani | IV.H.3 |
| Elmore, Monte | VIII.12 |
| Eudy, Leslie | VII.3 |
| F | |
| Fassbender, Linda | VIII.11 |
| Feng, Pingyun | IV.H.6 |
| Feng, Zhili | III.3 |
| Fenton, James | V.C.1 |
| Fletcher, Jim | V.G.2 |
| G | |
| Gallego, Nidia | IV.H.4 |
| Garzon, Fernando | V.D.7 |
| Gennett, Thomas | IV.C.6 |
| Ghirardi, Maria | II.G.1 |
| Goudy, Andrew | IV.A.7 |
| Graetz, Jason | IV.A.5, IV.H.12 |
| Greene, David | XI.6 |
| Gross, Karl | IV.E.2 |
| Grot, Stephen | V.C.4 |
| H | |
| Hamdan, Monjid | II.D.1 |
| Hancock, Dave | V.F.1 |
| Harris, Aaron | VIII.1, VIII.2, VIII.4, VIII.5 |
| Harrison, Kevin | II.D.3, VII.8 |
| Hennessy, Dan | XII.1 |
| Heshmat, Hooshang | III.8 |
| Heske, Clemens | II.F.4 |
| Heydorn, Ed | VII.2, VII.4 |
| Hicks, Mike | V.J.5 |
| Holladay, Jamie | IV.D.5 |
| Huda, Muhammad | II.F.7 |

XV. Primary Contacts Index

| | |
|-------------------------------------|----------------------|
| J | |
| James, Brian | IV.E.4, V.A.2, V.A.3 |
| Jaramillo, Thomas | II.F.1 |
| Jensen, Craig | IV.A.2, IV.B.4 |
| Johnson, Will | VI.1 |
| K | |
| Kenny, Kevin | XII.2 |
| Kerr, John | V.D.8 |
| King, David | II.A.1 |
| King, John | XII.4 |
| Kliever, Scott | XII.5 |
| Klingler, Jim | XII.6 |
| Knudsen, Jon | III.6 |
| Koh, Carolyn | IV.H.9 |
| Kurtz, Jennifer | V.A.1, VII.9, XII.3 |
| L | |
| Larsen, Brian | V.D.14 |
| Leavitt, Mark | VI.6 |
| Lewis, Michelle | II.E.2 |
| Lin, Zhenhong | XI.8 |
| Lipinska-Kalita, Kristina | IV.G.1 |
| Lipp, Ludwig | III.9, V.C.3 |
| Liu, Paul | II.C.1 |
| Liu, Shih-Yuan | IV.B.1, IV.B.3 |
| Long, Jeffrey | IV.C.8 |
| Lueking, Angela | IV.C.5, IV.H.10 |
| M | |
| Madan, Arun | II.F.5 |
| Mahadevan, Kathya | V.A.9 |
| Maness, Pin-Ching | II.G.2 |
| Markovic, Nenad | V.D.5 |
| McDaniel, Anthony | II.E.3 |
| Melaina, Marc | XI.3, XI.4, XI.9 |
| Melis, Tasios | II.G.4 |
| Ming, Quentin | V.J.4 |
| Mintz, Marianne | XI.11 |
| Mittelstadt, Cortney | V.C.2, V.F.6 |
| Mohapatra, Satish | VI.2 |
| Mondloch, Joseph | IV.C.10 |
| More, Karren | V.A.5 |
| Mukerjee, Sanjeev | V.D.11 |
| Mukundan, Rangachary | VE.5 |
| Murthi, Vivek | VD.2 |
| Myers, Deborah | VE.1 |
| N | |
| Nagle, Barbara | IX.3 |
| Newhouse, Norman | IV.D.10 |
| Norman, Timothy | II.H.1 |
| Norris, Bob | IV.F.1 |
| O | |
| Ogitsu, Tadashi | II.F.3 |
| Olsen, Raina | IV.C.9 |
| Owejan, Jon | V.F.7 |
| P | |
| Parilla, Phil | IV.C.11 |
| Patterson, Timothy | VE.4 |
| Pecharsky, Vitailij | IV.H.11 |
| Perry, Randy | VE.7 |
| Petrecky, James | XII.7, XII.8 |
| Petri, Randy | V.J.3 |
| Pfeifer, Peter | IV.C.3, IV.H.7 |
| Pivovar, Bryan | V.D.4 |
| Popov, Branko | V.D.13 |
| Power, Philip | IV.H.17 |
| R | |
| Ramanathan, Shriram | V.J.6 |
| Ramani, Vijay | V.D.10 |
| Ramsden, Todd | X.3 |
| Rawls, George | III.5 |
| Reiter, Joseph | IV.D.4 |
| Rinebold, Joel | IX.4 |
| Rivkin, Carl | VIII.6, VIII.7 |
| Roberts, Mike | II.B.1 |
| Robertson, Ian | IV.A.4 |
| Rocheleau, Richard | VII.5, X.1 |
| Rockward, Tommy | V.A.7, VIII.9 |
| Roger, Chris | V.G.1 |
| Ronnenbro, Ewa | IV.E.5 |
| Ruth, Mark | XI.7, XI.10 |

| | | | |
|---------------------|------------------|------------------|-----------------|
| S | | W | |
| Saur, Genevieve | II.D.4 | Wagener, Earl | VI.3 |
| Semelsberger, Troy | IV.D.3 | Wagner, Fred | V.D.12 |
| Simmons, Kevin | IV.F.4 | Walczyk, Dan | VI.3 |
| Singh, Prabhakar | V.K.4 | Wang, Conghua | V.H.1 |
| Smith, Barton | III.10, IV.F.2 | Wang, Michael | XI.2 |
| Sneddon, Larry | IV.H.18 | Wang, Yong | V.D.15 |
| Snurr, Randy | IV.C.4 | Warren, Dave | IV.F.3 |
| Somayazulu, Maddury | IV.H.8 | Weber, Adam | V.F.2 |
| Sprick, Sam | VII.10 | Wei, Max | V.A.10 |
| Stanfield, Eric | VI.4, VI.7, VI.8 | Weimer, Al | II.E.4 |
| Steward, Darlene | XI.5 | Weiner, Steven | VIII.10 |
| Storey, Robson | V.K.2 | Weisberg, Andrew | III.4 |
| St-Pierre, Jean | V.B.2 | Wessel, Silvia | VE.6 |
| Sullivan, Neal | V.K.3 | Weyman, Phil | II.G.3 |
| T | | Wipke, Keith | VII.1 |
| Taylor, Robin | II.E.1 | Wolverton, Chris | IV.H.13, IV.A.1 |
| Thornton, Matthew | IV.D.2 | X | |
| Tock, Kevin | V.J.1 | Xu, Liwei | II.F.6 |
| Turner, John | II.F.2, V.D.9 | Y | |
| U | | Yaghi, Omar | IV.C.2 |
| Udovic, Terry | IV.E.3 | Yildirim, Taner | IV.H.1 |
| Ulsh, Michael | VI.1 | Z | |
| V | | Zelenay, Piotr | V.G.3 |
| Vajo, John | IV.C.7 | Zhao, J.-C. | IV.A.3 |
| Valente, Pat | IX.2 | Zhou, Joe | IV.C.1 |
| Van de Walle, Chris | IV.H.14 | Zidan, Ragaiy | IV.A.6, IV.H.5 |
| van Hassel, Bart | IV.D.6 | | |
| Veenstra, Michael | IV.D.8 | | |

XVI. Hydrogen and Fuel Cells Program Contacts

Sunita Satyapal, Director

DOE Hydrogen and Fuel Cells Program
Fuel Cell Technologies Program
DOE Office of Energy Efficiency and Renewable Energy
Phone: (202) 586-2336
Email: Sunita.Satyapal@ee.doe.gov

Rick Farmer, Crosscutting Activities Team Leader

Fuel Cell Technologies Program
DOE Office of Energy Efficiency and Renewable Energy
Phone: (202) 586-1623
Email: Richard.Farmer@ee.doe.gov

John Vetrano

Materials Sciences and Engineering Division
Basic Energy Sciences Program
DOE Office of Science
Phone: (301) 903-5976
Email: John.Vetrano@science.doe.gov

Guido B. Dehoratiis, Jr.

Division of Advanced Energy Systems
DOE Office of Fossil Energy
Phone: (202) 586-2795
Email: Guido.B.Dehoratiis@hq.doe.gov

Carl Sink

Office of Gas Cooled Reactor Technologies
DOE Office of Nuclear Energy
Phone: (301) 903-5131
Email: Carl.Sink@nuclear.energy.gov

Hydrogen Production and Delivery

Sara Dillich, Acting Hydrogen Production and Delivery Team Leader

Fuel Cell Technologies Program
DOE Office of Energy Efficiency and Renewable Energy
Phone: (202) 586-7925
Email: Sara.Dillich@ee.doe.gov

Hydrogen Storage

Ned Stetson, Hydrogen Storage Team Leader
Fuel Cell Technologies Program
DOE Office of Energy Efficiency and Renewable Energy
Phone: (202) 586-9995
Email: Ned.Stetson@ee.doe.gov

Fuel Cells

Dimitrios Papageorgopoulos, Fuel Cells Team Leader
Fuel Cell Technologies Program
DOE Office of Energy Efficiency and Renewable Energy
Phone: (202) 586-5463
Email: Dimitrios.Papageorgopoulos@ee.doe.gov

Manufacturing R&D

Nancy Garland, Acting Manufacturing R&D Team Leader
Fuel Cell Technologies Program
DOE Office of Energy Efficiency and Renewable Energy
Phone: (202) 586-5673
Email: Nancy.Garland@ee.doe.gov

Technology Validation

Jason Marcinkoski, Acting Technology Validation Team Leader
Fuel Cell Technologies Program
DOE Office of Energy Efficiency and Renewable Energy
Phone: (202) 586-7466
Email: Jason.Marcinkoski@ee.doe.gov

Safety, Codes & Standards

Antonio Ruiz, Safety, Codes and Standards Team Leader
Fuel Cell Technologies Program
DOE Office of Energy Efficiency and Renewable Energy
Phone: (202) 586-0729
Email: Antonio.Ruiz@ee.doe.gov

Education

Gregory J. Kleen, Acting Education Team Leader
Fuel Cell Technologies Program
Department of Energy Golden Field Office
Phone: (720) 356-1672
Email: Gregory.Kleen@go.doe.gov

Market Transformation

Pete Devlin, Market Transformation and Interagency Coordination Manager
Fuel Cell Technologies Program
DOE Office of Energy Efficiency and Renewable Energy
Phone: (202) 586-4905
Email: Peter.Devlin@ee.doe.gov

Systems Analysis

Fred Joseck, Systems Analysis Team Leader
Fuel Cell Technologies Program
DOE Office of Energy Efficiency and Renewable Energy
Phone: (202) 586-7932
Email: Fred.Joseck@ee.doe.gov

American Recovery and Reinvestment Act (ARRA) Activities

Jim Alkire, Project Officer and Lead for Recovery Act Activities
Fuel Cell Technologies Program
DOE Office of Energy Efficiency and Renewable Energy
Phone: (720) 356-1426
Email: James.Alkire@go.doe.gov

XVII. Project Listings by State

Alabama

- V.F.5 CFD Research Corporation: Water Transport in PEM Fuel Cells: Advanced Modeling, Material Selection, Testing, and Design Optimization V-226
- V.F.5 ESI US R&D: Water Transport in PEM Fuel Cells: Advanced Modeling, Material Selection, Testing, and Design Optimization V-226

Arizona

- VI.3 Arizona State University: Adaptive Process Controls and Ultrasonics for High-Temperature PEM MEA Manufacture VI-17

Arkansas

- XII.4 FedEx Freight: Fuel Cell-Powered Lift Truck FedEx Freight Fleet Deployment XII-21

California

- II.C.1 University of Southern California, Los Angeles: Development of Hydrogen Selective Membranes/Modules as Reactors/Separators for Distributed Hydrogen Production II-23
- II.E.1 Science Applications International Corporation: Solar High-Temperature Water Splitting Cycle with Quantum Boost II-49
- II.E.1 Thermochemical Engineering Solutions: Solar High-Temperature Water Splitting Cycle with Quantum Boost II-49
- II.E.1 University of California, San Diego: Solar High-Temperature Water Splitting Cycle with Quantum Boost II-49
- II.E.3 Sandia National Laboratories: Solar Hydrogen Production with a Metal Oxide-Based Thermochemical Cycle. II-60
- II.F.1 Stanford University: Directed Nano-Scale and Macro-Scale Architectures for Semiconductor Absorbers and Transparent Conducting Substrates for Photoelectrochemical Water Splitting II-68
- II.F.1 Board of Trustees of the Leland Stanford Junior University: Directed Nano-Scale and Macro-Scale Architectures for Semiconductor Absorbers and Transparent Conducting Substrates for Photoelectrochemical Water Splitting II-68
- II.F.2 Stanford University: Semiconductor Materials for Photoelectrolysis II-74
- II.G.3 J. Craig Venter Institute: Hydrogen from Water in a Novel Recombinant Oxygen-Tolerant Cyanobacterial System. II-113
- II.G.4 University of California, Berkeley: Maximizing Light Utilization Efficiency and Hydrogen Production in Microalgal Cultures. II-118
- III.1 Sandia National Laboratories: Hydrogen Embrittlement of Structural Steels III-9
- III.3 Ben C. Gerwick Inc.: Vessel Design and Fabrication Technology for Stationary High-Pressure Hydrogen Storage. III-17
- III.4 Lawrence Livermore National Laboratory: Failure Analysis, Permeation, and Toughness of Glass Fiber Composite Pressure Vessels for Inexpensive Delivery of Cold Hydrogen III-22
- III.4 Spencer Composites Corporation: Failure Analysis, Permeation, and Toughness of Glass Fiber Composite Pressure Vessels for Inexpensive Delivery of Cold Hydrogen III-22
- III.7 HyGen Industries: Development of a Centrifugal Hydrogen Pipeline Gas Compressor III-35
- III.11 Lawrence Livermore National Laboratory: LLNL/Linde 875 bar Liquid Hydrogen Pump for High Density Cryogenic Vessel Refueling III-51
- III.11 Linde LLC: LLNL/Linde 875 bar Liquid Hydrogen Pump for High Density Cryogenic Vessel Refueling III-51

XVII. Project Listings by State

California (Continued)

| | | |
|---------|---|--------|
| IV.C.2 | University of California, Los Angeles: A Joint Theory and Experimental Project in the Synthesis and Testing of Porous COFs for Onboard Vehicular Hydrogen Storage | IV-67 |
| IV.C.6 | H2 Technology Consulting LLC: Weak Chemisorption Validation | IV-89 |
| IV.C.7 | HRL Laboratories, LLC: Room Temperature Hydrogen Storage in Nano-Confined Liquids | IV-95 |
| IV.C.8 | Lawrence Berkeley National Laboratory: Hydrogen Storage in Metal-Organic Frameworks | IV-97 |
| IV.C.11 | H2 Technology Consulting LLC: Hydrogen Sorbent Measurement Qualification and Characterization . . . | IV-109 |
| IV.D.1 | Jet Propulsion Laboratory: Hydrogen Storage Engineering Center of Excellence | IV-114 |
| IV.D.1 | California Institute of Technology: Hydrogen Storage Engineering Center of Excellence | IV-114 |
| IV.D.4 | Jet Propulsion Laboratory: Key Technologies, Thermal Management, and Prototype Testing for Advanced Solid-State Hydrogen Storage Systems | IV-129 |
| IV.D.4 | California Institute of Technology: Key Technologies, Thermal Management, and Prototype Testing for Advanced Solid-State Hydrogen Storage Systems. | IV-129 |
| IV.E.2 | H2 Technology Consulting LLC: Best Practices for Characterizing Engineering Properties of Hydrogen Storage Materials | IV-170 |
| IV.H.6 | University of California, Riverside: Synthetic Design of New Metal-Organic Framework Materials for Hydrogen Storage | IV-229 |
| IV.H.13 | University of California, Los Angeles: Theory of Hydrogen Storage in Complex Hydrides | IV-253 |
| IV.H.14 | University of California, Santa Barbara: Computational studies of hydrogen interactions with storage materials. | IV-256 |
| IV.H.17 | University of California, Davis: Heavy Cycloadditions: Reactions of Diagailene with Cyclic Polyolefins | IV-267 |
| IV.H.19 | Stanford University: Influence of Pressure on Physical Property of Ammonia Borane and its Re-Hydrogenation | IV-274 |
| V.A.8 | University of California, Irvine: Enlarging the Potential Market for Stationary Fuel Cells Through System Design Optimization | V-47 |
| V.A.10 | Lawrence Berkeley National Laboratory: A Total Cost of Ownership Model for Design and Manufacturing Optimization of Fuel Cells in Stationary and Emerging Market Applications | V-53 |
| V.A.10 | University of California, Berkeley: A Total Cost of Ownership Model for Design and Manufacturing Optimization of Fuel Cells in Stationary and Emerging Market Applications. | V-53 |
| V.D.1 | Jet Propulsion Laboratory: Advanced Cathode Catalysts and Supports for PEM Fuel Cells | V-84 |
| V.D.4 | Stanford University: Extended, Continuous Pt Nanostructures in Thick, Dispersed Electrodes. | V-107 |
| V.D.5 | Jet Propulsion Laboratory: Nanosegregated Cathode Catalysts with Ultra-Low Platinum Loading | V-111 |
| V.D.7 | University of California, Riverside: The Science and Engineering of Durable Ultralow PGM Catalysts. . . . | V-121 |
| V.D.8 | Lawrence Berkeley National Laboratory: Molecular-Scale, Three-Dimensional Non-Platinum Group Metal Electrodes for Catalysis of Fuel Cell Reactions. | V-126 |
| V.E.2 | Lawrence Berkeley National Laboratory: Durability Improvements through Degradation Mechanism Studies | V-175 |
| V.E.5 | Lawrence Berkeley National Laboratory: Accelerated Testing Validation. | V-190 |
| V.F.2 | Lawrence Berkeley National Laboratory: Fuel Cell Fundamentals at Low and Subzero Temperatures | V-211 |
| V.F.3 | Sandia National Laboratories: Development and Validation of a Two-Phase, Three-Dimensional Model for PEM Fuel Cells | V-217 |
| V.F.4 | Lawrence Berkeley National Laboratory: Transport Studies Enabling Efficiency Optimization of Cost-Competitive Fuel Cell Stacks | V-222 |
| V.J.1 | Intelligent Energy: Development and Demonstration of a New-Generation High Efficiency 10-kW Stationary Fuel Cell System. | V-272 |
| V.J.5 | University of California, Davis: Research and Development for Off-Road Fuel Cell Applications | V-289 |

California (Continued)

| | | |
|---------|--|---------|
| VI.6 | Quantum Fuel Systems Technologies Worldwide, Inc.: Development of Advanced Manufacturing Technologies for Low Cost Hydrogen Storage Vessels | VI-31 |
| VII.4 | University of California, Irvine: California Hydrogen Infrastructure Project | VII-26 |
| VII.4 | National Fuel Cell Research Center: California Hydrogen Infrastructure Project | VII-26 |
| VII.7 | California State University, Los Angeles: Sustainable Hydrogen Fueling Station, California State University, Los Angeles | VII-38 |
| VII.7 | Weaver Construction: Sustainable Hydrogen Fueling Station, California State University, Los Angeles. | VII-38 |
| VIII.1 | Sandia National Laboratories: Hydrogen Safety, Codes and Standards R&D – Release Behavior | VIII-9 |
| VIII.2 | Sandia National Laboratories: Risk-Informed Safety Requirements for H2 Codes and Standards Development. | VIII-15 |
| VIII.4 | Sandia National Laboratories: Hydrogen Materials and Components Compatibility. | VIII-22 |
| VIII.5 | Sandia National Laboratories: Component Testing for Industrial Trucks and Early Market Applications | VIII-25 |
| VIII.6 | Steele Consulting: National Codes and Standards Coordination | VIII-28 |
| VIII.10 | City of Santa Fe Springs: Hydrogen Safety Panel | VIII-45 |
| VIII.12 | California Fuel Cell Partnership: Hydrogen Emergency Response Training for First Responders | VIII-52 |
| IX.3 | University of California, Berkeley: Hydrogen Technology and Energy Curriculum (HyTEC) | IX-13 |
| IX.3 | Humboldt State University: Hydrogen Technology and Energy Curriculum (HyTEC) | IX-13 |
| X.3 | Oorja Protonics, Inc.: Direct Methanol Fuel Cell Material Handling Equipment Demonstration. | X-15 |
| XII.1 | Electricore, Inc.: Solid Oxide Fuel Cell Diesel Auxiliary Power Unit Demonstration. | XII-9 |
| XII.2 | Altery Systems, Folsom: Demonstrating Economic and Operational Viability of 72-Hour Hydrogen PEM Fuel Cell Systems to Support Emergency Communications on the Sprint Nextel Network. | XII-12 |

Colorado

| | | |
|---------|--|--------|
| II.A.2 | National Renewable Energy Laboratory: Distributed Bio-Oil Reforming | II-15 |
| II.D.3 | National Renewable Energy Laboratory: Renewable Electrolysis Integrated Systems Development and Testing | II-39 |
| II.D.3 | Spectrum Automation Controls: Renewable Electrolysis Integrated Systems Development and Testing | II-39 |
| II.D.4 | National Renewable Energy Laboratory: Hour-by-Hour Cost Modeling of Optimized Central Wind-Based Water Electrolysis Production. | II-43 |
| II.D.5 | Proton OnSite: Low-Cost Large-Scale PEM Electrolysis for Renewable Energy Storage | II-46 |
| II.E.3 | University of Colorado: Solar Hydrogen Production with a Metal Oxide-Based Thermochemical Cycle | II-60 |
| II.E.4 | University of Colorado: Solar-Thermal ALD Ferrite-Based Water Splitting Cycle | II-64 |
| II.F.2 | National Renewable Energy Laboratory: Semiconductor Materials for Photoelectrolysis. | II-74 |
| II.F.3 | Lawrence Livermore National Laboratory: Characterization and Optimization of Photoelectrode Surfaces for Solar-to-Chemical Fuel Conversion | II-79 |
| II.F.5 | MVSystems, Incorporated: Photoelectrochemical Hydrogen Production | II-89 |
| II.F.6 | National Renewable Energy Laboratory: Critical Research for Cost-Effective Photoelectrochemical Production of Hydrogen. | II-93 |
| II.G.1 | National Renewable Energy Laboratory: Biological Systems for Hydrogen Photoproduction | II-103 |
| II.G.2 | National Renewable Energy Laboratory: Fermentation and Electrohydrogenic Approaches to Hydrogen Production | II-108 |
| III.11 | Engineering, Procurement & Construction: LLNL/Linde 875 bar Liquid Hydrogen Pump for High Density Cryogenic Vessel Refueling | III-51 |
| IV.C.6 | National Renewable Energy Laboratory: Weak Chemisorption Validation | IV-89 |
| IV.C.11 | National Renewable Energy Laboratory: Hydrogen Sorbent Measurement Qualification and Characterization | IV-109 |

XVII. Project Listings by State

Colorado (Continued)

| | | |
|--------|--|---------|
| IV.D.1 | National Renewable Energy Laboratory: Hydrogen Storage Engineering Center of Excellence | IV-114 |
| IV.D.2 | National Renewable Energy Laboratory: System Design, Analysis, Modeling, and Media Engineering Properties for Hydrogen Energy Storage | IV-119 |
| IV.H.9 | Colorado School of Mines: Energy Storage in Clathrate Hydrogen Material. | IV-239 |
| V.A.1 | National Renewable Energy Laboratory: Analysis of Laboratory Fuel Cell Technology Status – Voltage Degradation. | V-11 |
| V.A.8 | National Renewable Energy Laboratory: Enlarging the Potential Market for Stationary Fuel Cells Through System Design Optimization | V-47 |
| V.B.1 | National Renewable Energy Laboratory: Effect of System Contaminants on PEMFC Performance and Durability | V-57 |
| V.B.1 | Colorado School of Mines: Effect of System Contaminants on PEMFC Performance and Durability | V-57 |
| V.D.4 | National Renewable Energy Laboratory: Extended, Continuous Pt Nanostructures in Thick, Dispersed Electrodes | V-107 |
| V.D.9 | National Renewable Energy Laboratory: Tungsten Oxide and Heteropoly Acid Based System for Ultra-High Activity and Stability of Pt Catalysts in PEM Fuel Cell Cathodes. | V-133 |
| V.D.9 | Colorado School of Mines: Tungsten Oxide and Heteropoly Acid Based System for Ultra-High Activity and Stability of Pt Catalysts in PEM Fuel Cell Cathodes | V-133 |
| V.D.9 | University of Colorado, Boulder: Tungsten Oxide and Heteropoly Acid Based System for Ultra-High Activity and Stability of Pt Catalysts in PEM Fuel Cell Cathodes | V-133 |
| V.D.14 | National Renewable Energy Laboratory: High Aspect Ratio Nano-Structured Pt-based PEM Fuel Cell Catalysts (EERE Post-Doc Fellowship) | V-159 |
| V.J.3 | Versa Power Systems: Advanced Materials for Reversible Solid Oxide Fuel Cell (RSOFC), Dual-Mode Operation with Low Degradation. | V-281 |
| V.K.3 | Colorado School of Mines: Biomass Fuel Cell Systems | V-305 |
| VI.1 | National Renewable Energy Laboratory: Fuel Cell Membrane Electrode Assembly Manufacturing R&D | VI-7 |
| VII.1 | National Renewable Energy Laboratory: Controlled Hydrogen Fleet and Infrastructure Analysis. | VII-11 |
| VII.3 | National Renewable Energy Laboratory: Technology Validation: Fuel Cell Bus Evaluations | VII-22 |
| VII.8 | National Renewable Energy Laboratory: Renewable Electrolysis Integrated System Development and Testing | VII-40 |
| VII.8 | Spectrum Automation Controls: Renewable Electrolysis Integrated System Development and Testing. | VII-40 |
| VII.9 | National Renewable Energy Laboratory: Stationary Fuel Cell Evaluation. | VII-44 |
| VII.10 | National Renewable Energy Laboratory: Next Generation H2 Station Analysis | VII-46 |
| VIII.3 | National Renewable Energy Laboratory: Component Standard Research and Development | VIII-18 |
| VIII.6 | National Renewable Energy Laboratory: National Codes and Standards Coordination | VIII-28 |
| VIII.6 | FP2 Fire Protection Engineering: National Codes and Standards Coordination | VIII-28 |
| VIII.6 | MorEvents: National Codes and Standards Coordination | VIII-28 |
| VIII.7 | National Renewable Energy Laboratory: Codes and Standards Outreach for Emerging Fuel Cell Technologies. | VIII-33 |
| VIII.7 | MorEvents: Codes and Standards Outreach for Emerging Fuel Cell Technologies | VIII-33 |
| X.3 | National Renewable Energy Laboratory: Direct Methanol Fuel Cell Material Handling Equipment Demonstration | X-15 |
| XI.1 | National Renewable Energy Laboratory: Infrastructure Analysis of Early Market Transition of Fuel Cell Vehicles. | XI-11 |
| XI.3 | National Renewable Energy Laboratory: Hydrogen Refueling Infrastructure Cost Analysis | XI-19 |
| XI.4 | National Renewable Energy Laboratory: Comparing Infrastructure Costs for Hydrogen and Electricity | XI-23 |

Colorado (Continued)

| | | |
|-------|--|--------|
| XI.5 | National Renewable Energy Laboratory: Infrastructure Costs Associated with Central Hydrogen Production from Biomass and Coal | XI-27 |
| XI.7 | National Renewable Energy Laboratory: Effects of Technology Cost Parameters on Hydrogen Pathway Succession | XI-35 |
| XI.9 | National Renewable Energy Laboratory: Resource Analysis for Hydrogen Production | XI-43 |
| XI.10 | National Renewable Energy Laboratory: Cost, Energy Use, and Emissions of Tri-Generation Systems | XI-47 |
| XII.1 | TDA Research, Inc.: Solid Oxide Fuel Cell Diesel Auxiliary Power Unit Demonstration. | XII-9 |
| XII.3 | National Renewable Energy Laboratory: Analysis Results for ARRA Projects: Enabling Fuel Cell Market Transformation | XII-16 |

Connecticut

| | | |
|---------|---|---------|
| II.D.2 | Proton OnSite: High Performance, Low Cost Hydrogen Generation from Renewable Energy | II-35 |
| II.H.2 | Proton Energy Systems: Hydrogen by Wire - Home Fueling System. | II-126 |
| III.9 | FuelCell Energy, Inc.: Electrochemical Hydrogen Compressor | III-44 |
| III.9 | Sustainable Innovations, LLC: Electrochemical Hydrogen Compressor | III-44 |
| IV.D.1 | United Technologies Research Center: Hydrogen Storage Engineering Center of Excellence | IV-114 |
| IV.D.6 | United Technologies Research Center: Advancement of Systems Designs and Key Engineering Technologies for Materials-Based Hydrogen Storage | IV-140 |
| V.B.2 | University of Connecticut: The Effect of Airborne Contaminants on Fuel Cell Performance and Durability | V-63 |
| V.B.2 | UTC Power: The Effect of Airborne Contaminants on Fuel Cell Performance and Durability. | V-63 |
| V.C.3 | FuelCell Energy, Inc.: High-Temperature Membrane with Humidification-Independent Cluster Structure. | V-76 |
| V.D.2 | UTC Power: Highly Dispersed Alloy Catalyst for Durability. | V-95 |
| V.E.1 | United Technologies Research Center: Polymer Electrolyte Fuel Cell Lifetime Limitations: The Role of Electrocatalyst Degradation. | V-168 |
| V.E.4 | UTC Power: Improved Accelerated Stress Tests Based on Fuel Cell Vehicle Data | V-186 |
| V.E.4 | United Technologies Research Center: Improved Accelerated Stress Tests Based on Fuel Cell Vehicle Data | V-186 |
| V.F.2 | United Technologies Research Center: Fuel Cell Fundamentals at Low and Subzero Temperatures | V-211 |
| V.J.6 | UTC Power: 150 kW PEM Stationary Power Plant Operating on Natural Gas | V-291 |
| V.K.4 | University of Connecticut: Improving Reliability and Durability of Efficient and Clean Energy Systems. | V-310 |
| VI.2 | UTC Power: Manufacturing of Low-Cost, Durable Membrane Electrode Assemblies Engineered for Rapid Conditioning. | VI-11 |
| VII.2 | FuelCell Energy, Inc.: Validation of an Integrated Hydrogen Energy Station | VII-18 |
| VIII.6 | Kelvin Hecht: National Codes and Standards Coordination. | VIII-28 |
| VIII.6 | GWS Solutions of Tolland, LLC: National Codes and Standards Coordination. | VIII-28 |
| VIII.10 | GWS Solutions of Tolland, LLC: Hydrogen Safety Panel. | VIII-45 |
| IX.4 | Connecticut Center for Advanced Technology, Inc.: State and Local Government Partnership | IX-16 |

Delaware

| | | |
|--------|--|-------|
| IV.A.7 | Delaware State University: Hydrogen Storage Materials for Fuel Cell-Powered Vehicles. | IV-39 |
| V.C.4 | Ion Power Inc.: Corrugated Membrane Fuel Cell Structures | V-80 |
| V.D.4 | University of Delaware: Extended, Continuous Pt Nanostructures in Thick, Dispersed Electrodes. | V-107 |
| V.E.2 | Ion Power Inc.: Durability Improvements through Degradation Mechanism Studies | V-175 |
| V.E.5 | Ion Power Inc.: Accelerated Testing Validation. | V-190 |

XVII. Project Listings by State

Delaware (Continued)

| | | |
|-------|---|-------|
| V.E.7 | E. I. du Pont de Nemours and Company: Analysis of Durability of MEAs in Automotive PEMFC Applications | V-201 |
| V.G.3 | University of Delaware: Advanced Materials and Concepts for Portable Power Fuel Cells | V-250 |
| VI.2 | University of Delaware: Manufacturing of Low-Cost, Durable Membrane Electrode Assemblies Engineered for Rapid Conditioning. | VI-11 |

Florida

| | | |
|---------|--|---------|
| IV.H.19 | Florida International University: Influence of Pressure on Physical Property of Ammonia Borane and its Re-Hydrogenation. | IV-274 |
| V.C.1 | University of Central Florida: Lead Research and Development Activity for DOE's High Temperature, Low Relative Humidity Membrane Program | V-68 |
| V.G.2 | University of North Florida: New MEA Materials for Improved Direct Methanol Fuel Cell (DMFC) Performance, Durability, and Cost. | V-246 |
| V.G.2 | University of Florida: New MEA Materials for Improved Direct Methanol Fuel Cell (DMFC) Performance, Durability, and Cost. | V-246 |
| VII.6 | University of Central Florida: Florida Hydrogen Initiative (FHI) | VII-33 |
| VII.6 | EnerFuels, Inc.: Florida Hydrogen Initiative (FHI). | VII-33 |
| VII.6 | Florida Atlantic University: Florida Hydrogen Initiative (FHI) | VII-33 |
| VII.6 | Florida Solar Energy Center: Florida Hydrogen Initiative (FHI) | VII-33 |
| VII.6 | SRT Group, Inc.: Florida Hydrogen Initiative (FHI). | VII-33 |
| VII.6 | Electrolytic Technologies Corporation: Florida Hydrogen Initiative (FHI) | VII-33 |
| VII.6 | Florida State University: Florida Hydrogen Initiative (FHI) | VII-33 |
| VII.6 | Bing Energy, Inc.: Florida Hydrogen Initiative (FHI). | VII-33 |
| VII.6 | Florida Institute of Technology: Florida Hydrogen Initiative (FHI). | VII-33 |
| VII.6 | University of South Florida: Florida Hydrogen Initiative (FHI). | VII-33 |
| VIII.10 | Addison Bain: Hydrogen Safety Panel. | VIII-45 |

Georgia

| | | |
|--------|--|--------|
| III.5 | Savannah River National Laboratory: Fiber Reinforced Composite Pipeline | III-27 |
| IV.A.6 | Savannah River National Laboratory: Electrochemical Reversible Formation of Alane | IV-35 |
| IV.H.5 | Savannah River National Laboratory: Elucidation of Hydrogen Interaction Mechanisms with Metal-Doped Carbon Nanostructures | IV-226 |
| V.E.6 | Georgia Institute of Technology: Development of Micro-Structural Mitigation Strategies for PEM Fuel Cells: Morphological Simulations and Experimental Approaches | V-195 |

Hawaii

| | | |
|--------|--|--------|
| II.F.5 | University of Hawaii at Manoa: Photoelectrochemical Hydrogen Production | II-89 |
| IV.A.2 | University of Hawaii: Fundamental Studies of Advanced High-Capacity, Reversible Metal Hydrides | IV-18 |
| IV.B.4 | Hawaii Hydrogen Carriers, LLC: Development of a Practical Hydrogen Storage System Based on Liquid Organic Hydrogen Carriers and a Homogeneous Catalyst | IV-55 |
| IV.C.6 | University of Hawaii: Weak Chemisorption Validation | IV-89 |
| V.B.1 | University of Hawaii: Effect of System Contaminants on PEMFC Performance and Durability | V-57 |
| V.B.2 | Hawaii Natural Energy Institute: The Effect of Airborne Contaminants on Fuel Cell Performance and Durability | V-63 |
| VII.5 | Hawaii Natural Energy Institute: Hawaii Hydrogen Power Park | VII-30 |
| X.1 | Hawaii Natural Energy Institute: Hydrogen Energy Systems as a Grid Management Tool. | X-7 |

Illinois

| | | |
|---------|--|--------|
| II.B.1 | Gas Technology Institute: One Step Biomass Gas Reforming-Shift Separation Membrane Reactor | II-19 |
| II.E.2 | Argonne National Laboratory: Membrane/Electrolyzer Development in the Cu-Cl Thermochemical Cycle. | II-56 |
| II.E.2 | Gas Technology Institute: Membrane/Electrolyzer Development in the Cu-Cl Thermochemical Cycle. | II-56 |
| III.2 | Argonne National Laboratory: Hydrogen Delivery Infrastructure Analysis | III-13 |
| IV.A.1 | Northwestern University: Efficient Discovery of Novel Multicomponent Mixtures for Hydrogen Storage: A Combined Computational/Experimental Approach | IV-11 |
| IV.A.4 | University of Illinois at Urbana-Champaign: Reversible Hydrogen Storage Materials - Structure, Chemistry, and Electronic Structure | IV-27 |
| IV.C.4 | Northwestern University: New Carbon-Based Porous Materials with Increased Heats of Adsorption for Hydrogen Storage | IV-78 |
| IV.C.10 | Northwestern University: Metal- and Cluster-Modified Ultrahigh-Area Materials for the Ambient Temperature Storage of Molecular Hydrogen | IV-105 |
| IV.E.1 | Argonne National Laboratory: System Level Analysis of Hydrogen Storage Options | IV-164 |
| IV.H.7 | Argonne National Laboratory: New Pathways and Metrics for Enhanced, Reversible Hydrogen Storage in Boron-Doped Carbon Nanospaces | IV-233 |
| IV.H.13 | Northwestern University: Theory of Hydrogen Storage in Complex Hydrides | IV-253 |
| V.A.4 | Argonne National Laboratory: Performance of Automotive Fuel Cell Systems with Low-Pt Nanostructured Thin Film Catalysts at High Power Densities | V-25 |
| V.D.1 | Argonne National Laboratory: Advanced Cathode Catalysts and Supports for PEM Fuel Cells. | V-84 |
| V.D.5 | Argonne National Laboratory: Nanosegregated Cathode Catalysts with Ultra-Low Platinum Loading. | V-111 |
| V.D.10 | Illinois Institute of Technology: Synthesis and Characterization of Mixed-Conducting Corrosion Resistant Oxide Supports. | V-138 |
| V.E.1 | Argonne National Laboratory: Polymer Electrolyte Fuel Cell Lifetime Limitations: The Role of Electrocatalyst Degradation. | V-168 |
| V.E.2 | Argonne National Laboratory: Durability Improvements through Degradation Mechanism Studies. | V-175 |
| V.E.3 | Argonne National Laboratory: Durability of Low Platinum Fuel Cells Operating at High Power Density | V-182 |
| V.E.7 | Illinois Institute of Technology: Analysis of Durability of MEAs in Automotive PEMFC Applications | V-201 |
| V.G.1 | Illinois Institute of Technology: Novel Materials for High Efficiency Direct Methanol Fuel Cells. | V-242 |
| V.H.1 | Gas Technology Institute: Low-Cost PEM Fuel Cell Metal Bipolar Plates | V-257 |
| XI.2 | Argonne National Laboratory: Life-Cycle Analysis of Vehicle and Fuel Systems with the GREET Model | XI-15 |
| XI.11 | Argonne National Laboratory: Employment Impacts of Early Markets for Hydrogen and Fuel Cell Technologies. | XI-52 |
| XI.11 | RCF Economic and Financial Consulting, Inc.: Employment Impacts of Early Markets for Hydrogen and Fuel Cell Technologies | XI-52 |

Iowa

| | | |
|---------|--|--------|
| IV.H.11 | Ames Laboratory: Complex Hydrides - A New Frontier for Future Energy Applications. | IV-245 |
|---------|--|--------|

Kansas

| | | |
|-------|---|--------|
| XII.2 | Black & Veatch Corporation: Demonstrating Economic and Operational Viability of 72-Hour Hydrogen PEM Fuel Cell Systems to Support Emergency Communications on the Sprint Nextel Network | XII-12 |
| XII.2 | Ericsson Services, Inc.: Demonstrating Economic and Operational Viability of 72-Hour Hydrogen PEM Fuel Cell Systems to Support Emergency Communications on the Sprint Nextel Network. | XII-12 |

XVII. Project Listings by State

Maryland

| | | |
|---------|--|---------|
| II.G.1 | Johns Hopkins University: Biological Systems for Hydrogen Photoproduction | II-103 |
| IV.C.8 | National Institute of Standards and Technology: Hydrogen Storage in Metal-Organic Frameworks | IV-97 |
| IV.E.3 | National Institute of Standards and Technology: Neutron Characterization in Support of the DOE Hydrogen Storage Sub-Program | IV-176 |
| V.A.6 | National Institute of Standards and Technology: Neutron Imaging Study of the Water Transport in Operating Fuel Cells | V-37 |
| V.I.1 | W. L. Gore & Associates, Inc.: Materials and Modules for Low-Cost, High-Performance Fuel Cell Humidifiers | V-261 |
| VI.2 | W. L. Gore & Associates, Inc.: Manufacturing of Low-Cost, Durable Membrane Electrode Assemblies Engineered for Rapid Conditioning | VI-11 |
| VI.4 | National Institute of Standards and Technology: Non-Contact Sensor Evaluation for Bipolar Plate Manufacturing Process Control and Smart Assembly of Fuel Cell Stacks | VI-24 |
| VI.7 | National Institute of Standards and Technology: Cause and Effect: Flow Field Plate Manufacturing Variability and its Impact on Performance | VI-36 |
| VI.8 | National Institute of Standards and Technology: Optical Scatterfield Metrology for Online Catalyst Coating Inspection of PEM (Fuel Cell) Soft Goods | VI-41 |
| VII.7 | General Physics Corporation: Sustainable Hydrogen Fueling Station, California State University, Los Angeles | VII-38 |
| VIII.10 | Energetics, Inc.: Hydrogen Safety Panel | VIII-45 |

Massachusetts

| | | |
|--------|--|--------|
| II.D.1 | Giner Electrochemical Systems, LLC: PEM Electrolyzer Incorporating an Advanced Low-Cost Membrane | II-31 |
| II.H.1 | Giner Electrochemical Systems, LLC: Unitized Design for Home Refueling Appliance for Hydrogen Generation to 5,000 psi | II-122 |
| III.7 | Concepts NREC: Development of a Centrifugal Hydrogen Pipeline Gas Compressor | III-35 |
| V.C.2 | Giner Electrochemical Systems, LLC: Dimensionally Stable High Performance Membrane (SBIR Phase III) | V-71 |
| V.D.6 | Massachusetts Institute of Technology: Contiguous Platinum Monolayer Oxygen Reduction Electrocatalysts on High-Stability Low-Cost Supports | V-117 |
| V.D.11 | Northeastern University: Development of Novel Non-PGM Electrocatalysts for Proton Exchange Membrane Fuel Cell Applications | V-143 |
| V.D.12 | Massachusetts Institute of Technology: High-Activity Dealloyed Catalysts | V-149 |
| V.D.12 | Northeastern University: High-Activity Dealloyed Catalysts | V-149 |
| V.E.1 | Massachusetts Institute of Technology: Polymer Electrolyte Fuel Cell Lifetime Limitations: The Role of Electrocatalyst Degradation | V-168 |
| V.E.3 | Nuvera Fuel Cells, Inc.: Durability of Low Platinum Fuel Cells Operating at High Power Density | V-182 |
| V.F.4 | Nuvera Fuel Cells, Inc.: Transport Studies Enabling Efficiency Optimization of Cost-Competitive Fuel Cell Stacks | V-222 |
| V.F.6 | Giner Electrochemical Systems, LLC: Transport in PEMFC Stacks | V-230 |
| V.F.6 | Tech-Etch: Transport in PEMFC Stacks | V-230 |
| V.F.6 | Ballard Material Products, Inc.: Transport in PEMFC Stacks | V-230 |
| V.G.2 | Northeastern University: New MEA Materials for Improved Direct Methanol Fuel Cell (DMFC) Performance, Durability, and Cost | V-246 |
| V.H.1 | IBIS Associates, Inc.: Low-Cost PEM Fuel Cell Metal Bipolar Plates | V-257 |
| V.I.2 | Protonex Inc.: Large Scale Testing, Demonstration and Commercialization of the Nanoparticle-Based Fuel Cell Coolant (SBIR Phase III) | V-266 |

Massachusetts (Continued)

| | | |
|---------|--|---------|
| V.J.2 | Acumentrics Corporation: Development of a Low-Cost 3-10 kW Tubular SOFC Power System | V-277 |
| VIII.10 | Firexplo: Hydrogen Safety Panel | VIII-45 |
| XI.3 | IDC Energy Insights: Hydrogen Refueling Infrastructure Cost Analysis | XI-19 |
| XI.4 | TIAX, LLC: Comparing Infrastructure Costs for Hydrogen and Electricity | XI-23 |

Michigan

| | | |
|---------|--|---------|
| III.3 | University of Michigan: Vessel Design and Fabrication Technology for Stationary High-Pressure Hydrogen Storage | III-17 |
| IV.C.8 | General Motors Company: Hydrogen Storage in Metal-Organic Frameworks | IV-97 |
| IV.D.1 | General Motors Company: Hydrogen Storage Engineering Center of Excellence | IV-114 |
| IV.D.1 | Ford Motor Company: Hydrogen Storage Engineering Center of Excellence | IV-114 |
| IV.D.1 | University of Michigan: Hydrogen Storage Engineering Center of Excellence | IV-114 |
| IV.D.7 | General Motors Company: Thermal Management of Onboard Cryogenic Hydrogen Storage Systems | IV-147 |
| IV.D.8 | Ford Motor Company: Ford/BASF SE/UM Activities in Support of the Hydrogen Storage Engineering Center of Excellence | IV-151 |
| IV.D.8 | University of Michigan: Ford/BASF SE/UM Activities in Support of the Hydrogen Storage Engineering Center of Excellence | IV-151 |
| V.C.4 | General Motors Company: Corrugated Membrane Fuel Cell Structures | V-80 |
| V.D.10 | Nissan Technical Center: Synthesis and Characterization of Mixed-Conducting Corrosion Resistant Oxide Supports | V-138 |
| V.D.11 | Michigan State University: Development of Novel Non-PGM Electrocatalysts for Proton Exchange Membrane Fuel Cell Applications | V-143 |
| V.D.11 | Nissan Technical Center: Development of Novel Non-PGM Electrocatalysts for Proton Exchange Membrane Fuel Cell Applications | V-143 |
| V.D.12 | General Motors Company: High-Activity Dealloyed Catalysts | V-149 |
| V.E.6 | Michigan Technological University: Development of Micro-Structural Mitigation Strategies for PEM Fuel Cells: Morphological Simulations and Experimental Approaches | V-195 |
| V.E.7 | Nissan Technical Center: Analysis of Durability of MEAs in Automotive PEMFC Applications | V-201 |
| V.H.1 | Ford Motor Company: Low-Cost PEM Fuel Cell Metal Bipolar Plates | V-257 |
| VIII.3 | SAE International: Component Standard Research and Development | VIII-18 |
| VIII.6 | Sloane Solutions: National Codes and Standards Coordination | VIII-28 |
| VIII.10 | General Motors Company: Hydrogen Safety Panel | VIII-45 |
| XII.1 | Delphi Automotive Systems, LLC: Solid Oxide Fuel Cell Diesel Auxiliary Power Unit Demonstration | XII-9 |

Minnesota

| | | |
|--------|--|-------|
| II.A.2 | University of Minnesota: Distributed Bio-Oil Reforming | II-15 |
| II.D.2 | Entegris, Inc.: High Performance, Low Cost Hydrogen Generation from Renewable Energy | II-35 |
| II.D.5 | 3M Company: Low-Cost Large-Scale PEM Electrolysis for Renewable Energy Storage | II-46 |
| V.D.1 | 3M Company: Advanced Cathode Catalysts and Supports for PEM Fuel Cells | V-84 |
| V.D.3 | 3M Company: Durable Catalysts for Fuel Cell Protection during Transient Conditions | V-100 |
| V.D.5 | 3M Company: Nanosegregated Cathode Catalysts with Ultra-Low Platinum Loading | V-111 |
| V.F.2 | 3M Company: Fuel Cell Fundamentals at Low and Subzero Temperatures | V-211 |
| V.J.5 | The Toro Company: Research and Development for Off-Road Fuel Cell Applications | V-289 |

Mississippi

| | | |
|-------|---|-------|
| V.K.2 | University of Southern Mississippi: Alternative Fuel Cell Membranes for Energy Independence | V-300 |
|-------|---|-------|

XVII. Project Listings by State

Missouri

| | | |
|---------|--|---------|
| IV.C.3 | University of Missouri: Multiply Surface-Functionalized Nanoporous Carbon for Vehicular Hydrogen Storage | IV-72 |
| IV.C.3 | Midwest Research Institute: Multiply Surface-Functionalized Nanoporous Carbon for Vehicular Hydrogen Storage | IV-72 |
| IV.H.15 | Washington University: In Situ NMR Studies of Hydrogen Storage Systems | IV-259 |
| IV.H.7 | University of Missouri: New Pathways and Metrics for Enhanced, Reversible Hydrogen Storage in Boron-Doped Carbon Nanospaces | IV-233 |
| VIII.10 | Becht Engineering: Hydrogen Safety Panel | VIII-45 |
| XII.2 | Burns & McDonnell Engineering Co., Inc.: Demonstrating Economic and Operational Viability of 72-Hour Hydrogen PEM Fuel Cell Systems to Support Emergency Communications on the Sprint Nextel Network | XII-12 |

Nebraska

| | | |
|---------|---|--------|
| III.6 | Lincoln Composites, Inc.: Development of High Pressure Hydrogen Storage Tank for Storage and Gaseous Truck Delivery | III-32 |
| IV.D.1 | Lincoln Composites, Inc.: Hydrogen Storage Engineering Center of Excellence | IV-114 |
| IV.D.10 | Lincoln Composites, Inc.: Development of Improved Composite Pressure Vessels for Hydrogen Storage | IV-160 |

Nevada

| | | |
|--------|---|--------|
| II.F.2 | University of Nevada, Las Vegas: Semiconductor Materials for Photoelectrolysis | II-74 |
| II.F.4 | University of Nevada, Las Vegas: Characterization of Materials for Photoelectrochemical (PEC) Hydrogen Production | II-84 |
| IV.G.1 | University of Nevada, Las Vegas: HGMS: Glasses and Nanocomposites for Hydrogen Storage | IV-208 |

New Jersey

| | | |
|--------|---|--------|
| IV.C.5 | Rutgers University: Hydrogen Trapping through Designer Hydrogen Spillover Molecules with Reversible Temperature and Pressure-Induced Switching | IV-82 |
| IV.H.2 | Rutgers University: Novel theoretical and experimental approaches for understanding and optimizing hydrogen-sorbent interactions in metal organic framework materials | IV-213 |
| V.D.11 | BASF Fuel Cell: Development of Novel Non-PGM Electrocatalysts for Proton Exchange Membrane Fuel Cell Applications | V-143 |
| V.H.1 | TreadStone Technologies, Inc.: Low-Cost PEM Fuel Cell Metal Bipolar Plates | V-257 |
| VI.5 | BASF Fuel Cell: High Speed, Low Cost Fabrication of Gas Diffusion Electrodes for Membrane Electrode Assemblies | VI-28 |
| XII.6 | Linde North America: GENCO Fuel Cell-Powered Lift Truck Fleet Deployment | XII-28 |

New Mexico

| | | |
|--------|---|--------|
| IV.B.2 | Los Alamos National Laboratory: Fluid Phase Chemical Hydrogen Storage Materials | IV-48 |
| IV.C.6 | University of New Mexico: Weak Chemisorption Validation | IV-89 |
| IV.D.1 | Los Alamos National Laboratory: Hydrogen Storage Engineering Center of Excellence | IV-114 |
| IV.D.3 | Los Alamos National Laboratory: Chemical Hydride Rate Modeling, Validation, and System Demonstration | IV-126 |
| V.A.7 | Los Alamos National Laboratory: Technical Assistance to Developers | V-43 |
| V.B.1 | Los Alamos National Laboratory: Effect of System Contaminants on PEMFC Performance and Durability | V-57 |
| V.D.4 | Los Alamos National Laboratory: Extended, Continuous Pt Nanostructures in Thick, Dispersed Electrodes | V-107 |

New Mexico (Continued)

| | | |
|--------|---|---------|
| V.D.7 | Los Alamos National Laboratory: The Science and Engineering of Durable Ultralow PGM Catalysts | V-121 |
| V.D.7 | University of New Mexico: The Science and Engineering of Durable Ultralow PGM Catalysts | V-121 |
| V.D.11 | University of New Mexico: Development of Novel Non-PGM Electrocatalysts for Proton Exchange Membrane Fuel Cell Applications | V-143 |
| V.D.11 | Los Alamos National Laboratory: Development of Novel Non-PGM Electrocatalysts for Proton Exchange Membrane Fuel Cell Applications. | V-143 |
| V.E.2 | Los Alamos National Laboratory: Durability Improvements through Degradation Mechanism Studies | V-175 |
| V.E.2 | University of New Mexico: Durability Improvements through Degradation Mechanism Studies | V-175 |
| V.E.3 | Los Alamos National Laboratory: Durability of Low Platinum Fuel Cells Operating at High Power Density | V-182 |
| V.E.4 | Los Alamos National Laboratory: Improved Accelerated Stress Tests Based on Fuel Cell Vehicle Data. | V-186 |
| V.E.5 | Los Alamos National Laboratory: Accelerated Testing Validation. | V-190 |
| V.E.6 | Los Alamos National Laboratory: Development of Micro-Structural Mitigation Strategies for PEM Fuel Cells: Morphological Simulations and Experimental Approaches | V-195 |
| V.E.6 | University of New Mexico: Development of Micro-Structural Mitigation Strategies for PEM Fuel Cells: Morphological Simulations and Experimental Approaches | V-195 |
| V.F.2 | Los Alamos National Laboratory: Fuel Cell Fundamentals at Low and Subzero Temperatures | V-211 |
| V.F.3 | Los Alamos National Laboratory: Development and Validation of a Two-Phase, Three-Dimensional Model for PEM Fuel Cells | V-217 |
| V.G.3 | Los Alamos National Laboratory: Advanced Materials and Concepts for Portable Power Fuel Cells | V-250 |
| VI.7 | Los Alamos National Laboratory: Cause and Effect: Flow Field Plate Manufacturing Variability and its Impact on Performance | VI-36 |
| VIII.8 | Los Alamos National Laboratory: Leak Detection and H ₂ Sensor Development for Hydrogen Applications | VIII-36 |
| VIII.9 | Los Alamos National Laboratory: Hydrogen Fuel Quality Research and Development | VIII-42 |
| XI.1 | Los Alamos National Laboratory: Infrastructure Analysis of Early Market Transition of Fuel Cell Vehicles. | XI-11 |

New York

| | | |
|---------|---|--------|
| II.C.2 | H ₂ Pump, LLC: Process Intensification of Hydrogen Unit Operations Using an Electrochemical Device | II-28 |
| II.E.1 | Electrosynthesis Co. Inc.: Solar High-Temperature Water Splitting Cycle with Quantum Boost | II-49 |
| III.8 | Mohawk Innovative Technologies, Inc.: Oil-Free Centrifugal Hydrogen Compression Technology Demonstration | III-40 |
| IV.A.5 | Brookhaven National Laboratory: Aluminum Hydride | IV-31 |
| IV.H.12 | Brookhaven National Laboratory: Atomistic Transport Mechanisms in Aluminum-Based Hydrides | IV-249 |
| V.B.1 | General Motors Company: Effect of System Contaminants on PEMFC Performance and Durability | V-57 |
| V.D.1 | General Motors Company: Advanced Cathode Catalysts and Supports for PEM Fuel Cells. | V-84 |
| V.D.2 | Brookhaven National Laboratory: Highly Dispersed Alloy Catalyst for Durability | V-95 |
| V.D.4 | State University of New York, Albany: Extended, Continuous Pt Nanostructures in Thick, Dispersed Electrodes. | V-107 |
| V.D.6 | Brookhaven National Laboratory: Contiguous Platinum Monolayer Oxygen Reduction Electrocatalysts on High-Stability Low-Cost Supports | V-117 |
| V.F.1 | Plug Power Inc.: Air-Cooled Stack Freeze Tolerance | V-206 |
| V.F.7 | General Motors Company: Investigation of Micro- and Macro-Scale Transport Processes for Improved Fuel Cell Performance | V-235 |
| V.F.7 | Rochester Institute of Technology: Investigation of Micro- and Macro-Scale Transport Processes for Improved Fuel Cell Performance. | V-235 |

XVII. Project Listings by State

New York (Continued)

| | | |
|-------|---|--------|
| V.F.7 | University of Rochester: Investigation of Micro- and Macro-Scale Transport Processes for Improved Fuel Cell Performance | V-235 |
| V.G.3 | Brookhaven National Laboratory: Advanced Materials and Concepts for Portable Power Fuel Cells | V-250 |
| V.H.1 | State University of New York, Stony Brook: Low-Cost PEM Fuel Cell Metal Bipolar Plates | V-257 |
| VI.3 | Rensselaer Polytechnic Institute: Adaptive Process Controls and Ultrasonics for High-Temperature PEM MEA Manufacture | VI-17 |
| XII.4 | Plug Power Inc.: Fuel Cell-Powered Lift Truck FedEx Freight Fleet Deployment | XII-21 |
| XII.5 | Plug Power Inc.: Fuel Cell-Powered Lift Truck Sysco Houston Fleet Deployment | XII-24 |
| XII.6 | Plug Power Inc.: GENCO Fuel Cell-Powered Lift Truck Fleet Deployment | XII-28 |
| XII.7 | Plug Power Inc.: Highly Efficient, 5-kW CHP Fuel Cells Demonstrating Durability and Economic Value in Residential and Light Commercial Applications | XII-30 |
| XII.8 | Plug Power Inc.: Accelerating Acceptance of Fuel Cell Backup Power Systems | XII-34 |

North Carolina

| | | |
|--------|--|--------|
| IV.H.2 | Wake Forest University: Novel theoretical and experimental approaches for understanding and optimizing hydrogen-sorbent interactions in metal organic framework materials. | IV-213 |
| V.C.1 | Scribner Associates, Inc.: Lead Research and Development Activity for DOE's High Temperature, Low Relative Humidity Membrane Program | V-68 |
| V.F.5 | Techverse: Water Transport in PEM Fuel Cells: Advanced Modeling, Material Selection, Testing, and Design Optimization | V-226 |

Ohio

| | | |
|---------|--|---------|
| II.F.6 | Midwest Optoelectronics, LLC: Critical Research for Cost-Effective Photoelectrochemical Production of Hydrogen | II-93 |
| II.F.6 | Xunlight Corporation: Critical Research for Cost-Effective Photoelectrochemical Production of Hydrogen | II-93 |
| II.F.6 | University of Toledo: Critical Research for Cost-Effective Photoelectrochemical Production of Hydrogen | II-93 |
| IV.A.3 | Ohio State University: Lightweight Metal Hydrides for Hydrogen Storage | IV-22 |
| V.A.9 | Battelle: Stationery and Emerging Market Fuel Cell System Cost Analysis | V-51 |
| V.C.4 | Graftech International Holdings Inc.: Corrugated Membrane Fuel Cell Structures | V-80 |
| V.K.1 | University of Akron: Development of Kilowatt-Scale Coal Fuel Cell Technology | V-295 |
| VI.5 | Case Western Reserve University: High Speed, Low Cost Fabrication of Gas Diffusion Electrodes for Membrane Electrode Assemblies. | VI-28 |
| VII.3 | Battelle: Technology Validation: Fuel Cell Bus Evaluations | VII-22 |
| VIII.6 | CSA Standards: National Codes and Standards Coordination | VIII-28 |
| VIII.10 | Powdermet Inc.: Hydrogen Safety Panel | VIII-45 |
| IX.2 | Ohio Fuel Cell Coalition: Raising H2 and Fuel Cell Awareness in Ohio | IX-11 |
| IX.2 | Edison Material Technology Center: Raising H2 and Fuel Cell Awareness in Ohio | IX-11 |

Oregon

| | | |
|--------|---|--------|
| II.B.1 | ATI Wah Chang: One Step Biomass Gas Reforming-Shift Separation Membrane Reactor | II-19 |
| IV.B.1 | University of Oregon: Hydrogen Storage by Novel CBN Heterocycle Materials | IV-44 |
| IV.B.3 | University of Oregon: Novel Carbon(C)-Boron(B)-Nitrogen(N)-Containing H2 Storage Materials | IV-51 |
| IV.D.1 | Oregon State University: Hydrogen Storage Engineering Center of Excellence | IV-114 |
| IV.D.9 | Oregon State University: Microscale Enhancement of Heat and Mass Transfer for Hydrogen Energy Storage | IV-156 |

Oregon (Continued)

| | | |
|-------|---|--------|
| V.J.5 | IdaTech, LLC: Research and Development for Off-Road Fuel Cell Applications | V-289 |
| X.2 | ClearEdge Power: Fuel Cell Combined Heat and Power Industrial Demonstration | X-10 |
| XII.7 | ClearEdge Power: Highly Efficient, 5-kW CHP Fuel Cells Demonstrating Durability and Economic Value in Residential and Light Commercial Applications | XII-30 |
| XII.8 | IdaTech, LLC: Accelerating Acceptance of Fuel Cell Backup Power Systems | XII-34 |

Pennsylvania

| | | |
|---------|---|---------|
| II.B.1 | National Energy Technology Laboratory: One Step Biomass Gas Reforming-Shift Separation Membrane Reactor | II-19 |
| II.B.1 | Schott North America: One Step Biomass Gas Reforming-Shift Separation Membrane Reactor | II-19 |
| II.C.1 | Media and Process Technology Inc.: Development of Hydrogen Selective Membranes/Modules as Reactors/Separators for Distributed Hydrogen Production | II-23 |
| II.D.2 | Pennsylvania State University: High Performance, Low Cost Hydrogen Generation from Renewable Energy | II-35 |
| II.E.2 | Pennsylvania State University: Membrane/Electrolyzer Development in the Cu-Cl Thermochemical Cycle | II-56 |
| II.E.3 | Bucknell University: Solar Hydrogen Production with a Metal Oxide-Based Thermochemical Cycle | II-60 |
| II.G.2 | Pennsylvania State University: Fermentation and Electrohydrogenic Approaches to Hydrogen Production | II-108 |
| IV.C.5 | Pennsylvania State University: Hydrogen Trapping through Designer Hydrogen Spillover Molecules with Reversible Temperature and Pressure-Induced Switching | IV-82 |
| IV.H.1 | University of Pennsylvania: From Fundamental Understanding to Predicting New Nanomaterials for High-Capacity Hydrogen Storage | IV-210 |
| IV.H.10 | Pennsylvania State University: Exploration of Novel Carbon-Hydrogen Interactions | IV-243 |
| IV.H.18 | University of Pennsylvania: Mechanistic Studies of Activated Hydrogen Release from Ammonia-Borane | IV-270 |
| V.D.5 | University of Pittsburgh: Nanosegregated Cathode Catalysts with Ultra-Low Platinum Loading | V-111 |
| V.F.2 | Pennsylvania State University: Fuel Cell Fundamentals at Low and Subzero Temperatures | V-211 |
| V.F.3 | Pennsylvania State University: Development and Validation of a Two-Phase, Three-Dimensional Model for PEM Fuel Cells | V-217 |
| V.F.4 | Pennsylvania State University: Transport Studies Enabling Efficiency Optimization of Cost-Competitive Fuel Cell Stacks | V-222 |
| V.F.7 | Pennsylvania State University: Investigation of Micro- and Macro-Scale Transport Processes for Improved Fuel Cell Performance | V-235 |
| V.G.1 | Arkema Inc.: Novel Materials for High Efficiency Direct Methanol Fuel Cells | V-242 |
| V.I.2 | Dynalene Inc.: Large Scale Testing, Demonstration and Commercialization of the Nanoparticle-Based Fuel Cell Coolant (SBIR Phase III) | V-266 |
| VII.2 | Air Products and Chemicals, Inc.: Validation of an Integrated Hydrogen Energy Station | VII-18 |
| VII.4 | Air Products and Chemicals, Inc.: California Hydrogen Infrastructure Project | VII-26 |
| VIII.6 | SAE International: National Codes and Standards Coordination | VIII-28 |
| VIII.10 | Air Products and Chemicals, Inc.: Hydrogen Safety Panel | VIII-45 |
| XII.2 | Air Products and Chemicals, Inc.: Demonstrating Economic and Operational Viability of 72-Hour Hydrogen PEM Fuel Cell Systems to Support Emergency Communications on the Sprint Nextel Network | XII-12 |
| XII.4 | Air Products and Chemicals, Inc.: Fuel Cell-Powered Lift Truck FedEx Freight Fleet Deployment | XII-21 |
| XII.5 | Air Products and Chemicals, Inc.: Fuel Cell-Powered Lift Truck Sysco Houston Fleet Deployment | XII-24 |
| XII.6 | GENCO Infrastructure Solutions: GENCO Fuel Cell-Powered Lift Truck Fleet Deployment | XII-28 |

XVII. Project Listings by State

Pennsylvania (Continued)

- XII.6 Air Products and Chemicals, Inc.: GENCO Fuel Cell-Powered Lift Truck Fleet DeploymentXII-28

Rhode Island

- V.D.5 Brown University: Nanosegregated Cathode Catalysts with Ultra-Low Platinum Loading V-111

South Carolina

- II.C.2 PBI Performance Products, Inc.: Process Intensification of Hydrogen Unit Operations Using an Electrochemical Device. II-28
- IV.D.1 Savannah River National Laboratory: Hydrogen Storage Engineering Center of Excellence IV-114
- V.B.1 University of South Carolina: Effect of System Contaminants on PEMFC Performance and Durability V-57
- V.D.13 University of South Carolina: Development of Ultra-Low Platinum Alloy Cathode Catalyst for PEM Fuel Cells. V-153
- V.F.6 University of South Carolina: Transport in PEMFC Stacks V-230
- VI.3 Tetramer Technologies, LLC: New High Performance Water Vapor Membranes to Improve Fuel Cell Balance of Plant Efficiency and Lower Costs (SBIR Phase I). V-270
- IX.1 South Carolina Hydrogen and Fuel Cell Alliance: Development of Hydrogen Education Programs for Government Officials IX-7
- IX.1 Greenway Energy: Development of Hydrogen Education Programs for Government Officials IX-7
- IX.1 Advanced Technology International: Development of Hydrogen Education Programs for Government Officials IX-7
- X.4 South Carolina Hydrogen and Fuel Cell Alliance: Landfill Gas-to-Hydrogen XI-1
- X.4 Advanced Technology International: Landfill Gas-to-Hydrogen XI-1

Tennessee

- II.D.2 Oak Ridge National Laboratory: High Performance, Low Cost Hydrogen Generation from Renewable Energy II-35
- III.3 Oak Ridge National Laboratory: Vessel Design and Fabrication Technology for Stationary High-Pressure Hydrogen Storage. III-17
- III.10 Oak Ridge National Laboratory: Composite Technology for Hydrogen Pipelines. III-47
- IV.C.9 Oak Ridge National Laboratory: The Quantum Effects of Pore Structure on Hydrogen Adsorption IV-100
- IV.F.1 Oak Ridge National Laboratory: High Strength Carbon Fibers IV-191
- IV.F.2 Oak Ridge National Laboratory: Lifecycle Verification of Polymeric Storage Tank Liners IV-197
- IV.F.3 Oak Ridge National Laboratory: Development of Low-Cost, High Strength Commercial Textile Precursor (PAN-MA) IV-200
- IV.H.4 Oak Ridge National Laboratory: Atomistic Mechanisms of Metal-Assisted Hydrogen Storage in Nanostructured Carbons IV-220
- IV.H.7 Oak Ridge National Laboratory: New Pathways and Metrics for Enhanced, Reversible Hydrogen Storage in Boron-Doped Carbon Nanospaces IV-233
- V.A.5 Oak Ridge National Laboratory: Characterization of Fuel Cell Materials. V-32
- V.D.3 Oak Ridge National Laboratory: Durable Catalysts for Fuel Cell Protection during Transient Conditions V-100
- V.D.4 Oak Ridge National Laboratory: Extended, Continuous Pt Nanostructures in Thick, Dispersed Electrodes. V-107
- V.D.4 University of Tennessee: Extended, Continuous Pt Nanostructures in Thick, Dispersed Electrodes V-107
- V.D.5 Oak Ridge National Laboratory: Nanosegregated Cathode Catalysts with Ultra-Low Platinum Loading V-111

Tennessee (Continued)

| | | |
|--------|---|-------|
| V.D.11 | University of Tennessee: Development of Novel Non-PGM Electrocatalysts for Proton Exchange Membrane Fuel Cell Applications | V-143 |
| V.E.2 | Oak Ridge National Laboratory: Durability Improvements through Degradation Mechanism Studies | V-175 |
| V.E.4 | Oak Ridge National Laboratory: Improved Accelerated Stress Tests Based on Fuel Cell Vehicle Data | V-186 |
| V.E.5 | Oak Ridge National Laboratory: Accelerated Testing Validation | V-190 |
| V.F.7 | University of Tennessee: Investigation of Micro- and Macro-Scale Transport Processes for Improved Fuel Cell Performance | V-235 |
| V.G.3 | Oak Ridge National Laboratory: Advanced Materials and Concepts for Portable Power Fuel Cells | V-250 |
| V.I.2 | University of Tennessee, Knoxville: Large Scale Testing, Demonstration and Commercialization of the Nanoparticle-Based Fuel Cell Coolant (SBIR Phase III) | V-266 |
| VI.2 | University of Tennessee: Manufacturing of Low-Cost, Durable Membrane Electrode Assemblies Engineered for Rapid Conditioning | VI-11 |
| XI.6 | Oak Ridge National Laboratory: Sensitivity Analysis of H ₂ -Vehicles' Market Prospects, Costs and Benefits | XI-31 |
| XI.6 | University of Tennessee, Knoxville: Sensitivity Analysis of H ₂ -Vehicles' Market Prospects, Costs and Benefits | XI-31 |
| XI.8 | Oak Ridge National Laboratory: Impact of DOE Program Goals on Hydrogen Vehicles: Market Prospect, Costs, and Benefits | XI-39 |

Texas

| | | |
|---------|--|---------|
| II.F.7 | University of Texas at Arlington: Photoelectrochemical Materials: Theory and Modeling | II-98 |
| III.7 | Texas A&M University: Development of a Centrifugal Hydrogen Pipeline Gas Compressor | III-35 |
| IV.C.1 | Texas A&M University: A Biomimetic Approach to Metal-Organic Frameworks with High H ₂ Uptake | IV-60 |
| IV.H.2 | University of Texas, Dallas: Novel theoretical and experimental approaches for understanding and optimizing hydrogen-sorbent interactions in metal organic framework materials | IV-213 |
| IV.H.12 | University of Texas, Dallas: Atomistic Transport Mechanisms in Aluminum-Based Hydrides | IV-249 |
| V.D.2 | Texas A&M University: Highly Dispersed Alloy Catalyst for Durability | V-95 |
| V.D.4 | University of Texas at Austin: Extended, Continuous Pt Nanostructures in Thick, Dispersed Electrodes | V-107 |
| V.E.1 | University of Texas at Austin: Polymer Electrolyte Fuel Cell Lifetime Limitations: The Role of Electrocatalyst Degradation | V-168 |
| V.F.5 | BCS Fuel Cells: Water Transport in PEM Fuel Cells: Advanced Modeling, Material Selection, Testing, and Design Optimization | V-226 |
| VIII.10 | William C. Fort: Hydrogen Safety Panel | VIII-45 |
| XII.5 | Sysco of Houston: Fuel Cell-Powered Lift Truck Sysco Houston Fleet Deployment | XII-24 |

Utah

| | | |
|-------|---|--------|
| III.3 | MegaStir Technologies: Vessel Design and Fabrication Technology for Stationary High-Pressure Hydrogen Storage | III-17 |
| XII.5 | Big-D Construction: Fuel Cell-Powered Lift Truck Sysco Houston Fleet Deployment | XII-24 |

Virginia

| | | |
|--------|--|--------|
| II.D.1 | Virginia Polytechnic Institute and State University: PEM Electrolyzer Incorporating an Advanced Low-Cost Membrane | II-31 |
| IV.E.4 | Strategic Analysis, Inc.: Hydrogen Storage Cost Analysis, Preliminary Results | IV-182 |
| IV.F.1 | Virginia Polytechnic Institute and State University: High Strength Carbon Fibers | IV-191 |
| IV.H.3 | Virginia Commonwealth University: Design and Synthesis of Chemically and Electronically Tunable Nanoporous Organic Polymers for Use in Hydrogen Storage Applications | IV-216 |

XVII. Project Listings by State

Virginia (Continued)

| | | |
|-------|--|--------|
| V.A.2 | Strategic Analysis, Inc.: Mass-Production Cost Estimation for Automotive Fuel Cell Systems | V-16 |
| V.A.3 | Strategic Analysis, Inc.: Stationary Fuel Cell System Cost Analysis | V-20 |
| V.F.6 | Virginia Polytechnic Institute and State University: Transport in PEMFC Stacks | V-230 |
| V.G.3 | Virginia Polytechnic Institute and State University: Advanced Materials and Concepts for Portable Power Fuel Cells. | V-250 |
| XI.7 | Strategic Analysis, Inc.: Effects of Technology Cost Parameters on Hydrogen Pathway Succession | XI-35 |
| XII.2 | Sprint Nextel: Demonstrating Economic and Operational Viability of 72-Hour Hydrogen PEM Fuel Cell Systems to Support Emergency Communications on the Sprint Nextel Network | XII-12 |

Washington

| | | |
|---------|---|---------|
| II.A.1 | Pacific Northwest National Laboratory: Biomass-Derived Liquids Distributed (Aqueous Phase) Reforming. | II-11 |
| III.3 | Global Engineering and Technology: Vessel Design and Fabrication Technology for Stationary High-Pressure Hydrogen Storage. | III-17 |
| IV.D.1 | Pacific Northwest National Laboratory: Hydrogen Storage Engineering Center of Excellence | IV-114 |
| IV.D.5 | Pacific Northwest National Laboratory: Systems Engineering of Chemical Hydride, Pressure Vessel, and Balance of Plant for Onboard Hydrogen Storage | IV-134 |
| IV.E.5 | Pacific Northwest National Laboratory: Early Market TRL/MRL Analysis | IV-186 |
| IV.F.4 | Pacific Northwest National Laboratory: Synergistically Enhanced Materials and Design Parameters for Reducing the Cost of Hydrogen Storage Tanks | IV-205 |
| IV.H.16 | Pacific Northwest National Laboratory: Activation of Hydrogen with Bi-Functional Ambiphilic Catalyst Complexes | IV-263 |
| V.D.15 | Pacific Northwest National Laboratory: Development of Alternative and Durable High Performance Cathode Supports for PEM Fuel Cells | V-162 |
| V.J.4 | InnovaTek: Power Generation from an Integrated Biomass Reformer and Solid Oxide Fuel Cell (SBIR Phase III) | V-285 |
| VI.6 | Boeing Research and Technology: Development of Advanced Manufacturing Technologies for Low Cost Hydrogen Storage Vessels | VI-31 |
| VI.6 | Pacific Northwest National Laboratory: Development of Advanced Manufacturing Technologies for Low Cost Hydrogen Storage Vessels | VI-31 |
| VIII.10 | Pacific Northwest National Laboratory: Hydrogen Safety Panel | VIII-45 |
| VIII.11 | Pacific Northwest National Laboratory: Hydrogen Safety Knowledge Tools. | VIII-49 |
| VIII.12 | Pacific Northwest National Laboratory: Hydrogen Emergency Response Training for First Responders | VIII-52 |
| VIII.12 | Hanford Fire Department: Hydrogen Emergency Response Training for First Responders | VIII-52 |
| VIII.12 | Hazardous Materials Management and Emergency Response Training and Education Center: Hydrogen Emergency Response Training for First Responders | VIII-52 |
| X.2 | Pacific Northwest National Laboratory: Fuel Cell Combined Heat and Power Industrial Demonstration | X-10 |
| XII.1 | PACCAR, Inc.: Solid Oxide Fuel Cell Diesel Auxiliary Power Unit Demonstration | XII-9 |
| XII.2 | ReliOn, Inc.: Demonstrating Economic and Operational Viability of 72-Hour Hydrogen PEM Fuel Cell Systems to Support Emergency Communications on the Sprint Nextel Network | XII-12 |
| XII.3 | Pacific Northwest National Laboratory: Analysis Results for ARRA Projects: Enabling Fuel Cell Market Transformation | XII-16 |

Washington, D.C.

| | | |
|--------|---|--------|
| IV.H.8 | Carnegie Institute of Washington: Novel Molecular Materials for Hydrogen Storage Applications | IV-236 |
| V.D.12 | George Washington University: High-Activity Dealloyed Catalysts | V-149 |

Wisconsin

- V.E.1 University of Wisconsin, Madison: Polymer Electrolyte Fuel Cell Lifetime Limitations: The Role of Electrocatalyst Degradation. V-168

Wyoming

- II.D.5 University of Wyoming: Low-Cost Large-Scale PEM Electrolysis for Renewable Energy Storage II-46

Foreign Countries**Canada**

- IV.D.1 Université du Québec à Trois-Rivières: Hydrogen Storage Engineering Center of Excellence IV-114
- IV.H.18 University of Ottawa: Mechanistic Studies of Activated Hydrogen Release from Ammonia-Borane. IV-270
- V.A.10 Ballard Power Systems: A Total Cost of Ownership Model for Design and Manufacturing Optimization of Fuel Cells in Stationary and Emerging Market Applications. V-53
- V.B.2 Ballard Power Systems: The Effect of Airborne Contaminants on Fuel Cell Performance and Durability. V-63
- V.D.1 Dalhousie University: Advanced Cathode Catalysts and Supports for PEM Fuel Cells. V-84
- V.D.3 Dalhousie University: Durable Catalysts for Fuel Cell Protection during Transient Conditions. V-100
- V.D.3 Automotive Fuel Cell Cooperation: Durable Catalysts for Fuel Cell Protection during Transient Conditions V-100
- V.D.7 Ballard Fuel Cells: The Science and Engineering of Durable Ultralow PGM Catalysts V-121
- V.D.15 Automotive Fuel Cell Cooperation: Development of Alternative and Durable High Performance Cathode Supports for PEM Fuel Cells V-162
- V.E.2 Ballard Power Systems: Durability Improvements through Degradation Mechanism Studies V-175
- V.E.5 Ballard Power Systems: Accelerated Testing Validation. V-190
- V.E.6 Ballard Power Systems: Development of Micro-Structural Mitigation Strategies for PEM Fuel Cells: Morphological Simulations and Experimental Approaches V-195
- V.E.6 Queen's University: Development of Micro-Structural Mitigation Strategies for PEM Fuel Cells: Morphological Simulations and Experimental Approaches V-195
- V.F.1 Ballard Power Systems: Air-Cooled Stack Freeze Tolerance V-206
- V.F.3 Ballard Power Systems: Development and Validation of a Two-Phase, Three-Dimensional Model for PEM Fuel Cells. V-217
- V.F.5 Ballard Power Systems: Water Transport in PEM Fuel Cells: Advanced Modeling, Material Selection, Testing, and Design Optimization V-226
- V.F.5 University of Victoria: Water Transport in PEM Fuel Cells: Advanced Modeling, Material Selection, Testing, and Design Optimization V-226
- V.I.1 dPoint Technologies, Inc.: Materials and Modules for Low-Cost, High-Performance Fuel Cell Humidifiers. V-261

France

- IV.C.6 Institut de Chimie et des Matériaux: Weak Chemisorption Validation IV-89
- IV.H.7 University Aix-Marseille: New Pathways and Metrics for Enhanced, Reversible Hydrogen Storage in Boron-Doped Carbon Nanospaces. IV-233
- IV.H.7 University Montpellier 2: New Pathways and Metrics for Enhanced, Reversible Hydrogen Storage in Boron-Doped Carbon Nanospaces. IV-233

Germany

- IV.C.6 Max Planck Institute: Weak Chemisorption Validation IV-89
- IV.D.8 BASF-SE: Ford/BASF SE/UM Activities in Support of the Hydrogen Storage Engineering Center of Excellence IV-151

XVII. Project Listings by State

Germany (Continued)

- V.D.12 Technical University Berlin: High-Activity Dealloyed Catalysts V-149
- V.F.5 SGL Carbon: Water Transport in PEM Fuel Cells: Advanced Modeling, Material Selection, Testing, and Design Optimization V-226
- V.G.3 SFC Energy: Advanced Materials and Concepts for Portable Power Fuel Cells V-250

Japan

- III.8 Mitsubishi Compressor Company: Oil-Free Centrifugal Hydrogen Compression Technology Demonstration III-40

Portugal

- IV.F.1 Fibras Sinteticas de Portugal, SA: High Strength Carbon Fibers IV-191

Russia

- II.G.1 Institute of Basic Biological Problems: Biological Systems for Hydrogen Photoproduction II-103

South Korea

- V.D.13 Yonsei University: Development of Ultra-Low Platinum Alloy Cathode Catalyst for PEM Fuel Cells. V-153

United Kingdom

- II.D.1 Parker Hannifin Ltd domnick hunter Division: PEM Electrolyzer Incorporating an Advanced Low-Cost Membrane II-31
- V.D.2 Johnson Matthey Fuel Cells: Highly Dispersed Alloy Catalyst for Durability. V-95
- V.D.6 Johnson Matthey Fuel Cells: Contiguous Platinum Monolayer Oxygen Reduction Electrocatalysts on High-Stability Low-Cost Supports V-117
- V.D.12 Johnson Matthey Fuel Cells: High-Activity Dealloyed Catalysts. V-149
- V.E.1 Johnson Matthey Fuel Cells: Polymer Electrolyte Fuel Cell Lifetime Limitations: The Role of Electrocatalyst Degradation. V-168
- V.F.4 Johnson Matthey Fuel Cells: Transport Studies Enabling Efficiency Optimization of Cost-Competitive Fuel Cell Stacks V-222
- V.G.2 Johnson Matthey Fuel Cells: New MEA Materials for Improved Direct Methanol Fuel Cell (DMFC) Performance, Durability, and Cost. V-246
- V.G.3 Johnson Matthey Fuel Cells: Advanced Materials and Concepts for Portable Power Fuel Cells. V-250

XVIII. Project Listings by Organization

3M Company

| | | |
|--------|--|-------|
| II.D.5 | Low-Cost Large-Scale PEM Electrolysis for Renewable Energy Storage | II-46 |
| V.D.1 | Advanced Cathode Catalysts and Supports for PEM Fuel Cells | V-84 |
| V.D.3 | Durable Catalysts for Fuel Cell Protection during Transient Conditions | V-100 |
| V.D.5 | Nanosegregated Cathode Catalysts with Ultra-Low Platinum Loading | V-111 |
| V.F.2 | Fuel Cell Fundamentals at Low and Subzero Temperatures | V-211 |

Acumentrics Corporation

| | | |
|-------|---|-------|
| V.J.2 | Development of a Low-Cost 3-10 kW Tubular SOFC Power System | V-277 |
|-------|---|-------|

Addison Bain

| | | |
|---------|-----------------------|---------|
| VIII.10 | Hydrogen Safety Panel | VIII-45 |
|---------|-----------------------|---------|

Advanced Technology International

| | | |
|------|---|------|
| IX.1 | Development of Hydrogen Education Programs for Government Officials | IX-7 |
| X.4 | Landfill Gas-to-Hydrogen | XI-1 |

Air Products and Chemicals, Inc.

| | | |
|---------|---|---------|
| VII.2 | Validation of an Integrated Hydrogen Energy Station | VII-18 |
| VII.4 | California Hydrogen Infrastructure Project | VII-26 |
| VIII.10 | Hydrogen Safety Panel | VIII-45 |
| XII.2 | Demonstrating Economic and Operational Viability of 72-Hour Hydrogen PEM Fuel Cell Systems to Support Emergency Communications on the Sprint Nextel Network | XII-12 |
| XII.4 | Fuel Cell-Powered Lift Truck FedEx Freight Fleet Deployment | XII-21 |
| XII.5 | Fuel Cell-Powered Lift Truck Sysco Houston Fleet Deployment | XII-24 |
| XII.6 | GENCO Fuel Cell-Powered Lift Truck Fleet Deployment | XII-28 |

Altery Systems

| | | |
|-------|---|--------|
| XII.2 | Demonstrating Economic and Operational Viability of 72-Hour Hydrogen PEM Fuel Cell Systems to Support Emergency Communications on the Sprint Nextel Network | XII-12 |
|-------|---|--------|

Ames Laboratory

| | | |
|---------|--|--------|
| IV.H.11 | Complex Hydrides - A New Frontier for Future Energy Applications | IV-245 |
|---------|--|--------|

Argonne National Laboratory

| | | |
|--------|--|--------|
| II.E.2 | Membrane/Electrolyzer Development in the Cu-Cl Thermochemical Cycle | II-56 |
| III.2 | Hydrogen Delivery Infrastructure Analysis | III-13 |
| IV.E.1 | System Level Analysis of Hydrogen Storage Options | IV-164 |
| IV.H.7 | New Pathways and Metrics for Enhanced, Reversible Hydrogen Storage in Boron-Doped Carbon Nanospaces | IV-233 |
| V.A.4 | Performance of Automotive Fuel Cell Systems with Low-Pt Nanostructured Thin Film Catalysts at High Power Densities | V-25 |
| V.D.1 | Advanced Cathode Catalysts and Supports for PEM Fuel Cells | V-84 |
| V.D.5 | Nanosegregated Cathode Catalysts with Ultra-Low Platinum Loading | V-111 |
| V.E.1 | Polymer Electrolyte Fuel Cell Lifetime Limitations: The Role of Electrocatalyst Degradation | V-168 |
| V.E.2 | Durability Improvements through Degradation Mechanism Studies | V-175 |

XVIII. Project Listings by Organization

Argonne National Laboratory (Continued)

| | | |
|-------|---|-------|
| V.E.3 | Durability of Low Platinum Fuel Cells Operating at High Power Density | V-182 |
| XI.2 | Life-Cycle Analysis of Vehicle and Fuel Systems with the GREET Model | XI-15 |
| XI.11 | Employment Impacts of Early Markets for Hydrogen and Fuel Cell Technologies | XI-52 |

Arizona State University

| | | |
|------|--|-------|
| VI.3 | Adaptive Process Controls and Ultrasonics for High-Temperature PEM MEA Manufacture | VI-17 |
|------|--|-------|

Arkema Inc.

| | | |
|-------|--|-------|
| V.G.1 | Novel Materials for High Efficiency Direct Methanol Fuel Cells | V-242 |
|-------|--|-------|

ATI Wah Chang

| | | |
|--------|--|-------|
| II.B.1 | One Step Biomass Gas Reforming-Shift Separation Membrane Reactor | II-19 |
|--------|--|-------|

Automotive Fuel Cell Cooperation

| | | |
|--------|---|-------|
| V.D.3 | Durable Catalysts for Fuel Cell Protection during Transient Conditions | V-100 |
| V.D.15 | Development of Alternative and Durable High Performance Cathode Supports for PEM Fuel Cells | V-162 |

Ballard Fuel Cells

| | | |
|-------|---|-------|
| V.D.7 | The Science and Engineering of Durable Ultralow PGM Catalysts | V-121 |
|-------|---|-------|

Ballard Material Products, Inc.

| | | |
|-------|-------------------------------------|-------|
| V.F.6 | Transport in PEMFC Stacks | V-230 |
|-------|-------------------------------------|-------|

Ballard Power Systems

| | | |
|--------|--|-------|
| V.A.10 | A Total Cost of Ownership Model for Design and Manufacturing Optimization of Fuel Cells in Stationary and Emerging Market Applications | V-53 |
| V.B.2 | The Effect of Airborne Contaminants on Fuel Cell Performance and Durability | V-63 |
| V.E.2 | Durability Improvements through Degradation Mechanism Studies | V-175 |
| V.E.5 | Accelerated Testing Validation | V-190 |
| V.E.6 | Development of Micro-Structural Mitigation Strategies for PEM Fuel Cells: Morphological Simulations and Experimental Approaches | V-195 |
| V.F.1 | Air-Cooled Stack Freeze Tolerance | V-206 |
| V.F.3 | Development and Validation of a Two-Phase, Three-Dimensional Model for PEM Fuel Cells | V-217 |
| V.F.5 | Water Transport in PEM Fuel Cells: Advanced Modeling, Material Selection, Testing, and Design Optimization | V-226 |

BASF Fuel Cell

| | | |
|--------|---|-------|
| V.D.11 | Development of Novel Non-PGM Electrocatalysts for Proton Exchange Membrane Fuel Cell Applications | V-143 |
| VI.5 | High Speed, Low Cost Fabrication of Gas Diffusion Electrodes for Membrane Electrode Assemblies | VI-28 |

BASF-SE

| | | |
|--------|--|--------|
| IV.D.8 | Ford/BASF SE/UM Activities in Support of the Hydrogen Storage Engineering Center of Excellence | IV-151 |
|--------|--|--------|

Battelle

| | | |
|-------|---|--------|
| V.A.9 | Stationery and Emerging Market Fuel Cell System Cost Analysis | V-51 |
| VII.3 | Technology Validation: Fuel Cell Bus Evaluations | VII-22 |

BCS Fuel Cells

- V.F.5 Water Transport in PEM Fuel Cells: Advanced Modeling, Material Selection, Testing, and Design Optimization. V-226

Becht Engineering

- VIII.10 Hydrogen Safety Panel VIII-45

Ben C. Gerwick Inc.

- III.3 Vessel Design and Fabrication Technology for Stationary High-Pressure Hydrogen Storage III-17

Big-D Construction

- XII.5 Fuel Cell-Powered Lift Truck Sysco Houston Fleet Deployment XII-24

Bing Energy, Inc.

- VII.6 Florida Hydrogen Initiative (FHI) VII-33

Black & Veatch Corporation

- XII.2 Demonstrating Economic and Operational Viability of 72-Hour Hydrogen PEM Fuel Cell Systems to Support Emergency Communications on the Sprint Nextel Network XII-12

Board of Trustees of the Leland Stanford Junior University

- II.F.1 Directed Nano-Scale and Macro-Scale Architectures for Semiconductor Absorbers and Transparent Conducting Substrates for Photoelectrochemical Water Splitting II-68

Boeing Research and Technology

- VI.6 Development of Advanced Manufacturing Technologies for Low Cost Hydrogen Storage Vessels VI-31

Brookhaven National Laboratory

- IV.A.5 Aluminum Hydride IV-31
 IV.H.12 Atomistic Transport Mechanisms in Aluminum-Based Hydrides IV-249
 V.D.2 Highly Dispersed Alloy Catalyst for Durability V-95
 V.D.6 Contiguous Platinum Monolayer Oxygen Reduction Electrocatalysts on High-Stability Low-Cost Supports. V-117
 V.G.3 Advanced Materials and Concepts for Portable Power Fuel Cells V-250

Brown University

- V.D.5 Nanosegregated Cathode Catalysts with Ultra-Low Platinum Loading V-111

Bucknell University

- II.E.3 Solar Hydrogen Production with a Metal Oxide-Based Thermochemical Cycle II-60

Burns & McDonnell Engineering Co., Inc.

- XII.2 Demonstrating Economic and Operational Viability of 72-Hour Hydrogen PEM Fuel Cell Systems to Support Emergency Communications on the Sprint Nextel Network XII-12

California Fuel Cell Partnership

- VIII.12 Hydrogen Emergency Response Training for First Responders VIII-52

California Institute of Technology

- IV.D.1 Hydrogen Storage Engineering Center of Excellence IV-114

XVIII. Project Listings by Organization

California Institute of Technology (Continued)

- IV.D.4 Key Technologies, Thermal Management, and Prototype Testing for Advanced Solid-State Hydrogen Storage Systems IV-129

California State University, Los Angeles

- VII.7 Sustainable Hydrogen Fueling Station, California State University, Los Angeles VII-38

Carnegie Institute of Washington

- IV.H.8 Novel Molecular Materials for Hydrogen Storage Applications IV-236

Case Western Reserve University

- VI.5 High Speed, Low Cost Fabrication of Gas Diffusion Electrodes for Membrane Electrode Assemblies VI-28

CFD Research Corporation

- V.F.5 Water Transport in PEM Fuel Cells: Advanced Modeling, Material Selection, Testing, and Design Optimization. V-226

City of Santa Fe Springs

- VIII.10 Hydrogen Safety Panel VIII-45

ClearEdge Power

- X.2 Fuel Cell Combined Heat and Power Industrial Demonstration X-10
XII.7 Highly Efficient, 5-kW CHP Fuel Cells Demonstrating Durability and Economic Value in Residential and Light Commercial Applications XII-30

Colorado School of Mines

- IV.H.9 Energy Storage in Clathrate Hydrogen Material IV-239
V.B.1 Effect of System Contaminants on PEMFC Performance and Durability V-57
V.D.9 Tungsten Oxide and Heteropoly Acid Based System for Ultra-High Activity and Stability of Pt Catalysts in PEM Fuel Cell Cathodes V-133
V.K.3 Biomass Fuel Cell Systems V-305

Concepts NREC

- III.7 Development of a Centrifugal Hydrogen Pipeline Gas Compressor. III-35

Connecticut Center for Advanced Technology, Inc.

- IX.4 State and Local Government Partnership IX-16

CSA Standards

- VIII.6 National Codes and Standards Coordination. VIII-28

Dalhousie University

- V.D.1 Advanced Cathode Catalysts and Supports for PEM Fuel Cells V-84
V.D.3 Durable Catalysts for Fuel Cell Protection during Transient Conditions V-100

Delaware State University

- IV.A.7 Hydrogen Storage Materials for Fuel Cell-Powered Vehicles IV-39

Delphi Automotive Systems, LLC

- XII.1 Solid Oxide Fuel Cell Diesel Auxiliary Power Unit Demonstration. XII-9

dPoint Technologies, Inc.

- V.I.1 Materials and Modules for Low-Cost, High-Performance Fuel Cell Humidifiers V-261

Dynalene Inc.

- V.I.2 Large Scale Testing, Demonstration and Commercialization of the Nanoparticle-Based Fuel Cell
Coolant (SBIR Phase III) V-266

E. I. du Pont de Nemours and Company

- V.E.7 Analysis of Durability of MEAs in Automotive PEMFC Applications V-201

Edison Material Technology Center

- IX.2 Raising H2 and Fuel Cell Awareness in Ohio IX-11

Electricore, Inc.

- XII.1 Solid Oxide Fuel Cell Diesel Auxiliary Power Unit Demonstration. XII-9

Electrolytic Technologies Corporation

- VII.6 Florida Hydrogen Initiative (FHI) VII-33

Electrosynthesis Co. Inc.

- II.E.1 Solar High-Temperature Water Splitting Cycle with Quantum Boost II-49

EnerFuels, Inc.

- VII.6 Florida Hydrogen Initiative (FHI) VII-33

Energetics, Inc.

- VIII.10 Hydrogen Safety Panel. VIII-45

Engineering, Procurement & Construction

- III.11 LLNL/Linde 875 bar Liquid Hydrogen Pump for High Density Cryogenic Vessel Refueling III-51

Entegris, Inc.

- II.D.2 High Performance, Low Cost Hydrogen Generation from Renewable Energy II-35

Ericsson Services, Inc.

- XII.2 Demonstrating Economic and Operational Viability of 72-Hour Hydrogen PEM Fuel Cell Systems
to Support Emergency Communications on the Sprint Nextel Network XII-12

ESI US R&D

- V.F.5 Water Transport in PEM Fuel Cells: Advanced Modeling, Material Selection, Testing, and Design
Optimization. V-226

FedEx Freight

- XII.4 Fuel Cell-Powered Lift Truck FedEx Freight Fleet Deployment. XII-21

Fibras Sinteticas de Portugal, SA

- IV.F.1 High Strength Carbon Fibers. IV-191

Firexplo

- VIII.10 Hydrogen Safety Panel. VIII-45

XVIII. Project Listings by Organization

Florida Atlantic University

| | | |
|-------|---|--------|
| VII.6 | Florida Hydrogen Initiative (FHI) | VII-33 |
|-------|---|--------|

Florida Institute of Technology

| | | |
|-------|---|--------|
| VII.6 | Florida Hydrogen Initiative (FHI) | VII-33 |
|-------|---|--------|

Florida International University

| | | |
|---------|---|--------|
| IV.H.19 | Influence of Pressure on Physical Property of Ammonia Borane and its Re-Hydrogenation | IV-274 |
|---------|---|--------|

Florida Solar Energy Center

| | | |
|-------|---|--------|
| VII.6 | Florida Hydrogen Initiative (FHI) | VII-33 |
|-------|---|--------|

Florida State University

| | | |
|-------|---|--------|
| VII.6 | Florida Hydrogen Initiative (FHI) | VII-33 |
|-------|---|--------|

Ford Motor Company

| | | |
|--------|--|--------|
| IV.D.1 | Hydrogen Storage Engineering Center of Excellence | IV-114 |
| IV.D.8 | Ford/BASF SE/UM Activities in Support of the Hydrogen Storage Engineering Center of Excellence | IV-151 |
| V.H.1 | Low-Cost PEM Fuel Cell Metal Bipolar Plates | V-257 |

FP2 Fire Protection Engineering

| | | |
|--------|---|---------|
| VIII.6 | National Codes and Standards Coordination | VIII-28 |
|--------|---|---------|

FuelCell Energy, Inc.

| | | |
|-------|---|--------|
| III.9 | Electrochemical Hydrogen Compressor | III-44 |
| V.C.3 | High-Temperature Membrane with Humidification-Independent Cluster Structure | V-76 |
| VII.2 | Validation of an Integrated Hydrogen Energy Station | VII-18 |

Gas Technology Institute

| | | |
|--------|---|-------|
| II.B.1 | One Step Biomass Gas Reforming-Shift Separation Membrane Reactor | II-19 |
| II.E.2 | Membrane/Electrolyzer Development in the Cu-Cl Thermochemical Cycle | II-56 |
| V.H.1 | Low-Cost PEM Fuel Cell Metal Bipolar Plates | V-257 |

GENCO Infrastructure Solutions

| | | |
|-------|---|--------|
| XII.6 | GENCO Fuel Cell-Powered Lift Truck Fleet Deployment | XII-28 |
|-------|---|--------|

General Motors Company

| | | |
|---------|--|---------|
| IV.C.8 | Hydrogen Storage in Metal-Organic Frameworks | IV-97 |
| IV.D.1 | Hydrogen Storage Engineering Center of Excellence | IV-114 |
| IV.D.7 | Thermal Management of Onboard Cryogenic Hydrogen Storage Systems | IV-147 |
| V.B.1 | Effect of System Contaminants on PEMFC Performance and Durability | V-57 |
| V.C.4 | Corrugated Membrane Fuel Cell Structures | V-80 |
| V.D.1 | Advanced Cathode Catalysts and Supports for PEM Fuel Cells | V-84 |
| V.D.12 | High-Activity Dealloyed Catalysts | V-149 |
| V.F.7 | Investigation of Micro- and Macro-Scale Transport Processes for Improved Fuel Cell Performance | V-235 |
| VIII.10 | Hydrogen Safety Panel | VIII-45 |
| VII.7 | Sustainable Hydrogen Fueling Station, California State University, Los Angeles | VII-38 |

George Washington University

| | | |
|--------|---|-------|
| V.D.12 | High-Activity Dealloyed Catalysts | V-149 |
|--------|---|-------|

Georgia Institute of Technology

| | | |
|-------|---|-------|
| V.E.6 | Development of Micro-Structural Mitigation Strategies for PEM Fuel Cells: Morphological Simulations and Experimental Approaches | V-195 |
|-------|---|-------|

Giner Electrochemical Systems, LLC

| | | |
|--------|---|--------|
| II.D.1 | PEM Electrolyzer Incorporating an Advanced Low-Cost Membrane | II-31 |
| II.H.1 | Unitized Design for Home Refueling Appliance for Hydrogen Generation to 5,000 psi | II-122 |
| V.C.2 | Dimensionally Stable High Performance Membrane (SBIR Phase III) | V-71 |
| V.F.6 | Transport in PEMFC Stacks | V-230 |

Global Engineering and Technology

| | | |
|-------|--|--------|
| III.3 | Vessel Design and Fabrication Technology for Stationary High-Pressure Hydrogen Storage | III-17 |
|-------|--|--------|

Graitech International Holdings Inc.

| | | |
|-------|--|------|
| V.C.4 | Corrugated Membrane Fuel Cell Structures | V-80 |
|-------|--|------|

Greenway Energy

| | | |
|------|---|------|
| IX.1 | Development of Hydrogen Education Programs for Government Officials | IX-7 |
|------|---|------|

GWS Solutions of Tolland, LLC

| | | |
|---------|---|---------|
| VIII.6 | National Codes and Standards Coordination | VIII-28 |
| VIII.10 | Hydrogen Safety Panel | VIII-45 |

H2 Technology Consulting LLC

| | | |
|---------|--|--------|
| IV.C.6 | Weak Chemisorption Validation | IV-89 |
| IV.C.11 | Hydrogen Sorbent Measurement Qualification and Characterization | IV-109 |
| IV.E.2 | Best Practices for Characterizing Engineering Properties of Hydrogen Storage Materials | IV-170 |

H2Pump, LLC

| | | |
|--------|---|-------|
| II.C.2 | Process Intensification of Hydrogen Unit Operations Using an Electrochemical Device | II-28 |
|--------|---|-------|

Hanford Fire Department

| | | |
|---------|---|---------|
| VIII.12 | Hydrogen Emergency Response Training for First Responders | VIII-52 |
|---------|---|---------|

Hawaii Hydrogen Carriers, LLC

| | | |
|--------|---|-------|
| IV.B.4 | Development of a Practical Hydrogen Storage System Based on Liquid Organic Hydrogen Carriers and a Homogeneous Catalyst | IV-55 |
|--------|---|-------|

Hawaii Natural Energy Institute

| | | |
|-------|---|--------|
| V.B.2 | The Effect of Airborne Contaminants on Fuel Cell Performance and Durability | V-63 |
| VII.5 | Hawaii Hydrogen Power Park | VII-30 |
| X.1 | Hydrogen Energy Systems as a Grid Management Tool | X-7 |

Hazardous Materials Management and Emergency Response Training and Education Center

| | | |
|---------|---|---------|
| VIII.12 | Hydrogen Emergency Response Training for First Responders | VIII-52 |
|---------|---|---------|

XVIII. Project Listings by Organization

HRL Laboratories, LLC

| | | |
|--------|--|-------|
| IV.C.7 | Room Temperature Hydrogen Storage in Nano-Confined Liquids | IV-95 |
|--------|--|-------|

Humboldt State University

| | | |
|------|---|-------|
| IX.3 | Hydrogen Technology and Energy Curriculum (HyTEC) | IX-13 |
|------|---|-------|

HyGen Industries

| | | |
|-------|---|--------|
| III.7 | Development of a Centrifugal Hydrogen Pipeline Gas Compressor | III-35 |
|-------|---|--------|

IBIS Associates, Inc.

| | | |
|-------|---|-------|
| V.H.1 | Low-Cost PEM Fuel Cell Metal Bipolar Plates | V-257 |
|-------|---|-------|

IdaTech, LLC

| | | |
|-------|--|--------|
| V.J.5 | Research and Development for Off-Road Fuel Cell Applications | V-289 |
| XII.8 | Accelerating Acceptance of Fuel Cell Backup Power Systems | XII-34 |

IDC Energy Insights

| | | |
|------|---|-------|
| XI.3 | Hydrogen Refueling Infrastructure Cost Analysis | XI-19 |
|------|---|-------|

Illinois Institute of Technology

| | | |
|--------|---|-------|
| V.D.10 | Synthesis and Characterization of Mixed-Conducting Corrosion Resistant Oxide Supports | V-138 |
| V.E.7 | Analysis of Durability of MEAs in Automotive PEMFC Applications | V-201 |
| V.G.1 | Novel Materials for High Efficiency Direct Methanol Fuel Cells | V-242 |

InnovaTek

| | | |
|-------|---|-------|
| V.J.4 | Power Generation from an Integrated Biomass Reformer and Solid Oxide Fuel Cell (SBIR Phase III) | V-285 |
|-------|---|-------|

Institut de Chimie et des Matériaux

| | | |
|--------|-------------------------------|-------|
| IV.C.6 | Weak Chemisorption Validation | IV-89 |
|--------|-------------------------------|-------|

Institute of Basic Biological Problems

| | | |
|--------|---|--------|
| II.G.1 | Biological Systems for Hydrogen Photoproduction | II-103 |
|--------|---|--------|

Intelligent Energy

| | | |
|-------|---|-------|
| V.J.1 | Development and Demonstration of a New-Generation High Efficiency 10-kW Stationary Fuel Cell System | V-272 |
|-------|---|-------|

Ion Power Inc.

| | | |
|-------|---|-------|
| V.C.4 | Corrugated Membrane Fuel Cell Structures | V-80 |
| V.E.2 | Durability Improvements through Degradation Mechanism Studies | V-175 |
| V.E.5 | Accelerated Testing Validation | V-190 |

J. Craig Venter Institute

| | | |
|--------|--|--------|
| II.G.3 | Hydrogen from Water in a Novel Recombinant Oxygen-Tolerant Cyanobacterial System | II-113 |
|--------|--|--------|

Jet Propulsion Laboratory

| | | |
|--------|---|--------|
| IV.D.1 | Hydrogen Storage Engineering Center of Excellence | IV-114 |
| IV.D.4 | Key Technologies, Thermal Management, and Prototype Testing for Advanced Solid-State Hydrogen Storage Systems | IV-129 |
| V.D.1 | Advanced Cathode Catalysts and Supports for PEM Fuel Cells | V-84 |
| V.D.5 | Nanosegregated Cathode Catalysts with Ultra-Low Platinum Loading | V-111 |

Johns Hopkins University

| | | |
|--------|--|--------|
| II.G.1 | Biological Systems for Hydrogen Photoproduction. | II-103 |
|--------|--|--------|

Johnson Matthey Fuel Cells

| | | |
|--------|---|-------|
| V.D.2 | Highly Dispersed Alloy Catalyst for Durability | V-95 |
| V.D.6 | Contiguous Platinum Monolayer Oxygen Reduction Electrocatalysts on High-Stability Low-Cost Supports | V-117 |
| V.D.12 | High-Activity Dealloyed Catalysts | V-149 |
| V.E.1 | Polymer Electrolyte Fuel Cell Lifetime Limitations: The Role of Electrocatalyst Degradation | V-168 |
| V.F.4 | Transport Studies Enabling Efficiency Optimization of Cost-Competitive Fuel Cell Stacks | V-222 |
| V.G.2 | New MEA Materials for Improved Direct Methanol Fuel Cell (DMFC) Performance, Durability, and Cost | V-246 |
| V.G.3 | Advanced Materials and Concepts for Portable Power Fuel Cells | V-250 |

Kelvin Hecht

| | | |
|--------|--|---------|
| VIII.6 | National Codes and Standards Coordination. | VIII-28 |
|--------|--|---------|

Lawrence Berkeley National Laboratory

| | | |
|--------|--|-------|
| IV.C.8 | Hydrogen Storage in Metal-Organic Frameworks. | IV-97 |
| V.A.10 | A Total Cost of Ownership Model for Design and Manufacturing Optimization of Fuel Cells in Stationary and Emerging Market Applications | V-53 |
| V.D.8 | Molecular-Scale, Three-Dimensional Non-Platinum Group Metal Electrodes for Catalysis of Fuel Cell Reactions | V-126 |
| V.E.2 | Durability Improvements through Degradation Mechanism Studies | V-175 |
| V.E.5 | Accelerated Testing Validation | V-190 |
| V.F.2 | Fuel Cell Fundamentals at Low and Subzero Temperatures | V-211 |
| V.F.4 | Transport Studies Enabling Efficiency Optimization of Cost-Competitive Fuel Cell Stacks | V-222 |

Lawrence Livermore National Laboratory

| | | |
|--------|---|--------|
| II.F.3 | Characterization and Optimization of Photoelectrode Surfaces for Solar-to-Chemical Fuel Conversion. | II-79 |
| III.4 | Failure Analysis, Permeation, and Toughness of Glass Fiber Composite Pressure Vessels for Inexpensive Delivery of Cold Hydrogen | III-22 |
| III.11 | LLNL/Linde 875 bar Liquid Hydrogen Pump for High Density Cryogenic Vessel Refueling | III-51 |

Lincoln Composites, Inc.

| | | |
|---------|--|--------|
| III.6 | Development of High Pressure Hydrogen Storage Tank for Storage and Gaseous Truck Delivery. | III-32 |
| IV.D.1 | Hydrogen Storage Engineering Center of Excellence | IV-114 |
| IV.D.10 | Development of Improved Composite Pressure Vessels for Hydrogen Storage | IV-160 |

Linde LLC

| | | |
|--------|---|--------|
| III.11 | LLNL/Linde 875 bar Liquid Hydrogen Pump for High Density Cryogenic Vessel Refueling | III-51 |
|--------|---|--------|

Linde North America

| | | |
|-------|---|--------|
| XII.6 | GENCO Fuel Cell-Powered Lift Truck Fleet Deployment | XII-28 |
|-------|---|--------|

Los Alamos National Laboratory

| | | |
|--------|---|--------|
| IV.B.2 | Fluid Phase Chemical Hydrogen Storage Materials | IV-48 |
| IV.D.1 | Hydrogen Storage Engineering Center of Excellence | IV-114 |
| IV.D.3 | Chemical Hydride Rate Modeling, Validation, and System Demonstration. | IV-126 |

XVIII. Project Listings by Organization

Los Alamos National Laboratory (Continued)

| | | |
|--------|--|---------|
| V.A.7 | Technical Assistance to Developers. | V-43 |
| V.B.1 | Effect of System Contaminants on PEMFC Performance and Durability | V-57 |
| V.D.4 | Extended, Continuous Pt Nanostructures in Thick, Dispersed Electrodes. | V-107 |
| V.D.7 | The Science and Engineering of Durable Ultralow PGM Catalysts | V-121 |
| V.D.11 | Development of Novel Non-PGM Electrocatalysts for Proton Exchange Membrane Fuel Cell Applications | V-143 |
| V.E.2 | Durability Improvements through Degradation Mechanism Studies | V-175 |
| V.E.3 | Durability of Low Platinum Fuel Cells Operating at High Power Density. | V-182 |
| V.E.4 | Improved Accelerated Stress Tests Based on Fuel Cell Vehicle Data | V-186 |
| V.E.5 | Accelerated Testing Validation | V-190 |
| V.E.6 | Development of Micro-Structural Mitigation Strategies for PEM Fuel Cells: Morphological Simulations and Experimental Approaches. | V-195 |
| V.F.2 | Fuel Cell Fundamentals at Low and Subzero Temperatures | V-211 |
| V.F.3 | Development and Validation of a Two-Phase, Three-Dimensional Model for PEM Fuel Cells | V-217 |
| V.G.3 | Advanced Materials and Concepts for Portable Power Fuel Cells | V-250 |
| VI.7 | Cause and Effect: Flow Field Plate Manufacturing Variability and its Impact on Performance | VI-36 |
| VIII.8 | Leak Detection and H ₂ Sensor Development for Hydrogen Applications | VIII-36 |
| VIII.9 | Hydrogen Fuel Quality Research and Development | VIII-42 |
| XI.1 | Infrastructure Analysis of Early Market Transition of Fuel Cell Vehicles | XI-11 |

Massachusetts Institute of Technology

| | | |
|--------|--|-------|
| V.D.6 | Contiguous Platinum Monolayer Oxygen Reduction Electrocatalysts on High-Stability Low-Cost Supports. | V-117 |
| V.D.12 | High-Activity Dealloyed Catalysts | V-149 |
| V.E.1 | Polymer Electrolyte Fuel Cell Lifetime Limitations: The Role of Electrocatalyst Degradation | V-168 |

Max Planck Institute

| | | |
|--------|---|-------|
| IV.C.6 | Weak Chemisorption Validation | IV-89 |
|--------|---|-------|

Media and Process Technology Inc.

| | | |
|--------|--|-------|
| II.C.1 | Development of Hydrogen Selective Membranes/Modules as Reactors/Separators for Distributed Hydrogen Production | II-23 |
|--------|--|-------|

MegaStir Technologies

| | | |
|-------|--|--------|
| III.3 | Vessel Design and Fabrication Technology for Stationary High-Pressure Hydrogen Storage | III-17 |
|-------|--|--------|

Michigan State University

| | | |
|--------|---|-------|
| V.D.11 | Development of Novel Non-PGM Electrocatalysts for Proton Exchange Membrane Fuel Cell Applications | V-143 |
|--------|---|-------|

Michigan Technological University

| | | |
|-------|--|-------|
| V.E.6 | Development of Micro-Structural Mitigation Strategies for PEM Fuel Cells: Morphological Simulations and Experimental Approaches. | V-195 |
|-------|--|-------|

Midwest Optoelectronics, LLC

| | | |
|--------|--|-------|
| II.F.6 | Critical Research for Cost-Effective Photoelectrochemical Production of Hydrogen | II-93 |
|--------|--|-------|

Midwest Research Institute

| | | |
|--------|---|-------|
| IV.C.3 | Multiply Surface-Functionalized Nanoporous Carbon for Vehicular Hydrogen Storage. | IV-72 |
|--------|---|-------|

Mitsubishi Compressor Company

| | | |
|-------|---|--------|
| III.8 | Oil-Free Centrifugal Hydrogen Compression Technology Demonstration. | III-40 |
|-------|---|--------|

Mohawk Innovative Technologies, Inc.

| | | |
|-------|---|--------|
| III.8 | Oil-Free Centrifugal Hydrogen Compression Technology Demonstration. | III-40 |
|-------|---|--------|

MorEvents

| | | |
|--------|--|---------|
| VIII.6 | National Codes and Standards Coordination. | VIII-28 |
| VIII.7 | Codes and Standards Outreach for Emerging Fuel Cell Technologies | VIII-33 |

MVSystems, Incorporated

| | | |
|--------|--|-------|
| II.F.5 | Photoelectrochemical Hydrogen Production | II-89 |
|--------|--|-------|

National Energy Technology Laboratory

| | | |
|--------|---|-------|
| II.B.1 | One Step Biomass Gas Reforming-Shift Separation Membrane Reactor. | II-19 |
|--------|---|-------|

National Fuel Cell Research Center

| | | |
|-------|--|--------|
| VII.4 | California Hydrogen Infrastructure Project | VII-26 |
|-------|--|--------|

National Institute of Standards and Technology

| | | |
|--------|--|--------|
| IV.C.8 | Hydrogen Storage in Metal-Organic Frameworks. | IV-97 |
| IV.E.3 | Neutron Characterization in Support of the DOE Hydrogen Storage Sub-Program | IV-176 |
| V.A.6 | Neutron Imaging Study of the Water Transport in Operating Fuel Cells | V-37 |
| VI.4 | Non-Contact Sensor Evaluation for Bipolar Plate Manufacturing Process Control and Smart Assembly of Fuel Cell Stacks | VI-24 |
| VI.7 | Cause and Effect: Flow Field Plate Manufacturing Variability and its Impact on Performance | VI-36 |
| VI.8 | Optical Scatterfield Metrology for Online Catalyst Coating Inspection of PEM (Fuel Cell) Soft Goods | VI-41 |

National Renewable Energy Laboratory

| | | |
|---------|---|--------|
| II.A.2 | Distributed Bio-Oil Reforming | II-15 |
| II.D.3 | Renewable Electrolysis Integrated Systems Development and Testing | II-39 |
| II.D.4 | Hour-by-Hour Cost Modeling of Optimized Central Wind-Based Water Electrolysis Production | II-43 |
| II.F.2 | Semiconductor Materials for Photoelectrolysis | II-74 |
| II.F.6 | Critical Research for Cost-Effective Photoelectrochemical Production of Hydrogen | II-93 |
| II.G.1 | Biological Systems for Hydrogen Photoproduction. | II-103 |
| II.G.2 | Fermentation and Electrohydrogenic Approaches to Hydrogen Production. | II-108 |
| IV.C.6 | Weak Chemisorption Validation | IV-89 |
| IV.C.11 | Hydrogen Sorbent Measurement Qualification and Characterization | IV-109 |
| IV.D.1 | Hydrogen Storage Engineering Center of Excellence | IV-114 |
| IV.D.2 | System Design, Analysis, Modeling, and Media Engineering Properties for Hydrogen Energy Storage | IV-119 |
| V.A.1 | Analysis of Laboratory Fuel Cell Technology Status – Voltage Degradation | V-11 |
| V.A.8 | Enlarging the Potential Market for Stationary Fuel Cells Through System Design Optimization | V-47 |
| V.B.1 | Effect of System Contaminants on PEMFC Performance and Durability | V-57 |
| V.D.4 | Extended, Continuous Pt Nanostructures in Thick, Dispersed Electrodes. | V-107 |
| V.D.9 | Tungsten Oxide and Heteropoly Acid Based System for Ultra-High Activity and Stability of Pt Catalysts in PEM Fuel Cell Cathodes | V-133 |
| V.D.14 | High Aspect Ratio Nano-Structured Pt-based PEM Fuel Cell Catalysts (EERE Post-Doc Fellowship) | V-159 |
| VI.1 | Fuel Cell Membrane Electrode Assembly Manufacturing R&D | VI-7 |

XVIII. Project Listings by Organization

National Renewable Energy Laboratory (Continued)

| | | |
|--------|--|---------|
| VII.1 | Controlled Hydrogen Fleet and Infrastructure Analysis | VII-11 |
| VII.3 | Technology Validation: Fuel Cell Bus Evaluations | VII-22 |
| VII.8 | Renewable Electrolysis Integrated System Development and Testing | VII-40 |
| VII.9 | Stationary Fuel Cell Evaluation | VII-44 |
| VII.10 | Next Generation H2 Station Analysis | VII-46 |
| VIII.3 | Component Standard Research and Development | VIII-18 |
| VIII.6 | National Codes and Standards Coordination | VIII-28 |
| VIII.7 | Codes and Standards Outreach for Emerging Fuel Cell Technologies | VIII-33 |
| X.3 | Direct Methanol Fuel Cell Material Handling Equipment Demonstration | X-15 |
| XI.1 | Infrastructure Analysis of Early Market Transition of Fuel Cell Vehicles | XI-11 |
| XI.3 | Hydrogen Refueling Infrastructure Cost Analysis | XI-19 |
| XI.4 | Comparing Infrastructure Costs for Hydrogen and Electricity | XI-23 |
| XI.5 | Infrastructure Costs Associated with Central Hydrogen Production from Biomass and Coal | XI-27 |
| XI.7 | Effects of Technology Cost Parameters on Hydrogen Pathway Succession | XI-35 |
| XI.9 | Resource Analysis for Hydrogen Production | XI-43 |
| XI.10 | Cost, Energy Use, and Emissions of Tri-Generation Systems | XI-47 |
| XII.3 | Analysis Results for ARRA Projects: Enabling Fuel Cell Market Transformation | XII-16 |

Nissan Technical Center

| | | |
|--------|---|-------|
| V.D.10 | Synthesis and Characterization of Mixed-Conducting Corrosion Resistant Oxide Supports | V-138 |
| V.D.11 | Development of Novel Non-PGM Electrocatalysts for Proton Exchange Membrane Fuel Cell Applications | V-143 |
| V.E.7 | Analysis of Durability of MEAs in Automotive PEMFC Applications | V-201 |

Northeastern University

| | | |
|---------|---|--------|
| V.D.11 | Development of Novel Non-PGM Electrocatalysts for Proton Exchange Membrane Fuel Cell Applications | V-143 |
| V.D.12 | High-Activity Dealloyed Catalysts | V-149 |
| V.G.2 | New MEA Materials for Improved Direct Methanol Fuel Cell (DMFC) Performance, Durability, and Cost | V-246 |
| IV.A.1 | Efficient Discovery of Novel Multicomponent Mixtures for Hydrogen Storage: A Combined Computational/Experimental Approach | IV-11 |
| IV.C.4 | New Carbon-Based Porous Materials with Increased Heats of Adsorption for Hydrogen Storage | IV-78 |
| IV.C.10 | Metal- and Cluster-Modified Ultrahigh-Area Materials for the Ambient Temperature Storage of Molecular Hydrogen | IV-105 |
| IV.H.13 | Theory of Hydrogen Storage in Complex Hydrides | IV-253 |

Nuvera Fuel Cells, Inc.

| | | |
|-------|---|-------|
| V.E.3 | Durability of Low Platinum Fuel Cells Operating at High Power Density | V-182 |
| V.F.4 | Transport Studies Enabling Efficiency Optimization of Cost-Competitive Fuel Cell Stacks | V-222 |

Oak Ridge National Laboratory

| | | |
|--------|--|--------|
| II.D.2 | High Performance, Low Cost Hydrogen Generation from Renewable Energy | II-35 |
| III.3 | Vessel Design and Fabrication Technology for Stationary High-Pressure Hydrogen Storage | III-17 |
| III.10 | Composite Technology for Hydrogen Pipelines | III-47 |
| IV.C.9 | The Quantum Effects of Pore Structure on Hydrogen Adsorption | IV-100 |

Oak Ridge National Laboratory (Continued)

| | | |
|--------|--|--------|
| IV.F.1 | High Strength Carbon Fibers | IV-191 |
| IV.F.2 | Lifecycle Verification of Polymeric Storage Tank Liners | IV-197 |
| IV.F.3 | Development of Low-Cost, High Strength Commercial Textile Precursor (PAN-MA) | IV-200 |
| IV.H.4 | Atomistic Mechanisms of Metal-Assisted Hydrogen Storage in Nanostructured Carbons | IV-220 |
| IV.H.7 | New Pathways and Metrics for Enhanced, Reversible Hydrogen Storage in Boron-Doped Carbon Nanospaces | IV-233 |
| V.A.5 | Characterization of Fuel Cell Materials | V-32 |
| V.D.3 | Durable Catalysts for Fuel Cell Protection during Transient Conditions | V-100 |
| V.D.4 | Extended, Continuous Pt Nanostructures in Thick, Dispersed Electrodes | V-107 |
| V.D.5 | Nanosegregated Cathode Catalysts with Ultra-Low Platinum Loading | V-111 |
| V.E.2 | Durability Improvements through Degradation Mechanism Studies | V-175 |
| V.E.4 | Improved Accelerated Stress Tests Based on Fuel Cell Vehicle Data | V-186 |
| V.E.5 | Accelerated Testing Validation | V-190 |
| V.G.3 | Advanced Materials and Concepts for Portable Power Fuel Cells | V-250 |
| XI.6 | Sensitivity Analysis of H ₂ -Vehicles' Market Prospects, Costs and Benefits | XI-31 |
| XI.8 | Impact of DOE Program Goals on Hydrogen Vehicles: Market Prospect, Costs, and Benefits | XI-39 |

Ohio Fuel Cell Coalition

| | | |
|------|--|-------|
| IX.2 | Raising H ₂ and Fuel Cell Awareness in Ohio | IX-11 |
|------|--|-------|

Ohio State University

| | | |
|--------|---|-------|
| IV.A.3 | Lightweight Metal Hydrides for Hydrogen Storage | IV-22 |
|--------|---|-------|

Oorja Protonics, Inc.

| | | |
|-----|---|------|
| X.3 | Direct Methanol Fuel Cell Material Handling Equipment Demonstration | X-15 |
|-----|---|------|

Oregon State University

| | | |
|--------|--|--------|
| IV.D.1 | Hydrogen Storage Engineering Center of Excellence | IV-114 |
| IV.D.9 | Microscale Enhancement of Heat and Mass Transfer for Hydrogen Energy Storage | IV-156 |

PACCAR, Inc.

| | | |
|-------|---|-------|
| XII.1 | Solid Oxide Fuel Cell Diesel Auxiliary Power Unit Demonstration | XII-9 |
|-------|---|-------|

Pacific Northwest National Laboratory

| | | |
|---------|--|---------|
| II.A.1 | Biomass-Derived Liquids Distributed (Aqueous Phase) Reforming | II-11 |
| IV.D.1 | Hydrogen Storage Engineering Center of Excellence | IV-114 |
| IV.D.5 | Systems Engineering of Chemical Hydride, Pressure Vessel, and Balance of Plant for Onboard Hydrogen Storage | IV-134 |
| IV.E.5 | Early Market TRL/MRL Analysis | IV-186 |
| IV.F.4 | Synergistically Enhanced Materials and Design Parameters for Reducing the Cost of Hydrogen Storage Tanks | IV-205 |
| IV.H.16 | Activation of Hydrogen with Bi-Functional Ambiphilic Catalyst Complexes | IV-263 |
| V.D.15 | Development of Alternative and Durable High Performance Cathode Supports for PEM Fuel Cells | V-162 |
| VI.6 | Development of Advanced Manufacturing Technologies for Low Cost Hydrogen Storage Vessels | VI-31 |
| VIII.10 | Hydrogen Safety Panel | VIII-45 |
| VIII.11 | Hydrogen Safety Knowledge Tools | VIII-49 |
| VIII.12 | Hydrogen Emergency Response Training for First Responders | VIII-52 |

XVIII. Project Listings by Organization

Pacific Northwest National Laboratory (Continued)

- X.2 Fuel Cell Combined Heat and Power Industrial Demonstration X-10
- XII.3 Analysis Results for ARRA Projects: Enabling Fuel Cell Market Transformation XII-16

Parker Hannifin Ltd domnick hunter Division

- II.D.1 PEM Electrolyzer Incorporating an Advanced Low-Cost Membrane II-31

PBI Performance Products, Inc.

- II.C.2 Process Intensification of Hydrogen Unit Operations Using an Electrochemical Device II-28

Pennsylvania State University

- II.D.2 High Performance, Low Cost Hydrogen Generation from Renewable Energy II-35
- II.E.2 Membrane/Electrolyzer Development in the Cu-Cl Thermochemical Cycle II-56
- II.G.2 Fermentation and Electrohydrogenic Approaches to Hydrogen Production. II-108
- IV.C.5 Hydrogen Trapping through Designer Hydrogen Spillover Molecules with Reversible Temperature and Pressure-Induced Switching IV-82
- IV.H.10 Exploration of Novel Carbon-Hydrogen Interactions IV-243
- V.F.2 Fuel Cell Fundamentals at Low and Subzero Temperatures V-211
- V.F.3 Development and Validation of a Two-Phase, Three-Dimensional Model for PEM Fuel Cells V-217
- V.F.4 Transport Studies Enabling Efficiency Optimization of Cost-Competitive Fuel Cell Stacks V-222
- V.F.7 Investigation of Micro- and Macro-Scale Transport Processes for Improved Fuel Cell Performance. V-235

Plug Power Inc.

- V.F.1 Air-Cooled Stack Freeze Tolerance V-206
- XII.4 Fuel Cell-Powered Lift Truck FedEx Freight Fleet Deployment. XII-21
- XII.5 Fuel Cell-Powered Lift Truck Sysco Houston Fleet Deployment XII-24
- XII.6 GENCO Fuel Cell-Powered Lift Truck Fleet Deployment XII-28
- XII.7 Highly Efficient, 5-kW CHP Fuel Cells Demonstrating Durability and Economic Value in Residential and Light Commercial Applications XII-30
- XII.8 Accelerating Acceptance of Fuel Cell Backup Power Systems. XII-34

Powdermet Inc.

- VIII.10 Hydrogen Safety Panel VIII-45

Proton Energy Systems

- II.H.2 Hydrogen by Wire - Home Fueling System. II-126

Proton OnSite

- II.D.2 High Performance, Low Cost Hydrogen Generation from Renewable Energy II-35
- II.D.5 Low-Cost Large-Scale PEM Electrolysis for Renewable Energy Storage II-46

Protonex Inc.

- V.I.2 Large Scale Testing, Demonstration and Commercialization of the Nanoparticle-Based Fuel Cell Coolant (SBIR Phase III) V-266

Quantum Fuel Systems Technologies Worldwide, Inc.

- VI.6 Development of Advanced Manufacturing Technologies for Low Cost Hydrogen Storage Vessels VI-31

Queen's University

- V.E.6 Development of Micro-Structural Mitigation Strategies for PEM Fuel Cells: Morphological Simulations and Experimental Approaches. V-195

RCF Economic and Financial Consulting, Inc.

- XI.11 Employment Impacts of Early Markets for Hydrogen and Fuel Cell Technologies XI-52

ReliOn, Inc.

- XII.2 Demonstrating Economic and Operational Viability of 72-Hour Hydrogen PEM Fuel Cell Systems to Support Emergency Communications on the Sprint Nextel Network XII-12

Rensselaer Polytechnic Institute

- VI.3 Adaptive Process Controls and Ultrasonics for High-Temperature PEM MEA Manufacture VI-17

Rochester Institute of Technology

- V.F.7 Investigation of Micro- and Macro-Scale Transport Processes for Improved Fuel Cell Performance. V-235

Rutgers University

- IV.C.5 Hydrogen Trapping through Designer Hydrogen Spillover Molecules with Reversible Temperature and Pressure-Induced Switching IV-82
- IV.H.2 Novel theoretical and experimental approaches for understanding and optimizing hydrogen-sorbent interactions in metal organic framework materials. IV-213

SAE International

- VIII.3 Component Standard Research and Development. VIII-18
- VIII.6 National Codes and Standards Coordination. VIII-28

Sandia National Laboratories

- II.E.3 Solar Hydrogen Production with a Metal Oxide-Based Thermochemical Cycle II-60
- III.1 Hydrogen Embrittlement of Structural Steels III-9
- V.F.3 Development and Validation of a Two-Phase, Three-Dimensional Model for PEM Fuel Cells. V-217
- VIII.1 Hydrogen Safety, Codes and Standards R&D – Release Behavior. VIII-9
- VIII.2 Risk-Informed Safety Requirements for H2 Codes and Standards Development VIII-15
- VIII.4 Hydrogen Materials and Components Compatibility VIII-22
- VIII.5 Component Testing for Industrial Trucks and Early Market Applications. VIII-25

Savannah River National Laboratory

- III.5 Fiber Reinforced Composite Pipeline III-27
- IV.A.6 Electrochemical Reversible Formation of Alane. IV-35
- IV.D.1 Hydrogen Storage Engineering Center of Excellence IV-114
- IV.H.5 Elucidation of Hydrogen Interaction Mechanisms with Metal-Doped Carbon Nanostructures. IV-226

Schott North America

- II.B.1 One Step Biomass Gas Reforming-Shift Separation Membrane Reactor. II-19

Science Applications International Corporation

- II.E.1 Solar High-Temperature Water Splitting Cycle with Quantum Boost II-49

XVIII. Project Listings by Organization

Scribner Associates, Inc.

- V.C.1 Lead Research and Development Activity for DOE's High Temperature, Low Relative Humidity Membrane Program V-68

SFC Energy

- V.G.3 Advanced Materials and Concepts for Portable Power Fuel Cells V-250

SGL Carbon

- V.F.5 Water Transport in PEM Fuel Cells: Advanced Modeling, Material Selection, Testing, and Design Optimization. V-226

Sloane Solutions

- VIII.6 National Codes and Standards Coordination. VIII-28

South Carolina Hydrogen and Fuel Cell Alliance

- IX.1 Development of Hydrogen Education Programs for Government Officials IX-7
X.4 Landfill Gas-to-Hydrogen XI-1

Spectrum Automation Controls

- II.D.3 Renewable Electrolysis Integrated Systems Development and Testing II-39
VII.8 Renewable Electrolysis Integrated Systems Development and Testing VII-40

Spencer Composites Corporation

- III.4 Failure Analysis, Permeation, and Toughness of Glass Fiber Composite Pressure Vessels for Inexpensive Delivery of Cold Hydrogen III-22

Sprint Nextel

- XII.2 Demonstrating Economic and Operational Viability of 72-Hour Hydrogen PEM Fuel Cell Systems to Support Emergency Communications on the Sprint Nextel Network XII-12

SRT Group, Inc.

- VII.6 Florida Hydrogen Initiative (FHI) VII-33

Stanford University

- II.F.1 Directed Nano-Scale and Macro-Scale Architectures for Semiconductor Absorbers and Transparent Conducting Substrates for Photoelectrochemical Water Splitting II-68
II.F.2 Semiconductor Materials for Photoelectrolysis II-74
IV.H.19 Influence of Pressure on Physical Property of Ammonia Borane and its Re-Hydrogenation IV-274
V.D.4 Extended, Continuous Pt Nanostructures in Thick, Dispersed Electrodes. V-107

State University of New York, Albany

- V.D.4 Extended, Continuous Pt Nanostructures in Thick, Dispersed Electrodes. V-107

State University of New York, Stony Brook

- V.H.1 Low-Cost PEM Fuel Cell Metal Bipolar Plates V-257

Steele Consulting

- VIII.6 National Codes and Standards Coordination. VIII-28

Strategic Analysis, Inc.

- IV.E.4 Hydrogen Storage Cost Analysis, Preliminary Results IV-182

Strategic Analysis, Inc. (Continued)

| | | |
|-------|--|-------|
| V.A.2 | Mass-Production Cost Estimation for Automotive Fuel Cell Systems | V-16 |
| V.A.3 | Stationary Fuel Cell System Cost Analysis | V-20 |
| XI.7 | Effects of Technology Cost Parameters on Hydrogen Pathway Succession | XI-35 |

Sustainable Innovations, LLC

| | | |
|-------|---|--------|
| III.9 | Electrochemical Hydrogen Compressor | III-44 |
|-------|---|--------|

Sysco of Houston

| | | |
|-------|---|--------|
| XII.5 | Fuel Cell-Powered Lift Truck Sysco Houston Fleet Deployment | XII-24 |
|-------|---|--------|

TDA Research, Inc.

| | | |
|-------|---|-------|
| XII.1 | Solid Oxide Fuel Cell Diesel Auxiliary Power Unit Demonstration | XII-9 |
|-------|---|-------|

Tech-Etch

| | | |
|-------|-------------------------------------|-------|
| V.F.6 | Transport in PEMFC Stacks | V-230 |
|-------|-------------------------------------|-------|

Technical University Berlin

| | | |
|--------|---|-------|
| V.D.12 | High-Activity Dealloyed Catalysts | V-149 |
|--------|---|-------|

Techverse

| | | |
|-------|---|-------|
| V.F.5 | Water Transport in PEM Fuel Cells: Advanced Modeling, Material Selection, Testing, and Design Optimization. | V-226 |
|-------|---|-------|

Tetramer Technologies, LLC

| | | |
|-------|--|-------|
| V.I.3 | New High Performance Water Vapor Membranes to Improve Fuel Cell Balance of Plant Efficiency and Lower Costs (SBIR Phase I) | V-270 |
|-------|--|-------|

Texas A&M University

| | | |
|--------|---|--------|
| III.7 | Development of a Centrifugal Hydrogen Pipeline Gas Compressor | III-35 |
| IV.C.1 | A Biomimetic Approach to Metal-Organic Frameworks with High H ₂ Uptake | IV-60 |
| V.D.2 | Highly Dispersed Alloy Catalyst for Durability | V-95 |

The Toro Company

| | | |
|-------|--|-------|
| V.J.5 | Research and Development for Off-Road Fuel Cell Applications | V-289 |
|-------|--|-------|

Thermochemical Engineering Solutions

| | | |
|--------|---|-------|
| II.E.1 | Solar High-Temperature Water Splitting Cycle with Quantum Boost | II-49 |
|--------|---|-------|

TIAX, LLC

| | | |
|------|---|-------|
| XI.4 | Comparing Infrastructure Costs for Hydrogen and Electricity | XI-23 |
|------|---|-------|

TreadStone Technologies, Inc.

| | | |
|-------|---|-------|
| V.H.1 | Low-Cost PEM Fuel Cell Metal Bipolar Plates | V-257 |
|-------|---|-------|

United Technologies Research Center

| | | |
|--------|--|--------|
| IV.D.1 | Hydrogen Storage Engineering Center of Excellence | IV-114 |
| IV.D.6 | Advancement of Systems Designs and Key Engineering Technologies for Materials-Based Hydrogen Storage | IV-140 |
| V.E.1 | Polymer Electrolyte Fuel Cell Lifetime Limitations: The Role of Electrocatalyst Degradation | V-168 |
| V.E.4 | Improved Accelerated Stress Tests Based on Fuel Cell Vehicle Data | V-186 |

XVIII. Project Listings by Organization

United Technologies Research Center (Continued)

- V.F.2 Fuel Cell Fundamentals at Low and Subzero Temperatures V-211

Université Aix-Marseille

- IV.H.7 New Pathways and Metrics for Enhanced, Reversible Hydrogen Storage in Boron-Doped Carbon
Nanospaces. IV-233

Université du Québec à Trois-Rivières

- IV.D.1 Hydrogen Storage Engineering Center of Excellence IV-114

University Montpellier 2

- IV.H.7 New Pathways and Metrics for Enhanced, Reversible Hydrogen Storage in Boron-Doped Carbon
Nanospaces. IV-233

University of Akron

- V.K.1 Development of Kilowatt-Scale Coal Fuel Cell Technology V-295

University of California, Berkeley

- II.G.4 Maximizing Light Utilization Efficiency and Hydrogen Production in Microalgal Cultures II-118
V.A.10 A Total Cost of Ownership Model for Design and Manufacturing Optimization of Fuel Cells in
Stationary and Emerging Market Applications V-53
IX.3 Hydrogen Technology and Energy Curriculum (HyTEC). IX-13

University of California, Davis

- IV.H.17 Heavy Cycloadditions: Reactions of Diagailene with Cyclic Polyolefins. IV-267
V.J.5 Research and Development for Off-Road Fuel Cell Applications. V-289

University of California, Irvine

- V.A.8 Enlarging the Potential Market for Stationary Fuel Cells Through System Design Optimization V-47
VII.4 California Hydrogen Infrastructure Project VII-26

University of California, Los Angeles

- IV.C.2 A Joint Theory and Experimental Project in the Synthesis and Testing of Porous COFs for Onboard
Vehicular Hydrogen Storage IV-67
IV.H.13 Theory of Hydrogen Storage in Complex Hydrides IV-253

University of California, Riverside

- IV.H.6 Synthetic Design of New Metal-Organic Framework Materials for Hydrogen Storage IV-229
V.D.7 The Science and Engineering of Durable Ultralow PGM Catalysts V-121

University of California, San Diego

- II.E.1 Solar High-Temperature Water Splitting Cycle with Quantum Boost II-49

University of California, Santa Barbara

- IV.H.14 Computational studies of hydrogen interactions with storage materials. IV-256

University of Central Florida

- V.C.1 Lead Research and Development Activity for DOE's High Temperature, Low Relative Humidity
Membrane Program V-68
VII.6 Florida Hydrogen Initiative (FHI). VII-33

University of Colorado

- II.E.3 Solar Hydrogen Production with a Metal Oxide-Based Thermochemical Cycle II-60
 II.E.4 Solar-Thermal ALD Ferrite-Based Water Splitting Cycle. II-64

University of Colorado, Boulder

- V.D.9 Tungsten Oxide and Heteropoly Acid Based System for Ultra-High Activity and Stability of
 Pt Catalysts in PEM Fuel Cell Cathodes V-133

University of Connecticut

- V.B.2 The Effect of Airborne Contaminants on Fuel Cell Performance and Durability V-63
 V.K.4 Improving Reliability and Durability of Efficient and Clean Energy Systems. V-310

University of Delaware

- V.D.4 Extended, Continuous Pt Nanostructures in Thick, Dispersed Electrodes. V-107
 V.G.3 Advanced Materials and Concepts for Portable Power Fuel Cells V-250
 VI.2 Manufacturing of Low-Cost, Durable Membrane Electrode Assemblies Engineered for Rapid
 Conditioning. VI-11

University of Florida

- V.G.2 New MEA Materials for Improved Direct Methanol Fuel Cell (DMFC) Performance, Durability,
 and Cost V-246

University of Hawaii

- IV.A.2 Fundamental Studies of Advanced High-Capacity, Reversible Metal Hydrides IV-18
 IV.C.6 Weak Chemisorption Validation IV-89
 V.B.1 Effect of System Contaminants on PEMFC Performance and Durability V-57

University of Hawaii at Manoa

- II.F.5 Photoelectrochemical Hydrogen Production II-89

University of Illinois at Urbana-Champaign

- IV.A.4 Reversible Hydrogen Storage Materials - Structure, Chemistry, and Electronic Structure IV-27

University of Michigan

- IV.D.1 Hydrogen Storage Engineering Center of Excellence IV-114
 IV.D.8 Ford/BASF SE/UM Activities in Support of the Hydrogen Storage Engineering Center of Excellence. . . . IV-151
 III.3 Vessel Design and Fabrication Technology for Stationary High-Pressure Hydrogen Storage III-17

University of Minnesota

- II.A.2 Distributed Bio-Oil Reforming II-15

University of Missouri

- IV.C.3 Multiply Surface-Functionalized Nanoporous Carbon for Vehicular Hydrogen Storage. IV-72
 IV.H.7 New Pathways and Metrics for Enhanced, Reversible Hydrogen Storage in Boron-Doped Carbon
 Nanospaces. IV-233

University of Nevada, Las Vegas

- II.F.2 Semiconductor Materials for Photoelectrolysis. II-74
 II.F.4 Characterization of Materials for Photoelectrochemical (PEC) Hydrogen Production II-84
 IV.G.1 HGMS: Glasses and Nanocomposites for Hydrogen Storage IV-208

XVIII. Project Listings by Organization

University of New Mexico

| | | |
|--------|---|-------|
| IV.C.6 | Weak Chemisorption Validation | IV-89 |
| V.D.7 | The Science and Engineering of Durable Ultralow PGM Catalysts | V-121 |
| V.D.11 | Development of Novel Non-PGM Electrocatalysts for Proton Exchange Membrane Fuel Cell Applications | V-143 |
| V.E.2 | Durability Improvements through Degradation Mechanism Studies | V-175 |
| V.E.6 | Development of Micro-Structural Mitigation Strategies for PEM Fuel Cells: Morphological Simulations and Experimental Approaches | V-195 |

University of North Florida

| | | |
|-------|---|-------|
| V.G.2 | New MEA Materials for Improved Direct Methanol Fuel Cell (DMFC) Performance, Durability, and Cost | V-246 |
|-------|---|-------|

University of Oregon

| | | |
|--------|--|-------|
| IV.B.1 | Hydrogen Storage by Novel CBN Heterocycle Materials | IV-44 |
| IV.B.3 | Novel Carbon(C)-Boron(B)-Nitrogen(N)-Containing H ₂ Storage Materials | IV-51 |

University of Ottawa

| | | |
|---------|---|--------|
| IV.H.18 | Mechanistic Studies of Activated Hydrogen Release from Ammonia-Borane | IV-270 |
|---------|---|--------|

University of Pennsylvania

| | | |
|---------|---|--------|
| IV.H.1 | From Fundamental Understanding to Predicting New Nanomaterials for High-Capacity Hydrogen Storage | IV-210 |
| IV.H.18 | Mechanistic Studies of Activated Hydrogen Release from Ammonia-Borane | IV-270 |

University of Pittsburgh

| | | |
|-------|--|-------|
| V.D.5 | Nanosegregated Cathode Catalysts with Ultra-Low Platinum Loading | V-111 |
|-------|--|-------|

University of Rochester

| | | |
|-------|--|-------|
| V.F.7 | Investigation of Micro- and Macro-Scale Transport Processes for Improved Fuel Cell Performance | V-235 |
|-------|--|-------|

University of South Carolina

| | | |
|--------|---|-------|
| V.B.1 | Effect of System Contaminants on PEMFC Performance and Durability | V-57 |
| V.D.13 | Development of Ultra-Low Platinum Alloy Cathode Catalyst for PEM Fuel Cells | V-153 |
| V.F.6 | Transport in PEMFC Stacks | V-230 |

University of South Florida

| | | |
|-------|---|--------|
| VII.6 | Florida Hydrogen Initiative (FHI) | VII-33 |
|-------|---|--------|

University of Southern California

| | | |
|--------|--|-------|
| II.C.1 | Development of Hydrogen Selective Membranes/Modules as Reactors/Separators for Distributed Hydrogen Production | II-23 |
|--------|--|-------|

University of Southern Mississippi

| | | |
|-------|---|-------|
| V.K.2 | Alternative Fuel Cell Membranes for Energy Independence | V-300 |
|-------|---|-------|

University of Tennessee

| | | |
|--------|---|-------|
| V.D.4 | Extended, Continuous Pt Nanostructures in Thick, Dispersed Electrodes | V-107 |
| V.D.11 | Development of Novel Non-PGM Electrocatalysts for Proton Exchange Membrane Fuel Cell Applications | V-143 |
| V.F.7 | Investigation of Micro- and Macro-Scale Transport Processes for Improved Fuel Cell Performance | V-235 |

University of Tennessee (Continued)

- VI.2 Manufacturing of Low-Cost, Durable Membrane Electrode Assemblies Engineered for Rapid Conditioning. VI-11

University of Tennessee, Knoxville

- VI.2 Large Scale Testing, Demonstration and Commercialization of the Nanoparticle-Based Fuel Cell Coolant (SBIR Phase III) V-266
- XI.6 Sensitivity Analysis of H₂-Vehicles' Market Prospects, Costs and Benefits XI-31

University of Texas at Arlington

- II.F.7 Photoelectrochemical Materials: Theory and Modeling II-98

University of Texas at Austin

- V.D.4 Extended, Continuous Pt Nanostructures in Thick, Dispersed Electrodes. V-107
- V.E.1 Polymer Electrolyte Fuel Cell Lifetime Limitations: The Role of Electrocatalyst Degradation V-168

University of Texas, Dallas

- IV.H.2 Novel theoretical and experimental approaches for understanding and optimizing hydrogen-sorbent interactions in metal organic framework materials. IV-213
- IV.H.12 Atomistic Transport Mechanisms in Aluminum-Based Hydrides IV-249

University of Toledo

- II.F.6 Critical Research for Cost-Effective Photoelectrochemical Production of Hydrogen II-93

University of Victoria

- V.F.5 Water Transport in PEM Fuel Cells: Advanced Modeling, Material Selection, Testing, and Design Optimization. V-226

University of Wisconsin, Madison

- V.E.1 Polymer Electrolyte Fuel Cell Lifetime Limitations: The Role of Electrocatalyst Degradation V-168

University of Wyoming

- II.D.5 Low-Cost Large-Scale PEM Electrolysis for Renewable Energy Storage II-46

UTC Power

- V.B.2 The Effect of Airborne Contaminants on Fuel Cell Performance and Durability V-63
- V.D.2 Highly Dispersed Alloy Catalyst for Durability V-95
- V.E.4 Improved Accelerated Stress Tests Based on Fuel Cell Vehicle Data V-186
- V.J.6 150 kW PEM Stationary Power Plant Operating on Natural Gas V-291
- VI.2 Manufacturing of Low-Cost, Durable Membrane Electrode Assemblies Engineered for Rapid Conditioning. VI-11

Versa Power Systems

- V.J.3 Advanced Materials for Reversible Solid Oxide Fuel Cell (RSOFC), Dual-Mode Operation with Low Degradation V-281

Virginia Commonwealth University

- IV.H.3 Design and Synthesis of Chemically and Electronically Tunable Nanoporous Organic Polymers for Use in Hydrogen Storage Applications IV-216

XVIII. Project Listings by Organization

Virginia Polytechnic Institute and State University

| | | |
|--------|---|--------|
| II.D.1 | PEM Electrolyzer Incorporating an Advanced Low-Cost Membrane | II-31 |
| IV.F.1 | High Strength Carbon Fibers | IV-191 |
| V.F.6 | Transport in PEMFC Stacks | V-230 |
| V.G.3 | Advanced Materials and Concepts for Portable Power Fuel Cells | V-250 |

W.L. Gore & Associates, Inc.

| | | |
|------|--|-------|
| VI.1 | Materials and Modules for Low-Cost, High-Performance Fuel Cell Humidifiers | V-261 |
| VI.2 | Manufacturing of Low-Cost, Durable Membrane Electrode Assemblies Engineered for Rapid Conditioning | VI-11 |

Wake Forest University

| | | |
|--------|---|--------|
| IV.H.2 | Novel theoretical and experimental approaches for understanding and optimizing hydrogen-sorbent interactions in metal organic framework materials | IV-213 |
|--------|---|--------|

Washington University

| | | |
|---------|---|--------|
| IV.H.15 | In Situ NMR Studies of Hydrogen Storage Systems | IV-259 |
|---------|---|--------|

Weaver Construction

| | | |
|-------|--|--------|
| VII.7 | Sustainable Hydrogen Fueling Station, California State University, Los Angeles | VII-38 |
|-------|--|--------|

William C. Fort

| | | |
|---------|---------------------------------|---------|
| VIII.10 | Hydrogen Safety Panel | VIII-45 |
|---------|---------------------------------|---------|

Xunlight Corporation

| | | |
|--------|--|-------|
| II.F.6 | Critical Research for Cost-Effective Photoelectrochemical Production of Hydrogen | II-93 |
|--------|--|-------|

Yonsei University

| | | |
|--------|---|-------|
| V.D.13 | Development of Ultra-Low Platinum Alloy Cathode Catalyst for PEM Fuel Cells | V-153 |
|--------|---|-------|